MMM INTERMAG 2025

New Orleans
LOUISIANA

January
13-17
2025

2025 Joint MMM-Intermag Conference

ABSTRACT BOOK

Jointly sponsored by AIP Publishing LLC and the IEEE Magnetics Society

IEEE MAGNETICS

AIP Publishing

Session TU
TUTORIAL: SYMMETRY IN MAGNETISM

Cindi Dennis, Chair
National Institute of Standards and Technology, Gaithersburg, MD, United States

INVITED PAPERS

TU-01. New Prospects of Symmetry in Magnetotransport Studies.
H. Chen[1] *1. Colorado State University, Fort Collins, CO, United States*

Using symmetry to analyze response properties of materials dates back to the 19th century. However, in recent decades, along with the prosperity of spintronics and subsequent variants of other "-tronics," the interplay of symmetry, electronic structure, and magnetic structure has continued to reveal novel phenomena that go beyond the traditional areas of magnetism and transport. In this tutorial, I will present a few hands-on examples that together offer a glimpse into an emerging landscape of novel transport phenomena enabled by new materials whose discovery is guided by symmetry. These include spin and charge transport phenomena in noncollinear antiferromagnets, characterized by unconventional spin order; in altermagnets, featuring unconventional electronic structures; and finally, the transport of orbital moments and multipole moments, representing unconventional response properties beyond charge and spin.

TU-02. How to Synthesize Magnetic Materials in Various Forms of Powder and Bulk.
Y. Hirayama[1] *1. Innovative Functional Materials Research Institute, National Institute of Advanced Industrial Science and Technology (AIST), Nagoya, Japan*

Pending

TU-03. Frustration in Magnetism: Misery Loves Company.
N. Leo[1] *1. Loughborough University, Loughborough, United Kingdom*

Frustration arises in systems in which not all interactions can be satisfied simultaneously. It is a phenomena that is ubiquitous in nature, and is relevant to the physical properties of water ice, protein folding pathways, and a key ingredient to unusual spin states, such as spin ices with correlated disorder and multiferroics with strong magnetoelectric coupling effects. This tutorial talk aims to give an overview over the relevant ingredients, the role that lattice symmetry and local environments play, and the fascinating emergent phenomena occurring in frustrated magnetic phases.

Session AA
SPIN CALORITRONIC METROLOGY
Joseph Barker, Chair
University of Leeds, Leeds, United Kingdom

INVITED PAPERS

AA-01. Nernst effect in topologically and magnetically non-trivial materials. *H. Reichlova[1] 1. Institute of Physics, Czech Academy of Sciences, Praha, Czechia*

The Nernst effect refers to transversal thermoelectric conversion, representing an elegant way to harvest heat. Its application potential is actively discussed, primarily focusing on the search for materials with high Nernst responses [1]. The anomalous Nernst effect, where time-reversal symmetry is broken by an internal magnetic order, also receives significant attention due to numerous studies observing large anomalous Nernst responses in emerging materials with complex spin structures [2, 3]. In this talk, I will present the large Nernst response in a family of van der Waals tellurides with topologically non-trivial band structures and discuss the possible origins of the enhanced Nernst signal. In the second part of the talk, I will focus on materials with compensated magnetic ordering, demonstrating that the anomalous Nernst effect can be present in various non-collinear antiferromagnets [4, 5], enabling novel magnetic microscopy techniques. In the final part, I will introduce the presence of the anomalous Nernst effect in an emerging class of compensated magnets known as altermagnets [6]. Despite their collinear spin arrangement, altermagnets open up a whole new family of materials for the search of efficient spin caloritronic devices.

[1] Pan et al., Nature Communications 13, 3909 (2022) [2] Ikhlas et al., Nature Physics 13, 1085–1090 (2017) [3] Pan et al., Nature Materials 21, 203–209 (2022) [4] Reichlova et al., Nature Communications 10, 5459 (2019) [5] Beckert et al., Physical Review B 108, 024420 (2023) [6] Badura et al., arXiv:2403.12929 (2024)

AA-02. Lock-in Thermography and Thermoreflectance for Imaging and Revealing Thermal Responses in Spin Caloritonic Structures. *R. Iguchi[1] 1. National Institute for Materials Science, Tsukuba, Japan*

Spin caloritronics is a branch of spintronics that combines the transport of spin and charge with the transport of heat. The field began with the observation of the spin Seebeck effect [1], which converts applied thermal gradients into spin currents. Therefore, most of the early studies in spin caloritronics have been devoted to the study of the effects induced by thermal gradients. These studies established an understanding of how thermal energy and spin dynamics are affected. As a consequence, it is expected for spin currents to induce a thermal response as a reciprocal process, as in the thermoelectric effects of electrons. By experimental advances, the temperature changes due to spin currents have been observed. It is first demonstrated by using thermography, where a heat current associated with a spin current composed of unidirectional spin waves generates heating at an edge of the system [2]. Subsequently, micro-fabricated thermocouple sensors identified the spin-dependent and spin Peltier effects [3,4] in nanostructures. While these effects demonstrate the ability to thermally manage devices based on spintronic principles, the measurements are not easy either due to a low signal-to-noise ratio of thermography or the necessity of making complicated structures. Thus, more convenient methods have been anticipated for accelerating spin caloritronic research. In this regard, we focused on the combination of thermography measurements and the lock-in technique for revealing the intricate thermal responses of spin caloritronic structures. Thermography reads the temperature by the emitted infrared intensity from the surface of materials, thus realizing a contactless and non-invasive approach to measure temperature variations induced by spin currents. The obtained detailed thermal distributions are crucial for distinguishing between different thermal contributions and isolating the effects induced by spin currents [5]. It allows for precise and systematic thermal measurements, thus facilitating a better understanding of the underlying mechanisms. For instance, the use of this method reveals the distribution of temperature change in the spin Peltier effect [6] and enables the observation of temperature change purely due to the anisotropic magneto-Peltier effect [7]. Another choice is the thermoreflectance method, which measures the temperature change by the change in reflectivity of a material with temperature. While it is widely used for measuring thermal diffusivity and conductivity in nanoscale devices by combining with the pump-probe technique, we demonstrated that by combining it with lock-in to an AC current, spin caloritronic phenomena can also be measured at frequencies higher than those achievable by the lock-in thermography method. The high-speed measurement for the spin Peltier effect reveals the μm-scale propagation of the heat current induced by the spin current [8]. In this talk, the basic procedures of lock-in thermography and thermo-reflectance for spin caloritronic phenomena will be introduced, followed by introducing a series of experiments. By using lock-in thermography and thermo-reflectance, thermal phenomena associated with the spin degrees of freedom can be investigated in depth, providing the basis for understanding the underlying physics and finding new functionalities for thermal management. We hope that these techniques will be useful for future research and development.

[1] K. Uchida, S. Takahashi, K. Harii et al., Nature Vol. 455, p.778 (2008) [2] T. An, V.I. Vasyuchka, K. Uchida et al., Nature Materials Vol. 12, p.549 (2013) [3] J. Flipse, F.L. Bakker, A. Slachter et al., Nature Nanotech Vol. 7, p.166 (2012) [4] J. Flipse, F.K. Dejene, D. Wagenaar et al., Physical Review Letters Vol. 113, p.027601 (2014) [5] K. Uchida and R. Iguchi, Journal of Physics Society Japan Vol. 90, p.122001 (2021) [6] S. Daimon, R. Iguchi, T. Hioki et al., Nature Communications Vol. 7, p.13754 (2016) [7] K. Uchida, S. Daimon, R. Iguchi et al., Nature Vol. 558, p.95 (2018) [8] T. Yamazaki, R. Iguchi, T. Ohkubo et al., Physical Review B Vol. 101, p.020415(R) (2020)

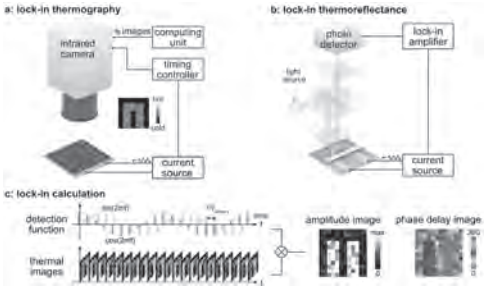

A and B: Typical setup for lock-in thermography (A) and lock-in thermoreflectance (B). C: analysis procedure for lock-in thermography

AA-03. Local Measurement of Thermal Spin Dynamics via NV Center Magnetometry. *N. Maksimovic*[1], R. Xue[1], P. Dolgirev[1], L. Xia[2], R. Kitagawa[3], A. Müller[4], F. Machado[5,1], D. Klein[2,6], D. MacNeill[2], K. Watanabe[7], T. Taniguchi[7], P. Jarillo-Herrero[2], M. Lukin[1], E. Demler[4] and A. Yacoby[1] *1. Harvard University, Cambridge, MA, United States; 2. MIT, Cambridge, MA, United States; 3. Tokyo Institute of Technology, Tokyo, Japan; 4. ETH Zurich, Zurich, Switzerland; 5. Harvard-Smithsonian Center for Astrophysics, Cambridge, MA, United States; 6. Weizmann Institute of Science, Rehovot, Israel; 7. National Institute for Materials Science, Tsukuba, Japan*

Central to spin caloritronic and spintronic technologies are the collective dynamics of thermal spin waves in magnets. New methods to quantitatively measure these dynamics, as well as novel regimes driven by strong spin wave interactions, are of particular interest. In this talk, I will discuss how nitrogen-vacancy (NV) centers in diamond can measure and image nanoscale spin dynamics in atomically-thin chromium trihalides. First, I'll demonstrate imaging of the critical slowing down of collective spin fluctuations across a magnetic freezing point. Second, I'll explain how noise magnetometry using NV centers can measure the diffusion constant of spin waves in the material. This technique allows us to experimentally distinguish between different spin transport regimes. In very spin isotropic materials like $CrCl_3$ monolayers, strong interactions between spin waves result in a hydrodynamic regime, where spin transport is governed by interactions between spin waves rather than with the atomic lattice. This hydrodynamic regime appears in our measurements as an enhancement of magnetic noise with decreasing temperature, an observation captured by our semi-classical microscopic model, which allows us to estimate the viscosity coefficient of the spin wave gas. Finally, NV sensing techniques can image not only equilibrium thermal fluctuations but also fluctuations generated by external spin pumping via RF drive fields. These advancements highlight the significant potential of NV centers in exploring and understanding spin dynamics, paving the way for future innovations in spin caloritronics and spintronics.

Xue, R., Maksimovic, N., et al. "Signatures of magnon hydrodynamics in an atomically-thin ferromagnet." arXiv preprint arXiv:2403.01057 (2024).

AA-04. Driving, transporting and sensing orbital currents at terahertz rates. *T. Seifert*[1] *1. Free University of Berlin, Berlin, Germany*

Terahertz emission spectroscopy (TES) is a powerful tool to reveal photocurrent dynamics with femtosecond time resolution [1]. An exciting application for TES arises in the emerging field of orbitronics that exploits the electron orbital momentum L for possible data-processing applications [2]. Compared to spin-polarized electrons, L may allow the transfer of magnetic information with considerably higher density over longer distances in more materials. However, direct experimental observation of L currents, their extended propagation lengths and their conversion into charge currents has remained challenging. Here, we optically trigger ultrafast angular-momentum transport in Ni|W|SiO2 thin-film stacks [3]. The resulting terahertz charge-current bursts exhibit a marked delay and width that grow linearly with the W thickness. We consistently ascribe these observations to a ballistic-like L current from Ni through W with a giant decay length (about 80 nm) and low velocity (about 0.1 nm per fs). At the W|SiO2 interface, the L flow is efficiently converted into a charge current by the inverse orbital Rashba–Edelstein effect, consistent with ab initio calculations. Our findings establish orbitronic materials with long-distance L transport as possible candidates for future efficient and ultrabroadband orbitronic terahertz emitters, and an approach to discriminate Hall-like and Rashba–Edelstein-like conversion processes.

[1] Leitenstorfer, Alfred, et al. "The 2023 terahertz science and technology roadmap." Journal of Physics D: Applied Physics 56, 223001 (2023). [2] Go, Dongwook, et al. "Orbitronics: Orbital currents in solids." Europhysics Letters 135, 37001 (2021). [3] Seifert, T.S., Go, D., Hayashi, H. et al. Time-domain observation of ballistic orbital-angular-momentum currents with giant relaxation length in tungsten. Nat. Nanotechnol. 18, 1132–1138 (2023).

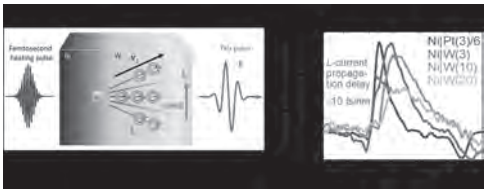

AA-05. Tunnel magneto-Seebeck effect and thermal conductivity of tunnel barriers. *T. Kuschel*[1] *1. Faculty of Physics, Bielefeld University, Bielefeld, Germany*

A magnetic tunnel junction (MTJ) that consists of an insulating tunnel barrier sandwiched by two magnetic electrodes is not only the main building block of magnetoresistive random-access memory (MRAM) devices, it is also the basis of potential spin caloritronic applications based on the tunnel magneto-Seebeck (TMS) effect. Here, a temperature gradient induces Seebeck voltages across the tunnel junction depending on the magnetization orientation of the two magnetic electrodes [1,2]. For example, the combination of TMS and the anomalous Nernst effect (ANE) in MTJs opens the possibility of detecting thermal gradients in three dimensions on the nano scale [3]. The thickness of the tunnel barrier and the choice of electrode material determines the TMS strength [4,5]. In addition, the thermal conductivity of the tunnel barrier also depends on the barrier's thickness and is a crucial quantity when Seebeck coefficients of MTJs have to be identified [3,6]. So far, estimates of thermal conductivity have been used such as values which are one order of magnitude below the thermal conductivity of bulk MgO or $MgAl_2O_4$ (MAO). However, only experimentally determined values for the thermal conductivity of tunnel barriers will result in reliable quantitative numbers for the TMS coefficients. Recently, several techniques have been utilized to determine the thermal conductivity of tunnel barriers. TMS measurements before and after the dielectric breakdown to get rid of parasitic AHE contributions have been conducted in combination with finite element modelling [7]. For example, here we extracted 0.7 W/(K m) for the thermal conductivity of ultra-thin MAO which is almost two orders of magnitude below the bulk value. In addition, ultrafast thermoreflectance and magneto-optic Kerr effect thermometry have been used to identify the thermal conductivity of ultrathin MgO and MAO [8]. The results of 0.4-0.6 W/(K m) now provide the basis for more accurate estimations of TMS coefficients. In my contribution, the TMS will be introduced and the determination of the thermal conductivity of ultrathin MgO and MAO will be presented. Finally, the impact of the barrier's thermal conductivity on the TMS is discussed.

[1] M. Walter et al., Nat. Mater. 10, 742 (2011); N. Liebing et al., Phys. Rev. Lett. 107, 177201 (2011). [2] T. Kuschel et al., J. Phys. D.: Appl. Phys. 52, 133001 (2018). [3] U. Martens, TK et al., Commun. Phys. 1, 65 (2018). [4] T. Huebner, TK et al., Phys. Rev. B 96, 214435 (2017). [5] A. Boehnke, TK et a., Nat. Commun. 8, 1626 (2017). [6] J. Zhang et al., Phys. Rev. Lett. 115, 037203 (2015). [7] T. Huebner, TK et al., J. Phys. D.: Appl. Phys. 51, 224006 (2018). [8] H. Jang, TK et al., Phys. Rev. Applied 13, 024007 (2020).

Session AB
ULTRAFAST SPIN-PHONON DYNAMICS

Oksana Chubykalo-Fesenko, Co-Chair
Instituto de Ciencia de Materiales de Madrid, CSIC, Madrid, Spain
Carl Simon Davies, Co-Chair
Radboud University, Nijmegen, Netherlands

INVITED PAPERS

AB-01. Ultrafast Phononic Switching of Magnetic Order. *A. Kirilyuk*[1]
1. FELIX Laboratory, Nijmegen, Netherlands

Excitations of the crystal lattice have a significant impact on the orbital dynamics of the electrons, and through it, also on spins. Recently, ultrafast optical techniques have provided new insights into the spin-lattice coupling including angular momentum transfer from magnetization to phonons [1,2]. It should therefore be possible to realize the opposite process, by driving the lattice and thus controlling the magnetization, on the same (femtosecond) time scale. We have recently demonstrated how the resonant excitation of circularly-polarized optical phonons in paramagnetic substrates can permanently reverse the magnetic state of the overlayer [3]. This was shown to be the result of a phono-magnetic effect, which is thus a low-frequency analogue of the inverse Faraday effect. With the handedness of the phonons steering the direction of switching, such effect offers a selective and potentially universal method for ultrafast non-local control over magnetic order. Moreover, a different and ultimately universal behaviour, characterized by displacive modification of crystal potentials, is driven by linearly-polarized excitation. The magnetic switching was shown to create very peculiar quadrupolar spatial patterns [4], confirming the mechanism. The mechanism appears to be very universal, and is shown to work in samples with very different crystallographic symmetry and magnetic properties, including weak ferromagnets and antiferromagnets, but also completely different systems such as ferroelectrics [5]. The dynamics of the domain formation was shown to proceed via a strongly inhomogeneous magnetic state resulting in a self-organization of magnon-polarons [6] and development of magneto-elastic solitons.

1. C. Dornes et al, Nature 565, 209 (2019). 2. S.R. Tauchert et al, Nature 602, 73 (2022). 3. C.S. Davies, F.G.N. Fennema, A. Tsukamoto, I. Razdolski, A.V. Kimel & A. Kirilyuk, Nature 628, 540 (2024). 4. A. Stupakiewicz, C.S. Davies, K. Szerenos, D. Afanasiev, K. S. Rabinovich, A. V. Boris, A.Caviglia,A.V.Kimel,A.Kirilyuk,Nat.Phys.17,489(2021).5.M.Kwaaitaal, D.G. Lourens, C.S. Davies & A. Kirilyuk, Nat. Photon. 18, 569 (2024). 6. M. Gidding, T. Janssen, C.S. Davies & A. Kirilyuk, Nat. Commun. 14, 2208 (2023).

AB-02. Polarized phonon-spin conversion in rare-earth and 2D materials. *H. Zhu*[1] *1. Rice University, Houston, TX, United States*

The electronic and magnetic properties of solids are fundamentally determined by the crystal structures. When the structure keeps evolving, the properties are usually determined by the instantaneous lattice configurations, but this may not always be true. Typical lattice vibration involves atoms oscillating back and forth around their equilibrium positions, and one would expect the perturbation on electronic properties to largely cancel out. But a qualitative change might be possible with coherent atomic circular motions, which break time-reversal symmetry and have been predicted to cause unexpected magnetic, topological, and transport phenomena. Notably, cirularly polarized phonons with quantized angular momentum are simply guaranteed by multi-fold rotational symmetry, and thus are rather common in materials. In this talk, I will first briefly explain the connection between circular polarization and the term "chiral" in phononic context. I will then give an example on chiral phonon-controlled spin polarization in rare earth halides, based on our recently developed time-resolved terahertz-optical spectroscopy, and evidence of cross-interface spin transfer. Finally, I will introduce quantum coherent spin-phonon coupling in 2D antiferromagnets, leading to magnon-phonon hybridization, nontrivial topology, and possible chiral edge states, showing phonons' impact on spin properties without any external fields. Together, these phenomena demonstrate a new paradigm of dynamic structural-property relationship in quantum materials, as well as possible routes towards low-loss bosonic transport.

1. Luo J, Lin T, Zhang J, Chen X, Blackert ER, Xu R, Yakobson BI, Zhu H "Large effective magnetic fields from chiral phonons in rare-earth halides." Science, 382(6671):698–702 (2023). https://doi.org/10.1126/science.adi9601 2. Luo J, Li S, Ye Z, Xu R, Yan H, Zhang J, Ye G, Chen L, Hu D, Teng X, Smith WA, Yakobson BI, Dai P, Nevidomskyy AH, He R, Zhu H "Evidence for Topological Magnon–Phonon Hybridization in a 2D Antiferromagnet down to the Monolayer Limit." Nano Letters, 23(5):2023–2030 (2023). https://doi.org/10.1021/acs.nanolett.3c00351

AB-03. Magnetophononics and the Chiral Phonon Misnomer. *R. Merlin*[1] *1. Physics, University of Michigan, Ann Arbor, MI, United States*

The direct, ultrafast excitation of polar phonons with electromagnetic radiation is a potent strategy for controlling the properties of a wide range of materials, particularly in the context of influencing their magnetic behavior. Here, we show that, contrary to common perception, the origin of phonon-induced magnetic activity does not stem from the magnetization due to the ion motion or the effect their motion exerts on the electron subsystem. Instead, through electron-phonon coupling, a coherent state of circularly polarized phonons generates significant non-Maxwellian fields that break time-reversal symmetry, effectively mimicking the effects of real magnetic fields. Remarkably, these effective fields can reach magnitudes up to 100 T, far exceeding the Maxwellian fields produced by the circular motion of ions. Since the light-induced non-reciprocal fields depend on the square of the phonon displacements, the chirality transferred by the photons to the ions does not play a role in magnetophononics.

AB-04. Magnon and Phonon Dynamics on Ultrafast Timescales. *U. Staub*[1] *1. Swiss Light Source, Paul Scherrer Institute, Villigen, Switzerland*

Manipulating the magnetization of antiferromagnets (AFs) is of great importance for spintronic applications. To do that with photons on ultrafast timescales, one either requires special materials or special concepts as the magnetic field is usually not a driving parameter in antiferromagnets. Here we address opportunities driving the spins on ultrafast timescales exciting magnons, phonons or orbitals. Discussed experiments are using ultrashort X-ray pulses created by an X-ray free-electron-laser (SwissFEL) that probe the sublattice magnetization, the orbitals and/or the crystal structure. In the

first example, I will show how one can resonantly drive an electromagnon and how to probe the phononic wave function of the electromagnon based on time resolved X-ray diffraction. This can be combined with the response of the spin system using time resolved resonant x-ray diffraction, which allows to disentangle phonoic and magnetic excitation in this composite mode. [1] The second example addresses the properties of direct driving of an orbital excitation using the magnetic field of the THz pulse. The response after the excitation results in quantum interference of the "two levels" seen through a time dependent antiferromagnetic signal with the frequency of two-level energy separation. [2] (See fig. 1) Last, chiral/circular phonons will be addressed and how the can be *seen by* circularly polarized x-rays, [3] how their time reversal symmetry breaking might couple to neutrons and how the atomic "circular" motion can be seen in real time.

[1] Hiroki Ueda, Roman Mankowsky, Eugenio Paris, Mathias Sander, Yunpei Deng, Biaolong, Liu, Ludmila Leroy, Abhishek Nag, Elizabeth Skoropata, Chennan Wang Victor Ukleev, Gérard Sylvester Perren, Janine Dössegger, Sabina Gurung, Cristian Svetina, Elsa Abreu, Matteo Savoini, Tsuyoshi Kimura, Luc Patthey, Elia Razzoli, Henrik Till Lemke, Steven Lee Johnson, and Urs Staub, Nature Commun. 14, 7778 (2023). [2] R. Mankowsky, M. Muller, M. Sander, S. Zerdane, X. Liu1, D. Babich, H. Ueda, Y. Deng, R. Winkler, B. Strudwick, M. Savoini, F. Giorgianni, S. L. Johnson, E. Pomjakushina, P. Beaud, T. Fennel, H.T. Lemke, and U. Staub, arXiv:2309.12751 (2023) [3] Hiroki Ueda, Mirian García-Fernández, Stefano Agrestini, Carl P. Romao, Jeroen van den Brink, Nicola A. Spaldin, Ke-Jin Zhou, and Urs Staub, Nature 618, 946 (2023).

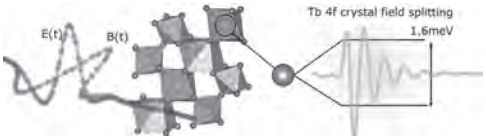

Fig.1. Sketch of THz driven orbital excitation and its quantum coherent magnetic response.

AB-05. Role of polarized phonons during ultrafast demagnetization.

U. Nowak[1] *1. Department of Physics, University of Konstanz, Konstanz, Germany*

Ultrafast demagnetization offers opportunities for rapid information processing or ultrafast spintronics. It is central to modern material research though a crucial question has remained elusive: If a material loses its magnetization within only femtoseconds, where is the missing angular momentum on such short time scales? We use molecular dynamics simulations to investigate the role of phonons during ultrafast demagnetization in nickel. For this purpose, we transfer angular momentum corresponding to the observed amount of demagnetization into the lattice and calculate the resulting changes in the diffraction pattern. Our results are in line with ultrafast electron diffraction measurements which show an almost instantaneous, long-lasting, non-equilibrium population of anisotropic high-frequency phonons that appear as quickly as the magnetic order is lost. Theory and experiment indicate a rotational lattice motion on atomic dimensions after the excitation with the laser pulse that takes up the missing angular momentum [1] before the onset of a macroscopic Einstein-de Haas rotation. In the second part of the talk we report on a new framework for spin-molecular dynamics that connects, on the one hand, to ab initio calculations of spin-lattice coupling parameters [2] and, on the other hand, to the magneto-elastic continuum theory. The derived Hamiltonian describes a closed system of spin and lattice degrees of freedom and explicitly conserves the total momentum, angular momentum and energy [3]. This framework allows us to use multi-scale modeling for investigating a broad range of spin-lattice dynamics phenomena from slow to ultrafast.

[1] S. R. Tauchert, M. Volkov, D. Ehberger, D. Kazenwadel, M. Evers, H. Lange, A. Donges, A. Book, W. Kreuzpaintner, U. Nowak, P. Baum: *Polarized phonons carry angular momentum in ultrafast demagnetization*, Nature 602, 73 (2022) [2] S. Mankovsky, S. Polesya, H. Lange, M. Weißenhofer, U. Nowak, and H. Ebert: *Angular Momentum Transfer via Relativistic Spin-Lattice Coupling from First Principles*, Phys. Rev. Lett. 129, 067202 (2022) [3] M. Weißenhofer, H. Lange, A. Kamra, S. Mankovsky, S. Polesya, H. Ebert, and U. Nowak: *Rotationally invariant formulation of spin-lattice coupling in multi-scale modeling*, Phys. Rev. B 108, L060404 (2023)

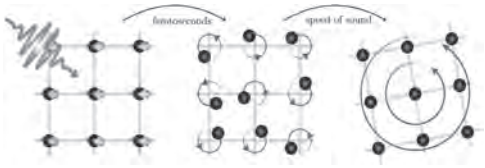

After the laser pulse has hit our magnetized sample, hot electrons and spins quickly couple to circularly polarized phonons that take up the angular momentum (middle panel). Only later, low-frequency shear waves mediate a macroscopic rotation of the sample (right panel).

Session AC
SPIN-ORBITRONICS I: ANGULAR MOMENTUM COMPENSATION, OUT-OF-PLAN TORQUES AND ENERGY EFFICIENT SWITCHING

Kai Litzius, Chair
University of Augsburg, Augsburg, Germany

INVITED PAPER

AC-01. Room temperature energy-efficient spin-orbit torque switching in two-dimensional van der Waals Fe_3GeTe_2 induced by topological insulators. *J. Zhang*[1], W. Xie[1] and T. Nie[1] *1. Beihang University, Beijing, China*

Spin-orbit torque (SOT)[1] writing methods compared to spin-transfer torque (STT) do not damage the tunnel barrier and can achieve faster operation speeds, better durability, and higher energy efficiency. Therefore, SOT-driven magnetization switching is expected to become the primary writing method for the next generation of MRAM[2-4]. Two-dimensional (2D) magnetic materials combine the advantages of high integration of 2D materials and low power consumption of spintronic materials, making them ideal for overcoming the "size scaling" and "power wall" bottlenecks to achieve high-performance SOT-MRAM. However, 2D materials struggle to maintain ferromagnetism at high temperatures. Research has shown that the Curie temperature of Fe_3GeTe_2 (FGT) can be raised to room temperature through interfacial effects[5], making it an ideal material for exploring SOT-driven magnetization switching. Although studies have used Pt as a spin current source to achieve SOT switching in FGT, the operating temperatures are below room temperature (<200K)[6,7]. All-van der Waals heterostructures can provide high spin transparency and improve SOT efficiency. Therefore, it is urgent to develop all-van der Waals (vdW) heterostructures that enable low-power SOT switching at room temperature to advance 2D spintronic devices. Firstly, we achieve spin-orbit torque-driven magnetization switching at room temperature[8]. We grow an all-van der Waals heterostructure of Bi_2Te_3/Fe_3GeTe_2 on a (0001) sapphire substrate by molecular beam epitaxy (MBE). The topological insulator Bi_2Te_3 not only elevated the Curie temperature of FGT through interfacial exchange coupling but also served as a spin current source, enabling FGT to switch at a low current density of approximately 2.2×10^6 A/cm^2. The measured SOT efficiency at room temperature was about 2.69. Our experiments demonstrated that the higher SOT efficiency mainly originates from the nontrivial topological characteristics of the heterostructure. Secondly, we quantitatively evaluated the SOT efficiency using harmonic Hall measurements and analyzed the differences between large-field power-law fitting and small-field derivation fitting. The results showed that the quality of the interface is crucial for achieving high spin transparency in constructing all-van der Waals heterostructures. Additionally, by adjusting the thickness of FGT, we optimized the thermal stability of the heterostructure, further confirming the key role of high-quality interfaces in achieving energy-efficient SOT switching. This lays a solid foundation for the future implementation of low-power, room-temperature all-van der Waals spintronic devices.

[1]Miron, I. M. *et al. Nature* 476 (2011) 189-193. [2]Manipatruni, S., Nikonov, D. E. & Young, I. A. *Nature Physics* 14 (2018) 338-343. [3] Ramaswamy, R., Lee, J. M. & Yang, H. *Applied Physics Reviews* 5 (2018) 031107. [4]Demidov, V. E., Urazhdin, S. & Demokritov, S. O. *Journal of Applied Physics* 127 (2020) 170901. [5]Wang, H. *et al. ACS Nano* 14 (2020) 10045-10053. [6]Alghamdi, M. *et al. Nano Letters* 19 (2019) 4400-4405. [7]Wang, X. *et al. Science Advances* 5 (2019) eaaw8904. [8]Wang, H., Wu, H., Zhang, J. *et al. Nature Communications* 14 (2023) 5173.

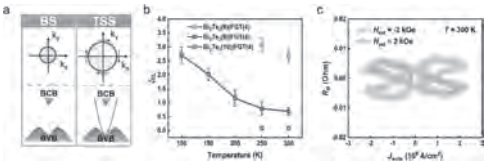

Figure.1 SOT efficiency characterization and current-induced room-temperature switching in Bi_2Te_3/Fe_3GeTe_2 heterostructures

CONTRIBUTED PAPERS

AC-02. Electrical mutual switching in Mn_3Sn/Mo/CoFeB heterostructure. *J. Yoon*[1], Y. Takeuchi[1,2], R. Takechi[1], J. Han[1], T. Uchimura[1], Y. Yamane[1], S. Kanai[1,4,5], J. Ieda[3], H. Ohno[1] and S. Fukami[1,6] *1. Tohoku University, Sendai, Japan; 2. National Institute for Materials Science, Tsukuba, Japan; 3. Japan Atomic Energy Agency, Tokai, Japan; 4. Japan Science and Technology Agency, Kawaguchi, Japan; 5. National Institute for Quantum Science and Technology, Takasaki, Japan; 6. Inamori Research Institute for Science, Kyoto, Japan*

The spin-orbit torque (SOT) provides a promising mechanism for electrically writing information in magnetic states [1-4]. Distinct from the existing schemes where the SOT is passively determined by the material and device structures, an active manipulation of the intrinsic SOT polarity, operated by electric current only, can open a new paradigm of programmable SOT devices. To achieve this goal, it is essential to electrically control the current-induced spin polarization of the spin source. In this work, we show a proof-of-concept of the programmable SOT device (Fig. 1) in a noncollinear-antiferromagnetic/nonmagnetic/ferromagnetic Mn_3Sn/Mo/CoFeB heterostructure, in which each magnetic layer works as both a reversible spin source and a target magnetic electrode, i.e., electrical mutual switching [5]. Figure 2 shows the R_H-I loops representing the electrical switching of CoFeB and Mn_3Sn. CoFeB undergoes current-induced switching due to the magnetic spin Hall torque (MSHT) arising from Mn_3Sn. The polarity depends on the magnetic orientation of Mn_3Sn, indicating the direct evidence of MSHT-induced switching [6] (Figs. 2(a), (b)). By properly tuning the driving current, the spin current from CoFeB further reverses the magnetic orientation of Mn_3Sn, which determines the polarity of the subsequent switching of CoFeB [7,8] (Figs. 2(c), (d)). This unprecedented scheme of mutual switching can be achieved in a spin-valve-like simple protocol because each magnetic layer serves as a reversible spin source and target magnetic electrode. It yields intriguing proof-of-concept functionalities for unconventional logic and neuromorphic computing. This work is partly supported by the JSPS Kakenhi, X-NICS, Iketani Science and Technology Foundation, and Casio Science and Technology Foundation.

[1] I. Miron et al., *Nature* Vol. 476, p.189 (2011). [2] L. Liu et al., *Science* Vol. 336, p.555 (2012). [3] S. Fukami et al., *Nat. Nanotechnol.* Vol. 11, p.621 (2016). [4] Q. Shao et al., *IEEE Trans. Magn.* Vol. 57, p.1 (2021). [5] J.-Y. Yoon et al., under review (2024). [6] M. Kimata et al., *Nature* Vol. 565, p.627 (2019). [7] A. Fert et al., *Rev. Mod. Phys.* Vol. 80, p.1517 (2008). [8] J.-Y. Yoon et al., *Nat. Mater.* Vol. 22, p.1106 (2023).

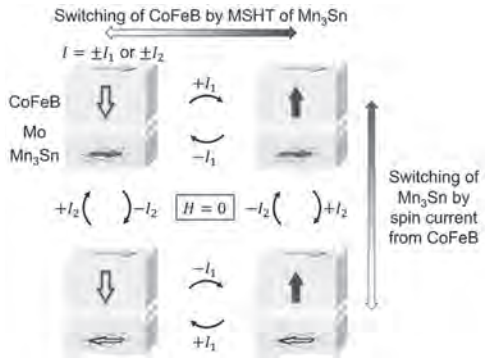

Fig. 1. Schematics of the electrical mutual switching between Mn_3Sn and CoFeB. $I_{1(2)}$ denotes the critical current to switch CoFeB (Mn_3Sn).

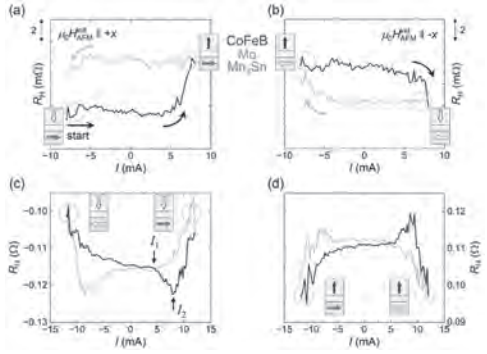

Fig. 2. R_H-I loops representing the electrical switching of (a,b (c,d)) CoFeB (Mn_3Sn) depending on the net magnetic orientation of Mn_3Sn (CoFeB). H_{AFM}^{init} denotes the magnetic field to initialize the magnetic orientation of Mn_3Sn.

AC-03. Alloying Rare Earth Nitrides for Angular Momentum Compensation. *E. Joshy*[1,2], J. Miller[1] and S. Granville[1,2] *1. Robinson Research Institute, Victoria University of Wellington, Wellington, New Zealand; 2. The MacDiarmid Institute for Advanced Materials and Nanotechnology, Wellington, New Zealand*

Rare earth nitrides (RENs), formed by the combination of lanthanides (or rare-earth ions) and nitrogen in a 1:1 ratio, exhibit a set of unique properties where their distinctive combinations enable them to function as ferromagnetic semiconductors, particularly suitable for spintronics applications [1]. The structural similarity of the RENs leads to the possibility of "solid solutions", which provides the flexibility to tune their magnetic properties and the interplay of both orbital angular momentum and spin angular momentum opens up possibilities for spintronics and spin-orbitronics applications. The solid solution $Gd_xSm_{1-x}N$ is a promising candidate because GdN is spin dominant with a saturation magnetisation of 7 μ_B/ion and SmN is orbital dominant with a very small magnetic moment of 0.035 μ_B/ion. The ferromagnetic exchange interaction aligns the spins of Gd^{3+} and Sm^{3+} ions, resulting in the opposition of total angular momentum for each ion in the solid solution [2]. This leads to magnetisation compensation and angular momentum compensation in the solid solution. A series of $Gd_xSm_{1-x}N$ thin films has been grown in an ultra-high vacuum environment, and their structural properties have been studied using X-ray diffraction (XRD). The composition of Gd and Sm in the solid solution was determined by using X-Ray Fluorescence (XRF) and magnetometry has been used to study the magnetic properties of the films. The magnetic saturation and coercive field can be tuned continuously between the GdN and SmN end-member values, shown in Figure 1. The magneto-transport measurements of solid solutions show the negative sign for anomalous Hall effect (AHE) resistivity, similar to GdN, which indicates the conduction electrons have spin moment that aligns parallel to the applied field, while the magnitude of AHE resistivity is similar to the SmN, for Sm rich solid solution [3].

[1] F. Natali, B. J. Ruck and N.O.V.Plank. *Prog Mater Sci*, vol. 58, no. 8, pp. 1316–1360(2013). [2] J. D. Miller, J.F.McNulty and B.J. Ruck, *Phys Rev B*, vol. 106, no. 17,p.174432 (2022). [3] J. D. Miller, H. J. Trodahl, M and Al Khalfioui, *Appl Phys Lett*, vol. 122, no. 9,p.092402 (2023)

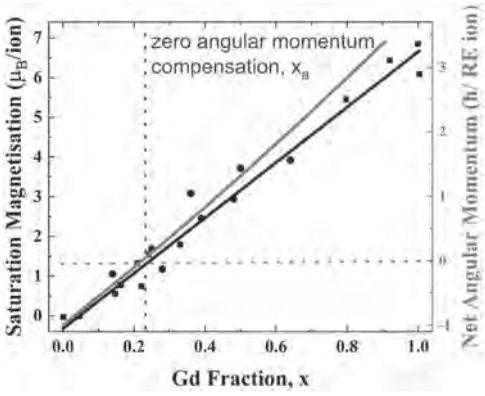

Fig.1: The change of 5 K saturation magnetisation (left axis) and net angular momentum (right axis) of $Gd_xSm_{1-x}N$ as function of Gd fraction, x, obtained from XRF. The zero angular momentum compensation is expected at nearly x_c=0.24.

AC-04. Optimization of orbital torques in ferrimagnets and relationship with Gilbert damping. S. Ding[1], W. Legrand[1], H. Wang[1], M. Kang[1], P. Noël[1] and *P. Gambardella*[1] *1. Department of Materials, Zurich, Switzerland*

The orbital magnetic moment of metals is usually quenched by electron delocalization and crystal field effects. However, the application of an electric field can induce a non-equilibrium movement of orbital angular momentum in conductive materials, particularly those with varying orbital characteristics across momentum space [1,2]. This phenomenon can lead to the generation of orbital current through an electric current in nonmagnetic layers, which can then diffuse into neighboring magnetic layers and interact with local magnetization [3]. In the first part of the presentation. I will talk about the efficiency of converting orbital momentum to spin momentum in ferrimagnetic materials, specifically in the RE-TM ferrimagnet Gd_yCo_{100-y} [4]. Our work underscores the underlying mechanisms that facilitate orbital-to-spin conversion within a magnetic layer at the atomic level. In the following part, I will present the study on the Gilbert damping parameter within the orbital torque system [5]. We found out that CoFe/CuO_x bilayers exhibit a favorable combination of effective orbital torque and minimal increase in Gilbert damping, suggesting promising prospects for implementing orbital torque oscillators with reduced damping compared to spin torque oscillators.

1. B. A. Bernevig, T. L. Hughes, and S. C. Zhang, Orbitronics: The Intrinsic Orbital Current in p-Doped Silicon, *Phys. Rev. Lett*. 95, 66601 (2005). 2. D. Go, D. Jo, K.-W. Kim, S. Lee, M.-G. Kang, B.-G. Park, S. Blügel, H.-W. Lee, and Y. Mokrousov, Long-Range Orbital Torque by Momentum-Space Hotspots, *Phys. Rev. Lett*. 130, 246701 (2023). 3. D. Lee et al., Orbital Torque in Magnetic Bilayers, *Nat. Commun*. 12, 6710 (2021). 4. S. Ding, M.-G. Kang, W. Legrand, and P. Gambardella, Orbital Torque in Rare-Earth Transition-Metal Ferrimagnets, *Phys. Rev. Lett.* 132, 236702 (2024). 5. S. Ding, H. Wang, W. Legrand, P. Noël, and P. Gambardella, Mitigation of Gilbert damping in CoFe/CuO_x orbital torque system, under review.

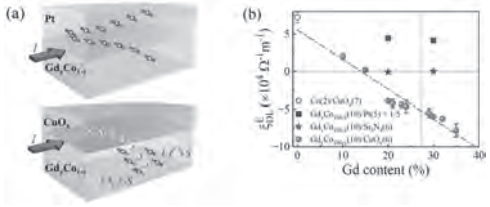

Figure 1. (a) Comparison of spin torque and orbital torque. The nonequilibrium orbital moment (*L*, circular arrows) diffuses into a Gd_yCo_{100-y} layer, where it is converted into a spin moment (*S*, straight arrows). The opposite spin-orbit coupling on the Co and Gd sites results in competing orbital-to-spin conversion. (b) Orbital torque efficiency vs Gd content.

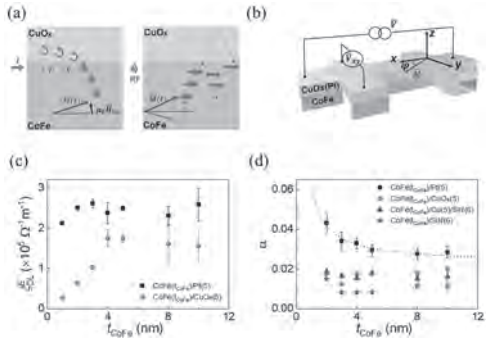

Figure 2 (a) Left: The nonequilibrium orbital moment (*L*) diffuses into the CoFe layer, where it is converted into a spin moment (*S*). Right: The precession of the magnetization in CoFe excites a spin and an orbital current that diffuse into CuO_x. (b) Schematic of the Hall bar (c) Damping-like spin-orbit efficiency in CoFe/Pt and CoFe/CuO_x as a function of the thickness of CoFe. (d) Thickness dependence of the Gilbert damping of CoFe with different nonmagnetic layers.

AC-05. Collinear spin current induced by artificial modulation of interfacial symmetry. *Z. Li*[1] and Z. Zhang[1] *1. Nanjing University, Nanjing, China*

Current induced spin-orbit torque (SOT) manipulation of magnetization is pivotal in spintronic devices. However, its application for perpendicular magnetic anisotropy magnets, crucial for high-density storage and memory devices, remains nondeterministic and inefficient. Here, we demonstrate a highly efficient approach to generate collinear spin currents by artificial modulation of interfacial symmetry, achieving 100% current-induced field-free SOT switching in CoFeB multilayers with perpendicular magnetization on stepped Al_2O_3 substrates. This field-free switching is primarily driven by the out-of-plane anti-damping SOT generated by the planar spin Hall effect (PSHE), resulting from reduced interface symmetry due to orientation-determined steps. Microscopic theoretical analysis confirms the presence and significance of PSHE in this process. Notably, our method for generating out-of-plane spin polarization along the collinear direction of the spin-current with artificial modulation of interfacial symmetry, overcomes inherent material symmetry constraints. Our findings provide a promising avenue for universal control of spin orbit torque, addressing challenges associated with low crystal symmetry and highlighting its great potential to advance the development of energy-efficient spintronic devices technology.

[1] Liu, L. *et al. Science* 2012, *336*, 555-558. [2] Yu, G. *et al. Nat. Nanotechnol.* 2014, *9*, 548-554. [3] Manchon, A., Koo, H. C., Nitta, J., Frolov, S. M. & Duine, R. A. *Nat. Mater.* 2015, *14*, 871-882. [4] Kim, J. *et al. Nat. Mater.* 2013, *12*, 240-245. [5] Meier, L. *et al. Nat. Phys.* 2007, *3*, 650-654. [6] Miron, I. M. *et al. Nature* 2011, *476*, 189-193. [7] Pai, C.-F., Mann, M., Tan, A. J. & Beach, G. S. D. *Phys. Rev. B* 2016, *93*, 144409. [8] van den Brink, A. *et al. Nat. Commun.* 2016, *7*, 10854. [9] Lau, Y. C., Betto, D., Rode, K., Coey, J. M. & Stamenov, P. *Nat. Nanotechnol.* 2016, *11*, 758. [10] Cui, B. *et al. ACS Appl. Mater. Interfaces* 2019, *11*, 39369-39375. [11] Cai, K. *et al. Nat. Mater.* 2017, *16*, 712. [12] Wang, M. *et al. Nat. Electron.* 2018, *1*, 582-588. [13] You, L. *et al. Proc. Natl. Acad. Sci. USA* 2015, *112*, 10310-10315. [14] Liu, L. *et al. Nat. Nanotechnol.* 2019, *14*, 939-944. [15] Ma, Q. *et al. Phys. Rev. Lett.* 2018, *120*, 117703. [16] Slonczewski, J. C. *J. Magn. Magn. Mater.* 1996, *159*, L1-L7. [17] Sun, J. Z. *Phys. Rev. B* 2000, *62*, 570. [18] Davidson, A., Amin, V. P., Aljuaid, W. S., Haney, P. M. & Fan, X. *Phys. Lett. A* 2020, *384*, 126228. [19] Ryu, J. *et al. Nat. Electron.* 2022, *5*, 217-223. [20] Yang, M. *et al. Nat. Commun.* 2024, *15*. [21] MacNeill, D. *et al. Nat. Phys.* 2016, *13*, 300-305. [22] Liu, Y. *et al. Phys. Rev. Appl.* 2019, *12*, 064046. [23] Chen, X. *et al. Nat. Mater.* 2021, *20*, 800-804. [24] Liu, L. *et al. Nat. Nanotechnol.* 2021, *16*, 277-282. [25] Baek, S. C. *et al. Nat. Mater.* 2018, *17*, 509-513. [26] Serlin., M. *et al. Science* 2020, *367*, 900-903. [27] He, W.-Y., Goldhaber-Gordon, D. & Law, K. T. *Nat. Commun.* 2020, *11*, 1650. [28] Li, T. *et al. Nat. Nanotechnol.* 2021, *16*, 1201-1207. [29] Liu, L., Lee, O. J., Gudmundsen, T. J., Ralph, D. C. & Buhrman, R. A. *Phys. Rev. Lett.* 2012, *109*, 096602. [30] Kong, W. J. *et al. Nat. Commun.* 2019, *10*, 233. [31] Li, Z. *et al. Appl. Phys. Lett.* 2023, *123*, 042404. [32] Murray, N. *et al. Phys. Rev. B* 2019, *100*, 104441. [33] An, S., Kim, J.-A., Lee, S., Lee, K.-S. & You, C.-Y. *Appl. Phys. Lett.* 2023, *123*, 062403. [34] Tao, Y. *et al. Appl. Phys. Lett.* 2022, *120*, 102405. [35] Zhang, J. *et al. ACS Appl. Mater. Interfaces* 2023, *15*, 49902. [36] Wu, H. *et al. Phys. Rev. B* 2019, *99*, 184403. [37] You, C.-Y., Lee, S., Park, S. & Falco, C. M. *Phys. Rev. B* 2004, *69*, 134402. [38] Okamoto, S., Nishiyama, K., Kitakami, O. & Shimada, Y. *J. Appl. Phys.* 2001, *90*, 4085. [39] Humphries, A. M. *et al. Nat. Commun.* 2017, *8*, 911. [40] Nan, T. *et al. Nat. Commun.* 2020, *11*, 4671. [41] Hu, S. *et al. Nat. Commun.* 2022, *13*, 4447 [42] Wang, M. *et al. Nat. Commun.* 2023, *14*, 2871. [43] Garello, K. *et al. Nat. Nanotechnol.* 2013, *8*, 587. [44] Hayashi, M., Kim, J., Yamanouchi, M. & Ohno, H. *Phys. Rev. B* 2014, *89*, 144425. [45] Kim, J. *et al. Nat. Mater.* 2013, *12*, 240. [46] Avci, C. O. *et al. Phys. Rev. B* 2014, *89*, 214419. [47] Cao, J. *et al. Sci. Rep.* 2018, *8*, 1355. [48] Pan, H., Liu, Z., Hou, D., Gao, Y. & Niu, Q. *Phys. Rev. Res.* 2024, *6*, L012034. [49] Song, P. *et al. Nat. Mater.* 2020, *19*, 292-298.

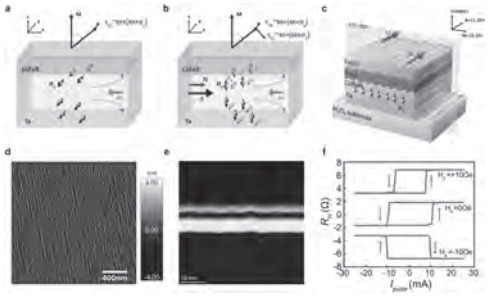

Fig. 1 SOT Switching of perpendicular magnetization by the z-polarized collinear spin current generated by step-shaped symmetry breaking.

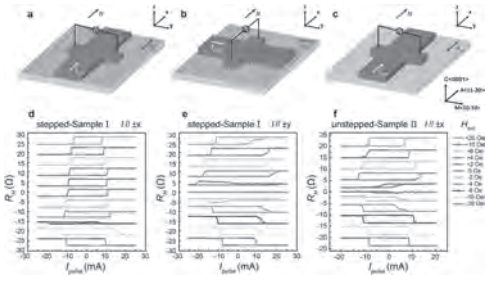

Fig. 2 Step-dependent (Symmetry-dependent) current-driven SOT switching measurement.

AC-06. Magnetization dynamics in beyond room temperature van der Waals magnet. *H. Bangar*[1], L. Pandey[1], B. Zhao[1] and S.P. Dash[1]
1. Department of Microelectronic and Nanotechnology, Chalmers University of Technology, Göteborg, Sweden

Van der Waals (vdW) magnetic materials represent an exciting new frontier in research due to their unique magnetic properties and potential applications in spintronics and quantum technologies [1]. These vdW magnets are made of two-dimensional (2D) layers of atoms bonded together by weak vdW forces, unlike the strong covalent bonds in conventional magnets. These materials possess layer-dependent magnetic interactions, providing novel ways to tune their properties [2,3,4,5]. Recent reports have shown beyond room-temperature ferromagnetism with tunable properties via alloying and doping Fe_5GeTe_2 with Ni or Co [6,7], with a record-high Curie temperature $T_c \sim 450$K in $(Ni_{0.4}Fe_{0.6})_5GeTe_2$ (NFGT) [8]. Although static magnetic properties of such magnets have been reported, spin-orbit torque (SOT) devices have not been investigated so far. Here, we report a large damping-like SOT in such high T_c vdW ferromagnet NFGT crystal using second harmonic Hall resistance measurements at room temperature. The interactions between the current-induced spin polarization in Pt and the intrinsic properties of the vdW magnet NFGT have the potential to produce strong SOT. The examination of second harmonic Hall resistance measurements (shown in Fig. 1) and angle-dependent data (Fig. 2) disclosed substantial damping-like and field-like torques due to the induced magnetization dynamics in NFGT/Pt heterostructures. The observation of linear enhancement in the strength of effective damping-like and field-like fields with the applied current clearly verifies the current induced SOT in NFGT/Pt system. Our results suggest that the large damping-like and field-like SOT in vdW magnets present opportunities for designing highly efficient magnetic memory and logic devices.

[1] S. Yang, et al., *Adv. Sci.* 8, 2002488 (2021). [2] B. Huang, et al., *Nature* 546, 270 (2017). [3] R. Ngaloy, et al. *ACS Nano* 18, 5240 (2024). [4] B. Zhao, et al. *Adv. Mater.* 35, 2209113 (2023). [5] B. Zhao, et al. arXiv preprint arXiv:2308.13408 (2023). [6] X. Chen, et al., *Phys. Rev. Lett.* 128, 217203 (2022). [7] M. Wang, et al., *Nano Lett.* 24, 4141 (2024). [8] B. Wang, et al., *Appl. Phys. Lett.* 123, 071902 (2023).

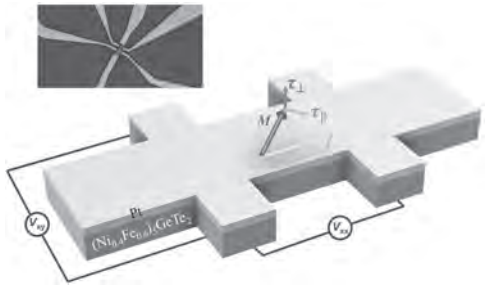

Fig. 1: Spin-orbit torque in $(Ni_{0.4}Fe_{0.6})_5GeTe_2$ (NFGT)/Pt heterostructure at room temperature. Schematic of the second harmonic Hall measurements configuration to evaluate spin-orbit torque in NFGT/Pt heterostructures and an optical image of the actual device.

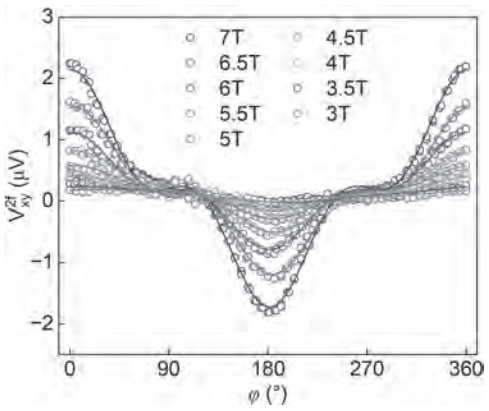

Fig. 2: Angle-resolved second harmonic Hall voltage at different magnetic fields (circles) and its corresponding fit (solid line).

AC-07. Temperature dependence of spin-orbit torque in $L1_2$-ordered Mn_3Pt. *C. Zhang*[1], Z. Tang[1], L. Yu[1], M. Al-Mahdawi[2] and M. Oogane[1,2]
*1. Department of Applied Physics, Tohoku University, Sendai, Japan;
2. Center for Science and Innovation in Spintronics, Tohoku University, Sendai, Japan*

Non-collinear antiferromagnets (AFMs) with topological spin structures has garnered significant interest recently[1-3]. The magnetic spin Hall effect in these materials allows for spin polarization manipulation by tuning the spin structure. Mn_3Pt is a well-known non-collinear AFM, in which current-induced *x*, *y*, *z* spin polarizations and the corresponding spin-orbit torques (defined here as *x*-, *y*-, *z*- SOTs) have been reported[4,5]. Understanding the underlying physics of these SOTs is essential, and one effective approach is to analyze their temperature dependence. However, there is still little experimental work focused on this issue. Here, we investigate SOT in $L1_2$-ordered Mn_3Pt under modified temperature T_{meas} and discuss the mechanism behind them. Mn_3Pt/Py stacks were deposited on MgO (001) substrates at a substrate temperature of 350 °C and subsequently annealed at 575 °C. Their structural properties were analyzed using X-ray diffraction. Peaks corresponding to (001) and (002) planes of $L1_2$-ordered Mn_3Pt were clearly observed. The ordering parameter, calculated from the ratio between the areas of these two peaks, was ~0.9, indicating that the long-range ordering has been obtained. We then investigated the SOT using harmonic Hall measurements. The ratio between the damping components of unconventional *x*-SOT and conventional *y*-SOT ($\tau_{x,DL}/\tau_{y,DL}$) at 300 K was 0.23±0.04, which is comparable to that measured using spin-torque ferromagnetic resonance measurements in our previous work[5]. In the range T_{meas} = 200-400K, $\tau_{x,DL}/\tau_{y,DL}$ rapidly decreased from 0.89±0.08 to 0.13±0.02, mainly due to the decrease of $\tau_{x,DL}$. This indicates that *x*-SOT originates from the magnetic spin Hall effect and is strongly influenced by the temperature dependence of spin structure in $L1_2$-ordered Mn_3Pt. The insights into the interplay between temperature and spin polarization in this study are expected to deepen the understanding of the magnetic spin Hall effect in non-collinear AFMs and contribute to the optimization of antiferromagnetic systems for future applications. This work was partially supported by the X-nics project, and CSIS, and CIES at Tohoku University, JSPS KAKENHI 24K17316, and research grants of Hirose Foundation.

[1] V. Baltz *et al.*, Rev. Mod. Phys. 90, 015005 (2018). [2] M. B. Jungfleisch, Phys. Lett. A 382, 865 (2018). [3] L. Šmejkal *et al.*, Nat. Phys. 14, 242 (2018). [4] H. Bai *et al.*, Phys. Rev. B 104, 104401 (2021). [5] L. Yu *et al.*, Appl. Phys. Express 15, 033002 (2022).

AC-08. Giant Spin Hall Effect with Multi-Directional Spin Components in Ni_4W. *Y. Yang*[1], S. Lee[1], Y. Chen[1], J. Qi[1], D. Sousa[1], M. Odlyzko[1], J. Garcia-Barriocanal[1], G. Yu[1], G. Haugstad[1], Y. Fan[1], Y. Huang[1], D. Lyu[1], Z. Cresswell[1], T. Low[1] and J. Wang[1] *1. University of Minnesota, Minneapolis, MN, United States*

Spin-orbit torque (SOT) is a promising approach to magnetization manipulation in spintronics devices. However, due to symmetry constraints, only in-plane spins are allowed for conventional SOT materials such as heavy metals and topological materials. Recently, unconventional spin currents with out-of-plane polarization have been demonstrated in SOT materials with low symmetries [1-5], enabling field-free deterministic switching of perpendicular magnetization. Despite this progress, the SOT efficiency of these materials has typically remained low, limiting their competitiveness in practical applications. Here, we report a giant SOT efficiency of 0.73 in sputtered Ni_4W/CoFeB heterostructure at room temperature, as evaluated by second harmonic Hall measurements [6]. In addition, due to the low crystal symmetry of Ni_4W, unconventional out-of-plane and Dresselhaus-like spin components were observed. Macro-spin simulations suggest that the multi-directional spins of Ni_4W collectively improve the magnetization switching efficiency by about an order of magnitude compared to other unconventional SOT materials, thus broadening the path towards energy-efficient spintronic devices using low-symmetry materials.

[1] D. MacNeill *et al.*, *Nature Physics,* vol. 13, pp. 300-305 (2017). [2] T. Nan *et al.*, *Nature Communications,* vol. 11, p. 4671 (2020). [3] L. Liu *et al.*, *Nature Nanotechnology,* vol. 16, pp. 277-282 (2021). [4] A. Bose *et al.*, *Nature Electronics,* vol. 5, pp. 267-274 (2022). [5] M. Dc *et al.*, *Nature Materials,* vol. 22, pp. 591-598, (2023). [6] J.-P. Wang *et al.*, US Patent, US20240172565A1 (2024).

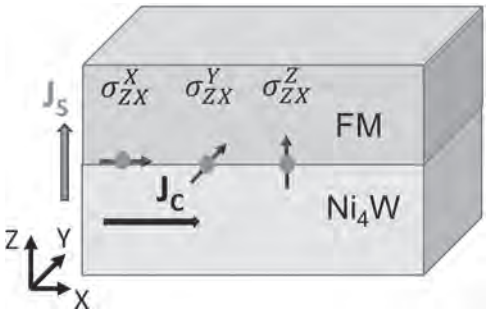

Fig. 1. Schematic of Ni_4W/CoFeB heterostructure. Spin current with spin polarizations along X, Y, Z directions are generated in Ni_4W and is injected to CoFeB layer.

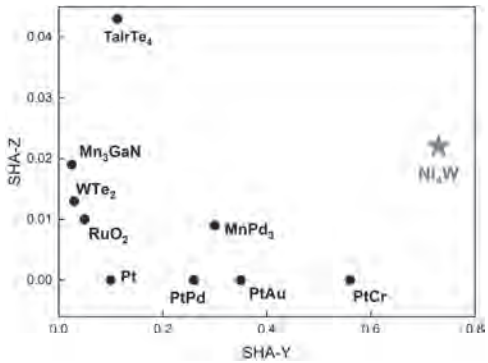

Fig. 2. Summary of conventional (SHA-Y) and out-of-plane (SHA-Z) spin Hall angle of conventional and unconventional SOT materials.

AC-09. Withdrawn

AC-10. Distinct Temperature Dependency of Charge to Spin Conversion from Rashba-Edelstein Effect. *J. Yoon*[1], J. Lee[2], M. Kim[1,3], S. Lee[1], K. Kim[4], Y. Choi[2], S. Park[2], D. Kim[3] and S. Choe[1] *1. Department of Physics and Astronomy, Seoul National University, Seoul, The Republic of Korea; 2. Division of Scientific Instrumentation and Management, Korea Basic Science Institute, Daejeon, The Republic of Korea; 3. Center for Spintronics, Korea Institute of Science and Technology, Seoul, The Republic of Korea; 4. Department of Physics, Yonsei University, Seoul, The Republic of Korea*

Spin-orbit torques (SOTs) possess the capability to manipulate magnets via charge-to-spin conversions[1]. The theoretical studies underpinning this phenomenon are rooted in both the spin Hall effect[2] (SHE) and the interfacial Rashba-Edelstein effect[3] (REE). However, the intricate nature of the conversion process introduces challenges, giving rise to persistent questions that hinder a comprehensive understanding of the origin of charge-to-spin conversion in the context of SOT, particularly in relation to SHE and REE. Here, we present evidence that SOT is directed by interface contributions of the REE. This is substantiated by the observation of two distinct temperature dependencies of field-like (FL) and damping-like (DL) SOTs, along with the identification of unidirectional magnetoresistance[4,5] in atomically thin quasi-two-dimensional ferromagnets. The results reveal a correlation

that seamlessly aligns with the underlying theoretical REE model[6]. These findings not only underscore the significance of the REE in fundamental physics but also shed light on the intricate impact of interfacial effects on magnetic materials.

1. Shao, Q. et al. IEEE Trans. Magn. 57, 800439 (2021). 2. Sinova, J. et al. Phys. Rev. Lett. 92, 126603 (2004). 3. Edelstein, V. M. Solid State Commun. 73, 233–235 (1990). 4. Avci, C. O., Mendil, J., Beach, G. S. D. & Gambardella, P. Origins of the Unidirectional Spin Hall Magnetoresistance in Metallic Bilayers. Phys. Rev. Lett. 121, 087207 (2018). 5. Vaz, D. C. et al. Phys. Rev. Mater. 4, 1–7 (2020). 6. Kurebayashi, H. et al. Nat. Nanotechnol. 9, 211–217 (2014).

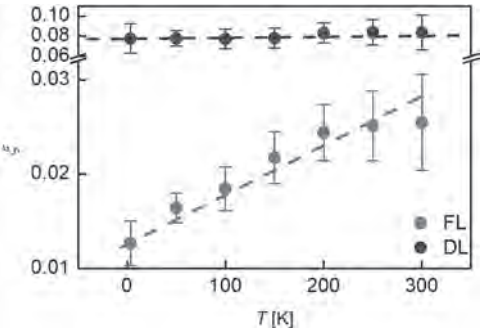

Temperature dependence of FL (red dot) and DL (blue dot) SOT efficiencies ξ. The dashed lines are guide for trends.

AC-11. Orbital-to-Spin Ratio of Dynamic Magnetization in Co/Pt.
O.A. Bakare[1], G.T. Street[1], R.E. Maizel[1], C. Klewe[2] and S. Emori[1]
1. Physics, Virginia Tech, Blacksburg, VA, United States; 2. Lawrence Berkeley National Laboratory, Berkeley, CA, United States

Recent theoretical work suggests that ferromagnets can pump orbital angular momentum ("orbital pumping") through resonant magnetization dynamics, which includes spin and orbital components [1,2]. Yet, it remains a challenge to disentangle the dynamics of orbital and spin moments quantitatively. In this study, we employ X-ray magnetic circular dichroism (XMCD) to quantify the orbital-to-spin moment ratio (μ_L/μ_S) of dynamic magnetization in Co/Pt, a widely used bilayer known for strong spin-orbit coupling [3]. Through our unique "dynamic XMCD" technique [4], we investigate whether non-equilibrium orbital dissipates differently from non-equilibrium spin. For instance, if orbital dissipates more quickly than spin, we might expect to see a smaller μ_L/μ_S for dynamic magnetization in Co (Fig. 1(b)) compared to static magnetization (Fig. 1(a)). Figure 1(c) shows the dynamic X-ray transmission response of the FMR-driven Co magnetization precession at different photon energies. Following the protocol in Ref. [4], the measured oscillation amplitude vs energy provides the dynamic XMCD spectrum (Fig. 2). Applying sum rule analysis to the integral of the dynamic XMCD gives $(\mu_L/\mu_S)_{dynamic} = 0.087 \pm 0.003$. This value is about 15% smaller than $(\mu_L/\mu_S)_{static} = 0.102 \pm 0.003$ from the static XMCD, acquired with the same sample holder and X-ray beam configuration as the dynamic XMCD. The error bars for $(\mu_L/\mu_S)_{dynamic}$ and $(\mu_L/\mu_S)_{static}$ capture the uncertainty associated with the processing of the background signal. The smaller $(\mu_L/\mu_S)_{dynamic}$ compared to $(\mu_L/\mu_S)_{static}$ suggests slightly faster orbital dissipation than spin dissipation in Co/Pt. Our present work contributes to the efforts to understand the fundamentals of non-equilibrium orbital angular momentum which is crucial for the development of advanced "orbitronic" devices.

[1] D. Go, K. Ando and A. Pezo, *arXiv preprint arXiv:2309*.14817 (2023). [2] H. Hayashi, D. Go and S. Haku, *Nature Electronics*, p.1-7 (2024). [3] J. Ryu, C.O. Avci and S. Karube, *Appl. Phys. Lett. Vol.* 114, 142402 (2019). [4] S. Emori, R. E. Maizel and G. T. Street, *Appl. Phys. Lett. Vol.* 124, 122404 (2024).

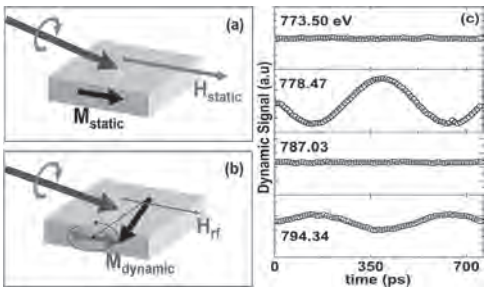

Fig.1: XMCD measurements with (a) static magnetization, M_{static} along the direction of the field (b) dynamic magnetization, $M_{dynamic}$ perpendicular to the field direction. (c) Dynamic transmission signal as a function of time at different photon energies.

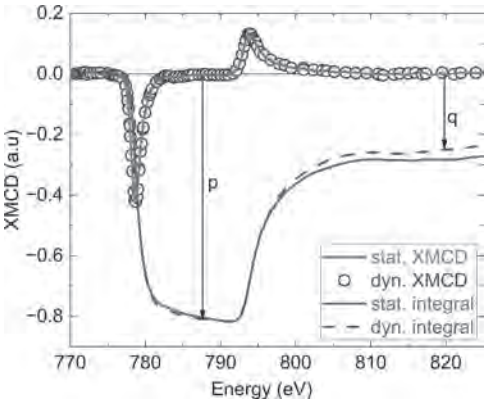

Fig.2: Static and dynamic XMCD at Co $L_{3,2}$ edges. The orbital-to-spin moment ratio was computed from the integral with $(\mu_L/\mu_s) = 2q / 3(3p - 2q)$.

AC-12. Out-of-Plane Spin Torque via Symmetry Engineering in an Oxide Polar Metal.
S. Zhou[1], J. Schimpf[2], H. Taghinejad[2], P. Meisenheimer[2], J. Analytis[2], S. Cheema[4], L. Martin[3] and L.M. Caretta[1] *1. Brown University, Providence, RI, United States; 2. UC Berkeley, Berkeley, CA, United States; 3. Rice University, Houstin, TX, United States; 4. Massachusetts Institute of Technology, Cambridge, MA, United States*

The field of spintronics is predicated on the ability to generate spin torques that can manipulate and switch the magnetization of magnetic nanobits for future applications in memory and logic, such as magnetic random access memory. Current-induced spin torques generated by materials with large spin-orbit coupling (SOC) are a promising approach. However, a significant challenge is generating spin torques (vector quantities) from charge currents (scalar quantities) with the correct orientation to deterministically switch perpendicularly oriented magnetic layers by 180 degrees. The orientation of the generated spin torque is set by the symmetry of the torque-producing material. Unfortunately, the high rotational and reflectional symmetry of conventional centrosymmetric spin torque metals, such as Pt, Ta, W, and topological insulators (e.g., Bi_2Se_3, Bi_2Te_3), lack the ability to efficiently switch the magnetization of perpendicularly magnetized nanomagnets without the additional assistance of an inefficient and unscalable magnetic field or another extrinsic source of symmetry breaking. Here, using $Pb_2Ir_2O_7$ (PIO) as a model system, we show that lattice mismatch strain and epitaxial growth of an oxide polar metal can be used to control the spin torque orientation via intrinsic symmetry engineering. Specifically, we demonstrate large out-of-plane spin torque efficiencies, and in orthorhombically distorted PIO. We hypothesize that the unconventional spin torques arise when the PIO asymmetry is engineered such that Dresselhaus and Rashba band structures are balanced. Our work provides a pathway to symmetry design of spin torques via epitaxy in complex oxides, as well as a pathway towards nonlinear or nonreciprocal spin current generation.

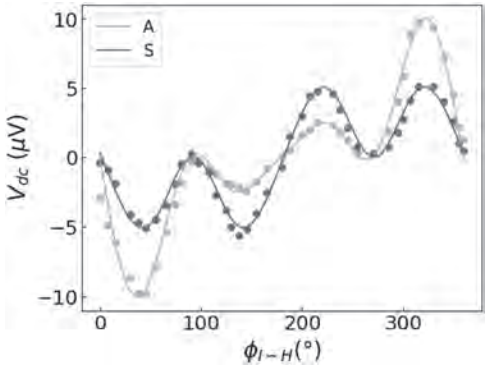

Fig.1 Angular dependent ST-FMR of PIO/Co/TiO_x thin film deposited on YSZ(110) showing a significant out-of-plane spin torque

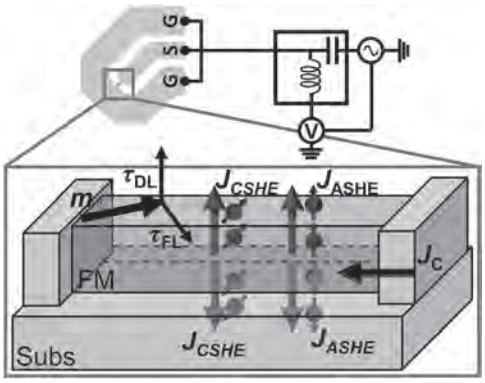

Fig.1 Schematics of ST-FMR measurement.

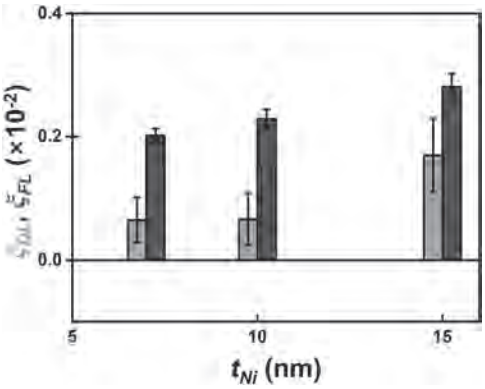

Fig.2 Damping-like and field-like torque efficiency in a Ni single layer.

AC-13. Conventional and Unconventional Spin-Orbit Torques in a Single Ferromagnetic Layer. *K. Han*[1,2], D. Yun[2], S. Jang[2,3], J. Ahn[1,2], Y. Nah[2,4], Y. Kim[2,4], M. Kang[2,5], S. Hong[2], O. Lee[2] and H. Koo[1,2]
1. KU-KIST Graduate School of Converging Science and Technology, Korea University, Seoul, The Republic of Korea; 2. Center for Semiconductor Technology, Korea Institute of Science and Technology, Seoul, The Republic of Korea; 3. Materials Science and Engineering, Seoul National University, Seoul, The Republic of Korea; 4. Electrical Engineering, Korea University, Seoul, The Republic of Korea; 5. Materials Science and Engineering, Korea University, Seoul, The Republic of Korea

The Spin Hall effect (SHE)[1], which occurs in non-magnetic heavy metals (HMs) with strong spin-orbit coupling (SOC), is the primary mechanism generating spin-orbit torque (SOT). In contrast, it had been considered that the SHE typically does not manifest in ferromagnetic materials (FMs). This is due to the exchange interaction between electron spins and the magnetization of material, which is much stronger than the SOC in FMs. This strong interaction suppresses the effect of SOC by inducing a spin-dephasing process among misaligned spins, aligning them with the direction of the magnetization. Recently, however, there has been substantial interest in the generation of transverse spin currents, similar to the SHE, within FMs[2-5]. These can be divided into conventional and unconventional spin Hall currents. Conventional spin Hall currents resemble the SHE in HMs, in which charge current, spin current, and spin polarization are mutually orthogonal. It could arise from the superposition of electric-field-induced eigenstates, which are resistant to spin dephasing. Unconventional spin Hall currents arise due to symmetry breaking induced by magnetization. According to the Curie symmetry principle[3], this reduced symmetry permits various spin polarization directions that are typically forbidden in symmetric materials. The physical mechanism remains under debate, but potential explanation involves spin precession around the magnetization. To detect these SOTs in FM, we employed angle-dependent Spin-Torque Ferromagnetic Resonance (ST-FMR) measurement on single Co, Ni, Py, CoFeB, and FeB layer with various interfacial layers. In this method, the transverse spin current can only be transferred to the substrate (or spin sink), resulting in spin accumulation on the other surface of the FM film. This accumulation creates both conventional and unconventional SOTs on the FM layer itself. The measurement data clearly show that SOT changes depend on the FM materials, the thickness of the FM layer, and interface materials, indicating that the generation of both conventional and unconventional SHE from the FM itself.

[1] J. Sinova, S. O. Valenzuela, J. Wunderlich, C. H. Back, and T. Jungwirth, Rev. Mod. Phys., vol. 87, no. 4, pp. 1213–1260, (2015) [2] V. P. Amin, J. Li, M. D. Stiles, and P. M. Haney, Phys. Rev. B, vol. 99, no. 22, p. 220405, (2019) [3] A. Davidson, V. P. Amin, W. S. Aljuaid, P. M. Haney, and X. Fan, Physics Letters A, vol. 384, no. 11, p. 126228, (2020) [4] K.-W. Kim, B.-G. Park, and K.-J. Lee, npj Spintronics, vol. 2, no. 1, p. 8, Apr. 2024, [5] F. Zheng et al., Phys. Rev. B, vol. 109, no. 22, p. 224401, (2024)

Session AD
MAGNETIZATION DYNAMICS AND MICROMAGNETICS I

Stavros Komineas, Co-Chair
University of Crete, Heraklion, Greece
Giovanni Finocchio, Co-Chair
University of Messina, Messina, Italy

INVITED PAPER

AD-01. Non-Hermitian dynamics on the Bloch sphere. *S. Komineas*[1,2] *1. Mathematics and Applied Mathematics, University of Crete, Heraklion, Greece; 2. Applied and Computational Mathematics, Foundation for Research and Technology, Heraklion, Greece*

A system of spins under spin-polarized currents is described using a complex functional, or a non-Hermitian (NH) Hamiltonian. A single spin under a magnetic field already presents non-trivial dynamics including periodic motion [1]. We will focus on the dynamics of two exchange-coupled spins m1, m2 on the Bloch sphere [2]. For uniaxial anisotropy, there are four fixed points for the dynamics. In the case of currents leading to Parity-Time (PT) symmetry, the nonlinear system is bistable for small currents and it exhibits stable oscillating motion. This is akin to synchronized spin-torque oscillators. Simple precessional (periodic) motion can be observed while a perturbation of this gives an additional frequency of oscillation as shown in the figure. An exceptional point that survives also in the nonlinear system is identified analytically. For the full nonlinear system, two conserved quantities are derived that furnish a geometric description of the spin trajectories in phase space, indicate stability of the oscillating motion, and make contact with the conservative (Hamiltonian) system. The progress in analytical results promise to support further work on the dynamics of NH systems that are defined on the Bloch sphere not only in magnetics but also in effective spin systems arising, e.g., in polariton Bose-Einstein condensates.

[1] A. Galda, V.M. Vinokur, Phys. Rev. B 94, 020408(R) (2016); A. Galda, V.M. Vinokur, Sci. Rep. 9, 17484 (2019). [2] S. Komineas, Phys. Rev. B 107, 094435 (2023).

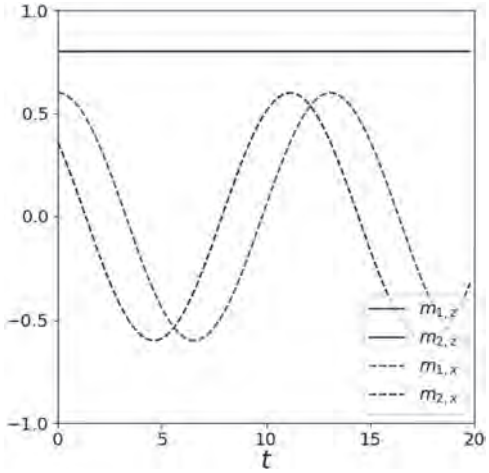

Fig. 1: Precessional oscillation of the two spins in the PT symmetric system.

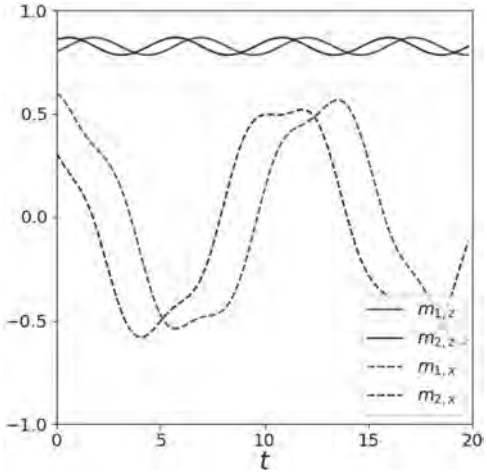

Fig. 2: A perturbation of the periodic motion leads to oscillation of the z components of the spins.

CONTRIBUTED PAPERS

AD-02. Deep Learning-Based Feature Engineering for Prediction of Magnetic properties of materials. *A. Kashyap*[1] and P. Joshi[1] *1. School of Physical Sciences, IIT Mandi, Mandi, India*

Magnetic properties arise from complex quantum mechanical interactions, including the spin and orbital contributions of electrons which are often difficult to model accurately and magnetic exchange interactions which are highly sensitive to the crystal structure and local atomic environments. Here in this study, we use a graph neural network-based approach which exploits the crystal information; Crystal Graph Convolutional Neural Networks (CGCNN) [1], to predict the magnetic properties of transition metal compounds. Numerous efforts have been done to deploy and improve CGCNN to predict the material properties like magnetic properties of organic and inorganic materials [2], elastic and mechanical properties of metals and alloys [3], charge density distribution [4] and so on. At the core of CGCNN is representation of the periodic crystal structures of materials as graphs where nodes correspond to atoms and edges to bonds. Node features can include atomic properties while edge features can include bond characteristics. Graph convolutional layers aggregates information from neighboring nodes and edges to update node features. Fully connected layers output the predicted material properties. But CGCNN also have its usual limitations including the accuracy dependence on feature representation. In this study, we report strategies for building a model by focusing on node features and data entropy. We have chosen datasets from the Materials Project [5] segmented based on magnetic ordering. Our approach involves extensive experimentation with different node feature combinations to identify the optimal set of atomic properties that best capture the magnetization characteristics of the materials. By comparing models that included magnetic moments derived from Density Functional Theory (DFT) calculations with

those using theoretical atomic magnetic moments from unpaired electrons, we report a methodology that reduces dependency on computationally intensive DFT calculations. Our results demonstrate the significance of detailed feature engineering in improving the accuracy of machine learning models for predicting material properties.

T. Xie and J. C. Grossman, Crystal Graph Convolutional Neural Networks for an Accurate and Interpretable Prediction of Material Properties, Phys. Rev. Lett. 120, 145301 (2018). Chi Chen, Weike Ye, Yunxing Zuo, Chen Zheng, and Shyue Ping Ong, Graph Networks as a Universal Machine Learning Framework for Molecules and Crystals, Chemistry of Materials 31 (9), 3564 (2019). Cheol Woo Park, Chris Wolverton Developing an improved Crystal Graph Convolutional Neural Network framework for accelerated materials discovery, Phys. Rev. Materials 4, 063801 (2020). Predicting charge density distribution of materials using a local-environment-based graph convolutional network Sheng Gong, 1 Tian Xie, 1 Taishan Zhu, 1 Shuo Wang, 2 Eric R. Fadel, 1 Yawei Li, 3 and Jeffrey C. Grossman1, Phy Rev B 100, 184103 (2019). A. Jain et al., "The Materials Project: A materials genome approach to accelerating materials innovation," APL Mater, 1, 11002, (2013).

AD-03. Shape Optimization of Tunneling Magnetoresistance Sensor Design via Automated Micromagnetic Simulations. *C. Fillies*[1], C. Wager[1], T. Schrefl[1], S. Tibus[2], S.J. Holt[3], A. Petrocchi[3], S.A. Pathak[3], M. Lang[3] and H. Fangohr[3] *1. Department für Integrierte Sensorsysteme, Universität für Weiterbildung Krems, Wiener Neustadt, Austria; 2. Robert Bosch GmbH, Reutlingen, Germany; 3. Structure and Dynamics of Matter, Max Planck Institute, Hamburg, Germany*

Tunneling magnetoresistance (TMR) sensors form the foundation of many electronic devices we rely on daily. TMR sensors operate on the principle that when two ferromagnets are magnetized in parallel, the tunneling probability of an electron is higher compared to when their magnetizations are antiparallel. The objective of this work is to identify a sensor shape and size that enable a large linear response in the hysteresis loop. The focus of this analysis is a sweep of the hard axis of the magnetic free layer of the sensor. [1] An automated optimization toolchain has been developed to test and propose new sensor shapes. This toolchain is based on four elementary steps: 1) Meshing the continuous sensor into a discrete mesh object. 2) Performing micromagnetic simulations on the mesh object via energy minimization. [2] 3) Post-processing to determine the linearity of the hysteresis loop. 4) Utilizing a Bayesian optimizer to suggest new shapes that likely have a highly linear hysteresis loop. [3] To facilitate parallelization and allow the simulation of different sensor shapes on multiple nodes simultaneously, all data is stored in a global database. This toolchain is implemented in Python, following the principles of object-oriented programming, to enable integration into a magnetic multiscale modeling suite (MaMMoS, Horizon Europe ID: 101135546). One of the main achievements was the automation of the entire process without the need for human interaction, while maintaining transparency and comprehensibility. Fig. 1 and Fig. 2 represent the same dataset where the lengths and widths of the free layer are optimized. Fig. 1 provides the improvement of the linear distanc of the hysteresis loop over the iterations of optimization. A plateau is reached after 20 iterations, indicating fast convergence. Fig. 2 shows the relationship between the design parameters and the linear range of the hysteresis loop. The results are promising as they indicate a convex relationship between the linear distance and the shape parameters.

[1] D. Suess, A. Bachleitner-Hofmann, A. Satz, Nature Electronics, Vol. 1, p.362-370 (2018). [2] L. Exl, J. Fischbacher, A. Kovacs, H. Oezelt, Computer Phys. Commun., Vol. 235, p.179-186 (2019). [3] F. Nogueira, "Bayesian Optimization: Open source constrained global optimization tool for Python", https://github.com/bayesian-optimization/BayesianOptimization (2014).

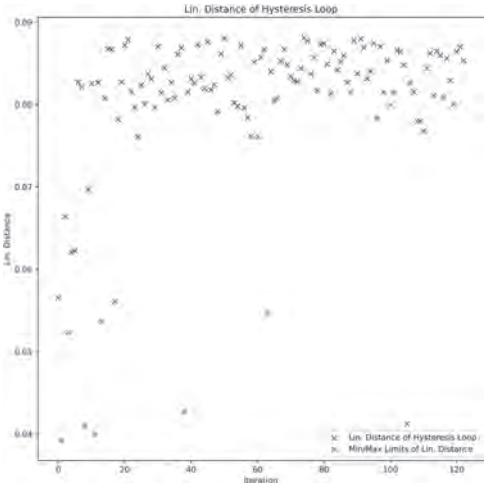

Fig. 1 shows the linear distances of the hysteresis loop over the iterations of optimization.

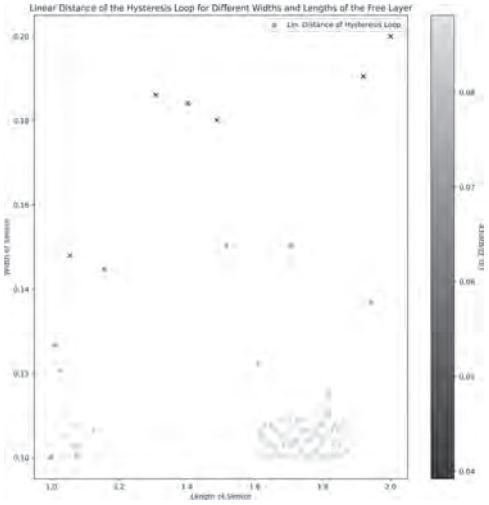

Fig. 2 shows the linear distance of the hysteresis loop for different lengths and widths of the free layer.

AD-04. Semi-classical derivation of a micromagnetic model for antiferromagnets and regularization of ill-posedness. *M. Hu*[1], E. Iacocca[2], M.J. Donahue[3] and M.A. Hoefer[1] *1. Applied Mathematics, University of Colorado Boulder, Boulder, CO, United States; 2. Department of Physics and Energy Science, University of Colorado Colorado Springs, Colorado Springs, CO, United States; 3. Applied and Computational Mathematics Division, National Institute of Standards and Technology, Gaithersburg, MD, United States*

A semi-classical derivation of a micromagnetic, continuum model for two-sublattice antiferromagnets (AFMs) is developed from a discrete spin lattice. To obtain the effective exchange field, all nearest-neighbor and next-nearest-neighbor exchange coupling with respect to the center spin in a magnetic unit cell are summed up to be the exchange Hamiltonian. Then the standard ferromagnetic (FM) micromagnetic exchange derivation [1] follows. Three exchange field terms are obtained in the long-wavelength regime: a spatially inhomogeneous FM exchange term, a spatially homogeneous AFM exchange term, and a spatially inhomogeneous AFM exchange term. By bridging the discrete, semi-classical atomic regime and the micromagnetic continuum regime, explicit relations between atomic exchange coupling and micromagnetic exchange stiffness constants are identified. Using spin wave stability analysis of the AFM ground states, unphysical short-wave instabilities are identified when the inhomogeneous AFM

exchange stiffness constant is larger than the inhomogeneous FM exchange stiffness constant, which is essentially the regime where the AFM exchange length scale is larger than the FM exchange length scale [2]. One implication of the short-wave instabilities is a restriction on the spatial discretization size in micromagnetic simulations. Furthermore, while a number of papers have been simulating the micromagnetic equations in the large FM exchange length regime [2-6], it is important to point out that the high-frequency instabilities suggest the ill-posedness of the initial-value problem of the model. To achieve well-posedness, as dictated by the physics, we propose two types of exchange regularization: 1) an additional higher-order exchange term, 2) modification of the inhomogeneous exchange terms with non-local operators. Both approaches effectively eliminate short-wave instabilities in the large AFM exchange length regime while preserving the second-order accuracy of the spin wave spectrum. We demonstrate the well-posedness of the regularized model by simulating domain walls where well-posedness is required for such magnetic textures with a narrow profile.

[1] Krawczyk, M., Sokolovskyy, M.L., Klos, J.W. and Mamica, S. On the formulation of the exchange field in the Landau-Lifshitz equation for spin-wave calculation in magnonic crystals. *Advances in Condensed Matter Physics*, 1, 764783 (2012). [2] Ntallis, N. and Efthimiadis, K. G., Micromagnetic simulation of an antiferromagnetic particle. *Computational Materials Science*, 97, 42–47 (2015). [3] Sánchez-Tejerina, L., Puliafito, V., Amiri, P. K. *et al.* Dynamics of domain-wall motion driven by spin-orbit torque in antiferromagnets. *Phys. Rev. B*, 101, 014433 (2020). [4] Shi, J., Lopez-Dominguez, V., Garesci, F. *et al.* Electrical manipulation of the magnetic order in antiferromagnetic PtMn pillars. *Nat Electron* 3, 92–98 (2020). [5] Zheng, Z., Zhang, Y., Lopez-Dominguez, V. *et al.* Field-free spin-orbit torque-induced switching of perpendicular magnetization in a ferrimagnetic layer with a vertical composition gradient. *Nat Commun* 12, 4555 (2021). [6] Schmitt, C., Sanchez-Tejerina, L., Filianina, M. *et al.* Identifying the domain-wall spin structure in antiferromagnetic NiO/Pt. *Phys. Rev. B*, 107, 184417 (2023).

AD-05. Withdrawn

AD-06. Periodic dispersion diagrams via finite element micromagnetics.

F. Ai[1], Z. Lin[1] and V. Lomakin[1] *1. University of California, San Diego, La Jolla, CA, United States*

Periodic dispersion diagrams (PDD) are important for understanding spin waves in magnetic materials and devices. Currently existing methods for calculating PDD have limitations in terms of the periodicity assumptions, accuracy, and applicability. For example, the plane-wave method assumes a homogeneity in the magnetization along non-periodic directions, a simplification that reduces problem dimensions but fails for many practical structures. Here, we propose a systematic solution to address all possible scenarios. We use an adaptation of a robust method to calculate the magnetostatic field under general periodicity settings [1]. We combine this approach with a fast eigenvalue solver that solves the eigen-states and eigen-frequencies [2] in the finite element method (FEM) based framework. We implement these methods as a module in the FEM-based FastMag micromagnetic simulator [3]. The presented framework allows computing PDD in general complex 3D problems with 1D, 2D, and 3D periodicities. The approach allows the magnetization to be non-uniform in any direction, allows for a high non-uniformities of the geometry and material composition, can handle problems where periodic and non-periodic directions are mixed, can handle periodic unit cells with large aspect ratios and irregularities, and can be extended to handle complex-valued dispersion diagrams in frequency and wavenumber. Figure 1 shows PDD of spin waves supported by a 2D periodic array of magnetic bubbles in an infinite large film (Fig. 1a). We find periodic bands of localized (flat curve 1) and propagating (curves 2 and 3) spin waves.

[1] F. Ai and V. Lomakin, Fast Fourier Transform periodic interpolation method for superposition sums in a periodic unit cell, Computer Physics Communications, https://doi.org/10.1016/j.cpc.2024.109291 [2] Lin, Z., Volvach, I., Wang, X., & Lomakin, V. (2022). Eigenvalue-Based Micromagnetic Analysis of Switching in Spin-Torque-Driven Structures. Phys. Rev. Appl., 17, 034016. [3] R. Chang, S. Li, M. V. Lubarda, B. Livshitz, V. Lomakin; FastMag: Fast micromagnetic simulator for complex magnetic structures (invited). J. Appl. Phys. 1 April 2011; 109 (7): 07D358. https://doi.org/10.1063/1.3563081

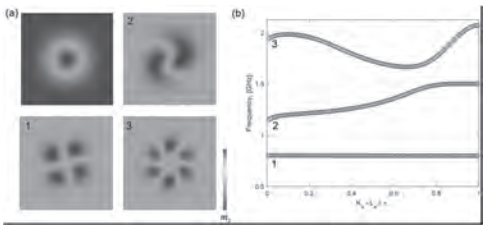

Figure 1. PDD for a 2D array of magnetic bubbles in a film. (a) The equilibrium state and 3 eigenstates of the lowest energy level. The first eigenstate is localized, where frequency is independent on the wave vector, the other two modes are propagating. (b) PDD of the 3 modes.

AD-07. Discretization Anisotropy In Micromagnetics. *S.J. Holt*[1,2], M. Lang[1,2], S.A. Pathak[1,2], A. Petrocchi[1,2] and H. Fangohr[1,2,3] *1. Max Planck Institute for the Structure and Dynamics of Matter, Hamburg, Germany; 2. Center for Free-Electron Laser Science, Hamburg, Dominican Republic; 3. University of Southampton, Southampton, United Kingdom*

The anisotropy in solutions of differential equations caused by discretization of these equations onto a regular lattice is a known phenomenon [1, 2, 3]. Despite this, the consequences of discretization anisotropy and how to mitigate against it are rarely discussed in the context of micromagnetics [4]. Micromagnetics models the physics of magnetic systems using a continuum approximation to express quantities such as the energy density and the effective field. These approximations take the form of differential equations, which need to be discretized onto a mesh to find a numerical solution. The impact of discretization anisotropy is extensive and includes phenomena such as the energy-minimizing rotation of magnetic structures, preferred directions, and creating artificial magnetization structures. Consequently, in many micromagnetic simulations involving exchange and DMI, magnetic structures can be observed propagating along preferred directions even when the systems are isotropic. More generally, discretization can lead to the formation of nonphysical magnetic structures, often reflecting the underlying symmetries of the discretization. A thorough understanding of these effects is important for the accurate interpretation of simulation results and for enhancing the overall fidelity of micromagnetic modeling. In this presentation we focus on these errors introduced by using finite difference approximations in micromagnetic simulations and their consequences in skyrmion hosting systems. This project has received funding from the European Union's Horizon 2020 research and innovation programme under the Marie Sklodowska-Curie grant agreement No 101152613 and MaMMoS No 101135546.

[1] A. Sescu, Advances in Difference Equations, Vol. 2015 (2015) [2] A. Kumar, Journal of Computational Physics, Vol. 201 (2004) [3] M. Donahue and R. D. McMichael, Physica B: Condensed Matter, Vol. 233 (1997) [4] M. J. Donahue and R. D. McMichael, IEEE Transactions on magnetics, Vol. 43 (2007)

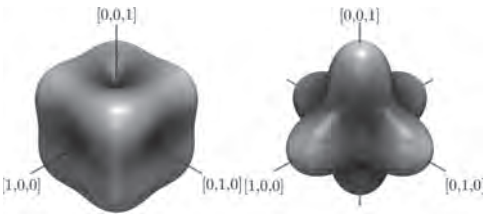

Anisotropy of the energy density of (left) exchange, (right) DMI, for a cubic discretization cell with a 3-point finite difference stencil. The radial distance from center represents the energy density magnitude in each direction.

AD-08. Micromagnetics of Nanoparticle Chains. *M.J. Donahue*[1], T.Q. Bui[2], F.M. Abel[3,4], S.I. Woods[2], E. De Lima Correa[4,5] and C. Dennis[4] *1. Information Technology Laboratory, National Institute of Standards and Technology, Gaithersburg, MD, United States; 2. Physical Measurement Laboratory, National Institute of Standards and Technology, Gaithersburg, MD, United States; 3. Physics, United States Naval Academy, Annapolis, MD, United States; 4. Material Measurement Laboratory, National Institute of Standards and Technology, Gaithersburg, MD, United States; 5. Theiss Research, La Jolla, CA, United States*

Magnetic particle imaging (MPI) is an important tool in biomedical and material science applications[1]. One aspect of colloidal nanoparticle systems receiving attention of late is signal enhancement due to formation of particle chains. The response of these systems increases at the millisecond time scale after the magnetic field is applied. Chain formation and growth have been suggested as a mechanism to explain this behavior[2], but micromagnetic simulations suggest that in AC fields chain rotation is the dominant mechanism. In the experimental data presented in Fig. 1, loops captured at 50 ms intervals gradually increase the hysteretic response. Micromagnetic simulations of chain growth do not match this behavior, but modeling a large population of fixed length chains rotating towards the applied field axis capture this trend, especially when combined with a background sub-population of unchained single superparamagnetic particles. The T=0 K simulations have larger H_c than the T=290 K experimental results. However, experimental studies at 10 K yield coercive fields similar to the simulations. Also, stochastic LLG simulations (Fig. 2) produce H_c values in line with the Fig. 1 experimental results. The thermal simulations consist of 32 separate trials at three reversal fields. The mean switching time at each field is computed from an exponential fit to the cumulative distribution function (CDF); this allows τ_N to be estimated even if some trials fail to reverse during the allocated run time (1000 μs). A decrease in τ_N from 27 ns at $\mu_0 H$=22 mT to 1500 ns at $\mu_0 H$=14 mT is consistent with a coercive field of ~10 mT at millisecond time scales.

[1] J. Kudr, Y. Haddad, L. Richtera, et al, Nanomaterials 7, 243 (2017). DOI: 10.3390/nano7090243 [2] C. Colson, K.L. Fung, J. Bryan, et al, bioRxiv (2022). DOI: 10.1101/2022.11.27.518061

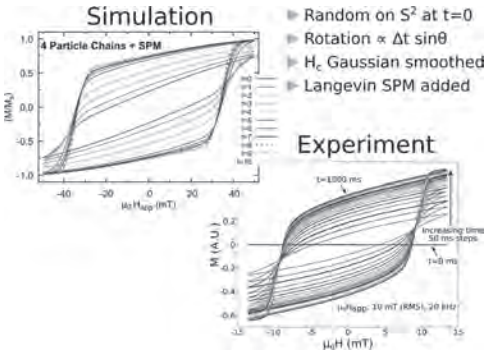

Fig. 1: Hysteresis loops of colloidal iron oxide nanoparticles (D≈18 nm). Lower right: Experimental results; individual loops taken at 50 ms increments. Upper left: Simulations of a population of nanoparticle chains randomly oriented at t=0, aligning towards the field axis at a rate proportional to the torque on the chain (Δt sinθ).

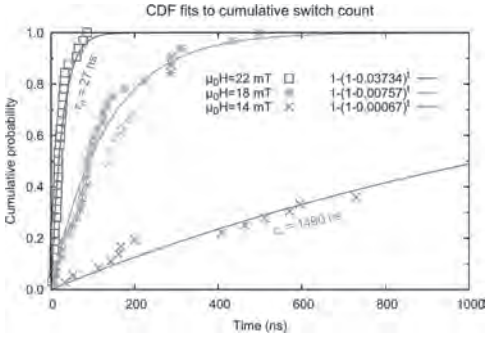

Fig. 2: Stochastic LLG simulations of Fe_3O_4 particle chains at 290 K in three reversing fields. Each symbol marks the time of reversal for one trial; 32 trials per field. Mean reversal time τ_N calculated from fit parameters (solid lines).

AD-09. Route to minimally dissipative switching in magnets via terahertz phonon pumping. M. Strungaru[1], M.O. Ellis[2], S. Ruta[3], R.F. Evans[4], R.W. Chantrell[4] and *O. Chubykalo-Fesenko[5] 1. Computer Science, University of Manchester, Manchester, United Kingdom; 2. School of Computer Science, University of Sheffield, Sheffield, United Kingdom; 3. College of Business, Technology and Engineering, Sheffield Hallam University, Sheffield, United Kingdom; 4. School of Physics, Engineering and Technology, University of York, York, United Kingdom; 5. Instituto de Ciencia de Materiales de Madrid, CSIC, Madrid, Spain*

The ability to manipulate and control magnetic properties via phonons could provide ultrafast, low energy switching mechanisms for storage applications. In order to investigate such a scenario, we have developed a spin-lattice dynamics framework (SLD) [1-2], able to treat both sub systems, spins (or magnons) and lattice (or phonons), in a self-consistent manner. The SLD model developed here allows for transfer of energy and angular momentum between the lattice and the spin system, with the latter realised by the pseudo-dipolar coupling form [3-4], which arises from the spin-orbit interaction and can be parameterised by magneto-elastic experiments. To model the effect of THz phonon excitation, we apply a periodic external force to each atom and for specific k-vectors and frequencies we observe precessional switching caused by the generation of magnetoelastic fields. We track the angular momentum transfer between sub-systems – Fig. 1 and conclude that the generated angular momentum during phonon excitation is not able to solely account for switching, and the switching mechanism relies on the generation of magneto-elastic fields. We are able to compute the switching phase diagram suggesting that ferromagnetic materials that present a flat phonon spectral region where a large number of phonon modes can be efficiently excited are good candidates for THz-assisted cold switching. The key factor is excitation with THz phonons with frequencies and k points at a maximum in the phonon density of states and no spin excitations. Since the heating resulting in our switching process is low (order of mK) our prediction may be of crucial importance for the next generation of eco-friendly storage devices, since heat production is one of the major problems for large data storage centers.

[1] Strungaru, Mara, et al. Physical Review B 109.22 (2024): 224412. [2] Strungaru, Mara, et al. Physical Review B 103.2 (2021): 024429. [3] A. I. Akhiezer, S. V. Peletminskii, and V. G. Baryakhtar, Spin Waves (North-Holland, Amsterdam, 1968). [4]S. Chikazumi and C. D. Graham, Physics of Ferromagnetism (Oxford University Press, Oxford, 1997), Vol. 94

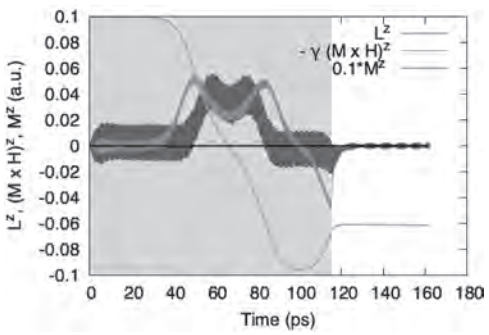

Evolution of the *z* component of angular momentum, magnetization and magnetic torque during THz phonon switching.

AD-10. Comprehensive Machine Learning Framework for Predicting Magnetic Properties and Identifying High-Performance Magnetic Materials. *S. Itani*[1], Y. Zhang[1,2] and J. Zang[1] *1. Physics and Astronomy, University of New Hampshire, Durham, NH, United States; 2. Chemistry, University of New Hampshire, Durham, NH, United States*

Magnetic materials are integral to modern science and technology, with applications spanning from data storage devices to energy technologies, medical equipment, and consumer electronics. However, the discovery of novel magnetic materials with a greater operating temperature range and optimized performance using more abundant elements remains a critical challenge. Traditional experimental approaches are time-consuming and expensive, while existing data driven methods are hindered by the lack of AI models trained on accurate, comprehensive, and feature-rich databases. This study addresses the challenge of accelerating this discovery process by developing accurate predictive models based on our comprehensive database generated by a novel approach that uses a Large Language Model (LLM) and conducting large-scale screening of the potential candidates. We constructed a database of 2,676 magnetic materials. Machine learning models, including Random Forest Classifier, Random Forest Regressor, XGBoost, and Neural Network were developed to classify materials and predict transition temperatures. These models were then applied to screen the Material Project database for potential high Curie temperature ferromagnetic materials. Our classification model achieved an accuracy of 90% in categorizing materials as FM, AFM, and NM. The best regression model predicted Curie temperature with R2 value of 0.86 and a mean absolute error of 62K. Our structured informed model achieved an R2 of 0.86 and a mean absolute error of 52K, demonstrating strong predictive performance. Screening of the Material Project database identified 15 promising ferromagnetic candidates with predicted Curie temperatures exceeding 600K. This work not only demonstrates the efficacy of a machine learning approach in accelerating the discovery of high-performance magnetic materials but also provides valuable resources for guiding experimental efforts in magnetic material research and development. This work was supported by the Department of Energy, Basic Energy Science under Grant No. DESC0020221.

Y. Zhang, S. Itani, and K. Khanal, Journal of Magnetism and Magnetic Materials, Vol. 597, p. 172001 (2024).

AD-11. Leveraging Parallel Computing for High-Performance Simulation of Magnetic Hysteresis and Eddy Current Losses. *J. Duan*[1] and V. Lomakin[1] *1. University of California, San Diego, San Diego, CA, United States*

We present a high-performance solver based on the finite element method (FEM) that enables computing the magnetization and electromagnetic field dynamics by combining the Landau-Lifshitz-Gilbert equation (LLGE) with Maxwell's equations (MEs). The solver simultaneously solves the LLGE and MEs and exchanges the magnetization and field information at every time step to result in a full two-way coupling between the equations. The main

contributions of this work are in an approach to solve MEs accounting for eddy currents with the ability to truncate the outgoing boundaries to any air box size and an approach to parallelize the LLGE and ME solvers on multi-GPU computing systems. Additionally, periodic boundary conditions (PBCs) are implemented in the FEM framework enabling using it in a broad range of problems with 1D, 2D, and 3D periodicities. The truncation boundary approach combined with the multi-GPU parallelization reduces the memory requirements per device and enables rapidly solving computationally large and complex problems. We demonstrate the use of the solver for computing the permeability and core loss in soft granular materials, which are used in various applications, such as electric motors and transformers. Modeling soft materials requires accounting for many grains or large size with PBCs. The solver can address many-grain models, with each grain of a several micron size. The calculations include obtaining equilibrium states, static hysteresis curves, and dynamic core loss, with and without including eddy current effects. The calculations provide insights into the physics of soft material operation, including different mechanisms of core loss. Figure 1a shows a periodic unit cell of a soft granular material model with grains separated by a small inter-granular distance. The grains have a cubic anisotropy and material parameters corresponding for ferrites. Figure 1b shows the core loss as a function of the applied field for different values of the conductivity. The core loss has multiple components, including the hysteresis, magnetic damping, and eddy current losses.

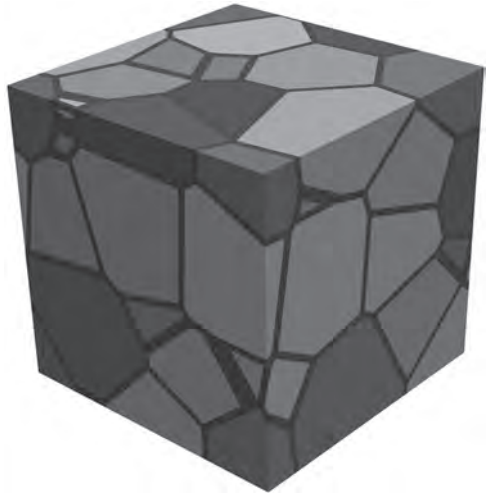

AD-12. Midpoint geometric integrators for inertial magnetization dynamics. M. d'Aquino[1], *S. Perna*[1] and C. Serpico[1] *1. DIETI, University of Naples Federico II, Naples, Italy*

The study of nanomagnetic systems' dynamics is crucial for recording, sensing, and low-power computing in information technologies[1]. The Landau-Lifshitz-Gilbert (LLG) equation is vital for analyzing these dynamics, capturing precessional motion influenced by external actions and spin interactions, leading to multistability, nonlinear resonance, and chaos[2]. In the last decade, the LLG equation was reformulated[3] with a correct inertial response predicting terahertz-range spin nutations, observed experimentally at 1 THz with a 10 ps damping time[4]. Previously, nutation-type magnetic motions were studied for symmetric nanomagnets subject to circularly-polarized microwaves[5]. Incorporating inertial effects augments the LLG equation, resulting in the inertial LLG (iLLG) equation. In this paper, we first show that the iLLG equation significantly differs from the classical LLG equation, demanding twice the number of state variables[6]. However, despite increased complexity, it exhibits remarkable conservation properties for magnetization amplitude and projection, and a Lyapunov structure under constant external magnetic fields[6]. Then, we propose two unconditionally-stable numerical schemes for time-integration of iLLG dynamics based on the implicit midpoint rule[7]. The first one notably preserves all properties but doubles the number of unknowns, requiring extensive changes in numerical codes. A second one retains the same computational cost as midpoint-discretized LLG[7] while preserving magnetization amplitude and projection[6]. Implementing the implicit midpoint rule involves solving a system of nonlinear equations, addressed with a fast quasi-Newton iterative technique[6]. Validation is made computing broadband frequency response of a ferromagnetic thin film magnetized along the easy direction[4] and subject to out-of-plane AC fields from GHz to THz. The numerical response compares with analytical solution for linear magnetization dynamics, revealing a 630 GHz peak indicative of ultrafast nutation dynamics and a ferromagnetic resonance peak at the Kittel frequency (see fig.1). The effectiveness of the second scheme is demonstrated with full micromagnetic simulation of inertial spin waves dynamics[8].

[1] B. Dieny, I.L. Prejbeanu, K. Garello, P. Gambardella, P. Freitas, R. Lehndorff, W. Raberg, U. Ebels, S.O Demokritov, J. Akerman, A. Deac, P. Pirro, C. Adelmann, A. Anane, A.V. Chumak, A. Hirohata, S. Mangin, S.O. Valenzuela, M.C. Onba?l?, M. d'Aquino, G. Prenat, G. Finocchio, L. Lopez-Diaz, R. Chantrell, O. Chubykalo-Fesenko, P Bortolotti, Nature Electronics 3 (8), 446-459, 2020. [2] E. A. Montoya, S. Perna, Y.-J. Chen, J. A. Katine, M. d'Aquino, C. Serpico, I. N. Krivorotov, Magnetization reversal driven by low dimensional chaos in a nanoscale ferromagnet, Nat. Comm. 10, 543, 2019. [3] Ciornei, M.-C., Rubí, J. & Wegrowe, J.-E. Magnetization dynamics in the inertial regime: Nutation predicted at short time scales. Physical Review B 83, 020410, 2011. [4] N. Kumar, N. Awari, S. Kovalev, D. Polley, N. Zhou Hagström, Sri Sai Phani Kanth Arekapudi, A. Semisalova, K. Lenz, B. Green, J.-C. Deinert, I. Ilyakov, M. Chen, M. Bowatna, V. Scalera, M. d'Aquino, C. Serpico, O. Hellwig, J.-E. Wegrowe, M. Gensch, S. Bonetti, Nat. Phys. 17, pp. 245-250, 2021. [5] C. Serpico, M. d'Aquino, G. Bertotti, and I. D. Mayergoyz, "Quasiperiodic magnetization dynamics in uniformly magnetized particles and films," J. Appl. Phys., vol 95, no. 11, pp. 7052–7054, 2004. [6] M. d'Aquino, S. Perna, C. Serpico, "Midpoint geometric integrators for inertial magnetization dynamics", arXiv:2310.09043, 2023. [7] M. d'Aquino, C. Serpico, and G. Miano, "Geometrical integration of Landau–Lifshitz–Gilbert equation based on the midpoint rule," J. Comput. Phys., vol. 209, no. 2, pp. 730–753, 2005. [8] M. d'Aquino, S. Perna, M. Pancaldi, R. Hertel, S. Bonetti, C. Serpico, "Micromagnetic study of inertial spin waves inferromagnetic nanodots", Physical Review B 107 (14), 2023.

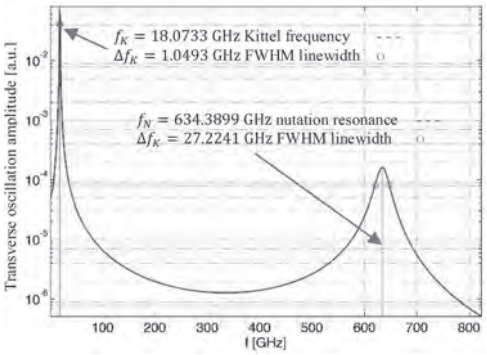

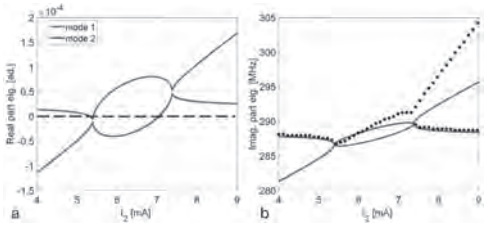

Real (a) and imaginary (b) parts of the eigenvalues of the linearized dynamics. Black dots refer to the peaks of the PSD computed from nonlinear oscillations of the coupled STVOs.

AD-13. Impact of exceptional points on nonlinear dynamics of coupled spin-torque oscillators. *S. Perna*[1], K. Ho[2], S. Wittrock[3], M. d'Aquino[1], R. Lebrun[2], V. Cros[2] and C. Serpico[1] *1. DIETI, University of Naples Federico II, Naples, Italy; 2. CNRS Thales, France, Palaiseau, France; 3. Helmholtz Institute, Berlin, Germany*

The coupling of several spin-torque vortex oscillators (STVO) promises to reach the required performances for future ICTs [1]. The initial step towards this direction is understanding the intricate nonlinear behavior that arises already when only two STVOs are interconnected. In this respect, a recent experimental investigation has revealed the emergence of amplitude death (AD) and exceptional points (EPs) as spin-polarized currents, that drive the dynamics of the two vortices, are changed in a proper range of values [2]. The study of two coupled STVOs in the presence of EPs requires a two-stage analysis. First, one studies the linearized dynamics of vortices around the respective ground states and ascertain the values of parameter values for which EPs are present. Subsequently, by combining numerical and analytical methods, one analyzes nonlinear regimes arising when coupled self-oscillations are set in. In this work, we carry on this study by focusing on the interplay between linear and nonlinear dynamics of the coupled STVO system, when the position of the EP in the parameters space is changed in a wide range of values. The system under investigation is similar to the one in ref[1]. The nonlinear dynamics of the coupled STVOs are investigated by numerical simulations where the DC spin-polarized currents exciting the vortex cores' motion and the coupling constant are appropriately changed[3]. For example, in the figure below the real (a) and imaginary part (b) of the eigenvalues of the linearized dynamics are shown when the STVO-1 is subject to a fixed DC current and the STVO-2 to a varying DC current. There are two EPs: one at I2=5.4 mA and the other at I2=7.3 mA. The connection between the analysis of linear and nonlinear dynamics is shown by comparing the eigenvalues with the peaks of the power spectral density (PSD) computed from the nonlinear dynamics of the coupled STVOs. The position of the peaks is also shown in Figure (b). This indicates that the occurrence of both EPs has a clear impact on the PSD of nonlinear oscillations.

[1] Dieny, B., Prejbeanu, I.L., Garello, K. et al. Opportunities and challenges for spintronics in the microelectronics industry. Nat Electron 3, 446–459 (2020) [2] S. Wittrock, et al. Non-hermiticity in spintronics: oscillation death in coupled spintronic nano-oscillators through emerging exceptional points, arXiv:2108.04804v2. [3] S. Perna, et al, Coupling-induced bistability in self-oscillating regimes of two coupled identical Spin-Torque Nano-oscillators, Physica B: Condensed Matter, vol. 674 (2024)

Session AE
ALTERMAGNETS AND ALTERMAGNETIC SPINTRONICS

Lukas Nadvornik, Chair
Charles University, Prague, Czechia

INVITED PAPER

AE-01. Unconventional magnetism: the emergence of nodal altermagnetism and beyond. *J. Sinova[1,2] 1. Johannes Gutenberg University Mainz, Mainz, Germany; 2. Texas A&M University, College Station, TX, United States*

Antiferromagnetic spintronics has been a very active research area of condensed matter in recent years. As we have learned how to manipulate collinear antiferromagnets actively and their emergent topology by means of new types of spin-orbit torques, a key problem remained: the inefficiency of relativistic mechanism. The necessity of relativistic effects to manipulate and detect Néel order arises from the spin degeneracy of collinear antiferromagnets in the non-relativistic limit – or at least it was thought. The discovery of d-wave magnetic order in momentum space motivated a closer look at the symmetry classification of collinear magnetic systems. This has emerged as the third basic collinear magnetic ordered phase of altermagnetism, which goes beyond ferromagnets and antiferromagnets. Altermagnets exhibit an unconventional spin-polarized d/g/i-wave band structure in reciprocal space, originating from the local sublattice anisotropies in direct space. This gives properties unique to altermagnets (e.g., the spin-splitter effect), while also having ferromagnetic (e.g., polarized currents) and antiferromagnetic (e.g., THz spin dynamics and zero net magnetization) characteristics useful for spintronics device functionalities. I will cover the basic introductory view to altermagnetism and its consequences to spintronics as well as new emerging exchange driven phenomena akin to spin-orbit coupling effects, such as p-wave magnetism, emerging from the basic concepts that gave rise to the discovery of altermagnetism.

[1] Libor Šmejkal, Rafael González-Hernández, T. Jungwirth and J. Sinova, Sci. Adv. 6, 23 (2020) [2] Libor Šmejkal, Jairo Sinova and Tomas Jungwirth, Phys. Rev. X 12, 031042 (2022) [3] Libor Šmejkal, Jairo Sinova and Tomas Jungwirth, Phys. Rev. X 12, 040501 (2022) [4] Zexin Feng, et al, Nature electronics 5, 735-743 (2022) [5] Libor Šmejkal, et al, Phys. Rev. X 12, 011028 (2022) [6] Rafael González-Hernández, et al, Phys. Rev. Lett. 126, 127701 (2021) [7] J. Krempaský, L. Šmejkal, et al, Nature 626, 517–522 (2024)

Fig. 1: The three collinear magnetic order classes – ferromagnetism, antiferromagnetism, and altermagnetism: (Left) Conventional FMs are ordered in space and have mostly an isotropic (*s*-wave) spin-polarization order parameter in the electronic structure. (Middle) AFMs are spin ordered in direct space but have no spin order, i.e., spin degenerate, in reciprocal space. In contrast, (Right) altermagnets have an anisotropic (*d*-wave illustrated, also possible *g,i*-wave symmetry) spin-polarization order, the naming arising from the alternating spin polarization.

CONTRIBUTED PAPERS

AE-02. Electrical detection of acoustic antiferromagnetic resonance in compensated synthetic antiferromagnets. *C. Song*[1], C. Chen[1], P. Liu[1] and F. Pan[1] *1. Tsinghua University, Beijing, China*

Synthetic antiferromagnets (SAFs) stand out as a seminal spintronic material, due to its combination of outstanding properties as antiferromagnets and comparatively easy manipulation and detection as ferromagnets. High-frequency antiferromagnetic resonance in SAFs, especially the optic mode (OM), is highly desired to attain fast operation speed in antiferromagnetic spintronic devices. SAFs exhibit ferromagnetic configurations above saturation field, however in that case, the intensity of OM is theoretically zero and hard to be detected in well-established microwave resonance experiments. To expose the hidden OM, the exchange symmetry between magnetic layers must be broken, inevitably introducing remanent magnetization. we report a feasible method to break the symmetry via surface acoustic waves with the maintenance of compensated SAF structure. By introducing an out-of-plane strain gradient inside the SAFs, we successfully reveal the hidden OM based on the method of direct-current electrical detection of surface-acoustic-wave-driven ferromagnetic resonance [1]. The OM intensity can be effectively modulated by controlling strain gradients in SAFs with different thicknesses, confirmed by finite-element simulations [2]. Our results provide a feasible scheme for detecting the concealed OM, which would trigger future discoveries in magnon-phonon coupling and hybrid quasiparticle systems [3].

[1] C. Chen, L. Han, C. Song, et al. Adv. Mater. 35, 2302454 (2023). [2] C. Chen, P. Liu, C. Song, et al. Phys. Rev. Lett. (in press). [3] C. Chen, M. Y. Ma, F. Pan, C. Song, Acta Physica Sinica, 73, 058502 (2024).

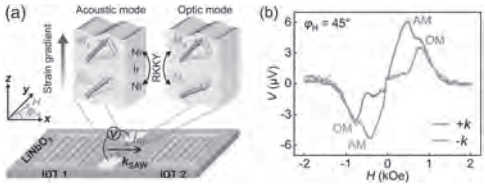

Fig. 1: Antiferromagnetic resonance in synthetic antiferromagnets. (a) Schematic of the magneto-acoustic hybrid device, where two antiferromagnetic resonance modes (the acoustic and optic mode) are included. (b) Magnetic field dependences of rectified voltage *V* at φ_H = 45° for acoustic wave propagating along +*k* and –*k*.

AE-03. Phenomenology of Altermagnets and Structure, Dynamics and Control of Altermanetic Textures. *O. Gomonay*[1], V. Kravchuk[2], K. Yershov[2], J. van den Brink[2] and J. Sinova[1] *1. Johannes Gutenberg University of Mainz, Mainz, Germany; 2. Leibniz Institute for Solid State and Materials Research in Dresden, Dresden, Germany*

We present a phenomenological theory of altermagnets, that captures their unique magnetization dynamics and allows modelling magnetic textures in this new magnetic phase. The main ingredient of the theory is an altermagnetic order parameter that describes the local environment of the magnetic atoms. In combination with the sublattice magnetizations of the Néel, this

order parameter allows to generalize a standard micromagnetic approach to the dynamics of altermagnetic systems and to predict non-trivial magnetic contributions in transport and optical tensors (e.g. crystal Hall conductivity or odd magneto-optical dichroism). We illustrate the application of the theory to the different types of altermagnets and show nontrivial altermagnetic effects that appear in the altermagnetic textures and their dynamics [3,4]. In particular, we can explain intuitively the characteristic lifted degeneracy of their magnon spectra, by the emergence of an effective sublattice-dependent anisotropic spin stiffness arising naturally from the phenomenological theory. We show that as a consequence the altermagnetic domain walls, in contrast to antiferromagnets, have a finite gradient of the magnetization, with its strength and gradient direction connected to the altermagnetic anisotropy, even for 180° domain walls. This gradient generates a ponderomotive force in the domain wall in the presence of a strongly inhomogeneous external magnetic field, which may be achieved through magnetic force microscopy techniques. The motion of these altermagentic domain walls is also characterized by an anisotropic Walker breakdown, with much higher speed limits of propagation than ferromagnets but lower than antiferromagnets. We also show that bending the film without stretching induces a local magnetization proportional to the gradient of the film curvature. The amplitude of the magnetization directly reflects the altermagnetic symmetry and depends on the direction of bending. Its angular distribution correlates with that of the altermagnetic splitting of the magnon and electronic bands.

[1] Šmejkal, L., González-Hernández, R., Jungwirth, T., & Sinova, J. (2020). Crystal time-reversal symmetry breaking and spontaneous Hall effect in collinear antiferromagnets. *Science Advances*, 6(23), eaaz8809. https://doi.org/10.1126/sciadv.aaz8809 [2] V.V. Eremenko & N.F. Kharchenko. Magneto-optics of antiferromagnets. (1987) *Phys. Rep.(*Review Section of Physics Letters) 155, 379. [3] O. Gomonay, V. P. Kravchuk, R. Jaeschke-Ubiergo, K. V. Yershov, T. Jungwirth, L. Šmejkal, J. van den Brink, J. Sinova (2024) Structure, control, and dynamics of altermagnetic textures arXiv:2403.10218 [4] K. Yershov, O. Gomonay, J. Sinova, J. van den Brink, V. Kravchuk. (2024) Curvature induced magnetization of altermagnetic films arXiv:2406.05103

AE-04. Demonstration of single-variant altermagnetic RuO_2(101) thin films on Al_2O_3 *r*-plane substrates. *Z. Wen*[1], C. He[1], J. Okabayashi[2], Y. Miura[1,3], T. Ohkubo[1], T. Seki[4,5], H. Sukegawa[1] and S. Mitani[1]
1. National Institute for Materials Science (NIMS), Tsukuba, Japan; 2. Research Center for Spectrochemistry, The University of Tokyo, Tokyo, Japan; 3. Kyoto Institute of Technology, Kyoto, Japan; 4. Institute for Materials Research, Tohoku University, Sendai, Japan; 5. Center for Science and Innovation in Spintronics, Tohoku University, Sendai, Japan

Altermagnetism represents a distinct magnetic phase separate from ferromagnetism and antiferromagnetism, characterized by large spin splitting yet zero net magnetization.[1-2] This unique property offers potential for spintronic applications such as spin-orbit torque (SOT) and magnetoresistive devices. Tetragonal RuO_2 has recently emerged as a notable altermagnet, confirmed through angle-resolved photoemission spectra. Particularly, the (101)-oriented RuO_2 film has demonstrated SOT-induced magnetization switching without an external magnetic field, thanks to tilted Néel vector orientations generating tilted spin currents. Crystallographically, RuO_2(101) has an equivalent variant RuO_2(with identical lattice planes and constants, while Néel vectors are oriented in mirror symmetry. The presence of two variants with different Néel vector orientations complicates material design and hinders precise control over spin transport properties. It is of importance to identify and utilize a single variant of RuO_2(101) to fully exploit its spin-splitting effect for spintronic applications. In this work, we fabricated epitaxial thin films of RuO_2(101) on Al_2O_3(102) *r*-plane substrates and employed comprehensive structural and magnetic characterization, including atomic-resolution scanning transmission electron microscopy and X-ray magnetic linear dichroism (XMLD), to confirm the presence of a single variant in the RuO_2(101) films. It is found that the matching oxygen atom arrangements on RuO_2(101) and Al_2O_3(102) surfaces play a critical role in determining the single-variant formation. XMLD analysis, sensitive to compensated magnetic structures and charge quadrupoles, undetectable by X-ray magnetic circular dichroism, revealed the direction of the Néel vector through probing charge distributions with linearly polarized synchrotron beams. This XMLD technique confirmed the single-variant altermagnetic RuO_2(101) film with finite charge quadrupole and spin moment, consistent with theoretical predictions. Moreover, we demonstrated unidirectional spin-splitting magnetoresistance in RuO_2(101)/CoFeB heterostructures, attributed to the distinct single variant and tilted spin current.

[1] L. Šmejkal, J. Sinova, and T. Jungwirth, *Phys. Rev. X* 12, 031042 (2022).
[2] L. Šmejkal, J. Sinova, and T. Jungwirth, *Phys. Rev. X* 12, 040501 (2022).

AE-05. Epitaxial growth and Observation of Time Reversal Symmetry Breaking in Altermagnetic RuO_2. *A. Akashdeep*[1], O. Fedchenko[1], J. Minár[2], Q.L. Nguyen[5], D. Kutnyakhov[4], M. Kläui[1], T. Jungwirth[3], G. Jakob[1], L. Smejkal[1,3], J. Sinova[1,3] and H. Elmers[1] *1. Institut für Physik, Johannes Gutenberg-Universität Mainz, Mainz, Germany; 2. New Technologies Research Center, University of West Bohemia, Piezen, Czechia; 3. Institute of Physics Academy of Sciences of the Czech Republic, Praha 6, Czechia; 4. Deutsches Elektronen-Synchrotron DESY, Hamburg, Germany; 5. Linac Coherent Light Source, SLAC National Accelerator Laboratory, Menlo Park, CA, United States*

Altermagnets, a promising new class of magnetic materials, have attracted considerable attention for their potential to revolutionize the development of innovative information technologies. These materials exhibit alternating spin polarization in both real and reciprocal space, giving them a unique combination of collinear antiferromagnetic and ferromagnetic properties [1]. Despite having a net magnetic moment of zero, altermagnets can generate both longitudinal and transverse spin currents and a spin-splitter torque with a component perpendicular to the interface [2]. This study focuses on the epitaxial growth of RuO_2, a prototypical material for altermagnets, using pulsed laser deposition. We characterize the epitaxial growth modes using reflection high-energy electron diffraction (RHEED), investigating both layer-by-layer and island growth modes. X-ray diffraction (XRD) analysis confirms the superior quality of films grown in the layer-by-layer mode compared to the island-growth mode. We observe time-reversal symmetry breaking in the band structure of altermagnetic RuO_2 by detecting magnetic circular dichroism in angle-resolved photoemission spectra [3]. Our experimental results, supported by ab initio calculations, provide the foundational electronic structure for various phenomena and applications. These applications span fields like topological matter and spintronics which are based on the unique time-reversal symmetry breaking found in altermagnets.

[1] L. Šmejkal, T. Jungwirth et al., Phys. Rev. X 12, 040501 (2022). [2] A. Bose, D. Ralph et al., Nat Electron 5, 267–274 (2022). [3] O. Fedchenko, H. J. Elmers et al., Sci Adv, 10(5), eadj4883 (2024).

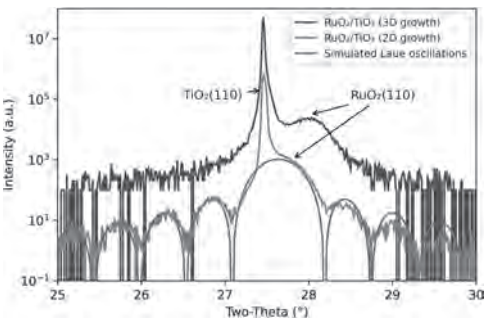

XRD for the layer by layer growth(2D) and island growth(3D)

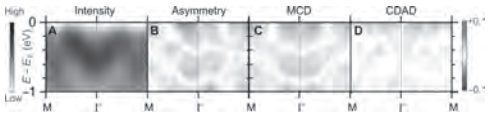

Experimental photoemission intensities map $I(E_B,0,k_y)$ revealing the energy dispersion of bands along the line M-Γ-M and asymmetries

AE-06. Manipulation of the Anomalous Hall Effect in MnTe Altermagnetic Thin Films. *S. Bey*[1], S. Fields[2], N. Combs[2], B.G. Márkus[3,1], D. Beke[3,1], J. Wang[1,4], L. Riney[1], K. Yoshimura[1], A. Ievlev[5], M. Zhukovskyi[6], T. Orlova[6], L. Forró[3,1], S.P. Bennett[2], X. Liu[1] and B.A. Assaf[1] *1. Dept. of Physics and Astronomy, The University of Notre Dame, Notre Dame, IN, United States; 2. Materials Science and Technology Division, U.S. Naval Research Laboratory, Washington, DC, United States; 3. Stavropoulus Center for Complex Quantum Matter, The University of Notre Dame, Notre Dame, IN, United States; 4. Materials Dept., UC Santa Barbara, Santa Barbara, CA, United States; 5. Center for Nanophase Materials Sciences, Oak Ridge National Laboratory, Oak Ridge, TN, United States; 6. Notre Dame Integrated Imaging Facility, The University of Notre Dame, Notre Dame, IN, United States*

Altermagnets are collinear magnets with zero net magnetization. Simultaneously, they feature properties typical of ferromagnets, such as the anomalous Hall effect and polarized spin currents. This combination makes them a promising candidate in the next generation of spintronics devices. Unlike in ferromagnets, the AHE in AMs is only allowed by symmetry for specific orientations of the Néel vector [1]. α-MnTe is a semiconductor predicted to host altermagnetism. Previous works in MnTe reported alternating spin polarization via ARPES, an AHE, and XMCD [2-5]. Due to the close lattice match, they mainly focus on thin films grown on InP(111). Given these results, the role of point defects and strain remains elusive and warrants further study. Studying α-MnTe grown on different substrates is vital to understanding the AHE's origin and its dependence on intrinsic material properties. This work achieves a substrate-dependent tuning of the anomalous Hall effect of AM MnTe by field cooling. We report the synthesis and magnetotransport of 100nm thick single-phase MnTe films on GaAs(111) and SrF2(111). We study magnetotransport in both films as a function of in-plane field cooling strength and direction. In MnTe on GaAs, we find that field cooling tunes the size and polarity of the AHE [6]. We hypothesize that field cooling favors the nucleation of a sizeable antiferromagnetic domain, satisfying the symmetry requirements to generate the AHE. However, in MnTe on SrF2, we only find a spontaneous AHE at low temperatures, which is insensitive to field cooling. We consider two key differences: surface analysis reveals a distinctive morphology in films on SrF2, while DFT calculations suggest that substrate-induced strain can influence the location of the valence band edge [7]. This work challenges prior work describing point defects as a potential origin for the AHE and highlights extrinsic and intrinsic effects tying the emergence of the AHE to the substrate.

[1] L. Šmejkal, J. Sinova, and T. Jungwirth, Phys Rev X, Vol. 12, no. 4, p. 040501 (2022) [2] J. Krempaský et al., Nature, vol. 626, no. 7999, pp. 517–522 (2024) [3] R. D. Gonzalez Betancourt et al., Phys Rev Lett, vol. 130, no. 3, p. 036702 (2023) [4] M. Chilcote et al., Adv Funct Mater, p. 2405829 (2024) [5] A. Hariki et al., Phys Rev Lett, vol. 132, no. 17, p. 176701 (2024) [6] D. Kriegner et al., Nat Commun, vol. 7, no. 1, p. 11623 (2016) [7] P. E. Faria Junior et al., Phys Rev B, vol. 107, no. 10, p. L100417 (2023)

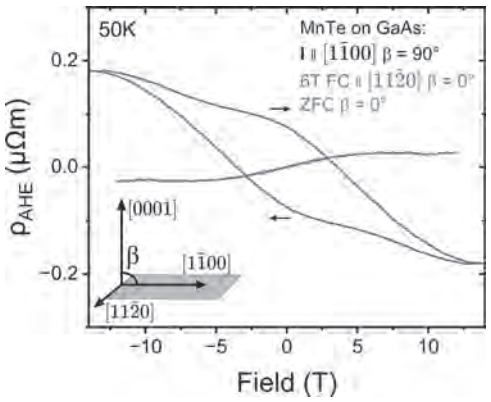

Fig. 1 AHE for MnTe on GaAs at 50K, for BFC = 6T ∥ hard axis and ZFC. I ∥ easy axis and B ⊥ to c-plane. The inset represents measurement geometry.

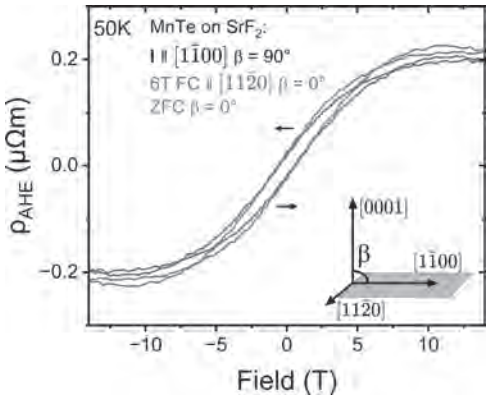

Fig 2. AHE for MnTe on SrF2 at 50K, following an identical procedure to Fig 1.

AE-07. Altermagnetic variants in thin films of Mn_5Si. *J. Rial*[1], M. Leiviskä[1,2], G. Skobjin[3], A. Badura[2,4], G. Gaudin[1], F. Disdier[1], R. Schlitz[3], I. Kounta[5], S. Beckert[6], D. Kriegner[2], A. Thomas[6,7], E. Schmoranzerová[4], L. Smejkal[2,8], J. Sinova[8,9], T. Jungwirth[2,10], L. Michez[5], H. Reichlova[2], S. Goennenwein[3], O. Gomonay[8] and V. Baltz[1] *1. SPINTEC, Grenoble, France; 2. Institute of Physics, Czech Academy of Sciences, Prague, Czechia; 3. Department of Physics, University of Konstanz, Konstanz, Germany; 4. Faculty of Mathematics and Physics, Charles University, Prague, Czechia; 5. Aix-Marseille University, Marseille, France; 6. Institute of Solid State and Materials Physics, TU Dresden, Dresden, Germany; 7. Leibniz Institute of Solid State and Materials Science, IFW Dresden, Dresden, Germany; 8. Institute for Physics, Johannes Gutenberg University Mainz, Mainz, Germany; 9. Department of Physics, Texas A&M University, Texas, TX, United States; 10. School of Physics and Astronomy, University of Nottingham, Nottingham, United Kingdom*

Altermagnetism describes an elementary compensated magnetic phase, which is based on spec the arrangement of magnetic moments with respect to crystalline symmetries. It has opened up new research path in several fields of condensed matter physics, like spintronics, valleytronics and superconductivity, along with expectations for the emergence of closely related technological applications [1]. Among the altermagnet candidates which have emerged, Mn_5Si_3 has attracted some attention, due to its composition of light-elements, with weak relativistic spin-orbit coupling, making it possible to unequivocally link its altermagnetic character to non-relativistic spin physics. Although theory and experimental findings together advocated the d-wave altermagnetic phase in thin films of Mn_5Si_3 [2-4], its presumed altermagnetic structure, giving rise to three options, or altermagnetic variants

(Figure 1), for the checkerboard distribution of the magnetic Mn atoms, had yet to be demonstrated. This work experimental demonstrates the so far presumed structure of the altermagnetic phase of thin films of Mn_5Si_3, via identification of altermagnetic variants [5]. Our experimental data revealed the symmetries of the system, at the nanoscale, through anisotropy of the anomalous Hall effect for nanometric devices. The spin orientation - crystal axes arrangement was reshuffled via field-driven variation of the order parameter, with an external magnetic field applied at several polar and azimuthal angles. The finding were corroborated by the results of a theoretical model accounting for the local environment of the magnetic sublattices, and returning the trajectories of the Néel vector and net magnetization due to DMI-induced canting. This study opens up prospects for the wide range of further fundamental research and practical applications in altermagnetism, where detecting and controlling altermagnetism is critical.

[1] Šmejkal et al., Phys Rev X. Vol. 12, p. 040501 (2022) [2] Kounta et al., Phys Rev Mat Vol. 7 (2), p. 024416 (2023) [3] Reichlova et al., Nat Commun Vol. 15, p. 4961 (2024) [4] Leiviskä et al., Phys. Rev. B vol. 109, p. 224430 (2024) [5] Rial et al., soon to be released in arXiv

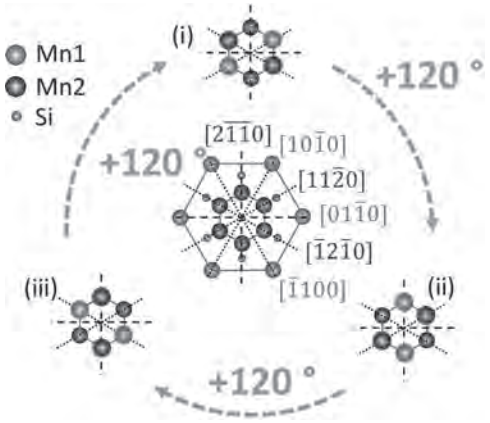

Fig.1 Representation of the hexagonal unit cell of the altermagnetic phase of Mn_5Si_3, consisting of two magnetically ordered opposite-spin sublattices of Mn2-atoms, highlighted in red and blue. The 3 possible variants rotated by 120° are shown.

AE-08. Observation of unconventional spin current in altermagnetic CrSb. *C. Tseng*[1], S. Karube[1,2], H. Narita[1], R. Hisatomi[1,2], D. Kan[1], Y. Shiota[1,2], Y. Shimakawa[1] and T. Ono[1,2] *1. Institute for Chemical Research, Kyoto University, Kyoto, Japan; 2. Center for Spintronics Research Network, Kyoto University, Kyoto, Japan*

Altermagnets (ATM)[1-4] have recently attracted significant attention due to unique properties such as giant spin splitting, spin-splitter effect (SSE), and a theoretically predicted high tunneling magnetoresistance ratio. In real space, the ATM behaves just like antiferromagnets without net magnetization. On the other hand, in reciprocal space, it interestingly exhibits an alternating band structure with spin-splitting originating from the anisotropic crystal field along different axes. In this study, an epitaxial CrSb(1-10) is deposited on a single crystal $LaAl0_3$(110) substrate using RF magnetron sputtering. In Fig. 1, the epitaxial structure has been confirmed through in-plane phi-scan measurement on the X-ray diffraction (XRD) which shows two-fold symmetry, consistent with the crystal symmetry of CrSb. The CrSb has been experimentally observed to have a large spin-split band structure of approximately 0.6 eV driven by the ATM utilizing soft X-ray angular resolved photoemission spectroscopy recently[5] while based on the band structure of CrSb, spin-splitter torque should be negligibly small[6]. We use the spin-torque ferromagnetic resonance method to evaluate each component's spin current[3]. When applying charge current along the X-axis, we observed a crystal direction-dependent spin current phenomenon not only for the Y-polarized current but surprisingly, also for the X-polarized current as shown in Fig. 2. The result is inconsistent with the traditional spin Hall effect and implies the existence of the unconventional spin-splitter effect in the CrSb. The detailed mechanism and further discussion will be provided during the conference.

1. Shao, D.-F., Zhang, S.-H., Li, M., Eom, C.-B. & Tsymbal, E. Y. Spin-neutral currents for spintronics. *Nature Communications* 12, 7061 (2021). 2. Šmejkal, L., Sinova, J. & Jungwirth, T. Beyond conventional ferromagnetism and antiferromagnetism: A phase with nonrelativistic spin and crystal rotation symmetry. *Physical Review X* 12, 031042 (2022). 3. Karube, S. *et al.* Observation of Spin-Splitter Torque in Collinear Antiferromagnetic RuO 2. *Physical review letters* 129, 137201 (2022). 4. Bai, H. *et al.* Efficient Spin-to-Charge Conversion via Altermagnetic Spin Splitting Effect in Antiferromagnet RuO 2. *Physical Review Letters* 130, 216701 (2023). 5. Reimers, S. *et al.* Direct observation of altermagnetic band splitting in CrSb thin films. *Nature Communications* 15, 2116 (2024). 6. Šmejkal, L., Sinova, J. & Jungwirth, T. Emerging research landscape of altermagnetism. *Physical Review X* 12, 040501 (2022).

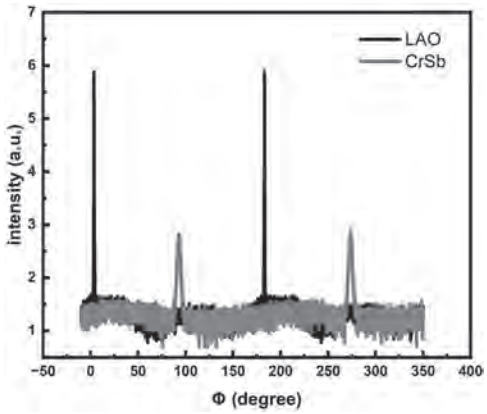

Fig.1 The XRD phi-scan of CrSb and LAO, both show two-fold symmetry which is consistent with the crystal symmetry.

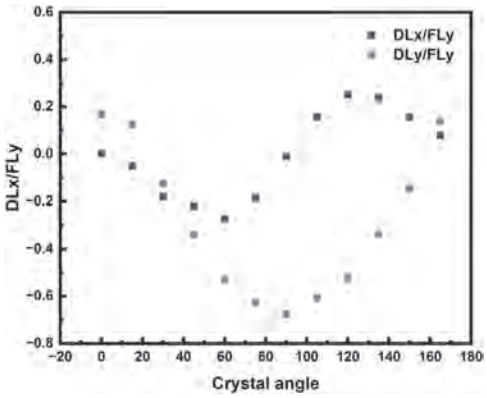

Fig.2 X and Y components of the damping-like torque in CrSb, 0 degree is perpendicular to the Neel vector direction[001] of CrSb. The data is divided by the Y component of the field like torque for normalization and they show clear crystal orientation dependent

AE-09. Anisotropic Spin to Charge Conversion in the Altermagnet RuO_2 Capped with YIG. *D. Qu*[1], Y. Wang[2], C. Liao[2], Y. Tien[2] and S. Huang[2] *1. Center for Condensed Matter Sciences, National Taiwan University, Taipei, Taiwan; 2. Department of Physics, National Taiwan University, Taipei, Taiwan*

The field of magnetism has seen a surge of interest in a novel classification known as altermagnetism over the past few years [1]. As a compensated collinear antiferromagnet with unique crystal symmetry, altermagnetic material exhibits time-reversal symmetry-breaking phenomena similar to that found in ferromagnet, known as the altermagnetic spin-splitting effect (ASSE). The non-relativistic ASSE enables the generation of a longitudinal spin polarized current and a transverse pure spin current upon the injection of a charge current along certain crystal orientations. However, experimentally establishing the transverse ASSE is challenging. This difficulty arises from the inevitable mixing of ASSE with the spin Hall effect (SHE) caused by the material's relativistic spin-orbit coupling. Moreover, the ASSE's dependence on the hard-to-probe and hard-to-control Néel vectors makes its observation and study even more difficult. This study [2] addressed these challenges by utilizing thermal spin injection from a top ferrimagnetic insulator yttrium iron garnet (YIG) layer. This approach allowed us to detect the inverse altermagnetic spin-splitting effect (IASSE) in high-quality epitaxial altermagnetic RuO_2 thin films grown on TiO_2 without the complication of a ferromagnetic metal. Our observations revealed a significant finding: the spin-to-charge conversion in the YIG/RuO_2/TiO_2 heterostructure is highly anisotropic. We attributed the anisotropy to an altermagnetic origin by ruling out the anisotropic SHE. We found that the IASSE exhibited an opposite sign compared to the inverse spin Hall effect (ISHE). Remarkably, the efficiency of the IASSE was found to be consistently 70% of that of the ISHE in RuO_2 for thicknesses ranging from 5 nm to 32 nm, as shown in Fig. 1. Furthermore, we demonstrated that the ASSE/IASSE effects are observable only when the Néel vectors are well-aligned by modifying the Néel vector domains via RuO_2 crystallinity through different substrates. Interestingly, the shape of the thermal voltage hysteresis loop is anisotropic and is broadened along the [001] RuO_2 orientation, which verifies the [001] orientations of the Néel vectors. Our study provides an alternative route in studying the altermagnet.

[1] Libor Šmejkal, Jairo Sinova, and Tomas Jungwirth, *Emerging Research Landscape of Altermagnetism.* Phys. Rev. X 12, 040501 (2022). [2] C.-T. Liao, Y.-C. Wang, Y.-C. Tien, S.-Y. Huang, and D. Qu, *Separation of Inverse Altermagnetic Spin-Splitting Effect from Inverse Spin Hall Effect in RuO_2.* Accepted by Phys. Rev. Lett. (2024), Editors' suggestion.

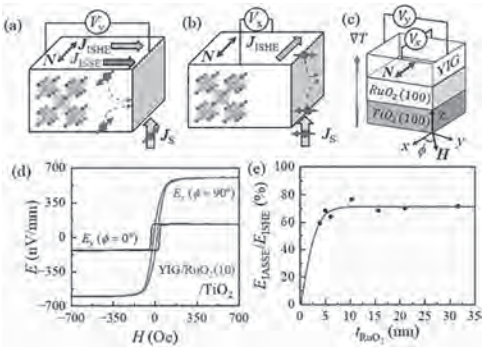

AE-10. Altermagnetism in the Hopping Regime. *E. Galindez Ruales*[1], L. Šmejkal[1,4], S. Das[1], C. Schmitt[1], F. Fuhrmann[1], E. Baek[2,1], A. Ross[1], R. Jaeschke Ubiergo[1], V. Bharadwaj[1], R. González-Hernández[3], A. Rothschild[5], J. Sinova[1,4], C. You[2], G. Jakob[1] and M. Kläui[1,6] *1. Institute of Physics, Johannes Gutenberg University Mainz, Mainz, Germany; 2. Department of Physics and Chemistry, DGIST, Daegu, The Republic of Korea; 3. Grupo de Investigacíon en Física Aplicada, Departamento de Física, Universidad del Norte, Barranquilla, Colombia; 4. Institute of Physics, Academy of Sciences of the Czech Republic, Prague, Czechia; 5. Department of Materials Science and Engineering, Technion-Israel Institute of Technology, Haifa, Israel; 6. Center for Quantum Spintronics, Norwegian University of Science and Technology, Trondheim, Norway*

Conventional AFMs exhibit time-reversal symmetry, resulting in a zero anomalous Hall coefficient. However, compensated magnets that are altermagnets can yield a nonzero anomalous Hall signal [1]. In high-symmetry systems, an isotropic Hall effect is expected, while low-symmetry systems, such as altermagnetic hematite, can demonstrate exceptional magnetotransport behavior. We present experimental evidence confirming the altermagnetic nature of doped hematite, showing that one cannot describe hematite as a conventional collinear antiferromagnet by revealing unique transport phenomena linked to altermagnetism [2]. Analysis of various Hall bar orientations relative to the crystallographic axis reveal robust Hall conductivity contributions deviating from the symmetry expected for collinear easy-axis antiferromagnets (Fig. 1). These contributions, arising from crystal symmetry and the magnetic order parameter, reveal a nondiagonal conductivity tensor component previously unexplained in conventional hematite. A key signature of altermagnetism is the sign inversion in the Hall effect every 60 degrees (Fig. 2). This behavior underscores altermagnetic properties' role in the Hall effect's crystal-direction dependence. The sign inversion suggests distinctive mechanisms governing the AHE, even in the probed hopping regime. In our samples, the hopping transport due to charge dopants aligns with predicted altermagnetic behavior. This provides the first experimental evidence of a Hall signal inversion in an altermagnetic material within the hopping regime. The observed anisotropic magnetotransport in doped hematite reinforces its classification as an altermagnet and paves the way for further exploration of altermagnetic materials and their unique transport properties.

[1] L. Šmejkal, et. al., Phys. Rev. X 12, 031042 (2022) [2] E. Galindez-Ruales, arXiv:2310.16907 (2024)

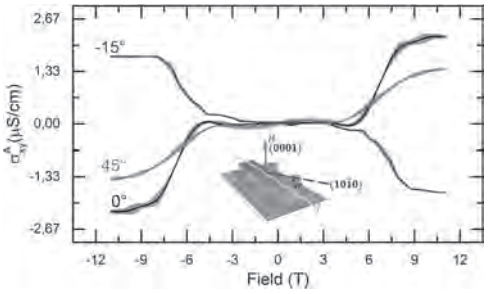

Fig. 1: Odd component of the transverse conductivity at 300 K of three different devices fabricated at selected angles relative to the in-plane crystallographic axis, denoted as a (10-10). A diagram illustrating a device with orientation α is provided below.

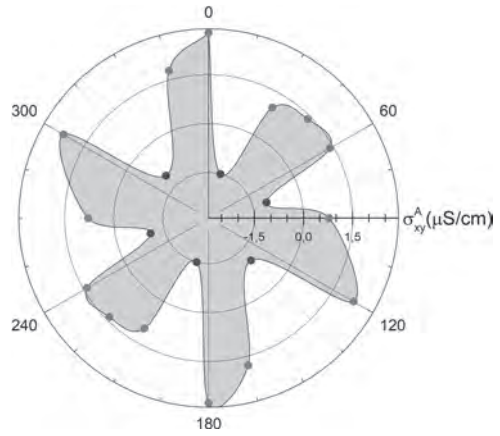

Fig. 2: Polar plot of the amplitude $^A\sigma_{xy}$ (H = 11T) as a function of the angle of the Hall bar. Red (blue) points represent a positive (negative) amplitude.

AE-11. Tunable Localized Currents at Crystallographic Domain Boundaries in Altermagnet RuO2. *G.M. Pantano*[1,2], E. Thareja[1], L. Smejkal[2,3], J. Sinova[2] and J.D. Gayles[1] *1. Department of Physics, University of South Florida, Tampa, FL, United States; 2. Institut für Physik, Johannes Gutenberg Universität Mainz, Mainz, Germany; 3. Institute of Physics, Czech Academy of Sciences, Prague, Czechia*

Interfacial phenomena in condensed matter physics has garnered significant interest due to the discovery of properties and phases distinct from the bulk, enabling the manipulation of materials for technological applications. In this work, we investigate novel effects arising from a chiral crystallographic domain boundary in the altermagnet ruthenium dioxide (RuO2) shown in Fig 1a. Altermagnets are characterized by a substantial non-relativistic spin splitting, as in Fig 1b, with compensated magnetic ordering. This unique spin splitting originates from the Heisenberg exchange interaction combined with the anisotropic octahedral crystal field, reducing the symmetry between the spin sublattices to a real-space rotation. This offers a new mechanism for controlling spin-dependent transport phenomena based on the crystal configuration, such as the crystal Hall effect in Fig 1c. Conventionally, these internal interfaces are seen as detrimental to transport due to increased scattering and the cancellation of opposite anomalous responses [1]. However, we uncover more intriguing phenomena at the interface. The green (right-handed chirality) and purple (left-handed chirality) unit cells are equivalent in Ru atomic positions and magnetic moment orientations (black vectors), but the isosurfaces are rotated by 90 degrees. We use first-principle calculations to characterize the interfacial states and their contribution to electronic transport. We observe enhanced anomalous transport along the interface due to an induced magnetization at the domain boundary related to the change of symmetry. We also theorize the localized currents are tunable by the direction of the magnetization at the interface. Our results improve our understanding of altermagnetic properties at interfaces with reduced dimensionality and symmetry, aiding in the development of sustainable, energy-efficient devices.

[1] I. I. Mazin, Phys. Rev. B, 107, L100418 (2023). [2] L. Smejkal, J. Sinova, and T. Jungwirth, Phys. Rev. X, 12, 040501 (2022). [3] E. W. Hodt, P. Sukhachov, and J. Linder, ArXiv (2024) URL: https://arxiv.org/abs/2406.07603.

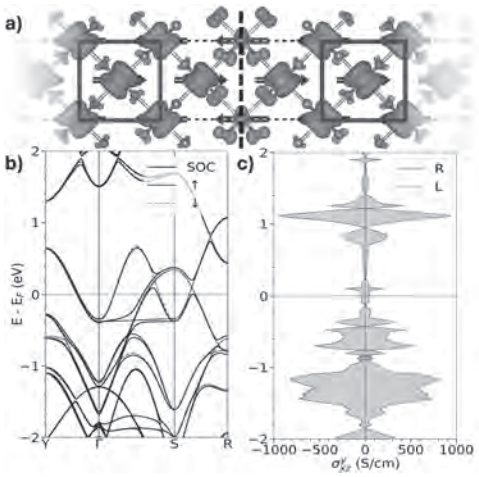

Fig. 1: a) Chiral crystallographic domain boundary formed by applying a [100] mirror symmetry operation reversing the local crystal chirality (purple) with projected spin magnetization density isosurfaces. b) and c) calculated electronic energy bands with and without spin-orbit coupling and anomalous Hall response for green and purple unit cells.

AE-12. Coexistence of Anomalous Hall Effect and Weak Magnetization in Nominally Collinear Antiferromagnet MnTe. *M. Sawicki*[1,2], K. Kluczyk[3], K. Gas[1,4], M.J. Grzybowski[3], P. Skupinski[1], M.A. Borysiewicz[5], T. Fas[3], J. Suffczynski[3], J.Z. Domagala[1], K. Grasza[1], A. Mycielski[1], M. Baj[3], K.H. Ahn[6], K. Vyborny[6] and M. Gryglas-Borysiewicz[3] *1. Institute of Physics, Polish Academy of Sciences, Warsaw, Poland; 2. Research Institute of Electrical Communication, Tohoku University, Sendai, Japan; 3. Faculty of Physics, University of Warsaw, Warsaw, Poland; 4. Center for Science and Innovation in Spintronics, Tohoku University, Sendai, Japan; 5. Lukasiewicz Research Network - Institute of Microelectronics and Photonics, Warsaw, Poland; 6. FZU-Institute of Physics of the Czech Academy of Sciences, Praha, Czechia*

Non-relativistic analysis based on spin group theory [1] has identified a class of collinear systems (called altermagnets) to exhibit spin-splitting of bands, while maintaining zero net magnetization in non-relativistic limit by symmetry. However, in real crystals the spin effects are always accompanied by the orbital ones and relativistic corrections cannot always be neglected. While in various material systems an antiferromagnetic (AFM) phase was found to coexist with a weak ferromagnetic (WFM) signal, symmetry-based theoretical predictions indicate a possibility of a non-zero anomalous Hall effect (AHE) even in the absence of sample magnetization. In particular hexagonal MnTe is a case of collinear AFM, where AHE and no detectable magnetization have been observed in thin film [2]. To solve the fundamental problem of origin of the AHE in antiferromagnets, we perform a comprehensive study of hexagonal MnTe samples combining experiment and theory [3]. We employ substrate-free bulk samples, in which undesired parasitic or background effects related to substrates are absent. We demonstrate that the existence of the AHE in the hexagonal MnTe (Fig. 1) is accompanied by the presence of a WFM signal, particularly easy to be measured in the remnant state (Fig. 2). We find this magnetisation to be oriented exclusively along the *c* axis of the hexagonal crystal, i.e. to be perpendicular to the Néel vector in MnTe [4], and to vanish precisely at the Néel temperature. We introduce a macrospin model involving the Dzyaloshinskii–Moriya type interaction, which explains the existence of a non-zero magnetic moment in the absence of external field. Moreover, by the Berry curvature analysis we show that the AHE in hexagonal MnTe is non-zero even when the magnetization vanishes. We argue that there is a common, symmetry-related origin of both the AHE and this weak FM signal.

[1] L. Šmejkal, J. Sinova, and T. Jungwirth, Phys. Rev. X 12, 040501 (2022). [2] R. D. Gonzalez Betancourt et al, Phys. Rev. Lett. 130, 036702 (2023). [3] K. P. Kluczyk et al., arXiv: 2310.09134 (2023). [4] D. Kriegner et al., Phys. Rev. B 96, 214418 (2017).

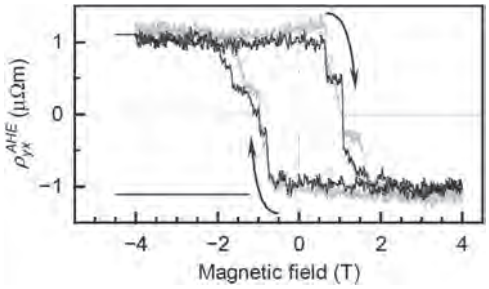

Fig. 1. The hysteresis ρ^{AHE} extracted from transverse magnetoresistance ρ_{xy}. The two curves come from two different pairs of contacts.

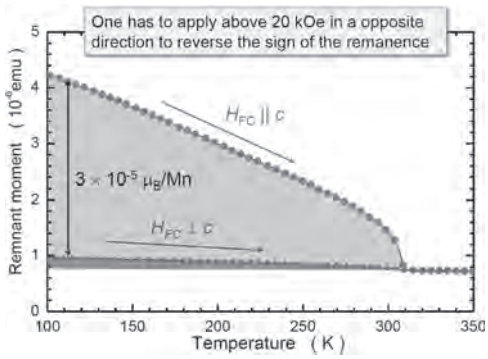

Fig. 2. Temperature dependence of the remnant moment measured along (red) and perpendicular (green) to the hexagonal *c* axis of MnTe. The orange area marks the magnitude of the WFM-like moment, vanishing at the Néel temperature

AE-13. Giant strain-induced spin splitting effect in MnTe, a *g*-wave altermagnetic semiconductor. *K. Belashchenko[1] 1. University of Nebraska-Lincoln, Lincoln, NE, United States*

Hexagonal MnTe is an altermagnetic semiconductor with *g*-wave symmetry of spin polarization in momentum space. In the nonrelativistic limit, this symmetry mandates that electric current flowing in any crystallographic direction is unpolarized. However, it is shown that elastic strain is very effective in inducing the spin splitting effect in MnTe. For this analysis, a spin-orbit-coupled k●p Hamiltonian for the valence band maximum at the A point is derived and fitted to eigenvalues calculated from first principles. The spin splitting angle is calculated using the Boltzmann approach in the relaxation-time approximation. The spin splitting gauge factor exceeds 20 near the valence band maximum. Thus, with suitable substrate engineering, MnTe can be used as an efficient source and detector of spin current in spintronic devices. Proper inclusion of the Rashba/Dresselhaus-like spin-orbit coupling is crucial for the correct description of the transport properties of MnTe.

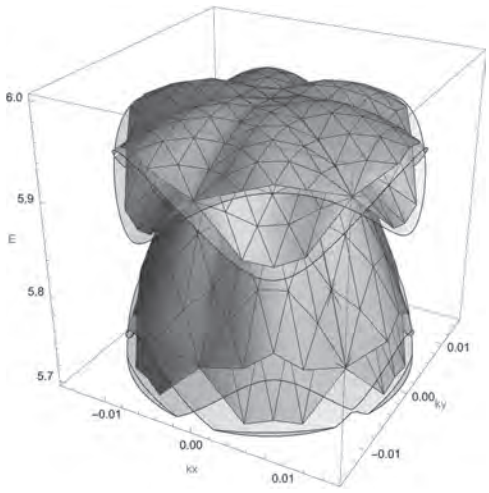

Band dispersion near the A point in MnTe with the Neel vector aligned along the y axis. Colored surfaces with mesh: calculated from first principles. Light transparent surfaces: fitted k●p Hamiltonian.

Session AF
STRUCTURED MATERIALS I

Cristina Gomez-Polo, Chair
Universidad Publica de Navarra, Pamplona, Spain

CONTRIBUTED PAPERS

AF-01. Design and control of three-dimensional topological magnetic fields using interwoven helical nanostructures. *J. Fullerton*[1] and C. Phatak[1,2] *1. Materials Science Division, Argonne national laboratory, Lemont, IL, United States; 2. Department of materials science and engineering, Northwestern University, Evanston, IL, United States*

The control of magnetic fields is of significant importance in many areas of physics, from fusion reactors to particle accelerators [1, 2], and has potential applications in pinning ultracold atoms and drug delivery [3, 4]. As such, it would be advantageous to gain control of localized magnetic fields on the nanoscale. It has recently been shown that three-dimensional (3D) magnetic nanostructures offer a promising platform to create localized topological stray field textures [5]. Focused electron beam induced deposition (FEBID) enables us a route towards the design and realization of functional 3D magnetic nanostructures [6, 7]. In this work, we will discuss the controlled formation of multiple topological stray field textures through reconfiguring the magnetization in a 3D nanostructure. We will outline complementary experimental and micromagnetic studies of nanostructures formed by several interconnected helical nanowires fabricated by FEBID (see example in figure 1a) and characterized by Lorentz transmission electron microscopy and off-axis electron holography. Through the application of a global magnetic field, the magnetization of the nanostructure can be reconfigured to form multi-domain or single domain states. Depending on the form of the magnetization, corresponding arrangements of magnetic charges will arise throughout the nanostructure, leading to unique forms of the emanating stray field. Figure 1b shows an example micromagnetic simulation of a sixfold multipole field cusp originating from an axial single domain magnetic state in an interwoven nanostructure. These results show a further development of how 3D nanostructures could be utilized in the creation of topological magnetic field textures and provide insight into how they can be controllably reconfigured and designed.

[1] J. Ongena, et. al., Magnetic-confinement fusion. *Nat. Phys.*, 12, 398 (2016). [2] M. Johansson, et. al., Magnet design for a low-emittance storage ring, *J. Synchrotron Radiat.*, 21, 884 (2014). [3] A. D. West, et al., Realization of the manipulation of ultracold atoms with a reconfigurable nanomagnetic system of domain walls, *Nano Lett.*, 12, 4065 (2012). [4] B. Wang, et. al., Trends in micro-/nanorobotics: Materials development, actuation, localization, and system integration for biomedical applications, *Adv. Mater.*, 33, 2002047 (2021). [5] C. Donnelly, et. al., Complex free-space magnetic field textures induced by three-dimensional magnetic nanostructures, *Nat. Nanotechnol.*, 17, 136 (2022). [6] L. Skoric, et. al., Layer-by-layer growth of complex-shaped three-dimensional nanostructures with focused electron beams, *Nano Lett*., 20, 184 (2020). [7] J. Fullerton, et. al., Understanding the effect of curvature on the magnetization reversal of three-dimensional nanohelices, *Nano. Lett.*, 24, 2481 (2024) This work was supported by the U.S. Department of Energy, Office of Science, Office of Basic Energy Sciences, Materials Sciences and Engineering Division. Use of the Center for Nanoscale Materials, an Office of Science user facility, was supported by the U.S. Department of Energy, Office of Science, Office of Basic Energy Sciences, under Contract No. DE-AC02-06CH11357.

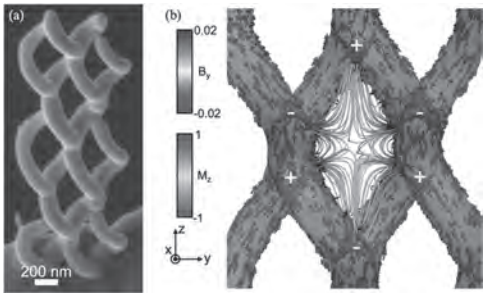

Figure 1: (a) An interwoven cobalt nanostructure fabricated by FEBID. (b) A micromagnetic simulation of the magnetization and resulting stray field in center gap in a single domain state. The magnetization is colored by the M_z component while the stray field is colored by the B_y component, and the purple and green isosurfaces represent areas of maximum and magnetic charge created by the diverging and converging magnetization.

AF-02. 3D Printing of Flexible Magnetic Nanocomposite via Selective Laser Sintering (SLS) with Magnetic Pole Patterning. *N. Tarabay*[1], M. Shakibmanesh[1] and C. Velez[2,1] *1. Department of Electrical Engineering and Computer Science, University of California, Irvine, Irvine, CA, United States; 2. Department of Mechanical and Aerospace Engineering, University of California, Irvine, Irvine, CA, United States*

We present a controllable method for 3D printing magnetic nanocomposites at a sub-millimeter scale using Selective Laser Sintering (SLS). The resulting nanocomposites contain NdFeB or AlNiCo38 nanoparticles (NPs) and Thermoplastic Polyurethane powder in weight ratios of 5-30%, achieving intrinsic coercivities of 0.15 and 1.45 T and $(BH)_{max}$ values of 0.05-0.1 and 0.1-0.5 kJ/m^3, respectively. Polymer-bonded magnetic nanocomposite 3D printing can produce structures with high magnetic properties and complex geometries [1] for various applications, including microrobotics [2], sensors [3], and actuators [4]. Post-printing magnetization has significantly enhanced $(BH)_{max}$ [5]. In this work, we leverage SLS advancements to achieve printed pixel sizes of 100 μm and finely tune the magnetic response by controlling the NPs and their concentration inside the polymer matrix and magnetically pattern poles in different directions. Compared with previous results reported at MMM [6], this method increased M_s by 218% and improved $(BH)_{max}$ by 250%. The effect of NPs concentration on magnetic properties was evaluated using a Vibrating Sample Magnetometer (VSM). We report a new method to assess composite morphology using nano-CT. Fig. 2 shows a 30% NdFeB sample with a volume fraction of 3.5% and a particle size of 40 μm, with no signs of aggregation. A 12 x 12 x 1.5 mm AlNiCo38 structure was also printed and magnetically patterned with ~3 mm alternating poles, as shown by scanning hall probe measurements in Fig. 2b. Our SLS printing method shows a 40% increase in volume fraction compared to DLP, expanding the potential for printing multiple ferromagnetic materials and selective magnetization of multiple pole directions.

[1] K. Schäfer, T. Braun and S. Riegg, *Materials Research Bulletin*., Vol. 158, p. 112051 (2023) [2] R. Li, M. Jiang and B. Liu, *Lab on a Chip.,* Vol. 24, no. 4, p. 832-842 (2024) [3] E. Fontana, L. Motyckova and C. Tomba, *IEEE*

Transactions on Magnetics., Vol. 58, no. 2, p. 1-5 (2021) [4] M. Khalid, Z. Arif and A. Tariq, *European Polymer Journal*., Vol. 205, p. 112718 (2024) [5] K. Gandha, L. Li and I. C. Nlebedim, *Journal of Magnetism and Magnetic Materials.,* Vol. 467, p. 8-13 (2018) [6] N. Tarabay, J. Lopez Medina and C. Velez, *Magnetism and Magnetic Materials Conference.,* (2023)

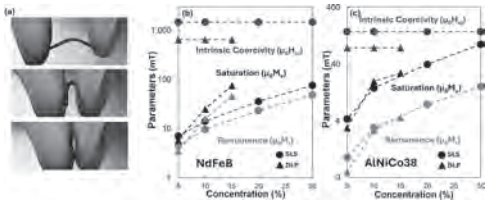

Fig.1 (a) Flexible printed magnetic nanocomposite (NdFeB 30%). Summary of the magnetic properties with weight percentage variation (a) NdFeB, (b) AlNiCo38.

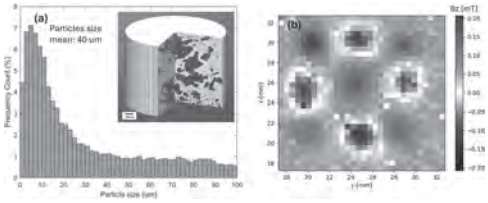

Fig.2 (a) Particle size distribution extracted from nano-CT showing an average particle size of 40 um. 3D constructed volume of the printed magnetic nanocomposite with polymer in white and NdFeB NPs in red (inset). (b) Gaussmeter scan of a 12 x 12 x 1.5 mm^3 printed AlNiCo38 structure, magnetically patterned with 9 distinct poles using a custom-made magnetization head.

AF-03. Soft X-ray Tomography of Curvilinear Spin Textures.
D.W. Raftrey[1,2], P. Fischer[1,2], O. Bezsmertna[3], R. Xu[3], D. Makarov[3], D. Bhattacharya[4], C. Langton[4], K. Liu[4] and A. Sorrentino[5] *1. Material Sciences Division, Lawrence Berkeley National Laboratory, Berkeley, CA, United States; 2. Physics, University of California, Santa Cruz, Santa Cruz, CA, United States; 3. Intelligent Materials and Systems, Helmholtz-Zentrum Dresden-Rossendorf, Dresden, Germany; 4. Physics, Georgetown University, District of Columbia, DC, United States; 5. MISTRAL beamline, ALBA Light Source, Cerdanyola del Vallès, Spain*

The curvature degree of freedom is of fundamental importance to the formation and structural properties of magnetic spin textures (1, 2). Here, soft x-ray tomography reveals three-dimensional spin textures on curved scaffolds at nanoscale resolution. We present results from experiments at the MISTRAL beamline of the ALBA synchrotron on a variety of curved geometries. Samples include a Co/Pd multilayer film grown over curved surfaces of Cu nanowire networks, and a nano-flower permalloy lattice hosting curvature-induced vortices (fig. 1). From tilt series of hundreds of individual projections, the data are analyzed in three dimensions. The circularly polarized images contain both the structural curvature information and the magnetic contrast from domain walls (XMCD). In the nanowire network, a quantitative three-dimensional analysis finds the Gaussian curvature couples asymmetrically to the spin texture in the curved Co/Pd films. Saddle points at the crossings of nano-wires with negative Gaussian curvature promote the formation of domain walls, while regions of positive Gaussian curvature in the network inhibit the formation of domain walls (fig. 2). The nano-flower samples host vortices deflected by the curvature. This lateral deflection is a consequence of curvature not observed in planar samples. These results demonstrate the effectiveness of a metal-on-scaffold approach to fabricating and characterizing curvilinear spin textures, opening a flexible design space for future experiments. This work was supported by the U.S. Department of Energy, Office of Science, Office of Basic Energy Sciences, Materials Sciences and Engineering Division under Contract No. DE-AC02-05-CH11231 within the Non-equilibrium Magnetic Materials Program. Work at GU was supported by the NSF (DMR-2005108)

1. Sheka, D. D. et al. Commun Phys 3 (2020) 2. Makarov, D. et al. Advanced Materials 34 (2022)

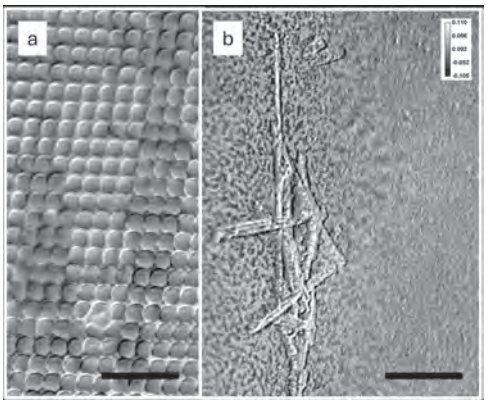

(a) Permalloy nano-flowers hosting magnetic vortices.(b) Co/Pd multilayer film grown over curved surfaces of Cu nanowire networks. All scale bars are 2 μm.

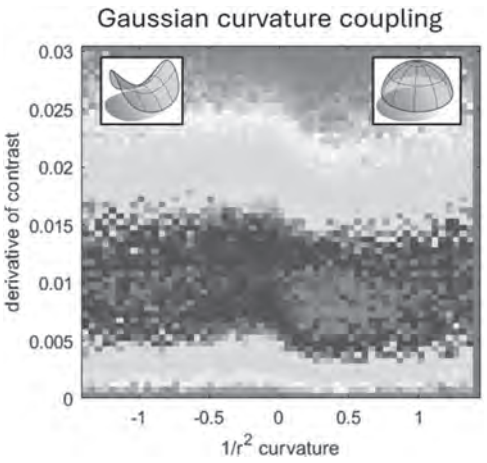

Quantified coupling between the derivative of XMCD contrast indicating magnetic domain walls and Gaussian curvature in a Co\Pd film coating a Cu nanowire network.

AF-04. Domain wall dynamics in cylindrical nanowires under high current pulses.
C. Bran[5], E. Saugar[6], S. Catalano[1], J. Marqués-Marchán[6], R. Perez Del Real[6], A. Asenjo[6], M. Foerster[2], M. Angel[2], A. Fraile Rodríguez[3], M. Vázquez[6], F. Casanova[4] and O. Chubykalo-Fesenko[6] *1. Centro de Física de Materiales CFM/MPC (CSIC-UPV/EHU), San Sebastian, Spain; 2. ALBA Synchrotron, Cerdanyola del Valles, Spain; 3. Universitat de Barcelona, Barcelona, Spain; 4. CIC nanoGUNE, San Sebastian, Spain; 5. Instituto de Nanociencia y Materiales de Aragón (INMA-CSIC), Universidad de Zaragoza, Zaragoza, Spain; 6. Institute of Materials Science of Madrid, Madrid, Spain*

Cylindrical magnetic nanowires are the basic examples of curved nanostructures that exhibit 3D textures and complex chiral domain walls [1,2]. Their domain walls (DWs) can be integrated into 3D spintronic architectures where they will act as information carriers. For future applications, understanding their dynamics under applied current is crucial. Here we report on the influence of current pulses and thermal gradients in Ni nanowires

with diameter of 100 nm. The magnetic texture of nanowires (NWs) before and after each applied current pulse was imaged by XMCD-PEEM. First, DWs were nucleated by high current pulses (>10 ^{12} A/m^2) which raise the temperature in the middle part of the NW above the Curie temperature and provide thermal nucleation [3]. The nucleated DWs, positioned towards the ends of the NW, are moved with low current pulses in the direction antiparallel to the applied current. The data show that for 20 ns current pulses of higher amplitude (7x10^{11} A/m^2) the DWs are moved in both directions, i.e, parallel and anti-parallel to the current. By applying repeatedly, the same pulse to the NW, the DWs are moving left and right around the initial position, bouncing from the nanowire ends (Fig. 1). We explain the origin of the observed behavior by a competition between the spin-transfer torque and the temperature gradient, created by Joule heating. Under the action of current and Oersted field, the DWs are pushed to the NW ends. After the pulse current is over, the temperature action moves DW back to the hotter region. The overall effect is a new DW position, different from the previous one. However, a large "bouncing" effect is produced only when the temperature goes close and even above the Curie temperature on ns timescale. In this case, for several ns the system gets almost demagnetized and DWs are almost destroyed but finally are re-nucleated under very strong thermal fluctuations. The results suggest that even strong current pulses are not able to remove DWs from the NW which may be very important for their potential applications.

[1]A. Fernández-Pacheco et al al., Nat. Commun, 8 (2017) 1 [2]R. Hertel, J. Phys. Condens. Matter 28 (2016), 483002. [3]C. Bran et al., Nanoscale 15 (2023), 8387.

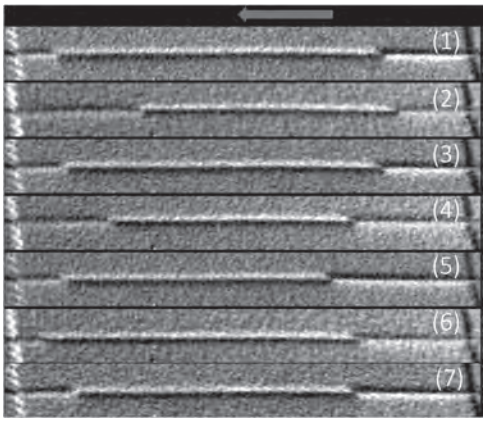

Fig.1. Sequence of XMCD-PEEM images taken after a current pulse was applied repeatedly along the NW.

AF-05. Interface Exchange Coupling in Hollow Nanostructures.
S. Slimani[1,2], M. Vasilakaki[3], K. Trohidou[3], N. Yaacoub[4] and D. Peddis[1,2]
1. Department of Chemistry and Industrial Chemistry, University of Genova, Genova, Italy; 2. Institute of Structure of Matter, National Research Council, Rome, Italy; 3. Institute of Nanoscience and Nanotechnology, NCSR "Demokritos", Attiki, Greece; 4. Institut Des Molécules Et Matériaux du Mans (IMMM) CNRS UMR, Le Mans, France

In the nanometer-scale regime, the surface to volume ratio (R=S/V) of nanoparticles becomes significantly large. This large R value has been proven to be a key factor for modified or novel magnetic properties of nanomaterials compared to those of the corresponding bulk materials. In this scenario, an interesting class of nanostructures, is the hollow nanoparticles (NPs), having both internal and external surfaces, which further amplifies the value of R [1]. Here, we present a comparative study of the morpho-structural and magnetic properties of full and hollow maghemite (γ-Fe_2O_3) nanoparticles, characterized by a big surface to volume ratio, of corresponding sizes 5.0(5) nm and 7.4(7) nm. These systems have been thoroughly characterized by means of DC and AC magnetization measurement and in field ^{57}Fe Mössbauer spectrometry. The in-field hyperfine structure analysis suggested the presence of a non-collinear structure for hollow NPs originated from the increased surface effects due to the hollow morphology. Interestingly, after field cooling, a horizontal shift of the hysteresis loop was observed. This exchange bias effect has been investigated as a function of the temperature and the cooling field. Monte Carlo (MC) simulations on assemblies of ferrimagnetic hollow nanoparticles show that the spins in the external thicker surface and at the interface are strongly exchange coupled. This strong exchange coupling enhances the antiferromagnetic character of the hollow nanoparticle, leading to the decrease of its saturation magnetization (M_s). At the interface, this strong exchange coupling results in a strong exchange bias inducing an increase of the coercive field, in agreement with the experimental findings.

[1]F. Sayed, N. Yaacoub, Y. Labaye, R.S. Hassan, G. Singh, P.A. Kumar, J.M. Greneche, R. Mathieu, G.C. Hadjipanayis, E. Agostinelli, D. Peddis. J. Phys. Chem. C. 122 (2018)

AF-06. Experimentally probed magnetic reversal modes in Fe_3O_4 magnetic nanotubes, including solid-state dewetting effects.
J.L. Palma[1,2], A. Pereira[3], E. Saavedra[4] and J. Escrig[4,2] *1. Engineering School, Universidad Central de Chile, Santiago, Chile; 2. Center for The Development of Nanoscience And Nanotechnology CEDENNA, Santiago, Chile; 3. Universidad Adolfo Ibañez, Santiago, Chile; 4. Physics Department, Universidad de Santiago de Chile, Santiago, Chile*

Our research involved the synthesis of magnetic nanotubes through atomic layer deposition (ALD) within alumina membranes. We varied the diameters of the pores while keeping other geometric parameters constant, such as the wall thickness of the nanotubes and the distance between them. We then synthesized magnetite (Fe3O4) nanotubes via ALD, resulting in a subsequent oxygen reduction. The morphology of the nanotubes was thoroughly investigated using electron microscopies, and energy dispersive spectroscopy analysis provided a detailed compositional analysis of the magnetic iron oxide. We studied the magnetization as a function of the externally applied magnetic field in a vibrating sample magnetometer at room temperature. Our findings revealed different magnetic behaviors in nanotubes with varying external diameters and constant wall thickness. A theoretical approach was used to explain these effects. Solid-state dewetting appears by the oxygen reduction [1], in which hematite (Fe2O3) is transformed into magnetite (Fe3O4), and close to 10% of the sample is loosed. Every nanopore created by solid-state dewetting acts as a nucleation point of the magnetization and creates a more active surface for biological applications. Despite the presence of multiple nucleation spots, our research demonstrates the ability to control the reversal of magnetization. We conducted micromagnetic simulations to gain a deeper understanding of the magnetization process. Theory suggests that the change in an individual nanotube's external radius directly influences its magnetic reversal mode, which is reflected in the macroscopic magnetic behavior of the entire sample [2]. The authors acknowledge the financial support from Fondecyt for projects 1240829, 1201491, EQM200216, EQM210088, and BASAL financing under project FB220001.

[1] A. P. Espejo, R. Zierold, and J. Gooth, Nanotechnology., Vol. 27, p.345707 (2016). [2] J. Escrig, J. Bachmann and J. Jing, Physical Review B., Vol. 77, p.214421 (2008).

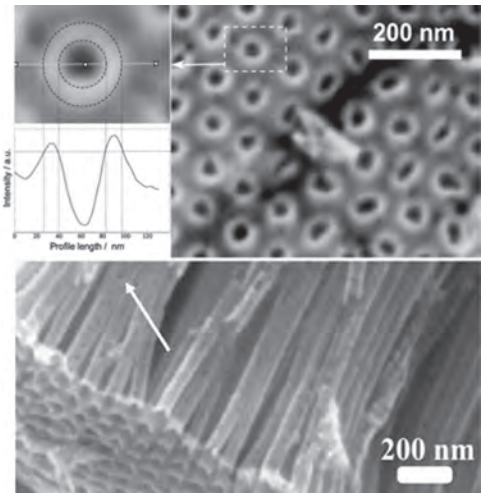

Fe_3O_4 Nanotubes in porous alumina membranes with 53 nm of pore diameter and wall thickness of 15 nm. (below) SEM image of nanotubes released from an alumina template.

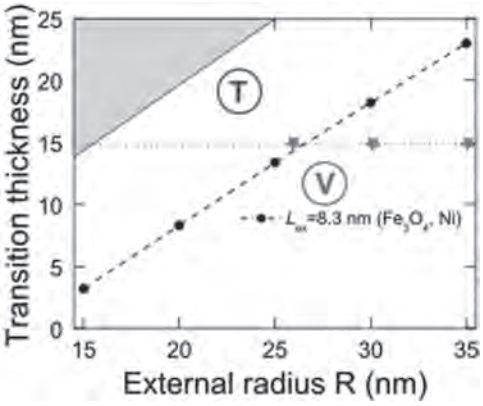

Trajectory of the transition thickness as a function of the external radius (R) for Fe3O4, black circles [4], and the three experimental cases synthesized for nanotubes of 25, 30 and 35 nm Radius.

AF-07. Magnetic field driven spatial light modulators made by giant vertically aligned nanocomposites of garnet and perovskite.

K. Hayashi[1], Y. Kunai[1,2], P.E. Lauer[1] and C.A. Ross[1] *1. Department of Materials Science and Engineering, Massachusetts Institute of Technology, Cambridge, MA, United States; 2. Advanced Research Core, Fujikura Limited, Kouto-ku, Japan*

Self-assembled vertically aligned nanocomposites (VANs) consisting of ferromagnetic pillars within a non-magnetic matrix have been studied extensively [1]. However, it is difficult to make giant VANs with a micrometer-thickness by self-assembly because self-assembly relies on elemental diffusion to form the pillars and matrix structure. We here propose a solution for making such thick VANs relevant to magneto-optical devices, which require micron-thick magnetic materials to provide a sufficient Faraday rotation [2]. We have found that films made by pulsed laser deposition (PLD) using a target composition of $A_3Fe_5O_{12}$ (A = Y, Bi or rare earth) form an epitaxial ferrimagnetic iron garnet on a $Gd_3Ga_5O_{12}$ (GGG) substrate but in contrast form a Fe-rich perovskite (Fe-rich $AFeO_3$) when grown on a $SrTiO_3$ (STO) substrate [3,4]. By defining pixel structures consisting of a patterned polycrystalline STO seed-layer on a GGG substrate, and then depositing a film with composition $A_3Fe_5O_{12}$, we fabricated 1~2 μm-thick garnet-perovskite VANs working as magnetic field driven spatial light modulators (SLMs). The garnet-perovskite VANs were made using electron-beam lithography (EBL) and PLD. The polycrystalline STO seed-layer was prepared by EBL on GGG substrates followed by the liftoff of a 10 nm amorphous STO film which is then crystallized. Then, a film with the composition of $Y_3Fe_5O_{12}$ (YIG) or $Bi_{1.5}Y_{1.5}Fe_5O_{12}$ (Bi-YIG) was deposited onto the STO/GGG template at 560~720°C substrate temperature. Figure 1 shows a cross-sectional SEM image of a YIG VAN with 1x1 um square YIG pixels separated by 2 μm of a Fe-rich YFO matrix, demonstrating that giant VANs can be fabricated by this method. A 1.5μm-thick Bi-YIG VAN with four pixels was fabricated on a double-sided polished GGG with an aluminum mirror on the backside. Interference patterns of reflected light through the Bi-YIG VAN with and without a perpendicular magnetic field (~0.07 T) are shown in Fig. 2. The interference patterns clearly change with and without the magnetic field, demonstrating that the Bi-YIG VAN functions as a magnetic field driven SLM. In the presentation, we will discuss in more detail the magnetic and magneto-optical properties of the VANs.

1: O. J. Lee, S. Misra, and J. L. MacManus-Driscoll, *APL Mater* 9, 030904 (2021). 2: S. Kharratian, H. Urey, and M. C. Onbashi, *Adv. Optical Mater.* 8, 1901381 (2020). 3: S. Ning, A. Kumar, and C. A. Ross, *Nat. Commun.* 12, 4298 (2021). 4: T. Su, S. Ning and C. A. Ross, *Phys. Rev. Mater.* 5, 094403 (2021).

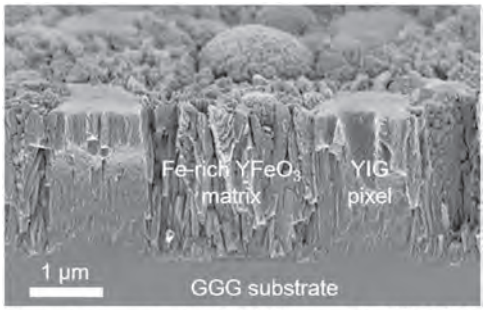

Figure 1: Cross-sectional SEM image of the YIG VAN.

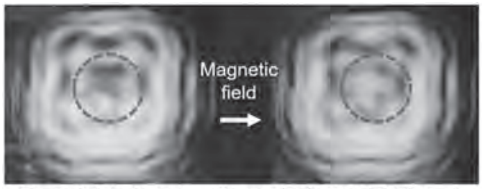

Figure 2: Interference patterns of reflected light through the Bi-YIG VAN with and without a perpendicular magnetic field (wavelength of the light is 532 nm).

AF-08. Engineering the Self-assembly of Epitaxial $CoFe_2O_4$ – $BiFeO_3$ Multiferroic Nanocomposites Using Focused Ion Beam Lithography.

R. Huynh[1], T. Su[1] and C.A. Ross[1] *1. Massachusetts Institute of Technology, Cambridge, MA, United States*

The coupling between ferroelectricity and ferromagnetism in magnetoelectric (ME) multiferroics enables the magnetization to be reorientated using electrical field and vice versa [1]. Hence, they are promising materials for low-power devices. Currently, one of the methods to create multiferroics is vertically aligned nanocomposites (VANs), which consist of magnetic nanopillars embedded in a ferroelectric matrix. The ME coupling is achieved via strain transfer at the interface, as in the epitaxial thin films consisting of ferrimagnetic spinel $CoFe_2O_4$ (CFO) and ferroelectric perovskite $BiFeO_3$ (BFO). Controlling the shape, geometry, and arrangement of CFO nanostructures is essential for implementation into devices [2]. Here we use focused ion beam (FIB) and pulsed laser deposition (PLD) to create ordered CFO/BFO VANs on a (111)-oriented conductive Nb-doped $SrTiO_3$ substrate and a (111)-oriented nonconductive $SrTiO_3$ substrate [3]. The process consists of three steps. First, Au-coated substrates are fabricated with different geometric patterns using FIB. They are then etched and annealed to develop an array of 2 nm deep trenches with spacings of 100 nm. Second, when CFO is deposited using PLD, CFO seeds preferentially nucleate inside the

patterned pits, forming 1 nm high fin-shaped structures. Third, BFO and CFO are co-deposited; BFO matrix forms on the mesa while CFO continues growing on top of existing seeds from previous deposition. Using this approach of patterning trenches in <110>-direction with PLD growth steps, alternating fin-shaped CFO/BFO structures are made in which the fins, of width 100 nm, lie parallel to <110> in plane directions. We then use probe microscopy to characterize ferroelectric, and magnetic properties. Specifically, magnetic domain structures of the CFO in the samples are imaged using magnetic force microscopy with and without an in situ in plane field of 2 kOe. At remanence, the CFO fins exhibit domains oriented parallel to the fins with head-to-head 180 degree domain walls, but a 2 kOe field saturates the magnetization in plane.

[1] N. A. Spaldin and R. Ramesh, *Nature Mater*, *18* (3), 203–212 (2019) [2] R. Comes, H. Liu and S. A. Wolf, *Nano Lett.*, *12* (5), 2367–2373 (2012) [3] T. Su, Y. Yu and C. A. Ross, *Nano Lett., 24 195* (2024)

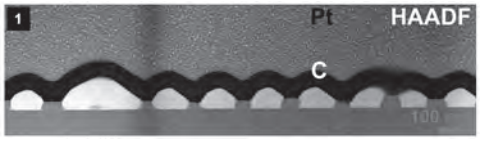

Fig.1 TEM cross section showing BFO (bright) and CFO (grey) fins on STO, with a C/Pt coating.

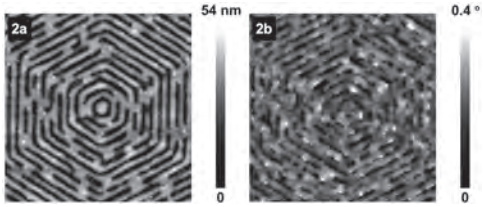

Fig.2 (a) AFM and (b) remanent MFM images of a hexagonal pattern.

AF-09. Withdrawn

AF-10. Surface Spin Configurations in Magnetic Nanoparticles. *N. Kim*[1], H. Wang[2], H. Chen[2] and S. Majetich[2,1] *1. Materials Science and Engineering, Carnegie Mellon University, Pittsburgh, PA, United States; 2. Physics, Carnegie Mellon University, Pittsburgh, PA, United States*

Both exchange interactions and anisotropy may differ for surface spins, relative to those in a nanoparticle interior. Understanding and finding the cause of the nanoscale spin configuration of magnetic nanoparticles has been challenging due to the gap in between the available simulations and the limitation of experiments. One of the few techniques that can reveal three-dimensional magnetic correlation lengths on a nanometer length scale is polarization-analyzed small-angle neutron scattering (PASANS) [1-2]. Three kinds of spinel ferrite nanoparticles [3-5] showed very different PASANS correlations. Here we describe a Fourier transform method that enables exploration of magnetic scattering from complex spin configurations from different proposed models [6], assuming the differences arise from variations in a shell of surface spins (Figure 1). Python was used to generate models of the surface spin configuration and calculate the projected Fourier transforms for conditions where the cores would be aligned in the x-direction by an external field. Simulations of the single particle M_x^2, M_y^2, and M_z^2 scattering intensities showed a unique signature for the M_x^2, M_y^2, and M_z^2 scattering intensities for the different models. Figure 2 shows the result of the shell simulation of M_x^2. The location of the dips distinguishes the spherical shell form factors for the different models. With the combination of simulation and experiment results, the unique spin configurations of the magnetic nanoparticles can be further explained. Fitting the experimental data requires additional consideration of the structure factor for the FCC assemblies of nanoparticles, and the spread of neutron wavelengths. Co ferrite [4] agrees best with uniformly magnetized particles, Fe_3O_4 [3] with a uniform but canted shell, and Fe_3O_4 core/Mn ferrite [5] with a throttle model.

[1] K. L. Krycka, et al., Physica B 404, 2561 (2009). [2] K. Krycka, et al., J. Appl. Crystallogr. 45, 554 (2012). [3] K. L. Krycka, et al., Phys. Rev. Lett. 104 207203 (2010). [4] K. Hasz, et al., Phys. Rev. B 90, 180405(R) (2014). [5] S. D. Oberdick, et al., Scientific Reports 8, 3425 (2018). [6] L. Berger, et al., Phys. Rev. B 77, 104431 (2008).

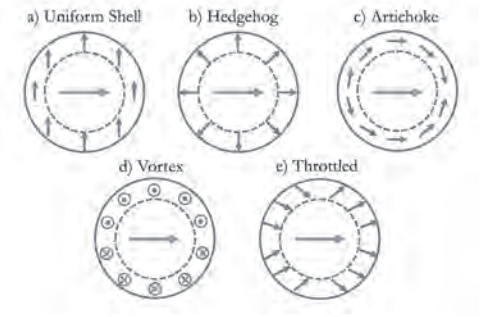

Fig 1: Schematics of the non-collinear nanoparticles simulated. The particles have core moments pointed to the right (gray) and the calculations for the shells alone have moments indicated in red.

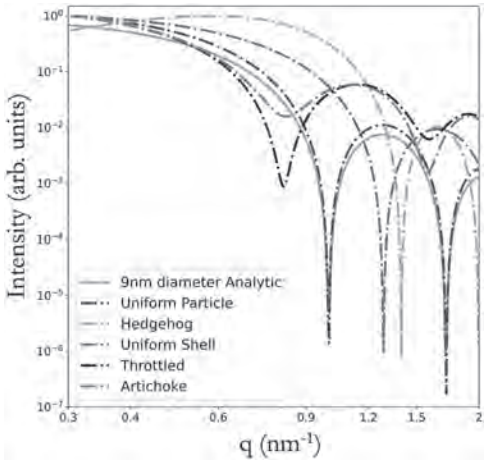

Fig 2: Single Particle intensity plot of M_x^2 vs. q of various spin configuration models (The vortex model does not have any magnetization pointing in the x-direction).

AF-11. DFT Guided Synthesis of Substituted Ferrite Magnetic Nanoparticles to Study Effective Magnetic Anisotropy. *A.D. Malaj*[1], C. Leies[1], S.S. Laha[1], V.R. Punyapu[2], R. Getman[2] and O.T. Mefford[1] *1. Materials Science and Engineering, Clemson University, Clemson, SC, United States; 2. William G. Lowrie Department of Chemical and Biomolecular Engineering, The Ohio State University, Columbus, OH, United States*

Multi-metallic nanoparticles have recently surged in interest to synthesize better catalysts, as increased catalytic activity in alcohol oxidation and dehydrogenation reactions have been reported from adding additional metals to the nanoparticles.[1] Catalytic activity, and the performance of these magnetic nanoparticles is highly dependent on their composition, morphology, and dimensions.[2] Specifically, tuning the magnetic anisotropy energy (K) and magnetic saturation (Ms) of superparamagnetic nanoparticles is highly sought after, as the optimal values for these properties will change depending on their application. Recently computational models were used to explore what effect tri-metallic substitutions have on the magnetic saturation and anisotropy energy for ferrite compositions.[3] A ferrite model was used based

on the calculated bulk unit cell of magnetite (Fe_3O_4). Eight repeats of the magnetite formula unit ($Fe_{24}O_{32}$) were used for many different ion substitutions. Among these bi-metallic and tri-metallic ion substitutions, magnetic saturation, magnetic anisotropy energy, and crystal structure were simulated. In this work, nanoparticles of $Fe_{3-x-y}Mn_xCo_yO_4$ were synthesized with targeted compositions based on the tertiary diagrams created from the computational models. The particles were synthesized an oleate precursor drip, following a modified thermal decomposition route based off the extended LaMer synthesis.[4] The nanoparticles' were monodisperse from transmission electron microscopy (TEM). Vibrating sample magnetometry (VSM) was used to experimentally obtain DC and AC magnetic data for each of the targeted compositions. The magnetic saturation (Ms) obtained from the DC magnetic experiments showed interesting correlations with the computationally derived values. The magnetocrystalline anisotropy values obtained from the AC magnetic data were also correlated with the computationally derived values. Additionally, AC magnetometric and calorimetric studies were conducted to evaluate the hyperthermia potential of the compositions.

1. S. A. Kondrat, P. J. Miedziak, M. Douthwaite, G. L. Brett, T. E. Davies, D. J. Morgan, J. K. Edwards, D. W. Knight, C. J. Kiely and S. H. Taylor, ChemSusChem 7 (5), 1326-1334 (2014). 2. J. W. Crawley, I. E. Gow, N. Lawes, I. Kowalec, L. Kabalan, C. R. A. Catlow, A. J. Logsdail, S. H. Taylor, N. F. Dummer and G. J. Hutchings, Chemical Reviews 122 (6), 6795-6849 (2022). 3. V. R. Punyapu, J. Zhu, P. Meza-Morales, A. Chaluvadi, O. T. Mefford and R. B. Getman, arXiv preprint arXiv:2309.09754 (2023). 4. B. D. Fellows, S. Sandler, J. Livingston, K. Fuller, L. Nwandu, S. Timmins, K. A. Lantz, M. Stefik and O. T. Mefford, IEEE Magnetics Letters 9, 1-5 (2017).

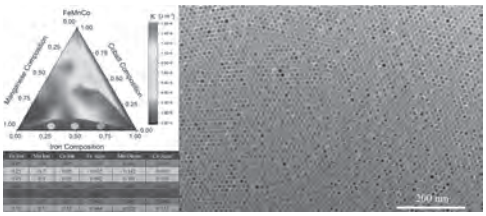

Figure 1. Tertiary diagram with metallic compositions depicted on the left. Representative TEM image of the nanoparticles on the right.

AF-12. Withdrawn

AF-14. Investigation of Element Mutual Interaction in Nanopatterned Ferromagnetic Thin Film Array. *H. Yin*[1] and A. El-Ghazaly[1] *1. Electrical and Computer Engineering, Cornell University, Ithaca, NY, United States*

Magnetic thin films have been widely incorporated in various microwave components including inductors [1], antennas [2], filters [3], phase shifters [4], etc., to increase inductance, miniaturize components for chip integration, and achieve magnetic tunability. Patterning magnetic thin film has been proposed to reduce eddy current loss and achieve higher quality factor at high frequencies [5], but without sufficient optimization of the pattern array, such an approach can in fact sacrifice magnetic permeability and inductance (though increase bandwidth) [6]. Additionally, while some previous works have exploited the shape anisotropy of patterns to design for specific ferromagnetic resonance (FMR) frequency based on the Kittel Equation [7], the effect of mutual interaction between the pattern elements is difficult to incorporate in two dimensions [8]. In this work, we systematically simulated the mutual interaction between elements of rectangular ferromagnetic ($Fe_{65}Co_{35}$) pattern arrays. We found that among the four nearest neighboring elements, the longitudinal elements (along the remanent magnetization direction) impose stronger ferromagnetic interaction field magnitudes than lateral elements, which contribute antiferromagnetic interaction. When a low external bias field (parallel to the magnetization) is applied, the interaction field lines become attracted by the longitudinal neighboring elements; at high bias fields where magnets are saturated, the returning flux results in a net antiferromagnetic interaction field, working to reduce the magnetization in laterally-adjacent patterns. For arrays covering the same percentage of the total area with the same gap length, patterns with higher aspect ratios have weaker longitudinal interactions. Therefore, we systematically show the influence of aspect ratio, proximity, and external bias on the magnetic interaction fields, and the resulting effects on higher FMR and permeability. Our study provides valuable guidance for designing magnetic thin film pattern arrays for radio frequency (RF) devices.

[1] T. Dastagir, W. Xu, S. Sinha, H. Wu, Y. Cao, and H. Yu, "Tuning the permeability of permalloy films for on-chip inductor applications," *Appl Phys Lett*, vol. 97, no. 16, p. 162506, Oct. 2010, doi: 10.1063/1.3502478. [2]

G.-M. Yang *et al.*, "Tunable Miniaturized Patch Antennas With Self-Biased Multilayer Magnetic Films," *IEEE Trans Antennas Propag*, vol. 57, no. 7, pp. 2190–2193, 2009, doi: 10.1109/TAP.2009.2021972. [3] B. Kuanr, Z. Celinski, and R. E. Camley, "Tunable high-frequency band-stop magnetic filters," *Appl Phys Lett*, vol. 83, no. 19, pp. 3969–3971, Nov. 2003, doi: 10.1063/1.1625424. [4] T. Wang *et al.*, "High-Performance Electrically Tunable RF Phase Shifter With the Application of PZT and Permalloy Thin-Film Patterns," *IEEE Trans Magn*, vol. 51, no. 11, pp. 1–4, 2015, doi: 10.1109/TMAG.2015.2446520. [5] T. Wang *et al.*, "Integrating Nanopatterned Ferromagnetic and Ferroelectric Thin Films for Electrically Tunable RF Applications," *IEEE Trans Microw Theory Tech*, vol. 65, no. 2, pp. 504–512, 2017, doi: 10.1109/TMTT.2016.2616869. [6] M. Yamaguchi, K. Yamada, and K. H. Kim, "Slit Design Consideration on the Ferromagnetic RF Integrated Inductor," *IEEE Trans Magn*, vol. 42, no. 10, pp. 3341–3343, 2006, doi: 10.1109/TMAG.2006.879636. [7] Y. Wu, Y. Yang, F. Ma, B. Zong, Z. Yang, and J. Ding, "Microwave permeability of stripe patterned FeCoN thin film," *J Magn Magn Mater*, vol. 426, pp. 467–472, 2017, doi: https://doi.org/10.1016/j.jmmm.2016.11.064. [8] V. Boucher, L.-P. Carignan, T. Kodera, C. Caloz, A. Yelon, and D. Ménard, "Effective permeability tensor and double resonance of interacting bistable ferromagnetic nanowires," *Phys Rev B*, vol. 80, no. 22, p. 224402, Dec. 2009, doi: 10.1103/PhysRevB.80.224402.

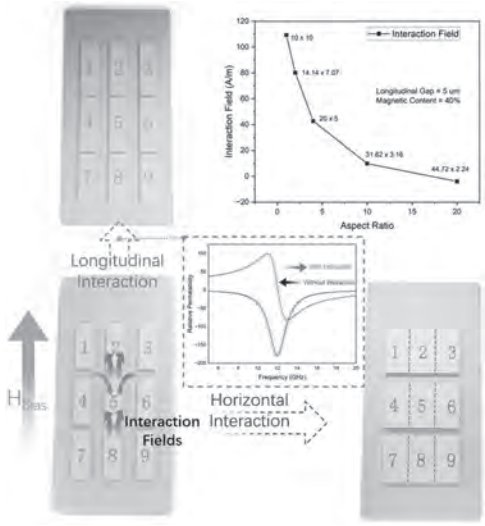

Fig. 1: Interaction fields in patterned magnetic arrays

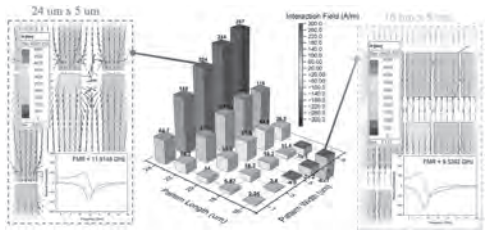

Fig. 2: Pattern dimensions vs interaction fields

AF-15. Tailoring Spin Textures in $La_{0.7}Sr_{0.3}MnO_3$-based Micromagnets.

D. Sasaki[1,2], T. Sahoo[1], I. Nihal[1], I. Snowden[1], M. Frame[1], S. Retterer[3], B. Achinuq[2], A. Scholl[2], P. Rickhaus[4], J. Lenz[4] and *Y. Takamura*[1]
1. Materials Science and Engineering, University of California, Davis, Davis, CA, United States; 2. Advanced Light Source, Lawrence Berkeley National Laboratory, Berkeley, CA, United States; 3. Center for Nanophase Materials Sciences, Oak Ridge National Laboratory, Oak Ridge, TN, United States; 4. QNami, Muttenz, Switzerland

The development of next-generation computing devices based on spintronics and magnonics requires an understanding of how magnetic spin textures can be tailored in patterned magnetic materials. Complex oxides such as $La_{0.7}Sr_{0.3}MnO_3$ (LSMO) offer a unique capability to tailor the observed spin textures due to their strong interactions between the lattice, charge, spin, and orbital degrees of freedom. In this work, an ion implantation-based patterning process was used to define magnetic islands embedded within a non-magnetic matrix [1] which results in a complex 3D strain state within the micromagnets involving tensile strain from the underlying $SrTiO_3$ (STO) substrate and lateral compressive strain from the surrounding implanted matrix. These LSMO micromagnets are defined into a variety of shapes (circles, squares, triangles, and hexagons with their edges oriented along different low index crystallographic directions) with and without their core regions removed (aka donut structures). The resulting spin textures are imaged using both x-ray photoemission electron microscopy (see Figure 1) and scanning N-V magnetometry. We find that the combined effects of the removal of the core region and the resulting strain profile affects the energetic balance between shape and magnetocrystalline anisotropy energies, which can be quantified through the ratio of vortex and Landau states.[2] These results demonstrate that complex oxide thin films and heterostructures serve as unique platforms for engineering spin textures for next generation spin-based devices.

[1] Y. Takamura *et al., Nano Letters,* 6 1287 (2006) [2] M.S. Lee, Y. Takamura *et al., ACS Nano,* 10, 8545 (2016)

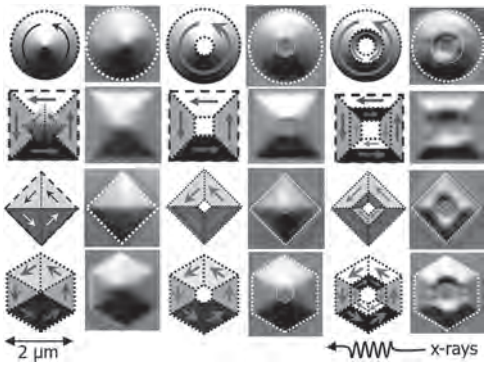

Figure 1: X-PEEM images of 2-micron wide micromagnets patterned into an LSMO thin film with and without their core regions removed. Schematics illustrate the corresponding ferromagnetic spin textures associated with each shape.

Session AG
ELECTRICAL MACHINES AND POWER ELECTRONICS I
Chins Chinnasamy, Chair
Oak Ridge National Laboratory, Knoxville, TN, United States

INVITED PAPER

AG-01. Development of inductor and transformer with both small iron loss and small copper loss for high frequency power converters.
T. Sato[1] and T. Mizuno[1] *1. Electrical and Computer Engineering, Shinshu University, Nagano, Japan*

1. Background Recently transformer and inductor have become a bottleneck when increasing both conversion efficiency and volumetric power density of the advanced power converters using SiC or GaN power device. Such the bottleneck is owing to the increase of both iron loss of the magnetic core material and ac copper loss of the winding at high frequency of hundreds of kHz or beyond. 2. Development of magnetic cores with small iron loss Fe-based nanocrystalline alloy has very small crystalline magnetic anisotropy and very small magnetostriction constant, these features conduct to very small hysteresis loss. Therefore, if the eddy current loss at high frequency can be reduced, small iron loss can be realized. As the first example, 18 um thick Co-Pd substituted FINEMET composition anisotropic ribbon [1] was fabricated for transformer core magnetized in the hard magnetization direction (i.e., the rotation magnetization reversal for getting minimum eddy current loss), which exhibited a relative permeability of about 10,000 at 100 kHz, 60% smaller iron loss compared to the conventional FINEMET ribbon and over 50 % smaller iron loss below 100 kHz compared to the Mn-Zn ferrite. As the second example, FINEMET composition plate-shape powder core was fabricated, which exhibited much smaller iron loss compared to the conventional polycrystalline Fe-Si, Ni-Fe and Fe-Al-Si spherical powder core. 3. Development of winding with small ac copper loss The ac copper loss is due to nonuniform current density in the winding conductor, where it is caused by eddy current induced by ac magnetic flux passing through the winding conductor, therefore, the magnetic flux path control (MPC) scheme [2] for reducing the magnetic flux through the winding conductor is necessary to realize small ac copper loss. Two types of MPC scheme were proposed. One was the conductor surrounded by magnetic material, such the magnetic sheath was MPC material with relative permeability lower than that of main magnetic core, the MPC material played a role of bypath of the ac magnetic flux passing through the conductor. The other was the planar winding molded by MPC material to fill the spacing between adjacent conductors, and the molded planar winding for planar device was put into inside the outer planar magnetic core. The MPC magnetic material played to reduce the ac magnetic flux (leakage component from the outer magnetic core) passing through the inner winding conductors. 4. Fabrication example of planar inductor The Fe-based nanocrystalline alloy ribbon core and plate-shape powder core have not yet been applied to transformer and inductor. Here, as a fabrication example, planar inductor with Fe-based amorphous spherical powder core and MPC planar winding. The main magnetic circuit consisted of powder core with 10 and 3 um size Fe-based amorphous spherical powders, which had a relative permeability of 31 constant up to around 10 MHz. The MPC material for planar winding was the composite consisting of 25 and 3 um size Fe-based nanocrystalline spherical powders and silicone resin, which exhibited a relative permeability of 25 constant up to around 10 MHz. Fig. 1 shows the schematic cross section and photo of the fabricated planar inductor. By introducing the MPC scheme, inductance increase of 37 %, ac resistance reduction of 50 % and Q-factor increase of 174 % were obtained. In case of planar magnetic circuit, Since there is a lot of leakage magnetic flux from the outer magnetic core, the MPC scheme is considered to be better at reducing the power loss than reducing the iron loss.

[1] Toshiro Sato et al., INTERMAG2023, HA-04 (invited), Sendai, Japan, May 2023. [2] Kazuhiro Shimura et al., IEEJ Trans. E. E. Engng., vol.18, No.9, pp.1533-1543, Sep. 2023.

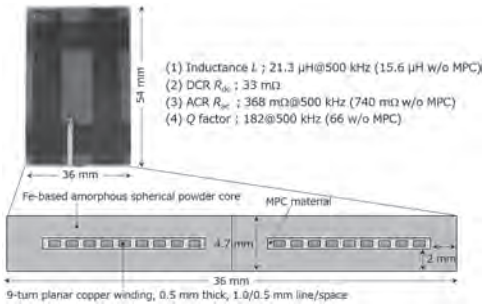

Fig.1 Fabrication example of planar inductor

CONTRIBUTED PAPERS

AG-03. Influences of magnetic property of beam electroplated with 3d ferromagnetic transition metal film on the output characteristics in perpendicular magnetic field assisted and inverse magnetostrictive electromagnetic vibration powered generators.
Y. Nakamura[1], S. Aketa[1], S. Kamiya[1], H. Kamogawa[1,2] and M. Ohtake[1] *1. Faculty of Engineering, Yokohama National University, Yokohama, Japan; 2. Technical Development Department, Kanto Kasei Co., Ltd., Yokosuka, Japan*

Electromagnetic vibration powered generators of inverse magnetostrictive type [1]–[3] and perpendicular magnetic field assisted type [4] have attracted attention as energy harvesters because of their low internal resistances, etc. Soft magnetic cantilever beam is a key component in both types of generators. $Fe_{81}Ga_{19}$ [1], $Fe_{30}Co_{70}$ [2], and Fe-Si-B [3] sheets of 25–1000 μm thicknesses bonded to base plates have been used as beams in inverse magnetostrictive type. However, the correlation of beam magnetic properties with output characteristic has not been made clear yet. In order to systematically vary the magnetic property, it is useful to employ beams electroplated with magnetic binary alloy films consisting of Fe, Co, and/or Ni, since the alloy composition can be easily varied. In the present study, Fe-Co and Fe-Ni alloy films of about 30 μm thickness are prepared on Cu base plates by electroplating and they are applied to beam materials in both types of generators. The influences of magnetic properties on the output characteristic are investigated. Fig. 1 shows our vibration powered generation characterization systems of beam material. Figs. 2(a)–(c) summarize the compositional dependences of magnetic properties. Fig. 2(d) shows the output characteristics in inverse magnetostrictive type generation. In the Fe-Co beams, a higher voltage is obtained around 30 at. % Co, though a larger magnetostriction is observed around 70 at. % Co. Furthermore, the Fe-Ni beams show higher voltages compared with the case of Fe-Co beams. These results show that not only large magnetostriction but also low coercivity are required in inverse magnetostrictive type. Fig. 2(e) shows the output properties in perpendicular magnetic field assisted type generation. For all the compositions except pure Ni, perpendicular magnetic field assisted type shows a higher output than inverse magnetostrictive type. The beams with low coercivity ($Fe_{66}Ni_{34}$–$Fe_{29}Ni_{71}$) show high voltages of 4.5–5.7 V. The result shows that low coercivity is

effective in perpendicular magnetic field assisted type. The present study has suggested that realization of low magnetic anisotropy brings out the potentials of both types of generations.

[1] T. Ueno and S. Yamada: *IEEE Trans. Magn.*, 47, 2407 (2011). [2] S. Yamaura, S. Makino, N. Kimura, M. Yokoyama, T. Kubota, and Y. Furuya: *Trans. Mat. Res. Soc. Japan*, 42, 127 (2017). [3] F. Osanai, S. Hashi, and K. Ishiyama: *The 2019 Annual Meeting record IEE Japan*, 146 (2019). [4] M. Ohtake, T. Kawai, and M. Futamoto: *Japanese Patent*, application no. 2022-086851 / publication no. 2023-174153 (2023).

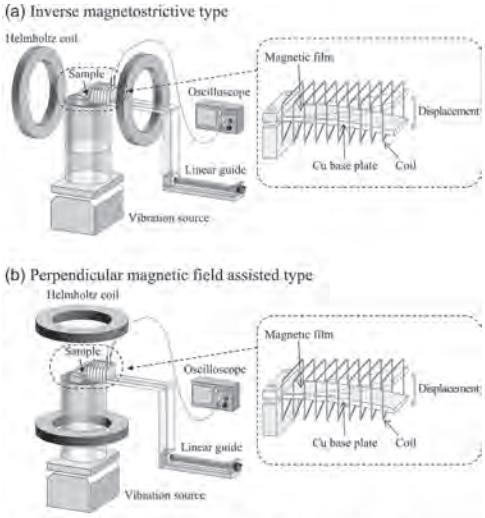

Fig. 1 Schematic diagrams of output characteristic measurement systems of (a) inverse magnetostrictive type and (b) perpendicular magnetic field assisted type vibration powered generations.

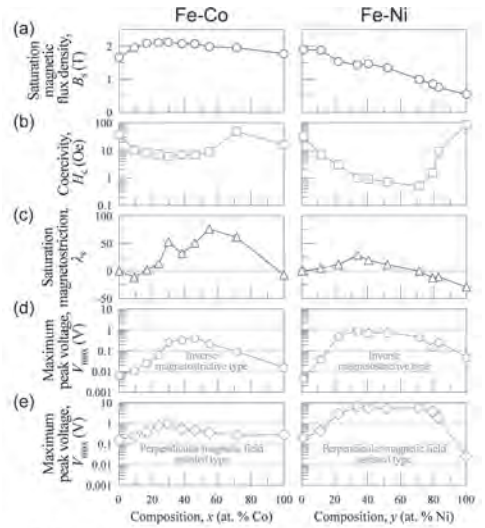

Fig. 2 Compositional dependences measured for Fe-Co and Fe-Ni alloy films of (a) saturation magnetic flux density, (b) coercivity, (c) saturation magnetostriction, and [(d),(e)] maximum peak voltages of (d) inverse magnetostrictive type and (e) perpendicular magnetic field assisted type vibration powered generators.

AG-05. Sensitivity analysis framework for a MIMO magnetic levitation actuator. *G. Zuidema*[1], D. Krop[1] and E. Lomonova[1] *1. Electrical Engineering, Eindhoven University of Technology, Eindhoven, Netherlands*

A novel multiple-input and multiple-output planar actuator is proposed, which utilizes mechanically driven stator magnet arrays to levitate a permanent magnet mover. A state of levitation and actuation is obtained by mechanically altering the orientation of the stator magnets to control the forces and torques on the levitating mover body. A drawback of using permanent magnets is the lack of magnetic field amplitude control which may result in a locally highly sensitive system that will limit the controllability of the actuator. In this study, a data-driven approach is proposed to suppress peak contributors while maximizing the force density of the system. The problem is first reduced to a two-body problem, consisting of a cylindrical stator magnet and a spherical mover magnet. The interaction between the two bodies is modeled using the equivalent surface charge model [1, 2] after which the solution of the potential magnetic energy of the two-body problem is fit by a feed-forward neural network for model acceleration [3]. Through superposition, a full actuation system is modeled within 1 s for 10^6 positions in 3D space. Data is generated by inserting 10^7 randomized angles to each of the 23 stator magnets while observing the magnetic potential energy on a levitating magnetic body, consisting of nine mover spheres, as shown in Fig. 1. Maximum relevance, minimal redundancy (MRMR) [4] feature selection methods are then used for the sensitivity analysis. Fig. 2 depicts the sensitivity of the system based on the MRMR feature importance score. For a translating mover body in the x-direction of the configuration of Fig. 1, at each position in x, six stator magnets are dominant inputs, resulting in a reduction of 17 dimensions in the optimization space.

[1] G. Akoun and J.-P. Yonnet, "3D Analytical Calculation of the Forces exerted between two cuboidal magnets," IEEE Transactions on Magnetics, vol. 20, no. 5, pp. 1962–1964, 1984. [2] J. W. Jansen, C. M. Van Lierop, E. A. Lomonova, and A. J. Vandenput, "Modeling of magnetically levitated planar actuators with moving magnets," IEEE Transactions on Magnetics, vol. 43, no. 1, pp. 15–25, 2007. [3] G. Zuidema, D. C. Krop, and E. A. Lomonova, "A neural network inverse problem solution for a mimo magnetic levitation actuator," International Journal of Applied Electromagnetics and Mechanics, vol. Preprint, pp. 1–8, 5 2024 [4] G. Darbellay and I. Vajda, "Estimation of the information by an adaptive partitioning of the observation space," IEEE Transactions on Information Theory, vol. 45, no. 4, pp. 1315–1321, 1999.

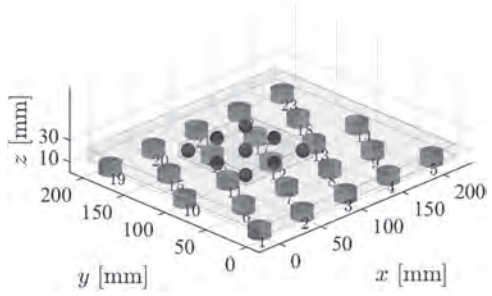

"Fig.1" The proposed MIMO permanent magnet based actuator with 23 cylindrical stator magnets and 9 spherical mover magnets in a north-south pattern. Red indicates the magnetic north and blue the magnetic south of a permanent magnet.

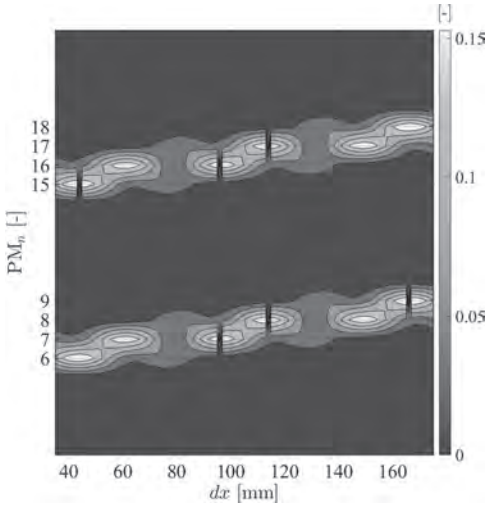

"Fig.2" MRMR-based sensitivity analysis for a translating mover in the x-direction, as seen in Fig. 1. At any position, a maximum of six stator magnets contribute to the potential magnetic energy of the actuator.

AG-06. Instrumentation and Characterization of Mixed GO Electrical Steel Magnetic Cores. *O. Dabaj*[1], C. Demian[1], J. Lecointe[1] and J. Blaszkowski[2] *1. Univ. Artois, UR 4025, Laboratoire Systèmes Électrotechniques et Environnement (LSEE), Béthune, France; 2. Thyssenkrupp Electrical Steel, Isbergues, France*

Abstract - This paper concerns a single-phase power transformer magnetic core composed of two different grades of grain-oriented electrical steel (GOES). It presents how the core is instrumented with B-coil and H-coil sensors to measure the local magnetic flux density and field strength distributions. *1. Introduction* The magnetic core performance of power transformers largely depends on the GOES grade. New EU regulations [1] aim at minimizing no-load losses in power transformers. Mixing different grades offers the possibility of balancing the cost and the efficiency [2][3][4]. A single-phase power transformer magnetic core using two different GOES grades is introduced, as well as its instrumentation. *2. Experimental apparatus and results* A previous paper [5] experimentally characterized a simplified mixed single-phase core with 40 laminations per limb and yoke. The specific iron losses decrease non-linearly with respect to the high-performance material grade. The scientific challenge is to study these phenomena in larger magnetic cores for power transformers. A 1 m x 1 m single-phase magnetic core with 560 laminations per limb and yoke, with mixed two GOES grades has been designed (Fig.1). Local magnetic properties in the middle of a limb are analyzed using calibrated B-coils and H-coils positioned inside the core using spacers. The goal is to analyze the effects of GOES grade mixing on the magnetic field and flux density distributions in the core. The methodology is validated using a simplified magnetic core before applying it to the power transformer core. The Fig.2 compares the local hysteresis cycle in the middle of a limb to the global cycle of the core at B =1.7 T. Local field strength (H) is lower for a given value of flux density (B) and values of B at saturation are the same. Coercive fields are similar in both cases. *3. In the full paper* The full paper will present a more detailed experimental analysis of mixed core, focusing on the B and H distribution in each grade, and the losses. It will make possible to explain the non-linear decrease of the losses observed in the simplified core.

[1] European Commission, "COMMISSION REGULATION (EU) No 548/2014 of 21 May 2014 on implementing Directive 2009/125/EC of the European Parliament and of the Council with regard to small, medium and large power transformers," Off. J. Eur. Union, vol. L 152, no. 2, pp. 1–15, 2014. [2] D. Snell and A. Coombs, "The influence of core materials and mix on the performance of a 100 kVA three phase transformer core," J. Magn. Magn. Mater., vol. 254–255, pp. 349–351, 2003, doi: 10.1016/S0304-8853(02)00847-8. [3] S. Magdaleno-Adame, Enrique Melgoza-Vazquez, Juan C. Olivares-Galvan, and Rafael Escarela-Perez, "Loss reduction by combining electrical steels in the core of power transformers," Int. Trans. Electr. energy Syst., vol. 26, no. 8, pp. 1737–1751, 2016. [4] T. D. Kefalas and A. G. Kladas, "Mixed Si-Fe Wound Cores Five Legged Transformer: Losses and Flux Distribution Analysis," IEEE Trans. Magn., vol. 48, no. 4, pp. 1609–1612, 2012. [5] O. A. Dabaj, R. Corin, J. philippe Lecointe, C. Demian, and J. Blaszkowski, "Impact of GOES grade mixing on the iron losses of single-phase magnetic cores," J. Magn. Magn. Mater., vol. 591, no. January, p. 171676, 2024, doi: 10.1016/j.jmmm.2023.171676.

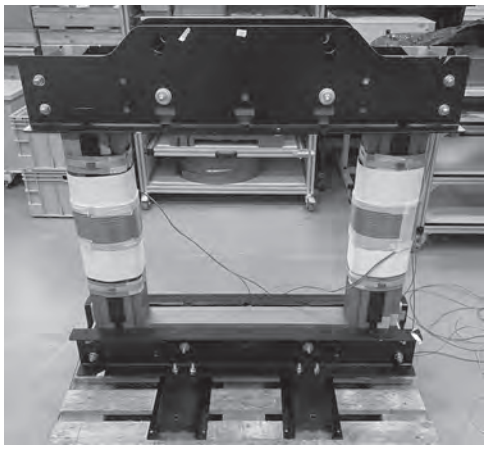

Power transformer single-phase magnetic core

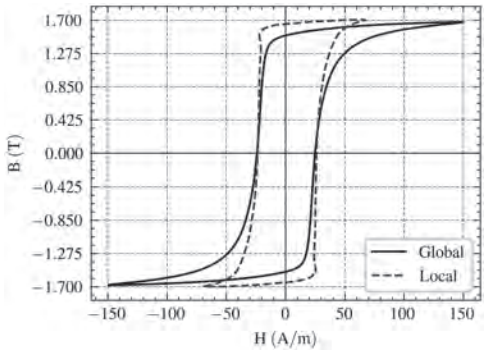

Comparison of local and global BH cycles at 1.7 T

AG-07. Fleet Digital Twin of Permanent Magnet Synchronous Motors: A Novel Approach for Virtual Validation. *M. Azeem*[1,2], M. Gulec[1,2], K. Vanthuyne[1,2] and P. Sergeant[1,2] *1. University of Ghent, Ghent, Belgium; 2. Flanders Make@UGent - MIRO, Ghent, Belgium*

Introduction: Digital twin of electric motors has been developed for parameter estimation, fault detection, and output quantity estimation [1]-[3]. However, gaps remain such as: 1) All these digital twins are being developed based on limited data from a single laboratory setup. 2) The digital twin approach to predict the efficiency of an electric motor under new load profiles—ones that have not yet been tested on the physical asset—has not been reported. It is often needed for researchers involved in motor development to investigate the efficiency of electric motors under new load profiles prior to field deployment. However, the experimental investigation is time-consuming and costly. Therefore, this study proposes a Fleet Digital Twin (FDT) to virtually estimate the efficiency of electric motors for new load profiles. *Method*: To develop a FDT, five identical PMSM setups are manufactured. Multiple New European Driving Cycle (NEDC) load profiles are run on four setups to collect data, as shown in Fig. 1(a). A fifth setup was reserved for validation purposes. The FDT creation process, as illustrated in Fig. 1(b), involves preparing a nominal model and importing experimental data into MATLAB. Subsequently, MATLAB codes, Simulink models, and

optimization software are configured to interoperate. The FDT relies on a stochastic approach, where the parameters such as d-axis inductance, q-axis inductance, PM flux linkage, stator resistance, eddy current loss coefficient, and hysteresis loss coefficient are determined through an optimization study using measured NEDC data from four setups. *Results*: The FDT aims to estimate the performance of new load profiles not used in training. Consequently, the efficiency of the Worldwide Harmonised Light Vehicle Test Procedure (WLTP) load profile is estimated using the FDT. To evaluate FDT performance, the WLTP load profile is experimentally tested on the 5th motor setup. Fig. 2(c) shows that the FDT efficiency predictions for both NEDC and WLTP closely match the experimental results, whereas the datasheet model predictions overestimate. Fig. 2(a) compares FDT and experimental results in the time domain for WLTP, and Fig. 2(b) does the same for NEDC.

(1) W. Song, Y. Zou, C. Ma and S. Zhang, "Digital Twin Modeling Method of Three-Phase Inverter-Driven PMSM Systems for Parameter Estimation," in IEEE Transactions on Power Electronics, vol. 39, no. 2, pp. 2360-2371, Feb. 2024. (2) B. Rodríguez, E. Sanjurjo, M. Tranchero, C. Romano and F. González, "Thermal Parameter and State Estimation for Digital Twins of E-Powertrain Components," in IEEE Access, vol. 9, pp. 97384-97400, 2021. (3) F. Tao, H. Zhang, A. Liu and A. Y. C. Nee, "Digital Twin in Industry: State-of-the-Art," in IEEE Transactions on Industrial Informatics, vol. 15, no. 4, pp. 2405-2415, April 2019.

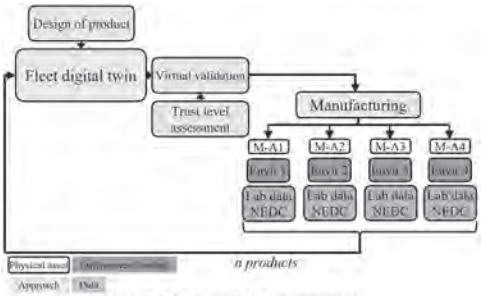

Fig. 1(a). Virtual validation approach

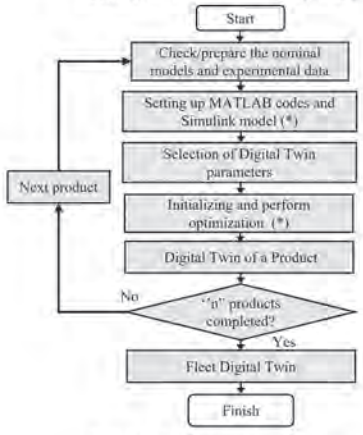

Fig. 1(b). Fleet digital twin process.

Fig. 1.

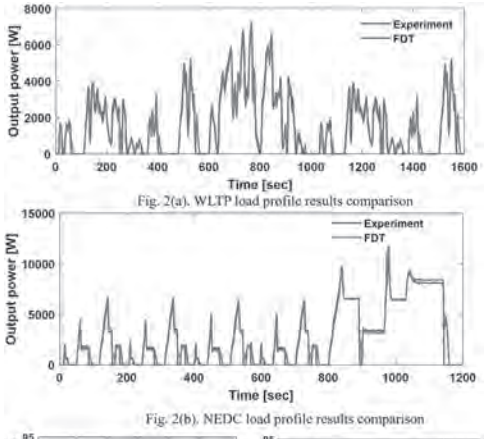

Fig. 2(a). WLTP load profile results comparison

Fig. 2(b). NEDC load profile results comparison

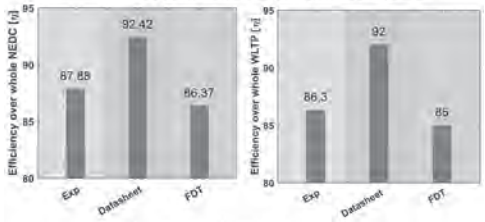

Fig. 2(c). WLTP and NEDC efficiency on whole drive cycle

Fig. 2.

AG-08. A Cost-Effective 12/10 Fractional Slot Concentrated Winding Synchronous Reluctance Motor for Electric Mid-Drive Two Wheeler Application. G. Shasikanth[1], *K. Anbukumar*[1] and M. Azhagar Raj[1]
1. Department of Electrical and Electronics Engineering, Anna University, Chennai, India

In this paper a 3.5kW Synchronous Reluctance Motor with Fractional Slot Concentrated Winding (FSCW) for a mid-drive electric two wheeler application is designed. The factors which affect the performance of the synchronous reluctance motor are cogging torque, torque ripple, unbalanced magnetic pull and vibration. Choosing the appropriate slot/ pole combinations plays a significant role in reducing the above factors and improvement in performance. Hence, among the possible slot/pole combinations under the Fractional Slot Concentrated Winding 12-slot/ 10-pole combination is chosen. For the mid-drive two wheeler electric vehicle application, the considered SynRM is not used anywhere before especially without using any Permanent Magnet Assistance, which for this application is a novel attempt. The design of the motor is carried out with five different rotor geometries and performance analysis is carried out for the rotor with the high average torque with less torque ripple by varying the number of barriers, tangential ribs, radial ribs and notches using 3D-FEM software. The shape of the barriers considered are circular and angular. Number of barriers in the rotor structure plays an important role in the torque performance of the motor while notch helps in reducing the torque ripple. Saliency Ratio of the motor is found out by applying d-axis and q-axis currents in the stator windings and obtaining L_d, L_q. Based on the extensive analysis of the five rotor geometries, it is seen that for the mid-drive electric two wheeler application the rotor with less number of barriers show superior performance. Among the rotor geometries, the one which produces maximum average torque with less torque ripple is chosen. For the above considered power rating and speed of 1200rpm, the chosen rotor achieves the desired average torque of 27.5 Nm with 13.8% torque ripple. Further the synchronous reluctance motor with the chosen rotor is subjected to thermal and vibrational analysis. Hence based on all the performance and mechanical analysis the motor with finalized rotor is fabricated for real-time testing and implementation in electric vehicle.

[1] C. M. Spargo, B. C. Mecrow and J. D. Widmer, "Application of fractional slot concentrated windings to synchronous reluctance machines," 2013 International Electric Machines & Drives Conference, Chicago, IL,

USA, 2013, pp. 618-625, doi: 10.1109/IEMDC.2013.6556159. [2] C. M. Spargo, B. C. Mecrow and J. D. Widmer, "Higher pole number synchronous reluctance machines with fractional slot concentrated windings," 7th IET International Conference on Power Electronics, Machines and Drives (PEMD 2014), Manchester, UK, 2014, pp. 1-6, doi: 10.1049/cp.2014.0279. [3] M. Murataliyev, M. Degano, M. Di Nardo, N. Bianchi and C. Gerada, "Synchronous Reluctance Machines: A Comprehensive Review and Technology Comparison," in Proceedings of the IEEE, vol. 110, no. 3, pp. 382-399, March 2022, doi: 10.1109/JPROC.2022.3145662. [4] M. A. Raj and A. Kavitha, "Effect of Rotor Geometry on Peak and Average Torque of External-Rotor Synchronous Reluctance Motor in Comparison With Switched Reluctance Motor for Low-Speed Direct-Drive Domestic Application," in IEEE Transactions on Magnetics, vol. 53, no. 11, pp. 1-8, Nov. 2017, Art no. 8209108, doi: 10.1109/TMAG.2017.2710191. [5] Marino, Luigi. "Design and Analysis of a Fractional-Slot Concentrated-Wound PM-Assisted Reluctance Motor." (2015). [6] S. Taghavi and P. Pillay, "A Sizing Methodology of the Synchronous Reluctance Motor for Traction Applications," in IEEE Journal of Emerging and Selected Topics in Power Electronics, vol. 2, no. 2, pp. 329-340, June 2014, doi: 10.1109/JESTPE.2014.2299235. [7] C. M. Spargo, B. C. Mecrow, J. D. Widmer, C. Morton and N. J. Baker, "Design and Validation of a Synchronous Reluctance Motor With Single Tooth Windings," in IEEE Transactions on Energy Conversion, vol. 30, no. 2, pp. 795-805, June 2015, doi: 10.1109/TEC.2014.2384476.

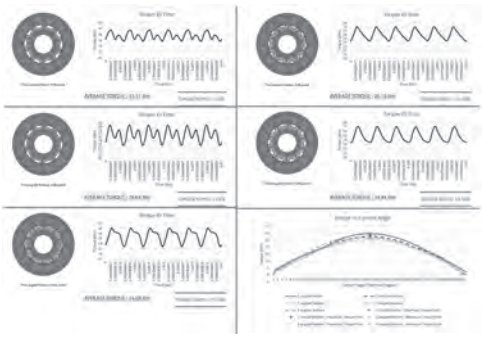

AG-09. Optimal Design Study for High Power Density of PMSM for Traction of Hydrogen Powered Train. *J. Lim*[1], C. Park[1], H. Lee[1], J. Lee[1], I. Jo[2] and S. Kim[2] *1. Korea National University of Transportation, Uiwang, The Republic of Korea; 2. Hanyang University, Seoul, The Republic of Korea*

Recently, South Korea has been studying the replacement of existing diesel powered train with hydrogen powered train [1]. However, hydrogen powered train are equipped with additional hydrogen tanks and fuel cells compared to existing diesel powered train, and require high power density of the propulsion system [2]. Therefore, the use of Permanent Magnet Synchronous Motor(PMSM), which are advantageous in high power density characteristics compared to Induction Motor(IM), has been considered for traction motor, and the model shown in Figure 1 is in application. However, it was necessary to increase the power density of the motor in Fig. 1, so an optimal design was performed according to the flow chart in Fig. 2. The conventional rotor size determination method using the magnetic and electrical load distribution method has limitations in determining the actual motor size. And the range of variables is different depending on the size of the rotor diameter. Therefore, several rotor sizes are derived within the category that is close to the target value based on the magnetic equivalent circuit. For example, 260mm and 300mm rotor diameters are satisfied with the target value. In this case, the design parameter range at 260mm is different from the range at 300mm. Therefore, the design parameter range of 260~270mm, 270~280mm, 280~290mm, 290~300mm, is divided to find the optimal model. The process of finding the optimal model is to determine the main factors through the design of experiments, generate and verify the surrogate gate model, apply the optimization algorithm, and derive the optimal model for each rotor diameter. The optimal models derived within each category are finally compared to derive the final model. For the final model, the power density is more than 0.54 kW/kg, and the power density is 0.78 kW/kg when changing from SUS304, which was previously used as a frame material, to aluminum, which is widely used recently. This is a significant level for total enclosed and self-ventilated traction motor. Therefore, the above contents will be discussed in full-manuscript.

[1] J. S. Lee, J. H. Ryu, "Hydrogen Fuel-Cell/Battery Hybrid Train", Journal Of The Korean Society For Railway, Vol. 22, No.1, pp.19-26 (2019) [2] J. H. Ryu, J. H. Lee, J. S. Lee, "Switching Frequency Determination of SiC-Inverter for High Eciency Propulsion System of Railway Vehicle", Energies, Vol. 13, No.19, pp.1-14 (2020)

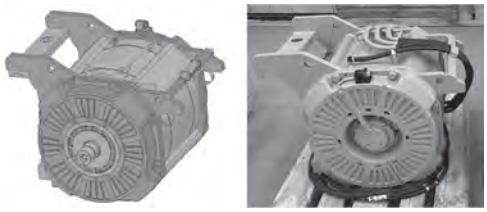

Fig.1. 332kW-class PMSM currently applied to hydrogen powered train

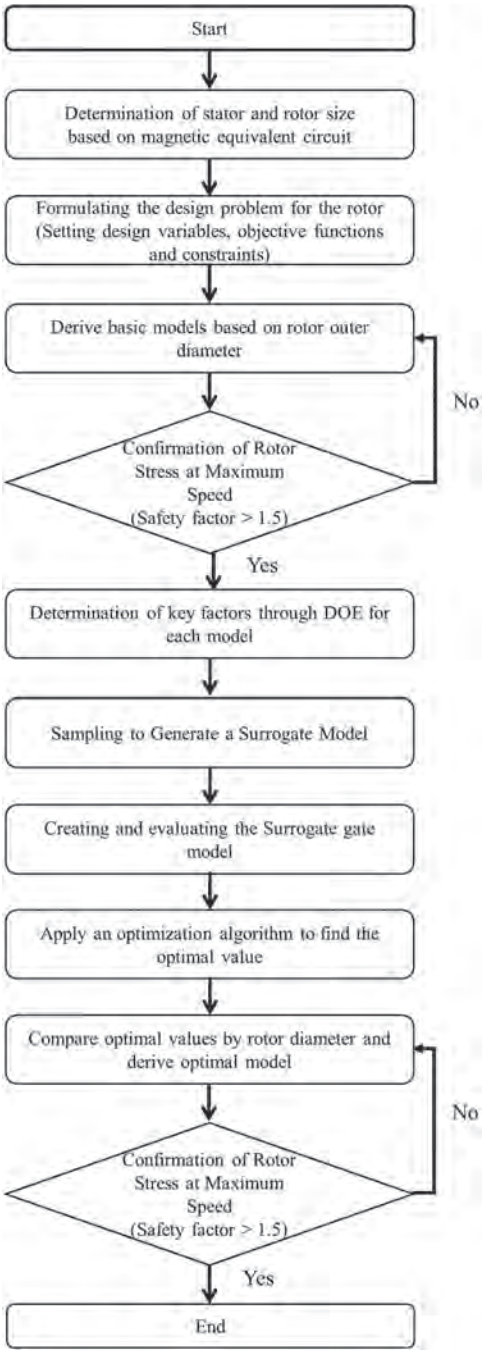

Flowchart for Improving the Power Density of Traction Motor

AG-10. Improvement of Torque and Efficiency of Magnetic-Geared Switched Reluctance Motor. *K. Iwaki*[1] and K. Nakamura[1] *1. Graduate School of Engineering, Tohoku University, Sendai, Japan*

Electric vehicles (EVs) have attracted great interest due to their potential to achieve zero carbon emissions. Moreover, in-wheel direct drive EVs have garnered significant attention [1] since they have traction motors in their driving wheel without any transmission elements, resulting in a compact size and ease of maintenance. Traction motors are required to have a wide speed-torque range, which means they must have large torque in low-speed regions and achieve high maximum speed. To achieve such characteristics, a novel magnetic-geared switched reluctance motor (MG-SRM) has been proposed in a previous paper [2]. The MG-SRM consists of a flux-modulated-type magnetic gear (MG) and a switched reluctance motor (SRM). In general, an SRM has a wide speed range but low torque, while an MG has high torque density. Thus, the MG-SRM in [2] was able to provide a wide speed-torque range. However, the torque of the MG-SRM at high-speed regions was small. Therefore, this paper focuses on improving torque and efficiency. Fig. 1(a) illustrates the specifications of the MG-SRM designed in [2], which features the 4-phase 16/20-pole outer-rotor SRM and the flux-modulated-type MG with a gear ratio of 9.25. Fig. 1(b) depicts the experimental setup of the MG-SRM. It consists of the prototype MG-SRM, the powder brake, the torque detector, and the 4-phase asymmetric half-bridge converter. Fig. 2(a) indicates the excitation start angle θ_s and the excitation end angle θ_e, according to the rotor position angle θ. In this paper, the rotor position angle θ is defined as 0 when a rotor pole is aligned with a stator pole. Thus, one cycle of the 4-phase 16/20-pole SR motor is $-9 \le \theta \le 9$ deg. In the conventional drive method, θ_s and θ_e are set at -9 deg. and -4.5 deg., respectively. On the other hand, in the improved drive method, θ_s is set at -10.5 deg. Fig. 2(b) shows the comparison of measured results when the rotational speed is 180 rpm. It can be seen from the figure that the torque is improved to 40 Nm, which is more than four times larger than that of the conventional method. Moreover, the efficiency is improved from 33% to 60%.

[1] Y. Yu, Y. Pei, F. Chai, and M. Doppelbauer, *IEEE Trans. Ind. Electron.*, vol. 70, no. 8, pp. 7761-7772 (2023). [2] K. Iwaki, K. Ito and K. Nakamura, *IEEE Trans. Magn.*, vol. 59, no. 11, 8202005 (2023).

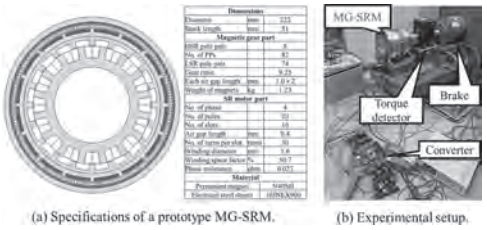

Fig.1 Specifications of MG-SRM and experimental setup.

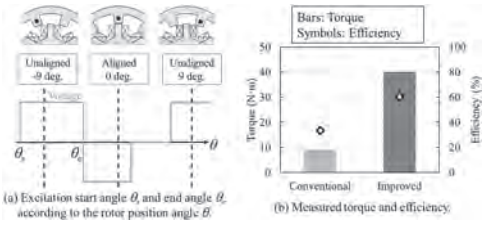

Fig.2 Condition of excitation and experimental results.

AG-11. Research on a new type of electrothermal multi-energy dual-stator motor and loss optimization. J. Yuan[1], *H. Wang*[1], H. Zhou[1] and B. Peng[1] *1. School of Electronic Engineering and Automation, Wuhan University, Wuhan, China*

At present, renewable energy, represented by wind energy, has become an effective alternative to traditional fossil energy. Renewable energy is clean and pollution-free, but because of wind energy's intermittent and fluctuating characteristics, it cannot be used as baseload energy.[1] Japanese scholars have proposed a wind powered thermal energy system (WTES), which is similar to concentrated solar power.[2] WTES converts all wind energy into thermal energy by heat generator, it solves the influence of wind energy characteristics on power system. But the conversion efficiency of heat to electrical energy is low, which limits the further development of the system. In the paper, a new type of electrothermal multi-energy dual-stator motor (ETDSM) is proposed to replace the initial heat generator, it can realize the simultaneous conversion of wind to electrical energy and thermal energy. It can directly meet a part of electrical demand and convert surplus wind energy into heat energy for utilization, improve the theoretical efficiency

of system. The topology of the device is shown in Fig.1(a), it includes the stator core, windings, rotor and permanent magnet. The outer stator is used to generate electricity, while the inner stator is used to generate heat. The heating part is made of low-carbon steel and the outside is excavated to enhance eddy current effect, the devices' output and loss of the device are shown in Fig.1(b). The heating power is only 20W when the heating part is made of silicon steel sheet material. As shown in Fig.2(1), under the rated condition, the iron loss of the device accounts for 66.1% of the electromagnetic loss of the device, it needs to be optimized. The low-loss silicon steel of JFE and the nano material NANOMET® are selected to replace the original stator core material DW315-50. As shown in Fig.2(2), the iron loss of materials under rated conditions is reduced by 34% and 70.7%. The new material has a good inhibition effect on iron loss. After replacing the new material, other electromagnetic losses of the device have not increased obviously, and the efficiency of the device has been further improved.

[1]Zhu H, Li H and Liu G, "Energy storage in high renewable penetration power systems: Technologies, applications, supporting policies and suggestions," CSEE Journal of Power and Energy Systems, vol. 9, no. 6, pp. 2099-2108, Nov. 2023. [2] Okazaki, T., Y. Shirai and T. Nakamura, "Concept study of wind power utilizing direct thermal energy conversion and thermal energy storage," Renewable Energy, vol.83, pp. 332 – 338, 2016.

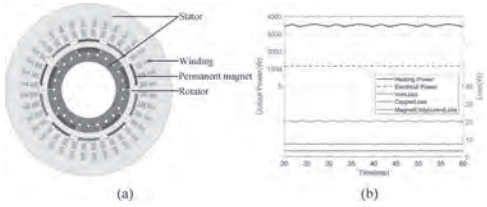

Fig.1 The device topology and simulation results

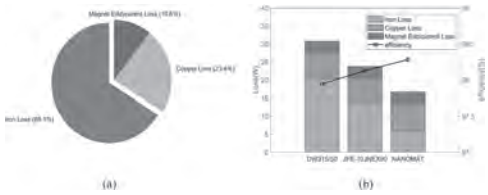

Fig.2 The device loss optimization result

AG-13. Design and Single Rotor Fault Analysis of A Magnetically Geared Segment Stator Contra-Rotating Switched Reluctance Motor for flying vehicles application. *S. Ip*[1] and K. Cheng[2] *1. Electrical and Electronic Engineering, The Hong Kong Polytechnic University, Hong Kong SAR, Hong Kong; 2. Electrical Engineering, University of California, Merced, Merced, CA, United States*

Flying vehicles is a novel idea for the rapid development of Low Altitude Economy which provides the possibility for both road and aerial transportation. Switched reluctance electric motors are generally favourable considering their low cost, simple structure and reliable performance under periodic shock experience during the take-off and landing cycle which is not favourable to permanent magnet motors. Additionally, contra-rotating propellers or axial compressors have shown attractive performance for flying vehicle applications. [1][2] Some research investigated double-rotor switched reluctance motors [3], [4], [5], [6] but none of them studied the torque distribution to two geared rotors [7] which is important for propeller matching for the engine. Therefore, a magnetically geared segment stator contra-rotating switched reluctance motor is proposed in this paper to power a contra-rotating propeller without a mechanical gearbox. The torque performance and flux distribution for the mentioned motor are analyzed. Moreover, the single-rotor fault operation performance characteristic is investigated to provide crucial knowledge when the flying vehicle has a partial failure in one of the rotors. during landing and require full power on a propeller to go around which has not been investigated by other double-rotor switched reluctance motor research.

[1] Y. Zhong, S. Huang, D. Luo, CES Transactions on Electrical Machines and Systems, Vol. 2, p. 220-225 (2018) [2] N. M. Nouri, S. Mohammadi, Ocean Engineering, Vol. 167, p. 397-404, (2018) [3] W. Uddin and Y. Sozer, 2015 IEEE Energy Conversion Congress and Exposition (ECCE), p. 3972-3978, (2015) [4] W. Sun, Q. Li, L. Sun and L. Li, IEEE Transactions on Transportation Electrification, Vol. 7, p. 754-765, (2021) [5] T. Guo, N. Schofield and A. Emadi, IEEE Transactions on Energy Conversion, Vol. 31, p. 1278-1286, (2016) [6] A. Ghaffarpour and M. Mirsalim, IEEE Transactions on Transportation Electrification, Vol. 8, p. 2400-2411(2022) [7] Y. Yang, N. Schofield and A. Emadi, IEEE Transactions on Energy Conversion, Vol. 30, p. 671-680, (2015)

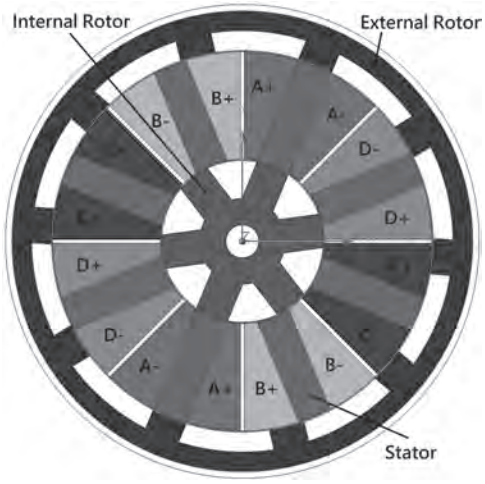

Fig.1 Cross-section of the Magnetically Geared Segment Stator Contra-Rotating Switched Reluctance Motor

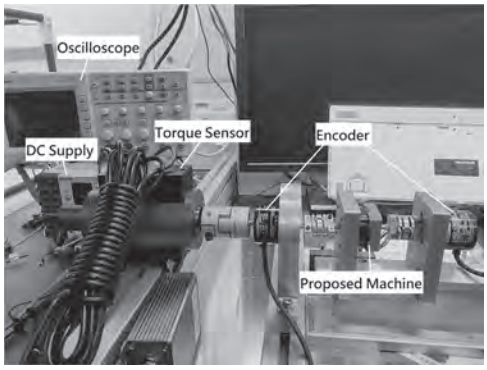

Fig.2 Test rig of the motor

Session AP
SPINTRONICS I
(Poster Session)

Jiahao Han, Chair
Tohoku University, Sendai, Japan

AP-01. Withdrawn

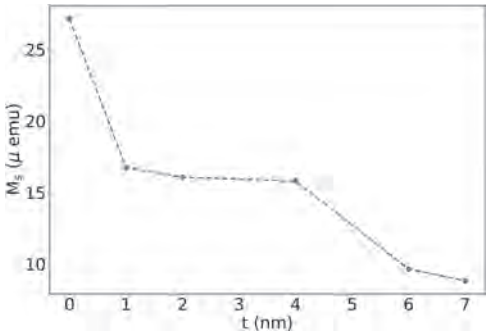

Saturation Magnetisation (Ms) for GdN(3)/FeMn thin film Hetrostructure recorded at 2 K for different FeMn thickness

AP-02. Harnessing Exchange Bias and Magnetic Proximity Effects for Superconducting Spintronics: A Novel GdN/FeMn Heterostructure. *V. Singhal*[1], P.K. Sharma[1], B. Dutta[1] and A. Pal[1] *1. MEMS, IIT Bombay, Mumbai, India*

Exchange bias after being first demonstrated in 1956 by Meiklejohn and Bean (M-B) [1,2] has Garnered significant attention due to its potential application in High density information storage[3]. Currently, most studies and devices incorporating exchange bias phenomena focus on ferromagnetic metals, which can suffer from eddy current losses at high frequencies. Therefore, the need for ferromagnetic insulators in exchange bias effects and their utilization in superconducting spintronics is highly desirable.[4] In this study, we present a novel exchange bias phenomenon in a ferromagnetic insulator, GdN (T_C ~ 35 K), and an antiferromagnet, FeMn (T_N ~ 470 K). Two intriguing points are highlighted: (1) the unconventional exchange bias in the T_C << T_N system, which exhibits a interplay of Type-I and Type-II coercivity[5,6] with varying FeMn thickness, and (2) the observed reduction in the saturation magnetization of GdN with increasing FeMn thickness. Concurrently, the exchange bias field increases with increasing FeMn thickness. Which eliminates the possibility of dead layer formation in GdN with increasing the FeMn thickness.

[1] W.H. Meiklejohn, C.P. Bean, Phys. Rev. 102 (1956) 1413. [2] W.H. Meikleiohn, C.P. Bean Phys. Rev. 105 (1957) 904. [3] H. Neal Bertram, Theory of Magnetic Recording, Cam-bridge University Press, Cambridge, 1994. [4] Appl. Phys. Lett. 115, 032403 (2019) [5] M. G. Blamire, M. Ali, C.-W. Leung, C. H. Marrows, and B. J. Hickey Phys. Rev. Lett. 98, 217202 [6] M. D. Stiles and R. D. McMichael, Phys. Rev. B 60, 12 950(1999); M. D. Stiles and R. D. McMichael, Phys. Rev. B 63, 064405 (2001).

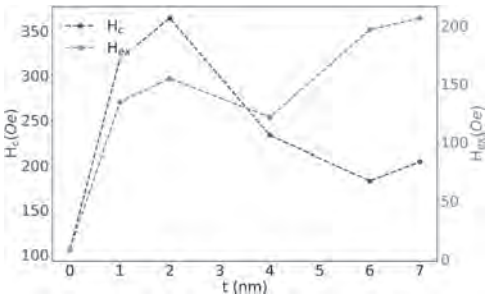

Exchange bias (Hex) and coercive field (Hc) for GdN(3)/FeMn thin film hetrostructure recorded at 2 K for different FeMn thickness.

AP-03. Direct X-PEEM imaging of the altermagnetic order of Hematite.
E. Galindez Ruales[1], C. Schmitt[1], R. González-Hernández[2], O. Gomonay[1], E. Golias[3], Y. Niu[3], A. Zakharov[3] and M. Kläui[1,4] *1. Institute of Physics, Johannes Gutenberg University Mainz, Mainz, Germany; 2. Grupo de Investigacíon en Física Aplicada, Departamento de Física, Universidad del Norte, Barranquilla, Colombia; 3. MAX IV Laboratory, Lund, Sweden; 4. Center for Quantum Spintronics, Norwegian University of Science and Technology, Trondheim, Norway*

Conventional antiferromagnets are known for their time-reversal symmetry in their electronic structure, which results in a zero anomalous Hall coefficient. In ferromagnets, the breaking of this symmetry is generated by internal magnetization, but this net magnetization can limit compatibility with other prominent phases like superconductors and topological insulators. The resulting stray fields from this magnetization limit device density and stability due to magnetic field interactions. Altermagnetism has recently been proposed to overcome these limitations by sharing the T-symmetry breaking characteristic of ferromagnetic while maintaining an antiparallel order of the magnetic sublattices leading to spin-polarized transport [1]. We demonstrate nanoscale imaging of altermagnetic order in Hematite using X-ray photoemission electron microscopy (X-PEEM) (Fig. 1). By leveraging the Anomalous Hall vector in X-ray magnetic circular dichroism (XMCD) and traditional collinear X-ray magnetic linear dichroism (XMLD), we realize detailed imaging of the Néel vector direction. This approach, previously applied to MnTe, reveals unique spin configurations and textures not seen in collinear ferromagnets [2]. In our case, this imaging reveals complex spin configurations and textures that conventional collinear ferromagnets do not exhibit. By correlating our information about the Néel vector distribution with first-principles calculations, we confirm that our imaging of the altermagnetic order follows the anomalus Hall conductivity symmetries. This research extends a new experimental field, making use of T-symmetry breaking, vanishing magnetization, and ultrafast dynamics resulting from the antiferromagnetic coupling of the sub-lattices. The ability to image the Néel vector direction is crucial for investigating other systems and holds promise for digital spintronics by overcoming current limitations in spatial, temporal, and energy scalability.

[1] L. Šmejkal, et. al., Phys. Rev. X 12, 031042 (2022) [2] O. J. Amin, et. al., arXiv:2405.02409(2024)

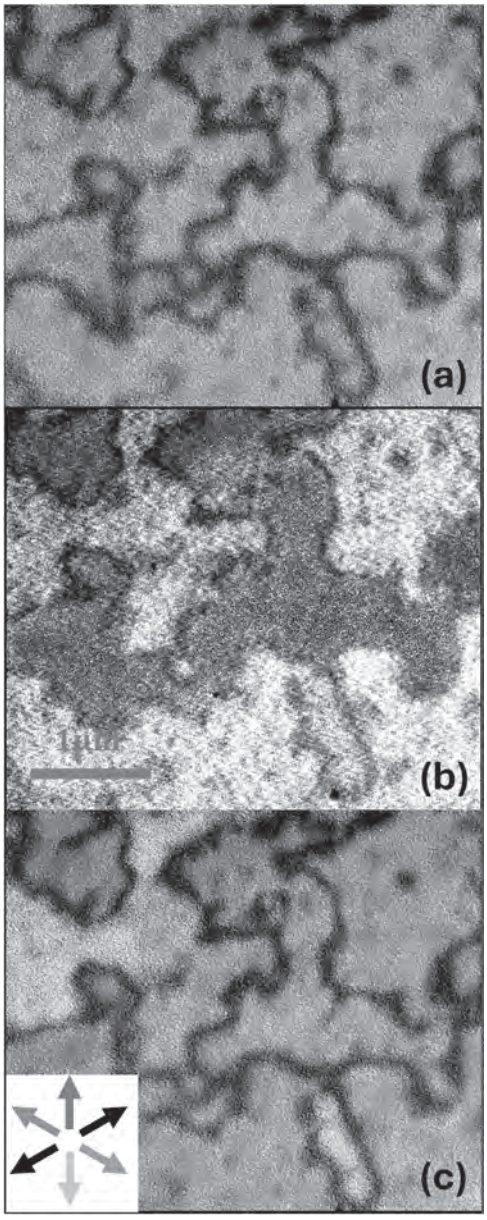

Room temperature X-ray photoemission electron microscopies (X-PEEM) of the altermagnetic hematite. (a) XMLD map, (b) XMCD, and (c) Extracted map of the absolute direction of the Néel vector obtained by combining the XMLD map and the XMCD image.

AP-04. Electric-field-controlled picosecond switching of antiferromagnets.
V. Lopez-Dominguez[1] *1. Institute of Advanced Materials, Universitat Jaume I, Castellon de la Plana, Spain*

Antiferromagnets (AFM) have attracted high attention for their unique properties and potential technological applications. Fundamentally, AFMs exhibit unconventional band topology, as observed in non-collinear AFMs[1,2] and the recently discovered altermangets[3]. As main consequence, both materials show a non-relativistic spin-momentum locking due to combined magnetic and lattice symmetries. Technogically, AFMs offer features like picosecond switching in magnetic memories (~100x faster than ferromagnetic memories)[4], immunity to external magnetic fields[5], high-density device arrays without inter-bit dipole interaction[2], and generation of Terahertz signals at the

nanoscale[6]. These properties have motivated extensive research into the electric control of AFMs[7], paving the path for highly integrable and ultrafast devices[8]. In this talk, I will review the electrical switching advances in AFMs grown by sputtering on silicon substrates, compatible with CMOS technology. The devices consist of micro and nanopillars of $PtMn$[5] and $IrMn_3$[9] on top of a Pt or Ta nanowires. The switching mechanism relies on the finite Spin Orbit Torque from the heavy metal layer, leading to a sizable switching at current densities ~10 MA/cm^2. Despite the successful control of the Néel vector in AFMs, high threshold currents complicate their integration in electronic circuits. Here, I will present, as an alternative approach, our latest numerical results on the electric field control of AFMs interfaced with a dielectric barrier such as MgO[4]. The dielectric barrier sets the Néel vector out of plane by an interfacial out of plane anisotropy. The application of voltage reconfigures the anisotropic energy barrier, inducing the Néel vector dynamics (voltage control of the magnetic anisotropy, VCMA). The reorientation of the magnetic moment of the AFM is dominated by the exchange interaction on the picosecond time scale, whereas the energy required to modify the AFM's anisotropy is comparable to ferromagnets. Consequently, VCMA switching represents a low energy consumption at ultra-fast speed. For example, the energy necessary for switching an AFM pillar is 250 aJ applying a voltage pulse of 30 ps in the absence of any current-induced torque.

1 Takeuchi, Y. *et al.* Chiral-spin rotation of non-collinear antiferromagnet by spin–orbit torque. *Nature Materials* 20, 1364-1370 (2021). 2 Shi, J. *et al.* Electrically Controlled All-Antiferromagnetic Tunnel Junctions on Silicon with Large Room-Temperature Magnetoresistance. *Advanced Materials* n/a, 2312008 (2024). 3 Leiviskä, M. *et al.* Anisotropy of the anomalous Hall effect in thin films of the altermagnet candidate ${\mathrm{Mn}}_{5}{\mathrm{Si}}_{3}$. *Physical Review B* 109, 224430 (2024). 4 Lopez-Dominguez, V., Almasi, H. & Amiri, P. K. Picosecond Electric-Field-Induced Switching of Antiferromagnets. *Physical Review Applied* 11, 024019 (2019). 5 Shi, J. *et al.* Electrical manipulation of the magnetic order in antiferromagnetic PtMn pillars. *Nature Electronics* 3, 92-98 (2020). 6 Tomasello, R. *et al.* Antiferromagnetic Parametric Resonance Driven by Voltage-Controlled Magnetic Anisotropy. *Physical Review Applied* 17, 034004 (2022). 7 Wadley, P. *et al.* Electrical switching of an antiferromagnet. *Science* 351, 587-590 (2016). 8 Jungwirth, T., Marti, X., Wadley, P. & Wunderlich, J. Antiferromagnetic spintronics. *Nature Nanotechnology* 11, 231-241 (2016). 9 Arpaci, S. *et al.* Observation of current-induced switching in non-collinear antiferromagnetic IrMn3 by differential voltage measurements. *Nature Communications* 12, 3828 (2021).

AP-05. Effect of controlled oxidation of Ni→NiO in YIG/Ta/Ni heterostructure. S.K. Jha[1,2], M. Sharma[1,3], N.K. Puri[2] and *B.K. Kuanr*[1] *1. Special Centre for Nanoscience, Jawaharlal Nehru University, New Delhi, India; 2. Applied Physics Department, Delhi Technological University, New Delhi, India; 3. Department of Physics, Deshbandhu College, University of Delhi, New Delhi, India*

This study used pulse-laser deposited epitaxial YIG thin-films on GGG substrates interfaced with Ta and Ni. Ni was further oxidized to NiO at 500 °C in the presence of oxygen. The intention of converting to NiO is to examine the prevalence of a favorable interface for the effective Spin backflow and spin-memory loss [1]. NiO enables the thermal magnon-mediated transmission of unity spin-current at room temperature due to considerably enhanced effective spin-mixing conductance at the interface. Heterostructure of GGG/YIG(90nm)/Ta(4nm)/Ni(20nm) have been fabricated. Thereafter, Ni was oxidized at 500 °C in O_2 atmosphere to convert Ni→NiO, hence to probe the spin transport in NiO which is mediated by coherent antiferromagnetic magnons [2-4]. Fig. 1(A), depicts the XRD data that confirm the formation of heterostructures and transition of Ni to NiO. Fig. 1(B) shows Raman spectra of YIG, YIG/Ta/Ni and YIG/Ta/NiO indicating transition of Ni to NiO. Atomic force microscopy measurements of bare YIG and YIG/Ta/NiO heterostructure revealed that root-mean-square roughness increased from 0.33nm to 1.89nm. Fig. 2(A) reveals the ferromagnetic resonance (FMR) spectra of YIG, YIG/Ta/Ni and YIG/Ta/NiO heterostructures. YIG shows a very sharp resonance at 2.5 kOe, whereas the YIG/Ta/Ni structure exhibit two distinct resonances for two magnetic layers (YIG and Ni) which are decoupled by 4nm Ta interlayer. Oxidizing Ni to NiO, Ni peak vanished due to the formation of antiferromagnetic NiO. The magnetization of the YIG layer is unaffected due to the presence of the protective Ta layer. At the same time YIG peak was broadened due to the presence of antiferromagnetic (AF) NiO which indicates spin transport through Ta. This can be explained as NiO enables short-range thermal magnon-mediated spin-transport. Magnons are the sole spin angular momentum carriers in NiO layer [1-2]. The parameters like Gilbert damping and zero-frequency linewidth (ΔH_0) retrieved from the fitting indicates increase in their values with oxidation.

[1] Zhu, L., et al. (2021). Physical Review Letters, 126(10), 107204. [2] Wang, H., et al. (2014). Physical review letters, 113(9), 097202. [3] Moriyama, T., et al. (2015). Applied Physics Letters, 106(16). [4] Wang, Y., et al. (2019). Science, 366(6469), 1125-1128.

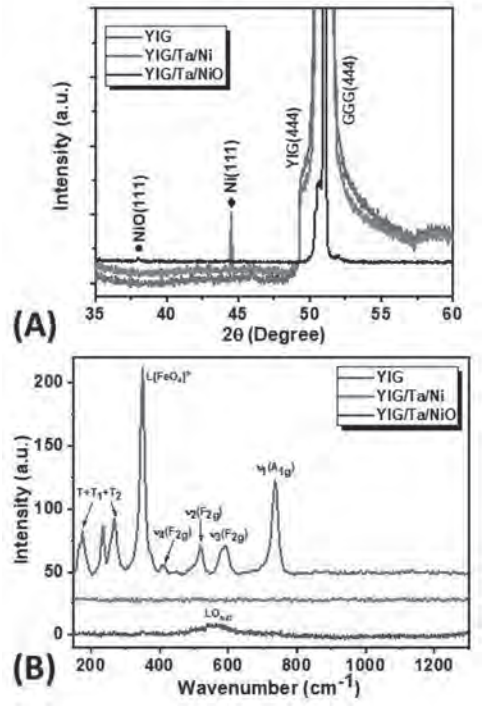

(A) XRD pattern (B) Raman Spectra, of YIG, YIG/Ta/Ni, and YIG/Ta/NiO thin films

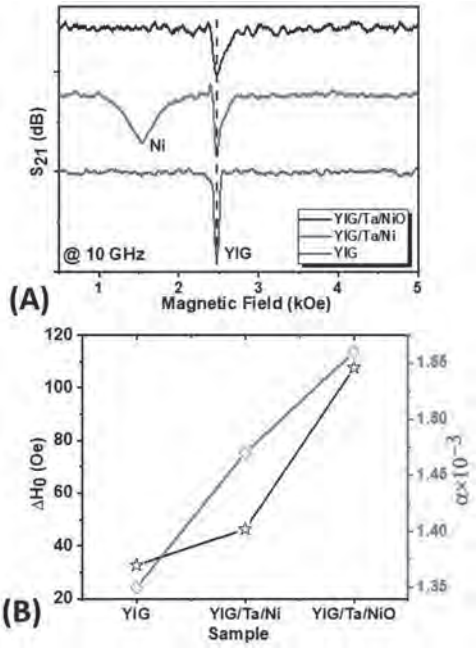

(A) FMR profile of heterostructures at 10 GHz (B) ΔH_0 and Gilbert damping of investigated samples

AP-07. Enhancing Magnetic Tunnel Junction-Based Molecular Spintronic Devices (MTJMSDs) Through Bottom Electrode Trenching for Small Molecule Attachment. *E. Peigney*[1], H. Brown[1], B. Sankhi[1] and P. Tyagi[1] *1. NSF CREST Center for Nanotechnology Research and Education, University of the District of Columbia, Washington, DC, United States*

Molecular spintronics devices (MSDs) offer solutions to downsizing and heat challenges in silicon-based technologies [1]. They adjust and control molecule spin states, opening possibilities for molecular magnets in quantum computing [2,3]. Synthetic antiferromagnetic materials can be generated by establishing robust exchange coupling between micro ferromagnetic electrodes [4,5], leading to novel devices such as spin-valves with multiple tunable states [4,6–8]. The quality and continuity of the insulator, or tunnel barrier, and the type of molecule used, are primary limitations [9]. Thiol groups often connect two metallic electrodes. The insulator layer's thickness and the nanogap between electrodes must allow current tunneling and molecule adhesion. Insulator layers typically range between 2 and 5 nm, limiting the use of molecules shorter than 2 nm. We overcame this by creating a trench within the bottom electrode, ensuring a controlled nanogap and an appropriately thick insulator layer. Trenches were fabricated using Focused Ion Beam (FIB) and Ar plasma etching in a bottom electrode of Ta(2 nm)/Co(5 nm)/NiFe(7 nm) deposited by sputtering (Fig. 1 and Fig. 2). Optimization of parameters (pressure, power, etc.) achieved clean trenches without defects. Challenges in depositing the insulator layer arose from spikes and notches (up to tens of nm) on cross-junction edges, blocking molecule bridging between electrodes. In this example, 1,10-decanedithiol molecules (1.6 to 1.8 nm long) effectively bridged the electrodes. This molecule's atomic insulator behavior enhances spin polarization by selectively allowing electrons with a certain spin orientation to flow, reducing spin relaxation and increasing polarization. This improvement could lead to more efficient spintronic devices like MRAM for data processing and storage. We conducted topological characterization of these devices using Atomic Force Microscopy (AFM) and electrical characterization with a custom I-V testing setup. Kelvin Probe Force Microscopy (KPFM) examined the influence of molecules on surface potential and the work function at the cross-junction.

[1] A. R. Rocha, V. M. García-suárez, S. W. Bailey, C. J. Lambert, J. Ferrer, and S. Sanvito, *Towards Molecular Spintronics*, Nature Mater 4, 335 (2005). [2] H. B. Heersche, Z. de Groot, J. A. Folk, H. S. J. van der Zant, C. Romeike, M. R. Wegewijs, L. Zobbi, D. Barreca, E. Tondello, and A. Cornia, *Electron Transport through Single Mn12 Molecular Magnets*, Phys. Rev. Lett. 96, 206801 (2006). [3] M. Affronte et al., *Single Molecule Magnets for Quantum Computation**, J. Phys. D: Appl. Phys. 40, 2999 (2007). [4] P. Tyagi and C. Riso, *Magnetic Force Microscopy Revealing Long Range Molecule Impact on Magnetic Tunnel Junction Based Molecular Spintronics Devices*, Organic Electronics 75, 105421 (2019). [5] S.-F. Shi and D. C. Ralph, *Atomic Motion in Ferromagnetic Break Junctions*, Nature Nanotech 2, 522 (2007). [6] E. G. Petrov, I. S. Tolokh, A. A. Demidenko, and V. V. Gorbach, *Electron-Transfer Properties of Quantum Molecular Wires*, Chemical Physics 193, 237 (1995). [7] E. G. Petrov, I. S. Tolokh, and V. May, *Magnetic Field Control of an Electron Tunnel Current through a Molecular Wire*, The Journal of Chemical Physics 108, 4386 (1998). [8] J. R. Petta, S. K. Slater, and D. C. Ralph, *Spin-Dependent Transport in Molecular Tunnel Junctions*, Phys. Rev. Lett. 93, 136601 (2004). [9] B. Hu, J. Yao, and B. J. Hinds, *Nanogap Electrodes Formed at the Exposed Edge of Au/Self-Assembled Monolayer/Al2O3/Au Tunnel Structures Grown by Atomic Layer Deposition*, Applied Physics Letters 97, 203111 (2010).

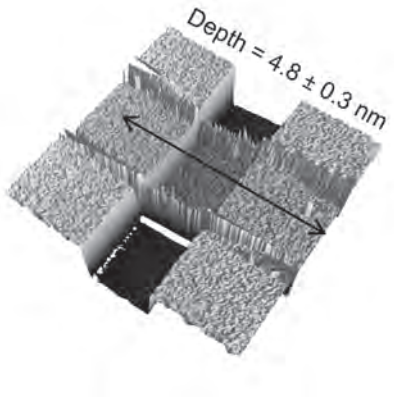

Fig. 1: AFM image of a trenched cross-junction.

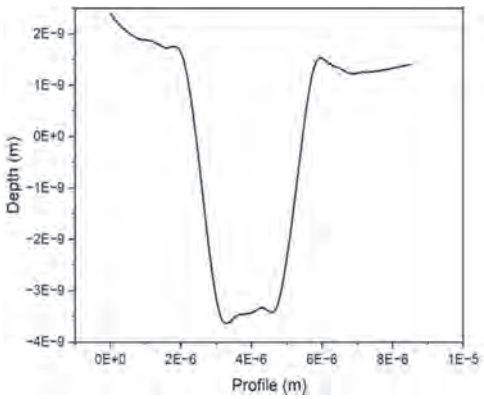

Fig. 2: Depth profile of the trenched cross-junction.

AP-08. Probing an amplified spin-orbit torque effect in antiferromagnetic oxide utilizing a magnetoresistance-based loop-shift method. H. Tseng[1] and *C. Yang*[1] *1. Materials Science and Engineering, National Yang Ming Chiao Tung University, Hsinchu, Taiwan*

Spin transport in antiferromagnets (AFMs) and the resulting spin torque effects have recently aroused significant interest due to their non-trivial physics involving long spin diffusion dynamics and low spin dissipation. Although recent studies have been devoted to focusing on spin transport within AFMs, few have effectively demonstrated the spin torque generated accordingly. This study attempts to correlate spin transport and the associated spin-orbit torque (SOT) effects in a Pt/NiO/CoFeB trilayer with varying NiO thicknesses. The characterization was performed using

angle-dependent magnetoresistance (ADMR) measurements and the magnetoresistance (MR)-based loop-shift method in a y-type geometry. It showed varying the NiO thickness in the trilayer allowed tailoring the robustness of NiO to promote the magnon transport through the spin fluctuation dynamics: Inserting an NiO layer of moderate thickness in the trilayer enables enhancing the SOT efficiency by threefold compared to the NiO-free stack. However, further increasing the NiO thickness appeared to reduce the SOT efficiency, as indicated by both ADMR and MR-based loop-shift measurements. The enhanced SOT efficiency quantitatively highlights the significance of AFM oxides for SOT devices together with the issues of spin transport modification, suggesting a pathway to reducing current density to meet low-power consumption SOT device technology.

[1] Chao-Yao Yang et al., Applied Physics Letters 118, 102403 (2021).
[2] Yan-Ting Liu et al., Anisotropy, Physical Review Applied 13, 044032 (2020).

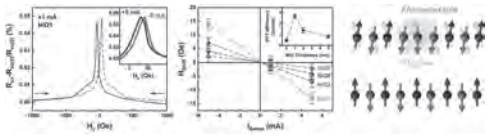

Session AQ
APPLICATIONS OF MAGNETIC MATERIALS AND DEVICES
(Poster Session)

Sevde Nur Arpaci, Chair
Northwestern University, Evanston, IL, United States

AQ-01. Additive Manufacturing of Stretchable Frequency-Reconfigurable Frequency Selective Surfaces with Split-Ring Resonators. *T. Boland*[1], C.S. Smith[1] and H. ElBidweihy[1] *1. Electrical and Computer Engineering, United States Naval Academy, Annapolis, MD, United States*

This study presents the fabrication and testing of a stretchable, frequency-reconfigurable frequency selective surface (FSS) using split ring resonators (SRRs). Utilizing additive manufacturing techniques, including stereolithography (SLA) 3D printing and aerosol jet printing (AJP), we created an FSS designed to filter at a center frequency of ~2.1 GHz. Frequency selective surfaces (FSS) are engineered metamaterials designed to filter specific frequencies of electromagnetic waves [1]. Traditional FSSs are fixed in their frequency response after fabrication, but recent advances have explored reconfigurable FSSs which can adapt their frequency response to changing conditions. Split-ring resonators (SRRs) are a common choice for FSSs due to their strong electric and magnetic responses, which allow for effective filtering [2]. In this study, we focus on mechanically reconfiguring an FSS by stretching its surface. When the FSS is stretched, the geometry of the SRRs change, altering their inductive and capacitive properties and thus their resonant frequency. The unit cells of the FSS were single square SRRs, chosen for their strong electric and magnetic responses, as illustrated with dimensions in Figure 1. The SRRs were printed on a flexible dielectric substrate fabricated using FormLabs Flexible 80A resin and an SLA printer. The conductive traces were printed using Creative Materials 127-30 flexible conductive ink and an aerosol jet printer. This combination ensured that the components of the FSS could stretch without degrading performance. The FSS's unit cell was characterized in a rectangular waveguide by straining it and measuring scattering parameters using a vector network analyzer (VNA). The SRR exhibited significant shifts in their resonant frequency when stretched, increasing by approximately 100 MHz per 20% strain--consistent with predictions seen in Figure 2 as simulated in COMSOL Multiphysics. The SRR maintained a strong filtering effect even under substantial deformation, proving its reconfigurability.

[1] R. Anwar, L. Mao, and H. Ning, Applied Sciences., Vol. 8, pp.1689 (2018) [2] H. Vani, Paramesha, and M. Goutham, International Journal of Advanced Research in Engineering and Technology., Vol. 9, pp.196 (2018)

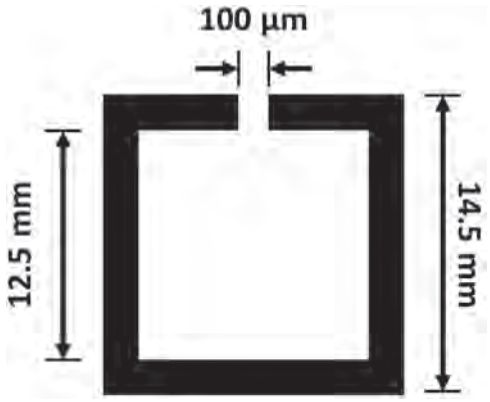

Fig. 1. Illustration and dimensions of the square split-ring resonator unit cell.

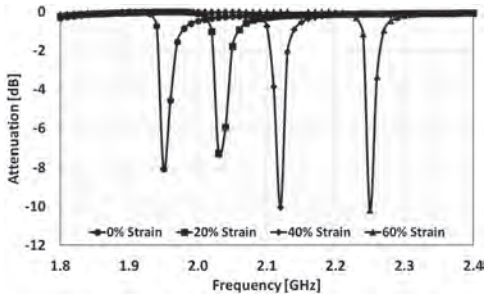

Fig. 2. Plot of resonant frequency peaks for a square split-ring resonator at 0-60% strain simulated in COMSOL Multiphysics.

AQ-02. Inspection of CFRP plate backside delamination using electromagnetic vibration and sound pressure measurement. *Y. Hosono*[1], S. Niwa[1], R. Takasugi[1], T. Ohashi[3] and Y. Gotoh[2] *1. Graduate School of Engineering, Oita University, Oita, Japan; 2. Faculty of Science and Technology, Oita university, Oita, Japan; 3. IHI Corporation, Yokohama, Japan*

1. Introduction Carbon Fiber Reinforced Plastic (CFRP) materials, primarily composed of carbon fibers and resin, are utilized in the automotive, mechanical, and aerospace industries due to their lightweight, high strength, and rigidity. Nondestructive testing is crucial for CFRP materials continuous and effective use [1-2]. Ultrasonic testing, a common method for nondestructive testing of CFRP materials [3-4], needs a moisture-containing contact medium to transmit waves to the material effectively. However, when CFRP materials are used in aircraft parts and other applications where pressure changes rapidly, the risk of internal damage increases due to the internal pressure changes caused by the state change of penetrated moisture within the CFRP material. This research proposes a new non-destructive testing method using low-frequency electromagnetic vibration to detect delamination in a single 0.14 mm thick prepreg layer on the backside of a 1.5 mm thick CFRP plate, which is used in certain parts of aircraft. The method's effectiveness is evaluated through experiments and 3D-FEM [5]. 2. Inspection method and experiment results Fig. 1 shows a model for inspecting delamination of a 0.14 mm-thick single-layer prepreg on the back side of a 1.5 mm-thick CFRP plate using electromagnetic vibration. This proposed sensor consists of a perforated permanent magnet wrapped with an AC excitation coil, a condenser microphone, and a thin steel sheet. The DC magnetic flux density from the permanent magnet and the eddy current from the AC excitation coil generate electromagnetic vibrations in the ± z-direction within a thin steel sheet via the Lorentz force [6], using a low vibration frequency of 6.7kHz. These vibrations are transmitted to the CFRP plate and detected as sound pressure by a condenser microphone on its surface. Fig.2 shows the measurement results of sound pressure at each position, denoting the measured sound pressure is increased around the backside delaminated area. This is because the macroscopic density in the CFRP material decreases in the backside delamination exists area. In the full paper, this phenomenon is evaluated using 3D-FEM for both electromagnetic force analysis and displacement analysis.

[1] C. E. Jones et al., "A Route to Sustainable Aviation: A Roadmap for the Realization of Aircraft Components with Electrical and Structural Multifunctionality," in IEEE Transactions on Transportation Electrification,

vol. 7, no. 4, pp. 3032-3049, (2021) [2] N. Takeichi, H. Senoh, T. Yokota, "Hybrid hydrogen storage vessel, a novel high-pressure hydrogen storage vessel combined with hydrogen storage material", International Journal of Hydrogen Energy, Vol.28, pp.1121-1129 (2002) [3] P. Shen, Y. Wu, Z. Luo, "Advanced Orthogonal Frequency and Phase Modulated Waveform for Ultrasonic Phased Array TFM Detection in CFRP Composites," in IEEE Transactions on Instrumentation and Measurement, vol. 73, pp. 1-10 (2024) [4] Cacciola, Matteo, Salvatore Calcagno, "Computational intelligence aspects for defect classification in aeronautic composites by using ultrasonic pulses.", IEEE transactions on ultrasonics, ferroelectrics, and frequency control 55, no. 4, pp. 870-878 (2008) [5] A. Hagisaka, S. Niwa, S. Shiota," Proposal of Detecting for Thickness Method of Hot Spring Scale inside Steel Pipes using Vibration", International Journal of Applied Electromagnetics and Mechanics, vol. 71, no. S1, pp. S483-S491 (2023) [6] S. Niwa, A. Hagisaka, I. Yamada, " Detection Method for Shrinkage Cavities Inside Spheroidal Graphite Cast Iron Using Vibration Measurement by Electromagnetic Force Excitation", Materials Transactions, vol.64, no. 2, pp.596-603 (2023)

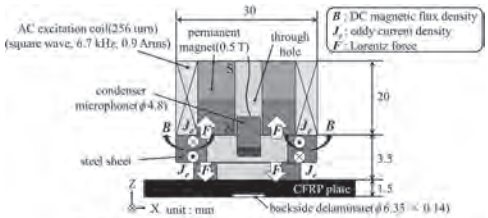

Fig.1 Inspection model for delamination on the back side of CFRP plate.

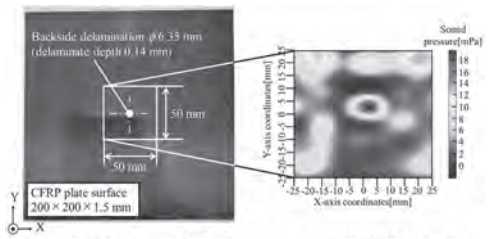

Fig.2 Evaluation result of 2 D scans around backside delamination

AQ-03. Micromagnetic Simulations of Concentration Detection Capability of Large Area Low Aspect Ratio GMR Sensors in Biomedical Diagnostics. *R.A. Mendonsa*[1], S. Liang[1], D. Tonini[1] and J. Wang[1] *1. University of Minnesota, Minneapolis, MN, United States*

Since the discovery of GMR [1,2], it has found many applications in sensors. One of these key areas is for biomedical sensing [3]. GMR biosensors with large area and low-aspect-ratio were demonstrated experimentally with ultra high sensitivity [4], followed by simplified theoretical explanation [5, 6]. This study presents a systematic micromagnetic simulation analysis of large-area and low-aspect-ratio GMR sensors, with a particular focus on two key regimes: the linear portion before saturation by the MNP interaction with the sensor and the flattening out due to sensor saturation. As shown in Fig. 1, magnetic nanoparticle (MNP) types, and critical spacings between MNPs and the sensor surface to optimize sensitivity and accuracy are explored. The systematic simulations compare material combinations and configurations, highlighting the impact of MNP characteristics and spacing on sensor performance across these regimes. The findings offer insights into the design and application of GMR sensors for detecting and quantifying different MNP concentrations as shown in Fig. 2, potentially enhancing diagnostic capabilities. This research advances the understanding of GMR sensor behavior and sets the stage for future experimental studies and developments in this promising field.

Binasch, Grünberg, et al. "Enhanced magnetoresistance in layered magnetic structures with antiferromagnetic interlayer exchange." Physical review B 39.7 (1989): 4828. Baibich, Mario Norberto, et al. "Giant magnetoresistance of (001) Fe/(001) Cr magnetic superlattices." Physical review letters 61.21 (1988): 2472. Baselt, David R., et al. "A biosensor based on magnetoresistance technology." Biosensors and Bioelectronics 13.7-8 (1998): 731-739. Srinivasan, B. et al. A detection system based on giant magnetoresistive sensors and high-moment magnetic nanoparticles demonstrates zeptomole sensitivity: potential for personalized medicine. Angew. Chem. Int. Ed. 48, 2764–2767 (2009). Su, Diqing, Kai Wu, and Jian-Ping Wang. "Large-area GMR bio-sensors based on reverse nucleation switching mechanism." Journal of Magnetism and Magnetic Materials 473 (2019): 484-489. Feng, Yinglong, et al. "Localized detection of reversal nucleation generated by high moment magnetic nanoparticles using a large-area magnetic sensor." Journal of Applied Physics 122.12 (2017).

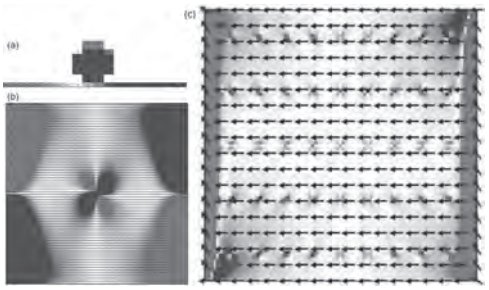

OOMMF simulation data showing a single MNP interacting with a thin film large area GMR sensor side view y axis zoomed in the center of the z plane (a) and top view z axis (b). The reverse nucleation site is clearly visible in the center of the thin film. (c) A 4umx4um sensor with 50 MNP's evenly dispersed.

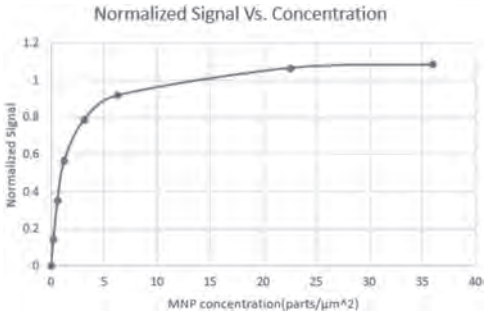

OOMMF simulation results converted to GMR effect plotted out with respect to concentration density of particles, showing the initial linear regime and the saturated regime.

AQ-04. Numerical analysis of inspection method of hot spring scale attached to steel pipes in geothermal power plants using electromagnetic vibration. *R. Takasugi*[1], H. Ikusada[1], Y. Hosono[1], S. Niwa[4], Y. Gao[2], T. Sasayama[3] and Y. Gotoh[2] *1. Division of Mechatronics, Graduate School of Engineering, Oita University, Oita, Japan; 2. Division of Intelligent Mechanical System, Faculty of Science and Technology, Oita University, Oita, Japan; 3. Graduate School of Information Science and Electrical Engineering, Kyushu University, Fukuoka, Japan; 4. Division of Mechanical Energy Engineering, Graduate School of Engineering, Oita University, Oita, Japan*

1. Introduction Steam from hot springs flows through the steel pipes at geothermal power plants [1]. In this steel pipe, components in the hot spring accumulate and form solid "hot spring scale," which can obstruct the flow of hot spring steam [2]. This paper proposes a method the pipe is vibrated electromagnetically without contact from the outside, and the thickness of hot spring scale on the inside of the steel pipe is measured from the vibration intensity. The inspection principle is clarified through 3-D FEM electromagnetic vibration displacement analysis considering hysteresis characteristics of the steel pipe. In addition, the results are compared with validation experiments. 2. Inspection model and Results The inspection model shown in Fig. 1 consisted of an actual steel pipe with the hot spring scale and an

electromagnetic force vibration device (EFVD), which includes three permanent magnets (PM), an AC excitation coil, a steel plate, and an acceleration sensor (AS). In this inspection method, the static magnetic field from the PM and the eddy currents from the AC excitation coil intersect orthogonally, generating Lorentz force inside the steel pipe. The distribution of this electromagnetic force is calculated by nonlinear electromagnetic field analysis using 3-D FEM with the "Play model" that takes into account for hysteresis characteristics inside the steel pipe. The vibration strength of the steel pipe obtained by the AS inside the EFVD is calculated by displacement analysis using 3-D FEM. Fig. 2 summarizes the vibration intensity versus the thickness of each hot spring scale measured by the AS inside of the EFVD and the results of analysis considering the initial magnetization curve and the hysteresis characteristics of the steel pipe. This figure illustrates that the vibration strength on the steel pipe is decreased when the hot spring scale thickness is increased. The effectiveness of the proposed inspection method was shown by the results of the analysis and the actual measurements, which showed a similar trend.

[1] K. Wang, B. Yuan, G. Ji, X. Wu, "A comprehensive review of geothermal energy extraction and utilization in oilfields", Journal of Petroleum Science and Engineering, vol. 168, pp. 635-638, 2018. [2] A. Hagisaka, S. Niwa, S. Shiota, Y. Gao, Y. Gotoh, "Proposal of detection for thickness method of hot spring scale inside steel pipes using vibration", International Journal of Applied Electromagnetics and Mechanics, vol. 71, no. S1, pp. S483-S491, 2023. [3] T. Matsuo, Y. Osaka, and M. Shimasaki, "Eddy-current analysis using vector hysteresis models with play and stop hysterons," IEEE Trans. Magn., vol. 36, no. 4, pp. 1172–1177, Jul. 2000.

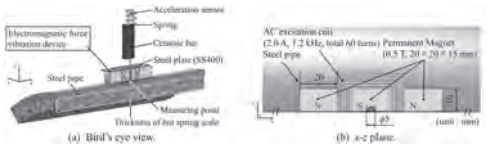

Fig. 1 Proposed inspection sensor and model (1/2 domain).

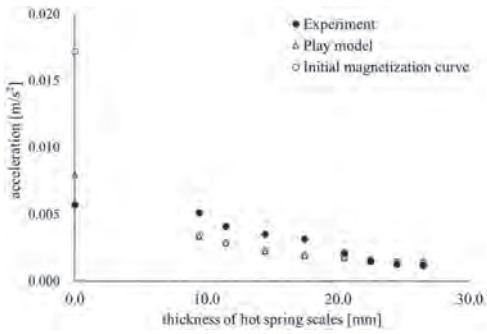

Fig. 2. Comparison of experiment and analysis. (Excitation current = 2.0 A (rms), excitation frequency = 1.2 kHz).

AQ-05. A Self-Assembled Magnetic Millirobot with an Elastic 3D Linear Structure for Minimally Invasive Medicine. *Y. Lee*[1], J. Lee[2] and S. Jeon[2] *1. Mechanical Engineering, Kongju National University, Cheonan, Chungnam, The Republic of Korea; 2. Mechanical and Automotive Engineering, Kongju National University, Cheonan, Chungnam, The Republic of Korea*

Small magnetic robots have been extensively studied as a potential alternative for minimally invasive surgery, offering numerous advantages, such as minimizing surgical risks while maximizing surgical outcomes [1-3]. Previously, we introduced a multi-modular magnetic millirobot (MMM) that can be inserted and retrieved through a medical syringe mechanism [4]. The MMM could change its equilibrium postures between the self-assembled and disassembled formations by applying different external magnetic fields. However, the MMM had limitations in extending to three-dimensional (3D) shapes because each module of the MMM was connected by pin joints [4]. To overcome these limitations, we propose a self-assembled magnetic millirobot (SAMM) composed of an elastic 3D linear structure and multiple magnets, as shown in Fig. 1. The SAMM is basically constructed to have no residual elastic energy in its initial formation, as shown in Fig. 1b and 1c. Thus, by combining the elastic bending moments of the elastic body and the magnetic interactive forces within the magnets, the SAMM can be constructed to have a variety of self-assembled 3D linear shapes capable of restoring its original formation even from the disassembled formations, as shown in Fig. 1b and 1c. Thus, the SAMM can be used as a minimally invasive medicine. In this study, we established theoretical conditions for the design parameters of the SAMM to be able to maintain its equilibrium formation under external forces and change its equilibrium formation between the self-assembled formation and the disassembled formation without causing a yield deformation. We then validated the proposed SAMM and the conditions by constructing the SAMM and demonstrating its controlled mechanical motions such as a self-assembly, disassembly, and locomotion actuated by an external magnetic field in a various in-vitro environments.

[1] B. J. Nelson, I. K. Kaliakatsos, and J. J. Abbott, *Annu. Rev. Biomed. Eng.*, Vol. 12, p. 55–85 (2010) [2] H. Gu *et al.*, *Nat. Commun.*, Vol. 14, no. 1 (2023) [3] T. Xu *et al.*, *Sci. Robot.*, Vol. 4, no. 29 (2019) [4] Y. Lee and S. Jeon, *AIP Adv.*, Vol. 14, no. 2 (2024)

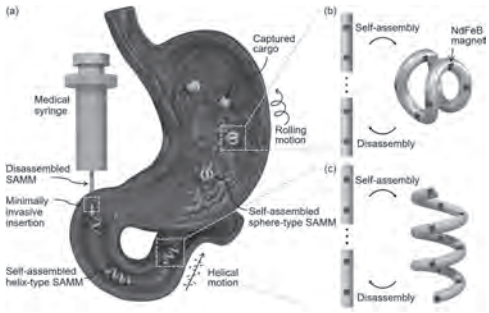

Fig. 1. (a) Schematic views of the SAMM's insertion, self-assembly, and locomotion in an intestinal organ. Self-assembled and disassembled formations of the (b) sphere-type and (c) helix-type SAMMs.

AQ-06. Hydrogen gas sensing using Pd coated spin-valve GMR with magneto-strictive FeSiB layer. *D. Oshima*[1], T. Kato[1,2] and S. Iwata[3] *1. Department of Electronics, Natoya University, Nagoya, Japan; 2. Institute of Materias and Systems for Sustainability, Nagoya University, Nagoya, Japan; 3. Nagoya Industrial Science Research Institute, Nagoya, Japan*

For utilizing hydrogen as a clean energy carrier, hydrogen sensors detecting leakage or accumulation of the hydrogen gas are required, which leads to an increased demand for developing low-power, cost-effective, and reliable hydrogen sensors. We have proposed a hydrogen sensor using a spin-valve giant magnetoresistance (GMR) strain gauge with a hydrogen-absorptive layer, because the GMR strain gauge can detect the strain as small as 10^{-6} [1] and also can be fabricated by sputtering and photolithography suitable for mass production, resulting in low-cost sensors. In this study, we investigated magnetoresistance (MR) properties of GMR wire with a hydrogen-absorptive Pd layer and a magneto-strictive FeSiB layer before and after hydrogen exposure. GMR films with a stack of substrate / NiFe(5) / MnIr(10) / $Co_{90}Fe_{10}$(3) / Cu(3) / $Co_{90}Fe_{10}$(1.5) / FeSiB(20) / Ta(2) / Pd(0 or 20) were fabricated using magnetron sputtering method. Numbers in parentheses are thicknesses in nanometer. Polyethylene naphthalate (PEN) was used as a substrate. GMR wires were fabricated using photolithography and Ar ion milling. MR properties were measured by a 4-probe method before and after exposing the sample to pure hydrogen with a pressure of 0.1 MPa. Figure 1 shows hard-axis MR curves of the GMR wire with Pd layer (a) before and (b) after H_2 exposure. The MR took maximum at ~100 Oe before the exposure, while it took maximum at ~160 Oe after the exposure. Coercivities of the pinned and free layers, an exchange bias field, and an interlayer coupling field estimated from the MR curves were almost unchanged by the H_2 exposure. Thus, the

change in the hard-axis MR curve is considered to be due to the change in the magnetic anisotropy field H_k of the FeSiB layer. The variation in the MR curve by the H_2 exposure was not observed in the GMR wire without Pd layer. These results indicated the GMR wire detected the Pd expansion by the H_2 absorption, showing the feasibility of the hydrogen sensor using the cost-efficient spin-valve GMR.

[1] Y. Hashimoto et.al., J. Appl. Phys. 123, 113903 (2018).

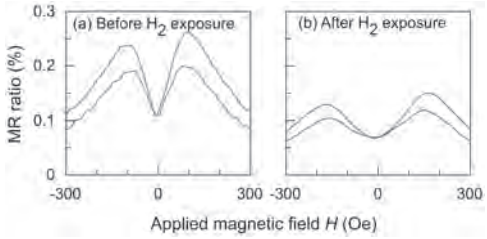

Fig. 1 Hard-axis MR curves of GMR wire (a) before and (b) after H_2 exposure.

AQ-07. Detecting and Differentiating Magnetic Signals from Moving Magnetic Nanoparticles for Enhanced Biosensing and Diagnostic Applications. *K. Hwang*[1], D. Brown[1], S. Attanayake[1], D. Luu[1], M. Nguyen[2], T. Lee[2] and M. Phan[1] *1. Physics, University of South Florida, Tampa, FL, United States; 2. Chemistry, University of Houston, Houston, TX, United States*

Magnetic nanoparticles are extensively utilized as biomarkers in various biomedical applications. Detecting and distinguishing magnetic signals from similarly sized moving magnetic nanoparticles in microfluidic systems is crucial yet challenging for biosensing. In this study, we have developed a novel method to detect and differentiate magnetic signals from moving superparamagnetic (SPM) and ferrimagnetic (FiM) nanoparticles of similar size. Our approach utilizes a highly sensitive magnetic coil-based sensor that exploits the combined effects of giant magnetoimpedance (GMI) and an LC-resonance circuit. Iron oxide nanoparticles of same size (160 nm) but different crystallite sizes (10 nm, 12 nm, and 15 nm for SPM particles; 19 nm and 26 nm for FiM particles) [1], which have similar saturation magnetization but different coercivities (zero for SPM particles and non-zero for FiM particles), flow through the magnetic coil at controlled velocities. Their distinct effects are analyzed through changes in the complex impedance of the sensing system. While SPM nanoparticles are found to show a similar response, FiM nanoparticles with varying coercivities demonstrate distinct signals. Our findings provide a new pathway for utilizing SPM and FM nanoparticles as innovative magnetic biomarkers to identify specific biological entities, thereby expanding their potential applications.

[1] Nguyen et al., "Magnetic Tunability via Control of Crystallinity and Size in Polycrystalline Iron Oxide Nanoparticles," SMALL, 2402940 (2024): doi.org/10.1002/smll.202402940

AQ-08. Magnetoconvection analysis of the cooling properties of magnetic nanoparticles in vegetable-based transformer oil. *H. Lee*[1] *1. Division of Smart Convergence Engineering, Changshin University, Changwon-si, The Republic of Korea*

This paper describes an investigation of the combined effects of magnetoconvection and an externally applied magnetic field on the thermal performance of vegetable oil-based magnetic nanofluids with different volume fractions of magnetic nanoparticles. Due to its high dielectric strength and good cooling performance under normal operating conditions, mineral-based oil has traditionally been used in power transformers. Environmentally friendly vegetable-based transformer oils have been substituted for mineral-based insulating oils because of their environmental impact. To date, the related studies have only reported on the characteristics of the dielectric breakdown in magnetic nanofluids based on vegetable oil, without the use of real electromagnetic systems. In addition, the thermal characteristics of vegetable oil-based magnetic nanofluids have not been fully investigated. Therefore, the aim of this study was to investigate the cooling performance by the addition of magnetic nanoparticles to vegetable transformer oil. In order to analyse this effect quantitatively, a multi-physics technique that incorporates magnetic-thermal-fluidic fields was developed on the basis of the quasi-static magnetic field approximation and conjugate heat transfer. Experiments were successfully carried out in a simple electromagnetic system with different insulating fluids to validate the numerical results.

[1] J. Patel, K. Parekh, R. V. Upadhyay, International Journal of Thermal Sciences, Vol. 103, p. 35-40, (2016) [2] Jian Li, Zhao-Tao Zhang, Ping Zou, Bin Du and Rui-Jin Liao, Modern Physics Letters B, Vol. 26, p. 1250095 (2012) [3] V. A. Primo, B. Garcia, R. Albarracin, Electrical Insulation Magazine IEEE, Vol. 34, p.13-26 (2018) [4] John Philip, P. D. Shima, and Baldev Raj, Applied Physics Letters, Vol. 92, p. 043108 (2008)

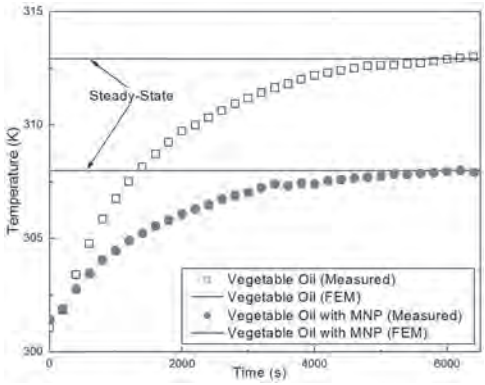

Temperature of conductors immersed in conventional vegetable oil and vegetable oil with a 7% volume fraction of magnetic nanoparticles as a function of time

Session AR
BIO-MAGNETISM AND BIOMAGNETIC APPLICATIONS
(Poster Session)

Ping Liu, Chair
University of Texas at Arlington, Keller, TX, United States

AR-01. Towards next-generation nerve repair: using glass-coated magnetic microwires to enhance and guide neurite outgrowth.
X. Zhang[1,2], K. Neuman[1], B.T. Lejeune[1], A. Koppes[1], R. Koppes[1], *M. Vázquez*[3] and L.H. Lewis[1,2,4] *1. Chemical Engineering, Northeastern University, Boston, MA, United States; 2. Mechanical and Industrial Engineering, Northeastern University, Boston, MA, United States; 3. Instituto de Ciencia de Materiales de Madrid, CSIC, Madrid, Spain; 4. Physics, Northeastern University, Boston, MA, United States*

The human nervous system, functioning as a complex electromagnetic network, presents opportunities for utilizing magnetic materials and phenomena to address various neurological issues and disorders. Peripheral nerve injuries, for example, are a leading cause of disability and can severely impact patients' quality of life. Current research in neuroregeneration encompasses strategies that use various types of external stimulations – chemical, electrical, topographical, *etc.* – to accelerate and guide nerve growth [1]. Here, we present encouraging results from a novel approach to guide neurite growth using magnetized glass-coated magnetic microwires that furnish a synergistic combination of magnetic and topographical stimulations. These microwires (dia~80 μm), comprised of a FeSiB metallic glass cylindrical core coated with a pyrex glass shell [2], possess an ultrasoft magnetic character, with the metallic core having a low coercivity of several A/m, high permeability up to 10^5, and saturation magnetization of ~1.5 T. In our investigations, rat dorsal root ganglia (DRG) neurons were cultured under various conditions, including on either magnetized magnetic microwires or inert glass fibers, with field-only and non-stimulated conditions serving as control groups (Fig). The DRG responses under each condition, including total neurite outgrowth and directionality, were compared. Our results suggest that the combination of magnetic and topographical stimulations significantly enhances and directs neurite outgrowth. Specifically, the employment of magnetic microwires under a magnetic field resulted in a 500% increase in total neurite outgrowth density and a 150% enhancement in neurite extension length compared to the non-stimulated controls. Additionally, the magnetic microwire significantly biased neurite outgrowth along the microwire, doubling the effect observed with glass fibers of the same dimensions. These findings pave the way for future exploration of biophysical stimulation techniques for peripheral nerve regeneration and deepen our understanding of material-tissue interactions. Acknowledgments: This work was funded by Fulbright España and Tufts CTSI S-GATS Award

[1] Neuman, K., et al. (2023). En route to next-generation nerve repair: static passive magnetostimulation modulates neurite outgrowth. Journal of Neural Engineering, 20(1), 016020. [2] Vázquez, M., 2007. Advanced magnetic microwires, in Handbook of Magnetism and Advanced Magnetic Materials, Ed. S. Parkin & H. Kronmuller, John Wiley Vol 4, 2192-2222

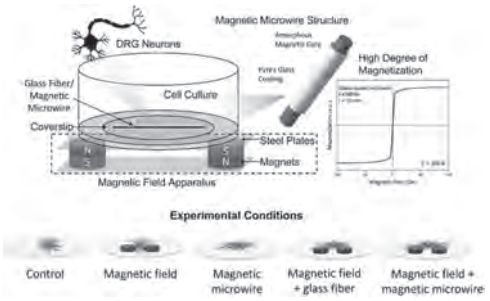

Schematic of the DRG culture setup

AR-02. Magnetic relaxation of Gd doped $MnFe_2O_4$ nanoparticles for MR effect and heat dissipation.
N. Kataoka[1,4], K. Aoki[1], A. Usui[3], T. Sakamoto[1], H. Amano[1], Y. Kusumoto[1] and Y. Ichiyanagi[1,2] *1. Physics, Yokohama National University, Yokohama, Japan; 2. Osaka University, Toyonaka, Japan; 3. Tohoku University, Sendai, Japan; 4. Sojitsu Corporation, Tokyo, Japan*

In the 1970s, MRI was developed to image the distribution of hydrogen content in the body, enabling the observation of tissue differences and the morphology and dynamics of lesions, which were difficult to observe with X-rays, with high contrast based on the hydrogen atom composition ratio. Nuclei have nuclear spins, which generate magnetic moments. Denoting the population of nuclear spins in a static magnetic field by M and the effective magnetic field in a rotational coordinate system by H, the magnetic moment moves according to the Bloch equation as $dM/dt = \gamma M \times H$ (1), where γ is a constant that varies depending on the atom, called the magnetic rotation ratio. The spin population is in precession, with only the component that contributes in the same direction as the external magnetic field remaining as the overall magnetization component, and its frequency follows Larmor's equation as $\omega_L = \gamma H$. In this study, $MnGd_xFe_{2-x}O_4$ nanoparticles (x = 0, 0.05, 0.10) encapsulated in amorphous SiO_2 were prepared by doping $MnFe_2O_4$ with a small amount of Gd ions, and their magnetic relaxation and MR effects were investigated. The samples were prepared by wet mixing of metal chlorides and sodium metasilicate solutions, and the particle size was controlled to 18 nm by adjusting the annealing temperature. T_1 and T_2 relaxation measurements were performed by spin-echo method and MR signals were measured. All samples showed a shortening effect of T_2 relaxation. These phenomena would be attributed to the strong effect of the magnetic moment of Gd, which has a maximum of seven unpaired electrons in the 4*f* orbitals, on the protons. A dominant shortening effect was also observed at T_1. Furthermore, it was confirmed that the material also has excellent heat dissipation properties as a medium for hyperthermia, and is expected to be used as a material with theranostic function in the future.

[1] Sota Hamada, Yuko Ichiyanagi, et al. *J. Magn. Magn. Mater.* 559 (2022) 169536. [2] S. S. Kelkar, T. M. Reineke, *Bioconjugate Chem.* 2011, 22, 1879–1903.

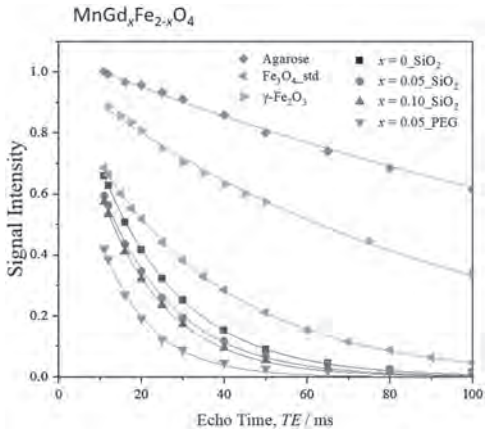

T_2 relaxation curves of various composition of 18-nm $MnGd_xFe_{2-x}O_4$ (x = 0, 0.05, 0.10) nanoparticles.

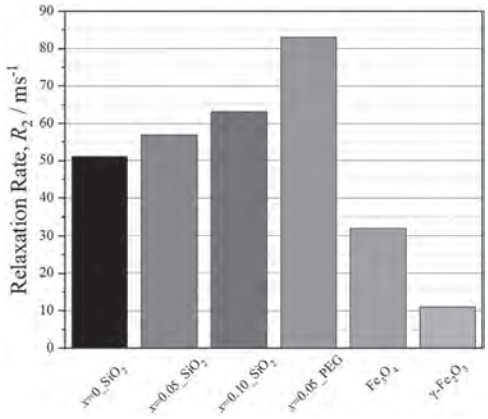

Relaxation rate R_2 of 18-nm $MnGd_xFe_{2-x}O_4$ (x = 0, 0.05, 0.10) nanoparticles.

AR-03. Directional Dependence of Moderate Magnetic Fields on HT22 Cell Proliferation. *M. Pirbhai*[1], N. Wagner[1], C. Ferguson[3] and A. Estevez[2] *1. Physics, St. Lawrence University, Canton, NY, United States; 2. Biology, St.Lawrence University, Canton, NY, United States; 3. Bioengineering, University of Oregon, Eugene, OR, United States*

Magnetotherapy has the potential to become a valuable tool in the biomedical field due to its minimally invasive therapeutic capabilities. However, our understanding of how static magnetic fields (SMFs) influence neural structure and growth remains incomplete. This study investigates the impact of magnetic field orientation on the proliferation of HT22 neural cells, a mouse hippocampal neuronal cell line. We explore how a 1 mT SMF, a strength comparable to moderate permanent magnets, affects cell proliferation when applied in different orientations. HT22 cells were exposed to a 1 mT magnetic field for 30 minutes outside the incubator. Control groups included cells left in the incubator and cells placed between the Helmholtz coils for 30 min without magnetic field exposure. Proliferation was measured by counting 12 random areas on a 20 mm diameter glass coverslip for 5 days. Our findings indicated a significant increase in cell proliferation in the presence of the magnetic field, with the highest proliferation, observed when the magnetic field was oriented vertically downward. This was followed by horizontal and vertically upward orientations, respectively. Both control groups exhibited lower proliferation rates compared to the magnetic field-exposed groups. To confirm the effect of the magnetic field, additional experiments were conducted: HT22 cells were grown on cell culture plastic dish, the media was changed to Locke's buffer during exposure, and the magnetic field exposure time was increased to 45 minutes. These variations altered the proliferation curve but consistently demonstrated that the vertically downward magnetic field produced the highest proliferation rate. This study highlights the directional dependence of moderate magnetic fields on HT22 cell proliferation, suggesting potential applications in cellular biology and therapeutic strategies. Further research is warranted to elucidate the underlying mechanisms driving this directional effect on cell proliferation. By delving into these interactions, we aim to provide insights that contribute to a more comprehensive understanding of magnetotherapy's potential role in neurobiology.

Xin Zhang, Kevin Yarema, and An Xu, Biological Effects of Static Magnetic Fields (2017) Xiaofei Tian, Dongmei Wang, and Meng Zha, Electromagnetic Biology and Medicine, Vol. 37, pg 114-125 (2018) Craig Jun Kit Wong, Yee Kit Tai, and Jasmine Lye Yee Yap, Biomaterials, Vol. 287 (2022)

AR-04. Optimization of a Quadrupole Magnetic Sorter for Continuous Flow Fractionation of Red Blood Cells from whole blood. *K. Paz Gonzalez*[1], S. Ciannella [1], L. Nguyen T. Tran[1], X. Wu[3], H. Choe[3], P. Iyer[3], K. Wu[2], J. Chalmers[3] and J. Gomez-Pastora[1] *1. Chemical Engineering, Texas Tech University, Lubbock, TX, United States; 2. Electrical and Computer Engineering, Texas Tech University, Lubbock, TX, United States; 3. William G. Lowrie Department of Chemical and Biomolecular Engineering, The Ohio State University, Columbus, OH, United States*

Depletion of Red Blood Cells (RBCs) from whole blood is crucial for accurate diagnostics and efficient therapeutic applications such as transfusions and stem cell transplants. Typically, RBCs are depleted using methods like RBC lysis, which can contaminate subsequent samples and cause cellular integrity loss [1]; density gradient centrifugation, which requires specialized equipment and may physically damage cells [1]; and antibody-labeled separation, which may impact cell viability and present a risk of non-specific binding [2][3]. This study focuses on optimizing a Quadrupole Magnetic Sorter (QMS) for continuous flow fractionation of RBCs, which in their deoxygenated state are inherently magnetic due to their hemoglobin content, allowing for their unlabeled separation from white blood cells (WBCs). The QMS, with a 10.2mm aperture and maximum magnetic field of 1.36 T, utilizes a quadrupole magnet array that creates a constant magnetic field gradient of 286 T/m essential for effective RBC separation [4]. A specially designed and 3D-printed manifold facilitates a continuous process by introducing the cell suspension and a buffer fluid at the inlets and the constant collection of RBC-enriched and RBC-depleted fractions at the outlets. Both fluids flow in parallel during magnetophoresis due to laminar flow inside the separator. RBCs diffuse into the buffer fluid by the motion caused by the magnetic force, which is perpendicular to the fluid flow direction. The annular flow channel, designed with an outer radius of 4.65mm and a varying inner radius determined by the rod used to exclude the volume near the center of the channel where the magnetic force is minimal, enables precise control of the cell suspension flow. We will evaluate system performance by varying total flow rates, flow rate ratios, and center rod radius to optimize the fractionation process. We anticipate conducting advanced RBC separation experiments with this new design, leveraging our findings to improve the QMS inlet and outlet design for practical applications. Our goal is to establish a reliable, label-free magnetic separation method for RBCs, providing significant benefits for diagnostic and therapeutic processes.

[1] HM. Shapiro, John Wiley & Sons., Ed. 4 (2005) [2] UO. Häfeli, J. Aue, J. Damani, Laboratory Techniques in Biochemistry and Molecular Biology. Vol. 32, p. 163-223 (2007) [3] JJ. Chalmers, Y. Xiong, X. Jin, Biotechnol Bioeng. Vol. 105. p. 1078–1093.(2010) [4] X. Wu, J. Gómez-Pastora, M. Zborowski, Separation and Purification Technology. Vol. 280, (2022)

AR-05. Conformable Electromagnetic Shielding Materials for Intentional Low to Medium Frequency Electromagnetic Interference in Brain Implants. *W. Lohr*[1], K. Feng[2], S. Smith[3] and R.L. Hadimani[2,4]
1. Department of Biomedical Engineering, Virginia Commonwealth University, Richmond, VA, United States; 2. Mechanical and Nuclear Engineering, Virginia Commonwealth University, Richmond, VA, United States; 3. Chemical & Life Science Engineering, Virginia Commonwealth University, Richmond, VA, United States; 4. Electrical and Computer Engineering, Iowa State University, Ames, IA, United States

Magnetic shielding from intentional electromagnetic interference (EMI) in deep brain stimulation (DBS) implants can be achieved via high permeability materials, but they are non-conformable and heavy. We made a conformable composite of polydimethylsiloxane (PDMS), permalloy nanoparticles and multi-walled carbon nanotubes (MWCNT). We tested the composite on a brain phantom with a DBS lead using transcranial magnetic stimulation (TMS) magnetic fields. TMS and DBS are FDA-approved treatments for depression and Parkinson's disease, respectively. DBS is susceptible to certain EMI. So, we evaluate how well a permalloy composite shielding cap blocks TMS pulses to ensure DBS safety. A 3D-printed brain mold is made using MRI images and filled with a PDMS and MWCNT composite, mimicking the electrical conductivity of the brain. A DBS lead is placed in the phantom's subthalamic nucleus. Tri-axial dipole probes are placed along the lead. The skull and skin are built as one layer of PDMS. The gap between the skull and the gray matter is filled with crayfish saline solution with an electrical conductivity of 1.4 S/m, similar to cerebrospinal fluid. The conformable magnetoelectric shielding cap is made of permalloy nanoparticles, PDMS, and MWCNT. Electric field readings are taken via dipole probes, with and without the cap. Hysteresis graphs of permalloy nanoparticles and composite films were taken at ~70°F (Fig.1). Readings were taken using a 9mm-thick composite film with a Gauss meter 15mm from the TMS coil. The average magnetic field amplitude with no shield was 0.7785 T (Fig. 2). With the film, it was 0.5805 T, giving a 52% shielding efficiency compared to solid permalloy. Our results show that the composite film has lower magnetization compared to pure permalloy nanoparticles. The composite film significantly blocks TMS pulses, suggesting that DBS leads can be protected by a composite cap. Further research can explore different shielding materials and thicknesses or other EMI sources.

1. Rahimpour, S., Kiyani, M., Hodges, S. E., & Turner, D. A. (2021). Deep brain stimulation and electromagnetic interference. Clinical Neurology and Neurosurgery, 203, 106577. https://doi.org/10.1016/j.clineuro.2021.106577 2. Cohen, S. L., Bikson, M., Badran, B. W., & George, M. S. (2022). A visual and narrative timeline of US FDA milestones for transcranial magnetic stimulation (TMS) devices. Brain Stimulation, 15(1), 73–75. https://doi.org/10.1016/j.brs.2021.11.010 3. Magsood, H., Syeda, F., Holloway, K., Carmona, I. C., & Hadimani, R. L. (2020). Safety Study of combination treatment: Deep brain stimulation and transcranial magnetic stimulation. Frontiers in Human Neuroscience, 14. https://doi.org/10.3389/fnhum.2020.00123 4. Glover, P. M., & Bowtell, R. (2007). Measurement of electric fields due to time-varying magnetic field gradients using dipole probes. Physics in Medicine and Biology, 52(17), 5119–5130. https://doi.org/10.1088/0031-9155/52/17/001

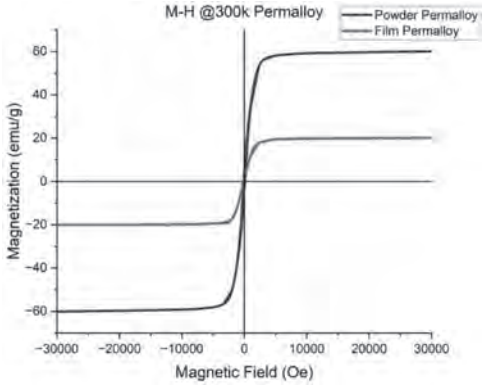

Fig. 1: Permalloy nanoparticle & composite film hysteresis graphs

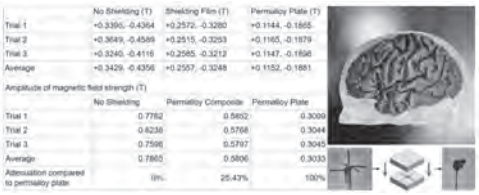

Fig. 2: TMS coil magnetic field strength with different shielding, brain phantom and dipole probe fabrication.

AR-06. Systematic Analysis of Transcranial Magnetic Stimulation Motor Response and EEG Functional Connectivity Relationship in Mild to Moderate TBI Patients. *E.R. Sprouse*[5], C.M. Harris[1,2], A. Jamil[3,6], L. Manning-Franke[4] and R.L. Hadimani[2,5] *1. Department of Life Sciences, Virginia Commonwealth University, Richmond, VA, United States; 2. Department of Mechanical and Nuclear Engineering, Virginia Commonwealth University, Richmond, VA, United States; 3. Massachusetts General Hospital, Boston, MA, United States; 4. Department of Physical Medicine and Rehabilitation, Virginia Commonwealth University, Richmond, VA, United States; 5. Department of Biomedical Engineering, Virginia Commonwealth University, Richmond, VA, United States; 6. Harvard Medical School, Boston, MA, United States*

Introduction Transcranial Magnetic Stimulation (TMS) is a neuromodulation procedure used to treat psychiatric and neurological disorders. When electroencephalography (EEG), a neuroimaging technique, is applied in conjunction with TMS, the analysis of resting-state EEG activity can be used to quantify functional connectivity (FC) in the brain. These modulations can then be related to a subject's resting motor threshold (RMT), a baseline parameter in TMS therapy that determines the treatment intensity (dose) of subjects undergoing TMS. Due to the highly variable nature of RMT, previous work has attempted to predict individual values by examining specific EEG nodes suspected to relate to motor activity, and their calculated average FC values to all other nodes [3]. We continue this with an investigation of the relationship of the FC values of a larger set of EEG scalp electrodes to RMT values collected from experimental participants. Methods We performed a post-hoc, time-frequency analysis of EEG data gathered in a previous experiment [2] via MATLAB[1]. A broad analysis of the global FC values of right-hemisphere EEG electrodes guided our pairwise FC analysis. We then fit linear regressions between pairs of EEG electrodes surrounding FC4 in the delta and alpha bands, as those are shown in previous work to be significant when predicting RMT [3]. Results Figure 1 shows a matrix of pairwise FC values and a map of the ROI pairs explored. When compared to the average FC of the FC4 node in the delta band, it is clear that the average FC value of the FC4 delta band alone is the strongest predictor of RMT. Figure 2 supports this finding by showing the negative correlation that the FC4 delta band has with RMT. Conclusion Understanding the relationship between neural synchronization and RMT could have clinical implications

for TMS, by providing an easy way to determine the optimal dosing parameters for treatment. Acknowledgments Authors acknowledge the NSF Grant #2349694 and VCU Breakthrough Grant #AP00001868.

[1] A. M. Bastos and J.-M. Schoffelen, "A tutorial review of functional connectivity analysis methods and their interpretational pitfalls", Frontiers Syst. Neurosci., vol. 9, pp. 175, Jan.2016. [2]Franke, Laura M., et al. "Randomized Trial of RTMS in Traumatic Brain Injury: Improved Subjective Neurobehavioral Symptoms and Increases in EEG Delta Activity." Brain Injury, vol. 36, no. 5, Apr. 2022, pp. 683–92, https://doi.org/10.1080/02699052.2022.2033845. [3]Hussain, Mishal Z., et al. "Investigation of EEG Neurophysiological Relationship to TMS Response in Mild Traumatic Brain Injury Patients." IEEE Transactions on Magnetics, vol. 59, no. 11, Nov. 2023, pp. 1–5, https://doi.org/10.1109/TMAG.2023.3282614.

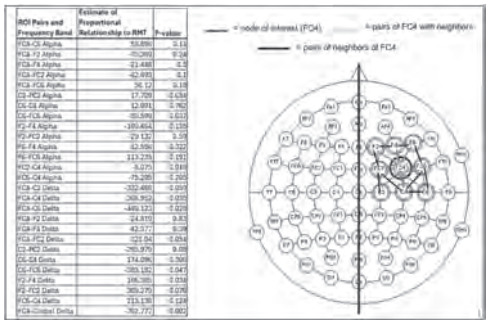

Figure 1. Regression results of FC between pairs of EEG nodes as RMT predictors (R-squared = 0.675, p = 0.047) and map of ROI pairs.

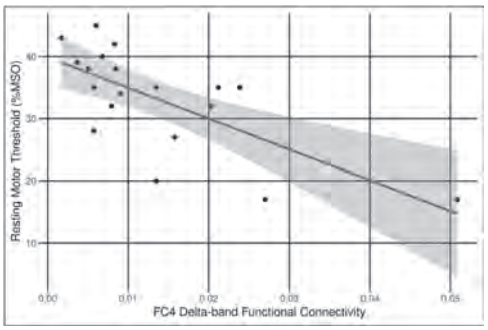

Figure 2. Linear regression between global FC4 Delta and RMT (R-squared = 0.457, p = 0.0009).

AR-07. Relationship of Motor Threshold in Transcranial Magnetic Stimulation with Quantitative Measures of White Matter Anisotropy.

C.M. Harris[4,1], C.J. Lewis[3,1], C.L. Peterson[3] and *R.L. Hadimani*[1,2]
1. Department of Mechanical and Nuclear Engineering, Virginia Commonwealth University, Richmond, VA, United States; 2. Department of Electrical and Computer Engineering, Iowa State University, Ames, IA, United States; 3. Department of Biomedical Engineering, Virginia Commonwealth University, Richmond, VA, United States; 4. Center for Biological Data Science, Virginia Commonwealth University, Richmond, VA, United States

Introduction: Transcranial magnetic stimulation (TMS) is a noninvasive neuromodulation technique in which dosage is determined via measurements of motor thresholds (MT) [1]. Previous studies have used model-based quantitative measures of white matter fiber tractography from diffusion magnetic resonance imaging (MRI), such as fractional anisotropy (FA), axial diffusivity (AD), radial diffusivity (RD), and mean diffusivity (MD), with respect to TMS [2-3]. We investigated model and model-free based dMRI metrics in corticospinal tracts to correlate with MT. Methods: 10 participants underwent first dorsal interosseous muscle TMS stimulation and dMRI [5]. Linear mixed-effects models were created with participants as random effects to predict active and resting motor thresholds (AMT and RMT) using model and model-free dMRI metrics and simulated TMS-induced electric field strengths. Results: Model derived dMRI metrics in corticospinal fiber tracts correlated with AMT in the models with brain-scalp distance (BSD) as a fixed effect. AMT correlated with the interaction between BSD and model derived measures of FA, MD, and AD. In models using the interactions of dMRI measures with simulated electric field strength instead, these measures were also significant. However, these effects were no longer significant after correction for multiple comparisons. Additionally, a multivariate regression analysis using model-free anisotropy measures showed no correlation between these measures and RMT. Conclusion: The use of certain dMRI-derived measurements of white matter microstructure could be another way to predict TMS responses. However, the use of model and model-free dMRI-derived measures in fiber tracts related to motor function cannot currently predict motor threshold alone, with anatomical measures remaining more significant. This work was supported by the VCU's Center for Rehabilitation Science and Engineering, Dean's Undergraduate Research Initiative, Commonwealth Cyber Initiative and VCU Breakthrough grant.

[1] S. Rossi, M. Hallett, P. M. Rossini, and A. Pascual-Leone, "Safety, ethical considerations, and application guidelines for the use of transcranial magnetic stimulation in clinical practice and research," *Clin. Neurophysiol.*, vol. 120, no. 12, pp. 2008–2039, 2009. [2] T. Herbsman *et al.*, "Motor threshold in transcranial magnetic stimulation: The impact of white matter fiber orientation and skull-to-cortex distance," *Hum. Brain Mapp.*, 30, 2044, 2009. [3] S. Klöppel *et al.*, "The cortical motor threshold reflects microstructural properties of cerebral white matter," *NeuroImage*, 40, 1782, 2008. [4] A. Hübers, J. C. Klein, J.-S. Kang, R. Hilker, and U. Ziemann, "The relationship between TMS measures of functional properties and DTI measures of microstructure of the corticospinal tract," *Brain Stimulat.*, 5, 297, 2012. [5] N. Mittal *et al.*, "Effect of neuroanatomy on corticomotor excitability during and after transcranial magnetic stimulation and intermittent theta burst stimulation," *Hum. Brain Mapp.*, 43, 4492, 2022.

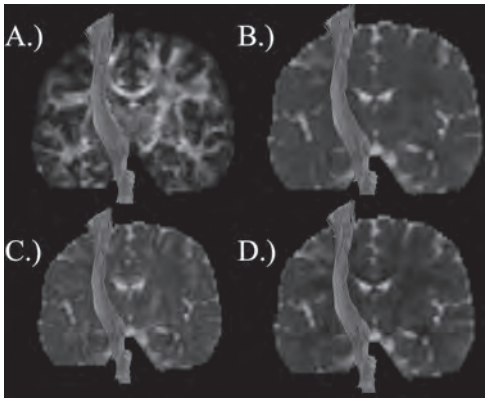

Fig 1. Diffusion Tensor Imaging derived corticospinal tractography of A.) FA B.) MD C.) AD D.) RD imaging for 1 participant.

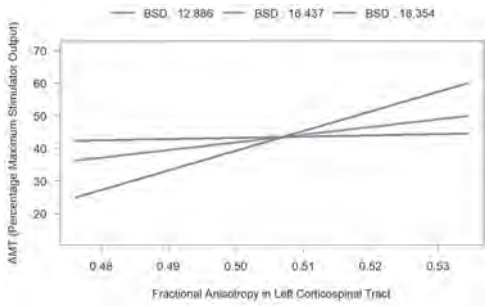

Fig 2. Linear mixed effects model of the correlation (R^2=0.306) between FA and AMT at varying BSD.

AR-08. Co-Fe nanowires for the destruction of cancer cells through magnetomechanical effect. H. Chiriac[1], A. Minuti[1], C. Stavila[1] and *N. Lupu*[1]
1. National Institute of Research and Development for Technical Physics, Iasi, Romania

Recent research has focused on using magnetic particles to destroy cancer cells through a mechanical process called the magnetomechanical effect [1]. This effect is achieved by rotating the magnetic particles using low-frequency magnetic fields, ultimately leading to the cells' death. High magnetic anisotropy is essential for magnetic nanostructures rotation, entirely under the influence of a rotating field. Various types of magnetic particles and nanowires are available for experimentation [2-4]. We proposed experimenting with Co-Fe nanowires (NW) and testing their viability with human osteosarcoma cells (HOS) to determine their effectiveness in destroying cancer cells through the magnetomechanical actuation (MMA). This study explores the potential use of Co-Fe nanowires for the targeted destruction of cancer cells through a magnetomechanical effect. Co-Fe nanowires, chosen for their high saturation magnetization and shape anisotropy, were tested against human osteosarcoma cells. Co-Fe nanowires were produced using electrodeposition in alumina membranes, with diameters of 200 nm and lengths of 2 μm. Co-Fe nanowires exhibited high saturation magnetization (165 emu/g) and significant shape anisotropy. Cell viability was assessed using the MTT assay and a custom-made rotating magnetic field system was employed to induce the magnetomechanical effect. HOS cell viability decreased significantly when exposed to MMA in the presence of Co-Fe nanowires, with values as low as 3%. The results demonstrated that Co-Fe nanowires significantly reduce cancer cell viability through magnetomechanical actuation. This study suggests that Co-Fe nanowires could be a viable tool in cancer therapy, leveraging their magnetic properties to target and destroy malignant cells.

[1] C. Naud *et al.*, "Cancer treatment by magneto-mechanical effect of particles, a review," *Nanoscale Adv.*, vol. 2, no. 9, pp. 3632–3655, Sep. 2020, doi: 10.1039/D0NA00187B. [2] L. Piraux, "Magnetic Nanowires," *Applied Sciences*, vol. 10, no. 5, Art. no. 5, Jan. 2020, doi: 10.3390/app10051832. [3] R. Jia, B. Ma, C. Zheng, X. Ba, L. Wang, and Q. Du, "Magnetic properties of micro-particles with different shapes and postures in the high precision particles detection," *Powder Technology*, vol. 356, pp. 628–639, Nov. 2019, doi: 10.1016/j.powtec.2019.08.044. [4] A. O. Fung, V. Kapadia, E. Pierstorff, D. Ho, and Y. Chen, "Induction of cell death by magnetic actuation of nickel nanowires internalized by fibroblasts," *Journal of Physical Chemistry C*, vol. 112, no. 39, pp. 15085–15088, Oct. 2008, doi: 10.1021/jp806187r.

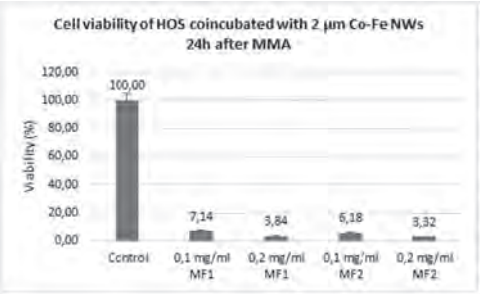

Figure 1. Viability of osteosarcoma cells after double magneto-mechanical actuation in the presence of 2 μm Co-Fe NW (MF1-one MMA treatment for 30 min; MF2- two MMA treatments for 30 min)

Session AS
ELECTRONIC STRUCTURE, MAGNETISM AND FUNDAMENTAL PHYSICAL PROPERTIES I (Poster Session)

Santosh KC, Co-Chair
San Diego State University, San Diego, CA, United States
Tej Nath Lamichhane, Co-Chair
University of Central Oklahoma, Edmond, Oklahoma, United States

AS-01. Modeling Magnetic Dipoles in Atoms Based on Hypothetical Magnetic Monopoles. *R.R. Morusupalli[1,2] 1. HP Inc, Palo Alto, CA, United States; 2. Formerly with Department of Materials Science and Engineering, Stanford, CA, United States*

Magnetic dipoles in atoms are traditionally explained by the intrinsic spin and orbital motion of electrons and their interactions with protons in the nucleus. The magnetic moment of an electron is typically modeled as arising from both its spin and its orbital motion around the nucleus, while protons contribute minimally due to their larger mass and smaller magnetic moment. This study investigates an alternative hypothesis where electrons and protons are treated as magnetic monopoles, proposing that an electron spinning clockwise acts as a magnetic north monopole (N) and a proton spinning clockwise acts as a magnetic south monopole (S). We aim to determine whether this hypothesis can still adequately explain the formation of magnetic dipoles in atoms. When considering the atom as a system of magnetic monopoles, the resultant magnetic dipole moment (μ_{atom}) would be influenced by the positions and orientations of these monopoles. The total magnetic dipole moment can be expressed as a vector sum: $\mu_{atom}=\mu_N+\mu_S$, where μ_N and μ_S are the magnetic moments due to the monopoles N and S, respectively. To analyze the net magnetic field (B) generated by the atomic system, we use the Biot-Savart law for monopoles: $B= (\mu_0 q_m v \times r) / 4\pi r^3$, where μ_0 is the permeability of free space, q_m is the magnetic charge, v is the velocity, and r is the distance vector. Integrating the contributions from both monopoles, we obtain the net magnetic field (B_{net}) and the resultant magnetic dipole moment (μ_{net}): $B_{net} = B_N + B_S$ and $\mu_{net} = \mu_N + \mu_S$ If the hypothesis that electrons and protons act as magnetic monopoles is correct, it could fundamentally change our understanding of atomic and molecular magnetism and Maxwell's equations would be rendered the symmetry that they currently lack. The hypothesis that electrons and protons can be modeled as magnetic monopoles presents an intriguing alternative to traditional approaches. More details and suggested experimental validations in manuscript.

D. J. Griffiths, Introduction to Electrodynamics, 4th ed. (Cambridge University Press, Cambridge, 2017). A. Rajantie, Contemporary Physics 53, 195–211 (2012). H. A. Enge, Introduction to Nuclear Physics (Addison-Wesley, Reading, MA, 1966). J. D. Jackson, Classical Electrodynamics, 3rd ed. (Wiley, New York, 1999). D. Gross, Proceedings Of The National Academy Of Sciences 93, 14256–14259 (1996). K. Milton, Reports On Progress In Physics 69, 1637 (2006).

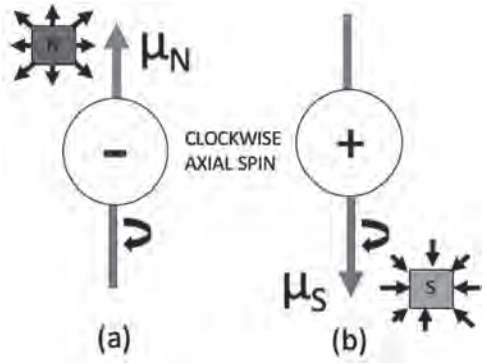

Hypothesized views: (a) An electron spinning clockwise is hypothesized as a magnetic monopole N. (b) A proton spinning clockwise is hypothesized as a magnetic monopole S.

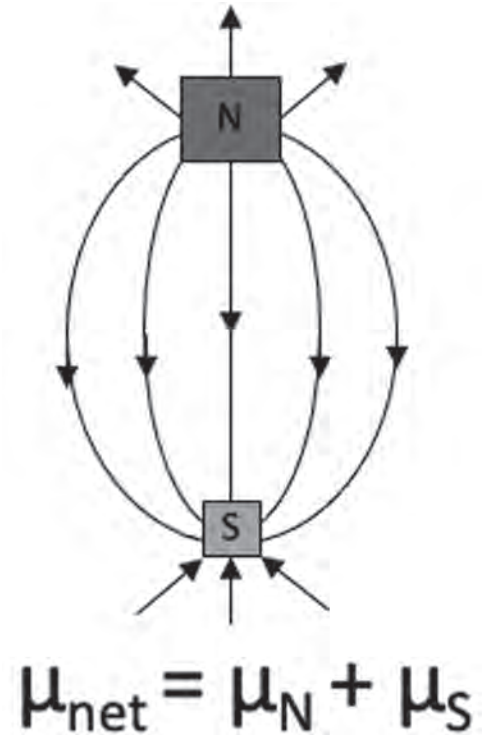

The monopoles shown with hypothesized magnetic field lines that may behave like a net dipole.

AS-02. Various magnetic properties and spin states of $Ba_3Co_{1-x}Ca_xRu_2O_9$ ($0 \le x \le 1$). *Y. Yasui*[1], A. Nagaya[1], A. Horie[1], I. Terasaki[2] and J. Kikuchi[1] *1. Physics, Meiji University, Kawasaki, Japan; 2. Physics, Nagoya University, Nagoya, Japan*

We have carried out the magnetic susceptibility and specific heat measurements on polycrystalline samples of $Ba_3Co_{1-x}Ca_xRu_2O_9$ as well as ^{101}Ru-NMR experiments of $Ba_3CaRu_2O_9$. The compounds with the general formula $Ba_3MRu_2O_9$ (M = Co, Ca, Zn, *etc*.) have the Ru_2O_9 dimers, made from face-shared RuO_6 octahedra, connected with corner-shared MO_6 octahedra to form triangular lattice in the *ab*-plane. $Ba_3MRu_2O_9$ exhibits various magnetic properties depending on the species of M^{2+} ions. In the case of M=Co, it is reported that Co^{2+} ($3d^7$) and Ru^{5+} ($4d^3$) ions have local spin and both spin systems exhibit an antiferromagnetic transition at $T_N \sim 100$ K [1]. On the other hand, $Ba_3CaRu_2O_9$ exhibits a non-magnetic state at low temperatures, where it was proposed that the S=3/2 spins of two Ru^{5+} ions become a dimer state through quantum mechanical singlet formation [2]. Recently, a novel type of spin liquid behavior has been proposed for $Ba_3ZnRu_2O_9$ [3]. We have controlled the magnetic ground state from an antiferromagnetic order to non-magnetic state by making a solid solution system $Ba_3Co_{1-x}Ca_xRu_2O_9$. The temperature dependences of the magnetic susceptibility and specific heat of $Ba_3Co_{1-x}Ca_xRu_2O_9$ indicate that an antiferromagnetic transition temperature T_N decreases with increasing x. With further increasing x, the magnetic ground state of the spin systems is changed to a spin-glass state at around $x \sim 0.55$. In the region of $x > 0.8$, the spin systems are found to be paramagnetic state of almost free spins. We have also studied spin states of $Ba_3CaRu_2O_9$ by using ^{101}Ru-NMR. The temperature dependences of both the Knight shift and the longitudinal relaxation rate are found to indicate a typical gap-like behavior with spin gap energy between ground state and first excited one, $E_g = 360 \pm 20$ K. In the presentation, we discuss the magnetic properties and spin states of $Ba_3Co_{1-x}Ca_xRu_2O_9$.

[1] P. Lightfoot *et al*.: J. Solid State Chem. 89 (1990) 174. [2] J. Darriet *et al*., J. Solid State Chem. 19 (1976) 213. [3] I. Terasaki *et al*.: J. Phys. Soc. Jpn. 86 (2017) 033702.

AS-03. Adsorption of Ag, Au, Cu, and Ni on MoS_2: theory and experiment. *A.J. Stollenwerk*[1], H. Harms[1], C.J. Cunningham[1], C. Sadler[1], E. O'Leary[2], T. Kidd[1] and P. Lukashev[1] *1. University of Northern Iowa, Cedar Falls, IA, United States; 2. Iowa State University, Ames, IA, United States*

We present the results of a computational and experimental study of the adsorption of various metals on MoS_2. In particular, we analyzed the binding mechanism of four metallic elements (Ag, Au, Cu, Ni) on MoS_2. Among these elements, Ni exhibits the strongest binding and lowest mobility on the surface of MoS_2. On the other hand, Au and Ag bond very weakly to the surface and have very high mobilities. Our calculations for Cu show that its bonding and surface mobility are between these two groups. Experimentally, Ni films exhibit a composition characterized by randomly oriented nanoscale clusters. This is consistent with the larger cohesive energy of Ni atoms as compared with their binding energy with MoS_2, which is expected to result in 3D clusters. In contrast, Au and Ag tend to form atomically flat plateaued structures on MoS_2, which is contrary to their larger cohesive energy as compared to their weak binding with MoS_2. Cu displays a surface morphology somewhat similar to Ni, featuring larger nanoscale clusters. However, unlike Ni, in many cases Cu exhibits small plateaued surfaces on these clusters. This suggests that Cu likely has two competing mechanisms that cause it to span the behaviors seen in the Ni and Au/Ag film morphologies. These results indicate that calculations of the initial binding conditions could be useful for predicting film morphologies. In addition, our calculations show that the adsorption of adatoms with odd electron number like Ag, Au, and Cu results in 100% spin-polarization and integer magnetic moment of the system. Adsorption of Ni adatoms, with an even electron number, does not induce a magnetic transition. Completion of experiments and analysis of the data was supported by Grant No. DE-SC0020334 funded by the U.S. Department of Energy, Office of Science. This work was supported in part by the National Science Foundation (Grant No. DMR-2300639).

AS-04. Effect of surface preparation on spin glass behavior at the Ni/MoS_2 interface. *H.A. Harms*[1], C.J. Cunningham[1], C. Hemesath[1], A.J. Stollenwerk[1], P. Lukashev[1], T. Kidd[1], B. Wei[2,3], L. Zhou[2,3], R. Prozorov[3,4] and P. Shand[1] *1. Physics, University of Northern Iowa, Cedar Falls, IA, United States; 2. Material Science and Engineering, Iowa State University, Ames, IA, United States; 3. Materials Sciences and Engineering, Ames National Laboratory, Ames, IA, United States; 4. Physics and Astronomy, Iowa State University, Ames, IA, United States*

Incorporating MoS_2 substrates into spintronic devices requires a thorough understanding of their interfacial properties with ferromagnetic metals. To this end, we investigated the magnetic properties of Ni/MoS_2 samples. Spin glass-like relaxation was observed in samples where Ni was deposited on MoS_2 annealed at 300°C as well as unannealed MoS_2. However, the relaxation rate of the magnetoresistance was found to be significantly greater in the annealed samples. Scanning tunneling microscopy images reveal that Ni forms granular structures with a diameter of two nanometers on both the annealed and unannealed samples. The similarity in cluster formation in both types of samples suggests that the system is not a standard 3D super spin glass. TEM images indicate a distinct difference at the interface: unannealed samples display regions of both structural order and disorder, whereas annealed samples exhibit a highly ordered interface. These results suggest that the spin glass-like behavior likely arises from the structural and magnetic disorder at the interface, including coupling between the Ni and Mo atoms. We hope that future magnetic force microscopy studies will shed additional light on this question. Completion of experiments and analysis of the data was supported by Grant No. DE-SC0020334 funded by the U.S. Department of Energy, Office of Science. This work was supported in part by the National Science Foundation (Grant No. DMR-2300639).

AS-05. Competing Antiferromagnetic Interactions and Associated Large Inverse Magnetocaloric Effect in TbSi and $TbSi_{0.6}Ge_{0.4}$. *A. Kumar*[1], P. Singh[1], A. Doyle[1], D. L. Schlagel[1] and Y. Mudryk[1] *1. Material Science Division, Ames National Laboratory, Ames, IA, United States*

The rare earth (RE) pseudo-binary compounds, RE-Si_xGe_{1-x}, have garnered considerable attention due to their intriguing fundamental and functional properties arising from the complex composition-structure (x-T) phase diagram. Among these compounds, $TbSi_xGe_{1-x}$($0 \le x \le 1$) stands out due to the significant orbital angular momentum (L = 3) and large single-ion anisotropy associated with Tb^{3+} ions [1, 2]. In this study, we first utilize density functional theory to unravel the dynamic stability of the $TbSi_{1-x}Ge_x$ (x = 0-1) pseudo-binary system, followed by an in-depth experimental exploration of the magnetization, specific heat, and crystallography of TbSi and $TbSi_{0.6}Ge_{0.4}$ compounds. Interestingly, both samples, despite having different crystal structures (FeB type for TbSi and CrB type for $TbSi_{0.6}Ge_{0.4}$), exhibit two similar antiferromagnetic transitions around $T_{N1} \approx 60$ K and $T_{N2} \approx 40$ K. We utilize point-by-point time-dependent analysis of the heating and cooling branches to obtain the high-resolution specific heat (C_P) data, thereby enabling us to probe the very small thermal hysteresis of less than 0.5 K associated with this transition. High-resolution C_P data show the second- and first-order nature of the magnetic transition at T_{N1} and T_{N2}, respectively, for both samples. Furthermore, we identify an additional magnetic phase in TbSi, situated between high- and low-temperature antiferromagnetic transitions, which also exhibits a first-order nature [3]. Of particular interest is $TbSi_{0.6}Ge_{0.4}$, which showcases very small thermal hysteresis (<0.4 K), minimal change in the unit cell volume at the transition, and significant broadening of the inverse magnetocaloric effect at the first-order magnetic transition. These characteristics open avenues for future research in similar rare-earth compounds for magnetocaloric applications. We construct comprehensive H-T phase diagrams for both samples (Fig. 1), shedding light on their complex magnetic behavior under varying temperatures and magnetic fields. Furthermore, our temperature-dependent x-ray diffraction measurements reveal notable magnetostriction and magnetoelastic coupling at the observed transition temperatures.

[1] P. Schobinger-Papamantellos and K. H. J. Buschow, Magnetic structure changes observed by neutron diffraction in the system $TbGe_{1-x}Si_x$ ($0.4 \leq x \leq 1.0$), J. Magn. Magn. Mater. 71, 134 (1988). [2] P. Schobinger-Papamantellos, T. Janssen, and K. H. J. Buschow, Thermal variation of incommensurate magnetic phases in TbSi as observed by neutron diffraction, J. Magn. Magn. Mater. 127, 115 (1993). [3] A. Kumar, P. Singh, A. Doyle, D. L. Schlagel, and Y. Mudryk, Multiple magnetic interactions and large inverse magnetocaloric effect in TbSi and $TbSi_{0.6}Ge_{0.4}$, Phys. Rev. B 109, 214410 (2024).

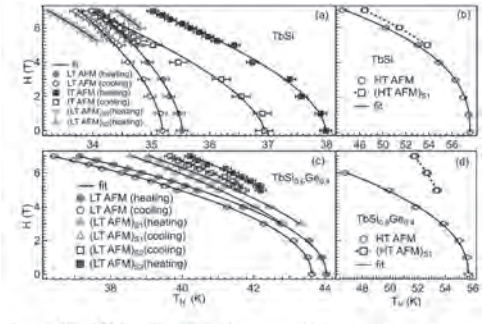

Figure 1: The field dependent shift in the various AFM transition temperatures measured in heating and cooling modes for (a, b) TbSi and (c, d) $TbSi_{0.6}Ge_{0.4}$.

AS-06. Novel Magnetic States in $Ba_3Zn_{1-x}Ca_xRu_2O_9$. *R. Sadamatsu*[1] and Y. Yasui[1] *1. Physics, Meiji University, Kawasaki, Japan*

$Ba_3MRu_2O_9$ (M=Zn, Ca, Co, *etc*.) have the Ru_2O_9 dimers, made from face-shared RuO_6 octahedra, connected with corner-shared MO_6 octahedra to form triangular lattice in the *ab*-plane. $Ba_3MRu_2O_9$ exhibits various magnetic properties depending on the species of M^{2+} ions. $Ba_3ZnRu_2O_9$ was reported as candidate of the quantum spin liquid system, where the magnetic susceptibility - temperature (χ -T) curve has not neither any traces of the Curie tail nor glassy behavior down to 50mK [1]. $Ba_3CaRu_2O_9$ exhibits a non-magnetic state at low temperatures. The mechanism of the non-magnetic state in $Ba_3CaRu_2O_9$ was proposed that the S = 3/2 spins of two Ru^{5+} ($4d^3$) ions become a dimer state through quantum mechanical singlet formation [2,3]. In the case of M=Co, the spin system exhibits an antiferromagnetic transition at T_N = 100 K [4]. The purpose of this study is to investigate the magnetic ground states of $Ba_3Zn_{1-x}Ca_xRu_2O_9$, which is solid solution between $Ba_3ZnRu_2O_9$ with a spin liquid state and $Ba_3CaRu_2O_9$ with a nonmagnetic state. In order to investigate the magnetic properties of $Ba_3Zn_{1-x}Ca_xRu_2O_9$ ($0 \leq x \leq 1$), we have carried out measurements of X-ray diffraction, magnetic susceptibility, and magnetic specific heat on the synthesized polycrystalline samples. The lattice constants of synthesized samples for x = 0, 0.05, 0.15, 0.25, 0.35, 0.50, and 1.00 have been evaluated from X-ray diffraction experiments, and have been found to linearly increase with increasing x in whole x-region. The magnetic susceptibility of samples with $0 < x < 1$ at $T < 200$ K exhibits the behavior of approximately interpolating between x = 0 and x = 1. In high temperature region, the χ -T curve of x = 0 has peak behavior at T_{peak} = 450 K. The peak temperature T_{peak} of the χ -T curves is found to increase with increasing x, and T_{peak} becomes to be 535 K for x = 1. From the change of the magnetic states, this result can be understood by considering that the substitution from Zn to Ca strengthens the intra-dimer interaction. In the presentation, we will discuss the changes in the magnetism of $Ba_3Zn_{1-x}Ca_xRu_2O_9$ based on the obtained results.

[1] I. Terasaki *et al*.: J. Phys. Soc. Jpn. 86 (2017) 033702. [2] J. Darriet *et al*.: J. Solid State Chem. 19 (1976) 213. [3] Y. Ochiai *et al*.: AIP Advances 14 (2024) 025211. [4] P. Lightfoot *et al*.: J. Solid State Chem. 89 (1990) 174.

AS-07. Effect of Hole Doping on the Structural, Electronic and Magnetic properties of CrAs. *B.S. Jacobs*[1] and A. Pandey[2] *1. Physics, University of Johannesburg, Johannesburg, South Africa; 2. School of Physics, University of the Witwatersrand, Johannesburg, South Africa*

Transition metal pnictides have garnered a lot of attention, especially after the discovery of high-temperature unconventional superconductivity (SC) in Fe-based pnictides where SC emerges in the vicinity of long-range antiferromagnetic (AF) ordered state [1-3]. The binary transition metal pnictide CrAs is an interesting system as it exhibits an interplay between lattice and magnetic structures and SC [4]. Pressure-induced spin reorientation transition in CrAs results in anti-parallel alignment of nearest neighbour spins in the vicinity of SC where bulk SC with T_c close to 2 K emerges at a critical pressure of 8 kbar where first order AF transition is completely suppressed, making it the first superconductor among Cr-based compounds [5]. The possibility of tuning the CrAs system towards SC using electron doping instead of pressure has been recently investigated in polycrystalline compositions $(Cr_{0.85}T_{0.15})As$ (T = Fe, Co, Ni) [6]. Although sizeable values of magnetic interactions were present in the compounds, no evidence of magnetic ordering and SC were observed down to the lowest temperature of measurement. Apparently, the AF transition present at $T_N \approx 270$ K in undoped CrAs gets suppressed in the electron-doped compositions. To get further insight into the interplay of interactions and properties of this system, investigations focused on the effect of partial substitution with hole-dopants are needed. In this investigation, we report the effect of hole-doping on structural, electronic, and magnetic properties of CrAs introduced via partial substitution of Cr with V and Ti.

1. J. Paglione and R. L. Greene, Nature Physics, Vol. 6, p.645 (2010) 2. D. C. Johnston, Advances in Physics, Vol. 59, p.803 (2010) 3. G. R. Stewart, Reviews of Modern Physics, Vol. 83, p.1589 (2011) 4. Y. Shen *et al*., Physical Review B, Vol. 93, p.060503(R) (2016) 5. W. Wu *et al*., Nature Communications, Vol. 5, p.5508 (2014) 6. B. S. Jacobs and A. Pandey, Journal of Magnetism and Magnetic Materials, Vol. 588, p.171397 (2023)

Session AT
FAST AND ULTRAFAST MAGNETISATION DYNAMICS
(Poster Session)

Carl Simon Davies, Chair
Radboud University, Nijmegen, Netherlands

AT-01. Spin-Orbit Torques in Te/Ferromangetic Devices. *S. Li*[1], A. Hoffmann[1], C. niu[2], R. Liu[1] and P. Ye[2] *1. University of Illinois at Urbana-Champaign, Urbana, IL, United States; 2. Purdue University, Lafayette, IN, United States*

Tellurium has a chiral helical structure. This chirality in tellurium breaks the inversion symmetry and results in a momentum-dependent radial spin texture at the Fermi level. With a charge current applied along the chirality direction, the Fermi level will be shifted and spins of electrons will be polarized either parallel or anti- parallel to the current (or chirality) direction depending on the handedness of the Te chirality [1]. This effect is similar to the Rashba-Edelstein effect. We are studying this chirality-induced spin polarizations by using spin-torque ferromagnetic resonance (ST-FMR) to observe the spin-orbit torques generated from single- crystalline Te flakes. In order to integrate Te samples into devices, we first deposited a 10-nm Permalloy (Py; $Ni_{80}Fe_{20}$) layer and used ion-milling and lithography to integrate Te/Py heterostructure into a coplanar waveguide for radio frequency (rf) measurements. We applied GHz rf currents through Te/Py devices and collect a dc mixing voltage (Vmix) due to the mixing of anisotropic magnetoresistance of Py and rf current [2]. We define the current direction to be along x direction and out-of-plane direction to be z. The characteristics of spin-orbit torque components generated by Te flakes can be obtained by studying the dependence of V_{mix} as a function of applied magnetic field direction. As shown in Fig.1, the antisymmetric component of V_{mix} from our measurements shows spin torques (τ_x) due to x spins, which are collinear with the current direction, in addition to the Oersted torques generated from the rf current, indicating chirality-induced spin polarizations from Te. At the same time, from the symmetric component, we also found substantial in-plane damping-like torques (τ_y) due to spins with polarizations along y direction, which originate from the spin Hall effect of the Te with large spin-orbit couplings [3]. We further calculated the spin-orbit torque efficiencies of chirality- induced torques τ_x and SHE-induced torques τ_y, and found them to be around 2.24 and 1.97 respectively.

[1] T. Furukawa, et al., Observation of current-induced bulk magnetization in elemental tellurium Nature Communications 8, 954 (2017) [2] L. Liu, et al., Spin-Torque Ferromagnetic Resonance Induced by the Spin Hall Effect, Phys. Rev. Lett. 106, 036601 (2011) [3] C. Niu, et al., Gate-tunable strong spin-orbit interaction in two-dimensional tellurium probed by weak antilocalization, Physical Rev. B 101, 205414 (2020)

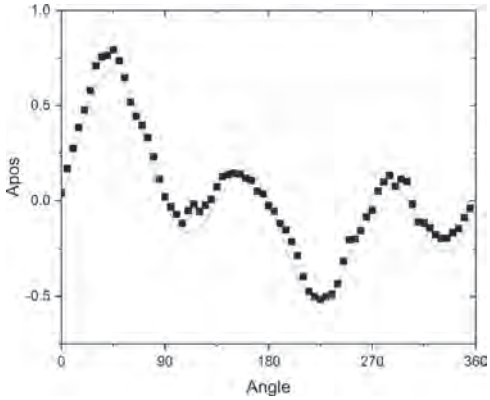

Fig.1 Antisymmetric angular dependencies, showing the extracted antisymmetric component at each angle between the rotating magnetic field and the rf current.

AT-02. Withdrawn

AT-03. Sub 100 ps Deterministic Switching of Synthetic Antiferromagnetic p-MTJ purely by the Electric Field. *J. Qi*[1], Y. Chen[1], Y. Lv[1], D. Zhang[1], O. Benally[1], Y. Huang[2], D. Lyu[1], S. Liang[1], Y. Yang[1] and B. Zink[1]
1. University of Minnesota, Minneapolis, MN, United States; 2. Chiao Tung University, Hsinchu, Taiwan

Achieving ultrafast switching of perpendicular magnetic tunnel junctions (pMTJs) has long been a challenging issue, particularly in the sub-200 picosecond (ps) range by the electric field effects. In this manuscript, we report a pMTJ structure with a synthetic antiferromagnet (SAF) free layer and a 2 nm MgO barrier. The SAF structure is designed and fine-tuned to allow the voltage-controlled exchange coupling (VCEC) [1]. The stack is patterned into a nanoscale pillar, exhibiting a resistance-area (RA) product of $3.93\times10^4\ \Omega\ \mu m^2$. By using the combination of VCEC and voltage-controlled magnetic anisotropy (VCMA), deterministic switching is achieved, with 50% switching occurring at 87.5ps and 94% switching at 100ps. An even faster result is expected with a higher applied voltage and high TMR ratio. This is the first report of pure electric field-controlled sub-100 ps deterministic switching of pMTJ with an industry-compatible stack structure.

1. Zhang, D. *et al. Nano Lett.* 22, 622–629 (2022).

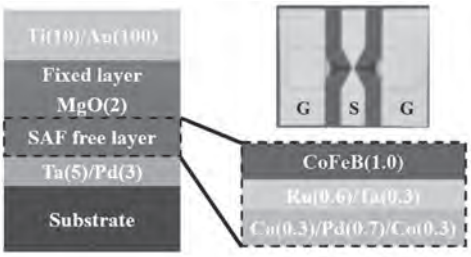

Fig. 1. Schematic illustration of the MTJ stack structure with the integration of a SAF free layer (thickness in nm) with the structure of Si/SiO2/Ta(5)/Pd(3)/[Co(0.3)/Pd(0.7)]/Co(0.3)/Ru(0.6)/Ta(0.3)/CoFeB(1)/MgO(2.0)/CoFeB(1.3)/Ta(0.7)/[Pd(0.7)/Co(0.3)]4/Pd(5). The top right shows the top view of the patterned device under the microscope. G and S are short for ground and signal respectively. The footprint is designed in such a way to have a minimum uverlap between the top and bottom electrode to make sure the parasitic capacitance in series with MTJ is small.

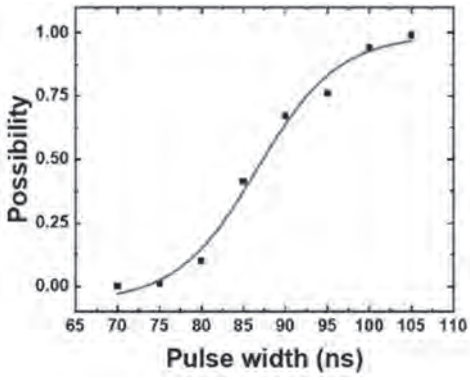

Fig. 2. The relation between switching probability and pulse width. After generating each pulse with a different pulse width, whether the MTJ is switched is checked by applying a small current. Each data point in the plot corresponds to 100 repetition trials under the same pulse width. The result shows that the switching probability increases as the pulse width is increased.

AT-04. Directional Damping in Co_2TiSn Thin Films. *A. Karki*[1], U. Karki[1], R. Nahar[1], R. Nold[1], B. Akintunde[1], N. Derksen[1], A. Hauser[1] and J. Mohammadi[1] *1. Physics and Astronomy, The University of Alabama, Tuscaloosa, AL, United States*

Co_2TiSn is of interest due to predictions of half-metallicity with full spin polarization at the Fermi level, which would make it highly desirable for spintronics applications [1]. In this project, 50 nm thick films of Co_2TiSn were grown on hexagonal Al_2O_3 (1120 and 0001) substrates with TiN buffer layers using the off-axis sputter beam epitaxy technique. In-plane, angle-dependent ferromagnetic resonance measurements at 20 GHz show six-fold anisotropy on films deposited on Al_2O_3(001)/TiN(111) substrate and buffer systems, whereas films grown on Al_2O_3(110)/TiN(111) show no significant anisotropy (see Fig 1(a),(c)). We characterized the Gilbert damping parameter in these films and confirmed anisotropic damping for Al_2O_3(001)/TiN(111) (Fig 1(b),(d)). FMR and magnetometry analysis find relatively low α x M_s values for both films, suggesting that the systems are potential candidates for magnetic devices such as pMTJs, where the critical current density for switching is directly proportional to damping and saturation magnetization [2,3].

[1] Y. Miura, M. Shirai, and K. Nagao; Ab initio study on stability of half-metallic Co-based full-Heusler alloys. *J. Appl. Phys*. 99, (2006) [2] A. Conca, T. Nakano, T. Meyer, Y. Ando, B. Hillebrands; CoFeAlB alloy with low damping and low magnetization as a candidate for spin transfer torque switching. *J. Appl. Phys.* 21 (2017). [3] R. Sbiaa, S. Y. H. Lua, R. Law, H. Meng, R. Lye, H. K. Tan; Reduction of switching current by spin transfer torque effect in perpendicular anisotropy magnetoresistive devices (invited). *J. Appl. Phys.* (2011).

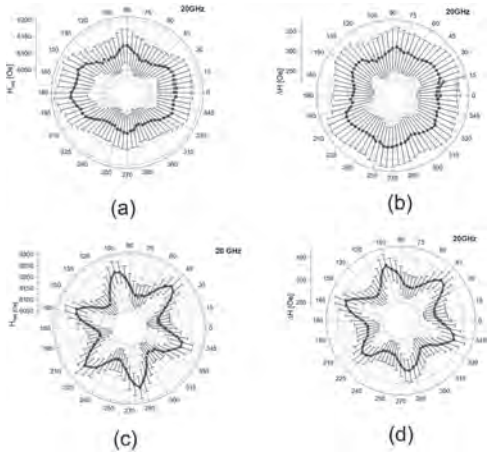

Fig 1: (a) Resonance field vs. ip rotation angle and (b) Linwidth vs. ip rotation angle of 50 nm Co_2TiSn film deposited on Al_2O_3 (110) (c) Resonance field vs. ip rotation angle and (d) Linwidth vs. ip rotation angle of 50 nm Co_2TiSn film deposited on Al_2O_3 (001).

AT-05. Magnetostriction dynamics in CoFe/Pt magnetic multilayers. *T. Fernandes*[1], F.M. Matinaga[2], L.H. de Andrade[1] and M. Martins[2]
1. SENAN, Centro de Desenvolvimento de Tecnologia Nuclear, Belo Horizonte, Brazil; 2. SEMAV, Centro de Desenvolvimento de Tecnologia Nuclear, Belo Horizonte, Brazil

Fs laser improved the generation and measurement technique of acoustic waves with ≤μm spatial resolution and frequency up to THz.[1,2] It was extended to generate and control magnons, i.e. strong coupling of phonon and spin wave enhance the precession amplitude, i.e., magnetic switching speeds.[3] We studied thin CoFe/Pt multi-layers with in(out) of plane magnetic anisotropy, whose properties was published previously.[4] Time resolved magneto optic Kerr effect (TRMOKE) and reflectance (TRR) were used to show spin precession under magnetostriction effects due to coherent and incoherent phonons generated by a 100 fs laser pulse excitation. Magnetic and phonons damped oscillations, amplitude and phase will

be analysed inview of the magnetostriction effect. Fig.1 shows a TRMOKE/ TRR for the in plane anisotropy sample, with a precession of 16GHz and a dumping time of 144ps. The TRR shows the phonon wave with a high attenuation. The behavior of those measurements as a function of the applied field H is shown on the inset picture. The zoom scale of those measurements are shown on fig.2, where the demagnetization (0,4ps) and remagnetization (1.6ps) is illustrated, and the phonon waves are clearly resolved, with the phonon and cavity (f_p,f_m) oscillation frequency are resolved by the Fourier transform (FFT) in inset figure. The f_p(180GHz) is generated on the metal by absorption of the laser pulse in the skin depth length, followed by the cavity mode f_m (247GHz), which were excited by the phonon wave amplitude tail. Those modes present yet beating period ~15ps. The fitting shows f_p(f_m) attenuation time of 9.5(10.2) ps respectively. The inverse magnetostriction effect were observed weakly on the TRMOKE(fig.1) besides the precession behavior, none interaction of the phonon wave & magnons could be observed here, since both frequency were too far with a cavity Q~3,5. All those analyses were done also for samples with magnetic anisotropy out of plane where similar behavior was observed.

[1] C. Thomsen, et.al., Coherent Phonon Generation and Detection by Picosecond Light Pulses, Phys. Rev. Lett., 53, 989-992 (1984). [2] Ji-Wan Kim, et al., Ultrafast Magneto-Acoustics in Nickel Films, Phys. Rev. Lett., 109, 166601-166610 (2011). [3] Zhang et al., High-frequency magnetoacoustic resonance through strain-spin coupling in perpendicular magnetic multilayers, Sci. Adv. 2020; 6 (2020). [4] F M. Matinaga, et al., Consequences on Magnetization Dynamics of Synthesizing [Co60Fe40/Pt]5 Multilayers over Varying Pt Buffer Structures, IEEE Trans. on Magnetics., 59, 11-16 (2023).

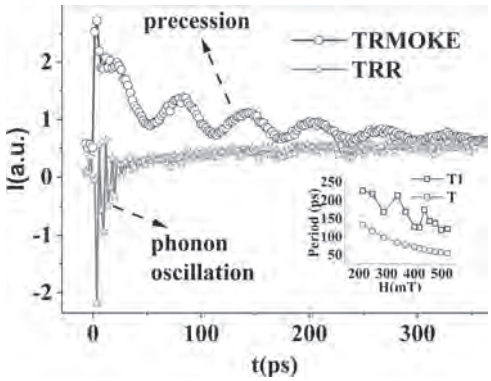

Fig. 1: TRMOKE (TRR) measurement, with the inset showing the precession period (T) and the dumping time (T1) as a function of external field H.

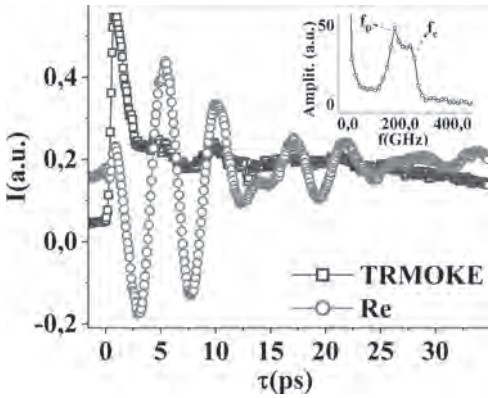

Fig. 2: TRMOKE (TRR) measured with resolution close to delay zero on fig.1. Inset shows the TRR FFT.

AT-06. Observation of coherently coupled cation spin dynamics in an insulating ferrimagnetic oxide. *C. Klewe*[1], P. Shafer[2,1], J. Shoup[3], C. Kons[3], Y. Pogoryelov[4], R. Knut[4], B.A. Gray[5], H. Jeon[6], B.M. Howe[5], O. Karis[4], Y. Suzuki[7,8], E. Arenholz[2,9], D.A. Arena[3] and S. Emori[10,7]
1. Advanced Light Source, Lawrence Berkeley National Laboratory, Berkeley, CA, United States; 2. National Synchrotron Light Source II, Brookhaven National Laboratory, Upton, NY, United States; 3. Department of Physics, University of South Florida, Tampa, FL, United States; 4. Department of Physics and Astronomy, Molecular and Condensed Matter Physics, Uppsala University, Uppsala, Sweden; 5. Materials and Manufacturing Directorate, Air Force Research Laboratory, Wright Patterson Air Force Base, WPAFB, OH, United States; 6. KBR, Beavercreek, OH, United States; 7. Geballe Laboratory for Advanced Materials, Stanford University, Stanford, CA, United States; 8. Department of Applied Physics, Stanford University, Stanford, CA, United States; 9. Pacific Northwest National Laboratory, Richland, WA, United States; 10. Department of Physics, Virginia Tech, Blacksburg, VA, United States

As existing CMOS-based microelectronics meet fundamental barriers, spintronics devices employing the electron spin rather than the electron charge are being developed into important new approaches to continue miniaturization and scaling. Particularly, the development and optimization of high-performance low damping oscillator materials for the generation, manipulation and detection of pure spin currents is a key area of fundamental research. However, many of the effects observed in these complex systems are notoriously difficult to resolve and their detection and disambiguation can present substantial challenges. The integration of ferromagnetic resonance (FMR) with X-ray absorption spectroscopy (XAS) as the underlying detection mechanism marks an important achievement for the exploration of magnetic interactions, as it extends the scope of X-ray magnetic circular dichroism (XMCD) to the dynamic range [1]. This enables the direct study of magnetization dynamics with element, site, and valence state specificity and may even be employed to disentangle spin and orbital contributions to the magnetic excitations [2]. By leveraging the element, site, and valence state specificity of time-resolved XMCD we examined the spin dynamics of individual cations (Fe2+, Fe3+, and Ni2+) on different sublattices in the highly diluted ferrimagnetic insulator NiZnAl-ferrite ($Ni_{0.65}Zn_{0.35}Al_{0.8}Fe_{1.2}O_4$) under continuous microwave excitation and tested whether they remain coherently coupled. A precise analysis of amplitude and phase of the magnetic precession (see Fig. 1) revealed that the cations' magnetic moments stayed tightly in sync and exhibited the same magnitude of spin relaxation within narrow limits of uncertainty. Thus, the oft-assumed "ferromagnet-like" dynamics remain robust in the ferrimagnetic oxide, even with high contents of nonmagnetic Zn2+ and Al3+ cations, notably reducing the exchange coupling [3].

[1] C. Klewe *et al.*, Synch. Rad. News 33, 12-19 (2020) [2] S. Emori *et al.*, Appl. Phys. Lett. 124, 122404 (2024) [3] C. Klewe *et al.*, Appl. Phys. Lett. 122, 132401 (2023)

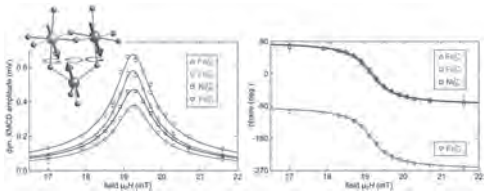

Fig. 1: Spin precession amplitude (left) and phase (right) displayed for individual cations on tetrahedral and octahedral sublattices.

AT-07. On the relevance of the Landau-Lifshitz-Gilbert equation in the optical limit. *B.J. Assouline*[1] and A. Capua[1] *1. Applied Physics, Hebrew University, Jerusalem, Israel*

Recently, we showed that optical pulses induce a torque on the magnetization, M, by merely considering the optical magnetic field, Hopt, in the Landau-Lifshitz-Gilbert (LLG) equation. The principle behind the interaction is that M is incrementally affected within each cycle, such that a significant torque builds up over the pulse duration in typical experimental conditions [1]. We found the strength of the interaction to be determined by $\eta=\alpha\gamma Hopt/fopt$, where fopt is the optical frequency and γ is the gyromagnetic ratio. Accordingly, the loss of spin angular momentum, represented by α, is key to the interaction. Moreover, we showed that for circularly polarized pulses, the polarity of the torque is determined by the optical helicity. Here, we discuss the relevance of the LLG equation on such fast timescales in light of these findings. Generally, the LLG equation assumes that the magnitude of M is preserved. Namely, the dynamics of the spins constituting M occur on slower timescales as compared to the spin-orbit and exchange interaction. When this assumption breaks down, such as in the ultrafast regime, the LLG equation should be applied locally, while macroscopically M nucleates and a texture arises. On a subdomain, the optical torque is uniform over all spins and the role of the exchange energy is less dominant. A second possible limitation is related to the characteristic time of the spin-orbit interaction that affects the ability to transfer spin angular momentum to the lattice and influences α. Moreover, thermal heating effects [2, 3] taking place within the pulse duration should also affect α [4, 5]. At this thermally activated limit, a more accurate description may require to account also for the longitudinal relaxation as in the Landau-Lifshitz-Bloch (LLB) equation [6, 7]. In a quantitative comparison between the prediction of the LLG equation [1] and experimental data [8], we show that the assumption that the magnitude of M is preserved is generally valid. Independently of the possible temporal variation of α, our calculations show the relevance of the Zeeman energy related to Hopt. Namely, even the simplest description of the magnetization dynamics in the optical regime yield a meaningful outcome.

[1] B. Assouline, A. Capua, Helicity-dependent optical control of the magnetization state emerging from the Landau-Lifshitz-Gilbert equation, Physical Review Research, 6 (2024) 013012. [2] E. Beaurepaire, J.C. Merle, A. Daunois, J.Y. Bigot, Ultrafast Spin Dynamics in Ferromagnetic Nickel, Physical Review Letters, 76 (1996) 4250-4253. [3] L. Avilés-Félix, L. Farcis, Z. Jin, L. Álvaro-Gómez, G. Li, K.T. Yamada, A. Kirilyuk, A.V. Kimel, T. Rasing, B. Dieny, R.C. Sousa, I.L. Prejbeanu, L.D. Buda-Prejbeanu, All-optical spin switching probability in [Tb/Co] multilayers, Scientific Reports, 11 (2021) 6576. [4] R. Hiramatsu, D. Miura, A. Sakuma, Temperature Variation of Gilbert Damping Constant in 3 d Transition Metals from First Principles, Journal of the Physical Society of Japan, 92 (2023) 044704. [5] S. Mankovsky, D. Ködderitzsch, G. Woltersdorf, H. Ebert, First-principles calculation of the Gilbert damping parameter via the linear response formalism with application to magnetic transition metals and alloys, Physical Review B—Condensed Matter and Materials Physics, 87 (2013) 014430. [6] D.A. Garanin, Fokker-Planck and Landau-Lifshitz-Bloch equations for classical ferromagnets, Physical Review B, 55 (1997) 3050. [7] T. Plefka, Nonlinear damping in spin systems: long range spin-spin interactions, Zeitschrift für Physik B Condensed Matter, 90 (1993) 447-454. [8] G.-M. Choi, A. Schleife, D.G. Cahill, Optical-helicity-driven magnetization dynamics in metallic ferromagnets, Nature Communications, 8 (2017) 15085.

Session AU
MACHINES OPTIMIZATION, MAGNETIC LOSS, AND THERMAL MODELING I (Poster Session)

Tsung Wei Chang, Chair
National Cheng Kung University, Tainan, Taiwan

AU-01. Modeling Approach for Ultra-Thin Wound Iron Cores Based on Equivalent Complex Permeability. *X. Li*[1,2], J. Yuan[1,2] and H. Zhou[1,2]
1. State Key Laboratory of Power Grid Environmental Protection, Wuhan University, Wuhan, China; 2. School of Electrical Engineering and Automation, Wuhan University, Wuhan, China

The anode saturation reactor is a vital component in high-voltage direct current (HVDC) transmission converter valve systems, protecting thyristors. Its core consists of silicon steel sheets, measuring 0.1 mm or thinner, to minimize eddy current losses from high-frequency excitations. However, finite element simulations of this device face challenge in directly solving multilayer thin sheets, including difficulties in mesh discretization, high dimensionality of matrix equations, and significant computational resource demands[1]. Thus, it is essential to explore modeling methodologies for the core. By implementing algorithmic improvements, memory consumption can be reduced while maintaining computational accuracy, thereby enhancing design and optimization efficiency. This study utilizes an equivalent complex permeability amplitude method that incorporates the skin effect to enhance traditional homogenization modeling. This approach improves the assessment of magnetic anisotropy in wound cores, enabling direct mesh discretization of the entire structure without requiring additional segmentation for the skin effect. A comparative analysis is conducted among the proposed method (d) and three existing methodologies: (a) isotropic homogenization modeling, (b) anisotropic homogenization modeling, and (c) thin sheet modeling. The electrical parameters and computational efficiencies of these models are evaluated, with experimental validation confirming the high reliability of loss calculations obtained through the new method. The simulation of the ASR's operating circuit integrates the core into a thyristor half-wave rectifier circuit, with a trigger angle of 60°, as shown in Fig. 1. Fig. 2 illustrates the electromagnetic response characteristics of the core under different modeling approaches. Notably, the improved modeling method results in a higher peak current, with computational results deviating from experimental values by no more than 7%. This method also significantly enhances computational efficiency compared to the other techniques used.

[1] Corcolle, Romain, and Laurent Daniel. "3-D semi-analytical homogenization model for soft magnetic composites." *"IEEE Transactions on Magnetics"*.57.7 (2021): 1-4.

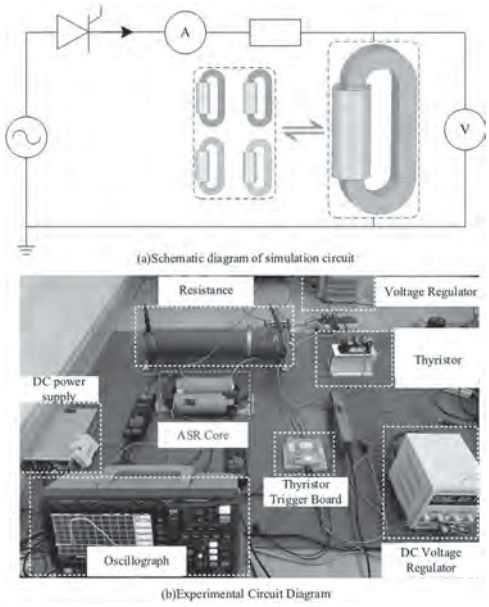

Fig. 1: Simulation Circuits

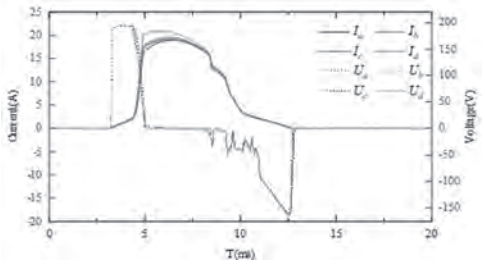

Fig. 2: Simulation Results

AU-02. Analysis of Core Loss of 10MW Direct Drive Permanent Magnet Synchronous Generator considering 3D Magnetic Flux Path and Rotor Overhang. *S. Kim*[1], H. Shin[2], K. Shin[3] and J. Choi[1] *1. Chungnam National University, Daejeon, The Republic of Korea; 2. Hyundai Mobis, Uiwang, The Republic of Korea; 3. Changwon National University, Changwon, The Republic of Korea*

Accurate prediction of electromagnetic losses is crucial to satisfying the efficiency requirements of generator design. Specifically, the accurate prediction of core losses requires consideration of magnetic field behavior. This study investigates the core loss of a 10 MW direct-drive permanent magnet synchronous generator (PMSG) with an overhang structure, considering the axial magnetic field behavior caused by the overhang. Figure 1(a) illustrates the 3D structure of the PMSG, Figure 1(b) depicts the split stator, Figure 1(c) shows the magnetic flux density, and Figure 1(d) shows the vector plot. The figures indicate significant saturation in the upper region from the overhang. Figure 1(e) presents the analysis model, and Figure 1(f) shows the actual model. To accurately predict core losses, both tangential and

radial magnetic field behaviors, as well as the axial magnetic field behavior induced by the overhang were considered. The stator was segmented and the magnetic field behaviors in all three directions were derived for each segment. Core losses were calculated using a modified Steinmetz equation to distinguish between alternating and rotating magnetic fields. The magnetic field behaviors in Regions 15 and 17 are presented in Figures 2(a) and 2(b), respectively. Figure 2(c) presents the core losses for each segment in the 2D model considering only the tangential and radial directions, whereas Figure 2(d) presents the core losses for each segment in the 3D model considering the axial direction, as well. In the figures, regions with alternating magnetic fields transform into regions with rotating magnetic fields when the axial direction is included, leading to increased core loss. Based on these results, a PMSG with an overhang, requires a comprehensive 3D core loss analysis to account for the axial magnetic field behavior. The detailed comparisons and analysis results are presented in the full paper.

[1] S.-M. Jang, K.-J. Ko, H.-K. Kim, S.-H. Lee, and T.-H. Sung, "An Analysis on Core Loss Characteristics for Permanent Magnet Synchronous Generator considering the Load Conditions", Transaction of the KIEE, vol. 2009, no. 4, pp. 55-57, Apr. 2009 [2] J.-H. Woo, T.-K. Bang, H.-K. Lee, K.-H. Kim, S.-H. Shin, and J.-Y. Choi, "Electromagnetic characteristic analysis of high-speed motors with rare-earth and ferrite permanent magnets considering current harmonics", IEEE Trans. Magn., vol. 57, no. 2, pp. 1-5, Feb. 2021 [3] C.-W. Kim, J.-M. Kim, S.-W. Seo, J.-H. Ahn, K. Hong, and J.-Y. Choi, "Core loss analysis of permanent magnet linear synchronous generator considering the 3-D flux path", IEEE Trans. Magn., vol. 54, no. 3, pp. 1-4, Mar. 2018

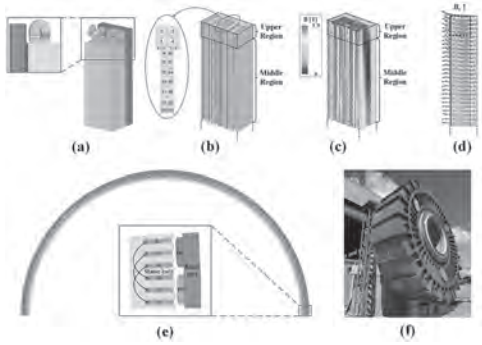

Fig.1 (a) 3D structure of the PMSG, (b) Split stator, (c) Magnetic flux density, (d) Vector plot, (e) Analysis Model, (f) Actual Model.

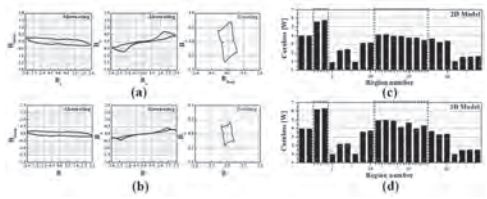

Fig.2 (a) Magnetic field behavior of region 15, and (b) region 17, (c) Core loss for each region obtained by 2D model, and (d) 3D model.

AU-04. Investigation of the contribution of Grain-Oriented Sheets to the performance of an Axial-Flux Switched-Reluctance Machine.
A. El Hajj[1], J. Drappier[1], *A. Tounzi*[1] and J. Korecki[1] *1. University of Lille, Lille, France*

The aim of this paper is to investigate the effect of using GO (Grain-Oriented) sheets into different parts of the machine. To do this, we will study an axial flux SRM (Switched-Reluctance Machine) with NO (Non-Oriented) laminations, which will be considered as a reference, then we will test the addition of rotor and stator teeth in GO, and finally when the entire machine is in GO. The studies will be carried out using 3D-FE (Finite Element) modelling where the anisotropic nature of the GO laminations is taken into account by a permeability tensor in the 3 directions while considering the non-linearity in the RD (Rolling Direction) and TD (Transverse Direction) directions using the following elliptical model: $B_{RD} = \mu_{RD}(H).H_{RD}$ $B_{TD} = \mu_{TD}(H).H_{TD}$ $H = \sqrt{(H_{RD}^2+H_{TD}^2)}$ $B_{ND} = \mu_{ND}.H_{ND}$, μ_{ND}=cst The following materials have been considered: - M400-50: isotropic NO sheets, with a thickness of 0.5 mm - HGO35: anisotropic GO sheets, with a thickness of 0.35 mm Their B-H curves are given in Fig. 1. In the case where the whole machine is made of GO, a specific cut-out is used to obtain the TD direction following the tangential direction. Contrary to what one might suppose, in the linear zone, as shown by the results in terms of electromagnetic torque (Fig. 2), the use of GOs makes no difference compared with NO insofar as the contribution of the RD is 'annihilated' by the limitation of the TD. More details about the simulations (model of the anisotropy, stator lamination, etc.), the parameters of the machine, and the field distribution will be given in the final version of this paper. Other operating conditions, with a more significant magnetic saturation effect, will also be discussed.

[1] J. Ma *et al.*, 'Optimal Design of an Axial-Flux Switched Reluctance Motor With Grain-Oriented Electrical Steel', *IEEE Transactions on Industry Applications*, vol. 53, no. 6, pp. 5327–5337, Nov. 2017, doi: 10.1109/TIA.2017.2727438. [2] R. Aydoun, G. Parent, A. Tounzi, and J.-P. Lecointe, 'Performance comparison of axial-flux switched reluctance machines with non-oriented and grain-oriented electrical steel rotors', *Open Physics*, vol. 18, no. 1, pp. 981–988, Jan. 2020, doi: 10.1515/phys-2020-0200.

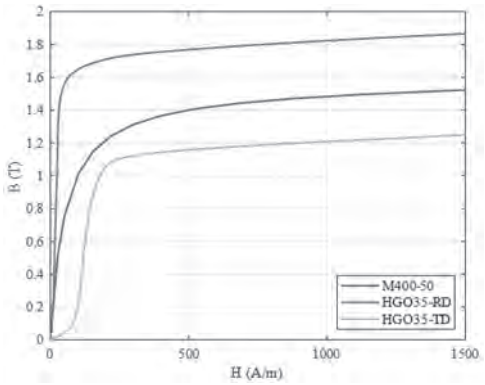

B-H curves of the studied materials

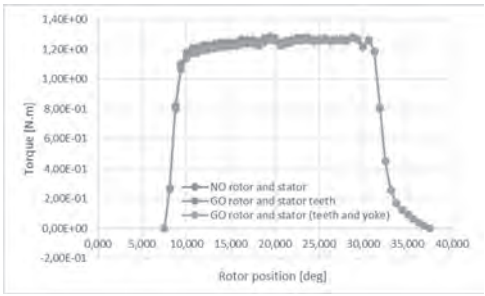

Variation of the electromagnetic torque with the rotor position

AU-05. A Frequency Independent Excess Loss Modeling for Arbitrary Waveforms.
T. Yamada[1], K. Semba[1], T. Sato[1] and H. Sano[1]
1. JMAG Business Company, JSOL Corporation, Tokyo, Japan

Accurate prediction of excess loss has become critical in electric machine design as the driving frequency of machines increases. A commonly used approach is employing the Bertotti model(1). Although the Bertotti model is generic, the resulting model's validity is limited by measurements that determine the model parameters as a function of magnetic flux density B and frequency(2)(3) and are difficult, especially in the high-frequency range. This is inconvenient for machine design, where complex fields with multiple frequency components and minor loops need to be dealt with. The limitation can be relaxed by removing the frequency dependency from the parameters. We investigated the possibility of a model that does not have frequency

dependency and is applicable to arbitrary waveforms. The results showed the possibility. The proposed model shares the general form of the Bertotti model, and excess loss P_{ex} is expressed as C*(dB/dt)^p. The key difference is that C depends not on frequency but only on B. Sets of C and p are identified to satisfy the measurement results changing frequency. If they do not have a frequency dependency, the resulting sets must coincide. The measurements are conducted on a ring core under biased AC fields with multiple frequencies (Fig.1). The target P_{ex} is carried out by subtracting hysteresis loss P_{hy} and classical eddy current loss P_{cl} from the measured loss P_{mes}. P_{hy} and P_{cl} are calculated using the Play model[4][5] and 1D FEA method[6] to reproduce minor loops and skin effects in the steel sheet. We found that a set of C and p exists that has a weak dependency on frequency when the shape of the steel sheet's magnetic susceptibility is used as C with an appropriate p (Fig.2). This was also observed with another steel sheet.

(1) G. Bertotti, "General properties of power losses in soft ferromagnetic materials," IEEE Trans. Magn., vol. 24, no. 1, pp. 621–630(1988) (2) D. Ionel, M. Popescu, and C. Cossar, "A General Model of the Laminated Steel Losses in Electric Motors with PWM Voltage Supply," IEEE Industry Applications Society Annual Meeting, pp. 1–7(2008) (3) T. Yoshioka, T. Tsuge, and Y. Takahashi, "Iron Loss Estimation Method for Silicon Steel Sheet Taking Account of DC-Biased Conditions," IEEE Tran. on Magn., vol. 55, no. 6, pp. 1–4(2019) (4) T. Matsuo, D. Shimode, Y. Terada, and M. Shimasaki, "Application of stop and play models to the representation of magnetic characteristics of silicon steel sheet," IEEE Tran. on Magn., vol. 39, no. 3, pp. 1361–1364(2003) (5) M. A. Krasnosel'skii and A. V. Pokrovskii, Systems with Hysteresis. Berlin, Heidelberg: Springer(1989)(6) O. Bottauscio, M. Chiampi, and D. Chiarabaglio, "Advanced model of laminated magnetic cores for two-dimensional field analysis," IEEE Trans. on Magn., vol. 36, no. 3, pp. 561–573(2000)

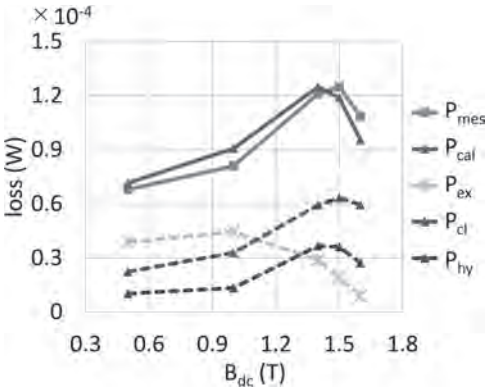

Fig.1 Loss variations regarding biased field B_{dc} at 5kHz The parameters C and p are determined to minimize the difference between P_{mes} and P_{cal}, which is the summation of P_{hy}, P_{cl}, and resulting P_{ex} at 1k, 5k, and 10k Hz with the AC amplitude of 0.2T.

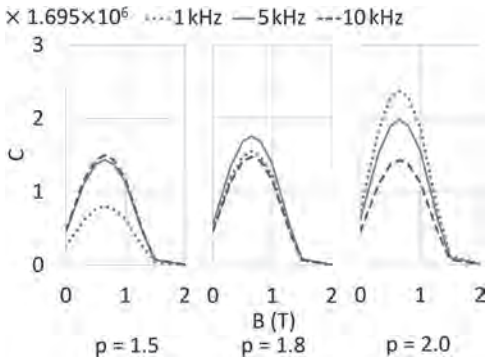

Fig.2 Frequency dependencies of C In the case of p=1.8, all C identified at different frequencies almost coincide. The shape of C is the same as the magnetic susceptibility. The steel is 35A210.

AU-06. Surrogate Model Based Drive Cycle Modelling and Optimization of Synchronous Reluctance Machines for Electric Vehicles. *Y. Gong*[1], A. Gneiting[1], S. Weigel[1], N. Parspour[1] and Z. An[1]
1. Institute of Electrical Energy Conversion (IEW), University of Stuttgart, Stuttgart, Germany

Design of traction machines for electric vehicles requires minimizing losses over the drive cycle [1], which is time-consuming to model. To achieve drive cycle-oriented optimization, recent works focus on various modeling methods, such as reduced-order Design of Experiment (DoE) for the flux & loss lookup table (LUT) [2], representative points from energy consumption distribution [3] or k-means clustering [4]. Additionally, surrogate models are growingly used in e-machine design [5] and drive cycle optimization [6]. However, two questions remain unresolved in drive cycle optimization using surrogate models: 1, How can FEA be used to precisely model losses at each operating point (OP) and determine the total energy loss for surrogate model training? 2. How can surrogate models predict the drive cycle losses more accurately in the optimization? This work investigates these questions using synchronous reluctance machines and Kriging models. For the first question, two methods for modeling loss energy are studied: 1. Establishing the iron loss map. 2. Calculating the loss for each OP separately. DoE methods for building the flux & loss LUT are also studied. Comparisons show that separate OP calculation with key value insertion in DoE provides the best accuracy. For the second question, the total loss energy is optimized using the strategy shown in Fig. 2, employing different prediction methods: 1. Direct prediction of the total loss energy from design variables - Direct Energy Loss Predictor (DELP). 2. Prediction of the flux & loss LUT to calculate the iron losses of each OP and the total loss energy – Lookup Based Sequential Loss Calculation Model (LSLCM). 3. Prediction of the total loss energy using a combination of design variables and the iron loss LUT as inputs - Hybrid Input Energy Loss Predictor (HIELP). The optimization results in Fig. 2 show that all three models achieve improved Pareto fronts compared to sampling. Among them, the LSLCM model yields the best results for total loss energy, while HIELP also outperforms DELP. Combining LSLCM with DELP or HIELP also improves the Pareto front, proving the effectiveness of LSLCM.

[1] L. A. D'Angelo, Z. Bontinck and S. Schöps, IEEE Transactions on Magnetics, vol. 56, no. 2, pp. 1–5 (2020) [2] B. Praslicka, C. Ma and N. Taran, IEEE Transactions on Industry Applications, vol. 59, no. 2, pp. 1351–1360 (2022) [3] P. Lazari, J. Wang and L. Chen, IEEE Transactions on Industry Applications, vol. 50, no. 5, pp. 3203–3213 (2014) [4] A. Gneiting, M. Waldhof, and N. Parspour, 2022 IEEE 7th Southern Power Electronics Conference (SPEC). IEEE, pp. 1–8 (2022). [5] Y. Gong and A. Gneiting, 2023 International Conference on Electrical Machines and Systems (ICEMS). IEEE, pp. 1284– 1290 (2023) [6] M. Djami, M. Hage-Hassan and C. Marchand, 2022 International Conference on Electrical Machines (ICEM). IEEE, pp. 251–256 (2022)

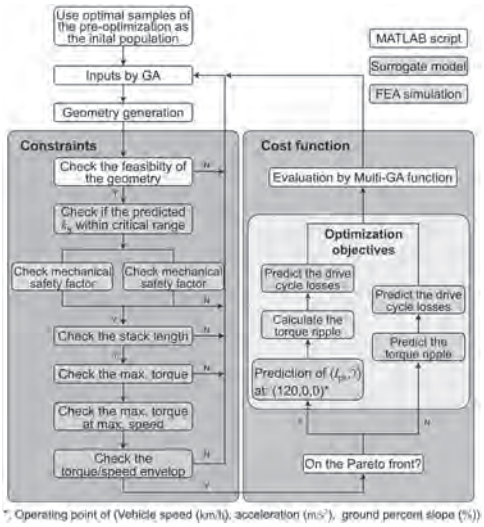

Fig. 1: Surrogate model-based drive cycle optimization strategy

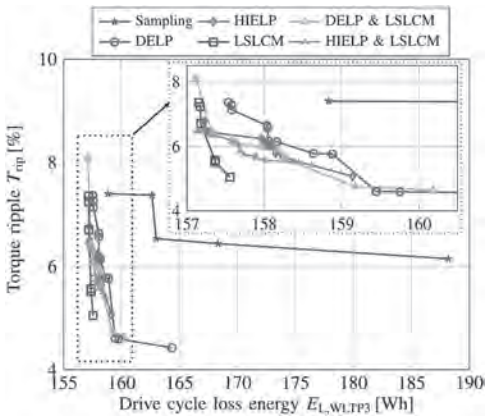

Fig. 2: Optimization results

AU-07. Effect of Laser Welding on Magnetic Properties of Laminated Cores of Non-Oriented Electrical Steel Sheets Cut by EDM and Laser Cutting. *Y. Tsuchida*[1] and K. Otsuka[1] *1. Oita University, Oita, Japan*

Differences in the manufacturing of laminated cores between motor prototyping and mass production have resulted in differences in the degree of degradation of the magnetic properties of laminated cores, causing difficulties in the development of new motors. Therefore, it is necessary to clarify the effects of cutting and stacking on the magnetic properties. Focusing on the cutting and stacking at the prototype stage, there have been no reports on the effects of laser welding on the magnetic properties of laminated cores (1, 2). Therefore, we investigated the magnetic properties of laminated cores fabricated using EDM and laser as cutting and laser welding as stacking. Ring-shaped laminated cores with a thickness of 4.9 mm were fabricated from non-oriented electrical steel sheets with a thickness of 0.35 mm, an outer diameter of 80 mm, and an inner diameter of 70 mm. Laminated Core-A was cut by EDM and welded by laser, and Laminated Core-B was cut by laser and welded by laser. For both cores, 1, 2, 4, 8, and 16 areas were joined by laser welding, as shown in Fig. 1. The effects of thermal stress caused by laser welding on the magnetic properties were investigated according to the number of welding areas. For the Core-A, the permeability becomes smaller at one laser welding than that at no welding, and the permeability is the smallest at 16 as shown in Fig. 2 (a). This is considered to be due to the thermal stress caused by laser welding, since the magnetic properties generally do not change much after EDM cutting. And for the Core-B, the permeability increases at one laser welding, and the magnetic properties are improved as shown in Fig. 2 (b). Unlike Core-A, the magnetic properties of Core-B are considered to have been improved because the thermal stress-affected zone during laser cutting was mitigated by the laser welding. The iron loss increased in the Laminated Core-A, however, decreased by about 7% in the Laminated Core-B. Details of the iron loss and its discussion will be presented in the full paper.

(1) A. Schoppa, J. Schneider, C. D. Wuppermann, and T Bakon, "Influence of welding and sticking of laminations on the magnetic properties of non-oriented steels", Journal of magnetism and magnetic materials", vol. 254-255, pp. 367-369 (2003) (2) H. Wang, Y. Zhang, and S. Li, "Laser welding of laminated electrical steels", Journal of Materials Processing Technology, vol. 230, pp. 99-108 (2016)

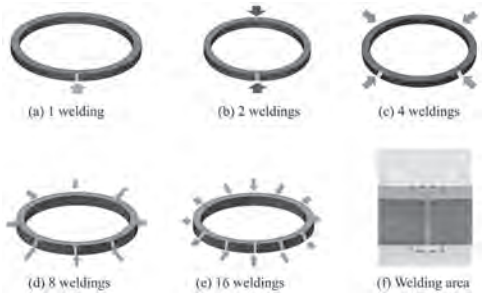

Fig. 1 Samples with laser welding after EDM- and laser-cutting and its welding area.

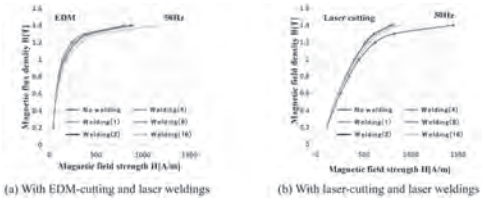

Fig. 2 B-H curves with some weldings after EDM- and Laser-cutting.

AU-08. Effect of Saturation Magnetic Flux Density on Cogging Torque of SPMSM According to Rolling Direction of Non-Oriented Electrical Steel. *J. Kim*[1], Y. Won[2], S. Park[3] and M. Lim[2] *1. Mechanical Engineering, Yeungnam University, Gyeongsan, The Republic of Korea; 2. Automotive Engineering (Automotive-Computer Convergence), Hanyang University, Seoul, The Republic of Korea; 3. Mechanical, Robotics and Energy Engineering, Dongguk University, Seoul, The Republic of Korea*

Surface-mounted permanent magnet synchronous motors (SPMSMs) have the advantage of being insensitive to manufacturing tolerances (MTs) due to the large effective air-gap and having small cogging torque and torque ripple [1]. Therefore, SPMSMs are widely used in applications where motor cogging torque needs to be minimized [2]. Cogging torque could become a critical performance metric for user convenience or for precise control. Cogging torque occurs at multiples of the least common multiple of the number of poles and slots [3]. However, when asymmetry occurs due to factors such as MTs, additional harmonic cogging torque is generated. Due to the MTs of the stator and rotor, cogging torque of the pole number order and slot number order is generated, respectively [4]. While studies on MTs and cogging torque abound, there has been little research analyzing the effect of saturation magnetic flux density according to the rolling direction (RD) of non-oriented electrical steel. Even non-oriented electrical steel exhibits differences in saturation magnetic flux density between the rolling & counter RD. While this does not significantly affect performance such as motor efficiency and average torque, it does impact cogging torque due to its high sensitivity. Therefore, in this study, the influence of saturation magnetic flux density according to RD of non-oriented electrical steel on cogging torque of 8-pole 12-slot SPMSM was investigated. After measuring the BH-curve according to the RD, as shown in Fig. 1, and applying it to 2D and 3D electromagnetic finite element analysis to analyze cogging torque, it was confirmed that the additional cogging torque harmonics at twice the pole

number significantly increased, as shown in Fig. 2. A notable observation was that stator tolerances have minimal impact on cogging torque harmonics at twice the pole number, whereas the anisotropic characteristics of electrical steel have a significant influence. Additionally, the effect of anisotropic characteristics of electrical steel on cogging torque was examined by varying the design variables of the SPMSM, and validation was conducted through experiments.

Y. -J. Won, J. -H. Kim, and S. -M. An, IEEE Transactions on Magnetics., Early Access. (2024) Y. -J. Won, J. -H. Kim, and S. -H. Park, IEEE Transactions on Magnetics., Vol. 59. (2023) S. Kim, S. -G. Lee, J. -M. Kim, IEEE Transactions on Energy Conversion., Vol. 35, pp. 2056-2065, (2020) S. -G. Lee, S. Kim, J. -C. Park, IEEE Transactions on Energy Conversion., Vol. 35, pp. 2076-2085, (2020)

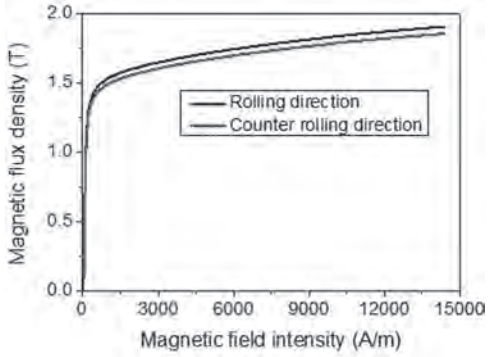

Fig. 1. BH-curve of non-oriented electrical steel according to rolling direction.

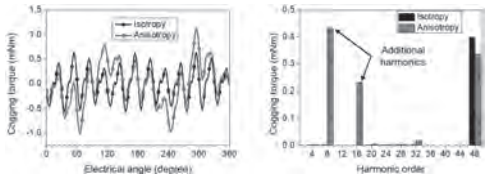

Session AV
ELECTRICAL MACHINES AND POWER ELECTRONICS II (Poster Session)

Christopher H. T. Lee, Chair
Nanyang Technological University, Singapore

AV-01. Electromagnetic Vibration and Torque Ripple Analysis of Multi-unit PMSMs. *Q. Wei*[1], l. Dong[1], W. Li[1], M. Andriollo[2] and D. Zeng[1]
1. Harbin Engineering University, Harbin, China; 2. University of Padova, Padova, Italy

Multi-unit permanent magnet synchronous motors (PMSMs) have many advantages such as high efficiency and high fault tolerance. Therefore, they have a broad application in the field of electric vehicles and high-power drives[1],[2]. With the continuous improvement of comfort and quietness of related equipment, vibration and noise control of multi-unit PMSMs is facing more and more stringent challenges[3]. Compared with the traditional three-phase PMSMs, the main advantage of multi-unit PMSMs is the use of multi-unit structure design, and each unit is independently controlled. This reduces the current power level requirements for switching devices and ensures their reliability[4],[5]. However, there are few researches on vibration and noise of multi-unit PMSMs. When a unit of a multi-unit PMSMs fails, it is usually directly cut out the faulty unit. The vibration and noise in this fault state have hardly been studied. In order to study the electromagnetic vibration and torque ripple of multi-unit PMSMs, an analytical magnetic field model under multi-unit operation is established in this paper. Firstly, the analytical models of loaded magnetic fields under the operation of 1 unit and k units are established. Then the vibration response of the missing element is theoretically derived and analyzed. Finally, the prototype is simulated and verified by experiments. The results show that the analytical model reveals the time-space distribution characteristics of the electromagnetic force and electromagnetic torque of the multi-unit PMSMs. The frequency distribution of the three components of the electromagnetic force under the operation of k unit motors meets $2\pi(2hf_e)$. The frequency of electromagnetic torque is $2\pi(6mf_e)$; When the unit is missing, the unbalanced magnetic pull results in additional electromagnetic force with different order frequencies and different frequency multiples. Its frequency distribution is $(2h\pm i)\omega_r$. The experimental results are shown in Fig. 1. Simulation and experimental results verify the above conclusions.

[1] M. Slunjski, O. Stiscia, and M. Jones, IEEE Trans. Ind. Electron., vol. 68, no. 8, pp. 6412-6423.2021. [2] X. Huang, A. Goodman, C. Gerada, and Y. Fang, IEEE Trans. Ind. Electron., vol. 59, no. 9, pp. 3532-3541.2012. [3] P. Xu et al., IEEE Trans. Ind. Electron., vol. 65, no. 3, pp. 1941-1954.2018. [4] D. Zeng, J. Zou, and Y. Xu, IEEE Trans. Ind. Electron., vol. 67, no. 4, pp. 2734-2743.2020. [5] G. Feng, C. Lai, and N. C. Kar, IEEE Trans. Energy Convers., vol. 35, no. 4, pp. 1796-1805.2020.

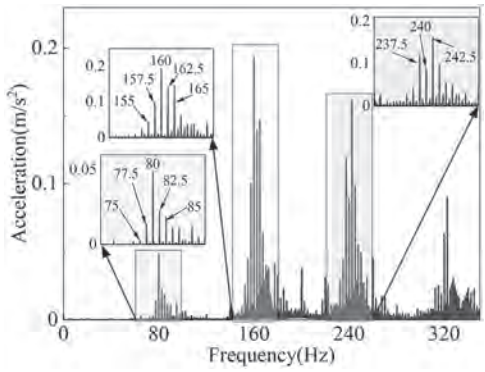

Fig.1 Experimental spectrum of vibration response when a unit motor is disconnected

AV-05. Research on reduction of cogging torque of spoke type generator using ferrite permanent magnets. *S. Kim*[1] and S. Jeong[2]
1. KETI, Gangju Metropolitan City, The Republic of Korea; 2. Gwangju University, Gangju Metropolitan City, The Republic of Korea

PM (Permanent Magnet) generators or motors using rare earth metals such as NdFeB (Neodymium Iron Boron) have the advantages of high power density and high efficiency. For this reason, many wind turbines and electric vehicle motors installed around the world are made using rare earth permanent magnets. However, as the name suggests, rare earth minerals are very rare among minerals on Earth and therefore have a high price range. In addition, because mining is concentrated in a specific region (China), rare earth metals are sometimes used to weaponize resources. For this reason, research on generators that use less or no rare earth metals has been actively conducted in recent years. Rare earth permanent magnets have a high residual magnetic flux density, making it possible to develop generators with large output in a small size. In contrast, ferrite has a residual magnetic flux density of about 1/3 that of rare earth permanent magnets. Therefore, to create a generator with equivalent performance, approximately three times the amount of ferrite magnets must be used. For this reason, generators using ferrite permanent magnets adopt a spoke-type rotor method that allows a large amount of ferrite to be used while maintaining the size of the generator as much as possible. For generators, it is very important to minimize cogging torque in order to easily start even in small winds. Cogging torque is generated by the suction force between the rotor permanent magnets and the stator core. Therefore, in order to reduce cogging torque, it is important to design the suction force to be constant. Therefore, in this paper, the structure of the permanent magnet guide for the 10-pole 24-slot and 10-pole 36-slot 2 models is designed asymmetrically to primarily reduce the cogging torque. In addition, by introducing multi-stage rotor skew, I would like to further compare the cogging torque and performance characteristics under load of the two models. The comparison is verified through numerical analysis through simulation, and a prototype for a case with 10 poles and 24 slots is produced to supplement the simulation results.

[1] D. Dorrell, L. Parsa, and I. Boldea, "Automotive electric motors, generators, and actuator drive systems with reduced or no permanent magnets and innovative design concepts," IEEE Trans. Ind. Electron., vol.61, no.10,

pp.5693–5695, Oct. 2014. [2] Sandra M. Castano; James Weisheng Jiang1; Berker Bilgin1; Hossein Dadkhah; Nitin Patel, "Design of a Spoke-Type Ferrite Magnet Generator for a Hybrid Electric Vehicle Application," in ITEC 2019, 19-21, June 2019. [3] Z. S. Du and T. A. Lipo, "Efficient utilization of rare earth permanent magnet materials and torque ripple reduction in interior permanent magnet machines," IEEE Transactions on Industry Applications, vol.53, no.4, pp.3485-3495, August 2017.

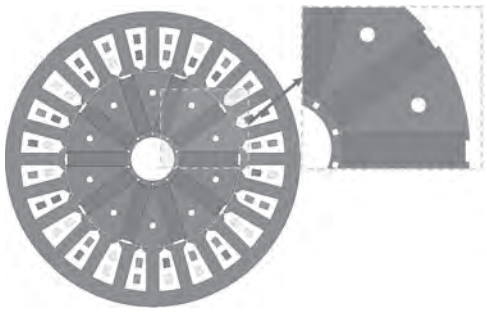

1. 10pole 24slot

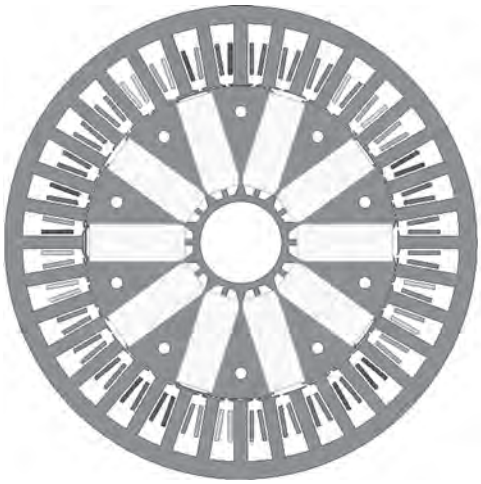

2. 10pole 36slot

AV-06. Design for Performance Improvement of PMa-SynRM with Asymmetric Rotor Shape Considering Mechanical stiffness. *S. Kim*[1], W. Jung[1], T. Kim[1], K. Shin[2] and J. Choi[1] *1. Department of Electrical Engineering, Chungnam National University, Daejeon, The Republic of Korea; 2. Department of Electrical Engineering, Changwon National University, Changwon, The Republic of Korea*

This paper proposes a design for Permanent Magnet-assisted Synchronous Reluctance Motor (PMa-SynRM) with an emphasis on mechanical robustness. The approach involves the asymmetric placemen t of rotor permanent magnets to shift the magnetic axis induced by the permanent magnets. This adjustment aligns the magnetic and reluctance torques within the same current phase. Figure 1(a) illustrates the conventional analytical model, and Figure 1(c) depicts the model with asymmetrically placed permanent magnets. Figures 1(b) and (c) compare the torque characteristics obtained using finite element analysis, thereby confirming the improved torque performance. However, employing an asymmetric structure may lead to increased torque ripple because of an imbalance in the magnetic field distribution despite the improvement in the overall torque. To address these challenges, this study employs a multi-objective algorithm to derive a motor topology that effectively reduces the torque ripple while maintaining or improving overall performance; however, the mechanical robustness inherent in the model with asymmetrically placed permanent magnets requires careful consideration. Figures 2 (a) and (b) demonstrate sufficient separation between the resonance and operating frequencies, ensuring adequate safety in rotor dynamics. The mechanical analysis of the asymmetric rotor and design considerations for the objective functions are extensively discussed throughout the paper. In conclusion, this study adopts an asymmetric rotor shape for PMa-SynRM motors and proposes a mechanically robust design using multi-objective algorithms that enhance electromagnetic performance. This contributes to more efficient and reliable motor designs capable of improving torque performance and reducing torque ripple, thereby benefiting various industrial and automotive applications.

Ying Xie, Jiawei Shao, Shoucong He, Bitian Ye, Fan Yang, Lijing Wang, IEEE Access, Vol. 10, p.79564-79573 (July 2022) Wenliang Zhao; Dezhi Chen; Thomas A. Lipo; Byung-Il Kwon, IEEE Trans. Magn. Vol. 51, NO. 11, p.8108504-8108504 (Nov 2015) Chengwu Diao, Wenliang Zhao, Yan Liu, and Xiuhe Wang, CES TEMS, Vol. 7, NO. 2, p. 179 - 186 (Jan 2023) T. Yanagisawa, Y. Yoshida, K. Tajima, J. Magn. Soc. Jpn., Vol. 44, NO. 2, p.45-51 (July 2020) Meimei Xu, Guohai Liu, Qian Chen, Jinghua Ji, Wenxiang Zhao, IEEE Trans. Transp. Electrif. Vol. 7, NO. 1, p.202-213 (Mar 2021)

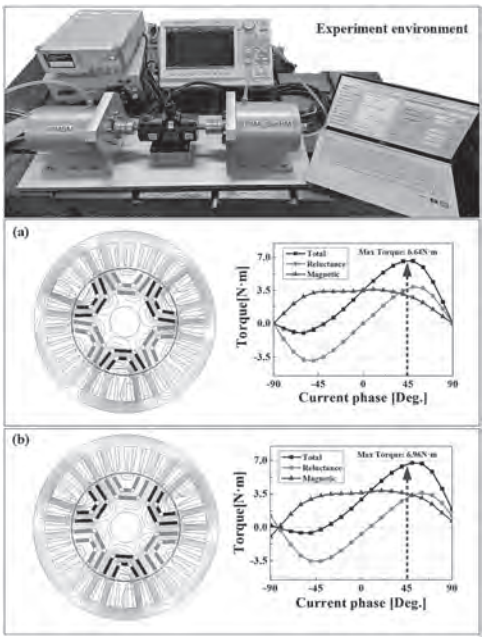

Fig. 1 Torque characteristics of PMa-SynRM by rotor geometry: (a) Conventional rotor model; (b) Asymmetric rotor model.

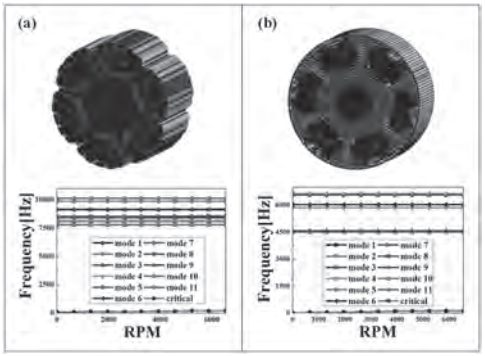

Fig. 2 Mechanical properties of the rotor at a maximum speed of 6540 rpm: (a) Stress analysis; (b) Campbell diagram analysis.

AV-07. Torque Improvement and Core Loss Reduction with Controllable Flux-Leakage Design in Spoke-Type Flux-Intensifying PM Motors. M.L. Duong[1], A.T. Huynh[2] and *M. Hsieh*[1] *1. Department of Electrical Engineering, National Cheng Kung University, Tainan, Taiwan; 2. Power Electronics and Machines Centre, Faculty of Engineering, University of Nottingham, Nottingham, United Kingdom*

I. Abstract This paper presents a novel approach for enhancing torque performance and reducing core loss in Spoke-type Flux-Intensifying Permanent Magnet (SFI-PM) motors using controllable magnetic flux leakage barriers. The SFI-PM motor design incorporates multiple flux barriers into a conventional Spoke-type Interior PM (SIPM) motor to increase d-axis inductance ($L_d > L_q$) and intensify magnetic flux density. However, this also reduces the output torque capacity compared to conventional SIPM motors. To mitigate this, magnetic flux leakage barriers are integrated into the *q*-axis of the SFI-PM motors, allowing control of the flux leakage bypass via the *q*-axis current. Then, under low-speed and heavy-load conditions, minimal leakage flux occurs within the rotor. Conversely, at high speed and light load, significant leakage flux reduces the flux-weakening current, enhancing output torque and efficiency across a wide speed range. To further optimize efficiency and torque, a multi-objective genetic algorithm (MOGA) is employed. The performance of the proposed Controllable Flux-Leakage SFI-PM (CFL-SFI-PM) motor is compared with conventional SIPM and SFI-PM motors and validated through Finite Element Analysis (FEA). II. Research Method and Analysis Results A 5kW CFL-SFI-PM motor model is developed from a conventional SIPM motor (Fig. 1). The rotor is enhanced with alternating flux barriers and magnetic flux leakage barriers in the q-axis to boost flux intensity and control leakage via q-axis current. The performance is compared with conventional SIPM (Fig. 1(a)) and SFI-PM motors in [1] (Fig. 1(c)). Efficiency and torque are further optimized using a MOGA method. Key specifications are provided in Table 1. The proposed model achieves an output torque of 23 Nm, slightly higher than the SFI-PM motor but lower than the SIPM motor. However, it boasts a better constant power speed range (CPSR) (Figs. 2(b)) and reduced high-speed iron loss, as shown in Fig. 3. Consequently, the efficiency map of the CFL-SFI-PM motor is improved (Fig. 3(c)). Detailed Finite Element Analysis (FEA) analysis and experiment will be reported in the whole paper.

[1] Min-Fu Hsieh, Anh Thanh Huynh, Viet-Vu Do, David Gerada, Chris Gerada, "Design Optimization of Spoke-type Flux-intensifying PM Motor with Asymmetric Rotor Configuration for Improved Performance," IEEE Transactions on Magnetics, Early Access, July 2024. DOI: 10.1109/TMAG.2024.3428416

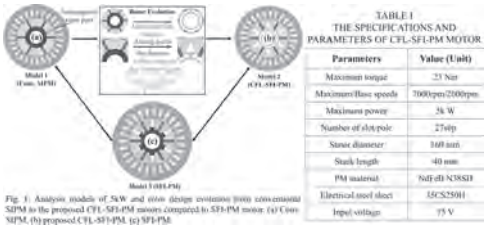

TABLE I
THE SPECIFICATIONS AND PARAMETERS OF CFL-SFI-PM MOTOR

Parameters	Value (Unit)
Maximum torque	23 Nm
Maximum/Base speeds	7000rpm/2000rpm
Maximum power	5k W
Number of slot/pole	27s6p
Stator diameter	169 mm
Stack length	40 mm
PM material	Nd Fe B N38SH
Electrical steel sheet	35CS250H
Input voltage	75 V

Fig. 1. Analysis models of 5kW and stator design systematic from conventional SIPM to the proposed CFL-SFI-PM motors compared to SFI-PM motor. (a) Conv. SIPM, (b) proposed CFL-SFI-PM, (c) SFI-PM.

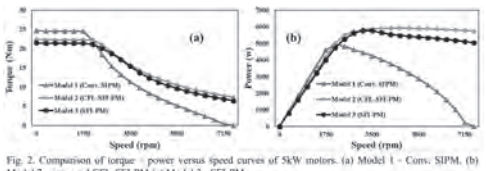

Fig. 2. Comparison of torque - power versus speed curves of 5kW motors. (a) Model 1 - Conv. SIPM, (b) Model 2 - proposed CFL-SFI-PM (c) Model 3 - SFI-PM.

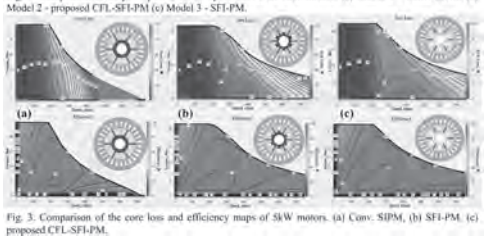

Fig. 3. Comparison of the core loss and efficiency maps of 5kW motors. (a) Conv. SIPM, (b) SFI-PM. (c) proposed CFL-SFI-PM.

AV-08. A Novel Traction Motor Design Approach Considering Efficiency Enhancing Current. *L.J. Caceres Vera*[1] and M. Hsieh[1] *1. Department of Electrical Engineering, National Cheng Kung University, Tainan, Taiwan*

Abstract This research aims to develop a design approach that incorporates the proposed Efficiency Enhancing Current (I_{Ee}) and Constant Power Speed Range (CPSR) early in the design stages to extend the high-efficiency area in the flux-weakening (FW) region. The method considers current limit circle, voltage limit ellipse, and constant torque curves in the id-iq plane, integrating the characteristic current (I_{ch}). These parameters significantly impact the CPSR and, consequently, the high-efficiency region. The paper includes both simulation and experimental validation. An interior permanent magnet synchronous motor (IPMSM) is designed and prototyped using this approach. Results show that early consideration of CPSR, $I_{ch,}$ and I_{Ee} are crucial to achieve high-efficiency are in the FW region. Proposed Method In electric motors, the stator inductance plays a critical role in defining the CPSR [1]. Traditional design methodologies focus on core dimensions and winding, neglecting CPSR, d-q axis inductances, and I_{ch}. These parameters are pivotal for extending CPSR and enhancing the high-efficiency area within the FW region. To address these shortcomings, this paper proposes a method that integrates current limit circle, voltage limit ellipse, and constant torque curves in the *id-iq* plane with I_{ch} and I_{Ee} (Fig. 1). This approach enables the estimation of I_{ch}, saliency, and d-q axis inductances necessary for an IPMSM to achieve maximum torque at both Maximum Torque Per Ampere (MTPA) and in the FW region. By incorporating these parameters in the design phase, the method ensures the motor design can attain an extended efficiency area in the FW region, thereby enhancing overall motor performance (Fig. 2). Conclusion This paper integrates the I_{Ee} into the design process and proposes a novel design method for extending the high-efficiency area in the FW region. Simulation and experimental results validate the effectiveness of this approach, demonstrating its potential to significantly improve motor performance. The findings highlight the importance of early consideration of CPSR, I_{ch}, and I_{Ee} in the design stages to enhance motor efficiency and performance.

[1] Y. Kim, B. Koo and K. Nam, "Induction Motor Design Strategy for Wide Constant Power Speed Range," in *IEEE Transactions on Industrial Electronics*, vol. 66, no. 11, pp. 8372-8381, Nov. 2019.

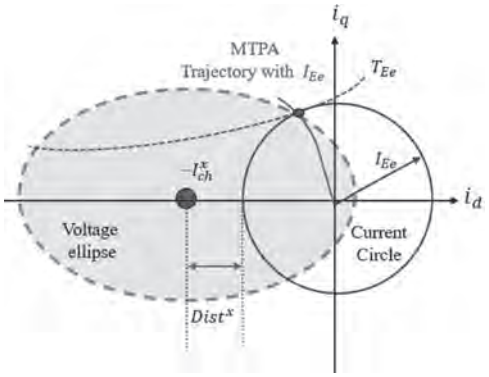

Fig. 1 Current circle and voltage ellipse

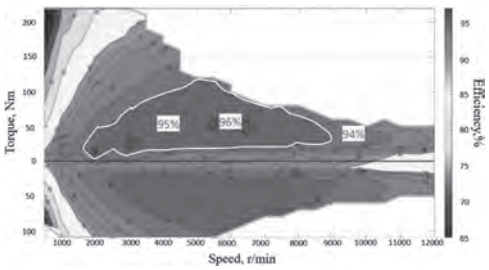

Fig. 2 Efficiency map (Experiment)

Session BA
FUNDAMENTALS AND ADVANCES IN 2D SPINTRONICS

Guoqiang Yu, Chair
Chinese Academy of Sciences, Beijing, China

INVITED PAPERS

BA-01. Observation of Quantum Spin Hall States in Monolayer $TaIrTe_4$. *Q. Ma[1] 1. Physics, Boston College, Chestnut Hill, MA, United States*

Introducing electron correlations to a quantum spin Hall (QSH) insulator can lead to the emergence of a fractional topological insulator and other exotic time-reversal-symmetric topological order, not possible in quantum Hall and Chern insulator systems. In this work, we report a dual QSH insulator within the intrinsic monolayer crystal of $TaIrTe_4$, arising from the interplay of its single-particle topology and density-tuned electron correlations [1]. At charge neutrality, monolayer $TaIrTe_4$ demonstrates the QSH insulator, manifesting enhanced nonlocal transport and quantized helical edge conductance. Interestingly, upon introducing electrons from charge neutrality, $TaIrTe_4$ only shows metallic behavior in a small range of charge densities but quickly goes into a new insulating state. This insulating state could arise from a strong electronic instability near the van Hove singularities, likely leading to a charge density wave. Remarkably, within this correlated insulating gap, we observe a resurgence of the QSH state. The observation of helical edge conduction in a (likely) CDW gap could introduce a new method for creating topological flat minibands via CDW superlattices, which offer a promising platform for exploring time-reversal-symmetric fractional phases and electromagnetism.

[1] J. Tang et. al., Nature 628, 515–521 (2024)

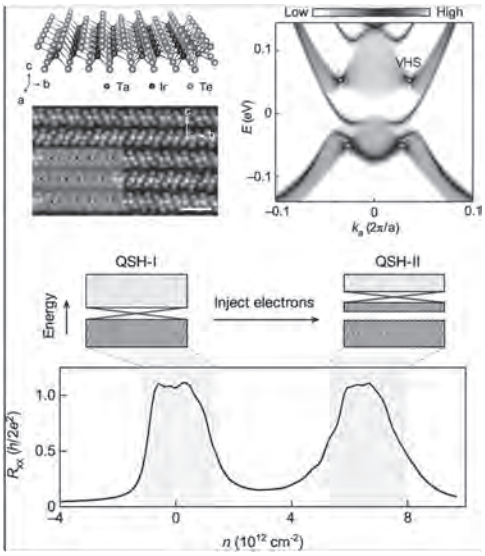

Dual quantum spin Hall states in monolayer $TaIrTe_4$

BA-02. Racetrack Memories enabled by novel spintronic materials and phenomena. *S. Parkin[1] 1. Max Planck Institute of Microstructure Physics, Halle (Saale), Germany*

Spintronics allows for advanced memory and storage technologies that go beyond today's charge-based devices. Most of these technologies are innately two-dimensional and rely on 2D arrays of individual memory and switches that are connected via multiple levels of complex wiring. Going beyond 2D is highly interesting. Magnetic Racetrack Memory (RTM) is a unique memory-storage device that relies on the current driven motion of domain walls along magnetic conduits. Chiral domain walls can be driven at speeds exceeding 1 km/s in synthetic antiferromagnetic racetracks by spin currents generated via the spin Hall effect in proximal metallic layers [1]. The scaling of 2D racetrack conduits to sub 80 nm wide dimensions is presented and the use of integrated anomalous Hall read sensors that allow for the detection of domain walls with ~10 nm spatial resolution is described [2]. We discuss several schemes for building prototype 3D racetracks. In one case freestanding membranes composed of atomically engineered thin film heterostructures that form the racetrack are formed on a sacrificial water-soluble sacrificial release layer. The freestanding membranes are transferred onto protrusions that have been pre-patterned on sapphire wafers to create 3D racetracks. The current induced domain wall motion is nearly identical in these structures as compared to the initial 2D layers [3]. In a second approach we fabricate 3D chiral magnetic racetracks via a novel state-of-the-art multi-photon super-resolution lithography system [4]. We show how the interplay between the geometrical chirality and the spin chirality of the individual domain walls allows for domain wall diode devices. Finally, we discuss how antiferromagnet materials can allow for novel racetracks and magnetic tunnel junction devices [5].

[1] S.-H. Yang, K.-S. Ryu, and S. S. P. Parkin, "Domain-wall velocities of up to 750 ms-1 driven by exchange-coupling torque in synthetic antiferromagnets," *Nat. Nanotechnol.,* vol. 10, pp. 221-226, 2015. [2] J.-C. Jeon, A. Migliorini, J. Yoon, J. Jeong, and S. S. P. Parkin, "Multi-core memristor from electrically readable nanoscopic racetracks," *Science* (accepted), 2024. [3] K. Gu *et al.*, "3D racetrack memory devices designed from freestanding magnetic heterostructures," *Nat. Nanotechnol.,* vol. 17, pp. 1065-1071, 2022. [4] A. Farinha, S.-H. Yang, J. Yoon, and S. S. P. Parkin, "Interplay of curvilinear twisting and spin chiralities in 3D twisted magnetic ribbons," *under review,* 2024. [5] Y. Chen *et al.*, "Twist-assisted all-antiferromagnetic tunnel junction in the atomic limit," *Nature (*2024).

BA-03. van der Waals Magnets and Antiferromagnets Interacting with Electron Spins. *D.C. Ralph[1]*, R. Jain[1], T.M. Cham[1], M. Roddy[1], B. Huang[1,4], V. Gupta[1,2] and Y.K. Luo[1,3] *1. Cornell University, Ithaca, NY, United States; 2. Yale University, New Haven, CT, United States; 3. Univ. of Southern California, Los Angeles, CA, United States; 4. Princeton University, Princeton, NJ, United States*

This talk will discuss two projects. The first concerns topological insulator/magnet samples made by mechanical stacking of exfoliated van der Waals flakes. The proximity interaction of the magnet with the topological surface state allows realization of the "parity anomaly" half-quantized Hall effect state at temperatures as high as 10 K, about a factor of 5 higher than for

any previous materials system. Capacitive measurements and thermal-activation transport studies both indicate a large value of the exchange gap of approximately 10 meV. Interaction with the topological surface state also induces a gate-dependent coercivity for the magnetic layer, as expected for interaction of a magnetic layer with a topological surface state. We speculate that in deposited samples even a small amount of disorder due to interfacial mixing can push the topological surface state away from the interface and thereby weaken the exchange coupling to the magnet. In contrast, the pristine interfaces formed by mechanical stacking of van der Waals layers eliminate intermixing, and we find that they provide much stronger interfacial exchange coupling within topological insulator/magnet heterostructures compared to samples made by top-down deposition The second project concerns 3-terminal tunnel junctions ($PtTe_2$/bilayer CrSBr/graphite) in which the A-type van der Waals antiferromagnet CrSBr acts as the tunnel barrier. Spin-filter tunneling through the CrSBr bilayer allows direct electrical measurements of antiferromagnetic resonance in the frequency domain. Furthermore, spin-orbit torque from the $PtTe_2$ electrode provides electrically-tunable control over the magnetic damping and resonance linewidth. We find the interesting result that the spin-orbit torque is highly local, with the spin current from the $PtTe_2$ electrode acting only on the individual spin sublattice layer adjacent to that electrode, with a negligible amount propagating to the next van der Waals layer.

BA-04. Withdrawn

BA-05. Field-free perpendicular magnetization switching by out-of-plane spins from two-dimensional materials. G. Shi[1] and *H. Yang*[1] *1. National University of Singapore, Singapore*

Field-free spin-orbit torque (SOT) switching of perpendicular magnetic anisotropy (PMA) is essential for the development of non-volatile spintronic devices, which have potential applications from embedded memories to the Internet of Things. Two-dimensional (2D) materials are particularly promising for creating high-density, miniaturized spintronic devices due to their efficient spin currents generation, highly controllable magnetism at the monolayer level, and the flexible integration of heterostructures [1]. Here, we experimentally demonstrate field-free SOT switching utilizing out-of-plane spins generated by 2D van der Waals materials, including WTe_2, $PtTe_2$/WTe_2, and $TaIrTe_4$. We fabricate wafer-scale 2D heterostructures consisting of low crystal-symmetry WTe_2 and the ferromagnet $CrTe_2$ with perpendicular anisotropy, achieving field-free switching of the $CrTe_2$ perpendicular magnetization [2]. However, due to the low Curie temperature of $CrTe_2$, this switching is performed below room temperature. To overcome this limitation, we further demonstrate field-free switching of PMA CoFeB at room temperature using 2D heterostructure $PtTe_2$/WTe_2 and single crystal flake $TaIrTe_4$. The high in-plane and out-of-plane spin Hall conductivities of $PtTe_2$/WTe_2 and $TaIrTe_4$ enable low-power SOT switching [3, 4]. Notably, the exceptional out-of-plane spin Hall conductivity of $PtTe_2$/WTe_2 bilayers is attributed to spin-to-spin conversion in WTe_2 induced by crystal asymmetry. Our findings pave the way for practical, low-power spintronic devices operating at room temperature, highlighting the potential of 2D materials in advancing next-generation spintronic applications.

1. H. Yang et al., “Two-dimensional Materials Prospects for Non-volatile Spintronic Memories” Nature 2022, 606, 663- 673. 2. G. Shi, et al. “Field-free manipulation of two-dimensional ferromagnet $CrTe_2$ by spin-orbit torques,” Nano Lett. under review. 3. Y. Liu, et al. “Field-free switching of perpendicular magnetization at room temperature using out-of-plane spins from TaIrTe4” Nat. Electron. 2023, 6, 732-738. 4. F. Wang, et al. “Field-free switching of perpendicular magnetization by two-dimensional $PtTe_2$/WTe_2 van der Waals heterostructures with high spin Hall conductivity” Nat. Mater. 2024, 23, 768-774.

Session BB
MAGNETICS FOR FUTURE TRANSPORTATION – FROM MEMORY TO MOTORS

Min-Fu Hsieh, Chair
National Cheng Kung University, Tainan, Taiwan

INVITED PAPERS

BB-01. Embedded STT-MRAM for Automotive Applications.
A. Wang[1], E. Chien[1], C. Chen[1], T. Chiang[1], *K. Huang*[1], R. Wang[1] and H. Chuang[1] *1. TSMC, Hsinchu, Taiwan*

MRAM is emerging as the leading candidate among various embedded memory technologies. STT-MRAM, with its scalable nature for high density, faster writing speed, and robust endurance, stands out as an ideal candidate for the rigorous demands of the automotive sector, particularly for Over-The-Air (OTA) updates towards autonomous driving future. This talk will address the ongoing technical challenges and necessary MTJ device breakthroughs required to achieve an reliable STT-MRAM solution that meets the stringent standards of the automotive industry. With implementing STT-MRAM in automotive production, underlinin its key role in the development of advanced automotive architectures, and its impact on the evolution of Software Defined Vehicle (SDV).

BB-02. About Multiphysic Modelling of High-Speed Electrical Machines for Elctric Powertrains.
L. Dahnoun[1], J. Fontchastagner[1] and *N. Takorabet*[1] *1. GREEN, Université de Lorraine, Nancy, France*

With the electrification of transportation systems, the race for the most efficient powertrains has become a major challenge for the transportation industry. The criterion of the highest power-to-weight ratio has become a real challenge especially for aeronautics transportation systems [1]. Under these conditions, electrical machines are subject to considerable mechanical and thermal stress. It is no longer possible to design an electrical machine without taking thermal and mechanical aspects into account, in addition to power supply aspects [2]. High-speed electrical machines present significant mechanical and thermal issues, in addition to strong electromagnetic stresses due to the high frequency of the power supply. Increased peripheral speeds lead to mechanical stresses on rotor components, such as the sleeves that maintain the permanent magnet on the rotor, or the cage bars in induction machines [2, 3]. High speeds lead designers to choose longer rotors to avoid high peripheral speeds. However, there are problems with the vibration of rotating structures, which affects the natural mechanical frequencies [4, 5]. Increasing power density in high-speed machines increases heat generation due to electrical, magnetic and mechanical losses. Characterizing these losses and extracting this heat remains a challenge [6,7]. All these contradictory physical aspects constitute a major challenge for multiphysics modeling and the design of electric machines with high power density and high operating speeds, to meet the future requirements of high-performance electric transport systems [8]. This paper will discuss a way of pre-designing electrical machines using coupled analytical models: magnetic-mechanical-thermal. Techniques of resolution of Partial Differential Equations are discussed according to the particularity of each physics. On Fig.1 and Fig.2 we can see how simplified analytical models are built-up for thermal and electromagnetic aspects. Under the assumed hypotheses, the models are validated by finite element codes. Thanks to their fastness, these multiphysic analytical models offer a first pre-optimization and estimation of design parameters of the machine, which can then be refined by finer numerical finite element models. Emphasis will be placed on induction machines, which are gaining renewed interest in the context of the growing use of magnet-free machines by automotive industry. For a given case study of high-speed machines, the multiphysics model is run to find optimal design that reduces the total mass of the machine that fulfills electrical, thermal and mechanical constraints. The optimized machine is modeled again with finite element codes (Electromagnetic, thermal and mechanical) so that the validation cans be confirmed. The approach presented in this paper can also be applied for permanent magnet machines where only electromagnetic model is adapted to account for the behavior of such machines with the presence of magnets in the moving rotor.

[1] D. Golovanov, L. Papini, D. Gerada, Z. Xu, C. Gerada, Multidomain Optimization of High-Power-Density PM Electrical Machines for System Architecture Selection, IEEE Transactions on Industrial Electronics, vol. 65, no. 7 2018 [2] A. Binder, T. Schneider, and M. Klohr, "Fixation of buried and surface-mounted magnets in high-speed permanent-magnet synchronous machines," IEEE Transactions on Industry Applications, vol. 42, no. 4, pp. 1031–1037, Jul. 2006, doi: 10.1109/TIA.2006.876072. [3] L. Dahnoun, T. Marcand, R. Rahouadj, C. Laurent, B. Dagusé, C-H. Bonnard, J. Fontchastagner, S. Mezani, N. Takorabet, Comparison Of Methods For Evaluating Mechanical Stress In The Rotor Of High-Speed Machines, 2022 International Conference on Electrical Machines ICEM, September 2022, Valencia, Spain [4] M. L. James, Vibration of Mechanical and Structural Systems: With Microcomputer Applications. Harper & Row, 1989. [5] Friswell, Michael & Penny, John & Garvey, Seamus & Lees, Arthur. (2010). Dynamics of Rotating Machines. 10.1017/CBO9780511780509. [6] Madhavan, S., Devdatta P B, R., Konda, Y.R. et al. Thermal management analyses of induction motor through the combination of air-cooling and an integrated water-cooling system. Sci Rep 13, 10125 (2023). https://doi.org/10.1038/s41598-023-36989-2. [7] A. Bourgault, O. Taqavi, Z. Li, G. Byczynski and N. C. Kar, "Advanced Lumped Parameter Thermal Network for Modeling of Cooling Solutions in Electric Vehicle Motor Applications," in IEEE Transactions on Magnetics, doi: 10.1109/TMAG.2024.3416096 [8] Z. Huang and J. Fang, "Multiphysics Design and Optimization of High-Speed Permanent-Magnet Electrical Machines for Air Blower Applications," in IEEE Transactions on Industrial Electronics, vol. 63, no. 5, pp. 2766-2774, May 2016, doi: 10.1109/TIE.2016.2518121

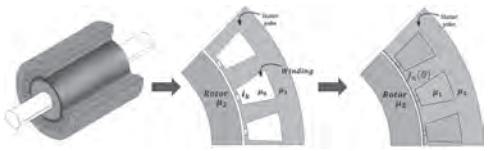

Fig.1. From physical device (Induction motor) to simplified analytical electromagnetic model

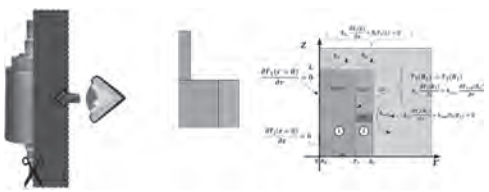

Fig.2. From physical device (Induction motor) to simplified analytical thermal model

BB-03. An adaptive hybrid magnetic sensing technology for enhanced electric vehicle applications. *M. Lai*[1] *1. iSentek, New Taipei City, Taiwan*

Electric vehicle (EV) applications require magnetic sensing technology with a broad dynamic sensing range and high sensitivity, which is crucial for accurately detecting current levels ranging from 10 mA to 600 A. Selecting a single magnetic sensing technology for such a wide range and high sensitivity is very challenging. This article suggests employing multiple magnetic sensing technologies as an alternate approach to fulfill the wide dynamic operating range and high sensitivity requirements for EVs. Challenges encompass expanding the linear sensing range, sensitivity, and maintaining the compact dimension. The semiconductor industry faces a crucial challenge of integrating diverse magnetic sensing technologies with ASICs. The present invention focuses on a design that integrates an adaptable algorithm with hybrid magnetic sensing components to attain a broad operating range and remarkable sensitivity. Further development involves integrating these heterogeneous magnetic sensing technologies into semiconductor-based solutions. These advancements elevate adaptive hybrid magnetic sensing technology, enhancing the performance and reliability of EV applications.

M. -H. Lai and K. -S. Chang, "AI Sensor Applications in Edge Computing," in IEEE Nanotechnology Magazine, vol. 17, no. 6, pp. 23-28, Dec. 2023. V. S. Luong *et al*., "Planarization, Fabrication, and Characterization of Three-Dimensional Magnetic Field Sensors," in *IEEE Transactions on Nanotechnology*, vol. 17, no. 1, pp. 11-25, Jan. 2018.

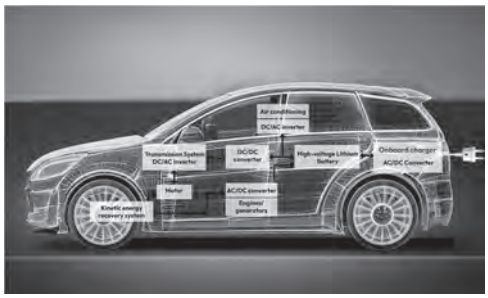

Fig. 1: This image offers detailed explanations of the use of magnetic sensing in electric vehicles.

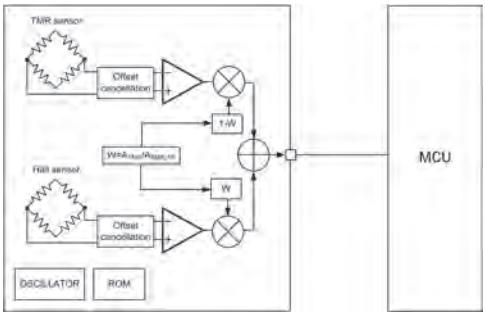

Fig. 2 illustrates the hybrid sensor structure with a built-in weighting function.

BB-04. High Frequency Magnetic Design for EV Fast Charging. *A. Knight*[1] *1. Electrical and Software Engineerign, University of Calgary, Calgary, AB, Canada*

Soft magnetic materials are playing an increasingly critical role in power electronic conversion for electric vehicles. At lower power levels, planar magnetics in high frequency transformers are a critical component in both DC-DC and AC-DC conversion for charging and on board power conditioning [1] [2]. With higher frequency high power switching made possible by wide bandgap devices, the need for high frequency magnetic components is growing rapidly [3]. Applications include filtering of conventional converter topologies, and the enabling of novel topologies. Key goals of these approaches include reduced component size and weight, reduced losses and thermal management as the converter volumes fall and heat loss becomes more concentrated. This presentation will review recent advances in power electronic circuits for electric vehicles that have been enabled by soft magnetic materials, advances in the magnetic devices, and challenges for future development.

[1] M. A. H. Rafi and J. Bauman, "A Comprehensive Review of DC Fast-Charging Stations With Energy Storage: Architectures, Power Converters, and Analysis," in *IEEE Transactions on Transportation Electrification*, vol. 7, no. 2, pp. 345-368, June 2021, doi: 10.1109/TTE.2020.301574 [2] S. Mukherjee and P. Barbosa, "Design and Optimization of an Integrated Resonant Inductor With High-Frequency Transformer for Wide Gain Range DC–DC Resonant Converters in Electric Vehicle Charging Applications," in *IEEE Transactions on Power Electronics*, vol. 38, no. 5, pp. 6380-6394, May 2023, doi: 10.1109/TPEL.2023.3243807 [3] S. Li, S. Lu and C. C. Mi, "Revolution of Electric Vehicle Charging Technologies Accelerated by Wide Bandgap Devices," in *Proceedings of the IEEE*, vol. 109, no. 6, pp. 985-1003, June 2021, doi: 10.1109/JPROC.2021.3071977

BB-05. Materials and Considerations for Motors to Support Efficient Transportation. *L.H. Lewis*[1] *1. Northeastern University, Boston, MA, United States*

Efficient and affordable electrification of the transportation sector, encompassing not only passenger cars but also larger transport vehicles, trains, aircraft, and ocean vessels, is an immense but highly impactful challenge.[1] An integral component of electric propulsion systems, the electric motor/generator, exhibits a variety of advantages and disadvantages that depend on the specific type and arrangement of magnets contained within. The overarching goal to minimize motor weight and size while maximizing performance requires the use of the highest-grade magnets available to manufacturers. To this end, this presentation provides an overview of existing high-performance magnets and discusses motivation and progress regarding the development of next-generation magnets necessary to support the projected immense growth in electrified mobility.

[1]. Fahimi, B., Lewis, L. H., Miller, J. M., Pekarek, S. D., Boldea, I., Ozpineci, B., ... & Patel, D. D. (2023). Automotive Electric Propulsion Systems: A Technology Outlook. *IEEE Transactions on Transportation Electrification*.

Session BC
SPIN-ORBITRONICS II: CHIRAL DEPENDENCE, QUANTUM SPIN TRANSFER AND UNCONVENTIONAL TORQUES

Yang Lv, Chair
University of Minnesota, Minneapolis, MN, United States

INVITED PAPER

BC-01. Chiral-induced Unidirectional Spin-to-charge Conversion.
A. Wittmann[1] *1. JGU Mainz, Mainz, Germany*

The observation of spin-dependent transmission of electrons through chiral molecules has led to the discovery of chiral-induced spin selectivity. [1] The remarkably high efficiency of the spin polarizing effect in chiral molecules has recently gained significant interest due to the high potential for novel sustainable hybrid chiral molecule magnetic applications. [2] However, the fundamental mechanisms underlying the chiral-induced phenomena at the hybrid molecule-metal interface remain to be understood fully. In our work, we explore the impact of chirality on spin angular momentum in hybrid metal/chiral molecule thin film heterostructures. For this, we inject a pure spin current from a ferromagnetic insulator at ferromagnetic resonance and investigate the effective interfacial spin-orbit coupling at the hybrid chiral interface. Notably, we observe a chiral-induced unidirectionality in the spin-to-charge conversion. [3] Furthermore, angle-dependent measurements reveal that the spin selectivity is maximum when the spin angular momentum is aligned with the chiral axis. Our findings validate the central role of spin angular momentum for the chiral-induced spin selectivity effect, paving the path toward three-dimensional functionalization of hybrid molecule-metal devices via chirality.

References [1] R. Naaman et al., Nat. Rev. Chem. 3, 250 (2019). [2] M. Ozeri, AW et al., J. Phys. Chem. Lett. 14, 4941 (2023). [3] A. Moharana, AW et al., arXiv:2402.19246 (2024)

CONTRIBUTED PAPERS

BC-02. Deterministic Switching of Noncentrosymmetric, Ferromagnetic Weyl Semimetals with Higher-order Spin-orbit Torque.
N. Fokkens[1], J. Shi[1] and F. Xue[1] *1. Physics, University of Alabama at Birmingham, Birmingham, AL, United States*

The unique topological effect and symmetry breaking of rare earth Weyl semimetals present substantial potential in spintronics applications. A particular example of such a material is PrAlGe, which is a noncentrosymmetric, ferromagnetic material.[1][2] The inversion symmetry breaking allows for the Weyl nodes to be stabilized and also allows direct control of magnetization order via spin-orbit torque. The C_4 rotational symmetry and two in-plane mirrors restrict the form of spin orbit torque and we find that not only the conventional results but new terms arise at the second order using conventional Cartesian methods. To illustrate the nature of high-order terms, we expand all orders of spin orbit torque in vector spherical harmonics basis [3][4]. The conventional view is that one in-plane mirror has to be broken to allow perpendicular switching because of the presence of a fixed point in the equator. However, we find that deterministic switching is possible when the higher order terms are comparable to lowest order terms, which indicates the importance of including these higher order terms to understand the magnetization dynamics in topological materials. In Weyl semimetals, spin-orbit coupling cannot be treated perturbatively near the Weyl points, thus resulting in plausible large higher-order terms that are also higher-order in spin-orbit coupling strength. This motivates us to perform first-principles calculations of spin-orbit torque in Weyl ferromagnet PrAlGe and resulting spin dynamics. The combination of these studies result in an understanding of the material's quantitative and qualitative spin orbit torque response, while also studying the interplay of topology in the presence of spin orbit torques.

[1] Chang G.,Singh, B., et al., Phys. Rev. B 97, 041104(R) (2018) [2] Sanchez, D. S., Chang, G., Belopolski, I., et al., Nature Communications, 10.1038 (2020) [3] Belashchenko, Kovalev, and Schilfgaarde, Phys. Rev. B 108, 020407 (2020) [4] Xue, F., Stiles, M. and Haney, P., Phys. Rev. B 108, 144422 (2023)

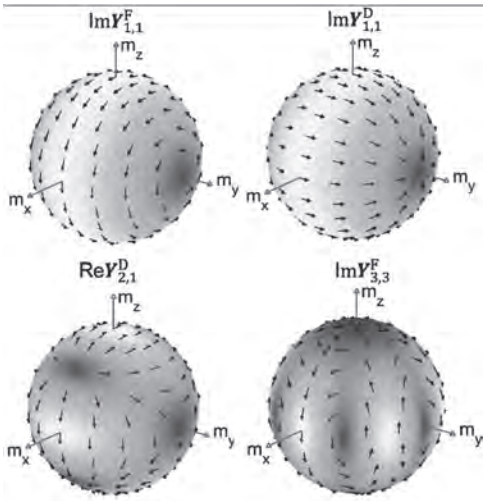

Fig. 1: Schematics of a few symmetry-allowed spin-orbit torques in tetragonal PrAlGe: conventional fieldlike and dampinglike (ImYF11\propto yxm, ImYD11\propto mx(yxm)) and two symmetry allowed higher order terms (ReYD21, IMYF33) used to study potential of deterministic switching

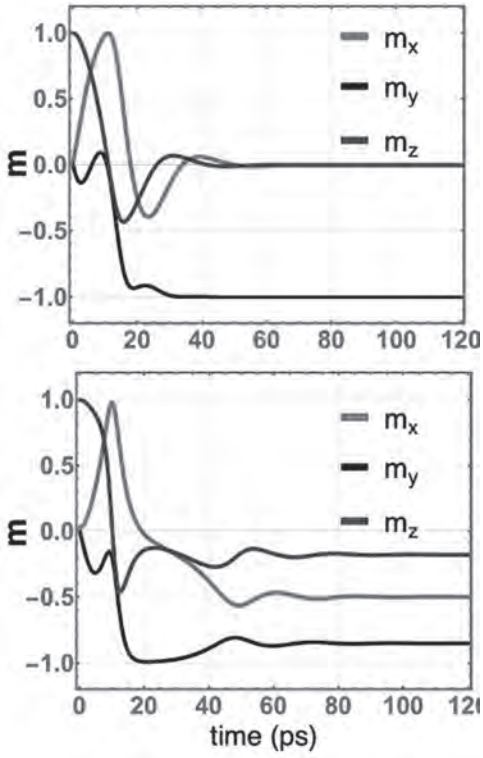

Fig. 2: Comparison of resulting magnetization at different combinations of terms. A smaller ratio (top) of higher order terms results in nondeterministic switching whereas a larger ratio (bottom) results in deterministic switching.

BC-03. Plasmonics for low energy and ultrafast creation of magnetic topological structures. *R. Sbiaa*[1], W.Z. Al Saidi[1], Y. Dusch[2] and N. Tiercelin[2] *1. Physics, Sultan Qaboos University, Al-Khoud, Oman; 2. CNRS, Centrale Lille, UMR 8520, IEMN, University of Lille, Lille, France*

Magnetic skyrmions, chiral nanoscale spin structures, exhibit topological protection [1] and hold promise for low-power, high-density memory devices and Neuromorphic computing. Their small size and stability make them attractive for various applications, and recent advancements have demonstrated their creation, displacement, and annihilation using magnetic fields [2], spin transfer torque [3], spin-orbit torque [4] and ultrafast heating pulses [5]. In this study, we demonstrate the possibility for skyrmion creation in magnetic thin films by plasmonic effect using nanoparticles (NPs). Although the laser used for the plasmonic effect has a large spatial covered due to the diffraction limit, skyrmions can be created only from the NPs deposited on the magnetic layer surface, leading to an accuracy in the created skyrmions positions. Fig. 1, shows the resonance wavelength dependence on the gold NP size. The inset of Fig. 1 is the cross-sectional view of the NP deposited on a 1 nm thick insulator. The thickness of the magnetic layer was fixed to 10 nm and protected against oxidation by 1 nm Pt thin film. Another advantage of this method is that the skyrmion is formed within a few tens of picoseconds as can be shown in Fig. 2. Although the creation time (t_{cr}) is exponentially reduced with the NP size, skyrmion within 60 ps can be created using NP with 25 nm radius. Details on the effect of the plasmonic resonance conditions and materials properties will be discussed and the efficiency of the plasmonic effect in creating ultrafast nanoscale skyrmions and skyrmioniums with low energy will be presented.

[1] O. Boulle *et al.*, Nature Nanotech. 11, 449 (2016). [2] A. Casiraghi *et al.*, Communications Physics 2, 145 (2019). [3] J. Masell *et al.*, Phys. Rev. B 101, 214428 (2020). [4] S. Woo *et al.*, Nature comm. 8, 15573 (2017). [5] S. G. Je *et al.*, Nano letters 18, 7362-7371 (2018).

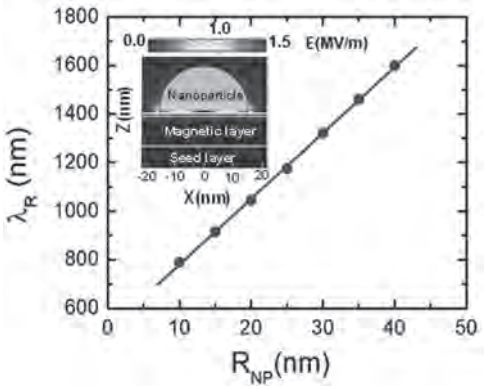

Resonance wavelength as a function of the radius of gold nanoparticle. Inset is the cross-section view of the investigated structure. The color code is the electric field distribution.

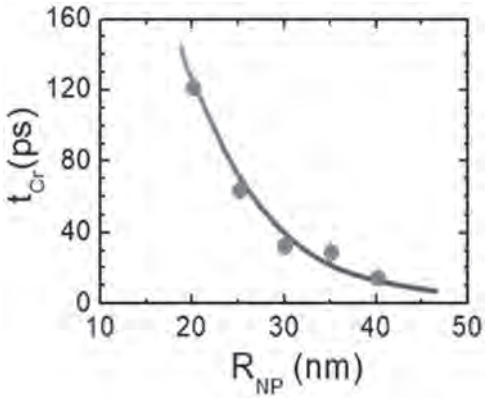

The time of the skyrmion creation versus the radius of the gold nanoparticle.

BC-04. Coexistence of Unconventional Spin Hall Effect and Antisymmetric Planar Hall Effect in IrO_2. *Y. Yang*[1], S. Nair[1], Y. Fan[1], Y. Chen[1], J. Qi[1], S. Lee[1], T. Low[1], B. Jalan[1] and J. Wang[1] *1. University of Minnesota, Minneapolis, MN, United States*

Unconventional spin Hall effect (USHE) in low-symmetry materials has attracted much attention in the spintronics field due to its potential in the reduction of energy consumption for logic or memory devices [1-3]. Recently, antisymmetric planar Hall effect (APHE) was discovered in rutile RuO_2 and IrO_2 (101) thin films, arising from the Lorentz force allowed by the symmetry [4]. Here, we observe the coexistence of USHE and APHE in IrO_2 (111) films by spin-torque ferromagnetic resonance (ST-FMR) and harmonic Hall measurements, respectively. Symmetric planar Hall effect (SPHE) with smaller magnitude is also observed along with the dominant APHE. The temperature dependence of SPHE and APHE is drastically different, suggesting different origins of the two components, which are the Dirac semimetal property and symmetry-induced Lorentz force, respectively. Our results indicate the potential interplay between USHE and APHE, opening the route for further understanding of the two effects and the exploration of new materials with the two features.

[1] D. MacNeill *et al.*, *Nature Physics,* vol. 13, pp. 300-305 (2017). [2] D. J. P. de Sousa *et al., Physical Review Applied,* vol. 18, p. 054020 (2022). [3] M. Patton *et al.*, *Advanced Materials,* vol. 35, no. 39, p. 2301608 (2023). [4] Y. Cui *et al.*, "Antisymmetric planar Hall effect in rutile oxide films induced by the Lorentz force", *Science Bulletin* (2024).

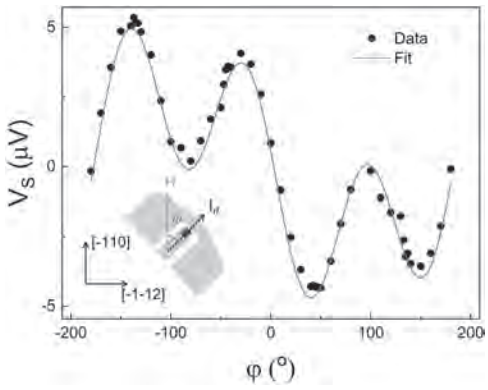

Fig. 1. Angular dependence of ST-FMR of IrO_2 (111) / CoFeB heterostructure, showing the existence of unconventional spin components.

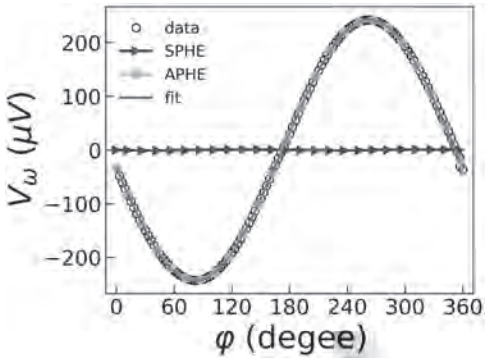

Fig. 2. Hall voltage of IrO_2 (111) thin film fitted as the sum of symmetric (SPHE) and antisymmetric (APHE) planar Hall components.

BC-05. Current-Induced Circular Dichroism on Metallic Surfaces: A First-Principles Study. *F. Mahfouzi*[1], P. Haney[1] and M. Stiles[1]
1. PML, National Institute of Standards and Technology, Gaithersburg, MD, United States

Circular dichroism, which is the difference in a system's response to left-hand and right-hand circularly polarized light can be used to characterize magnetic order. We use ab-initio calculations to investigate the current-induced optical response and orbital accumulation at the surfaces of metallic films. These are related by a sum rule that relates the circular dichroic absorption integrated over frequency to the gauge-invariant self-rotation contribution to the orbital magnetization, denoted by M_{SR}. In typical ferromagnets, M_{SR} is a good approximation to the total orbital magnetization. We compute the current-induced M_{SR} for a Pt thin film and compare it to the current-induced orbital accumulation calculated with the atom-centered approximation (ACA). We find significant differences: the size of M_{SR} is generally larger than the ACA orbital magnetization by an order of magnitude and includes substantial finite-size effects. The differences between the two quantities caution against interpreting optical measurements with models utilizing the ACA. Finally, we compute the total M_{SR} and ACA orbital magnetization accumulation as a function of layer thickness. For both quantities, the length scale at which the total surface accumulation saturates is on the order of the mean free path and longer than the length scale of their spatial profiles. Fig. 1 shows the current induced orbital accumulation for the self-rotating $\alpha_{SR}^{yx}=\delta M_{SR}^{y}/eE_x^{bias}$ and the ACA type $\alpha_{ACA}^{yx}=\delta M_{ACA}^{y}/eE_x^{bias}$ summed over half of the Pt film. The various curves represent different onsite random potential strengths with normal distributions. We observe that regardless of the impurity strength, both types of orbital accumulations increase monotonically with film thickness and decrease as impurity strength increases.

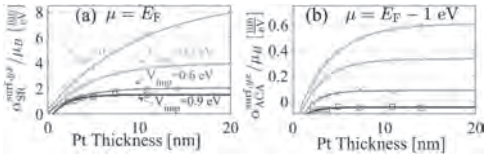

Figure 1. (a) Frequency-integrated, current-induced optical dichroic absorption versus Pt film thickness for various impurity strengths. (b) Current induced orbital accumulation summed over half of the film versus Pt film thickness at a shifted chemical potential.

BC-06. A spin-orbit torque knob to tailor stochasticity for physically secured applications. *M. Yang*[1] and C. Yang[1] *1. Materials Science and Engineering, National Yang Ming Chiao Tung University, Hsinchu, Taiwan*

The deterministic switching of spin-orbit torque (SOT) memory has long been the primary challenge for implementation. Conversely, stochastic switching has recently sparked significant interest for physically secured applications. This study investigated the effects of an external field (Hx) applied to break the SOT symmetry for deterministic switching in a Pt/Co bilayer with perpendicular anisotropy. This external field served as a tuning mechanism to adjust the stochasticity at the intermediate state during SOT switching. It was observed that moderate Hx could lead to a substantial variation in electrical output during the repeating write/read operations. In contrast, a large Hx enabled precise control over the intermediate states of the Pt/Co bilayer, effectively functioning as a memristor. The stochasticity derived from small Hx resulting from the dynamics of dendritic domain wall propagation during SOT switching. Herein, the oblique domain spiking from the initially reversed domain was notably influenced by the transverse component of SOT. Increasing Hx suppressed this oblique dendritic domain growth, allowing for controllable domain propagation and reducing stochasticity. By utilizing Hx as an external knob to tailor the stochasticity at the intermediate state, the high stochastic state can be employed as an ideal entropy source for an SOT-based random number generator.

1. Yi Cao et al., iScience 23, 101614 (2020). 2. Guoqiang Yu et al., Scientific Reports 6, 23956 (2016). 3. Young-Wan Oh et al., Nature Nanotechnology 11, 878 (2016). 4. Shunsuke Fukami et al., Nature Materials 15, 535 (2016). 5. Xiaomi Chen et al., AIP Advances 13, 105113 (2023). 6. Ssu-Yuan Wang et al., Advanced Electronic Materials 9, 2300472 (2023)

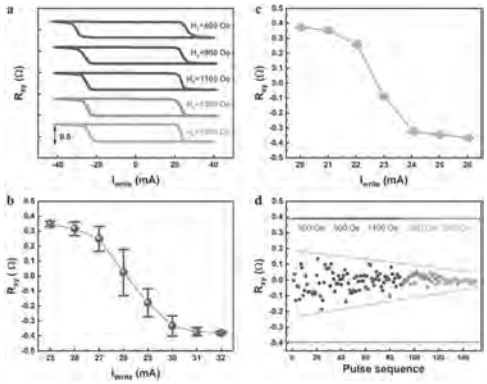

BC-07. Large Interfacial Rashba Torques in Atomically Thin Co|Al Systems. *N. Sebe*[1], S. Krishnia[2], S. Mallick[3], Y. Sassi[1], S. Collin[1], T. Denneulin[4], A. Kovács[4], R.E. Dunin-Borkowski[4], A. Fert[1], J. George[1], V. Cros[1] and H. Jaffrès[1] *1. Laboratoire Albert Fert, Palaiseau, France; 2. Institute of Physics, Johannes Gutenberg University Mainz, Mainz, Germany; 3. SRMIST, Chennai, India; 4. Forschungszentrum Julich, Jülich, Germany*

The developpement of SOT-MRAM requires higher energy efficiency in the control of magnetization dynamics. Spin Hall effects (SHE, Spin-Rashba) were the most investigated in that purpose. However, a new class of effects has risen interest: orbital effects leading to accumulation of angular momentum in orbital form. Contrary to spin effects, orbital Hall effect and orbital Rashba effect do not derive from spin-orbit coupling. Therefore, they are expected to occur in light metals. Our study examines to what extent a light metallic layer of Al can improve the spin-orbit torques (SOT) applied on an adjacent Co layer. In Ta|Pt|Co|Al|Pt multilayers, showing strong Perpendicular Magnetic Anisotropy (PMA) with ultrathin Co, we have measured the SOT for different thicknesses of the layers. Compared to reference samples where Al is replaced by Cu, we found large torques increase as well as a change of their geometry: the field-like component becomes prominent. We have developed a model explaining the experimental data by involving a strong (orbital) Rashba effect at the Co|Al interface. Still, SOT-MRAM devices, are composed of CoFeB alloys instead of sole Co. Hence we have grown stacks with CoFeB as ferromagnet layer. But those samples did not show PMA. In order to recover the effects measured with Co, we have sputtered dusting layers of cobalt at the interfaces of the ferromagnetic layer. Those series of samples (Ta|Pt|Co(0,3nm)|CoFeB|Al|Pt and Ta|Pt|Co(0,3nm)|CoFeB|Co(0,2nm)|Al|Pt) had PMA, though with a reduced anisotropy field than sole Co. Moreover, large SOT was also measured in those samples. Moreover, we measured current induced magnetization switching in our samples. A reduction of the critical currents was observed with the insertion of an Al layer. Still, since the Rashba effect promotes more the field-like torque than the damping-like, this reduction is observed slightly smaller than expected from the torque measurements.

D. Go and H.-W. Lee, "Orbital torque: Torque generation by orbital current injection," Phys. Rev. Res., vol. 2, p. 013177, Feb 2020. J. Kim, D. Go, et al, "Nontrivial torque generation by orbital angular momentum injection in ferromagnetic-metal/cu/al 2 o 3 trilayers," Physical Review B, vol. 103, no. 2, p. L020407, 2021. S. Ding, A. Ross, et al., "Harnessing orbital-to-spin conversion of interfacial orbital currents for efficient spin-orbit torques," Physical review letters, vol. 125, no. 17, p. 177201, 2020. S. Krishnia, ..., Nicolas Sebe, et al. "Large Interfacial Rashba Interaction Generating Strong Spin–Orbit Torques in Atomically Thin Metallic Heterostructures" Nano Letters 2023 *23* (15), 6785-6791

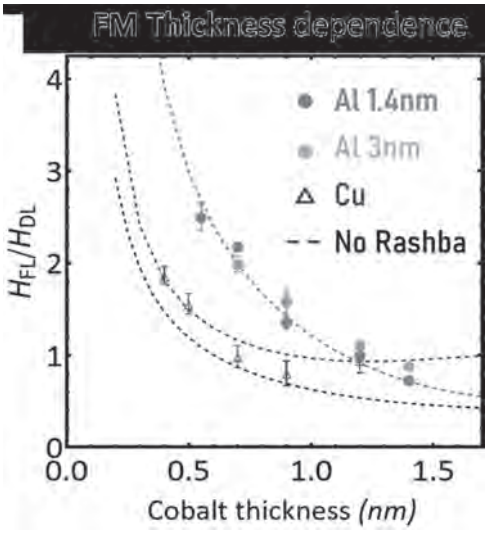

Field-like over damping-like ratio as a function of Co thickness. The large values of the ratio are a signature of Rashba effect.

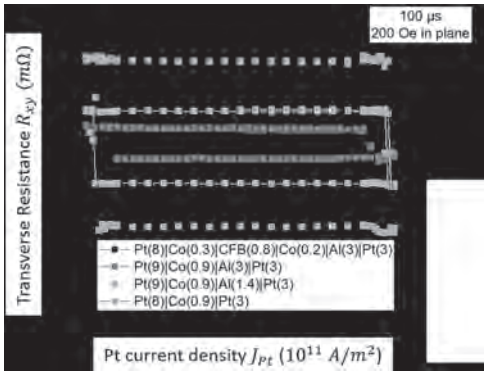

Current induced magnetisation switching cycles for different multilayers investigated.

BC-08. Design of an ultra-low magnetic field sensor based on spin Hall magnetoresistance. M. Kuepferling[1], W. Skowronski[2], E. Losero[1], P. Wisniowski[2], *A. Magni*[1], V. Basso[1], J. Langer[3] and B. Ocker[3] *1. INRiM, Torino, Italy; 2. AGH University of Science and Technology, Krakow, Poland; 3. Singulus Technologies AG, Kahl am Main, Germany*

Spin orbit torque (SOT) sensors are considered a low power alternative to conventional magnetoresistive sensors, having simpler device structure due to straightforward ways for sensor linearization or offset elimination [1]. Most commonly SOT is induced by the spin Hall effect, generated in heavy metal (HM)/ferromagnetic metal (FM) heterostructures. As an example, a spin Hall magnetoresistance (SMR) sensor with Wheatstone bridge design was recently shown to have an excellent detectivity (1nT/Hz$^{1/2}$) [2]. Ultra-low field (<nT) detection is becoming increasingly important (e.g. biomedical applications) with extremely challenging goals like detectivities down to 10fT/Hz$^{1/2}$ [3]. Here a Wheatstone bridge SMR sensor prototype was prepared, exploiting the in-plane anisotropy of FeCoB additionally to the SOT from HM for linearization. The bilayers made of HM wedge shaped films (Pt, Ta, W, Pt-Ti; 5-10nm) and a FM layer ($Fe_{60}Co_{20}B_{20}$; 2nm) were prepared using Singulus Timaris cluster tool system on oxidized Si wafers. The multilayers were patterned using optical lithography and ion-beam etching (see Fig. 1). An SMR of 0.3 and 0.08%, according to the HM material, was determined. The wedge design allows for a full characterization of the parameters in the spin diffusion model [4,5]. The different magnetoresistance contributions are distinguished by angle dependent measurements [6]. The full characterization of parameters and a theoretical analysis performed

by a thermodynamic model [7] allows the determination of the principal parameters influencing the performance and the power consumption. This will help to optimize the sensor design in terms of materials choice, layout, dimensions and film thickness. This research has been funded by the Italian Ministry of University and Research (MUR), "NEXT- GENERATION METROLOGY", FOE 2023 (Ministry Decree n. 789/2023). W.S. and P.W. acknowledge the program "Excellence initiative research university" for the AGH University of Krakow.

[1] Yihong Wu et al., J. Appl. Phys. 129, 060902 (2021); DOI: 10.1063/5.0039926 [2] Yanjun Xu et al., Appl. Phys. Lett. 115, 182406 (2019); DOI: 10.1063/1.5127838 [3] Chao Zheng et al., IEEE Trans Mag. 55 (2019); DOI: 10.1109/TMAG.2019.2896036 [4] Yan-Ting Liu et al Phys. Rev. Appl. 13, (2020), DOI: 10.1103/PhysRevApplied.13.044032 [5] A. Magni et al., IEEE Trans. Mag. 58, (2021), DOI: 10.1109/tmag.2021.3084866 [6] M. Althammer et al. Phys.Rev. B 87 (2013); DOI:10.1103/PhysRevB.87.224401 [7] V. Basso et al., J.Phys.D: Appl. Phys. 51, (2018), DOI:10.1088/1361-6463/aabc4c

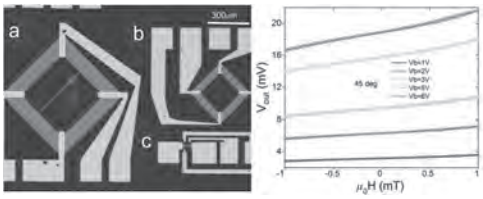

Fig.1: (Left) Wheatstone bridge sensors: stripes of a) 600x100μm and b) 300x50μm; c) Hall bar for the characterization of the SOT parameters (70x10μm). (Right) Output voltage as a function of the applied magnetic field at different bias voltages.

BC-10. Efficient magnetization switching and non-reciprocal magnon transport via orbital currents. *S. Krishnia*[1], O. Ledesma[1], R. Gupta[1], E. Galindez Ruales[1], F. Kammerbauer[1], A. Bose[1], C. Bouard[2], S. Martin[2], M. Drouard[2], D. Go[1], G. Jakob[1], Y. Mokrousov[1] and M. Kläui[1] *1. Institut für Physik, Johannes Gutenberg-Universität Mainz, Mainz, Germany; 2. Antaios, Meylan, France*

Spin-orbit interaction in metals and its ability to generate spin-currents have been a hallmark of spintronics over the last decade[1]. Beyond its fundamental interest, manipulating magnetization via the transfer of spin angular momentum has proven to be energy efficient for spin-based memory (e.g., SOT-MRAM[2]), skyrmion dynamics[3] and computing devices[4]. Conventionally, large spin currents have been achieved through two main charge-to-spin conversion mechanisms: the spin Hall effect and the Rashba-Edelstein effect, both intrinsically linked to strong spin-orbit coupling[1]. However, recent theories suggest that an electric current can also induce a transverse flow of orbital angular momentum, i.e., orbital current, in metals and/or at interfaces via the orbital Hall effect (OHE) and the orbital Rashba-Edelstein effect (OREE), even without a need of spin-orbit coupling[5]. The orbital current can then diffuse into adjacent metals and/or ferromagnets, exerting torques on the magnetic layer and significantly improving efficiencies[6]. Notably, we demonstrate that the orbital current generated at Cu/CuOx[7] and Co/Al[8] interfaces, enhances the torque efficiency by a factor of more than 10. We integrate the orbital Hall material Ru[9] into a judiciously chosen out-of-plane magnetic layer compatible with CMOS technology to perform the magnetization switching of 100 nm diameter magnetic memory bits for MRAM application. Our devices show a 60% reduction in power consumption, highlighting a significant improvement in magnetization switching efficiency in orbital current-based technologies[10]. Finally, we investigated the role of orbital current in magnon transport in an insulating magnet, YIG. We show non-reciprocal magnon generation and detection by adding Ru as a source of direct and inverse OHE. In particular, the generation of magnons via the combination of the spin Hall effect and OHE and their detection via the inverse spin Hall effect is 70% more efficient than the inverse process (see Fig. 1)[11].

1. A. Manchon *et al., Rev. Mod. Phys.* 91, 035004 (2019). 2. E. Grimaldi *et al., Nat. Nanotechnol.* 15, 111 (2020). 3. S. Woo *et al*., *Nat. Mater.* 15, 501 (2016). 4. K. Raab *et al., Nat. Commun.* 13, 6982 (2022). 5. D. Go et al., *Phys. Rev. Lett.* 121, 086602 (2018). 6. D. Go *et al., EPL* 135, 37001 (2021). 7. S. Ding *et al*., *Phys. Rev. Lett.* 125, 177201 (2020). 8. S. Krishnia *et al., Nano Lett.* 23, 6785 (2023). 9. A. Bose *et al., Phys. Rev. B* 107, 134423 (2023). 10. R. Gupta *et al*., *arXiv*:2404.02821 (2024). 11. O. Ledesma *et al.,* under review

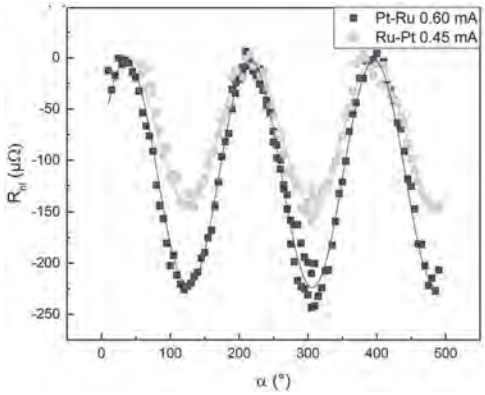

Comparison of the non-local resistance as a function of the angle between the injected current and magnetization direction, when current is injected into Pt (Ru) wire and voltage is detected in Ru (Pt) wire, depicted blue (green).

BC-11. Unconventional Spin-Orbit torques in Mn_3Pt. *R. Klause*[1] and A. Hoffmann[1] *1. Materials Science and Engineering and Materials Research Laboratory, University of Illinois Urbana Champaign, Urbana, IL, United States*

The spin-Hall effect is an efficient way to generate a spin accumulation from an electrical current, which can exert a torque on an adjacent ferromagnetic layer. For conventional spin-torque geometries in heavy metal/ferromagnet bilayers, the electrical current, spin current, and spin polarization are mutually perpendicular allowing only a magnetization collinear to the spin polarization to be switched efficiently and without applying an external magnetic field. Mn_3Pt is a metallic non-collinear antiferromagnet, that can give rise to unconventional spin-orbit torques due to its magnetic symmetry breaking. At high temperatures the magnetic phase transitions to a collinear antiferromagnet, where unconventional torques are not expected. Here we use angle dependent spin-torque ferromagnetic resonance to show that epitaxial Mn_3Pt thin films give rise to spin accumulations with spin polarization along the current direction, when current is applied along specific crystal directions. With current along 0°, 45°, and 90° with respect to the [100] crystal direction we only measure conventional torques, while with current along 15° and 30° we measure positive and along 60° and 75° we measure negative unconventional torques. Temperature dependent STFMR measurements will reveal whether the unconventional torques originate from the magnetic structure. This work was supported as part of Quantum Materials for Energy Efficient Neuromorphic Computing (Q-MEEN-C), an Energy Frontier Research Center funded by DOE BES under Award No. DE-SC0019273.

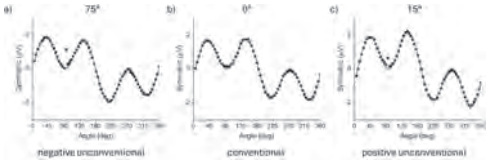

Symmetric component of the mixing voltage as a function of the angle between the current and magnetic field for three different current directions (75° (a), 0° (b), and 15° (c), where 0° corresponds to the [100] Mn_3Pt crystal direction). Unconventional torques with opposite sign are observed along 75° and 15°, while only conventional torques are observed along 0°.

BC-12. In Search of Quantum Spin Transfer in Spin-Orbit Bilayers. *G.T. Street*[1] and S. Emori[1] *1. Physics, Virginia Tech, Blacksburg, VA, United States*

Spins (s) injected into a ferromagnet generate a spin-transfer torque that can either enhance or reduce the thermal fluctuations of the magnetization (M) (Fig. 1a). At low temperatures with minimal fluctuations, no spin-transfer effects are expected with collinear s and M. However, recent studies predict "quantum spin transfer" via entanglement between collinear s and M [1, 2]. Here, we search for a DC transport signature of quantum spin transfer in a typical spin-orbit bilayer (Fig. 1c), where a current in Pt pumps *y*-polarized spins into y-magnetized permalloy. At room temperature, the DC resistance is mostly quadratic with current (Fig. 2a) as expected from Joule heating. Subtracting the quadratic background, we find a residual resistance monotonic with current and its slope reversing with the field polarity (Fig. 2c). This observation is consistent with the spin-orbit torque tuning the average y-component of M (captured by anisotropic magnetoresistance) by modulating the thermal fluctuations of M (Fig. 1a). At 7 K, the resistance response appears similarly quadratic (Fig. 2b). However, subtracting the quadratic background reveals a qualitatively distinct outcome: a pronounced V-shaped trend in residual resistance vs current, invariant with the field polarity (Fig 2d). This observation aligns with current- generated non-thermalized phonons at cryogenic temperatures [3], but not with quantum spin transfer whose electrical response should vary with field polarity [1]. Our work unveils coexisting fundamental transport signatures in spin-orbit nanostructures, which may find application in cryogenic devices.

[1] A. Zholud, R. Freeman, R. Cao, A. Srivastava, and S. Urazhdin, Phys. Rev. Lett., Vol. 119, p. 257201 (2017). [2] P. Mondal, U. Bajpai, M. D. Petrović, P. Plecháč, and B. K. Nikolić, Phys. Rev. B., Vol. 99, p. 094431 (2019). [3] G. Chen, R. Freeman, A. Zholud, and S. Urazhdin, Phys. Rev. X., Vol. 10, p. 011064 (2020).

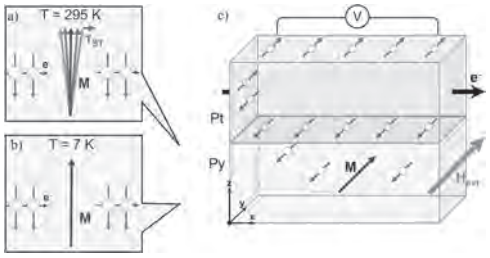

Fig 1: a) At 295 K, a spin-transfer torque acts on the fluctuating magnetization. b) At 7 K, thermal fluctuations are suppressed and no torque is applied. c) Spins are pumped from the spin-Hall Pt layer into the magnetized Py layer below.

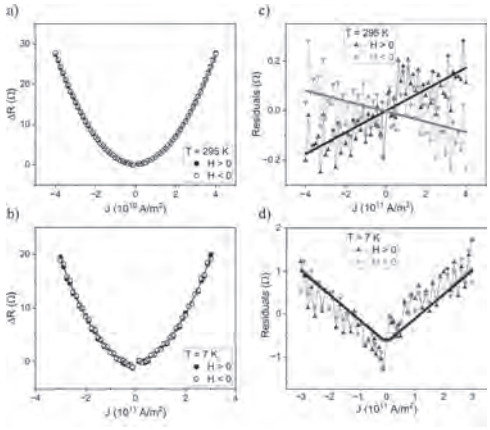

Fig 2: a) and b) Resistance (baseline set to zero) vs current density under a y-oriented field of 0.3 T. Quadratic fits are shown in blue. c) and d) Residual resistance responses with linear fits to highlight trends.

BC-13. Anti-damping Orbital Torque Driven by Inverse Orbital Rasha-Edelstein Effect in Co/Pt/CuOx. *P. Bissokarma*[1] and E. Montoya[1] *1. Department of Physics and Astronomy, University of Utah, Salt Lake City, UT, United States*

Recent theoretical[1,2] and experimental[3,4] studies have shown that non-equilibrium orbital angular momentum (OAM) can be used as a transport medium. The injection of non-equilibrium orbital current into a ferromagnet can excite the magnetization dynamics. Here we demonstrate that orbital angular momentum currents generated by the inverse Orbital Rashba Edelstein[5] (IOREE) effect can significantly enhance charge current-driven antidamping torques in multilayers with broken inversion symmetry. We use direct current bias dependent spin-torque ferromagnetic resonance (ST-FMR) measurement[6] to probe anti-damping torques in multilayer nanowires of Co/Pt and Co/Pt/CuOx, as shown in Fig. 1(a). CuOx is an as-grown metallic Cu layer that we have partially oxidized through a tunable thermally assisted process. Fig. 1 (b) shows an angular-dependent comparison of the strength of the antidamping torque as characterized by the change in FMR linewidth with applied bias current. These data show that the IOREE generated by the addition of the CuOx layer leads to significant enhancement of the total antidamping torque compared to the spin Hall torque coming from the Pt layer. We demonstrate that total anti-damping torque can be tuned by Pt thickness variation and degree of thermal oxidation of Cu.

1. Go, D., Jo, D., Kim, C. & Lee, *Phys. Rev. Lett.* 121, 086602 (2018). 2. Go, D. *et al., Phys. Rev. Research* 2, 033401 (2020). 3. Lee, D. *et al.*, *Nat Commun* 12, 6710 (2021). 4. Santos, E. *et al*., *Phys. Rev. Applied* 19, 014069 (2023). 5. El Hamdi, A. *et al.*, *Nat. Phys.* 19, 1855–1860 (2023). 6. Gonçalves, A. M. *et al*., *Applied Physics Letters* 103, 172406 (2013).

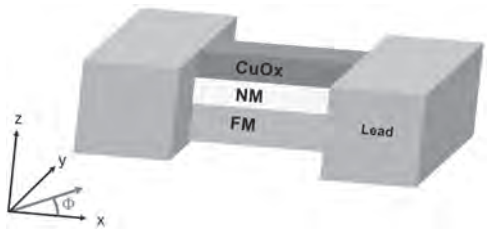

Fig.1(a) Schematic of Co/Pt/CuOx nanowire

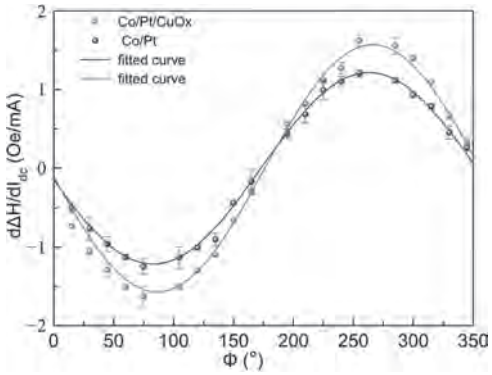

Fig. 1 (b) In-Plane (XY) angular dependence anti-damping torque for both Co/Pt (blue) and Co/Pt/CuOx (red) nanowires

Session BD
MAGNETIC RECORDING & SENSORS AND APPLICATIONS I

Ganping Ju, Chair
Seagate Technology, Fremont, CA, United States

INVITED PAPER

BD-01. Determination of oscillation state of a spin-torque oscillator fabricated in a MAMR head using injection locking. *Y. Nakagawa*[1], H. Suto[2] and T. Maeda[1] *1. Corporate Research and Development Center, Toshiba Corporation, Kawasaki, Japan; 2. Research Center for Magnetic and Spintronic Materials, National Institute for Materials Science (NIMS), Tsukuba, Japan*

Microwave-assisted magnetic recording (MAMR) using a spin-torque oscillator (STO) as a microwave field source is being developed to meet the ever-increasing demand for higher capacity HDDs [1,2]. We have invented a new STO structure with two field-generation layers (FGLs) (dual-FGL STO) [3,4], in which the two FGLs keep coupled antiparallelly during oscillation, leading to improved MAMR performance [5]. Our measurements of GMR spectra (electrical signal from STO's resistance oscillation) and analysis by micromagnetic simulations have supported the coupled oscillation in a dual-FGL STO [6]. However, an experimental method capable of detecting such an oscillation state has not been established. In this talk, a dual-FGL STO in a MAMR head is analyzed by injection locking method we recently developed [7]. In this technique (Fig. 1), the head position is first aligned on a coplanar waveguide (CPW) by using the reader part to detect the field from the current flowing in the CPW (1 kHz). Then a microwave electrical signal (GHz range) is introduced to the CPW, applying a microwave magnetic field to the STO. Injection locking occurs when the frequencies of the STO oscillation and microwave field are sufficiently close, resulting in the change in the STO resistance. We compare the results at a positive bias, where the coupled oscillation is excited, and at a negative bias, where the oscillation is excited in only one FGL. While no resistance change due to injection locking is observed at the peak frequency of GMR spectra at the positive bias (Fig. 2(a)), a clear locking effect [7] appears at the negative bias (Fig. 2(b)). Our method can determine the oscillation state based on the fact that the coupled oscillation is insensitive to external microwave field due to the cancellation of its effect within the two FGLs. Therefore, the absence of locking effect at the positive bias provides evidence of the coupled oscillation, a key factor for higher MAMR performance.

[1] J.-G. Zhu *et al*., *IEEE Trans. Magn.* 44, 125 (2008). [2] E. Roddick *et al*., *The 33rd Magnetic Recording Conference (TMRC)*, Milpitas, CA, USA, 2022, paper PB1 (doi: 10.1109/TMRC56419.2022.9918580). [3] M. Takagishi *et al.*, *IEEE Trans. Magn.* 57, 3300106 (2021). [4] Y. Nakagawa *et al.*, *IEEE Trans. Magn.* 58, 3201005 (2022). [5] Y. Nakagawa *et al.*, *IEEE Trans. Magn.* 60, 3200106 (2024). [6] Y. Nakagawa *et al.*, *Appl. Phys. Lett.* 122, 042403 (2023). [7] N. Asam *et al.*, *Appl. Phys. Lett.* 119, 142405 (2021). *Editor's Pick

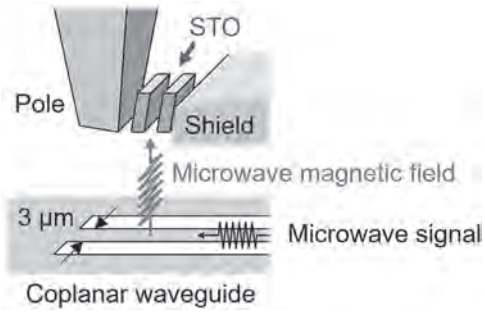

Fig.1 Measurement setup. CPW is aligned to the STO (~50 nm width) and generate a microwave magnetic field. In STO, only FGLs are shown.

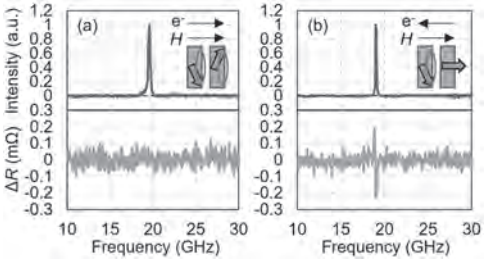

Fig.2 Experimental results. (a and b) GMR spectrum (top) and locking result (bottom) at a positive and negative bias, respectively.

CONTRIBUTED PAPERS

BD-02. Chemical Ordering of Sputtered FePt / *h*-BN Granular Media Using RF Substrate Bias. *B.L. Reese*[1,2], C. Aros-Caballero[1,2,3], E. Eleson[1,2,4], B. Turner[2,5], V. Bollapragada[2,5], D.E. Laughlin[1,2,5] and J. Zhu[1,2,5] *1. Materials Science and Engineering, Carnegie Mellon University, Pittsburgh, PA, United States; 2. Data Storage Systems Center, Carnegie Mellon University, Pittsburgh, PA, United States; 3. Materials Science and Engineering, University of Michigan, Ann Arbor, MI, United States; 4. Materials Science and Engineering, Pennsylvania State University, University Park, PA, United States; 5. Electrical and Computer Engineering, Carnegie Mellon University, Pittsburgh, PA, United States*

Recently hexagonal-BN (*h*-BN) / $L1_0$-FePt granular media has attracted significant attention regarding next generation heat assisted magnetic recording (HAMR) technologies [i], [ii]. The formation of crystalline *h*-BN at the FePt grain boundaries has resulted in significant enhancements to the sputtered media's microstructural and magnetic properties. While it has been shown that high temperature and RF substrate bias are necessary to achieve highly crystalline *h*-BN at the grain boundaries, limited discussion has been given to the broader impact of substrate bias on the FePt order of this system [iii]. To further evaluate the influence of RF substrate bias on sputtered *h*-BN / FePt granular media we have prepared several samples using different RF bias powers, 3 W / -20 V_{DC} to 8 W / -75 V_{DC}, on Corning NXT glass substrates. Samples grown via co-sputtering *h*-BN / FePt and pure FePt without a segregant were both investigated. Interestingly, it was found that the order of pure FePt deposited at 4 W and 8 W substrate bias remained relatively constant

and retained excellent texture, diffracted intensity ratios, $I_{(001)}/I_{(002)}$, were 2.92 and 2.78 respectively. However, as *h*-BN was added to the system the FePt ordering decreased monotonously with increased substrate bias, for the 8 W sample no (001) FePt superlattice reflection was observed in the x-ray diffraction (XRD) data. This behavior was confirmed in the magnetization data which also reflected a monotonous reduction of the out of plane coercivity from 32 kOe to 10 kOe for the 3 W and 8 W substrate bias samples respectively. Additionally, energy dispersive spectroscopy (EDS) was used to probe the composition of the deposited *h*-BN / FePt films. This data revealed a measurable reduction in the Fe-kα signal for increased bias powers suggesting that BN may change the deposited FePt composition and thereby influence the observed ordering. Relevant structural, microstructural, magnetic, and compositional data will be presented for the samples discussed above.

[i] C. Xu, B. S. D. C. S. Varaprasad, D. E. Laughlin and J.-G. Zhu, IEEE Trans. Mag., Vol. 59, p. 1-5 (2023) [ii] B. S. D. Ch. S. Varaprasad, C. Xu, M.-H. Huang, D. E. Laughlin and J.-G. Zhu, AIP Adv., Vol.13, p. 035002 (2023) [iii] C. Xu, B. S. D. C. S. Varaprasad, D. E. Laughlin and J.-G. Zhu, Sci. Rep., Vol. 13, p. 11087 (2023)

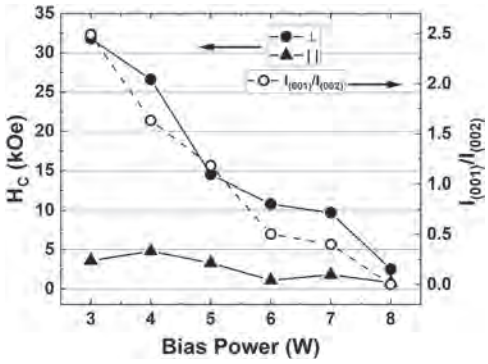

Diffracted intensity ratios, $I_{(001)}/I_{(002)}$, plotted against out-of-plane and in-plane coercive fields for *h*-BN / FePt granular media deposited using 3 W to 8 W substrate bias powers.

BD-03. Laser Current and Write Current Optimization Using DC Noise Measurement in Heat-Assisted Magnetic Recording Hard Disk Drives. *A. Sakoguchi*[1], J. Zhang[2] and J. Lee[2] *1. Western Digital Technologies GK, Fujisawa, Japan; 2. Western Digital Technologies, Irvine, CA, United States*

In Heat Assisted Magnetic Recording (HAMR), laser generates heat on media which helps write field-driven magnetization switching. Since both temperature and magnetic field influence on the write process, laser current and write current cannot be optimized independently. The mutual dependence of those parameters is clearly described in THMap as shown in Fig.1. It measures noise power after reverse DC write over saturated media to the opposite polarity as a function of laser current and write current which correspond to media temperature and magnetic field intensity [1]. The noise power is high in case magnetization of media grains partially switched. If we applied higher laser current and/or higher write current beyond the noise peak, it becomes low due to the magnetization saturation. High laser current and high write current are advantageous for saturation recording. They, however, contradict realizing narrow track pitch, and furthermore, maximum areal density [2]. Fig.2 shows write current dependence of bit error rate (BER) and THMap's noise power. Write current required for BER saturation was higher than that for the noise power saturation. It suggests that write current for the magnetization saturation is enough to achieve sufficient BER. In this study, we investigated a possibility of utilizing THMap for optimization of laser current and write current.

[1] P. O. Jubert *et al*., IEEE Trans. Magn., vol. 59, no. 3, p.1-5(2023). [2] C. Rea *et al*., IEEE Trans. Magn., vol. 50, no. 3, p.62-66 (2014)

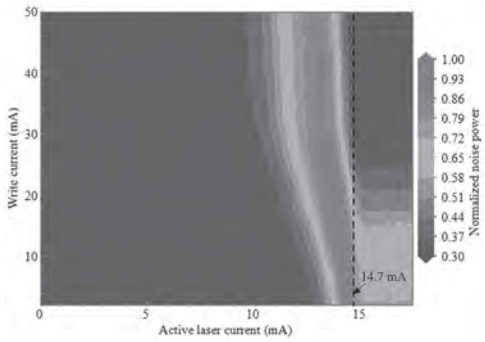

Fig.1. A THMap. Noise power after reverse DC write as a function of write current, and active laser current which is laser current above laser threshold. Initial noise power, which is low since media magnetization was saturated by applying sufficiently high laser current and write current beforehand, was remained in the large blue region. And the red ridge indicates that approximately half of grains have magnetization switched. Then, noise power became low again due to saturation in high laser current and write current condition.

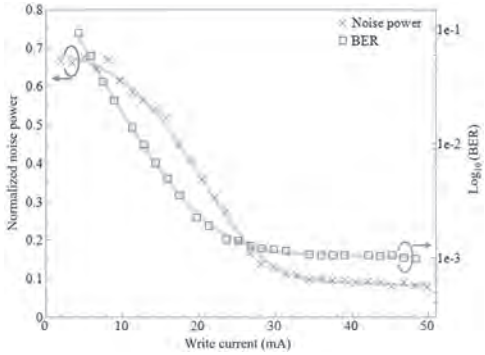

Fig.2. Write current dependence of BER and THMap's noise power. Active laser current 14.7 mA, which is shown as the dotted line in Fig.1, was applied. Noise power saturated before the BER saturation.

BD-04. Dual Layer Media Modeling for Heat Assisted Magnetic Recording. *A. Venugopal*[1], T.Y. Chang[1], P. Steiner[1] and P. Czoschke[1] *1. Seagate Technology LLC, Bloomington, MN, United States*

Heat assisted media recording (HAMR) is expected to provide immense advancements in hard-disk areal density capability (ADC) over the coming years. However, ADC improvements furthered by scaling alone would eventually be limited to ~ 5 Tbpsi due to the grain size limit of the magnetic recording media. Advanced designs are therefore crucial for continued ADC extension. Multi-layered media can potentially enable high areal densities in magnetic hard disk recording beyond such limits [1, 2]. In this work we look at the simplest of multi-layer recording-media concept – dual-layer media in the binary scheme. Here we use two parts of the grain – the top and the bottom - to increase the SNR and hence produce ADC improvements. The dual layer media grain consists of two parts with slightly different Curie temperature (Tc). It can be shown that effective zeros can be inserted in such a magnetic media when the write-field (the applied magnetic field) is switched (Fig. 1 (a)). The zeros, thus introduced, tend to be largely at/near the transitions. This 'zeroing' helps to reduce the transition noise [2]. The dependence of the width of the zero-insertion region on Tc difference between the layers is shown in Fig. 1(b). Also, plotted is the SNR of the media. In this work, we evaluate the ADC of the dual-layer media using micromagnetic simulations. The ADC calculations are performed using the variable bit aspect ratio (VBAR) algorithm. The impact of Tc differences between the two layers on ADC is evaluated to identify the optimal dual-layer design. The results are shown in Table I, which compares the bits per inch capability (BPIC), tracks per inch capability (TPIC), and ADC of the

dual layer media with single layer media. In addition, we look at techniques to improve ADC design in the presence of a vertical temperature gradient [3]. We achieve this by using Tc variation within the upper and the lower layers.

[1] P. Tozman, S. Isogami, I. Suzuki, et al., "Dual-layer FePt-C granular media for multi-level heat-assisted magnetic recording," *Acta Materialia*, Vol. 271, 2024, 119869, https://doi.org/10.1016/j.actamat.2024.119869. [2] T. Y. Chang et al., "Zero-State Insert Dual-Layer HAMR Media Recording," in IEEE Transactions on Magnetics, vol. 59, no. 3, pp. 1-7, March 2023, Art no. 3200107, doi: 10.1109/TMAG.2022.3206138. [3] A. Venugopal et al., "Temperature Performance of Dual-Layer Hamr Media," *2023 IEEE 34th Magnetic Recording Conference (TMRC)*, Minneapolis, MN, USA, 2023, pp. 1-3, doi: 10.1109/TMRC59626.2023.10264017.

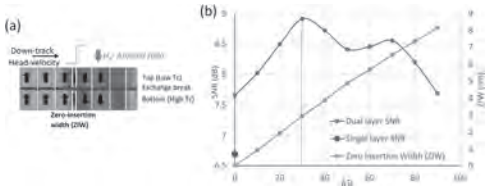

Fig. 1. (a) Zero grains are inserted when the magnetic field is switched, the width of the zero insertion is denoted by ZIW. (b) ZIW and SNR vs ΔTc. The max. SNR occurs when ΔTc ~ 30 K corresponding to a ZIW~3nm (~ half the grain-size).

SL	L1_Tc (K)	L2_Tc(K)	Tpeak -300(K)	BPIC	TPIC	ADC (Tbpsi)	Gain
SL	750	-	504	2560	1320	3.379	-
SL	720	-	464	2545	1329	3.382	(Base)
DL	750	750	488	2662	1304	3.471	+2.6%
DL	750	720	480	2850	1270	3.620	+7%
DL	750	700	473	2875	1175	3.378	-0.1%

Table. I Dual layer media ADC. (SL: Single layer; DL: Dual layer)

BD-05. Mutual Soft-Information Improvement Techniques for Lower Layer Performance Improving in Double-Layered Magnetic Recording Systems. *A. Khametong*[1], S. Greaves[2] and C. Warisarn[1] *1. College of Advanced Manufacturing Innovation, King Mongkut's Institute of Technology Ladkrabang, Bangkok, Thailand; 2. Research Institute of Electrical Communication (RIEC), Tohoku University, Sendai, Japan*

The emergence of DLMR [1] aims to further increase an AD by stacking media with more than one recording layer on the same platter. BPMR is another interesting alternative technology that uses nanoscale bit islands to enhance data storage density, reduce transition noise, and maintain thermal stability [2]. We construct DLMR bit-patterned media to increase AD. However, the use of these media is accompanied by signal processing challenges in separating the data from the different layers. Additionally [2]-[3], the lower layer can be far from the reader, making it difficult to retrieve the recorded bits, resulting in poor BER performance. We begin by arranging the bit islands in each layer into a rectangular array, while the bit islands between in different layers are arranged in a staggered array to reduce ILI, as shown in Fig. 1. Three readers read the data from the i-1th, i^{th}, and i+1th tracks, respectively. The i-1th and i+1th tracks belong to the upper layer, and the i^{th} track belongs to the lower layer. H-I and H-III are shifted closer together by 5% of the track pitch (T_z). This strategy not only reduces the ITI effect from neighboring tracks, but also facilitates signal processing. With this reading technique, we obtain three readback signals from three readers. We can produce three mutual data samples for each desired bit in the lower layer. To increase the soft-information reliability of the lower layer, therefore; this study proposes mutual soft-information improvement techniques (MIITs) that include maximum soft-information (MSI) and sum soft-information (SSI) schemes. MIITs can effectively improve the soft-information that passes from a SOVA detector through MSI and SSI schemes. Moreover, we also present three iterative systems based on the proposed MIIT, as shown in Fig. 2, which exchange the soft-information between SOVA and low-density parity check LDPC code. These proposed techniques can improve the BER performance of the lower layer, resulting in better BER performance for all three tracks compared to conventional systems under a single media layer at the same AD of 4 Tb/in^2.

[1] R. Wood, "The feasibility of magnetic recording at 1 terabit per square inch," IEEE Trans. Magn., vol. 36, no. 1, pp. 36–42, Jan. 2000. [2] N. Rueangnetr, S. Koonkarnkhai, P. Kovintavewat, and C. Warisarn, "Double layer magnetic recording with multilayer perceptron decoder for single reader/two-track reading in BPMR systems," AIP Adv. vol 13, 035104 (2023). [3] K. S. Chan, A. Aboutaleb, K. Sivakumar, B. Belzer, R. Wood, and S. Rahardja, "Data recovery for multilayer magnetic recording," IEEE Trans. Magn. 55, 6701216 (2019). [4] C. Buajong and C. Warisarn; "Recording media configurations for double-layered bit-patterned magnetic recording," AIP Adv. vol. 14, 015133 (2024).

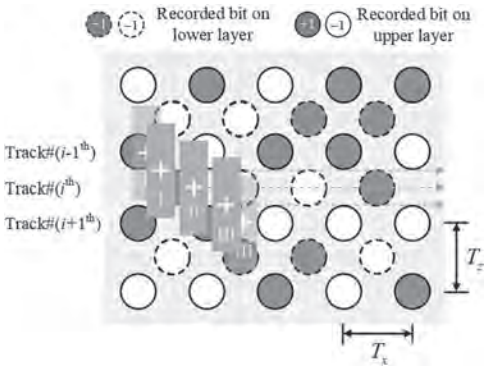

Fig. 1. Bit-pattered media DLMR with three readers.

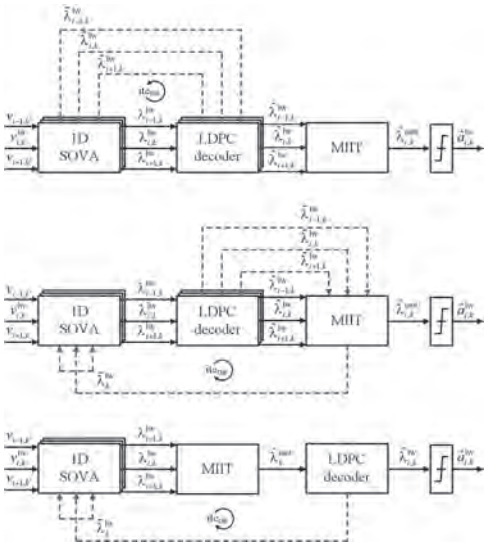

Fig. 2. The structures of three iterative systems combined with MIITs.

BD-07. Track Misregistration Estimation Technique based on Hybrid K-means and EM Algorithm in Bit-Patterned Media Recording Systems. P. Kochcha[1], *K. Kankhunthod*[1] and C. Warisarn[1] *1. College of Advanced Manufacturing Innovation, King Mongkut's Institute of Technology Ladkrabang, Bangkok, Thailand*

Bit-patterned media recording (BPMR) is an advanced technology designed to surpass the superparamagnetic limit, enabling hard disk drives to achieve areal densities (ADs) beyond 1 Tb/in^2. Increasing AD in BPMR systems by placing bit-islands closer together introduces significant inter-track interference (ITI) and inter-symbol interference (ISI), which degrade the bit-error rate (BER) during data detection [1-2]. Additionally, high AD exacerbates

track misregistration (TMR), where the reader deviates from the desired track centerline, leading to severe BER degradation. This work addresses this issue by proposing a hybrid TMR mitigation technique based on K-means [3] and expectation-maximization (EM) algorithms [4] to enhance TMR prediction accuracy and improve BER in multi-head multi-track BPMR systems. The block diagram of the proposed system is shown in Fig. 1. For an AD of 3.0 Tb/in^2, the track pitch (T_z) and bit period (T_x) are set to 14.5 nm. User bit sequences $a_{k,l\text{-}1}$, $a_{k,l}$, and $a_{k,l+1}$ are encoded with a low-density parity check (LDPC) encoder before recording. Readback sequences $r_{k,l\text{-}1}$, $r_{k,l}$, and $r_{k,l+1}$ are acquired by three readers and input into a hybrid K-means-EM-based TMR estimator. This estimator determines the TMR level by finding two sets of centroids for the readback signals using K-means and EM algorithms, dynamically selecting the estimated TMR output based on the predicted TMR range. Experiments show that K-means offers better accuracy at TMR levels of 0.5, 1.0, and 1.5 nm, while EM outperforms at 2.0, 2.5, and 3.0 nm. e.g., if estimated TMR values are 1.0 nm (K-means) and 1.5 nm (EM), the 1.0 nm value is chosen. Combining these algorithms achieves over 85% estimation accuracy across all TMR levels. For TMR mitigation, the appropriate 2D equalizer and 1D generalized partial response target coefficients for the SOVA detector are selected based on the estimated TMR level. The proposed system with TMR mitigation technique achieves BER performance close to an ideal system with 100% TMR estimation accuracy and significantly outperforms a conventional system without TMR mitigation with a performance gain up to 1.25 dB as shown in Fig. 2.

[1] W. Busyatras, C. Warisarn, Y. Okamoto, et al., AIP Advances., Vol. 7, No. 5, p. 056501-1, (2016) [2] K. Kankhunthod, C. Buajong, and C. Warisarn, IEEE Magn., Vol. 11, p. 1-5, (2020) [3] S. Jeong and J. Lee, IEEE Tran. Magn., Vol. 59, No. 3, p.1-5, (2023) [4] G. Kong, T. Kim, and M. Jung, IEEE Magn. Letters., Vol. 13, p. 1-5, (2022)

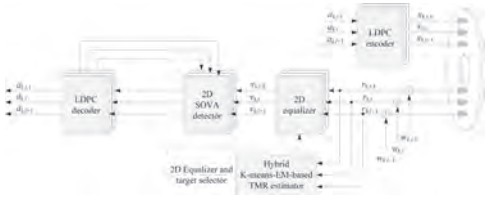

Block diagram of proposed system

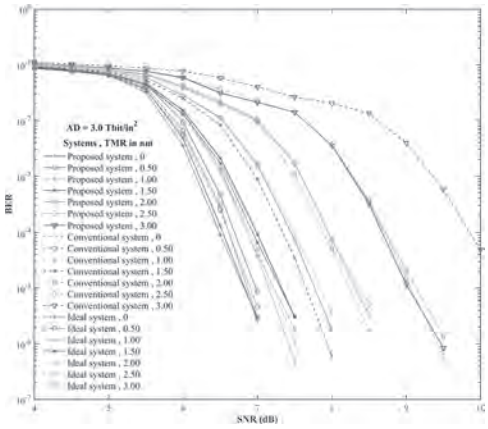

BER performance comparison

BD-08. Advancing Spatially Selective All-Optical Magnetic Switching in Nanomagnets for Magnetic Memory and Computing. *D. Bromley*[1], T. Farchy[1], J. Gartside[1], D. Cielecki[1], K.D. Stenning[1], A. Vanstone[1], H. Holder[1], T. Zheng[1], X. Xiao[2], R. Sapienza[1], R. Oulton[1] and W.R. Branford[1]
1. Physics, Imperial College London, London, United Kingdom;
2. Technology Innovation Institute, Abu Dhabi, United Arab Emirates

The realisation of spatially selective control of nanomagnets using pulsed lasers, specifically through all-optical magnetic switching, promises ultra-fast magnetisation control while circumventing the requirement for an external magnetic field, and addressing a longstanding goal in data storage and computational technologies. Traditional state-control approaches, utilising magnetic field and thermal protocols, access only a limited fraction of magnetic microstates, while alternative techniques, such as scanning magnetic tips[1], are impeded by slow setups and susceptibility to tip damage. Furthermore, existing methodologies relying on complex magnetic materials[2] underscore the need for a rapid and localised microstate control method across extensive nanomagnetic networks. Building on our prior breakthrough in all optical writing of single-layer NiFe nanomagnets within dense arrays[3] using continuous wave (CW) lasers, we have made significant progress in increasing the robustness, fidelity, and speed, and the complexity of the resulting magnetic textures. We observe that optimising the quality of the NiFe layer plays a crucial role in determining fidelity, even among samples with nearly identical coercive fields. NiFe is an exciting choice of material for AOMS technology. It is an affordable and non-toxic alloy, and eliminates the reliance on rare and geopolitically sensitive materials. Moreover, we have demonstrated that nanopatterned NiFe is highly amenable to optical writing using both continuous wave and fast pulsed laser illuminations. Additionally, our approach enables intricate microstate engineering of complex patterns to create magnetic images, greatly expanding potential applications in data storage and computational technologies.

1. Gartside, Jack C. Nature nanotechnology, 13.1 (2018): 53-58. 2. Igarashi, J. Nano Lett. 20, (2020): 8654–8660. 3. Stenning, Kilian D. Cell Reports Physical Science 4.3 (2023).

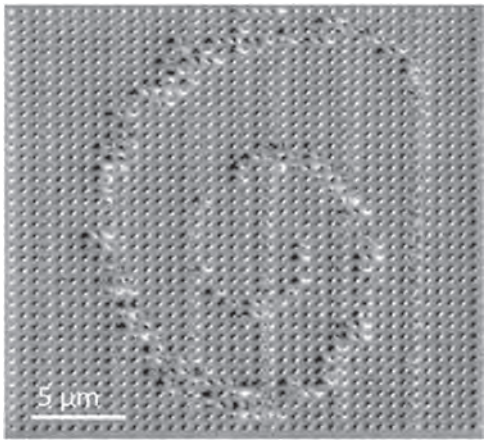

Magnetic force microscopy scan of a spiral pattern optically written on to a dense nanomagnetic array.

BD-09. Spin Transport Calculation in Aluminum Thin Film by Drift-Diffusion Equation. *R. Hao*[1] and R. Victora[1] *1. University of Minnesota, Minneapolis, MN, United States*

Previously we have shown that a sub-10 nm magnetic sensor based on a lateral spin valve (LSV) structure and using a synthetic antiferromagnet (SAF) for spin detection can perform well in gigahertz operations [1]. In our design (Fig. 1), the spin injection ferromagnet FM1 is near the recording media and the spin detection part is hundreds of nanometers away. FM1 injects spin-polarized electrons into Al through the left circuit, these electrons diffuse rightward along the Al channel to the right part for

magnetoresistance detection. Here we calculate spin transport along the Al channel with / without an electric field (E-field) applied using the one-dimensional drift-diffusion equation [2]. With the linear definition of the current spin polarization factor P as functions of spin-up electron density $n_\uparrow$ and spin-down electron density $n_\downarrow$, $P=(n_\uparrow-n_\downarrow)/(n_\uparrow+n_\downarrow)$, and assuming equal diffusion coefficients $D_\uparrow=D_\downarrow=D$ and equal mobilities $\mu_\uparrow=\mu_\downarrow=\mu$, we can write $\partial P/\partial t=D\partial^2 P/\partial z^2+\mu E\partial P/\partial z$ to calculate how current spin polarization in Al changes with time t and displacement z along the channel. E is amplitude of the applied electric field in z direction. We use FM1 magnetization dynamics as the input spin signal in Al, $P(z=0,t)=m_{z,\mathrm{FM1}}(t)$. We set the boundary conditions $P(z<0,t)=0$ and $P(z\to\infty,t)=0$, and the initial condition $P(z>0,t=0)=0$, then solve for $P(z,t)$. The equation can be solved using Laplace transform with respect to time [3], yielding an integral as the solution. Fourier transforms of the transmitted spin signal show that the high-frequency signal transmits less effectively than the low-frequency signal and requires a larger E-field for long-distance transmission. This effect leads to non-linear signal-to-noise ratio (SNR) of $P(z,t)$ with respect to E-field, see Fig. 2. Initially increasing E-field helps the ~1 GHz signal where information from FM1 lies, so SNR increases. When E-field is very large, there is little amplification of signal, only of noise: thus SNR decreases.

[1] R. Hao and R. H. Victora, *J. Magn. Magn. Mater.*, vol. 593, p. 171852 (2024). [2] S. Selberherr, *Analysis and Simulation of Semiconductor Devices*, Springer-Verlag Wien, New York, 1984, p. 16. [3] E. Butkov, *Mathematical Physics*, Addison-Wesley, New York, 1973, pp. 302-304.

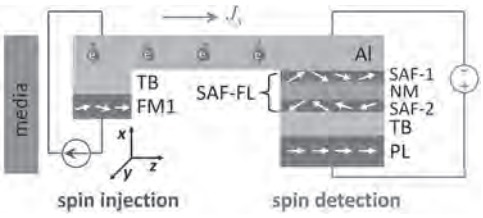

Fig. 1. Our magnetic sensor design based on a LSV structure. TB: tunnel barrier. SAF-FL: SAF used as free layer, SAF-1 and SAF-2 are ferromagnets, NM: nonmagnet. PL: pinned layer.

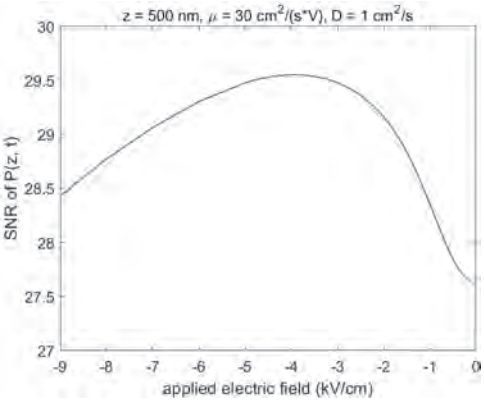

Fig. 2 SNR of transmitted spin signal at z=500 nm versus E-field in Al.

BD-10. Study on Planar Hall Magnetoresistive Sensor and its Application for Magnetic Encoder. *T. Jeon*[1], C. Jeon[1], J. Kim[1], B. Lim[2] and C. Kim[1] *1. Department of Physics and Chemisty, Daegu Gyeongbuk Institute of Science and Technology, Daegu, The Republic of Korea; 2. Department of Smart Sensor Engineering, Andong National Univerisity, Andong, The Republic of Korea*

We figured out the change in planar Hall magnetoresistive (PHMR) sensors performance in different specification, such as sensor layer thickness, geometry [1] and applied into magnetic encoder experiments. In this magnetic encoder application, PHMR sensor and permanent magnet was located near to steel gear to induce stray field from magnetized steel gear and detect the magnetic signal. PHMR signal was compared in different factors, such as distance between gear-sensor, distance between sensor-magnet or direction of sensor and magnet, etc. New ferromagnetic material and sensor geometry were applied to encoder sensors to enhance the main performance requirements such as total harmonic distortion (THD), signal amplitude and phase difference, and the experimental result was discussed in this speech.

T. Jeon, P. T. Das, M. Kim, C. Jeon, B. Lim, I. Soldatov, and C. G. Kim, *Sensors*, Vol. 20, no. 20, pp. 6891 (2019)

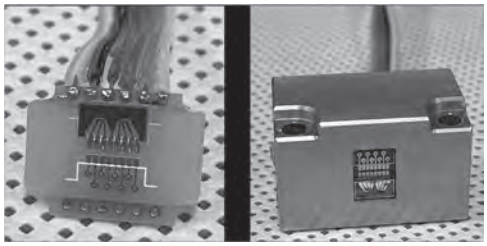

Fig. 1 Magnetic encoder using PHMR sensor on PCB (left) and in aluminum case (right).

BD-12. Design Optimization of a Position Sensor for Linearity Range Extension. M. Mirzaei[1], P. Ripka[1] and *J. Maier*[1] *1. Electrical Engineering, Czech Technical University, Prague, Czechia*

Position sensors are used for various industrial applications, including robotics, automotive, energy sectors, etc. The conventional position sensors have linear variable differential transformer (LVDT) configuration. Conventional LVDT position sensors have cylindrical structures with long solenoidal coils and short magnetic armature. Therefore, long coils make LVDT sensors become bulky for long-distance position measurement. Flat-type LVDT position sensors are appropriate options for position measurement, with flexible configurations for different applications [1]-[3]. This paper presents a design-optimized model of an LVDT sensor with short coils and long armatures. The sensor has one excitation coil and two antiserially connected pickup coils, which are located between two parallel armatures plates, as shown in Fig. 1. The 3D FEM is used for magnetic analysis and design optimization of LVDT sensors. The structure of the armatures is optimized to enhance the linearity range of the LVDT position sensor (Fig. 1). The rectangular shape of the armature [3] has been changed to a trapezoidal shape to decrease the nonlinearity error. Fig. 2 shows the 3D FEM and measurement results, which excellent linearity is shown for the simulation and measurement results. The linearity range increases by 15% with an allowable 2% nonlinearity error using trapezoidal shape armatures compared to rectangular shape armature LVDT sensors [3]. Various coils' dimensions and armature magnetic materials are investigated to improve further sensor performance in terms of higher sensitivity and lower nonlinearity error.

1. Y. Kano, S. Hasebe, and H. Miyaji, "New linear variable differential transformer with square coils", IEEE Trans. Magnetics, vol. 26, no. 5, pp. 2020 - 2022, Sep. 1990 2. M. Mirzaei, J. Machac, P. Ripka, A. Chirtsov, J. Vyhnanek, and V. Grim, "Design of a flat type magnetic position sensor using finite difference method", IET Sci. Meas. Technol., vol. 14, no. 5, pp. 514-524, July 2020 3. M. Mirzaei, P. Ripka, and V. Grim, "A position sensor with novel configuration of linear variable differential transformer", IEEE Sensors J., vol. 21, no. 20, pp. 22899 - 22907, Oct. 2021

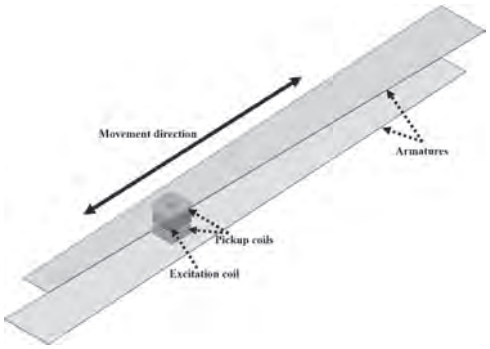

Fig. 1 The sensor model - a) excitation and pickup coils, b) armatures

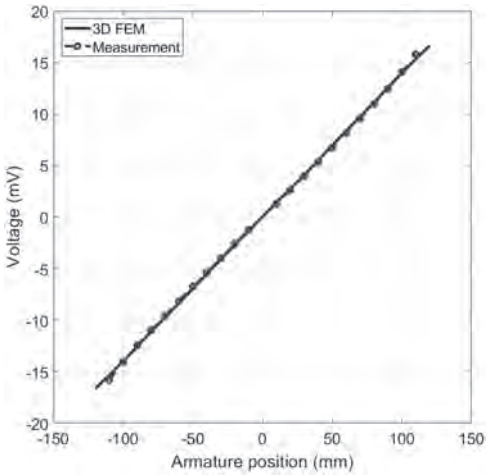

Fig. 2 The comparison between measurement and 3D FEM simulations at 1000 Hz– sensor voltage versus armature position

BD-13. An MLP-based ITI Suppression Method for Multi-Head Multi-Track Bit-Patterned Magnetic Recording. S. Koolkarnkhai[2], *C. Warisarn*[1] and P. Kovintavewat[2] *1. College of Advanced Manufacturing Innovation, King Mongkut's Institute of Technology, Ban, Thailand; 2. Department of Electrical Engineering, Nakhon Pathom Rajabhat University, Nakhon Pathom, Thailand*

Bit-patterned magnetic recording (BPMR) is a promising technology that can achieve an areal density (AD) of hard disk drives up to 5 Tb/in^2 [1]. However, it faces significant intertrack interference (ITI) issues at high ADs, which can degrade system performance. Various methods have been proposed to address ITI. For instance, Navabi [2] proposed a 2-dimensional (2D) equalizer and a 1D target for a 3-head 1-track (3H1T) BPMR system. This approach decodes only the main track and outperforms the system using a 1D equalizer and a 2D target. Karakulak [3] introduced the 2D Viterbi detector for the 2D target to counteract the ITI effect. Fig. 1 shows the 3H3T BPMR channel model with the proposed multilayer perceptron (MLP) -based ITI suppression method. An input sequence of the j-th track and the k-th bit $a_{j,k} \in \{\pm 1\}$ is sent to the channel matrix H [1] and corrupted by additive white Gaussian noise $\{n_{j,k}\}$ to obtain a readback signal $\{y_{j,k}\}$, where $j \in \{\pm 1, \pm 2, 0\}$. We assume the ITI in the readback signal is caused by only two adjacent tracks. Then, the readback signals $\{y_{-1,k}, y_{0,k}$, and $y_{1,k}\}$ are fed to an MLP-based estimator to approximate the ITI-unaffected signal of the main track $\{r_{0,k}\}$. This ITI suppression method uses an MLP with 27 input nodes and 5 hidden layers, each containing 100 nodes. All hidden nodes employ a leaky ReLU activation function, and the output node uses a linear activation function. The signal $\{r_{0,k}\}$ is scaled by a weighting factor w and subtracted from $\{y_{-1,k}\}$ and $\{y_{1,k}\}$ to lessen the ITI effect caused by the main track [4]. Hence, the refined signals $\{r_{-1,k}\}$ and $\{r_{1,k}\}$ will contain only the one-side ITI effect, which will be equalized by a 1D equalizer designed for the 2×3 2D target [4]. Conversely, the signal $\{r_{0,k}\}$ can be equalized by the 1D equalizer designed for the 1D target. Finally, the equalized signals $\{r_{-1,k}, r_{1,k}\}$ and $\{r_{0,k}\}$ are passed to the 2D and 1D Viterbi detectors to determine the most likely input sequences $\{a_{-1,k}, a_{1,k}\}$ and $\{a_{0,k}\}$, respectively. Fig. 2 compares the system performance at AD = 3 Tb/in^2. The proposed system performs better than the conventional systems presented in [2] "Conv 3H1T" and in [4] "Conv 3H3T."

[1] Y. Shiroishi, et al., "Future options for HDD storage," IEEE Trans. Magn., vol. 45, no. 10, pp. 3816–3822, October 2009. [2] S. Nabavi, "Signal processing for bit-patterned media channel with intertrack interference," Ph.D. dissertation, Dept. Elect. Eng. Comp. Sci., Carnegie Mellon University, Pittsburgh, PA, 2008. [3] S. Karakulak, "From channel modeling to signal processing for bit-patterned media recording," Ph.D. dissertation, Department of Electrical Engineering, University of California, San Diego, 2010. [4] S. Koonkarnkhai and P. Kovintavewat, "An iterative ITI cancellation method for multi-head multi-track bit-patterned magnetic recording systems," Digital Communication and Network, vol. 7, no. 1, pp. 96 - 101, 2021.

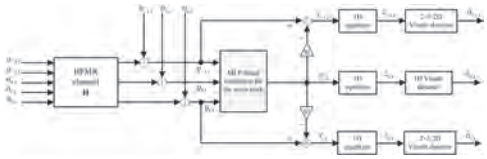

Fig. A proposed system.

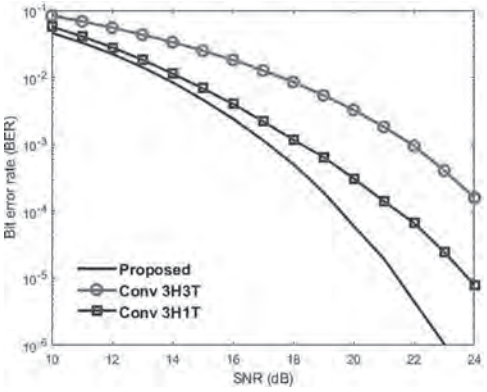

Fig. 2. Performance comparison.

Session BE
ANTIFERROMAGNETS AND FERRIMAGNETS

Xuemei Cheng, Chair
Bryn Mawr College, Bryn Mawr, PA, United States

INVITED PAPER

BE-01. Control of magnon spin transport in multiferroics. *T. Nan*[1]
1. Tsinghua University, Beijing, China

In-memory computing, utilizing non-volatile memories capable of performing both information storage and logic operations within the same device, holds the promise for empowering artificial intelligence with significantly reduced energy consumption. Existing logic-in-memory devices that have been implemented operate mainly based on charge transport, a process that inevitably gives rise to joule heating. On the other hand, information processing and transmission using magnons as information carriers is a promising route for developing spin-based logic and memory devices with low-dissipation, since magnons can transport spin in ferrimagnetic and antiferromagnetic insulators without involving moving electrons. Incoherent magnons can simply be electrically (and thermally) excited in dc electronic circuits, making them compatible with current semiconductor technology. For practical applications, the implementation of magnon logic operations using gate voltages is necessary. Current technology to manipulate magnon current transport at room temperature mainly relies on magnetic fields that can reorientate the magnetic ordering or modulate the magnetic domain structure. It remains challenging to develop a magnon-based logic due to the lack of efficient electrical manipulation of magnon transport. We presented a magnon logic-in-memory device in a spin-source/multiferroic/ferromagnet structure, where multiferroic magnon modes can be electrically excited and controlled. In this device, magnon information is encoded to ferromagnetic bits by the magnon-mediated spin torque. We showed that the ferroelectric polarization can electrically modulate the magnon spin-torque by controlling the non-collinear antiferromagnetic structure in multiferroic bismuth ferrite thin films with coupled antiferromagnetic and ferroelectric orders. By manipulating the two coupled non-volatile state variables—ferroelectric polarization and magnetization—we further demonstrate reconfigurable logic-in-memory operations in a single device. These findings highlight the potential of multiferroics for controlling magnon information transport and offer a pathway towards room-temperature voltage-controlled, low-power, scalable magnonics for in-memory computing.

1. Yuhan Liang, Dingsong Jiang, Yahong Chai, Yue Wang, Hetian Chen, Jing Ma, Pu Yu, Di Yi*, Tianxiang Nan*; Observation of Magnon Spin Transport in BiFeO3 Thin Films, Adv. Funct. Mater., 34, 2308944 (2023). 2. Yahong Chai, Yuhan Liang, Cancheng Xiao, Yue Wang, Bo Li, Dingsong Jiang, Pratap Pal, Yongjian Tang, Hetian Chen, Yuejie Zhang, Witold Skowronski, Qinghua Zhang, Lin Gu, Jing Ma, Pu Yu, Jianshi Tang, Yuan-Hua Lin*, Di Yi*, Daniel C. Ralph, Chang-Beom Eom, Huaqiang Wu, Tianxiang Nan*; Multiferroic Magnon Spin-Torque Based Reconfigurable Logic-In-Memory, arXiv:2309.14614.

CONTRIBUTED PAPERS

BE-02. Mechanisms Of Electrical Switching Of Ultrathin CoO/Pt Bilayers. *C. Schmitt*[1*], A. Rajan[1], G. Beneke[1], A. Kumar[1], T. Sparmann[1], H. Meer[1], B. Bednarz[1], R. Ramos[2,3], M. Angel[4], M. Foerster[4], E. Saitoh[3,5] and M. Kläui[1] *1. Johannes Gutenberg University Mainz, Mainz, Germany; 2. Universidade de Santiago de Compostela, Santiago de Compostela, Spain; 3. Tohoku University, Sendai, Japan; 4. ALBA Synchrotron Light Facility, Cerdanyola del Valles (Barcelona), Spain; 5. The University of Tokyo, Tokyo, Japan*

Insulating antiferromagnetic materials have attracted significant attention for their potential in spintronic applications due to their fast internal dynamics, sizeable spin-orbit coupling, and low Joule heating [1,2]. However, efficient electrical writing and reading of information is necessary for applications, but difficult to realize. It has been established that the orientation of the Néel vector can be read out via the spin Hall magnetoresistance (SMR) [3] and short current pulses can induce a reorientation of the antiferromagnetic order [4]. However, the underlaying switching mechanism is not yet well understood and mechanisms based on thermomagnetoelastic effects [5,6] and spin-orbit torques (SOTs) have been proposed [4,7,8]. Here, we investigate the electrical switching of ultrathin CoO(4 nm)/Pt(2 nm) bilayers and identify the switching mechanism using electrical and magneto-optical measurements of the antiferromagnetic domain structure for different current densities [9]. We apply alternating 1 ms long current pulses of varying current density to the perpendicular arms of a Hall cross structure. The resulting magnetic state is read electrically by SMR and compared to an image of the domain structure to unambiguously determine the switching mechanism. We find that electrical pulses along the same trajectory can lead to either an increase or a decrease of the SMR signal, depending on the current density of the pulse. By comparing the electrical results to imaging of the domain structure before and after the application of current pulses, we can understand how opposite changes in the SMR signal can result from a thermomagnetoelastic switching mechanism. Importantly, our spatially resolved imaging shows that regions where the current pulses are applied and regions further away exhibit different switched spin structures. This indicates the presence of a SOT based switching mechanism that can dominate in very thin films. These findings demonstrate the interplay of different switching mechanisms and thus motivate further research into thinner films.

[1] R. Lebrun, A. Ross, S.A. Bender, et al., *Nature* 561, 222–225 (2018). [2] S. Das, A. Ross, X.X. Ma, et al., *Nat. Commun*. 13, 6140 (2022). [3] G. R. Hoogeboom, A. Aqeel, T. Kuschel, et al., *Appl. Phys. Lett*. 111, 052409 (2017). [4] T. Moriyama, K. Oda, T. Ohkochi, et al., *Sci. Rep*. 8, 14167 (2018). [5] P. Zhang, J. Finley, T. Safi, et al., *Phys. Rev. Lett*. 123, 247206 (2019). [6] H. Meer, F. Schreiber, C. Schmitt, et al., *Nano Lett*. 21, 207204 (2021). [7] X. Z. Chen, R. Zarzuela, J. Zhang, et al., *Phys. Rev. Lett*. 120, 207204 (2018). [8] L. Baldrati, O. Gomonay, A. Ross, et al., *Phys. Rev. Lett.* 123, 177201 (2019). [9] C. Schmitt, A. Rajan, G. Beneke, et al., *Nano Lett.* 24, 1471–1476 (2024).

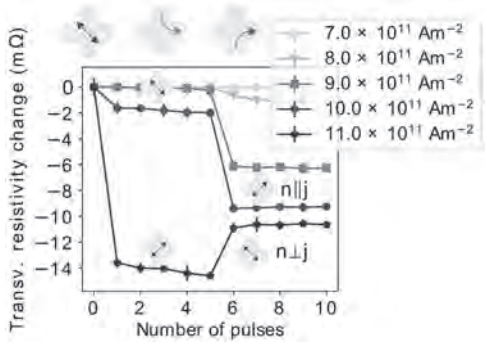

Fig. 1. Current density-dependent switching of the Néel vector n with respect to the current direction j in CoO(4 nm)/Pt(2 nm) thin-films.

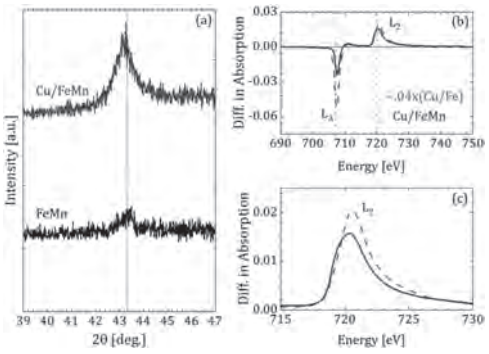

Fig. 1 (a) XRD for FeMn and Cu/FeMn. Bulk FeMn indicated at 43.31° (vertical line). (b,c) XMCD at 3 T field for Cu/BCC-Fe and Cu/FCC-FeMn (b) over wide energy range and (c) zoomed in around L_2 Fe edge.

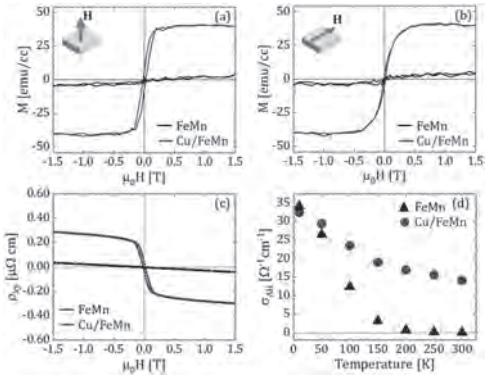

Fig. 2 (a,b) Magnetization curves (a) out-of-plane and (b) in-plane. (c) Hall resistivity vs applied field at room temperature. (d) AH conductivity vs temperature.

BE-03. Emergent Topological Magnetism in As-Grown Polycrystalline FCC FeMn. *R.E. Maizel*[1], C. Horn[2], M. Murayama[2], S. Channa[3], D. O'Mahoney[3], Y. Suzuki[3], C. Klewe[4], A.T. N'Diaye[4], R. Khatiwada[1], O.A. Bakare[1], G.T. Street[1], S. Abdizadeh[1], J. Zhao[5], M.F. Michel[5], J.J. Heremans[1] and S. Emori[1] *1. Physics, Virginia Tech, Blacksburg, VA, United States; 2. Material Science, Virginia Tech, Blacksburg, VA, United States; 3. Applied Physics and Geballe Laboratory for Advanced Materials, Stanford University, Stanford, CA, United States; 4. Advanced Light Source, Lawrence Berkeley National Laboratory, Berkeley, CA, United States; 5. Geoscience, Virginia Tech, Blacksburg, VA, United States*

Noncollinear antiferromagnets can exhibit intriguing topological phenomena, such as orbital magnetism and anomalous Hall (AH) effects [1-2]. However, topological antiferromagnetic films require growth or annealing at high temperatures [1-2], posing difficulty for device manufacturing. Here, we show net out-of-plane magnetism and AH response at room temperature in sputter-grown polycrystalline FCC FeMn *without any* high-temperature growth or annealing. Since FeMn is a widely used antiferromagnet for exchange-biasing, its potential as a topological material is attractive for practical applications. Theoretical works [3-4] predict topological magnetism and transport in FCC antiferromagnets with scalar spin chirality from the (111) orientation and uniaxial strain. The key to our (111) oriented FCC FeMn is an ultrathin Cu seed layer. X-ray diffraction confirms an FCC (111) texture for Cu/FeMn, and its absence without the Cu layer. Moreover, the (111) peak points to a strain of ~0.3% [5]. X-ray magnetic circular dichroism [Fig. 1(b,c)] indicates net magnetism in FCC FeMn, which cannot be explained by parasitic ferromagnetism from BCC Fe [6]. Room temperature magnetometry [Fig. 2(a-b)] shows spontaneous magnetization with easy axis out-of-plane in Cu/FeMn, whereas FeMn without Cu is paramagnetic. Hall measurements at high temperatures show a large AH response only in Cu/FeMn [Fig. 2(c-d)]. In summary, we attain robust net magnetization and AH effect in (111)-textured polycrystalline FCC FeMn films with no in-situ or post-annealing. Our work unlocks potential topological phenomena in commonplace antiferromagnets, compatible with practical device integration.

[1] Taylor, J. M., Markou, A., Lesne, E., et al., Physical Review B, Vol. 101, pgs. 094404, (2020) [2] Nakatsuji, S., Kiyohara, N., & Higo, T., Nature, Vol. 527, pgs. 212-215, (2015). [3] Hanke, J. P., Freimuth, F., Blügel, S., & Mokrousov, Y., Scientific Reports, Vol. 7, pg. 41078, (2017) [4] Kubler, J., -H.hock, K., Sticht, J., & Williams, A. R., Journal of Physics F: Metal Physics, Vol. 18, (1988) [5] Cankurtaran, M., Saunders, G. A., Ray, P., Wang, Q., Kawald, U., Pelzl, J., & Bach, H., Physical Review B, Vol. 47, pgs. 3161-3170, (1993). [6] Lang, L. L., Zhou, S. M., Fan, W. J., & Qiu, X. P., AIP Advances, Vol. 8, pg. 125220 (2018)

BE-04. Observation of Néel Vector Rotation in Amorphous Ferrimagnetic GdCo Thin Films. *T. Mandokoro*[1], Y. Shiota[1,2], T. Ito[1], H. Matsumoto[1], H. Narita[1], R. Hisatomi[1,2], S. Karube[1,2] and T. Ono[1,2] *1. ICR, Kyoto Univ, Uji, Japan; 2. CSRN, Kyoto Univniv, Uji, Japan*

Spin superfluidity is a novel phenomenon for a low-dissipation transport of spin angular momentum with a magnetization rotation in the plane [1,2]. Since the magnetic dipole interaction hinders the long-distance transport, antiferromagnetic materials serve a better platform to study the spin superfluidity. To observe this phenomenon, the antiferromagnetic Néel vector must be rotated in the magnetic easy plane [1,2], as shown in Fig. 1. While the control of the Néel vector by spin-orbit torque has been widely studied [3,4,5], the energy barrier of crystalline magnetic anisotropy hampers the Néel vector rotation [5]. To overcome this problem, we used an amorphous ferrimagnet GdCo with almost zero crystal magnetic anisotropy, where magnetic dipolar interaction almost is vanished at the magnetization compensation temperature (T_M). The magnetic moments of the two sublattices are confined to a plane perpendicular to the applied magnetic field (H_{ext}) when H_{ext} exceeds a spin-flop transition field H_{sf} near T_M, forming a virtual magnetic easy plane. We deposited a film stack of Ta(5)/$Gd_{0.28}Co_{0.72}$(3)/Pt(5) (unit: nm) tri-layer on a thermally oxidized Si substrate by using DC magnetron sputtering, followed by device processing. By performing anomalous Hall measurements with sweeping an external field, we confirmed that the GdCo film had an easy axis normal to the film plane. Next, we applied a pulse current of duration of 10 μs and measured the anomalous Hall resistance under the magnetic field of 8 T in the film plane, which is sufficient to induce spin-flop transition at 240 K. When the pulse current exceeds the threshold, the Néel vector rotates during the pulse current application and eventually relaxes along out-of-plane direction, pointing randomly either upward or downward. The result shown in Fig. 2 indicates changes in the

anomalous Hall resistance when the pulse current above 16 mA is applied, implying the signature of the Néel vector rotation. Our study provided a significant step toward demonstrating the spin superfluidity.

[1] E. B. Sonin, Adv. Phys. Vol. 59, p.181-255 (2008). [2] S. Takei *et al*., Phys. Rev. B Vol. 90, 094408 (2014). [3] P. Wadley *et al*., Science Vol. 351, p.587-590 (2016). [4] L. Han *et al*., Sci. Adv. Vol. 10, eadn0479 (2024). [5] P. Zhang *et al*., Phys. Rev. Lett. Vol. 129, 017203 (2022)

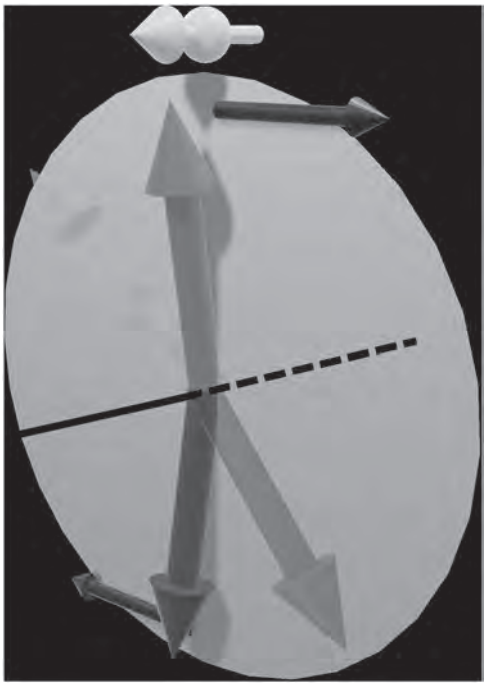

Fig. 1 Schematic illustration of the Néel vector rotation induced by spin-orbit torque.

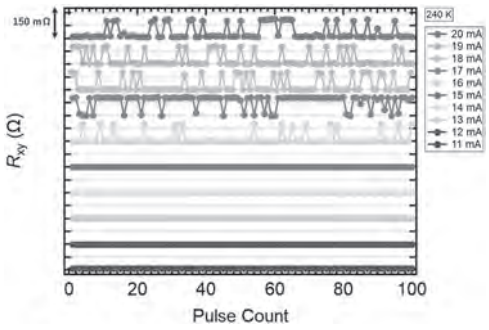

Fig. 2 Anomalous Hall resistance versus pulse number for various current amplitudes at 240 K and 8 T.

BE-05. Comparative investigation of temperature-dependent Gilbert damping in non-collinear antiferromagnetic Mn_3PtN and Mn_3Pt thin films. *N. Tripathi*[1], S. Mishra[1] and S. Isogami[2] *1. School of Materials Science & Technology, Indian Institute of Technology, IIT(BHU), Varanasi, India; 2. Research Centre for Magnetic and Spintronics Materials, National Institute of Materials Science, Tsukuba, Japan*

The influence of nitrogen has been investigated in the family of nitride-based antiferromagnets Mn3XN system, (X = Pt, Ir, etc.). The positive effects have been demonstrated such as showing large anomalous Hall effect due to enhanced Berry curvatures from Weyl points near the Fermi level [1,2]. Previous studies have shown that carbon can boost the anomalous Hall conductivity of CoMn thin films [3]. Whereas, boron can effectively modulate the spin structures and inter-band optical transitions of Mn4N thin film [4] and nitrogen can significantly increase the spin Hall angle in Mn3PtN in comparison to Mn3Pt [5]. The present study paves the way for the future tailoring of damping values using nitrogen in spintronic devices, such as spin-orbit torque magnetic random-access memories. We quantified the temperature-dependent effective Gilbert damping constant (αeff) and effective demagnetization field in Mn3PtN/CoFeB system on comparing with controlled sample Mn3Pt/CoFeB. The epitaxial samples consisting of Mn3PtN (5 nm)/CoFeB (3 nm)/MgO (3 nm), were deposited on MgO (001) substrates by DC/RF magnetron sputtering with a base pressure of 1×10–7 Pa. The FMR spectra were analysed using Kittel's formula assuming magnetic saturation along in-plane direction. Figure 1 shows the FMR spectra for the Mn3PtN/CoFeB bilayer with f = 7 GHz, indicating the behaviour of line width broadening for the 20K- 300K temperature range. Figure. 2 summarizes the temperature dependence of αeff compared with the controlled sample Mn3Pt to Mn3PtN sample, given by the FMR spectra in Fig. 1. It was revealed that the value was higher at 150 K, which is 1.25 times larger than the value at 300K which is 0.015(0.018) for Mn3Pt (Mn3PtN), and decreased with increasing te. In addition, we found negligible distribution of magnetic anisotropy in the bilayers. The magnetic transition from non-collinear to collinear antiferromagnetic spin structures influenced the exchange bias field. The effect of nitrogen on these characteristics will be more discussed for Mn3PtN/CoFeB and Mn3Pt/CoFeB bilayers at the conference [5].

[1] Zhou et al., Phys. Rev. B 101, 184403 (2020). [2] You et al., Nat. Comm. 12, 6524 (2021). [3] Isogami et al., Adv. Electron. Mater. 9, 2200515 (2023). [4] Sakaguchi et al., J. Phys. D: Appl. Phys (2023). [5] Tripathi et al., Phys. Rev. B 109, 224406 (2024).

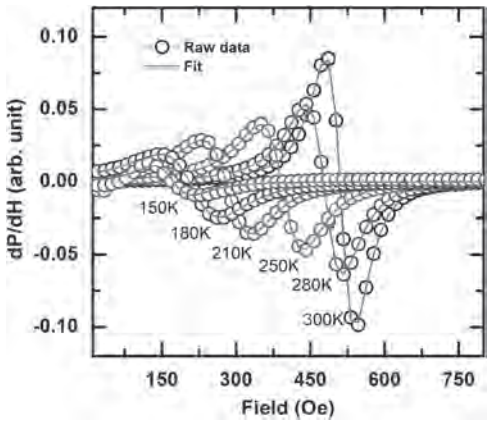

Fig.(1) FMR spectra for Mn3PtN/CoFeB measured at f = 7 GHz.

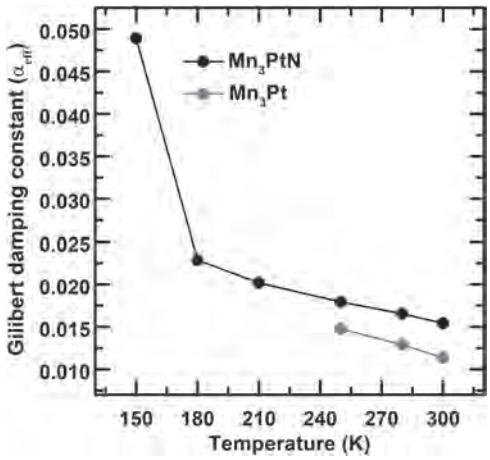

Fig. (2) comparative study of α_{eff} as a function of temperature.

BE-06. Withdrawn

BE-07. Magnetic Spin Hall Effect and Chirality Control of Antiferromagnetic Domain Walls in Compensated Ferrimagnets.

S. Ko[1], H. Kim[1], J. Kang[2], P. Cao Van[3], W. Choi[4], S. Kim[4], J. Jeong[3], B. Park[2], A.M. Park[1], K. Kim[5] and K. Kim[1,6] *1. Physics, Korea Advanced Institute of Science and Technology (KAIST), Daejeon, The Republic of Korea; 2. Material Science and Engineering, Korea Advanced Institute of Science and Technology (KAIST), Daejeon, The Republic of Korea; 3. Material Science and Engineering, Chungnam National University, Daejeon, The Republic of Korea; 4. Physics, University of Ulsan, Ulsan, The Republic of Korea; 5. Physics, Yonsei University, Seoul, The Republic of Korea; 6. Graduate School of Quantum Science and Technology, Korea Advanced Institute of Science and Technology (KAIST), Daejeon, The Republic of Korea*

The observation of the magnetic spin Hall effect (MSHE) has garnered significant attention due to its potential for generating z-spins [1,2] and enabling field-free spin-orbit torque switching [3]. However, MSHE has mainly been observed in non-collinear systems, and detecting it in collinear systems remains challenging. Although MSHE is considered a universal phenomenon, its clear identification in conventional collinear systems is complicated by the difficulty of distinguishing it from the anomalous Nernst effect (ANE). To address this, we deposited a ferrimagnetic GdCo bilayer with in-plane magnetic anisotropy by layering a Gd-rich top layer ($Gd_{30.4}Co_{69.6}$) over a Co-rich bottom layer ($Gd_{20.3}Co_{79.7}$). The antiparallel alignment of the Co moments in each layer cancels out the ANE signal and induces a natural antiferromagnetic domain wall. We discovered that the domain wall exhibits a Néel-like structure induced by the Dzyaloshinskii-Moriya interaction, resulting in an out-of-plane (OOP) magnetic moment [4]. This OOP moment generates a hysteresis loop in the anomalous Hall resistance when the magnetic field is swept along the in-plane direction. Notably, the polarity of this hysteresis loop is modulated by the in-plane current, indicating that the chirality of the domain wall can be effectively manipulated by the MSHE-induced spin current. Our findings reveal that compensated ferrimagnets serve as a unique platform for studying antiferromagnetic spintronics, providing a novel mechanism for controlling antiferromagnetic textures through MSHE.

[1] M. Kimata *et al*. *Nature* 565, 627-630 (2019). [2] K. Kondou *et al*. *Nature Communications* 12, 6491 (2021). [3] S. Hu *et al*. *Nature Communications* 13, 4447 (2022). [4] M. Bode *et al*. *Nature* 447, 190-193 (2007).

INVITED PAPER

BE-08. Manipulation of the quantum-metric structure in a topological chiral antiferromagnet. *J. Han*[1], T. Uchimura[1], Y. Araki[2], J. Yoon[1], Y. Takeuchi[1,3], Y. Yamane[1], S. Kanai[1,4,5], J. Ieda[2], H. Ohno[1] and S. Fukami[1,6] *1. Tohoku University, Sendai, Japan; 2. Japan Atomic Energy Agency, Tokai, Japan; 3. National Institute for Materials Science, Tsukuba, Japan; 4. PRESTO, Japan Science and Technology Agency, Kawaguchi, Japan; 5. National Institutes for Quantum Science and Technology, Takasaki, Japan; 6. Inamori Research Institute for Science, Kyoto, Japan*

The quantum metric and Berry curvature are two fundamental and distinct factors that describe the geometry of quantum eigenstates. While the role of the Berry curvature in governing various condensed-matter states has been investigated extensively [1,2], the quantum metric, which was also predicted to induce topological phenomena of equal importance [3], has rarely been studied. Recently, a breakthrough has been made in observing the quantum-metric nonlinear transport in a van der Waals magnet [4,5], but the effect is limited at cryogenic temperature and is tuned by strong magnetic fields of several teslas. In our study [6], we demonstrate room-temperature manipulation of the quantum-metric structure of electronic states through its interplay with the interfacial spin texture in a topological chiral antiferromagnet/heavy metal Mn_3Sn/Pt heterostructure (Fig. 1a), which is manifested in a time-reversal-odd second-order Hall effect (ScHE) (Figs. 1b and 1c). We show the flexibility of controlling the quantum-metric structure with moderate magnetic fields and verify the quantum-metric origin of the observed ScHE by theoretical modeling (Fig. 1c). Our results open the possibility of building applicable nonlinear devices by harnessing the quantum-metric structure of electronic states. A portion of this work is supported by JSPS Kakenhi Grant Nos. 19H05622, 22K03538, and 22KF0035, MEXT Initiative to Establish Next-Generation Novel Integrated Circuits Centers (X-NICS) Grant No. JPJ011438, and Casio Science and Technology Foundation Grant No. 40-4.

[1] D. Xiao, et al. *Rev. Mod. Phys.* 82, 1959 (2010). [2] L. Šmejkal, et al. *Nat. Phys.* 14, 242 (2018). [3] Y. Gao, et al. *Phys. Rev. Lett.* 112, 166601 (2014). [4] A. Gao, et al. *Science* 381,181 (2023). [5] N. Wang, et al. *Nature* 621, 487 (2023). [6] J. Han, et al. *Nat. Phys.* https://doi.org/10.1038/s41567-024-02476-2 (2024).

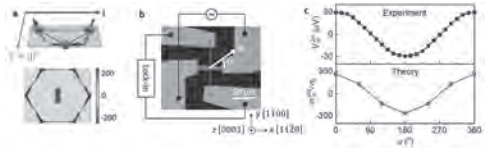

Fig. 1. a, Chiral-spin structure with out-of-plane canting in Mn_3Sn/Pt (upper panel), which leads to specific quantum-metric structure (lower panel) as the origin of the ScHE, that is, the Hall current j' is quadratic to the applied current j. b, Device connected to an alternating current source and a lock-in amplifier to measure the second-harmonic Hall signal to probe the ScHE. A magnetic field H that can rotate in the sample plane is applied. c, Experimental and theoretical ScHE as a function of the applied magnetic field angle. The field strength is fixed at 0.4 T.

CONTRIBUTED PAPERS

BE-09. Comparison of Magnetometry and Hall Transport in Ferrimagnetic Gd/Co Bilayers: Silent Spins and Altered Anisotropy. L. Hernandez[1], R.W. Greening[1], M.J. Roos[1], X. Fan[1] and *B.L. Zink*[1] *1. Physics & Astronomy, University of Denver, Denver, CO, United States*

Recently, transition metal (TM) rare earth metal (RE) ferrimagnetic (FIM) materials have seen a sharp increase in interest, since they offer unique tunability of the magnetization and offer potentially rapid magnetization dynamics. These systems have become an important focus in areas ranging from ultrafast all-optical magnetic switching, to "race-track" domain wall memories with increased speed, to current-driven switching in magnetic tunnel junctions via spin orbit torques. TM/RE ferrimagnetic systems have typically been explored both as alloys, and in layered structures with no intentional alloying. This second approach relies on strong antiferromagnetic interfacial exchange coupling of thin RE and TM films, forming a bilayer synthetic ferrimagnet. This has been particularly effective for all-optical switching, though still has open questions regarding the link between structure and composition of the layers and magnetic properties. Here we present a quantitative comparison of the anomalous Hall effect (AHE) and magnetic properties of Co/Gd bilayer synthetic ferrimagnets grown via sputtering at room temperature. As shown in Fig. 1, these samples have a magnetization compensation near 150 K, with diverging coercivity and a component of the SQUID measured magnetization that vanishes at the compensation temperature. However, as shown in Fig. 2, the ferrimagnet-like magnetic moment coexists with a second magnetic component that is entirely absent from the AHE signal near the compensation temperature. We suggest a possible origin for these electrically "silent" spins related to partial oxidation of the Gd layer [1]. We will also comment on a temperature dependent change in the magnetic anisotropy of similar bilayer FIM samples [2]. In contrast to the silent spins, this altered anistropy affects both AHE and the total sample magnetization.

1.) "Tunable temperature-driven magnetic switching and magnetic characterization of bilayer Gd/Co ferrimagnet heterostructures," L.Hernandez,R.W.Greening,M.J.Roos,X.Fan,andB.L.Zink,(submitted).2.) "Low temperature change of perpendicular magnetic anisotropy in synthetic bilayer ferrimagnet Pt-CoGd-Pt," L. Hernandez, R. W. Greening, M. J. Roos, X. Fan, and B. L. Zink (in preparation).

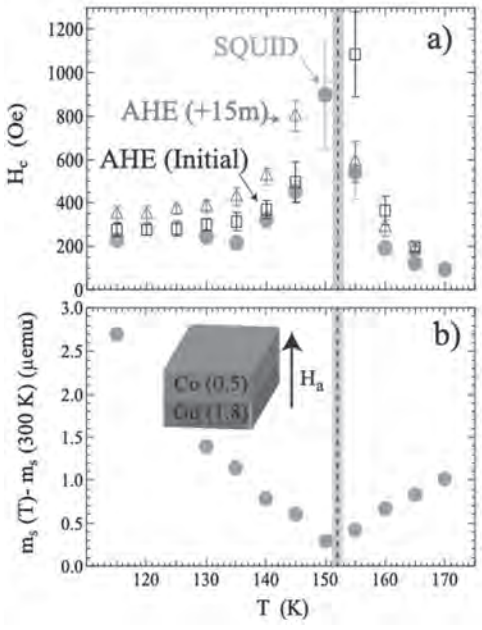

a) Coercive field vs. T for a Co/Gd bilayer ferrimagnet (with Pt over and underlayer). b) Isolating the FIM magnetic component, as shown in Fig. 2, shows vanishing M at compensation.

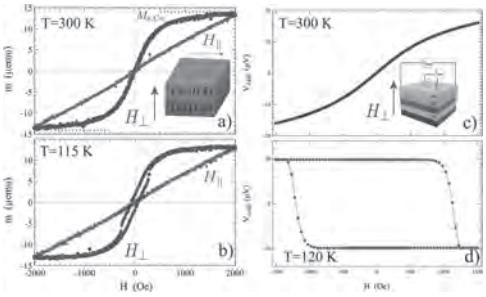

Comparison of SQUID measurements (a and b), and AHE on the same samples (c and d) shows that a large background component of magnetization from Co seemingly vanishes from AHE near compensation.

BE-10. Start-to-Finish Tuning of Magnetic Anisotropy in Iron Garnet Thin Films. *A. Kaczmarek*[1*], M. Aguiar[1], T.P. Grossmark[1], G. Beach[1] and C.A. Ross[1] *1. Materials Science and Engineering, Massachusetts Institute of Technology, Cambridge, MA, United States*

Iron garnet thin films ($IG, R_3Fe_5O_{12}$; R = Y, Eu, Tb, Dy, Tm, Lu, Bi) are desirable for spintronic devices, due to their highly engineerable magnetic anisotropy. While magnetic anisotropy in these films arises from many sources, most are predetermined by properties intrinsic to composition and substrate choice, and are not easily varied after growth. In contrast, magnetotaxial[1], or growth-induced, anisotropy arises from kinetically-controlled ordering of different R cations in nonequivalent dodecahedral sites at the growth surface and can be tuned during and after film growth. For any mixed-cation garnet, the degree of cation order (DCO), and thus magnetotaxial anisotropy, can be tuned three ways: (1) via substrate orientation and lattice parameter, which change the sites available to arriving cations; (2) via growth parameters to control the ordering kinetics; and (3) by annealing films to promote cation diffusion, reducing DCO and anisotropy. Here, we engineer magnetotaxial anisotropy in mixed (Bi, Lu, Y)IG thin films (~30 nm) made by pulsed laser deposition on (111)-oriented garnet substrates with a range of lattice constants. Structure and strain were measured by X-ray diffraction (XRD), and vibrating sample magnetometry and ferromagnetic resonance were used to determine saturation magnetization (~140 Ka/m) and anisotropy, with damping in the range of 0.001-0.0001. Cation order leads to the appearance of a normally forbidden (1-10) XRD peak, from which we quantify DCO. We find clear correlation of magnetotaxial anisotropy with DCO, confirming that R cation order produces anisotropy. DCO decreases linearly with increasing lattice mismatch in BiYIG films (Fig. 1). We also found that for LuYIG films, Lu and Y ordering has a nonmonotonic dependence on the growth rate, controlled via the laser repetition rate (Fig. 2). Lastly, we show that post-growth annealing reduces DCO and anisotropy in LuYIG films. This work facilitates the atom-by-atom engineering and development of new garnets for spintronic and magnonic devices.

A. Kaczmarek, E. Rosenberg, et al. *Nat. Commun.* 15, 5083 (2024).

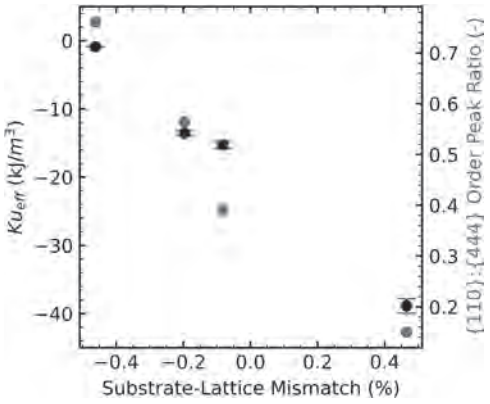

Fig. 1 Anisotropy and DCO for $Bi_{0.8}Y_{2.2}IG$ films grown on various substrates.

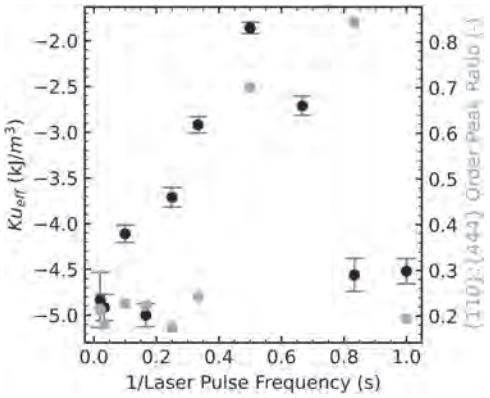

Fig. 2 Anisotropy and DCO vs. laser pulse rate for $Lu_{0.5}Y_{0.5}IG$ on (111) $Gd_3Ga_5O_{12}$.

BE-11. Strain Effects on Fluctuation Properties of Noncollinear Antiferromagnets for Probabilistic Computing Applications. *M. Rahman*[2,1] and M. Stiles[1] *1. Physical Measurement Laboratory, National Institute of Standards and Technology, Gaithersburg, MD, United States; 2. Department of Chemistry & Biochemistry, University of Maryland, College Park, MD, United States*

Noncollinear antiferromagnetic materials with D019 crystal symmetry (e.g., Mn3X; X=Sn, Ge, etc.) exhibit intriguing properties, positioning them as promising candidates for probabilistic computing. Despite being antiferromagnetic, the unique crystal symmetries in these systems allow phenomena such as tunneling magnetoresistance and the anomalous Hall effect, making them amenable to electrical readout techniques. Additionally, the competing magnetic interactions inherent in these systems give rise to an effective low-barrier system, a crucial element for accelerating existing probabilistic computing hardware. However, real-world samples of noncollinear antiferromagnets have not yet been developed into functional generators of randomness. This is speculated to be due to strain effects, which predominantly influence the material's pristine parameters [1, 2], thereby severely affecting their fluctuation properties. In this work, by combining density functional theory and micromagnetic simulations, we quantify the effect of epitaxial strain on the lattices of noncollinear antiferromagnets to predict their fluctuation properties. We find that strains typical of those due to substrates used to date increase the barrier high enough to drastically slow down the switching rate. These findings will not only help us design noncollinear antiferromagnets that are less susceptible to strain effects, leading to better p-bit candidates, but also develop novel methods for controlling and manipulating magnetism within this promising material platform.

[1] Higo, Tomoya, et al. Nature 607 (2022) 474 [2] Z. He, L. Liu, J. Appl. Phys. 135 (2024) 093902

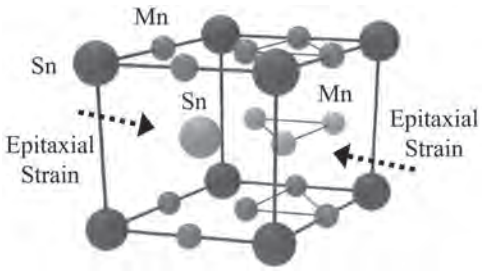

Epitaxial strain breaks crystal symmetry, modulating magnetic parameters that are symmetric in the pristine state. This results in a high-barrier system, which subsequently affects thermal stability of such magnets.

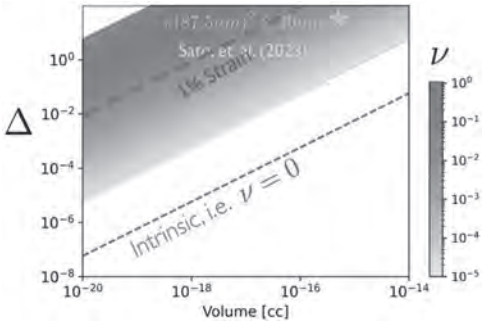

The thermal stability factor (Δ~Eb arrier/KT) is studied as a function of volume and ν, the exchange asymmetry constant that quantifies the degree of strain-induced symmetry breaking. Results suggest that strain can affect the thermal stability of these magnets, leading to a potential barrier-tuning mechanism using a controlled strain environment.

Session BF
HARD MAGNETS I
Ester M. Palmero, Chair
IMDEA Nanociencia, Madrid, Spain

INVITED PAPER

BF-01. Development of High-Performance Nd-Fe-B Based Magnet: Combating Materials Criticality. *X. Tang*[1], H. Sepehri-Amin[1], T. Ohkubo[1] and K. Hono[1] *1. National Institute for materials Science, Tsukuba, Japan*

In this talk, I will summarize our recent efforts in the development of high-performance Nd-Fe-B-based permanent magnets, with a focus on minimizing reliance on critical elements such as Dy and Nd. I will begin by introducing our recent fundamental research on the microstructural origins of high coercivity in (Nd,Dy)-Fe-B magnets. Contrary to conventional belief, this work reveals the role of Dy at grain boundaries in achieving high coercivity in Dy-containing magnets [1]. Based on this fundamental research, we employed a grain boundary diffusion process [2-3] to control the magnetism of the grain boundary phase, leading to the development of Dy-lean [4-5], Dy-free[6], and even Nd-lean [7-8] high-performance magnets. The magnets discussed in this talk exhibit attractive properties when benchmarked against those developed by industry and academia, while also reducing the usage of critical elements. Lastly, I will introduce the development of permanent magnets for a novel type of motor application [9].

[1] X. Tang et al, *NPG Asia Mater.*, 15, 50(2023). [2] H. Sepehri-Amin et al *Scri.Mater.* 63, 1124-1127 (2010). [3] H. Sepehri-Amin et al, *Acta Mater.* 61, 6622–6634 (2013) [4] X. Tang et al, *Acta Mater.* 203, 116479(2021). [5] M. Korent et al, *Scr. Mater.* 205, 114207(2021). [6] X. Tang, unpublished [7] X. Tang et al *Acta Mater.* 175, 1-10 (2019). [8] X. Tang et al *Acta Mater.* 190, 8-15 (2020). [9] X. Tang et al *Acta Mater.* 228, 117747 (2022).

CONTRIBUTED PAPERS

BF-02. Bulk Magnetic Hardening in $Sm(Fe,V)_{12}$ Alloys. Y. Xu[1], C. Han[2], C. Ni[2], A. Gabay[1] and *G. Hadjipanayis*[1,3] *1. Department of Physics and Astronomy, University of Delaware, Newark, DE, United States; 2. Department of Materials Science and Engineering, University of Delaware, Newark, DE, United States; 3. Department of Chemical Engineering, Northeastern University, Boston, MA, United States*

Cast Sm-Fe-V magnets with the tetragonal $ThMn_{12}$ type crystal structure were prepared with high coercivity through a two-step annealing. The annealing protocol used allowed us to produce a sufficient amount of non-magnetic Sm-rich grain-boundary phase for the efficient isolating of the 1:12 grains. As a result, a sample with composition $Sm_{11.1}Fe_{75.8}V_{13.1}$ achieved a coercivity of 3.6 kOe after the first annealing at 775 °C for 72 h and a record-high value of 6.7 kOe after an additional annealing at 825°C for 2 h. Scanning and transmission electron microscopy revealed that after the first annealing the Sm-rich phase is scarce and mostly concentrated in the triple junctions; after the second annealing, the phase is found at both the triple junctions and the grain boundaries (Fig. 1). The high coercivity, obtained without the use of powder metallurgy, has nearly doubled as compared to the highest previously reported value of 3.7 kOe [1]. This result opens a new pathway for enhancing the magnetic properties of rare-earth-lean permanent magnets, crucial for various technological applications where rare earth elements availability and cost are major concerns.

[1] S. Sugimoto, T. Shimono, H. Nakamura et al., Mater. Chem. Phys., Vol. 42, p. 298 (1995)

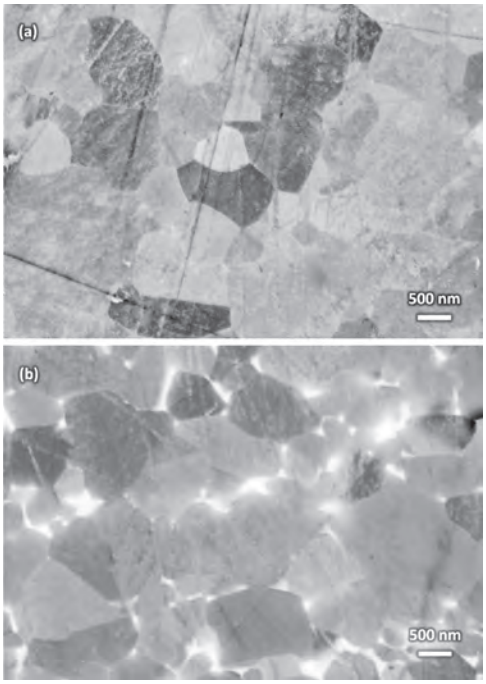

Fig. 1. Backscattered-electrons SEM micrographs (a) after annealing at 775 °C and (b) after additional annealing at 825 °C.

BF-03. Achieving high coercivity in post-sinter annealed Cu-doped $Sm(Fe,Ti,V)_{12}$-based sintered magnets. *J. Zhang*[1], X. Tang[1], T. Ohkubo[1], K. Hono[1] and H. Sepehri-Amin[1] *1. National Institute for Materials Science, Tsukuba, Japan*

Research on $SmFe_{12}$-based (1:12) compounds has been revived due to their excellent intrinsic magnetic properties [1]. However, how to transfer the intrinsic magnetic properties to the high extrinsic performance in bulk 1:12 magnet is still a major problem. Recent studies have been demonstrated coercivities of 0.8-1.0 T in textured 1:12 sintered magnets [2, 3]. Note that the reported coercivity is still less than 10% of the anisotropy field of the 1:12 phase. By introducing Cu, a record high coercivity of 1.4 T was obtained due to the formation of Cu-rich intergranular phases between 1:12 grains [4]. Therefore, microstructure engineering is essential to further realize high coercivity. Post-sinter annealing (PSA) is effective in forming the continuous grain boundary (GB) in Nd-Fe-B sintered magnets [5]. The question is whether PSA can further increase the coercivity in 1:12 sintered magnets. In this work, $Sm_8Fe_{77}Ti_5V_8Al_2$ (named Cu-free) and $Sm_8Fe_{76.5}Ti_5V_8Al_2Cu_{0.5}$ (named Cu-doped) sintered magnets were prepared by conventional powder processing method. The magnets were prepared by sintering at 1100 °C for 1.5 h, and followed by PSA at 500-1100 °C for 1.5 h. The coercivity of the Cu-doped magnet was significantly enhanced from 0.9 T to 1.48 T by PSA at 1100 °C for 1.5 h, compared to 0.93 T to 1.05 T in the referenced Cu-free magnet (Fig. 1a). Detailed microstructure characterizations were conducted

to understand the origin of the coercivity increase. The existence of ferromagnetic $SmFe_2$ in post-sinter annealed Cu-free sample was observed by XRD, TEM, and Lorentz microscopy while it could be fully eliminated in the optimally annealed Cu-doped sample. Moreover, thick and continuous Sm-rich intergranular phase with an excellent interconnection was observed in the optimally annealed Cu-doped magnet (Fig. 1c). Formation of thick intergranular phases can reduce the exchange-coupling between 1:12 grains resulting in a coercivity enhancement. This work indicates that the addition of Cu is beneficial to realize a large coercivity in optimally annealed 1:12 sintered magnets by suppressing the $SmFe_2$ phase and forming the Sm-rich intergranular phase.

[1] A. Gabay, G. Hadjipanayis, Recent developments in RFe_{12}-type compounds for permanent magnets, Scripta Materialia, 154 (2018) 284-288. [2] K. Otsuka, M. Kamata, T. Nomura, H. Iida, H. Nakamura, Coercivities of Sm-Fe-M sintered magnets with $ThMn_{12}$-type structure (M= Ti, V), Materials Transactions, 62 (2021) 887-891. [3] J. Zhang, X. Tang, H. Sepehri-Amin, A. Srinithi, T. Ohkubo, K. Hono, Origin of coercivity in an anisotropic $Sm(Fe,Ti,V)_{12}$-based sintered magnet, Acta Materialia, 217 (2021) 117161. [4] A. Srinithi, X. Tang, H. Sepehri-Amin, J. Zhang, T. Ohkubo, K. Hono, High-coercivity $SmFe_{12}$-based anisotropic sintered magnets by Cu addition, Acta Materialia, 256 (2023) 119111. [5] R.K. Mishra, J. Chen, G. Thomas, Effect of annealing on the microstructure of sintered Nd-Fe-B magnets, Journal of applied physics, 59 (1986) 2244-2246.

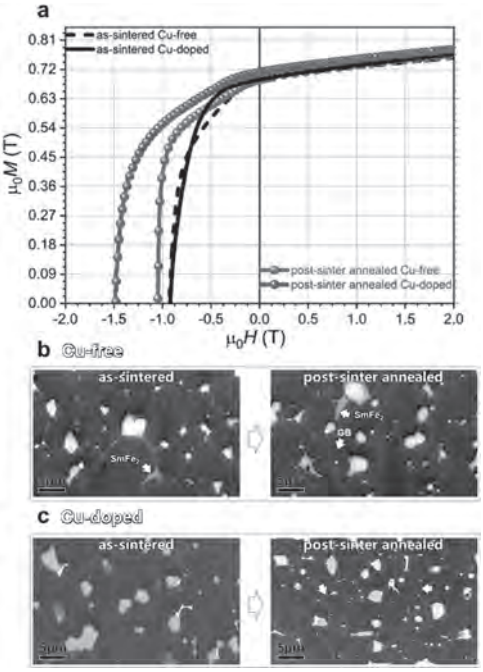

Fig. 1 Demagnetization curves and SEM images for Cu-free and Cu-doped magnets.

BF-04. Magnetic Properties and Microstructures of (Nd,Ce)-Fe-B Based HDDR Magnet Powders. *R. Shimbo*[1,2], T. Horikawa[1,2], M. Yamazaki[2], M. Matsuura[1], R. Kainuma[1] and S. Sugimoto[1] *1. Graduate School of Engineering, Tohoku University, Sendai-shi, Japan; 2. Aichi Steel Corporation, Tokai-shi, Japan*

Due to the recent increase in Nd demand, concerns about the Nd resource supply become an issue in Nd-Fe-B magnets. To solve this issue, it has been reported that a part of the Nd is replaced with abundant Ce, and the grain boundary diffusion (GBD) method is applied to form a core-shell structure to suppress the reduction of magnetic properties.[1)] However, there are few reports on such anisotropic (Nd,Ce)-Fe-B magnet powders produced by the HDDR method.[2-6)] In this study, we prepared three types of magnet powders with different amounts of Ce substitution and investigated their magnetic properties and microstructures. Starting powders of $(Nd_{1-x}Ce_x)_{12.5}Fe_{bal}B_{6.5}Nb_{0.2}$ with x=0 (Ce0), 0.5 (Ce50) and 1 (Ce100) were heated at 820°C under 30 kPa hydrogen for 3 h, followed by an evacuation to 1 kPa for 1.5 h (HDDR). Each of the obtained powders was then mixed with Nd-Cu-Al powder and subjected to GBD treatment at 800°C under vacuum for 1 h. The demagnetization curve after GBD of Ce50 showed a knick, which was not found in Ce0 and Ce100 (Fig. 1). From the results of XRD and SEM-EDX after HDDR of Ce50, ferromagnetic RFe_2 was found in the grain boundary in addition to $R_2Fe_{14}B$ and R-rich phase. Moreover, STEM-EDX results suggested that there is an inhomogeneous distribution of Ce within the $R_2Fe_{14}B$ grains, especially when RFe_2 was adjacent (Fig. 2 (a)). The RFe_2 is thought to be formed during the recombination stage in HDDR, in addition to that originally contained in the starting powder, and prevents the magnetically isolation of $R_2Fe_{14}B$ grains, resulting in a decrease in local H_{cJ}. Additionally, the above-mentioned compositional inhomogeneity in $R_2Fe_{14}B$ may occur at the recombination stage due to the difference in the pressure-temperature equilibrium curves (*P-T* curve) in HDDR between $Nd_2Fe_{14}B$ and $Ce_2Fe_{14}B$ (Fig. 2 (b))[7)]. Hence, the differences in the crystalline magnetic anisotropy within the $R_2Fe_{14}B$ grains are induced. Therefore, both RFe_2 and compositional inhomogeneity in $R_2Fe_{14}B$ grains induce the variation of H_{cJ}, which causes the knick in the demagnetization curve of Ce50.

1) M. Ito, M. Yano, N. Sakuma H. Kishimoto, A. Manabe, T. Shoji, A. Kato, N. M. Dempsey, D. Givord, and G. T. Zimanyi, *AIP Adv.*, Vol. 6, 056029 (2016) 2) T. Takeshita and R. Nakayama, *Proc. 10th Int'l. Workshop on Rare-Earth Magnets and Their Applications,* 551 (1989) 3) S. Sugimoto, H. Nakayama, K. Kato, D. Book, T. Kagotani, M. Okada and M. Homma, *J. Alloys Compd*., Vol. 293, 862 (1999) 4) C. Mishima, N. Hamada, H. Mitarai and Y. Honkura, *J. Magn. Soc. Jpn.*, Vol. 24, 407 (2000) 5) I. Poenaru, A. Lixandru, K. Güth, A. Malfliet, S. Yoon, I. Škulj and O. Gutfleisch, *J. Alloys Compd.*, Vol. 814, 152215 (2020) 6) M. Xing, J. Han, Z. Lin, F Wan, C. Li, S. Liu, C. Wang, J. Yang and Y. Yang, *J. Magn. Magn. Mater.*, Vol. 331, 140 (2013) 7) R. Shimbo, T. Horikawa, M. Yamazaki, M. Matsuura, R. Kainuma and S. Sugimoto, *Mater. Trans.*, Vol. 64, 266 (2023)

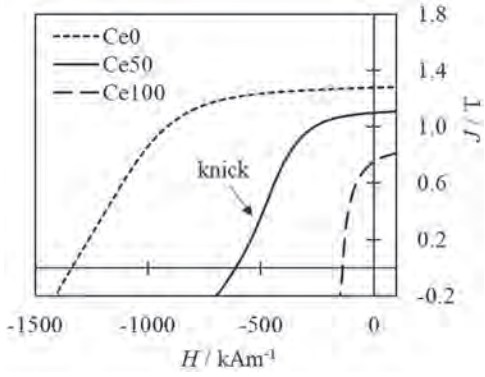

Fig. 1. Demagnetization curves of each Ce content after GBD

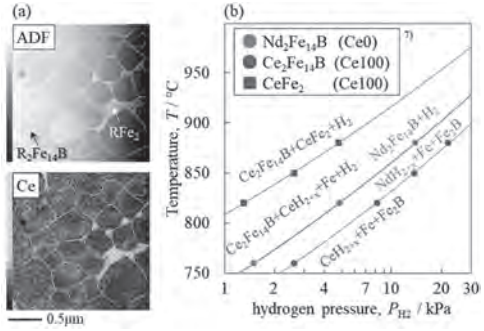

Fig. 2. (a) STEM-EDX mapping of Ce50 after HDDR (b) *P-T* curves in HDDR of Ce0 and Ce100

BF-05. 2- and 3-dimensional measurements of magnetic domain wall pinning in $Sm_2(CoFeCuZr)_{17}$. *A. Kovács*[1], A. Silinga[2], Y. Yang[3], T. Almeida[2], T. Smoliarova[4], B. Xu[3], K. Skokov[3], O. Gutfleisch[3], M. Farle[4] and R.E. Dunin-Borkowski[1] *1. Forschungszentrum Juelich, Juelich, Germany; 2. University of Glasgow, Glasgow, United Kingdom; 3. Technische Universität Darmstadt, Darmstadt, Germany; 4. University of Duisburg-Essen, Duisburg, Germany*

$Sm_2(CoFeCuZr)_{17}$ is a pinning-type high-performance magnet with outstanding thermal and chemical stability. The high coercivity results from the strong magnetic domain wall pinning at the phase boundaries between the hexagonal $SmCo_5$ and Sm_2Co_{17} phases. We use advanced off-axis electron holography, model-based reconstruction of the magnetisation and micromagnetic modelling to characterize the domain wall pinning properties in 2- and 3-dimensions. We investigate the correlation between the structure and magnetic field distribution around the domain wall using a sequence of experimental methods and micromagnetic simulations as shown in Figure 1. Conventional scanning transmission electron microscopy (S)TEM is used to map the phases around the domain wall that is imaged by Lorentz TEM (Fig.1a,b). The magnetic phase shift is then used to visualize the corresponding in-plane magnetic induction (Fig.1c) and to recover the magnetisation (Fig.1d) using a model-based iterative reconstruction. The TEM data are used as input for micromagnetic modelling (Fig.1e), which provides a representative analysis of the domain wall pinning. The 3-D characterisation is obtained by recording two orthogonal tilt series of electron holograms from a needle-shaped $Sm_2(CoFeCuZr)_{17}$ specimen. Following a tomographic reconstruction of the magnetisation, the 3-D field arrangement of the domain walls is obtained. The results are discussed in terms of the shape and the magnetocrystalline anisotropy of the sample, as well as local variations in its microstructure and chemical composition.

[1] This work is supported by Deutsche Forschungsgemeinschaft (DFG) through Project-ID 405553726, TRR270 HoMMage.

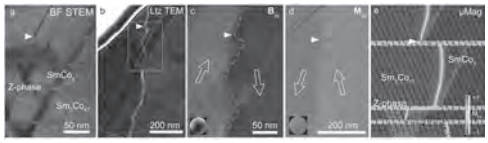

Figure 1. (a) BF STEM image of the Sm_2Co_{17}, $SmCo_5$ and Zr-rich Z-phase. (b) Defocused Lorentz TEM image, where the bright line is a domain wall. (c,d) Projected in-plane magnetic induction and magnetization maps extracted from off-axis electron holography and model-based reconstruction. (e) Micromagnetic modelling of the same geometry of phases extracted from TEM imaging. The white triangle mark the same region.

BF-07. Magnetic domain imaging for Sm-Fe-N powder by magnetic force microscopy. *Y. Hirayama*[1], W. Yamaguchi[1] and S. Okada[1] *1. Innovative Functional Materials Research Institute, Nagoya, Japan*

$Sm_2Fe_{17}N_3$ is a compound with high potential [1] as a post-Neodymium magnet. We have prepared high-performance $Sm_2Fe_{17}N_3$ fine powders by various methods [2]. Although the coercivity increases with decreasing particle size, fine powders prepared by different methods have different baselines of the relationship between particle size and coercivity. In particular, the reduction diffusion (RD) method can prepare much larger coercivity than powders obtained by the milling method, even with the same particle size distribution. One of the reasons for this is pointed out to be the good crystallinity and smooth surface of powders prepared by the RD method. On the other hand, for powders prepared by the milling method, damage accumulated on the surface during milling weakens the magnetism of the powder surface, causing a decrease in coercivity. However, there are few examples of direct observation of the magnetic domain structure inside the powder. Therefore, in this study, the magnetic domain state was investigated in detail using magnetic force microscopy (MFM). The anisotropic Sm-Fe-N powders were prepared by the jet milling and RD process. These powders were aligned and magnetized at 9 T in a resin. The flat surface was obtained using Ar mill. The magnetic domains in the state of remanent magnetization were observed in planes parallel and perpendicular to the c-axis. MFM (Nanosurf, DriveAFM) was used to observe the magnetic domains. The magnetic domains of SmFeN were observed while changing the magnetic field from the remanent magnetization state to -0.7 T. Even in the remanent magnetization state after magnetization at 9 T, numerous magnetic domains were observed within the grains, confirming a multidomain state. In particular, a maze pattern was observed for particles larger than 5 μm. Since the width of the magnetic domain was about 2 μm. Therefore, it was found that the particle diameter should be less than 2 μm to produce single-domain particles with better magnetic properties.

[1] T. Iriyama, K. Kobayashi, N. Imaoka, T. Fukuda, H. Kato, and Y. Nakagawa, "Effect of nitrogen content on magnetic properties of $Sm_2Fe_{17}N_x$ ($0<x<6$)," Magnetics, IEEE Transactions, 28 (1992) 2326-2331. [2] K. Takagi, Y. Hirayama, S. Okada, W. Yamaguchi, K. Ozaki, "Novel powder processing technologies for production of rare-earth permanent magnets" Science and Technology of Advanced Materials 22 (2021) 150-159.

BF-08. Progress towards Gas Atomized Feedstock to Substitute for Strip Casting in Scalable Manufacturing of Dy-free Ultrafine Grained Nd-Fe-B Magnets. *B. Finney*[2,1], M.J. Kramer[2], W. Tang[2], B. Cui[2], J. Cui[2,1] and I.E. Anderson[2,1] *1. Materials Science and Engineering, Iowa State University, Ames, IA, United States; 2. Ames National Laboratory, Ames, IA, United States*

Strong permanent magnets are increasingly important with the continued development of electric vehicles. The superior ambient temperature magnetic strength of Nd-Fe-B has been well-known since their development/discovery in the early 1980s. Dy additions provide the thermal stability for these permanent magnets to be used at motor operation temperatures (150-180C). However, using this heavy rare-earth (HRE) is not sustainable and must be replaced with an alternate way to provide thermal stability. Research from Hono shows that an ultrafine (<2-3 μm) grain size also improves high-temperature magnetic properties. Coercivity can be enhanced, especially if grains are sufficiently isolated from magnetic interaction (inhibiting domain switching). Domain switching can also be caused by microstructure "contamination" from free iron (a soft magnetic phase) in the magnets that can form during solidification. Both the alloy choice and solidification rate of the Nd-Fe-B alloy must be considered to effectively eliminate the ferritic Fe phase from the solidification microstructure of the magnet alloy. Conventional Nd-Fe-B magnet alloy feedstock is hydrogen decrepitated and milled from strip-cast stock with a composition designed to eliminate free-Fe for strip-cast solidification. Substituting gas atomized feedstock requires an alloy compatible with rapid solidification during gas atomization to maximize usable powder yield, like strip casting. An analysis of the pseudo-binary equilibrium phase diagram considered a metastable field construction where free-Fe can nucleate as a primary phase from the melt but not excessively to reduce the magnetic saturation of resulting magnets. Thus, we tried to eliminate free-Fe in solidified powders. This work was done in conjunction with GKN Hoeganaes, who made a powder composition series in the GKN labs with an EIGA (electrode induction melting gas atomization) that was studied initially with X-ray diffraction. Subsequent SEM and XRD revealed differences with our conventional gas-atomized powder of the same size class. Supported by USDOE-EERE-VTO through Ames National Laboratory contract DE-AC02-07CH11358.

1. (figure 1) M. Sagawa, S. Hriosawa, H. Yamamoto, S. Fujimura, Y. Matsuura. B-Fe-Nd Phase Diagram. ASM Alloy Phase Diagram Center. 1987 2. (figure 2) Hono K, Sepehri-Amin H. Strategy for high-coercivity Nd-Fe-B magnets. Scr Mater. 2012 Sep;67(6):530–5.

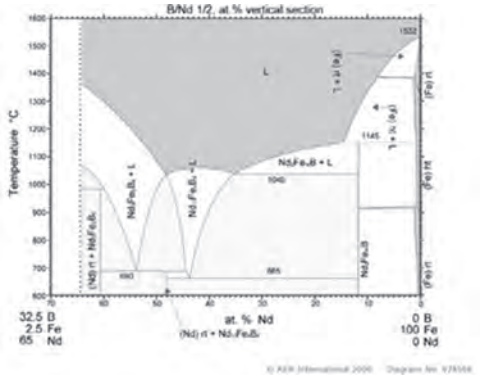

Phase diagram of Nd-Fe-B magnets

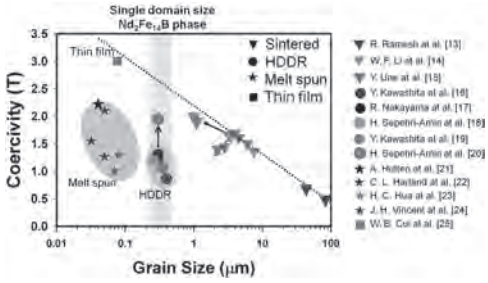

Coercivity vs. grain size for sintered magnets

BF-09. Increase of energy products of $Sm_2Fe_{17}N_3$ sintered magnet using novel sintering aid. *Y. Iida*[1,2], A. Hosokawa[2], W. Yamaguchi[2] and Y. Hirayama[2] *1. Niterra Co., Ltd., Komaki, Japan; 2. National Institute of Advanced Industrial Science and Technology (AIST), Nagoya, Japan*

The $Sm_2Fe_{17}N_3$ compound is one of prospective candidates for next generation permanent magnets because of its high saturation magnetization and coercivity as well as high Curie temperature [1]. However, $Sm_2Fe_{17}N_3$ has not been sintered densely due to the constraints of decomposition temperature (620°C). It has been reported that Zn (melting point, T_m = 420°C) bonded magnets improved density and coercivity [2]. Unfortunately, during the sintering process, the lower magnetization phase was formed at the interface of $Sm_2Fe_{17}N_3$ and Zn, which reduced the squareness and maximum energy product [2,3]. Therefore, it is necessary to develop novel sintering aids other than Zn to improve the performance of $Sm_2Fe_{17}N_3$ sintered magnet. We newly discovered one of the promising metals containing alkaline earth metals with low T_m as a sintering aid, which can achieve the high density and energy product for $Sm_2Fe_{17}N_3$ sintered magnet. Commercial coarse $Sm_2Fe_{17}N_3$ powder pulverized by jet-milling under argon atmosphere inside a glove box and obtained the low oxygen content fine powder (D_{50} = 2–3 μm). For sintering aids, we chose the Ba-based alloy and obtained the fine powder (D_{50} = 2–3 μm) by planetary ball-milling after arc melting. The magnetic alignment was conducted under 2 T at room temperature. The mixed powder was sintered at 450°C for 2 min under the vacuum below 0.5 Pa with applying a pressure of 1200 MPa. The magnetic properties of sintered magnets were characterized by using the PPMS-VSM (Quantum Design inc.). It was confirmed that the T_m of the Ba-based alloy powder was 440°C by differential scanning calorimetry. We succeeded in obtaining $Sm_2Fe_{17}N_3$ sintered magnets with a relative density of 90.2 % with developed sintering aid. Furthermore, the remanence improved with densification and no decrease in squareness was confirmed. The maximum energy product of the $Sm_2Fe_{17}N_3$ magnets with the addition of sintering aid was 195 kJ/m^3, whereas that without the addition of sintering aid was 170 kJ/m^3.

[1] T. Iriyama, K. Kobayashi, N. Imaoka, *IEEE Trans. Magn.*, 28, p.2326-2331 (1992) [2] M. Matsuura, N. Tezuka, S. Sugimoto, *J. Magn. Magn. Mater.*, 467, p.64-68 (2018) [3] M. Matsuura, N. Tezuka, S. Sugimoto, *J. Magn. Magn. Mater.*, 510, p.166943 (2020)

BF-10. Metal coating of $Sm_2Fe_{17}N_3$ powder to realize heat-resistant resin-bonded magnet applications. *W. Yamaguchi*[1], K. Takagi[1], A. Hosokawa[1] and Y. Hirayama[1] *1. National Institute of Advanced Industrial Science and Technology (AIST), Nagoya, Japan*

$Sm_2Fe_{17}N_3$ is recognized as a competent material for anisotropic bonded magnets, but its potential has not been fully exploited yet. $Sm_2Fe_{17}N_3$ has magnetization comparable to that of $Nd_2Fe_{14}B$, and its Curie temperature is much higher than that of $Nd_2Fe_{14}B$, so it should have occupied an important position as a heat-resistant magnet. However, due to the significant drops in coercivity at elevated temperatures, its use as a high heat-resistant powder has not realized. Since it has been proven that the coercivity degradation is caused by a redox reaction between the magnet phase and the iron oxides contained in the surface oxide layer [1], it is expected that the problem can be solved by forming an oxidation-resistant film on the surface of each particle. The coating material should be free of oxygen itself, dense, and have the ability to stop oxidation from progressing inward. In the present study, we are establishing a technology to form a uniform metal film on the surface of oxide-free powder, and are searching for materials that prevent oxidation. $Sm_2Fe_{17}N_3$ fine powders with oxide-free surfaces were prepared by jet-milling a coarse powder in a purified Ar atmosphere [2]. Coating the powders with various metals was carried out by a magnetron sputtering technique while stirring the powder in a vacuum chamber [3]. The coated and uncoated powders were subjected to heat treatment at 300 °C for 2h in the air. Magnetic property of the powders with and without coating after the heat treatment were measured using a vibrating sample magnetometer. Microstructures around the surface of the coated particles were observed using a transmission electron microscope (TEM). Coercivity of the as-coated powders increased or decreased depending on the coating material. Degradation in the coercivity and the remanence caused by heating in the air was significantly suppressed for some coating materials. TEM observations confirmed that the $Sm_2Fe_{17}N_3$ phase and the covering layer formed an oxide-free, direct metal-to-metal interface. For the powders with improved heat resistance, penetration of oxygen was limited within the covering layer, even after the heat-treatment in the air.

[1] W. Yamaguchi, R. Soda, K. Takagi, Role of Surface Iron Oxides in Coercivity Deterioration of $Sm_2Fe_{17}N_3$ Magnet Associated with Low Temperature Sintering, Mater. Trans. 60 (2019) 479-483. [2] R. Soda, K. Takagi, M. Jinno, W. Yamaguchi, and K. Ozaki, Anisotropic $Sm_2Fe_{17}N_3$ sintered magnets without coercivity deterioration, AIP Advances 6 (2016) 115108. [3] W. Yamaguchi, R. Soda, K. Takagi, Metal-coated $Sm_2Fe_{17}N_3$ magnet powders with an oxide-free direct metal-metal interface, J. Magn. Magn. Mater. 498 (2020) 166101.

BF-11. Synthesis Optimization for $Sm_2Fe_{17}N_3$ for Bulk Magnet Fabrication. *R. Kuchi*[1], I.Z. Hlova[1], X. Liu[1], O. Palasyuk[1], D. Schlagel[1], A. Peirsol[2] and M.J. Kramer[1] *1. Ames National Laboratory, Ames, IA, United States; 2. Iowa State University, Ames, IA, United States*

High-performance permanent magnets play a crucial role in efficient energy conversion in high-power density electric motors and generators. Currently, Nd-Fe-B-based magnets doped with Dy are commonly used for these applications. However, the high cost and criticality of Nd/Dy present significant obstacles to meet the increasing demand in permanent magnets due to anticipated growth in electric vehicles and the planned expansion of offshore wind turbines. While some manufacturers have started incorporating low-performance critical-element-free magnets into traction motors, a more promising solution could be the development of thermally stable Sm-Fe-N-based material for manufacturing of fully dense sintered permanent magnets with properties comparable to Nd-based magnets that has the potential to transform the automotive permanent magnet industry. Both thermal instability and surface oxidation have been identified as major reasons for the reduction in coercivity during sintering thus hindering the widespread adoption and implementation of high-performance sintered Sm-Fe-N-based magnets. The innovative reduction-diffusion synthesis that directly converts Sm_2O_3 into Sm_2Fe_{17} followed by nitrogenation and washing produces a low-oxygen

thermally stable material that, upon sintering, does not exhibit signs of deterioration. Our bottom-up synthesis produces powders with ~< 1 μm grains demonstrating H_{ci} ~ 14.3 kOe and M_s of 143 emu/g. Our top-down approach forms larger grains > 10 μm but when milled produces H_{ci} of ~ 6.7 kOe but higher M_s (159 emu/g) and better remanence (M_r ~ 140 emu/g) with an energy product of 22.4 MGOe.

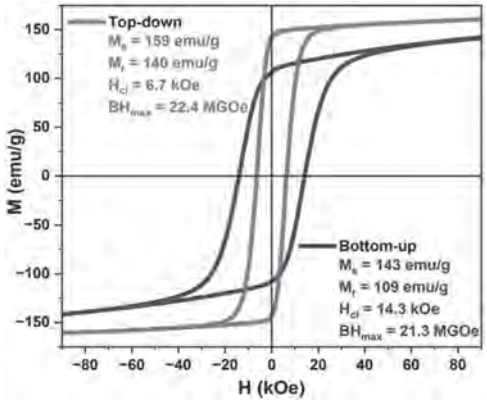

BF-12. Fe based approaches for rare-earth reduced and free permanent magnets. *L. Alff*[1] *1. TU Darmstadt, Darmstadt, Germany*

Iron is the most abundant ferromagnetic element on earth. Due to its extraordinary chemical versatility, it can be used in various compounds to achieve sustainable high-performance permanent magnetic materials. In this contribution, we investigate the role of Fe as substitution for Co in 1:5 compounds [1,2] where also Sm is replaced by so-called free rare earth elements such as La and Ce. The second iron based approach is interstitial design using nitrogen and boron to induce tetragonality and magnetic anisotrop in standard bcc iron. Our most recent key achievement is that we have introduced more nitrogen interstitials into Fe as previously reported record values in literature [3]. We are using thin film deposition by molecular beam epitaxy to achieve atomic control of the materials and to correlate magnetic properties to their atomistic origins.

[1] G. Gkouzia et al., Inorg. Chem. 62, 16354–16361 (2023) [2] S. Sharma et al., ACS Appl. Mater. Interfaces 13, 32415–32423 (2021) [3] D. Gölden et al., J. Magn. Magn. Mater. 422, 407-411 (2017)

Session BG
MAGNETOIONIC AND MAGNETOELECTRIC MATERIALS

Christian Rinaldi, Chair
Politecnico di Milano, Milano, Italy

INVITED PAPER

BG-01. Recent Progress in Nitrogen Magneto-ionics: New Materials and Phenomena for Brain-inspired Memory Devices. *J. Sort*[1,2], N. López[1], A. Arredondo[1], Z. Tan[1], Z. Ma[1], I. Spasojevic[1], P. Monalisha[1], N. Casañ-Pastor[3], A. Quintana[3], E. Pellicer[1], C. Jensen[5,7], Z. Chen[5], F. Celegato[6], K. Liu[5], J. Nogués[4,2] and E. Menéndez[1] *1. Universitat Autonoma de Barcelona, Bellaterra, Spain; 2. ICREA, Barcelona, Spain; 3. Institut de Ciència de Materials de Barcelona (ICMAB-CSIC), Bellaterra, Spain; 4. Catalan Institute of Nanoscience and Nanotechnology (ICN2), Bellaterra, Spain; 5. Georgetown University, Washington, DC, United States; 6. INRIM, Torino, Italy; 7. NIST, Gaithersburg, MD, United States*

Magneto-ionics refers to voltage-driven changes in the magnetic properties of materials as a result of electric-field-induced ion transport and redox changes in mixed ionic-electronic conductors. In a similar way as bringing spin to electronics has led to the revolutionary field of spintronics, merging magnetism with voltage-triggered ion motion (iontronics) has large potential for the development of analog magnetic memories and their application in emerging research areas such as synaptic devices and in-memory computing. In most systems, magneto-ionics relies on controlled migration of oxygen, hydrogen or lithium ions. Here, we will show that voltage-driven transport of nitrogen ions (*i.e*., nitrogen magneto-ionics) can be triggered at room temperature in transition metal nitride (CoN, FeN, CoMnN, FeCoN) films via liquid or solid electrolyte gating [1-7]. Nitrogen magneto-ionics can induce reversible ON-OFF transitions of ferromagnetic states, with adjustable magnetization and coercivity, at faster rates and lower threshold voltages than oxygen magneto-ionics [1,2]. In this talk we will review the recent progress in voltage-driven ion motion in transition-metal nitrides, a particular class of materials where ferromagnetic, paramagnetic and antiferromagnetic phases can coexist depending on the alloy composition and the nitrogen concentration [5]. Remarkably, and in contrast to oxygen magneto-ionics, nitrogen transport tends to occur uniformly through a plane-wave-like migration front, an effect particularly interesting for the implementation of multilayer memory devices. We will show strategies to further increase the magneto-ionic switching rates in this class of materials, as well as cyclability. Several synaptic characteristics can be emulated through voltage-driven ion motion: potentiation/depression, spike-time dependent plasticity, amplitude-dependent plasticity, or multilevel memory, amongst others [6]. By cumulative effects of pulsed voltage actuation (at frequencies in the 1 – 100 Hz range), learning by maturity (post-stimulated potentiation) can be also mimicked in some specific systems [3]. We will also show that some of these effects can be induced without any wire connection to the sample, through a phenomenon called bipolar electrochemistry [4]. Finally, new physical phenomena arising in patterned nanoscale magneto-ionic systems will also be described. In particular, in arrays of FeCoN sub-micron disks, a tunable and reversible transition between different states can be induced by varying the voltage actuation protocol. Miniaturization of nitrogen magneto-ionic systems offers future prospects for analog computing and brain-inspired devices, where multiple synapses will need to be interconnected to perform logic operations. Acknowledgements: This work has been supported by the European Research Council (2021-ERC-Advanced REMINDS Grant no. 101054687), the Spanish Agencia Estatal de Investigación (PID2020-116844RB-C21 PID2021-123276OB-I00, MCIN/AEI/10.13039/501100011033 & "European Union NextGenerationEU/PRTR" grant CNS2022-135230, CEX2023-001263-S, and CNS2022-135230), and US AFOSR (FA9550-23-1-0497).

[1] J. de Rojas et al., *Nat. Commun.*, vol. 11, p. 5871 (2020). [2] J. de Rojas et al., *Appl. Phys. Lett.*, vol. 120, p. 070501 (2022). [3] Z. Tan et al., *Mater. Horiz.*, vol. 10, p. 88 (2023). [4] Z. Ma et al., *Nat. Commun.*, vol. 14, p. 6486 (2023). [5] N. López-Pintó et al, *Adv. Funct. Mater*. (early view), p. 2404487 (2024). [6] P. Monalisha et al., *Adv. Electron. Mater*. 9 (2023) 2300249. [7] Z. Ma et al., *J. Materiomics*, vol. 10, p. 870 (2024).

CONTRIBUTED PAPERS

BG-02. Correlations between Defect Density and Magnetic Properties of Heusler Alloy Films. C. Leung[2], Y. Ling[2], H. Koizumi[1], S. Panda[3], A. Markou[3], E. Lesne[3], C. Felser[3] and *A. Hirohata*[1,3] *1. Center for Science and Innovation in Spintronics, Tohoku UNiversity, Sendai, Japan; 2. Department of Material Science and Engineering, City University of Hong Kong, Kowloon, Hong Kong; 3. Max-Planck-Institut für Chemische Physik fester Stoffe, Dresden, Germany*

In spintronics, it is crucial to make a half-metallic ferromagnetic film for the improvement of signal-to-noise ratios with further miniaturisation [1]. Among such films, a Heusler alloy film holds the greatest potential to exhibit 100% spin polarisation at room temperature [2] [3]. In this presentation, we have investigated Heusler alloy films with different compositions to reveal the roles of antisite disordering for device implementation. Two sets of Heusler alloy films were epitaxially grown on MgO(001) substrates by ultrahigh vacuum sputtering; $Mn_2Rh_{1-x}Ir_xSn$ (60)/*a*-Si (3) (x=0 and 0.32) and $Co_2Mn_{1\pm\delta}Ga$ (40)/*a*-Si (3) or Pt (4) (thickness in nm). Their temperature dependence of saturation magnetisation and damping constant was measured for the formation of magnetic skyrmions [4]. The first set crystallised as a tetragonal inverse Heusler alloy. By cross-sectional transmission electron microscopy (TEM) with energy dispersive X-ray spectroscopy (EDX), the correlation between the changes in the atomic distance and the deficiency of an element was analysed. As shown in Fig. 1, high-angle annular dark field (HAADF) scanning TEM images show atomic displacements as yellow or red circles, either contraction or expansion, respectively. We found that the film with x=0 shows atomic displacements in several grains, while the film with x=0.32 exhibits broader distribution of the displacements. For the film with x=0, the main cause of such displacements is induced by Mn excess, which may induce long-range deformation up to 8 atomic layers. For the x=0.32 film, on the other hand, the displacement is generated mainly by Rh excess, followed by Sn excess. Such a displacement may lead to the reduction in the spin polarisation. This study was supported by the Advanced Grant (SAHAJ) from the European Research Council and the Cooperative Research Project from the Center for Science and Innovation in Spintronics (Core Research Cluster) of Tohoku University.

[1] A. Hirohata *et al.*, *J. Magn. Magn. Mater.* 509, 166711 (2020). [2] C. Felser and A. Hirohata (Eds.), *Heusler Alloys* (Springer, Berlin, 2016). [3] K. Elphick *er al.*, *Sci. Technol. Adv. Mater.* 22, 235 (2021). [4] A. K. Sharma *rt al.*, *Adv. Mater.* 33, 2101323 (2021). [5] J. Jena *et al.*, *NanoLett.* 20, 59 (2020).

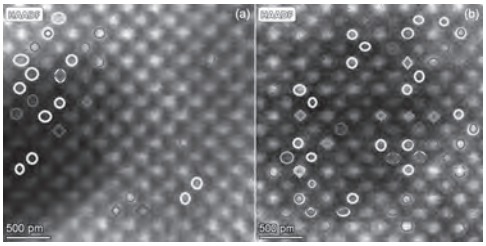

Fig. 1 HAADF TEM images on $Mn_2Rh_{1-x}Ir_xSn$ (60) films with (a) x=0 and (b) 0.32. Excess of atoms measured by EDX is indicated as blue, purple, pink and green rhombus symbols for Mn, Sn, Ir and Rh, respectively.

BG-03. Control of perpendicular anisotropy and compensation behaviour in Tb_xCo_{1-x} with Hydrogen ion implantation. *R.G. Hunt*[1], D. Moldarev[1], M.P. Grassi[1], D. Primetzhofer[1] and G. Andersson[1]
1. Physics and Astronomy, Uppsala University, Uppsala, Sweden

Magneto-ionic devices utilize the motion of ionic elements to continuously and deterministically adjust device-relevant magnetic properties such as perpendicular magnetic anisotropy (PMA)[1], interlayer coupling [2], and the Dzyaloshinskii-Moriya interaction [3]. Recently, it was also shown that in ferrimagnetic materials that the compensation behaviour can be controlled using a solid-state source of hydrogen ions [4] with ~μs charging times making them an exciting candidate for future devices. In this work, we investigate the hydrogen-induced change in ferrimagnetic behaviour in thin-film Tb_xCo_{1-x} alloys using ion implantation. Figure 1 shows the change in compensation composition (x_c) and in-plane (IP) transition points with increasing hydrogen dose. For a dose with an approximate H-to-metal atom ratio of 1:4.5, the IP transition point and x_c both move by approximately 6 at.% and show minimal change with a higher implantation dose. The seeming insensitivity to significantly increased dosages suggests that there is a threshold above which there would be diminishing returns in material tunability and hydrogen sensitivity. Further investigation of the saturation magnetization (Ms) can relate this to the atomic Tb and Co moments. We consider two models: one in which the atomic moments are considered constant for all compositions, and one in which the atomic moments vary with the composition. In both models we determine that the Tb sublattice moment experiences a drastic decrease of either 22 or 24%. The origin of this reduction may be structural in nature, with the magnitude of the exchange interaction being reduced as the relative Tb-Co bond lengths increase, however it could also be explained by an increase in the sperimagnetic cone angle exhibited in these alloys. Further experiments are needed to fully understand this observation.

[1] - R. Pachat, D. Ourdani, M. Syskaki, et al., Advanced Materials Interfaces, Vol 9, Issue 36, (2022) [2] - M. Ameziane., R. Rosenkamp, L. Flajšman, et al., Applied Physics Letters, Vol. 122, Issue 23, (2023) [3] - L. Herrera Diez, Y.T. Liu, D.A. Gilbert, et al., Physical Review. Applied, 12 (3), (2019). [4] - M. Huang, M.U. Hasan, K. Klyukin, et al., Nature Nanotechnology 16, p.981-988 (2021).

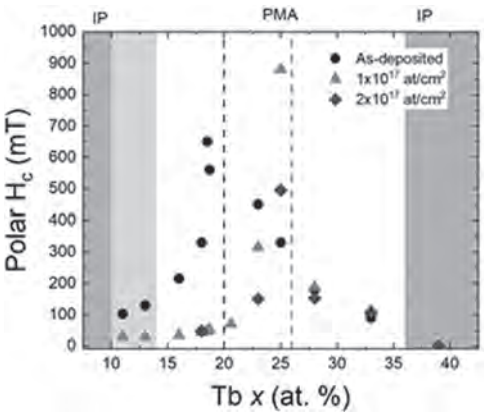

Fig. 1. Magnetic coercivity extracted from Kerr effect hysteresis loops for series of samples with increasing hydrogen dose (in at/cm²). Dashed lines indicate position of x_c, shaded regions indicate IP anisotropy.

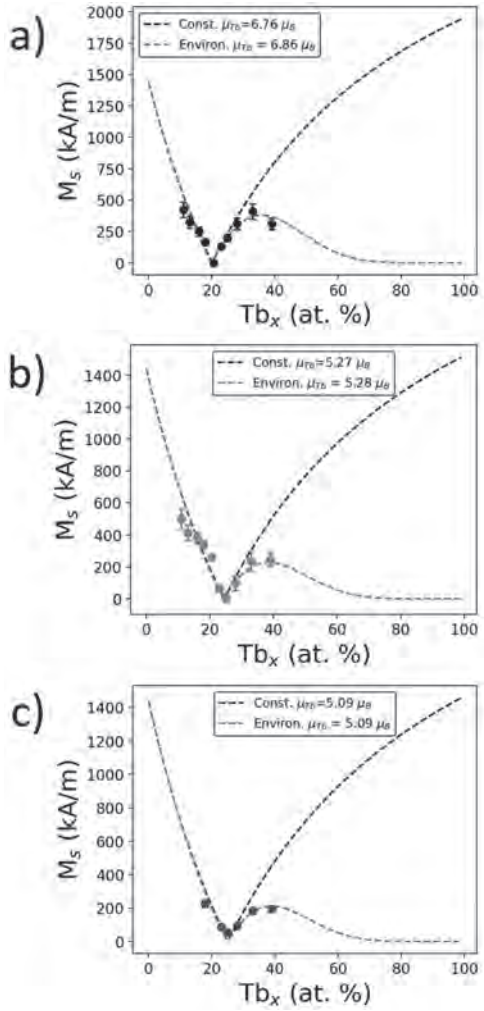

Fig. 2. Magnetometry data for a) the as-deposited, b) 1 x 10^{17}, and c) 2 x 10^{17} at/cm2 samples. Dashed lines are fit to the constant model (black) and environment model (red).

BG-04. Regulating the Magnetic Properties of $La_{0.5}Sr_{0.5}FeO_{3-\delta}$ Through Voltage-Controlled Oxygen Content. P. Nizet[2], F. Chiabrera[2], *N. López-Pintó*[1], N. Alayo[2], P. Langner[2], F. Baiutti[2], A. Morata[2], J. Sort[1,3] and A. Tarancon[2,3] *1. Universitat Autonoma de Barcelona (UAB), Barcelona, Spain; 2. Institut de Recerca en Energia de Catalunya (IREC), Barcelona, Spain; 3. ICREA, Barcelona, Spain*

Unveiling the interplay between changes in the concentration of mobile defects (such as oxygen vacancies) and functional properties in relevant materials represents a step forward in both fundamental research and potential applications. In this work, we focus on thin films of mixed ionic-electronic conductor $La_{0.5}Sr_{0.5}FeO_{3-\delta}$ (LSF50), a perovskite oxide which has shown interesting optical, electric and magnetic properties in previous studies, and finds application in solid oxide fuel cell electrodes, as a catalyst in oxygen evolution reactions, or as a functional material in computing devices.[1,2,3] However, precise and continuous control of the oxygen stoichiometry, a reversible way of tuning the vacancy content after the synthesis of the film, has yet not been fully studied. For this reason, the oxygen content of a LSF50 film was controlled by means of low voltage modulation (<1 V). Its functional properties were tailored as function of the oxygen content, revealing a strong correlation between electrical conductivity an magnetic order transition in the material. To display the potential of the LSF50, a gold rail-like design was patterned on top of a LSF50 film (see figure). This configuration allowed for a high throughput range of oxidation states within the same film after voltage treatment. Subsequently, a ferromagnetic (FM) 2.5-nm Co layer was deposited on top, and coupled through a field cooling (FC) from 325 K. The T_N was expected to progressively decrease along the rails, which was confirmed by a gradual decrease in the Co coercivity (H_C) after the point where T_N was meant to be close to RT. The H_C of the FM, which depended on the oxidation state of the AFM LSF50 buried underneath, could be used as a reference to assess the electric and optical properties of the LSF50, therefore providing a contactless way of reading the information stored in the LSF50, which ultimately can be utilized to read information from spintronic and neuromorphic devices.

[1] S. P. Simner, et al., *Electrochem. Solid St.,* 5 *(2002),* DOI: 10.1149/1.1483156
[2] Z. Shen, et al., *J. Mater. Chem. A,* 8 *(2020),* DOI: 10.1039/C9TA13313E
[3] A. Krick, et al., *APL Mater.,* 5 *(2017),* DOI: 10.1063/1.4982249

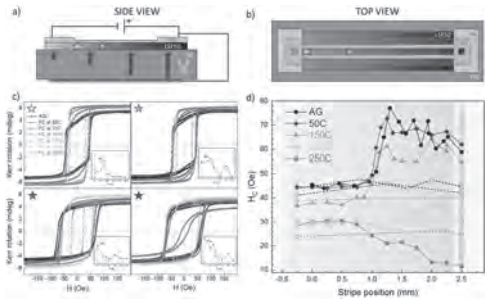

a-b) Side and top view, of the microfabricated gold rail and adjacent FM Co layer. c) Loops after FC at several temperatures at the marks. d) H_C along the stripe, after each FC.

BG-05. Ionically Driven Synthesis of Compensated Ferrimagnet $Mn_{4-x}Co_xN$ with Giant Exchange Bias. *Z. Chen*[1], C. Liu[2], X. Zhang[2] and K. Liu[1] *1. Physics, Georgetown University, Washington, DC, United States; 2. King Abdullah University of Science & Technology, Thuwal, Saudi Arabia*

Compensated ferrimagnets, which combine the benefits of both ferromagnets and antiferromagnets, present a promising platform for spintronics applications. Among these, the manganese nitride ferrimagnet Mn_4N stands out as a particularly intriguing rare-earth-free spintronic material due to its uniaxial anisotropy, low saturation magnetization, high thermal stability, and high domain wall velocity. Additionally, nitrogen-based magneto-ionics offer an innovative alternative to traditional oxide-based systems [1-4]. Recently, we have achieved high-quality Mn_4N films by sputtering Mn directly onto an Mn_3N_2 seed layer at elevated temperatures, leveraging the chemically induced nitrogen ionic motion [5]. In this study, we have synthesized compensated $Mn_{4-x}Co_xN$ by doping Co. X-ray diffraction confirms that Co has been incorporated into the Mn_4N structure. As Co concentration increases, room-temperature anomalous Hall effect measurements also show the sign of the Hall angle changes from negative to positive once the compensation point is crossed near $x = 1.00$ (Fig. 1). Low-temperature magnetometry reveals that the saturation magnetization is the lowest at $x = 1.00$ (Fig. 2). A giant exchange bias of over 1.5 T and coercivity of over 2.0 T at $x = 1.00$ (near the compensation point) were also observed at 5 K after field cooling. The large exchange anisotropy is attributed to the exchange interaction between the compensated $Mn_{4-x}Co_xN$ and ferrimagnetic Mn_4N. Our results demonstrate a promising rare-earth-free and heavy-metal-free compensated ferrimagnetic platform with remarkable tunability for spintronic and magneto-ionic applications. This work has been supported in part by the NSF (ECCS- 2151809) and AFOSR (FA9550-23-1-0497).

[1]. D. A. Gilbert et al, Nat. Commun. 7, 11050 (2016). [2]. J. de Rojas et al, Nat. Commun. 11, 5871 (2020). [3]. P. D. Murray et al, ACS Appl. Mater. Interfaces 13, 38916 (2021). [4]. C. J. Jensen et al, ACS Nano 17, 6745 (2023). [5]. Z. Chen et al, Appl. Phys. Lett. 123, 082403 (2023).

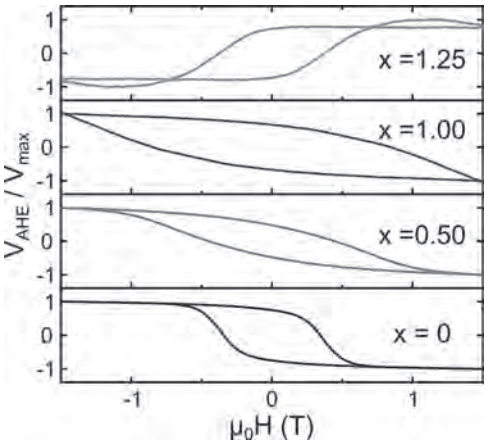

Fig. 1. Anomalous Hall effect on samples with different Co concentrations (x in $Mn_{4-x}Co_xN$).

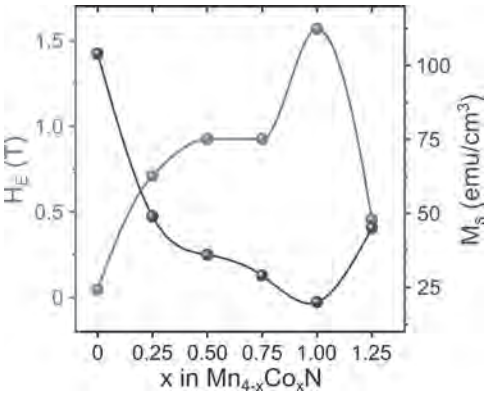

Fig. 2. Trends of exchange field and saturation magnetization measured at 5 K for samples with different Co concentrations.

Now VP13-10

BG-06. Magneto-Ionic Vortices: Voltage-Controlled Curling-Spin Analog-Memory Nanomagnets. *I. Spasojević*[1], Z. Ma[1], A. Barrera[2], F. Celegato[3], A. Palau[2], P. Tiberto[3], K. Buchanan[5] and J. Sort[1,4] *1. Physics Department, Autonomous University of Barcelona, Bellaterra, Spain; 2. Institute of Materials Science of Barcelona (ICMAB), Bellaterra, Spain; 3. Advanced materials and Life science Division, Istituto Nazionale di Ricerca Metrologica (INRIM), Turin, Italy; 4. Catalan Institution for Research and Advanced Studies (ICREA), Bellaterra, Spain; 5. Physics Department, Colorado State University, Fort Collins, CO, United States*

Control of magnetism through electric-field-induced ion motion (*magneto-ionics*) is poised to reshape existing voltage actuation approaches, aimed at bolstering energy efficiency across a diverse spectrum of spintronics and magnetically driven devices. However, despite the pressing need for strategies to control magnetic states at the *nanoscale*, most magneto-ionic studies to date have focused on continuous films [1-4]. Here we will demonstrate *in-situ* probing of ion motion in nanometer-sized structures, revealing the presence of *dynamically evolving spin configurations*, strongly dependent on the gating duration. More precisely, we will introduce a so far unexplored nanoscale magnetic object: *an analog magnetic vortex controlled by electric-field-driven ion motion* (*i.e.*, *magneto-ionic vortex* or, for simplicity, "*vortion*") [5]. This state is generated from a paramagnetic material (in our case FeCoN) *via in-situ* voltage application and subsequent gradual extraction of N^{3-} ions within *patterned nanodots*. What distinguishes *vortions* from conventional magnetic vortex states is that their key properties, such as amplitude of magnetization, nucleation and annihilation fields, coercivity, remanence and anisotropy, can be *controlled* and *fine-tuned* in an *analog* and *reversible* manner using an *energy-conscious* voltage gating process. This manipulation occurs post-synthesis, obviating the need for energy-demanding methods like laser pulses or spin-torque currents. By taking an advantage of a so far overlooked aspect of N^{3-} magneto-ionics—occurrence of a planar ion migration front —control of the magnetic layer's thickness is achieved in the nanodots, enabling reversible transitions among paramagnetic, single-domain, and vortion states, offering future prospects for analog computing, in e.g. brain-inspired devices.

[1] U. Bauer et al., Nat. Mater., vol 14, p. 174-181 (2015). [2] J. De Rojas et al., Nat. Commun., vol. 11, p. 5871 (2020). [3] A. Quintana et al., ACS Nano, vol 12, p. 10291-10300 (2018). [4] K. Duschek et al., J. Mater. Chem. C., vol 6, p. 8411-8417 (2018). [5] I. Spasojevic et al., arXiv:2403.13722 [cond-mat.mtrl-sci] (2024). (at review stage) Acknowledgements This work has been supported by the European Research Council (2021-ERC-Advanced REMINDS Grant N 101054687).

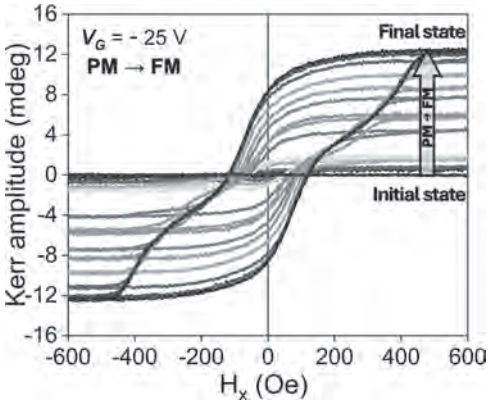

Fig 1. Evolution of MOKE hysteresis loops during negative voltage actuation of FeCoN nanodots starting from a paramagnetic state, showing a transition in shape from square-like to constricted.

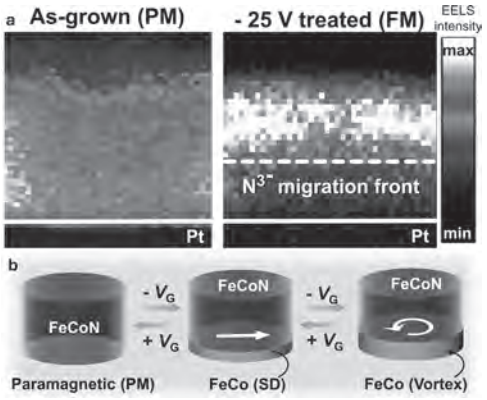

Fig 2. a) Nitrogen EELS compositional mapping of as-grown and voltage treated FeCoN nanodot, b) Schematic of the transition between paramagnetic, single domain and magneto-ionic vortex states driven by N^{3-} ion migration.

BG-07. Magnetic Phase Diagram of Non-collinear Antiferromagnet $Mn_{3+x}Sn_{1-x}$ Thin Films. *K. Gas*[1,2], J. Yoon[1], Y. Sato[1], H. Kubota[1], J.Z. Domagala[2], P. Dluzewski[2], Y.K. Edathumkandy[2], Y. Takeuchi[1,3], S. Kanai[1,4,5], H. Ohno[1], M. Sawicki[2,1] and S. Fukami[1] *1. Tohoku University, Sendai, Japan; 2. Institute of Physics, Polish Academy of Sciences, Warsaw, Poland; 3. National Institute for Materials Science, Tsukuba, Japan; 4. PRESTO, Japan Science and Technology Agency (JST), Kawaguchi, Japan; 5. National Institutes for Quantum Science and Technology, Takasaki, Japan*

The non-collinear antiferromagnetic $D0_{19}$-$Mn_{3+x}Sn_{1-x}$ exhibits various intriguing properties akin to ferromagnets, such as a large anomalous Hall effect (AHE) arising from the Berry curvature associated with Weyl points [1]. Since its properties are expected to significantly change with the Mn content x through the position of the Fermi level [2] as well as other factors [3,4], the development of a systematic knowledge of the role of x in $Mn_{3+x}Sn_{1-x}$ on its physical properties is timely and important. We comprehensively study the structural (XRD, TEM), magnetic, and magnetotransport properties of m-plane-oriented epitaxial $Mn_{3+x}Sn_{1-x}$ ($-0.03 \le x \le +0.23$) thin layers deposited by magnetron sputtering [5]. The wide temperature range of our studies (4 – 400 K) allows us, for example, to construct an x-dependent magnetic phase diagram (Fig. 1). The most profound feature is the disappearance of the transition (at temperature T_1) between an anti-chiral commensurate phase (hosting inverse triangular antiferromagnetic order) and a non-coplanar modulated incommensurate phase [6] for $x \ge +0.15$. This leads to observing a sizable AHE below 100 K in Mn-rich $Mn_{3+x}Sn_{1-x}$ (Fig. 2), which retains its high-temperature chirality down to the liquid He temperatures. We also find that the Néel temperature (T_N) depends on the Mn composition and correlates with the simultaneous change in the in-plane lattice parameter. Our work broadens the understanding of the correlation between the structural and magnetic characteristics of Mn_3Sn thin films towards developing novel devices. Acknowledgments: This study has been partly supported by TUMUG Support Program from Center for Diversity, Equity, and Inclusion, Tohoku University, and by JSPS Kakenhi 19H05622, 21J23061, 24KJ0432, 24H00039, 24H02235.

[1] S. Nakatsuji *et al.*, Nature, 527, 212 (2015). [2] K. Kuroda *et al.*, Nat. Mater., 16, 1090 (2017). [3] J.-Y. Yoon *et al.*, AIP Advances, 11, 065318 (2021). [4] T. Uchimura *et al.*, Appl. Phys. Lett., 120, 172405 (2022). [5] J.-Y. Yoon *et al.*, Appl. Phys. Express, 13, 013001 (2020). [6] Y. Chen *et al.* arXiv:2306.07822v3

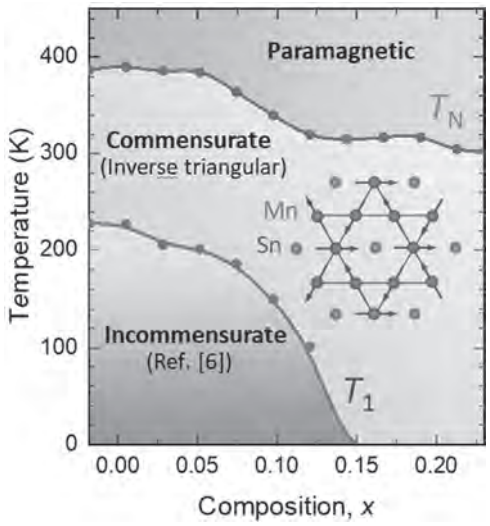

Fig. 1 Mn composition dependent magnetic phase diagram of $D0_{19}$-$Mn_{3+x}Sn_{1-x}$ epitaxial thin layers. The cartoon shows the spin arrangements in the inverse triangular spin structure of Mn_3Sn.

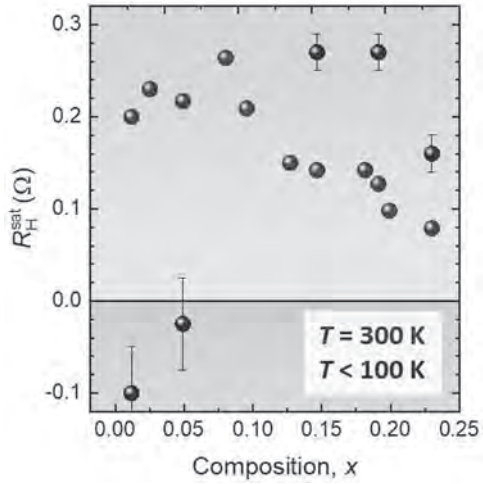

Fig. 2 Saturated values of AHE at T = 300 K (reddish bullets) and at low temperature, T < 100 K, (navy bullets). Note that for x > 0.15 large magnitudes of AHE retain the same chirality (indicated by the sign of R_H) as typically found at room temperature for this material.

BG-08. Bipolarity of anomalous Nernst effect in quaternary equiatomic Heusler alloys. A. Chanda[1], J. Nag[2], N. Schulz[1], A. Alam[2], K. G. Suresh[2], M. Phan[1] and *H. Srikanth*[1] *1. Physics, University of south Florida, Tampa, FL, United States; 2. Physics, Indian Institute of Technology Bombay, Bombay, India*

The anomalous Nernst effect (ANE) is an emergent branch of spintronics wherein a transverse electric voltage is generated in a magnetic material orthogonal to both the applied thermal gradient and the magnetization directions of the material. Like the thermoelectric generators based on the Seebeck thermopiles composed of conventional *p*-type and *n*-type semiconductors with opposite polarities of the longitudinal Seebeck coefficients, combining materials with large positive and negative ANE coefficients would lead to the development of large scale ANE-based thermopile devices with highly efficient thermoelectric conversion compared to the Seebeck based thermopiles [1]. However, while most of the magnetic materials show positive ANE, only limited number of materials exhibit negative ANE [2]. Furthermore, majority of the materials showing negative ANE have low Curie temperatures (T_C). On this context, quaternary Heusler alloys with high Curie temperatures and large spin polarizations would be promising candidates for room temperature ANE-based thermopile device applications. Here, we demonstrate that high-T_C quaternary equiatomic Heusler alloys CrRu*X*Ge (*X* = Co or Mn) with large spin-polarizations can exhibit both positive and negative ANE coefficients depending on their chemical compositions and hence, can be potential candidates for developing efficient room temperature ANE-based thermopiles [3]. We found that CrRuCoGe shows positive anomalous Nernst coefficient whereas CrRuMnGe exhibits a negative at room temperature, which has been attributed to the dominating contribution of the anomalous transverse thermoelectric conduction. Our detailed analysis indicates that the origin of the observed ANE in both these samples is dominated by the asymmetric skew scattering of charge carriers in the measured temperature regime. The sign change and tunability of ANE presented in this study provide a step forward towards the development of ANE-based efficient thermopile devices operating at room temperature utilizing the equiatomic quaternary Heusler alloys.

[1] S Noguchi *et al*., *Nat. Phys.,* Vol. 20, p.254-260 (2024). [2] K. Ito *et al*., *Phys. Rev. Appl.,* Vol. 21, p. 54012 (2024). [3] A. Chanda *et al*., *Phys. Rev., B* Vol. 109, P. 224415 (2024).

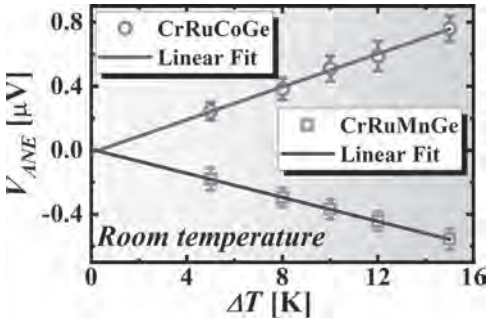

ANE voltage as a function of applied temperature gradient for CrRuCoGe and CrRuMnGe

BG-09. Electric Field Control of Magnetization in FeGa microstructures on PMN-PT. *G. Pradhan*[1,2], F. Celegato[1], A. Magni[1], G. Barrera[1], M. Coisson[1], P. Rizzi[2] and P. Tiberto[1] *1. INRIM, Turin, Italy; 2. UNITO, Turin, Italy*

The recent era of information technology largely focusses on energy saving and cost efficiency. Manipulation of magnetic state of a micro element solely with the use of electric fields has attracted new attention due to its potential ability to be used in low-power magneto-electronics [1,2]. Artificial magnetoelectric materials are suitable candidates due to its coupling between magnetization and electric-field induced strain, which consumes less power and reduces heat losses [3,4,5,6]. In the framework of artificial multiferroic heterostructures and their interfacial magnetoelectric interplay, we have investigated the properties of FeGa microstructures fabricated on PMN-PT (Fig. 1(a)). The in-plane strains (ε_x, ε_y) generated in the PMN-PT substrate were measured using a strain gauge (Fig. 1(b)). Due to the [011] crystal orientation, the in-plane strains are anisotropic resulting in significant difference in remnant strain values marked by the blue and red dots. The magnetic hysteresis of elliptical disks (long axis of 5 μm) were recorded using Magneto-Optic Kerr effect (MOKE) as represented by the -0 and +0 kV/cm curves in figure 1(c) (remanent strain states at zero electric field). A difference in the shape of the hysteresis is observed which marks the rotation of anisotropy of the system. A vortex domain state is observed in reversal at -0 kV/cm whereas a S-shaped multidomain is recorded at +0 kV/cm. This influence in domain patterns marks the presence of strain-induced anisotropy in the system. Further, an electric field pulse of a magnitude of 6 kV/cm was applied to the magnetic remanence state. A single domain state is observed before application of electric field (Fig. 1(d)). Under electric field application of 6 kV/cm, the magnetic state changes to a S-shaped multidomain state which remains stable even after the field is removed. This marks the manipulation of magnetic state with the sole use of electric field.

1. N. A. Spaldin and R. Ramesh, *Nature materials,* 18.3, 203-212 (2019) 2. S. Manipatruni, et al., *Nature,* 565.7737, 35-42 (2019) 3. T. H. Lahtinen, K. J. Franke, and S. van Dijken, *Scientific reports,* 2.1, 258 (2012) 4. R. Lo Conte, et al., *Nano letters,* 18.3, 1952-1961 (2018) 5. Q. Li, et al., *Applied Physics Letters,* 110.26 (2017) 6. M. G. De Jesus, et al., *Smart Materials and Structures,* 31.3, 035005 (2022)

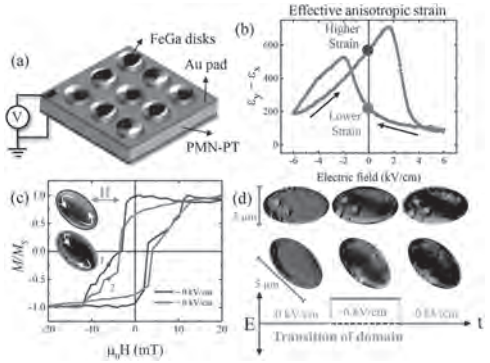

Fig. 1. (a) Schematic of FeGa/PMN-PT heterostructure for voltage application. (b) Effective strain measured in PMN-PT. (c) Magnetic hysteresis and domains structures recorded at remanent strain states. (d) Evolution of magnetic state under application of electric field pulse.

BG-10. Controlling Magneto-Ionics by Defect Engineering Through Light Ion Implantation. *Z. Ma*[1], S. Martins[1], Z. Tan[1], S. Chen[2], E. Monteblanco[3], M. Liedke[4], M. Butterling[4], A. Attallah[4], E. Hirschmann[4], A. Wagner[4], D. Ravelosona[3], J. Sort[1] and E. Menéndez[1] *1. Universitat Autònoma de Barcelona, Barcelona, Spain; 2. Université Paris-Saclay, Paris, France; 3. Spin-Ion Technologies, Paris, France; 4. Helmholtz-Zentrum Dresden – Rossendorf, Dresden, Germany*

Magneto-ionics, a phenomenon that relies on the voltage-driven transport of ions and redox processes to modify magnetic properties, has emerged as a promising avenue for energy-efficient manipulation of magnetism in next-generation memory and computing devices. As a diffusion-controlled mechanism, defects play a central role in determining ion motion and, hence, magneto-ionic response. Here, the potential of ion implantation is exploited to engineer depth-resolved defect type and density with the aim to control the magneto-ionic behavior of Co_3O_4 thin films. We show that through a single implantation process of light ions (He^+) at 5 keV, the magneto-ionic response of a nanostructured 50 nm thick Co_3O_4 film, in terms of rate and amount of induced magnetization, at short-, mid-, and long-term voltage actuation, can be controlled by varying the generated collisional damage through the ion fluence [1]. Specifically, compared with the as-grown film, while mild collisional damage, characterized by a maximum displacement per atom (dpa) of around 0.01 upon implanting with 10^{14} ion cm^{-2}, results in larger vacancy clusters along the top 35 nm, intermediate collisional damage with a maximum dpa of 0.1 (implanting with 10^{15} ion cm^{-2}) leads to an increased density of mixed vacancy clusters across the bottom 15 nm. The former promotes ion motion at an early stage of voltage actuation, whereas the latter leads to an increased density of mixed vacancy clusters, thereby a larger number of sites that can be activated at long-term voltage actuation, and subsequently, an enhanced induced magnetization is observed. Further increase in fluences (i.e., 10^{16} ion cm^{-2}, which yields a maximum dpa of 1) tends to depress magneto-ionics due to pronounced defect size reduction. These results constitute a proof-of-principle that paves the way to further use ion implantation (tuning the ion nature, energy, fluence, target temperature, or using multiple implantations) to enhance performance in magneto-ionic systems, with implications in ionic-based devices.

Z. Ma et al, *Adv. Funct. Mater.* (early view), p. 2312827 (2024).

BG-12. Tuning the type of magnetic order through the Cr-substitution in $Co_3O_2BO_3$ Ludwigite. *D.L. Mariano*[1], D.R. Candela[2], D.C. Freitas[2], C.S. Mejia[4], M.A. Continentino[3] and L. Ghivelder[1] *1. physics, Universidade Federal do Rio de Janeiro, Rio de Janeiro, Brazil; 2. physics, Universidade Federal Fluminense, Niteroi, Brazil; 3. physics, Centro Brasileiro de Pesquisas Físicas, Rio de Janeiro, Brazil; 4. physics, Helmholtz-Zentrum Dresden-Rossendorf, Dresden, Germany*

Ludwigites have formula unit $M_2M'O_2BO_3$, where M and M' are transition metals. These compounds may exhibit different physical properties ranging from structural ordering, charge ordering, coexistence of magnetic order and paramagnetism, metamagnetic transition, magnetocaloric effect, dimensional crossover, spin crossover and spin-glass. This variety of physical behavior has been attributed to a combination of strong correlation and low-dimensional effects. So, these materials offer a unique opportunity to study the correlation between magnetism and dimensionality. The homometallic $Co_3O_2BO_3$ ludwigite, with high-spin (HS) Co^{2+} and low-spin (LS) Co^{3+}, shows an AFM ordering at 42 K [1,2]. When the compound is doped with non-magnetic ions, in most cases, andcontrary to expected, the magnetic interactions are strengthened and the magnetic transition temperature increases. On the other hand, when doped with magnetic ions, such as Fe^{3+}, Mn^{3+}, magnetic disorder leads the system to a spin-glass state, except for Cr, which occupies a unique site in the structure [3,4,5]. Particularly, when $Co_3O_2BO_3$ is doped with Cr^{3+}, forming the $Co_{2.5}Cr_{0.5}O_2BO_3$, the magnetic interactions are strengthened, and T_M rises to 76 K [5]. Despite the presence of three different magnetic ions, Co^{2+}, Co^{3+} and Cr^{3+}, in the HS states, no frustrated magnetic interactions are established. The magnetic dimensionality increases from 2D in $Co_3O_2BO_3$ to 3D in $Co_{2.5}Cr_{0.5}O_2BO_3$. Here we extend our study of Cr-doped ludwigite $Co_{3-x}Cr_xO_2BO_3$, comprising a broader range of Cr contents to understand the role of Cr, which yield changes of the magnetic structure and dimensionality in these compounds. XRD results show that Cr^{3+} occupy manly sites 4 and gradually expand the unit cell, favoring the appearance of HS Co^{3+}. The T_M increases gradually with the increase of Cr content, reaching 115 K for x=1.0. We show that depending on the Cr concentration, the compound adopts different spin structures. It goes from AFM for low Cr content, through ferrimagnetic (FIM) for intermediate concentrations, and back to AFM for high Cr contents.

[1] D. C. Freitas, M. A. Continentino,* R. B. Guimarães, and J. C. Fernandes Phys. Rev. B 77, 184422 (2008). [2] D. C. Freitas, C. P. C. Medrano, D. R. Sanchez, M. Nuñez Regueiro, J. A. Rodríguez-Velamazán, and M. A. Continentino, Phys. Rev. B 94, 174409 (2016). [3] D. C. Freitas, M. A. Continentino, R. B. Guimarães, J. C. Fernandes, E. P. Oliveira, R. E. Santelli, J. Ellena, G. G. Eslava, and L. Ghivelder, Phys. Rev. B 79, 134437 (2009). [4] M. A. V. Heringer, D. L. Mariano, D. C. Freitas, E. Baggio-Saitovitch, M. A. Continentino, and D. R. Sanchez, Phys. Rev. Materials 4, 064412 (2020). [5] D. L. Mariano, M. A. V. Heringer, D. C. Freitas, E. Baggio-Saitovitch, M. A. Continentino, E. C. Passamani, and D. R. Sanchez Phys. Rev. B 102, 064424 (2020).

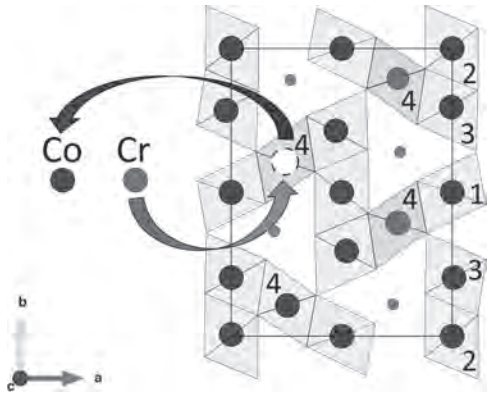

Crystallographic structure of $Co_{3-x}Cr_xO_2BO_3$ Ludwigite.

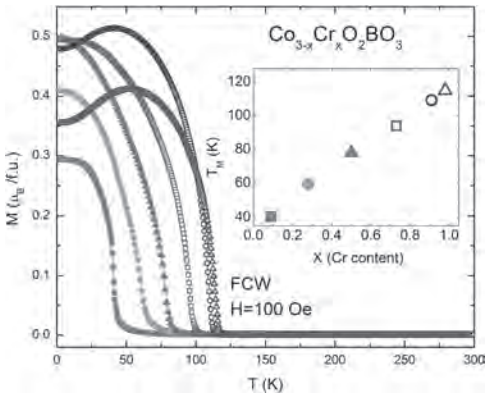

M vs.T measurements for $Co_{3-x}Cr_xO_2BO_3$ ludwigites under an applied field of 100 Oe.

BG-13. Giant magnitude of ultraviolet magnetic circular dichroism in thin film $Co_2MnGa_{1-x}Ge_{1-x}$ Heusler alloys. *S. Granville*[1,2], Y. Zhang[1], Y. Yin[3] and H. Shu[4] *1. Robinson Research Institute, Victoria University of Wellington, Lower Hutt, New Zealand; 2. MacDiarmid Institute for Advanced Materials and Nanotechnology, Wellington, New Zealand; 3. Department of Materials Science & Engineering, Monash University, Clayton, VIC, Australia; 4. Department of Applied Physics, National Pingtung University, Pingtung, Taiwan*

Ferromagnetic Weyl semi-metal Heusler alloy Co_2MnGa has been shown to have very large values for a range of magnetoelectronic properties such as large anomalous Hall [1,2], anomalous Nernst [3,4], and spin Hall [5] coefficients, related to the large Berry curvature in this material's electronic structure. The strongly spin-polarised band structure might be expected to show up in spin-selective optically-excited transitions between the states, which may have applications in magneto-optics, however optical and magneto-optical studies of Co_2MnGa are much less common [6,7]. In this presentation we will show a giant difference in the absorption of right- and left-circularly polarised UV light in $Co_2MnGa_{1-x}Ge_{1-x}$ thin films, reversible with a magnetic field. This magnetic circular dichroism (MCD) reaches over 25 mdeg/nm, almost as large as the strongest UV MCD in rare-earth-containing ferromagnets such as CoTb or GdFeCo. The MCD has the same magnetic field dependence as the anomalous Hall effect, evidence it is linked to the electronic band structure. From calculations of the spin-polarised density of states, we link the MCD to optical transitions between hybridised Co-Mn 3d minority states. Substituting Ge for Ga broadens the large MCD response to cover a wide range of UV energies, 3.5 – 4.5 eV. Our results demonstrate these materials are a promising way to achieve large and broad MCD for applications with immunity to temperature variation.

[1] A. Markou, D. Kriegner, J. Gayles et al., Phys. Rev. B Vol. 100, 054422 (2019). [2] Y. Zhang, Y. Yin, G, Dubuis et al., Npj Quantum Mater. 6, 17 (2021). [3] A. Sakai, Y. P. Mizuta, A. A. Nugroho et al., Nature Phys. 14, 11 (2018). [4] J. Hu, Y. Zhang, X. Huo et al., IEEE Magnetics Letters 13, 4503605 (2022). [5] L. Leiva, S. Granville, Y. Zhang et al., Phys. Rev. B 103, 4 (2021). [6] E. I. Shreder, A. A. Makhnev, K. G. Suresh et al., Mod. Phys. Lett. B 36, 2150573 (2022). [7] B. Mallett, Y. Zhang, C. Pot et al., Phys. Rev. Mater. 7, 094203 (2023).

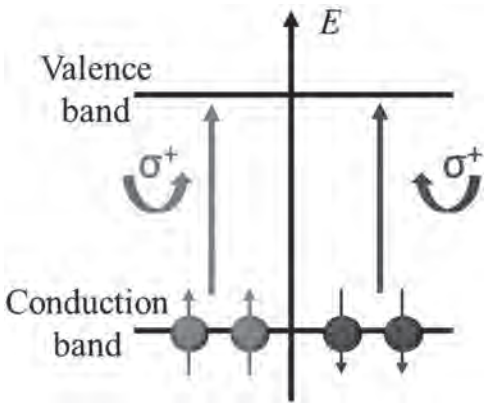

Figure 1: Spin-selective optical absorption.

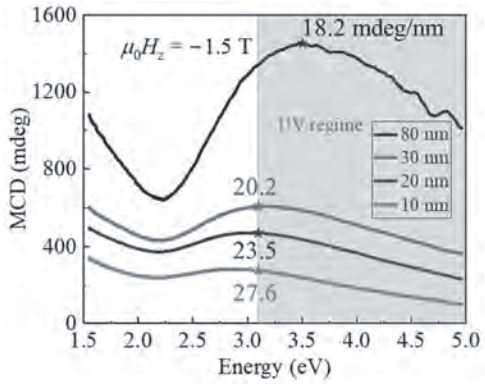

Figure 2: Magnetic circular dichroism (MCD) of Co_2MnGa thin films with large magnitude in the UV range.

Session BP
SPINTRONICS II
(Poster Session)

Tobias Wagner, Chair
Johannes Gutenberg University Mainz, Mainz, Germany

BP-01. 10 MHz Polarization Control in Spintronic Terahertz Emitters.

G. Lezier[1], J. Lampin[2], M. Vanwolleghem[2] and *N. Tiercelin*[1]
1. AIMAN-FILMS, Universite de Lille, CNRS, Centrale Lille, Universite Polytechnique des Hauts-de-France, UMR 8520-IEMN, Lille, France; 2. Photonique THz, Universite de Lille, CNRS, Centrale Lille, Universite Polytechnique des Hauts-de-France, UMR 8520-IEMN, Lille, France

Since the seminal paper from Seifert et al. [1], Inverse Spin Hall Effect Spintronic THz Emitters (ISHE STE) have shown to be efficient sources for pulsed terahertz generation [2]. Besides their broad gapless spectrum, and given the strict orthogonality of the magnetic state and the emitted THz waves polarization, these emitters allow for the control of said polarization at the source, which is of prime interest for applications in Polarization spectroscopy and THz ellipsometry [3,4,5]. In previous works we demonstrated quasi-static control of the polarization using varying magnetic fields [6] or magnetoelectric effect [7]. Dynamic control up to 10KHz was demonstrated by Gueckstock et al. [8], but no higher frequency has been demonstrated up to now. In this work, we have shown a polarization control up to 10 MHz. This was achieved in W/FeCo/Pt ISHE STEs possessing an in-plane magnetic anisotropy enabling the use of a field induced spin reorientation transition (SRT) [9], which strongly increase the magnetization sensitivity to the external driving field that is generated using a high-frequency electromagnet on a ferrite core (inset Fig. 1). The THz emission is characterized in a Time Domain Spectroscopy setup, and a Zurich high frequency lock-in amplifier allows for the detection of the 10MHz modulated THz signal. In a first experiment, Fig. 1 shows the temporal spectrum measured at 10 MHz with no bias and a H_{Dyn} field amplitude higher than the coercive field of the emitter. Since we desire a polarization rotation rather than a 180° flipping, the bias field is applied so that magnetization oscillates around the x axis. As evidenced on Fig. 2, the maximum THz amplitude is obtained when the bias reaches the anisotropy field of the layer, where the SRT takes place. Details of the sample preparation, measurement setup, results, interpretation and outlook will be presented.

[1] T. Seifert, S. Jaiswal, U. Martens, J. Hannegan, L. Braun, P. Maldonado, F. Freimuth, A. Kronenberg, J. Henrizi, I. Radu, E. Beaurepaire, Y. Mokrousov, P. M. Oppeneer, M. Jourdan, G. Jakob, D. Turchinovich, L. M. Hayden, M. Wolf, M. Münzenberg, M. Kläui, and T. Kampfrath, Nat. Photonics, Vol. 10, 483–488 (2016). [2] E. Papaioannou and R. Beigang, Nanophotonics, Vol. 10, no. 4, p.1243 (2021) [3] S. Dhillon et al., J. Phys. D: Appl. Phys. Vol. 50, p.043001 (2017) [4] A. Leitenstorfer et al., J. Phys. D: Appl. Phys. Vol. 56, p.223001 (2023) [5] S. Watanabe, Photonics, Vol. 5(4), p.58 (2018) [6] P. Kolejak, G. Lezier, K. Postava, J-F. Lampin, N. Tiercelin, M. Vanwolleghem, ACS Photonics, Vol. 9(4), p.1274 (2022) [7] G. Lezier, P. Koleják, JF. Lampin, K. Postava, M. Vanwolleghem, N. Tiercelin, Appl. Phys. Lett., Vol. 120, p.152404 (2022) [8] O. Gueckstock, L. Nádvorník, T. Seifert, M. Borchert, G. Jakob, G. Schmidt, G. Woltersdorf, M. Kläui, M. Wolf, T. Kampfrath, Optica, Vol. 8(7) p. 1013 (2021) [9] N. Tiercelin, J. Ben Youssef, V. Preobrazhensky, P. Pernod, H. Le Gall, Journ of Mag. & Mag. Mat, Vol. 249(3), pp519 (2002).

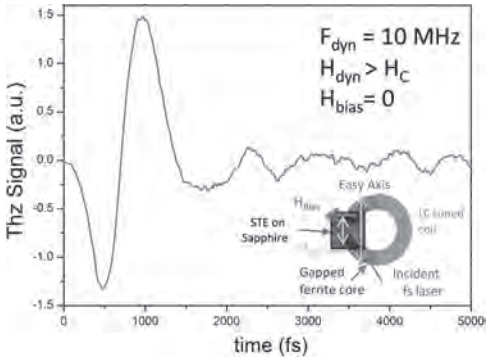

Fig.1: Time domain spectrum of the emitted signal measured while flipping magnetization at 10 MHz along the hard axis with a synchronous detection at the same frequency. Inset shows the configuration.

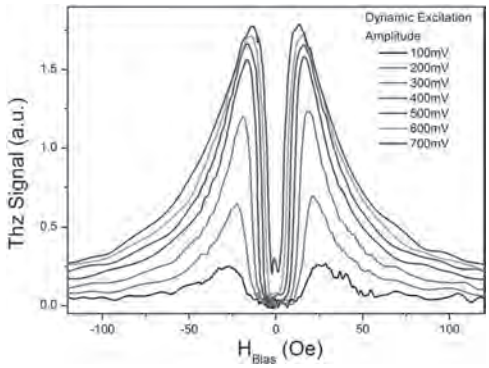

Fig.2: Maximum amplitude of the THz signal while sweeping the bias field H_{Bias} for increasing amplitudes of dynamic excitation H_{Dyn}.

BP-02. Thermal stability of epitaxial and polycrystalline Mn_3Sn nanodots.

Y. Sato[1,2], H. Kubota[1,2], Y. Takeuchi[3,4], Y. Yamane[1,5], J. Yoon[1,2], S. Kanai[1,2,4], J. Ieda[6], H. Ohno[1,4,7] and S. Fukami[1,2,4] *1. Laboratory for Nanoelectronics and Spintronics, RIEC, Tohoku Univ., Sendai, Japan; 2. Graduate School of Engineering, Tohoku Univ., Sendai, Japan; 3. ICYS, NIMS, Tsukuba, Japan; 4. WPI-AIMR, Tohoku Univ., Sendai, Japan; 5. FRIS, Tohoku Univ., Sendai, Japan; 6. ASRC, JAEA, Ibaraki, Japan; 7. CSIS, Tohoku Univ., Sendai, Japan*

Antiferromagnets have attracted great interest owing to their unique properties, such as high-speed dynamics and negligible stray field [1,2]. In particular, non-collinear antiferromagnets exhibit intriguing topological phenomena [3,4]. Further, recent studies showed current-induced switching [5-7] and rotation of spin structures [8], and observed tunneling magnetoresistance [9,10] in thin-film systems. Meanwhile, the stability of the collective antiferromagnetic state against thermal fluctuation has not been studied well despite its importance as a figure of merit of the retention time. Here, we study the thermal stability *D* in non-collinear antiferromagnetic Mn_3Sn nanodots with various sizes [11]. We prepare stacks consisting of MgO(110) sub./W(2)/Ta(3)/Mn_3Sn(20)/MgO(1.3)/Ru(1) and Si/SiO_2

sub./Ta(7)/Mn_3Sn(30)/MgO(1.3)/Ru(1) [in nm] using sputtering, leading to a formation of -oriented epitaxial and polycrystalline Mn_3Sn structures, respectively [12]. Stacks are processed into circular dot devices by electron beam lithography and Ar ion milling. Figure 1 shows the measurement circuit with the scanning electron microscopy (SEM) image of the nanodot device and the Hall resistance R_H versus out-of-plane magnetic field H for typical samples. We measure D from switching probability P versus amplitude of pulse H with the pulse duration of 1 s [Fig. 2(a), (b)] [11]. Figure 2(c) shows the dot size D dependence of the evaluated D. In both epitaxial and polycrystalline samples, D maintains similar values down to D ~ 300 nm, below which it decreases with decreasing D. At D > 300 nm, Δ values of 30-nm-thick polycrystalline Mn_3Sn (~ 50–100) are smaller than that of 20-nm-thick epitaxial ones (~ 90–170), indicating a more thermally active nature in polycrystalline Mn_3Sn. Our result provides a basis for the design of reliable and efficient antiferromagnetic spintronics devices. This work was partly supported by JSPS Kakenhi, MEXT X-NICS, and RIEC Cooperative Research Projects.

[1] T. Jungwirth *et al*., Nat. Nanotechnol. 11, 231 (2016). [2] V. Baltz *et al*., Rev. Mod. Phys. 90, 015005 (2018). [3] S. Nakatsuji *et al*., Nature 527, 212 (2015). [4] A. Nayak *et al*., Sci. Adv. 2, e1501870 (2016). [5] H. Tsai *et al*., Nature 580, 608 (2020). [6] T. Higo *et al*., Nature 607, 7919(2022). [7] J.-Y. Yoon *et al*., Nat. Mater. 22, 1106(2023). [8] Y. Takeuchi *et al*., Nat. Mater. 20, 1364 (2021). [9] X. Chen *et al*., Nature 613, 492 (2023). [10] P. Qin *et al*., Nature 613, 485 (2023). [11] Y. Sato *et al*., Appl. Phys. Lett. 122, 122404 (2023). [12] J.-Y. Yoon *et al*., Appl. Phys. Express 13, 013001 (2020).

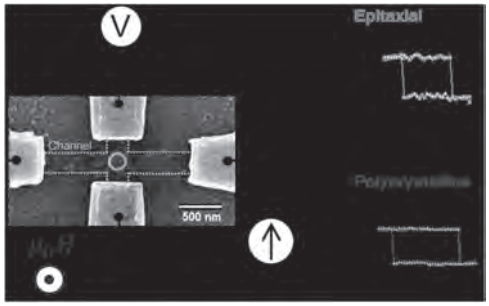

Fig.1 Measurement circuit with SEM image of a nanodot device and R_H-H curves for epitaxial and polycrystalline Mn_3Sn nanodots.

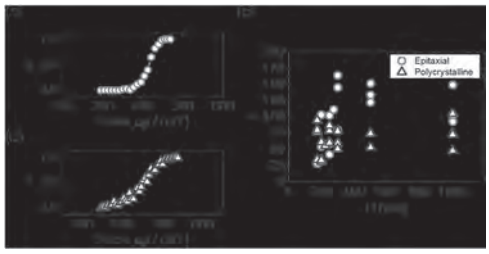

Fig.2 P versus H for (a) epitaxial and (b) polycrystalline Mn_3Sn nanodots. (c) D versus D in Mn_3Sn nanodots.

BP-03. Enhanced THz Emission in Magnetic Hybrid Nanostructures with $L1_0$ Interfacial FePt layer. *O. Crisan*[1], A. Crisan[1] and E. Papaioannou[1,2]
1. National Institute for Materials Physics, Magurele, Romania;
2. Aristotle University of Thessaloniki, Thesssaloniki, Greece

The formation of hybrid nanostructures in spintronic devices has been investigated as a response to specific needs especially in nanoelectronics or adjacent fields where combined optical and magnetic response to various excitations is required for various types of sensing. While spin phenomena have long been investigated within the context of conventional ferromagnetic materials, the study of spin generation, relaxation, and spin-orbit coupling in layered systems took off only recently with the advent of hybrid spintronics. Here we present initial approach to nanostructuring of hybrid structures based on magnetic FePt-based bilayers, as well as their response to the optical excitation of magnetization, in view of potential applications as THz spintronic emitters. Indeed, spintronic THz emitters made of $L1_0$ phase ferromagnetic/non-magnetic bilayers, can exhibit spin-to-charge current transition, resulting in controlled and tunable THz pulse emission. We have synthesized magnetic bilayers made of Si(001) / Fe(2 nm) / Pt(3 nm) and by appropriate annealing we have engineered at the Fe / Pt interface an area of alloying made of $L1_0$ phase FePt. Upon optical pumping with a femtosecond laser pulse, we have found that the THz signal emitted from the heterostructure is highly enhanced in the presence of the $L1_0$ interfacial area, compared with the case where the alloying at the interface is not manifested.

BP-04. Investigating Magnetic Ordering in Proposed Altermagnetic RuO_2 Thin Films. S. Bhatt[1], *F.M. Abel*[2,3], T. Adel[3], D.T. Plouff[1], X. Wang[1], V. Sharma[4], S. Jois[4], G.M. Stephen[4], A. Friedman[4], R. Torsi[3], M. Munoz[3], D. Wines[3], A.R. Hight Walker[3], B. Donavon[2], M.E. Jamer[2] and J.Q. Xiao[1]
1. University of Delaware, Newark, DE, United States; 2. United States Naval Academy, Annapolis, MD, United States; 3. National Institute of Standards and Technology, Gaithersburg, MD, United States;
4. Laboratory of Physical Sciences, College Park, MD, United States

Recent studies on RuO_2 have demonstrated that the existence of magnetic ordering in this compound is controversial and inconsistent. Computational results have suggested a fragile nature to the magnetic ordering that is possibly related to Ru vacancies [1]. Based on several recent studies, the properties of RuO_2 grown on various substrates may be antiferromagnetic/altermagnetic-like [2,3] or even superconducting [4], possibly due to small changes in the crystal structure. Interestingly, the bulk RuO_2 shows no magnetic [5,6] or superconducting properties [2], which makes the thin film properties more interesting to tune. In this study, RuO_2 is grown on MgF_2 substrates with and without a NiFe capping layer. We observe a thickness dependent unidirectional exchange bias which emerges below 10 K in 10 nm to 100 nm of RuO_2 films interfaced with about 10 nm of NiFe. The largest exchange bias measured for both 100 nm (110) and (100) oriented films is shown in the Fig. 1. To investigate the emergence of exchange bias below 10 K we plan to perform temperature dependent magneto-Raman to deduce the origin of the exchange bias effect and magnetic ordering observed in these films by considering changes in the phonon and possible magnon modes between 2 K and 20 K.

[1] Smolyanyuk, A., Mazin, I. I., Garcia-Gassull, L., & Valentí, R. (2024). Fragility of the magnetic order in the prototypical altermagnet RuO_2. *Physical Review B*, *109*(13), 134424. [2] Feng, Z., Zhou, X., Šmejkal, L., Wu, L., Zhu, Z., Guo, H., ... & Liu, Z. (2022). An anomalous Hall effect in altermagnetic ruthenium dioxide. *Nature Electronics*, *5*(11), 735-743. [3] Bai, H., Han, L., Feng, X. Y., Zhou, Y. J., Su, R. X., Wang, Q., ... & Song, C. (2022). Observation of spin splitting torque in a collinear antiferromagnet RuO_2. *Physical Review Letters*, *128*(19), 197202. [4] Ruf, J. P., Paik, H., Schreiber, N. J., Nair, H. P., Miao, L., Kawasaki, J. K., ... & Shen, K. M. (2021). Strain-stabilized superconductivity. *Nature Communications*, *12*(1), 59. [5] Hiraishi, M., Okabe, H., Koda, A., Kadono, R., Muroi, T., Hirai, D., & Hiroi, Z. (2024). Nonmagnetic Ground State in RuO_2 Revealed by Muon Spin Rotation. *Physical Review Letters*, *132*(16), 166702. [6] Keßler, P., Garcia-Gassull, L., Suter, A., Prokscha, T., Salman, Z., Khalyavin, D., ... & Moser, S. (2024). Absence of magnetic order in RuO_2: insights from μSR spectroscopy and neutron diffraction. *arXiv preprint arXiv:2405.10820*.

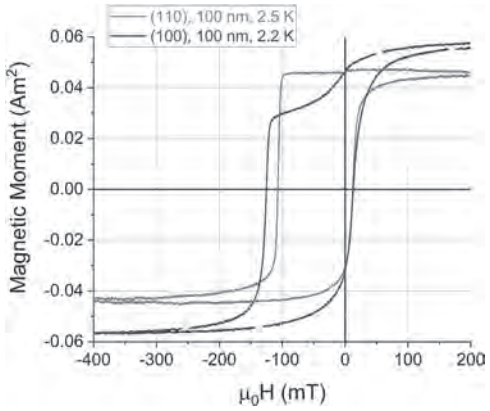

Fig. 1. MgF_2/RuO_2 (100 nm)/NiFe (10 nm)/ Al(5 nm) hysteresis after annealing at 400 K for 1 hour and field cooling in a 1 Tesla field.

BP-05. Enhancing the Magneto-Optical Kerr Effect in Non-collinear Antiferromagnets via a Dielectric Layer. *E. Gong*[1], M. Yoo[1] and A. Hoffmann[1] *1. Materials Science and Engineering, University of Illinois at Urbana-Champaign, Urbana, IL, United States*

Non-collinear antiferromagnets, such as Mn_3Sn and Mn_3Ge, have magnetic moments arranged at 120° angles to each other, resulting in unique magnetic properties, such as the anomalous Hall effects and the magneto-optical Kerr effect (MOKE) [1, 2]. These materials are promising for spintronics due to their significant interactions with electric currents and light, which are determined by the orientation of magnetic octupole moments [3]. However, the lack of net magnetization of the octupole moments poses challenges for magneto-optical observations. Here we demonstrate the enhancement of the magneto-optical Kerr effect (MOKE) in a non-collinear antiferromagnet, Mn_3Sn, with a carefully selected thickness of a dielectric material, MgO, by creating constructive interference with the reflected light. First, we determined the complex refractive index by ellipsometry measurements, and then we performed subsequently numerical calculations using this parameter to determine how the Kerr amplitude varies with different thicknesses of a MgO layer [4]. The calculation results show that the Kerr amplitude has a sinusoidal-like dependence on the MgO thickness and is maximized at the optimized thickness. Next, we measured the Kerr amplitude across a range of MgO layer thicknesses using a polar MOKE system. The measured data show a sinusoidal periodic trend with a doubling of the Kerr amplitude at an optimized MgO thickness compared to the case without the dielectric layer. The experimental results show good agreement with our numerical calculations (Fig. 1). This study will improve the detection of magnetic domain structures with high sensitivity and contrast, which is essential for exploring antiferromagnetic spintronics. This work was supported by the NSF through the Illinois MRSEC (DMR-1720633).

[1] S. Nakatsuji et al., Nature., 527, 212 (2015). [2] T. Higo et al., Nat. Photonics., 12, 73 (2018). [3] T. Chen et al., Nat. Commun., 12, 572 (2021). [4] D. Kim, YW. Oh and J.U. Kim, Nat Commun., 11, 5937 (2020).

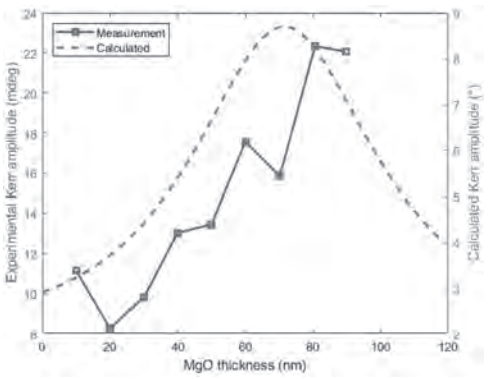

Fig. 1: Measured Kerr amplitude as a function of MgO layer thickness (left y-axis), compared with the trend from numerical calculations (right y-axis).

BP-06. Effect of strain on altermagnetic properties of Mn_5Si_3. A. Badura[1,2], *E. Schmoranzerová*[2], Z. Sadeghi[2], P. Nemec[2], Z. Soban[1], M. Leiviska[1], H. Reichlova[1,3], S. Beckert[3], V. Baltz[4], I. Kounta[5], L. Michez[5], L. Smejkal[6], J. Sinova[6], S. Goennenwein[7] and D. Kriegner[1] *1. Institute of Physics ASCR v.v.i, Prague, Czechia; 2. Faculty of Mathematics and Physics, Charles University, Prague, Czechia; 3. Technical University Dresden, Dresden, Germany; 4. SPINTEC, Univ. Grenoble Alpes, CNRS, CEA, Grenoble, France; 5. Aix Marseille University, CNRS, IM2NP, Marseille, France; 6. Institute of Physics, Johannes Gutenberg University Mainz, Mainz, Germany; 7. Department of Physics, University of Konstanz, Konstanz, Germany*

Altermagnets are a newly emerging class of materials where the crystal symmetry breaking leads to a non-relativistic spin splitting in the band structure [1]. Among materials exhibit this new type of magnetic ordering is the metallic compound Mn_5Si_3 in form of thin films [2, 3]. Bulk Mn_5Si_3 does not display altermagnetic ordering due to a doubling of unit cells [4] which preserves the time reversal combined with translation (Tt) symmetry (Fig. 1(a)) In contrast, in the epitaxial layers, the difference in thermal expansion coefficient of Si substrate and Mn_5Si_3 results in tensile strain upon cooling and enforces hexagonal crystal symmetry, which prevents the unit cell doubling [2,3]. Consequently, the Tt symmetry is broken and Mn_5Si_3 thin films become altermagnetic. The presence of the Anomalous Hall Effect (AHE) has been established in connection with altermagnetism [2], however, the exact relationship between the epitaxial strain and the AHE is not understood. To investigate the role of strain in the magnetotransport response, we measured the AHE signal of Mn_5Si_3 epitaxial films as a function of applied external strain. External strain was introduced by gluing the samples to a support material with a distinct thermal expansion coefficient from that of the Si substrate. By cooling such a stack below Néel temperature, where a compensated collinear altermagnetic order is present, the different thermal expansion creates either tensile or compressive strain (see Fig. 1(b)). In Fig. 1(c) (right part) a difference between the strained and unstrained AHE loop is shown. The external strain leads to a reduction (compressive) or enhancement (tensile) of the coercive field of the hysteresis loops, and the same trend can be identified for the AHE amplitude. These observations are in accord with the expected role of tensile strain in stabilizing the altermagnetic order.

[1] J. Šmejkal, J. Sinova, & T. Jungwirth, Phys. Rev. X, vol.12, p. 040501 (2022). [2] H. Reichlová et al., Nat.Comm., vol. 15, p. 4961 (2024) [3] M. Leiviska et al., Phys. Rev. B, vol. 109, p. 224430 (2024) [4] C.Sürgers, W. Kittler, T. Wolf, & H.V. Löhneysen, AIP Adv., vol. 6, p. 055604 (2016).

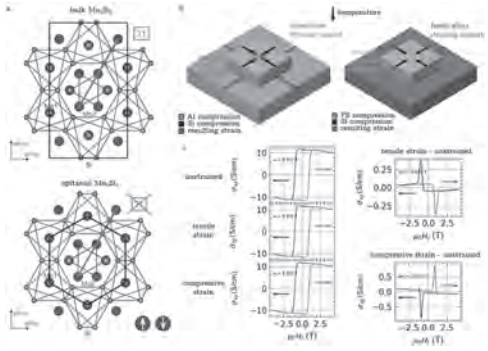

Fig. 1: **a) structure of Mn_5Si_3 as a bulk and epitaxial layer. b) Schematics of straining method by gluing to Al and fused silica supports. c) Left: AHE hysteresis loops measured at 80 K. Right: Difference between the AHE on strained and unstrained samples for applied tensile/ compressive strain.**

BP-07.Withdrawn

BP-08.*Withdrawn*

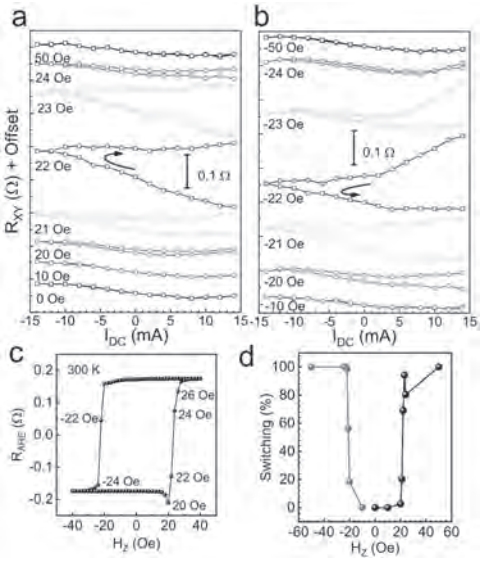

Fig. 2. Magnetization switching at various fields with DC. The R_{XY}-I_{DC} plots at different out-of-plane magnetic bias fields (H_Z) for (a) positive and (b) negative field direction of H_Z. The curved arrow shows the current direction. (c) EHE loop for comparing the current-induced switching. The magnetic field values are written corresponding to data points on the curve. (d) Percentage magnetization switching estimated from (a) and (b) for various bias fields.

Session BQ
SENSORS AND APPLICATIONS II
(Poster Session)

Alexandria Will-Cole, Chair
Sandia National Laboratories, Albuquerque, NM, United States

BQ-01. Effects of wire diameter on the sensitivity of output voltages for amorphous wire–based magnetic sensors. *F. Akagi*[1], S. Yamada[1], Y. Honkura[2] and S. Honkura[2] *1. Kogakuin University, Tokyo, Japan; 2. MagneDesign corporation, Aichi, Japan*

1. Introduction: Gigahertz (GHz) spin rotation sensors using FeCoSiB amorphous wires with zero-magnetostriction have shown high sensitivity because GHz pulsed currents passing through these wires generate strong circular magnetic fields in the wire surface, exclusively producing spin magnetization rotations at GHz angular velocities that do not affect inner domains [1]. In this study, we investigated the relationship of the diameter of an amorphous wire with the sensitivity of output voltages using the Landau–Lifshitz–Gilbert equation, which considers eddy currents. 2. Calculation model The calculation model of the amorphous wire is shown in Fig. 1. The magnetic properties included a saturation magnetization of 1.0 T, a magnetic anisotropy constant of 250 J/m^3 [2]. The easy axis of magnetization in the amorphous wire was presumed to be oriented circumferentially at the surface due to the tension during the manufacturing process. Conversely, the wire core was assumed to have an axial orientation. The sensitivity of the output voltage was defined as the output voltage gradient at nearly zero external magnetic field. 3. Results Figure 2 shows the relationship between the sensitivity of the output voltage observed during the rising and falling times of the pulse current and the wire diameter. The sensitivity of the output voltage during the falling time remained nearly constant regardless of the wire diameter. Conversely, the sensitivity of the output voltage during the rising time increased with decreasing wire diameter. However, when the wire diameter was very small, the voltage remained nearly constant regardless of the external magnetic field, hindering the determination of the output voltage gradient. This can be attributed to a decrease in the demagnetization fields in the axial direction of the wire with decreasing wire diameter, which causes the spin angle of the magnetization reversal to remain constant regardless of the wire diameter.

[1] Y. Honkura, and S. Honkura, *J. Magn. Magn. Mater.*, 513, 167240, (2020). [2] F. Akagi, T. Kaneko, H. Kan, Y. Honkura, and S. Honkura, *Sensors*, 23, 2786 (2023).

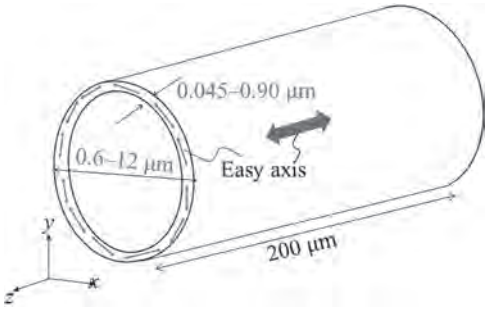

Fig. 1 Calculation model of FeCoSiB amorphous wire.

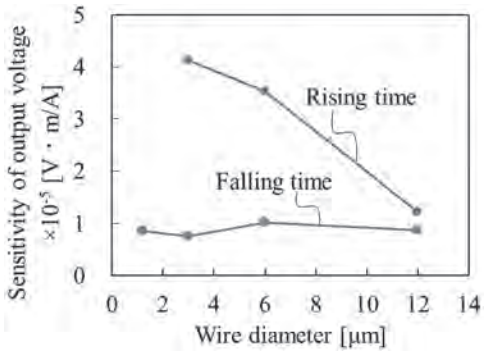

Fig. 2 Relationship between sensitivity of output voltage observed during the rising and falling times of the pulse current and wire diameter.

BQ-02. Method for Estimating Crack Length and Depth using RBF in Eddy Current Testing. *D. Kosaka*[1], H. Hanawa[2] and T. Hirano[3] *1. Polytechnic University, Kodaira-shi, Japan; 2. The Japanese Association for Non-Destructive Testing Industry, Chiyoda-ku, Japan; 3. Hazardous Materials Safety Techniques Association, Minato-ku, Japan*

The welded-steel tanks require periodic maintenance to prevent weld cracks caused by the weight of amounts of oil. The Magnetic flux leakage inspection or the magnetic particle inspection[1] is commonly used for the crack detection. The repair decisions are based on estimates of crack length obtained from the inspections resulting from the magnetic particle inspection. However, this method requires removing coatings from oil tanks to protect them from corrosion. This results in a significant amount of waste generated from sound coatings due to the need for repeated removal and reapplication of coatings for each inspection. The Eddy Current Testing (ECT) is widely known as an inspection can detect cracks over the coating. While ECT has the advantage of easily recording measurement results and quickly detecting minute cracks, it has limitations in accurately estimating the shape of cracks[2]. This is because the effects of crack length and depth, respectively cannot be separated from the amplitude of the ECT detection signals. We propose a new method for estimating crack length and depth using the response width as defined in ISO 15548-2:2019 and the maximum amplitude value of the ECT detection signal[3]. Response width is the length between -6 dB of the maximum amplitude when the length in the scanning direction is on the horizontal axis and the amplitude of the detection signal is on the vertical axis. The effectiveness of the proposed method was verified using the finite element method. The simulation model used is shown in Fig. 1. Fig. 2 shows the simulation results of plotting the “maximum value of the crack signal” and the “response width” of the reference cracks (depths of 0.5, 1, 1.5, and 2 mm and lengths of 3, 4, and 5 mm) and the estimated crack (depth of 1.7 mm and length of 4.5 mm) on an amplitude-response width plane. The result of estimating a crack of 4.5 mm in length by radial prescriptive function interpolation using nine reference cracks was 4.4 mm. In the presentation, we will show the measured results of applying the proposed method to defects with known geometry created by machining.

[1] Bouteille, Patrick, M. Finckbohner and S. Lugin, QIRT congress proceeding (2012) [2] Noritaka Yusa, Haoyu Huang and Kenzo Miya, NDT & E International, Vol. 40, No. 3, pp. 185-191 (2007) [3] Hazardous Materials Safety Techniques Association, https://khk-syoubou.or.jp/pdf/guide/research/20_2024-03-et.pdf, in Japanese (2024)

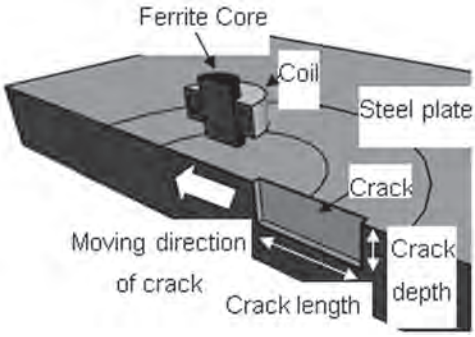

Fig. 1 Simulation model.

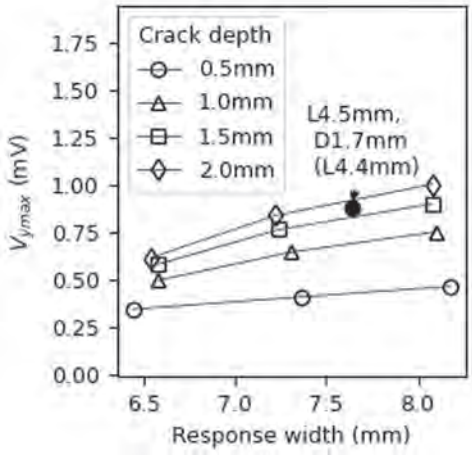

Fig. 2 Simulated crack signals on the amplitude vs response width plane.

BQ-03. Material-Dependent Sensitivity Degradation of Magnetoelastic Torque Transducers Under Cyclic Torsional Stress. *R. Kari*[1] and M. Callahan[1] *1. MagCanica, Inc., San Diego, CA, United States*

Magnetoelastic torque transducers are used in numerous applications spanning automotive, commercial, and aerospace sectors; however, they typically require the application of a significant number of full-load torque cycles to stabilize the transducer transfer function. The transducer material and magnitude of torsional stresses applied during the stabilization process are critical factors influencing the number of loading cycles required for stability and consequence of overloads, impacting the reliability of transducers when deployed in real-world systems. This study explores the potential for developing mathematical relationships and associated metrics that can be used to ascertain transducer stability and quantify the consequences of applying stresses beyond the calibration range. Magnetoelastic materials with varying Nickel and Chromium including those shown in Table 1 were investigated. Fig. 1 provides the physical characteristics of the shafts and illustrates the typical sensitivity change, showing a rapid initial decrease followed by a gradual approach to stability. Sensitivity was defined as the transfer function of axial magnetic field measured with a flux-gate magnetometer versus applied torsional stress, and was evaluated at regular intervals (e.g. after each full-scale torque cycle) by applying four subscale torque cycles of 20MPa. Each shaft was magnetized in a local region with oppositely oriented circumferential bands to enable common mode rejection. Varying degrees of nominal sensitivity and degradation were observed across the materials tested, with the results shown in Table 1. The results reveal a clear correlation between material composition, applied stress, degradation in sensitivity, and the number of cycles required for stabilization. Based on our findings, it is observed that the degradation follows a typical first order non-linear relationship. This relationship can be used to develop metrics associated with the number of cycles required to stabilize the system, develop new magnetization and calibration processes to minimize the cycles required, and evaluate the consequence of overloads in real-world applications to determine if the system needs to be recalibrated.

I.J. Garshelis, Journal of Applied Physics, Vol. 85, pp 5468-5470 (1999) M. Boley, D. Franklin, D. Rigsbee, Journal of Applied Physics, Vol. 87, pp 7073-7075 (2000) R. Kari, R. Alvi, M. Callahan, SAE Technical Paper 2022-01-0375 (2022)

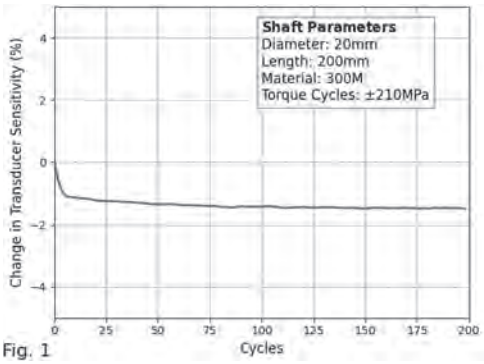

Fig. 1

Table 1
Degradation of Magnetoelastic Torque Transducers Under Different Cycles and Applied Stresses

Applied Stress [MPa]	Material	Initial Sensitivity [A/m]	Degradation [%]	Degradation [%]	Degradation [%]	Degradation [%]
			Cycles = 2	Cycles = 20	Cycles = 60	Cycles = 100
105	300M	1.7	-0.2	-0.2	-0.2	-0.2
210	300M		-1.3	-1.8	-1.9	-1.9
315	300M		-3.7	-5.3	-5.9	-6.2
105	Ferrium M54	4.9	-2.0	-2.3	-2.5	-2.5
210	Ferrium M54		-9.1	-13.1	-14.0	-15.1
315	Ferrium M54		-22.7	-32.8	-36.4	-37.8
105	MLX17	8.0	-21.4	-31.6	-34.8	-36.1
210	MLX17		-54.6	-70.5	-74.7	-76.1
315	MLX17		-70	-84.4	-87.6	-88.7

BQ-04. Expanding the Field Range of PHE Sensors for Increased Industrial Applicability. *D. Lahav*[1], M. Schultz[1], S. Amrusi[2], A. Grosz[2] and L. Klein[1] *1. Physics, Bar Ilan Institute of Nanotechnology and Advanced Materials, Department of Physics, Bar-Ilan University, Ramat Gan, Tel Aviv 52900, Israel; 2. Department of Electrical and Computer Engineering, Ben-Gurion University of the Negev, Beer-Sheva, Israel*

A recent comprehensive review of planar Hall effect (PHE) sensors [1] underscores the growing interest in these sensors and identifies numerous opportunities for further enhancements that could broaden their application scope. However, PHE sensors have a notable limitation: they typically operate within a magnetic field range of hundreds of microteslas (μT) [2]. This restriction poses challenges for applications requiring broader field ranges, such as in the automotive industry. To meet the increasing demand for highly sensitive magnetic sensors with larger measuring field range across industrial, scientific, and consumer sectors, it is essential to expand the field range of PHE sensors and evaluate the impact of such an expansion on their equivalent magnetic noise (EMN) [3]. Previous attempts to increase the field range of magnetoresistive sensors included modifications to the ferromagnetic layer and variations in the thicknesses of spacer and capping layers. Here, we achieve an increase of more than an order of magnitude in the field range by manipulating the shape-induced magnetic anisotropy [3]. We present measurements of elliptical PHE sensors with uniaxial magnetic anisotropy ranging from less than mT to more than 10 mT, and show that an EMN of less than 10 nT/ √ Hz at 10 Hz is achieved for anisotropy field exceeding 4 mT (Fig.1). Additionally, by measuring the PHE resistance (R_{PHE}) in a field range where the sensor response in linear, descending from a high positive field (R^{+}_{PHE}), and ascending from a low negative field (R^{-}_{PHE}), we show that sensors with larger field range exhibit negligible

hysteresis, associated with their effective single magnetic domain behaviour (Fig.2). We discuss the potential industrial applications of PHE sensors with extended field range and compare their performance with other commonly used sensors in similar applications. In addition, we discuss promising routes to further expand the field range while minimizing detrimental effects on resolution.

[1] A. Elzwawy, L. Marnitz, A. Moskaltsova, O. Gurel, and J.-M. Schmalhorst, Journal of Physics D, vol. 54, no. 35, p. 353002, (2021). [2] H. Nhalil, T. Givon, P. T. Das, V. Mor, M. Schultz, S. Amrusi, L. Klein, and A. Grosz, IEEE Sensors Letters, vol. 3, no. 12, pp. 1–4, (2019). [3] D. Lahav, M. Schultz, S. Amrusi, A. Grosz, and L. Klein, Sensors, vol. 24, no. 13, (2024).

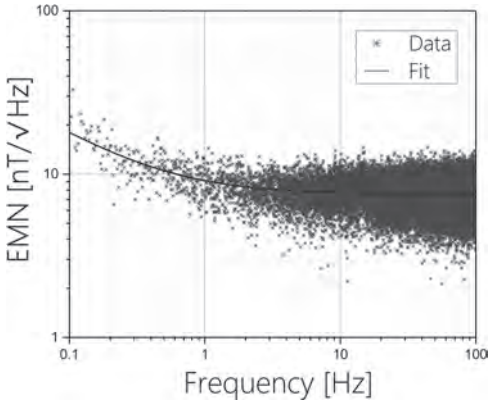

Figure 1: EMN vs. frequency of a PHE sensor with an anisotropy field of 4.2 mT.

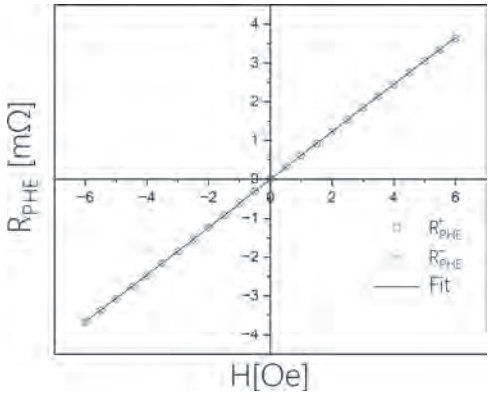

Figure 2: R^{+}_{PHE} and R^{-}_{PHE} vs applied field parallel to the hard axis of the ellipse of a PHE sensor with an anisotropy field of 4.2 mT.

BQ-05. Localization of multiple cracks in a cylindrical ferromagnetic rod based on the Fourier coefficients of the radial leakage magnetic flux. *K. Shiku*[1] and T. Nara[1] *1. The University of Tokyo, Bunkyo-ku, Japan*

Magnetic flux leakage testing (MFLT) is necessary before induction hardening of cylindrical ferromagnetic rods because cracks would extend in the process. Although conventional MFLT uses an array of magnetic sensors to measure the leakage magnetic flux (LMF) [1], such arrays have difficulty in calibration. In contrast, we proposed a crack localization method using only two coils ("Fourier coils") [2], which measure the first-order Fourier coefficients. However, estimating multiple crack circumferential positions was impossible if they were at the same axial positions. This study proposes a method to estimate multiple crack circumferential positions in a rod based on measuring the circumferential multiple-order Fourier coefficients of the radial LMF. As shown in Fig. 1, for the case when two cracks are located at the circumferential positions φ_1 and φ_2 with the same z-axis coordinates, we derived algebraic equations $c_m = \sum^{2}_{k=1} p_k e^{-im\varphi_k}$, $m = 0,1,2$ where c_m and p_k are, respectively, the m th-order Fourier coefficient and a magnetic dipole moment relevant with the crack size and shape. This form of equations are called a moment problem [3], and φ_k with p_k are algebraically obtained from measurements of c_m. Theoretically, this formulation can easily be extended to any number of cracks. Since c_1 can be measured using the coils in [2], we developed sensors that directly measure the zeroth (c_0) and the second order (c_2) Fourier coefficients of the radial LMF in this research. The magnified photo in Fig. 1 shows the proposed sensor that measures Re c_2, the second-order Fourier cosine coefficient, by winding the coil in the repeated figure-of-eight form, whose width is $2w|cos\ 2\varphi|$ at circumferential position φ, where $2w$ is the maximum width. Im c_2 can be measured using the same coil rotated with 90 degrees. c_0 is measured by the coil whose width is $2w$ at any φ. Fig. 2 shows the estimation results of the two crack locations using the proposed sensors. The maximum error was 22.5°, showing that the proposed method can estimate two crack positions.

[1] Z. Zhou and Z. Liu, IEEE Transactions on Industrial Electronics., vol. 68, pp. 2543–2553 (2021) [2] K. Shiku, T. Nara, and Y. Gotoh, IEEE Transactions on Magnetics., vol. 59, pp. 1–5 (2023). [3] T. Nara and S. Ando, Journal of Inverse and Ill-posed Problems., vol. 15, pp. 403–418 (2007)

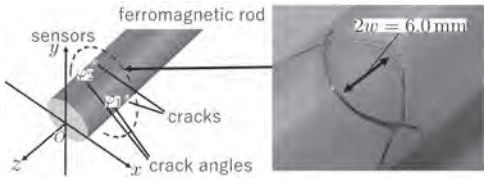

Problem setting and proposed sensor that measures the second-order Fourier cosine coefficient.

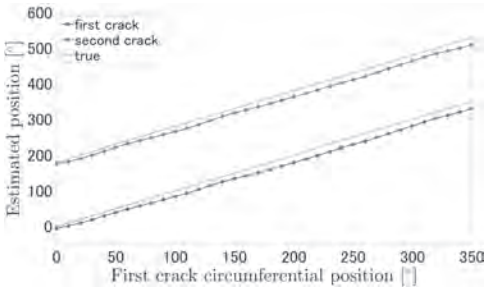

Estimation results of the two crack circumferential positions.

BQ-06. Optimal Design of Dual Induction Eddy Current Probe for Vibration Suppression. *K. Matsushima*[1], D. Kosaka[1] and Y. Kumakura[2] *1. Polytechnic University, Kodaira, Japan; 2. Tex Riken Co., Ltd, Nishinomiya, Japan*

In comparison to other non-destructive testing methods, eddy current testing (ECT) can detect minute surface defects that occur during the manufacturing process of metal parts. However, this method is also highly sensitive to vibrations that occur during product transportation in the manufacturing process, and vibration signals can interfere with the detection of minute flaw signals. Methods that employ uniform eddy currents[1] or self-differential probes[2], as well as methods that necessitate signal processing, such as multi-frequency methods [3] and frequency filters, have been proposed to attenuate signals other than flaw signals. The authors proposed an electromagnetically passive method that employs dual induction, which simultaneously utilizes self-induction and mutual induction, to suppress solely vibration signals without attenuating flaw signals [4]. In this paper, we discuss how to design a dual-guidance probe. Fig. 1 shows a simulation model of a dual induction differential ECT probe. This probe comprises four coils, designated L_1 to L_4. L_2 and L_3 are designated as the internal coils, while L_1 and L_4 are designated as the external coils. The distances between L_1 and L_2 and between L_3 and L_4 are always identical. This distance is defined as the coil distance. Since the appropriate coil distance differs depending on the test conditions, there is a need for a cost-saving method to determine the suitable coil distance that does not rely on trial and error through numerical

experiments or prototyping. Fig. 2 shows the outcomes of a simulation investigating the relationship between skin depth and optimal coil spacing. It can be observed that the optimal coil spacing is contingent on the skin depth. This indicates that it is suitable to determine the coil spacing based on the skin depth matching to the flaw depth. It was elucidated that the coil spacing of the dual induction probe should be determined from the skin depth, which matches the depth position of the flaw in the object to be detected, rather than considering the excitation frequency and conductivity separately. The results of the measurement experiment will be presented orally.

[1] Ageng S. Repelianto and Naoya Kasai, Sensors, Vol. 19, No. 2, 397 (2019) [2] B. Wincheski, J. P. Fulton, S. Nath and M. Namkung, Materials Evaluation, Vol. 52, No. 1, pp. 22–26 (1994) [3] Don E. Bray and Roderic K. Stanley, CRC Press, pp. 418-419 (1997) [4] Daigo Kosaka, Yuji Kumakura, and Fumio Kojima, IEEE Transactions on Magnetics, Vol. 59, No. 11, pp. 1-6 (2023)

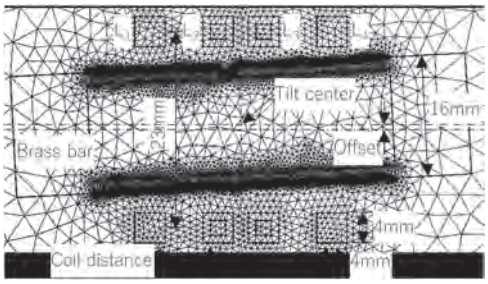

Fig. 1 Simulation model.

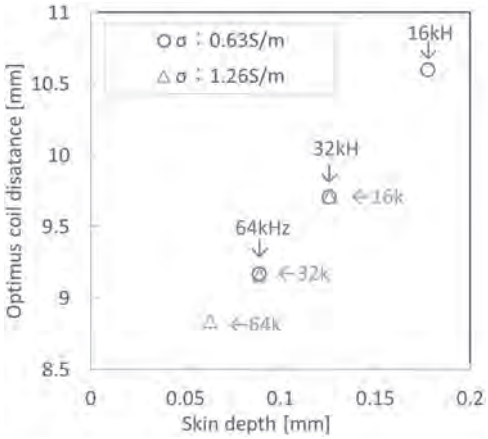

Fig. 2 Simulated optimus coil distance.

Session BR
BIOMAGNETICS AND EMERGING TOPICS RELATED TO MAGNETISM
(Poster Session)

Shin Yabukami, Co-Chair
Tohoku University, Sendai, Japan
Xian Wu, Co-Chair
The Ohio State University, Burlington, MA, United States

BR-01. Advancing Single-Cell Hematological Analysis: A Microfluidic Approach to Measure RBC Physical Properties. *L. Nguyen T. Tran*[1], K. Paz Gonzalez[1], H. Choe[2], X. Wu[2], P. Iyer[2], K. Wu[3], J. Chalmers[2] and J. Gomez-Pastora[1] *1. Chemical Engineering, Texas Tech University, Lubbock, TX, United States; 2. Chemical and Biomolecular Engineering, The Ohio State University, Columbus, OH, United States; 3. Electrical and Computer Engineering, Texas Tech University, Lubbock, TX, United States*

Hematological analysis is crucial for diagnosing and monitoring blood-related disorders, such as anemia [1]. However, the limitations of commercially available hematology analyzers, including high cost and substantial space and weight requirements, restrict their deployment to specific laboratory settings. Herein, we develop a novel cell tracking velocimetry (CTV) device designed to precisely measure the physical properties of individual particles and cells, such as magnetic susceptibility, size/volume, or density. The device consists of a microfluidic chamber made of a square glass tubing positioned between an assembly of permanent magnets, creating a well-defined magnetic field gradient. A portable microscope camera captures particle and cell motion as they traverse the channel, enabling accurate trajectory tracking. Post-image processing is performed using ImageJ's FIJI plug-in, TrackMate. By analyzing the velocity profiles and employing mathematical models, the properties of the particles and cells can be determined with high precision [2]. To validate the CTV system accuracy, we are conducting experiments using polystyrene beads of known size, density, and magnetic properties. Following the validation with synthetic particles, the CTV system will be then applied to analyze fresh human red blood cells (RBCs). We will measure several hematological parameters from fresh human blood samples, as well as their iron and hemoglobin concentration, by correlating the magnetophoretic velocity of RBCs to these factors [3]. This single-cell analysis aims to determine key hematological parameters such as mean corpuscular hemoglobin concentration (MCHC) and cellular iron content, potentially providing more comprehensive information than traditional averaged measurements. Our CTV device offers a quick, label-free, and non-invasive method for analyzing magnetic properties of particles and individual cells, with proven applications in hematology and anemia diagnosis, as well as potential uses in cancer research, promising to enhance our understanding of disease mechanisms and contribute to the development of better diagnostic and treatment approaches.

[1] Monique Pinto, Jhenifer, Leilismara Sousa Nogueira, and Danyelle Romana Alves Rios. "Hematological parameters: is there a difference between those released by the hematological analyzer and to the customer?." Einstein (16794508) 21 (2023). [2] Kim, James, et al. "Quantification of the mean and distribution of hemoglobin content in normal human blood using cell tracking velocimetry." Analytical chemistry 92.2 (2019): 1956-1962. [3] Gómez-Pastora, Jenifer, et al. "Potential of cell tracking velocimetry as an economical and portable hematology analyzer." Scientific reports 12.1 (2022): 1692.

BR-02. Study of Oversized SPIO Nanoparticles with a Magnetic Particle Spectrometer for Suitability as MPI Tracers. *C. Bastajian*[1,2], C. McDonough[1], C. Hunt[1,3] and A. Tonyushkin[1] *1. Physics, Oakland University, Rochester, MI, United States; 2. Electrical Engineering, Oakland University, Rochester, MI, United States; 3. Mechanical Engineering, Oakland University, Rochester, MI, United States*

Magnetic Particle Spectrometry (MPS) is a sensitive analytical method that evaluates the magnetic response of superparamagnetic iron oxide nanoparticles (SPIO) under AC magnetic fields [1]. Our group has constructed a custom MPS system for characterization of SPIO. SPIO, known for their advantageous characteristics such as non-linear excitation, high saturation amplitude, and absence of remnant magnetization, are commonly used in targeted drug delivery and magnetic particle imaging (MPI) [2]. Traditionally, single-core SPIO Vivotrax (Magnetic Insight) has been widely used in the MPI community, but recently, the nanoflower-shaped cluster SPIO SynomagD 70 nm (Micromod) has become a popular MPI tracer due to superior performance. This study explores the suitability of oversized sphere shell SPIO clusters for MPI, specifically Magnefy and ProMag (BangsLab) with a hydrodynamic diameter ~1 μm, as these particles haven't been thoroughly explored for MPI applications. Our MPS technique involves applying 1 kHz AC magnetic fields with a rms value of 25 mT to the SPIO and detecting their magnetization responses M(H) in the frequency domain, described by Langevin theory. Standard NMR tubes with 100 μl of SPIO solution with a concentration of 5.5 mg/mL are placed in the MPS system inside a gradiometer receive coil connected to the low-noise preamplifier (SR560, Stanford Research). A DAQ card (National Instrument) digitizes the data, to be analyzed by custom software focusing on the third harmonic response, which forms the signal for our single-sided MPI scanner [3]. The resulting M(H) curves (Fig.1) demonstrate that SynomagD and Vivotrax exhibit steep magnetization, corroborating exceptional MPI performance. In contrast, the M(H) curves of the oversized SPIO do not show sufficient steepness for the third harmonic to be detected at lower field values ≤ 5 mT. Specifically, ProMag and Magnefy exhibit negligible third harmonic magnitudes compared to SynomagD's magnitude at ~1.6 mT (Fig. 2), the setting used in our scanner. While the oversized SPIO show potential for use in preclinical MPI systems [4] with high excitation magnetic fields, they are not suitable as tracers at low fields typically employed in emerging clinical systems.

[1] N. Garraud, et. al., "Design and validation of magnetic particle spectrometer for characterization of magnetic nanoparticle relaxation dynamics," AIP Advances 1 May 2017; 7 (5): 056730. [2] J. W. Bulte, "Superparamagnetic iron oxides as MPI tracers: A primerand review of early applications," Ad. Drug Del. Rev., vol. 138, pp. 293–301, 2019. [3] C. McDonough, J. Chrisekos, and A. Tonyushkin, "Tomographic Magnetic Particle Imaging with a Single-Sided Field-Free Line Scanner," IEEETrans. on Biomedical Engineering, jul 15, 2024. doi:10.1109/TBME.2024.3427665. [4] J. Guzy, et. al., "Complex Relationship between Iron Oxide Nanoparticle Degradation and the Signal Intensity in Magnetic Particle Imaging," ACS Applied Nano Materials 2020 3 (5), 3991-3999.

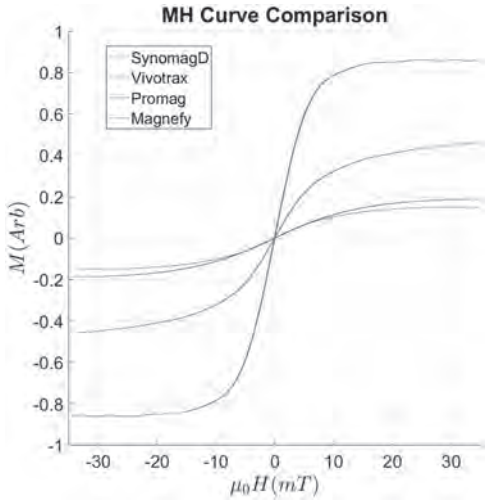

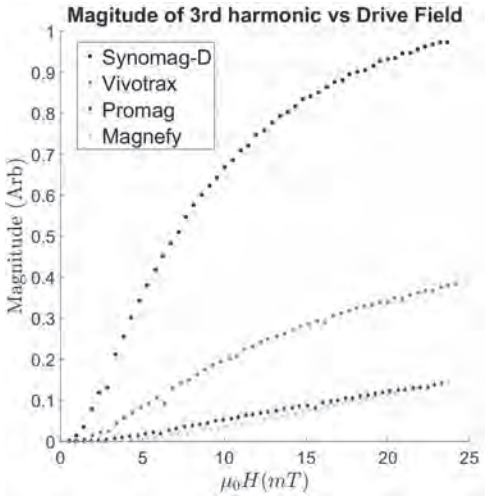

BR-03. Tuning Excitation Field Amplitude for Higher Magnetic Particle Imaging Resolution: A Modeling Study. *E. Azizi*[1], B. Rezaei[1], S. Mostufa[1], C. Li[1], J. Gomez-Pastora[2], R. He[1] and K. Wu[1] *1. Electrical and Computer Engineering, Texas Tech University, Lubbock, TX, United States; 2. Chemical Engineering, Texas Tech University, Lubbock, TX, United States*

Magnetic particle imaging (MPI) has been actively studied and applied to biomedical imaging and will reach to clinical stage soon. To further push the limit of spatial resolution in MPI, researchers have been working towards optimizing the image reconstruction algorithms, excitation field profiles, MNP tracer designs, etc. Recent studies reported that lower excitation field amplitudes can improve spatial resolution, though this comes at the expense of lower tracer sensitivity.[1,2] Different excitation field profiles directly affect the relaxation times of MNPs and thus, change the collective dynamic magnetizations recorded by the receive coils in MPI. However, there is a gap between understanding the field-caused relaxation dynamics of MNP tracers and the resulting MPI spatial resolution. Herein, we apply a stochastic Langevin function with coupled Brownian and Néel relaxations to model the dynamic magnetizations of MNP tracers in liquid subjecting to an excitation field. We assumed an ensemble of 1,000 non-interacting iron oxide MNPs with varying magnetic core sizes are subjected to different excitation fields that have a fixed frequency of 25 kHz and varied amplitude from 1 to 20 mT/μ_0. The collective time-domain dynamic magnetizations (M-t curves), magnetization-field hysteresis loops (M-H curves), and point spread functions (PSFs, dM/dH-H curves) are collected from these MNP tracers. The full width at half maximum (FWHM) from PSF profiles is used as a parameter to evaluate the intrinsic MPI spatial resolution for different MNPs.[3,4] Fig 1 shows an example of 30 nm MNPs subjected to varying excitation fields. In addition, we collected the harmonic spectra of MNPs, analyzing the signal-to-noise ratio (SNR) at varying excitation field amplitudes. This work provides insights into the interplay between tracers' dynamics and excitation field profiles.

[1] C. Kuhlmann, A.P. Khandhar, R.M. Ferguson, S. Kemp, T. Wawrzik, M. Schilling, K.M. Krishnan, and F. Ludwig, "Drive-Field Frequency Dependent MPI Performance of Single-Core Magnetite Nanoparticle Tracers," IEEE Transactions on Magnetics 51(2), 1–4 (2015). [2] L.R. Croft, P.W. Goodwill, J.J. Konkle, H. Arami, D.A. Price, A.X. Li, E.U. Saritas, and S.M. Conolly, "Low drive field amplitude for improved image resolution in magnetic particle imaging: Low drive field amplitude for improved image resolution," Med. Phys. 43(1), 424–435 (2015). [3] T. Jiang, W. Yi, Z. Du, and W. Liu, "An improved point spread function for complex susceptibility-based magnetic particle imaging," Measurement Science and Technology 33(9), 095402 (2022). [4] K. Murase, "Simultaneous correction of sensitivity and spatial resolution in projection-based magnetic particle imaging," Medical Physics 47(4), 1845–1859 (2020).

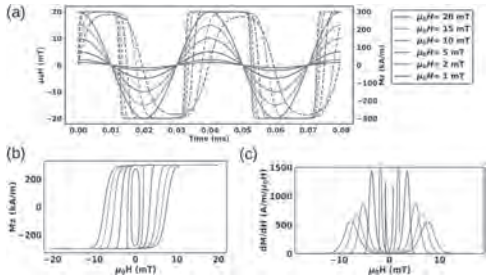

Fig 1. Simulated dynamic magnetization responses of 30 nm MNP tracers subjected to an excitation field of 25 kHz and varying amplitudes from 1 to 20 mT/μ_0. (a) M-t curves. As a reference, the excitation field is also plotted. (b) and (c) are M-H curves and PSF profiles, respectively.

BR-04. Experimental investigation of magnetic microbead recovery using a quadrupole magnetic field: insights toward process intensification. S. Ciannella[1], X. Wu[2], *H. Choe*[2], K. Wu[3], J. Chalmers[2] and J. Gomez-Pastora[1] *1. Department of Chemical Engineering, Texas Tech University, Lubbock, TX, United States; 2. William G. Lowrie Department of Chemical and Biomolecular Engineering, The Ohio State University, Columbus, OH, United States; 3. Department of Electrical and Computer Engineering, Texas Tech University, Lubbock, TX, United States*

The use of functionalized magnetic particles for detecting or separating multiple chemicals and biomolecules from fluid samples is a growing area of interest, particularly in biomedicine and environmental applications, such as water and wastewater treatment[1-3]. Surface-functionalized magnetic beads (MBs) can be recovered through magnetophoresis after incubation with target substances, for their analysis, removal of pollutants, contaminants, and pathogens, or diagnostic purposes. The recovery of MBs using microdevices with permanent magnets is gaining attention[4,5], however, there is limited information on the processing capacity and performance of permanent-magnet continuous flow devices at high flow rates, with recent studies using a computational fluid dynamics (CFD) approach[6-8]. Process intensification focuses on developing smaller, cleaner, and more energy-efficient technologies through device miniaturization and novel separation techniques[9], for example. Following this premise, we present an experimental study of the recovery of commercially available amine-coated magnetic beads (MBs) (Ocean Nanotech, CA, USA) of various sizes using a customized quadrupole magnetic sorter (QMS) device, which operates without a power source and features a compact, portable design with a vertical, annular microchannel surrounded by four permanent magnets in a quadrupolar orientation. A constant magnetic field gradient within the microchannel exerts a magnetophoretic force on flowing particles that redirects their trajectory toward regions of higher magnetic potential, where they

are retained. MB recovery is evaluated by the percentage of beads retained in the QMS microchannel after a certain residence time in a flow-through configuration. The concentration (particles *per* mL) of MBs dispersed in a biocompatible fluid is quantified before and after magnetic exposure using a Multisizer 4e Coulter Counter (Beckman Coulter, CA, USA) to estimate particle recovery. Based on previous investigations[10-12], we expect to identify statistically significant correlations between flow rates, particle sizes, and recovery performance to advance the field toward practical aspects of process intensification using a QMS.

(1) Amesh, P.; Suneesh, A. S.; Robert Selvan, B.; Venkatesan, K. A.; Chandra, M. Magnetic assisted separation of uranium(VI) from aqueous phase using diethylenetriamine modified high capacity iron oxide adsorbent. *Journal of Environmental Chemical Engineering* 2020, *8* (2), 103661. DOI: 10.1016/j.jece.2020.103661. (2) Li, W.; Yang, L.; Liu, H.; Li, X.; Liu, Z.; Wang, F.; Sui, N.; Xiao, C. Rapid and large scale separation of magnetic nanoparticles by low field permanent magnet with gas assistance. *AIChE Journal* 2014, *60* (9), 3101-3106. DOI: 10.1002/aic.14533. (3) Mariani, G.; Fabbri, M.; Negrini, F.; Ribani, P. L. High Gradient Magnetic Separation of pollutant from wastewaters using permanent magnets. *Separation and Purification Technology* 2010, *72* (2), 147-155. DOI: 10.1016/j.seppur.2010.01.017. (4) Zhu, Y.; Zhang, B.; Gu, J.; Li, S. Magnetic beads separation characteristics of a microfluidic bioseparation chip based on magnetophoresis with lattice distributed soft magnets. *Journal of Magnetism and Magnetic Materials* 2020, *501*, 166485. DOI: 10.1016/j.jmmm.2020.166485. (5) Dalili, A.; Samiei, E.; Hoorfar, M. A review of sorting, separation, and isolation of cells and microbeads for biomedical applications: microfluidic approaches. *Analyst* 2018, *144* (1), 87-113, 10.1039/C8AN01061G. DOI: 10.1039/c8an01061g. (6) González-Fernández, C.; Gomez Pastora, J.; Basauri, A.; Fallanza, M.; Bringas, E.; Chalmers, J. J.; Ortiz, I. Continuous Flow Separation of Magnetic Particles from Biofluids: How Does the Microdevice Geometry Determine the Separation Performance? In *Sensors*, 2020; Vol. 20. (7) González-Fernández, C.; Gomez-Pastora, J.; Bringas, E.; Zborowski, M.; Chalmers, J. J.; Ortiz, I. Recovery of Magnetic Catalysts: Advanced Design for Process Intensification. *Ind Eng Chem Res* 2021, *60* (46), 16780-16790. DOI: 10.1021/acs.iecr.1c03474. (8) Karampelas, I. H.; Gómez-Pastora, J. Novel Approaches Concerning the Numerical Modeling of Particle and Cell Separation in Microchannels: A Review. In *Processes*, 2022; Vol. 10. (9) Kopac, T. Research Progress on Process Intensified Water Treatment Applications. In *Separations*, 2022; Vol. 9. (10) Chong, P. H.; Tan, Y. W.; Teoh, Y. P.; Lim, C. H.; Toh, P. Y.; Lim, J.; Leong, S. S. Continuous Flow Low Gradient Magnetophoresis of Magnetic Nanoparticles: Separation Kinetic Modelling and Simulation. *Journal of Superconductivity and Novel Magnetism* 2021, *34* (8), 2151-2165. DOI: 10.1007/s10948-021-05893-z. (11) Samanta, A.; Ganguly, R.; Datta, A.; Modak, N. Separation of magnetic beads in a hybrid continuous flow microfluidic device. *Journal of Magnetism and Magnetic Materials* 2017, *427*, 300-305. DOI: 10.1016/j.jmmm.2016.10.143. (12) Khashan, S. A.; Dagher, S.; Alazzam, A.; Mathew, B.; Hilal-Alnaqbi, A. Microdevice for continuous flow magnetic separation for bioengineering applications. *Journal of Micromechanics and Microengineering* 2017, *27* (5), 055016. DOI: 10.1088/1361-6439/aa666d.

BR-05. Basic Study on the Application of Wireless Power Transfer to Sensing Systems related to functionalized petri dishes. *R. Jomae*[1], Y. Hara[1], M. Yokosawa[1], F. Sato[1], O. Ito[1], K. Sagara[2] and S. Sasaki[2]
1. Tohoku Gakuin University, Sendai, Japan; 2. Hikaridenshi, Osaki, Japan

In recent years, with the outbreak of the pandemic caused by COVID-19 and the demand for the extension of healthy life expectancy due to the declining birthrate and aging population, the rapid development of the fields of drug discovery and regenerative medicine has led to an increase in social demand for cell culture. In order to solve this problem, automatic cell culture devices that replace the manual work of skilled technicians with robot arms, such as Kawasaki Heavy Industries' cell culture robots, have also been developed. Therefore, in this study, we propose a functionalized petri dish that enables individual management of various parameters of cultured petri dishes, and aim to establish elemental technologies. We will conduct a basic study on the application of wireless power transfer as a power supply method to the sensing system installed in the petri dish. By using wireless power transfer, it is possible to supply power to multiple units at the same time without the complexity of wires, and there is no need to replace batteries when monitoring over a long period of time is required. In this system, the purpose is to simultaneously supply power to multiple petri dishes for one power supply system, and it is necessary to generate a uniform magnetic field over a wide area. Therefore, a Helmholtz coil is used, which has the characteristic of making it possible to widen the range in which the magnetic field is uniform. Normally, Helmholtz coils use circular coils, but in this study, we propose a Helmholtz-shaped coil using a square coil with a larger area in the coil than a circular coil, and compare two types of coils, a circular coil and a square coil. As a study method, electromagnetic field analysis simulation is performed to compare the range of uniform magnetic fields between a square coil and a circular coil. As a result of the simulation, it was found that the range of uniform magnetic fields is wider in the square Helmholtz coil than in the circular Helmholtz coil. Therefore, in order to supply power to the sensing system of a wider range and more petri dishes, a square Helmholtz coil is considered to be suitable.

K. Yamaoka, K. Kuwana, Y. Ohta, M. Kotani, T. Dohi, LIFE2014., GS8-4-1-GS8-4-2(2014) H. Kubo, The Japanese journal of medical instrumentation, Vol.81, No.6, p439-444(2011)

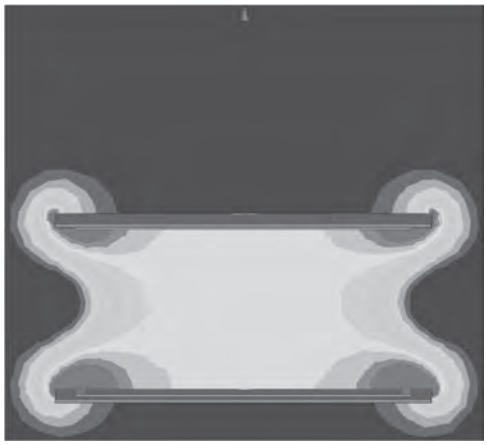

Fig.1 Magnetic field in a square coil

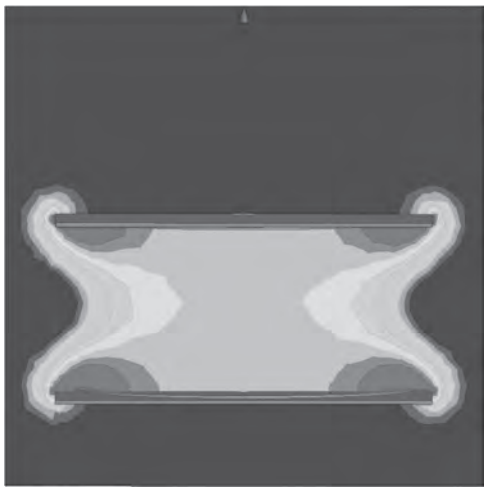

Fig.2 Magnetic field in a circular coil

BR-06. Impact of Number of Paramagnetic Nanostructure Coupled with Two Ferromagnetic Electrodes of a Cross-Junction Shaped Molecular Spintronics Device at Different Thermal Energies. C. D'Angelo[1] and *P. Tyagi*[1] *1. University of the District of Columbia, Washington, DC, United States*

Nanoscale spintronics devices can revolutionize computer logic and memory units. Interestingly, paramagnetic nanostructures, such as molecules, strongly exchange coupled with two ferromagnetic electrodes can yield novel forms of magnetic materials. However, there is a knowledge gap about the role of the number of paramagnetic nanostructures on the various properties of whole spintronics devices. It is also not clear if a single molecule-based device will be stable over a period of time as compared to devices with higher molecular channels present between the two ferromagnetic electrodes. We focus on the magnetic tunnel junction (MTJ) based spintronics device (MTJMSD) architecture to make this study relevant to the experimentally attainable device structure [1-3]. We designed an analogous Heisenberg model to simulate the effect of molecular nanostructures present along the perimeter of MTJ. Under this approach, varying populations of paramagnetic nanostructures are placed along the MTJ perimeter to simulate the magnetic properties of the ferromagnetic electrodes and overall MTJMSD. We assume that the tunnel barrier of the MTJ does not allow any leakage current or exchange coupling, and paramagnetic nanostructures dictate the exchange coupling between the ferromagnetic electrodes. Also, the width of the ferromagnetic electrodes is governed by the number of paramagnetic nanostructures. This study systematically varied the number of nanostructures from 1 to 625 (25 x 25). Single molecule-based MTJMSD exhibited lower stability as compared to devices involving a higher molecule population. Interestingly, the magnetic moment of molecular nanostructure started exhibiting decoherence beyond a certain limit of molecular population. Thermal energy also impacted the response from varying molecular populations sandwiched between the two ferromagnetic electrodes of an MTJMSD. This paper will discuss the impact of molecular population and thermal energy on the MTJMSD properties by investigating the magnetic moment of the individual components. We will also discuss the impact on spatial correlation between molecule magnetic properties and ferromagnetic electrodes.

[1] S. Yuasa and D. Djayaprawira, "Giant tunnel magnetoresistance in magnetic tunnel junctions with a crystalline MgO (0 0 1) barrier," *J. Phys. D: App. Phys.,* vol. 40, p. R337, 2007. [2] W. J. Gallagher, S. S. P. Parkin, J. C. Slonczewski, and J. Z. Sun, "Magnetic tunnel junctions with controlled magnetic response," US 5650958 A, 1997. [3] P. Tyagi, "Systems and Methods of Fabricating Gate Electrode on Trenched Bottom Electrode based Molecular Spintronics Device.," USA Patent US20210111274A1, 2023.

BR-07. Magnetic Field-Flow Fractionation of Diamagnetic Particles. *N. Carlstedt*[1], P. Brungi[1], P. Wang[1] and P. Andrei[1] *1. Florida State University, Tallahassee, FL, United States*

Field-flow fractionation is a flow-based separation technique in which a generalized force is applied in the direction perpendicular to the flow of the fluid to move the particles that need to be separated towards the boundaries of the flow channel. Since the fluid velocity decreases when the particles approach the boundary of the flow channel, flow-field fractionation can be used efficiently to separate the particles that interact with the applied generalized force from the particles that do not interact with this force. In the case of magnetic field-flow fractionation (MFFF), the generalized force is the magnetophoretic force, which acts on the magnetic particles in the liquid and can be used to separate them from other non-magnetic particles [1], [2]. In this presentation we propose for the first time an MFFF system that is specifically designed to separate weakly magnetic diamagnetic particles (such as Y(III) and La(III)) from other non-magnetic or paramagnetic particles. As far as we know, all of the the existing MFFF systems proposed in the literature so far have been designed for paramagnetic particles but not for diamagnetic particles, which have relatively small magnetic susceptibility of around -10^{-5} M^{-1}. Our MFFF system is based on using a matrix of parallel magnetic and non-magnetic wires that is placed in a uniform magnetic field to produce values of (larger than 10^5 T^2/m in order to attract the magnetic particles. The system is designed in such a way that only the diamagnetic particles are being attracted by the wires, while the paramagnetic particles are being pushed away (non-magnetic particles are being unaffected), in this way achieving an efficient separation. At the conference, we will present simulation results obtained by solving the Navier-Stokes equations for fluid flow coupled with the drift-diffusion equations for magnetic particles [3]. The limitations of the MFFF system will be analyzed by looking at the minimum size and magnetic susceptibility at which the particles can be fractionated, for various values of the design parameters, flow rate and external magnetic field. Practical designs will also be discussed.

[1] S. Kim, Y. Okimoto, S. Murase, S. Noguchi, and H. Okada, "Characteristics of magnetic separation for magnetic particle and ion by magnetic chromatography with novel magnetic column," *IEEE Trans. Appl. Supercond.*, vol. 19, no. 3, pp. 2152, (2009). [2] M. Manouchehri, S. Seidi, and F. O. Abdullah, "Application of magnetic nanomaterials in magnetic-chromatography: A review," *Talanta*, vol. 229, p. 122273 (2021). [3] P. Andrei and N. Carlstedt, "Modeling of magnetic separation of metal ions in aqueous solutions", Intermag 2024, Rio de Janeiro, Brazil (2024).

BR-08. Synthesized and Commercial Iron Sulfide Particles as Contaminant Sorbents. *N. Shuvo*[1,3], J. Bussey[2,3], A. Lere-Adams[2,3], M. Dixon Wilkins[3], S. Karcher[3] and J. McCloy[1,2,3] *1. Chemistry, Washington State University, Pullman, WA, United States; 2. School of Mechanical and Materials Engineering, Washington State University, Pullman, WA, United States; 3. Institute of Materials Research, Washington State University, Pullman, WA, United States*

Magnetic nanoparticles are used for wastewater treatment, chemical separation, and theranostic medicine. Their magnetic nature allows particle movement after capturing or delivering chemical agents. Normally for magnetic separation, iron oxide (usually magnetite) or zero-valent iron particles with surface-attached ligands are used. Bare particles have advantages, however, preventing moment reduction by ligands and allowing access to the reducing nature of iron species on the surface. Herein, nanoparticles of iron sulfide, nominally greigite (Fe_3S_4) but including other iron sulfides (pyrite, pyrrhotite), target the removal of radionuclide elements from aqueous solutions simulating radioactive liquid waste. Target radioisotopes, ^{99}Tc and ^{129}I, are highly mobile in groundwater at contaminated sites, and their half-lives drive long-term environmental doses for some radioactive waste disposal sites. Thus, it is advantageous to separate them from liquid streams and sequester them elsewhere. Greigite particles here are synthesized by several methods – a) mechano-synthesis, b) hydrothermal, c) solvothermal, and d) biological routes. Synthesized particles are compared with commercially obtained iron sulfides, for phase fractions via X-ray diffraction (XRD), magnetic properties via vibrating sample magnetometry (VSM), and morphologies via scanning electron microscopy (SEM), Fig. 1. Select Fe-S material shows sorbing of perrhenate (pertechnetate surrogate) as evidenced Raman vibrational modes of dissolved ions, Fig 2a,b. Additionally, tests investigating sorbent effects on iodate solution showed a strong reduction by Fe-S, changing the solution from clear to red, producing I_3^- ions and some FeI_2 precipitate, Fig. 2c.

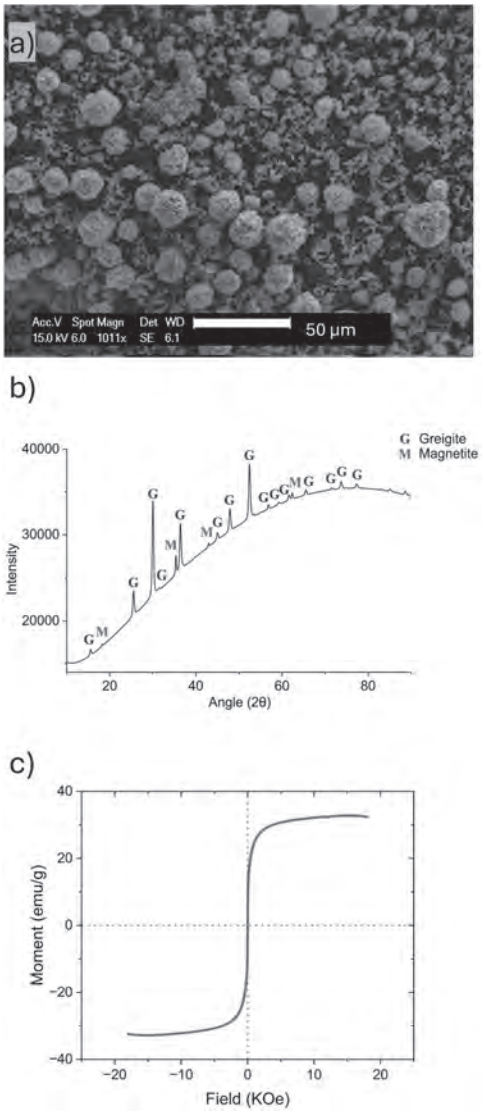

Fig. 1. Fe-S from hydrothermal synthesis: a) SEM showing clusters and small particles; b) XRD showing greigite and minor magnetite phase; c) VSM showing low coercivity and high magnetization.

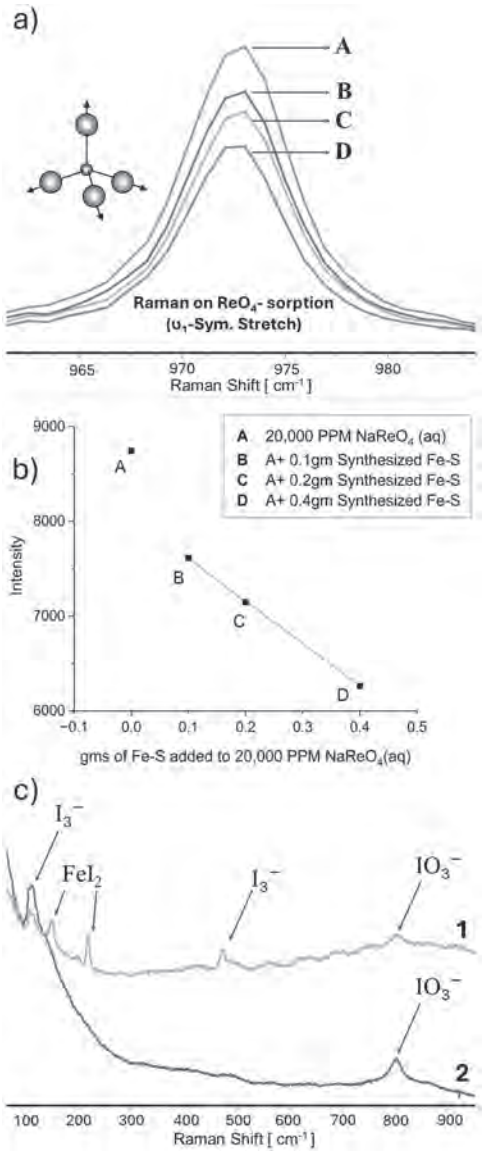

Fig. 2. Demonstrated sorbent action for Fe-S: a) decrease in ReO_4^- Raman symmetric stretch and b) signal intensity reduction versus added Fe-S; c) Raman spectra of 1) precipitate formation containing I_3^- along with FeI_2 and, 2) reaction of Fe-S with iodate solution and reduction to I_3^-.

Session BS
ELECTRONIC STRUCTURE, MAGNETISM AND FUNDAMENTAL PHYSICAL PROPERTIES II (Poster Session)

Arti Kashyap, Co-Chair
Indian Institute of Technology Mandi, Mandi, India
Hari Paudyal, Co-Chair
University of Iowa, Ames, IA, United States

BS-01. Probing Magnetic Anisotropy and Switching Fields in $TbMn_6Sn_6$ Kagome Quantum Magnet: Impact of Spin Reorientation. *D. Le*[1], R. Roy Chowdhury[1], W. Zhao[2], J. Karel[2], H. Srikanth[1], J.D. Gayles[1] and M. Phan[1] *1. Department of Physics, University of South Florida, Tampa, FL, United States; 2. Monash University, Melbourne, VIC, Australia*

Recent advancements in understanding topological magnetism have highlighted the potential of Kagome magnets to host flat bands, Dirac cones, and topological Weyl points, leading to intriguing quantum phenomena suitable for spintronics. $TbMn_6Sn_6$, a heavy rare-earth-based Kagome magnet, exhibits exotic topological Chern phases induced by spin-orbit interactions at low temperatures [1], and displays magnetic Skyrmions in the vicinity of its spin reorientation (SR) temperature, T_{SR} ~ 315 K [2], making it a prominent candidate in the Kagome family. However, the effect of SR on magnetic anisotropy and its temperature evolution in this material remains inadequately understood. Through combined magnetometry and radio-frequency (RF) transverse susceptibility (TS) measurements, we observe strong variations in magnetic anisotropy and switching fields in $TbMn_6Sn_6$ around its T_{SR}, particularly in the temperature region of 310-330 K where Skyrmions have been detected [1]. These variations stem from distinct temperature and field responses of the Tb and Mn magnetic moments, along with their competing magnetic interactions. The TS peak height notably drops sharply by an order of magnitude at T_{SR}, indicating significant alterations in spin dynamics as the magnetization vector rotates from the ab-plane to the c-axis direction. Furthermore, density functional theory calculations consistently validate these changes in magnetic anisotropy during the SR process. Our findings underscore the profound impact of spin reorientation on the complex interplay between Tb spins and the frustrated Mn Kagome lattice in $TbMn_6Sn_6$.

[1] Li et al., *Advanced Materials* 35, 2211164 (2023). [2] Mielke III et al., *Communications Physics* 5, 107 (2022).

BS-02. Challenges of Using FeMn for Magnetic Tunnel Junction-Based Molecular Spintronics Devices (MTJMSD). *B. Sankhi*[1] and P. Tyagi[1] *1. Mechanical Engineering, University of District of Columbia, Washington, DC, United States*

Magnetic Tunnel Junction-based Molecular Spintronics Devices (MTJMSD) hold significant promise for the next generation of low-power memory and logic devices, applicable from conventional computers to quantum computing systems [1]. The fabrication scheme and selection of electrode materials are critical for these devices [2]. In this study, we explore the use of antiferromagnetic FeMn alloy, known for its zero net magnetization, high exchange bias, and minimal stray fields, as one of the electrodes in MTJMSDs. The material stack employed was Ta (5 nm)/FeMn (5 nm)/AlOx (2 nm)/NiFe (5 nm)/Ta (5 nm) on a thermally oxidized silicon substrate, with NiFe serving as the other electrode and a 2 nm AlOx insulating layer in between. We successfully characterized the device at both room and low temperatures, observing excellent tunneling behavior. Moreover, the incorporation of single-molecule magnets significantly enhanced the current, transforming the MTJ into an MTJMSD. However, after a period of one month, the FeMn electrode exhibited significant degradation, likely due to surface interactions, while the NiFe electrode remained stable. Atomic Force Microscopy (AFM) revealed considerable surface roughness and material accumulation on the FeMn electrode, indicating susceptibility to environmental factors. This transient behavior of the FeMn-based MTJ contrasts with the expected robustness of MTJ devices. For developing commercially viable MSDs, it is crucial to establish a fabrication scheme that addresses the susceptibility of antiferromagnetic-ferromagnetic electrodes to oxidation, chemical etching, and stress-induced deformations during both fabrication and usage. Our study provides insights into the selection and optimization of material systems for the successful development of MTJMSDs, emphasizing the need for improved surface stability and durability in antiferromagnetic materials.

[1] M. N. Leuenberger and D. Loss, "Quantum computing in molecular magnets," Nature, vol. 410, no. 6830, pp. 789-793, 2001. [2] P. Tyagi, E. Friebe, and C. Baker, "Addressing the challenges of using ferromagnetic electrodes in the magnetic tunnel junction-based molecular spintronics devices," Journal of Nanoparticle Research, vol. 17, pp. 1-13, 2015.

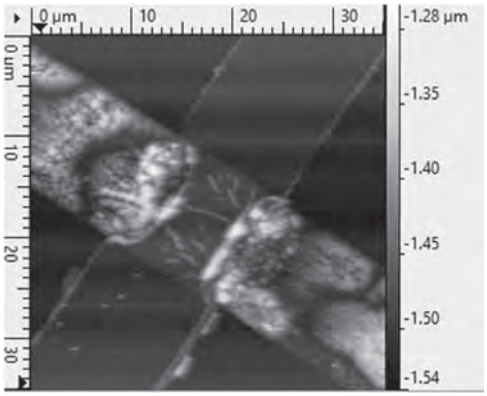

Fig.1 Atomic force microscopy image of one junctions of the molecule treated magnetic tunnel Junction after the time duration of a month.

BS-03. Using the critical behavior to probe the relationship between quasi-two-dimensional and three-dimensional spin-glasses. *T.M. Pekarek*[1], I. Miotkowski[2] and A. Ramdas[2] *1. Physics, University of North Florida, Ja, FL, United States; 2. Physics, Purdue University, West Lafayette, IN, United States*

Single-crystalline $Zn_{1-x}Mn_xTe$ is a three-dimensional (3D) monochalcogenide system that exhibits a prominent spin-glass transition at low-temperatures. This system is based on the host ZnTe semiconductor where Mn goes into the lattice substitutionally at the Zn lattice site. Spin-glass systems are being investigated for applications in short-term, low-energy memory and processing power that makes these materials important for further study. The host ZnTe is also being investigated for applications in solar cell structures. We report on the critical behavior in the 3D $Zn_{0.49}Mn_{0.51}Te$ system. We utilized the scaling equation of state and the relation $\chi_{nl} = C_1 H^{(2/\delta)}$ describing Zn0.49Mn0.51Te's spin-glass transition at 20.8 K. We extracted the critical exponents δ = 5.5 +/- 0.5 and φ = 4.8 for $Zn_{0.49}Mn_{0.51}Te$. We explored the sensitivity of the value extracted for δ to the critical temperature T_c.

We then compared these results for our 3D system with the strikingly similar values for the critical exponents describing the spin-glass behavior in the quasi-two-dimensional spin-glass system $Ga_{1-x}Mn_xS$ that has been reported to exhibit an anomalous spin-glass transition. *The authors would like to thank G. Williams of the University of Manitoba for his useful discussions. The authors would like to thank J.H. Blackburn. This research was supported by UNF's Terry Presidential Professorship, a Purdue Univ. Academic Reinvestment Program, and by the National Science Foundation (NSF) Grants No. DMR-16-26332 and DMR-14-29428.

BS-04. Muon Probing and Magnetism in Cuprate Superconductors.
C. Boekema[1,2] 1. Physics, San Jose State, San Jose CA 95106, CA, United States; 2. Ad Fysi Care, Los Gatos CA 95032, CA, United States

There are still questions as to how and where the muon probes magnetism in cuprates. Shekhter *et al* [1] found that using a *metal* approach, the muon charge reduces or destroys pseudogap loop currents. [2] Yet, Dawson's muon-site search [3] indicated candidates only in *insulating* regions of these quasi-2-dim superconductors $RBa_2Cu_3O_{7-d}$ (RBCO). Sio *et al* [4] studied the muon sites in GdBCO by using Maximum Entropy [5] (MaxEnt, ME) to analyze transverse field (TF) muon-spin-rotation (μSR) GdBCO data. We have improved upon this MEμSR study. The Balmer (B1 & B2) sites and Lin (L1, L2 & L3) sites are located in RBCO, ~1 Å away from O^{2-} ions. B1 & B2 are near the BaO layer; [3] B2 is the favorite site. L1, L2 and L3 are near or in the CuO-chain layer. [4,6] At & below RT, muons localize at these B/L sites, depending on local potential energy and their thermal hopping energy. For both underdoped GdBCO (d1, T_c = 81 K) and optimal doped GdBCO (d0; T_c = 93 K) TFμSR data [7] were recorded at and below RT at 100-Oe and 1-kOe fields. MEμSR analysis (being more sensitive [5] than FT & curve fitting) is performed. The best ME fits include two Lorentzians (Lor) & one Gaussian (Gau) for the grain boundary. These ME results are consistent with muon occupancy of B2 and B1/Lin sites. [3,8] When B1 and Lin *positions* are near a positive O vacancy (repelling m^+ probes) these sites become less stable in underdoped GdBCO(d1). As T increases, this effect is more pronounced. At 120 K three signals are visible in underdoped GdBCO(*d* 1), yet at RT only one dominant signal remains. In contrast, two Lorentzian signals are present at 120 K and at RT for GdBCO(*d*0), where there are significantly *less* O vacancies. Thus, the muon localizes in an undisturbed *insulating* environment away from the CuO_2 planes and measures (weak) magnetic fields of Sharma's pseudogap loop currents. [2,6,8,9]

[1] A Shekhter *et al*, Phys Rev Lett 101 (2008) 227004. [2] CM Varma, PRL 83 (1999) 3538; ME Simon & CM Varma, PRL 89 (2002) 247003; IM Vishik *et al,* Proc Nat Acad Sci 109 (2012) 18332. [3] WK Dawson *et al*, J Appl Phys 64 (1988) 5809; Hpf Int 63 (1990) 219. [4] H Sio, MC Browne *et al*, APS March meeting (2011) & SJSU internal report. [5] C Boekema and MC Browne, MaxEnt 2008, AIP Conf Proc #1073 pp260-267.r [6] C Boekema *et al,* Physica C493 (2013) 136. [7] DW Cooke *et al*, Phys Rev B37 (1988) 9401. [8] T Songatikamas *et al*, J Spcd & Nvl Magn 23 (2010) 793. [9] C Boekema *et al*, J Modern Physics B29 (2015) 1542026.

BS-05. Anomalous magnetic behavior and large exchange bias in non-centrosymmetric Sm_7Pd_3.
A. Biswas[1], *A. Kumar*[1], D.L. Schlagel[1] and Y. Mudryk[1] *1. Ames National Laboratory, Ames, IA, United States*

Recently, materials exhibiting a combination of long-range magnetic ordering with nearly zero magnetic moment and large magnetic anisotropy have been under intense scrutiny due to their possible potential applications in spintronics and memory devices [1,2]. We report such a highly desirable magnetic state, comprising very low saturation magnetization (M_s) and exceptionally large magnetic coercivity (H_C) in a 4*f*- intermetallic Sm_7Pd_3. The polycrystalline sample stabilizes with a non-centrosymmetric Th_7Fe_3-type crystal structure at room temperature and undergoes a symmetry-invariant magnetoelastic transition at T_C=169 K into a non-collinear magnetic state [3]. The temperature dependence of magnetization revealed a very unusual scenario of manifestation of negative magnetization below T_C when magnetic measurement was carried out after cooling the material at zero field (ZFC). The signature of negative magnetization in the ZFC curves was prominent even in the presence of magnetic field as large as 20 kOe. The magnetic field dependence of magnetization study indicates that H_C increases rapidly below 50 K and it exceeds 130 kOe at 2 K albeit the M_S remains below 0.1 m_B/ Sm. While it is generally believed that the presence of multiple magnetic rare-earths (RE) leading to magnetic compensation is necessary for realization of exchange bias (EB) in case of 4*f* -intermetallic compounds [4,5], our present polycrystalline sample shows quite large EB effect (H_{EB} = 2.6 kOe for a cooling field of 90 kOe at T=10 K) despite having single type RE (Sm) atom. We also extended our study to the pulsed-laser deposited thin films having thickness ~ 150 nm, where the magnetic behavior is markedly modified. Although a sharp magnetic transition at T_C ~ 169 K was evident in the thin-film, interestingly, it does not exhibit any noticeable magnetic hysteresis in contrary to its bulk polycrystalline counterpart. Acknowledgements: This work was supported by the Division of Materials Science and Engineering of the Office of Basic Energy Sciences, Office of Science of the U.S. Department of Energy (DOE). Ames National Laboratory is operated for the U.S DOE by Iowa State University under Contract No. DE-AC02-07CH11358.

[1] S. K. Kim, G. S. D. Beach, K. Lee, T. Ono, T. Rasing, H. Yang, Nature Materials, V-21, 24 (2022). [2] V. Baltz, A. Manchon, M. Tsoi, T. Moriyama, T. Ono, T. Tseekovnyak, Review of Modern Physics, V-90, 015005 (2018). [3] A. Biswas, R. K. Chouhan, O. Dolotko, P. Manfrinetti, S. Lapidus, D. L. Schlagel, Y. Mudryk, Acta Materiallia, V- 265, 119630 (2024). [4] P.D. Kulkarni, U.V. Vaidya, S.K. Dhar, P. Manfrinetti, A.K. Grover, Journal of Physics D: Applied Physics V-42, 082001 (2009). [5] T. Del Rose, Y. Mudryk, D. Haskel, A. Pathak, V. Pecharsky, "*Physical Review Materials,* 6, 044413 (2022).

BS-07. Spin-resolved Electronic Structure of the Ferromagnetic Triple-layered Ruthenate $Sr_4Ru_3O_{10}$.
P. Ngabonziza[2], J. Denlinger[1], A. V. Fedorov[1], G. Cao[3], G. Gebreyesus[4], J. Allen[6] and R. Martin[5] *1. Advanced Light Source, Lawrence Berkeley National Laboratory, California, CA, United States; 2. Physics, Louisiana State University, Baton Rouge, LA, United States; 3. Physics, University of Colorado at Boulder, Boulder, CO, United States; 4. Physics, University of Ghana, Accra, Ghana; 5. Physics, University of Illinois at Urbana-Champaign, Champaign–Urbana, IL, United States; 6. Randall Laboratory of Physics, University of Michigan, Michigan, MI, United States*

We report spin-resolved electronic band structure studies of the triple-layered ruthenate $Sr_4Ru_3O_{10}$. Although the band structure of $Sr_4Ru_3O_{10}$ has been the subject of recent experimental and theoretical investigations [1,2,3]; there have been no reported spin-resolved experimental studies that explore in more detail the complex magnetism of $Sr_4Ru_3O_{10}$. In this poster presentation, we will report on the first combined spin- and angle-resolved photoemission (SARPES) study of $Sr_4Ru_3O_{10}$ [4]. Our SARPES data reveal major effects of spin polarization in different parts of the Brillouin zone. We resolve two separate strong intensity narrow bands with opposite spin-polarization at 30 meV below the Fermi-level, which exhibit surprisingly dramatic temperature-dependent amplitude changes upon warming to the Curie temperature of the $Sr_4Ru_3O_{10}$ system. We will discuss a comparison between the SARPES data to spin-resolved density functional theory (DFT) calculations.

[1].P.Ngabonziza*,E.Carleschi,V.Zabolotnyy,A.Taleb-Ibrahimi,F.Bertran, R. Fittipaldi, V. Granata, M. Cuoco, A. Vecchione, and B. P. Doyle* *Fermi surface and kink structures in $Sr_4Ru_3O_{10}$ revealed by synchrotron-based ARPES*; *Scientific Reports 10, 21062 (2020)* [2] G. H. Gebreyesus*, P. Ngabonziza*, J. Nagura, S. Nicola, O. Akin-Ojo, and R. M. Martin* *Electronic structure and magnetism of the triple-layer ruthenate $Sr_4Ru_3O_{10}$; Physical Review B 105, 165119 (2022)* [3]. C. A. Marques, P. A. E. Murgatroyd, R. Fittipaldi, W. Osmolska, B. Edwards, I. Benedičič, G.-R. Siemann, L. C. Rhodes, S. Buchberger, M. Naritsuka, E. Abarca-Morales, D. Halliday, C. Polley, M. Leandersson, M. Horio, J. Chang, R. Arumugam, M. Lettieri, V. Granata, A. Vecchione, P. D. C. King and P. Wahl *Spin-orbit coupling induced Van Hove singularity in proximity to a Lifshitz transition*

in Sr4Ru3O10; npj Quantum Materials 9, 35 (2024) [4] P. Ngabonziza*, J. D. Denlinger*, A. V. Fedorov, G. Cao, J. W. Allen, G. Gebreyesus, and R. M. Martin; Layer-dependent spin-resolved electronic structure of ferromagnetic triple-layered ruthenate $Sr_4Ru_3O_{10}$; arXiv:2305.07222 (2023)

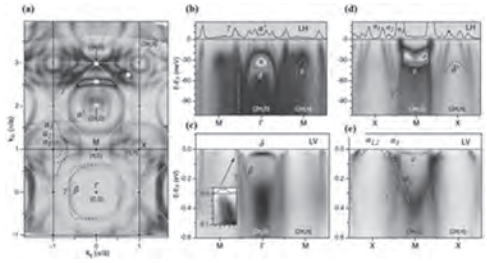

Figure 1: Spin-integrated ARPES electronic structure of low temperature $Sr_4Ru_3O_{10}$. Figure from Ref. [4]

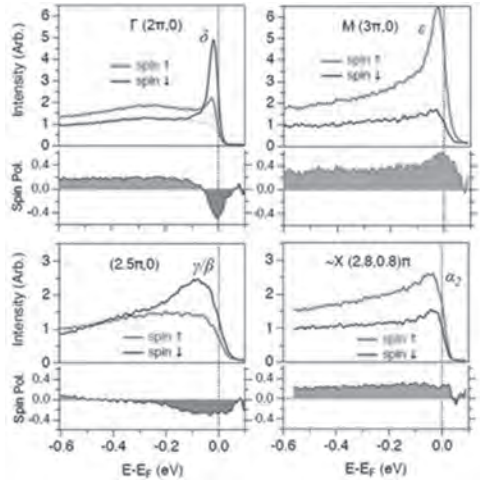

Figure 2: Spin-resolved ARPES at low temperature. Figure from Ref. [4]

BS-08. Transition Phase and Magnetic Properties of $LaTiO_3$ Perovskite Under Hydrostatic Pressure. J. Cervantes[1], J. Antonio[2], H. Muñoz[3], A. Torres[3] and *E. Carvajal*[3] *1. Universidad Nacional Autónoma de México, Instituto de Investigaciones en Materiales, Ciudad de México, Mexico; 2. Universidad Nacional Autónoma de México, Facultad de Ciencias, Ciudad de México, Mexico; 3. Instituto Politécnico Nacional, ESIME-Cul., Ciudad de México, Mexico*

The impact of the hydrostatic pressure on the transition phase, and the magnetic properties of the $LaTiO_3$ perovskite (LTO) was studied for this work. Calculations were performed in the theoretical framework of the Density Functional Theory (DFT), using the Hubbard-corrected Local Density Approximation (LDA+U). For the LTO crystal with the Pbnm (62) space group, the energy band gap decreases as the hydrostatic pressure increases. This is linked to the Ti-*d* and O-*p* orbitals greater overlap, and the resulting decrease of the Ti-O bond lengths. Furthermore, the magnetic moment of the Ti-*d* electrons decreases as pressure increases, while the G-type antiferromagnetic order remains. Finally, the hydrostatic pressure-induced phase transition (P_T) from perovskite to post-perovskite (Pbnm to Cmcm) will be determined through enthalpy calculations. Also, the magnetic properties of the LTO Cmcm bulk phase were calculated [1].

[1] J. M. Cervantes, *et al*., J. Electrochem. Soc. 170(11), 110528 (2023). doi:10.1149/1945-7111/ad0b76.

Session BT
2D SPINTRONICS AND TOPOLOGICAL MATERIALS I & DOMAIN WALLS (Poster Session)

Qiming Shao, Chair
The Hong Kong University of Science and Technology, Kowloon, Hong Kong

BT-01. 2D magnetism in layered systems with honeycomb lattice: A theoretical calculation. *K. Pokhrel*[1] and K. Carva[1] *1. Condensed matter, Charles University, Prague, Czechia*

Two-dimensional (2D) materials have attracted interest in many applications, and have emerged as a unique family of nano-materials in physics and materials science. The ability to control the electronic states of two-dimensional (2D) materials is expected to lead to new physical phenomena and device concepts. Graphene is one of the most interesting 2D materials because of its unique band structure leading to electrons behaving like massless particles. There is a large number of materials composed of layers coupled by weak van der Waals forces, which allow for easy layer separation and arbitrary stacking of these. Even more recently, 2D materials with magnetism have been discovered. FM order has been found to exist even in an atomically thin layer in CrI3 [1]. Key property here is the magnetic anisotropy, and among layered systems one can find representatives whose magnetism is described more or less accurately by either the Heisenberg, Ising, or XY model. In layered vdW magnets, like vanadium triiodide (VI3), the exchange coupling between layers is rather weak and can be relatively easily modified. Regime of weak inter-layer coupling represents transition between the more explored cases of isotropic bulk-like magnets and the ideal 2D limit (monolayer) [2]. In this study, we explore the general characteristics of VX3 (eg: VI3, VCl3, VBr3) by analyzing its finite temperature magnetic order. We utilize atomistic spin dynamics methods, specifically implementing the stochastic Landau-Lifshitz-Gilbert (LLG) equation, to investigate the behavior of the spin system in VX3. This includes a detailed analysis of the inter-layer exchange interactions and single ion anisotropy, which play a crucial role in the magnetic phase transitions and the overall behavior of the system as it moves towards the 2D limit. The method is applied to systems with honeycomb lattice, where also the most well-known 2D magnet example – CrI3 - belongs. We study how is the ordering temperature affected by inter-layer coupling and other properties in these systems, and how much this solution differs from the mean-field approach results.

[1]: B. Huang, etal., Nature 546 (2017) 270 [2] :Torelli and Olsen, 2D Mater. 6 (2019) 015028

BT-02. Superparamagnetic Properties of Metal-free Nitrogen-doped Graphene Quantum Dots. *M. Sultan*[1], W. Jadwisienczak[2], B. Weiner[3] and G. Morell[1] *1. Department of Physics, University of Puerto Rico - Rio Piedras, San Juan, PR, United States; 2. School of Electrical Engineering and Computer Science, Ohio University, Athens, OH, United States; 3. Department of Chemistry, University of Puerto Rico - Rio Piedras, San Juan, PR, United States*

This article reports the superparamagnetic behavior of metal-free nitrogen-doped graphene quantum dots (N-GQDs). The pulsed laser ablation (PLA) method was utilized to synthesize N-GQDs with an average diameter of 3.45 nm and a high doping level (N/C) of 1.4. The magnetic properties of as-synthesized N-GQDs were explored by performing magnetization vs. magnetic field (M-H) and magnetization vs. temperature (M-T) measurements. M-H plots measured in a temperature range of 2–300 K revealed the superparamagnetic behavior of N-GQDs. The value of saturation magnetization was found to be directly correlated to nitrogen concentration, and a saturation magnetization up to 28.7 emu/g was obtained at room temperature (300 K). M-T measurements with zero-field-cooled (ZFC) and field-cooled (FC) conditions were employed to study anisotropy energy barriers and blocking temperature. A variation in the blocking temperature (TB) from 288 to 61 K was observed when the external magnetic field (H) was changed from 0.1 to 0.6 T. The origin of superparamagnetism was attributed to the presence of graphitic nitrogen bonding configuration and defect states. The observed superparamagnetic properties, along with the optical properties of N-GQDs, create an opportunity for developing materials for biomedical applications and data recording devices.

BT-03. Investigation of Ferromagnetism Induced in Gamma-Ray Irradiated Molybdenum Disulfide Nano-Thin Films. *C. Wang*[1] and C. Lee[1] *1. Department of Engineering and System Science, National Tsing Hua University, Hsinchu City, Taiwan*

Two-dimensional semiconductor molybdenum disulfide (MoS_2) has been considered a promising material for applications in electronics and photonics. Furthermore, the van der Waals interface of two-dimensional materials has also been suggested for integration in spintronics [1-3]. Recently, Anbalagan *et al*. reported that defects in MoS_2 thin films created with gamma-ray radiation can induce magnetization of approximately 610 emu/cm^3 at room temperature [4]. In this research, MoS_2 nano-thin films on SiO_2/Si substrates with thicknesses of 0.6 nm, 4 nm, and 8 nm were prepared using reactive magnetron sputtering [5] and irradiated with gamma-rays of both 1.1732 MeV and 1.3325 MeV from a ^{60}Co source. The positive correlation between the magnitude of magnetization and radiation dose suggests that the origin of magnetic moments results from the number of defects. Additionally, the trend of increasing magnetization with decreasing thickness suggests an extraordinary exchange interaction in the thin film. The results are not consistent with models of vacancy or phase transformation [6]. X-ray photoelectron spectroscopy (XPS) measurements reveal that both Mo and S atoms are oxidized after gamma-ray irradiation. The 0.6-nm MoS_2 monolayer shows the most prominent oxidation compared to thicker MoS_2 nano-thin films, suggesting that thicker MoS_2 can resist radiation damage better than thinner ones. It can be inferred that the magnetic moments are contributed by oxygen atom substitution or interstitials in the lattice.

[1] J.-F. Dayen *et al*., Applied Physics Reviews, vol. 7, no. 1 (2020). [2] W. Zhang *et al*., APL Materials, vol. 4, no. 3 (2016). [3] Q. Xie *et al*., Advanced Materials, vol. 31, no. 21 (2019), p. 1900776. [4] A. k. Anbalagan *et al*., ACS Nano, vol. 17, no. 7 (2023), pp. 6555-6564. [5] C.-C. Wang *et al*., Applied Surface Science, vol. 659, no. 30 (2024), p. 159889. [6] L. Cai *et al*., Journal of the American Chemical Society, vol. 137, no. 7 (2015), pp. 2622-2627.

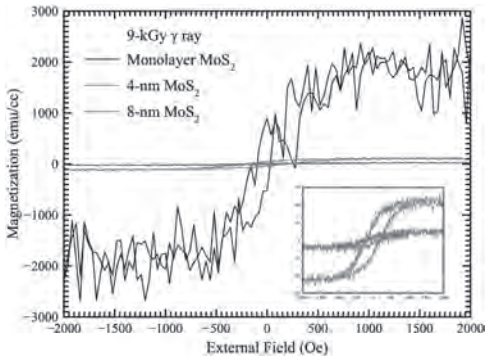

Magnetization of 0.6-nm, 4-nm, and 8-nm MoS_2 thin films with a dose of 9000 Gy.

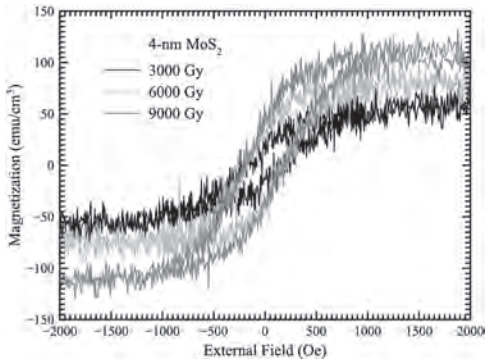

Magnetization of 4-nm MoS_2 Thin Films with Doses of 3000, 6000, and 9000 Gy.

BT-04. Graphene Induced Invertible Magnetoresistance in Variable Phase Iron Oxides. *N. Schulz*[1], D. DeTellem[1], G. Datt[2], A. Chanda[1], R. Roy Chowdhury[1], A.I. Ojo[1], T. Sarkar[3], H. Rodríguez Gutiérrez[1], S. Witanachchi[1], D.A. Arena[1], M. Venkata Kamalakar[2], M. Phan[1] and H. Srikanth[1] *1. University of South Florida, Tampa, FL, United States; 2. Department of Physics and Astronomy, Upsala University, Upsala, Sweden; 3. Department of Materials Science and Engineering, Upsala University, Upsala, Sweden*

Iron oxides exist as one of the oldest magnetic systems in history and have been studied extensively due to their phase-tunable magnetic and electronic properties. The combination of ferrimagnetic half-metallic magnetite (Fe_3O_4) with antiferromagnetic insulating hematite (α-Fe_2O_3) forms a so-called bi-phase iron oxide (BPIO) system that exhibits highly tunable magnetic and spintronic properties controllable through varying the respective phase volume fractions[1]. Here, the interfacial physics between variations of these phases of iron oxide and atomically thin layers of hexagonally bonded carbon atoms, graphene (Gr), is studied by comparing heterostructures of 100 nm thick single-phase iron oxide or BPIO with monolayer Gr and a capping layer of Pt. Combined temperature-dependent magnetometry and surface-sensitive magnetoresistance measurements were utilized to study the bulk and surface sensitive magnetic properties. It is found that the inclusion of graphene in these heterostructures induces an inversion in the sign of magnetoresistance at finite temperature. This phenomenon is explained through an effective percolative transport model, which describes the combined action of the distinct interfacial physics occurring for iron oxide in insulating and conducting temperature regimes, identified through a peak in the resistivity versus temperature[2]. Interestingly, the switching temperature and the sharpness of the transition are controllable by varying the phase volume fractions of the iron oxide layer, as well as the crystallinity. The BPIO films, which grow naturally on Si substrates, exhibit the highest switching temperature. These observations underscore the ability to induce magnetoresistive switching in abundant iron oxide grown on cost-effective, CMOS-compatible substrates via the inclusion of a single layer of Gr with potential applications in modern devices and neuromorphic computing.

[1] A. Chanda, C.-M. Hung, A. Tuan Duong, S. Cho, H. Srikanth, and M.-H. Phan, "Magnetism and spin-dependent transport phenomena across Verwey and Morin transitions in iron oxide/Pt bilayers," *J Magn Magn Mater*, p. 170370, Jan. 2023, doi: 10.1016/j.jmmm.2023.170370. [2] N. Schulz *et al.*, "Surface Termination-Enhanced Magnetism at Nickel Ferrite/2D Nanomaterial Interfaces: Implications for Spintronics," *ACS Appl Nano Mater*, vol. 6, no. 12, pp. 10402–10412, Jun. 2023, doi: 10.1021/acsanm.3c01352.

Now VP14-10

BT-05. Exchange effects from a magnetic substrate in transition metal dichalcogenides zigzag ribbons. *M.M. Salazar Cardona*[1], O. Avalos Ovando[2,3] and J.P. Ramos Andrade[1] *1. Physics, University of Antofagasta, Antofagasta, Chile; 2. Physics and Astronomy, Ohio University, Athens, OH, United States; 3. Nanoscale and Quantum Phenomena Institute, Athens, OH, United States*

Majorana zero modes (MZMs) have been predicted in semiconductor materials in the presence of an external magnetic field and proximitized to a superconductor. Nevertheless, controlling laboratory conditions to observe MZMs and their interesting non-Abelian properties remains challenging [1]. In this scenario, 2D transition metal dichalcogenides (TMDs) proximitized with ferromagnetic insulators emerge as an interesting alternative due to their properties, such as strong and intrinsic spin-orbit coupling [2]. We propose a comparative study of the effects of exchange and Rashba interactions on tungsten diselenide (WSe2) and tungsten ditelluride (WTe2) placed on top of europium oxide (EuO). As a first step, we explore the emergence of spin-polarized edge states in a zigzag TMD ribbon proximitized with a ferromagnetic substrate. In both cases, we demonstrate the capability of breaking time-reversal symmetry in the dichalcogenides through different magnitudes of Rashba and exchange fields. Additionally, the case of the WSe2/EuO zigzag ribbon shows isolated edge states in the material's band gap, indicating that these states are likely more accessible experimentally. With our study, we pave the way for proposing new observations of MZMs in TMDs.

[1] Lutchyn, R. M., Bakkers, E. P., Kouwenhoven, L. P., Krogstrup, P., Marcus, C. M., & Oreg, Y. (2018). Majorana zero modes in superconductor–semiconductor heterostructures. Nature Reviews Materials, 3(5), 52-68. [2] Cortés, N., Ávalos-Ovando, O., Rosales, L., Orellana, P. A., & Ulloa, S. E. (2019). Tunable spin-polarized edge currents in proximitized transition metal dichalcogenides. Physical Review Letters, 122(8), 086401.

BT-06. Thermal magnetization fluctuation in geometrically constrained magnetic domain wall on the ferromagnetic nanowire. *S. Ahn*[1] *1. POSTECH, Pohang, The Republic of Korea*

The structure and properties of a geometrically constrained magnetic domain wall (MDW) in constrictions like notches, protrusions, and functional structures is very interesting because it differs considerably from those of an unconstrained MDW like the well-known Bloch and Néel walls [1]. Furthermore, the thermal fluctuations in such geometrically constrained MDWs are critical to understand the switching of the magnetic domains and MDWs as inputs for a random variable generator for probabilistic computing [2]. In this study, the constrained MDWs at the nanowire have been numerically investigated based on thermal fluctuation of the 2D magnetization (M) vector, $\underline{M}$ (r, t) =M_x (r, t) $\underline{x}$ + M_y (r, t) $\underline{y}$ [3]. Figure 1(a) shows noise spectra in magnetization components of the constrained MDW at specific frequencies of 4 kinds of modes. Figure 1(b) depicts schematics of thermal M fluctuation at each frequency corresponding to Fig. 1(a), which means the red region indicates the highest magnetization fluctuation at each mode. Figure 2 shows RMS (root mean square) amplitudes of M_x and M_y at specific frequencies under H_T. Especially, the M_x and M_y show stepwise reductions at 1.52 (Mode 1) and 3.58 GHz (Mode 3) with increasing transverse field, H_T in the negative direction. It is caused by transverse magnetizations of constrained vortex-type MDWs at notches [4]. Thus, it is clearly seen that the specific modes of thermal M fluctuations in the MDWs exist and the

strength of the thermal M fluctuations in the MDWs depends on each mode. Besides, the thermal fluctuation at a single domain of nanowire shows a nonlocal distribution in the nanowire as shown in inset (i) at 6.0 and (ii) at 8.0 GHz, respectively.

[1] P. Bruno, Phys. Rev. Lett. 83, 2425 (1999). [2] K. Everaert *et al*., Appl. Phys. Lett. 122, 211902 (2023) [3] S.-M. Ahn *et al*., J. Nanosci. Nanotechnol. 11, 6472 (2011). [4] N. Smith, J. Appl. Phys. 90, 5768 (2001).

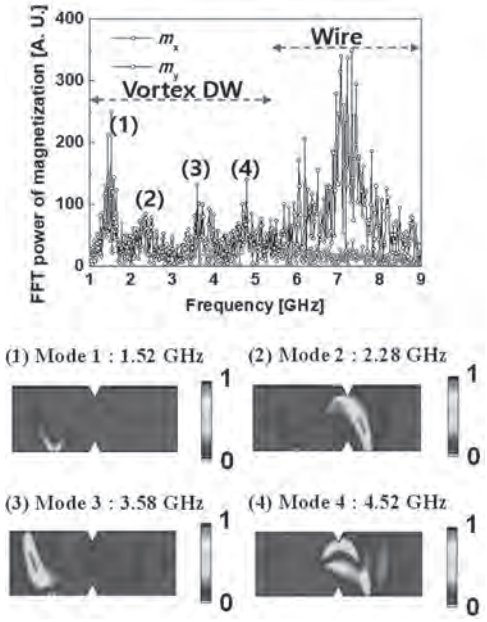

Fig. 1 (a) Noise spectra in magnetization components (M_x and M_y) of MDWs and (b) 4 modes (calculated) of thermal magnetization fluctuations at notches on nanowire at specific frequencies.

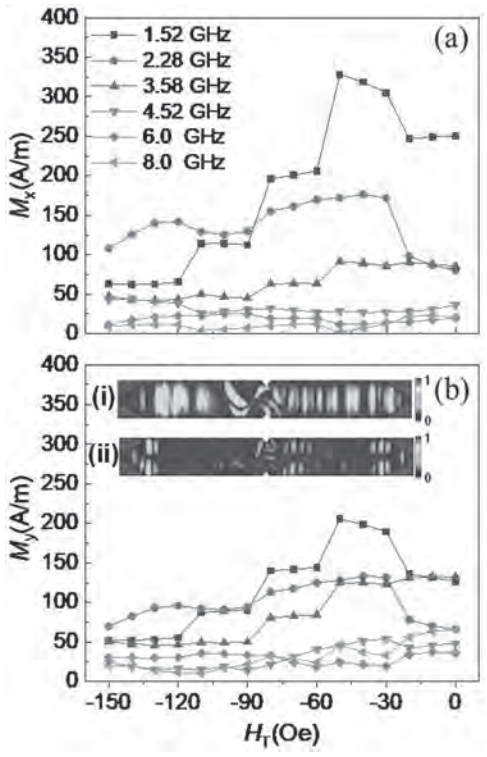

Fig. 2 RMS values of (a) M_x and (b) M_y of the DWs and nanowire domains at specific frequencies with respect to H_T. Inset: nonlocal thermal fluctuations of nanowire domains at (i) 6.0 GHz and (ii) 8.0 GHz.

Now VP12-09

BT-07. Dipolar Field-assisted Domain Wall Depinning in Trilayer Structures. *X. Chen*[2], W. Liu[1] and M. Bryan[3] *1. Electrical Engineering and Electronics, University of Liverpool, Brownlow Hill, United Kingdom; 2. Physics, Royal Holloway, University of London, Egham, United Kingdom; 3. Electrical Engineering, Royal Holloway, University of London, Ehgam, United Kingdom*

Control over domain wall (DW) positioning in nanoscale magnetic structures is fundamental to racetrack memory.[1] Pinning strength in a planar nanowire can be tailored by varying notches,[2] this approach limits device performance due to Walker breakdown when moving DW undergo changes in magnetization.[3] To suppress Walker breakdown, 3D systems like cylindrical and trilayer structures have been developed.[4,5] Cylindrical geometries are challenging to produce using planar lithographic techniques, hindering integration with peripheral electronics infeasible. Previously, we showed that trilayers can mimic dynamic behavior seen in nanotubulars, allowing standard manufacturing to access the novel properties of curved geometries.[5] Here, we reveal an intriguing pinning behavior of the dipolar-coupled DW from notches in a trilayer structure, showing that pining strength can be propagation order-dependent. Trilayers consisting of 2 nm Permalloy/1 nm spacer/2 nm Permalloy (100 nm width) were modelled with triangular notches using OOMMF. Coupling DWs in the top and bottom layers exhibited opposing magnetizations, resulting in either clockwise (CW) [Fig. 1(a)] or anti-clockwise (ACW) [Fig. 1(b)] circulation. Three distinct phases occurred when propagating DWs toward a notch: no depinning (P_0), only one wall depinning (P_1), and both walls depinning (P_2). Depinning thresholds in the trilayer were lower than in isolated layers, due to the transverse component of the stray field. The notch, acting as a magnetization filter, strongly influenced the transition field from P_1 to P_2. The P_1-P_2 boundary required up to 170% higher fields for CW wall pairs than ACW walls [Fig. 1(c-d)], due to flux closure effect, which induced a slight offset between individual walls within the trilayer, influencing the magnetization of the leading wall. Our findings underscore the necessity of considering stray field and flux closure effects when studying DW dynamics in 3D nanowires, as these phenomena cannot be directly extrapolated from single-layer systems.

1. S.S.P.P. Parkin, M. Hayashi, and L. Thomas, Science, 320 (5873), 190 (2008) 2. D.M. Burn, and D. Atkinson, Sci Rep 6, 34517 (2016) 3. H. Tanigawa, T. Koyama, and M. Bartkowiak, Phys Rev Lett 101, 207203 (2008) 4. J.A. Fernandez-Roldan, A. De Riz, and B. Trapp, Sci Rep 9, 5130 (2019) 5. X. Chen, T.J. Hayward, and W. Liu, J. Appl. Phys. 130, 223901 (2021)

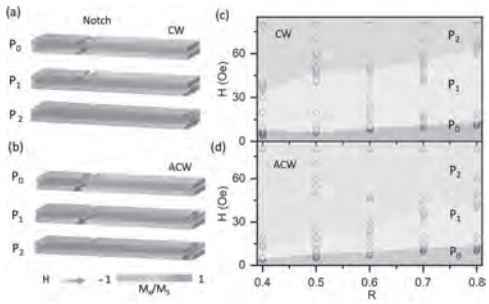

Fig. 1. Schematic diagrams showing three pinning states for (a) CW-DWs and (b) ACW-DWs. Phase diagrams of wall pinning for (c) CW-DWs and (d) ACW-DWs as a function of the depth-to-wire width ratio, R.

BT-08. Impact of Inertial and Nonlinear Damping Effects on the Strain-induced Domain Wall Motion in Bilayer Composite Structure. *S. Dolui*[1] and S. Dwivedi[1] *1. Mathematics, National Institute of Technology Andhra Pradesh, Tadepalligudem, India*

This article analytically investigates the combined impact of inertial and nonlinear damping (viscous and dry friction) effects on the strain-controlled dynamic features of domain walls in an isotropic, linearly elastic hybrid bilayer piezoelectric-magnetostrictive composite structure. To be precise, we perform the analysis under the one-dimensional inertial Landau-Lifshitz-Gilbert

equation, considering the influences of stresses induced by a piezoelectric actuator. By employing the classical traveling wave ansatz, this study explores how various factors, such as magnetostriction, magnetoelasticity, viscous, dry friction, and inertial damping effects, characterize the motion of the magnetic domain walls in both the steady-state and precessional dynamic regimes. The results exhibit valuable insights into how these key parameters can effectively modulate dynamic features such as domain wall width, velocity, mobility, threshold, and Walker breakdown limits. The obtained analytical results are further numerically illustrated for metallic and semiconductor ferromagnet, and a qualitative comparison with recent observations is also presented.

Session BU
ENERGY HARVESTING, VIBRATION ANALYSIS AND ADVANCED MATERIALS MANUFACTURING (Poster Session)

Dushyant Kumar, Chair
Netaji Subhas University of Technology, New Delhi, India

BU-01. Distribution characterization of magnetic flux density variation in soft magnetic rectangular beam during perpendicular magnetic field assisted electromagnetic vibration powered generation. *Y. Nakamura*[1], S. Kamiya[1] and M. Ohtake[1] *1. Faculty of Engineering, Yokohama National University, Yokohama, Japan*

Electromagnetic vibration powered generators with types of movable magnet [1] and inverse magnetostriction [2]–[5] have attracted much attention as energy harvesters. Recently, we have proposed a new type of electromagnetic generator named perpendicular magnetic field assisted type [6]. The generator consists of a soft magnetic cantilever beam, an electromagnetic coil, and a pair of magnets applying perpendicular magnetic field, as shown in Fig. 1. When the beam is bent either up or down by vibration, the angle of magnetic field with respect to the surface of beam tip is slightly varied from 90°. Consequently, in-plane alternating magnetic field is produced in the beam along the length direction and causes the magnetization reversal, which generates electromotive force through the coil. In order to enhance the output characteristic, it is necessary to consider the distribution of magnetic flux density variation, ΔB, in beam, which is influenced by the shape magnetic anisotropy. In the present study, the ΔB distribution in beams made of non-oriented silicon steel plates is characterized during vibration powered generation. The influence of beam shape (width) is investigated. Here, the width is varied in a range of 5–50 mm to change the influence of shape magnetic anisotropy, whereas the length and the thickness are respectively fixed at 50 mm and 350 μm to maintain the resonance frequency at about 140 Hz. The ΔB is measured by tracing a search coil along the length direction, as shown in Figs. 2(a) and (b). Figs. 2(c-1) and (d-1), respectively, show the beam length dependence of output voltage of search coil and the distribution of ΔB, when the beam of 20 mm width is used. The ΔB increases with approaching the center of beam. The distribution is attributed with the shape anisotropy, which is supported by micromagnetic simulation result shown in Fig. 2(e-1). Fig. 2 (d-2) shows the ΔB distribution in beam of 10 mm width. A higher ΔB is obtained when compared with the case of 20 mm width, since the beam is more easily magnetized due to increase in shape magnetic anisotropy. The present study has shown that control of shape anisotropy is important in achieving a higher output property.

[1] C. B. Williams and R. B. Yates: *Sens. Actuators, A*, 52, 8 (1996). [2] T. Ueno and S. Yamada: *IEEE Trans. Magn.*, 47, 2407 (2011). [3] S. Fujieda, S. Suzuki, A. Minato, T. Fukuda, and T. Ueno: *IEEE Trans. Magn.*, 50, 2505204 (2014). [4] S. Yamaura, S. Makino, N. Kimura, M. Yokoyama, T. Kubota, and Y. Furuya: *Trans. Mat. Res. Soc. Japan*, 42, 127 (2017). [5] F. Osanai, S. Hashi, and K. Ishiyama: *The 2019 Annual Meeting record IEE Japan*, 146 (2019). [6] M. Ohtake, T. Kawai, and M. Futamoto, Japanese Patent, application no. 2022-086851 / publication no. 2023-174153 (2023).

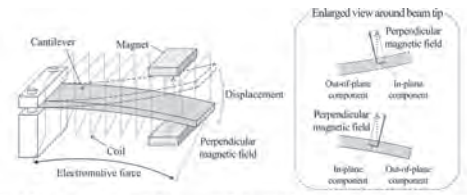

Fig. 1 Schematic diagram of perpendicular magnetic field assisted electromagnetic vibration powered generator.

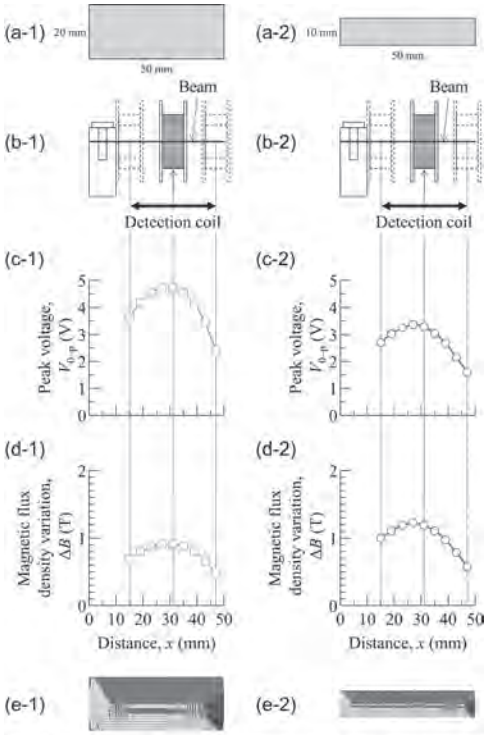

Fig. 2 (a) Schematic diagrams of beam shape, (b) cross-sectional diagrams of positional relationship between beam and coil, [(c),(d)] distributions of (c) peak voltage and (d) magnetic flux density variation, and (e) magnetization distributions from a micromagnetic simulation for beams of [(a-1)–(e-1)] 20 mm and [(a-2)–(e-2)] 10 mm width.

BU-02. Integrated Micro-Generator Design for Energy Harvesting in Smart Flow Meters. *P. Liao*[1] and M. Tsai[1] *1. Mechanical Engineering, National Cheng Kung University, Tainan, Taiwan*

Smart flow meters have emerged as a key trend for the future. These devices automatically provide feedback on usage and intelligently detect fluid leakage issues such as in water or gas systems, enabling effective management of fluid resources and information. They require low internal working voltage, primarily to support periodic data transmission to the cloud and sensors. Thus, utilizing micro-energy generated directly at the measurement site has become increasingly important. Achieving low power consumption and efficient energy harvesting is now a primary goal. Some literature proposed microgenerators [1] that use traditional surface-mounted permanent magnet (SPM) generators. This results in increased rotor size and inertia, leading to excessive rotor load, which is unsuitable for installation in small-flow smart flow meters. Therefore, this study, using an impeller-type flow meter as an example, proposes a 5-volt, 1-watt flux-switching permanent magnet (FSPM) [2] microgenerator. Its rotor is a single magnetic conductor without magnets, which is simpler in structure, lighter in weight, and more structurally robust than typical SPM generators. Furthermore, considering the costs of magnets and coils, this study compares a multi-tooth structure

[3] and traditional FSPM generators. Different tooth and slot numbers are introduced into finite element software for simulation to identify designs that offer optimal characteristics at lower costs. Finally, due to the small height of the magnetic conductor components, which are challenging to produce with traditional silicon steel sheets, selective laser melting is employed to fabricate the prototype of the magnetic conductor. The characteristics of the proposed design are then verified via empirical testing.

[1] Z. C. Shen, Y. Yao, Q. L. Wang, L. Lu, and H. X. Yang, "A novel micro power generation system to efficiently harvest hydroelectric energy for power supply to water intelligent networks of urban water pipelines," Energy, vol. 268, Apr, 2023. [2] Z. Zhu, "Switched flux permanent magnet machines—Innovation continues." 2011 International Conference on Electrical Machines and Systems, Beijing, China, Aug. 20-23, 2011. [3] Z. Q. Zhu, J. T. Chen, Y. Pang, D. Howe, S. Iwasaki, and R. Deodhar, "Analysis of a Novel Multi-Tooth Flux-Switching PM Brushless AC Machine for High Torque Direct-Drive Applications," IEEE Transactions on Magnetics, vol. 44, no. 11, pp. 4313-4316, 2008.

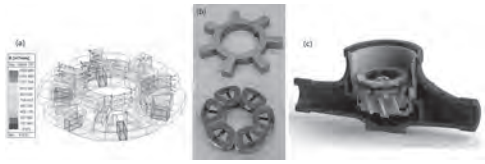

Fig. 1. Hydropower Generator Design for Smart Flow Meters: (a) Magnetic flux direction in FSPM, (b) Prototype of FSPM, (c) FSPM micro generator in smart flow meters

BU-03. Robotic End Effector for Magnetic Sample Colleciton. *L. Schorr*[1], I. Scaparo[1], J.P. Nunez[1], I. Thakur[1], F. Hanna[1] and R.L. Hadimani[1,2]
1. Department of Mechanical Engineering, Virginia Commonwealth University, Richmond, VA, United States; 2. Department of Biomedical Engineering, Virginia Commonwealth University, Richmond, VA, United States

Magnetic materials are a vital part of many key technologies and industries, creating an increase in demand for magnetic materials, which pose several supply chain issues. Namely, high-energy product magnetic materials rely on rare earth elements (REEs) to achieve high magnetic anisotropy. These REEs, including neodymium or samarium, are considered critical materials [1], which has motivated significant research investigating rare-earth-free magnets, such as the mineral tetrataenite. Tetrataenite, while difficult to synthesize on Earth, is readily found in asteroids. To facilitate collection in the aerospace environment, a robotic end effector capable of automating aspects of the process was designed. Our proposed design uses a set of permanent magnet linear Halbach arrays for use in handling of magnetic materials. The arrays can be rotated 180° to switch between the high and low strength sides of the array to pick up and drop objects, respectively. Additionally, the arrays will be mounted on a parallel robotic end effector to accommodate various sizes of magnetic materials. This design can hold magnetic materials using the magnetic force of the arrays rather than relying on the compressive force exerted by a gripping end effector. As the design does not require active energy input for continual grasping of the material, only to release it, this would be well employed in conditions such as space where energy is a premium [2]. With these in mind, we determined an ideal design to have the following characteristics: 1. relatively uniform magnetic field to allow grasping anywhere along the gripper, 2. able to both transport heavy magnetic objects while simultaneously able to drop light magnetic objects, and 3. be reasonably manufacturable. Our fabricated prototype was able to meet all of these requirements, with a maximum payload of approximately 2.5kg and the ability to drop objects weighing less than 30g. Additionally, this technology has applications well beyond aerospace, including in post-processing for metal additive manufacturing and grasping of slick materials in traditional manufacturing.

[1] Notice of Final Determination on 2023 DOE Critical Materials List. Notice 88 FR 51792. Federal Register, July 28, 2023, pp. 51792–51798. [12] Aiming Liu et al. "Energy consumption modeling of industrial robot based on simulated power data and parameter identification". In: Advances in Mechanical Engineering 10.5 (May 1, 2018). Publisher: SAGE Publications, p. 1687814018773852.

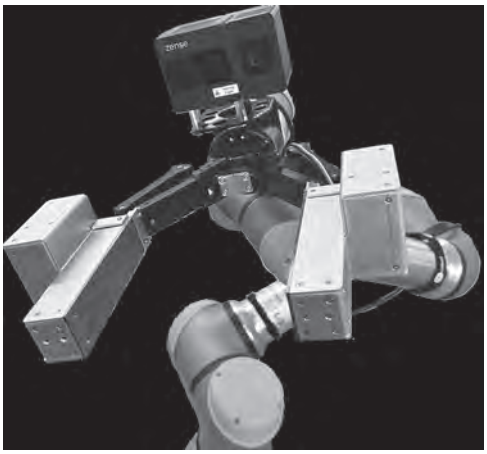

Robot with magnetic gripper and 3D camera

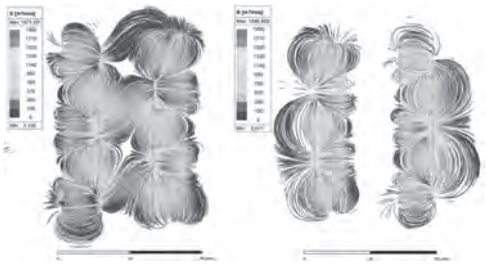

Flux diagram pointing for grasping (left) and dropping (right)

BU-04. Exploring the Magnetic and Magnetocaloric Properties of PLA Composite Filaments of $Mn_{0.5}Fe_{0.5}Ni_{0.95}Cr_{0.05}Si_{0.95}Al_{0.05}$ for Additive Manufacturing. *T.F. McKenzie*[1], J.R. DeFeo[2], A. Bhatta[1], J. Casey[2], V. Yenugonda[2], S. Mukaddaskhonov[1], G. Toromani[1], A.K. Pathak[2] and M. Khan[1] *1. Physics, Miami University, Oxford, OH, United States; 2. Physics, SUNY Buffalo State University, Buffalo, NY, United States*

$Mn_{0.5}Fe_{0.5}Ni_{0.95}Cr_{0.05}Si_{0.95}Al_{0.05}$ that belongs to the $Mn_{1-x}Fe_{x-\delta}Ni_{\delta}Si_{1-y}Al_y$ intermetallic family [1, 2] exhibits a first-order phase transition at ~325 K on heating [3]. For field changes of 20 kOe and 50 kOe peak entropy changes of -16 J kg^{-1} K^{-1} and -42 J kg^{-1} K^{-1}, respectively, have been reported for the compound. Like the other members of the $Mn_{1-x}Fe_{x-\delta}Ni_{\delta}Si_{1-y}Al_y$ family, $Mn_{0.5}Fe_{0.5}Ni_{0.95}Cr_{0.05}Si_{0.95}Al_{0.05}$ physically deteriorates to powder form over a few thermal cycles due to the large thermal expansion that accompanies the first order phase transition. This makes this material, in bulk form, unsuitable for application in magnetocaloric cooling. Additive manufacturing is an emerging method that can be utilized to fabricate polylactic acid (PLA)-based composite filament for fused deposition modeling [4]. This method allows design of parts of various shapes that are physically stable over many thermal cycles. Here we present an experimental study on the structural and magnetocaloric properties of PLA-based composite filaments containing nominal (27, 54, and 57) wt.% of $Mn_{0.5}Fe_{0.5}Ni_{0.95}Cr_{0.05}Si_{0.95}Al_{0.05}$ powder. X-ray diffraction patterns confirmed that powder and filament exhibited the hexagonal and orthorhombic crystal structures at room temperature. The magnetization data over a temperature range, M(T), showed a first-order magnetic phase transition accompanied by thermal hysteresis in all samples. The entropy changes evaluated from the magnetization data peaked at 302 K for the powder sample and 322 K for filament with 57 wt.% powder during warming. For a field change of 5T, peak entropy changes of -5.5 J kg^{-1} K^{-1} and -1.2 J kg^{-1} K^{-1} were observed for powder and filament, respectively. The work at State University of New York (SUNY), Buffalo State University, was supported by the National Science Foundation Award No. DMR-2213412.

[1] A. Biswas, A.K. Pathak, N.A. Zarkevich, Acta Mater., Vol. 180, p.341 (2019) [2] Jacob Casey, Babajide Akintunde, Ranjit Chandra Das, J. Magn. Magn.Mater., Vol.579, 170862(2023)[3]A.Bhatta, J.Casey, S.Bhattacharjee, AIP Advances., Vol. 14, 015336 (2024) [4] Á. Díaz-García, J.Y. Law, A. Cota, ScienceDirect., Vol. 24, 101049 (2020)

FIG. 1: Printed object using (a) PLA (b) PLA+ Mn0.5Fe0.5Ni0.95Cr0.05Si0.95Al0.05 composite filaments.

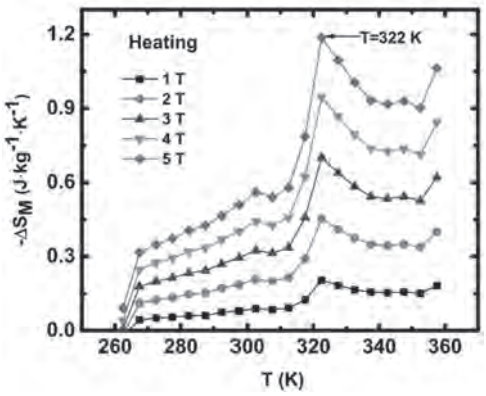

FIG. 2: The temperature dependence of the isothermal entropy changes, ΔS_T (T), for nominal 57 wt.% powder composite filament.

BU-06. Beyond 1-watt energy harvester based on beam vibration and electromagnetic induction. *H. Kijima-Aoki*[1] and H. Masumoto[1] *1. Tohoku University, Sendai, Japan*

Following the trend toward automating maintenance with sensor device networks for aging infrastructures, developing a stand-alone environmental power source to replace batteries and commercial power sources is urgent. Although a 1-3W power supply needs multi-functional sensors that satisfy human inspection criteria, the output level of environmental power generation is in the order of 100 mW, excluding solar power generation. Vibration power generation, which converts unwanted environmental vibrations into electric power, is expected to be adapted to different environments from solar power generation. This study aims to achieve more than a 1-watt outcome by developing an electromagnetic induction vibration power generator using beam resonance. The electromagnetic vibrating power generator consists of the soft magnetic core plate (50-layered MaDC-A®, PROTERIAL) inserted in 1000 turn-coil (90 ohms), which is attached to a free end of the non-magnetic cantilever beam. A pair of permanent magnets were fixed with back yoke or non-magnetic fixture (hereafter "without BY"). The vibration test was performed under 10-30 Hz with accelerations of 1G. From the time-dependent V and P (Fig.2), the beam resonated at 14Hz with an amplitude of free end position of 20 mm. To our knowledge, the V_{p-p} and V_{rms} of both devices are the highest value for magnetic vibrating power generators. The peaks are decreased and broadened in the case of the device without BY. The V was maximized when the resonated beam passed across the inverse polar of two permanent magnets with maximum speed. The role of BY is to control the magnetic flux distribution to prevent the soft magnetic core from sticking with permanent magnets. Since the order of power generation is more than 2 W, our electromagnetic vibrating power generator is expected to meet the requirements as an environmental power supply for multi-functional sensor devices.

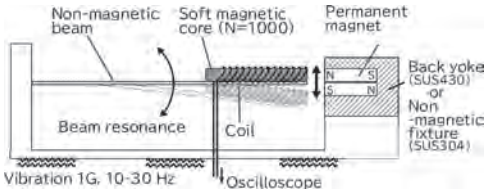

Fig.1 Schematic illustration of electromagnetic vibrating power generator

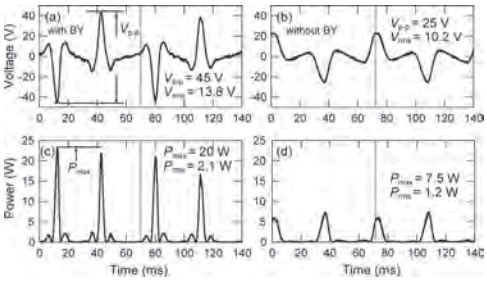

Fig.2 Time-dependent output voltage (V) and power (P) of device with BY((a) and (c)), and without BY((b) and (d)). Dotted line indicate the single oscillation period of free end of cantilever beam.

BU-07. Quantum scattering interference process that enhances the thermoelectric efficiency in quantum dot systems: Its manifestation in photoemission and inverse photoemission spectroscopy. *R. Franco Peñaloza*[1], J. Silva-Valencia[1], E. Ramos Rodriguez[2], R. Cortes-Santamaria[3] and M. Figuiera Da Silva[4] *1. Departamento de Física, Universidad Nacional de Colombia, Bogotá, Colombia; 2. Vicerrectoria de Investigaciones, Universidad Manuela Beltran, Bogotá, Colombia; 3. Condensed Matter Group, International Centre for Theoretical Physics-ICTP, Trieste, Italy; 4. Instituto de Física, Universidade Federal Fluminense, Niterói, Brazil*

Recently we employed universality properties over the linear thermoelectric transport coefficients -as temperature function- for the single impurity Anderson model, associated to the presence of a quantum scattering center -in the electron hole symmetric point- [1], to explore the conditions that in a system of two coupled serial quantum dots (QDs) permits achive a very high value for the thermoelectric efficiency. We identify the presence of quasi BICs as associated with the improving of the thermoelectric efficiency at low and high temperatures and a quantum scattering interference process that involves charge fluctuations in a QD, these quasi BICs are manifested in the density of states, transmission coefficient and quantum phase shifts [2]. In the actual work we obtain the manifestations of the conditions that improves the thermoelectric efficiency in optical properties -Photoemission spectroscopy (PES) and Inverse Photoemission spectroscopy (IPES)- in the system of two coupled QDs studied in our previous paper; additionally we study the arise of a non-Fermi Liquid (NFL) behavior as associated to this enhancing process over the thermoelectric efficiency, we show this by the presence of a minimum in the imaginary part of the self-energy at the Fermi level and the behavior of the electrical resistivity as temperature function in the conditions where the thermoelectric efficiency is enhanced [3]. Our results shows that the thermoelectric efficiency improving at high temperatures is associated to the presence of a BIC-thermally activated, linked to a many-body state in the QDs.

[1] D. F. Aranguren-Quintero, E. Ramos, J. Silva-Valencia, M. S. Figueira, L. N. Oliveira and R. Franco, Phys. Rev. B. 103, 085112 (2021). [2] R. S. Cortes-Santamaria, J. A. Landazabal-Rodríguez, J. Silva-Valencia, E. Ramos, M. S. Figueira and R. Franco. Scipost Physics to be published (2024)- https://scipost.org/submissions/scipost_202312_00043v2/, https://arxiv.org/abs/2302.09099. [3] G. R. Stewart- Rev. Mod. Phys. 73, 793 (2001).

BU-08. Fast Performance Analysis of Coreless Axial-Flux PMSM Based on Hybrid Equivalent Circuit and Harmonic Interaction Model.

L. Dai[1], S. Niu[1], Z. Li[1] and *F. Ni*[1] *1. Department of Electrical and Electronic Engineering, The Hong Kong Polytechnic University, Hong Kong, Hong Kong*

I. Introduction The coreless axial flux permanent magnet synchronous machine (AFPMSM) is characterized by double-side rotors and a middle layer stator winding in the axial direction [1]. Fig. 1 provides an illustration of the machine's structure. This design offers several notable advantages, including the absence of cogging torque, low vibration noise, low torque ripple, and low core loss. Traditionally, performance calculations for coreless AFPMSMs have relied heavily on the time-consuming three-dimensional finite element method (3D FEM). It typically takes several hours to calculate a single operating case. Although previous studies have made some progress in expediting the calculation, such as the quasi-3D FEM [2], significant computational requirements still persist. To address the urgent need for fast and accurate analysis of coreless AFPMSMs, as well as to facilitate large-scale design optimization, this paper proposes a hybrid analytical model that combines the magnetic equivalent circuit (MEC) and the harmonic interaction model (HIM). The MEC enables fast and efficient calculation of magnetic properties, while the HIM accurately accounts for additional effects resulting from harmonic interactions. By integrating these two models, the proposed hybrid approach offers a balance between computation speed and accuracy, making it suitable for efficient analysis and optimization of coreless AFPMSMs. II. Proposed Analytical Model Fig. 2 illustrates the proposed calculation process for coreless AFPMSM, which utilizes the MEC model to compute the magnetic distribution within the motor. Subsequently, a harmonic FFT analysis is conducted to extract the harmonic components. By leveraging the HIM, the motor's overall performance can be accurately calculated based on these harmonic interactions.

[1] B. Gao et al., "Optimal Design of PCB Coreless Axial Flux Permanent Magnet Synchronous Motor With Arc Windings," in IEEE Transactions on Energy Conversion, vol. 39, no. 1, pp. 567-577, March 2024, doi: 10.1109/TEC.2023.3315413. [2] J. H. Kim et al., "3D Hybrid Segmented Layer Modeling of On-Load Magnetic Fields and Torques for Coreless Axial-Flux Permanent Magnet Synchronous Motor," in IEEE Transactions on Energy Conversion, vol. 38, no. 3, pp. 1815-1826, Sept. 2023, doi: 10.1109/TEC.2023.3240168.

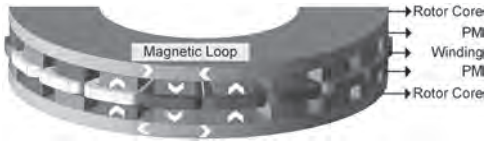

Fig. 1. Structure presentation of coreless AFPMSM.

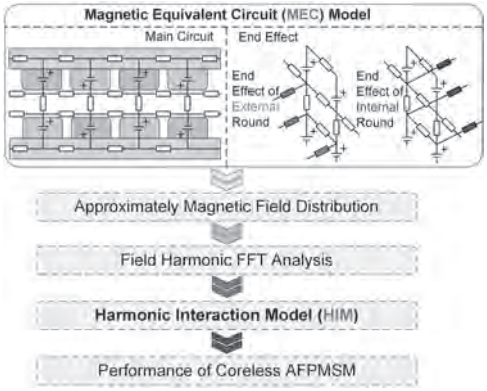

Fig. 2. Illustration of the proposed calculation process.

Session BV
ELECTRICAL MACHINES AND POWER ELECTRONICS III (Poster Session)

Massimo Pasquale, Chair
INRIM, Torino, Italy

BV-01. Study on an Assistance Yoke Structure for Improving Magnetization Performance Through Post-Assembly Magnetization.
J. Hwang[1], T. Kim[1], J. Moon[1] and D. Kang[1] *1. Energy Conversion System Lab(ECSL), Keimyung University, Daegu, The Republic of Korea*

The hybrid vehicle (HEV) market is experiencing an increase in demand due to high fuel efficiency and environmental regulations [1]. To address this, the automotive industry uses the post-assembly magnetization process to improve productivity and reduce manufacturing costs [2]. However, during the post-assembly magnetization process, the thin inner and outer diameter structure of the hybrid drive motor rotor leads to magnetic flux density saturation in the rotor core, causing incomplete magnetization in local parts of the permanent magnet. To fully magnetize these incompletely magnetized parts, it is essential to use a power supply with higher current and specifications than necessary, which results in saturation of the magnetizing yoke and heating of the winding, leading to a decrease in stability [3]. This study proposes an Assistance Yoke structure that reduces the magnetic flux density saturation of the rotor inserted into the inner diameter of the magnetizing yoke, allowing the permanent magnet to be magnetized with a lower magnetizing magnetic field. The Assistance Yoke structure is inserted into the inner diameter of the hybrid drive motor rotor and effectively changes the path of the magnetizing magnetic field without distortion. By doing so, the Assistance Yoke structure can magnetize the permanent magnet with a lower magnetizing magnetic field compared to the existing magnetizing yoke, enhancing the stability of the magnetizer and reducing the size of the magnetizer by avoiding the need to increase the outer diameter of the magnetizing yoke to apply an unnecessarily high magnetizing magnetic field.

[1] Z. Yang, F. Shang and M. Krishnamurthy, "Comparative Study of Interior Permanent Magnet, Induction, and Switched Reluctance Motor Drives for EV and HEV Applications," in IEEE Trans. Transport. Electrific, vol. 1, no. 3, pp. 245-254, Oct. 2015 [2] Q. Wang, H. Ding and L. Li, "Study of a Post-Assembly Magnetization Method of a V-Type Rotor of Interior Permanent Magnet Synchronous Motor for Electric Vehicle," in IEEE Trans. Appl. Supercond vol. 30, no. 4, pp. 1-5, June 2020. [3] D. G. Dorrell, M. -F. Hsieh and Y. -C. Hsu, "Post Assembly Magnetization Patterns in Rare-Earth Permanent-Magnet Motors," in IEEE Trans Mag, vol. 43, no. 6, pp. 2489-2491, June 2007

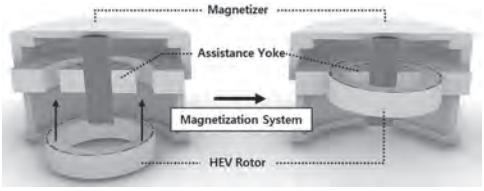

Fig. 1. Assistance Yoke and Magnetizer Assay

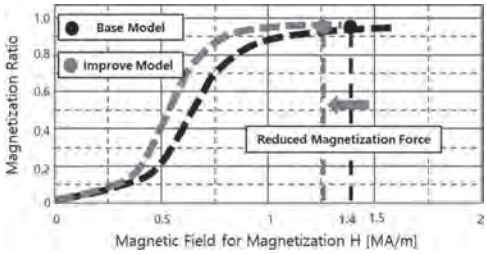

Fig. 2. Comparison of Magnetic Field for Magnetization

BV-02. Design and Analysis for Improved Efficiency Based on Design Variables and Performances Considering the Nonlinear Core Material of IPMSM.
S. Lee[1], T. Kim[1], Y. Choi[1], K. Shin[2] and J. Choi[1]
1. Chungnam National University, Daejeon, The Republic of Korea;
2. Changwon National University, Changwon, The Republic of Korea

Interior permanent magnet synchronous motors (IPMSM) are widely used in automotive parts and electric vehicles (EVs) because of their wide operating range and high efficiency. Vector control of the current is crucial for the efficient use of IPMs, with the inductance being the most critical parameter. However, the magnetic saturation caused by high currents can make model parameter tracking challenging. This study creates a 3D map of inductance and flux linkage to track performance, which is essential for predicting model performance at various current operating points. The parameters and performance of models with two different rotor shapes were compared, with the flux saturation achieving high tracking accuracy. The 3D shape and experimental apparatus of the IPMSM used in this study are displayed in Figures 1(a) and (b), respectively. Figure 1(c) depicts the required performance curve of the model. The analysis results indicate that the efficiency at the main operating point is lower than that at the maximum efficiency point. Figure 1(d) shows the impact of each design variable on output performance, confirming that the difference between d- and q-axis inductances significantly affects the torque. Therefore, the design variables for the improved model were selected accordingly. The parameters and output performances of the existing and improved models are compared in Figures 2(a), (b), and (c), indicating that the improved model has enhanced parameters. The efficiency maps are compared in Figures 2(d) and (e), showing that the efficiency at the main operating point has increased from 90.86% to 91.62%. The efficiency maps were derived analytically using parameters that considered core nonlinearity. The detailed process of selecting model design variables and analytic derivation of the efficiency maps are presented through experiments and comparisons.

[1] Z. Liu, X. Fan, W. Kong, L. Cao, and R. Qu, "Improved small-signal injection-based online multiparameter identification method for IPM machines considering cross-coupling magnetic saturation," IEEE Trans. Power Electron., vol. 37, no. 12, pp. 14362–14374, Dec. 2022. [2] J.-C. Park et al., "Design Optimization Using Asymmetric Rotor in IPMSM for Torque Ripple Reduction Considering Forward and Reverse Directions," IEEE Trans. Magn., vol. 59, no. 11, pp. 1-5, 2023. [3] H. -J. Kim and C. -S. Lee, "Shape Parameters Design for Improving Energy Efficiency of IPM Traction Motor for EV," in IEEE Transactions on Vehicular Technology, vol. 70, no. 7, pp. 6662-6673, July 2021.

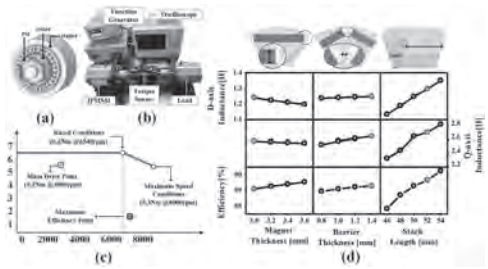

Fig.1 (a) 3D structure of analysis model, (b) Experimental apparatus, (c) Required performance curve of the motor (d) Design factor analysis graph.

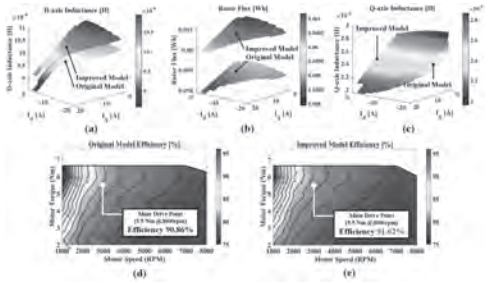

Fig.2 Comparison of Parameters and Performance (a) D-axis Inductance, (b) Rotor Flux, (c) Q-axis Inductance, (d) Efficiency Map of Original Model Based on Equations (e) Efficiency Map of Improved Model Based on Equations.

BV-03. Design and Experimental Verification of a Surface-Mounted Permanent Magnet Synchronous Machine with Bread-Loaf Shape Magnets Considering Multi-physics Analysis. *S. Kim*[1], S. Kim[1], W. Jung[1], K. Shin[2] and J. Choi[1] *1. Chungnam National University, Daejeon, The Republic of Korea; 2. Changwon National University, Changwon, The Republic of Korea*

Permanent Magnet Synchronous Machines (PMSMs) offer high power density, high efficiency, compactness, and lightweight characteristics, making them suitable for various applications. In military applications, high power density and low cogging torque are particularly important. This paper analyzes a bread-loaf-shaped magnet for a Surface Permanent Magnet Synchronous Machine (SPMSM) with the purpose of reducing cogging torque, considering multi-physics analysis. Fig. 1(a) shows the 2D shapes of the SPMSM used in this study and the design variables of the bread-loaf-shaped magnet. Fig. 1(b) shows the cogging torque comparison graphs for each model, and Fig. 1(c) shows the no-load FFT results. The bread-loaf-shaped magnet design shows lower THD and reduced cogging torque. This confirms that the bread-loaf-shaped magnet is more beneficial compared to the conventional magnet shape. Fig. 2(a) shows the results of the modal analysis in the mechanical analysis of the designed bread-loaf-shaped SPMSM, demonstrating that it has been sufficiently optimized to avoid resonance at specific frequencies. Fig. 2(b) shows the temperature rise over time, indicating that the heat generated during SPMSM operation remains within the target temperature range. This indicates that the designed bread-loaf-shaped magnet structure provides efficient thermal management. Fig. 2(c) shows the stator and rotor manufactured based on the experimental equipment and design model. This visually validates the implementation and verification of the research findings. Finally, Fig. 2(d) shows experimental results, comparing analysis data to substantiate the validity of the design. The analysis and experimental results confirm that the bread-loaf-shaped SPMSM is suitable for military applications. Additionally, the full paper provides a detailed analysis of the design techniques based on theoretical derivation for the bread-loaf-shaped magnets and their multi-physics analysis.

[1] W. Zhao, X. Wang, C. Gerada, H. Zhang, C. Liu, and Y. Wang, "Multi-physics and multi-objective optimization of a high-speed PMSM for high-performance applications," IEEE Trans. Magn., vol. 54, no. 11, pp. 1–5, Nov. 2018 [2] S.-W. Hwang, J.-W. Chin, M.-S. Lim, and J.-P. Hong, "Electromagnetic and thermal multi-physics design of SPMSM for wearable robot," in Proc. Int. Conf. Electr. Mach. (ICEM), Alexandroupoli, Greece, 2018. [3] S. Zhu, W. Zhao, J. Ji, G. Liu, Y. Mao, and T. Liu, "Investigation of bread-loaf magnet on vibration performance in FSCW PMSM considering force modulation effect," IEEE Trans. Transp. Electrific., vol. 7, no. 3, pp. 1379–1389, Sept. 2021. [4] M. Zhou, X. Zhang, W. Zhao, J. Ji, and J. Hu, "Influence of magnet shape on the cogging torque of a surface-mounted permanent magnet motor," *Chinese Journal of Electrical Engineering*, vol. 5, no. 4, pp. 40–50, Dec. 2019.

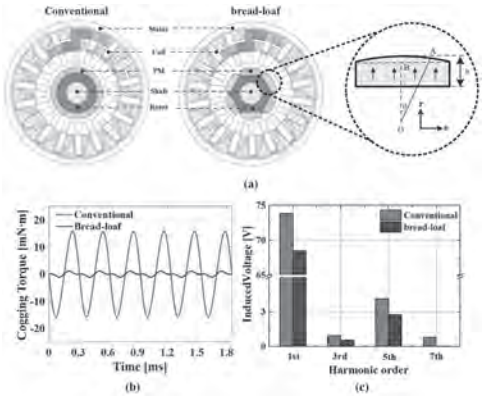

Fig. 1. Analysis model and results of SPMSM: (a) 2D model and design variable (b) Cogging Torque, (c) No-load induced voltage FFT

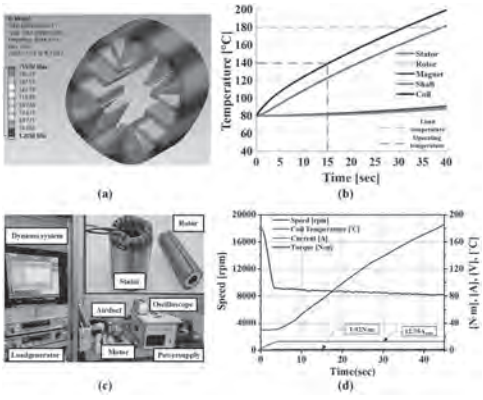

Fig. 2. Analysis results of bread-loaf shape with SPMSM: (a) Mechanical analysis, (b) Thermal analysis, (c) Experimental setup, (d) Experimental results

BV-04. Electromagnetic Analysis of AFPM based on Quasi-3D FEM Considering End Effects. *J. Jang*[1], J. Yang[1], H. Ban[1], K. Shin[2] and J. Choi[1] *1. Department of Electrical Engineering, Chungnam National University, Daejeon, The Republic of Korea; 2. Department of Electrical Engineering, Changwon National University, Changwon, The Republic of Korea*

Axial-flux permanent magnet (AFPM) motors offer a compact axial structure and high torque density, making them highly valuable in electric vehicles and various other applications. Finite element method (FEM) enables accurate analysis by considering the nonlinearity of materials. However, for AFPM motors, which involve complex three-dimensional (3D) geometrical structures, this approach is often time-consuming. This paper proposes a new Quasi-3D analysis technique that uses correction functions to efficiently and accurately interpret the electromagnetic characteristics of AFPM motors, accounting for end effects. Fig. 1(a) shows the 3D model of the AFPM. The Quasi-3D modeling approach illustrated in Fig. 1(b) divides the model into *n* independent computational regions. Each region is analyzed individually, as illustrated in Fig. 1(c) and Fig. 1(d), and the results are combined to derive the overall performance of the AFPM motor. Fig. 2(a)

shows the prototype model used in the experiment, which replicates the actual operating conditions to verify the accuracy of the Quasi-3D analysis method. Fig. 2(b) shows parameters of planes of radius. Fig. 2(c) shows the distribution of the correction function, which reflects the changes in the magnetic flux distribution between the rotor and stator. Fig. 2(d) illustrates the no-load back electromotive force (EMF) waveform without considering the end effects. Fig. 2(e) displays the no-load back EMF waveform with the end effects considered using the correction function. The Quasi-3D method incorporating end effects shows a no-load back EMF magnitude with an error rate within 3% compared with the experimental results. This confirms the accuracy of the proposed Quasi-3D method in accounting for end effects. This study provides a detailed theoretical analysis and examination of the electromagnetic characteristics under load conditions.

[1] A. Parviainen, M. Niemela, and J. Pyrhonen, "Modeling of axial flux permanent-magnet machines," *IEEE Transactions on Industry Applications,* vol. 40, no. 5, pp. 1333-1340, 2004. [2] J. Azzouzi, G. Barakat, and B. Dakyo, "Quasi-3-D analytical modeling of the magnetic field of an axial flux permanent-magnet synchronous machine," *IEEE Transactions on Energy Conversion,* vol. 20, no. 4, pp. 746-752, 2005. [3] T. Zou, D. Li, R. Qu, J. Li, and D. Jiang, "Analysis of a dual-rotor, toroidal-winding, axial-flux vernier permanent magnet machine," *IEEE transactions on industry applications,* vol. 53, no. 3, pp. 1920-1930, 2017.

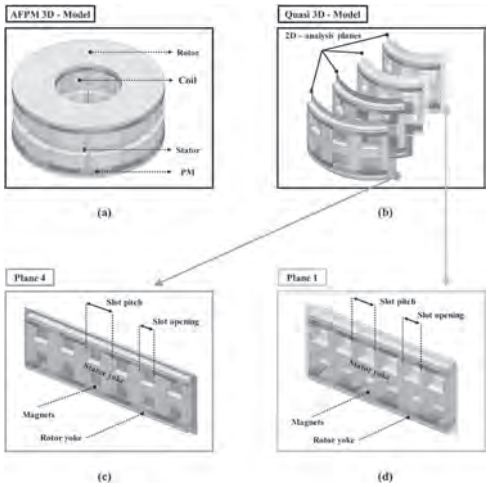

Fig.1 Analysis Model: (a) AFPM 3D, (b) 2-D analysis plane, 2-D analysis plane with a radius (c) 44mm and (d) 30.5mm.

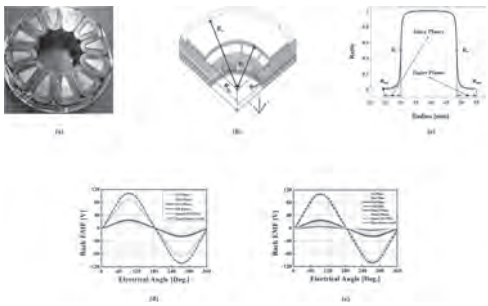

Fig.2 (a) Prototype machine, (b) Parameters of AFPM, (c) Distribution of correction function according to radius of planes, Comparison of Back EMF (d) Without considered end effect (e) Considered end effect.

BV-05. Optimal Split Ratio Design of Outer Rotor SPMSM Considering Variations in Magnetic Properties of Ferrite PM within the Same Grade. *K. Kim*[1], Y. Bai[1], J. Kim[2] and M. Lim[1] *1. Automotive engineering, Hanyang University, Seoul, The Republic of Korea; 2. Mechanical Engineering, Yeungnam University, Gyeongsan, The Republic of Korea*

Within the same grade, the coercive force of ferrite PM decreases as the residual magnetic flux density increases. The outer rotor surface-mounted permanent magnet motor (SPMSM) can enhance torque density as the split ratio (SR) between the stator and the rotor increases under limited outer diameter conditions. However, as the SR increases, the thickness of the PM decreases. If ferrite PM with high residual magnetic flux density is used within the same grade, irreversible demagnetization may occur due to its low coercivity. Consequently, the available ferrite PM material may vary depending on the SR, affecting the torque density of the outer rotor SPMSM accordingly. In this article, a design method is presented that considers the material characteristics of four types of grade 7 ferrite PMs and the electromagnetic characteristics according to the SR of the outer rotor SPMSM. Using a theoretical approach of the outer rotor SPMSM, the airgap magnetic flux density (AMFD) and back electromagnetic force (BEMF) are analyzed as functions of the SR. Fig. 1 shows the magnetic characteristics of grade 7 ferrite PMs and the variations in AMFD and BEMF according to SR. The initial design, aiming for high efficiency and high power density using ferrite PM materials and the SR, is evaluated through 2D Finite Element Analysis (FEA). Additionally, the issue of low-temperature irreversible demagnetization of ferrite PMs is reviewed. Based on the initial design results, the ferrite PM material is selected, and the SR range for design is determined. Fig. 2 shows the core stack length, PM thickness, PM material, load characteristics, and demagnetization ratio according to the SR. Subsequently, the optimal SR, ensuring high efficiency and power density, is selected through the optimal design. The design results are compared and validated through experiments conducted on the manufactured motor.

[1] H. Moayed-Jahroni, A. Rahideh, and M. Mardaneh, "2-D Analytical Model for External Rotor Brushless PM Machines," *IEEE Trans. Energy Convers.,* vol. 31, no. 3, pp. 1100-1109, Sep. 2016. [2] A. Isfanuti, L. Tutelea, I. Boldea, T. Staudt and P. da Silva, "Outer Ferrite-PM-Rotor BLAC Motor Characterization: FEM-Assisted Optimal Design and Preliminary Experiments," *IEEE Trans. Ind. Appl.,* vol. 56 no. 3, pp. 2580-2589, May-Jun. 2020. [3] H. Kim, J. Jeong, M. Yoon, J. Moon, and J. Hong, "Simple Size Determination of Permanent-Magnet Synchronous Machines," *IEEE Trans. Ind. Electron.,* vol. 64 no. 10, pp. 7972-7983, Oct. 2017. [4] Y. Shen and Z. Zhu, "Analytical Prediction of Optimal Split Ratio for Fractional-Slot External Rotor PM Brushless Machines," *IEEE Trans. Magn.,* vol. 47 no. 10, pp. 4187-4190, Oct. 2011.

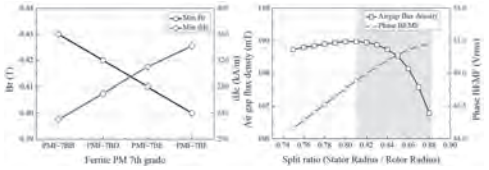

Fig. 1. 7th grade ferrite PM magnetic characteristics and AFD & BEMF according to SR.

SR	Stack length (mm)	PM thickness (mm)	PM Characteristics			Load (Same current)		Demagnetization ratio (%)
			grade	Br @RT (T)	iHc @RT (kA/m)	Average torque (Nm)	Torque ripple (%)	
0.81	43.5	12.06	720H	0.41	334	17.36	4.84	0.049
0.82	43	11.12				17.29	4.70	0.069
0.83	42	10.18				17.27	4.88	0.08
0.84	42	9.24				17.28	4.83	0.173
0.85	44.5	8.3	710H	0.4	382	17.24	4.43	0.1
0.86	47.5	7.36				17.23	4.49	0
0.87	50	6.42				17.24	4.62	0
0.88	-	5.49	Irreversible demagnetization					

Fig. 2. Stack length, PM thickness, PM material properties, load characteristics, and demagnetization ratio according to SR.

BV-06. Analysis of Magnetic Field Behavior and Core Losses in Permanent Magnet Synchronous Generators for Wave Energy Converter according to Load Conditions. *W. Jung*[1], J. Park[1], S. Kim[1], K. Kim[2], J. Park[2], K. Shin[3] and J. Choi[1] *1. Chungnam National University, Daejeon, The Republic of Korea; 2. Korea Research Institute of Ships and Ocean Engineering, Daejeon, The Republic of Korea; 3. Changwon National University, Changwon, The Republic of Korea*

Multi pole permanent magnet synchronous generator(PMSG), suitable for a wide range of high-speed operations, feature a simple magnetic circuit design, fast response, and linear torque-current and speed-voltage characteristics. However, variability in generation conditions and output limits renewable energy generation. Therefore, analyzing the electromagnetic and loss characteristics of the generator in different regions is essential. This study investigated the electromagnetic loss characteristics of PMSG under AC and DC load. The DC and AC loads produced square-wave and sinusoidal currents, respectively; the harmonics of the current differed by load type, necessitating an accurate core loss analysis considering the current harmonics. The Steinmetz equation was modified to include the ideal eddy current loss coefficient. The loss coefficients were derived by curve fitting the core loss of electrical steel at different frequencies. The magnetic field behavior in different regions was analyzed to determine core loss. Fig. 1(a) shows the 2D finite element method(FEM) analysis model. Fig. 1(b) shows the experimental setup, including DC and AC load banks and generator. Fig. 1(c) show the curve-fitting applied to manufacturer-provided core loss data, used to derive hysteresis, eddy-current, and ideal eddy-current loss coefficients. Fig. 1(d) show the distribution of core loss for each load condition. Fig. 2(a) and 2(b) show circuit diagrams and current waveforms for AC and DC load, respectively. Fig. 2(c) show the magnetic field behavior during AC load. The fields were classified into alternating and rotational magnetic fields to derive more accurate core loss values. The experimental data, FEM results, and values derived from the modified Steinmetz equation under different load conditions were compared to validate the study's accuracy (Fig. 2(d)). More detailed data and discussions will be presented in the full paper.

[1] Tae-chul Jeong, Won-Ho Kim, Mi-Jung Kim, IEEETransactions on magnetics, Vol. 49, No. 5, 2343, (2013) [2] Jong-Hyeon Woo, Tae-Kyoung Bang, Hoon-Ki Lee, IEEE Trans. Magn., Vol. 57, No. 2, pp. 1-5, (2021) [3] Sang-Hyeop Kim, Jong-Hyeon Woo, Yong-Joo Kim, AIP Adcances, Vol. 14, No. 1, 015322, (2024) [4] D. Gerada, A. Mebarki, N. L. Brown, IEEE Transactions on Industrial Electronics Vol. 61 No. 6, pp. 2946–2959, (2014) [5] G. Bramerdorfer, J. A. Tapia, J. J. Pyrhönen, IEEE Transactions on Industrial Electronics Vol. 65, No. 10, pp. 7672–7684, (2018)

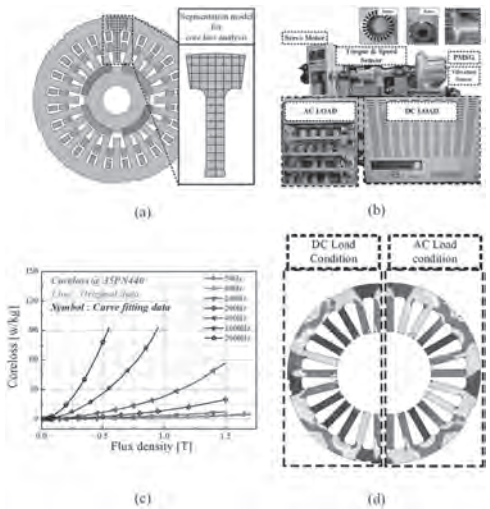

Fig.1 (a) 2D FEM model, (b) experimental setup, (c) core loss data curve-fitting for 35PN250, (d) core loss distribution of DC and AC load conditions.

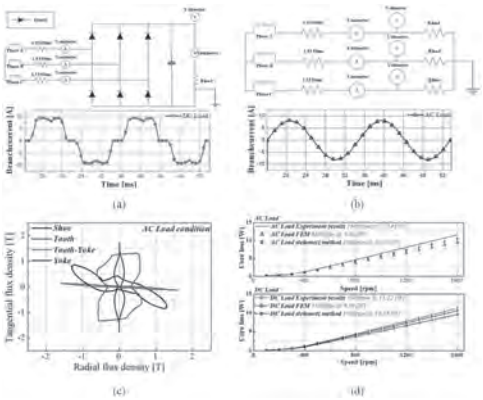

Fig.2 Load circuit and current: (a) DC, (b) AC, (c) Magnetic field behavior under AC load, (d) Analysis and experimental results under DC and AC loads.

BV-08. Temperature Performance of SmFe12 Permanent Magnets in Electric Motors. *H. Baldino*[2], D. Hedlund[1] and P. Kulik[1] *1. Electrical and Computer Engineering, University of Central Florida, Orlando, FL, United States; 2. Material Science and Engineering, University of Central Florida, Orlando, FL, United States*

Rare-earth-lean Sm1Fe12 (1-12) based compounds demonstrate high-temperature performance that surpasses that of NdFeB permanent magnets. In this work, the performance of various 1-12 compositions in an electric motor are investigated with COMSOL, assuming ideal conditions, and compared to motors simulated with NdFeB and ferrite magnets. Results show that 1-12 magnets have better output power at higher rotational speeds compared to other permanent magnets. Magnetic, electrical, and thermodynamic data were collected from existing literature sources for 1-12 materials in addition to data collected from sputtered thick film samples. Simplifications for the coercivity and its temperature response in the 1-12 system were done by extrapolating from the anisotropy field and $4\pi M_s$ providing an estimate in the range of 1 to 2 Tesla. The efficiency, the output power, and the torque produced by an electric motor designed with and without cooling under currents between 0.5 and 10 A were simulated. Results show that a similar efficiency is achieved between 1-12 and NdFeB magnets when cooled to room temperature. However, the higher Curie temperature of the 1-12 magnets lead to higher efficiency, total output power, and torque when simulated at operating temperatures (see Fig. 1 for an example at 5A). In conclusion, electric motors designed with 1-12 magnets at their core show better temperature dependent performance than ones designed with NdFeB. Future work is needed to validate these simulation results with bulk 1-12 magnets produced with adequate coercivity to understand its response with temperature.

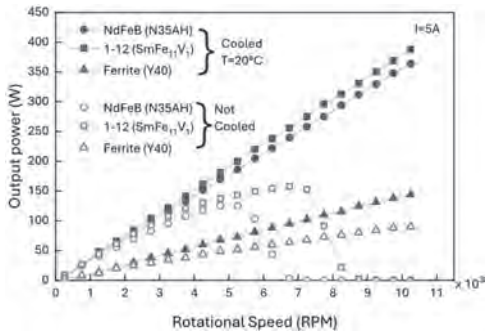

Fig.1 Output power of simulated electric motor (I=5A) with various permanent magnets of the same size under cooled (solid lines), to 20 °C, and uncooled (dashed lines) conditions. SmFe11V shows the same output power profile as the N35AH (highest temperature performing NdFeB magnet) when maintained at room temperature. With no cooling the higher temperature resistance of the 1-12 magnet shows a better power output at higher RPM. The ferrites strong electrical resistivity and low thermal conductivity leads it to retain a linear power gain to high RPM but underperforms in total power output compared to the 1-12 and NdFeB designs.

CELESTIN D

Session

EVENING SESSION: SCIENCE AND HISTORY OF ROCK AND ROLL

Amal El-Ghazaly, Co-Chair
Cornell University, Ithaca, NY, United States
Vivek Amin, Co-Chair
Indiana University
Matt Sakakeeny, Co-Chair
Tulane University

Session CA
TOPOLOGICAL THERMOELECTRICS: UTILIZING TOPOLOGY AND SPIN FOR NEXT-GENERATION ENERGY CONVERSION

Sarah Watzman, Chair
University of Cincinnati, Cincinnati, OH, United States

INVITED PAPERS

CA-01. Topology for energy efficient spintronics and energy conversion. *C. Felser*[1] *1. Topological Quantum Chemistry, Max Planck Institute Chemical Physics of Solids, Dresden, Germany*

Topology, a mathematical concept, recently became a hot and truly transdisciplinary topic in condensed matter physics, solid state chemistry and materials science. All 200 000 inorganic materials were recently classified into trivial and topological materials, such as topological insulators, Dirac, Weyl and nodal-line semimetals, and topological metals [1]. More than 25% of all materials host topological bands around the Fermi energy. Beyond the single particle picture, we have identified first antiferromagnetic topological materials [2]. Experimentally, we have realized ferromagnetic materials, examples are Co_2MnGa and $Co_3Sn_2S_2$. Surprisingly all crossings in the band structure of ferromagnets are Weyl nodes or nodal lines [3]. Mn_3Sn and $YbMnBi_2$ are examples of non collinear antiferromagnetic Weyl semimetals, which show giant values for the anomalous Hall and Nernst effect [4]. Kagome lattice even beyond $Co_3Sn_2S_2$ and Mn_3Sn have tunable properties based on the unique band structure with van Hove singularities, Weal points and flatbands. There is a large class of materials of the composition 1:6:6 (RET_6Z_6 RE=rare earth, T=transition metal, Z=main group metal), which allows a flexible design of the electronic structure additional to charge density wave instabilities. In the context of real space topology, skyrmions and antiskyrmions are a possible new direction for new data storage [5]. Our goal is to identify new quantum-materials for highly efficient spintronics, quantum computing and energy conversion.

1 Bradlyn *et al.*, Nature 547, 298, (2017), Vergniory, *et al.,* Nature 566, 480 (2019), Vergniory, *et al*., Science (2022). 2. Xu et al. Nature 586, 702 (2020). 3. Liu, et al. Nature Physics 14, 1125 (2018), Belopolski, et al., Science 365, 1278 (2019), Guin, et al. Advanced Materials 31 (2019) 1806622, Liu, et al., Science 365, 1282 (2019), Morali, et al., Science 365, 1286 (2019) 4. Pan, et al., Nature Materials 21 (2022) 203, Kübler and Felser, EPL 120 (2017) 47002 and EPL108 (2014) 67001, Nayak, et al. Science Advances 2 (2016) e1501870 5. Nayak et al., Nature 548 (2017) 561

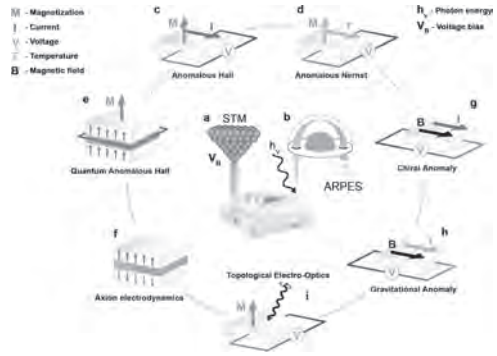

CA-02. Withdrawn

CA-03. Thermoelectric Properties of Thin Films of Cadmium Arsenide. *S. Stemmer*[1] *1. University of California, Santa Barbara, Santa Barbara, CA, United States*

Bulk cadmium arsenide (Cd_3As_2) hosts topologically non-trivial bands in its electronic structure. In thin films, it can be engineered to a variety of new topological phases. In this talk, we will discuss different types of topological phases observed in high-quality quantum wells of Cd_3As_2, which we grow by molecular beam epitaxy. We show that these phases can be identified via Landau level spectroscopy and their quantum Hall effects. We also discuss measurements of the Seebeck coefficient using gated, thermoelectric Hall bars with resistive heaters and thermistors. We discuss the interplay of topology, electron correlations, and spin-orbit coupling that gives rise to unusually large thermoelectric effects both with and without externally applied magnetic fields.

CA-04. Record-Breaking Nernst Thermopower and Thermal Hall Angle in YbMnBi2. J. Wen[1], K. Manna[2,3], D. Vu[4,5], Y. Pan[2,6], C. Felser[2], B. Skinner[7] and *J.P. Heremans*[1,4,7] *1. Department of Materials Science and Engineering, The Ohio State University, Columbus, OH, United States; 2. Max Planck Institute for Chemical Physics of Solids, Dresden, Germany; 3. Department of Physics, Indian Institute of Technology Delhi, New Delhi, India; 4. Department of Mechanical and Aerospace Engineering, The Ohio State University, Columbus, OH, United States; 5. Department of Applied Physics, Yale University, New Haven, CT, United States; 6. Center of Quantum Materials & Devices, Chongqing University, Chongqing, China; 7. Department of Physics, The Ohio State University, Columbus, OH, United States*

Transverse thermoelectrics (TE) simplify the construction of TE modules. They can be based on various principles, such as on materials that have Seebeck coefficients of different polarities along different crystallographic direction or the spin-Seebeck effect or the Nernst effect. Nernst effects are typically maximized in semimetals, where they are labeled the "ordinary Nernst effet (ONE), and in magnetic or topological materials where they are due to the effect of the Berry curvature, the "anomalous Nernst effect (ANE)". We demonstrate that the magnetic Weyl semimetal $YbMnBi_2$, characterized by low Hall density and a chemical potential near Weyl points, exhibits the highest Nernst thermopower (Sxy) dominated by ANE among magnetic materials. Specifically, Syx reaches approximately 110 μV K-1 at 254 K under an applied magnetic field ($5\ T \leq |\mu_0 H| \leq 9\ T$ along the spin canting direction). This high thermopower arises from the interplay of contributions from filled electron bands, topologically induced large Hall conductivity, and substantial resistivity anisotropy. Additionally, a significant thermal Hall angle of $0.02 < Grad_y\ (T) / Grad_x\ (T) < 0.06$ at 9T was observed over the temperature range of 40 K to 310 K.

CA-05. Unusual transport properties of TiSe2 and GeTe for Solid-State Cooling. *M. Zebarjadi*[1], S. Akhanda[1] and S. Das[1] *1. University of Virginia, Charlottesville, VA, United States*

Topological semimetals are demonstrated promising for thermoelectric, thermomagnetic, and recently Thomson solid-state cooling. In this talk, I will summarize some of the relevant theoretical and experimental work on a series of materials with an emphasis on TiSe2 and GeTe. Single crystals of 1T-TiSe2 were studied focusing on their thermoelectric and thermomagnetic properties around the charge density wave (CDW) transition (≈ 200 K). The abrupt Fermi surface reconstruction associated with this transition leads to an exceptional peak in the Thomson coefficient (τ) of 450 $\mu V.K^{-1}$ at 184 K, surpassing the Seebeck coefficient (S). Thermally-induced phase changes were shown in the past to result in sharp changes in the Seebeck coefficient and therefore large Thomson coefficients ($\tau = TdS/dT$, T is temperature). These large Thomson values, however, have been limited to a narrow temperature range. Here, we show that 1T-TiSe2 exhibits a remarkably broad temperature range (170 – 400 K) with a Thomson coefficient exceeding 100 $\mu V.K^{-1}$, a characteristic highly desirable for the development of practical Thomson coolers with extended operational ranges. Additionally, the Nernst coefficient exhibits an unusual temperature dependence, increasing with temperature in the normal phase, which we attribute to bipolar conduction effects. The combination of solid-solid pure electronic phase transition to a semimetallic phase with bipolar transport is identified as responsible for the unusual Nernst trend and the unusually large Thomson coefficient over a broad temperature range. On the second part of the talk, I will discuss our findings relevant to GeTe-alloys and the relations between chemical bonding and physical properties. We observe that Pb-doped GeTe exhibits low lattice thermal conductivity due to weak p-p orbital interactions, whereas In-doping boosts lattice thermal conductivity by reinforcing the chemical bonds, as elucidated by Crystal Orbital Hamilton Population (COHP) analysis. Weak s-p interactions in Bi-, Sb-, and Pb-doped GeTe, and strong s-p interactions in In-doped GeTe compared to the pure GeTe, as probed by Projected Density of State (PDOS), is correlated to the experimentally observed high power factor and enhanced zT in Bi, Sb, and Pb doping in contrast to In-doping.

Session CB
WHEN MAGNONS MEET QUANTUM SPINS

Gianluca Gubbiotti, Chair
IOM-CNR, Perugia, Italy

INVITED PAPERS

CB-01. Quantum magnonics via color centers. *Y. Tserkovnyak*[1]
1. Physics and Astronomy, University of California, Los Angeles, Los Angeles, CA, United States

I will review our recent work that aims at harvesting quantum fluctuations of magnetic systems, with both quantum information and many-body physics in mind. Focusing on magnons as building blocks of collective spin dynamics in magnetic insulators, I will discuss the prospects of their scalable integration with proximal color centers, such as nitrogen-vacancy impurities, using the latter as either quantum sensors, which can be operated in a range of different physical modalities, or qbits, whose entangled dynamics is governed by the common dissipative magnonic environment. Recent experiments on using color centers as spectrally-resolved sensors of magnetic dynamics demonstrate their strong coupling with a range of 2D materials. Inspired in part by the ideas from quantum optics, we are now pursuing the inverse functionality: imprinting collective noise of the tunable environment onto emergent many-body properties of color-center ensembles.

CB-03. Using spins and microwaves to probe an ultra-low damping organic-based ferrimagnet. *G. Fuchs*[1] *1. Cornell University, Ithaca, NY, United States*

As quantum technologies emerge, there is a growing realization that coupling distinct quantum systems into hybrid platforms is interesting for combining the best physical characteristics. Although magnetic materials are typically too lossy for quantum applications, the loss in magnetic insulators has no well-understood lower limit at cryogenic temperatures. In this presentation I will discuss progress integrating the ultra-low damping organic-based ferrimagnet vanadium tetryacyanoethylene, $V[TCNE]_x$, into hybrid magnonic systems. I will focus on two experiments. First, we strongly couple a $V[TCNE]_x$ microstructure to a superconducting microwave resonator. This hybrid magnonic system has a cooperativity exceeding 1000 at 0.44 K with spin wave mode linewidths as narrow as 1 MHz [1]. Second, following our theoretical efforts to understand strong coupling between diamond nitrogen-vacancy (NV) spins and $V[TCNE]_x$ magnons [2], we fabricate $V[TCNE]_x$ microdisks on diamond and use NV center spins to study their magnetic excitations. We demonstrate an ferromagnetic resonance echo protocol to study $V[TCNE]_x$ magnons at arbitrary magnetic fields, even when the two spin systems are not in resonance [3].

[1] Q. Xu *et al.*, Advanced Science 11, 2310032 (2024). [2] D. R. Candido, G. D. Fuchs, E. Johnston-Halperin, and M. E. Flatté, Materials for Quantum Technology 1, 011001 (2020). [3] B. A. McCullian *et al*., in preparation (2024).

CB-04. Withdrawn

CB-05. Nonlinear spin dynamics in magnon/nitrogen-vacancy hybrid system. *Z. Hu*[1], Z. He[1], Q. Wang[1], C. Chou[1], J. Hou[1] and L. Liu[1]
1. Massachusetts Institute of Technology, Cambridge, MA, United States

Nitrogen-vacancy (NV) centers have been traditionally utilized as sensors for probing low frequency magnetic fields, which have limited capabilities in detecting spin wave dynamics (around GHz). Expanding quantum spin sensing beyond the conventional linear regime could broaden the frequency range, opening up opportunities for various microwave and quantum applications [1-2]. Recently we demonstrate that the intrinsic nonlinear dynamics in NV spins can facilitate magnetic sensing across a wide spectrum [3], with various multi-photon magnetic resonance achieved. Furthermore, we show that this capability can be further enhanced by exploiting the nonlinear spin dynamics in hybrid systems formed by NV and ferri- or ferro-magnetic thin films [4]. By studying the frequency mixing effect in the hybrid NV/magnon systems, we reveal that magnons not only amplify the intensity of nonlinear resonance signals intrinsic to NV spins, but also enable novel frequency mixings through parametric pumping and nonlinear magnon scatterings. The insights into magnetic nonlinearities in hybrid NV/magnon system establish them as a promising candidate for advanced magnetic sensing with a broad frequency range, particularly meaningful for nanoscale, dynamical, and non-invasive material characterization.

[1] G. Wang *et al.*, Phys. Rev. X 12, 021061 (2022) [2] J. J. Carmiggelt *et al.*, Nat. Commun. 14, 490 (2023) [3] Z. Hu *et al.*, Phys. Rev. Applied 21, 044057 (2024) [4] Z. Hu *et al.*, arXiv:2405.02474

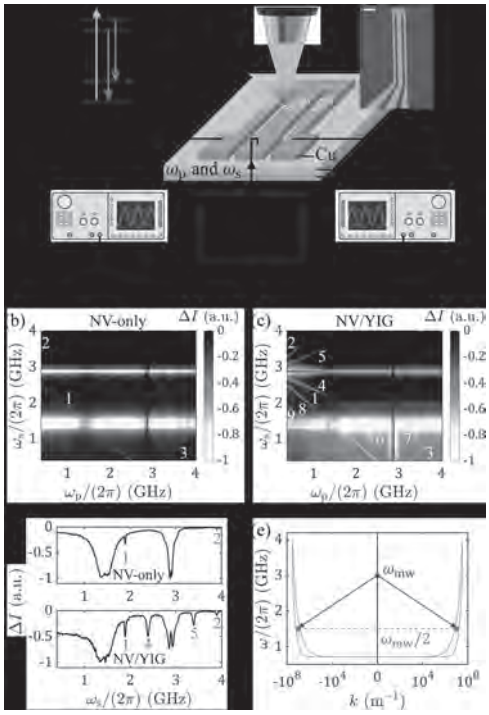

(a) Experimental scheme for nonlinear magnetic sensing in a hybrid NV/YIG system. (b) Resonance spectra of an NV-only system. (c) Resonance spectra of the NV/YIG system. (d) Top and bottom show single cut in (b) and (c), respectively. (e) Illustration of parametric pumping process inside YIG.

Session CC
2D SPINTRONICS AND TOPOLOGICAL MATERIALS II

Guoqiang Yu, Chair
Chinese Academy of Sciences, Beijing, China

INVITED PAPER

CC-01. Proximity Phenomena in Van der Waals Heterostructures.
J. Svetlik[2], T. Guillet[2], V. Zatko[2], F. Herling[2], R. Galceran[3], W. Savero Torres[2], L. Camosi[2], M. Jamet[4], F. Bonell[4], J. Sierra[2] and *S.O. Valenzuela*[1,2]
1. ICREA, Barcelona, Spain; 2. ICN2 - Catalan Institute of Nanoscience and Nanotechnology, Bellaterra, Spain; 3. University of Barcelona, Barcelona, Spain; 4. SPINTEC, Grenoble, France

Van der Waals (vdW) heterostructures, including those incorporating topological insulators (TIs) from the Bi_2Te_3 family of materials, have transformative potential for magnetic random-access memory applications [1]. Furthermore, the atomically thin nature of vdW materials allows for property design through proximity effects, stemming from short-range interactions [2]. This designer approach is particularly appealing for spintronics devices, which harness functionalities from thin layers of magnetic and non-magnetic materials and their interfaces [1,2]. In this presentation, I will explain how to identify proximity effects in graphene by means of spin transport dynamics, such as spin relaxation anisotropy [3] and charge-to-spin interconversion [4]. I will discuss the significance of crystal symmetry and how systems with reduced symmetry can lead to unconventional charge-to-spin conversion components, as well as methods to determine their origins [5]. Additionally, I will highlight the importance of boundary states and preserving the quality of the TI/ferromagnet (FM) interface to maximize spin orbit torques (SOT). I will demonstrate that introducing a non-magnetic metallic [6] or graphene [7] interlayer between the TI and FM, when FM is a transition metal, can significantly alter the nature and increase the efficiency of the SOTs [6,7]. I will further show that similar enhancements are observed with sharp interfaces between the TI and a vdW FM [8]. Acknowledgements: This research was supported by MICIU/AEI/10.13039/501100011033 through Grant No. PID2022-143162OB-I00.

[1] H. Yang et al., *Nature* 606, 663 (2022) [2] J. F. Sierra *et al*., *Nature Nano*. 16, 856–868 (2021) [3] L. A. Benítez *et al*., *Nature Phys.* 14 (2018); *APL Materials* 7, 120701 (2019) [4] L. A. Benítez *et al*., *Nature Mater.* 19, 170 (2020) [5] L. Camosi *et al.*, *2D Mater*. 9, 035014 (2022) [6] F. Bonell *et al*., *Nano Lett.* 20, 5893 (2020) [7] R. Galceran *et al*., *Adv. Mater. Interfaces* 9, 2201997 (2022) [8] T. Guillet *et al., Nano Lett.* 24, 822 (2024)

CONTRIBUTED PAPERS

CC-02. Withdrawn

CC-03. Thickness-Dependent Behavior of Magnetic Domains in van der Waals Fe_3GeTe_2 during Magnetization Reversal.
J. Garland[1,2], J. Fullerton[2], P. Cai[3], Y. Li[2], E. Santos[3], C. Phatak[2,4] and A. Petford-Long[2,4]
1. Applied Physics Program, Northwestern University, Evanston, IL, United States; 2. Materials Science Division, Argonne National Laboratory, Lemont, IL, United States; 3. School of Physics and Astronomy, University of Edinburgh, Edinburgh, United Kingdom; 4. Materials Science and Engineering Department, Northwestern University, Evanston, IL, United States

The van der Waals (vdW) ferromagnet Fe_3GeTe_2 (FGT) has attracted interest for studying 2D magnetism due to its relatively high Curie temperature (200 - 220 K) [1] and demonstrated ability to host Bloch- and Néel-type skyrmions [2,3]. Characterization of emerging magnetic vdW materials is

essential for understanding fundamental magnetic behavior and achieving precise control of magnetic domains for potential applications in data storage and magnetic sensing. In these materials, external stimuli such as applied magnetic field and parameters such as sample thickness affect the intrinsic energy terms governing the formation and behavior of domains and nontrivial topological spin textures. Lorentz transmission electron microscopy (LTEM) enables high-resolution observation of magnetic domains while varying key conditions such as temperature and magnetic field. In this work, we use in-situ cryo-LTEM to image the field-driven evolution of magnetic domains in an exfoliated FGT flake with thickness from 20-100 nm. First, we apply a field-cooling procedure to nucleate Néel skyrmions, then we apply field in the negative direction to study the magnetization reversal. We observe the formation of skyrmion lattices and their growth into unique faceted domain states. In thicker regions, initial skyrmion lattices are denser with smaller radii, and stronger fields are necessary to increase domain size and reach uniform reversal. Micromagnetic simulations closely reproduce the spin-reversal effect, highlighting the interplay between anisotropy, magnetic field, and field-cooling conditions. Our systematic study demonstrates high control of skyrmion size, density, and transitions to novel phases by tuning applied field and sample thickness of FGT, as well as contributing to a better understanding of the governing energy terms during magnetization reversal. This work was supported by the U.S. Department of Energy (DOE), Office of Science, Office of Basic Energy Sciences (BES), Materials Sciences and Engineering Division. Use of the Center for Nanoscale Materials, an Office of Science user facility, was supported by the U.S. DOE, Office of Science, BES, under Contract No. DE-AC02-06CH11357.

[1] H. J. Deiseroth, K. Aleksandrov, C. Reiner, et al., Eur. J. Inorg. Chem., Vol. 2006, p.1561-1567 (2006). [2] B. Ding, Z. Li, G. Xu, et al., Nano Lett., Vol. 20, p.868-873 (2020). [3] C. Liu, J. Jiang, C. Zhang, et al., Adv. Sci., Vol. 10, 2303443 (2023).

CC-04. Origin and Thermal Evolution of Exchange Bias in $MnPS_3/Fe_3GeTe_2$ antiferromagnetic/ferromagnetic van der Waals Heterostructures. *A. Puthirath Balan*[1], A. Kumar[1], P. Reiser[2], J. Vas[3], T. Denneulin[3], D. Le[4], T. Saunderson[1,10], M. Tschudin[2], C. Pellet-Mary[2], D. Dutta[2], C. Schrader[2], T. Scholz[5], J. Geuchies[6], S. Fu[6], H. Wang[6], A. Bonanni[7], B. Lotsch[5], U. Nowak[8], G. Jakob[1], J.D. Gayles[4], A. Kovács[3], R.E. Dunin-Borkowski[3], P. Maletinsky[2] and M. Kläui[1,9] *1. Institute of Physics, Johannes Gutenberg University Mainz, Mainz, Germany; 2. Department of Physics, University of Basel, Basel, Switzerland; 3. Ernst Ruska-Centre for Microscopy and Spectroscopy with Electrons and Peter Grünberg Institute, Forschungszentrum Jülich, Julich, Germany; 4. Department of Physics, University of South Florida, Florida, FL, United States; 5. Max Planck Institute for Solid State Research, Stuttgart, Germany; 6. Max Planck Institute for Polymer Research Mainz, Mainz, Germany; 7. Johannes Kepler University Linz, Linz, Austria; 8. Department of Physics, University of Konstanz, Konstanz, Germany; 9. Centre for Quantum Spintronics, Department of Physics, Norwegian University of Science and Technology, Trondheim, Norway; 10. Peter Grünberg Institut and Institute for Advanced Simulation, Forschungszentrum Jülich and JARA, Julich, Germany*

Van der Waals materials, with their layered structures, provide an excellent platform to study exchange bias, but controlling it effectively remains challenging. Here we investigate exchange bias in $MnPS_3/Fe_3GeTe_2$ van der Waals heterostructures, showing nearly a 1000% variation through thermal cycling [1]. Despite the compensated interfacial spin configuration of $MnPS_3$ [2,3], a 170 mT exchange bias is observed at 5 K, one of the largest in van der Waals heterostructures. We find that this significant exchange bias is linked to weak ferromagnetic ordering in $MnPS_3$ below 40 K [4,5]. The tunability of exchange bias during thermal cycling is associated with amorphization and changes in the van der Waals gap during field cooling. Detailed interface analysis reveals atom migration between layers, forming amorphous regions. This highlights the need to characterize interfaces in van der Waals heterostructures as they are more complex than generally expected.

[1] A. Puthirath Balan, A. Kumar, M. Kläui, Advanced Materials, 2403685 (2024). [2] P. A. Joy, S. Vasudevan, Physical Review B, 46, 5425 (1992). [3] G. Long, H. Henck, A. F. Morpurgo, Nano Letters, 20, 2452 (2020). [4] H. Han, H. Lin, H. Li, Physical Review B, 107, 075423 (2023). [5] S. Chaudhuri, C. N. Kuo, J. G. Lin, Physical Review B, 106, 094416 (2022).

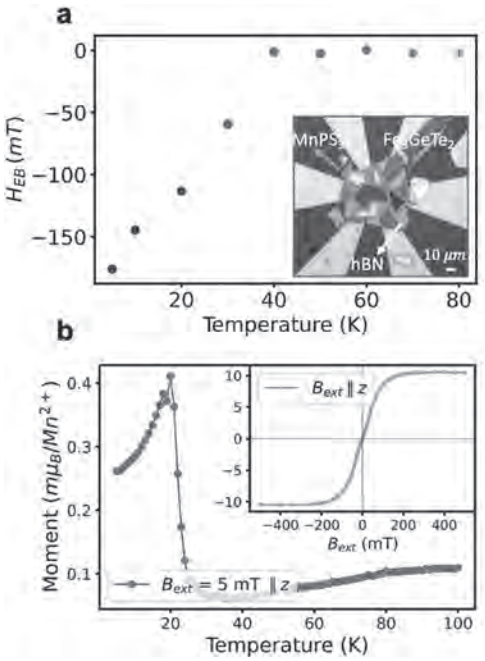

Fig.1 a. The exchange bias (H_{EB}) as a function of temperature observed in $hBN/MnPS_3/Fe_3GeTe_3$ heterostructures (inset) reveals the blocking temperature of $MnPS_3$ to be nearly 40 K, b. The *M* versus *T* curve measured for the bulk $MnPS_3$ crystal in an OOP orientation indicates a clear onset of magnetization below 40 K that coincides with that of H_{EB} *vs. T* curve, and the inset displays an isothermal *M* versus *H* curve at 5 K.

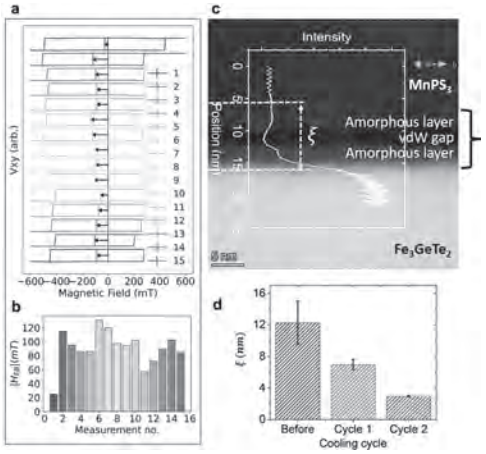

Fig. 2 a. The AHE hysteresis loops measured after each field-cooling cycle consecutively for 15 times, b. The magnitude of EB varies between 25 and 132 mT, c. A high-resolution STEM image of the $MnPS_3/Fe_3GeTe_2$ interface at room temperature, and d. A bar graph summarizing the observed modification of intercrystalline distances, before and after two consecutive thermal cycles.

CC-05. Gilbert damping in large-area CVD monolayer MoS_2/permalloy heterostructures. *H. De Libero*[1], E. Chalmers[1], N. Natera Cordero[1], A. Strudwick[1], I. Vera Marun[1] and T. Thomson[1] *1. University of Manchester, Manchester, United Kingdom*

The understanding of Gilbert damping in NM/FM heterostructures is critical for the advancement of next-generation spintronic devices [1]. While damping mechanisms in conventional NM/FM heterostructures are well-studied, 2D-material/FM heterostructures are an emerging field. Transition metal dichalcogenides (TMDs), notable for their high spin-orbit coupling and charge-to-spin conversion capabilities, have garnered significant interest for spintronic applications [2] and advances in fabricating large-area TMDs demonstrate a viable route towards applications [3]. However, key mechanisms in charge-spin conversion and spin relaxation need further study. Here, we report on Gilbert damping in large-area CVD-grown monolayer MoS_2/permalloy heterostructures using broadband VNA-FMR spectroscopy. Permalloy (NiFe) was deposited on MoS_2 via DC magnetron sputtering, with monolayer MoS_2 confirmed through x-ray reflectometry and Raman spectroscopy. By varying the NiFe thickness, we explored both bulk and surface contributions to Gilbert damping [4]. Notably, our results show no enhancement in effective damping due to spin pumping. However, the bulk damping contribution to the effective damping in NiFe increased when interfaced with monolayer MoS_2 compared to SiO_2 (Fig. 1). X-ray diffraction analysis indicated an increase in (220) and a decrease in (111) crystallite grains for NiFe grown on MoS_2 (Fig. 2), suggesting a link between crystallinity and bulk damping via spin-lattice scattering. Atomic force microscopy also revealed an increased surface roughness for the MoS_2/NiFe samples. Additionally, the reduced variation in Raman linewidth across the sample suggests fewer defects in our MoS_2 samples compared to other studies, correlating with the lack of extrinsic spin-orbit coupling enhanced damping [5]. These results highlight the significance of optimizing ferromagnet growth parameters on large-area TMDs to control Gilbert damping, which is crucial for the development of efficient spintronic devices.

[1] A. A. Serga, A. V. Chumak and B. Hillebrands, J. Phys. D: Appl. Phys., vol. 43, pp. 264002 (2010) [2] S. Husain, R. Gupta, A. Kumar, et. al., Appl. Phys. Rev., vol. 7, pp. 041312 (2020) [3] Y. H. Lee, X. Q. Zhang, W. Zhang, et. al., Adv. Mater., vol. 24 (17), pp. 2320-2325 (2012) [4] Y. Zhao, Q. Song, S. H. Yang, et. al., Scientific Reports, vol. 6 (1), pp. 22890 (2016) [5] R. Bansal, A. Kumar, N. Chowdhury et. al., J. Magn. Magn. Mater., vol. 476, pp. 337-341 (2018)

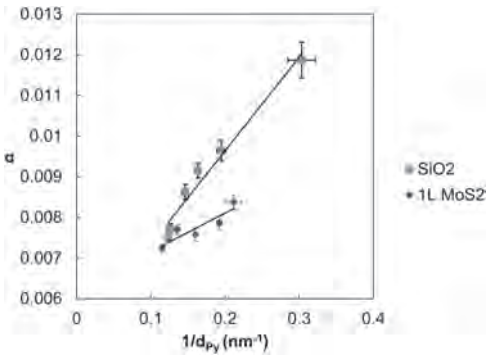

Fig. 1. Gilbert damping against permalloy thickness deposited on SiO_2 and 1L MoS_2.

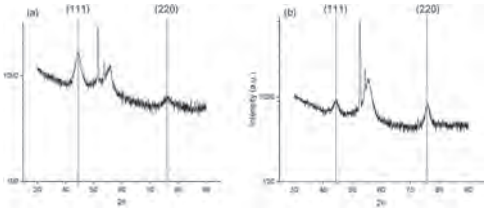

Fig. 2: Grazing-incidence XRD for 8 nm of permalloy grown on SiO_2 (a) and 1L MoS_2 (b). Vertical lines indicate powder diffraction peaks for permalloy.

CC-06. Phase and compositional influence on the magnetic properties of atmospheric chemical vapour deposition (APCVD) grown $FeTe_x$ ($1 \le x \le 2$) system. *B.P. Jena*[1] and S. Chandran[1] *1. Physics, IIT Madras, Chennai, India*

Phase, composition and thickness control on the magnetic behaviour in two-dimensional (2D) iron-based tellurides provides ample opportunity to tune the magnetic properties for potential application in spintronics [1]–[3]. Here, we report the structural, vibrational and magnetic property studies of iron telluride crystals with varying Te to Fe stoichiometry [$FeTe_x$: $1 \le x \le 2$] synthesized via atmospheric pressure chemical vapour deposition (APCVD) with and without potassium iodide salt as a catalyst. Magnetic property studies are performed on three samples, denoted as FTS1, FTS2 and FTS3, with an average composition of $x \sim 1$, 1.5 and 2, respectively. The composition of three samples is examined using scanning electron microscopy coupled with energy-dispersive X-ray spectroscopy and X-ray photoelectron spectroscopy. Subsequent magnetic characterization is performed through temperature-dependent magnetization measurements and hysteresis loop analyses at 10 K and 300 K, revealing a synergic effect of the magnetic properties with the varying composition of $FeTe_x$. Our findings highlight the impact of the non-stoichiometry composition of x in $FeTe_x$ on the magnetic behaviour compared to the pristine antiferromagnetic FeTe and ferromagnetic $FeTe_2$ systems. This investigation is of paramount importance as the existing literature neglects the non-stoichiometric effect on the magnetic properties. Additionally, the importance of achieving micron-sized $FeTe_x$ crystals using salt-assisted over conventional APCVD process will be addressed. This study emphasizes the importance of non-stoichiometric composition $FeTe_x$ in inducing the ferromagnetic behaviour in an antiferromagnetic system (FeTe), providing a platform to explore spintronics devices by tuning multiple magnetic phases of iron telluride.

[1]. Kang, L.; Ye, C.; Zhao, X, *Nat. Commun*., vol. 11, p. 1–9 (2020) [2]. Petrovic, C.; Capitano, D.; Zhixiang, H, *ACS omega*., vol. 6, p. 10537–10546 (2021) [3]. Wu, H.; Feng, Z.; Pal, A.; *Chem. Mater.*, vol.*33*, p. 4927–4935 (2021)

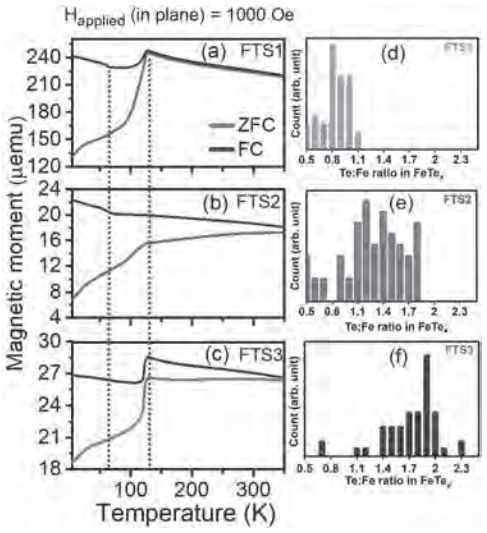

Fig.1 Magnetization (M) versus temperature (T) measurements in the zero field-cooled (ZFC) and field-cooled (FC) conditions performed with an applied field (H) of 1000 Oe in the in-plane direction. (a) FTS1, (b) FTS2 and, (c) FTS3 samples are grown by slow-cooled APCVD process. (d, e, f) Histogram plots show the distribution of composition *x* in $FeTe_x$ crystals for three samples FTS1, FTS2, FTS3, respectively.

CC-07. Room Temperature 2D Ferromagnetism in Chromium doped Transition-Metal Dichalcogenide $PdTe_2$. *S. Cheng*[1], H. Shiu[1], Y. Lai[1], W. Tseng[1], W. Chen[1], T. Chuang[1], D. Wei[1], C. Lue[2] and Y. Hsu[1,3]
1. National Synchrotron Radiation Research Center, Hsinchu, Taiwan; 2. Department of Physics, National Cheng Kung University, Tainan, Taiwan; 3. Department of Photonics, National Cheng Kung University, Tainan, Taiwan

Doping Two-dimensional (2D) materials with impurities or transition metals has emerged as a promising strategy to improve magnetic anisotropy and magnetic exchange interaction strength. Specifically, 2D transition-metal dichalcogenides are of particular interests due to their potential to provide larger magnetic anisotropy. In our study, we utilized argon ion bombardment to create defect vacancies or dangling bonds on the superconductor, palladium ditelluride ($PdTe_2$) surface without destroying its crystallinity. This was followed by the deposition of a chromium layer with a nominal thickness of 2 monolayers. Subsequently, the Cr-doped $PdTe_2$ was annealed at temperatures near its phase transition. Structural changes in the Cr/$PdTe_2$ lattice were characterized using Raman scattering spectroscopy and grazing incident X-ray diffraction. The XRD analyses show that all Cr-doped $PdTe_2$ samples maintain a hexagonal structure, with the *a*-axis (or *c*-axis) lattice constants becoming shorter due to the smaller ionic size of Cr ions compared to Pd and Te ions. We observed changes in the Raman spectra upon doping with Cr ions. Figure 1(a) shows the Raman spectra of pristine $PdTe_2$ crystal, which displays two distinct modes: one at 55 cm^{-1} (E_g, in-plane) and another at 122 cm^{-1} (A_{1g}, out-of-plane). After doping Cr ions into $PdTe_2$, three new Raman peaks appear at 71 cm^{-1}, 110 cm^{-1} and 137 cm^{-1}. These Raman results are consistent with previously reported data for $CrTe_2$ powder. Additionally, our magnetic experimental results further reveal a significant ferromagnetic response in $PdTe_2$ material at room temperature as the Cr doping concentration increase (as depicted in Figure 2). Based on the mentioned findings, we have successfully developed a method to induce room-temperature ferromagnetism in 1T-$PdTe_2$ single crystals. The detail results will be presented in our forthcoming reports.

J. Qiao et al., *J. Mater. Chem. C*, 2023, 11, 13438.

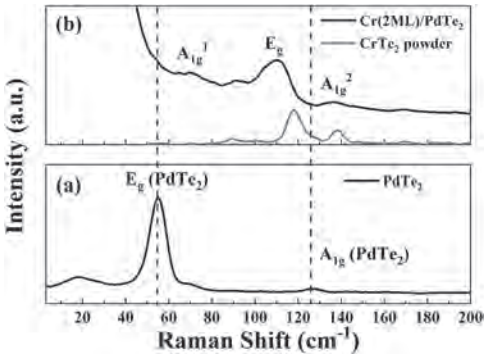

Raman Spectra of (a) pristine $PdTe_2$ single crystal and (b) Cr(2ML)/ $PdTe_2$ and $CrTe_2$ powder.

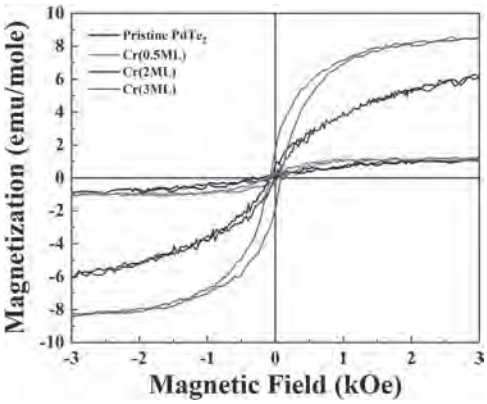

M-H curves of pristine $PdTe_2$ and Cr-doped $PdTe_2$ samples were measured at room temperature under an in-plane magnetic field.

INVITED PAPER

CC-08. *C*-paired spin-valley locking in layered van der Waals antiferromagnetic materials. *J. Liu*[1] *1. Physics, Hong Kong University of Science and Technology, Kowloon, Hong Kong*

Antiferromagnetic (AFM) materials hold great promises in the next-generation information technology due to the zero stray field and ultra-fast dynamics, and how to detect and manipulate the AFM orders been becoming one of the bottlenecks. In this talk, I will present our works about our recently proposed new type of spin-valley locking (SVL), named C-paired SVL, which enables both static and dynamical controls of AFMs to realize a multifunctional antiferromagnetic material. Compared to the spin structure of 2D materials and the surface states of topological materials, C-paired SVL is enabled by a crystal symmetry instead of the time-reversal symmetry, and the large spin splitting is from the exchange coupling between itinerant electrons and local magnetic moments instead of spin-orbit coupling. Thus, both spin and valley can be accessed by simply breaking the corresponding crystal symmetry. Typically, one can use a strain field to induce a large net valley polarization/ magnetization and use a charge current to generate a large noncollinear spin current. Based on symmetry analysis and first-principles calculations, we also predicted C-paired SVL can exist in layered van der Wasls materials V_2Se_2O and V_2Te_2O and also in experimentally verified 3D AFM materials MnTe, RuO_2, MnF_2, $NaOsO_3$, $LaMnO_3$, $LaCrO_3$, $TbFeO_3$, FeF_2, CoF_2, NiF_2, etc. All these predicted phenomena have been confirmed in recent experiments in RbV_2Te_2O, RuO_2 and MnTe [*Nat. Commun. 12, 2846 (2021)*]. These properties can also help us realize the electric readout and 180° deterministic switching of the Néel order, which has also been confirmed in our recent experimental work [*Sci. Adv. 10, eadn0479 (2024)*]. Due to the unique properties distinct from conventional ferromagnet and antiferromagnet,

these materials were proposed to belong to a third type of magnets, named altermagnet in 2022 [*Phys. Rev. X 12, 040501 (2022)*].

1. Fayuan Zhang, Xingkai Cheng, Zhouyi Yin, et al. Crystal-symmetry-paired spin-valley locking in a layered room-temperature antiferromagnet (under preparation) 2. Lei Han, Xizhi Fu, Rui Peng, et al. Sci. Adv. 10, eadn0479 (2024) 3. Haiyang Ma, Mengli Hu, Nana Li, et al. Multifunctional Antiferromagnetic Materials with Giant Piezomagnetism and Noncollinear Spin Current, Nat. Commun. 12, 2846 (2021)

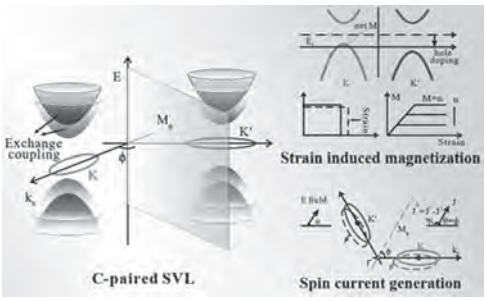

C-paired spin-valley or spin-momentum locking and the piezomagnetism and noncollinear spin current.

CONTRIBUTED PAPERS

CC-09. Valley-spin-polarization of MoS_2 monolayer induced by ferromagnetic order of an antiferromagnet. C. Chan[1] and *C. Yang*[1]
1. Materials Science and Engineering, National Yang Ming Chiao Tung University, Hsinchu, Taiwan

Transition metal dichalcogenides (TMDs) monolayers exhibit unique valleytronics properties due to the dependency of the coupled valley and spin state at the hexagonal corner of the first Brillouin zone. Precisely controlling valley spin-polarization via manipulating the electron population enables its application in valley-based memory or quantum technologies. This study uncovered the uncompensated spins of the antiferromagnetic oxide (NiO) serving as the ferromagnetic (FM) order to induce valley spin-polarization in molybdenum disulfide (MoS_2) monolayers via the magnetic proximity effect (MPE). A spin-resolved photoluminescence spectroscopy (SR-PL) was employed to observe MoS_2, where the spin-polarized trions appear to be responsible for the MPE, leading to a valley magnetism. Results indicate that local FM order from the uncompensated surface of NiO could successfully induce significant valley spin-polarization in MoS_2 with the depolarization temperature approximately at 100 K, which is relatively high compared to related literature. This study reveals new perspectives and potential of AFM materials in the field of exchange-coupled van der Waals heterostructures.

1. Y. Liu *et al.,* Valleytronics in transition metal dichalcogenides materials. *Nano Research 12*, 2695-2711 (2019). 2. C. Y. Yang *et al.,* Phase-driven magneto-electrical characteristics of single-layer MoS_2. *Nanoscale8*,5627-5633(2016).3.K.F.Maketal.,Controlofvalleypolarization in monolayer MoS_2 by optical helicity. *Nat Nanotechnol 7*, 494-498 (2012). 4. G. Kioseoglou *et al.,* Valley polarization and intervalley scattering in monolayer MoS_2. *Applied Physics Letters 101, 221907* (2012).

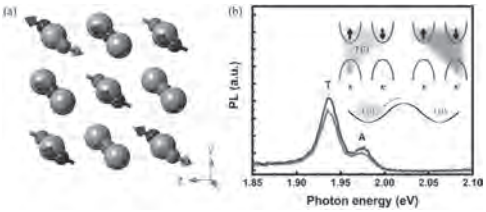

CC-10. Enhanced Controllability of Valley Polarization in ML-WSe_2 Using the Single-Contact Method. *J. Siao*[1], H. Lin[1], T. Lin[1], Y. Chu[1] and M. Lin[1,2,3] *1. Physics, National Taiwan University, Taipei, Taiwan; 2. Atomic and Molecular Sciences, Academia Sinica, Taipei, Taiwan; 3. Research Center for Applied Sciences, Academia Sinica, Taipei, Taiwan*

Manipulation of valley pseudospins in monolayer transition metal dichalcogenides (ML-TMDs) has garnered significant attention for its potential in valleytronics. However, achieving controllable valley polarization (VP) using circularly polarized photoluminescence (CPPL) remains challenging at high temperatures and with off-resonance excitation. To address this, we introduce a novel design, termed the single-contact structure, which employs a special electrostatic doping modulation circuit to ML-WSe_2. The voltage-control surpasses traditional back-gate modulation in PL and VP enhancement under off-resonance conditions. High on/off trion VP (3 to 16%) can be achieved at 8 K, and distinguishable states remain observable up to 225 K. The proposed electrostatic doping model is supported by measurements of varied contact conditions and temperatures. These findings pave the way for efficient valley pseudospin control via electrostatic doping, advancing the practical applications of valleytronics and optoelectronics in TMD monolayer.

CC-11. Withdrawn

Session CD
MAGNONICS I: MAGNON MANIPULATION AND APPLICATION

Jacob J Wisser, Chair
National Institute of Standards and Technology, Broomfield, CO, United States

INVITED PAPER

CD-01. Reconfigurable standalone magnonic devices exploiting micromagnets and MEMS. *R. Bertacco*[1] *1. Department of Physics, Politecnico di Milano, Milano, Italy*

The advancement of integrated magnon technology for high-frequency signal processing [1] is facing significant challenges, such as the integration of low-power solutions for applying a bias field and the tuning of the local effective field controlling spin waves (SWs) propagation. Here we report on a novel technology platform for realizing magnonic devices which are: (i) self-standing (i.e. not requiring external bias fields by bulky magnets), (ii) fully integrated (i.e. compatible with usage as stand-alone devices inside consumer electronics, with electric inputs and output), (iii) reconfigurable. The basic concept is exploiting permanent micro-magnets mounted on movable parts of microelectromechanical systems (MEMS) to apply the bias field to a magnonic conduits placed in proximity. The bias field, and thus the spin-wave dispersion in the conduit, can be effectively tuned by changing the distance between the micromagnets and the conduit. In this way fundamental signal processing units (frequency filters, phase shifters and time delay lines) with tunable features can be implemented. In the talk I'll first describe a first demonstration, by Brillouin Light Scattering, of the feasibility of coupling CoFeB magnonic conduits to SmCo micromagnets, at variable distances, to modulate the frequency and phase of spin-waves modes. [2] Then I'll report on the first example of stand-alone fully integrated magnonic device which does not need any external electromagnet to operate in the 2-6 GHz frequency range and can be integrated on a silicon chip. This proof-of-concept device features a CoFeB conduit flanked by NiFe flux concentrators and SmCo permanent micromagnets capable to apply a variable field (up to about 25 mT) in the central region of the conduit, depending on the distance between the flux concentrators and the permanent magnets. Inductive antennas are then used to implement the electric input and output of the RF signals (see figure 1). By combined VNA and BLS measurements we demonstrate that the device can be operated as a tunable phase shifter with a phase change of about 180 deg for a relative displacement of 10 mm of the flux concentrators and permanent micromagnets. Finally, I'll report on first hybrid magnonic devices implementing on-chip reconfigurability of RF signal processing. This work has been carried out in the framework of the EU M&MEMS project [3].

[1] A. Barman et al., "The 2021 magnonic roadmap", 2021 J. Phys.: Condens. Matter 33, 413001. [2] M. Cocconcelli et al., "Tuning magnonic devices with on-chip permanent micromagnets", https://arxiv.org/abs/2406.03206 [3] https://mandmems.eu/ (EU Project 101070536 — MandMEMS)

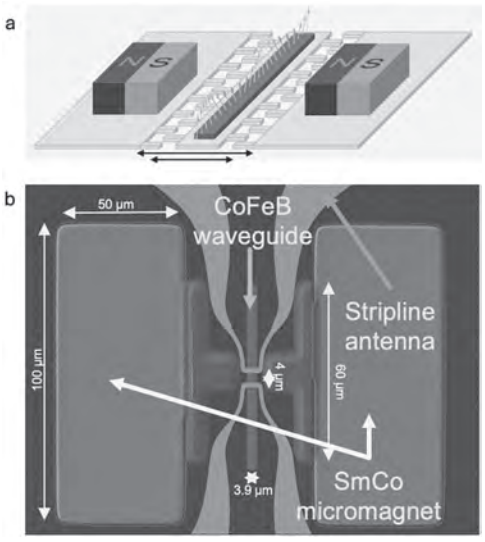

Figure 1: a) Concept of hybrid magnonic-MEMS devices; b) SEM image of a standalone magnonic device integrated on silicon with full electric-in electric-out RF signals.

CONTRIBUTED PAPERS

CD-02. Magneto-ionic voltage control of spin-wave phase with negligible amplitude modulation. *L. Flajsman*[1], M. Ameziane[1], R. Mansell[1] and S. van Dijken[1] *1. Aalto University, Espoo, Finland*

Precise manipulation of spin-wave phases is crucial for the development of various wave-based computing architectures in the field of magnonics [1]. This study introduces a novel approach for achieving deterministic, fully reversible voltage control over the phase of propagating spin waves using lithium-ion-based magneto-ionics. We perform detailed voltage-gated spin-wave analysis by employing super-Nyquist sampling magneto-optical Kerr effect microscopy on CoFeB/LiPON structures. The material stack consists of Ta 0.5 nm/CoFeB 12 nm/Ti 1.5 nm/LiPON 70 nm/Pt 6 nm with cobalt iron boron film as the spin-wave medium and a solid-state lithium phosphorus oxynitride electrolyte as a gate. We accomplish cyclable phase shifts larger than 2π at 2.25 V (Fig. 1a), while preserving the spin-wave amplitude (Fig. 1b) and propagation length. The voltage-programmable phase shift is attributed to alterations in the spin-wave dispersion relation within the gated region of the CoFeB film. This is a result of reversible electrochemical intercalation and deintercalation of lithium ions, a phenomenon previously utilized to manipulate magnetization direction, skyrmion numbers, and the strength of Ruderman-Kittel-Kasuya-Yosida (RKKY) coupling [2-4]. Notably, the magneto-ionic process does not involve significant redox reactions, as confirmed by cyclic voltammetry measurements, ensuring that the tuning of the spin-wave phase is both durable and rapid. Using lock-in techniques we are able to measure the realtime effects of pulsed gate voltages on the spin wave propagation. In Fig. 2 we show that, at 7 V, spin waves can be controlled within a millisecond timescale. Our findings are promising for the advancement of integrated magnonic circuitry with low-power on-chip programmability in a scalable and robust system.

[1] A. Mahmoud, F. Ciubotaru, F. Vanderveken, A. V. Chumak, S. Hamdioui, C. Adelmann, and S. Cotofana, Appl. Phys. Lett. 128, 161101 (2020). [2] M. Ameziane, R. Mansell, V. Havu, P. Rinke, and S. van Dijken, Adv. Funct. Mater. 32, 2113118 (2022). [3] M. Ameziane, J. Huhtasalo, L. Flajšman, R. Mansell, and S. van Dijken, Nano Lett. 23, 3167 (2023). [4] M. Ameziane, R. Rosenkamp, Lukas Flajšman, S. van Dijken, and R. Mansell, Appl. Phys. Lett. 122, 232401 (2023).

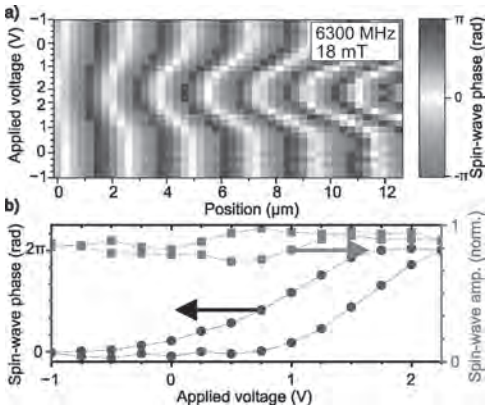

Fig. 1: (a) 1D spin-wave phase scan as a function of applied voltage. (b) Extracted phase shift (black circles) and spin-wave amplitude (red rectangles) 7 μm from the excitation antenna (0 μm). The spin waves are in the Damon-Eshbach configuration.

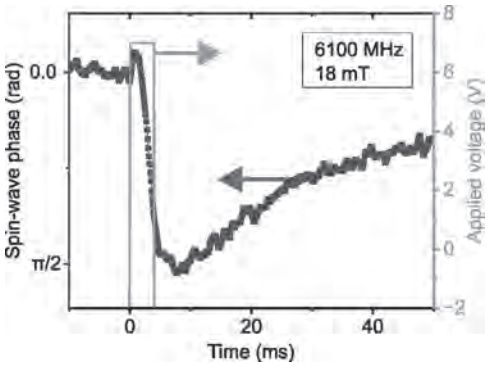

Fig. 2: Response of the spin-wave phase in a CoFeB/LiPON structure to a 3 ms voltage pulse. The width of the LiPON electrolyte gate is 5 μm, the pulse amplitude is 7 V.

CD-03. Withdrawn

CD-04. On-chip integrated spin-wave transducers: optimization and nonlinear limits. F. Kohl[1], M. Wagner[1], B. Heinz[1] and *P. Pirro*[1]
1. Physics, RPTU Kaiserslautern, Kaiserslautern, Germany

In recent years, magnonics has emerged as a promising candidate for integrated microwave devices. The excitation and manipulating of spin waves has shown promise for integrated microwave devices like delay lines, filters and isolators since it is providing inherent non-reciprocity and reconfigurability over several GHz spans. Ongoing research aims to bridge the gap between theoretical feasibility and practical implementation, with a particular focus on advancing on-chip integrated spin-wave devices. While dynamic Oersted-driven spin-wave transducers are commonly used in micro-structured devices, the performance currently achieved demands substantial improvements to compete with established technologies. To address these challenges, a basic spin-wave transducer, composed of microstructured input and output antennas atop of Yttrium-Iron-Garnet (YIG) films with various thicknesses, serves as an exemplary testbed for integrated magnon-based RF devices with an active region significantly smaller than 0.1mm^2. In a comprehensive study, we assess insertion losses, bandwidths, group delays, nonlinear effects and their respective tuneability by external magnetic fields, considering various key parameters such as magnetic material properties and spin-wave dispersion relations. Leveraging propagating spin-wave spectroscopy and Brillouin light scattering spectroscopy, we measure spin-wave transmission and interpret results, providing valuable insights into the system's behavior and key parameters influencing device efficiency. Through reduction of reflection and dissipation losses, we achieve record transmission efficiency for on-chip integrated spin-wave devices. Using systematic power dependent studies, we explore the nonlinear effects limitng the power transmission and characterize their YIG thickness dependence. Additionally, we leverage inherent non-reciprocity to enhance isolation

within the device, rendering it suitable for applications akin to a microwave diode. This work represents a crucial step towards realizing the full potential of magnonics in practical applications. This research is funded by the European Union within HORIZON-CL4-2021-DIGITAL-EMERGING-01 (No. 101070536,MandMEMS)

CD-05. Very Narrow Linewidth of Propagating Magnons with Submicron-Scale Wavelength and Associated Damping. *J. Lim*[1], T. Lo[1], R. Klause[1], Y. Li[2], V. Novosad[2] and A. Hoffmann[1] *1. Materials Science and Engineering, University of Illinois Urbana-Champaign, Urbana, IL, United States; 2. Materials Science Division, Argonne National Laboratory, Lemont, IL, United States*

Yttrium iron garnet (YIG) is a well-known material for its exceptionally low magnetic damping, which is manifested in a very narrow linewidth (smaller than 10 MHz of full-width at half maximum, FWHM) of the ferromagnetic resonance mode (the Kittel mode, which is a spatially uniform mode) in the microwave frequency range [1]. Magnetic damping associated with the Kittel mode has been extensively studied in various setups [2], but the study of magnetic damping associated with a propagating spin wave with a definite wavelength has been more scarce [3]. A magnon, a quantum of a spin wave, has recently been proposed as an information carrier in quantum circuits [4-6] because magnons have unique properties: 1) non-reciprocity due to broken time-reversal symmetry, and 2) the ability to miniaturize systems due to their much shorter wavelength compared to microwave photons at the same frequency. In this study, we observed a very narrow linewidth (less than 5 MHz of FWHM) for a spin wave resonance with a 1 μm wavelength in the Damon-Eshbach geometry, where the magnetic field H is perpendicular to the wavevector k in a 100 nm-thick YIG film. Fig.1 shows a microwave spectrum at a magnetic field H = 1470 Oe. The linewidths of the Kittel mode and the spin wave were 50 MHz and 4 MHz, respectively. The damping of the Kittel mode and the spin wave is expected to be $(0.7 \pm 0.3) \times 10^{-4}$ and $(0.7 \pm 0.4) \times 10^{-4}$, respectively. A ladder-shaped, multi-element antenna with a submicron-scale period was fabricated using e-beam lithography on top of a sputter-grown YIG film. The multi-element part was integrated with the central conductor of a photolithographically fabricated coplanar waveguide for microwave transmission. Fig.2 shows the multi-element part of the antenna. Since the spin wave resonance has low damping, a very narrow linewidth, and a definite wave vector, it can serve as a suitable entity to study microwave photon-propagating magnon coupling (propagating magnon-polariton) in superconducting resonator-YIG waveguide structures for quantum information applications. This work was supported by DOE BES under contract No. DE-SC0022060.

[1] C. Hauser, T. Richter, N. Homonnay, C. Eisenschmidt, M. Qaid, H. Deniz, D. Hesse, M. Sawicki, S.G. Ebbinghaus, G. Schmidt, Sci. Rep., 6 (2016). [2] G. Schmidt, C. Hauser, P. Trempler, M. Paleschke, E.T. Papaioannou, Physica Status Solidi B-Basic Solid State Physics, 257 (2020). [3] Q.W. Fu, Y. Li, L.N. Chen, F.S. Ma, H.T. Li, Y.B. Xu, B. Liu, R.H. Liu, Y.W. Du, Chinese Phys Lett, 37 (2020). [4] Z.H. Jiang, J. Lim, Y. Li, W. Pfaff, T.H. Lo, J.C. Qian, A. Schleife, J.M. Zuo, V. Novosad, A. Hoffmann, Appl. Phys. Lett., 123 (2023). [5] Y. Li, J.C. Qian, Z.H. Jiang, T.H. Lo, D. Ding, T. Draher, T. Polakovic, W. Pfaff, A. Schleife, J.M. Zuo, W.K. Kwok, V. Novosad, A. Hoffmann, Int El Devices Meet, DOI 10.1109/Iedm45625.2022.10019460(2022). [6] Y. Li, W. Zhang, V. Tyberkevych, W.K. Kwok, A. Hoffmann, V. Novosad, J. Appl. Phys., 128 (2020).

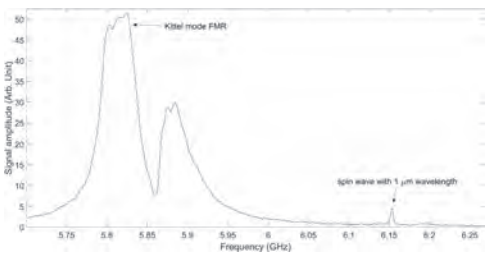

Fig. 1. FMR spectrum at H=1470 Oe.

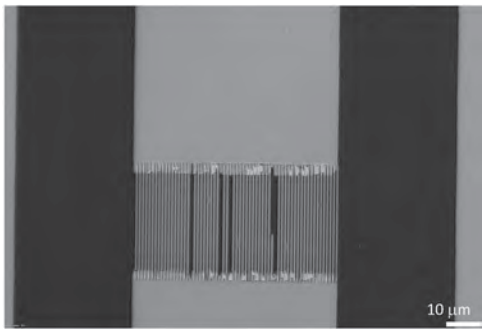

Fig. 2. Optical microscope image of the antenna with 1 μm period.

CD-06. Spin pumping driven by magnon-photon polaritons in a ferromagnet-coplanar superconducting resonator hybrid system. *D. Wagle*[1*], Y. Li[2], A. Rai[1] and B. Jungfleisch[1] *1. Physics and Astronomy, University of Delaware, Newark, DE, United States; 2. Argonne National Labortory, Lemont, IL, United States*

Combining the strengths of quantum-coherent systems with complementary functionalities can create robust and versatile hybrid systems, which hold great potential for applications in quantum information processing and transduction. High-quality coplanar superconducting resonators can facilitate the (ultra-) strong coupling between microwave photons and magnons due to their low loss and high sensitivity. Here, we demonstrate spin pumping driven by a strongly coupled magnon-photon system using a ferromagnet-coplanar superconducting resonator hybrid system at 1.4 K. For this purpose, a high-quality NbN superconducting resonator loaded with a macroscopic yttrium iron garnet /Pt bilayer sample in a flip-chip configuration is used [Fig. 1]. Electrical readout via the inverse spin-Hall effect reveals characteristic coupling features, including avoided level crossing and linewidth broadening, demonstrating the electrical detection of strong coupling between microwave photons and magnons [Fig. 2]. The microwave photon-magnon coupling strength obtained by combined spin pumping and inverse spin-Hall effect measurements is compared to microwave transmission experiments. Microwave power-dependent measurements reveal a decrease in the coupling strength with increasing microwave power alongside the onset of nonlinearities of the superconducting resonator above a critical threshold of the microwave power.

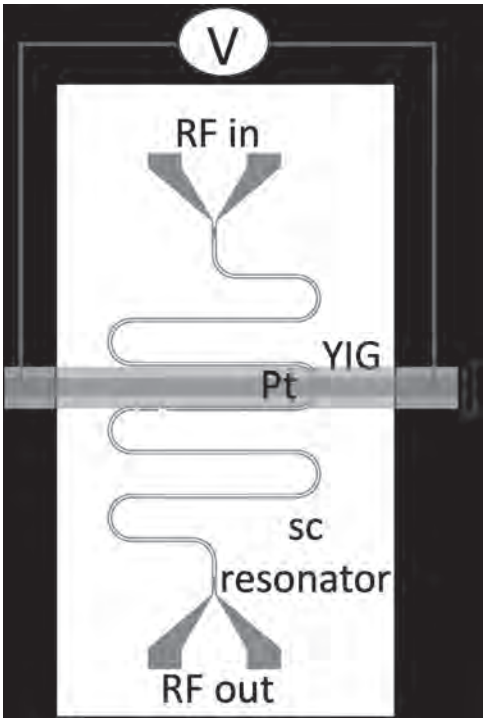

Schematic illustration of experimental setup.

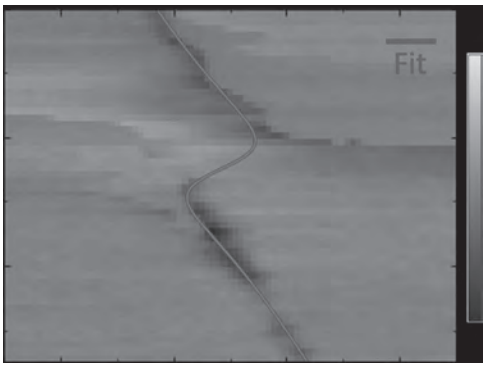

The spin pumping voltage spectra as a function of field and frequency.

CD-07. Magnon lifetimes in YIG spheres for quantum magnonics at millikelvin temperatures. R. Serha[1,2], K. McAllister[3], D. Schmoll[1,2], P.E. Schmidt[8], I.Y. Yang[5,6], M. Trupke[8,7], S. Knauer[1], T. Reimann[4], C. Dubs[4], C. Gonzalez Ballestero[9], M. Aspelmeyer[7,8], G. Kirchmair[5,6], *D.A. Bozhko*[3] and A. Chumak[1] *1. Faculty of Physics, University of Vienna, Vienna, Austria; 2. Vienna Doctoral School in Physics, University of Vienna, Vienna, Austria; 3. Department of Physics and Energy Science, University of Colorado Colorado Springs, Colorado Springs, CO, United States; 4. INNOVENT e.V. Technologieentwicklung, Jena, Germany; 5. Institute for Quantum Optics and Quantum Information, Austrian Academy of Sciences, Innsbruck, Austria; 6. Institute for Experimental Physics, University of Innsbruck, Innsbruck, Austria; 7. Vienna Center for Quantum Science and Technology (VCQ), Faculty of Physics, University of Vienna, Vienna, Austria; 8. Institute for Quantum Optics and Quantum Information (IQOQI) Vienna, Austrian Academy of Sciences, Vienna, Austria; 9. Institute for Theoretical Physics, Vienna University of Technology, Vienna, Austria*

Magnonics is the field of science that deals with data carried by spin waves and their quanta, magnons, in magnetically ordered media [1]. The ferrimagnet yttrium iron garnet (YIG) is known for its exceptionally low magnetic damping and long magnon lifetimes, making it a preferred material for experiments and RF technologies [2]. The magnon lifetime is crucial for quantum magnonics, as recent advancements in the excitation and detection of single magnons [3] and the measurement of the Wigner function of a single magnon [4] via a superconducting qubit have highlighted. It has been reported that with decrease in temperature the magnetic damping increases in YIG, which is associated with chemical contamination and purity of the single crystal [5,6,7]. We report on the magnetic damping of three 300 μm-diameter YIG spheres of varying chemical purity. The first YIG is a common and commercially available material (@RT $\alpha = 11*10^{-5}$), the second is of high-quality (@RT $\alpha = 4*10^{-5}$) and the third is an ultra-pure YIG (@RT $\alpha = 8*10^{-5}$). Stripline ferromagnetic resonance (FMR) spectroscopy was performed for frequencies up to 40 GHz in a physical property measurement system (PPMS) and a dilution refrigerator in the temperature range from 30 mK to 300 K. In the following, the anti-crossing of the YIG sphere FMR with superconducting resonators of different U-shaped configurations (inspired by [8]) was studied to optimize the coupling. At frequencies commonly used for superconducting qubits (≈ 5 GHz), the damping reaches a maximum at about 40 K, before decreasing steadily at lower temperatures (see Fig. 1). At 2 K, the ultra-pure sphere shows the longest magnon lifetime of about 440 ns (corresponding to $\alpha = 2*10^{-5}$), while the lifetime in the high-quality YIG sphere drops down to 50 ns. The understanding of the damping mechanisms at mK temperatures allows for the quantum single magnon experiments with long-living magnons.

[1] A. Barman and *et al*., J. Phys. Condens. Matter, Vol. 33, p. 413001 (2021) [2] V. Cherepanov, I. Kolokolov and V. L'vov, Phys. Rep., Vol. 229, p. 81 (1993) [3] D. Lachance-Quiron, S. P. Wolski, Y. Tabuchi and *et al.*, Science, Vol. 367, p. 425 (2020) [4] D. Xu, X.-K. Gu, H.-K. Li and *et al*., Phys. Rev. Lett., Vol 130, p. 193603 (2023) [5] L. Mihalceanu, V. I. Vasyuchka, D. A. Bozhko and *et al*., *Phys. Rev. B*, Vol. 97, p. 214405 (2018) [6] S. Kosen, A. F. van Loo, D. A. Bozhko and *et al*., APL Mater., Vol 7, p. 101120 (2019) [7] H. Maier-Flaig, S. Klingler, C. Dubs and *et al*., Phys. Rev. B, Vol. 95, p. 214423 (2017) [8] Y. Li, V. G. Yefremenko, M. Lisovenko and *et al*., Phys. Rev. Lett., Vol 128, p. 047701 (2022)

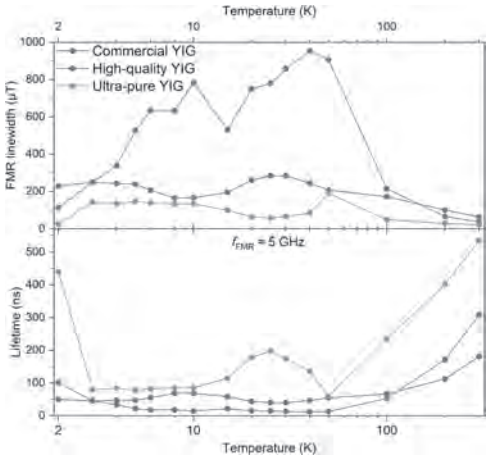

Fig.1: FMR linewidths and magnon lifetimes of three different YIG spheres vs temperature in logarithmic scale for a FMR frequency of about 5 GHz. The error bars are smaller then the measurement markers.

CD-08. Shaping non-reciprocal caustic beams. *V. Vlaminck*[1,2], D. Stoeffler[4], D. Wagle[3], V.M. Castel[1,2], L. Temdie-Kom[1,2], M.T. Kaffash[3], H. Majjad[4], Y. Henry[4], B. Jungfleisch[3] and M. Bailleul[4] *1. MO, IMT Atlantique, Brest, France; 2. Lab-STICC, Brest, France; 3. University of Delaware, Newark, DE, United States; 4. IPCMS, Strasbourg, France*

Spin waves constitute the building blocks of novel wave computing methods such as spectral analysis [1], and neuromorphic computing [2], which are all interference-based techniques. Recently, basics concepts of optics applied to spin waves demonstrated the possibility to shape and steer spin wave

beams, suggesting prominent performance in particular tasks such as image processing and speech recognition [3]. However, The complexity of spin dynamics, inherently due to its dependence to numerous parameters, and the intricacy of magnon-magnon interactions, requires heavy computational methods, which can limit the scope of study. In this context, we developed an efficient tool to study the near-field diffraction (NFD) patterns of spin wave in homogeneous out-of-plane magnetized thin films for arbitrary distribution of excitation fields [4, 5]. Here, we present the adaptation of our NFD model to in-plane magnetized thin films, and reveal how caustic spin-wave beams can be directly emitted from a sharply constricted stripline. We show in particular the importance of not only meeting the suitable caustic conditions of field and frequency, but also having of a seemingly punctual source for shaping the caustic beam [6]. Using spatially resolved micro-focused Brillouin light spectroscopy on various constriction sizes, we satisfyingly verify our predictions (see Fig. 1), and explore further the steerability as well as the caustic beams properties (see Fig. 2). These findings have important implications for future development of magnonic devices such as spin wave splitters, passive spin-wave frequency-division demultiplexers, and wave-based computing building blocks for neuromorphic architecture. This work was supported by the French ANR projects “MagFunc”, and ANR-22-EXSP-0004 “SWING”, the U.S. Department of Energy, Office of Basic Energy Sciences, Division of Materials Sciences and Engineering under Award DE-SC0020308, and the Transatlantic Research Partnership, a program of FACE Foundation and the French Embassy.

[1] A. Papp, W. Porod, A.J. Csurgay, G. Csaba, “Nanoscale spectrum analyzer based on spin-wave interference”, Scientific Reports 7, 9245, (2017). [2] A. Papp, W. Porod, G. Csaba, “Nanoscale neural network using non-linear spin-wave interference”, Nature Communications 12, 6422, (2021). [3] E. Albisetti, S. Tacchi, R. Silvani, G. Scaramuzzi, et al., “Optically inspired nanomagnonics with nonreciprocal spin waves in synthetic antiferromagnets”, Advanced Materials 32, 1906439, (2020). [4] L. Temdie, V. Castel, M. Jungfleisch, R. Bernard, H. Majjad, D. Stoeffler, Y. Henry, M. Bailleul, and V. Vlaminck. “Probing spin wave diffraction patterns of curved antennas”, Phys. Rev. Appl. 21, 014032 (2024). [5] V. Vlaminck, L. Temdie, V. Castel, M.B. Jungfleisch, D. Stoeffler, Y. Henry, M. Bailleul, “Spin wave diffraction nmodel for perpendicularly magnetized films”, Journal of Applied Physics 133, 053903, (2023). [6] D. Wagle, D. Stoeffler, L. Temdie, M. T. Kaffash, V. Castel, H. Majjad, R. Bernard, Y. Henry, M. Bailleul, M. B. Jungfleisch, and V. Vlaminck, “Shaping non-reciprocal caustic spin-wave beams”, arXiv:2404.15011 (2024)

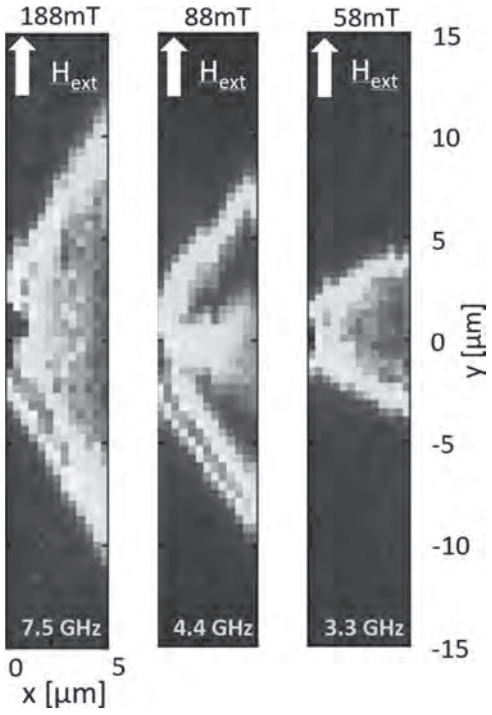

Fig.1: BLS measurement of swpin wave caustic beam from a constricted stripline

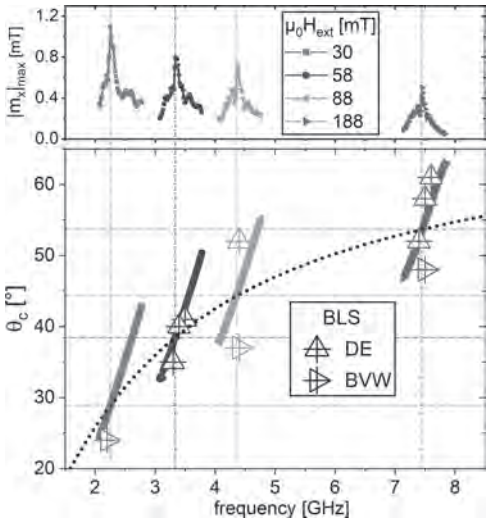

Fig. 2: Frequency dependence of the caustic angle and amplitude.

CD-09. Mutual nonlinear interactions between parametrically excited spin-wave modes in a YIG microdisk. *G. Soares*[1], R. Lopes Seeger[1,2], A. Kolli[1], M. Massouras[2], N. Beaulieu[3], J. Ben Youssef[3], M. Muñoz[4], P. Che[6], A. Anane[6], S. Perna[5], M. d'Aquino[5], C. Serpico[5], T. Srivastava[2], H. Merbouche[1], J. Kim[2] and G. de Loubens[1] *1. Service de Physique de l'État Condensé, CEA Paris-Saclay, Université Paris-Saclay, CNRS, Gif-sur-Yvette, France; 2. Centre de Nanosciences et de Nanotechnologies, Université Paris-Saclay, CNRS, Palaiseau, France; 3. LabSTICC, CNRS, Université de Bretagne Occidentale, Brest, France; 4. Instituto de Tecnologías Físicas y de la Información (CSIC), Madrid, Spain; 5. Department of Electrical Engineering and ICT, University of Naples Federico II, Napoli, Italy; 6. Laboratoire Albert Fert, CNRS, Thales, Univ. Paris-Saclay, Palaiseau, France*

Hardware based neuromorphic computing (HNC) has been proposed as a potential solution for the exponential increase in energy cost of training deep neural networks. Recently, HNC leveraging in nonlinear magnetization dynamics has been successfully implemented in magnon reservoirs[1-3]. However, reservoirs have few means of network customization. In magnetic microstructures, all the spin-wave eigenmodes (SWM) excited non-linearly are mutually coupled. Thus, by defining the neural network in the k-space, the result is a fully interconnected and tunable network of neurons (SWM) and synapses (mutual couplings) – with minimal nanofabrication required. We have previously demonstrated that parallel parametric pumping allows the efficient excitation of a large number of SWM in a YIG microdisk with a stripline[4]. Here, we use frequency multiplexing to parametrically excite several SWM and study their mutual interactions. Fig.1a shows a two-tone microwave magnetic resonance force spectroscopy experiment. The total SWM magnon count is shown as a function of frequencies f_A and f_B, with the pulses delayed by a few μs. Clear signatures of nonlinear interactions between SWM are observed on this diagram: at the mode crossings, the total magnon count is not the sum of the respective single tone experiments. Nonlinear frequency shifts (Fig.1b), and, strikingly, non-commutativity are also observed (Fig.1c), with the final dynamic state depending on the order of the microwave pulses. These phenomena are successfully explained by a normal mode model[5], where the key ingredients governing the response of the system are the self and mutual nonlinear frequency shifts of the SWM and the supercriticality of the parametric excitations. Additional measurements where three excitations are multiplexed with variable relative delays demonstrates a large amount of distinct dynamic states with little change in experimental conditions. These results open exciting new possibilities of exploiting mutual interactions of parametrically excited SWM for fundamental magnetism, neuromorphic computing and beyond.

[1] A. Papp, W. Porod, and G. Csaba, "Nanoscale neural network using non-linear spin-wave interference", Nature Commun. 12, 6422 (2021) [2] A. Allwood, et al. "A perspective on physical reservoir computing with nanomagnetic devices". *Appl. Phys. Lett.* 23122 (4): 040501 (2023) [3] L. Körber, et al., "Pattern recognition in reciprocal space with a magnon-scattering reservoir", Nature Commun. 14, 3954 (2023) [4] T. Srivastava, et al., "*Identification of a Large Number of Spin-Wave Eigenmodes Excited by Parametric Pumping in Yttrium Iron Garnet Microdisks",* Phys. Rev. Appl. 19, 064078 (2023) [5] S. Perna et al., "Computational micromagnetics based on normal modes: bridging the gap between macrospin and full spatial discretization", J. Magn. Magn. Mater. 546, 168683 (2022)

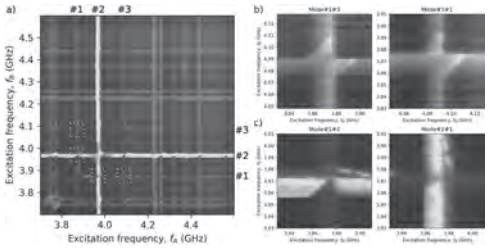

Fig.1 Two-tone parametric spectroscopy map (a) zoom at the mode crossings with nonlinear frequency shifts (b) and non-commutativity (c).

CD-10. Three-dimensional nanoscale control of magnetism in crystalline Yttrium Iron Garnet for magnonics. V. Levati[1], *M. Vitali*[1], A. Del Giacco[1], N. Pellizzi[1], R. Silvani[2], L. Ciaccarini Mavilla[2], M. Madami[2], I. Biancardi[1], D. Girardi[1], M. Panzeri[1], P. Florio[1], D. Breitbach[3], P. Pirro[3], G. Corrielli[4], R. Osellame[4], R. Bertacco[1], V. Russo[1], A. Li Bassi[1], S. Tacchi[5], D. Petti[1] and E. Albisetti[1] *1. Politecnico di Milano, Milan, Italy; 2. Università di Perugia, Perugia, Italy; 3. RPTU Kaiserslautern-Landau, Kaiserslautern, Germany; 4. CNR-IFN, Milan, Italy; 5. CNR-IOM, Perugia, Italy*

Yttrium Iron Garnet is key across spintronics and photonics, due to its exceptional magnetic and magneto-optical properties. The record-low magnetic damping of crystalline YIG, for example, allows the propagation of spin waves across millimeter distances, making it the material of choice for low-power-dissipation transmission and computing in the field of magnonics [1], for the study of fundamental physical phenomena such as Bose-Einstein condensation, and quantum computing. For all these applications, the possibility of designing and studying enhanced functionalities by manipulating magnetism in three-dimensions has sparkled the interest towards novel nanofabrication methodologies [2, 3, 4]. Yet, currently, high-quality YIG nanopatterning presents formidable challenges and is mostly limited to two-dimensional geometries. In this work, we show that by irradiating single-crystal YIG films with a focused UV laser, we drive a giant stable enhancement of the perpendicular magnetic anisotropy, in nanoscale regions confined in three-dimensions and whose extension within the volume of the system can be finely controlled (Figure 1). By harnessing these three-dimensional anisotropy profiles, we demonstrate a fine tuning of the spin-wave band structure, of the spatial localization of the spin-wave modes within the volume of the film, and the control of spin-wave non-reciprocity, realizing proof-of-principle magnonic materials and three-dimensional magnonic crystals (Figure 2). The straightforward, single-step nanofabrication of three-dimensional magnetic systems based on crystalline YIG opens the way to a new class of magnonic and magneto-optic devices where functionality arises from tailored three-dimensional magnetic properties profiles.

[1] P. Pirro et al., Advances in coherent magnonics. Nat Rev Mater 6, 1114–1135 (2021). [2] Three-Dimensional Magnonics: Layered, Micro- and Nanostructures. Routledge & CRC Press (2019) [3] A. Fernández-Pacheco et al., Three-dimensional nanomagnetism. Nat Commun 8, 15756 (2017). [4] V. Levati et al., Adv Mater Technol, 8, 2300166 (2023).

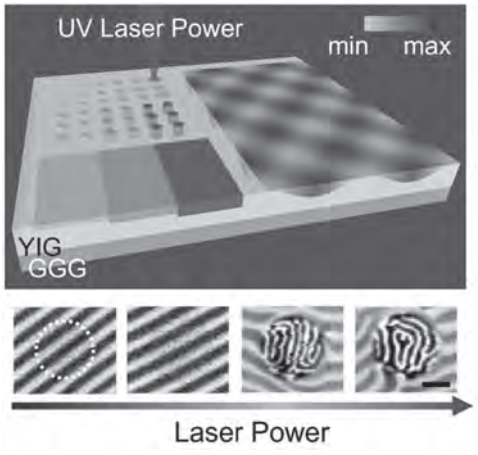

Figure 1. Sketch of the laser irradiation process and of the three-dimensional magnetic properties profiles induced in YIG (top panel). Magnetic force microscopy images of the domain structure of YIG increasing the laser power from left to right. Scale bar 2 um.

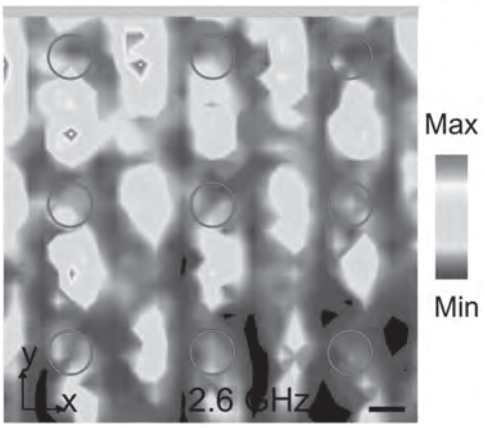

Figure 2. Spatial map of the spin-wave intensity in a 3D magnonic crystal measured via Brillouin Light Scattering microscopy. Irradiated regions are marked by red circles. Microwave antenna in yellow. Scale bar 500 nm.

CD-11. Fabrication and Characterization of Suspended YIG Microstructures. *S.W. Kurfman*[1], F. Heyroth[2] and G. Schmidt[1,2] *1. Institute for Physics, Martin Luther University Halle-Wittenberg, Halle (Saale), Germany; 2. Interdisziplinäres Zentrum für Materialwissenschaften, Martin Luther University Halle-Wittenberg, Halle (Saale), Germany*

Efficient coupling between magnetic excitations and acoustic modes is hindered by enhanced phonon loss into the substrate bulk. These losses can be minimized through the fabrication of suspended magnonic microstructures where the acoustic modes of the magnonic material are isolated from the substrate. Here, we demonstrate the fabrication of low-loss suspended YIG microstructures with a single attached support point. We additionally show characterization of excited magnon modes via optical techniques (e.g. TR-MOKE) and inductive measurements. Due to confinement effects, these structures exhibit acoustic resonant modes in the GHz regime and therefore provide an avenue towards efficient coupling of magnetic and acoustic modes. In conjunction with optical techniques (e.g. Brillouin Light Scattering) to measure the acoustic modes, these YIG microstructures promise application potential ranging from efficient microwave-to-optical light frequency conversion [1] to quantum systems utilizing coherent multipartite coupling [2].

[1] Engelhardt *et al., Phys. Rev. Appl.* 18 (2022) 044059. [2] Lachance-Quirion *et al., Appl. Phys. Express* 12, (2019) 070101.

CD-12. Imaging of magnon modes in a YIG microdisk with a magnetic vortex. *L. Peeters*[1], L. Flajsman[1] and S. van Dijken[1] *1. Applied Physics, Aalto University, Espoo, Finland*

The excitation of magnon modes in magnetic microstructures is of significant interest for applications in neuromorphic computing [1] and microwave-to-optics transduction in hybrid quantum systems [2]. Microdisks with a magnetic vortex are particularly attractive for the excitation of confined magnon modes due to their complex mode structure and nonlinear dynamics [3,4]. In this study, we employ super-Nyquist sampling magneto-optic Kerr effect (SNS-MOKE) microscopy to image magnon modes in 63-nm-thick yttrium iron garnet (YIG) microdisks. The microdisks are fabricated using e-beam lithography and pulsed laser deposition (PLD) at room temperature. Post-patterning, the YIG disks are crystallized through annealing in an oxygen atmosphere. Magnon modes are excited during SNS-MOKE imaging by Ω-shaped microwave antennas, which are patterned concentrically around the disks with a width of 1 μm. Figure 1 presents an example of magnon mode imaging on a YIG disk with a diameter of 5 μm, subjected to a microwave excitation power of 2 dBm. The excitation frequency is fixed at 1.271 GHz while the in-plane magnetic bias field is varied. At zero magnetic field, the disk displays a magnetic vortex, and the magnon mode is radially symmetric. Applying a magnetic field along the positive *x*-direction gradually shifts the vortex core, altering the mode profile. At 4 mT, the vortex is annihilated, resulting in uniform magnetization. In this presentation, we will provide a detailed discussion on the dependence of magnon modes in YIG microdisks on frequency, magnetic field, and excitation power.

[1] L. Körber, C. Heins, T. Hula *et al.*, *Nat. Commun.* 14, 3954 (2023). [2] K. Wang, Y.P. Gao, R. Jiao *et al.*, *Front. Phys.* 17, 42201 (2022). [3] L. Körber, C. Heins, I. Soldatov *et al.*, *Appl. Phys. Lett.* 122, 092401 (2023). [4] K. Schultheiss, R. Verba, F. Wehrmann *et al.*, *Phys. Rev. Lett.* 122, 097202 (2019).

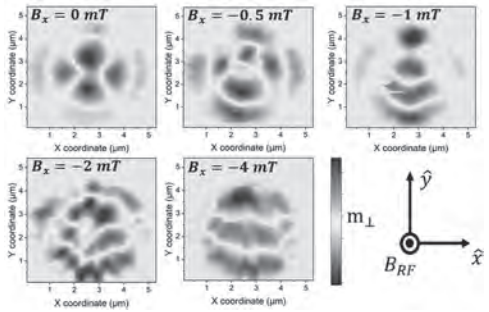

Figure 1: Magnetic field dependence of the magnon mode profile in a 5-μm-diameter YIG disk at 1.271 GHz with an excitation power of 2 dBm. The magnetic bias field is applied in the positive *x*-direction.

CD-13. Manipulation of Spin-wave Transport in a YIG Film by an Array of Magnetic Vortices. *J. Hyun*[1], N. Kuznetsov[1], L. Flajsman[1] and S. van Dijken[1] *1. Department of Applied Physics, Aalto University, Espoo, Finland*

Effective information encoding and processing in magnonic systems necessitates active control of spin-wave transport [1,2]. In this study, we report on the manipulation of propagating spin waves in a hybrid magnonic system composed of a 70 nm YIG film with an array of 50 nm CoFeB nanodisks patterned on top, separated by a 4 nm Ta spacer. In the absence of an external magnetic field, the CoFeB nanodisks exhibit a vortex state. Utilizing broadband spin-wave spectroscopy, we demonstrate that dipolar coupling between the YIG film and the magnetic vortices in the disks introduces two distinct gaps in the spin-wave transmission spectrum (Fig.1). Super-Nyquist sampling magneto-optical Kerr (SNS-MOKE) microscopy visualizes the rejection of spin waves at specific frequencies (Fig.2). The frequency, width, and depth of the spin-wave transmission gaps can be adjusted by varying the diameter of the CoFeB disks (d = 120, 180, 240, 320 nm) or the period of the disk array (p = 390, 470, 550, 630 nm). Applying an external magnetic field shifts the transmission gap frequencies by modifying the spin-wave dispersion in the YIG film and moving the vortex core within the CoFeB disks. The annihilation of the vortices at a critical field changes the spin-wave transmission spectrum abruptly. In addition to magnetic-field control, we explore the manipulation of spin-wave transport using nanosecond laser pulses. By leveraging plasmon excitations in the CoFeB nanodisk arrays, we alter the magnetic properties through rapid thermoplasmonic heating. The complex interplay between spin-wave transport in the YIG film, the micromagnetic state of the CoFeB nanodisks, and thermoplasmonic heating is further analyzed using micromagnetic and finite-difference time-domain simulations.

[1] A. Barman et al., J. Phys.: Condens. Matter, Vol. 33, p. 413001 (2021) [2] A. V. Chumak et al., IEEE Trans. Magn., Vol. 58, pp. 1-72 (2022)

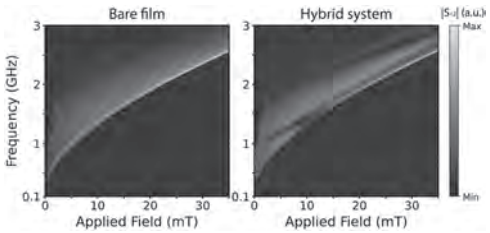

Fig.1: Contour plot of the S_{12} amplitude as a function of magnetic field for a 70 nm bare YIG film and the same YIG film with an array of 50 nm CoFeB nanodisks (d = 180 nm, p = 470 nm).

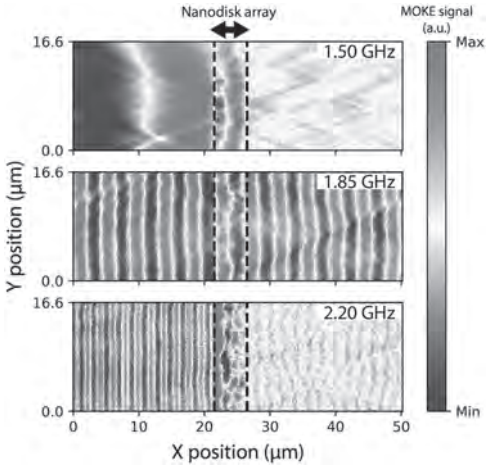

Fig.2: SNS-MOKE microscopy images of spin-wave transport in a 70 nm YIG film with an array of CoFeB nanodisks recorded at 1.50 GHz, 1.85 GHz, and 2.20 GHz. The dashed lines indicate the position of the disk array. A magnetic field of 11.3 mT is oriented along the y-axis.

Session CE
MAGNETORESISTIVE SENSORS

Victor Lopez-Dominguez, Chair
Universitat Jaume I, Castellon de la Plana, Spain

INVITED PAPER

CE-01. TMR Sensors on the Edge: non-invasive and agnostic monitoring of Industrial Tools. *R. Ferreira*[1], E. Paz[1], A. Talantsev[1], A. Araújo[1], E. Iranmehr[1] and T. Boehnert[1] *1. INL - International Iberian Nanotechnology Laboratory, Braga, Portugal*

Over several decades, magnetic information storage technology was a strong driving force for a significant development of magnetoresistive sensors starting from hall sensors, to AMR, GMR and finally TMR sensors [1]. Since then, these sensors have been finding new uses in a large number of non-storage applications that have very different challenges [2]. The progression from early MTJ structures to present day high performance magnetic field sensors required significant progress in what concerns the mechanisms used to obtain highly linear transfer curves [3], with well controlled stray fields [4] and a manageable 1/f noise [5] which is still a large challenge in TMR sensors compared to other types of spintronic sensors and one that is particularly important in most non-storage related real world applications. Despite the hurdles, a careful choice of designs [6] and materials [7] make it possible to produce nowadays sensors with magnetic field detection limits approaching $1pT/Hz^{0.5}$ at 1Hz at room temperature, with devices that are small enough to be mass produced at wafer level, straightforward to integrate homogeneously or heterogeneously with standard CMOS electronics, with good yields and good uniformities. Furthermore, MTJ sensors have an outstanding sensitivity compared to other spintronic sensors which means that very weak magnetic fields can generate large electrical signals that can measured with modest electronics and signal conditioning at very fast data rates. This technological capability opens prospects that are not limited to the mere detection of magnetic fields. A good magnetic field sensor is an equally good sensor of any other physical quantity that can be mediated by a magnetic field. To illustrate this point, this presentation will provide the example of a magnetic field sensor acting as a position sensor when combined with a reference permanent magnet and capable of achieving displacement resolutions of the order of 10nm [8]. Furthermore, this system will be used as a transducer of mechanical vibrations in real world industrial tools [9]. This approach makes it possible to obtain information very similar to that of conventional MEMS based sensors [10], with the important advantage of allowing a non-local, non-contact and non-invasive monitoring of the internal components of a machine without prior knowledge of the machine architecture and over a wide range of frequencies. This novel and completely agnostic approach to the monitoring of industrial tools can be combined with equally agnostic and totally unsupervised machine learning algorithms to extract useful data about the condition of industrial machines [11] or even the behaviour of their users [12] in a wide context that covers predictive maintenance, production line control and automation, quality control, user safety, etc... The presentation will end with a short description of ongoing efforts and prospects to combine MTJ sensors together with other spintronic technologies towards a full spintronic solution for smart sensing on the edge.

[1] "Magnetoresistive sensors", P. Freitas, R. Ferreira, S. Cardoso and F. Cardoso, J. Phys.: Condens. Matter 19 pp.165221, (2007), doi: 10.1088/0953-8984/19/16/165221 [2] "Spintronic Sensors", P. P. Freitas, R. Ferreira and S. Cardoso, Proceedings of the IEEE, vol. 104, no. 10, pp. 1894-1918, (2016), doi:10.1109/JPROC.2016.2578303 [3] "Linearization of magnetic sensors with a weakly pinned free-layer MTJ stack using a three-step annealing process", E. Paz, R. Ferreira and P. P. Freitas, IEEE Transactions on Magnetics, vol. 52, no. 7, pp. 1-4, (2016), Art no. 4002104, doi:10.1109/TMAG.2016.2525772 [4] "Impact of the Synthetic Antiferromagnet in TMR Sensors for Improved Angular- Dependent Output", P. D. R. Araujo et al., IEEE Sensors Journal, vol. 24, no. 11, pp. 17588-17595, (2024), doi:10.1109/JSEN.2024.3389732. [5] "1/f noise in linearized low resistance MgO magnetic tunnel junctions", J. M. Almeida; R. Ferreira; P. P. Freitas; J. Langer; B. Ocker; W. Maass, J. Appl. Phys. 99, 08B314, (2006), doi:10.1063/1.2172179 [6] "Sub-pT magnetic field detection by tunnel magneto-resistive sensors", Mikihiko Oogane et al, Appl. Phys. Express 14 123002, (2021), doi:10.35848/1882-0786/ac3809 [7] "Low frequency noise in arrays of magnetic tunnel junctions connected in series and parallel", R. Guerrero; M. Pannetier-Lecoeur; C. Fermon; S. Cardoso; R. Ferreira; P. P. Freitas, J. Appl. Phys. 105, 113922 (2009), doi:10.1063/1.3139284 [8] "Magnetic tunnel junction platforms for linear positioning and nanoscale displacement sensing", Artem Talantsev, Elvira Paz, Tim Böhnert, André Araújo, Ricardo Ferreira, Measurement 223, pp. 113663 (2023), doi:10.1016/j.measurement.2023.113663 [9] "Magnetoresistive Sensors and Piezoresistive Accelerometers for Vibration Measurements: A Comparative Study", R. Dionísio et al., J. Sens. Actuator Netw., 10(1), 22, (2021), doi:10.3390/jsan10010022 [10] "Method and system for non-invasive vibration-based condition monitoring of a machine", R. Ferreira, T Böhnert, E. Paz, US Patent App. 17/996,081(2023) [11] "Unsupervised Extraction of Shape-Based Signal Patterns for Incoming Signal Recognition", E. Iranmehr, T. Böhnert, E. Paz, M. Martins and R. Ferreira, IEEE Sensors Journal, vol. 23, no. 11, pp. 11992-12007,(2023), doi:10.1109/JSEN.2023.3268540 [12] "Spintronic Sensors Based on Magnetic Tunnel Junctions for Wireless Eye Movement Gesture Control", A. Tanwear et al., IEEE Transactions on Biomedical Circuits and Systems, vol. 14, no. 6, pp. 1299-1310, (2020), doi:10.1109/TBCAS.2020.3027242.

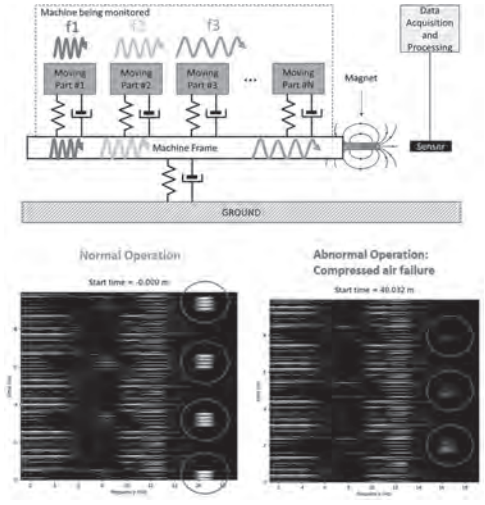

CONTRIBUTED PAPERS

CE-02. Arrays of coupled magnetic tunnel junctions for sensor applications. *A. Meo*[1], F. Garesci[2], A. Grimaldi[2,3], D. Rodrigues[1], M. Carpentieri[1] and G. Finocchio[3] *1. Department of Electrical and Information Engineering, Politecnico di Bari, Bari, Italy; 2. Department of Engineering, University of Messina, Messina, Italy; 3. Department of Mathematical and Computer Sciences, Physical Sciences and Earth Sciences, University of Messina, Messina, Italy*

Magnetic tunnel junction (MTJs) are the most promising spintronic device thanks to their compatibiility with CMOS technology, scalability and low power consumption. We have designed a spintronic accelerometer exploiting a system of MTJs in which the MTJs, working as spin-toque oscillators (STOs) and spin-torque diodes (STDs), are integrated on excitable substrates, such as microelectromechanical systems (MEMS), that can transduce the external stimulus (a_{ext}) into a mechanical excitation. This translates into an excitation of the magnetic system via the stray field that couples the MTJs. When the distance between the MTJs changes, this displacement reflects into a variation of the dipolar coupling between the MTJs that results in a change in the output voltage generated by the MTJs working as STD, via spin diode effect [1]. By exploiting the different timescales characterising the coupled magneto-mechanical system, this change in the output voltage allows to extract the acceleration directly [2,3]. We extend the original design to an array of magnetic tunnel junctions, exemplified in Fig.1. Arrays of MTJs allow to extend the detection from 1D to 2D and can yield an improvement of the sensitivity and energy efficiency of the accelerometer. Furthermore, this design could also be exploited in other applications, such as microwave amplifiers and reservoir computing. Here we explore different design configurations and perform systematic studies on the dynamics of the array of MTJs, both mechanical and magnetic, to find those conditions that yield a stable synchronisation between the MTJs, a linear output signal from the fixed-MTJs and allows to maximise the output sensitivity. This work was supported under the project number 101070287 – SWAN-on-chip – HORIZON-CL4-2021-DIGITAL-EMERGING-01; the MUR-PNRR project SAMOTHRACE (ECS00000022), funded by European Union (Next-Generation EU); the projects PRIN 2020LWPKH7 – The Italian factory of micromagnetic modeling and spintronics and PRIN_20225YF2S4 – Magneto-Mechanical Accelerometers, Gyroscopes and Computing based on nanoscale magnetic tunnel junctions (MMAGYC), funded by the Italian Ministry of University and Research.

1. Finocchio, G. *et al.* Appl. Phys. Lett. 118 (2021), 160502. 2. Meo, A. *et al*, Phys. Rev. Appl. 20 (2023), 034003. 3. Meo, A. *et al*, Solid-State Electronics 208 (2023), 108727.

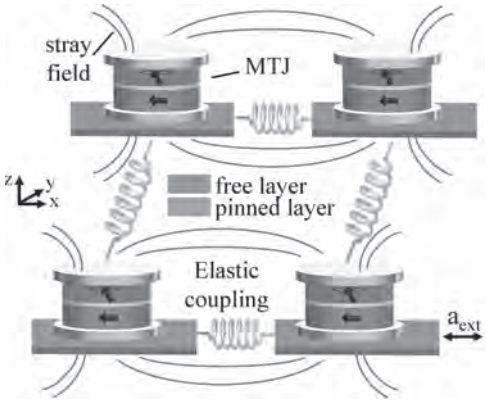

Sketch of the accelerometer design.

CE-03. Withdrawn

CE-04. Flexible planar-Hall magnetometer with nT resolution at extremely low frequencies. *J. Schmidtpeter*[1,2], P.T. Das[1], P. Makushko[1], E. Oliveros-Mata[1], Y. Zabila[1], C. Schubert[1], T. Wondrak[2] and D. Makarov[1] *1. Institute of Ion Beam Physics and Materials Research, Helmholtz-Zentrum Dresden-Rossendorf e.V., Dresden, Germany; 2. Institute of Fluid Dynamics, Helmholtz-Zentrum Dresden-Rossendorf e.V., Dresden, Germany*

Flexible and stretchable magnetic sensors have attracted a lot of attention recently as they have unique properties, being ultra-thin, lightweight, highly flexible and stretchable. They can provide new opportunities in human health monitoring, wearable electronics, and other fields such as process monitoring. In recent years, therefore, considerable research efforts have been made to develop flexible and stretchable magnetic sensors to meet the requirements of future technologies, and significant progress has been made [1-3]. Moreover, the magnetic properties of these sensors are comparable to those of industry standard rigid magnetic field sensors, with the added ability to adapt to complex surface geometries and to scan in direct contact with the sample surface [4,5]. In the present study, highly flexible exchange biased planar-Hall sensors on different polymer substrates are fabricated and the most important optimization steps required to increase their resolution in nT level are identified for extremely low frequencies (<10 Hz). In order to achieve this, the role of other key parameters such as layer stacks, sensor geometries, substrates and fabrication steps have also been investigated. Moreover, the effects of repeated bending cycles on sensor sensitivity, linearity and noise performances are investigated to determine the long-term stability and reliability of the manufactured devices. Finally, the sensor performance is evaluated with rigorous bending and fatigue tests, that simulate real-world conditions encountered in wearable applications. This research contributes to the advancement of flexible sensor technology by providing insight into the material and sensor performance under mechanical stress, paving the way for reliable and high-performance flexible sensor systems.

[1] Wang, Zhiguang, et al. *Adv.Mater. (Deerfield Beach, Fla.)* 28.42 (2016): 9370. [2] Granell, Pablo Nicolás, et al. *npj Flex. Electron.* 3.1 (2019): 3. [3] Melzer, Michael, et al. *Adv. Mater.* 27.7 (2015): 1274. [4] Nhalil, Hariharan, et al. *Appl. Phys. Lett.* 123.2 (2023). [5] Kim, Mijin, et al. *IEEE Magn. Lett.* 11 (2020): 1-5.

CE-05. Multi-Functional Flexible Planar Hall Effect Sensors.

D. Lahav[1], H. Nhalil[1], M. Schultz[1], S. Amrusi[2], A. Grosz[2] and L. Klein[1]
1. Physics, Bar Ilan Institute of Nanotechnology and Advanced Materials, Department of Physics, Bar-Ilan University, Ramat Gan, Tel Aviv 52900, Israel; 2. Electrical and Computer Engineering, Ben-Gurion University of the Negev, Beer-Sheva, Israel

Magnetic sensors are essential in various technological applications, including navigation, medical diagnostics, industrial automation, consumer electronics, and more. Among magnetoresistive sensors, planar Hall effect (PHE) sensors, in particular, offer significant advantages such as ultra-low equivalent magnetic noise (EMN) in the range of pT/√Hz, straightforward design, and cost-effectiveness. In previous studies we have presented rigid elliptical PHE sensors with EMN of 24 pT/√Hz at 50 Hz [1]. Furthermore, by integrating magnetic flux concentrators (MFCs) an EMN of 5 pT/√Hz at 10 Hz was achieved [2]. Recently, we have reported flexible elliptical PHE sensor (Fig.1) with EMN of ~200 and ~300 pT/√Hz at 10 Hz, in flat and bent states, respectively [3]. These EMN values represent a major improvement compared to other flexible magnetic field sensors. Here, we report a significant step forward and present a multi-functional flexible PHE sensor, that can be used not only for measuring magnetic fields but also for measuring minute strains. We will present our latest results which indicate that flexible elliptical PHE sensor have the potential of serving as strain gauges with the ability to detect few percents of micro-strain.

[1] H. Nhalil, P. T. Das, M. Schultz, S. Amrusi, A. Grosz, and L. Klein, Applied Physics Letters, vol. 117, no. 26, p. 262403 (2020). [2] H. Nhalil, T. Givon, V. Mor, M. Schultz, S. Amrusi, L. Klein, and A. Grosz, IEEE Sensors Letters, vol. 3, no. 12, pp. 1–4 (2019). [3] H. Nhalil, D. Lahav, M. Schultz, S. Amrusi, A. Grosz, and L. Klein, Applied Physics Letters, vol. 123, p. 024102 (2023).

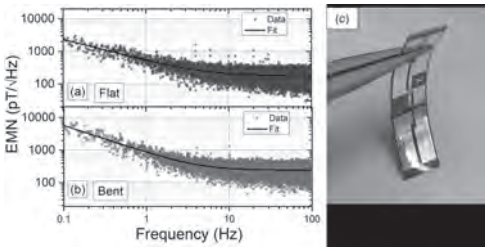

Figure 1: EMN of flexible elliptical PHE sensors vs. frequency in (a) flat and (b) bent states. (c) A photo of a flexible elliptical PHE sensor

CE-06. Optically Broadband Piezo-Optomechanical Magnetometer.

Z. Castillo[1,2], *B.P. Smith*[1], A. Will-Cole[1], M. Dong[3], K. Bussmann[4], P. Finkel[4] and M. Eichenfield[1,5] *1. Sandia National Laboratories, Albuquerque, NM, United States; 2. Department of Physics and Astronomy, University of New Mexico, Albuquerque, NM, United States; 3. The MITRE Corporation, Bedford, MA, United States; 4. US Naval Research Laboratory, Washington, DC, United States; 5. Wyant College of Optical Sciences, University of Arizona, Tucson, AZ, United States*

Precision sensing of magnetic fields has numerous applications spanning navigation [1], geology [2], and biology [3]. Optomechanical magnetometers are of particular interest due to their low power, miniaturization, scalability, and sensitivities of pT/√Hz or better without the need for external magnetic shielding or cryogenic cooling [4]. Here we demonstrate a magnetic field peak sensitivity of ~52 pT/√Hz using an optically broad band device, an important advancement due to the dramatically relaxed requirements for laser stability and linewidth. The optomechanical device also includes piezoelectric actuation that enables the sensor to be tuned to its optimal sensing point despite fabrication errors and environment conditions. Our sensor, shown in Fig. 1, uses the piezo-optomechanical Mach-Zehnder interferometers described in [5]. The addition of sputtered $Fe_{0.5}Co_{0.5}$/Ag multilayers on a single modulator arm makes the device sensitive to magnetic fields in proportion to the piezomagnetic coefficient, which quantifies the change in strain per change in magnetic field, as shown in Fig. 2. Additionally, electrical modulation of the piezoelectric actuator can frequency shift the signal of interest by creating a phase modulated local oscillator that frequency mixes with the magnetically modulated signal phase due to the square law nature of the photodetection. This frequency shifting has several advantages: electronic *1/f* noise as well as other technical noise is avoided, shot noise is readily achieved, and the sensitive mechanical modes of the device that exist at megahertz frequencies may be used to measure lower frequency fields [6].

[1] J. S. Bennett et al., "Precision Magnetometers for Aerospace Applications: A Review," Sensors, vol. 21, no. 16, 2021 [2] E. A. Lima and B. P. Weiss, "Ultra-high sensitivity moment magnetometry of geological samples using magnetic microscopy," Geochemistry, Geophysics, Geosystems, vol. 17, no. 9, pp. 3754–3774, 2016 [3] A. Borna et al, "Non-Invasive Functional-Brain-Imaging with an OPM-based Magnetoencephalography System," PLOS ONE, vol. 15, no. 1, pp. 1–24, Jan. 2020 [4] B.-B. Li et al., "Ultrabroadband and sensitive cavity optomechanical magnetometry," Photon. Res., vol. 8, no. 7, pp. 1064–1071, Jul. 2020 [5] M. Dong et al., "Piezo-optomechanical cantilever modulators for VLSI visible photonics," APL Photonics, vol. 7, no. 5, p. 051304, May 2022 [6] M. J. D'Agati et al., "High-Q Factor, Multiferroic Resonant Magnetic Field Sensors and Limits on Strain Modulated Sensing Performance," Journal of Microelectromechanical Systems, vol. 32, no. 1, pp. 91–102, 2023

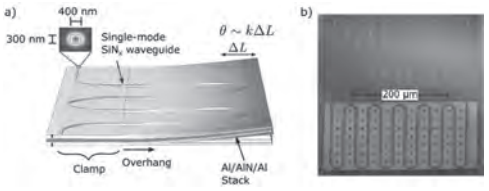

Fig. 1. a) CAD rendering of the piezo-optomechanical magnetometer with magnetostricitve material (teal) and buried piezoelectric layer (fuchsia). b) SEM image of the sensor with magnetostricitve film (lighter shade). Interference between the upper and lower paths imprints the strain induced phase modulations into amplitude fluctuations of the output intensity.

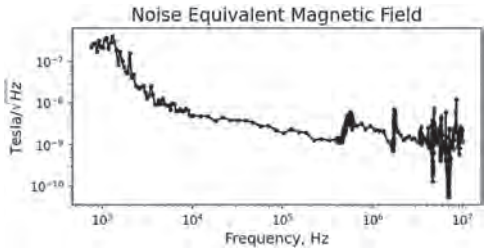

Fig. 2. Results of direct readout of the amplitude modulated optical signal. Mechanical resonances of the structure beyond 1 MHz enhance the minimum detectable signal, allowing an optimal sensitivity at 52 pT/√Hz near 6 MHz.

CE-07. Organic Solvent Chemical Sensing with various Magnetic Tunnel Junction based Molecular Spintronics Device Configurations.

H. Brown[1] and P. Tyagi[1] *1. University of The District of Columbia, Washington, DC, United States*

In an era where precision and sensitivity in chemical sensing are paramount, our innovative integration of organic molecules into magnetic tunnel junctions heralds a transformative advancement in spintronics-based applications. The demand for novel, low-power, robust, nanoscale chemical sensors is a critical topic of interest for many groups [1-3]. The aim of this research is to develop magnetic tunnel junction based molecular spintronics devices (MTJMSD) as a system to achieve commercially adaptable nanoscale chemical sensors. In this study we use a "pillar" and "hole" array MTJMSD configuration where various organic molecules terminating in thiol

functionalized groups covalently bond to ferromagnetic electrodes separated by a thin insulating layer of 1-2 nm via electrochemical functionalization [4]. Utilizing common semiconductor fabrication techniques and spin-dependent transport measurements, we explore using MTJMSD's as nanoscale sensors. Our results highlight the robust functionality of our bare MTJ followed by appreciable differences in electron spin resonance (ESR), vibrating sample magnetometer (VSM), and magnetic force microscopy (MFM) measurements after molecular functionalization. The sensor was exposed to ethanol, acetone, IPA (Isopropyl alcohol), and dichloromethane highlighting its discrimination functionality. These findings solidify the MTJMSD as a reliable spintronic applications test bed while displaying novel chemical sensing capabilities. This work paves the way for future research in molecular spintronics-based applications broadly and highlights their potential to revolutionize nanoscale chemical detection specifically.

[1] D. Zappa, "Low-power detection of food preservatives by a novel nanowire-based Sensor Array," *Foods*, vol. 8, no. 6, p. 226, Jun. 2019. doi:10.3390/foods8060226 [2] J. Li, D. Powell, S. Getty, and Y. Lu, "High sensitivity, low power nano sensors and devices for chemical sensing - NASA technical reports server (NTRS)," NASA, https://ntrs.nasa.gov/citations/20050082006 (accessed Jul. 23, 2024). [3] D. Mandler and S. Kraus-Ophir, "Self-assembled monolayers (sams) for electrochemical sensing," *Journal of Solid State Electrochemistry*, vol. 15, no. 7–8, pp. 1535–1558, Jul. 2011. doi:10.1007/s10008-011-1493-6 [4] P. Tyagi, E. Friebe, and C. Baker, "Advantages of prefabricated tunnel junction-based molecular spintronics devices," *Nano*, vol. 10, no. 04, p. 1530002, Jun. 2015. doi:10.1142/s1793292015300029

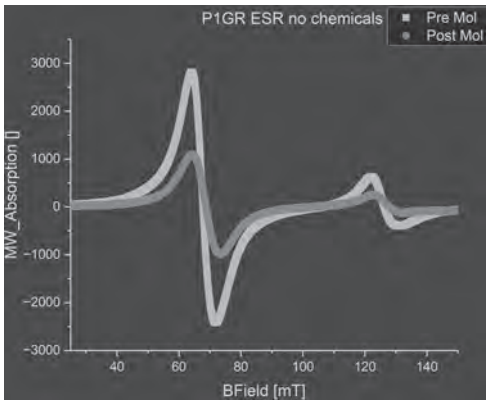

Figure 1: Pre-molecule and post-molecule in-plane ESR signals show a distinct change in absorbed microwave radiation resulting from molecular effect

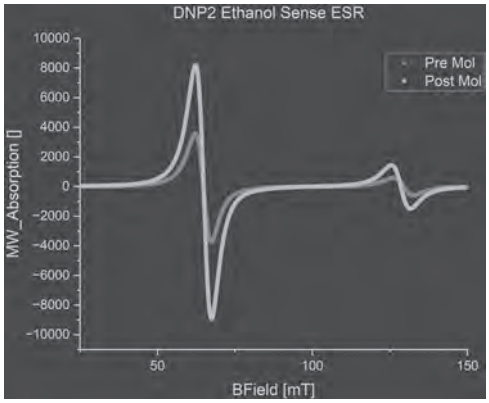

Figure 2: In-plane ESR spectrum showing distinct microwave absorption in the presence of ethanol between a pre-molecule MTJ, and a post-molecule treated MTJ

CE-08. Gain Enhancement and Ground Plane Immunity of Mechanically Driven Thin-Film Bulk Acoustic Wave Resonator Magnetoelectric Antenna Arrays. *B. Luo*[1*], X. Liang[1], H. Chen[1], N. Sun[1], H. Lin[2] and N.X. Sun[1] *1. Electrical and computer engineering, Northeastern University, Boston, MA, United States; 2. Winchester Technologies, Burlington, MA, United States*

In recent decades, the escalating demand for compact, low-profile, and high-gain antennas has been driven by the proliferation of applications such as Internet-of-Things (IoTs), 5th generation (5G) wireless systems, and implantable medical devices [1-2]. Conventional electrical antennas face challenges such as large size, detuned impedance, degraded gain, and poor radiation efficiency when mounted on a ground plane. These limitations arise from their reliance on electromagnetic resonance and electrical dipole radiation. In contrast, ME antennas leverage electromechanical resonance, ME coupling, and magnetic dipole radiation, offering ultra-compact sizes comparable to acoustic wavelengths and enhanced radiation performance on ground planes [3-7]. This paper presents groundbreaking advancements in magnetoelectric (ME) antenna technology, demonstrating significant antenna gain improvements and ground plane immunity by utilizing thin-film bulk acoustic wave resonator (FBAR) ME antenna arrays [8]. Our study explores parallel and series array topologies to achieve substantial gain and radiation efficiency enhancement without compromising impedance matching and quality factor of ME resonators. A notable 10 dBi gain enhancement is observed in a 3×3 FBAR ME array, achieving a peak antenna gain of –17.3 dBi (Fig. 1), which is 50 dBi higher than the start-of-art loop or dipole electrical antennas with comparable sizes [4] [8]. We have also experimentally demonstrated the ground plane immunity of FBAR ME antenna arrays, showing a 3 dBi gain enhancement when mounted on various ground planes (Fig. 2). The demonstrated ground plane immunity and gain enhancement make FBAR ME antenna arrays promising ultra-compact platform-independent conformal antenna candidates for portable electronic and implantable biomedical devices, wireless communication, and wireless power transfer.

[1] W. Hong, Z.H. Jiang, C. Yu, *et al.*, *IEEE Transactions on Antennas and Propagation*, Vol. *65*, p.6231-6249 (2017). [2] A. Kiourti and K. S. Nikita, *IEEE Antennas and Propagation Magazine*, Vol. *54*, p. 210-228 (2012). [3] C. Dong, Y. He, M. Li, N. X. Sun *et al.*, *IEEE Antennas and Wireless Propagation Letters*, Vol.*19*, p.398-402 (2020). [4] T. Nan, H. Lin, Y. Gao, N. X. Sun *et al.*, *Nature Communications*, Vol. *8*, 296 (2017). [5] M. Zaeimbashi, M. Nasrollahpour, A. Khalifa, N. X. Sun *et al.*, *Nature Communications*, Vol. *12*, 3141 (2021). [6] X. Liang, H. Chen, N. Sun, B. Luo, N. X. Sun *et al.*, *Advanced Engineering Materials*, Vol. *25*, p.2300425 (2023). [7] B. Luo, A. Will-Cole, C. Dong, N. X. Sun *et al*., *Nature Reviews Electrical Engineering* Vol.*1*, 317-334 (2024). [8] B. Luo, X. Liang, H. Chen, N. X. Sun *et al.*, *Advanced Functional Materials*, p.2403244 (2024).

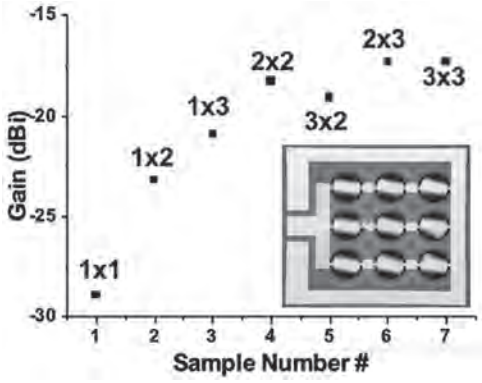

Figure 1 Antenna gain versus ME antenna array topology and number. The inset shows the optical image of the 3x3 ME antenna array.

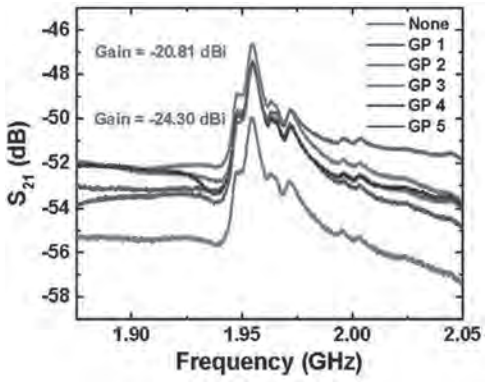

Figure 2 Experimental demonstration of ground plane immunity of ME antenna array. 3-dBi gain enhancement was demonstrated in S_{21} measurements in different sizes of ground planes (GPs 1~5) over a plastic substrate (None).

CE-11. Multichannel Giant Magnetoresistance Eddy-Current Probes with Dynamic Liftoff Correction. *L. Bui*[1,2], J. Jeng[1], H. Huang[1] and T. Nguyen[1] *1. Department of Mechanical Engineering, National Kaohsiung University of Science and Technology, Kaohsiung, Taiwan; 2. Faculty of Mechanical Engineering, Hung Yen University of Technology and Education, Hung yen, Vietnam*

This work presents a technique to overcome defect signal discrepancies at different liftoff levels for the eddy-current (EC) array probes based on giant-magnetoresistance (GMR) sensors. The relationship between flaw signals at different liftoff distances is explored by employing the excitation coil as a displacement sensor to detect the liftoff distance. The schematic diagram for the dynamic liftoff correction system is shown in Fig. 1. The GMR chip is the GF708 bare die from Sensitec GmbH combined with the tiny excitation coil with a feature size of 2.8 mm [1]. Fig. 2(a) shows the aluminum sample with six artificial slots, #1 to #6, of which the depths are 0.1, 0.3, 0.5, 1.0, 1.5, and 1.8 mm, respectively. Each defect is 0.5 mm in width, and the adjacent cracks are 14.3 mm apart. Fig. 2(b) shows the phasor diagram of in-phase and quadrature EC signals from a one-dimensional scan over the six cracks. The excitation frequency is 45 kHz, and liftoff distances are 0.1, 0.2, and 0.3 mm, respectively. It is evident that the signals for different crack depths may overlap when the liftoff distances change from 0.1 to 0.3 mm. As the liftoff distance increases, the signal amplitude diminishes, and the phase difference increases. The correction factors are calculated using the quadratic polynomial regression method based on the data taken by the GMR EC probe and displacement sensors. By using the correction factors, the EC data are rescaled and rotated based on the measured liftoff distance to eliminate the liftoff effect, as shown in Fig. 2(c). It is found that the defect signal at a liftoff distance of 0.1 mm is restored from those at liftoff distances of 0.2 and 0.3 mm. The corrected signals at various liftoff distances overlap well, indicating that the suggested method can efficiently recover the defect signals within an adequate liftoff range. The proposed method is valuable for quantitative EC imaging of surface defects on high conductivity samples

[1] L.-V. Bui *et al.*, "High-Resolution Flaw Detection Using Eddy-Current Probe Array Based on Giant Magnetoresistance Sensors," *IEEE Transactions on Magnetics,* pp. 1-1, 2024, doi: 10.1109/tmag.2024.3402331

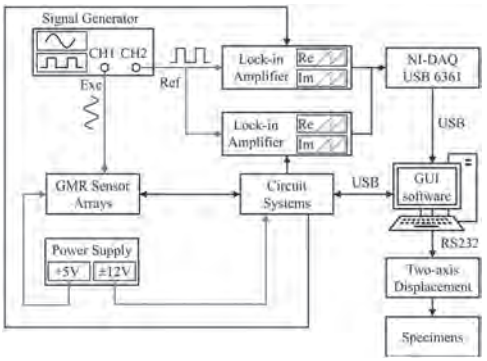

Fig. 1. Functional diagram of the GMR EC probe array flaw imaging system with dynamic liftoff correction

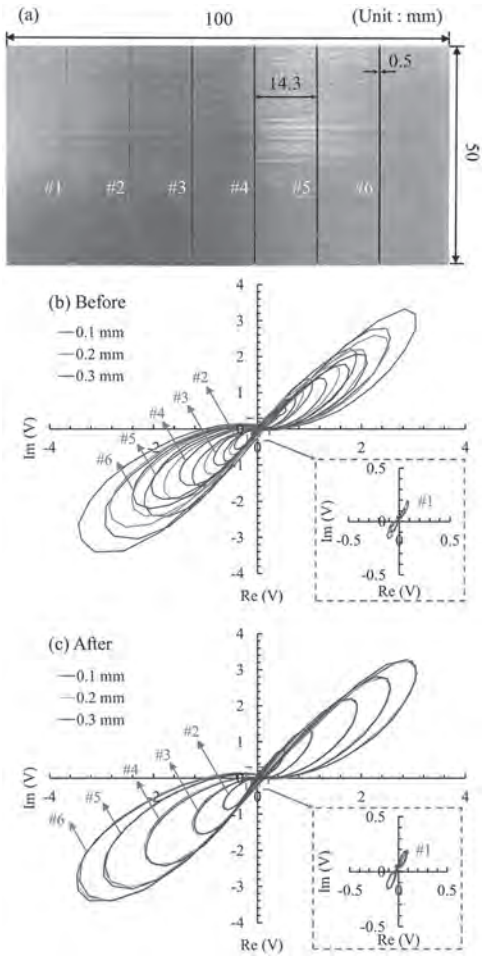

Fig. 2. EC signals before and after liftoff correction for cracks on an aluminum: (a) photograph of the sample; (b) the results before, and (c) after liftoff correction

CE-12. Noise Characterization of Spin-Transfer-Torque-based Magnetic Field Sensor. *K. Komuro*[1], H. Nicolas[2], B. Dieny[3], D. Oshima[1], T. Kato[4] and R. Sousa[3] *1. Electronics, Graduate School of Engineering, Nagoya University, Nagoya, Japan; 2. University of Strasbourg, Strasbourg, France; 3. IRIG, Spintec, Grenoble, France; 4. IMaSS, Nagoya University, Nagoya, Japan*

In this study, we examined the signal-to-noise ratio (SNR) of magnetic field sensors based on spin transfer torque (STT) switching of magnetic tunnel junctions (MTJs) with perpendicular anisotropy. By applying a bias voltage to the MTJ, the magnetization of the free layer can be switched due to STT. The STT-based field sensor can detect the external field by measuring the change in switching voltage, since it depends on the external field applied to MTJ. The STT-based sensor has been demonstrated in Ref. [1], and reported a noise level of 21.8 $\mu T/Hz^{1/2}$. To understand the origin of the noise in the sensor, we have analyzed the STT switching behavior of MTJ pillars having different thermal stability factors Δ. The applied voltage dependence of the switching probability in each pillar was determined from at least 1000 pulse switching trials under varying external fields. The duration of the applied voltage pulses was 1 μs. The SNR was defined as the square of the voltage signal at a 50% switching probability, divided by its variance. The solid circles in Fig. 1 show the experimental SNR obtained from different samples as a function of Δ where no external field was applied. The SNR data confirms a monotonous increase for larger Δ. This suggests that the stochastic magnetization reversal dominates the noise of the STT-based MTJ sensor. The solid green and dashed blue lines show the theoretical calculation based on the stochastic reversal and the fitting as a function of Δ^2, respectively. The experimental results were reproduced well by the theoretical calculation and were confirmed to roughly vary as Δ^2. From these results, we found that adjusting Δ of MTJ is effective in achieving a large signal and low stochastic noise simultaneously. Acknowledgment: This work was partially supported by the European Research Council via grant reference ERC-2022-PoC2 (NANOSENSE No. 101100599).

[1] H. Nicolas *et al*., IEEE Sensors Journal, 23, pp. 5670-5680 (2023).

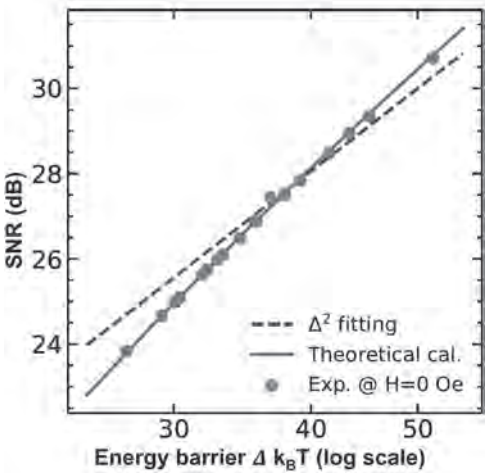

Fig. 1. Δ dependence of SNR of STT-based MTJ sensors under zero applied field (solid circles). The green solid and blue dashed lines represent the theoretical calculation results and the Δ^2 fittings, respectively.

CE-13. Simultaneous measurements of magnetomyographic and magnetocardiographic signals using SQUIDs and relocatable magnetoresistive-device-based flux sensors. *Y. Adachi*[1], T. Tatsuoka[2], T. Fukui[3], T. Shibuya[4] and S. Kawabata[5] *1. Applied Electronics Laboratory, Kanazawa Institute of Technology, Kanazawa, Japan; 2. METOOL Inc., Tokyo, Japan; 3. LibreFields LLC, Tokyo, Japan; 4. TDK Corp., Tokyo, Japan; 5. Department of Advanced Technology in Medicine, Tokyo Medical and Dental University, Tokyo, Japan*

INTRODUCTION: Magnetoresistive (MR) sensors are being used to detect biomagnetic signals alongside traditional superconducting quantum interference device (SQUID) sensors. MR sensors have a magnetic field resolution on the order of pT, while SQUID sensors typically achieve resolutions better than several fT. Although MR sensors have inferior magnetic flux resolution compared to SQUID sensors, they offer high flexibility for sensor placement. This study employed a relocatable MR sensor array alongside a SQUID biomagnetometer to simultaneously record biomagnetic signals, such as magnetomyographic (MMG) and magnetocardiographic (MCG) signals, to examine for any interference between the two systems. METHOD: A relocatable sensor array of three MR sensors (Nivio-xMR, TDK Corp., Japan) arranged with 40-mm intervals was used in conjunction with a 132-channel SQUID biomagnetometer system [1]. MMG measurements from the tibialis anterior (TA) and abductor pollicis brevis (APB) muscles of a subject, evoked by repetitive electric current pulses applied to the peroneal nerve at the knee and the median nerve at the wrist, respectively, were examined using both sensor arrays. Aside from MMG, MCG signals were also collected with the SQUID sensors positioned along the dorsal side and the MR sensors positioned along the ventral side of the body surface of a subject in the supine position. In both MMG and MCG measurements, the relative position and orientation of the MR sensor array to the SQUID sensor array were determined using marker coils. RESULT: Although each MR sensor was equipped with a flux concentrator composed of a magnetic material to enhance its magnetic field sensitivity, there was minimal interference with the SQUID performance. Both the MMG and MCG signals were successfully detected by SQUIDs and MR sensors as shown in Figs. 1-2. CONCLUSION: The two sensor arrays of SQUIDs and MR sensors could simultaneously measure of MMG and MCG signals with less mutual interference. These sensor types can complement each other's strengths and weaknesses, thereby enhancing the range of applications for biomagnetic measurements.

[1] Y. Adachi et al., Supercond Sci Tech, vol. 30 (2017) 063001, doi: 10.1088/1361-6668/aa66b3.

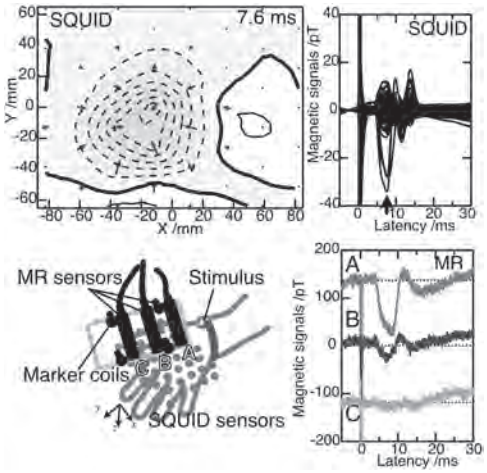

MMG measurement from APB by SQUID and MR sensors.

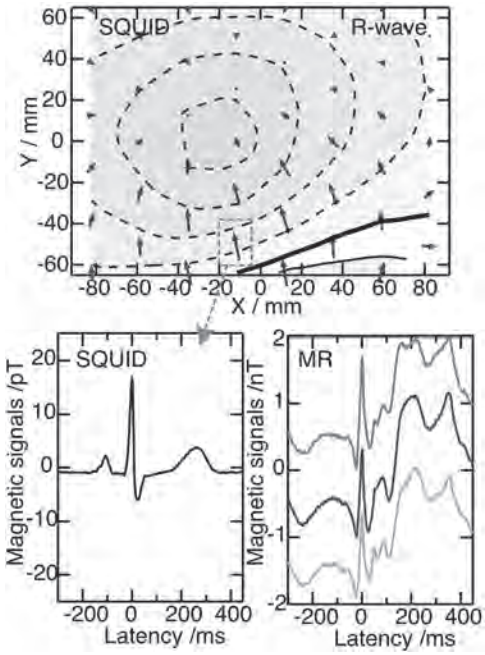

MCG signals simultaneously recorded SQUID and MR sensors.

Session CF
HARD MAGNETS II

George Hadjipanayis, Chair
University of Delaware, Newark, DE, United States

CONTRIBUTED PAPERS

CF-01. Assessing Induced Short-Range Order and Magnetocrystalline Anisotropy in Equiatomic FeNi. *L.H. Lewis*[1], P. Stamenov[2], P. Henry[3], J. O'Brien[2] and S. Langridge[3] *1. Northeastern University, Boston, MA, United States; 2. Trinity College, Dublin, Ireland; 3. Rutherford Appleton Laboratory, Didcot, United Kingdom*

Tetrataenite, the mineral name for atomically ordered FeNi, is of exploratory interest as a permanent "gap" magnet. This compound, which is only found naturally in extraordinarily slowly cooled meteorites, possesses an atomically layered structure (Strukturbericht designation $L1_0$, AuCu structural prototype) that can donate appreciable magnetocrystalline anisotropy energy (MAE) to furnish a theoretical energy product between that of the weaker oxide ferrimagnets and the strongest rare-earth "supermagnets". While indeed a promising material, engineering tetrataenite into a permanent magnet requires an immense acceleration of its formation to industrially relevant timescales. Further, the constituent Fe and Ni atoms in the crystal lattice must undergo substantial segregation into layers to realize a high MAE[1]. Approaching these objectives, tailored processing of disordered, highly strained FeNi alloys employing thermal energy augmented by strain and magnetic energies is found to induce local atomic order in only 6 weeks. This outcome is confirmed by simultaneous conversion X-ray and backscattered g-ray ^{57}Fe Mossbauer spectroscopy[2] and by neutron scattering. Analyses of data returned by these probes inform the extent, distribution and degree of atomic order conferred by the specialized processing protocol, and suggests improvements for future efforts to realize FeNi-based permanent magnets.

[1]. Woodgate, C. D., Patrick, C. E., Lewis, L. H., & Staunton, J. B., "Revisiting Néel 60 years on: The magnetic anisotropy of $L1_0$ FeNi (tetrataenite)", *J. Appl. Phys*., 134(16) (2023) [2]. Lewis, Laura H., and Plamen S. Stamenov. "Accelerating Nature: Induced Atomic Order in Equiatomic FeNi." *Advanced Science* (2023): 2302696.

CF-02. Withdrawn

CF-03. Influence of Strain and Applied Field on the $L1_0$ Atomic Ordering and Subsequent Hard Magnetic Properties of Near-Equiatomic FeNi. *C.D. Woodgate*[1,2], L.H. Lewis[3,4] and J.B. Staunton[1] *1. Department of Physics, University of Warwick, Coventry, United Kingdom; 2. H. H. Wills Physics Laboratory, University of Bristol, Bristol, United Kingdom; 3. Department of Chemical Engineering, Northeastern University, Boston, MA, United States; 4. Department of Mechanical and Industrial Engineering, Northeastern University, Boston, MA, United States*

The ever-growing demand for advanced permanent magnets is accompanied by a pressing need for materials of reduced critical element content, including rare earth elements, which carry concerns around price volatility, geopolitical sensitivities, and significant environmental impact. One rare-earth-free magnetic material of current interest is atomically ordered FeNi [1], which crystallizes in the $L1_0$ structure and is commonly referred to by its meteoritic mineral name, tetrataenite [2]. However, a low atomic ordering temperature and consequently sluggish kinetics make this material challenging to synthesize in industrially relevant timeframes. Here, new results dervied from first-principles computational approaches will be presented examining the combined impacts of mechanical strain, applied magnetic field, and varying Fe:Ni ratio on the $L1_0$ ordering temperature of this material (Fig. 1). These results are in alignment with recent experimental outcomes reporting induced atomic order in bulk specimens, given suitable processing conditions [3]. Our DFT-based methodology [4,5] enables holistic modelling of both atomic ordering and associated magnetocrystalline anisotropy—including the effects of finite temperature —within the same computational framework. These results suggest new routes by which bulk synthesis of this material could potentially be achieved. [Research supported by the U.S. Department of Energy, Office of Basic Energy Sciences under Award Number DE SC0022168 (for atomic insight) and by the UK Engineering and Physical Sciences Research Council, Grant No. EP/W021331/1 and the U.S. National Science Foundation under Award ID 2118164 (for advanced manufacturing aspects).]

[1] L. Neel *et al.*, J. Appl. Phys. 35, 873 (1964). [2] L. H. Lewis *et al.*, J. Phys.: Condens. Matter 26, 064213 (2014). [3] L. H. Lewis, P. S. Stamenov, Adv. Sci. 2302696 (2023). [4] C. D. Woodgate *et al.*, J. Appl. Phys. 134, 163905 (2023). [5] C. D. Woodgate *et al.*, arXiv:2401.02809 (2024).

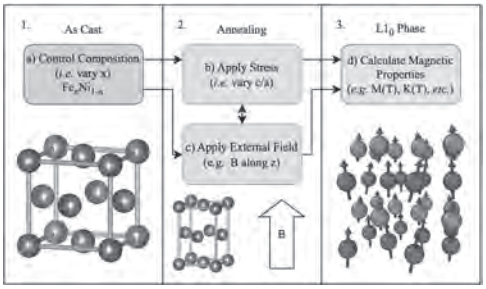

Figure 1: Potential processing routes to accelerate formation of the atomically ordered $L1_0$ phase of FeNi.

CF-04. Synthesis of Fe_5C_2 nanocrystals with enhanced anisotropy.
P. Joshi[1], H. Abbas[1], T. Karki[1], J. Mohapatra[1] and P. Liu[1] *1. Department of Physics, University of Texas at Arlington, Arlington, TX, United States*

Fe_5C_2 exhibits a monoclinic crystal structure with significant magnetocrystalline anisotropy (1.04 MJ/m^3) [1]. In this study, we achieved anisotropic Fe_5C_2 nanocrystals with an anisotropy field exceeding 10 kOe by modulating their aspect ratios from 1 to 2.7. To assess anisotropy in the solution-phase synthesized samples, we measured hysteresis loops along both the parallel and perpendicular directions relative to the alignment (with sample packing fraction < 5%). Notably, for samples with aspect ratios of 2.7, the hysteresis loop measured along the alignment direction exhibited an enhanced coercivity of 725 Oe and a remanence-to-saturation magnetization (M_s/M_r) ratio of 0.62. On the contrary, along the perpendicular direction, we observed decreased coercivity (670 Oe) and a lower M_s/M_r ratio (0.22). Interestingly, as the aspect ratio decreased to 1.8 and 1, we not only observed reduced coercivity along the alignment direction but also found that the parallel and perpendicular hysteresis loops coincided at fields below 8 kOe. Although this approach does not directly evaluate the anisotropy field, the consistent shift of the coincide point of the parallel and perpendicular hysteresis loops suggests that we successfully induced high anisotropy in Fe_5C_2 nanocrystals through aspect ratio modulation.

[1] L. Yin, R. Juneja, L. Lindsay, T. Pandey, and D. S. Parker, *Semihard Iron-based Permanent-Magnet materials*, Phys. Review Applied., 2021, 15, 024012.

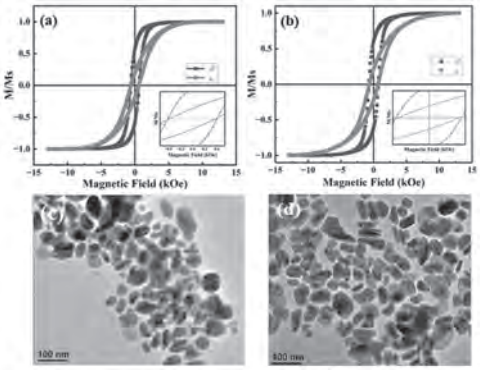

Figure 1: Room temperature hysteresis loops of aligned samples and corresponding TEM images with aspect ratios of (a, c) 1.8 and (b, d) 2.7.

CF-05. A novel ferromagnetic phase Fe_3Cu exhibiting high anisotropy.
H. Abbas[1], P. Joshi[1], T. Karki[1], J. Mohapatra[1] and P. Liu[1] *1. Physics, University of Texas at Arlington, Arlington, TX, United States*

In this study, we report the fabrication of a novel ferromagnetic phase of Fe_3Cu using a chemical synthesis approach. XRD pattern shows that Fe_3Cu exhibits a tetragonal crystal structure (Fig. 1). This structure's theoretically calculated anisotropy constant is 0.42 MJ/m^3 [1]. The rod-shaped morphology of nanostructures was observed, beneficial for adding shape anisotropy. The zero field-cooled and field-cooled magnetization curves showed that the blocking temperature lies above the room temperature which is the signature of the highly anisotropic nanostructures (Fig. 2 (a)). To measure the magnetic anisotropy, M-H loops of aligned samples were taken when their easy axis of magnetization was aligned parallel/perpendicular to the applied magnetic field (Fig. 2 (b)). A coercivity of 710 Oe and 620 Oe was observed at room temperature when the sample was aligned parallel and perpendicular to the magnetic field, respectively. The remanence to saturation magnetization ratio of cubic structure (or any randomly aligned structure) is usually observed to be 0.5. Here, we observed the remanence to saturation magnetization ratio as 0.68 and 0.24, when the sample was aligned parallel and perpendicular to the applied magnetic field, respectively. These results correspond to the magneto crystalline anisotropy due to the tetragonal phase and shape anisotropy due to the rod shape of nanostructures. The higher concentration of nanorods and higher aspect ratio benefit the anisotropy.

1. https://magmat.herokuapp.com/query?select_type=reduced_formula&in_string=Fe3Cu.

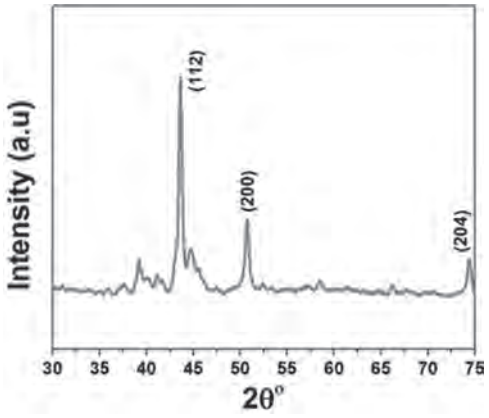

Figure 1: XRD pattern for Fe_3Cu nanoparticles

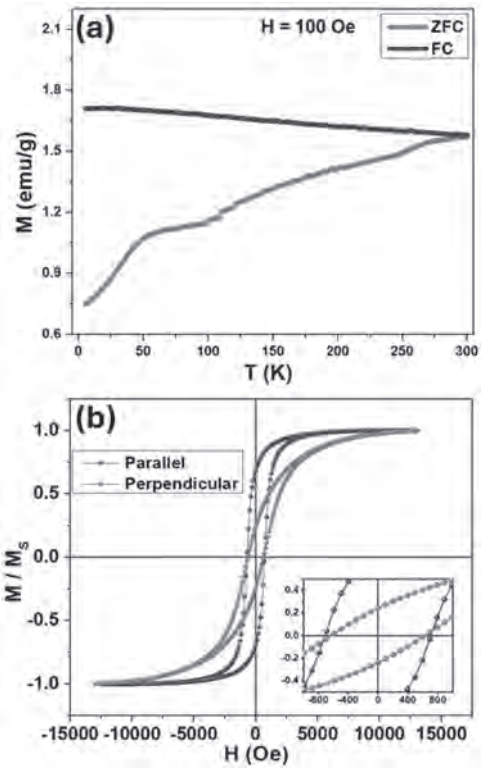

Figure 2: (a) ZFC-FC magnetization curve at 100 Oe, (b) M-H loop at 300 K when the sample was aligned parallel and perpendicular to the magnetic field.

CF-06. Process-Structure-Property Relationships in Additively Manufactured Alnico Permanent Magnets. *A.R. Duong*[1], I.M. Smith[3], K. Snyder[2], S. Sarker[1], O. Bishop[1,2], E. Carpenter[3] and R. Barua[1]
1. Mechanical Engineering, Virginia Commonwealth University, Richmond, VA, United States; 2. Commonwealth Center for Advanced Manufacturing, Disputanta, VA, United States; 3. Chemistry, Virginia Commonwealth University, Richmond, VA, United States

As the United States aims for net-zero carbon emissions by 2050, demand for rare-earth-free permanent magnets is expected to rise globally [1]. Among alternatives, Alnico alloys are promising, especially for high-temperature applications. Alnico's exceptional magnetic properties come from its unique microstructure, featuring periodically distributed, crystallographically oriented ferromagnetic (Fe-Co)-rich nanostructures in an (Al-Ni)-rich matrix formed by spinodal decomposition. Metal additive manufacturing technologies offer new options for tailoring the microstructure of Alnico alloys. This study is focused on examining process-structure-property correlations in Co-free Alnico-3 alloys fabricated using magnetic-field-assisted direct energy deposition (DED). Gas atomized pre-alloyed Alnico powders were built into an array of ~90 samples (~5x5x10mm) wherein laser operating parameters (power P, speed v, beam radius D) and the powder mass flow rate during printing were varied systematically across the build. Subsequently, select specimens were heat-treated in an inert atmosphere at about 850 °C for 10 minutes, then slow-cooled to 550-800 °C for four hours [2]. Results show grain morphology and micro segregation in the nanostructured samples can be tailored by undercooling. In particular, higher energy density during deposition (E) increases the melt pool size, leading to larger grains and increased secondary phase nucleation due to slower cooling rates, Fig 1. In the as-printed state, coercivity (Hc) increases with increase in E monotonically. Intriguingly, following heat treatment, samples deposited with E<1.1 J*s/kg*mm^3 demonstrate an increase in Hc, while those deposited with E>1.1 J*s/kg*mm^3 show a distinct decrease. These results will be discussed in the context of micromagnetic simulations that reveal that the magnetic properties of DED-processed Alnico magnets are closely linked to the morphology and dimensions of the spinodal decomposed phases.
Acknowledgment: U.S. National Science Foundation (Award No. 2310234)

[1] - Coey, J. M. D. "Perspective and prospects for rare earth permanent magnets." *Engineering* 6.2 (2020): 119-131. [2] - Zhang, C., Li, Y., Han, X. H., Du, S. long, Sun, J. bing, & Zhang, Y. (2018). Structure and magnetic properties of Alnico ribbons. *Journal of Magnetism and Magnetic Materials*, *451*, 200–207. https://doi.org/10.1016/j.jmmm.2017.11.045

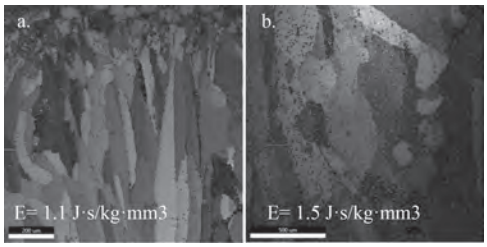

a) Low laser power sample demonstrates smaller grains and less precipitates, b) High laser power sample demonstrates larger grains and more precipitates.

CF-07. Influence of Nitrogen Stoichiometry on the Crystal Structure and Magnetic Properties of Antiperovskite Mn_3GeN. *S. O'Donnell*[1,2], C.E. Regier[2], S. Mahatara[1], S. Lany[1], S. Bauers[1], R.W. Smaha[1] and J.R. Neilson[2] *1. National Renewable Energy Laboratory, Golden, CO, United States; 2. Chemistry, Colorado State University, Fort Collins, CO, United States*

Nitride antiperovskites are an intriguing family of compounds that host a plethora of functional magnetic properties, ranging from hard permanent magnets to magnetocalorics. Within these compounds, the nitrogen stoichiometry can often vary based on synthesis conditions. However, the effects of varying nitrogen stoichiometry on the crystalline structure and magnetic properties are rarely studied. Here, we examine how altering the nitrogen stoichiometry in antiperovskite Mn_3GeN leads to not only a change in crystalline structure but also to substantial impacts on its hard magnetic properties. We show that the nitrogen stoichiometry can effectively be tuned based on synthesis conditions, where higher temperatures and inert atmospheres or vacuum leads to nitrogen-deficient compounds. Under appropriate conditions, a fully denitrided Mn_3Ge phase is obtained in a new metastable polymorph. We find that the magnetic hardness is substantially increased with decreasing nitrogen stoichiometry. Interestingly, the room temperature magnetization shows complex behavior that is non-linear with nitrogen stoichiometry. While intermediate amounts of nitrogen lead to a significant decrease in saturation magnetization, the magnetization is nearly fully recovered in the fully denitrided phase. These results clearly demonstrate the critical role nitrogen plays in determining both the crystalline structure and magnetic properties and is very likely applicable to the entire nitride antiperovskite family.

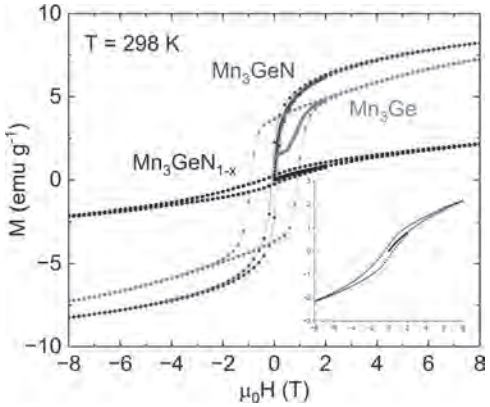

Magnetization as a function of applied field for Mn_3GeN, Mn_3GeN_{1-x}, and Mn_3Ge at T = 298 K.

CF-08. Densification of Nitride Permanent Magnet Nanoparticles. *R.W. Smaha*[1,2], S. O'Donnell[1,2], R. Kuchi[1,3], Y. Wu[1,4], R. Kinner[1,5], S. Bauers[1,2], F. Johnson[1,4], I.Z. Hlova[1,3] and M.J. Kramer[1,3] *1. Critical Materials Innovation Hub, U.S. Department of Energy, Ames, IA, United States; 2. National Renewable Energy Laboratory, Golden, CO, United States; 3. Ames National Laboratory, Ames, IA, United States; 4. Niron Magnetics, Minneapolis, MN, United States; 5. Powdermet, Euclid, OH, United States*

Several nitride-based compounds show great promise as permanent magnets containing little or no rare-earth elements. α″-$Fe_{16}N_2$ exhibits a magnetization in excess of the Slater-Pauling limit,[1] and $Sm_2Fe_{17}N_3$ is promising for high-temperature applications.[2] In particular, nanoparticles of these materials exhibit high magnetization and a promising magnetocrystalline anisotropy.[3] However, challenges exist in forming dense, grain-aligned magnets of these materials due to the low thermal stability of the nitride phases. We will discuss recent developments in densifying nanoparticle magnets of $Fe_{16}N_2$ and $Sm_2Fe_{17}N_3$ using low-temperature, high pressure methods, focusing on maintaining their coercivity and magnetization during processing steps including alignment and compaction. Isolating single-crystal nanograins and aligning them in a magnetic field without decomposition become more difficult with smaller grain sizes. Metallization of the intergranular regions aids in controlling the growth and stability of the grain boundary phases that form during these processing steps and is key to unlocking the potential of these materials as rare-earth-free or rare-earth-lean permanent magnets.

[1] J.P. Wang, Journal of Magnetism and Magnetic Materials., Vol. 497, p.165962 (2020). [2] J.M.D. Coey and H. Sun, Journal of Magnetism and Magnetic Materials., Vol. 87, p.L251 (1990). [3] R. Kuchi, et al., Journal of Alloys and Compounds., Vol. 980, p.173532 (2024).

CF-09. Giant coercivity in Manganese Substituted Strontium M-type Hexaferrite Nanopowders. *A. Sassi*[1,2], A. Pasko[1], S. Gam-Derouich[4], V. Yenugonda[2], F. Mazaleyrat[1] and A. Pathak[2,3] *1. SATIE, CNRS, Université Paris-Saclay, ENS Paris-Saclay, Gif-sur-Yvette, France; 2. Department of Physics, SUNY Buffalo State, Buffalo, NY, United States; 3. One Research Circle, GE Aerospace Research, Niskayuna, NY, United States; 4. ITODYS, UMR CNRS 71086, Université Paris Diderot, Sorbonne Paris Cité, Paris, France*

Nanopowders of manganese substituted strontium M-type hexagonal ferrites $SrMn_xFe_{12-x}O_{19}$ with $1 \leq x \leq 6$ were successfully synthesized using the citrate precursor sol-gel method [1]. The pH during the preparation was set to 6. The obtained powders were calcined at 900°C and at 950°C. XRD analysis at room temperature and magnetometry in a maximum field of 6 T at temperatures ranging from 5 to 393 K were performed. SEM and EDX analyses were also done in order to correlate the different parameters with the magnetic properties. XRD analyses showed that a calcination temperature of 950°C was necessary for the obtention of monophasic $SrMn_xFe_{12-x}O_{19}$ nanopowders (Figure 1). This temperature is higher than that needed for the formation of unsubstituted monophasic $SrFe_{12}O_{19}$ around 800°C. EDX analyses revealed that the obtained powder compositions correspond to the targeted compositions. When the Mn content increases, saturation magnetization, M_s decreases and thus going from 72 Am^2/kg for $x = 0$ to 32 Am^2/kg for $x = 6$. This can be explained by the replacement of Fe ions by Mn ions in parallel spin sites (*2a*, *2b* and *12k*) [2]. H_c on the other hand increases monotonically by increasing Mn content and reaches 1.14 T for $x = 6$. This important increase in coercivity might be explained by the effect of Mn on the particle size and shape which is supported by the SEM analyses. The latter showed that the particle size decrease by increasing Mn content while remaining under the single domain size, and the high Mn content particles tend to have platelet-like shapes. This study revealed the importance of conducting further investigation to improve the magnetic properties of $SrMn_xFe_{12-x}O_{19}$ and to better understand the effect of Mn on the high H_c values. Acknowledgements: This work was performed at the State University of New York (SUNY), Buffalo State University, and was supported by the National Science Foundation (Award No. DMR-2213412).

[1] A. K. Pathak and A. Sassi, Magnet powder and sintered magnet of strontium and barium M-type modified hexagonal ferrite, Pat. Ref. 160-2251P0, US Pat. No.: 63/600,105 [2] Kim, M., Lee, H. and Kim, J. (2020) 'Magnetic properties of Mn substituted strontium ferrite powders synthesized by the molten salt method', *AIP Advances*, 10(1). doi:10.1063/1.5129909.

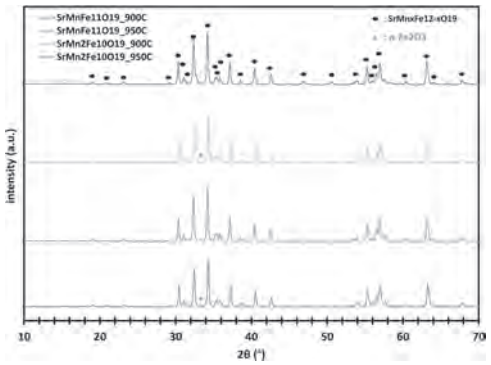

Figure 1: XRD patterns of SrM hexaferrite nanopowders after a calcintion at 900°C and 950°C.

CF-10. $L1_0$ FeNi films synthesized through denitriding of reactively sputtered FeNiN. *W. Beeson*[1], C. Jensen[2], V. Stanic[3], J. Jordan-Sweet[3], H. Zhang[4], S. Krylyuk[4], A. Davydov[4], J. Borchers[2], A.J. Grutter[2], C. Kinane[5], A. Caruana[5] and K. Liu[1] *1. Department of Physics, Georgetown University, Washington, DC, United States; 2. NIST Center for Neutron Research, National Institute of Standards and Technology, Gaithersburg, MD, United States; 3. IBM T.J. Watson Research Center, Yorktown Heights, NY, United States; 4. Materials Science and Engineering Division, National Institute of Standards and Technology, Gaithersburg, MD, United States; 5. ISIS, Rutherford Appleton Lab, Didcot, United Kingdom*

$L1_0$ FeNi is a potential rare-earth free high magnetic anisotropy material with large saturation magnetization. Due to its low order-disorder transition temperature and low diffusivity, the A1 to $L1_0$ transformation is kinetically limited, severely preventing its formation over laboratory timescales using conventional processing methods. Recent studies have provided a route to circumvent the kinetic limitations: denitriding of the more readily fabricated tetragonal FeNiN, often formed by molecular epitaxy (MBE) or insertion of N into FeNi.[1][2][3] In this work, we demonstrate synthesis of FeNiN films using reactive nitride sputtering on both STO and thermally oxidized Si/SiO_2 substrates, and subsequent denitriding to obtain $L1_0$ FeNi films. The 20 nm as-grown

films are non-magnetic, as shown in Fig. 1, and found to be single-phase tetragonal FeNiN by X-ray diffraction (XRD). After denitriding, the films become ferromagnetic and exhibit a large increase in coercivity, up to 1.6 kOe in the case of the films grown on Si/SiO_2. The $L1_0$ ordering of denitrided films was confirmed by detection of the (001) superlattice peak in XRD using synchrotron radiation, as shown in Fig. 2. Polarized neutron reflectometry measurements further explored N extraction as a function of time and the resulting structural and magnetic depth profile change. This study presents a promising industry-compatible fabrication route towards rare-earth-free and precious-metal-free high magnetic anisotropy materials. This work has been supported by the NSF (ECCS- 2151809).

[1] S. Goto, et al., Sci. Rep. 7, 13216 (2017) [2] K. Ito, et al., Appl. Phys. Lett. 116, 242404 (2020) [3] T. Nishio, et al., APL Mater. 9, 091108 (2021)

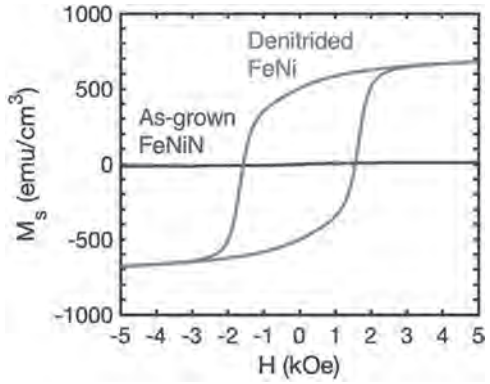

Figure 1. In-plane hysteresis loops of as-grown FeNiN and denitrided FeNi films.

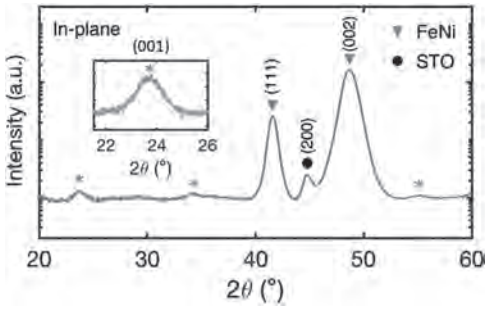

Figure 2. In-plane XRD θ-2θ scans of 20 nm denitrided FeNi films on STO, measured using synchrotron radiation with a photon energy of 8.33 keV. The asterisks denote the positions of $L1_0$ FeNi superlattice peaks. The inset shows an enlarged view of the FeNi (001) superlattice peak.

CF-11. Optimization of Coercivity and Price of a Permanent Magnet considering the Microstructure. *C. Wager*[1,2], C. Fillies[1], T. Schrefl[1,2], A. Kovacs[1,2], H. Oezelt[1], D. Böhm[1], Q. Ali[1], H. Yamano[3], M. Yano[3], N. Sakuma[3], A. Kinoshita[3], T. Shoji[3] and A. Kato[3] *1. Department of Integrated Sensor Systems, University for Continuing Education Krems, Wiener Neustadt, Austria; 2. Christian Doppler Laboratory for magnet design through physics informed machine learning, Wiener Neustadt, Austria; 3. Toyota Motor Corporation, Shizuoka, Japan*

Coercivity is the most important extrinsic property in permanent magnet applications. Microstructural parameters such as grain size and surface defects are important considerations in the production of permanent magnets. Yet the relationship between coercivity and microstructure remains in need of further exploration. [1] In this work we optimize the chemical composition of a $(Nd,Ce,La,Pr,Tb,Dy)_2(Fe,Co,Ni)_{14}(B,C)$ permanent magnet aiming for high coercivity and low price. To account for the microstructure, we compute the coercive field from the anisotropy field and the magnetization using the microstructural parameters α and N_{eff} [2]. Starting point for the optimization is a set of measured intrinsic material properties for different chemical compositions and temperatures. The design space is explored using a genetic algorithm, NSGA-II [3], which considers many different material designs per generation. The objective functions are evaluated by two surrogate models based on Gaussian Process Regression [4] which also estimate model uncertainty. The regressors were trained on measurement data and are used to predict the intrinsic magnetic properties (magnetization and anisotropy field) and the price for the chemical composition. Our results indicate that the optimal chemical composition for reaching a certain coercivity at lowest price depends on the microstructure. To reach the same coercive field with increasing N_{eff} the Neodymium content or the heavy rare earth content must be increased for room temperature and for 453 K, respectively. Figure 1 shows an example of the pareto front obtained from the multi-objective optimization for 453 K, α=0.45 and N_{eff}=0.91. Along the pareto front we identify three different regions: 1) Neodymium free, 2) Neodymium based but heavy rare earth free and 3) heavy rare earth containing magnet designs. Table 1 gives the chemical composition for pareto optimal designs with a coercivity of at least 1.5 Tesla for different temperatures and microstructural parameters.

[1] J. Li, H. Sepehri-Amin, T. Sasaki, et al., Science and Technology of Advanced Materials., Vol. 22, p. 386 (2021) [2] S. Bance, B. Seebacher, T. Schrefl, et al., Journal of Applied Physics., Vol. 116 (2014) [3] K. Deb, A. Pratap, S. Agarwal, et al., IEEE Transactions on Evolutionary Computation, Vol. 6, p. 182 (2002) [4] F. Pedregosa, G. Varoquaux, A. Gramfort, et al., Journal of Machine Learning Research., Vol. 12, p. 2825 (2011)

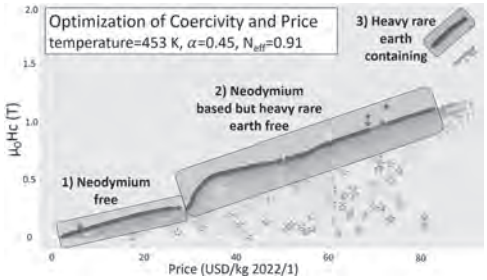

Fig.1: Designs evaluated during optimization. The stars are the initial population.

temp(K)	α	N_{eff}	chemical composition	$\mu_0 H_c$(T)	price(USD/kg)
300	0.42	0.25	$(Nd_{0.13}Ce_{0.54}La_{0.29}Pr_{0.07})_2Fe_{14}B_{0.95}C_{0.05}$	1.50	15.73
300	0.43	0.38	$(Nd_{0.28}Ce_{0.44}La_{0.23}Pr_{0.04})_2Fe_{14}B_{0.95}C_{0.05}$	1.51	20.61
300	0.45	0.91	$(Nd_{0.81}Ce_{0.25}La_{0.13}Pr_{0.81})_2Fe_{14}B$	1.51	38.55
300	0.45	1.22	$(Nd_{0.78}La_{0.20}Dy_{0.02})_2Fe_{14}B_{0.98}C_{0.02}$	1.50	50.73
453	0.42	0.25	$(Nd_{0.88}La_{0.08}Dy_{0.04})_2Fe_{14}B_{0.98}C_{0.02}$	1.50	59.61
453	0.43	0.38	$(Nd_{0.92}Ce_{0.01}La_{0.05}Tb_{0.01})_2(Fe_{0.95}Co_{0.05})_{14}B$	1.50	68.18
453	0.45	0.91	$(Ce_{0.56}La_{0.01}Dy_{0.43})_2Fe_{14}B$	1.66	82.55
453	0.45	1.22	$(Ce_{0.01}Pr_{0.03}Dy_{0.44})_2Fe_{14}B$	1.50	84.82

Tab.1: This table lists a selection of magnet designs with a coercivity of at least 1.5 Tesla and a price in USD/kg from 2022/1.

CF-12. FeCo nanowire – strontium ferrite composites: an alternative for the fabrication of rare-earth-free permanent magnets. *L. Perez*[1,2], A. Berja[3], L. Álvaro-Gómez[1], L. Gómez-Cruz[2], L. Lorenzo[2], C. Granados Miralles[3], C. Salazar[4], A. Pérez[4], C. Garijo[4], C. Fernández[4] and A. Quesada[3] *1. Fisica de Materiales, Universidad Complutense de Madrid, Madrid, Spain; 2. IMDEA Nanociencia, Madrid, Spain; 3. Instituto de Cerámica y Vidrio - CSIC, Madrid, Spain; 4. Lurederra Technological Center, Los Arcos, Navarra, Spain*

Due to their capacity to transform electrical energy into mechanical and vice versa, permanent magnets are key elements for the transition to a sustainable green future. High-performing technologies employ REE magnets, as they allow for lighter and more efficient devices. Unfortunately, REEs are critical raw materials and there is a strong demand for the development of alternative REE-free magnets. One of the routes explored in the past years consists in fabricating composite materials by combining soft and hard magnetic phases. We recently reported a composite bonded magnet based on strontium hexaferrite and electrodeposited FeCo metallic nanowires that present

a 48% improved energy product with respect to ferrite magnets [1]. The main bottleneck toward industrial implementation of these systems is the low yield and large production cost of electrodeposited nanowires [2]. In this work, we present our recent findings on the road towards the implementation of these composites in real applications. On the one hand, we have developed model systems using electrodeposited nanowires. In particular, considering that Co is also a critical raw material, we have partially substituted Co with Ni, increasing the nanowires content in the composite up to 50% to keep the remanence higher and, thus, the energy product. On the other hand, we propose a novel technology for the synthesis of metallic nanowires, based on Flame Spray Pyrolysis. This technology is broadly used in the industry for the synthesis of nanoparticles. We explore a modification of the technique, introducing a permanent magnetic field in the reaction chamber, as a potential method to produce ferromagnetic nanowires [3]. The new research findings, along with this new technological approach, have made these composites a viable alternative for the development of novel REE-free permanent magnets, with competitive performance for their use in green technologies. This research was funded by the European Commission through the Project BEETHOVEN (101129912). Views and opinions expressed are however those of the author(s) only and do not necessarily reflect those of the European Union or HADEA. Neither the European Union nor the HADEA can be held responsible for them.

[1] J.C. Guzmán-Mínguez et al. ACS Appl. Nano Mater. 3 (10) 9842 (2020) [2] C. Fernández-González et al. Nanomaterials 11 1657 (2021) [3] E K Athanassiou et al. Nanotechnol. 18 165606 (2007)

CF-13. First-Principles Study of Influence of Nitrogen Stoichiometry on Magnetic Ordering in Mn_3AN (A = Ge, Ga). *S. Mahatara*[1], S. O'Donnell[1,2], R.W. Smaha[1], J.R. Neilson[2], S. Bauers[1] and S. Lany[1]
1. MCCS, National Renewable Energy Laboratory, Golden, CO, United States; 2. Department of Chemistry, Colorado State University, Fort Collins, CO, United States

Nitride antiperovskites (APs), in which the cation-anion positions of the perovskite structure are inverted, have attracted considerable interest in recent years because of their remarkable properties ranging from permanent magnetism to piezomagnetism. The nitrogen stoichiometry in these compounds can vary depending on the synthesis conditions. However, it is unclear how compositional changes in these APs influence their atomic and/or magnetic structures. Experimental techniques such as neutron diffraction can be used to identify the magnetic structures at various N-stoichiometries, but they are resource-limited and require complex structure refinement protocols. On the other hand, computational approaches such as DFT alone pose challenges of identifying magnetic ground states from a combinatorially large set of possibilities. To this end, we perform magnetic ground state searches on two APs, Mn_3GeN and Mn_3GaN based on first principles Monte Carlo simulations, where the acceptance criteria are evaluated based on DFT energies in supercells of APs. Our results will elucidate how varying nitrogen stoichiometry in these APs affects their magnetic properties, along with the structural changes during denitrification.

CF-14. Enhancing magnetic properties and Curie temperature of 4d and 5d transition metal and p-block element co-doped Fe_2P alloys. K. Baatartsogt[1], T. Namsrai[2], J. Narmandakh[1], U. Enkhnaran[1], S. Deleg[1], O. Narantogtokh[2], S. Dorj[2], O. Tumentsereg[3], O. Khorgolkhuu[4] and *O. Dorj*[3] *1. Functional Materials Laboratory, Institute of Physics and Technology, Mongolian Academy of Sciences, Ulaanbaatar, Mongolia; 2. Physics, National University of Mongolia, Ulaanbaatar, Mongolia; 3. Physics, Incheon National University, Incheon, The Republic of Korea; 4. National Institute for Computational Sciences, Oak Ridge, TN, United States*

Fe_2P alloys are among the standout contenders to fill the gap magnets between hard ferrite and rare-earth based permanent magnet (PM) applications. In this work, we examine if its Curie temperature, one of the major problems with Fe_2P based alloys for permanent magnet applications, can be increased though specific selection of doping compositions: $M_{0.04}Fe_{2-x}P_{y-1}Z_y$ (M = 4d and 5d heavy transition metals, and Z = p-block elements such as B, C, N for 2nd row, Al, Si and S for 3rd row and Ga, Ge, As and Se for 4th row). Calculations using the Density Functional Theory (DFT) method show that doping with Os, 5d heavy transition metal, enhances magneto-crystalline anisotropy of $Os_{0.04}Fe_{2-x}P_{y-1}Z_y$ up to 3.32 MJ/m^3, 10% higher than that of the pristine Fe_2P alloy, due to the spin-orbit coupling of high nuclear charge and close to the half-filled electron configurations. Increase in the Curie temperature (T_c), magnetic saturation (M_s) and energy product (BH_{max}) of $M_{0.04}Fe_{2-x}P_{y-1}Z_y$ (M = Ru, Os, Pt and Z = B, Al, Ga) is also observed. In particular, Ru and Os, co-doped with the B group elements increases the $(BH)_{max}$ at all the concentrations, reaching maximum value of 38 MGOe for $Os_{0.04}Fe_{1.96}P_{0.84}B_{0.16}$. This is 40% increase compared with pristine Fe_2P (27 MGOe) and comparable with that of hard magnets. Furthermore, the saturation magnetization increases 17% (1.21 T), and the Curie temperature to 400K compared to the pristine Fe_2P for $Ru_{0.04}Fe_{1.96}P_{0.84}B_{0.16}$ and $Pt_{0.04}Fe_{1.96}P_{0.84}Ga_{0.16}$. The results suggest the co-doping Fe_2P with 4d, 5d transition metals along with group B elements could be a novel approach to designing permanent magnet candidates. Acknowledgements: This work is supported by the US Office of Naval Research (ONR), Office of Naval Research Global (ONRG) and Army International Technology Center, Indo-Pacific (ITC-PAC) under the ONRG grant N62909-22-1-2045.

CF-15. Hot Axial Pressure during Quenching of Bulk Millimetric $(Mn_{0.6}Al_{0.4})_{98}C_2$: Influence on their Hard Magnetic Properties. V. Madurga[1], J. Vergara[1,2] and *C. Favieres*[1,2] *1. Laboratory of Magnetism, Department of Science, Physics, Public University of Navarre, Pamplona, Spain; 2. IMANAT^2. Institute for Advanced Materials and Mathematics, Public University of Navarre, Pamplona, Spain*

In this work, cylindrical pellets of $(Mn_{0.6}Al_{0.4})_{98}C_2$, typically 16 mm in diameter and 5 mm in height, were fabricated starting from the powder elements, Mn and C, and small pieces of laminated Al. The mixed elements were cold-pressed at 400 kg/cm^2. The resulting cylinders were heated to 1300 °C in an NB crucible. At this temperature, an axial pressure of 0.4 kg/cm^2 was applied to the molten cylinder while it was cooled to room temperature at ≈ 70 °C/s. These bulk samples were found to be ferromagnetic at room temperature exhibiting hard magnetic hysteresis loops, reinforced by the observation of the magnetic τ–phase MnAl on their X-ray diffractograms. The influence of the applied hot axial pressure on the samples was investigated. When no pressure was applied during melting and quenching of the samples, the percentage of magnetic τ–phase present in these samples was significantly different from that corresponding to the samples melted and quenched under hot pressure: For the samples obtained without pressure, this percentage is ≈ 10 %, while for the samples melted and quenched under pressure, it is increased to ≈ 20 %. The hysteresis loops measured with a maximum applied field of 1 T revealed values of the coercive field Hc ≈ 650 Oe and magnetization M ≈ 60 emu/g for the samples obtained with no pressure, whereas Hc ≈ 1200 Oe for the samples melted and quenched with pressure and M ≈ 110 emu/g.

[1] Yuxiao Jia, Yuye Wua, Shuang Zhao, Jingmin Wang and Chengbao Jiang, *Relation between solidification microstructure and coercivity in MnAl permanent-magnet alloys*. Intermetallics 96, 41 (2018) [2] Dong Liang, Tao Zhu, Zhuyin Shao, Shunquan Liu, Jingzhi Han, Honglin Du, Qing Xu, Changsheng Wang, Wenyun Yang and Jinbo Yang, *Study on the relationship between structure and magnetic properties of τ-phase MnAl prepared by cryo-milling*. AIP Advances 14, 015227 (2024)

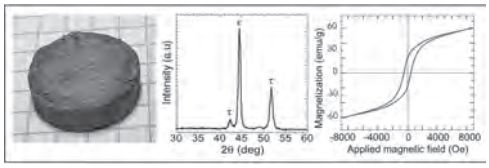

Figure 1. Left: $(Mn_{0.6}Al_{0.4})_{98}C_2$ cylindrical pellet, melted and quenched with axial pressure. Center: X-ray diffractogram corresponding to this $(Mn_{0.6}Al_{0.4})_{98}C_2$ pellet obtained by hot axial pressure during quenching, showing the presence of the magnetic τ–phase MnAl. Right: Room temperature hysteresis loop corresponding to a $(Mn_{0.6}Al_{0.4})_{98}C_2$ pellet obtained with no pressure during melting and quenching, exhibiting a coercive field Hc ≈ 650 Oe and magnetization M ≈ 60 emu/g.

Session CG
MAGNETOELECTRIC MATERIALS AND PHENOMENA I
Paola Tiberto, Chair
INRIM, Torino, Italy

INVITED PAPER

CG-01. Chirality: a new degree of freedom for skyrmionics.
C. Gueneau[1], F. Ibrahim[1], J. Fischer[1], C. Fillion[1], L. Vojáček[1], R. Kumar[1], A. Fassatoui[2], S. Pizzini[2], L. Ranno[2], D. Ourdani[3], M. Belmeguenai[3], Y. Roussigné[3], S. Chérif[3], S. Auffret[1], J. Faure-Vincent[1], I. Joumard[1], O. Boulle[1], G. Gaudin[1], L.D. Buda-Prejbeanu[1], M. Chshiev[1,4], C. Baraduc[1] and *H. Béa*[1,4] *1. Spintec, Grenoble, France; 2. Néel Institute, Grenoble, France; 3. Laboratoire des Sciences des Procédés et des Matériaux, Villetaneuse, France; 4. Institut Universitaire de France, Paris, France*

In ultrathin magnetic films with perpendicular magnetic anisotropy (PMA), an antisymmetric exchange interaction, called Dzyaloshinskii-Moriya Interaction (DMI) [1] may exist due to interfaces and spin-orbit coupling. DMI may stabilize Néel domain walls (DWs) with a given sense of rotation (chirality) leading to non-trivial magnetic skyrmions [2] (Fig.1 top). Skyrmions move under current due to spin-orbit torques [3], which make them interesting for spintronics. This motion depends on the DW texture and chirality, defined by DMI sign and amplitude, respectively. We have studied skyrmion [4] and domain wall chirality in the PMA region [5] of double wedge stacks of Ta/FeCoB/TaO_x (Fig.2). To do so, we used a polar magneto-optical Kerr effect microscope (MOKE) to track the current-induced motion of skyrmions and DWs and deduce their chirality. We observed that DMI sign changes as a function of the oxidation state of FeCoB/TaO_x interface, but also with FeCoB thickness (red line in Fig.2). This behavior is reproduced by our *ab-initio* calculations of a simplified Fe/TaO_x interface [5]. In particular, we attribute the change of DMI sign with Fe thickness to a variation of interatomic distance between Fe and Ta at the interface. Additionnally, the use of a gate voltage can invert locally and dynamically the chirality of magnetic skyrmions and DWs by tuning the sign of the DMI coefficient D [6]. We used Brillouin Light Scattering to measure DMI coefficient as well as MOKE through a transparent electrode to observe skyrmion motion under current. We attribute this control of chirality to a tuning with the gate voltage of the oxidation state at the top FeCoB/TaO_x interface (Fig.1 bottom), which controls DMI sign [4] [7]. Micromagnetic simulations show that this chirality control is downscalable to nanometric skyrmions [6]. This local and dynamic reversal of DW chirality is a new degree of freedom towards an efficient and individual control of skyrmions, enabling new functionalities for spintronic logic devices and memories.

[1] I. E. Dzyaloshinskii, *J. Exptl. Theoret. Phys*., 46 (1964) 960; T. Moriya, *Phys. Rev*. 120 (1960) 91 [2] A. Fert, et al., *Nature Review Materials*, 46 (2017) 17031 [3] A. Thiaville et al., *Europhys. Lett.,* 100 (2012) 57002; S. Emori et al., *Nat. Mater*.12 (2013) 611 [4] R. Kumar et al., *Phys. Rev. Appl.,* 19 (2023) 024064; [5] C. Gueneau et al., to be submitted, (2024) [6] C. E. Fillion, et al., *Nat. Commun.,* 13 (2022) 1 [7] M. Arora, et al., *Physical Review B*, 101 (2020) 054421

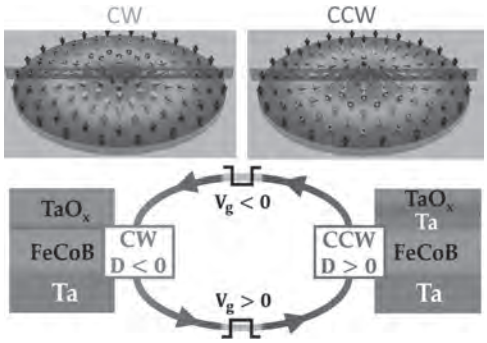

(top) Representation of clockwise (CW) and counterclockwise (CCW) Néel skyrmions. (bottom) Inversion of skyrmion and domain wall chirality by a gate voltage, induced by oxygen ion migration effects in Ta/FeCoB/TaO_x stack.

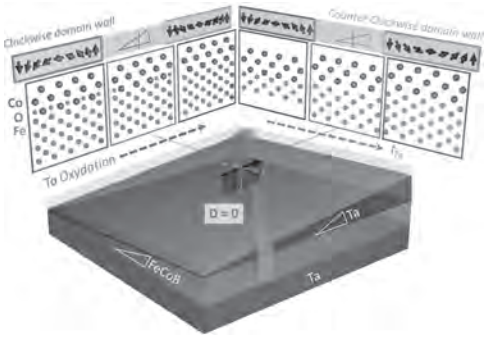

Schematics of our Ta/FeCoB/TaO_x double wedge with an experimental change of DMI sign with both TaO_x oxidation and FeCoB thickness (red line), reproduced by *ab-initio* calculations.

CONTRIBUTED PAPERS

CG-02. Epitaxial Strain Induced Enhancement of Dielectric Constant and VCMA Effect in MgO Based Magnetic Tunnel Junctions.
T. Nozaki[1], H. Onoda[1], S. Tamaru[1], H. Nakayama[1], M. Konoto[1], T. Nozaki[1] and S. Yuasa[1] *1. Research Center for Emerging Computing Technologies, National Institute of Advanced Industrial Science and Technology (AIST), Tsukuba, Japan*

Voltage controlled magnetic anisotropy (VCMA) effect has received much attentions as a magnetization control technique with ultra-low power consumption. Attempts have been made to incorporate high-*k* dielectrics as a tunnel barrier to obtain a larger charge accumulation and thus an enhanced VCMA effect[1]. However, achieving both a large dielectric constant (ε_r) and a large tunnel magnetoresistance (TMR) ratio is challenging. On the other hand, MgO tunnel barrier itself has a potential for a larger ε_r. In this study, we experimentally investigated the ε_r of MgO tunnel barrier in epitaxial stacks (MgO sub./MgO (5 nm)/Cr (50 nm)/Fe (0.9 nm)/Ir (0.06 nm)/Co (0.1 nm)/MgO (t_{MgO} nm)/cap structures) and discussed the origin of the enhanced ε_r of MgO tunnel barrier. For epitaxial stack with thin MgO ($t_{MgO} \leq 3$ nm), we

demonstrated a large $\varepsilon_r \geq 15.9$, which is apparently larger than those of polycrystalline MgO tunnel barrier ($\varepsilon_r = 11.9$) and bulk MgO ($\varepsilon_r = 10$). By investigating epitaxial stacks with thick MgO ($4 \leq t_{MgO} \leq 10$ nm), we observed a compression of lattice parameter *a* and simultaneous enhancement of ε_r of the MgO tunnel barrier with decreasing t_{MgO} (Fig. 1). We interpreted the large ε_r of epitaxial MgO tunnel barrier in terms of a compressive strain induced enhancement of ε_r[2]. We also confirmed that the VCMA coefficient of the epitaxial stacks increases as the ε_r increases (Fig. 2). This study demonstrates the controllability of ε_r through strain engineering. This study also provides a new perspective to the large VCMA effect observed in the epitaxial magneti tunnel junctions (MTJs)[3]. This work was partly based on results obtained from a project, JPNP16007, commissioned by the New Energy and Industrial Technology Development Organization (NEDO).

[1] H. Onoda et al., Phys. Rev. Materials 6, 104406 (2022). [2] E. Bousquet et al., Phys. Rev. Lett. 104, 037601 (2010). [3] T. Nozaki et al., APL Mater. 8, 011108 (2020).

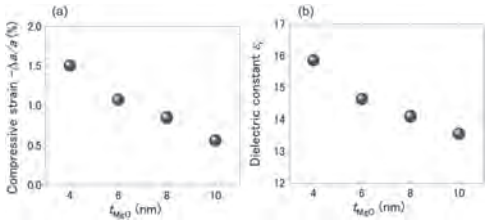

Fig. 1 t_{MgO} dependence of (a) compressive strain ($-\Delta a/a$) and (b) ε_r of MgO tunnel barrier for the epitaxial stacks with thick MgO tunnel barrier.

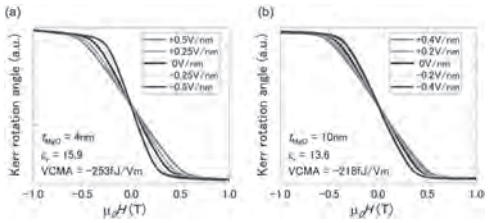

Fig. 2 Magnetization curves under electric field for the epitaxial stack with t_{MgO} = (a) 4 nm and (b) 10 nm, measured by MOKE.

CG-04. RIXS-MCD of Multiferroic ε-Fe_2O_3 Nanoparticles. *R. Nickel*[1], G. Buccoliero[1], M. dos Reis Cantarino[1] and K. Kummer[1] *1. ESRF, Grenoble, France*

Magnetoelectric materials have a significant role to play in the development of new technologies due to the inherent possibilities of controlling a magnetic state with an electric field and *vice versa*. However, optimizing the applications of such materials requires an understanding of their underlying magnetic and electronic interactions. ε-Fe_2O_3 is a hard ferrimagnetic material that exhibits strong magnetoelectric coupling at room temperature.[1] Its simple composition, with only Fe and O ions, avoids the stoichiometry challenges that can hamper other perovskite oxides such as $BiFeO_3$.[2] However, this phase does come with its own unique challenges. For example, ε-Fe_2O_3 exists only in the nanoscale. As a result, experimental techniques that require single crystal samples cannot be used and size effects are convolved with the measured properties.[3] From a fundamental point of view, the fact that all four cation sites are occupied by Fe3+ creates a challenge in resolving the electronic structure. Conventional techniques such as soft x-ray absorption spectroscopy (XAS) with x-ray magnetic circular dichroism (XMCD) fail to identify a unique structure due to the overlap between spectral components. Instead, a more complex approach is required. Resonant inelastic x-ray scattering (RIXS) is a photon-in photon-out technique able to detect elementary excitations in a material. Additional information is obtained via RIXS-MCD spectra, which measures the dichroism in these excitations and can be used to differentiate between similar sites. Here we present the results of 9T RIXS-MCD maps of ε-Fe_2O_3 measured at ID-32 of the ESRF and discuss new insights into the electronic structure of multiferroic ε-Fe_2O_3.

[1] M. Gich *et al.* Nanotechnology, 2006, 17, 687. [2] L. Dedon *et al.* Chem. Mater, 2016, 28, 5952. [3] R. Nickel *et al.* Nanoscale, 2023, 23, 7845.

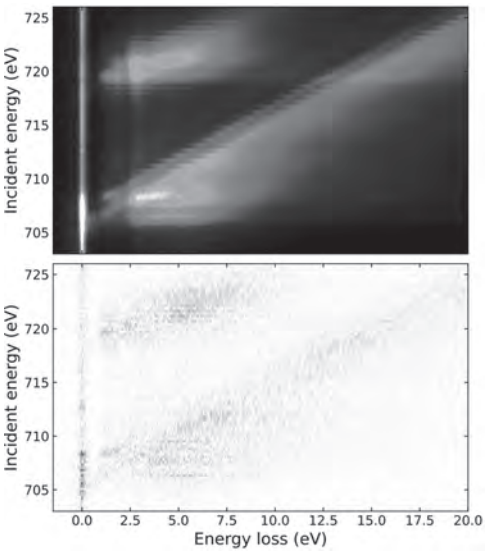

RIXS-MCD map of ε-Fe_2O_3 at 9T, 300K.

CG-05. Withdrawn

CG-07. Electrically Controlled Dzyaloshinskii–Moriya Interaction via Magnetic Textures in a Weyl Semimetal. *Y. Semenov*[1] and K.W. Kim[1] *1. North Carolina State University, Raleigh, NC, United States*

In this work, we demonstrate that purely electrical generation of indirect Dzyaloshinskii–Moriya interaction (DMI) in Weyl semimetal (WSM) can be achieved through non-homogeneous textures. This approach is founded upon the recently discovered asymmetrical indirect spin-spin interaction mediated by Weyl fermions in WSM [1]. A sizable effect of an indirect DMI needs in imbalance of fermion populations of Weyl nodes, a consequence of the axial anomaly in WSM influenced by non-orthogonal electric and magnetic fields. While the applied bias generates an electric field, the superimposition of the required magnetic field demands a specific technological sophistication [2].

In contrast, we leverage the intrinsic axial magnetic field inherent in an inhomogeneous magnetic texture of WSM. In practical structures, such chiral anomalies can be achieved in twisted textures akin to ferromagnetic domain walls. Thereby, the DMI affects the DW, allowing its width to be controlled in an electric field. As another example, we investigate formation of magnetic domain interfacing with a ferromagnetic environment (Fig. 1). It requires the supplementary effect of spin-transfer torque (STT). Application of STT to a conventional ferromagnet (FM) can create domains, mimicking the operation of racetrack memory. The WSMs enhance spin torque via electrically induced DMI. Numerical estimations (Fig. 2) highlight advantages in the creation of the magnetic textures in WSM vs to conventional FM, enabling practical implementation in racetrack memory devices.

1. P. Nikolic, Phys. Rev. B Vol. 103, p. 155151 (2021). 2. Y. G. Semenov and K. W. Kim, Phys. Rev. B Vol. 107, p. 094434 (2023).

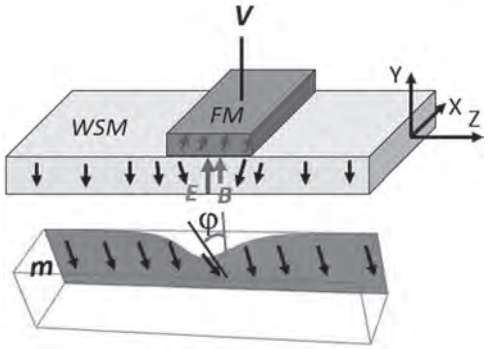

Schematics of the magnetic WSM/auxiliary FM layer composite. The top metallic layer is a hard FM with magnetization tilted to z axis. Voltage V applied to FM contact generates a STT and mediates electric field evoking a DMI in the WSM with magnetization deviation φ from equilibrium state.

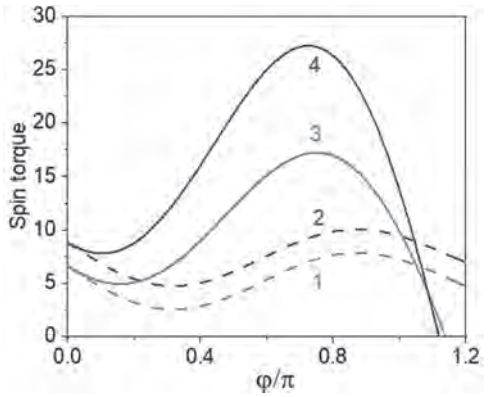

Spin torque as it appears at typical material parameters applied to magnetic domain of the 48 nm length with magnetization twisting φ in conventional FM (dashed lines) affected by STT in the electric fields E_1 =30 kV/cm (curve 1) and E_2 =40 kV/cm (curve 2). Solid lines (curve 3 for E_1 and 4 for E_2) represent the effect of DMI enhanced the spin torques.

CG-08. Compositional Tuning of Magnetic and Magnetotransport Properties of $Co_2MnGa_{1-x}Ge_x$ Heusler alloys thin films - from a Weyl semi-metal to a Half-metal. *B. Patel*[1,2], Y. Zhang[1] and S. Granville[1,2]
1. Robinson Research Institute, Victoria University of Wellington, Wellington, Netherlands; 2. MacDiarmid Institute for Advanced Materials and Nanotechnology, Wellington, New Zealand

Compositional tuning of Heusler alloys to take advantage of their outstanding electronic properties, such as a large anomalous Hall effect or high spin polarisation, is highly desirable [1]. Co_2-based Heusler alloys Co_2MnGa, which is a Weyl semi-metal with a large anomalous Hall effect [2], and Co_2MnGe, which is a half-metal with high spin polarisation [3], are interesting as they have very similar electronic band structures. Ga and Ge are next to each other in the periodic table, so it may be possible to tune the band structure and topological Weyl properties through gradual compositional variation in $Co_2MnGa_{1-x}Ge_x$. Such types of tunable ferromagnets offer great opportunities for controlling spin currents and torques [4]. Here, I will present work on the successful modification of composition between Co_2MnGa and Co_2MnGe in thin films made via the magnetron sputtering technique with co-sputtering of targets. Moreover, XRD confirmed all films are in the ideal Heusler $L2_1$ structure with lattice parameters varying from 5.763 Å for Co_2MnGe to 5.760 Å for Co_2MnGa. Magnetic and electrical properties vary smoothly as Ge% increases from 0 to 100: saturation magnetisation (at 10 K) increases from 727 emu/cc to 801 emu/cc, resistivity (at 300 K) decreases from 170 μΩcm to 22 μΩcm and anomalous Hall resistivity (at 300 K) decreases from 6.63 μΩcm to 0.03 μΩcm. The continuous variation of magnetic and electronic properties demonstrates that simultaneous tuning of spin polarisation and anomalous Hall effect tuning are feasible in $Co_2MnGa_{1-x}Ge_x$ and potentially other Heusler alloys.

(1) Simon Trudel et al. J. Phys. D: Appl. Phys., vol. 43, p. 193001 (2010) (2) Zhang, Y., Yin, Y., Dubuis, G., *et al. npj Quantum Mater.* vol. 6, p. 17 (2021) (3) Chatterjee, Samanta, Ghosh and Mandal. Physical Review B, vol. 108, no. 20, p. 205108 (2023) (4) Kim, KW., Park, BG. & Lee, KJ. *npj Spintronics,* vol. 2, no. 8 (2024)

CG-10. Ferroelectric control of magnetic anisotropy in the layered multiferroic Co/$Hf_{0.5}Zr_{0.5}O_2$. G. Gandini[1], J. Hertel[2], G. Spaccia[1], D. Benettin[1], F. Fagiani[1], M. Cantoni[1], T. Gurieva[2], C.A. Durner[2], M. Lederer[2], B. Lilienthal-Uhlig[2], A. Manchon[3] and *C. Rinaldi*[1]
1. Physics, Politecnico di Milano, Milano, Italy; 2. Center Nanoelectronic Technologies (CNT), Fraunhofer IPMS, Dresden, Germany; 3. Aix-Marseille Université, CNRS, CINAM, Marseille, France

Magnetoelectric multiferroics are promising candidates for energy-efficient in-memory computing, both in single-phase or composites comprising ferroelectric/ferromagnetic coupled films. While many systems are based on materials not suitable for industrial processes, doped hafnia stands out as one of the few CMOS-compatible ferroelectrics enabling the creation of non-volatile spin-orbit devices on silicon [1, 2]. Here, we present the excellent magneto-electric properties of perpendicularly magnetized cobalt thin films on Zr-doped hafnia ($Hf_{0.5}Zr_{0.5}O_2$ - HZO) over silicon We show the conditions for achieving perpendicular magnetic anisotropy; thus, we provide recipes to achieve optimal magnetic and ferroelectric properties versus annealing and ferroelectric training. The proposed approach allows for saturation polarizations of up to 20 μC/cm^2. The variations of magnetic anisotropy versus voltage are studied by *in-operando* magneto-optical Kerr microscopy on fabricated micro-capacitors. By comparing remanence and DC measurements, we demonstrated a pure ferroelectric control of the magnetic coercivity in Co thin films (Fig. 1 and 2), with a negligible role of the voltage-controlled magnetic anisotropy (VCMA) at variance with other reports [3, 4]. A significant retention is demonstrated, and finally, some insights on the interfacial properties of the system based on calculations are presented. The results indicate the artificial multiferroic Co/HZO as a promising candidate for voltage-controlled spin-based computing. C.R. acknowledges the PRIN 2022 project SORBET (grant no. 2022ZY8HJY) funded by MUR.

[1] T. Zakusylo *et al.*, Materials Horizons, Vol. 11, p. 2388 (2024). DOI: 10.1039/D3MH01966G [2] S. Lancaster *et al.*, ACS Applied Materials and Interfaces, Vol. 15, p. 16963 (2023). DOI: 10.1021/ACSAMI.2C22205 [3] B. Vermeulen *et al.*, ACS Applied Materials and Interfaces, Vol. 11, p. 34385 (2019). DOI: 10.1021/ACSAMI.9B07973 [4] B. Zhangeta *et al.*, Applied Physics Letters, Vol. 119 (2021). DOI: 10.1063/5.0054593/40821

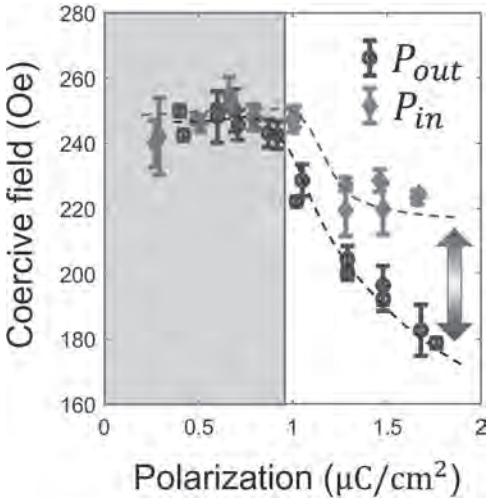

Coercive field versus polarization strength for the two polarization states. Red and blue dots refer to inward (P_{in}) and outward (P_{out}) polarizations. The graph shows a general reduction of the coercivity versus the modulus of the polarization. Above a certain P, a modulation of the coercivity appears and attests at around 25% for P of about 1.8 μC/cm^2.

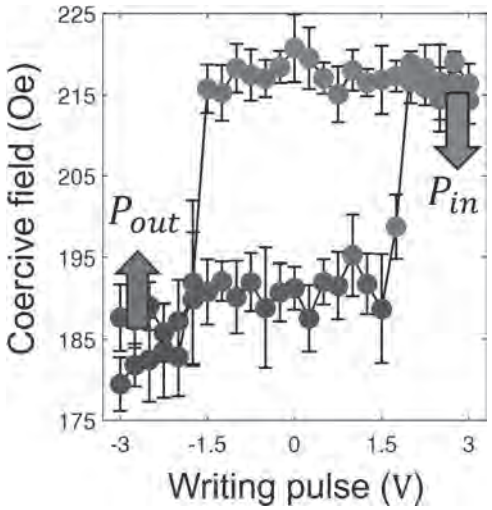

Magnetic coercive field versus the amplitude of the voltage pulse used to set the polarization state.

INVITED PAPER

CG-09. Voltage control of spin-to-charge interconversion in Mn_2Au films. *C. Song*[1], X. Chen[1], L. Huang[1] and F. Pan[1] *1. Tsinghua University, Beijing, China*

Compared with ferromagnets, antiferromagnets (AFM) have huge potential in high-density information storage and Teraherz nano-oscillator because of their ultrafast spin dynamics and vanishingly small stray field. How to manipulate antiferromagnetic moments and achieve ultrafast detection of antiferromagnetic spins has become the frontier and hotspot of research in

the field of spintronics. Based on the local inversion symmetry breaking of Mn_2Au thin films, we observed the mutual conversion between out-of-plane spin-polarized spin current and charge current, which is strongly dependent on the antiferromagnetic moments. Thus, such spin-charge interconversion processes are termed as antiferromagnetic spin Hall effect and antiferromagnetic inverse spin Hall effect [1,2]. The reciprocity phenomena of Néel spin-orbit torque effect [3.4], so-called spin-charge interconversion, are observed in the Mn_2Au single layer. The antiferromagnetic moments and corresponding spin-charge conversion can be modulated by applying voltage. They also demonstrate that the optical spin-orbit torque induced by circularly polarized laser can be used to drive the antiferromagnetic oscillations with a frequency of 2 THz in Mn_2Au films. Due to the local inversion symmetry breaking of Mn_2Au, an a.c. current is generated via spin-to-charge conversion, which can be detected through free-space terahertz emission.

[1] X. Chen, C. Song, et al. Nat. Mater. 20, 800 (2021). [2] L. Huang, C. Song, et al. Adv. Mater., 34, 220598 (2022). [3] X. Chen, C. Song, et al. Nat. Mater. 18, 931 (2019). [4] L. Huang, C. Song, et al. Nat. Commun. 15, 4270 (2024). [5] L. Huang, C. Song, et al. 2nd review process in Nat. Commun..

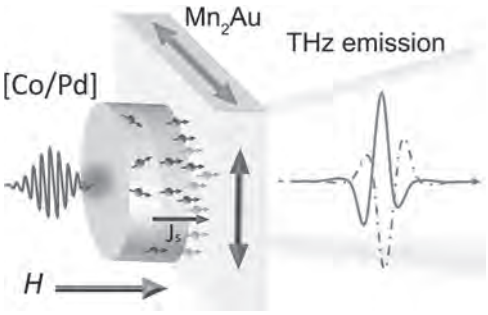

Inverse spin Hall signals dependent on the antiferromagnetic Néel vector in Mn_2Au/[Co/Pd] heterostructures.

CONTRIBUTED PAPER

CG-11. Magnetic and Structural Polymorphism of CuMnSb Thin Films. *M. Sawicki*[1,2], A. Ciechan[1], P. Dluzewski[1], S. Kret[1], K. Gas[1,3], L. Scheffler[4,5], C. Gould[4,5], J. Kleinlein[4,5], L.W. Molenkamp[4,5] and P. Boguslawski[1] *1. Institute of Physics, Polish Academy of Sciences, Warszawa, Poland; 2. Research Institute of Electrical Communication, Tohoku University, Sendai, Japan; 3. Center for Science and Innovation in Spintronics, Tohoku University, Sendai, Japan; 4. Physikalisches Institut (EP3), Universitaet Wuerzburg, Wuerzburg, Germany; 5. Institute for Topological Insulators, Universitaet Wuerzburg, Wuerzburg, Germany*

Heusler alloys allow for studying the origin of the transition between magnetic phases because they offer a wide spectrum of functionalities [1]. Indeed, Heusler alloys exhibit ferromagnetic (FM), antiferromagnetic (AFM), and canted ferromagnetic order. This indicates that different types of magnetic coupling are competing in this family. Moreover, some of its members display structural polymorphism, which permits analyzing relationships between the crystalline phase, the magnetic phase, and the corresponding electronic structure. Our combined high-resolution transmission electron microscopy and magnetometry shows that epitaxial CuMnSb films exhibit a coexistence of two magnetic phases, coherently intertwined in nanometric scales [2]. The films are deposited by MBE technique on matching GaSb substrates [3]. The dominant α phase is a half-Heusler cubic AFM with the Nèel temperature of 62 K, i.e., the equilibrium structure of bulk CuMnSb. The secondary phase is its tetragonal β polymorph (present as ~50 nm pseudomorphic inclusions) with the FM Curie temperature of about 90 K. First principles calculations provide a consistent interpretation of experiment, since the total energy of β-CuMnSb is higher than that of α-CuMnSb only by 0.12 eV per formula unit. This allows for epitaxial stabilization of β-CuMnSb, and its metallic character favors RKKY-type FM coupling. The calculated magnetic moment of Mn ions is close to the measured value. Combined, the findings highlight a practical route towards fabrication of functional materials in which coexisting polymorphs provide complementing functionalities in one host.

[1] L. Wollmann, A.K. Nayak, S.S.P. Parkin, and C. Felser, Ann. Rev. Mater. Res. 47, 247 (2017). [2] A. Ciechan, P. Dluzewski, S. Kret, K. Gas, L. Scheffler, C. Gould, J. Kleinlein, M. Sawicki, L.W. Molenkamp, and P. Boguslawski, Phys. Rev B, accepted. [3] L. Scheffler et al, Appl. Phys. Lett. 121, 012401 (2022). [4] Similar magnetic properties were observed in: L. Scheffler et al, Phys. Rev. Mater. 4, 114402 (2020).

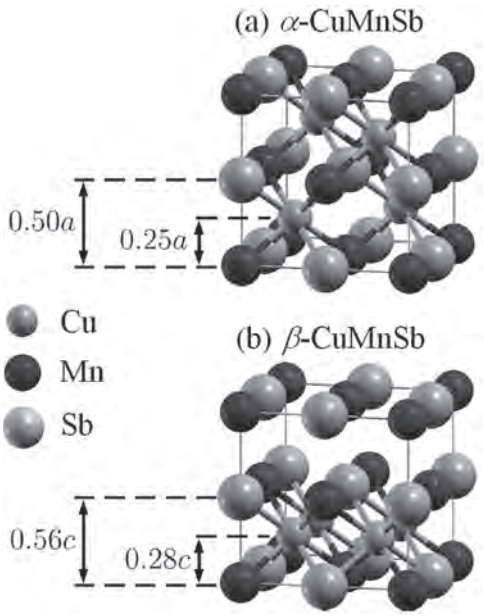

Fig. 1. Crystal structures of (a) α-CuMnSb with the cubic lattice parameter *a*, (b) tetragonal β-CuMnSb with the lattice parameters *a* in the (x, y) plane and *c* in the [001] direction.

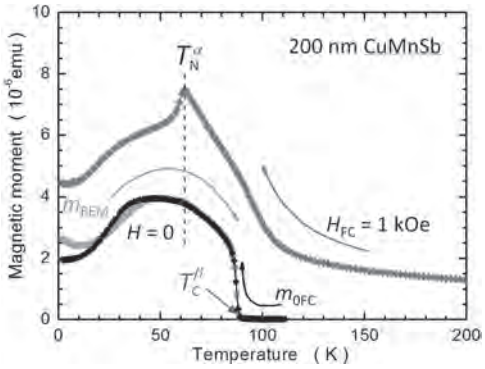

Fig. 2. Temperature dependence of the magnetic moment of CuMnSb. Red diamonds: initial cooling in H_{FC} = 1 kOe. The cusp at 62 K indicates the Neel transition of α-CuMnSb. Orange bullets: *T* dependence of the remnant moment during warming (m_{REM}), whereas the black diamonds are obtained during subsequent cooling at the same $H = 0$ (m_{0FC}). The red arrow indicates the Curie temperature of the FM β-CuMnSb at 88 K.

Session CP
SOFT MAGNETIC MATERIALS I
(Poster Session)

Frank M Abel, Chair
United States Naval Academy, Annapolis, MD, United States

CP-01. Magnetic, structural, and morphological properties behavior of $Ni_{1-x}Co_xFe_2O_4$ magnetic nanoparticles: theoretical and experimental study. *J.A. Lopez Medina*[2], C. Velez[1], N. Tarabay[3], D. Dominguez Vargas[4], S. Sharma[2], P. Piza[5], J. Guerrero[4], S. Aguila Puentes[4], M. Farias[4], G. Soto[4] and R. Ponce[4] *1. Department of Mechanical and Aerospace Engineering- University of California, Irvine, Irvine, CA, United States; 2. CONAHCYT – IxM - Centro de Nanociencias y Nanotecnología, Universidad Nacional Autónoma de México, Ensenada, Mexico; 3. Department of Electrical Engineering and Computer Science- University of California, Irvine, Irvine, CA, United States; 4. Centro de Nanociencias y Nanotecnología, Universidad Nacional Autónoma de México, Ensenada, Mexico; 5. Centro de Investigación en Materiales Avanzados, Chihuahua, Mexico*

In this work, we synthesized nanoparticles of the $Ni_{1-x}Co_xFe_2O_4$ (with x= 0.25, 0.50, and 0.75) inverse spinel by the hydrothermal method. Scanning transmission electron microscopy (STEM) analysis and elemental characterization revealed the formation of nanoparticles of the order of ~ 3 nm with a homogeneous distribution of their constituents, denoting the correct material synthesis. The results show that as the Co content increases, the structures' cell parameters increase and the crystal size decreases. Besides, the magnetic characterization exhibits an increase in the saturation magnetization as the Co content moves from x=0.25 to x=0.75, on the other hand, the coercive field decreases, which is attributed to the superparamagnetic behavior of the structures. Density Functional Theory (DFT) calculation demonstrates that the inverse spinel is the most favorable configuration for $NiFe_2O_4$ and $CoFe_2O_4$ compounds. Besides, by first-principles thermodynamics, we have shown that Co tends to occupy the Ni sites as the most favorable configuration, with an increase in the cell parameter and total magnetization as Co content increases, in excellent agreement with experimental measurements. Our findings demonstrate that Co-Ni-based ferrites are soft magnetic materials, which are suitable candidates for devices requiring rapid magnetization and demagnetization. Acknowledgments This work was partially supported DGAPA-UNAM, through research projects: PAPIIT IN110424, IA100624, and IG101124. Calculations were performed in the DGCTIC-UNAM Supercomputing Center projects LANCAD-UNAM-DGTIC-286, LANCAD-UNAM-DGTIC-368, and LANCAD-UNAM-DGTIC-422. The authors acknowledge the use of facilities and instrumentation at the UC Irvine Materials Research Institute (IMRI) supported in part by the National Science Foundation Materials Research Science and Engineering Center program through the UC Irvine Center for Complex and Active Materials (DMR-2011967).

1. S. Khan, S. Mansoor, Z. Rafi, B. Kumari, A. Shoaib, M. Saeed, S. Alshehri, M. M. Ghoneim, M. Rahamathulla, U. Hani and F. 2. Shakeel, J. Mol. Liq., 2022, 348, 1–15. 3. M. Tiwari, N. Bangruwa and D. Mishra, Talanta Open, 2023, 8, 100257. 4. X. Batlle, C. Moya, M. Escoda-Torroella, Ò. Iglesias, A. Fraile Rodríguez and A. Labarta, J. Magn. Magn. Mater.S. J. Salih and W. M. Mahmood, Heliyon, 2023, 9, 1–25. 5. M. Samadishadlou, M. Farshbaf, N. Annabi, T. Kavetskyy, R. Khalilov, S. Saghfi, A. Akbarzadeh and S. Mousavi, Artif. Cells, Nanomedicine Biotechnol., 2018, 46, 1314–1330.

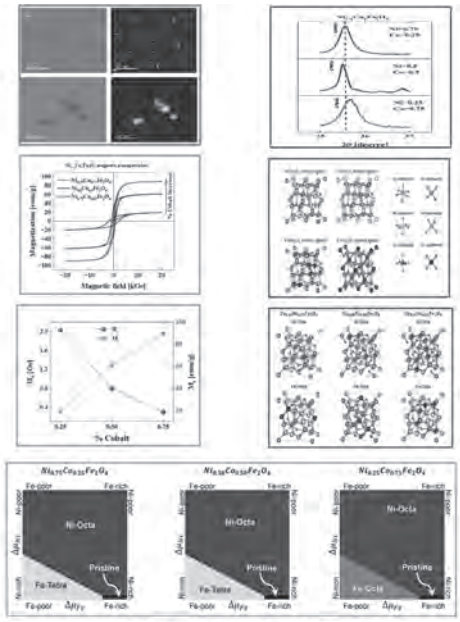

DFT and first-principles thermodynamics establish that Co^{2+} occupies Ni sites, promoting that the a and M_s changes as Co^{2+} rises

CP-02. Effect of Cerium Doping and Two-step Annealing on Terbium Iron Garnet on Si. *P. Liu*[1], K. Srinivasan[2,3] and B. Stadler[3,1] *1. Chemical Engineering and Materials Science, University of Minnesota, Minneapolis, MN, United States; 2. Electrical and Computer Engineering, Boise State University, Boise, ID, United States; 3. Electrical and Computer Engineering, University of Minnesota, Minneapolis, MN, United States*

Cerium-doped terbium iron garnet (CeTbIG) thin films have been investigated as effective magneto-optical (MO) claddings on waveguides in integrated optical isolators due to their high Faraday rotation and compatibility with non-garnet substrates like silicon.[1-4] However, most research discussing the cerium content in CeTbIG thin films has focused only on Faraday rotation values, without systematic study of grain size and magnetic properties such as the ratio of remanent magnetization (Mr) to saturation magnetization (Ms). These factors are also crucial for isolator design, especially for 1-D mode conversion isolators which can operate at remanence without external magnetic fields.[5] Furthermore, the regular post-anneal temperature for CeTbIG thin films is 900°C or higher, limiting their application in the integration of electronic and photonic devices. Therefore, in this work, we deposited garnet thin films on silicon wafers by RF sputtering and conducted a systematic study on the relationship between Ce content (Ce/Ce+Tb = R_2) and grain size, as well as the M_r/M_s value, with different thicknesses and rare-earth content (Ce+Tb/Fe = R_1). Fig. 1 shows that the grain size generally increases as the Ce content increases. The largest mean grain size of 6.22 μm was obtained at R_1 = 0.70 and R_2 = 0.25. Additionally, the M_r/M_s values range from 0.50 to 0.70 by in-plane room-temperature magnetic hysteresis measurement, which is suitable for developing a field-free isolator in tiny photonic devices. Furthermore, the two-step annealing, involving a first low-temperature anneal and a second crystallization treatment, offers an

effective method to lower the annealing temperature from 900°C to 800°C.[6] Fig. 2 shows that a first anneal of 400°C increases the Faraday rotation of films annealed at 800°C by approximately 33%.

1. K. Srinivasan and B.J. H. Stadler, Review of integrated magneto-optical isolators with rare-earth iron garnets for polarization diverse and magnet-free isolation in silicon photonics, Opt. Mater. Express Vol. 12, p. 697-716 (2022) 2. K. Srinivasan, C. Zhang, and B.J. H. Stadler, High-Gyrotropy Seedlayer-Free Ce:TbIG for Monolithic Laser-Matched SOI Optical Isolators. *ACS Photonics*, Vol. 6, p. 2455–2461 (2019). 3. T. Fakhrul, B. Khurana, and C. A. Ross, High Figure of Merit Magneto-Optical Ce- and Bi-Substituted Terbium Iron Garnet Films Integrated on Si. *Adv. Opt. Mater*., Vol. 9, p. 2100512 (2021). 4. P. Dulal, A.D. Block, and B.J.H. Stadler, Optimized Magneto-optical Isolator Designs Inspired by Seedlayer-Free Terbium Iron Garnets with Opposite Chirality. *ACS Photonics*, Vol. 3, p. 1818–1825 (2016). 5. C. Zhang, P. Dulal, and B.J.H. Stadler, Monolithically-Integrated TE-mode 1D Silicon-on-Insulator Isolators using Seedlayer-Free Garnet. *Sci Rep*, Vol. 7, p. 5820 (2017) 6. T.E. Gage, P. Dulal, and B.J.H. Stadler, Si-integrated ultrathin films of phase-pure $Y_3Fe_5O_{12}$ (YIG) via novel two-step rapid thermal anneal, *Mater. Res. Lett*., Vol. 5, p. 379-385 (2017)

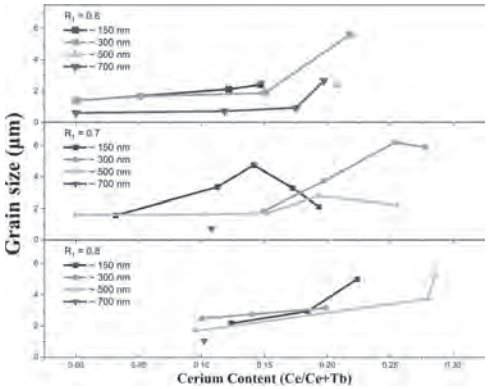

Fig. 1 Plot of grain size versus cerium content (Ce/(Ce+Tb) = R_2) with different thicknesses and rare-earth content (Ce+Tb/Fe = R_1).

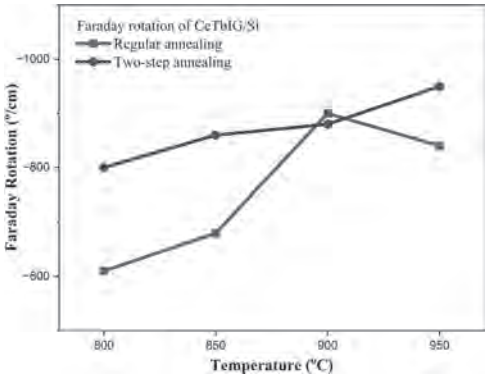

Fig. 2 Plot of Faraday rotation versus annealing temperatures by both regular and two-step annealing. Note: The two-step annealing involves a 5-minute pre-anneal at 400°C followed by a regular anneal at temperatures ranging from 800°C to 950°C for an additional 5 minutes.

CP-03. A systematic study on the influence of the microscopic structures on FMR of YIG based iron garnet dots. *Y. Omori*[1], H. Someya[1] and M. Ishida[1] *1. NEC Corporation, Minato-ku, Japan*

We studied the influence of the microscopic structure on Ferromagnetic Resonance (FMR) on YIG-based Iron Garnet (IG) films. IGs such as Yttrium Iron Garnet (YIG: $Y_3Fe_5O_{12}$) are attractive type of magnets for the use of applications due to their low Gilbert damping [1]. Recently it is suggested that the YIG dots' parametric excitation have a potential to be used for probabilistic bit operation or more quantum-like calculations [2,3]. For those applications, it is important to have stable characteristics and low dispersion of Ferromagnetic Resonance (FMR) in the dots. To understand and control the influence of the microscopic shape or structure is required. In this study, we performed systematic experiments of FMR. The YIG or other IG films were grown on 1-inch GGG (111) substrate with magnetron sputtering techniques. The films were fabricated to 100~1000 dot shapes with 10-100μm radius and put electrodes. In the fabrication process, systematic differences were given to each sample. For instance, we measured the dependence of FMR on the geometrical factor such as thickness, radius, and the electrodes shape. Also, we gave the dots designed damages and measured the dependence of FMR on the damage size and the number of the damages (Fig.1). The FMR signals were measured with using the Vector Network Analyzer and the semi-Auto probing system. The size seems to be more dominant on the HWHM. The more detailed discussion will be presented at the conference. This work was supported by JST-CREST (JPMJCR20C1).

[1] L. J. Cornelissen, et al., Nature Physics 11, 1022-1026 (2015). [2] T. Makiuchi, et al., Appl. Phys. Lett. 118, 022402 (2021). [3] T. Makiuchi, et al., Nature Materials 23, 627–632 (2024).

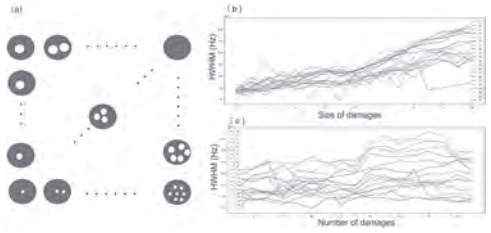

Fig. 1: (a) Schematic of the designed damage experiments on YIG dots. Different size and number of damages are given to the dots. The HWHM of FMR dependence on (b) size and (c) number of the damages.

CP-04. Additive Manufacturing of Soft Magnetic Material with Insulator Characteristic. *T. Chang*[1] and P. Huang[2] *1. Electric Motor Technology Research Center, National Cheng Kung University, Tainan, Taiwan; 2. Mechanical Engineering, National Cheng Kung University, Tainan, Taiwan*

Iron loss significantly impact the performance of magnetic components. In traditional soft magnetic composite molding processes, insulating layer are used to coat the grains, that effectively reduces loss. However, conventional mold manufacturing is costly and time-consuming in prototyping stages. Additive manufacturing enables rapid prototyping of magnetic components but lacks the capability to create insulating layers. This study explores the formation of insulating layers in NiFe material with different growth directions using additive manufacturing and compares measurement. Previous research [1] observed that controlling the chamber atmosphere forms an insulating layer on the surface, as the cross-section shown in Fig 1, effectively reducing eddy currents. Other studies suggested that creating gaps during additive manufacturing can also mitigate iron loss [2]. Therefore, insulating layers remains crucial in iron loss. This study compares Pcv (iron loss) of samples manufactured with different growth directions at 0°, 45°, and 90°, as shown in Fig. 2(a). Fig. 2(b) shows the orientation of the magnetic field after winding and the different directions of insulating layer formed via additive manufacturing. Additionally, ring-shaped samples were manufactured for subsequent measurements using additive manufacturing technology, as shown in Fig. 2(c). The Pcv measurements at different frequencies, shown in Fig. 2(d), reveal that Pcv increases linearly with frequency. Moreover, the orientation of the insulating layer relative to the magnetic flux generated by the measuring coil influences the Pcv value. When the insulating layer is horizontal to the direction of the magnetic flux generated by the measuring coil, the Pcv value is the highest; conversely, when vertical to the magnetic flux direction, the Pcv value is the lowest. The results show that different insulating layer directions affects iron losses; hence, the component placement angle can be adjusted according to the desired Pcv value during the additive manufacturing of magnetic components.

[1] K.J. Jhong, T.W. Chang, W.H. Lee, M.C. Tsai, and I.H. Jiang, "Characteristic of high frequency Fe-Si-Cr material for motor application by selective laser melting," AIP Advances, vol. 9, no. 3, 2019. [2] D. Goll, D. Schuller, G. Martinek, T. Kunert, J. Schurr, C. Sinz, T. Schubert, T. Bernthaler, H. Riegel, and G. Schneider, "Additive manufacturing of soft magnetic materials and components," Additive Manufacturing, vol. 27, pp. 428-439, 2019.

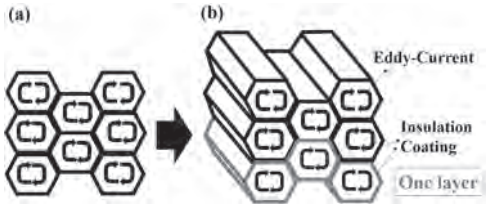

Fig.1 Cross-section view at(a) 0° (b) 45°

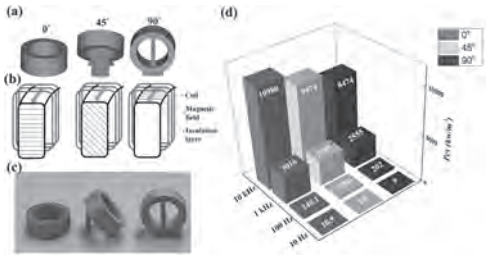

Fig.2 (a) Growth directions at 0°, 45°, and 90° (b)Directions of magnetic field and insulating layer (c)Samples (d) Pcv measurement.

CP-05. Magnetic and Thermal Properties of Hybrid Soft Magnetic Composites with Ferrite. *J. Fuzer*[1], S. Vovk[1], S. Dobák[1], P. Kollár[1], R. Bureš[2], M. Fáberová[2], V. Tsakaloudi[3] and V. Zaspalis[3] *1. Institute of Physics, P.J. Šafárik University in Košice, Košice, Slovakia; 2. Institute of Materials Research, Slovak Academy of Sciences, Košice, Slovakia; 3. Department of Chemical Engineering, Centre for Research and Technology-Hellas, Thessaloniki, Greece*

Soft magnetic composites are composed of magnetic powders and insulating medium using powder metallurgy where the basic idea of the soft magnetic composite is to limit the eddy currents circulating in the cross-section of the sample having the main influence on the significant frequency-dependent increase of energy loss [1-2]. Multicomponent magnetic phases with hybrid composite design consisting of the ferromagnetic major composite phase coated with insulating ferrimagnetic material can be one of the ways in the development of new magnetic materials. This approach provides the benefit of magnetic moment of ferrite insulation contributing to the effective magnetization of composite while maintaining high electrical resistivity. The warming at high frequency conditions can change the magnetic properties of the material, which makes it necessary to consider the temperature effect in the process of permeability and core loss prediction [3]. Therefore, the thermal analysis will be one of the important issues not only in high-speed motor design. This study with different content of Mn-Zn ferrite demonstrates a notable advantage of the coating, which is based on the SiO_2 layer and sintered Mn-Zn spinel ferrite. This design facilitates the preservation of soft magnetic properties even after thermal cycling up to 200°C. Considering specific operational frequency requirements, the optimal ferrite concentration for the composite ranged between 2 % and 4 %. Nevertheless, the composite demonstrated stable permeability and relaxation dispersion profiles even after thermal cycling under operational conditions. Higher concentrations of ferrite (> 3 wt%) led to a decrease in the DC component of real permeability, while magnetic loss decreased across the frequency spectrum up to 100 kHz with increasing ferrite content, peaking at 4 %. The factors contributing to energy include hysteresis losses, intra-particle eddy current losses localized within the conductive iron grains, inter-particle eddy current losses resulting from electrical connections among particles, and additional losses near mobile domain walls. The study emphasized the significant impact of excess loss, particularly in the medium-frequency range.

[1] E.A. Périgo, B. Weidenfeller, P. Kollár and J. Füzer, Appl. Phys. Rev., vol. 5, pp. 031301 (2018) [2] K.J. Sunday and M.L. Taheri, Metal Powder Report, vol. 72, pp. 425-429 (2017) [3] S. Vovk, J. Füzer, S. Dobák et. al., Ceram. Int., vol. 49(18), pp. 30137-30146, (2023)

CP-06. Fabrication of Buffer Layers for Highly Sensitive TMR Sensors with Co-based Heusler alloy electrodes. *H. Hamasaki*[1], T. Hojo[1], M. Tsunoda[2] and M. Oogane[1] *1. Department of Applied Physics, Graduate School of Engineering, Tohoku University, Sendai, Japan; 2. Development of Electronic Engineering, Graduate School of Engineering, Tohoku University, Sendai, Japan*

Introduction TMR sensor is a magnetic field sensor based on the tunnel magnetoresistance (TMR) effect. Due to their highly sensitivity, magnetocardiography (MCG) measurements at room temperature have been reported [1]. However, detecting smaller magnetic fields like magnetoencephalography (MEG) requires a larger TMR ratio and a smaller anisotropy magnetic field H_k (= $2K_1/Ms$). We fabricated Co-based Heusler alloy $Co_2FeAl_xSi_{1-x}$ thin films, which are expected to have a large TMR ratio at room temperature due to their half-metallicity and revealed that K_1 changes from positive to negative value with increasing Al component x around 0.33 [2]. To apply to TMR sensor, high B2 ($L2_1$) ordering, excellent (001) crystalline orientation and low K_1 are required. To this end, we deposited Co_2FeAl, Co_2FeSi, and their intermediate composition $Co_2FeAl_{0.33}Si_{0.67}$ thin films on Cr/Ag buffer layers and systematically investigated their K1 and B2 ($L2_1$) ordering and (001) crystalline orientation. Experimental On single crystalline MgO (001) substrates, Cr (60 nm)/Ag (20 nm) buffer layers were fabricated using the sputtering method. Then, 50 nm thick Co_2FeAl, Co_2FeSi, and $Co_2FeAlSi$ were fabricated at room temperature, followed by Ru (2 nm) layer to prevent oxidation. After deposition, post-annealing was performed at temperatures Ta=300–700°C. Results All the samples showed Ag(002) peaks in 2θ/ω scan [see Fig. 1], indicating fcc Ag epitaxially grown on bcc Cr. B2 and $L2_1$ ordering parameter of $Co_2FeAlSi$ thin film were approximately 90% and 40%. Co2FeAlSi grown on the Cr/Ag buffer achieved higher B2 ordering than the sample without buffer. This improvement is attributed to the lattice mismatch relaxation between the substrate and $Co_2FeAlSi$ thin films. In addition, (001)-orientation of $Co_2FeAlSi$ layer was improved due to Cr/Ag layer. Figs. 2 shows the angular dependence of resonance field and linewidth of the $Co_2FeAlSi$ thin film measured by out-of-plane FMR measurement. the magnetic damping constant was 4.9×10^{-3}, and this value was relatively small compared to previously reported value for $Co_2FeAlSi$ thin films.

[1] A. Kanno et al., Sci. Reo. 12, 6106 (2022) [2] T. Hojo et al., J. Magn. Magn. Mater. 601 172144 (2024)

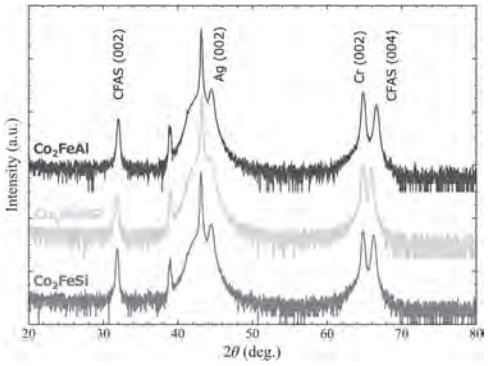

Fig.1 2θ/ω scan of Heusler alloy thin films grown on the CrAg buffer layer

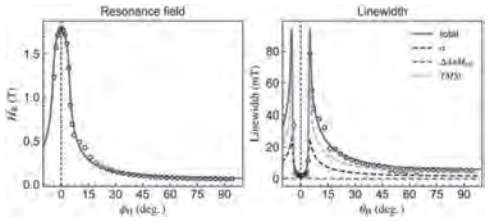

Fig.2 Resonance field and linewidth of the $Co_2FeAlSi$ thin film

CP-07. Chiral Induced Anisotropy in Soft Magnetic Films. R. Pasnak[1], M. Hasan[1] and *L.M. Malkinski*[1,2] *1. Department of Physics, University of New Orleans, New Orleans, LA, United States; 2. Advanced Materials Research Institute, University of New Orleans, New Orleans, LA, United States*

Uniaxial magnetic anisotropy can be induced in magnetic materials by applying magnetic field or tensile stresses during magnetic sample annealing or growth. We used a novel method of sample fabrication by changing the direction of magnetic field relative to the substrate position during thin film deposition. Consequently, the direction of the easy anisotropy axis rotated layer by layer and formed a chiral induced anisotropy. Sputtering of permalloy (Py) Fe_80Ni_{20} was used to deposit continuous films, arrays of circles of diameter of 5 μm and ellipses (5x25 μm) with the chiral anisotropy. After each layer of 5 or 10 nm the Si substrate placed in the uniform field of external coils was rotated by 10 degrees. The total change of the angle of the field relative to the sample was 180 degrees. The reference samples with the same patterns were deposited without field and in the presence of uniform field of 75 Oe at fixed direction relative to the substrate. The chiral anisotropy was found to have marked influence on the magnetization processes. Magnetic measurements were made at the angles of 0, 45 and 90 degrees relative to the patterned arrays using vibrating sample magnetometer (MircroMag). Examples of magnetic hysteresis loops of the arrays of circles deposited without field and in the rotating field are presented in Fig.1. They show a significant reduction of coercivity of the sample with chiral anisotropy Fig 1b) as compared to the isotropic sample deposited without field. It is believed that reduction of coercivity is due to enhanced reversible magnetization rotation processes or vortex type magnetization processes at weak fields as opposed to domain wall movements in the isotropic sample. The new method may potentially lead to fabrication of magnetic skyrmions which occur in the systems with chiral magnetocrystalline anisotropy.

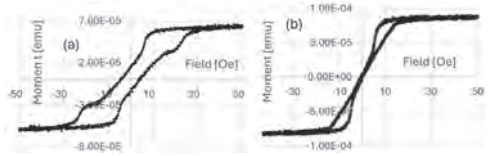

Fig.1 Hysteresis loops of an array of Py circles: a) of an isotropic sample and b) of a sample with chiral anisotropy

CP-08. Single domain wall propagation in Co-rich magnetic microwires with graded magnetic anisotropy. P. Corte-Leon[1,2,3], *V. Zhukova*[1,2,3], J. Blanco[2,3] and A. Zhukov[1,2,4] *1. Polym. and Adv. Mater., Univ. Basque Country, UPV/EHU, San Sebastian, Spain; 2. Appl. Phys., University of Basque Country, EIG, UPV/EHU, San Sebastian, Spain; 3. EHU Quantum Center, University of the Basque Country, UPV/EHU, San Sebastian, Spain; 4. IKERBASQUE, Basque Foundation for Science, Bilbao, Spain*

Studies of amorphous magnetic wires have attracted great interest owing to outstanding magnetic properties, like the giant magnetoimpedance (GMI) or the magnetic bistability and related single domain wall (DW) propagation [1,2]. The so-called Taylor-Ulitovsky technique allows manufacturing glass-coated amorphous magnetic wires (GCAMW) of the widest diameters range (from 200 nm up to 100 μm) coated with an insulating and flexible glass-coating [1,2]. The DW velocities observed in amorphous microwires with magnetic bistability are generally an order of magnitude superior to that of planar nanowires [2]. For proposed applications the degree of the DW dynamics control is essentially relevant. The controllable DW nucleation and propagation have been predicted in magnetic materials with graded magnetic anisotropy obtained using rather complex techniques [3]. Recently we proposed simple method to prepare Fe-rich GCAMW with graded magnetic anisotropy by stress-annealing at variable temperature [2]. On the other hand, hysteresis loops of Co-rich microwires can be substantially tunned by annealing conditions: annealing temperature and time [4]. Accordingly, we studied the effect annealing at variable T_{ann} on hysteresis loops and dependence of DW velocity, v, versus magnetic field, H, in $Fe_{3.6}Co_{69.2}Ni_1B_{12.5}Si_{11}Mo_{1.5}C_{1.2}$ microwire. The DW dynamics was studied using modified Sixtus-Tonks method using 3 pick-up coils placed along the studied microwire. In such Co-rich microwire we observed a gradual modification of the hysteresis loops along the microwire length (Fig. 1). As earlier predicted, in the region with graded anisotropy we observed unusual DW propagation where the DW velocity is non-uniform along the microwire (Fig.2b). While in the region annealed at constant T_{ann}, the DW velocity values between the pick-up coils 1-2 and 2-3, $v_{1\text{-}2}$ and $v_{2\text{-}3}$ respectively are almost the same (Fig.2a). Resuming, have proposed rather simple method to design graded magnetic anisotropy in Co-rich magnetic microwire by annealing of microwires with a temperature gradient.

1. H. Chiriac, S. Corodeanu, M. Lostun, etc. J. Appl. Phys. 107, 09A301 (2010) 2. V. Zhukova, P. Corte-Leon, L. González-Legarreta, etc. Nanomaterials 10, 2407 (2020) 3. R. Skomski, T.A. George, and D.J. Sellmyer, J. Appl. Phys. 103, 07F531 (2008) 4. L. Gonzalez-Legarreta, P. Corte-León, V. Zhukova, etc. J. Alloys Compd. 830, 154576, (2020)

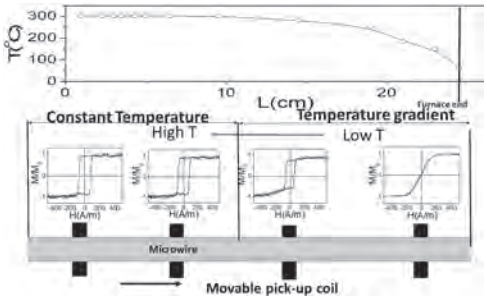

Hysteresis loops of studied microwire annealed at temperature gradient.

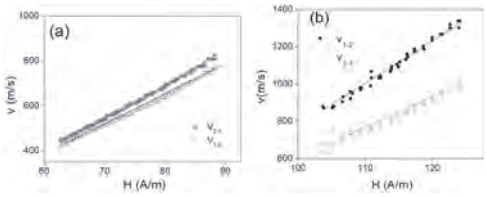

***v(H)* dependencies in annealed at constant (a) and variable T_{ann} (b) microwire.**

Session CQ
MAGNONICS II
(Poster Session)

Olivier Boulle, Chair
SPINTEC, Grenoble, France

CQ-01. Proposal of Spin Auto-Oscillation Based on Nonlinear Gain-Driven Magnon-Polaritons. *R. Suzuki*[1], T. Chiba[1,2] and H. Matsueda[1,3]
1. Tohoku University, Sendai-shi, Japan; 2. FRIS, Sendai-shi, Japan; 3. CSIS, Sendai-shi, Japan

Recently, cavity magnonics that manipulate magnon-polariton (MP) have attracted broad interest in modern quantum physics and quantum information technology. Very recently, an ultrastrong coupling (USC) of MPs at room temperature has been experimentally and theoretically demonstrated by using a metamaterial consisting of a coil and inserted magnet [1-3] termed as a dynamical inductor. Utilizing the magnon-photon coupling, a maser based on gain-driven polariton (GDP) where an MP combined with a gain resource has been demonstrated[4,5]. Considering the potential of GDP to induce magnon excitation, GDP will have significant implications for spintronic oscillator devices. There are several challenges to realize the spin-oscillation based on GDP. Firstly, the GDP demonstrated in the previous study accompanies a nontrivial fluctuation with a sub-microsecond period to stabilize the emission [5]. Additionally, magnon has an intrinsic nonlinearity which should be taken into consideration in auto-oscillation phenomena. In this study, we theoretically investigate nonlinear magnon dynamics based on GDP. As shown in Fig (a), we model a GDP based on an electric circuit model. By combining the Kirchhoff circuit equation and the Landau-Lifshitz-Gilbert (LLG) equation, we simulate the nonlinear dynamics of the ultrastrongly coupled GDP. Figure (b) shows the result of numerical simulations. In this figure, we are focusing on the x component of the magnon. Comparing the strong coupling regime with the USC regime, in the USC regime the nontrivial fluctuation becomes lower. Based on the results so far, magnons can automatically oscillate by the gain of the photonic system through the magnon-photon coupling. This principle paves the way for utilizing a gain from arbitrary oscillator systems which can combine with magnon.

[1] T. Chiba *et al.*, Appl. Phys. Lett. 124, 012402 (2024). [2] T. Chiba *et al.*, J. Magn. Soc. Jpn., 48, 2 (2024). [3] K. Mita *et al.*, arXiv:2406.19046 [4] J. T. Hou *et al.*, Phys. Rev. Appl. 16, 034034 (2021). [5] B. Yao *et al.*, Phys. Rev. Lett. 130, 146702 (2023).

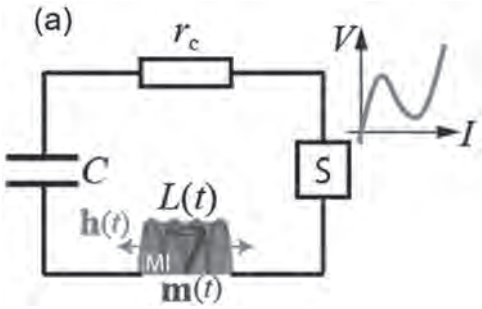

(a) Schematics of an RLC circuit with gain (S component is a negative resistance element that can cancel out the circuit's intrinsic damping) and dynamical inductor represented gray box.

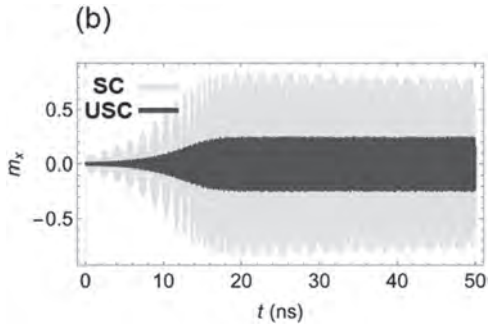

(b) The time evolution of magnon (m_x). SU represents a strong coupling.

CQ-02. Contribution of Three-magnon Scattering to Gilbert Damping at Elevated Temperatures. *Y. Chen*[1] and R. Victora[1] *1. University of Minnesota, Minneapolis, MN, United States*

Gilbert damping is a key parameter representing the energy loss in the Landau-Lifshitz-Gilbert equation, which describes the dynamics of magnetization and is crucial in micromagnetic simulations. We have developed an analytical method to calculate Gilbert damping, based on the contributions from the three-particle magnon scattering process [1]. By incorporating the exchange, anisotropic, and demagnetization energies, we applied this method to determine Gilbert damping at different temperatures. Our calculation shows that, near the Curie temperature, the calculated damping equals around 80% of the results obtained from the coarse-graining method proposed by Feng and Visscher in 2001[2], which means three-magnon scattering gives a dominant contribution to Gilbert damping. This research may give useful insights into the relationship between Gilbert damping and magnons.

[1] Qu, Tao, et al. "Oscillations and confluence in three-magnon scattering of ferromagnetic resonance." Physical Review B 107.6 (2023): L060401. [2] Feng, Xuebing, and P. B. Visscher. "Coarse-graining Landau–Lifshitz damping." Journal of Applied Physics 89.11 (2001): 6988-6990.

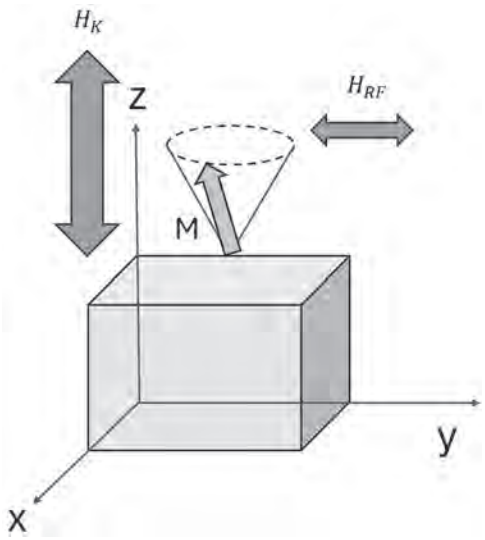

Sample and field geometry. H_k is the anisotropy field and H_{RF} is the applied microwave field along y-direction that dynamically excites the magnetization and makes it precess

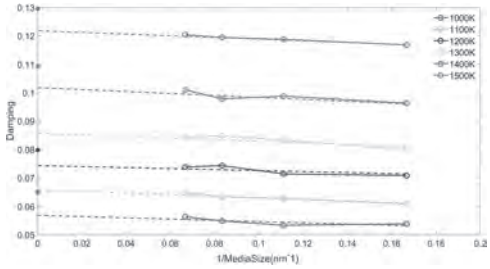

Damping vs.1/Sample-Size using coarse-graining method (scattered data points at y-axis) and three-magnon scattering model(curves), at different temperatures.

CQ-03. Thickness and Width Dependence of Spin Wave Propagation in Permalloy Microstripe Waveguides. *D. M S*[1], S.N. Adithya[1], M. Kuchibhotla[1], A.O. Adeyeye[2] and A. Haldar[1] *1. Physics, Indain institute of technology Hyderabad, Hyderabad, India; 2. Physics, Durham university, Durham, United Kingdom*

Engineering magnonic devices for efficient information transport using spin wave-based spin currents has garnered significant attention recently[1]. An integral part of any magnonic device is a waveguide, and spin wave propagation in these waveguides is highly sensitive to their geometry[2,3]. Here, we have conducted a comprehensive analysis of the combined effect of the width and thickness of the permalloy microstripe waveguide on spin wave propagation using analytical calculations and experiments. Permalloy stripes of widths(w) varying from 2 to 4 μm are fabricated for two thicknesses(t): 5 nm and 20 nm. A shorted coplanar waveguide with a stripe width of 1 μm is used to excite the spin waves. The nanoscale imaging of spin waves is performed using the micro-Brillouin light scattering technique. The dispersion calculations shown in Fig.1(a) and (b) reveal a fourfold increase in the group velocity of spin waves with an increase in the thickness. The increase in thickness has also broadened the accessible frequency range from 0.6 to 2.5 GHz. Additionally, the spin wave mode frequencies show an increasing trend with width, owing to the reduction in demagnetizing fields, as displayed in Fig.1(c) and (d). We also noticed a remarkable decrease in the linewidth of the BLS signal with thickness. The spatially resolved measurements show that changes in both thickness and width significantly affect the decay length, with spin waves propagating longer distances in wider and thicker waveguides (Fig.1(e) and 1(f)). The decay length exhibits a fourfold increase with the thickness, which is consistent with our analytical calculations. Our findings have potential implications for the development of future magnonic devices.

[1] A. V. Chumak, V.I. Vasyuchka, A.A. Serga et.al, Nat Phys 11(6), 453–461 (2015). [2] V.E. Demidov, S.O. Demokritov, K. Rott, et.al, Appl Phys Lett 91(25), (2007). [3] V.E. Demidov, J. Jersch, S.O. Demokritov, et.al, Phys Rev B Condens Matter Mater Phys 79(5), (2009).

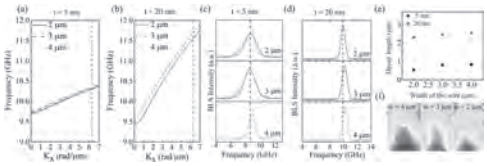

Fig.1 The dispersion characteristics of spin waves at 110 mT for various widths of stripe for thickness (a) 5 nm and (b) 20 nm. BLS spectra for various widths for thickness (c) 5 nm and (d) 20 nm. (e) Variation of decay length of propagating spin waves as a function of width for t = 5, 20 nm. (f) 2D map of spin wave intensity obtained from space-resolved measurements for microstripes of various widths of t = 20 nm, carried out at 110 mT. Blue indicates minimum, and red indicates maximum absorption.

CQ-05. Spin Wave Dynamics in Bicomponent Sierpinski Square. *R. Mehta*[1] and S. Saha[1] *1. Department of Physics, Ashoka University, Sonipat-131029, India*

Quasiperiodic magnonic crystals, unlike their periodic counterparts, lack strict periodicity which gives rise to complex and localized spin wave spectra characterized by numerous band gaps [1]. Fractals, with their self-similar structures across different length scales exemplifying dilation symmetry, are observed in nature through examples like lightning, snowflakes, broccoli, and coastlines. It has been reported that magnetostatic mode formation in an artificial magnetic fractal structure is related to their geometric scaling [2]. Moreover, the spin wave dynamics in Sierpinski triangle show the appearance of frequency gap with the iteration number exceeding a certain value and its tunability with the orientation and strength of the external magnetic field, proposing their application in magnonic filters [3]. In this work, we have studied the magnetization dynamics of a square-shaped deterministic magnonic fractal known as the Sierpinski square (BSQ) which is composed of two different magnetic materials, specifically NiFe and CoFe alloys. For such BSQ structure, the spinwave propagation is modified by the exchange interaction between two different magnetic materials. To investigate the spinwave dynamics the Landau-Lifshitz-Gilbert equation is solved using micromagnetic simulations. A complex evolution of the spin-wave modes has been observed as the iteration number increased with the presence of mini-frequency gaps [Fig. 1(a)]. The magnetization dynamics have also been calculated for bicomponent periodic arrangement of squares (BPS) having the same base length of Sierpinski square and are differ significantly from BSQ [Fig. 1(b)]. It is interesting to note that spatial profile of spin wave mode for BSQ shows the formation of nanochannels extended through the structure, while these extended nanochannels are missing for periodic arranged structure [Fig. 1(c, d)]. The observation of extended nanochannels for BSQ may propose their potential application in magnonic devices.

1) S. Watanable, V. Bhat, K. Baumgaertl, and D. Grundler, Adv. Funct. Mater. 30, 2001388 (2020). 2) J. Zhou, M. Zelent, Z. Luo, V. Scagnoli, M. Krawczyk, L. J. Heyderman, and S. Saha, Phys. Rev. B 105, 174415 (2022) 3) R. Mehta, M. Moalic, M. Krawczyk and S. Saha, Journal of Physics: Condensed Matter 35, 324002 (2023)

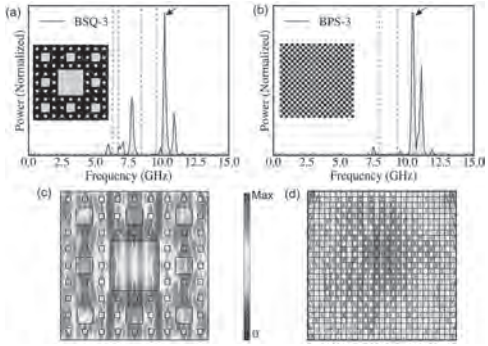

Fig. 1: (a) FFT spectra of the simulated time-domain magnetization for 3rd iteration of (a) BSQ and (b) BPS at H_{ext} = 0.1 T and φ = 0°. The spatial profile of spin wave mode at the highest intensity peak around 10 GHz for (c) BSQ-3 and (d) BPS-3.

CQ-06. Magneto-Raman spectroscopy of spin waves in bulk CrI_3 with Ni. *C.J. Cunningham*[1], G. Ye[2], C. Nnokwe[2], T. Nguyen[2], C. Sadler[1], K. Wu[2], W. Liu[3], B. Lv[3], P. Lukashev[1], P. Shand[1], A.J. Stollenwerk[1] and R. He[2] *1. Department of Physics, University of Northern Iowa, Cedar Falls, IA, United States; 2. Department of Electrical and Computer Engineering, Texas Tech University, Lubbock, TX, United States; 3. Department of Physics, University of Texas at Dallas, Richardson, TX, United States*

A spin wave describes the spin dynamics of magnetic ordering when excited and its frequency determines the ultimate switching speed of state-of-the-art spintronic devices. To realize the application of van der Waals magnets in spintronic applications, a complete description of the 2D magnetic phase is needed, which requires not only the identification of the ordered ground state, but also the understanding of the excitations, i.e., spin waves, or equivalently, magnons. Magneto-Raman spectroscopy is a powerful tool for studies of spin waves as spin wave modes usually display Zeeman shifts as a function of applied magnetic field. By comparing ultra-low frequency (<10 cm^{-1}) Raman spectra of spin wave modes from pristine bulk CrI_3 [1] and from bulk CrI_3 with a thin layer of Ni on the surface, we see that CrI_3 with Ni on the surface shows only a single spin wave branch at magnetic field up to 7T (Fig. 1), suggesting the existence of only a ferromagnetic phase. This is distinct from pristine CrI_3 whose spin wave spectra show three branches below 2T from a mixed state of antiferromagnetism on the surface and ferromagnetism in deeper bulk layers (Fig. 2). Our studies show that the magnetic phase of CrI_3 can be controlled through deposition of thin metal layers on the surface. Completion of experiments and analysis of the data was supported by Grant No. DE-SC0020334 funded by the U.S. Department of Energy, Office of Science. This work was supported in part by the National Science Foundation (Grant No. DMR-2300639).

[1] Siwen Li, Zhipeng Ye, Xiangpeng Luo, Gaihua Ye, Hyun Ho Kim, Bowen Yang, Shangjie Tian, Chenghe Li, Hechang Lei, Adam W. Tsen, Kai Sun, Rui He, and Liuyan Zhao, "Magnetic field-induced quantum phase transitions in a van der Waals magnet," Physical Review X., Vol. 10, 011075 (2020).

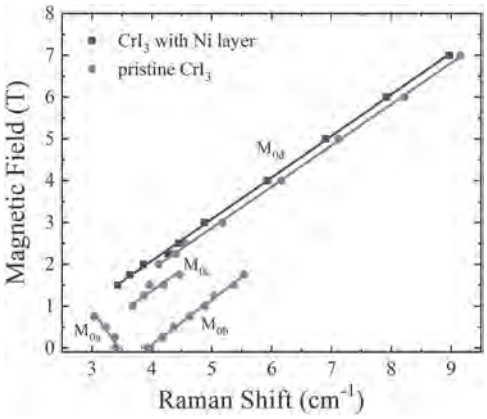

Fig. 1: Magnetic field dependence of spin wave mode frequencies from pristine CrI_3 and CrI_3 with Ni on surface. The M_{0a} and M_{0b} are two branches from surface AFM and M_{0c} is the branch from bulk FM in pristine CrI_3. M_{0d} is the branch from CrI_3 with Ni on the surface. All data were measured at 11 K using a co-circularly polarized 633 nm laser.

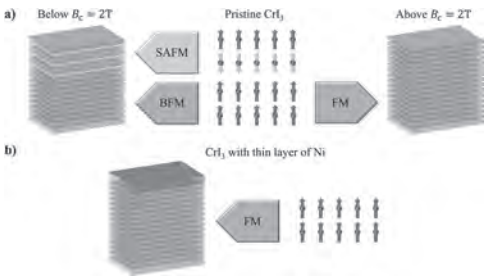

Fig. 2: (a) Schematic illustration of magnetic states in pristine CrI_3 below and above the critical field of 2T. SAFM and BFM refer to surface AFM and bulk FM, respectively. (b) Magnetic states in CrI_3 with Ni thin layer on surface.

CQ-07. Thickness Dependence of Spin-wave Propagation in Low-damping CoFe Thin Films. *M. Kiechle*[1], J.J. Wisser[1], W.K. Peria[1], J.M. Shaw[1] and H.T. Nembach[1] *1. Physical Measurement Laboratory, National Institute of Standards and Technology, Boulder, CO, United States*

We investigate spin-wave propagation in Cobalt-Iron thin films across a broad frequency range exceeding f = 30 GHz and wavevectors k > 100 rad/μm using micro-focused Brillouin Light Scattering (μBLS). The $Co_{0.25}Fe_{0.75}$ alloy [1] has highly favorable magnetic properties, including high saturation magnetization Ms and low magnetic damping. While CoFe's Gilbert damping is comparable to that of heavily researched sputtered garnets, the CMOS compatibility of metallic magnetic systems is highly advantageous for Spintronics. Moreover, the nearly tenfold higher M_s leads to larger group velocities crucial for computational speed, positioning CoFe as a promising material for enabling efficient spin transport and manipulation. We carefully deconvolute the different contributions to the spin-wave propagation length λ_d: First, the magnetic relaxation rate, which has been shown in the past to have k^2 contributions [2], and second, the spin-wave velocity, which depends on M_s and film thickness t. For this, we sputter-deposited a CoFe thickness series ranging from t = 2 nm to 20 nm of Ta(1)/Cu(1)/Co0.25Fe0.75(t)/Cu(1) and patterned them into spin-wave conduits. A microstrip line is used for spin-wave excitation, and λ_d is determined from the spatial distribution of the spin-wave amplitude obtained from BLS linear scans (Fig. 1). The measured λ_d is then analyzed in relation to t and f, and compared to the calculated k-dependence from the spin-wave dispersion. In addition to the damping characterization of a thickness series, we also investigate the feasibility of manipulating the intrinsic damping torque by the spin-Hall effect, i.e., injecting spin current through an adjacent large spin-Hall angle metal (we use 6 nm of Pt). This task is particularly

challenging in magnetic metals, as the electric current is shunted by the magnetic layer itself, resulting in reduced current densities in the spin-orbit materials.

[1] Schoen, M., Thonig, D., Schneider, M. et al. Ultra-low magnetic damping of a metallic ferromagnet. Nature Phys 12, 839–842 (2016) [2] Nembach, Hans T., Justin M. Shaw, Carl T. Boone, and Thomas J. Silva. Mode-and Size-Dependent Landau-Lifshitz Damping in Magnetic Nanostructures: Evidence for Nonlocal Damping." Physical review letters 110, no. 11 (2013): 117201.

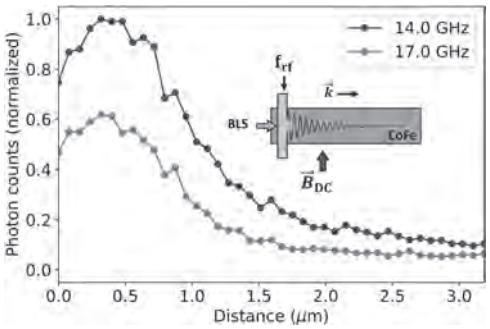

BLS line scan of RF-excited spin waves in a 2 nm thin film and the illustrated measurement configuration (B_{DC} = 56 mT) starting on the antenna edge. The intensity profiles are modeled with a point-wise convolution of an exponential decay and the Gaussian beam profile to extract λ_d.

CQ-08. Brillouin Light Scattering measurements of Dzyaloshinskii Moriya Interaction: reproducibility and uncertainty. *M. Madami*[1], S. Tacchi[2], C. Marrows[3], E. Darwin[3], B.J. Hickey[3], A. Huxtable[3], A. Magni[4], A. Di Pietro[4], G. Durin[4], M. Kuepferling[4] and G. Carlotti[1] *1. Department of Physics and Geology, University of Perugia, Perugia, Italy; 2. CNR - Istituto Officina dei Materiali, Perugia, Italy; 3. School of Physics and Astronomy, University of Leeds, Leeds, United Kingdom; 4. Istituto Nazionale di Ricerca Mertologica (INRiM), Torino, Italy*

Brillouin light scattering (BLS) is a well-established technique to measure spin waves (SWs) in magnetic materials due to its high sensitivity in a wide range of wave vectors and a relatively simple experimental apparatus and it has become one of the most straightforward and reliable techniques to measure the DMI constant [1]. This is possible because SWs propagating in opposite directions have opposite chiralities and the DMI contribution would either decrease or increase the SW frequency resulting in an intrinsic nonreciprocity of the SW propagation which is revealed by BLS as a Stokes/Anti-Stokes (A/AS) peak asymmetry [2], as shown in Fig.1. Nonetheless the problem of the measurement's reproducibility as well as the uncertainty on the determination of the DMI constant remains an open problem. As a matter of fact, in the scientific literature there are several examples of inconsistent results about DMI properties, obtained on nominally identical samples with different experimental techniques and, sometimes, even with the same experimental technique from different groups [3]. In the present study we investigated, by means of BLS, the DMI on ferromagnetic/heavy-metal multilayers, like Pt(3.0nm)/Co(0.8nm), with emphasis on the reproducibility of the measurements and on the uncertainty on the extracted value of the DMI constant. For this experimental analysis we repeated the BLS measurements in different regions of the same sample to obtain a reasonable statistic to extract the value of the DMI constant with a reliable uncertainty, as shown in Fig.2. The results of this study show how the DMI constant can sometimes vary even in regions of the sample which are very close to one another, like 1-2 mm, by a substantial amount. We point out the importance to understand if and how these fluctuations can be explained by statistical uncertainty or by an actual difference in the local sample properties. The final aim of this work is to try and establish good practices in the experimental determination of DMI constant by means of BLS.

[1] K. Di, V. L. Zhang, H. S. Lim, et al., Appl. Phys. Lett. 106, 052403 (2015). [2] A. Zheludev, S. Maslov, G. Shirane, et al., Phys. Rev. B 59, 11432–11444 (1999). [3] M. Kuepferling et al., Reviews of Modern Physics, vol. 95, no. 1. American Physical Society (APS), Mar. 22, (2023).

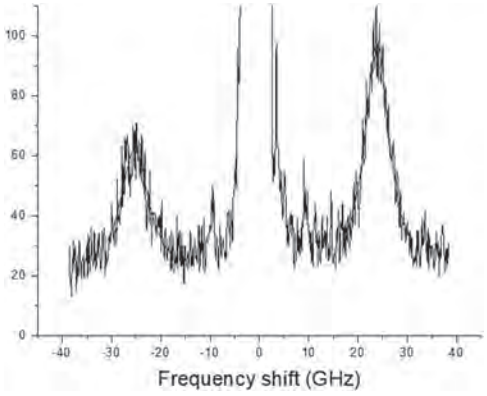

BLS spectrum measured on a Pt(3.0nm)/Co(0.8nm) sample

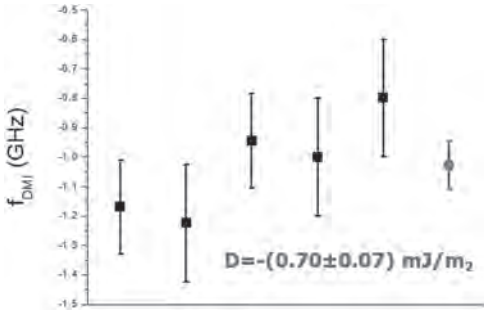

S/AS frequency asymmetry measured in different regions of the Pt(3.0nm)/Co(0.8nm) sample and its mean value with correct uncertainties

Session CR
BIOMEDICAL THERAPIES AND OTHER BIOMEDICAL APPLICATIONS
(Poster Session)

Samuel Oberdick, Chair
National Institute of Standards and Technology, Boulder, CO, United States

CR-01. A Hybrid Machine Learning Algorithm for Predicting Resting Motor Thresholds in Patients with Schizophrenia and Healthy Individuals Undergoing Transcranial Magnetic Stimulation.
Y.R. Saxena[1,2], C.J. Lewis[3], M. Alam[1], J. Atulasimha[1,4], U.M. Mehta[5] and *R.L. Hadimani*[1,3,6] *1. Mechanical and Nuclear Engineering, Virginia Commonwealth University, Richmond, VA, United States; 2. Electrical Engineering and Computer Science, University of California at Berkeley, Berkeley, CA, United States; 3. Biomedical Engineering, Virginia Commonwealth University, Richmond, VA, United States; 4. Electrical and Computer Engineering, Virginia Commonwealth University, Richmond, VA, United States; 5. National Institute of Mental Health and Neurosciences, Bangalore, India; 6. Electrical and Computer Engineering, Iowa State University, Ames, IA, United States*

Transcranial magnetic stimulation (TMS) is an FDA-approved method for treating neurological and psychiatric disorders [1]. It is currently being tested as an experimental treatment for patients with schizophrenia. Due to the complex and varied neuroanatomy and functional states of brains, it is difficult to predict the resting motor threshold (RMT) needed for treatment with TMS. Our prior research has shown that anatomical parameters like coil-to-cortex distance (CCD), grey matter volume (GMV), and depolarized grey matter volume (DGMV) are all associated with RMT [2]. Additionally, connectivity derived from functional magnetic resonance imaging (fMRI) is also associated with RMT [3]. Previous studies have used linear regression modeling to analyze the associations of parameters with RMT; however, machine learning has not been used to directly predict the RMT from these parameters. This study investigates the use of machine learning in predicting the RMT from functional connectivity and anatomical data. For 54 subjects with schizophrenia and 43 healthy subjects, fMRI Blood Oxygen Level Detection (BOLD) in 25 brain regions were turned into time series with 300 timestamps and fed into a Long Short-Term Memory (LSTM) model. The outputs of the LSTM are concatenated with the CCD, GMV, and percentages of voxels in the grey matter over 50 V/m (DGMV50) and 100 V/M (DGMV100) and then fed into an artificial neural network (ANN) that predicted the RMT. With 50 epochs, the training loss and the testing loss are 0.0366 and 0.0228[SA1] respectively. In addition, the training and testing MAEs are 0.1474 and 0.1280 respectively, corresponding to errors of 4.5694% and 3.9680% of the maximum stimulator output (%MSO) in the predicted RMT values.

[1] B. R. Mishra, S. Sarkar, and S. K. Praharaj, Annals of Indian Academy of Neurology, Vol 14(4), p. 245-251 (2011) [2] C. J. Lewis, L. M. Franke, J. V. Lee, N. Mittal, G.T. Gitchel, R. A. Perera, K. L. Holloway, W. C. Walker, C. L. Peterson, R. L. Hadimani, AIP Advances, Vol 13 (2) (2023) https://doi.org/10.1063/9.0000567 [3] C. J. Lewis, N. Mittal, A. K. Pandurangi, U. M. Mehta, R. L. Hadimani, AIP Advances, Vol 14 (1) (2024)

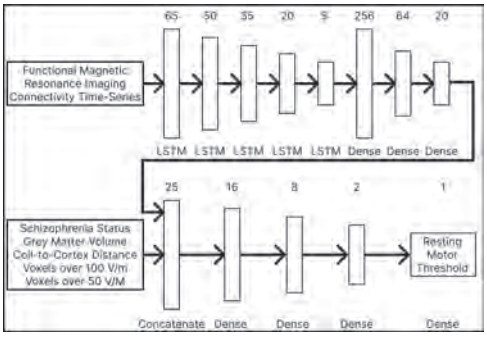

Fig 1. Diagram of Hybrid Machine Learning Algorithm Architecture

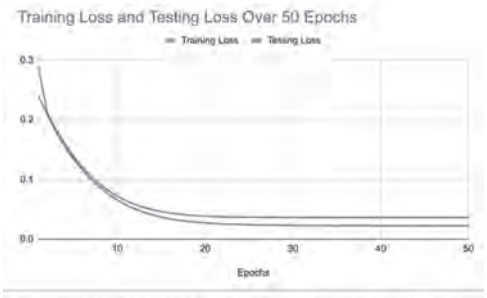

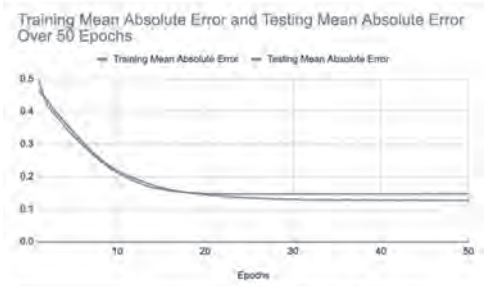

	Model Loss	Model Mean Absolute Error	True Error
Training	0.0366	0.1474	4.5694
Testing	0.0228	0.128	3.968

Fig 2. Diagram of Training and Testing Loss and Mean Absolute Error Over 50 Epochs of Training and Table of Training and Testing Loss and Mean Absolute Error After 50 Epochs of Training

CR-02. Optimization of pulse magnetic field for effective magnetic hyperthermia treatment.
A. Kuwahata[1], Y. Adachi[1], E. Nakamura[2] and S. Yabukami[1] *1. Tohoku University, Sendai, Japan; 2. High Energy Accelerator Research Organization (KEK), Tsukuba, Japan*

The heating efficiency and cancer treatment effect of magnetic hyperthermia (MH) strongly depends on the magnetic relaxation of magnetic nanoparticles (MNPs) because the mechanism behind heat generation is based on the MNP dynamics under the application of alternating magnetic fields (AMF) [1]. Although the conventional sinusoidal wave can generate heat, there is a lack

of heating efficiency due to a slow steep of magnetic field changing. Thus, we proposed the pulse magnetic field (PMF) and numerically and experimentally demonstrated the rapid changes of the magnetic field, achieving 400% heating efficiency [2,3] to overcome the limitation of the conventional wave. In this study, we optimized the parameters, such as capacitance, inductance, frequency, and pulse width, of the PMF to enhance the heating efficiency. Figure 1(a) presents the experimental setup for a pulse generator and heating efficiency evaluation system for the MH operation. The charged electric energy is rapidly released, and the inductive coil generates the PMF Typical waveforms of PMF (200 and 400 kHz) are shown in Figs. 1(b) and (c). Figure 2(a) shows the specific loss power (SLP) and unconditional loss power (ULP) we proposed [2,3] of PMF with the repetitive frequencies of 200 and 400 kHz. We observed the enhancement of SLP for a higher frequency and the same value of ULP for both frequencies. The practical heating power is calculated by SLP times ULP. The results indicate the enhancement of 200% heating efficiency. The pulse magnetic field technology will facilitate the development of a compact MH system for the installation of medical sites. We will develop a pulse transformer system to enhance much heating efficiency and demonstrate cancer treatment in mouse animal experiments.

[1] D. Chang *et al.*, Front. Pharmacol. 9, 386237 (2018). [2] A. Kuwahata *et al.*, AIP Advances 13, 025145 (2023). [3] Y. Adachi *et al.,* AIP Advances 14, 015144 (2024).

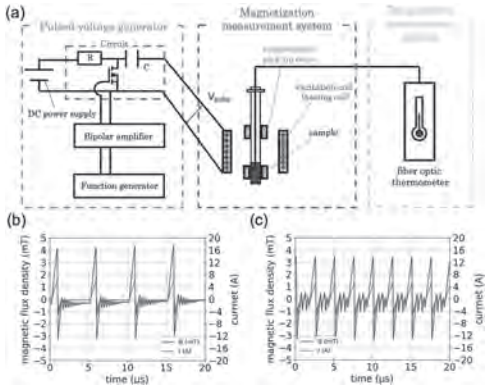

(a) Experimental setup for a pulse generator and heating efficiency evaluation system. Typical waveforms of pulse magnetic fields with the frequency of (a) 200 and (b) 400 kHz.

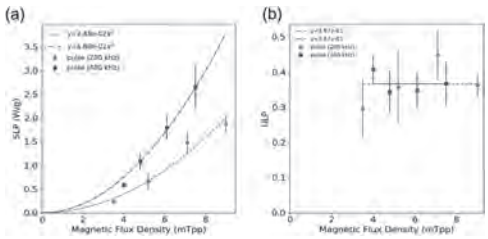

(a) Specific loss power (SLP) and (b) unconditional loss power (ULP) [2,3] of pulse magnetic fields with the repetitive frequency of 200 (red lines) and 400 kHz (blue lines).

CR-03. Development of magnetic hyperthermia coil system for wide treatment temperature area on breast and neck cancer patients.
A. Yamazaki[1], T. Kagami[2], A. Kuwahata[1,2] and S. Yabukami[1,2] *1. Graduate School of Engineering, Tohoku University, Sendai, Japan; 2. Graduate School of Biomedical Engineering, Tohoku University, Sendai, Japan*

Magnetic hyperthermia (MH) based on magnetic heat generation of the magnetic relaxation mechanisms of magnetic nanoparticles (MNPs) under alternating magnetic fields (AMF) is a promising cancer treatment technology due to non-invasiveness compared with other treatment methods such as radiation, microwave irradiation, and chemotherapy [1]. To enhance the treatment effect produced by a wider area where heating up to treatment temperature (43°C), the spatial distribution of the magnetic field generated by the magnetic coil should be optimized [2]. However, the conventional coils, such as solenoid and Helmholtz coils [3,4], cannot controlled the field distribution for practical/clinical applications. In this study, we developed and evaluated the magnetic hyperthermia coil system for generating the wider treatment temperature area on breast and neck cancer patients. Fig. 1 illustrate the magnetic coil design of the conventional solenoid, breast and neck coils for practical clinical applications. The proposed breast and neck coil can fit the shape of each body part. We employ COMSOL Multiphysics® and calculate the spatial distribution of magnetic field and treatment temperature area on based on magnetic heating a finite element method [4]. Fig. 2 shows the field distribution and treatment area. The uniformities of magnetic field of the conventional, breast, and neck coils are 0.3%, 26.7%, and 15.8%, respectively. The proposed breast and neck coils generate much better uniformity. In addition, the area of treatment temperature of the conventional, breast, and neck coils are 7.4%, 71.1%, and 62.9%, respectively. The proposed breast and neck coils achieved a wider treatment area. The results indicates that our proposed coil system provide the enhancement of cancer treatment effect on specific cancer patients. We will fabricate a prototype coil system and perform animal experiments in murine tumor model.

[1] Suriyanto *et al.*, Biomedical engineering online, 16, 36 (2017). [2] L. Wu *et al.*, IEEE Trans Magn, 51, 2 (2015). [3] L. Shoshiashvili *et al.*, Cancers 15, 1672 (2023). [4] T. Kagami *et al.*, IEEJ Trans. (2024).

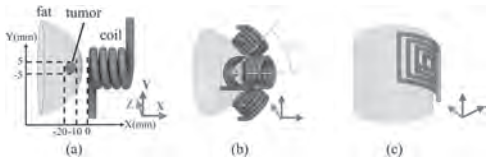

Fig. 1. Magnetic coil design of (a) conventional solenoid, (b) breast and (c) neck coils for practical clinical applications.

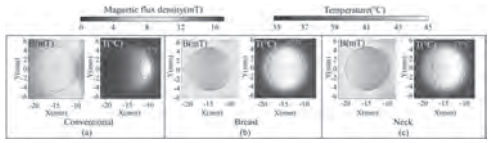

Fig. 2. Spatial distribution of magnetic fields and treatment temperature area in the vicinity of tumor location for (a) conventional solenoid, (b) breast, and (c) neck coil.

CR-04. Magnetic Hyperthermia Performance of Commercial Iron Oxide Magnetic Nanoparticles.
B. Rezaei[1], S. Mostufa[1], E. Azizi[1], Y.A. Wang[2], C. Li[1], J. Gomez-Pastora[3], R. He[1] and *K. Wu*[1] *1. Department of Electrical and Computer Engineering, Texas Tech University, Lubbock, TX, United States; 2. Ocean Nano Tech LLC, San Diego, CA, United States; 3. Department of Chemical Engineering, Texas Tech University, Lubbock, TX, United States*

Magnetic hyperthermia therapy (MHT) is an evolving treatment for tumors where magnetic nanoparticles (MNPs) are directed to the tumor and exposed to an alternating magnetic field (AMF). This induces localized heating, causing the apoptosis of cancer cells. Monitoring heat delivery in a non-invasive, real-time manner is crucial for predicting clinical outcomes. This precise control over the hyperthermia process allows for targeted temperature adjustments in the range of 42-46 °C, effectively targeting cancer cells while minimizing damage to surrounding healthy tissue.[1,2] Factors like MNP size, media viscosity, and AMF frequency and amplitude influence MHT. Optimizing these factors enhances heat dissipation through mechanisms like hysteresis loss, and Néel and Brownian relaxations, improving the specific absorption rate (SAR) and intrinsic loss power (ILP) of the MNPs.[3] In this study, we meticulously measure the temperature-time curves (Fig 1) and ILP values of several commercially available iron oxide MNP products, specifically, 50 nm multi-core carboxyl-coated MNPs and 15 – 30 nm

single-core amine-coated MNPs. These measurements are conducted under different AMF frequencies and amplitudes to evaluate the impact of AMF on the heating efficiency of the nanoparticles. By systematically varying the concentration and magnetic core size of the MNPs and tuning the frequency and amplitude of the AMF, we aim to elucidate how these factors collectively influence heat dissipation. This, in turn, enhances our understanding of the optimal conditions for *in-vivo* hyperthermia treatment. Our results indicate that among the MNP products tested, the single-core amine-coated nanoparticles with a size of 30 nm exhibited the highest ILP. Additionally, for different MNP concentrations, the multi-core MNPs show the highest ILP at a concentration of 2 mg/mL (see Fig 1).

[1] S. Moise, J.M. Byrne, A.J. El Haj, and N.D. Telling, "The potential of magnetic hyperthermia for triggering the differentiation of cancer cells," Nanoscale 10(44), 20519–20525 (2018). [2] H. Gavilán, S.K. Avugadda, T. Fernández-Cabada, N. Soni, M. Cassani, B.T. Mai, R. Chantrell, and T. Pellegrino, "Magnetic nanoparticles and clusters for magnetic hyperthermia: optimizing their heat performance and developing combinatorial therapies to tackle cancer," Chem. Soc. Rev. 50(20), 11614–11667 (2021). [3] B.B. Lahiri, S. Ranoo, A.W. Zaibudeen, and J. Philip, "Magnetic hyperthermia in magnetic nanoemulsions: Effects of polydispersity, particle concentration and medium viscosity," Journal of Magnetism and Magnetic Materials 441, 310–327 (2017).

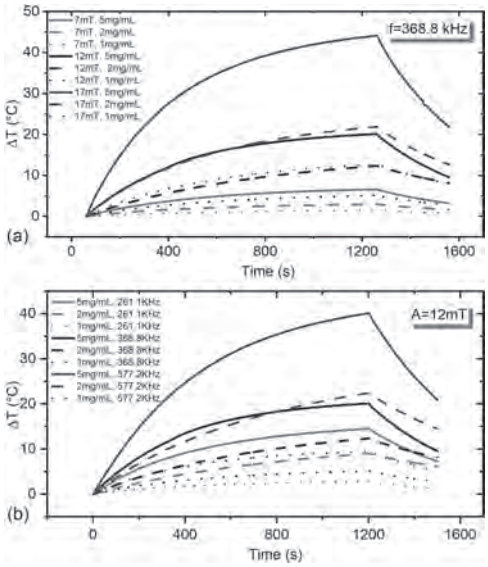

Fig 1. The temperature-time curves of 1 mg/mL, 2 mg/mL, and 5 mg/mL 50 nm multi-core carboxyl group-coated MNPs subjected to (a) 368.8 kHz AMF with varying field amplitudes of 7 mT, 12 mT, and 17 mT. (b) 12 mT AMF with varying field frequencies of 261.1 kHz, 368.8 kHz, and 577.2 kHz.

CR-05. Gd-Doped Cobalt Ferrite Nanoparticles: Structural, Magnetic, and Cytotoxicity Studies for Improved Hyperthermia Therapy.
S. Attanayake[1], *S. Jan*[1], Ç. Demirci[2,3], T. Demircan[4], H. Srikanth[1] and M. Phan[1] *1. Physics, University of South Florida, Tampa, FL, United States; 2. Physics, Mugla Sitki Kocman University, Mugla, Turkey; 3. The Center of Research Laboratories, Mugla Sitki Kocman University, Mugla, Turkey; 4. Department of Medical Biology, Mugla Sitki Kocman University, Mugla, Turkey*

Doping spinel ferrites with transition metals and rare-earth elements is critical for enhancing their magnetic properties for biomedical applications, including magnetic hyperthermia therapy. Here, we synthesized Cobalt ferrite ($CoFe_2O_4$ or CFO) nanoparticles doped with the high magnetic moment rare-earth metal Gadolinium (Gd), forming the series $CoFe_{2-x}Gd_xO_4$ with $0.00 \leq x \leq 0.20$, to explore the correlation between the dopant and the magnetic characteristics of the parent system. A combination of analytical techniques including X-ray diffraction, Energy Dispersive Spectroscopy, Raman Spectroscopy, and Transmission Electron Microscopy confirmed the phase purity of the synthesized nanostructures with excellent crystallinity. Magnetization measurements showed an enhancement in saturation magnetization with up to 15% Gd doping in the $CoFe_{2-x}Gd_xO_4$ samples. Hyperthermia measurements demonstrated improved heating efficiency under an alternating magnetic field, where a magnetic field of 800 Oe was sufficient to achieve therapeutic temperatures in two different carrier media (water and agar). Assessment of cytotoxicity using human breast cell lines revealed that Gd-doped CFO nanoparticles exhibited lower toxicity compared to undoped ones, showing higher biocompatibility across the cell lines. These findings underscore the potential of doping CFO-based nano-systems to tailor their magnetic properties, addressing challenges such as heating efficiency and cytotoxicity. This advancement highlights the promise of Gd-doped spinel ferrites in advancing cancer therapy applications.

CR-06. Effects of X-ray Irradiation on Self-Regulating Hyperthermia Magnetic Nanoparticles of Gadolinium Silicide.
S. Smith[1], S.B. Naranjo[2], J.R. Marin[2] and R.L. Hadimani[2] *1. Chemical and Life Science Engineering, Virginia Commonwealth University, Richmond, VA, United States; 2. Mechanical and Nuclear Engineering, Virginia Commonwealth University, Richmond, VA, United States*

Magnetic hyperthermia treatment materials, such as gadolinium silicide (Gd5Si4), have been proposed as potential candidates in nanomedicine due to their self-regulating nature of heating using tunable transition temperature which protects against overheating. [1],[2] With biocompatible capabilities of Gd5Si4 nanoparticles, possibility of exposure to X-Ray irradiation for medical imaging or irraditation therapies opens questions on potential changes in magnetic properties which may change self-regulating heating safety. This study investigates the effects of high dose (120 Gy/min) X-Ray irradiation on Gd5Si4 nanoparticles. Gd5Si4 nanoparticles were prepared using the procedure reported in [1]. An X-RAD 225XL Precision X-Ray was used to irradiate a sample with a X-Ray dosage of ~120 Gy/min over 5 hours. The study produced results which showed observable effects to the magnetic properties of the material when exposed to X-Ray irradiation. XRD analysis was carried out before and after irradiation which showed no observable changes in the XRD peaks. A vibrating sample magnetometer (VSM, Quantum Design, 3 T VersaLab) was used to measure magnetization (M) of Gd5Si4 from 200K to 400K at an applied magnetic field of 100 Oe and with applied magnetic fields from -3 T to 3 T at 300K. Fig.1(a) shows M-T data from 200K to 400K before irradiation and Fig.1(b) shows M-T data after irradiation. A small change is seen in the transition temperature of 1K-3K, and a change in magnetization (M) of the samples is present. Fig.2(a) and Fig.2(b) present hysteresis graphs at 300K. Change in saturation is present in post-irradiation graphs with increase in magnetization in irradiated samples. These results indicate that irradiation affects magnetic hyperthermia treatment by changing the magnetization of the samples and the transition temperature without having an effect on structural properties.

[1] Z. Boekelheide, Z. A. Hussein, S. M. Harstad, A. A. El-Gendy and R. L. Hadimani, "Gd5Si4 Micro- and Nano-Particles for Self-Regulated Magnetic Hyperthermia," in IEEE Transactions on Magnetics, vol. 53, no. 11, pp. 1-4, Nov. 2017, Art no. 5400204, doi: 10.1109/TMAG.2017.2708688. [2] A. A. El-Gendy et al., "Ferromagnetic Gd5Si4 Nanoparticles as T2 Contrast Agents for Magnetic Resonance Imaging," in IEEE Magnetics Letters, vol. 8, pp. 1-4, 2017, Art no. 1507504, doi: 10.1109/LMAG.2017.2728503.

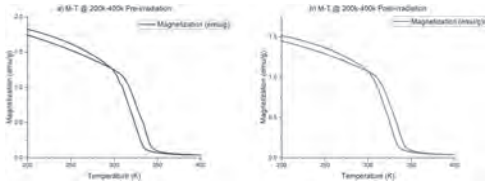

Fig.1 MT(a) Data from 200K to 400K at 100 Oe applied magnetic field before irradiation.(b)MT post irradiation data demonstrates change in magnetization (M) and a change of 1K-3K in transition temperature.

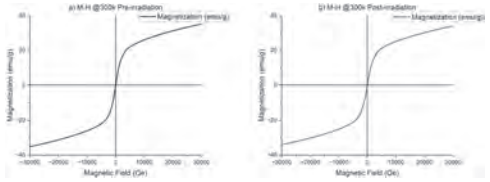

Fig.2 MH(a) hysteresis data from -3T to 3T at 300K before irradiation.(b) MH hysteresis data after irradiation showcasing decreased magnetization.

CR-07. Evaluation of cytokeratin in lymph node metastasis using magnetic nanoparticles and protein aggregates. *S. Yabukami*[1,2], T. Murayama[1], K. Kaneko[2], A. Ban[1], Y. Ozawa[3], H. Okamoto[3] and T. Kamei[3] *1. Graduate School of Biomedical Engineering, Tohoku University, Sendai, Japan; 2. Graduate School of Engineering, Tohoku University, Sendai, Japan; 3. Graduate School of Medicine, Tohoku University, Sendai, Japan*

In this study, we aim to apply protein sensors to rapid intraoperative diagnosis of lymph node metastasis. The advantage of intraoperative diagnosis of lymph node metastasis is that by determining the presence or absence of metastasis during surgery, extensive lymph node dissection, which was previously considered necessary when metastasis was negative, can be omitted. This is an extremely useful diagnostic method that reduces surgical invasiveness for patients, shortens surgical time, and reduces medical costs. In the present study, cytokeratin, which is a biomarker of lymph node metastasis, was bound to protein G-coated magnetic nanoparticles (FG beads, 180 nmΦ) via primary antibody (Anti-Cytokeratin AE1/AE3 Antibody (Monoclonal Mouse IgG1)). Figure 1 shows the magnetic response which was evaluated under the switching magnetic field [1]. The magnetic signal clearly increased as the increase of cytokeratin, because the cytokeratin aggregated magnetic nanoparticles. Figure 2 shows the comparison of magnetization between two cancer patients and non-cancer patients. Lymph nodes were obtained from two esophageal cancer patients and one non-cancer patient (corrosive esophagitis). The collected lymph nodes were homogenized in PRO-MEASURE Protein Measurement Solution using a bio masher, diluted 10-fold, and the supernatant was collected. The antigen-antibody reaction was allowed to proceed for 30 minutes, and then, without washing, the magnetic responses were evaluated by the same method as Fig. 1. Lymph nodes from cancer patients contain cytokeratin, which promotes the aggregation of magnetic nanoparticles and increases the magnetic signal. Statistically significant differences could be assessed between some cancer and non-cancer patients, suggesting the potential of intraoperative rapid diagnosis.

[1] S. Yabukami, T. Murayama, K. Kaneko, J. Honda, L. Tonthat, K. Okita, "Magnetic response of aggregation mixed with magnetic nanoparticles and protein for simultaneous protein detection", *AIP Advances*, 14 (3), 035102 (2024).

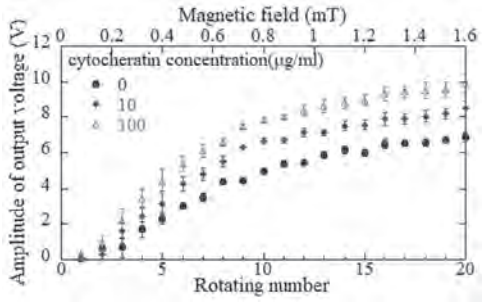

Fig.1 A magnetic response to cytokeratin (0, 10, 100 μg/ml) when the magnetic field increased.

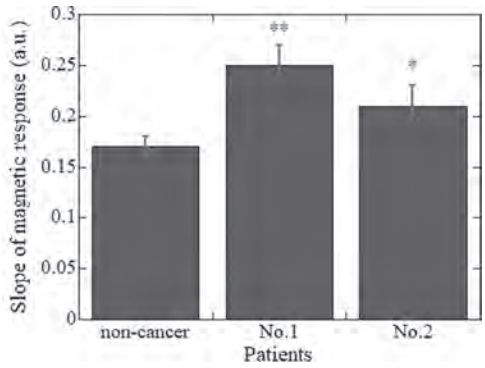

Fig. 2 The comparison of magnetic response between two cancer patients and a non-cancer patient. Significant differences between non-cancer and cancer patients were evaluated by t-tests individually. The vertical axis shows standard error **, *, for $p<0.01$ and $p<0.05$, respectively.

CR-08. Polyol-Mediated Synthesis of Iron Oxide Nanoflowers for Biomedical Applications. *A.D. Malaj*[1], S.S. Laha[1] and O.T. Mefford[1] *1. Materials Science and Engineering, Clemson University, Clemson, SC, United States*

Iron oxide nanostructures have played a significant role in advancing many biomedical fields, including magnetic hyperthermia, advanced drug delivery, and MRI imaging.[1-3] Recently, clustered nanoparticles, commonly referred to as iron oxide nanoflowers (IONFs), were shown to have higher intrinsic loss parameters compared to their unclustered forms due to the high magnetic interactions between the individual particles.[4] They also uniquely remain superparamagnetic even though their cluster sizes can exceed the superparamagnetic size limit of ~25 nm, due to their nearly zero remanence and coercivity, which can benefit their colloidal stability due to less agglomeration.[5] In this work, iron oxide nanoflowers were synthesized following a polyol-based synthetic route described elsewhere.[6] The particles were produced using iron acetylacetonate as a precursor and triethylene glycol (TEG) as a dispersing medium, allowing them to be water-dispersible after synthesis. Polyacrylic acid (PAA) is also used as a surface directing agent, causing the nanoparticles to cluster into shapes resembling flowers. These nanoflowers were shown to have controllable average cluster diameters ranging from 40-50 nm based on the amount of PAA used (Figure 1A). The DC and AC magnetic properties of these nanoflowers were extensively characterized. From the DC magnetic data, the saturation magnetization was estimated to be approximately 60 emu/g (Figure 1B). From the AC susceptibility data, low-temperature relaxation features below 50 K and high-temperature blocking phenomena around 200 K were reported (Figure 1C). The broadening of the blocking peak suggests polydispersity in the crystallite sizes of the individual particles. This also suggests that the blocking temperature of the entire nanoflower is heavily dictated by the size of the individual particles that comprise it. Additionally, AC magnetometric and calorimetric studies were conducted to evaluate the hyperthermia potential of these nanoflowers.

1. R. Hachani et. al., Nanoscale 8 (6), 3278-3287 (2016). 2. Y. Bao, J. Sherwood and Z. Sun, Journal of Materials Chemistry C 6 (6), 1280-1290 (2018). 3. S. Laurent et. al., International journal of molecular epidemiology and genetics 2 (4), 367 (2011). 4. C. Blanco-Andujar et. al., Nanoscale 7 (5), 1768-1775 (2015). 5. F. Hu et. al., Chemical communications 46 (1), 73-75 (2010). 6. J. Van der Zee, Annals of oncology 13 (8), 1173-1184 (2002).

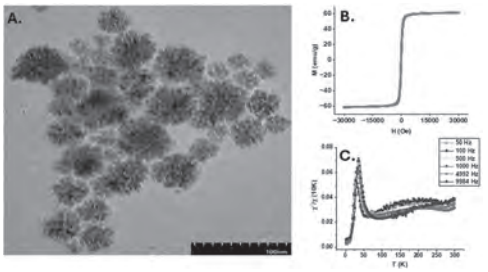

Figure 1: A. TEM image of iron oxide nanoflowers synthesized with 750 mM PAA. B. Magnetization (M) vs. applied field (H) loop of the nanoflowers at 300 K. C. AC susceptibility plot of the nanoflowers at six different frequencies.

Session CS
MATERIALS WITH COUPLED MAGNETIC PHENOMENA I
(Poster Session)

Vijaysankar Kalappattil, Chair
Northeastern University, Burlington, MA, United States

CS-01. Noncollinear Interlayer Exchange Coupling Across IrFe Spacer Layers. *J. Lisik*[1], S. Myrtle[1] and E. Girt[1] *1. Department of Physics, Simon Fraser University, Burnaby, BC, Canada*

Antiferromagnetic interlayer exchange coupling between two ferromagnetic layers across a nonmagnetic spacer layer is incorporated into almost all spintronic devices. Recently, we discovered that the coupling angle between two Co layers can be precisely controlled between 0° (ferromagnetic alignment) and 180° (antiferromagnetic alignment) by adding a magnetic material, Fe or Co, to a nonmagnetic Ru spacer layer [1,2]. This is desired, as the optimal design of spintronic devices almost always requires noncollinear alignment between ferromagnetic layers. Ru and Ir spacer layers provide the first and second strongest antiferromagnetic coupling, respectively [3]. For this reason, we built on our RuFe and RuCo work by studying noncollinear coupling between Co layers across IrFe spacer layers [4]. Notably, we achieved the largest antiferromagnetic coupling strength ever observed across spacer layers of 0.6 nm or thicker, with J_1 peaking at 3.4 mJ/m^2 for Co | $Ir_{50}Fe_{50}$ | Co. The Fe concentration and IrFe thickness regions for which the coupling is ferromagnetic, antiferromagnetic, and noncollinear are shown in Fig. 1(a). Figure 1(c) shows that the noncollinear coupling region of Co | IrFe | Co is significantly larger than that of Co | RuFe | Co or Co | RuCo | Co. The coupling regions after annealing the samples at 350°C for 1 hour, which is typical for device fabrication [5], are shown in Fig. 1(b). The half-filled circles represent samples with a coupling angle of 90° ± 20°, revealing that orthogonal coupling is favoured across the majority of the annealed samples. Moreover, orthogonally-coupled samples with IrFe thicknesses from 0.5 to 0.7 nm and Fe concentrations above 50 at.% have a strong biquadratic coupling strength, with J_2 ranging from 1.3 to 3.4 mJ/m^2. Since the highest sensitivity of magnetic sensors is achieved through orthogonal alignment of neighbouring magnetic layers, IrFe could enable new designs for sensors.

[1] Z. R. Nunn, C. Abert, D. Suess, and E. Girt, Sci. Adv., Vol. 6, p.eabd8861 (2020) [2] Z. R. Nunn, J. Lisik, P. Omelchenko, et al., J. Appl. Phys., Vol. 133, p.123901 (2023) [3] S. S. P. Parkin, Phys. Rev. Lett., Vol. 67, p.3598 (1991) [4] J. Lisik, S. Myrtle, and E. Girt, J. Mag. Mag. Mat., Vol. 585, p.171109 (2023) [5] K. Yakushiji, A. Fukushima, H. Kubota, et al., Appl. Phys. Express, Vol. 6, p.113006 (2013)

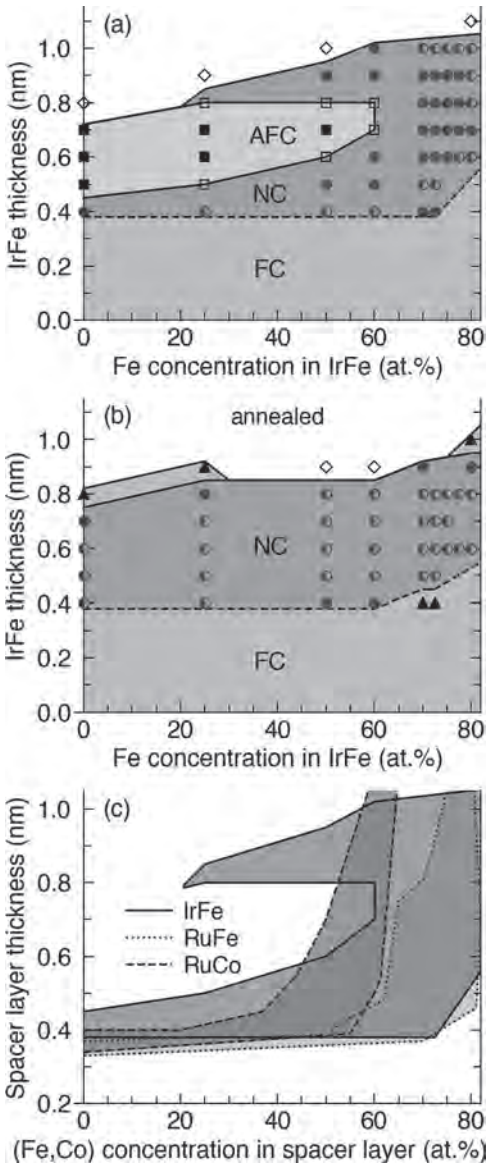

Fig. 1: Ferromagnetic (FC), antiferromagnetic (AFC), and noncollinear (NC) coupling regions of Co | IrFe | Co (a) before and (b) after annealing, where each marker represents a measured sample. (c) NC regions of Co | (IrFe, RuFe, RuCo) | Co before annealing.

CS-02. Field-induced transformation of complex spin ordering and magnetodielectric and magnetoelastic coupling in MnGeTeO6. *A. Pal*[1]
1. Faculty of Science and Engineering, University of Groningen, Groningen, Netherlands

Geometrically frustrated magnets have garnered widespread attention from the scientific community. These materials exhibit numerous fascinating low-temperature phenomena arising from their diverse magnetic interactions. Notable examples include exotic quantum states such as spin liquids, spin ice, and magnetization plateaus. In this context, the layered triangular lattice antiferromagnet (TLAF) system, $MnGeTeO_6$ (MGTO), emerges as an intriguing candidate for investigating the properties outlined above. Its crystalline structure belongs to a non-centrosymmetric (NCS) trigonal system with space group *P*312. The coexistence of a spin-frustrated triangular lattice with an NCS polar crystal structure triggered the emergence of complex noncollinear and noncoplanar spin structures, alongside intriguing magnetoelectric (ME) properties in this system. Our magnetization and specific heat studies suggest that this compound $MnGeTeO_6$ undergoes a long-range antiferromagnetic transition below the Néel temperature (T_N) ~ 9 K, which is further validated in the neutron powder diffraction (NPD) study. In the absence of an external magnetic field (*H*), analysis of NPD data reveals a complex incommensurate spin structure, characterized by a mixture of helical and cycloidal spin orderings with a propagation vector of k = (1/3, 1/3, 0.184). Upon the application of *H*, this spin ordering transforms into a conical spin structure, which is manifested as a metamagnetic transition in the isothermal magnetization (*M*) curve when *H* exceeds ~ 0.9 T. Total energy calculations and estimation of various exchange interaction energies (*J*) by Density Functional Theory calculations also support the formation of such a complex spin ordering. Moreover, a pronounced dielectric (ε′) anomaly is observed near T_N, which is suppressed considerably under *H*. The variation of ε′ with increasing *H* closely reflects the M^2 scaling behavior in the low *H* regime, thus indicating a higher-order magnetoelectric coupling. Moreover, synchrotron x-ray diffraction reveals an isostructural distortion below T_N, suggesting magnetoelastic coupling as a trigger for the dielectric anomaly.

CS-03. Magnetism and magnetocaloric effect of multicomponent rare earth intermetallic compound hydride $Gd_{0.2}Tb_{0.2}Dy_{0.2}Ho_{0.2}Er_{0.2}NiH_{1.4}$. *A. Mohapatra*[1], D. A. R[1], A. Chelvane[2], A. Morozkin[3], R. S[1] and R. Nirmala[1] *1. Physics, Indian Institute of Technology Madras, Chennai, India; 2. Defence Metallurgical Research Laboratory, Hyderabad, India; 3. Moscow Lomonosov State University, Moscow, Russian Federation*

Rare earth intermetallic compounds with equiatomic composition of heavy rare earths (R = Gd, Tb, Dy, Ho and Er) and nickel order ferromagnetically at low temperatures (T_C) and exhibit large magnetocaloric effect (MCE) near T_C [1]. Substitution with equimolar amounts of five magnetic rare earths at the R-site has led to the synthesis of multicomponent compound $Gd_{0.2}Tb_{0.2}Dy_{0.2}Ho_{0.2}Er_{0.2}Ni$ (Space group *Pnma*, No. 62). This compound orders ferromagnetically at 66 K and shows interesting metamagnetic transition at 2 K. The compounds RNi (R = Gd, Tb and Dy) are known to react with the hydrogen at ambient temperature and pressure conditions [2]. Hydrogen insertion in the lattice of RNi compounds leads to increase in unit cell volume and weakens the indirect exchange interaction and results in reduced T_C while preserving large MCE. In the present study, $Gd_{0.2}Tb_{0.2}Dy_{0.2}Ho_{0.2}Er_{0.2}NiH_{1.4}$ has been synthesized and characterized by magnetization measurements. The hydride sample has broadened peaks in the powder X-ray diffraction pattern yielding average crystallite size value of about 7 nm. The transmission electron microscopy image confirms that the sample is nanostructured upon hydrogenation. Magnetization of $Gd_{0.2}Tb_{0.2}Dy_{0.2}Ho_{0.2}Er_{0.2}NiH_{1.4}$ has been measured as a function of temperature from 5 K to 300 K in applied magnetic field of 5 kOe [Fig. 1a]. This sample remains a paramagnet down to 5 K. Magnetization shows a tendency to saturate in fields of 70 kOe at 5 K. Isothermal magnetic entropy change (ΔS_m) has been calculated from the field dependent magnetization data from 5 K to 30 K [Fig. 1b] and the maximum value of ΔS_m is found to be -9.8 $Jkg^{-1}K^{-1}$ for a field change of 50 kOe at 8 K for the hydride sample, $Gd_{0.2}Tb_{0.2}Dy_{0.2}Ho_{0.2}Er_{0.2}NiH_{1.4}$. This value is little lower than -13 $Jkg^{-1}K^{-1}$ obtained for the same field change in parent $Gd_{0.2}Tb_{0.2}Dy_{0.2}Ho_{0.2}Er_{0.2}Ni$ compound around its T_C ~66 K.

1. Aparna Sankar, J. Arout Chelvane, A. V. Morozkin, A. K. Nigam, S. Quezado, S. K. Malik and R. Nirmala, AIP Advances 8 (2018) 056208 and references therein. 2. S. Tereshina, A.Yu. Karpenkov, A.A. Kurganskaya, V.B. Chzhan, S.A. Lushnikov, V.N. Verbetsky, E.S. Kozlyakova, A.N. Vasiliev, J. Magn. Magn. Mater. 574 (2023) 170693

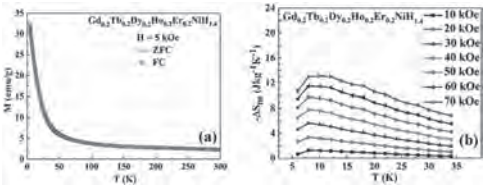

Fig. 1 (a) Magnetization vs temperature and (b) isothermal magnetic entropy change vs temperature of $Gd_{0.2}Tb_{0.2}Dy_{0.2}Ho_{0.2}Er_{0.2}NiH_{1.4}$.

CS-06. Effects of Boron Content on Magnetostriction and Temperature Dependent Magnetic Damping in FeGaB Thin Films. *Z. Zhang*[1] and A. Hoffmann[1] *1. Materials Science and Engineering, University of Illinois Urbana-Champaign, Urbana, IL, United States*

Due to their short wavelengths and long propagation distances, surface acoustic waves are promising candidates for miniaturizing microwave devices such as isolators and circulators, which rely on large nonreciprocity and low propagation loss facilitated by low damping and large magnetoelastic coupling. $Fe_{80}Ga_{20}$ is a popular choice for the magnetoelastic layer due to its high magnetoelastic response in the disordered A2 phase [1]. In this work, we stabilized this disordered phase by boron doping. Subsequently we studied the influence of boron concentration on magnetoelastic coupling and temperature dependent damping. $(Fe_{80}Ga_{20})_{1-x}B_x$ films with boron content from 2% to 16% were synthesized by co-sputtering. Structural characterization by x-ray diffraction reveals a reduction in the Fe (100) Bragg peak when increasing B from 2% to 8%, and a vanishing of the peak at 10% B, indicating gradually stabilized disorder. The magnetostriction was measured by cantilever deflection in a rotating magnetic field, as shown in Fig. 1(a). Fig. 1(b) shows that the saturation magnetostriction increases with B concentration until reaching a peak at 10% B. Boron doping effect on the magnetic damping was studied by field modulation ferromagnetic resonance (FMR). The damping decreases with B concentration, as shown in Fig. 2(a), with the lowest damping of 5.8×10^{-3} achieved at 12% B. Additionally, temperature dependent FMR was performed on 6% and 10% B doped $Fe_{80}Ga_{20}$ to analyze the damping as a function of temperature, as shown in Fig. 2(b). Both samples show a damping peak upon cooling down to 50 K. The damping peak for 10% B sample represents 61.38% increase relative to room temperature damping, while such increase in the 6% sample is mitigated to 26.67 %. This suggests that the damping peak at around 50 K may have a large contribution from magnetoelastic coupling. This work was supported by DOE BES under contract No. DE-SC0022060.

[1] P. Meisenheimer, R. Steinhardt, S. Sung, Nature Communications 12, 2757 (2021).

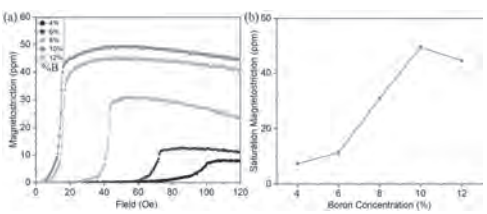

Fig. 1: (a) Magnetostriction vs. field for $Fe_{80}Ga_{20}$ with different B doping; (b) Saturation magnetostriction as a function of B concentration.

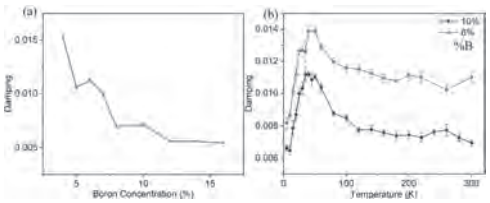

Fig. 2: (a) Gilbert damping at room temperature as a function of B concentration; (b) Gilbert damping vs. temperature for $(Fe_{80}Ga_{20})_{94}B_6$ and $(Fe_{80}Ga_{20})_{90}B_{10}$.

CS-07. On correctly assessing the reversibility of the magnetocaloric effect. *R. Kiefe*[1] and J. Amaral[1] *1. Physics, University of Aveiro, CICECO, Aveiro, Portugal*

Certain materials exhibit a temperature change when subjected to a magnetic field — the magnetocaloric effect (MCE), forming the basis for magnetic refrigeration. The MCE is a reversible process, and so, under adiabatic conditions, applying and removing an external magnetic field will keep the system at its starting temperature. The adiabatic temperature change (ΔT_{ad}) will depend on the magnetocaloric material (refrigerant) used, and it largely dictates the performance of such devices. Analysis of magnetic refrigeration systems requires either estimating ΔT_{ad} from indirect measurements (the refrigerant's magnetization and specific heat at different temperatures and external magnetic fields) or by direct measurement of ΔT_{ad}, which poses its own challenge. Correctly estimating ΔT_{ad} by these indirect measurements is then crucial to properly describe and design refrigeration systems. Estimating an adiabatic temperature change (ΔT_{ad}) from indirect measurements - magnetization and specific heat - using direct integration is an approximation [1], and is often stated as a rigorous approach [2,3]. Yet, this approximation not only does not describe a reversible process, but also deviates from more accurate estimates. We propose an alternative approach grounded in the same thermodynamic principles, providing a more accurate estimation of ΔT_{ad}. This method involves considering small steps in magnetic field change (δH) and calculating corresponding temperature changes (δT) through iteration across the entire magnetic field change. The proposed procedure yields a reversible adiabatic temperature change and with more accuracy, deviating from estimates by direct integration by more than 10%.

[1] Smith A., Bahl C. R., Bjørk R., Engelbrecht Advanced Energy Materials, 2(11):1288–1318 (2012) [2] Pecharsky, V. K. and Gschneidner, K. A., J. Journal of Applied Physics, 86(1):565–575 (1999) [3] Franco V., Blázquez J., Ipus J., Law, J. Progressin Materials Science, 93:112–232 (2018)

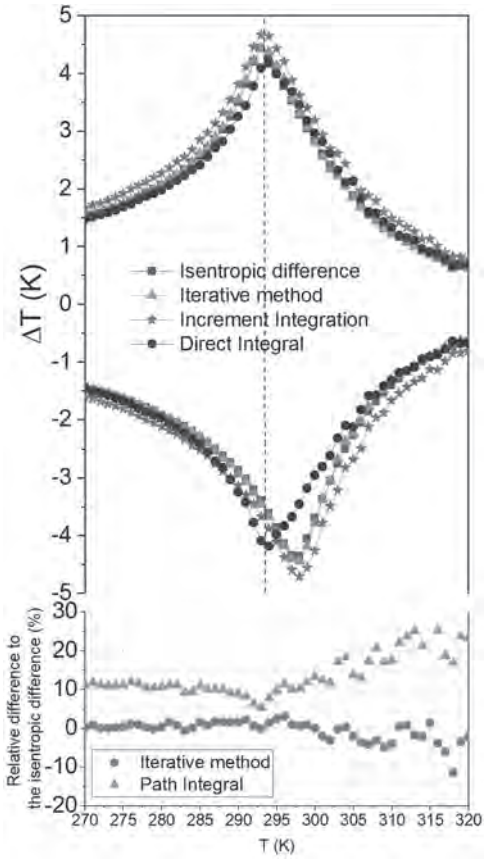

Top - ΔT_{ad} from field application estimated from entropy and by iterative methods. Bottom - Relative diference between ΔT_{ad} estimated by the isentropic difference and by the numerical methods.

CS-08. Phase Transitions and Magnetic Properties of Cu and Fe Doped $Ni_2Mn_{0.55}Cu_{0.35}Fe_{0.10}Ga$ Heusler Alloy. *H.A. Adedo*[1], J.R. DeFeo[2], V. Yenugonda[2], S. Rahman[1], A.K. Pathak[2] and M. Khan[1] *1. Department of Physics, Miami University, Oxford, OH, United States; 2. Department of Physics, SUNY Buffalo State University, Buffalo, NY, United States*

The Ni_2MnGa based Heusler alloys are extensively studied for the numerous multifunctional properties they exhibit. Many of these properties, like magnetocaloric effect, are associated with the first order martensitic phase transition that can be precisely controlled by varying the stoichiometry and by atomic doping [1, 2]. Upon heating, a first order coupled magnetostructural phase transformation is observed near 345 K in $Ni_2Mn_{0.70}Cu_{0.30}Ga$, a Cu-doped derivative of the Heusler alloy Ni_2MnGa [3]. A partial decoupling of the phase transitions occurs during cooling resulting in a large variation in the magnetocaloric properties of the material when the measurements are done while heating and cooling [3]. Here, we present a study on the phase transitions and associated magnetic properties of $Ni_2Mn_{0.55}Cu_{0.35}Fe_{0.10}Ga$, a Fe doped derivative of $Ni_2Mn_{0.70}Cu_{0.30}Ga$. X-ray diffraction data showed a tetragonal structure at room temperature. The temperature dependence of magnetization data obtained while heating revealed two distinct transitions at 338 K and 368 K. On cooling the transitions were observed at 333 K and 355 K. The lower temperature transition showed a thermal hysteresis of ~5 K while the higher temperature transition exhibited a thermal hysteresis of ~13 K. The magnetic entropy changes obtained from isothermal magnetization data indicated that transition at 338 K is a second order transition while the one at 368 K is a first order phase transition. Peak entropy changes of -8 J kg^{-1} K^{-1} have been observed. The experimental data suggested

that the martensitic phase transition occurred in a paramagnetic state in $Ni_2Mn_{0.55}Cu_{0.35}Fe_{0.10}Ga$. The work at State University of New York (SUNY), Buffalo State University, was supported by the National Science Foundation Award No. DMR-2213412.

[1] M. Khan, I. Dubenko, S. Stadler and N. Ali, J. Phys. 97, 10M304 (2005). [2] S. Stadler, M. Khan, J. Mitchell, and N. Ali, Appl. Phys. Lett. 88, 192511 (2006). [3] S. A. Agbo, S. Bhatt, and M. Khan, Intermetallics 138, 107322 (2021).

Session CT
DOMAIN WALLS AND SKYRMIONS I
(Poster Session)

Davi Rodrigues, Co-Chair
Politecnico di Bari, Bari, Italy
Lucas Perez, Co-Chair
Universidad Complutense de Madrid, Madrid, Spain

CT-01. Possibility of Achieving Both Skyrmion Stability and High-Speed Transport on W/CoFeB. *T. Cheng*[1], L. Zhang[1], R. Satone[1], Y. Kurokawa[1], K. Tokunaga[1] and H. Yuasa[1] *1. Graduate school and Faculty of Information Science and Electrical Engineering, Kyushu University, Fukuoka, Japan*

Skyrmion, a quasi-particle, is attracting a lot of attention for its topological stability, small size and high transport velocity under spin orbit torque (SOT). However, they cannot be realized at the same time resulting in a trilemma. [1] To overcome the trilemma, intrinsic parameters such as SOT efficiency and Dzyaloshinskii-Moriya interaction (DMI) constant could be improved by structural and material engineering. In this computational study, the usable area map for stable skyrmion and skyrmion transport velocity was estimated on a β-W/CoFeB system, which had been reported to have a high spin Hall angle θ_{SH} in the range of 0.33 to 0.41. [2,3] Skyrmions were first generated by flipping the magnetization with an external magnetic field antiparallel to the initially uniform out-of-plane magnetization. Fig. 1 indicates the usable area in terms of the DMI constant and external field, where colour shows the diameter of the skyrmion. The DMI energy tends to minimize the system energy by enlarging the skyrmion while the Zeeman energy counteracts the DMI energy resulting in smaller skyrmions. The generated skyrmions were then transported by a spin polarized current under θ_{SH} from 0.1 to 0.5. The velocity shown in Fig. 2 verifies the proportionality between the skyrmion size and transport velocity for all θ_{SH}. As expected, the velocity decreases with a decreasing skyrmion size. Complicating matters further, at the limit of 20 nm diameter, the skyrmion was not moved at $\theta_{SH} = 0.1$ and was destroyed at higher θ_{SH}. On the other hand, a clear trend of increase in velocity with the increase in θ_{SH} can be observed for skyrmions over 30 nm diameter.

[1] Y. Liu, N. Lei and C. Wang, Physical Review Applied, 11, 014004 (2019) [2] K. Demasius, T. Phung and W. Zhang, Natural Communications, 7, 10644 (2016) [3] H. Fulara, M. Zahedinejad and R. Khymyn, Science Advances, 5(9), eaax8467 (2019)

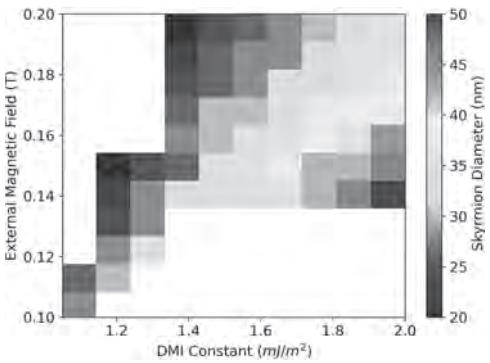

Fig. 1 Diameters of the skyrmion generated under varying external field strength and DMI constant.

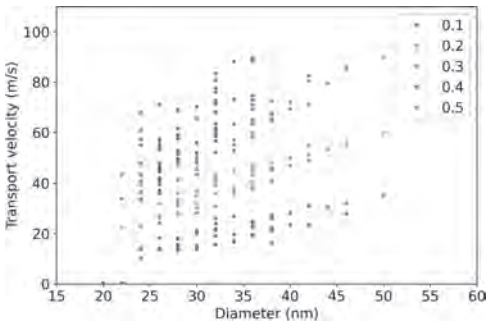

Fig. 2 Relationship between skyrmion transport velocity and diameter under different spin Hall angles θ_{SH}.

CT-02. Theoretical study of current induced domain wall motion in perpendicularly magnetized nanotubes in three-dimensional magnetic shift register. *N. Umetsu*[1], H. Tokuhira[1], M. Quinsat[1], S. Hashimoto[1], T. Kondo[1] and M. Kado[1] *1. Frontier Technology R&D institute, Kioxia Corporation, Yokohama, Japan*

The three-dimensional (3D) magnetic domain wall (DW) shift register is considered as one of the potential candidates for ultra-high density data-storage units [1, 2]. Recently, we proposed a tube-type 3D shift register memory [3]. Tubes are particularly suitable for high-density applications because the width of the DW can be reduced by orienting the magnetic easy axis in a direction perpendicular to the tube axis. In this study, our focus is on tubes made of materials with perpendicular magnetic anisotropy (PMA), as shown in Fig.1. In PMA-tubes, both spin transfer torque (STT) and spin orbit torque (SOT) can be utilized for DW shift, unlike azimuthal magnetic anisotropy-tubes [4]. We aim to investigate the shape effects on DW motion under the influence of both STT and SOT. To analyze the current-induced DW motion in PMA-tubes, we employed micro-magnetic simulation (μM) based on the finite volume method [5]. Fig. 2 shows the current density dependence of DW velocity for both tubes and ribbons. The DW velocity in tubes is higher in the presence of SOT, which can be attributed to the presence of effective magnetic fields specific to PMA-tubes. These include not only the curvature-induced anisotropy field [4] but also the stray field inside the tube. These effective fields were calculated from the magnetic energy and incorporated into the one-dimensional model (1DM) [6], resulting in good agreement with the results of μM, as shown in Fig. 2. Based on these findings, we conclude that optimizing the shape effects of PMA-tubes in SOT-driven DW is a promising technique for future 3D shift register memory.

[1] S. S. P. Parkin, M. Hayashi and L. Thomas, Science, Vol. 320, p.190 (2008). [2] Y. Kurokawa and H. Yuasa, J. J. Appl. Phys., Vol. 62, p.SC1070 (2023). [3] M. Quinsat, et al., submitted to IEDM 2024. [4] J. Hurst et al., Phys. Rev. B, Vol. 103, p.024434 (2021). [5] K. Rupp et al., SISPAD, p.365 (2014). [6] E. Martinez and O. Alejos, J. Appl. Phys., Vol. 116, p.023909 (2014).

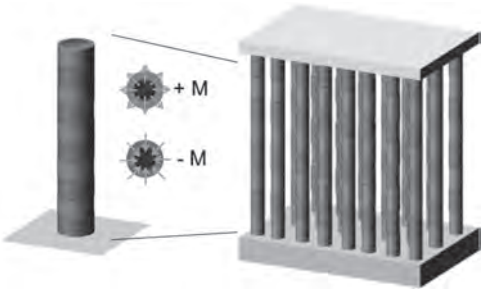

Fig.1 Schematic illustration of PMA-tube DW memory.

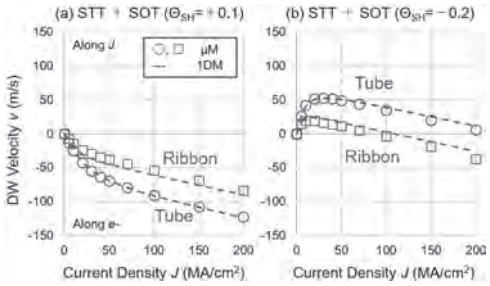

Fig.2 Current density dependence of DW velocity. Diameter of tube and width of ribbon are both 50 nm, and thickness of both films is also 1 nm. The saturation magnetization is 1000 emu/cm^3, the perpendicular magnetic anisotropy is 8.3 Merg/cm^3, the exchange stiffness is 1 uerg/cm, the Gilbert damping is 0.2, the spin polarization is 0.5, the Dzyaloshinskii-Moriya interaction constant is 0.2 erg/cm^2, and the spin Hall angles are (a) +0.1 and (b) -0.2.

CT-03. Kinematic Model of Magnetic Domain Wall Motion for Fast, High-Accuracy Simulations. *A.J. Edwards*[1], K. Doleh[1], L. Humphrey[1], C.M. Linseisen[1], M.D. Kitcher[2], J.M. Martin[1], C. Cui[3], J.C. Incorvia[3], F. García Sánchez[4], N. Hassan[1] and J.S. Friedman[1] *1. Electrical and Computer Engineering, The University of Texas at Dallas, Richardson, TX, United States; 2. Materials Science & Engineering, Carnegie Mellon University, Pittsburgh, PA, United States; 3. Electrical and Computer Engineering, The University of Texas at Austin, Austin, TX, United States; 4. Departemento de Fisica Aplicada, Universidad de Salamanca, Salamanca, Spain*

Domain wall (DW) devices have garnered recent interest for diverse applications including memory [1], logic [2], and neuromorphic primitives [3]; fast, accurate device models are therefore imperative for large-scale system design and verification. Extant DW motion models are sub-optimal for large-scale system design either over-consuming computing resources with physics-heavy equations [4, 5] or oversimplifying the physics, drastically reducing model accuracy [6, 7]. We propose a DW model inspired by the phenomenological similarities between motions of a DW and a kinematic object being acted on by forces like air resistance or static friction. We therefore define DW displacement according to x″(t) = v′(t) = a(t) = a_J(t) + a_damp(t) + a_pin(t), where x is DW displacement, v is DW velocity, and a_J, a_damp, and a_pin are the accelerations due to spin-orbit torque current (J), damping, and pinning. The accelerations are defined according to a_J = k4 J^4 + k3 J^3 + k2 J^2 + k1 J + k0, a_damp = -v * (d1 + d2 |J|) [mimicking stokes drag], and a_pin = {-a_J when |J| < p, |v| < p2 and 0 otherwise}. Fitting parameters k0-k4, d1, d2, p1, and p2 are extracted from mumax3 [8] simulations, and Fig. 1 illustrates that, once trained, the kinematic model predicts domain wall motion very closely for a wide range of stimulating current densities. Additionally, the model was trained across 32 micromagnetic parameter combinations, predicting DW motion within 1.2\% error on average compared with micromagnetic simulations that are 400 times slower. As illustrated in Fig. 2, our model is seven times faster than extant collective coordinate (1DCC) models and 14 times more accurate than extant hyper-reduced models (refs) making it an essential tool for large-scale DW circuit design and simulation. The model is publicly posted along with scripts that automatically extract model parameters from user-provided simulation or experimental data to extend the model to alternative micromagnetic parameters.

[1] S. S. P. Parkin, M. Hayashi, and L. Thomas, Science 320, 190–194 (2008). [2] T. P. Xiao, C. H. Bennett, X. Hu, et. al., IEEE JXCDC 5, 2, 188--196 (2019). [3] N. Hassan, X. Hu, L. Jiang-Wei, et. al., Journal of Applied Physics 124, 152127 (2018). [4] C. Wang, Z. Wang, M. Wang, et. al., IEEE TED 67, 2621–2626 (2020). [5] M. Wang and Y. Jiang, IEEE TMAG, 58, 8, 1-5 (2022). [6] W. S. Zhao, J. Duval, D. Ravelosona, et. al., Journal of Applied Physics 109, 07D501 (2011) [7] X. Hu, A. J. Edwards, T. P. Xiao, et. al., proc. IEEE ISCAS 2020 1-5 (2020). [8] A. Vansteenkiste, J. Leliaert, M. Dvornik, et. al., AIP Advances 4, 107133 (2014).

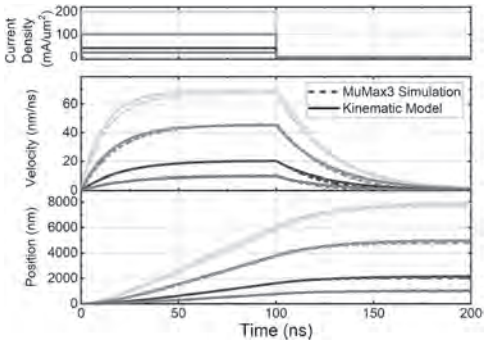

Fig. 1. Mumax3 and kinematic model predictions of DW velocity and position in response to spin-orbit torque stimulation.

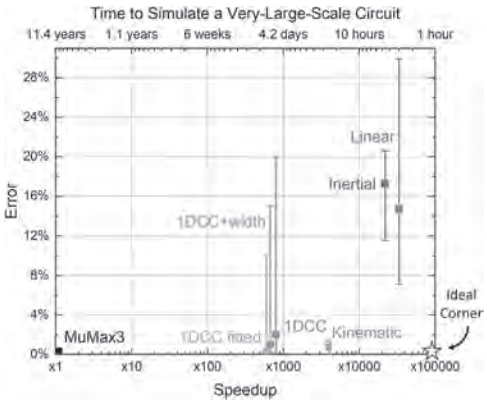

Fig. 2. Accuracy and speedup of kinematic model relative to other models in the literature.

CT-04. Micromagnetic Study of the Controlled Conversion of a 360 deg DW to Pairs of Bimeron – Antibimeron. *P. Babu*[1] and J. Sinha[1] *1. Physics and Nanotechnology, SRM Institute of Science and Technology, Chennai, India*

A thorough understanding of the mechanism involved in the stabilization and efficient manipulation of non-trivial topological spin textures, such as magnetic bimerons is crucial to achieve potential applications in storage and logic devices. Here, we perform micromagnetic simulations using mumax3 to investigate the conversion process of a 360 deg domain wall (DW) to pairs of bimeron and antibimeron under the simultaneous influence of spin transfer torque (STT) and out of plane bias field. The DW is stabilized in a square shaped sub-micron dot of side length 512 nm and thickness of 4 nm in a ferromagnetic background having in-plane magnetic anisotropy and a current density of 70 MA/cm^2 is subsequently applied along – x direction. We consider the material parameters corresponding to Pt/Co/AlO_x and D = 4mJ/m^2. Our results show that the DW acquires a deformed shape with time and depins from the lower boundary of the sub–micron dot when it is

subjected to a sufficient homogeneous current. Under the continuous action of STT and other competing terms such as DMI, exchange and Zeeman interactions, the spins along the boundary of the depinned stripe domain undergoes rotation to form a non-coplanar structure with a non-zero topological charge. As a consequence, we observe the transformation of the domain (Q = 0) into pairs of bimeron and antibimeron (cf. Fig 1a). The temporal evolution of the total energy during this conversion process is shown in Fig 1b. Further, by applying an additional bias field in the xz plane of varying intensity and inclination angle results in energy efficient and faster conversion rates of the DW. In particular, we observe that the total energy of the system reduces drastically with increasing bias field strength at a constant inclination angle. Similarly, for a constant bias field intensity, varying the inclination angle between 0 deg to 40 deg shows that the time required to stabilize the first bimeron is significantly reduced by ~ 3 ns.

[1] B. Göbe, M. Alexander, H. Jürgen et al., Phys. Rev. B. 99, 060407 (2019) [2] P. Babu, H.P Perumal et al., ACS Appl. Electron. Mater. 6, 221 (2024) [3] K. Ohara et al., Nano Lett. 22, 8559 (2022) [4] A. Vansteenkiste at al., AIP Adv. 4, 107133 (2014)

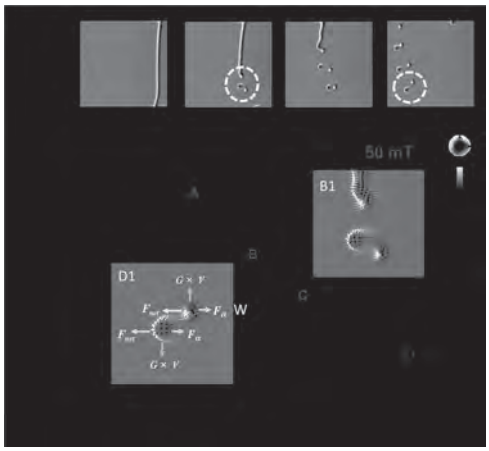

Fig 1: (a) Top view snapshots of the spin configuration describing the dynamical conversion process from a Neel stripe domain to pairs of bimeron-antibimeron. (b) Plot of total energy density as a function of time.

CT-06. Enhanced High Harmonic Generation Beamline for Ultrafast Resonant Magnetic Scattering. *I. Binnie*[1], J. Thurston[1], D. Morrill[1], G. Gui[1], C. Klein[1], Y. Li[1], H. Fang[1], H.C. Kapteyn[1] and M.M. Murnane[1]
1. University of Colorado, Boulder, Boulder, CO, United States

Resonant magnetic scattering (RMS) is a powerful tool for probing the structure and dynamics of magnetic textures. Here, we present an extreme UV (EUV) source and beamline optimized for ultrafast RMS studies at the magnetic M-edge. The experiment uses a coherent quantum process known as high harmonic generation (HHG) to produce bright coherent EUV beams that can be tuned across the M edges of magnetic materials. Additionally, bright HHG results from phase matched upconversion of femtosecond lasers: thus, by adjusting the interaction geometry and pulse shape of the driving laser, both the HHG linewidth and central photon energy can be tuned while preserving short pulse durations (~10fs). Finally, HHG provides a unique degree of control over the phase and polarization properties by tailoring the spin and orbital angular momentum of the driving beam. These unique properties of HHG are ideal for implementing ultrafast RMS in a flexible tabletop setting. In this experiment, we collect on-resonance scattering from magnetic samples in a pump-probe configuration. The beamline is engineered to maximize the on-resonance flux and therefore improve signal-to-noise in RMS. The light source is an EUV HHG beam driven by a near-IR amplified pulsed laser. The driving laser phase is optimized via spatial light modulation prior to amplification to tune the brightness and location of a particular EUV harmonic. In addition, the HHG process is driven in a newly engineered waveguide that reduces reabsorption in the gas HHG medium, thereby increasing the EUV flux. This new beamline operates in transmission and is optimized for thin-film magnetic samples with features on the order of 100 nm. The excitation mechanism is ultrafast demagnetization after irradiating with a ~30fs near-IR laser beam. Our preliminary experiments probed FeGd multilayers supporting a dipole-stabilized skyrmion lattice. This topological feature demonstrates stability over long time scales at environmental conditions. The dynamics of their creation, annihilation, and phase transition are an important topic of study for spintronics. This enhanced RMS beamline will enable the study of skyrmions and other topological magnetic lattices at their fundamental time scales.

S. A. Montoya et al., Phys. Rev. B 95, 1-13 (2017). D. Zusin, Physics Graduate Thesis, University of Colorado, Boulder (2018). A. Rundquist et al., Science 280(5368), 1412–1415, (1998). Hernández-García, et al., Phys. Rev. Lett. 111, 083602 (2013).

CT-07. Formation Process of Dipole Antiskyrmions in Fe/Gd Multilayers. *J.A. Reddinger*[1] and B. McMorran[1] *1. Physics, University of Oregon, Eugene, OR, United States*

Magnetic skyrmions and antiskyrmions are magnetic solitons with integer topological charges. Due to an energetic stability associated with nontrivial skyrmion number, skyrmions and antiskyrmions are of particular interest for use as bits in spintronics devices. Fe/Gd multilayers have demonstrated the capacity to host a wide variety of magnetic textures, including chiral/achiral stripe domains, bubbles, skyrmions, and antiskyrmions. Fe/Gd multilayers do not rely on the Dzyaloshinskii-Moriya interaction (DMI) to stabilize spin textures. Instead, competition between the dipole and exchange energies stabilizes what are referred to as dipole solitons [1]. While the dipole skyrmion formation process in Fe/Gd multilayers is reproducible and well understood, that of the dipole antiskyrmion is not. The dipole antiskyrmion consists of 4 Bloch lines (BL), features along the domain wall (DW) of the texture where the DW chirality switches smoothly. Due to the lack of DMI, the shape of the dipole antiskyrmions exhibit energy-minimizing, symmetry-breaking deformations (Fig. 1). The relative complexity of the dipole antiskyrmion's structure limits the likelihood of successful formation during magnetic field sweeps from saturation. Successful formation requires isolating 4 alternating chirality BLs. One possible precursor state is the H stripe structure (Fig. 2). However, reliably generating a configuration featuring H stripe structures from saturation is difficult. By using micromagnetic simulation [2] on seeded magnetizations generated from a custom tool, any configuration of stripe domain magnetization can be generated. The tool allows full domain wall editing via chirality flipping and BL placing in order to prepare a physically credible initial state. The tool also recreates the Neel cap structure found in Fe/Gd textures, further reducing the energy of the initial magnetization and increasing the feasibility of the seed. This tool is used to prepare and test a variety of stripe configurations and their propensity for antiskyrmion formation.

S. A. Montoya, S. Couture, and J. J. Chess, Physical Review B, Vol. 95 (2017) A. Vansteenkiste, J. Leliaert, and M. Dvornik, AIP Advances, Vol. 4 (2014)

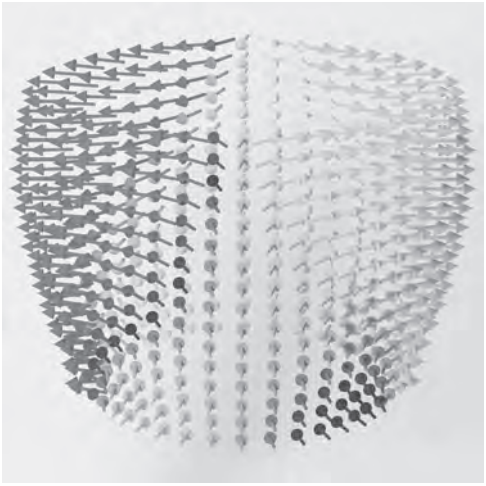

DW of simulated dipole antiskyrmion in Fe/Gd multilayers.

H stripe structure magnetization. Red/blue is out of/into the plane. White arrows indicate DW chirality.

CT-08. Theoretical Insights into Square Skyrmion Lattice Origin in $GdRu_2Si_2$ and Uniaxial Pressure Effects. *R. Pathak*[1], S. Sarkar[1], O. Eriksson[1,2] and V. Borisov[1] *1. Physics and Astronomy, Uppsala University, Uppsala, Sweden; 2. Wallenberg Initiative Materials Science for Sustainability, Uppsala University, Uppsala, Sweden*

A magnetic skyrmion is a topological spin texture generally found in magnetic materials lacking a center of symmetry, but recently, they have also been observed in centrosymmetric crystals. The miniaturization of skyrmion size holds promise for high-density memory technology applications [1]. This study delves into the electronics and magnetic properties of the GdRu2Si2 alloy, experimentally known to host nanometer-sized square skyrmion lattices within specific magnetic fields and temperature ranges [2]. Employing the first-principle density functional theory (DFT) calculations [3] and atomistic spin dynamics simulations [4, 5], we aim to understand the microscopic origins of the formation of square skyrmion lattices. Our investigation reveals that the interplay between frustration in exchange interactions, long-range dipolar interaction and uniaxial anisotropy plays an essential role in determining the generation of the square skyrmion lattice. Additionally, we intend to explore the impact of uniaxial pressure on exchange interactions and magnetic anisotropy, thereby examining alterations to the magnetic phase diagram. We found uniaxial pressure helped stabilize the skyrmions up to a certain point.

[1] Göbel, B., Mertig, I., Tretiakov, O. A. Beyond skyrmions: review and perspectives of alternative magnetic quasiparticles. Phys. Rep. 895, 1–28 (2021). [2] Khanh, N. D.; Nakajima, T.; Yu, X.; Gao, S.; Shibata, K.; Hirschberger, M.; Yamasaki, Y.; Sagayama, H.; Nakao, H.; Peng, L.; Nakajima, K.; Takagi, R.; Arima, T.-h.; Tokura, Y.; Seki, S. Nanometric square skyrmion lattice in a centrosymmetric tetragonal magnet. Nat. Nanotechnol. 15, 444–449 (2020). [3] Wills, J. M.; Alouani, M.; Andersson, P.; Delin, A.; Eriksson, O.; Grechnyev, O. Full-Potential Electronic Structure Method (Springer, 2010) [4] Eriksson, O., Bergman, A., Bergqvist, L., & Hellsvik, J. Atomistic Spin Dynamics: Foundations and Applications (Oxford University Press, 2017). [5] Skubic, B., Hellsvik, J., Nordström, L. & Eriksson, O. A method for atomistic spin dynamics simulations: implementation and examples. J. Phys. Condens. Matter 20, 315203 (2008).

Session CU
ELECTRICAL MACHINES AND HIGH SPEED ELECTRICAL MACHINES (Poster Session)

Anh Thanh Huynh, Chair
University of Nottingham, Nottingham, United Kingdom

CU-01. Novel Dual Inverter Two-Layer Sub-Harmonic Vernier Machine. *S. Rafin*[1], Q. Ali[2], H. Hussein[1] and O.A. Mohammed[1]
1. Electrical and Computer Engineering, Florida International University, Miami, FL, United States; 2. Electrical Engineering, Sukkur IBA University, Sukkur, Pakistan

This study introduces a novel dual-inverter 2-layer sub-harmonic vernier machine (DI2L-SHVM) with an outer rotor configuration designed to address the limitations of existing vernier machine technologies. The proposed machine aims to enhance performance and resolve unbalanced heating issues in brushless wound rotor vernier machines (BL-WRVMs) presented in [1] for electric vehicle applications. Existing vernier machines face limitations: PMVMs suffer from high costs, low power factors, and core losses at high speeds, while VRMs have lower torque density and poor power factors [2]. The DI2L-SHVM, as illustrated in Figure 1, employs two CSIs driving separate ABC and XYZ stator windings in a two-layer configuration. The top layer contains only ABC, while the bottom alternates between ABC and XYZ, as shown in Figure 2. The rotor features field and harmonic windings connected via a diode bridge rectifier, enabling the generation of fundamental and sub-harmonic magnetomotive force (MMF) components for enhanced performance and control. The DI2L-SHVM features 4 stator poles, 24 stator slots, and 44 rotor poles & slots. Its dimensions include a 238 mm stator outer diameter, 300 mm rotor outer diameter, 30 mm stack length, and 0.5 mm air gap. The machine operates at a base speed of 300 rpm. The specifications are tailored to meet the requirements of in-wheel motor applications in electric vehicles. The novel topology enables precise control over field excitation and efficiently utilizes sub-harmonic MMF effects. The novel design offers improved performance over traditional vernier machines, generating 18.17 Nm average torque from a compact 1.5 kW vernier motor. To validate the novelty of the proposed design, thorough simulations and analyses were conducted using Ansys Electronic Desktop software. These studies encompassed various aspects of the machine's performance, including electromagnetic characteristics, thermal behavior, and overall efficiency. The DI2L-SHVM design advances torque generation and reduces ripple. Its dual-inverter topology and 2-layer winding arrangement overcome existing limitations, providing an innovative solution for transportation electrification.

[1] Qasim Ali, Asif Hussain, Noman Baloch, and Byung Il Kwon. 2018. "Design and Optimization of a Brushless Wound-Rotor Vernier Machine" Energies 11, no. 2: 317. https://doi.org/10.3390/en11020317.
[2] S. S. H. Bukhari et al., "Novel Self-Excited Brush-Less Wound Field Vernier Machine Topology," in IEEE Access, vol. 10, pp. 97868-97878, 2022, doi: 10.1109/ACCESS.2022.3206381.

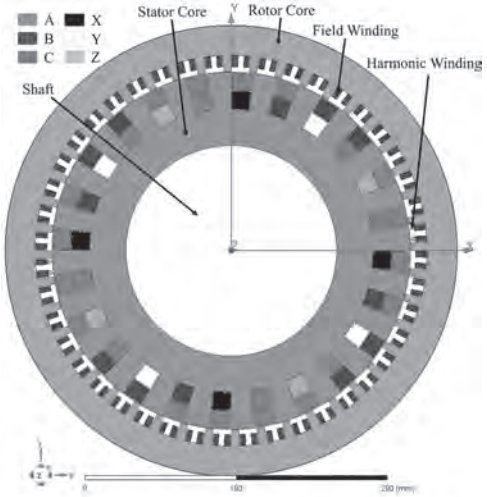

Fig. 1. Dual inverter 2-layer sub-harmonic vernier machine layout.

Fig. 1

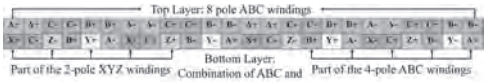

Fig. 2. 2-layer and 24-slot ABC and XYZ stator winding layout.

Fig. 2

CU-02. Optimized Design of Sub-Harmonic Synchronous Machines. *S. Rafin*[1], Q. Ali[2], H. Hussein[1] and O.A. Mohammed[1] *1. Electrical and Computer Engineering, Florida International University, Miami, FL, United States; 2. Electrical Engineering, Sukkur IBA University, Sukkur, Pakistan*

This study addresses torque ripple challenges in sub-harmonic synchronous machines (SHSMs). SHSMs offer adjustable excitation and high-power density without rare-earth materials but produce higher torque ripple than wound rotor synchronous machines (WRSMs) [1, 2]. The research optimizes 2-layer (2L) and 3-layer (3L) SHSM designs to minimize torque ripple while maintaining performance [3, 4], as illustrated in Fig. 1. A novel approach combines a new harmonic winding arrangement with optimized rotor design using segmented positioning and skewing techniques. The optimization uses the Parametric FEA and Ansys Maxwell simulations. The study compares optimized 2L-SHSM and 3L-SHSM designs against predecessors and conventional WRSMs, as shown in Table I. The machines are 8-pole 48-slot configurations rated at 1.3 kW and 900 rpm. The analysis explores continuous and discrete skewing methods with inclination angles from 0° to 10°. Results show significant torque ripple reduction in both optimized designs. The 2L-SHSM achieves an 83.94% reduction compared to its predecessor, while the 3L-SHSM shows an 86.84% reduction. These improvements maintain comparable average torque and improved efficiency. For the 2L-SHSM, an 8° continuous skew yields 5.22% torque ripple and 11.98 Nm average torque, while a 6° discrete skew provides 5.46% ripple and 11.96 Nm torque. The 3L-SHSM performs better, with a 6° discrete skew resulting in 4.21%

ripple and 12.32 Nm torque and a 7° continuous skew producing 4.57% ripple and 12.33 Nm torque. The optimized designs outperform conventional WRSMs and previous SHSM iterations across all performance criteria. This research presents a promising solution for electric vehicle applications requiring low torque ripple and robust performance, addressing PMSM limitations while offering benefits to brushless wound rotor technology. Finally, this study demonstrates the effectiveness of combining novel harmonic winding arrangements with optimized rotor designs and skewing techniques in reducing SHSM torque ripple. The results suggest that these optimized 2L-SHSM and 3L-SHSM designs could advance electric vehicle technology and improve performance, efficiency, and manufacturability.

[1] T. A. Lipo and Z. S. Du, "Synchronous motor drives-a forgotten option," *2015 Intl Aegean Conference on Electrical Machines & Power Electronics, 2015 Intl Conference on Optimization of Electrical & Electronic Equipment & 2015 Intl Symposium on Advanced Electromechanical Motion Systems*, Side, Turkey, 2015, pp. 1-5. [2] S. M. S. H. Rafin and O. A. Mohammed, "Novel Dual Inverter Sub-Harmonic Synchronous Machines," in *IEEE Transactions on Magnetics*, vol. 59, no. 11, pp. 1-5, Nov. 2023, Art no. 8202605. [3] S. M. S. H. Rafin, Q. Ali, and T. A. Lipo, "A novel sub-harmonic synchronous machine using three-layer winding topology," *World Electric Vehicle Journal*, vol. 13, no. 1, pp. 16, 2022. [4] S. M. S. H. Rafin, Q. Ali, S. Khan, and T. A. Lipo, "A novel two-layer winding topology for sub-harmonic synchronous machines," *Electrical Engineering*, vol. 104, no. 5, pp. 3027-3035, Oct 2022.

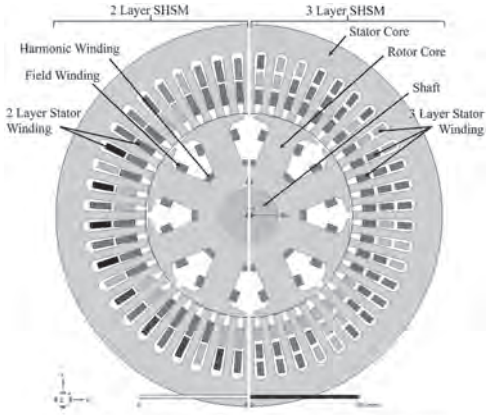

Fig. 1. 2-layer and 3-layer sub-harmonic synchronous machine layout.

Fig. 1

TABLE I
PERFORMANCE COMPARISON BETWEEN WRSM, PREVIOUS AND OPTIMIZED 2L-SHSM AND 3L-SHSM

Indicator	WRSM	Previous Design		Optimized Design	
		2L-SHSM	3L-SHSM	2L-SHSM	3L-SHSM
Stator current ($I_{s,rms}$)	4.50	4.5	4.5	4.5	4.5
Field current (I_{exc})	9.50	17.18	20.23	18.63	18.64
Harmonic current ($I_{s,rms}$)	-	14.78	14.05	18.16	18.17
Terminal voltage (V_{ph})	68.10	91.75	113.89	72.73	75.75
Average torque (N_{av})	7.30	12.03	12.53	11.96	12.32
Torque ripple (%)	16.67	34.00	32.00	5.46	4.21
Efficiency (%)	81.53	81.03	82.11	83.74	84.62

TABLE I

CU-03. Analysis of Electromagnetic Characteristic of Hybrid-Type Double-Cage Induction Motor Using Subdomain Method. *S. Eom*[1], H. Ban[1], K. Yu[1], J. Yang[1], K. Shin[2] and J. Choi[1] *1. Chungnam National University, Daejeon, The Republic of Korea; 2. Changwon National University, Changwon-si, The Republic of Korea*

With the recent resurgence of interest in non-rare-earth motors, induction motors are being reevaluated across various fields. This has led to ongoing research on the accurate prediction of their performance. Among them, the double-cage induction motor(DCIM) features a high starting torque owing to the high resistance of the inner rotor slots and a low starting current owing to the low resistance of the outer rotor slots. Additionally, its low resistance during normal operation results in reduced losses and high efficiency, making it widely used in many applications. One of the most widely used and reliable methods for analyzing DCIM is the finite element method (FEM). Although the FEM provides highly accurate results, it involves the computation of transient states until steady-state performance is achieved, leading to very long computation times. In such cases, using an analytical approach with the subdomain method can significantly reduce computation time compared with the FEM while maintaining high accuracy. Figure 1 (a) shows a 3D representation of the DCIM used in the analysis. Figure 1 (b) shows a simplified representation of the rotor of the DCIM, where the upper and lower parts are made of copper and aluminum, respectively. Figure 1 (c) presents a simplified view of the motor stator. Figure 2 (a) shows the radial air-gap flux density, Figure 2 (b) shows the tangential air-gap flux density, Figure 2 (c) shows the torque-slip charateristics, and Figure 2 (d) shows the output power-speed charateristics. Based on the results of the analysis, it can be concluded that using the subdomain method to compute the magnetic field of a DCIM is both efficient and accurate. Further details and results concerning the electromagnetic characteristics of the DCIM are presented in the full paper.

[1] K. Boughrara, N. Takorabet, R. Ibtiouen, O. Touhami and F. Dubas, "Analytical analysis of cage rotor induction motors in healthy defective and broken bars conditions", IEEE Trans. Magn., vol. 51, no. 2, pp. 1-17, Feb. 2015. [2] E. Devillers, J. Le Besnerais, T. Lubin, M. Hecquet and J. P. Lecointe, "An improved 2-D subdomain model of squirrel-cage induction machine including winding and slotting harmonics at steady state", IEEE Trans. Magn., vol. 54, no. 2, Feb. 2018. [3] H. Chen, J. Zhang, J. Zhao, S. Qu and Y. Zhou, "Analytical calculations of magnetic fields induced by MMF spatial harmonics in multiphase cage rotor induction motors", IEEE Trans. Magn., vol. 57, no. 10, Oct. 2021.

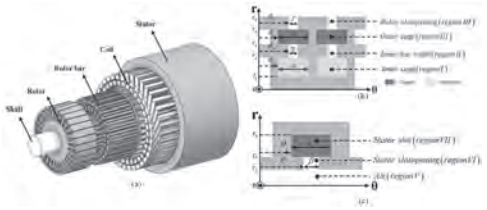

Fig. 1. Structure of inductom motor (a) 3D exploded view, (b) Simplified rotor slot, (c)Simplified stator slot

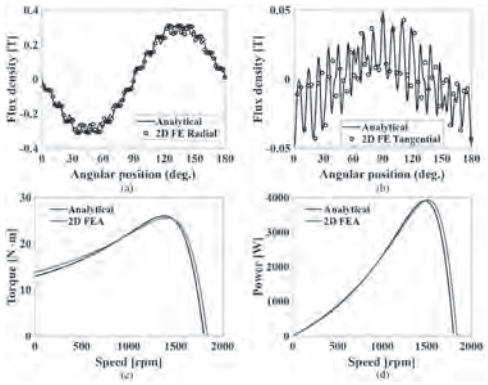

Fig. 2. Comparison of analytical predictions with FEM: (a)Air-gap flux density of the radial component, (b)Air-gap flux density of the tangential component, (c)Torque-slip characteristics, (d)Output power-slip characteristics

CU-04. AC loss of high-speed permanent magnet synchronous motor according to winding type considering current harmonics. *Y. Choi*[1], K. Kwak[1], S. Kim[1], S. Lee[1], K. Shin[2] and J. Choi[1] *1. Chungnam National University, Daejeon, The Republic of Korea; 2. Changwon National University, Changwon, The Republic of Korea*

During high-speed rotation, high-frequency AC power is applied to stator windings, resulting in significant eddy current and AC copper loss. Therefore, most high-speed machines use litz windings. However, litz windings are disadvantaged in terms of poor manufacturability. For hairpin windings, DC copper loss has been reduced in contrast to that of litz windings. However, the AC copper loss significantly increased owing to proximity and skin effects. Regardless, because of its excellent manufacturability, it is necessary to compare the loss with that of the litz winding and to investigate its application for high-speed machines. Therefore, in this study, the electromagnetic characteristics and loss of a litz-wound high-speed permanent-magnet synchronous motor, considering current harmonics, were analyzed and verified through experimental results of a manufacturing model. Subsequently, a hairpin-wound model was designed and its performance was compared to that of the litz-wound model. Fig. 1 illustrates (a) the model geometry, (b) skin and proximity effects, (c) applied current waveform, (d) experimental equipment used, and (e) experimental data obtained. Fig. 2 illustrates (a) the current density, (b) loss density distribution for each winding, and (c)–(d) show the loss data when current is applied. As a result of comparing the model loss for each winding, it was confirmed that although AC copper loss accounts for a significant portion of the hairpin winding, the difference in total loss was approximately 1.5 [W], which is insignificant. Therefore, the utilization of hairpin windings in high-speed machines is expected to increase in the future. Finally, this paper presents an in-depth analysis alongside experimental results, including a discussion on thermal characteristics according to the winding type for each model.

[1] W. Yu, W. Hua, Z. Zhang, Z. Wu, P. Wang and W. Xia, "Comparative Analysis of AC Copper Loss With Round Copper Wire and Flat Copper Wire of High-Speed Stator-PM Flux-Switching Machine," *in IEEE Trans. on Ind. Appl.*, vol. 58, no. 6, pp. 7131-7142, Nov.-Dec. 2022 [2] H. Jiang, J. Zhang, Z. Zhang and G. Hu, "Equivalent 2-D FEA Modeling Method for AC Loss Analysis of High-Speed Electrical Machines With Litz Winding Considering Incomplete Transposition," *in IEEE Trans. on Magn.*, vol. 59, no. 11, pp. 1-6, Nov. 2023 [3] Y. Zhao, D. Li, T. Pei and R. Qu, "Overview of the rectangular wire windings AC electrical machine," *in CES Trans. on Electrical Machines and Systems*, vol. 3, no. 2, pp. 160-169, June 2019

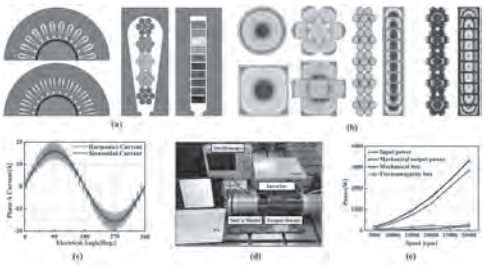

Fig. 1. (a) High-speed PMSM structure according to winding pattern, (b) distribution of current and copper loss densities, (c) sinusoidal and harmonic current, (d) experimental equipment, (e) experimental data.

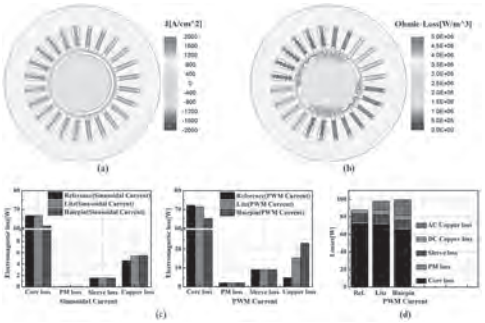

Fig. 2. (a) Current density distribution (b) loss density for each model, (c) loss when applying sinusoidal and harmonic currents, (d) total loss data under harmonic current application.

CU-05. Characteristic Analysis and Optimal Design for Efficiency Improvement of Wound Field Synchronous Machine with Grain-Oriented Electrical Steel. *K. Yu*[1], W. Jung[1], M. Nguyen[1], S. Eom[1], H. Ban[1], K. Shin[2] and J. Choi[1] *1. Chungnam National University, Daejeon, The Republic of Korea; 2. Changwon National University, Changwon, The Republic of Korea*

In this study, to reduce losses and improve the power density and efficiency of the wound field synchronous machine (WFSM), a combined design of grain-oriented (GO) and non-grain-oriented (NGO) electrical steel was developed and analyzed at various operating points. Considering the anisotropic characteristics of GO steel according to the magnetic flux path, four specific design cases were analyzed, as shown in Fig. 1(a). GO steel is designed to be easily magnetized in the rolling direction; therefore, it exhibits excellent magnetic properties when magnetic flux flows in this direction [1]. However, as shown in Fig. 1(b), the magnetic properties are poorer in the direction perpendicular to the rolling direction. Figs. 1(c) and 1(d) show the magnetic flux density over time at each point. The magnitude of the magnetic flux density at the tooth point varies for both cores, with the direction remaining relatively constant. Therefore, using GO steel for each rotor and stator tooth can result in excellent electromagnetic performance. Electromagnetic performance and mechanical analyses were conducted using finite element analysis (FEA). Stability was confirmed through the mechanical analysis of Case D, which had the most assembly parts. After selecting the best case based on the analysis results, optimization was performed. Optimization was carried out through the flow chart in Fig. 2(a). The performance of the optimal model was compared with that of Case A, thereby confirming that both power density and efficiency were improved. Accordingly, considering the direction of the magnetic flux and the application of the GO steel in appropriate locations, excellent performance is expected from various applications. The analysis techniques, various design variables, and electromagnetic performance of the WFSM are presented in detail in the paper.

[1] W. Geng, J. Hou, and Q. Li, "Electromagnetic analysis and efficiency improvement of axial-flux permanent magnet motor with yokeless stator by using grain-oriented silicon steel," IEEE Transactions on Magnetics, vol. 58, no. 2, pp. 1-5, 2021. [2] J. Ma et al., "Optimal design of an axial-

flux switched reluctance motor with grain-oriented electrical steel," IEEE Transactions on Industry Applications, vol. 53, no. 6, pp. 5327-5337, 2017.

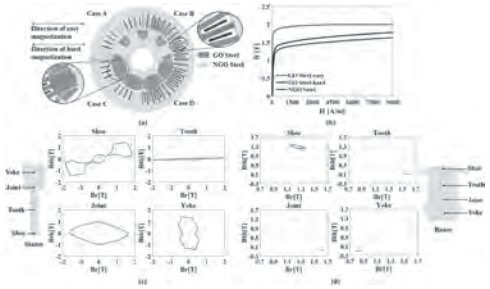

Fig. 1. Analysis models and characteristic of GO and NGO steel, (a) B-H curve, (b) analysis models, (c) and (d) variation of core flux density over time.

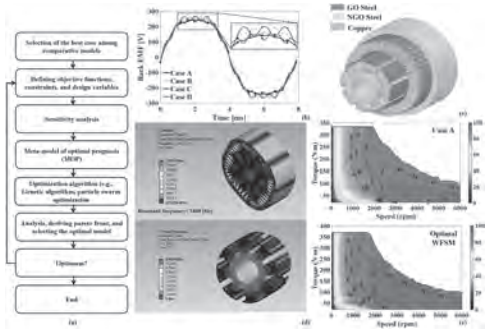

Fig. 2. (a) Flow chart of optimization, (b) back EMF at no-load condition, (c) structure of optimal WFSM, (d) FEA mechanical analysis results of Case D, and (e) comparison of efficiency maps between Case A and optimal WFSM.

CU-08. Rotor Design Process of Ultra-High-Speed Permanent Magnet Synchronous Motor Considering Rotor Interference Fit Tolerance.

J. Kim[1] and D. Kim[2] *1. Mechanical Engineering, Yeungnam University, Gyeongsan, The Republic of Korea; 2. Automotive Engineering, Honam University, Gwangju, The Republic of Korea*

Ultra-high-speed permanent magnet synchronous motors (UHS PMSMs) are actively studied for their high-power density and compact size [1]. Typically, UHS PMSMs are manufactured by interference-fitting a retainer sleeve (RS) around the permanent magnet (PM) to prevent PM scattering during high-speed rotation [2]. A large interference fit can damage the RS, while a small interference fit can cause large tensile stress to the PM. Thus, determining the appropriate interference fit is crucial when designing the rotor of a UHS PMSM. The interference fit has tolerances based on the outer diameter tolerance of the PM and the inner diameter tolerance of the RS. This study proposes a rotor design process for UHS PMSM that considers interference fit tolerances. The mechanical stress of the PM and RS was analytically derived concerning temperature, speed, and interference fit. Assuming the total thickness of the shaft, PM, and RS remains constant, we investigated how mechanical stress changes with temperature, speed, and interference fit. The maximum speed is 90 krpm, temperature range is -40-200°C, and interference fit tolerance is ±0.01 mm. For the PM, mechanical stress increases with higher temperature and speed and as the interference fit tolerance moves in the negative direction, as shown in Fig. 1. For the RS, mechanical stress increases with lower temperature, higher speed, and as the interference fit tolerance moves in the positive direction, as shown in Fig. 1. Therefore, under worst-case conditions for PM and RS, stress can be calculated to ensure a safety factor of at least 1.1. Then, to consider electromagnetic characteristics, the air-gap magnetic flux density was calculated using space harmonic analysis techniques [3]. The rotor design should be carried out where the air-gap magnetic flux density is maximized within the mechanically safe area, as shown in Fig. 2. Additionally, we designed a motor including a stator and compared characteristics such as torque density and efficiency based on rotor radius. Efficiency was highest with a small rotor radius, while torque density was highest with a large rotor radius. Detailed results will be provided later due to space limitations.

D. -M. Kim, J. -H. Kim, S. -G. Lee, IEEE Transactions on Magnetics., Vol. 57, pp. 1-5 (2021) J. -H. Kim, S. -Y. Im, S. -M. An, IEEE Transactions on Magnetics., Vol. 59, pp. 1-5 (2023) J. -H. Kim, D. -M. Kim, Y. -H, Jung, IEEE Transactions on Energy Conversion., Vol. 36, pp. 2850-2860 (2021)

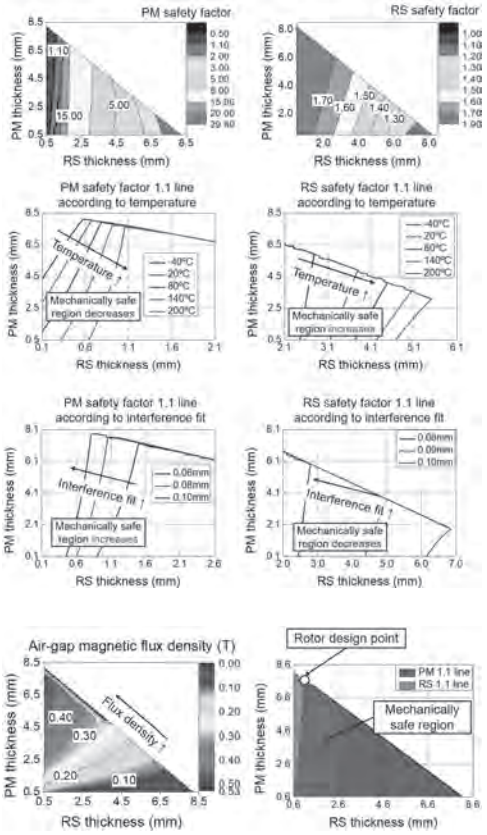

Session CV
ELECTRICAL MACHINES AND POWER ELECTRONICS IV (Poster Session)

Christopher H. T. Lee, Chair
Nanyang Technological University, Singapore

CV-01. Design of Magnetization Yoke to Reduce the Number of Double Spoke Type PMSM Magnetization Using I-Core. *D. Choi*[1], D. Nam[1], Y. Lee[1], N. Jo[1] and W. Kim[2] *1. Next Generation Smart Energy System Convergence, Gachon University, Seongnam, The Republic of Korea; 2. Electrical Engineering, Gachon University, Seongnam, The Republic of Korea*

This paper conducted a study on the reduction of the number of split Magnetization and the prevention of irreversible demagnetization using the I-Core of a double spoke type motor. Recently, as interest in spoke-type motors using ferrite permanent magnets has increased, the need for research on magnetization and irreversible demagnetization in double spoke-type rotor shapes has emerged. Ferrite magnets have the advantage of being much less expensive than rare earth magnets. However, in the existing spoke-type rotor shape, the magnet was deeply embedded in the rotor, making it difficult to magnetization. As it is important to use permanent magnets excluding rare earths in the future, the use of spoke-type motors becomes important, and design to consider magnetization and prevent irreversible demagnetization accordingly is important. Therefore, this paper proposed a magnetization yoke shape design in consideration of magnetization and irreversible demagnetization on using I-Core of Double Spoke type PMSM to solve this problem.

[1] H. S. Seol, T. C. Jeong, H. W. Jun, J. Lee, D. W. Kang, "Design of 3-Times Magnetizer and Rotor of Spoke-Type PMSM Considering Post-Assembly Magnetization", IEEE Transactions on Magnetics, vol. 53, no 11, pp. 1-5, Nov 2017 [2] Q. Wang, H. Ding, H. Zhang, Y. Lv, H. Guo and L. Li, "Study of a Post-Assembly Magnetization Method of a V-Type Rotor of Interior Permanent Magnet Synchronous Motor for Electric Vehicle," in IEEE Transactions on Applied Superconductivity, vol. 30, no. 4, pp. 1-5, June 2020 [3] D. -W. Nam, K. -B. Lee, and W. -H. Kim, "A study on Core Skew considering manufacturability of double-layer spoke-type PMSM," Energies 2021, 14, 610, Jan. [4] H. S. Seol, "Design strategy of magnetizer for post-assembly magnetization of spoke-type ferrite magnet motor" J. Electron. Mater. vol. 48 no. 3 Mar. 2019. [5] M. F. Hsieh Y. C. Hsu and D. G. Dorrell "Design of large-power surface-mounted permanent-magnet motors using post assembly magnetization" IEEE Trans. Ind. Electron. vol. 57 no. 10 pp. 3376-3384 Oct. 2010.

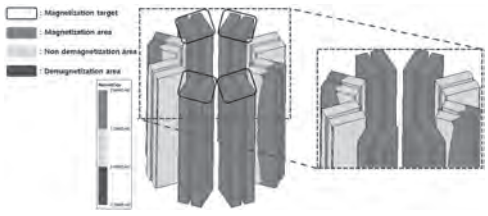

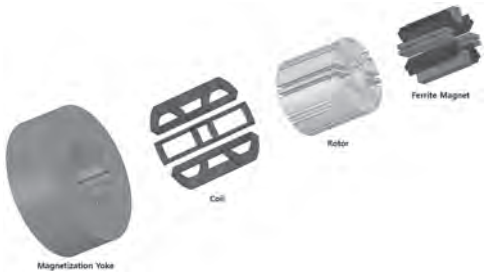

CV-02. A study on Performance Improvement of Axial Flux Motor Through Halbach Array and Same Direction Skew. M. Hong[2], W. Kim[1], N. Jo[1], *J. Kim*[1] and S. Ko[1] *1. Electrical Engineerering, Gachon University, Seongnam, The Republic of Korea; 2. Electrical Engineerering, Hangyang University, Seoul, The Republic of Korea*

In this paper, methods to reduce iron loss through same direction skew and Halbach array by utilizing the shape freedom of 3D printing are proposed. Axial flux motors have a higher power density than radial flux motors and are advantageous in a multi-pole structure. However, in the case of an axial flux motor, it is difficult to manufacture through electrical steel sheet lamination for iron loss reduction. As a method for reducing iron loss in existing axial flux motors, manufacturing through core-loss type, armor force steel plate, and powder material rolling is mainly used. However, in the case of the armor force steel plate, there is a disadvantage in that it is difficult to manufacture, and in the case of manufacturing through rolling, high-cost mold manufacturing is essential. It is possible to overcome the disadvantages of the existing manufacturing method when manufacturing a motor by utilizing the shape freedom, which is an advantage of 3D printing technology. However, cores manufactured using 3D printing currently have high iron loss characteristics, which is a fatal disadvantage to motor output. To reduce iron loss, a combination of pole numbers and slots with a small number of poles can be selected, but a combination with a small number of poles opposes the characteristics of an axial flux motor. Through the same direction skew and Halbach array, the performance of an axial flux motor can be increased even in a combination with a small number of poles. The validity of the proposed model was reviewed through finite element analysis.

[1] M. Aydin and M. Gulec, "A New Coreless Axial Flux Interior Permanent Magnet Synchronous Motor With Sinusoidal Rotor Segments," in IEEE Transactions on Magnetics, vol. 52, no. 7, pp. 1-4, July 2016, Art no. 8105204, doi: 10.1109/TMAG.2016.2522950 [2] H. -J. Pyo, J. W. Jeong, J. Yu, S. G. Lee and W. -H. Kim, "Design of 3D-Printed Hybrid Axial-Flux Motor Using 3D-Printed SMC Core," in IEEE Transactions on Applied Superconductivity, vol. 30, no. 4, pp. 1-4, June 2020, Art no. 5202004, doi: 10.1109/TASC.2020.2973364.

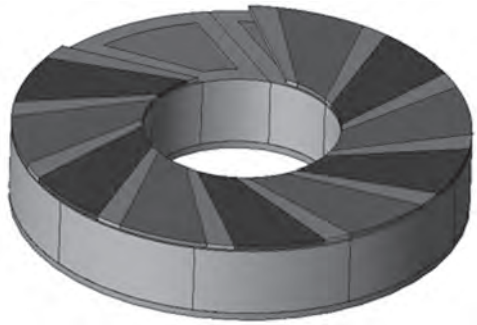

CV-03. Study on axial flux motor using pcb stator for collaborative robot joint electric motor using Halbach array and slit structure.
M. Hong[1], N. Jo[1], H. Kim[1], *J. Kim*[1] and W. Kim[1] *1. Electrical Engineererring, Hanyang University, Seoul, The Republic of Korea*

Axial flux motors have a pancake-like structure with a stack length shorter than the diameter, and have an advantageous structure for increasing output compared to radial flux motors. Axial flux motors can be classified into cored type and coreless type depending on the presence or absence of core. The cored type has the advantage of concentrating magnetic flux compared to the coreless type. However, considering the afpm structure in which magnetic flux flows in the axial direction, it is difficult to manufacture a stator by stacking electrical steel sheets based on one axial direction. Additionally, the stator core can be manufactured by rolling insulated soft magnetic powder material for each particle. there is. When using soft magnetic composite powder, the magnetic and mechanical properties are lower than those of laminated steel sheets and mass production is difficult. Due to these shortcomings, various studies have been conducted recently to replace the stator of AFPM using printed circuit boards without a core. In this paper, we propose a motor structure that uses a pcb board to manufacture an AFPM stator. A halbach array was applied to reduce magnetic flux concentration and back yoke saturation, and a slit structure was implemented to reduce ac loss. The suggestions were verified through finite element analysis.

[1] M. Aydin and M. Gulec, "A New Coreless Axial Flux Interior Permanent Magnet Synchronous Motor With Sinusoidal Rotor Segments," in IEEE Transactions on Magnetics, vol. 52, no. 7, pp. 1-4, July 2016, Art no. 8105204, doi: 10.1109/TMAG.2016.2522950 [2] H. -J. Pyo, J. W. Jeong, J. Yu, S. G. Lee and W. -H. Kim, "Design of 3D-Printed Hybrid Axial-Flux Motor Using 3D-Printed SMC Core," in IEEE Transactions on Applied Superconductivity, vol. 30, no. 4, pp. 1-4, June 2020, Art no. 5202004, doi: 10.1109/TASC.2020.2973364

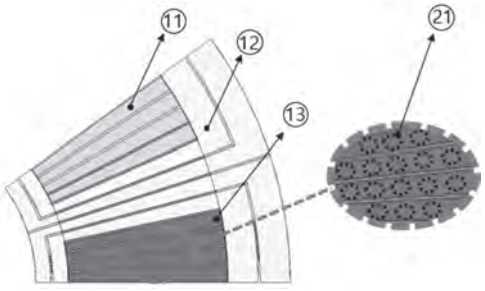

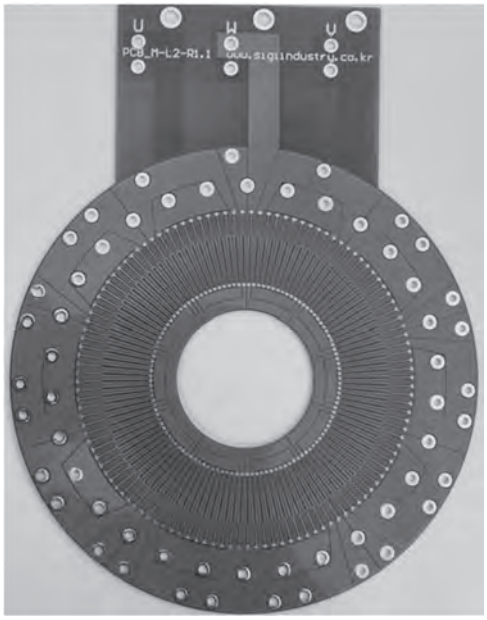

CV-05. Modal Analysis of Electromagnetic Vibrations in Switched Reluctance Machines.
O. Naderi Samani[1], S. Taghipour Boroujeni[1] and *N. Takorabet*[2] *1. Engineering Dep., Shahrekord University, Shahrekord, The Islamic Republic of Iran; 2. GREEN, Université de Lorraine, Nancy, France*

The vibrations of Switched Reluctance Machines (SRMs) are studied. For this purpose, a static 2D subdomain based analytical model is developed. Validity of the obtained model and accuracy of the presented studies are investigated by means of FEA. Using the obtained static model, the spectrum of magnetic pressure in different mechanical modes are obtained. As an index of the machine vibration, the spectrum of the air gap magnetic pressure is used to study the SRM vibrations in different conditions of the rotor speed and the generated electromagnetic torque. As a good alternative of PM machines, Switched Reluctance Machines (SRMs), attract a lot of attention [1-5]. However, due to the double-salient air gap of SRMs, they suffer from torque ripple, mechanical vibration and acoustic noise [6]. Some studies are carried out by means of multi-physics Finite Element Analysis (FEA) [7-8] on vibrations of SRM. As well as, FEA experimental based approaches [9,10] is used to study the vibrations in SRMs. As a fact, FEA requires time-consuming computations, and measurement is an expensive approach. As a fast-computational method, providing an analytical model for SRMs is helpful to study the vibration in SRMs. Some analytical models that are based on magnetic equivalent circuit method are presented in for SRMs. They are capable of considering magnetic saturation [11], however harmonic component of air gap flux density could not be exactly estimated in these methods and consequently the predicted vibrations are not exact. As well as the mentioned analytical models, sub-domain analysis method is to solve Poisson's equation in the machine air gap [12-13]. In II, the natural frequencies are obtained. After that, by using the sub-domain analysis technique, the radial electromagnetic pressure in Switched Reluctance Machines (SRMs) are obtained in III. The proposed model is verified in section IV. Based on the developed model, in section V, the vibrations of SRM in different conditions of the electromagnetic torque and rotor speed are studied.

1 - B. Bilgin and A. Emadi, "Electric motors in electrifed transportation: A step toward achieving a sustainable and highly efficient transportation system," IEEE Power Electron. Mag., vol.1, no.2, pp.10–17, Jun.2014. 2 - E. Bostanci, et al.: 'Opportunities and challenges of switched reluctance motor drives for electric propulsion: a comparative study', IEEE Trans. Transp. Electrif., vol.3, no.1, pp. 58–75, 2017. 3 - M. Castano, B. Bilgin, E. Fairall, and A. Emadi, "Acoustic Noise Analysis of a High-Speed High-Power Switched Reluctance Machine: Frame Effects," IEEE Trans.

Energy Convers., vol. 31, no. 1, pp. 69-77, March 2016. 4 - M. Michon, S. D. Calverley, K. Atallah, "Operating strategies of switched reluctance machines for exhaust gas energy recovery systems," IEEE Trans Ind. Appl., vol. 48, no. 5, pp.1478–1486, 2012. 5 - G. Li, J. Ojeda, S. Hlioui, E. Hoang, M. Lecrivain and, M. Gabsi, "Modification in rotor pole geometry of mutually coupled switched reluctance machine for torque ripple mitigating," IEEE Trans. Magn., vol. 48, no. 6, pp. 2025–2034, 2012. 6 - J. O. Fiedler, K. A. Kasper, and R. W. D. Doncker, "Calculation of the Acoustic Noise Spectrum of SRM Using Modal Superposition," IEEE Trans Ind. Appl., vol. 57, no. 9, pp. 2939–2945, 2010. 7 - X. Liang, et al., "Comparative study of classical and mutually coupled switched reluctance motors using multiphysics finite-element modelling", IEEE Trans. Ind. Electron. Vol. 61, no.9, pp. 5066–5074, 2014 7 - X. Q. Guo, R. Zhong, D. S. Ding, M. S. Zhang, W. J. Shao, and W. F. Sun, "Origin of resonance noise and analysis of randomizing turn on angle Method in switched reluctance motor," IET Elect. Power Appl., vol.11, pp.1324–1332, 2017. 8 - D. Torregrossa, B. Fahimi, F. Peyraut, and A. Miraoui, "Fast computation of electromagnetic vibrations in electrical machines via field reconstruction method and knowledge of mechanical impulse response," IEEE Trans. Ind. Electron., vol. 59, no.2, pp.839–847, 2012. 9 - X. Q. Guo, R. Zhong, L. P. Zhao, J. Yin, and W. F. Sun, "Method for radial vibration modelling in switched reluctance motor," IET Elect. Power Appl., vol. 10, pp.834–842, 2016. 10 - M. Moallem and G. E. Dawson, "An improved magnetic equivalent circuit method for predicting the characteristics of highly saturated electromagnetic devices," IEEE Trans. Magn., vol. 34, no. 5, pp. 3632–3635, 1998. 11 - Q. Yu, X. Wang and Y. Cheng ' Magnetic Modeling of Saliency Effect for Saturated Electrical Machines With a New Calculation Method," IEEE Trans. Magn., vol. 52, no. 6, p. 8001106, 2016. 12 - S. T. Boroujeni, S. P. Emami, N. Takorabet, A. Mahmoudi, "Analytical investigation of the armature current influence on the torque and radial force in eccentric consequent pole PM machines" IET Electric Power Applications, vol.15, no.4, 2021, pp. 441-452. 14 - S. Taghipour*, P. Emami and P. Jalai, "Analytical Modeling of Eccentric PM-inset machines with a Slotless Armature", IEEE Trans. Energy Conversion, vol. 34, no 3, pp.1466-1474.

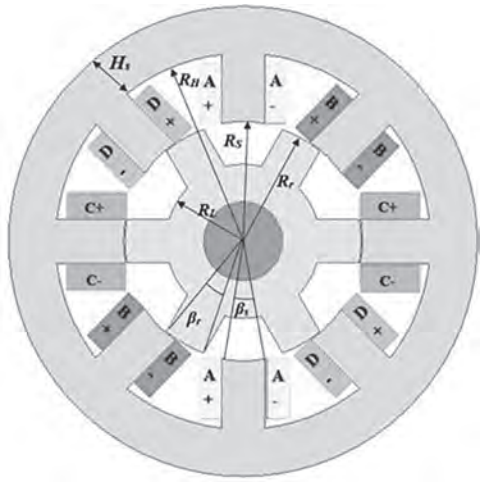

Fig. 1: Geometry and used variables for the studied 8/6 SRM

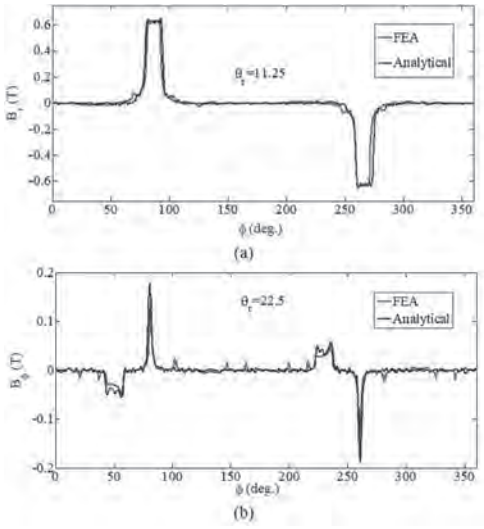

Fig. 2: Flux density components for i_a=1A obtained by the proposed model and FEA (a) Radial; (b) and tangential

CV-06. A Study on the Analysis of Reluctance Torque Based on Rotor I-Core Thickness in Double Spoke Type PMSM. N. Jo[1], D. Nam[1], *Y. Lee*[1], M. Hong[2] and W. Kim[1] *1. Gachon University, Gyeonggi-do, The Republic of Korea; 2. Hanyang University, Seoul, The Republic of Korea*

his study focuses on the rotor shape of the Double Layer Spoke motor, one of the flux-concentrating models. Due to its characteristics, the flux-concentrating model simultaneously utilizes both reluctance torque and magnetic torque. This paper analyzes the reluctance torque in relation to the core thickness between the magnets, and through finite element analysis, it was confirmed that the reluctance torque increases as the core thickness between the magnets increases. Due to mechanical friction between the brush and the commutator during rotation, dust is generated from the brush, leading to mechanical wear, a limited lifespan, or potential failures. Consequently, there has been active research on Brushless Alternating Current (BLAC) motors, and interest in permanent magnets is increasing. However, rare earth elements are predominantly produced by China, which accounts for the largest proportion globally. To mitigate this dependency on Chinese rare earth permanent magnets, the Spoke Type Permanent Magnet Synchronous Motor (PMSM) can be used. This motor has a structure that concentrates magnetic flux density, allowing the use of Ferrite permanent magnets as a substitute for rare earth permanent magnets. The Ferrite Spoke Type motor includes Single Layer Spoke Type and Double Layer Spoke Type motors. The Single Layer Spoke Type motor does not exhibit a significant difference in inductance between the d-axis and q-axis, resulting in limited utilization of reluctance torque. In contrast, the Double Layer Spoke Type motor has a q-axis magnetic barrier between the magnets, enabling greater utilization of reluctance torque compared to the Single Layer Spoke Type motor. Therefore, the Double Layer Spoke Type motor generates more copper losses due to the higher magnetic torque usage compared to the Single Layer Spoke Type motor of the same output. Based on this, an analysis of reluctance torque was conducted by varying the core thickness between the magnets.

[1] M. Onsal, B. Cumhur, Y. Demir, E. Yolacan and M. Aydin, "Rotor Design Optimization of a New Flux-Assisted Consequent Pole Spoke-Type Permanent Magnet Torque Motor for Low-Speed Applications," in *IEEE Transactions on Magnetics*, vol. 54, no. 11, pp. 1-5, Nov. 2018 [2] D. Cui, L. Max, C. Boström and B. Ekergård, "Design of Spoke Type Traction Motor with Ferrite Material for EV Application," *2022 International Conference on Electrical Machines (ICEM)*, Valencia, Spain, 2022

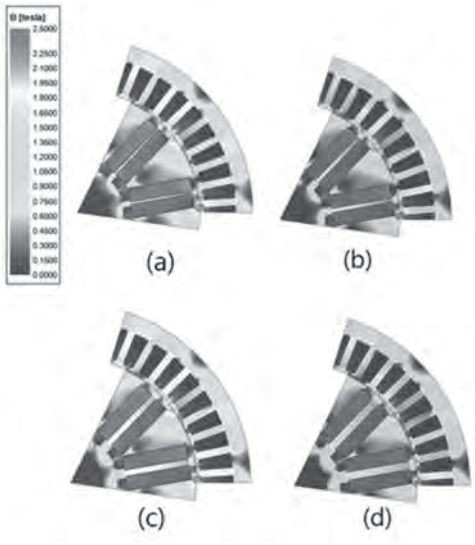

Saturation of Magnetic Flux Density for Different I-Core Thicknesses (a) 1mm; (b) 2mm; (c) 3mm; (d) 4mm

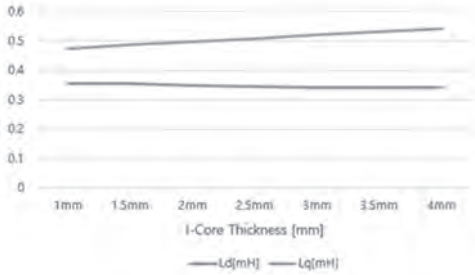

Comparison of d-axis and q-axis Inductance Based on I-Core Thickness

CV-07. A Study on the Design of Axial Flux Motor for Increased Power Density Compared to Radial Flux Motor. M. Youn[1], J. Kim[1], *Y. Song*[1], Y. Lee[1] and W. Kim[1] *1. Gachon University, Seongnam, The Republic of Korea*

The Electric Water Pump (EWP) motor for automotive applications is essential for effectively circulating coolant to maintain the temperature of the engine or battery, both in electric vehicles and internal combustion engine vehicles. Typically, AFPM (Axial Flux Permanent Magnet) motors offer higher electromagnetic torque and torque density compared to RFM (Radial Flux Motor) motors [1]. Accordingly, this paper proposes a method to replace the existing RFPM motor with an AFPM motor that has a higher output density and improve its performance. Initially, volume optimization was achieved through a slim design, and the radial dimensions of the AFPM were increased to obtain higher output. This allowed for efficient utilization of space within the cooling system. Furthermore, various design parameters were adjusted and optimized to enhance the motor's performance. The performance of the designed models was evaluated, and a comparison with the existing RFM was conducted to confirm the performance improvement and increased output density of the motor. This research is expected to enhance the efficiency of the automotive cooling system through the improvement of the EWP motor's performance.

A. Cavagnino, M. Lazzari, F. Profumo and A. Tenconi, "A comparison between the axial flux and the radial flux structures for PM synchronous motors," in IEEE Transactions on Industry Applications, vol. 38, no. 6, pp. 1517-1524, Nov.-Dec. 2002, doi: 10.1109/TIA.2002.805572. J. A. Bala, N. O. Kalu, S. U. Hussein and T. A. Folorunso, "A Fuzzy Logic Control Scheme for Electric Automotive Water Pumps," 2022 IEEE Nigeria 4th International Conference on Disruptive Technologies for Sustainable Development (NIGERCON), Lagos, Nigeria, 2022, pp. 1-5, doi: 10.1109/NIGERCON54645.2022.9803074. C. Zhang, K. J. Tseng and T. D. Nguyen, "Analysis and comparison of axial flux PM synchronous motor and induction motor," 2010 Conference Proceedings IPEC, Singapore, 2010, pp. 572-577, doi: 10.1109/IPECON.2010.5697060. Sung Chul Oh and A. Emadi, "Test and simulation of axial flux-motor characteristics for hybrid electric vehicles," in IEEE Transactions on Vehicular Technology, vol. 53, no. 3, pp. 912-919, May 2004, doi: 10.1109/TVT.2004.827165. Jacek F. Gieras, Rong-Jie Wang and Maarten J. Kamper, Axial Flux Permanent Magnet Brushless Machines, Springer, 2008. F. Profumo, Zheng Zhang and A. Tenconi, "Axial flux machines drives: a new viable solution for electric cars," in IEEE Transactions

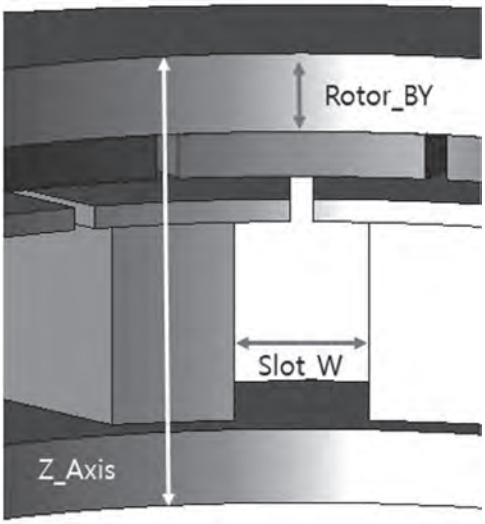

Session DA
MAGNETIC BRAIN STIMULATION AND IMAGING

Nian X Sun, Chair
Northeastern University, Boston, MA, United States

INVITED PAPERS

DA-01. Multi-Magnetic Material Coils and Prediction of Stimulation Strength Using Machine Learning in Transcranial Magnetic Stimulation.

R.L. Hadimani[1,2] 1. Department of Mechanical and Nuclear Engineering, Virginia Commonwealth University, Richmond, VA, United States; 2. Department of Electrical and Computer Engineering, Iowa State University, Richmond, VA, United States

Transcranial Magnetic Stimulation (TMS) can tune brain functions non-invasively, safely, and effectively without the need for surgery or drugs. Thus, it can enable the treatment of several debilitating neurological and psychiatric disorders and enhance cognitive capabilities 1-3]. TMS coils suffer from lack of focal stimulation in the deeper parts of the brain due to rapid decay of magnetic field from the source. Focality on the cortical surface can be improved by using high magnetic permeability and high saturation flux ferromagnetic cores. For deeper stimulation even the ferromagnetic cores suffer from the spread of the magnetic field. My lab has designed and fabricated several novel focal and deep brain stimulation coils based on novel soft ferromagnetic and diamagnetic materials as shown in Fig.1 [4-5]. We have experimentally verified some of the results from coil design in rats in collaboration with the Department of Neurology at VCU and Richmond Veteran Hospital. My team has also designed a TMS coil configuration that can stimulate multiple sites simultaneously and vary sites of stimulation without moving the coils physically. We have also investigated a feasibility study of combined TMS and DBS using brain phantom in collaboration with the VCU Department of Neurosurgery [6]. *We have successfully conducted human subject studies on healthy population and used a deep convolution neural network to predict the stimulation strengths in the brains of patients with mild traumatic brain injury in the form of induced electric fields as shown in Fig. 2*. We are currently working to *predict TMS treatment responses in humans by using deep machine learning algorithms considering anatomical and functional variables using MRI, fMRI, DTI and EEG*. These new machine-learning algorithms will enable prediction of the TMS treatment outcomes of patients and determine the dose-response curves before the treatment begins in the future.

D. Kumbhare, M. A. Azam, R. Hadimani, G. Weistroffer, J. Atulasimha, and M. S. Baron, "Healthy and pathological pallidal regulation of thalamic burst versus tonic mode firing: a computational simulation," *Neuro Report*, vol. 34, no. 16, p. 773, Nov. 2023. L. M. Franke, G. T. Gitchel, R. A. Perera, R. L. Hadimani, K. L. Holloway, and W. C. Walker, "Randomized trial of rTMS in traumatic brain injury: improved subjective neurobehavioral symptoms and increases in EEG delta activity," *Brain Injury*, vol. 36, no. 5, pp. 683–692, Feb. 2022 N. Mittal, B. Thakkar, C. B. Hodges, C. Lewis, R. L. Hadimani, and C. L. Peterson, "Effect of neuroanatomy on corticomotor excitability during and after transcranial magnetic stimulation and intermittent theta burst stimulation," *Human Brain Mapping*, vol. 43, no. 14, pp. 4492–4507, 2022, I. C. Carmona, O. F. Afuwape, D. C. Jiles, and R. L. Hadimani, "Estimation of the Focality of Coils and Quality of Stimulation of Biological Tissues During Transcranial Magnetic Stimulation," *IEEE Transactions on Magnetics*, vol. 58, no. 2, pp. 2022. M. Tashli, A. Mhaskar, G. Weistroffer, M. S. Baron, and R. L. Hadimani, "Novel multi-magnetic material transcranial magnetic stimulation coils for small animals application," *AIP Advances*, vol. 14, no. 1, p. 015324, Jan. 2024

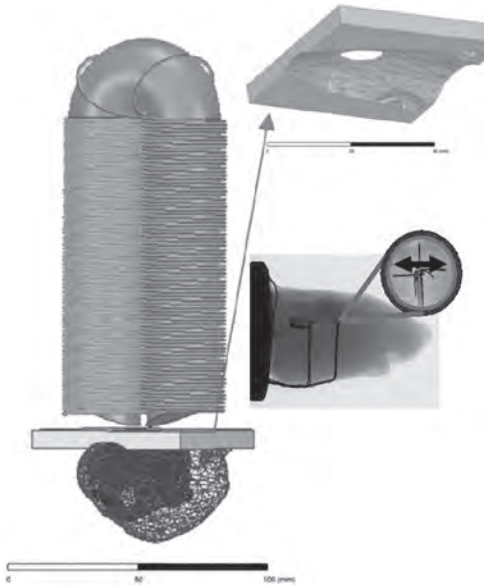

Fig. 1 Novel Parabolic Ferromagnetic Core (PFC) TMS coil with highly diamagnetic pyrolytic graphite shielding plate for a focused stimulation of the primary motor cortex (M1) of a rat's brain.

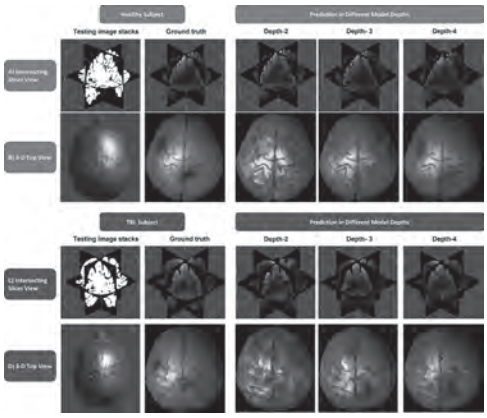

Fig. 2. Prediction of induced electric field in mild to moderate traumatic brain injury patients (bottom) with a DCNN model that is trained on healthy subjects (top).

DA-02. Enabling a Wireless Non-invasive Two-Way Brain-Machine Interface with Magnetoelectric Nanoparticles. P. Liang[3], E. Zhang[1], S. Chen[4], M. Abdel-Mottaleb[5], V. Andre[5], M. Shotbolt[5], J. Tian[1], A. Scott-Vandeusen[5], E. Zhu[5] and *S. Khizroev*[1,2] *1. Electrical and Computer Engineering, University of Miami, Coral Gables, FL, United States; 2. Biochemistry and Molecular Biology, University of Miami, Miami, FL, United States; 3. Cellular Nanomed, Irvine, CA, United States; 4. Chemical, Environmental and Materials Engineering, University of Miami, Coral Gables, FL, United States; 5. Biomedical Engineering, University of Miami, Coral Gables, FL, United States*

It is commonly believed that high-resolution wireless and non-invasive two-way brain machine interface (BMI) will revolutionize many aspects of our lives, ranging from information processing to energy and medicine [1]. However, to date, such technology has not been made available. Arguably, the most developed technology today would be optogenetics. However, optogenetics is limited by the need for genetic modification of the brain tissue and the difficulty to transmit light through the skull and tissue [2]. MagnetoElectric NanoParticles (MENPs) were proposed as a solution more than a decade ago [3]. Due to their magnetoelectric (ME) effect, MENPs convert wirelessly applied magnetic fields into local electric fields which in turn provide targeted electric modulation of neural activity. Figure 1A shows a transmission electron microscopy (TEM) image of a 30-nm $CoFe_2O_4$@ $BaTiO_3$ core-shell MENP with a magnetoelectric effect of over 1 V/cm/Oe, a saturation magnetization of <1 emu/g, and a coercivity of over 700 Oe. Figure 1B shows an optically measured calcium ion signal from a rat brain hippocampus cell culture, clearly showing an action potential triggered in response to application of 1-second long 50-Hz 1,200-Oe-magnetic field pulses. Reciprocally, MENPs can convert electric fields due to local neural activity into magnetic moment changes that in turn could be used for wireless recording. However, to fully realize the enormous potential of this approach, several technological roadblocks need to be overcome. Besides the need to further maximize the magnetoelectric effect, these roadblocks relate to the capability to target the neuronal membrane, minimize the nanoparticles' agglomeration, and control the magnetic field energy localization with metastable physics. This presentation discusses in vitro and in vivo studies to demonstrate the wireless targeted deep brain stimulation with MENPs. It also gives a perspective on the future potential impacts of this technology, particularly with respect to the wireless non-invasive recording aspect. To realize the latter, MENPs will need to be integrated with high-resolution magnetic imaging technologies such as magnetic resonance imaging (MRI) or the recently emerged magnetic particle imaging (MPI). Furthermore, having the potential to enable a two-way wireless BMI with high spatial and temporal resolutions, MENPs have the potential to shed light on the computing architecture of the brain as well as revolutionize the state of treatment of currently untreatable neurological diseases and brain and other tumors.

[1] S. Rajangam *et al.*, *Sci Rep* vol. 6 (ARTN 22170) (2016). [2] O. Yizhar, L. E. Fenno, T. J. Davidson, M. Mogri, and K. Deisseroth, *Neuron,* vol. 71 (1), 9-34 (2011). [3] K. Yue, R. Guduru, J. M. Hong, P. Liang, M. Nair, and S. Khizroev, *Plos One,* vol. 7 (ARTN e44040) (2012)

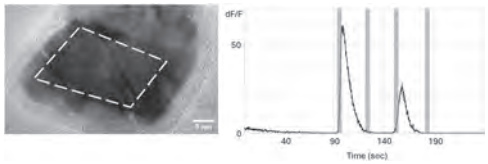

(Left) TEM image of a 30-nm $CoFe_2O_4$@$BaTiO_3$ core-shell MENP. The yellow broken line highlights the cobalt ferrite core. (Right) Optically measured calcium ion signal from hippocampus rat cell culture, with 1 ug of MENPs per a dish with 100,000 cells, in response to application of 1-second long 50-Hz 1,200-Oe-magnetic field pulses. To provide the optical response, the cell culture was tagged with a calcium ion sensitive fluorescent dye Cal520.

DA-03. Cellular Mechanisms of Transcranial Magnetic Stimulation in Cerebellar Cortex. *P. Sundaram*[1] *1. Radiology, MGH/Martinos Center, Boston, MA, United States*

In this talk, I will describe how my lab is developing a cellular level understanding of how TMS activates neurons in the cerebellum of humans. For this we use (1) electrophysiology experiments in an *in vitro* cerebellum model and computational modeling the induced electric fields in the tissue and (2) TMS-EEG-MEG studies in human cerebellum in vivo. Since the local anatomy and electrophysiology of the cerebellum are evolutionarily conserved, the fundamental neural dynamics will generalize. The combination of invasive electrophysiology in the *in vitro* cerebellum, the *in vivo* human TMS studies combined with electric field simulations will likely allow better understanding of the cellular basis/biophysics of TMS, opening new applications of TMS for studying the role of the cerebellum in human brain function.

DA-04. Engineering Magnetic Particles for Positive MRI Contrast. *S. Oberdick*[4,2], S. Dodd[1], G. Erich[2], A. Hunter[3], K. Jordanova[9,2], K. Keenan[2], A. Koretsky[1], J. Lundstrom[4,2], O.T. Mefford[3], G. Parigi[5,6,7], M. Poorman[8] and G. Zabow[2] *1. LFMI, NINDS, NIH, Bethesda, MD, United States; 2. NIST, Boulder, CO, United States; 3. Dept. of Mat. Sci. and Eng., Clemson University, Clemson, SC, United States; 4. Dept. of Physics, University of Colorado, Boulder, Boulder, CO, United States; 5. CERM, University of Florence, Sesto Fiorentino, Italy; 6. Dept. of Chem. "Ugo Schiff", University of Florence, Sesto Fiorentino, Italy; 7. CIRMMP, Sesto Fiorentino, Italy; 8. Hyperfine, Inc., Guilford, CT, United States; 9. Radiology, Stanford University, Palo Alto, CA, United States*

Magnetic resonance imaging (MRI) is a non-invasive technique that produces three-dimensional visualizations of human anatomy. MR images can be enhanced using contrast agents, which are exogenous magnetic materials that interact with resonant protons in tissue and modify image characteristics. Generally, contrast agents can be categorized as positive or negative, depending on whether they increase or decrease signal, respectively. Magnetic particles are usually thought of as negative contrast agents because they dephase signal from water protons at common magnetic field strengths, resulting in a region of decreased signal on an MR image. However, new technological advancements related to low field MRI scanners and, separately, microfabrication of magnetic particle constructs, have created new opportunities for contrast generation that move beyond negative contrast. In this talk, I will describe new pathways for magnetic particle-based positive MRI contrast using low field MRI and, also, "color" contrast with geometrically engineered magnetic microstructures. First, I will describe possibilities for using magnetic nanoparticles (MNPs) as positive contrast agents with low field MRI (LF-MRI). LF-MRI scanners require less infrastructure than clinical MRI scanners and can be wheeled next to a patient's bedside, creating revolutionary possibilities for point-of-care diagnostics. Previous work demonstrated that iron oxide-based MNPs have desirable properties for positive T1 contrast at emerging field strengths used for LF-MRI [1]. The T1 contrast at fields used for LF-MRI is modulated by the diffusion of protons near MNPs and can be affected by magnetic and structural properties of the particles. To better understand the relationship between MNP characteristics and resultant T1 contrast, we measured MNPs with variations in size and surface coatings using an FDA-approved 64 mT MRI scanner. Figure 1 shows an example of MNPs used in the study. We also varied the diffusion coefficient of water in sample environments to understand how biologically relevant diffusion conditions affect T1 contrast. Secondly, I will describe how hollow cylinder shaped MNP-polymer microparticles (Figure 2a) can be used as radio frequency (RF) multispectral MRI contrast agents [2]. Multispectral, or "color" contrast is a unique form of contrast that uses three-dimensional magnetic microstructures to produce a distinct frequency readout [3]. I will describe techniques for producing MNP-polymer microparticles which generate spectral shifts which are tens of times larger than familiar NMR chemical shifts, providing an RF-identifier that is spectrally distinct from the environment. These contrast agents can also be used as biosensors by using shape reconfigurable "smart" hydrogels that expand

or shrink in response to environmental conditions (Figure 2b). The change in shape causes a corresponding shift in the proton resonance, producing an MRI-addressable readout of the microenvironment. I will show proof-of-principle experiments demonstrating a multispectral response to changes in pH (Figure 2c and 2d).

1. Oberdick, S. D. et al., Sci. Rep., Vol. 13, p. 11520 (2023) 2. Oberdick, S. D. et al., ACS Sens., Vol. 9, p. 42–51 (2024) 3. Zabow, G. et al., Nature, Vol. 453, p. 1058–1063 (2008)

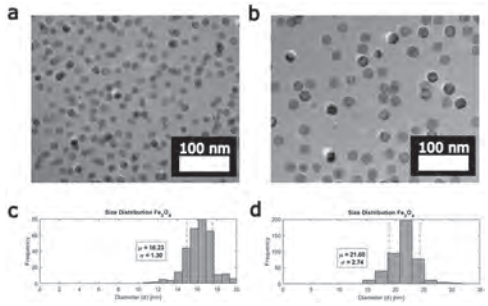

Figure 1. Transmission electron microscope (TEM) images of MNPs with sizes of (a) 16 nm and (b) 22 nm, which were functionalized with PEG coatings and used for LF-MRI contrast agent studies. The histograms beneath each TEM image show the size distributions for the (c) 16 nm and (d) 22 nm particles, measured using TEM.

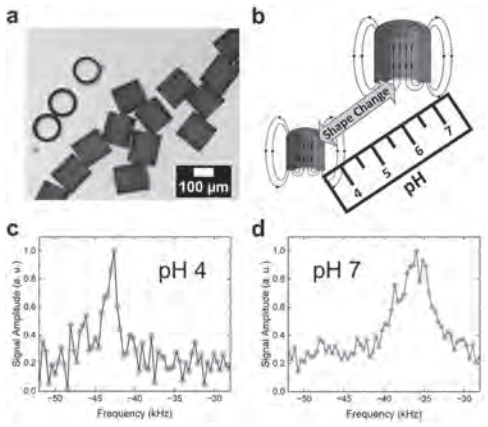

Figure 2. (a) Optical microscope image of magnetic hydrogel particles with a hollow cylinder geometry used for multispectral or "color" contrast generation. (b) Physical changes in the contrast agents, caused by pH-induced hydrogel swelling, can be used to modify the magnetic fields within the cylinder. (c) When the contrast agents are in a contracted state at pH 4, they produce a frequency readout of -43 kHz. (d) At pH 7, the contrast agents expand, producing a shift in the frequency readout to -36 kHz.

DA-05. MRI and Safety - Focusing on High Static Magnetic Fields. *S. Yamaguchi-Sekino[1] 1. National Institute of Information and Communications Technology (NICT), Koganei, Japan*

MRI is a non-invasive method for visualizing internal structures and is essential in clinical practice. MRI devices are crucial for diagnosing diseases and are also important partners in elucidating brain function through imaging techniques such as fMRI, which visualizes functional activity in the brain, and MR spectroscopy, which evaluates the dynamics of biomolecules within the brain and body. The technical characteristics of MRI devices is its use of variety electromagnetic sources - such as strong static magnetic fields, pulsed magnetic fields, and high-frequency electromagnetic fields. Consequently, extensive safety research has been conducted concerning the biological effects of these electromagnetic fields. On the other hand, increasing the static magnetic field strength improves image quality, leading to the advancement of MRI devices from 1.5 T to 3 T and from 3 T to 7 T. In 7 T MRI, due to the fact that the signal to noise ratio (SNR) is proportional to the magnetic field strength, resulting in an increased SNR with higher magnetic fields [1]. Therefore, 7 T MRI systems enable high resolution and high contrast imaging at the level of several hundred micrometers. Additionally, high-field MRI offers the advantage of improved spectral resolution when evaluating the dynamics of biomolecules within the body, such as in MR spectroscopy [1]. Although there are operational technical challenges such as heating and image inhomogeneity, the benefits of high-field MRI, particularly in brain function imaging, are receiving significant attention. A whole-body MRI system with even higher magnetic fields, such as 11.7 T, have recently begun operating [2]. This presentation focuses on evaluating the safety of high-intensity static magnetic fields, starting with the introduction of high field MRI in brain imaging. Consequently, safety issues related to high static magnetic fields such as effects on stem cells [3], measurement results [4][5] and effects on humans [6], and the impact on MRI operators during pregnancy and childbirth [7] will be discussed.

[1] P. Balchandani, P. Naidich, Am J Neuroradiol, Vol. 36 No. 7, pp.1204-15 (2015) [2] N. Boulant, L. Quettier; Iseult Consortium, MAGMA, Vol. 36 No. 2, pp.175-189 (2023) [3] S. Yamaguchi-Sekino, T. Kira, M. Sekino et al., Bioelectromagnetics, Vol.40, No.1, pp.16–26 (2019) [4] S. Yamaguchi-Sekino, T. Nakai, S. Imai et al., Bioelectromagnetics, Vol. 35, 70-75 (2014) [5] S. Yamaguchi-Sekino, M. Sekino, T. Nakai, IEEE Transactions on Magnetics, Vol. 51, No. 11, pp.1-4 (2015) [6] S. Yamaguchi-Sekino, K. Iwakiri, M. Sekino et al., IEEJ TRANSACTIONS ON ELECTRICAL AND ELECTRONIC ENGINEERING, Vol.17, Issue 7, pp.981-985 (2022) [7] S. Yamaguchi-Sekino, N. Kojimahara, Magn Reson Med Sci, Vol. 23, No. 1, pp.122-126 (2024)

Session DB

ADVANCED MAGNETIC MATERIALS & MANUFACTURING FOR FUTURE ELECTRIC MOTORS AND POWER ELECTRONICS

Yacine Amara, Co-Chair
Université Le Havre Normandie, Le Havre, France
Masahiro Yamaguchi, Co-Chair
Tohoku University, Sendai, Japan
Johannes JH Paulides, Co-Chair
Advanced Electromagnetics Group, Waalwijk, Netherlands

INVITED PAPERS

DB-01. Design Freedoms and Challenges in Additively Manufacturing Electrical Machines. *A. Kallaste*[1] *1. Electrical Power Engineering and Mechatronics, Tallinn University of Technology, Tallinn, Estonia*

The traditional landscape of designing and manufacturing electrical machines has encountered a plateau. However, a transformative shift has emerged with the advent of additive manufacturing technology (AM), unlocking unprecedented opportunities for electrical machine design and production. Additive manufacturing technology, has the potential to revolutionize machine design by enabling the creation of complex structures and the utilization of advanced topology optimization tools [1]. Ongoing research in electrical machines using AM technology explores diverse avenues to enhance machine components. This research focuses on developing better magnetic cores, more efficient windings, improved heat exchangers, and innovative solutions to reduce machine weight [2]. By leveraging AM, it is possible to enhance machine performance, making them lighter and more efficient. One of the significant advantages of AM in electrical machine design is its ability to produce complex geometries that are otherwise challenging or impossible to achieve with traditional manufacturing methods. This capability allows for the integration of intricate cooling channels within heat exchangers, leading to more efficient thermal management [3]. Moreover, AM facilitates the development of magnetic cores with optimized shapes and material distributions [4]. This optimization can reduce magnetic losses and improve the overall efficiency of electrical machines. The flexibility of AM also enables the production of customized windings that enhance the performance of electric motors and generators. These windings can be tailored to specific electromagnetic requirements, resulting in improved torque, power density, and energy efficiency. However, from a design perspective, there is considerable research to be done on how to consider the asymmetry in machine design. The development of effective design methodologies and constraints remains an ongoing challenge, requiring refinement of design tools and techniques. Material properties of AM materials may not yet meet the stringent mechanical, thermal, or electrical requirements necessary for optimal machine performance. For example, magnetic material losses, especially eddy current losses, need to be addressed to maximize the efficiency of AM-produced electrical machines. Dimensional limitations inherent in AM technologies may constrain the scalability of electrical machines, demanding advancements in process capabilities and equipment. Surface quality issues, can affect the performance and reliability of AM-produced components. Therefore, post-processing techniques and surface treatments are often required to achieve the desired quality and functionality. Despite these challenges, the potential benefits of AM in electrical machine production are significant. By overcoming material limitations, surface quality issues, and dimensional constraints, AM can unlock new possibilities for electrical machine design and manufacturing. The ability to rapidly prototype and customize machines opens up opportunities for innovation and allows for the development of customized machines for niche applications. In conclusion, additive manufacturing technology presents a transformative opportunity for the design and production of electrical machines. Its ability to create complex structures, enable rapid prototyping, and customize machines for specific applications has the potential to revolutionize the field. However, to fully exploit this potential, it is necessary to address the challenges related to material properties, surface quality, dimensional limitations, and design methodologies. Overcoming these challenges will pave the way for widespread adoption of AM in the production of next-generation electrical machines, facilitating advancements in performance, efficiency, and customization across various industries.

1. M. U. Naseer, A. Kallaste, B. Asad, "A Review on Additive Manufacturing Possibilities for Electrical Machines," Energies 2021, vol. 14, no. 7, p. 1940 (2021) 2. S. Hussain, A. Kallaste, and T. Vaimann, "Recent Trends in Additive Manufacturing and Topology Optimization of Reluctance Machines," *Energies 2023, Vol. 16, Page 3840*, (2023) 3. P. S. Ghahfarokhi *et al.*, "Opportunities and Challenges of Utilizing Additive Manufacturing Approaches in Thermal Management of Electrical Machines," *IEEE Access*, vol. 9, pp. 36368–36381, 2021, doi: 10.1109/ACCESS.2021.3062618 4. M. U. Naseer *et al.*"Design procedure and preliminary analysis for the introduction of axial asymmetry in the synchronous reluctance machines," in 2023 IEEE WEMDCD, (2023)

DB-02. High Power Density Motor Equipped with Additively Manufactured Windings. *A. El-Refaie*[1] *1. Marquette University, Milwaukee, WI, United States*

This presentation will cover the design and analysis details of a high-specific power 250 kW direct-drive electric drivetrain system intended for hybrid/electric propulsion applications. The system includes a motor equipped with additively-manufactured hollow windings integrated with heat pipes, a tightly integrated modular power electronics and a shared thermal management system. The tradeoff studies and optimization of the motor design will be presented. Details of the electromagnetic, thermal and mechanical analysis will be covered. Sub-components characterization including thermal and electrical characterization of the additively-manufactured coils, heat pipes, and motorette will be also presented, In addition details about the drive design and the overall system integration and cooling options will also be presented.

DB-03. Novel Applications of Additive Manufacturing for Improved Electrical Machine Design and Performance. M. Tsai[1], *P. Wang*[1] and T. Chang[2] *1. Mechanical Engineering, National Cheng Kung University, Tainan, Taiwan; 2. Electric Motor Technology Research Center, National Cheng Kung University, Tainan, Taiwan*

Additive manufacturing is renowned for reducing production time and costs. Beyond these benefits, advancements in additive manufacturing have significantly improved the performance and design of components. While most research focuses on non-ferrite applications, our research is centered on

ferrite-based applications, such as electrical machines and magnetic components. Traditional electric motors are mostly made from laminated 2D electrical steel sheets. The selective laser melting (SLM) technology, combined with ferrite-based soft magnetic composite (SMC) powder, enables the creation of intricate and complex electrical machine structures that are challenging or difficult to the traditional manufacturing processes. This approach also eliminates the need for mold design and development time required in conventional methods. A key contribution of our research is improving magnetic permeability and reducing core losses in motor cores, which are significant challenges in metal 3D additive manufacturing. A notable feature of the SLM technology presented in this research is its ability to enhance the functional properties of magnetic materials by introducing oxygen into the cavities of the iron-based SMC during the SLM process, forming an insulating layer [1]. Figs. 1(a) and (b) show the microscopic structures of silicon steel sheets and SMC powder (FeSiCr). Prototypes utilizing this manufacturing technique include the honeycomb structure of the line-start synchronous reluctance motor (LSSynRMs) [2] shown in Fig. 1(c). The LSSynRMs rotor features intricate ribs, flux barriers, and cages. Fig. 1(d) shows the prototype of LSSynRM rotor made from SMC powder via SLM. Additionally, Fig. 2(a) shows an integrated fan-rotor electric motor [3] design which combines traditional fan blades with the motor rotor into a single unit. This integration significantly reduces the motor size while enhancing power density. Such a conceptual design is realized through the SLM process as shown in Figs. 2(b) and (c). Our research demonstrated the practical possibilities of employing a combination of SLM and SMC to create high-performance magnetic material and intricate, complex motor structures.

[1] K.J. Jhong, T.W. Chang, W.H. Lee, M.C. Tsai, and I.H. Jiang, "Characteristic of high frequency Fe-Si-Cr material for motor application by selective laser melting," *AIP Advances,* vol.9, no.3, pp.035317, 2019. [2] P.W. Huang, M.C. Tsai, and I.H. Jiang, "3-D structure line-start synchronous reluctance motor design based on selective laser melting of 3-D printing," *IEEE Transactions on Magnetics,* vol.54, no.11, pp.1-4, 2018. [3] S.T. Wu, P.W. Huang, T.W. Chang, I.H. Jiang, and M.C. Tsai, "Application of magnetic metal 3-D printing on the integration of axial-flow impeller fan motor design," *IEEE Transactions on Magnetics,* vol.57, no.2, pp.1-5, 2020.

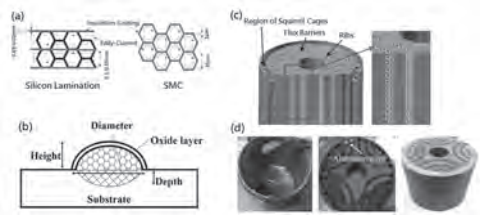

Fig. 1. (a) Microscopic structures of silicon lamination and SMC powder for motors. (b) Melted FeSiCr powder treated by SLM process. (c) 3D grid structure in the rotor of new LSSynRM. (d) Prototype of new LSSynRM.

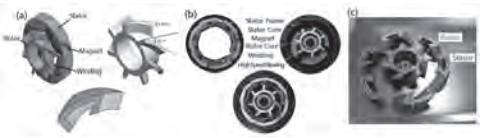

Fig. 2. (a) Integrated fan-motor with airfoil-shaped rotor: motor, fan-rotor, and stator. (b) Complete fan-motor prototypes. (c) Stator and rotor prototype manufactured by SLM.

DB-04. Novel approaches of nanocrystalline alloys with large saturation magnetization for next-generation power-electronics applications.
S. Okamoto[1], A. Urata[2], H. Oikawa[2], S. Hiramoto[1], N. Ono[1], R. Gautam[3], H. Sepehri-Amin[3], T. Ohkubo[3] and T. Ogasawara[4] *1. Tohoku University, Sendai, Japan; 2. Tokin Corp., Shiroishi, Japan; 3. NIMS, Tsukuba, Japan; 4. AIST, Tsukuba, Japan*

Due to the recent strong demands of downsized and high-efficiency energy conversion power-electronics systems, it has been expected to develop soft magnetic materials with large saturation magnetization M_s and low core loss for magnetic passive devices such as transformers and inductors used in power-electronics systems. Therefore, some of soft magnetic nanocrystalline alloys with large M_s have been newly developed such as Fe-Si-B-P-Cu (NANOMET) [1], Fe-Si-B-Cu [2], Fe-B based [3] alloys. However, there are some drawbacks of these alloys for the practical application, such as brittleness and requirement of rapid thermal annealing. These factors make it very difficult to fabricate powder and wound cores with high-packing density. In this work, we have studied novel approaches to overcome these obstacles for both the powder and wound core applications using NANOMET based alloys. For powder core application, hot-press process was applied to the NANOMET based powder cores. As a result, this process enables us to simultaneously realize high-packing density and well-nanocrystallization of this powder material. Consequently, the packing density the hot-pressed core increases to 89 % from 70 % of the conventional cold-pressed powder core, resulting in the high core M_s of 1.55 T. Moreover, the core loss at the frequency of 100 kHz and the excitation flux density of 100 mT decreased down to 146 kW/m^3 from 852 kW/m^3 of the conventional cold-pressed powder core. These properties are extremely superior compared with the widely used commercial cores, such as Sendust and Fe-Si powder cores, for power-electronics applications. On the other hand, for wound core application of rapid quenched amorphous ribbon of NAMET based precursor alloy, after a careful control of crystallinity, we have successfully developed a novel approach to realize the very low iron loss comparable to that of FINEMET with keeping the elasticity and unnecessarily of rapid thermal annealing. At the onset of nanocrystallization, the iron loss decreases significantly, and simultaneously the very narrow stripe magnetic domain structure with several mm in width is observed, which is quite different magnetic domain structure from that of the conventional soft magnetic ribbons. From the iron loss analysis based on the magnetization reversal process [4,5], this stripe magnetic domain structure leads the change in the magnetization process from the conventional magnetic domain wall displacement to magnetization rotation, leading to the very low excess loss of this material. This work was supported by MEXT-Programs for INNOPEL (JPJ009777) and DXMag (JPMXP1122715503).

[1] A. Urata, H. Matsumoto, S. Yoshida, and A. Makino, IEEE Trans. Magn. 47, 3177 (2011). [2] M. Ohta and Y. Yoshizawa, Appl. Phys. Lett. 91, 062517 (2007). [3] K. Suzuki, R. Parsons, B. Zang, K. Onodera, H. Kishimoto, and A. Kato, Appl. Phys. Lett. 110, 012407 (2017). [4] N. Ono, Y. Uehara, Y. Endo, S. Yoshida, N. Kikuchi, H. Oikawa, and S. Okamoto, IEEE Trans. Magn. 59, 6301305 (2023). [5] N. Ono, Y. Uehara, T. Onuma, T. Taniguchi, N. Kikuchi, and S. Okamoto, J. Magn. Magn. Mater. 603, 172222 (2024).

DB-05. Metrology for Steel Laminations and Power Electronics Magnetic Cores: Loss Measurement Techniques and Uncertainties from DC to the Microwave Regime.
M. Pasquale[1], C. Beatrice[1], E. Ferrara[1], N. Banu[1], F. Fiorillo[1], C. Ragusa[2] and L. Solimene[2] *1. Advanced Materials Metrology and Life Sciences, INRIM, Torino, Italy; 2. Department of Energy, Politecnico di Torino, Torino, Italy*

Magnetic laminations and cores for power electronics play a crucial role in modern energy conversion systems, enabling efficient and reliable power transfer. Accurate measurements of the magnetic properties and losses in these laminations and cores is essential for optimal design and performance of electrical machines and power electronics devices. This work provides an overview of the available international measurement standards, as well

as examples of hysteresis loops and power loss figures obtained by broadband measurements on steel laminations, ferrite, nanocrystalline, and amorphous magnetic cores, encompassing different experimental setups and methods. The measurement techniques discussed in this presentation allow for dynamic *B-H* measurement at different induction levels up to the 10 kHz range in steel laminations, and up to the MHz range in cores, where permeability evaluation is also possible up to the GHz range. The energy losses are analysed by the loss separation method, considering the eddy current and spin damping dissipation mechanism, besides the magnetic flux penetration issues. They are posed in direct relationship with the real and imaginary permeability components, by discriminating between domain wall and rotational contributions. Available measurement standards are discussed, and the analysis of the measurement uncertainties is provided. Calibration procedures to assess and reduce the uncertainties arising from circuitry, instrument resolution, temperature, and environmental effects are considered. Since the DC-MHz frequency range is particularly relevant for power electronics, the power loss measurement techniques here discussed, and the related uncertainties specifically address the challenges associated with this frequency range. Through their comprehension, engineers and researchers involved in the design and optimization of power electronics devices can make well-informed decisions. The insights provided in this presentation may directly contribute to the reduction of uncertainties in power electronics measurements, facilitating the development of more efficient and reliable energy conversion systems.

1. Stuart Harmon, M. Pasquale et al “Comparisons of total power loss measurements performed on ring samples from 10 kHz to 1 MHz at room temperature”. HEFMAG Report 2023 DOI 10.5281/zenodo.8304981 2. O. de la Barrière, E. Ferrara, A. Magni, A. Sola, C. Ragusa, C. Appino, and F. Fiorillo Skin Effect and Losses in Soft Magnetic Sheets: From Low Inductions to Magnetic Saturation IEEE TRANSACTIONS ON MAGNETICS, VOL. 59, NO. 11, NOVEMBER 2023 6301211 3. S Dobák, C Beatrice, V Tsakaloudi, F Fiorillo - Magnetic losses in soft ferrites Magnetochemistry, 2022 4. N Banu, E Ferrara, M Pasquale, F Fiorillo, O De la Barrière, D Brunt Temperature and frequency dependence of magnetic losses in Fe-Co IEEE Access 2023

Session DC
2D SPINTRONICS AND TOPOLOGICAL MATERIALS III

Zhenchao Wen, Chair
National Institute for Materials Science (NIMS), Tsukuba, Japan

CONTRIBUTED PAPERS

DC-02. Quantum Transport in Sputtered Topological Semimetal α-Sn Thin Films. *V. Kalappattil*[1], C. Liu[1], M. Mehraeen[2], R. Li[2], Z. Chen[3], S. Zhang[2], K. Liu[3] and M. Wu[1] *1. Department of Physics, Northeastern University, Boston, MA, United States; 2. Department of Physics, Case Western Reserve University, Cleveland, OH, United States; 3. Department of Physics, Georgetown University, Washington, DC, United States*

Topological Dirac semimetals represent a relatively newly discovered topological quantum phase. In comparison with other topological Dirac semimetals, α-Sn is much more attractive since it's a single-element topological material and can transform into other topological phases, such as a Weyl semimetal or a topological insulator, under certain strain or field conditions[1,2]. Thin-film topological quantum materials are predominantly prepared by molecular-beam epitaxy and mechanical exfoliation, but those techniques are intrinsically incompatible with mature semiconductor technologies. In this work (111)-oriented thin films of topological Dirac semimetal α-Sn are grown on silicon, a common semiconductor substrate, by sputtering, a mainstream semiconductor growth technique, at a temperature achievable by cooling water. Transport measurements show for the first time the surface states-associated quantum oscillations in the α-Sn. The Berry phase deduced from the quantum oscillation data is 3.29 (or 1.05π). This value is close to π and thereby confirms the topologically non-trivial nature of the surface states. The data analyses revealed the effective mass, quantum lifetime, and quantum mobility of the TSS as 0.14 m_e, 0.343 ps, and 4500 cm^2/ (V.s) respectively. The transport data also reveal a negative magnetoresistance in the films, which has been theoretically predicted to occur in α-Sn as a result of the chiral anomaly but has never been experimentally observed. Taken together, the results demonstrate the first realization of epitaxy-grade thin-film topological materials via an integrable and scalable sputtering technique and pave the way for future applications of topological Dirac semimetal α-Sn in information control and storage devices in particular. This work has been supported partially by the U.S. Department of Energy (DE-SC0018994) and the U.S. National Science Foundation (DMR-2005108).

1. C.-Z. Xu, Y.-H. Chan, Y. Chen, P. Chen, X. Wang, C. Dejoie, M.-H. Wong, J. A. Hlevyack, H. Ryu, H.-Y. Kee, N. Tamura, M.-Y. Chou, Z. Hussain, S.-K. Mo, and T.-C. Chiang, Elemental Topological Dirac Semimetal: α -Sn on InSb(111), Phys. Rev. Lett. 118, 146402 (2017). 2. Y. Zhang, V. Kalappattil, C. Liu, S. S.-L. Zhang, J. Ding, U. Erugu, Z. Chen, J. Tian, K. Liu, J. Tang, and M. Wu, Large magneto-electric resistance in the topological Dirac semimetal α -Sn, Science Advances, 8 (30), eabo0052 (2022).

DC-03. Probing Intrinsic Magnetization Dynamics of the $Y_3Fe_5O_{12}/Bi_2Te_3$ Interface at Low Temperature. *A. Will-Cole*[1,2], V. Lauter[3], A.J. Grutter[4], C. Dubs[5], J.L. Hart[6], D.A. Lidsky[1], M. Lindner[5], T. Reimann[5], N. Bhattacharjee[2], T. Lu[1], P. Sharma[1], N.R. Valdez[1], C.J. Pearce[1], T.C. Monson[1], J. Cha[6], D. Heiman[2] and N.X. Sun[2] *1. Sandia National Laboratories, Albuquerque, NM, United States; 2. Northeastern University, Boston, MA, United States; 3. Oak Ridge National Laboratory, Oak Ridge, TN, United States; 4. National Institute of Standards and Technology, Gaithersburg, MD, United States; 5. Innovent, Jena, Germany; 6. Cornell University, Ithaca, NY, United States*

Topological insulator-magnetic insulator (TI-MI) heterostructures hold significant promise in the field of spintronics, offering the potential for manipulating magnetization through topological surface state-enabled spin orbit torque.[1] However, many TI-MI interfaces are plagued by issues such as contamination within the magnetic insulator layer and the presence of a low-density transitional region of the topological insulator. [2-4] These interfacial challenges often obscure the intrinsic behavior of the TI-MI system. In this study, we addressed these challenges by depositing sputtered Bi_2Te_3 on liquid phase epitaxy grown $Y_3Fe_5O_{12}/Gd_3Ga_5O_{12}$. The liquid phase epitaxy grown $Y_3Fe_5O_{12}$ has exceptional interface quality, without an extended transient layer derived from interdiffusion processes of the substrate or impurity ions, thereby eliminating rare-earth impurity-related losses in the MI at low temperatures. [5] At the TI-MI interface, high resolution depth-sensitive polarized neutron reflectometry confirmed the absence of a low-density transitional growth region of the TI. By overcoming these undesirable interfacial effects, we isolate and probe the intrinsic low-temperature magnetization dynamics and transport properties of the TI-MI interface. Our findings revealed strong spin pumping at low temperatures, accompanied by an additional in-plane anisotropy. The enhanced spin pumping at low temperatures is correlated with the observed suppression of bulk conduction and the weak-antilocalization in the TI film, highlighting the interplay between the transport and spin pumping behavior in the TI-MI system.

1. Y. Wang, and H. Yang, *Acc. Mater. Res.*, 3, 1061, (2022). 2. A. Mitra, O. Cespedes, Q. Ramasse, M. Ali, S. Marmion, M. Ward, R. M. D. Byrdson, C. J. Kinane, J.F.K. Cooper, S. Langridge, and B. J. Hickey, *Sci. Rep.*, 7, 11774 (2017). 3. J.F.K. Cooper, C. J. Kinane, S. Langridge, M. Ali, B. J. Hickey, T. Niizeki, K. Uchida, E. Saitoh, H. Ambaye, and A. Glavic, *Phys. Rev. B.,* 96, 104404 (2017). 4. L. Riddiford, A. Grutter, T. Pillsbury, M. Stanley, D. Reifsnyder Hickey, P. Li, N. Alem, N. Samarth, and Y. Suzuki, *Phys. Rev. Lett.*, 128, 126802, (2022). 5. A. R. Will-Cole, James L. Hart, Valeria Lauter, Alexander Grutter, Carsten Dubs, Morris Lindner, Timmy Reimann, Nichole R. Valdez, Charles J. Pearce, Todd C. Monson, Judy J. Cha, Don Heiman, and Nian X. Sun, *Phys. Rev. Materials*, 7, 054411, (2023).

INVITED PAPER

DC-05. Electronic Structure and Magnetism of Fe_3GaTe_2. *J. Lee*[1,2,3] *1. Advanced Light Source, Lawrence Berkeley National Laboratory, Berkeley, CA, United States; 2. Max Planck POSTECH, Pohang, The Republic of Korea; 3. Department of Physics, UC Berkeley, Berkeley, CA, United States*

A van der Waals (vdW) ferromagnet with a high Curie temperature (T_C) has been highly pursued, with the goals of understanding robust long-range spin orders in low-dimensional systems and exploring its potential application in spintronic devices. Among the known vdW ferromagnets, the newly discovered Fe_3GaTe_2 exhibits intrinsic ferromagnetism above room temperature, necessitating a detailed investigation into the microscopic origins of its ferromagnetism and the mechanism behind its higher T_C. Here, we present a comprehensive study of the electronic structure of Fe_3GaTe_2 in its ferromagnetic ground state and its temperature-dependent evolution using angle-resolved photoemission spectroscopy (ARPES) and theoretical calculations. Our results highlight two key observations: notable shifts in the chemical potential of Fe_3GaTe_2 compared to its sister material Fe_3GeTe_2, and significant band shifts around the Fermi level with temperature. Combined with theoretical calculations, we demonstrate the critical contribution of Heisenberg exchange interactions to developing high T_C ferromagnetic ordering in Fe_3GaTe_2. Furthermore, our study elucidates the distinct contributions to the ferromagnetism from Fe atoms in different sites, revealing a complex mixed nature of the localized and itinerant spin behaviors in Fe_3GaTe_2.

CONTRIBUTED PAPERS

DC-06. Emergent Spin Textures and Magnetoresistive Anomalies in Doped Fe_3GeTe_2: Unraveling Complexities in 2D Ferromagnets. *R. Roy Chowdhury*[1], H. Srikanth[1], R. Singh[2] and M. Phan[1] *1. Department of Physics, University of South Florida, Tampa, FL, United States; 2. Department of Physics, Indian Institute of Science Education and Research Bhopal, Bhopal, India*

Magnetism in two-dimensional (2D) van der Waals (vdW) materials has emerged as a new paradigm enunciating new condensed matter phenomena, with significant potential for advancing spintronic and quantum computing technologies [1]. Among 2D vdW ferromagnets, Fe_3GeTe_2 (FGT) stands out due to its high Curie temperature, distinctive uniaxial magnetic anisotropy, and the presence of an unusual magnetic ground state. However, consensus is lacking on the underlying micromagnetic interactions *viz.* magnetic anisotropy, exchange, dipole-dipole, and possible *Dzyaloshinskii–Moriya interaction*. These interactions are crucial for understanding the stabilization of the unusual magnetic ground state in FGT. Here, we elucidate the underlying physics responsible for the nontrivial ground state and demonstrate the ability to tune emergent properties by substituting elements at either magnetic (Fe) or nonmagnetic (Ge) sites. Single crystals of FGT, Co (45%) and As (40%) -doped FGT were grown by a chemical vapor transport method. Transverse resistivity measurements under H ∥ *c*-axis reveal a sizeable anomalous Hall effect, and H ⊥ *c*-axis exhibits unconventional magnetoresistive behavior with a prominent cusp-like feature respectively [2,3]. Radio-frequency transverse susceptibility (TS) measurements reveal a reduction in effective magnetic anisotropy field with Co/As-doping. Relative to FGT, the TS spectra of Co-doped FGT show significant broadening, indicating varying local distributions of anisotropy with doping at the magnetic site. While the TS spectra in both FGT and Co-doped FGT exhibit distinct asymmetries, indicative of a complex magnetic ground state at low temperatures, the introduction of As doping suppresses this asymmetry. This observation underscores the contrasting effect of non-magnetic doping on the magnetic order within FGT. Concomitant magneto-optical imaging confirms the presence of aggregates resembling skyrmion-like structures with sizes varying with the type and concentration of doping. Our findings advance the current understanding of emergent behaviors arising from intricate spin textures, holding promise for applications in topological magnetism and spintronic devices based on non-collinear spin textures.

[1] K. S. Burch *et al.*, *Nature* 563, 47 (2018). [2] R. Roy Chowdhury *et al.*, *Sci. Rep.* 11, 14121 (2021). [3] R. Roy Chowdhury *et al.*, *Phys. Rev. Mater.* 6, 014002 (2022).

DC-08. Exciton-Activated Giant Phonon Magnetic Moment in Monolayer MoS_2. *H. Mustafa*[3], G. Ye[1], C. Nnokwe[1], M. Fang[2], S. Chaudhary[6], D. Smirnov[4], J. Yan[5], K. Law[3], M. Mahjouri-Samani[3], K. Wu[1], E. Yang[2], G.A. Fiete[6], R. He[1] and W. Jin[3] *1. Texas Tech University, Lubbock, TX, United States; 2. Stevens Institute of Technology, Hoboken, NJ, United States; 3. Auburn University, Auburn, AL, United States; 4. National High Magnetic Field Laboratory, Tallahassee, FL, United States; 5. Towson University, Towson, MD, United States; 6. Northeastern University, Boston, MA, United States*

The concept of chirality has been extended to the description of circularly polarized phonons in which the atomic circular motions produce nonzero angular momentum. Transition metal dichalcogenides host chiral phonons at high symmetry points of the Brillouin zone, providing an ideal platform to explore the interplay between chiral phonons and valley degree of freedom through optical excitation. In this work, we present helicity-resolved magneto-Raman studies of monolayer MoS_2, in which a doubly degenerate chiral phonon mode is found at ~270 cm^{-1}. Our wavelength- and temperature-dependent measurements show that this chiral phonon is activated through the resonant excitation of A exciton. Under an out-of-plane magnetic field, the chiral phonon exhibits giant Zeeman splitting, which corresponds to an effective magnetic moment of ~2.5μ_B [1]. We attribute such effective magnetic moment to the coupling between the orbital excitation and the chiral phonon, forming hybrid orbital-lattice modes [2]. The hybrid states manifest themselves as the mode with primarily phononic character () at ~270 cm^{-1} and the mode with primarily electronic character (Ω_{ph}) at ~30 cm^{-1}. Our study provides important insights into lifting the chiral phonon degeneracy in an achiral covalent material, paving a route to excite and control chiral phonons.

[1] Chunli Tang *et al*., Phys. Rev. B 109, 155426 (2024) [2] S. Chaudhary *et al*., arXiv: 2306.11630v1 (2023)

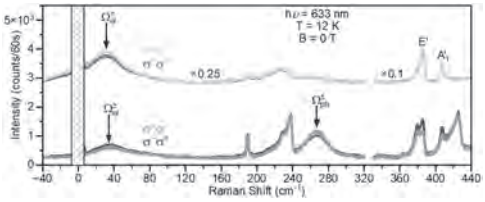

Fig.1. The helicity selection rule in monolayer MoS_2 is demonstrated in the on-resonant excitation of 633 nm (1.96 eV) at 12 K and zero external magnetic field. The helicity-conserved $\sigma^+\sigma^+$ (yellow) and $\sigma^-\sigma^-$ (green) channels show the widely studied E′ and A_1' phonon modes at ~384.3 cm^{-1} and ~405.4 cm^{-1}, respectively. The helicity-changed $\sigma^+\sigma^-$ (orange) and $\sigma^-\sigma^+$ (blue) channels show the doubly degenerate chiral phonon mode at ~270 cm^{-1}. In addition to the phonon modes, a low-frequency mode at ~35 cm^{-1} is observed in all four polarization configurations.

DC-09. Intrinsic Ferromagnetism in Liquid Phase Exfoliated 2D van der Waals $CrCl_3$. F.A. Silva[5,6,2], H. Chang[2], *L.A. Hernandez*[2], J.H. Warner[3], J.R. Fernandes[4], S.G. Santos[1,7], F.D. Magalhães[5,6], A.M. Pinto[5,6,1] and J.C. Incorvia[2] *1. Instituto de Investigação e Inovação em Saúde, Universidade do Porto, Porto, Portugal; 2. Electrical and Computer Engineering, University of Texas at Austin, Austin, TX, United States; 3. Mechanical Engineering, University of Texas at Austin, Austin, TX, United States; 4. Centro de Química Vila Real, Departamento de Física, Universidade de Trás-os-Montes e Alto Douro, Vila Real, Portugal; 5. Laboratory for Process Engineering, Environment, Biotechnology and Energy, Universidade do Porto, Porto, Portugal; 6. Associate Laboratory in Chemical Engineering, Universidade do Porto, Porto, Portugal; 7. Instituto de Engenharia Biomédica, Universidade do Porto, Porto, Portugal*

Transition metal trihalides, such as $CrCl_3$, are 2D van der Waals (vdW) materials with unique magnetic properties at the monolayer limit. Their intralayer ferromagnetism (FM) and interlayer antiferromagnetism (AFM) offer useful applications in low dimensional spintronics, optoelectronics, and biomedicine, since traditionally studied 2D materials lack intrinsic magnetism. Recent work on vdW $CrCl_3$ has focused on mechanical exfoliation, while liquid phase exfoliation (LPE) is still being explored and is important for solution-based applications like Magnetic Hyperthermia Therapy and MRI.[1] LPE with surfactant containing solutions, such as polyvinylpyrrolidone (PVP10) and sodium dodecyl sulfate (SDS), are used to exfoliate flakes from bulk $CrCl_3$ to lower the tendency to aggregate compared to that of IPA, NMP or urea. In this work,[2] 2D vdW $CrCl_3$ nanoflakes are produced through LPE using PVP10 and SDS and characterized through various means, with this presentation focusing on the magnetic properties. M vs. T measurements in Fig 1 show a FM phase transition below 50 K with an AFM transition at T_N = 15 K for both samples. A Curie-Weiss (CW) analysis shows a small difference in CW temperatures, $CrCl_3$ + PVP10 θ_{CW} = 33.29 K ± 1.90 K; $CrCl_3$ + SDS θ_{CW} = 29.12 K ± 1.25 K, and effective moments, $CrCl_3$ + PVP10 μ_{eff} = 4.20 μ_B ± 0.63 μ_B; $CrCl_3$ + SDS μ_{eff} = 3.95 μ_B ± 0.49 μ_B, closely aligning with recent work.[3,4] An XPS analysis confirms that deviations are attributed to other Cr ions present such as Cr(II) and Cr(VI). M vs. H loops indicate a significant moment is generated below ordering temperature as visualized in Fig 2, with a stronger magnetic susceptibility in $CrCl_3$ + PVP10 χ = 1.018 emu/mol-Oe than in $CrCl_3$ + SDS χ = 0.936 emu/mol-Oe at 5 K. Although both samples display positive θ_{CW}, it is evident that using PVP10 results in a larger magnetic susceptibility and harbors more intrinsic ferromagnetism than that of SDS.

1. L. S. Pires, F. D. Magalhães, and A. M. Pinto. *Polymers*. 14, 1464 (2022). 2. F. A. L. S. Silva, H. P. Chang, L. A. Hernandez, *et al*. *ACS Appl. Nano Mater.* In preparation. 3. N. Bykovetz, A. Hoser, and C. L. Lin. *AIP Advances*. 9, (3): 035029 (2019). 4. S. Mondal, *et al*. *Appl. Phys. Lett.* 117, 092405 (2020).

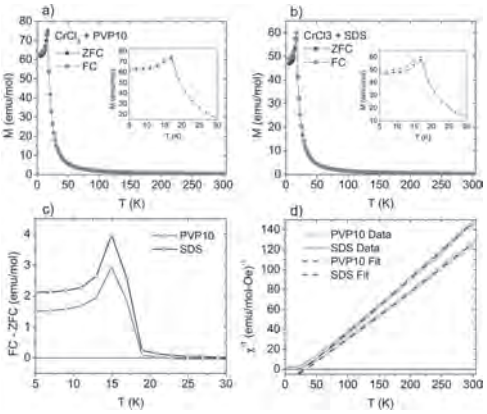

Fig 1. M vs. T for $CrCl_3$ a) + PVP10 and b) + SDS with *Insets:* a closer look at the phase transition. c) FC–ZFC plotted vs. T. d) Inverse Susceptibility vs. T with Curie-Weiss fits.

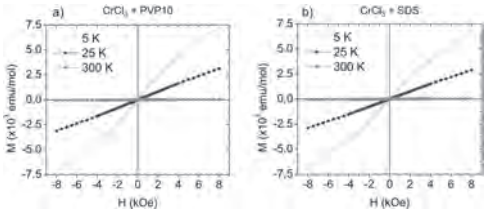

Fig 2. M vs. H for $CrCl_3$ a) + PVP10 and b) + SDS at 5 K, 25 K and 300 K.

DC-11. Gate-tunable ferromagnetic transport properties in monolayer graphene/Fe_3GeTe_2 heterostructures. *M. Aoki*[1], V. Zatko[1], T. Guillet[1], M. Shiraishi[2,4], J. Sierra[1] and S.O. Valenzuela[1,3] *1. Catalan Institute of Nanoscience and Nanotechnology, Barcelona, Spain; 2. Electronic Science and Engineering, Kyoto University, Kyoto, Japan; 3. Catalan Institution for Research and Advanced Studies, Barcelona, Spain; 4. CSRN, Kyoto University, Kyoto, Japan*

Van der Waals (VdW) heterostructures with graphene have attracted considerable interest due to the tunability of graphene's properties via the proximity effect[1]. Introducing magnetism into graphene by overlaying a ferromagnet (FM) is particularly intriguing. This graphene/FM heterostructure combines graphene's gate-tunability with the non-volatility of magnetization, creating multifunctional and reconfigurable devices. The recent discovery of VdW FMs, enabling atomically flat interfaces between graphene and FM, has further sparked interest in fundamental physics and applications for ultra-compact devices[2]. In this work, we investigate the magneto-transport properties of a heterostructure composed of monolayer graphene (MLGr) and the van der Waals ferromagnet Fe_3GeTe_2, encapsulated with hexagonal boron nitride. The heterostructure was fabricated using a dry transfer method and shaped into a Hall bar structure via reactive ion etching and e-beam lithography, followed by the creation of one-dimensional contacts[3]. The inset of Fig. 1 shows typical transversal resistance R_{xy} as a function of the out-of-plane magnetic field B. Alongside the ordinary Hall effect originating from MLGr, a hysteretic anomalous Hall effect (AHE) is observed. Figure 1 illustrates the AHE amplitude R_{AHE} at zero magnetic field as a function of the back-gate voltage V_g. Remarkably, the AHE is enhanced by more than a factor of 3 around the MLGr charge neutrality point (CNP), indicating strong tunability by electrostatic gating. The gate dependence of the AHE does not align with that of the resistance or the Hall effect, indicating that the increase of the AHE cannot be explained by either the modulation of current distribution or the interplay between the Hall effect and the stray field. In this presentation, I will discuss the origin of the gate-tunable AHE. This work is supported by MICIU/AEI/10.13039/501100011033 through Grant No. PID2022-143162OB-I00. M.A. acknowledges financial support from the JSPS Overseas Research Fellowship.

[1] J. F. Sierra, J. Fabian, R. K. Kawakami, S. Roche and S. O. Valenzuela, Nature Electronics, Vol. 16, p. 856 (2021). [2] B. Huang, M. A. McGuire, A. F. May, D. Xiao, P. Jarillo-Herrero and X. Xu, Nature Materials, Vol. 19, p. 1276 (2020). [3] L. Wang, I. Meric, P. Y. Huang, Q. Gao, Y. Gao, H. Tran, T. Taniguchi, K. Watanabe, L. M. Campos, D. A. Muller, J. Guo, P. Kim, J. Hone, K. L. Shepard and C. R. Dean, Science, Vol. 342, p. 614 (2013).

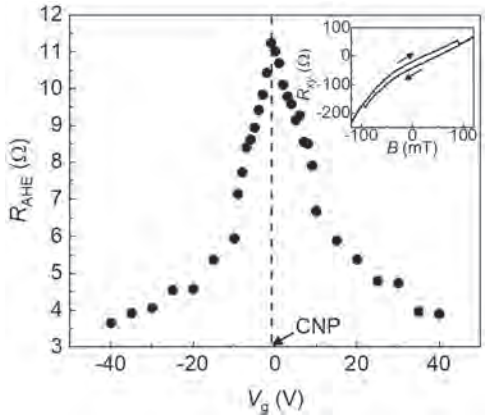

Fig.1. R_{AHE} as a function of V_g. Inset: R_{xy} as a function of B at V_g = 0 V. Measurements were implemented at 100 K.

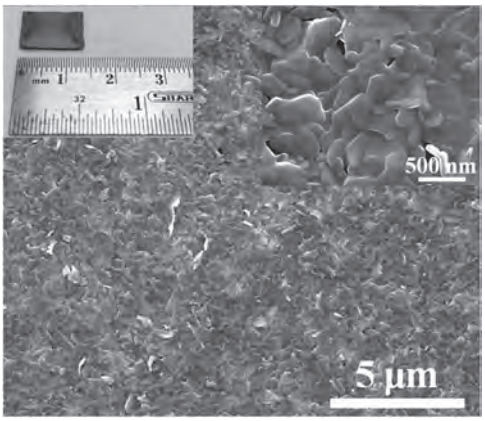

Fig.1 SEM image of VSe_2 thin film on Si/SiO_2 substrate. Inset shows a CVD-grown sample (~ 1cm × 1cm).

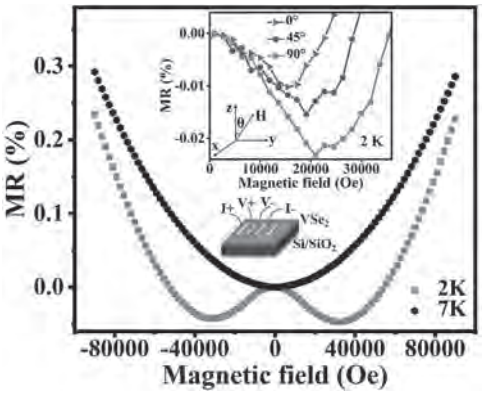

Fig.2 Negative MR at low fields observed at 2K, diminishes at higher temperature (7 K). Inset shows dependence of MR (at 2 K) for different angles between applied field and sample surface.

DC-12. Kondo Effect in CVD-Grown Large Area Continuous 2D VSe_2 Thin Film. *V. Samanta*[1] and S. Chandran[1] *1. Physics, Indian Institution of Technology Madras, Chennai, India*

Two-dimensional (2D) transition metal dichalcogenides have attracted significant research interest across diverse fields, including electronics, spintronics and energy applications. Recently, VSe_2 has garnered extensive attention due to its unique physical and chemical properties, such as high electrical conductivity [1], charge density wave (CDW) [1] and intrinsic ferromagnetism in mono to few-layers [2], distinct from bulk form. However, synthesizing high-quality continuous 2D VSe_2 thin film for potential applications remains a significant challenge. Here, we present a method to grow a large area (~ 1cm × 1cm), continuous 1T-VSe_2 thin film on Si/SiO_2 by chemical vapor deposition (CVD). Structural and spectroscopic analyses indicate a highly crystalline thin film with no impurity phases. Scanning electron microscopy images confirm the continuous growth of VSe_2 on the substrate with a uniform distribution of V and Se elements throughout the film. Temperature-dependent resistivity measurements using the four-probe method show the metallic nature of 1T-VSe_2, with an anomaly around 100 K attributed to CDW ordering [1]. Low temperature magneto-transport studies demonstrate the presence of Kondo effect in metallic multilayer VSe_2 thin film. The localized magnetic moments, mainly originating from the interlayer V ions, play a crucial role in scattering of conduction electrons in Kondo effect [3]. The presence of Kondo effect is confirmed by observing negative magnetoresistance (MR) at low magnetic field (< 4T) below Kondo temperature. This negative MR is observed irrespective of the magnetic field's orientation relative to the electric current, confirming the isotropic nature of the Kondo effect. Moreover, VSe_2 thin film exhibits soft ferromagnetic behaviour at room temperature, likely originating from the interlayer V ions. The large area continuous VSe_2 thin film holds promise for next-generation electronics and spintronic devices.

[1] Y. Xue, Y. Zhang, H. Wang, *Nanotechnology*, vol. 31, p. 1-8 (2020) [2] M. Bonilla, S. kolekar, Y. Ma, *Nat. Nanotechnol.*, vol. 13, p. 289–293 (2018) [3] S. Barua, M. C. Hatnean, M. R. Lees, *Sci. Rep.*, vol. 7, p. 1-10 (2017)

Session DD
DOMAIN WALLS AND SKYRMIONS II

Christopher Marrows, Chair
University of Leeds, Leeds, United Kingdom

INVITED PAPER

DD-01. Highly efficient current-driven magnetic octupole domain-wall motion in noncollinear antiferromagnets. *Y. Otani[1,2,3] 1. ISSP, University of Tokyo, Kashiwa, Japan; 2. CEMS, RIKEN, Wako, Japan; 3. Trans-Scale Quantum Science Institute, University of Tokyo, Tokyo, Japan*

Antiferromagnets (AFMs) have the natural advantages of terahertz spin dynamics and negligible stray fields, thus appealing for domain-wall applications. However, it has been challenging due to their insensitive magneto-electric responses. Recent research on noncollinear chiral AFMs Mn_3X (X = Sn, Ge) enabled us to detect and manipulate their magnetic octupole domain states. Here, we demonstrate a current-driven fast magnetic octupole domain-wall (MODW) motion in Mn_3X. The magneto-optical Kerr observation reveals the Néel-like MODW of Mn_3Ge can be accelerated up to 750 m s^{-1} with a current density of only 7.56×10^{10} A m^{-2} under no magnetic field. The MODWs show extremely high mobility with a small critical current density. Moreover, our theory reveals that the MODW motion in noncollinear AFMs is driven by the spin-transfer torque derived from the current-induced nonequilibrium spin accumulation. Our results open a new route to developing a mechanism for antiferromagnetic domain-wall-based applications.

1. M. Wu, K. Kondou, Y. Nakatani, T. Chen, H. Isshiki, T. Higo, S. Nakatsuji, & Y. Otani, "Magnetic octupole domain evolution and domain-wall structure in the noncollinear Weyl antiferromagnet Mn_3Ge", APL Mater. 11, 081115 (2023). 2. M. Wu1, T. Chen1, T. Nomoto, H. Isshiki, Y. Nakatani, T. Higo, T. Tomita, K. Kondou, R. Arita, S. Nakatsuji, & Y. Otani, "Current-driven fast magnetic octupole domain-wall motion in noncollinear antiferromagnets", Nature Communications 15, 4305 (2024)

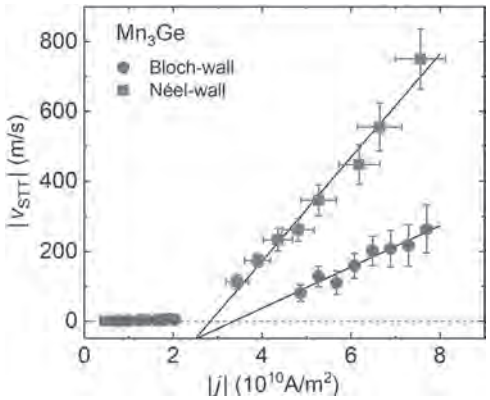

Figure 1: Bloch- and Néel- like MODW speeds $|v_{STT}|$ as a function of the injected current in |j| in Mn_3Ge.

CONTRIBUTED PAPERS

DD-02. Numerical calculations of collective octupole dynamics in noncollinear antiferromagnets. *M. Yoo[1]* and A. Hoffmann[1] *1. University of Illinois at Urbana-Champaign, Urbana, IL, United States*

$D0_{19}$-type noncollinear antiferromagnets, such as Mn_3Sn and Mn_3Ge, exhibit significant transport and optical responses despite their negligible net magnetization [1, 2]. These properties are governed by the orientation of the magnetic octupole moment, which is analogous to the magnetic dipole moment in ferromagnets [3]. In general, the static and dynamic behavior of octupole moments has been studied by numerical calculations using atomistic models [4, 5]. However, the study of non-uniform octupole configurations in submicron or larger systems is practically challenging due to computational limitations. In this study, we investigate the collective dynamics of octupoles in non-uniform configurations by adapting a micromagnetic approach. First, we derived a governing equation for the collective octupole vector and the exchange interaction among the octupoles, analogous to the micromagnetic models in ferromagnetic systems [Fig. 1]. Using the results, we numerically calculated the profiles and dynamics of the domain walls in the micrometer scale [Fig. 2]. The results are in good agreement with the numerical results obtained from the atomistic-spin model. Our study improves the theoretical understanding of non-uniform configurations in micrometer-scale antiferromagnets, and furthermore paves the way for the development of next-generation spintronic devices using non-collinear antiferromagnets. This work is supported by the NSF through the Illinois MRSEC (DMR-1720633).

[1] S. Nakatsuji et al., Nature Vol. 527, p.212 (2015) [2] T. Higo et al., Nat. Photonics Vol. 12, p.73 (2018) [3] T. Chen et al., Nat. Commun. Vol. 12, p.572 (2021) [4] S. Sugimoto et al., Commun. Phys. Vol. 3, p.111 (2020) [5] H. Tsai et al., Nature Vol. 580, p.608 (2020)

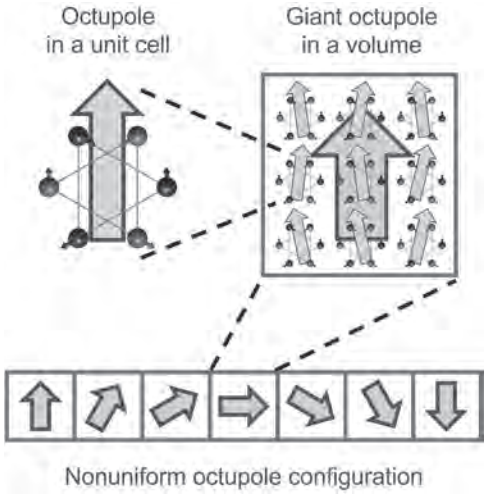

Schematic of the micromagnetic model for noncollinear antiferromagnets.

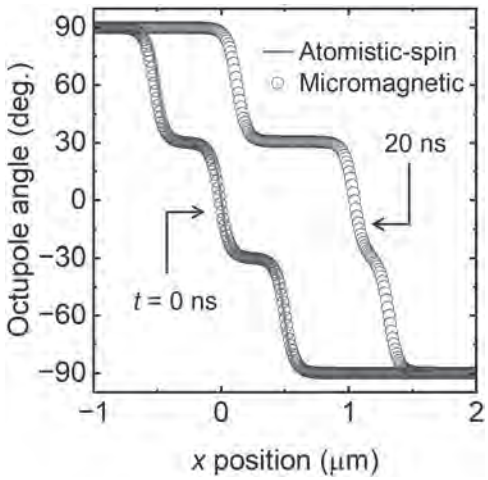

180° domain wall profiles calculated from the atomistic-spin model (line) and the micromagnetic model (symbol) at the initial state (t = 0 ns) and during the motion under the y-directional field, $\mu_0 H_y$ = 1 mT, at t = 20 ns.

DD-03. Direct Evidence for Magnetic Bloch Point Quadrupoles Constituting Hybrid Topological Strings. *F.S. Yasin*[1,2], J. Masell[3,2], Y. Takahashi[4], T. Akashi[4], N. Baba[5], K. Karube[2], D. Shindo[2], T. Arima[2,6], Y. Taguchi[2], Y. Tokura[2,7,8], T. Tanigaki[4] and X. Yu[2] *1. Center for Nanophase Materials Sciences, Oak Ridge National Laboratory, Oak Ridge, TN, United States; 2. Center for Emergent Matter Science, RIKEN, Wako, Japan; 3. Institute of Theoretical Solid State Physics, Karlsruhe Institute of Technology (KIT), Karlsruhe, Germany; 4. Research and Development Group, Hitachi Ltd., Hatoyama, Japan; 5. Research Institute for Science and Technology, Kogakuin University, Hachioji, Japan; 6. Department of Advanced Materials Science, University of Tokyo, Tokyo, Japan; 7. Department of Applied Physics, University of Tokyo, Tokyo, Japan; 8. Tokyo College, University of Tokyo, Tokyo, Japan*

We employ off-axis electron holography configured for vector field electron tomography (VFET) [1,2] to image the 3D structure of a hybrid antiskyrmion present in an $(Fe_{0.63}Ni_{0.3}Pd_{0.07})_3P$ nanoplank at room temperature and zero field. These measurements unveil four (anti)BPs present along the antiskyrmion's Bloch lines which topologically transform the hybrid texture from skyrmion at the surfaces to antiskyrmion within the bulk of the nanoplank. Slices of the 3D magnetic field of a micromagnetically simulated skyrmion, antiskyrmion, and hybrid antiskyrmion are shown in Fig. 1. The dipole-dipole energy facilitates the Néel domain wall twists at the textures' surfaces linking the spin textures' cores and peripheral spins to form a dipole flux-closure. As shown in the xy-slices of the antiskyrmion (Fig. 1e-g), however, the presence of Bloch lines near the surface drives the domain walls to severely deform. Hybrid antiskyrmion strings exhibit no such deformation due to the transition to surface skyrmion textures, and our energy density calculations reveal that these hybrid textures are the lowest energy spin texture configuration in this uniaxial ferromagnet for a wide range of applied magnetic fields and sample thicknesses. These calculations suggest that the dipolar and DMI energy terms are leading contributors in stabilizing topologically complex hybrid antiskyrmions over their conventional counterparts, and that the thickness-averaged topological charge may be tuned via application of an external magnetic field or with varying thickness [3].

[1] G. Lai, T. Hirayama, A. Fukuhara, K. Ishizuka, T. Tanji, and A. Tonomura, Journal of Applied Physics 75, 4593 (1994). [2] S. J. Lade, D. Paganin, and M. J. Morgan, Optics Communications 253, 382 (2005). [3] F. S. Yasin et al., Advanced Materials 36, 2311737 (2024).

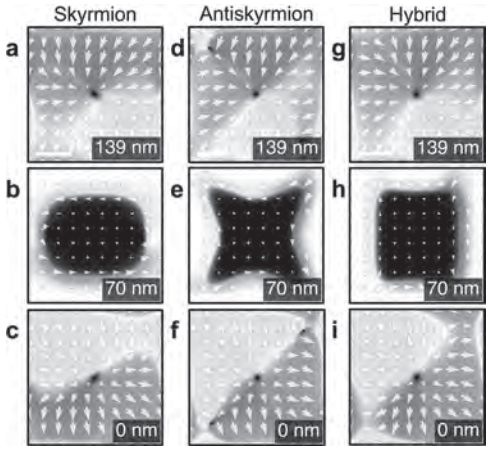

Figure 1. Comparison of simulated spin textures. Selected slices of the simulated magnetic field for a (a-c) skyrmion string, (d-f) antiskyrmion string and (g-i) hybrid antiskyrmion string. The -slices at the (a, d, g) top surface, (b, e, h) middle, and (c, f, i) bottom surface are plotted side by side for comparison. Note the deformation at the antiskyrmion string's center (e) induced by the domain walls pinching along opposing Bloch lines at the antiskyrmion string's surfaces (d, f). Scalebars 100 nm. Reprinted with permission from the supplementary information of [3], Figure S2.

DD-04. Spin Textures and Magnetization Dynamics in Cylindrical Nanowires. *L. Perez*[1,2], L. Gómez-Cruz[2], L. Álvaro-Gómez[1], S. Ruiz Gómez[3], C. Fernandez Gonzalez[3], L. Aballe[3], E. Pereiro[3], N. Mille[4], R. Belkhou[4], C. Thirion[5], D. Gusakova[6], A. Masseboeuf[6] and O. Fruchart[6] *1. Física de Materiales, Universidad Complutense de Madrid, Madrid, Spain; 2. Fundación IMDEA Nanociencia, Madrid, Spain; 3. Alba Synchrotron, Cerdanyola del Valles, Spain; 4. Synchrotron SOLEIL, Gif-sur-Yvette, France; 5. Univ. Grenoble Alpes, CNRS, Institut Neel, Grenoble, France; 6. SPINTEC, Grenoble, France*

Magnetic cylindrical nanowires provide an optimal platform for exploring 3D nanomagnetism. In such systems, magnetostatic interactions induce curling magnetization [1], which is reflected both in the spin textures of domains [2] and in domain walls (DWs), such as in the Bloch Point Wall (BPW) [3]. Therefore, a significant impact of the Oersted field is expected when driving these systems by current pulses, and this impact is strongly influenced by the spin textures stabilized in the nanowires. We have explored Permalloy cylindrical nanowires with periodic $Fe_{70}Ni_{30}$ chemical modulations with two different diameters: 120 nm, where the magnetization is axial in the domains, and 200 nm, which displays azimuthal domains. For the case of lower diameter nanowires, we focus our investigation on the interplay between the magnetization curling in the chemical modulations and in the DWs. This interaction strongly depends on their relative magnetization circulation, being attractive when both magnetic textures have the same circulation and repulsive in the opposite case, paving the way towards using chemical modulations as polarizers for DWs. Additionally, when a current pulse is injected through the system, the circulation of the Oersted field impacts both the modulation and DW, which allows us to propose the use of nanowires in logic devices. When driving DW motion by current pulses in systems with axial magnetization, it is difficult to disentangle the effects of spin-transfer torque, the Oersted field, and Joule heating on magnetization dynamics. Therefore, we have also studied larger-diameter nanowires, which display azimuthal domains. In such systems, the effect of the Oersted field is enhanced. We have observed deterministic DW motion driven by nanosecond current pulses with an amplitude as low as 10^{10} A/m^2, which is two orders of magnitude lower than previously reported in the literature [4], with DW speeds up to 2 km/s. Our results clearly demonstrate that the Oersted field is the main driving force of domain wall dynamics in these systems.

[1] Laura Álvaro-Gómez et al. Phys. Rev. B 106 054433 (2022) [2] Sandra Ruiz-Gómez et al. Nanoscale 12, 17880 (2020) [3] S. da Col et al. Phys. Rev. B. 89 180405 (2014) [4] M. Schöbitz, et al. Phys. Rev. Lett. 123 217201 (2019).

DD-05. Complex dynamics of Bloch point domain walls in cylindrical magnetic nanowires. *O. Chubykalo-Fesenko*[1], E. Saugar[1], F. Tejo[2] and K. Gusliyenko[3] *1. Instituto de Ciencia de Materiales de Madrid, CSIC, Madrid, Spain; 2. Universidad Central de Chile, Santiago de Chile, Chile; 3. Universidad del Pais Vasco, San Sebastian, Spain*

Magnetic cylindrical nanowire are promising candidates for future 3D nanoscale applications such as Internet of nanothings. Thus, it is important to understand the possibility to manipulate domain wall dynamics in cylindrical geometry, which are different from that in planar nanostripes. Indeed, cylindrical magnetic nanowires possess a very special topologically non-trivial domain wall of the Bloch point type (BP-DW)[1]. It has a large mobility in response to external magnetic field [2] Also, in cylindrical geometry the absence of the Walker breakdown phenomenon has been predicted [1] and thus, very high velocities can be expected. On the other hand, recent simulations and experiments [3] have shown that during dynamics the BP-DW is converted to the vortex-antivortex (V-AV) domain wall. Thus, the possibility to drive stationary BP-DWs in cylindrical geometry is an open question which we discuss here. Our analytical approach, based on the Thiele equation and a rigid ansatz, allows to conclude that BP-DW has non-zero gyrovector. Consequently, it cannot move straight with a steady velocity and escapes towards the nanowire surface. The escape time depends on the material parameters and nanowire geometry. In simulations this corresponds to the BP-DW conversion into the V-AV domain wall. Under applied field, the V-AV pair rotates around the nanowire and the DW velocity is low [4]. A remarkable effect occurs for higher fields, especially for nanowires with large saturation magnetisation [5]. Simulations show that BP-DW acquires a conical shape with the Bloch point at the cone vertex. Under applied field the DW cone elongates. The obtained DW velocities are much higher than the "magnonic limit", estimated in Fe close to 2 km/s. We associate the giant velocities (up to 14km/s in Fe) to the jet-propulsion effect by a constant ejection of new Bloch points from DW (see Figure).

[1] R. Hertel, J. Phys.: Condens. Matter 28, 483002 (2016) [2] R. Wieser, et al, Phys. Rev. B 69, 064401 (2004) [3] A. Wartelle, et al Phys. Rev. B 99, 024433 (2019) [4]G. H. R. Bittencourt et al J.Appl. Phys 135, 063906 (2024) [5] F. Tejo et al Nanosclale 2024, 16, 10737 (2024)

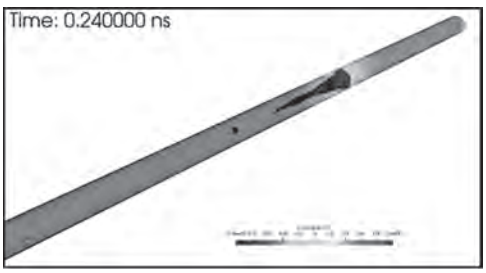

Snapshot of domain wall dynamics in Fe cylindrical nanowire of 60 nm diameter under applied field B=60mT, showing the conical shape and and ejection of a pair of Bloch points.

DD-06. Energy Landscape and Pinning Fields of Bloch-Point Domain Walls in Curved Nanowires. *C. Abert*[1], S. Ruiz-Gomez[2,3], P. Morales Fernandey[2], S. Koraltan[1], L. Danesi[1], A. Hierro-Rodriguez[5], A. Fernández-Pacheco[4], C. Donnelly[2] and D. Suess[1] *1. University of Vienna, Vienna, Austria; 2. Max Planck Institute for Chemical Physics of Solids, Dresden, Germany; 3. ALBA Synchrotron Light Source, Barcelona, Spain; 4. TU Wien, Vienna, Austria; 5. Universidad de Oviedo, Oviedo, Spain*

Soft-magnetic nanowires can promote the formation of stabl e Bloch-point domain walls depending on their material parameters and size. Motivated by experimentally measured pinning fields in curved nanowires [1], we investigate the energy landscape and pinning by means of micromagnetic simulations. In the context of numerical micromagnetics, the singular nature of the Bloch point requires special care since it violates the prerequisite of a smooth magnetization distribution that is assumed in the micromagnetic theory. Depending on the discretization strategy this has various implications that have to be handled carefully. In the case of finite-difference micromagnetics, simulations are based on a regular mesh with a mesh size usually chosen in the dimension of the matierial's exchange length. This discretization underestimates the magnetization gradient of the Bloch point and thus its energy. As a consequence, this modeling approach also underestimates pinning effects at the atomic lattice [2]. In the case of finite-element micromagnetics, simulations are based on an irregular mesh. This allows for the accurate modeling of curved surfaces as required by the investigated nanowires. However, due to varying cell sizes of the mesh, the energy of the Bloch point strongly fluctuates depending on its position leading to spurious pinning sites. In this work, we combine finite-difference simulations with finite-element simulations to obtain a complete picture of domain wall pinning effects in curved nanowires due to curvature, see Fig. 1, and lattice pinning, see Fig. 2. Our simulations match the experimental findings obtained on Cobalt nanowires with varying curvature and deliver a deep understanding for the origin of the different contributions that act as pinning sources.

[1] Ruiz-Gomez, Sandra, et al. "Tailoring the energy landscape of a Bloch point singularity with curvature." *arXiv preprint arXiv:2404.06042* (2024). [2] Kim, Se Kwon, and Oleg Tchernyshyov. "Pinning of a Bloch point by an atomic lattice." *Physical Review B—Condensed Matter and Materials Physics* 88.17 (2013): 174402.

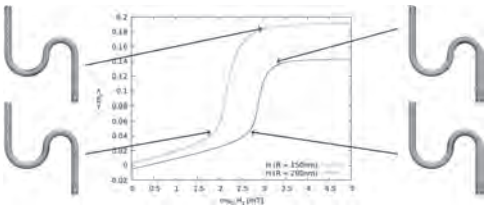

Depinning of Bloch-point domain walls in curved nanowires. The wall pins in the streigth part of the wire. Pinning depends on the radius of the curvature and increases with decreasing radius.

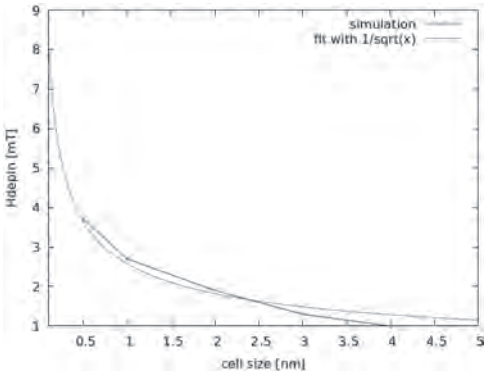

Finite-difference simulation of the lattice pinning of a Bloch-point wall in a straight nanowire using different cell sizes.

DD-07. Current-induced domain wall dynamics for Fe-based amorphous microwires. E. Calle[1], M. Vázquez[2] and *R. Perez Del Real*[2] *1. Universidad Autónoma de Madrid, Madrid, Spain; 2. Institute of Materials Science of Madrid, Madrid, Spain*

The propagation of a single domain wall (DW) is crucial for enhancing DW logic devices. Fe-rich amorphous glass-coated microwires are ideal for this study as their magnetization involves a single DW moving at velocities over 1 km/s [1]. While many studies focus on DW dynamics under an axial magnetic field, few address applied current [2,3]. This work examines DW dynamics with current pulses. The microwire here studied ($Fe_{75}Si_{10}B_{15}$, 18,6 mm of metallic nucleus, 21,6 mm total diameter and 42 cm length) shows an intrinsic torsion related to their manufacturing process, as a result of which the application of a current induces a change in the longitudinal component of magnetization. Depending on whether the orientation of the circular field is parallel or antiparallel to the Mφ component of the domain, the application of a current to the microwire (constant for the duration of wall propagation) results in an increase or decrease in the velocity of the DW with respect to its value in absence of current (a bias DC magnetic field is applied as well). Besides, the ability to induce wall movement has been shown under the action of only a current pulse applied to the wire when the pulse magnitude is above a certain threshold value (7.3 mA). The study of the dynamics of the wall has revealed the existence of two propagation regimes. For current pulse amplitudes below 10 mA, the velocity shows a dependence on the pulse width that can be described by a power law, corresponding to an intermittent movement of the wall as a consequence of the strong interaction with the defects, so analogous to what occurs in the low axial field regime. For higher amplitudes above 10 mA, the velocity increases linearly with the current, as also happens in the viscous regime of motion induced by axial field. The mobility obtained in the case of the viscous regime turns out to be approximately 8 times less in the case of current-induced motion than in the case of movement induced by axial field. This difference is expected due to the predominantly axial magnetoelastic anisotropy caused by tensile stresses in the metallic core.

[1]] H. Chiriac and T. A. Ovari, Prog. Mat. Sci. 40(5), 333 (1996) [2] V. Zhukova, J. M. Blanco, A. Chizhik, M. Ipatov and A. Zhukov, AIP Advances 7, 056026 (2017) [3] S. Corodeanu, H. Chiriac, A. Damian, N. Lupu, T. Óvári, Sci. Rep. 9, 5868 (2019)

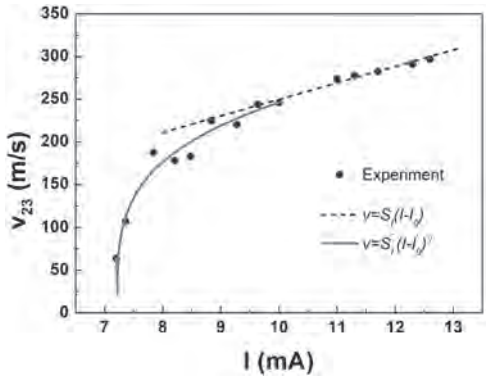

Fig 1. Domain wall velocity as a function of the applied current

INVITED PAPER

DD-08. Helimagnet-Based Spintronics: Control and Detection of Magnetic Chirality. *H. Masuda*[1] *1. Institute for Materials Research, Tohoku University, Sendai, Japan*

Helimagnetic structures, in which the magnetic moments are spirally ordered, host an internal degree of freedom called chirality (or helicity) corresponding to the handedness of the spiral (Figure 1). Since the chirality does not couple to the magnetic field and is invariant under any translation and rotation, it seems quite robust against disturbances and is therefore promising for next-generation magnetic memory. Chiraity control was recently achieved in a centrosymmetric metallic helimagnet MnP by the magnetic field sweep with the application of an electric current at low temperatures [1]. Although this result implies the possibility of spintronics based on helimagnetic chirality, problems such as cumbersome control and detection methods, low working temperatures, and the microfabricated bulk form of the sample have to be solved for practical applications. In this study, utilizing an epitaxial film of room-temperature helimagnetic conductor $MnAu_2$, we demonstrate the chirality switching by the electric current pulses under magnetic fields [2]. Moreover, we have succeeded in detecting the chirality at zero magnetic fields by means of simple transverse resistance measurement in a bilayer device composed of $MnAu_2$ and a spin Hall material Pt, utilizing the spin accumulation effect arising from the spin Berry phase. The simplified control and detection methods, theroom-temperature operation, and the thin film form of the device may pave the way to future helimagnet-based spintronics.

[1] N. Jiang, Y. Nii, H. Arisawa, E. Saitoh, Y. Onose, Nat. Commun. 11, 1601 (2020). [2] H. Masuda, T. Seki, J. Ohe, Y. Nii, H. Masuda, K. Takanashi, Y. Onose, Nat. Commun. 15, 1999 (2024).

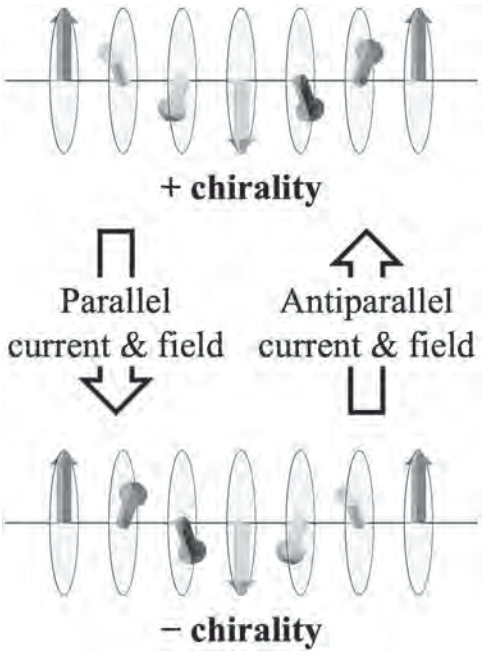

Figure 1. Concept of the helimagnet-based spintronics. Chirality, the handedness of the helimagnetic spiral, is controlled by the electric current and the magnetic field.

CONTRIBUTED PAPERS

DD-09. Decoupling the influences of chiral damping and Dzyaloshinskii-Moriya interaction in chiral magnetic domain walls.
C.A. Akosa[1,2,3], G. Tatara[2], A. Manchon[4] and M. Mochizuki[1] *1. Applied Physics, Waseda University, Tokyo, Japan; 2. CEMS, RIKEN, Wako, Japan; 3. Theoretical & Applied Physics, AUST, Abuja, Nigeria; 4. CNRS, CINaM, Aix-Marseille Université, Marseille, France*

We revisit the nature and impact of both the chiral damping (CD) and Dzyaloshinskii-Moriya interaction (DMI) in uniaxial chiral ferromagnetic nanowires with broken inversion symmetry. We propose that CD, akin to its chiral energy counterpart (DMI), can be described in terms of the Lifshitz invariants permissible by the underlying symmetry of the system. This representation offers a clearer foundation for integrating CD into the dynamics of various chiral magnetic textures. We theoretically investigate the current-induced motion of chiral domain walls (DWs), driven by both spin-transfer torque and the spin Hall effect in the presence of CD. We demonstrate that it is possible to unambiguously separate the influence of CD from that of DMI by analyzing the current-induced dynamics. In particular, below the Walker breakdown (WB), the DMI does not affect the DW velocity, whereas increases in the strength of CD result in a decrease in the DW velocity. Moreover, for the spin- orbit torque driven motion, while the DMI enhances both the WB current density and the maximum attainable velocity below the WB, the CD only enhances the WB without affecting the maximum attainable velocity below the WB. Our findings open up intriguing opportunities for exploitation in exotic magnetic textures.

C. A. Akosa, G. Tatara, A. Manchon, and M. Mochizuki, Phys Rev. B 110, 024420 (2024).

DD-10. X-ray Scattering Studies on the Phase Transitions of the Nematic Magnetic Helical Phase in Amorphous FeGe.
Z. Tumbleson[4,1], S.A. Morley[1], E. Hollingworth[2], A. Singh[1], T. Bayaraa[1], N. Burdet[3], A. Us-Saleheen[1], M. McCarter[1], D.W. Raftrey[4,1], R. Pandolfi[1], V. Esposito[3], G. Dakovski[3], F. Decker[3], A. Reid[3], T. Assefa[3], P. Fischer[1,4], S. Griffin[1], S. Kevan[1], F. Hellman[2,1], J.J. Turner[3] and S. Roy[1,4] *1. Lawrence Berkeley National Laboratory, Berkeley, CA, United States; 2. University of California, Berkeley, Berkeley, CA, United States; 3. SLAC National Accelerator Laboratory, Menlo Park, CA, United States; 4. University of California, Santa Cruz, Santa Cruz, CA, United States*

A nematic phase describes a system in which translational symmetry is preserved while orientational symmetry is broken. While ubiquitous in the research field of liquid crystals, the extension of this phase to magnetic systems is extremely limited. Here, I present on the thermodynamic phase transitions of the helical phase of amorphous FeGe and show that there exists striking similarities between magnetic helices and nematic directors when viewed through the lens of liquid crystals. I will present coherent X-ray scattering results that directly probe the spatio-temporal order parameters of the magnetic spin texture.

DD-11.Withdrawn

Session DE
SPINTRONIC DEVICES I: MRAM, SENSOR AND ENERGY EFFICIENT COMPUTING

Deyuan Lyu, Chair
University of Minnesota, Minneapolis, MN, United States

INVITED PAPER

DE-01. Magnetics for the next-computing era. *K. Lee*[1] *1. Samsung Electronics, Yongin-si, The Republic of Korea*

The rapid evolution of computing technologies demands innovative solutions to address the increasing need for performance, efficiency, and data storage. Magnetic materials and devices are poised to play a pivotal role in the next computing era, offering promising advancements in several key areas. This talk reviews the roles and potentials of magnetics and spintronics to enablethe next-generation energy-efficient computing solutions for edge AI and data center applications, including spin-transfer-torque MRAM (STT-MRAM), magnetic inductor, and spin-based probabilistic computing. Foredge AI, the rend of software-defined vehicles (SDV) and the use of STT-MRAM represent signifcant advancedments in the automotive industry. Due to small cell size, reliable operations at 150C and high endurance > 1M cycles, STT-MRAM is well-positioned to supportvarious automotive grade-1 applications in the SDV era [1], providing the best embedded non-volatile memory (eNVM) solution for code/data storage at FinFET nodes. For data center applications, we are also looking at various opprotunities for magnetics fromthe point of optimizing the system-level power consumption. Integrated voltage regulators equiped with embedded magnetic inductors are likely to become one of the key technology elements for future data center applications. High-bandwidth and low-power STT-MRAM with nearly unlimited endurance [2] can also pave a way for energy-efficient AI computing by minimizing IO transactions between computing units and external memory. Lastly, we also review the potential of the latest advanced spintronics such as spin-basedprobablistic computing from the viewpoint of energy efficiency.

[1] Kangho Lee, et al., "22-nm FD-SOI Embedded MRAM Technology for Low-Power Automotive-Grade-l MCU Applications, "IEDM 2018 [2] T. Y. Lee, et al., "World-most energy-efficient MRAM technology for non-volatile RAM applications," IEDM 2022

CONTRIBUTED PAPERS

DE-02. Exploring Ge_xSn_yTe for Energy-Efficient Computing Devices Using Ferroelectric Rashba Semiconductors. *F. Fagiani*[1], L. Nessi[1], G. Gandini[1], S. Cecchi[2], F. Delodovici[4], G. Vinai[3], I. Vobornik[3], K. Rohit[5], A. Rubano[5], M. Fiebig[6], S. Picozzi[4], M. Cantoni[1], R. Bertacco[1] and C. Rinaldi[1] *1. Physics, Politecnico Milano, Milano, Italy; 2. Università Bicocca, Milano, Italy; 3. CNR-IOM, Trieste, Italy; 4. CNR-SPIN, Chieti, Italy; 5. Università Federico II, Napoli, Italy; 6. ETH Zürich, Zurigo, Switzerland*

The energy consumption of information and communication technology is predicted to reach 50% of the total electricity produced yearly by 2040: a trend that dictates an acceleration toward beyond-CMOS technologies. A thrilling path towards super energy efficient non-volatile transistors was proposed by Intel [1], suggesting non-volatile devices that exploit collective phenomena such as ferroelectricity and ferromagnetism, and endowed with spin-based read-out mechanisms for computing. Such a transition is a tough journey that requires significant material advancements to ensure high performance and controllability [2]. Ferroelectric Rashba semiconductors (FERSC) stand out as materials endowed by non-volatility, voltage control and spin-based processing capability. We demonstrated that ferroelectric polarization in epitaxial thin films of GeTe can be reversed by electric pulses, and this, in turn, changes the sign of the spin-to-charge current conversion (S2CCC) of the semiconductor, enabling the realization of the so-called ferroelectric spin-orbit transistor [3,4]. However, achieving low switching voltage and large S2CCC is crucial for applications. Here, we show that alloying GeTe and SnTe in the ternary $Ge_xSn_{(1-x)}Te$ allows for engineering the band structure, ferroelectric properties and S2CCC. The giant Rashba effect in GeSnTe persists above room temperature (Fig. 1) [5]. The inclusion of tin allows to reduce the ferroelectric switching field, that can enter the sub-1V range, as demonstrated by electro-resistance measurements (Fig. 2). Preliminary spin transport measurements will also be presented. Our findings offer new perspectives on engineering FERSC for advanced beyond-CMOS logic-in-memory devices. We acknowledge the PRIN 2022 project SORBET (grant no. 2022ZY8HJY) funded by MUR.

[1] S. Manipatruni., *Nature*, 565, 35 (2019) [2] D.C. Vaz, F. Casanova *et al.*, *Nat. Commun.,*15, 1902 (2024) [3] S. Varotto *et.al.*, *Nat. Electron.*, 4, 740 (2021) [4] D. Di Sante *et al.*, *Adv. Mater.*, 25, 509 (2013) [5] E. Plekhanov, S. Picozzi, *Phys. Rev. B*, 90, 161108R (2014)

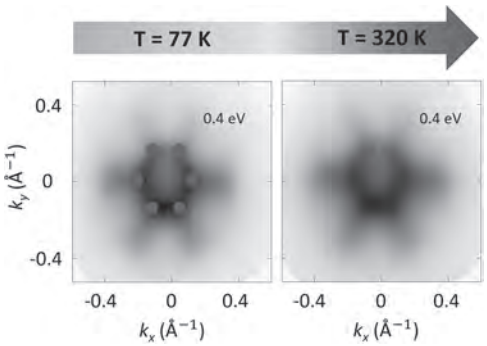

The Rashba contour of the material persists at room temperature, suggesting a rather high critical temperature. The red dots indicate the bulk bands re-entering.

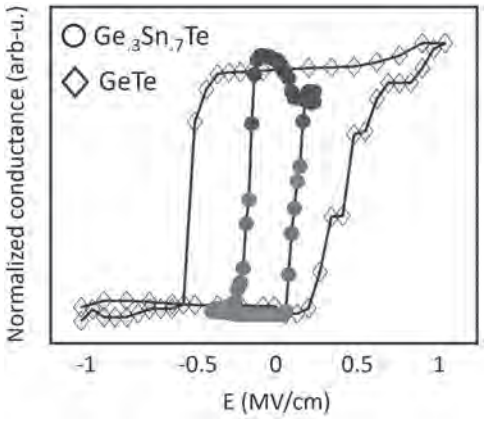

Ferroelectric hysteresis loops of GeTe and GeSnTe through electroresistive measurements.

DE-03. Temperature dependent spin dynamics in LSMO/Pt bilayer.

B. Sahoo[1,2], A. K[3], K. Matthews[2], S. Petit-Watelot[3], J. Rojas-Sanchez[3], A. Frano[2], S. Das[2] and E. Fullerton[1,2] *1. Center for Memory and Recording Research, University of California, San Diego, San Diego, CA, United States; 2. Physics, University of California, San Diego, San Diego, CA, United States; 3. Physics, Institut Jean Lamour Université Lorraine - CNRS (UMR 7198) Campus Artem, Nancy Cedex, France*

Energy efficient oscillators are essential for the development of low-power neuromorphic computing systems. Commonly used oscillator material systems are all metallic bilayers of Ferromagnet(FM)/ Heavy metal or non-magnetic metal (HM or NM) (FM=CoFeB, Py; NM=Pt, Pd Ta, W) with a relatively high intrinsic Gilbert damping of the order of 10-2 and FMR linewidths of the order of 50 Oe or more [1] [2] [3] [4]. High spin-charge conversion, low damping, and small resonance linewidth are essential constituents for development of energy efficient oscillators. In this regard, complex ferromagnetic oxides namely LSMO ($La_{0.67}Sr_{0.33}MnO_3$) offer a unique pathway for creating energy efficient nano-oscillators. LSMO has half metallicity, high spin polarization, sharp resonance linewidth, low damping and a large anisotropic magnetoresistance (AMR) response. This, combined with Pt, a proven material with high spin-charge conversion effi-ciency, can potentially be used to create robust nano-oscillators. In this experiment, we probe the magnetization dynamics and spin transport in NGO(110)/LSMO(13 nm)/Pt(0 and 5 nm) thin films at various temperatures ranging from 300K to 90K via ferromagnetic resonance (FMR) and spin-pumping FMR (SP-FMR) measurements. We find that the bilayer system exhibits a low damping (0.002) and small linewidth (12Oe) and a large spin Hall angle (≈ 3.5%) at 170K, making it the best working temperature for spin Hall nano-oscillators made out of this system.

J.-C. Rojas-Sánchez, N. Reyren, P. Laczkowski, W. Savero, J.-P. Attané, C. Deranlot, M. Jamet, J.-M. George, L. Vila and H. Jaffrès, "Spin Pumping and Inverse Spin Hall Effect in Platinum: The Essential Role of Spin-Memory Loss at Metallic Interfaces," *Physical Review Letters,* vol. 112, p. 106602, March 2014. K. Ando and E. Saitoh, "Inverse spin-Hall effect in palladium at room temperature," *Journal of Applied Physics,* vol. 108, December 2010. S.-I. Kim, D.-J. Kim, M.-S. Seo, B.-G. Park and S.-Y. Park, "Dependence of inverse-spin Hall effect and spin-rectified voltage on tantalum thickness in Ta/CoFeB bilayer structure," *Applied Physics Letters,* vol. 106, January 2015. C.-F. Pai, L. Liu, Y. Li, H. W. Tseng, D. C. Ralph and R. A. Buhrman, "Spin transfer torque devices utilizing the giant spin Hall effect of tungsten," *Applied Physics Letters,* vol. 101, p. 122404, September 2012.

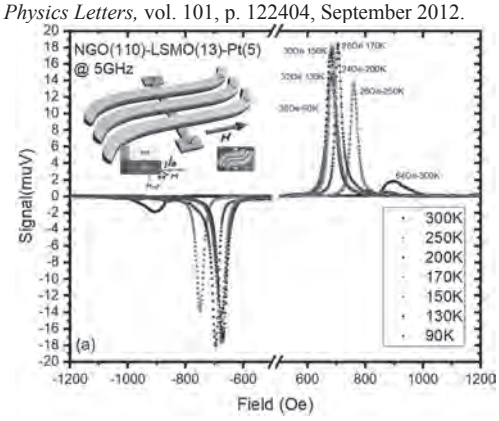

Figure 1 a) shows a spin pumping dominated spin rectification signal from LSMO/Pt, which increases with decrease in temperature. Inset shows the device schematic for the measurement

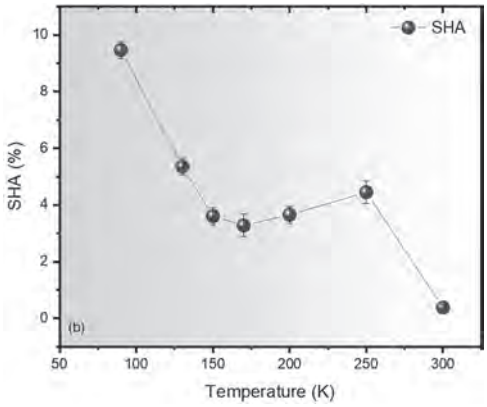

(b) shows the variation of calculated spin Hall angle with temperature. A nominal value of 3.5 to 4% is achieved in the range of 250 to 150K

DE-04. Withdrawn

DE-05. Non-Local Spin Valve Optimization *via* Wide-Range Interfacial Resistance Tuning: Toward Spin Accumulation Sensors. B. Kaiser[1], J. Ramberger[1], M. Norum[1], N. Nandakumaran[1], J. Dewey[1] and *C. Leighton*[1]
1. University of Minnesota, Minneapolis, MN, United States

Due to continued scaling, reader sensors in hard disk drives face pressing challenges related to rising electrical resistance and thus impedance mismatch issues. All-metal, or at least low-resistance, field sensors are thus of high interest to displace current magnetic tunnel junction heads. Spin accumulation sensors based on metallic non-local spin valves (NLSVs) are promising candidates but need further signal optimization, particularly in the ultrathin limit required for applications. Here, we report on a wide-ranging study of spin signal optimization in ultrathin $Al/AlO_x/Co_{75}Fe_{25}$-based NLSVs (Fig. 1), using interfacial resistance-area-product (*RA*) tuning to mitigate spin back-diffusion [1]. The Al-oxidation-controlled *RA* is tuned over 8 orders of magnitude, providing a complete picture of the evolution of interfacial transport mechanism, spin signal, and non-local background. Signal improvements up to factors of almost 10^3 are obtained over transparent-interface devices (to ~0.15 Ω, Fig. 2), and the upper limit of feasible resistance-area product in NLSVs (~1 kΩμm^2) is established. Most significantly, the spin signals in such NLSVs at application-relevant resistances still lie substantially (1-2 orders of magnitude) beneath theoretical limits (Fig. 2), due to diminished tunneling spin polarization. Connecting tunneling devices to the transparent limit, a universal spin polarization *vs*. *RA* relation is thus uncovered in AlO_x-based devices, over almost 12 orders of magnitude in *RA*, highlighting the specific issue limiting technological progress in this area. Strategies to achieve further gains will be discussed. Work supported by Seagate Technology Inc., NSF (DMR-2103711), and ASRC. Parts of this work were conducted in the Minnesota Nano Center, supported by NSF (ECCS2025124), and in the UMN Characterization Facility, supported by NSF MRSEC (DMR-2011401).

[1] B. Kaiser, J. Ramberger, M. Norum, N. Nandakumaran, J. Dewey, and C. Leighton, submitted (2024).

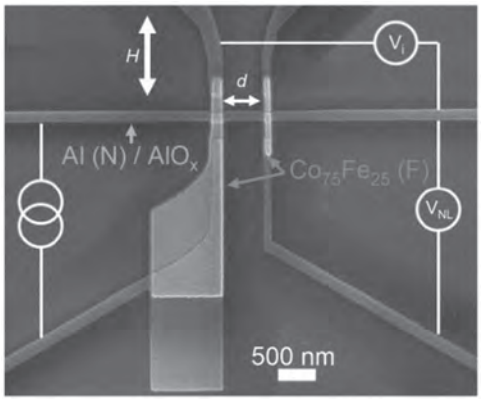

Fig. 1. Scanning electron micrograph of a typical NLSV studied in this work, showing the Al channel, $Co_{75}Fe_{25}$ injector/detector, applied magnetic field *H*, and wiring configuration.

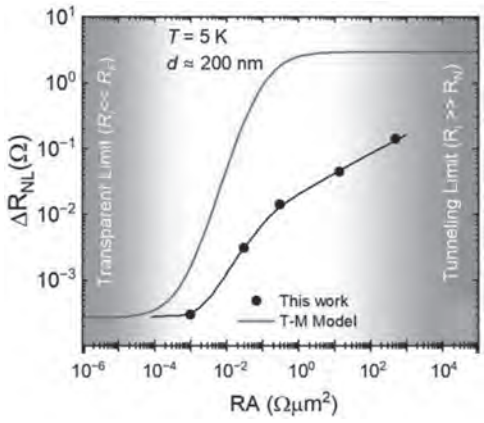

Fig. 2. NLSV spin signal ΔR_{NL} *vs*. resistance-area product *RA*, comparing our experimental results to the Takahashi-Maekawa (T-M) model.

DE-06. Magnetic tunnel junction implementations of unconventional computing. *D. Rodrigues*[1], E. Raimondo[2,3], R. Tomasello[1], M. Carpentieri[1] and G. Finocchio[3] *1. Department of Electrical and Information Engineering, Politecnico di Bari, Bari, Italy; 2. Istituto Nazionale di Geofisica e Vulcanologia, Roma, Italy; 3. Department of Mathematical and Computer Sciences, Physical Sciences and Earth Sciences, University of Messina, Messina, Italy*

Magnetic tunnel junctions (MTJs) offer promising solutions for improving the performance and efficiency of hardware implementations in unconventional computing [1,2]. Their electrically readable magnetization dynamics, characterized by nonlinearity and nonvolatility, make MTJs highly suitable for neuromorphic computing. We propose three MTJ designs optimized for specific tasks within neural networks (NNs), for drop-in replacements in neuromorphic systems, see Figure: (a) spiking neurons for spiking neural networks [3]; (b) dynamic neurons [4]; and (c) components for implementing nonlinear activation functions and their gradients. First, we present an MTJ-based spiking neuron that emulates the bio-realistic Hodgkin-Huxley model, capable of tonic spiking and leaky integrate-and-fire behavior. The MTJ achieves GHz spiking rates at applied voltages around 200 mV by combining magnetization dynamics and thermal fluctuations. Second, we propose spin-transfer nano-oscillators as dynamic neurons. Similar to reservoir computing, these neurons dynamically project inputs into an output space where classification is easily performed by linear regression. However, dynamic neurons can be tuned via dynamical control parameters, allowing for optimized task performance. Training of these control parameters is achieved via optimal control theory. Finally, we demonstrate how MTJs can implement nonlinear activation functions and their gradients in

conventional neural networks, thereby allowing for efficient forward and backward propagation. We show that discrepancies between device-obtained and software-generated activation curves do not significantly affect the performance of the backpropagation algorithm. The robustness, scalability, and low power requirements of MTJ implementations make them ideal for deploying deep neural networks in edge applications. Our work [5], coupled with advances in MTJs and spintronic technologies, promises to significantly improve the performance of NNs and address current challenges that hinder their widespread adoption.

[1] Finocchio, Giovanni, et al., Nano Futures 8.1 (2024): 012001. [2] Grollier, Julie, et al., Nature electronics 3.7 (2020): 360-370. [3] Rodrigues, Davi R., et al., Physical Review Applied 19.6 (2023): 064010. [4] Rodrigues, Davi R., et al., IEEE Transactions on Nanotechnology 22 (2023): 800-805. [5] This work was supported by the project PRIN 2020LWPKH7 "The Italian factory of micromagnetic modeling and spintronics" and the project PRIN20222N9A73 "SKYrmion-based magnetic tunnel junction to design a temperature SENSor-SkySens", funded by the Italian Ministry of University and Research (MUR) and by the PETASPIN Association (www.petaspin.com). DR, RT and MC acknowledge the support of the project PE0000021, "Network 4 Energy Sustainable Transition - NEST", funded by the European Union - NextGenerationEU, under the National Recovery and Resilience Plan (NRRP), Mission 4 Component 2 Investment 1.3 - Call for Tender No. 1561 dated 11.10.2022 of the Italian MUR (CUP C93C22005230007). DR also acknowledges the support of the project D.M. 10/08/2021 n. 1062 (PON Ricerca e Innovazione), financed by the Italian MUR, and ER acknowledges the support of the project PON Capitale Umano (CIR_00030), financed by the Italian MUR.

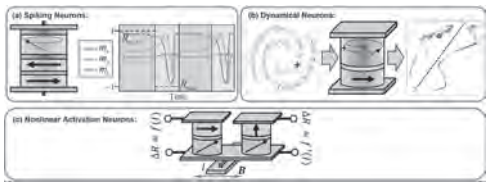

Implementations of MTJs for unconventional computing: (a) spiking neurons; (b) dynamic neurons; and (c) nonlinear activation neurons.

DE-07. Spin-Orbit Torque Magnetic Tunnel Junctions at Cryogenic Temperatures. *K. Senapati*[1], A. Fassatoui[1], L. Vila[1], A. Kandazoglou[1], G. Gaudin[1], S. Rao[2], S. Couet[2] and K. Garello[1] *1. SPINTEC, Grenoble, France; 2. Interuniversitair Micro-Elektronica Centrum, Leuven, Belgium*

Magnetoresistive RAM (MRAM) is gaining traction in embedded memory technology due to its lower power consumption, high speed, scalability, and endurance. MRAM utilizes magnetic tunnel junctions (MTJs) and the tunnel magneto-resistance (TMR) effect for reading data. While spin transfer torque and toggle MRAM are commercially available with write time > 10 ns, spin orbit torque (SOT) MRAM, currently in the research stage, demonstrates sub-ns writing speeds and higher endurance. This positions SOT-MRAM as a promising candidate for future energy-efficient, fast embedded memory solutions [1]. Currently, there is increasing interest in evaluating the behavior of memories at cryogenic temperatures (77K, 4K) for high-performance and quantum computing applications [2]. However, the behavior of SOT-MRAM at low temperatures is under-explored. We will report in this presentation about cryogenic properties of 300mm integrated W-based SOT-MTJs [1]. First, we will introduce the magnetic tunnel junction characteristics (TMR, B_c, B_k, B_{off}, Δ, R_{SOT}) variations with temperature down to 50 K, for various MTJ diameters (50 to 100 nm). Fig. 1 shows a typical R-H curve at 50K and 300K where one can clearly observe expected increase of the coercivity (B_c), as well as of TMR that is consistent with the inelastic electron tunneling model [3]. Additionally, we will discuss the temperature and field dependence of the SOT critical switching current (DC) down to 11 K, as shown in Fig. 2. We will present switching distribution probabilities from pulsed currents as fast as 250 ps, down to 77 K. This analysis allows us to study the intrinsic critical switching current and energy conservation parameters versus temperature, which are crucial for benchmarking SOT-MTJ systems [4]. Our results establish an initial benchmark for SOT-MTJ technology for cryogenic applications and help identify pathways to leverage SOT physics in low-temperature environments.

1. K. Garello, F. Yasin, S. Couet, *et al. 2018 IEEE Symposium on VLSI Circuits*, 81–82 (2018) 2. S. Alam, M.S. Hossain, S.R. Srinivasa, *et al. Nat Electron* 6, 185–198 (2023) 3. K. Cao *et al. IEEE Transactions on Magnetics*, vol. 55, no. 3, pp. 1-4, March 2019 4. V. Krizakova, M. Perumkunnil, S. Couet, *et al.* Journal of Magnetism and Magnetic Materials 562, 169692 (2022)

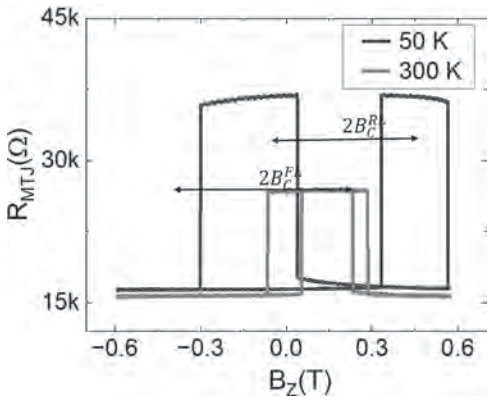

R-H loops obtained from 60nm based MTJ at 300K and 50K

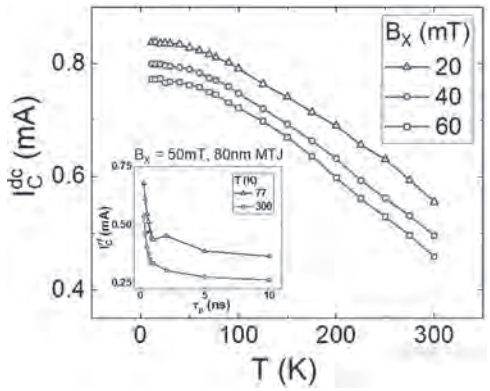

Critical switching current (DC) versus temperature for an 80nm based SOT-MTJ at varied external fields. Inset shows critical switching current (*rf*) versus pulse width curves down to 250ps pulses for an 80nm based SOT-MTJ at T = 300K and 77K

DE-08. Spin transmission through NiO in Pt/NiO/NM/Py heterostructure. *B. Sahoo*[1,2], C. Safranski[2], G. Hu[2], J. Liang[2], M. Robbins[2], P. Hashemi[2] and J.Z. Sun[2] *1. Physics, University of California, San Diego, San Diego, CA, United States; 2. IBM T.J. Watson Research Center, Yorktown Heights, NY, United States*

Efficient operation of spin orbit torque magnetic random-access memories (SOT-MRAM) requires separation of the spin- and charge-current pathways [1] [2]. NiO is an electrically insulating, but spin conducting material. By interfacing it with a heavy metal spin current generator (Pt in this case), one can confine the charge current flow to Pt, while transmitting spin current through NiO into the adjacent layer [3] [4] [5] [6] [7] [8] [9]. We use d.c. bias spin torque ferromagnetic resonance (ST-FMR) on 600 nm 1800 nm nano-bridge patterned from Pt/NiO/NM/Py (Py=permalloy) thin film stack to evaluate the spin current received by the Py layer. Here the non-magnetic metal (NM)=Cu,Ag, … is a layer for spin conduction but disrupts direct exchange coupling between the ferromagnetic detector (Py) and the antiferromagnetic NiO. The NiO thickness is varied while all other layers are kept at constant thickness. The samples considered are Ta(5) |Pt(50)

|NiO (x=0,12.5,15,20,25) |NM(20) |Py(50) |MgO(15) |TaN(20) and, Ta(5) |NM(20)|Py(50) |MgO(15) |TaN(20) where the numbers indicate thickness in angstroms. These samples are named S1 to S5 and S0 respectively. We observe robust spin transmission (>40%) even at 25 Å NiO thickness. The spin-transmissivity's NiO thickness dependence is nearly exponential for samples with NM. Shown in Fig.1(a-b) are its SOT channel current dependence-based spin-transmissivity vs NiO thickness. For samples with direct NiO/Py interface however, a faster NiO-thickness dependence is seen. An insertion of a well grown NM between NiO and Py increases the decay length compared to Pt/NiO/Py (Figure 1(b)). These experiments provide an existence proof of a materials stack that allows charge- and spin-current separation without direct exchange coupling with the ferromagnet.

[1] R. Andrawis, A. Jaiswal and K. Roy, "Design and comparative analysis of spintronic memories based on current and voltage driven switching," *IEEE Transactions on Electron Devices,* vol. 65, p. 2682–2693, 2018. [2] M. Kazemi, G. E. Rowlands, S. Shi, R. A. Buhrman and E. G. Friedman, "All-Spin-Orbit Switching of Perpendicular Magnetization," *IEEE Transactions on Electron Devices,* vol. 63, p. 4499–4505, November 2016. [3] H. Wang, C. Du, P. C. Hammel and F. Yang, "Antiferromagnonic Spin Transport from Y3Fe5O12 into NiO," *Physical Review Letters,* vol. 113, p. 097202, August 2014. [4] T. Moriyama, S. Takei, M. Nagata, Y. Yoshimura, N. Matsuzaki, T. Terashima, Y. Tserkovnyak and T. Ono, "Anti-damping spin transfer torque through epitaxial nickel oxide," *Applied Physics Letters,* vol. 106, April 2015. [5] Y. Wang, D. Zhu, Y. Yang, K. Lee, R. Mishra, G. Go, S.-H. Oh, D.-H. Kim, K. Cai, E. Liu, S. D. Pollard, S. Shi, J. Lee, K. L. Teo, Y. Wu, K.-J. Lee and H. Yang, "Magnetization switching by magnon-mediated spin torque through an antiferromagnetic insulator," *Science,* vol. 366, p. 1125–1128, November 2019. [6] L. Zhu, L. Zhu and R. A. Buhrman, "Fully Spin-Transparent Magnetic Interfaces Enabled by the Insertion of a Thin Paramagnetic NiO Layer," *Physical Review Letters,* vol. 126, p. 107204, March 2021. [7] Y.-M. Hung, C. Hahn, H. Chang, M. Wu, H. Ohldag and A. D. Kent, "Spin transport in antiferromagnetic NiO and magnetoresistance in Y3Fe5O12/NiO/Pt structures," *AIP Advances,* vol. 7, December 2016. [8] W. Lin, K. Chen, S. Zhang and C. L. Chien, "Enhancement of Thermally Injected Spin Current through an Antiferromagnetic Insulator," *Physical Review Letters,* vol. 116, p. 186601, May 2016. [9] H. Meer, O. Gomonay, A. Wittmann and M. Kläui, "Antiferromagnetic insulatronics: Spintronics in insulating 3d metal oxides with antiferromagnetic coupling," *Applied Physics Letters,* vol. 122, February 2023. [10] J. Dong, C. Cheng, J. Wei, H. Xu, Y. Zhang, Y. Wang, Z. Zhu, L. Li, H. Wu, G. Yu and X. Han, "Enhancement of interfacial spin transparency in Py/NiO/Pt heterostructure," *Applied Physics Letters,* vol. 122, March 2023.

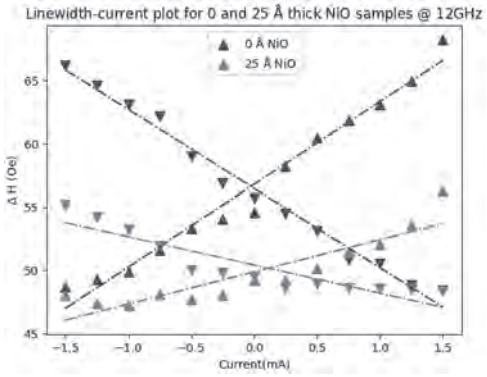

Figure 1 (a) Linewidth (ΔH) vs the applied current for Pt/NM/Py (blue) and Pt/NiO(25)/NM/Py (red). Δm is the averaged slope for the positive field (up triangles) and negative field (down triangles).

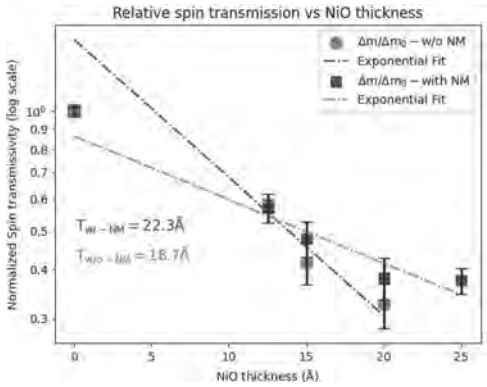

(b) shows the relative spin transmission from Pt to Py through varying NiO thickness. Insertion of NM layer (blue squares) increases the decay length as compared to samples without the NM spacer (red dots).

DE-09. Strong antiferromagnetic interlayer exchange coupling caused by small amounts of Re addition in synthetic AF system with Ir-Re spacer. *Y. Saito*[1], T. Roy[2], S. Ikeda[1,2,3], M. Shirai[2,3], H. Honjo[1], H. Inoue[1] and T. Endoh[1,2,4] *1. Center for Innovative Integrated Electronic Systems, Tohoku University, Sendai, Japan; 2. Center for Science and Innovation in Spintronics, Tohoku University, Sendai, Japan; 3. Research Institute of Electrical Communication, Tohoku University, Sendai, Japan; 4. Department of Electrical Engineering, Graduate School of Engineering, Tohoku University, Sendai, Japan*

Synthetic antiferromagnetic (AF) pinned layer is widely used in order to reduce the stray field of the pinned layer and stabilize the magnetic alignment of the pinned layer in the perpendicular magnetic tunnel junctions (MTJs) [1]. A major obstacle to reliable and fast spin-orbit-torque (STT) switching is a phenomenon known as back hopping [2-4]. This phenomenon is related to the undesired switching of the pinned layer, which then induces fast perpetual cyclic switching of both free and pinned layers in STT-MTJs called back hopping. Oscillation period and magnitude of interlayer exchange coupling (($|J_{ex}|$)) in the pinned layer depend on the nonmagnetic spacer material, and nonmagnetic spacer layers such as Ru and Ir are representative materials of nonmagnetic spacer layers in the synthetic AF pinned layer with strong interlayer exchange coupling [5 - 7]. To solve the issue of back hopping in miniaturized spin devices and to achieve stable operation of STT magnetic-random-access memories (MRAM), a material that provides stronger AF interlayer exchange coupling is necessary. In this work, detailed Re concentration (C_{Re}) dependence of the $|J_{ex}|$ in the synthetic AF system with Ir-Re spacer layer is conducted. We observed strong AF interlayer exchange coupling caused by small amounts of Re addition and phase shift of AF peak to thinner spacer layer region in synthetic AF system with Ir-Re spacer (Figs. 1(a) – 1(c)). The synthetic AF system with Ir-Re spacer has tolerance of the strong AF interlayer exchange coupling and perpendicular magnetic anisotropy up to 673K annealing (Figs. 1(a) – 1(c)). First-principles calculations show nearly consistent results with experiments, which show a peak of $|J_{ex}|$ around Re concentration of less than 5% (Figs. 2(a) and 2(b)). These results show the importance of preparing synthetic AF systems with thin spacer layer thickness for obtaining a strong AF interaction. This work was supported by the CIES Consortium, X-NICS (No. JPJ011438), and JSPS KAKENHI (JP24H00030, JP21K18189).

[1] S. Ikeda et al., Nature Mater. 9, 721 (2010). [2] T. Min et al., J. Appl. Phys. 105, 07D126 (2009). [3] T. Devolder et al., Phys. Rev. B 102, 184406 (2020). [4] W. Kim et al., IEEE Trans. Magn. 52, 3401004 (2016). [5] D. C. Worledge et al., Appl. Phys. Lett. 98, 022501 (2011). [6] Y, Saito et al., Phys. Rev. B 104, 064439 (2021). [7] Y. Saito et al., Appl. Phys. Lett. 119, 142401 (2021).

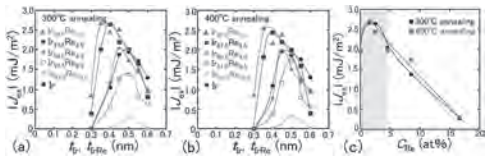

Plot of the magnitude of $|J_{ex}|$ as functions of Ir and IrRe thicknesses for (a) 573K and (b) 673K annealing samples. (c) Dependence of the maximum values of $|J_{ex}|$ on C_{Re}.

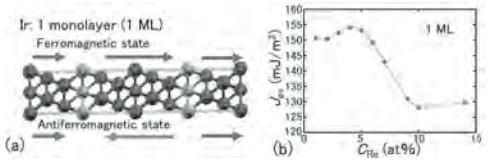

Result of first-principles calculations.

DE-10. Thermal Effects on Damping Determination of Perpendicular MRAM Devices by Spin-Torque Ferromagnetic Resonance.
H.J. Richter[1], R.V. Chopdekar[1], G. Mihajlović[1], J. Gibbons[1], N. Davila[1], M.K. Grobis[1] and T. Santos[1] *1. Research, Western Digital, San Jose, CA, United States*

The Gilbert damping plays an important role for understanding the switching behavior of perpendicular magnetic random-access memory (MRAM) cells. Damping measurements are typically made on full films of the free layer materials rather than on finished devices. It is to be expected that the damping is different between the device and the film level measurements [1,2,3]. Here we report on device level damping measurements using spin-torque driven ferromagnetic resonance. For all free layer materials investigated, we find that the extracted damping increases with decreasing device size and is higher than the respective film level values (Fig. 1). It is worked out that thermal agitation disturbs the resonance and causes an increase of the apparent damping. The effect is modeled by Langevin dynamics and good agreement with a variety of experimental details is obtained. An illustration of the thermal effect is shown in Fig. 2. For MRAM sizes bigger than about 55nm, the thermal agitation effect becomes negligible. Beyond the increase caused by thermal agitation, we believe that the device level damping is still somewhat higher than the film-level damping

[1] O. Ozatay et al., *Nat. Mater. 7*, 567 (2008). [2] H.T. Nembach et al., *Phys. Rev. Lett,* 110, 117201 (2013) [3] L. Thomas et al., *IEEE International Electron Devices Meeting (IEDM)*, San Francisco, CA, USA, 2017, pp. 38.4.1-38.4.4, (2017)

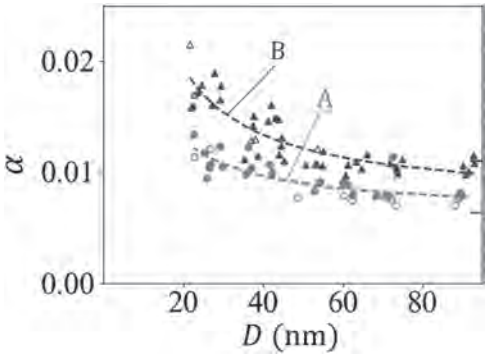

Fig. 1: ***Extracted damping for two free layers across multiple sizes. The markers on the right show the respective film level damping. The dashed lines are guides to the eye.***

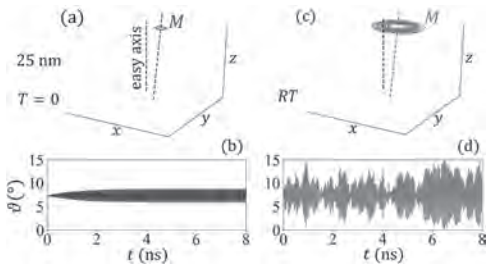

Fig. 2: Illustration (simulation result) of the effect of thermal agitation on ferromagnetic resonance: polar diagrams (a) and (c) and time traces (b) and (d) for a 25nm cell with free layer A at resonance; with (right) and without (left) thermal agitation, respectively.

DE-11. Nonlinear amplification of microwave signals in spin-torque oscillators.
K. Zhu[1], *M. Carpentieri*[4], L. Zhang[1], B. Fang[1], J. Cai[1], R.V. Verba[2], A. Giordano[3], V. Puliafito[4], B. Zhang[1], G. Finocchio[5] and Z. Zeng[1] *1. Suzhou Institute of Nano-Tech and Nano-Bionics, Nanofabrication Facility, Chinese Academy of Sciences, Suzhou, China; 2. Institute of Magnetism, Kyiv, Ukraine; 3. Engineering, University of Messina, Messina, Italy; 4. Electrical and Information Engineering, Politecnico di Bari, Bari, Italy; 5. Mathematical and Computer Sciences, Physical Sciences and Earth Sciences, University of Messina, Messina, Italy*

Spintronics-based microwave devices, such as oscillators and detectors, have been the subject of intensive investigation in recent years owing to the potential reductions in size and power consumption. However, only a few concepts for spintronic amplifiers have been proposed, typically requiring complex device configurations or material stacks. The concept of microwave amplification based on spin-transfer torque in a three-terminal device was proposed by Slonczewski in one of his patents[1]. Recently microwave amplification has been demonstrated with two terminal MTJs biased with a direct current (dc) and designed with materials that have a large heat-to-spin conversion[2]. Here, we demonstrate a spintronic amplifier based on two-terminal magnetic tunnel junctions (MTJs) produced with CMOS-compatible material stacks that have already been used for spin-transfer torque memories[3]. We achieve a record gain ($|S11| > 2$) for input power on the order of nW(<–40 dBm) at an appropriate choice of the bias field direction and amplitude. Based on micromagnetic simulations and experiments, we describe the fundamental aspects driving the amplification and show the key role of the co-existence in microwave emissions of a dynamic state of the MTJ excited by a dc current and the injection locking mode driven by the microwave input signal. Our work provides a way to develop a class of compact amplifiers that can impact the design of the next generation of spintronics-CMOS hybrid systems. Acknowledgements This work was supported under the project PRIN 2020LWPKH7 “The Italian factory of micromagnetic modelling and spintronics”, and the “Network 4 Energy Sustainable Transition - NEST” project (MIUR project code PE000021, Concession Degree No. 1561 of October 11, 2022), in the framework of the NextGenerationEu PNRR plan, and by PETASPIN association (www.petaspin.com).

[1] Slonczewski, J. C. Electronic device using magnetic components. U.S. Patent 5695864A (1997). [2] Goto, M. et al., Nat. Nanotechnol. 14 (2018): 40-43. [3] Zhu K., Carpentieri M. et al., Nat. Communications 14 (2023): 2183-1-9.

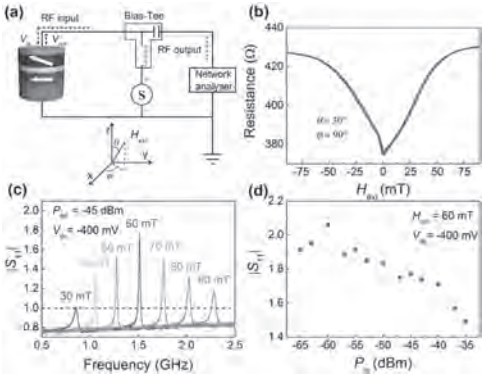

Microwave amplification with amplification measurement. a) A schematic diagram of the measurement systems. B) Magnetoresistance-field curves of one MTJ device. c) Amplification parameter |S11| as a function of frequency under different values of external field ranging from 30 to 90mT. d) |S11| as a function of the input microwave power.

DE-12. Field-free deterministic spin-orbit torque switching in all-2D van der Waals heterostructures at room temperature. *L. Pandey*[1], B. Zhao[1], P. Rout[1], H. Bangar[1], R. Ngaloy[1], M. Abdel-Hafiez[2], H. Chang[3] and S.P. Dash[1,4] *1. Department of Microtechnology and Nanoscience, Chalmers University of Technology, Göteborg, Sweden; 2. Department of Applied Physics and Astronomy, University of Sharjah, Sharjah, United Arab Emirates; 3. School of Materials Science and Engineering, Huazhong University of Science and Technology, Hubei, China; 4. Graphene Centre, Chalmers University of Technology, Göteborg, Sweden*

The emerging all-van der Waals (vdW) heterostructure, with control over the crystal symmetries and magnetic anisotropies, provides a new platform for generating unconventional spin polarization and efficiently controlling the magnetization dynamics [1]. Specifically, vdW heterostructure of topological quantum material with current-induced out-of-plane spin polarization and ferromagnet with out-of-plane magnetization are promising candidates for tunable, compact and energy-efficient spintronic memory technologies [2]. However, in all-vdW heterostructures, the generation of efficient out-of-plane spin polarization is limited and achieving energy-efficient and field-free magnetization switching of out-of-plane magnetization due to unconventional spin-orbit torque (SOT) phenomena remains challenging [3]. Here, we demonstrate the field-free SOT switching in an all-vdW heterostructure combining topological Weyl semimetal candidate $TaIrTe_4$ [4] and the ferromagnet Fe_3GaTe_2, which exhibits out-of-plane magnetic anisotropy above room temperature (Fig 1). Deterministic field-free switching of $TaIrTe_4/Fe_3GaTe_2$ is observed at room temperature with a low current density of, an order of magnitude smaller than that of conventional heavy metal/ferromagnet thin films. Furthermore, the second harmonic angle and field sweep Hall voltage measurements are performed at room temperature to calculate the SOT efficiency. The ratio of damping-like torque to current density (H_{DL}/J) is estimated to be around. From the switching experiments, the ratio of easy axis coercive field (H_z^{coer}) to switching current is found to be around. These findings on all-vdW heterostructures indicate the presence of unconventional out-of-plane anti-damping torque from the adjacent $TaIrTe_4$ layer, offering a promising route to energy-efficient and external field-free spintronic devices.

[1] H. Kurebayashi et al., Nat. Rev. Phys. 4, 150-166 (2022). [2] H. Yang et al., Nature 606, 663–673 (2022). [3] B. Zhao et al., arXiv:2308.13408 [4] L. Bainsla et al., Nat. Commun. 15, 4649 (2024)

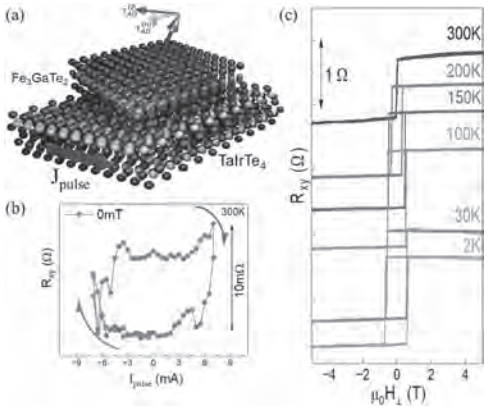

Field-free deterministic spin-orbit torque switching in $TaIrTe_4/Fe_3GaTe_2$ all van der Waals heterostructures at room temperature.

DE-13. Magnetic domain wall type Spin-Memristor for neuromorphic computing. *T. Gushi*[1], S. Yamada[1], I. Shinto[1], T. Shibata[1] and S. Tomoyuki[1] *1. Advanced Products Development Center, Technology & Intellectual Property HQ, TDK corporation, Ichikawa, Japan*

In recent years, an increase in power consumption for computation related to AI technology is becoming a new social issue. Analogue neuromorphic computing has been expected to solve this problem. A memristor, which stores analog resistance value as a weight of neural network, is a basic element for analogue neuromorphic computing devices [1]. Magnetic domain wall (DW) type memristor, named Spin-Memristor, is highly anticipated as an ideal element due to its linear and symmetric response to writing pulses [2]. Spin-Memristor has 3-terminal structure and 3 different fixed magnetization direction layers. One of the issues with Spin-Memristor is the difficulty to form such fixed portions [3]. We report fabrication process and properties of bottom-pinned type Spin-Memristor (Fig. 1), which is expected to realize stable fabrication of these portions at both ends of DW layer compared to top-pinned type structure. To confirm the concept of the bottom-pinned type structure, current induced DW motion (CIDWM) and formation of magnetic fixed portions were evaluated by using Anomalous Hall Effect (AHE) elements. The stacking film consisting of CoFeB layer, [Co/Pd] system DW layer and synthetic anti-ferromagnetic (SAF) - fixed layer was deposited on Si wafer and processed into Hall bar structure. Electron beam lithography and Ar ion milling were used to fabricate the elements with 3 standards of width, followed by SEM observation. Magnetization fixed portions were put on both ends of the DW layer to keep DW stably. Figure 2 shows the probability of CIDWM monitored by depinning from the Hall bar portion. The threshold current density (j_{th}), defined by 50% probability, showed clear width dependence and j_{th} was reduced from 1.09×10^{12} to 0.72×10^{12} A/m^2 with reducing element width from 163 nm to 63 nm. In addition, temperature dependence of CIDWM will be reported in the presentation. We also confirmed the functionality of magnetic fixed portions by monitoring the DW formation and propagation properties. Two types of magnetic fixed portions having opposite magnetization directions could be formed at each end of the DW layer.

[1] G. W. Burr *et. al.*, Adv. Phys. X 2, 89 (2017). [2] T. Shibata *et al*., APEX 13, 043004 (2020). [3] T. Ashida et al., Jpn. J. Appl. Phys., 59, 078002 (2020).

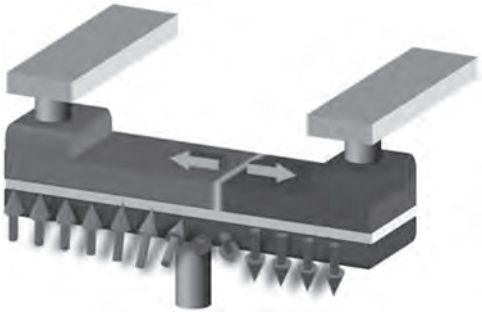

Fig. 1 Structure of Bottom-pinned type Spin-Memristor.

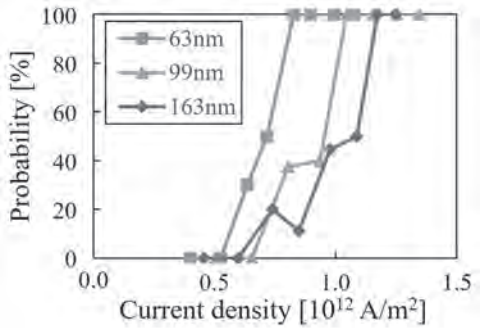

Fig. 2 Element width dependency of CIDWM probability.

Session DF
MAGNETOCALORIC MATERIALS AND REFRIGERATION
Manh-Huong Phan, Chair
University of South Florida, Tampa, FL, United States

INVITED PAPER

DF-01. Hysteresis, Reversibility, and Partial Transformations in Magnetocaloric Materials: a Combined Analysis Using TFORC and Thermography. *V. Franco*[1], J. Revuelta-Losada[1], A.N. Khan[1], L.M. Moreno-Ramírez[1] and J. Law[1] *1. University of Seville, Seville, Spain*

Reduction of the carbon footprint of our activities has a different implication depending on the sector. While the situation in transportation can be as simple as changing the mode of transport (e.g., from plane to train) whenever reasonable, temperature control systems do not allow us to replace air conditioners and refrigerators with different devices with a comparable temperature span; our only option is to replace the technology with a more environmentally friendly one. Caloric refrigeration would allow us to make this transition, but hysteresis and lack of reversibility in cyclic operation are important hurdles that need to be overcome without reducing the performance of materials. The magnetocaloric effect is maximised for first-order thermomagnetic phase transitions, but the price is hysteresis and irreversibility. Here we present the physics behind the recently proposed temperature-FORC (TFORC) technique for magnetocaloric systems [1], its use to identify detailed information of phase transitions, and for predicting the thermomagnetic response of a material in arbitrary conditions. The reversible response under cyclic excitations can also be independently determined by thermography [2], showing that some of the simple approximations present in the literature should be used with caution. Examples are presented for Heusler, MM'X, and high-entropy alloys. The methodology presented here will be instrumental in the implementation of more efficient caloric refrigeration devices.

[1] V. Franco, T. Gottschall, K. P. Skokov and O. Gutfleisch, "First-Order Reversal Curve (FORC) Analysis of Magnetocaloric Heusler-Type Alloys", *IEEE Magnetics Letters*, 7, (2016) 6602904. [2] J. Revuelta-Losada, A.N. Khan, L.M. Moreno-Ramírez, J.Y. Law, V. Franco, "Reversible Magnetocaloric Effect Characterized by Low-Cost Lock-In Infrared Thermography", submitted.

CONTRIBUTED PAPERS

DF-02. Understanding the microscopic origin of the relation between magnetoelasticity and magnetic damping constant in $Fe_{4x}Co_{4-4x}N$. *I. Kurniawan*[1], K. Ito[2], T. Seki[2,3], K. Masuda[1] and Y. Miura[1,4] *1. National Institute for Materials Science, Tsukuba, Japan; 2. Institute for Materials Research, Tohoku University, Sendai, Japan; 3. Center for Science and Innovation in Spintronics, Tohoku University, Sendai, Japan; 4. Kyoto Institute of Technology, Kyoto, Japan*

Magnetostrictive materials exhibit lattice parameter changes parallel to the magnetic field, which is useful for flexible spintronics [1]. Recent experiments reported a large negative magnetostriction (λ) in Fe_4N [2], with Co substitution reversing its sign. A strong relationship between λ and the magnetic damping constant (α) was observed. Since λ is proportional to the strain (ε) dependence of magnetic anisotropy energy (MAE) [3], which corresponds to the magnetoelastic coupling, this study focuses on microscopic origin of relation between magnetoelasticity and the damping constant. In this study, we focused on $Fe_{4x}Co_{4-4x}N$ structures and carried out first-principles calculations based on density-functional theory. We calculated MAE by including the spin-orbit interaction self-consistently. The α is calculated using the torque correlation model [4]. To identify the dominant contributions to the MAE, we performed second-order perturbation analysis [5], decomposing the MAE by spin transition processes, atomic sites and orbitals. Our calculation results agree well with the experimental observations for the compositional dependence of λ (Fig. 1) and α (Fig. 2). A slight shift in the theoretical calculations suggests that the experimental samples may be electron-doped. Further analysis shows that the magnetoelasticity is mainly dominated by spin-conserving ($\downarrow\Rightarrow\downarrow$) and spin-flip ($\uparrow\Rightarrow\downarrow$) electron scattering around the Fermi level. The inclusion of Co changes the slope of $d\mathrm{MAE}(\downarrow\Rightarrow\downarrow)/d\varepsilon$ from negative to positive while keeping the positive behavior of the $d\mathrm{MAE}(\uparrow\Rightarrow\downarrow)/d\varepsilon$, leading to a sign change in λ. On the other hand, α is proportional to the density of states at the Fermi level, which is mainly contributed to minority spin states. These results highlight the crucial role of minority spin states in the simultaneous control of λ and α. This work was partly supported by Grants-in-Aid for Scientific Research (Grants No. 22H04966) from the Japan Society for the Promotion of Science and the Japan Science and Technology Agency (JST) CREST.

[1] S. Ota, A. Ando, and D. Chiba, Nat Electron 1, 124 (2018). [2] K. Ito *et al*., arXiv:2403.16679. [3] R. Wu, L. Chen, and A. J. Freeman, J Magn Magn Mater 170, 103 (1997). [4] V. Kamberský, Czechoslovak Journal of Physics 26, 1366 (1976). [5] Y. Miura and J. Okabayashi, Journal of Physics: Condensed Matter 34, 473001 (2022).

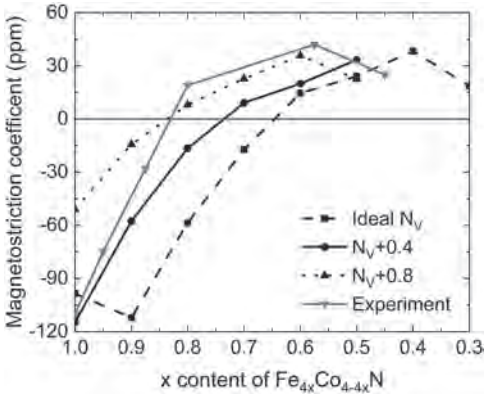

Fig. 1. Compositional dependence of the experimental and theoretical λ. Different values of the total number of electrons are considered in the calculation.

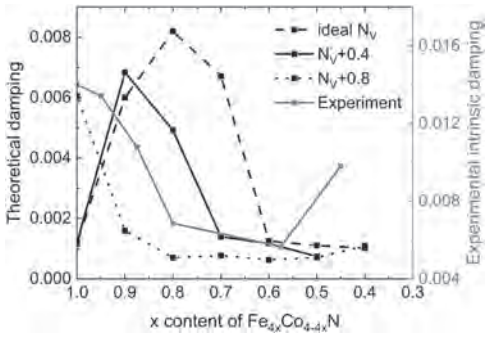

Fig. 2. Same as Fig. 1 but for α.

DF-03. Magnetocaloric effect in the full hydrogen liquefaction range in Gd_3Ni_6XY. I. Aseguinolaza[1], A. Herrero[1], A. Garcia-Adeva[1], E. Apiñaniz[1], A. Garshev[2,3], A. Morozkin[2] and *A. Oleaga*[1] *1. University of the Basque Country, Bilbao, Spain; 2. Department of Chemistry, Moscow State University, Moscow, Russian Federation; 3. Faculty of Materials Science, Moscow State University, Moscow, Russian Federation*

Hydrogen storage and transport require the development of new efficient and environmentally friendly refrigeration techniques in the region 20-77 K. Magnetocaloric refrigeration stands out as one of the most promising, provided a new generation of materials with high magnetic entropy changes and refrigerant capacities are developed in that region. We present a broad table-like magnetocaloric effect in the quasiternary intermetallic family Gd_3Ni_6XY {X, Y = Si, Al and Ga}, spanning over the full hydrogen liquefaction range. In the present work, a full crystallographic, magnetic and magnetocaloric study has been performed on three compounds of the Gd_3Ni_6XY family: Gd_3Ni_6AlGa, Gd_3Ni_6SiAl and Gd_3Ni_6SiGa. All the compounds present a cubic unit cell with $Ce_3Ni_6Si_2$-type structure (space group *Im-3m*, N 229, *cI*44). In all of them, a first paramagnetic to ferromagnetic phase transition takes place (T_C) whose position can be tuned by playing with the p-block elements (105 K for AlGa, 63 K for SiAl, 60 K for SiGa), surely due to the smallest radius of Si, as it has been observed with other families [1]. At low magnetic field there are no additional transitions but, as the field is slightly increased, a metamagnetic transition introduces a second spin reorientation transition (T_M), whose relevance is shown in the magnetic entropy change as a sustained direct magnetocaloric effect (see Fig. 1). The maximum of the magnetic entropy change is (at $\mu_0\Delta H$ = 0-5T) 4.7, 6.0, 5.9 J kg^{-1} K^{-1}, for Gd_3Ni_6AlGa, Gd_3Ni_6SiAl and Gd_3Ni_6SiGa, respectively, while TEC(10) are 4.6, 6.0, 5.6 J kg^{-1} K^{-1}. The fact that the magnetocaloric effect is well sustained along a wide temperature region makes this family promising for real magnetocaloric systems following Ericsson cycles. The study is completed with a critical behavior study of the paramagnetic to ferromagnetic transitions in the three compounds, retrieving the critical exponents β, γ, δ whose values are well supported by the scaling of the magnetocaloric variables; Fig. 2 shows, as an example, the Modified Arrott plot for Gd_3Ni_6AlGa, from where β and γ are obtained.

[1] A. Herrero, I.R. Aseguinolaza, A. Oleaga, A.J. Garcia-Adeva, E. Apiñaniz, A.V. Garshev, V. O. Yapaskurt, A.V. Morozkin, Dalton Transactions 52 (2023) 5780

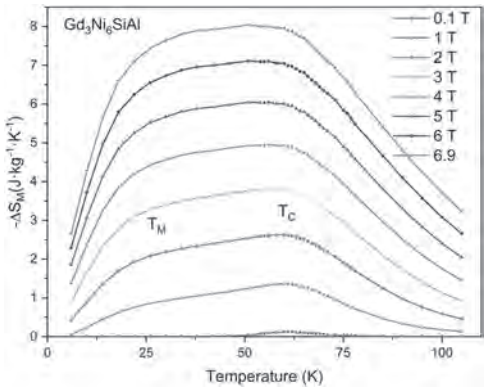

Fig. 1: Magnetic entropy change of Gd_3Ni_6SiAl for $\mu_0\Delta H$=0-6.9T

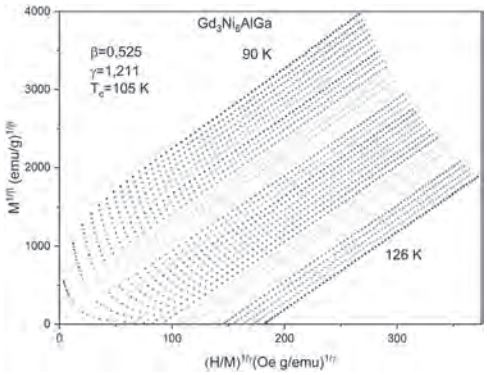

Fig. 2: Modified Arrott Plot for PM-FM transition in Gd_3Ni_6AlGa.

DF-04. FEMCE - A 3D Finite Element Simulation Tool for Magnetic Refrigerants. *R. Kiefe*[1] and J. Amaral[1] *1. Physics, University of Aveiro, CICECO, Aveiro, Portugal*

The magnetocaloric effect (MCE) is typically induced via an applied magnetic field change on the magnetic refrigerant. This is achieved by displacing either the magnetic field source or the magnetic refrigerant itself. A less explored method to induce the MCE is via a change of the demagnetizing field of the refrigerant, rotating the refrigerant between two directions with different shape-induced demagnetizing factors. To our knowledge, the first report on this approach was by Barclay et al., in a patent filed in 1984 [1], where a sheet of Gadolinium with undisclosed dimensions was rotated under an applied magnetic field of 0.3 T, showing a peak MCE value of 0.8 K. This value is sufficiently high to raise questions on the applicability of this approach in magnetic refrigeration devices. The main advantage would be lowering the power requirements of the movement, which is simply the rotation of the refrigerant within a homogeneous field. This improvement can be particularly relevant, as the energy cost of movement/rotation in current magnetic refrigeration device prototypes can amount up to 78% of the total [2,3]. An improvement in the compactness of the refrigeration device, compared to the usual design, is also a possibility. In this work, we revisit the demagnetizing field induced MCE, by comparing experimental measurements with simulations. A finite-element approach allows to go beyond the approximation of a homogeneously magnetized refrigerant, showing the temperature profile of the refrigerant in different geometries. Experimental measurements were made on thin plates of Gd, rotated under an applied field of 1.2 T. The temperature profile of the experimental and simulated ΔT_{ad} (T) data show good agreement. Exploring finite-element simulations for Gd sheets, we find the demagnetizing field induced MCE reaches peak maximum ΔT_{ad} (T) for applied fields below 0.5 T

[1] Barclay et al., Magnetic Refrigeration Apparatus and Method, US Patent 4459811 (1984) [2] Tura et al., Int. J. Refrig. 34 628 (2011) [3] Masche et al., Appl. Therm. Eng. 204 117947 (2022)

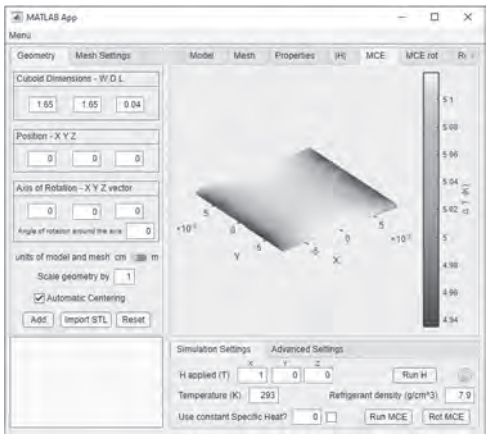

FEMCE interface exhibiting the temperature change estimated for a sheet of gadolinium (1.65x1.65x0.04 cm) under an horizontal magnetic field of 1 T.

DF-05. Direct Measurement of the Rotative Magnetocaloric Effect of Anisotropic Magnetic Materials. *O.L. Bernard*[1,2,3], P. Fournier[1,2,3] and M. Balli[4] *1. Physic, Université de Sherbrooke, Sherbrooke, QC, Canada; 2. Institut Quantique, Sherbrooke, QC, Canada; 3. Regroupement Québécois sur les Matériaux de Pointe, Sherbrooke, QC, Canada; 4. Physic, Ecole Supérieure d'Ingénierie des Energies, International University of Rabat, Rabat, Morocco*

The rotative magnetocaloric effect has gained popularity in the scientific community as an alternative to the direct magnetocaloric effect for an eventual implementation in simpler cooling devices [1]. Its appeal comes from the fact that one may use refrigeration schemes where the anisotropic active material rotates in a uniform field rather than moving in and out of a magnet to produce the cooling/warming cycles required for magnetic refrigeration, such as the one proposed by Balli *et al.* [2]. Since that proposal, several magnetic materials with very large anisotropy of the magnetic entropy change have been explored. However, few studies of the effect using direct measurements have been reported so far[3]. This study presents an experimental method to directly measure the temperature change of an anisotropic magnetic material as it rotates in a uniform magnetic field. The setup includes a thermometer attached to the sample that is suspended in a vacuum in a net with poor thermal conductance to the bath. As the sample rotates in a uniform field, its magnetic entropy varies, leading to cooling or warming depending on the direction of rotation between the easy and the hard magnetization axes. As shown in the figures, it enables the real-time monitoring of temperature changes as a function of various experimental controlling parameters such as the magnetic field, the angular velocity, and the direction of rotation. A model explaining most of the features observed will be presented alongside real-time direct measurements of ΔT for a $TmMnO_3$ single crystal. * Work supported by the NSERC under grant RGPIN-2018-06656, CFREF, FRQNT and U. de Sherbrooke.

[1] M. Balli et al., Appl. Phys. Rev., Vol 4, p.021305 (2017) [2] M. Balli et al., Appl. Phys. Lett., Vol 104, p.232402 (2014) [3] R. Almeida et al., J. Phys. Energy, Vol 6, p.015020 (2024)

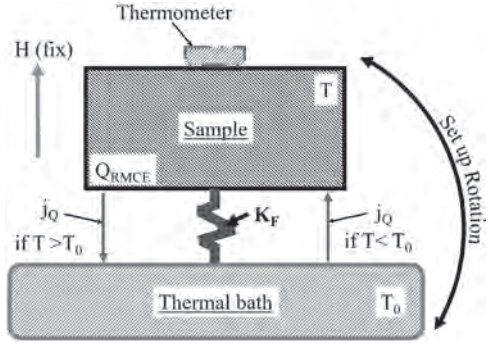

Fig. 1 Schematization of the experimental set up composed of a thermometer on a sample held in a nylon net and a sample holder.

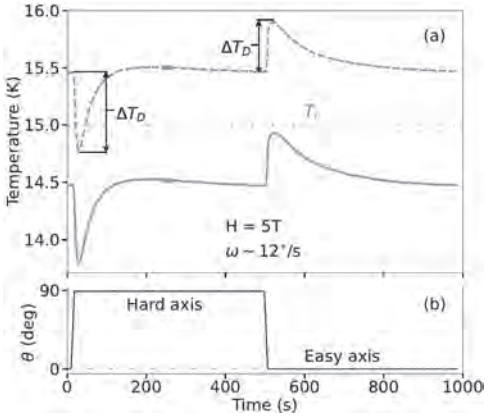

Fig. 2 (a) Two direct measurement of the RMCE of $TmMnO_3$ sample with the definition of ΔT_D. The error on the data is represented by a few bars around 250s. (b) Rotation sequence of the measurements.

DF-06. Enhancing Magnetocaloric Properties of Ni-Mn-In by Sn Doping. *S. Aksoy Esinoglu*[1] and M. Acet[2] *1. Physics Engineering Department, Istanbul Technical University, Istanbul, Turkey; 2. Faculty of Physics, Duisburg-Essen University, Duisburg, Germany*

Ferromagnetic Ni-Mn-In based Heusler alloys exhibit a first-order structural transformation that leads to various properties, including magnetic shape memory, magnetic field-induced strain, and reverse magnetocaloric effects [1]. When Sn is doped to $Ni_{50}Mn_{34}In_{16}$, the valence electron concentration increases without changing the martensite transition temperature (M_S) and the Curie temperature T_C. The total entropy change at the transition ΔS of the Sn-doped Heusler alloy becomes nearly 20.6 J $kg^{-1}K^{-1}$. The adiabatic temperature change ΔT_{ad} is nearly -6.5 K when an applied magnetic field is increased from 0 to 5 T, and it is nearly 5 K when the magnetic field is decreased from 5 to 0 T as shown in the Fig. 1. The isothermal magnetization curves display significant hysteresis when the magnetic field is applied and removed. We report on the temperature dependence of ferromagnetic resonance in this material in both the martensite and austenite states to investigate the magnetic properties around the transformation region [2]. Our findings reveal that below M_S both ferromagnetic and anti-ferromagnetic interactions are present which gives rise to magnetocaloric properties.

[1] T. Krenke, E. Duman, M. Acet et al., Phys. Rev. B, 75, 104414 (2007). [2] S. Aksoy, O. Posth, M. Acet et at., Journal of Physics: Conference Series, 200, 092001 (2010).

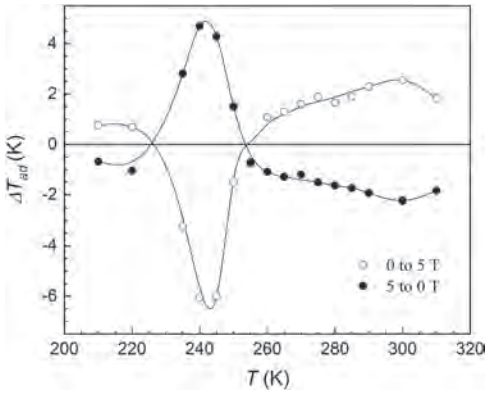

Fig. 1. The adiabatic temperature change induced by a magnetic field change of 5 T of $Ni_{50}Mn_{34}In_{15}Sn_1$. Hollow and full circles represent measurements in increasing and decreasing field. Prior to each measurement, the sample was taken initially to 210 K.

DF-07. Prospects and Challenges: Magnetic-field-assisted Direct Ink Writing of Magnetocaloric Heat Exchange Structures. V. Sharma[1], K. Bhandari[1], H. Zhao[1] and *R. Barua*[1] *1. Mechanical and Nuclear Engineering, Virginia Commonwealth University, Richmond, VA, United States*

Magnetic heat pumping (MHP) is an energy-efficient, eco-friendly alternative to traditional vapor-compression technologies; however, manufacturing challenges persist, particularly in shaping the brittle magnetocaloric alloys into thin-walled structures essential for effective heat transfer in an active magnetic regenerator AMR [1]. To this end, a magnetic-field-assisted direct ink writing additive manufacturing (AM) method has been developed whose novelty lies in a proprietary ink made of magnetocaloric powders, a polymer binder, and solvents optimized for shear-thinning properties essential for printing [2,3]. Acting as a sacrificial binding agent, the polymer initially holds the 3D-printed structure in place but is later removed using a carefully designed two-step heat-treatment process. Research on AM process development using three precursor magnetocaloric powders - $La_{0.6}Ca_{0.4}MnO_3$, $AlFe_2B_2$, and $La(Fe_xCo_ySi_{1-x-y})_{13}$ - will be discussed [4]. The effect of various process parameters, such as powder-binder ratio, the viscosity of printing ink, powder size, shape and internal porosity etc., on the geometrical and mechanical characteristics of green parts will be discussed. In addition, the effects of sintering and printing parameters on the quality of the densified magnetocaloric structures will be deliberated upon, ultimately demonstrating the feasibility of printing heat exchange structures with microchannels as small as 150 μm. These results offer insights into the process–structure-property relationships and provide guidelines for minimizing porosity and related microstructural defects in the 3D printed magnetocaloric parts. Acknowledgement: Research Funded by the VCU College of Engineering and the Venturewell Foundation E-teams Program

[1] Funk, Alexander, et al. “Getting magnetocaloric materials into good shape: Cold-working of La (Fe, Co, Si) 13 by powder-in-tube-processing.” *Materials today energy* 9 (2018): 223-228. [2] Sharma, Vaibhav, et al. “Room-temperature Polymer-assisted Additive Manufacturing of Microchanneled Magnetocaloric Structures.” *Journal of Alloys and Compounds* (2022): 165891. [3] Sharma, Vaibhav, et al. “Influence of powder feedstock characteristics on extrusion-based 3D printing of magnetocaloric structures.” *Materials Research Express* 11.4 (2024): 046101. [4] Sharma, Vaibhav. “Extrusion-based Additive Manufacturing of Magnetic Heat Exchange Structures for Caloric Applications.” (2024).

DF-08. Extending the revolutionary high entropy design concept to tune the critical crossover point of magnetocaloric materials. *J. Law*[1], Z. Tian[2,3], L.M. Moreno-Ramírez[1], V. Franco[1], F. Hu[2,3] and B. Shen[2,3,4] *1. University of Seville, Seville, Spain; 2. Beijing National Laboratory for Condensed Matter Physics & State Key Laboratory of Magnetism, Institute of Physics, Chinese Academy of Sciences, Beijing, China; 3. School of Physical Sciences, University of Chinese Academy of Sciences, Beijing, China; 4. Ningbo Institute of Materials Technology & Engineering, Chinese Academy of Sciences, Zhejiang, China*

The recent surge of interest in using the magnetocaloric effect (MCE) for gas liquefaction has increased the search for cryogenic magnetocaloric materials, revitalizing even the extensively studied systems. The classic RCo_2 Laves phase compounds (R represents a lanthanide) have been a focal point, which undergo first- (FOMT) or second-order thermomagnetic phase transitions (SOMT) depending on the R selection. Excitingly, those with R = Dy, Ho, or Er, show FOMT behavior with remarkable MCE, while those with R elements before Dy in the periodic table exhibit SOMT. Thus, the critical composition, also known as the threshold where FOMT transits to SOMT, is projected to lie between neighboring Dy and Tb in the lanthanide row of the periodic table. Magnetocaloric high-entropy alloys (HEAs) have emerged as an intriguing material family in the last five years [3,4]. They combine multiple principal elements to maximize configurational entropy for new properties. Though their MCE performance was reported suboptimal, we used a targeted search approach and unveiled the sweet spot within the vast compositional space, unlocking their MCE potential [5]. This work takes a step forward by applying the HEA concept at the R-site in RCo_2, finding a shift in the critical crossover point and a larger MCE in multiprincipal-R-Co_2 avoiding detrimental hysteresis. Exponent *n* criterion [6,7] is used for evaluating the critical point and the order of thermomagnetic phase transition, settling long-standing controversies in the reports for RCo_2 family. The findings reveal new compositions within the Laves phase family and mark a significant shift in HEA design methodology away from the conventional focus on the center of the multiprincipal elements phase diagram. Supported by the Clean Hydrogen Partnership, HyLICAL project (Grant no. 101101461), the European Innovation Council via project CoCoMag (Grant no. 101099736), the Research Council of Norway within LIQUID-H project, EMERGIA 2021 fellowship (Ref. EMC21_00418) from Junta de Andalucia and the Chinese Academy of Sciences President’s International Fellowship Initiative (PIFI) for visiting scientists (Grant No. 2024VMA0021, 2024VMC0006).

[1] C. Romero-Muñiz, J.Y. Law, et al., The Innovation Materials, 1(3) (2023) 100045. https://doi.org/10.59717/j.xinn-mater.2023.100045 [2] J.Y. Law, V. Franco, Handbook on the Physics and Chemistry of Rare Earth Elements, Volume 64 (2023) 175-246. *Commemorative Volume to V.K. Pecharsky*. https://doi.org/10.1016/bs.hpcre.2023.10.004 [3] J.Y. Law, V. Franco, Journal of Materials Research, 38(1) (2023) 37-51. https://doi.org/10.1557/s43578-022-00712-0 [4] J.Y. Law, V. Franco, APL Materials, 9(8) (2021) 080702. https://doi.org/10.1063/5.0058388 [5] J.Y. Law, Á. Díaz-García, et al., Acta Materialia 212 (2021) 116931. https://doi.org/10.1016/j.actamat.2021.116931 [6] J.Y. Law, V. Franco, et al., Nature Communications, 9(1) (2018) 2680. https://doi.org/10.1038/s41467-018-05111-w [7] V. Franco, J.Y. Law, et al., Journal of Physics D: Applied Physics, 50(41) (2017) 414004.

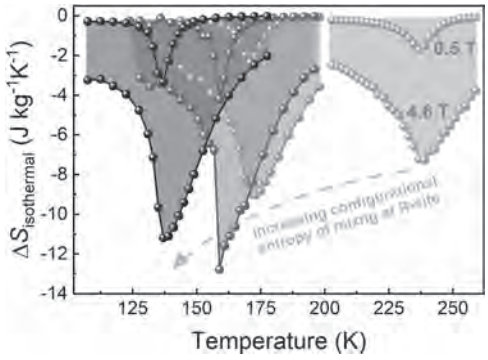

MCE of multiprincipal-R-Co_2

DF-09. Field induced change in the behavior of magnetic transition in Eu_2In. *A. Kumar*[1], A. Biswas[1] and Y. Mudryk[1] *1. Material Science Division, Ames National Laboratory, USA, Ames, IA, United States*

The R_2In (R = rare earth) compounds have attracted the scientific community in recent years due to their intriguing changes in crystal structure and magnetic response. In this family, R = Eu and Pr are of particular interest due to their large magnetic entropy change (ΔS_M) at the first-order ferromagnetic (FM) to paramagnetic (PM) transitions, even with a small change in the magnetic field (ΔH), making them interesting candidates for magnetocaloric applications [1, 2]. Surprisingly, the magnetocaloric response of these compounds deteriorates at higher fields, where the rate of increase in the maximum magnetic entropy change (ΔS_M^{max}) decreases for ΔH > 2-3T. Recent theoretical investigations predict a field-induced change from the first-order to the second-order nature of FM to PM transition in Eu_2In for H > 2.5T [3]. In the present study, we thoroughly investigate the magnetization and specific heat of Eu_2In across the FM to PM transition in applied magnetic fields up to 7 T. A notable change in the behavior of the field exponent of magnetic entropy (*n*) and the rate of dispersion in the universal master curve of $\Delta S_M(H, T)$ data has been observed at this critical magnetic field of H_C = 2.5T, in agreement with theory [3]. The specific heat measurements show a clear splitting of the zero-field sharp peak into a doublet with an increase in the magnetic field. Based on the field evolution of the strength and position of these features, we propose the evolution of an additional structural transition that is decoupled from the main magnetic transitiona for H>2.5T. In addition, the specific heat measurements show significant broadening accompanied by a decrease in the strength of the peak at the magnetic phase transition with an increase in the magnetic field. Following this observation, we use three different approaches to examine the robustness of the first-order nature of this phase transition in the high-field regime using the magnetization measurements. The overshot of *n* above 2, dispersion of the scaling behavior, and nonlinearity in the modified Arrott plots, even for H = 60-70 kOe magnetic fields, clearly indicate the overall first-order nature of this phase transition up to 70 kOe.

[1] F. Guillou, A. K. Pathak, D. Paudyal, Y. Mudryk, F. Wilhelm, A. Rogalev, and V. K. Pecharsky, Non- hysteretic first-order phase transition with large latent heat and giant low-field magnetocaloric effect, Nat Commun 9, 2925 (2018). [2] A. Biswas, N. A. Zarkevich, A. K. Pathak, O. Dolotko, I. Z. Hlova, A. V. Smirnov, Y. Mudryk, D. D. Johnson, and V. K. Pecharsky, First-order magnetic phase transition in Pr_2In with negligible thermomagnetic hysteresis, Phys. Rev. B *101*, 224402 (2020). [3] B. P. Alho, P. O. Ribeiro, P. J. Von Ranke, F. Guillou, Y. Mudryk, and V. K. Pecharsky, Free-energy analysis of the nonhysteretic first-order phase transition of Eu_2In, Phys. Rev. B 102, 134425 (2020).

DF-10. Transition from Ferromagnetic to Noncollinear to Paramagnetic State with Increasing Ru Concentration in FeRu Films. *J. Lisik*[1], M. Rojas[1], S. Myrtle[1], D.H. Ryan[2], R. Hübner[3], P. Omelchenko[1], C. Abert[4], A. Ducevic[4], D. Suess[4], I. Soldatov[5], R. Schaefer[5], J. Seyd[6], M. Albrecht[6] and E. Girt[1] *1. Department of Physics, Simon Fraser University, Burnaby, BC, Canada; 2. Physics Department and Centre for the Physics of Materials, McGill University, Montreal, QC, Canada; 3. Institute of Ion Beam Physics and Materials Research, Helmholtz-Zentrum Dresden-Rossendorf, Dresden, Germany; 4. Physics of Functional Materials, University of Vienna, Vienna, Austria; 5. Leibniz Institute for Solid State and Materials Research Dresden, Dresden, Germany; 6. Institute of Physics, University of Augsburg, Augsburg, Germany*

Fe, having the largest room-temperature saturation magnetization of all elements, is a crucial component of magnetic devices. Thin-film magnetic devices make extensive use of not only Fe but also Ru layers. Thus, it is important to understand how the presence of Ru in Fe affects the magnetic and structural properties of Fe. X-ray diffraction and transmission electron microscopy show that the crystal structure of our $Fe_{100-x}Ru_x$ films is predominantly body-centered cubic (bcc) for x<13 and gradually transitions to hexagonal close-packed (hcp) in the range of approximately 13≤x≤20. We found that the hcp phase is paramagnetic while the bcc phase is magnetic. The magnetic properties of the bcc phase in our films were characterized by Mössbauer spectroscopy, magnetometry, magneto-optical Kerr effect microscopy, and Lorentz transmission electron microscopy. Despite significant in-plane shape anisotropy, the magnetic moments in $Fe_{100-x}Ru_x$ films with 4≤x≤18.5 are not bound to the film plane at zero external magnetic field. Instead, there are large out-of-plane magnetization components distributed both above and below the film plane. Figure 1 shows the evolution of the *M(H)* measurements as Ru is added to Fe. The remanent-to-saturation magnetization ratio, M_r/M_s, quickly decreases from 0.96 for a single Fe layer to 0.32 for $Fe_{92}Ru_8$, while the saturation field increases with concentration of Ru in Fe. The presence of large out-of-plane magnetization components, high saturation fields, and low M_r/M_s observed in our films suggest that bcc FeRu has noncollinear magnetic order. We use a simple atomistic model to show that noncollinear order in cubic FeRu structures can be induced by the competition between ferromagnetic Fe-Fe coupling and antiferromagnetic coupling between Fe atoms separated by Ru atoms. The simulation results, as shown in Fig. 2 for $Fe_{90}Ru_{10}$, are in agreement with our experimental findings.

(J. Lisik, M. Rojas), S. Myrtle, et al., Phys. Rev. B, Vol. 110, p.104429 (2024).

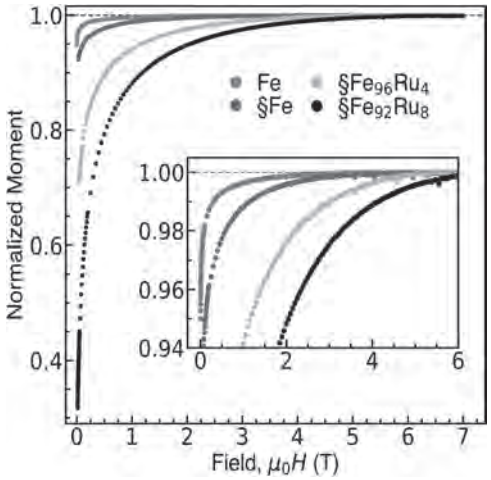

Fig. 1: Normalized *M(H)* measurements with magnetic field applied in-plane of a single Fe layer and of §$Fe_{100-x}Ru_x$ (x = 0, 4, 8), where the § signifies that the layer is grown on top of Ta │ Ru and capped with Ru.

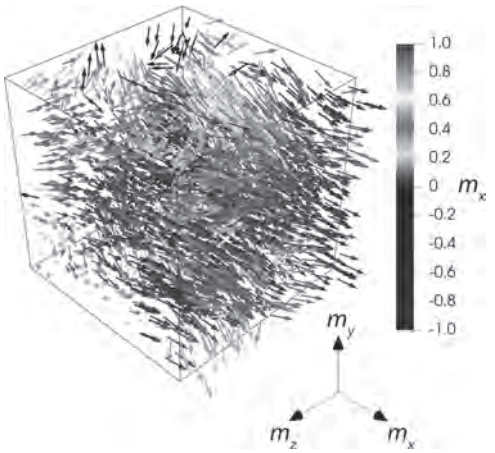

Fig. 2: Simulated magnetic moment distribution of an $Fe_{90}Ru_{10}$ film after magnetic field along x-axis is removed.

DF-11. Magnetic Field-Induced Thermal Behavior and Sedimentation of Strontium Ferrite-PDMS Composites for Actuator Applications.

M. Islam[1], M. Kashem[2], W. Li[2] and W. Geerts[1,3] *1. MSEC, Texas State University, San Marcos, TX, United States; 2. Chemical Engineering, Texas Tech University, Lubbock, TX, United States; 3. Physics, Texas State University, San Marcos, TX, United States*

Abstract: Magnetic composite polymers combine the properties of both magnets and polymers, which enables the production of complex-shaped magnetic components. These materials have potential applications ranging from microfluidics to vibration dampers, actuators, and minimally invasive medical devices because, with an applied magnetic field, they can change shape precisely, quickly, and consistently. Our study investigates the dispersion of strontium ferrite particles ($SrO(Fe_2O_3)_6$) suspended in the polydimethylsiloxane (PDMS) matrix and how that is effected by gravity, an applied magnetic field, or vacuum. The time-dependent behavior of composites in a magnetic field during the curing process was also explored. Particle density and orientation in the cured composite were determined from hysteresis curves measured with a MicroSense EZ9 VSM. A punching tool was used to take samples from a 40-mm-long cylindrical sample. We found well-distributed strontium ferrite (SF) particles in PDMS when curing the composite without a magmatic field. However, during curing in the presence of a magnetic field provided by a Halbach cylinder, the particles align along the field lines, leaving a clear SF particle-depleted PDMS layer on the surfaces. A similar effect was observed when the suspension was cured in vacuum, while very little sedimentation due to gravity was reported. Furthermore, the time-dependence of the magnetic moment vector in an applied magnetic field during the curing process was measured using the method of Ahmed [1]. The magnetic moment transient as a function of curing time and temperature was measured with the biaxial VSM. At lower temperatures, the transient had a small time constant due to the lower dynamic viscosity of the uncured specimen. Hysteresis analysis and time-dependent studies after various temperature treatments showed a notable change in curing at approximately 55 °C, indicating the transition from a magneto-rheological fluid to a magnetorheological elastomer. The fraction of SF particles and saturation magnetization were correlated, while coercivity was field-angle independent and remanence was field-angle-dependent. This work was in part supported by NSF (grant 2216440).

[1] Tanjina N. Ahmed et al. AIP Adv. 13, 025024 (2023).

DF-12. Direct determination of carrier parameters in indium tin oxide nanocrystals using concepts from magnetoplasmonics.

A. Gabbani[1,2], E. Della Latta[1], X. Li[3], M. Kociak[3], M. Geppi[1], S. Borsacchi[4] and *F. Pineider*[1,2] *1. Department of Chemistry and Industrial Chemistry, University of Pisa, Pisa, Italy; 2. Department of Physics and Astronomy, University of Florence, Sesto Fiorentino (FI), Italy; 3. Laboratorie de Physique des Solides, University of Paris-Saclay, Orsay, France; 4. ICCOM, CNR, Pisa, Italy*

Indium Tin Oxide (ITO) is the prototype conductive oxide, which has recently gathered interest in nano-optics,[1] owing to the excellent plasmonic properties displayed by ITO nanocrystals (NCs) in the infrared spectral region. Unlike noble metals, the plasmonic resonance frequency in spherical ITO NCs can be tuned synthetically by controlling the tin content.[2] Nanostructuration typically introduces several challenges in the characterization of electronic parameters in NCs, hampering advanced material design. Indeed, while films of doped oxides are routinely studied through electrical experiments, these cannot be reliably applied to NCs, since the insulating ligand layer forces charge hopping and results in a complex behaviour. Moreover, the surface potential creates a depletion region near the surface, which typically requires core@shell models with a purely dielectric shell to fit the extinction spectrum.[3] In this work,[4] we present an integrated approach (Figure 1) based on magneto-optics, single-particle Electron Energy Loss (EELS) spectroscopy and ^{119}Sn Solid State Nuclear Magnetic Resonance (SSNMR) spectroscopy to extract the fundamental electronic parameters of a series of ITO NCs with variable tin doping. Our methodology overcomes the limitations of standard fitting approaches based on extinction spectroscopy, which can only determine the ratio between carrier density and mass. Conversely, exploiting concepts from magnetoplasmonics[5,6] we determined the carrier effective mass directly on the NCs, discarding the use of literature values. The effective mass was found to deviate from the parabolic approximation at high carrier density. This approach can be generalized to other plasmonic heavily-doped semiconductor nanostructures and represents, to the best of our knowledge, the only method to date to characterize the full Drude parameter space of 0-D nanosystems. This research has received funding from the EU through Horizon 2020 program (grant agreement No. 823717 –ESTEEM3), and from the MUR through PRIN Project 2017CR5WCH Q-Chiss.

[1] A. Agrawal, *et al.*, Chem. Rev., Vol. 118 (6), p. 3121 (2018,) [2] A. Mazzotta, *et al.*, ACS Appl. Mater. Interfaces, Vol. 14 (30), p. 35276 (2022) [3] S. L. Gibbs, *et al.,* Acc. Chem. Res., Vol. 52 (9), p. 2516 (2019) [4] A. Gabbani, *et al.*, ACS Nano, Vol. 1, p. 15139 (2024) [5] A. Gabbani, *et al.*, Nano Lett., Vol. 22 (22), p. 9036 (2022) [6] A. Gabbani, *et al.*, J. Appl. Phys., Vol. 129 (21), p. 211101 (2021)

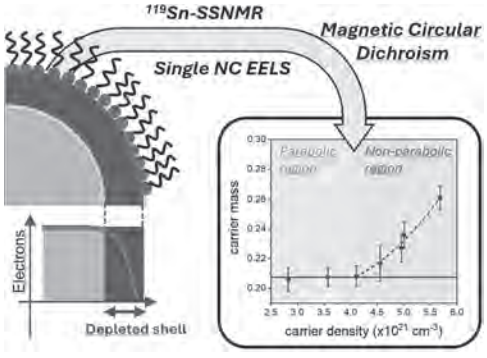

Figure 1: The multitechnique approach employed to extract the relation between carrier mass and carrier density in a series of chemically prepared ITO NCs with variable Sn content.

DF-13. Modelling of Nonlinear Magneto-Thermo-Mechanical Behaviour of Magnetostrictive Materials Subjected to Prestress and Thermal Load. *S. Somavarapu*[1], P. Kondaiah[1] and K. Deepak[2] *1. Mahindra University, Hyderabad, India; 2. Indian Institute of Technology (BHU) Varanasi, Varanasi, India*

Magnetostrictive material is a type of smart materials by the coupling of magnetic, mechanical and thermal ferroic orders. These materials exhibit the villari effect and conversely joule effect. The nonlinear magnetostrictive material properties are enabling the different applications like sensor, actuator including vibrational energy harvesting applications. Metglas is soft ferromagnetic nonlinear magnetostrive material stands out due to high magnetic saturation point comparing with other magnetostrictive materials, and its low cost which makes the suitable for mass production and cost-effective battery-powered solutions. The nonlinear magnetostrictive material properties, such as magnetization and total strain which comprising of magnetostrictive strain and mechanical strain developed by external magnetic field, prestress and temperature which needs to be characterized effectively for Metglas. Considering that, the present work focuses on investigating these nonlinear magnetostrictive properties of Metglas using combined multiloading of prestress and temperature along with the external magnetic field using finite element method. A three-dimensional magnetostrictive material is adopted and further implemented with user defined nonlinear constitutive relations to investigate the magnetostrive behaviour under magneto-thermo-mechanical loadings using COMSOL Multiphysics. Prior to conduct the present study the analytical nonlinear constitutive models of magneto-thermo-mechanical magnetostrictive material are modelled and validated with good agreement. The results showed that the magnetostrictive strain increases from 39.7 ppm to 45.2 ppm by increasing the compressive stresses from 0 MPa to -40 MPa and 39.7 ppm to -110 ppm by increasing temperature from 0°C to 80°C respectively. The developed Finite Element Model is used to predict the material parametric and stimulation parametric study to find and optimize the Metglas magnetostrictive material under magneto-thermo-mechanical loading.

V. S. Elakkiya, S. Sudersan, and A. Arockiarajan, "Stress-dependent nonlinear magnetoelectric effect in press-fit composites: A numerical and experimental study," *European Journal of Mechanics - A/Solids*, vol. 93, p. 104536, May 2022, doi: 10.1016/j.euromechsol.2022.104536. X. Liu and X. Zheng, "A nonlinear constitutive model for magnetostrictive materials," *ACTA MECH SINICA*, vol. 21, no. 3, pp. 278–285, Jun. 2005, doi: 10.1007/s10409-005-0028-8. X. J. Zheng and L. Sun, "A nonlinear constitutive model of magneto-thermo-mechanical coupling for giant magnetostrictive materials," *Journal of Applied Physics*, vol. 100, no. 6, p. 063906, Sep. 2006, doi: 10.1063/1.2338834. X. Gao, Y. Pei, and D. Fang, "Experimental Study on Magneto-thermo-mechanical Behaviors of Terfenol-D," *JMMP*, vol. 4, no. 6, pp. 652–657, 2010, doi: 10.1299/jmmp.4.652.

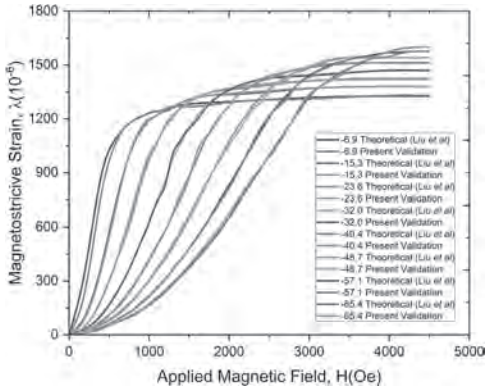

Fig.1. Validation of magnetostrictive starin for prestress along with magnetic field with theoretical results of Liu *et al*

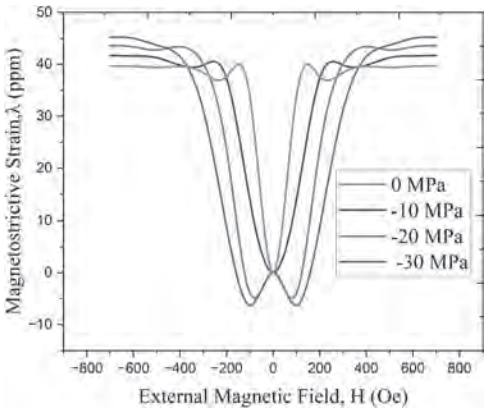

Fig.2. Variation of Magnetostrictive starin for combined magnetic field and prestress

Session DG
THIN FILMS, MULTILAYERS, AND EXCHANGE BIAS SYSTEMS I

Sarah Watzman, Chair
University of Cincinnati, Cincinnati, OH, United States

CONTRIBUTED PAPERS

DG-01. Magnetotransport properties of epitaxial films and Hall bar devices of $Sr_3Ru_2O_7$. P. Ngabonziza[1,2], A. Sharma[1], A. Scheid[3], *S. Sajeev*[1], P. A. van Aken[3] and J. Mannhart[3] *1. Physics and Astronomy, Louisiana State University, Baton Rouge, LA, United States; 2. Physics, University of Johannesburg, Auckland Park, South Africa; 3. Max Planck Institute for Solid State Research, Stuttgart, Germany*

The perovskite structured strontium ruthenates of the Ruddlesden-Popper family ($Sr_{n+1}Ru_nO_{3n+1}$) are a class of materials in the realm of 4d transition metal oxides that are attractive for both fundamental and applied research. The physics of these materials is remarkably rich for it exhibits interesting electric and magnetic properties and are peculiar among strongly correlated electron systems. There are several reported studies on the novel properties of these systems (on single crystals and thin films), but fewer attempts have been made on epitaxially grown phase-pure thin films and especially on devices of $Sr_3Ru_2O_7$ and $Sr_4Ru_3O_{10}$[1][2]. In this presentation, I will discuss our recent results on the structural and magnetotransport properties of epitaxially grown $Sr_3Ru_2O_7$ thin films and Hall bar devices patterned side by side on the same film[3]. This approach is advantageous over single crystal samples since a comparative study of transport properties could be done on the same film that were grown under similar conditions. Firstly, we optimized the pulsed laser deposition growth conditions to obtain the phase pure films of $Sr_3Ru_2O_7$. Structural properties investigated by X-ray diffraction and STEM revealed that these epitaxial films are phase pure [Fig.1]. Secondly, we performed magnetization measurements on these films which revealed no sign of ferromagnetic transition in the entire measured temperature range [Fig.2]. Thirdly, we fabricated several Hall bar devices of several widths of the active channel on which we performed electronic transport measurements. These revealed an inverse relation of the sheet resistance with active channel width. Lastly, from comparative magnetoresistance measurements performed on thin films and Hall bar devices for field along c-axis, a positive magnetoresistance of 10% was measured for unpatterned films, whereas for Hall bar devices of channel widths of 10 and 5 μm, MR values of 40% and 140% were measured respectively. These films showed switching behaviors from positive to negative MR that are controlled by the direction of the applied magnetic field.

[1]. P. B. Marshall, K. Ahadi, H. Kim, and S. Stemmer, Phys. Rev. B 97, 155160 (2018) [2]. W. Tian, J. H. Haeni, D. G. Schlom, E. Hutchinson, B. L. Sheu, M. M. Rosario, P. Schiffer, Y. Liu, M. A. Zurbuchen, and X. Q. Pan, Appl. Phys. Lett. 90, 022507 (2007). [3]. P. Ngabonziza, A. Sharma, A. Scheid, S. Sajeev, P. A. van Aken, and J. Mannhart, Phys. Rev. Mater. 8, 044401 (2024).

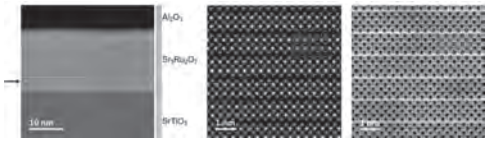

STEM image of $Sr_3Ru_2O_7$ in [100] zone axis orientation[3].

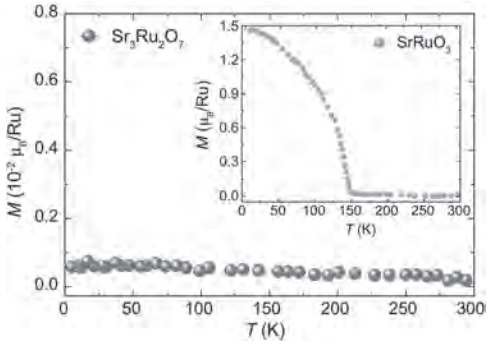

Magnetization vs Temperature graph of $Sr_3Ru_2O_7$ film. Inset-Magnetization data of $SrRuO_3$[3]

DG-02. Fast spin precession in ferrimagnetic Mn_4N thin films with perpendicular magnetic anisotropy. *S. Granville*[1,2] and Y. Zhang[1] *1. Robinson Research Institute, Victoria University of Wellington, Wellington, New Zealand; 2. MacDiarmid Institute for Advanced Materials and Nanotechnology, Wellington, New Zealand*

Ferrimagnets composed of two antiferromagnetically-coupled magnetic sublattices have attracted much attention recently due to the easily controlled and detected net magnetization and a fast magnetic dynamic behavior [1]. In particular, ferrimagnetic thin films with perpendicular magnetic anisotropy (PMA) show great potential for high-density spintronics devices [2]. Currently, most work focuses on rare earth-transition metal ferrimagnetic alloys such as GdFeCo and TbCo. However, the magnetization of these materials is sensitive to temperature and composition [3]. Antiperovskite Mn_4N is a rare-earth-free ferrimagnet with PMA, high thermal stability (T_C = 740 K), high spin polarization and low saturation magnetization, all highly attractive qualities for practical spintronics devices [4]. Crystalline thin films of Mn_4N have previously been deposited on MgO substrates, however there is a large lattice mismatch of -6% [5]. Here, we introduced a Pd buffer layer to improve the lattice matching and perpendicular magnetic anisotropy of the Mn_4N films. We prepared stacks of MgO(substrate)/Pd(t = 0, 2 and 8 nm)/Mn_4N(80 nm)/Ta(3 nm) by reactive magnetron sputtering. The Pd buffer layer results in a higher crystalline quality Mn_4N film with lower tetragonal distortion. The magnetisation is reduced with increasing Pd buffer layer thickness, however the coercive field is increased from ~ 400 mT to ~ 800 mT [Fig. 1(b)], resulting from an enhancement of PMA from ~2.2×10^4 Jm^{-3} to 3.4×10^4 Jm^{-3}. Time-resolved magneto-optical Kerr effect measurements show a fast precessional frequency of ~100 GHz and a high damping ~ 0.2, potentially useful for fast-switching magnetic structures.

[1] S. K. Kim, G. S. D. Beach, K.-J. Lee et al., Nat. Mater. 21, 24 (2022) [2] B. Dieny and M. Chshiev, Rev. Mod. Phys. 89, 025008 (2017) [3] H. Bai, T. Xu, Y. Dong et al., Adv. Electron. Mater. 8, 2100772 (2022) [4] Z. Zhang and W. Mi, J. Phys. D: Appl. Phys. 55 013001 (2022) [5] T. Hirose, T. Komori, T. Gushi et al., AIP Adv. 10, 025117 (2020)

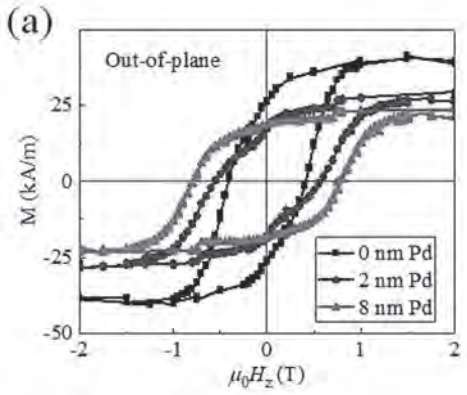

Figure 1: Pd thickness dependence of magnetization of Mn_4N in an out-of-plane magnetic field.

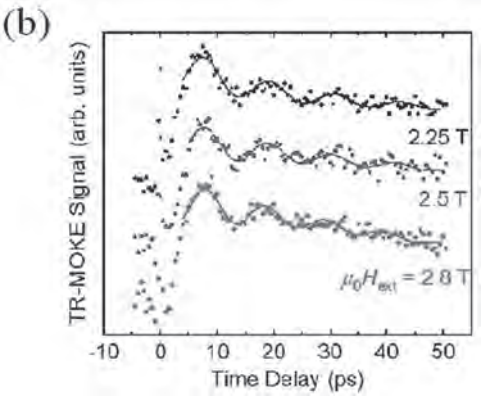

Figure 2: Time-resolved MOKE measurements of Mn_4N with optimised 8 nm Pd buffer layer.

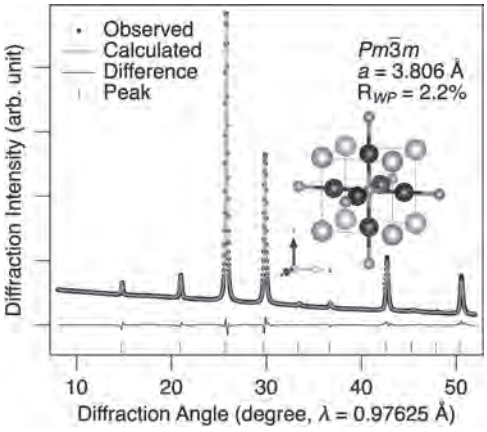

Synchrotron diffraction pattern and Lebail fit of a polycrystalline Co_3PdN thin film.

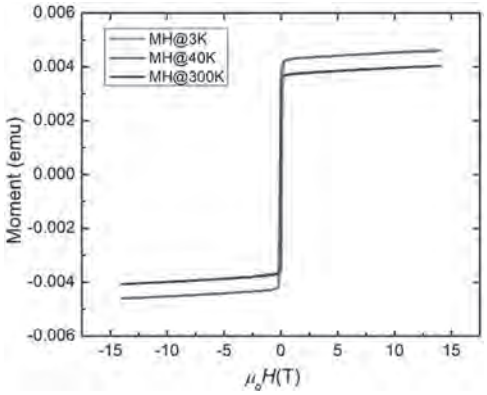

Magnetic hysteresis curves collected from a polycrystalline Co_3PdN thin film at various temperatures.

DG-03. Experimental realization of the recently predicted magnetic antiperovskite Co_3PdN. *S. Bauers[1] 1. National Renewable Energy Laboratory, Golden, CO, United States*

Nitrides of the form X_3AN (where X is a 3d metal Mn, Fe, Ni, Co) are subset of antiperovskite materials with exciting properties. Examples of magnetic antiperovskites include: Co_3FeN, which has been reported as half-metallic, Fe_3FeN (i.e., Fe_4N) and its N-vacancy ordered derivative $Fe_{16}N_2$, which is the strongest known ferromagnet, and Mn_3CuN, which exhibits a giant magnetostrictive effect. Recently, several Co-containing antiperovskites, including Co_3PdN and Co_3PtN were predicted to be stable, despite no experimental reports. We study the synthesis, stability, and magnetic properties of Co_3PdN thin films prepared using magnetron sputtering. We find that the antiperovskite structure persists across a relatively large range of Co:Pd ratios. Synchrotron X-ray diffraction from stoichiometric Co_3PdN is fit to a cubic antiperovskite structure with a lattice constant of a = 3.806 Å. Prior computational works assumed a ferromagnetic ground state, and we confirm these results by comparing the total energy of ferromagnetic Co_3PdN to several antiferromagnetic configurations, which are all at least +88 meV/atom higher in energy. Experimentally, we find that Co_3PdN is a soft magnetic material with a low-temperature (3 K) coercive field of H_C = 800 Oe. The stability of Co_3PdN is assessed using both high-temperature magnetometry and temperature-dependent X-ray diffraction. We find a Curie temperature of $T_C \approx 550$ K, and a decomposition temperature of around 600 K. We also discuss magnetotransport collected from epitaxial thin films of Co_3PdN grown on $SrTiO_3$ and MgO substrates. We compare Co_3PdN to Co_3PtN which, despite also being predicted as stable, does not adopt the antiperovskite structure. This work represents experimental confirmation of Co_3PdN antiperovskite and should motivate further study of this material's magnetoelectric functionality as well as exploration of similar Co_3AN compounds awaiting experimental realization.

DG-04. Interfacial Alloying Induced Magnetic Proximity Effect in Platinum/Dysprosium Iron Garnet Heterostructures. *M.J. Gross[1], J. Herrero-Martín[2], S. Valencia[3], A.J. Grutter[4], J. Borchers[4], Y. Choi[5], G. Fabbris[5], A. Kossak[6], A. Kaczmarek[6], S. Kundu[7], S. Ghosh[7], A. Mykhoyan[7], A. Wittmann[8] and C.A. Ross[6] 1. Electrical Engineering and Computer Science, Massachusetts Institute of Technology, Cambridge, MA, United States; 2. ALBA Synchrotron Light Source, Barcelona, Spain; 3. Helmholtz-Zentrum Berlin für Materialien und Energie, Berlin, Germany; 4. NIST Center for Neuron Research, National Institute of Standards and Technology, Gaithersburg, MD, United States; 5. Advanced Photon Source, Argonne National Laboratory, Argonne, IL, United States; 6. Materials Science and Engineering, Massachusetts Institute of Techonology, Cambridge, MA, United States; 7. Chemical Engineering and Materials Science, University of Minnesota, Twin Cities, MN, United States; 8. Physics, Johannes Gutenberg University Mainz, Mainz, Germany*

The magnetic proximity effect (MPE) contributes to the magnetic behavior of heavy metal/magnetic insulator heterostructures. MPE influences a range of spin transport phenomena emphasizing its relevance to spintronic device applications. The existence and origins of MPE in heavy metals interfaced with insulating rare earth iron garnets (REIGs) has been controversial due to the low ferrimagnetic moment of REIGs and the presence of roughness and intermixing at the interface [1],[2]. Previously, we reported MPE in a 9 nm sputtered Pt layer grown without breaking vacuum ("in-situ" growth) atop a layer of dysprosium iron garnet ($Dy_3Fe_5O_{12}$, DyIG) [3]. Polarized neutron reflectometry (PNR) measured across the compensation temperature of DyIG showed a magnetic signal within the top 9 nm thick Pt grown that scaled with the DyIG net moment. However, no x-ray magnetic circular dichroism (XMCD) was detected in the Pt L_2 edge, which was initially

attributed to the interfacial location of the induced magnetic moment and averaging over the 9 nm thick layer. To clarify the origin of the magnetic signal, we measured XMCD at the Fe L_3 edge. Comparison of the XMCD spectra obtained at different temperatures reveal a metallic Fe magnetic signature present at 15 K, see Fig 1. We propose that the source of the magnetic signal within the Pt layer is a FePt alloy created at the interface due to intermixing. The PNR data is consistent with this interpretation if an interfacial FePt alloy is considered in which the magnetization originates from 3.5% Fe intermixed within the first 4 nm of the Pt layer, Fig 2. Transport of Ions in Matter simulations confirm the plausibility of intermixing originating from bombardment by high energy Pt and Ar atoms during the film growth process. These results underscore the influence of film growth on interface structure and magnetic properties.

[1] Y. M. Lu et al., Phys Rev Lett 110, 147207 (2013). [2] S. Geprägs et al., ArXiv:1307.4869 [Cond-Mat.Mtrl-Sci] (2013). [3] J. J. Bauer et al., Phys Rev B 104, 094403 (2021).

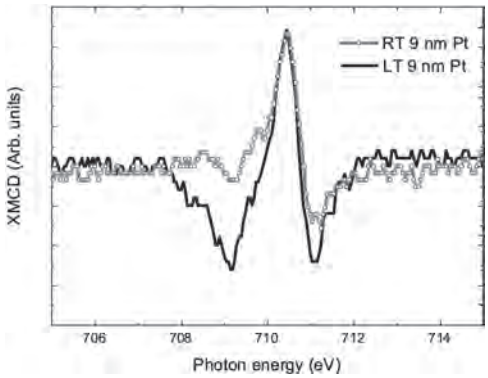

XMCD of the Fe L3 edge taken at 15 K (LT) and 300 K (RT) of the 9 nm Pt/DyIG sample. The LT XMCD curve has been inverted to compare to the RT curve.

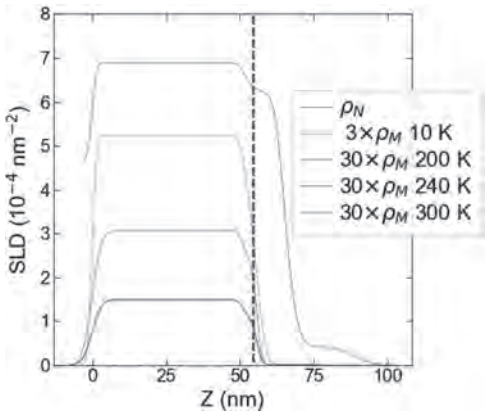

PNR scattering length density: magnetization ρ_M at 10 K, 200 K, 240 K, and 300 K as well as density ρ_N vs depth. Dashed blue line represents the interface between the DyIG and Pt.

DG-05. Co/Gd-based Synthetic Ferrimagnets with PMA for Magneto-Photonic Integration: Growth, Magnetostatics and Modeling.

T.J. Kools[1], J. Hintermayr[1], B. Koopmans[1] and R. Lavrijsen[1] *1. Applied Physics, Eindhoven University of Techology, Eindhoven, Netherlands*

Synthetic ferrimagnets (sFiMs) with perpendicular magnetic anisotropy (PMA) based on Co and Gd exhibit a host of fascinating physical phenomena like all-optical switching of the magnetization[1], fast domain-wall motion [2], and therefore are a candidate for integrated magneto-photonics [3]. Adding to all the progress that has been made in demonstrating their applicability, we will show that there are also still several interesting physical questions remaining in the magnetostatics of this kind of ultrathin system, with the proximity induced magnetization at the Co/Gd-interface taking center stage. This becomes apparent when we consider the simplest Co-Gd-Based sFiM with PMA: the Pt/Co/Gd trilayer. In Fig. 1, we show a scan of the polar MOKE remanence of a typical Pt/Co/Gd sample where, in orthogonal directions, we vary the thickness of the Co- and Gd layer. With increasing Co-thickness, we observe the non-magnetic to OOP to in-plane regimes for the magnetization typical for the Pt/Co system. However, the behavior as a function of Gd thickness is not trivial, showing its impact on the magnetic properties far beyond the thicknesses where one would expect the morphology of the Co/Gd interface to still be affected, but also a significantly decreasing effective anisotropy in the ultrathin regime, and compensation. In this contribution, we will unravel this interesting magnetostatic behavior, which we believe to be caused by two distinct phenomena. Namely, the interplay between sputter-induced intermixing, and changes in the global Curie temperature with increasing Gd thickness. We will discuss the extensive MOKE and SQUID experiments we have done to substantiate this claim, and support it with kinetic simulations describing the growth (Fig. 2) and an analytical model describing the induced magnetization at the Co/Gd interface. In short, we will shed light on the physics governing the magnetic behavior of ultrathin SFiMs and demonstrate how the Gd thickness may be used as a knob to tune its basic properties.

[1]: M. Lalieu, M, Peeters, S. Haenen *et al*., *Phys. Rev. B*., Vol. 96, p.220411 (2017) [2]: P. Li, T. Kools, B. Koopmans *et al*., *Adv. Electron. Mater.*, Vol. 9, p.200613 (2023) [3]: H. Pezeshki, P. Li, R. Lavrijsen *et al.*, *Phys. Rev. App.*, Vol. 19, p.054036 (2023)

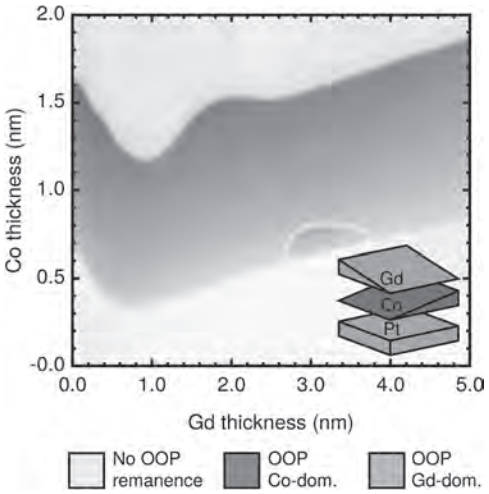

Fig 1: Polar MOKE measurement of the remanence of a Pt/Co(y)/Gd(x) bilayer sample.

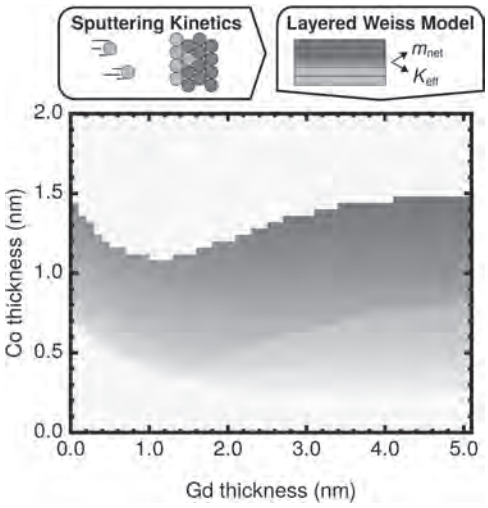

Fig. 2: Schematic overview of the simulation procedure addressing sputter-induced intermixing and a typical resulting phase diagram.

DG-06. Skyrmions in Biased Ferromagnetic and Antiferromagnetic Coupled Multilayers. *E. Darwin*[1], R. Tomasello[2], M. Carpentieri[2], G. Finocchio[3] and H.J. Hug[1,4] *1. Empa, Zurich, Switzerland; 2. Politecnico di Bari, Bari, Italy; 3. University of Messina, Messina, Italy; 4. University of Basel, Basel, Switzerland*

Synthetic antiferromagnets (SAFs) are an attractive and advantageous material platform, promising to improve the performance of spintronic devices[1]. When placing a non-magnetic spacer between two ferromagnetic (FM) materials, the FM layers can experience interlayer exchange coupling (IEC)[2]. Particular spacers, such as Ir and Ru, cause either FM or antiferromagnetic (AFM) coupling depending on their thickness, via the Ruderman–Kittel–Kasuya–Yoshida (RKKY) interaction[3]. AFM-IEC promotes the formation of a SAF. SAFs are appealing for device applications such as spin orbit torque magnetoresistive random access memory (SOT-MRAM) and skyrmion applications due to the suppression of the skyrmion Hall effect (SkHE)[4]. Recent studies have experimentally stabilized skyrmions in SAFs being driven with smaller current densities than their FM counterparts and with a negligible SkHE[5,6]. In this work, we advance the knowledge of SAF systems and test the limits of the SAF when coupling together different amounts of magnetic material or when increasing number of repetitions[7]. We use this knowledge to design a SAF bias layer, consisting of two Co layers, to be more robust and stable against external fields. This SAF bias layer was used to bias skyrmions in a ferromagnetic multilayer, the sample as shown in Figure 1a. Figure 2a shows an MFM image of dense skyrmions of around 75 nm in diameter at 0 mT. This method was also used to bias the multilayer SAF as shown in Figure 1a. Figure 2b shows an MFM image of less dense skyrmions of around 40 nm at 0 mT. The skyrmions in the multilayer SAF have low contrast compared to the FM multilayer, indicative of their SAF nature. This research paves the way for more efficient and practical applications of SAF skyrmions in future spintronic devices.

[1] R. A. Duine, et al., Synthetic antiferromagnetic spintronics, Nat. Phys. 14 (2018) 217–219. [2] P. Bruno, Theory of interlayer magnetic coupling, Phys. Rev. B 52 (1995) 411–439. [3] K. Yosida, Magnetic properties of Cu-Mn alloys, Phys. Rev. 106 (1957) 893–898. [4] X. Zhang, et al., Magnetic bilayer-skyrmions without skyrmion Hall effect, Nat. Commun. 7 (2016) 10293. [5] T. Dohi, et al., Formation and current-induced motion of synthetic antiferromagnetic skyrmion bubbles, Nat. Commun. 10 (2019) 5153. [6] V. T. Pham, et al., Fast current-induced skyrmion motion in synthetic antiferromagnets, Science 384 (2024) 307-312. [7] E. Darwin, et al., Antiferromagnetic interlayer exchange coupled Co68B32/Ir/Pt multilayers, Sci. Rep. (2024) 1–10.

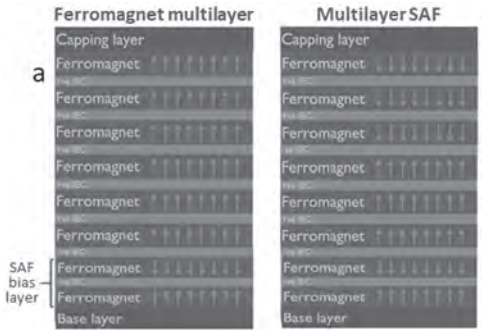

Figure 1: a) FM multilayer with six repetitions, biased via a two repetition SAF. Two three-repetition multilayers coupled together antiferromagnetically, biased via a two repetition SAF.

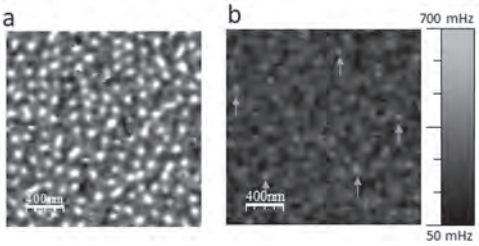

Figure 2: a) MFM image of the ferromagnetic multilayer showing a skyrmion lattice at 0 mT. b) Multilayer SAF MFM image showing skyrmions (some examples indicated with an arrow) at 0 mT. Both images are on the same contrast scale.

DG-08. Effect of oxygen pressure and layer thickness on the magnetic properties of iron garnet superlattices. *T.P. Grossmark*[1], A.C. Kaczmarek[1], B. Khurana[1] and C.A. Ross[1] *1. The Department of Materials Science and Engineering, The Massachusetts Institute of Technology, Cambridge, MA, United States*

Complex oxide multilayers can exhibit a wide variety of rich magnetic phenomena, yet there have been few reports of the synthesis or properties of garnet superlattices with layer thicknesses approaching the unit cell dimension of 1.2 nm [1]. We recently synthesized superlattices made from rare earth (RE = Tm, Tb, Eu, Lu) iron garnets (IGs) using pulsed laser deposition. Atom probe tomography and transmission electron microscopy revealed composition modulation without dislocations, and layer thicknesses as low as 0.45 nm, less than half a unit cell. TmIG/TbIG superlattices exhibit perpendicular magnetic anisotropy that is qualitatively different from the in-plane anisotropy of the solid solution. [2]. In this work, we describe the role of oxygen pressure on the structure and magnetic properties of garnet superlattices. In-situ reflection high energy electron diffraction during growth was used to evaluate the surface roughness and to demonstrate sub-unit cell layer by layer growth. Lower growth pressures lead to improved interface sharpness and multilayer quality in TbIG/TmIG superlattices, evident from the lower surface roughness, higher intensity satellite peaks from X-ray diffraction and a lower coercivity hysteresis loop from vibrating sample magnetometry. This is attributed to an increase in the energy of the species arriving at the substrate. YIG/LuIG superlattices were then prepared with layer thicknesses varying from tens of nanometers to a quarter of a unit cell. YIG and LuIG have very low ferromagnetic resonance (FMR) linewidths, and the anisotropy was extracted from the field-dependence of the resonance frequency. The contributions to anisotropy were evaluated as a function of layer thickness. In particular, the growth-induced anisotropy resulting from the intermixed Y and Lu at the interfaces [3] becomes important at low layer thicknesses. By pushing the limits of multilayer thickness and quality, we demonstrate tunability of the electronic and magnetic properties of garnet heterostructures.

[1] M. Y. Chern et al., Appl. Phys. Lett. 69, 854 (1996). [2] B. Khurana et al., submitted (2024). [3] A. Kaczmarek et al, Nat. Commun. 15, 5083 (2024)

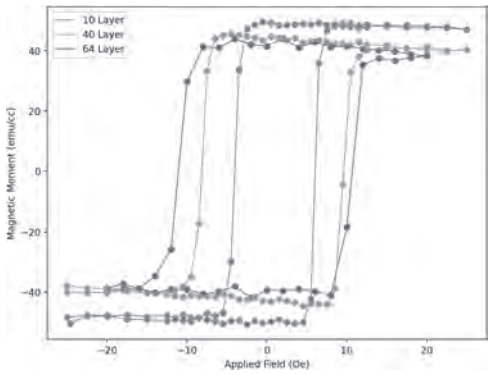

Fig 1. VSM of TbIG/TmIG multilayers grown at different pressures.

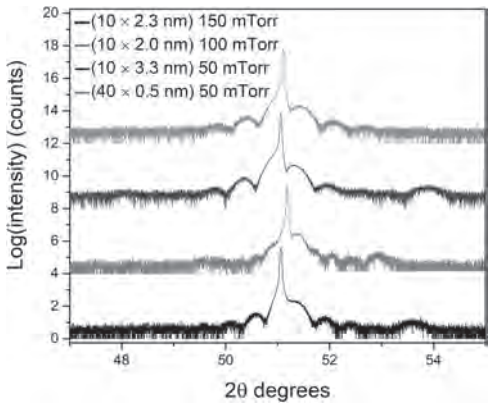

Fig 2. Pressure dependent XRDs of TbIG/TmIG multilayers. Labels: (Layer number x thickness).

DG-09. Enhancement of Magnetic Stability in Antiferromagnetic CoO Films byAdsorption of Organic Molecules. *I. Bergenti*[1], L. Gnoli[1], C. Del Conte[5], M. Benini[1], K. Lin[2], G. Fratesi[3], S. Achilli[3], E. Molteni[3], V. Dediu[1] and M. Cinchetti[4] *1. CNR-ISMN, Bologna, Italy; 2. National Chung Hsing University, Taichung, Taiwan; 3. University of Milan, Milan, Italy; 4. TU Dortmund, Dortmund, Germany; 5. University of Bologna, Bologna, Italy*

The possibility of tuning some intrinsic AF properties, such as ultra-fast magnetization dynamics and magnon-mediated spin transport, by the absorption of molecules is expected to lay the basis for a multifunctional antiferromagnetic spintronics thanks to the ability of molecules to respond to external stimuli. In this work, we investigated the effect of the absorption of C_{60} molecules on the well known antiferromagnetic CoO. We first demonstrate that molecular adsorption on CoO ultra thin films determines an interfacial charge re-distribution that affects the Co-O-Co superexchange interaction generating an increase of the AFM stability and a shift of the Néel temperature[1]. By analyzing the effect at different CoO thin film thicknesses, we have found that the effect is not confined to the interfacial layer but extend to at least to 10 unit cell from the surface. To explore the effect of light excitation of the C_{60} on the CoO, we exchange coupled it to a Co layer. In an optical pump and probe scheme, we investigated the TR-Moke of the multilayer Co/CoO/C_{60}. By exciting C_{60} near the absorption edge with a laser at 380nm, the magnetization precession frequency increases with respect the Co/CoO bare layer. This difference is larger below the blocking temperature of the AFM CoO. Such increase in precession frequencies is attributed to an increase in anisotropy. A numerical estimation of the difference in anisotropy field is provided by the comparing the data corresponding to similar pump power reaching the Co layer with and without C60.

[1] L. Gnoli et al., ACS Appl. Electron.Mater. 2024,6,3138

DG-10. Angular-Dependent Magnetic Properties in V_2O_3/Ni Hybrid Heterostructures. *K. Ignatova*[1] and U. Arnalds[1] *1. The Institute of Physical Sciences, Physics Division, University of Iceland, Reykjavík, Iceland*

Vanadium sesquioxide (V_2O_3) is an intriguing material that has gathered significant attention in the field of condensed matter physics and material science. It exhibits multiple simultaneous phase transitions, including a metal-insulator transition, structural phase transition (SPT), and paramagnetic/antiferromagnetic (PM/AFM) transition at a critical temperature of around 150 K [1-4]. In this work we present the in-plane angle and temperature dependence of coercivity and exchange bias (EB) in a V_2O_3/Ni magnetic bilayer across the SPT of V_2O_3. Distinct variations are observed in coercivity and exchange bias field across the SPT in V_2O_3, depending on in-plane angles and different field cooling (FC) states. A peak in coercivity, occurring at a temperature corresponding to the phase coexistence region of the V_2O_3 transition, is observed only along the main easy axis (0°/ 180°) of the film, disappearing at other angles and remaining independent of the FC state (see insets Fig. 1). Temperature-dependent measurements, with the applied cooling field along different angles, revealed that the onset of EB at the SPT of V_2O_3 occurs irrespective of the FC state, yet demonstrates a complex in-plane angular dependence based on the orientation of the applied cooling field. The cooling field orientation influences the exchange bias's anisotropy, magnitude, and direction. Notably, when the cooling field is applied along the secondary easy axis (90°/ 270°), coinciding with the alignment of the V magnetic moments, EB displays a characteristic unidirectional symmetry (Fig. 2, right). Cooling with the applied magnetic field along main axis (0°/ 180°) introduces additional and intricate anisotropic behavior of EB (Fig. 2, left).

[1] A. S. McLeod, E. Van Heumen, J. G. Ramirez, Nature Physics, Vol. 13, p. 80-86 (2017) [2] R. Moon, Journal of Applied Physics, Vol. 41, p. 883 (1970) [3] K. Ignatova, E. B. Thorsteinsson, U. B. Arnalds, Journal of Physics: Condensed Matter, Vol. 34, p. 495001 (2022) [4] K. Ignatova, E. Vlasov, U. B. Arnalds, APL Materials, Vol 12 (2024)

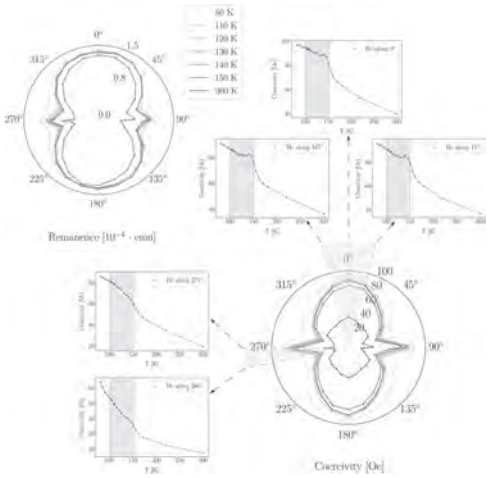

Temperature and azimuthal angular dependence of coercivity and remanent magnetization for the V_2O_3/Ni film. The graph insets show detailed coercivity behavior across the SPT of the V_2O_3 along different angles. Cyan dashed line areas indicate phase coexistence regions in the V_2O_3 during the SPT.

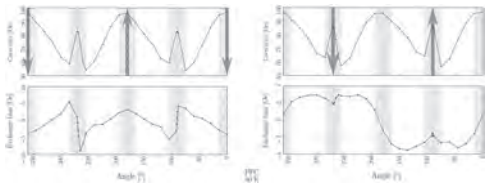

Coercivity and exchange bias in Oe at 80 K for two positive FC states along the primary and secondary easy axes as a function of in-plane angle. Arrows represent the FC direction. Dashed green lines denote the easy axes.

DG-11. Complex Exchange Bias driven by Natural Oxide Layers in $CrPS_4/Fe_3GeTe_2$ Antiferromagnetic/Ferromagnetic van der Waals Heterostructures. *A. Puthirath Balan*[1], A. Kumar[1], T. Scholz[2], Z. Lin[3], A. Shahee[1], S. Fu[4], T. Denneulin[5], J. Vas[5], A. Kovács[5], R.E. Dunin-Borkowski[5], H. Wang[4], J. Yang[3], B. Lotsch[2], U. Nowak[6] and M. Kläui[1,7] *1. Institute of Physics, Johannes Gutenberg University Mainz, Mainz, Germany; 2. Max Planck Institute for Solid State Research, Stuttgart, Germany; 3. School of Physics, Peking University, Beijing, China; 4. Max Planck Institute for Polymer Research Mainz, Mainz, Germany; 5. Ernst Ruska-Centre for Microscopy and Spectroscopy with Electrons and Peter Grünberg Institute, Forschungszentrum Jülich, Julich, Germany; 6. Department of Physics, University of Konstanz, Konstanz, Germany; 7. Centre for Quantum Spintronics, Department of Physics, Norwegian University of Science and Technology, Trondheim, Norway*

Two-dimensional van der Waals heterostructures potentially provide an excellent platform to study exchange bias due to their single crystalline, atomically flat interfaces. Chromium thiophosphate ($CrPS_4$), an antiferromagnetic material with uncompensated magnetic spins, is promising to explore exchange bias phenomena [1]. Recent research shows that naturally oxidized vdW ferromagnetic Fe_3GeTe_2 exhibits exchange bias, due to the antiferromagnetic coupling of its ultrathin surface oxide layer (O-FGT) with the underlying Fe_3GeTe_2 [2]. Anomalous Hall measurements examine exchange bias in the $CrPS_4$/(O-FGT)/Fe_3GeTe_2 heterostructure, considering contributions from the $CrPS_4$ layer and the oxide layer [3]. A distinct, nonmonotonic exchange bias trend is observed below 140 K. The exchange bias induced by a "preset field" suggests that the prevailing phase in the surface oxide is ferrimagnetic Fe_3O_4 [4]. Additionally, a thin FeO underlayer and $CrPS_4$ that form a heterostructure lead to a significant modulation of the exchange bias, highlighting the intricate nature of exchange coupling in vdW heterostructures and their potential for tailored manipulation.

[1] R. Wu, A. Ross, M. Kläui, Physical Review Applied, 17, 064038 (2022). [2] H. K. Gweon, S. Y. Lee, J. W. Choi, Nano Letters, 21, 1672– 1678 (2021). [3] A. Puthirath Balan, A. Kumar, M. Kläui, ACS Nano, 18, 8383-8391 (2024). [4] J. Dho, Applied Physics Letters, 106, 202405 (2015).

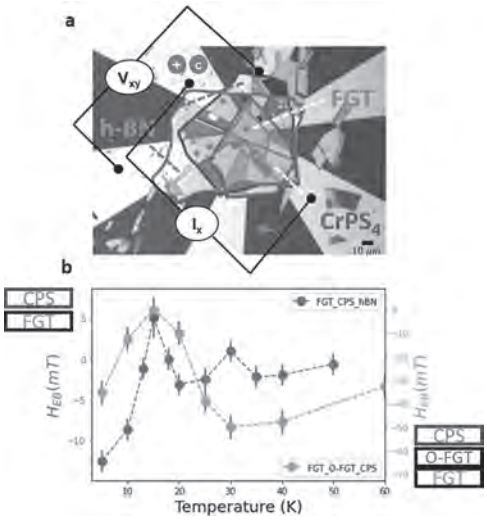

Fig. 1 a. The optical micrograph of a h-BN/$CrPS_4$/Fe_3GeTe_2 device (scale bar 10 μm), and b. Comparison of H_{EB} for a pristine (blue) and for oxygen-exposed (orange) devices for + 8 T field-cooling.

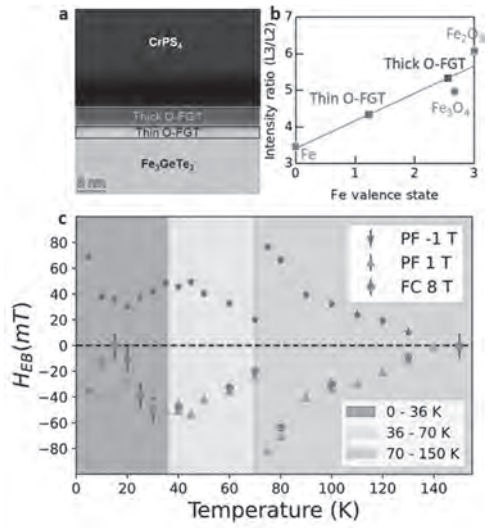

Fig. 2 a. The STEM image of the surface of the FGT sample, b. Fe L3/L2 intensity ratios as a function of Fe valence state. Gray line is a linear fit obtained using three reference spectra of Fe, Fe_3O_4 and Fe_2O_3. The L3/L2 ratio is larger in the Fe rich thick O-FGT compared to the thin O-FGT indicating a higher valence state. c. Trend of exchange bias field calculated as a function of temperature for both positive (orange) and negative (blue) 1 T preset field (PF) experiments as well as for the + 8 T field-cooled (FC) experiments (green).

DG-12. Understanding All-Optical Exchange Bias Reversal by Phase Space Exploration. *F. van Riel*[1], S. Vercruysse[1], B. Koopmans[1] and D. Leitao[1] *1. Applied Physics, Eindhoven University of Technology, Eindhoven, Netherlands*

Exchange bias (EB) arises at a ferromagnetic/antiferromagnetic interface, where it induces a preferential magnetization direction in the ferromagnet. Magnetoresistive (MR) sensors ubiquitously use EB for referencing in individual sensing elements. New technological opportunities, such as local vector field detection[1], would be enabled by controlling the reference. Hence, we explore methods for fast and field-free dynamical EB reorientation, in particular via all-optical helicity-independent switching (AOS) in ferrimagnetic Co/Gd compounds[2]. By using single femtosecond laser pulses (first harnessed by Guo et al.[3]) we show for the first time a full

field-free reversal of the EB-induced preferential magnetization direction in stacks (Fig. 1) containing IrMn and Co/Gd multilayers[4]. Each laser pulse toggles between positive and negative EB, while always satisfying unidirectionality at zero field. By exploring a phase space of three key parameters (laser fluence F, IrMn thickness t_{IrMn} and external field H), both experimentally and with simulations, we identified distinct regimes corresponding to different physical mechanisms. Fig. 2a,b shows an experimental phase diagram and highlights two critical fluence regimes. F_{FM} corresponds to the AOS threshold fluence, which is dependent[5] on H. F_{AFM} corresponds to the exceedance of the IrMn blocking temperature T_b and is independent of H. To further back up this claim, Fig. 2c shows how F_{AFM} varies with t_{IrMn} and that it follows the same trend as T_b. Simulations describing exchange-driven and temperature-driven dynamics on both the ultrashort and longer timescales show good qualitive agreement with both our own data (Fig. 2b) as well as measurements by others[3], providing us with tunable parameters to deliver optimized performance in MR sensor applications.

[1] C. Zheng, K. Zhu, S. Cardoso de Freitas et al., IEEE Transactions on Magnetics, Vol. 55(4), p.1-30 (2019) [2] I. Radu, K. Vahaplar, C. Stamm et al., Nature, Vol. 472(7342), p.205 (2011) [3] Z. Guo, J. Wang, G. Malinowski et al., Advanced Materials, Vol. 36(21), p.2311643 (2024) [4] M. L. M. Lalieu, M. J. G. Peeters, S. R. R. Haenen et al., Physical Review B, Vol. 96(22), p.220411 (2017) [5] M. J. G. Peeters, Y. M. van Ballegooie and B. Koopmans, Physical Review B, Vol. 105(1), p.014429 (2022)

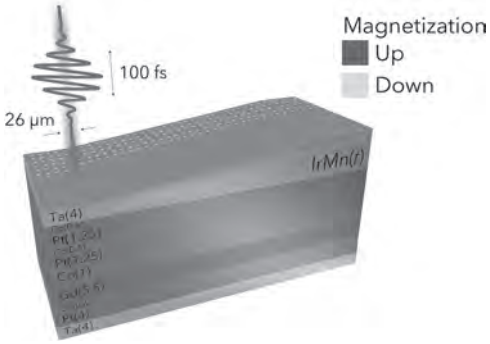

Fig. 1: Overview of the sample stack and methodology. IrMn is grown as a wedge with thickness $0 < t_{IrMn} < 15$nm. Each laser pulse is fired with different F and H.

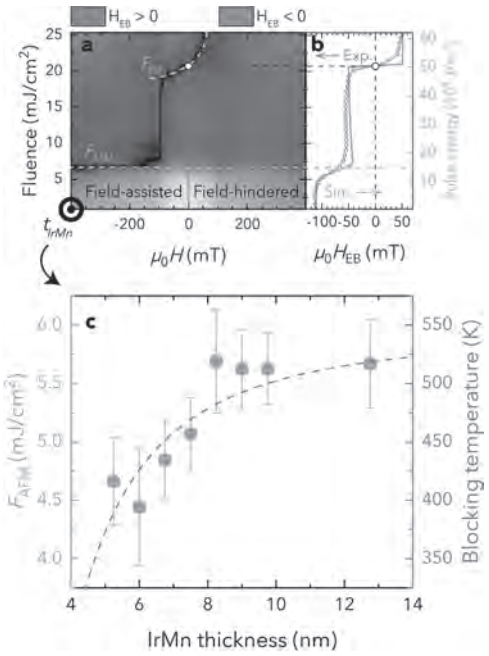

Fig. 2: (a) 2D slice from 3D experimental phase diagram of EB after laser excitation. (b) Cross-section from (a) at zero field with simulation comparison. (c) Dependence of F_{AFM} on t_{IrMn}. The red dashed line is fitted to experimental T_b data.

DG-13. Magneto-Ionically Tuning the Magnetization and Exchange Bias in all-solid-state CoMnN Heterostructures. *N. López-Pintó*[1], C. Jensen[2,3], Z. Chen[2], Z. Tan[1], Z. Ma[1], M. Liedke[4], M. Butterling[4], A. Wagner[4], J. Herrero-Martín[6], E. Menéndez[1], J. Nogués[5,7], K. Liu[2] and J. Sort[1,7] *1. Fisica de materials II, Universitat Autonoma de Barcelona, Barcelona, Spain; 2. Georgetown University, Washington, DC, United States; 3. NIST center for neutron research, Gaithesburg, MD, United States; 4. Helmholtz-Zentrum Dresden, Rossendorf, Germany; 5. Institut Catala de Nanociencia i Nanotecnologia (ICN2), Barcelona, Spain; 6. ALBA synchrotron, Barcelona, Spain; 7. ICREA, Barcelona, Spain*

The rapid growth of nanoelectronics and integration of artificial intelligence on the internet of things demand innovative materials for faster, energy-efficient data storage and processing. Magnetism is central for this purpose, as typically devices switch between two states. Magnetic fields or spin polarized electric currents are commonly employed for the purpose, both of which have considerable energy losses by heat dissipation. To minimize these detrimental effects recent research explores the use of electric fields as an alternative. Magneto-ionics (MI) has proven successful in tuning magnetic properties in a remarkable, non-volatile manner. MI has been broadly investigated in oxygen-based systems, despite other mobile ions (H^+, OH^-, Li^+ or N^{3-}) also showing potential. For instance, nitrogen-based MI induces larger changes with lower threshold voltages than its oxygen counterpart when gated in propylene carbonate-based electrolytes.[1,2] Nonetheless, solid-state structures are preferred for device applications, a domain where nitrogen MI lacks research. In this work, we report a 110% increase in saturation magnetization in an all-solid-state Ta/$Co_{0.55}Mn_{0.45}$N/Ta heterostructure by means of voltage-driven nitrogen ion transport towards the bottom Ta reservoir layer, correlating the observed magnetic changes to the structural and chemical modification of the ternary phase.[3] Furthermore, the sample exhibits exchange bias (EB) below 30 K, confirming the presence of multiple nitride phases, which are modified upon gating. Additional compositions were also studied, which, after being coupled to a Co FM layer, exhibited variable EB at room temperature or below, depending on the composition. The EB was later modified following a voltage treatment, showing a modest modification of the interfacial phenomenon at RT, while a large change is observed at low temperatures (down to 100 K). Further experiments are currently being

carried out to fully understand the coupling behavior after voltage treatment. These findings suggest a pathway for non-volatile control of magnetic properties in nitride compounds, which is appealing for energy-efficient spintronic devices compatible with CMOS technology.

[1] J. de Rojas, et al., *Nat. Commun.* 11, 5871 (2020). [2] Z. Tan, et al., *ACS Appl. Mater. Interfaces* 14, 44581 (2022). [3] N. López-Pintó, et al., Adv. Func. Mater., 2024, 2404487.

DG-14. Flexible Exchange-Biased Films with Superior Strain Stability.
H. Yang[1], X. Bao[1], Y.l. Xie[1] and R. Li[1] *1. Ningbo Institute of Materials Technology and Engineering, Chinese Academy of Sciences, Ningbo, China*

Flexible magnetic films and devices are attractive for developing wearable electronics with low power consumption, high sensitivity, and multifunctionality.[1-4] The exchange bias (EB) effect plays an undisputed role in the state-of-art spintronic devices. However, the poor stability of EB under mechanical strain is detrimental to the construction of reliable flexible spintronic devices for potential wearable applications. Our previous work revealed an enhancement of stress stability in flexible Co/Pt multilayers with strong perpendicular magnetic anisotropy (PMA),[5] here we show that the strain-induced variation of EB field could be greatly suppressed by engineering flexible IrMn/$[Co/Pt]_3$ systems featured with PMA. MOKE measurements indicate a decrease of the perpendicular exchange bias field (H_{PEB}) and an increase of the coercive field (H_C) under tensile strain. The reduction of H_{PEB} could be engineered by the crystal structure of IrMn layer, and upon the application of 2% tensile strain, H_{PEB} drops by only 25% in system with poorly crystallized IrMn due to a lower strain transfer efficiency. In addition, as the PMA enhances, the reduction of H_{PEB} at 2% tensile strain drops from ~ 50% to ~ 20%. Moreover, by cycling hysteresis loops under a certain tensile strain, we demonstrate that by a proper alignment of the interfacial magnetization moments, the strain-driven training effect can be largely eliminated, resulting in a greatly enhanced stability of PEB under tensile strain. Our results provide design rules for prospective flexible spintronic devices with stable performance under mechanical deformations.

1. Huali Yang, Yali Xie, Zengxing Lu, Zhiming Wang, Run-Wei Li. Research progress of flexible magnetic films and devices. Acta Phys. Sin. 71, 097503 (2022). 2. Gilbert Santiago Cañón Bermúdez, Denys Makarov. Magnetosensitive E-Skins for Interactive. Adv. Funct. Mater. 31, 2007788 (2021). 3. Pavlo Makushko, Eduardo Sergio Oliveros Mata, Gilbert Santiago Cañón Bermúdez, et al., Gaspare Varvaro, Denys Makarov. Flexible Magnetoreceptor with Tunable Intrinsic Logic for On-Skin Touchless Human-Machine Interfaces. Adv. Funct. Mater. 31, 2101089 (2021). 4. Huali Yang, Shengbin Li, Yuanzhao Wu, Xilai Bao, Ziyin Xiang, Yali Xie, Lili Pan, Jinxia Chen, Yiwei Liu, Run-Wei Li. Advances in Flexible Magnetosensitive Materials and Devices for Wearable Electronics. Adv. Mater. https://doi.org/10.1002/adma.202311996 (2024). 5. Mengchao Li, Huali Yang, Yali Xie, Kai Huang, Lili Pan, Wei Tang, Xilai Bao, Yumeng Yang, Jie Sun, Xinming Wang, Shenglei Che, and Run-Wei Li. Enhanced Stress Stability in Flexible Co/Pt Multilayers with Strong Perpendicular Magnetic Anisotropy. Nano Lett. 23, 8073–8080 (2023).

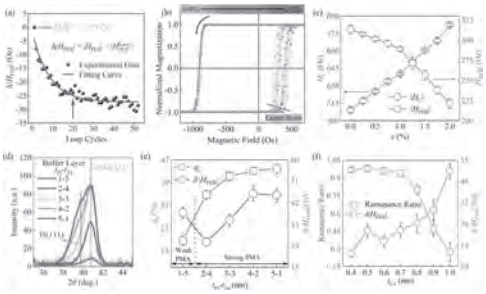

a) Loop cycles dependence of $\Delta|H_{PEB}|$. b) OOP hysteresis loops under strain. c) Strain dependence of H_C and $|H_{PEB}|$. d) XRD scans. e) Buffer layer controlled strain transfer efficiency and $\delta|H_{PEB}|$. f) Dependence of the remanence ratio and $\delta|H_{PEB}|$ on Co thickness.

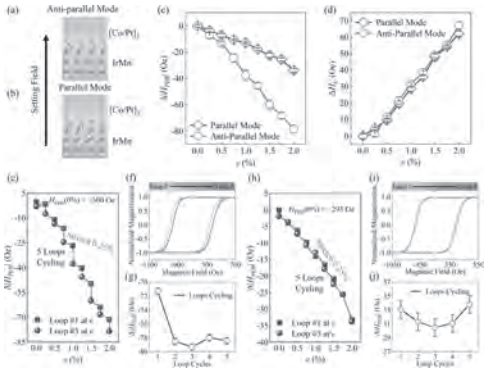

(a) Anti-parallel mode. (b) Parallel mode. c-d) Tensile strain dependence of $\Delta|H_{PEB}|$ and ΔH_C. Dependence of $\Delta|H_{PEB}|$ on strain and loop cycles in (e-g) anti-parallel and (h-j) parallel mode.

DG-15. An phase of elongated magnetic bubbles by imprinting a magnetic vortex on the $FeGeTe_2$ (FGT) stripe phase.
A.T. N'Diaye[1], T. Wang[2], A. Scholl[1], X. Huang[2], H. Zhang[2], X. Zhang[3], C. Hwang[4], R. Ramesh[5], M. Crommie[2] and Z.Q. Qiu[2] *1. Advanced Light Source, Lawrence Berkeley National Lab, Berkeley, CA, United States; 2. UC Berkeley, Berkeley, CA, United States; 3. King Abdullah Univ of Sci & Tech (KAUST), Thuwal, Saudi Arabia; 4. Quantum Technology Institute, Korea Reserach Institute of Standards and Science, Daejeon, The Republic of Korea; 5. Rice University, Houston, TX, United States*

The study of magnetic spin textures is deeply connected to fundamentally new physics and at the same time inspires novel applications. Thin films and, more recently, Van der Waals materials are fascinating and promising material systems for the study of such textures. C obalt thin films are a prototypical magnetic system in which the stripe phase and thickness dependent spin reorientation transition have been extensively studied. [1] When combined with suitable interfaces, these films can show chiral stripe phases and skyrmion spin textures, or, within proper confinement, be locked in a switchable magnetic vortex state. [2] The van der Waals ferromagnet $FeGeTe_2$ (FGT), just as cobalt, can also exhibit a chiral stripe phase that can be transformed into a magnetic skyrmion phase. [3] Using x-ray-photoemission electron microscopy (x-ray PEEM) with x-ray circular dichroism (XMCD), we study the interaction of the cobalt vortex state with the FGT stripe phase. Magnetic vortices are formed in micron sized Co disks grown by physical vapor deposition using a shadow mask and covered with a spacer layer. Subsequently, FGT flakes are deposited through a dry transfer method. While the cobalt vortex phase remains largely unaltered, the FGT stripe phase melts into a an elongated bubble state with some imprint of the rotational symmetry of the underlying vortex. With varied spacer thicknesses and FGT thicknesses we study details of the interlayer coupling. Micromagnetic simulations with MuMax3 are used to validate our understanding of the mechanisms behind the formation of the elongated bubble phase. Our findings provide a novel spin texture phase in van der Waals magnetic materials.

[1] Farid El Gabaly et al New J. Phys. 10 073024 (2008) https://doi.org/10.1088/1367-2630/10/7/073024 [2] Qian Li et al Appl. Phys. Lett. 110, 262405 (2017) https://doi.org/10.1063/1.4990987 [3] Mengmeng Yang et al Science Adv. 6, 36 (2020) https://doi.org/10.1126/sciadv.abb5157

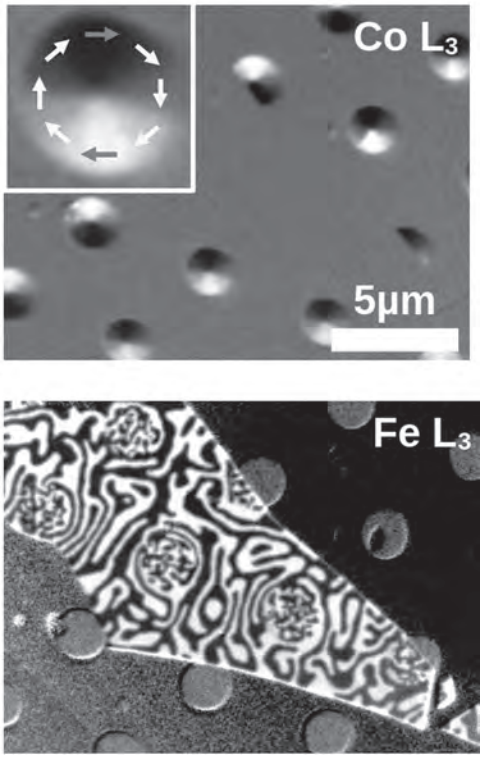

XMCD PEEM images of the magnetic stripe phase in FGT on the vortex state in Co discs of 2µm diameter. Both images show the same area. The image on the top shows the Co vortex state, the image on the bottom shows the FGT stripe phase with elongated bubbles on the areas covering the disks.

Session DP
SOFT MAGNETIC MATERIALS II
(Poster Session)

Jiahao Han, Chair
Tohoku University, Sendai, Japan

DP-01. Analysis and Design of Current Transformers for Low-Frequency Transmission Systems Using Hybrid Magnetic Materials. M. Xu[1], Z. Li[1], S. Lu[1], T. Huang[1], *G. Ma*[2,3], H. Zhou[2] and J. Yuan[2] *1. State Grid Jiangsu Electric Power Co., Ltd. Marketing Service Center, Nanjing, China; 2. Electrical Engineering and Automation, Wuhan University, Wuhan, China; 3. Department of Electrical and Electronic Engineering, The Hong Kong Polytechnic University, Hong Kong, China*

With the advancement of fractional frequency transmission, offshore wind power will be transmitted by low power frequencies around 10~30Hz. However, traditional current transformers face saturation distortion issues at low frequencies. Utilizing materials with high magnetic saturation intensity could add measurement errors. This paper proposes a transformer structure that maintains accuracy at low frequencies. This structure comprises two iron cores: one made of conventional silicon steel with an air gap, and the other made of nanocrystalline alloy material without air gap. These iron cores are concentrically placed, with the coils connected in series. According to the equivalent circuit, when the nanocrystalline alloy is saturated, its permeability becomes smaller, and the silicon steel core will share secondary induced voltage. In this case, transformers with hybrid materials will have better accuracy under low-frequency occasions. Fig. 1 illustrates the structure of the proposed transformer. The transformer body consists of two concentrically placed iron cores. The inner core is silicon steel, while the outer core is nanocrystalline alloy. The silicon steel core includes an air gap with a width of δ. The secondary windings with N_2 turns are connected in series. Fig. 2 compares the measurement results between the proposed and traditional transformers under 10Hz. The black waveform represents the primary side current, while the orange one denotes the secondary side of the proposed transformer. The blue waveform corresponds to the secondary side waveforms of conventional single-core silicon steel transformers. The secondary side current has been adjusted according to the turn ratio (N_2/1). It is evident that the traditional transformer exhibits distortion due to low-frequency saturation, whereas the new transformer maintains high measurement accuracy. Data analysis indicates that the ratio error of the new transformer is about 0.14% at 10Hz, which means it achieves an accuracy level of 0.5.

Sehloff, David, and Line A. Roald. “Low frequency AC transmission upgrades with optimal frequency selection.” IEEE Transactions on Power Systems, Vol. 37.2, p.1437-1448 (2021).

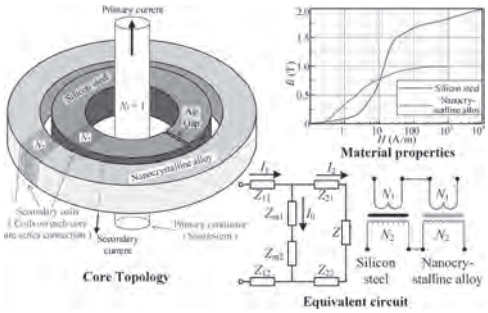

Fig. 1. Structure of new transformer.

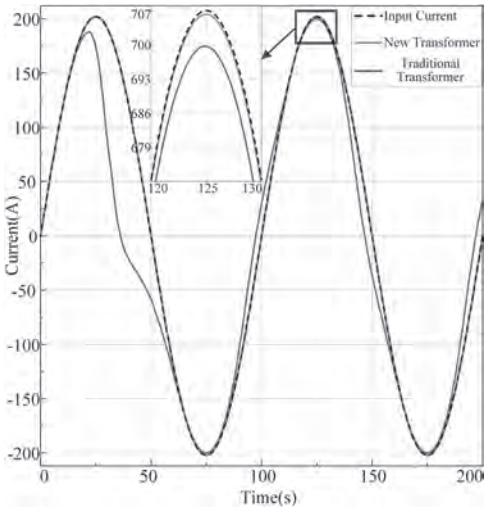

Fig. 2. Comparison of current waveforms between new and traditional transformers at 10Hz.

DP-02. The varying magnetic properties of different doping concentration of MnO doped C_4AF. *L. Huang*[1], A. Baral[2], C. Pesce[3], N. Morley[1] and T. Hanein[2] *1. University of Sheffield, Sheffield, United Kingdom; 2. University of Leeds, Leeds, United Kingdom; 3. earth4Earth, Sheffield, United Kingdom*

$Ca_4Fe_2Al_2O_{10}$ (C_4AF, 4CaO-Al_2O_3-Fe_2O_3) is one of the phases of cement, which is ferrite-rich and magnetic. [1, 2] Recycling the UK iron wastes for C_4AF production can reduce the CO_2 emissions, but other components such as MnO doping will change the magnetic properties of the C_4AF products. [2] Application of magnetic cements with higher magnetic moments can provide a stronger signal difference between uniform wall and cracks during the magnetic flux leakage testing for detecting structural defects in industry.[3] [N1] The Mn ions prefer to replace the Fe ions in C_4AF crystal structure due to lower defect formation energies of Mn ions-doping.[4] When the Fe ion is fully replaced by the Mn ion, $Ca_4Al_2Mn_2O_{10}$ is antiferromagnetic [5] while the pure C_4AF is paramagnetic (Fig. 1a). Powder samples of ferrites C_4AF with different MnO doping concentration (0 wt.% - 4.5 wt.%) with 1350 °C sintering temperatures were prepared and measured by SQUID. When the doping concentration of the MnO is higher than 3. 5 wt.%, the paramagnetic state starts to be replaced by the antiferromagnetic state. The higher magnetic moments were observed for higher MnO doping. In Fig. 1b, the magnetic moments at low temperatures [5 K, 100 K] show an increasing tendency to the higher MnO doped weight of C_4AF. The moment of the MnO doped samples have values higher than the theoretical moment of both Fe and Mn with the low spin state but lower than the magnetic moment with all Fe ions in the high spin state at room temperature. These indicated that the doped Mn ions help the Fe ions partially change from the low spin state to the high spin state and change the alignment between spins in the crystal structure. This adjustable magnetic properties of MnO doped C_4AF can rise more potential of the application of the magnetic cements

1. Elakneswaran, Yogarajah, et al. “Characteristics of ferrite-rich Portland cement: Comparison with ordinary Portland cement.” *Frontiers in Materials* 6 (2019): 97. 2. Riley, Alex L., et al. “Legacy iron and steel wastes in the UK: Extent, resource potential, and management futures.” *Journal of Geochemical Exploration* 219 (2020): 106630. 3. Guanyang He et al. “Magnetic tunnel junction based gradiometer for detection of cracks in cement.” *Sensors and Actuators A: Physical* 331 (2021): 112966. 4. Qixiang Wu et al. “ Revealing the mechanism of manganese doping in sulphoaluminate cement clinker.” *Journal of Molecular Structure* 1301 (2024): 137305. 5. Wright, Adrian J., et al. “Structures and magnetic ordering in the brownmillerite phases, Sr_2MnGaO_5 and Ca_2MnAlO_5” *Journal of Materials Chemistry* 12.4 (2002): 978-982.

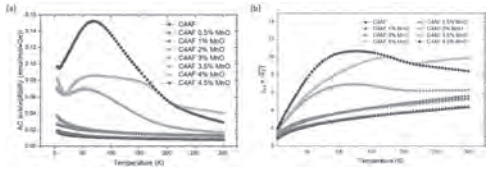

Fig. 1 (a) AC susceptibility of different MnO doping concentration samples. (b) Magnetic moment of the different MnO doped C4AF samples.

DP-03. Research on Vibration Characteristics and Suppression Measure of Saturation Core Fault Current Limiter Based on Nanocrystalline Materials. *J. Yuan*[1,2], Y. Liu[1,2], Y. Sun[3], X. Li[1,2] and H. Zhou[1,2] *1. State Key Laboratory of Power Grid Environmental Protection, Wuhan University, Wuhan, China; 2. School of Electrical Engineering and Automation, Wuhan University, Wuahn, China; 3. State Grid Hubei Electric Power Co., LTD. Wuhan Power Supply Company, Wuhan, China*

With the rapid development of HVAC system and renewable energy sources, the level of short-circuit current in power grids has escalated significantly, establishing the Saturation Core Fault Current Limiter (SCFCL) as a promising solution for current limitation[1]. Traditional SCFCLs use silicon steel sheets as their core material, which has a high magnetostriction coefficient, leading to severe core vibrations during fault current limitation[2]. The vibration may cause internal components to loosen or even break, generate significant noise, thereby compromising equipment and system safety[3]. This paper proposes a novel topology of a composite material-based SCFCL (NSCFCL) to address these issues. We begin by introducing the working principle of the NSCFCL and analyzing its vibration characteristics. Subsequently, we demonstrate the effectiveness of the proposed topology through finite element simulations. The basic structure of NSCFCL is depicted in Figure 1(a), comprising cores, permanent magnets, and AC/DC coils. Specifically, the cores are made of iron-based nanocrystalline alloy materials. Figure 1(b) illustrates the 3D model of the NSCFCL in COMSOL, showcasing its magnetic flux density distribution, which demonstrates alternating desaturation of the core on both sides during short-circuit fault. Figures 2(a) and 2(b) present vibration displacements at various measurement points for the two core materials, highlighting Point B as experiencing the most significant vibration. Notably, the maximum vibration displacement of the NSCFCL is reduced by 78% compared to the conventional SCFCL, due to factors such as core saturation level, magnetic state variations, and external constraints. Additionally, Figures 2(c) and 2(d) compare the acceleration at Point B for both core materials, showing a 71% reduction in acceleration for the NSCFCL, demonstrating its ability to significantly mitigate core vibration force without compromising current limitation performance.

[1] J. Yuan, Y. Sun, W. Zhang, et al, “A novel hybrid magnetic material based on three-phase saturated core fault current limiter,” AIP Advances, vol. 14 (2): 025301(2024). [2] T. Ben, L. Hou, L. Chen, et al, “The Vector Electromagnetic Vibration of Magnetically Controlled Reactor Considering the Vector Hysteretic Magnetostriction Effect,” IEEE Transactions on Magnetics, vol. 58, no. 9, pp. 1-5(2022). [3] P. Zhang, L. Li, Z. Cheng, et al, “Study on Vibration of Iron Core of Transformer and Reactor Based on Maxwell Stress and Anisotropic Magnetostriction,” IEEE Transactions on Magnetics, vol. 55, no. 2, pp. 1-5(2019).

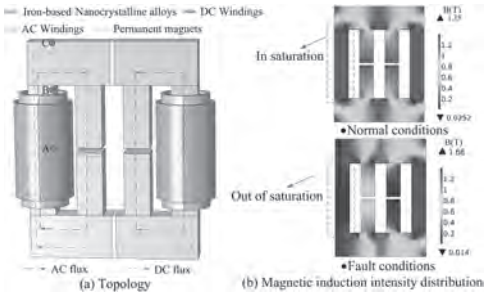

Fig. 1 Configuration of NSCFCL and flux results

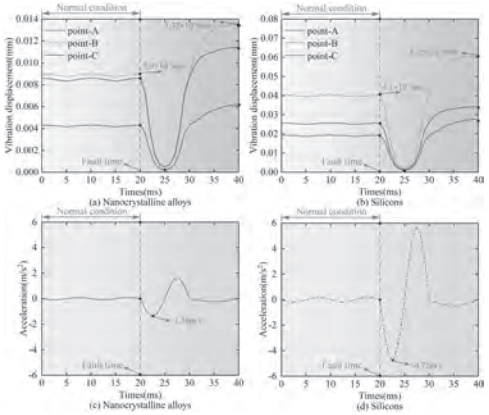

Fig. 2 Comparison results of vibration displacement and acceleration

DP-04. AC electrical property and generation of extra eddy current loss in Mn-Zn ferrites in the high frequency range. *Y. Ying*[1] and Z. Li[1] *1. Zhejiang University of Technology, Ha, China*

In this work, AC conductivity, complex impedance and power loss (P_{cv}) in the Ta_2O_5 doped Mn-Zn ferrites have been comprehensively investigated. In the high frequency range, AC conductivity increases remarkably with increasing frequency. It is found that the traditional loss separation method underestimates eddy current loss (P_{ev}) and overestimates residual loss (P_{rv}) due to no consideration of the frequency influence on conductivity. Based on the analysis of AC conductivity, the generation mechanism of P_{ev} in the high frequency range has been clarified and the loss separation method has been modified. The new loss separation method could be more accurate to guide the development of low-P_{cv} Mn-Zn ferrites for high frequency applications. The Ta_2O_5 addition effectively reduces all three parts of loss including hysteresis loss (P_{hv}), P_{ev} and P_{rv}, and the Mn-Zn ferrite with low P_{cv} in the frequency range of 1-3 MHz is developed. The optimal sample shows P_{cv} at room temperature as low as 15, 65 and 359 kW/m^3 at 1MHz/30mT, 2MHz/30mT and 3MHz/30mT, respectively. The mechanism of Ta_2O_5 influence on P_{hv} and P_{rv} has also been clarified. Fig. 1. Angular frequency dependence of the AC conductivity of MnZn ferrites with the Ta2O5 content: (a) 0, (b) 300, (c) 600 and (d) 900 ppm at different temperatures. Fig. 2. Frequency dependence of P_{cv}/f of Mn-Zn ferrites with the Ta2O5 content: (1) 0, (2) 300, (3) 600 and (d) 900 ppm. The contribution of each part of loss on P_{cv} is also illustrated.

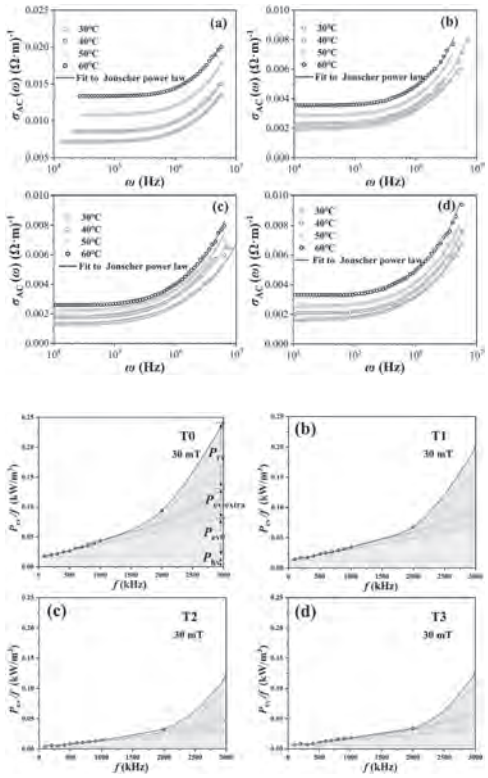

DP-06. Band-structure and ferromagnetism of the GaMnAsP epitaxial layers. *N. Tataryn*[1], O. Yastrubchak[1], S. Mamykin[1], V. Romanyuk[1], O. Kondratenko[1], B.A. Assaf[2], J. Furdyna[2], X. Liu[2], G. Schönhense[3], H. Elmers[3], K. Medjanik[3], R. Serha[4], K. Levchenko[4], M. Sawicki[5] and K. Gas[5] *1. V. E. Lashkaryov Institute of Semiconductor Physics, National Academy of Sciences of Ukraine, Kyiv, Ukraine; 2. Department of Physics and Astronomy, University of Notre Dame, Notre Dame, IN, United States; 3. Institut für Physik, Johannes Gutenberg-Universität, Mainz, Germany; 4. Faculty of Physics, Nanomagnetism and Magnonics, University of Vienna, Vienna, Austria; 5. Institute of Physics, Polish Academy of Sciences, Warsaw, Poland*

Dilute magnetic semiconductors (DMSs) represent a class of alloys that combine semiconductor properties with magnetism integrated into a single material. Their magnetic properties arise from transition metal ions introduced into the semiconductor host lattice. The combination of electronic and magnetic properties results in entirely new physical properties that are of interest in basic science and hold promise for a wide range of device applications referred to as spintronics [1-5]. The impact of P and Mn incorporation into GaAs layers on their electronic- and band-structures and magnetic and structural properties has been studied. The (Ga,Mn)(P,As) epitaxial layers on GaAs thus harbor ferromagnetism with perpendicular magnetic anisotropy, rendering them suitable for observing crucial phenomena such as the anomalous Hall effect (AHE). Additionally, co-doping Mn and P facilitates independent adjustment of magnetic and electrical properties within this system [6], thereby enabling modulation of the exchange interaction between Mn spins mediated by itinerant holes, which dictate the magnetism in these materials. We have investigated $Ga_{1-x}Mn_xP_yAs_{1-y}$ layers doped with x = 0 - 0.08 of Mn and y = 0.12 - 0.32 of P, grown on (001)-oriented GaAs substrates at 230°C by low-temperature molecular-beam epitaxy. All Mn and P content and layer thicknesses were verified during growth by reflection high-energy electron diffraction (RHEED) intensity oscillations. After the growth, the (Ga,Mn)(P,As) epitaxial layers were annealed at the temperature of 250°C to improve the magnetic and transport properties of the layers by promoting out-diffusion of Mn ions from the interstitial positions [7]. Hard-X-ray angular-resolved photoemission spectroscopy (HARPES) reveals that a strongly dispersing band crosses the Fermi energy in the highly doped samples. This is a consequence of the high concentration of Mn-induced itinerant holes in the valence band of the III-V semiconductor host. The spectroscopic ellipsometry (SE) and photo-reflectance spectroscopy results confirmed the modification of the valence band of the epitaxial layers. The micro-Raman and magnetometry measurements supported this study [8-13].

1. Ohno H., Making nonmagnetic semiconductors ferromagnetic // Science.-1998.-281.-P. 951-956. 2. Tataryn N., et al., Valence Band Dispersion in Bi Doped (Ga,Mn)As Epitaxial Layers // *IEEE Transactions on Magnetics*.-2023.-59.-P. 1-5. 3. Yastrubchak O., et al., Band Engineering of Magnetic (Ga,Mn)As Semiconductors by Phosphorus Doping // *IEEE Transactions on Magnetics*.-2023.-59.-P. 1-6. 4. Yastrubchak O., et al., Influence of Bi doping on the electronic structure of (Ga,Mn)As epitaxial layers // Scientific Reports.-2023.-13.-P. 17278. 5. Medjanik K., et. al., Site-specific atomic order and band structure tailoring in the diluted magnetic semiconductor (In,Ga,Mn)As // Phys. Rev. B.-2021.-103.-P. 075107. 6. Lemaître A., et al., Strain control of the magnetic anisotropy in (Ga,Mn)(As,P) ferromagnetic semiconductor layers // Appl. Phys. Lett.-2008.-93.-P. 021123. 7. Yastrubchak O., et al., Effect of low-temperature annealing on the electronic- and band-structures of (Ga, Mn) As epitaxial layers // J. Appl. Phys.-2014.-115.-P. 012009. 8. Yastrubchak O., et al., Strain release in InGaAs/InxAl1−xAs/InP heterostructures // Physica B: Condensed Matter.-2003.-340.–342.-P. 1082-1085. 9. Yastrubchak O., et al., Electronic and band-structure evolution in low-doped (Ga,Mn)As // J. Appl. Phys.-2013.-115.-P. 053710. 10. Yastrubchak O., et al., Anisotropic strain relaxation in lattice mismatched III–V epitaxial layers // Phys. Stat. Sol. (c),-2005.-2.-P. 1943-1947. 11. Gluba L., et al., On the nature of the Mn-related states in the band structure of (Ga, Mn) As alloys via probing the E_1 and $E_1+\Delta_1$ optical transitions, // Appl. Phys. Lett.-2014.-105.-P. 032408. 12. Dmitruk N. L., et al., Multilayer diffraction gratings Al/GaAs as polaritonic photodetectors // Phys. Stat. Sol. (a).-2001.-184.-P. 165-174. 13. Dmitruk N. L., et al., Ultraviolet responsivity control in Schottky barrier heterostructures with textured interface // Thin Solid Films.-2000.-364.-P. 280-283.

DP-07. Domain Wall Depinning in Rapidly Quenched Submicrometric Amorphous Wires. *T.A. Ovari*[1], S. Corodeanu[1], G. Ababei[1], H. Chiriac[1] and N. Lupu[1] *1. National Institute of Research and Development for Technical Physics, Iasi, Romania*

Rapidly quenched cylindrical amorphous wires exhibit excellent soft magnetic properties due to the lack of magnetocrystalline anisotropy and to the superior symmetry. Most studied ones have diameters in the range of micrometers, and, more recently, even below 1 μm, i.e., from 80 to 900 nm [1]. Ultrathin amorphous wires present a one-step axial magnetization reversal, called magnetic bistability, which appears when the applied field is larger than a threshold, called switching field [2]. Submicrometric wires are bistable irrespective of the sign and magnitude of their magnetostriction, as opposed to typical micrometric samples, where only highly positive magnetostrictive ones are bistable. They have a single domain structure with an axial easy axis and with end domains having reverse magnetization, due to demagnetization. The related end domain walls suffer depinning and propagate when the applied field is equal to the switching field. A similar process is expected in both low magnetostrictive, e.g., Co-Fe-Si-B, and highly magnetostrictive, e.g., Fe-Si-B, submicrometric amorphous wires, although the switching field values are significantly different (see Table I). Here, we focused on explaining such differences, by using inductive axial hysteresis loop measurements, Sixtus-Tonks-type measurements of the domain wall propagation speeds, and Lorentz transmission electron microscopy (LTEM) imaging of the domain walls, to understand their behavior at depinning. The results show that only in highly magnetostrictive samples, the domain walls elongate before complete depinning, prior to propagation, as illustrated in Fig. 1. This behavior has been attributed to the large magnetoelastic contribution. No such elongation has been observed in low magnetostrictive amorphous samples. The results are important for applications of submicrometric amorphous wires in magnetic microsensors and domain wall-based logic devices. Acknowledgments - Work supported by the Romanian Ministry of Research, Innovation and Digitalization through the NUCLEU Program - Contract 18N/2023, Project PN23 11 01 01.

[1] T.-A. Óvári, G. Ababei, G. Stoian, S. Corodeanu, H. Chiriac, and N. Lupu, Sci. Rep. 14, 5728, Mar 2024. [2] A. Zhukov, P. Corte-Leon, L. Gonzalez-Legarreta, M. Ipatov, J.M. Blanco, A. Gonzalez, and V. Zhukova, J. Phys. D: Appl. Phys. 55, 253003, Jun 2022.

Composition	Diameter (nm)	Switching Field (A/m)
$(Co_{0.94}Fe_{0.06})_{72.5}Si_{12.5}B_{15}$	300	990
$(Co_{0.94}Fe_{0.06})_{72.5}Si_{12.5}B_{15}$	450	650
$Fe_{77.5}Si_{7.5}B_{15}$	100	13300
$Fe_{77.5}Si_{7.5}B_{15}$	300	4970

Table I. Sample characteristics and switching field values.

Fig. 1. Elongated domain wall in a highly magnetostrictive Fe-Si-B sample (LTEM).

DP-08. Exploratory synthesis and characterization of Mn-based chiral nanomagnets, thin films and multi layers. *J. Moore*[1] *1. School of Engineering, University of Central Oklahoma, Edmond, OK, United States*

Chirality refers to single handedness in physical properties of materials that lack mirror symmetry in their crystal structure. Mn-ions are known dopants for the optical chiral property development in nanomaterials, organic-inorganic hybrids and thin films[1, 2]. Additionally, bulk Mn-based materials such as MnSi[3] and Mn3X (Sn, Ge)[4] also exhibit chiral magnetism. Chiral nanomagnets and heterostructures are promising platforms for chiral magneto-optical applications which are greatly limited with low Curie temperatures. We will review the status of Mn-based chiral magnetic materials in bulk, nanomaterials and thin films and present an exploratory electrochemical synthesis[5] and characterization report of high Curie temperature Mn based magnetic materials thin films. We will demonstrate the application of design of experiment (DOE) concept to control the involved parameters optimization in the experiment.

1. Wang, C., et al., Efficient Photoluminescence of Manganese-Doped Two-Dimensional Chiral Alloyed Perovskites. The Journal of Physical Chemistry Letters, 2021. 12(50): p. 12129-12134. 2. Wang, B., et al., Environmental-friendly lead-free chiral Mn-based metal halides with efficient circularly polarized photoluminescence at room temperature. Journal of Alloys and Compounds, 2022. 910: p. 164892. 3. Karhu, E.A., et al., Chiral modulations and reorientation effects in MnSi thin films. Physical Review B, 2012. 85(9): p. 094429. 4. Chen, T., et al., Anomalous transport due to Weyl fermions in the chiral antiferromagnets Ge. Nature Communications, 2021. 12(1): p. 572. 5. Pappaianni, G., et al., Electrodeposition of MnAs-Based Thin-Film as a Possible Promising Candidate in Spintronics Applications. Journal of The Electrochemical Society, 2024. 171(6): p. 062502.

Session DQ
MAGNONICS III
(Poster Session)

Vincent Vlaminck, Chair
IMT Atlantique, Nantes, France

DQ-01. Dipole-exchange spin waves in van der Waals Néel-type antiferromagnetic films and nanoribbons. *B. Hussain*[1] and M.G. Cottam[2]
1. University of Michigan, Dearborn, MI, United States; 2. University of Western Ontario, London, ON, Canada

In the last decade two-dimensional (2D) magnetic materials have been of intense interest following the discovery of van der Waals ferromagnetic and antiferromagnetic materials [1]. These compounds, where the magnetic ions typically lie on a honeycomb lattice, exhibit a spontaneous magnetic order and existence of spin-wave (SW) excitations below a stable critical temperature. Here we present a theoretical study for the effects of the long-range magnetic dipole-dipole interactions on the SWs in monolayer van der Waals antiferromagnets with a Néel-type ordering (see Fig. 1), following the microscopic (or Hamiltonian-based) formalism previously developed for the ferromagnetic case [2]. The dipole-dipole interactions give an extra anisotropy in these materials, along with the Ising-exchange anisotropy and/or single-ion anisotropies that stabilize the 2D magnetic ordering. Analytical expressions are obtained for the SW energies $E(\mathrm{k})$ at any 2D wave vector k, and numerical applications are made for a general model system and specifically to $MnPS_3$ [3,4]. Two cases are considered: complete films, where there are no edge effects, and finite-width nanoribbons (or stripes) with zigzag edges. It is found, in general, that the bulk SW energies are shifted upwards due to the dipole-dipole interactions. For the nanoribbon geometry, we predict edge modes that are localized at the lateral edges in addition to the bulk-like standing modes (see Fig. 2 for a numerical example of a zigzag nanoribbon with finite width in the x direction). These edge modes show different characteristics from those predicted in [5], where localization effects were studied due to Dzyaloshinskii-Moriya interactions.

[1] J.-U. Lee *et al.* (2016). Nano Lett. 16, 7433. [2] B. Hussain and M. G. Cottam (2022). J. Phys. Condens. Matter 34, 445801. [3] A. R. Wildes *et al.* (1998). J. Phys.: Condens. Matter 10, 6417. [4] T. Olsen (2021). J. Phys. D: Appl. Phys. 54, 314001. [5] D. Ghader and A. Khater (2019). Nature Sci. Rep. 9, 15220.

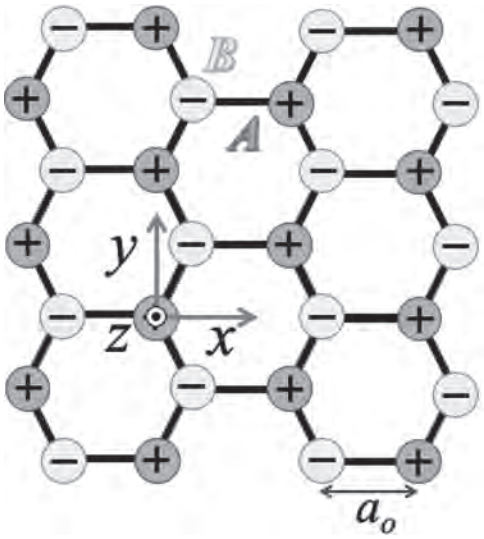

Schematic illustration of a van der Waals antiferromagnet with Néel-type ordering, showing the spin-up (+) and spin-down (-) sublattice orientations (along z).

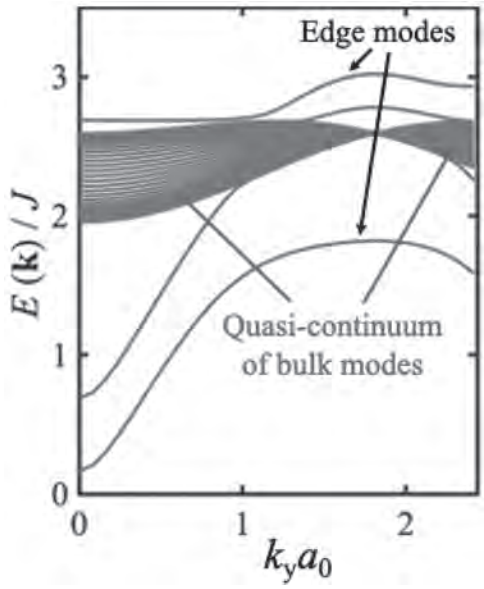

Dispersion relations for the SW energy $E(\mathrm{k})$, relative to the nearest-neighbor exchange J, plotted versus dimensionless longitudinal wave vector. The quasi-continuum of closely spaced bulk SW modes and the edge SW modes are shown for a nanoribbon with $N = 60$ lines of atoms.

DQ-02. Spin-Wave Dispersion in a Skyrmion Chain. K. Zulfiqar[1,2,5], *S.J. Holt*[1,5], M. Lang[1,5], S.A. Pathak[1,5], E. Vinas Bostroem[3,5] and H. Fangohr[1,4,5] *1. SSU-CS, Max Planck Institute for Structure and Dynamics of Matter, Hamburg, Germany; 2. University of Hamburg, Hamburg, Germany; 3. Theory, Max Planck Institute for Structure and Dynamics of Matter, Hamburg, Germany; 4. University of Southampton, Southampton, United Kingdom; 5. Center for Free-Electron Laser Science, Hamburg, Germany*

A magnon is a quantized spin wave, representing a collective excitation of electron spins in a magnetic material. In principle, information coded in magnons can propagate through a magnetic material over long distances due to small dissipation [1]. The interaction of spin waves with topological structures, such as skyrmions, provides rich physics and potential for future applications [2]. Recent research demonstrates the practical implementation of skyrmion-based magnonic crystals, offering dynamic control by tuning bandgaps using a magnetic field or spin current [3]. In this study, we extend previous research [3] on skyrmion chain systems and investigate spin-wave propagation in a confined track geometry of a non-centrosymmetric ferromagnet. Finite difference micromagnetic simulations [4] are performed on a strip with dimensions of $1000 \times 100 \times 10$ nm^3. To obtain the magnon dispersion relation, the system in equilibrium is exposed to a spatially varying time-dependent external excitation and dispersion curves are extracted through Fourier transforms [5, 6]. We find that the frequency $\omega = 5.8$ GHz corresponds to an out-of-phase breathing mode of the skyrmions, while the frequency $\omega = 115$ GHz depicts an in-phase gyrotropic dynamics of skyrmions. Focusing on the standing wave position, $k_x = 0$, we observe coherent oscillations of the skyrmion cores in the y direction for all magnon bands. This work is supported by the Marie Sklodowska-Curie grant agreement No. 101152613 and the funding provided by MaMMoS, Horizon Europe grant ID: 101135546.

1. H. Yuan, Y. Cao, et al., Physics Reports, Vol. 965, p. 1-74 (2022). 2. A. Fert, V. Cros, J. Sampaio, Nature Nanotechnology, Vol. 8, p. 152-156 (2013). 3. Z. Chen, F. Ma, Journal of Applied Physics, Vol. 130, p. 090901 (2021). 4. M. Beg, M. Lang, H. Fangohr, IEEE Transactions on Magnetics, Vol. 58, p. 1-5 (2022). 5. G. Venkat, B. Kumar, et al., IEEE Transactions on Magnetics, Vol. 49, p. 524-529 (2013). 6. D. Kumar, O. Dmytriev, et al., Journal of Physics D: Applied Physics, Vol. 45, p. 015001 (2012).

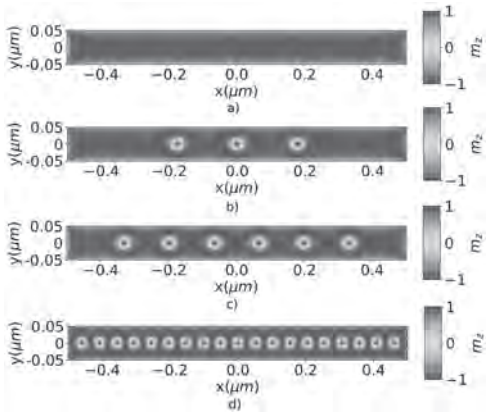

We progessively add skyrmions to the FeGe strip: Starting from a uniform magnetic state (a), an increasing number of skyrmions are nucleated with (b) have odd numbers of skyrmions, (c) have even numbers of skyrmions and (d) has the maximum number of skyrmions sampled within the confined geometry.

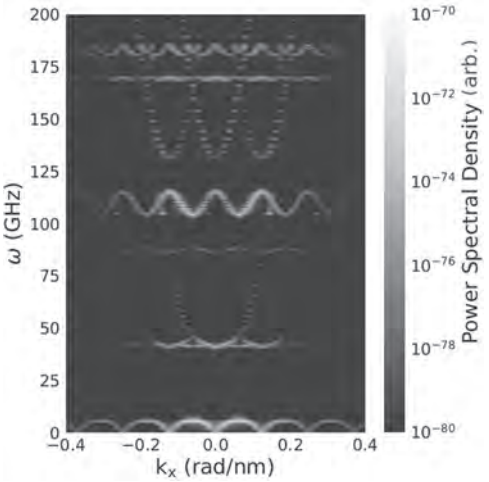

Spin-wave dispersion plot of the m_x component of magnetisation in an FeGe skyrmion chain configuration strip

DQ-03. A Modified Model Based on Boltzmann Approach for Studying Viscous Fluid Transport of Magnons. *X. Liu*[1], Y. Li[1], C. Chen[1] and J. Zhang[1] *1. Tongji University, Shanghai, China*

Since the giant magnetoresistance (GMR) effect was discovered between 1986 and 1989[1], the development of spintronics greatly changed the modern semiconductor and information industries. Among the subject, the magnon transport problem is one of the most important topics due to its excellent spin transmission properties. In 2015, L. J. Cornelissen and B. J. van Wees et al. found that high-frequency magnons can be excited directly through electron current and transported over long distances in magnetic insulator yttrium iron garnet (YIG)[2]. Model for the magnon transport phenomena was proposed, however, it has difficulty in situations such as the YIG is not thin enough. To these problems, we propose a modified model based on the existing theories and experimental phenomena. In this paper, within the framework of non-equilibrium Boltzmann transport, we address on the physical mechanism of how coupled phonons regulate and enhance the effects of magnon flow and propagation distance; as well as, the conversion mechanism of spin/magnon/phonon in magnetic multilayer film materials. We also study frequencies of coupled phonons that affect magnon's relaxation in k-space and by using external gradient field methods to control magnon transport. Moreover, based on quantum exchange interaction, We introduce a new scattering process which makes the magnon transport exhibit a fluid-like property that can be captured by a viscous fluid transport equation[3,4]. Our work is an improvement and supplement to the existing magnon transport model.

[1] I. Zutic, J. Fabian, and S. D. Sarma, Reviews of Modern Physics 76, 323 (2004). [2] Cornelissen, L.J., et al., Nature Physics, 2015. 11(12): p. 1022-1026. [3] Liu, T., W. Wang, and J. Zhang, Physical Review B, 2019. 99(21). [4] Y. Li, C. Chen, J. Zhang, et al., AIP Advances 12, 035154 (2022).

DQ-04. Enhanced Magnon-Magnon Coupling in Artificial Square Ice with Perpendicular Magnetic Anisotropy. *S. Sankaran Kunnath*[1], M.K. Zelent[1], M. Moalic[1] and M. Krawczyk[1] *1. Faculty of Physics, Institute of Spintronics and Quantum Information, Adam Mickiewicz University, Poznan, Poland*

The study of magnetization dynamics in artificial spin ices (ASI) has recently garnered significant attention due to their intriguing physics and potential applications in reprogrammable memory, logic, and reconfigurable magnonics [1]. ASIs are geometrically ordered arrays of magnetic nanoislands, with magnetization states governed by exchange and dipolar interactions, enabling the exploration of emergent magnetic phenomena and complex behaviors. Numerous experimental and theoretical studies have

investigated magnetization dynamics across various lattice geometries, including square, Kagome, as well as other geometries composed of in-plane nanomagnets [2]. Here, we explore the in-plane magnetized ASI lattices but embedded in a perpendicularly magnetized matrix to combine the benefits of those classic planar ASIs with increased dynamic interactions between nanoelements through a ferromagnetic matrix for use in magnonics. With micromagnetic modelling we study static properties and spin-wave (SW) dynamics of Co/Pd multilayers, where the in-plane nanoelements can be present due to controlled FIB irradiation. Each element in the square array is 200nm long, 75nm wide, and 13.2nm thick. Our results reveal 4 standard for ASI types of magnetization configuration in in-plane nanoelements with a rich mode spectrum featuring distinct high-frequency dynamics, with various SW localizations and mode quantization (Fig.1). Interestingly, we observe strong magnon-magnon coupling, attributed to the hybridization of confined modes from the nanoelements and the perpendicularly magnetized matrix. Notably, reducing the vertex gap intensifies the dipolar interactions between nanoelements, which causes the magnetization at the edges to bend and leads to an enhancement in coupling strength. Our findings offer a new approach toward tunable magnon-magnon coupling in ASI for magnonic applications.

[1] S Gliga et al., APL Mater. 8, 040911 (2020) [2] S Lendinez et al., J. Phys. Condens. Matter 32, 013001 (2020)

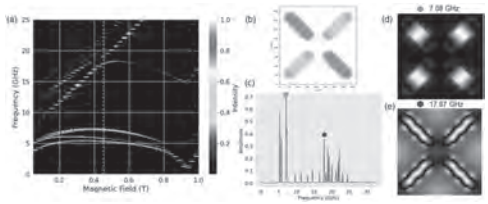

Fig. 1 (a) Evolution of the SW resonance spectra for the ASI with a 100 nm vertex gap as a function of out-of-plane field. (b) Static spin configuration and (c) FFT spectra at 0.45 T (Δf minimum). (d) Spatial distribution of the in-plane dynamical magnetization component for SW modes corresponding to nanoelements, and (e) ASI-bulk matrix.

DQ-05. Effect of Ru underlayer on magnetic anisotropy and magnetization reversal in CoFeB thin film structures. *S. Sahu*[1,2] and G. Basheed[1,2] *1. Indian Reference Material, CSIR National Physical Laboratory, New Delhi, India; 2. Academy of Scientific and Innovative Research (AcSIR), Ghaziabad, India*

We investigated the in-plane magnetic anisotropy (IPMA) and magnetization reversal mechanisms in DC magnetron sputtered $Co_{20}Fe_{60}B_{20}$ single and bilayer CoFeB/Ru/CoFeB magnetic thin films with CoFeB thicknesses of 15 and 20 nm grown on Si/SiO_2 substrates. Broadband (5-40GHz) ferromagnetic resonance and longitudinal magneto-optical Kerr effect (L-MOKE) measurements were employed to extract these properties. All CoFeB thin films exhibited variations in remanent magnetization (M_r) and coercive field (H_c) with (θ_H), the angle between the magnetic field and the easy axis, indicating the presence of in-plane uniaxial magnetic anisotropy (UMA) with an easy axis along $\theta_H = 0^\circ$. The angular dependence of H_c and the remanent ratio (M_r/M_s) in all CoFeB thin film were well-described by a Two-Phase pinning (TP) model, revealing two distinct UMAs (UMA1 >> UMA2) in single layer CoFeB (15nm and 20 nm) thin films, whereas observed single UMA in CoFeB/Ru/CoFeB structures with same thicknesses. MOKE domain imaging confirmed the magnetization reversal processes in all films. Broadband CPW FMR measurements revealed that Gilbert damping (α) in CoFeB films with a Ru underlayer (CoFeB/Ru/CoFeB) was reduced by approximately 60% for a 15 nm thickness and by about 45% for a 20 nm thickness compared to the single-layer CoFeB thin films. This reduction is attributed to strong ferromagnetic coupling, aligning the magnetic moments of both CoFeB layers, causing synchronous precession and reducing overall damping. These findings offer crucial insights into the magnetic behavior of CoFeB thin films, which can improve the performance of magnetic storage and spintronic devices.

1.T. McKinnon, E. Girt, Appl. Phys. Lett. 113 (19), 192407 (2018) 2. B. K. Hazra, S. N. Kaul, S. Srinath 2020 AIP Adv. 10, 065017 (2020) *3.S. Chen, M. Tang, Appl. Phys. Lett.* 103, 032402 (2013) 4.C. Kittel Phys. Rev. 73(2), 155 (1948)

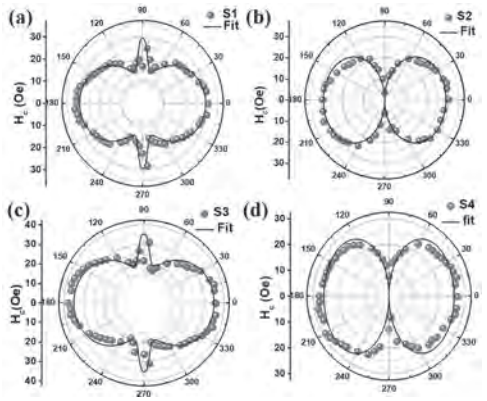

Fig.1: Variation of Hc with in-plane angle (θ_H) for (a) S1: CoFeB (15 nm) (b) S2: CoFeB (15 nm)-Ru-CoFeB (15 nm) (c) S3: CoFeB (20 nm) (b) S4: CoFeB (20 nm)-Ru-CoFeB (20 nm) thin films. The solid symbols and blue continous lines denote the raw data and theoretical fits respectively.

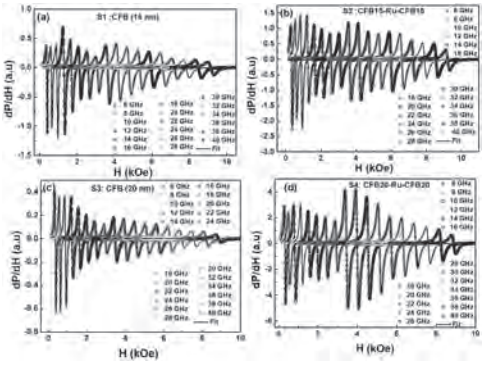

Fig.2: Experimental CPW-FMR spectra (open symbols) with fit (solid lines) for (a) S1: CoFeB (15 nm) (b) S2: CoFeB (15 nm)-Ru-CoFeB(15 nm) (c) S3: CoFeB (20 nm) (b) S4: CoFeB (20 nm)-Ru-CoFeB(20 nm) thin films in the frequency range of 6 -40 GHz.

DQ-06. Hybrid Spin-Photon Systems: Exploring the Purcell Effect. *S. Verma*[1], A. Maurya[1], R. Singh[1] and B. Bhoi[1] *1. Department of Physics, Indian Institute of Technology (BHU) Varanasi, India, Varanasi, India*

The Purcell effect, a key concept in cavity quantum electrodynamics refers to the modification of the spontaneous emission lifetime of a quantum source induced by its interaction with the environment [1]. Although the Purcell effect is well-explored in quantum systems, its realization, optimization, and application in classical systems still require significant investigation [2]. In this paper, we introduce a novel approach for observing the Purcell effect in a classical system using a microwave photon-magnon hybrid system consisting of a yttrium iron garnet (YIG) and a planar hexagonal ring resonator (HRR). Numerical simulations with CST Microwave Studio, varying the YIG film's damping constant α from 1.4×10^{-5} to 2.1×10^{-2}, reveal an enhanced spontaneous emission rate of microwave photons when coupled to lossy magnons. To theoretically validate these findings, we developed a quantum model that very accurately reproduced the observed Purcell phenomena observed in photon-magnon coupled anti-crossing dispersion spectra as shown in Fig. 1 (a) and (b). By demonstrating the Purcell effect's role in enhancing decay rates and revealing the relationship between coupling strength, linewidth, and magnon decay, our findings offer new insights into photon-magnon interactions in a planar hybrid system which opens up new avenues for future research into the Purcell effect's potential in magnonic devices and quantum technologies.

1. E. M. Purcell,"Spontaneous Emission Probabilities at Radio Frequencies," Phys. Rev. 69, 681 (1946). 2. X. Zhang, C.-L. Zou, L. Jiang and H. Tang,"Strongly Coupled Magnons and Cavity Microwave Photons," Phys. Rev. Lett. 113, 156401 (2014).

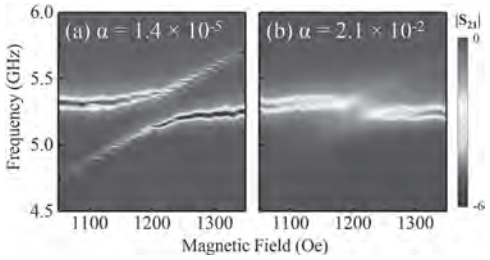

Fig. 1. $|S_{21}|$ power as a function of the applied field and microwave frequency, when the damping constant of YIG is (a) $\alpha = 1.4 \times 10^{-5}$, and (b) 2.1×10^{-2}.

DQ-07. Rotational Dependence of Photon-Magnon Coupling in a Planar ELCR-YIG System. *A. Maurya*[1], S. Verma[1], R. Singh[1] and B. Bhoi[1] *1. Department of Physics, Indian Institute if Technology (BHU) Varanasi, India, Varanasi, India*

In this work, we present a planar hybrid system comprising an electric-field-coupled resonator (ELCR), which exhibits a purely electric response with no magnetoelectric coupling and a yttrium iron garnet (YIG) film to investigate the interaction between photons and magnons at room temperature. The simulations were performed using the commercial electromagnetic full-wave simulator CST Microwave Studio, and the schematic representation of our planar system is shown in Fig. 1(a). The transmission spectra were recorded as a function of microwave frequency for various strengths of the bias magnetic field (H). In this setup, when the split gap of the ELCR is perpendicular to the microstrip line, only one resonance peak (photon mode) is observed at 4.06 GHz. However, upon rotating the ELCR, as shown in the Fig. 1(b), the intensity of this peak decreases while a new resonance peak (photon mode) at 5.74 GHz appears. Further rotation, until the split gap is parallel to the microstrip line, causes the first peak to disappear completely. The interaction of both photon modes with the magnon mode (quanta of spin wave in YIG) results in coupling strengths of 33 MHz and 58 MHz, respectively. We have also verified our results theoretically. The theoretical analysis involved considering the concept of traveling photons and developing a quantum model for the 3-mode system, which fully corroborated our simulation results. These findings have significant implications for advancing microwave quantum photonic devices, developing magnetically tunable metamaterials, and exploiting the strong coupling between magnons and microwave photons.

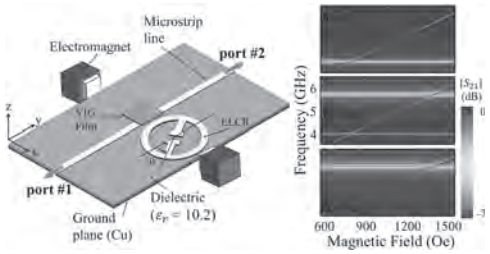

Fig. 1 (a) The simulation setup for investigating photon-magnon coupling, involves a planar geometry with an ELCR (photon mode) structure and a YIG (magnon mode) film. A static applied magnetic field H_{dc} is generated by an electromagnet oriented in the x-direction. The YIG film is positioned on the microstrip line adjacent to the ELCR. (b) The transmission spectra plotted for the rotation angle 0,60 and 90.

DQ-08. Magnon-Polaron Excitations in Olivine-Type Silicates. *A.B. Niraula*[1], Q. Huang[1], Y. Cheng[3], G. Granroth[3], H. Zhou[2] and X. Bai[1] *1. Physics and Astronomy, Louisiana State University, Baton Rouge, LA, United States; 2. Physics and Astronomy, University at Tennessee, Knoxville, TN, United States; 3. Neutron Scattering Division, Oakridge National Laboratory, Oak Ridge, TN, United States*

Collective excitations known as phonons and magnons result from long-range orderings of the lattice degrees of freedom and spin in a crystal. Since these low-energy modes frequently have very weak couplings, they can be viewed as free quasi-particles and treated independently in theories using harmonic approximations. The degeneracies at the crossing points of overlapping magnon and phonon bands may be lifted with strong magnetoelastic coupling, giving rise to a novel class of hybridized quasi-particles known as magnon-polarons. A model material with strong magnetoelastic couplings but simple chemical and structural features is highly needed for quantitative analysis and neutron scattering experiments. One of the most interesting observations of magnon-polarons was made within the olivine-type silicates M_2SiO_4 (M = Co and Fe)[1,2]. The initial findings[1,2] demonstrate avoid-crossing because of the high magnetoelastic connection. So far, however, no additional experimental or theoretical research has been carried out to verify the existence of hybrid magnon-polarons and comprehend the underlying mechanism. In my poster, I'll demonstrate how most of the characteristics of the magnetic and phonon spectra at the base temperature of Co_2SiO_4 can be captured using density functional calculations and linear spin-wave theory. I'll also show group-theoretical analysis, identify the symmetry characteristics that allow selection rules to lift the accidental degeneracy, and use that information to introduce particular exchange-striction or single-ion magneto-striction types of magnetoelastic coupling terms.

[1] Schmidt, et al. *Journal of magnetism and magnetic materials*, 140, 1989-1990(1995). [2] Schmidt, et al. *Journal of Magnetism and Magnetic Materials*, 104, 1049–1050 (1992). [3] Cheng, et al. *J. Chem. Theory Comput.* 15, 1974−1982 (2019).

Fig.1. Single-crystal (13.4g) mount of Co_2SiO_4, co-aligned in (hk0)-scattering plane

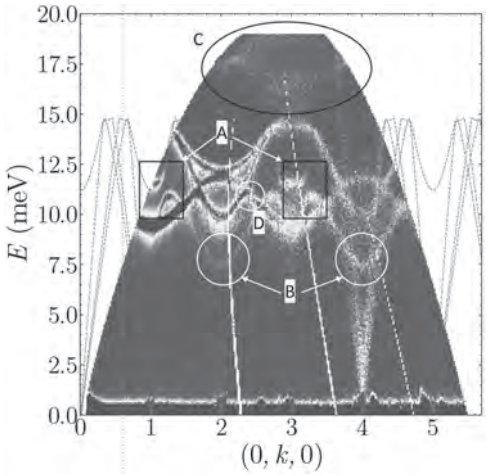

Fig.2. INS data collected at ARCS with incident neutron energy of 20meV overlapping with theoretical calculation of phonon-spectra (dotted red lines). Regions A, B and D are the indication of magnon-phonon coupling. Region C will be investigated.

Session DR
MAGNETIZATION DYNAMICS & MATERIALS WITH COUPLED MAGNETIC PHENOMENA II (Poster Session)

Jinho Lim, Chair
University of Illinois Urbana-Champaign, Urbana, IL, United States

DR-01. Strain-induced annihilation of dipolar skyrmions in uniaxial ferromagnet Fe-Sn. *M. Charilaou*[1] *1. Physics, University of Louisiana at Lafayette, Lafayette, LA, United States*

Recent experimental observations of dipolar skyrmions in the uniaxial ferromagnet Fe_3Sn_2 at room temperature have sparked interest in this material due to the potential in the judicious control of nanoscale magnetization textures. In this study, micromagnetic simulations of Fe-Sn thin films, with size and geometry comparable to samples used in transmission electron microscopy experiments, show that at remanence, there is a mixed state containing dipolar skyrmions and stripe domains. Application of tensile strain leads to a gradual modification of the magnetic state via the annihilation of the dipolar skyrmions and the formation of domain walls perpendicular to the strain axis, with the magnetization remaining out-of-plane. Once the strain reaches a threshold value, the magnetization switches abruptly towards an in-plane configuration with domain walls parallel to the strain axis. If the strain is decreased back to zero, the material returns to an out-of-plane configuration. These results can be used to design and interpret imaging experiments and they indicate that strain can be used to control the shape of dipolar skyrmions in this uniaxial ferromagnet and that depending on the level of strain, a variety of magnetic states can be achieved.

DR-02. Highly Tunable of Electronic States near Chirality-reversed Planar Defect with Magnetic Interstitial Atomic Layer in Magnetic Weyl Semimetals. *E. Thareja*[1], J.D. Gayles[1] and I. Vekhter[2] *1. Department of Physics, University of South Florida, Tampa, FL, United States; 2. Department of Physics and Astronomy, Louisiana State University, Baton Rouge, LA, United States*

Topological features in electronic band structure are robust against many types of disorder, which makes materials such as topological insulators and Weyl semimetals promising for low-power spintronics and quantum computing. Weyl semimetals possess topologically protected linear band crossings, called Weyl nodes, that always arise in pairs. The electronic excitations near these nodes have spin-momentum locking that can be characterized by a chiral charge, with individual nodes having opposite chirality [1], see Fig. 1a. While non-magnetic candidates for Weyl semimetals have been known for about a decade, their magnetic counterparts (which typically have fewer Weyl node pairs) have only been identified recently [2,3,4]. Weyl semimetals, like other materials, have planar defects such as twin boundaries. In this work, we show using a continuum model planar defect between chirality-reversed (due to magnetization-reversal) regions will host bound states, in agreement with [5], see Fig 1b. Moreover, we demonstrate that in the presence of magnetic interstitial atomic layer at the planar defect the dispersion and spin texture of these states is highly tunable. These properties have periodic dependence on electrostatic potentials (U_0), from the defect, due to the Weyl character of the electronic states. Another consequence of Weyl character is that magnetic potential from interstitial layer pointing out of the defect plane (U_x) do not affect physical observables. While in-plane magnetic potential components parallel to the vector connecting the Weyl nodes (U_z) is inconsequential for bound states, it strongly scatters the bulk states, Fig. 2. In-plane component perpendicular to the Weyl node splitting (U_y) on the other hand affects both bound states and scatters bulk states, see Fig. 2. Hence, we provide a comprehensive picture of how electrostatic and magnetic potentials from interstitial layer can be used to tune chirality-reversed planar defect states in magnetic Weyl semimetals.

[1] N. P. Armitage, E. J. Mele, and A. Vishwanath, Rev. Mod. Phys. 90, 015001 (2018). [2] Liu, D. F., A. J. Liang, E. K. Liu, et al. Science 365, 6459 (2019). [3] S. Nie, T. Hashimoto, and F. B. Prinz, Phys. Rev. Lett. 128, 176401 (2022) [4] Yao, X., Gaudet, J., Verma, R., Phys. Rev. X 13, 011035 (2023). [5] Y. Araki, A. Yoshida, and K. Nomura, Phys. Rev. B 98, 045302 (2018).

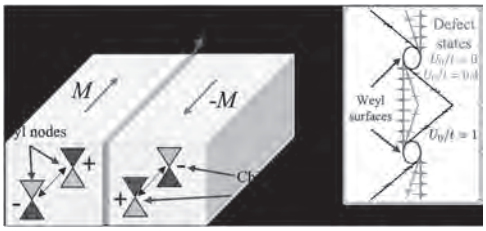

Fig. 1 (a) Chirality-reversed planar defect with interstitial layer (b) Bound states at the planar defect (red, green, black)

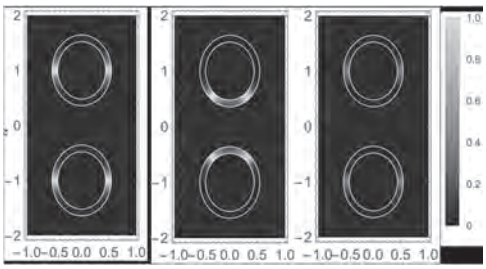

Fig. 2 Transmission probability of bulk states across the planar defect

DR-04. Geometrically Tunable Spin Superfluidity and a Spin Pumping–Induced Magnetoresistance Enabled by Spontaneous Symmetry Breaking in Easy-Plane Magnets. *M.D. Kitcher*[1] and G. Beach[1] *1. Materials Science and Engineering, Massachusetts Institute of Technology, Cambridge, MA, United States*

Spin superfluidity (SSF) inovles the near-dissipationless transport of spin angular momentum across a magnetic material via a coherently precessing spin spiral [1], making it a promising route towards magnetic analogs of superconducting devices, as well as novel spintronics devices [2]. While conventional easy-plane magnets can exhibit SSF in theory [3], the required device geometries are incompatible with current fabrication methods and/or spin injection via the spin Hall effect (SHE) in an adjacent heavy metal. Considering the ideal case of an insulating magnet, we analyze the nonlocal spin and charge transfer efficiencies of SSF devices with a lateral geometry [4], which has been underexplored due to an absence of compatible materials. Using a hydrodynamic formulation of the Landau–Lifshitz–Gilbert equation in conjunction with magneto-circuit theory, we show that the spin transfer efficiency is maximized when the area of the injector is much larger than the combined area of the detector and transport channel. Moreover, we relate the charge transfer efficiency and the nonlocal resistance at the detector to the conventional spin magnetoresistance (SMR) at the heavy

metal/insulator interface and consider its geometrical tunability. Our analysis demonstrates that beyond mediating SSF, spontaneous symmetry breaking in easy-plane magnets can engender spin-pumping–induced SMR, the previously unrecognized Onsager reciprocal of conventional SMR.

[1] E. B. Sonin, Sov. Phys. JETP 47, 1091 (1978); Adv. Phys. 59, 181 (2010) [2] D. Hill, S. K. Kim, and Y. Tserkovnyak, Phys. Rev. Lett. 121, 037202 (2018) [3] S. Takei and Y. Tserkovnyak, Phys. Rev. Lett. 112, 227201 (2014) [4] H. Skarsvåg, C. Holmqvist, and A. Brataas, Phys. Rev. Lett. 115, 237201 (2015)

DR-05. Quantum Landauer Erasure using Magnetic Tunneling Junctions. *C. Wang*[1], X. Li[2] and J. Hong[3] *1. School of Sciences, Hubei Institute of Technology, Wuhan, China; 2. Huazhong University of Science and Technology, Wuhan, China; 3. UC Berkeley, Berkeley, CA, United States*

Recently, the research of Landauer's principle in information technology has been a hot topic. [1-3] The theory states that there must be an energy dissipation of at least kTLn(2) of dissipation from a memory bit when a binary bit of data is removed from the hot bath contact memory at a given temperature. The Landauer limit has long been proven to be applicable in a wide range of classical systems. In recent years, there has also been evidence that this theory is also applicable to the quantum realm. [4-5] However, despite the good applicability of Landauer's principle to information technology, there is still some controversy among scholars. In this talk, a widely used digital memory technology is used to carry out the limit through theoretical simulation analysis and experimental investigation on the phenomenon of self-selected transmission torque magnetic tunnel pairing as shown in Fig 1. The findings (described in Fig 2) show that there is a convergence to the Landauer limit in heat dissipation during the adiabatic erasure of the nanoscale single-domain magnetic free layer of magnetic tunneling junctions, which proves the applicability of the Landauer principle to information technology, and lays a foundation for the further development of practical information processing technology, while approaching the basic limit of energy dissipation.

[1] Landauer, R. IBM J. Res. Develop. 5, 183–191 (1961) [2] Meindl, J.D., Davis, J.A. IEEE J. Solid-state Circuits 35, 1515–1516 (2000) [3] Berut, A., Arakelyan, A., Petrosyan, A. Nature 484, 187–190 (2012) [4] Gaudenzi, R., Burzuri, E. Nature Physics 14,565-568(2018) [5] Hong, J., Lambson, B., Dhuey, S. Science Advances 2(3) (2016)

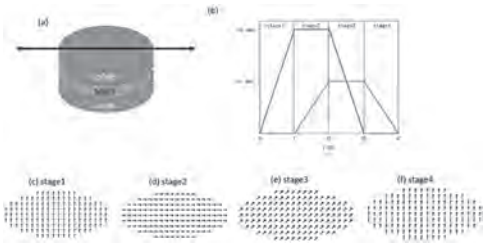

Figure1. (a) A schematic of MTJ structure (b) Magnetization as a function of applied field. (c)-(f) steps 1-4 in the process to perform Landauer test.

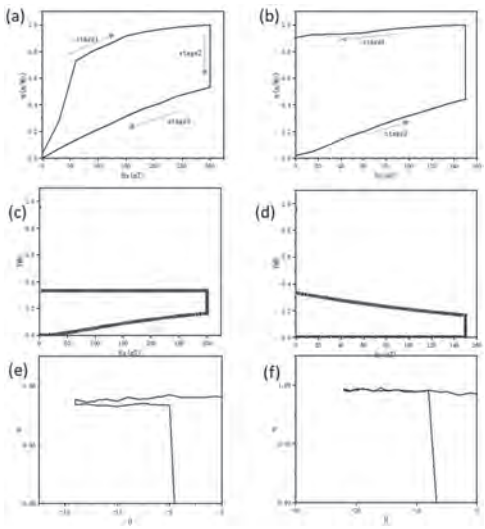

Figure2. (a) X-axis and (b) Y-axis hysteresis loops of a magnetic tunneling junction during the "restore to one" operation at 0 K. (c) the magnetoresistance (MR) on the X-axis. (d) the MR on the Y-axis. (e) the MR loops in x-axis and (f) the y-hysteresis curves of MR

DR-06. An Ultrasensitive Molecular Detector for Direct Sensing of Spin Currents at Room Temperature. T. Feggeler[1,2], R. Meckenstock[3], T. Strusch[3], M.V. Efremova[4], M. Farle[3] and *U. Wiedwald*[3] *1. Department of Physics, University of California, Berkeley, CA, United States; 2. Advanced Light Source, Lawrence Berkeley National Laboratory, Berkeley, CA, United States; 3. Faculty of Physics, University of Duisburg-Essen, Duisburg, Germany; 4. Department of Applied Physics, Eindhoven University of Technology, Eindhoven, Netherlands*

The experimental analysis of pure spin currents at interfaces is one major goal in the field of magnonics and spintronics. Complimentary to the established Spin-Hall effect [1] to use spin pumping from ferromagnetic interfaces for information processing, we present a novel approach based on the spin pumping detection by an interfacial, resonantly excited molecular paramagnet adsorbed to the surface of the spin current generating magnet [2]. We show that the sensitivity of this electron paramagnetic resonance (EPR) detector can be enhanced by orders of magnitude through an intramolecular transfer of spin polarization at room temperature. Our proof-of-principle sample consists of ferrimagnetic Fe_3O_4 octahedral nanoparticles covered by oleic acid which has two paramagnetic centers S1 and S2. Here, S1 arises from the chemisorption with and is located directly at the interface to Fe_3O_4. S2 is located in the center of the molecule close to the double bond of oleic acid and not influences by the chemisorption. Using ferromagnetic resonance excitation of the Fe_3O_4 nanoparticles to pump spins into S1 a population inversion of the spin-split levels of S2 is formed vastly enhancing the detection sensitivity on the atomic scale. Fig. 1 displays the peak-to-peak amplitude of signal S2 in SPC (black) and in-plane (red) configurations as function of microwave power. The S2 amplitude is decreasing with increasing power due to the larger population inversion. We detect a minimum of the S2 line intensity at 30 mW for SPC as compared to 80 mW for the in-plane configuration. Therefore, the effect is stronger in SPC as compared to the in-plane configuration. Due to the additional S1 EPR excitation by spin pumping from FMR, more S1 excited states are available leading to enhanced stimulated emission of S2, thus decreasing the absorption of externally fed microwaves. Our stimulated emission-based detection scheme is a broadly applicable, non-invasive technique for the direct and remote measurements of spin currents without electrical contacts.

[1] J. Sinova, S.O. Valenzuela, J. Wunderlich et al., Reviews of Modern Physics 87, 1213-1259 (2015). [2] T. Feggeler, Ralf Meckenstock, Tanja Strusch, Maria V. Efremova, Michael Farle, Ulf Wiedwald, ACS Applied Materials Interfaces, in revision.

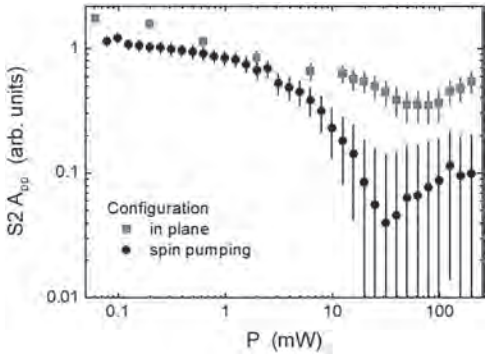

Peak-to-peak amplitude A_{pp} of S2 for in-plane and spin-pumping configuration as function of microwave power in double logarithmic representation.

DR-07. Sputter Deposited Magnetostrictive $Fe_{(100-x)}$ Al_x Alloy on Flexible Substrate. P. Kumar[1,4,3], R. Kumar[1], S. [1], *V. Sharma*[2], M.K. Khanna[1] and B.K. Kuanr[3] *1. Department of Electronic Science, University of Delhi, New Delhi, India; 2. Department of Physics, Northeastern University, Boston, MA, United States; 3. SCNS, Jawaharlal Nehru university, New Delhi, India; 4. Physics, Motilal Nehru College, University of Delhi, New Delhi, India*

$Fe_{(100-x)}$ Al_x thin films, composed of iron (Fe) and aluminum (Al), represent an intriguing class of materials known for their unique magnetic, electrical, and mechanical properties. These thin films are extensively studied for their potential applications in various technological fields, including spintronics, magnetic sensors and storage, and protective coatings[1]. In this investigation, using co-sputtering FeAl thin films of two different compositions $Fe_{65}Al_{35}$ and $Fe_{75}Al_{25}$ were deposited on two different flexible substrates such as Kapton (marked K1,K2) and mica (M1,M2) respectively. The XRD plot (Fig. 1) of all films confirm the formation of a disordered ferromagnetic A2 phase. The effective magnetization (M_{eff}) were determined from Hr vs frequency plot (Fig. 2(a)) from ferromagnetic resonance (FMR) experiments. Almost same M_{eff} values are obtained (14.60 kOe and 14.50 kOe) both for M1 and K1 films. As the Fe concentration increases the M_{eff} increased to 16.89 kOe and 17.04 kOe for M2 and K2, respectively. To determine the magnetostrictive effect, bending strain was applied. This investigation have been performed using bended microstrip line based FMR. Figure 2(b-c) displays FMR spectra obtained applying stress. The value of isotropic magnetostriction coefficient (λ) is related as $K_u \approx 3/2\lambda\ \sigma_{xx}$ and $H_u = 2K_u/M_S$ (where each term has its usual meaning) [2]. The determined λ is observed to increase in Fe concentration for kapton and decrease for mica. Their values are 27.57 PPM and 29.59 PPM for K1 and K2, respectively. For mica, the λ values are 29.90 PPM and 27.88 PPM for M1 and M2, respectively. Our research has demonstrated that the magnetization of FeAl deposited on a flexible substrate, may readily be controlled by magnetostriction. The left-shift of FMR spectra is due to tensile stress. Similarly, with compressive stress we have observed right-shift of FMR spectra which was possible with flexible substrates.

1. M. Gueye, F. Zighem, M. Belmeguenai, M. S. Gabor, C. Tiusan, and D. Faurie, J Phys D; Appl Phys 49, (2016). 2. M. Gueye, B. M. Wague, F. Zighem, M. Belmeguenai, M. S. Gabor, T. Petrisor, C. Tiusan, S. Mercone, and D. Faurie, Appl Phys Lett 105, (2014).

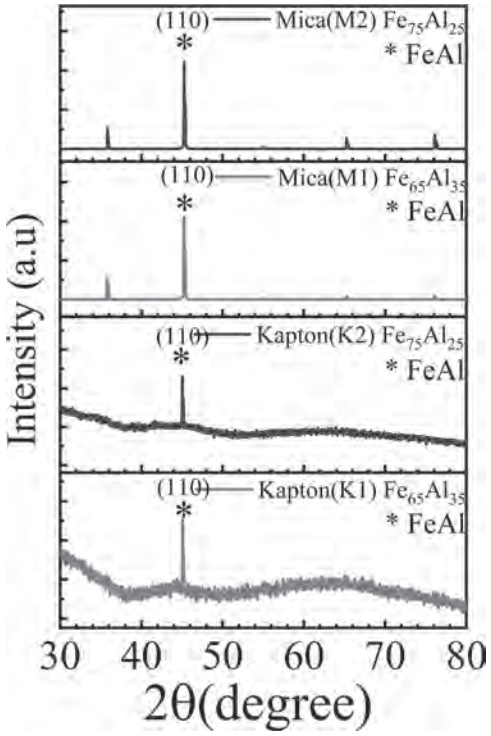

Figure 1 XRD pattern of different compositions of FeAl on flexible Mica and Kypton Substrate

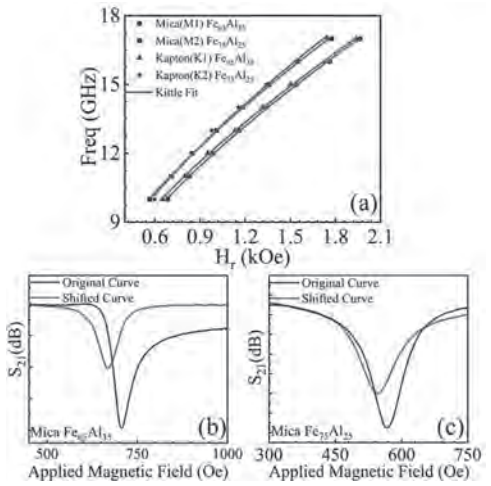

Figure 2 (a) Hr Vs Freq plot of two different composition of FeAl on Mica and Kapton (b-c) shift in Hr position of FMR on Mica for FeAl (75:25 and 65:35)

DR-08. The Effect of Cu Doping on the Magnetic and Magnetocaloric Properties of $Al_{1.2}Si_{0.15}Fe_{2-x}Cu_xB_2$. *S. Rahman*[1], J.R. DeFeo[2], H.A. Adedo[1], V. Yenugonda[2], A.K. Pathak[2] and M. Khan[1] *1. Department of Physics, Miami University, Oxford, OH 45056, USA, Oxford, OH, United States; 2. Department of Physics, SUNY Buffalo State University, Buffalo, NY 14222, USA, Buffalo, NY, United States*

Due to the large entropy changes it exhibits near room temperature, the intermetallic compound $AlFe_2B_2$ has gained much attention in recent years [1, 2]. The material crystallizes in a *Cmmm* orthorhombic structure and exhibits a ferromagnetic transition between T_C = 274 K – 320 K. Peak entropy changes between -2.1 J/kg K and -4.4 J/kg K have been reported for a field change of 2 T. Partial doping of Si for Al in $Al_{1.2-x}Si_xFe_2B_2$ significantly increases the magnetocaloric properties of the system. For a field change of 5 T, a peak

magnetic entropy change of -7.4 J/kg K has been observed in the system for $x = 0.15$ [3]. Here we present an experimental study on the effect of Cu doping on the magnetic and magnetocaloric properties of $Al_{1.2}Si_{0.15}Fe_{2-x}Cu_xB_2$. X-ray diffraction, dc magnetization, and resistivity measurements have been performed on the system for x=0.05, 0.1, 0.15. Although the orthorhombic phase was dominant the system the percentage of FeB phase increased in the samples with increasing Cu concentration. The T_C also decreased from ~308 K (x = 0.05) to ~300 K (x=0.15) with increasing Cu concentration. Peak entropy changes of more than -5 J/kg K along with a refrigeration capacity of 160 J/K were observed in the system. The experimental results will be presented and discussed in detail. The work at State University of New York (SUNY), Buffalo State University, was supported by the National Science Foundation Award No. DMR-2213412.

1) X. Tan, P. Chai, C. M. Thompson and M. Shatruk, J. Am. Chem. Soc., Vol. 135, p.9553 (2013) 2) A. E. Boukili, N. Tahiri and E. Salmani, Intermetallics., Vol. 104, p.84 (2019) 3)Md Sakhawat Hossain, Kyra Stillwell and S. Agbo, Journal of Magnetism and Magnetic Materials., Vol. 571, 170576 (2023)

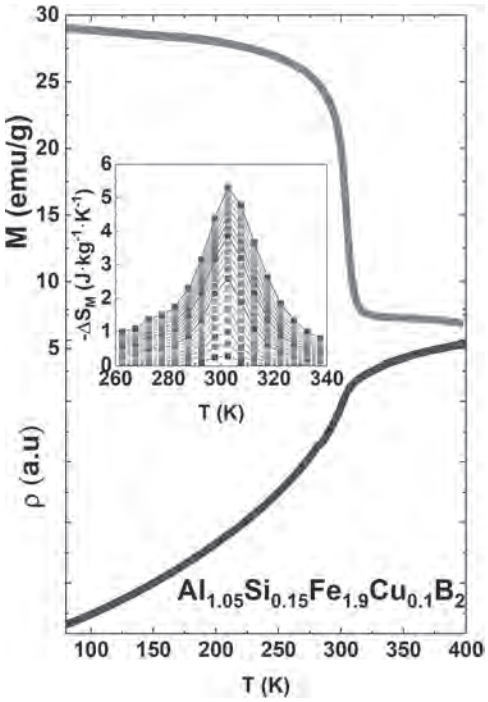

Fig.1. Temperature dependence of magnetization, resistivity, and magnetic entropy changes in $Al_{1.2}Si_{0.15}Fe_{2-x}Cu_xB_2$ (x = 0.10).

Session DS
MAGNETOELECTRIC MATERIALS AND PHENOMENA II
(Poster Session)

Lucas Caretta, Co-Chair
Brown University, Providence, RI, United States
Kai Litzius, Co-Chair
University of Augsberg, Augsberg, Germany

DS-01. Investigating Physical Properties and Evolution of Griffiths Phase in $Tb_2Ni_{1-x}Co_xMnO_6$ Double Perovskites. *A. Raghu*[1] and S.D. Kaushik[1] *1. Physics, UGC DAE CSR Mumbai Centre, Mumbai, India*

Magnetic materials are at forefront of material science research due to their crucial role in various cutting-edge applications. Besides, magnetic properties study enriches our understanding of fundamental physical principles and leads to development of advanced materials. Double perovskites are fascinating class of materials which are derived out of simple perovskite ABO_3, where A and B site can be large electropositive cation and small transition metal anion. These materials exhibit unique structural and physical properties like ferroelectricity, electrical conductivity, magnetoresistance etc [1]. In rare earth based double perovskites, combination of valency of ions at B site is key factor in ascertaining physical properties. La_2NiMnO_6 and La_2CoMnO_6 are case in point where former is a ferromagnetic insulator with magneto-dielectric behavior while later shows higher magnetoresistance, magnetocapacitance with two ferromagnetic phase transitions [2,3]. Here, we discuss results on $Tb_2Ni_{1-x}Co_xMnO_6$ double perovskite where substitution of $Ni2^+$ by Co^{2+} has been explored to understand role of ionic radii on structural and magnetic properties by subjecting them to XRD, neutron diffraction (ND) and magnetization study. Polycrystalline $Tb_2Ni_{1-x}Co_xMnO_6$ were synthesized by solid state route using high purity (≥ 99.9%) precursors in stochiometric ratio with calcination and intermediate grinding with final sintering at 1250°C. Phase formation was confirmed by XRD and ND recorded at PD-3, Dhruva, India [4]. Figs shows Rietveld refined XRD and ND patterns of $Tb_2Ni_{1-x}Co_xMnO_6$ (x = 0, 1) fitted with monoclinic $P2_1/n$ space group by employing Fullprof suite along with crystal structure [5]. Magnetization study carried out by employing PPMS in VSM mode (M/s. Quantum Design) on $Tb_2Ni_{1-x}CoxMnO_6$ (x = 0) ascertain, paramagnetic to antiferromagnetic transition at 112 K. Isothermal magnetization at 5 K, 50 K and 300 K further elucidate ordering. Physical and structural properties are further being comprehended by temperature dependent neutron diffraction, dielectric, specific heat, AC Susceptibility study which will clearly depict role of Ni and Co ion in tailoring properties and magnetic structure of $Tb_2Ni_{1-x}Co_xMnO_6$.

[1]. S. Otsuka and Y. Hinatsu, J. Solid State Chem., 227, 132-141(2015). [2]. D N Singha, P Sinha, D K Mahato, Mater Today Proc., 45640 (2017). [3]. Y. Mao, J. Parsonsa, J.S Mcloy, Nanoscale., 5, 04720(2013). [4]. V. Siruguri, P.D. Babu, M. Gupta et al., Pramana., 71. 1197–1202(2008). [5]. J. Rodriguez Carvajal, Physica B., 192, 55(1993).

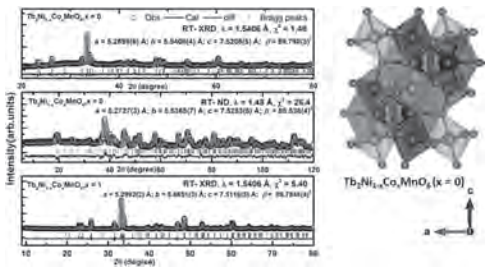

Fig1

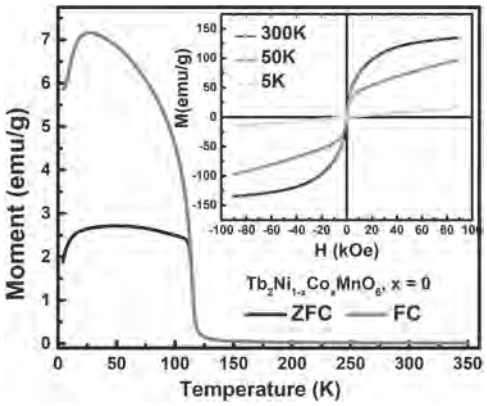

Fig2

DS-02. Tuning Magnetocaloric Effect at Constant Temperature in $Ho_{36}Co_{64-x}Al_x$ Multiphase Alloys. *E.A. Balfour*[1], H. Fu[2], D. Ami-Erigo[1], J.S. Bayor[1] and R.L. Hadimani[3] *1. Applied Physics, C. K. Tedam University of Technology and Applied Sciences, Navrongo, Ghana; 2. School of Physics, University of Electronic Science and Technology of China, Chengdu, China; 3. Department of Mechanical and Nuclear Engineering and Department of Biomedical Engineering, Virginia Commonwealth University, Richmond, VA, United States*

Tuning magnetocaloric effect (MCE) at fixed temperature under given magnetic change has been a challenge. For various reasons including medical, MCE may be required to be tuned at a fixed temperature to a desired magnitude. Unfortunately, this has not yet been possible. Although magnetic entropy change (MEC) and other accompanying properties are known to be tuned by varying the composition of magnetocaloric materials (MCMs), the changes in MEC do not occur at fixed temperature. For instance, depending on the Fe content in the $Mn_{1-x}Fe_xAs$ alloys, MEC magnitude ($-\Delta S_M$) decreases with increasing temperature (from 285 K to 310 K) [1]. In the case of $Tb_{1-x}Y_xCoC_2$ the MCMs are single phases that maintain their parent structures within the limits of the composition variation. Their $-\Delta S_M$ peaks decrease with decreasing temperature under magnetic field changes of 0 to 2, 3, 5 T for x=0.0 to x=0.4 [2]. In this work, we report the tuning of magnetocaloric effect under fixed magnetic field change at constant temperature in the $Ho_{36}Co_{64-x}Al_x$ multiphase alloys by composition variation. Fig. 1, shows that $-\Delta S_M$ is enhanced from 12.1 J/kg K to 16.7 J/kg K under the field change of 5 T for the MCM compositions of x=19 to x=22, respectively. The tuning of the $-\Delta S_M$ occurs at the fixed temperature of 31.5 K. However, for the compositions x<19 and x>22, the $-\Delta S_M$ peaks shift to higher and lower temperatures respectively. The properties of the alloy system have been analysed and the behaviour of the 19≤x≤22 composition alloys is explained based on the structure, magnetic and magnetocaloric properties of their component phases. The ability to significantly adjust the $-\Delta S_M$ at constant temperature is unique and an important development. These systems are technologically promising in hyperthermia treatment and other magnetically sensitive technological applications that require tuning $-\Delta S_M$ to a desired magnitude at constant temperature under suitable magnetic field change.

[1] A. de Campos, D. L. Rocco, A. M. G. Carvalho, et al., *Nat. Mat.* 5, 802 (2006). [2] Z.G. Xie, B. Li, J. Li, et al., *Phys. B* 405, 2133 (2010).

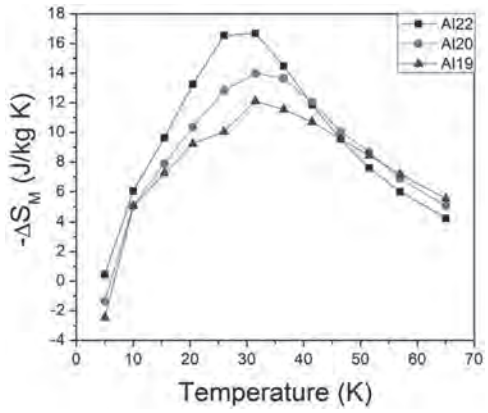

Figure 1. Variation of -ΔS_M at 31.5 K under magnetic field change of 5 T for the composition variations of x=19, 20 and 22 designated as Al19, Al20 and Al22, respectively.

DS-03. Visualizing Domain Structures in Multiferroic ε-Iron Oxide Thin Films. *D. DeTellem*[1], S. Witanachchi[1] and M. Phan[1] *1. Physics, University of South Florida, Tampa, FL, United States*

With the ever-increasing demand for fast and robust electronics, multiferroic materials continue to be a promising avenue for the future of nonvolatile high-speed memory. One promising candidate for this research direction is epsilon Fe_2O_3 - an intriguing, room-temperature, multiferroic semiconductor. Possessing a magnetization of 40 emu/cc and a bulk coercivity of ~2T, it is an ideal material for robust magnetic memory. Because it also possesses ferroelectric ordering, it may also be possible to control its magnetic properties via an electric field, allowing its application to be extended toward the exciting area of magnetoelectric spin-orbit logic devices. We report here the pulsed laser deposition (PLD) growth of epitaxial thin films of epsilon Fe_2O_3 on strontium titanate and niobium-doped strontium titanate substrates. Through careful tuning of parameters, we present the results of high-quality films that are remarkably free of particulates, allowing the magnetic domain structure of epsilon Fe_2O_3 to be investigated by magnetic force microscopy for the first time. The evolution of the magnetic domain structure with temperature correlates with the temperature-dependent magnetization measured through magnetometry. We also present piezo response microscopy images showing the polarization of the films over a larger area than has been shown previously.

DS-04. Realization of Perpendicular Magnetic Anisotropy of (001) $Mn_{1.5}Ga$ on SiO_2 substrate. *N. Zahrin*[1], K. Tokunaga[1], Y. Kurokawa[1] and H. Yuasa[1] *1. Kyushu University, Fukuoka, Japan*

The half metals with perpendicular magnetic anisotropy (PMA) material are desirable as they can be utilized for novel data processor or storage, for example, MTJ for MRAM, domain wall racetrack memories, and skyrmion devices. The MnGa film on a MgO substrate is one of the candidates due to sufficient PMA and the high spin polarization [1]. For wide applications, however, SiO_2 substrate is more realistic than MgO substrate. Therefore, we fabricated MnGa film on SiO_2 substrate by introducing MgO buffer layer. Here, we inserted additional Co buffer layers between MgO and MnGa to reduce the lattice mismatch and investigated the crystalline structure and magnetic property. We compared two samples, S1 without Co buffers and S2 with Co buffers shown in Fig. 1. They were prepared by sputtering and annealed at 673 K for 1h. The X-ray diffraction pattern and diffraction peaks of $L1_0$- $Mn_{1.5}Ga$ (002) and MgO (002) were observed in Fig. 1 for both samples, indicating that $Mn_{1.5}Ga$ films formed a [001] oriented films. We can obtain the crystallized $Mn_{1.5}Ga$/MgO on SiO_2 substrate and post annealing for the first time although it has been difficult to obtain the well-crystalline structure without the combination of the MgO single crystal substrate and the in-site annealing during deposition [2,3]. Fig. 2 shows the magnetization curves under (a) in-plane and (b) perpendicular magnetic fields. Both samples showed PMA and S2 showed higher magnetization than S1, which suggests that Co buffers improve the magnetic polarization of $Mn_{1.5}Ga$. However, the coercivity increased by Co buffers. Our result suggests that simple structure of (001) oriented in Co-inserted $Mn_{1.5}Ga$/MgO may provide future prospect of a p-MTJ material.

[1] X. P Zhao, J Lu and S W Mao, J. Phys. D: Appl. Phys. 50, 285002 (2017) [2] Weinan Zhou, Keisuke Masuda and Yuya Sakuraba, Appl. Phys. Lett. 118, 152406 (2021) [3] K. Hasegawa, M. Mizuguchi and Y. Sakuraba, Appl. Phys. Lett. 106, 252405 (2015)

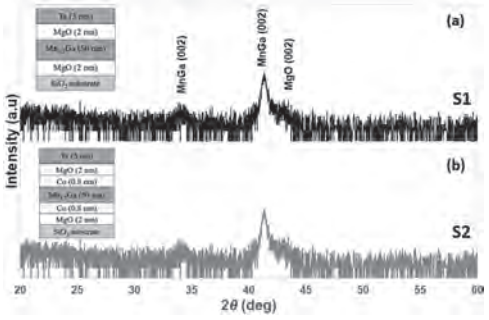

Fig.1. XRD pattern alongside the stacking structure for sample (a) without Co layer (S1) and (b) with Co-layer (S2)

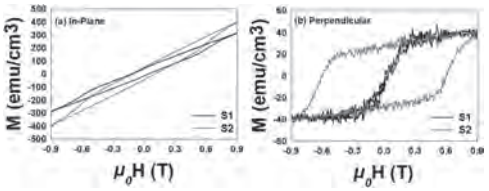

Fig.2 M-H curves for S1 and S2 under (a) in plane and (b) perpendicular magnetic field

DS-05. Exploring spin-gapless semiconducting properties of FeVTaAl and FeCrZrAl. *C. Sadler*[1], S. Smith[2], B. Schmidt[1], P. Kharel[3], P. Shand[1] and P. Lukashev[1] *1. Physics, University of Northern Iowa, Cedar Falls, IA, United States; 2. Cedar Falls High School, Cedar Falls, IA, United States; 3. Chemistry, Biochemistry and Physics, South Dakota State University, Brookings, SD, United States*

Here, we present results of a computational study of electronic, magnetic, and structural properties of FeVTaAl and FeCrZrAl, quaternary Heusler alloys exhibiting nearly spin-gapless semiconducting behavior. Our calculations indicate that these materials may crystallize in regular Heusler cubic structure, which has a significantly lower energy than the inverted Heusler cubic phase. Both compounds exhibit ferromagnetic alignment, with an integer magnetic moment per unit cell at equilibrium lattice parameter. While both FeVTaAl and FeCrZrAl have been reported recently to exhibit spin-gapless semiconducting electronic structure, a closer inspection of their band structures shows that FeVTaAl is a half-metal, while FeCrZrAl is magnetic semiconductor at their optimal lattice constants. Our calculations indicate that while expansion of the unit cell volume enhances these properties for both compounds, mechanical pressure ultimately destroys half-metallicity of FeVTaAl (Fig. 1 (a)) and magnetic semiconductivity of FeCrZrAl (Fig. 1 (b)). Thus, both of these alloys may be potentially useful for practical applications in spin-based electronics, but one should avoid implementing them in situations where their unit cell volume may be reduced, e.g. in thin-film applications with substrates of larger lattice constants. We hope that these results will stimulate experimental efforts to synthesize these materials. Acknowledgments This research is supported by the *National Science Foundation* (NSF) under Grant Numbers 2003828 and 2003856 via DMR and EPSCoR.

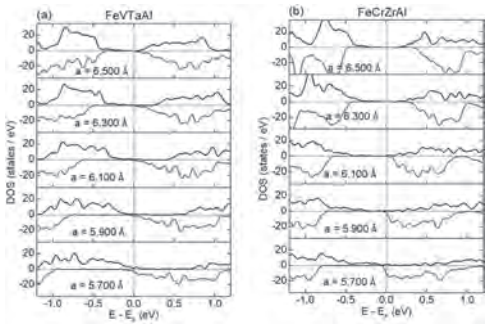

Figure 1: Calculated total density of states (DOS) of FeVTaAl (a) and FeCrZrAl (b) for different values of lattice parameters (indicated in the figure) calculated at uniform pressure. The vertical line corresponds to the Fermi level. Positive (black line)/negative (red line) DOS represents spin-up/spin-down states, correspondingly.

DS-06. Synthesis of Regular and Iron-Doped Lanthanum Calcium Manganese Oxide Nanoparticles for Magnetic Refrigeration.

I.M. Smith[1], J. Ahmed[1], P. Moberg[1] and E. Carpenter[1] *1. Chemistry, Virginia Commonwealth University, Richmond, VA, United States*

Vapor phase refrigeration has been a ubiquitous method for cooling for over a hundred years. However, it is inefficient and uses environmentally unfriendly refrigeration gases like fluorocarbons. There is a growing need for alternative cooling methods like solid-state cooling which could be more efficient and environmentally friendly. While thermoelectrics or magnetostriction methods have shown promise, magnetocaloric has the greatest potential. Magnetic refrigeration uses magnetic nanoparticles that utilize the magnetocaloric effect, allowing for an efficient and rapid change in temperature when subjected to a magnetic field. Such materials require reduced electrical consumption and lower operational costs, besides reducing the greenhouse gas emissions from conventional systems. While most magnetocalorics utilize rare-earth containing elements, other rare-earth free oxides like (La,Ca)MnO3 (LCMO) have shown great promise. Utilizing a modified Pechini sol-gel synthesis method, we present an improvement to the previously reported LCMO and Iron-doped Lanthanum Calcium Manganese Oxide (LCMFO) nanoparticles for magnetic refrigeration. The iron-doped nanoparticles were designed to improve the electron alignment capability of the original powder, subsequently increasing the entropy (ΔS), which is an essential parameter for an efficient magnetic refrigerant. Studies of the nanoparticle scale and the effective magnetocaloric effect of both nanopowders have been undertaken to prove the potential scalability, environmental sustainability, and refrigeration potential for the replacement of conventional refrigeration methods.

DS-08. Enhancing Magnetic and Insulating Properties of $BiFeO_3$-Based Multiferroic Thin Films via B-Site Dual Substitution of Ni and Co along with Oxygen-Rich Target for Magnetic Memory Device Applications.

S.S. Das[1,2], Y. Suzuki[1], S. Ratha[1], G. Egawa[1] and S. Yoshimura[1]
1. Graduate School of Engineering Science, Akita University, Akita, Japan; 2. Department of Material Science, Akita University, Akita, Japan

$BiFeO_3$ (BFO) based materials, known for their ferromagnetic and ferroelectric properties, are promising candidates for efficient magnetic memory devices with reduced power consumption. We successfully demonstrated magnetization switching [1] and magnetization transfer [2] by applying electric field in BFO based materials, highlighting their potential in magnetic memory device application. The reported BFO based thin films have not so good magnetic properties like saturation magnetization (M_s), perpendicular magnetic anisotropy (PMA) and insulating properties which necessitates refinement, especially for memory device applications. To obtain good magnetic properties, we substituted Co or Ni in the B-site of BFO [3]. Co substitution was effective for improving M_s whereas Ni substitution resulted in good PMA. Therefore, in this study, both Co and Ni were discussed as dual B-site dopants at different concentrations in $(Bi,La)(Fe,(Co,Ni))O_3$ (BLFNCO) for the further improvement in the magnetic properties. To improve the insulating property, a newly designed sputtering target with higher oxygen concentration is discussed. We explored on BLFNCO thin film at different Co and Ni atomic concentrations in the B-site of BFO. This strategy led to a notable improvement in M_s with maintaining relatively high $S_\perp/S_{//}$ (PMA), making the thin films highly suitable for magnetic memory device applications as shown in Fig. 1 and Fig. 2. This study emphasizes the crucial role of appropriate B-site element substitution in BFO to enhance magnetization and PMA. To achieve good insulating property, a special sputtering target with higher oxygen concentration was designed to combat the oxygen vacancy during the film fabrication. In the case of normal sputtering target, $LuFeO_3$ (Lu:O=1:3) and others are used as base material. However, in the case of newly developed oxygen rich target, $Lu_3Fe_5O_{12}$ (Lu:O=1:4) is used. The thin films fabricated by oxygen rich target showcase 2 times higher breakdown voltage than the normal sample. These results show that not only the material composition but also the preparation method of the sputtering target contributes greatly for improving the properties of thin films.

[1] M. Kuppan, D. Yamamoto, G. Egawa, S. Kalainathan and S. Yoshimura. *Scientific Reports*, *11*(1) (2021). [2] S. Yoshimura, N. Oshita, G. Egawa and M. Kuppan, *Nanotechnology* 34 465703 (2023). [3] Y. Suzuki, T. Ozeki, G. Egawa, and S. Yoshimura, *J. Soc. Mater. Eng. Resour. Jpn.*, vol.33-1/2, pp.12-17 (2023).

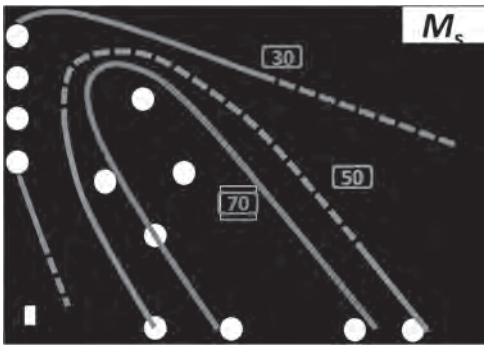

Fig 1. M_s of BLFNCO

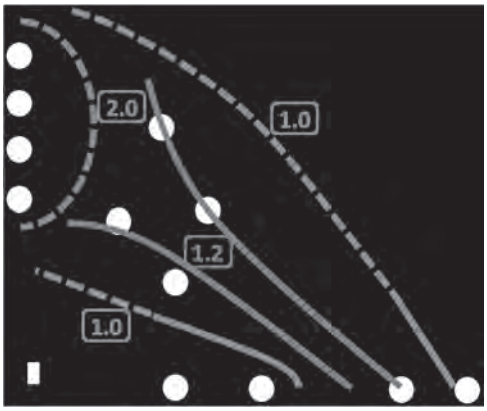

Fig 2. $S_\perp/S_{//}$ of BLFNCO

Session DT
MAGNETORESISTANCE & DOMAIN WALLS
(Poster Session)

Myoung-Woo Yoo, Chair
University of Illinois Urbana-Champaign, Champaign, IL, United States

DT-01. Tunnel magnetoresistance up to 405% at room temperature in exchange-spin-valve CoFeB/MgO/CoFeB junctions by *in-situ* MgO annealing. *H. Sukegawa*[1], T. Scheike[1], J. Uzuhashi[1], Z. Wen[1], S. Kasai[1], T. Ohkubo[1] and S. Mitani[1] *1. National Institute of Materials Science, Tsukuba, Japan*

MgO-based magnetic tunnel junctions (MTJs) are commonly used for practical spintronic devices, including magnetoresistive random access memories. Recently, we have demonstrated a tunnel magnetoresistance (TMR) ratio of 631% at room temperature (RT) by developing an epitaxial CoFe/MgO/CoFe(001) MTJ structure [1]. The giant TMR ratio was attributed to the improvement of the CoFe/MgO barrier interface structures. In this study, to improve the TMR ratio at RT of practical polycrystalline MTJs, we introduce the *interface engineering* used in the epitaxial MTJ to an exchange-spin-valve type CoFeB/MgO/CoFeB structure. In-plane magnetized CoFeB/MgO/CoFeB with an exchange-spin-valve structure were deposited by ultra-high vacuum magnetron sputtering. The typical structure is: (Si/SiO_2) substrate/(Ta/Ru) buffer/CoFeB (4)/CoFe (1)/MgO (1-1.5)/CoFeB (3-5)/CoFe (0.7)/Ru (1.3)/CoFe (3)/IrMn (8)/Ru cap (unit: nm). *In-situ* post-annealing was introduced to improve the MgO(001) texture, which was monitored by reflection high-energy electron diffraction (RHEED). TMR properties were characterized at RT by dc four probe method after MTJ patterning into an area of ~40 mm^2. Figure 1 shows a RHEED pattern of the MgO barrier after annealing temperature at 500°C. A clear (001) texture was observed. After further interfacial modification by annealing process and thickness, a TMR ratio of up to 405% was observed as shown in Fig. 2 due to the improvement of spin-dependent coherent tunneling effect. The TMR ratio exceeds the previous report of 365% in the exchange spin-valve CoFeB/MgO/CoFeB MTJ [2]. This work was supported by JSPS KAKENHI 22H04966, 24K00948, 24H00408, and MEXT Program: Data Creation and Utilization-Type Material Research and Development Project JPMXP1122715503.

[1] T. Scheike *et al.*, Appl. Phys. Lett. 122, 112404 (2023). [2] Y.M. Lee *et al.*, Appl. Phys. Lett. 89, 042506 (2006).

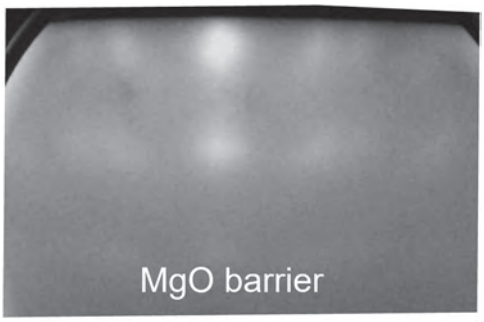

Figure 1. RHEED pattern of MgO(001) textured barrier deposited on a CoFeB layer.

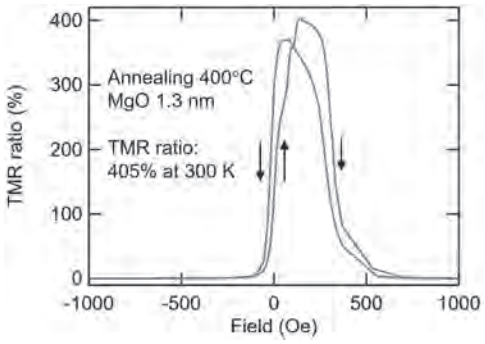

Figure 2. TMR ratio as a function of magnetic field of a CoFeB/MgO/CoFeB spin-valve MTJ.

DT-02. Interfacial Contributions to the Anisotropic Magnetoresistance in FeRh Films Capped with Pt or SiN_x. *A. Tsai*[1], E. Eremina[1], T. Wing[1], S.K. Patel[2], E. Fullerton[2] and J.C. Eckert[1] *1. Physics, Harvey Mudd College, Claremont, CA, United States; 2. CMRR, UCSD, San Diego, CA, United States*

FeRh is a material of interest because of its tunable first-order hysteretic phase transition near room temperature from a low-temperature antiferromagnetic (AF) phase to a high-temperature ferromagnetic (FM) phase, with accompanying large change in resistivity and lattice parameter. It has been reported that the electronic band structure in collinear AF materials can be significantly affected by changes in spin orientation such as spin canting, resulting in complex transport properties. For an FeRh/Pt bilayer, observations of unidirectional magnetoresistance, which increases strongly with magnetic field and decreasing temperature, have been attributed to the interplay of the Rashba spin-orbit coupling at the AF-heavy metal interface and the AF spin canting of FeRh or to a field-induced change in the Fermi surface morphology [2]. In this work, we conduct measurements of the anisotropic magnetoresistance (AMR) of FeRh films with thickness ranging from 10nm to 100nm and capped with Pt or SiN_x at various temperatures and fields. Thicker FeRh films show AMR with two-fold symmetry, however lower symmetries begin to emerge as the FeRh film is thinned, and the symmetry of films capped with Pt diverges from that of films capped with SiN_x. We will discuss the possible origins and the role of the capping layers on these phenomena.

1. S. Shim, et al., Phys. Rev. X 12, 021069 (2022). 2. J Sklenar, et al., Communications Physics 6 (1), 241 (2023).

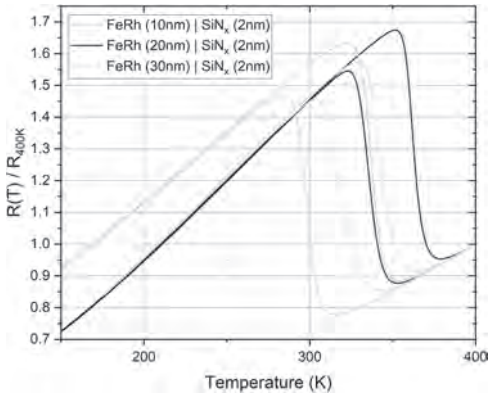

Resistance vs. temperature for FeRh films of different thicknesses capped with SiN_x. Current was directed along FeRh(100) with a 1T, field applied perpendicular to the current.

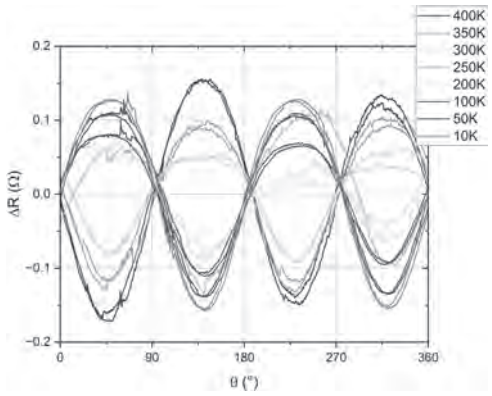

Angular dependence of the AMR at different temperatures for a 30nm FeRh film capped with 2nm SiN_x. Current was directed along FeRh(100) with an 8T field. Mean value of each resistance curve was subtracted to center curves around 0.

DT-03. Longitudinal and transverse conductivity measurements across the Verwey transition in Fe_3O_4 thin film. *N. Bano*[1], A. Tripathy[1], H. Singh[1] and D.K. Shukla[1] *1. Physics, UGC-DAE CSR, Indore, Indore, India*

The Fe_3O_4, an inverse spinal compound, also known as magnetite has received a lot of attention due to the combination of several interesting properties, such as high spin-polarized current [1], and high Curie temperature ~ 858 K etc. It exhibits a first order metal-insulator transition, which is widely known as Verwey transition (VT), T_V, at ~ 120 K [2]. The VT is linked to the charge ordering of the Fe^{2+} and the Fe^{3+} ions, as well as a structural transition (high temperature cubic to low temperature monoclinic structure), and electron-phonon coupling [2,3]. It has been reported that, the Fe_3O_4 exhibits a strong correlation between longitudinal conductivity and anomalous Hall effect (AHE). A. Fernández-Pacheco *et al.,* reported the universal scaling behavior, $\sigma_{xy} \propto \sigma^{1.6}_{xx}$, over four decades of the longitudinal conductivity [4]. The scaling suggested a common underlying mechanism for electrical, electronic and magnetic properties in this compound and the origin of the AHE may include contributions from skew scattering, and side jump. However, understanding of the relation between longitudinal and transverse conductivity across Verwey transition, and contributions of the electrical, electronic and magnetic properties in the same, is still an open problem. Here, we report longitudinal conductivity and AHE measurements on pulsed laser deposition grown single crystalline Fe_3O_4 thin film (on LAO substrate). Grown thin film exhibits T_V ~ 120 K, and about three orders of magnitude change in resistivity across T_V, confirming the high-quality of the sample. The AHE data at room temperature is consistent with previous reports [4]. However, AHE signal does not scale with magnetization when approaching T_V, moreover, transverse conductivity measurements across T_V reveals that the carrier type changes from electron to electron and hole both.

1. A. Yanase *et al.,* "J. Phys. Soc. Jpn" 53, 312 (1984). 2. Verwey *et al.,* "Nature" 144, 327-328 (1939). 3. Imada *et al.,* "Review of Modern Physics" 70, 1039-1263 (1998). 4. A. Fernández-Pacheco *et al.,* "Physical Review B" 78, 212402 (2008).

DT-04. Spin-Valve-Like Magnetoresistance in MnZnSb Single Crystal. *J. Dev*[1,2], S. Sardar[1,2], S. Singh[1] and P. Kushwaha[1] *1. CSIR-National Physical Laboratory (NPL), New Delhi, India; 2. Academy of Scientific and Innovation Research (AcSIR), Ghaziabad, India*

The Spin-Valve-like Magnetoresistance (SVMR) exhibits asymmetric behaviour with two distinct resistance states that switch with the direction of the magnetic field. Spin-valves have empowered the spintronics devices to have memory, which can be achieved through spin-dependent scattering in typically ferromagnetic (FM) layers. Typically observed in magnetic thin-film multilayer structures, SVMR is rare in bulk materials. This study explores the existence of SVMR in an intermetallic alloy, MnZnSb. A single crystal of MnZnSb was grown using modified Bridgeman techniques and thoroughly characterised using XRD, SEM/EDAX, elemental mapping, and laue diffraction measurements. All characterization techniques show that the prepared sample was crystallised in P4/nmm crystal structure, single phase (MnSb impurity less than 3%) and homogenous in nature. Anisotropic studies have been performed by applying a magnetic field in different crystallographic directions. Detailed magnetization and electrical transport measurements suggest a T_C ~315K, with an additional hump like broad hysteretic transition near 120K, which appears only when H is applied parallel to the c-axis (Fig. 1). Isothermal magnetic relaxation data collected at low temperatures was well-fitted with a combination of power law and stretched exponential equations, suggesting the coexistence of two magnetic states in the form of magnetic clusters. Isothermal magnetoresistance measurement shows asymmetric behaviour that arises only below 150K (Fig. 2). The appearance of such SVMR has been suggested on the basis of forming FM clusters along with antisite spin disorder, which affects electron scattering at the interface of the two magnetic phases.

1. Dieny, B. *et al. Phys Rev B* vol. 43 (1991). 2. Chappert, C.et al. *Nat Mater* 6, 813–823 (2007). 3. Agarwal, S. *et al. Phys Rev B* 97, (2018). 4. Singh, S. *et al. Phys Rev Lett* 109, (2012). 5. Manekar, M.et al. *Journal of Physics Condensed Matter* 23, (2011). 6. Chen, J. et al. *Mater Res Lett* 5, 329–334 (2017).

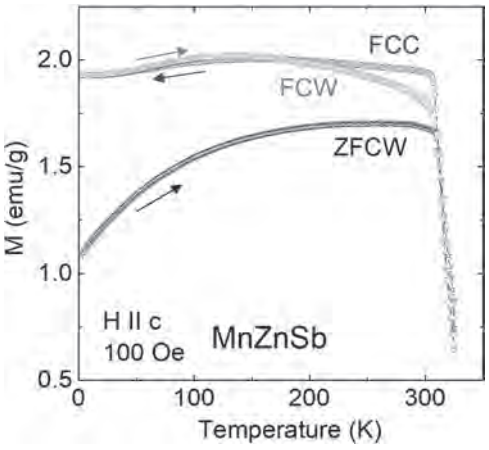

Temperature dependent magnetization at 100 Oe (In ZFC and FC mode) with H II c-axis.

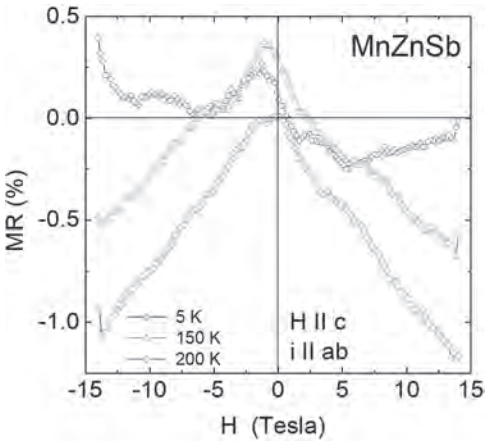

Field dependent isothermal MR (%) at different temperatures.

DT-05. Magnetotransport in van der Waals ferromagnet Fe_3GeTe_2 bulk with current out of plane. R. Jhang[1], N. Hai[1], *L. Tsai*[1], R. Jain[1], K. Raju[1], R. Sankar[1], J. Liang[2] and S. Lee[1] *1. Institute of Physics, Academia Sinica, Taipei, Taiwan; 2. Department of Physics, Fu Jen Catholic University, Taipei, Taiwan*

Fe_3GeTe_2 (FGT) has recently received worldwide attention because it is not only a 2D van der Waals (vdW) system but also exhibits intriguing physical properties of topological ferromagnet [1,2]. Here, we investigate the temperature dependence of the anomalous Hall effect (AHE) and longitudinal magnetoresistance (MR) of FGT to explore anisotropy in magnetotransport behavior. We grow FGT single-crystal by chemical vapor transport and define the shape of device by employing the dual-beam focused ion beam. The Cu electrodes are defined by lithography and ion-beam milling techniques. The direction parallel to the long axis of the sample, into the paper plane, and perpendicular to the vdW layers are defined as a, b and c axis, respectively (Fig. 1). AHE hysteresis loops, as a function of the magnetic field (H) along a and c axes at different temperatures (from 10K-200K) are shown in Fig 2 (a and b). For H\\ a-axis (or b-axis), the coercive field H_c reaches a maximum value of 10068 Oe at 10K. For H\\ c-axis, the squareness of AHE hysteresis loop is enhanced. The H_c (8 Oe) at 10K, is much less than in the case of H//a-axis, indicating that c-axis is the easy axis. Fig. 2 (c and d) displays the variation of MR with respect to H. We observe the negative linear MR in the wide range of temperatures (10-200K) in the case of H// c-axis. However, for H// a-axis, the MR signal exhibits a shift from negative to positive when T < 50K and H < 50000 Oe. Although the electron-magnon scattering assumption has been proposed to interpret this intriguing phenomenon [3], there remain several open questions on their transport mechanisms causing the MR dependence on the orientation of the applied field. In our viewpoint, since FGT possesses both magnetic and topological behavior, the effect from intrinsic Berry curvature should be taken into account. Based on first-principle calculations, we study the role of electron-magnon scattering and the Berry phase on MR behavior. Comparison to the current in a-axis data will be given.

1. Kim, K., Seo, J., Lee, E. et al. Nature Mater 17, 794–799 (2018). 2. Deng, Y., Yu, Y., Song, Y. et al. Nature 563, 94–99 (2018) 3. P. Saha, M. Singh, V. Nagpal, P. Das, and S. Patnaik, Phys. Rev. B 107, 035115 (2023)

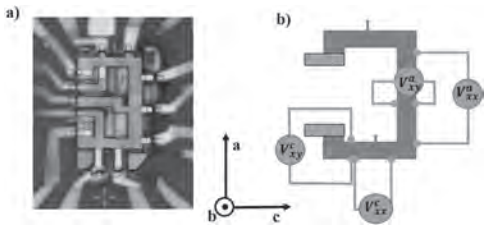

Fig 1: a) Optical image of FGT device. b) Schematic illustration of measurement setup

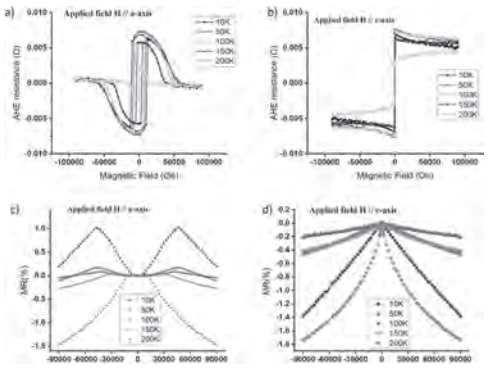

Fig 2: Anomalous Hall resistance (a)-(b) and magnetoresistance (c)-(d) as a function of field measured at different temperatures.

DT-06. Observation of Magnetoresistance Effect in $Ni_{78}Fe_{22}$/Erq_3/FeCo Organic Spin Valves. *R. Miyamoto*[1], M. Matsuzaka[1], M. Taniguchi[1], T. Ueda[1], C. Hashimoto[1], K. Kashima[1], K. Ando[1,2] and H. Kaiju[1,2] *1. Faculty of Science and Technology, Keio University, Yokohama, Japan; 2. Center for Spintronics Research Network, Keio University, Yokohama, Japan*

Molecular spintronics has attracted significant interest because molecules, composed of light elements, exhibit long spin diffusion lengths and they are suitable for spin transport layers. Recently, a large magnetoresistance (MR) effect was observed in devices using molecules composed of atoms with small nuclear spins[1]. Here we focus on tris-(8-hydroxy-quinoline) erbium (Erq_3), in which Al is replaced by Er in tris-(8-hydroxyquinoline) aluminum (Alq_3)[2],[3]. The nuclear spin of Al is 5/2, while that of Er is 0. The small nuclear spin can provide a weak hyperfine interaction, leading to the suppression of spin scattering. In this study, we fabricate $Ni_{78}Fe_{22}$ (Py)/ Erq_3/FeCo crossbar organic spin valves (OSVs) (Fig. 1(a)), and investigate their spin transport properties. The crossbar OSVs were prepared using DC magnetron sputtering and Ar ion milling for FeCo, thermal evaporation for Erq_3, and DC magnetron sputtering through a shadow mask for Py layer. The microstructures of OSVs were evaluated by transmission electron microscopy (TEM). The magnetic properties were measured by focused magneto-optical Kerr effect. The MR curves were measured by DC four-probe method under a magnetic field. As depicted in Fig. 1(b) and (c), the cross-sectional TEM images reveal well-defined interfaces and long-range homogeneity in the entire region of OSV layers. These clear interfaces can suppress the spin scattering in the OSVs. Fig. 2(a) shows the magnetization curves of Py and FeCo electrodes of OSVs. The coercivity of Py thin films is different from that of FeCo thin films, indicating the realization of parallel and antiparallel magnetization states in OSVs. Fig. 2(b) shows MR curves in OSVs at 200 K. A negative MR effect is observed in accordance with the magnetization states of OSVs. This means that we can successfully observe a spin signal through Erq_3 layer with a thickness of 29 nm. These results may open new avenues to the development of organic spintronics based on nuclear spins of molecules.

[1] D. Sun, E. Ehrenfreund and Z. V. Vardency, Chem. Commun., Vol. 50, p. 1781 (2014) [2] Z. H. Xiong, D. Wu and Z. V. Vardency, Nature, Vol. 427, p. 821 (2004) [3] I. Angervo, M. Saloaro and H. Huhtinen, Appl. Surf. Sci., Vol. 589, 152854 (2022)

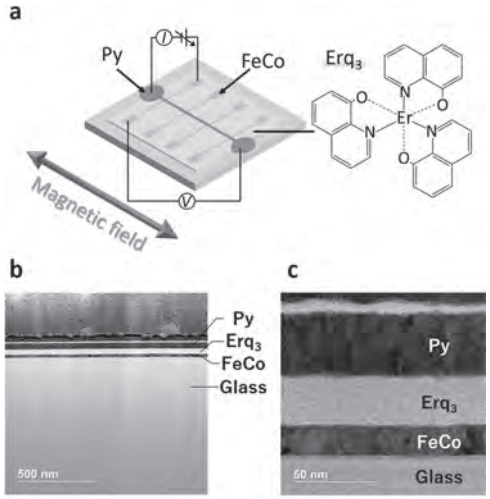

Fig. 1 (a) Schematic illustration and (b) wide and (c) local areas of cross-sectional TEM images of Py/Erq$_3$/FeCo OSVs.

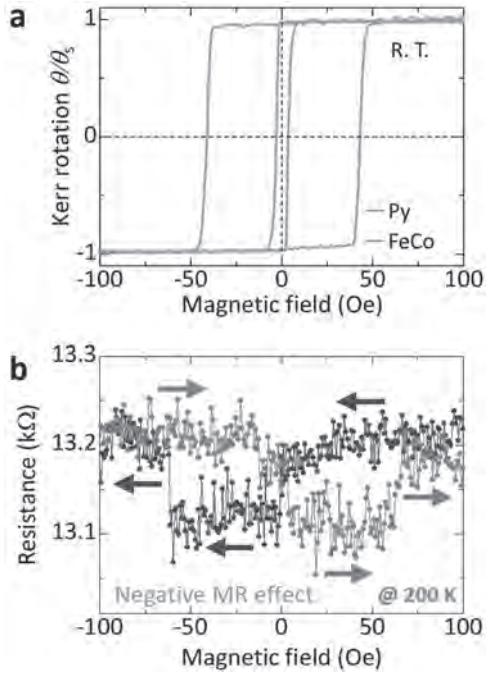

Fig. 2 (a) Magnetization curves of Py and FeCo and (b) MR effect observed in OSVs.

DT-07. A temperature sensor based on magnetic skyrmions. D. Kechrakos[1], *M. Lianeris*[2], D. Rodrigues[2], A. Meo[2], M. Carpentieri[2], R. Tomasello[2] and G. Finocchio[3] *1. Physics Laboratory, School of Pedagogical and Technological Education, Athens, Greece; 2. Department of Electrical and Information Engineering, Politecnico di Bari, Bari, Italy; 3. Department of Mathematical and Computer Sciences, Physical Sciences and Earth Sciences, University of Messina, Messina, Italy*

The interplay of temperature and topology has so far led to successful proof-of-concept of skyrmion-based applications, as a reshuffler, Brownian reservoir computing [1] and low-power information transport, giving rise to the emerging field of Skyrmion Caloritronics [2,3]. In this work, we use massive micromagnetic simulations, to present a proof-of-concept of a skyrmion-based temperature-sensor based on a magnetic tunnel junction that exhibit a spin-transfer diode (STD) effect, namely the generation of a rectified (dc) voltage as a response to a spin-polarized microwave (ac) current. At low current densities, the skyrmion breathing mode is excited that modulates periodically the MTJ resistance, leading to a (partially) rectified output voltage (V_{dc}) that is maximum at resonance. Furthermore, thermal effects, cause a linear shift of the resonance frequency and the rectified voltage V_{dc} with increasing temperature. The resonant voltage-vs-temperature linear relation constitutes the basis of the proposed temperature sensor (Fig.1). Using realistic material parameters for the simulated CoFeB/MgO/CoFeB MTJ [4]with a stabilised Neel skyrmion in the free layer (FL) we find a resonant frequency response in the range of 6-7 GHz for a device operating close to room temperature (250-350K) and subject to a field ranging from zero to 300mT. Our results could encourage a novel application of finite-temperature skyrmion dynamics, as they demonstrate for the first time the feasibility of a skyrmion-based temperature sensor with advantages in terms of low-power consumption, CMOS integrability, small area occupancy, and high detectivity. Work supported by PRIN 20222N9A73 "SKYrmion-based magnetic tunnel junction to design a temperature SENSor" (Italian Ministry of Research), by PE0000021, "Network 4 Energy Sustainable Transition – NEST" (European Union – NextGenerationEU, National Recovery and Resilience Plan, Mission 4 Comp. 2 Inv. 1.3 - Call for tender No. 1561 of 11.10.2022 of MUR (CUP C93C22005230007) and by PETASPIN association (www.petaspin.com).

[1] Raab, K., Brems, M.A., Beneke, G. et al. "Brownian reservoir computing realized using geometrically confined skyrmion dynamics" Nature Comm. 13, 6982 (2022). [2] E. Raimondo, E. Saugar, J. Barker, et al. "Temperature-gradient-driven magnetic skyrmion motion" Phys. Rev. Applied, 18 024062 (2022). [3] C. Back, V. Cros, H. Ebert, "The 2020 skyrmionics roadmap," J. Phys.D: Applied Physics, 53, 363001 (2020). [4] Y. Guang, L. Zhang, J. Zhang, et al., "Electrical Detection of Magnetic Skyrmions in a Magnetic Tunnel Junction", Adv. Electron. Mater. 9, 2200570 (2023)

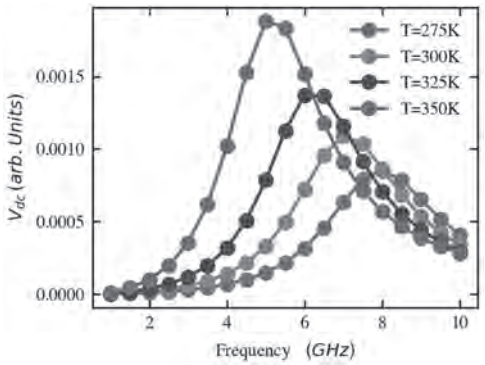

Figure 1. Frequency dependence of rectified voltage at various temperatures and zero field.

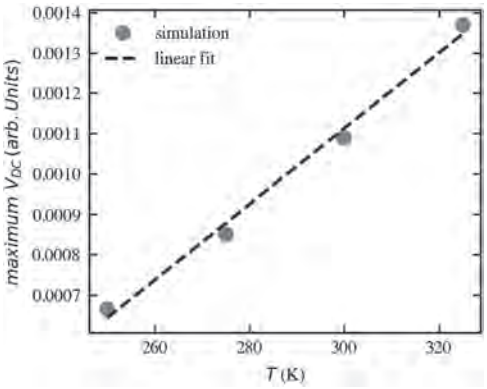

Figure 2. Linear temperature dependence of maximum rectifying voltage at zero field.

DT-08. Strain-induced ultrafast magnetization dynamics in cubic magnetostrictive materials with inertial and nonlinear dissipative effects. *S. Dolui*[1] and S. Dwivedi[1] *1. Mathematics, National Institute of Technology Andhra Pradesh, Tadepalligudem, India*

This article focuses on the analytical investigation of strain-induced ultrafast magnetic domain wall motion in a bilayer structure composed of piezoelectric and magnetostrictive materials. We perform the analysis within the framework of the inertial Landau-Lifshitz-Gilbert equation, which describes the evolution of magnetization in cubic magnetostrictive materials. By employing the classical traveling wave ansatz, the study explores how various factors such as magnetoelasticity, dry-friction, inertial damping, chemical composition, crystal symmetry, and tunable external magnetic field influence the motion of the domain walls in both steady-state and precessional dynamic regimes. The results provide valuable insights into how these key parameters can effectively modulate dynamic features such as domain wall width, threshold, Walker breakdown, and domain wall velocity. The obtained analytical results are further numerically illustrated, and a qualitative comparison with recent observations is also presented.

Session DU
ELECTRONIC STRUCTURE, MAGNETISM AND FUNDAMENTAL PHYSICAL PHENOMENA
(Poster Session)

Arti Kashyap, Co-Chair
Indian Institute of Technology Mandi, Mandi, India
Hari Paudyal, Co-Chair
University of Iowa, Ames, IA, United States

DU-01. Awake and Walking ICUs: Revolutionizing Critical Care Medicine. *K. Dayton[1] 1. CEO, Dayton ICU Consulting, Spokane, WA, United States*

The standardization of automatic sedation and immobility for every intubated patient on mechanical ventilation comes at a high price to patients, staff, and healthcare systems. The ABCDEF Bundle can help ICU teams overcome decades of culture and antiquated traditions to implement evidence-based sedation and mobility practices and become Awake and Walking ICUs (Dayton, 2024). Nurses are key in leading this revolution of patient care and are beneficiaries through improved workplace environment, improvement in burn out, and having the joy of helping patients survive and thrive. The bundle guides a change in patient-management that results in a transformation in patient outcomes. The ABCDEF decreases 7-day mortality by 68% decrease in 7-day mortality, delirium by 25-50%, ICU readmission by 46%, restraints use by 60%, and discharge to care facility by 36%(Pun, 2019). Mobility within 48 hours after intubation improves return baseline function by discharge by 24% (Schweikert, 2009) and cognitive function by 20% 1 year after discharge (Patel, 2022). Creating Awake and Walking ICUs requires adequate staffing but is also the best way to advocate for safe staffing and utilize staffing resources. The ABCDEF Bundle ICU decreases ICU costs by 30% (Hseih, 2019). This due to the impact on delirium and ICU-Acquired weakness (ICUAW). Delirium increases costs by 39% (Milbrandt, 2004) and ICU length of stay by 4.77 days (Dziegielewski, 2021). ICUAW alone increases costs by 30.5% (Hermans, 2015). Being free of sedation decreases time on the ventilator by 4.2 days and time in the hospital by 1.52-9.09 days (Strom, 2010). For every unit of out of bed mobility, there is a 10% decrease in time on the ventilator (Fazio, 2024), and for each additional 10 minutes of mobility there is a 1.2 day decrease in hospital length of stay (Jenkins, 2023). Delirium is a psychological burden (Schmitt, 2019), doubles RN hours required for care (Seiler, 2021), increases workplace violence (Jakobsson, 2020), falls, and self-extubation (Kwon, 2017). The ABCDEF bundle saves lives, money, and clinicians. It is time for nurses to arise and advocate for patients and clinicians by revolutionizing critical care medicine to standardize Awake and Walking ICUs.

Dayton, K., Hudson, M., & Lindroth, H. AACN Advanced Critical Care, 34, p.4 (2023) Fazio, et al. American Journal of Critical Care: an Official Publication, American Association of Critical-Care Nurses, 33, p.3 (2024) Hseih, et al. Critical Care Medicine, 47, p. 7 (2019) Jenkins, et al. PM&R: The Journal of Injury, Function, and Rehabilitation, 16, p. 219 (2024) Patel, et al. The Lancet. Respiratory Medicine, 11, p.6 (2023) Pun, et al. Critical Care Medicine, 47, p.1 (2019) Strøm, T., Martinussen, T., & Toft, P. Lancet, 375, p. 475. (2010)

Fig.1

Fig.2

DU-02. High-Throughput Studies of Novel Magnetism in Borides. *Z. Zhang[1], A. Kutepov[2], K. Belashchenko[2] and V. Antropov[1,3] 1. Iowa State University, Ames, IA, United States; 2. University of Nebraska-Lincoln, Lincoln, NE, United States; 3. Ames National Laboratory, Ames, IA, United States*

Boride systems are known for their diverse structures and versatile properties. In this work, we do high-throughput searches and studies for novel magnetism and magnetic materials in borides. Materials' formation energy and magnetism are calculated from first principles. Here, we unveil a family of dimerized quantum magnets (DQM) in the $YCrB_4$-type structure [1] and a family of altermagnets in the $FeMo_2B_2$-type structure. DQM are exotic crystals where Bose-Einstein condensation of magnetic excitations can happen. However, known DQM are only a few oxides and halides. We identify 9

DQM and 11 conventional antiferromagnets (AFM) in $YCrB_4$-type borides, where 3d transition metal atoms (T) are arranged in structural dimers. Quantum magnetism in these compounds is dominated by strong AFM interactions between Cr within the dimers, with much weaker interactions between the dimers. These systems are proposed to be close to a quantum critical point between a disordered singlet spin-dimer phase, with a spin gap, and the ordered conventional Néel AFM phase. Conventional AFM in these compounds is dominated by ferromagnetic (FM) Mn interactions within the dimers. They provide a platform to tune the magnetic exchange coupling by doping and study the unconventional quantum phase transition and conventional magnetic transitions. Altermagnetism (AM) is a novel class of magnetism exhibiting momentum-dependent electronic band spin splitting, typical of FM, and zero net magnetization, typical of AFM. However, AM has not been reported in borides. We identify 27 magnets in $FeMo_2B_2$-type borides, of which 11 are AM. AM ordering in these compounds is dominated by FM-coupled *T* chains formed by *T* nearest neighbors along [001] and AFM interactions between the nearest chains. Apart from electronic band splitting, chiral magnons and the origin of magnon chiralities are reported for this family of AM. Possible applications and challenges for such metallic AM borides are discussed. Acknowledgment This work is supported by the U.S. Department of Energy (DOE) Established Program to Stimulate Competitive Research (EPSCoR) Grant No. DE-SC0024284.

[1] Zhen Zhang *et al.*, Unveiling a family of dimerized quantum magnets, conventional antiferromagnets, and nonmagnets in ternary metal borides, Journal of the American Chemical Society 146, 16878 (2024).

DU-03. Prediction of Magnetic Order and Dimensionality in Cerium-Based Compounds Guided by Structural Characteristics and Tri-Critical Exponents. *J.A. Torres*[1], A.S. Poulo[1], T. Lamichhane[1], J. Littleton[1] and J. Moore[1] *1. Engineering Physics, University of Central Oklahoma, Edmond, OK, United States*

Josh Torres, Jeffery Moore, Jayce Littleton, Anjali Poulo and Tej Nath Lamichhane Department of Engineering & Physics, University of Central Oklahoma Ce is the most abundant element and exhibits the most diverse chemical and physical properties among the lanthanides. It has immense potential to solve the looming raw materials crisis in high performance magnets industry providing new compounds for gap magnets[1, 2]. The prediction of magnetic order and dimensionality in cerium-based compounds represents a crucial area of research due to its unique magnetic and electronic properties. Here we use structural characteristics and tri-critical exponents to identify the key parameters influencing their magnetic order. By integrating these structural insights with tri-critical exponents derived from experimental and theoretical studies, we develop a predictive model that can accurately determine the magnetic dimensionality and ordering phenomena. Our findings highlight the pivotal role of lattice symmetry, valency, bond lengths, and coordination environments in shaping the magnetic properties. The proposed model not only elucidates the fundamental mechanisms driving magnetic order in cerium-based compounds but also provides a robust comparison framework for designing and comparing new lanthanides[3] and actinides[4] materials with tailored magnetic properties. This approach paves the way for advancements in materials science, particularly in the development of novel magnetic materials alloy for technological applications.

1. Lamichhane, T.N., et al., *Single-Crystal Permanent Magnets: Extraordinary Magnetic Behavior in the Ta, Cu Fe-doped CeCo5 Systems.* Physical Review Applied, 2019. 11(1): p. 014052. 2. Lamichhane, T.N., et al., *Ce3-xMgxCo9: Transformation of a Pauli Paramagnet into a Strong Permanent Magnet.* Physical Review Applied, 2018. 9(2): p. 024023. 3. Churna Bhandari, G.N.N., Jonathan D.H. Smith, Durga Paudyal, *Accurate Machine Learning Predictions of Coercivity in High-Performance Permanent Magnets.* 2023. 4. Broyles, C.C., William; Sheng Ran, *Structure-Driven Prediction of Magnetic Order in Uranium Compounds.* 2024.

DU-04. High-Throughput Computational Approach to Designing Unconventional Magnets: Transition Metal Phosphates T_2PO_5. Y. Jia[1], A. Alsaad[2], *R. Sabirianov*[3], A. Kutepov[4], K. Belashchenko[4], Z. Zhang[5] and V. Antropov[5] *1. UCSD, San Diego, CA, United States; 2. JUST, Irbid, Jordan; 3. UNO, Omaha, NE, United States; 4. UNL, Lincoln, NE, United States; 5. ISU, Ames, IA, United States*

In this work, we present an examination of the altermagnetism in the T2PO5 family (T = Fe, Co, Ni, Cr, Mn) within the C2/c and I4_1/amd crystal structures. We studied the magnetic properties of T2MPO5 (TM = 3d element) systems using various electronic structure methods, including LDA/PBE, LDA/PBE+U, QSGW, GW, and Hartree-Fock. For the T = Fe and Co systems, altermagnetic behavior was observed in the tetragonal, monoclinic, and orthorhombic crystalline structures, exhibiting large magnetic moments and significant momentum-dependent spin splitting. The system with Ni showed much weaker magnetic properties. A noticeable difference between different Fe atoms was obtained in the orthorhombic and monoclinic structures in the insulating states, while the metallic state significantly suppressed this difference. Our calculations also revealed the coexistence of stable magnetic states in the monoclinic structure of Fe2PO5: semiconducting and metallic, both with similar magnetic properties. We demonstrated that Co2PO5 has a mechanically stable structure in both C2/c and I4_1/amd, with antiferromagnetic (AFM) ordering in the ground state. We found that the C2/c structure is more stable relative to I4_1/amd and has higher formation energy. Starting from the structure of Fe2PO5 in I4_1/amd, we replaced the Fe atoms with other transition metals (T = Co, Ni, Cr, Mn) to obtain the initial atomic structures of T2PO5. Both the lattice parameters and atomic positions were relaxed until the residual forces were less than 0.02 eV/Å. The optimized lattice parameters are listed in Table 1. The predicted magnetic properties in these materials, including the large momentum-dependent spin splitting, can be verified experimentally. We further studied the exchange couplings in these systems, showing the existence of chiral magnons in the Heisenberg model and their interactions with the corresponding chiral Stoner decays. This work is supported by the U.S. Department of Energy (DOE) Established Program to Stimulate Competitive Research (EPSCoR) Grant No. DE-SC0024284. Computations were performed at the High Performance Computing facility at Iowa State University and the Holland

Table 1. Crystal and magnetic structure in T2PO5, energy difference $\Delta E = E_{AFM} - E_{FM}$ between ferromagnetic (FM) and antiferromagnetic(AFM) states, as well as relative stability of $C2/c$ and $I4_1/amd$ systems, $\Delta E_{I4_1/amd} - E_{C2/c}$.

Compound	Stable phase	Stable ordering in $C2/c$	ΔE in $C2/c$ (eV/f.u.)	Stable ordering in $I4_1/amd$	ΔE in $I4_1/amd$ (eV/f.u.)	ΔE_1 in FM ordering (eV/f.u.)	ΔE_1 in AFM ordering (eV/f.u.)
Cr2PO5	C2/c	FM	0.012	—	—	—	—
Mn2PO5	C2/c	FM	0.026	—	—	—	—
Fe2PO5	C2/c	AFM	-0.058	AFM	-0.056	-0.010	0.005
Co2PO5	I4_1/amd & C2/c	AFM	-0.114	AFM	-0.064	0.153	0.181
Ni2PO5	I4_1/amd & C2/c	FM	0.032	FM	0.045	0.491	0.501

DU-05. Intrinsic Magnetism and Thermal Stability of Transition Metal and Rare-Earth Adatoms on $MoSe_2$ monolayer. N. Batnyam[1], B. Odontuya[2], G. Munkhsaikhan[2] and *D. Odkhuu*[1] *1. Department of Physics, Incheon National University, Incheon, The Republic of Korea; 2. Department of Physics, Mongolian University of Science and Technology, Ulaanbaatar, Mongolia*

Semiconducting two-dimensional (2D) materials doped with transition metal or rare-earth atoms have potentials for spintronic applications due to their ferromagnetism and semiconducting behavior. In this presentation, we report our recent results of the intrinsic magnetic properties of 3*d* transition metal (Fe and Co as examples) and 4*f* rare-earth atoms (Nd and Sm) on $MoSe_2$ monolayer obtained from density functional theory plus U, Monte Carlo, and molecular dynamic simulations. Herein, we have systematically considered both substitution and adsorption doping approaches, and various amounts of dopant atoms. It is found that as a generic, the adsorbate metal dopant atoms energetically prefer atop site of Mo atom rather than the other Se top and hollow sites while the substitutes can replace for the Mo in $MoSe_2$ monolayer, in agreement with the relevant experimental and previous theoretical studies. We further demonstrate that, as the concentration of either substitutional or adsorption dopant atoms increases, spin magnetic moment always

decreases while the perpendicular magnetocrystalline anisotropy (PMA) increases, reaching large PMA energy values of about 3 meV per Fe and 35 meV per Sm atom. The underlying mechanism of these results is illustrated in terms of single-particle *d*- and *f*-electron energy spectrum analysis. Moreover, the temperature dependent intrinsic magnetic properties of metal and rare-earth doped $MoSe_2$ monolayers and their Curie temperatures will be discussed in comparison with the available experimental results. This work is supported by the US DOD Office of Naval Research Global under award No. N62909-23-1-2035.

DU-06. Models of spin-split bands in antiferromagnets. G. Bednik[1] and *R. Sabirianov*[1] *1. Physics, University of Nebraska Omaha, Omaha, NE, United States*

We propose two models of one-dimensional antiferromagnetism, whose electronic bands break Kramers degeneracy and thus host spin-splitting. Specifically, we consider models whose unit cells have two magnetic atoms ordered antiferromagnetically, and their symmetries are lowered by two additional non-magnetic atoms. In the first model, we propose an antiferromagnet, in which two magnetic sublattices are not related to each other by symmetries. In the second model, we consider antiferromagnet, in which two magnetic sublattices are related by a combination of time reversal with translational symmetry while lacking inversion. We find that if the magnetic and non-magnetic atoms form a 'ladder', then Kramers degeneracy can be lifted by adding staggered magnetic field to certain plaquettes of the lattice. This work is supported by the U.S. Department of Energy (DOE) Established Program to Stimulate Competitive Research (EPSCoR) Grant No. DE-SC0024284. Computations were performed at the High Performance Computing facility at Iowa State University and the Holland Computing Center at the University of Nebraska.

DU-07. Observed Frustrated Antiferromagnetism in Ni-Mn-Based Functional Heusler Alloys. *S. Aksoy Esinoglu*[1] and M. Acet[2] *1. Physics Engineering Department, Istanbul Technical University, Istanbul, Turkey; 2. Faculty of Physics, Duisburg-Essen University, Duisburg, Germany*

Ni-Mn-*X* based Heusler alloys (*X*: In, Sn, Sb) exhibit martensitic transformation below room temperature. They are ferromagnetic or nearly ferromagnetic in the austenite state. Through the martensite transition temperature M_s, a sudden drop is observed in the magnetization as the temperature decreases. Modulated martensite structures such as 5M and 7M occurring below the M_s are not stable and inter-martensitic transitions with a temperature-hysteresis ranging up to 100 K can take place. These modulated structures can be incommensurate with the lattice periodicity, whereby the modulation vector q is also temperature-dependent. We undertake temperature-dependent neutron polarization analysis experiments on $Ni_{50}Mn_{40}Sb_{10}$, $Ni_{50}Mn_{37}Sn_{13}$, and $Ni_{50}Mn_{34}In_{16}$ to understand the cause of the drop and the nature of the magnetic coupling in martensitic state where modulated structures prevail [1]. The wave-vector dependence of the magnetic scattering cross-section shows that the magnetic correlations just below M_s are of a short-range frustrated antiferromagnetic type with a correlation length of several Angstroms. This is akin to the cases observed in spin-ice, Kagome lattices, and β-Mn; all of which show a similar wave-vector dependence in their magnetic scattering cross-sections [2]. In these systems a long-range antiferromagnetic structure cannot be established within the unit cell of either commensurate or incommensurate modulated martensite structure in Ni-Mn-*X*.

[1] Aksoy S., Acet M., Deen P et al., Physical Review B, 79, 21 (2009) [2] Mondelli C., Anderson K., Mutka H. et al., Physica B, 267-268, 139 (1999)

DU-08. Withdrawn

Session DV
ANALYSIS AND DESIGN FOR ELECTRICAL MACHINES
(Poster Session)

Ants Kallaste, Co-Chair
Tallinn University of Technology, Tallinn, Estonia
Anh Thanh Huynh, Co-Chair
University of Nottingham, Nottingham, United Kingdom

DV-01. Model Order Reduction of Bidirectional CLLLC Converter for Flywheel Energy Storage System. *K. Xu*[1], Y. Zhu[1], Y. Guo[1], G. Lei[1] and J. Zhu[2] *1. School of Electrical and Data Engineering, University of Technology Sydney, Sydney, NSW, Australia; 2. School of Electrical and Information Engineering, The University of Sydney, Sydney, NSW, Australia*

Advancements in power electronics and new materials, especially SiC and GaN, have enabled devices to achieve higher switching frequencies and power densities. This increase complicates the transient electromagnetic processes in power electronics systems, leading to challenges in circuit simulation and the coupling of electromagnetic and thermal fields [1]. Model order reduction (MOR) techniques are introduced to minimize the computational complexity of power electronic systems. These reduced-order models retain dependency on design parameters without requiring repeated reductions for each parameter variation. Conventional MOR methods include finite element-based models, Krylov subspace methods, proper orthogonal decomposition for nonlinear systems, and trajectory piecewise linear model reduction. However, these methods do not produce universal models when system parameters change [2]. Simulating the CLLLC converter is particularly challenging due to its highly non-linear operation and sensitivity to parasitic elements. It's crucial to analyze the impact of parameter changes on the stability of both the reduced-order model and the closed-loop system, as inductances and transformer leakage inductance are challenging to measure accurately and can vary due to factors like core material nonlinearity. In Fig.1, the high-fidelity model of a CLLLC converter with nonlinear inductors is presented. Thus, efficient order reduction techniques are necessary to analyze high-fidelity models that account for parasitic elements quickly [3][4]. This paper proposes an efficient MOR method for the CLLLC converter. The CLLLC is simplified to an equivalent resonant tank, and small-signal modeling is performed for its switching, resonant, and rectifier networks, considering circuit parasitic parameters. Sensitivity analysis is then conducted to calculate the participation coefficients of each variable. Finally, a reduced-order model is constructed using a hybrid modeling method, capturing the fast, slow, and interactive transient behaviors of the system based on its time constants.

1. Y. Gu, N. Bottrell and T. C. Green, "Reduced-Order Models for Representing Converters in Power System Studies," in *IEEE Transactions on Power Electronics*, vol. 33, no. 4, pp. 3644-3654, April 2018. 2. X. Dong, A. Griffo and J. Wang, "Multiparameter Model Order Reduction for Thermal Modeling of Power Electronics," in *IEEE Transactions on Power Electronics*, vol. 35, no. 8, pp. 8550-8558, Aug. 2020. 3. S. A. Nahvi, M. A. Bazaz and H. Khan, "Model order reduction in power electronics: Issues and perspectives," *2017 International Conference on Computing, Communication and Automation (ICCCA)*, Greater Noida, India, pp. 1417-1421, 2017. 4. Q. Cossart, F. Colas and X. Kestelyn, "Model reduction of converters for the analysis of 100% power electronics transmission systems," *2018 IEEE International Conference on Industrial Technology (ICIT)*, Lyon, France, pp. 1254-1259, 2018.

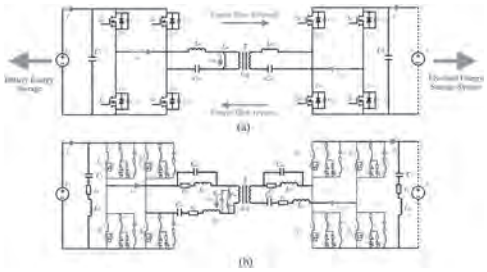

High-fidelity model of a CLLLC converter with nonlinear inductors. (a) Circuit schematic. (b) Detailed high-order model.

DV-02. Synergetic Optimization Based on Doubly Salient Pole-changing Machine for Torque Ripple Reduction. W. Wenjie[1], S. Niu[1] and *M. Jiang*[1] *1. EEE, Hong Kong Polytechnic University, Hong Kong, Hong Kong*

I. Introduction In recent years, the prospects of doubly salient machine in application fields such as electric vehicles have received widespread attention due to its higher torque density. Based on the doubly salient structure, a new doubly salient pole-changing machine is proposed to further extend the speed range. Due to the more harmonics generated by the doubly salient structure, its torque ripple is larger than other modulation machines. In order to reduce torque ripple, some effective methods have been presented in [1]. However, it is difficult to simultaneously reduce the torque ripples in normal and flux-weakening states for the proposed machine. To overcome this problem, this paper presents a synergetic optimization method from three different perspectives, which including skewing poles, notching teeth and excitation sources. Through the synergetic optimization of three different parts, the torque ripples of the proposed doubly salient pole-changing machine are simultaneously decreased in different operating states. II. Proposed optimization method Fig. 1 presents the overall synergetic optimization process. It is shown that the proposed optimization method can be divided into three main parts, which can be involved as follow: Skewing poles optimization: The step skewing rotor is applied and optimized to reduce the cogging torque. Notching teeth optimization: The notching teeth is arranged and optimized on main rotor modulation teeth to adjust the flux field harmonic amplitude and phase. Excitation sources optimization: The PM and DC excitation source requires to be optimized to ensure the balance of the flux field polarity. The different optimal key parameters that affect these three parts are selected corresponding with optimal objectives in different operating states. With the help of the multi-objective optimization algorithm, the final doubly salient machine is optimized with the lower torque ripple. Fig. 2 illustrates the comparison results of torque waveforms between the original and optimized machines.

[1] Z. Zhang, P. Wang, W. Hua, T. Zhang, G. Wang and M. Hu, "Comprehensive Investigation and Evaluation of Cogging Torque Suppression Techniques of Flux-Switching Permanent Magnet Machines," *IEEE Trans. Transport. Electrific*., vol. 9, no. 3, pp. 3894-3907, Sept. 2023.

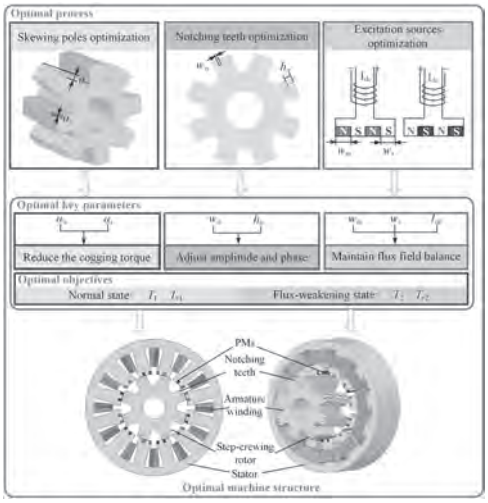

Fig. 1. The overall flowchart of the proposed synergetic optimization for torque ripple reduction.

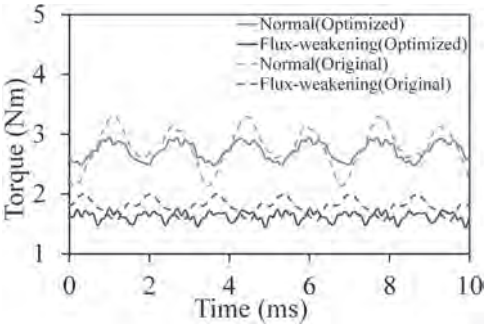

Fig. 2. Torque waveform comparison between optimized and original designs.

DV-03. Improved Analytical Technique for Electromagnetic Analysis of Axial Flux Permanent Magnet Motor Considering 3D Leakage Flux.
J. Yang[1], T. Kim[1], K. Shin[2] and J. Choi[1] *1. Electrical Engineering, Chungnam National University, Daejeon, The Republic of Korea; 2. Electrical Engineering, Changwon National University, Changwon, The Republic of Korea*

The axial flux permanent magnet (AFPM) motor is increasingly utilized due to its compact structure, high power density, and efficiency. It is suitable for applications such as in-wheel motors and fan motors, where the diameter is larger than the axial length. Structurally, AFPM motors require 3D analysis. However, the analysis process using the finite element method (FEM) is time-consuming and complicates determining the physical relationships between design variables, necessitating extensive trial and error during initial design. The subdomain method employs Fourier series and governing equations, simplifying the correlation between design variables. It provides analysis results comparable to FEM but in a shorter time. However, assumptions made to simplify the model can hinder accurate 3D evaluation. Specifically, for AFPM motors, the influence of leakage magnetic flux due to end effects is significant, necessitating consideration for precise analysis. This study presents a method to derive the electromagnetic characteristics of AFPM motors using a subdomain method accounting for 3D leakage flux. Figure 1 (a) shows the analytical model of the AFPM motor, and Figure 1 (b) depicts the simplified model for application to the subdomain method. The conventional subdomain method was enhanced to consider leakage flux due to end effects. Figure 1 (c) illustrates the leakage flux loops at the outer and inner diameters of the magnet, and Figure 1 (d) shows a magnetic equivalent circuit (MEC) used to compensate for the leakage flux. The electromagnetic analysis results obtained through the improved method, incorporating the leakage flux coefficient, are presented in Figure 2 (a) and (b). Figures 2 (c) and (d) depict the experimental setup for measurements of the prototype. Detailed theory and experimental results will be provided in the full paper.

[1] A. Cavagnino, M. Lazzari and F. Profumo, *IEEE trans. Ind. Appl.*, Vol. 38, no. 6, pp. 1517-1524 (2002) [2] Ronghai Qu and T. A. Lipo, *IEEE trans. Ind. Appl.*, Vol. 40, no. 1, pp. 121-171 (2004) [3] J. Zhao, T. Ma and X. Liu, *IEEE Trans. Energy Convers.*, Vol. 36, no. 3, pp. 2120-2130 (2021) [4] J. Azzouzi, G. Barakat and B. Dakyo, *IEEE Trans. Energy Convers.*, Vol. 20, no. 4, pp. 746-752 (2005) [5] K. -H. Shin, J. -H. Lee, S. Sung, IEEE Trans. Magn., Vol. 59, no. 11, pp. 1-5 (2023)

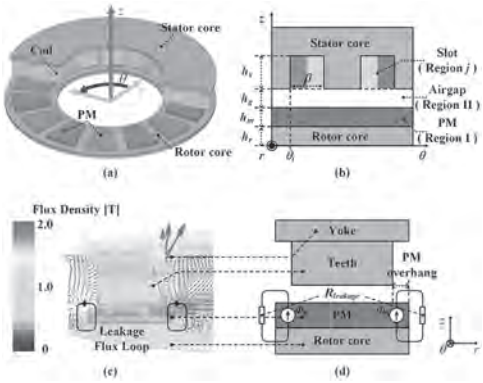

Fig. 1. Axial flux permanent magnet motor: (a) analysis model, (b) simplified analytical model, (c) leakage magnetic flux loop caused by end effects, and (d) simplified leakage flux loop through magnetic equivalent circuit

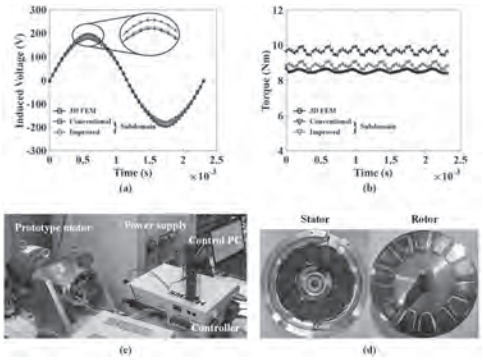

Fig. 2. Analysis results of analysis model ((a) phase induced voltage and (b) torque), (c) experimental setup, and (d) actual manufactured stator and rotor

DV-04. 3D FEM Calculation of Eddy Current Losses in Clamping Structures Considering Stator End-Windings of High-Power Electrical Machines.
W.M. Mohand Oussaid[1,2], *A. Tounzi*[1], A. Benabou[1], J. Korecki[1], R. Romary[2], W. Boughanmi[3] and D. Laloy[3] *1. L2EP, Univ. Lille, Arts et Métiers Institute of Technology, Centrale Lille, Junia, ULR 2697 - L2EP, Lille, France; 2. Univ. Artois, UR 4025, Laboratoire Systèmes Électrotechniques et Environnement (LSEE), Béthune, France; 3. R&D, Jeumont Electric, Jeumont, France*

Eddy current losses in clamping plates and fingers contribute to additional losses in electrical machines. These losses, caused by the magnetic leakage flux from the stator end-windings, are challenging to quantify and are often approximated or underestimated, thereby negatively impacting the machine's efficiency and overall performance. While some recent studies attempt to address this issue using analytical approaches combined to 2D Finite Element Analysis (FEA) [1], most studies employ 3D Finite Element Method (FEM) [2-3]. [2] proposes a calculation of eddy current losses in the clamping plates and fingers of an induction machine using 3D FEM with

non-conformal meshing. However, the computation time remains significant. The findings in [3] demonstrate that end clamping plates significantly influence the magnetic field and performance of induction machines. For the 3D magnetostatic FEA, only one-eighth (1/8) of the model is considered. This study uses Code_Carmel [4], an in-house 3D FEM software, to calculate eddy current losses in the clamping devices considering the stator end-windings of a high-power electrical machine, comparing results between a full model and a reduced model. As shown in Fig. 1, and following the approach in [3], one-eighth of the model is used to solve a 3D magnetodynamic problem in time domain. Unlike the previous study, this investigation focuses on a magnetodynamic rather than a magnetostatic problem. Eddy current losses are calculated in an aluminum clamping structure. An anti-periodic symmetry boundary condition is applied to replicate the stator winding current densities of the full model, by imposing identical source terms (KI) in T-Ω formulation on the anti-periodic faces. The calculations are compared to those obtained with the full model. Table 1 shows a good correlation between the two methods, with an error of less than 1.8%. This result is highly satisfactory, as it leads to a significant reduction in model size and, consequently, calculation time.

[1] T. Fricke, B. Schwarz and B. Ponick, "A Fast Calculation Approach for Pressure Finger Losses in Large Salient-Pole Synchronous Machines," in IEEE Transactions on Magnetics, vol. 57, no. 8, pp. 1-7, Aug. 2021. [2] A. Stermecki, O. Biro and I. Bakhsh, "3-D Finite Element Analysis of Additional Eddy Current Losses in Induction Motors," in *IEEE Transactions on Magnetics*, vol. 48, no. 2, pp. 959-962, Feb. 2012. [3] J. Yan, C. Di and X. Bao, "Influence of End Region Structure on the Equivalent Circuit Based on Frozen Permeability for Induction Machines," 2023 26th International Conference on Electrical Machines and Systems (ICEMS), Zhuhai, China, 2023, pp. 1016-1020. [4] *Code_Carmel,* LAMEL (L2EP & EDF R&D), temporal version 2.3.0, https://code-carmel.univ-lille.fr/

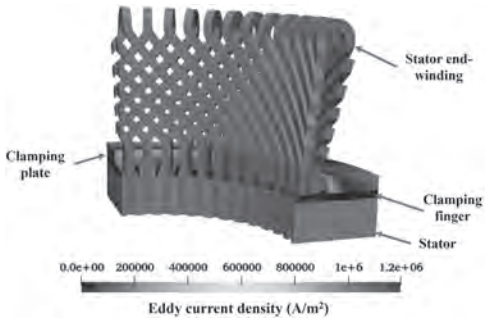

Fig. 1. Eddy current density in aluminum clamping structure considering only one-eighth of the model.

Model	Full model	Reduced model (1/8)
Number of mesh elements	4 244 964	555 776
Eddy current losses (W)	9.57	9.74
Calculation time	6h 41min	35min

Table 1. Comparison of eddy current losses calculated in aluminum clamping devices between the full model and the reduced model.

DV-06. Analytical and Experimental Approaches to Predicting Magnetic Field Asymmetry and Electromagnetic Forces in Slotted Surface-Mounted Permanent Magnet Machines with Rotor Eccentricity.

Y. Kim[1], *J. Yang*[1], K. Shin[2] and J. Choi[1] *1. Chungnam National University, Daejeon, The Republic of Korea; 2. Changwon National University, Changwon, The Republic of Korea*

Rotor eccentricity caused by defects in the manufacturing or operational processes of motors affects electromagnetic performance. The deviation in the air-gap flux density due to rotor eccentricity affects the back electromotive force (EMF) and cogging torque. Although rotor eccentricity can be identified using finite element analysis (FEA), the analysis is time-consuming, and understanding the direct physical relationship between eccentricity and design variables is challenging. Therefore, an analytical approach based on the electromagnetic governing equations was employed to analyze the impact of eccentricity on the design variables. Figure 1(a) shows a simplified subdomain model of surface-mounted permanent magnet synchronous motor (SPMSM), and Fig.1 (b) illustrates the coordinate system transformation of the stator and rotor. In Fig. 1(b), the coordinate systems of the stator and rotor are represented as (X-Y) and (x'-y'). Fig. 1(c) shows the experimental setup used to validate the proposed subdomain method. Fig. 1(d) depicts the FE anlysis model. Using perturbation and electromagnetic field theories, the governing equations for the air gap region were derived, and the air gap flux density was determined using the magnetic vector potential and boundary conditions, as shown in Fig. 2(a). The perturbation of the magnetic flux density due to the rotor eccentricity ratio is shown in Fig. 2(b). Fig. 2(c) shows the back-EMF. The flux density was then applied to the Maxwell stress tensor to obtain the magnetic pull-force (MPF) distribution, as shown in Fig. 2(d). The results were validated through comparisons with experimental data and FEA results, thereby confirming the asymmetry caused by rotor eccentricity. The details of the subdomain method, perturbation theory, analysis results, and design specifications of the SPMSM are provided in the full paper.

[1] A. Rahideh, M. Mardaneh, T. Korakianitis, "Analytical 2-D Calculations of Torque, Inductance, and Back-EMF for Brushless Slotless Machines With Surface Inset Magnets," *IEEE Trans. Magn*, vol. 49, no. 8, Aug, 2013. [2] T. Du, H. Geng, Y. Zhang, "Exact Analytical Method for Active Magnetic Bearings With Rotor Eccentricity," *IEEE Trans. Magn*, vol. 55, no. 12, Dec, 2019. [3] A. Vahaj, A. Rahideh, T. Lubin, "General Analytical Magnetic Model for Partitioned-Stator Flux-Reversal Machines With Four Types of Magnetization Patterns," *IEEE Trans. Magn*, vol. 55, no. 11, Nov, 2019. [4] V. Z. Faradonbeh, A. Rahideh, M. M. Ghahfarokhi, "Analytical Modeling of Slotted, Surface-Mounted Permanent Magnet Synchronous Motors With Different Rotor Frames and Magnet Shapes," *IEEE Trans. Magn*, vol. 57, no. 1, Jan, 2021 [5] H. K. Lee, K. H. Shin, T. K. Bang, "Experimental Verification and Analytical Study of Influence of Rotor Eccentricity on Electromagnetic Characteristics of Permanent Magnet Machine," *IEEE Trans. Appl*, vol. 30, no. 4, Jun, 2020.

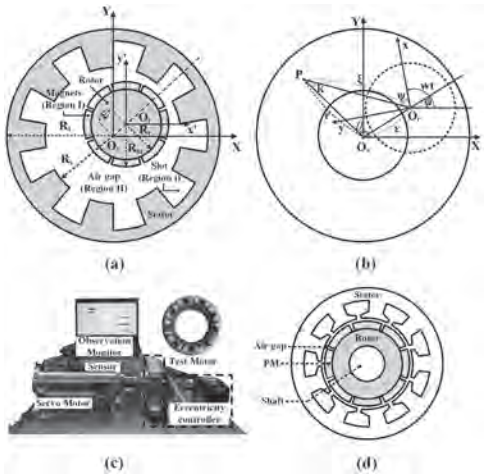

Fig. 1. Analysis model of SPMSM: (a) simplified subdomain model, (b) coordinate systems of the stator and rotor, (c) experimental setup, (d) FE analysis model

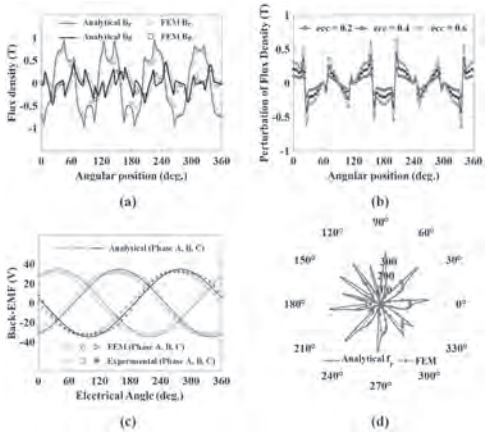

Fig. 2. Analysis results of analysis model: (a) magnetic flux density, (b) perturbance of magnetic flux density due to the rotor eccentricity ratio, (c) back-EMF, (d) MPF distribution in radial direction

DV-07. Novel Electromagnetic Analysis Method for a YASA Motor Based on Multi-Dimensional Hybrid FEA. *J. Son*[1] and D. Lim[1]
1. Department of Electrical, Electronic, and Computer Engineering, University of Ulsan, Ulsan, The Republic of Korea

Recently, an axial flux permanent magnet motor (AFPMM) has been received more attention due to high torque density [1], [2]. When analyzing the electromagnetic characteristics of the AFPMM, 3D periodic finite element analysis (P-FEA) is required to consider the complex magnetic flux distribution [2]. However, time-consuming 3D FEA is unsuitable for the design process as the repetitive analysis and comparison on various design variables are needed [3]. In this paper, multi-dimensional hybrid FEA (MD-FEA) method is proposed to alleviate the time cost of the AFPMM design. As shown in Fig. 1, the MD-FEA consists of the 2D FEA of the quasi 3D model and static FEA (S-FEA) of the 3D model, and the final results can be obtained by post-processing the analysis results of each method. For the quasi 3D method, the equivalent analysis results of the 3D model can be obtained by combining the results of the multiple 2D models, and the calculation time can be drastically reduced. Moreover, pulsation characteristics can be considered, as the cross sectional 2D models reflect the structure of the 3D model. However, the quasi 3D method has limitations in the accuracy, as the edge effects at the internal and external regions and flux between each cross section cannot be considered. The MD-FEA overcomes the limitations of the conventional quasi 3D method through the 3D S-FEA. The torque and voltage of the motor can be calculated using the phase flux linkage values obtained through the S-FEA, and reliable accuracy with the acceptable analysis time can be resulted as the 3D FEA is conducted only at the initial rotor position. However, the S-FEA cannot consider the pulsation characteristics as the other periodic part is neglected. Therefore, the MD-FEA combines two methods to ensure accuracy while considering the pulsation characteristics and reducing analysis time. Fig. 2 shows the analysis result at the operating point, and the MD-FEA shows superior performance on both calculation time and analysis accuracy. Detailed explanations on the MD-FEA, target YASA AFPMM, performance verification, and experimental validation will be described at the full paper.

[1] W. Cheng, G. Cao, and Z. Deng, IEEE Transactions on Magnetics, vol. 57, no. 2, pp. 1-5 (2021) [2] F. Yi, C. Zhang, and S. Qiu, L, IEEE Transactions on Magnetics, vol. 59, no. 12, pp. 1-10 (2023) [3] A. Gu, B. Ruan, and W. Cao, IEEE Access, vol. 7, pp. 180251-180257 (2019)

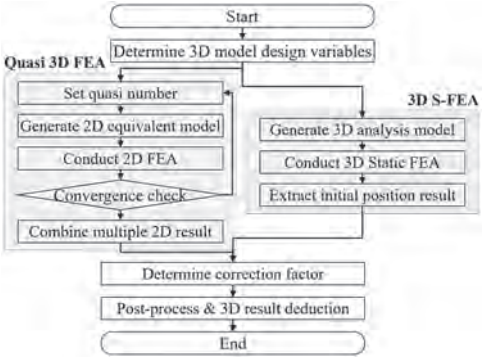

Fig. 1. Flow chart of the MD-FEA

	3D P-FEA	MD-FEA	Comparison
Average torque [Nm]	239.32	237.89	-0.60 %
Torque ripple [%]	7.26	7.68	+0.42 %p
Phase voltage [V_{rms}]	176.62	179.27	+1.50 %
Calculation time [Sec]	3,895	461	-88.16 %
Memory usage [GB]	5.71	2.58	-54.82

Fig. 2. Operating point analysis result

DV-08. A Method of Deriving Electromagnetic Characteristics of a SPMSM Based on Two-Stage Magnetostatic FEA. *J. Lee*[1] and D. Lim[1]
1. Department of Electrical, Electronic, and Computer Engineering, University of Ulsan, Ulsan, The Republic of Korea

This paper proposes a new strategy to quickly review the output and vibration characteristics of a surface mounted permanent magnet synchronous motor (SPMSM) by the two-stage magneto-static finite element analysis (TSS-FEA). In general, methods of evaluating motor performance are divided into finite element analysis (FEA) and analytical method (AM). The FEA has high accuracy, but it takes a lot of time. On the other hand, the AM is less accurate than the FEA, but motor performance can be quickly derived [1]. Meanwhile, electric motors have recently been used in various fields. Some applications, require high output density and low vibration at the same time [2]. The TSS-FEA aims to identify the time-varying electromagnetic force with magneto static FEA (MS-FEA) and derive torque and voltage. The flowchart of TSS-FEA is shown in Fig. 1. First, MS-FEA is performed under no-load conditions to derive air-gap permeance, and the air-gap magnetic flux density is calculated through the derived permeance and the magnetomotive force (MMF) calculated by the equation, and the electromagnetic forces are calculated as the magnetic flux density using the maxwell stress tensor [3]. Next, MS-FEA is performed under load conditions to derive voltage and torque. To derive the torque and voltage with reliable accuracy, the flux-linkage is obtained MS-FEA at the initial rotor position, and calculated with the torque and voltage equations using flux-linkage [4]. The results and analysis time obtained through this were compared with time-varying FEA (T-FEA) and summarized in Fig. 2, and it was confirmed that results with reliable accuracy were derived at the reduced calculation time. Since the technique proposed in this paper has reliable accuracy based on MS-FEA and can quickly derive output and electromagnetic forces, it can be used when examining the performance of many design variables in the initial design stage of SPMSM that requires both high output performance and low vibration characteristics. In addition, if the air gap MMF is calculated by an analytical method, it can be applied to any shape, so it can be extended to various shapes of SPMSM.

[1] Z. Pan and S. Fang, IEEE Journal of Emerging and Selected Topics in Power Electronics, vol. 10, no. 2, pp. 1800-1812 (2022) [2] Y. -H. Jung, M. -R. Park and M. -S. Lim, IEEE Transactions on Energy Conversion, vol. 35, no. 2, pp. 928-937 (2020) [3] Z. Xing, X. Wang and W. Zhao, *IEEE Transactions on Transportation Electrification*, vol. 8, no. 4, pp. 4337-4347 (2022) [4] J. -C. Son and D. -K. Lim, IEEE Transactions on Magnetics, vol. 58, no. 8, pp. 1-6 (2022)

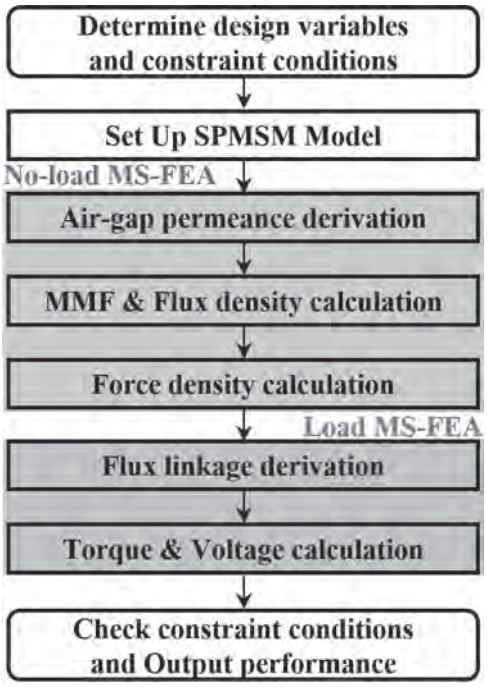

Fig.1. Flowchart of the TSS-FEA

	T-FEA	TSS-FEA	Comparison [%]
Average Torque [Nm]	65.67	66.54	1.32
Voltage [V]	343.09	346.87	1.10
6^{th} Force density [kNm/m^2]	39.14	37.30	-4.68
36^{th} Force density [kNm/m^2]	4.42	4.51	2.00
Calculation Time [s]	171.29	64.10	62.58

Fig.2. Comparison of calculation results

Session XA
21ST-CENTURY PERMANENT MAGNETS: HOW TO TAKE IT TO THE NEXT LEVEL? A PANEL/AUDIENCE DIALOG

Laura H Lewis, Chair
Northeastern University, Boston, MA, United States

INVITED PAPERS

XA-01. $Sm(Fe,Co)_{12}$-based Hard Magnetic Materials: Perspective 1.
G. Hadjipanayis[1,2], C. Han[3] and C. Ni[3] 1. Department of Physics and Astronomy, University of Delaware, Newark, DE, United States; 2. Department of Chemical Engineering, Northeastern University, Boston, MA, United States; 3. Department of Materials Science and Engineering, University of Delaware, Newark, DE, United States

The development of $Sm(Fe,M)_{12}$ permanent magnets (M = Ti, V, Cr, Mo, …), advertised as a superior replacement for the Nd-Fe-B, has yet to meet most of the optimistic expectations. Despite the 18.7 kOe [1] and 14.0 kOe [2] coercivities H_c, which were realized, respectively, in $Sm(Fe,Co)_{12}$ thin films and $Sm(Fe,Ti,V,Al)_{12}$ sintered magnets, the prospects of the functional 1:12 magnet with a high energy storage capacity are rather uncertain. On the fundamental side, it has been recently demonstrated [3], that the probabilistic nature of the M substitutions in the $Sm(Fe,M)_{12}$ crystal lattice may lead to large fluctuations of the local magnetocrystalline anisotropy, likely holding back the H_c values. Our latest HRTEM analysis of the calcium-reduced submicron $(Sm,Zr)(Fe,Co,Ti)_{12}$ particles [4] exhibiting a broad range of H_c values, up to 16.3 kOe, provides an insight into the effect of synthesis conditions on the homogeneity of the 1:12 crystal structure. The sintering of magnets has been successful only with 15-18 at.% of the nonmagnetic M including at least 8 at.% of V [2]; however, this large substitution decreases the magnetization significantly and severely restricts the stored magnetic energy. We have unsuccessfully attempted sintering the 1:12 alloys with only 7-8 at.% M = Ti at 1200 °C, taking advantage of the equilibrium existing at this temperature between the 1:12 phase and a Sm-rich liquid phase [5]. The phase transformations occurring between room temperature and 1200 °C appear to compromise not only the magnetic insulation of the 1:12 grains, but even the crystallographic pre-alignment of these grains. The high samarium vapor pressure further complicates the liquid-phase sintering and often leads to an inhomogeneity of the resulting composition. While most of the researchers pursuing the development of anisotropic $Sm(Fe,Co,M)_{12}$ magnets understandably attempt to reproduce the technology and the microstructure of Nd-Fe-B, we should remain open-minded with respect to the manufacturing methods not involving powder metallurgy, such as "bulk" magnetic hardening [6]. The work was supported by the U.S. Department of Energy under Award Number DE SC0022168.

[1] Y. Mori, S. Nakatsuka, S. Hatanaka et al., J. Magn. Soc. Japan, Vol. 48, p. 17 (2024) [2] A. Srinithi, X. Tang, H. Sepehri-Amin et al., Acta Mater., Vol. 256, 119111 (2023) [3] C. Patrick, Y. Huang, L. Lewis and J. Staunton, Phys. Rev. Lett., Vol. 132, 056703 (2024) [4] A. Gabay and G. Hadjipanayis, Scr. Mater., Vol. 196, 113760 (2021) [5] A. Gabay, C. Han, C. Ni and G. Hadjipanayis, J. Alloys Compd., Vol. 965, 171444 (2023) [6] Y. Xu, C. Han, C. Ni et al., J. Magn. Magn. Mater., Vol. 603, 172223 (2024)

XA-02. Sm(Fe,Co)12-based and its relative magnetic materials: Perspective 2.
Y. Takahashi[1] 1. NIMS, Tsukuba, Japan

Extensive effort for developing new permanent magnetic materials beyond $Nd_2Fe_{14}B$ have been done to meet the demand for coming motorized society. Sm-based compound with $ThMn_{12}$ structure is one of the candidates for next generation permanent magnet because of highest molar fraction of Fe and expected high saturation magnetization (μ_0Ms) in the rare-earth containing compound. However, the addition of nonmagnetic element is necessary to stabilize the structure at RT because 1-12 system is high temperature metastable phase. The addition of the non-magnetic phase stabilizing element causes the reduction of μ_0Ms. Low coercivity (μ_0Hc) is another reason that 1-12 phase did not receive an attention up to recently. We have successfully prepared epitaxial $Sm(Fe_{0.7}Co_{0.3})_{12}$ thin film by a sputtering method and demonstrated the high μ_0Ms of 1.78 T, anisotropy field (μ_0Hk) of 8.2 T and Curie temperature (Tc) of 859 K [1] which are superior to those of $Nd_2Fe_{14}B$. By introducing B into $Sm(Fe_{0.7}Co_{0.3})_{12}$ film, high μ_0Hc of 1.2 T was achieved due to the formation of nanogranular microstructure [2]. Although B addition causes the enhancement of μ_0Hc in the thin film, it is not the case of bulk sample because it forms boride with the phase stabilizing element such as Ti. Therefore, getting high μ_0Hc in the bulk form is thermodynamically difficult because there is no equilibrium nonmagnetic phase in $Sm(Fe_{0.7}Co_{0.3})_{12}$. Recently, Srinithi et al reported high μ_0Hc of 1.4 T by introducing Fe-lean intergranular phases by the microstructure engineering [3]. Another candidate with high Fe content is the metastable TbCu7 type Sm-Fe (1-7) compound of hexagonal crystal structure. In a 1-7 structure, Sm atoms are randomly substituted by Fe dumbbells in a disordered manner. This disordered structure of the 1-7 compound makes it interesting because the Fe atoms in the 1-7 structure can be beyond the stoichiometry of SmFe7, i.e., Fe/Sm > 7. Thus, μ_0M_s in the 1-7 compound can be increased. 1-7 compounds acquire uniaxial anisotropy after the nitrization. The maximum μ_0Ms of 1.7 T is achieved in the 1-7 compounds, which is higher than that of Nd-Fe-B. Moreover, unlike the 1-12 compound, the 1-7 compound is advantageous as it can be stabilized in bulk form by non-equilibrium processing, such as, melt-spinning, rapid quenching, HDDR, and mechanical alloying, without the addition of stabilizing elements. Overall, the high Fe content and a resulting high magnetization along with the ability to be processed in bulk form without the need for stabilizers make the SmFe7-based compound a potential candidate for the development of alternative permanent magnetic material, which can be processed into anisotropic bonded magnets and sintered magnets. However, this compound is not well explored, and its intrinsic magnetic properties are unknown. We recently have demonstrated the formation of single phase SmFe8.8N1.1 compound with TbCu7 type structure in the thin film form [4]. Firstly, we optimized the composition of SmFez (z=5~12) in the high throughput combinatorial method. We chose SmFe9 composition due to the high and low volume fractions of TbCu7 phase and a-Fe, respectively. After nitriding, it shows strong perpendicular anisotropy with high μ_0Hk of 22 T, high μ_0Ms of 1.64 T and high Tc of 770 K which are superior to those of Nd2Fe14B. The benchmark is shown in Fig.1. In the discussion, I would like to the prospect of Sm-based high Fe concentration permanent magnetic and other possible candidates.

[1] Y. Hirayama et al., Scripta Mater138, 62 (2017). [2] H. Sepehri-Amin et al., Acta Mater194, 337 (2020). [3] A.K. Srinithi et al., Acta Mater256, 119111 (2023.) [4] A.R. Dilipan et al., Acta Mater274, 119996 (2024).

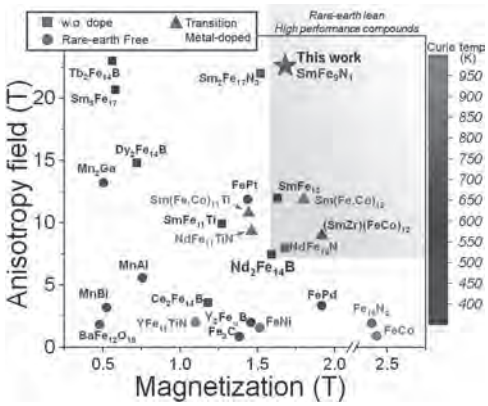

XA-03. Progress and Prospects of Hard Hexaferrites for Permanent Magnet Applications. *C. de Julián Fernández*[1] *1. Institute of Materials for Electronics and Magnetism C.N.R., Parma, Italy*

Permanent magnets (PMs) are key elements in technologies like electric mobility and the wind turbines that are pillars of the Green Transition. These technologies use high performing rare earth (RE) magnets, mainly NdFeB ones. However, the China's monopoly in all the RE magnets production chain and supply constitute a strong handicap for the Green Transition. This problem drives to the innovation and research in the ambit of PMs, in particular to develop new RE-free or lean PMs [1-3]. On the other hand, hard hexaferrite magnets constitute nowadays the most produced PMs in the world, and they are in second position in economic importance after the RE PMs [3]. In fact, NdFeB magnets and Sr-hexaferrite ceramic ones dominate the PM market due to the high performances of the first ($(BH)_{max}$ up to 400 kJm^{-3}) and the lower cost and average performances ($(BH)_{max}$ up to 38 kJm^{-3}) of the second. Even the big gap in the properties of these two materials, and driven the criticality of the RE supply, the fluctuations of the RE costs and by the low costs of the ceramic magnets, there is strong interest in the substitution of RE magnets by ceramic ones [4,5]. In my presentation, I will illustrate different studies oriented to increase the magnetization and/or the coercive field of hard ferrites with the purpose to obtain novel ceramic magnets that can substitute RE PMs in particular applications. I will show that the increase of the coercive field of hexaferrites and Cobalt ferrite in nanoscale is possible thanks to the optimization of size, composition and strain [6-8]. In addition, different types of novel hybrid ferrite materials have been synthesized with the aim to obtain high remnant magnetization [9-11]. These materials are typically composed by a Sr hexaferrite or Cobalt ferrite hard phase and a high magnetization phase and both moieties are coupled by exchange or dipolar mechanisms. Finally, I will discuss on the development of bulk magnets from single nanophase and hybrid composites illustrating also several cases of prototypes [12-14]. This research was developed in the framework of the PRIN 2022 PNRR project HyPerMag "HYbrid ferrite nanocomposites for novel Rare-earth free PERmanent MAGnets" that is financed by the European Union –NextGenerationEU.

[1] O. Gutfleisch et al. Advanced Materials 23 (2011) 821. [2] L. H. Lewis and F. Jimenez-Villacorta. Metall, Mater Trans A 44, (2013) 2. [3] M. Coey Engineering 6 (2020) 119 [4] C. Granados-Miralles, P. Jenuš. J. Phys. D Appl. Phys. 54 (2021) 303001. [5] C. de Julián Fernández et al. J. Phys. D Appl. Phys. 54 (2021), 15300 [6] A. López-Ortega et al., Chem. Mater. 27 (2015) 4048. [7] E. Lottini et al. Chemistry of Materials. 28 (2016), 4214. [8] B. Muzzi et al. ACS Appl. Nano Mater. 5 (2022) 14871. [9] J. Guzman-Minguez ACS Appl. Nano Mater. 3 (2020) 9842. [10] B. Muzzi et al. Small (2022) 2107426 [11] P. Maltoni et al. Scientific Reports 11 (2021) 23307 [12] P. Jenuš et al. J. Phys. D Appl. Phys. 54 (2021) 204002 [13] A. Serrano et al. J. European Cer. Soc. 42 (2022) 1014. [14] J. Guzman-Minguez et al. Nanomaterials 13 (2023) 2097.

XA-04. Synthetic $L1_0$-FeNi: Achievements and Challenges. I.Z. Hlova[1], O. Dolotko[1], M. Abramchuk[1], A. Biswas[1] and *Y. Mudryk*[1] *1. Ames National Laboratory of the US Department of Energy, Ames, IA, United States*

An ordered tetragonal $L1_0$-FeNi, also known as meteoritic mineral tetrataenite – a promising rare-earth-free hard-magnetic compound – has been synthesized starting from a mechanochemically-activated disordered cubic $A1$-FeNi via formation of a chemically-ordered FeNiN intermediate and its subsequent denitrogenation and further purification of the product [1]. Refining the synthesis conditions is crucial for improving the hard-magnetic properties of $L1_0$-FeNi (BH^*_{max} = 56 MGOe). Mechanochemical processing facilitates the formation of highly active fine particles, improving nitrogenation/denitrogenation and enhancing coercivity. Nature of a process control agent employed during the mechanochemical activation of $A1$-FeNi and ammonia flow velocity during the synthesis of the intermediate are two of the main factors controlling the nitrogenation. Denitrogenation with hydrogen at elevated pressures and at temperatures substantially below the order-disorder transition preserves the chemical order established in the intermediate. Post-synthesis refinement of the $L1_0$-FeNi product includes removal of residual nitrides with a dilute acid to further improve hard-magnetic properties of the material. The thus synthesized $L1_0$-FeNi powders exhibit coercivity as high as 2.3 kOe and maximum energy product reaching 6 MGOe – the highest values ever reported for a synthetic tetrataenite. This work provides significant insights into the synthesis parameters and optimization of the synthesis of $L1_0$-FeNi, advancing its potential as a rare-earth-free permanent magnet, and highlights the anticipated challenges on the way to its widespread application. This work was performed at the Ames National Laboratory of the US Department of Energy and supported by the Critical Materials Innovation Hub, and Energy Innovation Hub funded by the US Department of Energy, Office of Energy Efficiency and Renewable Energy, Advanced Manufacturing and Materials Technologies Office (AMMTO). Ames National Laboratory is operated for the U.S. DOE by Iowa State University under contract DE-AC02-07CH11358.

[1] I.Z. Hlova, O. Dolotko, M. Abramchuk, A. Biswas, Y. Mudryk, V.K. Pecharsky, J. Alloys Compd., 981 (2024) 173619.

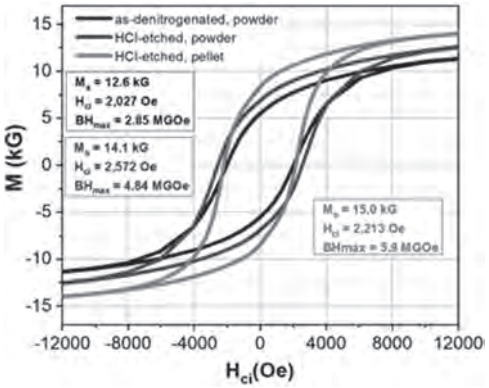

Figure: Magnetization of both the as prepared $L1_0$-FeNi powder and material obtained after HCl etching as a function of applied magnetic field.

XA-05. Development of Sustainable Rare Earth-free Permanent Magnets based on MnAlC through Conventional and Advanced Manufacturing. *E.M. Palmero*[1], C. Muñoz Rodriguez[1], L. Feng[2], T. Mix[2], J. Rial[1], J. de Vicente[1], T. Woodcock[2] and A. Bollero[1] *1. Group of Permanent Magnets and Applications, IMDEA Nanociencia, Madrid, Spain; 2. Institute of Metallic Materials, Leibniz IFW Dresden, Dresden, Germany*

Nowadays, permanent magnets (PMs) play a key role in different applications such as electromobility, energy and many domestic appliances. For a high magnetic performance, the most extended choice is PMs containing

rare-earths (REs). Alternative RE-free PMs are investigated to plug the gap between ferrites and NdFeB magnets [1,2]. MnAlC alloy is a promising RE-free PM candidate due to its theoretical $(BH)_{max}$ of 12 MGOe, high availability of constituent elements and diminished environmental impact [3]. A controlled microstructure and phase transformation is critical for developing its PM properties [4,5]. Research along the last decades shows the efforts on obtaining fully dense MnAl-based permanent magnets using conventional fabrication (e.g., hot extrusion and deformation) [6]. Alternatively, advanced fabrication such as additive manufacturing is attracting much interest as it allows for fabricating complex and high-performance objects with tailored properties and a minimal waste generation [2]. The main challenges to fabricate PMs by 3D-printing are that it requires high PM particles loading and no deterioration of the PM properties along the processing. Herein, the results obtained using conventional and advanced fabrication techniques to obtain MnAl-based magnets will be discussed. To fabricate highly dense bulk magnets by hot compaction, our starting material was gas-atomized ε-phase MnAlC powder. By applying an optimal combination of pressure and temperature, hot-pressing the ε-phase MnAlC alloy was able to manage simultaneously (i.e., single step process) the ε-to-τ phase (only ferromagnetic phase of the system) transformation and the powder compaction to end with a high-density (93%) magnet [7]. An increase in the coercivity of up to 25% was observed for the hot-pressed magnet by comparison with the annealed gas-atomized loose powder (Fig. 1), due to the formation of β-Mn and Mn_3AlC phases, a reduced mean crystallite size and induced strain during compaction [7]. Hard magnetic objects were fabricated by extrusion-based 3D-printing using composites based on gas-atomized τ-MnAlC particles embedded in polymer and synthesized by solution casting (Fig. 2) [8]. The particle size, polymer and fabrication parameters are key factors to be optimized for obtaining flexible and continuous filaments with high particle loading. By optimizing the fine-to-coarse particles ratio, it was possible to obtain homogeneous highly loaded composites and flexible filaments, i.e., leading to an enhanced effectiveness of the extrusion process. The magnetic characterization showed that the properties are not deteriorated in any of the steps of the fabrication process [8]. These routes are promising and cost-efficient ways which open the path to new possibilities for the fabrication of MnAlC-based magnets. *Acknowledgements* Authors acknowledge Höganäs AB (Sweden) for providing the gas-atomized MnAlC particles by an industrial IMDEA-Höganäs collaboration, and support from EU M-ERA.NET, MINECO and MICINN by projects NEXMAG (PCIN-2015-126), 3D-MAGNETOH (MAT2017-89960-R) and NEXUS (PID2020-115215RB-C21), the "Severo Ochoa" Programme for Centers of Excellence in R&D (CEX2020-001039-S), and by Regional Government of Madrid through *NANOMAGCOST* project (S2018/NMT-4321). E.M.P. acknowledges support from AEI by the JdC-I program (IJC2020-043011-I/MCIN/AEI/10.13039/501100011033) and EU by NextGenerationEU/PRTR. *Present address (A. Bollero):* Advanced Technologies and Micro Systems, Robert Bosch GmbH, 70839 Stuttgart, Germany

[1] J.M.D. Coey, IEEE Trans. Magn., 47, 4671 (2011) [2] A. Bollero and E.M. Palmero, "Recent advances in hard - ferrite magnets" in Modern Permanent Magnets, J.J. Croat and J. Ormerod, Eds. Elsevier, pp. 65-112 (2022) [3] H. Kono, J. Phys. Soc. Japan, 1444-1451 (1958); L.H. Lewis et al., Metall. Mater. Trans. A, 44, 2-20 (2013) [4] V. Øygarden et al., J. Alloys Compd., 779, 776 (2019) [5] J. Rial et al., Acta Mater., 157, 42 (2018); Engineering, 6 (2), 173 (2020) [6] T. Ohtani et al., IEEE Trans. Magn. 13 (5), 1328 (1977); L. Feng et al., Acta Mater. 199, 155 (2020) [7] C. Muñoz-Rodríguez et al., J. Alloys Compd., 847, 156361 (2020) [8] E.M. Palmero et al., Sci. Technol. Adv. Mater. 19, 465 (2018); Addit. Manuf. 33, 101179 (2020)

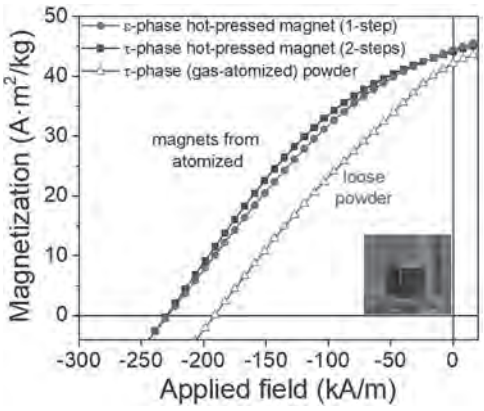

Fig. 1. Room temperature hysteresis loops (second quadrant) of the loose annealed powder (ε transformed into τ-phase) and the magnets obtained by hot-pressing the ε- and τ-phase powders. Inset shows the resulting compacted MnAlC magnet.

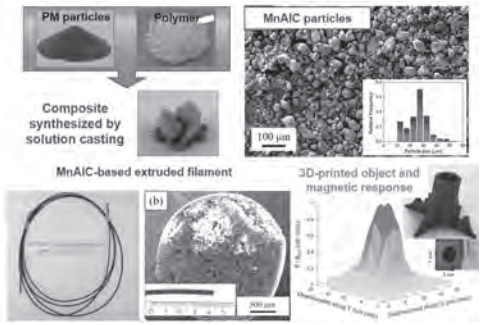

Fig. 2. Gas-atomized MnAlC particles, polymer, MnAlC-based composite and filament, and 3D-printed object with the 3D plot of the magnetic flux density at the 3D-printed MnAlC-based disc surface.

XA-06. Computational Insight into $L1_0$ FeNi optimization.

J.B. Staunton[1], C.D. Woodgate[1,2], G.A. Marchant[1] and L.H. Lewis[3,4]
1. Physics, University of Warwick, Coventry, United Kingdom; 2. Physics, University of Bristol, Bristol, United Kingdom; 3. Chemical Engineering, Northeastern University, Boston, MA, United States; 4. Mechanical and Industrial Engineering, Northeastern University, Boston, MA, United States

$L1_0$-FeNi-based materials are promising 'gap' magnets which require their intrinsic magnetic properties, such as magnetic anisotropy, to be improved, their chemical ordering temperatures to be raised and better kinetics [1]. Computational materials modelling [2] is useful in this context by providing insight into the fundamental physics. This talk will discuss how modelling has resolved apparent literature discrepancies in the value of the uniaxial magnetic anisotropy (MAE) of $L1_0$ FeNi (tetrataenite) in both natural and synthetic samples. The effects of both imperfect atomic long-range order and finite temperature are included (Figure). Initially the computational results [3] appear to undershoot the measured values but scrutiny of Néel et al.'s original analysis [4] reveals the importance of the nanoscale polycrystalline, multivariant nature of experimental samples. The modelling also demonstrates the impact of magnetic order on the development of atomic order and the efficacy of annealing samples in an applied magnetic field. We further describe an integrated, first-principles-based modelling approach [4] for studying both chemical order and subsequent magnetic properties. We consider introducing a variety of additives into the Fe-Ni system at low concentrations to promote $L1_0$ order and enhance its MAE. Crucially, our modelling predicts both the nature of any chemical order and the MAE for the given system [5]. The ordering behaviour with these additives is rich and its effect of the predicted MAE varies. Interestingly, we find that it is often the addition of light elements such as Al which enhances the MAE the most.

[Research supported by the U.S. Department of Energy, Office of Basic Energy Sciences under Award Number DE SC0022168 (for atomic insight) and by the UK Engineering and Physical Sciences Research Council, Grant No. EP/W021331/1 and the U.S. National Science Foundation under Award ID 2118164 (for advanced manufacturing aspects).]

[1] N. Maat et al., Acta Mat. 196, 776 (2020). [2] J.B. Staunton et al., Phys. Rev. B 74, 144411 (2006). [3] C.D. Woodgate et al., Journal of Applied Physics 134, 163905 (2023) [4] L. Néel et al., J. Appl. Phys. 35, 873 (1964) [5] C.D. Woodgate et al., arXiv preprint arXiv:2401.02809

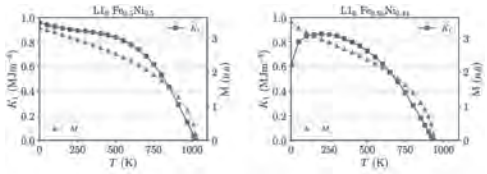

Anisotropy constant K_1 and magnetiization M calculated as a function of temperature for crystals of $L1_0$ $Fe_{0.5}Ni_{0.5}$ and $L1_0$ $Fe_{0.56}Ni_{0.44}$. It can be seen that K_1 remains high up to and beyond room temperature.

Session EA
NOVEL MAGNETIC TUNNEL JUNCTION MECHANISMS FOR MULTIFUNCTIONAL MEMORIES

Christopher H Bennett, Chair
Sandia National Laboratories, Albuquerque, NM, United States

INVITED PAPERS

EA-01. Complex Spintronic Synapses Exploiting Magnetoionics. *D. Querlioz*[1] and L. Herrera Diez[1] *1. Univ. Paris-Saclay, CNRS, Palaiseau, France*

Synapses of the brain are complex objects, where biophysical processes are modulated by biochemistry. This complexity provides high adaptability to the brain and enables different forms of learning. Magnetoionic gating, can tune and modulate the physical properties of spintronic devices and presents a striking similarity with the modulation of biophysics by biochemistry in biology. In this talk, I will demonstrate how magnetoionic can be harnessed to develop complex spintronic synapses. Such devices can be leveraged to address the challenge of catastrophic forgetting —the phenomenon where artificial intelligence systems lose previously acquired knowledge when learning new tasks. I will explain the mathematical roots and the key elements for allowing this effect and will show the implications of these results to allow embedded systems that learn continuously.

EA-02. Measurement-driven modeling of superparamagnetic tunnel junctions for computing applications. *M. Daniels*[1] *1. Physical Measurement Laboratory, National Institute of Standards and Technology (NIST), Gaithersburg, MD, United States*

As unconventional computing systems utilizing superparamagnetic tunnel junction grow in size and complexity, accurate compact models will become essential for the engineering work required to realize prototype systems. In this talk, we describe a data-driven methodology for modeling these devices based on observed experimental data. In particular, we argue that macrospin models are insufficiently complex to serve as accurate computational models, and more general Langevin dynamical frameworks should be used in their stead. We also discuss programmatic efforts at NIST to scale up characterization techniques for novel nanodevices like superparamagnetic tunnel junctions, and talk about the challenges and opportunities as the community moves toward more and more mature demonstrations and prototypes.

L. Pocher, T. N. Adeyeye, S. Gibeault, et al., arXiv:2403.11988 (2024)

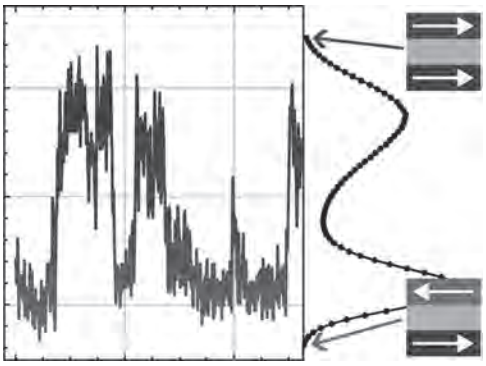

Measurements of real superparamagnetic tunnel junctions show that, unlike in a macrospin, the maximally magnetized states are not the most energetically favorable.

EA-03. Experimental Demonstration of Magnetic Tunnel Junction-Based Computational Random-Access Memory. *Y. Lv*[1], B. Zink[1], R. Bloom[1], H. Cilasun[1], P. Khanal[2], S. Resch[1], Z. Chowdhury[1], A. Habiboglu[2], W. Wang[2], S. Sapatnekar[1], U. Karpuzcu[1] and J. Wang[1] *1. Department of Electrical and Computer Engineering, University of Minnesota, Minneapolis, MN, United States; 2. Department of Physics, University of Arizona, Tucson, AZ, United States*

Recent advances in machine intelligence have been placing growing demands on our computing systems, especially for implementations with artificial neural networks. The conventional Von Neumann computer architecture suffers from the well-known "memory bottleneck" issue due to the inherent physical segregation of logic and memory components. This results in constant data transfers between logic and memory components, leading to performance and energy penalties. To address this challenge, besides the near-memory computing[1] and in-memory computing[2], [3] approaches, another one, which is often referred to as "true" in-memory computing, emerged recently. Computational random-access memory (CRAM)[4], [5] is one such example. Logic is performed natively by the memory cells; the data for logic operations never has to leave the memory. Additionally, CRAM offers unique features such as random access of data and operands, massive parallel computing capabilities, and reconfigurability of operations[4], [5]. CRAM operates in a fully digital fashion. CRAM benefits further from the adoption of emerging memory devices, including magnetic tunnel junctions (MTJs) and memristors, which offer significantly improved performance and energy efficiency. Both two-terminal or three-terminal memory devices can be adopted by CRAM variants. Benchmarking studies show that CRAM has the potential to deliver significant gains in performance and power efficiency[6], particularly for data-intensive, memory-centric, or power-sensitive applications, such as bioinformatics, image and signal processing, neural networks, and edge computing. However, there has been no experimental study of CRAM yet. In this talk, we present our recent work on the first ever experimental demonstration of a CRAM array hardware[7]. This work provides a proof of concept as well as a platform to study key aspects of the technology experimentally. We also provide detailed projections and guidelines for future CRAM design and development. Figure 1 shows the hardware portion of experimental setup. It is built with a so-called 'circuit-around-die' approach[8]: semiconductor circuitry is built with commercially available components around the MTJ dies. This approach offers a more rapid development cycle and the flexibility needed for exploratory experimental studies on CRAM arrays. The hardware is a 1×7 CRAM array, with the design of cells taken from the 2T1M CRAM cells[4], [5], and modified for simplified memory access. MTJs with perpendicular interfacial anisotropy, diameter of 100 nm, low resistance-area product, and high TMR ratio, are used for the CRAM hardware. One of the key results is CRAM's 2-input logic operation, as shown in Fig. 2, demonstrating CRAM's fundamental capability of computation. The Boolean logic state of the output of a CRAM logic operation is denoted as D_{out}. Experiments measure the statistical average of D_{out}, $\langle D_{out} \rangle$, at various amplitudes of the voltage pulse (V_{logic}) applied to the two input CRAM cells during the logic operation. At 0.62 V, there is a margin for V_{logic} to produce $\langle D_{out} \rangle$ close to '0' when the input is '11' and '1' for the rest of the input states. This matches the expected behavior of a NAND gate. The 'NAND margin' indicates the range of V_{logic} to achieve a NAND operation. Similarly, setting V_{logic} to 0.55 V transforms

the CRAM logic operation into a NOR gate. This demonstrates the reconfigurability of CRAM logic operations, enabled by tuning V_{logic} and/or the duration of the logic operation voltage pulse. Further results and discussions will be presented in the talk.

[1] J. T. Pawlowski, in *2011 IEEE Hot Chips 23 Symposium (HCS)*, May 2011, pp. 1–24. [2] S. Matsunaga *et al.*, *Appl. Phys. Express*, vol. 1, p. 091301 (2008). [3] J. Borghetti *et al.*, *Nature*, vol. 464, no. 7290, pp. 873–876 (2010). [4] J.-P. Wang and J. D. Harms, *US Patent*, US9224447B2 (2015). [5] Z. Chowdhury *et al.*, *IEEE Comput. Archit. Lett.*, vol. 17, no. 1, pp. 42–46 (2018). [6] M. Zabihi *et al.*, *IEEE Trans. Comput.*, vol. 68, no. 8, pp. 1159–1173 (2019). [7] Y. Lv *et al.*, *arXiv Prepr.*, 2312.14264 (2023), to appear in *npj Unconventional Computing*. [8] Y. Lv, R. P. Bloom, and J.-P. Wang, *IEEE Magn. Lett.*, vol. 10, pp. 1–5 (2019).

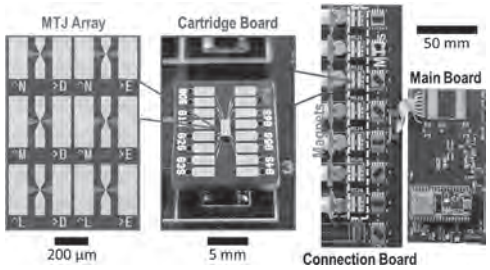

Fig. 1. Experimental setup of CRAM demonstration.

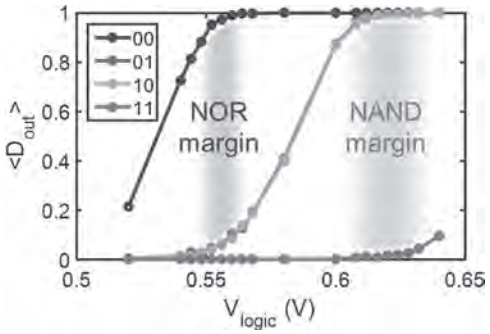

Fig. 2. Experimental results for 2-input CRAM logic operation. Plots show output logic average, $< D_{out} >$, vs. logic voltage, V_{logic}. Each curve corresponds to a specific input state. The separation between the $< D_{out} >$ curves indicates the margins for NOR or NAND operation, highlighted in blue and red, respectively.

EA-04. Nanomagnetic and Skyrmion Devices: Hardware AI and Quantum Control. *J. Atulasimha*[1] *1. Mechanical and Nuclear Engineering; Electrical and Computer Engineering; Physics, Virginia Commonwealth University, Richmond, VA, United States*

Our group studies energy efficient electrical control of magnetization in nanomagnets [1] and skyrmions [2] with applications to computing. We will discuss realizing AI hardware with such nanomagnetic devices. Specifically, multi-state nanoscale domain wall racetracks can be used as highly quantized synapses in deep neural networks [3] and convolutional neural networks [4], with overall improvement in area, energy, and latency by 13.8, 9.6, and 3.5 times respectively [4] compared to purely CMOS implementations. Additionally, interacting nanomagnets can be used for low Size Weight and Power (SWaP) analog [5] and digital reservoir computing [6]. The dynamics of confined skyrmions in patterned dots can also be used for reservoir computing for long-term prediction of temporal data [7]. Furthermore, by driving the magnetization of nanomagnets electrically, highly confined microwaves can be generated at the Larmor precession frequency of proximally located spins. This can implement single-qubit quantum gates with fidelities approaching state-of-the-art [8] in a scalable manner. Further confinement of microwaves using convergent-divergent skyrmion devices can implement even more localized and low footprint quantum control of spins [9]. New experimental and simulation results in these directions will be discussed. Recent work presented here was supported by NSF grants CCF-1909030, EECS 1954589, ExpandQISE 2231356 and Virginia Commonwealth Cybersecurity Initiative (CCI) grants.

References: [1] *Nano Letters*, 16, 1069, 2016. [2] *Nature Electronics* 3, 539, 2020. [3] *IEEE Access*, 10, 84946, 2022. [4*] IEEE Transactions on Neural Networks and Learning Systems* (early access), 2024, 10.1109/TNNLS.2024.3369969 [5] *Appl. Phys. Lett.* 121, 102402, 2022. [6] *Communication Physics* 6, 215, 2023. [7] *IEEE Access, 11,*124725, 2023. [8] *Communication Physics* 5, 284, 2022. [9] https://arxiv.org/abs/2401.00573

EA-05. Advances in Antiferromagnetic Tunnel Junctions. *S. Arpaci*[1,2] *1. Department of Electrical and Computer Engineering, Northwestern University, Evanston, IL, United States; 2. Applied Physics Program, Northwestern University, Evanston, IL, United States*

Antiferromagnetic (AFM) spintronics is emerging as a key technology for the next generation of memory and computing devices, as well as terahertz detectors and emitters. AFM devices potentially offer very high speed, energy efficiency, and bit density in memory applications, along with the absence of dipole interactions between neighboring bits [1]. This talk will discuss the latest breakthroughs in all-AFM tunnel junctions (ATJs), particularly focusing on the Mn_3X family of noncollinear antiferromagnets, sputter-deposited on silicon substrates. These devices exhibit large tunneling magnetoresistance (TMR) effects at room temperature that can be used to electrically detect (i.e., read) AFM order in an efficient manner, while also allowing for electrical manipulation (i.e., writing of information) via spin-orbit torque (SOT) [2]. As such, ATJs represent a new direction for spintronics that can enable a wide range of applications. The Mn_3X family of AFM materials possess a noncollinear magnetic order which results in a spin-split band structure and helicity of spin polarization in momentum space. The resulting momentum-dependent spin polarization has been recently predicted to cause significant variation in tunneling conduction based on the Néel vector orientation in noncollinear AFM-based tunnel junctions, representing the fully antiferromagnetic equivalent of the TMR effect. Recent research demonstrated the use of electric currents to control magnetic order in AFM structures [3-6]. These advances were followed by recent reports that demonstrated TMR in noncollinear AFM tunnel junctions [7,8]. However, these devices relied on external magnetic fields for manipulation and were not yet realized on silicon, whereas practical memory devices require all-electrical protocols for reading and writing information. This talk will showcase AFM tunnel junctions simultaneously exhibiting electric current-induced switching and large TMR effects, realized on silicon, eliminating the need for external magnetic fields [2]. The experimental setup involves AFM tunnel junctions in a double cross geometry. The noncollinear $PtMn_3$ can be grown preferentially with a (111) texture using a Pt seed on silicon substrates. This device structure allows us to perform both tunnelling magnetoresistance measurements and control experiments on an adjacent non-magnetic arm of the device. We utilize the first cross containing the AFM tunnel junction by applying the write current between bottom electrodes through the underlying Pt layer in opposite directions and exerting spin-orbit torque on the bottom $PtMn_3$ free AFM layer, and reading the tunnelling resistance through top and bottom contacts. The second cross without the junction is used for control experiments to verify that the observed switching signals originate from the $PtMn_3$. Our detailed measurements revealed significant TMR effects (up to ~100%) and successful electric current-induced switching. We will discuss the effect of lateral dimensions on the device behavior, prospects for nanoscale AFM tunnel junctions, comparison of alternative AFM materials, the role of the upper fixed AFM layer, and devices utilizing epitaxially grown AFM films, aiming to enhance device performance and integration into existing semiconductor technology. The potential applications of these

advancements in computing, memory storage, and terahertz technology will be explored, highlighting the transformative impact of AFM materials in the next generation of spintronic devices.

[1] P. Khalili Amiri, C. Phatak and G. Finocchio, Vol. 54, *Annual Review of Materials Research* (2016) [2] J. Shi, S. Arpaci, et al., *Advanced Materials*, 2312008 (2024) [3] J. Shi et al., *Nature Electronics 3*, 92-98 (2020) [4] S. Arpaci, et al., *Nature Communications 12*, 3828 (2021) [5] S. DuttaGupta, et al., *Nature communications 11*, 1-8 (2020) [6] A. Du, et al., *Nature Electronics 6*, 425–433 (2023) [7] P. Qin, et al., *Nature 613*, 485-489 (2023) [8] X. Chen, et al., *Nature 613*, 490-495 (2023)

Session EB
SPIN-ORBIT TORQUES AND SPIN DYNAMICS IN 2D SYSTEMS

Simranjeet Singh, Chair
Carnegie Mellon University, Pittsburgh, PA, United States

INVITED PAPERS

EB-01. Lossless Spin-Orbit Torque in layered Antiferromagnetic Topological Insulators. *R. Cheng*[1,2,3] and J. Tang[2] *1. Electrical and Computer Engineering, University of California Riverside, Riverside, CA, United States; 2. Physics and Astronomy, University of California Riverside, Riverside, CA, United States; 3. Materials Science and Engineering, University of California Riverside, Riverside, CA, United States*

Spintronics is an essential upgradation of electronics where the quantum spin of electrons becomes a central quantity of interest. A prevailing pursuit of spintronics is to effectively control magnetism and magnetic dynamics through electrical stimuli, which can be realized in a heterostructure composed of a magnet and a non-magnetic driver operated by electric currents. This archetypal setup, however, suffers from two fundamental problems: 1) The transfer of spin angular momenta is greatly inhibited by the interface; 2) The input power is mostly dissipated through Joule heating, rendering the overall efficiency surprisingly low. The discovery of intrinsic magnetic topological insulators (iMTIs) opened a unique physical platform to address the above issues. Thanks to the intertwined topological electrons and magnetic ordering, an iMTI driven by electric fields can generate non-equilibrium spins on its own, which in turn drives its magnetic dynamics internally without the aid of other materials. Such a monostructural system can function as an electrical actuator and a magnetic oscillator simultaneously, obviating the undesirable interface in heterostructures. Furthermore, the spin generation and transfer processes do not rely on Ohm's currents but are instead enabled by the "adiabatic currents" arising from the Berry curvature crosslinking the crystal momentum and magnetic orientation. Because adiabatic currents do not incur Joule heating, they can convert 100% of the input electric power into magnetic dynamics, marking a transformative boost of operational efficiency compared to established approaches. In this presentation, I will introduce the intriguing physics underlying a series of compelling functionalities of monostructural spintronics based on iMTIs, which heralds a new paradigm featuring lossless power conversion in the absence of interfaces, heterostructures, and other common complications.

[1] J. Tang and R. Cheng, Phys. Rev. Lett. 132, 136701 (2024). [2] J. Tang and R. Cheng, Phys. Rev. B 106, 054418 (2022).

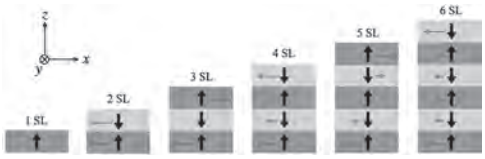

Illustration of layer-resolved SOT (red arrows) for $MnBi_2Te_4$ of 1 to 6 septuple layers. Black arrows indicate the magnetic moment of each septuple layer.

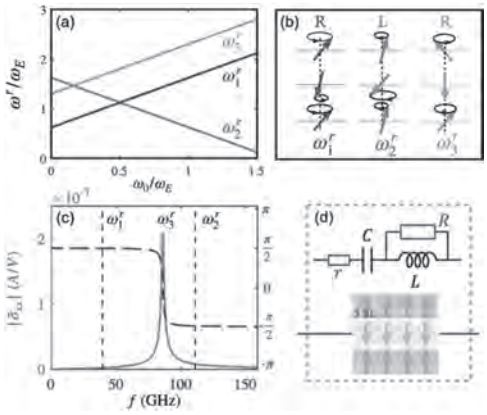

SOT-induced antiferromagnetic resonance of a 3-SL $MnBi_2Te_4$. (a) Resonance frequencies as functions of an applied magnetic field normal to the plane (with a strength scaled into angular frequency). (b) SL-specific magnetic precessions in each eigenmode. (c) Longitudinal electrical admittance as a function of the driving frequency for a 3-SL $MnBi_2Te_4$, where only a single peak at around the mode appears. (d) Effective circuit incorporating the combined effects of SOT and topological charge pumping.

EB-02. Real-Space Investigation of the Stability, Nucleation and Sub-nanosecond Dynamics of Chiral Topological Spin Textures. *K. Litzius*[1] *1. University of Augsburg, Augsburg, Germany*

In the pursuit of advancing applications in memory and logic, the investigation into noncolinear spin textures, specifically chiral magnetic solitons such as domain walls and skyrmions, has emerged as a promising avenue of research. While current-driven devices show potential, their practical implementation in one- and two-dimensional devices and controlled creation and excitation remain challenging, requiring a deeper understanding of spin texture dynamics in multidimensional space. This talk will discuss our recent advances towards such control of chiral magnetic textures in two dimensions and on short time scales. We address the challenge of free two-dimensional manipulation of skyrmions and chiral domain walls through an exploration of the displacement of chiral solitons in ferrimagnetic films, utilizing ultrafast laser pulses to enable motion over arbitrary distances and directions with well-defined reproducibility. The central focus is on understanding the role of the Dzyaloshinskii-Moriya interaction (DMI) in ensuring such reproducible ultra-fast domain wall motion, thereby preventing destabilization and domain randomization induced by precessional dynamics. Furthermore, in that light, we discuss transiently chaotic dynamics induced by spin-orbit torques around an artificial anisotropy-engineered defect to disclose a regime of violent picosecond fluctuations, including topological instabilities that, remarkably, result in deterministic final configurations. Overall, our findings contribute to a deeper understanding of spin texture dynamics in multidimensional space, opening new avenues for the advancement of spintronics.

[1] L. Caretta et al., Nat. Nanotechnol. 13, 1154–1160 (2018). [2] J. Gorchon et al. Phys. Rev. B 94, 184406 (2016). [3] Y. Quessab et al. Phys. Rev. B 97, 054419 (2018). [4] L.-M. Kern et al. ArXiv: 2401.12130 (2024).

EB-03. Resonant optical detection of 2D spin textures. *X. Zhang*[1]
1. University of Florida, Gainesville, FL, United States

The recently discovered atomically-thin magnetic crystals provide a unique playground for understanding magnetization in 2D confinement and developing new approaches to manipulating magnetism for novel spintronic devices. In particular, antiferromagnets (AFMs) are promising for realizing high-speed information processing given their THz magnetic resonance frequency. However, they are also less sensitive to optical and electrical detection due to their net zero magnetization. In this talk, I will discuss our recent results on 2D AFM transition-metal trichalcogenides, where we couple the magnetic transitions into the mechanical degree of freedom. We observed the expected steady-state spin transitions based on magnetostriction effects and also saw signatures of additional transition points related to the magnetic domain dynamics.

EB-04. Quantum Noise Spectroscopy of Critical Dynamics in Two-dimensional Magnets. *S. Chatterjee*[1], F. Machado[2], M. Ziffer[3], N. Yao[2], E. Demler[4], E. Davis[5] and A. Pasupathy[3] *1. Physics, Carnegie Mellon University, Pittsburgh, PA, United States; 2. Harvard University, Cambridge, MA, United States; 3. Columbia University, New York City, NY, United States; 4. ETH Zurich, Zurich, Switzerland; 5. New York University, New York City, NY, United States*

Imaging spatial and temporal correlations of spins in two-dimensional (2d) magnets presents a significant challenge, since traditional scattering and spectroscopic tools do not apply. In this talk, I will propose and analyze a new technique based on quantum states of 'color defects' in solid state materials, such as nitrogen-vacancy (NV) sensors in diamond, to probe spin-correlations with energy and momentum resolution in 2d magnets. Specifically, I will argue that the decoherence of the defect 'probe qubit' due to magnetic noise, caused by spin fluctuations in a proximate 2d magnetic flake, can provide valuable information about phase transitions in 2d magnets. I will show that such decoherence-based noise spectroscopy directly targets slow critical dynamics in 2d magnets, and can hence be used to diagnose the universality class associated with the magnetic transition and extract critical exponents via a scaling analysis. Finally, to illustrate the ability of magnetic noise spectroscopy to identify the nature of critical fluctuations in magnets, I will discuss its recent application to trilayer CrSBr, a truly two-dimensional magnet that undergoes a magnetic phase transition around 140 K.

F. Machado, E. A. Demler, N. Y. Yao and S. Chatterjee, Phys. Rev. Lett., 131, 070801 (2023) M. E. Ziffer, F. Machado, B. Ursprung, A. Lozovoi, A. B. Tazi, Z. Yuan, M. E. Ziebel, T. Delord, N. Zeng, E. Telford, D. G. Chica, D. W. deQuilettes, X. Zhu, J. C Hone, K. L Shepard, X. Roy, N. P. de Leon, E. J. Davis, S. Chatterjee, C. A. Meriles, J. S. Owen, P. J. Schuck and A. N. Pasupathy, arXiv:2407.05614 (2024)

EB-05. Quantum spintronics with graphene-based magnetic heterostructures. *T. Ghiasi*[1] *1. Harvard University, Cambridge, MA, United States*

A new paradigm for spintronic devices is recently developed by exploiting proximity effects in graphene-based van der Waals heterostructures. Through proximity effects, the superior spin and charge transport properties of graphene are enriched by induced spin-orbit couplings [1-2] and magnetic exchange interactions [3-4]. Our recent spin transport measurements in magnetic graphene-based heterostructures, in particular, have shown a strong spin polarization of conductivity in graphene, resulting in an active role of the magnetic graphene in the electrical and thermal generation of spin currents [3]. We further evaluate the charge transport in magnetized graphene in the quantum Hall regime, where the magnetic orbital and exchange interactions result in an energy modulation of the Landau levels and allow for the detection of spin-polarized edge states at zero external magnetic field [4]. The preserved long-distance spin transport in both diffusive and quantum Hall regimes at zero external magnetic fields makes magnetic graphene ideal for ultra-thin magnetic memory and sensory devices with applications in quantum spintronic circuitries.

[1] Ghiasi, TS, et al. Nano Letters 17, 7528 (2017) [2] Ghiasi, TS, et al. Nano Letters 19, 5959 (2019) [3] Ghiasi, TS, et al. Nature Nanotechnology 16, 788 (2021) [4] Ghiasi, TS, et al. arXiv:2312.07515 (2023)

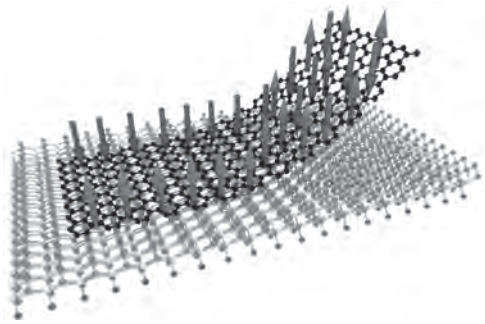

The emergence of topological spin transport in graphene by the magnetic proximity effect

Session EC
MAGNETORESISTANCE, SPIN CALORITRONICS, AND DAMPING

William K Peria, Chair
National Institute of Standards and Technology, Boulder, CO, United States

CONTRIBUTED PAPERS

EC-01. Enhancement of tunnel magnetoresistance in fully perpendicular MnGa-based magnetic tunnel junctions with metastable bcc CoMnFe interlayer. *D. Kumar*[1], N. Kamata[2,1], K. Hyeokjin[2,1] and S. Mizukami[1,3]
1. WPI Advanced Institute for Materials Research, Tohoku University, Sendai 980-8577, Japan, Sendai, Japan; 2. Department of Applied Physics, Tohoku University, Sendai 980-8579, Japan, Sendai, Japan; 3. Center for Science and Innovation in Spintronics, Tohoku University, Sendai 980-8577, Japan, Sendai, Japan

Magnetic tunnel junctions with crystalline MgO barriers utilizing perpendicularly magnetized magnetic materials as electrodes (*p*-MTJs) have significant potential for applications such as spin-transfer torque magnetoresistive random access memory. Tetragonal Heusler alloys (Mn-X; X= Ga, Ge etc.) have great attention considering their unique physical properties, such as large perpendicular magnetic anisotropy (PMA), low magnetization and low Gilbert damping constant [1]. A significant challenge is experimentally obtaining a high TMR effect in those MTJs. Inserting a thin 3d transition ferromagnetic metal/alloy layer between the MgO and bottom electrode enhances the TMR ratio. Recently, we observed a significant improvement in the TMR ratio using metastable bcc CoMn as an interlayer in MnGa-based *p*-MTJs [2], owing to intriguing properties of CoMn alloys [3,4]. Since CoMn shows a much higher TMR ratio via the addition of Fe [5], as compared to CoMn [3,4], we further investigated MTJs using metastable bcc CoMnFe as an interlayer to increase their TMR ratio. The MTJs were prepared using ultrahigh vacuum magnetron sputtering. MTJs stacking structure was MgO subst./Cr(40)/MnGa(30)/Mg(0.4)/CoMnFe(*d*)/Mg(0.4)/MgO(2)/CoFeB(1.2)/Ta(3)/Ru(5) (thickness is in nm). Microfabrication was performed using optical lithography with Ar ion etching. MTJs were annealed in a vacuum furnace with different temperatures (T_a). Transport measurements were performed using four-probe method at 300K. Fig. 1(a) and 1(b) show TMR curves for *p*-MTJs without and with CoMnFe interlayers. MR ratio of 7% was observed for *p*-MTJ without interlayer, while the MR ratio of ~110% was observed for 1.2-nm thick CoMnFe interlayer at T_a=300°C. A clear change was observed in MR curve from standard TMR curve to the inverted type due to the insertion of CoMnFe interlayer, which is associated with the antiferromagnetic coupling between the bottom electrode MnGa and CoMnFe interlayers, as observed in the similar *p*-MTJ with CoMn interlayer [2]. Results obtained further demonstrate the effectiveness of metastable bcc Co-based alloys for Mn-based *p*-MTJs, and detailed data will be presented.

1. X. Zhao and J. Zhao, Adv. Mater. Interfaces 9, 2201606 (2022). 2. K. Z. Suzuki et al., Appl. Phys. Lett. 118, 172412 (2021); AIP Advances 13, 035225 (2023). 3. K. Kunimatsu et al., Appl. Phys. Express 13, 083007 (2020). 4. K. Elphick et al., Phys. Rev. Appl. 16, 054052 (2021). 5. T. Ichinose et al., J. Alloys. Comp. 960, 170750 (2023).

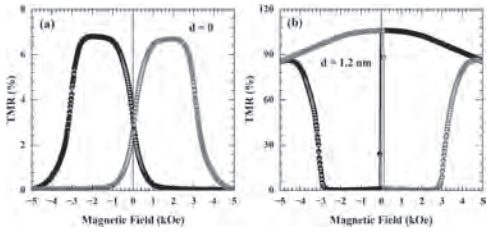

TMR curves for MnGa *p*-MTJs (a) without and (b) with 1.2nm-thick CoMnFe interlayer

EC-02. Tunnel Magnetoresistance in Fully Epitaxial CoPt/MgO/CoPt(111) Perpendicular Magnetic Tunnel Junctions. *J. Song*[1,2], T. Scheike[1], C. He[1], Z. Wen[1], T. Ohkubo[1], K. Kim[3], H. Sukegawa[1] and S. Mitani[1,2] *1. National Institute for Materials Science, Tsukuba, Japan; 2. Graduate School of Science and Technology, University of Tsukuba, Tsukuba, Japan; 3. Samsung Advanced Institute of Technology, Suwon, The Republic of Korea*

Magnetoresistive random access memories (MRAMs) play a considerable role with the memory cell consisting of magnetic tunnel junctions (MTJs). For scaling down the element size below 10 nm, a giant tunnel magnetoresistance (TMR) ratio alongside a large perpendicular magnetic anisotropy (PMA) is crucial. The conventional bcc(001) MTJ employs the Δ_1 coherent tunneling mechanism with interface-induced PMA to meet this requirement with a typical CoFeB/MgO/CoFeB structure. However, the presence of fcc(111)-Co-based hard layers promoted the magnetic coupling but crystallographically inconsistent structure, leading to the complexity in manufacturing [1]. Recently, a new concept known as fcc(111) MTJ structure with the Co-based alloys such as CoPt predicts a large bulk PMA energy and giant TMR ratio exceeding 2000% due to the interfacial resonant tunneling mechanism [2]. However, the experimental TMR demonstration for epitaxial CoPt/MgO/CoPt(111) perpendicular MTJs (p-MTJs) was yet to be performed. In this work, the p-MTJ stack with the structure of sapphire(0001) substrate/Ru (40)/CoPt multilayer (ML) (4)/Ru (0.9)/CoPt ML (4)/Co (0.6)/MgO (1.6)/CoPt ML (5.2)/Ru (12) (units in nm) (Fig. 1) was deposited using magnetron sputtering with a base pressure less than 9×10^{-7} Pa. The bottom layer utilized the synthetic antiferromagnetic (SAF) structure. The CoPt layers were prepared by repeating of a (Co/Pt) monolayer unit. Microstructural analysis including X-ray diffraction, etc. confirmed the fully (111) epitaxial growth of CoPt/MgO/CoPt. The patterned MTJs have a TMR ratio up to 15 % at room temperature as shown in Fig. 2. We observed symmetric bias voltage dependences for TMR ratio and differential conductance, indicating that the similar interface quality between top and bottom MgO side was achieved. Although further improvement of interface states is needed to activate the resonant tunneling mechanism for giant TMR, our demonstration highlighted the potential of this novel structure beyond the conventional (001) p-MTJs.

[1] K. Yakushiji, H. Kubota, A. Fukushima, and S. Yuasa, Appl. Phys. Express., Vol. 8, p.083003 (2015) [2] K. Masuda, H. Itoh, Y. Sonobe, H. Sukegawa, S. Mitani, and Y. Miura, Phys. Rev. B., Vol. 103, p.064427 (2021)

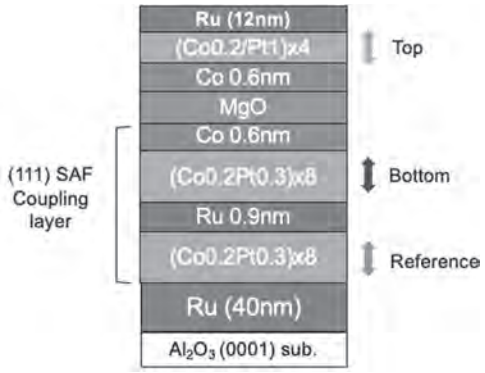

FIG. 1. Schematic illustration of epitaxial fcc(111) p-MTJ stack.

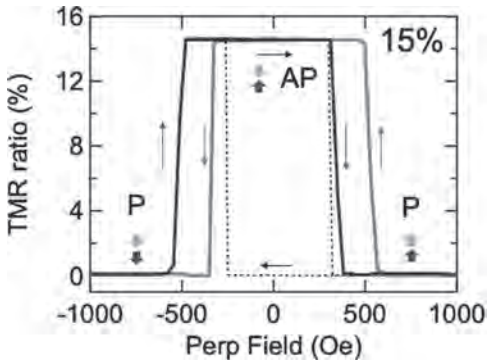

FIG. 2. TMR-field curves at room temperature. The dashed line indicates the minor loop for top CoPt ML.

EC-03. Tunnel magnetoresistance enhancement by ultrathin MgO insertions in Fe/$MgGa_2O_4$/Fe(001) magnetic tunnel junctions.
R.R. Sihombing[1], T. Scheike[1], Z. Wen[1], J. Uzuhashi[1], T. Ohkubo[1], S. Mitani[1] and H. Sukegawa[1] *1. CMSM, National Institute of Materials Science, Tsukuba, Japan*

Magnetic tunnel junctions (MTJs) are widely utilized in spintronic applications, such as tunneling magnetoresistive (TMR) heads in hard disk drives and magnetoresistive memory cells. To maintain the scaling of these devices, the development of low-barrier height materials for the MTJ barrier is strongly required. $MgGa_2O_4$ (MGO) is a promising candidate for a low *RA* barrier due to its low band gap (~4.7 eV) and large TMR ratios of 121% at room temperature (RT) [1]. Recently, CoFeB/MgO/MGO/MgO/CoFeB MTJs have shown an improved interfacial perpendicular magnetic anisotropy at the MGO/CoFeB interfaces due to the MgO insertions [2]. However, the mechanism of the improvements has yet to be determined. In this study, we developed epitaxial Fe/MgO/MGO/MgO/Fe(001) MTJs to improve the TMR ratios and explore the effect of the MgO sub-nanometer insertion. MTJ stacks were deposited using ultra-high vacuum magnetron sputtering. The typical stack structure is MgO(001) substrate/Cr buffer/Fe (50)/bottom MgO (0.3)/MGO (1.7)/top MgO (0.3)/Fe (5)/IrMn (10)/Ru (10), (unit: nm) as shown in Fig. 1. The MgO and MGO layers were deposited using MgO and $MgGa_2O_4$ sintered targets. The stacks were post-annealed at 200°C with a magnetic field of 2 kOe. Magnetotransport properties were characterized by the DC four-probe method after patterning into micrometer-scale MTJs. Figure 2 shows the TMR-field curve of the MTJ pillar measured at RT (upper) and 5 K (lower). A TMR ratio of 151% (291%) was observed at RT (5 K), which is larger than 121% (196%) in Fe/MGO/Fe without MgO nano-insertions [1] indicating the enhancement of coherent tunneling by the MgO insertion (as observed by bias voltage spectra). Scanning transmission electron microscopy and energy dispersive X-ray spectroscopy of the MTJ cross-section revealed that the 0.3-nm-MgO suppresses Ga diffusion from the MGO to the Fe layers, leading to the improvement of the TMR ratio.

This work was supported by KIOXIA Corporation, MEXT Program: Data Creation and Utilization-Type Material Research and Development Project JPMXP1122715503, and JSPS KAKENHI 22H04966, and 24H00408.

[1] H. Sukegawa *et al.*, Appl. Phys. Lett. 110, 122404 (2017). [2] S. Mertens *et al.*, Appl. Phys. Lett. 118, 172402 (2021).

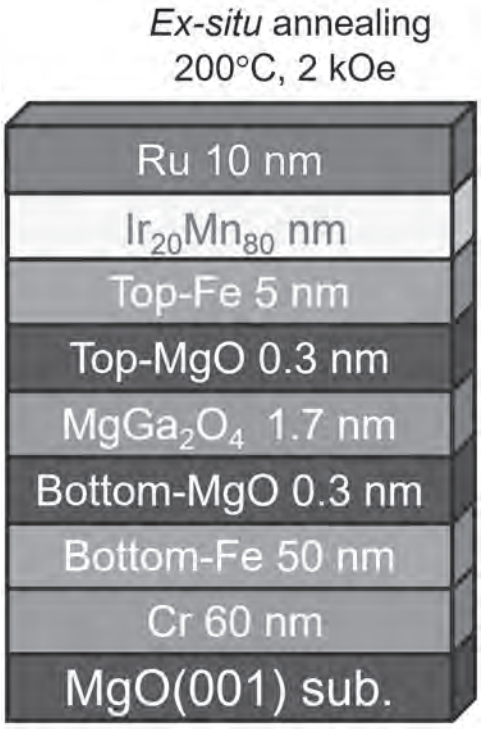

Fig. 1. The MTJ design

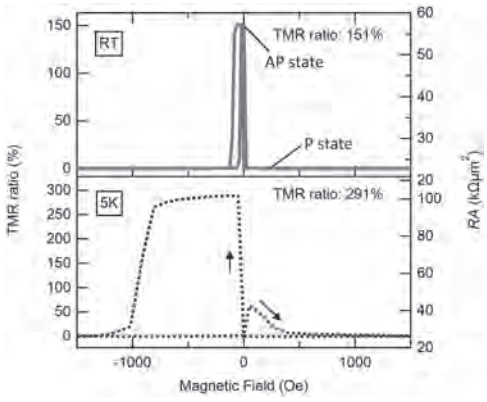

Fig. 2. TMR ratio and *RA* vs magnetic field of Fe/MgO (0.3)/MGO (1.7)/MgO (0.3 nm)/Fe MTJ at RT and 5 K

EC-04. Theory for the TMR oscillation as a function of the barrier thickness.
K. Masuda[1], T. Scheike[1], H. Sukegawa[1], Y. Kozuka[1], S. Mitani[1] and Y. Miura[1,2] *1. National Institute for Materials Science, Tsukuba, Japan; 2. Kyoto Institute of Technology, Kyoto, Japan*

The oscillation of the tunnel magnetoresistance (TMR) ratio as a function of the insulating barrier thickness has been universally observed in crystalline magnetic tunnel junctions (MTJs) [1-3] and is now recognized as the "TMR oscillation." However, the physical origin of this phenomenon has yet to be clarified, although previous theoretical studies have considered several effects based on the Δ_1 coherent tunneling theory [4,5]. To solve this long-standing problem will advance our understanding on the TMR effect and

provide guiding principles for achieving higher TMR ratios. In this work, we provide a possible explanation for the TMR oscillation [6]. The key of our idea is to consider a superposition of wave functions with opposite spins and different Fermi momenta. Focusing on a typical Fe/MgO/Fe(001) MTJ, we solve the tunneling problem assuming a superposition of the majority-spin Δ_1 and minority-spin Δ_2 wave functions as the transmission wave function. We show that the obtained conductances in the parallel and antiparallel magnetizations states and the resultant TMR ratio oscillate with a period of ~3Å by varying the MgO thickness, consistent with experimental observations. Our analytical expression clarifies that the period of the TMR oscillation is determined by the difference in the Fermi momenta between the majority-spin Δ_1 and minority-spin Δ_2 states. We finally compare the present calculation results with our experimental results obtained for the high-quality single-crystalline MTJ. We find that the calculation results [Fig. 1] can reproduce the characteristic sawtooth-like shape of the TMR oscillation observed in experiments [Fig. 2]. This work was supported by Grant-in-Aids for Scientific Research (22H04966, 23K03933, and 24H00408) and MEXT Program: Data Creation and Utilization-Type Material Research and Development Project (JPMXP1122715503).

[1] S. Yuasa *et al*., Nat. Mater. 3, 868 (2004). [2] R. Matsumoto *et al*., Appl. Phys. Lett. 90, 252506 (2007). [3] T. Scheike *et al*., Appl. Phys. Lett. 120, 032404 (2022). [4] W. H. Butler *et al*., Phys. Rev. B 63, 054416 (2001). [5] X.-G. Zhang *et al*., Phys. Rev. B 77, 144431 (2008). [6] K. Masuda *et al*., arXiv:2406.07919.

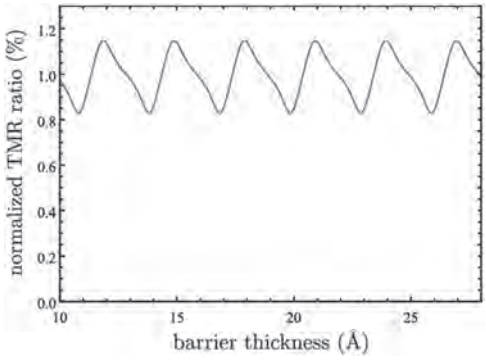

Theoretically calculated TMR ratios as a function of the insulating barrier thickness, adapted from Ref. [6].

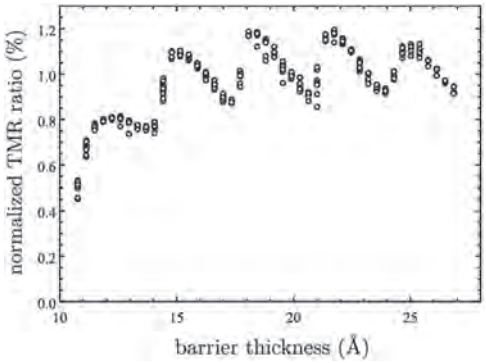

Experimentally obtained TMR ratios as a function of the insulating barrier thickness, adapted from Ref. [6].

EC-05. Observed Perpendicular Magnetic Anisotropy in $CoFe_2O_4$/ $MgO/ZnFe_2O_4$ Magnetic Tunnel Junction: X-ray Magnetic Circular Dichroism Study. R. Charak[1], *S. Gautam*[2], S. Garg[2], P. Thakur[3], N. Goyal[4], Y. Kim[5] and K. Chae[6] *1. Energy Research Centre, Panjab University, Chandigarh, India; 2. Dr. SSB Univ Inst Chem Engg & Tech, Panjab University, Chandigarh, India; 3. Beamline Division, Diamond Light Source Ltd., Didcot Oxfordshire, United Kingdom; 4. Department of Physics, Panjab University, Chandigarh, India; 5. Pohang Accelerator Lab, POSTECH, Pohang, The Republic of Korea; 6. Advanced Analysis & Data Center, Korea Institute of Science and Technology, Seoul, The Republic of Korea*

Magnetic tunnel junctions (MTJs) have been studied for decades as spintronic devices with two ferromagnetic electrodes separated by an insulating layer. This study explores the use of an antiferromagnetic material as one electrode paired with a ferromagnetic electrode to understand variations in perpendicular magnetic anisotropy (PMA) and tunnel magnetoresistance (TMR). The multilayer, consisting of CoFe2O4 (40nm)/MgO (20nm)/ZnFe2O4 (40nm), is also irradiated with swift heavy ions to sharpen the interface between the layers. We investigate the spin-orbital magnetic moment, PMA, and TMR of the MTJ using angle-dependent X-ray magnetic circular dichroism (XMCD) with element-specific hysteresis loops at the Fe L-edge. Our results clearly show PMA for both pristine and irradiated samples, with a decrease in XMCD spectra intensity for out-of-plane measurements. This intensity decrease is linked to spin polarization, indicating a direct relationship with TMR. Furthermore, TMR is inversely proportional to the increasing angle in both pristine and irradiated MTJs, as observed in XMCD measurements. The out-of-plane hysteresis loop in the irradiated stack resembles giant magnetoresistance (GMR) behavior, attributed to interface sharpening. In summary, this research highlights how examining the spin-orbital magnetic moment, PMA, and magnetoresistive properties in CoFe2O4/MgO/ZnFe2O4 MTJs can significantly advance the development of reliable and efficient magnetic storage devices.

1. Samanta, Kartik, et al., *Phys. Rev. B* 109.17 (2024): 174407. 2. Garg, Shaffy, et al., *Mater. Lett.* 349 (2023): 134738. 3. Kim, D. H., et al., *J. Mag. Magn. Mater.* 432 (2017): 450-454. 4. Yang, Chao-Yao, et al., *Scientific Rep.* 5.1 (2015): 17169. 5. Park, Byong Guk, et al., *Nature Mate.* 10.5 (2011): 347-351.

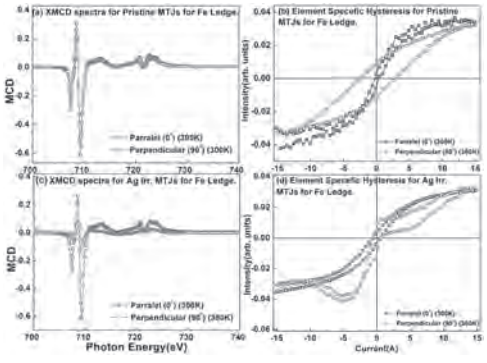

Angle dependent XMCD/element specific hysteresis curves: (a) XMCD spectra at Fe L-edge for CoF/MgO/ZnF MTJ with in-plane and perpendicular measurements at 300 K, (b) Element specific hysteresis loop at Fe L-edge for CoF/MgO/ZnF MTJ with in-plane and perpendicular measurements, (c) XMCD spectra at Fe L-edge for Ag irradiated CoF/MgO/ZnF MTJ with in-plane and perpendicular measurements at 300 K, (d) Element specific hysteresis loop at Fe L-edge for Ag irradiated CoF/MgO/ZnF MTJ with in-plane and perpendicular measurements.

EC-06. Spin-selective transport in chiral molecular junctions on semiconductors. *Y. Adhikari*[1], T. Liu[2], H. Wang[3], Z. Hua[1], H. Liu[1], P. Schlottmann[1], H. Gao[1], P. Weiss[2], B. Yan[4], J. Zhao[3] and P. Xiong[1]
1. Department of Physics, Florida State University, Tallahassee, FL, United States; 2. Department of Chemistry and Biochemistry, University of California, Los Angeles, Los Angeles, CA, United States; 3. State Key Laboratory of Superlattices and Microstructures, Institute of Semiconductors, Chinese Academy of Sciences, Beijing, China; 4. Department of Condensed Matter Physics, Weizmann Institute of Science, Rehovot, Israel

Electrical generation and transduction of polarized electron spins in semiconductors (SCs) via *nonmagnetic* means are of broad interest in spintronics and quantum information science. One such pathway exploits chiral/helical spin textures in electronic structures; a contrasting approach utilizes the interplay of electron spin with chirality in real space. One prominent manifestation of such effects of is chirality-induced spin selectivity (CISS), where real-space structural chirality induces spin polarization of electrons from a nonmagnetic (NM) electrode[1]. CISS has far-reaching fundamental implications involving intricate interplays among structural chirality, topological states, and electronic spin and orbitals. However, definitive understanding of its physical origin remains elusive. We have studied the CISS effect through measurement of spin-selective transport in chiral molecular junctions comprising a NM normal metal electrode and a self-assembled monolayer of chiral molecules (α-helix L-polyalanine) on magnetic (GaMnAs) or nonmagnetic (*n*-GaAs) SCs, where the spin polarization is detected via measurements of spin-valve and Hanle effect, respectively. The pronounced CISS effect in robust SC-based molecular device platform enabled systematic and rigorous examination of its dependences on the molecular structure, normal metal material, and bias current. The results reveal several key characteristics of the CISS effect: i) nontrivial linear-response magnetoconductance (MC) in two-terminal CISS spin valves, in apparent violation of the Onsager reciprocal relation[2]; ii) crucial role of the spin-orbit coupling in the normal metal electrode, suggesting the importance of orbital polarization in the chiral molecules[3]; iii) spin generation by CISS in SCs[4]. Our experiments have provided significant new insights on CISS and demonstrated its potential for enabling semiconductor spintronics free of any magnetic materials. *Work supported by NSF grants DMR-1905843 and DMR-2325147

[1] B.P. Bloom, *et. al*., *Chem. Rev*. 124, 1950 (2024). [2] T. Liu, *et. al*., *ACS Nano* 14, 15983 (2020). [3] Y. Adhikari, T. Liu, *et. al*., *Nat. Commun*. 14:5163 (2023). [4] T. Liu, Y. Adhikari, H. Wang, *et. al*., *Adv. Mater*. 2406347 (2024).

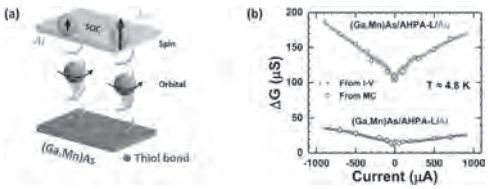

Fig. 1 (a) Mechanism for orbital to spin polarization conversion. (b) Bias dependence of spin-valve MC with Au and Al contacts. [3]

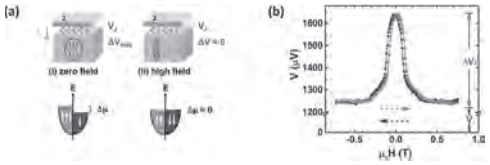

Fig. 2 (a) Depiction of spin accumulation and Hanle effect in molecular junction. (b) Representative Hanle curve. [4]

EC-07. Colossal anisotropic absorption of spin currents induced by chirality. *R. Sun*[1], Z. Wang[2], B.P. Bloom[3], A.H. Comstock[1], C. Yang[2], A. McConnell[1], C. Clever[3], M. Molitoris[3], D. Lamont[4], Z. Cheng[5], Z. Yuan[5,7], W. Zhang[6], A. Hoffmann[8], J. Liu[2], D.H. Waldeck[3] and D. Sun[1]
1. Physics, North Carolina State University, Raleigh, NC, United States; 2. Department of Mechanical and Aerospace Engineering, North Carolina State University, Raleigh, NC, United States; 3. Department of Chemistry, University of Pittsburgh, Pittsburgh, PA, United States; 4. Petersen Institute of Nanoscience and Engineering, University of Pittsburgh, Pittsburgh, PA, United States; 5. Institute of Physics, CAS, Beijing, China; 6. Department of Physics and Astronomy, University of North Carolina at Chapel Hill, Chapel Hill, NC, United States; 7. Department of Physics, Beijing Normal University, Beijing, China; 8. Department of Materials Science & Engineering and Materials Research Laboratory, University of Illinois at Urbana-Champaign, Urbana, IL, United States

Spin currents are essential for the development of modern spintronics concepts (*1*) (*2*). Via spin pumping, the flow of spin current across the FM/NM interface can be probed by examining the phenomenological Gilbert damping factor, α, and it constitutes one of the key parameters describing the dynamics of FM materials and the spin-related characteristics of an adjacent NM. The enhanced damping Δα is typically determined by the material parameters for a prepared FM/NM interface and is isotropic regardless of the spin polarization orientations (Fig. 1A). The chiral induced spin selectivity (CISS) effect, where the structural chirality of a material determines the preference for the transmission of electrons with one spin orientation over that of the other, is emerging as a design principle for creating next-generation spintronic devices (3). Recent work suggests that chiral matter displays large effective SOC, and manifests efficient 'spin filtering' when a charge current passes along the chiral axis of materials. According to the generalized Landau-Lifshitz-Gilbert equation, the Gilbert damping factor is treated as a tensor, implying that control over the rotational or orientational anisotropy could play a crucial role in directing spin current (Fig.1 B) (4). The combination of structural chirality and enhanced SOC presents an exciting opportunity to engineer the anisotropy of the Gilbert damping factor through the CISS effect. Here, we find that the Gilbert damping in a chiral cobalt oxide film exhibits a maximum (minimum) value when the direction of the spin polarization is parallel (perpendicular) to the chiral axis, whereas an achiral analogue of the cobalt oxide film shows isotropic damping. By rotating the magnetization orientation of the FM from the in-plane to the out-of-plane direction, a twofold symmetry of the anisotropic damping manifests and displays a maximum-minimum ratio of ten times. This effect is attributed to the strong spin-flip process arising from chirality-induced band spin-splitting, which yields a reciprocal large spin transmission probability along the chiral axis. These studies reveal a pathway for tailoring anisotropic non-local Gilbert damping through structural chirality.

1. A. Hoffmann, S. D. Bader, Opportunities at the Frontiers of Spintronics. *Phys.Rev. Applied* 4, 047001 (2015). 2. J. Puebla, J. Kim, K. Kondou, Y. Otani, Spintronic devices for energy-efficient data storage and energy harvesting. *Comm. Mater.* 1, 24 (2020). 3. R. Naaman, Y. Paltiel, D. H. Waldeck, Chiral molecules and the electron spin. Nat. Rev. Chem. 3, 250-260 (2019). 4. R. Sun, Z. Wang, B. P. Bloom, A. H. Comstock, C. Yang, A. McConnell, C. Clever, M. Molitoris, D. Lamont, Z.-H. Cheng et al. Colossal anisotropic absorption of spin currents induced by chirality. Sci. Adv. 10, eadn3240 (2024)

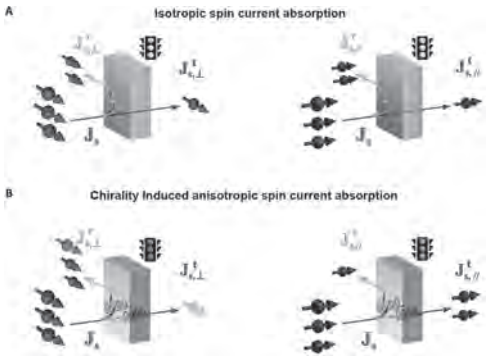

Fig.1 A & B

EC-08. Observations of Non-Local Spin-Valve Signal and Hanle Signal in Perpendicularly Magnetized Mn/Co/n-GaAs Junctions via All Electrical Methods. *M. Ogawa*[1], K. Nara[1], M. Yamanouchi[1] and T. Uemura[1] *1. Grad. School of Information Science and Technology, Hokkaido University, Sapporo, Japan*

All electrical generation and detection of perpendicularly polarized spins in semiconductors are important techniques for realizing high-performance spin transistors. Although there have been many reports on all electrical spin injection and detection using in-plane magnetized ferromagnets, such as Fe, CoFe and Co_2MnSi, there has been no report on that using out-of-plane magnetized ferromagnets with non-local geometry. In this study, we demonstrated a spin injection from perpendicularly magnetized Mn/Co bilayer [1] into n-GaAs through non-local spin-valve and Hanle measurements. The bilayer consisting of a 1.7-nm-thick Mn and a 1.0-nm-thick Co was grown on n-GaAs. An anomalous Hall effect measurement showed a clear perpendicular magnetic anisotropy of the Mn/Co bilayer with its coercivity $\mu_0 H_c$ of approximately 0.41 T at 77K, where μ_0 is the permeability of the vacuum. The sample was processed into a four-terminal lateral spin-valve device to evaluate spin injection characteristics. The non-local resistance R_{NL} measured at 77 K exhibited sharp changes at $\mu_0 H_z \approx \pm 0.4$ T, which is close to $\mu_0 H_c$ of the Mn/Co bilayer, where H_z is an out-of-plane external magnetic field (Fig. 1). The change of R_{NL} is caused by the switching between parallel (P) and anti-parallel (AP) magnetization configuration between injector and detector contacts (spin-valve effect). Furthermore, clear Hanle signal was observed: The R_{NL} for the P (AP) configuration gradually decreased (increased) as $|\mu_0 H_x|$ increased, and merged at $|\mu_0 H_x| > 40$ mT, where H_x is an in-plane magnetic field (Fig. 2). The observations of spin-valve signal and Hanle signal provide the direct evidence of injection, transport, and detection of perpendicularly polarized spins in Mn/Co/n-GaAs lateral junctions. This work was supported in part by JSPS KAKENHI (22K18961), MEXT X-NICS (JPJ011438), MEXT ARIM (JPMXP1224HK0020), JST CREST (JPMJCR22C2), and JST SPRING (JPMJSP2119).

[1] R.K. Han *et al*., Phys. Rev. Applied. 19, 024033 (2023).

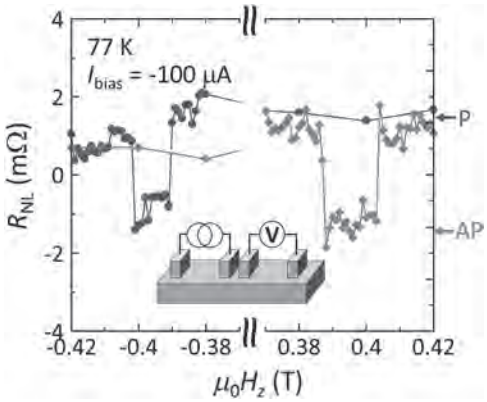

Fig. 1. Non-local resistance R_{NL} as a function of out-of-plane external magnetic field H_z. The red (blue) plots indicate that H_z was swept from -0.5 (+0.5) T to +0.5 (-0.5) T.

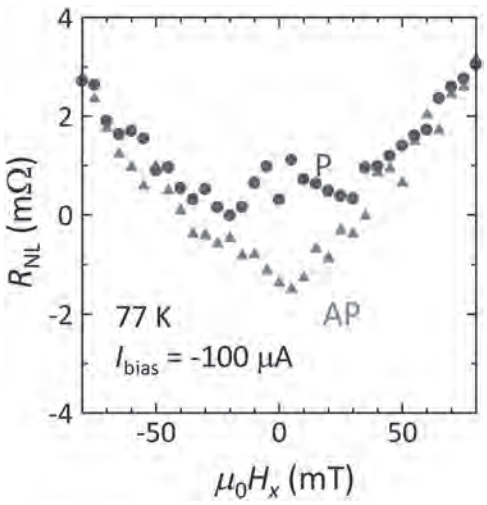

Fig. 2. R_{NL} as a function of in-plane magnetic field H_x in both the P and AP configuration.

EC-09. Low spin-flip probability of the Kondo scattering in Cu channels with dilute Fe impurities. *Y. Ji*[1] and X. Shen[1] *1. University of Delaware, Newark, DE, United States*

The Kondo effect originates from the antiferromagnetic exchange interaction between the itinerant electrons and the localized spins of magnetic impurities. [1] It is generally accepted that the Kondo scattering process is associated with a high probability of spin flip. In Kondo's original calculation, the spin flip probability is shown to be 2/3 assuming a spherical Fermi surface. The measurement of the Kondo spin flip probability is fundamentally intriguing but had been experimentally challenging. The nonlocal spin valve (NLSV) system in spintronics provides an effective approach to investigate the spin relaxation process in nonmagnetic materials. In Cu channels with dilute Fe impurities, the Kondo spin relaxation rate as well as the Kondo spin-flip probability have been studied. However, different works have reported markedly varied spin-flip probabilities. [2-4] In addition, it is important to note that while the spin relaxation rate and spin flip rate are often used interchangeably, there is actually a difference by a factor of 2. In this study, we experimentally determine the Kondo spin flip probability in Cu-based NLSVs with Fe impurities. The impurity concentration is varied by both intentional and unintentional doping. Six sets of NLSVs are studied and each set contains 8 to 15 devices. The widths and thicknesses of all Cu channels are either 300 nm or 500 nm. The Kondo spin-flip probability, determined for each set, decreases from 0.14 to 0.03 as the Kondo resistivity varies from < 0.001 to 0.009 μΩcm. The corresponding impurity concentration is

between < 1 and 9 ppm. Our study reveals that contrary to the conventional wisdom, the Kondo spin-flip probability is not a constant and can be much lower than unity even in dilute Kondo alloy. The original Kondo calculation assumes the interaction of conduction electrons with a single impurity spin. However, even at 1 ppm concentration, there are multiple impurities with randomly oriented spins within the radius of the Kondo screening cloud. We hypothesize a cancellation effect and construct an intuitive physical picture using the Kondo screening cloud.

[1] J. Kondo, Prog. Theor. Phys. 32, 37 (1964). [2] K. W. Kim et al, Phys. Rev. B 95, 104404 (2017). [3] J. T. Batley et al, Phys. Rev. B 92, 220420(R) (2015). [4] X. Y. Shen and Y. Ji, Phys. Rev. B 104, 085101 (2021).

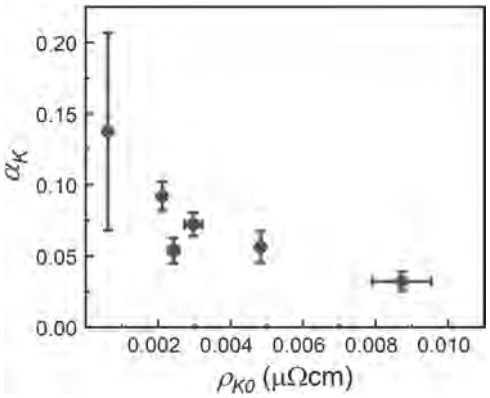

EC-11. Influence of oxidic and metallic interfaces and spacers on the magnetic damping of Permalloy thin films. *V. Ney*[1], K. Lenz[2], R. Hübner[2], F. Ganss[2], R. Salikhov[2], O. Hellwig[2], J. Lindner[2] and A. Ney[1] *1. Solid State Physics Devision, Johannes Kepler University Linz, Linz, Austria; 2. Helmholtz Zentrum Dresden Rossendorf, Dresden, Germany*

A thorough understanding of magnetic damping in ferromagnetic materials is of importance in spintronics from both a fundamental and a practical point of view. The phenomenological Gilbert parameter α [1] in the Landau-Lifshitz equation is central to quantify the magnetic damping, which can be measured with ferromagnetic resonance (FMR). Permalloy (Py = $Ni_{80}Fe_{20}$) is one of the model systems with low magnetic damping. The ferromagnetic metal is well-understood, but surprisingly the available data for α spreads from $4\text{-}9\times10^{-3}$ [2,3]. To find the reason for these variations is crucial, since an increase of α is often used as an indication for spin pumping. It has to be distinguished between influences like oxidation, roughness - two magnon processes - and real spin pumping. Here, we report on a systematic study of the temperature and frequency dependence of the FMR linewidth of Py, which was grown on typical substrates (silicon and sapphire) and capped with materials commonly used for preventing oxidation (Ta, Al, and SiO_x). The resulting frequency and temperature dependence of the FMR linewidth deviates significantly from the expected Gilbert-like behavior. Unwanted non-Gilbert-like contributions appear, especially at low temperatures, and particularly for oxidic interfaces [4]. In contrast, metallic capping layers avoid non-Gilbert-like contributions. Special focus was paid to the influence of the Al spacer thickness which was varied between 1 and 10 nm [5]. In particular, Py sandwiched in between a metallic Al cap and a thin spacer layer (shown in Fig. 1), exhibits negligible inhomogeneous FMR linewidth broadening and a very small, purely Gilbert-like contribution of α = 0.0068(2) down to the lowest temperature [4,5], as shown in Fig. 2. First results on the spin pumping of these systems into Pt will also be shown.

[1] T. L. Gilbert, IEEE Trans. Magn. 40, p.3443 (2004) [2] A. A. Starikov et al., Phys. Rev. Lett. 105, p.236601 (2010) [3] M. A. W. Schoen et al., Phys. Rev. B 95, p. 134411 (2017) [4] V. Ney et al., Phys. Rev. Materials 7, p. 124403 (2023) [5] V. Ney et al., to be submitted

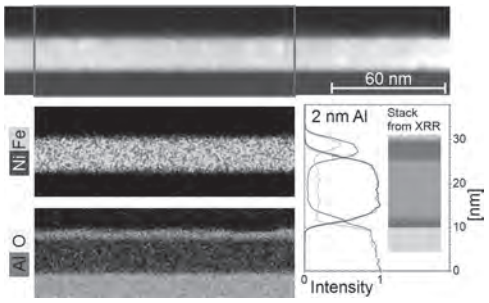

Fig. 1: HAADF-STEM images and element distribution maps of Fe/Ni and Al/O for a Py sample with an Al cap and a 2 nm Al spacer. The line profiles are shown scaled to the model stack derived by XRR.

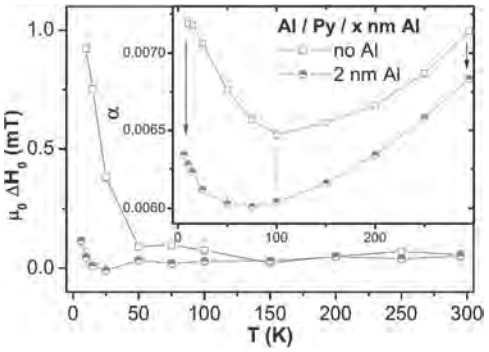

Fig. 2: Inhomogeneous broadening ΔH_0 and homogeneous Gilbert-like damping α (inset) derived from the linear fit of the frequency dependence of the FMR linewidth ΔH for all measured temperatures.

EC-12. Observation of the Transverse Thomson Effect. *A. Takahagi*[1], T. Hirai[2], A. Alasli[1], S.J. Park[2], H. Nagano[1] and K. Uchida[2,3] *1. Department of Mechanical Systems Engineering, Nagoya University, Nagoya, Japan; 2. National Institute for Materials Science, Tsukuba, Japan; 3. Department of Advanced Materials Science, The University of Tokyo, Kashiwa, Japan*

The thermoelectric effects have attracted attention as principles for energy harvesting and thermal management technologies. The Seebeck, Peltier, and Thomson effects, which are known as longitudinal thermoelectric effects, have been systematically studied for many years. The Seebeck and Thomson effects are related to each other through the so-called Kelvin relation, where the Thomson coefficient is determined by the temperature derivative of the Seebeck coefficient. Although the transverse thermoelectric effects including the Nernst and Ettingshausen effects have also been investigated for a long time, the transverse Thomson effect (TTE) has only been predicted theoretically and has not yet been observed experimentally.[1] According to the analogy with the Thomson effect, the TTE should be related to the temperature derivative of the Nernst coefficient. Therefore, observing the TTE is expected to systemize the transverse thermoelectric effects and demonstrate a new principle of thermal control. In this study, we have directly observed the temperature response due to the TTE using the thermoelectric imaging technique based on the lock-in thermography.[2-4] We measured the spatial distribution of temperature change of a nonmagnetic conductor when a charge current, temperature gradient, and magnetic field are applied orthogonally to each other. The temperature change was observed to increase with increasing charge current and temperature gradient, consistent with the predicted TTE trend but different from the conventional Ettingshausen effect. The numerical calculations based on the thermoelectric transport model closely matched the experimental results. Therefore, we confirmed that this observed temperature change is due to the TTE and experimentally clarified its fundamental properties. This result fills a missing piece in transverse thermoelectrics and will bring new developments in spin caloritronics.

[1] L. D. Landau, E. M. Lifshitz, and L. P. Pitaevskii, *Electrodynamics of Continuous Media* (Pergamon Press, Oxford, 1984) [2] S. Daimon, R. Iguchi, T. Hioki, E. Saitoh, and K. Uchida, Nat. Commun., Vol. 7, 13754 (2016) [3] K. Uchida, S. Daimon, R. Iguchi, and E. Saitoh, Nature, Vol. 558, p.95-99 (2018) [4] K. Uchida, M. Murata, A. Miura, and R. Iguchi, Phys. Rev. Lett., Vol. 125, 106601 (2020)

EC-13. Temperature gradient-driven motion of domains in a chiral magnetic metal multilayer. L. Huang[1,2], L. Kailas[1], S. Connell[1], G. Burnell[1] and *C. Marrows[1] 1. School of Physics and Astronomy, University of Leeds, Leeds, United Kingdom; 2. School of Material Science, University of Sheffield, Sheffield, United Kingdom*

Spin textures, such as domain walls [1] (DWs) and skyrmions [2], have been shown to move in response to temperature gradients. The flow of electrons or magnons induced by the spin Seebeck effect [3] can exert spin transfer torques [4]. Entropic forces arise owing to gradients in the micromagnetic parameters [5], which can either enhance or oppose the STTs [6]. There are conflicting experimental results for skyrmions. Conventional cold to hot motion was observed in insulating CuoSeO [7], but motion from hot to cold has been observed in Pt/CoFeB/MgO [2]. Experiments on DWs are few. In Ref. [1] a DW in the magnetic insulator YIG was reported to move towards the hot end of the system. In metals, DWs in in-plane magnetised Py wires showed this as an additional effect to current-driven motion [8]. Here we report experiments on the motion of domains in Pt/CoB/Ir metallic multilayers in a temperature gradient. The multilayers support both PMA and a chiral DMI [9] and were patterned into 10 μm wide tracks. The domain locations were determined using magnetic force microscopy (see Fig. 1) before and after a two minute heat pulse was applied to an electrically isolated Pt heater wire (purple area in schematic, SiO_2 insulator in green) crossing a magnetic track (red). The heat pulse was generated by flowing a dc current through the heater, which generates a temperature gradient along the track. We estimate that the temperature in the region shown in Fig. 1 varies from about 340 K to 300 K across the area that was imaged during heating. After accounting for Oersted field effects by measuring average domain displacements for both directions of heater current and both senses of applied field, we find that the domains always move towards the heater. We find velocities ~1 nm/s in a temperature gradient of ~20 K/μm.

[1] W. Jiang, P. Upadhyaya, Y. Fan, et al. Phys. Rev. Lett. 110, 177202 (2013). [2] Z. Wang, M. Guo, H.-A. Zhou, et al., Nature Electron. 3, 672 (2020). [3] D. Hinzke and U. Nowak, Phys. Rev. Lett. 107, 027205 (2011). [4] P. Yan, X. S. Wang, and X. R. Wang, Phys. Rev. Lett. 107, 177207 (2011). [5] F. Schlickeiser et al., Phys. Rev. Lett. 113, 097201 (2014). [6] E. Raimondo, et al., Phys. Rev. Applied 18, 024062 (2022). [7] X. Yu, F. Kagawa, S. Seki, et al., Nature Comms. 12, 5079 (2021). [8] J. Torrejon et al., Phys. Rev. Lett. 109, 106601 (2012). [9] K. Zeissler et al., Nature Commun. 11, 428 (2020).

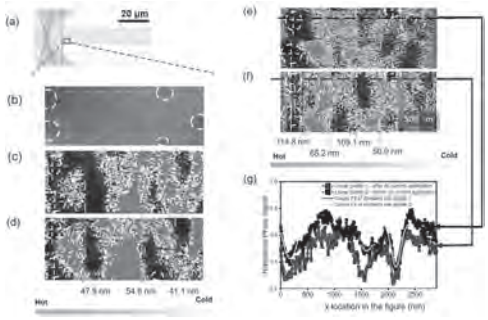

MFM imaging. (a) Schematic showing imaged region of track. (b) Full saturation at +600 Oe. Dark regions (marked with dashed yellow circles) are defects used as references. Example MFM images in +30 Oe field: (c) and (d) before and after a + 30 mA current was applied to the heater. (e) and (f) Before and after a -30 mA current. Dashed green lines show domain motion. (g) MFM image line sections.

EC-14. Spin caloritronics in topological and nonunitary superconductors. T. Matsushita[2], T. Mizushima[3], Y. Masaki[4], S. Fujimoto[3] and *I. Vekhter[1] 1. Department of Physics and Astronomy, Louisiana State University, Baton Rouge, LA, United States; 2. Department of Physics and Yukawa Institute, Kyoto University, Kyoto, Japan; 3. Department of Materials Engineering Science, Osaka University, Osaka, Japan; 4. Department of Applied Physics, Tohoku University, Sendai, Japan*

Interplay between superconductivity and magnetism and has generated significant interest in exotic superconductors as potential platform for studying the magneto-superconducting phenomena and applications in superconducting spintronics. A major obstacle is the paucity of reliable tests for materials that are time-reversal preserving yet exhibit topological and non-unitary superconducting orders that enable spin-polarized transport. We argue that the spin currents driven by thermal gradients provide a sensitive probe of the nature of the pairing in such superconductors. We show that nonvanishing spin-Nernst effect stemming from spin-anisotropic scattering of quasiparticles on non-magnetic impurities can be used to identify helical Cooper pairs [1], while finite superconducting spin-Seebeck and spin-Nernst signals together can be used to identify spin-polarized Cooper pairs in the momentum space and hence pinpoint non-unitary superconductors [2]. To determine the spin Seebeck signal it is essential to account for the counter-flow of the electron pairs induced by the thermal gradient: while the charge thermoelectric current vanishes in the superconducting state, the spin current of partially polarized pairs does not. We provide the estimate of the magnitude of this effect in candidate materials to show that such measurements are within the range of experiments in near future. Our work establishes spin caloritronics as a probe of exotic superconducting orders.

[1] T. Matsushita et al., Phys. Rev. Lett. 128, 097001 (2022) [2] T. Matsushita et al., arXiv:2404.02633 (unpublished)

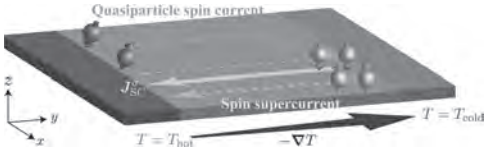

Illustration of the superconducting spin Seebeck effect in non-unitary superconductors. The spin supercurrent is generated to cancel the dissipative electric current carried by quasiparticles.

EC-15. Nernst Effect in Bismuth at Different Crystal Orientations. *A. Sola*[1], E.S. Olivetti[1] and V. Basso[1] *1. INRIM, Torino, Italy*

Several physical effects have been discovered thanks to studies on elemental bismuth because of the peculiarity of its electronic structure [1]. In the field of thermoelectricity, the importance of bismuth is given by its large transverse (Nernst) and longitudinal (Seebeck) figure of merit ZT, which is maximal among all the elemental metals [2]. Although these properties have been known for decades, some details about the electronics structure such as the spin and the valley degrees of freedom have fostered a renewed fundamental interest on this topic [3]. In this work we investigate the ordinary Nernst voltage as a function of the magnetic field on a bismuth single crystal. We compare the cases where the magnetic field is applied along the binary, the bisectrix and the trigonal directions of the crystal, while keeping the directions of the voltage and temperature gradients perpendicular to each others and in turn to the direction of the magnetic field, as provided for a Nernst effect measurement. The case with the magnetic field applied along the binary axes is compatible with previous literature results [4]. For other orientations, we find strikingly different magnetic field dependencies (see figure). The Nernst vs. magnetic field characteristic of polycrystalline bismuth and the related deviation from linearity observed at low fields [5,6] is compatible with the superimposition of all the contributions to the Nernst thermopower that we measure on single crystal. This study provides details for the benefit of the design of devices such as transverse thermoelectric modules based on the coupled effect of permanent magnets and ordinary-Nernst-effect materials [7].

[1] Fuseya, Y., et. al. *Journal of the Physical Society of Japan* 84.1 (2015): 012001. [2] Gallo, C. F., et. al. *Journal of Applied Physics* 34.1 (1963): 144-152. [3] Behnia, Kamran. *Journal of Physics: Condensed Matter* 21.11 (2009): 113101. [4] Michenaud, J. P., et al. "Korenblit et al." *Solid State Communications* 9 (1971): 1433-1435. [5] Zhang, J., et al. *Journal of Applied Physics* 117.17 (2015). [6] Parzer, M., et al. *Review of Scientific Instruments* 95.4 (2024). [7] Murata, Masayuki, et al. *Applied Physics Letters* 124.19 (2024).

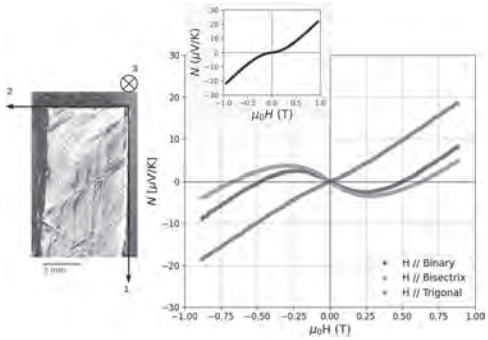

Left: magnified picture of the bismuth single crystal sample under test with a sketch of the binary (1), bisectrix (2) and trigonal (3) directions. Right: ordinary Nernst coefficient as a function of the applied magnetic field in the following measurement configurations: H ‖ binary, ∇T ‖ trigonal, ∇V ‖ bisectrix (blue line). H ‖ bisectrix, ∇T ‖ trigonal, ∇V ‖ binary (orange line). H ‖ trigonal, ∇T ‖ binary, ∇V ‖ bisectrix (green line). In the inset, the Nernst vs. H characteristic of a polycrystalline sample is reported.

Session ED
SKYRMIONS

Claas Abert, Chair
University of Vienna, Vienna, Austria

INVITED PAPER

ED-01. Experimental Visualizations of Three-Dimensional Skyrmion Topological Transition and Stabilization Pathways. *M. Henderson*[1]
1. Neutron Scattering Division, Oak Ridge National Laboratory, Oak Ridge, TN, United States

Magnetic skyrmions define a unique class of topological object, characterized by a multi-directional twisting of spins which nucleate and annihilate on magnetic singularities, called Bloch points. In three dimensions, their stabilization into flexible tubes introduces enhanced dimensionalities and emergent phenomena which endows them with superior functionalities as information carriers in future spintronic devices. Unfortunately, a lack of bulk probes has prevented their complete characterization in three dimensions, inhibiting the development of modern skyrmion device architectures. Here, we present the first experimental visualizations of three-dimensional skyrmion topological transition pathways across nucleation and annihilation phase trajectories in a bulk triangular lattice skyrmion host. Reconstructed spin textures uncover novel skyrmion formation pathways through field-perpendicular tubes, while stabilized tubes exhibit exotic periodic modulations and coexistences with unprecedented three-dimensional topological objects. We explore skyrmion phase energetics and topological stability through tunable magnetic field sequences, highlighting skyrmion nucleation and ordering phenomena through conical and defect-mediated pathways, respectively. Our results provide unprecedented access to three-dimensional topological phenomena which overturn previous architectures of skyrmion nucleation and manipulation, reimagining spintronic frameworks through new control pathways and encoding structures.

CONTRIBUTED PAPERS

ED-02. Skyrmion, stripe domain, and sublattice skyrmion spin textures in synthetic antiferromagnetic multilayers. C. Barker[1,2], R. Aboljadayel[1], R. Peremadathil-Pradeep[3], K. Fallon[4], Z. Tumbleson[5], S.A. Morley[6], S. McVitie[4], H.J. Hug[3] and *C. Marrows*[1] *1. School of Physics and Astronomy, University of Leeds, Leeds, United Kingdom; 2. National Physical Laboratory, Teddington, United Kingdom; 3. EMPA, Dübendorf, Switzerland; 4. SUPA, School of Physics and Astronomy, University of Glasgow, Glasgow, United Kingdom; 5. University of California Santa Cruz, Santa Cruz, CA, United States; 6. Advanced Light Source, Lawrence Berkley National Laboratory, Berkeley, CA, United States*

Synthetic antiferromagnets (SAFs) make use of indirect exchange coupling across metal spacer layers to achieve an antiferromagnetic ground state in a magnetic multilayer. SAFs are predicted to [1], and experimentally show [2] reduced skyrmion Hall angle [3] and fast skyrmion [4] and DW motion [5]. Here we study spin-textures generated during the field-induced transition [6] from the SAF to saturated state. Here we report on studies of SAFs based on the repeat unit [Pt(8)/ CoB(16)/ Ru(7)/ Pt(8)/ CoFeB(10)/ Ru(7)], with layer thicknesses in Å. Our chosen multilayer stack has ultrathin CoB layers so properties are dominated by interfaces, indirect exchange coupling acoss Ru spacers to enforce AF ordering, Pt layers to induce perpendicular anisotropy (PMA) and Dzyaloshinskii-Moriya interaction (DMI). The CoB and CoFeB layer thicknesses were chosen to give moments are equal and thus cancel owing to the coupling through the Ru spacers, thus forming the sublattices of a SAF structure with zero net moment. We report the evolution of spin textures in our perpendicularly magnetised SAF Ta/Ru/{Pt/CoFeB/Ru/Pt/CoB/Ru}x5}Ta multilayers as observed by Lorentz microscopy, soft x-ray resonant magnetic scattering, and magnetic force microscopy. The hysteresis loop in Fig. 1(a) shows a region of zero moment around remanance (the SAF state) and magnetic saturation above about 80 mT. The magnetization in the all of the layers is laterally uniform in this state, as it is when magnteically saturated by an applied field. As we reduce the field from saturation we observe a variety of spin textures during the transition to the SAF ground state by MFM: conventional skyrmions with core opposed to field direction (Fig. 1(b)); stripe domain states(Fig. 1(c)); and skyrmions with a core along the field direction (Fig. 1(d)). Weak Lorentz contrast, the presence of scattering features only when tuning to the Fe L3 edge (not Co) lead us to conclude that these exist in only one sublattice and hence present a 3D character: the other sublattice is uniform.

[1] J. Barker and O Tretiakov, Phys. Rev. Lett. 116, 147203 (2016); X. Zhang et al., Nature Commun. 7, 10293 (2016); F. Büttner, et al., Sci. Rep. 8, 4464 (2018); E. Haltz, CHM et al., arXiv:2309.03697. [2] W. Legrand, et al., Nature Mater. 19, 34 (2020); R. Juge et al., Nature Commun. 13, 4807 (2022). [3] T. Dohi et al., Nature Commun. 10, 5153 (2019). [4] V. T. Pham et al., Science 384, 307 (2024). [5] C. E. A. Barker et al., J. Phys. D: Appl. Phys. 56, 425002 (2023). [6] C. E. A. Barker et al., Phys. Rev. B 109, 134437 (2024). [7] M. J. Benitez, CHM et al., Nature Commun. 6, 8957 (2015).

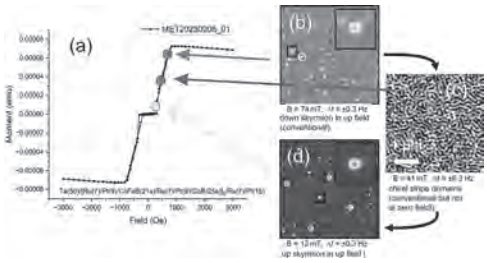

SAF behavior under field. (a) Hysteresis loop measured by SQUID-VSM. MFM images at (b) 74 mT; (c) 41 mT; and (d) 12 mT. The reversal of the skyrmion core polarity is evident in panels (b) and (d).

ED-03. Topological spin-torque diode effect in skyrmion-based magnetic tunnel junctions. *R. Tomasello*[1], B. Fang[2], M. Carpentieri[1], E. Darwin[3], W. Jiang[4], X. Zhang[5], G. Finocchio[6] and Z. Zeng[2]
1. Politecnico di Bari, Bari, Italy; 2. Nanofabrication Facility, Suzhou Institute of Nano-Tech and Nano-Bionics, Chinese Academy of Sciences, Suzhou, China; 3. Swiss Federal Laboratories for Materials Science and Technology, EMPA, Dubendorf, Switzerland; 4. State Key Laboratory of Low-Dimensional Quantum Physics and Department of Physics, Tsinghua University, Beijing, China; 5. Physical Science and Engineering Division, King Abdullah University of Science and Technology, Thuwal, Saudi Arabia; 6. University of Messina, Messina, Italy

Magnetic skyrmions have reached a great success as information carriers in next-generation of data storage (racetrack memory)[1], and unconventional computing[2]. The recent room-temperature observation of skyrmions in magnetic tunnel junctions (MTJs)[3–5] has opened the way to the combination of Spintronics and Topology to expand the possible applications of

skyrmions. However, a skyrmion-based microwave technology has been only theorized up to now[6], and the electrical manipulation of skyrmions in MTJs has been used only to prove static properties[3,4,5]. Here, we design MTJ devices hosting room-temperature magnetic skyrmions with a diameter <300nm[7]. We perform experimental spin-torque diode measurements, by which we identify three modes (Fig. 1): 1 mode at frequency of 4 GHz and low field, which we refer to the skyrmion breathing mode; 1 mode at frequency of 5 GHz at high field with red-shift we associate to the MTJ reference layer (RL) dynamics; and 1 mode at frequency of 8 GHz at high field with blue shift we relate to the uniform dynamics of the free layer (FL). To confirm the origin of these modes, we use two strategies. One is to grow an MTJ without the skyrmion-hosting layer. The second is to perform state-of-the art micromagnetic simulations of the whole device magnetic stack with layer dependent parameters and direct and forward spin-transfer torque in the free and reference layer of the MTJ respectively. By engineering the material properties of the MTJ free layer and of the skyrmionic layer, the simulations confirm, both qualitatively and quantitatively, the different origin of the three modes. Work supported by the projects PRIN 2020LWPKH7, PRIN 20222N9A73 funded by the Italian Ministry of Research, PE0000021, "Network 4 Energy Sustainable Transition – NEST", funded by the European Union – NextGenerationEU, Mission 4 Component 2 Investment 1.3 - Call for tender No. 1561 of 11.10.2022 of Ministero dell'Università e della Ricerca (MUR) (CUP C93C22005230007), and by PETASPIN association (www.petaspin.com).

[1] B. He, R. Tomasello et al. Nano Lett. 23, 9482 (2023). [2] S. Li et al. Mater. Horizons 8, 854 (2021). [3] S. Kasai et al. Appl. Phys. Express 12, 83001 (2019). [4] Y. Guang et al. Adv. Electron. Mater. 9, 2200570 (2023). [5] S. Chen et al. Nature 627, 522 (2024). [6] G. Finocchio et al. Appl. Phys. Lett. 107, 262401 (2015). [7] B. Fang, R. Tomasello et al. arXiv:2405.10753 (2024).

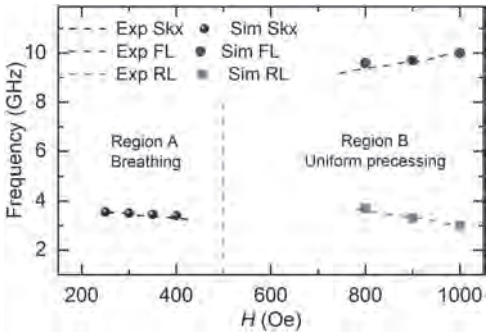

Figure 1: Frequency of the excited modes as a function of the applied field H for tilted of θ = 30° from the z-axis. Symbols are micromagnetic simulations results, dashed lines are experimental results.

ED-05. Realizing Quantitative Quasi-Particle Modeling of Skyrmion Dynamics in Arbitrary Potentials. *M.A. Brems*[1], T. Sparmann[1], S.M. Fröhlich[1], J. Rothörl[1], F. Kammerbauer[1], E.M. Jefremovas[1], O. Farago[2], M. Kläui[1] and P. Virnau[1] *1. Institute of Physics, Johannes Gutenberg University Mainz, Mainz, Germany; 2. Biomedical Engineering Department, Ben Gurion University of the Negev, Be'er Sheva, Israel*

Magnetic skyrmions in thin films can be treated as two-dimensional magnetic quasi-particles that are exciting as model systems for fundamental physics as well as for novel devices due to their topologically enhanced stability and easy electrical manipulability. Skyrmions have been shown to exhibit thermal diffusion in a spatially inhomogeneous effective energy landscape that stems from pinning effects caused by random material defects [1, 2]. We experimentally exploit the diffusion of magnetic skyrmions in arbitrary pinning potentials to realize fully quantitative Thiele model simulations on experimentally relevant large length and time scales [3]. We overcome the previous limitation of Thiele model simulations to qualitative predictions as we ascertain the two key missing parameters for calibration of the experimental and simulation time scales and current-induced forces. Simultaneously, we demonstrate how to leverage skyrmion systems to finally study diffusion in arbitrary potentials experimentally, as our complete spatial map of skyrmion pinning energy enables the treatment of such systems in the Lifson-Jackson framework [4]. Current-induced spin-torques act as a bias to the diffusion as they result in a deterministic force acting on the skyrmion [5]. We develop a method to isolate the effects of the pinning potential and the current-induced bias by exploiting their different behavior under current inversion. Thereby, we can directly ascertain the total force acting on the skyrmion at a given current density. Compared to conventional methods, we determine current-induced forces via stochastic dynamics rather than deterministic motion. Consequently, our method is sensitive even to ultra-low current-densities (~10^6 A/m^2) at which the issue of skyrmion deformation, which only occurs at higher current densities and makes the analysis less robust [5], is effectively avoided.

[1]: J. Zázvorka et al., Nat. Nanotechnol. 14, 658 (2019) [2]: R. Gruber et al., Nat. Commun. 13, 3144 (2022) [3]: M. A. Brems et al., Under Review, (2024) [4]: S. Lifson and J. L. Jackson, J. Chem. Phys. 36, 2410 (1962) [5]: K. Litzius et al., Nat. Electron. 3, 30–36 (2020)

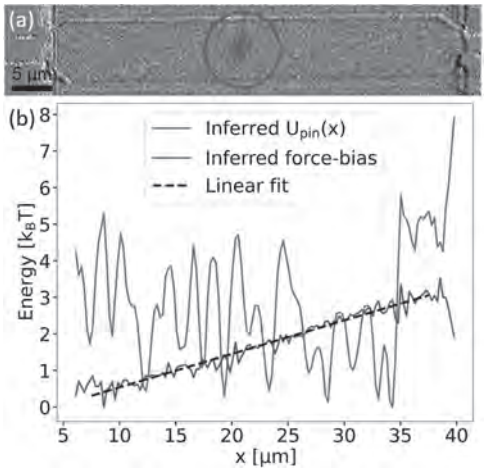

Fig. 1 a) Kerr-microscopy image of the experimental setup. A single skyrmion (dark spot highlighted by a red circle) is confined within a wire with contacts at both ends. b) The inferred pure pinning-potential and current-bias for a fixed current density. The slope of the current bias (dashed line) is equal to the force on the skyrmion.

ED-06. Slow Ordering Kinetics of Magnetic Skyrmions. N. Liyanage[1], N. Tang[1], R. Dally[2], L. Quigley[1], C.C. Buchanan[1], G. Shu[3], N. Butch[2], K. Krycka[2], M. Bleuel[2], J. Borchers[2], L. DeBeer-Schmitt[4] and *D.A. Gilbert*[1] *1. University of Tennessee, Knoxville, TN, United States; 2. National Institute of Standards and Technology, Gaithersburg, MD, United States; 3. National Taiwan University, Taipei, Taiwan; 4. Oak Ridge National Laboratory, Oak Ridge, TN, United States*

Magnetic skyrmions are topologically protected, nanoscale whirls of the spin configuration that tend to form hexagonally ordered arrays. As a topologically non-trivial structure, the nucleation and annihilation of the skyrmion, as well as the interaction between skyrmions, varies from conventional magnetic systems. Recent works have suggested that the ordering kinetics in these materials occur over millisecond or longer timescales, which is unusually slow for magnetic dynamics. The current work investigates the skyrmion ordering kinetics, particularly during lattice formation and destruction, using time-resolved small angle neutron scattering (TR-SANS). Evaluating the time-resolved structure and intensity of the neutron diffraction pattern reveals the evolving real-space structure of the skyrmion lattice and the timeframe of the formation. Measurements were performed on three prototypical B20 skyrmion materials: MnSi, (Fe,Co)Si, and Cu2OSeO3. To probe lattice formation and destruction kinetics, the system was prepared in the stable skyrmion state, and then a square-wave magnetic field modulation

was applied. The measurements show that the skyrmions form ordered domains very quickly, with a significant distribution in lattice parameters, which then converge to the final structure; the results confirm the slow kinetics, with formation times between 10 ms and 99 ms. Comparisons are made between the measured formation times and the fundamental material properties, suggesting the ordering temperature, saturation magnetization and magnetocrystalline anisotropy may be driving the timeframes. Micromagnetic simulations were also performed and support a scaling of the kinetics with sample volume, an artifact which is caused by the reconciling of misaligned domains.

WLNC Liyanage et al., Nanoscale 16, 10715 (2024) T. Nakajima, et al., Phys. Rev. B, 98, 014424 (2018) L. J. Bannenberg, et al., Phys. Rev. B, 96, 184416 (2017) C. J. Glinka, et al., J. Appl. Cryst. 53, 598 (2020)

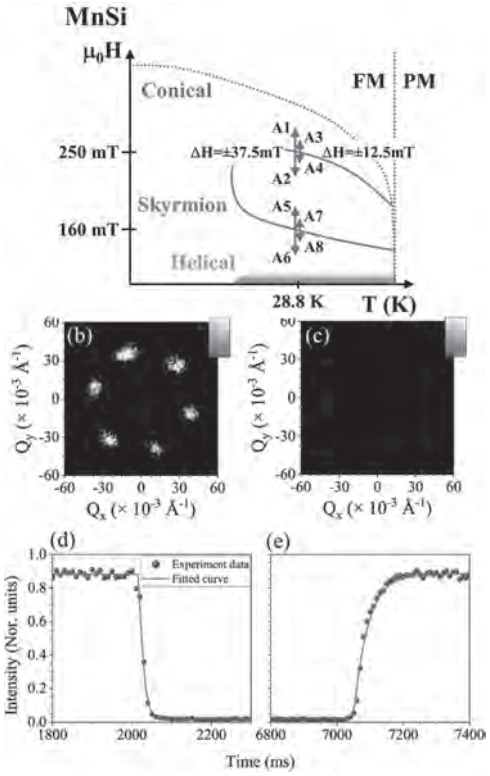

ED-07. Curvature-induced enhancement of thermal stability of skyrmions. A.G. Silva-Junior[1], J.M. Fonseca[1], J.I. Costilla[1], M.M. Amaral[1], *A. Riveros*[2] and V. Carvalho[1] *1. Departamento de Física, Universidad Federal de Visosa, Visosa, Brazil; 2. Escuela de Ingeniería, Universidad Central de Chile, Santiago, Chile*

Geometry plays an important role in the nucleation, stabilization, and manipulation of magnetization patterns within magnetic nanoelements [1-3]. This work analyzes the impact of curvature on the thermal stability of skyrmions hosted on Gaussian-shaped nanoshells. The curvature is controlled by τ, which sets the bump height and convexity type: $\tau > 0$ indicates convexity (Fig. 1a), while $\tau < 0$ signifies concavity (Fig. 1b). Based on annihilation processes observed in flat nanoparticles, three distinct annihilation processes - skyrmion contraction, expansion, and displacement towards the nanodot border - are analyzed. We show that the curvature-induced effective interactions significantly alter the energy barriers associated with these annihilation processes. The changes in the energy are related to the relative alignment between the skyrmion core and the direction normal to the surface, highlighting the presence of favorable and unfavorable chiralities for skyrmion stabilization in curved nanodots. By mapping the energy landscape of the system as a function of skyrmion radius and position (Fig. 1c), we identified saddle points that delineate skyrmion and uniform states. We show that unlike the obtained for flat nanodots [4], the lowest energy barrier reaches values that ensure their lifetimes at room temperature to months without external additional stimuli, in curved nanodots before thermal fluctuations annihilate it (Fig. 2). This underscores the impact of curvature on the dynamic behavior and thermal stability of skyrmions and suggests new opportunities for designing and controlling magnetic devices based on skyrmions [5]. Acknowledgements: This work was financed by the Coordenação de Aperfeiçoamento de Pessoal de Nível Superior Brasil (CAPES) Finance Code 001, by CNPq (Grant Nos. 309032/2021-0 and 305256/2022-0), FAPEMIG and by CIP2022036.

[1] A. M. Turner, V. Vitelli and D. R. Nelson, Reviews of Modern Physics., Vol. 82, p.1301 (2010). [2] T. Lopez-Leon, V. Koning and K. B. S. Devaiah, Nature Physics., Vol. 7, p.391 (2011). [3] D. D. Sheka, Applied Physics Letters., Vol. 118, p.230502 (2021). [4] A. Riveros, F. Tejo and J. Escrig, Physical Review Applied., Vol. 16, p.014068 (2021). [5] A. G. Silva Jr., J. M. Fonseca and J. I. Costilla, Journal of Applied Physics., Vol. 136, p.043902 (2024).

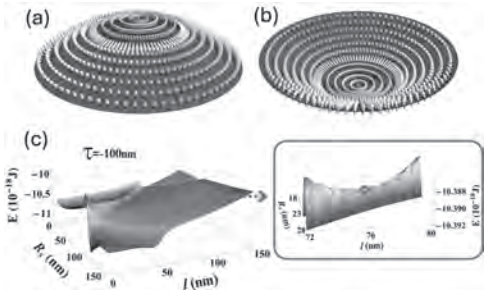

Skyrmion within a convex (a) and a concave (b) Gaussian surface. (c) Skyrmion energy as a function of the skyrmion radius (R_s) and position (l) in the concave nanoshell. The saddle point is identified in the zoomed-in view.

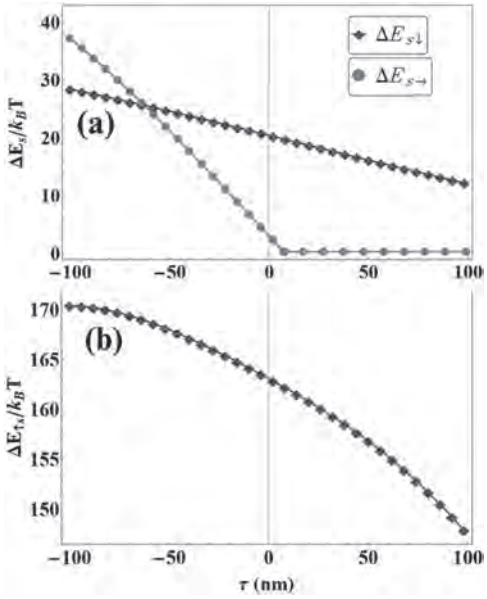

Energy barriers for skyrmion annihilation as a function of τ, illustrating scenarios of core contraction(s↓), displacement (s→), and expansion (s↑).

ED-09. Topological Melting of a 2D Skyrmion Lattice. R. Gruber[1], M.A. Brems[1], F. Kammerbauer[1], J. Rothörl[1], O. Farago[2], P. Virnau[1] and *M. Kläui*[1,3] *1. Physics, Johannes Gutenberg University Mainz, Mainz, Germany; 2. Biology, Ben Gurion University of the Negev, Beer Sheva, Israel; 3. Center for Quantum Spintronics, NTNU, Trondheim, Norway*

Magnetic skyrmions are chiral, quasi-particle spin textures with exciting properties resulting from their topology. Beyond technological applications, skyrmions in thin films have attracted significant interest for exhibiting 2D phase behavior – different from 3D systems [1-4]. Between the solid state with long-range translational order and the unordered liquid state, 2D systems can show the intermediate hexatic phase with quasi-long-range orientational but lacking translational order [5]. Skyrmions in thin films are of special interest since they exhibit Brownian diffusion with rich dynamics, which is directly accessible in real-time and real-space by Kerr microscopy [2,3]. However, pinning effects [4] have been a main factor preventing dense skyrmion arrangements from crystallization to a solid state [3]. Here, we report the observation of topological melting of an ordered skyrmion lattice into a liquid while reducing the skyrmion density by tuning the external magnetic field. We use magnetic field oscillations to reduce pinning effects [6] and achieve improved average ordering. However, remaining pinning effects confine polycrystalline skyrmion domains randomly, thus hampering a true single crystal formation. To obtain external control over the domain dimensions, we tailor the boundary conditions by confining the system to a hexagonal shape. In this finite system, the ordering becomes so robust that the ordering criteria of the solid, hexatic and liquid phase from the continuous KTHNY theory are realized. Our system then allows us the resolve the transitions between the phases as melting and condensation processes and the resulting lattice dynamics in real time and real space. Skyrmion lattices are thus ideal to observe melting of 2D lattices on finite scales. We identify the role of the energy landscape and the topological nature of the phases by following skyrmions individually to elucidate the topological two-step melting.

[1] P. Huang, T. Schönenberger, M. Cantoni, L. Heinen, A. Magrez, A. Rosch, F. Carbone, and H. M. Rønnow, Melting of a Skyrmion Lattice to a Skyrmion Liquid via a Hexatic Phase, Nature Nanotechnology 15, 9 (2020). [2] J. Zázvorka et al., Thermal Skyrmion Diffusion Used in a Reshuffler Device, Nat. Nanotechnol. 14, 658 (2019). [3] J. Zázvorka, F. Dittrich, Y. Ge, N. Kerber, K. Raab, T. Winkler, K. Litzius, M. Veis, P. Virnau, and M. Kläui, Skyrmion Lattice Phases in Thin Film Multilayer, Advanced Functional Materials 30, 2004037 (2020). [4] R. Gruber et al., Skyrmion Pinning Energetics in Thin Film Systems, Nat. Commun. 13, 1 (2022). [5] M. Kläui et al., Freezing and melting skyrmions in 2D, Nat. Nanotechnol. 15, 726 (2020) [6] R. Gruber et al., 300-Times-Increased Diffusive Skyrmion Dynamics and Effective Pinning Reduction by Periodic Field Excitation, Adv. Mater. 35, 2208922 (2023)

INVITED PAPER

ED-08. Experimental observation of current-driven antiskyrmion sliding in stripe domains. *Y. Zhang*[1] *1. Chinese Academy of Science, Institute of Physics, Beijing, China*

Magnetic topological spin textures such as skyrmions and antiskyrmions emerge as promising candidates for information carriers in high-density memory, neuromorphic computing applications, and logic components due to their unusual topological properties and emergent electromagnetic phenomenon. Here, we have experimentally demonstrated the current-driven dynamics of antiskyrmions in a $Mn_{1.4}PtSn$ chiral magnet at room temperature, without the requirement for an external magnetic field. This is realized by embedding antiskyrmions in helical stripe domains, which naturally provide one-dimensional (1D) straight tracks along which the antiskyrmion sliding can be easily launched with low current density and without transverse deflection from the antiskyrmion Hall effect. The dominant factors for the higher mobility of antiskyrmion embedded in helical stripes are discussed, manifesting the contribution of increased driving force and averaged pinning potential as unravelled by micromagnetic simulation and the collective pinning theory. We further show that our method can be applied to the sliding motion of merons in stripe domains. Our findings provide clear demonstration and comprehensive understanding of antiskyrmion gliding along natural stripe tracks under a low current density.

Zhidong He, ... Shi-Zeng Lin*, Ying Zhang* and Baogen Shen, Nature Materials, 2024, https://doi.org/10.1038/s41563-024-01870-8

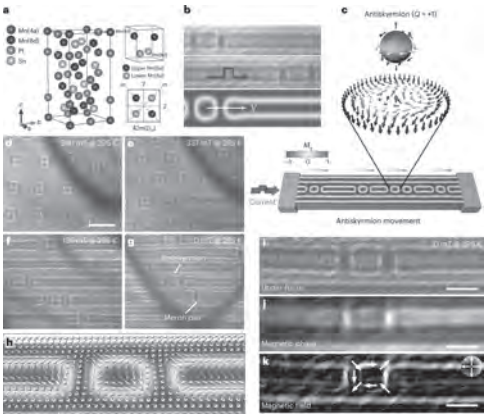

Fig. 1 Realization of room-temperature antiskyrmions with different magnetization states and their straight current-driven behavior along the naturally helical stripes at zero field in $Mn_{1.4}PtSn$ chiral magnet.

CONTRIBUTED PAPERS

ED-10. Multidimensional Soliton Lattices in Iron-Gadolinium Thin Films. *C.C. Buchanan*[1], N. Tang[1], N. Liyanage[2], S. Montoya[3], E. Fullerton[3], D.A. Gilbert[1,2] and L. DeBeer-Schmitt[4] *1. Materials Science and Engineering, University of Tennessee, Knoxville, TN, United States; 2. Physics and Astronomy, University of Tennessee, Knoxville, TN, United States; 3. Center for Memory and Recording Research, University of California San Diego, La Jolla, CA, United States; 4. Neutron Scattering Division, Oak Ridge National Laboratory, Oak Ridge, TN, United States*

Skyrmions are swirling magnetic spin structures characterized by complete rotation of the magnetic moments across the skyrmion diameter such that the moments at the core and edge are oriented in opposite out of plane directions. Continuous wrapping of the spin moments makes skyrmions topologically non-trivial and gives them stability in a range of temperatures and fields [1]. This stability makes skyrmions attractive for applications in data storage and spintronic devices, particularly since skyrmions are much smaller than modern magnetic domains in hard drives and require only a fraction of the energy to be moved [2]. We have used small angle neutron scattering (SANS) to characterize skyrmion lattices in Fe/Gd thin film heterostructures. Due to the layered film structure this system has perpendicular magnetic anisotropy which allows stabilization of room temperature skyrmion lattices. We have analyzed three magnetic states using SANS, including an ordered stripe state, an ordered skyrmion lattice state, and a disordered skyrmion lattice state. Using the SANS data we were able to see the length scale and periodicity of each of the states as they were deformed by the applied field. The q spacing, intensity, and period of the stripe state and disordered skyrmions follows chiral soliton theory under positive applied field. Under the negative field, none of the states align with the soliton theory. In contrast to previous work [3], we see smooth (as opposed to stepwise) changes in q spacing and intensity with applied field. Additionally, we see third order peaks in the intensity measurements of the ordered stripe state.

[1] T. B. Winkler et al., Phys. Rev. Appl. 16 (2021). [2] F. Büttner, I. Lemesh, and G. Beach. Scientific reports 8, no. 1 (2018): 4464. [3] A. Singh et al. Phys. Rev. B 105, no. 9 (2022): 094423.

ED-11. Propagation and interaction of skyrmions in antiferromagnets.
S. Komineas[1,2] and G. Theodorou[1,2] *1. Mathematics and Applied Mathematics, University of Crete, Heraklion, Greece; 2. Foundation for Research and Technology, Heraklion, Greece*

Skyrmions in antiferromagnets (AFM) with the Dzyaloshinskii-Moriya (DM) interaction are expected to exist for essentially the same reasons as in DM ferromagnets (FM). We show that AFM skyrmions can be traveling as solitary waves with velocities up to a maximum value that depends on the DM parameter [1]. Their configuration is found numerically and we explore their particle-like character by giving the energy-momentum dispersion based on exact relations. The solitonic behavior of skyrmions in AFM is in stark contrast to the dynamical behavior of their FM counterparts. We further consider head-on collision events between two skyrmions [2]. We find numerically that the result of the collision depends on the initial velocity of the skyrmions. For small velocities, the skyrmions are shrinking as they are approaching, as shown in the figure, they subsequently bounce back eventually acquiring almost their initial speed. For larger velocities, the skyrmions approach each other and shrink until they become singular points that are eventually annihilated. An analytical description indicates two processes that play a major role in determining the dynamics: (a) the Interaction potential between the skyrmions that depends on the distance between them and also on their size, and (b) the internal potential energy of the skyrmions that is known to give breathing oscillations of the skyrmion size [3]. Analytical relations for both processes are obtained and the numerical results are reproduced by a collective coordinate approach that takes into account the varying skyrmion size. The possibility of skyrmion annihilation through breathing-type oscillations is explained based on the internal potential energy whose features are analytically derived. It leads to a prediction of skyrmion collapse and subsequent annihilation events due to excitation of large amplitude breathing oscillations [3]. We find the counter-intuitive property that the skyrmion possesses a nonzero kinetic energy at the instance of its annihilation. We acknowledge support from the E.U. Horizon Europe Programme under Grant Agreement No. 101119608 (project TOPOCOM).

[1] S. Komineas and N. Papanicolaou, SciPost Phys. 8, 086 (2020). [2] G. Theodorou, S. Komineas, arXiv.org:2305.13515 (2023). [3] S. Komineas and P. E. Roy, Phys. Rev. Res. 4, 033132 (2022).

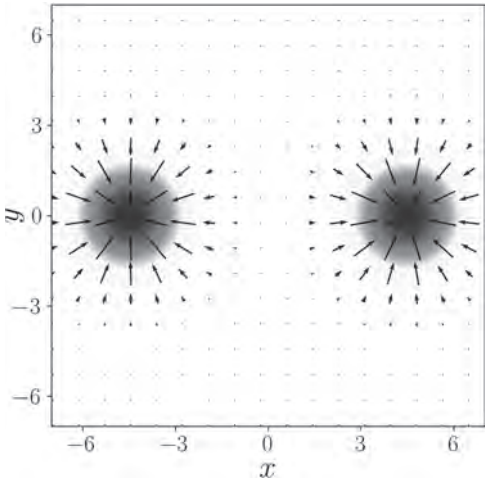

Two skyrmions initially set in a head-on collision course.

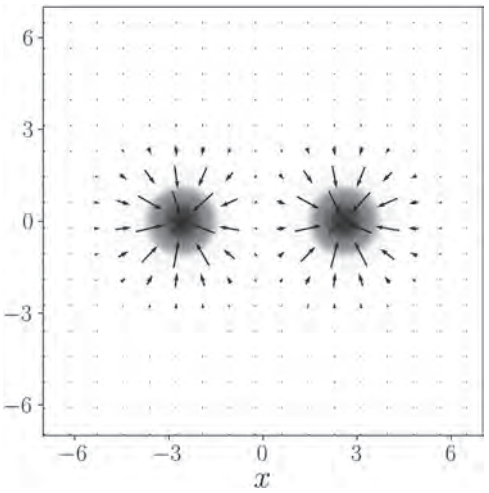

The skyrmions decelerate and also shrink in size as they approach. They eventually stop momentarily and bounce back.

Session EE
SPINTRONIC DEVICES II: ANTIFERROMAGNETISM, VOLTAGE-CONTROLLED EFFECTS, DOMAIN WALL LOGIC AND PROBABILISTIC SWITCHING

Fei Xue, Chair
University of Alabama at Birmingham, Birmingham, AL, United States

CONTRIBUTED PAPERS

EE-01. Toggle SOT-MRAM Architecture with Self-Terminating Write Operation. *E.C. Usih*[1], N. Hassan[1], A.J. Edwards[1], F. García Sánchez[2], P. Khalili[3] and J.S. Friedman[1] *1. Electrical and Computer Engineering, The University of Texas at Dallas, Richardson, TX, United States; 2. Departamento de Fisica Aplicada, Universidad de Salamanca, Salamanca, Spain; 3. Electrical and Computer Engineering, Northwestern University, Evanston, IL, United States*

Toggle spin-orbit torque (SOT) driven magnetoresistive random-access memory (MRAM) with perpendicular anisotropy has a simple material stack and is more robust than directional SOT-MRAM [1]. However, a read-before-write operation is required to utilize the toggle SOT-MRAM for directional switching, which threatens to increase the write delay. To resolve these issues, we propose a high-speed memory architecture for toggle SOT-MRAM that includes a minimum-sized bit cell and a custom read-write driver. The proposed driver induces an analog self-terminating SOT current that functions via an analog feedback mechanism that can read and write the toggle SOT-MRAM bit cell within a single clock cycle. As the read and write operations are completed within 492ps this memory architecture provides the first viable solution for non-volatile L3 cache. Compared to other works [2] based on the area-energy-delay-product metric, our work achieves about a 2.8x improvement on the next best alternative.

[1] N. Hassan, S. P. Lainez-Garcia, F. Garcia-Sanchez and J. S. Friedman, "Toggle spin-orbit torque {MRAM} with perpendicular magnetic anisotropy," *IEEE Journal on Exploratory Solid-State Computational Devices and Circuits,* vol. 5, no. 2, pp. 166-172, 2019. [2] F. Oboril, R. Bishnoi, M. Ebrahimi and M. B. Tahoori, "Evaluation of Hybrid Memory Technologies Using SOT-MRAM for On-Chip Cache Hierarchy," *IEEE Transactions on Computer-Aided Design of Integrated Circuits and Systems,* vol. 34, no. 3, pp. 367-380, 2015.

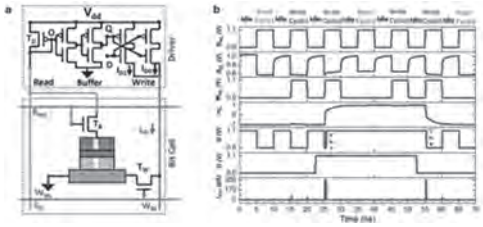

Figures showing a) The proposed bit cell structure, b) Functionality of the bit cell.

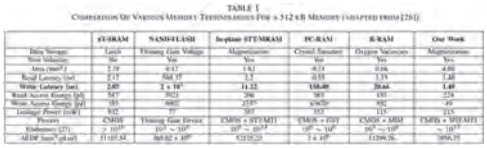

EE-02. Withdrawn

EE-03. Precise quantification of ferromagnetic exchange in thin films via Brillouin light scattering. *J.J. Wisser*[1], M. Tanksalvala[1], J.S. Harms[2], M. Kiechle[1], W.K. Peria[1], R.A. Duine[3], J.M. Shaw[1] and H.T. Nembach[1,4] *1. NIST, Boulder, CO, United States; 2. University of Konstanz, Konstanz, Germany; 3. Utrecht University, Utrecht, Netherlands; 4. University of Colorado, Boulder, CO, United States*

The exchange stiffness constant, A_{ex}, is a fundamental property of magnetic materials, but there are significant challenges to accurately measure this property in technologically-relevant magnetic ultra-thin films. As such, models predicting magnetic RAM (MRAM) performance suffer from significant inaccuracies and require the fabrication of fully functional devices for testing. This is a slow and expensive process, and a method for quantifying exchange at the film level would greatly reduce the industry's reliance on such a trial-and-error process. We have developed an experimental technique for precisely determining A_{ex} at the film level utilizing Brillouin light scattering (BLS) spectroscopy. [1] Through the use of a unique optical setup based on [2], we are able to map the full spin wave dispersion in both the Damon-Eshbach (DE) and backward volume (BV) geometries without moving the laser on the sample surface (see Figure 1). This ensures a uniform magnetic field at the laser spot and minimizes the drift in laser focus between angles. We combine our powerful experimental technique with a closed form solution for the spin wave dispersion in both the DE and BV geometries to cut down on computationally-expensive simulations and assumptions often utilized in exchange calculations. An example measured dispersion curve with the fit for the exchange is shown in Figure 2 for a 10 nm thick permalloy (Py) film. By simultaneously fitting the DE and BV branches we are able to obtain excellent agreement between experiment and theory with an exchange stiffness of 8.0 pJ/m. This work dramatically increases the throughput of magnetic exchange measurements and provides more precise inputs for modeling of spintronic device performance.

[1] G. A. Riley, J. M. Shaw, T. J. Silva, and H. T. Nembach, Applied Physics Letters 120, 112405 (2022). [2] D. A. Bozhko, H. Y. Musiienko-Shmarova, V. S. Tiberkevich, A. N. Slavin, I. I. Syvorotka, B. Hillebrands, and A. A. Serga, Phys. Rev. Res. 2, 023324 (2020). [3] B. Kalinikos and A. Slavin, Journal of Physics C: Solid State Physics 19, 7013 (1986).

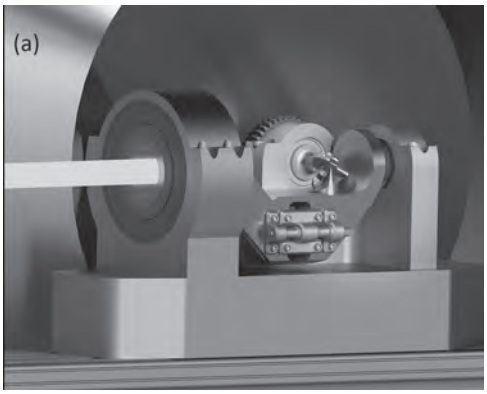

Figure 1. Experimental setup for measuring ferromagnetic exchange. The laser spot does not move as the sample is rotated.

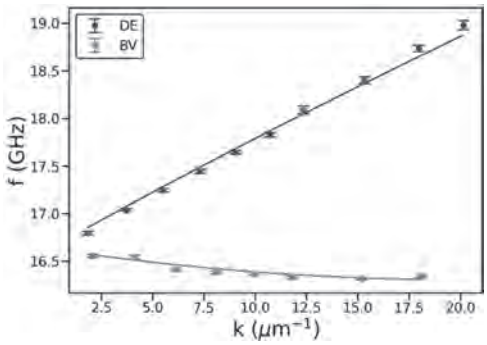

Figure 2. Dispersion in both the DE (blue) and BV (red) configurations for a 10 nm Py film. The fits are shown in the solid lines. Note: these fits are to the dispersion by Kalinikos and Slavin. [3]

EE-04. Error-Free and Current-Driven Synthetic Antiferromagnetic Domain Wall Memory Enabled by Channel Meandering. *P. Zhang*[1,3], W. Haensch[1,3], C. Phatak[1,2] and S. Guha[1,3] *1. Materials Science Division, Argonne National Laboratory, Lemont, IL, United States; 2. Materials Science and Engineering, Northwestern University, Evanston, IL, United States; 3. Pritzker School of Molecular Engineering, University of Chicago, Chicago, IL, United States*

We propose a new type of multi-bit and energy-efficient magnetic memory based on current-driven, field-free, and highly controlled domain wall motion [1]. A meandering domain wall channel with precisely interspersed pinning regions provides the multi-bit capability of a magnetic tunnel junction. The magnetic free layer of the memory device has perpendicular magnetic anisotropy and interfacial Dzyaloshinskii-Moriya interaction, so that spin-orbit torques induce efficient domain wall motion. Using micromagnetic simulations, we find two pinning mechanisms that lead to different cell designs: two-way switching and four-way switching. The memory cell design choices and the physics behind these pinning mechanisms are discussed in detail. Furthermore, we show that switching reliability and speed may be significantly improved by replacing the ferromagnetic free layer with a synthetic antiferromagnetic layer. Switching behavior and material choices will be discussed for the two implementations.

[1] P. Zhang, W. Haensch, C. M. Phatak, and S. Guha, arXiv:2405.18261 (2024)

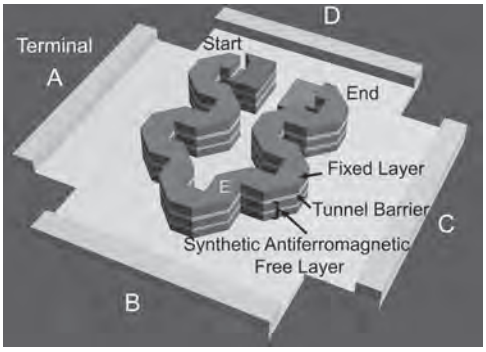

Conceptual schematic of 4-way switching device. Write currents are sent through the four side terminals, and the magnetic domain wall is moved by the spin-orbit torque in discrete steps, following the meandering domain wall channel. Each turn requires changing the write current direction, resulting in a precise control of the domain wall location. Read is done simply by a magnetic tunnel junction.

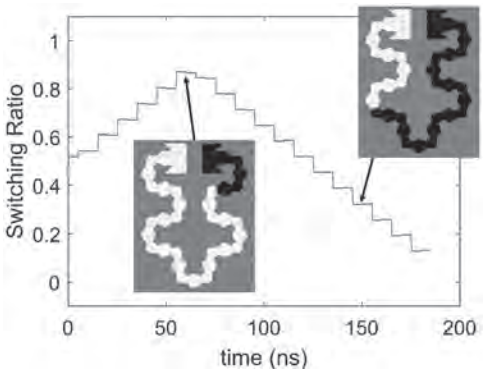

Testing of the 4-way switching device using micromagnetic simulation. The inset figures are the magnetic states of the upper layer during the operation. By controlling applied current directions, the device resistance states can be tuned freely and reversibly.

EE-05. Effects of Temperature on the Performance of STT-MRAM Devices with Different Thicknesses. S. Mangadahalli Siddaramu[1], M. Hindenberg[1], M. Wagner-Reetz[1], J. Müller[2] and *J. Chatterjee*[1]
1. Fraunhofer Institute for Photonic Microsystems, CNT, Dresden, Germany; 2. GlobalFoundries Fab1 LLC and Company KG, Dresden, Germany

Spin-transfer torque magnetoresistive random-access memory (STT-MRAM) is being investigated for automotive applications. To qualify for automotive applications, it is important to understand the thermal variation of retention and switching characteristics of STT-MRAM, devices such as thermal stability factor (Δ), critical switching current (I_C), and STT efficiency. Therefore, we have investigated these characteristics as a function of temperature from -25 °C to 150 °C for four different storage layer (SL) thicknesses. Primarily, Δ values have been extracted by using both macrospin (MS), and domain wall nucleation and propagation (DW) models and their thermal variation have been modeled accordingly [1]. Fig.1 shows a significant decrease in Δ with increasing temperature. At higher temperatures, Δ converges to a similar value for all SLs' thicknesses, suggesting pronounced thermal variation with thicker SL. As a result, the Blocking temperature is larger for thicker SL. The Gilbert damping constant (α), domain wall width (δ_w), and domain wall energy density (σ_w) have also been extracted from the DW model and shown in Fig.2. The σ_w decreases monotonically with temperature indicating a decrease in the stability of the domain walls at higher temperatures (Fig. 2). Therefore multidomain nucleation could potentially be the dominant reversal mechanisms, at higher temperature [2]. The thermal variation of I_C, α, TMR, and also the practical switching efficiency will also be discussed. This study will, therefore, bring further insight into understanding the STT-MRAM performance in a wide temperature range which is important for automotive applications.

[1] J. M. Iwata-Harms et al., Scientific Reports, Vol. 8, p.14409 (2018).
[2] G. Vértesy and I. Tomáš, J Appl Phys, Vol. 93, p.4040-4044 (2003).

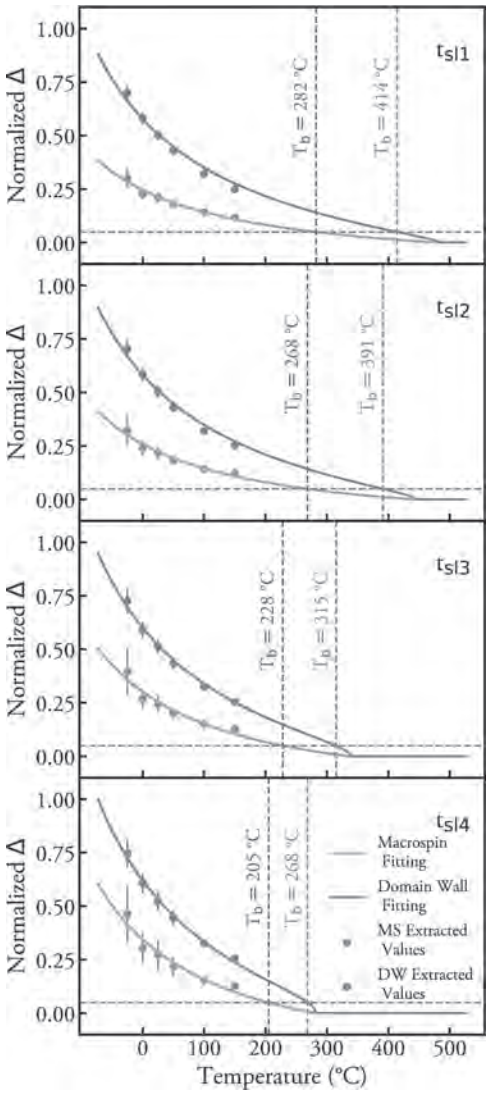

Average of Δ from 120 MTJ cells as a function of temperature. Extrapolation to higher temperature gives blocking temperature (T_b)

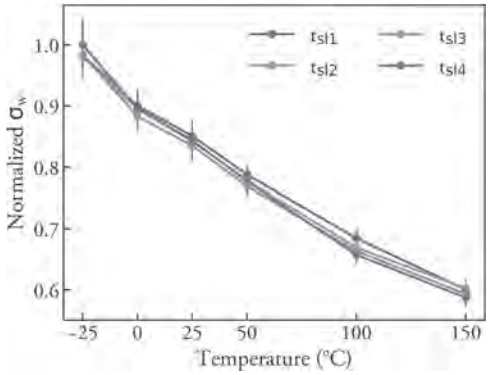

Average σ_w as a function of temperature.

EE-06. Withdrawn

EE-07. Ultrafast Coupled Domain Wall Motion in Mn_2Au-Permalloy. S. Jenkins[1], *T. Wagner*[2*], O. Gomonay[2] and K. Everschor-Sitte[1] *1. Faculty of Physics and Center for Nanointegration Duisburg-Essen (CENIDE), University of Duisburg-Essen, Duisburg, Germany; 2. Institute of Physics, Johannes Gutenberg University Mainz, Mainz, Germany*

Mn_2Au is a very attractive antiferromagnet due to its high temperature stability, THz dynamics and metallic conductivity. Additionally, the Néel vector in Mn_2Au can be controlled electrically, because Néel spin-orbit torques are allowed by symmetry and have been observed experimentally [1]. By using atomistic spin dynamics simulations and a phenomenological model, we show that interface exchange coupling in the antiferromagnetic-ferromagnetic hybrid system Mn_2Au-Permalloy enables the controlled reading, writing, and manipulation of antiferromagnetic domains. The domain wall patterns in the Mn_2Au are imprinted on the permalloy and, therefore, allow for the indirect imaging of the Néel order parameter [2]. Furthermore, it has been observed that the strong interface exchange coupling leads to coupled dynamics in the bilayer system [3]. Our simulations show that the coupled domain wall structures in Mn2Au-Py bilayers can be manipulated by either acting on the Néel order parameter via Néel spin-orbit torques or by acting on the magnetization (the ferromagnetic order parameter) via magnetic fields. In both cases, we predict ultrahigh domain wall speeds on the order of 8.5 km/s, as shown in Fig. 2 [4]. Thus, employing a thin ferromagnetic layer has the potential to easily control the Néel order parameter in antiferromagnets even where Néel spin-orbit torques are forbidden by symmetry. The controlled manipulation of the antiferromagnetic order parameter paves the way for the development of high-density storage and efficient computing technologies working in the THz regime.

[1] S. Reimers et al., Nat. Commun. 14, 1861 (2023). [2] S. P. Bommanaboyena et al., Nat. Commun. 12, 6539 (2021). [3] H. Al-Hamdo, T. Wagner et al., Phys. Rev. Lett. 131, 046701 (2023). [4] S. Jenkins, T. Wagner et al., Phys. Rev. B 109, 224431 (2024).

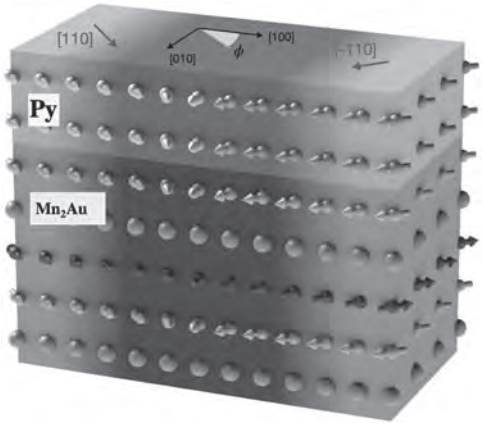

Fig. 1: Schematic diagram of a 90-degree domain wall in an Mn_2Au-Permalloy bilayer. The Mn_2Au layer is shown in blue and is capped by the Permalloy shown in gray.

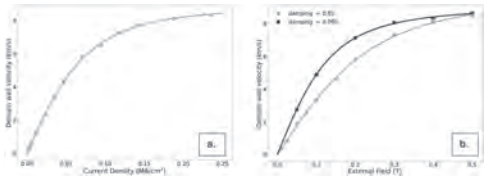

Fig. 2: a. Domain wall velocity of the coupled bilayer magnetization as a function of the applied current. b. Domain wall velocity of the coupled bilayer magnetization as a function of the applied field.

EE-08. Energy-Efficient Manipulation of Stochastic Switching Behavior by Voltage Controlled Exchange Coupling in Magnetic Tunnel Junctions. *J. Qi*[1], B. Zink[1], O. Benally[1], D. Zhang[1], Y. Lv[1], D. Lyu[1] and J. Wang[1] *1. University of Minnesota, Minneapolis, MN, United States*

Magnetic tunnel junctions (MTJs) have emerged as promising candidates for generating stochastic signals, making them ideal for stochastic computing (SC) and neuromorphic computing due to their inherent randomness[1]. By leveraging the competition between spin transfer torque (STT) and the external magnetic field, the average switching rate and output level can be independently adjusted[2,3], thus addressing device variation issues from the fabrication process. However, the energy consumption increases significantly when biasing all MTJs in an array network due to each device's limited current spin conversion efficiency, undermining the overall benefits. In this study, we validate the existence of voltage-controlled exchange coupling (VCEC) in MTJ with a single SAF structure by analyzing the switching polarization and the spin torque property. The effect is utilized instead of STT to maintain the tunability of stochastic switching, achieving energy consumption as low as ~100nW, which is roughly ten times lower than in previous dual-biased STT-MTJ studies. The switching rate, on the other hand, could be manipulated by the VCMA effect by two orders of magnitude. The current impact from the underneath layer is found to be added linearly on top, mainly due to the thermal effect. A simplified model is provided to underscore the necessity of the VCEC effect. Our results demonstrate the feasibility of using VCEC in dual-biased MTJs, marking a significant advancement for MTJ applications in stochastic computing.

1. Zink, B. R., Lv, Y. & Wang, J.-P. *IEEE Journal on Exploratory Solid-State Computational Devices and Circuits* 8, 173–184 (2022). 2. Zink, B. R. & Wang, J.-P. *IEEE Magnetics Letters* 12, 1–5 (2021). 3. Zink, B. R., Lv, Y. & Wang, J.-P. *Journal of Applied Physics* 124, 152121 (2018).

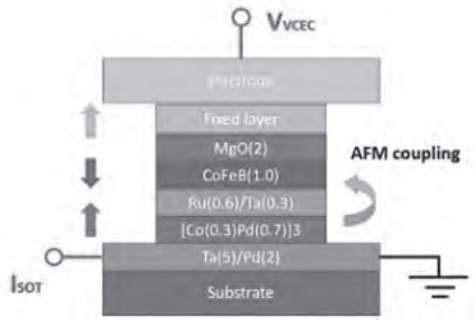

Fig. 1. Schematic illustration of the MTJ stack structure with the integration of a SAF free layer.

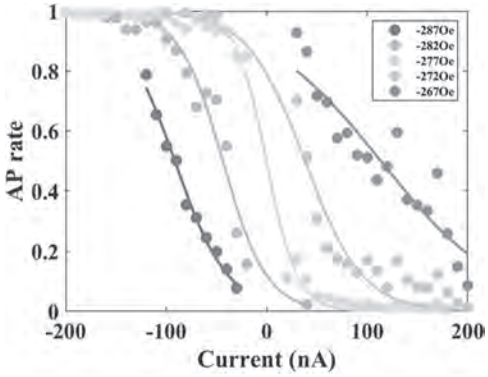

Fig. 2. AP rate manipulated by the current under different magnetic fields.

EE-09. Numerical analysis of vortex spin torque oscillator with an additional free layer. *K. Horizumi*[1], T. Chiba[2,3] and T. Komine[1] *1. Graduate School of Science and Engineering, Ibaraki University, Hitachi, Japan; 2. Department of Applied Physics, Graduate School of Engineering, Tohoku University, Sendai, Japan; 3. Frontier Research Institute for Interdisciplinary Sciences(FRIS), Tohoku University, Sendai, Japan*

A vortex spin torque oscillator (VSTO) is a nanoscale device generating high-frequency signals [1]. There is a threshold current to establish a stable motion of vortex core depending on both the damping and the magnetostatic potential [2]. In this study, we investigate the effect of the potential shape on vortex core dynamics by changing the free layer structure with an additional ferromagnetic disk. Thiele equation describing the vortex core dynamics in the free layer was numerically solved [3,4]. The VSTO consists of a ferromagnetic/non-magnetic multilayer, as shown in the inset of Fig.1. The free layer has a radius of 187.5 nm and a thickness of 5 nm. An additional disk attached to the free layer can deform the potential shape. The additional disk has a thickness of 1.5 nm, and the radius is 20 or 40 nm. Figure 1 shows the micromagnetically calculated potentials with/without the additional disk. With the additional disk, the potential energy has two minima at both the center of the free layer and the edge of the additional disk. Figure 2 shows the vortex core displacement as a function of drive current when the initial core position is set to the disk center. The threshold current changes with the additional disk and is significantly reduced when the radius is 20 nm. This calculation results agree with the threshold currents estimated by fitting the sum of quadratic and quartic functions near the disk center [4]. This is because the threshold current density almost depends on the quadratic curvature of the potential. On the other hand, when the initial position s (t = 0) of the vortex core is set to the potential minimum at the additional disk edge, the vortex motion is hooked in the potential energy minimum, and stable gyration is kept out, even if the current density is much less than the threshold current density. The vortex dynamics for various potentials will also be discussed in the presentation.

[1] V. S. Pribiag, I. N. Krivorotov, G. D. Fuchs, P. M. Braganca, O. Ozatay, J. C. Sankey, D. C. Ralph, and R. A. Buhrman, *Nat. Phys.* Vol. 3, pp. 498-503 (2007). [2] K. Yu. Guslienko, X. F. Han, D. J. Keavney, R. Divan, and S. D. Bader, *Phys. Rev. Lett*. Vol. 96, 67205 (2006). [3] A. V. Khvalkovskiy, J. Grollier, A. Dussaux, Konstantin A. Zvezdin, and V. Cros, *Phys. Rev. B* Vol. 80, 140401(R) (2009). [4] Y. Imai, K. Nakajima, S. Tsunegi, and T. Taniguchi, *Sci. Rep.* Vol. 12, 21651 (2022).

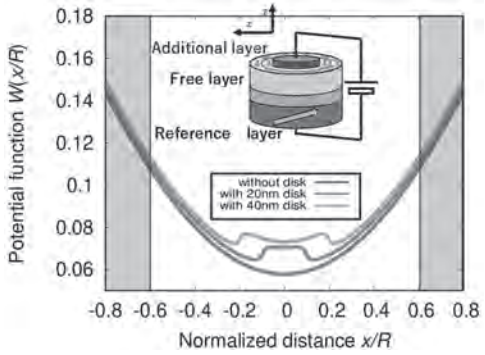

Fig1. Potentials for micromagnetic models. The inset illustrates VSTO with a double-disk free layer.

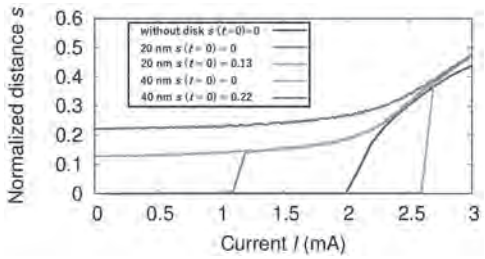

Fig2. Current dependences of normalized vortex core distance s for various potentials, where s (t =0) is the initial core distance far from the disk center.

EE-10. Withdrawn

EE-11. Voltage-Gated Spin-Orbit Torque for Selective Data Writing in IrMn-Based Perpendicular Magnetic Tunnel Junction Arrays.
Z. Liu[1], W. Li[1], S. Peng[1], J. Lu[1], J. Liu[1], X. Li[1], S. Lu[1], Y. Otani[2] and W. Zhao[1] *1. Fert Beijing Institute, School of Integrated Circuit Science and Engineering, Beihang University, Beijing, China; 2. Institute for Solid State Physics, University of Tokyo, Tokyo, Japan*

Magnetic random-access memory (MRAM) holds immense potential as a mainstream memory technology of the next generation owing to its fast speed, non-volatility, and high density. SOT-induced deterministic perpendicular magnetization switching necessitates an in-plane external field, which limits its practical application. One approach involves changing the SOT channel material from heavy metals to antiferromagnets, where field-free SOT switching can be achieved by leveraging in-plane exchange bias (EB) [1-3]. Nevertheless, challenges such as high power consumption and the three-terminal requirement still hinder the energy efficiency and integration density of SOT-MRAM. One potential solution is to introduce the voltage-controlled magnetic anisotropy (VCMA) effect, which can reduce the energy barrier during SOT switching, and thus reduce power consumption [4-7]. In this paper [8], we first experimentally demonstrate field-free voltage-gated SOT switching in IrMn-based perpendicular magnetic tunnel junctions (MTJs) with a diameter of 80 nm, and we fabricate a memory array that integrates multiple MTJs on a shared IrMn strip, as illustrated in Fig. 1. When a gate voltage of 0.8 V is applied to an MTJ in the array, the SOT critical current density decreases by 70%, resulting in a substantial 91% reduction in total power consumption (Fig. 2a). In addition, we plot the cumulative distribution function (CDF) and probability density function (PDF) of the switching probability for MTJ2, showing a clear operation window for selective writing (Fig. 2b). Through this voltage-gated SOT switching, selective data writing in the MTJ array is accomplished. Moreover, the endurance of more than 1×10^{12} and the write error rate below 8×10^{-5} are achieved. These findings demonstrate the high performance of voltage-gated SOT devices and contribute to its practical application in MRAM.

[1] Y. W. Oh, S. Chris Baek, Y. M. Kim, Nat. Nanotechnol., Vol. 11, no. 10, p. 878-884(2016) [2] S. Peng, D. Zhu, W. Li, Nat. Electron., Vol. 3, no. 12, p. 757-764(2020) [3] W. Li, S. Peng, J. Lu, Phys. Rev. B, Vol. 103, no. 9, Art. no. 094436(2021) [4] S. Peng, J. Lu, W. Li, in Proc. IEEE Int. Electron Devices Meeting, p. 28.6.1-28.6.4(2019) [5] J. Lu, W. Li, J. Liu, Appl. Phys. Lett., Vol. 122, no. 1, Art. no. 012402 (2023) [6] Y. C. Wu, K. Garello, W. Kim, Phys. Rev. Appl., Vol. 15, no. 6, Art. no. 064015(2021) [7] K. Cai, S. Van. Beek, S. Rao, in Proc. Symp. VLSI Circuits, p. 375-376(2022) [8] W. Li, Z. Liu, S. Peng, IEEE Electron Device Lett., Vol. 45, no. 5, p. 921–924(2024).

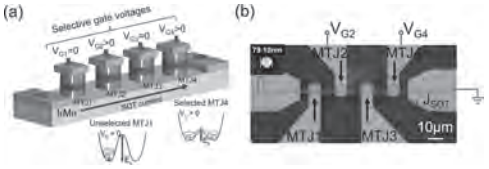

Fig. 1 (a)Schematic of selective switching operation in IrMn-based pMTJ array. (b)An optical image of the pMTJ array with diameters of 80 nm and its electrical measurement setup.

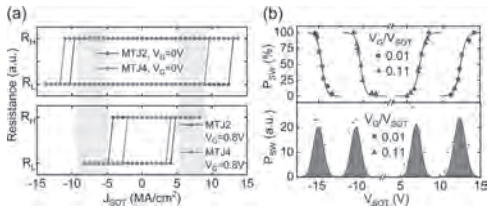

Fig. 2 (a)Voltage-gated SOT switching of MTJ2 and MTJ4 with a pulse width of 40 ms. (b)CDF and PDF of voltage-gated SOT switching probability for MTJ2 with a pulse width of 15 ns.

EE-12. Towards an Ising Machine Simulator based on Spintronic Oscillator Digital Twins.
C. Chopin[1], A. Hakam[1], M. Ibarra Gomez[1], L.D. Buda-Prejbeanu[1], S. de Wergifosse[2], F. Abreu Araujo[2], E. Aubouin[3], L. Hutin[3], F. Badets[3], P. Talatchian[1] and U. Ebels[1] *1. Univ. Grenoble Alpes, CEA, CNRS, Grenoble-INP, SPINTEC, Grenoble, France; 2. Institute of Condensed Matter and Nanosciences, Université Catholique de Louvain, Louvain-la-Neuve, Belgium; 3. Univ. Grenoble Alpes, CEA, LETI, Grenoble, France*

Ising machines (IMs) are gaining interest as specialized systems designed to efficiently solve widespread combinatorial optimization problems (COPs). IMs leverage the Ising model, where a network of binary-valued spins with specific spin coupling interactions seeks its lowest energy state or ground state, which represents the COP solution. Several hardware implementations [1] are under study; ours leverages the stochastic IM's cost-free thermal noise, exploring complex energy landscapes while escaping local minima. Spin-torque nano-oscillators (STNOs) are perfect candidates for such stochastic IMs [2, 3]: (i) when injection-locked to a microwave signal at twice its frequency, the STNO's phase Φ becomes binarized; (ii) thermal noise stochastically triggers transitions between those two phase states, see fig.1; (iii) several controllable coupling mechanisms exist to adjust Ising spin interactions. While these requirements have been verified experimentally [2], setting coupling weights that encode a COP in IMs remains challenging. Indeed, they depend significantly on the STNO's output power, which varies from device to device, possibly impacting COP resolution. Therefore, it is crucial to fully understand the impact of those couplings on the dynamics of an STNO array. This calls for a digital twin to precisely model experimental STNO output signals within large arrays. Ongoing experiments [2] make use of vortex-based STNOs, that can be well modeled by the stochastic Thiele equation approach (sTEA) [4, 5]. We successfully reproduced experimental results where the phase α of an additional rf signal Λ emulating an STNO array controls the probability of being preferentially in one of the two phase states, see fig.2. Combining these sTEA results with our experimental data-driven approach [5] is key to build an IM simulator close to experimental challenges. It is a major asset to determine experimental couplings and finally solve a given COP.

[1] Y. Zhang, Y. Deng, Y. Lin *et al.*, Micromachines 13(7), 1016 (2022) [2] N.-T. Phan, N. Prasad, A. Hakam *et al.*, Phys. Rev. Applied 21, 034063 (2024) [3] D. I. Albertsson, M. Zahedinejad, A. Houshang *et al.*, Appl. Phys. Lett. 118, 112404 (2021) [4] A. A. Thiele, Phys. Rev. Lett. 30, 230 (1973) [5] F. Abreu Araujo, C. Chopin, S. de Wergifosse, ArXiv, 2206.13596 (2022)

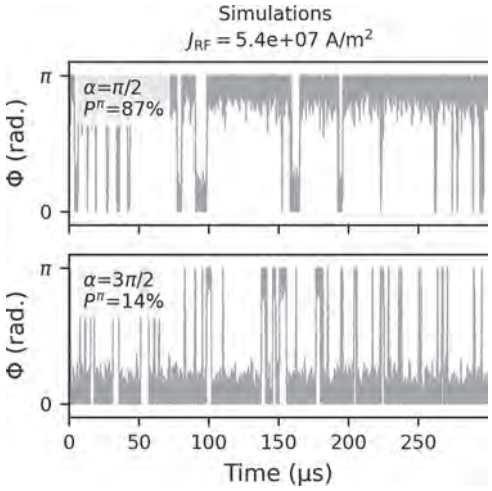

Fig.1: Simulated STNO phase Φ-time traces for Λ with a fixed amplitude J_{RF} and different phases α.

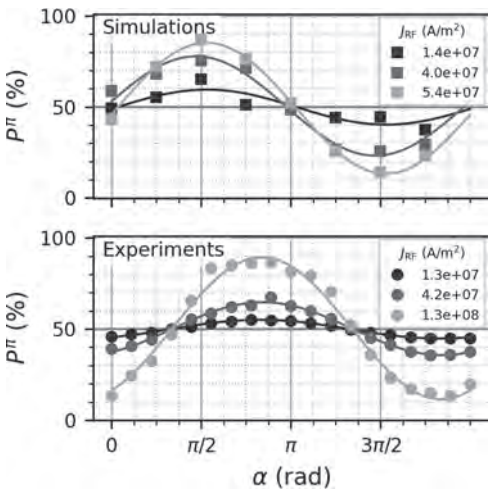

Fig.2: Probability $P^π$ of being in the π state vs. Λ phase α for different amplitudes J_{RF}. Simulations (a) reproduce nicely experiments (b). Solid lines are sinusoidal fits.

Now VP23-10

EE-14. Large spin orbit torque induced by high temperature annealed BiSb topological insulator on oxidized Si substrates. *H. Ho*[1], W. Li[1], S. Takahashi[2], Y. Hirayama[2], Y. Kato[2] and H.N. Pham[1] *1. Electrical and Electric Engineering, Tokyo Institute of Technology, Meguro, Japan; 2. Samsung Japan Corp., Yokohama, Japan*

BiSb topological insulator is a promising spin-orbit torque (SOT) material thanks to its colossal spin Hall angle θ_{SH} [1] and high electrical conductivity σ [2] for ultrafast [3] and ultralow power [4] SOT memory devices. Although hisgh crystal quality BiSb thin films have been studied so far on single crystalline substrates [2-7], realizing high quality of BiSb with high θ_{SH} and high σ on amorphous Si substrate is mandatory for realistic SOT spintronic applications. Furthermore, high temperature endurance during fabrication is also critical for integration with CMOS electronics. In this work, we aim to realize BiSb topological insulator thin films with high θ_{SH} and high σ on thermally oxidized Si/SiO_x substrate using oxide buffer layers and high temperature post annealing. We first deposited a thick TiO_x layer which can block O_2 migration from SiO_x to BiSb during annealing and an optional TaO_x oxide buffer layer on Si/SiO_x substrates. Both oxide layers are deposited by reactive sputtering of a Ti and Ta target. Next, we sputtered a 10 nm-thick BiSb on top of the oxide layers and a 3-nm Ti protection layer. After cooling the substrate in ultrahigh vacuum to room temperature, we deposited ferromagnetic multilayers for SOT evaluation. The schematic structure of sample A-TiO_x/BiSb/Ti/Pt/Co/Pt, sample B-TiO_x/TaO_x/BiSb/Ti/Ta/CoFeB/MgO and their θ-2θ X-ray diffraction (XRD) spectra are shown in Fig. 1. Single phase BiSb (012) and (011) are confirmed in sample A and B, respectively. By high temperature annealing, we improved BiSb conductivity up to 1.1×10^5 $\Omega^{-1}m^{-1}$ and achieved a relatively high θ_{SH} ~ 1.7 – 5. In Fig.2, we demonstrate type-z SOT magnetization switching of CoFeB in sample B with a low BiSb current density of 2.2 MA/cm² which is an order smaller than that of heavy metals. Our results show that it is possible to achieve high performance BiSb on Si/SiO_x substrates by employing oxide buffer layers and high temperature annealing.

1. N. H. D. Khang, Y. Ueda, P. N. Hai, Nature Mater. 17, 808 (2018). 2. Y. Ueda, N. H. D. Khang, K. Yao, et al., Appl. Phys. Lett. 110, 062401 (2017). 3. N. H. D. Khang, T. Shirokura, T. Fan, et al., Appl. Phys. Lett. 120, 152401 (2022). 4. H. Wu, A. Chen, P. Zhang, et al., Nature Commun. 12, 6251 (2021). 5. K. Yao, N. H. D. Khang, P. N. Hai, J. Cryst. Growth 511, 99 (2019). 6. T. Fan, M. Tobah, T. Shirokura, et al., Jpn. J. Appl. Phys. 59, 063001 (2020). 7. K. Ueda, Y. Hadate, K. Suzuki, et al., Thin Solid Films 713, 1383 (2020).

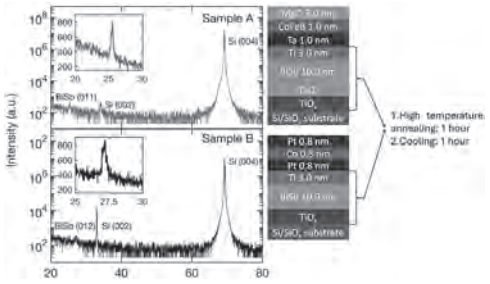

Schematic structure and wide-view (main figures) and narrow-view (insets) XRD spectra of the stacks.

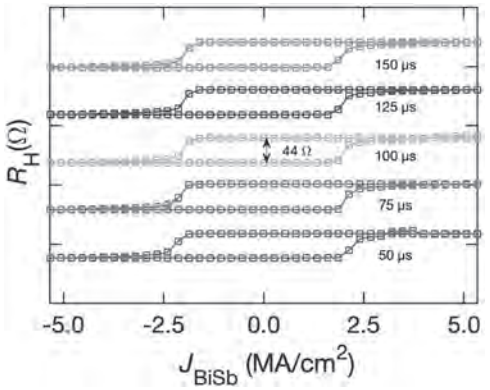

Type-z SOT magnetization switching of CoFeB in sample B by low BiSb current density.

EE-15. Magnetic and Transport Properties of Altermagnetic Candidate GdAlSi. *J. Shi*[1], N. Fokkens[1] and F. Xue[1] *1. Physics, University of Alabama at Birmingham, Birmingham, AL, United States*

Since experiment observations strongly support emerging altermagnetic band structure in metallic RuO_2 and semiconductor MnTe, a broad class of materials are predicted to be altermagnets, which has induced significant interest in the condensed-matter research community. Compared to materials with standard ferromagnetic (FM) and antiferromagnetic (AFM) orders, altermagnets exhibit strong time-reversal symmetry-breaking response and spin-polarization accompanied by antiparallel collinear magnetic order with vanishing net magnetization. In this work, we focus on the magnetic and electronic properties of a promising altermagnet candidate: GdAlSi. Its crystalline forms a body-centered tetragonal structure, belonging to the non-centrosymmetric

space group $I4_1md$ (109). Here, we consider three magnetic configurations in GdAlSi: non-magnetic, FM, and AFM. Our *ab initio* calculations confirm the presence of a collinear AFM ordering in GdAlSi as the most stable ground state among these three configurations. The band structure without spin-orbit coupling (SOC) reveals the emergence of a hole pocket along Γ-$\sum^1$ path, suggesting a semi-metallic nature. With the incorporation of SOC in the band structure, we confirm that the degeneracy occurs along the Γ-Z^1 path in reciprocal space due to C_{4z} rotational symmetry. GdAlSi has been discovered to host many Weyl points near the Fermi level, and it is beneficial to investigate how the spin-orbit torque (SOT) effect is enhanced near these Weyl points. Due to the global inversion symmetry breaking in GdAlSi, the SOT is also symmetry-allowed and can be efficient in driving the Néel order dynamics. We calculate the SOT for two magnetization sublattices in GdAlSi using the ab initio tight-binding Hamiltonian after Wannierization. We will discuss how the crystal symmetry and existence of Weyl points affect the spin-orbit torque properties.

[1]Cartesian coordinate of high symmetry points: Γ (0, 0, 0); $\sum$ (-0.6969784122 0.0000000000 -0.4333231264); Z (0.0000000000 0.0000000000 0.4333231264)

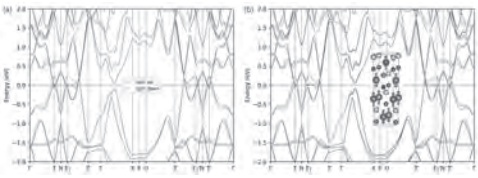

Figure 1. The bulk band structures without SOC (a) and with SOC (b) for AFM configuration. The AFM orders are shown in the inset figure in (b).

EE-13. Investigation and design of Magnetic Tunnel Junction Molecular Spintronic Devices based Solar Cells via Monte Carlo Simulation.

O. Kirkland[1] and P. Tyagi[1] *1. University of the District of Columbia, Washington, DC, United States*

This talk will present the results of a theoretical study towards the design of a spin-based photovoltaic array. The construction of this device will advance the established research on the molecular tunnel junction molecular spintronic devices (MTJMSD). These devices are made by bridging two ferromagnetic electrodes (FMs) with an insulating barrier by chemically bonding the exposed edges with a paramagnetic molecule. [1] These devices exhibit high levels of exchange coupling at room temperature, high stability, reproducibility, and are made from simple photolithographic methods out of cheap earth-abundant materials. [2] Recently, MTJMSDs have been shown to generate a reproducible spin-based photocurrent. [3], [4] A solar cell made of such a device, will be significantly cheaper than those made of silicon and may allow absorption of wavelengths that are not accessible with silicon. This theoretical study used Monte Carlo calculations to produce a 3d Heisenberg model of spin orientation of the two FMs. An example of this is shown in Fig. 1. This representation is the result of 300 million iterations of the calculation of the magnetic moment for each atom of the electrodes in the model, as well as the sum magnetic moment of the device overall. The time evolution of this is shown in Fig 2. This method has previously been used to successfully model the exchange coupling of MTJMSDs. [5], [6] In this study we have controlled for the exchange coupling through the bridging molecule, the temperature, as well as the anisotropy and size of the bottom electrode. Our aim was to answer the questions: What is the effect of increasing the number of molecules in the junction, by increasing the length of the exposed edge, on exchange coupling? What effect does anisotropy have on designing reproducible electrodes. Our future work will focus on determining the ideal distance between adjacent electrodes. The answers to these questions are critical towards the design of a large scale MTJMSD based solar cell.

[1] P. Tyagi, D. Li, S. M. Holmes, J Am Chem Soc., vol. 129, p. 4929 (2007) [2] P. Tyagi, C. Baker, and C. D'Angelo, Nanotechnology, vol. 26, p. 305602 (2015) [3] P. Tyagi and C. Riso, Nanotechnology, vol. 30, p. 495401, (2019) [4] M. Savadkoohi, D. Gopman, P. Suh, ACS Appl Electron Mater, vol. 5, p. 3333 (2023) [5] M. Savadkoohi; Dahal, B. R.; Grizzle, A.;J. Magn. Magn. Mater. vol. 529, p. 167902 (2021) [6]Dahal, B. R.; Savadkoohi, M.; Grizzle, A.; Scientific Reports, vol. 12, p. 5721 (2022)

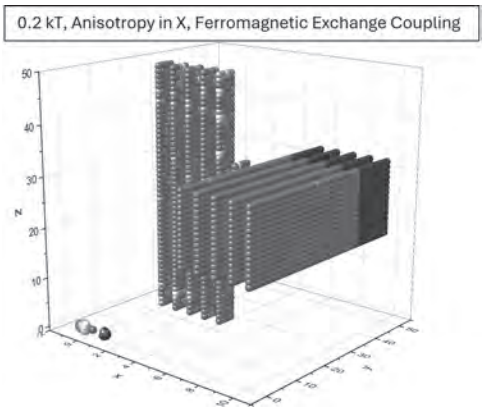

Fig. 1. 3d Heisenberg Model Plot of Magnetic Moment in the X direction of the 50 by 15 bottom electrode.

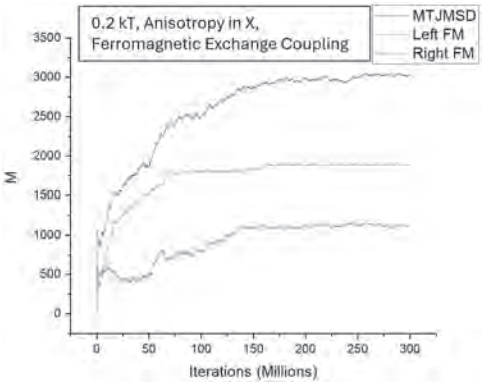

Fig. 2. Magnetic moment *(M)* vs. simulation count of the MTJMSD, left and right ferromagnetic electrodes.

Session EF
SOFT AND HARD MAGNETS

Xiaoyu (Criss) Zhang, Co-Chair
Northeastern University, Boston, MA, United States
Ravi Gautam, Co-Chair
National Institute for Materials Science (NIMS), Tsukuba, Japan

CONTRIBUTED PAPERS

EF-01. High-temperature phase transition during hydrogen disproportionation of Nd-Fe-B alloys. G. Bacchetta[1], F. Orlandini Keller[1], C. Flament[1], L. Magnier[1], *S. Luca*[1], J. Garandet[1] and C. Rado[1]
1. Univ. Grenoble Alpes, CEA LITEN, Grenoble, France

Hydrogen induced phase transformation of Nd-Fe-B alloys has been extensively studied, especially for the development of Hydrogenation Disproportionation Desorption Recombination (HDDR), allowing to obtain sub-micrometric grains while keeping the crystallographic orientation of the precursor grains, resulting in highly coercive and anisotropic powders. Several phase diagrams, exploring temperature and H_2 pressure, were proposed [1-3] to describe the domains of stability of the disproportionated and recombined states. While a wide range of H_2 pressure was explored in the literature, temperatures above 900 °C are rarely reported. In addition, most of the studies focus on simple ternary Nd-Fe-B alloys. In this study, we report on the microstructural evolution and phase equilibria of high-temperature hydrogenation-disproportionation of Nd-Fe-B strip cast alloys, widely used for high performance magnet manufacturing. The upper domain of the phase diagram of such alloys under hydrogen is, to the best of our knowledge, not reported in the literature. Structural and microstructural characterizations of disproportionated NdFeB based Dy-free and Dy-rich powders showed the presence of an hydrogen induced phase transition at high temperatures, implying the presence of four thermodynamically stable phases: REH_{2+x}, α-Fe, $RE_2Fe_{14}B$ and $RE_{1.1}Fe_4B_4$. To the best of our knowledge, this is the first published evidence of such a phase transition, which seems to be influenced by the presence of the Heavy RE element Dy. This study covers the phase transition temperatures, microstructures and kinetics aspects for two compositions of strip cast alloys typically used for Nd-Fe-B magnet fabrication. The main finding of this work is the occurrence of a phase transition at high temperatures leading to the formation of four thermodynamically stable phases. This happens before the expected recombination into $RE_2Fe_{14}B$, similarly to what is documented for Co-rich alloys [4-5]. The stability domain of these phases and their chemical compositions is discussed regarding the initial composition of the alloy.

[1] H. Nakamura, K. Kato, D. Book, S. Sugimoto, M. Okada, and M. Homma, *J. Magn. Soc. Jpn.*, vol. 23, no. 1_2, pp. 300–305, 1999, [2] T. Horikawa, M. Matsuura, S. Sugimoto, M. Yamazaki, and C. Mishima, *IEEE Trans. Magn.*, vol. 51, no. 11, pp. 1–4, Nov. 2015, [3] M. Szymanski, B. Michalski, E. Jezierska, M. Leonowicz, and Z. Miazga, *Journal of Rare Earths*, vol. 34, no. 8, pp. 843–849, Aug. 2016, [4] M. Uehara, P. Choi, T. Tomida, H. Tomizawa, S. Hirosawa, and Y. Maehara, *IEEE Trans. Magn.*, vol. 31, no. 6, pp. 3632–3634, Nov. 1995, [5] T. Tomida, P. Choi, Y. Maehara, M. Uehara, H. Tomizawa, and S. Hirosawa, *Journal of Alloys and Compounds*, vol. 242, no. 1–2, pp. 129–135, Sep. 1996

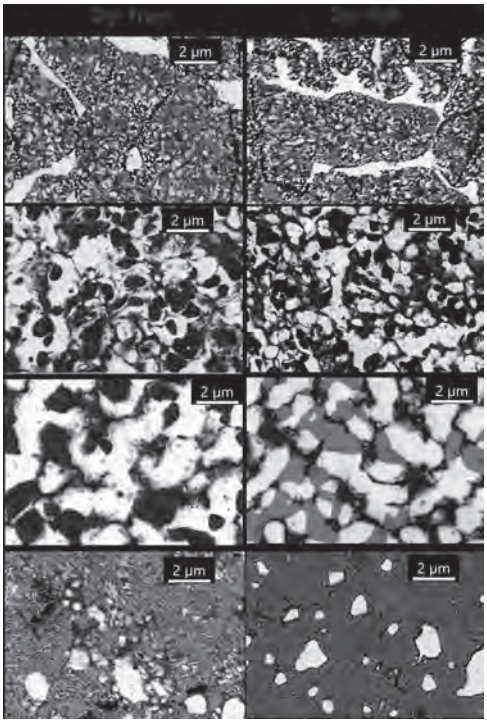

EF-02. Controlling High Dense Particle Settling for 3D Printing of Functional Objects by Vat Photopolymerization. C.E. Frank[1], *E.M. Palmero*[1], C.M. Montero[1] and A. Bollero[1] *1. Group of Permanent Magnets and Applications, IMDEA Nanociencia, Madrid, Spain*

The use of advanced fabrication such as additive manufacturing (AM) for fabricating devices attracts much interest in many high-tech sectors such as energy, transport, or biomedicine. This is due to the possibility to obtain functional 3D objects with complex shapes, tailored properties, high performance and minimal waste [1]. The manufacturing of functional 3D objects by AM requires high filling factors of the functional material (e.g., with magnetic, electrical or thermal conductive) in the matrix and no deterioration of the properties along processing [2, 3]. Herein, rheological additives and particle surface treatments were used to stabilize the highly dense particles (gas-atomized NdFeB particles) in suspension and control the printed concentration gradient in the objects fabricated by vat-photopolymerization [4]. The density of the NdFeB particles was 7.43 g/cm^3 and the one for the UV-curable resin 1.10 g/cm^3, this large difference originating a particles settling during the process (Fig. 1). Settling tests and vibrating sample magnetometry (Fig. 1) were used to determine the influence of the additives concentration (thixotropic and wetting agents, TA and WA) on the concentration gradient in the 3D-printed part. The combination of 6.0 wt% TA + 4.4 wt% WA was found to produce the most uniform concentration

along the part (Fig. 2) [4]. The results obtained show a suitable and promising route for its application in developing a new generation of functional objects by 3D-printing. *Acknowledgements* Authors acknowledges support from MICINN by the projects NEXUS (PID2020-115215RB-C21) and 3D4ENERGY (CNS2023-145011), and the "Severo Ochoa" Programme for Centers of Excellence in R&D (CEX2020-001039-S). E.M.P. acknowledges support from AEI by the JdC-I program (IJC2020-043011-I/MCIN/AEI/10.13039/501100011033) and EU by NextGenerationEU/PRTR. *Present address (A. Bollero):* Advanced Technologies and Micro Systems, Robert Bosch GmbH, 70839 Stuttgart, Germany

[1] L.E. Murr, J. Mater. Sci. Technol. 32, 987 (2016) [2] E.M. Palmero and A. Bollero, "3D and 4D printing of functional and smart composite materials" in Encyclopedia of Materials: Composites – Materials Science and Materials Engineering, Vol. 2, pp. 402-419, Elsevier (2021). [3] E.M. Palmero et al., Sci. Technol. Adv. Mater. 19, 465 (2018); IEEE Trans. Magn. 55, 2101004 (2019); Addit. Manuf. 33, 101179 (2020) [4] C.E. Frank, E.M. Palmero et al., *To be submitted* (2024)

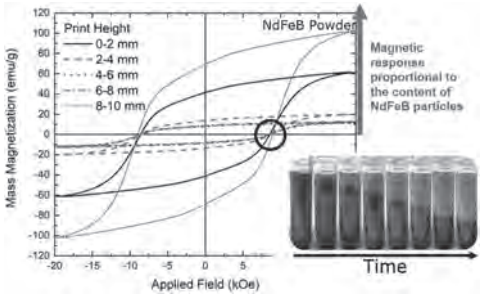

Fig. 1. Hysteresis loops of the 3D-printed parts measured at different print heights to quantify the particle settling effect.

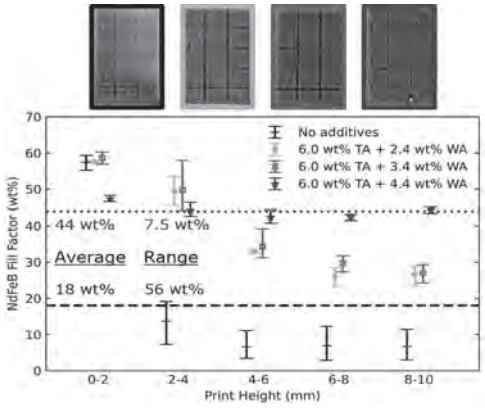

Fig. 2. Concentration gradient of the NdFeB particles in the 3D-printed parts for different combinations of additives in the suspension.

EF-03. Magnetic properties of RE-Co_5 intermetallic compounds.

V. Antropov[1], Z. Zhang[1] and L. Pourovskii[2] *1. Ames National Laboratory, Ames, IA, United States; 2. CPHT, CNRS, École Polytechnique, Institut Polytechnique de Paris, Paris, France*

We studied magnetic moments, critical temperature of magnetic phase transition and magnetic anisotropy of RECo5 (R= rare earth atom) intermetallic compounds using different electronic structure methods and theoretical methods. First, we performed constrained LDA and LDA+U calculations for the different magnetic configurations of RE to demonstrate how the ratio between crystal field, exchange and spin orbit splitting is changing depending on the position and width of 4f-levels of RE atoms. This comparison establishes what type of perturbation theories should be used for the description of different properties determined by these f-electrons. We show that while constrained magnetic states can possess some properties similar to the experimentally observed (i.e. magnetic anisotropy) many other properties of such excited states cannot describe the experiment. In cases where crystal field theory is applicable, we further perform series of studies using combinations of LDA+U and DMFT methods with Hubbard I approximation on RE site to obtain parameters of crystal field theory. These approaches produced similar results for the spectral properties, magnetic moments, anisotropies and demonstrate a most stable ferrimagnetic alignment of the 3d and 5d spin densities for the magnetic states with the overall best agreement with the experiments.

EF-04. Withdrawn

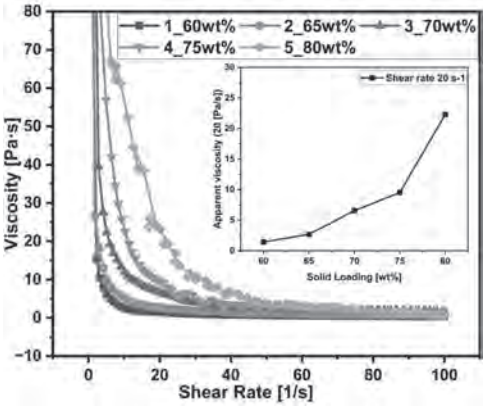

Viscosity vs Shear rate for varying Solid Loading from 60wt% to 80wt%.

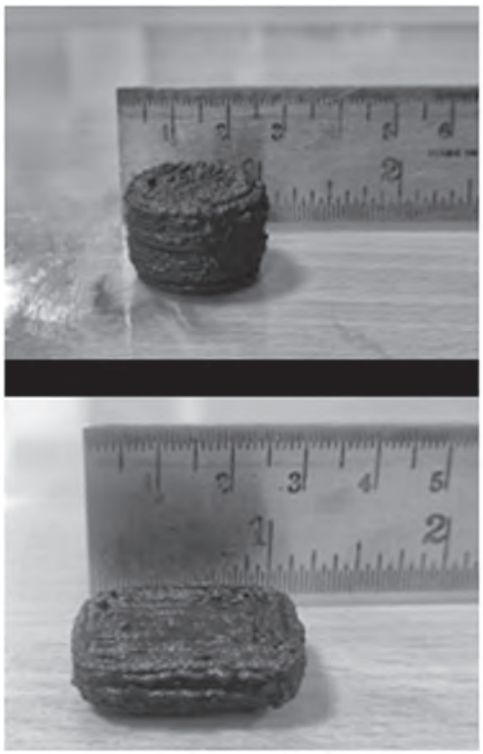

After Printing (Green Pellet)

EF-05. A material processing prospective on exchange-spring permanent magnets. A.S. Poulo[1], J.A. Torres[1], J. Littleton[1], J. Moore[1] and *T. Lamichhane*[1] *1. University of Central Oklahoma, Edmond, OK, United States*

Exchange coupling between proximal hard and soft magnetic layers to enhance the magnetic energy product is an overarching principle of exchange-spring permanent magnet which has potential to design critical rare-earth free permanent magnets. Although it can be easily demonstrated in thin film technology, it is very challenging in bulk polycrystalline permanent magnets to achieve high energy density. This presentation will investigate the current status of both thin films based and polycrystalline based exchange-spring permanent magnet systems, compare most successful materials systems and their processing technologies. Finally, an outlook is presented for critical rare earth free (La & Ce-based) polycrystalline exchange spring permanent magnet systems.

EF-06. Electrically Switchable Magnetic Elastomer. *O. Sodomka*[1] and F. Mach[1] *1. Department of Electrical and Computational Engineering, University of West Bohemia in Pilsen, Pilsen, Czechia*

The electropermanent magnet is a device that can have its external magnetic field switched on and off by an electrical pulse [1] which consists of two permanent magnets with similar B_r and different H_c. The presented electrically switchable magnetic elastomer or electropermanent elastomer (EPE) is a composite material with distributed microparticles in its volume. The distributed character makes it behave like the electropermanent magnet, however, it is more compact, scalable and possible to fine-tune the targeted properties during production. The pulse control requiring low power consumption and the resulting power density make the device energy efficient. The schematic of the composite is depicted in Fig. 1. The electropermanent effect is achieved by composition of two ferromagnetically hard materials with different magnetic coercivity and remanent flux density. The particles used are NdFeB microparticles (H_{cNd}) and strontium ferrite microparticles (H_{cSF}), where $H_{cNd}>H_{cSF}$. The particles are homogeneously dispersed in a silicone matrix (Fig. 1 right). The operation principle is presented in Fig. 2. The hysteresis loops were measured by a DC hystograph on a single material sample. The blue loop is acquired by measuring the full loop (reaching the H_{sFull}) of the composite elastomeric material. The subsequent hysteresis loops (positive and negative) are representing the working cycle of switching the EPE. The saturation of these subsequent loops has to be lower than the full loop (about $H_{sON} = H_{sFull} / 3$) to keep the primary magnetization of the NdFeB particles. Using pulses of the external magnetic field, reaching H_{sON} and H_{sOFF} (both $< H_{sFull}$), switches the magnetization of the strontium ferrite microparticles, resulting in zero or non-zero remanent flux density (B_{rON} is not 0 and $B_{rOFF} = 0$).

[1] A. Knaian. Electropermanent magnetic connectors and actuators: devices and their application in programmable matter. PhD thesis, Massachusetts Institute of Technology, 2010.

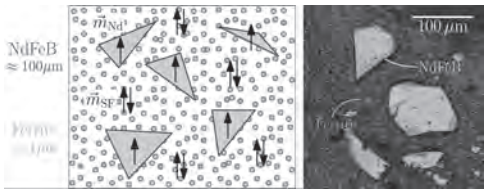

Fig. 1 Schematic diagram of the EPE material cell. Distribution of the filling and magnetic moments inside the material with the comparison of the average particle size. SEM image of the sample.

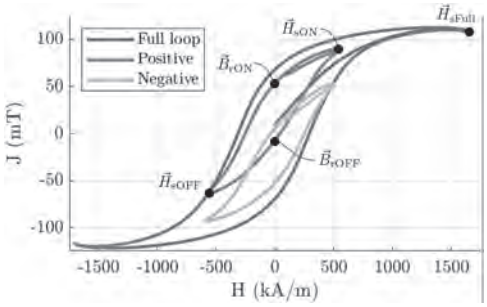

Fig. 2 Measured data illustrating the operating principle of the EPE. Blue loop is the measured full loop of the composite. Positive and negative loops are measured with lower external field saturations representing the working cycle.

EF-07. Influence of Cationic Distribution on the Magnetic and Electromagnetic Properties of Substituted Barium Hexaferrite within X-band (8.2 GHz-12.4 GHz). *K. Rana*[1], M. Tomar[1,2] and A. Thakur[3]
1. Physics, Electronic Materials and Device Laboratory, New Delhi, Delhi, India; 2. Physics, Miranda College, Delhi, India; 3. Applied Physics, Amity University, Gurugram, India

Cobalt substituted M-type barium hexaferrite with nominal composition BaCoxFe(12-x)O19 (0.0≤x≤1.0) in the steps of 0.2 were prepared via the chemical co-precipitation technique. Thermal analysis was performed on pure BaM before undergoing thermal treatments to extract beneficial information about its crystallization point. From TGA/DTA analysis, it was confirmed that 900 °C was an ideal sintering temperature for the pure BaM ferrite sample. On that basis, all six samples were sintered at the same temperature. XRD confirmed the formation of the M phase in all the samples, whereas the morphology of all the samples was investigated by using the FESEM technique. Magnetic parameters like saturation magnetization (M_s), coericivity (H_c), and squareness ratio (SQR) were examined using VSM. The value of M_s was found to decrease from 65.74 emu/g to 54.30 emu/g at the very initial stage (x = 0.2) due to the small amount of dopant, but after that, with an increase in the dopant content, the M_s value was found to increase up to x = 0.8 and reach 65.39 emu/g. A moderate Ms value with a higher coericivity H_c of 3784 Oe was obtained for x = 0.8. On the other hand, the variation of complex permittivity and complex permeability with composition were investigated over the X-band frequency range (8.2 GHz–12.4 GHz). Reliable and sustainable values of permittivity (more than 10) and magnetic loss $Tan\delta_m$ (at x = 0.021) at x = 0.8 make this composition suitable for high-frequency applications as well as electromagnetic shielding.

1. S Kumar, S Supriya and R Pandey, Journal of Magnetism and Magnetic Materials., 458, 30.38 (2018). 2. R Meena, S Bhattacharya and R Chatterjee, Materials Science and Engineering B., 171, 133-138 (2010)

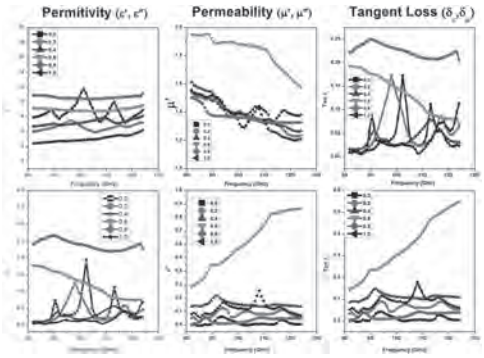

Fig.1 Complex permitivity, permeability and tangent losses of $BaCo_xFe_{(12-x)}O_{19}$ (0.0○C within the K-band frequency range.

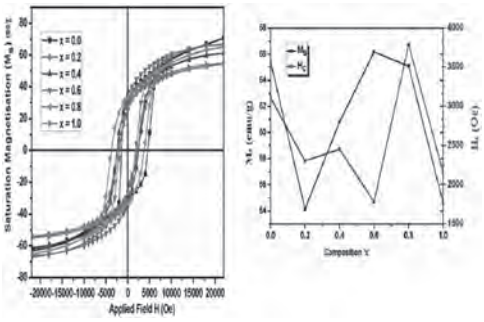

Fig.2 M-H loops of $BaCo_xFe_{(12-x)}O_{19}$ (0.0 < x < 1 with step 0.2) sintered at 900 °C and the variation of M_s and H_c with the composition x

EF-08. Nonreciprocity of surface acoustic waves coupled to spin waves propagating in a ferromagnetic bilayer having non-collinear magnetizations of layers. L. Ushii[1], *A.N. Slavin*[2], V. Tyberkevych[2] and R.V. Verba[1]
1. Institute of Magnetism, Kyiv, Ukraine; 2. Physics, Oakland University, Rochester, MI, United States

Nonreciprocity of propagation of surface acoustic waves (SAWs) in a microwave frequency band can be achieved using magnetoelastic interaction of SAW with spin waves (SWs) propagating in magnetic heterostructures [1,2]. Recent works have shown that ultimate isolation of counter-propagating hybridized SAW/SW is achieved in heterostructures consisting of a synthetic antiferromagnet – ferromagnetic (FM) bilayer with antiferromagnetic RKKY interlayer coupling – placed on top of a piezoelectric acoustic waveguide [3]. In this work, we study in details a more practical and technologically simpler system based on an FM bilayer, where layers are coupled by only dipole-dipole interaction, and having non-collinear magnetizations of the FM layers, similar to the system studied experimentally in [4,5]. We show that the in-plane magnetic anisotropy with non-collinear easy axes in the FM layers is the only essential factor for the realization of strongly nonreciprocal propagation of hybridized SAW/SW. We formulate requirements to relative orientation of the layer's magnetizations and wave propagation direction necessary for the realization of an efficient SAW isolator. We also demonstrate examples of SAW transmission characteristics which prove the possibility of achieving an isolation exceeding 40 dB for sub-mm long FM bilayer with insertion losses of just a few dB larger than those of a pure SAW device. In addition to relative fabrication simplicity, the proposed heterostructure exhibits a reasonable robustness in respect to deviations of the anisotropy axes and/or bias field direction – an additional benefit for mass-production.

[1] M. Weiler et al., Elastically Driven Ferromagnetic Resonance in Nickel Thin Films, Phys. Rev. Lett. 106, 117601 (2011). [2] R. Verba, et al., Nonreciprocal Surface Acoustic Waves in Multilayers with Magnetoelastic and Interfacial Dzyaloshinskii-Moriya Interactions, Phys. Rev. Applied 9, 064014 (2018). [3] R. Verba, V. Tiberkevich, and A. Slavin, Wide-Band Nonreciprocity of Surface Acoustic Waves Induced by Magnetoelastic Coupling with a Synthetic Antiferromagnet, Phys. Rev. Applied 12, 054061 (2019). [4] P. J. Shah et al., Giant nonreciprocity of surface acoustic waves enabled by the magnetoelastic interaction, Sci. Adv. 6, eabc5648 (2020). [5] D. A. Bas et al, Nonreciprocity of Phase Accumulation and Propagation Losses of Surface Acoustic Waves in Hybrid Magnetoelastic Heterostructures, Phys. Rev. Appl. 18, 044003 (2022).

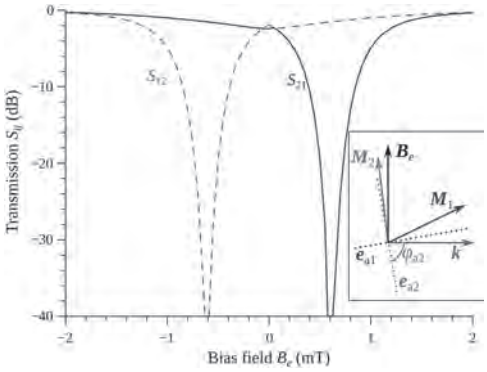

Calculated transmission of a SAW/SW isolator based on a 100 microns long FeGaB(20)/Al_2O_3(5)/FeGaB(20) (thickness in nm in parenthesis) bilayer on top of $LiNbO_3$ crystall at the frequency of 1.5 GHz. Losses at the excitation and reception SAW transducers are not accounted for. Inset shows orientation of the wave vector *k*, anisotropy axes e_{a1}, e_{a2}, bias field B_e, as well as the layers static magnetizations M_1 and M_2. Anisotropy axes are tilted of the *k* direction by φ_{a1} = 10 deg and φ_{a2} = -80 deg, bias field B_e is perpendicular to the wave vector *k*.

EF-09. Garnet Microcavity Using Ce:YIG and GGG Showing Perpendicular Magnetic Anisotropy. *T. Goto*[1], Y. Yoshihara[1], T. Koguchi[1], T. Watanabe[2], K. Mori[1], H. Miyashita[1], C.A. Ross[3] and K. Ishiyama[1]
1. Tohoku University, Sendai, Japan; 2. Shin-Etsu Chemical, Annaka, Japan; 3. Massachusetts Institute of Technology, Canbridge, MA, United States

Magnetooptical devices, such as Q-switched lasers [1], optical isolators [2], and magnetic holographic memory, have garnered substantial interest due to their distinct properties. Key parameters in these applications are a high magnetooptical response and minimal magnetic domains. Achieving these parameters simultaneously in magnetic films is challenging because film thickness, magnetooptical response, perpendicular magnetic anisotropy (PMA), and magnetic domain width are interrelated. As film thickness increases, magnetooptical response improves; however, PMA diminishes due to strain relaxation between the film and substrate, causing the magnetization's easy axis to shift in-plane, which eliminates magnetic domains. To address this, we utilized a microcavity structure to achieve both a significant magnetooptical response and small magnetic domains, facilitated by PMA. We epitaxially grew magnetic garnet films on a gadolinium gallium garnet (GGG) substrate using RF ion beam sputtering at 900°C [3]. Alternating layers of cerium-substituted yttrium iron garnet (Ce:YIG) and GGG formed Bragg mirrors (Fig. 1), with a defect layer double the thickness within the Bragg mirror to create a localized mode within a photonic band gap, enhancing the Faraday rotation (FR). The transmissivity of 48.3% and FR of –4.2° at a wavelength of 1111 nm were obtained. This configuration, known as a microcavity or magnetophotonic crystal, leverages the slight lattice constant differences between Ce:YIG and GGG to induce lattice strain, PMA, and magnetic domains. Magnetooptical microscopy revealed that the magnetic domain width in the Bragg mirror and microcavity was less than 500 nm, with domain wall widths under 100 nm. The microcavity resonance at a near-infrared wavelength amplified the FR, enabling the all-garnet magnetooptical microcavity sample to achieve both large magnetooptical responses and small magnetic domain structures simultaneously. This research was partially funded by JSPS KAKENHI (Nos. 20H02593, 20K20535, 23H01439, 23K17758), NEDO No. 23200047-0, and the Inamori Foundation. We also acknowledge support from CINTS, LNS, and FTCTU.

[1] T. Goto, et al., Opt. Express 24, 17635-17643 (2016). [2] T. Goto, et al., Opt. Express 22, 19047-19054 (2014). [3] Y. Yoshihara, et al., Appl. Phys. Lett. 123, 112404 (2023).

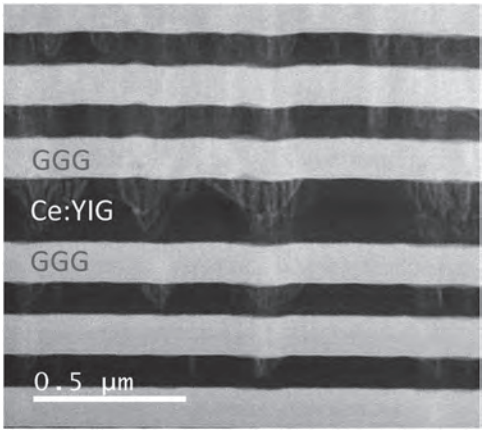

Fig. 1. Cross-sectional TEM image of a part of the fabricated garnet microcavity.

EF-10. FeGa Thin Film Coupled to a Network of Photoresponsive Liquid Crystals: Control of Magnetic Properties by Light Irradiation. G. Barrera[1], F. Celegato[1], D. Martella[2,4], M. Coisson[1], C. Parmeggiani[2,3], N. Fuochi[2,4], D. Wiersma[2,3] and *P. Tiberto*[1] *1. Advance Materials and Life Sciences, INRIM, Torino, Italy; 2. European Laboratory for Non Linear Spectroscopy (LENS), Sesto Fiorentino (FI), Italy; 3. Physics and Astronomy Department, University of Florance, Sesto Fiorentino, Italy; 4. Chemistry "Ugo Schiff" Department, University of Florence, Firenze, Italy*

Composite magnetic materials with multiple responses to environmental stimuli have a significant impact on various applications, particularly in sensing and actuation systems. The combination of a 30 nm magnetostrictive FeGa layer with soft photo-responsive polymers, specifically liquid crystalline network (LCN) containing an azobenzene dye is here studied. This composite structure allows to finely tune the film magnetic properties through light irradiation and without the need for a magnetic field. Specifically, UV light irradiation leads to polymer contraction along the x-axis and expansion along the y-axis, exploiting the isomerisation of the dye in the LCN. The photo-actuation transfers a mechanical stress to the magnetostrictive FeGa thin film, whose magnetic domains rearrange under the effect of uniaxial stress anisotropy. As a result, FeGa magnetic properties depend on the duration and intensity of UV irradiation. Conversely, irradiation with green light is able to restore the original molecular order in the polymer, gradually releasing the stress in the FeGa thin film and, consequently, recovering its pristine magnetic properties. Room-temperature hysteresis loops of the FeGa/LCN photoresponsive sample were measured by applying a magnetic field H in the film plane along both *x* and *y*-directions after irradiation with UV (see Figure 1a) and green lamps for a selected time. Magnetic parameters, including normalized magnetization remanence (M_r/M_s), coercive field (H_c) and magnetic susceptibility (χ_{Hc}) have been evaluated as a function of the duration and intensity of the light illumination. To assess the actuation mechanism, magnetoresistance measurements were performed under opto-mechanical control of the magnetization. Specifically, the ΔR/R value is recorded for an interval of time during which UV light and green light are properly switched on and off, revealing a magnetic memory effect (see Figure 1b). The coupling between the opto-mechanical properties of the substrate and the magnetostrictive behavior of the FeGa layer is here discussed.

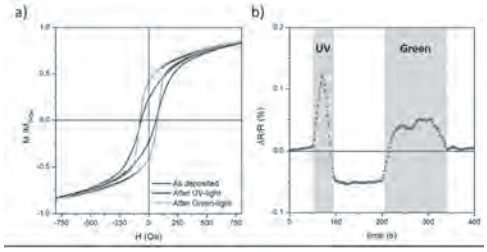

FeGa/LCN hysteresis loop in as-deposited state and after light irradiation; b) Time evolution of the ΔR/R curve triggered by UV irradiation and green light.

EF-11. Anomalous Optical Properties of Single-Molecule Magnet (SMM) Modified Magnetic Tunnel Junction (MTJ) at Room Temperature. J.E. Hernandez[1], J. Martinez-Lillo[2] and *P. Tyagi*[1]
1. University of the District of Columbia, Washington, DC, United States; 2. Universitat de València, Valencia, Spain

Magnetic tunnel junctions (MTJs) are well known for their applications in spin-valve and magnetic random access memory(MRAM) applications [1,2]. This paper will provide our experimental studies that MTJ is also an excellent test bed for making MTJ-based molecular spintronics devices (MTJMSD) and magnetic metamaterials (Fig.1). We utilize custom-designed single-molecule magnets (SMM) to form molecular spin channels along the perimeter of MTJ comprising of Co/NiFe/AlOx/NiFe pillar form thin film stack. We simultaneously grew ~20,000 MTJs and transformed them into

MTJMSD. Spectroscopic optical measurements were performed to compare the optical properties of MTJs before and after transforming into MTJMSD. A drastic difference in reflectance versus wavelength was observed on MTJMSD. Surprisingly, despite being made up of metallic films, MTJMSD started absorbing>70% of the light radiation (Fig. 2). Electron spin resonance(ESR) was conducted to investigate the effect of the SMM on the MTJ. ESR studies revealed that SMM channels have impacted acoustic and optical modes' typical amplitude and position, confirming the impact on the nature of inter-layer coupling. SMM-induced coupling dominated the weak magnetic interaction present on MTJ via the insulating tunnel barrier. Notably, the anomalous light absorption provides an essential insight into the spin photovoltaic effect we have reported in our recent studies [3,4]. This paper will compare the response from two types of SMM and elaborate on the impact of molecular structure on the optical response from MTJMSD at room temperature. This study can be useful in exploring the utility of MTJ beyond conventional use, leading to the new direction of magneto-optical properties.

[1] X. Fan, R. Cao, T. Moriyama, W. Wang, H.W. Zhang, J.Q. Xiao, App. Phys. Lett., 95 (2009) 122501. [2] A. Grizzle, C. D'Angelo, J. Martínez-Lillo, P. Tyagi, RSC Advances, 11 (2021) 32275-32285. [3] P. Tyagi, C. Riso, Nanotechnology, 30 (2019) 495401. [4] M. Savadkoohi, D. Gopman, P. Suh, C. Rojas-Dotti, J. Martínez-Lillo, P. Tyagi, ACS Applied Electronic Materials, 5 (2023) 3333-3339.

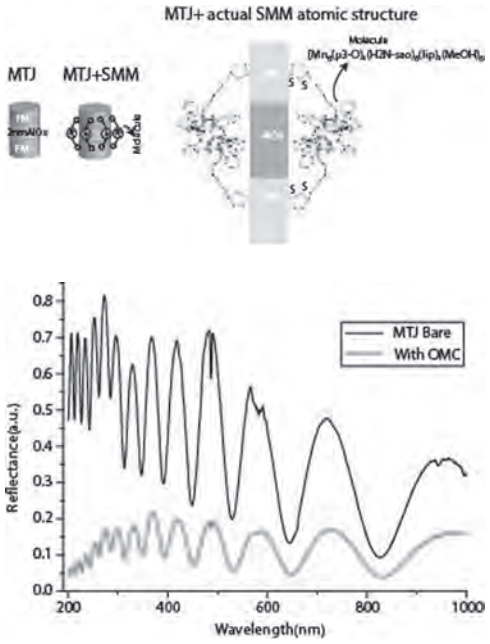

EF-12. Hybrid magnon-phonon cavity realized in a magnetoelastic heterostructure. *C. Tang*[1,2], H. Goyal[1,2], D. Sasaki[3], Y. Xiong[4], M. Mahjouri-Samani[1], M. Adams[1], Y. Takamura[3], W. Zhang[4] and W. Jin[2,1]
1. Department of Electrical and Computer Engineering, Auburn University, Auburn, AL, United States; 2. Department of Physics, Auburn University, Auburn, AL, United States; 3. Department of Materials Science and Engineering, University of California, Davis, Davis, CA, United States; 4. Department of Physics and Astronomy, University of North Carolina at Chapel Hill, Chapel Hill, NC, United States

Strong coupling between two quantized excitations leads to a hybridized state that allows to explore new phenomena and technologies. Phononic excitations, such as long-lived, high-overtone bulk acoustic waves (BAWs) [1, 2], can host many well-isolated modes at the same frequency. Meanwhile, magnetic excitations or magnons in magnetically-ordered materials show frequency tunability and can strongly couple with photons and phonons [3-7]. In this work, we study magnon-phonon dynamics in $La_{0.7}Sr_{0.3}MnO_3/SrTiO_3$ (LSMO/STO) heterostructures using ferromagnetic resonance (FMR). LSMO is a half-metallic ferromagnetic oxide with low magnetic damping rate, and it was epitaxially grown on STO - a prototypical perovskite substrate with a structural phase transition at $T_S \sim 105$ K. First, we demonstrate coupling between magnon and longitudinal/transverse acoustic-phonons as evidenced by avoided crossings in the FMR spectra at 250 K shown in Fig. 1 and the cooperativity (C) of the avoided crossings falls in the strong coupling regime (C>1). As temperature decreases, the number of avoided crossings monotonically increases. Remarkably, below T_S, perpendicular standing spin wave bands appear and they all strongly couple with high-overtone BAW phonons, forming a hybrid magnon-phonon network. These results resemble the picture of a hybrid magnon-phonon cavity realized through the magnetoelastic coupling between LSMO and STO. Our work highlights high-quality magnetoelastic heterostructures as a suitable material platform to implement magnon-phonon hybrids, holding the promise of storing, encoding, and transducing coherent information between phonon and magnon modes.

[1] Y. Chu, P. Kharel, and W. H. Renninger, Science 358, 199 (2017). [2] Y. Chu, P. Kharel, and T. Yoon, Nature 563, 666 (2018). [3] D. D. Awschalom, C. R. Du, and R. He, IEEE Transactions on Quantum Engineering 2, 1 (2021). [4] Y. Li, W. Zhang, and V. Tyberkevych, Journal of Applied Physics 128 (2020). [5] H. Yuan, Y. Cao, and A. Kamra, Physics Reports 965, 1 (2022). [6] D. Lachance-Quirion, Y. Tabuchi, and A. Gloppe, Applied Physics Express 12, 070101 (2019). [7] B. Flebus, D. Grundler, and B. Rana, Y. Otani, Journal of Physics: Condensed Matter (2024).

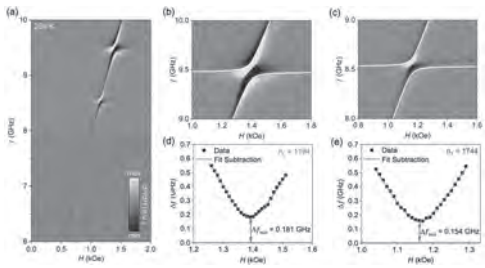

FIG. 1. Magnon-phonon coupling FMR spectra and characterization. (a) Spectral intensity of the FMR signal at T = 250 K. Close-ups of avoided crossing at (d) f = 9.47 GHz, H = 1.4 kOe, and (e) f = 8.53 GHz, H = 1.2 kOe. The white curves show the fitted avoided crossings. (f) and (g) show the corresponding splitting energy Δf for avoided crossings in (d) and (e), respectively.

EF-13. Magnetoplasmonic Nanocolumnar Films Fabricated by Sputtering. M. Garrido-Segovia[1,2], E. Navarro[2,3], A. Espinosa[4] and *J. García-Martín*[1] *1. Instituto de Micro y Nanotecnología, CSIC, Tres Cantos, Spain; 2. Depto. Física de Materiales, UCM, Madrid, Spain; 3. Instituto de Magnetismo Aplicado, Las Rozas, Spain; 4. Instituto de Ciencia de Materiales de Madrid, CSIC, Madrid, Spain*

In recent decades, sputtering has proven to be a versatile and efficient technique for the production of thin films. This widely used fabrication method is compatible with glancing angle deposition (GLAD), and, under appropriate growth conditions, can produce nanocolumnar films. Previous studies on iron nanocolumns have demonstrated that their magnetic properties depend on the morphology of the nanocolumns, which is determined by the deposition parameters [1,2]. Additionally, research on nanocolumns of plasmonic materials, such as gold, has revealed the presence of localized surface plasmon resonances [3]. The combination of magnetic materials, such as iron, and plasmonic materials, such as gold, is of great interest due to the wide range of applications that these magnetoplasmonic nanostructures can support. In this study we present, for the first time, bimetallic nanocolumnar films of gold and iron fabricated by GLAD sputtering. We have fabricated two types of bimetallic nanocolumnar films: one with gold nanocolumns (NCs) at the bottom and iron NCs at the top, and another with the opposite configuration. Morphological characterization of the samples was conducted

using scanning electron microscopy (SEM), where backscattered electrons (whose number depends on the atomic mass of the element) highlighted the different materials, see Fig. 1. The crystalline and electronic structures were evaluated via X-ray diffraction. Additionally, the optical properties of these films were examined using spectral reflectivity measurements and their magnetic properties were analyzed using a vibrating sample magnetometer. The results demonstrate the potential of these nanostructures for applications in sensing, as well as in magnetic and photothermal cancer therapies.

[1] E. Navarro et al., Nanomaterials, *12*, 1186 (2022). [2] M. Garrido-Segovia et al., Chapter in Functional Magnetic and Spintronic Nanomaterials, NATO Science for Peace and Security Series B: Physics and Biophysics, Springer, 2024 (accepted). [3] G. Barbillon et al., Nanomaterials, 12, 4157 (2022).

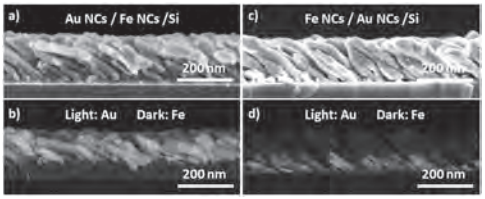

Figure 1: Cross-sectional SEM images with secondary electrons (top row) and backscattered electrons (bottom row) of gold NCs above iron NCs (a and b) and of iron NCs above gold NCs (c and d).

EF-15. Effect of Rare-Earth Doping on Magnetic Softness and Magnetization Dynamics of Fe-Ga Films. *S. Ajia*[1], R. Nishina[1], T. Miyazaki[2], S. Muroga[1] and Y. Endo[1,3] *1. Department of Electrical Engineering, Tohoku University, Sendai, Japan; 2. School of Engineering, Tohoku University, Sendai, Japan; 3. CSIS, Tohoku University, Sendai, Japan*

Fe-Ga binary alloys have been attracted great attention for various magneto-electrical applications because of high magnetostriction and large saturation magnetization [1-3]. Doping Fe-Ga with a third element is known to modify the magnetostriction [4]. Several groups reported that the addition of B into Fe-Ga films causes refined grain size and diminished magnetocrystalline anisotropy, which led to increased magnetostriction and excellent magnetic softness [5-7]. On the other hand, there are little reports for the effect of rare-earth (RE) element doping on magnetic properties of Fe-Ga films. Herein, we selected Y, Ce, and Pr as the third elements to dope into the $Fe_{71}Ga_{29}$ alloy. We investigated the effect of RE elements doping on the magnetic softness and dynamic properties of a series of $(Fe_{0.71}Ga_{0.29})_{100-x}RE_x$ (Fe-Ga-RE) films in detail. The coercivity (H_c) of each Fe-Ga-RE film was summarized in Fig. 1(a) as a function of RE content (x) from their hysteresis loops. In each Fe-Ga-RE film, H_c showed a decreasing tendency as x increased. In particular, in case of Ce doping, H_c value was reduced from 59.3 Oe (x = 0 at.%) to about 30 Oe for x > 1.4 at.%, and reached 11.4 Oe at x = 6.7 at.%. Thus, the low H_c might result from strain release and refinement of grain size of $Fe_{71}Ga_{29}$ film by doping of RE elements. Fig. 1(b) showed the relationship between the effective in-plane damping constant (α) vs saturation magnetostriction (λ_s) for all films. α decreased as λ_s increased for Y and Pr doped film, while fluctuated as λ_s increased for Ce doped one. These relationships may be derived from the localized strain and magnetic anisotropy induced by RE dopant. Also, similar to our previous study of doping La into Fe-Ga alloy [8], a small amount of Pr doping is effective for obtaining larger λ_s (52.8 ppm) with lower α (0.0151). Therefore, the combination of these properties makes Fe-Ga-RE films promising candidates to apply in magnetoelectric devices and microwave magnetic devices. This study was supported by X-NICS, CSIS, CSRN, and CIES of Tohoku University; MEXT, Japan (No. JP011438); and ASRC, Japan.

[1]B. K. Kuanr, *et al*., J. Appl. Phys., Vol. 115, p.17C112 (2014) [2] W. Jahjah, *et.al*., *Phys. Rev. Appl.,* Vol. 12, p.024020 (2019) [3]Y. Kawabe, *et.al*., T. Magn. Soc. Jpn., (Special Issues) Vol. 3, p.34 (2019) [4] E.M. Summers, *et al.*, J. Mater. Sci., Vol. 42, p.9582 (2007) [5]J. Lou, *et al*., Appl. Phys. Lett, Vol. 91, p.182504 (2007) [6]S. Muramatsu, *et.al*., AIP Advances, Vol. 11, p.025114 (2021) [7]K. Yadagiri, *et al.*, J. Mater. Sci., Vol. 58, p.11327 (2023) [8]R. Nishina, *et.al*., T. Magn. Soc. Jpn., (Special Issues) Vol. 8, p.10 (2024)

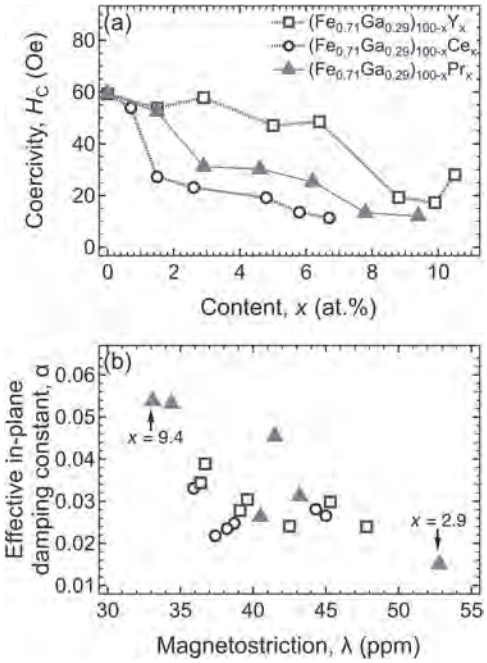

Fig. 1(a) Change in H_c with the content of RE, and (b) relationship between λ_s and α for all RE doped films.

Session EG
MAGNETIC CRYSTALLINE ALLOYS

Nicoleta Lupu, Chair
National Institute of R&D for Technical Physics, Iasi, Romania

CONTRIBUTED PAPERS

EG-01. Interplay Between Magnetism and Short-Range Order in Medium- and High-Entropy Alloys: CrCoNi, CrFeCoNi, and CrMnFeCoNi. *C.D. Woodgate*[1,2], L.H. Lewis[3,4] and J.B. Staunton[1]
1. Department of Physics, University of Warwick, Coventry, United Kingdom; 2. H. H. Wills Physics Laboratory, University of Bristol, Bristol, United Kingdom; 3. Department of Chemical Engineering, Northeastern University, Boston, MA, United States; 4. Department of Mechanical and Industrial Engineering, Northeastern University, Boston, MA, United States

We present computational results suggesting a potential route for tuning atomic ordering in medium- and high-entropy alloys, by annealing samples in an applied magnetic field and thus altering the magnetic state. Controlling atomic order is critical for tuning materials properties, and our approach is anticipated to open up new routes for discovery of novel materials. Specifically, the impact of magnetism on predicted atomic short-range order in Ni-based high-entropy alloys is studied using a first-principles, all-electron, Landau-type linear response theory, coupled with lattice-based atomistic modelling [1,2]. We perform two sets of linear-response calculations: one in which the paramagnetic state is modelled within the disordered local moment picture, and one in which systems are modelled in a magnetically ordered state. We show that the treatment of magnetism can have significant impact both on the predicted temperature of atomic ordering and also the nature of atomic order itself [3]. In CrCoNi, we find that the nature of atomic order changes from being $L1_2$-like when modelled in the paramagnetic state to $MoPt_2$-like when modelled assuming the system has magnetically ordered. In CrFeCoNi, atomic correlations between Fe and the other elements present are dramatically strengthened when we switch from treating the system as magnetically disordered to magnetically ordered. Our results show it is necessary to consider the magnetic state when modelling multicomponent alloys containing mid- to late-3*d* elements, and we suggest that, potentially, there could be a variety of multicomponent alloy compositions containing 3*d* transition metals that will exhibit specific atomic ordering when thermally treated in an applied magnetic field. [We acknowledge the support of the UK Engineering and Physical Sciences Research Council, the US Department of Energy, and the US National Science Foundation.]

[1] C. D. Woodgate and J. B. Staunton, Phys. Rev. B 105, 115124 (2022).
[2] C. D. Woodgate and J. B. Staunton, Phys. Rev. Mater. 7 013801 (2023).
[3] C. D. Woodgate D. Hedlund, L. H. Lewis, J. B. Staunton, Phys. Rev. Mater. 7, 053801 (2023).

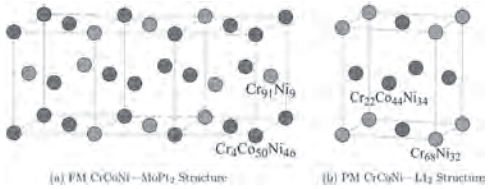

Competing chemical orderings in the medium-entropy alloy CrCoNi. In the paramagnetic state, it is $L1_2$-like order (right) which dominates, but once magnetic order has established, it is $MoPt_2$-like order (left) which is preferred.

EG-02. Relationship between chemical bonding state, magnetostrictive coefficient, and Gilbert damping coefficient in Fe-Al-N alloy system. *K. Imamura*[1], T. Sato[1], S. Isogami[2], N.H. Oono[1] and M. Ohtake[1] *1. Faculty of Engineering, Yokohama National University, Yokohama, Japan; 2. Research Center for Magnetic and Spintronic Materials, National Institute for Materials Science, Tsukuba, Japan*

Soft magnetic materials have been used in a wide range of applications from electric machines to electronic thin film devices. Low magnetostrictive coefficient (λ) is generally required, since the residual strain degrades the permeability due to inverse magnetostrictive effect. Recently, a correlation between λ and Gilbert damping coefficient (α) has been suggested in some materials [1]-[3], though these properties are quite different in time scale and the mechanism has not been made clear. However, its employment may enable high throughput screening for development of new soft magnetic materials, since the α can be evaluated for small samples prepared by combinatorial synthesis. In order to consider its availability, relationship between λ and α needs experimentally determining for various kinds of material systems. Fe-Al alloy is one of high permeability materials and its chemical bonding state seems to be controllable by addition of N atom. In the present study, $(Fe_{0.8}Al_{0.2})_{100-x}N_x$ (at. %) single-crystal films of bcc(001) orientation are prepared by varying the N content from $x = 0$ to 8.2. The structure is characterized by RHEED, XRD, HR-TEM, and XPS. The λ and α are investigated by cantilever method and time-resolved magneto-optical Kerr effect. Fig. 1 shows the XPS spectra. As the N content increases, Al atom tends to be bonded to N rather than Fe atom. The result also shows that 2p electrons of Al atom, which is free in Fe-Al binary system, is localized around N atom. Fig. 2(a) shows the N content dependence of λ. The λ decreases with increasing the N content. Localization of Al-2p electron might to be related with weakening coupling between magnetic moment and crystal lattice. Fig. 2(b) shows the N content dependence of α. The α decreases with increasing the N content. The reason is due to that energy dissipation from magnetization precession to lattice vibration decreases as the coupling is weakened. Fig. 2(c) summarizes the relationship between $|\lambda|$ and α. The α seems to be correlated with the $|\lambda|$. The present study has shown that measurement of α could lead to indirect evaluation of λ even for alloy systems involving light elements.

[1] R. Bonin, M. L. Schneider, T. J. Silva, and J. P. Nibarger: *J. Appl. Phys.*, 98, 123904 (2005). [2] Y. Endo, Y. Mitsuzuka, Y. Shimada, and M. Yamaguchi, *J. Appl. Phys.*, 109, 07D336 (2011). [3] S. Umetsu, M. Sato, Y. Takahashi, N. Inaba, F. Kirino, M. Ohtake, and M. Futamoto, *IEEE Trans. Magn.*, 59, 2900205 (2023).

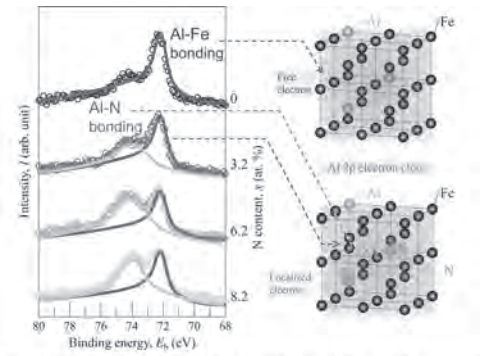

Fig. 1 XPS spectra of Al 2p measured for $(Fe_{0.8}Al_{0.2})_{100-x}N_x$ films with N contents of 0–8.2 at. % and schematic illustration of chemical bonding state between Fe, Al and N atoms.

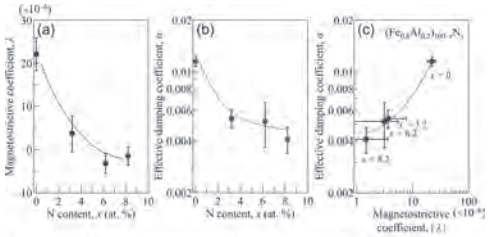

Fig. 2 [(a),(b)] N content dependences of (a) magnetostrictive coefficient λ and (b) effective damping coefficient α of $(Fe_{0.8}Al_{0.2})_{100-x}N_x$ film. (c) Relationship between α and $|\lambda|$.

EG-03. Synthesis and Magnetic Properties of Fe-Co-N-based Magnetic Materials. *T. Tabata*[1], Y. Asari[1], M. Noujima[1] and S. Terada[1] *1. Research & Development Group, Hitachi Ltd., Hitachi, Japan*

Fe-Co alloys are known as the soft magnetic materials (SMMs) with the highest magnetization [1]. Therefore, Fe-50Co alloy, known as Permendur, has been used as SMMs for downsizing and increasing the performance of power electronics. However, Co is known to be a very expensive element. In addition, the reduction of Co from 50 at.% decreases the permeability of the material [2]. Therefore, it is necessary to develop materials that exhibit excellent soft magnetic properties while reducing the amount of Co. On the other hand, iron nitrides have been reported to exhibit different magnetic properties. Among them, α''-$Fe_{16}N_2$ shows higher saturation magnetization and γ'-Fe_4N has lower magnetocrystalline anisotropy than α-Fe, indicating that the introduction of nitrogen is a promising method to solve the problem of reducing the amount of Co in Fe-Co alloys [3]-[5]. Therefore, we investigated the synthesis and magnetic properties of Fe-Co-N alloys. Fe-Co foils with a thickness of about 100 μm were prepared by cold rolling. In our previous work, we confirmed that Fe-Co-N can be formed by heating the prepared Fe-Co foil in a nitriding furnace under an ammonia gas atmosphere [6]. In addition, we reported that gas nitriding at low temperatures below 700°C is desirable to promote nitrogen diffusion and the formation of the γ' phase [7]. The composition of the surface phase of the Fe-Co-N foil was evaluated by X-ray diffraction (XRD). Fig.1 shows the XRD pattern of the prepared Fe-Co-N foil. As shown in this Fig.1, we confirmed that the Fe-Co-N foil was composed of the mixture of α-Fe-Co (bcc) and nitride phase ε (hcp) and γ' (fcc). Furthermore, we confirmed that the nitride phase was uniformly distributed in this foil by EPMA measurement. In this study, we investigate the magnetic properties of this nitrided foil and study in detail the effects of nitrogen introduction and its microstructure on the magnetic properties. This research is partially based on results obtained from Green Innovation Fund Projects (JPNP21026) commissioned by the New Energy and Industrial Technology Development Organization (NEDO).

[1] D. I. Bardos, J. Appl. Phys., Vol. 40, p. 1371 (1969) [2] G. W. Elmen, Trans. AIEE, Vol. 54, p. 1292 (1935) [3] B. C. Frazer, Phys. Rev., Vol. 112, p. 751 (1958) [4] Y. Sugita, K. Mitsuoka, M. Komuro, et al., Appl. Phys. Lett., Vol. 20, p. 492 (1971) [5] Y. Sugita, K. Mitsuoka, M. Komuro, et al., J. Appl. Phys., Vol. 70, p. 5977 (1991) [6] T. Tabata, M. Komuro, Y. Asari, et al., AIP Advances, Vol. 14, p. 065217 (2024) [7] T. Tabata, Y. Asari, M. Nojima, et al., INTERMAG2024, Rio de Janeiro, Brazil (2024)

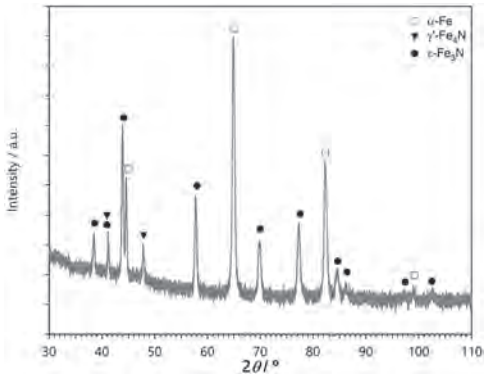

Fig. 1 X-ray diffraction pattern of the surface of the fabricated nitride foil

EG-04. Anisotropy of Losses in Non-Segmented Assemblies of Grain-Oriented Steel with Circular Easy Axis Distribution. *S. Dobák*[1], J. Fuzer[1], I. Petryshynets[2], P. Kollár[1] and F. Kováč[2] *1. Institute of Physics, Faculty of Science, P. J. Safarik University in Kosice, Kosice, Slovakia; 2. Institute of Materials Research, Slovak Academy of Sciences, Kosice, Slovakia*

A few studies have demonstrated that grain-oriented (GO) steel rings, when stacked with their rolling directions (RDs) shifted by a constant angle θ (Fig. 1), facilitate the transfer of magnetic flux between laminations under both unidirectional and rotating fields [1,2]. This unconventional approach reduces magnetic losses by directing the flux along the RD in the layers, enabling the construction of energy-efficient GO cores for AC rotating machines with reduced noise [3]. Our latest research quantified this phenomenon by examining the domain wall (d.w.) phase-specific distribution of pinning and interaction fields [4]. In this study, we decompose the losses into hysteresis W_{hyst}, classical W_{class}, and excess W_{exc} components as functions of frequency f, peak induction B_p, and angle θ. We applied the Statistical Theory of Losses (STL) to derive the parameters defining the statistics of generalized magnetic objects under DC and AC regime. This approach elucidates the reduction in losses at specific circular anisotropy, particularly when the θ is near the hard magnetization axis, $\theta \approx 55°$, in adjacent sheets. The transitions between 180° and 90° d.w. phases from the in-plane [001] easy axis to the out-of-plane [100] and [010] axes result in a deviation of W_{exc} from the usual $f^{0.5}$ dependence. Beyond the applicability of STL up to a few hundred hertz, the hysteresis loops become reentrant, indicating a nucleation-type process. The hard axis compensation, which interferes with the homogenization of the magnetization process at increasing f, can be distinctly analyzed by identifying the mechanisms governed by quasi-static and dynamic d.w. motion. The extracted quantities enable us to measure the evolution of eddy current (e.c.) and excess fields over the time, capturing the widening of the hysteresis loop attributed to classical e.c.s and d.w. motion. An example of this loop decomposition, along with its prediction, is illustrated in Fig. 2. *Funded by the EU NextGenerationEU through the Recovery and Resilience Plan for Slovakia under the project No. 09I03-03-V04-00008.*

[1] R. Penin, J.-P. Lecointe, G. Parent., et al., IEEE Trans. Ind. Electron., Vol. 61, No. 8, p. 4374 (2014). [2] S. Lopez, B. Cassoret, J.-F. Brudny, et al., IEEE Trans. Magn., Vol 45, No. 10, p. 4161 (2009). [3] C. Demian, B. Cassoret, J.-F. Brudny, et al., IEEE Trans. Magn., Vol. 48, No. 4, p. 1409 (2012). [4] S. Dobák, J. Füzer, I. Petryshynets, et al., Appl. Phys. Lett., Vol. 123, Art. No. 242406 (2023).

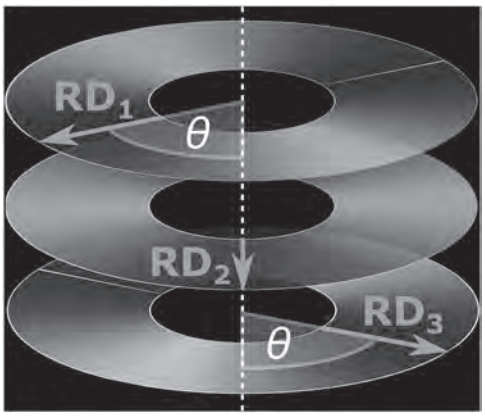

Fig. 1. Core configuration with RDs shifted by angle θ.

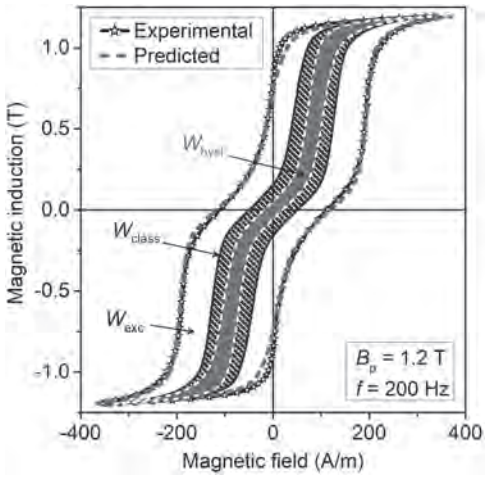

Fig. 2. Decomposed AC hysteresis loop measured in assembly with θ = 0° and its prediction by STL.

EG-05. Enhanced permeability of high-frequency $Nd_2Fe_{17}N_3$ magnetic powder with a reduced surface iron oxide layer by inert gas annealing.
J. Akamatsu[1], S. Abe[1] and N. Imaoka[1] *1. Magnet Material Development Dept., Nichia Corporation, Anan, Japan*

Our previous study [1] demonstrated that phosphoric acid coating and annealing $Nd_2Fe_{17}N_3$ in air improves both μ' and tanδ. However, the magnetic bonds between the powder particles were weak because the a-Fe_2O_3 layer on the top surface exhibited weak ferromagnetism. To solve this problem, we attempted to improve its magnetic properties by performing additional annealing after the aforementioned process. Additional annealing was tested at 420 °C with varying treatment times (15 min to 8 h) and atmospheres (Ar, H_2, N_2, and NH_3). Annealing in Ar or N_2 improved μ′ without degrading tanδ. The μ′ of the sample annealed at 420 °C for 4 h in Ar at 10 MHz increased from 10.39 to 12.81 after treatment (Fig. 1). In addition, X-ray diffraction analysis of the powder annealed in Ar showed that the 104 diffraction line at 33° for a-Fe_2O_3 weakened with increasing treatment time, and new diffraction lines appeared at approximately 57°. The peak of a-Fe_2O_3 almost disappeared after annealing for > 4 h. Through the conversion electron collection method, the Fourier-transformed radial distribution function of the Fe K-edge-extended X-ray absorption fine structure spectra of these powders revealed that the waveform of a-Fe_2O_3 was consistent with that of the pre-treated sample, whereas that of the sample annealed for 4 h in Ar was consistent with that of Fe_3O_4 (Fig. 2). Furthermore, the valence state of Fe in the annealed powder was confirmed by X-ray photoelectron spectroscopy, and both trivalent and divalent Fe were present. These results show that annealing in a gas with no reducing effect, such as Ar, reduces the a-Fe_2O_3 on the surface to Fe_3O_4 using $Nd_2Fe_{17}N_3$ itself, increasing the volume of the magnetic material in the powder, further promoting magnetic bonding between the powders, and improving magnetic permeability.

J. Akamatsu, S. Abe, and N. Imaoka, "High-Frequency Magnetic Properties of Nd $_2$ Fe $_{17}$ N $_3$ Magnetic Powders With Nano-α-Fe Phase-Separated Surface Layers", *IEEE Trans. Magn.*, Vol. 59, 2300405 (2023)

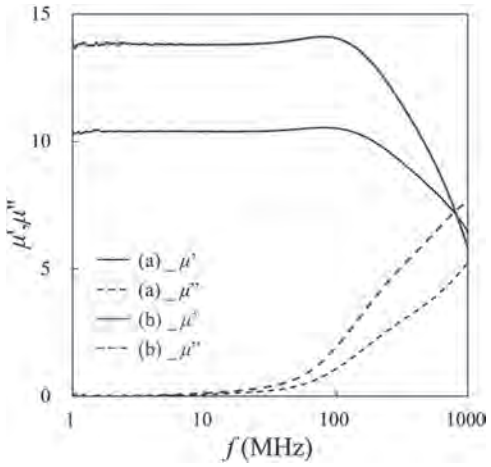

Fig. 1. Comparison of the complex permeability of $Nd_2Fe_{17}N_3$ samples before and after additional annealing in Ar: (a) before additional annealing; and (b) after additional annealing.

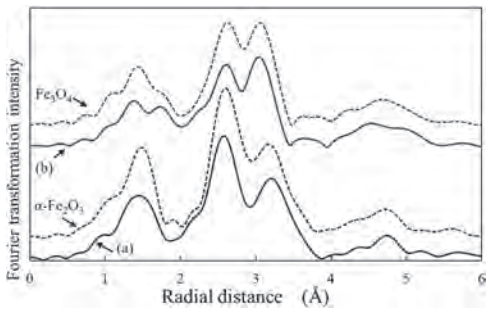

Fig. 2. Radial distribution function of the $Nd_2Fe_{17}N_3$ powders by X-ray absorption fine structure spectroscopy: (a) before additional annealing; and (b) after additional annealing.

EG-06. Statistical modeling of soft magnetic composites' permeability.
F. Mazaleyrat[1] *1. SATIE CNRS, ENS Paris-Saclay, Gif-sur-Yvette, France*

Soft magnetic composites (SMC) also known as powder cores are widely used in many applications because of their linearity, controllable permeability and isotropy. Because of the distributed air gap, the permeability is governed by the inner demagnetizing fields. To model the permeability dependence on the filling fraction, essentially two approaches are used both based on spatial periodicity hypothesis: the non magnetic grain boundary model [1] and the effective medium theory [2]. Actually, the first one works only for dense materials and the second works at low concentration. Both need fitting of two parameters, the inner demagnetizing factor and the particle susceptibility, just because the periodicity hypothesis is never verified for magnetic filling factors larger than 20%. A breakaway model is proposed based on the computation of mathematical esperance of the statistical distribution of magnetic chains and the subsequent determination of demagnetizing coefficient of an ellipsoid of equivalent aspect ratio. The model is collated with permeability data from the literature for spherical or non-spherical particles based SMCs and shows a excellent agreement with only one or even without fitting parameter in the whole concentration range.

[1] M. Johnson, E. Visser, A coherent model for the complex permeability in polycrystalline ferrites, IEEE transactions on magnetics 26 (5) (1990) 1987–1989. [2] J.-L. Mattei, A. Konn, M. Le Floc'h, Magnetic behavior of heterogeneous magnetic materials, IEEE Trans Instrum Meas 42 (2) (1993) 121–125.

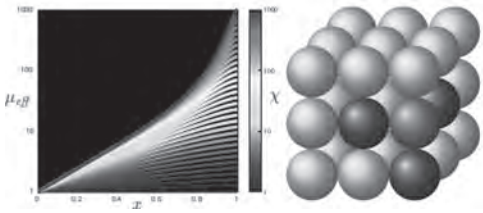

Effective permeability dependence on the magnetic particles volume fraction and intrinsic suceptibility.

EG-07. The Impact of the Physical, Electrical and Magnetic Properties of Ferromagnetic Materials on their Excess Loss. *S. Jacobs*[1] and J. Rens[2] *1. ArcelorMittal Global R&D, Zwijnaarde, Belgium; 2. ArcelorMittal Global R&D Gent, Zwijnaarde, Belgium*

The excess loss (Pexc) in a ferromagnetic material is linked to the eddy currents generated due to the domain wall movements during the subsequent magnetising and demagnetising fields in AC applications [1]. Theory [2] describes a dependency of this Pexc to the frequency with a power of 1.5. This implies the Pexc does not increase as fast with the frequency as the induced eddy current loss, but it does bring a substantial loss component in high speed automotive and flight powertrain applications. The Pexc of a series of electrical steels (ES) with different thickness, electrical resistivity, texture and grain size, is studied in an Epstein frame set-up. The total measured losses are split between hysteresis loss (corrected for flux redistribution), eddy current loss (corrected for flux redistribution and edge effects due to the lamination width), resulting in a Pexc matrix per material over a frequency and polarisation range, that is matching machine exploitation conditions. The loss models [2,3,4] are the basis for describing the dependency of the Pexc, on physical parameters such as thickness, grain size, texture. The Pexc description is performed in the time domain, to integrate all wave forms occurring at different depths in the lamination thickness. The model improvement is based on integrating the maximum permeability as parameter that differentiates the domain wall movement in the magnetisation behaviour. Further analysis identifies the number of domain walls throughout the thickness of the lamination. It proves the impact of the flux redistribution on the excess loss. Fig. 1 shows for a semi-processed (SP) ES the waveforms in the lamination at different working points. Fig. 2 shows both the evolution of the number of domain walls and Pexc, from the center of the lamination to its outer skin, for the same working points. The model is further deployed on other ES examples and interpreted to their physical properties.

[1] R. Bozorth, Ferromagnetism, IEEE Press, edition of 1993 [2] G. Bertotti, "General Properties of Power Losses in Soft Ferromagnetic Materials", IEEE Transaction on Magnetics, vol. 24, no. 1, January 1988 [3] I.D. Mayergoyz, "Dynamic Preisach Models of Hysteresis", IEEE Transactions on Magnetics, vol. 24, no. 6, November 1988 [4] S.E. Zirka et al., " Measurement and Modeling of B-H Loops and Losses of High Silicon Nonoriented Steels", IEEE Transactions on Magnetics, vol. 42, no. 10, October 2006.

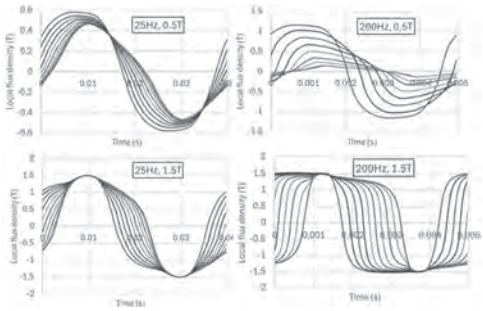

Local polarisation waveforms through the lamination thickness, for average flux densities of 0.5 and 1.5 T and frequencies of 25 and 200 Hz, for a SP ES.

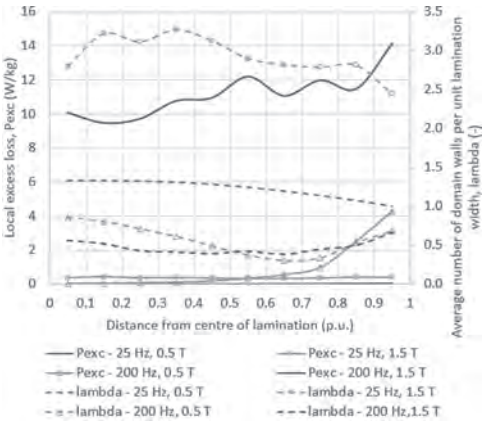

Evolution of the number of domain walls and the excess loss, through the lamination thickness, for the working points and ES of Fig. 1.

EG-08. Development of Co-rich glass-coated microwires with high GMI effect. A. Gonzalez Villegas[1,2], P. Corte-Leon[1,2,4], V. Zhukova[1,2], J. Blanco[2,3] and *A. Zhukov*[1,2,3] *1. Department Polymers and Advanced Materials, University of Basque Country, San Sebastian, Spain; 2. Department Applied Physics, University of Basque Country, San Sebastian, Spain; 3. Ikerbasque, Bilbao, Spain; 4. Department of Materials Science & Metallurgy, University of Cambridge, Cambridge, United Kingdom*

In the past years, studies of glass-coated amorphous microwires have attracted attention, due to their versatility in multiple sensing capabilities such as their magnetic softness and magnetic bistability, the Giant Magneto-Impedance (GMI) effect, and good mechanical properties and high corrosion resistance [1,2]. The fabrication technique allows the preparation of amorphous microwires with diameters from 100 nm to 100 μm [2]. The main interest in GMI effect is related to its giant sensitivity to applied magnetic field, H: experimentally observed above 600 % change of impedance, Z, under applied magnetic field about 800 A/m [3]. The performance of sensors and devices utilizing the GMI effect is critically affected by the GMI ratio value. Accordingly, we studied the effect of annealing (up to 350 °C) on the hysteresis loops and GMI ratio, $\Delta Z/Z$, of $Co_{72}Fe_4B_{13}Si_{11}$ glass-coated microwire prepared using Taylor-Ulitovsky method with metallic nucleus diameter about 40 μm and total diameter 45 μm. Using X-ray diffraction we observed and prepared materials are amorphous. Low and negative magnetostriction coefficient of as-prepared microwires is obtained using the small-angle magnetization rotation method. Even as-prepared microwire presents rather soft magnetic properties: coercivity, H_c, about 20 A/m and magnetic anisotropy field, H_k, about 170 A/m (see Fig.1a). After annealing we observed that the main change of the hysteresis loops consists of a decrease in H_k –value up to $H_k \approx 75$ A/m, while the H_c remains almost unchanged ($H_c \approx 24$ A/m, see Figs 1b-d). High GMI ratio ($\Delta Z/Z \approx 400$ %) is observed in as-prepared sample. A remarkable GMI ratio improvement up to above 700% is observed after annealing at appropriate conditions (see Fig.2b-d).

The observed change in the hysteresis loop shape and in ΔZ/Z - value and magnetic field dependence upon annealing are discussed in terms of the internal stresses relaxation and modification in the magnetostriction coefficient sign and values.

[1] H Chiriac, T.A. Óvári, Amorphous glass-covered magnetic wires: preparation, properties, applications, Progr. Mater. Sci. 40 (5) (1996) 333-407. [2] A. Zhukov, M. Ipatov, P. Corte-León, L. Gonzalez- Legarreta, M. Churyukanova, J.M. Blanco, J. Gonzalez, S. Taskaev, B. Hernando and V. Zhukova, J. Alloys Compd. 814 (2020) 152225.

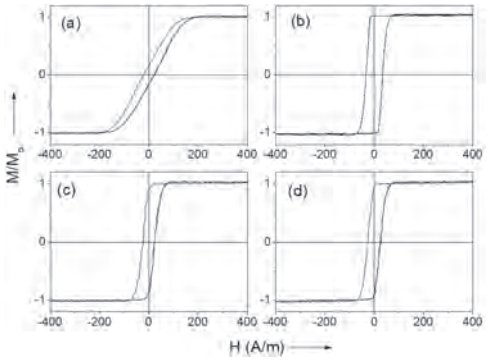

Fig. 1. Hysteresis loops of as-prepared (a) and annealed at T_{ann}= 275 °C (b), T_{ann}= 300 °C (c) and T_{ann}= 350 °C (d) $Co_{72}Fe_4B_{13}Si_{11}$ sample.

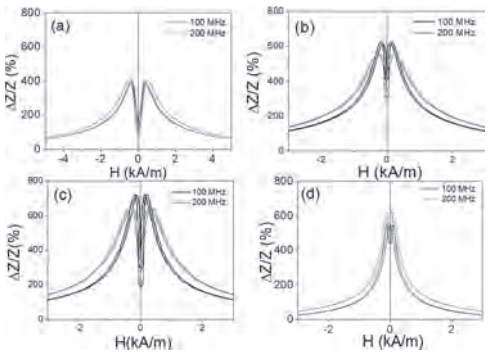

ΔZ/Z(*H*) dependencies measured in as-prepared (a) and annealed at 275 °C (b); 300 C(c) and 350 °C (d) microwires.

EG-09. Magnetic, structural, and transport properties of Heusler alloy Cr_2FeSn. *G. Karthik*[1] and R. Kuppan[1] *1. Department of Nuclear Physics, University of Madras, Chennai, India*

The study of magnetic properties of Heusler alloys have attracted immense attention in recent times due to their fascinating properties such as high spin polarization, half metallicity, crystalline ordering and low damping constant which makes them potential applicants in ultralow power spintronic devices [1,2]. In this study, we have explored how the structural disorderness of Heusler alloy Cr_2FeSn (CFS) influences its physical transport characteristics. The full Heusler alloy was synthesized by vacuum arc melting followed by vacuum annealing. In order to investigate the structure and composition of the prepared CFS sample, X-ray diffraction and electron microscopy analysis has been carried out. We infer that the sample has a disordered phase of the $L2_1$ type, with secondary phases of FeSn and Sn. Further, local electrode atom probe (LEAP) analysis was performed and we see that the elements are homogeneously distributed in the full Heusler phase. Magnetic measurements performed using SQUID suggest that the alloy is soft ferromagnetic in nature having low coercive field values with a saturation magnetization of 1.5 μ/f.u. (at 4K) and a Curie temperature of 375K. The intrinsic structural disorder dramatically affects the thermal and electrical transport in the sample. At the high-Sn end, strange thermal transport behavior with unusually low thermal conductivity ~7.6 W/mK at 8K is observed for CFS. By analyzing transport properties of CFS, we observe that the linear magnetoresistance obtained is mainly dominated by the high-mobility bulk electron carriers present in the sample. Also, we notice that the secondary phase of non-cubic FeSn intermetallic is highly anisotropic in behaviour at low temperatures. We further predict that the reduced electrical conductivity can be correlated with the microstructure of the sample. We believe that these findings are useful for further investigation towards the design of potential bulk materials for magnetic Heusler alloy applications and also allow us to comprehend the effect of the kind and degree of disorder on its functional properties.

Zhang, Xiaoqian, et al. “Direct observation of high spin polarization in Co2FeAl thin films.” Scientific Reports 8.1 (2018): 8074. Feng, Yu, et al. “Ultrahigh spin transport performance in Ti2CoGe based magnetic tunnel junction.” Journal of Magnetism and Magnetic Materials 492 (2019): 165669. Karati, Anirudha, et al. “Ti2NiCoSnSb-a new half-Heusler type high-entropy alloy showing simultaneousincrease in Seebeck coefficient and electrical conductivity for thermoelectric applications.” Scientific reports 9.1(2019): 1-12.

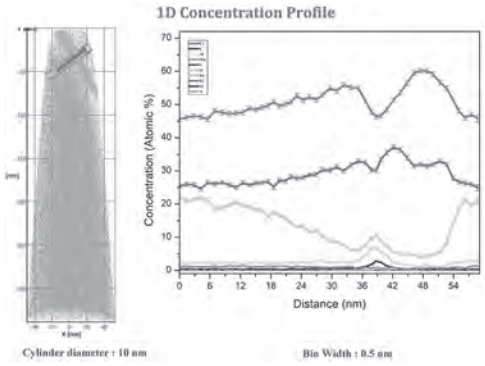

Fig.1 APT study showing composition profile of Cr_2FeSn alloy.

EG-10. Effects of Isothermal Aging on the Magnetic Properties of Non-Oriented Electrical Steels: Interpretation Based on the Iron Loss Separation Approach. *L. Saleh*[1], O. Messal[1], A. Benabou[1] and M. Dumont[2] *1. Electrical Engineering and Power Electronics Laboratory, University of Lille, Lille, France; 2. Mechanics, Surfaces and Materials Processing (MSMP), Ecole Nationale Supérieure d’Arts et Métiers, Lille, France*

Non-oriented (NO) electrical steels (ES) are used in numerous applications, from electrical motors and generators to various magnetic components in electrotechnical equipment. During their life-cycle, these ES are subjected to high temperatures due to the working conditions as well as iron and Joule losses. High temperatures over time can activate the unwanted magnetic aging phenomenon, i.e., the irreversible impairment of the ES magnetic properties. Indeed, in the presence of excess carbon, the latter precipitates as iron carbides that impede the domain wall motion during magnetization. The major effect of magnetic aging in terms of the ES usage properties is the increase in iron losses [1] - [4]. In this work, the effects of isothermal aging on a commercial NO ES are investigated and interpreted through the changes in iron losses as well as the nature and the underlying causes of these losses. An experimental study was performed on a set of NO ES samples of the same grade. Each sample underwent an isothermal heat treatment at one of the 3 temperatures 160, 180 and 200°C for up to 300 hours which consisted of multiple heating intervals interrupted by air-cooling stages to measure the sample magnetic properties at RT using a single strip tester. Almost 50,000 B-H hysteresis loops were measured along the rolling direction under B sine waveform over the magnetizing frequency range of 10 to 100 Hz for induction peak values in the range 0.025 T - 1.75 T. Then, using the acquired measurements, the loss separation approach [5] in which the specific losses are separated into 3 components (hysteresis, classical and excess losses) was performed. The effects of aging on each loss component were then examined as a function of time, aging temperature, peak induction value, and

frequency. The results reveal that the increase in iron losses is mainly due to hysteresis losses while the excess losses are less sensitive to aging [Fig.1]. In contrast, the eddy current losses are insensitive to aging time. These results are to be further employed in an iron loss separation based-modeling approach to predict the iron loss evolution with aging time.

[1] S. K. Ray and O. N. Mohanty, "Magnetic ageing characteristics of low silicon electrical steels", J. Magn. Magn. Mater., Vol. 28, no. 1–2, p. 44–50 (1982) [2] M. F. De Campos, M. Emura, and F. J. G. Landgraf, "Consequences of magnetic aging for iron losses in electrical steels", J. Magn. Magn. Mater., Vol. 304, no. 2, p. e593–e595 (2006) [3] G. M. R. Negri, N. Sadowski, N. J. Batistela *et al.*, "Magnetic Aging Effect Losses on Electrical Steels", IEEE Trans. Magn., Vol. 52, no. 5, p. 1–4 (2016) [4] H. Helbling, M. Toto-Jamil, M. Dumont, *et. al.*, "Temperature-dependent modelling of magnetic ageing of FeSi electrical steels", Journal of Magnetism and Magnetic Materials, Vol. 564, p. 170051 (2022) [5] G. Bertotti, "Hysteresis in magnetism: for physicists, materials scientists, and engineers", Academic Press (1998).

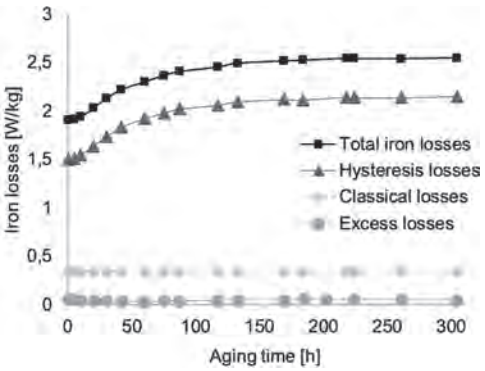

Iron losses vs. time at 1 T, 50 Hz, for an aging temperature of 180°C

EG-11. Permeability enhancement and eddy current suppression of the bioinspired nacre structural soft magnetic composites for high frequency application. *W. Li*[1], W. Xiang[1], H. Cai[1], Y. Ying[1] and S. Che[1]
1. Zhejiang University of Technology, Hangz, China

The bioinspired nacre structural soft magnetic composites are fabricated by the highly planar arrangement of flaky-Sendust (thickness ~1μm) and flaky nanocrystalline particles (thickness ~20μm) respectively. These composites, characterized by densely planar-oriented particles, exhibit exceptionally high permeability and low loss, making them highly suitable for high-frequency energy transformation applications. The flaky nanocrystalline particles, due to their hardness, were hot-pressed in the supercooled liquid region to achieve high density, simultaneously forming nanocrystals within the amorphous matrix. The internal structures/microstructure evolution of the flaky nanocrystalline particles has been thoroughly studied. While the flaky-Sendusts were cold pressed. The novelty textured nacre structural flaky nanocrystalline composite exhibits a high maximum permeability of 2170 (at 1000 Hz) and low magnetic loss of 41.61 W/kg (at 1.0 T and 1000 Hz), surpassing the frequency performance of silicon steel. While flaky-Sendust composites exhibit the high permeability up to 600 at 1 MHz which is ten times of the common Sendust composites. The total loss is reduced to 470.82 and 1162.60 kW/m^3 at 100 and 200 kHz stimulated at 100 mT. This remarkable performance is attributed to the anisotropic demagnetizing factor for the laminated structure of the flaky particles. The total loss is significantly reduced for the suppressed eddy current due to the thin thickness less than the skin depth. Compared to the traditional SMC and silicon steel, these novel SMCs exhibits great porential in high frequency power switching device, noise filter and electric machines.

[1] Wangchang Li, Yang Zheng, Yue Kang, Ansar Masood, Yao Ying, Juan Li, Shenglei Che. Magnetic behavior of soft magnetic composites constructed by rapidly quenched flake-like FeSiAl alloy. Journal of Alloys and Compounds 819 (2020) 153028. [2] Wangchang Li, Haowen Cai, Yue Kang, Yao Ying, Jing Yu, Jingwu Zheng, Liang. Qiao, Ye Jiang, Shenglei Che, High permeability and low loss bioinspired soft magnetic composites with nacre-like structure for high frequency applications, Acta Materialia 167 (2019) 267-274.

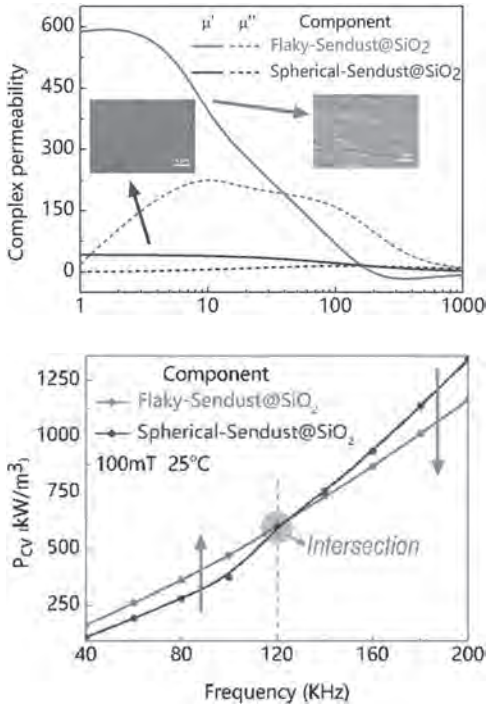

EG-13. Quaternary magnetic semiconductors for photonic and spintronic applications. *O. Yastrubchak*[2], N. Tataryn[1], S. Mamykin[1], V. Romanyuk[1], O. Kondratenko[1], O. Kolomys[2], L. Borkovska[3], L. Khomenkova[3], J. Furdyna[4], B.A. Assaf[4], X. Liu[4] and Y. Ichiyanagi[5]
1. Department of Kinetic Phenomena and Polaritonics, V. E. Lashkaryov Institute of Semiconductor Physics, National Academy of Sciences of Ukraine, Kyiv, Ukraine; 2. Optical Submicron Spectroscopy Lab, V. E. Lashkaryov Institute of Semiconductor Physics, National Academy of Sciences of Ukraine, Kyiv, Ukraine; 3. Department of Sensor Systems, V. E. Lashkaryov Institute of Semiconductor Physics, National Academy of Sciences of Ukraine, Kyiv, Ukraine; 4. Department of Physics and Astronomy, University of Notre Dame, Notre Dame, IN, United States; 5. Department of Physics, Graduate School of Engineering Science, Yokohama National University, Yokohama, Japan

Dilute ferromagnetic semiconductors (DFMSs) are a class of alloys that merge semiconductor traits with magnetism within a single material [1]. Their magnetic characteristics stem from the inclusion of transition metal ions (Mn) into the parent lattice of the semiconductor (GaAs). The distinguishing feature of spintronic devices based on DFMSs lies in their ability to generate spin-polarized currents. Besides the generation of spin current, which is pertinent to spintronics, it is anticipated that modifications in the band structure due to the presence of additional doping ions such as In, P, or Bi in the (Ga,Mn)As matrix will engender innovative DFMS device concepts [2-5]. The spin-orbit coupling engenders numerous phenomena in magnetic materials such as (Ga,Mn)As, including anisotropic magnetoresistance (AMR), planar Hall effect (PHE), and spin-orbit torque. We have investigated (Ga,Mn)(P,As), (Ga,Mn)(Bi,As), and (In,Ga,Mn)As and reference GaAs and Ga(P,As), Ga(Bi,As) and (In,Ga)As layers, grown on (001)-oriented GaAs substrates at 230°C by low-temperature molecular-beam epitaxy. The spectroscopy results are consistent with the valence-band model of hole-mediated ferromagnetism in the (Ga,Mn)(Bi,As) and (In,Ga,Mn)As layers. They reveal a downward shift of the chemical potential for Mn-doped epilayers, and a highly dispersed band crossing the Fermi

level for high Mn contents. It is found that Bi and In ions cause significant modifications to the spin-split-off band. The optical gap of as grown (Ga,Mn)(As,P) is slightly smaller than that of Ga(As,P). These observations can be interpreted by considering a Mn impurity band that pins Fermi level above the valence band edge in as grown samples. The quaternary (Ga,Mn)(Bi,As), (In,Ga,Mn)As, and (Ga,Mn)(P,As) combine the properties of (Ga,Mn)As, Ga(Bi,As), (In,Ga)As and Ga(P,As) ternary compounds respectively and offer the possibility of tailoring the band-gap structure to the requirements of novel device functionalities for future spintronic and photonic applications [5-13]. This work was sponsored by the CRDF grant - RFP DE-01-2023 'Ukraine Cybersecurity and Alternative Energy Research Competition (G-202401-71628).

1. Ohno H., Making nonmagnetic semiconductors ferromagnetic // Science.-1998.-281.-P. 951-956. 2. Tataryn N., et al., Valence Band Dispersion in Bi Doped (Ga,Mn)As Epitaxial Layers // *IEEE Transactions on Magnetics*.-2023.-59.-P. 1-5. 3. Yastrubchak O., et al., Band Engineering of Magnetic (Ga,Mn)As Semiconductors by Phosphorus Doping // *IEEE Transactions on Magnetics*.-2023.-59.-P. 1-6. 4. Yastrubchak O., et al., Influence of Bi doping on the electronic structure of (Ga,Mn)As epitaxial layers // Scientific Reports.-2023.-13.-P. 17278. 5. Medjanik K., et. al., Site-specific atomic order and band structure tailoring in the diluted magnetic semiconductor (In,Ga,Mn)As // Phys. Rev. B.-2021.-103.-P. 075107. 6. Lemaître A., et al., Strain control of the magnetic anisotropy in (Ga,Mn)(As,P) ferromagnetic semiconductor layers // Appl. Phys. Lett.-2008.-93.-P. 021123. 7. Yastrubchak O., et al., Effect of low-temperature annealing on the electronic- and band-structures of (Ga, Mn) As epitaxial layers // J. Appl. Phys.-2014.-115.-P. 012009. 8. Yastrubchak O., et al., Strain release in InGaAs/InxAl1−xAs/InP heterostructures // Physica B: Condensed Matter.-2003.-340.–342.-P. 1082-1085. 9. Yastrubchak O., et al., Electronic and band-structure evolution in low-doped (Ga,Mn)As // J. Appl. Phys.-2013.-115.-P. 053710. 10. Yastrubchak O., et al., Anisotropic strain relaxation in lattice mismatched III–V epitaxial layers // Phys. Stat. Sol. (c),-2005.-2.-P. 1943-1947. 11. Gluba L., et al., On the nature of the Mn-related states in the band structure of (Ga, Mn) As alloys via probing the E_1 and $E_1+\Delta_1$ optical transitions, // Appl. Phys. Lett.-2014.-105.-P. 032408. 12. Dmitruk N. L., et al., Multilayer diffraction gratings Al/GaAs as polaritonic photodetectors // Phys. Stat. Sol. (a).-2001.-184.-P. 165-174. 13. Dmitruk N. L., et al., Ultraviolet responsivity control in Schottky barrier heterostructures with textured interface // Thin Solid Films.-2000.-364.-P. 280-283.

EG-14. Theoretical and experimental investigation of half-metallic properties in V_2CoAl. P. Kharel[1], C. Brown[1], B. Schmidt[2], C. Sadler[2], S. Diallo[2], M. Anas[1], P. Shand[2] and *P. Lukashev*[2] *1. Chemistry, Biochemistry and Physics, South Dakota State University, Brookings, SD, United States; 2. Physics, University of Northern Iowa, Cedar Falls, IA, United States*

We present results of a combined experimental and computational investigation of electronic, magnetic, and structural properties of V_2CoAl, a Heusler compound exhibiting nearly half-metallic electronic structure at equilibrium. Our calculations indicate that this alloy crystallizes in inverted Heusler cubic structure. The magnetic alignment of this material is ferrimagnetic, due to the anti-aligned magnetic moment of two vanadium sub-lattices. V_2CoAl retains its nearly perfect spin polarization under compression of the unit cell volume. At the same time, the spin polarization is strongly reduced under expansion of the unit cell volume. The reduction of the spin polarization at larger lattice constants is due to the rigid shift of the spin-up states, which results in modified exchange splitting. Although the perfectly ordered cubic structure is assumed in the theoretical calculations, the bulk sample prepared using arc melting and annealing crystallizes in the disordered cubic structure. With proper annealing conditions (700 °C for 1 week), samples with B2 type disorder have been obtained. The disordered sample shows ferrimagnetic order with a Curie temperature of about 80 K (see Fig. 1), and high-field (H = 9 T) magnetization at 2K of 0.6 emu/g. In this presentation, we will also discuss the computational results on the effect of disorder and the electrical transport properties measured on the disordered samples. This research is supported by the *National Science Foundation* (NSF) under Grant Numbers 2003828 and 2003856 via DMR and EPSCoR. Mohd Anas is supported by DOE EPSCoR (DE-SC0024284) grant.

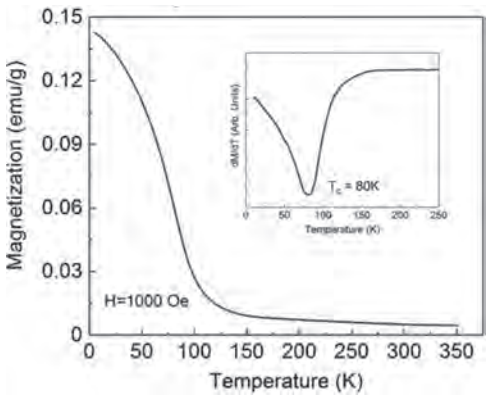

Thermomagnetic curve of V_2CoAl. The inset shows the dM/dT versus T curve indicating the Curie temperature.

EG-15. Ultra-stable Weyl topology in association with magnetic textures in shandite compound $Co_3Sn_2S_{(2-x)}Se_x$. *D. Le*[1], B. Konushbaev[1], G.M. Pantano[1], Y. Mokrousov[3,2], M. Phan[1] and J.D. Gayles[1] *1. Department of Physics, University of South Florida, Tampa, FL, United States; 2. Institute of Physics, Johannes Gutenberg University Mainz, Mainz, Germany; 3. Peter Grünberg Institut and Institute for Advanced Simulation, Forschungszentrum Jülich and JARA, Jülich, Germany*

The shandite compounds $Co_3Sn_2S_2$ and $Co_3Sn_2Se_2$ have garnered great interest due to a large momentum space Berry curvature that drives topological phenomena. One significant aspect of the Berry curvature is its role in the anomalous Hall and Nernst effects, which are maximized at the Weyl nodes [1]. On the other hand, the presence of inversion symmetry results in the Berry curvatures of the Dzyaloshinkii-Moriya interactions (DMI) summing to zero. Therefore, it is unexpected to observe topological textures, such as skyrmions, at finite temperatures. Nevertheless, there is experimental evidence that $Co_3Sn_2S_2$ can host a skyrmionic A phase where still preserving inversion symmetry [2]. Moreover, while the fabrication of $Co_3Sn_2Se_2$ remains challenging, experimental results have demonstrated the stability of a metastable state in Co_3Sn_2SeS a new shandite candidate [3]. However, there is current limited theoretical understanding of the magnetic and electronic structure required to investigate the stability of Weyl crossings and the hosting of skyrmions. In this study, we employ first principles, tight binding calculations and symmetry analysis to compare the effects of varying the composition of $Co_3Sn_2S_{(2-x)}Se_x$ compounds. Specifically, $Co_3Sn_2S_2$ and $Co_3Sn_2Se_2$ (x=0 or 2, respectively) retain inversion symmetry, whereas Co_3Sn_2SeS (x=1) lacks inversion symmetry. Our results illustrate the phase transition for the ultra-stable Weyl crossings with distinct magnetic textures, as show in Fig. 1. We investigate the impact of magnetic structures on the topological electronic structures, thereby formulating a complete diagram of this system. Despite Co_3Sn_2SeS favoring DMI which aids in stabilizing topological structures, we find that topological-chiral interactions play a predominant role. The $Co_3Sn_2S_{(2-x)}Se_x$ compounds will thus serve as one of the pioneering real systems capable of simultaneously hosting both skyrmions and ultra-stable Weyl features. This opens future possibilities for manipulating intrinsic skyrmions via the chiral anomalous effects.

[1] Liu, Enke, et al. Nature physics 14.11 (2018): 1125-1131. [2] Wu, H. C., et al. Materials Today Physics 12 (2020): 100189. [3] Shin, Dong-Hwa, et al. arXiv preprint arXiv:2105.03892 (2021).

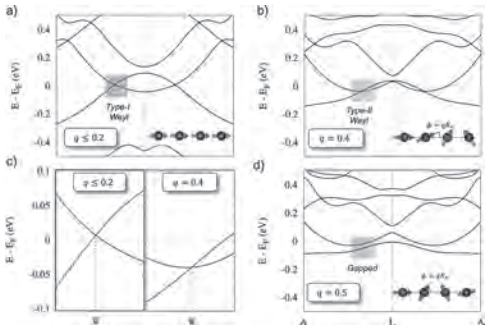

Fig 1. Phase transition in $Co_3Sn_2S_2$ band structures. (a) Type-I Weyl in red, (b) Type-II Wey in green, (c) Zoom-in Weyl crossing of (a) and (b), respectively, and (d) Gapped in blue.

Session EP
HARD MAGNETS III
(Poster Session)

Xin Tang, Chair
National Institute for Materials Science (NIMS), Tsukuba, Japan

EP-01. Aluminum praseodymium doped M type ferrite for replacing rare earth magnets in EVS motor applications. *D. Sharma*[1], A. Dogra[2] and M. Singh[1] *1. Physics, Himachal Pradesh University, Shimla, India; 2. Physics, CSIR NPL, Delhi, India*

The growing demand for electric vehicles, driven by the need for increased efficiency, has spurred efforts to find alternatives to costly rare earth magnets such as NdFeB. One promising solution is M-type strontium ferrite, which offers favorable magnetic properties suitable for electric vehicle motors at a lower cost. This study aims to synthesize and characterize $SrFe_{12-x}Al_2O_{19}$ and $Sr_{1-x}Pr_xFe_{10}Al_2O_{19}$ (with x = 0.05 - 0.20 representing Pr substitution) hexaferrites. Utilizing the auto-combustion sol-gel technique, ferrite nanoparticles were prepared, benefiting from straightforward preparation, chemical uniformity, and a well-defined crystalline structure. XRD structural analysis confirmed the formation of single-phase M-type hexaferrite in all samples, with some impurity phases at higher Pr-Al concentrations. The addition of Al-Pr in pure M-type ferrite led to a reduction in lattice constant and cell volume. SEM images verified the samples' surface morphology. Magnetic studies via VSM showed that Al^{3+} doping increased coercivity from 5500 Oe to 10500 Oe, mainly due to reduced grain size and enhanced magneto-crystalline anisotropy. Pr doping had a nuanced effect on magnetic properties, raising the remanence from 17 emu/g to 23.05 emu/g. These findings suggest that precise control of dopant levels in M-type hexaferrites can significantly enhance their magnetic properties, presenting them as promising alternatives to rare earth magnets in electric vehicle applications.

EP-02. Facile synthesis and magnetic characterization of FeNi magnetic alloys. *P. Agoeyevu*[1], M. Jiang[2] and E. Carpenter[1] *1. Chemistry, Virginia Commonwealth University, Richmond, VA, United States; 2. Department of Chemical and Life Science Engineering, Virginia Commonwealth University, Richmond, VA, United States*

Iron – Nickel alloys have been a persistent magnetic alloy for many decades. In recent years, has received new attention due to the discovery of the mineral tetrataenite in meteorites. This L10 phase of iron–nickel possesses good magnetic properties that could rival those of rare-earth- based magnets. Herein, we report the attempted synthesis of tetrataenite from Iron Nickel Oxalate microspheres. The microsphere precursor was synthesized using an innovative and easily scalable continuous flow process resulting in highly uniform homogeneous precursors which once annealed under 10% hydrogen, convert to the $L1_0$ phase of iron-nickel alloy. Using an in-situ high-temperature stage on a PANalytical X'Pert Pro diffractometer, we were able to watch the evolution of the crystal phase as the sample was heated from 25 C to 900 °C. The XRD patterns and elemental composition measured by EDS showed that the Fe – Ni particles were mainly composed of cubic $Fe_{0.56}$ $Ni_{0.44}$ at 900 having an average particle size of 51.3 nm. The magnetic properties showed a saturation magnetization of 150.10 emu/g and a coercivity at room temperature of 19.89 emu/g. This innovative approach shows great promise as a means to synthesize magnetic alloys.

EP-03. Theoretical Estimate of Thermal Stability Range of α''–$Fe_{16}N_2$ Within the Iron Nitride Binary Phase Diagram. *P. Stoeckl*[1] and J. Wang[2,1] *1. Physics, University of Minnesota, Minneapolis, MN, United States; 2. Electrical and Computer Engineering, University of Minnesota, Minneapolis, MN, United States*

α''–$Fe_{16}N_2$ has been investigated as one of promising candidates for environment-friendly magnets. While giant saturation magnetization has previously been experimentally observed in α''–$Fe_{16}N_2$, its magnetic anisotropy and structural stability leave room for improvement. Recent theoretical studies have considered alloying $Fe_{16}N_2$ with various elements to improve the magnetic properties and/or stability against decomposition. However, estimates of stability in particular are typically restricted to simple ground-state-energy comparisons, effectively taken at 0 K. For a more practical measure of stability, we therefore extend ground-state energies, obtained with the plane-wave density-functional theory (DFT) code Quantum ESPRESSO, with appropriate empirical and/or statistical corrections to obtain free energies at arbitrary temperature. We then compare the stability of $Fe_{16}N_2$ against the neighboring phases and phase combinations in the Fe-N binary system within the Compound Energy Formalism, to estimate the range of temperatures at which it is stable. Depending on choice of correction terms, $Fe_{16}N_2$ may be predicted to persist well above 800 K with simple corrections, or limited to < 450 K yielding to α–Fe + ε–Fe_3N at higher temperatures with more advanced terms. We compare against experimental observations of formation enthalpies and the Fe–N phase diagram, and discuss the effect and relative accuracy of different correction terms.

[1] P. Stoeckl, P. Swatek, & J.-P. Wang, *AIP Advances* 14(1), 015047 (2024). See also, *e.g.*: [2] M. H. Han et al., J. Phys.: Cond. Mat. 32(3), 035801 (2019). [3] Z. You et al., J. Phase Equilib. Diffus. 39, 650–677 (2018)

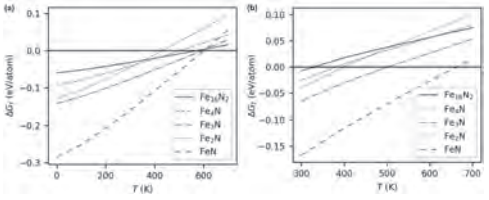

Free energies of formation of ordered Fe–N phases from ΔE_{DFT} plus corrections – (a) empirical *T*-dependent terms, (b) statistical correction terms. Adapted from previous work in ref. [1].

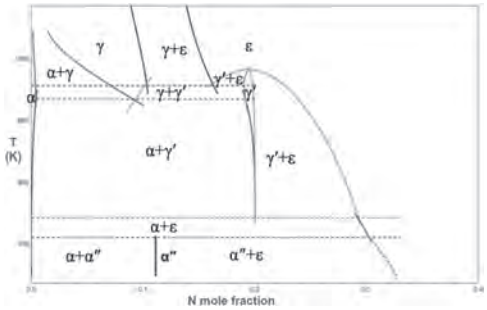

Prospective phase diagram for binary Fe–N including ordered α''–$Fe_{16}N_2$ (ab-initio plus statistical correction terms). Preliminary result.

EP-05. Sm-Fe-N Bulk Magnets Prepared by Hot Pressing Using Zn-Coated Magnetic Powder by Electrodeposition. *S. Che*[1], D. Shi[1] and J. Zheng[1] *1. Research Center of Magnetic and Electronic Materials, Zhejiang University of Technology, Huzhou, China*

Sm-Fe-N has comparable saturation magnetization intensity together with a magnetic anisotropy field three times higher and a Curie temperature 160 K higher than those of Nd-Fe-B. However, Sm-Fe-N decomposes around 620 °C, resulting in the disappearance of permanent magnetic properties, so it is impossible to prepare bulk magnets by high-temperature sintering like Nd-Fe-B. The use of low melting point metals such as Zn as bonding materials to prepare high-density all-metal bulk Sm-Fe-N magnets is a useful choice. To increase the (BH)max of the Sm-Fe-N magnets, adequate dispersion of Sm-Fe-N magnetic powders and Zn powders with limited content is the key. However, magnetic powder is mixed directly with Zn powder in most studies at present, which is difficult to achieve a uniform mixing. In this paper, a uniform and low-oxygen-content Zn coating was electrodeposited on the surface of Sm-Fe-N magnetic powders in an ionic liquid by a homemade magnetic stirring fluidized bed electrodeposition equipment. Subsequently, Sm-Fe-N/Zn composite magnets were obtained by hot pressing. It is shown that the Zn content adjustments can be effectively realized by electrochemical amounts of electricity, and with the increase of Zn content, the intrinsic coercivity Hcj and the compressive strength δs of the magnet increase. Compared to directly mixing commercial Zn powders and Sm-Fe-N powders, The hot-pressed magnet prepared by electrodeposited magnetic powders has higher coercivity and compressive strength even though the Zn content is lower. This is attributed to the improved dispersion uniformity of the Zn powders with the magnetic powders, as well as the reduced oxygen content of the powders. During hot pressing, the electrodeposited Zn particles melt at high temperatures and flow around the magnetic powder to form a "core-shell" structure. The properties of Sm-Fe-N bulk magnets obtained by hot pressing with magnetic powders containing 7.06 wt.% Zn coated are: (BH) max= 25.74 MGOe, HCj= 5.68 KOe, δs=174 MPa.

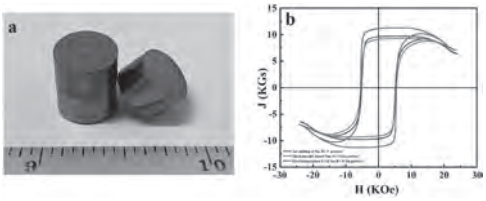

Physical diagram of Sm-Fe-N composite magnets obtained by hot pressing and the hysteresis line diagrams of composite magnets obtained by hot pressing with different raw materials.

EP-06. Understanding Structure-Composition-Property Relations in Manganese Zinc Nitride Antiperovkites. *C.E. Regier*[2], S. O'Donnell[1], S. Mahatara[1], R.W. Smaha[1], S. Lany[1] and J.R. Neilson[2,3] *1. National Renewable Energy Lab (NREL), Golden, CO, United States; 2. Chemisty, Colorado State University, Fort Collins, CO, United States; 3. Materials Science, Colorado State University, Fort Collins, CO, United States*

Permanent magnets are crucial to the increasing demand for renewable energy technologies. Currently, permanent magnets rely on rare-earth elements for high energy densities, but concerns with extraction procedures, and abundance have pushed for the discovery of new ferromagnetic materials. Transition metals have garnered interest as candidates due to their low cost, abundance, and paramagnetic nature. However, increasing both the magnetization and anisotropy of transition metal-based ferromagnets remains challenging. Therefore, our research proposes understanding crystal chemistry's role in influencing the magnetic anisotropy in 3*d* element-based ferromagnets. Antiperovskite nitrides with the general formula M_3AN, (*M* is a transition metal and *A* is a metal or metalloid) provide a chemical framework to investigate relationships between composition, crystalline anisotropy, and magnetic anisotropy. As presented here, Mn_3ZnN is paramagnetic at room temperature and exhibits complex phase transitions to an antiferromagnetic ground state. Deliberate topochemical denitridation, Mn_3ZnN_{1-x}, retains the crystalline arrangement of Mn and Zn but modifies the electron count in the material to produce a ferromagnet at room temperature. These relationships provide new approaches for high-energy density, transition-metal-based magnet discovery.

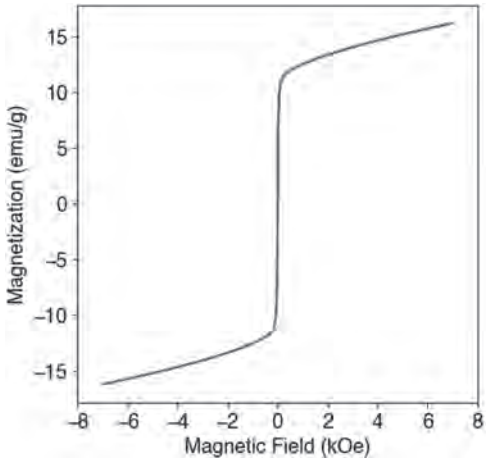

Figure 1: Magnetization vs Field for Mn_3ZnN_{1-x} at T = 2 K illustrating soft ferromagnetic behavior.

EP-07. Unusually High Coercivity of Sputtered $Fe_{16}N_2$ Thin Films. *E. Gokce-Polat*[1,3], B. Wolf[1], A. DeRuiter[2], W. Echtenkamp[1], H. Kim[4] and J. Wang[1] *1. Department of Electrical and Computer Engineering, University of Minnesota, Minneapolis, MN, United States; 2. Department of Chemical Engineering and Materials Science, University of Minnesota, Minneapolis, MN, United States; 3. Department of Engineering Physics, Istanbul Medeniyet University, Istanbul, Turkey; 4. Hyundai Motor Company, Uiwang-Si, The Republic of Korea*

In recent years, research into rare-earth-free permanent magnets (PM) has gained significant importance for the clean and renewable energy industries due to supply constraints and environmental concerns associated with rare-earth materials [1, 2]. Among the most promising candidates for new PM are $Fe_{16}N_2$ based systems, composed of abundant and environmentally friendly elements, offering high saturation magnetization(Ms) [3, 4]. However, a PM has not only a high Ms but also a reasonably high coercivity, which corresponds to resistance to demagnetization, is desired. Therefore, understanding and improving the coercivity mechanism of $Fe_{16}N_2$ is essential for its use as a substitute for rare-earth magnets in industrial applications such as electric vehicles[3]. In this study, $Fe_{16}N_2$ thin films have been fabricated epitaxially on MgO (001) single-crystal substrates via Fe (001) seed layers using a facing target sputtering system. Systematically investigated the thickness-dependent magnetic and structural properties in $Fe_{16}N_2$ thin films. The degree of N ordering in the α''- $Fe_{16}N_2$ (the N-disordered phase is α'-Fe_8N) reached 0.44 for the samples. The saturation field (Hs) reached approximately 7,200 Oe with increasing film thickness, indicating the formation of out-of-plane oriented domains and the existence of perpendicular magnetic anisotropy in the $Fe_{16}N_2$ films. In our study, it was observed that the coercivity is directly proportional to the Ms up to the critical thickness of 25 nm, whereas for thicker films (greater than 25 nm), the coercivity is inversely proportional to the Ms. At the critical thickness, a significant coercivity value of 884 Oe was obtained, which is considerably higher than that of a pure Fe sample at room temperature (Fig. 1). Furthermore, as the temperature decreases, the coercivity increases, reaching up to 980 Oe at 10 K (Fig. 2). The reasonably high coercivity found indicates that the $Fe_{16}N_2$ films possess hard magnetic properties, making them highly promising for advanced PM applications.

[1] J.M.D. Coey, Scripta Materialia Volume 67, Issue 6, September 2012, Pages 524-529 [2] J. Cui, M. Kramer, L. Zhou, F. Liu, ..., and, D. Sellmyer, Acta Materialia Volume 158, 1 October 2018, Pages 118-137. [3] J.-P. Wang, Journal of Magnetism and Magnetic Materials Volume 497, 1 March 2020, 165962 [4] N. Ji, Y Wu, and J.P. Wang, J. Appl. Phys. 109, 2011, 07B767.

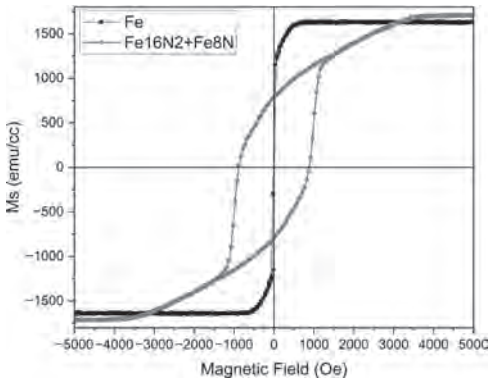

Fig. 1. In-plane M-H loops of samples Fe(16nm)MgO and (10nm) Fe-N(25nm)Fe(3.6nm)MgO) at room temperature

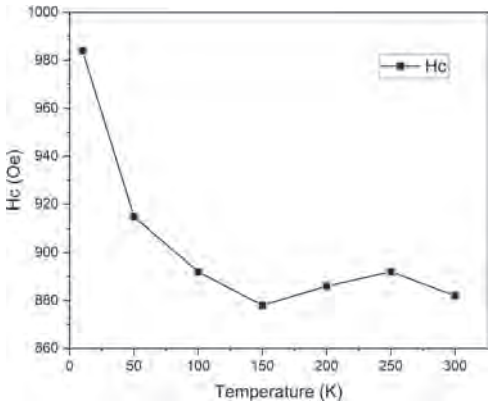

Fig. 2. Temperature dependence of the coercive field for sample Cr (10nm)Fe-N(25nm)Fe(3.6nm)MgO)

EP-08. Rare-earth free permanent magnet – triple-doped iron phosphide (Fe_2P). O. Narantogtokh[1], T. Namsrai[1], S. Dorj[1,2], J. Narmandakh[2], K. Baatartsogt[2], U. Enkhnaran[2], S. Deleg[2], O. Tumentsereg[3], *O. Dorj*[3] and O. Khorgolkhuu[4] *1. Department of Physics, National University of Mongolia, Ulaanbaatar, Mongolia; 2. Functional Material Laboratory, Institute of Physics and Technology, Mongolian Academy of Sciences, Ulaanbaatar, Mongolia; 3. Department of Physics, Incheon National University, Incheon, The Republic of Korea; 4. National Institute for Computational Sciences, Oak Ridge, TN, United States*

Iron phosphide (Fe 2 P) in hexagonal structure has attracted attention for permanent magnetic applications due to its large uniaxial magneto-crystalline anisotropy (2.32-2.68 MJ/m 3). This research aims to investigate the effects of alloying substitutions on Curie's temperature, which is the main limitation of Fe 2 P alloys for permanent magnet application while retaining its high magneto-crystalline anisotropy. We present our approach to designing new rare-earth free permanent magnets comparable to Nd 2 Fe 14 B in performance. The Density-functional Theory calculations on Fe 2 (P 1-x B x), Fe 2 (P 1-x-y B x Si y) and Fe 2-z (P 1-x-y B x Si y) alloys with x=0.04, y=0.04 to 0.16 and z=0.04 show that for the triple-doped Fe 2 P alloys, saturation magnetization is enhanced from μ 0 M S = 1.05 T to 1.14 T, coercivity from Ku = 2.99 MJ/m 3 to 1.10 MJ/m 3 and (BH) max from 27.90 MGOe to 32.82 MGOe. The Curie temperature exhibited a notable increase of approximately 37% (T C =450 K) at the low fraction of Mn, B and Si. In addition, the calculated thermodynamic stability of the alloys are -0.48 eV/atom, -0.46 eV/atom, and -0.48 eV/atom indicating that the compositions are stable within a triple-doping Mn-B-Si in Fe 2 P alloy.

[1] Yangkun He et al. Adv. Funct. Mater. 2021, 2107513 [2] R. Wäppling et al. J. Solid State Chemistry 3, 276 (1971). [3] D. Bellavance et al. J. Solid State Chem. 2 (1970) 285 [4] R. Fruchart et al. J. Applied Physics 40, 1250 (1969). [5] S. Chiba et al. J. Physical Society of Japan 15, 581 (1960). [6] M. Sagawa et al. J. Appl. Phys. 57, 4094 (1985).

Session EQ
MAGNONIC AND RF SENSORS
(Poster Session)

Anjan Soumyanarayanan, Chair
National University of Singapore, Singapore

EQ-02. Coupled Spin Wave-Surface Acoustic Wave Interactions Supported in a Scandium-Doped Aluminum Nitride-Silicon Carbide Acoustic Platform. *A. Will-Cole*[2], X. Du[1], J.E. Shoup[3], B. Luo[4], V. Lauter[5], A.J. Grutter[3], O. Pitcl[6], M. Miller[2], B.P. Smith[2], L. Hackett[2], Y. Deng[2], N.X. Sun[4], D.B. Gopman[3], R. Olsson[1] and M. Eichenfield[2,6] *1. University of Pennsylvania, Philadelphia, PA, United States; 2. Sandia National Laboratories, Albuquerque, NM, United States; 3. National Institute of Standards and Technology, Gaithersburg, MD, United States; 4. Northeastern University, Boston, MA, United States; 5. Oak Ridge National Laboratory, Oak Ridge, TN, United States; 6. University of Arizona, Tucson, AZ, United States*

Acoustically driven magnetic resonance (ADMR) is a phenomenon whereby phonons and magnons (spin wave quanta) couple to form hybrid magneto-acoustic modes. While phonons are inherently reciprocal (linear non-magnetic materials), nonreciprocal transmission emerges in coupled magnon-phonon systems due to the helicity mismatch between surface acoustic waves and spin waves [1]. Enhanced nonreciprocity can be achieved through integration of magnetic heterostructures with strong asymmetry in their spin wave dispersion, i.e., synthetic antiferromagnetic heterostructures, and those with interfacial Dzyaloshinskii-Moriya interactions [2-6]. This results in both nonreciprocal acoustic power transmission and phase accumulation, the latter of which shows promise for radiofrequency (RF) front end devices, such as isolators and circulators [6]. To date, ADMR devices predominantly utilize bulk single crystal piezoelectric substrates, have been limited to coupling with the Rayleigh mode, have been plagued by high insertion losses, and excited only through narrowband resonances [7]. Here we present on several ADMR devices based on scandium-doped aluminum nitride film on silicon carbide. Our scandium-doped aluminum nitride film on silicon carbide platform has high piezoelectric transduction efficiency for the Sezawa acoustic mode with isotropic acoustic propagation in the plane, which eases on-chip design compared to anisotropic platforms e.g., lithium niobate and lithium tantalate [8]. In addition, we have optimized and explored wide bandwidth ADMR excitation through tapered interdigital transducers. The monolithic integration of magnetic films on this state-of-the-art acoustic platform may enable the next generation of ADMR-based RF front end devices and circuits. SNL is managed and operated by NTESS under DOE NNSA contract DE-NA0003525.

[1] M. Kuß, M. Albrecht, and M. Weiler, *Front. Phys*., 10, 981257, (2022). [2] M.F. Lewis and E. Patterson, *Appl Phys Lett,* 20, 276–8., (1972). [3] R. Sasaki, Y. Nii, Y. Iguchi, Y. Onose, *Phys Rev B*, 95, 020407, (2017). [4] M. Xu, K. Yamamoto, J. Puebla *et al*., *Sci Adv,* (2020). 6:eabb1724. [5] P.J. Shah, D.A. Bas, I. Lisenkov *et al*, *Sci. Adv*., 6, eabc5648, (2020). [6] D. A. Bas, R. Verba, P.J. Shah *et al*., *Phys. Rev. Applied*., 18, 044003, (2022). [7] M. Kuß, S. Glamsch, Y. Kunz *et al, ACS Appl. Electron. Mater*., 5, 5103, (2023). [8] L. Hackett et al, *Appl. Phys. Lett.*, 124, 113503 (2024).

EQ-04. Multilayer Garnet Integrated Tunable Resonators. *N. Gagnon*[1], H. Baldino[2], Z. Franz[1], D. Evans[1], D. Hedlund[1] and P. Kulik[1] *1. Electrical and Computer Engineering, University of Central Florida, Orlando, FL, United States; 2. Material Science and Engineering, University of Central Florida, Orlando, FL, United States*

Current MEMS-based resonators face a restricted operational frequency span and require complex designs for tunability. Additionally, to achieve varying frequency resonances multiple geometries are needed or resonators must be independently biased. These hurdles impose significant design restrictions and require time consuming and often difficult processes to fabricate. As an alternative, an Al/YIG/GGG/YIG/Al (aluminum, yttrium iron garnet, and gadolinium gallium garnet) double sided tunable resonator was designed and is to be fabricated using rapid laser lithography. By utilizing a simple geometry on a two-sided YIG stack, we have achieved two-separate resonances using a single static magnetic bias through the use of neighboring permanent magnets. The ferromagnetic resonance of each independent resonator due to a change in applied magnetic field (Hex) can be found through FMR=γH–μoMs, where Ms, H, γ is the saturation magnetization, magnetic anisotropy field and gyromagnetic ratio respectively [1,2]. The out of-plane magnetic field applied by the magnet simultaneously biases both resonators, resulting in two separate resonances. These two separate resonances can then be coupled together using inter-resonator coupling to create a magnetically tunable bandpass filter or operate independently of one another to make two separate magnetically tunable oscillators [3]. Our simulated double-sided resonator exhibits a resonance frequency of 2.63GHz with a magnetic bias of 880Oe applied and 2.71GHz with a bias of 980Oe applied. Solving Kittel's equation for out of plane FMR, we see that these results closely match the calculated values. Observing figure 1, the resonator geometry is closely impedance matched to 50 ohms and displays a large impedance shift at the point of resonance. To simplify testing of our device, fabrication of the two-sided resonator geometry will utilize vias to connect the bottom probe pads with the top surface for ease of measurement and will be completed utilizing our rapid laser lithography. Future efforts will involve maximizing the Q factor, reducing the scale, and improving flux directionality to increase the range of tunability.

1. Dai, S., Bhave, S. A. & Wang, R. Octave-Tunable Magnetostatic Wave YIG Resonators on a Chip. IEEE Trans. Ultrason. Ferroelectr. Freq. Control 67, 2454–2460 (2020). 2. Costa, J. D. et al. Compact tunable YIG-based RF resonators. Appl. Phys. Lett. 118, (2021). 3. Du, X., Idjadi, M. H., Ding, Y., Zhang, T., Geers, A. J., Yao, S., Pyo, J. B., Aflatouni, F., Allen, M., & Olsson, R. H. (2024). Frequency tunable magnetostatic wave filters with zero static power magnetic biasing circuitry. Nature Communications, 15(1).

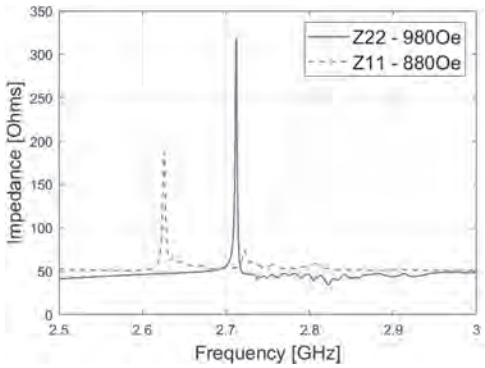

Fig 1: Double Sided Resonator Graph

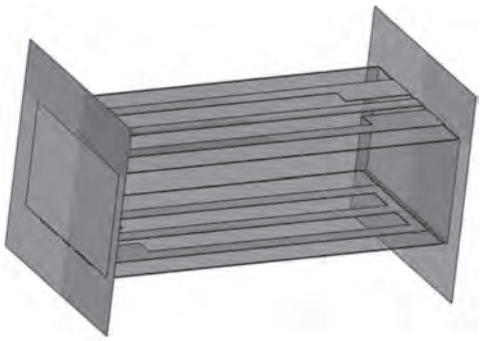

Fig 2: Double Resonator Geometry

EQ-05. Giant Non-Reciprocity Driven by Strong Magnon-Phonon Coupling in Low-Loss Fundamental Mode Surface Acoustic Wave Magnetoacoustic RF Devices. *B. Luo*[1], A. Winkler[2], H. Schmidt[2], Y. Liu[1], B. Davaji[1] and N.X. Sun[1] *1. Electrical and Computer Engineering, Northeastern University, Boston, MA, United States; 2. SAWLab Saxony, Dresden, Germany*

Integrated nonreciprocal isolators and circulators have revolutionized wireless communication and sensing [1]. However, they exhibit high power usage of 40mW~200mW and are not suitable for low-power applications [1]. Recently, magnetoacoustic non-reciprocal RF devices exhibit substantial nonreciprocity with remarkable power efficiency and CMOS compatibility, making them ideally suited for low-power and wideband full-duplex wireless radio systems [2-4]. Non-reciprocal magnetoacoustic devices consist of a magnetic stack between two interdigital transducers (IDTs) on a piezoelectric substrate. By applying RF voltage on IDTs, the induced surface acoustic wave (SAW) propagates and interacts with spin wave (SW) in the magnetic stack. The strong magnon-phonon coupling leads to hybrid magnetoacoustic waves that exhibit a much higher backward loss rate than the forward one or vice versa [2]. Ongoing research strives to enhance non-reciprocity strength and bandwidth while maintaining high transmission [2]. Despite successful demonstrations of magnitude or phase non-reciprocity in magnetic multilayers such as FeGaB/Al_2O_3/FeGaB [3-4], the insertion loss is still high (>50 dB) owing to low transmission efficiency of SAW harmonics. Here we demonstrate a low-loss magnetoacoustic non-reciprocal RF device driven by SAW fundamental mode at 2.87 GHz. The 10-dB low insertion loss (Fig. 1) and sharp acoustic resonance lead to strong magnon-phonon coupling [5-8]. The consequent giant non-reciprocity of 200 dB/mm (Fig. 2) make the device potential for integrated compact, power-efficient, CMOS-compatible RF isolators and circulators.

[1] A. Nagulu and H. Krishnaswamy, *IEEE Journal of Solid-State Circuits*, Vol. 54, p.1288-1303 (2019). [2] R. Verba, V. Tiberkevich and A. Slavin, *Physical Review Applied*, Vol. 12, p.054061 (2019). [3] P. J. Shah *et al.*, *Science Advances*, Vol. 6, p.eabc5648 (2020). [4] D. A. Bas *et al*, *Physical Review Applied*, Vol.18, p.044003 (2022). [5] Y. Hwang *et al.*, *Physical Review Letters*, Vol.132, p.056704 (2024). [6] C. Berk *et al.*, *Nature Communication*, Vol. 10, p.2652 (2019). [7] K. An *et al.*, *Physical Review B*, Vol. 101, p.060407 (2020). [8] F. Godejohann *et al.*, *Physical Review B*, Vol. 102, p.144438 (2020).

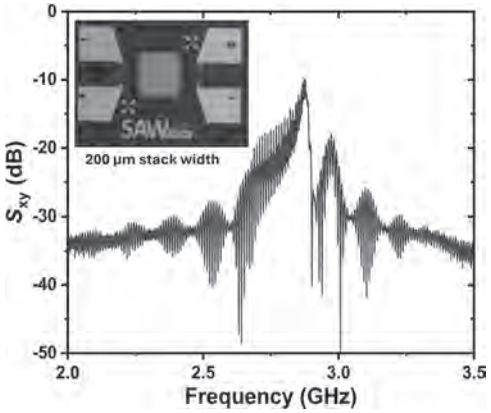

Figure 1. Transmission coefficient S_{xy} of the magnetoacoustic RF device with a low insertion loss of 10 dB. The inset shows the optical picture of the device composed of two 2.87 GHz Interdigital Transducers (IDTs) and a 200 μm×200 μm FeGaB\SiO_2\FeGaB magnetic stack with non-reciprocal spin wave spectrum.

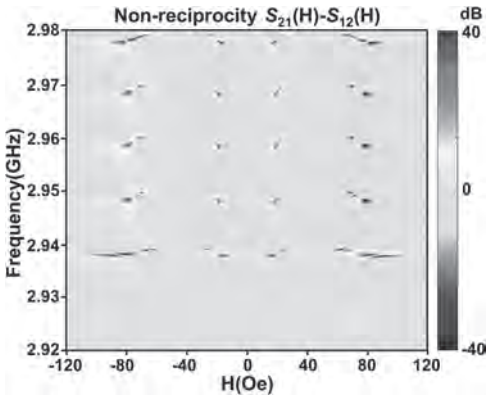

Figure 2. Non-reciprocity versus RF frequency and bias magnetic field at 168 degrees to SAW propagation. 40 dB strong (~200 dB/mm) non-reciprocity is realized near the anti-crossings due to strong magnon-phonon coupling, which is ~10 times that in the 7th order mode SAW driven magnetoacoustic device [3].

EQ-06. Comprehensive investigation of magnetoimpedance on micromachined soft magnetic material. *H. Kikuchi*[1] and Z. Wang[1] *1. Iwate University, Morioka, Japan*

Magnetoimpedance (MI), utilizes the skin effect and ferromagnetic resonance via permeability changes [1], is used in highly sensitive sensors and for a qualification of soft magnetic materials. So far, element length is over several mm (2–10mm, typical), while we have miniaturized element to less than 1 mm using thin-film [2]. However, when length becomes below 100 μm, a demagnetizing effect reduces the sensitivity, impedance changes and makes controlling anisotropy difficult. In this study, we explored the feasibility of fabricating thin-film elements having several μm thick, wide, and less than 100 μm long, with a nearly 1:1 sectional aspect ratio, using photolithography and focused ion beam techniques, then their MI properties were examined. To control anisotropy, we adopted Joule heating [3], as static field annealing is ineffective for these sizes due to the demagnetizing effect. Applying Joule heating to such small volumes is also challenging. Fig. 1 shows the applied field dependence of impedance for micromachined elements with and without Joule heating. The element dimensions are 2μm-thick/wide, 100μm-long, made of amorphous CoZrNb. Impedance was measured at

1 GHz with -20 dBm. The as-deposited state shows a discontinuous jump, typical of properties with inclined easy axis from width direction due to shape anisotropy. After Joule heating with 20 mA, those properties changed to preferable profiles for sensing application, showing a double peak profile due to easy directions parallel to width direction. Additionally, when 0 dBm power was applied to the element, the profile was similar to that after Joule heating, indicating the potential for controlling anisotropy with relatively higher power—a new finding in this study. However, this also suggests the need to carefully manage input power for small volume elements as shown in Fig 2, the results of the elements with 1μm-thick /wide, 30μm-long. The impedance changes when the input power is -20 dBm, while showing no changes with 0 dBm due to the crystallization of the element. Throughout this study, the maximum change ratio of 78% was also obtained.

[1] L. V. Panina, K. Mohri, Appl. Phys. Lett. 65 (1994) 1189–1191. [2] H. Kikuchi et al., IEEE Magn. Lett., 10 (2019) 8107205. [3] H. Kikuchi et al., IEEE Trans. Magn., 58 (2022) 2000905.

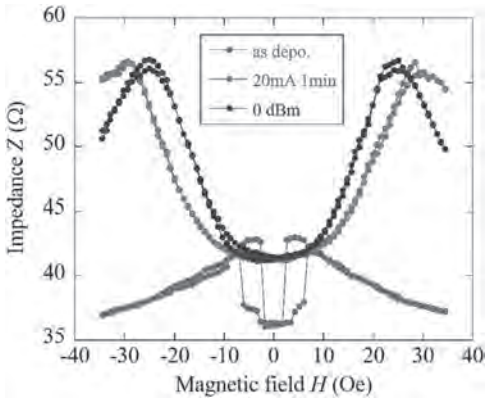

Fig. 1 Example of field dependence of impedance.

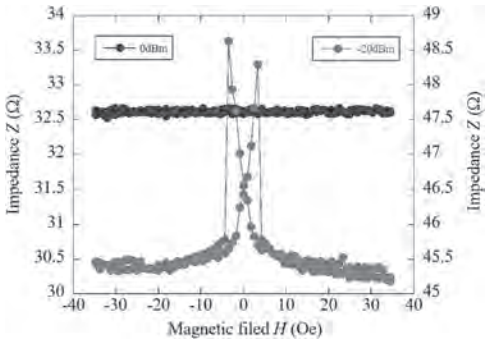

Fig. 2 Field dependence of impedance for small volume element.

EQ-07. Modeling Magnetic Field in Racetrack-Core Fluxgates at High Excitation Frequency. *J. Maier*[1], P. Ripka[1] and M. Mirzaei[1]
1. Department of Measurement, Czech Technical University in Prague, Prague, Czechia

A miniaturized fluxgate sensor was developed by our team [1]. The sensor uses an 8 mm long racetrack-shaped core made of 25 μm thick sheet of VITROVAC6025F. FEM simulations were used in the design process. The simulation model did not include eddy currents and was performed at an excitation frequency of 100 kHz. While the measurements at 100 kHz matched simulation results very well, further testing showed that significantly higher excitation frequencies are needed to reach optimal performance. The maximum sensitivity is reached at 1.5 MHz excitation, but the noise and perming (remanence) are worse than desired at such high frequencies. Pulse excitation [2] was used to reach a higher peak excitation current while maintaining reasonable power dissipation. However, no improvement in perming and noise was observed. We suspected that the higher frequency components of the pulse signal are unable to saturate the internal volume of the core due to skin effect and eddy currents. We might calculate the penetration depth based on the properties of the material (μr = 70 000, σ = 740 000 S/m), which is 2.2 μm at 1 MHz. As the surface saturates, the permeability decreases, supposedly leading to an increase in penetration depth. We used an improved FEM simulation model to gain more insight into this problem. Eddy current AC simulations were performed with sinusoidal excitation of 200 mA amplitude (141 mA RMS, which is near the maximum that can practically be used with the micro-fluxgate). The model consists of the racetrack core and excitation coils. Due to technological reasons, the micro-fluxgate was designed with excitation coils located only at the ends of the straight segments, while the middle part is used for sensing the coil. Results in Fig. 1 show that despite the high excitation amplitude, frequencies of 500 kHz and higher cannot fully saturate the core. This problem is most prominent in the center of the straight segments (highest distance from the excitation coils). At frequencies above 1 MHz, the saturation only reaches about 6 μm under the surface as seen in Fig. 2.

[1] J. Maier, P. Ripka and P. Chen, "CMOS-based Micro-fluxgate with Racetrack Core and Solenoid Coils", subm. Sensors and Actuators [2] P. Ripka, S. O. Choi, A. Tipek et al., "Pulse excitation of the micro-fluxgate sensors," IEEE Transactions on Magnetics, vol. 37, no. 4, Part 1, pp. 1998–2000, July 2001.

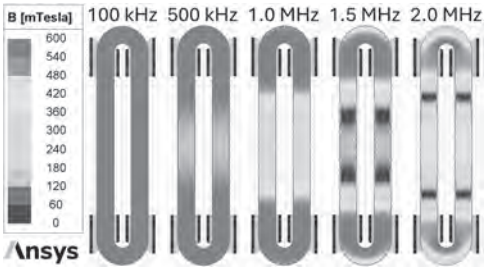

Fig. 1: Horizontal slice through the middle of the core's thickness

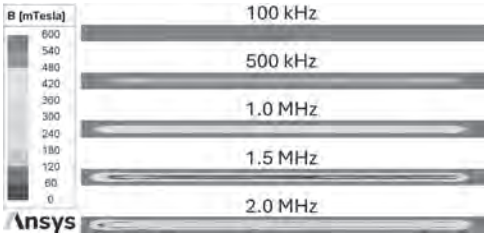

Fig. 2: Vertical slice through the middle of the core's straight segment

EQ-08. MR-scanner Independent Three-dimensional Magnetic Field Mapping System of RF Coil with Phantom Loading. M. Takahashi[1], *A. Kuwahata*[1], M. Fushimi[2], M. Sekino[2] and S. Yabukami[1] *1. Tohoku University, Sendai, Japan; 2. The University of Tokyo, Tokyo, Japan*

The fundamental issue in magnetic resonance imaging (MRI) is improving the signal-to-noise ratio (SNR) of the received signal to obtain images with high spatial resolution. We can maximize the SNR of the received signal by numerically designing the proper radiofrequency (RF) coil [1, 2]. However, practical performance test requires experimental evaluations by utilizing MR-scanner, resulting time consuming and some effort. In this study, we developed magnetic field mapping system with high resolution for an MRI RF coil with a curved shape under a bio-mimicking loading. Figure 1 shows the three-dimensional magnetic field mapping system by using a two-port network analyzer and three actuators including a stepping motor for the magnetic field mapping of the MRI RF coil. Two circular loop coils are used to measure x- and y-component of the magnetic field. The MRI RF receive coil sensitivity is evaluated by $|B_1| = |(B_{1,x}\text{-}iB_{1,y})^*/2|$ for a static magnetic field along the z-axis. Figure 2 shows the spatial distribution of $|B_{1,S21}|$ measured by the proposed system, magnetic field $|B_{1,calc}|$ calculated by the finite element method (ANSYS HFSS), and signal intensity $|B_{1,MRI}|$

obtained by 7 T MR-scanner (Biospec 70/20, Bruker) on xy- and xz-plane. The spatial distribution of $|B_{1,S21}|$ (Fig. 2(a)) was similar to $|B_{1,calc}|$ (Fig. 2(b)) and $|B_{1,MRI}|$ (Fig. 2(c)). The quantitative evaluation, the linear regression between the data measured by the mappings system, calculated by RF simulation, and obtained by 7 T MR-scanner revealed that the developed system worked well with acceptable margin of error. Our method will enable evaluate a RF surface coil for practical application on MRI without MR-scanner.

[1] D. Hernandez and K.-N. Kim, Investig. Magn. Reason. Imaging 24, 95 (2020). [2] M. Takahashi *et al.*, AIP Adv. 14, 015216 (2024).

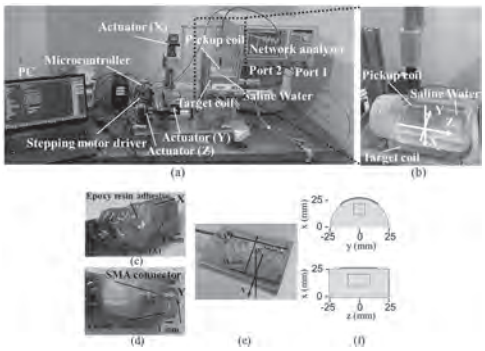

Experimental setup for the magnetic field mapping system. (a) whole view, (b) magnified view of phantom, (c) Bx pickup coil (d) By pickup coil, (e) RF coil, and (f) location of phantom and RF coil.

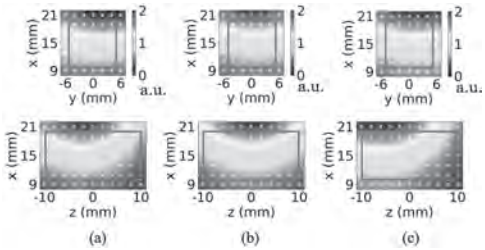

Distribution of (a) normalized magnetic field $|B_{1,S21}|$ measured by the developed system, (b) calculated magnetic field $|B_{1,calc}|$, and (c) MR signal intensity $|B_{1,MRI}|$. The upper and bottom row corresponds to xy- and xz-plane, respectively.

Session ER
SPINTRONIC DEVICES III: CPP-GMR, SOT-MRAM AND SPIN-TORQUE OSCILLATORS (Poster Session)

Ravi Kumar Bandapelli, Chair
Carnegie Mellon University, Pittsburgh, PA, United States

ER-01. Magnetoresistance Effect Based on Spin-Selective Transport in Nano-Devices Using Chiral Molecules. *M. Matsuzaka*[1], R. Miyamoto[1], K. Kashima[1], T. Ueda[1], K. Terai[1], T. Yamamoto[1], K. Sambe[2], T. Akutagawa[2] and H. Kaiju[1,3] *1. Faculty of Science and Technology, Keio University, Yokohama, Japan; 2. Institute of Multidisciplinary Research for Advanced Materials, Tohoku University, Sendai, Japan; 3. Center for Spintronics Research Network, Keio University, Yokohama, Japan*

Molecular spintronic nano-devices are expected to provide a high spin polarization, leading to a large magnetoresistance (MR) effect [1]. We have successfully observed MR effect in nano-devices using high-mobility molecules at room temperature [2]. Recently, chirality induced spin selectivity (CISS) effect has been observed in the chiral molecules [3–6] and attractive for the application to the MR devices. CISS effect was observed in the micro-devices using chiral molecules sandwiched between magnetic and non-magnetic electrodes under a high magnetic field H of ~5 kOe at a certain voltage [5, 6]. In this study, we fabricate the nano-devices, consisting of chiral molecules, *N*-(3*S*)-3,7-dimethyloctyl[1]benzothieno[3,2-*b*]benzothiophene-2-carboxyamide (*S*-BTBT-CONHR) sandwiched between Au and $Ni_{78}Fe_{22}$ (Py) thin-film edges (Fig. 1), and investigate their spin transport properties under low magnetic field at both positive and negative bias voltages. The fabrication method of our proposed devices mainly consists of sputtering, thermal pressing, mechanical cutting, polishing and spin-coating techniques [2]. The magnetic properties were evaluated by magneto-optic Kerr effect. The MR curves were measured by a 4-probe method under a magnetic field of ~±190 Oe at room temperature. Fig. 2 shows the magnetization curves of Py thin films and MR curves in Au/*S*-BTBT-CONHR/Py devices. The MR curves correspond to the magnetization states of Py electrodes, in which the coercivity is ~39 Oe. This means that MR effect based on CISS effect is observed in nano-devices using chiral molecules under low magnetic field. The MR curves exhibit the same polarity at both positive and negative bias voltages. This fact indicates that the sign of spin selectivity is independent of the spin injection direction in the devices, which is consistent with previous results obtained by the magnetic-conductive atomic force microscopy [3–6]. This study can lead to the realization of the nanoscale MR devices with high magnetic sensitivity and provide a new insight into CISS effect for spintronic device application.

[1] C. Barraud, P. Seneor and R. Mattana, Nat. Phys., Vol. 6, p. 615 (2010) [2] M. Matsuzaka, Y. Sasaki and K. Hayashi, Nanoscale Adv., Vol. 4, p. 4739 (2022) [3] B. Göhler, V. Hamelbeck and T. Z. Markus, Science, Vol. 331, p. 894 (2011) [4] Z. Xie, T. Z. Markus and S. R. Cohen, Nano Lett., Vol. 11, p. 4652 (2011) [5] M. Suda, Y. Thathong and V. Promarak, Nat. Commun., Vol. 10, 2455 (2019) [6] C. Kulkarni, A. K. Mondal and T. K. Das, Adv. Mater., Vol. 32, p. 1904965 (2020)

Fig. 1 Schematic of Au/*S*-BTBT-CONHR/Py devices.

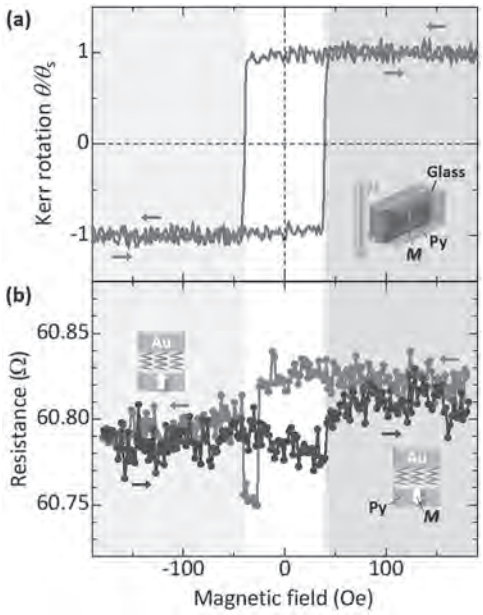

Fig. 2 (a) Magnetization curves of Py electrodes and (b) MR curves in Au/*S*-BTBT-CONHR/Py devices.

ER-02. Spin Transfer Torque assisted Field-Free Spin Orbit Torque Switching in CPP-GMR with Antiferromagnetically Coupled Perpendicularly Magnetized Co/Pd Memory Layer. *D. Pan*[1], D. Oshima[1], B. Zhu[1] and T. Kato[1] *1. Electronics, Nagoya University, Nagoya, Japan*

To solve the difficulties on storage density of future magnetic random access memory (MRAM), a novel magnetic memory known as 3-dimensional domain wall magnetic memory (3D-DWMM) has been proposed [1]. A synthetic antiferromagnetic (SAF) structure is suitable for 3D-DWMM

because SAF has a smaller stray field compared to traditional ferromagnetic (FM) structures. For the data writing process, magnetization switching via the combination of spin transfer torque (STT) and spin orbit torque (SOT) enables deterministic switching without an external magnetic field, which is a promising candidate for 3D-DWMM. In this study, we fabricated GMR devices having SAF memory layer of $[Co(0.4)/Pd(0.2)]_1/Co(0.4)/Ru/Co(0.3)/[Pd(0.2)/Co(0.3)]_1$ with pillar diameter of 180 nm or 200 nm. The STT and SOT switching of the CPP-GMR nanopillars was successfully observed by injecting current through the pillar or in the 4 μm width Pt bottom electrodes, respectively. The STT assisted SOT switching was confirmed by applying both STT and SOT currents in the zero field. Figure 1 shows the SOT switching *I-R* loop. An in-plane external magnetic field of –1.0 kOe was applied during the switching. A perpendicular external magnetic field was applied to the device prior to the measurement to create a parallel initial state. Arrows in Fig. 1 represent the magnetization of the lower $[Co(0.4)/Pd(0.2)]_1/Co(0.4)$ and the upper $Co(0.3)/[Pd(0.2)/Co(0.3)]_1$ in the SAF memory layer, respectively. The current density required for switching from P to AP is nearly identical to that needed for switching from AP to P. By introducing STT current from SAF reference layer, the field free SOT switching was observed. Figure 2 shows the dependence between SOT current density and STT current density. The STT and SOT current densities were normalized by their respective critical switching densities, which were determined from the STT and SOT *I-R* loops. By comparing with GMR with FM Co/Pd memory layer [2, 3], we found that the efficiency of STT assistance in SAF memory structures is lower than that in ferromagnetic coupled memory structures.

[1] Hung. Y.M et al., Applied Physics Express 14(2) (2021). [2] D. Pan et al., IEEE Trans. Magn., 59, 3284862 (2023). [3] D. Pan et al., IEEE Transactions on Magnetics, doi: 10.1109/TMAG.2024.3416759.

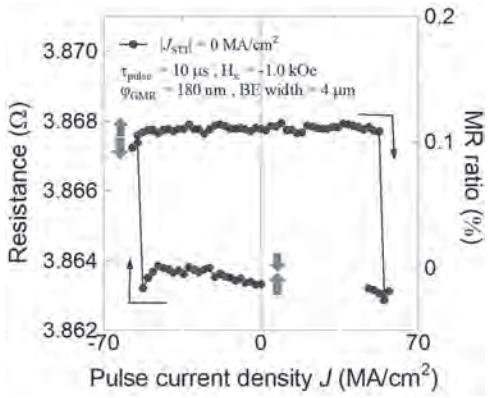

Fig.1 SOT switching of GMR with SAF memory layer.

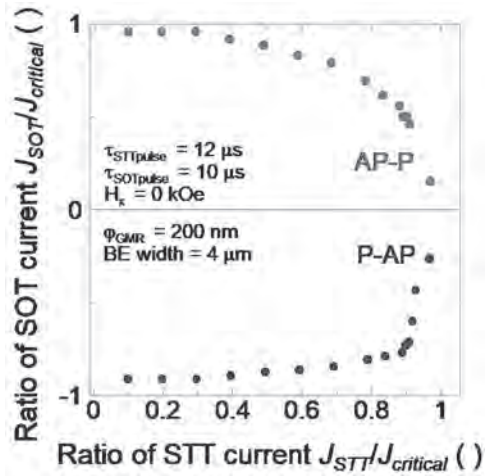

Fig.2 STT assisted field-free SOT switching current density with SAF memory layer.

ER-03. Spin-torque diode effect driven by magnetization phase-transitions: a theoretical analysis. *M. Lianeris*[1], A. Meo[1], M. Carpentieri[1], R. Tomasello[1] and G. Finocchio[2] *1. Department of Electrical and Information Engineering, Polytechnic University of Bari, Bari, Italy; 2. Department of Mathematical and Computer Sciences, Physical Sciences and Earth Sciences, University of Messina, Messina, Italy*

Spin torque diodes (STDs) are currently among the most widely studied spintronic devices thanks to their capabilities, among which we list the frequency response that can be resonant or broadband depending on the system properties and the excitation [1]. Metamaterials, such as FeRh, that exhibit a temperature-induced first order antiferromagnetic (AFM)-to-ferromagnetic (FM) phase transitions have recently attracted attention as alternative materials for spintronic applications. In FeRh this phase transition occurs close to room temperature, and it can be induced by Joule heating via electrical current injection. Moreover, this system also exhibits two resistance states depending on the magnetic phase [2]. In this work we occur phase transitions in a STD. We develop a two-sublattice model to investigate systematically the STD response induced by these phase transitions in FeRh. We first analyze the phase diagram describing the equilibrium magnetization state as a function of the perpendicular magnetic anisotropy constant (K_u) and the inter-sublattice exchange constant (A_0), as shown in Figure 1. We identify three regions: i) AFM, where the two sublattices are in the AFM state; ii) FM, where the two sublattices are in the FM state; iii) FM/AFM, where the equilibrium state depends on the initial state. We characterise the phase transition and find that it occurs when the anisotropy energy balances the energy of the inter-sublattice exchange, given by the condition: $K_u=4A_0\alpha_0^{-2}$, where α_0 is the lattice constant of the material. We then focus on the dynamical response of FeRh when subjected to an ac current with variable frequency to excite the STD phenomenon. To describe the effect of the temperature, we extract the temperature scaling of the magnetic properties from atomistic spin simulations and include within the macrospin approach. Our results show a broadband response in a large range of frequencies Figure 2. These results are promising and can be useful for the design of alternative energy harvest systems. Supported By (i) PRIN "SkySens" (ii) "NEST", and (iii) PETASPIN association.

[1] G. Finocchio, R. Tomasello, B. Fang, A. Giordano, V. Puliafito, M. Carpentieri, and Z. Zeng, "Perspectives on spintronic diodes," Applied Physics Letters, vol. 118, no. 16, p. 160502, 04 2021. [Online]. Available: https://doi.org/10.1063/5.0048947 [2] H. Wu, H. Zhang, B. Wang, F. Groß, C.-Y. Yang, G. Li, C. Guo, H. He, K. Wong, D. Wu et al., "Current-induced neel order switching facilitated by magnetic phase transition," Nature communications, vol. 13, no. 1, p. 1629, 2022.

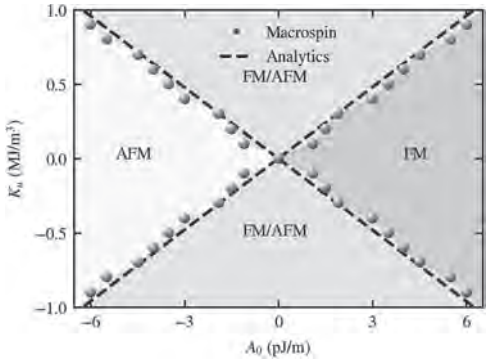

Figure.1: Phase diagram of the equilibrium magnetization state.

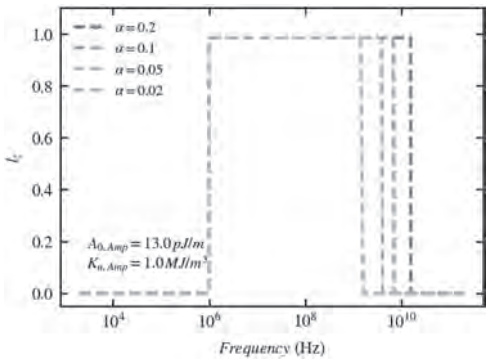

Figure.2: The broadband response of the Néel-vector-z

ER-04. BEOL-compatible, 5 ns-fast, single pulse field-free switching 50 nm AFM(PtMn)-TopSOT-MRAM. *C. Lin*[2,1], K. Li[1], J. Shieh[1], Y. Chen[1], C. Hsu[1], W. Chen[1,3], C. Shen[1], T. Hou[1], J. Sun[1,4], D. Tang[5], C. Hsin[3] and C. Lai[2,6] *1. Taiwan Semiconductor Research Institute, Hsinchu, Taiwan; 2. College of Semiconductor Research, National Tsing Hua University, Hsinchu, Taiwan; 3. Department of Electrical Engineering, National Taiwan University, Taipei, Taiwan; 4. Industry-Academia Innovation School, National Yang Ming Chiao Tung University, Hsinchu, Taiwan; 5. Industrial Technology Research Institute, Hsinchu, Taiwan; 6. Department of Materials Science and Engineering, National Tsing Hua University, Hsinchu, Taiwan*

We introduce a cutting-edge structure known as AFM-Top-SOT-MRAM, utilizing antiferromagnetic principles, specifically designed for Z-type field-free switching and superior scalability. The 50 nm AFM-Top-SOT-MRAM device offers thermal stability equivalent to traditional long magnetic channels but in a significantly compact form factor. This design minimizes stray fields affecting adjacent devices, thereby enhancing overall scalability. Notably, our AFM-Top-SOT-MRAM achieves an impressive 101% TMR ratio and facilitates field-free SOT switching with speeds as rapid as 5 ns. Our approach leverages Co's robust exchange anisotropy in conjunction with a thin PtMn layer and an ultra-thin Ru seed layer. This combination optimizes the W spacer to generate high spin currents while effectively reducing switching current density. Importantly, the 50 nm device demonstrates excellent thermal stability and compatibility with BEOL processes up to 400°C, ensuring robust performance in diverse operating environments. Experimental results highlight the potential of our technology in delivering high-performance, scalable field-free SOT MRAM solutions.

[1] S. Couet et al., VLSI, 2021. [2] K. Garello et al., VLSI, 2019. [3] D.Q. Zhu et al., IEDM, 2021. [4] H. Honjo et al., IEDM, 2019. [5] N. Sato et al., VLSI, 2020. [6] Y.-J. Tsou et al., VLSI, 2021. [7] Y.-J. Tsou et al., TED, 2021. [8] W.-J. Chen et al., SISPAD, 2021. [9] W. Cai et al., EDL, 2021. [10] K. Cai et al., IEDM, 2022. [11] K. -S. Li et al., IEDM, 2023.[12] C.-F. Pai et al., Physical Review B, 2016. [13] Z. Wen et al., AIP Advances, 2016.

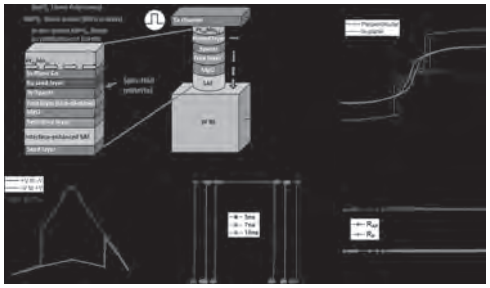

(a) The film stacks and device structure. The in-plane Co pinned by PtMn provides ferromagnetic coupling for perpendicular CoFeB. (b) Magnetic properties of AFM-Top-SOT. (c) STT-RV curve with 101% TMR. (d) 5ns fast field-free switching with 42MA/cm^2 current density. (e) 10^{10} cycle time of AFM-Top-SOT device.

ER-05. Swift Skyrmion as True Random Number Generator. *A. Joy*[1,2] *1. Physics, Indian Institute of Science Bangalore, Bangalore, India; 2. NISE, Max Planck Institute for Microstructure Physics, Halle, Germany*

The next-generation data storage devices using skyrmions is based on their motion through nanowires consisting of metallic multi-layers with high spin-orbit coupling and DMI(Dzyaloshinskii Moriya Interaction). Skyrmions are quantized swirling spin structures observed in many systems even at room temperatures. Our system with suitably controlled magnetic anisotropy and inter-skyrmion repulsion helped to move the skyrmion at a velocity of 260 m/s at room temperature. In addition, we present a method for generating random numbers using these exceptionally fast skyrmions at room temperature. In a world that revolves around one-time-passwords and cryptocurrencies, a massive amount of random number generations with higher efficiency is a requisite. Using the newly introduced method, 10 million truly random numbers per second can be generated. These results identify ferromagnetic ultrafast skyrmions as an intriguing candidate for true random number generation.

1. Nagaosa Naoto and Tokura Yoshinori. Topological properties and dynamics of magnetic skyrmions. Nat. Nanotechnol 8(12):899, 2013. 2. Bogdanov and A. Hubert. Thermodynamically stable magnetic vortex states in magnetic crystals. J.Magn.Magn. Mat 138(3):269, 1994. 3. Shijiang Luo and Long You. Skyrmion devices for memory and logic applications. APL Mat., 9(5):050901, 2021. 4. T.H.R. Skyrme. A unified field theory of mesons and baryons. Nucl. Phy 31:556–569, 1962. 5. Stuart Parkin and See-Hun Yang. Memory on the racetrack. Nat.Nanotechnol., 10:195–8, 2015. 6. Stuart S. P. Parkin, Masamitsu Hayashi, and Luc Thomas. Magnetic domain-wall racetrack memory. Science, 320(5873):190–194, 2008. 7. Berk Sunar. True Random Number Generators for Cryptography, pages 55–73. Springer US, Boston, MA, 2009. 8. Mario Stip cevi c and C etin Ko c. True Random Number Generators, pages 275–315. Nov 2014.

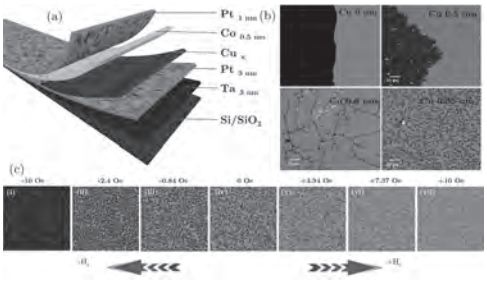

(a) Illustration of different layers deposited in the skyrmion system. (b) Magnetic domain Images of the samples T a3nmP t3nmCuxCo0.5nmP t1nm with x values 0, 0.5, 0.6, and 0.65 nm, captured using Kerr Microscope. (c) Variation of the domain texture corresponding to the sample $Ta_{3nm}Pt_{3nm}Cu_{0.65nm}Co_{0.5nm}Pt_{1nm}$ on applying out of plane field varied from -10 Oe to +10 Oe. These images represent domain images corresponding to the hysteresis.

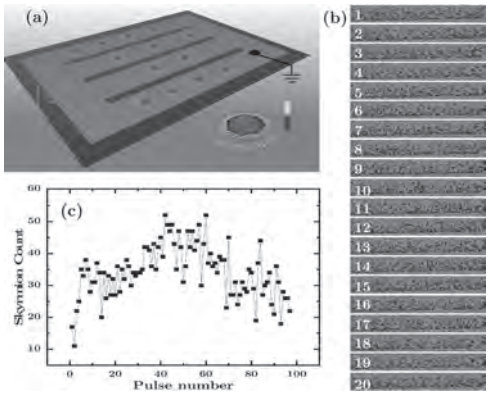

(a) Illustration showing the generation of a four digit number using a single pulse. (b) Kerr Microscope images of the sample upon applying current pulses subsequently with high enough strength to push skyrmions entirely out of the track. The skyrmions are newly generated in each pulse at a current density of 2.65 × 1011A/m2 and a pulse width of 60 ns. Out of the series of images, twenty of them are shown here. The randomness of the result is tested using JavaScript E-labs learning objects associated with Professor Hossein Arsham. (c) The number of skyrmions counted is plotted against the number of pulses, which shows the distribution. The plot shows the number of skyrmions for 100 consecutive electrical current pulses.

ER-06. Coupling of Self-Generated Spin Waves and Spin Transfer Torque Driven Oscillations in Biquadratic Coupled Orthogonal Magnetization Disks. *T. Cheng*[1], C. Liu[1], Y. Kurokawa[1] and H. Yuasa[1]
1. Graduate School and Faculty of Information Science and Electrical Engineering, Kyushu University, Fukuoka, Japan

The magnetization dynamics of spin torque oscillators (STOs) formed by two biquadratically magnetic coupled orthogonal layers had been revealed in this computational study. It had been previously established that the biquadratic magnetic coupling between two orthogonal magnetisation layers of an out-of-plane fixed (FePt) and in-plane free layer ($Co_{90}Fe_{10}$) can offer a high frequency oscillation when excited by Slonczewski spin transfer torque. [1] In this structure, the demagnetisation field of the fixed layer forces the edge of the free layer to point out-of-plane indicated in Fig. 1a. This results in a spin wave generated at the edge propagating towards the center once a current is applied as shown in the 0.1 ns and 10 ns snapshot of the free layer magnetization shown in Fig. 1b and c respectively. Further investigation was done by varying the diameter of the disk and a Fourier Transform analysis for each of the simulation cell to reveal small oscillations in z-direction. The resulting spectrum is shown in Fig. 2, where the oscillations in the z-direction was split into multiple distinctive lines. When overlayered with the oscillation frequency of average y-direction magnetization (STO frequency), the overall oscillations coupled to one of the lines in the spectrum resulting in a periodic change in frequency until the influence from the edge became less apparent to the overall area after the diameter = 600 nm. The result indicates complex dynamics are involved in biquadratically coupled orthogonal STO, whereas imperfection in fabrications could dramatically change the generation of the spin waves so as the STO oscillation frequency. On the other hand, the result suggests a possibility of engineering an STO frequency by shape besides external stimulation such as applied field, microwave signal or electrical current density.

[1] C. Liu, Y. Kurokawa and N. Hashimoto, Scientific Reports, 13, 3631 (2023)

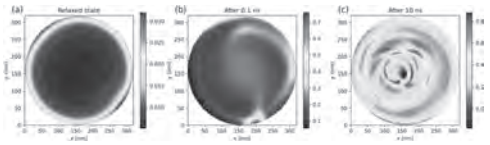

Fig. 1 Z-Direction magnetization of the orthogonal biquadratic coupled STO (a) after relaxation and (b) 0.1ns and (c) 10ns after application of the spin polarized current.

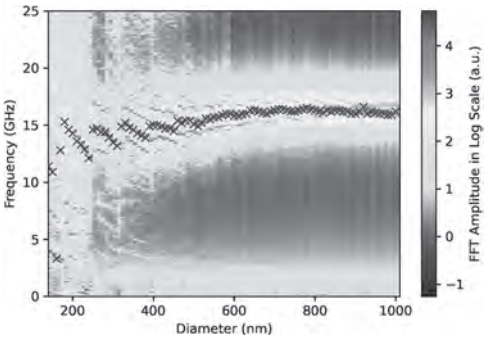

Fig. 2 Spectrum of z-direction oscillations in log scale. Marked with crosses indicating the peak frequency of the y-direction average magnetization (STO operating frequency).

ER-07. Imaging of dispersion relation of magnetoelastic waves in epitaxial ferromagnetic Heusler alloys using multiple-overtones surface acoustic wave. *K. Yamanoi*[1], S. Yamada[2], K. Hamaya[2] and Y. Nozaki[1]
1. Keio University, Yokohama, Japan; 2. Osaka University, Toyonaka, Japan

Recent studies highlighted the significance of magnon-phonon coupling, formed between spin waves and surface acoustic waves (SAWs), in the development of magnon-based logic device. This coupling occurs at the intersection points of the dispersion relations for the spin waves and SAWs, making it crucial to investigate both the intersection conditions and the coupling strength. In this work, we present a multiple overtone SAW device capable of evaluating multiple intersection conditions within a single device, successfully visualizing the dispersion relations of magnon-phonon coupling at different SAW excitation frequencies. We fabricated a pair of interdigital transducers (IDTs) consisting of a Ti(2 nm)/Al(50 nm)/Ti(2 nm) multilayer structure on a $LiNbO_3$ substrate using conventional lift-off technique. A Heusler ferromagnetic alloy Co_2FeSi/V films, known for its high spin polarization, was deposited between the IDTs via molecular beam epitaxy. Figure 1(a) shows the transmission signal of our multiple overtones SAW device, measured with a vector network analyzer. The fundamental SAW frequency at approximately 0.193 GHz matched well with the predicted SAW excitation frequency based on the IDT's structural period of 20 μm. Remarkably, higher-order SAWs up to the 29th overtone (5.6 GHz) was successfully excited. By measuring the magnetic field dependence of the SAW propagation signal, we observed the energy dispersion due to the magnon-phonon coupling at each SAW peak signal. Figure 1 (b) shows a heatmap of the energy dispersions as a function of SAW frequencies and in-plane magnetic fields parallel to the SAW propagation direction. These results clearly visualize the relationship between the resonance field and SAW frequencies, elucidating the intersection conditions for magnons and phonons in the Co_2FeSi film. At lower frequencies, a single peak due to magnon-phonon coupling was observed, whereas at higher frequencies, two magnon-phonon couplings were observed. This was found to be due to the magnetic state of the Co_2FeSi alloy.

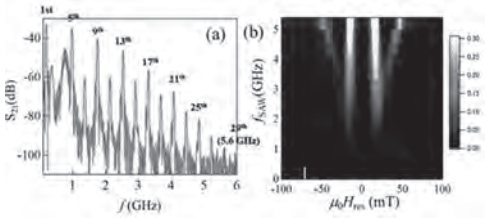

Figure 1(a) Frequency dependence of the transmission signal for multiple overtones SAW device. (b) Visualization of magnon-phonon intersection conditions using multiple overtones SAW.

ER-08. Anharmonic potential induced chaotic dynamics of spintronic oscillator. *R. Tatsumi*[1], T. Chiba[1,2], T. Komine[3] and H. Matsueda[1,4]
1. Engineering, Tohoku University, Sendai, Japan; 2. FRIS, Sendai, Japan; 3. Engineering, Ibaraki University, Hitachi, Japan; 4. CSIS, Sendai, Japan

Recently, physical reservoir computing, which is a neural network based on the nonlinear dynamics of physical systems, has received much attention from information science and nonlinear physics. As a promising resource, spintronic devices have been actively studied, because the magnetization dynamics allow low power consumption and nanosecond-scale response on the device operation. It is known that reservoir computing shows high performance at the so-called "edge of chaos", which is a transient state between the periodic phase and the chaotic phase [1]. Accordingly, the chaotic dynamics of spin torque oscillator (STO) are theoretically investigated [2,3]. However, it is still veiled the reason why the magnetization dynamics exhibit chaotic dynamics. Therefore, it is highly desirable to reveal the principle of chaotic magnetization dynamics. In this study, we propose a spintronic Duffing oscillator that exhibits chaotic magnetization dynamics in the spin-torque ferromagnetic resonance. Figure 1 shows a schematic illustration of our model characterized by the magnetic potential with the uniaxial magnetic anisotropy. The shape of the potential is similar to that of the Duffing equation which represents chaotic dynamics in a particle system. That is the key to realizing the chaotic dynamics. We find that the trajectory of magnetization in the phase space is similar to that of the Duffing equation. In this context, the Duffing equation and Landau-Lifshitz-Gilbert (LLG) equation have a mathematically equivalent structures. Based on the LLG equation, we investigated the magnetization dynamics by means of the Lyapunov exponent (fig. 2). Figure 2 shows that chaotic dynamics occur when the spin torque-induced effective field is around 20 mT, which is approximately one order of magnitude smaller than the uniaxial magnetic anisotropy field. In the presentation, we will discuss how to tune the potential shape.

[1] R. Legenstein *et al.*, Neural Networks 20, 323-334 (2007). [2] T. Taniguchi *et al.*, J. Magn. Magn. Mater. 563, 170009 (2022). [3] T. Yamaguchi *et al.*, Phys. Rev. B 100, 224422 (2019).

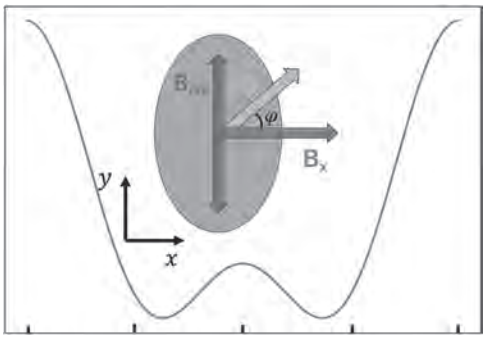

The shape of magnetic potential for the magnetization angle and a schematic illustration of our model. The external magnetic fieldis 165 mT. The magnetic anisotropy field along y-axisis 200 mT.

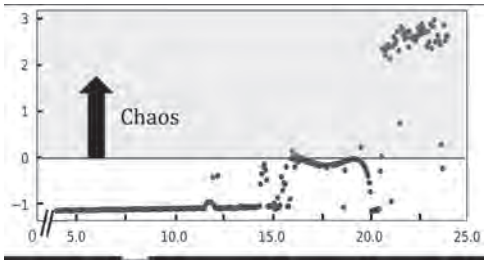

Lyapunov exponent as a function of the magnitude of spin torque induced effective fields with the resonance frequency 3.22 GHz

Session ES
MAGNETOELECTRIC DEVICES AND APPLICATIONS
(Poster Session)

Pedram Khalili, Chair
Northwestern University, Evanston, IL, United States

ES-01. Demonstration of Spintronic Devices and Arrays Based on Field-Free Voltage-Gated Spin-Orbit Torque Switching. *Z. Liu*[1], H. Zhang[1], J. Liu[1], Y. Zhang[1], W. Li[1], J. Lu[1] and S. Peng[1] *1. Fert Beijing Institute, School of Integrated Circuit Science and Engineering, Beihang University, Beijing, China*

Spin-orbit torque magnetic random-access memory (SOT-MRAM) attracts extensive attention due to its advantages of high speed, separate read/write path, etc. However, its practical application is hindered by issues like the need for an in-plane magnetic field for perpendicular MTJs (p-MTJs) and high power consumption. By using the in-plane exchange bias field generated at the antiferromagnetic/ferromagnetic interface, the issue of requiring an in-plane field for p-MTJs can be resolved. Additionally, the voltage-controlled magnetic anisotropy (VCMA) effect can reduce the power consumption [1-5]. In this paper, we investigate low-power field-free data writing in pMTJs and pMTJ arrays. Firstly, we deposited a perpendicularly magnetized IrMn/CoFeB/MgO trilayer film and patterned it into Hall bar devices. Field-free SOT switching is achieved with the assistance of an in-plane exchange bias, while the VCMA effect is utilized to reduce the critical switching current density. Next, we deposited a full film stack of IrMn-based pMTJs and manufactured pMTJ devices with diameters of 3μm and 5μm. By inserting a thin W layer at the IrMn/CoFeB interface, we increased the annealing temperature beyond 350°C and achieved a high tunnel magnetoresistance (TMR) ratio exceeding 100%. Finally, we reduced the device size to 80 nm (Fig. 1a) and fabricated a memory array with multiple pMTJs (Fig. 1b). The ns-scale SOT switching and selective data writing were realized in the array through voltage-gated SOT switching. When a gate voltage of 0.6V is applied, the critical switching current density dramatically decreases, creating a switching window highlighted by a green rectangle in Fig. 2a. In addition, the cumulative distribution function (CDF) of the switching probability for MTJ2 and MTJ3, as shown in Fig. 2b, confirms the feasibility of selective writing. These findings highlight the potential of voltage-gated SOT devices and arrays for practical MRAM applications [6-8].

[1] Y. W. Oh, S. Chris Baek, Y. M. Kim, Nat. Nanotechnol., Vol. 11, no. 10, p. 878-884(2016) [2] S. Peng, D. Zhu, W. Li, Nat. Electron., Vol. 3, no. 12, p. 757-764(2020) [3] W. Li, S. Peng, J. Lu, Phys. Rev. B, Vol. 103, no. 9, Art. no. 094436(2021) [4] Y. C. Wu, K. Garello, W. Kim, Phys. Rev. Appl., Vol. 15, no. 6, Art. no. 064015(2021) [5] K. Cai, S. Van. Beek, S. Rao, in Proc. Symp. VLSI Circuits, p. 375-376(2022) [6] S. Peng, J. Lu, W. Li, in Proc. IEEE Int. Electron Devices Meeting, p. 28.6.1-28.6.4(2019) [7] J. Lu, W. Li, J. Liu, Appl. Phys. Lett., Vol. 122, no. 1, Art. no. 012402 (2023) [8] W. Li, Z. Liu, S. Peng, IEEE Electron Device Lett., Vol. 45, no. 5, p. 921–924(2024)

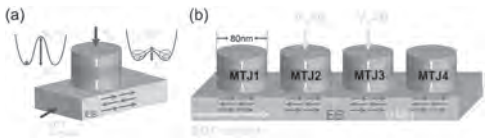

Fig. 1 (a) Schematic of voltage-gated SOT switching in a pMTJ device. (b) Schematic of selective switching operation in IrMn-based pMTJ array.

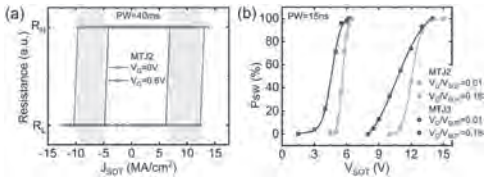

Fig. 2 (a) Voltage-gated SOT switching experiment of MTJ2. (b) CDF of voltage-gated SOT switching probability for MTJ2 and MTJ3.

ES-02. Voltage-controlled magnetic anisotropy driven non-linear parametric resonance. *A. Giordano*[1], A. Grimaldi[1], R. Sharma[2], E. Raimondo[4], R. Tomasello[3], M. Carpentieri[3], H. Yang[2] and G. Finocchio[1] *1. University of Messina, Messina, Italy; 2. University of Singapore, Singapore; 3. Politecnico di Bari, Bari, Italy; 4. INGV, Messina, Italy*

Spintronic diodes (STDs) exhibit potential advantages over the semiconductor counterpart. They are compact (nanoscale size), CMOS-compatible, energy-efficient [1][2]. In addition, the STDs can be measured as a response of different driving forces such as spin-transfer-torque, magnetic field and voltage controlled magnetic anisotropy(VCMA) [3]. We have performed a systematic study of the resonance response of the MTJ as a function of spin-transfer torque and VCMA amplitudes. In particular, the dynamics is driven by the presence of VCMA and simultaneity by spin-transfer-torque driven by an ac in-plane spin-polarized current density (Jac =0.1MA/cm). Our results predicted a fractional parametric resonance response driven by the simultaneous excitation of VCMA and ac spin-transfer torque for spintronic diodes working in the passive regime which has been also confirmed experimentally in magnetic tunnel junctions enabling the simultaneous excitation of spin-transfer torque and VCMA. At low VCMA, the resonance is characterized by ferromagnetic resonance curves which can be coupled with a parametric excitation once a dc current is also supplied. At larger value of the VCMA we found that parametric excitation at twice the value of resonance frequency can be achieved at zero dc current and a non-linear parametric response is observed, and it is characterized by several harmonic at fractional peaks, all of which are an integer fraction of the main resonance frequency. At large VCMA we found the excitation of high order parametric resonance characterized by the excitation of harmonics at 2, 3 and 4 times the ferromagnetic resonance. This work opens a new direction for the use of spintronic diodes in the field of communication, as a single device would have the ability to detect more information carriers. ACKNOWLEDGEMENTS This work was supported under the project number 101070287 -- SWAN-on-chip - HORIZON-CL4-2021-DIGITAL-EMERGING-01, by the Italian Ministry of University and Research through the project “SkySens” PRIN_20222N9A73_002, PRIN 2020LWPKH7 (IT-SPIN), the MUR-PNRR project SAMOTHRACE (ECS00000022) by European Union (NextGeneration EU) and by the PETASPIN association (www.petaspin.com).

[1] G. Finocchio et al., “Perspectives on spintronic diodes,” Applied Physics Letters, vol. 118, no.16. 2021, doi: 10.1063/5.0048947. [2] P. N. Skirdkov and K. A. Zvezdin, “Spin-Torque Diodes: From Fundamental Research to Applications,”Annalen der Physik, vol. 532, no. 6. Wiley-VCH Verlag, Jun. 01, 2020, doi: 10.1002/andp.201900460 [3] Y. J. Chen et al., “Parametric resonance of magnetization excited by electric field,” Nano Lett., vol. 17, no. 1, pp. 572–577, Jan. 2017, doi: 10.1021/acs.nanolett.6b04725

ES-03. Towards Cancer Theragnostics using Magnetoelectric Nanoparticles. *V. Andre*[1], M. Abdel-Mottaleb[1], S. Chen[1], M. Shotbolt[1], S. Khizroev[1] and P. Liang[2] *1. University of Miami, Miami, FL, United States; 2. Cellular NanoMed Inc, Irvine, CA, United States*

This study investigates the theragnostic capabilities of Magnetoelectric Nanoparticles (MENPs) using magnetic resonance imaging (MRI) in a murine pancreatic adenocarcinoma model. MENPs exploit the magnetoelectric effect to convert magnetic fields into local electric fields, and apply this to cancer biology by inducing irreversible electroporation (IRE) in tumor cell membranes while sparing healthy cells. Additionally, MENPs enhance MRI by modulating T2 relaxometry. The research involved a pilot study with 21 mice and a confirmatory study with 27 mice. MENPs, administered at doses of 300 μg or higher and exposed to MRI magnetic fields, achieved a mean three-fold reduction in tumor volume (62.3% vs. 188.7%, $p<0.001$). A significant correlation was observed between the decrease in T2 relaxation time on MRI and tumor volume reduction ($r=0.351$, $p=0.039$), confirming the predictive diagnostic potential of MENPs. Notably, six out of 17 mice in the confirmatory study's experimental arms achieved a stable clinical complete response, highlighting the potential for durable treatment outcomes. Importantly, MENPs were not associated with any discernible clinical toxicities. This study presents the first in vivo evidence of an externally controlled, MRI-based theragnostic agent capable of targeting and treating solid tumors through IRE, representing a novel and promising approach to cancer therapy.

Khizroev, S. & Liang, P. Engineering Future Medicines With Magnetoelectric Nanoparticles: Wirelessly controlled, targeted therapies. *Ieee Nanotechnol Mag* 14, 23-29 (2020). https://doi.org:10.1109/Mnano.2019.2952227 Smith, I. T. *et al.* Nanomedicine and nanobiotechnology applications of magnetoelectric nanoparticles. *Wires Nanomed Nanobi* (2022). https://doi.org:ARTN e184910.1002/wnan.1849 Rodzinski, A. *et al.* Targeted and controlled anticancer drug delivery and release with magnetoelectric nanoparticles. *Sci Rep-Uk* 6 (2016). https://doi.org:ARTN 2086710.1038/srep20867 Martin, R. C., 2nd *et al.* Treatment of 200 locally advanced (stage III) pancreatic adenocarcinoma patients with irreversible electroporation: safety and efficacy. *Ann Surg* 262, 486-494; discussion 492-484 (2015).

ES-04. High Data-Rate VLF Magnetoelectric Communications with Single-Side-Band Nonlinear Antenna Modulation. *Y. Liu*[1], T. Noochan[1], B. Luo[1] and N.X. Sun[1] *1. Electrical and Computer Engineering, Northeastern University, Boston, MA, United States*

Very Low Frequency (VLF) electromagnetic waves show great potential in underground and underwater communication owing to their strong penetration depth in lossy media like seawater [1]. However, the long wavelength of VLF signals requires antennas that are large in size and have high power consumption. At the same time, state-of-the-art VLF communication systems suffer from low data rates of ~200 bit/s. Recent research demonstrated that magnetoelectric (ME) antennas leveraging electromechanical resonance(EMR) could reduce VLF antenna size by several orders of magnitude [1-4]. Despite this advancement, the bandwidth and efficiency of VLF ME antennas are limited by relatively low resonance frequencies at VLF. Recently, a double-side-band Nonlinear Antenna Modulation (DSB-NAM) technique with carrier frequency equal to the electromechanical resonance frequency ($f_{carrier} = f_{EMR}$), has been utilized to overcome this limitation, but it suffers from high power consumption and weak signals (Fig. 1, Fig. 2a and b) [1-4]. In this work, we demonstrate a new modulation technique for VLF ME antennas, the single-side-band Nonlinear Antenna Modulation (SSB-NAM), which offers higher signal-to-noise ratio (SNR) with over 10 kb/s data rates, and much stronger modulation output. Unlike DSB-NAM [1-4], where the carrier signal frequency is equal to the EMR frequency(f_{EMR}) of VLF ME antennas, the $f_{carrier}$ in SSB-NAM is adjusted with the baseband data frequency ($f_{baseband}$), ensuring that $f_{carrier} + f_{baseband} = f_{EMR}$ (Fig 1, Fig. 2c and d). In both DSB-NAM and SSB-NAM, no mixer is used before feeding the baseband data and carrier signal into ME antennas; instead, the modulation output signal was directly produced due to the intrinsic nonlinearity of ME antennas. The spectrum reveals three peaks at $f_{carrier} - f_{baseband}$, $f_{carrier}$, and f_{EMR} (Fig. 2c). Our findings indicate that the modulated output at f_{EMR} remains stable and strong across $f_{baseband}$ range from 0.5 kHz to 10 kHz, maintaining around 4 nT (Fig. 2d). These results demonstrate that robust transmission and wide bandwidth capabilities are achieved for advanced VLF underwater and underground communications.

1. B. Luo, AR Will-Cole, C. Dong, NX Sun, Nature Reviews Electrical Engineering, 1, 317-334 (2024). 2. C. Dong, Y. He, X. Liu, and N. X. Sun, New York, NY, USA, 2022: ACM, pp. 1-5. 3. C. Dong *et al.*, *IEEE Antennas and Wireless Propagation Letters,* 19, 398-402 (2020). 4. Y. He, PhD Dissertations, 2023.

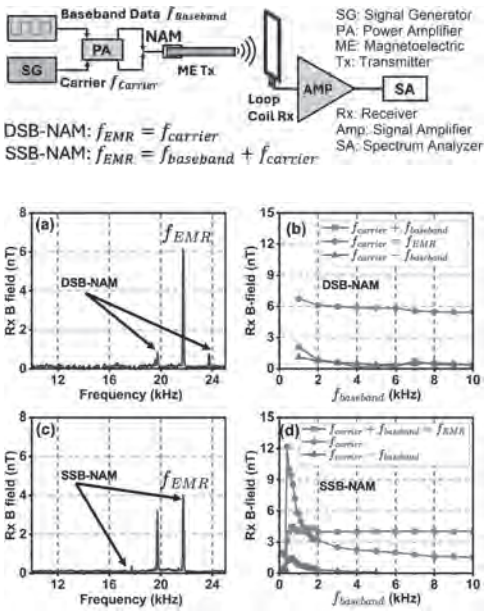

ES-05. Electric Field Controlled Nanowire Based Domain Wall Logic Device. *J. Weng*[1], P. Zhang[1] and J. Hong[2] *1. School of Sciences, Hubei University of Technology, Wuhan, China; 2. UC Berkeley, Berkeley, CA, United States*

Magnetic domain walls (DWs) based device structures have significant potential applications as information carriers for novel high-density, high-speed spintronic devices with non-volatility. [1,2] However, in most previous studies of magnetic domain wall logic devices, the propagation of the magnetic domain walls has been dependent on the control field of an external field, which is particularly problematic in large-scale applications. A multiferroic system consists of a piezoelectric substrate coupled to a ferromagnet, which offers the possibility to control the magnetisation by magnetoelastic coupling and by an electric field. [3-5] This talk presents strain induced anisotropic tilting of the magnetisation can control the DW motion. We propose a method for performing all-electric logic operations using such systems. As shown in Fig 1, ferromagnetic coupling between adjacent magnetic domains induced by electric field-controlled strain has been used to facilitate non-collinear spin alignment, which is used to implement the fundamental building blocks in all implementations of Boolean logic, including DW generation, propagation and fixation, paving the way for scalable logic memory applications.

[1] Lahtinen, T., Franke, K., van Dijken, S. Sci Rep 2, 258 (2012). [2] Beach, G., Nistor, C., Knutson, C. Nature Mater 4, 741–744 (2005). [3] Yin, Z. W., Luo, H. S., Wang, P. C. Ferroelectrics, 229(1), 207–216 (1999). [4] Consolo, G., Valenti, G. J. Appl. Phys. 121, 043903 (2017). [5] Yu, G., Shi, S. Journal of Magnetism and Magnetic Materials 552 (2022).

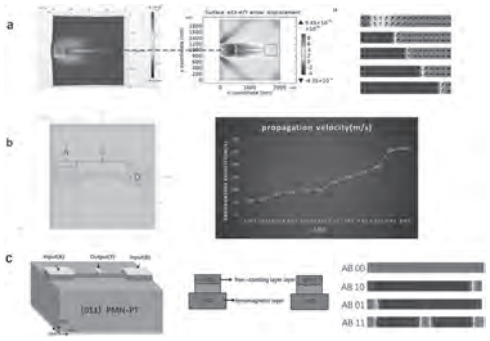

Fig. 1 a, The process for realizing the propagation of magnetic domain walls along nanowires. b, Effect of different sizes of electrodes and nanowires on the propagation rate of magnetic domain walls. c, Structure and principle of the XOR/XNOR logic gate.

ES-06. Boron Doping and Voltage Effects on Spin Reversal of Antiferromagnetic Domains in Cr_2O_3 Thin Films and Devices.
A. Erickson[1], S. Shah[1], A. Mahmood[1], P. Buragohain[1], I. Fescenko[2], A. Gruverman[1], C. Binek[1] and *A. Laraoui*[1] *1. University of Nebraska-Lincoln, Lincoln, NE, United States; 2. University of Latvia, Riga, Latvia*

Chromia (Cr_2O_3) is a magnetoelectric antiferromagnetic (AFM) oxide that allows voltage-control of the Néel vector under the presence of a magnetic field [1]. Boron doping of Cr_2O_3 increases the Néel temperature from 307 to 400 K [2] and it is believed to break the local symmetry giving rise to transient polarization under an applied electric field, allowing for purely voltage control of the Néel vector [2]. Here, we use NV magnetometry [3-4] to image the stray fields resulting from single layers of uncompensated spins on the surface and interface of Cr_2O_3 with the substrate [5]. The acquired image confirms the presence of homogeneously AFM domains (size ~ 50 – 300 nm) that depends strongly on the film thickness, explained by the increase of nucleation site density using Avrami phase transformation model [6]. Reconstruction of the surface magnetization from the NV stray-field maps unveils a clear difference between the pure and B-doped Cr_2O_3 films, *i.e.*, 90° between stable Néel vectors in B-doped films, and 180° for pure films. We discuss results on voltage induced Néel vector 90° spin reversal in B:Cr_2O_3/V_2O_3 devices [6], a promising result for AFM spintronics. Acknowledgments: This work is supported by the National Science Foundation/EPSCoR RII Track-1: Emergent Quantum Materials and Technologies (EQUATE), Award OIA-2044049. I. F. acknowledges support from the Latvian Quantum Initiative under European Union Recovery and Resilience Facility project no. 2.3.1.1.i.0/1/22/I/CFLA/001. The research was performed in part in the Nebraska Nanoscale Facility: National Nanotechnology Coordinated Infrastructure and the Nebraska Center for Materials and Nanoscience (and/or NERCF), supported by the National Science Foundation under Award ECCS: 2025298, and the Nebraska Research Initiative.

[1] N. Wu, et *al.*, *Physical Review Letters* 106, 087202 (2011). [2] A. Mahmood, et *al.*, *Nature Communications* 12, 1674 (2021). [3] S. Lamichhane, A. Laraoui et *al.*, *ACS Nano* 17, 9, 8694–8704 (2023) [4] R Timalsina, A Laraoui, et *al.*, *Advanced Electronic Materials* 10 (3), 2300648 (2024) [5] A. Erickson, A. Laraoui. et *al.*, *RSC Advances* 13, 178-185 (2023). [6] A. Erickson, A. Laraoui, et *al.*, *Advacned Functional Materials,* under review, https://doi.org/10.48550/arXiv.2405.11122.

ES-07. Electric field effect on exchange coupling induced T_c-modulation in superconducting spin valves.
T. Kikuta[1], S. Komori[1], K. Imura[2] and T. Taniyama[1] *1. Department of Physics, Nagoya University, Nagoya, Japan; 2. ILAS, Nagoya University, Nagoya, Japan*

In a superconducting spin valve (ferromagnet/superconductor/ferromagnet), proximity effects (e.g. spin scattering of spin-polarized quasiparticles and exchange coupling between spins of Cooper pairs and spins in a ferromagnet) modulate the superconducting transition temperature (T_c). These proximity effects are controllable by manipulating the magnitude and orientation of the magnetization. Generally, a magnetic field is used to control the magnetization. However, a new method for controlling the magnetization without a magnetic field is required for its application to electronics. Here, we report electric field effect on the proximity effects in superconducting spin valves. We have fabricated a $Pr_{0.8}Ca_{0.2}MnO_3$ (PCMO) (50 nm) /$YBa_2Cu_3O_7$ (YBCO) (15 nm) /PCMO (100 nm) superconducting spin valve on a $Pb(Mg_{1/3}Nb_{2/3})O_3$-$PbTiO_3$ (PMN-PT) (001) substrate using pulsed laser deposition. Figure 1 shows the magnetoresistance of the superconducting spin valve at 0 and 4 kV/cm. An increase in the electrical resistance indicates a suppression of superconductivity and a decrease means a liberation from the suppression. The suppression of T_c due to exchange coupling is maximized (minimized) when the magnetization alignment of the two ferromagnetic layers is parallel (antiparallel). Therefore, the effect gives dips in the magnetoresistance curve in the antiparallel configuration. The magnitude of the dips changes in an electric field, indicating that the T_c-modulation via exchange coupling can be manipulated by an electric field. The results potentially provide a new method for controlling the proximity effects and are promising for the electric field control of superconducting spintronic devices. We discuss the details of the mechanisms of the electric field effect with our previous work on a superconducting spin valve consisting of $La_{0.67}Ca_{0.33}MnO_3$ and $YBa_2Cu_3O_7$[1]. Work supported by JSPS KAKENHI (23KK0086, 24H00380, 24KJ1306), JST FOREST (JPMJFR212V), and Iketani Science and Technology Foundation.

[1] T. Kikuta, S. Komori, K. Imura, T. Taniyama, APL Materials Vol. 12, 071115 (2024)

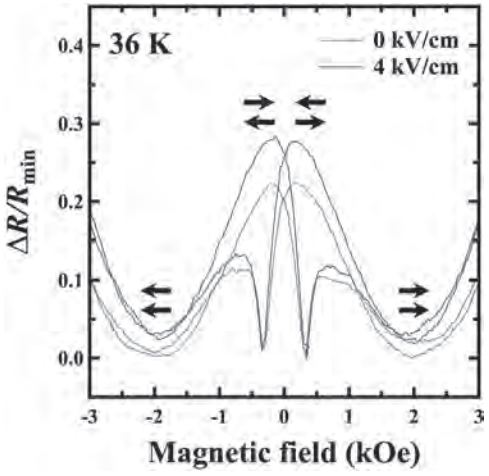

Fig. 1: In-plane magnetoresistance for a PCMO (50 nm) /YBCO (15 nm)/ PCMO (100 nm) superconducting spin valve on a PMN-PT (001) substrate at 0 kV/cm (red curves) and 4 kV/cm (blue curves).

ES-08. Stabilizing Topological Non-collinear Magnetoelectric Textures at Room Temperature.
A. Ghosal[1], S. Zhou[2], M. Ramesh[8], S. Husain[4], H. Zhang[4], C. Klewe[7], J. Mundy[6], D. Schlom[8], P. Stevenson[3], R. Ramesh[5,4] and L.M. Caretta[1] *1. School of Engineering, Brown University, Providence, RI, United States; 2. Department of Physics, Brown University, Providence, RI, United States; 3. Department of Physics, Northeastern University, Boston, MA, United States; 4. Department of Materials Science and Engineering, University of California, Berkeley, Berkeley, CA, United States; 5. Department of Materials Science and Nanoengineering, Rice University, Houston, TX, United States; 6. Department of Physics, Harvard University, Cambridge, MA, United States; 7. Lawrence Berkeley National Laboratory, Berkeley, CA, United States; 8. Department of Materials Science and Engineering, Cornell University, Ithaca, NY, United States*

Topological solitons, such as skyrmions, Bloch points, and merons, have been touted as information carriers in future memory, logic, and quantum information science applications[3,6]. In this regard, antiferromagnets[4,5] possess a number of advantages, such as immunity to stray fields and

ultrafast dynamics. Likewise, ferroelectric topologies have been shown to exhibit interesting phenomena like negative capacitance[1] and emergent chirality[2]. While both topological antiferromagnetic and polar solitons have recently been observed[2] a key challenge is to stabilize topological textures with co-existing order parameters and manipulate them on-demand with ultralow power. Magnetoelectric materials, which exhibit coupling between simultaneous ferroelectric and magnetic ordering, are a promising pathway, as they enable low-voltage electric field nucleation and manipulation of magnetism. Here, we experimentally demonstrate a pathway to stabilizing multiferroic topological solitons in thin films of the model magnetoelectric $BiFeO_3$ (BFO) at room temperature. By engineering epitaxial strain and electrostatic boundary conditions in BFO, we stabilize topological singularities at instabilities at multiferroic domain boundaries. We confirm the magnetic order of these textures through vector photoemission electron microscopy and scanning nitrogen vacancy magnetometry and correlate this to polar order via piezoresponse force microscopy and transmission electron microscopy (Figure 1). Our results illustrate a significant step towards the realization of magnetoelectric topology.

1. Das, S., Hong, Z., Stoica, V.A. et al. Local negative permittivity and topological phase transition in polar skyrmions. Nat. Mater. 20, 194–201 (2021). 2. Das, S., Tang, Y.L., Hong, Z. et al. Observation of room-temperature polar skyrmions. Nature 568, 368–372 (2019). 3. Fert, A., Ramesh, R., Garcia, V., et al. Electrical Control of Magnetism by Electric Field and Current-Induced Torques. Rev. Mod. Phys. 96, 015005 (2024) 4. Jani, H., Harrison, J., Hooda, S. et al. Spatially reconfigurable antiferromagnetic states in topologically rich free-standing nanomembranes. Nat. Mater. 23, 619–626 (2024). 5. Jani, H., Lin, JC., Chen, J. et al. Antiferromagnetic half-skyrmions and bimerons at room temperature. Nature 590, 74–79 (2021). 6. Junquera, J., Nahas, Y., Prokhorenko, S., et al. Topological phases in polar oxide nanostructures. Rev. Mod. Phys. 95, 025001 (2023).

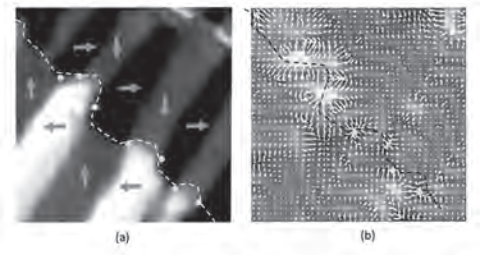

Figure 1: Correlated (a) piezoresponse force microscopy and b) scanning nitrogen vacancy (NV) magnetometry at a multiferroic domain boundary in $BiFeO_3$ (white dashed line) illustrating multiferroic singularities.

Session ET
THIN FILMS, MULTILAYERS, AND EXCHANGE BIAS SYSTEMS II
(Poster Session)

Juan Luis Palma, Chair
Universidad Central de Chile, Santiago, Chile

ET-01. Structural and Magnetic Properties of Fe_xSn_{1-x} Thin Films.

C. Brennan-Rich[1], T. Almeida[2], S. McVitie[2], S. Collins[3,4], R. Drummond-Brydson[4] and C. Marrows[1] *1. School of Physics and Astronomy, University of Leeds, Leeds, United Kingdom; 2. School of Physics and Astronomy, University of Glasgow, Glasgow, United Kingdom; 3. School of Chemistry, University of Leeds, Leeds, United Kingdom; 4. School of Chemistry and Process Engineering, University of Leeds, Leeds, United Kingdom*

The Fe-Sn intermetallic alloys form layered structures that have distinct magnetic properties. FeSn is an antiferromagnet [1] while Fe_3Sn_2 is a frustrated ferromagnet [2]: these differ only in their layer stacking sequence. Fe_3Sn_2 has also been identified as a candidate for hosting magnetic skyrmions stabilised by frustration [3]. Such stabilisation allows for a free chirality [4,5] and therefore could act to store bits in a spintronic device [6]. Here we report epitaxial growth of Fe-Sn thin films on sapphire with phase content adjusted by controlling the relative Fe and Sn fluxes. Characterisation of these films was achieved through Cu K-α X-ray diffraction (XRD) and Scanning Transmission Electron Microscopy (STEM) with quality comparable to films in the literature grown by MBE techniques [7]. Fig. 1(a) shows an XRD pattern of a 30 nm film grown on sapphire with a Pt seed layer. The Fe sputter power used was 31 W and the Sn power 11 W. Fig. 2 shows the Fe_xSn_{1-x} film imaged through STEM imaging. These data show that an Fe_3Sn_2 (0009) peak, with associated Laue oscillations indicating a good crystallographic order, as well as the absence of strong FeSn peaks is not sufficient to conclude that the resulting film is phase pure. Fig. 1 (a) contains these features, but under STEM imaging a phase mixture of FeSn and Fe_3Sn_2 is still present in Fig. 2. Fig. 1(b) shows how the film properties change as the Fe power is varied for a fixed Sn power of 11 W. The variation in position of the XRD peak near 40° is shown: a combination of FeSn (0002) and Fe_3Sn_2 (0009). Since, for the powers considered, Fe content is linearly proportional to Fe power the movement of this peak follows Vegard's law for lattice parameters in a solid solution of FeSn to Fe_3Sn_2. Magnetic data was gathered using SQUID magnetometry. The saturation magnetisation as a function of Fe deposition power is also plotted in Fig. 1(b) When the Bragg peak is close to the (0009) position for Fe_3Sn_2, for an Fe sputter power of 29 W, the magnetisation matches the literature value for that Fe_3Sn_2 [7,8]. We have therefore shown that the magnetisation of Fe_xSn_{1-x} films is consistent with the mixture of ferromagnetic and antiferromagnetic phases that they contain.

[1] H. Inoue et al., Molecular beam epitaxy growth of antiferromagnetic kagome metal FeSn, Appl. Phys. Lett. 115, 072403 (2019) [2] C. Lee et al., Spin wavepackets in the Kagome ferromagnet Fe3Sn2: Propagation and precursors. PNAS. 120 (21) e2220589120 (2023) [3] L.A. Fenner, A.A. Dee and A.S. Wills, Non-collinearity and spin frustration in the itinerant kagome ferromagnet Fe_3Sn_2. J. Phys.: Cond. Matt. 21, 452202 (2009) [4] Z. Hou et al., Current-Induced Helicity Reversal of a Single Skyrmionic Bubble Chain in a Nanostructured Frustrated Magnet, Adv. Mater. 32, 1904815, 2020 [5] D. Zhang, Z. Hou and W. Mi, Anomalous and topological Hall effects of ferromagnetic Fe3Sn2 epitaxial films with kagome lattice. Appl. Phys. Lett. 120, 232401 (2022) [6] C. Wang et al., Manipulating and trapping skyrmions by magnetic field gradients, New J. Phys. 19 083008 (2017) [7] S. Cheng et al., Atomic layer epitaxy of kagome magnet Fe_3Sn_2 and Sn-modulated heterostructures, APL Mater. 10, 061112 (2022) [8] K. Khan et al., Intrinsic anomalous Hall effect in thin films of topological kagome ferromagnet Fe_3Sn_2, Nanoscale, 14, 8484 (2022) [9] H. Giefers and M. Nicol, High pressure X-ray diffraction study of all Fe–Sn intermetallic compounds and one Fe–Sn solid solution, Journal of Alloys and Compounds, Volume 422, Issues 1–2, Pages 132-144 (2006)

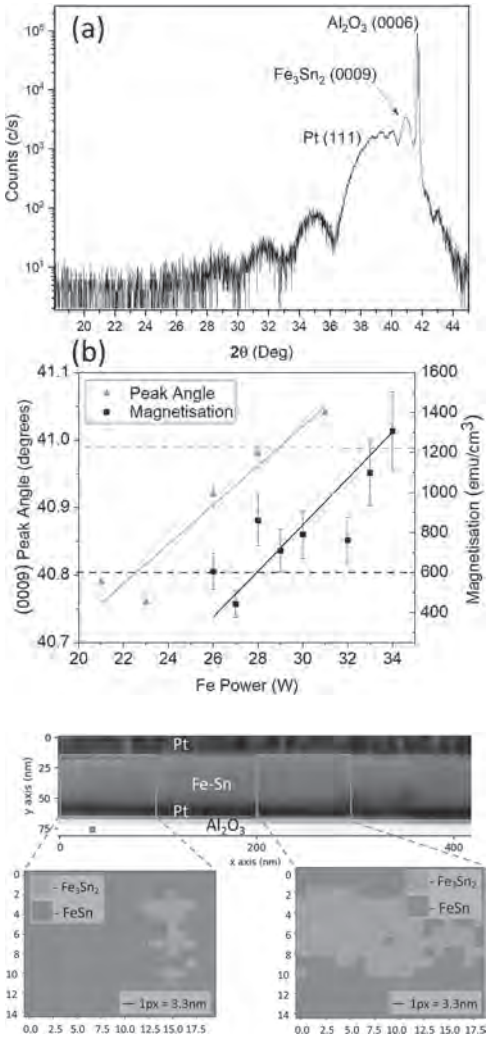

ET-02. Investigation of Curie Temperature and Gilbert Damping of Magnetron Sputtered $Al_{0.25}CrFeCoNi$ Thin Films. *M. Noor*[1], T. Das Gupta[1], A. Vasdev[2,3], M. Detisch[4], L. De-Long[5], W. Gannon[5], B. Jungfleisch[6], T. Balk[1], T. Hastings[2] and P. Rottmann[1] *1. Chemical and Materials Engineering, University of Kentucky, Lexington, KY, United States; 2. Electrical and Computer Engineering, University of Kentucky, Lexington, KY, United States; 3. Materials Science Division, Argonne National Laboratory, Lemont, IL, United States; 4. Electron Microscopy Center, University of Kentucky, Lexington, KY, United States; 5. Physics & Astronomy, University of Kentucky, Lexington, KY, United States; 6. Physics and Astronomy, University of Delaware, Newark, DE, United States*

Ferromagnetic Multi-Principal Component Alloys (MPCAs) are emerging materials systems that offer tunable magnetic properties with tailored mechanical and electrical properties. $Al_xCrFeCoNi$, a promising soft magnetic MPCA, has been predicted to exhibit compositionally tunable Gilbert Damping (GD) with a minimum near $Al_{0.25}CrFeCoNi$, where the density of states is minimized at the Fermi level [1]. To evaluate the suitability of $Al_{0.25}CrFeCoNi$ for functional nanomagnetic and magnonic systems it's important to establish its magnetic properties e.g., GD in thin film form. Although related MPCAs have been prepared by arc or induction melting, sputtering or pulsed laser deposition [2], no prior studies of magnetic behavior of $Al_{0.25}CrFeCoNi$ thin films have been identified. This study investigates $Al_{0.25}CrFeCoNi$ thin films synthesized via magnetron sputtering, employing comprehensive characterization techniques e.g. XRD, FIB/SEM, EDS to analyze structure and composition. The choice of this composition aims to balance soft magnetic properties with lower GD compared to permalloy. Magnetic properties were thoroughly investigated using SQUID magnetometry. M-H hysteresis loops were measured to determine key parameters such as saturation magnetization and coercive field. Additionally, temperature-dependent magnetization measurements in zero-field cooling and field cooling states were performed to identify curie temperatures and potential spin glass behavior. To evaluate the dynamic magnetic properties, broadband FMR spectroscopy was employed. This technique allowed for the assessment of GD through resonance linewidth analysis across a wide frequency range. Efforts are underway to fabricate $Al_{0.25}CrFeCoNi$ artificial spin ices, nanopatterned magnetic lattices with emerging applications in magnonic and reservoir/neuromorphic computing. This will allow us to investigate the impact of reduced GD, a spin glass transition, and the potential for hierarchical magnetic frustration. The study bridges the gap between materials science and advanced computing, paving the way for the development of novel magnetic materials tailored for specific computational architectures.

[1] J. Kudrnovský, V. Drchal, F. Máca, I. Turek, and S. Khmelevskyi, "Electron transport in high-entropy alloys: $Al_xCrFeCoNi$ as a case study", Physical Review B 100, 014441 (2019). [2] P. Kumari, A. K. Gupta, R. K. Mishra, M. S. Ahmad, and R. R. Shahi, "A comprehensive review: recent progress on magnetic high entropy alloys and oxides", Journal of Magnetism and Magnetic Materials 554, 169142 (2022)

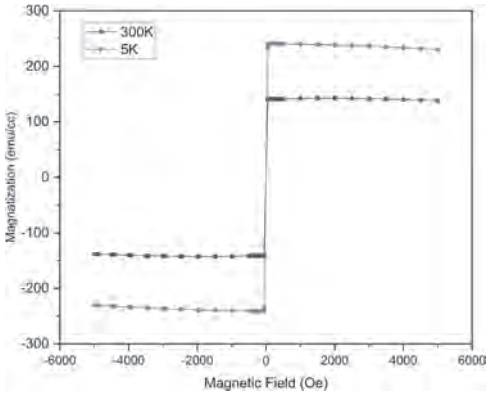

Hysteresis Loops Recorded by SQUID at 300K and 5K

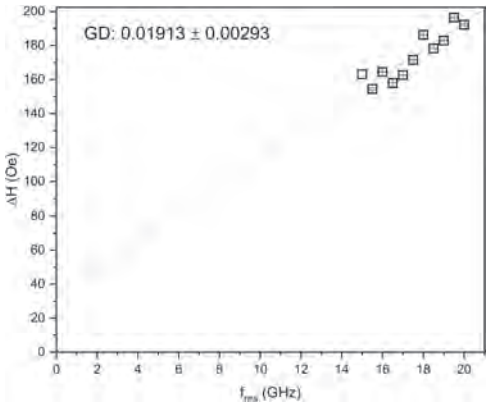

GD Parameter Derived from Linewidth (ΔH) and Resonance Frequency (f_{res})

ET-03. Thin film synthesis, structural analysis and magnetic properties of novel ternary transition metal nitride $MnCoN_2$. S. Dugu[1], R.W. Smaha[1], A. Treglia[2], S. Lany[1] and *S. Bauers*[1] *1. National Renewable Energy Laboratory, Golden, CO, United States; 2. Colorado State University, Fort Collins, CO, United States*

Transition metal (*TM*) nitrides have potential in industrial applications due to their outstanding properties such as high hardness, strength, excellent thermal conductivity, and unique electrochemical properties. In 2019, Sun *et al* [1] constructed a stability map of inorganic ternary metal nitrides using high-throughput computational methods. While this work predicted hundreds of new ternary nitrides, only one new chemical space was predicted to contain a previously unknown compound comprising nitrogen and two *TM*s: $MnCoN_2$. In this study, a series of Mn-Co-N thin films were synthesized and characterized for structural and magnetic properties. Combinatorial Mn-Co-N thin films are deposited using reactive cosputtering at different temperatures ranging from 25–450˚C and various process pressures. The phase of the as-grown material is checked by XRD. Survey density function theory total energy calculations are performed in parallel on five prototype structures based on zincblende or rocksalt lattices. Comparing the calculated structures with experimental diffraction patterns, the synthesized films better match rocksalt-derived structures, withvlower formation energy than zincblende candidates. However, only the primary diffraction peaks are seen, suggesting a large amount of cation anti-site disorder. Mn and Co concentrations are checked by XRF and N concentration is checked by RBS, confirming nearly 1:1:2 concentrations of Mn:Co:N with some reduced N due to O impurity. SEM and EDS are also performed, which illustrated the presence of all elements at their respective energy level. Magnetic properties for $MnCoN_2$ films have been studied by SQUID magnetometer which demonstrates that the film possesses a weak canted antiferromagnetic moment of remnant magnetization 0.01 emu/gm and coercive field of 0.5 T with Tc ~ 10 K. XAS shows Mn and Co exhibit octahedral coordination with N confirming rock-salt structure. Our experimental confirmation of this new TM_1–TM_2–N motivates renewed effort in new materials prediction and discovery in similar ternary spaces. In ongoing computation search, few more TM_1–TM_2–N have been predicted such as Ti-Co-N, Zn-Co-N, Nd-Mn-N, Mn-Sn-N etc which we look forward to synthesizing in near future.

1. Sun, W. *et al,* A map of the inorganic ternary metal nitrides. *Nat. Mater.* 18, 732–739 (2019)

ET-04. Exchange-Bias Effects in the Hysteresis Losses of Core-Shell Nanoparticles. *C. de Julián Fernández*[1], A. López-Ortega[2], E. Lottini[3], B. Muzzi[4], M. Albino[4] and C. Sangregorio[4] *1. Institute of Materials for Electronics and Magnetism C.N.R., Parma, Italy; 2. Departamento de Ciencias, Universidad Pública de Navarra, Pamplona, Spain; 3. INSTM- Università di Firenze, Florence, Italy; 4. Institute of Chemistry and Organometallic Compounds CNR, Florence, Italy*

In this work we investigate the effect of the exchange bias (EB) in the hysteresis losses of different core-shell nanoparticles. This effect produces the shift of the hysteresis loop of the composite after the field cooling (FC) from certain order or relaxation temperature. This appears mainly in hybrid nanostructures composed by antiferromagnetic (AFM) and ferro or ferrimagnetic (FiM) moieties that are exchange coupledby their interfaces. The hypothesis of employing EB to develop performing magnets [1-3] has been considered. Here we investigate the EB mechanisms in these nanostructures considering the change of energy losses (Wls). Wls are correlated to irreversible processes in the demagnetization processes, being particularly important for soft materials and for evaluating hyperthermia effects, and they should be a fingerprint of the exchange coupling of the two moieties. However, Studies on Wls are absent in EB literature. In this work, we investigate a series of 3 type of AFM core and FiM shell (CoxFe1−xO rock-salt core, and cubic spinel CoxFe3−xO4) with average total size of 6 nm, 9 nm and 18 nm and the FiM shell thickness is 2-3 nm in all cases [3]. The Zero Field cooling (ZFC) coercive fields of the three CS NPs are very similar (1.37 T -1.26 T), while the FC coercive field and exchange field are, 0.32,0.82 and 0.55 T for the first and 1.5 T, 1.9 and 1.6 T for the second, corresponding to the 6, 9 and 18 nm size NPs, respectively. Hence, the effect of the EB in the 9 nm CS NPs produces the larger shift of the hysteresis. The Wls were calculated integrating normalized hysteresis loops. The variation of FC Wls orespect to the ZFC Wls is 20% in the 6 nm NPs and larger but similar, 40% and 37%, for the 9 nm and 18 nm NPs. This indicates a different behavior of the EB considering the magnetic losses. In other to understand these differences, the EB loops were measured decreasing the FC temperature. The correlation between the energy losses and the coercive field under the FC and ZFC will be shown. This work was developed in the framework of the PRIN-PNRR project HyperMag (prot. P2022RRRT4) and supported by European Union – NextGenerationEU.

[1] A. P. Malozemoff, Phys. Rev B 37 (1988) 7673 [2] L. H. Lewis Metall, Mater Trans A 44, (2013) 2. [3] E. Lottini Chem. Mater. 2016, 28, 4214–4222

ET-05. Temperature Dependence of the Interlayer Exchange Coupling in Epitaxial Fe/MgO/Fe (001) Heterostructures. *A.I. Ojo*[1], A. Ravensburg[2], M.P. Grassi[2], V. Kapaklis[2] and D.A. Arena[1] *1. Department of Physics, University of South Florida, Tampa, FL, United States; 2. Department of Physics and Astronomy, Uppsala University, Uppsala, Sweden*

The discovery of large tunneling magnetoresistance (TMR) in epitaxial Fe/MgO heterostructures has ignited a wave of research into factors influencing the antiferromagnetic interlayer exchange coupling (IEC) such as tunnel barrier thickness [1], Fe layer thickness [2], and the number of repetitions [3]. However, limited experimental work has been done to understand the temperature dependence of the coupling while probing different crystallographic directions. In this study, we investigate the temperature dependence of the IEC in epitaxial Fe/MgO/Fe bilayers using broadband ferromagnetic resonance (FMR), with the applied magnetic field oriented along the Fe [100], [110], and [001] directions. The thicknesses of the Fe and MgO layers are ~2nm each. The FMR spectra of the coupled system reveal two distinct eigenmodes: a low-field (acoustic - LFR) mode and a high-field (optic - HFR) mode. The presence of the optic mode is attributed to slight dissimilarities in the magnetic layers. The relative positions (δ) of the acoustic and optic modes indicate a negative sign of the IEC, further confirming that the coupling is antiferromagnetic. As the temperature decreases, the ratio of the LFR to the HFR amplitude increases, indicating an enhancement of the coupling strength. Consequently, below 180K, only the acoustic mode is observed in the FMR spectra. These results provide valuable insights into the temperature-dependent behavior of IEC in Fe/MgO heterostructures and superlattices, with potential implications for developing and optimizing spintronic devices.

[1] T. Katayama, S. Yuasa, J. Velev, M. Y. Zhuravlev, S. S. Jaswal, and E. Y. Tsymbal, Applied Physics Letters 89, 112503 (2006). [2] A. L. Ravensburg, M. P. Grassi, B. Hjörvarsson, and V. Kapaklis, Physical Review B 109, 224404 (2024). [3] T. Warnatz, F. Magnus, N. Strandqvist, S. Sanz, H. Ali, K. Leifer, A. Vorobiev, and B. Hjörvarsson, Scientific Reports 11, 1942 (2021).

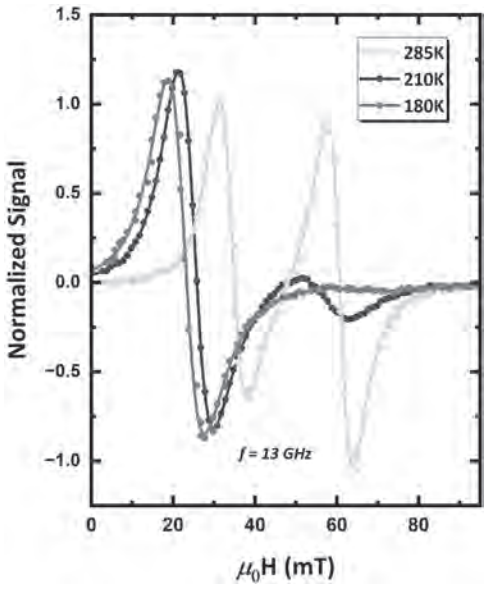

Fig. 1. Fe easy axis FMR spectra at 13 GHz across different temperatures.

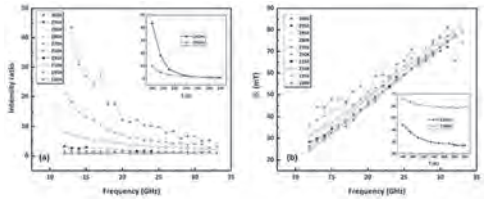

Fig. 2 (a) The ratio of the intensity of the low-field mode to the high-field mode as a function of frequency. The inset shows the temperature variation of the intensity ratio. (b) The absolute value of the relative positions (|δ|) of the low-field and high-field modes as a function of frequency. The inset shows the temperature variation of |δ|.

ET-06. Exploring FeCo-based nanogranular thin film with reduced eddy current loss. G. Wei[1], A. Masood[1], R. Anjum[1] and *R. Sai*[1] *1. Tyndall National Institute, Cork, Ireland*

The advent of PwrSoC and PwrSiP featuring thin film inductors - either integrated on power management IC die at back-end-of-the-line fabrication process or embedded in glass/organic interposer during 2.5D packaging - intensified the quest for miniaturization and efficiency in integrated inductors. Higher converter switching frequency (beyond 100 MHz) lowers the required inductance value, which in turn enables miniaturization of the inductor. However, owing to the dominating eddy current and anomalous losses in the magnetic core at high frequency, state-of-the-art low-resistivity magnetic thin film materials such as CoZrTa and CoZrTaB turn out to be practically untenable. Need of the hour is a high-resistivity magnetic thin film material. Nanogranular soft magnetic yet high resistivity thin film materials are promising for the development of next-generation magnetic thin films [1-2]. In this work, the relationship between the texture of a FeCoX (X: B and/or N) based granular films and their electrical resistivity is examined using COMSOL. The most influential physical parameters are identified.

Three design space studies are undertaken: the effect of grain size, grain boundary width, and grain boundary resistivity of a nanogranular films on their overall sheet resistance. Meshing was done by generating Voronoi diagram (Fig. 1a) based on various SEM images (Fig. 1b) of the nanogranular thin films studied here. Fig. 1c combines the effect of grain sizes (red dots), grain boundary width (blue dots), and the conductivity of grain boundary (black dots) regions on the electrical resistivity of a ferromagnetic nanogranular film. Both magnetic grain size decrease and grain boundary width increase eventually augment the overall grain boundary region (mentioned as dielectric vol.%). The resistivity of the grain boundary region has a profound effect on the overall resistivity of the film. Accordingly, by controlling sputtering pressure and power, 10X enhancement of resistivity (>1000 μΩ-cm) over traditional CoZrTa film has been achieved in B- and N-doped FeCo granular soft-magnetic thin film.

[1] H. Kijima-Aoki, et.al, AIP Advances 12, 035229 (2022); [2] D. Cronin, et.al., J. Appl. Phys. 127, 243903 (2020).

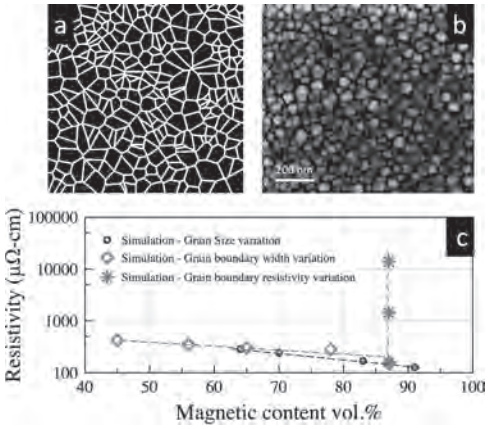

Fig. 1: (a) Voronoi diagram based mesh structure, (b) SEM image, and (c) effect of various structural parameters on film resistivity

ET-07. Unveiling the magnetic and optical properties of one-step grown, epitaxial $SmCrO_3$ thin films. *M. Madaan*[1], A. Jain[2] and V. Malik[1]
1. Physics, Indian Institute of Technology Roorkee, Roorkee, India; 2. Solid State Physics Division, Bhabha Atomic Research Centre, Mumbai, India

In the era of multifunctional materials featuring the coupled order parameters, rare earth orthochromites ($RCrO_3$, where R stands for rare-earth) exhibit captivating characteristics such as magnetization reversal, spin reorientation, multiferroicity, and magnetoelectric coupling etc [1-4]. These properties find various insightful applications in fields spanning spintronics, fast magnetic storage devices, refrigeration[5], sensors [6] and other related research areas. Herein this work, we present investigations of magnetic and optical properties of pulsed laser deposited (PLD) grown $SmCrO_3$ (SCO) thin films on single-oriented STO (100) substrate. High-resolution x-ray diffraction (HRXRD) confirms the epitaxial nature of the film. Magnetization studies, conducted in the temperature range of 2K to 300K under a 50Oe magnetic field using a dc SQUID magnetometer identify specific magnetic transitions and their corresponding temperatures. The magnetization (M) vs. temperature T) reveals signatures of spin canted antiferromagnetic (AFM) - paramagnetic (PM) transition in the vicinity of 195K (T_N), followed by spin reorientation transition near 35K (T_{SR}), consistent with bulk $SmCrO_3$ [7]. Magnetic isotherms after deduction of dominating diamagnetic part in high fields also indicate the growth of ferromagnetic component below T_N. To explore the multiband optical transition features in SCO thin film, room temperature spectroscopic ellipsometry was performed in wavelength ranging 250-1600 nm. Optical constants derived from fitting the optical absorption spectrum data implying multilayer model system with Lorentzian oscillators. It depicts peaks refering optical transitions, intra $t_{2g} - e_g$, inter $t_{2g} - t_{2g}$ and O 2p – Cr 3d charge transfer gap, akin to $YCrO_3$[8], $LaCrO_3$ [9] thin films. Hence, these properties critically are tuned with lattice strain in films, highlighting opportunities of multifunctional heterostructures. These findings encourage the future exploration of photovoltaics, and optoelectronics for rare-earth orthochromite systems.

[1] H. Zhang et al.,*Solid State Sci*, vol. 125, (2022); [2] B. Rajeswaran et al.,*Phys Rev B Condens Matter Mater Phys*, vol. 86, no. 21, (2012);[3] T. Sau *et al.*, *Phys Rev B*, vol. 103, no. 14, (2021); [4] M. Tripathi et al., *Phys Rev B*, vol. 96, no. 17, (2017); [5] T. Sau *et al.*, *Phys Rev B*, vol. 106, no. 6, p. 064413, (2022); [6] M. Tripathi et al., *RSC Adv*, vol. 6, no. 93, pp. 90255–90262, (2016); [7] P. Gupta et al., *J Phys D Appl Phys*, vol. 48, no. 2, (2015); [8] Y. Sharma *et al.*, *Nanomaterials*, vol. 10, no. 10, pp. 1–8, (2020); [9] Y. Sharma *et al.*, *Appl Phys Lett*, vol. 119, no. 7, (2021)

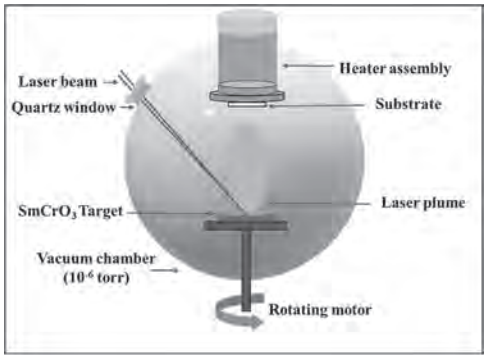

Fig. 1 Schematic of pulsed laser depostion (PLD) system

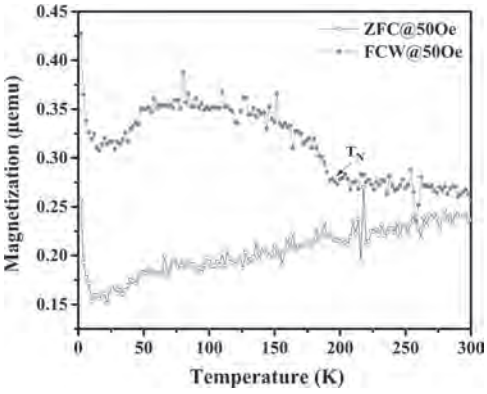

Fig. 2 Magnetization curves for $SmCrO_3$/ STO film under 50 Oe magnetic field.

ET-08. Focused Ion Beam Milling of Ta/Co/NiFe Magnetic Tunnel Junction based Molecular Spintronics Device. *H. Brown*[1], E. Mutunga[1] and P. Tyagi[1] *1. University of The District of Columbia, Washington, DC, United States*

In the realm of molecular spintronics, fabricating magnetic tunnel junctions (MTJs) with traditional techniques often encounters challenges in achieving precision and uniformity. This study introduces an advanced method using focused ion beam (FIB) milling with Gallium ions to enhance the fabrication of Ta/Co/NiFe/AlOx/NiFe magnetic tunnel junction-based molecular spintronics devices (MTJMSD). Our research aims to refine the fabrication process, focusing on the junction area, to improve the interaction between ferromagnetic electrodes (FMEs) and molecular transport channels. The current MTJMSD configuration requires a 2 nm insulating layer, where defects can cause short-circuits. Maintaining a short separation between FMEs while incorporating an insulating layer of 5-10 nm minimizes short-circuit risks and facilitates molecular connection. Plasma ion etching presents challenges such as over-etching and lack of uniformity. These limitations are particularly pronounced in MTJs, where junction area precision is crucial.

To address these challenges, our approach leverages the high-resolution capabilities of Gallium Ion FIB milling. This technique allows for precise etching of the junction area, enhancing the interface between FMEs and the insulating barrier, a critical factor for optimal MTJMSD performance. In our methodology, the FIB dose varied from 4.1E-12 to 8.8E-11 pC/μm^2 to investigate its impact on etching depth within the FME layers. Key parameters such as beam energy, current, diameter, and overlap percentage were kept constant to isolate the effects of the FIB dose. We observed that the FIB etch depth exhibited linear scaling with dosage, highlighting the precision and predictability of the FIB milling process. We achieved precise and uniform milling depths from 1 to 28 nm, demonstrating the efficacy of FIB milling in achieving controlled etching at the nanoscale. This research marks a significant improvement in the precision and control of MTJ fabrication and underscores the potential of Gallium Ion FIB milling as a transformative technique in manufacturing advanced molecular spintronics devices.

[1] Tyagi, P. (2011). Multilayer Edge Molecular Electronics Devices: A Review. *Journal of Materials Chemistry*, *21*(13), 4733. https://doi.org/10.1039/c0jm03291c [2] V. Milosavljević and P. J. Cullen, "Spatial phase-resolved optical emission spectroscopy for understanding plasma etching uniformity," *EPL (Europhysics Letters)*, vol. 110, no. 4, p. 43001, May 2015. doi:10.1209/0295-5075/110/43001 [3] M. Urbánek *et al.*, "Focused ion beam fabrication of spintronic nanostructures: An optimization of the milling process," *Nanotechnology*, vol. 21, no. 14, p. 145304, Mar. 2010. doi:10.1088/0957-4484/21/14/145304

Session EU
STRUCTURED MATERIALS II
(Poster Session)

Olin Thompson Mefford, Chair
Clemson University, Clemson, SC, United States

EU-01. Evaluating the Heating Efficacy of Short Nanowires Produced by Improved Multilayered Template-assisted Electrodeposition.
R. Kolisnyk[2], A. Harpel[1], A. Afful[2] and B. Stadler[2,1] *1. Chemical Engineering and Material Science, University of Minnesota, Minneapolis, MN, United States; 2. Electrical and Computer Engineering, University of Minnesota, Minneapolis, MN, United States*

Various metallic or oxide nanoparticles are widely used for magnetic hyperthermia and nanowarming of cryopreserved biospecies under an alternating magnetic field. Magnetic nanowires (MNWs) under the same concentration can beneficially contribute to the heating rate due to coupled hysteresis and resistive losses compared to other nanoparticles. One of the limitations is upscaling the production of such particles to meet the demand for high concentration. Typically, MNWs are synthesized through template-assisted electrodeposition, and their aspect ratio is determined by porous template parameters. It is worth mentioning that for bioapplication nanoparticles' dimensions are limited. Considering this and the industrial approach of a porous template manufacturing process, in the case of short nanowires mass production around 90-95% of template thickness would not be used, which is ineffective. Thus, two cases are available: 1-decreasing template thickness, which has processing restrictions and confined application; 2- filling pores with stacked nanowires. The later case is discussed further. Firstly, this study investigates the possibility of upscaling the production of short cobalt, nickel, and iron MNWs synthesized through a standard template-assisted process and the additional introduction of sacrificial copper interlayers. They are subsequently chemically etched, using as oxidizers iron(III) nitrate, ammonium hydroxide, and ammonium chloride of different concentrations, to yield high aspect ratio MNWs. Secondly, it is determined how the synthesis and etching conditions affect MNWs' heating efficacy in terms of reproducibility. While nickel MNWs during the template release process and following copper interlayers etching undergo surface passivation ($\delta_{NiO} \approx 5$nm) and show fairly high repeatability, the iron and cobalt MNWs are sensitive to both successive processes and their repeatability and heating efficiency are highly susceptible to treatment condition (e.g etching agent and its concentration, treatment time). In conclusion, the potential process of upscaling the synthesis of short nickel, cobalt, and iron nanowires has been studied and the consequent their heating application has been discussed.

EU-02. Importance of Magnetic Anisotropy in Determining Heating and Imaging Performance of Magnetic Nanoflower Colloids.
J. Borchers[1], K. Krycka[1], B.B. Santos[2], E. De Lima Correa[2], A. Sharma[3], H. Carlton[3], Y. Dang[2], M.J. Donahue[4], C. Gruettner[5], R. Ivkov[3,6,7] and C. Dennis[2] *1. NIST Center for Neutron Research, National Institute of Standards and Technology, Gaithersburg, MD, United States; 2. Material Measurement Laboratory, National Institute of Standards and Technology, Gaithersburg, MD, United States; 3. Department of Radiation Oncology and Molecular Radiation Sciences, Johns Hopkins University School of Medicine, Baltimore, MD, United States; 4. Information Technology Laboratory, National Institute of Standards and Technology, Gaithersburg, MD, United States; 5. micromod Partikeltechnologie, GmbH, 18057 Rostock, Germany; 6. Department of Oncology, Sydney Kimmel Comprehensive Cancer Center, Johns Hopkins University, Baltimore, MD, United States; 7. Department of Mechanical Engineering, Johns Hopkins University, Baltimore, MD, United States*

Functionalized magnetic nanoparticles have recently demonstrated efficacy in biomedical applications, such as magnetic nanoparticle hyperthermia (MNPH) and magnetic particle imaging (MPI). The composition, surface stabilization, and nanoparticle structure are all key to determining their performance. Here, we examine two compositions (ferrite and cobalt ferrite) of nanoflowers that consist of a central core with granular "petals." The magnetic nanoflowers (MNFs) have different surface treatments (ionic surfactant or dextran coating) designed to stabilize them in water via electrostatic or steric repulsion, respectively. To determine the correlation between their structure and function, we characterized the MNFs using techniques including specific loss power (SLP), point spread function, AC susceptibility, small angle neutron scattering (SANS), and torque measurements. For both nanoflower compositions, choice of coating has little effect on MNPH and MPI, but the heating output and the imaging tracer quality of the cobalt ferrite MNFs are greatly reduced relative to the ferrite MNFs. We first determined from SANS that uncoated MNFs form multi-pole-like clusters and loose chains. In contrast, the coated nanoflowers form dipoles with branched chains that tilt in increasing magnetic field. Polarized SANS further reveals that while the magnetization in the ferrite MNFs is uniform, the cobalt ferrite MNFs have a core/shell magnetic structure with a magnetization that is reduced significantly relative to bulk. The shell formation leads to frustration that reduces the effective magnetic anisotropy and the maximum heat generated in MNPH. The reduction in magnetic anisotropy then leads to a more linear response of the magnetic moment of the MNFs to magnetic field, which results in minimal MPI signal. Overall, the magnetic anisotropy, as influenced by the MNF composition, is of primary importance, relative to surface stabilization and colloidal structure, for optimizing performance of these nanoparticles in biomedical applications.

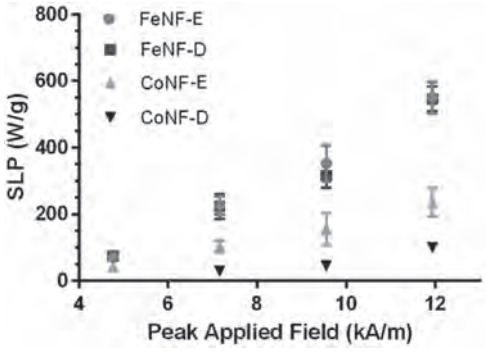

Fig. 1: SLP for coated (D) and uncoated (E) iron oxide (FeNF) and cobalt oxide (CoNF) nanoflowers

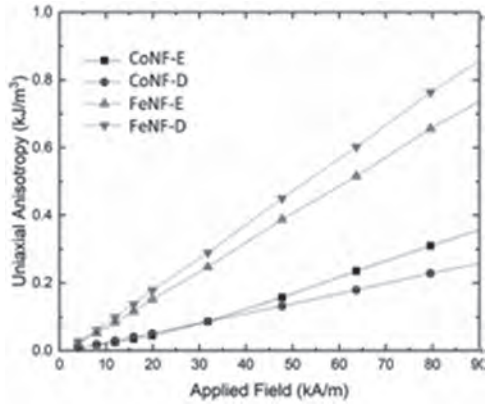

Fig. 2: Effective magnetic anisotropy measured from torque magnetometry for the nanoflower series

EU-03. Growth Mechanism of One-Dimensional Assemblies Consisting of Silica-Coated Magnetic Nanoparticles. *C. Oka*[1], T. Shiojima[1], J. Sakurai[1] and S. Hata[1] *1. Department of Micro-Nano Mechanical Science and Engineering, Nagoya University, Nagoya, Japan*

Magnetic nanoparticles (MNPs) with a high aspect ratio have attracted attention in fields such as cancer treatment, magnetic recording, and magnetic fluids because of their magnetic anisotropy, but their synthesis requires vacuum, reduction, and/or high temperature conditions. Hence, we have focused on one-dimensional (1D) assemblies of MNPs, which are expected to exhibit magnetic anisotropy as well as the high-aspect-ratio MNPs, and we have manufactured the 1D assemblies of MNPs under atmospheric pressure and room temperature conditions by silica coating of MNPs in a chain-like alignment under a uniform magnetic field [1]. In the present study, we investigated a mechanism of the growth of the 1D assemblies with the duration of the magnetic field application for the chain alignment. We calculated the length of 1D assemblies of MNPs without silica coating using MagChain [2] and compared it with the length of our 1D assemblies with silica coating. Fig. 1 shows the results of experimental and calculated lengths of 1D assemblies of MNPs with and without silica coating, respectively, depending on the duration of magnetic field application. The experimental and calculated lengths are in relatively good agreement up to 240 s, but after 240 s, the experimental length possesses larger values than the calculated length. This would be because the MNP alignment and the silica deposition occur simultaneously in addition to the experimental length including the thickness of the silica coating. Under conditions where the magnetic field application time is relatively long, as shown in Fig. 2, the 1D assemblies of MNPs coated with silica are connected leading to the form of long 1D assemblies. Therefore, since the experimental length includes the thickness of silica not only at the surface but also at gaps between short MNP chains, the length would be larger than the calculated length.

[1] T. Shiojima et al., Japanese Journal of Applied Physics, Vol. 63, 03SP77 (2024) [2] J.S. Andreu et al., Physical Review E, Vol. 85, 036709 (2012)

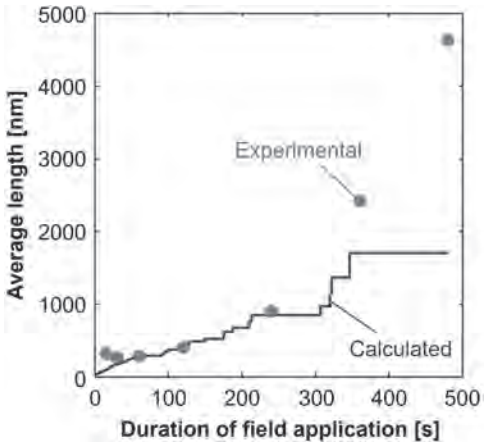

Fig. 1 The length of 1D assemblies vs duration of magnetic field application.

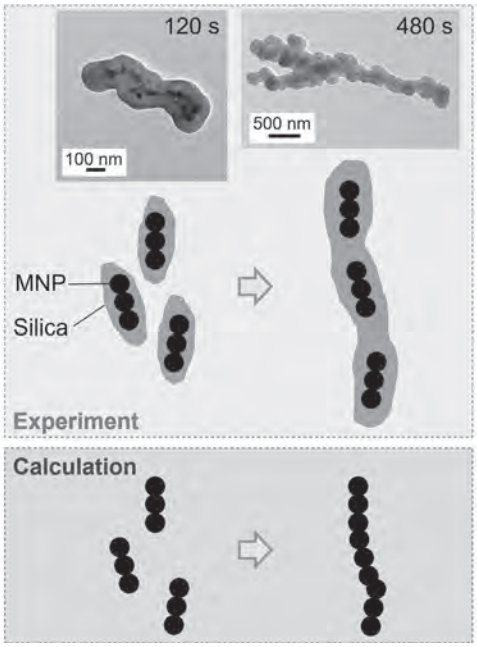

Fig. 2 Schematic illustrations and TEM images of 1D assemblies.

EU-04. High Magnetoresistance in Magnetic Polymer Nanocomposites Comprising Fe Nanoparticles and PEDOT: PSS. *S. Liang*[1], R.A. Mendonsa[2], V.K. Chugh[2], D. Su[1], K. Wu[3] and J. Wang[1,2] *1. Chemical Engineering and Materials Science, University of Minnesota, Minneapolis, MN, United States; 2. Electrical and Computer Engineering, University of Minnesota, Minneapolis, MN, United States; 3. Electrical and Computer Engineering, Texas Tech University, Lubbock, TX, United States*

Magnetic polymer nanocomposites (PNCs), comprising magnetic nanoparticles dispersed within a polymer matrix, exhibit unique electrical and magnetoresistive properties. However, achieving high magnetoresistance (MR) under low magnetic fields at room temperature remains challenging for reported magnetic PNCs, limiting their potential applications.[1-3] Herein, we present a novel magnetic PNC consisting of carbon-coated iron magnetic nanoparticles (Fe MNPs) and poly(3,4-ethylenedioxythiophene): poly(styrene sulfonate) (PEDOT: PSS). Fe MNPs were selected for their high magnetic moment, while PEDOT: PSS (1.1 wt.% in H_2O) was chosen for its well-studied conductive properties and tunable conductivity. Fe MNPs, with an average particle size of 22 nm, were evenly dispersed in PEDOT: PSS via wet ball milling to form a mixture. This mixture was drop-cast on a Si substrate and air-dried under a fixation magnetic field of 5000 Oe. The resulting film (see Fig. 1a) exhibited chain-like structures of

Fe MNPs, which have been reported to potentially enhance the MR ratio in similar magnetic PNCs.[1] As depicted in Fig. 1b, the MR ratio (defined as $[R(H) - R_{max}]/R_{max}$) of the resultant magnetic PNC thin films was measured to be 82% under a magnetic field of 700 Oe. Additionally, Fig. 1c illustrates the MR curves of four repeated measurements, demonstrating the cycle-by-cycle repeatability of the MR behavior. The high MR ratio achieved at a low magnetic field, coupled with the intrinsic flexibility and biocompatibility of PEDOT: PSS, suggests promising applications for PEDOT: PSS/MNPs composites in next-generation MR sensors, such as flexible and wearable magnetic sensors.

[1] J. Meyer, T. Rempel, M. Schäfers, *et al.*, Smart materials and structures., *22*(2), p.025032(2013) [2] B.H. Zhou, and J.D. Rinehart, ACS Applied Electronic Materials., 1(7), p.1065-1069(2019) [3] R. Wirecka, K. Maćkosz, A. Zywczak, *et al.*, Nanomaterials., 13(5), p.879.(2023)

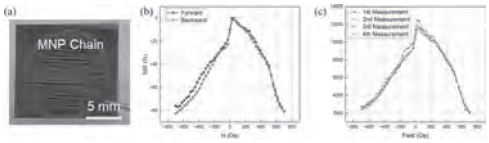

Fig.1 (a) Photograph of the Fe MNP/PEDOT: PSS (mass ratio 10:1) magnetic PNCs. (b) MR curves of the magnetic PNC thin films (forward: -700 Oe to 700 Oe, backward: 700 Oe to -700 Oe). (c) Iterative MR measurements from the same sample at the same location.

EU-05. Magnetization Dynamics in Co-$CoFe_2O_4$ Based Nanostructures: A Multimodal Characterizations Study to Understand Interparticle Interactions. *S. Jan*[1], S. Attanayake[1], N. Schulz[1], H. Khurshid[2], M. Phan[1], D.A. Arena[1] and H. Srikanth[1] *1. Department of Physics, University of South Florida, Tampa, FL, United States; 2. Department of Applied Physics and Astronomy, University of Sharjah, Sharjah, United Arab Emirates*

Core-shell nanoparticles have been proven to be a versatile platform for the tailoring of electronic and magnetic properties [1, 2]. In this work, we synthesize Co-$CoFe_2O_4$ (Co@CFO) core-shell nanostructures to expand the potential applications of the traditionally hard inverse spinel ferrite, CFO, via the inclusion of high saturation magnetization, magnetically soft Co. To confirm the morphology, chemical composition, and crystal structures, we employed a combination of analytical techniques, including transmission electron microscopy, energy dispersive spectroscopy, and X-ray diffraction. The results indicate that the synthesized nanostructures are highly crystalline with a core of elemental Co encapsulated with a shell of CFO. Static and dynamic magnetic measurements indicate robust magnetic ordering across a broad frequency range, underscoring the potential applicability of these nanostructures in high-frequency applications. Low temperature magnetic exchange bias is observed. The respective contributions from the magnetically hard and soft phases were deconvoluted to determine the intrinsic and extrinsic magnetic properties, and a novel parameter, denoted as the exchange dispersion (δ), is introduced to describe how the coercivity varies across the hard and soft phases as the temperature is varied. These results underscore the potential of the inclusion of elemental Co in core-shell nanostructures to tune the magnetic properties for applications in high-density magnetic storage, microwave absorbers and shielding, magnetic resonance imaging, magneto-optical devices, spintronics and magnetic sensors.

1. H. Khurshid, R. Yoosuf, and H. Zafar, From multi-segmented to core/shell nanorods: Morphology evolution in Fe–Au nanorods by tuning fabrication conditions, *Nanotechnology,* 34 (18), 185602 (2023). 2. A. López-Ortega, M. Estrader, and G. Salazar-Alvarez, Applications of exchange coupled bi-magnetic hard/soft and soft/hard magnetic core/shell nanoparticles, *Physics Reports,* 553, 1-32. (2015).

EU-06. Withdrawn

EU-07. Emergent Ferromagnetism and Phase Coexistence in 3D-Printed CrMnFeCoNi High Entropy Alloys. *V. Mishra*[1], N. Mudiyanselage[1], D. DeTellem[1], M. Jin[2], S. Witanachchi[1], M. Pham[2] and M. Phan[1] *1. Physics, University of South Florida, Tampa, FL, United States; 2. Department of Materials, Imperial College London, London, United Kingdom*

3D printing of high entropy alloys (HEAs) like CrMnFeCoNi has led to the creation of diverse novel structures with exceptional mechanical properties, making them suitable for a wide array of applications [1]. While the magnetic properties of non-printed CrMnFeCoNi alloys have been extensively studied [2], the influence of 3D printing on their magnetic behavior remains largely unexplored. In this study, we utilized 3D printing techniques to fabricate three samples under different conditions and compared their magnetic properties to those of their non-printed counterparts. X-ray diffraction analysis revealed that, in addition to the expected FCC phase, all samples exhibited a structurally disordered Mn-rich BCC phase. The crystallite size, particularly across the (111) superlattice reflection, was larger in the non-3D printed sample compared to the others. However, the opposite trend was observed for the (200) reflection associated with Co and Ni. Magnetization measurements revealed a magnetic glass-like behavior at low temperatures (< 100 K) for all samples, although this behavior was notably suppressed in the 3D-printed samples. Interestingly, the 3D-printed samples exhibited emergent ferromagnetism, which correlates with the variation in the (111) to (200) peak ratio. Analysis using Curie-Weiss fitting of inverse magnetic susceptibility versus temperature yielded negative values of Curie-Weiss temperature (θ_{CW}) for all samples, indicating the presence of predominant antiferromagnetic interactions. The variation in θ_{CW} correlated with the presence of the Mn-rich BCC phase. These findings underscore the impact of varying 3D printing parameters on the structure and magnetic properties of CrMnFeCoNi high entropy alloys.

[1] M. Jin, E. Hosseini, S.R. Holdsworth, M.S. Pham, "Thermally activated dependence of fatigue behaviour of CrMnFeCoNi high entropy alloy fabricated by laser powder-bed fusion," Additive Manufacturing 51, 102600 (2022). [2] Schneeweiss et al., "Magnetic properties of the CrMnFeCoNi high-entropy alloy," Phys. Rev. B 96, 014437 (2017).

EU-08. Static magnetic field modulates spinodal decomposition in Cu-Ni-Fe system. *X. Zhang*[1,2], C. Woodgate[3], G. Hadjipanayis[1,4], J.B. Staunton[3] and L.H. Lewis[1,2,5] *1. Chemical Engineering, Northeastern University, Boston, MA, United States; 2. Mechanical and Industrial Engineering, Northeastern University, Boston, MA, United States; 3. Physics, University of Warwick, Coventry, United Kingdom; 4. Physics and Astronomy, University of Delaware, Newark, DE, United States; 5. Physics, Northeastern University, Boston, MA, United States*

Electric machines with improved efficiency and performance require ferromagnetic materials with optimized structures and properties, which are sensitive to specific aspects of material processing. In this study, structural and magnetic attributes of the spinodal alloy CuNiFe subjected to magnetic-field-assisted annealing are investigated from combined experimental and computational perspectives. We demonstrate that the application of a modest, static magnetic field during thermal treatment promotes spinodal elemental redistribution in the alloy, impacting the resulting phase distribution, scale, and extrinsic magnetic response. Ribbons of composition $Cu_{40}Ni_{42}Fe_{18}$ were synthesized by melt-spinning into a uniform, FCC-structured solid solution phase and were subsequently annealed at 500°C for up to 200 hours with or without a magnetic field ($\mu_0 H$ = 60 mT)[1]. All annealed specimens exhibit nanoscale (~10 nm) periodic chemical segregations into Cu-rich and FeNi-rich regions within a coherent FCC lattice along <100> direction, with the wavelength and amplitude of the chemical periodicity increasing with annealing time. This spinodal decomposed structure results in increased magnetic hardness. It is found that magnetic field annealing

modulates spinodal structure by promoting the amplitude of chemical fluctuations up to three-fold, resulting in higher coercivity and lower initial susceptibility relative to the zero-field-annealed counterparts (Fig.1). Contributing fundamental insight into these outcomes, first-principles DFT calculations[2] suggest that long-range ferromagnetic order induced by an external magnetic field substantially alters the strength and nature of atomic interactions (Fig.2), impacting the stability of the initial solid solution phase. These results suggest that annealing with engineering-approachable magnetic fields can achieve controlled microstructures of alloys, resulting in modified magnetic anisotropy and responses. Acknowledgments: US Department of Energy, UK Engineering and Physical Sciences Research Council, National Science Foundation

[1] N. Maât, I. McDonald, R. Barua, et al., Acta Materialia, 196, 776-789 (2020). [2] C. D. Woodgate, D. Hedlund, L. H. Lewis, J. B. Staunton, Physical Review Materials 7, 053801 (2023).

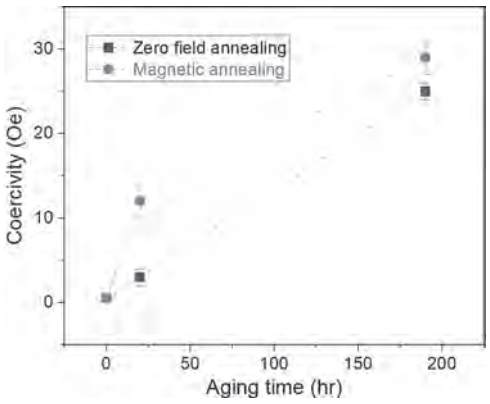

Coercivity of annealed CuNiFe vs. annealing time

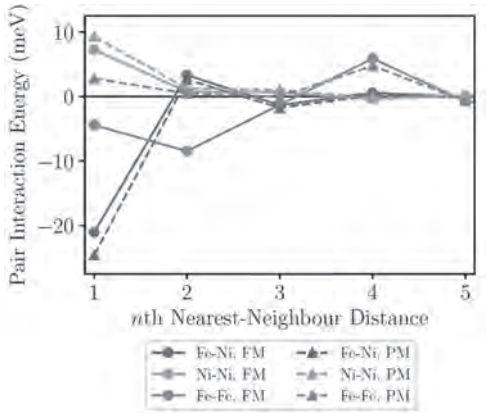

Effective atomic interaction energy vs. nth nearest neighbor modeled in ferro- (FM) or paramagnetic (PM) state

Session EV
MACHINES OPTIMIZATION, MAGNETIC LOSS, AND THERMAL MODELING II (Poster Session)

Po-Wei Huang, Chair
National Cheng Kung University, Tainan, Taiwan

EV-01. Investigation on the Steel Sheet Subdivision and Orientation Potentials of the Stator Core of an Axial Flux Machine. *S. Weigel*[1], A. Schaefer[1] and N. Parspour[1] *1. Institute of Electrical Energy Conversion, University of Stuttgart, Stuttgart, Germany*

A double sided axial flux machine with a yokeless and segmented armature (YASA) can be manufactured with different soft magnetic materials in the stator core. The options are soft magnetic composite materials (SMC) and different configurations of steel sheet packages for the guidance of magnetic flux in three dimensions [1]. However, these approaches exhibit disadvantages regarding magnetic properties or geometric freedom. Therefore, a novel approach to setup up the soft magnetic stator core is simulatively investigated. Instead of constructing the core segments from a continuous sheet metal package, it is to be constructed from several differently oriented sheet metal packages. To evaluate the theoretical potential of this approach the subdivisions and directions of the steel sheets in the tooth tip of the stator are varied and the influences on the torque and the iron losses of the machine are investigated by numerical magnetic field simulation (Fig. 1). For the simulation each steel sheet package is modelled as a homogenized region with anisotropic material properties and the iron losses are computed in post processing using Bertotti parameters and considering alternating, rotational magnetization as well as the DC offset of the magnetic flux density. The genetic multi objective algorithm from the global optimization toolbox in MATLAB is used to find the pareto front of the two objectives (torque and iron losses in Fig. 2). Moreover, the torque ripple of the final pareto front is computed and analyzed, showing a configuration with a minimum of torque ripple. In addition to that several tooth tip concepts on the pareto front are discussed. In general, the tooth tip concepts with many horizontal steel sheet segments at the considered speed have advantages regarding both optimization goals. The stacking factor of the steel sheet package has a strong influence on the ability to guide the magnetic flux of each configuration. When the saturation flux density is reached in the middle of the stator core, configurations with many horizontal steel sheet segments gain the highest mean torque values.

[1] L. Svensson, K. Frogner, P. Jeppsson, Journal of Magnetism and Magnetic Materials., Vol. 324, p.2717-2722 (2012)

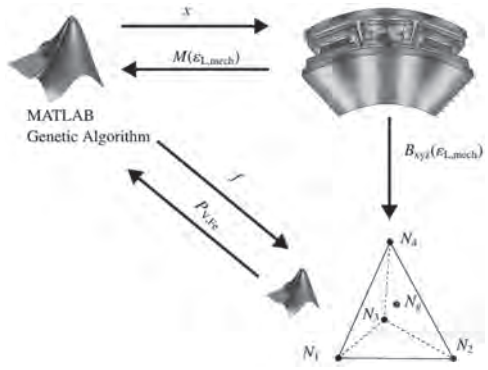

Fig. 1 Transfer of values between the different computing environments

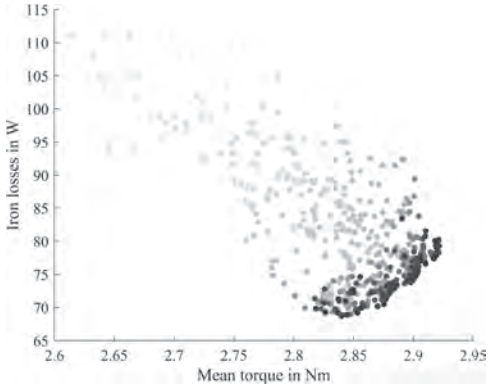

Fig. 2 Development of the scores of the individuals

Now VP2-13

EV-02. Vibration Analysis of Permanent Magnet Synchronous Motors Considering Magneto-Thermal Coupling and Structural Deformation. *H. Cao*[1,4], D. Zeng[2], Y. Li[3], Z. Sun[4], X. Wang[1,4] and C. Jiang[1,4] *1. College of Energy, Xiamen University, Xiamen, China; 2. Harbin Engineering University, Harbin, China; 3. Four Academies and Four Departments of Aerospace Science and Industry, Beijing, China; 4. Innovation Laboratory for Sciences and Technologies of Energy Materials of Fujian Province (IKKEM), Xiamen, China*

As the demand for environmental comfort increases, the vibration noise of permanent magnet synchronous motors(PMSM) is receiving more attention[1][2]. The permanent magnet and other structures in PMSM are susceptible to temperature changes. The variation in temperature distribution within the motor can affect the spatiotemporal distribution of the electromagnetic field, thereby altering the motor's vibration state[3]. Changes in the motor's electromagnetic performance can also affect the temperature distribution. Additionally, thermal stress can cause structural deformation and displacement, further impacting the spatiotemporal distribution of the electromagnetic field[4]. Currently, research on the characteristics of temperature rise and structural changes in PMSM, and how these changes lead to alterations in motor vibration, is still insufficient. This paper investigates a 4-unit PMSM by establishing a 2D model of the motor's electromagnetic field and a 3D finite element model of its temperature field. The study explores the impact of magnetic-thermal coupling on the calculation of electromagnetic excitation in the PMSM. Furthermore, a 3D structural finite element model of the motor is developed to examine the effects of temperature load on the motor's structure. The electromagnetic field is reconstructed after calculating structural displacement and the electromagnetic excitation force is solved. Simulations of the motor's electromagnetic vibration are performed using the results from the uncoupled electromagnetic field, magnetic-thermal coupling, and reconstructed electromagnetic force calculations as excitations. Temperature rise tests, structural modal tests, and vibration response tests of the motor are conducted to verify the model's accuracy. The results indicate that accounting for magnetic-thermal coupling reduces the simulation error in the response of radial electromagnetic force wave harmonics. Considering the influence of electromagnetic field reconstruction improves the accuracy of the motor housing vibration calculation in some frequencies.

[1] Wang S, Hong J, Sun Y, et al. Exciting force and vibration analysis of stator permanent magnet synchronous motors[J]. IEEE Transactions on Magnetics, 2018, 54(11): 1-5. [2] Ballo F, Gobbi M, Mastinu G, et al. Noise and vibration of permanent magnet synchronous electric motors: A simplified analytical model[J]. IEEE Transactions on Transportation Electrification, 2022, 9(2): 2486-2496. [3] Si J, Zhao S, Feng H, et al. Analysis of temperature field for a surface-mounted and interior permanent magnet synchronous motor adopting magnetic-thermal coupling method[J]. CES Transactions on Electrical Machines and Systems, 2018, 2(1): 166-174. [4] Fan J, Zhang C, Wang Z, et al. Thermal analysis of permanent magnet motor for the electric vehicle application considering driving duty cycle[J]. IEEE Transactions on Magnetics, 2010, 46(6): 2493-2496.

Fig.1 Temperature field and structural displacement result

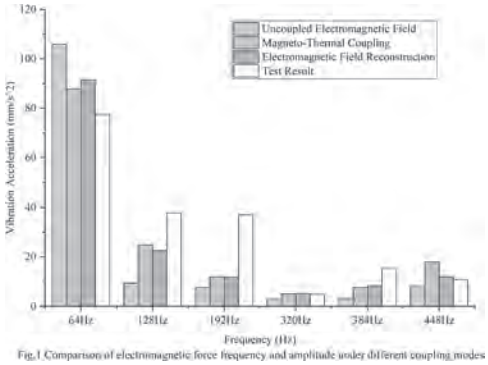

Fig.2 Comparison of electromagnetic force frequency and amplitude under different coupling modes

Now VP2-12 **EV-03. BH curve normalization method for semi-infinity silicon steel sheets model based on vector magnetic circuit theory.** W. Qin[1], *X. Ma*[1], M. Cheng[1], Z. Wu[1] and X. Zhu[2] *1. Southeast University, Nanjing, China; 2. North China Electric Power University, Baoding, China*

The BH curve, also known as the magnetization curve, is a essential concept in the study of magnetic materials in the field of electromagnetism. It describes the relationship between the peak magnetic induction B_m and the peak magnetic field strength H_m of magnetic materials [1]. Due to the skin effect of magnetic flux, these magnetic circuit parameters not only vary with the B of the magnetic circuit but also change with the frequency [2]. Therefore, for the same magnetic material, the magnetic circuit parameters corresponding to different frequencies exhibit variations, resulting in BH curves that differ at different frequencies. Currently, research on the measurement and simulation methods of BH curves for magnetic materials at different frequencies is relatively limited. Obtaining BH curves at different frequencies requires sequential measurements at each frequency, which is not only time-consuming but also requires specialized high-frequency experimental equipment. Prof Cheng proposed a method to extrapolate BH curves based on the concept of magductance and experimental analysis. While this method shows some feasibility in practical applications, it lacks reliable theoretical derivation. Therefore, building upon this foundation, this paper conducts a systematic theoretical derivation. It proposes an infinite thickness model for silicon steel sheets and, based on this, a method to extrapolate and deduce BH curves. With this method, given the BH curve at a certain frequency, one can deduce BH curves at different frequencies using vector magnetic circuit theory [3]. The proposed BH curve method not only aligns with theoretical validation from literature references but also conforms to experimental measurement results [4]. The formulae for calculating magnetic reluctance and magductance can be derived based on the semi-infinite model of silicon steel sheets. According to the formulas, it is evident that reluctance is directly proportional to $f^{0.5}$, while magductance is inversely proportional to $f^{0.5}$. Based on this relationship, a method for extrapolating BH curves is proposed, as shown in Fig. 1. The reliability of this extrapolation method has been validated through relevant experiments, as depicted in Fig. 2.

[1] S. K. Sahdev. Electrical machines[M]. Cambridge: Cambridge University Press, 2018. [2]M. K. Kazimierczuk. High-frequency magnetic components, 2nd edition[M]. New York: Wiley, 2014. [3] M. Cheng, W. Qin, X. Zhu, "Magnetic-Inductance: Concept, Definition, and Applications," IEEE Transactions on Power Electronics, vol. 37, no. 10, pp. 12406–12414, Oct. 2022. [4] W. Qin, M. Cheng, Z. Wang, Vector magnetic circuit analysis of silicon steel sheet parameters under different frequencies for electrical machines[J]. IET Electric Power Application. 2024, 1–14.

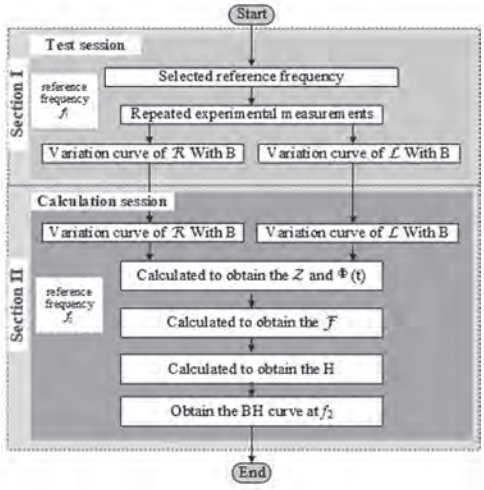

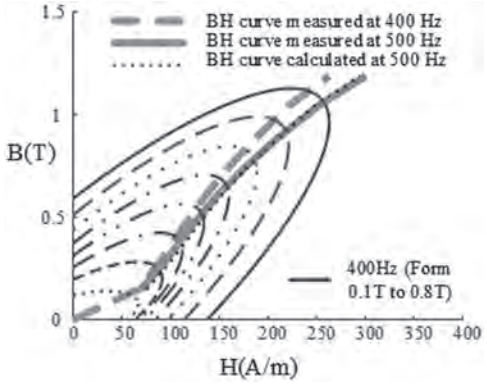

EV-04. Optimal Design of a Six-Phase Motor for Large Ships to Reduce Cogging Torque and Torque Ripple. *D. Choi*[1], H. Han[1], H. Kim[1], S. Jeon[1] and W. Kim[2] *1. Next Generation Smart Energy System Convergence, Gachon University, Seongnam, The Republic of Korea; 2. Electrical Engineering, Gachon University, Seongnam, The Republic of Korea*

Currently, environmental pollution and noise are significant global concerns, and large ship are not exempt from these issues. Traditional mechanical systems in large ship, which rely on fossil fuels, cause environmental pollution and generate substantial noise upon entering ports. As a result, various regulations have been imposed. These regulations have led to the development of eco-friendly ship systems utilizing electric motors. However, large ships require extremely high power output, unlike conventional motors. Additionally, motor durability is critical during ship operation. The solution to these challenges lies in multiphase motors; by adopting multiphase

motors over traditional three-phase motors, higher output can be achieved. However, multiphase motors require a larger number of slots, making them suitable for large motor applications. This paper proposes an optimal design methodology to address the issues of cogging torque and torque ripple in a six-phase motor designed for large vessels. By transitioning from a three-phase to a six-phase motor and optimizing the pole-slot combination of the final model, we aim to mitigate these problems. Through the application of advanced design techniques, we propose a six-phase motor that maximizes power factor and efficiency.

1. G. -D. Nam, H. -J. Sung, C. Kim, M. Park and I. -K. Yu, "Design and Characteristic Analysis of a 1 MW Superconducting Motor for Ship Propulsions," in IEEE Transactions on Applied Superconductivity, vol. 29, no. 5, pp. 1-5, Aug. 2019, Art no. 5203305, doi: 10.1109/TASC.2019.2902872. 2. E. Yolacan, M. K. Guven, M. Aydin and A. M. El-Refaie, "Modeling and Experimental Verification of an Unconventional 9-Phase Asymmetric Winding PM Motor Dedicated to Electric Traction Applications," in IEEE Access, vol. 8, pp. 70182-70192, 2020, doi: 10.1109/ACCESS.2020.2985669. 3. W. Li, G. Feng, Z. Li, J. Tjong and N. C. Kar, "Multireference Frame Based Open-Phase Fault Modeling and Control for Asymmetrical Six-Phase Interior Permanent Magnet Motors," in IEEE Transactions on Power Electronics, vol. 36, no. 10, pp. 11712-11725, Oct. 2021, doi: 10.1109/TPEL.2021.3072947. 4. S. Paul and K. Basu, "Overmodulation Techniques of Asymmetrical Six-Phase Machine With Optimum Harmonic Voltage Injection," in IEEE Transactions on Industrial Electronics, vol. 68, no. 6, pp. 4679-4690, June 2021, doi: 10.1109/TIE.2020.2989709.

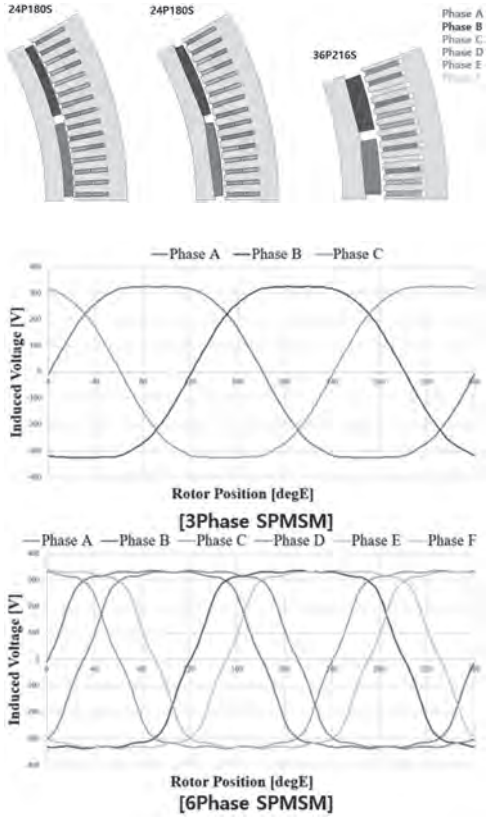

EV-05. A Study on the Support Structure for the Improvement of Counter Torque Strength of Urban Small Wind Power Generator with Block Coil. H. Kim[1], M. Hong[2], *S. Ko*[1], D. Jung[3] and W. Kim[4]
1. Next Generation Energy System Convergence, Gachon University, Seongnam, The Republic of Korea; 2. Electrical Engineering, Hanyang Unversity, Seongdong-gu, The Republic of Korea; 3. Department of Electrical and New Materials Engineering, Andong National University, Andong-si, The Republic of Korea; 4. Electrical Engineering, Gachon University, Seongnam, The Republic of Korea

This paper proposes a support structure for Axial Flux type wind turbine of Double Rotor Single Stator type using block coil winding technology with zero cogging characteristics. Small-scale wind power generation applied in urban centers is continuously increasing worldwide. This is because small wind power generation is easy to install as long as the wind conditions are favorable, with less environmental damage and less restrictions on installation conditions, and the spread of small wind power along with photovoltaics can increase energy independence and contribute to the construction of a decentralized power system. Accordingly, it is necessary to improve the technology of the most important generator in wind power generation to miniaturize, lighten, and increase the efficiency of wind power systems. The winding technology with zero cogging characteristics is mainly adopted for urban small wind turbines that require high power density for reasons such as drive and noise reduction. However, when the generator is driven, the winding generates a counter torque that is the opposite of the torque received by the rotor, so a structural design that considers this is also required. Therefore, this paper studies the counter torque resistance through 3D stiffness analysis and proposes a support structure to improve the counter torque resistance accordingly. Considering the electronic and structural characteristics of the block coil generator, a counter torque characteristic analysis method was established through multiphysics interlocking analysis, and the stress and deformation between the block coil winding and core were analyzed based on the counter torque mapped through the electronic analysis. In the case of the Axial Flux generator, unlike the Radial Flux type, the counter torque support structure can be designed by utilizing the space between the block coils by utilizing the stator plate on the inner side of the block coil, and the counter torque support structure is designed in a position that does not affect the electromagnetic performance of the generator.

[1] J. H. J. Potgieter and M. J. Kamper, "Torque and Voltage Quality in Design Optimization of Low-Cost Non-Overlap Single Layer Winding Permanent Magnet Wind Generator," IEEE Trans. on Ind. Electron., vol. 59, no. 5, May 2012, pp. 2147-2156 [2] J. Y. Choi, S. H. Lee, K. J. Ko, and S. M. Jang, "Improved Analytical Model for Electromagnetic Analysis of Axial Flux Machines With Double-Sided Permanent Magnet Rotor and Coreless Stator Windings," IEEE Trans. on Magn., vol. 47, No. 10, Oct. 2011, pp. 2760-2763. [3] Hong. D.-K, "Design, Analysis, and Experimental Validation of a Permanent Magnet Synchronous Motor for Articulated Robot Applications," IEEE Trans. Magn., vol. 54, no. 3, pp. 1-4, March 2018.

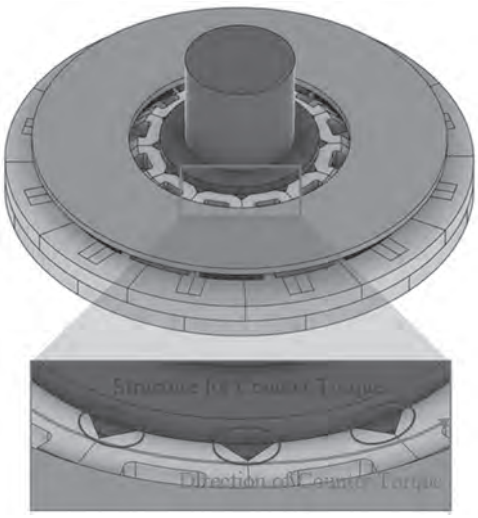

Fig. 1 Structure for Counter Torque

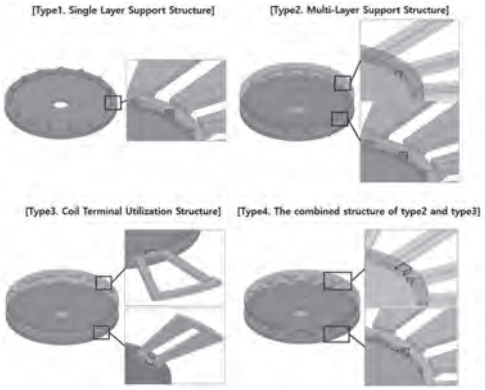

Fig. 2 Support Structure Concept

EV-06. Density-Based Rotor Topology Optimization of High-Power Density Wound-Field Flux-Switching Machine for Traction Applications.
M. Fereydoonian[1] and W. Lee[1] *1. Elmore Family School of Electrical and Computer Engineering, Purdue University, West Lafayette, IN, United States*

Externally excited synchronous machines (EESMs) have garnered interest in the passenger car sector in recent years due to their potential to eliminate RE magnets, deliver high efficiency at low torque and high-speed conditions, enhancing vehicle range during highway driving, an essential aspect of customer satisfaction. This work presents a density-based topology optimization method for a 12/10 stator/rotor pole wound-field flux-switching machine (WFFSM). The integrated stator structure of WFFSM and the coexisting field and armature windings in the stator lead to a complex and inefficient magnetic flux path generation that does not directly contribute to torque generation. This longer and inefficient magnetic flux path results in higher self– and mutual inductance of armature winding, which degrades net torque. Additionally, the flux switching in the rotor causes significantly higher rotor core loss than regular EESMs, further reducing efficiency. The rotor geometry is crucial in influencing the flux linkage between field and armature windings and, consequently, the electromagnetic performance. Therefore, the primary objective of this paper is to design a novel rotor design that facilitates an optimal magnetic flux path, leading to higher torque, lower core loss, and higher efficiency. The study employs a density-based rotor topology optimization to determine the optimal steel distribution within the rotor, minimizing voltage THD and maximizing average torque. The resulting design features a modular U-shape rotor structure with flux barriers positioned centrally within each rotor tooth to guide the flux along the optimal magnetic path, illustrated in Fig. 1. The effectiveness of the optimized modular rotor WFFSM is presented in Fig. 2, showing significant improvements in motor performance. For the optimized rotor WFFSM, core loss decreased by 27%, with torque and efficiency increasing by 9% and 1.7%, respectively. The final paper will provide a detailed analysis of torque enhancements, core loss reduction, and the efficiency map.

[1] A. Shoeb and S. Xue, "Topology Optimization of Axial Flux Machines with a Simplified 2D Finite Element Approximation," *2023 IEEE Energy Conversion Congress and Exposition (ECCE)*, Nashville, TN, USA, 2023, [2] Théodore Cherrière, Sami Hlioui, L. Laurent, François Louf, Hamid Ben Ahmed, and M. Gabsi, "Multi-material topology optimization of a flux switching machine," *Science and technology for energy transition*, vol. 78, pp. 41–41, Jan. 2023, doi: https://doi.org/10.2516/stet/2023037. [3] M. Fereydoonian, K. Lee, G. Choi, and W. Lee, "Rotor Saliency Optimization for High-Power Density Wound-Field Flux-Switching Machines," *in Proc. IEEE Energy Convers. Cong. and Expo. (ECCE)*, Nashville, TN, USA, 2023, pp. 3867-3874. [4] Z. -Q. Zhu and Y. Xiao, "Novel Magnetic-Field-Shifting Techniques in Asymmetric Rotor Pole Interior PM Machines With Enhanced Torque Density," in *IEEE Transactions on Magnetics*, vol. 58, no. 2, pp. 1-10, Feb. 2022, Art no. 8100610

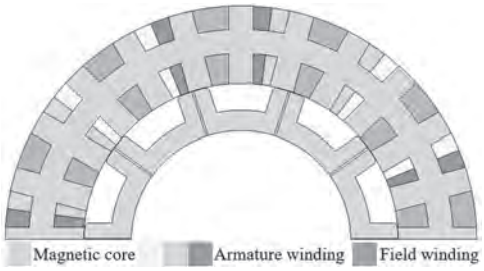

Fig 1. 2D view of the optimized modular rotor WFFSM.

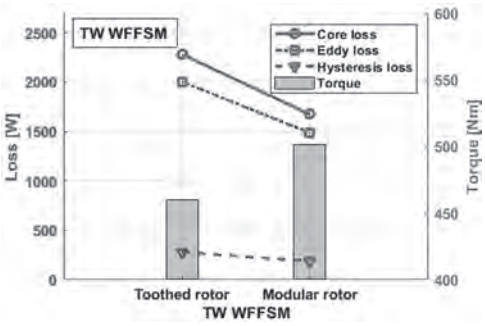

Fig. 2. Comparison of torque and losses for the toothed and the optimized modular rotor TW WFFSM (J_{dc} = 8.5 A/mm², J_{ac} = 8.5 A/mm²).

EV-07. Efficient and Versatile Anhysteretic Magnetization Models for Soft Magnetic Materials in FEA and Circuit Simulations.
A. Schaefer[1], S. Weigel[1] and N. Parspour[1] *1. Institute of Electrical Energy Conversion (iew), University of Stuttgart, Stuttgart, Germany*

For the efficient simulation and optimization of electrical machines, the soft magnetic behavior of core materials is typically represented by the magnetization curve rather than complex hysteresis models and hysteresis losses are calculated and accounted for in post-processing instead. Currently, either interpolation methods or phenomenological magnetization models are used to describe the magnetization curve. However, existing methods [1, 2, 3, 4] exhibit several disadvantages concerning identification, comparability, implementation, and the resulting behavior of the nonlinear solver. Based on these identified disadvantages, a set of criteria for magnetization models is developed. An analysis of the state of the art reveals that existing methods do not meet these criteria. Therefore, three novel models are proposed to advance the state of the art: a simple algebraic model, a special arc tangent model, and a special hyperbolic tangent model. To evaluate these models, the Langevin function, which describes anhysteretic behavior based on a physical approach in models such as the Jiles-Atherton model [5], is used. The new methods are fitted to the anhysteretic Langevin functions of

different materials and show excellent agreement in regression as well as improved computational efficiency compared to the Langevin function. The regression performance of the best models is depicted in Fig. 1, with an R-squared value exceeding 0.9 for M350-35A and over 0.99 for the other four materials. In particular, the algebraic and arc tangent models exhibit excellent regression performance, rendering them viable alternatives to existing models for magnetization curves in technical simulations.

[1] J. Brauer, IEEE Trans. Magn., Vol. 11 (1), p. 81 (1975) [2] K. Mandal, S. K. Ghatak, Journal of Magnetism and Magnetic Materials, Vol. 167 (3), p. 264–268 (1997) [3] R. Szewczyk, JAMRIS, Vol. 10 (2), p. 3–8 (2016) [4] M. Mirzaei, P. Ripka, IEEE Trans. Magn., Vol. 54 (11), p. 1–5 (2018) [5] D. C. Jiles; D. L. Atherton, Journal of Magnetism and Magnetic Materials. Vol. 61 (1-2), p. 48–60 (1986)

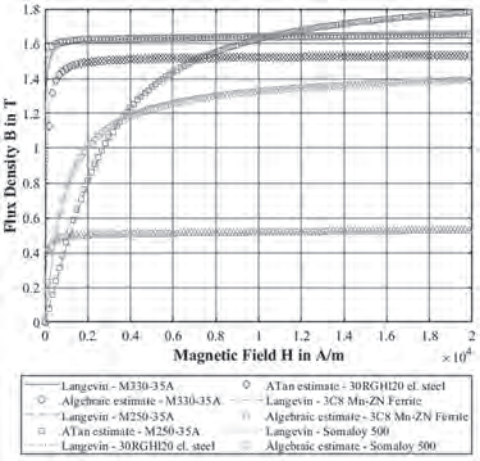

Fig. 1 Regression performance of the novel magnetization models for different soft magnetic materials

EV-08. Design and analysis of a novel watch speaker using top magnets structure for a thinner smart watch. *Y. Oh*[1], Y. Jung[1], K. Park[1], Z. Jiang[1] and S. Hwang[1] *1. Mechanical Engineering, Pusan National University, Pusan, The Republic of Korea*

With the evolution of wearable devices, the consumer demand for slim designs, has increased. This necessitates thinner microspeakers, which are crucial for evaluating smartwatch performance. This study focused on developing a thinner micro speaker while maintaining a performance comparable to that of existing watch speakers. The position of the sound hole in the smartwatch requires the speaker to be mounted at 90°. Therefore, it is crucial to reduce the width of the watch speaker, to reduce the smartwatch thickness. As shown in Fig. 1, the dimensions of the existing watch speaker (prototype) are 15.0 × 5.8 × 3.6T (mm), whereas those of the newly designed speaker are 16.8 × 5.2 × 3.4T (mm). The reduction in width by 0.6 mm enables the development of thinner smartwatches. The new design incorporates top magnets by replacing a portion of the conventional PC frame. This has been enabled by advancements in insert molding technology. The study also investigated the optimal magnetization polarity of the top magnets in a new magnetic structure to maximize the force factor. Simulations were conducted for three polarities, and the polarity with the best performance was selected. The magnetic flux density, force factor, and sound pressure level (SPL) were simulated using electromechanical–acoustic coupling analysis using finite element analysis. The new design was analyzed and optimized by modifying the thicknesses of the yoke, top plates, main magnets, and top magnets. The analysis was validated through a B&K experiment. The SPL measurements were conducted in a closed box of volume 3 with an input voltage of 3.1 V, ranging from 100 Hz to 20k Hz at a distance of 10 cm. Fig. 2 shows that the SPL of the new design at resonant frequency (1400 Hz) is 91.42 dB. This is almost equal to that of the prototype (91.72 dB). Furthermore, the new design outperformed the prototype in the 100–500 Hz range (Fig. 2). By employing top magnets with appropriate polarity, the new magnetic structure with reduced width exhibited a performance equivalent to that of the prototype.

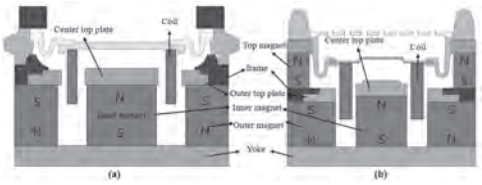

Fig. 1 The comparison of magnetic circuits: (a) prototype; and (b) new design

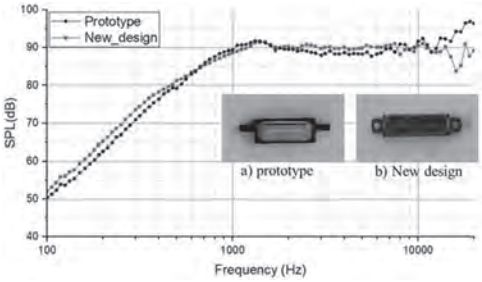

Fig. 2 SPL comparison between the prototype and New design

Session FP
HARD MAGNETS IV
(Poster Session)

Jiasheng Zhang, Chair
National Institute for Materials Science (NIMS), Tsukuba, Japan

FP-01. Withdrawn

FP-02. Coercivity enhancement in heavy rare earth free Nd-Fe-B

FP-03. Spark Plasma Sintered Manganese Substituted Strontium M-type Nanohexaferrite. *A. Sassi*[1,2], A. Pasko[1], S. Amara[4], C. Florica[5], V. Yenugonda[2], G. Setti[4], F. Mazaleyrat[1] and A. Pathak[2,3] *1. SATIE, CNRS, Université Paris-Saclay, ENS Paris-Saclay, Gif-sur-Yvette, France;*

2. Department of Physics, SUNY Buffalo State, Buffalo, NY, United States; 3. One Research Circle, GE Aerospace Research, Niskayuna, NY, United States; 4. Computer, Electrical and Mathematical Sciences and Engineering, King Abdullah University of Science and Technology, Thuwal, Saudi Arabia; 5. Nanofabrication Core Lab, King Abdullah University of Science and Technology, Thuwal, Saudi Arabia

La-Co substitued hexaferrites are the most performant ferrites in the market of permanent magnets [1]. However, La and Co belong to the family of rare earth and strategic elements and to avoid their usage, nanostructuring ferrites which improve high H_c [2] is being studied as a possible alternative. Nanopowders of manganese substituted strontium M-type hexagonal ferrites $SrMn_xFe_{12-x}O_{19}$ with x = 0, 4, 5 and 6 were successfully synthesized using the citrate precursor sol-gel method [3]. The obtained nanopowders were calcined at 950°C and then were Spark Plasma Sintered at 800°C. XRD analysis at room temperature and magnetometry in a maximum field of 6 T at temperatures ranging from 5 to 375 K were performed on the nanopowders as well as on their sintered pellets. Figure 1 represents M_s, M_r, H_c and M_r/M_s of the nanopowders and their sintered pellets. While M_s, M_r, H_c and M_r/M_s decrease by increasing the Mn content in both the nanopowders and their sintered pellets, due to the replacement of the Fe ions by the Mn ions in parallel spin sites, coercivity increases reaching as high as 0.76 T in the sintered (x = 6) pellet. The sintering process seems to have no effect on M_s and M_r since they have almost the same values in the loose nanopowders and in their sintered pellets. While H_c is almost the same between the powder and the sintered pellet for x = 0, it drastically decreases after sintering reaching 67% of the H_c of the starting loose powder for x = 6. Interestingly, M_r/M_s shows a different behavior since it considerably increases in the sintered pellets reaching 0.58 for x = 4 then it drastically drops to 0.34 for x = 6. Further investigation is needed in order to improve the performance of $SrMn_xFe_{12-x}O_{19}$ for the high potential it has as an alternative in a variety of applications. Acknowledgements: This work was performed at the State University of New York (SUNY), Buffalo State University, and was supported by the National Science Foundation under Award No. DMR-2213412.

[1] F. Kools, A. Morel, R. Grössinger, J. M. Le Breton, P. Tenaud, J. Magn. Magn. Mat., Vol. 242-245, p. 1270-1276 (2002) [2] F. Mazaleyrat, A. Pasko, A. Bartok, M. Lobue, Journal of Applied Physics., Vol. 109, 07A708 (2011) [3] A. K. Pathak and A. Sassi, Magnet powder and sintered magnet of strontium and barium M-type modified hexagonal ferrite, Pat. Ref. 160-2251P0, US Pat. No.: 63/600,105

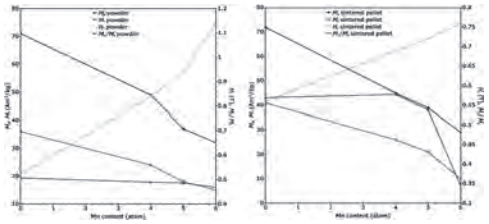

Figure 1: Mn effect on the magnetic properties of SrM powders and sintered pellets.

FP-04. Withdrawn

FP-05. Evaluating the disordering kinetics of tetrataenite, employing integrated magnetic and metallurgical perspectives. *X. Zhang*[1,2], E. Dos Santos[3], J. Gattacceca[4] and L.H. Lewis[1,2,5] *1. Chemical Engineering, Northeastern University, Boston, MA, United States; 2. Mechanical and Industrial Engineering, Northeastern University, Boston, MA, United States; 3. Instituto de Ciência e Tecnologia, Universidade Federal dos Vales do Jequitinhonha e Mucuri (UFVJM), Diamantina, Brazil; 4. Centre de Recherche et d'Enseignement des Géosciences de l'Environnement (CEREGE), Aix-en-Provence, France; 5. Physics, Northeastern University, Boston, MA, United States*

A high degree of atomic ordering in ferromagnetic $L1_0$-type compounds donates substantial magnetocrystalline anisotropy, making these materials good candidates for permanent magnets. While it remains highly challenging to obtain the "holy grail" $L1_0$ FeNi compound (*aka*, tetrataenite) due to its extremely sluggish formation below its reported ordering temperature (320°C), it is possible to investigate the kinetics of the inverse transformation – disordering of tetrataenite – in some natural meteorites to understand the phase stabilities. Here, new and quantified insight into the kinetics of the disordering process that transforms $L1_0$-structured tetrataenite to A1 (FCC)-structured taenite is obtained through a re-evaluation of published data collected from Santa Catharina meteorite samples annealed under varying temperature-time conditions [1]. The original work utilized coercivity and remanence to track the presence of the hard magnetic tetrataenite after annealing for various durations. Building upon this work, we delve deeper into quantitative aspects of tetrataenite disordering using metallurgical-inspired approaches applied to the original magnetic datasets. Specifically, time- and temperature-dependent disordering transformation profiles were constructed based on derived magnetocrystalline anisotropy constants that start at estimated values of 0.5 – 0.6 MJ/m^3 in the ordered state and decrease monotonically with annealing time to stabilize below 0.2 MJ/m^3, Fig. Analyzed data indicate that the A1 (taenite) phase emerges from pre-existing nuclei and grows in an interface-controlled manner. Further, the activation energy associated with the disordering increases monotonically from 250 (±20) kJ/mol at the beginning of the process to 320 (±10) kJ/mol towards the end, consistent with a progressively sluggish disordering process. These results are anticipated to guide the laboratory synthesis of the $L1_0$ FeNi phase, which holds great potential as an advanced permanent magnet. Acknowledgments: This work was supported by the US Department of Energy and the National Science Foundation.

[1] Dos Santos, E., Gattacceca, J., Rochette, P., Fillion, G., & Scorzelli, R. B. (2015). Journal of Magnetism and Magnetic Materials, 375, 234-241.

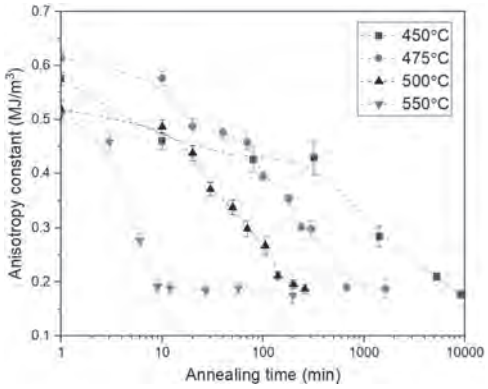

Magnetic anisotropy constant of the meteorite specimen vs. annealing time at various temperatures

FP-06. Effect of Mn Substitution on Coercivity of $SrFe_{8-x}Mn_xAl_4O_{19}$ Nanoparticles. *P. Joshi*[1], H. Abbas[1], T. Karki[1], J. Mohapatra[1] and P. Liu[1] *1. Department of Physics, University of Texas at Arlington, Arlington, TX, United States*

Nanoparticles of hard magnetic ferrites have found more applications [1]. In this research work, we investigated the effect of Mn substitution on magnetic properties of M-type $SrFe_8Al_4O_{19}$ nanoparticles. The samples ($SrFe_{8-x}Mn_xAl_4O_{19}$ with x=0, 0.25, 0.5, 0.75, and 1) were synthesized using sol-gel technique. The average particle size was found to be in the range of 27-32 nm using Scherrer formula in the XRD peaks. Further, the XRD pattern (Figure 1) indicates that Mn substitution does not change the crystal structure and not induce any secondary phase. The crystal structure was observed to be hexagonal. Zero-field-cooling curve depicts that the blocking temperature lies around 230 K and plateau in field-cooling curve at low temperatures indicates the presence of strong inter-particle interactions (Figure 2 (a)). Figure 2 (b) shows that coercivity of 12.5 kOe was observed for x =0, for x = 0.25, it sharply decreased to 8.8 kOe, and then increased with x. This is likely due to the reduction in magnetocrystalline anisotropy [2]. For larger Mn concentrations, it may create distortion in the structure thereby increasing the coercivity afterwards.

[1]. C de Julián Fernández *et al,* Progress and prospects of hard hexaferrites for permanent magnet applications, 2021 *J. Phys. D: Appl. Phys.* 54 153001.
[2]. JN Dahal et al., *Synthesis and magnetic properties of $SrFe_{12-x-y}Al_xCo_yO_{19}$ nanocomposites prepared via autocombustion technique.* Journ. Alloys Comp., 2014, 595(9):213-220.

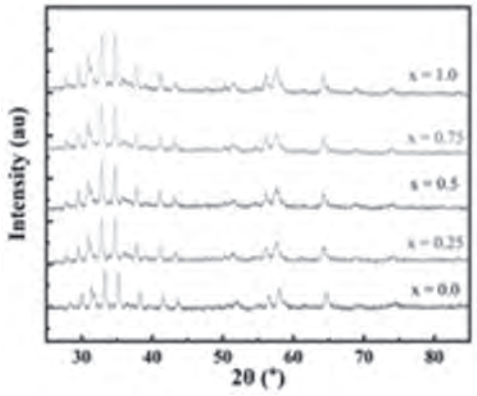

Figure 1: XRD pattern for $SrFe_{8-x}Mn_xAl_4O_{19}$ with x = 0, 0.25, 0.5, 0.75, and 1.

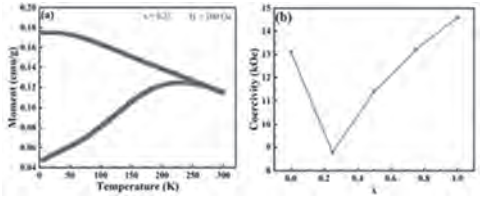

Figure 2: (a) ZFC-FC at 100 Oe for x = 0.25, (c) Variation in coercivity and magnetization with x.

FP-07. Thermodynamics of materials synthesis under applied magnetic fields. *A. Rauf*[1] and W. Sun[1] *1. Materials Science and Engineering, University of Michigan, Ann Arbor, MI, United States*

In the same way that high temperature stabilizes metastable high-entropy materials, magnetic fields can potentially stabilize metastable high-magnetic moment materials. Here we quantitatively analyze the thermodynamic contributions of magnetic field during the synthesis of ferromagnetic materials, with a goal of designing synthetic pathways to new permanent magnets. In general, we find that the magnetic field contribution to the free energy of chemical phase transformations is very weak under typical materials synthesis conditions. However, magnetic fields can still induce structural distortions, which may affect electronic and magnetic properties of materials. We conclude with a broad computational screen of metastable ferromagnetic materials that could potentially be synthesized under large applied magnetic fields.

FP-08. Computational search of alpha″-$Fe_{16}N_2$ inspired nitrides for novel permanent magnets. A. Rauf[1] and *W. Sun*[1] *1. Materials Science and Engineering, University of Michigan, Ann Arbor, MI, United States*

The iron nitride α″-$Fe_{16}N_2$ has a very high reported magnetic moment for a permanent magnet with no rare earth elements. However, it is metastable and difficult to synthesize, and also has low coercivity. Here, we search for other metal-rich nitrides that may possess similar structural or electronic structure aspects as α″-$Fe_{16}N_2$ that could serve as viable good candidates for new permanent magnets. In particular, we examine the effect of chemical substitutions on a vacancy-ordered double perovskite prototype structure, and its effect on thermodynamic stability, synthesizability, and magnetic properties.

Session FQ
MAGNETIC DEVICES FOR SENSING AND RECORDING & THIN FILMS, MULTILAYERS, AND EXCHANGE BIAS SYSTEMS III
(Poster Session)

Zhenchao Wen, Chair
National Institute for Materials Science (NIMS), Tsukuba, Japan

FQ-01. Development of Flexible Sendust Composite Sheets with Enhanced Magnetic Permeability for Microwave Absorbers and Antennas. *M.P. Whalen*[1], D.T. Plouff[2], N.B. Shevchenko[3], M. Mirotznik[4] and J.Q. Xiao[2] *1. Quantum Science and Engineering Program, University of Delaware, Newark, DE, United States; 2. Department of Physics and Astronomy, University of Delaware, Newark, DE, United States; 3. Center for Composite Materials, University of Delaware, Newark, DE, United States; 4. Department of Electrical and Computer Engineering, University of Delaware, Newark, DE, United States*

The demand for soft magnetic composites with high magnetic permeability at high frequencies is escalating, driven by the need for next-generation microwave absorbing materials and magnetodielectric antennas[1-3]. While significant efforts have been directed towards enhancing the permeability of these composites[4-8], the challenge of improving their flexibility for conformal applications while maintaining high permeability remains underexplored. In this study, we present the development of flexible composite sheets utilizing FeSiAl Sendust flakes embedded in a matrix comprising acrylic rubber, epoxy resin, and a curing agent. The composites were fabricated through a hot-pressing technique, which induced strong alignment of the flakes, as evidenced by the (400) to (220) peak ratio improvement from 0.5 to 7.9 post hot pressing as shown in Fig. 1. This alignment resulted in a composite exhibiting high relative permeability that is maintained at elevated frequencies, with relative permeability μ_r' of 14.8 and μ_r'' of 20.4 at 1 GHz (Fig. 2). Notably, a high mass fraction of flakes, exceeding 90%, and volume fraction of flakes of approximately 38% was achieved as confirmed by VSM analysis, contributing to the composite's significant saturation magnetization of 118 emu/g and low coercivity of 1.9 Oe. Moreover, the innovative approach allows for the curing of multiple layers of the composite sheet during hot pressing, enabling the creation of thickness-tunable composites without compromising permeability. This work establishes a robust platform for the advancement of soft magnetic composites, particularly tailored for conformal applications, paving the way for their integration into cutting-edge microwave absorbing and antenna technologies.

1. E. A. Périgo, B. Weidenfeller, and P. Kollár et al, Appl. Phys. Rev, Vol. 5 (2018) 2. N. Ahmed and G. J. Atkinson, International Conference on Electrical Machines ICEM (2022) 3. T. Yousefi, T. Sebastian and R. E. Diaz, IEEE Transactions on Antennas and Propagation, Vol. 64, p. 2784-2796, (2016) 4. C, Liu, J. Cai, and Y. Duan et al, Journal of Magnetism and Magnetic Materials, Vol. 458, p. 116-122 (2018) 5. K. K. Oh, H. Lee, and W. S. Lee et al, Journal of Magnetism and Magnetic Materials, Vol. 321, p. 1295-1299 (2009) 6. K. Oh, S. M. Hong and Y. Seo, Polymers Advanced Technologies, Vol. 25, p. 1366-1370 (2014) 7. S. Shin, J. Park, and J. Ro et al, J Mater Sci: Mater Electron, Vol. 32, p. 20164–20176 (2021) 8. Z. Yuan, L. Wu, and M. Yi et al, Journal of Magnetism and Magnetic Materials, Vol. 543 (2022)

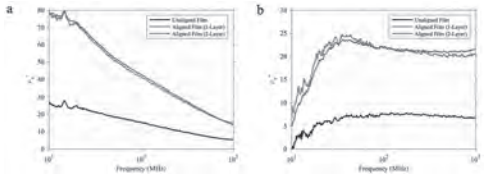

Fig. 1 Frequency dependence of the complex relative permeability on flake alignment in composite films; (a) real part of permeability, (b) imaginary part of permeability.

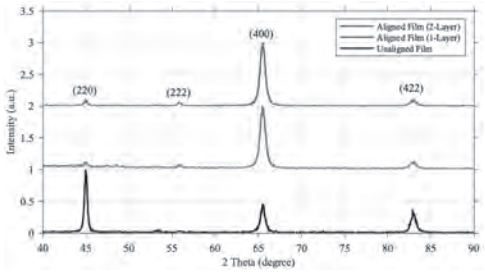

Fig. 2 XRD data of composite films with varying alignment and layer configurations.

FQ-02. Innovative assessment of carburized steel hardness profiles using low-frequency magnetic incremental permeability. H. Lberni[1], *B. Ducharne*[2], H. Petitpré[1], J. Mogniotte[3], Y. Tene Deffo[4], F. Zhang[1] and C. Gallais[5] *1. CETIM, Senlis, France; 2. Tohoku University, Sendai, Japan; 3. INSA Lyon, Villeurbanne, France; 4. University of Buea, Buea, Cameroon; 5. Safran Transmission Systems, Collombes, France*

LF-MIP is an innovative, non-destructive evaluation technique used to assess carburization treatments on steel components. Carburization is essential for enhancing surface hardness and wear resistance, but improper treatment can lead to mechanical failures. Traditional evaluation methods are often destructive and costly [1]. LF-MIP uses the relationship between a material's magnetization properties and its mechanical characteristics. It involves slowly magnetizing the sample while applying Eddy Current Testing at low frequencies [2]. The technique is efficient at evaluating deep carburization due to its deep penetration capability, which allows it to assess layers that are not reachable by other methods. In previous work, we described a simulation method combining the Dodd & Deeds analytical expression with the Jiles-Atherton theory to simulate the relation between the carburization treatment case depth and LF-MIP measurements [3, 4]. In this new work, we went beyond. We used a 3D Finite Element Model (3D-FEM) to simulate all LF-MIP experimental situations, providing precise 3D magnetic field distributions and scanned depths up to the whole carburization treatment trajectory. We used 16NiCrMo13 martensitic stainless steel specimens that were categorized based on varying degrees of carburizing treatment time. The hardness profiles of these specimens were measured and compared with simulations based on an analytical expression inspired by Fick's laws of diffusion [5, 6]. A series of pre-calculated hardness profiles were then plotted, and the physical properties' profiles, such as conductivity and

permeability, were computed, assuming they followed similar trajectories. Comsol simulations were performed with a coil above a conductive material divided into layers of adjustable thickness and properties. The results were used to create an impedance distribution chart that could estimate unknown hardness profiles based on LF-MIP characterization. The method's predictions were validated by comparing them with experimental measurements, achieving an error of less than 6% for various treated specimens.

[1] I. McCue, E. Benn, and B. Gaskey, [1] G. Parrish, "Carburizing: microstructures and properties," ASM International, 1999. [2] B. Gupta, T. Uchimoto, B. Ducharne, G. Sebald, T. Miyazaki, and T. Takagi, "Magnetic incremental permeability non-destructive evaluation of 12 Cr-Mo-WV Steel creep test samples with varied ageing levels and thermal treatments," *NDT&E International*, 104, pp.42-50, 2019. [3] B. Ducharne, Y.A.T. Deffo, G. Sebald, T. Uchimoto, C. Gallais, and O. Ghibaudo, "Low-frequency incremental permeability for the evaluation of deep carburization treatments: Theoretical understanding," *Journal of Magnetism and Magnetic Materials*, *586*, p.171236, 2023. [4] B. Ducharne, Y.A.T. Deffo, S. Zhang, G. Sebald, M. Lallart, T. Uchimoto, C. Gallais, and O. Ghibaudo, "Carburization depth evaluation from magnetic non-destructive testing," *NDT&E International*, 137, p.102864, 2023. [5] A. Paul, T. Laurila, V. Vuorinen, S.V. Divinski, A. Paul, T. Laurila, V. Vuorinen, V. and S.V. Divinski, "Fick's laws of diffusion. *Thermodynamics, diffusion and the kirkendall effect in solids*," pp.115-139.T, 2014. [6] J. Philibert, "One and a half century of diffusion: Fick, Einstein before and beyond," 2006.

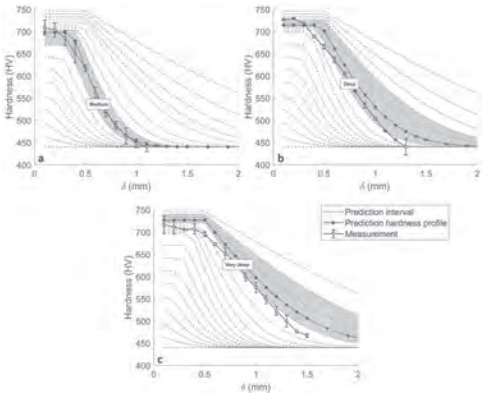

Comparisons between the measured hardness trajectories, the mean predictions, and their corresponding ranges.

FQ-03. Flexible Polymer/Ferrite Composites for Millimeter Wave Applications. *B.M. Mears*[1], G. Macedo[1], V.S. Peytchev[1] and D. Arnold[1]
1. Electrical and Computer Engineering, University of Florida, Gainesville, FL, United States

Flexible magnetic composites are critical for 5th and 6th generation (5G/6G) communications and millimeter wave applications. Detailed knowledge of their electromagnetic properties is necessary to inform design of structures and devices, such as electromagnetic absorbers [1], circulators [2], and other radio-frequency components. A variety of flexible magnetic composite materials, such as shown in fig. 1, are fabricated and characterized for millimeter wave systems and applications. The electromagnetic properties, including ferromagnetic resonance and complex permittivity and permeability, are determined in the range of 33 – 50 GHz. Commercially available M-type barium ferrite (BaM), M-type strontium ferrite (SrM), and yttrium iron garnet (YIG) nanoparticles (particle sizes of 500 nm, 2 um wide and 50 nm thick, and <100 nm respectively) are individually mixed into a matrix of the polymer polydimethylsiloxane (PDMS) at three different ratios: 20 wt%, 40 wt%, and 60 wt%. Each composite mixture is then cast in 0.5-mm-thick WR-22 rectangular waveguide shims (cross section of 5.69 mm x 2.84 mm) and cured at 85° C for two hours in the presence of an out-of-plane magnetic field. The fabrication process is noteworthy for being low temperature, low cost, and short duration. The final structures can be fabricated on a variety of substrates and exhibit high mechanical flexibility. Electrical measurements are performed by using a vector network analyzer (VNA) to obtain the two-port scattering (S) parameters of a rectangular waveguide loaded with each composite material. Complex permittivity and permeability are extracted from the measured S parameters based on the Nicolson-Ross-Weir (NRW) algorithm [3]. As an example, the real and imaginary permeabilities for 60 wt% BaM, SrM, and YIG composites are shown in fig. 2. The full manuscript will present a comprehensive catalog of the electromagnetic properties of these composites in the 33 – 50 GHz range.

[1] B. Mears, F. Freeman, and D. Arnold, Advanced Engineering Materials., Vol. 26, Issue 9 (2024) [2] H. Kim, R. Bowrothu, and Y. Yoon, IEEE 35th International Conference on Micro Electro Mechanical Systems Conference (MEMS)., pp. 1034-1037 (2022) [3] O. Luukkonen, S. Maslovski, and S. Tretyakov, IEEE Antennas and Wireless Propagation Letters., Vol. 10, pp. 1295-1298 (2011)

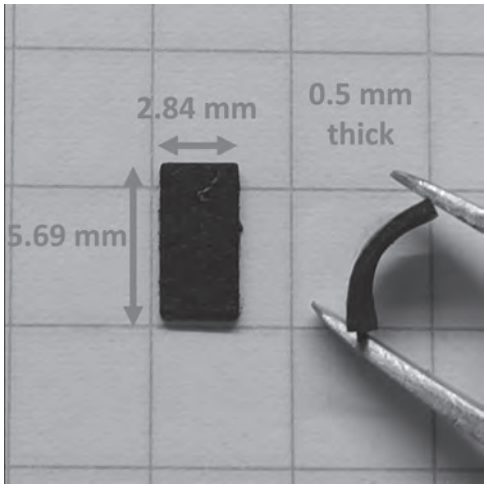

Fig. 1 Photograph showing the size and flexibility of the composites, specifically an SrM composite.

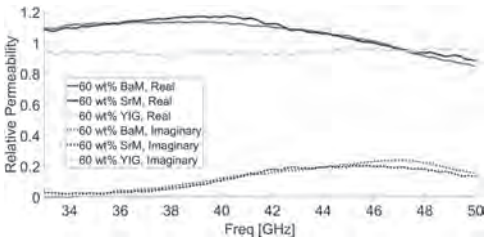

Fig. 2 Complex permeability of 60 wt% BaM, SrM, and YIG composites versus frequency. Solid lines are real parts of permeability, and dotted lines are imaginary parts.

FQ-04. Development of a tri-axis concentric fluxgate magnetometer with high orthogonality and high linearity. T. Nguyen[1], J. Jeng[1] and *L. Bui*[1,2] *1. Department of Mechanical Engineering, National Kaohsiung University of Science and Technology, Kaohsiung, Taiwan; 2. Faculty of Mechanical Engineering, Hung Yen University of Technology and Education, Hung Yen, Vietnam*

This study fabricates and characterizes a concentric tri-axis fluxgate magnetometer. The vector magnetometer consists of a tubular soft flux chopper with a toroidal coil and three concentric pick-up coils. The Z-axis pick-up coil is placed in the cavity of the flux chopper to reduce the size of the sensor. With the X and Y-axis pick-up coils enclosing the flux chopper and the Z-axis coil at the center, the three sensing axes are concentric and the overall size of the vector magnetometer is no more than 10 mm×15 mm×15 mm. The concentric coils ensure a single field point for the X, Y, and Z- sensing axes while achieving high orthogonality. The achieved non-orthogonality errors are less than ±1°. The three-axis fluxgate control circuit

based on second harmonic detection and magnetic field feedback is also developed to improve the non-linearity. The built circuit can generate an AC excitation signal and efficiently demodulate the three-axis outputs of the concentric fluxgate sensor to produce three separate DC voltage signals in proportion to the external quasi-static magnetic field. With feedback, the average non-linearity is less than 0.1% in the ±60 μT range. The proposed design concept is valuable for developing the compact and sensitive vector magnetometer for applications regarding precise geomagnetic measurement.

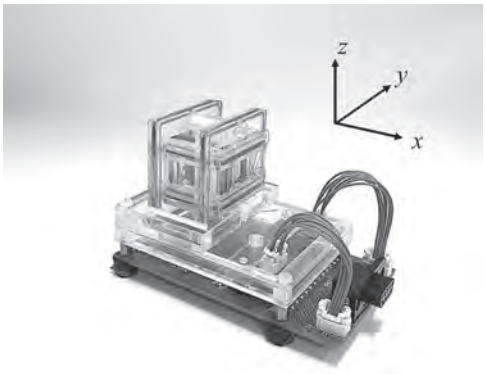

Fig. 1. The photograph of the tri-axis concertric fluxgate magnetometer wtih a Helmholtz-coil feedback system

FQ-06. Combined and Separated Signal Processing Techniques for Dual Layer Bit-Patterned Magnetic Recording. N. Rueangnetr[1], S. Greaves[2] and *C. Warisarn*[1] *1. College of Advanced Manufacturing Innovation, King Mongkut's Institute of Technology, Bangkok, Thailand; 2. Research Institute of Electrical Communication (RIEC), Tohoku University, Sendai, Japan*

A combination of BPMR [1] and MLMR [2-3], which is known as dual-layer BPMR, has been proposed [4-5] to overcome the super-paramagnetic limitation of current recording technology. However, it is crucial to solve challenges such as the difficulty in retrieving data from the lower recording layer due to its distance from the read/write head, and to develop effective signal processing methods to distinguish between data from the upper and lower layers within a single readback waveform. Therefore, this study presents a new dual-layer BPMR structure as shown in Fig. 1, which was used to generate readback signals, and then proposes combined and separated signal processing techniques. At the receiver, the noisy readback signal was oversampled at a rate of $0.5kT_x$, where T_x is the bit period, giving a data sequence, $r[k]$, comprising signals from the upper and lower layers at alternating sampling positions. Next, for the combined signal processing technique (System-A), shown in Fig. 2, $r[k]$ was filtered using a 1-D MMSE equalizer designed to obtain the equalized sequence $z[k]$. The recorded bits in the upper and lower layers, i.e., $a_1[k]$ and $a_2[k]$, were arranged in alternating positions as the odd and even bits in the equalizer design process. The SOVA was then used to detect the equalized sequence $z[k]$ and produce the soft-information, before separating the data sequences for the upper and lower layers. These two sequences were sent to individual LDPC decoders to determine the estimated recorded bits. For the separated signal processing technique (System-B), the data sequence, $r[k]$, was first separated into odd and even sequences, i.e., $r_1[k]$ and $r_2[k]$, corresponding to the two recording layers. The two data sequences were then used separately for target and equalizer design, as shown in Fig. 2. We analyzed a system with AD of 4.0 Tb/in^2 and found that our proposed systems offer greater performance improvements than the system proposed in [4]. Furthermore, the separated technique can yield improved performance over the combined technique of around 3.0 dB at a BER of 10^{-4}.

[1] B. Terris, T. Thomson, and G. Hu, "Patterned media for future magnetic data storage," Microsyst. Technol., vol. 13, no. 2, pp. 189–196, April 2006. [2] Y. Nakamura, M. Nishikawa, and Y. Okamoto, "Performance Improvement of Dual STO Reading With AM–FM Combined Detection for 3-D Magnetic Recording," in IEEE Transactions on Magnetics, vol. 57, no. 3, pp. 1-5, March 2021, Art no. 3000205. [3] Y. Nakamura, M. Nishikawa, Y. Kanai, and Y. Okamoto, "A study of three-dimensional equalization for reproducing a double-layer magnetic recording medium," IEEE Trans. on Magn., vol. 58, no. 8, pp. 1-4, Aug. 2022. [4] N. Rueangnetr, C. Warisarn, and S. J. Greaves, "Optimization of layer thicknesses for dual-layer bit-patterned media recording (BPMR) systems," in IEEE Transactions on Magnetics, doi: 10.1109/TMAG.2024.3410296. [5] A. Khametong and C. Warisarn, "A study of iterative signal processing schemes for double-layered bit-patterned recording," in IEEE Transactions on Magnetics, doi: 10.1109/TMAG.2024.3402184.

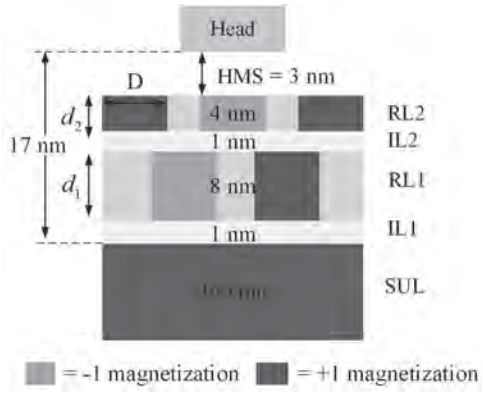

Fig. 1. Geometry of the dual-layer BPMR medium in cross-sectional view at total AD = 4.0 Tb/in^2.

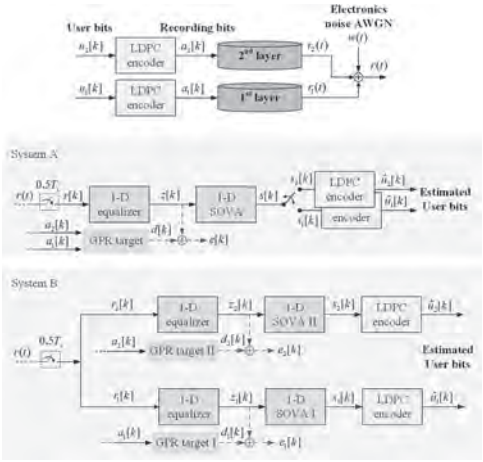

Fig. 2. Block diagram of dual-layer BPMR channel model.

FQ-07. Development of highly conductive $SrMoO_3$ epitaxial thin films for advanced spintronic applications. *M. Roy Chowdhury*[1,2], C. He[2], K. Tang[2], H. Koizumi[2], Z. Wen[2], S. Thota[1], H. Sukegawa[2] and S. Mitani[2] *1. Physics, Indian Institute of Technology Guwahati, Guwahati, India; 2. National Institute for Materials Science, Tsukuba, Japan*

Perovskite transition-metal oxides (TMO) have emerged as prominent spin-Hall candidates with high spin-Hall angle and low resistivity, paving the path for low-power magnetoelectric switching and improved spintronic devices [1,2]. $SrMoO_3$ (SMO) is one such attractive TMO with a cubic (*Pm-3m*) perovskite structure and a remarkably low room-temperature resistivity (~ 5.1 μΩ-cm) in the bulk form [3]. For use in modern technology, scalable, low-cost deposition of SMO thin films must be feasible. However, the growth of conductive single-phase SMO films by sputtering faces two challenges: (i) formation of $SrMoO_4$ as an impurity and (ii) need for H_2 in the sputtering mixture to prevent $SrMoO_4$ growth. In this work [4], we developed a RF sputtering technology to achieve conductive SMO thin films from an insulating $SrMoO_4$ target in a H_2-free, pure Ar ambience with no secondary

phase. SMO films were deposited on $SrTiO_3$(001) substrates at 624°C in an UHV (~10^{-7} Pa) sputtering chamber with pure Ar (10 Pa) by tuning the sputtering parameters. The significance of controlling the target-substrate distance (TSD) between 1-15 cm was demonstrated by a drastic change in resistivity from 1.46×10^5 μΩ-cm to 310 μΩ-cm via plasma-assistance. A TSD of 2.5 cm yielded a single-phase SMO film with the lowest resistivity (Fig.1) and its XRD pattern exhibited the Bragg peaks corresponding to SMO(001) and SMO(002) lattice planes along with the $SrTiO_3$(001) substrate (Fig. 2). Cross-sectional microstructural analyses verified epitaxy and atomically-resolved single crystalline structures. Temperature-dependent DC-resistivity and ordinary Hall measurements revealed metallic behavior (inset of Fig. 2), high carrier concentration and moderate mobility for the optimized sample. Thus, our sputtering approach achieved H_2-free, low-cost, scalable deposition of pure, conductive SMO thin films for use in spintronic devices with future scope for sputter deposition of other thermodynamically unstable TMO. This work was partially supported by JST CREST (Grant No. JPMJCR19J4).

[1] H. Chen and D. Yi, APL Mater. *9*(6) (2021) [2] D.C. Vaz, A. Barthélémy, and M. Bibes, Jpn. J. Appl. Phys. *57*, p.0902A4 (2018) [3] I. Nagai, N. Shirakawa, S.I. Ikeda, et al. Appl. Phys. Lett., 87, 024105 (2005) [4] M. Roy-Chowdhury et al. Sci. Tech. Adv. Mater., in-press.

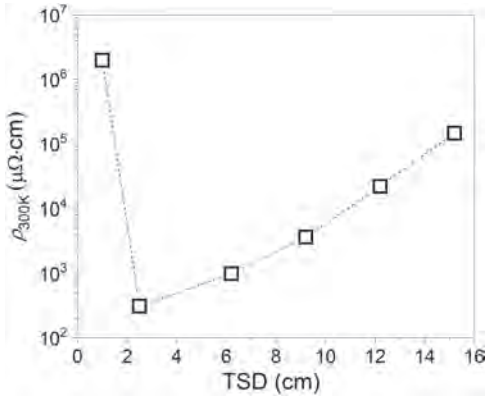

Fig. 1. TSD dependence of the resistivity of SMO films at 300 K.

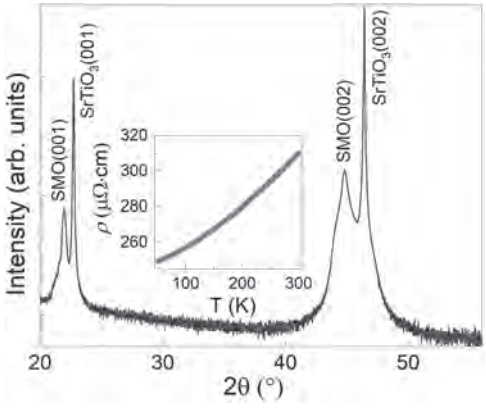

Fig. 2. XRD pattern for SMO film obtained at optimum TSD = 2.5 cm. The inset shows the temperature dependence of resistivity.

FQ-08. Massive replacement of Cu in FePt-Carbon ultra-thin buffer layer for K_u enhancement of FePt granular films. *K. Tham*[1], D. Miyazaki[1] and S. Saito[2] *1. Material Company, TANAKA KIKINZOKU KOGYO K. K., Tsukuba, Japan; 2. Electronic Engineering, Graduate School of Engineering, Tohoku University, Sendai, Japan*

To ensure that hard disk drive (HDD) remains competitive in the data storage, recently a new design of magnetic recording technology, heat assisted magnetic recording (HAMR) has been launched into the market to replace currently commercialized perpendicular magnetic recording. The $L1_0$ type FePt phase which has high uniaxial magneto-crystalline anisotropy energy (K_u) of 5×10^7 erg/cm^3 at room temperature is a promising material for the HAMR medium. Regarding nanostructure of the medium, a granular structure with fine columnar and isolated magnetic grains, small angular distribution of *c*-axis, and high degree of order are desirable, however these goals are still unaccomplished. Based on our previous study in $K_{u\perp}^{film}$ of FePt granular film, there is a disorder portion at the initial growth region which deteriorate $K_{u\perp}^{film}$ of the film[1, 2]. Therefore to suppress the disorder portion we have conducted an investigation of employing a buffer layer (BL) in between the FePt granular film and the MgO underlayer. In this paper, we will report the evaluation result of nanostructure and magnetic properties of the granular films deposited on a $Fe_{35}Pt_{35}Cu_{30}$-carbon BL. Fig. 1 shows in-plane XRD profiles for FePt-B_2O_3 granular films with various $Fe_{35}Pt_{35}Cu_{30}$-30vol%C BL thicknesses. For all films, mainly, the (110), (200), and (220) diffractions from $L1_0$-FePt phase are observed, which indicates that FePt grains have *c*-plane sheet texture. At BL thickness from 0.4 to 0.6 nm, significant increase in integral intensity of (110) diffraction is observed. Fig. 2 shows dependence of M_s^{film} and $K_{u\perp}^{film}$ of FePt-B_2O_3 granular film on FePtCu-C BL thickness at various Cu content. At Cu content of 30at.%, when BL thickness is varied, M_s^{film} shows no obvious change. On the other hand, $K_{u\perp}^{film}$ shows a significant increase from 0.78 to 1.70×10^7 erg/cm^3 at BL thickness from 0 to 0.6 nm. These results suggest that the initial growth region becomes ordered due to the employment of a FePtCu-C BL, which leads to the enhancement of $K_{u\perp}^{film}$.

1) T. Saito et al., *AIP Advances*, 11, 015310 (2021). 2) D. Isurugi et al., *IEEE Trans. Magn.*, 59, 3201304 (2023).

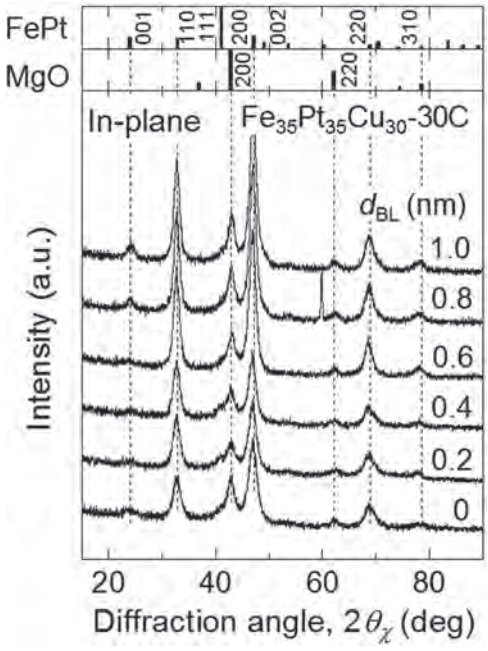

In-plane XRD profiles for FePt-B_2O_3 granular film with various $Fe_{35}Pt_{35}Cu_{30}$-30vol%C BL thickness.

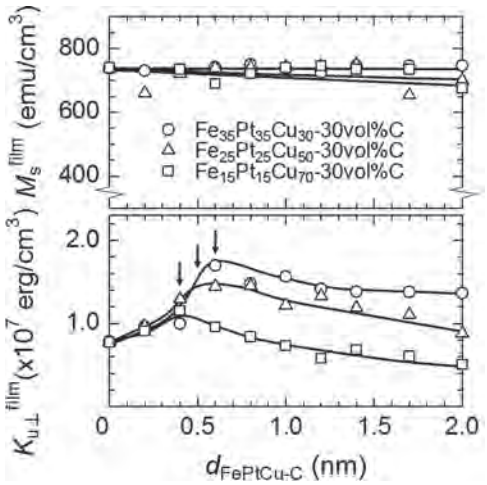

Dependence of M_s^{film} and $K_{u\perp}^{film}$ of FePt-B_2O_3 granular film on FePtCu-C BL thickness at various Cu content.

Session FR
SPINTRONIC DEVICES IV: STT/SOT MRAMS AND SWITCHING DYNAMICS (Poster Session)

Sachin Krishnia, Chair
Johannes Gutenberg University Mainz, Mainz, Germany

FR-01. Magnetization States and Switching Dynamics of Noncollinear Spin-Torque Devices. *A. Terko*[1], G. Lertzman Lepofsky[1], P. Flauger[2], D. Suess[2], E. Girt[1] and C. Abert[2] *1. Department of Physics, Simon Fraser University, Burnaby, BC, Canada; 2. Faculty of Physics, University of Vienna, Vienna, Austria*

State-of-the-art MRAM devices are usually composed of three layers: two hard ferromagnetic layers comprising a synthetic antiferromagnet reference layer and a free ferromagnetic layer. Such designs rely on a collinear alignment between the free and the hard layers, which limits the switching performance of these devices [1,2]. Instead, noncollinear coupling has been shown to improve writing performance by ensuring a non-stochastic spin-torque on the free layer [3,4]. This work employs micromagnetic simulations [5] to investigate the relaxed magnetization states of a FM1/SL/FM2/MgO/FM3 STT-MRAM design. The ferromagnetic (FM) layers have perpendicular-to-plane magnetic anisotropy and the SL mediates noncollinear interlayer coupling between FM1 and FM2 of the reference layer [6], shown in Fig. 1. We show that our previous conclusions made when simulating only the reference system [6] must be modified when the free layer (FM3) is introduced. The effect of the varying stray field from FM3 tends to change the orientation of the reference system, FM1 and FM2. Fig. 1 shows a phase diagram of the interlayer angle between FM2 and FM3 after relaxation, as a function of the interlayer exchange coupling constants J_1 and J_2, across the SL. On the right of the figure, we show two examples of the alignment of the FM layers for J_1 = 1.0 mJ/m^2 and J_2 = 1.5 mJ/m^2. These illustrate the differences in the alignment of the magnetic moments in all FM layers depending on orientation of the free layer. We show that decreasing the thicknesses and saturation magnetization of the FM layers, while keeping the anisotropy of FM2 larger than that of FM1, serves to minimize the effect of the stray field. We will also present results from simulating the current-mediated reversal dynamics of the free layer. To do this, we construct a model of the field- and damping-like torque components of the spin-torque using voltage-dependent parabolic functions [7] extracted from measurements of CoFeB/MgO spacer layers [8].

[1] S. Mangin, D. Ravelosona, J. A. Katine, et al., Nat. Mater. 5, p.210 (2006). [2] A. D. Kent and D. C. Worledge, Nat. Nanotechnol., Vol. 10, p.187 (2015). [3] R. Sbiaa, J. Phys. D: Appl. Phys., Vol. 46, 395001 (2013). [4] Z. R. Nunn, C. Abert, D. Suess, and E. Girt, Sci. Adv., Vol. 6, eabd8861 (2020). [5] C. Abert, L. Exl, F. Bruckner, J. Magn. Magn. Mater., Vol. 345, p.29 (2013). [6] G. Lertzman-Lepofsky, A. Terko, S. Koraltan, Phys. Rev. B., Vol. 109, 224421 (2024). [7] P. Flauger, C. Abert and D. Suess, Phys. Rev. B., Vol. 105, 134407 (2022). [8] H. Kubota, A. Fukushima, K. Yakushiji, et al., Nature Phys., Vol. 4, p.37–41 (2008).

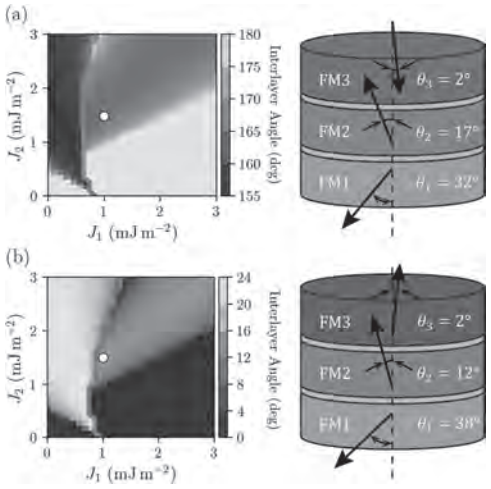

Fig. 1 Interlayer angle, the angle between the FM2 and FM3 layers, as a function of J_1 and J_2 in FM1/SL/FM2/MgO/FM3 for (a) parallel alignment and (b) antiparallel alignment of FM2 and FM3.

FR-02. Energy Landscape of Noncollinear Exchange Coupled Magnetic Multilayers. *G. Lertzman Lepofsky*[1], A. Terko[1], S. Koraltan[2], D. Suess[2], E. Girt[1] and C. Abert[2] *1. Department of Physics, Simon Fraser University, Burnaby, BC, Canada; 2. Faculty of Physics, University of Vienna, Vienna, Austria*

Spin-transfer and spin-orbit torque magnetic random-access memory (STT/SOT-MRAM) designs promise to combine the density and low-cost of dynamic RAM, the performance of static RAM, and the non-volatility of traditional magnetic hard drives [1], and yet the switching currents and write-error-rates of state-of-the-art devices remain unacceptably large [2,3]. In this work [4], we conduct an exploration of the energy landscape of two coupled ferromagnetic layers with perpendicular-to-plane uniaxial anisotropy, K_u, using finite-element micromagnetic simulations [5]. These multilayers can be used to produce noncollinearity in the reference layers of STT/SOT-MRAM cells [6], which has been shown to increase the performance of these classes of MRAM by ensuring a non-zero spin-torque at the beginning of switching processes [7]. We show that there exists a range of values of the interlayer exchange coupling constants, J_1 and J_2, for which the magnetic state of these multilayers can relax into either one or two energy minima, depending on the initial conditions of the multilayer, parallel (PP) or antiparallel (AP), Fig. 1. A noncollinear antiparallel state with one minimum is optimal for use in STT/SOT devices and Fig. 1(c) shows that there is a wide range of experimentally achievable coupling constants that can produce such alignment. This range increases with the difference in the ferromagnetic layer anisotropies. We further investigate the thermal stability of the structures in the two minima regions, using string method simulations to determine the energy barriers. We show that the stabilities of the minima increase with increasing difference in the anisotropy of the ferromagnetic layers. Finally, we provide an analytical solution to the location of the minima in the energy landscape of coupled macrospins, which has good agreement with our micromagnetic results for a simplified case involving ferromagnetic layers with the same thickness and anisotropy.

[1] A. V. Khvalkovskiy, D. Apalkov, S. Watts, et al., J. Phys. D: Appl. Phys., Vol. 46, p.074001 (2013). [2] A. D. Kent and D. C. Worledge, Nat. Nanotechnol., Vol. 10, p.187 (2015). [3] D. C. Worledge, 2023 IEEE International Reliability Physics Symposium (IRPS), p.1 (2023) [4] G. Lertzman-Lepofsky, A. Terko, S. Koraltan, Physical Review B, Vol. 109, p.224421 (2024). [5] C. Abert, L. Exl, F. Bruckner, J. Magn. Magn. Mater., Vol. 345, p.29 (2013). [6] Z. R. Nunn, C. Abert, D. Suess, and E. Girt, Sci. Adv., Vol. 6, p.eabd8861 (2020). [7] R. Sbiaa, J. Phys. D:Appl. Phys., Vol. 46, p.395001 (2013).

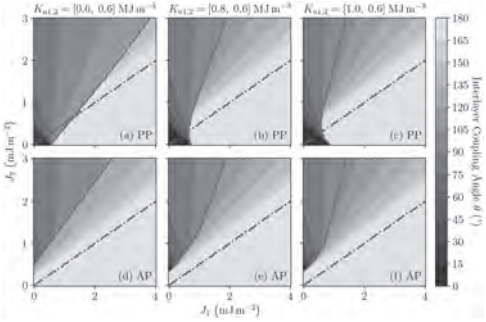

Fig. 1 Interlayer coupling angles for simulations with PP [(a) to (c)] and AP initial conditions [(d) to (f)] for varying J_1, J_2, and K_{u1}. Structures left of the red line are noncollinear and collinear PP, structures right of the red line are noncollinear and collinear AP.

FR-03. Anomalous Hall Resistance in Ta/$Co_{40}Fe_{40}B_{20}$/MgO/Ta for Constructing Physical Unclonable Function. *D. Divyanshu*[1], M. Tang[1], A.H. Lone[1], S. Amara[1] and G. Setti[1] *1. CEMSE (Integrated Intelligent Systems (I2S)), King Abdullah University of Science and Technology, Thuwal, Saudi Arabia*

Physical Unclonable Functions (PUFs) enhance device authenticity and resist cloning by generating unique identifiers. Spintronics-PUF devices, with key advantages for hardware security, have gained significant interest [1]-[4]. In this work, we experimentally demonstrate Ta (5nm)/ $Co_{40}Fe_{40}B_{20}$ (0.85nm)/ MgO (2nm)/ Ta (2nm) Hall bar devices as spintronic PUFs, considering process-induced device-to-device (D2D) variation in the critical spin-orbit torque (SOT) switching current. PUF tokens are fabricated under similar conditions to account for actual process variation during the fabrication process. The single PUF token size is 510 μm*510 μm. The anomalous Hall effect loops and the current-induced magnetization switching loops demonstrate good perpendicular magnetic anisotropy (PMA) and D2D variation. Fig 1 shows the detailed block diagram of the setup used. Measurements were performed in a magnetic field environment at room temperature. A constant DC read current of 60 μA is used. A fixed write current of ±1.72 mA, Hx = +400 Oe, for this setup, is used to generate the challenge-response (CRP) pairs. Obtained anomalous Hall resistance (R_H) is converted into response bits, which include appropriate normalization and offset. The challenge set consists of 300 bits in matrix form, and the corresponding response set consists of 300 bits. The obtained CRP data set is then evaluated for PUF performance metrics using Python and NIST SP 800-22 statistical suit. Several key PUF performance metrics are calculated, as shown in Fig 2. Our results indicate good performance in terms of uniformity (45.167%), response complexity, and repeatability for the selected main PUF tokens. However, the obtained uniqueness value is inferior due to the chosen biasing point. Overall, this work demonstrates a promising initial performance for spintronic PUFs, which can be further optimized.

[1] S. Gosh, *Proc. IEEE Inst. Electr. Electron. Eng.*, vol. 104, no. 10, pp. 1864–1893 (2016). [2] G. Finocchio *et al.*, *J. Appl. Phys.*, vol. 128, no. 3, p. 033904 (2020). [3] D. Divyanshu, *et. al, IEEE Access*, vol. 10, pp. 93029–93038 (2022). [4] S. Zhang *et al.*, *Sci. China Inf. Sci.*, vol. 65, no. 2 (2022).

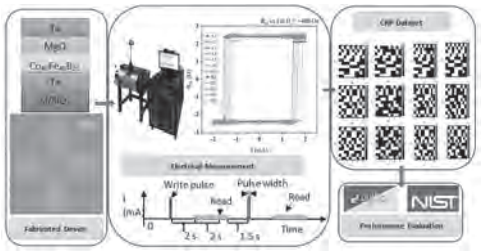

Detailed block diagram of steps involved for R_H based PUF metrics evaluation.

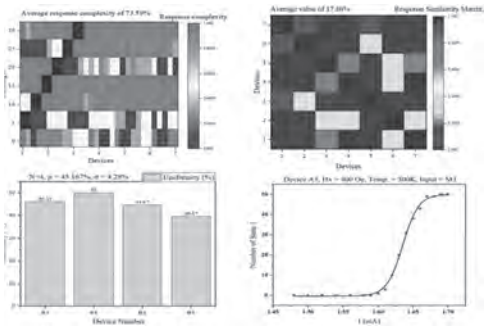

PUF performance metrics calculation and behaviour results.

FR-04. Fabrication of high aspect ratio magnetic dot array with honeycomb structure. *Y. You*[1], K. Yamanoi[1] and Y. Nozaki[1] *1. Department of Physics, Keio University, Yokohama, Japan*

Recently, phononic crystals(PnCs) have been investigated to realize nontrivial topological modes. For instance, acoustic topological edge modes were demonstrated in a honeycomb PnC of metallic nanopillars on a $LiNbO_3$(LN) substrate[1]. In such devices, nanopillars are utilized for resonating local oscillation of surface acoustic waves(SAWs). It is noted that there are some resonant modes with finite angular momentum, which is coupled with electron spins via gyromagnetic effect[2], implying that topological PnC could advance spintronic devices. In this work, we numerically examined optimum design of honeycomb PnC consisting of metallic nanopillars with high aspect ratio for emerging strong gyromagnetic effect. According to the numerical result, we produced honeycomb PnC composed of magnetic dots with perpendicular magnetic anisotropy(PMA), aiming to realize magnetization reversal via acoustic gyromagnetic effect. Figure 1 shows the dispersion relations of SAW propagation in a honeycomb PnC calculated using COMSOL Multiphysics. Here, eigenmodes for each wave vector were calculated under the Floquet periodic boundary condition for a unit cell with honeycomb PnC. The dot diameters for A- and B-sites in a unit cell were 0.6 and 0.5 μm, respectively. The unit cell size and dot height were respectively fixed at 1.2 μm and 0.14 μm. Rotational mode appears at 1.50, 1.85 and 2.06 GHz, although an in-plane vibrating mode can be simultaneously observed at 1.85 and 2.06 GHz. These rotational modes are eliminated when the diameters of A- and B-sites are identical, because modes with positive and negative angular momentum are degenerated at K point. According to the numerical analysis of the rotational modes, we fabricated honeycomb PnC. We deposited Ta(100 nm)/[Pt(3 nm)/Co(0.95 nm)]$_{10}$/Pt(3 nm) on LN substrate. Magneto-optical Kerr loop showed a PMA. The film was patterned into honeycomb PnC using focused ion beam lithography. Figure 2 shows the atomic force micrograph(AFM) for our device. The dot diameters in A- and B-sites were 0.5 and 0.45 μm, respectively, and the height was 0.14 μm, whose dimensions were optimized for 1.85 GHz-SAW to excite rotational modes.

[1] Y. Nii and Y. Onose, Phys. Rev. Appl. 19, 014001 (2023) [2] Y. Kurimune, M. Matsuo, and Y. Nozaki, Phys. Rev. Lett. 124, 217205 (2020)

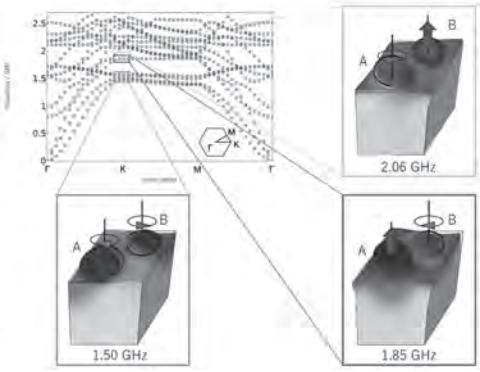

Numerical dispersion relation for our device.

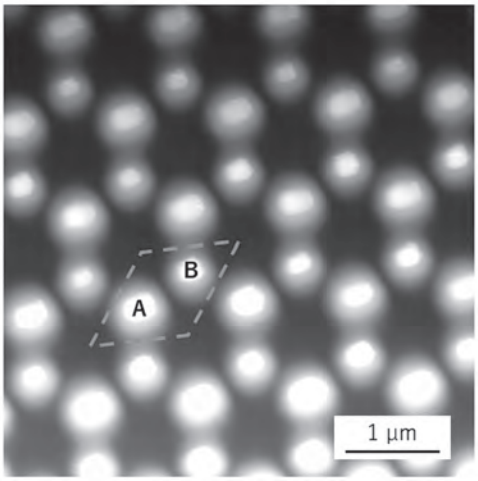

AFM image of our device.

FR-05. Coherent Spin-Orbit Torque Magnetization Switching of Ring-Shaped MTJ for High-Density SOT-MRAM. *M. Yoshikawa*[1], M. Koike[1], N. Umetsu[1], T. Li[1] and M. Quinsat[1] *1. Frontier Technology R&D Institute, Kioxia Corporation, Yokohama, Japan*

Spin-orbit torque (SOT) magnetization switching [1,2] is most promising as next-generation technology for magnetic random access memory (MRAM) to achieve high-speed writing, low power consumption and high endurance [3]. However, magnetic stability and immunity are critical factors in high-density MRAM. In this study, we propose a magnetically stable cell architecture with a ring-shaped magnetic tunneling junction (Rs-MTJ) for high-density SOT-MRAM. The understanding of the SOT switching behavior in the Rs-MTJ is limited so far. Thus, it is investigated using the micro-magnetic simulation based on the Landau-Lifshitz-Gilbert (LLG) equation. Additionally, the magnetic stability is estimated by the analytical energy calculation of the various static magnetic states of the Rs-MTJ. Our newly proposed SOT-MRAM cell architecture, illustrated in Fig. 1, basically consists of an Rs-MTJ, an Rs-selector, a write transistor and a vertical SOT line with a tubular structure. Due to the formation of a closed magnetic circuit in the Rs-MTJ, it is expected to enhance magnetic stability in the static state and improve magnetic immunity. From the LLG based micro-magnetic simulation analysis of the storage layer (SL) of the Rs-MTJ, we observe coherent SOT magnetization reversal in a ring radius of 20 nm. Fig. 2 shows that the SOT switching current-density (J_{sw}) is inversely proportional to the SOT switching time (t_{sw}). It indicates that the SOT switching behavior of the Rs-MTJ is consistent with the macro-spin model and the formation of the multi magnetic domain state is not favored in the structure. The results obtained from the analytical energy calculation suggest that optimizing of the SL dimensions leads to increased stability of the closed magnetic state. Using a practical Co-based material, the SL of the Rs-MTJ exhibits a retention energy over 60 k_BT down to a ring radius of 20 nm. Based on these results, it is found that the Rs-MTJ enhances magnetic stability and is promising for high-density SOT-MRAM.

[1] L. Liu, *et al.*, Science Vol.336, p.555 (2012). [2] I. M. Miron, *et al.*, Nature Vol.476, p.189 (2011). [3] K. Garello, *et al.*, IEEE IMW, pp.101 (2019).

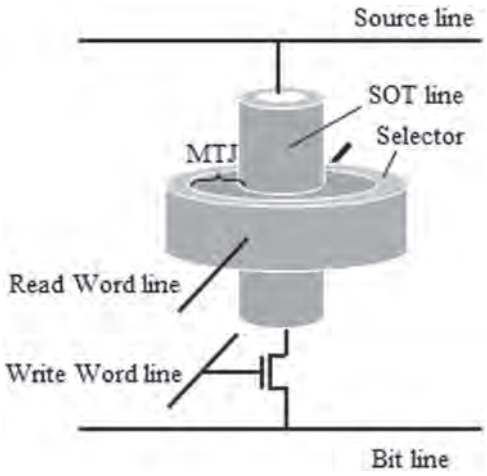

Fig. 1 Schematic SOT-MRAM cell architecture with Rs-MTJ.

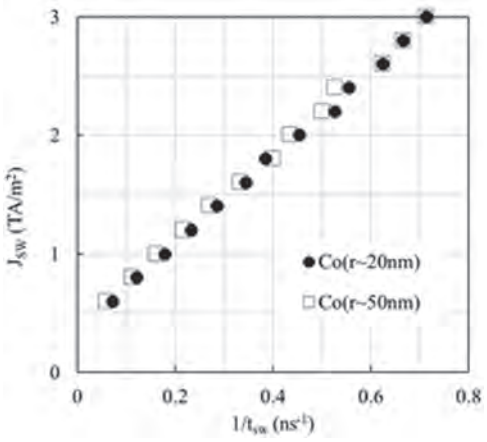

Fig. 2 Relationship between SOT switching time(t_{sw}) and SOT switching current density(J_{sw}).

FR-06. Understanding stability and behavior of Magnetic Tunnel Junction (MTJ) using Electron Spin Resonance (ESR). *J.E. Hernandez*[1], P. Tyagi[1], B.N. Mengesha[1] and A. Feutmba[1] *1. University of the District of Columbia, Washington, DC, United States*

Magnetic tunnel junctions (MTJs) have significant potential for various applications. They consist of two ferromagnetic electrodes separated by a thin insulating layer, allowing tunable properties through material selection and insulator thickness design. MTJs are a promising platform for next-generation MTJ-based molecular spintronics devices (MTJMSDs). The impact of molecular spin channels on MTJs' stability, especially along exposed sides, remains unexplored. This study investigates the thermal stability of MTJMSDs with varying insulator thicknesses. Fabrication involves photolithography, thin film sputtering, and forming molecular channels. Single Molecule Magnets (SMMs) create channels on the MTJ's exposed edges, connecting the top and bottom electrodes. To assess thermal response, samples were heated incrementally from room temperature to 190°C in 20°C intervals. Magnetic resonance variations were evaluated using Electron Spin Resonance (ESR). Initial ESR measurements at room temperature provided a baseline, while subsequent measurements revealed changes in magnetic resonance properties due to temperature fluctuations. ESR results showed

that the two modes corresponding to the MTJ's ferromagnetic electrodes varied with temperature changes. The thermal stability of two different devices is shown in Figures 1 and 2, with 1. a thinner insulator (0.5nm) and 2. a thicker insulator (1.5nm). Our findings demonstrate that MTJMSDs with thinner insulators exhibit superior thermal stability compared to isolated ferromagnetic electrodes and untreated MTJs. This enhanced stability is due to the molecular channels between the ferromagnetic electrodes, fostering strong coupling and improving thermal resilience in MTJMSDs. This study advances the development of thermally stable MTJMSDs, crucial for reliable and consistent performance in practical applications.

X. Fan, R. Cao, T. Moriyama, W. Wang, H. W. Zhang, and J. Q. Xiao, "Magnetic tunnel junction based microwave detector," *App. Phys. Lett.,* vol. 95, p. 122501, 2009. A. Grizzle, C. D'Angelo, J. Martínez-Lillo, and P. Tyagi, "Spin state of a single-molecule magnet (SMM) creating long-range ordering on ferromagnetic layers of a magnetic tunnel junction – a Monte Carlo study," *RSC Advances,* vol. 11, pp. 32275-32285, 2021.

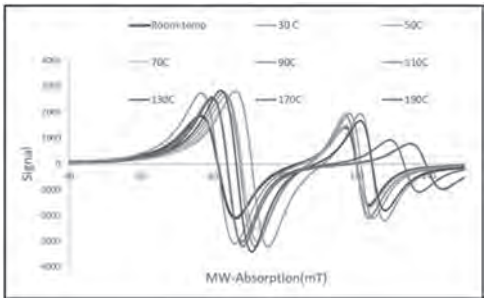

Figure 1. 0.5nm insulator thickness AlOx-based MTJMSD sample's Spin Resonance response under all the temperature increments.

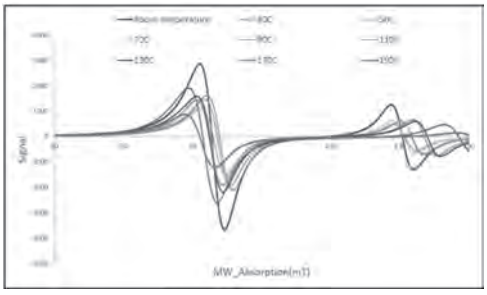

Figure 2. 1.5nm insulator thickness AlOx-based MTJMSD sample's Spin Resonance response under all the temperature increments.

FR-07. Correlation between the top electrode size and the spin orientations in T-shaped Magnetic Tunnel Junction Based Molecular Spintronic Devices (MTJMDS). *J.E. Hernandez*[1], P. Tyagi[1], H. Brown[1] and B. Sankhi[1]
1. University of the District of Columbia, Washington, DC, United States

This study investigates the magnetic behavior of Magnetic Tunnel Junction-Based Molecular Spintronic Devices (MTJMSDs). Using Monte Carlo Simulation, it explores the impact of coupling strengths and interactions between magnetic molecules and ferromagnetic electrodes at different top electrode sizes in T-shaped MTJMSDs. Variations in top electrode size directly affect the number of attached molecules and their impact on the samples. The Monte Carlo Simulation method replicates diverse MTJMDS samples, manipulating parameters such as JmL (Heisenberg exchange coupling), molecular junction area, maximum magnitude of spin fluctuation, and anisotropy. Conducted over 200 million iterations for a stable low-energy state, this simulation reveals the effects of these parameters on free electron distribution and magnetic moment stability within MTJMDS. The molecular junction area is a pivotal factor in determining top electrode size. Changes in Heisenberg exchange coupling, anisotropy, and maximum magnitude of spin fluctuation are crucial for determining spin alignment. Simulations reveal the intricate relationship between these parameters, impacting the magnetic and electrical properties of the samples. The primary outcome is a three-dimensional image, depicting constituent atom spins as vectors under different alignments with the x, y, and z axes. This insight provides a foundational understanding of the interplay between molecular structure, magnetic interactions, and electronic transport characteristics in nanoscale MTJMDS, offering valuable insights for developing practical devices. Table 1 shows the values changed during the simulations. The Heisenberg exchange coupling varies between -1, 0, and 1. The molecular junction area ranges from 1, 3, 5, 7, 9, 11, to 21 (top electrode size x 50 bottom electrode size). The Maximum Magnitude of Spin Fluctuation changes between 1 and 0. Anisotropy, which has a vector value, changes in the x-direction from 1,0,0 to 0,0,0, and then in the y-direction from 0,0,0 to 0,1,0, with changes made in steps of 0.2.

1 Tyagi, P., Baker, C., and D'Angelo, C.: 'Paramagnetic Molecule Induced Strong Antiferromagnetic Exchange Coupling on a Magnetic Tunnel Junction Based Molecular Spintronics Device', Nanotechnology, 2015, 26, pp. 305602 2 Tyagi, P.: 'PhD Thesis: Fabrication and Characterization of Molecular Spintronics Devices, University of Kentucky (http://archive.uky.edu/handle/10225/878)', 2008 3 Tyagi, P.: 'Trenched Bottom Electrode and Liftoff based Molecular Devices. US Patent Application No. 16/102,732.' 2020 4 Savadkoohi, M., D'Angelo, C., Grizzle, A., Dahal, B., & Tyagi, P. (2022). Spatial influence of paramagnetic molecules on magnetic tunnel junction-based molecular spintronic devices (MTJMSD). Chemical Physics Letters, 800, 139667. https://doi.org/10.1016/j.cplett.2022.139667

Thickness/length (both electrodes)	Anisotropy	Temperature(K)	JmL/JmR	Molecular junction area	FL=FR=Fm
5/50	AL= 1.0,0 to 0,0,0 in 0.2 steps; 0,0,0 to 0,1,0 in 0.2 steps	0.1	JmL=1.0, 1 JmR=1	1x50, 3x50,5 x 50, 7x50,9x50, 11x50, 21x50	1 and 0

Table 1. Parameters used in the simulations.

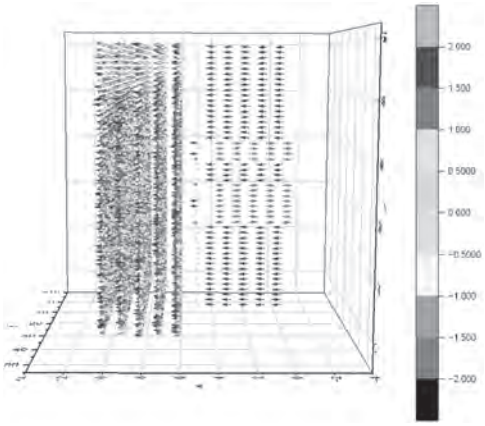

Figure 1. T-shaped MTJMDS simulation showing the spin of the atoms as vectors, showing the alignment in the x-axis.

FR-08. Influence of Ferromagnetic Interlayer Exchange Coupling on Current-Induced Magnetization Switching and Dzyaloshinskii-Moriya Interaction in Co/Pt/Co Multilayer System. *K. Grochot*[1], P. Ogrodnik[2], J. Mojsiejuk[1], P. Mazalski[3], U. Guzowska[3], W. Skowronski[1] and T. Stobiecki[1]
1. Institute of Electronics, AGH University of Krakow, Kraków, Poland;
2. Faculty of Physics, Warsaw University of Technology, Warsaw, Poland;
3. Faculty of Physics, University of Bialystok, Bialystok, Poland

Spin-orbit torque induced current magnetization switching (SOT-CIMS) provides an energy-efficient way of manipulating the magnetization in the ferromagnetic layers, which may lead to potential applications in storage devices. We present a detailed study the relationship among interlayer exchange coupling (IEC), Dzyaloshinskii-Moriya interaction (DMI), and multilevel magnetization switching within a Ti(2)/Co(1)/Pt(0- 4)/Co(1)/MgO(2)/Ti(2) (thicknesses in nanometers) patterned into micrometer-sized Hall-bar devices. Here, the Pt is used as a source of the spin current, and as a nonmagnetic spacer whose variable thickness enables the magnitude of the

ferromagnetic IEC to be effectively tuned [1]. From anomalous Hall effect (AHE), anisotropic magnetoresistance (AMR) and spin Hall magnetoresistance (SMR) measurements, we found that the increase in Pt thickness (t_{Pt}) leads to the reorientation of Co-magnetizations from the in-plane to the perpendicular direction at $t_{Pt} \approx 1.3$ nm. Further increase in Pt thickness, over 3 nm, reduces the ferromagnetic coupling and, consequently, two weakly coupled Co layers become magnetized orthogonally to each other. From analysis of the Stokes and anti-Stokes peaks (Fig.1a) spectra measured by the Brillouin light scattering (BLS), we quantify the effective DMI (Fig. 1b), and explore its potential role in magnetization dynamics and multilevel magnetization switching. Experimental findings show four distinct resistance states under an external magnetic field and spin Hall effect related spin current (Fig.1c). We explain this phenomenon based on the asymmetry between Pt/Co and Co/Pt interfaces and the interlayer coupling, which, in turn, influences DMI and subsequently impacts the magnetization dynamics. Numerical simulations, including macrospin, 1D domain wall, and simple spin wave models, further support the experimental observations of multilevel switching and help uncover the underlying mechanisms. Our proposed explanation [2], supported by magnetic domain observation using polar-magnetooptical Kerr microscopy, offers insights into both the spatial distribution of magnetization and its dynamics for different IECs, thereby shedding light on its interplay with DMI.

[1] P. Ogrodnik et al., *ACS Appl. Mater. Interfaces* 13, 47019 (2021) [2] K. Grochot et al., *Sci Rep* 14, 9938 (2024)

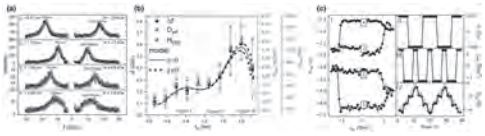

Session FS
SPINTRONIC NEURAL COMPUTING
(Poster Session)

Helena Reichlova, Co-Chair
Institute of Physics of the Czech Academy of Sciences, Praha, Czechia
Davi Rodrigues, Co-Chair
Politecnico di Bari, Bari, Italy

FS-02. All-Magnonic Neurons Based on Chiral Magnonic Resonators. K. Fripp[1], A. Shytov[1] and *V. Kruglyak*[1] *1. University fo Exeter, Exeter, United Kingdom*

We demonstrate chiral magnonic resonators [1,2] as building blocks of artificial neural networks. Using micromagnetic simulations and analytical modelling, we show that chiral magnonic resonators can concentrate energy of incident linear spin waves, leading to a strongly nonlinear response of the resonators' confined modes to the excitation. For modest excitation levels, the effect is described in terms of a nonlinear shift of the resonant frequency ('detuning'), which results in amplitude-dependent scattering of monochromatic spin waves. We show how this behavior can be harnessed to realize a sigmoid-like activation and so to implement artificial neurons in a deep neural network linked by spin waves propagating in a linear medium. Figures 1 and 2 exemplify a numerically simulated linear excitation pattern and the corresponding nonlinear response, respectively, of a magnonic neuron formed by a Permalloy nanodisk placed above a YIG film (inset in Fig.1). Our numerical results are in good agreement with a phenomenological model in which the nonlinear detuning of the confined mode is quadratic in its amplitude, while the propagation in the medium is linear. The research leading to these results has received funding from the UK Research and Innovation (UKRI) under the UK government's Horizon Europe funding guarantee (Grant No. 10039217) as part of the Horizon Europe (HORIZON-CL4-2021-DIGITAL-EMERGING-01) under Grant Agreement No. 101070347. Yet, views and opinions expressed are those of the authors only and do not necessarily reflect those of the EU, and the EU cannot be held responsible for them.

[1] V. V. Kruglyak, Appl. Phys. Lett. 119, 200502 (2021). [2] K. G. Fripp, Y. Au, A. V. Shytov, and V. V. Kruglyak, Appl. Phys. Lett. 122, 172403 (2023).

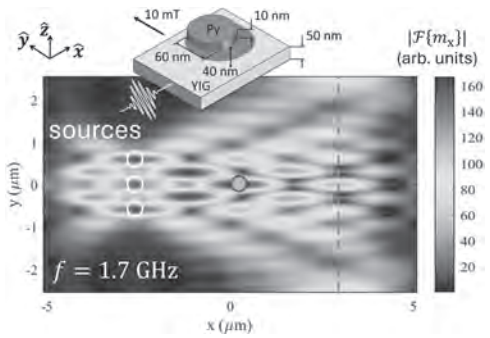

Fig. 1 The linear spin wave pattern created by three Gaussian magnonic sources in a YIG medium and incident on a neuron, i.e. a Permalloy (Py) disk acting as a chiral magnonic resonator (inset). The dashed line shows the position of the next neural layer.

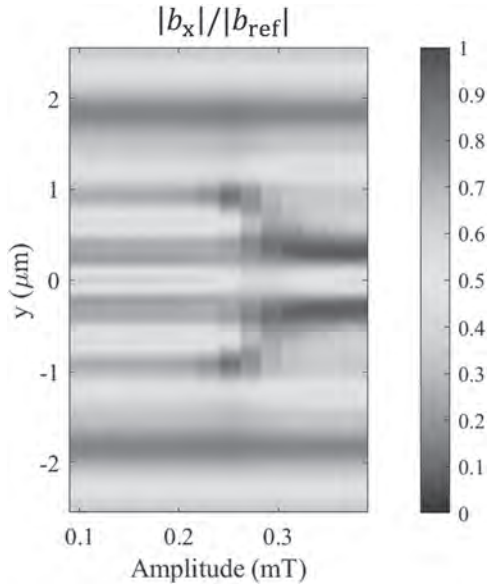

Fig. 2 The dynamic stray magnetic field of the spin waves scattered by the neuron and detected at the next neural layer is shown as a function of the incident spin wave amplitude. The field is normalized by the value of that created by the incident spin waves at the position of the neuron.

FS-03. Computing with Magnetic Tunnel Junction Based Sigmoidal Activation Functions. *Y. Bao*[1], S. Yang[1], Z. Yao[1] and H. Yang[1] *1. Department of Electrical and Computer Engineering, National University of Singapore, Singapore*

Artificial neural networks (ANNs) are powerful tools used in science and engineering, but their scalability is limited by increasing energy and area demands. The implementation of nonlinear activation functions in ANNs is crucial, as it directly influences the energy, area, and overall performance of the computing system. Implementing sigmoidal functions, which are the most commonly used activation functions, in digital hardware is challenging due to the exponentiation and division terms involved. The magnetic tunneling junction (MTJ), originally designed for memory applications, shows promise for computing. However, most current uses of MTJs for implementing sigmoidal functions are based either on simulations or extracted experimental data. In this work, we first configure an energy- and area-efficient MTJ-based unit (consisting of 1 MTJ, 1 NMOS transistor, and 1 resistor) for implementing sigmoidal functions. We then build a system with three MTJ cells (Fig. 1a) and train a simple neural network for speech separation tasks. During ten speech separation experiments, we observe the exceptional endurance of MTJs, generating 10^9 bits per MTJ. Our results (Fig. 1b) highlight the potential of our MTJ-based system to enhance energy and area efficiency, along with algorithm performance, compared to traditional computing systems. When compared to state-of-the-art digital implementations, our scalable circuit has the potential to consume up to 383 times less energy and occupy 7354 times less area. The algorithm performance

metric, maximum signal-to-distortion ratio (SDR), is 16.9% higher. This performance variance is due to random noise during the physical switching process. These findings pave the way for more efficient computing systems in the future. Our work is fully hardware-based and utilizes spin-transfer-torque MTJ (STT-MTJ) which offers scalability [1], unlike previous fully hardware-based studies that used stochastic MTJ and suffered from substantial device variation and lack of scalability [2,3].

[1] Y. Bao, S. Yang, Z. Yao *et al.*, *Appl. Phys. Lett.*, vol. 124, no. 24, p. 242403 (2024) [2] W. A. Borders, A. Z. Pervaiz, S. Fukami *et al.*, *Nature*, vol. 573, no. 7774, pp. 390–393 (2019) [3] J. Si, S. Yang, Y. Cen *et al.*, *Nat. Commun.*, vol. 15, no. 1, p. 3457 (2024)

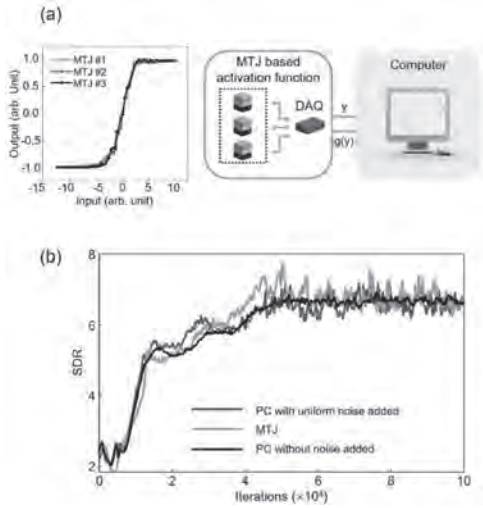

Fig. 1 (a) Sigmoidal curves of three MTJ computing units after calibration (left) and system data flow during experiments (right). (b) Averaged SDR curves from ten speech separation experiments.

FS-04. Development of zero-field skyrmionic devices. W. Griggs[1], I. Charalampidis[1], V. Pavlidis[1] and *C. Moutafis*[1] *1. University of Manchester, Manchester, United Kingdom*

The recent proliferation of highly resource-intensive artificial intelligence has underscored the growing need for innovative computational approaches with enhanced performance and efficiency. Magnetic skyrmions have emerged as promising candidates for use as information carriers in next-generation computational devices, owing to their stability, nanoscale size, and high mobility. However, for skyrmionic devices to be useful, skyrmions must be stabilized without external magnetic fields. Several approaches have been explored, such as by tuning interlayer exchange coupling [1] or through geometrical confinement [2]. Here we demonstrate the ability to stabilize room temperature, zero-field skyrmions in two nanoscale systems. First, we stabilize zero-field skyrmions in nanodisk arrays (Fig. 1a), and show that it is possible to tune their nucleation probability through tilted field pulses. We explore the roles of diameter and field pulse angle on the domain state of the disks, and demonstrate a skyrmion nucleation probability ranging from zero to 88%. Thus, through materials engineering and confinement we demonstrate the generation of stable skyrmions at zero field with a modifiable nucleation yield. This system may offer an interesting approach to probabilistic computing, wherein the ability to tune the relative distribution of bistable states is essential. We furthermore stabilize a population of skyrmions in partitioned nanotrack devices (Fig. 1b). These devices may perform the role of multibit artificial synapses for neuromorphic computing [3]. The devices are characterised through magnetic force microscopy (MFM) with custom-engineered in-situ magnetic fields. We demonstrate that a population of skyrmions can manifest in our device at zero applied field (Fig. 1b) and show progress towards modifying the population of skyrmions either side of the device through applied programming current pulses.

[1] Y. Guang, et al., Nat. Commun., 11, 949 (2020). [2] P. Ho et al., Phys. Rev. Applied, 11, 24064 (2019). [3] R. Chen et al., Phys. Rev. Applied 14, 014096 (2020).

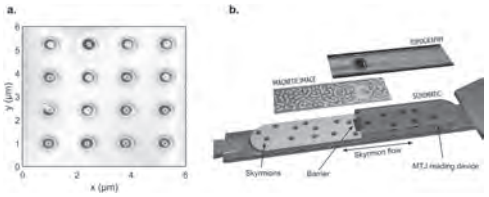

Fig. 1. a. MFM scan of an array of nanodisks in which zero-magnetic field skyrmions are stabilized at room temperature. b. (Bottom layer): A schematic of a skyrmionic synapse device. (Middle layer): MFM image from a nanofabricated synapse at zero magnetic field. (Top layer): The corresponding synapse topography.

FS-05. Restricted Boltzmann Machine for Modeling Complex Physical Systems: A Case Study in Artificial Spin Ice. *R.B. Popy*[1], M. Hamdi[1] and R.L. Stamps[1] *1. Physics and Astronomy, University of Manitoba, Winnipeg, MB, Canada*

Restricted Boltzmann machines are powerful tools in the field of generative, probabilistic learning, capable of capturing complex dependencies in data[1]. By understanding their architecture and operational principles, one can employ them for diverse purposes such as dimensionality reduction, feature learning and even representing and analyzing various physical systems[2]. This work aims to provide insights into the capabilities and limitations of restricted Boltzmann machines in modelling complex physical systems in the context of artificial spin ice[3]. Geometrical frustration in artificial spin ice systems creates degeneracies leading to complex states and collective dynamics. From reconfigurable magnonics to neuromorphic computing, artificial spin systems are emerging as versatile functional platforms that go beyond simply imitating naturally occurring materials. Using out of equilibrium data from Monte Carlo simulations of artificial spin ice geometries, this work demonstrates the sensitivity of learning artificial spin ice state distributions with restricted Boltzmann machines. Results indicate that careful application of the restricted Boltzmann machine algorithm can reduce the training data required for feature extraction, which can be used for faster sample generation[4]. Additionally, we demonstrate how the restricted Boltzmann machine can distinguish different artificial spin ice geometries by identifying their respective state distribution features.

[1] Paul Smolensky et al. Information processing in dynamical systems: Foundations of harmony theory. Department of Computer Science, University of Colorado, Boulder, 1986. [2] David Yevick and Roger Melko. The accuracy of restricted Boltzmann machine models of Ising systems. Computer Physics Communications, 258:107518, 2021. [3] Sandra H Skjærvø, Christopher H Marrows, Robert L Stamps, and Laura J Heyderman. Advances in artificial spin ice. Nature Reviews Physics, 2(1):13–28, 2020. [4] Rehana Begum Popy, Mahdis Hamdi, and Robert L. Stamps. Restricted Boltzmann machine for modeling complex physical systems: A case study in artificial spin ice. arXiv Preprint, arXiv:2407.11165, 2024.

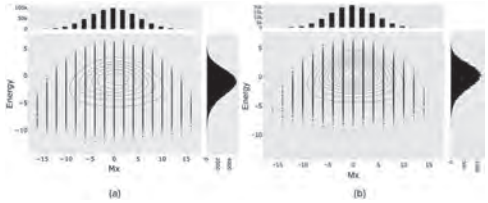

2D histogram contour plots showing the distribution of states in energy magnetization space for a) 600,000 Monte Carlo realizations of a 6x6 pinwheel ASI at T=3.5 D/k_B and b) 120,000 Monte Carlo sampled pinwheel ASI data (at T=3.5 D/k_B) trained RBM reconstruction. The summed energy and magnetization histograms display the energy and magnetization values frequencies. Even though the RBM is trained on relatively fewer samples, its reconstruction captures the essence of pinwheel ASI data distribution, including the spread of data points and most probable states. A slight shift in the energy range can be observed.

FS-06. Domain Wall and Skyrmion Devices-based Spiking Neural Networks. *A.H. Lone*[1], D.N. Rahimi[1], M. Tang[1], D. Divyanshu[1], S. Amara[1] and G. Setti[1] *1. CEMSE (Integrated Intelligent Systems (I2S)), King Abdullah University of Science and Technology, KAUST, Thuwal, Saudi Arabia*

Using domain walls and skyrmions in Spintronic devices has emerged as a promising avenue for advancing energy-efficient data storage and non-conventional computing architectures[1-4]. Leveraging magnetic multilayer structures (shown in Fig. 1(a)), our study showcases the realization of a magnetic field-gated and current-controlled Leaky Integrate and Fire (LIF) neuron device. The measured magnetic hysteresis loop demonstrates a multi-domain magnetic profile (see Fig. 1(b). The functionality of these devices resembles that of gate-controlled LIF neurons, as shown in Fig. 1(c), resembling spintronic Mem-transistor devices. The current pulses facilitate domain wall motion, whereas the external magnetic field serves as the bias for tuning neuron firing properties. Our investigation demonstrates the controllability of neuron spiking rates through current and magnetic field modulation, as shown in Fig. 2(c). We have developed a comprehensive LIF neuron model(shown in Fig. 1(c)) based on measurements, showcasing the seamless integration of these devices within system-level SNN frameworks as shown in Fig. 2. Furthermore, we propose a scaled version of multilayer spintronic domain wall MTJ as LIF neurons, LIF characteristics is achieved through a combination of spin-orbit torque (SOT) and manipulation of demagnetization energy within thin films. Subsequently, we integrate both experimentally derived and simulated neuron models into a 3-layer SNN (Fig. 2(a)) and Convolutional Spiking Neural Network (CSNN) (Fig. 2(b)) framework, demonstrating their efficacy in accurately classifying MNIST and FMNIST datasets, achieving classification accuracies surpassing 96% (shown in Fig. 2(d)). These findings underscore the potential of the presented devices as viable alternatives for neuromorphic computing applications, owing to their commendable system-level performance, Mem-transistor attributes, and prospects for scalability.

References: [1] Kyung Mee Song et al., "Skyrmion-based artificial synapses for neuromorphic computing. Nat Electron," 3(3):148–155, March 2020. [2] Abhronil Sengupta et al., "Spin-orbit torque induced spike-timing dependentplasticity,"AppliedPhysicsLetters,106(9):093704,March2015.[3] Xing Chen et al. "A compact skyrmionic leaky–integrate–fire spiking neuron device," Nanoscale, 10:6139–6146, 2018. [4] Aijaz H. Lone et al., "Skyrmion-Magnetic Tunnel Junction Synapse With Long-Term and Short-Term Plasticity for Neuromorphic Computing," IEEE Trans. Electron Devices, 70(1):371–378, January 2023

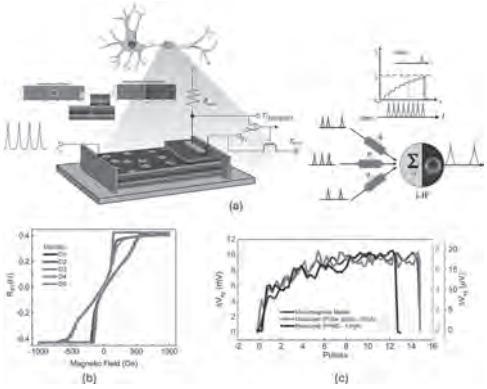

Fig. 1(a) Magnetic domain wall/skyrmion LIF neuron device. (b) Magnetic hysteresis shows multidomain characteristics. (c) LIF characteristic

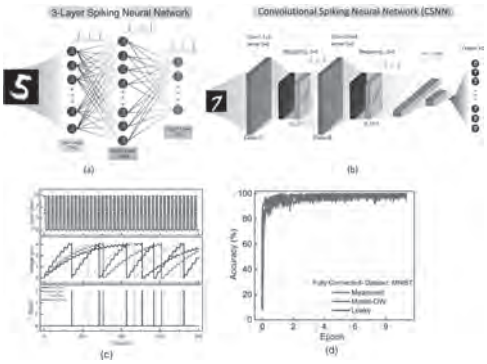

Fig. 2(a) 3-Layer SNN architecture. (b) CSNN architecture. (c) Current controlled spike rate. (d) Recognition accuracy on MNIST dataset.

FS-07. On-Chip Learning of UNet Architecture Using Spintronic Devices for Image Segmentation. V. Vadde[1], B. Muralidharan[1] and *A. Sharma*[2] *1. Department of Electrical Engineering, Indian Institute of Technology Bombay, Mumbai, India; 2. Department of Electrical Engineering, Indian Institute of Technology Ropar, Rupnagar, India*

Image segmentation is a crucial machine-learning task that involves classifying and clustering each pixel in an image to identify objects. Segmentation has substantial uses in self-driving cars, analyzing medical and satellite images [1]. UNet has become the prominent architecture for segmentation tasks. In this work, we design spintronic hardware for various layers of the UNet architecture, including convolution, deconvolution, activation, and pooling functions. We implement these layers by employing a hybrid of orthogonal current-injected magnetic tunnel junction (MTJ) and domain wall MTJs (DW-MTJ). Leveraging the linear behavior [2] of orthogonal current-injected MTJs, we demonstrate the implementation of the rectified linear unit (ReLU) activation function and the max-pooling function. By utilizing the synaptic properties of DW-MTJs, we achieve the realization of convolution and deconvolution operations [3]. We simulate these devices using a hybrid simulation platform that couples micromagnetic simulations, the Landau-Lifshitz-Gilbert-Slonczewski (LLGS) equations, non-equilibrium Green's function, SPICE circuit simulation, and machine learning network implementation. We demonstrate the efficiency of our proposed network by testing it on the Cambridge-driving labeled video (CamVid) dataset, achieving an accuracy of 83.71%, comparable to that of the software implementation. Furthermore, we demonstrate that by utilizing unstable ferromagnets, the network's energy consumption can be reduced by up to an order of magnitude, decreasing from 821 mJ to 85.79 mJ.

[1] Liu, X., Deng, Z., & Yang, Y. Artificial Intelligence Review, 52, 1089-1106, (2019). [2] Vadde, V., Muralidharan, B., & Sharma, A. IEEE Transactions on Electron Devices, 70(7), 3943-3950, (2023). [3] Vadde, V., Muralidharan, B., & Sharma, A. APL Machine Learning, 2(3), 036101 (2024).

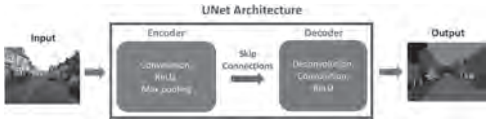

Fig. 1: The UNet architecture comprises an Encoder, Decoder, and skip connections. It contains convolution, deconvolution, ReLU, and max-pooling layers terminated with a softmax function. An example input image with its corresponding output from the CamVid database is shown.

FS-08. Ultrafast Skyrmions for Neuromorphic Computation. *A. Joy*[1,2], S. Satheesh[1] and P. Anil Kumar[1] *1. Physics, Indian Institute of Science Bangalore, Bangalore, India; 2. NISE, Max Planck Institute for Microstructure Physics, Halle, Germany*

The human brain processes information efficiently due to the dynamics of neurons and synapses, which can inspire effective artificial Spiking Neural Networks (SNN). Spintronic devices are ideal for neuromorphic computing, with skyrmions as effective information carriers due to their topological protection and particle-like nature. Ferrimagnet and antiferromagnet-based spintronics have previously enabled artificial synapses and neurons. We propose a ferromagnetic device ($Ta_{3nm}Pt_{3nm}Cu_{0.65nm}Co_{0.5nm}Pt_{1nm}$) that simulates artificial neurons and synapses ultrafast due to high-velocity skyrmions. Electrical pulses control skyrmion accumulation and dissipation, analogous to synaptic weight changes. Lateral Structure Inversion Asymmetry (SIA) enables field-free, energy-efficient switching. This device reproduces neuron and synapse functionalities with superior time scales, making ferromagnet-based skyrmions viable for ultrafast neuromorphic spintronics, capable of highly efficient cognitive tasks.

1. M.-K. Kim, Y. Park, I.-J. Kim, and J.-S. Lee, Emerging materials for neuromorphic devices and systems, iScience 23, 101846 (2020). 2. S. Fukami and H. Ohno, Perspective: Spintronic synapse for artificial neural network, Journal of Applied Physics 124, 151904 (2018). 3. M. Pfeiffer and T. Pfeil, Deep learning with spiking neurons: Opportunities and challenges, Frontiers in Neuro-science 12, (2018). 4. N. Nagaosa and Y. Tokura, Topological properties and dynamics of magnetic skyrmions, Nat Nanotechnol 8, 899, (2013). 5. M. Weißenhofer and U. Nowak, Diffusion of skyrmions: the role of topology and anisotropy, New Journal of Physics 22, 103059 (2020). 6. S. Lepadatu, Effect of inter-layer spin diffusion on skyrmion motion in magnetic multilayers, Sci Rep 9, 9592 (2019). 7. J. Grollier, D. Querlioz, K. Y. Camsari, K. Everschor- Sitte, S. Fukami, and M. D. Stiles, Neuromorphic spintronics, Nat Electron 3 (2020). 8. I. Dzyaloshinsky, A thermodynamic theory of "weak" ferromagnetism of antiferromagnetics, J. Phys.Chem.Sol. 4, 241 (1958).

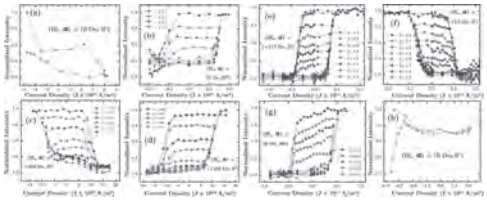

Memristor action measurements. (a)-(d) Memristor action for 50μs pulses. (a) Non-deterministic field-free switching (α=0°). (b) Hysteresis curve showing multiple non-volatile memory states without Hx (α = 90°), indicating memristor realization via MOKE. (c) Hysteresis curve (α=0°) with Hx=-400 Oe for deterministic switching. (d) Hysteresis curve (α=0°) with Hx=400 Oe for deterministic switching. (e)-(h) Memristor action for ns pulses (60 ns width). (e) Current density vs. Intensity with Hx=+110 Oe (α=0°) for deterministic switching using Kerr Microscope. (f) Current density vs. Intensity with Hx=-110 Oe (α=0°) for deterministic switching using Kerr Microscope. (g) Hysteresis curve (α = 90°) without Hx, showing memristor realization via MOKE. (h) Non-deterministic field-free switching (α=0°)

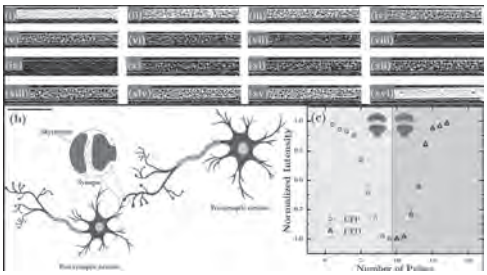

Implementation of an artificial synapse using ferromagnet-based system. (a)[i-xvi] Successive Kerr microscope images show 900 nm skyrmions after unipolar current pulses. The first six images show potentiation; the last six show depression. (b) Schematic of a skyrmion-based synapse, with weights adjusted by skyrmion modulation via current. (c) Normalized intensity vs current pulses:blue triangles show LTD, red circles show LTP. LTP and LTD are manipulated by pulse amplitude.

Session FT
THIN FILMS, MULTILAYERS, AND EXCHANGE BIAS SYSTEMS IV (Poster Session)

Anna Giordano, Chair
University of Messina, Messina, Italy

FT-01. Chiral Magnonic Crystals Induced by Periodically Tailoring Interfacial Dzyaloshinskii-Moriya Interaction. F. Wei[1], Y. Zhou[1], *W. Zhang*[2] and S. Kang[1] *1. Shandong University, Jinan, China; 2. Weifang University, Weifang, China*

Artificially introducing periodic patterns into magnetic materials can manipulate spin waves, creating structures known as magnonic crystals (MCs) that exhibit rich band structures. Incorporating a magnetochiral mechanism into MCs unlocks nonreciprocal properties in spin waves, further enhancing their potential applications in spintronic devices with ultra-low power consumption. Here, we comprehensively investigate the spin wave band structures of bicomponent chiral MCs by periodically tailoring the intensity of the interfacial Dzyaloshinskii-Moriya interaction (i-DMI) in ferromagnetic and heavy metal trilayer systems (HM_1/FM/$HM_{1(2)}$). The band structures strongly depend on the i-DMI, lattice periods, and/or external magnetic field. Interestingly, increasing the effective i-DMI energy induces a flat band structure with zero group velocity, which originates from the robust localization of magnon modes. Meanwhile, the nonreciprocal properties in these MCs can be significantly enhanced with increasing the effective i-DMI energy, facilitating the unidirectional propagation of spin waves. Moreover, the width and position of the indirect band gap in our MCs are easily tuned and closely related to the i-DMI, lattice period, and/or external magnetic field. The wavevector difference between the top of the first band and the bottom of the second band increases linearly with the effective i-DMI energy (see Fig.1 a). Both frequency-domain finite-element method (FDFEM) calculations and finite-difference time-domain (FDTD) micromagnetic simulations agree well with the experimental observations. This study offers a convenient method to design and tailor magnetic band structures, facilitates controlled manipulation of quasi-particles, and provides insights and methodologies for designing spin wave-based nanodevices

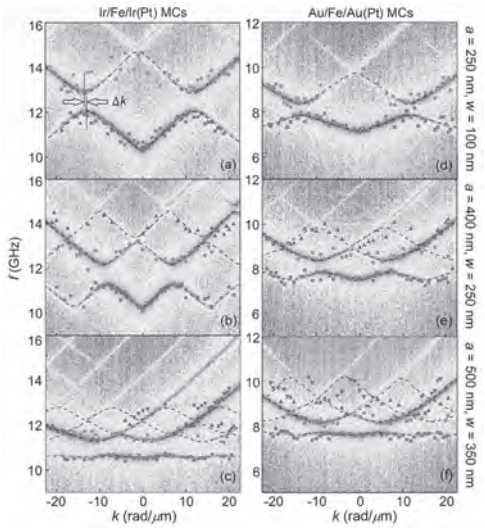

Figure 1 Band structures of spin waves in chiral MCs with different periods for Ir/Fe/Ir(Pt) and Au/Fe/Au(Pt) chiral MCs. The background intensity plots are simulated using MuMax3. The solid symbols represent the dispersion branches extracted from the BLS spectra, and the dashed lines depict the FDFEM calculations.

FT-02. Magnetic and Transport Properties of $LaSrMnRuO_6$ Double Perovskite Thin Films. *A. Kumar*[1,2], D. Palai[3], D. Samal[3] and P. Santhosh[1,2] *1. Department of Physics, IIT Madras, Chennai, India; 2. Functional Oxide Research Group, IIT Madras, Chennai, India; 3. Department of Physics, Institute of Physics, Bhubaneswar, India*

Double perovskite (DPs) oxides have general formula $A_2BB'O_6$ or $AA'BB'O_6$. They show various interesting properties such as ferromagnetism, antiferromagnetic, tunnelling-type magnetoresistance (TMR) with half metallicity and some unusual magnetic state such as spin glass [1-3]. $LaSrMnRuO_6$ (LSMRO) has an orthorhombic structure with a *Pnma* space group and Mn/Ru disorder at B-site [4]. However, B-site ordered double perovskites are considered to be better for improving magnetic and transport properties such as curie temperature and magnetization etc [5]. In this work, we have carried out fabrication of LSMRO thin films followed by detailed study of structural, magnetic and transport properties. Presence of superlattice peak in XRD pattern at 19° confirms ordering in LSMRO thin films. A detailed analysis to understand the magnetization data as well as transport properties in the LSMRO thin films will be presented.

1.K. L. Kobayashi et al., Nature 395, 677 (1998). 2.J. Willem et al., J. Mater. Chem. 15, 715 (2005). 3.B. D. Battle et al., J. Solid St. Chem. 78, 281 (1989). 4.P. M. Woodward et al., J. Am. Cerum. Soc. 96 (6), 1796 (2008) 5.J. E. Kleibeuker et al., NPG Asia Material 9, 406 (2017).

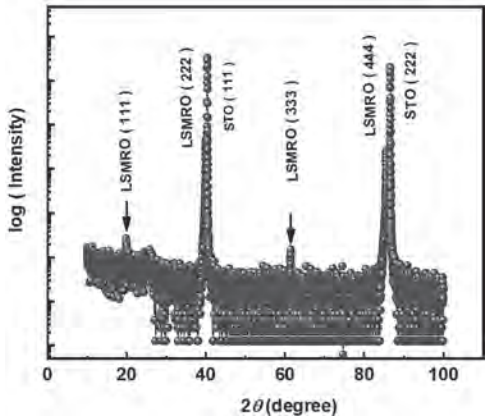

θ-2θ XRD plot of LSMRO thin film on STO (111) substrate, and arrow at 19° and 61° indicate B-site ordering peak

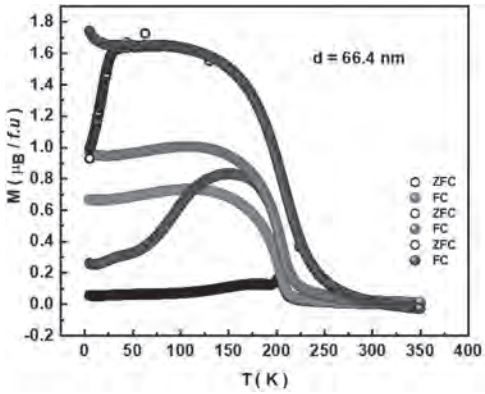

Thermal variation of magnetization under ZFC and FC protocol in 100 Oe, 1000Oe and 10000Oe magnetic fields

FT-03. Hydrogen-Mediated Spin-Orbit Torque and Voltage-Controlled Magnetic Anisotropy in $[Tb/Co]_3$/PtTb Structures. B. Chen[1], *C. Lin*[2] and C. Lai[1] *1. Material Science and Enigneering, National Tsing Hua University, Hsinchu, Taiwan; 2. College of Semiconductor Research, National Tsing Hua University, HsinChu, Taiwan*

High threshold switching currents pose a significant obstacle to the realization of Spin-Orbit Torque MRAM (SOT-MRAM). To address this challenge, various approaches have been proposed, such as enhancing extrinsic scattering via high spin-orbit coupling (SOC) materials alloyed with light metals or tuning the heavy metal/ferromagnet (HM/FM) interface to increase spin transparency. However, most of these methods are intrinsic to the material, limiting their applicability. Here, we propose modulating spin-orbit torque in a perpendicular sub//$[Tb/Co]_3$/PtTb structure via external atmospheres, introducing a magneto-ionic concept to enhance feasibility. PtTb alloy serves as a spin current source and has high affinity for hydrogen. Initially, we applied different atmospheres in enclosed cells and conducted harmonic measurements to obtain SOT efficiency. The results showed that damping-like efficiency (ξ_{DL}) and anisotropy (H_k) both decayed with increasing H_2 pressure, with a more significant change observed in H_k, leading to a decrease in threshold current. Hydrogen incorporation modulates the coupling strength between RE and TM atoms, which changes H_k and also influences the spin transparency at the HM/FM interface, leading to a decrease in ξ_{DL}. This characteristic enables H_2-sensing functionality. To further enhance the multifunctionality of our structure, we leveraged the hydrogen affinity of Pt and Tb to create an intrinsic hydrogen ion reservoir via reactive sputtering, forming a metal hydride in PtTb layer. We then achieved ion migration by applying different voltages on a typical Hall cross configuration with a top voltage gate oxide SiO_2. The anomalous Hall effect (AHE) signal decreased with applying the positive voltage, as shown in Fig. 1. The Tb hydride was reported to stabilize H^-. Therefore, applying a positive voltage on the top gate oxide forms negative charge accumulation at the PtTb/SiO_2 interface, which repels H^- in PtTb into $(Tb/Co)_3$ and reduces the perpendicular anisotropy and magnetization. Our results indicate the potential for multifunctionality in $[Tb/Co]_3$/PtTb structures for memory and sensor applications.

W. Zhang *et al.*, *Nature,* vol. 616, no. 7955, pp. 73-76, (2023) H. An, S. Haku, Y. Kageyama, *Advanced Functional Materials,* vol. 30, no. 30, p. 2002897, (2020) S. Akamaru, H. Yamamoto, and M. Hara, vol. 47, no. 11, pp. 7491-7498 (2022) L. Zhu, D. C. Ralph, and R. A. Buhrman, *Applied Physics Reviews,* vol. 8, no. 3, (2021)

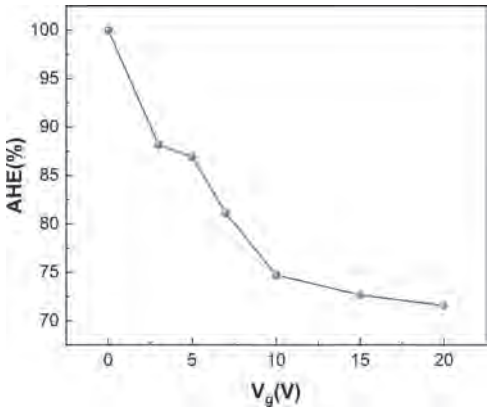

Fig.2 Variations of AHE signal with applied voltage (each sequence is 120sec)

FT-04. Conductivity-like Gilbert damping for iron-rich Fe-Si thin films at low temperature. *Y. Jiang*[1], T. Miyazaki[2], S. Ajia[1], S. Muroga[1] and Y. Endo[1,3] *1. Department of Electrical Engineering, Graduate School of Engineering, Tohoku University, Sendai, Japan; 2. Faculty of Engineering, Tohoku University, Sendai, Japan; 3. Center for Science and Innovation in Spintronics (CSIS), Tohoku University, Sendai, Japan*

The Gilbert damping constant (α), which describes the strength of the damping torque in the Landau-Lifshitz-Gilbert (LLG) equation, is one of the dominant parameters to predict the magnetization dynamics in magnetic films, and is also closely related to the performance of spintronic devices [1, 2]. To realize ultra-low-power consumption in these devices, understanding the mechanism of α is required. Until now, we reported that the in-plane effective damping constant ($\alpha_{\parallel}$) became higher than the out-of-plane effective damping constant ($\alpha_{\perp}$) for $Fe_{100-x}Si_x$ (Fe-Si) polycrystalline films at room temperature, indicating that intrinsic damping overlapped with extrinsic damping [3]. Herein, to further understand the mechanism of $\alpha_{\perp}$ in Fe-Si polycrystalline films, we investigated the electrical and magnetic properties of these films at various low temperatures in detail. Fig. 1 shows the temperature dependence of relative resistivity ($\rho/\rho_{100\,k}$) for 75 nm-thick Fe-Si films with various Si compositions (x). For x = 9.7 and 13.7, $\rho/\rho_{100\,k}$ decreased slightly and then increased as the temperature increased, whereas for x = 21.7, it decreased monotonically with the increase of temperature. These results reveal that the electrical properties of these films change from metallic behavior to semiconductive one as x increases. Fig. 2 shows the temperature dependence of $\alpha_{\perp}$ for these films. For x = 9.7 and 13.7, $\alpha_{\perp}$ increased and then decreased as the temperature increased from 10 K to 100 K. On the other hand, for x = 21.7, $\alpha_{\perp}$ increased monotonically as the temperature increased. These behaviors are opposite to that of $\rho/\rho_{100\,k}$, indicating a reverse correlation between α and ρ for Fe-Si films at low temperatures. They could be explained by Kambersky's breathing Fermi surface model [4]. Therefore, these results demonstrate that the Gilbert damping at low temperatures for Fe-Si films is derived from a conductive behavior.

[1] T. L. Gilbert, IEEE Trans. Magn., Vol. 40, p.3443 (2004) [2] S. Bhatti, R. Sbiaa, A. Hirohata et al., Mater. Today, Vol. 20, p.530 (2017) [3] Y. Jiang, S. Muroga, T. Miyazaki et al., IEEE Trans. Magn., Vol. 59, p.1 (2023) [4] M. Fähnle, J. Seib, C. Illg, Phys. Rev. B, Vol. 82, p.144405 (2010)

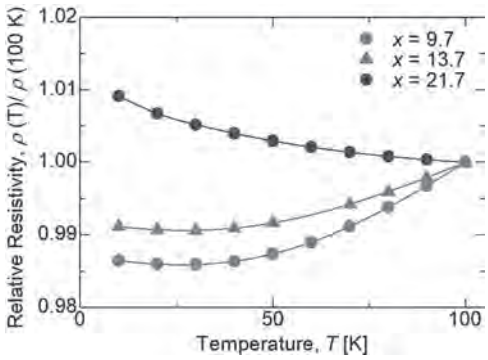

Temperature dependence of relative resistivity ($\rho/\rho_{100\,k}$) for 75 nm-thick Fe-Si films with various Si compositions (x).

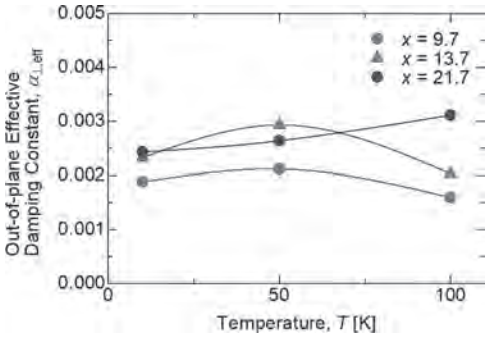

Change in out-of-plane effective damping constant ($\alpha_\perp$) of 75-nm-thick Fe-Si films with temperature.

FT-05. Evidence of bilinear coupling in IrMn/Co/Cu/NiFe spin valves. *B.R. de Castro*[1], M.G. Silva[1], A.C. Krohling[1], L.H. de Andrade[1] and M. Martins[1] *1. Centro de Desenvolvimento da Tecnologia Nuclear, Belo Horizonte, Brazil*

Spintronics devices have been extensively studied due to the wide range of applications in industry. An interesting device illustration is the spin valves (SV) heterostructures which combine magnetoresistance, exchange bias and exchange coupling between ferromagnetic layers that play a crucial role in GMR devices [1-2]. In this work magnetic properties of IrMn/Co/Cu/NiFe spin valves are studied through magneto-optic Kerr effect (MOKE). The spin valve heterostructures were prepared onto a naturally oxidized Si[110] substrate. All the layers depositions were made without spinning the sample holder, resulting in the shadow effect and Cu and NiFe (permalloy – Py) elongated grains being coherently grown in the same direction [3]. The Cu spacer, Co and IrMn layers were deposited with morphologies rotated with respect to the Cu/Py bilayer and a sketch of the resulting sample is shown in figure 1. The MOKE measurements were carried in longitudinal geometry and s-polarization at 670 nm. We report the magnetic response shown in figure 2 in the case of magnetic field H applied parallel to Co and Py easy axes and perpendicular to substrate Si[110] direction. The results indicate an easy-like magnetization feature with the two square-like loops shifted relative to the origin. The loop shifted towards negative external fields is due to the exchange bias effect on Co/IrMn layer, while the right shifted loop is a permalloy loop modified by the bilinear coupling due to small separation (3 nm) between the ferromagnetic layers. In case H field is applied parallel to Si[110] direction, a symmetric single-like loop with small coercivity appears due to hard axes of Co and Py (insert of figure 2). In conclusion, the magneto-optic measurements confirm the easy axes magnetization of ferromagnetic layers as predetermined in the synthesis, also the exchange bias and bilinear coupling of the spin valve.

[1] V. P. Ningrum, B. Liu and W. Wang, Research, Vol. 2020, p. 1 (2020)
[2] Y. Liu, F. Wang and D. Kong, Physics Letter A, Vol. 381, p. 1732 (2017)
[3] A. C. Krohling, C. H. Verbeno, T. E. P. Bueno, Journal of Magnetism and Magnetic Materials, Vol. 512, p. 166985 (2020)

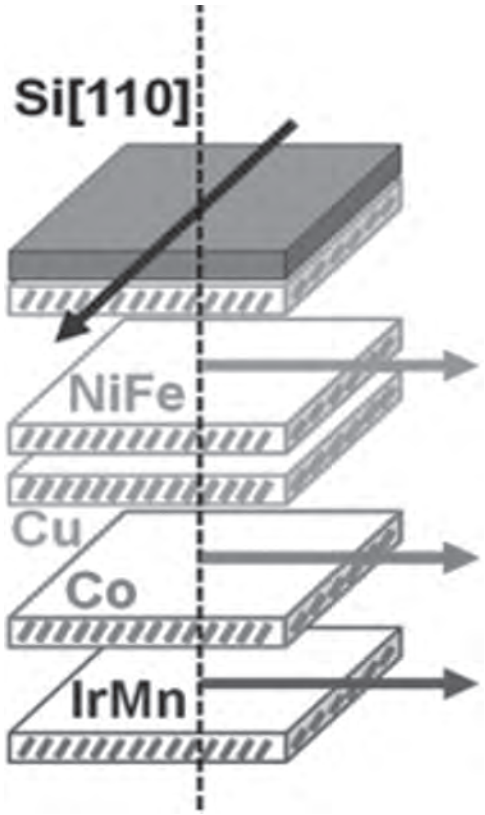

Fig. 1. Diagram of spin valve layers. The green/red arrows indicate the anisotropies axes, blue the unidirectional anisotropy and black the Si[110] direction.

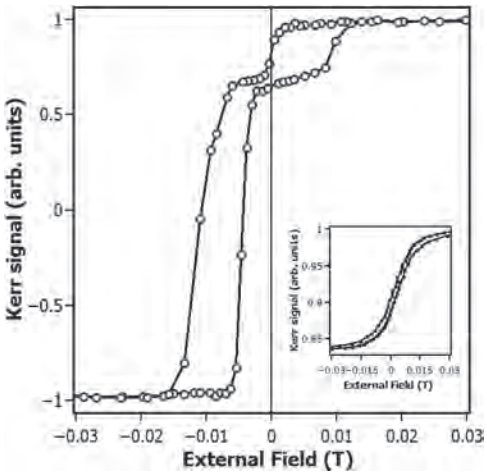

Fig. 2. Spin valve hysteresis show the left shifted loop due the exchange bias of Co/IrMn layer and second loop of permalloy NiFe.

FT-07. Anomalous Temperature Dependence of Magnetic Damping in $La_{0.5}Sr_{0.5}MnO_3$ Thin Films. *R. Arakawa*[1], T. Onogi[1], S. Komori[1] and T. Taniyama[1] *1. Physics, Nagoya University, Nagoya, Japan*

$La_{1-x}Sr_xMnO_3$ exhibits ultralow magnetic damping due to a high spin polarization at the Fermi level, which is highly attractive for achieving long-range spin wave propagation. However, the temperature and thickness dependence of the Gilbert damping constant α in $La_{1-x}Sr_xMnO_3$ thin films have yet to be fully understood, particularly near the ferromagnetic-antiferromagnetic phase boundary x=0.5. Here we report an anomalous temperature dependence of α in $La_{0.5}Sr_{0.5}MnO_3$ (LSMO) thin films on Nb-doped $SiTiO_3$ (Nb:STO), where

α exhibits a minimum at ~100 K. We discuss the underlying mechanism of this anomalous behavior. The temperature dependence of magnetization of a 38-nm-thick epitaxial LSMO film shows a noticeable bump at 118 K (Fig. 1), in close proximity to the structural phase transition temperature of Nb:STO (121 K) [1], indicating the emergence of secondary ferromagnetic phases induced by strain transfer due to the structural phase transition of Nb:STO. Figure 2 illustrates the temperature dependence of α evaluated by the ferromagnetic resonance linewidth (ΔH) versus resonance frequency (f_r) relationship, fitting $\Delta H=\Delta H_0+2\pi f_r\alpha/g$ [2]. An increase in α is clearly seen in the low-temperature (10-100 K) and high-temperature (150-300 K) regions, whereas the temperature dependence is independent of film thickness. This is in contrast to the results of $La_{0.7}Sr_{0.3}MnO_3$ reported previously, in which α increases with decreasing film thickness due to spin pumping associated with the presence of a magnetically active dead layer [3]. We attribute this anomalous temperature-dependent and film thickness-independent behavior of α in our LSMO samples to the Kamberský type spin damping in conjunction with spin pumping into secondary magnetic phases induced by the structural phase transition of Nb:STO. The results could open a way to control the magnetic damping for magnonic applications by strain engineering, which creates a new magnetic phase in LSMO as a spin sink. Work supported by JSPS KAKENHI (23KK0086, 24H00380, 24KJ1306), JST FOREST (JPMJFR212V) and Iketani Science and Technology Foundation.

[1] Z. Zhang, P. Qian, and X. Yang, Sci. Rep., Vol. 12, 2499 (2022) [2] Y. Wang, X. Fan, and X. Feng, Appl. Phys. Lett., Vol. 123, 112403 (2023) [3] V. Haspot, P. Noël, and J. P. Attané, Phys. Rev. Mater., Vol. 6, 024406 (2022)

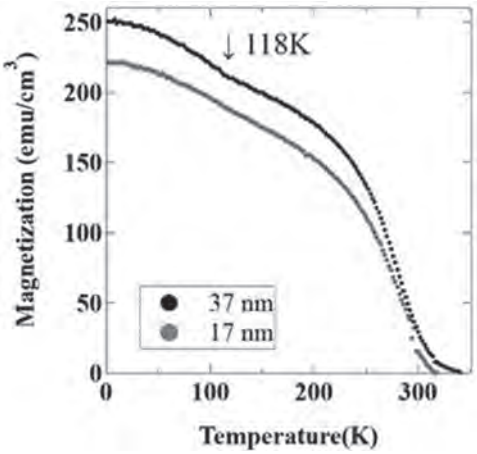

Fig. 1 Temperature dependence of the magnetization of LSMO thin films.

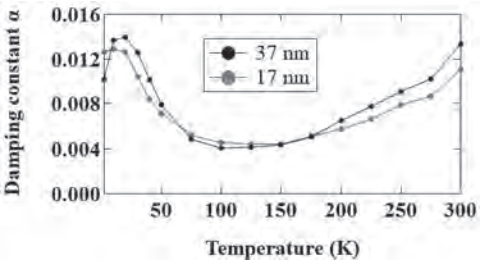

Fig. 2 Temperature dependence of the α of LSMO thin films.

FT-08. Exploring Interfacial Effects in Transition Metal Dichalcogenide / Ferrimagnetic Alloy Heterostructure. *L. Ramos*[1], D.A. Arena[1], A.I. Ojo[1], Y. Wadumesthri[1] and H. Rodríguez Gutiérrez[1] *1. Physics, University of South Florida, Tampa, FL, United States*

Ferrimagnetic materials and 2-dimensional transition-metal dichalcogenide (TMDs) materials have recently attracted attention as promising candidates for spintronics applications due to their tunable magnetic properties [1] and proximity effect [2], respectively. We are particularly interested in the magnetic behavior of the WSe_2/FeCoGd heterostructure system, as there is limited research on the effect of TMDs seed layer on the magnetic properties of FeCoGd. In this study, we explore the influence of film thickness and specific TMD substrates on the magnetic properties of amorphous ferrimagnetic FeCoGd alloy thin films. A set of FeCoGd thin films in the range of 4-32nm, with a composition of $Fe_{73}Co_8Gd_{19}$, were fabricated using the magnetron sputtering technique on various substrates: Si, Si/WSe_2 bilayer, and Si/WSe_2 monolayer. A 5 nm capping layer of Ta was deposited to protect the films from oxidation and contamination. Structural analysis via X-ray diffraction (XRD) confirmed the amorphous nature of the FeCoGd films, while energy-dispersive spectroscopy (EDS) verified their elemental composition. Raman spectroscopy was employed to investigate the chemical structure of the Si/WSe_2/FeCoGd, revealing the characteristic WSe_2 peak at ~250cm^{-1} and demonstrating that the sputtering process preserved the properties of the WSe_2 seed layer. Magnetic properties, assessed using a vibrating-sample magnetometer (VSM), indicated a significant dependence on film thickness and substrate. Our findings reveal a soft magnetic phase, in-plane magnetic anisotropy, and tunability of the saturation magnetization and coercive field of FeCoGd thin films with varying thickness and substrate, as shown in Figures 1a & 1b. Additionally, a proximity effect of WSe_2 on FeCoGd is observed where saturation magnetization and coercivity depend on the WSe_2 seed layer. These results demonstrate the potential of 2D WSe_2 and amorphous ferrimagnetic FeCoGd alloy thin film heterostructures for modifying the magnetic properties for spintronic device applications.

[1] K. Wang, L. Wu, Z. Xu, Z. Lu, R. Xiong, Extraordinary Hall effect of sputtered amorphous ferrimagnetic GdFeCo alloy films, Mater. Today Commun. 35 (2023) 106023 [2] N. Zibouch, A. Kuc, J. Musfeldt, T. Heine, Transition-metal dichalcogenides for spintronic applications, Ann. Phys. 526 (2014) 201400137

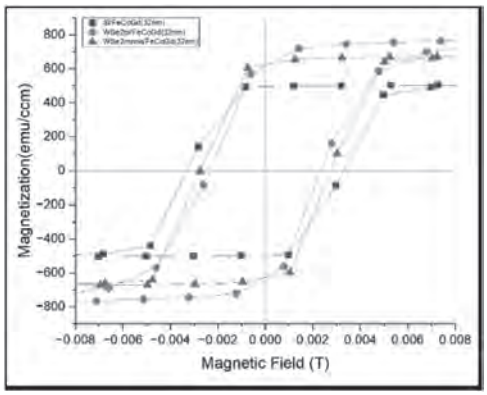

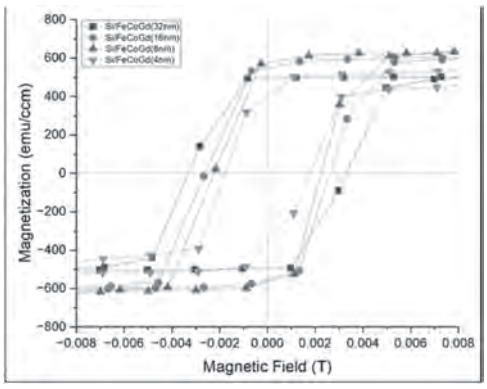

Session FU
MICROSCOPY, IMAGING, AND MAGNETIC CHARACTERIZATION I (Poster Session)

Sophie A. Morley, Chair
Lawrence Berkeley National Laboratory, Berkeley, CA, United States

FU-01. Modular Cryogenic Piezoelectric Scanner for Scanning SQUID Microscopy. *J. Bedard*[1], J.D. Franklin[1], Z. Ritchey[1], M. Roshdy[3], O.R. Bilal[3,4], M. Jain[1,2,4] and I. Sochnikov[1,2,4] *1. Department of Physics, University of Connecticut, Storrs, CT, United States; 2. Department of Material Science & Engineering, University of Connecticut, Storrs, CT, United States; 3. School of Mechanical, Aerospace, and Manufacturing Engineering, University of Connecticut, Storrs, CT, United States; 4. Institute of Material Science, University of Connecticut, Storrs, CT, United States*

Scanning Superconducting QUantum Interference Device (SQUID) microscopy uses the unparalleled magnetic flux sensitivity of SQUIDs to image magnetic, superconducting, and topological materials and devices [1]. Typical scanning SQUID microscopes utilize either commercial piezoelectric nano-positioners or lab-made "s-bender" scanners, named after the s-like motion of the piezoelectric bimorphs. The advantages of s-bender based scanners are large scanning areas and maintaining sample to sensor alignment. However, the design of these scanners results in a low resonate frequency, leaving measurements susceptible to vibrational noise [2,3]. Here, we designed and tested a cryogenic scanner based on modular sets of parallel piezoelectric bimorphs offering an alternative to s-benders. The modularity of the scanners allows replacements and alternative experimental configurations. The device was installed in a dilution refrigerator and has a scan range of 160μm at 20mK without noticeable heating or vibration effects. The scanner's capabilities are demonstrated by scanning SQUID images of magnetic domains in a $EuTiO_3$ thin film. Our design ensures precise orthogonal motion along x-y-z motion with no sensor tilting, while providing additional stiffness to reduce the impacts of vibrations. The scanner could find applications in a variety of scanning probe microscopes or techniques that require a large-range nano positioning, especially at low temperatures. Distribution A. Approved for public release: distribution unlimited. (AFRL-2024-3423) Date Approved 06-27-2024

[1] E. Persky, I. Sochnikov, B. Kalisky, Annual Review of Condensed Matter Physics 13, 385-405 (2022). [2] J. Siegel, J. Witt, N. Venturi, S. Field, Review of Scientific Instruments 66, 2520-2523 (1995). [3] G. Björnsson, B. Gardner, J. Kirtley, K. Moler, Review of Scientific Instruments 72, 4153-4158 (2001).

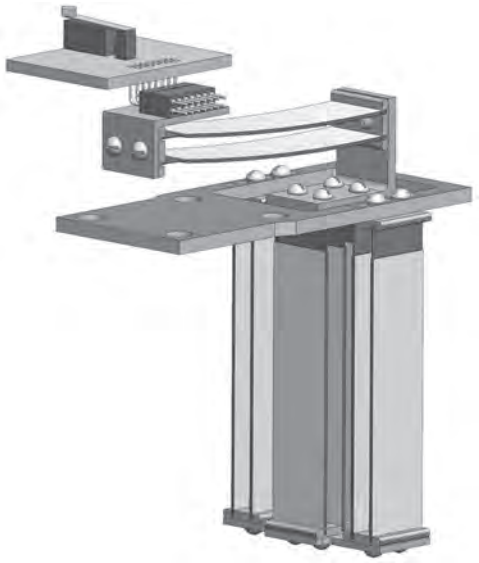

Fig.1 CAD model of the modular cryogenic scanner.

FU-03. Nondestructive Ferromagnetic Resonance as a Tool to Evaluate Quality in Samples with Perpendicular Magnetic Anisotropy. *A. Harpel*[1], M. Anas[2], A. Wege[2], R. Franklin[2] and B. Stadler[2,1] *1. Chemical Engineering and Materials Science, University of Minnesota, Minneapolis, MN, United States; 2. Electrical and Computer Engineering, University of Minnesota, Minneapolis, MN, United States*

Samples with perpendicular magnetic anisotropy (PMA) are particularly popular today for various computing and spintronic applications [1], [2], [3], [4], but to make the transition from research labs to industry, tight quality control is needed. However, because many measurements have factors such as porosity and magnetization that scale together (e.g.: measurements of total sample magnetization), there is a dearth of quick, non-destructive, low-cost methods to effectively quantify quality. Here, to create a wide range of controlled samples with perpendicular magnetic anisotropy, MNWs were fabricated in anodized aluminum oxide templates [5]. The deposition quality is evaluated by common, but qualitative or semi-quantitative methods, which are then compared to the quantitative values for fill factor (FF) and saturation magnetization (M_S) measured using a nondestructive ferromagnetic resonance (FMR) method. Of note, seeding Co MNWs with Cu before fabrication is shown to improve FF while maintaining MNW quality, demonstrating that this method has a sensitivity to FF and M_S that allows for measurement differentiation at practicable values. For the seeded sample, FMR measured FF at 12.3 ± 0.4 %, with a M_S of 1.64 ± 0.10 T. For the sample without a seed, FMR measured FF at 9.0 ± 0.4% with a M_S of 1.62 ± 0.13 T. These quantitative measurements were corroborated by all the qualitative and semi-quantitative results, indicating that nondestructive FMR is a viable method to quantify fill factor and quickly evaluate the quality of templated MNWs. Importantly, fill factor (or sample porosity) and magnetization can be separately analyzed by this method.

[1] D. Apalkov, B. Dieny, and J. M. Slaughter, *Proc. IEEE*, vol. 104, no. 10, pp. 1796–1830, (2016). [2] B. Dieny and M. Chshiev, *Rev. Mod. Phys.*, vol. 89, no. 2, p. 025008, (2017). [3] I. Tudosa, J. A. Katine, S. Mangin, and E. E. Fullerton, *IEEE Trans. Magn.*, vol. 46, no. 6, pp. 2328–2330, (2010). [4] J. J. Bauer *et al.*, *Adv Elect Materials*, vol. 6, no. 1, p. 1900820, (2020). [5] L. Sun, Y. Hao, C.-L. Chien, and P. C. Searson, *IBM J. Res. & Dev.*, vol. 49, no. 1, pp. 79–102, (2005).

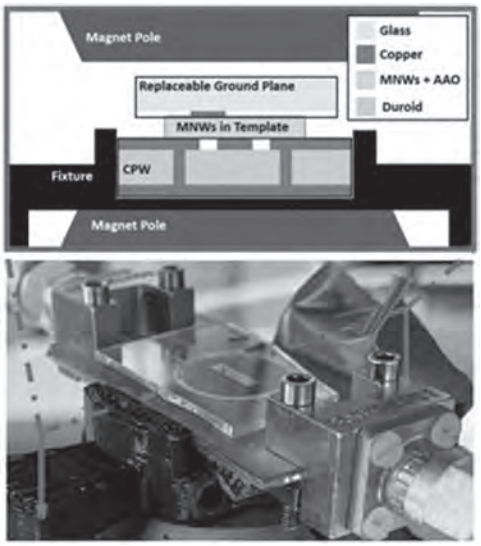

Fig. 1: Nondestructive FMR measurement setup

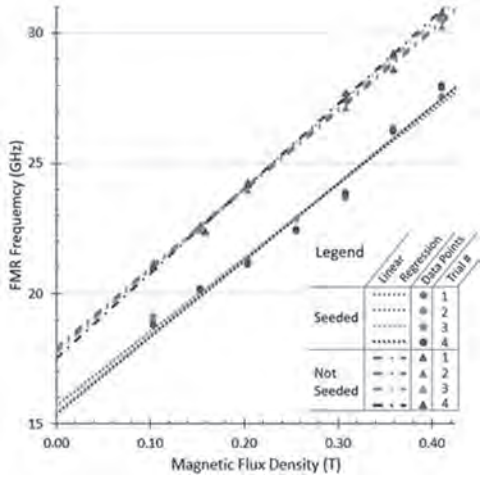

Fig. 2: Results comparing the FMR response of templated Co MNWs are shown for the cases with and without a Cu seed layer.

FU-04. Estimation of Rebar Corrosion Level using Magnetic Sensor Array with Convolutional Neural Network. *Y. Ogata*[1,2], T. Yanagida[1], B. Kakinuma[1] and K. Kobayashi[2] *1. Advantest Laboratories Ltd., Sendai, Japan; 2. Graduate School of Science and Engineering, Iwate University, Morioka, Japan*

The deterioration of reinforced concrete structures caused by rebar corrosion is a serious problem. Non-destructive testing to detect rebar corrosion at an early stage has shown promise [1], particularly eddy current-based methods utilizing excitation coil [2]. However, no research has measured the 3-axis magnetic signal over a wide spatial range around the coil. In this study, we therefore compared the magnetic signal of the sensor above the coil with that of a sensor distant from the coil using a 3-axis 100-channel (10×10) magnetic sensor array. We also utilized a convolutional neural network (CNN) [3] to estimate the corrosion level of a rebar whose depth is unknown. Four types of corroded rebar were prepared: Rebar A (no corrosion) and Rebars B, C, and D (6, 12, and 24 hours of electrolytic corrosion, respectively). A coil with an 80-Hz current flow was placed below the sensor on the center of the array, and rebars were positioned below the coil. The X- and Z-axes correspond to the longitudinal direction of the rebar and the normal direction of the coil. Measurements were performed ten times after rotating the rebars a few degrees. Figure 1 shows the magnitude amplitude of 3-axis sensors when the rebar depth was 40 mm. When the sensor was above the coil, amplitude variance was large, and when it was 80 mm away, amplitude was clearly separated into the four types of rebar. This finding indicates that rebar corrosion is easier to detect by measuring the magnetic signal over a wide spatial range. Next, we trained a CNN using the amplitude when the rebar depths were 20, 25, 30, 40, and 50 mm and evaluated its accuracy using the amplitude when depths were 22, 27, 32, 35, 37, 42, 45, and 47 mm. As shown in Fig. 2, the average accuracy of the 3-axis input data was better than that the single axis, which means that estimation of rebar corrosion is possible even if the rebar depth is unknown. Overall, our findings demonstrate that multi-axis and multi-array magnetic measurements are effective in estimating rebar corrosion.

[1] R. Rodfigues, S. Gaboreau, J. Gance, et al., Construction and Building Materials, Vol. 269, 12140, (2021) [2] D. F. He, S. Takaya, N. Tsutsumi, et al., 2019 PhotonIcs & Electromagnetic Research Symposium Spring, (2019) [3] J. Gu, Z. Wang, J. Kuen, L. Ma, et al., Pattern Recognition, Vol. 77, pp. 354-377, (2018)

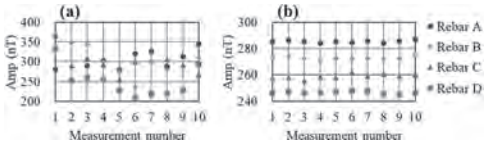

Fig. 1. Magnitude of (a) sensor above coil and (b) sensor 80 mm away from coil.

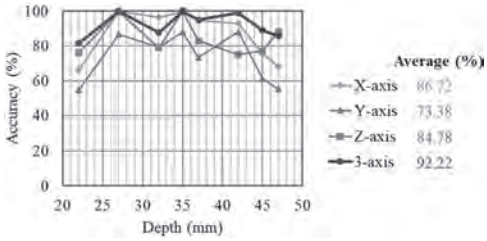

Fig. 2. CNN accuracy of 4 types of input data.

FU-05. In-situ correlative facility for advanced magnetic materials. *S. Ruiz Gómez*[1], A. Arché[1], W. Khaliq[1], A. Garcia de Herreros[1], N. Bagués[1] and L. Aballe[1] *1. ALBA Synchrotron, Barcelona, Spain*

ALBA Synchrotron is developing tools open to all the scientific community for research in advanced magnetic materials in order to address the scientific challenges of fields like spintronics, 2D materials or green energies. New instruments to be installed in the ALBA premises are a high resolution (scanning) transmission electron microscope for in situ studies including gas, liquid, temperatures and bias environments. Complementary to this new high resolution electron microscopes, we are carrying out the adaptation of existing beamlines (PEEM, TXM, XAS, XRD) to perform correlative experiments. Compatible operando sample environments for complementary characterization tools together with advanced data analysis will provide excellent opportunities for true multi-modal and multi-length scale characterization of magnetic materials. While (S)TEM microscopies offer unsurpassed spatial resolution and a variety of contrast mechanisms, X-ray-based techniques provide highly specific chemical, structural, electronic and magnetic information with high efficiency so that larger fields of view, thicker samples

and faster processes can be studied. This works reviews the available techniques at ALBA Synchrotron, showcasing examples that demonstrate how the integration of multiple imaging approaches not only facilitates the study of complex magnetic systems but also opens avenues for the potential characterizations of in-operando devices.

[1] https://www.cells.es/en/instrumentation [2] https://www.cells.es/en/instrumentation/incaem

FU-06. Withdrawn

FU-07. Characterization of Magnetic Core-Shell Nanoparticles in Carbon Matrices. *V. Pena Perez*[1], C.R. Gonzalez[1], E. Villegas[1], J. Baughman[1], F. Iglesias[1], A. Khodagulyan[1], O. Bernal[1] and A.N. Kocharian[1] *1. Department of Physics and Astronomy, California State University Los Angeles, Los Angeles, CA, United States*

This article presents a comprehensive study on the synthesis and characterization of metallic magnetic and non-magnetic nanoparticles, including Iron, Copper, Nickel, Zinc, Cobalt, and Ferrocene, and their enhanced magnetic properties. The research delves into the nanostructure images and size-dependent properties of these nanoparticles, utilizing techniques such as powdered X-ray diffraction (PXRD), scanning electron microscopy (SEM), and high-resolution transmission electron microscopy (HR-TEM) for detailed size and structural analysis. A novel algorithm is introduced for the accurate morphological analysis of these nanoparticles, focusing on their crystallinity and amorphous regions. The figure below of the magnetic measurements for FePc indicates to be the most saturated, whereas FeTCPP seems the most coercive. NiTPP seems to be the midpoint showing average saturation and coercivity, and CuTPP seems to be the least responsive to magnetic behavior. The study establishes a correlation between the structural properties using data SEM and HR-STEM images and magnetic characteristics of the nanoparticles, as assessed through physical property measurement system (PPMS) and electron paramagnetic resonance (EPR). The findings underscore the significance of advancing the magnetic properties of graphene itself and in synthesis of magnetic nanoparticles in carbon matrix for biomedicine applications, offering new perspectives for future research in nanotechnology and materials science. This work is supported by grants from the American National Science Foundation, catsus grant No. HRD-1547723 and No. HRD-2112554, as well as the National Institute of Health, grant No. T34-GM08228.

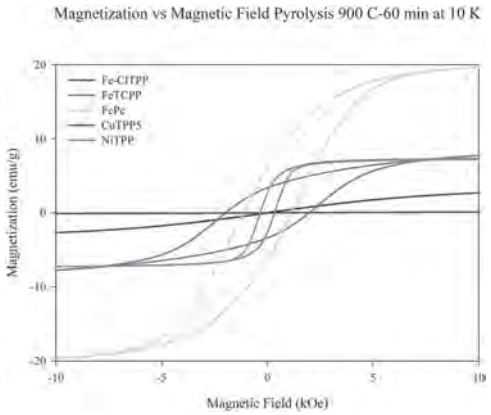

Figure 1

Session FV
MAGNETIC ASPECTS RELATED TO ELECTROMECHANICAL CONVERSION, TRANSFORMERS AND INDUCTORS (Poster Session)

Johannes JH Paulides, Chair
Advanced Electromagnetics Group, Waalwijk, Netherlands

FV-01. Influence of Particle Size and Fabrication Conditions on Magnetic Properties of Dust Cores Composed of Iron Powders. *Y. Kodama*[1], S. Ajia[1], T. Miyazaki[2], S. Muroga[1] and Y. Endo[1,3] *1. Graduate School of Engineering, Tohoku University, Sendai, Japan; 2. Faculty of Engineering, Tohoku University, Sendai, Japan; 3. Center for Science and Innovation in Spintronics, Tohoku University, Sendai, Japan*

Recently, passive devices such as inductors, transformers, and so on, are required to downsize and reduce the iron loss[1], and so the development of soft magnetic materials used in these devices with higher saturation magnetic flux density and lower iron loss are necessiated. Dust cores have attracted much attention as one of the candicates for these materials because of their high saturation magnetic flux density and high electrical resistance[2]. Herein, we fabricated the dust cores composed of spherical shaped iron powders with median sizes (D_{50}) of 9.3, 12.0 and 39.4 mm, and investigated their structures, electrical properties, and magnetic one. We also systematically evaluated magnetic properties of the dust cores with various resin contents and annealing temperatures, and discussed the most suitable fabirication conditions of dust cores. Fig. 1 shows relationships between the core losses per one cycle at the maximum flux density of 100 mT and the frequency of 100 kHz and D_{50} of powders for the dust core with various resin contents. The dynamic loss (P_{dyn}/f) lowered with the decrease of D_{50}, which might be attributed to the suppression of the eddy current loss by the smaller cross-sectional area. As for the resin contents, in case of all D_{50}, the hysteresis loss (P_{hys}/f) lowered as resin contents were decreased. This is because the gaps between the particles became narrower and the core density increased as the resin contents were decreased. On the other hand, P_{dyn}/f was independent of resin contents at Core A and B. This indicates that the eddy current loss between particles can be suppressed in the dust cores with the resin content of approximately 0.3 wt%. Therefore, these results suggest that iron loss of the dust core can reduce by modifying the particle size and the fabrication conditions. This work was supported in part by MEXT Program for Creation of Innovative Core Technology for Power Electronics Grant Number JPJ009777. This work was also supported in part by CSIS, CSRN, and CIES, Tohoku University.

[1] J. Biela, U. Badstubner, J.W. Kolar, IEEE Transaction on Power Electronics, Vol. 24, p. 288 (2009) [2] H. Shokrollahi, K. Janghorban, Journal of Materials Processing Technology, Vol. 189, p. 1 (2007)

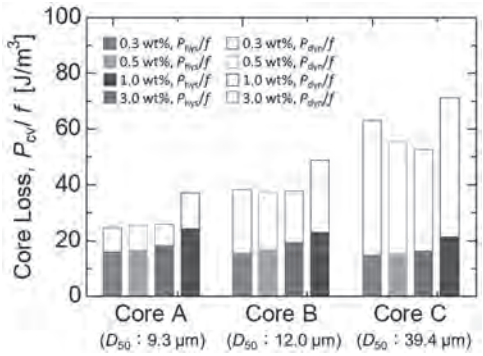

Fig. 1 Relationships between the core losses per one cycle at the maximum flux density of 100 mT and the frequency of 100 kHz and the median size of powders for the dust core with various resin contents.

FV-02. Development of dual-spring linear resonant actuator for improved haptic performance. *K. Park*[1], Z. Jiang[1], Y. Oh[1], Y. Jung[1] and S. Hwang[1] *1. Mechanical Engineering, Pusan National University, Pusan, The Republic of Korea*

With the rapid development of the electromagnetic industry, improving the haptic performance has become a crucial aspect to consider in smartphones, automobiles, and haptic controllers that are used frequently. Currently, haptic controllers have transitioned from eccentric rotating mass motors (ERMs) to linear resonant actuators (LRAs) owing to their fast response times, long lifetimes, and low power consumption compared with those of ERMs. However, the limited space of 10 × 10 × 10 mm hinders the achievement of sufficient acceleration and displacement control. Therefore, this study proposes a new type that has a smaller displacement and higher acceleration performance than the prototype while maintaining the same size and resonance frequency. An electromagnetic–mechanical (E–M) coupling method was employed to analyze the LRA. The acceleration and displacement were analyzed using the E–M coupling method. Fig. 1 shows schematics of the prototype and new type. The main differences between the prototype and new types are in the spring and shaft. The prototype uses one spring, one mass (tungsten), and one shaft for control and provides stability to the system. However, the new type uses two springs and two masses without a shaft. This design allows for a larger moving mass and permanent magnet compared with the prototype. Additionally, the system is more stable. This approach enables a higher acceleration performance and improved displacement control. The force factor is a critical parameter in E–M coupling; it is defined as the product of the magnetic flux density on the coil (B) and total coil length (L). It was calculated as 0.835 N/A and 1.015 N/A for the prototype and new type, respectively. Fig. 2 shows the displacement and acceleration of the prototype and new type. The new type achieved a 0.3 mm decrease in displacement and 0.35 G increase in acceleration at an same resonance frequency compared with the prototype. The samples are currently being fabricated; the acceleration and displacement will be measured using experimental equipment. These results will be included in the full paper.

Jiang. Z.X, 'Design and Analysis of Wide-bandwidth Actuator for Haptic Controller With Novel Magnetic Circult', IEEE Transcation on Magnetics, Vol. 59, Issue. 12 (2023)

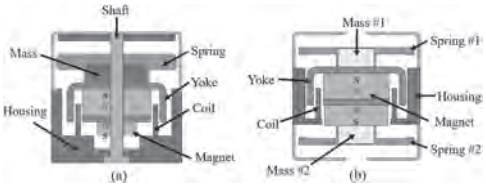

Fig. 1 Design comparison: (a) prototype, (b) new type.

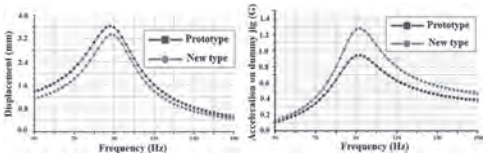

Fig. 2 Comparison of: (a) displacement, (b) acceleration.

FV-03. Loss estimation for toroidal cores composed by electrolytic iron powder based on machine learning. *S. Muroga*[1], S. Ajia[1], Y. Kodama[1], S. Matsumoto[2] and Y. Endo[1,3] *1. Graduate School of Engineering, Tohoku University, Sendai, Japan; 2. School of Engineering, Tohoku University, Sendai, Japan; 3. Center for Science and Innovation in Spintronics, Tohoku University, Sendai, Japan*

Toroidal cores composed of soft magnetic powders have been investigated to realize next-generation high-frequency passive components [1]. These cores possess high saturation magnetic flux density but generate large losses in the high-frequency range. Reducing core loss is one of the major challenges because it is necessary to simultaneously consider multiple complex parameters [2-4]. In this study, a method for estimating AC losses using variables including process conditions was investigated for developing design guidelines. Nine types of magnetic cores [4] with different shapes of electrolytic iron powders, different process conditions were used for evaluation. Fig. 1 shows an overview of the AC loss estimation method using a regressor. The objective variables were set to AC loss, which was calculated from the area of the hysteresis loop measured by a B-H analyzer. The explanatory variables were set to the amplitude and frequency of the applied flux density of the B-H analyzer, the pressure and heat treatment temperature during core fabrication, the measured resistivity of the core, etc. In addition, the principal component scores extracted from the magnetization curves and the dimension-reduced information from the magnetization curves were used. The total number of data was 354; 75% were used to train regressors based on Lasso, Random Forest, and Gaussian Process models. 25% were used for testing. As a result of the training, the AC loss was expressed as a function using variables such as the applied flux density, frequency, and annealing temperature. Fig. 2 shows an example of the Lasso regression results. The coefficient of determination was 0.96, indicating high accuracy. The results demonstrate the usefulness of this method for the design of low-loss powder cores. This work was supported in part by MEXT-Program for Creation of Innovative Core Technology for Power Electronics (JPJ009777); MEXT-Data Creation and Utilization-Type Material Research and Development Project (JPMXP1122715503); RIEC, CSIS, CSRN, and CIES, Tohoku University; Tohoku University-NICT Research Support Project.

[1] H. Shokrollahi, K Janghorban, "Soft magnetic composite materials (SMCs)," J. Mater. Process. Technol., vol. 189, no. 1-3, #6, 2007. [2] T. Takashita, N. Nakamura, Y. Ozaki, "Influence of Particle Shape on Microstructure and Magnetic Properties of Iron Powder Cores," Mater. Trans., vol. 57, no. 11, pp. 1859-1867, 2016. [3] T. Saito, H. Tsuruta, A. Watanabe, T. Ishimine, T. Ueno, "Pure-iron/iron-based-alloy hybrid soft magnetic powder cores compacted at ultra-high pressure," AIP Advances, vol. 8, no. 4, 2017. [4] Y. Kodama, P. Nguyen, T. Miyazaki, Y. Endo, "Study on Magnetic Properties of Toroidal Cores Composed by Electrolytic Iron Powder with Different Shapes," IEEE Trans. Magn., vol. 59, no. 11, pp. 1-5, Art. no. 6100505, 2023.

An overview of the AC loss estimation method.

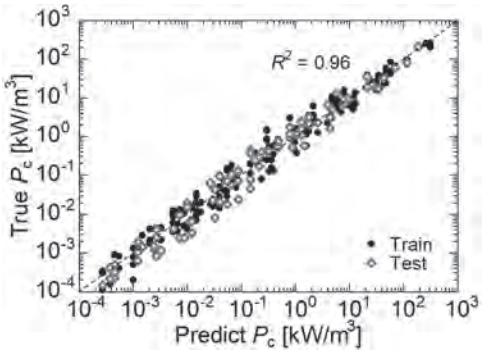

Fig.2 Examples of estimation result (Lasso regression).

FV-06. Novel Zero-Sequence Current Excited Double-Sided Vernier Reluctance Linear Machine with High-Order -Harmonic Toroidal Winding. Z. Li[1], *F. Ni*[1] and S. Niu[1] *1. Department of Electrical and Electronic Engineering, The Hong Kong Polytechnic University, Hong Kong, Hong Kong*

Double-sided vernier reluctance linear machine (DS-VRLM) is suitable for long stroke applications, taking advantages of magnet-free design, eliminated magnetic pull and high thrust force density. Aiming to eliminate the DC coils in DS-VRLM, and further boost the thrust force density of it, a novel integrated non-overlapped toroidal winding design excited by zero-sequence current utilizing high-order harmonic of excitation magnetic field is proposed. The key to achieve it is instead of using DC winding to provide field excitation, the proposed machine is driven by integrated toroidal winding whose field excitation is generated by zero-sequence current. Fig.1.(a) shows the winding configuration of newly proposed DS-VRLM. Two coils in the same phase are arranged in the same slot but divided into winding 1 and winding 2, which have different polarities of zero-sequence current. Fig. 1.(b) illustrates the speed control scheme for the proposed DS-VRLM. According to the special arrangement of equivalent field current, which is distributed alternatively every two slots as shown in Fig.1, higher-order harmonics of field current, especially third-order harmonic, could be utilized to generate working harmonics [1]. Taking machine with 12/7 slot/pole combination as example, the gear ratio of the working harmonic can be improved from 1.75 to 3.5 compared with machine using conventional fundamental harmonic. To illustrate the advantages of the proposed design, the proposed machine is also compared with 12/10 full-pitched variable flux reluctance linear machine (VF-RLM), and switched reluctance linear machine (SRLM) [2] under the same copper loss (240W) and dimension (initial design parameter) for fair comparison. As shown in Fig.2, the VF-LRM could achieve lowest force ripple (3.76% at rated condition) but also with the lowest output thrust force in average (67.34N). The proposed design could obtain approximately the same output force (133.7N) as SRLM (144.3N), but with much lower force ripple ratio (27.5%) than SRLM at different excitation conditions.

[1] Z. Li, X. Zhao and S. Niu, "Novel High-Order-Harmonic Toroidal Winding Design Approach for Double-Sided Vernier Reluctance Linear Machine," in IEEE Transactions on Industrial Electronics [2] J. Du, D. Liang and X. Liu, "Performance Analysis of a Mutually Coupled Linear Switched Reluctance Machine for Direct-Drive Wave Energy Conversions," in IEEE Transactions on Magnetics, vol. 53, no. 9, pp. 1-10, Sept. 2017, Art no. 8108110.

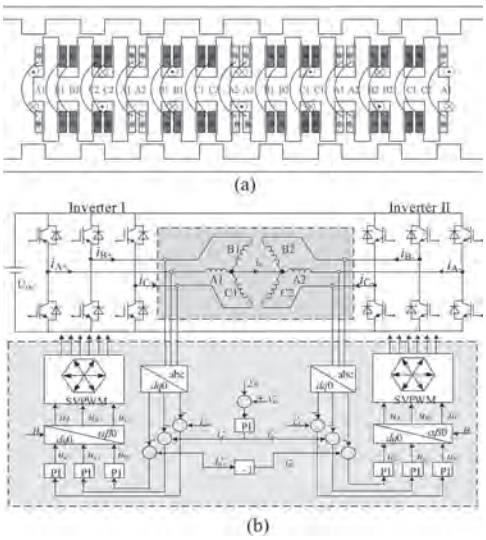

Fig. 1. The proposed DS-VRLM. (a) Winding configuration. (b) Control scheme.

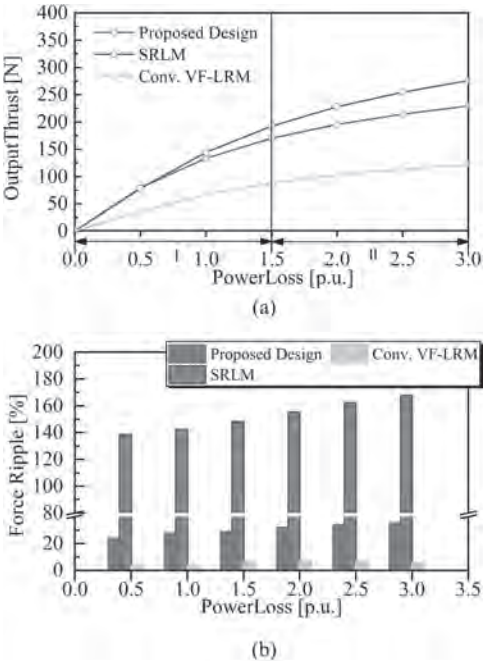

Fig. 2. Result of simulation (a) The average force. (b) Thrust force ripple

FV-07. Novel Transverse-Flux Tubular Linear Reluctance Machine with Dynamic DC-Saturation-Relieving Function. Z. Li[1], *F. Ni*[1] and S. Niu[1] *1. Department of Electrical and Electronic Engineering, The Hong Kong Polytechnic University, Hong Kong, Hong Kong*

Due to variable DC saturation under different load conditions, the DC-saturation issue cannot be perfectly addressed with constant PM (CPM) when the motor is overloaded, causing serious leakage flux in the air gap. The low coercivity PM (LC-PM) is known as memory material, whose magnetic status is relatively easy to change via pulsing magnetizing current (PMC) [1]. LC-PM has been proven effective for dynamic PM excitation adjustment in PM synchronous machines for a wider speed range, but its effectiveness in relieving DC saturation is less discussed. This paper presents a novel transverse-flux tubular linear reluctance machine (TF-TLRM) with dynamic DC-relieving ability. It employs low-coercivity permanent magnets (LC-PMs) in the stator slots instead of rare-earth magnets. The single-phase topology of the proposed TF-TLRM is presented in Fig.1.(a). The motor's mover consists of three separate stator parts. One mover core has 12 teeth wound alternately with armature coils, field coils, and magnetizing coils, as shown in Fig. 1(b). The parts for phases B and C are aligned with phase A, with a distance of $2kt+2/3t$, where k is an integer, and t is the pole pitch of the motor. The stator is composed of the laminations with stack thickness of t, and switched by 60 mechanical degrees every t distance. The hysteresis model in Fig. 1(c) intuitively demonstrates the operation points of the LC-PMs, which can be determined by magnetic field intensity H_{mk} and the load line together. In coordinate with different excitation modes, the operation points of the slot PM can be switched among P_1, P_2, and P_3 by applying magnetizing/demagnetizing current. The performance and validity of the proposed design are verified and compared with design with CPM, which are illustrated in Fig. 2. The overload capability of the proposed design is furtherly improved about 36.2% and detent force ripple is reduced by 53.8% under over-load condition.

[1] H. Yang, H. Zheng, and Z. Q. Zhu, "Comparative Study of Partitioned Stator Memory Machines with Series and Parallel Hybrid PM Configurations," IEEE Transactions on Magnetics, vol. 55, no. 7, pp. 1-8, 2019.

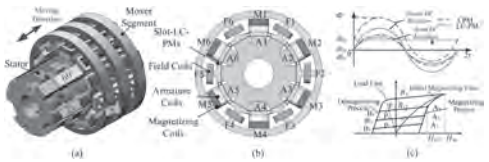

Fig. 1. The proposed TF-TLRM. (a) Three-dimensional assembling diagram. (b) Cross-sectional view. (c) Dynamic DC-relieving mechanism.

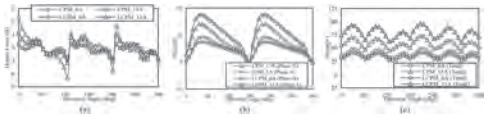

Fig. 2. Performance comparison. (a) Detent force. (b) Output thrust of phase A. (c) Thrust of three phases.

FV-08. Fundamental Study of Factors Leading to Performance Variations in Cancellation Coil Systems for Wireless Power Transfer. *M. Yokosawa*[1], F. Sato[1], S. Miyahara[1], H. Matsuki[2], K. Inada[3], T. Abe[3] and S. Sasaki[4] *1. Tohoku Gakuin University, Sendai, Japan; 2. Tohoku University, Sendai, Japan; 3. NITTOKU, Saitama, Japan; 4. Hikaridenshi, Osaki, Japan*

In recent years, factory automation (FA) has been attracting attention from the viewpoints of labor cost reduction and efficiency improvement. Automated guided vehicles (AGVs) are used to transport and tow loads, and their use is increasing. However, the current charging methods, plug-in and battery replacement systems, are not efficient enough because of the non-operating time and the need to manually replace batteries. Sometimes, a wireless power supply is used while the AGV is stopped, but the configuration must be such that the AGV remains in place. To improve work efficiency, we have adopted a "non-contact power supply system on the move" to supply power during work or while the machine moves. In this system, a power transmission device is installed in the moving range of the AGV, so that power can be supplied simply by passing in the vicinity of the AGV. Because of the characteristics of this system to stably supply power over a long section, the transmission coils are long, and the leakage magnetic field becomes large, especially in places where there is no power receiving device facing it, because there is nothing to obstruct the magnetic field. For industrial use, electromagnetic noise to peripheral devices must be suppressed to a certain value. Therefore, we studied a system that can feed power while reducing the leakage of magnetic field using electromagnetic field simulation. Fig. 1 shows a diagram of the installation of the power transmission coils and cancellation coils. Fig. 2 shows a graph of the leakage magnetic field measured at different distances. In this study, various factors that affect the performance of the cancellation coil system are examined through simulations and actual measurements. The factors will include the presence or absence of coils on the receiving side, the use of ferrite tiles, and the size of the power transmission section.

[1]M. Yokosawa, H. Kojima, S. Miyahara., "Study on the characteristics of power transmission side of leaky magnetic field canceling coil for non-contact power transfer while in operation,". AIP Advances 2024; 13, 025231. [2] A. Mahesh, B. Chokkalingam, L.Mihet-popa, "Inductive Wireless Power Transfer Charging for Electric Vehicles–A Review" IEEE, Access, Volume:9, 137667-137713, (2021) [3]Brain. S, and, other "Optimisation of Magnetic Material Placement in IPT PAD for EV Charging " 2022 Wireless Power Week (WPW), (2022) [4] Y. Ota, T. Takura, F. Sato., "Wireless Power Transfer by Low Coupling Electromagnetic Induction-LC booster" 2012 IEEE, MTT-S International Microwave Workshop Series on Innovative Wireless Power Transmission: Technologies, Systems, and Applications (IMWS-IWPT 2012) Proceedings, pp. 175-178, 2012 [5]AOKI Syuta, and other: "Reduction of Leakage Electromagnetic Field from Feeding Coil for Contactless Charging System for Moving Electric Vehicle", IEICE technical report 115(82),43-48,(2015)

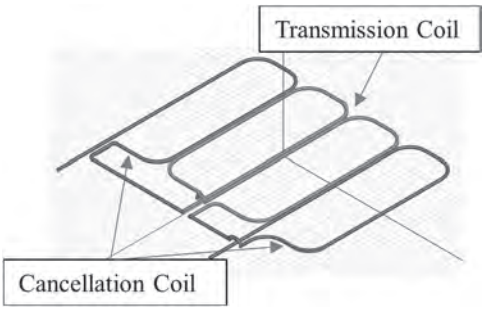

Fig.1 Arrangement of power transmission coils and cancellation coils

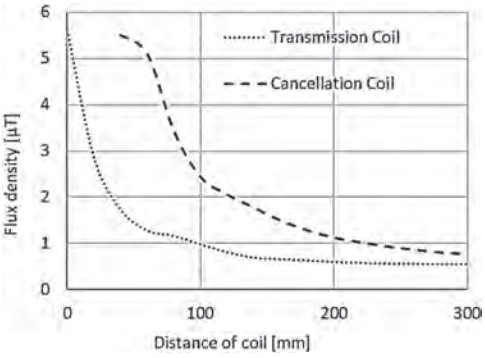

Fig.2 Comparison of leakage magnetic field between conventional feeding system and cancellation coil system

Session FA
IMAGING NANOSCALE MAGNETIZATION DYNAMICS AND SPIN FLUCTUATIONS

Peter Fischer, Chair
Lawrence Berkeley National Laboratory, Berkeley, CA, United States
Sujoy Roy, Co-Chair
Lawrence Berkeley National Laboratory, Berkeley, CA, United States

INVITED PAPERS

FA-01. Time-Resolved Magnetic Imaging Using Electrons and Extreme-Ultraviolet Photons. *C. Ropers[1,2] 1. Ultrafast Dynamics, MPI-NAT, Göttingen, Germany; 2. University of Göttingen, Göttingen, Germany*

Time-resolved and *in-situ* experimental techniques are essential in the mapping of non-equilibrium spin structures and dynamics. This talk will discuss the development and application of two complementary approaches to ultrafast nanoscale magnetic imaging, based on spatially coherent sources of pulsed electrons and photons. Specifically, Fresnel-mode Lorentz microscopy is applied in the study of current-driven vortex dynamics and pinning [1], as well as in the imaging of laser-created skyrmions and antiskyrmions [2]. Furthermore, ultrafast high-harmonic microscopy [3] provides element-specific imaging of spin textures with combined femtosecond temporal and sub-20 nm spatial resolutions. Using this technique, high-contrast maps of domain wall dynamics yield stringent limits on phenomena such as domain wall broadening and motion upon ultrafast laser demagnetization [4].

[1] M. Möller et al., Phys. Rev. Research 4 013027 (2022). [2] T. Titze, M. Möller et al. (unpublished (2024). [3] S. Zayko et al., Nat. Comm. 12, 6337 (2021). [4] H.-T. Chang. S. Zayko et al., unpublished (2024).

FA-02. Neutrons and Skyrmions: Unraveling the Spin-tastic Mysteries of Magnetic Materials. *L. DeBeer-Schmitt[1] 1. Neutron Science Division, Oak Ridge National Laboratory, Oak Ridge, TN, United States*

Neutron scattering, particularly small-angle neutron scattering (SANS), is a powerful tool for probing material structural and magnetic properties. This presentation will showcase its application in studying magnetic skyrmions and other long-range magnetic ordering. For applications, Skyrmion-based devices will require materials that can host these magnetic spin textures at ambient conditions (i.e. zero applied magnetic field and at room temperatures and above). Amorphous Fe/Gd multilayer thin films are one way to reach this goal. Recently, we have demonstrated the use of SANS, and later SAXS, to investigate the dynamic behaviors of skyrmions in Gd/Fe multilayers under microwave excitations, uncovering complex structure in the spin waves and providing insights into their nanoscale dynamics. These findings highlight the versatility of SANS in exploring both static and dynamic magnetic phenomena.

Ryan D. Desautels, Lisa DeBeer-Schmitt, Sergio A. Montoya, Julie A. Borchers, Soong-Geun Je, Nan Tang, Mi-Young Im, Michael R. Fitzsimmons, Eric E. Fullerton, and Dustin A. Gilbert, "Realization of ordered magnetic skyrmions in thin films at ambient conditions", Phys. Rev. Materials 3, 104406 – Published 10 October 2019 W. L. N. C. Liyanage, Nan Tang, Lizabeth Quigley, Julie A. Borchers, Alexander J. Grutter, Brian B. Maranville, Sunil K. Sinha, Nicolas Reyren, Sergio A. Montoya, Eric E. Fullerton, Lisa DeBeer-Schmitt, and Dustin A. Gilbert, "Three-dimensional structure of hybrid magnetic skyrmions determined by neutron scattering ", Phys. Rev. B 107, 184412 – Published 5 May 202 N. Tang, W. L. N. C. Liyanage, S. A. Montoya, S. Patel, L. J. Quigley, A. J. Grutter, M. R. Fitzsimmons, S. Sinha, J. A. Borchers, E. E. Fullerton, L. DeBeer-Schmitt, D. A. Gilbert, Skyrmion-Excited Spin-Wave Fractal Networks. Adv. Mater. 2023, 35, 2300416. https://doi.org/10.1002/adma.202300416

FA-03. Time resolved scanning Kerr microscopy: a flexible probe of magnetization dynamics for challenging sample environments. *R. Hicken[1] 1. Physics and Astronomy, University of Exeter, Exeter, United Kingdom*

Time resolved scanning Kerr microscopy is a highly flexible tool for the investigation of spatially resolved magnetization dynamics. With femtosecond laser sources readily available, a variety of resonant and non-resonant magnetic processes may be accessed through stroboscopic measurements, with temporal resolution limited by the pulse duration and the timing jitter between the optical probe and the pump mechanism. Typically, the optical probe is focused to a small diameter stationary spot using a high numerical aperture microscope objective, with the sample or device structure mounted on a translation stage so that its position can be scanned to form a time resolved image. This approach has enabled the detection of precessional dynamics within microscale elements, imaging of confined spin wave excitations, and observation of collective modes of nano-element arrays [1], in response to excitation by pulsed magnetic fields. Use of phase-locked microwave excitations enables measurements of time domain ferromagnetic resonance (FMR) [2], spin-orbit torque (SOT)-FMR [3], and spin transfer oscillators in an injection-locked state [4], while enhanced spatial resolution can be obtained through incorporation of an atomic force microscope with a plasmonic antenna at its tip [5]. However, the standard measurement configuration is difficult to implement in environments where variable temperature and/or large AC and DC magnetic fields are required. Instead, it has been found that beam scanning using galvanometer mirrors provide an effective solution, and that depolarization of the moving beam on the curved optical surfaces may be overcome. The efficacy of this approach is demonstrated in a microscope that can image the high frequency magnetization dynamics of magnetic nanoparticles (MNPs) within biological tissue that are implanted to induce magnetic hyperthermia [6]. A typical image is shown in Figure 1 in which cells have been incubated with MNPs that tend to aggregate within intra-cellular lysosomes. Dynamic hysteresis loops may be recorded at selected positions to understand how the magnetic response is affected by the local environment. Kerr microscopy is also ideally suited to the study of flakes of few-layer van der Waals bonded material at low temperature, with all-optical switching being demonstrated in WSe_2/CrI_3 bilayers [7]. Most recently, a beam scanning microscope that incorporates a fixed optical pump beam has been constructed to explore the underlying magnetization dynamics of flakes that are just a few μm in lateral size, at low temperatures and high fields within a superconducting magnet system [8]. Figure 2 shows the time resolved response of two $Cr_2Ge_2Te_6$ flakes where the time dependence of the optically induced demagnetization and subsequent remagnetization is strongly dependent upon the flake thickness.

1. V. V. Kruglyak, P. S. Keatley, A. Neudert et al., Phys. Rev. Lett. 104, 027201 (2010) 2. P. S. Keatley, P. Gangmei, M. Dvornik et al., Phys. Rev. Lett. 110, 187202 (2013) 3. P. S. Keatley, K. Chatzimpaloglou, T. Manago et al., Appl. Phys. Lett. 118, 122405 (2021) 4. T. M. Spicer, P. S. Keatley, M. Dvornik et al., Appl. Phys. Lett. 113, 192405 (2018) 5. P. S. Keatley, T. H. J. Loughran, E. Hendry et al., Rev. Sci. Instrum. 88, 123708 (2017) 6. M. E. Sharifabad, R. Soucaille, X. Wang et al., ACS Nano 18, 5297 (2024) 7. M. Dabrowski, S. Guo, M. Strungaru et al., Nature Commun. 13: 5976 (2022) 8. M. Dabrowski, S. Haldar, S. Khan et al., (submitted for publication)

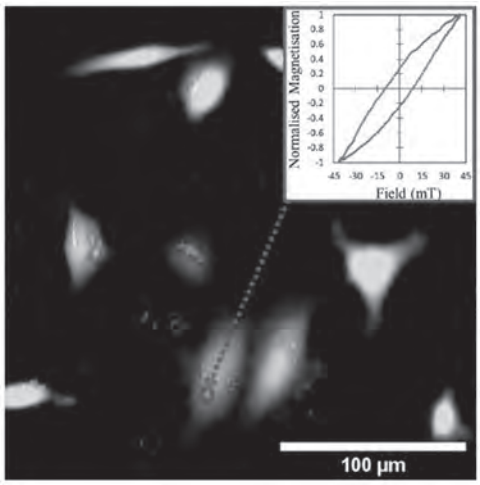

Figure 1. Correlative image of fluorescence from live HeLa cells (green) and ac susceptibility amplitude from magnetic nanoparticles (red), at 65 kHz frequency and 22 mT field amplitude. The inset shows a point source AC hysteresis loop again at 65 kHz.

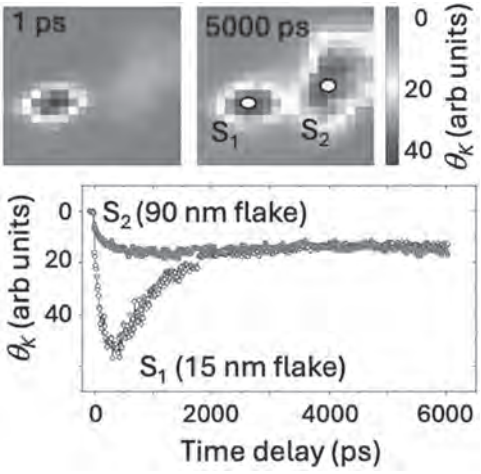

Figure 2. Time resolved Kerr rotation (θ_K) images (8µm x 8 µm) from $Cr_2Ge_2Te_6$ flakes (15 and 90 nm thickness) with out of plane magnetization at 1 and 5000 ps time delay, and time dependent measurements at selected spots shaded yellow. Measurements were performed at a temperature of 6 K in an out of plane field of 0.5 T.

Session FB
2025 IEEE CLEDO BRUNETTI AWARD SYMPOSIUM

Giovanni Finocchio, Chair
University of Messina, Messina, Italy

INVITED PAPERS

FB-01. Development of Embedded Spin-Transfer-Torque MRAM. *D. Worledge*[1], G. Hu[1], S. Brown[1], C.P. D'Emic[1], M.G. Gottwald[1], P. Hashemi[1], J.Z. Sun[1] and P.L. Trouilloud[1] *1. IBM-Samsung MRAM Alliance, Yorktown Heights, NY, United States*

Embedded Spin-Transfer Torque Magnetoresistive Random Access Memory (STT-MRAM) has now replaced embedded Flash memory below the 28 nm node at all advanced foundries. Embedded Flash became too expensive to develop and manufacture, requiring over 12 mask adders (additional lithography levels, beyond the standard CMOS flow), compared to 3 mask adders for embedded STT-MRAM. No foundry has developed, or plans to develop, embedded Flash below the 28 nm node. Embedded STT-MRAM has been in production at the 28 nm node since 2019 [1], and is currently being developed for the 14 nm and 16 nm nodes, with automotive micro-controller products expected there in the next few years [2]. Future growth of STT-MRAM for use as an embedded non-volatile memory appears strong. For example, Samsung has announced plans for embedded STT-MRAM at the 8 nm node in 2026 and 5 nm node in 2027 [3]. This talk will give an overview of what STT-MRAM is and how it works, including the basic building blocks of spin-transfer torque and perpendicular magnetic anisotropy, and describe some of the applications in which it is used. I'll review some of the early scientific work at IBM developing the first perpendicularly magnetized CoFeB-based tunnel junctions [4] with stable perpendicularly magnetized Co-multilayer-based reference layers [5], and the first demonstration of reliable STT-MRAM [6]. Then I will review some of the technology development work in the IBM-Samsung MRAM Alliance to develop STT-MRAM into a useful embedded technology, including scaling down to 11 nm junctions, understanding the key dependencies of the switching current on materials and device parameters, demonstrating reliable switching using 2 ns write pulses, and developing double magnetic tunnel junctions to reduce the switching current.

[1] https://news.samsung.com/global/samsung-electronics-starts-commercial-shipment-of-emram-product-based-on-28nm-fd-soi-process [2] https://www.eenewseurope.com/en/nxp-tsmc-bring-embedded-mram-to-automotive-mcus/ [3] https://news.samsung.com/global/samsung-electronics-unveils-automotive-process-strategy-at-samsung-foundry-forum-2023-eu [4] D. C. Worledge, G. Hu, David W. Abraham, J. Z. Sun, P. L. Trouilloud, J. Nowak, S. Brown, M. C. Gaidis, E. J. O'Sullivan, and R. P. Robertazzi, Spin torque switching of perpendicular Ta|CoFeB|MgO-based magnetic tunnel junctions, Appl. Phys. Lett. 98, 022501 (2011) [5] G. Hu, T. Topuria, P. M. Rice, Jean Jordan-Sweet, and D. C. Worledge, Optimization of tunneling magnetoresistance in perpendicular magnetic tunnel junctions with Co|Pd reference layers, IEEE Mag. Lett. 4, 3000104 (2013) [6] D. C. Worledge, G. Hu, P. L. Trouilloud, D. W. Abraham, S. Brown, M. C. Gaidis, J. Nowak, E. J. O'Sullivan, R. P. Robertazzi, J. Z. Sun, and W. J. Gallagher, Switching distributions and write reliability of perpendicular spin torque MRAM, 2010 International Electron Devices Meeting, 2010, 12.5.1 (2010)

FB-02. From Niche to Mainstream: MRAM Innovations and Application Expansion. *G. Koh*[1] *1. Sungkyunkwan Uiniversity, Suwon, The Republic of Korea*

In the early 2000s, concerns about the scaling limitations of traditional memories such as DRAM and Flash grew, leading to the emergence of new memory technologies such as MRAM, PRAM, FRAM, and ReRAM. These new technologies attracted significant interest and expectations, prompting active research in both industry and academia. Among them, MRAM was considered the most promising candidate to potentially replace DRAM due to its comparable speed and write endurance. Additionally, MRAM's nonvolatile memory characteristics suggested it could also replace Flash memory, and its high-speed operation made it a potential candidate to replace SRAM, raising hopes for it to become a universal memory solution. MRAM first entered mass production in 2006 but was limited to niche markets due to its higher cost compared to existing memory technologies. As MRAM fell short of initial expectations, skepticism began to grow, and as a result, the development boom of MRAM slightly cooled down in the late 2000s. However, continuous technological innovations in MRAM improved its competitiveness, leading to the realization of its expanded applications. The initial MRAM technology, which was based on field switching methods, was fundamentally vulnerable to cell size reduction. However, the introduction of Spin-Transfer-Torque (STT) switching technology enabled innovations in reducing cell size and switching current. Additionally, the development of MTJ (Magnetic Tunnel Junction) technology utilizing perpendicular magnetic anisotropy further enhanced cell size reduction and improved cost competitiveness. Samsung has been involved in MRAM development from its early stages, accumulating expertise and focusing on developing mass production technology for MRAM based on the new perpendicular STT-MRAM technology throughout the 2010s. The company established a collaboration and communication system encompassing research institutions like IBM, the MRAM academic community, and equipment companies, strengthening the MRAM development ecosystem. In 2019, Samsung began mass production of embedded MRAM products, replacing conventional embedded Flash, marking MRAM as a key product technology in the Foundry business. Since then, through continuous innovations in MTJ material technology, patterning technology, and related process integration, Samsung has achieved higher integration density, lower power consumption, longer endurance, faster operation speeds, and higher temperature retention characteristics, driving the expansion of MRAM applications. In this presentation, I will review these development achievements and discuss the future direction.

FB-03. Spin-Transfer-Torque MRAM for Last-Level Cache Applications. *G. Hu*[1], C. Safranski[1], M.G. Gottwald[1], P.L. Trouilloud[1], L. Rehm[1], G. Kim[1], S. Brown[1], J. Bruley[1], C.P. D'Emic[1], C. Lavoie[1], J. Liang[1], M. Robbins[1], J.Z. Sun[1], P. Hashemi[1] and D. Worledge[1] *1. IBM T J Watson Research Center, Yorktown Heights, NY, United States*

STT-MRAM has emerged as a promising non-volatile memory technology, with both standalone STT-MRAM and eMRAM (as an eFlash replacement) now commercially available [1-2]. Optimization of conventional CoFeB-based single Magnetic Tunnel Junction (MTJ) devices is anticipated to meet the

performance requirements for next-generation eMRAM used in non-volatile working memory applications. To broaden eMRAM's application to last-level-cache, it is essential to explore new material systems beyond CoFeB or innovative device structures beyond single MTJs to meet stringent requirements for switching current, switching speed, and endurance. In this presentation, I will review our recent advancements in device structures and materials to reduce switching current and enhance the high-speed switching performance of STT-MRAM devices. By utilizing a novel double spin-torque MTJ (DS-MTJ) device structure, we achieved up to a 2x reduction in switching current and reliable sub-nanosecond switching. This was accomplished by harnessing spin torques from both the top and bottom interfaces of the free layer in DS-MTJs with a second reference layer [3-4]. Furthermore, we developed magnetic ordered-alloys with low moment and strong bulk perpendicular magnetic anisotropy (PMA) as replacements for conventional CoFeB-based free layer materials. STT-MRAM devices based on these new materials showed superior device properties, exhibiting high coercivity (H_c > 8 kOe), high energy barrier (E_b > 80 k_BT), and sub-5 nanosecond switching simultaneously, overcoming the fundamental trade-off between high energy barrier and high-speed switching found in CoFeB-based devices using interface PMA [5].

[1] S. Aggarwal, et al., "Demonstration of a Reliable 1 Gb Standalone Spin-Transfer Torque MRAM For Industrial Applications," 2019 IEEE International Electron Devices Meeting (IEDM), 2019, pp. 2.1.1-2.1.4 [2] K, Lee, et al., "1Gbit High Density Embedded STT-MRAM in 28nm FDSOI Technology," 2019 IEEE International Electron Devices Meeting (IEDM), 2019, pp. 2.2.1-2.2.4 [3] G. Hu et al., "Double spin-torque magnetic tunnel junction devices for last-level cache applications," 2022 IEEE International Electron Devices Meeting (IEDM), 2022, pp. 10.2.1-2.2.4 [4] C. Safranski et al., "Reliable Sub-nanosecond MRAM with Double Spin-torque Magnetic Tunnel Junctions," 2022 Symposium on VLSI Technology, 2022, T01-4 [5] M. Gottwald et al., "First demonstration of high retention energy barriers and 2 ns switching, using magnetic ordered-alloy-based STT MRAM devices," 2024 Symposium on VLSI Technology, 2024, T10-4

Session FC
UNCONVENTIONAL COMPUTING WITH MAGNETISM AND MAGNETIC MATERIALS

Miguel Romera, Chair
Universidad Complutense de Madrid, Madrid, Spain

INVITED PAPER

FC-01. Physics and engineering of stochastic magnetic tunnel junction for probabilistic computer. *S. Fukami[1] 1. Tohoku University, Sendai, Japan*

Today's electronics are built on sophisticated CMOS computers consisting of deterministic devices where stochastic behavior is attempted to be minimized. In the meantime, it is known that there are several kinds of hard problems for today's CMOS computers to address efficiently, such as machine learning, combinatorial optimization, and quantum simulation. As a result, there has been an increasing demand for the development of domain-specific computers designed to readily address these problems. Notably, since these hard problems can often be solved with vast numbers of random numbers, probabilistic computing hardware consisting of inherently stochastic elements is expected to be promising. Spintronics offers a promising platform for this purpose, and recent studies have successfully demonstrated proof-of-concepts of the spintronics-based probabilistic computers [1-4]. In this talk, after a brief overview of the spintronics-based probabilistic computing, I will elaborate on the physics and engineering of the stochastic magnetic tunnel junction (MTJ) that is the key component of the probabilistic computer. To make the probabilistic computer high-performance and reliable, the stochastic MTJ needs to satisfy several requirements, some of which involve unexplored physics in the studies of conventional nonvolatile MTJs for MRAM applications. For example, the high-speed generation of random telegraph noise, which is critical for short time-to-solution, can be achieved by not only reducing the energy barrier between the two magnetization directions but also reducing the attempt time of the magnetization switching. We found that these two criteria can be simultaneously achieved with in-plane easy-axis MTJ [5,6]. We also quantified the attempt time by measuring the temperature dependence of the properties of stochastic MTJs and found that spin-wave excitation plays a crucial role there [7]. In addition, insensitivity against the external magnetic fields and bias voltage is also an important metric, which has been found to be achieved by utilizing synthetic antiferromagnetically coupled free layer [8,9] and double-free-layer structures [9-11], respectively. If time allows, the physics governing the properties of stochastic magnetic tunnel junctions will be discussed [12-13]. These studies are carried out in collaboration with H. Ohno, S. Kanai, W. A. Borders, K. Hayakawa, K. Kobayashi, R. Ota, H. Kaneko, S. Datta, and K. Y. Camsari, and were partly supported by JST-CREST JPMJCR19K3, JST-ASPIRE JPMJAP2322, MEXT X-NICS JPJ011438 and RIEC Cooperative Research Projects.

W. A. Borders et al., Nature 573, 390 (2019). J. Kaiser et al., Phys. Rev. Appl. 17, 014016 (2022). A. Grimardi et al., IEEE IEDM 2022, 22.4 (2022). N. A. Singh et al., IEEE IEDM 2023, 12.1 (2023). S. Kanai et al., Phys. Rev. B 103, 094423 (2021). K. Hayakawa et al., Phys. Rev. Lett. 126, 117202 (2021). H. Kaneko et al., Appl. Phys. Express, 17, 053001 (2024). K. Kobayashi et al., Phys. Rev. Appl., 18, 054085 (2022). K. Selcuk et al., Phys. Rev. Appl. 21, 054002 (2024). K. Y. Camsari et al., Phys. Rev. Appl. 15, 044049 (2021). R. Ota et al., arXiv:2405.20665 (2024); to be published in Appl. Phys. Lett. doi: 10.1063/5.0219606. K. Kobayashi et al., Appl. Phys. Lett. 119, 132406 (2021). T. Funatsu et al., Nat. Commun., 13, 4079 (2022).

CONTRIBUTED PAPERS

FC-02. Probability fluctuations in fast true random number generators based on perpendicular magnetic tunnel junctions. *A. Sidi El Valli[1]*, M. Tsao[1] and A.D. Kent[1] *1. New York University, New York, NY, United States*

Pseudorandom numbers play an important role in stochastic simulations. They are used extensively in Monte-Carlo and AI applications [1]. However, the cost of their generation in hardware remains a challenge [2]. A potential solution is to use true random number generators (TRNGs) drawn from physical noise. In this work we investigate TRNGs based on perpendicular magnetic tunnel junctions (pMTJ) [3,4]. To generate random numbers, we use magnetically stable devices, in contrast to superparamagnetic MTJs, and operate them with short write pulses with a switching probability of p~0.5 [5]. This approach offers better stability to external perturbations and was demonstrated to yield a variation of probability with temperature of $dp/dT \sim 0.006$ K-1 [6]. To generate a single bit, we send a sequence of three voltage pulses to the pMTJ (i) to set the device into a known state, (ii) stochastically switching the junction state about 50% of the time, and finally (iii) reading the resulting MTJ state. The total sequence duration is 9.6 ns, corresponding to 104 Mb/s. To extract the random bits, we use a Teledyne FPGA 14-bit digitizer (ADQ7) to read the final state voltage and assign "0" or "1" depending on whether it is low or high. To study the probability deviations in bitstreams we recorded the average probability of 100 million bits every 30 minutes. The results are depicted in the bottom plot in Figure 1a. The dashed lines in Figure 1 marks a pause of 12 hours in measurements. This helps in assessing the remanence of the previous probability value. The results show an increase in the probability with a maximum deviation of ~ 3% that is followed by a decrease towards 0.5. Interestingly the antiparallel state resistance extracted during the same measurements show similar behavior with time; see top plot in Figure 1a and Figure 1b. These observations show that device characteristics and probability bias are correlated and suggest that pMTJ characteristics change during electrical actuation.

*Acknowledgment: We acknowledge support from ONR Award No. N00014-23- 1-2771 and DOE Office of Science (ASCR/BES) Microelectronics Co-Design project COINFLIPS. [1] B. P. Kersevan et al., "The Monte Carlo event generator AcerMC versions 2.0 to 3.8 with interfaces to PYTHIA 6.4, HERWIG 6.5 and ARIADNE 4.1," Comput. Phys. Commun 184, 919–985 (2013). [2] S. Misra et al., "Probabilistic neural computing with stochastic devices," Adv. Mater. 35, 2204569 (2023). [3] A. D. Kent et al., "A new spin on magnetic memories," Nat. Nanotechnol. 10, 187 (2015). [4] R. B. Goldfarb et al., "Introduction to magnetic random access memory," John Wiley & Sons, 2016. [5] L. Rehm et al., "Stochastic magnetic actuated random transducer devices based on pMTJs," Phys. Rev. Applied 19, 024035 (2023). [6] L. Rehm et al., "Temperature-resilient random number generation with stochastic actuated magnetic tunnel junction devices," Appl. Phys. Lett. 124, 052401 (2024).

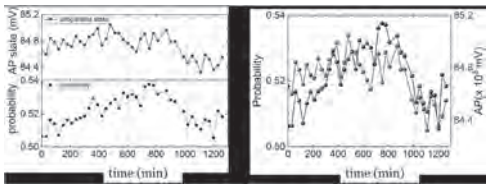

Figure 1: AP state and probability versus time. a) The average probability of 100 million bits and antiparallel resistance (in mV) as a function time. b) Two y-axis plots of the measurements in (a) showing the correlations.

FC-03. Quantized Neural Networks using MRAM-based Stochastic Computing Units. *S. Sabyasachi*[1], W. Al Misba[1], Y. Shao[2], P. Khalili[2] and J. Atulasimha[1] *1. Department of Mechanical & Nuclear Engineering, Virginia Commonwealth University, Richmond, VA, United States; 2. Department of Electrical and Computer Engineering, Northwestern University, Evanston, IL, United States*

Artificial Neural Networks (ANN) have a tremendous potential for future applications. However, several challenges are encountered while designing ANN. An ANN architecture involves a very large number of multiplications and additions, requiring high energy and resulting in large footprint devices for inference. Stochastic Computing (SC) offers less resource intensive ANN implementation with minimal accuracy loss [1]. Tunable True Random Number Generators (TRNG) is required to implement SC in hardware which can be realized through Magnetoresistive Random Access Memory (MRAM) bits- i.e. Magnetic Tunnel Junctions (MTJ) [2]. We study the use of SC for arithmetic operations, specifically multiply and accumulate- the most resource intensive operation in a typical ANN to reduce area, power and latency using experimentally obtained MRAM bitstreams [2]. The key finding from this work is that using a limited number of discrete quantized states for both weights and hidden layer nodes in an ANN can further reduce latency and power in SC, while preserving accuracy to a great extent. We examined the inference accuracy with SC for the MNIST dataset after training with quantized states and investigated whether inference accuracy is improved if training with quantized states incorporates SC as well. Bitstream lengths of 100, 200, 300, 400 and 500 were investigated. Higher accuracy was obtained in all cases when both training and inference incorporated SC, rather than only inference utilizing SC. Yixin et al. reported 95% accuracy for 1024-bit long stream [2]. We obtained comparable accuracy with much shorter bitstreams (fig. 1, 2). For 11 quantized states with a one hidden layer architecture, highest inference accuracy of 94.33% was obtained for 500 bits (fig.1) while for a three hidden layers architecture, highest obtained accuracy was 96.82% for 400 bits (fig.2). Using quantized states and shortening bitstreams reduce latency and power consumption as well. Preliminary investigations demonstrate at least 5X improvement in latency and power of implementing an ANN compared to SC without quantization. Acknowledgement: NSF grant ECCS: #1954589 and Convergence Lab Initiative (CLI).

[1] A. Ren, Z. Li, C. Ding, Q. Qiu, Y. Wang, J. Li, X. Qian, and B. Yuan, ACM, ASPLOS, Part F1271, p.405 (2017). [2] Y. Shao, S. L. Sinaga, I. O. Sunmola, A. S. Borland, M. J. Carey, J. A. Katin, V. Lopez-Dominguez, and P. K. Amiri, IEEE Magnetics Letters, vol. 12 (2021).

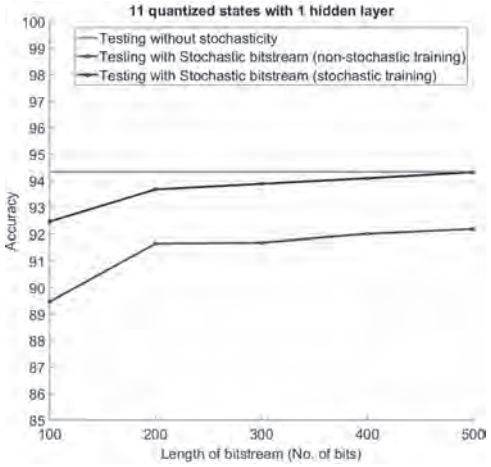

Fig. 1: one hidden layer

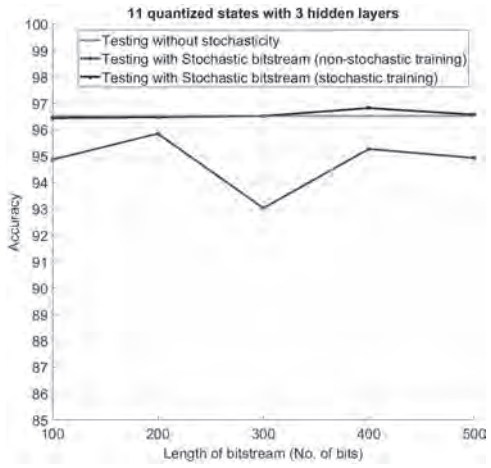

Fig. 2: three hidden layers

FC-04. Identifying Angular Dependent States in Superparamagnetic Artificial Spin Ice with Tunnel Magnetoresistance. *C. Sullivan*[1], H. Chen[2], B. Fang[3], X. Zhang[3] and S. Majetich[2] *1. Materials Science and Engineering, Carnegie Mellon University, Pittsburgh, PA, United States; 2. Physics, Carnegie Mellon University, Pittsburgh, PA, United States; 3. Materials Science and Engineering, King Abdullah University of Science and Technology, Thuwal, Saudi Arabia*

Artificial spin ice (ASI), which consists of magnetostatically coupled nanomagnets, has been proposed for non-traditional computing devices [1-2]. To enable electrical control and increase response speed, the ASI is formed from a square array of in-plane superparamagnetic tunnel junctions. Tunnel magnetoresistance (TMR) measurements suggest nearly field free telegraphing in a checkerboard-like magnetization pattern. Fig. 1(a-b) shows two types of characteristic behavior that arise from magnetostatic stray field interactions. Fig 1(c) shows TMR vs. time measurements for an x device that exhibits nearly symmetric two-state telegraphing. Fig. 1(d) shows TMR vs. time for a y device that demonstrates a continuous shift in baseline TMR with discrete spikes to lower resistance. Considering the nature of TMR along a hard axis, changes in the baseline suggest y devices are more susceptible to changes in local fields resulting in a spin canting mechanism. Using an empirical cosine law [3-4], the angular dependence of spin canting was characterized. Fig. 2 shows the distribution of angles in an (a) x device, and (b-c) a y device over equal time windows. Schematics of angular dependence are shown to the right of each. X devices demonstrate two state behavior, while y devices show variability in the average angular position (φ) and relative noise width (w). Although the time average position is about $\varphi = \pi/2$,

changes in the local magnetostatic field drive the state to canted positions. Spikes in TMR of y devices are characteristic of magnetization switching into an unstable state, suggesting y devices also telegraph with an effective energy barrier. Preliminary Mumax3 simulations show y devices have an angular dependent relationship with the effective magnetostatic field for high energy ASI configurations.

[1] W. Hu, Z. Zhang, and Y. Liao, *Nature*, 14, 2562 (2023). [2] K. Hon, Y. Kuwabiraki, M. Goto, *Applied Physics Express*, 14, 033001 (2021). [3] J. S. Moodera and L. R. Kinder, *Journal of Applied Physics*. 79, p. 4724 (1996). [4] H. Chen, B. Parks, and Q. Zhang, *Applied Physics Letters*, 120, 212401 (2022).

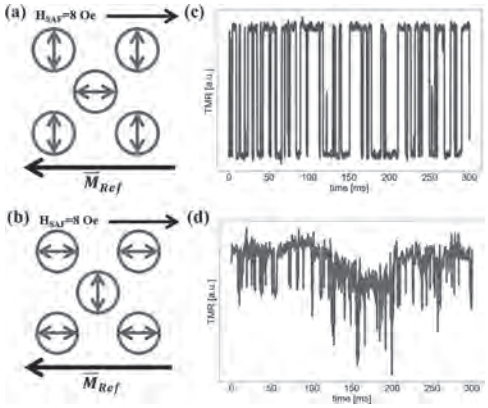

Fig. 1 Schematic of the device and nearest neighbors for (a) x device and (b) y device with effective reference layer contributions. TMR vs time behavior for (c) x device and (d) y device.

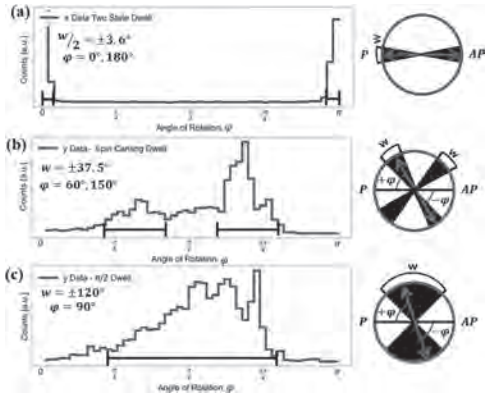

Fig. 2 Histogram and corresponding schematic of angular distributions for (a) two state x device and (b-c) variable spin canting for y devices. φ is the angular position for a spin state and w is the width of the angular distribution.

FC-05. Deterministic and stochastic SOT-driven switching in Pt/Co bilayers by DMI modulation. *R.I. Salinas*[1] and C. Lai[1] *1. Materials Science and Engineering, National Tsing Hua University, Hsinchu, Taiwan*

The Dzyaloshinskii-Moriya Interaction (DMI), a chiral magnetic interaction that arises in systems with strong spin-orbit coupling and broken inversion symmetry, favors non-collinear alignment of neighboring spins, leading to the formation of chiral magnetic structures such as skyrmions and Néel-type domain walls. The interfacial DMI plays a significant role in stabilizing these spin textures, making it a critical parameter for developing spintronic devices. In thin film heterostructures like Pt/Co bilayers, the extent of this interaction depends on the proximity of the Co atoms to the Pt interface. As Co thickness increases, only the spins near the interface are strongly influenced by the interfacial DMI [1]. When the DMI is small, the resulting domain walls are more stable and less prone to rapid propagation. This stability facilitates multilevel states where the magnetization can be precisely controlled to represent different levels. Such multilevel states are crucial for applications in data storage and neuromorphic computing, where analog switching is required. On the other hand, large DMI results in fast domain wall propagation, which introduces a stochastic element to the spin-orbit torque (SOT) driven switching process due to the dynamic and unstable nature of the domain walls, as depicted in Fig.1. This stochastic switching behavior is advantageous for probabilistic computing and random number generation, where randomness and variability are essential for efficient computation. In this study, we show that by carefully tuning the DMI in Pt/Co bilayers and the application of SOT, it is possible to tailor the switching dynamics, enabling both deterministic and stochastic switching regimes, as shown in Fig. 2, which provides significant flexibility for designing multi-functional spintronic devices. This capability enhances learning algorithms, improves pattern recognition, and supports cognitive functions, paving the way for advanced neuromorphic systems that closely mimic the complex behavior of the human brain [2].

1. D. Khadka, S. Karayev, and S. X. Huang, Journal of Applied Physics 123, 123905 (2018) 2. R. I. Salinas, P. C. Chen et al., Materials Research Letters, 11(5), 305–326 (2022)

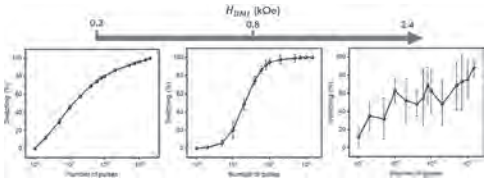

Fig.1. Transition from deterministic to stochastic SOT-driven switching by increasing DMI.

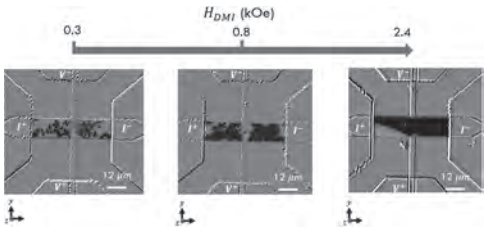

Fig. 2. Kerr microscope images of SOT-driven switching dynamics with increasing DMI.

FC-06. Experimental implementation of a programmable Ising Machine using vortex-based Spin-Torque Nano-Oscillators. *A. Hakam*[1], L. Martins[1], L. Hutin[2], F. Badets[2], L. Benetti[3], A. Jenkins[3], R. Ferreira[3], P. Talatchian[1] and U. Ebels[1] *1. Univ. Grenoble Alpes, CEA, CNRS, Grenoble INP, SPINTEC, 38000, Grenoble, France; 2. Université Grenoble Alpes, CEA, LETI, 38000, Grenoble, France; 3. International Iberian Nanotechnology Laboratory (INL), 4715-31, Braga, Portugal*

Ising machines (IMs) are physics-inspired computing systems that can efficiently solve combinatorial optimization problems (COPs). IMs emulate a binary-valued spin-lattice that inherently seeks to minimize its total energy, where spin-coupling interactions can encode a COP and lowest energy states represent COP solutions. Instead of fine-tuning annealing schemes [1] to gradually stabilize the system onto the ground state, we aim to use the IM's thermal noise to stochastically explore the spin state configurations and infer the lowest energy states from the maxima of the resolved probability distribution. Spin-torque nano-oscillators (STNOs) are excellent candidates for building IMs [1], as they do not suffer from the limitations of other proposed technologies, which are often restricted to time-multiplexing proof of concepts [2], cryogenic temperatures [3], or macroscopic-sized spins [4]. Leveraging CMOS compatibility, nanoscale size, and the rich nonlinear dynamics at MHz-GHz frequencies, STNOs have been used for neuromorphic computing with frequency encoding schemes [5]. However, the theoretically

predicted potential of phase encoding [6] remains largely unexplored in experiments. We aim to implement a spatial and programmable IM operating through the stochastic phase dynamics of coupled vortex-based STNOs (frequency f~200MHz). To emulate a binary spin, we use the fact that when the STNO is synchronized to a microwave signal at 2f, its phase adopts two perfectly equiprobable states [7]. We demonstrated experimentally that an external microwave signal at f disrupts this equiprobability, the key for controlling spin's probability state. As a first proof of concept consisting of a two-spin IM (N=2), we demonstrate programmable coupling via an adjustable resistance representing the spin-coupling strength, see Fig.1. We show that increasing the coupling resistance decreases the correlation between the STNO phases and alters its sign, see Fig. 2. Further results will be discussed to scale to larger arrays (N>2) to build a full spatial and programmable stochastic IM using vortex-based STNOs.

[1] D. I. Albertsson, M. Zahedinejad, A. Houshang et al., Appl. Phys. Lett., Vol. 118, p. 112404 (2018). [2] A. Litvinenko, R. Khymyn, V. H. González et al., Commun Phys, Vol. 6, 227 (2023). [3] M. W. Johnson, M. H. S. Amin, S. Gildert et al., Nature, Vol. 473, p. 194–198 (2011). [4] P. L. McMahon, A. Marandi, Y. Haribara et al., Science, Vol. 354, p. 614–617 (2016). [5] M. Romera, P. Talatchian et al., Nature, Vol. 563, p. 230–234 (2018). [6] D. E. Nikonov, G. Csaba, W. Porod et al., IEEE Journal on Exploratory Solid-State Computational Devices and Circuits, Vol. 1, p. 85-93 (2015). [7] N.-T. Phan, N. Prasad, A. Hakam et al., Phys. Rev. Applied, Vol. 21, p. 034063 (2024).

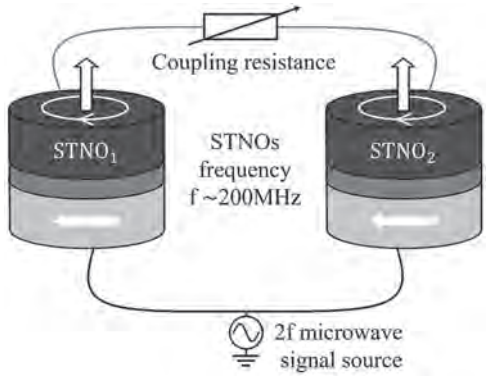

Fig.1: Schematic of an STNO-based two-spin IM.

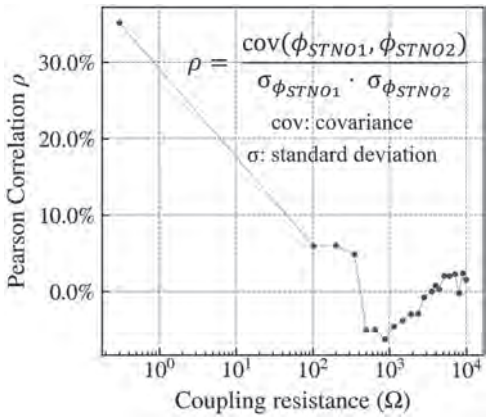

Fig.2: Pearson correlation between the two STNO phases vs. coupling resistance.

FC-07. Solving Combinatorial Optimization Problems through Stochastic Landau-Lifshitz-Gilbert Dynamical Systems. *D. Chen*[1], A.D. Kent[1], D. Sels[1,2] and F. Morone[1] *1. Physics, New York University, New York, NY, United States; 2. Center for Computational Quantum Physics, Flatiron Institute, New York, NY, United States*

Magnetic Tunnel Junctions (MTJs) hold significant potential for innovative computing applications due to their rich dynamics and stochastic nature. One prominent application in computing is finding solutions to NP-Hard combinatorial optimization problems. Most optimization paradigms using MTJs are based on the energy and annealing models, where the true solution to an optimization problem is mapped to the ground state of the system's Hamiltonian. The optimization task then becomes a physical process of finding the system's ground state. While experiments have been conducted with arrays of (<100) MTJs to factor semiprimes and solve small optimization problems, comprehensive theoretical and numerical studies on the advantages of these systems compared to established classical optimization methods are needed to fully understand their potential and limitations. We present numerical studies modeling a system of macrospins governed by Landau-Lifshitz-Gilbert (LLG) dynamics, capturing the essential physical characteristics of MTJ's free magnetic layer [1]. We apply this system to solve the Sherrington-Kirkpatrick (SK) model, which serves as an ideal benchmark due to having an exact solution in the thermodynamics limit as system size $n\to\infty$. To compare our results with classical optimization protocols, we benchmark against the Glauber dynamics of Ising spins. We compute the disorder-average energy per spin $\langle E\rangle/n$ of the SK model at the end for system sizes ranging from n=40 to 2000. Plotting the $\langle E\rangle/n$ against $n^{-2/3}$, our results are shown in Fig.1. We observe the LLG dynamics consistently finds a lower energy state than the Glauber dynamics, and the LLG results extrapolate to $\langle E\rangle/n=-0.762(1)$ as $n\to\infty$, which is very close to the exact optimal value $\langle E\rangle/n=-0.763$. Our results demonstrate the potential of using magnetization dynamics of coupled macrospins to solve NP-hard optimization problems.

[1] Dairong Chen, Andrew D. Kent, Dries Sels, and Flaviano Morone, arXiv:2407.00530 (2024)

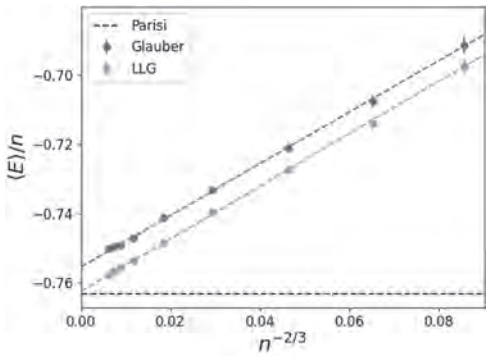

Fig.1 Average ground state energy per spin $\langle E\rangle/n$ as a function of $n^{-2/3}$ for Glauber (blue line) and LLG (orange line) dynamics. The horizontal dashed line represents the asymptotic $n\to\infty$ exact ground state energy obtained by Parisi. Error bars indicate the standard error of the mean energy per spin.

FC-09. Optimization of a GPU-accelerated Ising Machine for the solution of very large problems based on the synchronization of oscillators. L. Mazza[1], M. Carpentieri[1], G. Finocchio[2] and *V. Puliafito*[1] *1. Politecnico di Bari, Bari, Italy; 2. University of Messina, Messina, Italy*

Heuristic paradigms like Ising Machines (IMs) are recently gaining interest in both academia and industry for their capability of finding good solutions, in limited time, for NP combinatorial optimization problems. Conventional algorithms, in fact, process such problems with time and memory requirements scaling more than linearly with their size, making them ineffective for large-scale applications. In this work, we present an optimization strategy for an algorithmic implementation of an IM to solve sparse and extremely large

(up to 20M nodes) Max-Cut problems. The IM is based on the synchronization of nonlinear oscillators, like spintronic ones, simulated by means of the integration of coupled differential equations on GPU [1]. Evaluating the Max-Cut of an undirected and weighted graph corresponds with the binarization of the starting network into two groups in such a way that the cut connections are maximized. In our approach, the starting graph is encoded into a network of oscillators that is randomly initialized and that evolves towards a local minimum, corresponding to a solution of the problem. The binarization of the oscillators happens considering the in phase and out of phase ones, which is achieved through the injection locking of an ac signal tuned with their second harmonic [2-3]. We simulated numerous problems of different size and density. In particular, we solved a cubic system, having three connections for each node, with twenty million oscillators, which is the largest Max-Cut problem ever solved by means of our knowledge. We did a systematic statistical analysis for the quality of the solutions obtained for several problems of the G-set, achieving accuracies on average higher than 99.5%. Regarding solving times, our algorithm turns out much faster than deterministic approaches [4], for instance a cubic problem with 1K nodes requires ten hours to be solved with the deterministic solver and less than one second with the proposed approach, which achieved a solution for the 20M-node cubic problem in 8 minutes. A novel strategy, which makes use of a segmentation process in the IM algorithm, is presented for maximizing the accuracies for time-constrained applications.

[1] T. Wang and J. Roychowdhury, "OIM: Oscillator-Based Ising Machines for Solving Combinatorial Optimisation Problems," in Lecture Notes in Computer Science, vol. 11493 LNCS, Springer International Publishing, 2019, pp. 232–256. [2] A. Grimaldi et al., "Evaluating spintronics-compatible implementations of Ising machines," Phys. Rev. Applied, vol. 20, 024005, 2023. [3] L. Mazza, E. Raimondo, A. Grimaldi, and V. Puliafito, "Simulated Oscillator-Based Ising Machine for two Million Nodes Max-Cut Problems," in 2023 IEEE 23rd International Conference on Nanotechnology (NANO), Jul. 2023, pp. 1037–1041. [4] D. P. Williamson and M. Goemans, "Improved Maximum Approximation Algorithms for Using Cut and Satisfiability Programming Problems Semidefinite," Science (80)., vol. 42, no. 6, pp. 1115–1145, 1994.

FC-10. Effect of device-to-device variation in spintronic probabilistic ising machines. *E. Raimondo*[1,2], E. Garzòn[3], Y. Shao[4], A. Grimaldi[2], S. Chiappini[1], R. Tomasello[5], N. Davila[6], J. Katine[6], M. Carpentieri[5], M. Chiappini[1], M. Lanuzza[3], P. Khalili[4] and G. Finocchio[2] *1. Istituto Nazionale di Geofisica e Vulcanologia, Rome, Italy; 2. University of Messina, Messina, Italy; 3. University of Calabria, Rende, Italy; 4. Northwestern University, Evanston, IL, United States; 5. Politecnico di Bari, Bari, Italy; 6. Western Digital, San Jose, CA, United States*

Ising machines (IMs) are a promising hardware-friendly unconventional computing paradigm for solving of combinatorial optimization problems (COPs)[1]. IMs search for the ground state of an Ising Hamiltonian. Among of several paradigms of IMs, this study focuses on probabilistic IMs (PIMs). In PIMs the Ising spin is the probabilistic bit (p-bit), a bistable tunable stochastic unit that exhibits a sigmoidal behavior. The p-bit can be naturally implemented in hardware, particularly using spintronic devices such as magnetic tunnel junctions (MTJs) [2-4]. A hardware implementation of a PIM involves considering the inherent device-to-device variations. Experimental observations of the p-bit behavior using MTJs indicate that these variations are mainly reflected in slight differences in the slope (α) of the sigmoidal curve. To emulate hardware PIMs, we assign at each p-bit a different α value sampled from a Gaussian distribution with mean of one and standard deviation σ (see inset of Fig. 1). We study the effect of this non-ideal behavior on the success probability (SP) of solving the instance of maximum satisfiability problem (Max-SAT) "s3v70c700-1.cnf" and we compare the three well-known energy minimization algorithms: simulated annealing (SA), parallel tempering (PT) and simulated quantum annealing (SQA). Fig. 1 shows the SP as a function of σ for the three algorithms. The SQA shows not only impressive ideal performance (higher than PT and SA), but also remarkable robustness to even extreme variations in the slope of the p-bits. This finding suggest that SQA is the best choice for hybrid PIMs.

[1] N. Mohseni, Nat. Rev. Phys. 4, 363 (2022). [2] K. Y. Camsari, Phys. Rev. X 7, 031014 (2017). [3] G. Finocchio, J. Magn. Magn. 521, 167506 (2021). [4] A. Grimaldi, Phys. Rev. Appl. 17, 024052 (2022). [5] Acknowledgements: This work has been supported by project number 101070287 — SWAN-on-chip — HORIZON-CL4-2021-DIGITAL-EMERGING-01, the projects PRIN 2020LWPKH7, PRIN_20225YF2S4, PRIN20222N9A73, PON Capitale Umano (CIR_00030), funded by the Italian Ministry of University and Research (MUR), and by the PETASPIN association (www.petaspin.com). R.T. acknowledge support from the Project PE0000021, The work at Northwestern University was supported by the National Science Foundation (NSF), Division of Computing and Communication Foundations (CCF), under award number 2322572.

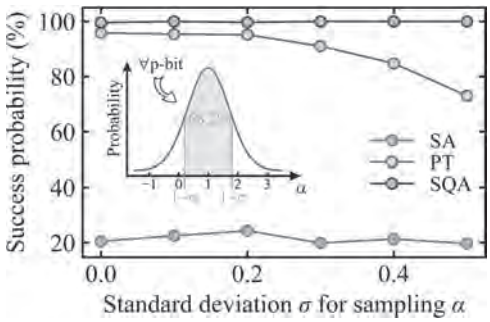

Fig. 1: Success probability over 1000 runs per point as a function of the standard deviation σ of the normal distribution used to sample the slope of each p-bit's sigmoidal curve, for the Max-SAT instance "s3v70c700-1.cnf". The problem is tested with SA (red), PT (green), and SQA (blue). 1000 replicas are used.

FC-11. A Time- and Energy-Efficient Ising Machine Based on Voltage-Controlled Magneto-Resistive Devices. Z. Tong[1], Y. Hou[1], Y. Jiang[1], Z. Xiao[1], X. Wu[1], A. Lee[2], D. Wu[2] and *Q. Shao*[1,3] *1. Department of Electronic and Computer Engineering, The Hong Kong University of Science and Technology, Clear Water Bay, Hong Kong; 2. InstonTech, Suzhou, China; 3. Department of Physics, The Hong Kong University of Science and Technology, Clear Water Bay, Hong Kong*

Combinatorial optimization (CO), defined as the approach to finding the optimal combinations from a finite set of objects, is widely used in various industries. In many scenarios, CO mathematically relies on solving non-deterministic polynomial-time-complete (NP-complete) problems, which are regarded as the most challenging problems for conventional computers. Ising machines, inspired by the fundamentals of statistical mechanics and micromagnetics, are adept at solving complex optimization problems by mapping the problems to the coupling relationships within the Ising model and seeking solutions through the evolution and convergence of the model. In recent years, voltage-controlled magneto-resistive devices have garnered significant attention due to their fast operation speed, low power consumption, and highly-tunable switching probability. In this work, we utilize voltage-controlled magneto-resistive devices to construct a fully-connected Ising machine capable of solving various classical CO problems, including max-cut and traveling salesman problems. Furthermore, we propose a novel method that employs a crossbar array to facilitate on-chip updates of device manipulation, thereby enhancing the time and energy efficiency of the Ising machine. Our approach demonstrates significant improvements in both computational speed and energy consumption, making it a feasible solution for real-time and large-scale optimization challenges.

Session FD
MAGNONICS IV: FUNDAMENTAL MAGNONIC PROPERTIES AND INTERACTIONS

Edoardo Albisetti, Co-Chair
Politecnico di Milano, Milano, Italy
Philipp Pirro, Co-Chair
RPTU Kaiserslautern-Landau, Kaiserslautern, Germany

CONTRIBUTED PAPERS

FD-01. Spin Nutation Driven Non-Resonantly in Ferromagnets.
J. Schlegel[1], A. De[2], A. Lentfert[2], L. Scheuer[2], B. Stadtmüller[2], P. Pirro[2], G. von Freymann[3], M. Aeschlimann[2] and U. Nowak[1] *1. Department of Physics, University of Konstanz, Konstanz, Germany; 2. OPTIMAS, RPTU Kaiserslautern-Landau, Kaiserslautern, Germany; 3. Fraunhofer ITWM, Kaiserslautern, Germany*

The understanding of ultrafast magnetization dynamics and its manipulation is crucial for developing future spintronic devices. In this context, ferromagnets with their finite magnetization offer an easily accessible order parameter which can be manipulated with an external magnetic field, but the speed of their dynamics is limited by a precession frequency in the lower GHz regime. However, a much faster type of magnetic dynamics has been theoretically predicted and experimentally confirmed: nutation [1,2]. In analogy to a mechanical gyroscope nutation leads to significantly higher frequencies and thus can overcome the precessional limit [3]. In this work we investigate nutation in ferromagnetic permalloy [4]. A laser pump pulse excites the magnetic film thermally, leading to a rapid change of the effective field direction away from the initial equilibrium condition. This triggers both precession and nutation on ultrashort time scales. On the basis of a Heisenberg model we simulate the magnetization dynamics of such a non-resonantly excited spin model [5]. The dynamics is described by the inertial Landau-Lifshitz-Gilbert equation of motion (iLLG), which is an extended form of the standard LLG and contains an additional second order time derivative term. The simulated magnetization dynamics unveils a nutational mode in the regime of hundred gigahertz, way above the precessional mode in the single gigahertz domain. Moreover, we show that the nutation leads to a separation of the angular momentum and magnetization vectors with the magnetization nutating around the angular momentum of the spin system. Our simulation results are compared to current pump-probe measurements. They show that the experimental findings cannot be explained by the standard LLG equation of motion but can be attributed to an additional inertial contribution in the equation of motion. The fact that ultrafast demagnetization, nutation and precession can be triggered non-resonantly will have profound implications for the field of ultrafast spintronics.

[1] Mondal et al., JMMM, Vol. 579, 170830 (2023) [2] Neeraj et al., Nat. Phys., Vol. 17, 245-250 (2020) [3] Winter et al., Phys. Rev. B., Vol. 106, 214403 (2022) [4] De et al., arXiv:2405.01334 (2024) [5] Hinzke et al., Phys. Rev. B, Vol. 92, 054412 (2015)

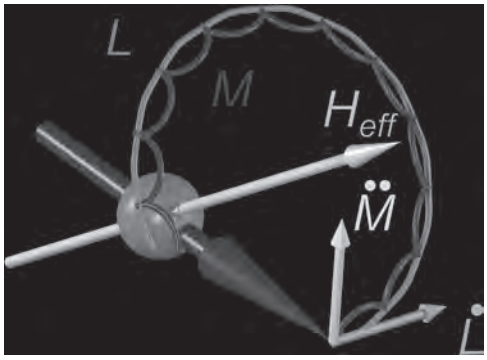

Fig.1: Sketch of magnetization and angular momentum dynamics after a tilting of the effective field

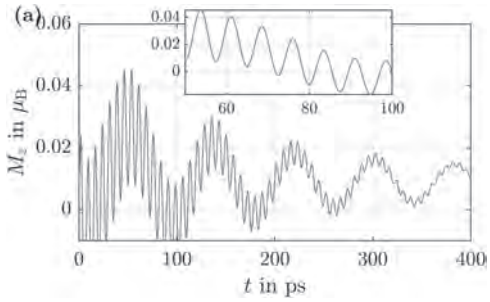

Fig.2: Simulated magnetization dynamics after the excitation, showing both precession and nutation.

FD-02. Non-bosonic damping of spin waves at elevated temperatures in van der Waals ferromagnetic films. *M.G. Cottam*[1] and B. Hussain[2] *1. University of Western Ontario, London, ON, Canada; 2. University of Michigan, Dearborn, MI, United States*

The magnetization dynamics in van der Waals magnets is a topic of intense interest [1,2]. Here the spin-wave (SW) renormalization processes in a monolayer van der Waals ferromagnet are studied using a non-bosonic diagram technique. Specifically, the contributions to the spin-spin Green's functions are evaluated by the drone-fermion perturbation method within a high-density $1/z$ perturbation expansion (see [3,4]), where z is the number of spins interacting with any given spin. Our focus is on calculating the spin-wave (SW) damping at any temperature below the Curie temperature T_C. In addition to the three- and four-magnon processes, which typically dominate at relatively low temperatures, as expected from traditional boson expansion methods, an additional mechanism is found that becomes important only at temperatures above about $0.5T_C$. This is a "spin-disorder" damping, which was mainly studied previously in bulk magnetic materials [3]; it was successful in explaining experiments for neutron scattering linewidths in EuO [5] and for asymmetrically broadened lineshapes in Raman scattering

in FeF_2 [6]. The mechanism involves a SW being scattered by the instantaneous disorder produced when a longitudinal spin component undergoes large thermal fluctuations, and so it is formally analogous to the so-called two-magnon damping discussed by McMichael et al. [7], occurring when a magnon scatters off static spatial inhomogeneities in a magnetic sample. Numerical estimates are presented here for the honeycomb lattice of van der Waals ferromagnets (see Fig. 1) with numerical estimates being made for $Cr_2Ge_2Te_6$. The behavior of the SW damping is shown in Fig. 2 at various elevated temperatures and small wave vectors (where damping is small compared to the SW energy).

[1] M. Gibertini et al. (2019), Nat. Nanotech. 14, 408. [2] V. V. Mkhitaryan and L. Ke (2021), Phys. Rev. B 104, 064435. [3] G. C. Psaltakis and M.G. Cottam (1981), J. Phys. A 14, 2149. [4] M. G. Cottam and Z. Haghshenasfard (2021) J. Phys. Condens. Matter 33, 235802. [5] T. L. Reinecke and R.B. Stinchcombe (1978), J. Phys. C 7, 527. [6] D. J. Lockwood et al. (1984) J. Phys. C 17, 6009. [7] R. D. McMichael et al. (2003) Phys. Rev. Lett. 90, 227601.

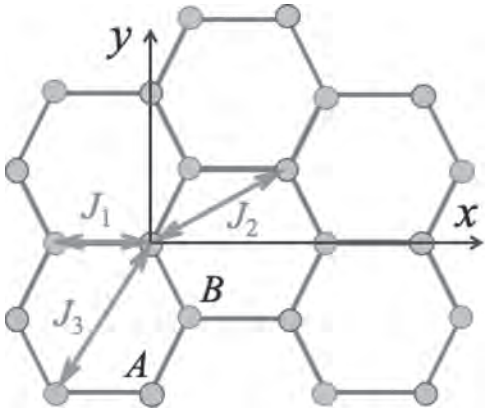

Honeycomb lattice of a van der Waals ferromagnet, showing the *A* and *B* sublattice sites and the exchange interactions between nearest, next-nearest, and third-nearest neighbors. The spin orientations are in the out-of-plane (*z*) direction.

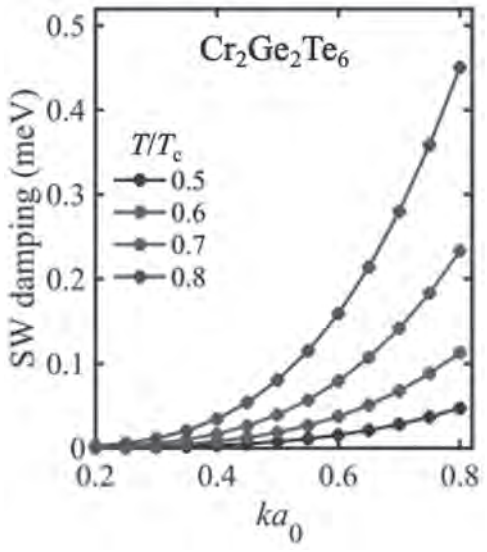

Estimates for the SW damping due to the spin-disorder scattering in a $Cr_2Ge_2Te_6$ monolayer, plotted versus the magnitude $k = |\mathbf{k}|$ of the in-plane wave vector at several elevated temperatures for T/T_C.

FD-03. Study of Spin-Wave Transport Properties in Thin Thulium Iron Garnet Films Grown on GGG and sGGG Substrates. R. Timalsina[1], B. Giri[1], H. Wang[1], A. Erickson[1], S. Sarin[1], S. Lamichhane[1], S. Liou[1], J. Shield[1], X. Xu[1] and *A. Laraoui*[1] *1. University of Nebraska-Lincoln, Lincoln, NE, United States*

Thulium iron garnet (TmIG), a rare-earth iron garnet with a ferromagnetic behavior, has attracted huge interest recently due to its successful growth down to a few nanometers [1], along with observations of perpendicular magnetic anisotropy (PMA) [1], topological Hall effect, indicative of the presence of topological spin textures [2]. Despite these advancements, comprehensive studies of its spin wave (SW) transport properties are lacking. Here, we use spin-wave electrical transmission spectroscopy (SW-ETS) in combination with nitrogen vacancy (NV) magnetometry to study SW propagation properties of TmIG thin films (thickness of 7 – 34 nm) grown on GGG and sGGG substrates. SW-ETS measurements unveil the propagation of nonreciprocal magnetostatic surface spin waves (MSSWs) on TmIG/GGG films up to distances of 80 μm with a SW group velocity of 2 – 8 km/s [3]. TmIG/sGGG films have PMA and reciprocal forward volume magnetostatic spin waves with a propagation length up to 32 μm [3]. Furthermore, by using NV magnetometry, we directly image MSSWs of wavelengths 0.8 – 2 μm, with decay lengths up to 50 μm [4]. These findings lay the groundwork for using spin waves in TmIG films for applications in magnon spintronics [5]. Acknowledgements: This material is based upon work supported by the NSF/EPSCoR RII Track-1: Emergent Quantum Materials and Technologies (EQUATE) Award OIA-2044049 and NSF award# 2328822. The research was performed in part in the Nebraska Nanoscale Facility: National Nanotechnology Coordinated Infrastructure and the Nebraska Center for Materials and Nanoscience (and/or NERCF), which are supported by NSF under Award ECCS: 2025298, and the Nebraska Research Initiative.

[1] C.N. Wu, et *al.*, *Scientific Report* 8, 11087 (2018). [2] A. S. Ahmed, et *al.*, *Nano Letters* 19(8), 5683 (2019). [3] R. Timalsina, A. Laraoui, et *al.*, *Advanced Electronic Materials,* under review. https://doi.org/10.48550/arXiv.2405.10740 (2024). [4] R. Timalsina, A. Laraoui, et *al.*, *Advanced Electronic Materials* 10, 2300648 (2024). [5] A.V. Chumak, et *al.*, *Nature Physics* 11(6):453 (2015).

Now VP12-10

FD-04. Unveiling the Origins of Strong Magnetostriction in Cobalt Ferrite Using Neutron Scattering. *G. Kaur*[2], H. Lane[1], C. Stock[2] and P. Gehring[3] *1. Physics and Astronomy, St Andrews, Edinburgh, United Kingdom; 2. Physics and Astronomy, The University of Edinburgh, Edinburgh, United Kingdom; 3. National Institute of Standards and Technology, Gaithersburg, MD, United States*

Cobalt ferrite ($CoFe_2O_4$, CFO) stands out among advanced functional materials due to its exceptional magnetostrictive behavior. This property allows its shape to be influenced by its magnetic state, making it desirable for various technological applications such as electronic devices, ferrofluids, magnetic drug delivery, microwave devices, and high-density information storage[1-3]. Here we use neutron diffraction to characterize the interplay between CFO's nuclear and magnetic structures[4] from 1.5 K to 900 K. This study complements our recent inelastic neutron scattering (INS) experiments on single crystal and powder samples[5]. The combined diffraction data, along with our INS findings, and with linear spin wave theory, will provide a deeper understanding of the underlying mechanism responsible for CFO's strong magnetostrictive effect. This knowledge will be valuable for designing novel materials with precisely controlled magnetostrictive properties for applications in areas like sensors and actuators[6].

1) Slonczewski J C, Phys. Rev. 110 1341 (1958). 2) Zheng H et al., Science 303 661 (2004). 3) Bhame S D et al., J. Appl. Phys. 100 113911 (2006). 4) Teillet et al., J. Mag. Magn. Mater. 123, 93 (1993). 5) Lane H et al., in preparation. 6) Chen Y, et al., IEEE Trans. Magn. 35 3652 (1999).

FD-05. Magnetoelastic Coupling between Surface Acoustic Waves and Backward Volume Spin Waves. *N. Homrocky*[1], C. Trevillian[1], A.N. Slavin[1] and V. Tyberkevych[1] *1. Oakland University, Rochester, MI, United States*

Hybrid magnetoelastic (ME) waves are interesting for applications in microwave signal processing and wave-based computing. An important parameter of ME interaction is the coupling rate between different acoustic and spin wave modes that considers spatial profile of interacting waves. Here, we theoretically calculate ME coupling rate between surface acoustic waves (SAW) and backward volume spin waves (BVSW) propagating in YIG/GGG bilayers. The BVSW properties were calculated using the Kalinikos-Slavin theory of dipole-exchange spin waves [1] takes includes exchange corrections to the profile and dispersion of spin waves. Figure 1 shows the dependence of the SAW-BVSW coupling rate on the bias magnetic film for different YIG thicknesses. Generally, the coupling rate increases with increasing field, which is related to the increase of the resonant wavevector at which dispersions of two waves cross. However, for very large fields and, respectively, wavevectors, the SAW localization depth becomes smaller than YIG thickness and the coupling rate decreases. The maximum achievable coupling rate is inversely proportional to YIG thickness and can exceed 100 MHz for sub-mm thicknesses. Figure 2 shows an example of numerically calculated spectrum of hybrid ME waves in the considered geometry. The SAW and the lowest BVSW branches cross around wavevector 1 rad/mm (wavelength 6 mm), at which point a clearly visible anti-crossing region appears due to ME interaction. Since SAW and BVSW modes have opposite signs of group velocity, their interaction creates a *frequency gap* in the spectrum of hybrid waves, in which no propagating modes exist. This property is in striking contrast to coupling of waves with the same sign of group velocity (e.g., SAW and surface spin waves) and can be used to design SAW-BVSW converters having 100% conversion efficiency.

Kalinikos, B. A., and A. N. Slavin. "Theory of dipole-exchange spin wave spectrum for ferromagnetic films with mixed exchange boundary conditions." *J. Phys. C: Solid State Phys.* 19 (1986): 7013.

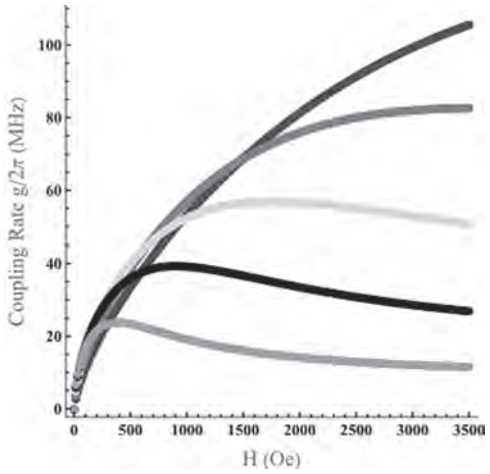

SAW-BVMSW coupling rate as a function of bias magnetic field strength for different YIG film thicknesses (from top to bottom: 250 nm, 500 nm, 1 mm, 2 mm, and 5 mm).

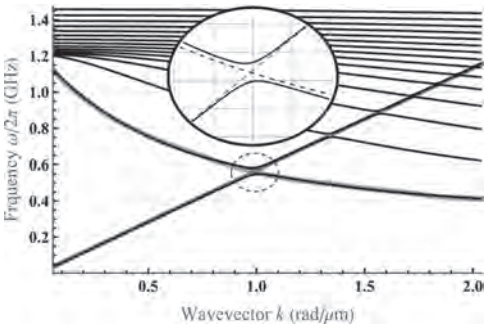

Spectrum of the hybrid ME system in YIG/GGG bilayer. Highlighted branches correspond to SAW (red) and BVSW (blue). Parameters: YIG thickness 5 μm, bias magnetic field 100 Oe.

FD-06. Backward Volume Spin Waves in Graded Magnonic Media. K. Fripp[1] and *V. Kruglyak*[1] *1. University of Exeter, Exeter, United Kingdom*

We have modelled numerically backward-volume dipole-exchange spin waves (BVDESWs) in graded profiles of the bias magnetic field. We demonstrate spin-wave wavelength conversion upon the wave's reflection from turning points due to the two characteristic minima ("U-points") occurring in their dispersion (Fig. 1) at finite (non-zero) wave vectors. As a result, backward-volume dipole-exchange spin waves confined in "spin-wave wells" either form Möbius modes (Fig. 2), making multiple real-space turns for each reciprocal-space roundtrip, or split into pairs of degenerate modes in the valleys near the two U-points. The latter modes may therefore be assigned a pseudospin. We show that the pseudospin can be switched by scattering the spin wave from decreases of the bias magnetic field, while it is immune to scattering from field increases. Pseudospin creation and read-out can be accomplished using chiral magnonic resonators [1-3]. Taken together, the possibility of pseudospin creation, manipulation and read-out suggests a path to development of a spin-wave version of valleytronics ("magnon valleytronics"), in which the pseudospin (rather than amplitude or phase) of spin waves would be used to encode data. Our results are not limited to graded bias magnetic field [4] but can be generalized to other magnonic media with spatially varying characteristics, produced using the toolbox of graded index magnonics.

[1] V. V. Kruglyak, Appl. Phys. Lett. 119, 200502 (2021). [2] K. G. Fripp, A. V. Shytov, and V. V. Kruglyak, Phys. Rev. B 104, 054437 (2021). [3] K. G. Fripp, Y. Au, A. V. Shytov, and V. V. Kruglyak, Appl. Phys. Lett. 122, 172403 (2023). [4] K. G. Fripp and V. V. Kruglyak, Phys. Rev. B 103, 184403 (2021).

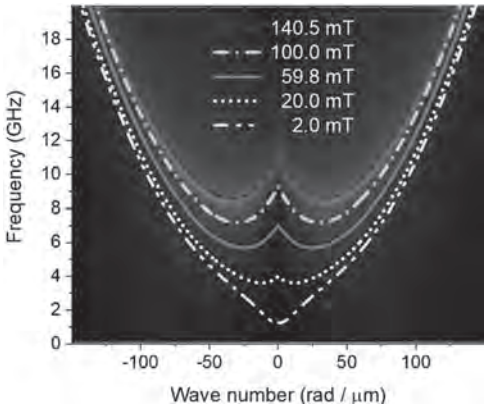

Fig. 1 The lines show the dispersion relation of BVDESWs for the indicated values of the bias magnetic field. The background shows the dispersion for the field of 140.5 mT obtained by Fourier-transforming results of the micromagnetic simulations.

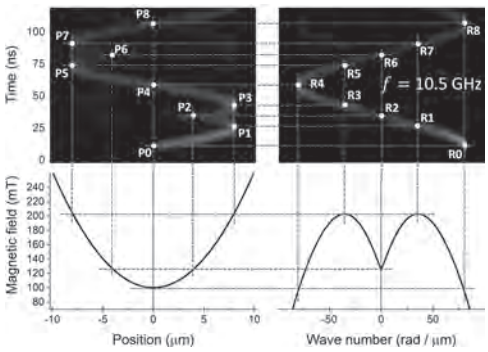

Fig. 2 The wave-packet trajectories (top row) and corresponding magnetic field profiles (bottom row) are shown in the real (left column) and reciprocal (right column) space for the central frequency of 10.5 GHz. The brighter color corresponds to greater spin-wave amplitude. The dashed lines and points at their crossings show the correspondence between features from the different panels.

FD-07. Spin wave band structure in ferromagnetic waveguides with a sinusoidal magnetization distribution. P. Micaletti[1], A. Roxburgh[2], M. Marzolla[3], E. Iacocca[2] and *F. Montoncello*[1] *1. Department of Physics and Earth Sciences, University of Ferrara, Ferrara, Italy; 2. Department of Physics, University of Colorado at Colorado Springs, Colorado Springs, CO, United States; 3. Department of Information Science and Engineering, University of Bologna, Bologna, Italy*

In 3D Magnonics [1], a ferromagnetic film layer (waveguide) can have a non-uniform magnetization due to the vertical interaction with other layers of different geometry [2]. Here, we study a film with a periodic magnetization, implemented as a sine function with variable amplitude (Fig. 1-a). Through micromagnetic simulations [3], we obtain the sinusoidal magnetization after relaxation of a uniform state to an applied sinusoidal magnetic field. The sinusoidal field simulates the vertical interaction with an overlayer of appropriate geometry. By Fourier analysis [4], the SW dispersion relations were obtained, together with the mode spatial profiles. We discuss the occurrence of band gaps at the zone boundary as a function of the sinusoidal field magnitude. Then we show how a periodic uniaxial magnetic anisotropy Ku can also attain such a sinusoidal magnetization, the amplitude of which can be varied through Ku. This anisotropy simulates a ferroelectric overlayer interacting via inverse-magnetostriction with the ferromagnetic film. We show how by tuning Ku it is possible to switch the magnonic gap from zero to about 1 GHz, turning the magnonic waveguide behavior from metallic (crossing dispersions) to insulating (anti-crossing) (Fig. 1b,c). We suggest applications of our findings to sensing activity (nanoparticles adsorbed onto the overlayer can modify Ku and hence dynamic properties like the gap or the frequency of localized modes) and to magnon stimulated adiabatic Raman passage (where Ku can modify the waveguide coupling strength and hence the magnon population transfer) [5]. PM and FM acknowledge support by the Department of Physics and Earth Sciences-University of Ferrara Grant FIRD 2023, as well as the CINECA award under the ISCRA initiative, for the availability of high performance computing resources and support. A.R. and E.I. acknowledge support by the National Science Foundation under Grant No. 2205796.

[1] G. Gubbiotti in "Three-Dimensional Magnonics: Layered, Micro and Nanostructures", Jenny Stanford Publishing, Singapore (2019). [2] R. Negrello et al., APL Materials10, 091115 (2022). [3] A. Vansteenkiste et al., AIP Advances 4, 107133 (2014). [4] B. Van de Wiele and F. Montoncello, J. Phys. D: Appl. Phys. 47, 315002 (2014). [5] Q. Wang, T. Brächer, M. Fleischhauer, B. Hillebrands, P. Pirro, Appl. Phys. Lett. 118, 182404 (2021).

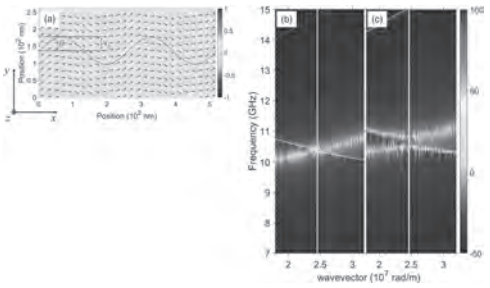

Fig. 1: (a) Magnetization distribution, Y_0 is the undulation amplitude. (b) Band structure along x-axis when Ku=0.8 kJ/m^3, showing zero gap at the Brillouin zone boundary (metallic behavior). (c) Band structure along x-axis when Ku=5.0 kJ/m^3, showing a gap of 0.350 GHz (insulating behavior).

FD-08. Mode Crossing in Interface-coupled TmIG/CoFeB Bilayers with Perpendicular Magnetization. W. Al Misba[1], J.E. Shoup[2], M.J. Gross[3], K. Hayashi[4], C.A. Ross[4], J. Atulasimha[1] and *D.B. Gopman*[2] *1. Department of Mechanical and Nuclear Engineering, Virginia Commonwealth University, Richmond, VA, United States; 2. Materials Science and Engineering Division, National Institute of Standards and Technology, Gaithersburg, MD, United States; 3. Department of Electrical Engineering and Computer Science, Massachusetts Institute of Technology, Cambridge, MA, United States; 4. Department of Materials Science and Engineering, Massachusetts Institute of Technology, Cambridge, MA, United States*

Magnetic bilayers offer versatile opportunities to tailor functional properties. For example, a metallic ferromagnet may serve as the second layer for compatibility with magnetic tunnel junctions (MTJs) to sense the magnetization of a complex oxide. This second layer may effect changes into the bilayer's micromagnetic properties, ranging from vertical domain walls [1]; domain structure and coercivity modification to Gilbert damping enhancement [2] and mutual resonance effects [3] like avoided crossings. We present static and dynamic properties of one such heterostructure - a $Tm_3Fe_5O_{12}$ (TmIG) / $Co_{20}Fe_{60}B_{20}$ (CoFeB) bilayers – as an advance toward integrating perpendicular magnetic anisotropy (PMA) garnets with MTJs. 40 nm thick TmIG films grown on (111)-cut GGG substrates were coated with ion beam sputtered CoFeB films using the stacking structure (numbers in parentheses reflect thicknesses in nm): CoFeB(x)/W(0.4)/CoFeB(0.8)/MgO(1)/W(5); x = 0.8 nm; 1 nm; 3 nm and 4 nm. Post-annealing at 300 °C was carried out to enhance PMA in the CoFeB layer. Static magnetic properties change significantly between the two thinner films (x = 0.8 nm, 1 nm) and the thicker films (x = 3 nm, 4 nm). We observe PMA with larger coercivity in the thinner films as compared to uncoated TmIG, whereas the thicker films undergo a two-step reversal: irreversible TmIG switching followed by CoFeB rotation. Kerr microscopy reveals a transition from labyrinth domains to dendritic patterns (Fig. 1 (a)-(c)) as the demagnetization penalty of the CoFeB overlayer modifies the magnetic microstructure. We see clear dynamic coupling in the thickness-dependent enhancement of TmIG Gilbert damping, increasing as much as 50 %. This damping enhancement arises from spin pumping between two non-collinear magnetizations (TmIG and CoFeB). Angular dependent ferromagnetic resonance reveals a mode crossing where this damping enhancement is minimized (Fig. 2(a)-(b)) for both modes as the effective fields merge. Our study sheds light on engineering spintronic devices via interfacial damping control.

[1] Z. R. Nunn, C. Abert, and D. Suess, Sci. Adv. Vol 6, p. eabd8861 (2020) [2] P. Hyde, L. Bai, and D. M. J. Kumar, Phys. Rev. B Vol 89, p. 180404(R) (2014) [3] S. Klingler, V. Amin, and S. Geprägs, Phys. Rev. Lett. Vol 120, p.127201 (2018) Partial funding is acknowledged from the following sources: NSF EECS 1954589, 1954606, 2152825 NSF CCF 1909030 National Institute of Standards and Technology of the US Department of Commerce

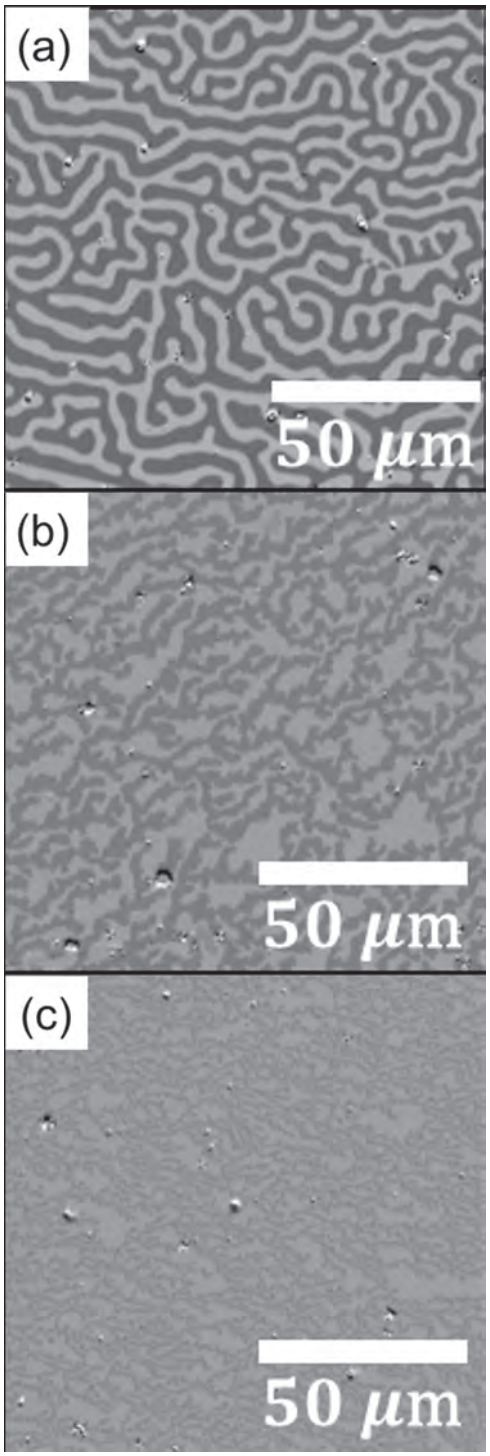

FIG 1. Magnetic domain images for (a) pristine TmIG; (b) x = 1 nm; (c) x = 3 nm.

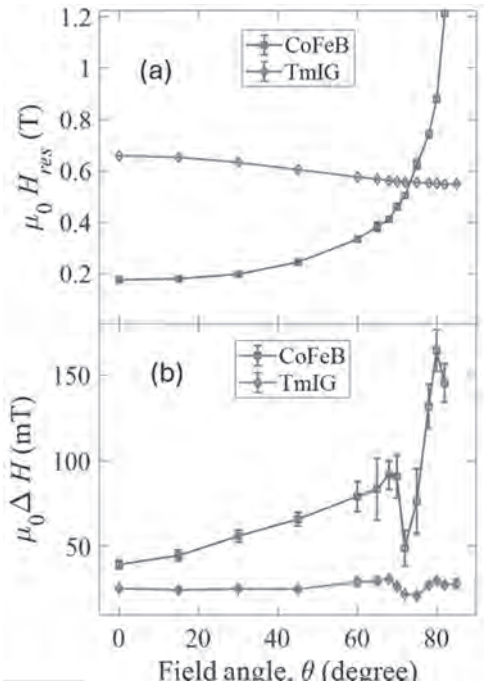

FIG 2. Resonance field (a) and linewidth (b) for TmIG and CoFeB modes at 14 GHz for x = 3 nm.

FD-09. Creation of Bose-Einstein condensate of magnons in antiferromagnet using rapid cooling. P. Artemchuk[1], V. Tyberkevych[1] and *A.N. Slavin*[1] *1. Department of Physics, Oakland University, Rochester, MI, United States*

It was shown experimentally that magnons in a ferromagnet (FM) can undergo a process of Bose-Einstein condensation (BEC) at room temperature [1]. The magnonic BEC in FM [1] was achieved by increasing the number of magnons using parametric pumping [1, 2]. Later, BEC of magnons in an FM sample was created when sample was, first, heated by a current pulse, and, then, rapidly cooled when the current pulse ends [3]. It would be interesting to observe BEC of magnons in antiferromagnets (AFM), and theories of magnonic BEC in AFM using the application of a magnetic field [4] or creation of a spin accumulation [5] were proposed. We propose to use the method of rapid cooling [3] to achieve BEC of magnons in an AFM. We assume that a heating pulse creates a gas of thermal magnons in an AFM sample (we consider NiO), while no coherent magnons are excited. We describe the gas of thermal magnons in AFM using thermodynamic parameters: total energy E and total number of magnons N. To study the temporal evolution of the magnon gas in AFM we consider the system of equations that accounts for the interaction of the gas of magnons with the AFM crystal lattice. This system allows us to calculate the temporal evolution of the total energy and number of magnons in the rapid cooling process. We also calculated evolution of the chemical potential μ and temperature T of the gas (see Fig.1), and estimated the fraction of magnons N_{BEC}/N in the condensed (BEC) state (see Fig.2). The results shown in Figs. 1, 2 were obtained for the heating temperature 360 K, room temperature 280 K and cooling time 0.1 ns. They demonstrate that the lifetime of BEC in an AFM is much shorter than in FM, and that BEC formation in an AFM requires much shorter cooling time (0.1 ns in AFM compared to ~ 1 ns in FM). We believe that the obtained results will be useful for the planning of experiments to observe BEC of magnons in AFM crystals.

[1] S. O. Demokritov, V. E. Demidov, O. Dzyapko, et al., Nature 443, 430-433 (2006). [2] A. A. Serga, V. S. Tiberkevich, C. W. Sandweg, et al., Nat. Commun. 5, 3452 (2014). [3] M. Schneider, T. Brächer, D. Breitbach, et al., Nature Nanotech. 15, 457 (2020). [4] T. Giamarchi, C. Rüegg and O. Tchernyshyov, Nature Phys. 4, 198-204 (2008). [5] E. L. Fjærbu, N. Rohling, and A. Brataas, Phys. Rev. B 95, 144408 (2017).

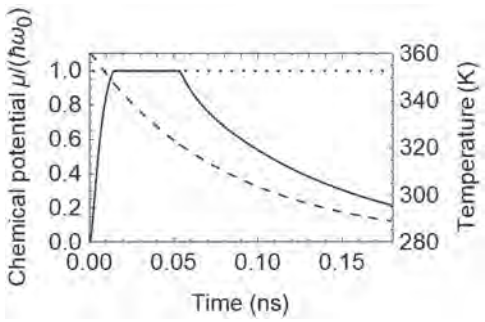

Fig. 1. Change of chemical potential μ (solid line), normalized by the minimum energy of magnons (dotted line), and temperature *T* (dashed line) of the magon gas during rapid cooling process.

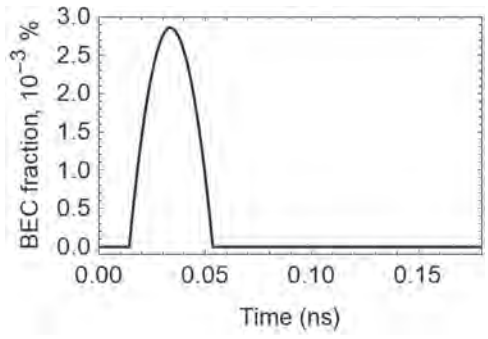

Fig. 2. Change in time of the fraction of magnons N_{BEC}/N in the state of Bose-Einstein condensate.

FD-10. Exotic antiferromagnetic magnons on a Möbius strip: Topology-induced symmetry breaking. *K. Deng*[1] and R. Cheng[1,2,3] *1. Electrical and Computer Engineering, University of California Riverside, Riverside, CA, United States; 2. Physics and Astronomy, University of California Riverside, Riverside, CA, United States; 3. Materials Science and Engineering, University of California Riverside, Riverside, CA, United States*

Topological effects in solid-state systems are largely enabled by symmetry properties, typically arising from interactions. On the other hand, the impact of real-space topology beyond what is normally derivable from a periodic boundary condition has been overlooked. Recent studies of non-trivial real-space topological structures (such as Möbius strips) primarily focused on local curvature effects under a continuous geometry, while it remains mysterious if there are any residual effects solely attributed to the non-trivial boundary condition even in the absence of local curvature. Here, using antiferromagnetic (AFM) magnons on a Möbius strip, we demonstrate a hitherto unknown mechanism dubbed topology-induced symmetry breaking, wherein certain local symmetry preserved by the Hamiltonian is broken in the excited eigenstates due to topological constraints. The AFM magnons exhibit linear polarization of the Néel vector devoid of chirality and form two non-degenerate branches that cannot be smoothly connected to or be decomposed by the circularly-polarized magnons commonly seen in AFM materials. Only one branch of the exotic magnons supports standing-wave formation on the Möbius strip while the other does not, owing to its spectral shift incurred by the boundary condition. Our findings not only showcase the significant influence of real-space topology on the physical nature of magnons but also inspire new research directions in the broad pursuit of topological effects in physics.

[1] K. Deng and R. Cheng, arXiv:2403.07846.

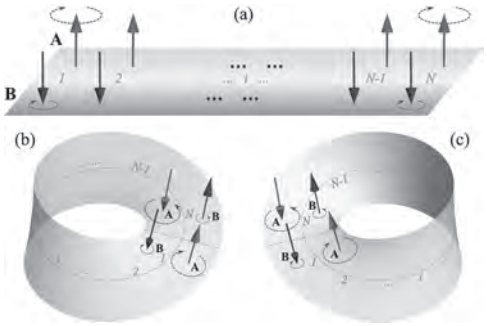

(a) AFM nanoribbon consists of two ferromagnetic spin chains, where the red (blue) arrows show the equilibrium spins on the A (B) sublattice. The black arrows indicate the spin precessions associated with the left-handed mode. (b) and (c) depict the two distinct ways of creating a Möbius strip by the nanoribbon. While the AFM ground state is compatible with the twisted boundary condition, the excited states in the form of circularly-polarized magnons are radically disrupted.

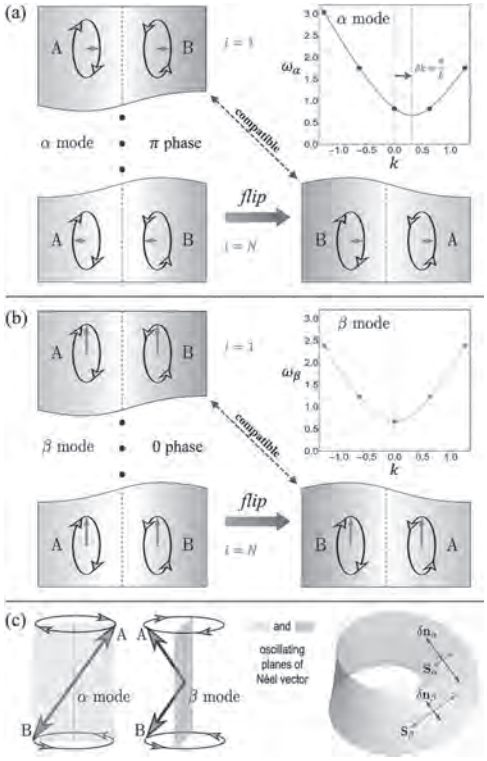

(a) and (b) illustrate the α and β modes at k=0, and the spectra of the lowest few modes on each branch. (c) Left: 3D perspective of the spin precessions in each mode. Right: illustration of the oscillating Néel vector and the total spin vector.

FD-13. Thickness crossover from two- to three-dimensional magnon transport properties. *C.M. Webb*[1] and S. Zhang[1] *1. Physics, University of Arizona, Tucson, AZ, United States*

Magnon transport properties are highly dependent on dimensionality. In thermal equilibrium, the magnon number in a 2D system diverges as the effective magnetic field approaches zero, while in a 3D system, it is nearly independent of magnetic anisotropy and external field. Consequently, magnon magnetoresistance in 2D can reach several thousand percent at moderate external field strengths, whereas it is much smaller in 3D systems. For an

ultrathin magnetic film composed of only a few monolayers, magnon transport exhibits both 2D and 3D characteristics. We theoretically identify the crossover thickness for both ferromagnetic and antiferromagnetic materials, below which the equilibrium and transport properties of magnons are 2D-like. We find the crossover thickness ranges from one monolayer to several monolayers, depending on the parameters. Our identified crossover thickness can serve as a guideline for determining the film thickness at which a material can be approximately treated as 2D. This work is supported by NSF-ECCS.

Session FE
BIOMEDICAL THERAPIES, DIAGNOSIS AND NANOMEDICINE

Kai Wu, Chair
Texas Tech University, Lubbock, TX, United States

INVITED PAPER

FE-01. Magnetoplasmonic Nanocapsules as Wirelessly Controlled Nanotherapies. *J. Nogués*[1,2], A. Lafuente[1], A. Flucksman[3], A. Gómez Roca[1], J. Sort[4,2], C. Nogues[4], O. Benny[3] and B. Sepulveda[5] *1. Catalan Institute of Nanoscience and Nanotechnology (ICN2), Bellaterra, Spain; 2. ICREA, Barcelona, Spain; 3. Institute for Drug Research, The Hebrew University of Jerusalem, Jerusalem, Israel; 4. Universitat Autonoma de Barcelona, Bellaterra, Spain; 5. Instituto de Microelectronica de Barcelona (IMB-CNM, CSIC), Bellaterra, Spain*

Advanced nanobiomedical applications have been traditionally based on chemically synthesized single-phase inorganic or organic nanoparticles. Here, we present a novel type of structure especially suited for diverse biomedical uses: magnetoplasmonic nanodomes [1,2]. The nanodomes are composed of magnetoplasmonic semishells deposited onto 100-200 nm diameter polymer beads. The very high plasmonic absorption of the nanodomes in the near-infrared is used for very efficient local optical heating for cancer treatment [1]. The nanodomes exhibit a magnetic vortex configuration which, due to its vanishing remanent magnetization, results in virtually no dipolar interactions between particles, leading to an outstanding colloidal stability of the nanoparticles despite their size [1]. Importantly, their strong magnetic character allows remote manipulation to easily concentrate them in the site of action and regulate the level of photo-hyperthermia. Moreover, due to their asymmetric shape, the nanodomes exhibit strong optic and magnetic anisotropies. Thus, rotation of the nanodomes through alternating magnetic fields can be tracked optically using their different absorption depending on the orientation. Since the rotation of the nanoparticles depends strongly on the viscosity of the medium, which in turn depends on the temperature, the optical tracking of the rotation can be used to accurately determine the local temperature change around nanodomes [2], allowing in-situ tracking of the photo-hyperthermia treatments. The same nanodome concept can be extended to drug delivery, where the semishell allows for remote control of the nanocapsule, or MRI tracking of the beads [3]. This concept of magnetoplasmonic nanocapsules loaded with paclitaxel drug has enabled complete eradication of the tumors in vivo in mice by combining magnetic concentration and photothermal actuation, using a drug concentration between 200 and 500-fold lower than the therapeutic window of the free drug (Figure 1) [3]. We have extended this nanocapsules concept to generate enhanced tunable synergistic nanotherapeutic actuation, for example, combining simultaneous photodynamic and photothermal therapies for enhanced antibiotic effects [4].

[1] Z. Li et al. Appl. Mater. Today 12, 430 (2018). [2] Z. Li et al. Small, 14, 1800868 (2018). [3] A. Flucksman et al. ACS Nano 17, 1946 (2023). [4] A. Flucksman et al. ACS Appl. Mater. Interfaces 15, 50330 (2023).

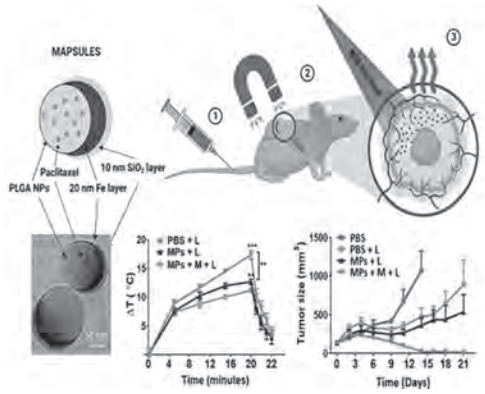

Schematic representation of the efficient tumor eradication at ultralow drug concentration via externally magnetic concentration and photothermal actuation.

CONTRIBUTED PAPERS

FE-02. Analyzing the magnetic properties of iron oxide nanorods for biomedical applications. *S.S. Laha*[1], E. Odion[1] and O.T. Mefford[1] *1. Materials Science and Engineering, Clemson University, Clemson, SC, United States*

Recent studies focusing on shape-modified nano-magnetite have witnessed significant developments in cancer nanomedicine research, including magnetic hyperthermia, targeted drug delivery, and advanced imaging techniques such as magnetic resonance imaging (MRI) and magnetic particle imaging (MPI). In this regard, iron oxide nanorods, with exciting magnetic properties, have emerged as a favorable candidate both from the standpoint of fundamental physics and practical applications. Magnetite (Fe_3O_4) nanorods of various aspect ratios, were fabricated using a typical hydrothermal procedure (with minor modifications) as described by Das *et al.*[1] The precursors, containing iron pentacarbonyl, oleic acid, and hexadecylamine, were dissolved in a high boiling point solvent, namely, 1-octanol and heated in a Teflon-lined autoclave chamber at ~220 °C, for several hours to produce rod-like structures of magnetite. The DC magnetic measurements, M vs. H and M vs. T, conducted on one such sample (L=42.06 ± 7.90; W= 4.17 ± 0.77; Figure 1A) report the formation of particles exhibiting saturation magnetization of ~60 emu/g at 300 K (Figure 1B). Furthermore, the zero-field cooled (ZFC) magnetization (M) vs. temperature (T) measurements (applied *dc* field =100 Oe) clearly show evidence of Verwey transition (VT), a typical metal-insulator transition corresponding to the magnetite phase, near ~ 120 K (Figure 1C), without any clear evidence of blocking transitions. Interestingly, the AC magnetic studies, for example, $c^{//}$ (out-of-phase susceptibility) vs. T measurements (Figure 1D), performed at three different frequencies of 100 Hz, 1000 Hz, and 10000 Hz under an AC magnetic field amplitude of 10 Oe, do show distinct blocking signatures near 200-250 K, along with low-temperature glassy features < 50 K, as reported earlier for magnetite particles.[2-4]

1. R. Das, J. Alonso, Z. Nemati Porshokouh, V. Kalappattil, D. Torres, M.-H. Phan, E. Garaio, J. Á. García, J. L. Sanchez Llamazares and H. Srikanth, The Journal of Physical Chemistry C 120(18), 10086-10093 (2016).

2. R. Das, J. A. Cardarelli, M.-H. Phan and H. Srikanth, Journal of Alloys and Compounds 789, 323-329 (2019). 3. S. Laha, R. Regmi and G. Lawes, Journal of Physics D: Applied Physics 46 (32), 325004 (2013). 4. S. S. Laha, E. Abdelhamid, M. P. Arachchige, A. Kumar and A. Dixit, Journal of the American Ceramic Society 100 (4), 1534-1541 (2017).

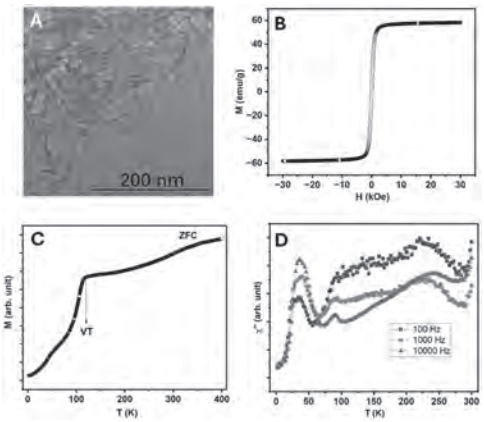

Figure 1: A. TEM image of Fe_3O_4 nanorods; B. Magnetization (M) *vs* Applied field (H) plot at 300K; C. Magnetization (M) *vs*Temperature (T) plot under a DC applied field of 100 Oe, VT represents the Verwey transition near 120 K; D. Out-of-phase ($c^{//}$) susceptibility vs T plots at three different frequencies of 100 Hz, 1000 Hz and 10000 Hz at 10 Oe field amplitude, of Fe_3O_4 nanorods.

FE-03. Highly Uniform Star-shaped Multifunctional Magnetic-plasmonic Au-Fe_3O_4 Nano-heterostructures. B. Muzzi[1], M. Albino[1,2], E. Balica[2], A. Omelyanchik[3], A. Gabbani[4,1], A. Laurenzana[5], F. Pineider[4] and *C. Sangregorio[1,2] 1. ICCOM-CNR, Sesto Fiorentino (FI), Italy; 2. Dept. of Chemistry U.Schiff, Univ. of Florence, Sesto Fiorentino (FI), Italy; 3. Dept. of Chemistry and Industrial Chemistry, Univ. of Genova, Genova, Italy; 4. Dept. of Chemistry and Industrial Chemistry, Univ. of Pisa, Pisa, Italy; 5. Dept. of Experimental and Clinical Biomedical Sciences, Univ. of Florence, Florence, Italy*

Multifunctional hybrid nanoparticles have attracted enormous interest for the possibility to combine two or more functionalities from different inorganic materials in the same nanostructure. Within this framework, magnetic-plasmonic nanoparticles (MP-NP) are characterized by a unique combination of magnetic and optical properties[1,2], which can provide a multifunctional theranostic platform for biomedicine. Here we present the synthesis of an Au@Fe3O4 core@shell system with a highly uniform unprecedent star-like shell morphology with combined plasmonic and magnetic properties. [3] An advanced electron microscopy characterization allowed assessing the multifaced nature of the Au core and its role in the growth of the peculiar epitaxial star-like shell with excellent crystallinity and homogeneity. Magnetometry and magneto-optical spectroscopy revealed a pure magnetite shell, with a superior saturation magnetization compared to similar Au@ Fe3O4 heterostructures reported in the literature, ascribed to the star-like morphology, as well as to the large thickness of the shell. Of note, Au@ Fe3O4 nanostars loaded cancer cells displayed magneto-mechanical stress under a low frequencies external alternating magnetic field (few tens of Hz). On the other hand, such a uniform, homogeneous, and thick magnetite shell enables the shift of the plasmonic resonance of the Au core to 640 nm, which is the largest red-shift achievable in Au@Fe3O4 homogeneous core@ shell systems, prompting application in photothermal therapy and optical imaging in the first biologically transparent window. Preliminary experiments performed irradiating a stable water suspension of the nanostar and Au@ Fe3O4 loaded cancer cell culture suspension at 658nm, confirmed their optical response and their suitability for photothermal therapy. The outstanding features of the prepared system can be thus potentially exploited as multifunctional platform for magnetic-plasmonic applications.

[1] Espinosa, A.; Reguera, J.; Curcio, et al. Small 16 (2020) 1. [2] Li, Z.; Jin, J.; Yang, Nat. Commun. 11 (2020) 1. [3] Muzzi, B.; Albino, M.; Omelyanchik, A. et al. ACS Adv. Mater. Inter. 5 (2022) 1471.

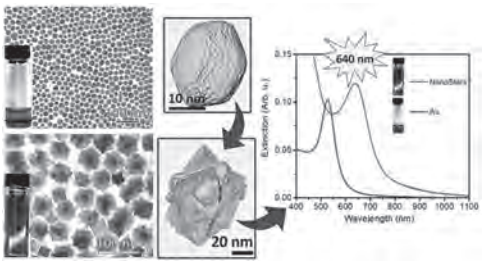

FE-04. Withdrawn

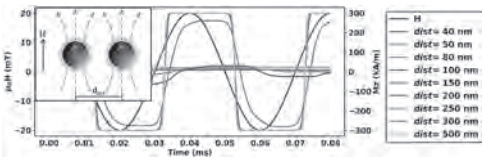

Fig 1. Dynamic magnetization responses of 30 nm SPIONs subjected to an excitation field of 25 kHz and amplitude of 20 mT/μ_0. The average inter-particle distance is varied from 40 nm to 500 nm. SPIONs are assumed in the field-free region.

FE-05. Enhanced Imaging Capabilities of a Single-Sided Magnetic Particle Imaging Scanner for Large Phantoms. *C. McDonough*[1], M. Jurj[1] and A. Tonyushkin[1] *1. Physics, Oakland University, Rochester, MI, United States*

Magnetic Particle Imaging (MPI) detects superparamagnetic iron oxide (SPIO) tracers, offering exceptional contrast, sensitivity, and quantification [1]. Conventional closed-bore MPI scanners restrict imaging volume, our single-sided MPI scanner design [2] allows for an unrestricted imaging volume, uniquely enabling the imaging of objects larger than those accommodated by commercially available MPI scanners. Our single-sided MPI scanner employs a 0.58-0.84T/m field-free line (FFL) and a 25kHz drive field with a 1.6mT amplitude [3]. The FFL offers advantages over field-free point scanners [4,5], including higher sensitivity due to integration along FFL, and compatibility with well-established image reconstruction techniques like filtered backprojection (FBP). Here, we demonstrate our scanner's capabilities by imaging a large (16cm x 12cm x 6cm) anatomical breast phantom (SynDaver) that exceeds the size limits of commercial small animal systems, targeting applications for breast cancer detection. In the experiment, two model "tumors" of 18µl spherical volumes filled with undiluted SynomagD embedded 13mm apart and 6mm deep in the breast phantom. We performed FBP imaging in the coronal plane and 2D projection imaging in the axial plane at the maximum resolutions of 4mm and 2mm in the horizontal and the vertical planes, respectively. The reconstructed FBP and projection images revealed distinct point sources with clear separation. Spatial resolution in the coronal plane, based on the point-spread function, was measured to be 6mm full-width at half maximum, achieving sub-centimeter performance comparable to clinical nuclear medicine. These results validate our single-sided MPI scanner's unique ability to image objects larger than those compatible with the existing commercial systems, while maintaining acceptable resolution. In the future, by modifying the current setup with the scanner rotation will eliminate the need for a subject turntable thus lifting the limit on the overall subject size. This advancement opens new possibilities for applications requiring larger imaging volumes, particularly in clinical diagnostic imaging.

1. B. Gleich and J. Weizenecker, "Tomographic imaging using the nonlinear response of magnetic particles," Nature, vol. 435, no. 7046, pp. 1214–1217, 2005. 2. J. Pagan, C. McDonough, T. Vo, and A. Tonyushkin, "Single-sided magnetic particle imaging device with field-free-line geometry for in vivo imaging applications," IEEE Transactions on Magnetics, vol. 57, no. 2, p. 5300105, 2021. 3. C. McDonough, J. Chrisekos, and A. Tonyushkin, "Tomographic Magnetic Particle Imaging with a Single-Sided Field-Free Line Scanner," IEEE Trans. on Biomedical Engineering, doi:10.1109/TBME.2024.3427665. 4. T.F. Sattel, et. al., "Single-sided device for magnetic particle imaging," J of Phys D: Appl Phys, vol. 42, no. 2, p. 022001, jan 2009. 5. K. Grafe, et. al., "2D Images Recorded With a Single-Sided Magnetic Particle Imaging Scanner," IEEE Trans. on Medical Imaging, vol. 35, no. 4, pp. 1056–1065, apr 2016.

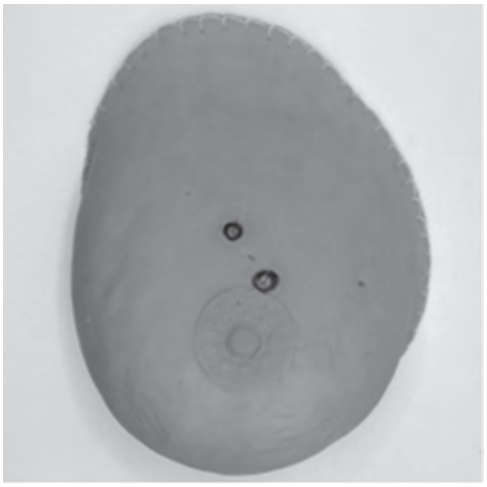

Breast phantom with two artificial SPIO tumors.

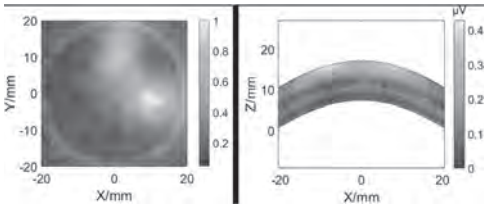

Coronal and axial MPI image of SPIO breast tumors.

FE-06. Magnetic position determination with giant-magnetoresistance and moving field-free point in catheter. *L. Paquet*[1,2,3], A. Solignac[4], K. Tse Ve Koon[1], M. Ohta[3,5], N. Tsuruoka[6], Y. Haga[5,6], C. Fermon[4], M. Pannetier-Lecoeur[4] and B. Ducharne[2,7] *1. CREATIS, Université Lyon 1, CNRS UMR5220, INSERM U1206, INSA-Lyon, Lyon, France; 2. ELyTMaX, IRL3757, Univ Lyon, INSA-Lyon, CEntrale Lyon, Université Claude Bernard Lyon 1, Tohoku University, Sendai, Japan; 3. Institute of Fluid Science, Tohoku University, Sendai, Japan; 4. SPEC, CEA, CNRS, Université Paris-Saclay, CEA-Saclay, Gif-Sur-Yvette, France; 5. Graduate School of Biomedical Engineering, Tohoku University, Sendai, Japan; 6. Graduate School of Engineering, Tohoku University, Sendai, Japan; 7. Université de Lyon, INSA-Lyon, LGEF EA682, Lyon, France*

X-ray fluoroscopic imaging is the standard method to obtain catheter position during catheterization procedures, a minimally invasive surgery for diagnostic and treatment of the vascular network [1]. However, this method exposes both patients and doctors to ionizing radiation. To address this issue, we propose a new method to track the catheter by installing a magnetic sensor at the catheter tip and generating a known magnetic field (MF) around the operative zone. Due to the mandatory small size of the catheter, we utilized micrometer-sized giant-magnetoresistance (GMR) sensors for this tracking system [2, 3]. GMR sensors require only two connection wires, have a wide bandwidth that allows flexibility in selecting the working frequency and can detect low-intensity MFs down to the nano Tesla range [4]. In this work, a 300µm x 700µm GMR chip (shown Fig.1b) is prepared and characterized (Fig 1.a). It is then installed on a catheter to show the integration feasibility. The presented results are obtained with GMRs connected in a Wheatstone bridge configuration in a larger chip for ease of manipulation. Both present a similar magnetic response. Our novel tracking method is based on the time detection of a moving null MF, known as the Field-Free Point (FFP) inspired by Magnetic Particle Imaging (MPI) [5]. Rather than measuring the MF intensity to compute the position [6], the time detection of the FFP gives the information on the position. We constructed an experimental setup to demonstrate the feasibility of this method in one dimension. On a 1D setup, along a line from -15cm to 15cm, we measure the positions and standard variations every cm. The results are shown in Fig 2. The average of

all standard deviation is 1.3mm with an average deviation from the actual position of 4.9% showing promising results for further steps.

[1] C.J Davidson and R.O Bono, 1997. Cardiac catheterization. *Libby P*, *10*, p.18. [2] C Chopin, J Torrejon, A Solignac et al, 2020. Magnetoresistive sensor in two-dimension on a 25 μm thick silicon substrate for in vivo neuronal measurements. *ACS sensors*, *5*(11), pp.3493-3500. [3] S.H.N Kouakeuo, A Solignac, R.V Sabariego et al, 2022. Internal characterization of magnetic cores, comparison to finite element simulations: a route for dimensioning and condition monitoring. *IEEE Transactions on Instrumentation and Measurement*, *71*, pp.1-10. [4] J Moulin, A Doll, E Paul et al, 2019. Optimizing magnetoresistive sensor signal-to-noise via pinning field tuning. *Applied Physics Letters*, *115*(12). [5] B Gleich and J Weizenecker, 2005. Tomographic imaging using the nonlinear response of magnetic particles. *Nature*, *435*(7046), pp.1214-1217. [6] H.A Jaeger, A.M Franz, K O'Donoghue et al, 2017. Anser EMT: the first open-source electromagnetic tracking platform for image-guided interventions. *International journal of computer assisted radiology and surgery*, *12*, pp.1059-1067.

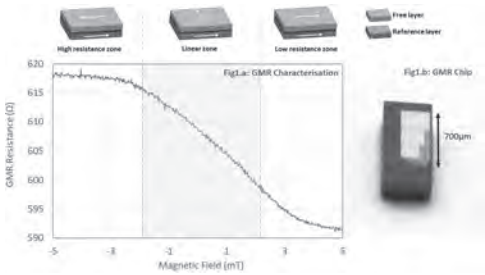

Figure 1: 1a – Resistance of the GMR alone vs. an external magnetic field. The top sketches show the corresponding ferromagnetic layers' magnetic orientations 1b. Manufactured chip with 2 GMRs

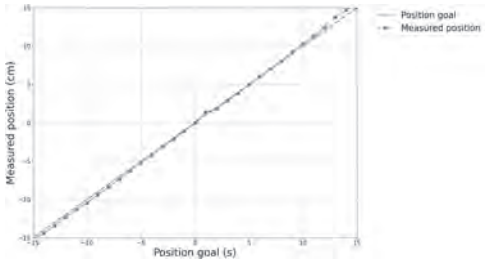

Figure 2: Comparison between the position goal and the measured positions

FE-07. Novel Smart Implants for Brain Aneurysms. *P. Velvaluri*[1], B. Luo[1], E. Spetzler[2], E. Mackensen[2], J. McCord[2], E. Quandt[2], D. Meyners[2] and N.X. Sun[1] *1. Northeastern University, Boston, MA, United States; 2. Kiel University, Kiel, Germany*

Brain aneurysms, characterized by balloon-like disfigurations along blood vessels, pose a significant risk if untreated, potentially leading to rupture, brain hemorrhage, and death. Current implants for aneurysm treatment aim to reduce blood flow into the aneurysm but sometimes fail, resulting in regrowth and further complications. Often, such failures are detected too late, complicating retreatment and increasing health risks. Smart implants capable of signaling their dysfunctionality could allow for timely medical intervention, preventing side effects and enabling effective retreatment. Recent advancements in fabrication of implants using microsystem technology allow for a significant overhaul of implant design, providing safer treatment options. Our research has demonstrated the versatility of this approach using NiTi-based shape memory alloys to create implants with several advantages[1,2]. Additionally, this technology enables the development of 'smart implants' equipped with on-board electronics for communication. Magnetoelectric (ME) antennas, consisting of magnetostrictive and piezoelectric layers, have demonstrated significant miniaturization potential compared to conventional electromagnetic antennas, operating at their acoustic resonance rather than electromagnetic resonance[3]. These compact ME antennas, when integrated on implant surfaces, offer an optimal solution for wireless data transmission in smart implants. Despite their robustness and size advantages, ME-based Solidly Mounted Resonator (SMR) antennas have lower S_{11} compared to other ME antenna variants[3]. To enhance their performance for implant applications, reducing magnetic noise is crucial. The application of exchange-biased layers, which stabilize the magnetic layers by coupling antiferromagnetic and ferromagnetic layers[4,5] shows promise for achieving deterministic switching and significantly reducing magnetic noise. In this work we demonstrate the fabrication and characterization of exchange bias-based low-noise ME SMR antennas on NiTi substrates for smart implant applications. Integrating such advanced on-board electronics in implants heralds a new era of active, responsive medical devices, revolutionizing the treatment of vascular diseases.

[1] Prasanth Velvaluri, Arun Soor, … Eckhard Quandt: Origami-inspired thin-film shape memory alloy devices. Scientific Reports 11 (2021). [2] Prasanth Velvaluri, Mariya S. Pravdivtseva, … Eckhard Quandt: Thin-film patient-specific flow diverter stents for the treatment of intracranial aneurysms. Advanced materials technologies, 6 (2021). [3] Xianfeng Liang, Huaihao Chen, … Nian X. Sun: Mechanically Driven Solidly Mounted Resonator (SMR)-Based Nanoelectromechanical Systems Magnetoelectric Antennas. Adv. Eng. Mater., 25 (2023). [4] Enno Lage, … Eckhard Quandt, and Dirk Meyners: Exchange biasing of magnetoelectric composites, Nature Materials 11 (6) (2012), 523-529. [5] Viktor Schell, … Eckhard Quandt, and Dirk Meyners: Exchange biased surface acoustic wave magnetic field sensors. Scientific Reports 13, 8446 (2023).

FE-08. Advanced Magnetoelectric Neuromodulation: Remote control over multiple channels. *E. Zhang*[1], V. Pustovalov[1], H. Ye[1], S. Sevim[1], B. Nelson[1] and S. Pané[1] *1. MAVT, ETH Zurich, Zurich, Switzerland*

Numerous cellular functions are heavily dependent on manipulating electric fields. As such, applied currents delivered through implanted wires have proven to be powerful tools for combating diseases[1] such as Parkinson's. However, the risks and difficulties associated with the inherently invasive methodology has driven increasing research into minimally invasive or non-invasive techniques, but their clinical successes have been limited. Approaches based on remotely induced electric fields through eddy currents or guided electric currents have shown strong functional capability[2], but they have limited ability to safely target deep brain areas without triggering overly large volumes of brain tissue. Optogenetic and magnetothermal stimulation methods are highly selective[3], but their surgical and genetic modification requirements complicate the clinical picture. Magnetic fields are an attractive approach to delivering energy within the body due to their low interaction with biological tissue, but they need a minimally or entirely non-invasive means to convert that energy to biologically relevant stimuli. We achieve this with highly efficient, core-shell magnetoelectric nanoparticles (MENPs), which act as hyperlocal transducers for magnetic fields into electric fields. When smaller than 50nm, they can be guided into place with magnetic fields and cross the blood brain barrier[4]. Other groups and I have already shown that properly applied MENPs can perform neuromodulation[5], stem cell differentiation[6], and guided growth in vitro[7], but the larger picture in vivo remains mixed[8]. Current studies have relied on tertiary indicators of brain activity that measure general increases in neural activity without determining whether nonspecific MENP stimulation effects primarily excitatory or inhibitory networks in the brain. In this research, we demonstrate how near-uniformly applied magnetoelectric nanoparticles can nevertheless differentially and repeatably activate subsets of neuron populations through improved manipulation of several non-linear factors in both the particle properties and the biological physics. In doing so, we clear a significant hurdle in understanding the role MENPs can play in treating neurological diseases.

[1] J.M. Bronstein et al., Arch. Neurol. 68(2), (2011). [2] M. Hallett et al., Neuron 55(2), 187–199 (2007). [3] K. Deisseroth et al., Nat. Methods 8(1), 26–29 (2011). [4] M. Pardo et al.,Nanomed.: Nanotech., Bio and Med. 32, (2021) [5] E. Zhang et al., Brain Stimulat. 15(6), 1451–1462 (2022). [6] M. Dong et al., Adv. Funct. Mats. 30(17) (2020) [7] F. Mushtaq et al., Appl. Mats. Today. 16, 290-300 (2019). [8] K.L. Kozielski et al., Sci. Adv. 7(3), eabc4189 (2021).

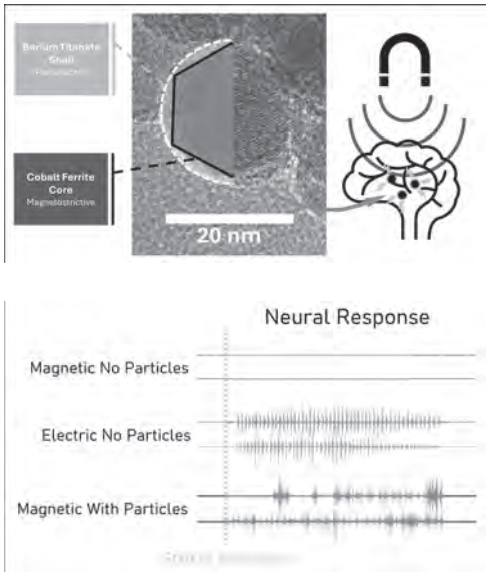

FE-09. Development of a Portable Cell-on-Chip Platform Using Advanced Magnetophoresis Technology. *B. Lim*[1], Y. Kang[2] and C. Kim[2] *1. Department of Smartsensor Engineering, Andong National University, Andong, The Republic of Korea; 2. Department of Physics and Chemistry, DGIST, Deagu, The Republic of Korea*

This study proposes a new magnetic manipulation technology using two-step lithography and permanent magnets to overcome the limitations of existing magnetic actuation technologies and develop a portable cell-on-chip platform. Customized nano-sized notches are created on micro-disc magnets using two-step optical and thermal lithography to precisely control the magnetic orientation and energy distribution. This technology provides a platform capable of effectively separating and capturing cells even under relatively weak magnetic fields. Such a platform has the potential to develop cost-effective, on-site systems capable of single-cell level diagnostics and analysis. This represents a significant advancement for more sophisticated cell-on-chip applications and is expected to contribute to real-time biomedical diagnostics and treatments.

[1] J. Yoon, Y. Kang, H. Kim, A. Ali, K. Kim, S. R. Torati, M.-Y. Im, C. Jeon, B. Lim, C. Kim, "Tailored Micromagnet Sorting Gate for Simultaneous Multiple Cell Screening in Portable Magnetophoretic Cell-On-Chip Platforms." Adv. Funct. Mater. (2024) 2312875

FE-10. Designing Magnetic Pathways for Precise Microrobot Navigation and Bio-applications. *Y. Kang*[1], A. Ali[1], H. Kim[2], B. Lim[3] and C. Kim[1] *1. DGIST, Daegu, The Republic of Korea; 2. National Nanofab Center, Daejon, The Republic of Korea; 3. Andong University, Andong, The Republic of Korea*

As microrobotic research advances in biomedical engineering, technologies capable of precisely controlling micro-sized particles or cells are essential. However, magnetic field-based controls constrain all microrobots to move in a coordinated manner, limiting their functions and independent behaviors. This study presents a design principle for achieving precise navigation of microrobots using an asymmetric magnetic pathway. A specific geometry of NiFe thin film was designed to mimic a train on a railway track, was fabricated via photolithography and sputtering. Under a rotating magnetic field (strength of 7 mT and rotating frequency of 0.1Hz), an asymmetric magnetic energy distribution along the axis allowed continuous movement of microrobots in a fixed direction, regardless of magnetic field rotation, clockwise (CW) or counterclockwise (CCW), as shown in Fig.1. This system facilitated precise control, enabling path switching at bifurcation points based on the rotation direction of the magnetic field. Moreover, the integrated radial pathways, combining bidirectional and unidirectional properties, efficiently gathered dispersed particles and controlled their extraction. We demonstrated that nanoparticles also could be manipulated by forming clusters and fulfilling functions in the same manner as microparticles. Based on the observed manipulation functions of proposed magnetic pathways, we showed that the system also facilitated the isolation of labeled cells from free particles and demonstrated potential in drug delivery applications using drug-loaded nanoparticles (Fig.2). We employed pH-dependent DOX as the drug, and with the integrated radial pathway for particle collector, magnetic particles labeled with THP-1 cells were trapped at a specific location. At the same time, drug-loaded nanoparticle clusters were transferred precisely to these locations, illustrating the possibility of localized drug delivery. Therefore, the proposed magnetic pathways have performed complex individual control, indicating significant potential for expansion to bio-applications based on Lab-on-a-chip technology.

B. Lim, V. Reddy and C. Kim, *Nat. Commun.*, 5, 3846 (2014) B. Lim, S. R. Torati and C. Kim, *NPG Asia Mater.*, 9, e369 (2017) A. Ali, H. Kim and C. Kim, *Small.*, 20, 2305528 (2024)

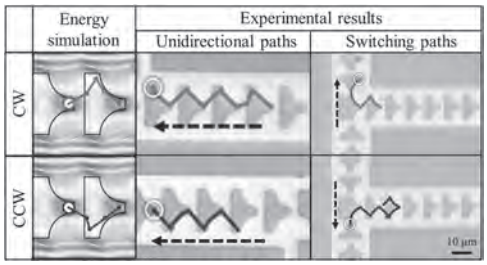

Fig.1 Directional navigation

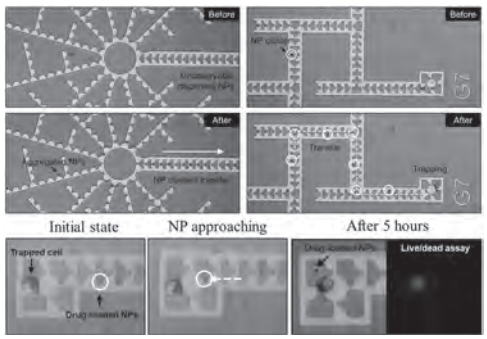

Fig.2 Nanoparticle clusters manipulation and drug delivery experiment

FE-11. Prediction of resting motor threshold using machine learning on multimodal data in transcranial magnetic stimulation. *M. Garcia*[1,2], M. Tashli[3], C.M. Harris[3,4], J. Coleman[1], A. Jamil[1,2], L. Manning-Franke[4], B. Wade[1,2] and R.L. Hadimani[3,5] *1. Psychiatry, Massachusetts General Hospital, Boston, MA, United States; 2. Harvard Medical School, Boston, MA, United States; 3. Mechanical and Nuclear Engineering, Virginia Commonwealth University, Richmond, VA, United States; 4. Physical Medicine and Rehabilitation, Virginia Commonwealth University, Richmond, VA, United States; 5. Electrical and Computer Engineering, Iowa State University, Ames, IA, United States*

Resting Motor Threshold (RMT) is a key personalized dosing metric in transcranial magnetic stimulation (TMS), expressed as a percentage of maximum stimulator output (MSO), to ensure safe and effective stimulation. Predicting RMT can improve TMS efficiency by reducing manual calibration time and enhancing dosing precision. While our previous research has linked RMT to brain anatomy[4,5], functional connectivity[3] and simulated e-field features[4,5] also play a role. This study used machine learning to identify key features for predicting RMT. We analyzed data from 17 participants who

underwent electroencephalography (EEG) and structural T1-weighted MRI for TMS treatment[2]. Features included brain-scalp distance[4], neuroanatomical parameters (via Freesurfer 7.3.2[1]), EEG connectivity across frequency bands[3], simulated e-field strengths[4], depolarized gray matter volume[4,5], age[4], and gender. Given the limited sample size and high dimensionality, we used logistic regression, random forests, and support vector machines, with various sampling methods for robust model estimation and feature importance assessment. Data were split into 80% train and 20% test sets. Models were trained to classify high, medium, and low RMT values using repeated stratified 4-fold cross-validation (CV), evaluated by mean accuracy. Permutation tests identified the best predictors of RMT across all models. CV accuracies (max = 69.2%) showed that certain feature groups reliably predicted RMT levels. Key predictors included Delta power band connectivity (0.5–3 Hz) at channel FCz and anatomical features of the inferior parietal cortex (thickness, volume, and folding index) (Fig. 1 and Fig. 2). These Delta band results and the importance of channels FC4 and P4 align with findings in [3]. Our study identified key features for predicting RMT from multimodal data, showing potential for enhancing TMS dosing accuracy and understanding magnetic neuromodulation, leading to more precise models. Further work should add features like connectivity matrices, and replicate findings with a larger sample.

[1] C. Destrieux, B. Fischl, A. Dale, and E. Halgren, “Automatic parcellation of human cortical gyri and sulci using standard anatomical nomenclature,” Neuroimage, vol. 53, no. 1, pp. 1–15, Oct. 2010, doi: 10.1016/j.neuroimage.2010.06.010. [2] L. M. Franke, G. T. Gitchel, R. A. Perera, R. L. Hadimani, K. L. Holloway, and W. C. Walker, “Randomized trial of rTMS in traumatic brain injury: improved subjective neurobehavioral symptoms and increases in EEG delta activity,” Brain Injury, vol. 36, no. 5, pp. 683–692, Apr. 2022, doi: 10.1080/02699052.2022.2033845. [3] M. Z. Hussain, C. J. Lewis, A. Jamil, L. M. Franke, J. A. Camprodon, and R. L. Hadimani, “Investigation of EEG Neurophysiological Relationship to TMS Response in Mild Traumatic Brain Injury Patients,” IEEE Transactions on Magnetics, vol. 59, no. 11, pp. 1–5, Nov. 2023, doi: 10.1109/TMAG.2023.3282614. [4] C. J. Lewis et al., “The relationship of neuroanatomy on resting motor threshold and induced electric field strength on treatment outcomes in mild to moderate traumatic brain injury patients during transcranial magnetic stimulation,” AIP Advances, vol. 13, no. 2, p. 025260, Feb. 2023, doi: 10.1063/9.0000567. [5] N. Mittal, C. Lewis, Y. Cho, C. L. Peterson, and R. L. Hadimani, “Effect of Fiber Tracts and Depolarized Brain Volume on Resting Motor Thresholds During Transcranial Magnetic Stimulation,” IEEE Transactions on Magnetics, vol. 58, no. 8, pp. 1–6, Aug. 2022, doi: 10.1109/TMAG.2022.3148214.

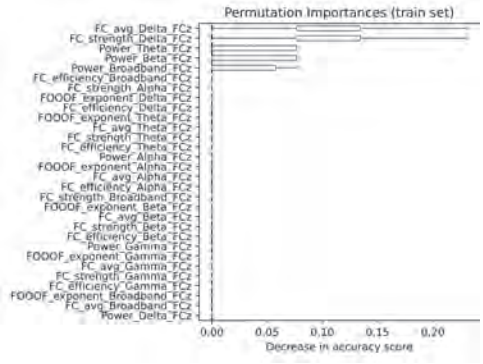

Fig. 1. Permutation test outcomes on channel FCz extracted features.

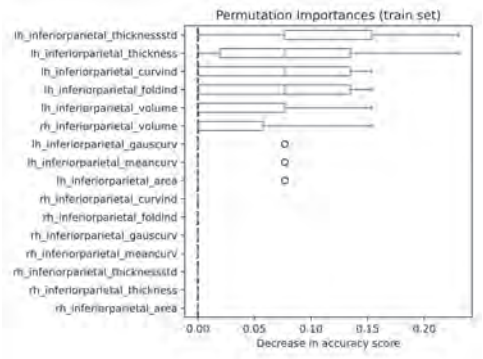

Fig. 2. Permutation test outcomes on inferior parietal cortex anatomical features.

Session FF
SOFT MAGNETIC MATERIALS III
Arkady Zhukov, Chair
Basque Foundation for Science, San Sebastian, Spain

INVITED PAPER

FF-01. High-Frequency Core Loss Reduction in Fe-Based Soft Magnetic Ribbons: A Microstructural Approach. *R. Gautam*[1], S. Hiramoto[2], H. Mamiya[1], T. Ogasawara[3], S. Okamoto[2], T. Ohkubo[1] and H. Sepehri-Amin[1] *1. National Institute for Materials Science, Tsukuba, Japan; 2. Tohoku University, Sendai, Japan; 3. National Institute of Advanced Industrial Science and Technology, Tsukuba, Japan*

Soft magnets are crucial for efficient energy conversion in modern power electronics, especially with the advent of wider bandwidth semiconductors such as SiC and GaN, which require minimal core losses at higher frequencies. Fe-based soft magnets, such as Nanomet, prepared by rapid solidification are well-known for their excellent soft magnetic properties such as large saturation magnetization and low coercivity [1,2]. However, the core losses in these materials need to be reduced in the 10-100 kHz region for power electronics applications. The microstructure of as-spun ribbons can be optimized by optimal annealing that results in different functionalities in these materials [3]. Our study focuses on how nanostructure engineering minimizes core losses in Fe-based amorphous materials. We prepared $Fe_{84.6}Si_{0.5}B_{9.4}P_{3.5}Cu_{0.8}C_{1.2}$ ribbons using melt spinning and annealed at 400-480 °C for 10-60 s to obtain different microstructures. The as-spun ribbons were observed to be amorphous, with an onset of crystallization at 394 °C. Microstructural analysis using XRD, TEM, and APT revealed the formation of α-Fe(Si) nanocrystals (< 20 nm) in the amorphous matrix. Magnetic domain observations were conducted using the magneto-optical Kerr effect (MOKE) and Lorentz microscopy. Figure 1(a) depicts the total core loss of ribbons, as measured at 1.0 T and 10 kHz, as a function of the volume fraction of α-Fe(Si) crystals. TEM images of the selected samples indicated in Fig. 1(a) are presented in Fig. 2(b), revealing a fully amorphous structure in the as-spun ribbon and the presence of α-Fe(Si) crystals within the residual amorphous matrix in the sample with low core loss. Our findings indicate that optimal annealing reduced the core losses from 165 W/kg in the amorphous state to 75 W/kg, correlating with 4-7 vol% of α-Fe(Si) crystals in the amorphous matrix. However, further crystallization leads to increased losses. Detailed analysis of the core losses reveals the minimal contributions of hysteresis and eddy current losses and identifies excess losses as the major contributor. Changes in magnetic domain shape and their movement under an AC magnetic field, as observed through MOKE, were key factors in the core loss reduction. This approach was validated for several nanocrystalline soft magnetic materials, emphasizing the importance of precise microstructure engineering to achieve minimal core losses. The detailed mechanism underlying core loss reduction will be discussed in detail.

A. Urata, H. Matsumoto and S. Yoshida *et. al.*, IEEE Trans. Magn., 47, 3177 (2011). A. D. Setyawan, Kana Takenaka and Parmanand Sharma *et. al.*, *J. Appl. Phys.,* 17B715, 117 (2015). Ravi Gautam, Takamasa Hirai and Abdulkareem Alasli *et. al.*, *Nat. Commun.,* 15, 2184 (2024).

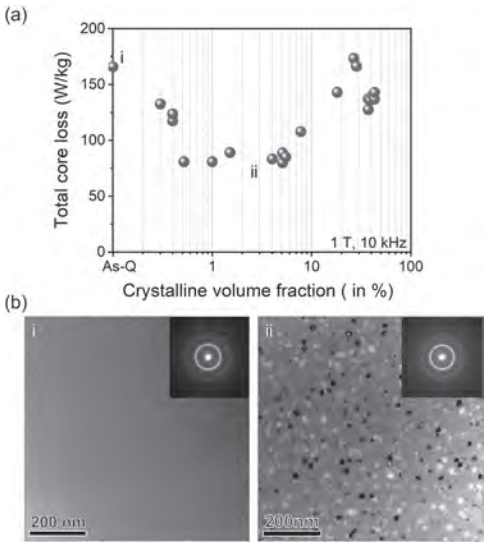

Fig. 1. (a) Total core loss of Fe-based soft magnetic ribbons plotted against the volume fraction of α-Fe(Si) crystals. (b) TEM images of the samples labeled in (a) show the presence of α-Fe in the residual amorphous matrix.

CONTRIBUTED PAPERS

Now VP19-10

FF-02. Soft magnetic composites casted from ferrites and construction binders with lowest core loss for high-efficient wireless charging. *M. Esguerra*[1], I.R. Ellithy[1] and R. Radhakrishnan[1] *1. Magment GmbH, Munich, Germany*

Transport decarbonization requires electrification with an efficient and widespread charging infrastructure. Road electrification with dynamic wireless charging can help to reduce the size of batteries reducing significantly the environmental impact of lithium mining. Robust and low-loss magnetic materials are required to allow for high-efficient inductive transmission comparable to plug-in charging with an added convenience which accelerates the adoption of electric vehicles. Traditional ferrites used, for example, in wireless power transfer, experiences a compressive pressure yielding a significant transmission efficiency drop, which makes it unsuitable for embedding them in load-bearing structures. Soft Magnetic Composites cast with recycled ferrites and cement, or asphalt, are highly robust and possess the lowest core losses at flux densities up to 50 mT in the range of up to 100kHz in a wide temperature range. This paper will show how by refining the particle size distribution of the aggregates and using precision-enhanced magnetic testing and sophisticated hysteresis modelling, the performance of these materials could be significantly improved with respect to the stress effect on losses. By correlating processing steps to a multi-linear regression model, the optimum particle size distribution is found, yielding a material grade with minimal losses. Compared to conventional best-in-class powder cores (containing Nickel), these composites feature lower core losses at a fraction of the cost. Industrialization based on existing building materials methods and equipment secures global high scalability.

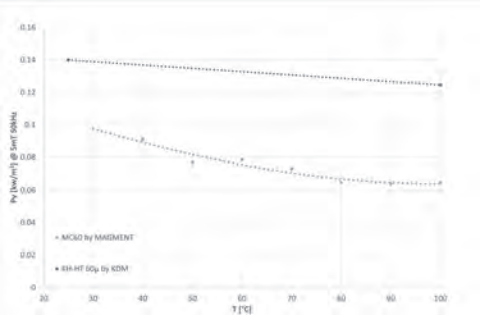

Fig.1 Benchmark of core loss over temperature for magnetizable concrete MC60 vs. high flux powder core KH-HT 60µ at 5mT, 50kHz.

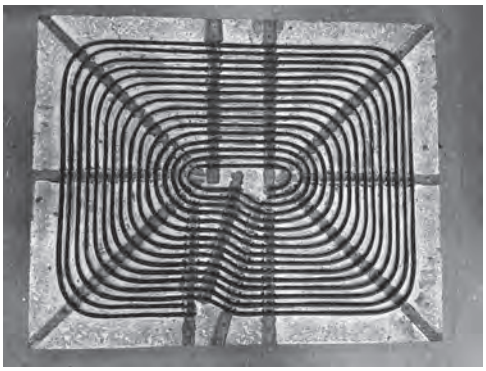

Fig 2. Wireless charging ground pad with an embedded coil in MC60 magnetizable concrete.

FF-03. Withdrawn

FF-04. Superior Stability and Enhanced Heating Performance in Mn- and Zn-Substituted Ferrite-Based Fluids for Magnetic Hyperthermia with Improved Biocompatibility. *P. Kumar*[1,2,3], A. Singh[2,4], S. Pathak[5] and R. Pant[2] *1. Department of Physics, RMIT University, Melbourne, VIC, Australia; 2. Indian Reference Materials Divisions, CSIR-NPL, New Delhi, Delhi, India; 3. Indian Reference Materials Divisions, ACSIR, Delhi, India; 4. Department of Physics, IIT JAMMU, JAMMU, India; 5. Department of Material Sciences and Engineering, Seoul National University, Seoul, Korea (the Democratic People's Republic of)*

This study presents significant advancements in magnetic hyperthermia based cancer treatment through the development of ultrahigh specific absorption rate (SAR) performance in Zn- and Mn-substituted magnetite superparamagnetic (SPM) nanoparticles. While MHT shows promise for cancer therapy, clinical applications face challenges such as low heating performance,

agglomeration of magnetic nanoparticles (MNPs) in blood vessels, cytotoxicity, and hemocompatibility. To address these issues, we adopted a reverse micelles-based coprecipitation synthesis approach to prevent MNP agglomeration and optimized the substitution of Zn and Mn ions in magnetite. For Zn-substituted magnetite, we achieved significant SAR improvements with values of 325 W/g and 579 W/g using the initial slope method (ISM) and Box Lucas method (BLM), respectively, for $Zn_{0.3}Fe_{2.7}O_4$ MNPs. This represents over a 300% increase compared to pure magnetite, attributed to enhanced saturation magnetization (174–257 kA/m) and magneto-crystalline anisotropy (12–24 kJ/m^3). The increase in saturation magnetization is due to the higher magnetic moment with increased Zn concentration, strengthening the JAB interaction, although further Zn increases lead to decreased magnetization explained by the Yafet-Kittle model. Similarly, for Mn-substituted magnetite, we achieved a remarkable 181% increase in SAR (510 kW/kg) using the BLM, attributed to elevated saturation magnetization from optimal Mn ion distribution and increased spin relaxation time, enhancing energy dissipation and resulting in higher SAR values. Biocompatibility assessments showed minimal hemolysis rates (<5%) in hemolysis assays with red blood cells and high cytocompatibility (>92% cell viability) in MTT assays for both Zn- and Mn-substituted magnetite NPs, confirming their suitability for clinical applications. The improved heating performance allows for lower MNP concentrations, reducing potential toxicity effects. This study offers a promising approach to enhancing SAR performance in magnetite SPM nanoparticles through Zn and Mn ion substitution, with significant improvements in heating performance and excellent biocompatibility, making them strong candidates for MHT-based cancer treatment.

1. A. Hajalilou, L. Ferreira, M.M. Jorge, C. Reis, M. Cruz, J. Magn. Magn. Mater. 537 (2021), 168242. 2. V. Pilati, G. Gomide, R.C. Gomes, G.F. Goya, J. Depeyrot, Langmuir 37 (2021) 1129–1140.

FF-05. Minnealloy: An Ultra-High Saturation Magnetization Soft Ferromagnet. *A.S. Padgett*[1], J. Wang[2], S.R. Bishop[1], W. Echtenkamp[2], P.F. Weck[1], L.J. Treadwell[1], J.D. Boissiere[1], C.R. Riley[1] and D.R. Lowry[1]
1. Sandia National Laboratories, Albuquerque, NM, United States; 2. Department of Electrical and Computer Engineering, University of Minnesota, Minneapolis, MN, United States

Industry, telecommunications, and electrical grid technology rely on magnetic components such as inductors and transformers. However, the cores for many of these components contain critical materials [1] that are susceptible to availability and supply chain risks. A rare-earth and critical material free alternative called Minnealloy, α''-$Fe_{16}NC$, is being developed to replaced grain oriented electrical steel (GOES), non-oriented electrical steel (NOES), and amorphous metal (AM). Minnealloy's small magnetic coercivity (197 A/m bulk phase, ~5 A/m engineered [2,3]), intermediate resistivity ($\geq 30 \times 10^{-8}$ Ωm) and gargantuan magnetic flux density ($\geq$ 2.47T) result in low losses and more power transferred per cycle than any existing transformer core material for a given *mass or volume* [4,5,6,7]. It is predicted to operate at higher frequencies (> 100 MHz) and known to operate at higher power, with comparable hysteresis and lower eddy current losses, than GOES, NOES, and AM. Replacing a silicon steel transformer core with Minnealloy will result in up to a 33% *volume and weight* reduction; replacing a high-frequency ferrite transformer core with Minnealloy will result in an 80% volume reduction. However, achieving high phase purity in bulk samples to demonstrate the expected material performance remains a challenge. In this talk, and accompanying conference paper, we will discuss powder and ribbon fabrication routes, magnetic properties measurements, density functional theory modeling, and a path to higher phase purity for commercial application. *Sandia National Laboratories is a multimission laboratory managed and operated by National Technology & Engineering Solutions of Sandia, LLC, a wholly owned subsidiary of Honeywell International Inc., for the U.S. Department of Energy's National Nuclear Security Administration under contract DE-NA0003525.*

[1] D. J. Bauer, R. T. Nguyen, and B.J. Smith, "Critical Materials Assessment," U.S. Department of Energy, Washington D.C., Rep. DOE/EE-2756, July 2023. [2] H. Giselher, "Modern soft magnets: Amorphous and nanocrystalline materials," *Acta Mater.*, vol. 61, pp. 718-734, Feb. 2013. [3] F.C. Li, T. Liu, J.Y. Zhang, S. Shuang, Q. Wang, A.D. Wang, J.G. Wang, and Y. Yang, "Amorphous–nanocrystalline alloys: fabrication, properties, and applications," *Mater. Today Adv.*, vol. 4, Dec. 2019. [4] M. D. Mehedi, Y. Jiang, P. K. Suri, D. J. Flannigan, and J-P Wang, "Minnealloy: a new magnetic material with high saturation flux density and low magnetic anisotropy," *J. Phys. D: Appl. Phys.*, vol. 50, no. 37, Aug. 2017. [5] X. Zhang and J-P Wang, "High saturation magnetization and low magnetic anisotropy Fe-CN martensite thin film," *Appl. Phys. Lett.,* vol. 114, iss. 15, Apr. 2019. [6] G. Guo, J. Liu, and JP Wang, "Carbon and microstructure effects on the magnetic properties of Fe–CN soft magnetic materials (Minnealloy)," *TMS 2020 149th Annual Meeting & Exhibition Supplemental Proceedings*, pp. 1841-1852, Feb. 2020. [7] Y. Sugita, H. Takahashi, M. Komuro, M. Igarashi, R. Imura, and T. Kambe "Magnetic and electrical properties of single phase, single crystal Fe16N2 films epitaxially grown by molecular beam epitaxy," *J. Appl. Phys.*, vol. 79, pp. 5576-5581, Apr. 1996.

FF-06. Stability and Evolution of Induced Anisotropies in Nanocrystalline Soft Magnetic Alloys for Extreme Temperature Application. *T. Paplham*[1], A. Leary[2] and P. Ohodnicki[1,3,4] *1. Mechanical Engineering and Materials Science, University of Pittsburgh, Pittsburgh, PA, United States; 2. NASA Glenn Research Center, Cleveland, OH, United States; 3. Electrical and Computer Engineering, University of Pittsburgh, Pittsburgh, PA, United States; 4. Physics and Astronomy, University of Pittsburgh, Pittsburgh, PA, United States*

The development of the FeCo-based (HiTPerm) and Co-rich sytems has previously enabled nanocrystalline inductor solutions for applications > 150 °C in aerospace and deep-well drilling. However, next generation electric aircraft and more ambitious aerospace applications such as a planned Venus surface lander have ambient temperatures approaching 500 °C [1,2]. These extreme environments place strict demands on the stability and performance of the nanocrystalline inductor core. Additional challenges lie at the device scale, where the low decomposition temperature of typical potting resins eliminates the possibility of traditional gapped inductor topologies [1]. Gapless inductors, which achieve low effective permeability through a field- or stress-induced magnetic anisotropy rather than a cut gap, are highly promising for these applications [3]. However, development of a successful gapless inductor requires that the magnetic properties, particularly the induced magnetic anisotropy, be stable for extended periods at the operating temperature. Here we investigate the stability of field- and stress-induced anisotropies in Co-rich alloys over extended periods at temperatures of 400 °C and greater. Evolution over time will be assessed and quantified from an energetics-based perspective using a kinetic model, with the effect of varying temperature considered in terms of distributions in relaxation times and anisotropy fields [4,5]. Observed differences between the stabilities of field- and stress-induced anisotropies will be analyzed and rationalized on a physical basis. Strong understanding of the evolution of an induced anisotropy and the underlying physics as a function of temperature is critical for success in extreme temperature inductor implementation.

[1] A. Vannini, A. Marfoli, L. Papini, IEEE Work. Electr. Mach. Des. Control Diagnosis, Vol. 2021, p.101-106 (2021) [2] P. Beauchamp, M.S. Gilmore, R.J. Lynch, IEEE Aerosp. Conf. Proc., Vol. 2021, p.1-18 (2021) [3] A. Leary, V. Keylin, A. Devaraj, J Mater. Res., Vol. 31, p.3089-3107 (2016) [4] K.Y. Ho, P.J. Flanders, C.D. Graham, J Appl. Phys., Vol. 53, p.2279-2281 (1982) [5] V. Franco, C.F. Conde, A. Conde, J Magn. Magn. Mat., Vol. 185, p.353-389 (1998)

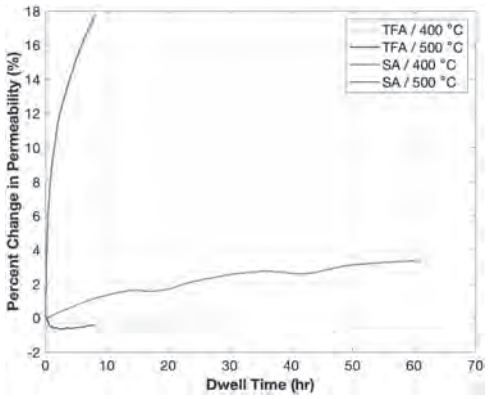

Fig. 1: Evolution of permeability along the ribbon axis of a transverse field annealed (TFA) and stress annealed (SA) Co-rich nanocrystalline alloy over time, measured *in-situ* at high temperature.

FF-07. Fe_3CoC nanocrystals with high magnetization. *H. Abbas*[1], P. Joshi[1], T. Karki[1], J. Mohapatra[1] and P. Liu[1] *1. Physics, University of Texas at Arlington, Arlington, TX, United States*

In this study, we synthesized Fe_3CoC nanoparticles using the chemical solution approach and melt-spinning technique. The surfactant (CTAB) amount was varied in the chemical approach to obtain different-size nanoparticles. The average crystallite size was calculated from XRD patterns and found to be 19 nm, 26nm, 27nm, and 29 nm for chemically synthesized nanoparticles and 23 nm for crystallites in melt-spun ribbons. The crystal planes (110), (200), and (211) in the XRD pattern (Figure 1) belong to the Fe_3Co cubic phase, however, the peaks with an asterisk (*) show the presence of carbon atoms in the structure, resulting in a possible distorted cubic structure. The same diffraction peaks were observed in the XRD pattern for crystallites in melt-spun ribbons. The morphology of nanoparticles was observed to be spherical. ZFC magnetization curve (Figure 2 (a)) shows that the blocking temperature lies above the room temperature and FC curve indicates the existence of strong inter-particle interactions between nanoparticles. The inset to Fig. 2 (a) shows the MH loops of the aligned sample, parallel and perpendicular to the magnetic field. These results indicate the presence of considerable anisotropy in the system. Figure 2 (b) shows the magnetic susceptibility curves for 29 nm nanoparticles and melt-spun ribbons. High magnetization (1930 emu/cm^3) and magnetic susceptibility were observed for melt-spun ribbons as compared to nanoparticles due to their surface spin disorder and interparticle interactions.

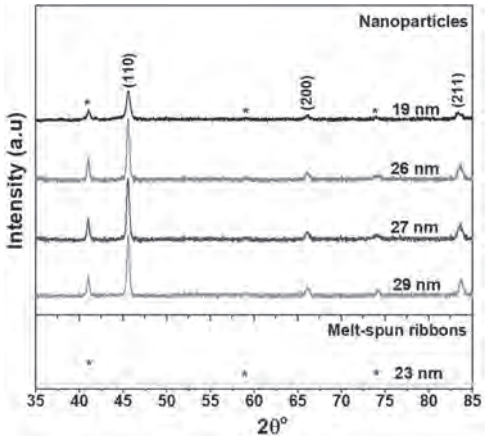

Figure 1: XRD patterns for Fe_3CoC nanoparticles, and melt-spun ribbons

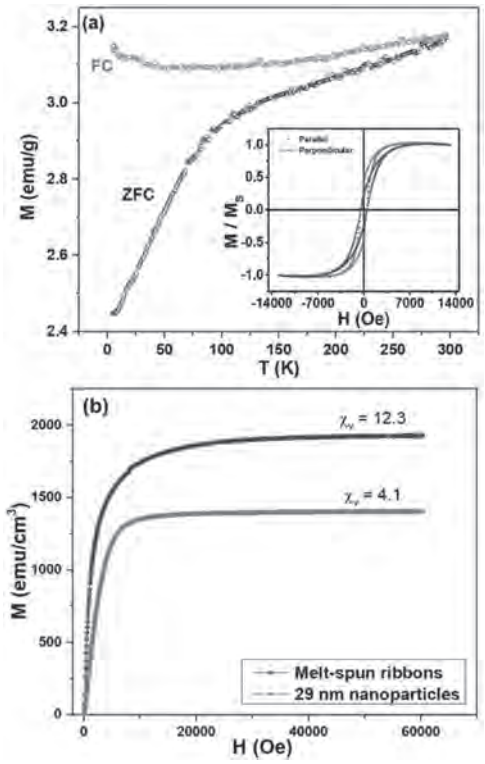

Figure 2: (a) ZFC-FC magnetization curve at 100 Oe, inset shows the MH loops of aligned samples, parallel and perpendicular to the magnetic field, and (b) Magnetic susceptibility curves for 29 nm nanoparticles and melt-spun ribbons.

FF-08. Advanced Magnetic Anisotropy Engineering in Soft Magnetic Co-Based Amorphous Wires for Enhanced Performance. H. Chiriac[1], M. Lostun[1], S. Corodeanu[1], T.A. Ovari[1] and *N. Lupu*[1] *1. National Institute of Research and Development for Technical Physics, Iasi, Romania*

The circular symmetry of Fe-based and Co-based soft magnetic amorphous and nanocrystalline wires, along with their anisotropies, plays a crucial role in determining their macroscopic response and enhanced performance. In this work, we explore the potential to precisely control magnetic anisotropy of amorphous wires with a nominal composition of $Co_{68.15}Fe_{4.35}Si_{12.5}B_{15}$ and diameters of 120 μm, produced using in-rotating water spinning, with a saturation magnetization of 0.68 T, a coercive field of less than 8 A/m, and magnetic permeabilities of up to 200,000 at low magnetic fields (a few A/m). Certain applications require controlled, constant values of magnetic permeability over a range of magnetic fields. This behavior can be achieved through thermal treatments under longitudinal stresses. The shape and inclination of the longitudinal B-H curves (Fig. 1) indicate induced perpendicular anisotropy in stress-annealed wires, with its magnitude depending on the annealing temperature/current and applied longitudinal stress. This anisotropy was found to be reversible after subsequent heat treatment. The observed creep-induced anisotropy originates from the orientational ordering of small clusters in the amorphous matrix, creating anelastic strains perpendicular to the tensile stress applied during annealing. Our research has revealed a prolonged relaxation phenomenon lasting several days. To mitigate this effect, we aimed to reduce microscopic non-uniformities in the wires that contribute to creep-induced anisotropy. These changes are also evident in the magnetostrictive behavior of the wires, with λ_s varying from slightly negative values (-0.7 x 10^{-6}) in the as-cast state to slightly positive values (+0.35 x 10^{-6}) after inducing perpendicular anisotropy. Understanding these aspects is essential for advancing cutting-edge sensing applications. *Financial support from NUCLEU Programme - Contract No. 18N/01.01.2023, Project PN23 11 01 01 is highly acknowledged.*

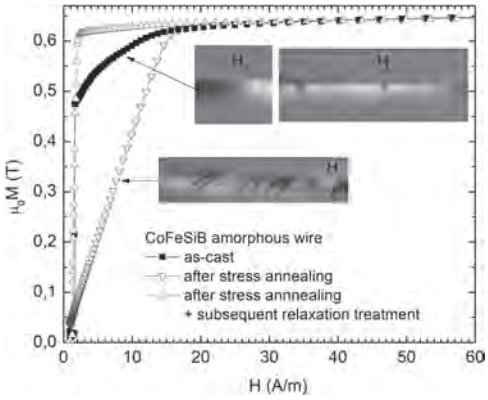

The magnetization curves and magnetic domain structures of Co-based nearly zero magnetostrictive amorphous wires demonstrate the presence of induced perpendicular anisotropy in stress-annealed wires and the reversibility of magnetization processes with annealing.

FF-09. Fabricating and characterizing soft ferromagnetic Fe-CN (Minnealloy) ribbons for use in efficient high frequency transformer cores. *W. Echtenkamp*[1], A.S. Padgett[2], S. House[2], S.R. Bishop[2], D.R. Lowry[2] and J. Wang[1] *1. Electrical and Computer Engineering, University of Minnesota, Minneapolis, MN, United States; 2. Sandia National Laboratories, Albuquerque, NM, United States*

Soft ferromagnetic materials play a crucial role in the world's electrical system, in particular serving as essential components of all transformers, electrical motors, and generators. We develop and evaluate Minnealloy, α''-$Fe_{16}(NC)$, a novel soft magnetic material composed only of Fe-N-C. Rising to prominence only in the last decade, Minnealloy has the benefit of being free of the critical elements cobalt, nickel or silicon, while providing performance superior to today's soft magnetic materials. It has been shown that the saturation flux density is 27% higher than pure iron, and the coercivity can be maintained around 10 Oe.[1-3] Minnealloy ribbons have been fabricated by melt-spinning, a manufacturing compatible and scalable process. An oxidation/reduction/nitriding process is used which significantly changed the microstructure of the ribbon, introducing many vacancies and microchannels which facilitated the diffusion of nitrogen through the ribbon, yielding higher nitride volume. The effects of the post melt-spinning processes on the stoichiometry, phase purity, microstructure, and magnetization are studied and the feasibility of using Minnealloy ribbon in high frequency transformer cores is explored.

1. Md Mehedi, Yanfeng Jiang, Pranav Kumar Suri, David J. Flannigan and Jian-Ping Wang, Journal of Physics D: Applied Physics 50 (37), 37LT01 (2017). 2. Guannan Guo, Jinming Liu and Jian-Ping Wang, TMS 2020 149th Annual Meeting & Exhibition Supplemental Proceedings, 1841-1852 (2020). 3. M. Tobise, Y. Nomura, M. Kodama, T. Murakami and S. Saito, IEEE Transactions on Magnetics 58 (8), 1-5 (2022).

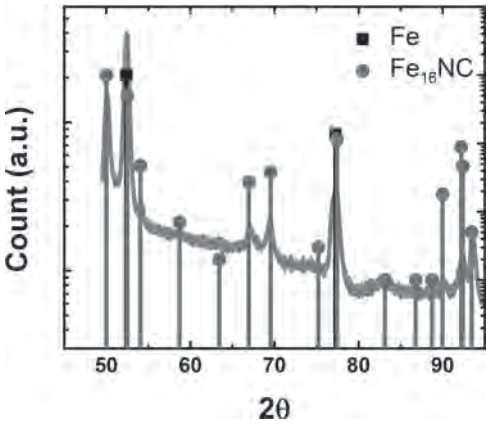

Figure 1: X-ray diffraction pattern of the ribbon as prepared. Fe and $Fe_{16}NC$ peaks are marked.

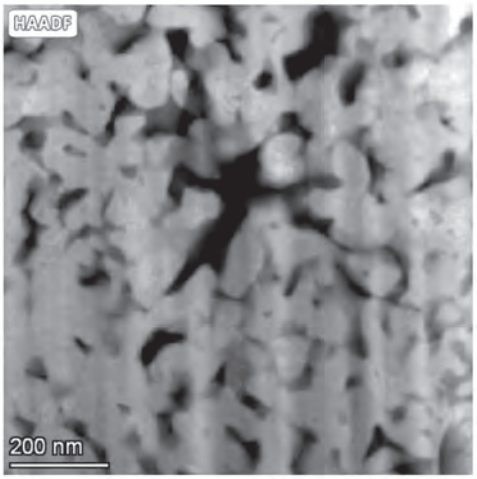

Figure 2: High-angle annular dark-field imaging image showing the microstructure of the ribbon.

FF-10. Analysis of iron loss and complex permeability using Cole-Cole diagram for Fe-based nanocrystalline core. *Y. Tomita*[1], T. Iriyama[1] and H. Takabayashi[1] *1. Corporate Research & Development center, Daido Steel. co., ltd., Nagoya, Japan*

Along with the increase of a driving frequency for power electronics devices, more and more development of higher performance soft magnetic material with low iron loss and high permeability at high frequency will be expected. It is important to understand the mechanism of the iron loss or permeability for the development of new soft magnetic materials. In this study, we tried to adopt Cole-Cole relaxation equation for the analysis of the complex permeability spectra and iron loss in reversible process with the Fe-based nanocrystalline core. The iron loss and complex permeability spectra of the Fe-based nanocrystalline core were measured by B-H analyzer and impedance analyzer, respectively. The reversible permeability was calculated with a procedure proposed by Beatrice[1)]. Then, we analyze the permeability spectra and iron loss using the Cole-Cole diagram, which is used in the field of electrochemistry to analyze permittivity spectra[2)]. Fig.1 shows the Cole-Cole diagram of measured μ' and μ''. It shows a circular arc shape. For dielectric permittivity, it is known that the circular arc Cole-Cole diagram can be expressed by the Cole-Cole relaxation equation[2)]. Here, we replaced permittivity by permeability as follows, $\mu=1+(\mu_{DC}-1)/\{1+(if/f_p)^{1-\alpha}\}$, $\alpha=(2/\pi)\arctan\{(\mu_{DC}^2-4\mu''^2_{max})/(4\mu_{DC}\mu''_{max})\}$ where i is imaginary unit, μ_{DC} is DC permeability, f_p is peak frequency of μ'', and μ''_{max} is the maximum value of μ''. parameter α can be calculated based on the geometrical relationship in the Cole-Cole diagram. Fig.2 shows the measured and calculated values

of the permeability and iron loss. The iron loss P was calculated from the following equation, $P=\mu'' B_m^2 f/(2\mu_r^2)$ $P=\cos(\alpha\pi/2)B_m^2 f^{2-\alpha}/(2\mu_{DC} f_p^{1-\alpha})$ where μ'' and μ_r is imaginary part and norm of complex permeability. It can be seen that the calculated values coincide well with the measured values. From these results, it is thought that the analysis using the Cole-Cole diagram is an effective method to understand the mechanism of magnetization process in soft magnetic properties.

1) C. Beatrice, et al., J. Magn. Magn. Mater., Vol.429 p.129 (2017) 2) K. Cole, H. Cole, J. Chem. Phys., Vol.9, p.341 (1941)

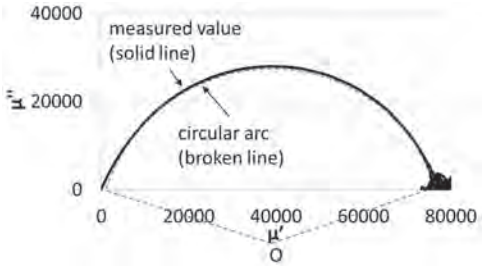

Fig.1 Cole-Cole diagram of the permeability for nanocrystalline core

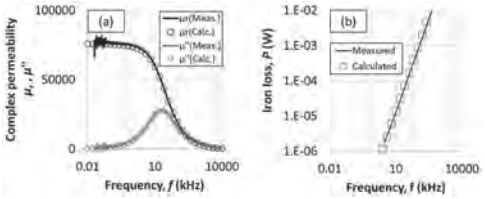

Fig.2 Measured and calculated values of the (a) permeability spectra and (b) iron loss with the nanocrystalline core

Session FG
VAN DER WAALS MATERIALS

Ethan Ahn, Chair
George Mason University, Fairfax, VA, United States

INVITED PAPER

FG-01. Gate tunable spin transport in a two-dimensional semiconductor. *A. Avsar[1,2,3] 1. Materials Science and Engineering, National University of Singapore, Singapore; 2. Department of Physics, National University of Singapore, Singapore; 3. Center for Advanced 2D Materials, National University of Singapore, Singapore*

Exploitation of the intrinsic spin of an electron, spintronics, facilitates the development of multifunctional and novel devices which could play an important role in the Beyond-CMOS era. Two-dimensional (2D) crystals and their van der Waals heterostructures are particularly promising for spintronics device applications due to their unique properties, including strong responses to field effect gating and proximity interactions, which may enable new functionalities that are not possible with conventional bulk materials [1]. Black phosphorus is a particularly promising 2D semiconducting material for spintronics research due to its high charge mobilities, low atomic mass, and puckered crystalline structure, which are expected to lead to anisotropic spin transport with nanosecond spin-lifetimes. In this seminar, I will introduce ultra-thin BP as a unique platform for studying rich spin-dependent physics. Firstly, I will show that BP supports all electrical spin injection, transport, precession and detection up to room temperature [2]. Then, I will present our recent findings on the impact of the unique crystal structure of BP on its spin dynamics, revealing strong anisotropic spin transport along three orthogonal axes [3]. The exceptional spin transport and its strong gate-tunability together with the strong spin-lifetime anisotropy we observe in BP add to the growing body of evidence for the potential of 2D materials in functional spin-based device applications.

[1] A. Avsar, H. Ochoa, F. Guinea, B. Özyilmaz, B. J. van Wees, and I. J. Vera-Marun, "Spintronics in graphene and other two-dimensional materials", *Review of Modern Physics* 92 (2), 021003 (2020), [2] A. Avsar, J. Y. Tan, M. Kurpas, K. Watanabe, T. Taniguchi, J. Fabian and B. Özyilmaz, "Gate Tunable Black Phosphorus Spin Valve with Nanosecond Spin Lifetimes", *Nature Physics*, 13, 888-894 (2017). [3] L. Cording, J. Liu, J. Tan, K. Watanabe, T. Taniguchi, A. Avsar*, B. Özyilmaz*, "Highly anisotropic spin transport in ultrathin black phosphorus", *Nature Materials*, 23 (4), 479-485 (2024).

CONTRIBUTED PAPERS

FG-02. Anomalous Hall Effect in Cr_2Te_3/Pt Heterostructures. *C. Huai[1], M. Bian[1], K. He[2], A. Mucchietto[3], E. Kirstein[3], R. Sabirianov[4], S. Crooker[3], J. Bird[2] and H. Zeng[1] 1. Physics, University at Buffalo, Buffalo, NY, United States; 2. Electrical Engineering, University at Buffalo, Buffalo, NY, United States; 3. National High Magnetic Field Laboratory, Los Alamos National Lab, Los Alamos, NM, United States; 4. Department of Physics, University of Nebraska-Omaha, Omaha, NE, United States*

Unconventional anomalous Hall effect (AHE), characterized by additional humps and dips near the coercive field in AHE hysteresis, has been observed in Cr_2Te_3 thin films grown by molecular beam epitaxy. We attribute the origin of this unconventional AHE to an intrinsic mechanism dictated by the self-intercalation in the covalent 2D magnet[1]. This mechanism is distinctly different from previously proposed mechanisms such as topological Hall effect, or two-channel AHE arising from spatial inhomogeneities. In this work, we report the discovery of similar unconventional AHE in a Cr_2Te_3/Pt heterostructure, as shown in Fig. 1. Its origin remains to be elucidated. We found that the conductivity of the Cr_2Te_3/Pt heterostructure is an order of magnitude higher than that of Cr_2Te_3 layer alone. We therefore conclude that the carrier transport in the heterostructure is dominated by the Pt layer, similar to that of a ferromagnetic insulator/Pt bilayer. AHE has been observed in such systems, and can be attributed to magnetic proximity effect[2] and/or spin Hall effect (SHE) [3] [4]. We used X-ray magnetic circular dichroism (XMCD) to probe any possible induced magnetic moment in Pt. XMCD results showed the absence of induced moment, suggesting that magnetic proximity effect plays an insignificant role in the AHE observed in the heterostructure. The imaginary part of the spin mixing conductance can also lead to an AHE signal in a magnetic insulator/Pt heterostructures, known as the spin-Hall AHE. To investigate the presence of SHE, we measured the Spin Hall Magnetoresistance (SMR) [5] by varying the relative orientation between the magnetization of the Cr_2Te_3 film and the current direction. As seen in Fig. 2, we observed that the device resistance depends on the relative orientation, confirming the presence of SHE and the crucial role it plays in the unconventional AHE behavior in the heterostructure. Our work provides insight into the intricate interplay between spin and charge currents in magnetic/non-magnetic heterostructures, which is important for spintronic device applications.

[1] Bian, M., et al., *Unconventional Anomalous Hall Effect Driven by Self-Intercalation in Covalent 2D Magnet Cr2Te3*. 2024. submitted. [2] Huang, S.-Y., et al., Physical review letters, 2012. 109(10): p. 107204. [3] Hirsch, J., *Spin hall effect.* Physical review letters, 1999. 83(9): p. 1834. [4] Hahn, C., et al., Physical Review B—Condensed Matter and Materials Physics, 2013. 87(17): p. 174417. [5] Nakayama, H., et al., Physical review letters, 2013. 110(20): p. 206601.

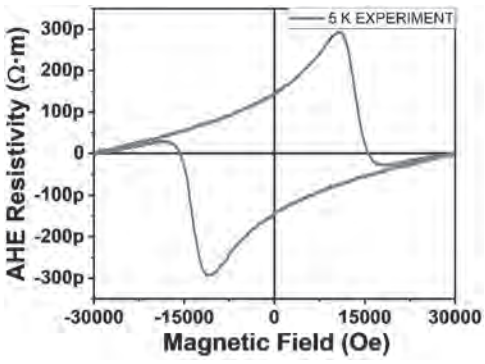

Fig. 1 AHE resistivity of Cr_2Te_3/Pt measured at 5K.

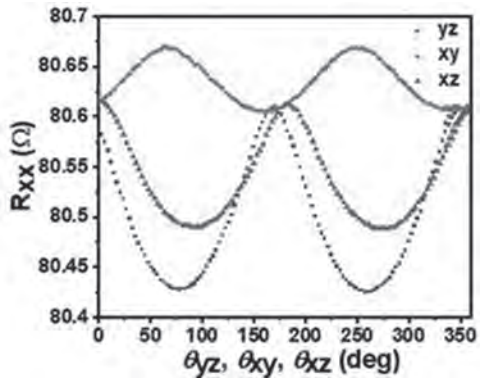

Fig. 2 SMR measurements of Cr_2Te_3/Pt.

FG-04. Spin- and orbital-charge conversion at the surface states of $Bi_{1-x}Sb_x$ topological insulator. *A. Pezo*[1], J. George[1] and H. Jaffrès[1] *1. Laboratoire Albert Fert, Essone, France*

Topological insulators are quantum materials characterized by Time-reversal protected surface states (TSS) which make them appealing candidates for the design of next generation of highly efficient spintronic devices. The very recent demonstration of large transient spin-charge conversion (SCC) and subsequent powerful THz emission from $Co|Bi_{1-x}Sb_x$ bilayers clearly demonstrate such potentiality and feasibility for the near future [1-3]. Amongst the exotic properties appearing in and at the surface of such quantum materials, spin-momentum locking (SML) remains as a key ingredient to effectively convert the spin degree of freedom into a charge or a voltage signal. In that sense, in this work we will provide some clear theoretical and numerical insights implemented by multiorbital and multi-layered tight-binding methods (TB). These developments clarify our recent experimental results obtained by THz-TDS spectroscopy techniques in the time domain [2]; and allows us to disentangle the various magnetic SCC contributions. Taking advantage of their spin-momentum locking property, we also postulate the occurrence of Orbital-to-charge conversion (OCC) taking place also in these aforementioned experiments at equal footing to SCC. By extending the spin-to-charge conversion theory, we postulate the emergence of its orbital counterpart, namely the Orbital-charge conversion (OCC), covering different contributions in terms of the orbital degree of freedom. Our results unveil the interest and prospects for the use of specific materials as source of both spin and orbital current (as Ni); and we may anticipate the advantage of using lighter elements with the restricting requirement of large SOC would be avoided in the latter case. Furthermore, given that physical degrees of freedom as photons are able to also carry orbital angular momentum we comment on recent theoretical efforts to opto-electronic properties in our system.

[1] H. Park et al., Topological Surface-Dominated Spintronic THz Emission in Topologically Nontrivial $Bi_{1-x}Sb_x$ Films. *Adv. Sci.* 2022, 9, 2200948 [2] E. Rongione et al., Spin-Momentum Locking and Ultrafast Spin-Charge Conversion in Ultrathin Epitaxial $Bi_{1-x}Sb_x$ Topological Insulator. *Adv. Sci.* 2023, 10, 2301124. [3] S. Rho et al., Exceptional Spin-to-Charge Conversion in Selective Band Topology of $Bi/Bi_{1-x}Sb_x$ with Spintronic Singularity. Adv. Funct. Mater., 33: 2300175. [4] T. Adamantopoulos, M. Merte, D. Go, F. Freimuth, S. Blügel, and Y. Mokrousov. Orbital Rashba Effect as a Platform for Robust Orbital Photocurrents. Phys. Rev. Lett. 132, 076901.

INVITED PAPER

FG-05. Twist-angle tunable spin texture in WSe_2/graphene van der Waals heterostructures. *F. Casanova*[1,2] *1. CIC nanoGUNE, San Sebastian, Spain; 2. IKERBASQUE, Bilbao, Spain*

2D materials are an exciting new material family in which the proximity effect is especially important and opens ways to transfer useful spintronic properties from one 2D material into another. For instance, transition metal dichalcogenides (TMD) can be used to enhance the spin-orbit coupling of graphene. The spin-orbit proximity in such graphene/TMD van der Waals heterostructures leads to spin-charge interconversion of out-of-plane spins due to spin Hall effect, first observed experimentally by using MoS_2 as the TMD [1], of in-plane spins perpendicular to the charge current due to the Rashba-Edelstein effect (REE), first observed by using WS_2 as the TMD [2], or to coherent spin precession with electrical control by using WSe_2 as the TMD [3]. Recent theoretical works have predicted the modulation of spin texture in graphene-based heterostructures by twist angle [4], although an experimental verification is missing. We demonstrate the tunability of the spin texture and associated REE with twist angle in WSe_2/graphene heterostructures by spin precession experiments [5]. For specific twist angles, we experimentally detect a spin component radial with the electron's momentum (an "unconventional" REE), in addition to the standard orthogonal component (conventional REE) and show that the helicity of the spin texture can be reversed by angle twisting, paving the way for the development of novel spin-twistronic devices.

[1] C.K. Safeer et al., Nano Lett. 19, 1074 (2019). [2] T.S. Ghiasi et al., Nano Lett. 19, 5959 (2019); L.A. Benitez et al., Nat. Mater. 19, 170 (2020). [3] J. Ingla-Aynés et al., PRL 127, 047202 (2021). [4] S. Lee et al., PRB 106, 165420 (2022); K. Zollner et al., PRB 108, 235166 (2023). [5] H. Yang et al., arXiv:2312.10227, accepted in Nat. Mater.

CONTRIBUTED PAPERS

FG-06. Quantized transport in one-dimensional nanowire-graphene spin injectors. D. Burrow[1], J. Toscano-Figueroa[1], V. Guarochico Moreira[1], K. Omari[1], I. Grigorieva[1], T. Thomson[1] and *I. Vera Marun*[1] *1. The University of Manchester, Manchester, United Kingdom*

The potential of 2D (van der Waals) materials for spintronics has been recognized since graphene was first isolated [1]. However, realizing the early promise of low-power spintronics for next generation classical and quantum computation has proved challenging, in part due to the nature of the interface between a ferromagnetic metal needed to spin polarize injected electrons into the graphene transport layer and spin transport in the graphene layer. Encapsulating graphene in h-BN provides a platform that allows mobilities in excess of 100 000 cm2 V−1 s−1 and spin diffusion lengths approaching 20 μm [2]. In this presentation we report recent advances in high-mobility spintronics by building on our developed architecture [2, 3, 4] which has shown spin-polarized contacts at the 1D edge of h-BN encapsulated graphene. We demonstrate the detection of quantized conductance in the absence of an applied magnetic field, and quantum Hall transport, at one-dimensional spin injecting contacts between magnetic nanowires and record high-mobility graphene spin transistors. The nanowires define an effective quantum point contact at the graphene edge, even in the absence of any constriction in the graphene itself. The demonstration of ballistic spin injection is a milestone in the development of 2D ballistic spintronics.

[1] E.W. Hill et al., IEEE Trans. Magn., 42, 2694 (2006) [2] V.H. Guarochico-Moreira et al., Nano Letters, 22, 935–941 (2022) [3] C.R. Anderson et al., Sci Rep 13, 10343 (2023) [4] J. C. Toscano-Figueroa *et al.*, arXiv, May 30, 2024. doi: 10.48550/arXiv.2405.20491. (Accepted in NPJ Spintronics).

FG-07. Unidirectional Magnetoresistance in Heterostructures of Weyl Semimetal and Ferromagnetic Insulator. *R. Bandapelli*[1], I. Kao[1], J. Tang[2], S. Xu[3], Q. Ma[2], J. Katoch[1] and S. Singh[1] *1. Physics, Carnegie Mellon University, Pittsburgh, PA, United States; 2. Physics, Bostan College, Chestnut Hill, MA, United States; 3. Department of Chemistry and Chemical Biology, Harvard University, CAMBRIDGE, MA, United States*

Unidirectional magnetoresistance (UMR) in heterostructures, consisting of ferromagnetic insulators (FMIs) and Weyl semimetals (WSMs), refers to a nonlinear longitudinal resistance, which changes sign upon the reversal of charge current polarity or the magnetization. This effect typically originates from the interaction of spin polarization and magnetization at the interface [1]. WSMs, such as $TaIrTe_4$, offer unconventional charge-to-spin conversion capabilities (i.e., the ability to generate out-of-plane spins), which can be harnessed for developing bi-stable memory and logic devices with perpendicular magnetization. Two-dimensional (2D) FMIs, such as $Cr_2Ge_2Te_6$ (CGT), have the potential to enhance functionalities in spin-orbit torque (SOT) devices through electric field tunable magnetism. Previously, the electrical readout of magnetization in a 2D FMI, i.e., CGT, has been demonstrated by coupling it with heavy metals and topological insulators [2-4]. However, the results are limited to Anomalous Hall effect. In this work, we demonstrate proximity-induced UMR that is sensitive to both out-of-plane and in-plane magnetization. Utilizing the gate tunability of 2D materials, we realized sign switching of UMR due to the change of electron chemical potential in $TaIrTe_4$. Our results show highly tunable UMR in $TaIrTe_4$/ CGT heterostructures opens an exciting avenue for novel magnetic readout in future 2-terminal SOT devices.

1. C. O. Avci et al., Nature Physics 11, 570 (2015). 2. M. Lohmann et al., Nano Lett., 19, 2397 (2019). 3. V. Gupta et al., Nano Lett., 20, 7482 (2020). 4. M. Mogi et al., Phys. Rev. Lett. 123, 016804 (2019).

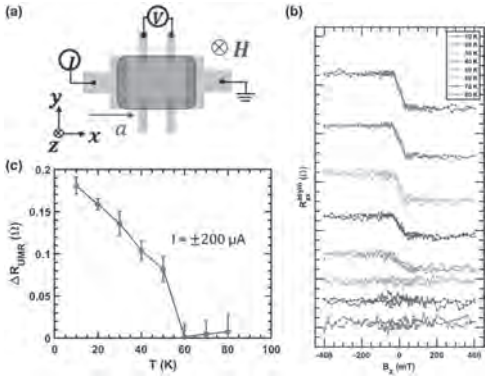

Fig. 1: (a) Schematic of the device configuration where the charge current is applied along the a-axis of $TaIrte_4$, and longitudinal resistance (R_{xx}) is measured in the same direction while the out-of-plane magnetic field is applied. (b) Asymmetric component of R_{xx} as a function of out-of-plane magnetic field at different but fixed temperatures. (c) UMR as a function of the temperature.

FG-08. Unidirectional magnetoresistance in van der Waals antiferromagnet. *L. Jia*[1], Z. Zheng[1] and J. Chen[1] *1. National University of Singapore, Singapore*

Unidirectional magnetoresistance (UMR), a type of nonlinear transport phenomenon, has attracted intensive interest due to its diverse physical mechanisms in different systems [1–3]. The recent discovery of UMR in antiferromagnetic (AFM) heterostructures has highlighted the role of Rashba spin-orbit coupling (SOC) [4,5]. This effect significantly influences the sign and magnetic field dependence of UMR by connecting momentum-dependent transport to the spin degree of freedom. Although a generalized tight-binding Hamiltonian model has provided some understanding of the physical mechanism, the relation between AFM UMR and the exact interfacial band structure as well as the spin distribution, remains incomplete. In this study, we explore the complex UMR behaviour in a van der Waals AFM heterostructure $CrPS_4$/Pt (Figure 1) for the first time, from both the perspective of theoretical model and experimental implementation. In our experiment, we measured the second harmonic longitudinal/Hall voltage and extracted the precise amplitude of AFM UMR by excluding the contribution of magneto-thermal effect. We observed two different magnetic-field-dependent UMR tendencies in $CrPS_4$/Pt devices, as shown in Figure 2. For the theoretical analysis, we developed a comprehensive Hamiltonian model based on density functional theory. The existence of different UMR tendencies can be well explained, and the physical mechanism is attributed to the selection of interfacial chemical potential and various type of spin distribution corresponding to the electron bands. Our work demonstrates the complexity of the band structure and spin distribution at the heterostructure interface of the van der Waals AFM semiconductor and heavy metal. This allows for deeper understanding of the characteristics of nonlinear transport phenomena in van der Waals magnetic materials.

[1] C. O. Avci, K. Garello, A. Ghosh, M. Gabureac, S. F. Alvarado, and P. Gambardella, *Unidirectional Spin Hall Magnetoresistance in Ferromagnet/Normal Metal Bilayers*, Nature Phys 11, 570 (2015). [2] C. O. Avci, J. Mendil, G. S. D. Beach, and P. Gambardella, *Origins of the Unidirectional Spin Hall Magnetoresistance in Metallic Bilayers*, Phys. Rev. Lett. 121, (2018). [3] G. Liu, X. Wang, Z. Z. Luan, L. F. Zhou, S. Y. Xia, B. Yang, Y. Z. Tian, G. Guo, J. Du, and D. Wu, *Magnonic Unidirectional Spin Hall Magnetoresistance in a Heavy-Metal–Ferromagnetic-Insulator Bilayer*, Phys. Rev. Lett. 127, 207206 (2021). [4] S. Shim, M. Mehraeen, J. Sklenar, J. Oh, J. Gibbons, H. Saglam, A. Hoffmann, S. S.-L. Zhang, and N. Mason, *Unidirectional Magnetoresistance in Antiferromagnet/Heavy-Metal Bilayers*, Phys. Rev. X 12, 021069 (2022). [5] Z. Zheng et al., *Coexistence of Magnon-Induced and Rashba-Induced Unidirectional Magnetoresistance in Antiferromagnets*, Nano Lett. 23, 6378 (2023).

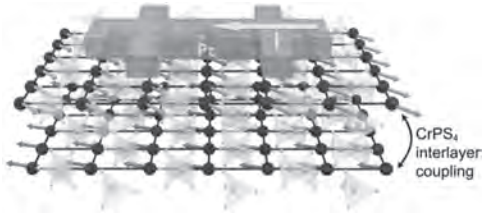

Schematic of $CrPS_4$/Pt heterostructure.

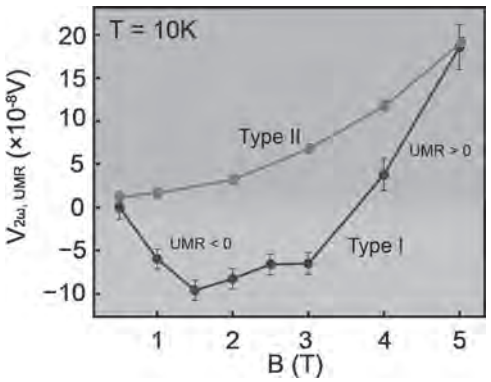

Two different tendencies of the UMR component versus the magnetic field.

FG-09. Magnonic Otto thermal machine. *N. Vidal-Silva*[1], F. Peña[2], R. Troncoso[3] and P. Vargas[2] *1. Universidad de La Frontera, Temuco, Chile; 2. Universidad Técnica Federico Santa María, Valparaiso, Chile; 3. Universidad Adolfo Ibañez, Santiago, Chile*

We propose a quasi-static magnon-based Otto thermal machine in two-dimensional (2D) magnetic insulators. The quasi-static thermodynamical cycles are engineered by exposing a magnon spin system to thermal baths at different temperatures and tuning the Dzyaloshinskii-Moriya (DM) interaction. We find that a thermal gas of magnons converts a fraction of heat into energy in the form of work, where the efficiency is maximized for specific values of DM, reaching the corresponding Carnot efficiency. We witness a positive to negative net work transition during the cycle that marks the onset of a refrigerator-like behavior. The work produced by the magnonic Otto engine enhances the magnon chemical potential. The last enables a spin accumulation that might result in the pumping of spin currents at the interfaces of metal-magnet heterostructures. Therefore, we unveil the spin pumping mediated by quasi-static thermodynamic cycles in magnonic systems. Our work opens new possibilities for the efficient leverage of conventional two-dimensional magnets.

Vidal-Silva, N., Peña, F. J., Troncoso, R. E., & Vargas, P. Magnonic Thermal Machines. *arXiv preprint arXiv:2404.08153 (2024)*

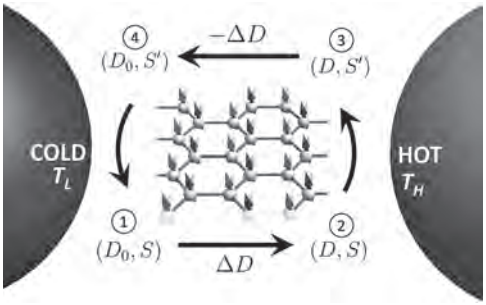

Schematic of the magnonic Otto cycle based on a magnetic honeycomb lattice with fluctuating spins. The cycle operates between hot (T_H) and cold (T_C) temperatures. In the horizontal processes, the entropy S (S′) holds fixed, while the DM parameter D (D_0) holds unchanged in the vertical processes.

IEEE AWARDS CEREMONY

Adekunle Adeyeye, Co-Chair
Durham University, Durham, United Kingdom
Atsufumi Hirohata, Co-Chair
Tohoku University, Sendai, Japan

Session PL
PLENARY SESSION

Mark Stiles, Chair
NIST, Gaithersburg, MD, United States

INVITED PAPER

PL-01. Innovation of Magnetics in Data Storage and Magnetoresistance: Past, Present, and Future. *Y. Tanaka[1] 1. Tohoku University, Sendai, Japan*

This plenary talk will focus on magnetics innovation both on the data storage and use of magnetoresistance as part of the "Year of Tunneling Magnetoresistance".

Session GA
ADVANCED MATERIALS AND DEVICES FOR ENERGY HARVESTING AND CONVERSION

Mario Carpentieri, Chair
Politecnico di Bari, Bari, Italy

INVITED PAPERS

Now VP13-09

GA-01. Nonlinear Spintronics: Unveiling Quantum Rectenna for Sensing and Energy Applications. *D. Kumar*[1,2], R. Sharma[3,2] and H. Yang[2] *1. Physics, Netaji Subhas University of Technology, New Delhi, India; 2. Electrical and Computer Engineering, National University of Singapore, Singapore; 3. Electrical Engineering, Indian Institute of Technology Ropar, Rupnagar, India*

Nonlinear spintronic phenomena are emerging in inversion-asymmetric spin-polarised nonmagnetic materials with high spin-orbit coupling and nonlinear transport effects. A second-order nonlinearity such as nonlinear magnetoresistance [1], nonlinear Hall effect (NLHE) [2] manifests in two distinct components; a voltage oscillating at twice the frequency (2ω) of the driving alternating current and a dc component that is generated due to the rectification effect. As a result, the realm of nonlinear spintronics, influenced by quantum properties, becomes applicable in scenarios necessitating frequency doubling or rectification. This has implications for energy harvesting, wireless communications, and terahertz detection. Among these quantum phenomena, the NLHE, which enables the generation of a transverse voltage without an applied magnetic field, is a potential alternative for energy harvesting. Recently, for the first time, we reported the room temperature NLHE in a type-II Weyl semimetal $TaIrTe_4$ [3]. We also observed a temperature-induced sign change in the NLHE, which is attributed to the sign change in Berry curvature dipole. More significantly, we harnessed this room temperature quantum effect to demonstrate wireless RF-rectification without the need for external bias or magnetic fields. The presentation will delve into an in-depth exploration of this accomplishment, elaborating on its intricacies and discussing recent efforts in nonlinear spintronics for energy harvesting.

[1] P. He et al., Nat. Phys. 14, 495 (2018). [2] P. He et al., Phys. Rev. Lett. 123, 016801 (2019). [3] D. Kumar et al., Nat. Nanotechnol. 16, 425 (2021).

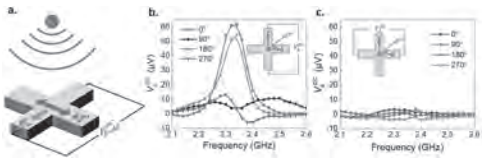

Rectification demonstration based on the nonlinear Hall effect in $TaIrTe_4$. (a) Schematic of the rectifier fabricated on Td-$TaIrTe_4$. A patch antenna with a high directivity and gain of 3 dBi at ~2.4 GHz was used as the electromagnetic radiation source. The Hall bar device, utilizing the room-temperature NLHE in $TaIrTe_4$, rectifies the incident electric field along a-axis (Eω) and generates a d.c. signal along the transverse direction b-axis. The rectified d.c. voltage measured along the b-axis (b) and along the a-axis (c) as a function of frequency while aligning the incident electric field at four different angles (θ = 0, 90, 180, and 270°) relative to the a-axis. Maximum rectification occurs when the electric field is parallel to the a-axis (θ = 0°) and the voltage is measured along the b-axis, consistent with the symmetry constraints of the NLHE.

GA-02. High-Performance Thermomagnetic Generator Controlled by a Magnetocaloric Switch. *H. Zhang*[1], X. Liu[1], H. Chen[1], K. Qiao[1], Z. Yu[1], L. Xie[1], R. Ramanujan[2], F. Hu[3], K. Chu[4] and Y. Long[1] *1. School of Materials Science and Engineering, University of Science and Technology Beijing, Beijing, China; 2. School of Materials Science and Engineering, Nanyang Technological University, Singapore; 3. Institute of Physics, Chinese Academy of Sciences, Beijing, China; 4. School of Materials Science and Engineering, Lanzhou Jiaotong University, Lanzhou, China*

Low grade waste heat accounts for ~65% of total waste heat, but few technologies can efficiently convert low-temperature waste heat into electricity[1]. Conventional waste heat recovery technologies, such as thermoelectric generator (TEG) and pyroelectric generator (PEG), exhibit low conversion efficiency for low-grade waste heat recovery. In contrast, thermomagnetic generator (TMG) has much higher conversion efficiency at low grade waste heat range[2]. However, the practical performance of previous TMGs is still far below the theoretical value. In this work, we designed a novel TMG for low-temperature waste heat recovery[3], in which the magnetocaloric material acts as a switch that controls the magnetic circuit, unlike its usual role as the coil core in previous TMGs[4-5]. The magnetic flux in the induction coil change between the negative and positive maximum values. Thus, the induced power increases by a factor of four compared to previous TMGs in which the flux only changes between zero and the maximum value. This topology has other advantages, e.g., higher maximum flux density in the iron yoke, avoiding magnetic stray fields and the hysteresis effect. It overcomes a key drawback of the pretzel-like topology by utilization of all the flux change in the conductive magnetic circuit[6]. The effects of key structural and system parameters on the TMG performance were studied through a combination of experiments and finite element simulations. The optimized TMG performance is 2 to 3 orders of magnitude higher than those of other active TMGs. It is also higher than those of TEGs and PEGs. Such a colossal TMG performance proves the effectiveness of our topology design of magnetic circuit with MCS. Furthermore, a LED light is successfully lit up, and a TMG array is proposed as a potential utilization scenario to harvest the low-grade waste heat.

[1] H. D. Chen, Z. H. Ma, and H. Zhang*. Evaluation of thermomagnetic generation performance of classic magnetocaloric materials for harvesting low-grade waste heat. *Appl. Energy* 306, 117999 (2022). [2] X. L. Liu, Z. H. Ma, and H. Zhang*. High-Performance Thermomagnetic Generator Controlled by a Magnetocaloric Switch. *Nat. Commun.* 14, 4811 (2023). [3] W. H. Chen, Y. B. Chiou, and R. Y. Chein. Power generation of thermoelectric generator with plate fins for recovering low-temperature waste heat. *Appl. Energy* 306, 21 (2022). [4] Z. H. Ma, H. D. Chen, and H. Zhang*. Thermomagnetic generation performance of Gd and La(Fe, Si)13Hy/In material for low-grade waste heat recovery. *Adv. Sustain. Syst.* 5, 2000234 (2021). [5] X. L. Liu, H. Zhang*, and H. D. Chen. Significant optimization of active thermomagnetic generator for low-grade waste heat recovery. *Appl. Therm. Eng.* 221, 119827 (2023). [6] A. Waske, D. Dzekan, and K. Sellschopp. Energy harvesting near room temperature using a thermomagnetic generator with a pretzel-like magnetic flux topology. *Nat Energy* 4, 68-74 (2019).

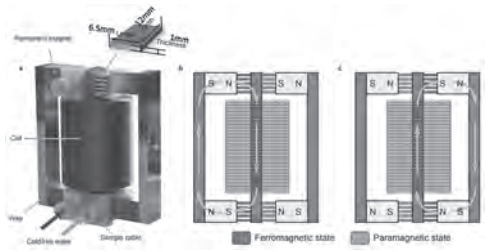

GA-03. Design and Optimization of Small Electromagnetic Harvesters for Vibrational Energy Scavenging. *C. Gomez-Polo*[1,2], I. Royo-Silvestre[1,2], D. Gandia[1,2], E. Garaio[1,2] and J. Beato-Lopez[1,2] *1. Departamento de Ciencias, Universidad Pública de Navarra, Pamplona, Spain; 2. Institute for Advanced Materials and Mathematics (INAMAT2), Universidad Pública de Navarra, Pamplona, Spain*

Electromagnetic vibrating harvesters are low-cost devices that collect environmental vibrational energy (civil infrastructures, transportation, human motion, etc.,) and convert it into electrical energy. Particularly, small devices can be employed to feed low power electric systems, such as wireless sensor networks (WSNs) specifically useful in applications with difficult access (e.g., remote locations or on moving parts of machinery) avoiding battery replacement. In this work two types of electromagnetic harvesters will be presented based on the classical electromagnetic induction law: (i) magnetic levitation vibration harvesters [1] and (ii) U-shaped cantilevers [2]. In both cases, the main challenge is to control the characteristic resonant frequency to fit it within the low frequency range of environmental vibrations (1–100 Hz) while keeping relative high output power densities (≈ 1 mW/cm^3). For this purpose, the development of experimental prototypes is guided and analyzed employing Finite Element Analysis (FEA). Particularly, an algorithm based on analytical equations has been implemented to design magnetic springs in levitation-based harvesters operating at very low frequencies (≈ 2 Hz) [3]. A prototype consisting of a fixed ferrite and a mobile rare-earth magnet was designed and experimentally tested, where the semi-analytical optimum solution was properly modified via FEA. For cantilever harvesters, a steel ferromagnetic U-frame including a NdFeB magnet and a ferrite magnet used as "magnetic tip mass" was prototyped and tested. FEA and Magnetic Circuit analysis were used to optimize magnetic flux changes under low-frequency vibrations (< 100 Hz). The size (mass) of the ferrite magnet allowed control of the resonance frequency (51-77 Hz) without appreciable changes in the generated voltage. *Acknowledgements.*- This work has been developed under the project TED2021130884B-I00 funded by MCIN/AEI/10.13039/501100011033 and European Union "Next Generation EU/PRTR".

[1] J.J. Beato-López, I. Royo-Silvestre, J.M. Algueta-Miguel, C. Gómez-Polo, Sensors, 20(7) (2020) 1873; https://doi.org/10.3390/s20071873. [2] D. Gandía, E. Garaio, I. Royo-Silvestre, J.J. Beato-López, C. Gómez-Polo, 2024 IEEE International Magnetic Conference. DOI: 10.1109/INTERMAG-ShortPapers61879.2024.10577076. [3] I. Royo-Silvestre, J.J. Beato-López, C. Gómez-Polo, Appl. Energy, 360 (2024) 122778. https://doi.org/10.1016/j.apenergy.2024.122778.

GA-04. Recent Advances in Enabling Soft Magnetics Technology for WBG and UWBG Power Electronics Applications. *P. Ohodnicki*[1], T. Paplham[1], S. Mullurkara[1], L. Wewer[1], Y. Wang[1], B. Bhandari[1], C. Zheng[1], B. Grainger[1] and M. Ghosh[1] *1. University of Pittsburgh, Pittsburgh, PA, United States*

Numerous trends are driving needs for advances in electrical power conversion technologies, including rapid deployment of renewables in the electric power grid and electrification of the transportation sector. Soft magnetics technologies play a critical role as an enabler for state-of-art power electronics conversion and systems able to fully exploit the latest advances in wide bandgap (WBG) and ultra-wide bandgap (UWBG) semiconductor-based switching devices. Current commercial soft magnetic materials and manufacturing solutions are not optimized for these new application requirements. Amorphous and nanocrystalline soft magnetic alloys have emerged as the premier solution for many WBG-based power electronics converter applications, including medium frequency transformers and inductors, as a result of increased saturation flux densities relative to ferrites and reduced eddy current losses compared to electrical steels. In case of future UWBG power electronics, alternative soft magnetic materials and manufacturing pathways are required for unprecedented combinations of power, voltage, and switching frequencies. In addition, novel soft magnetic materials and manufacturing pathways can play a critical role in high performance electric motor technologies which represent a major fraction of electrical energy utilization. This presentation will provide an overview of recent advances in soft magnetic materials and advanced manufacturing processes, targeting to address these demanding application requirements. More specifically, the presentation will discuss advances related to nanocrystalline soft magnetic alloys for WBG power electronics applications: (1) recent advances in nanocrystalline alloy chemistry optimization to enable unprecedented high temperature stability approaching operational temperatures of 500C and (2) advanced processing concepts to enable rapid thermal processing of amorphous alloys using electromagnetic field assisted techniques for spatially controlled microstructure and magnetic property optimization. Advances in ferrite-based material chemistry and processing for future UWBG applications will also be discussed: (1) synthesis of nanocomposite metal and ferrite composite systems through harvesting thermodynamic and kinetic pathways and (2) additive manufacturing of ferrite-based components for scalability and novel microstructure engineering routes for high power applications. Important component level design considerations dictating the preferred core selection between nanocrystalline, and ferrite based magnetic components for high power and medium frequency applications representative of both near-term WBG and future UWBG power electronics applications will also be discussed, highlighting the importance of considering device and system level impacts in materials and manufacturing research.

[1] Ohodnicki, P., Kautz, E., Devaraj, A. *et al. Journal of Materials Research* 36, 105–113 (2021). https://doi.org/10.1557/s43578-020-00066-5. [2] Paplham, T.W., Wang, Y., Greve, D.W. *et al. Journal of Materials Research* 38, 780–788 (2023). https://doi.org/10.1557/s43578-022-00862-1. [3] A. Talaat, J. Egbu, C. Phatak, K. Byerly, M.E. McHenry, P.R. Ohodnicki, Materials Research Bulletin, Volume 152, 2022, 111839, ISSN 0025-5408, https://doi.org/10.1016/j.materresbull.2022.111839. [4] Ahmed Talaat, David W. Greve, M.V. Suraj, Paul R. Ohodnicki, Journal of Alloys and Compounds, Volume 854, 2021, 156480, ISSN 0925-8388, https://doi.org/10.1016/j.jallcom.2020.156480. (https://www.sciencedirect.com/science/article/pii/S0925838820328449) [5] A. Talaat, M.V. Suraj, K. Byerly, A. Wang, Y. Wang, J.K. Lee, P.R. Ohodnicki, Journal of Alloys and Compounds, Volume 870, 2021, 159500, ISSN 0925-8388, https://doi.org/10.1016/j.jallcom.2021.159500. [6] M. K. Ghosh, C. Bracken, M. Juds, B. R. Andapally, B. Grainger and P. R. Ohodnicki, *2023 IEEE Electric Ship Technologies Symposium (ESTS)*, Alexandria, VA, USA, 2023, pp. 107-114, doi: 10.1109/ESTS56571.2023.10220567. [7] Zheng, Chuyuan and Bhandari, Bishal and Mullurkara, Suraj Venkateshwaran and Mandal, Dipika and Bracken, Chris and Pierce, Alex and Ohodnicki, Paul R., Binder Jet 3d Printing of Mn-Zn Ferrite Soft Magnet Toroidal Cores. Available at SSRN: https://ssrn.com/abstract=4672911 or http://dx.doi.org/10.2139/ssrn.4672911.

GA-05. Novel functional magnetic materials from high-throughput studies. *H.C. Herper*[1], A. Vishina[1], M. Marathe[2] and O. Eriksson[1] *1. Physics and Astronomy, Uppsala University, Uppsala, Sweden; 2. KTH, Stockholm, Sweden*

Striving to reduce the CO_2 emission and to fight global warming, it needs new functional materials which make electric transportation, wind power etc. cost effective and really sustainable. Magnetic materials used in these applications turn out to be a bottleneck in this scenario by containing rare earths

(RE) or other critical raw materials. Some improvements have been made by reducing critical raw materials [1], but more is needed. We aim to identify new materials with the efficiency of the current ones while surpassing them ecologically and economically. In this talk, the focus will be on (semi) hard magnets and their intrinsic magnetic properties. Thus, the key elements which provide magnetism will be 3d elements. To identify new materials 'tailored' for a specific application materials design based on ab initio methods combined with thermodynamic modelling will be used. Various methodologies, including big data searches intertwined with high-throughput calculations, will be presented and their efficiency and accuracy discussed. Our investigations start either with a large body of systems provided by a structural data base [2] or with novel structures generated by machine learning software [3]. While in the database driven searches the focus is on existing phases that have not been explored regarding their potential for PM. Machine learning based methods generate completely new structures, however, similar screening criteria are used in both methods. Depending on the requirements for the magnetic material a set of selection rules is defined. Phases that pass all the filter criteria are investigated in detail using a combination of first principles electronic structure methods and thermodynamic modelling [3-5] and can then be synthesized. Results from database driven high-throughput searches for rare-earth-free permanent magnets are shown in Fig. 1(a). The filled symbols denote the systems which passed the filters and were investigated in detail by ab initio methods and Monte Carlo simulations. Systems of interest for permanent magnets are shown in the shaded right corner, i.e. magnetization and magnetocrystalline anisotropy (MCA) are above the threshold values 1T and 1MJ/m^3 [1,6]. Open symbols mark known systems which were also found in the search and can be viewed as proof of principle. The hexagonal Co_3Mn_2Ge system could be synthesized and uniaxial MCA was confirmed (Fig 1(b)). To explore the phase space beyond the known phases we looked for binary Fe-Ta systems using machine learning tools. [3] The 5d element Ta was expected to boost the MCA due to its large spin-orbit coupling. Three of the newly generated phases where particularly interesting showing uniaxial MCA with high values up to 10 MJ/m^3 and being very close to the hull curve. How and whether these phases might be stabilized will be discussed. Funded by MaMMoS (EU HORIZON), NOVAMAG (HORIZON 2020), Olle Engkvist stiftelse, Swedish Strategic Research Foundation (SSF), STandUp, National Academic Infrastructure for Supercomputing in Sweden (NAISS former SNIC)

[1] A.M. Schönhöbel et al. Journal of Alloys and Compounds 786, 969 (2019) [2] A. Vishina. et al., Physical Review B 101, 094407 (2020) [3] S. Arapan, P. Nieves, H. C. Herper, and D. Legut, Physical Review B 101, 014426 (2020) [4] A. Vishina, O. Eriksson, and H. C. Herper, Materials Research Letters 11 (1), 76-83 (2023) [5] M. Marathe and H. C. Herper, Physical Review B 107, 174402 (2023) [6] A. Vishina et al, Acta Materialia 212, 116913 (2021)

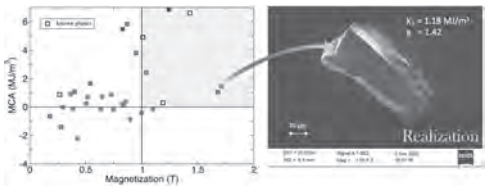

a) Candidate phases for PM predicted from database-driven high-throughput studies (Ref. [1], [6]). The filled symbols mark the calculated MCA vs. the magnetization. Open symbols are known phases which turned up in our calculations and can be viewed as proof of principle. (b) SEM graph of the synthesized sample of one candidate phase (Co_3Mn_2Ge).

Session GB
NEW CHALLENGES IN NANOMAGNETISM FROM TOPOLOGY TO THE THIRD DIMENSION

Riccardo Tomasello, Chair
Politecnico di Bari, Bari, Italy

INVITED PAPERS

GB-01. Scientific and technological challenge and opportunities with 3-dim nanomagnetism. *P. Fischer[1,2] 1. LBNL, Berkeley, CA, United States; 2. UC Santa Cruz, Santa Cruz, CA, United States*

The scientific and technological exploration of three-dimensional magnetic nanostructures is an emerging research field with exciting novel physical phenomena, originating from the increased complexity in spin textures, topology, and frustration in three dimensions. The concept of chirality which requires three dimensions, is essential to understand e.g., fundamental interactions in cosmology and particle physics, the evolution of life in biology, or molecular chemistry, but has recently also attracted enormous interest in the magnetism community. Tailored three-dimensional nanomagnetic structures, including in artificial spin ice systems or magnonics will enable novel applications in magnetic sensor and information processing technologies with improved energy efficiency, processing speed, functionalities, and miniaturization of future spintronic devices. Another approach to explore and harness the full three-dimensional space is to use curvature as a design parameter, where the local curvature impacts physical properties across multiple length scales, ranging from the macroscopic to the nanoscale at interfaces and inhomogeneities in materials with structural, chemical, electronic, and magnetic short-range order. In quantum materials, where correlations, entanglement, and topology dominate, the local curvature opens the path to novel phenomena that have recently emerged and could have a dramatic impact on future fundamental and applied studies of materials. Particularly, magnetic systems hosting non-collinear and topological states and 3D magnetic nanostructures strongly benefit from treating curvature as a new design parameter to explore prospective applications in the magnetic field and stress sensing, micro-robotics, and information processing and storage. Exploring 3d nanomagnetism requires advances in modelling/theory, synthesis/fabrication, and state-of-the-art nanoscale characterization techniques to understand, realize and control the properties, behavior, and functionalities of these novel magnetic nanostructures. I will summarize and review the challenges but also the opportunities ahead of us in the future exploration of nanomagnetism in three dimensions. Work supported by DOE BES MSE Contract DE-AC02-05-CH11231

2024 Roadmap on 3D Nano-magnetism, G Gubbiotti, A. Barman eds, Journal of Physics C: Condensed Matter (2024) submitted A. Fernández-Pacheco, R.Streubel,O.Fruchart,R.Hertel,P.Fischer,R.P.Cowburn,*Three-dimensional nanomagnetism,* Nature Comm 8:15756 (2017) S. Ladak, A. Fernandez-Pacheco, P. Fischer, *Science and Technology of 3D Magnetic Nanostructures (Editorial),* APL Materials 10 120401 (2022) R. Streubel, E. Tsymbal, P. Fischer, *Perspective: Magnetism in Curved Geometries,* JAP 129 210902 (2021) P. Fischer, D. Sanz-Hernández, R. Streubel, A. Fernández-Pacheco, *Research update: Launching a new dimension with 3D magnetic nanostructures,* APL Materials 8 010701 (2020)

GB-02. Tailoring the energy landscape of a Bloch point singularity in a 3D nanostructure. *S. Ruiz Gómez[1,2], C. Abert[3], P. Morales Fernandey[2], C. Fernandez Gonzalez[1,2], S. Koraltan[3], L. Danesi[3], D. Suess[3], M. Foerster[1], M. Angel[1], A. Mandziak[4], D. Wilgocka-Slezak[4,5], P. Nita[4,5], M. Koenig[2], A. Hierro-Rodriguez[6], A. Fernandez-Pacheco[7] and C. Donnelly[2] 1. ALBA Synchrotron, Madrid, Spain; 2. Max Planck Institute for Chemical Physics of Solids, Dresden, Germany; 3. Faculty of Physics, University of Vienna, Vienna, Austria; 4. SOLARIS Synchrotron light Sources, Krakow, Poland; 5. Jerzy Haber Institute of Catalysis and Surface Chemistry, Krakow, Poland; 6. Universidad de Oviedo, Oviedo, Spain; 7. Institute of Applied Physics, Vienna, Austria*

Topological defects, or singularities, play a crucial role in the statics and dynamics of complex systems. In magnetism, Bloch point singularities are point defects that facilitate the nucleation of textures such as skyrmions and hopfions[1]. These textures are typically stabilized in chiral magnets, though the impact of chirality on Bloch point singularities remains largely unexplored. In this work, we use advanced three-dimensional nanofabrication techniques, specifically Focused Ion Beam Induced Deposition (FEBID), to investigate how curvature-induced symmetry breaking affects Bloch point singularities within a ferromagnetic nanowire[2,3]. By combining X-ray magnetic microscopy with in situ magnetic field application[4], we found that domain walls containing Bloch point singularities stabilize in specific regions of the nanowires where the energy is minimized. Moreover, we demonstrate that curvature modulation can be employed to manipulate the energy landscape of Bloch points. This enables the creation of pinning sites and asymmetric potential wells, facilitating the realization of a robust Bloch point shift-register that exhibits non-reciprocal behavior. These findings highlight the influence of symmetry and chirality on singularities, presenting a method for the controlled nucleation and propagation of topological textures. This opens up new avenues for developing logic and computing devices based on these principles.

[1] Birch, M.T., et al. Commun Phys 4, 175 (2021). [2] Skoric, L. et al. *Nano Lett*. 20, 184-191 (2020). [3] Ruiz- Gomez, S. et al. arXiv: 2404.06042. (2024). [4] Foerster, M. et al. Ultramicroscopy. 171, 63, (2016).

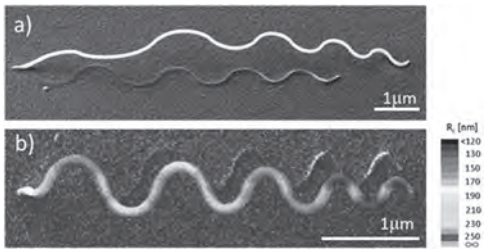

Fig. 1. Fabrication of 3D undulating nanostructures. a) SEM image taken at 45° tilt of the undulating structure fabricated with FEBID using $Co_2(CO)_8$ precursor on a Si substrate. b) top view of the same structure with a color map superposed where the colors indicates the radius of curvature along the structure.

GB-03. All-Electrical Control of Magnetic Skyrmions via Interlayer Exchange Coupling. *A. Soumyanarayanan[1,2] 1. Physics, National University of Singapore, Singapore; 2. Institute of Materials Research and Engineeering, Agency for Science, Technology and Research, Singapore*

Topological spin textures such as magnetic skyrmions represent the smallest realizable emergent magnetic entities in functional materials [1,2]. Their ease of tunability and electrical mobility in multilayer films [3-5] offers considerable promise as nanometre-scale bits for sustainable computing. However, the instability of skyrmions at the ultrathin limit, coupled with the absence of robust electrical readout and deterministic manipulation, have presented longstanding roadblocks to unleashing their potential [2]. Here, we engineer interlayer exchange coupling (IEC) in chiral multilayers to achieve all-electrical control of skyrmions. First, we demonstrate the use of IEC to systematically tailor the energetics and kinetics of skyrmion formation in ultrathin multilayers [6]. This enables the generation of robust, zero-field skyrmions with tunable configurations and densities. Next, we employ IEC to integrate a chiral layer with conventional magnetic layers to develop a nanoscale magnetic tunnel junction (MTJ) hosting a single skyrmion [7]. Using a suite of electrical and imaging techniques, we show that the MTJ nucleates skyrmions of fixed polarity, whose large readout signal corresponds directly to skyrmion size. The MTJ exploits complementary mechanisms to stabilize distinctly sized skyrmions at zero field, realizing three non-volatile electrical states. Crucially, the MTJ can electrically write and delete skyrmions to both uniform states with switching energies 1,000 times lower than state-of-the-art. In contrast to conventional MTJs, the applied voltage emulates a magnetic field. This reshapes both the energetics and kinetics of the switching transition, which is stabilized by IEC effects. The established large-readout, efficient switching, and lateral manipulation on our wafer-scale stack [7] provides a much-anticipated platform for all-electrical skyrmionics. Finally, the unique attributes of skyrmionic MTJs are promising for unconventional computing, including via designer IEC architectures.

[1] A. Soumyanarayanan *et al.*, Nature 539, 509 (2016). [2] A. Fert *et al.*, Nature Reviews Materials 16, 898 (2017). [3] A. Soumyanarayanan *et al.*, Nature Materials 16, 898 (2017). [4] X. Chen *et al.*, Advanced Science 9, 2103978 (2022). [5] A.K.C. Tan, P. Ho *et al.*, Nature Communications 12, 4252 (2021). [6] X. Chen, T. Tai, H.R. Tan *et al.*, Advanced Functional Materials 34, 2304560 (2023). [7] S. Chen, J. Lourembam, P. Ho *et al.*, Nature 627, 522 (2024).

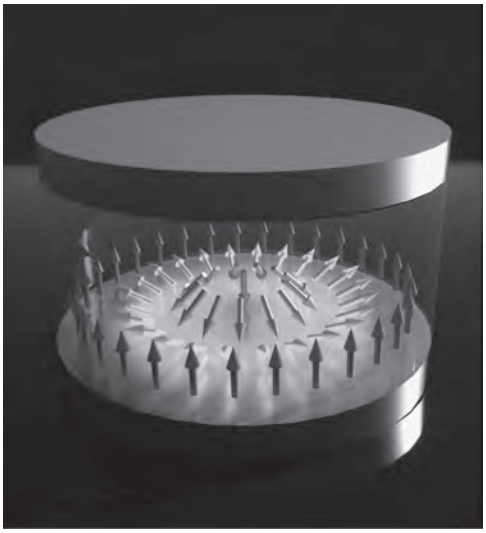

Schematic of a skyrmionic MTJ

GB-04. Skyrmions in synthetic antiferromagnets and their fast current induced dynamics. *O. Boulle[1] 1. Spintec, Grenoble, France*

Skyrmions are topological spin textures which hold great promise as nanoscale bits of information in memory and logic devices [1]. Although room-temperature ferromagnetic skyrmions and their current-induced manipulation have been demonstrated [2,3], their velocity has been limited to about 100 meters per second [3,4]. In addition, their dynamics are perturbed by the skyrmion Hall effect, a motion transverse to the current direction caused by the skyrmion topological charge. Antiferromagnetic skyrmions allow these limitations to be lifted owing to their vanishing magnetization and net zero topological charge, promising fast dynamics without skyrmion Hall effect. In this talk, I will address the stabilization and current induced manipulation of skyrmions in compensated synthetic antiferromagnetic (SAF). I will first show that skyrmions can be stabilized at room temperature in Pt/Co/Ru based compensated SAFs and nucleated using local current injection and ultrafast laser pulses [5]. I will then show that SAF skyrmions can be moved by current at velocities over 900 m/s without skyrmion Hall effect [6]. Micromagnetic simulations and analytical models using experimental parameters show that this enhanced skyrmion velocity can be explained by the compensation of the gyrotropic force in the synthetic antiferromagnet. I will conclude the talk with recent results on the electrical nucleation and detection of a skyrmion in magnetic tunnel junctions, which is another important milestone for skyrmion based devices [7]. Our results open important paths toward the realization of logic and memory devices based on the fast manipulation of skyrmions.

[1] A. Fert, V. Cros, and J. Sampaio, Nat. Nano. 8, 152 (2013). [2] O. Boulle *et al.*, Nature Nano., 11, 449 (2016) [3] A. Fert, N. Reyren and V. Cros, Nat Rev Mater 2, 17031 (2017). [4] R. Juge, S-G. Je *et al.*, Phys. Rev. Appl. 12, 044007 (2019) [5] R. Juge, N. Sisodia *et al.*, Nature Comm., 13, 4807 (2022) [6] V.T Pham, N. Sisodia, I. Di Manici, J. Urrestarazu Larranaga *et al.*, Science, 384, 6693 (2024) [7] J. Urrestarazu Larranaga, N. Sisodia, R. Guedas, Nano Letters, 24, 3557 (2024)

GB-05. Hopfions in Magnetic Crystals. N. Kiselev[1] and *P. Rybakov[2] 1. Peter Grüngerg Institute, Forschungszentrum Jülich, Jülich, Germany; 2. Uppsala University, Uppsala, Sweden*

Magnetic solitons are localized magnetization field configurations in crystals that possess properties similar to ordinary particles, allowing them to move and interact with each other and the environment. These characteristics make them promising candidates for information transfer and data storage applications. The most well-known magnetic solitons, such as skyrmions in 2D materials and skyrmion strings in bulk samples, represent quasi-two-dimensional configurations. We present the experimental discovery of 3D topological magnetic solitons, also known as hopfions [1]. Hopfions can be understood as closed twisted skyrmion strings, which, in the simplest case, form toroidal or ring-like structures localized in a small volume of the magnetic sample [2]. We observed hopfions linked with skyrmion strings in B20-type FeGe plates through high-resolution transmission electron microscopy. In this talk, I will discuss several aspects of hopfion rings, including the diversity of configurations of hopfion rings linked with one or a few skyrmion strings, a highly reproducible protocol for hopfion ring nucleation, the hopfion ring zero modes, and the topological analysis of these configurations. Additionally, I will discuss other perspective systems where theory predicts statically stable hopfions.

[1] Zheng, F. et al., Nature 623, 718 (2023). [2] Rybakov, F. N. et al. APL Mater. 10, 111113 (2022).

Session GC
NEUROMORPHIC AND RESERVOIR COMPUTING

Martina Kiechle, Chair
National Institute of Standards and Technology, Boulder, CO, United States

INVITED PAPER

GC-01. Reliable Edge Neuromorphic Systems Based on Multi-Level SOT Spintronic Devices. *L. Anghel*[1] *1. SPINTEC, Grenoble, France*

Internet of Things (IoT) and smart wearable devices for personalized healthcare will require storing and computing ever-increasing amounts of data. The key requirements for these devices are ultra-low-power, high-processing capabilities, autonomy at low cost, as well as reliability and accuracy to enable Green AI at the edge. Artificial Intelligence (AI) models, especially Bayesian Neural Networks (BayNNs) are resource-intensive and face challenges with traditional computing architectures due to the memory wall problem. Computing-in-Memory (CIM) with emerging resistive memories offers a solution by combining memory blocks and computing units for higher efficiency and lower power consumption. However, implementing BayNNs on CIM hardware, particularly with spintronic technologies, presents technical challenges due to variability and manufacturing defects. Our solutions aim to address these challenges through full-stack hardware and software co-design, developing novel algorithmic and circuit design approaches to enhance the performance, energy-efficiency and robustness of BayNNs on sprintronic-based CIM platforms.

CONTRIBUTED PAPERS

GC-02. Analog Magnetic Tunnel Junctions with Antiferromagnet/Ferromagnet Stack Controlled by Spin-Orbit Torque for Neuromorphic Computing. *A. Lagarrigue*[1], K. Vihanga De Zoysa[1], S. Varaganti[1], S. Kanai[1], S. Moriya[1], S. Sato[1], Y. Horio[1], H. Ohno[1] and S. Fukami[1] *1. Tohoku University, Sendai, Japan*

As conventional computing struggles to address several tasks with high energy efficiency, significant efforts have been devoted to neuromorphic computing. This promising alternative aims to mimic the physiological behavior of biological neurons and synapses using solid-state components. Synaptic plasticity, a prevalent characteristic of the human brain, can be approximated as a memristor—a device whose resistance can switch between non-volatile states while retaining memory of previous states, allowing the storage of analog weights of neural networks in a single device. Such analog-like behavior was observed in spin-orbit torque (SOT) based devices (Hall bars and nanodots) with antiferromagnet/ferromagnet heterostructures [1,2], leading to a demonstration of associative memory where the weight is stored as the multidomain structure [3]. However, the small anomalous Hall resistance variations (in the mΩ range) and the 4-terminal Hall bar geometry are not optimal for practical applications, motivating the present study. In the current work, we study 3-terminal perpendicular magnetic tunnel junctions (MTJs) with diameter D_{MTJ} ranging from 200 nm to 10 μm, patterned on top of an antiferromagnetic PtMn channel. The write operation is performed by applying a current pulse I_{CH} (t = 0.1 s) through the channel [Fig. 1(a)], while the read operation is conducted through tunnelling magnetoresistance (TMR) measurements [Fig. 1(b)]. The MTJ's stack structure is shown in Fig. 1(c). We demonstrate analog and field-free SOT switching of the MTJ's resistance. Figure 2(a) shows $R_{MTJ}(I_{CH})$ with several intermediate non-volatile resistive states and a resistance variation of > 100 Ω. The availability of the intermediate states is demonstrated in Fig. 2(b) where excited states can be accessed with single pulses. In-depth measurements with magnetic field reveal the potential to achieve even higher resistance change with TMR > 100%. This result paves the way for energy-efficient artificial synapses for neuromorphic applications.

[1] S. Fukami, C. Zhang, S. Duttagupta *et al., Nature Mater.,* Vol. 15, p. 535–541 (2016) [2] A. Kurenkov, C. Zhang, S. DuttaGupta *et al.*, *Appl. Phys. Lett.,* Vol. 110, p. 092410 (2017) [3] W. A. Borders, H. Akima, S. Fukami *et al.*, *Appl. Phys. Express.,* Vol. 10, p. 013007 (2017)

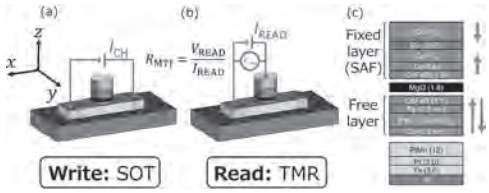

Fig 1: Device schematics with electrical configuration in (a) write and (b) read modes. (c) MTJ's stack structure.

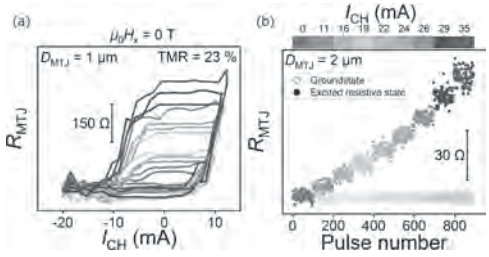

Fig. 2: (a) Field-free switching of R_{MTJ}. (b) Accessibility of intermediate states.

GC-04. Demonstration of Leaky-Integrate-Fire Behavior in Domain Wall Magnetic Tunnel Junction Neuromorphic Devices. *N. Zogbi*[1], T. Leonard[1], S. Liu[1], V.C. Rogers[1], C.H. Bennett[2] and J.C. Incorvia[1] *1. Electrical and Computer Engineering, The University of Texas at Austin, Austin, TX, United States; 2. Sandia National Laboratories, Albuquerque, NM, United States*

Neuromorphic computing seeks to emulate the behavior of biological synapses and neurons to increase speed and efficiency of neural networks. The domain wall-magnetic tunnel junction (DW-MTJ) has a unique ability to emulate this behavior with the same thin film stack, by modulating the DW, allowing for a monolithically integrated system [1, 2]. This is enabled by placing an MTJ on the ferromagnetic track and sensing the change in resistance with varying inputs applied to the device. Previous simulation work has predicted that modifying the shape anisotropy of the ferromagnetic track can implement intrinsic leaking to achieve the bio-realistic Leaky, Integrate, and Fire (LIF) behavior, which is highly desirable due to its broad applications in neural networks [3]. Here, we experimentally show DW-MTJs with LIF behavior based on shape anisotropy (Fig. 1). This structure initializes a DW on either side of the ferromagnetic track allowing for both integration and leaking to be performed. To perform leaking, a field is used to saturate the MTJ to its P or AP state, then, by pulsing current through

the Oe line on the larger portion of the track, the DW is initialized. The anisotropy causes the DW to leak to the smaller portion of the trapezoidal track to achieve the lowest magnetostatic energy. This leaking procedure and measurement results of 75 cycles are shown in Fig. 2. Furthermore, we explore integration on these devices and combine these two behaviors to demonstrate LIF on a DW-MTJ. These results show that the shape anisotropy-based system can allow for monolithically integrated neural networks using DW-MTJs. SNL is managed and operated by NTESS under DOE NNSA contract DE-NA0003525.

[1] T. Leonard, S. Liu and M. Alamdar, Advanced Electronic Materials., Vol. 8, (2022) [2] T. Leonard, S. Liu and H. Jin, Applied Physics Letters., Vol. 112, (2023) [3] W. H. Brigner, J. S. Friedman and N. Hassan, IEEE Transactions on Electron Devices., Vol. 88, p.4970 (2019)

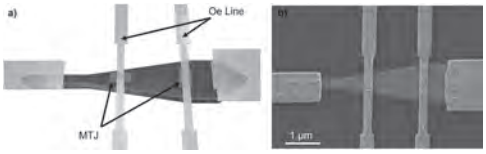

Fig. 1: Device Design. (a) Shape anisotropy based DW-MTJ with trapezoidal DW track (blue), MTJs for resistance readout (red), and Oersted field lines to nucleate DWs. (b) SEM image of DW-MTJ.

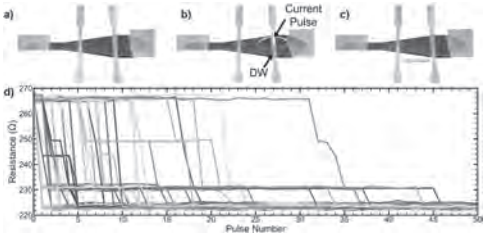

Fig. 2: Leaking experiment with protocol and data. (a) Saturation of DW-MTJ configuring the MTJ to be AP. (b) Initialization of DW with Oe line. (c) Spontaneous leaking of DW observed by change in resistance of left MTJ. (d) Measurement of left MTJ after a-c sequence over many cycles, showing stochastic relaxation to the P state as the DW leaks.

INVITED PAPER

GC-05. Fast Excitation Dynamics in Artificial Spin Ice Made from Magnetic Tunnel Junctions. *S. Majetich*[1] *1. Physics, Carnegie Mellon University, Pittsburgh, PA, United States*

Artificial Spin Ice (ASI) consists of magnetostatically coupled nanomagnets where frustration leads to multiple low energy states and propagating excitations [1]. These excitations, or emergent magnetic monopoles, are due to fictitious magnetic charges with a non-zero sum at the nodes between nanomagnets. Here the ASI is formed from the free layers of magnetic tunnel junctions (MTJs), which have faster dynamics than the larger patterns of traditional ASI, and offer the potential to inject excitations on one side of the array using spin transfer torque, and detect them on the other side via tunnel magnetoresistance (TMR). The free layers of the CoFeB-based MTJs are patterned into square arrays of 60 nm circular nanomagnets with a 90 nm pitch, as shown in Fig. 1 (a). The MTJs had in-plane magnetization, and a 7 Oe fringe field from the pinned synthetic antiferromagnet (SAF) reference layer breaks symmetry. Conductive atomic force microscopy of individual MTJs (Fig. 1 (b) reveals a pattern of alternating easy axis directions, like that seen with larger ASI nanomagnets. Time-dependent TMR depends on the angle between the SAF field and the easy axis. If parallel there is zero field telegraphing between q = 0 and 180°, but if perpendicular there is significant spin canting relative to an average angle of ± 90°. Changes in the effective energy barrier are used to identify whether a particular nanomagnet is part of an emergent magnetic monopole excitation. Non-trivial propagation through the frustrated lattice, necessary for neuromorphic computing, has been achieved by applying an external field diagonal to the square ice pattern [2]. Here a rotated SAF field [3], relative to the ASI orientation, is used to favor a general propagation direction while allowing for non-linear response when excitations interact.

1. R. F. Wang, et al., Nature 439, 303 (2006). 2. Y. Perrin, et al., Nature 540, 410 (2016). 3. H. Chen, et al., Appl. Phys. Lett. 120, 212401(2022).

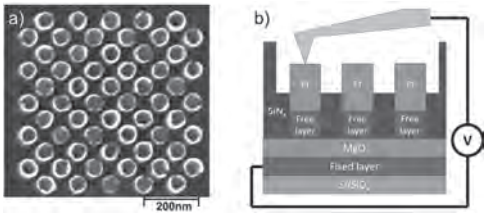

Figure 1. (a) Scanning electron microscopy image of square ASI showing the patterned free layers of the MTJs. (b) Schematic of the CAFM measurement of TMR in individual MTJs.

CONTRIBUTED PAPER

GC-07. Magnonic Resonators as Building Blocks of Scalable Magnonic Logic Circuits and Reservoir Computers. *A. Shytov*[1], O. Kyriienko[1], K. Fripp[1] and V. Kruglyak[1] *1. University fo Exeter, Exeter, United Kingdom*

We report on nonlinear magnonic resonators as viable building blocks of unconventional computing architectures. Via micromagnetic simulations, we demonstrate that the spin-wave modes confined in magnonic resonators [1-3] exhibit a strongly nonlinear response owing to energy concentration when resonantly excited by incident linear spin waves [4]. We use this nonlinearity to design and optimize (i) magnonic logic gates, and (ii) nonlinear magnonic reservoirs for data processing in the time domain. The developed gates include NAND (with fidelity of better than 95%, which can be improved further albeit at the expense of unwanted phase variation), as well as AND (93%) and NOR (92%). The designed reservoirs consist of one or more resonators coupled either actively (via an additional microwave feedback ring) or passively (via multiple spin wave reflections between the resonators). Their performance is analyzed for a range of benchmark tests on analog and noisy binary data, using standard time-multiplexing protocols for realistic device parameters informed by the micromagnetic simulations. Our tests reveal that the passive reservoirs can show superior performance for simple short memory tasks, such as retrieving previous / predicting next sample, parity checks and majority gates, simple arithmetic operations. For binary inputs, fidelity of better than 99% may be achieved even for noise levels of up to 10%. At the same time, the actively coupled reservoirs perform better on more complex tasks, such as NARMA10 or NARMA20 time series prediction, while the feedback coefficient proves a useful handle for fine-tuning the reservoir. Our magnonic devices, both gates and reservoirs, may be concatenated to form more complex and powerful logic circuits and reservoir computing architectures. The research leading to these results has received funding from the UK Research and Innovation (UKRI) under the UK government's Horizon Europe funding guarantee (Grant No. 10039217) as part of the Horizon Europe (HORIZON-CL4-2021-DIGITAL-EMERGING-01) under Grant Agreement No. 101070347. Yet, views and opinions expressed are those of the authors only and do not necessarily reflect those of the EU, and the EU cannot be held responsible for them.

[1] V. V. Kruglyak, Appl. Phys. Lett. 119, 200502 (2021). [2] K. G. Fripp, A. V. Shytov, and V. V. Kruglyak, Phys. Rev. B 104, 054437 (2021). [3] H. Qin, et al, Nature Commun. 12, 2293 (2021). [4] K. G. Fripp, Y. Au, A. V. Shytov, and V. V. Kruglyak, Appl. Phys. Lett. 122, 172403 (2023).

INVITED PAPER

GC-06. Nonlinear Magnonic Hardware for Pattern Recognition.
C. Heins[1,2], L. Körber[1,2,3], J. Kim[4], T. Devolder[4], S. Thlang[4], J. Mentink[3], A. Kákay[1], J. Fassbender[1,2], H. Schultheiss[1] and *K. Schultheiss[1] 1. Institut für Ionenstrahlphysik und Materialforschung, Helmholtz-Zentrum Dresden-Rossendorf, Dresden, Germany; 2. Fakultät Physik, Technische Universität Dresden, Dresden, Germany; 3. Institute of Molecules and Materials, Radboud University, Nijmegen, Netherlands; 4. Centre de Nanosciences et de Nanotechnologies, CNRS, Université Paris-Saclay, Palaiseau, France*

Neural networks are powerful tools to learn patterns and make inferences in complex problems. However, they rely on a massive number of neurons and interconnecting weights which require extensive training using a large dataset. To compensate for this, reservoir computing is based on recurrent neural networks with randomly fixed weights. Thereby, only the output weights require training for a particular task, reducing the training to a simple linear regression. Recently, there has been a shift towards physical reservoir computing, offering potential advantages in speed, energy efficiency, and hardware simplicity. Physical reservoir computing utilizes the inherent nonlinearity of physical systems to map the input into a higher-dimensional space in which different input patterns become linearly separable. New advancements and experimental implementations use diverse physical substrates, including mechanical structures, optical systems, and spintronic devices. In our work, we take advantage of the rich nonlinear dynamics inside magnetic vortices. Their eigenmode system comprises the gyrotropic motion of the vortex core as well as magnon modes with well-defined radial and azimuthal quantization in the vortex's skirt. Harnessing the nonlinear interactions between these different vortex eigenmodes in reciprocal space, it is possible to perform temporal information processing and pattern recognition without relying on information transport in real space [1]. This presentation will give a comprehensive overview of experimental results and numerical simulations demonstrating the capabilities and advantages of magnon reservoir computing. Additionally, the mutual nonlinear interactions between the magnon modes and the vortex core gyration lead to a much richer set of eigenstates, extending the dimensionality of the magnon scattering reservoir. This work has received funding from the EU Research and Innovation Programme Horizon Europe under grant agreement no. 101070290 (NIMFEIA).

[1] L. Körber, et al., "Pattern recognition in reciprocal space with a magnon-scattering reservoir" *Nature Communications*, 14, 3954 (2023).

CONTRIBUTED PAPER

GC-09. Brownian reservoir computing approach for Gesture recognition by using geometrically confined skyrmion dynamics.
G. Beneke[1], T. Winkler[1], K. Raab[1], M.A. Brems[1], F. Kammerbauer[1], P. Gerhards[2], K. Knobloch[2], S. Krishnia[1], J. Mentink[3] and *M. Kläui[1,4] 1. Institut für Physik, Johannes Gutenberg-Universität Mainz, Mainz, Germany; 2. Infineon Technologies Dresden, Dresden, Germany; 3. Institute for Molecules and Materials, Radboud University, Nijmegen, Netherlands; 4. Center for Quantum Spintronics, Norwegian University of Science and Technology, Trondheim, Norway*

Physical Reservoir Computing (RC) is a novel computing paradigm that goes beyond traditional von Neumann architectures by exploiting the dynamic properties of complex physical systems, known as reservoirs, to efficiently process information in tasks such as pattern recognition. This hardware-centric approach has the potential for a significant reduction in training effort as well as a substantial reduction in power consumption. Magnetic skyrmions, which are topological, particle-like spin textures, are particularly promising candidates for non-conventional computing and especially reservoir computing, due to their non-linear interactions and established methods for low-power manipulation coupled with thermally excited dynamics [1,2]. Traditional spin-based reservoir computing has primarily been used for static detection or relied on the intrinsic magnetization dynamics timescales, necessitating cumbersome rescaling of typically slower real-world data. In this study, we exploit the capabilities of time-multiplexed skyrmion RC by aligning the intrinsic timescales of the reservoir with those of real-world temporal patterns [3]. Specifically, we use millisecond-scale hand gestures recorded with range-doppler radar and recognize them by feeding the data as time-dependent voltage excitations directly into our device. By observing the temporal evolution of the skyrmion trajectory through read-outs at one or multiple positions of the reservoir. This can be achieved with multiple magnetic tunnel junctions, allowing the device to be scaled down to the nanometer scale. Our hardware solution demonstrates competitive or even superior performance compared to state-of-the-art, energy-intensive software-based neural networks [3]. The key advantage of our approach lies in its ability to integrate data from sensors without the need for temporal conversion, thanks to the time-dependent input and the adjustable intrinsic timescales of the skyrmion dynamics within the reservoir. This capability allows for real-time data feeding into the reservoir, paving the way for a wide range of applications.

[1] K. Raab *et al. Brownian reservoir computing realized using geometrically confined skyrmion dynamics*. Nat. Commun. 13, 6982 (2022). [2] J. Zázvorka *et al. Thermal skyrmion diffusion used in a reshuffler device.* Nat. Nanotechnol. 14, 658–661 (2019). [3] G. Beneke et. al., submitted, arXiv 2403.01877 (2024)

Session GD
MICROSCOPY, IMAGING, AND MAGNETIC CHARACTERIZATION II

Shawn Pollard, Chair
The University of Memphis, Memphis, TN, United States

INVITED PAPER

GD-01. Unraveling stochasticity and fluctuations in magnetic thin films using coherent X-ray scattering. *S. Roy*[1], A. Singh[2], E. Hollingworth[3], S.A. Morley[1], A. Us-Saleheen[1], Z. Tumbleson[2], M. McCarter[1], S. Kevan[1], P. Fischer[2] and F. Hellman[3] *1. Advanced Light Source, Lawrence Berkeley National Laboratory, Berkeley, CA, United States; 2. Materials Sciences Division, Lawrence Berkeley National Laboratory, Berkeley, CA, United States; 3. Dept. of Physics, University of California Berkeley, Berkeley, CA, United States*

Fluctuation and stochasticity are characteristics of material complexity that have been enduring themes in condensed matter and statistical physics research. Fluctuation provides basis for phase transitions and critical phenomena in statistical mechanics, order parameter field theories in quantum criticality etc. It is conceivable that fluctuations also play an important role in stabilizing the topological skyrmion phase in a magnetic system. Recently a new beamline/endstation has been successfully commissioned at the Advanced Light Source (ALS); the Cosmic-Scattering endstation. Cosmic-Scattering is a state-of-the-art UHV compatible coherent soft X-ray endstation that uses high brilliance of synchrotron radiation to carry out these fluctuation based measurements. In this talk I will describe the development of this uniquely powerful experimental method. Among several results, I will focus on two recent experiments where we worked at the interface of condensed matter and statistical physics using coherent X-ray scattering, and obtain information about local events that provides pathway for phase transition. Amorphous FeGe (*a*-FeGe) thin films show interesting stripe and skyrmion phases [1,2]. We show that phase transition in *a*-FeGe involve existence of nanoscale fluctuation "hot-spots" whose origin lies in local non-equilibrium states [3]. The fluctuating hot spots start over a small fraction of the domains at random length scales, and the fluctuating population gradually grows non-linearly into collective fluctuations. The growth of the fluctuation population resembles dynamic coherence length which forms the basis of phase transition. We also studied the distribution of the fluctuation amplitude and it followed a gaussian distribution implying ergodic dynamics whereas few kelvins below this transition temperature the distribution becomes skewed or asymmetric due to non-ergodic behavior. Our approach provides a new way to evaluate the statistics of the fluctuations in many classes of heterogeneous materials. Work supported by US DOE.

[1]. D. S. Bouma, Z. Chen, B. Zhang, F. Bruni, M. E. Flatté, A. Ceballos, R. Streubel, L. W. Wang, R. Q. Wu, F. Hellman, Phys. Rev. B 2020, 101, 014402. [2]. R. Streubel, D. S. Bouma, F. Bruni, X. Chen, P. Ercius, J. Ciston, A. T. N'Diaye, S. Roy, S. D. Kevan, P. Fischer, F. Hellman, Adv. Mater. 2021, 33, 2004830. [3]. A. Singh, E. Hollingworth, S. A. Morley, X. M. Chen, A. Us Saleheen, R. Tumbleson, M. M. McCarter, P. J. Fischer, F. Hellman, S. D. Kevan, and S. Roy, "Characterizing Temporal Heterogeneity by Quantifying Nanoscale Fluctuations in Amorphous Fe-Ge Magnetic Films", Adv. Funct. Mater. (2023), 2300224, DOI: 10.1002/adfm.202300224.

CONTRIBUTED PAPERS

GD-02. Direct Imaging of Room Temperature Magnetic Skyrmions in Gradient-DMI Engineered CoPt Single Layers. A. Erickson[1], Q. Zhang[2], H. Vakili[1], S. Lamichhane[1], L. Jia[2], I. Fescenko[3], E. Schwartz[1], S. Liou[1], A. Kovalev[1], J. Chen[2,4] and *A. Laraoui*[1] *1. University of Nebraska-Lincoln, Lincoln, NE, United States; 2. National University of Singapore, Singapore; 3. University of Latvia, Riga, Latvia; 4. National University of Singapore (Suzhou) Research Institute, Suzhou, China*

Topologically protected magnetic skyrmions can be stabilized by interfacial or bulk Dzyaloshinskii-Moriya interaction (DMI) and/or dipolar interactions. Interfacial DMI decays with increase of the magnetic layer thickness in just a few nanometers and bulk DMI typically only stabilizes magnetic skyrmions at low temperatures [1]. Consequently, more flexibility in manipulation of DMI is required for utilizing nanoscale skyrmions in energy efficient memory and logic devices at room temperature (RT). Recently, considerable bulk DMI was achieved at room temperature (RT) by a compositional gradient engineering in CoPt single layer films, referred to as gradient DMI (g-DMI) [2]. Here, we demonstrate the observation of RT skyrmions stabilized by g-DMI in composition gradient engineered CoPt single layer films by employing topological Hall effect, magnetic force microscopy, and nitrogen vacancy magnetometry [3-5]. Skyrmions remain stable at a wide range of applied magnetic fields. Using micromagnetic simulation and analytical magnetization reconstruction, we explore the helicity as a competition between g-DMI and dipolar interactions [6]. Furthermore, we observe skyrmion pairs which may be explained by skyrmion-antiskyrmion interactions [6]. Acknowledgments:This work is supported by the National Science Foundation/EPSCoR RII Track-1: Emergent Quantum Materials and Technologies (EQUATE), Award OIA-2044049. I. F. acknowledges support from the Latvian Quantum Initiative under European Union Recovery and Resilience Facility project no. 2.3.1.1.i.0/1/22/I/CFLA/001. The research was performed in part in the Nebraska Nanoscale Facility: National Nanotechnology Coordinated Infrastructure and the Nebraska Center for Materials and Nanoscience (and/or NERCF), supported by the National Science Foundation under Award ECCS: 2025298, and the Nebraska Research Initiative. The research performed in the National University of Singapore was supported by the Singapore Ministry of Education MOE-T2EP50121-0011, MOE Tier 1: 22-4888-A0001.

[1] A. Fert, et *al.*, *Nature Review Materials* 2, 1–15 (2017). [2] Q. Zhang et. *al.*, *Physical Review Letters* 128, 167202 (2022). [3] A Laraoui, K Ambal, *Applied Physics Letters* 121, 060502 (2022) [4] A. Erickson, A. Laraoui, et *al.*, *RSC Advances* 13, 178-185 (2023). [5] R. Timalsina, et *al.*, *Advanced Electronic Materials* 2300648 (2023). [6] A. Erickson, A. Laraoui, et *al.*, *ACS Nano*, under review, https://doi.org/10.48550/arXiv.2405.09632.

GD-03. Magnetic domain structures of rare-earth metal surfaces. *P. Härtl*[1], M. Leisegang[1] and M. Bode[1] *1. Experimental Physics 2, University of Würzburg, Würzburg, Germany*

Rare earth metals (REMs) are difficult, if not impossible, to clean as bulk materials due to their extreme reactivity. Therefore, films of REMs are studied to explore their rich magnetic properties, which are primarily influenced by the element-specific sign and wavelength of the RKKY interaction. Based

on their complex cleaning procedure, the magnetic behavior of REM(0001) surfaces remains a subject of ongoing debate [1,2], while it is still unknown for most of them. Here we present investigations of complex magnetic structures on epitaxial REM films grown on W(110) using spin-polarized scanning tunneling microscopy (SP-STM). In a recent study of the thickness-dependent domain structures of Gd(0001) films, we confirmed a spin reorientation transition [3], where the easy magnetization axis changes from in-plane to out-of-plane at a critical thickness $\Theta_{crit} \approx (100\pm20)$ atomic layers (AL) [1]. Below Θ_{crit}, we observed μm-sized in-plane domains aligned along the [1-10] direction of W(110). Above Θ_{crit}, out-of-plane magnetized zig-zag-shaped stripe domains become dominant. The magnetic domain structure of Tb(0001) films produces a sixfold magnetic contrast, consistent with the expected in-plane orientation of magnetic domains, similar to earlier findings in Dy(0001)/W(110) [4]. We find that the density of structural defects and dislocations decreases with increasing Tb film thickness, leading to the formation of larger domains. Analysis of the domain walls reveals their Néel character, with widths of approximately 1.4 nm, 2.5 nm, and 3.0 nm for 60°, 120°, and 180° domain walls, respectively.

[1] P. Härtl *et al*., Phys. Rev. B 105, 174431 (2022). [2] P. Härtl *et al*., Phys. Rev. B, submitted July 2024. [3] A. Berger *et al*., Phys. Rev. B 52, 1078 (1995). [4] L. Berbil-Bautista *et al.*, Phys. Rev. B 76, 064411 (2007). [5] J. E. Prieto, *et al*., Phys. Rev. B 94, 174445 (2016).

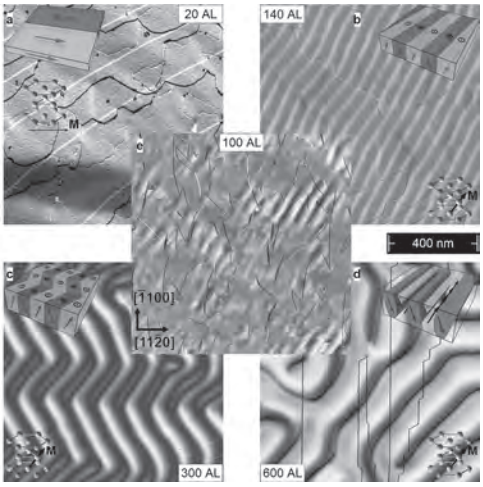

Fig. 1: SP-STM study of coverage-dependent magnetic domain structures of Gd(0001)/W(110) for films with a thickness of a 20 AL, b 140 AL, c 300 AL, d 600 AL and e 100 AL [1]. The insets show qualitative models of the observed domain structures.

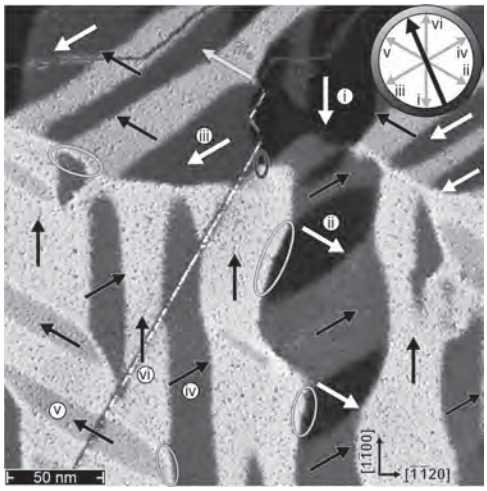

Fig. 2: SP-STM map of a 90 AL thick Tb(0001)/W(110) film [2]. The black and white arrows indicate the sample's local magnetization directions with respect to the tip magnetization (thick black arrow) in the inset. The green (120°) and blue (180°) ellipses represent domain walls that differ from the 60° rotation domain walls. The cyan arrow displays the sample's magnetization direction [5].

GD-04. Scanning SQUID Characterization of Strained Multiferroic Iron Substituted Gadolinium Orthochromite Thin Film. *J. Bedard*[1], J. Pfund[1], M. Jain[1,2,3] and I. Sochnikov[1,2,3] *1. Department of Physics, University of Connecticut, Storrs, CT, United States; 2. Department of Material Science & Engineering, University of Connecticut, Storrs, CT, United States; 3. Institute of Material Science, University of Connecticut, Storrs, CT, United States*

Multiferroic gadolinium perovskites $GdCrO_3$ and $GdFeO_3$ exhibit large magnetocaloric and magneto-electro-caloric effects and are promising materials for low temperature magnetic refrigeration technologies [1,2]. Iron substitution of gadolinium orthochromite increases both the ferroelectric and canted antiferromagnetic ordering temperatures beyond room temperature, although magnetic and ferroelectric properties depend on crystallographic quality [3,4]. We synthesized and characterized magnetic properties of an oriented, single-phase $GdFe_{0.5}Cr_{0.5}O_3$ thin film on a $SrTiO_3$ substrate using chemical solution deposition and spin coating techniques. Using a scanning Superconducting QUantum Interference Device (SQUID) microscope, we characterized the texture and strength of antiferromagnetic domains at temperatures ranging from 6K to 74K. Weak ferromagnetism resulting from canting of iron and chromium moments diminishes at much lower temperatures than in polycrystalline films grown on platinized silicon [4]. However, magnetocaloric properties of the material improved in comparison [4]. We will discuss the effects of strain and epitaxy on magnetocaloric properties and interactions between gadolinium, iron, and chromium moments. In addition to ion substitution, strain engineering could be one method to optimize magnetocaloric or magnetoelectric properties. Distribution A. Approved for public release: distribution unlimited. (AFRL-2024-3434) Date Approved 06-27-2024

[1] Y. Zhu, P. Zhou, T. Li, J. Xia, S. Wu, Y. Fu, K. Sun, Q. Zhao, Z. Li, Z. Tang, Y. Xiao, Z. Chen, H. Li, Physical Review B 102, 144425 (2020). [2] M. Das, S. Roy, R. Mandal, Physical Review B 96, 174405 (2017). [3] J. Shi, M. Johnson, M. Zhang, P. Gao, M. Jain, APL Materials 8, 031106 (2020). [4] J. Shi, M. S. Seehar, Y. Dang, S. Suib, M. Jain, Journal of Applied Physics 129, 243904 (2021)

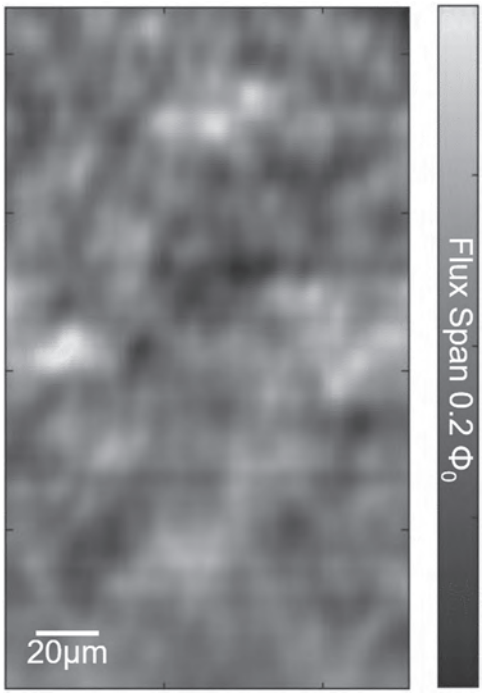

Fig. 1 Magnetic flux image showing canted antiferromagnetic domains in a $GdFe_{0.5}Cr_{0.5}O_3$ thin film at 32.6K

GD-05. Visualization of Anomalous Nernst Effect Using Probe-Induced Local Temperature Gradients. *H. Isshiki*[1], N.D. Budai[1], M.R. Ullerithodi[1], A. Kobayashi[1], Z. Zhu[1], R. Uesugi[1,3], T. Higo[1,3], S. Nakatsuji[1,3] and Y. Otani[1,2] *1. Institute for Solid State Physics, Univ. of Tokyo, Kashiwa, Japan; 2. CEMS, RIKEN, Wako, Japan; 3. Department of Physics, Univ. of Tokyo, Tokyo, Japan*

The anomalous Nernst effect (ANE) generates an electric field perpendicular to both the magnetization and the temperature gradient in ferromagnetic materials. This transverse thermoelectric effect has recently garnered significant attention, as it enables efficient thermoelectric conversion with a very simple structure: the anomalous Nernst thermopile. While scanning anomalous Nernst effect microscopy with laser and lock-in thermography are methods used to visualize thermoelectric effects, they suffer from very poor spatial resolution (~1 μm). We have developed a novel method to visualize ANE using an atomic force microscope (AFM) [1]. As shown in Fig. 1, a local temperature gradient is created by contacting a standard AFM probe to a heated sample wire, allowing us to map the ANE voltage at both ends of the wire. We achieved a spatial resolution of approximately 80 nm. This method is applicable not only to ordinary ferromagnetic materials but also to films with perpendicular magnetization and antiferromagnetic Weyl semimetals. For instance, Fig. 2 shows the results of applying this method to polycrystalline Mn_3Sn. As seen in Figs. 2(b) and 2(c), the local ANE corresponding to the distribution of magnetic polarization in Mn_3Sn was observed in both the initial and residual states [2]. Furthermore, we can apply this technique to anomalous Nernst thermopiles, allowing us to visualize multi-domain structures and thermoelectric effects in junction areas within the device.

[1] N. Budai, H. Isshiki, Z. ZHu et al. Appl. Phys. Lett. 122, 102401 (2023) [2] H. Isshiki, N. Budai, A. Kobayashi et al. Phys. Rev. Lett. 132, 216702 (2024)

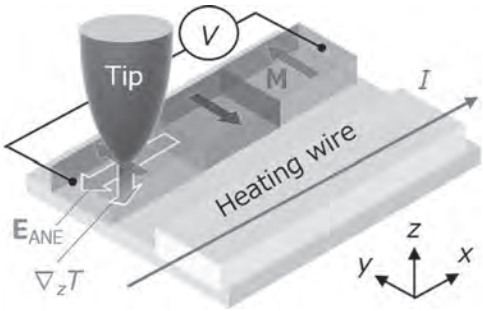

Fig.1 Schematic drawing of our technique.

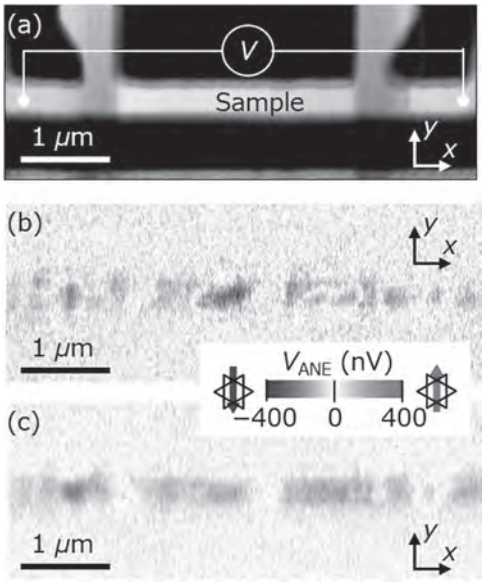

Fig. 2 (a) Topography of the Mn_3Sn wire. (b), (c) Local anomalous Nernst voltages before and after applying an external magnetic field. The Seebeck signals have been removed.

GD-06. Synthesis of Magnetic Nanostructures in Porphyrin and Phthalocyanine Matrices. V. Pena Perez[1], C. Reynaga Gonzales[1], E. Villegas[1], J. Baughman[1], T. Chung[1], F. Iglesias[1], A. Khodagulyan[1], O. Bernal[1] and *A.N. Kocharian*[1] *1. Department of Physics and Astronomy, California State University Los Angeles, Los Angeles, CA, United States*

This study explores the innovative use of carbon matrixes in the synthesis of magnetic nanographite, layered graphene stacks and graphene coated magnetic nanoparticles, with a focus on their morphological, structural, and magnetic properties. To obtain a deeper insight into the influences of impurities in graphene matrix on magnetic properties of synthesized by pyrolysis, the two different metal free modifications of porphyrin such as tetraphenyl porphyrin (TPP) and tetra(4-carboxyphenyl) porphyrin (TCPP) with oxygen content (radical) were synthesized by subsequential post annealing with oxygen and nitrogen, to characterize and investigate the role of oxygen and nitrogen content in graphene environment. The research highlights the significance of porphyrin and phthalocyanine precursors and their metal counterparts for use as carbon matrixes, examining their unique characteristics and applications in nanoparticle synthesis by sequential annealing. Employing advanced characterization techniques such as high-resolution transmission electron microscopy (HR-STEM) and powdered X-ray diffraction (PXRD), Raman and Fourier-transform infrared (FTIR) spectroscopies we analyze the graphitization and porosity effects and layer sizes of nanographite and their impact on magnetic properties. A novel algorithm, integrating node extraction and 2D Gaussian mapping, is developed to enhance the accuracy of morphological analysis. Our findings reveal the critical role of graphene,

and effect of oxygen and nitrogen impurities in influencing the magnetic behavior of carbon matrix and embedded nanoparticles, providing valuable insights into the design and development of advanced magnetic nanomaterials. This work is supported by grants from the American National Science Foundation, catsus grant No. HRD-1547723 and No. HRD-2112554, as well as the National Institute of Health, grant No. T34-GM08228

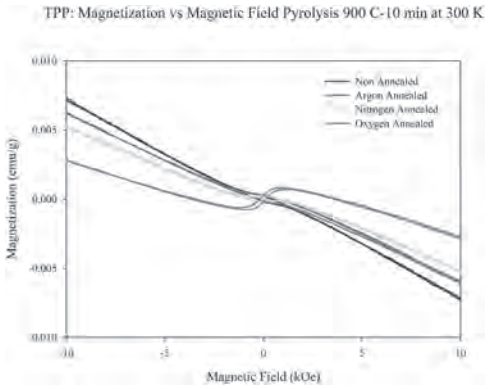

Figure 1

GD-07. A quantum sensing metrology for magnetic memories.
P. Rickhaus[1], V.J. Borras[1], R. Carpenter[2], S. Couet[2], U. Celano[3], O. Pylypovskyi[4], L. Zaper[1], A. Stark[1], *M. Munsch*[1], M. Nordmann[1], C. Adelmann[2], P. van der Heide[2], P. Maletinsky[5] and D. Makarov[4]
1. Qnami AG, Muttenz, Switzerland; 2. IMEC, Leuven, Belgium; 3. ASU, Tempe, AZ, United States; 4. Helmholtz-Zentrum Dresden-Rossendorf, Dresden, Germany; 5. University of Basel, Basel, Switzerland

For a wide variety of magnetic devices, such as spin-transfer-torque magnetic random access memory (STT-MRAM), the devices performance has been characterized mostly electrically. While the electrical performance is what ultimately matters, its assessment requires electrical contacts and can only be performed at the end of a fabrication cycle. Here we show that ultrasensitive stray-field measurements with Scanning Nitrogen-Vacancy Magnetometry (SNVM) can reveal important information of magnetic storage devices, such as bit-to-bit variation. For the case of STT-MRAM, we demonstrate magnetic reversal characterization in individual, < 60 nm sized bits, to extract key magnetic properties, thermal stability, and switching statistics, and thereby gauge bit-to-bit uniformity. We showcase the performance of our method by benchmarking two distinct bit etching processes immediately after pattern formation. In contrast to ensemble averaging methods such as perpendicular magneto-optical kerr effect, we show that it is possible to identify out of distribution (tail-bits) bits that seem associated to the edges of the array, enabling failure analysis of tail bits. We also broaden the scope and indicate the relevance of nanoscale magnetic inhomogeneities for race-track memory nanowires and antiferromagnetic Bit-patterned memory devices. Our findings highlight the potential of nanoscale quantum sensing, opening an entire field of precharacterization possibilities for magnetic devices.

V.J. Borràs, *et al.* A quantum sensing metrology for magnetic memories. *npj Spintronics* 2, 14 (2024) P. Maletinsky, et al., *A robust scanning diamond sensor for nanoscale imaging with single nitrogen-vacancy centres*, Nature Nanotechnology 2012 7:5 7, 320–324 (2012). S. Rao, et al., *Stt-mram array performance improvement through optimization of ion beam etch and mtj for last-level cache application*, IMW 10.1109/IMW51353.2021.9439592. (2021), Celano U., et al., *Probing Magnetic Defects in Ultra-Scaled Nanowires with Optically Detected Spin Resonance in Nitrogen-Vacancy Center in Diamond*. Nano Lett. 21, 24, 10409–10415 (2021) P. Rickhaus et.al, *Antiferromagnetic nanoscale bit arrays of magnetoelectric Cr2O3 thin films*, arXiv: 2406.19085 (2024)

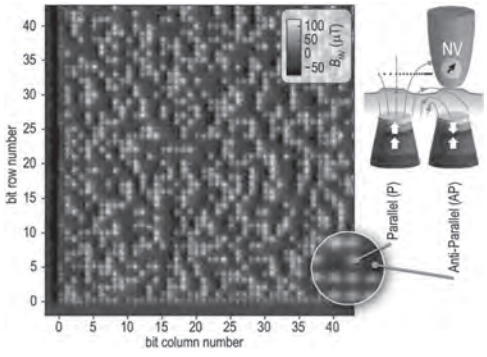

Fig.1: SNVM map of 45 × 45 bits (10 × 10 μm) after encapsulation. Bits in the anti-parallel (AP) state appear dark, bits in the parallel (P) state appear bright. The P and AP bit configurations generate distinct stray field patterns (gray lines). The NV probe measures their projection onto the NV quantization axis (black arrow) at the flying distance of the NV probe.

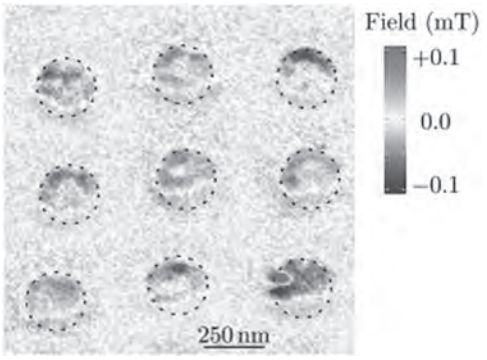

Fig.2: Stray field maps and domain structure of AFM bits (250 nm in diameter) in magnetically disordered state measured with SNVM. The dashed lines are guides to the eye and depict the selected bit position. The color bar shows the change of the stray field in the range between –0.1 and +0.1 mT

GD-08. Control of the Antiferromagnetic Configuration in $La_{0.55}Sr_{0.45}MnO_3$ Ultrathin Films.
C.A. Vaz[1] and G. Panchal[1]
1. Swiss Light Source, Paul Scherrer Institut, Villigen PSI, Switzerland

Antiferromagnetic (AFM) materials have been drawing significant interest as building blocks for spintronics on account of their faster spin dynamics compared to conventional ferromagnets (in the THz instead of GHz range), the absence of stray fields and their immunity to external magnetic field perturbations [1]. However, a major challenge remains the control of the antiferromagnetic domain state, since antiferromagnetic systems tend to exhibit complex multidomain configurations, even in thin films of simple collinear antiferromagnetic materials [2]. Such complex domain states are surprising, since they cost exchange and magnetocrystalline energy at no magnetostatic energy gain and are thought to arise from local variations in the magnetic anisotropy induced by strain from local defects that pin the antiferromagnetic domains as the system is cooled from above the Néel temperature [3]. However, controlling the antiferromagnetic domain structure is critical for device applications, an aspect that has been less well addressed in the literature. Here, we present our recent results of the antiferromagnetic domain structure of ultrathin $La_{0.45}Sr_{0.55}MnO_3$ (LSMO)/$SrTiO_3$(001) films as a function of thickness and post-growth annealing, measured with x-ray photoemission electron microscopy (XPEEM). Our results show that the average domain size decreases as the LSMO film thickness increases from 15 uc to 50 uc. In addition, we find that the antiferromagnetic domain structure of the 15 uc film exhibits much larger domains after ex situ annealing in air. These results show that the AFM domain size can be tuned by the film thickness and suggests that the reduction in local defects, such as oxygen vacancies,

have a strong impact on the AFM domain structure. These observations have clear implications for size scaling of AFM domains for antiferromagnetic spintronics applications.

[1] Baltz et al, Rev. Mod. Phys. 90:015005, 2018. [2] Moriyama et al, Scientific Reports, 8:14167, 2018. [3] Gomonay, Loktev, Low Temp. Phys. 30:804, 2004.

GD-09. Wide-field MOKE microscopy and magnetometry on $Cr_2Ge_2Te_6$ exfoliated van-der-Waals flakes. I. Soldatov[1], B. Özer[1], L. Veyrat[2], B. Buchner[1] and *R. Schaefer*[1] *1. Leibniz Institute for Solid State and Materials Research Dresden, Dresden, Germany; 2. Nano & semiconductor group, LNCMI-Toulouse, Toulouse, France*

Since their discovery [1], ferromagnetic two-dimensional (2D) van-der-Waals (vdW) materials, exfoliated via adhesive tape, are intensively explored [2]. They often have Curie temperatures below room temperature and are characterized by a uniaxial magnetic anisotropy perpendicular to the film plane. As for most magnetic materials, hysteresis measurements and domain research also play crucial roles in the characterization of vdW material. Hysteresis loops are mostly obtained by laser-based magneto-optical Kerr effect (MOKE) magnetometry or by anomalous Hall effect measurements, while for domain imaging primarily Lorentz Transmission Electron Microscopy, Nitrogen-Vacancy Microscopy and X-ray based imaging are applied [2]. Wide-field MOKE microscopy, a common imaging technique for general domain research [3], has hardly been used. Using $Cr_2Ge_2Te_6$ flakes in the 10 nm thickness range, we explore the potential of this method for the characterisation of low-dimensional crystals. By plotting the Kerr intensity at selectable sample areas as a function of magnetic field, hysteresis loops at specific thicknesses are obtained. Pinched loops with a characteristic shoulder are typically measured, indicating the nucleation of perpendicularly magnetized band and bubble domains. Such domain patterns, however, *cannot* be seen in the Kerr microscope, probably owed to the resolution limit of cryo-Kerr microscopy (~ 500 nm). The method is nevertheless useful as it detects how the flakes, which usually consist of differently thick areas, are magnetised locally. We further verify a thickness- and light colour dependent sign inversion of the Kerr signal [4] and explain it by a Fresnel-type depth sensitivity concept [5]. Accordingly, the Kerr contrast is governed by the relative phase of the Kerr amplitude that can be freely adjusted by a rotatable compensator. A thickness-dependent magneto-optical Voigt parameter [6] or multilayer interference [4] are not required to explain the sign in-versions. The compensator is thus the decisive optical element in (general) MOKE magnetometry and microscopy on low-dimensional vdW materials. It needs to be appropriately aligned to avoid a cancelation of the Kerr contrast and to maximise the Kerr signal.

[1] C. Gong et al.: Discovery of intrinsic ferromagnetism in two-dimensional van der Waals crystals. *Nature* 546, 265–269 (2017). [2] Q.H. Wang et al., The Magnetic Genome of Two-Dimensional van der Waals Materials. ACS Nano, 16, 5, 6960–7079 (2022) [3] R. Schäfer and J. McCord: Magneto-Optical Microscopy. In: Franco, V., Dodrill, B. (eds) Magnetic Measurement Techniques for Materials Characterization. Springer, Cham. (20219, https://doi.org/10.1007/978-3-030-70443-8_9 [4] Z. Ma et al., Micro-MOKE with optical interference in the study of 2D $Cr_2Ge_2Te_6$ nanoflakes based magnetic heterostructures. AIP Advances 9, 5, 125116 (2019) [5] W. Kuch et al.: Magnetic Microscopy of Layered Structures, Springer (2015) [6] O. Maximova et al.. The Magneto-Optical Voigt Parameter from Magneto-Optical Ellipsometry Data for Multilayer Samples with Single Ferromagnetic Layer. Physics of the Solid State 63(10), 1485–1495 (2021)

GD-10. Magneto-Optical Kerr Effect Characterisation of Static and Dynamic Processes in a Thulium Iron Garnet Film. *P.S. Keatley*[1], M.J. Gross[2], J.J. Bauer[3], M.F. Chowdhury[4], J. Atulasimha[4], C.A. Ross[3] and R. Hicken[1] *1. Department of Physics and Astronomy, University of Exeter, Exeter, United Kingdom; 2. Electrical Engineering and Computer Science Department, Massachusetts Institute of Technology, Cambridge, MA, United States; 3. Department of Materials Science and Engineering, Massachusetts Institute of Technology, Cambridge, MA, United States; 4. Department of Mechanical and Nuclear Engineering, Virginia Commonwealth University, Richmond, VA, United States*

Thulium Iron Garnet (TmIG) films have recently shown promise for ultralow switching current density in spintronic applications[1] due to efficient spin transport at TmIG/Pt interfaces[2]. Understanding the TmIG equilibrium state and corresponding sub-nanosecond magnetization dynamics will allow further optimisation for spintronic devices. Here we use a combination of wide-field and time-resolved scanning Kerr microscopies to characterise the ferrimagnetic domain structure and magnetization dynamics of 6.4 nm thick TmIG grown by pulsed laser deposition on a (111)-oriented Gadolinium Gallium Garnet (GGG) substrate, as in [2]. The GGG substrate was not pre-annealed so that the effect of interface defects could be explored. Out-of-plane and in-plane magnetometry (hysteresis loops and domain imaging) was carried out for two principal wavelengths of 400 nm and 520 nm to identify the optimum magneto-optical contrast. The resonance frequency as a function of in-plane magnetic field was then extracted from time-resolved measurements at the optimum wavelength. Hysteresis loops showed an out-of-plane magnetic anisotropy with a low coercivity below 1 mT. However, the magnetization could be pulled in-plane with only moderate applied fields indicating that the perpendicular magnetic anisotropy was low. Furthermore, domain images (Fig. 1) reveal a combination of large area uniform magnetization domains punctuated with regions of finer labyrinth-type domains that are correlated with surface defects that may introduce local strain, for which TmIG has a significant dependence[1]. Such variations would not be readily detectable in bulk characterisation techniques. Time-resolved measurements of precession of the magnetization biased in-plane (Fig. 2) show an almost linear dependence on in-plane magnetic field, and a low precession frequency into the sub-GHz regime with long relaxation time as expected for the low damping of TmIG previously reported ~1×10^{-3} [1-3]. These results show that magneto-optical Kerr effect measurements will be a critical tool for the continued optimisation of such materials for spintronic applications.

[1] C. N. Wu *et al*., Sci Rep 8, 11087 (2018). [2] A. Quindeau *et al*., Adv. Electron. Mater., 3, 1600376 (2017). [3] R. Timalsina *et al*., Adv. Electron. Mater., 10, 2300648 (2024). This work was funded by NSF ECCS-EPSRC collaborative research grants 2152601, 2152528 and EP/X036715/1.

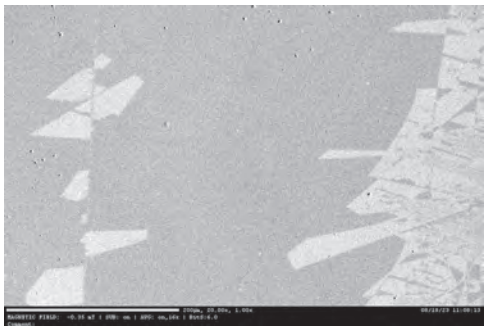

Fig. 1. Wide field polar Kerr image (scale bar 200 μm).

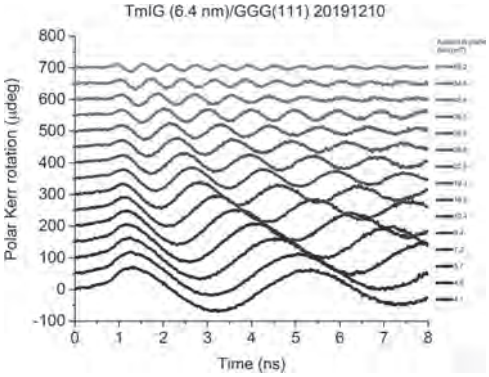

Fig. 2. Time-resolved polar Kerr signals.

GD-11. Strain induced magnetic effects in thin films studied by transmission electron microscopy. *A. Kovács*[1], M. Charilaou[2], D. Kong[1], I. Kézsmárki[3], X. Han[4] and R.E. Dunin-Borkowski[1] *1. Ernst Ruska-Centre, Forschungszentrum Juelich, Juelich, Germany; 2. University of Louisiana at Lafayette, Lafayette, LA, United States; 3. University of Augsburg, Augsburg, Germany; 4. Southern University of Science and Technology, China, China*

Controlling magnetism by strain offers an innovative pathway to modulate magnetic states and domain configurations, making it a promising strategy for manipulating nanoscale magnetic structures. In this work, we have made a direct observation of the magnetoelastic coupling between tensile strain and magnetization in a soft magnetic nickel [1] and a kagome-type iron-tin single crystal thin films. Magnetic imaging of the focused ion beam prepared samples are carried out using Fresnel defocus imaging and off-axis electron holography in an aberration-corrected transmission electron microscope. Tensile strain is applied using either a custom-made bimetallic device or a dedicated MEMS-based device (BestronST). Experimental magnetic imaging results are compared with micromagnetic simulations to quantify the strain-induced anisotropy field and the magnetoelastic energy density. Figure 1 shows bright field TEM image of the nickel sample in unstrained and strained conditions and the corresponding magnetic induction maps. The unstrained sample has a magnetic domain structure with low angle (<90°) magnetic domain walls (DWs) (Fig.1b). Strikingly, when the tensile strain is increased, the magnetic field lines become perpendicular to the direction of the tensile strain. The low angle DWs transform into 180° walls, which are perpendicular to the strain axis (Fig.1d). When the strain is reduced to 0%, the magnetic domains return to their original state, suggesting a reversible magnetoelastic process up to 0.20% strain. The measurements of the domain wall widths and the micromagnetic simulation are used to quantitatively describe the magnetoelastic effect. A similar methodology has been applied to iron-tin single crystals containing dipolar skyrmions, which transform into periodic stripe domains before the magnetization rotates to the in-plane direction. Quantitative analyses of strain-induced effects show that a change in interatomic spacing associated with strain induces a substantial anisotropy that can lead to a transformative change in the magnetic state and magnetic hardening, as well as controlling the direction of the magnetization.

[1] D. Kong et al., Nature Communications 14 (2023) 3963. [2] This work is supported by ERC under the EU's Horizon 2020 Research and Innovation Programme (Grant No. 856538, project "3D MAGiC") and DFG through Project-ID 405553726, TRR270 "HoMMage".

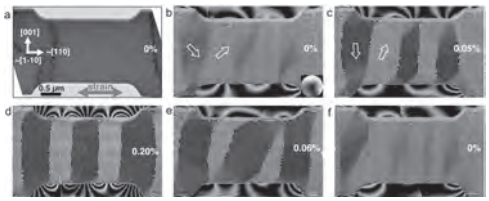

GD-12. Probing Complex Spin Fluctuations by Megahertz X-ray Photon Correlation Spectroscopy. *L. Shen*[1,2], Z. Tumbleson[3,4], R. Plumley[1], C. Peng[1], S.A. Morley[3], G. Mercurio[5], A. Scherz[5], S. Roy[3], E. Blackburn[2] and J.J. Turner[1] *1. SLAC National Accelerator Laboratory, Menlo Park, CA, United States; 2. Lund University, Lund, Sweden; 3. Lawrence Berkeley National Laboratory, Berkeley, CA, United States; 4. UC Santa Cruz, Santa Cruz, CA, United States; 5. European XFEL GmbH, Hamburg, Germany*

Megahertz X-ray Photon Correlation Spectroscopy (MHz-XPCS) is an innovative technique enabled by second-generation X-ray Free-electron Lasers (XFELs) [1]. In this study, we employ MHz-XPCS to investigate the spontaneous microsecond fluctuations of spins in the amorphous magnetic superlattice Fe/Gd. These fluctuations, which can span timescales of several decades, exhibit complex behavior [2-4]. We have developed a protocol based on the over-sampling of spin fluctuations, enabling us to classify distinct dynamical heterogeneities within the sample and, more importantly, to analyze their correlations. These observations are supported by micromagnetic simulations.

[1] F. Lehmkühler *et al*., PNAS 117, 24110 (2020) [2] M. H. Seaberg *et al*., Phys. Rev. Lett. 119, 067403 (2017) [3] A. Singh *et al*., Adv. Funct. Mater. 33, 2300224 (2023) [4] R. Tumbleson *et al*., arXiv:2404.13212

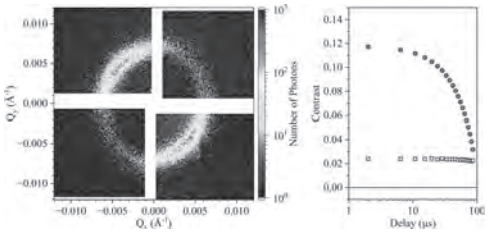

LHS: Resonant X-ray Scattering Profile of the Spin Stripes in Fe/Gd at the Gd M_5-edge. RHS: Intensity-intensity autocorrelation function showing the decorrelation, i.e. reduction in contrast, as a function of time. This probes the spin fluctuations.

GD-13. Domain wall curvature effects on the measurement of the Dzyaloshinskii Moriya interaction strength in the creep regime. *A. Magni*[1], A. Di Pietro[1], G. Carlotti[2], G. Durin[1], M. Madami[2], C. Marrows[3], S. Pizzini[4], L. Ranno[4], S. Tacchi[5], E. Darwin[6], A. Huxtable[3], B.J. Hickey[3] and M. Kuepferling[1] *1. INRIM, Torino, Italy; 2. Physics and Geology, Università di Perugia, Perugia, Italy; 3. University of Leeds, Leeds, United Kingdom; 4. Insitut Néel, Grenoble, France; 5. Consiglio Nazionale delle Ricerche, Perugia, Italy; 6. EMPA, Duebendorf, Switzerland*

The measurement of the interfacial Dzyaloshinskii Moriya interaction (DMI) strength D via domain wall (DW) velocity in the creep regime is a versatile technique that allows access to this important quantity through magneto-optical experiments [1]. The downside of this method is that it sometimes lacks agreement in the value of D with other measurement methods such as the Brillouin light scattering (BLS) technique [2]: it has been recently shown that the value of D can be underestimated by up to 8 times is samples with large DMI [3]. A possible cause and important factor in accurately determining the DMI strength in the creep regime is the radius dependence of magnetic domain wall velocity in bubbles, but up to now few works have analyzed this aspect [4]. In this work we address the radius dependence of the DW velocity in thin film Pt(3)/Co(0.8)/Ir(1) samples. We measure (see Fig. 1) a significant radius dependence of the DW velocity and discuss how this could be due to the pinning characteristics of the considered sample. We support our findings by using an adapted version of the analytical model by Je et al. [1] for DW motion in the creep regime in the presence of IP fields and DMI. We emphasize the effect of this radius dependence of the velocity on the experimentally measured values of the DMI strength, demonstrating how disregarding the bubble radius can cause a systematic measurement underestimation (up to 30% - See Fig. 2). We conclude that an accurate DMI strength evaluation in the creep regime requires a preliminary analysis of the radius dependence of the DW velocity.

[1] S.-G. Je, D.-H. Kim, and S.-C. Yoo, Physical Review B, vol. 88, p. 214401 (2013). [2] M. Kuepferling, G. Carlotti, and A. Casiraghi, Reviews of Modern Physics, vol. 95, p. 15003 (2023). [3] A. Magni, G. Carlotti, and A. Casiraghi, IEEE Transactions on Magnetics, vol. 58, pp. 1–16 (2022). [4] X. Zhang, Y. Zhou, and M. Ezawa, Physical Review Applied, vol. 9, p. 24032 (2018).

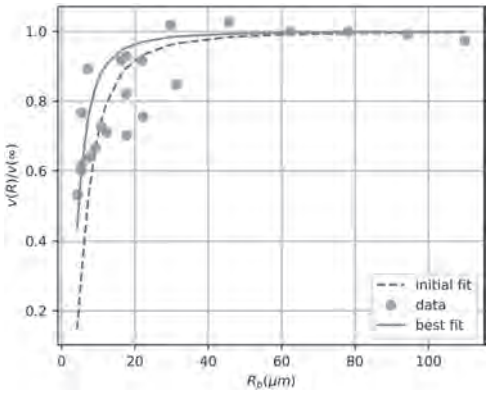

Fig. 1: Value of the ratio between the velocity of a bubble of radius R_b and the velocity in the limit of an infinite-size bubble, as a function of the bubble radius R_b. Best fit obtained with model [1].

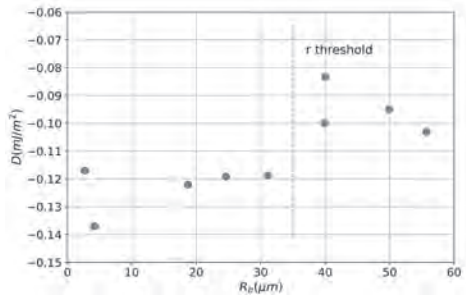

Fig. 2: DMI value obtained by the bubble expansion method, for different values of R_b. The r threshold represents the radius above which the DW velocity stabilizes to a constant value.

Session GE
ANALYSIS AND DESIGN FOR HIGH-PERFORMANCE MAGNETIC SYSTEMS

David Lowther, Chair
McGill University, Montreal, QC, Canada

INVITED PAPERS

GE-01. Overview of Permanent Magnet Wind Power Generators.
M. Jiang[1], S. Niu[1] and K. Chau[1] *1. Department of Electrical and Electronic Engineering, The Hong Kong Polytechnic University, Kowloon, Hong Kong*

The global transition towards renewable energy sources has been motivated by concerns regarding energy security and environmental pollution associated with fossil fuels. Among these sources, wind power generation has experienced remarkable growth and has become a significant provider of clean electricity. Initially, non-permanent magnet (PM) machines, such as squirrel cage induction generators (SCIGs) were commonly used, but has limitations such as high starting current and low power factor. To address these limitations, wound rotor induction generators (WRIGs) and electrically excited synchronous generators (EESGs) are invented. However, both WRIGs and EESGs relied on brushed slip rings, necessitating regular maintenance. To address these challenges, notable interest has been expressed in implementing PMs in generators, eliminating the need for brushes and slip rings. This advancement enables a brushless system for the entire generator. Furthermore, PM generators offer benefits such as compact size, high efficiency, and high power density. This paper presents a comprehensive overview of existing topologies of permanent magnet wind power generators (PMWPGs). As depicted in Fig. 1, the paper categorizes PMWPGs into four main types based on their power ports: electrical ports (EPs) and mechanical ports (MPs). Each category is further divided based on the operating principle, distinguishing between conventional types and emerging types that utilize modern flux modulation theories. The key features of PMWPGs, including torque/power density, efficiency, and cost, are compared and summarized. Control strategies for various types of PMWPGs are introduced. The paper addresses the challenges and difficulties encountered in the field. Finally, the paper highlights the emerging trends and opportunities for further development in wind power generation. It provides insights into the advancements and potential areas for improvement in this rapidly evolving field.

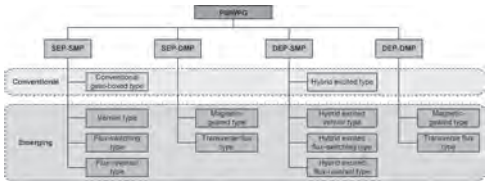

Fig. 1: Classification of PMWPGs

GE-02. Advanced Electric Machines and Drives for Wind Power Generation.
Z. Dong[1,2], R. Huang[1,2], Y. Liu[1,2] and *C. Liu*[1,2] *1. School of Energy and Environment, City University of Hong Kong, Hong Kong, China; 2. Shenzhen Research Institute, City University of Hong Kong, Shenzhen, China*

GLOBAL ENERGY security and environmental issues promote the utilization of renewable energies. Wind power is one of the potential candidates for technical implementation [1] and commercial utilization [2] due to its simple capture and huge amount around the world. However, the requirements of wind generation can be summarized as high power density, high efficiency, high reliability, reasonable cost, more flexibility, redundancy, etc. Thus, advanced electric machines and drives are expected and propsoed in this work. In the typical wind power generation systems, both electric machines and power converters play a crucial role in wind power generation. To this end, this paper mainly focuses on these two key components. Before the specific discussion, the general configurations of wind power generation systems should be introduced. They put forward different requirements for the electric machines and the power converters. According to the criterion of speed control, the configuration of wind power generation system can be classified into two types: Fixed-speed and Variable-speed systems. More comparison results and figures about the configurations of wind power generation will be presented in the full paper. First, the emerging electric machine topologies for wind power generation will be reviewed. Due to the limited axial space in the wind turbine, it is better to space the corresponding space by replacing the conventional radial-flux electric machine with non-radial-flux electric machines, i.e., axial-flux electric machines and transverse-flux electric machines [3]. Not limited to these two types, the conventional radial-flux electric machine can also be combined with the axial-flux electric machine to further improve the torque density. Besides, these non-radial-flux topologies also provide better heat dissipation. These selected emerging electric machines are depicted in Fig.1, more types of electric machines for wind power generation will be demonstrated in the full paper, and their performance comparison and suitable power level, drive mode (indirect and direct drive), cost, and so on will also be presented. Then, the emerging power converter topologies for wind power generation will be discussed. To settle the high-power stress, both series connection and parallel connection of several power converters can be the candidates, as shown in Fig.1. They can provide higher power level with several limit power rating converters. From another perspective, under the same power capacity, the power rating requirements for the power devices can be reduced, which will reduce the general cost under a certain level. Besides, the additional converters also provide the redundancy of the system, thus bringing better reliability. For both primary-side converter (connected to generator, AC to DC) and secondary-side inverter (connected to transformer/grid, DC to AC), the typical winding connection pattern is star-connected. Open-end winding connection can also be adopted [4], as shown in Fig.2. It not only provides reliability, but also doubles the dc-link voltage utilization, which can reduce the size of the step-up transformer, or even eliminate it. Moreover, to eliminate the dc-link capacitor between the primary and secondary sides, the matrix converter can be employed [5]. The generated AC power from the generator can be directly transferred to the transformer/grid, thus simplifying the system structure and reducing the power losses during the power conversion. This work was supported in part by NSFC grants (Ref No. 52077186 and 52377069), China; in part by a RGC CRF (Ref. No.: C1052-21GF), Hong Kong SAR; and in part by RGC RFS (Ref. No.: RFS2223-1S05), Hong Kong SAR. (Corresponding author: Chunhua Liu; chunliu@cityu.edu.hk)

Wind Turbine Systems," *IEEE Trans. Ind. Appl.,* vol. 48, no. 2, pp. 708-719, 2012. [2] S. Chatterjee, and S. Chatterjee, "Review on the techno-commercial aspects of wind energy conversion system," *IET Renewable Power Generation,* vol. 12, no. 14, pp. 1581-1608, 2018. [3] R. Huang, Z. Song, H. Zhao *et al.*, "Overview of Axial-Flux Machines and Modeling Methods," *IEEE Trans. Transport. Electrific.,* vol. 8, no. 2, pp. 2118-2132, 2022. [4] F. Zhang, L. Zhu, S. Jin *et al.*, "Controller Strategy for Open-Winding Brushless Doubly Fed Wind Power Generator With Common Mode Voltage

Elimination," *IEEE Trans. Ind. Electron.,* vol. 66, no. 2, pp. 1098-1107, 2019. [5] C. N. El-Khoury, H. Y. Kanaan, I. Mougharbel *et al.*, "A review of matrix converters applied to PMSG based wind energy conversion systems." pp. 7784-7789.

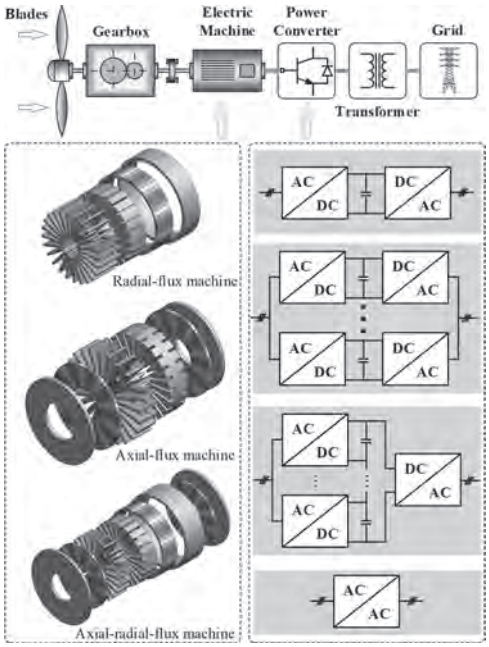

Fig.1 Configuration of typical wind power generation and the key equipment in electric machines and power converters

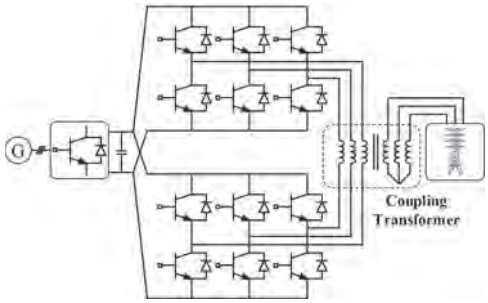

Fig.2 Open-end winding topology for the power inverter with transformer/grid

GE-03. Magnetic materials as key drivers for a sustainable electrification. *A. Bollero*[1], L. Powalla[1], M. Köhne[1] and W. Rammaier[1]
1. Advanced Technologies and Microsystems, Robert Bosch GmbH, Sector Research and Advance Engineering, 71272 Renningen, Stuttgart, Germany

Strong efforts run to address urgent environmental issues through consolidation of a sustainable electrification path. Magnetic materials are at the core of this development. A permanent-magnet synchronous motor (PMSM) -motor type dominating the electromobility market- makes a perfect example of the combined interplay between hard and soft magnetic materials: permanent magnets and electrical steel. Composition, morphology and microstructure will primarily define the materials characteristics (mainly, magnetic and mechanical properties), and it will be their interaction which will determine the machine performance. This presentation will focus on the magnetic material characteristics and not on advanced motor concepts, but under the premise that innovation in materials and design in e-drives must go necessarily together to match optimum performance, improved sustainability, diminished CO_2 footprint and reduced cost (mandatory requirement to make the technology widely affordable to enable achievement of zero-emission targets in a near future). Rare earth (RE)-based permanent magnets integrated in the rotor are nowadays the only possible choice for high-performance and efficient (minimized energy loss) electric drive solutions in PMSM. A decrease in the operation temperature of the magnets in the rotor might allow the use of more sustainable alternatives (e.g. by reducing or even removing the heavy RE content). However, an e-vehicle includes additional applications (e.g. small motors and actuators), which might also profit from the integration of improved RE-free magnets with no need to match the high energy density values of sintered Nd-Fe-B magnets. Examples of approaches followed towards the development of alternative permanent magnet materials will be discussed by considering La-, Co-free hexaferrite nanocomposites and MnAlC powder with coercivity above 475 kA/m [1,2] to be used as precursors for magnet fabrication [1,3] by addressing identified challenges [4]. Electrical steel is the soft magnetic material used as lamella stacks in the fabrication of the rotor (integrating the magnets) and the stator. Power density and machine efficiency are determined by a maximized magnetic saturation and minimized magnetic losses under variable operation conditions. Mechanical strength needs to be also addressed to guarantee workability, which makes necessary to find a tradeoff between mechanical and magnetic properties [5]. In addition, a proper understanding on the detrimental impact of manufacturing (e.g. stamping and stacking) on the magnetic properties will help to take countermeasures to mitigate it. The possibility of using non-grain oriented e-steel with thickness below 0.25 mm opens the possibility to reduce further magnetic losses and enhance the motor performance, but brings also technological challenges that will be briefly discussed.

[1] A. Bollero and E.M. Palmero, Recent advances in hard ferrite magnets, in J.J. Croat and J. Ormerod (eds.) Modern Permanent Magnets, pp. 65-112, Elsevier (2022). [2] J. Rial *et al.*, Acta Mater. 157, 42 (2018); Engineering 6 (2), 173 (2020). [3] T. Ohtani *et al.*, IEEE Trans. Magn., MAG-13, 1328 (1977); L. Feng *et al.*, Acta Mater. 199, 155 (2020). [4] J. Yuxiao *et al.*, Acta Mater. 245, 118654 (2023); C. Muñoz-Rodríguez *et al.*, J. Alloys Compd. 847, 156361 (2020). [5] N. Leuning *et al.*, J. Magn. Magn. Mater. 567, 170322 (2023).

CONTRIBUTED PAPERS

Now VP4-10

GE-04. High Power Density PM Motor for Electric Aircraft Propulsion Utilizing Litz Wire and Hairpin Winding Technologies. *A.T. Huynh*[1], H. Huang[1], J. Jiang[1], T. Zou[1], D. Gerada[1], T. Yang[1] and C. Gerada[1]
1. Power Electronics and Machines Centre, Faculty of Engineering, University of Nottingham, Nottingham, United Kingdom

Choosing the right winding technology is crucial for enhancing power density and efficiency in aircraft propulsion systems. This paper compares 1MW-class PM motors with Litz wire and hairpin winding technologies. Models with 72 slots/12 poles are optimized using a MOGA method to maximize power density and efficiency. The impact on power density, loss distribution, efficiency, and thermal performance is thoroughly investigated. Results show significant power density improvement with hairpin winding due to shorter stack and reduced end-winding lengths, despite higher AC copper losses limiting the high-efficiency region. To mitigate copper losses and further improve efficiency, optimization through a new motor constant is applied to the design of hairpin winding and stator slots. Finally, FEA validates the machine's performance and confirms the effectiveness of the optimization. Fig. 1 (a) and (b) depict models of 1MW class PM machines with 5-stage Halbach PM utilizing Litz wires and Hairpin windings. The machines are designed with identical specifications, featuring 72 slots/12 poles and the same stator outer diameter. The study employs the Multi-Objective Genetic Algorithm (MOGA) to optimize both designs, maximizing power density and efficiency while satisfying specified constraints. Subsequently, the new motor constant combined with a Genetic Algorithm (GA) is employed to optimize the design parameters of the hairpin winding and stator slot to maximize the high-efficiency operating region. Fig. 2 shows the optimization outcomes from a MOGA for a 1MW-class PM machine with Litz wire and hairpin winding. The Litz wire machine achieves 30 kW/kg

power density and 98% efficiency (Fig. 3a). In contrast, the hairpin winding machine attains 38.7 kW/kg power density with the same efficiency (Fig. 3b) due to reduced stack and end-winding lengths. Fig. 3 shows the results of optimizing hairpin winding and stator slot design using a new motor constant and Genetic Algorithm (GA). The 1MW PM motor's power density remains 38.7 kW/kg, while efficiency increases to 98.5% due to reduced copper losses from 33 kW to 27 kW. The full paper will present a detailed analysis.

[1] European Commission, Flightpath 2050: *Europe's vision for aviation; maintaining global leadership and serving society's needs; report of the High-Level Group on Aviation Research*. Luxemburg: Publications Office of the European Union, 2012 [2] W. Cao et al., "Overview of electric motor technologies used for more electric aircraft (MEA)," *IEEE Trans. Ind. Electron*., vol. 59, no. 9, pp. 3523–3531, Sep. 2012. [3] E. Preci et al., "Rectangular and Random Conductors: AC Losses Evaluations and Manufacturing Considerations," IECON 2020 The 46th Annual Conference of the IEEE Industrial Electronics Society, Singapore, 2020, pp. 1076-1081. [4] A. Bardalai et at., "AC loss Analysis in Winding of Electrical Machines with varying Strands-in-hand and Bundle Shapes," *2020 23rd International Conference on Electrical Machines and Systems (ICEMS*), Hamamatsu, Japan, 2020, pp. 845-850. [5] T.A. Huynh, V.H. Che, M.-F. Hsieh, "Maximization of High-efficiency Operating Range of Spoke-type PM E-bike Motor by Optimization through New Motor Constant," *EEE Trans. Ind.Appl.,* vol. 59, no. 2, pp. 1328 - 1339, 2023.

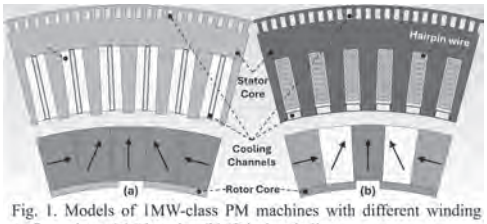

Fig. 1. Models of 1MW-class PM machines with different winding configurations. (a) Litz wire, (b) Hairpin winding.

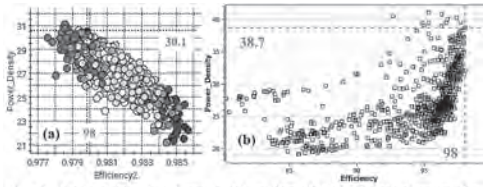

Fig. 2. Multi-Objective Genetic Algorithm (MOGA) optimization for 1MW PM motors. (a) Litz wire, (b) Hairpin Winding.

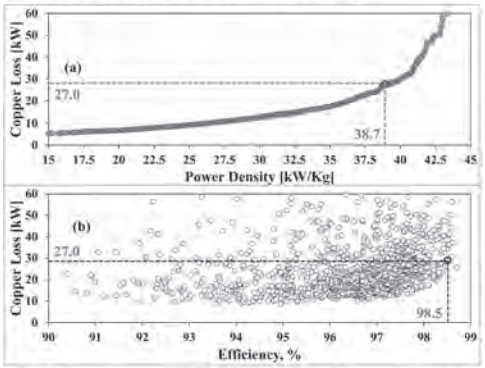

Fig. 3. Genetic Algorithm (GA) optimization for Hairpin Winding. (a) Copper loss versus power density, (b) Copper loss versus efficiency.

GE-05. Investigation of High Pass-Through-Flux and Sputtering Performance of Ferromagnetic Sputtering Targets. *Q. Zeng*[1], D. VanHeerden[1], J. Wagner[1], G. Wiehl[1] and S. Kennedy[1] *1. Materion Corp., Brewster, NY, United States*

One critical measurable property that determines the strength of the projected magnetic field of the sputter cathode is the so-called "Pass-Through-Flux (PTF)". In this study, we investigate the effect of varied mechanical work as well as the resulting microstructure on the PTF of ferromagnetic sputtering targets. Commercial high purity magnetic materials were subjected to a series of thermomechanical processes. A portion of these materials were subjected to recrystallization annealing for different grain size, as well as stress relief anneal to differentiate the effect of strain and grain size. The PTF of the resulting materials was measured both parallel and perpendicular to target surface. In addition, in order to mimic the use of these materials in a sputter tool, the materials were subjected to various magnetic fields to analyze their impact on PTF. The results show that the PTF is significantly influenced by thermomechanical processing, the external magnetic field strength, the thickness of the target, as well as magnetization direction. Figure 1 shows the color-coded PTF maps, which indicate that an optimally-worked (enhanced) target exhibits a much higher mean PTF, but a less uniform PTF across the target surface versus a typically-processed target. DC magnetron sputtering trials were executed on sputtering targets fabricated with varied conditions. As shown in Figure 2, some thermomechanical processing has significantly improved PTF, sputtering performance and lifetime of the targets. The impactors of PTF go well beyond the expected grain size refinement. To understand the underlying mechanisms, microstructure and grain texture of both target and thin film will be examined by SEM, XRD and EBSD analysis. We will also measure intrinsic magnetic properties, such as coercivity and precise permeability data at similar sputtering field strengths by using VSM, to correlate with target's PTF.

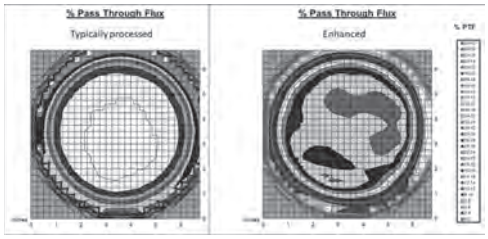

Fig. 1: PTF uniformity map comparison of typical and enhanced Dia.177.8 mm x 3.81 mm thick targets

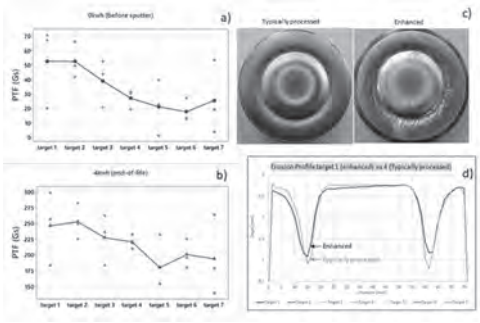

Fig. 2: PTF tested in a sputter tool and corresponding eroded target surfaces ("racetracks"). a) before sputter, b) end-of-life, c) spent target photographs, and d) cross-sectional erosion profiles after sputtering

GE-06. Fractional operators for the analytical expressions of the dynamic magnetic power loss. *B. Ducharne*[1,2] and G. Sebald[2]
1. INSA Lyon, Villeurbanne, France; 2. Tohoku University, Sendai, Japan

We introduce a novel analytical approach for predicting the dynamic magnetic power loss in ferromagnetic materials subjected to alternating or rotating magnetic fields [2]. The proposed method utilizes fractional derivative analytical expressions of trigonometric functions [2-4], providing a computationally efficient and accurate tool for core loss prediction. The resulting analytical expressions are validated against a large amount of experimental data from state-of-the-art setups [5, 6], demonstrating a high level of accuracy with a relative Euclidean distance below 5% for most tested materials and consistently below 10% (Fig. 1). Key findings include the observation that the dynamic power loss contribution under a rotating magnetic field is precisely two times higher than that under an alternating field under standard sinusoidal flux density conditions. This insight is crucial for the design and optimization of electromagnetic converters such as transformers, inductors, and motors, where magnetic losses can significantly impact efficiency, performance, and reliability. The research also highlights that by understanding the material's electrical conductivity, the dynamic magnetic power loss can be simplified to a single parameter—the fractional order—which is consistent for both rotational and alternating contributions. The paper further discusses the implications of these findings on the selection of appropriate ferromagnetic materials for specific applications, contributing to the development of environmentally friendly technologies that consume less energy and reduce the overall environmental impact. The study confirms the viscoelastic behavior of the magnetization process in ferromagnetic materials, thereby validating the use of fractional derivative operators for their simulation. This work offers a significant advancement in the understanding and prediction of magnetic losses in electromagnetic systems, with potential applications in various industries where compact and lightweight converters are critical, such as in portable electronic devices and aerospace systems.

[1] Bertotti, G., 1998. *Hysteresis in magnetism: for physicists, materials scientists, and engineers*. Gulf Professional Publishing. [2] Hilfer, R. ed., 2000. *Applications of fractional calculus in physics*. World scientific. [3] Ducharne, B. and Sebald, G., 2022. Fractional derivatives for the core losses prediction: State of the art and beyond. *Journal of Magnetism and Magnetic Materials*, p.169961. [4] Ducharne, B., Zurek, S. and Sebald, G., 2022. A universal method based on fractional derivatives for modeling magnetic losses under alternating and rotational magnetization conditions. *Journal of Magnetism and Magnetic Materials*, *550*, p.169071. [5] Appino, C., de La Barrière, O., Beatrice, C., Fiorillo, F. and Ragusa, C., 2014. Rotational magnetic losses in nonoriented Fe–Si and Fe–Co laminations up to the kilohertz range. *IEEE Transactions on Magnetics*, *50*(11), pp.1-4. [6] Zurek, S., 2017. *Characterisation of soft magnetic materials under rotational magnetisation*. CRC Press.

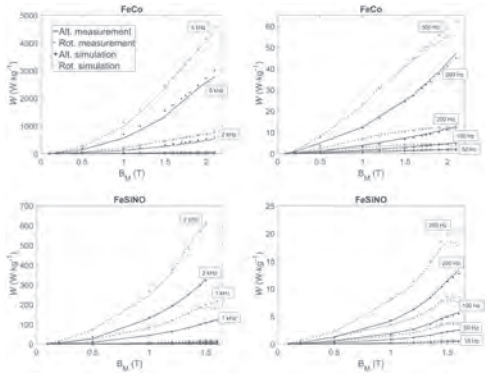

Fig. 1: Comparisons simulation/measurement under alternating and rotational magnetization for FeCo (top) and NOFeSi (bottom) materials

GE-07. Withdrawn

GE-08. Coil Design for a Moving-Magnet Planar Motor Using the Stream-Function Method. *B. Kuijpers*[1], J. Jansen[1] and E. Lomonova[1]
1. Eindhoven University of Technology, Eindhoven, Netherlands

This paper describes the design of a coil for a moving-magnet planar motor using the stream-function method. The stream-function method, commonly used in gradient-coil design [1]-[3], is an inverse boundary element method that synthesizes a conductor layout on a meshed surface with minimized power dissipation considering constraints on the force exerted on the mover. It has recently been applied to the design of coreless linear motors [4]. Typically, for the design of coils for a moving-magnet planar motor, a racetrack shaped coil is parameterized and its dimensions are optimized [5]. The force exerted on the magnet array by a coil with constant current is sinusoidally varying with the x-position. Since the magnetic flux density is not symmetric at all positions underneath the magnet array, a small force ripple is always present. Further decoupling of the force production in x-, and y-directions by reducing the inherited force ripple is necessary to improve the position accuracy of the planar motor. The stream-function method gives extra degrees of freedom in the coil design because it is not limited by a racetrack shape. It reduces the force ripple by restricting the bounds on the force constraints, but compromises the power dissipation. Fig. 1 shows a north-south magnet array with a classical racetrack coil and a meshed surface used in the stream-function method with the resulting coil shape defined by the iso-contour lines. The meshed surface has the same length and width as the racetrack coil. The Fourier transform is calculated for the force over a three period long square grid of positions with a fundamental frequency of twice the magnet pitch τ. The harmonic spectrum of the force in x-, y-, and z-directions are shown in Fig. 2. For equal amplitude of the desired harmonic (1,0) of the force in x, and z-directions, the large unwanted harmonics (0,1), (2,1), and (1,2) are reduced by the coil optimized with the stream-function method with 83%, 97%, and 97%, respectively.

[1] C.C. Sanchez, M.F. Pantoja and M. Poole, IEEE Transactions on Magnetics, Vol. 48, p.1967-1975 (2012) [2] E. Smith, F. Freschi and M. Repetto, IEEE Transactions on Biomedical Engineering, Vol. 63, p.924-932 (2016) [3] Y. Wang, Q. Wang and L. Guo, IEEE Transactions on Biomedical Engineering, Vol. 66, p.3339-3345 (2019) [4] B.J.A. Kuijpers, J.W. Jansen and E.A. Lomonova, IEEE Transactions on Magnetics, Vol. 59, p.1-9 (2023) [5] J.W. Jansen, C.M.M. van Lierop and E.A. Lomonova, IEEE Transactions on Industry Applications, Vol. 44, p.1108-1115 (2008)

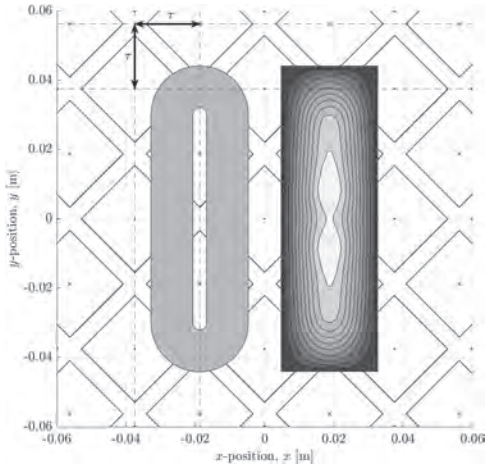

Fig. 1. The magnet array underneath the racetrack coil and the coil optimized by the stream-function method defined by the iso-contour lines.

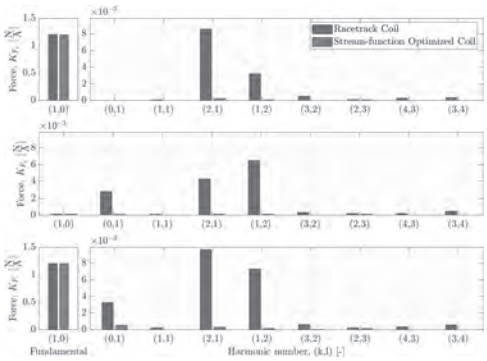

Fig. 2. Harmonic spectrum of the force for the racetrack coil and the stream-function optimized coil.

GE-09. Design of an Electromagnetic Reaction Wheel with Halbach Array. K. Liu[1], S. Lin[1], K. Peng[1] and *J. Chang*[1,2] *1. Department of Power Mechanical Engineering, National Tsing Hua University, Hsinchu, Taiwan; 2. Department of Mechanical and Computer-Aided Engineering, National Formosa University, Yunlin, Taiwan*

This article presents an advanced methodology for optimizing magnetic field design based on coil sets analysis findings of the electromagnetic reaction wheel (ERW) architecture [1], which incorporates both a Halbach array configuration [2] and a ferrite core. The stability of reaction wheels largely depends on the design of the electromagnets within the structure. Therefore, a strong electromagnetic field is usually employed to drive the internal carrier along their tracks. However, this design often fails for space applications where weight and power consumption are strictly regulated [3,4]. Moreover, a weaker magnetic field would result in unstable motion of the carrier. To solve this critical issue, this paper proposes two novel designs using Halbach array coil sets and ferrite cores to enhance the magnetic flux density. Based on the conventional design constraints derived from the finite element process, the magnetic flux density within the model is used as a nominal parameter to describe the reliability issue, as shown in Fig. 1. This issue is then addressed using Halbach array coil sets, constructed with the same tube model but including two on-tube coils and three inside coils filled with ferrite cores to optimize the parameter values. The magnetic flux density behavior is illustrated through simulation in Fig. 2. Additionally, results show that the Halbach array increases the flux density from 11 gauss to 23 gauss at the unstable point, and after further verification, the magnetic force was enhanced by 337.2%. This improvement significantly enhances the ERW's performance by optimizing the distribution of the rotating mass and eliminating the need for bearings. The findings suggest that the Halbach array ERW offers a more efficient, reliable, and durable solution for satellite attitude control, making it a superior alternative to traditional reaction wheels. This innovation has the potential to enhance the performance of future satellite missions, particularly for 1U CubeSats.

[1] H. S. Chen, K. Y. Peng, and J. Y. Chang, *2023 IEEE International Magnetic Conference - Short Papers (INTERMAG Short Papers)*, p. 1-2, (2023) [2] D. L. Trumper, M. E. Williams, and T. H. Nguyen, *Conference Record of the 1993 IEEE Industry Applications Conference Twenty-Eighth IAS Annual Meeting*, vol.1, p. 9-18 (1993) [3] I. M. da Fonseca, P. M. Bainum, and A. R. da Silva, *Acta Astronautica,* vol. 60, no. 10, p. 865-872 (2007) [4] G. A. Macala, A. Y. Lee, and E. K. Wang, *Journal of Spacecraft and Rockets,* vol. 51, no. 2, p. 574-585 (2014)

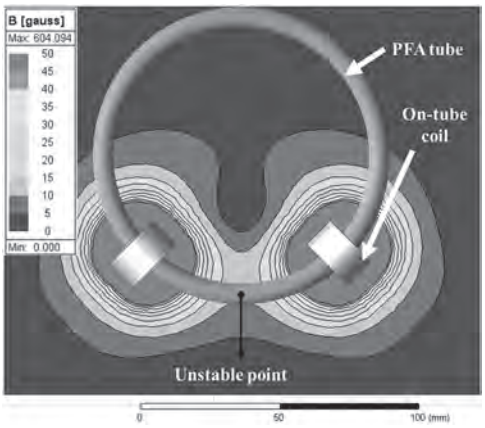

Fig. 1 In the conventional coil set model, the flux density at the unstable point is 11 gauss.

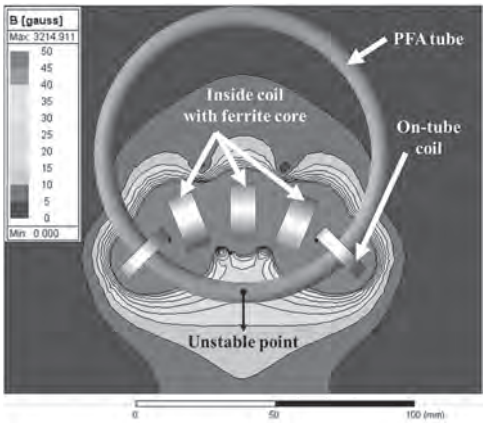

Fig. 2 By optimizing the coil set model using the Halbach array, the flux density at the unstable point was enhanced to 23 gauss.

Session GF
ULTRAFAST MAGNETISATION DYNAMICS AND SWITCHING

Andrei Kirilyuk, Chair
Radboud University, Nijmegen, Netherlands

INVITED PAPER

GF-01. Ultra-Fast All Optical Switching in Spintronic Devices.

J. Gorchon[1], T. Hauet[1], M. Hehn[1,2], J. Hohlfeld[1], G. Malinowski[1] and *S. Mangin[1,2] 1. Institut Jean Lamour, Université de Lorraine, Nancy, France; 2. CSIS, Tohoku University, Sendai, Japan*

In 1996, Bigot et al. made a significant discovery that established the new field of ultra-fast magnetism. They demonstrated that excitation with a femtosecond laser pulse could induce sub-picosecond demagnetization of a thin Ni film [1]. However, it was not until ten years later that Theo Rasing's group in Nijmegen demonstrated complete deterministic all-optical switching (AOS) using circularly polarized laser pulses on a GdFeCo ferrimagnetic alloy [2]. This phenomenon was subsequently termed all-optical helicity-dependent switching (AO-HDS) [3], observable in a wide range of samples [4,5]. A major drawback of AO-HDS in most magnetic films is its requirement for a large number of pulses, rendering the process relatively slow [6]. Conversely, single-pulse all-optical helicity-independent switching (AO-HIS) emerges as a more promising approach for practical applications, owing to its need for just one laser pulse and significantly quicker response [7]. However, in the case of metallic samples, AO-HIS appears to be restricted to Gd-based materials (alloys and multilayers) [8-11] and MnRuGa [12]. Recently, another type of single-pulse all-optical switching has been observed, attributed to magnetization precession during anisotropy reorientation [13,14]. Despite its novelty, this all-optical precessional switching process is comparatively slow, occurring over several hundred picoseconds. During the seminar we will examine magnetization reversal resulting from the direct interaction between the ultra-short laser pulse and the magnetization. Additionally, we will discuss how light can produce heat pulses or spin-polarized femtosecond current pulses which can then be exploited to reverse the magnetization of thin ferromagnetic films and magnetic heterostructures [15,16,17]. Part of the ultra-fast magnetism community is now focusing on deterministic magnetization switching induced by single femtosecond or picosecond laser pulses in spintronic devices, such as spin valves [18-24] and tunnel junctions [25,26]. During the talk we will show recent results on ultra-fast magnetization reversal (starting within less than one picosecond) in various ferrimagnetic and ferromagnetic spin-valve structures as shown in figure 1, both perpendicularly magnetized [18-23] and in-plane magnetized [24]. Concerning perpendicularly magnetized systems, we have recently demonstrated optically induced ultrafast magnetization reversal occurring in less than a picosecond in rare-earth-free archetypal spin valves ([Pt/Co]/Cu/[Co/Pt]) commonly utilized for current-induced spin-transfer torque (STT) switching [23]. We discovered that the magnetization of the free layer can be switched from parallel to antiparallel alignment, akin to STT switching, revealing the presence of an unexpected, intense, and ultrafast source of opposite angular momentum in our structures. Additionnaly, we will also show results on ultrafast optical control of exchanged biased structures. Indeed, we have shown that for an exchanged biased IrMn/GdCo bilayer, not only can a single laser pulse switch the ferrimagnetic GdCo layer, but it can also change the sign of the exchange bias, demonstrating that the magnetic configuration in the antiferromagnetic IrMn layer is affected by the laser pulse [27]. These findings pave the way for ultrafast magnetization control by combining concepts from spintronics and ultrafast magnetism.

[1] E. Beaurepaire, J. C. Merle, A. Daunois, and J. Bigot, Phys. Rev. Lett. 76, 4250 (1996). [2] C. D. Stanciu, et al, Phys. Rev. Lett. 99, 047601 (2007). [3] M. S. El Hadri, et al, Phys. Rev. B 94, 064412 (2016). [4] S. Mangin et al., Nat. Mater. 13, 286 (2014). [5] C.-H. Lambert et al.,Science 345, 1337 (2014). [6] M. S. E. Hadri, et al J. Phys. Appl. Phys. 50, 133002 (2017). [7] I. Radu et al., Nature 472, 205 (2011). [8] T.A. Ostler et al. Nat. Commun. 2012, 3, 666 (2012) [9] M. Beens et al. Phys. Rev. B 100, 220409(R) 2019 [10] J. Wei et al. Phys. Rev. Appl 15, 054065 (2021). [11] W. Zhang et al Phys. Rev. B 109 (9), 094412 (2024). [12] C. Banerjee, et al. Nat. Commun. 11, 4444 (2020). [13] L. Avilés-Félix, et al. Sci Rep 10, 5211 (2020) [14] Y. Peng et al. Nat Com 14 (1), 5000 (2023), Y. Peng et al Appl. Phys. Letters 124 (2) (2024) [15] Y. Xu and S. Mangin, J. Magn. Magn. Mater. 564, 170169 (2022). [16] J. Gorchon, et al J. Magn. Magn. Mater. 563, 169919 (2022). [17] P. Scheid et al J. Magn. Magn. Mater 560, 169596 (2022). [18] Q. Remy, et al Nature Com 14 445 (2023) [19] S. Iihama, et al Adv. Mater. 30, 1804004 (2018). [20] J. Igarashi, et al Nano Lett. 20, 8654 (2020). [21] Q. Remy, et al Adv. Sci. 7, 2001996 (2020). [22] Q. Remy, Phys. Rev. B 107, 174431 (2023) [23] J. Igarashi et al, Nature Mat, 114 36(2023) [24] J.X Lin et al under review (2024) [25] J.Y. Chen Phys. Rev. Appl 7 021001 (2017) [26] D. Salomoni Phys. Rev. Appl 20 034070 (2023) [27] Z. Guo Adv. Mater 36 (21) 2311643 (2024)

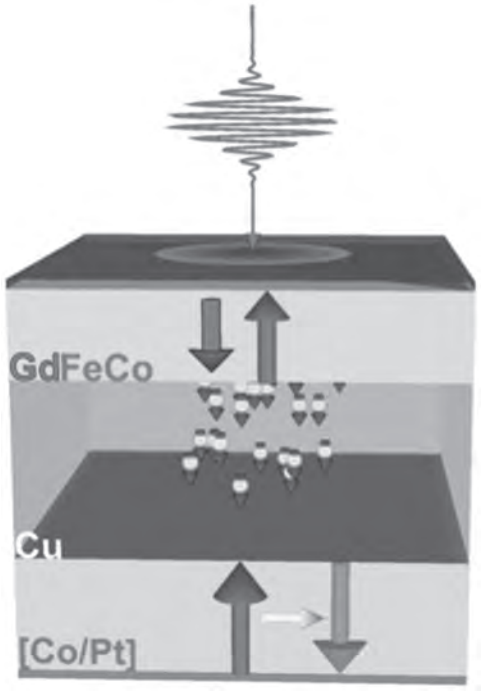

Fig.1 Sketch of a spin-valve structure used to demonstrate femto-second single pulse switching of each magnetic layer independently. The generation of femto-second spin current is shown to play a major role [17-23].

CONTRIBUTED PAPERS

GF-02. Measuring the Intrinsic Timescales of Ultrafast Spin Reorientation with Extreme Ultraviolet Light. *A. Grafov*[1], S.A. Ryan[1], N. Li[1], H.T. Nembach[2], J.M. Shaw[2], H. Bhandari[3], T. Kafle[1], R. Sapkota[1], H.C. Kapteyn[1,4], N.J. Ghimire[3] and M.M. Murnane[1] *1. JILA, University of Colorado Boulder, Boulder, CO, United States; 2. NIST, Boulder, CO, United States; 3. University of Notre Dame, Notre Dame, IN, United States; 4. KMLabs Inc., Boulder, CO, United States*

Optical excitation can enable ultrafast manipulation of spin states in magnetic materials. Spin reorientation materials are of particular note as they can change magnetization direction with respect to their crystollographic axes due to changes in temperature. While the mechanisms of the spin-reorientation transition have been studied in the quasi-static limit, the intrinsic timescales of this transition have previously not been determined. Here we present the first measurement of the intrinsic timescale of the spin-reorientation transition in a Kagome ferromagnet. The ferromagnet is optically excited through the transition using an ultrafast visible pump pulse, and the time-dependent magnetization of the material is probed with extreme ultraviolet light using the Magneto-Optical Kerr Effect. By pumping the material with a range of fluences and comparing our experimental results with theoretical models, we are able to measure the intrinsic timescales of ultrafast spin reorientation, demagnetization, and recovery.

Ryan et al., in prep (2024) Jones et al. (2022) arXiv:2203.17246v1

GF-03. Ultrafast Spin Dynamics across Metal/Semiconductor Interfaces: All-Optical Injection of Spin Currents in Silicon. *S. Laterza*[1], A. Caretta[1] and M. Malvestuto[1,2] *1. Elettra Sincrotrone Trieste S.C.p.A., Trieste, Italy; 2. Istituto Officina Dei Materiali-CNR, Trieste, Italy*

Integrating magnetic properties in the current semiconductor technology is the aim of Spintronics. The increased ability to tailor hybrid metal-semiconductor heterostructures made possible to use them as building blocks for spintronic devices based on current semiconductor technology. Furthermore, these systems still allow to gain intriguing insights from the complex interplay of different mechanisms, both from the fundamental and applied physics point of view. However, a viable Spintronic technology requires the effective generation, transport, manipulation, and detection of spins in solid-states devices. A path towards the generation and transport of spin currents in silicon will be proposed via the propagation of a superdiffusive spin pulse triggered by the ultrafast demagnetization of a magnetic film [1]. The system under study - a nickel thin film grown on a passivated silicon substrate [2] - offers a benchmark for investigating the interaction between optical, magnetic, and electric properties in a simple device.

[1] S. Laterza, A. Caretta, R. Bhardwaj *et al.*, Optica 9, 12 (2022). [2] P. Rajac, R. Ciancio, A. Caretta *et al.*, Appl. Surf. Sci, 623 (2023) 156986. [3] A. Caretta, S. Laterza, V. Bonanni *et al.*, Struct. Dynam. 8 (2021), 034304. [4] M. Malvestuto, A. Caretta, R. Bhardwaj *et. al.*, Rev. Sci. Instrum. 93 (2022), 115109. [5] S. Laterza, A. Caretta, R. Bhardwaj *et al.*, Sci. Rep. 14 (2024), 1329.

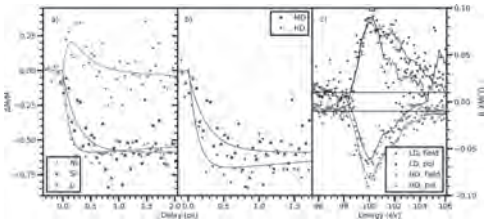

Fig. 1: a) RMOKE magnetic dynamics [3,4] at the Ni $M_{2,3}$ and Si $L_{2,3}$ edges (red and blue) measured in saturation field. The solid lines represent the fitting from which the characteristic demagnetization times are extracted. The difference $(\Delta M/M)_{js}$ is also shown (gray). b) RMOKE magnetic dynamics at the Si $L_{2,3}$ edge on two heterostructures varying only for the doping of the Si substrate (medium and high-doped in blue and magenta respectively). c) Reflectivity XMCD both at opposite fields and helicities on the low and high-doped samples at the Si $L_{2,3}$ edge [5].

Fig. 2: Si static magnetism can be explained both by the diffusion through the barrier of spin-polarized thermal electrons from the Ni film into the substrate (a) and by the existence of a chemical potential splitting induced by the proximity effect due to the presence of an interface with a ferromagnet (b). The magnetic dynamics triggered by the optical pump pulse arrival causes contemporary a quenching of the magnetization in Ni and therefore in Si, as well as the generation and propagation of a spin current in Si (c). The overall observed dynamics is a competition between the demagnetization and the transient superdiffusive spin current.

GF-04. Withdrawn

GF-05. Ultrafast Spin Dynamics in Fe-Gd Ferrimagnetic Alloys Investigated with Near-Fermi Level Probes. S. Saha[1,2], R. Knut[2], N. Alzahrani[3,4], J.E. Shoup[4,5] and *D.A. Arena*[4] *1. Physics, Ashoka University, Haryana, India; 2. Physics, Uppsala University, Uppsala, Sweden; 3. Physics, University of Jeddah, Jeddah, Saudi Arabia; 4. Physics, University of South Florida, Tampa, FL, United States; 5. Materials Science and Engineering Division, National Institute of Standards and Technology, Gaithersburg, MD, United States*

Elemental spins in ferrimagnetic rare earth / transition metal (RE/TM) alloys display a rich set of dynamics that reflect the complex, multi-sublattice and temperature-dependent spin arrangements, differing spin magnitudes, and dissimilar gyromagnetic ratios on the RE and TM sites. Ultrafast and high-energy element resolved probes indicate that in Fe-Gd or FeCo-Gd alloys, the Gd 4*f* spins exhibit a demagnetization / remagnetization dynamics that are distinct from the behavior of the Fe 3*d* states; generally, Gd 4*f* derived x-ray absorption or scattering signals indicate a longer demagnetization time for Gd than for Fe [1,2]. In this work, we examine relatively low energy, element resolved dynamics of Fe and Gd using a table-top high harmonic generation (HHG) extreme ultra-violet (EUV) source. We examine two Fe-Gd samples where the Gd concentration was varied to modify the magnetization compensation temperature from above to below room temperature. Broadband, synchrotron based static reflectivity measurements from 20 eV to 70 eV confirm the anti-ferromagnetic alignment of the Fe and Gd spins and the static EUV-HHG asymmetry spectra across the same energy range mimic the overall trends of the synchrotron spectra. Pump-probe ultrafast, element-resolved studies using the EUV-HHG source indicate that both the Fe and the Gd sub-lattices demagnetize by about 20% - 30% under relatively modest pump fluences. For both samples (above and below magnetization compensation), the magnetization dynamics on the Fe and Gd sites exhibit a similar demagnetization profile and recovery time. The results suggest that

in RE/TM alloys, the dynamics of Gd 5*d* states are in line with the dynamics of the Fe 3*d* electronic manifold, and thus the dynamics of Gd states closer to E_F may be distinct from the more tightly bound 4*f* states.

[1] I. Radu *et al.*, "Transient ferromagnetic-like state mediating ultrafast reversal of antiferromagnetically coupled spins," *Nature*, vol. 472, no. 7342, pp. 205–208, 2011. [2] C. E. Graves *et al.*, "Nanoscale spin reversal by non-local angular momentum transfer following ultrafast laser excitation in ferrimagnetic GdFeCo," *Nat. Mater.*, vol. 12, no. 4, pp. 293–298, Mar. 2013.

GF-07. Probing Ultrafast Spin Excitations in Magnetic Alloys Using Extreme Ultraviolet Spectroscopy. *N. Li*[1], A. Grafov[1], S.A. Ryan[1], M.F. Elhanoty[2], O. Grånäs[2], E. Lesne[3], C. Felser[3], H.C. Kapteyn[1] and M.M. Murnane[1] *1. JILA, University of Colorado, Boulder, CO, United States; 2. Department of Physics and Astronomy, Uppsala University, Uppsala, Sweden; 3. Max Planck Institute for Chemical Physics of Solids, Dresden, Germany*

Harnessing and controlling spin dynamics are promising routes for revolutionizing data storage and transfer. One avenue involves using very short laser pulses to directly excite or manipulate spins, potentially allowing control on femtosecond or even attosecond timescales. However, advancing this technology requires a deeper understanding of the mechanisms by which light can manipulate spins, and what are the different competing microscopic processes. This motivates the development of better probe techniques with high time-resolution and signal-to-noise ratio in order to capture element-specific spin dynamics on short timescales. These capabilities are particularly useful for studying new materials such as Kagome ferrimagnets, antiferromagnets, and spin-engineered multilayers, to help with the development of energy-efficient spintronic devices. Here, we present a noise-canceled, tabletop, extreme ultraviolet (EUV) magneto-optic spectroscopy setup that is optimized for probing laser-excited magnetic materials. By measuring element-specific dynamics across the entire M-edges of several elements within a single alloy with few-femtosecond resolution, we uncover the processes governing optically induced spin evolution on timescales of 100 fs or less. We also use this new beamline to explore spin dynamics in the Heusler alloy Co_2MnGa, where optical excitation channels can be spin-selective due to its half-metallic band structure. Through careful comparison of comprehensive data sets with time-dependent density functional theory, we can distinguish the different competing microscopic mechanisms: same-site Co-Co spin transfer, inter-site Co-Mn spin transfer, and ultrafast spin flips mediated by spin-orbit coupling. The spin transfer dominates in the first 80 fs, inducing a transient enhancement of Co magnetization. Demagnetization pathways such as spin-flips dominate later, inducing a reduction in the magnetization of both elements. And the spin transfer has highly energy-dependent behavior. Compared with dynamics in pure Co, we find the prevalence of spin-transfer-related enhancements depends on an intricate relationship between spin-polarization, spin-lifetimes, crystalline disorder, and the density of states.

[1] A. Kimel, A. Zvezdin, S. Sharma *et al.*, "The 2022 magneto-optics roadmap," *J. Phys. D: Appl. Phys.*, 55, 443003 (2022). [2] S. A. Ryan, P. C. Johnsen, M. F. Elhanoty *et al.*, "Optically controlling the competition between spin flips and intersite spin transfer in a Heusler half-metal on sub–100 fs time scales," *Sci. Adv. 9, eadi1428(2023).* [3] P. C. Johnsen, S. A. Ryan, C. Gentry et al, "A beamline for ultrafast extreme ultraviolet magneto-optical spectroscopy in reflection near the shot noise limit," *Rev. Sci. Instrum. 94, 033001 (2023).*

GF-08. All-optical switching in Pt/Co multilayers: from helicity dependent switching to bubble domains. *A. Villar*[1], D. Doménech[1], R. Montero[2], A. Devishvili[3], R. Morales[1,4,5], P. Vavassori[5,6] and J. Porro[1,5] *1. BCMaterials, Basque Centre for Materials, Applications & Nanostrcutures, Leioa, Spain; 2. Laser Facility, SGiker, Leioa, Spain; 3. Institut Laue-Langevin, Grenoble, France; 4. Chemical-Physics, UPV/EHU, Faculty of Science and Technology, Leioa, Spain; 5. IKERBASQUE, Basque Foundation for Science, Bilbao, Spain; 6. CIC nanoGUNE BRTA, Donostia-San Sebastián, Spain*

The need for ultrafast and highly efficient magnetic memory storage technologies, driven by multiple factors such as the increasing numbers of data centres or high-performance computation, has focused the research in state-of-the-art opto-spintronics. In this area, we can find the All-Optical Switching (AOS) phenomena, which consists in the deterministic ultrafast magnetization reversal of a magnetic material induced by femtosecond laser pulses[1] and includes helicity dependent AOS (AOS-HD), in which final magnetization depends on the sign of the circularly polarized laser pulses [Fig. 1]. Since its discovery in 2007 in GdFeCo alloy thin films[2], AOS has been observed in ferrimagnetic[3] and ferromagnetic alloys and multilayer[4] thin films. In the present work we study Co/Pt multilayer thin films with perpendicular magnetic anisotropy that undergo AOS-HD. The ferromagnetic/heavy metal interface generates a spin-orbit coupling from which the AOS-HD phenomenon arises. This interaction is critically dependent on the sample's parameters, such as Co and Pt layers' thickness, roughness, texture and possible interdiffusion events between Co and Pt layers. The fine tuning of the parameters of the sample (i.e. layer thicknesses, growth deposition rates and compositions) and the laser (i.e. energy per pulse, pulse repetition rate and pulse duration), enables the enhancement of the AOS-HD phenomenon. Furthermore, when specific sample with strip domains and laser pulse characteristics are met, the AOS turns into the creation of circular shape magnetic domains, called bubble-domains [Fig. 2]. Here we present a study that relates the magnetic depth profile, the quality of interfaces and layer interdiffusion with the observed AOS-HD phenomenon in different samples, as derived from polarized neutron reflectometry experiments.

[1] G. Kichin., M. Hehn, J. Gorchon et al. Phys. Rev. Appl. Vol. 12, p.024019 (2019) [2] C. D. Stanciu, F. Hansteen, A. V. Kimel et al. Phys rev. Lett. Vol. 99, p.047601 (2007) [3] L. Avilés-Félix, A. Olivier, G. Li et al. Sci. Rep., Vol. 10, p.5211 (2020) [4] Y. Quessab, R. Medapalli, M. S. El Hadri, et al. Phys. Rev. B, Vol. 97, p.054419 (2018)

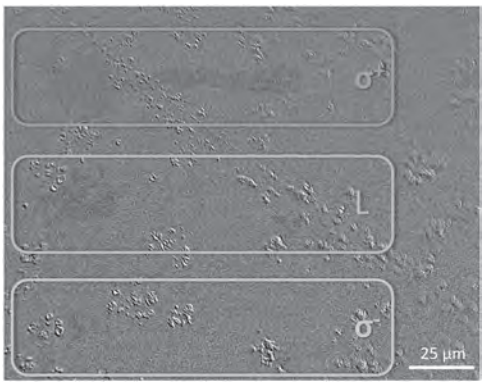

Fig. 1: Magneto-Optic Kerr Effect microscopy image demonstrating photon helicity-dependent AOS by femtosecond laser pulses' sweeping the surface of the sample with three different polarizations: circular dextrogyre (σ+, top), levogyre (σ-, bottom), and linear (L, centre).

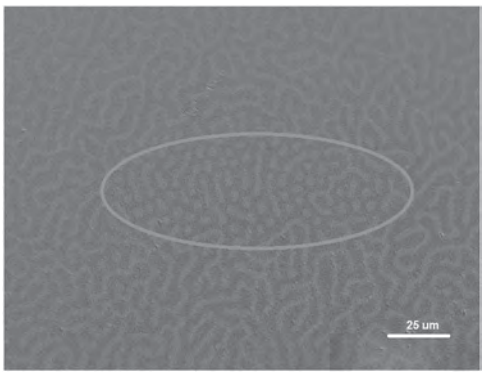

Fig. 2: Magneto-Optic Kerr Effect microscopy image showing bubble domains after a femtosecond laser pulse sweeps over the sample's surface.

GF-10. Light-helicity induced orbital angular momentum transfer torque in ferromagnetic metals. *K. Nukui*[1,2], S. Iihama[3,2], K. Ishibashi[1,2], S. Yamashita[1], A. Sakuma[1], P. Scheid[4], G. Malinowski[4], M. Hehn[4,5], S. Mangin[4,5] and S. Mizukami[2,5] *1. Department of Applied Physics, Tohoku University, Sendai, Japan; 2. WPI-AIMR, Tohoku University, Sendai, Japan; 3. FRIS, Tohoku University, Sendai, Japan; 4. CNRS, Institut Jean Lamour, Université de Lorraine, Nancy, France; 5. CSIS, Tohoku University, Sendai, Japan*

Photon carries spin angular momentum in circularly-polarized light, and the utilization of the photon's spin angular momentum is one of the key issues in spintronics. It is known that the circularly-polarized light induces magnetization in various matters via the inverse Faraday effect or absorption of photon angular momentum [1, 2, 3]. Recent theoretical study suggested that the inverse Faraday effect or absorption of photon angular momentum induce orbital angular momentum [4, 5]; however it is not well studied experimentally. To gain insight into this orbital physics, we investigated photon-helicity-induced magnetization precession in $Co_{1-x}Pt_x$ alloy thin films [6]. The 5-nm-thick $Co_{1-x}Pt_x$ (x = 0 - 0.7) alloy films were fabricated on thermally-oxidized Si substrates using ultra-high vacuum magnetron sputtering. We measured the magnetization precession dynamics induced by circularly-polarized light pulse using a time-resolved magneto-optical Kerr effect (TRMOKE) based on a pump-probe technique (Fig. 1). In addition to field-like torque, attributable to magnetic field generation owing to the inverse Faraday effect, we observed non-trivial and large damping-like torque which has never been discussed for single ferromagnetic layer (Fig. 2). The composition dependence of those two torques was elucidated via a model that considers mutual coupling via spin-orbit interaction between magnetization and the electronic orbital angular momentum induced by circularly-polarized light pulse. This work enhances our understanding of the physics relevant to the interplay of photon-helicity and magnetization in magnetic metals [6].

[1] J. P. van der Ziel *et al.,* Phys. Rev. Lett. 15, 190 (1965). [2] G. M. Choi, A. Schleife, and D. G. Cahill, Nat. Commun. 8, 15085 (2017). [3] P. Němec *et al.,* Nat. Phys. 8, 411–415 (2012). [4] M. Berritta *et al.,* Phys. Rev. Lett. 117, 137203 (2016). [5] P. Scheid, S. Mangin, and S. Lebègue, arXiv:2311.14774. [6] K. Nukui *et al.,* arXiv:2405.07405.

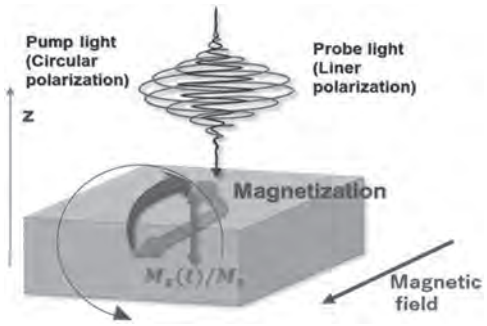

Fig. 1 Schematic of measurement for circularly-polarized light-induced magnetization dynamics.

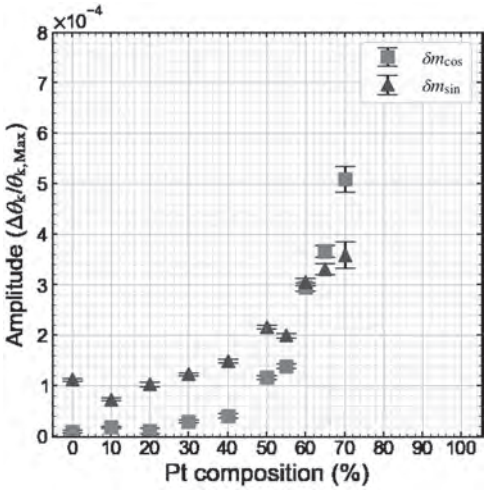

Fig. 2 The amplitude of field-like and damping-like torque (δm_{sin} and δm_{cos}) as a function of the Pt composition.

GF-11. Substrate-Mediated Phononic Switching of Magnetization Using Transient Polarization Gratings. F.G. Fennema[1,2], A. Tsukamoto[3], A. Kirilyuk[1,2] and *C.S. Davies*[1,2] *1. HFML-FELIX, Radboud University, Nijmegen, Netherlands; 2. Radboud University, Institute for Molecules and Materials, Nijmegen, Netherlands; 3. Nihon University, Chiba, Japan*

In the last half-decade, groundbreaking experiments have shown that the nascent process of ultrafast demagnetization involves the flow of angular momentum from the rapidly-quenched magnetization to circularly-polarized optical phonons [1]-[2]. Reciprocally, it is also viable for circularly-polarized optical phonons – when excited at resonance – to give rise to a transient magnetization [3]-[4]. Very recently, it has been demonstrated that such phonon-created emergent magnetization in paramagnetic substrates can even be used to remotely switch the magnetization of a magnetic heterostructure mounted atop the said substrate [5]. Here, we explore the more general spectral dependence of phononic switching of magnetization via the ultrafast Barnett effect. In our experiments, we spatiotemporally interfere two orthogonally-polarized infrared pulses under an angle, thus forming a transient grating that is spatially modulated in terms of polarization. We scan this excitation across heterostructures comprised of GdFeCo and Si_3N_4 nanolayers grown on paramagnetic Al_2O_3 and ZnO substrates, and magneto-optically image the magnetization of the magnetic overlayer. As shown in Fig. 1a, we observe for specific pumping wavelengths that one optical helicity σ^+ switches the magnetic ordering in the substrate-mounted heterostructure, while the other helicity σ^- does not. In contrast, when using a different pumping wavelength, the polarization grating leaves only demagnetization in its wake (Fig. 1b). By tuning the central wavelength of the pump pulses, we find that the quality of switching scales with the population of doubly-degenerate transverse-optical phonon modes in the substrate, proving

the vital role of the substrate in this process. Moreover, since the transient polarization grating is formed irrespective of the pumping wavelength, the quality of magnetic switching can be assessed across a much larger spectral range in alternative paramagnetic substrates, compared to the approach used in Ref. [5].

[1] C. Dornes *et al*, Nature 565, 209 (2019) [2] S. R. Tauchert *et al*, Nature 602, 73 (2022) [3] J. Luo *et al*, Science 382, 698 (2023) [4] M. Basini *et al*, Nature 628, 534 (2024) [5] C. S. Davies *et al*, Nature 628, 540 (2024)

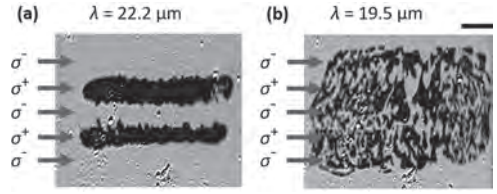

Fig. 1: (a)-(b) Typical background-corrected magneto-optical images of the magnetization taken after scanning - from left to right - a polarization grating across the magnetic heterostructure mounted atop c-cut sapphire. Scale bar, 50 µm.

GF-13. Withdrawn

Session GG
ELECTRONIC STRUCTURE AND FUNDAMENTAL PROPERTIES

Jinke Tang, Co-Chair
University of Wyoming, Laramie, WY, United States
Durga Paudyal, Co-Chair
University of Iowa, Iowa City, IA, United States

CONTRIBUTED PAPERS

GG-01. Magnetic Properties of the Metallic Delafossite Triangular-Lattice Antiferromagnet $PdCrO_2$ and its Anomalous Hall Effect. *Y. Tao*[1], Y. Zhang[1], F. Tutt[1], A. Paul[2], E. Ritz[1], J. Garcia-Barriocanal[3], T. Birol[1] and C. Leighton[1] *1. Chemical Engineering and Materials Science, University of Minnesota, Minneapolis, MN, United States; 2. Indian Institute of Technology Jammu, Jammu and Kashmir, India; 3. Characterization Facility, University of Minnesota, Minneapolis, MN, United States*

Metallic delafossites (ABO_2) are of high interest due to fascinating physical properties, such as record-breaking oxide electrical conductivity [1], emergent magnetic states, and anomalous magnetotransport related to geometrical frustration. A notable example is $PdCrO_2$, consisting of triangular-lattice layers of Pd and CrO_2 alternating along the *c*-axis. While the Pd layers are metallic and host exceptional conductivity, the CrO_2 layers are Mott-insulating with antiferromagnetic (AF) order below $T_N \approx 38$ K. $PdCrO_2$ also exhibits an unconventional anomalous Hall effect, although much remains to be understood regarding its magnetic and magnetotransport behavior. We address this here through wide-temperature-range X-ray diffraction, magnetometry, heat capacity, and magnetotransport on high-quality chemical vapor transport (CVT)-grown $PdCrO_2$ single crystals [2]. We find that $PdCrO_2$ is the first metallic delafossite to exhibit a large and unusual *c*-axis negative thermal expansion (-5 ppm/K) up to ~300 K, likely related to short-range magnetic fluctuations well above T_N. Magnetic susceptibility measurements show no bifurcation of ZFC and FC curves (Fig. 1), in contrast to prior work, suggesting that CVT crystals are less prone to magnetic impurity phases. Specific heat data allow accurate separation of electronic, phononic, and magnetic contributions (Fig. 1), indicating 3D magnon excitations in $PdCrO_2$. Most surprisingly, the anomalous Hall effect in $PdCrO_2$ persists well above T_N, connecting to the negative thermal expansion and suggesting a possible role for chiral spin-clusters (Fig. 2). Work supported by DOE through the University of Minnesota (UMN) Center for Quantum Materials (DE-SC0016371). Parts of this work were conducted in the UMN Characterization Facility, supported by NSF MRSEC (DMR-2011401).

[1] Y. Zhang, F. Tutt, G. N. Evans, P. Sharma, G. Haugstad, B. Kaiser, J. Ramberger, S. Bayliff, Y. Tao, M. Manno, J. Garcia-Barriocanal, V. Chaturvedi, R. M. Fernandes, T. Birol, W. E. Seyfried Jr., and C. Leighton, *Nat. Commun*. 15, 1399 (2024). [2] Y. Tao, Y. Zhang, F. Tutt, A. Paul, E. Ritz, J. Garcia-Barriocanal, T. Birol, and C. Leighton, unpublished (2024).

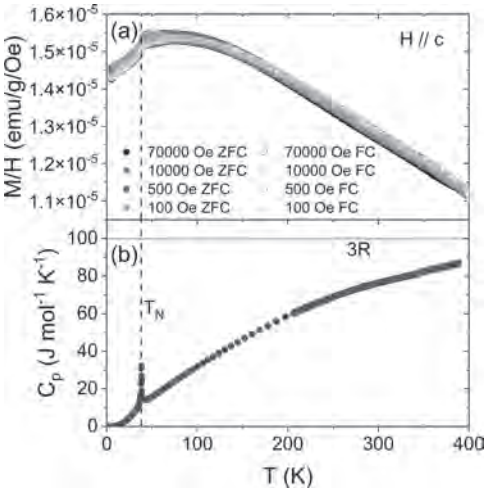

Fig. 1. Temperature (*T*) dependence of the magnetic susceptibility *M*/*H* and specific heat C_p of a CVT-grown $PdCrO_2$ single crystal.

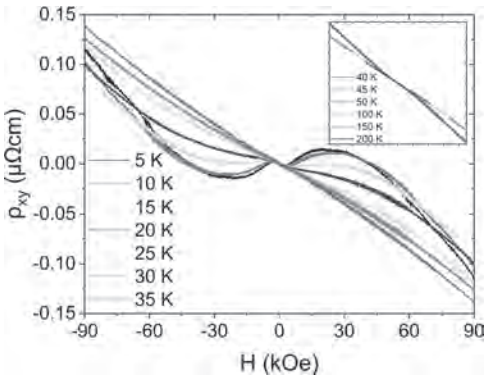

Fig. 2. Field (*H*) dependence of the Hall resistivity ρ_{xy} for a CVT-grown $PdCrO_2$ single crystal between 5 and 200 K.

GG-02. First-principle Calculations of Magnetic Properties of $Dy_6(Fe,Mn)Bi_2$ Compounds for Magnetic Refrigeration Applications. A. Garcia-Adeva[1], F. Ramón-García[1], *E. Apiñaniz*[1], A. Herrero[2], I. Aseguinolaza[2] and A. Oleaga[2] *1. Física Aplicada, Universidad del País Vasco (UPV/EHU), Vitoria-Gasteiz, Spain; 2. Física Aplicada, Universidad del País Vasco (UPV/EHU), Bilbao, Spain*

Ternary intermetallic compounds have received a great deal of attention, since these compounds show interesting magnetic properties that are of interest for refrigeration applications. In particular, our research group has pursued a comprehensive study of the intermetallic family R_6TX_2, where R is a rare earth element, T is a transition metal, and X is either of Bi, Te, or

Sb [1, 2, 3, 4, 5]. Many members of this family exhibit two magnetic phase transitions with relevant magnetocaloric effect that extend, in some cases, around room temperature. They also possess very complex magnetic properties, which is a subject of fundamental interest in itself. Indeed, most of these compounds exhibit a paramagnetic (PM) to ferromagnetic (FM) phase transition at an intermediate temperature. Moreover, there is a second phase transition at very low temperature to a non-collinear spin order. It is specially striking the fact that the PM to FM transition temperature in this family of compounds spans by more than 200 K upon Fe substitution by Mn [1, 2,3]. These facts led us to investigate microscopic models on the framework of the density functional theory that allow us to understand these intriguing magnetic properties and act as a guide in the search of novel materials which possess adequate magnetic properties for refrigeration applications. Initially, we studied the magnetic properties of Ho6(Fe,Mn)Bi_2 crystals [5] and, in the present work, we extend this study to the Dy_6MnBi_2 and Dy_6FeBi_2 crystals in order to furher understand the magnetic behavior of the R_6TX_2 intemetallics. The equation of state (Fig. 1), magnetic moments, and total (Fig. 2) and projected magnetic densities of states have been calculated. Also, by using a combination of both first principle calculations and simple analytical mean field theory, the exchange couplings between magnetic ions and the corresponding Curie temperatures of the magnetic phase transition have been calculated and a reasonable agreement with our previous experimental results is found.

[1] A. Herrero, A. Oleaga, A. Salazar, et al, Journal of Alloys and Compounds 821 (2020) 153198. doi:10.1016/j.jallcom.2019.153198. [2] A. Oleaga, A. Herrero, A. Salazar, et al, Journal of Alloys and Compounds 843 (2020) 155937. doi:10.1016/j.jallcom.2020.155937. [3] A. Herrero, A. Oleaga, I. Aseguinolaza, et al, Journal of Alloys and Compounds 890 (2022) 161849. doi:10.1016/j.jallcom.2021.161849. [4] A. Herrero, I. R. Aseguinolaza, A. Oleaga, et al, Dalton Transactions 52 (17) (2023) 5780–5797. doi:10.1039/D3DT00223C. [5] A. J. Garcia-Adeva, E. Apiñaniz, A. Herrero, et al, Rare Metals (accepted).

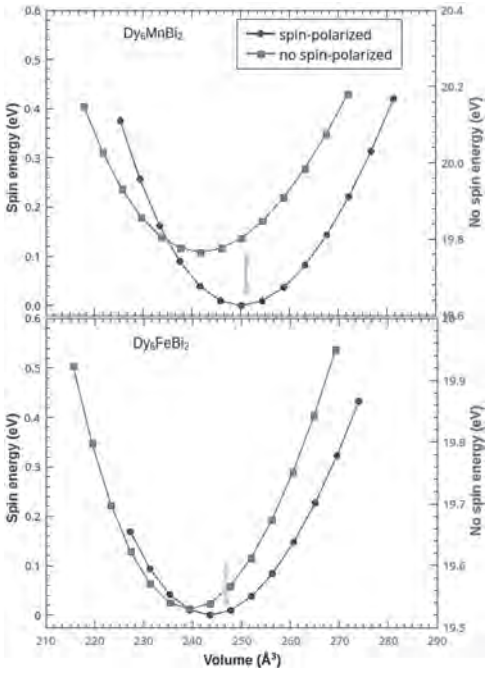

Fig. 1: Equation of state

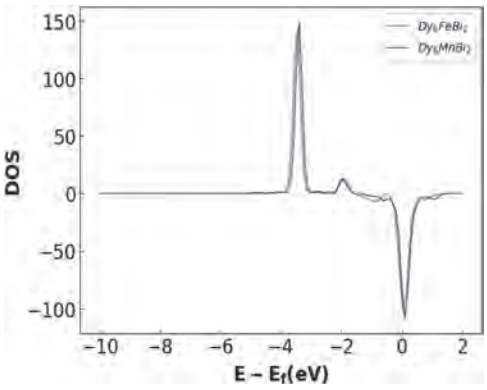

Fig. 2: Electronic density of states

GG-03. Superconducting diode effect without magnetic field in layered superconductor $FeTe_{0.6}Se_{0.4}$. *U. Nagata*[1], M. Aoki[1,2], A. Daido[3], R. Ohshima[1,2], S. Kasahara[4], Y. Kasahara[3], Y. Ando[1,2], Y. Matsuda[3], Y. Yanase[3,2] and M. Shiraishi[1,2] *1. Electronic Science and Engineering, Kyoto University, Kyoto, Japan; 2. CSRN Kyoto University, Kyoto, Japan; 3. Science, Kyoto University, Kyoto, Japan; 4. Research Institute for Interdisciplinary Science, Oakyama University, Okayama, Japan*

Since FeTeSe is a layer superconductor and a candidate of topological superconductor (TSC), much effort has been so far paid to explore its nature as TSC [1,2]. FeTeSe also collects great attention from spintronic viewpoints [3,4] because characteristic spin texture can be created as reported in the work exerting angle-resolved photo emission spectroscopy [1], of which spin functions can be utilized in the field. Thus, FeTeSe is one of the significant materials in a broad range of condensed matter physics. The superconducting diode effect (SDE) [5], where nonreciprocal supercurrent flow takes place, has been intensively investigated from both experimental and theoretical approaches in spintronics as a novel physical effect. Meanwhile, underlying physics of the SDE is somewhat elusive, and especially, the role of time-reversal symmetry is under debate [6]. In this study, we investigated the SDE in $FeTe_{0.6}Se_{0.4}$ (FTS). Inset of Fig.1 shows an optical image of the fabricated device. The FTS was exfoliated and transferred on a thermally oxidized Si substrate and the Au/Co electrodes were fabricated. Electric current was flowed between electrodes 1 and 4, and a four-terminal voltage was measured between electrodes 2 and 3. Figure 1 shows the *I-V* characteristics at around the critical current under positive (black) and negative (red) electric current, respectively, at 12 K without an external magnetic field. We clearly observed the difference of the critical current, ΔI_c, indicating existence of the field-free SDE. More importantly, the sign of ΔI_c is independent of the external magnetic field as shown in Fig.2, which is different from the conventional aspect of the SDE that requires broken time-reversal symmetry induced by either a magnetic field or magnetization of ferromagnet [5,7]. Systematic investigation revealed that the origin is strong thermal response of the FTS and thermal gradient in the FTS film caused by inhomogeneous device geometry [8]. Detailed discussion will be introduced in the presentation.

[1] P. Zhang et al., Science, Vol. 360, p.182 (2018) [2] T. Machida et al., Nat. Mater., Vol. 18, p.811 (2019) [3] K. Ohnishi, M. Shiraishi et al., APEX, Vol. 14, p.093002 (2021) [4] K. Ohnishi, M. Shiraishi et al., under review [5] F. Ando et al., Nature, Vol. 584, p.373 (2020) [6] H. Wu et al., Nature, Vol. 604, p.653 (2022) [7] H. Narita et al., Nat. Nanotechnol., Vol. 17, p.823 (2022) [8] U. Nagata, M. Shiraishi et al., under review

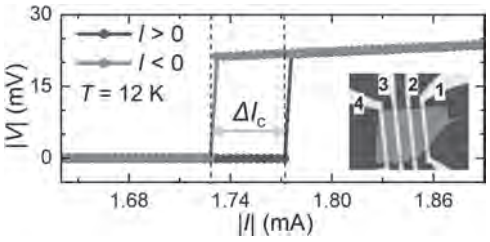

Fig.1 *I-V* characteristics of the FTS without magnetic field. Inset is an optical image of the device.

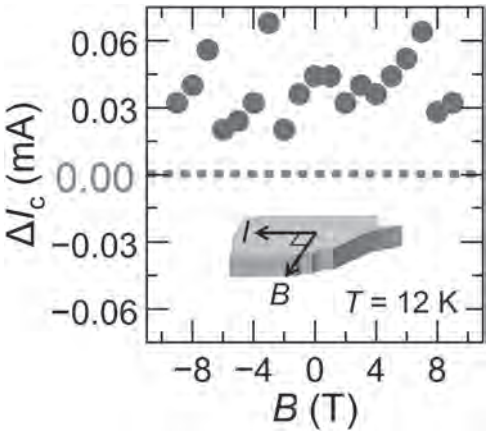

Fig.2 External magnetic field (*B*) dependence of ΔI_c. Inset shows a schematic of measurement geometry.

GG-04. Non-trivial Spin Structures and Multiferroic Properties of the DMI-Compound $Ba_2CuGe_2O_7$. *P. Wild*[1], K. Fellner[1], M. Dembski-Villalta[1] and S. Mühlbauer[1] *1. TUM/MLZ, Garching, Germany*

Incommensurate spiral magnets have raised tremendous interest in recent years, mainly motivated by their wealth of spin structures with potential non-trivial topology, such as skyrmions. A second field of interest is multiferroicity. Antiferromagnetic $Ba_2CuGe_2O_7$, characterized by a quasi-2D structure with Dzyaloshinskii-Moriya interactions (DMI), is interesting in both of these regards and combines them with a variety of unconventional magnetic phase transitions. $Ba_2CuGe_2O_7$ is an insulator characterized by a tetragonal, non-centrosymmetric space group (P-42_1m) with a = 8.466 Å and c = 5.445 Å. The main features of the magnetic structure are due to the Cu2+ ions in a square arrangement in the tetragonal (a,b) plane with dominant nearest-neighbor AF exchange along the diagonal in the plane and much weaker FM exchange between planes, leading to a quasi-2D behaviour. Below the Néel temperature T_N = 3.05K, the DMI term is responsible for a long-range incommensurate, almost AF cycloidal spin spiral with the spins (almost) confined in the (1,-1,0) plane in the ground state. At zero external field, neutron diffraction is used for a careful examination of the distribution of critical fluctuations in reciprocal space, associated with the paramagnetic to helimagnetic transition of $Ba_2CuGe_2O_7$. Caused by the reduced dimensionality of $Ba_2CuGe_2O_7$, a crossover from incommensurate antiferromagnetic fluctuations to 2D AF Heisenberg fluctuations is observed. Recently, a new phase with a vortex-antivortex magnetic structure has been theoretically described. It has been experimentally confirmed in a pocket in the phase diagram at around 2.4K and an external field along the crystalline c-axis of around 2.2T. A lack of evidence for a thermodynamic phase transition towards the paramagnet in specific heat measurements and a finite linewidth in energy and momentum of the incommensurate peaks in neutron scattering, as opposed to the cycloidal ground state, seem to mark the vortex phase as a slowly fluctuating structure at the verge of ordering. Polarization measurements and neutron experiments including electrical field are already planned for further pinning down of the multiferroic properties.

[1] M. Mostovoy. Phys. Rev. Lett., 96:1–4, 2006. [2] S. Mühlbauer *et al,* Rev. Mod. Phys, 91, 015004 (2019) [3] A. Zheludev *et al.* Phys. Rev. B, 54 (21):15163- 15170, (1996). [4] B. Wolba. PhD thesis, KIT, 2021. [5] H. Murakawa *et al.* Phys. Rev. Lett., 103(14):2–5,2009.

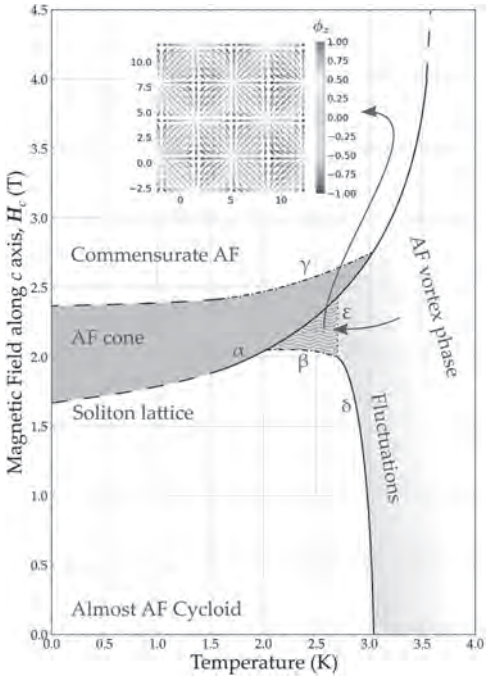

Fig.1: Magnetic phase diagram of $Ba_2CuGe_2O_7$

GG-05. Transition metals: Matching microscopic quantum dynamics with macroscopic magnetic order. *V. Janiš*[1] and M. Khanore[1] *1. Institute of Physics, Czech Academy of Sciences, Praha, Czechia*

Metals may show long-range magnetic order if the electron correlations are sufficiently strong. This metallic magnetism does not fit the Pauli or Stoner pictures. Static, weak-coupling theories with no local magnetic moments do not account for the Curie-Weiss behavior of the magnetic susceptibility if the critical temperature lies below the Fermi energy of the degenerate Fermi gas. The first theory that qualitatively correctly reproduces the Curie-Weiss law in weak ferromagnetic metals was proposed by Moriya and collaborators [1]. This theory describes consistently only the critical behavior above the transition temperature. It suffers, as other dynamical approximations, from a serious drawback when continued into the ordered phase. The transition point derived from the vanishing of magnetization is not identical to the critical point of the magnetic susceptibility in the paramagnetic phase. The reason for this mismatch is the discrepancy between the microscopic quantum dynamics and the macroscopic thermodynamic order. A generic feature of all dynamical approximations such as RRPA, FLEX, or parquets is the impossibility of simultaneously conforming the quantum dynamical Schwinger-Dyson equation with the thermodynamic conservation laws [2]. It means that the two-particle vertex from the Schwinger-Dyson equation differs from that in the Ward identity guaranteeing that the long-range order emerges at the critical point of the magnetic susceptibility [3]. We found that to match the vanishing of magnetization with the critical point of the magnetic susceptibility one has to suppress specific non-conserving processes in the ordered phase. We demonstrate the proper continuous extension of the dynamical approximations into the ordered phases suppressing the non-conserving diagrams on the half-filled Hubbard model at intermediate coupling within the dynamical mean-field approximation.

[1] T. Moriya, *Spin Fluctuations in Itinerant Electron Magnetism,* Springer Verlag, Berlin, Heidelberg (1985) [2] V. Janiš, P. Zalom, V. Pokorný and A. Klíč, Phys. Rev. B 100, 195114 (2019) [3] V. Janiš, V. Pokorný, and Š. Kos, Phys. Rev. B 109, 075171 (2024)

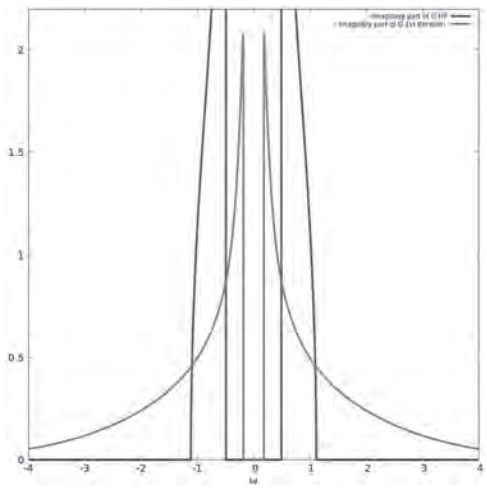

Fig.1: Normal spectral function of the antiferromagnetic solution of the zero-temperature half-filled Hubbard model for *U=2* and semi-elliptic DoS. Self-consistent second-order local approximation (green) was compared to the Haretree-Fock solution (magenta). The dynamical corrections decrease the energy gap and extend the outer band edges.

GG-06. Spin fluctuation driven magnetoresistance, domain re-distribution and anomalous Hall effect in helical antiferromagnetic Eu metal thin films. N. Shrestha[1] and *J. Tang*[1] *1. Department of Physics and Astronomy, University of Wyoming, Laramie, WY, United States*

Europium (Eu) metal has a body centered cubic crystal structure which, upon a paramagnetic-to-helical magnetic phase transition, undergoes a body centered tetragonal distortion. The magnetic helix appears below a Néel temperature (T_N) of ~90 K, and an applied magnetic field gives rise to conical magnet structure. We have prepared Eu metal thin films on Si (001) substrates using Eu metal as a target by pulsed laser deposition (PLD) and studied the transport properties by a four-probe method. The resistance shows a sudden slope change at T_N of 88 K. The magnetoresistance (MR) is positive at temperatures below 30 K and exhibits negative values above that. Our analyses show that the positive MR at low temperatures originates from magnetic field induced spin fluctuation, and the negative MR at higher temperature is a result of suppression of critical spin fluctuation of the Eu spins by the magnetic field. The Eu film also shows hysteretic MR behaviors in mid field range, which is a result of re-distribution of the helical antiferromagnetic domains by the magnetic fields. We have also studied the transverse magnetotransport in the Eu thin films. The observed anomalous Hall effect (AHE) is believed to be associated with the magnetic moment induced by the field or due to the helical spin structure of Eu itself. Acknowledgement This work was supported by the National Science Foundation (Grant No. 2228841) and the US Department of Energy, Office of Basic Sciences, Division of Material Sciences and Engineering (DE-SC0020074 and DE-SC0021281).

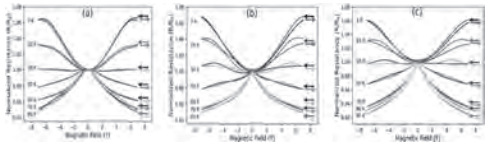

Fig. 1 MR of Eu thin films at different temperatures and field directions (a) out-of-plane (H_z), (b) in-plane (H_x) and (c) in-plane (H_y) with current in the x-direction.

GG-07. Comprehensive Study of GGA+*U* Approach to Modeling Electronic Structure of α″–$Fe_{16}N_2$. *P. Stoeckl*[1], P. Swatek[2] and J. Wang[1,2] *1. Physics, University of Minnesota, Minneapolis, MN, United States; 2. Electrical and Computer Engineering, University of Minnesota, Minneapolis, MN, United States*

Within the framework of density-functional theory (DFT), a common extension to the usual generalized-gradient approximation (GGA) exchange-correlation functional is the inclusion of Hubbard parameters *U* (,*J*) as GGA+*U*. In the study of the iron nitride phase α″–$Fe_{16}N_2$, first-principles calculations have yielded inconsistent results for its giant magnetic moment and reasonably high magnetocrystalline anisotropy (MCA). Several previous works have applied the GGA+*U* approach to α″–$Fe_{16}N_2$ to improve agreement with these experimental observations, each with unique methodology for selecting Hubbard parameters. While this approach has yielded increased magnetic moments and MCA over GGA, it typically falls short of experimental moments. This work employs the plane-wave DFT code Quantum ESPRESSO to more comprehensively investigate the influence of Hubbard parameters *U*, *J* on the electronic structure and resultant magnetic properties of α″-$Fe_{16}N_2$. We survey a broad range of values for *U* and *J*, and compare to values from first principles, e.g. self-consistent linear-response calculations. MCA varies significantly with *U*, *J* including changes in sign, whereas magnetic moments remain inline with previous GGA+U calculations. These values are compared against experimental ranges to determine which *U*, *J* yield the best agreement. To elucidate these results, we consider band structures and density of states to provide a deeper understanding of the magnetic behavior in α″–$Fe_{16}N_2$.

[1] P. Stoeckl, P. Swatek, & J.-P. Wang, *AIP Advances* 13(2), 025014 (2023). [2] P. Stoeckl, P. Swatek, & J.-P. Wang, *AIP Advances* 11(1), 015039 (2021). [3] J.-P. Wang, *J. Magn. Magn. Mat.* 497, 165962 (2020). See also: [4] R. Islam & J. P. Borah, *J. Appl. Phys.* 128(11), 114902 (2020). [5] X. Li *et al., phys. stat. solidi (RRL)* 13(7), 1900089 (2019). [6] W. Zhou *et al., Phys. Lett. A* 378(11-12), 909-14 (2014). [7] H. Sims *et al., Phys. Rev. B* 86(17) (2012). [8] N. Ji *et al., New J. Phys* 12(6), 063032 (2010). [9] W. Y. Lai *et al., J. Phys.: Cond. Mat*. 6(18), L259-64 (1994).

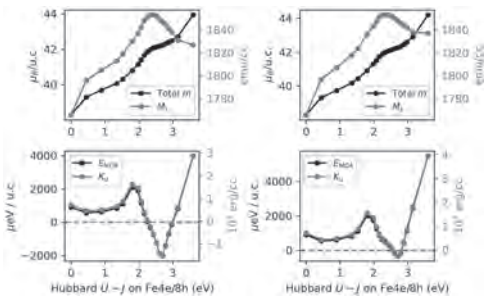

Fig.1: Magnetic properties of $Fe_{16}N_2$ as function of *U–J* on Fe4e/8h (N nearest neighbors), with *U–J* = 0.9 eV fixed on Fe4d (away from N). Left: *J* = *U*/10; Right: *J* = 0. Adapted from previous work in ref. [1].

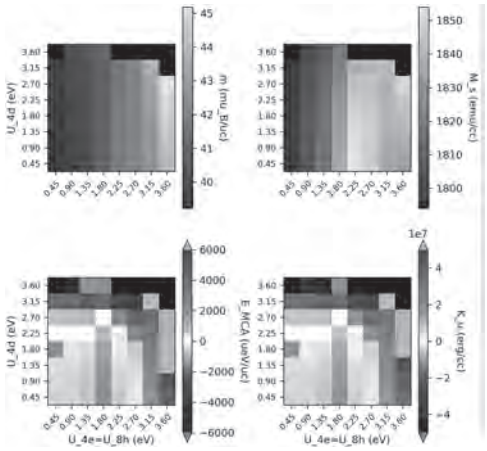

Fig. 2: Magnetic properties of $Fe_{16}N_2$ as function of *U* on Fe4e/8h vs. *U* on Fe4d sites (*J*=0 throughout). Preliminary results.

GG-08. Signatures of Magnetic Glassiness in Zinc Ferrite: Low-Temperature Fast "Rejuvenation" versus Room-Temperature Slow Relaxation and Memory-Effect. *A. Ney*[1], J. Lumetzberger[1], V. Ney[1], D. Primetzhofer[2], A. Zakharova[3], N. Daffe[3], F. Wilhelm[4] and A. Rogalev[4]
1. Solid State Physics Division, Johannes Kepler Univ, Linz, Austria; 2. Uppsala Univ, Uppsala, Sweden; 3. Swiss Light Source, Villigen, Switzerland; 4. ESRF, Grenoble, France

Zinc ferrite ($ZnFe_2O_4$, ZFO) in thin-film form possesses a range of possible applicationsas an interesting semiconducting material in spintronics with tunable magnetic properties including unconventional magnetic order due to intrinsic or extrinsic frustration. ZFO belongs to the family of normal spinels of the form AB_2O_4. In bulk form ZFO is known to be antiferromagnetic with a low Néel-temperature [1]. The magnetic properties significantly change as a thin film, especially for a finite degree of inversion and/or off-stoichiometry where ferro(i) magnetic order up to room temperature can be found, e.g. [2]. In contrast, other studies report the existence of a spin-glass or cluster-glass behavior under various conditions in bulk [3] or in thin films [4] exhibiting a wide range of spin freezing temperatures. Here we present a systematic study of epitaxial, stoichiometric ZFO thin films prepared using reactive magnetron sputtering over a wide range of preparation conditions which exhibit signatures of magnetic glassiness up to room temperature [5]. Figure 1 shows an example of a ZFO film grown at high sputter power where even for short waiting times t_{wait} a clear increase of ΔM is visible at low temperatures. In contrast the common "hole burning effect" around the waiting temperature T_{wait} is only present for long waiting times. While the former effect is present irrespective of sputter power, the latter is only observed for high sputtering powers. Using soft x-ray magnetic circular dichroism we can provide evidence for a finite degree of inversion accompanied by the formation of Zn on octahedral lattice sites as well as a finite magnetic polarization of Zn. In addition, hard x-ray linear dichroism allows a correlation of magnetic glassiness with disorder in the Zn cationic sublattice, which can be induced by increasing the sputtering power, thus further elucidating the microscopic origin for magnetic glassiness at unusually high temperatures up to room temperature.

[1] J. M. Hastings and L. M. Corliss, Rev. Mod. Phys. 25, 114 (1953) [2] V. Zviagin, M. Grundmann, and R. Schmidt-Grund, Phys. Status Solidi B 257, 1900630 (2020) [3] M. A. Hakim, M. Manjurul Haque, M. Huc, and P. Nordblad, Phys. B: Condens. Matter 406, 48 (2011) [4] Y. Yamamoto, H. Tanaka, and T. Kawai, Jpn. J. Appl. Phys. 40, L545 (2001) [5] J. Lumetzberger, V. Ney, A. Zakharova, N. Daffe, D. Primetzhofer, F. Wilhelm, A. Rogalev, and A. Ney, Phys. Rev. B 107, 144416 (2023)

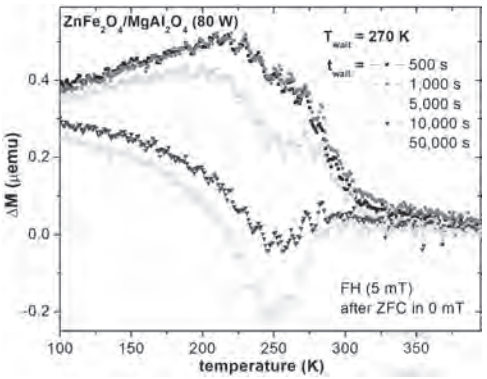

Fig.1: Difference of magnetization ΔM for an epitaxial zinc ferrite film taken between field heated (FH) magnetization curves recorded after zero-field cooling (ZFC) with and without waiting time t_{wait} at the waiting temperature T_{wait} for various t_{wait}.

GG-09. Withdrawn

GG-10. Frustration driven low-temperature spin dynamics in magnetically diluted Co-based glassy spinel systems. *M. Roy Chowdhury*[1], T. Sarkar[2], E.S. Choi[3] and S. Thota[1] *1. Physics, Indian Institute of Technology Guwahati, Guwahati, India; 2. Department of Materials Science and Engineering, Uppsala University, Uppsala, Sweden; 3. National High Magnetic Field Laboratory, Tallahassee, FL, United States*

Magnetically diluted spinels can be experimentally derived from conventional long-range ordered systems (e.g. Co_3O_4) by elemental substitution at the tetrahedral (*A*) and/or octahedral (*B*) sites of the spinel lattice [1]. Such systems provide a unique platform to study the effect of magnetic frustration, leading to loss of long-range magnetic order and emergence of a spin-glass (SG) phase. In this work, we investigated two doubly-diluted derivatives of long-range ordered antiferromagnetic Co_3O_4: $ZnTiCoO_4$ (ZTCO) and $ZnMnCoO_4$ (ZMCO). These systems were synthesized by replacing all the *A*-sites by nonmagnetic Zn^{2+} and 50% of the *B*-sites by nonmagnetic Ti^{4+} or magnetic Mn^{3+} respectively, such that both possess only one magnetic cation. Polycrystalline ZTCO and ZMCO were confirmed to be isostructural to cubic Co_3O_4 (*Fd*-3*m*) by x-ray diffraction. Although they appear quite simple at first glance, their magnetism is quite complex as revealed by detailed studies. Temperature and field dependent DC and *ac* magnetic measurements established a 'hierarchically organized' cluster SG ground state in both systems. Frequency dispersion of *ac*-susceptibility and a non-exponential time evolution of isothermal remanent magnetization also confirmed the cluster SG state. Absence of a λ-like peak in the specific heat data near the magnetic transitions validated the presence of only short-range ordering in both systems [2]. Differential DC magnetic susceptibility plots revealed another transition above the cluster SG phase in both cases; a short-ranged antiferromagnetic phase (T_N = 14K) in ZTCO while ZMCO exhibited ferrimagnetic behavior (T_{FN} = 38K) with short-range magnetic correlations as shown in Fig. 1. A field-induced transition was also observed for ZMCO but absent in ZTCO. Thus, probing the role of elemental substitution in magnetically diluted spinels provided valuable insights on frustration driven spin dynamics in complex oxides which is a crucial step in effectively tuning their properties for technological advancements. This work is partially supported by by Ministry of Education, India by PMRF fellowship.

[1] R.J. Hill, J.R. Craig, and G.V. Gibbs, Physics and chemistry of minerals, 4(4), pp.317-339 (1979) [2] M.R. Chowdhury, M.S. Seehra, P. Pramanik, et al., Journal of Physics: Condensed Matter, 34(27), p.275803 (2022)

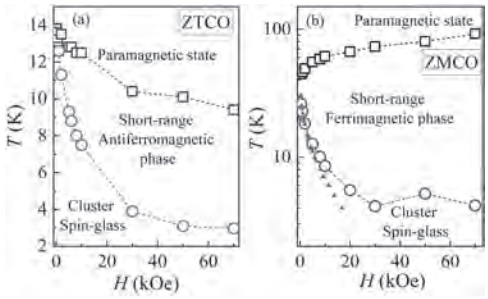

Fig. 1. The magnetic phase diagram of (a) ZTCO and (b) ZMCO on the *T-H* plane depicting major phase transition lines.

GG-11. Single Molecule Magnet's (SMM) Effects on Antiferromagnet-based Magnetic Tunnel Junction. *B. Sankhi*[1] and P. Tyagi[1] *1. Mechanical engineering, University of the district of Columbia, Washington, DC, United States*

The integration of single-molecule magnets (SMMs) into magnetic tunnel junctions (MTJs) offers significant potential for advancing molecular spintronics, particularly for next-generation memory devices, quantum computing, and energy storage technologies such as solar cells [1,2]. In this study, we present the first demonstration of SMM-induced spin-dependent properties in an antiferromagnet-based MTJ molecular spintronic device (MTJMSD). We engineered cross-junction-shaped devices comprising FeMn/AlOx/NiFe MTJs. The AlOx barrier thickness at the intersection between exposed junction edges was comparable to the SMM length, facilitating the incorporation of SMM molecules as spin channels for spin-dependent transport. The SMM channels enabled long-range magnetic moment ordering around molecular junctions, which were precisely engineered via fabrication processes. The SMM [3], composed of a $Mn6(\mu_3\text{-}O)_2(H_2N\text{-}sao)_6(6\text{-}atha)2(EtOH)_6$ [H_2N-saoH=salicylamidoxime, 6-atha=6-acetylthiohexanoate] complex, featured thiol groups at the ends to form bonds with the magnetic electrodes. SMM-treated junctions demonstrated a significant current enhancement, reaching up to 7 μA at an input voltage of 40 mV. Furthermore, SMM-doped junctions exhibited current stabilization in the μA range at lower temperatures, whereas the bare electrodes showed current suppression to the picoampere range. Magnetization measurements conducted at 55 K and 300 K on pillar-shaped devices revealed a reduction in magnetic moment at low temperatures. Additionally, Kelvin probe atomic force microscopy (KPAFM) measurements confirmed that SMM integration transformed the electronic properties over long ranges. These findings are attributed to the spin channels formed between magnetic metal electrodes, which enhance spin polarization at each magnetic electrode. Our research highlights the potential of using antiferromagnetic materials, characterized by minimal stray fields and zero net magnetization, to transform MTJMSD devices.

[1] M. N. Leuenberger and D. Loss, "Quantum computing in molecular magnets," *Nature,* vol. 410, no. 6830, pp. 789-793, 2001 [2] M. Savadkoohi, D. Gopman, P. Tyagi, "Spin solar cell phenomenon on a single-molecule magnet (SMM) impacted CoFeB-based magnetic tunnel junctions," *ACS Applied Electronic Materials,* vol. 5, no. 6, pp. 3333-3339, 2023. [3] C. Rojas-Dotti and J. Martínez-Lillo, "Thioester-functionalised and oxime-based hexametallic manganese (III) single-molecule magnets," *RSC advances,* vol. 7, no. 77, pp. 48841-48847, 2017.

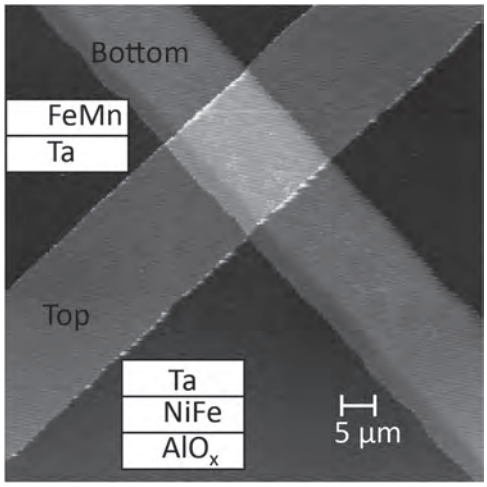

Fig.1 Atomic force microscopy image of one the junction of Bare Mgnetic Tunnel Junction

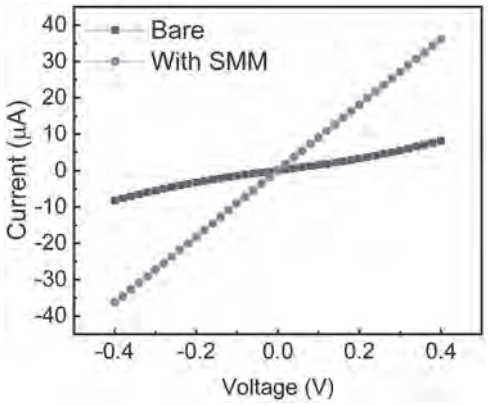

Fig.2 Transport measurement before and after the SMM treatment.

GG-12. Self-consistent magnetic dynamic susceptibility in the itinerant magnets. M. Auslender[1] and *V. Antropov*[2] *1. Ben-Gurion University of the Negev, Be'er Sheva, Israel; 2. Ames National Laboratory, Ames, IA, United States*

We propose a novel linear response approach for studying magnetic excitations in itinerant magnets using spin dynamic susceptibility. The method is self-consistent and based on the Mori correlation function theory. The self-consistency is obtained directly using corresponding spin-spin, spin-spin current and spin current-spin current correlators. With such approach no introduction of any enhancement factor aka Stoner parameter is needed. We discuss the advantages of such an approach relative to traditional standard linear response schemes. The density functional studies of magnetic excitations in ferromagnetic Ni metals will be presented and compared with earlier results.

*Work at Ames Laboratory was supported by the U.S. Department of Energy (DOE), Office of Science, Basic Energy Sciences, Materials Science and Engineering Division. Ames Laboratory is operated for the U.S. DOE by Iowa State University under contract # DE-AC02-07CH11358.

GG-13. Enhanced cooperativity in photon magnon hybrid system using nested meta-resonator: insights of coherent and dissipative coupling. S. Yadav[1], P. Kumar[1], M. Sharma[1,2] and *B.K. Kuanr*[1] *1. Special Centre for Nanoscience, Jawaharlal Nehru University, South West Delhi, India; 2. Department of Physics, Deshbandhu College, University of Delhi, New Delhi, India*

Recently, hybrid systems between a mechanical oscillator and atomic spins have been extensively studied to explore potential applications in classical and quantum information transfer. Strong coupling interaction can be influenced by the position of magnetic material on the resonator. In the present work, the correlation between the coupling strength (g) and photon/magnon dissipation rate (k_p/k_m) at different position of the hybrid system have been investigated based on the strong coupling regime($g>k_p,k_m$) and Purcell regime ($k_m>g>k_p$). Control of different coupling interaction was achieved via a 5 GHz photon mode (nested meta-resonator Split Ring Resonator, SRR) to the spinwave magnon mode (Yttrium Iron Garnet bulk). A new meta-resonator structure was designed to achieve high Q factor and high electric field density by using multi-ring with an extended length of single SRR as shown in Fig. 1. In Fig. 2, Positions A, B and C are selected to demonstrate strong coherent and dissipative photon-magnon coupling. When YIG disc was positioned at A and B (Fig. 2(a-b)), rf-magnetic field of the nested SRR reaches its maximum, a strong coherent coupling strength of 474 MHz and 699MHz respectively was obtained due to the direct overlap of the nested SRR and magnon modes. To achieve strongly dissipative photon-magnon coupling, we consider the interaction of traveling waves with the magnon modes. For this purpose, we place the YIG disc near the output microstrip line of the design (Fig. 2(c)). In this configuration, the direct coherent coupling is suppressed, while the in direct dissipative coupling (g=378 MHz) is sustained by traveling waves in the output microstrip line. Hence, the dissipative coupling does not give the strong coupling regime in passive magnonic systems. This was further justified by determining the cooperativity (C) of different hybrid subsystems. We observed that for coherent coupling C >1 whereas for dissipative coupling C <1 as obtained for position A (C=2.2), position B (C=1.56) and position C (C=0.82), respectively.

[1] Rao, J et.al, (2023). *Physical Review Letters*, *131*(10), 106702. [2] Kaffash, M. et.al, (2022). *Quantum Science and Technology*, *8*(1), 01LT02. [3] Ma, Z., et.al, *Applied Physics Letters*, *121*(19).

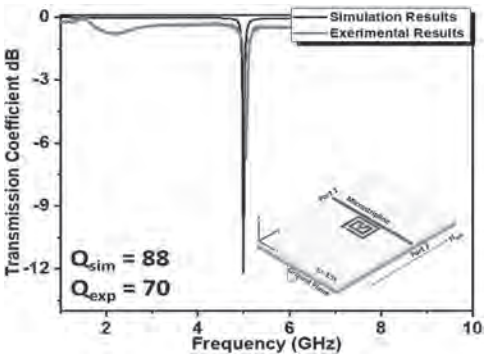

Fig. 1: Experimental and simulated response of nested meta-resonator (inset: designed diagram)

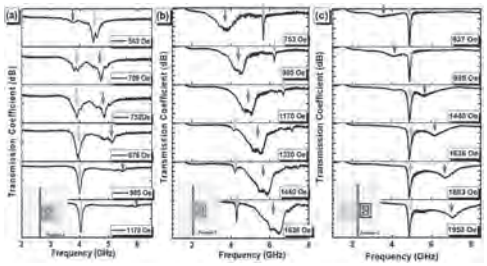

Fig. 2: (a-c). Transmission Coefficient of the hybrid system at different position A, B, C (as shown in inset)

GG-14. Spin Dynamics in the Floating Phase of a Frustrated Spin-5/2 Chain Magnet. *Q. Huang*[1], A.B. Niraula[1], D. Dahlbom[2], B. Thipe[1], G. Granroth[2], B. Winn[2], A. Aczel[2], J. Chen[1], S. Stadle[1], D. Young[1], K. Barros[3], X. Tao[4,5], J. Zhang[6], S. Calder[2], C. Batista[7] and X. Bai[1] *1. Department of Physics and Astronomy, Louisiana State University, Baton Rouge, LA, United States; 2. Oak Ridge National Laboratory, Oak Ridge, TN, United States; 3. Los Alamos National Laboratory, Los Alamos, NM, United States; 4. State Key Laboratory of Crystal Material, Jinan, China; 5. Institute of Crystal Materials, Jinan, China; 6. Shandong University, Jinan, China; 7. Department of Physics and Astronomy, University of Tennessee, Knoxville, TN, United States*

The antiferromagnetic Heisenberg spin chain is one of the most important models in quantum magnetism. Frustration induced by competing interactions is the key to the formation of novel phases and new quantum critical points. For instance, the J1-J2 spin-1/2 chain realizes a dimerized phase when the ratio of J2/J1 is larger than 0.24 [1]. While in the spin-1 chain, the same frustrated J1-J2 model does not produce a dimerized phase. Instead, it realizes the topologically non-trivial Haldane phase at small J2 [2], and an exotic ground state associated with two inter-twinned Haldane chains at large J2 [3]. Conventional wisdom is that large spin leads to classical behavior. This might be the case for three-dimensional systems, but the physics of quantum spin chains is qualitatively different. There has been a steady stream of theoretical studies for frustrated spin chains with large spins. A very recent

DMRG study for spin-5/2 chains predicted a critical floating phase, which is primarily a consequence of J1-J2 frustration [4]. This phase is characterized by quasi-long-range incommensurate correlations and the dominant wave vector is not "frozen" to any specific value, but so-called "floats" or changes continuously all over the phase. The nature of its elementary excitations is largely unknown, except that it should be gapless. We identified Bi3FeMo2O12 (BMFO) as an ideal candidate for performing inelastic neutron scattering (INS) and gaining further insight into the collective spin dynamics in the floating phase. In this talk, we will present the results of INS measurements on BFMO across various temperatures. A Heisenberg model was used to simulate the INS data with linear spin-wave theory (LSWT). As shown in Fig. 1, the INS spectra at the base temperature of 1.5 K revealed a continuum feature, indicating possible quantum fluctuations in this large-spin system. Additionally, the spectra at higher temperatures displayed the temperature evolution of the spin dynamics, enabling a discussion of the phase transitions within the system.

[1] Okamoto, K. and Nomura, K. Physics Letters A, 169(6), 433-437 (1992). [2] Haldane, F.D.M. Physics Letters A, 93(9), 464-468 (1983). [3] Kolezhuk, A.K. and Schollwöck, U. Physical Review B, 65(10), 100401, (2002) [4] Chepiga, N., Affleck, I. & Mila, F. arXiv 2202.05087

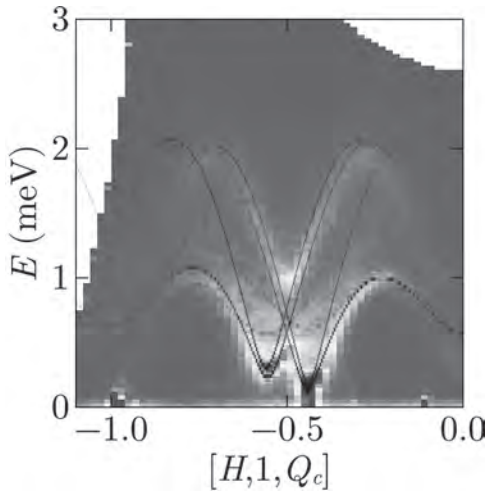

Fig. 1 The INS spectra along [H 0 0] direction measured at 1.5 K. The black lines represent the results of LSWT simulation with a Heisenberg model.

GG-15. Reexamination of the Electronic Phase Diagram of Doped NiS_2: Electronic, Magnetic, and Structural Inhomogeneity across the Mott Insulator-Metal Transition. *Y. Tao*[1], B. Das[1], S. Calder[2], E. Day-Roberts[1], M. Maiti[1], Y. Lee[1], C. Komar[1], T. Birol[1] and C. Leighton[1]
1. Chemical Engineering and Materials Science, University of Minnesota, Minneapolis, MN, United States; 2. Neutron Scattering Division, Oak Ridge National Laboratory, Oak Ridge, TN, United States

Pyrite-structure NiS_2 is a model antiferromagnetic (AF) Mott insulator that can be electron doped, hole doped, and bandwidth controlled. Despite decades of study, the electronic and magnetic behavior of NiS_2 have proven challenging to understand. Here, we build on recent advances establishing surface conduction in NiS_2 [1-3] to completely reexamine the electronic phase behavior of electron- and hole-doped $Ni_{1-x}Cu_xS_2$ and $Ni_{1-x}Co_xS_2$ [4]. Single-crystal magnetometry, heat capacity, neutron diffraction, and electronic transport measurements suggest that prior work overlooked vital details of the magnetic ordering in this system. While electron and hole doping rapidly increase the AF ordering temperature (T_{ND}) by ~4-fold at $x \approx 0.1$, signatures remain of AF and weak ferromagnetic (WF) ordering at the same temperatures (T_N and T_{wf}) as in undoped NiS_2 (Fig. 1). As T_N and T_{wf} remain constant, the associated magnetic moments (M_{wf}, Fig. 1) are diminished by doping, strongly implicating electronic/magnetic phase coexistence across the Mott insulator-metal transition (Fig. 2). Substantial structural changes and inhomogeneity accompany these evolutions, highlighting the importance of structural-chemical-electronic-magnetic coupling in NiS_2. The insulator-metal transition is also strongly electron/hole asymmetric (Fig. 1), which we interpret *via* dynamical mean-field theory results. These findings significantly revise and advance our understanding of the electronic phase behavior of this prototypical Mott insulator, highlighting the essential role of electronic, magnetic, structural, and chemical inhomogeneity across the Mott transition. Work supported by DOE through the University of Minnesota (UMN) Center for Quantum Materials (DE-SC0016371), and ENRTF. Parts of this work were conducted in the UMN Characterization Facility, supported by NSF MRSEC (DMR-2011401).

[1] S. El-Khatib, B. Voigt, B. Das, A. Stahl, W. Moore, M. Maiti, and C. Leighton, *Phys. Rev. Mater.* 5, 115003 (2021). [2] R. Hartmann, M. Hogen, D. Lignon, A. K. C. Tan, M. Amado, S. El-Khatib, M. Egilmez, B. Das, C. Leighton, M. Atature, E. Scheer, and A. Di Bernardo, *Nanoscale* 15, 10277 (2023). [3] S. El-Khatib, F. Mustafa, M. Egilmez, B. Das, Y. Tao, M. Maiti, Y. Lee, and C. Leighton, *Phys. Rev. Mater.* 7, 104401 (2023). [4] Y. Tao, B. Das, S. Calder, M. Maiti, Y. Lee, C. Komar, T. Birol, and C. Leighton, unpublished (2024).

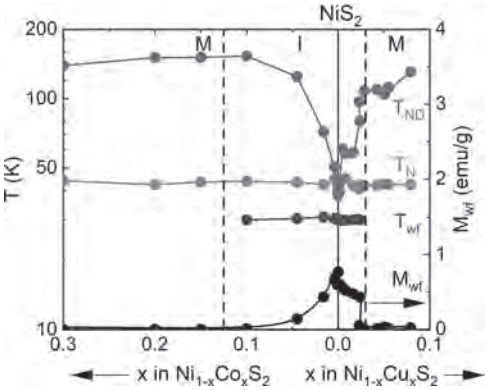

Fig. 1. New magnetic phase diagram of hole (Co) and electron (Cu) doped NiS_2. T_{wf}, T_N, and T_{ND} are plotted. The right axis shows M_{wf}. Vertical dashed lines mark the Mott insulator (I)-metal (M) transition boundaries.

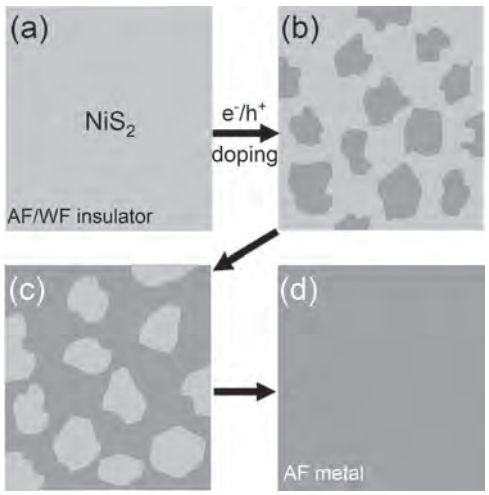

Fig. 2. Schematics of the proposed phase evolution of NiS_2 with electron or hole doping, through a regime of electronic/magnetic phase coexistence.

Session GP
HARD MAGNETS IV & MATERIALS WITH COUPLED MAGNETIC PHENOMENA II (Poster Session)

Christopher D. Woodgate, Chair
University of Warwick, Coventry, United Kingdom

GP-01. Intrinsic hard magnetic properties and thermal stability of a $ThMn_{12}$-type permanent magnet. *N. Batnyam*[1] and D. Odkhuu[1]
1. Physics, Incheon National University, Yeoun-su, The Republic of Korea

Titanium is known to be the most favorite stabilizing element in replacing Fe within the $ThMn_{12}$-type permanent magnets; however, it degrades the permanent magnetic properties rapidly. Consequently, minimizing the amount of Ti is imperative for tailoring the desired magnetic properties in $Sm(Fe,Ti)_{12}$ magnets while retaining the structural stability. In this presentation, the density functional theory, density functional perturbation theory, and Monte Carlo simulations are systematically used to investigate the impact of additional M substitutional elements on the thermodynamic stability and intrinsic magnetic properties in $SmFe_{11}Ti_{0.5}M_{0.5}$ phase (M is a 3*d* or 3*p* metal element). It is predicted that Ni and Al, among the M substitutional atoms, not only stabilize the $ThMn_{12}$ phase but also enhance saturation magnetization $\mu_0 M_s$ and magnetocrystalline anisotropy K_u, and thus the maximum energy density product $(BH)_{max}$. More specifically, $SmFe_{11}Ti_{0.5}Al_{0.5}$ phase exhibits the highest $\mu_0 M_s$ value of 1.4 T and K_u of 16.3 MJ m^{-3}, which are higher than those of $SmFe_{12}$ (1.6 T and 12.3 MJ m^{-3}) and $SmFe_{11}Ti$ (1.3 T and 10.1 MJ m^{-3}). Furthermore, the temperature dependent intrinsic magnetic properties and Curie temperatures of $SmFe_{12}$, $SmFe_{11}Ti$, $SmFe_{11}Ti_{0.5}Co_{0.5}$, and $SmFe_{11}Ti_{0.5}Al_{0.5}$ compounds will be discussed in comparison with the available experimental data. This work is supported by the US Office of Naval Research (ONR), Office of Naval Research Global (ONRG) and Army International Technology Center, Indo-Pacific (ITC-PAC) under the ONRG grant N62909-22-1-2045.

GP-02. Bulk Anisotropic Nanograin $Sm_{0.4}Pr_{0.6}Co_5$ Magnets with Excellent Energy Product. W. Liu[1], L. Zhang[1], Z. Wang[1], L. Liu[1], *Y. Li*[1] and M. Yue[1] *1. Beijing University of Technology, Beijing, China*

Rare earth permanent magnet materials are widely used in various modern scientific and technological fields. In recent years, the rapid development of application fields such as wind power generation and electric vehicles requires permanent magnets to bear high coercivity and good thermal stability. Nanocrystalline permanent magnets have attracted the attention of researchers due to their strong pinning and easy acquisition of high coercivity, as well as their rich magnetic behavior, which also provides ideas for the development of new rare earth permanent magnet materials. The $SmCo_5$ compound shows superior magnetocrystalline anisotropy field and good thermal stability. However, its saturation magnetization (10.4 kG) is low, which is not conducive to obtaining high magnetic energy product, which will restrict the miniaturization of corresponding devices. In this study, nanograined $(Sm,Pr)Co_5$ magnet was prepared by replacing some Sm with Pr, due to the $PrCo_5$ compound has a high saturation magnetization of 12.5 kG[1-3]. The anisotropic $Sm_{1-x}Pr_xCo_5$ (x=0.2-0.6) magnets were prepared by hot pressing and hot deformation method. In general, $I_{(002)}/I_{(111)}$ peak intensity contrast can be used to quantify the c-axis texture strength of $RECo_5$ magnet. According to the XRD pattern, with the substitution amount x increases, $I_{(002)}/I_{(111)}$ increases, the maximum value was 3 at x=0.6, and the c-axis texture increases. Hence, the hot deformed magnet with a substitution amount of 60% exhibits optimal c-axis texture. As x increases, the remanence of the magnet gradually increases, due to the improvement of saturation magnetization and the optimization of c-axis texture. Besides, as x increases, the coercivity gradually decreases due to the lower magnetocrystalline anisotropy field of $PrCo_5$ compared to $SmCo_5$. As a result, the hot-deformed $Sm_{0.4}Pr_{0.6}Co_5$ magnets bear maximum energy product of 22 MGOe and a higher coercivity of 12 kOe. Our findings can provide reliable references for the development of high-performance nanocrystalline permanent magnet materials.

[1] O. Gutfleisch, M.A. Willard, E. Bruck, Magnetic materials and devices for the 21st century: stronger, lighter, and more energy efficient, Adv. Mater. 23, 821–842 (2011). [2] S.Q. Liu, Sm-Co high-temperature permanent magnet materials, Chin. Phys. B 28, 017501(2019). [3] A.M. Gabay, Y. Zhang, G.C. Hadjipanayis, Hot-pressed and die-upset Pr-co magnets produced from mechanically activated alloys, J. Magn. Magn. Mater. 294, 287–293(2005).

GP-03. Enhancing intrinsic permanent magnetic properties of $ThMn_{12}$-type $Sm(Fe_{1-x}Co_x)_{11.5}Ti_{0.5}$ through interstitial B, N, and C elements. *S. Dorj*[1,2], T. Namsrai[1], J. Narmandakh[2], O. Tumentsereg[3], O. Khorgolkhuu[4] and O. Dorj[1,3] *1. Department of Physics, National University of Mongolia, Ulaanbaatar, Mongolia; 2. Institute of Physics and Technology, Mongolian Academy of Sciences, Ulaanbaatar, Mongolia; 3. Department of Physics, Incheon National University, Incheon, The Republic of Korea; 4. National Institute for Computational Sciences, Oak Ridge, TN, United States*

The $ThMn_{12}$-type $SmFe_{11}Ti$ has been recognized as a possible contender for high-performance permanent magnets thanks to its saturation magnetization, uniaxial magnetocrystalline anisotropy, Curie temperature, and anisotropy field. The early transition metal Ti stabilizes the $ThMn_{12}$ phase but significantly reduces its permanent magnet performance, thus needs to be minimized. In this presentation, we report the crucial effects of interstitial B, N, and C atoms on the intrinsic permanent magnetic properties and thermal stability of $SmFe_{11.5}Ti_{0.5}$ alloy with reduced Ti content using the density functional theory, density functional perturbation theory and Monte Carlo simulations. It is predicted that the presence of all interstitial elements considered (B, N, and C) can improve the permanent magnetic properties of $SmFe_{11.5}Ti_{0.5}$ phase, including saturation magnetization up to about 10%, while maintaining thermal stability, which are superior to those of the well explored $SmFe_{11}Ti$ phase. Our calculations further demonstrate that the permanent magnetic properties of $SmFe_{11.5}Ti_{0.5}B_{0.5}$ and $SmFe_{11.5}Ti_{0.5}N_{0.5}$ alloys can also be enhanced by replacing Fe with Co, in agreement with an experiment. The underlying mechanism of these results is illustrated in terms of single-particle energy spectrum analyses, and the intrinsic magnetic properties at an elevated temperature and Curie temperature are discussed in comparison with the available experimental results.

Hirayama, Y., Takahashi, Y.K., Hirosawa, S., & Hono, K. (2017). Intrinsic hard magnetic properties of Sm(Fe1-xCox)12 compound with the ThMn12 structure. *Scripta Materialia*, 138, 62-65. Ochirkhuyag, T., Hong, S.C., & Odkhuu, D. (2022). Intrinsic hard magnetism and thermal stability of a ThMn12-type permanent magnet. *npj Computational Materials*, 8, 193. Saito, T., Watanabe, F., & Nishio-Hamane, D. (2019). Magnetic properties of SmFe12-based magnets produced by spark plasma sintering method. *Journal of Alloys and Compounds*, 773, 1018-1022. Y.K. Takahashi, H. Sepehri-Amin & T. Ohkubo (2021): Recent advances in SmFe12-based permanent magnets, Science and Technology of Advanced Materials, DOI: 10.1080/14686996.2021.1913038 Tozman, P., Sepehri-Amin, H.,

Takahashi, Y.K., Hirosawa, S., & Hono, K. (2018). Intrinsic magnetic properties of Sm(Fe1-xCox)11Ti and Zr-substituted Sm1-yZry(Fe0.8Co0.2)11.5Ti0.5 compounds with ThMn12 structure toward the development of permanent magnets. *Acta Materialia*. https://doi.org/10.1016/j.actamat.2018.05.008

GP-04. Anisotropic nanocrystalline $(Sm_{0.4}Pr_{0.6})Co_5$ permanent magnets with controllable magnetic properties. L. Liu[1], W. Liu[1], *Y. Li*[1], L. Zhang[1], Z. Wang[1] and M. Yue[1] *1. Beijing University of Technology, Beijing, China*

The development of rare earth permanent magnet materials is crucial for achieving miniaturization and light weighting of electric electromechanical devices. SmCo-based compounds possess high magnet crystalline anisotropy fields and high Curie temperatures, making them highly suitable for high-temperature applications. Newly developed nanocrystalline permanent magnets can more effectively utilize their intrinsic magnetic properties, as the abundant grain boundaries in nanocrystalline magnets can act as pinning sites to achieve high coercivity (H_{ci}). Therefore, the development of high-performance nanocrystalline SmCo permanent magnets is crucial for further promoting their high-temperature applications. In previous work, a low-temperature deformation technology was developed, achieving strong magnetic anisotropy and high coercivity through this method. However, the introduction of Sm-rich nano precipitates reduced M_r, resulting in a maximum magnetic energy product [$(BH)_{max}$] of only 14.1 MGOe [1, 2]. Another approach is to optimize the composition, utilizing the PrCo5 compound, which more easily forms c-axis textures through deformation and has a higher saturation magnetization than that of $SmCo_5$. The prepared anisotropic $(Sm,Pr)Co_5$ magnets showed magnetic properties with M_r of 9.38 kG, H_{ci} of 17.2 kOe, and $(BH)_{max}$ of 21.1 MGOe [3, 4]. Therefore, combining low-temperature deformation technology and Pr substitution is expected to further optimize the magnetic properties of nanocrystalline anisotropic magnets. This study significantly improved the magnetic properties of hot-deformed (HD) $(Sm_{0.4}Pr_{0.6})Co_5$ magnets through systematic deformation process optimization. The optimal H_{ci} and $(BH)_{max}$ of the hot-deformed magnets at 300K reached 19.7 kOe and 22.4 MGOe, respectively. At 573 K, the HD magnets still maintained a high coercivity of 9.5 kOe, with a coercivity temperature coefficient $\beta(H_{ci})$ of -0.189 %/°C and a remanence temperature coefficient $\alpha(B_r)$ of -0.031%/°C. The study also shows that by adjusting the deformation process, the HD $(Sm_{0.4}Pr_{0.6})Co_5$ magnets can achieve controllability magnetic properties, which enables the HD magnets, more flexible and adaptable for practical applications.

[1]X. C. Xu, Y. Q. Li and Z. H. Ma, Scripta materialia., Vol.178, p.34-38 (2020) [2] Y. Teng, Y. Q. Li and W. Q. Liu, Journal of Rare Earths., (2023) [3] X. C. Xu, H. G. Zhang and T. Wang, Journal of alloys and compounds., Vol.699, p.262-267 (2017) [4] X. C. Xu, Y. Q. Li and Y. Teng, Materials characterization., Vol.173, p.110942 (2021)

GP-06. Magnetic properties of $Sm_2Fe_{17}N_3$ at low temperature. I. Nlebedim[1] and *X. Liu*[1] *1. Division of Critical Materials, Ames National Laboratory, Ames, IA, United States*

Although Nd-Fe-B is the most powerful magnet, its Curie temperature (586K) and spin re-orientation (136K) limit the suitability for applications above 400K or below150K. In this work, we have evaluated the low-temperature hard-magnetic performance of $Sm_2Fe_{17}N_3$, with typical grain size of 2-3mm. From 295–20K and 20K, the coercivity increases linearly from 12–30kOe. The correlation between coercivity and the magnetocrystalline anisotropy field can be described by a 'Kromuller formula' ($H_{ci}(T) = \alpha H_A(T) - N_{eff} M_s(T)$) microstructure parameter(α)=0.156; effective demagnetization constant(N_{eff})=0.7. Combining experiments and micromagnetic simulation, we identified that the coercivity in $Sm_2Fe_{17}N_3$ particles is controlled by nucleation of the reversal magnetic domain. Also, the maximum energy product increases from 35–41MGOe with a decreasing temperature (295–145K), and remains almost unchanged afterwards. Therefore, in addition to its suitability for applications around room temperature, $Sm_2Fe_{17}N_3$- based magnet also has potential for low-temperature applications such as magnetic refrigeration for the liquefaction of natural gas and hydrogen.

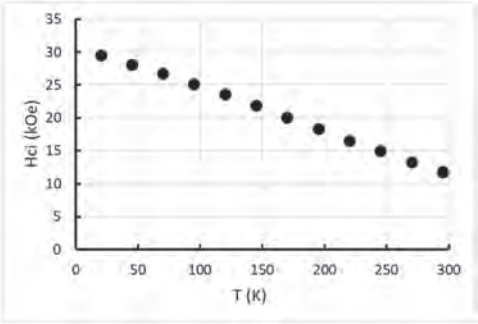

Fig. 1

Session GQ
SPIN-ORBITRONICS II: ANTIFERROMAGNETS, DMI AND UNCONVENTIONAL TORQUES (Poster Session)

Daniel B. Gopman, Chair
National Institute of Standards and Technology, Gaithersburg, MD, United States

GQ-01. Current-induced field-free magnetization switching in the MXene-based Cr_2N/(Co/Pt) multilayer structure. *P. Kumar*[1] and S. Isogami[1] *1. National Institute for Materials Science, Tsukuba, Japan*

In recent decades, transition metal (M = Ti, Cr, Fe, etc.) metalloids (X = C, N, B) compounds have attracted attention owing to their properties, suitable for spintronics application[1]. For example, a higher anomalous Hall conductivity, modulation of spin structures, and inter-band optical transitions are found for Co_2Mn_2C and $(Mn_4N)B$[2,3]. Considering these appealing properties, we focus on the atomically layered 2D MXene phases $M_{n+1}X_n$ (n = 1, 2, 3), which have recently grabbed attention due to a tunable bandgap, large/robust spin-orbit coupling, a stable magnetic ground state, and stable half-metallic transport properties[4]. The Cr_2N, one of the MXene phases, shown in Fig. 1, has the following properties: (i) an out-of-plane spin structure, (ii) an antiferromagnetic magnetic ground state from 85 to 500 K, and (iii) a layered structure on a suitable substrate with high crystallinity[5]. The 2D spin-orbit torque (SOT) devices are promising for high integration circuits, and the TMDC (WTe_2)[6]/graphene-based SOT devices[7,8] have been demonstrated so far. In contrast to these pioneering works, we investigated the effect of MXene as a spin source layer for the current-induced magnetization switching (CIMS), in our study. As a result, we successfully demonstrated the *field-free* CIMS at room temperature in the Hall bar devices, leading to a highly dense 2D-SOT device in the future. A multilayer film; Al_2O_3(0001) sub.// Cr_2N(5)/[Co(0.35)/Pt(0.3)]$_{x3}$/MgO(2) (in nm) was deposited using the DC/RF magnetron sputtering systems, and its CIMS is investigated with applied magnetic field (H_x) along the current channel of the Hall bar devices. The magnetization switching states are consistent with the AHE (Fig. not shown here). A typical dependency of critical switching current (J_c) on the H_x is shown in Fig. 2. We found full CIMS at $H_x \neq 0$ kOe, as shown in the inset of Fig. 2. However, the occurrence of CIMS at $H_x = 0$ kOe indicates that Cr_2N is effective for a *field-free* CIMS, which is unique to our results. Further, a detailed experimental result emphasizing such origin will be presented.

[1] Shinji Isogami *et al*., Adv. Electron. Mater. 9, 2200515 (2023). [2] Shinji Isogami *et al*., Phys. Rev. Mater. 7, 014411 (2023). [3] Shinji Isogami *et al*. J. Appl. Phys. 131, 073904 (2022). [4] Tahata Amrillah *et al*., Phys. Chem. Chem. Phys. 25, 18584 (2023). [5] Sandra Julieta Gutiérrez-Ojeda *et al*., ACS Omega 7, 33884 (2022). [6] Peng Li *et al*., Nat. Commun. 9, 3990 (2018). [7] Haozhe Yang *et al*., Nano Lett. 23, 4406 (2023). [8] Aurélien Manchon *et al*., Rev. Mod. Phys. 91, 035004 (2019).

Fig. 1: A schematic 2D layered structure for Cr_2N.

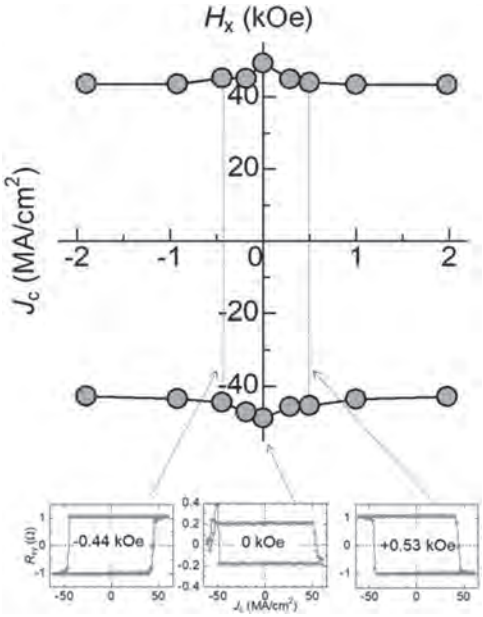

Fig. 2: J_c-H_x plot from the CIMS measurements. The inset shows CIMS hysteresis loops.

GQ-02. Enhancing Unconventional Spin-Orbit Torque Efficiency: Unraveling the Role of Polycrystalline Effects in Low-Symmetry Materials. *Y. Yang*[1] and J. Wang[1] *1. University of Minnesota, Minneapolis, MN, United States*

Unconventional spin Hall conductivity (USHC) has been observed in spin-orbit torque (SOT) materials with low crystal or magnetic symmetries [1-5]. Compared to conventional SHC, USHC exhibits higher switching efficiency for a ferromagnet with perpendicular magnetic anisotropy and enables field-free switching [6]. However, the USHC values of materials discovered so far remain low, with one significant reason being the polydomain nature of the SOT materials. Here, we discuss the influence of in-plane crystallographic orientations of SOT materials on the (U)SHC values, using Pt and Mn_3GaN as case studies. Effective (U)SHC values, considering the polycrystalline domains in a textured SOT material, are calculated based on a theoretical Gaussian orientation distribution function. The SHC of Pt remains constant regardless of the degree of polycrystallinity. In contrast, the SHC values are significantly affected for unconventional materials such as Mn_3GaN. We find that conventional SHC is less affected compared to USHC for Mn_3GaN, with a conventional SHC drop of 19% versus an out-of-plane SHC drop of 40% for an in-plane Gaussian distribution with a standard deviation of 60 degrees. This discussion provides guidance for the exploration and development of unconventional SOT materials with low symmetries, aiming to achieve higher unconventional SOT efficiency in spintronic device applications.

[1] D. MacNeill et al., Nature Physics, vol. 13, pp. 300-305 (2017). [2] T. Nan et al., Nature Communications, vol. 11, p. 4671 (2020). [3] L. Liu et al., Nature Nanotechnology, vol. 16, pp. 277-282 (2021). [4] A. Bose et al., Nature Electronics, vol. 5, pp. 267-274 (2022). [5] M. Dc et al., Nature Materials, vol. 22, pp. 591-598, (2023). [6] D. J. P. de Sousa et al., Physical Review Applied, vol. 18, p. 054020 (2022).

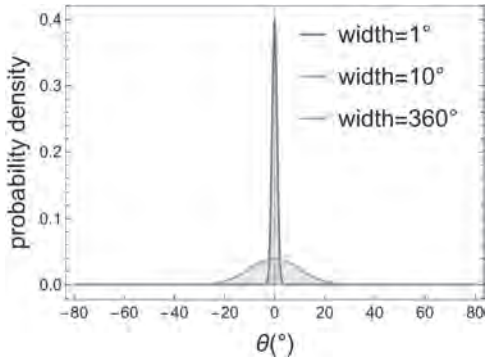

Fig. 1. Illustration of a Gaussian-shape in-plane orientation distribution function with standard deviation (width) of 1°, 10° and 360°, representing a single-crystal, textured polycrystal and random polycrystal, respectively. θ represents the orientation of grain relative to the central grain direction.

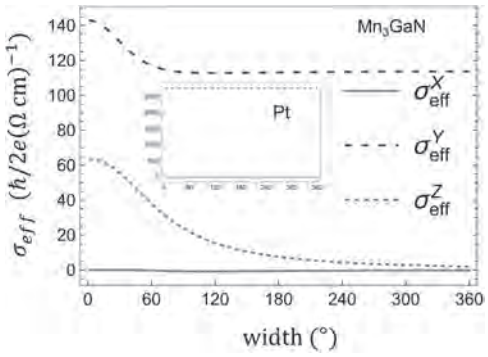

Fig. 2. Effective spin Hall conductivities of Mn_3GaN and Pt with X, Y or Z spin polarization as a function of width of the polycrystal grain distribution, where X is the charge current direction, Y is the transverse direction and Z is the out-of-plane direction. Effective spin Hall conductivity is calculated considering the polycrystalline effect, with in-plane orientation of grains following Gaussian distribution.

GQ-03. Spin Transport in Antiferromagnetic CoO Thin Films. *C. Schmitt*[1], E. Galindez Ruales[1], H. Meer[1], T. Kikkawa[2], A. Akashdeep[1], T. Kuschel[1,3], E. Saitoh[2,4] and M. Kläui[1] *1. Johannes Gutenberg University Mainz, Mainz, Germany; 2. The University of Tokyo, Tokyo, Japan; 3. Bielefeld University, Bielefeld, Germany; 4. Tohoku University, Sendai, Japan*

Insulating antiferromagnetic materials are of particular interest for the development of low power devices, as their low damping allows for the transport of pure spin currents over long distances [1, 2]. However, the efficient control of the magnetization state and spin transport in insulating antiferromagnets can be challenging due to their lack of net magnetization. In particular, the vanishing net magnetization also prevents many conventional read-out mechanisms that are based on sensing stray fields or spin-polarized currents including for instance conventional tunnelling magnetoresistance effects. However, it has been established that the readout of the orientation of the Néel vector can be realized via the spin Hall magnetoresistance (SMR) [3]. SMR depends sensitively on the interface including local proximity moments and there are different reports about the sign of the SMR for antiferromagnets. Here, we investigate angular-dependent SMR measurements in a bilayer of epitaxial CoO(001) thin films and Pt. We find that in comparison to works on NiO(001) thin films [4] the electrical signal is not a purely antiferromagnetic SMR and the interpretation of the signal and the extraction of the Néel vector can thus be challenging. We observe that contributions in addition to the antiferromagnetic SMR, such as field-induced anisotropy effects due to the unquenched orbital moments in CoO [5], exist and additional effects at the CoO/Pt interface need to be considered. It is particularly impressive that the electrical signal can be strongly altered by changing the interface properties of the CoO/Pt when inserting a Cu interlayer. This observation makes CoO a promising material for non-local spin transport experiments, especially in combination with the large unquenched orbital momentum that theoretically allows for large orbital-currents in CoO thin films.

[1] R. Lebrun, A. Ross, S.A. Bender, et al., *Nature* 561, 222–225 (2018). [2] S. Das, A. Ross, X.X. Ma, et al., *Nat. Commun*. 13, 6140 (2022). [3] G. R. Hoogeboom, A. Aqeel, T. Kuschel, et al., *Appl. Phys. Lett.* 111, 052409 (2017). [4] L. Baldrati, A. Ross, T. Niizei, et al., *Phys. Rev. B* 98, 024422 (2018). [5] M. J. Grzybowski, C. F. Schippers, O. Gomonay, et al., *Phys. Rev. B* 107, L060403 (2023).

GQ-04. ST-FMR Investigations of a WSe_2 Spin Sink. *Y. Chu*[1], K. Chiu[1] and M. Lin[1,2,3] *1. Department of Physics, National Taiwan University, Taipei, Taiwan; 2. Institute of Atomic and Molecular Sciences, Academia Sinica, Taipei, Taiwan; 3. Research Center for Applied Sciences, Academia Sinica, Taipei, Taiwan*

Spin-orbit torques (SOTs) from spin injection based on spin-orbit coupling (SOC) have become mainstream in modern spintronics. To achieve more efficient SOT effects, versatile approaches, such as material selection and interface engineering, have been attempted, which bring stronger bulk or interfacial SOC effects to the devices. Among the tactics, the reduction of spin backflow with transition metal dichalcogenides (TMDCs) underlayers as spin sinks was proposed and demonstrated along with improved device performance[1]; however, the reduction has not yet been directly verified. In this work, we demonstrate spin-torque ferromagnetic resonance (ST-FMR) studies on Pt/permalloy (Py) heterostructures with and without thick WSe_2 underlayers. Extracting the field-like and damping-like torque efficiencies as well as spin mixing conductance from Py-thickness-dependent ST-FMR measurements, we apply the spin transparency model and quantitatively acquire the spin backflow factor.[2] The results show that the backflow factor is reduced after the addition of the WSe_2 spin sink while the Pt/Py interfaces remain unaltered. Our work solidly clarifies the role of TMDC underlayers in SOT devices, which should benefit the optimization and designs of TMDC-based SOT devices. The work was supported by the National Science and Technology Council in Taiwan through grant No. NSTC 112-2112-M-002-046-MY3.

[1] H. Xue, M. Tang, Y. Zhang, Z. Ji, X. Qiu, and Z. Zhang, Adv. Electron. Mater. 8, 2100684 (2022). [2] H. Moriya, A. Musha, and K. Ando, Appl. Phys. Express 14, 063001 (2021).

GQ-05. Study of Dzyaloshinskii Moria Interaction on Magnetic Tunnel Junction-Based Molecular Spintronics Devices (MTJMSD). *B. Sankhi*[1] and P. Tyagi[1] *1. Mechanical engineering, University of the District of Columbia, Washington, DC, United States*

Magnetic Tunnel Junction-based Molecular Spintronics Devices (MTJMSD) offer significant potential for linking molecules with ferromagnetic electrodes, creating a variety of metamaterials with unique magnetic properties[1]. Understanding the complex interactions between molecules and electrode materials is essential for the progress of molecular spintronics. In this study, we utilized Monte Carlo Simulation (MCS) to explore the impact of Dzyaloshinskii-Moriya Interaction (DMI) on the MTJMSD system. Our findings indicate that DMI-treated electrodes exhibited oppositely aligned magnetic moments organized into uniform alternating bands. The molecules displayed short-range interactions with electrode spins, leading to modifications in this banded structure. Remarkably, high DMI levels resulted in the loss of net magnetization in one of the ferromagnetic electrodes, aligning with previous experimental observations[2,3]. Furthermore, we examined the

time evolution of energy for each electrode, the entire MTJMSD system, and the magnetic moments of the molecules. It was observed that the magnetic moments of the molecules significantly decreased with increasing DMI, suggesting extensive interactions between the molecules and DMI-treated electrodes. Our study underscores the importance of investigating antisymmetric interactions, such as DMI, within the MTJMSD system, highlighting their critical role in defining the magnetic and electronic properties of these advanced spintronic devices.

[1] P. Tyagi, "Multilayer edge molecular electronics devices: a review," *Journal of Materials Chemistry,* vol. 21, no. 13, pp. 4733-4742, 2011. [2] M. Savadkoohi, C. D'Angelo, A., P. Tyagi, "Impact of ferromagnetic electrode length and thickness on Magnetic Tunnel Junction-Based Molecular Spintronic Devices (MTJMSD)," *Organic Electronics,* vol. 102, p. 106429 [3] E. Mutunga, C. D'Angelo, and P. Tyagi, "Magnetic molecules lose identity when connected to different combinations of magnetic metal electrodes in MTJ-basedmolecular spintronics devices (MTJMSD)," *Scientific Reports,* vol. 13, no. 1, p. 16201, 2023.

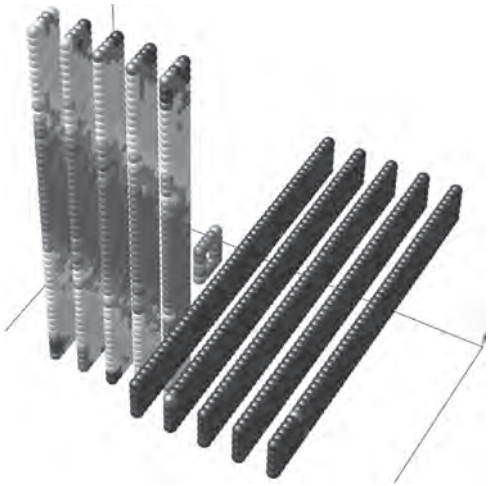

Fig.1 Simulated 3D Lattice plots of magentic tunnel junction based moelcular spintronics device (MTJMSDs) at equilibrium for DMI=0.1, Molecule-left elctrode exchange interaction (J_{mL})=1 and molecule-right electrode exchange interation (J_{mR})=-1. In this configuration, square shaped molecule is placed in between left and right electrodes.

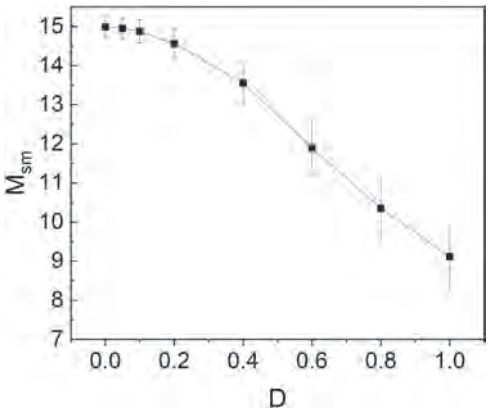

Fig.2 Molecular spin moments as a funtion of DMI values.

GQ-06. Median Mishaps between Chirality and Spin-Orbit Torques via Asymmetric Hysteresis. M. Kim[1,2] and *D. Kim*[1] *1. Korea Institute of Science and Technology, Seoul, The Republic of Korea; 2. Seoul National University, Seoul, The Republic of Korea*

Averaged observations of physical phenomena have been utilized for comprehending specific occurrences in nature; however, these may overlook the crucial characteristics of individual events, thereby leading to diverse conclusions. For example, individual wave occurrences such as superposition and interference yield markedly divergent outcomes when viewed in detail. Similarly, this study enhances the comprehensive framework of spin-orbit torque (SOT) within the hysteresis loop shift measurement by employing the average of effective magnetic fields arising from two distinct magnetic reversals. This approach facilitates the presentation of a physically descriptive SOT model, previously characterized only by single chirality qualitatively. By integrating this model with established measurement methodologies and theoretical paradigms, we advance a theoretical framework based on the magnetic domain-wall chirality of individual polarizations and aim to elucidate the phenomena of SOT with clarity. The anticipated outcomes include the rectification of inaccuracies in widely employed measurement methodologies and the enhancement of our comprehension of the fundamental physics, which are expected to propel advancements in next-generation spintronics materials and devices.

GQ-07. Spin-Orbit Torques in Permalloy Films with Shape-Induced High-Order Magnetic Anisotropy. *A. Zaig*[1] *1. Physics, Bar-Ilan University, Ramat Gan, Israel*

Using bilayer films of β-Ta (5 nm)/$Ni_{0.8}Fe_{0.2}$ (2 nm), we fabricate structures with various types of shape-induced anisotropy. The structures are in the form of a single ellipse, two crossing ellipses and three crossing ellipses that exhibit effective uniaxial, bi-axial, and tri-axial magnetic anisotropy, respectively [1, 2]. We study spin-orbit torques (SOTs) in these devices with first- and second-order harmonic Hall measurements for current flowing along the long axis of the ellipses and an external magnetic field applied in the film plane. Previously we have shown that in the single ellipse the SOT efffective field exhibits giant enhancement associated with magnetization reversal, and we derived a modified equation that considers the low-field limit where the magnetization does not align with the direction of the applied field. Fig. 1 below displays our main results, a giant response to the SOT field, by the sharp spikes of the second-order harmonic Hall signal around the transition as predicted from Stoner's Wahlfarth model of single-domain ferromagnets. Here, we study the applicability of the modified equation for the structures consisting of two and three crossing ellipses where the magnetic anisotropy is of higher order and the magnetization is not uniform. We discuss whether it is enough to consider the non- uniformity of the magnetization by averaging or rather the existence of magnetization gradients has by itself a noticeable effect on the measured SOTs.

[1] Shubhankar Das, Ariel Zaig, *Scientific Reports* volume 9, Article number: 20368 (2019). [2] Shubhankar Das, Ariel Zaig, *Appl. Phys. Lett.* 116, 262405 (2020). [3] Zaig Ariel, Das Shubhankar, Physical Review B 106, 214401 (2022).

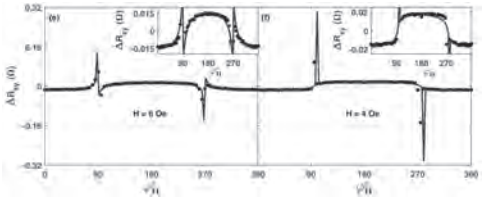

Fig. 1: The second-order harmonic Hall signal as a function of external magnetic field angle. The insets present the harmonic Hall signal without the transitions regimes.

GQ-08. Temperature Dependence of Dzyaloshinskii-Moriya Interaction in Pt/Co/Gd Thin Films. F. Wei[1], Y. Zhou[1], W. Zhang[2] and *S. Kang*[1]
1. Shand University, Jinan, China; 2. Weifang University, Weifang, China

Magnetic skyrmions generated in an antiferromagnetically (AFM) coupled system have attracted considerable interest and offer potential advantages for spintronic devices. Due to negligible dipolar fields, these skyrmions enable reduced skyrmion-Hall effects and smaller skyrmion sizes for ultra-high-density information storage. However, the Dzyaloshinskii-Moriya interaction (DMI) is a crucial factor in such materials, determining the stability and dynamic characteristics of chiral spin structures like skyrmions. Here, we focus on a Pt/Co/Gd trilayer thin film system with AFM coupling and investigate the temperature dependence of DMI using a wavevector-resolved Brillouin light scattering (BLS) spectrometer. Fig. 1a illustrates the magnetization of Pt(4 nm)/Co(1 nm)/Gd(2 nm) films. Due to the AFM coupling between Co and Gd layers, the total magnetization decreases with decreasing temperature. The compensation temperature, where the total magnetization exhibits a minimum value, is around 50K. As the temperature further decreases, the total magnetization starts to increase as the magnetization of Gd increases more rapidly compared to that of Co. Fig. 1b shows the temperature dependence of interfacial DMI in the Pt(4 nm)/Co(1 nm)/Gd(2 nm) film. It is clear that the interfacial DMI intensity initially increases with decreasing temperature, peaking at around 45K with a maximum value of approximately 3.21 mJ/m^2. We further clarify that this behavior is strongly related to the temperature-driven perpendicular anisotropy in this system by anomalous Hall effect (AHE) measurements. Moreover, our results can qualitatively explain the observed most stable skyrmions in Co/Gd/Pt multilayers at the low temperature of 70K[1].

[1] X. Wang et al., Phys. Rev. Mater. 6, 084412 (2022).

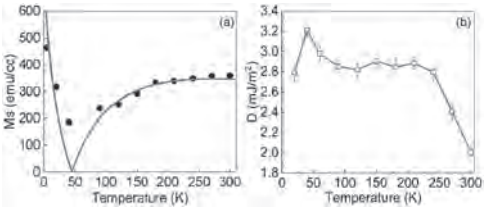

Figure 1 (a) the total magnetization and (b) interfacial DMI energy of Pt(4 nm)/Co(1 nm)/Gd(2 nm) trilayer system as a function of temperature.

Session GR
MAGNETOELECTRIC MATERIALS AND PHENOMENA III & SPINTRONIC DEVICES III: STT/SOT MRAMS AND SWITCHING DYNAMICS
(Poster Session)

Xiaoyu (Criss) Zhang, Chair
Northeastern University, Boston, MA, United States

GR-01. Room Temperature Ferromagnetism in Transition-Metal-Doped ZnO Semiconductors Induced by Tunable Bound Magnetic Polarons.
A. Alsmadi[1] and B. Salameh[1] *1. Physic Department, Kuwait University, Sabah Al Salem University City. Kuwait, Kuwait*

Searching for semiconductor materials with tunable room-temperature ferromagnetism (RTFM) remains an outstanding goal for future spintronic devices. Previous investigations have confirmed the observation of RTFM in ZnO-based magnetic semiconductors, but the role of the intrinsic defects in mediating this ferromagnetism is still debated [1-3]. In this work, we prepared a series of high-quality TM-doped ZnO films (TM = Ni, Co, Mn, Cu) and investigated the role of these complex defect states on their magnetic ordering. The defect states were analyzed through systematic photoluminescence and X-ray photoelectron spectroscopy measurements. The concentrations of the defects were controlled by annealing the prepared films in different atmospheres (vacuum, hydrogen-rich, and oxygen-rich). Our new results showed that vacuum and hydrogen annealing enhanced oxygen vacancies (V_O) and zinc interstitials (Zn_i), leading to improved and tunable RTFM, while oxygen-rich annealing reduced V_O and Zn_i, resulting in weaker RTFM. The magnetic ordering mechanism is explained by the Bound Magnetic Polarons (BMPs) model, with long-range ferromagnetic coupling between TM ions mediated by intrinsic V_O and Zn_i defects through TM^{+2}-V_O-TM^{+} and TM^{+2}-Zn_i-TM^{+} defect complexes.

[1] T. Dietl, et. al., Science 287, 1019-1022 (2000) [2] A. M. Alsmadi, et. al., J. Phys. Chem. C 124, 16116 (2020) [3] A. M. Alsmadi, et. al., Phys. Rev. B 108, 054444 (2023)

GR-02. Magnetotransport Properties of $NiFe_{1+x}Mn_{1-x}Al$ Heusler Alloys.
S. Diallo[1], P. Shand[1], P. Lukashev[1], P. Kharel[2], G. Baker[2], J. Wysong[2] and B. Schmidt[1] *1. Physics, University of Northern Iowa, Cedar Falls, IA, United States; 2. Chemistry, Biochemistry and Physics, South Dakota State University, Brookings, SD, United States*

Heusler alloys have undergone extensive examination over the past two decades, both experimentally and theoretically, owing to their promising applications in the burgeoning field of spintronics. This presentation discloses the outcomes of a comprehensive investigation into the Heusler compound Nickel Iron Manganese Aluminum ($NiFe_{1+x}Mn_{1-x}Al$), which integrates theoretical analyses and calculations with experimental findings. This study compares the magnetic and electronic properties of NiFeMnAl for x = 0 and x = 0.25. In NiFeMnAl (x = 0), a dramatic increase in longitudinal resistance is observed at approximately 350 K, while for x = 0.25, this increase is absent. Additionally, the magnetoresistance is negative at lower temperatures for x = 0 but gradually becomes positive as the temperature approaches the upturn in resistance. In contrast, for x = 0.25, the magnetoresistance remains negative throughout the entire temperature range. It is likely that the change in the sign of magnetoresistance in the x = 0 sample is associated with the sharp upturn in longitudinal resistance. Furthermore, the sign of the current carriers also changes near the resistance upturn in the x = 0 sample. It is hypothesized that these changes in carrier sign and magnetoresistance are due to a significant shift in the distribution of current carriers of both signs, influenced by the band structure of the materials. Anticipated to be valuable for researchers actively involved in the practical implementation of spin-based electronics, this study contributes to the evolving understanding of Heusler alloys and underscores $NiFe_{1+x}Mn_{1-x}Al$'s potential candidacy for advancements in spintronics, offering a promising avenue for future research and application development.

GR-04. Anomalous Hall Effect in a Room Temperature Magnetic High Entropy Alloy.
R. Roy Chowdhury[1], N. Schulz[1], E. Kasotakis[2], M. Farle[2], N. Shkodich[2], M. Phan[1] and H. Srikanth[1] *1. Department of Physics, University of South Florida, Tampa, FL, United States; 2. Universität Duisburg-Essen, Duisburg, Germany*

High entropy alloys (HEAs), composed of five or more principal elements in equiatomic or nearly equiatomic ratios in a solid solution with a high symmetry crystal structure has attracted considerable interest for their potential to design novel materials with tailored emergent properties [1]. Among them, magnetic HEAs containing one or more 3*d*-transition metals are emerging candidates owing to their versatile and tunable magnetic properties, while maintaining excellent mechanical responses such as high strength, fracture toughness, and thermal stability [2]. For designing a magnetic HEA with optimal magnetic and electronic characteristics, a clear understanding of its key properties *viz*. saturation magnetization (M_S), coercive field (H_C), and electronic resistivity is extremely important. Here, we demonstrate CoCrNiFeGa as a novel room temperature magnetic HEA and elucidate its magnetic and electronic properties. Polycrystalline CoCrNiFeGa was synthesized using high-energy ball milling of constituent elements followed by spark plasma sintering [3]. Room temperature X-ray diffraction analysis reveals that the alloy consists of 70% volume fraction of BCC ($a = b = c = 2.88$ Å) and 30% of FCC phase ($a = b = c = 3.61$ Å) respectively. Temperature (T) dependent magnetic susceptibility measurements show a Curie temperature of ~ 812 K. Spin freezing behavior below $T \sim 50$ K under applied magnetic field (H) ~ 100 Oe is also observed. Magnetic hysteresis curves show a soft magnetic behavior, with $M_S \sim 2.85$ μ_B/f.u. and coercivity $H_C \sim 70$ Oe at $T = 5$K. Saturation magnetic polarization at $T = 5$ K amounts to 0.48 T. The longitudinal resistivity exhibits metallic behavior across the entire T range. Interestingly, the Hall conductivity (σ_H) under applied H shows a saturation-like behavior, suggesting the presence of an anomalous Hall effect (AHE). $_H$ versus M_S at various T shows a linear behavior, indicating the Karplus-Luttinger origin of AHE. Furthermore, $_H$ is independent of longitudinal conductivity, hinting towards an intrinsic origin of AHE. These experimental findings introduce a novel candidate in the magnetic HEA family with intrinsic AHE, showcasing potential for HEA-based spintronics devices and applications.

[1] E. P. George, D. Raabe, and R. O. Ritchie, *Nat. Rev. Mater.* 4, 515 (2019). [2] T. Zuo, M. C. Gao, and L. Ouyang, *Acta Mater.* 130, 10 (2017). [3] N. Shkodich, F. Staab, and M. Spasova, *Materials* 15(20), 7214 (2022).

GR-05. Role of texture breaking layer on the reference layer stability of STT-MRAM devices. *J. Chatterjee*[1], S. Rao[1], R. Carpenter[1], K. Wostyn[1], A. Palomino Lopez[1] and S. Couet[1] *1. IMEC, Leuven, Belgium*

STT-MRAM devices are being investigated for last-level cache applications for which it is essential to achieve less than 1E-6 write error rate [1] for a relatively thinner magnetic tunnel junction (MTJ) stack for easy integration. Upon spin-polarized current excitation, an MTJ cell can undergo dynamic back hopping causing a write error if the reference layer (RL) is not stable. Hence the RL's stability against the applied spin torque should be improved by improving the perpendicular magnetic anisotropy and it's pinning energy with the hard layer. We will discuss the role of three different types of texture breaking layers (TBLs), such as (A) paramagnetic element, W; (B) alloy or nanolaminates between W and ferromagnetic elements (W-FM); and (C) alloy or nanolaminates between W, ferromagnetic elements, and boron (W-FM-B); on the RL's stability as well as magneto-transport properties of MTJ stack (see Fig. 1(a)) and patterned devices. It can be seen from the table (Fig 1b) that for 2.5 Å W, the pinning field of the RL ($H_{ex\text{-}PostAnneal}$) is the largest, 10780 Oe, which is reduced to 9810 Oe after patterning the MTJ stack due to process induced defect creation or interdiffusion. Fig. 1(c) exhibits canted RL reversals for both 2.5 Å W and W-FM-B based TBLs. W-FM TBLs improves the PMA of RL and a sharper RLs' reversal can be observed. Moreover, W-FM TBL helps to improve the TMR keeping a relatively large $H_{ex\text{-}PostAnneal}$. Therefore, W-FM based TBL is the best in terms of TMR, PMA and Hex of the RL. One can notice from the R(H) loops shown in Fig. 2, that W-FM-B based TBLs exhibits, a canted branch in the antiparallel resistance states indicates a weaker RL. Upon using W TBLs, the R(H) loops has become square because of improved RL's stability. Pulsed-current induced STT switching including WER characteristics for the three different flavors of TBLs will be investigated to get further insights about the RL's stability.

[1] G. Hu et al. IEDM p. 2.6.1 2019; J. G. Alzate et al. IEDM p. 2.4.1 2019.

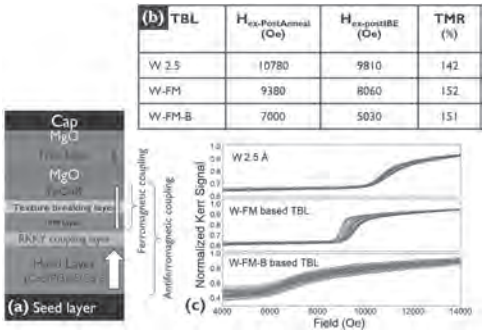

Fig.1: (a) Schematics of MTJ stacks. (b) Table listing $H_{ex\text{-}PostAnneal}$, $H_{ex\text{-}PostIBE}$ and TMR after 400°C anneal. (c) RL reversal in the descending branch of the MOKE-hysteresis loops measured 49 points across 300 mm wafer.

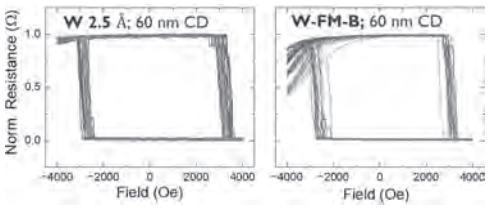

Fig.2: Normalized Average R(H) loops of 20 devices with 60 nm CD.

GR-06. Investigation of the origin of enhanced spin-orbit torque efficiency in strained Py/Pt bilayer. *A. Chouhan*[1], H.A. Mendonca[1], S. Dutta[1], A. Shukla[1], R.R. Pandey[1] and A.A. Tulapurkar[1] *1. Department of Electrical Engineering, Indian Institute of Technology Bombay, Mumbai, India*

Enhanced damping-like spin-orbit torque efficiency (ξ_{DL}) of 0.193 was observed in Py/Pt bilayers deposited on flexible polyimide substrate on application of 0.312% tensile strain [1] as shown in Fig. (1). We attempted to investigate the origin of this increase in ξ_{DL} by investigating the effect of tensile strain on spin hall conductivity (SHC) of Platinum [1], as ξ_{DL} magnitude is dependent on SHC of heavy metal which in turn is dependent on bulk properties such as Berry Curvature of band structure and extrinsic scattering effects. Using Kubo formalism [2][3], *ab-initio* calculations were performed through QUANTUM ESPRESSO package [4]. A deformative strain (ε) of 1% was applied on the FCC unit cell of Pt, to understand SHC variation with strain. Effect of strain on SHC was observed by varying Fermi energy of Pt, as is shown in Fig. (2). The calculations were carried out for three different cases – (1) no strain, ($\varepsilon_{xx} = \varepsilon_{yy} = \varepsilon_{zz} = 0$), (2) ($\varepsilon_{xx} = 0.01$, $\varepsilon_{yy} = \varepsilon_{zz} = 0$), (3) ($\varepsilon_{xx} = 0.01$, $\varepsilon_{yy} = \varepsilon_{zz} \neq 0$), ($\sigma_{xx} \neq 0$, $\sigma_{yy} = \sigma_{zz} = 0$) where σ_{xx}, σ_{yy} and σ_{zz} are the diagonal elements of the stress tensor matrix. An almost negligible 1.2% change in SHC was observed for 1% strained case compared to the non-strained case. This suggests a minimal role of strained bulk Pt and a significant role of modulated interface in enhanced values of ξ_{DL} and ξ_{FL} in strained Py/Pt bilayer as found experimentally in ref. [1]. Also, experimental results showing the role of strained Pt layer to cause switching in Perpendicular Magnetic Anisotropy systems will be presented.

[1] A. Chouhan, H. A. Mendonca, et al., "Enhanced spin–orbit torques in strained nife/pt bi-layers on flexible substrate", J.Magn.Magn.Mater. 587, 171337 (2023) [2] J. Qiao, J. Zhou, et al., "Calculation of intrinsic spin hall conductivity by wannier interpolation", Phys. Rev. B 98, 214402 (2018) [3] G.-Y. Guo, S. Murakami, et al., "Intrinsic spin hall effect in platinum: First-principles calculations", Phys. Rev. Lett. 100, 096401 (2008) [4] P. Giannozzi, S. Baroni, et al., "Quantum espresso: a modular and open-source software project for quantum simulations of materials", J. Phys.: Condens. Matter 21, 395502 (2009)

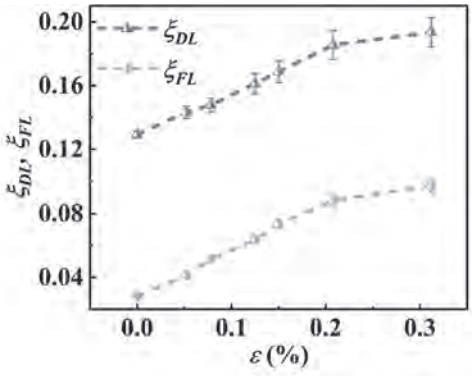

Fig. 1 ξ_{DL} and ξ_{FL} as a function of tensile strain [1]

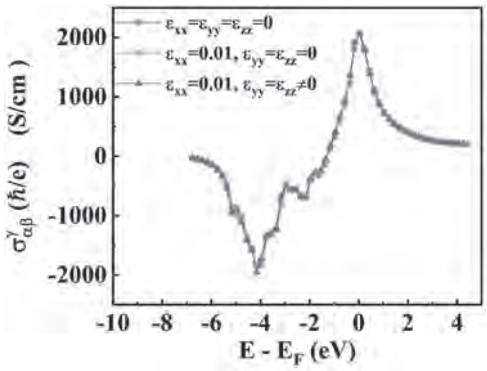

Fig. 2 SHC of Pt as a function of Fermi energy where α is the spin current direction, γ is the spin polarization direction and β is the charge current direction [1]

GR-07. Tailoring the Structural and Magnetic Properties of $LaNiO_3$ Perovskite Nanostructure via Mn Doping for Spintronic Applications.

S. K[1,2], M. Swalihu[3,4] and R. N E[1] *1. Department of Physics, Farook College, Calicut, India; 2. Department of Physics, Providence Women's College, Calicut, India; 3. Department of Physics, Catholicate College, Pathanamthitta, India; 4. International and Interuniversity Center for Nanoscience and Nanotechnology, Mahatma Gandhi University, Kottayam, India*

Lanthanum nickel oxide (LaNiO3) is a member of the perovskite oxide family. It is highly regarded for its distinctive features, including its crystal structure, high electronic conductivity, and catalytic activity.[1-6] The Mn-doped $LaNiO_3$ samples are intriguing because of the inconsistency in the valence states.[7] We investigates the structural and magnetic properties of $LaNiO_3$ and $LaNi_{0.7}Mn_{0.3}O_7$ nanoparticles. Samples were synthesised using a modified solgel method which incorporates polyvinyl alcohol as a complexing agent. An X-ray diffractometer (PANalytical) was used to study the structure. Rietveld refinement was done using the Full Prof software. Fig. 1 shows the refined XRD pattern, confirming the presence of rhombohedral form with space group R-3c. The observed peaks in the XRD patterns match the reference pattern of ICSD ref. ID no. 01-079-2451. Magnetization measurements of were carried by using a SQUID magnetometer (Quantum Design MPMSXL). At room temperature, the undoped sample exhibits no hysteresis, which suggests paramagnetic properties. Remarkably, we discovered that the doped sample demonstrates hysteresis at room temperature. Fig. 2 displays both loops, which validate the ferromagnetic characteristics of $LaNi_{0.7}Mn_{0.3}O_3$ at temperatures of 50K and 300K. In this case, the low spin and high spin states of Mn and Ni lead to both a Mn-O-Mn and Ni-O-Ni exchange interaction, as well as a Mn-O-Ni super exchange interaction, which contribute to the ferromagnetic effect. The temperature-dependent magnetization curves, were measured by following the zero-field cooled (ZFC) and field cooled (FC) protocols with 1000Oe applied fields on the sample. The result indicates the presence of ferromagnetic behaviour below 300K. Hence, it is apparent that the Curie temperature is in close proximity to 300 K. Therefore, it is feasible to tailor the magnetic state within the $LaNiO_3$ structure by using a suitable dopant in the precise composition. This manipulation results in the acquisition of outstanding magnetic properties, which hold great potential for advanced spintronic research.

[1] R. Riedel, and I.-W. Chen, Ceramics Science and Technology, Volume 2: Materials and Properties (John Wiley & Sons, 2011). [2] A. Wold, B. Post, and E. Banks, Journal of the American Chemical Society 79(18), 4911–4913 (1957). [3] F. Mahmoudi, K. Saravanakumar, V. Maheskumar, Journal of Hazardous Materials, 129074 (2022). [4] J. Zhu, H. Li, L. Zhong, Acs Catalysis 4(9), 2917–2940 (2014). [5] J.X. Flores-Lasluisa, F. Huerta, D. Cazorla-Amorós Environmental Research 214, 113731 (2022). [6] G. Sai Gautam, E.B. Stechel, and E.A. Carter, Chemistry of Materials 32(23), 9964–9982 (2020). [7] J. Sunarso, A.A. Torriero, W. Zhou, The Journal of Physical Chemistry C 116(9), 5827–5834 (2012).

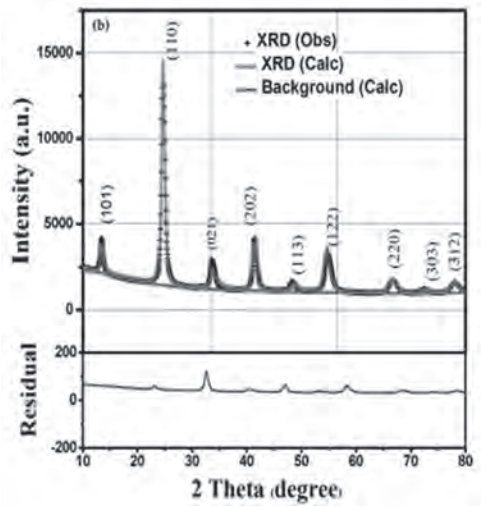

Fig. 1 XRD pattern of $LaNi_{0.7}Mn_{0.3}O_3$

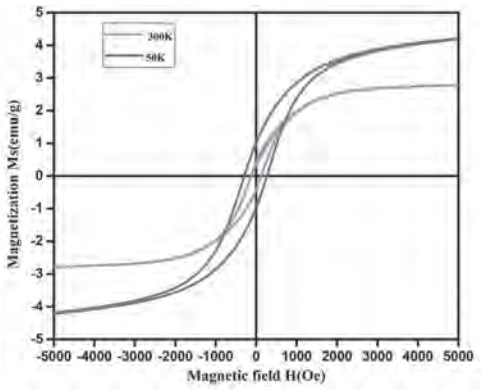

Fig. 2 M–H loops of $LaNi_{0.7}Mn_{0.3}O_3$ at 50 K and 300 K

GR-08. Innovative Trenched Bottom Electrode Molecular Devices with Gate Electrodes: Advances and Applications in Spintronics.

E. Peigney[1], H. Brown[1], B. Sankhi[1] and P. Tyagi[1] *1. NSF CREST Center for Nanotechnology Research and Education, University of the District of Columbia, Washington, DC, United States*

In traditional silicon-based microelectronic devices, high-speed data processing and storage rely on electronic switches, which control transport between source and drain by applying electric field stimuli to a gate terminal. Creating gate-controlled devices at the molecular level remains challenging even after three decades [1]. It is crucial to insulate the gate from the molecule and the source/drain electrodes to ensure the gate terminal establishes only an electrostatic coupling with the molecule to minimize gate leakage and maximize the electric field affecting the molecule. Traditional methods suffered from a low device yield (<10%) and are restricted to the use of gold [2–5]. A recent patent introduced an innovative method for fabricating gate-controlled molecular devices using standard microfabrication techniques similar to those used in CMOS devices [6]. This method, compatible with existing manufacturing industries, involves photolithography, thin layer deposition through sputtering, and argon etching. The invention specifies two potential gate locations, both involving a trench: (a) beneath the bottom electrode and (b) within the drain (see Fig. 1a and b). Molecules are positioned along the exposed trench edges. Depending on the type of molecules used, the final product can exhibit a range of properties. Single-Molecule Magnets (SMMs) were employed, imparting magnetic characteristics to the gated device. Composed of a magnetic materials stack (NiFe, Co, etc.), these devices were characterized topologically using Atomic Force Microscopy (AFM) and electrically using a custom I-V testing setup. I-V tests revealed multi-state CMOS-like behavior influenced by gate voltage. Kelvin

Probe Force Microscopy (KPFM) characterized the influence of molecules on surface potential and work function at the drain/source junction. Special attention was given to the tunnel barrier thickness, aiming to enhance the electric field and minimize leakage current.

[1] G. Ke, C. Duan, F. Huang, and X. Guo, *Electrical and Spin Switches in Single-Molecule Junctions*, InfoMat 2, 92 (2020). [2] W. Liang, M. P. Shores, M. Bockrath, J. R. Long, and H. Park, *Kondo Resonance in a Single-Molecule Transistor*, Nature 417, 6890 (2002). [3] J. A. Mol, C. S. Lau, W. J. M. Lewis, H. Sadeghi, C. Roche, A. Cnossen, J. H. Warner, C. J. Lambert, H. L. Anderson, and G. A. D. Briggs, *Graphene-Porphyrin Single-Molecule Transistors*, Nanoscale 7, 13181 (2015). [4] J. Park et al., *Coulomb Blockade and the Kondo Effect in Single-Atom Transistors*, Nature 417, 722 (2002). [5] H. Song, Y. Kim, Y. H. Jang, H. Jeong, M. A. Reed, and T. Lee, *Observation of Molecular Orbital Gating*, Nature 462, 1039 (2009). [6] P. Tyagi, *Trenched Bottom Electrode and Liftoff Based Molecular Devices*, US10833162B2 (10 November 2020).

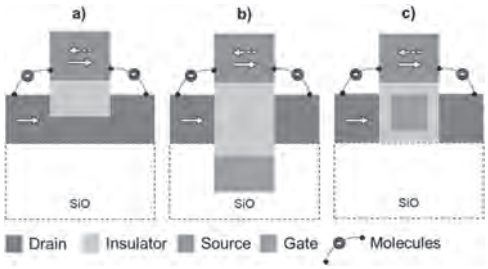

Fig. 1: Scheme of: a trenched bottom electrode device a) without and with a gate electrode b) below the bottom electrode, c) encapsulated within the drain electrode.

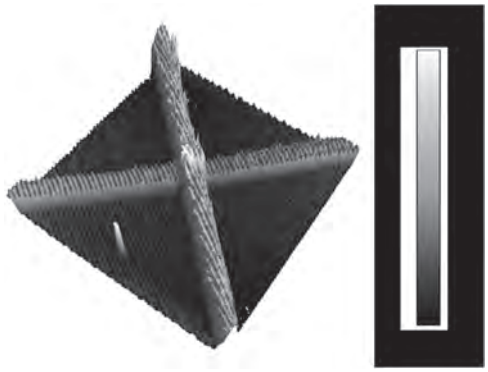

Fig. 2: AFM image of the full stack of the Fig. 1b) design.

Session GS
EMERGING COMPUTING USING MAGNETIC AND SPINTRONIC MATERIALS (Poster Session)

Gregory M Stephen, Chair
Laboratory for Physical Sciences, College Park, MD, United States

GS-02. Using Machine Learning Algorithms to Predict the Magnetic Susceptibility of Rare Earth Ions. *P. Brungi*[1], N. Carlstedt[1] and P. Andrei[1]
1. Department of Electrical and Computer Engineering, Florida State University, Tallahassee, FL, United States

Calculating the magnetic susceptibility of rare earth (RE) compounds is inherently challenging due to their complex yet similar electronic structures. In this presentation, we employ machine learning techniques to develop models that predict the magnetic susceptibility of RE compounds. Using a limited dataset of various RE halides, oxides, sulfates, and sulfides, we examine the potential of two machine learning algorithms (deep neural networks and linear regression algorithms) to uncover relationships between compound characteristics and their magnetic properties. We compare the accuracy of these algorithms and discuss the findings. The results indicate that while neural networks require extensive datasets for effective training and to avoid overfitting, linear regression provides a robust and interpretable solution for smaller datasets. Linear regression's simplicity not only facilitates easier interpretation of the results but also provides insights into the relative importance of different factors influencing magnetic susceptibility. Both algorithms incorporate various features (i.e. fingerprints) of the RE compounds, including SMILES, compound type, ionization number, and composition, to predict magnetic susceptibility. More information about how the dataset was built, the features that were used and the accuracy of the models will be discussed at the meeting. We assess the models' performance using standard metrics, emphasizing their ability to generalize across different types of RE compounds. By leveraging machine learning to analyze existing data on RE compounds, we aim to enhance our understanding of the relationships between compound characteristics and magnetic properties. This approach could accelerate the discovery and design of new materials with specific magnetic properties, opening avenues for future research and applications in material science [1]. It also underscores the value of data-driven approaches, even with constrained datasets. Future work will focus on expanding the dataset, adding more features to the models, and exploring the potential of other machine learning algorithms such as random forests, boosting, and support vector machines as more data becomes available.

[1]Y. Zhang, S. Xing, L. Wei, and T. Shi, 'Utilizing Machine Learning Models for Predicting Diamagnetic Susceptibility of Organic Compounds', *ACS Omega*, vol. 9, no. 12, pp. 14368–14374, 2024.

GS-03. Operational window of inverse temperature for accurate probabilistic computing with stochastic magnetic tunnel junctions. *H. Kaneko*[1], S. Kanai[1,2,3], H. Ohno[1] and S. Fukami[1,4] *1. Tohoku Univ., Sendai, Japan; 2. National Institutes for Quantum Science and Technology, Takasaki, Japan; 3. Japan Scienceand Technology Agency, Kawaguchi, Japan; 4. Inamori Research Institute for Science, Kyoto, Japan*

Probabilistic computing/computer (p-computing/computer) with stochastic magnetic tunnel junctions (s-MTJs) shows promise to address some computationally hard problems for conventional deterministic computers [1,2]. In p-computing, the Ising model is often used to solve problems, where the "inverse temperature" has to be set to an appropriate value; however, its guideline has not been established. Here, we study the operational window of the inverse temperature by examining the accuracy of p-computing for various types of random telegraph noise (RTN) of s-MTJs [3-8]. We investigate the accuracy of computing based on the Ising model in terms of (i) the frequent appearance of the lowest energy (E) states (correct solutions) compared to the incorrect ones in the statistics and (ii) the low variation of probabilities among the lowest energetically equivalent states. We simulate the NAND-gate operation [9] using experimentally obtained RTN of s-MTJs [8] with various statistical properties (amplitude, distribution, etc.). We also test two extreme cases: binary and continuous random numbers [Fig. 1]. The interaction between bits is implemented by sending a signal given by $-I_0\partial E/\partial x_i$ to the ith bit, where I_0 corresponds to the inverse temperature and x_i is the binary state of the ith bit. For the case of too high I_0, the system tends to stick in local minima in solution space, whereas the contrast between correct and incorrect solutions becomes weak for the case of too low I_0, giving the upper and lower bound of I_0 ($I_{0\,\mathrm{max}}^{*}$ and $I_{0\,\mathrm{min}}^{*}$, respectively). Figure 2 shows the main result of this work. Key features include (i) the operational window of I_0 decreases with decreasing the amplitude of RTN and (ii) it depends on the nature of the random telegraph noise. The obtained results provide a guideline to design the s-MTJs and operate the p-computer. This work is supported in part by JST-CREST JPMJCR19K3, JST-PRESTO JPMJPR21B2, JST-ASPIRE JPMJAP2322, and Takano Research Foundation.

[1] K. Y. Camsari *et al*., Phys. Rev. X 7, 031014 (2017)., [2] W. A. Borders *et al*., Nature 573, 390 (2019). [3] S. Kanai *et al.*, Phys. Rev. B 103, 094423 (2021)., [4] K. Hayakawa *et al.*, Phys Rev. Lett. 126, 117202 (2021). [5] K. Kobayashi *et al.*, Phys. Rev. Appl. 18, 054085 (2022)., [6] K. Y. Camsari *et al*., Phys. Rev. Appl. 15, 044049 (2021). [7] K. Selcuk *et al.*, Phys. Rev. Appl. 21, 054002 (2024)., [8] R. Ota *et al*., Appl. Phys. Lett. 125, 022406 (2024). [9] N. A. Aadit *et al.*, Nat. Electron. 5, 460 (2022).

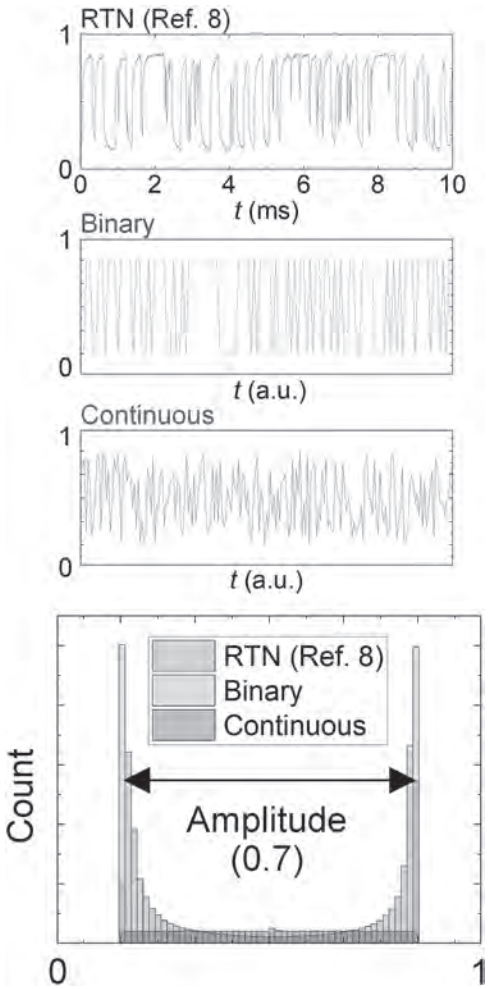

Fig. 1 Histogram and cumulative probability of RTN and binary/continuous random number.

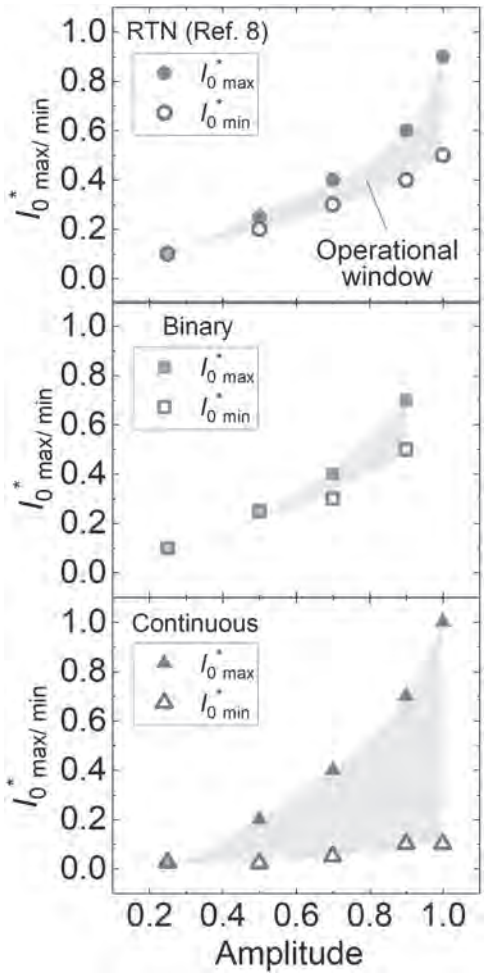

Fig. 2 Operational window of inverse temperature for various amplitudes of RTN and binary/ continuous random numbers.

GS-04. Simulation of Error Rate of and Logic Gates Made from Stochastic MTJs. S. Endo[1] and *S. Greaves*[1] *1. RIEC, Tohoku University, Sendai, Japan*

Introduction Stochastic magnetic tunnel junctions (MTJs) may be used for random number generation, or as components in a low-energy probabilistic computer [1]. Two streams of random numbers, generated by two individual MTJs, can be multiplied together using an AND logic gate. Such a gate can be implemented using a third MTJ. In this work we model the error rate of these logic gates. The model A schematic of the model is shown in fig. 1. Three identical MTJs, with a diameter of 10 nm, a pinned layer thickness of 1 nm and a free layer thickness of 2 nm were modelled using LLG micromagnetics with a Slonczewski spin torque term. The MTJs were sufficiently far apart that magnetostatic interactions were negligible. MTJs with perpendicular and in-plane anisotropy were compared. Currents J_1 and J_2 were equal and were chosen to give a 50% probability that the free layer magnetisation, M, would be less than zero when measured along the easy axis at any given time. The free layer magnetisation of MTJ1 and MTJ2 was sampled at regular intervals. The sampling interval was chosen to give statistically random bit sequences, where 0 corresponds to $M < 0$ and 1 to $M > 0$. The currents $J_{1,3}$ and $J_{2,3}$ were negative when $M < 0$ and positive for $M > 0$. J_3 was a constant current equal to J_1 - $|J_{1,3}|$. Results Fig. 2 shows the error rate of the AND gate at 300 K as a function of the currents $J_{1,3}$ and $J_{2,3}$. When $J_{1,3}$ and $J_{2,3}$ were zero the magnetisation of MTJ3 was uncorrelated with MTJ1 and MTJ2 and the error rate was around 0.5. As $J_{1,3}$ and $J_{2,3}$ increased the error rate decreased. At 300 K the minimum error rate was around 6% for MTJs with perpendicular anisotropy and 9% for MTJs with in-plane anisotropy. The in-plane MTJs had a higher error rate as larger currents were required

to ensure the free layer magnetisation remained in the intended direction. The error rate can be reduced by lowering the temperature, but this also lowers the operational speed as magnetisation fluctuations become less frequent.

[1] B. R. Zink, Y. Lv and J. -P. Wang, IEEE Journal on Exploratory Solid-State Computational Devices and Circuits, 8(2), 173-184, (2022).

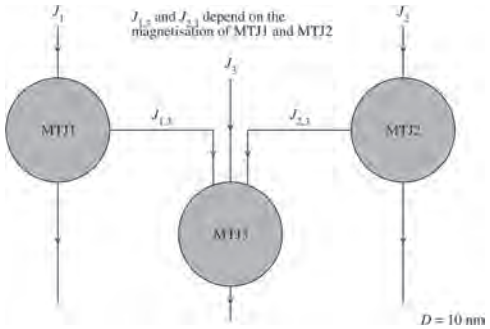

Fig. 1 Schematic of AND gate using three stochastic MTJs

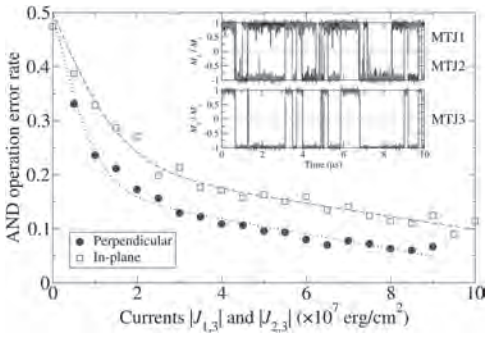

Fig. 2 AND operation error rate vs. currents $J_{1,3}$ and $J_{2,3}$ for MTJs with perpendicular and in-plane anisotropy at 300 K. Inset: example of perpendicular MTJ free layer magnetisation at 80 K

GS-05. Design of a High-Speed Vacuum Pump Motor Applying 6Phase and Harmonic Reduction. H. Han[1], I. Yang[2], D. Choi[1], S. Lee[1] and *W. Kim*[3] *1. Next Generation Smart Energy System Convergence, Gachon University, Seongnam-si, The Republic of Korea; 2. Electrical Engineering, Hanyang University, Seoul, The Republic of Korea; 3. Electrical Engineering, Gachon University, Seongnam-si, The Republic of Korea*

Recently, the semiconductor and display industries have become core sectors of the economy, focusing on maintaining high production volumes and technological prowess. In the case of vacuum pump motors, miniaturization through high power density is important which is why PMSM (Permanent Magnet Synchronous Motor) is predominantly used [1][2]. Not only high power density but also high-speed operation is a crucial factor for vacuum pump motors. High-speed vacuum pump motors can provide faster and more stable vacuum environments, thereby improving the quality and productivity of manufacturing processes. However, as the speed increases, the motor voltage also rises proportionally. This creates a trade-off relationship between voltage limitations and speed. This paper proposes a method to convert a 3phase motor for vacuum pumps into a 6phase motor to alleviate voltage limitations and enable high torque at high speeds. The 6phase can be divided into two main types [3][4][5]. the symmetric method, where each phase from Phase A to Phase F has a phase difference of 60degE (electrical degree). And the asymmetric method, where [Phase A, Phase B, Phase C] form set 1 and [Phase D, Phase E, Phase F] form set 2, with phases within each set having a phase difference of 120 degE and a phase difference of 30 degE between the sets. In the symmetric, the line voltage differs from that of a 3phase. In a 3phase system, the phases are electrically 120 degE apart, resulting in a line voltage that is √3 times the phase voltage. However, in 6phase, the phases are 60degE apart, making the line voltage that is 1 time the phase voltage. However, when converting the motor to a 6phase, new harmonics are formed in the line voltage at odd multiples of 3. To address this issue, as shown in Fig. 1, tapering of the rotor was implemented to increase the resistance of the q-axis magnetic flux path, thereby reducing these harmonics. This design change helps to mitigate the unwanted harmonics introduced by the 6phase configuration. As a result, as illustrated in Fig.1 and Fig. 2, we can observe both superior operating characteristics at high speeds and a significant reduction in harmonics.

[1] J. Fang and S. Xu, "Effects of Eddy Current in Electrical Connection Surface of Laminated Cores on High-Speed PM Motor Supported by Active Magnetic Bearings," in *IEEE Transactions on Magnetics*, vol. 51, no. 11, pp. 1-4, Nov. 2015, Art no. 8207604, doi: 10.1109/TMAG.2015.2449905. [2] M. Wei, Y. Chang, X. Song and L. Ye, "Design and thermal analysis of Permanent Magnet Synchronous Motor of Dry Vacuum Pump for Semiconductor Equipment," *2022 23rd International Conference on Electronic Packaging Technology (ICEPT)*, Dalian, China, 2022, pp. 1-6, doi: 10.1109/ICEPT56209.2022.9873510. [3] M. Onsal, Y. Demir and M. Aydin, "A New Nine-Phase Permanent Magnet Synchronous Motor With Consequent Pole Rotor for High-Power Traction Applications," in *IEEE Transactions on Magnetics*, vol. 53, no. 11, pp. 1-6, Nov. 2017, Art no. 8700606, doi: 10.1109/TMAG.2017.2709788. [4] Y. Demir and M. Aydin, "A Novel Dual Three-Phase Permanent Magnet Synchronous Motor With Asymmetric Stator Winding," in *IEEE Transactions on Magnetics*, vol. 52, no. 7, pp. 1-5, July 2016, Art no. 8105005, doi: 10.1109/TMAG.2016.2524027. [5] Jedryczka, C.; Mysinski, M.; Szelag, W. Development and Analysis of Six-Phase Synchronous Reluctance Motor for Increased Fault Tolerance Capabilities. Energies 2024, 17, 2351.

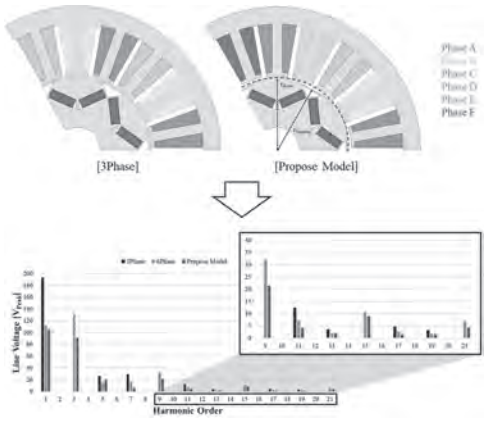

Fig. 1: Propose model geometry and harmonic analysis

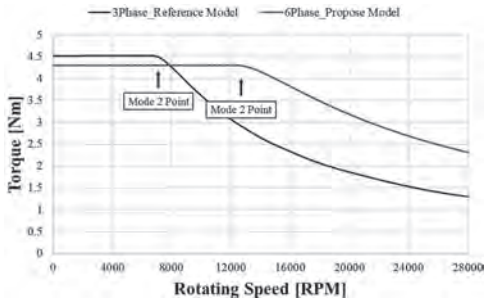

Fig. 2: Compare T-N Curve

GS-06. Research on Reducing Cogging Torque and Torque Ripple by Changing the Shape of Permanent Magnet in Large Ship Motor.
S. Jeon[1], D. Choi[1], Y. Song[1], S. Lee[1] and *W. Kim*[1] *1. Next Generation Smart Energy System Convergence Major, Gachon University, Seongnam, The Republic of Korea*

As global energy consumption increases and environmental regulations become stricter, the need for high-performance, efficient electric motors is growing. Motors used in large ships require high torque and output, making PMSMs (Permanent Magnet Synchronous Motors) suitable for these applications. This study focuses on optimizing the design of an SPMSM (Surface Permanent Magnet Synchronous Motor) for large ships to minimize cogging torque and reduce torque ripple. Generally, cogging torque and torque ripple are influenced by factors such as teeth width, yoke length, and the shape of permanent magnets. The objective of this study is to minimize cogging torque and reduce torque ripple by modifying the shape of the permanent magnets. Increases in cogging torque and torque ripple lead to electromagnetic vibration and noise in the motor. To address these issues, this study proposes the following measures. The IPMSM (Interior Permanent Magnet Synchronous Motor) is known to have lower cogging torque compared to the SPMSM because the rotating rotor experiences less magnetic resistance between the permanent magnets and the stator. Therefore, the basic model of SPMSM was replaced with an IPMSM for optimal design. Cogging torque is generated by the attraction between the rotor's permanent magnets and the stator teeth as the rotor rotates. To further reduce cogging torque beyond the conventional Side Tapering technique, a new design method called Asymmetry Double-Side Tapering was applied to the rotor's permanent magnets. The Asymmetry Double-Side Tapering optimal design technique involves asymmetrically tapering both sides of the permanent magnets and adjusting the tapering angles to further decrease the attraction between the permanent magnets and the stator teeth during rotor rotation. This minimizes cogging torque and reduces torque ripple. The results of this study were validated through FEA(Finite Element Analysis).

1. G. Sooriyakumar, R. Perryman and S. J. Dodds, "Improved Cogging Calculation Methods for Surface Mounted Permanent Magnet Synchronous Motors," Proceedings of the 41st International Universities Power Engineering Conference, Newcastle upon Tyne, UK, 2006 2. M. Zhou, X. Zhang, W. Zhao, J. Ji and J. Hu, "Influence of magnet shape on the cogging torque of a surface-mounted permanent magnet motor," in Chinese Journal of Electrical Engineering, vol. 5, no. 4, pp. 40-50, Dec. 2019 3. Z. Cao, Z. Zhang and J. Liu, "Techniques of Torque Ripple Reduction for Outer-rotor Surface-mounted Permanent Magnet Synchronous Motor," 2020 23rd International Conference on Electrical Machines and Systems (ICEMS), Hamamatsu, Japan, 2020

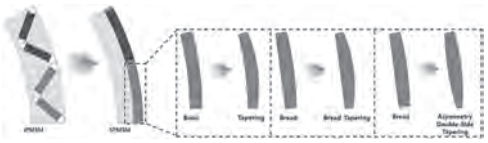

Fig. 1: Step-by-step design process of SPMSM model

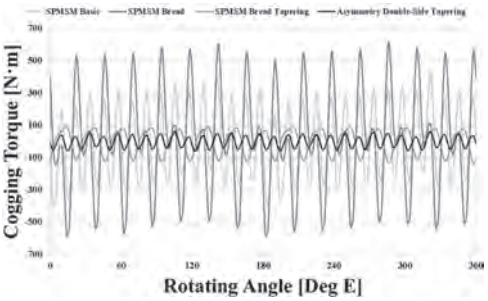

Fig. 2: Basic, Bread, Bread Tapering, Asymmetry Double-Side Tapering Coggig Torque

GS-07. Performance Prediction of Coaxial Magnetic Gear Based on Ring Specimen Test Result.
S. Lee[1], S. Im[1], B. Bae[1] and M. Lim[1] *1. Automotive Engineering (Automotive-Computer Convergence), Hanyang University, Seoul, The Republic of Korea*

Coaxial magnetic gear (CMG) offers many advantages over mechanical gear, such as high torque density, high efficiency, low noise, and no tooth wear. To predict the performance of CMG through finite element analysis (FEA), it is essential to know the magnetic properties of the electrical steel sheets. The Epstein frame test (EFT) is widely used to obtain magnetic properties. However, for small geometry rotating machines the ring specimen test (RST) is preferred due to its simplicity and geometric similarity. Fig. 1 shows the fabricated ring specimens and magnetic properties data obtained by RST. Using this magnetic property data, the performance of the CMG is predicted through three-dimensional (3D) FEA. In 3D FEA, the high-speed rotor (HSR) and the low-speed rotor (LSR) are analyzed separately using EFT data and RST data, respectively. During this process, the pole piece is fixed using EFT data. As shown in Fig. 2, the 3D FEA results using EFT data indicate torques of 2.47 Nm (HSR) and 17.2 Nm (LSR), with an iron loss of 1.15 W. Using RST data, the torques are 2.44 Nm (HSR) and 16.9 Nm (LSR), with an iron loss of 1.59 W. Additionally, the HSR torque predicted from the 3D FEA results is 2.49 Nm using EFT data and 2.46 Nm using RST data. The equation used for predicting HSR torque through 3D FEA is shown in Fig. 2. Finally, to validate the CMG performance predicted based on the 3D FEA results, experiments are conducted. The experimental setup and results are shown in Fig. 2. The experimental results show that the HSR torque is 16.8 Nm and the LSR torque is 2.45 Nm. The torque prediction errors compared to the experimental results are 1.57 % for HSR and 2.38 % for LSR using EFT data, and 0.31 % for HSR and 0.6 % for LSR using RST data. This demonstrates that the accuracy of CMG performance predictions is superior when utilizing RST data compared to EFT data.

S. -H. Lee, S. -Y. Im, J. -Y. Ryu and M. -S. Lim, "Optimum Design Process of Coaxial Magnetic Gear Using 3D Performance Prediction Method Considering Axial Flux Leakage," *IEEE Trans. Ind. Appli*., vol. 60, no. 2, pp. 3075-3085, (2024). D.-M. Kim, J.-W. Chin, J.-P. Hong, and M.-S. Lim, "Performance prediction of surface-mounted permanent magnet synchronous motor based on ring specimen test result," *IET Electric Power Appl.*, vol. 13, no. 9, pp. 1280–1286, (2019). M. S. Lim, J. H. Kim, and J. P. Hong, "Experimental characterization of the slinky-laminated core and iron loss analysis of electrical machine," *IEEE Trans. Magn*., vol. 51, no. 11, (2015).

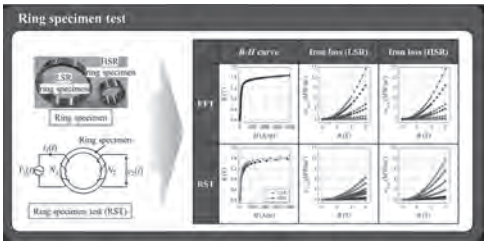

Fig. 1. Magnetic properties obtained by RST.

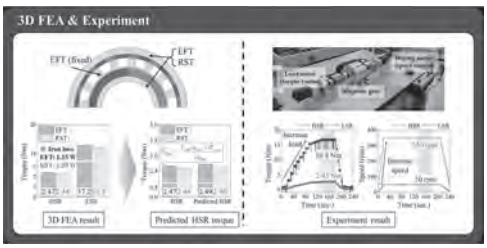

Fig. 2. 3D FEA result, predict HSR torque, and experiment result.

Session GT
MAGNETIZATION DYNAMICS AND MICROMAGNETICS II (Poster Session)

Michael Joseph Donahue, Co-Chair
National Institute of Standards and Technology, Gaithersburg, MD, United States
Jonathan Leliaert, Co-Chair
Ghent University, Ghent, Belgium

GT-01. Temperature-Based Frequency Tunability in Spin-Torque Vortex Nano Oscillators for Neuromorphic Computing System.
S. Soni[1,2], *S. Shreya*[1], Y. Rezaeiyan[1], H. Farkhani[1], B.K. Kaushik[2] and F. Moradi[1] *1. Electrical and Computer Engineering Department, Aarhus University, Aarhus, Denmark; 2. Electronics and Communication Engineering Department, Indian Institute of Technology Roorkee, Roorkee, India*

Spin-torque vortex nano-oscillators (SVNOs) stand out among spin-based nano-oscillators due to their enhanced frequency tunability, wide linewidth, and high output power, making them ideal for several applications such as microwave frequency signal generation, frequency detection, and neuromorphic computing system (NCS) [1-3]. In this work, we have investigated the frequency tunability due to varying temperature effects on SVNOs for temperature-based NCS [2]. We explore how temperature or temperature gradient variations affect the oscillation frequency and output power of SVNOs, which holds potential for applications in spintronics-optical NCSs. We define a temperature gradient from 390K at the surface to 300K at the SVNO nanopillar to examine thermal effects, which reveals that temperature fluctuations disrupt the magnetization of SVNO, leading to changes in the power spectral density (PSD) and oscillation frequency as shown in Fig.1. The frequency and output power are 154MHz and -6.53dBm without temperature effects whereas 128MHz and -5.78dBm with applied temperature gradient, respectively, indicating reduced frequency and increased output power. Moreover, the energy landscape is studied to investigate the variation in energy component interplay which plays a major role in the formation of magnetic vortex core [3], which has been analytically analyzed shown in the inset of Fig. 2. Moreover, Fig. 2 illustrates the increase in exchange and thermal energy due to temperature effects, while demagnetization energy remains almost unchanged. As a result, the total energy increases from 3.90×10^{-18}J without temperature to 232×10^{-18}J demonstrating a rise in the ground energy state of the vortex core. Additionally, we utilize an in-house physics-based Verilog-A model of SVNO, incorporating temperature effects to implement NCS [4]. By integrating insights from the device-level analysis, we aim to develop efficient systems capable of performing pattern recognition tasks leveraging temperature-based frequency tunability of SVNO NCSs.

[1] S. Shreya *et al.*, *Scientific Reports*, vol. 13, (2023). [2] R. Li *et al., Sci Rep* Vol. 14, 10043 (2024). [3] S. Shreya *et al.*, *2023 IEEE International Magnetic Conference*, Sendai, Japan, 2023, pp. 1-2. [4] S. Shreya *et al.*, *IEEE Transactions on Electron Devices*, vol. 69, pp. 4651–4658, (2022).

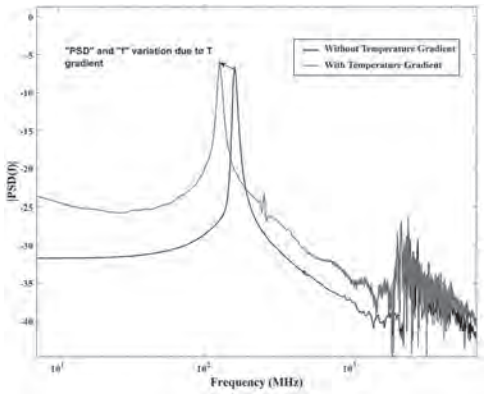

Fig. 1. PSD vs frequency variation of SVNO due to temperature-effect

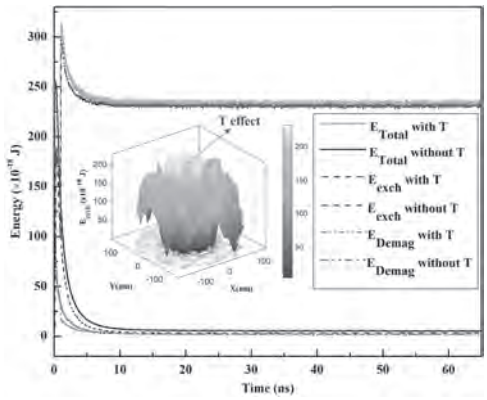

Fig. 2: Variation in the energy components of SVNO due to the temperature effect and the inset shows energy landscape.

GT-02. Effect of Tracer Size Distribution on Magnetic Particle Imaging Resolution.
E. Azizi[1], B. Rezaei[1], S. Mostufa[1], S. Liang[2], Y.A. Wang[3], J. Wang[2], C. Li[1], J. Gomez-Pastora[4], R. He[1] and K. Wu[1] *1. Electrical and Computer Engineering, Texas Tech University, Lubbock, TX, United States; 2. Electrical and Computer Engineering, University of Minnesota, Minneapolis, MN, United States; 3. Ocean Nano Tech LLC, San Diego, CA, United States; 4. Chemical Engineering, Texas Tech University, Lubbock, TX, United States*

Iron oxide magnetic nanoparticles (MNPs) are favored as tracers for magnetic particle imaging (MPI) due to their high biocompatibility, low cost, and ease of preparation. The tracers' magnetic core sizes and their surface coating layers significantly affect MPI signals. Most modeling works reported to date have assumed an ensemble of MNP tracers with identical sizes, ignoring the fact that artificially synthesized MNPs typically follow a log-normal size distribution, which can deviate results from real cases. Herein, using a stochastic Langevin function[1,2], we investigated the effect of MNP tracers' size distribu-

tion on their collective dynamic magnetizations and the point-spread functions (PSF) in MPI. We first characterized the log-normal size distributions of four commercial MNP products from Ocean Nano Tech, SHP15, SHP25, IPG30, and SHS30, using transmission electron microscopy (TEM) and determined their averaged magnetic core sizes (D_c) and standard deviations (σ), see Fig. 1. Their surface coating layer thickness is obtained from hydrodynamic sizes by a dynamic light scatter (DLS). Subsequently, we modeled an ensemble of 1,000 non-interacting MNPs in a field-free region. By deteriorating (2σ, 5σ, 10σ) and improving (0.1σ, 0.2σ, 0.5σ) the size uniformity (i.e., varying the standard deviations from actual value σ) of these MNPs, we recorded their dynamic magnetization responses. Fig. 2 shows an example of the simulation results on SHP15 MNPs, with an average magnetic core size of 12.42 nm, a non-magnetic coating layer thickness of 8 nm, and varying σ from 0.011 to 1.1. For x-space MPI, the imaging resolution is correlated to the full width at half maximum (FWHM) in the PSF profiles. Our study provides valuable insights into how the size distribution of tracers can affect the intrinsic spatial resolution of MPI.

[1] S.A. Shah, D.B. Reeves, R.M. Ferguson, J.B. Weaver, and K.M. Krishnan, "Mixed Brownian alignment and Néel rotations in superparamagnetic iron oxide nanoparticle suspensions driven by an ac field," Physical Review B 92(9), 094438 (2015). [2] N. Usov, and B.Y. Liubimov, "Dynamics of magnetic nanoparticle in a viscous liquid: Application to magnetic nanoparticle hyperthermia," Journal of Applied Physics 112(2), 023901 (2012).

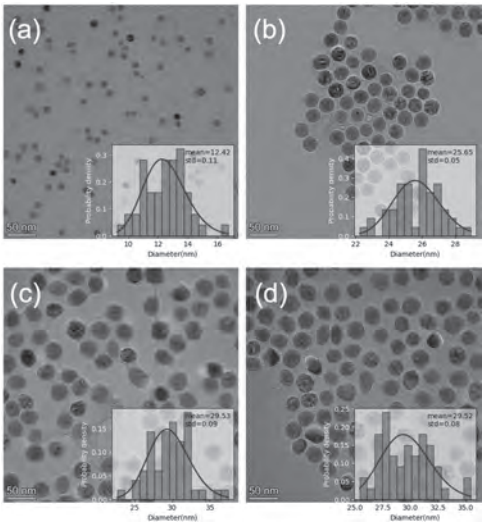

Fig 1. TEM images and histograms of magnetic core size distributions of (a) SHP15, (b) SHP25, (c) IPG30, and (d) SHS30 MNPs.

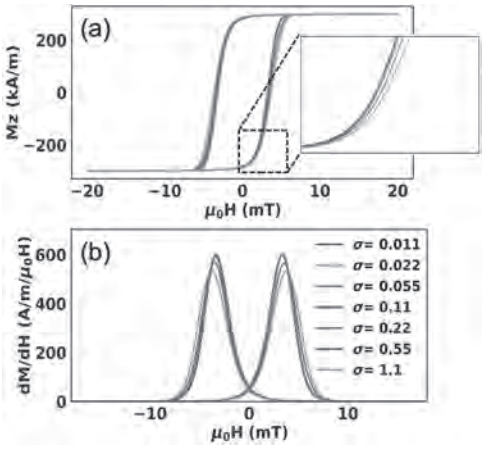

Fig 2. Simulated dynamic magnetization responses of SHP15 MNPs with varied core size standard deviation σ, subjected to an excitation field of 25 kHz and 20 mT/μ_0. σ=0.11 is the measured standard deviation from MNPs. (a) and (b) are M-H curves and PSF profiles, respectively.

GT-03. Fast Identification of the Jiles-Atherton-Model Parameters and the Electric Conductivity Based on Gaussian Process Regression.

A. Schaefer[1], Y. Gong[1] and N. Parspour[1] *1. Institute of Electrical Energy Conversion (iew), University of Stuttgart, Stuttgart, Germany*

For the identification of the Jiles-Atherton hysteresis model (JA model) [1], a variety of different approaches already exist. In most cases, parameter determination is based on an optimization algorithm [2-4]. During the optimization, the deviation of the hysteresis curves from the required reference trajectory is minimized, thereby approximating the suitable parameters. Depending on the implementation of the JA model and the optimization algorithm used, this approach can be very computationally and time-intensive. Therefore, a data-driven approach based on gaussian process regression (GPR) is being investigated. Using numerical simulations, BH curves of toroidal core samples made from solid material are initially generated. Hysteresis and eddy current effects are considered through the use of electromagnetically coupled Maxwell equations and the JA model. By varying the JA parameters and the electrical conductivity of the toroidal core sample, the behavior of different materials is simulated, and the corresponding BH loops are stored in a dataset. Additionally, the parameters of the core geometry and electrical excitation are varied, enabling the novel approach to robustly estimate the resulting parameters for different excitations. The resulting dataset is used as a basis of the GPR with the parameters of the hysteresis curve as input and the JA parameters as well as the electrical conductivity as output. The complete process from data generation to prediction is depicted in Fig. 1. The GPR model achieves strong regression performance with R-squared values of at least 0.9999. Overall, this approach can reliably estimate the JA parameters and the conductivity of the material based on the hysteresis curve as well as the geometric and electrical boundary conditions. The estimation of the parameters occurs with minimal temporal delay and is universally applicable for various excitations.

[1] D. C. Jiles; D. L. Atherton, Journal of Magnetism and Magnetic Materials. Vol. 61 (1-2), p. 48–60 (1986) [2] K. Chwastek and J. Szczyglowski, Journal of Magnetism and Magnetic Materials, Vol. 314, p. 47-51 (2007). [3] M. Hamimid, M. Feliachi and S. M. Mimoune, Physica B: Condensed Matter, Vol. 405, p. 1947-1950 (2010). [4] S. Liu, R. Liu, D. Liang and G. Yu, IOP Conf. Ser.: Mater. Sci. Eng., Vol. 199, p. 12145 (2017).

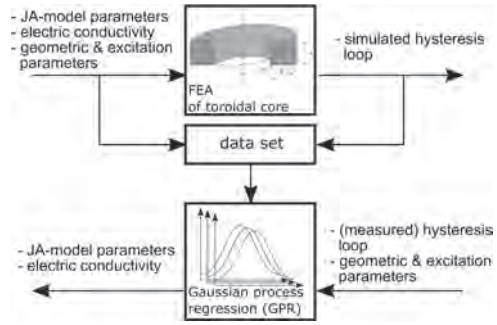

Fig. 1: Flow chart of data generation and gaussian process prediction for JA parameter and conductivity estimation

GT-04. Kolmogorov-Arnold Network for 2-D Magnetostatic Fields Solving. *Y. Zhu*[1], K. Xu[1], B. Wan[1], G. Lei[1] and J. Zhu[2] *1. School of Electrical and Data Engineering, University of Technology Sydney, Ultimo, NSW, Australia; 2. School of Electrical and Computer Engineering, University of Sydney, Camperdown, NSW, Australia*

The data-driven machine-learning approach has significantly advanced the development of computational electromagnetics. Numerous research highlight the successful utility of magnetic materials and field modelling or prediction. Most current studies present multilayer perception (MLP) leveraged physics-informed neural network (PINN) to integrate empirical data and available physical prior knowledge into the machine learning process. However, the MLP-based PINN may face intensive computation resource limitations from its fixed activation function, particularly in large-scale fitting tasks [1]. This study introduces the development and application of Kolmogorov-Arnold Networks (KAN) as a novel method to overcome these limitations. Unlike MLP-PINN, KAN uses the learnable activation functions associated with network edges and eliminates linear weights. Univariate functions parameterized by B-spline have been employed to construct the activation function in KAN's architecture [2]. This study presents two illustrative examples of solving magnetostatic field problems grounded in electromagnetic theory. It established the partial differential equation (PDE) of the magnetic vector potential A expression under a given current density. The analysis includes the magnetic vector potential A in two geometrical settings: square and circular regions. The KAN is compared with finite difference methods (FDM) and MLP-PINN, which approve of its performance while magnetostatic field fitting. The results indicate that the KANs can achieve higher accuracy with less computational overhead when predicting magnetic potentials. The following Fig.1 states the fitting result of KAN and disturbing error with FDM. Fig. 2 shows the MLP-PINN required more epochs than KAN, which reached the same training loss level.

[1] H. Wang, L. Lu, S. Song and G. Huang, Communications in Computational Physics., Vol. 34, p. 869-906 (2023) [2] Z. Liu et al., arXiv preprint., arXiv:2404.19756 (2024)

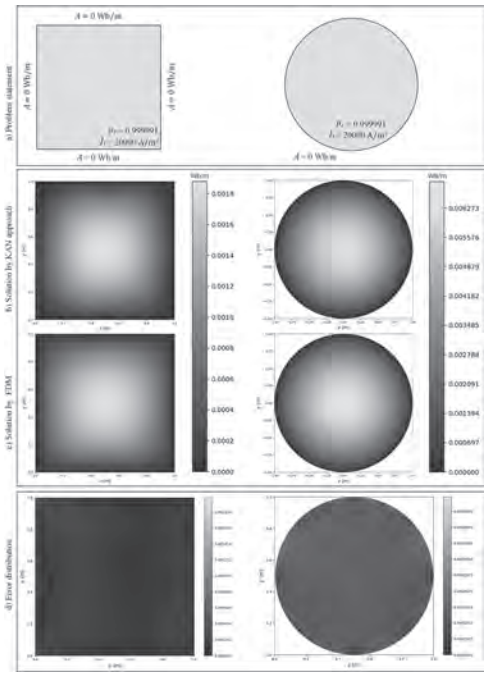

Fig.1. The comparative study result overview for magnetostatic fields problems. a) Problem statement; b) Solution of vector potentials by KAN approach in square geometry (left) and circular geometry (right); c) Solution by FDM approach; d) KAN approach (absolute) error distribution compare with FDM.

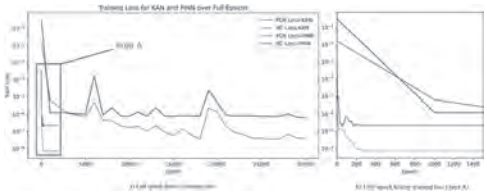

Fig.2. Training loss for KAN (extended into 1500 epoch) and MLP-PINN (30000 epoch). a) Full epoch history; b) 1500 epoch history.

GT-06. Comprehensive Database of Magnetic Materials Using AI-Driven Methodologies. *Y. Zhang*[1,2], S. Itani[1] and J. Zang[1] *1. Physics, University of New Hampshire, Durham, NH, United States; 2. Chemistry, University of New Hampshire, Durham, NH, United States*

Magnetic materials play an indispensable role in modern science and engineering domains. In the realm of magnetic materials, predicting new material materials poses significant challenges. The recent explosion of machine learning in material prediction is rapidly changing the landscape of materials science. Although there are many databases of materials derived from DFT calculations, machine learning models trained on experimental data can more accurately predict properties and closely match real-world outcomes. To address this need, we introduce a novel automated workflow leveraging large language models (LLMs) to extract key information from scientific literature. Our system analyzed articles from Elsevier's collection of journals, including the Journal of Magnetism and Magnetic Materials, generating a database with 26,706 magnetic materials. Each including chemical compositions, structural information (space group, crystal structure, lattice parameters, etc.), magnetic phase transition temperatures (Curie, Néel, and Curie-Weiss temperatures), and magnetic properties (Magnetic Moment, Coercivity, etc.). Building on our initial success, we are continuously expanding the extraction process to include more relevant literature. This ongoing effort is expected to further enhance the database, providing an even more robust resource for the magnetic materials community. The resulting database is hosted on our website https://magneticmaterials.org, where it is available for download by

researchers. We continuously update the website and database, and plan to add more features, such as machine learning models for predicting material properties and APIs for easy access to specific types of materials. This work was supported by Department of Energy, Basic Energy Science under Grant No. DESC0020221

Yibo Zhang, et al. Journal of Magnetism and Magnetic Materials., Vol. 597, p.172001 (2024)

GT-07. Clustering Vector Fields Using Unsupervised Machine Learning. S.A. Pathak[1,2], S.J. Holt[1,2], *A. Petrocchi*[1,2], M. Lang[1,2] and H. Fangohr[1,2,3] *1. Max Planck Institute for the Structure and Dynamics of Matter, Hamburg, Germany; 2. Center for Free-Electron Laser Science, Hamburg, Germany; 3. Faculty of Engineering and Physical Sciences, University of Southampton, Southampton, United Kingdom*

The study of nanoscale magnetic materials has gained significant attention due to their diverse applications. Understanding magnetization states and their behavior is crucial for advancing this field. However, in-depth studies generate vast amounts of data, requiring considerable effort for evaluation. In our previous research, we automated this process using unsupervised machine learning (ML) to analyze 2D magnetization vector fields, each representing an isolated state [1]. In this study, we extend our approach to a 3D system with periodic boundary conditions. By varying the Dzyaloshinskii–Moriya interaction (DMI) constant and external magnetic field in a micromagnetic simulation, we obtained equilibrium states and aimed to cluster them within a phase diagram. Direct clustering of the high-dimensional feature space (2.5 million dimensions) of the magnetization fields resulted in poor performance. To address this, we first used a Variational Autoencoder (VAE) [2] to reduce the dimensionality to a 9-dimensional latent space, then applied KMeans for clustering. Our approach identified four primary clusters: helical, skyrmion, saturation, and mixing of the three former states (Fig. 1), which are well-studied [3, 4]. We note that the clusters are not completely separated, however, the overwhelming majority of the vector fields within a cluster belong to a given magnetization state. The algorithm successfully clusters known states and demonstrates stability even when the magnetizations show a significant amount of disorder. The VAE's generative capability also allows extending the phase diagram by generating new realistic states. This study shows the potential of unsupervised ML in assisting researchers with evaluating extensive magnetization data. We could effectively cluster thousands of simulation results with minimal human intervention. The model showed robustness against perturbations within clusters, and thus, holds promise for handling noisy experimental data. We acknowledge support from the MaMMoS project, Horizon Europe ID: 101135546 and the Marie Sklodowska-Curie grant agreement ID: 101152613.

[1] S. A. Pathak *et al.*, *AIP Adv.* 14, no. 2 (2024) [2] D. P. Kingma *et al.*, *arXiv*:1312.6114 (2013) [3] S. A. Pathak *et al.*, *Phys. Rev. B* 103, no. 10 (2021) [4] B. Göbel *et al.*, *Phys. Rep.* 895, pp. 1-28 (2021)

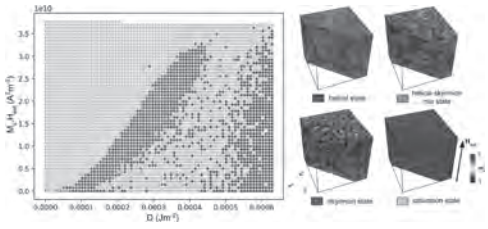

Fig.1 Phase diagram showing different clusters and their majority magnetization field examples.

GT-08. Physics Informed Neural Networks Based on Unsupervised Learning for Multidomain Electromagnetic Analysis. *B. Wan*[1], G. Lei[1], Y. Zhu[1], K. Xu[1], Y. Guo[1] and J. Zhu[2] *1. School of Electrical and Data Engineering, University of Technology Sydney, Ultimo, NSW, Australia; 2. School of Electrical and Information Engineering, University of Sydney, Camperdow, NSW, Australia*

1.Introduction Physics informed neural networks (PINNs) have recently been introduced to solve electromagnetic problems, mainly single domain problem [1]-[2]. PINNs based on unsupervised learning can successfully solve single domain problems without value of physical quantity, which is seen as ground truth. However, it cannot solve multidomain problems because they cannot fit physical quantity in the interface. Therefore, a novel method to employ PINNs based on unsupervised learning to solve multidomain problems is proposed. The feasibility of the method is investigated by solving two problems and TEAM benchmark problem 22. Results are compared and discussed. 2.PINN based on unsupervised learning for multidomain problem First, discretized direct boundary integral equations of domains and interfaces are assembled and solved [3]. Those equations can be defined as $1/2u+\Sigma Hu=\Sigma Gq$, where H and G can be calculated from integration on boundary elements Γ, which can be defined as $H=\int_\Gamma q^* ds$ and $G=\int_\Gamma u^* ds$, where u^* and q^* are the fundamental solution and its derivative of the Laplace equation. The values of physical quantity and its derivatives can be solved for every boundary and interface. Then, the multidomain problem can be transformed into multiple single domain problems. The PINN based on unsupervised learning can be utilized to solve the single domain problem. The loss function of PINN can be defined as $L=MSE_p+MSE_b$, where $MSE_p=MSE[\varepsilon(d^2u_p/dx^2+d^2u_p/dy^2)]$, and ε and u_p are the relative dielectric constant and predicted value of PINN.MSE_b is the RMS for the difference between the predicted and given boundary conditions. 3. Case study and conclusion 2-D square and multi-domain electrostatic problems are defined as problems 1 and 2. Laplace equation is the control equation, and the boundary condition are presented in Fig.1. The TEAM problem 22 will be included in the full text. Results are presented in Fig.2. The max error between FEA and PINN is 0.50 for problem 1, attributed to mutation points at (0,1) and (1,1). However, when the region containing mutation points is excluded, the max error decreases to 0.11 within y=[0,0.85]. The max error between FEA and PINN is 0.12 for problem 2.

[1] C. Liu, K. Yang, J. Bao, W. Yu, J. You, L. Li, and T. Cui, "Recent Progress in Intelligent Electromagnetic Computing," *Journal of Radars,* vol. 12, no. 4, pp. 657-683, 2023. [2] A. C. Polycarpou, *Introduction to the finite element method in electromagnetics*. Springer Nature, 2022. [3] J. T. Katsikadelis, *The boundary element method for engineers and scientists: theory and applications*. Academic Press, 2016.

Fig.1 Definition of problems

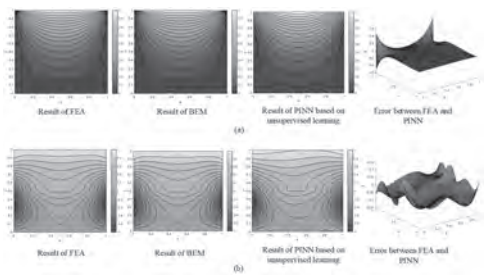

Fig.2 Results and comparison. (a)problem1. (b)problem2

Session GU
MICROSCOPY, IMAGING, AND MAGNETIC CHARACTERIZATION III (Poster Session)

Sascha Schäfer, Chair
University of Regensburg, Regensburg, Germany

GU-01. Antiferromagnetism in $La_{0.8}Sr_{0.2}MnO_3$ Ultrathin Films Driven by Interfacial Charge Doping. G. Panchal[1], F. Stramaglia[1] and *C.A. Vaz*[1] *1. Swiss Light Source, Paul Scherrer Institut, Villigen PSI, Switzerland*

The interface between complex oxide materials have since long been recognised as a site for the emergence of novel phenomena as a consequence of the break in crystal symmetry and charge exchange occurring at the interface region. In particular, the interfaces of the mixed valence manganites have been shown to be specially sensitive to charge and strain transfer, given their sensitivity to charge, spin, orbital order and lattice distortions [1]. In this work, we show that nominally ferromagnetic $La_{0.8}Sr_{0.2}MnO_3$ ultrathin films interfaced with antiferromagnetic $La_{0.45}Sr_{0.55}MnO_3$ buffer layers adopt an antiferromagnetic ground state at small thicknesses. Specifically, we use x-ray photoemission electron microscopy (XPEEM) combined with the circular and linear x-ray magnetic dichroic effects, to determine the evolution of the magnetic ground state of ultrathin $La_{0.8}Sr_{0.2}MnO_3$ films 0–10 unit cells (uc) thick deposited on antiferromagnetic $La_{0.45}Sr_{0.55}MnO_3$/$SrTiO_3$(001). We observe no ferromagnetic contrast, but instead large antiferromagnetic domains for $La_{0.8}Sr_{0.2}MnO_3$ thicknesses up to 3 uc, showing that nominally ferromagnetic $La_{0.8}Sr_{0.2}MnO_3$ is antiferromagnetic. For thicknesses above 3 uc, ferromagnetic domains emerge, confirming that the additional layers revert to the ferromagnetic ground state. We find a drastic increase in the complexity of the domain configuration between 3 and 5 uc, which we attribute to competing magnetic and electronic ground states in the system. We attribute the interfacial modified magnetic ground state to charge sharing at the interface due to the chemical potential mismatch, which leads to hole doping at the $La_{0.8}Sr_{0.2}MnO_3$ interface [3]. Our results indicate that the screening of the contact potential occurs within three unit cells and represents another example of intrinsic charge doping at oxide interfaces leading to modified interfacial electronic and magnetic properties [4]. The present work sheds light on the impact of charge sharing at the interface of complex oxide materials, in particular on the magnetic and electronic states, and presents a strategy for modulating the electronic ground state properties at metallic interfaces.

[1] C. A. F. Vaz et al., J. Phys.: Condens. Matter 27 (2015) 123001. [2] F. Stramaglia et al., ACS Appl. Mater. Interfaces 16 (2024) 4138. [3] G. Panchal, F. Stramaglia, C. A. F. Vaz, APL Mater. 12 (2024) 061117. [4] Z. Zhong and P. Hansmann, Phys. Rev. X 7 (2017) 011023.

GU-02. High-Gradient Magnetic Separation and Phenotypic Characterization of Sickle RBCs. *J. Chalmers*[1], P.R. Iyer[1], J. Strayer[1], X. Wu[1], H. Choe[1], A. DeBastiani[1], B. Karakuzu[1,2], J. Gomez-Pastora[3], K. Wu[4], A. Palmer[1], M. Zborowski[5] and P. Desai[6] *1. Chemical and Biomolecular Engineering, Ohio State University, Columbus, OH, United States; 2. Bioengineering, Izmir Institute of Technology, Izmir, Turkey; 3. Chemical Engineering, Texas Tech University, Lubbock, TX, United States; 4. Electrical and Computer Engineering, Texas Tech University, Lubbock, TX, United States; 5. Biomedical Engineering, Cleveland Clinic Lerner Research Institute, Cleveland, OH, United States; 6. Levine Cancer Institute, Charlotte, NC, United States*

Sickle cell disease (SCD) results from a β-globin gene mutation, resulting in hemoglobin self-polymerization (HbS) and the subsequent sickling of red blood cells (RBCs). This reduces the oxygen-binding affinity of RBCs, impairing their ability to bind to oxygen. In SCD patients suffering severe sickle crises, RBC exchange transfusions are carried out to reduce the concentration of the sickle RBCs in the blood and improve the overall oxygen-carrying capacity of RBCs. Unfortunately, over 40% of SCD patients experience RBC alloimmunization, in which the body produces antibodies against allogeneic donor RBCs. The current method of matching RBC antigen profiles to mitigate the effect of alloimmunization faces significant challenges regarding cost and supply chain demand. As a result, there is a clear need for novel technologies that can minimize the number of allogenic RBC units required for efficient transfusion management of SCD patients. A potential strategy is to selectively deplete HbS RBCs by their magnetophoretic behavior correlated with oxygen binding affinity. We conducted high gradient magnetic separation of oxygenated RBCs from healthy and SCD patients' blood samples with a Miltenyi MiniMACS™ column inserted into a custom-made Halbach array magnet designed to boost the magnetic separation efficiency. Cell tracking velocimetry (CTV) and imaging flow cytometry (IFC) were employed for single-cell magnetic and phenotypic characterization. CTV integrates microscopy and microfluidics to assess magnetic behavior under a well-defined magnetic field gradient. IFC combines microscopy and flow cytometry to analyze RBC morphology and biomarker expression (e.g., CD47 and CDC71). CD47 regulates cell clearance, and CD71 indicates reticulocyte count. We aim to correlate the expression of CD47 and CD71 with the magnetic characterization from CTV to establish the separation of sickle RBCs from healthy RBCs. This study highlights the potential of magnetic separation techniques combined with CTV and IFC to enhance the efficacy of RBC transfusions for SCD patients and provide critical insights into RBCs' magnetic and phenotypic characteristics.

1. J. Howard, Hematology., Vol. 2016, p.625-631 (2016) 2. P. J. Derry, A. T. T Vo, A. Gnanansekaran, J. Mitra, A. V. Liopo, M. L. Hegde, A-L. Tsai, J. M. Tour, and T. A. Kent, Frontiers in Cellular Neuroscience., Vol. 14, p.603043 (2020) 3. M. Weigand, J. Gómez-Pastora, J. Strayer, X. Wu, H. Choe, S. Lu, E. Plencner, K. Landes, A. Palmer, M. Zborowski, P. Desai. J. Chalmers, IEEE Transactions on Biomedical Engineering., Vol. 69, p.3582-3590 (2022) 4. T. Özpolat, T. C. Chang, X. Wu, A. E. St. John, B. A. Konkle, J. Chen, J. A. López, Cytometry Part A., Vol 101, p.448-457

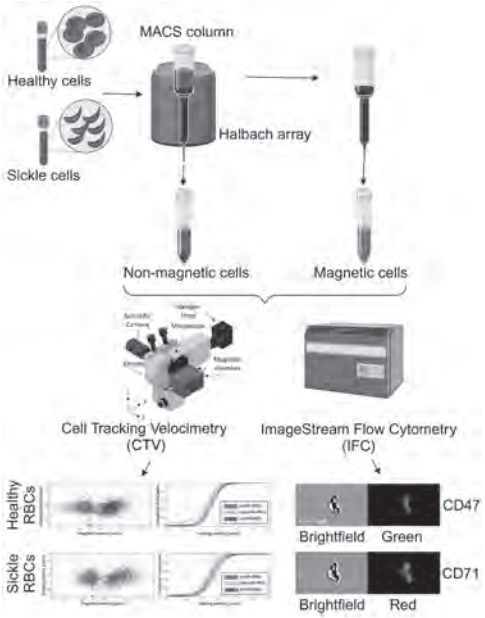

Fig. 1: Illustration of magnetic separation and phenotypic characterization of sickle RBCs

GU-03. Numerical Analysis of Hybrid Electromagnetic Coil Systems for Efficient Gradient Field Generation in Human-Sized Magnetic Particle Imaging. *S. Mostufa*[1], E. Azizi[1], B. Rezaei[1], C. Li[1], J. Gomez-Pastora[2], R. He[1] and K. Wu[1] *1. Department of Electrical and Computer Engineering, Texas Tech University, Lubbock, TX, United States; 2. Department of Chemical Engineering, Texas Tech University, Lubbock, TX, United States*

Magnetic particle imaging (MPI) is a tracer-based imaging modality first reported in 2005.[1] In an MPI system, an alternating magnetic field (AMF) periodically magnetizes the magnetic nanoparticle (MNP) tracers and causes the nonlinear magnetic responses recorded by a receive coil. Spatial encoding is realized by a gradient field that selectively 'enables' the magnetic responses of tracers in a field-free region (FFR), while 'disables' (magnetically saturating) tracers outside this FFR. Reported gradient field strength is typically in the range of 1 to 7 T/m/μ_0 [2]. The field of view (FOV) is determined by the ratio of AMF field amplitude to gradient field strength. A higher gradient field strength improves imaging resolution but reduces the FOV.[3] For larger objects, like a human-sized scanner, focus fields are added to increase coverage. One major challenge for clinical MPI use is achieving a sufficient bore size. Preclinical MPI systems have bore sizes between 3 cm and 12 cm,[4] which is limited by the power consumption for the current-carrying coils. Increasing the bore size causes a lower gradient field strength and as a result, worsens the imaging resolution. Herein, we designed and simulated electromagnetic coils with various core materials and shapes, keeping the coil windings (4680 with 40 layers), bore size (20 cm), and current (45 A) fixed. The hybrid electromagnetic coil system with a cone-shaped NdFeB core showed the highest gradient field and field uniformity. Fig. 1 shows schematic diagrams of different coil designs and their magnetic flux density profiles. Fig. 2 presents the simulation results for magnetic flux density B and Bz, field-free points (FFP), and gradient field profiles along the coil axis.

[1] B. Gleich, and J. Weizenecker, "Tomographic imaging using the nonlinear response of magnetic particles," Nature 435(7046), 1214–1217 (2005) [2] Rezaei B, Tay Z W, Mostufa S, Manzari O N, Azizi E, Ciannella S, Moni H, Li C, Zeng M, Gómez-Pastora J and Wu K 2024 Magnetic nanoparticles for magnetic particle imaging (MPI): design and applications *Nanoscale* [3] T. Knopp, and T.M. Buzug, *Magnetic Particle Imaging: An Introduction to Imaging Principles and Scanner Instrumentation* (Springer Science & Business Media, 2012) [4] T. Knopp, N. Gdaniec, and M. Möddel, "Magnetic particle imaging: from proof of principle to preclinical applications," Phys. Med. Biol. 62(14), R124–R178 (2017)

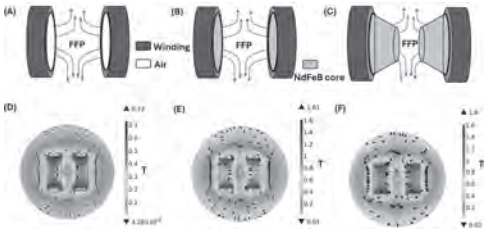

Fig 1. Schematic diagrams in COMSOL simulation for three hybrid electromagnetic coil systems with cores such as (A) air, (B) NdFeB, and (C) cone-shaped NdFeB magnetic flux concentrator. (D) – (F) are the magnetic flux density distributions of these hybrid electromagnetic coil systems in (A) – (C).

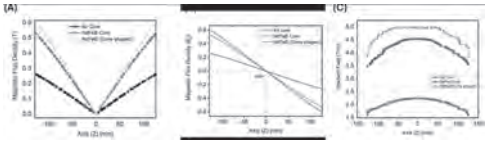

Fig 2. The COMSOL simulation results of (A) magnetic flux density B, (B) B_z, and (C) the gradient field profiles along the coil axis, generated by different hybrid electromagnetic coil designs.

GU-04. Method to Measure the Mass and Particle Size of Rare Earth Materials in Aqueous Solutions. *A. Igboanugo*[1] and P. Andrei[1] *1. Florida State University, Tallahassee, FL, United States*

Recent advances in high-precision mass measurement instruments that are available commercially for both industrial and academic research applications, have opened new avenues for the development of magnetic characterization methods for magnetic materials [1]. In this presentation we investigate the possibility to use a high-precision mass balance and permanent magnets to measure the amount (mass) and particle size of rare-earth elements in aqueous solutions. The technique is based on measuring the apparent weight of the aqueous solution as a function of time and the distance between a neodymium magnet placed in the proximity of the solution and the solution itself. Using both computational methods and experiments, it is shown that the apparent weight of the solution can change significantly to be accurately measured when a strong permanent magnet is brought near the solution. If we extract the effects of the solvent (in our case water, which is diamagnetic) and of the cuvette (usually paramagnetic), the initial change in the apparent weight is due to the magnetostatic force between the permanent magnet and the rare earth particles in the solution. This magnetostatic force can be used with finite element calculations to determine the mass of rare earth particles in the solution. The particle size of the rare-earth particles in the solutions can be determined from the rate at which the apparent weight of the solution changes with respect to time, after the application of the magnetic field. Larger particles are attracted towards the magnet faster than smaller magnetic particles [2]. Once they approach the magnet, the magnetostatic force between the magnet and solutions increases even more, in this way decreasing the apparent weight of the solution. Therefore, the rate at which the apparent weight of the solution changes with respect to time is a direct indication of the particle size in the solution. Experimental measurements and how they are used together with finite element simulations to determine the mass of rare earth materials in aqueous solutions will be presented at the meeting. The limitations of the method will also be discussed.

[1] K. Wojtaszek, A. Cristofolini, A. Popoli, K. Kolczyk-Siedlecka, and M. Wojnicki, "A Novel Approach for Quantifying Magnetic Susceptibility of Aqueous and Organic Solutions," J. Phys. Chem. A, vol. 128, no. 2, pp. 488–499, 2024. [2] P. Andrei and N. Carlstedt, "Modeling of Magnetic Separation of Metal Ions in Aqueous Solutions", Intermag 2024, Rio de Janeiro, Brazil, Ma 2024.

GU-06. An XPEEM Study of Voltage-induced Magnetic Domain Separation in a $La_{0.7}Sr_{0.3}MnO_3$ Thin Film. T. Chen[1], D. Sasaki[2], *B. Achinuq*[3], N. Ghazikhanian[4], P. Salev[5], H. Ohldag[3], A. Scholl[3], I.K. Schuller[4], Y. Takamura[2] and A.D. Kent[1] *1. Department of Physics, New York University, New York, NY, United States; 2. Department of Materials Science and Engineering, University of California Davis, Davis, CA, United States; 3. Advanced Light Source, Lawrence Berkeley National Laboratory, Berkeley, CA, United States; 4. Department of Physics, University of California San Diego, La Jolla, CA, United States; 5. Department of Physics and Astronomy, University of Denver, Denver, CO, United States*

$La_{0.7}Sr_{0.3}MO_3$ (LSMO) is a transition metal oxide that is a ferromagnetic metal at low temperatures and a paramagnetic insulator above its Curie temperature. It exhibits both resistive and magnetic switching properties[1,2]. Unlike most phase-change resistive switching materials that transition from an insulator to a metal at elevated temperatures[3-6], LSMO transitions from a metal to an insulator as the temperature increases. Applying a voltage bias above a critical value to a fabricated LSMO thin film device can induce phase separation, forming a paramagnetic insulating barrier. In this study, we employed X-ray magnetic circular dichroism-photoemission electron microscopy (XMCD-PEEM) to observe magnetic domain configurations as a function of bias voltage. For voltages exceeding a certain threshold, magnetic domains segregate into two distinct regions: one displaying clear white/black contrast, indicative of well-defined micron-scale magnetic domains, and the other showing intermediate gray contrast, characteristic of regions with reoriented magnetization. Significant changes in magnetic domain configurations were observed only in the gray areas. Furthermore, this voltage-induced phase separation was found to depend on bias polarity, with the gray area expanding from the opposite sample edge when the applied voltage was reversed. These findings demonstrate the intricate voltage-induced domain dynamics in phase-change materials.

1. C. Zener, Physical Review, 82, 403 (1951). 2. P. W. Anderson and H. Hasegawa, Physical Review, 100, 675 (1955). 3. M. D. Pickett and R. S. Williams, Nanotechnology, 23, 215202 (2012). 4. S. Kumar, Z. Wang, N. Davila, N. Kumari, K. J. Norris, X. Huang, J. P. Strachan, D. Vine, A. D. Kilcoyne and Y. Nishi, Nature communications, 8, 658 (2017). 5. A. Asamitsu, Y. Tomioka, H. Kuwahara and Y. Tokura, Nature, 388, 50-52 (1997). 6. S. Mercone, A. Wahl, C. Simon and C. Martin, Physical Review B, 65, 214428 (2002).

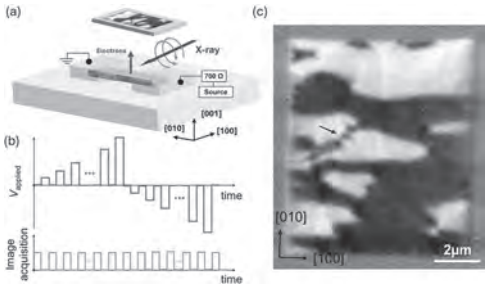

Figure 1. (a) Schematic of XMCD-PEEM experiment setup at the ALS. (b) Measurement sequence of the voltage and image acquisition. At 110 kelvin, a bias voltage was first applied and then turned off, and an image was recorded afterwards. (c) XMCD-PEEM image of LSMO device prior to voltage application. The black arrow points out the cross type of domain structure.

Session GV
ELECTRICAL MACHINES, POWER ELECTRONICS & ELECTROMECHANICAL CONVERSION (Poster Session)

Abdelmounaim Tounzi, Chair
Université de Lille, Villeneuve d'Ascq, France

GV-03. Design and Analysis of an Interior Permanent Magnet Synchronous Motor with a Carbon Fiber-Reinforced Plastic Sleeve Based on Electromagnetic-Mechanical Coupled Analysis. *K. Kwak*[1], Y. Choi[1], M. Koo[2], H. Shin[3], K. Shin[4] and J. Choi[1] *1. Electrical Engineering, Chungnam National University, Daejeon, The Republic of Korea; 2. Purpose Built Mobility Group, Korea Institute of Industrial Technology, Gwangju, The Republic of Korea; 3. Specialized Machinery and Robotics Group, Korea Institute of Industrial Technology, Gimje, The Republic of Korea; 4. Electrical Engineering, Changwon National University, Changwon, The Republic of Korea*

Interior permanent magnet synchronous motors (IPMSMs), which are primarily used as traction motors, encounter mechanical problems in their rotors during high-speed operation. To address this issue, this paper presents the design and analysis of an IPMSM rotor with a carbon fiber-reinforced plastic (CFRP) sleeve based on electromagnetic-mechanical coupled analysis. The design focuses on the considerations necessary for designing and manufacturing the rotor, which is complicated by the inclusion of a sleeve, thereby differentiating it from typical IPMSMs. Fig. 1 shows the shapes and flux lines of (a) a typical IPMSM; (b) a model with the rib removed and the sleeve applied; (c) a model with both the rib and bridge removed, and the sleeve applied; and (d) a model with the rib, bridge, and gap between magnets removed, and the sleeve applied. Among the different models, model (d) in Fig. 1 has the lowest leakage flux, indicating the best electromagnetic performance. Fig. 2 (a) shows the variables considered when designing an IPMSM with a CFRP sleeve. Figs. 2 (b) and 2 (c) show the cogging torque and torque ripple, respectively, according to the notch size. Fig. 2 (d) shows the cogging torque according to the notch angle. Figs. 2 (e) and 2 (f) show the mechanical analyses of a typical IPMSM and an IPMSM with a CFRP sleeve, respectively. Therefore, an IPMSM with a CFRP sleeve must be designed by considering various design variables based on electromagnetic and mechanical analyses. The detailed design and experimental verification are presented in this paper.

[1] M. Clauer and A. Binder, *Elektrotech. Inftech*., Vol. 140, p.302-313 (2023) [2] G. Du, H. Yan, N. Li, L. Li, Y. Chen, G. Lei and J. Zhu, *IEEE Trans. Transp. Electrif.*, p.1-1 (2024)

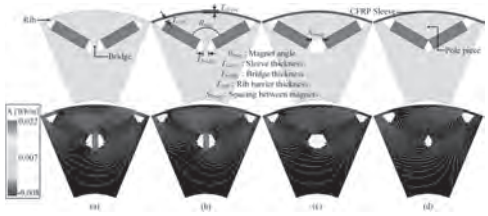

Fig. 1. Shapes and flux lines of (a) a typical IPMSM; (b) a model with the rib removed and the sleeve applied; (c) a model with both the rib and bridge removed, and the sleeve applied; and (d) a model with the rib, bridge, and the gap between magnets removed and the sleeve applied.

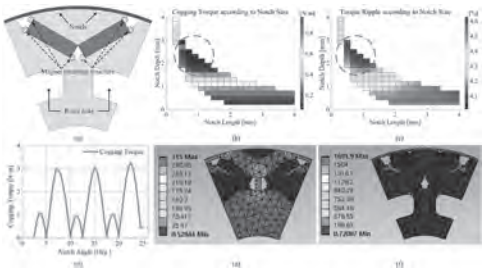

Fig. 2. (a) Design variables to consider when designing an IPMSM with a CFRP sleeve, (b) cogging torque according to notch size, (c) torque ripple according to notch size, (d) cogging torque according to notch angle, (e) mechanical analysis of a typical IPMSM, and (f) mechanical analysis of an IPMSM with a CFRP sleeve.

GV-07. High Efficiency Rotary Transformer Design Based on Modular Core. *P. Huang*[1], T. Chang[2], I. Lu[2] and M. Tsai[1] *1. Mechanical Engineering, National Cheng Kung University, Tainan, Taiwan; 2. Electric Motor Technology Research Center, National Cheng Kung University, Tainan, Taiwan*

In recent years, wound rotor synchronous motors (WRSMs) have garnered significant attention due to their independence from permanent magnets. This independence allows for the adjustment of the air gap magnetic field and speed range by manipulating the rotor winding current, thereby broadening their applicability across various working environments. However, WRSM rotors rely on slip rings and brushes to transfer electrical energy, which can cause sparks and wear due to continuous friction. As a result, the use of rotary transformers (RTs) for contactless energy transfer has become an attractive alternative. Current RTs require the flux to flow both axially and radially due to the rotational action. This necessitates a flux path that traditional steel sheet stacking processes, typically used for fixed transformers, cannot efficiently support, as some stacking directions may oppose the desired flux direction, resulting in low energy transmission. Consequently, most literature suggests the use of soft magnetic composite (SMC) materials or a combination of SMC and steel sheets. However, challenges such as complex assembly and low permeability persist. To address these issues, this study proposes a novel RT design with high magnetic permeability, leveraging the properties of adhesive steel sheets. Through finite element analysis (FEA) simulation and prototype implementation, the design was validated by integrating it into a WRSM for experimental verification. As illustrated in the accompanying figure, this study proposes an RT composed entirely of steel sheets, with the stacked orientation perfectly parallel to the flux path. These sheets are stacked, bonded, wire-cut, and finally assembled into the RT core. Additionally, a 300W, three-phase, four-pole, 18-slot WRSM was designed to validate the feasibility of the proposed RT. Using the model for simulation, the comparison table reveals that the proposed RT made of steel sheets induces a higher voltage on the secondary side at low frequencies compared to the same model made of SMC. Conversely, at high frequencies, the trend is reversed. Thus, the design proposed in this study is more suitable for the operational range of typical low-frequency industrial motors.

[1] Y. Zhang, J. Yang, D. Jiang, D. Li and R. Qu, "Design, Manufacture, and Test of a Rotary Transformer for Contactless Power Transfer System," in IEEE Transactions on Magnetics, vol. 58, no. 2, Art no. 8400206, Feb. 2022, doi: 10.1109/TMAG.2021.3094135. [2] T. Raminosoa and R. Wiles, "Contactless Rotor Excitation for Traction Motors," 2018 IEEE Energy Conversion Congress and Exposition (ECCE), Portland, OR, USA, 2018, pp. 6448-6453, doi: 10.1109/ECCE.2018.8557553.

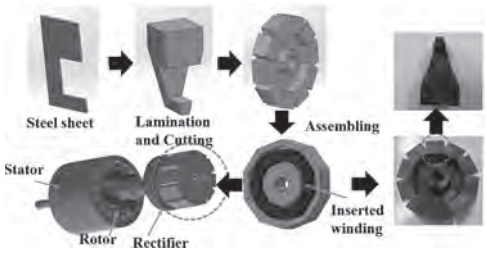

Figure

Material	Primary side (V)	Secondary side (V)	Frequency
Ferrite powder	30	11.3	60 Hz
Ferrite powder	30	29.7	1000 Hz
Steel sheet	30	23.5	60 Hz
Steel sheet	30	29	1000 Hz

Table

GV-08. A Study of Roadside Coil Configuration in Wireless Power Transfer System for EVs Using Repeater Coils. *A. Saito*[1], S. Miyahara[1], F. Sato[1] and H. Matsuki[2] *1. Tohoku Gakuin University, Sendai, Japan; 2. Tohoku University, Sendai, Japan*

In recent years, EVs have become increasingly popular around the world, and research on wireless power supply technology for EV driving has been active in line with this trend. To realize this wireless power transfer system for EVs on a real scale, it is necessary to increase the length of the power transfer section per power supply unit, and to secure a sufficient power transfer section with a small number of power supply units as a whole. A single coil method that extends a single coil has been proposed as a method to solve this problem. However, since the resistance loss increases as the coil length increases, resulting in a decrease in efficiency, it is necessary to propose a method that can extend the feeding section while keeping the coil length constant to some extent. We have therefore proposed a repeater coil method. This method extends the feed section by inserting a Booster repeater coil between each transmission coil, which acts as a bridge between the two coils. This allows the use of a minimum length of coils, which leads to a reduction in efficiency due to resistance loss. In addition, this in-transit power supply system must also take into account transient phenomena that may occur when the EVs to be supplied are out of the supply lane. For this reason, we have proposed a new repeater coil configuration for the transmission side that assumes no-load conditions. In this study, we proposed a new repeater coil system that combines a rectangular coil and a direct-wound coil, which enables stable feeding of EVs with a rectangular coil and can also handle transient phenomena, and conducted experiments. Figures 1 and 2 show a schematic diagram of the system used in the experiment and the experimental results. In this study, a spiral coil is assumed to be used for the receiving coil on the EV side. The results confirm that the newly proposed repeater system, which takes advantage of the characteristics of rectangular and spiral coils and repeaters the current from the transmission coil to which the power supply is connected, has narrowed the range in which the power supply efficiency drops significantly and also provides a stable power supply.

[1] T. Misawa, T. Takura, F. Sato, IEICE Technical Report, pp.13-18, (2012) [2] Dukju Ahn, Songcheol Hong, IEEE Trans, Vol 60, No.1, pp.1373-1382, (2013) [3] Takehiro Imura, Electrical Engineering in Japan, Vol.183, No.1, pp.51-62, (2013) [4] Y. Ota, N. Aruga, F. Sato, J. Magn. Soc. Jpn., 39, pp25-28, (2015) [5] H. Abe, IEICE Technical Report, WPT2020-28, (2020)

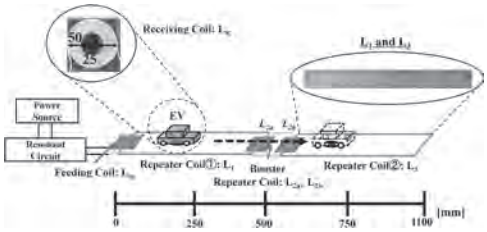

Fig. 1 System overview diagram

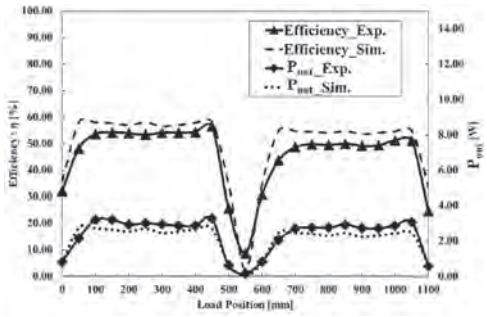

Fig. 2 Experimental results

Session HA
CAVITY MAGNONICS AND NON-RECIPROCAL SPIN WAVE PROPAGATION

Can-Ming Hu, Chair
University of Manitoba, Winnipeg, MB, Canada

INVITED PAPERS

HA-01. Anomalous Long-Distance Coherence in Critically Driven Cavity Magnonics. *Y. Yang*[1], J. Yao[1], Y. Xiao[2], P. Fong[3], H. Lau[3,4] and C. Hu[1] *1. Physics, University of Manitoba, Winnipeg, MB, Canada; 2. Physics, Nanjing University of Aeronautics and Astronautics, Nanjing, China; 3. Physics, Simon Fraser University, Burnaby, BC, Canada; 4. Quantum Algorithms Institute, Surrey, BC, Canada*

Developing quantum networks necessitates coherently connecting distant systems via remote strong coupling. Here, we demonstrate long-distance coherence in cavity magnonics operating in the linear regime. By locally setting the cavity near critical coupling with traveling photons, nonlocal magnon-photon coherence is established via strong coupling over a 2-m distance. We observe two anomalies in this long-distance coherence: first, the coupling strength oscillates twice the period of conventional photon-mediated couplings; second, clear mode splitting is observed within the cavity linewidth. Both effects cannot be explained by conventional coupled-mode theory, which reveals the tip of an iceberg of photon-mediated coupling in systems under critical driving. Our Letter shows the potential of using critical phenomena for harnessing long-distance coherence in distributed systems.

Y. Yang, J. Yao, Y. Xiao, et al, Physical Review Letters, Vol. 132, no. 20, p.206902(2024)

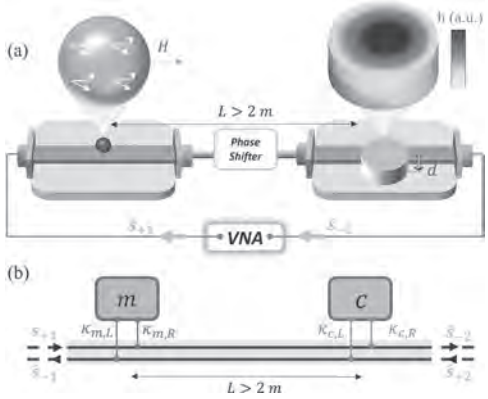

Fig.1 Setup.

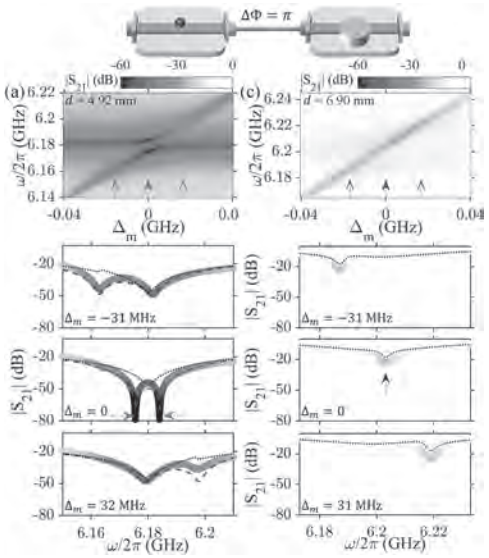

Fig. 2 Long-distance coupling: the field dependency.

HA-02. Spin-Wave Edge and Cavity Modes in a Moiré Magnonic Crystal. *G. Gubbiotti*[1] *1. IOM, CNR, Perugia, Italy*

Moiré superlattices, which consist of twisted layers of van der Waals materials [1] exhibit extraordinary electronic behaviors such as superconductivity and correlated topological states. Moiré physics has recently been applied in photonics to reconstruct photonic band structures that enable novel functionalities such as magic-angle lasers. So far, moiré physics in magnonic systems has only been studied from a theoretical point of view [2]. In this work, we use micromagnetic simulations to report magnon flat-band formation in twisted bilayer magnonic crystals at the optimal "magic angle" and interlayer exchange coupling combination. At the flat-band frequency, magnons undergo a strong two-dimensional confinement with a lateral scale of about 185 nm. The magic-angle magnonic nanocavity occurs at the *AB* stacking region of a moiré unit cell, unlike its photonic counterpart which is at the *AA* region, due to the exchange-induced magnon spin torque. The magnon flat band originates from band structure reformation induced by interlayer magnon-magnon coupling. [3] We also investigate the confinement of spin waves in a nano magnonic waveguide integrated on top of a magnetic moiré superlattice. Our numerical analysis reveals a magnonic flat-band at the center of the Brillouin zone, created by a 3.5-degree twist in the moiré superlattice. The flat band, characterized by a high magnon density of states and a zero group velocity, allows for the confinement of magnons within the *AB* stacking region. From the experimental point of view, we have fabricated nanostructured moiré magnonic crystals based on low-damping yttrium iron garnet thin films. We report the experimental observation of spin-wave moiré edge and cavity modes using Brillouin light scattering spectro-microscopy in a nanostructured magnetic moiré lattice consisting of two triangular antidot lattices based on a yttrium iron garnet thin film. Spin-wave moiré edge modes are

detected at an optimal twist angle and with a selective excitation frequency. At a given twist angle, the magnetic field acts as an additional degree of freedom for tuning the chiral behavior of the magnon edge modes. Micromagnetic simulations indicate that the edge modes emerge within the original magnonic band gap and at the intersection between a mini-flat band and a propagation magnon branch. [5] G.G. acknowledges funding from the European Union – Next Generation EU – "PNRR – M4C2, investimento 1.1 – "Fondo PRIN 2022" – TEEPHANY– ThreEE-dimensional Processing tecHnique of mAgNetic crYstals for magnonics and nanomagnetism ID 2022P4485M CUP B53D23002820006.

[1] Y. Cao and et al, Nature 556, 43–50 (2018). [2] Y.-H. Li and et al, Phys. Rev. B 102, 094404 (2020). [3] J. Chen et al, Phys. Rev. B 105, 094445 (2022). [4] J. Chen et al, submitted. [5] H. Wang et al, Phys. Rev. X 13, 021016 (2023).

HA-03. The Toroidal Moment in Nanomagnets and its Connection with Nonreciprocal Magnonics. F. Brevis[1], L. Körber[2,3], R. Gallardo[1,4], A. Kákay[3] and *P. Landeros*[1,4] *1. Departamento de Física, Universidad Técnica Federico Santa María, Valparaíso, Chile; 2. Institute of Molecules and Materials, Radboud University, Nijmegen, Netherlands; 3. Institut für Ionenstrahlphysik und Materialforschung, Helmholtz-Zentrum Dresden - Rossendorf, Dresden, Germany; 4. Center for the Development of Nanoscience and Nanotechnology (CEDENNA), Santiago, Chile*

Nonreciprocal magnonics is a field of research focused on manipulating and controlling magnons in magnetic materials. It specifically aims to achieve nonreciprocal behavior, meaning that the spin-wave propagation is different in opposite directions. Over the past decade, numerous nonreciprocal magnonic systems have been theoretically anticipated, and some have been successfully demonstrated in experiments [1], with some even showing frequency shifts on the order of several GHz. Nonetheless, for more complex magnonic systems (such as graded films, multilayers, nanotubes, and curved shells) or in cases where the equilibrium magnetization is nonuniform, numerical methods are required to estimate the frequency shift among counterpropagating spin waves. Consequently, and given the relevance of nonreciprocal and unidirectional wave propagation for magnon-based technological devices (such as magnonic diodes, circulators, isolators, etc.), there is a pressing need for novel approaches to predict the existence of spin-wave nonreciprocity. One of these approaches involves the toroidal moment τ. Proposed by Dubovik and Tugushev [2] from multipole expansions of the vector potential, the toroidal moment can be understood by considering an electric current moving along the meridians of a toroid, which in turn generates a magnetic field and a circular magnetization through the center of the toroid; this emerging magnetization generate a τ perpendicular to the plane of the toroid. In ferromagnetic systems lacking external electric or polarization currents, the volume-bound current (the curl of the magnetization) can generate a toroidal moment. Therefore, the existence of magnetic textures promotes the creation of such a moment. However, there are a few definitions of τ [3], and their interrelation is investigated theoretically. It is found that the term that links them corresponds to a surface toroidal moment originated by surface-bound currents. The surface and volume toroidal moments for different well-known magnetic textures, such as conical-helix and skyrmionic/vortex classes, are calculated, and the relevance of each contribution is discussed [4]. The surface toroidal moment is generally parallel in direction to the volume toroidal moment but may differ in magnitude and sign. Considering the surface term can broaden the discussion around the toroidal moment and emphasize surface phenomena when examining magnetic materials. The significance of the toroidal moment in the context of nonreciprocal magnonics [1] is discussed in various scenarios, such as the current-induced spin-wave Doppler shift in thin films [5], different magnetic textures (such as conical-helical, skyrmionic, meron, and bimerons), magnetization-graded films [6], magnetic bilayers [7], and films with interfacial and bulk DMI. The toroidal moment accounts for the spatial symmetry breaking of the magnetization in such a way that, if the wave vector k has a nonzero projection along the toroidal moment, $\tau \cdot k \neq 0$, nonreciprocal spin-wave propagation is then permitted, with physical origin on the magnetostatic interaction [8]. Here, we elucidate the correct formulation of the toroidal moment that is suitable for predicting nonreciprocal behavior. We also address the appropriate selection of the origin of the coordinate system, as the toroidal moment generally depends on it. Furthermore, we illustrate the relationship between the toroidal moment and nonreciprocity in various magnetic systems that have been previously examined, suggesting a strategy for anticipating reciprocal or nonreciprocal behavior. The significance of this research lies in the fact that, through straightforward calculations, it is feasible to a priori estimate the presence of nonreciprocity in these systems by solely considering the geometry and the equilibrium static magnetization. The validation of these findings could be achieved through magnetization dynamics calculations and micromagnetic simulations.

[1] B. Flebus et al., J. Phys.: Condens. Matter 36, 363501 (2024). [2] V. Dubovik and V. Tugushev, Phys. Rep. 187, 145 (1990). [3] N. A. Spaldin, M. Fiebig, and M. Mostovoy, J. Phys.: Condens. Matter 20, 434203 (2008). [4] F. Brevis, L. Körber, A. Kákay, R. A. Gallardo, and P. Landeros, in preparation. [5] J. Fernández-Rossier et al, Phys. Rev. B 69, 174412 (2004). [6] R. A. Gallardo et al., New J. Phys. 21, 033026 (2019). [7] R. A. Gallardo et al., Phys. Rev. Appl. 12, 034012 (2019). [8] L. Körber et al., Phys. Rev. B 106, 014405 (2022).

Session HB
INTERDISCIPLINARY AND EMERGING TOPICS

Alpha T N'Diaye, Co-Chair
Lawrence Berkeley National Laboratory, Berkeley, CA, United States
Cinthia Piamonteze, Co-Chair
Paul Scherrer Institut, Villigen PSI, Switzerland

CONTRIBUTED PAPERS

HB-02. High-Gradient Magnetic Chromatography of Rare-Earth Elements. P. Brungi[1], N. Carlstedt[1] and *P. Andrei*[1] *1. Florida State University, Tallahassee, FL, United States*

High-gradient magnetic chromatography (HGMC) is a relatively new technique that refers to the chromatographic separation of a mixture of magnetic particles (MPs) using high-gradient magnetic separation (HGMS) systems [1,2]. However, unlike HGMS which is currently being used on a large scale to separate magnetic from non-magnetic particles, the goal of HGMC is to separate different types of magnetic particles which have different but relatively close magnetic susceptibility, mass and volume. Both methods (HGMS and HGMC) are using a matrix of soft magnetic wires situated in a uniform magnetic field in order to create large magnetic field gradients to attract the MPs. In the case of HGMS experiments the MPs are removed simultaneously during the release phase, while in HGMC experiments the MPs are being removed gradually from the chromatographic column by slightly changing the conditions of the experiment. In this presentation we will discuss and compare two types of HGMC systems: magnetic field-controlled HGMC and flow rate-controlled HGMC. In magnetic field-controlled HGMC we first apply a strong magnetic field to capture the MPs on the wires then, we decrease the magnetic field slowly and keep the flow rate constant until all the MPs are released from the wires. In flow rate-controlled HGMC we first capture the particles using a very slow flow rate and keeping the value of the magnetic field constant; then, we increase the flow rate slowly while the MPs are gradually released from the wires. Similar to the case of magnetic field-controlled HGMC, the MPs with a lower magnetic are released first followed by the MPs with higher magnetic susceptibility. In the full presentation we will discuss possible designs of HGMC systems. We will also introduce the new concept of stability curves [2], that is instrumental in the design of the separation process (for instance, Fig. 1 shows the stability curves for three types of magnetic particles with slightly different magnetic susceptibilities). In addition, we will derive analytical equations that take into consideration thermal diffusion, drag, gravitation and magnetic forces, and can be used to calculate the recovery and grade of the separation process.

[1] L. Kuger and M. Franzreb, "Design of a Magnetic Field-Controlled Chromatography Process for Efficient and Selective Fractionation of Rare Earth Phosphors from End-of-Life Fluorescent Lamps," ACS Sustainable Chem. Eng., vol. 12, no. 8, pp. 2988 (2024). [2] P. Andrei and N. Carlstedt, "High-Gradient Magnetic Chromatography: Modeling, Simulation, and Design", IEEE Trans. Magn., submitted, (2024)

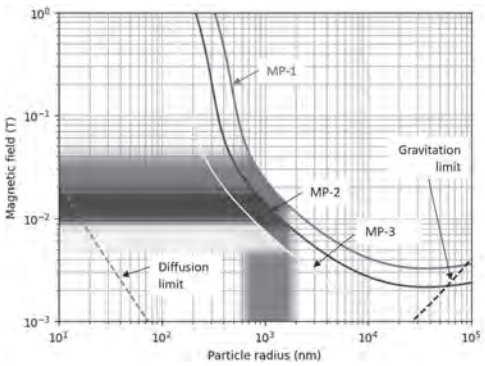

Figure 1

HB-03. Numerical simulations of magnetic packed columns for biological cell separation. *H. Choe*[1], J. Chalmers[1], J. Strayer[1], X. Wu[1], P. Iyer[1], A. DeBastiani[1], B. Karakuzu[1,2], J. Gomez-Pastora[3], M. Zborowski[4] and K. Wu[5] *1. William G. Lowrie Department of Chemical and Biomolecular Engineering, The Ohio State University, Columbus, OH, United States; 2. Department of Bioengineering, Izmir Institute of Technology, Izmir, Turkey; 3. Department of Chemical Engineering, Texas Tech University, Lubbock, TX, United States; 4. Department of Biomedical Engineering, Cleveland Clinic, Cleveland, OH, United States; 5. Department of Electrical and Computer Engineering, Texas Tech University, Lubbock, TX, United States*

Magnetic separation or purification is widely used in variety of fields including mineral recovery, coolant cleaning/monitory, and biological cell separation. While electromagnetic systems are popularly used, permanent magnets are continuing to increase in power and, relatively speaking, decrease in price which allows further development and applications. Among various magnetic separator designs, the magnetic packed column presents the potential to create the highest magnetic energy gradients, which translates to the potential to separate a wider range of targets. This high magnetic energy gradients are achieved by the column packing distorting and strengthen the local magnetic field gradient when the packed column is exposed to an external magnetic field. Therefore, the combination of external magnetic field strength, and the shape, material, and packed position of the magnetic beads can enhance separation. Correspondingly, the efficiency of a magnetic separator depends on several factors, such as the external magnetic field gradient or strength, magnetic properties of the beads, and other physical properties of the fluid and particles, including viscosity, density, and size. To address this comprehensive effect, in this study, COMSOL Multiphysics software was used to analyze the magnetic force in gradients in various magnetic separation environment, such as fluid flow and external magnetic field strength. Moreover, the simulation results suggest the prediction of particle movements using particle trajectories. This application of simulation provides insight into designing new magnetic separator and improving their separation efficiency.

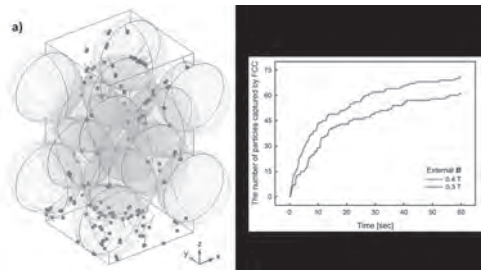

Fig. 1: COMSOL simulation of magnetic packed column with different external magnetic flux density (*B*), a) an example of simulation geometry and particle trajectory and b) the number of particles attached to the surface of magnetized bead.

HB-04. Wirelessly Measuring Brain Activity Using Magnetoelectric Nanoparticles as an Amplifier of Neuron Signals. *S. Chen*[1], E. Zhang[2], J. Tian[3] and S. Khizroev[3] *1. Chemical, Environmental, and Materials Engineering, University of Miami, Coral Gables, FL, United States; 2. MAVT, ETH Zurich, Zurich, Switzerland; 3. Electrical Engineering, University of Miami, Coral Gables, FL, United States*

Wirelessly measuring the brain's activity is a very challenging problem, due to the limited density of information to record and the natural barriers between the brain and any receiver. While there are many current methods, such as functional magnetic resonance imaging (fMRI), electroencephalography (EEG), and Magnetoencephalography (MEG), all of them suffer from certain drawbacks. In the case of an fMRI, although a powerful method capable of fully imaging the brain[1], it is limited by the time it takes to resolve an image, preventing it from achieving real time measurement. EEGs can measure electrical signals detected through the scalp in real time, and while in a smaller form factor, lack the penetrative capability to measure deep brain activity, as electrical signals from further within the brain will be screened away by the conductive brain tissues. MEG overcomes some of these issues, by offering both the ability to measure in real time and provide spatial detection like an fMRI[2]. However, MEG is reliant on extremely small fields emanating from the whole brain, in the sub-1-nOe range, and thus requires increasingly complex detection mechanisms, making it another extremely costly method. And as with any surface detection method, it suffers from the realities of the inverse problem of extracting volumetric data from surface measurements. Here we propose a method to detect the electrical signal from brain activity within a small 3D volume, by utilizing magnetoelectric nanoparticles (MENPs) to convert induced electrical fields in the brain into detectable magnetic fields. This allows magnetic measurement of neural activity deep in the brain. Previously, we demonstrated the ability to stimulate neurons using a magnetic field and a magnetostrictive core-piezoelectric shell MENPs[3]. As the MENPs rely on the magnetoelectric effect, the converse holds true, allowing MENPs to convert neuronal electrical signals into magnetic fields[4]. By placing MENPs in certain locations of the brain (or throughout using an intravenous injection), the combined magnetic field from the MENPs can be read at high temporal and spatial resolution with more easily available smaller, and ever increasingly sensitive TMR sensors, significantly reducing the hardware requirements.

1. Glover GH. Overview of Functional Magnetic Resonance Imaging. *Neurosurg Clin N Am*. 2011;22(2):133-139. doi:10.1016/j.nec.2010.11.001 2. Fred AL, Kumar SN, Kumar Haridhas A, et al. A Brief Introduction to Magnetoencephalography (MEG) and Its Clinical Applications. *Brain Sci*. 2022;12(6):788. doi:10.3390/brainsci12060788 3. Zhang E, Abdel-Mottaleb M, Liang P, et al. Magnetic-field-synchronized wireless modulation of neural activity by magnetoelectric nanoparticles. *Brain Stimulat*. 2022;15(6):1451-1462. doi:10.1016/j.brs.2022.10.004 4. Bok I, Haber I, Qu X, Hai A. In silico assessment of electrophysiological neuronal recordings mediated by magnetoelectric nanoparticles. *Sci Rep*. 2022;12(1):8386. doi:10.1038/s41598-022-12303-4

HB-05. Characterizing the Physicochemical Properties of Magnetic Nanoparticles by a Surface Plasmon Resonance Approach. *S. Mostufa*[1], B. Rezaei[1], E. Azizi[1], Y.A. Wang[2], C. Li[1], J. Gomez-Pastora[3], R. He[1] and K. Wu[1] *1. Department of Electrical and Computer Engineering, Texas Tech University, Lubbock, TX, United States; 2. Ocean Nano Tech LLC, San Diego, CA, United States; 3. Department of Chemical Engineering, Texas Tech University, Lubbock, TX, United States*

Magnetic nanoparticles (MNPs) are widely recognized as effective signal amplifiers for surface plasmon resonance (SPR)-based biosensors. Herein, we report that SPR sensors can be a useful tool to characterize the physicochemical properties of protein-functionalized MNPs. In this work, a Kretschmann configuration-based SPR sensing platform with a scanning angular range of up to 17° is employed to identify the resonance conditions of different iron oxide nanoparticle suspensions. We demonstrate the feasibility of SPR for differentiating protein coating layers on MNPs, such as amine, biotin, and streptavidin, as well as distinguishing different MNP magnetic core sizes (from 15 nm to 30 nm) and MNP concentrations (from 0.013 mg/mL to 2.5 mg/mL). The SPR resonance angle shift, $\Delta\theta$, is used as a crucial parameter for characterizing these physicochemical properties of MNPs. Standard characterization techniques[1] rely on costly and bulky equipment, which is not easily accessible and requires well-trained personnel. Our work reports that the SPR sensor can effectively identify various physicochemical properties of MNPs. We highlight that SPR sensors hold significant potential as they might become a reliable method for characterizing MNPs in future research and applications. Fig 1 shows the working principle SPR platform for characterizing three commercial MNP products from Ocean Nano Tech (i.e., SHA25, SHS25, SHB25). Fig 2 is an example showcasing that different surface protein coatings on MNP can cause unique resonance angle shifts in SPR.

[1] Rezaei B, Mostufa S and Wu K 2024 Chapter 6 - Characterization methods for magnetic nanoparticles *Woodhead Publishing Series in Electronic and Optical Materials* ed K Wu and J-P B T-M N in N Wang (Woodhead Publishing) pp 155–77

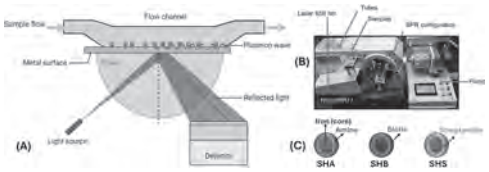

Fig 1. (A) Schematics of the SPR system setup and detection approach. (B) Photograph of the NanoSPR77 device and the peristaltic pump (C) Schematics of SHA, SHB, and SHS series MNPs that have iron cores coated by amine, biotin, and streptavidin proteins, respectively. Figure (A) was created with BioRender.com.

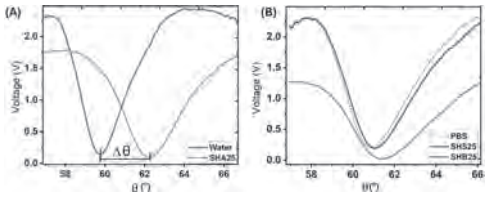

Fig 2. SPR curves of (A) deionized water and SHA25; (B) PBS, SHS25, and SHB25. The deionized water and PBS serve as references to obtain the resonance angle shift, Δθ. SHS25, SHB25, and SHA25 share identical iron oxide core sizes and nanoparticle concentrations but different surface protein coatings.

HB-06. Magnetic Force Microscopy Revealing Long-range Room Temperature Stable Molecule Bridge Induced Magnetic Ordering on Magnetic Tunnel Junction (MTJ). *P. Tyagi*[1] *1. University of the District of Columbia, Washington, DC, United States*

Magnetic tunnel junctions (MTJs) can integrate novel single molecular device elements to overcome long-standing fabrication challenges, thus unlocking their novel potential. This study employs magnetic force microscopy (MFM) to demonstrate that organometallic molecules, when placed between two ferromagnetic electrodes along cross-junction shaped MTJ edges (Fig.1), dramatically altered the magnetic properties of the electrodes, affecting areas several hundred microns in size around the molecular junction vicinity at room temperature (Fig. 1). These findings are supported by magnetic resonance and magnetometer studies on ~7000 MTJ pillars. MFM on the pillar sample showed an almost complete disappearance of the magnetic contrast. Spatial magnetic image suggests that molecular channels significantly impacted the spin density of states in the ferromagnetic electrodes (Fig. 2). The molecular channels forming the bridges along the cross-junction area (Fig.1) also produced in the magnetic electrodes influence MTJ transport properties, stabilizing currents up to six orders of magnitude smaller at room temperature. This advancement in MTJ-based molecular devices paves the way for a new generation of commercially viable logic and memory devices controlled by molecular quantum states at near-room temperatures.

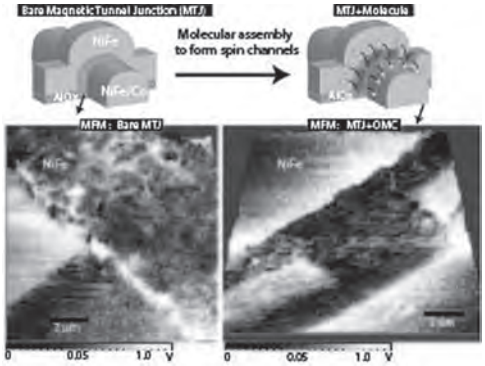

Fig. 1

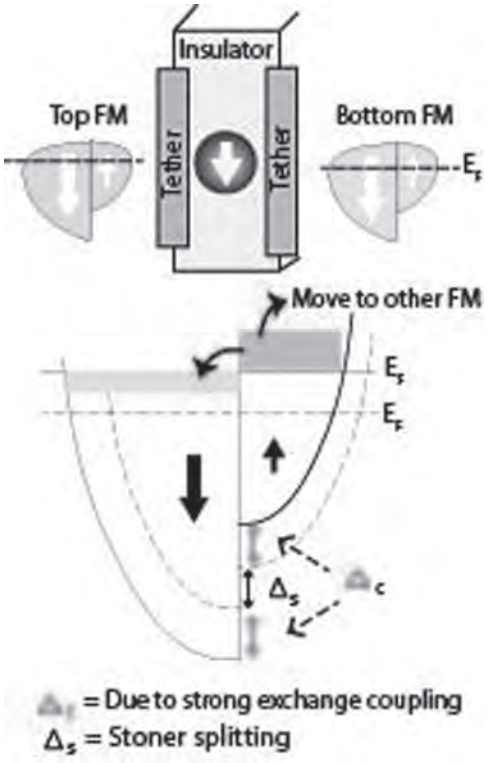

Fig. 2

HB-07. Ultrastrongly-coupled magnon-polaritons in magnetochiral meta-molecules. *S. Tomita*[1], K. Mita[1], T. Kodama[1], T. Ueda[2], T. Nakanishi[3], K. Sawada[4] and T. Chiba[1] *1. Tohoku University, Sendai, Japan; 2. Kyoto Institute of Technology, Kyoto, Japan; 3. Kyoto University, Kyoto, Japan; 4. RIKEN SPring-8 Center, Sayo, Japan*

A magnon, a quantized elementary excitation in magnets, can be transformed to magnon-polariton when it is coupled to alternating current (AC) electromagnetic fields, namely photons [1]. The magnon-polariton has gained attention particularly in spintronics and quantum information technology for applications to hybrid quantum systems [2]. A coherent and ultrastrong magnon-photon coupling is indispensable toward the quantum regime. Furthermore, the ultrastrongly-coupled magnon-polariton is inherently non-reciprocal owing to the breaking of time-reversal symmetry by magnetization or magnetic fields. The non-reciprocity results in a transmission amplitude (and phase) difference depending on the propagation direction and polarization of photons. However, such a directionally non-reciprocal optical phenomenon has yet to be observed in ultrastrongly-coupled systems, except for dissipative or strong magnon-photon coupling. Here, we demonstrate ultrastrong-couplings of the directionally non-reciprocal magnon-polaritons in a single magnetochiral (MCh) metamolecule at room temperature. The MCh metamolecule consists of a polycrystalline yttrium-iron garnet (YIG) cylinder as a magnetic meta-atom inserted in a right-handed helix made of copper (Cu) as a chiral meta-atom placed in a microwave waveguide [3]. As in Fig. 1, the metamolecule exhibits magnon-polariton with a coupling ratio larger than 0.2, indicating the ultrastrong-coupling regime. The ultrastrong coupling is achieved by direct interaction between microwave photons in the Cu chiral structure and magnons in the YIG cylinder. Moreover, the magnon-polariton has directional non-reciprocity. These experimental results are reproduced well via numerical simulations and theoretical consideration [4]. This work is financially supported by JST-CREST (JPMJCR2102) and KAKENHI(22K14591,23K13621). The authors are grateful to H. Kurosawa for instructing the numerical calculation.

[1] Harder et al., Journal of Applied Physics 129, 201101 (2021). [2] Lachance-Quirion et al., Applied Physics Express 12, 070101 (2019). [3] Tomita et al., Physical Review Letters 113, 235501 (2014). [4] Mita et al., arXiv:2406.19046.

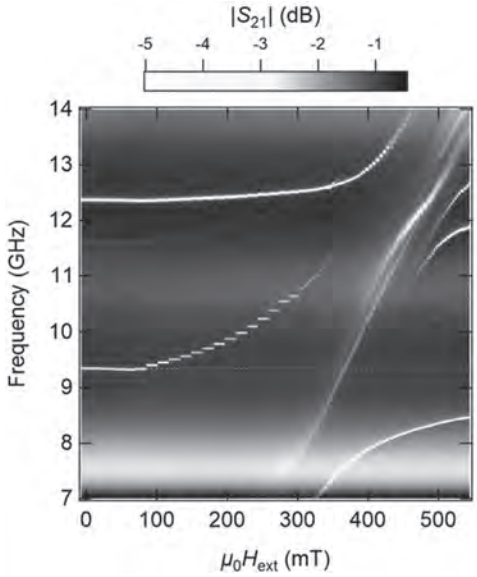

Fig.1 Measured 2D plots of $|S_{21}|$ of the metamolecule as functions of applied external DC magnetic field and frequency.

HB-08. Magnetic Tunnel Junction Testbed Based Molecular Spintronics Devices: A Method of Solving 70-Year-Old Challenge in Making Molecular Devices. *P. Tyagi*[1] and C. Riso[1] *1. University of the District of Columbia, Washington, DC, United States*

For >70 years, efforts have been made to include molecules in devices, but without much progress toward mass-producible and robust devices. Molecule-based devices may govern the advancement of logic and memory devices for next-generation computers and may be suitable for quantum computation. Molecules are unparalleled nanostructures that serve as device elements because chemists can mass-produce a variety of molecules with unique optical, magnetic, and transport characteristics. However, the biggest challenge is to connect two or three metal electrodes to the molecule (s) and develop a robust and versatile device fabrication technology that can be adopted for commercial-scale mass production (Fig.1). Utilizing tunnel junctions as a testbed for making molecular devices solves many critical problems [1]. We focused on producing magnetic tunnel junction-based molecular devices (MTJMSD). This talk will show that an MTJMSD evolves when molecules are bridged along the exposed side edges of a tunnel junction. With the MTJMSD approach, many unprecedented advantages have become available to researchers. MTJMSD enables the connection between ferromagnetic electrodes and a variety of molecules with the spin state. For the first time, the MTJMSD approach enabled magnetic measurements and conventional transport studies[1]. Magnetic studies showed that molecules could transform the magnetic[2] and transport properties of the MTJs[3] at room temperature.

1. P. Tyagi, "Multilayer edge molecular electronics devices: a review," *J. Mater. Chem.,* vol. 21, pp. 4733-4742, 2011. 2. P. Tyagi, C. Baker, and C. D'Angelo, "Paramagnetic Molecule Induced Strong Antiferromagnetic Exchange Coupling on a Magnetic Tunnel Junction Based Molecular Spintronics Device," *Nanotechnology,* vol. 26, p. 305602, 2015. 3. P. Tyagi and E. Friebe, "Large Resistance Change on Magnetic Tunnel Junction based Molecular Spintronics Devices," *J. Mag. Mag. Mat.,* vol. 453, pp. 186-192, 2018.

HB-09. Electronic and Magnetic Structure Study of Multiwalled Carbon Nanotubes for Spintronics Applications Using X-ray Absorption and Magnetic Circular Dichroism Spectroscopy. *S. Gautam*[1], P. Thakur[2], S. Augistine[3], N. Brookes[4] and K. Chae[5] *1. Dr. SSB Univ Inst Chemical Engg & Tech, Panjab University, Chandigarh, India; 2. Beamline Division, Diamond Light Source, Oxfordshire, United Kingdom; 3. Department of Physics, Deva Matha College, Kottayam, India; 4. ESRF, Grenoble, France; 5. Advanced Analysis & Data Center, Korea Institute of Science & Technology, Seoul, The Republic of Korea*

Multi-walled carbon nanotubes (MWCNTs) fabricated using the catalytic technique of microwave plasma-enhanced chemical vapor deposition (MPCVD) have been extensively investigated to understand their electronic and magnetic structures. These investigations employed near-edge X-ray absorption fine structure (NEXAFS) and X-ray magnetic circular dichroism (XMCD) spectroscopy. NEXAFS analysis at the Fe and Co L-edges reveals the presence of divalent ions in an octahedral symmetry. Additionally, the emergence of two distinct NEXAFS peaks between the pi and sigma^\ast transitions indicates the 1s to sp3 hybridization resulting from Fe^{2+} and Co^{2+} ions attached to the carbon nanotubes. The Raman spectra of MWCNTs further support these findings, showing characteristic features that confirm the presence of Co-C and Fe-C bonds. Moreover, element-specific hysteresis loops and XMCD spectra demonstrate that MWCNTs exhibit room temperature ferromagnetism, which is primarily attributed to the Fe-C and Co-C bonding within the nanotubes. This intrinsic ferromagnetism, combined with the high aspect ratio and unique electronic properties of MWCNTs, suggests significant potential for their integration into spintronics storage devices.

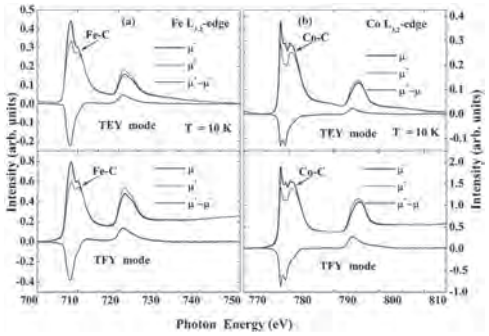

Fig. 1

Session HC
COMPUTING WITH SPIN DYNAMICS
Matthew Daniels, Chair
National Institute of Standards and Technology, Gaithersburg, MD, United States

INVITED PAPER

HC-01. Neuromorphic Computing with Networks of Interconnected Magnetic Tunnel Junctions. A. López[1], D. Costa[2], T. Böhnert[2], P.P. Freitas[2], R. Ferreira[2], J. Camarero[3,4], C. León[1], J. Grollier[5] and *M. Romera*[1] *1. Complutense University of Madrid, Madrid, Spain; 2. International Iberian Nanotechnology Laboratory, Braga, Portugal; 3. IMDEA Nanociencia, Madrid, Spain; 4. Universidad Autónoma de Madrid, Madrid, Spain; 5. Unité Mixte de Physique CNRS, Thales, Université Paris-Sud, Université Paris-Saclay, Palaiseau, France*

A promising branch of neuromorphic computing aims to perform cognitive operations in hardware by leveraging the physics of efficient and well-established nano-devices. Spintronic devices are promising candidates as building blocks for these neuromorphic networks due to their multifunctionality, reprogrammable nature, and memory. In this presentation, an overview of recent work based on networks of spintronic nano-oscillators capable of learning vowel recognition [1] and binding temporal events [2] through synchronization will be presented. I will then discuss how spintronic nano-devices identical to those employed in industrial spin-transfer-torque magnetic random-access memories (STT-MRAM) can be used as interconnected processing units capable of learning pattern recognition. To this end, a reconfigurable classifier based on a network of electrically connected magnetic tunnel junctions that categorizes information encoded in the amplitude of input currents through the spin-torque-driven magnetization switching output configuration [3] will be presented. These results, obtained using the same working principle employed in STT-MRAM memories, constitute an important step towards the development of large-scale neuromorphic networks based on well-established technology. Finally, I will discuss recent results on a three-terminal synaptic transistor, which uses a half-metallic ferromagnet as the transistor channel and implements important synaptic properties related to short-term and long-term memory and plasticity [4].

[1] M. Romera, P. Talatchian, S. Tsunegi *et al., Nature* 563, 230 (2018). [2] M. Romera, P. Talatchian, S. Tsunegi *et al., Nature Communications* 13, 883 (2022). [3] A. Lopez, D. Costa, T. Bohnert *et al*., *Physical Review Applied*, in press (2024). [4] A. Lopez, J. Tornos, A. Peralta *et al*., Advanced *Electronic Materials* 9, 2300007 (2023).

CONTRIBUTED PAPERS

HC-02. A Neuromorphic Computational Model for Spintronics-based Hopfield Oscillatory Neural Network. S. Soni[1,2], Y. Rezaeiyan[1], T. Boehnert[3], R. Ferreira[3], B.K. Kaushik[2], F. Moradi[1] and *S. Shreya*[1] *1. Electrical and Computer Engineering Department, Aarhus University, Aarhus, Denmark; 2. Electronics and Communication Engineering Department, Indian Institute of Technology Roorkee, Roorkee, India; 3. Spintronics, International Iberian Nanotechnology Laboratory (INL), Braga, Portugal*

The human brain is competent in information processing and learning, largely due to the coordinated activity of neuronal populations. These populations exhibit rhythmic fluctuations in activity known as oscillatory dynamics, observed across different brain regions [1]. These oscillations are crucial in various cognitive functions, such as memory consolidation, sensory processing, and motor control. This work proposes a novel neuromorphic computational (NC) model comprising analytical derivation for a spintronics-based Hopfield oscillatory neural network (HONN) employing frequency coupling inspired by the brain's oscillatory dynamics applicable for tasks such as pattern recognition, image denoising, and so on. Similar to the Kuramoto model which represents the phase-based coupling of two oscillators [2, 3], this work presents a detailed mathematical analysis of frequency and phase-based coupling mechanism along with the Theile equation of the magnetic vortex core dynamics applicable to our proposed HONN. This approach uses spin-torque vortex nano-oscillators (SVNOs) as neurons [4] connected via resistive synapses representing coupling strength. The model describes the analytical relation of the oscillators and the synaptic element and how it influences the synchronized frequency (f_{sync}). Stronger coupling aligns f_{sync} closer to the higher gyrotropic frequency of the magnetic vortex core within the network, while weaker coupling promotes f_{sync} closer to the lower one as shown in Fig.1. This phenomenon is utilized in a four-SVNO neuron coupling network design to illustrate the testing an image denoising pattern flow in the HONN, where Hebbian learning rules update synaptic connections. These connections transition between low resistance (LRS) and high resistance (HRS) states mimicking biological brain plasticity. This model validates the HONN hardware architecture comprising SVNOs and CMOS components, as shown in Fig. 2, and helps mitigate challenges in developing large-scale complex HONN hardware.

[1] I. E.J. de Vries *et al.*, *Trends in Cognitive Sciences*, vol. 24, (2020). [2] Y. Kuramoto, Chemical oscillations, waves, and turbulence (1984). [3] S. Y. Ha et *al.*, *Physics. D, Nonlinear Phenomena*, vol. 239, (2010). [4] S. Shreya et *al.*, *IEEE TED*, vol. 69, no. 8, pp. 4651-4658, (2022).

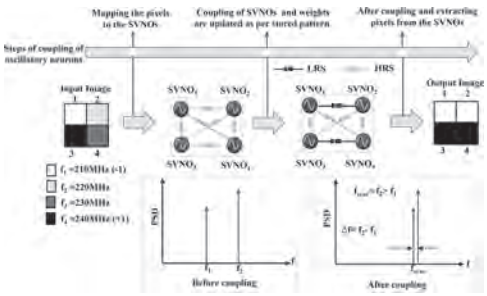

Fig.1. Pattern denoising process flow using 4 SVNOs neuron HONN, showing the before and after coupling mechanism states between two SVNOs.

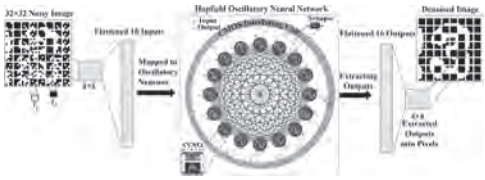

Fig.2. HONN hardware architecture for image denoising tasks using 16 SVNOs.

HC-03. Real time machine learning with spintronic enhanced Generative Adversarial Network. *S. Gupta*[1], A. Abhinandan[2], V. Vadde[1], B. Muralidharan[1] and A. Sharma[2] *1. Electrical Engineering, Indian Institute of Technology Bombay, Mumbai, India; 2. Electrical Engineering, Indian Institute of Technology Ropar, Ropar, India*

Achieving real-time machine learning tasks such as text-to-image generation, data augmentation, and image-to-image translation involves advanced neural network architectures [1] like Generative Adversarial Networks (GANs). GANs [2] architectural guidelines facilitate new data creation using competing generator and discriminator neural networks. We present the first-ever spintronic implementation of DCGAN for image generation implemented via blocks such as a generator, discriminator, ReLU, and Leaky ReLU using spintronic devices. In the generator network, deconvolution block inputs are zero-padded to achieve up-sampling followed by a convolution operation, reducing boundary effects and maintaining spatial information to transform random noise into synthetic data. The deconvolution is implemented using our proposed skyrmion based cross bar [3] array with an ultra-low write energy of 2.0 fJ/unit to store the kernel values. Additionally, we designed a hybrid CMOS-domain wall-based ReLU circuit with a power consumption of 4.7μW. We also propose a modified CMOS hybrid domain wall circuit to implement the leaky ReLU activation function and employ the skyrmion based crossbar array for the convolution block of the discriminator network. The leaky ReLU functionality is achieved via modified uniaxial anisotropy profile of the domain wall. We further optimized Image generation using hyperparameters such as learning rate, batch size, number of epochs, and activation functions. Our proof-of-concept demonstration, as shown in Fig. 1, paves the way toward a comprehensive spintronic hardware-aware GAN. This development is highly promising for energy-efficient GANs implemented using skyrmion and domain wall devices, capturing spatial hierarchy and local dependencies in image data, and generating high-quality synthetic data that resembles real data for efficient real-time machine learning.

[1] Goodfellow, I., Pouget-Abadie, J., Mirza, M., Xu, B., Warde-Farley, D., Ozair, S., Courville, A. and Bengio, Y., 2020. Generative adversarial networks. *Communications of the ACM*, *63*(11), pp.139-144. [2] Dewi, C., 2024. Generative Adversarial Network for Synthetic Image Generation Method: Review, Analysis, and Perspective. *Applications of Generative AI*, pp.91-116. [3] Gupta, S., Vadde, V., Muralidharan, B. and Sharma, A., 2024. A Comprehensive Convolutional Neural Network Architecture Design using Magnetic Skyrmion and Domain Wall. *arXiv preprint arXiv:2407.08469*.

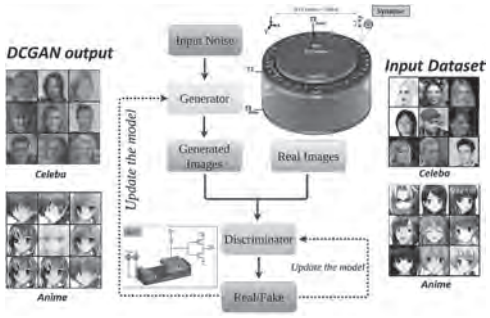

Block Diagram of Generative Adversarial Network with skyrmionic synapse and hybrid CMOS domain wall ReLU.

HC-04. Physical reservoir computing (PRC) utilizing a solid-state magneto-ionic platform. *M. Rajib*[1], D. Bhattacharya[2], M.F. Chowdhury[1], S. Sarker[1], C. Jensen[2], G. Chen[3], K. Liu[2] and J. Atulasimha[1,4] *1. Mechanical and Nuclear Engineering Department, Virginia Commonwealth University, Richmond, VA, United States; 2. Department of Physics, Georgetown University, DC, DC, United States; 3. Nanjing University, Nanjing, China; 4. Electrical and Computer Engineering, Virginia Commonwealth University, Richmond, VA, United States*

Recently, magneto-ionic control of interfacial magnetism has emerged as an ultra-energy-efficient method of controlling magnetization, leading to the proposal of various low-power spintronic devices. Magneto-ionics involves the migration of ions through electrolytes at the interface between magnets and electrolytes, modifying physical properties like perpendicular magnetic anisotropy (PMA) and the Dzyaloshinskii-Moriya Interaction (DMI) [1-3]. By applying a voltage pulse that moves oxides away from the interface, the PMA of the magnetic layer can be reduced (see Fig. 1). Conversely, applying a voltage of opposite polarity reintroduces oxide ions onto the magnetic layer, thereby increasing the PMA. However, changes in PMA are volatile due to ion diffusion processes, which exhibit a key characteristic of physical reservoir computing known as short-term memory. While several magneto-ionic devices have been proposed exploiting their energy-efficiency, a proof-of-concept magneto-ionic physical reservoir has yet to be demonstrated. In this study, we experimentally demonstrate that a magneto-ionic heterostructure can achieve the recognition of sine and square pulses from a small number of randomly distributed pulse train, as shown in Fig. 2, with 100% accuracy. Furthermore, besides illustrating the short-term memory capability of the magneto-ionic device, we quantify two performance metrics—namely, short-term memory (STM) and parity check capacity (PC)—which show promising values (1.44 and 2, respectively). Our work paves the way for exploiting relaxation dynamics of magneto-ionic devices and developing energy-efficient magneto-ionic devices. Acknowledgement: This work has been supported in part by the NSF (CCF-1909030, ECCS-2151809 and DMR- 2005108).

[1] Bauer et al. Nature Mater 14, 174–181 (2015). [2] Chen et al, Nat. Comm. 13, 1350 (2022). [3] Fillion et al, Nat. Comm. 13, 5257 (2022).

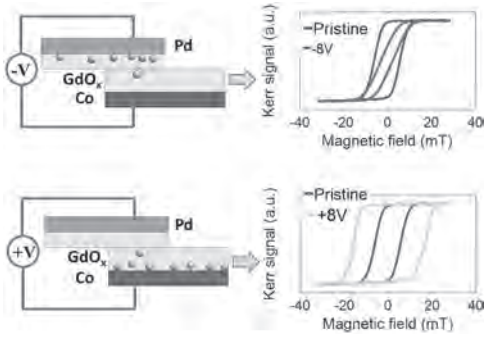

Fig. 1: Magneto-ionic control of PMA in a Co/Ni thin film with positive and negative voltage pulse.

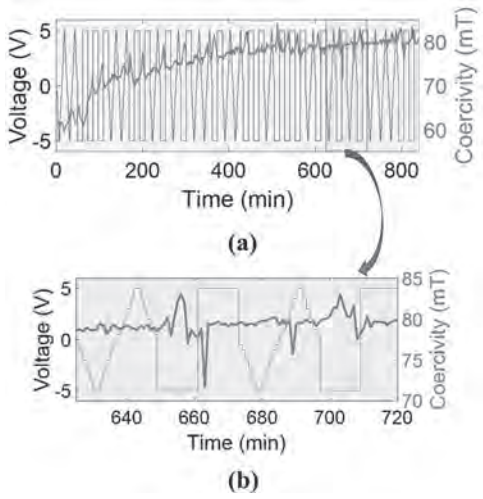

Fig. 2: (a) Coercivity changes induced by randomly distributed 35 sine and square voltage pulses. (b) Coercivity changes for pulses 27th to 30th are displayed (marked by green color in (a)). A distinct pattern emerges in the coercivity changes observed for sine and square pulses, with the square pulse demonstrating sharper peaks in comparison to the sine pulse.

HC-06. Implementing a Fault Tolerant Spin Ensemble Qubit with Exchange Coupling. *A. Chakraborty*[1], M.F. Chowdhury[1], M. Niknam[2,3], L. Bouchard[2] and J. Atulasimha[1] *1. Department of Mechanical and Nuclear of Engineering, Virginia Commonwealth University, Richmond, VA, United States; 2. Department of Chemistry and Biochemistry, University of California Los Angeles, Los Angeles, CA, United States; 3. Center for Quantum Science and Engineering, University of California Los Angeles, Los Angeles, CA, United States*

A qubit can potentially be realized as an ensemble of spins consisting of rare earth (RE) ions with long coherence time e.g., up to 3 ms for Yb^{3+} [1] or transition metal (TM) ions in a matrix. Previously we showed that, qubit consisting of widely separated and noninteracting ensemble of spins can be proximally controlled by the magnetic field generated from a nanomagnet or magnetic skyrmion with high fidelity although due to spatial variation of control field at 0-1 K [2][3]. Closely positioned spins induce significant exchange interaction that may help mitigate dephasing due to spatial field inhomogeneities. However, with the decrease of spin distance the dipolar interaction also increases. The latter causes significant dephasing [4]. Here, we have simulated spin dynamics for different spin arrangements with varying exchange interaction mitigating the effect of dipolar interaction, spatial field gradient and random noise. Our results indicate that although isotropic exchange improves fidelity to some extent through partially reducing decoherence due to the dipolar interaction, the anisotropic exchange Hamiltonian mostly mitigates the dephasing due to the dipolar interaction and hence improve the fidelity and coherence time (Figure-A). Isotropic exchange can entirely overcome the fidelity loss due to spatial variation of the control field. Moreover, with appropriate selection of isotropic exchange, the improvement in fidelity can be observed under moderate thermal (1K~16K) conditions (Figure B). By carefully choosing both isotropic and anisotropic exchange coefficients it is possible to obtain quantum gates with fidelity above 99.87% even in the presence of dipolar interactions, spatial gradient of control field and thermal noise that is comparable to single spin qubit fidelity 99.89%. Acknowledgement: NSF ExpandQISE grant #2231356.

1. Nature, 580, 201, 2020 2. Communications Physics 5, 284 no. 1 (2022). 3. arXiv:2401.00573 4. Proceedings of the National Academy of Sciences 119.15 (2022).

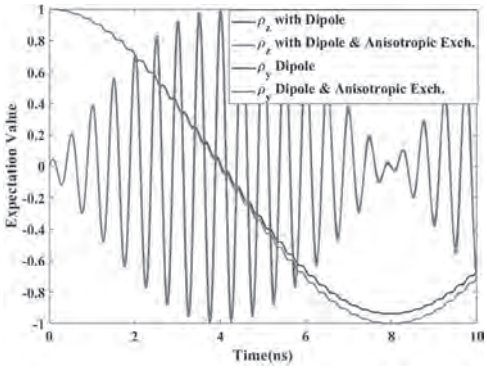

Figure (A): Comparison of Rabi oscillations with mw control field in Lab Frame and in non-thermal condition of four spins chain with dipole and anisotropic exchange interaction.

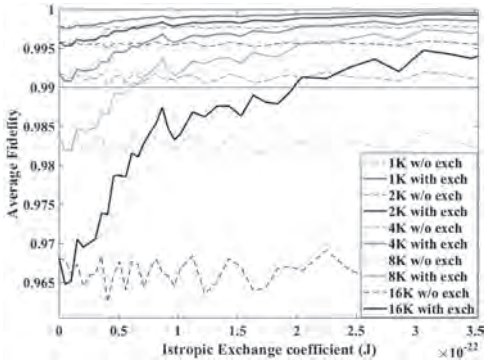

Figure (B): Average fidelity vs isotropic exchange coefficient plot for different temperatures.

HC-07. Pipelined Voltage-Propagated Skyrmion Logic with High Thermal Stability. *B. Walker*[1], K. Muthukrishnan[1], R. Thapa[1], E. Rivas[1], X. Hu[1], M. Frank[2], F. García Sánchez[3], A.J. Edwards[1] and J.S. Friedman[1] *1. Electrical and Computer Engineering, University of Texas at Dallas, Richardson, TX, United States; 2. Sandia National Laboratories, Albuquerque, AZ, United States; 3. Departamento de Fisica Aplicada, Universidad de Salamanca, Salamanca, Spain*

Previous works have demonstrated the feasibility and efficiency of skyrmions in cascaded logic structures inspired by reversible computing, either by pipelining the skyrmions with inefficient electronic current [1-3] or moving them individually with the highly efficient voltage-controlled magnetic anisotropy (VCMA) effect [4]. However, previous works had yet to demonstrate the pipelining of cascaded logic structures using VMCA propagation. In this work, we perform the first demonstration of pipelining with VCMA propagation, illustrated for a full adder that simultaneously performs three distinct addition tasks. Further, we provide insight into the extrinsic causes of dissipation that can be improved to help skyrmion logic approach the limit predicted by the Landauer principle.

[1]: M. Chauwin et al., Physical Review Applied 12 (2019) 064053 [2]: B. W. Walker et al., Applied Physics Letters 118 (2021) 192404 [3]: X. Hu et al., IEEE Magnetics Letters 13 (2022) 4503805 [4]: B. W. Walker et al., ArXiv Preprint, (2023), doi:10.48550/arXiv.2301.10700

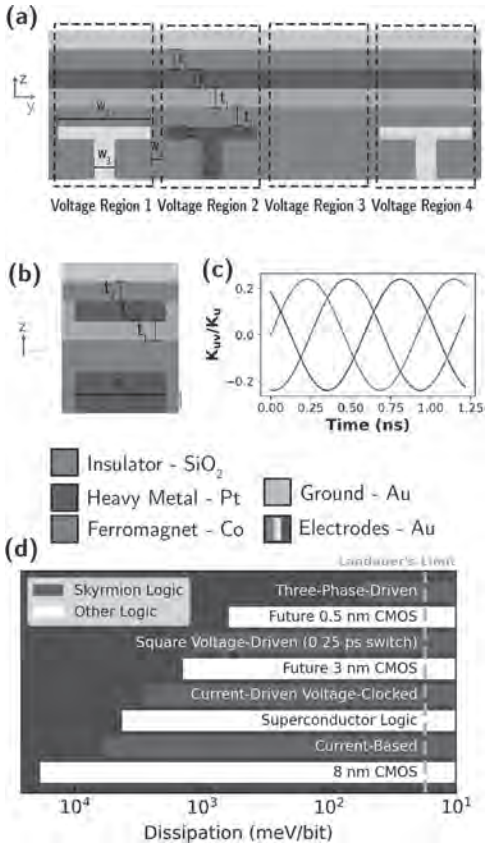

Figure 1. Three-phase VCMA propagated skyrmion logic operation. (a) YZ Cross Section. An electric field is applied across a Co/Pt interface (teal/purple) via electrodes (red/green/blue) separated by SiO2 (grey). The skyrmion exists in the ferromagnet layer. (b) XZ Cross Section (w_1=19 nm, w_2=1 nm, w_3=11 nm, w_4=20 nm, t_1=0.8 nm, t_2=0.5 nm) (c) VCMA anisotropy waveform applied to electrodes of corresponding color. (d) Comparison of total dissipation per bit processed for skyrmion logic technologies (red) and other logic technologies (white) relative to the room temperature Landauer limit (gold line).

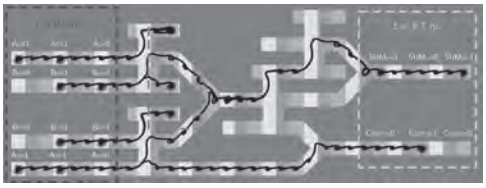

Figure 2. Micromagnetic simulation of pipelined full adder. Skyrmions are pipelined into the full adder form the left, encoding inputs (A_0=0, B_0=1; A_0=0, B_0=1; A_1=1, B_2=1; A_3=1, B_3=0). Black lines represent their trajectories, and skyrmions are propagated according to the respective VCMA regions (light red/green/blue) using the VCMA waveform shown in Fig. 1(c). At t=0 ns (blue), the skyrmions are initialized and propagated rightward to the correct logical outputs at t=8.7 ns (green).

Session HD
STATICS AND DYNAMICS OF MAGNETIC TEXTURES

Alejandro Riveros, Chair
Universidad Central de Chile, Santiago, Chile

INVITED PAPER

HD-01. Unraveling Optically Induced Ultrafast Modification of Nanoscale Magnetic Textures. *R. Jangid*[1,2], N. Zhou Hagström[1,3], M. Madhavi[1], K. Rockwell[4], J.M. Shaw[5], J. Brock[6], M. Pancaldi[7], D. De Angelis[7], F. Capotondi[7], E. Pedersoli[7], H.T. Nembach[8,9], M. Keller[5], S. Bonetti[3,10], E. Fullerton[6], E. Iacocca[4], R. Kukreja[1] and T. Silva[5]
1. University of California Davis, Davis, CA, United States; 2. Synchrotron Light Source II, Brookhaven National Laboratory, Upton, NY, United States; 3. Department of Physics, Stockholm University, Stockholm, Sweden; 4. Center for Magnetism and Magnetic Nanostructures, University of Colorado Colorado Springs, Colorado Springs, CO, United States; 5. Quantum Electromagnetics Division, National Institute of Standards and Technology, Boulder, CO, United States; 6. Center for Memory and Recording Research, University of California, San Diego, La Jolla, CA, United States; 7. Elettra Sincrotrone Trieste S.C.p.A., Trieste, Italy; 8. Department of Physics, University of Colorado, Boulder, CO, United States; 9. Physical Measurement Laboratory, National Institute of Standards and Technology, Boulder, CO, United States; 10. 'Department of Molecular Sciences and Nanosystems, Ca' Foscari University of Venice, Venezia, Italy

Ultrafast control of magnetization has emerged as a new paradigm for the next generation memory and data storage devices. Numerous studies have been performed to understand the mechanism of transfer of angular momentum at such fast timescales. However, it has been recently recognized that nanoscale heterogeneities can play a critical role in dictating the ultrafast behavior. I will discuss our recent experimental results at x-ray free electron laser (XFEL) sources where we uncovered magnetic texture dependent magnetization dynamics at ultrafast timescales. These experimental findings have been possible due to recent advances in x-ray and extreme ultraviolet sources which combine the power of coherent x-rays with femtosecond (fs) temporal resolution. Our results shows that the symmetry of magnetic texture dictates the magnitude and timescale of the ultrafast response [1-2]. These results clarify the previous controversy in the literature for time-resolved magnetic studies for different samples showing distinct responses. We also observed fluence threshold dependence for distortions of diffraction pattern which are not seen for magnetization quenching, consistent with a picture of domain wall motion with pinning sites. Supported by simulations, we show that a speed of ~66 km/s for highly curved domain walls can explain the experimental data [2]. We show that far from equilibrium behavior can be used to manipulate spin degrees of freedom at mesoscopic lengthscales.

1. Nanna Zhou Hagström et al. PRB 106, 224424 (2022) 2. Rahul Jangid et al. PRL 131, 256702 (2023)

CONTRIBUTED PAPERS

HD-02. Co/Gd based nanofilm engineering for the ultrafast field-free optical writing of nanometer-scale skyrmion bubbles. *M. van der Schans*[1] and B. Koopmans[1] *1. Applied Physics and Science Education, Eindhoven University of Technology, Eindhoven, Netherlands*

Silicon transistors form the basis of today's information society. However, there is an increasing demand for more efficient and powerful computing. An option for satiating this demand can be found in magnetic skyrmions, as their topological protection and mobility are excellent for usage in data storage and transmission. More specifically, optical nucleation and/or toggle switching of skyrmions could be highly beneficial because of its ability to be implemented in photonic integrated chips. Nanofilms with Co as a core ferromagnetic material have been shown, recently, to allow for the stochastic optical nucleation of skyrmions with a supporting external field [1]. Alternatively, Co/Gd based structures display deterministic All-Optical Switching (AOS) of, albeit micrometer-scale, magnetic domains [2]. In this work, we try to profit from both developments. By specially engineered magnetic nanofilms, we aim at optically generating single bubble skyrmions, that remain stable without the addition of an external field. First, we've shown that it is possible to nucleate an ensemble of quasi-randomly distributed skyrmions. We did so by growing a Pt/Co/Ir nanofilm near the Spin-Reorientation Transition (SRT) from Out-Of-Plane (OOP) to In-Plane (IP) magnetization. The origin of this behaviour seems to lie in the ultrafast phase transition from OOP to IP as the system is heated by a femtosecond laser pulse, and successively quenches back to the OOP configuration while cooling down. Secondly, experiments on optically writing and annihilating skyrmionic bubbles in a fully deterministic fashion without an external field are in progress. Preliminary experiments on a Pt/Co/Gd/Co/Pt/Co/Ir stack have shown regimes with larger AOS domains and regimes with smaller stochastically nucleated skyrmions, depending on the laser fluence, but the combination of the two has not yet been achieved. These results are seen as a stepping stone towards achieving the deterministic writing and annihilation of single skyrmions for computational purposes.

[1] : K. Gerlinger, B. Pfau and F. Büttner, Apply. Phys. Lett., Vol 118, p.192403 (2021) [2] : M. L. M. Lalieu, M.J.G. Peeters and S. R. R. Haenen, Phys. Rev. B, Vol 96, p.220411 (2017)

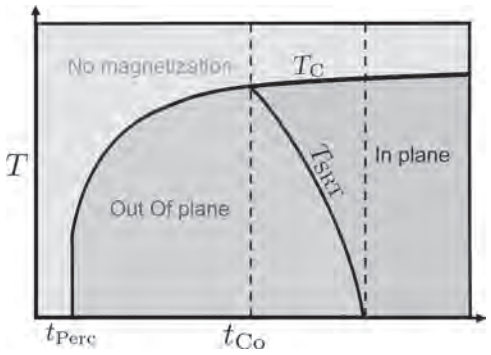

Fig. 1: Phase diagram of the magnetic state of Pt/Co/Ir as a function of temperature T and Co thickness t_{Co}

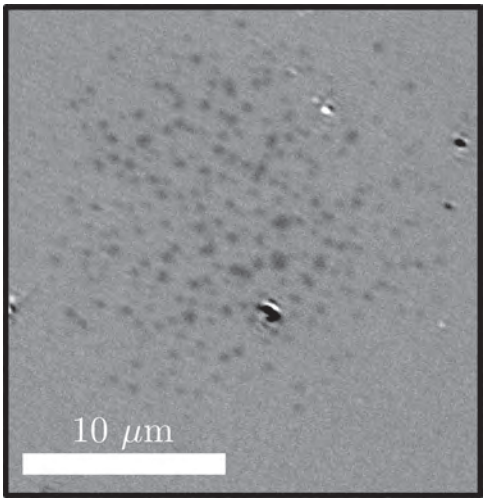

Fig. 2: Kerr microscopy image of an optically nucleated ensemble of skyrmions in Pt/Co/Ir.

HD-03. From Ferromagnetic Magnetostatics to Antiferromagnetic Topology: Antiferromagnetic Vortex States in NiO-Fe Nanostructures. M. Slezak[1], *T. Wagner*[2], V. Bharadwaj[2], O. Gomonay[2], A. Koziol Rachwal[1], T.O. Mentes[3], A. Locatelli[3], M. Zajac[4], D. Wilgocka-Slezak[5], P. Drozdz[6] and T. Slezak[1] *1. Faculty of Physics and Applied Computer Science, AGH University of Science and Technology, Krakow, Poland; 2. Institute of Physics, Johannes Gutenberg University Mainz, Mainz, Germany; 3. Elettra - Sincrotrone Trieste S.C.p.A., Trieste, Italy; 4. National Synchrotron Radiation Centre SOLARIS, Jagiellonian University, Krakow, Poland; 5. Jerzy Haber Institute of Catalysis and Surface Chemistry PAS, Krakow, Poland; 6. Institute of Physics, Maria Curie-Sklodowska University, Lublin, Poland*

Magnetic vortices are topological spin structures commonly found in ferromagnets. However, they are novel for antiferromagnets, which promise faster intrinsic dynamics compared to ferromagnets. In particular, Wu et al. observed the interface-exchange-coupling-dependent transfer of the Fe vortex state to the coupled CoO or NiO layer for patterned microstructures [1]. We experimentally demonstrate that in a nanostructured antiferromagnetic-ferromagnetic hybrid bilayer, a magnetic vortex naturally stabilizes by magnetostatic interactions in the Fe(110) and imprints onto the adjacent NiO(111) via interface exchange coupling, as shown in Fig. 1. We assume the coupling to be collinear, as recently reported in continuous NiO(111)-Fe(110) bilayers by Slezak et al. [2]. Our micromagnetic simulations elucidate the mechanism for the existence of antiferromagnetic vortex states [3]. Visualizations of our micromagnetic simulations shown in Fig. 2 indicate good correspondence with the experimental results. We find that the interplay between the interface exchange coupling and the antiferromagnetic anisotropy plays a crucial role in locally reorienting the Néel vector out-of-plane in the prototypical in-plane antiferromagnet NiO and thereby stabilizing the vortices in the antiferromagnet.

[1] Wu, J. et al. Nat. Phys. 7, 303-306 (2011). [2] Slezak, M. et al. Nanoscale 12, 18091-18095 (2020). [3] Slezak, M., Wagner, T. et al., arXiv:2403.05151 (2024).

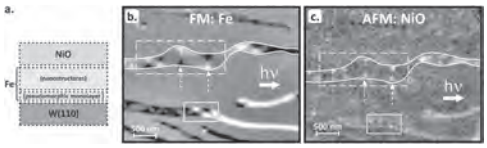

Fig. 1: a) Schematic representation of the NiO-Fe bilayer structure. b,c) XMCD- and XMLD-PEEM images of a typical 4μm×3.0μm region which includes several NiO-Fe nanostructures. Dashed arrows indicate the position of vortex states.

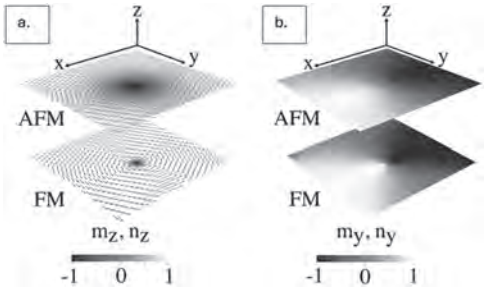

Fig. 2: a, b) Magnetization (m) and the Néel vector (n) configuration in the z and y components. The upper layer represents the AFM Néel vector, while the lower layer represents the FM magnetization. The color codes indicate the magnitude of the selected order parameter. In a) the arrows indicate the in-plane components of the magnetization and of the Néel vector.

HD-04. Demonstration of the Current-induced Creation and Motion of Magnetic Vortex-Antivortex Pairs. *J. Yang*[1], T. Lee[1], S. Ko[1], K. Moon[2], S. Lee[3], M. Shin[4], S. Kim[5] and K. Kim[1] *1. Physics, Korea Advanced Institute of Science and Technology, Daejeon, The Republic of Korea; 2. Quantum Spin Team, Korea Research Institute of Standards and Science, Daejeon, The Republic of Korea; 3. Electronic Engineering, Gachon University, Seongnam, The Republic of Korea; 4. Electrical Engineering, Korea Advanced Institute of Science and Technology, Daejeon, The Republic of Korea; 5. Physics, University of Ulsan, Ulsan, The Republic of Korea*

Topological spin textures in magnetic materials, such as domain walls (DWs), skyrmions, and Bloch lines have been receiving significant attentions owing to their extraordinary stability based on the topological arguments [1, 2]. The topology of the spin textures is characterized by non-trivial topological charge, which is conserved and topologically protected in a continuous magnetic system [3]. These intriguing properties have led to extensive research on the topological spin textures, paving the way for technological applications in future spintronic devices such as DW-based and skyrmion-based racetrack memory. In in-plane magnetized systems, vortex and antivortex structures are also topologically non-trivial spin textures with curling magnetic configurations around their cores [4-6], leading to a stable state by reducing the magnetostatic energy. The vortex-antivortex (V-aV) pairs can be stabilized in the patterned in-plane ferromagnet by forming a sequential chain within the DW, which is also called a cross-tie wall [7]. In this work, we investigate the current-induced creation and motion of the V-aV pairs in in-plane magnetized Permalloy (Py) thin film. A 40-nm-thick Py film is patterned into a trapezoidal structure, which enables the DW to be stably positioned at the center of the patterned element. We find that the V-aV pairs are generated and shifted within the DW by nanosecond current pulses, and we analyze their dynamic behaviors using magneto-optical Kerr effect (MOKE) microscopy and MuMax3 micromagnetic simulations [8]. Our results suggest that the dynamics of V-aV pairs can be utilized as a next-generation racetrack memory beyond the DW- and skyrmion-based racetrack memory.

[1] N. D. Mermin, Rev. Mod. Phys. 51, 591 (1979) [2] H. B. Braun, Adv. Phys. 61, 1 (2012) [3] N. Nagaosa, and Y. Tokura, Nat. Nanotechnol. 8, 899 (2013) [4] M. Löhndorf, A. Wadas, and R. Wiesendanger, Appl. Phys.

Lett. 68, 3635 (1996) [5] A. Hubert, and R. Schäfer, Magnetic Domains: The Analysis of Magnetic Microstructures, Springer (1998) [6] K. Shigeto, T. Okuno, and T. Ono, Appl. Phys. Lett. 80, 4190 (2002) [7] S. Middelhoek, J. Appl. Phys. 34, 1054 (1963) [8] A. Vansteenkiste, J. Leliaert, and B. V. Waeyenberge, AIP Adv. 4, 107133 (2014)

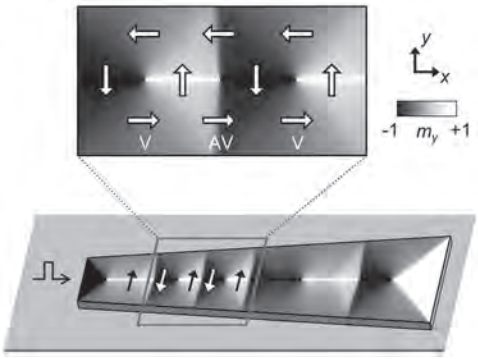

Fig. 1. Schematic illustrations of vortex-antivortex (V-aV)-based race-track memory. The detailed magnetization profile is shown in the zoomed image, indicating the sequential chain of V-aV pairs.

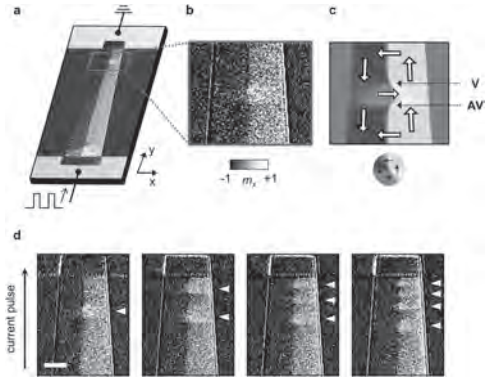

Fig. 2. Current-induced multiple V-aV creation. (a) Py trapezoidal device structure and MOKE image after the creation of a single V-aV pair. (b) The zoomed MOKE image and (c) corresponding simulated image of a V-aV pair. (d) MOKE image sequence of current-induced multiple V-aV creation, as indicated by yellow wedges. Scale bar is 10 μm.

HD-05. Modulated Effective Exchange in PyGd Alloys Probed through Vortex Annihilation Processes. *L. Jacob*[1], H. Han[2], M. Im[3] and S. Pollard[1] *1. Department of Physics and Materials Science, University of Memphis, Memphis, TN, United States; 2. Department of Materials Science and Engineering, Korea National University of Transportation, Chungju, The Republic of Korea; 3. Advanced Light Source, Lawrence Berkeley National Laboratory, Berkeley, CA, United States*

Magnetic vortices represent promising magnetic structures with applications ranging from novel memory and logic devices to biomedical fields. Owing to their stable, quasiparticle nature, they also provide tools in which to study fundamental magnetic interactions in thin films. The vortex has been previously broadly studied in ferromagnetic materials such as permalloy [1-4]. However, significantly less work has focused on ferrimagnetic systems. Recently, ferrimagnetic thin films have garnered interest due to their potential in ultrafast, energy efficient spintronic devices, owing to the negative exchange interaction between disparate magnetic sublattices [5]. In rare earth (RE)/transition metal (TM) ferrimagnetic alloys, further control of the vortex comes from tunable sublattice interactions. In this work, we utilize transmission x-ray magnetic circular dichroism (XMCD) to understand the impact of Gd concentration on the reversal process in Py_xGd_{1-x} alloys, and link these changes to the well-understood change in saturation magnetization with RE concentrations, as well as changes in the effective exchange stiffness. Discs with a diameter of 4 μm and a net thickness of 100 nm were patterned on Si_3N_4 membranes using electron beam lithography. Alloyed films were grown by co-sputtering Py and Gd with a fixed Py deposition power while varying the Gd sputter power. Gd concentrations varied from 0-30%. The vortex annihilation process was imaged using full-field transmission soft X-ray microscopy (XM-1, BL 6.1.2) at room temperature (Fig. 1). A significant decrease in the vortex annihilation field is found (Fig. 2) which cannot be explained solely by a decrease in saturation magnetization. By fitting measured and simulated annihilation behavior using micromagnetic modelling, the effect of Gd concentration on the effective exchange stiffness is investigated. Further, these changes are linked to a transition from nanocrystalline Py films to an amorphous PyGd system and compared to results in PyGd multilayers extracted by Lapa et al [6]. Funding from the NSF (ECCS-2138271) and the DOE (Contract No. DE-ACO2-05CH11231) are gratefully acknowledged.

[1] K. Guslienko, K. Metlov, Physical Review B., Vol. 63 (2001) [2] S. Kim, Y. Choi, and K. Lee, Applied Physics Letters., Vol. 91 (2007) [3] D. Kim, E. Rozhkova, and I. Ulasov, Nature Materials., Vol. 9 (2010) [4] C. Holl, M. Knol, and M. Pratzer, Nature Communications., Vol. 11 (2020) [5] S. Kim, G. Beach, and K. Lee, Nature Materials., Vol. 21, p. 24-34 (2022) [6] P. Lapa, J. Ding, and C. Phatak, Journal of Applied Physics., Vol. 122 (2017)

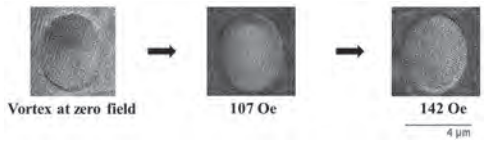

Fig. 1 XM-1 Imaging of Vortex

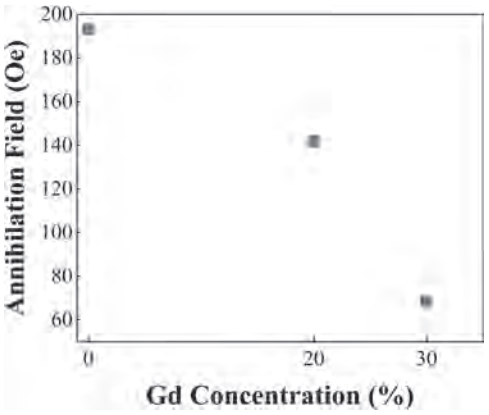

Fig. 2 Gd Concentration vs. Annihilation Field

HD-06. Computational studies of novel Dzyaloshinsky-Moriya interactions. *S.J. Holt*[1,2], S.A. Pathak[1,2], M. Lang[1,2] and H. Fangohr[1,2,3] *1. Max Planck Institute for the Structure and Dynamics of Matter, Hamburg, Germany; 2. Center for Free-Electron Laser Science, Hamburg, Germany; 3. University of Southampton, Southampton, United Kingdom*

The exploration of magnetic phases in chiral magnets has gathered significant interest due to the unique physics and potential applications of these materials. A key factor in these systems is the Dzyaloshinsky-Moriya Interaction (DMI) [1, 2], which arises from the asymmetric environment of interacting magnetic spins and is linked to non-centrosymmetric crystallographic point groups. While a few point groups have had their DMI extensively studied, many remain unexplored [3]. In this talk, we present results which start to address this gap by computationally investigating these relatively unexplored DMI terms. These novel terms have been integrated into micromagnetic simulation tools, and made available as open-source resources. We systematically explore the multidimensional parameter space of these new DMI terms

to identify magnetic phases and classify new ones By leveraging Machine learning algorithms, such as clustering and autoencoders, have been using to automate this process, rapidly identifying and cluster similar magnetic phases across vast parameter spaces. As a result, we have generated detailed phase diagrams for select crystallographic point groups and obtained novel and complex magnetic structures such as Figure 1. This project has received funding from the European Union's Horizon 2020 research and innovation programme under the Marie Sklodowska-Curie grant agreement No 101152613 and MaMMoS No 101135546.

[1] I. Dzyaloshinsky, Journal of Physics and Chemistry of Solids, Vol. 4, (1958) [2] T. Moriya, Physical Review, Vol. 120 (1960) [3] I. A. Ado, A. Qaiumzadeh, A. Brataas, and M. Titov, Physical Review B, Vol. 101 (2020)

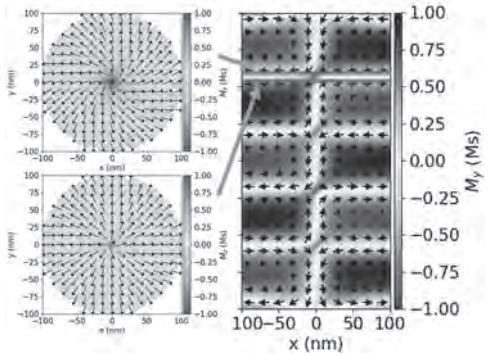

Fig.1: Micromagnetic simulation for D_n n ≥ 3 crystallographic point group showing a stacked vortex structure with stable Bloch points. The images in the left represent cross-sections at the positions of the red lines shown on the right.

HD-07. Finite Element Method Modeling of Magnetoelastic Dynamics.

E. Savostin[1] and V. Lomakin[1] *1. Materials Science, University of California San Diego, La Jolla, CA, United States*

This work explores the implementation of finite element method (FEM) modeling for fully coupled magnetoelastic formulation, incorporating the Landau-Lifshitz-Gilbert (LLG) and displacement wave elastic equations. Given the stiff nature of the elastic equations, partially integrated elements such as TET10, HEX8, and HEX20 are utilized. The Ritz method is employed for the variational formulation. The Newmark method is used for the time stepping of the elastic equations. Backward differentiation and midpoint rule are used for the time stepping of the LLG equation. The magnetization and displacements are updated via non-linear iterations to provide self-consistent magnetoelastic solutions. The magnetoelastic equations encompass both direct and reverse magnetostriction effects, enabling the simulation of the magnetization dynamics, such as skyrmions and spin-transfer torque (STT) oscillators, where strain fields drive their behavior. Furthermore, we demonstrate that strain-dependent Dzyaloshinskii-Moriya interaction can amplify the nonlinear breathing modes of skyrmions. Figure 1 shows spatial distribution of 1D magnetoelastic waves in thin ferromagnetic film.

[1] R. Ludwig and W. Lord, "A finite-element formulation for the study of ultrasonic NDT systems," in *IEEE Transactions on Ultrasonics, Ferroelectrics, and Frequency Control*, vol. 35, no. 6, pp. 809-820, 1988. [2] E. Savostin and V. Lomakin, "Giant phonon-skyrmion coupling in ferromagnet/heavy metal heterostructures", PRB, 2024.

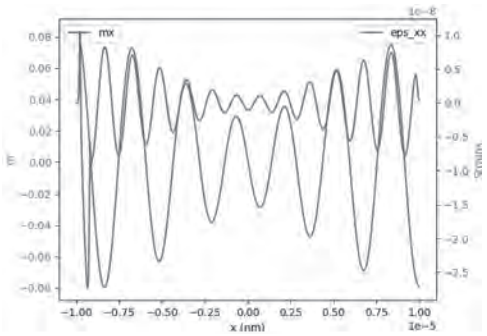

Fig. 1

Session HE
SENSORS AND APPLICATIONS III

Andrea Meo, Chair
Politecnico di Bari, Bari, Italy

INVITED PAPER

HE-01. Magnetic Layering for Low Detectability Magnetoelectric Magnetic Sensors. *J. McCord*[1] *1. Department of Materials Science, Kiel University, Kiel, Germany*

Magnetic field sensors are devices that detect and measure magnetic fields around permanent magnets, electrical conductors, and electrical devices. As such, they are particularly relevant for applications in IoT, 5G, smartphones, energy, and biomedical engineering. In this context, dedicated research is carried out on novel thin film composite magnetoelectric sensor concepts for the detection of magnetic fields down to the picotesla range. Advanced magnetooptical Kerr effect microscopy with high temporal resolution is used to study local effects in operating magnetoelectric composite sensor structures. Together with supporting electrical measurements, the realized magnetospatial analysis of working devices sheds light on magnetization changes due to domain nucleation, domain wall resonances, domain wall bending modes, and spin-wave-like phenomena. Each of these is specific to different types of composite magnetoelectric sensors, ranging from resonance to modulated to ΔE to SAW sensor systems excited from the kHz to the GHz regime. Complementary electrical noise and detection limit analyses reveal the different noise mechanisms, both electrical and magnetic, for the different sensors. By understanding the complex magnetic interactions, strategies and implementations are identified to optimize magnetic sensor structures. Various general concepts of magnetic layering for single domain behavior are presented. Based on the various examples, the design and application of flux-closed and magnetically domain-engineered multilayer structures with minimal noise in magnetoelectric sensors will be discussed. Layer-wise control of magnetic anisotropy is the key to sensor optimization in terms of detectability and efficient fabrication. By introducing special magnetic sensing layers with individual parallel, antiparallel or noncolinear magnetization arrangements, the influence of the existing carrier signals on the magnetic noise is strongly reduced. In particular, the absence of domain walls or pinned domain walls leads to a strong noise reduction and thus to a significant improvement of the detectability. Magnetostatically stabilized but still responsive single magnetic domain layers are the basis for low noise sensors. The applied magnetic lamination paves the way for ultra-low noise magnetoelectric sensor applications capable of detecting picotesla magnetic fields. Limits to sensitivity enhancement due to additional magnetoelastic domain effects leading to self-emergence of periodic magnetic domain structures in low anisotropy magnetic films are discussed. Further limitations arise from nonlinear magnetoelastic effects. With recent improvements due to magnetic layering, low-noise sensor detectabilities are now approaching fundamental limits. Funding by the DFG for the CRC 1261 “Magnetoelectric Sensors: From Composite Materials to Biomagnetic Diagnostics” is highly acknowledged. The contributions of a large number of collaborators within the CRC and of Roland Mattheis are very much appreciated.

[1] L. Thormählen, P. Hayes, E. Elzenheimer, et al., Applied Physics Letters Vol. 124, p.17 (2024) [2] E. Spetzler, B. Spetzler, and J. McCord, Advanced Functional Materials, Vol. 34, p.2309867 (2024) [3] V. Schell, E. Spetzler, N. Wolff, et al., Scientific Reports, Vol. 13, p.8446 (2023) [4] C. Müller, P. Durdaut, R.B. Holländer, et al., Advanced Electronic Materials, Vol. 8, p.2200033 (2022) [5] P. Durdaut, C. Müller, A. Kittmann, et al., Sensors, Vol. 21, p.5631 (2021) [6] N.O. Urs, E. Golubeva, V. Röbisch, et al., Physical Review Applied, Vol. 13, p.024018 (2020) [7] M. Jovičević Klug, L Thormählen, V Röbisch, et al., Applied Physics Letters, Vol. 114, p.192410 (2019) [8] P Hayes, M Jovičević Klug, S Toxværd, et al., Scientific Reports Vol. 9, p.16355 (2019)

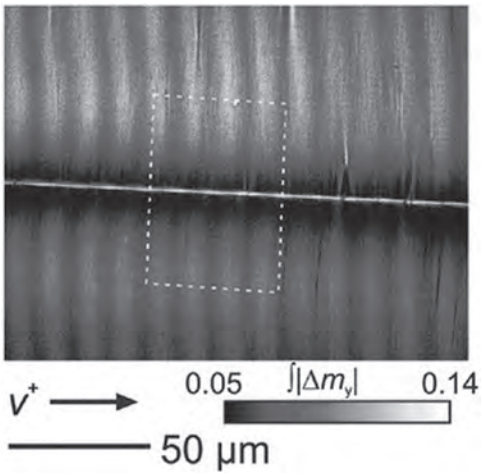

Figure 1. Operando time-resolved magnetooptical noise imaging of propagating surface acoustic wave amplitude variation in a magnetoelectric SAW sensor device, showing uncorrelated magnetic noise signatures at the domain walls (from [4]).

CONTRIBUTED PAPERS

HE-02. Utilizing Field Gradient Measurements for Object Tracking in Permanent Magnet Based Manipulation Systems. *J. Davy*[1], M. Brockdorff[1] and P. Valdastri[1] *1. School of Electronic Engineering, University of Leeds, Leeds, United Kingdom*

Advancements in magnetically actuated medical robots have driven the development of sophisticated magnetic manipulation systems [1]. These systems manipulate the magnetic field within a workspace, enabling the precise application of forces and torques to targeted magnetic robots within the body. A notable approach utilizes permanent magnets around the patient, creating a large workspace with high field strength [2]. For clinical applications, precise localization of the robot is crucial, necessitating reliable tracking methods as the system moves internally within the patient. Recent research has focused on localization systems that use measurements of the actuation magnetic field to estimate the robot’s pose. Previous studies have demonstrated effective 6-DoF (Degree of Freedom) localization using a combination of a single field sensor and an accelerometer. However, the rotational symmetry of a magnetic dipole creates a singularity plane, potentially causing erroneous localization and drift [3]. Additionally, these methods suffer from reduced accuracy in low magnetic fields due to the sensors’ decreased sensitivity. Where others have utilized field gradient localization in electromagnetic coil based actuation systems, this work explores their use in tracking during permanent magnet actuation [4]. Our approach extends existing methodologies by incorporating multiple field sensors and estimating gradients using finite differences. Given the relatively large gradients in permanent magnet actuation, we demonstrate that

our method is robust and resistant to singularities, effectively localizing with 6-DoF. We apply this technique to platforms utilizing one or multiple external permanent magnets and validate it through simulations and experimental studies, confirming our system's accuracy and robustness (Fig. 1 and 2). Our findings suggest that using field gradient measurements can enhance the precision of localization systems in permanent magnet actuation, eliminating the need for additional sensors or time-varying fields.

[1] Nelson, B.J., 2024. An electromagnetic robot for navigating medical devices. *Nature Reviews Bioengineering*, *2*(5), pp.370-371. [2] Pittiglio, G., Brockdorff, M., da Veiga, T., Davy, J., Chandler, J.H. and Valdastri, P., 2022. Collaborative magnetic manipulation via two robotically actuated permanent magnets. *IEEE Transactions on Robotics*, *39*(2), pp.1407-1418. [3] da Veiga, T., Pittiglio, G., Brockdorff, M., Chandler, J.H. and Valdastri, P., 2023. Six-degree-of-freedom localization under multiple permanent magnets actuation. *IEEE Robotics and Automation Letters*, *8*(6), pp.3422-3429. [4] Fischer, C., Quirin, T., Chautems, C., Boehler, Q., Pascal, J. and Nelson, B.J., 2022. Gradiometer-based magnetic localization for medical tools. *IEEE Transactions on Magnetics*, *59*(2), pp.1-5.

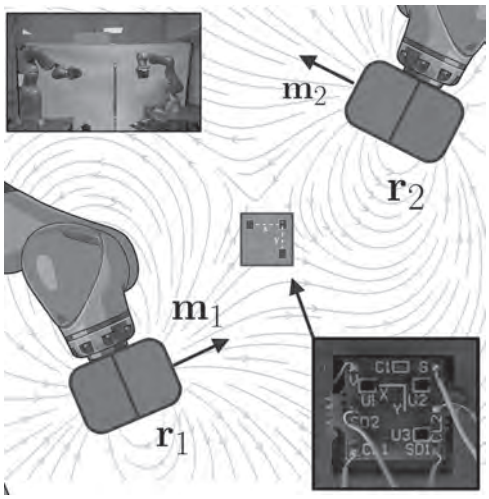

Fig 1. Diagram of gradient measurement by finite differences under multple manipulated magnet actuation.

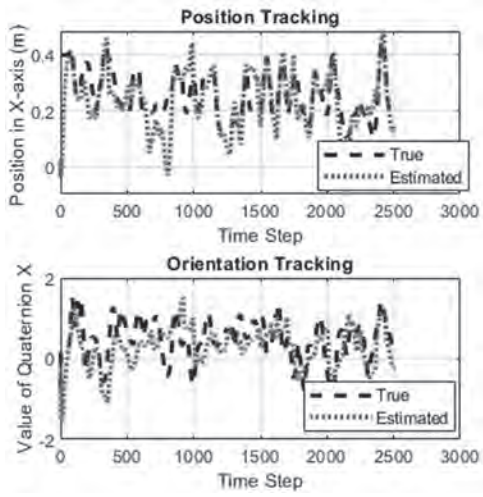

Fig 2. Pose tracking utilizing gradient measurements for a singular external magnet.

HE-03. Observation of magnetic nanoparticles-protein aggregates and highly sensitive protein detection. K. Kaneko[1], A. Ban[2], T. Murayama[2], L. Tonthat[1], *S. Yabukami*[2,1], M. Tanaka[3], Y. Tanaka[3] and T. Abe[2]
1. Graduate School of Engineering, Tohoku University, Sendai, Japan; 2. Graduate School of Biomedical Engineering, Tohoku University, Sendai, Japan; 3. Graduate School of Life Sciences, Tohoku University, Sendai, Japan

There is substantial demand for the rapid detection of proteins that can act as biomarkers for diagnosing metastatic cancer, mitochondrial disease, hypertension, etc. We developed a quick and easy detection system of protein. The increase of the protein aggregated the magnetic nanoparticles and enhanced the signal-to-noise ratio [1]. To obtain evidence for this hypothesis, we have observed magnetic nanoparticles and protein aggregates by a Transmission Electron Microscope (TEM, JEM-1400 Plus). Fig. 1 shows the TEM image of magnetic nanoparticles and protein aggregate with and without GDF-15. For this sample, the magnetic nanoparticles (Nanomag-D, average particle size 130 nmΦ) to which protein A was added were bound to the primary antibody (GDF-15 antibody). Then the antigen-antibody reaction with the antigen protein (GDF-15) was carried out. The GDF-15 concentrations were 0 and 1000 ng/ml. The number and size of aggregates on the images were analyzed by the software MIPAR. As a result, the percentage of aggregates larger than 0.03 μm^2 was approximately 5.8% at a concentration of 1000 ng/ml and approximately 4.2% at 0 ng/ml, and the value was higher when GDF-15 was included at 1000 ng/ml. It is thought that cross-bridges between the antigen and the magnetic nanoparticles occur, causing the size of the aggregates to increase. TEM observation and magnetic response revealed that the protein promotes the aggregation of magnetic nanoparticles. Fig. 2 shows the magnetic response as a function of the concentration of GDF-15 (0, 10, 30, and 100 pg/ml) when the switching magnetic field was applied [1]. We succeeded in detecting a protein (GDF15) in synthetic urine (including Creatinine of 7.6 mg/dL, BZ344, Chemazone Inc), achieving a high sensitivity of 10 pg/ml. The output voltage at 10 pg/ml increased 1.75 times higher than without antigen.

[1] Shin Yabukami, Toru Murayama, Koki Kaneko, Junichi Honda, Loi Tonthat, Kazuhiko Okita, "Magnetic response of aggregation mixed with magnetic nanoparticles and protein for simultaneous protein detection", *AIP Advances*, 14 (3), 035102 (2024).

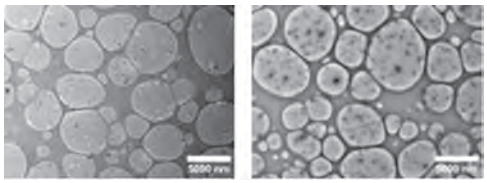

Fig. 1 TEM image of samples. (a)GDF-15 of 0 ng/ml. (b)GDF-15 of 1000 ng/ml.

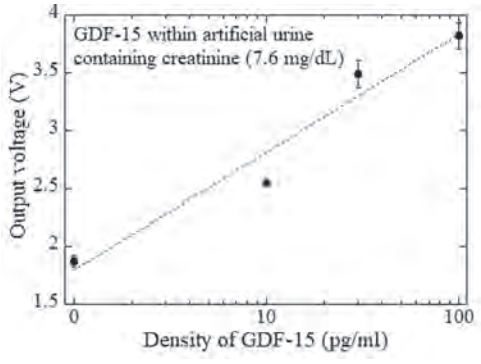

Fig. 2 Successful detection of protein (GDF15) in synthetic urine with a high sensitivity of 10 pg/ml.

HE-05. A machine learning powered wearable imaging sensor for cancer detection. *Z. Sun*[1], R. Hong[2,3], Q. Chen[4], H. Chang[3] and J. Hong[4]
1. Hubei University of Technology, Wuhan, China; 2. Albany High School, Albany, CA, United States; 3. Lawrence Berkeley National Lab, Berkeley, CA, United States; 4. UC Berkeley, Berkeley, CA, United States

Considerable progress has been achieved in the development of functional flexible materials, forming the foundation of flexible and wearable electronics. [1-3] These materials have undergone substantial advancements over the past decade. Based on this, we have designed a versatile multifunctional wearable imaging system with machine-learning algorithm for cancer detection as shown in Fig 1. The data services to enable sensor imaging and optimize pre- and post-operative care decisions for breast cancer will be provided in the future. Here, we present findings concerning the design and efficacy of a wearable, wireless patch designed for real-time imaging, employing flexible magnetoelectric nanoparticle (MENP) technology. [4,5] It integrates advanced magnetoelectric sensors for real-time imaging, capable of capturing highly detailed images that can be used for early detection of breast cancer. The device marks a substantial breakthrough in wearable sensing technology, offering direct practical applications in medical device market. It aims to minimize discomfort, increase screening frequency options, and improve early diagnosis in the future. As shown in Fig 2, sensor signals are acquired via ADC, processed, and converted into DAC output amplitudes to achieve real-time updates of DAC outputs. With further optimization, the system can integrate machine learning algorithms and this wearable devices to deliver appropriate and actionable data in 3D format to the patients and physicians.

[1] Li, W., Liu, H., Wu, F. 2023 8th International Conference on Information Systems Engineering (ICISE), Dalian, China, 2023, pp. 167-170, doi: 10.1109/ICISE60366.2023.00041. [2] He, T., C. Lee, C. IEEE Open Journal of Circuits and Systems, vol. 2, pp. 702-720, 2021, doi: 10.1109/OJCAS.2021.3123272. [3] Meng, H., Zhong, W., Ma, K. Engineered Regeneration, vol. 5, issue 2, pp. 186-198, 2024, ISSN 2666-1381, doi: 10.1016/j.engreg.2024.03.003. [4] Song, X. ACS Nano 18(26): 16648-16657, 2024. [5] Tu, J., Min, J., Song, Y. Nat. Biomed. Eng., vol. 7, pp. 1293-1306, 2023. [6] Park, H. IEEE Transactions on Biomedical Circuits and Systems, vol. 17, no. 5, pp. 889-899, Oct. 2023, doi: 10.1109/TBCAS.2023.3288126.

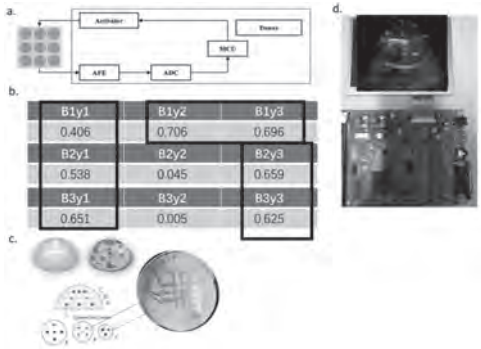

Fig 1. (a) The wearable sensing system by combining the sensors with a in-house built PCB. (b) The signal average in different areas of breast phantom which illustrates the differences in signals between cancer and normal cells. The shaded portion indicates signals from cancer cells. (c) The positions of cancer cells and normal cells. (d) During the scanning, changes in the spin-echo signal were observed.

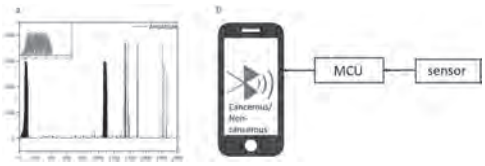

Fig 2 (a) The converted amplitudes to modulate the amplitude of the DAC output waveform. (b) how the final output signal changes received by a mobile APP. The wearable imaging system harnesses the sensors for real-time image acquisition, with the controller utilizing ATSAMV71Q21B for sensor signal processing. [6]

HE-06. Low Loss Phononic Phase Shifter Mediated by Acoustic Driven Magnetic Resonance. *A. Will-Cole*[1], A. Franson[2], A. Wendt[3], P. Shah[2], L. Hackett[1], M. Miller[1], M. Newburger[2], M. Page[2] and M. Eichenfield[1,3]
1. Sandia National Laboratories, Albuquerque, NM, United States;
2. Air Force Research Laboratory, Fairborn, OH, United States;
3. University of Arizona, Tucson, AZ, United States

A key advantage of operating in the acoustic domain for high frequency applications is that there is significant velocity reduction when converting between the electromagnetic to acoustic domain leading to a 10^5 increase in the delay per unit length. Reconfigurable phononic integrated circuits are desirable for a plethora of applications ranging from radiofrequency front ends, neuromorphic computing, to quantum computing and memory storage based on phonons. A phononic phase shifter is a critical component for these future reconfigurable phononic integrated circuitry, however there are limited mechanisms to achieve acoustic phase shifts. Current acoustic phase shifts are achieved via the electro-acoustic effect such that the change in the elasticity of a solid due to an applied voltage to cause a change in the phase velocity of travelling acoustic waves.[1] However, the electro-acoustic effect is very weak enabling only small phase shifts, therefore requiring longer delay lengths to achieve π phase shifts which means more propagation loss incurred. Recently acoustic driven magnetic resonance (ADMR) whereby magnetic spin waves are coupled to surface acoustic waves, have shown magnetically tunable, non-reciprocal transmission of acoustic power and phase accumulation. [2]-[5] Typically, ADMR devices are based on bulk ferroelectric substrates, such as LiNbO3. Here we fabricated and characterized Ni-based ADMR delay lines on an acoustic platform of LiNbO3 film integrated on a silicon substrate. We studied coupling to several acoustic modes – Rayleigh, spurious Rayleigh, and a Shear Horizontal surface acoustic wave mode – and identified magnetically tunable switching paths with unprecedentedly short propagation lengths and corresponding ultralow loss to achieve π phase shifts. We have found that these ADMR modes can achieve the desired tunability of wave velocity without large coupling losses, therefore this platform is technologically relevant for phonon phase shifting applications. SNL is managed and operated by NTESS under DOE NNSA contract DE-NA0003525.

[1] L. Shao, D. Zhu, M. Colangelo *et al. Nat Electron,* 5, 348–355 (2022). [2] J. Shah et al, Sci. Adv. 6, eabc5648, (2020). [3] D.A. Bas et al, Phys. Rev. Appl., 18, 044003 (2022). [4] M. Kuß et al, Phys.Rev. B,107, 0244, (2023). [5] M. Kuß et al, ACS Appl. Electron. Mater., 5, 9, 5103, (2023).

HE-07. Urban Traffic Vehicle Speed Estimation Solutions Using Dual-Axis Magneto-Impedance Sensors. *R. Yao*[1] and T. Uchiyama[1]
1. Graduate School of Engineering, Nagoya University, Nagoya, Japan

With the rapid development of automated driving, urban vehicle speed estimation faces new challenges: the real-time monitoring area needs to be expanded significantly. However, traditional vehicle detection devices (such as traffic cameras, infrared, and ultrasonic sensors) are costly and cannot be deployed over large areas quickly. Therefore, we propose a vehicle speed estimation system using low-cost, high-accuracy Magneto-Impedance (MI) sensors, which serve as Vehicle-to-Infrastructure (V2I) devices to

estimate the speed of moving vehicles in real time. Mainstream vehicle speed estimation methods based on magnetic sensors primarily use time-domain signal processing [1], [2]. By utilizing multiple sensors, speed is estimated by analyzing the magnetic signatures of the signals and the time differences between them. However, variations in driving conditions, vehicle loads, and sensor setups can lead to significant errors. To address these issues, we analyzed the magnetic signatures of various vehicle types and different measurement scenarios, optimizing the experimental setup. We achieved a 97% average accuracy in speed estimation (± 3 km/h) using the time difference method with sensor spacing of 1.6 m and a placement height of 0.66 m. Nevertheless, time-domain methods often require multiple sensors and straight roads. In real-world scenarios, not all roads meet these conditions. To maximize the speed measurement range, we propose a speed estimation method using a single MI sensor based on frequency-domain signals. We analyzed the dominant frequencies of vehicles driving on straight and curved roads and trained magnetic models using deep learning to validate the results. The trained magnetic model of passenger cars is shown in Fig. 1. This frequency-domain method achieved a measurement accuracy of 93.6% within a 5 km/h error range.

[1] D. Obertov, V. Bardov and B. Andrievsky, 2014 6th International Congress on Ultra Modern Telecommunications and Control Systems and Workshops (ICUMT), pp. 111-117, doi: 10.1109/ICUMT.2014.7002088.
[2] K. Wang, H. Xiong, and J. Zhang, IEEE Internet of Things Journal, vol. 8, no. 22, pp. 16666-16679, 15 Nov.15, 2021, doi: 10.1109/JIOT.2021.3074907.

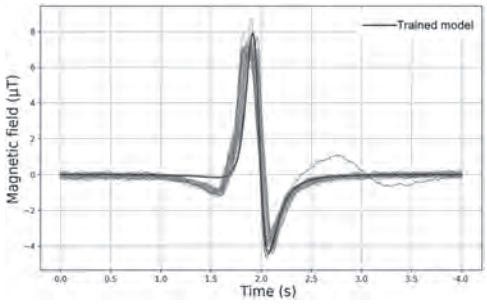

Fig. 1: Trained magnetic model of passenger cars.

Session HF
TERAHERZ ANTIFERROMAGNETIC SPINTRONICS

Vito Puliafito, Chair
Politecnico di Bari, Bari, Italy

INVITED PAPER

HF-01. Terahertz antiferromagnetic dynamics induced by ultrafast spin currents. *J. Chauleau[1] 1. SPEC, CEA-Saclay, Gif-sur-Yvette, France*

Insulating antiferromagnets have emerged as significant players in the realm of ultrafast spintronics. Their intrinsic terahertz spin dynamics (see for example [1]) and their capacity to convey spin currents (see for example [2]) make them highly promising for processing spin information at terahertz rates. This capability opens up new perspectives for tomorrow's ultrafast devices. However, the direct transfer of spin angular momentum to an antiferromagnetic insulator at picosecond and sub-picosecond time scales has yet to be conclusively demonstrated. In this presentation, I will address this issue, specifically discussing our experimental evidence that the transfer of ultrafast spin angular momentum to an antiferromagnetic texture can generate coherent terahertz antiferromagnetic excitations [3]. We achieve this through a combination of advanced time-resolved magneto-optical experiments on ferromagnetic/antiferromagnetic bilayers and state-of-the-art mastering of thin epitaxial layer antiferromagnetic textures [4,5]. These findings underscore the efficiency of ultrafast spin transfer torque in triggering antiferromagnetic dynamics and, more broadly, confirm that magnetic information can indeed be propagated into antiferromagnetic spin waves at picosecond timescales.

[1] T. Kampfrath et al. *Nat. Photon*. 5, 31 (2011) [2] R. Lebrun et al. *Nature*, 561 222 (2018) [3] S. René et al, arXiv:2407.14787 [4] P. Dufour et al., *Nanoletters*, 23, 2073 (2023) [5] J.-Y. Chauleau et al., *Nat. Mater.* 19, 386 (2020)

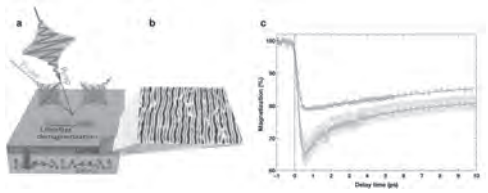

Fig. 1: a) Schematic representation of the Tr-MOKE experimental configuration. The large bi-color double arrow stands for the ultrafast exchanges of angular momentum between the ferromagnet and the antiferromagnet. b) Scanning nitrogen-vacancy magnetometry image of the single AF cycloidal state present in the epitaxial $BiFeO_3$ layer with a typical period of 67 nm. c) Ultrafast magnetization dynamics of the CoFeB/$BiFeO_3$ bilayer (orange dots) and the CoFeB reference layer (blue dots). The CoFeB magnetization and the probe incidence plane are along the $BiFeO_3$ cycloid plane or the $DyScO_3$ a-axis and the probe is p-polarized. The magnetization dynamics is presented as in percent (%) of variation.

CONTRIBUTED PAPERS

HF-02. Distortion-free sampling of ultrabroadband terahertz electric fields by spin accumulation. A. Chekhov[1,2], Y. Behovits[1,2], J. Heitz[1,2], M. Syskaki[3], S. Jaiswal[3], *O. Gueckstock*[1,2], B. Serrano[1,2], A. Ruge[1,2], J. Kredl[4], M. Wolf[2], M. Münzenberg[4], G. Jakob[3], M. Kläui[3], T. Seifert[1,2] and T. Kampfrath[1,2] *1. Freie Universität Berlin, Berlin, Germany; 2. Fritz-Haber-Institut der Max-Planck-Gesellschaft, Berlin, Germany; 3. Institute of Physics, Johannes Gutenberg University, Mainz, Germany; 4. Institute of Physics, Greifswald University, Greifswald, Germany*

In spintronics, FM|HM stacks consisting of a ferromagnetic-metal (FM) and a heavy-metal (HM) layer are versatile model systems with elementary functionalities like spin transport, spin-charge interconversion and torque [1]. Excited by femtosecond laser pulses, FM|HM stacks emit ultrabroadband terahertz electromagnetic pulses that have sizeable amplitude and carry unique information on ultrafast processes inside the stack [2,3]. However, in contrast to the generation of terahertz fields, their spintronic detection has not yet been addressed. Here, we apply intense terahertz pulses to FM|HM stacks and probe the resulting optical birefringence. Strikingly, the signal odd in the FM magnetization agrees excellently with the shape of the incident terahertz electric field over the full bandwidth 1-13 THz (see Fig. 1). Analysis indicates that the birefringence arises from the terahertz-field-driven spin accumulation at the FM/HM interface through the spin Rashba-Edelstein effect [5], which decays by electron velocity relaxation in <10 fs. A possible contribution by the spin Hall effect is minor as it would be longer-lived. Our results demonstrate spintronic detection of intense ultrabroadband terahertz fields with extremely flat amplitude and phase response and, thus, no need for deconvolution procedures. Our experiment provides time-domain signatures of the spin Rashba-Edelstein effect and can be viewed as an implementation of interface-specific terahertz-optical sum-frequency generation.

1. Seifert, T. S., Cheng, L., Wei, Z., Kampfrath, T. & Qi, J. *Appl Phys Lett* 120, 180401 (2022). 2. Rouzegar, R., Chekhov A.L. *et al. Phys Rev Appl* 19, 034018 (2023). 3. Rouzegar, R. *et al. Phys Rev B* 106, 144427 (2022). 4. Chekhov A.L. *et al. Phys Rev Appl* 20, 034037 (2023) 5. Manchon, A. *et al. Rev Mod Phys* 91, 035004 (2019).

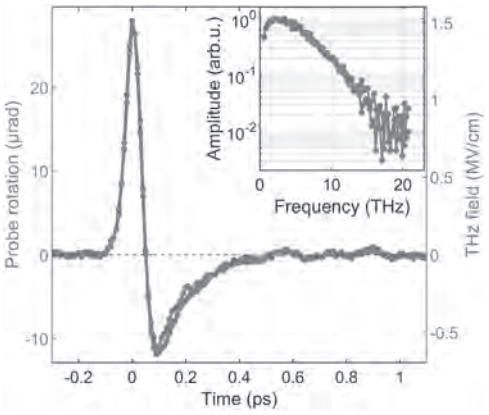

THz-induced optical birefringence signal in CoFeB(3nm)|Pt(3nm) sample (blue) and the driving THz field (red) measured by Zeeman torque sampling [4]. The inset shows spectral amplitudes of the signals.

HF-03. Ultrafast collapse of octupole order in chiral antiferromagnetic Mn_3Sn films with perpendicular magnetic anisotropy. *Z. Jin*[1,2], K. Nukui[1,2], K. Ishibashi[1,2], S. Iihama[3], M. Ishibashi[2] and S. Mizukami[2,4]
1. Department of Applied Physics, Tohoku University, Sendai, Japan; 2. WPI-AIMR, Tohoku University, Sendai, Japan; 3. Department of Materials Physics, Nagoya University, Nagoya, Japan; 4. CSIS, Tohoku University, Sendai, Japan

In typical ferromagnets, magnetic order can be reduced and quenched within sub-picosecond timescales by ultrashort laser pulse irradiation, known as ultrafast demagnetization, which has garnered significant attention in recent decades. A fundamental question is how fast magnetic order can change in antiferromagnets (AFMs). Noncollinear AFM Mn_3Sn is particularly interesting due to its Néel temperature (T_N) above room temperature (~420 K) and notable magneto-optical Kerr effect (MOKE) due to its magnetic-octupole order and topological Weyl nature. While many studies focus on magnetic-octupole dynamics, the ultrafast dynamics of magnetic-octupole order in Mn_3Sn is less explored. We investigate this in Mn_3Sn films with a magnetic easy plane oriented perpendicular to the film surface, prepared using magnetron sputtering. The film stacking structure is MgO (110) sub./ W(2) / Ta(3) / Mn_3Sn(30) / MgO(1.3) / Ru(1) (thickness in nm). Ultrafast dynamics of magnetic-octupole order were measured using time-resolved MOKE (TRMOKE). Fig. 1 shows the schematic measurement configuration, detecting the out-of-plane component of the magnetic-octupole by polar MOKE geometry with a probe pulse. Fig. 2 shows typical TRMOKE data, where the magnetic signal was extracted by taking the difference of signals measured with an applied magnetic field of ±2 T. We observed ultrafast reduction of magnetic-octupole order to about 60% within 0.1 ps and quick recovery, with a timescale similar to that observed in Ni or Co with higher magnetic ordering temperatures Tc. No critical slowing down was observed, contrasting with low Tc ferromagnets. Ultrafast quenching up to 100% was also observed at 1.3 mJ/cm^2, demonstrating the ultrafast manipulation of octupole order via laser pulse. This work is partially supported by JST PRESTO (No. JPMJPR22B2), JSPS KAKENHI (21H05000, 24K21234), and S.M. thanks to CSRN. Z.J. thanks to SPRING(JST), X-NICS(MEXT), GP-Spin at Tohoku Univ. We would like to thank T. Uchimura and S. Fukami at Tohoku Univ. for help in the preparation and basic characterization of samples.

[1] B. Koopmans et al., *Nat. Mater.* 9, 259 (2010). [2] T. Higo et al., *Nat. Photon.* 12, 73 (2018). [3] S. Miwa et al. *Small Sci.,* 1, 2000062 (2021), for example. [4] J.-Y. Yoon et al., *Nat. Mater.* 22, 1 (2023). [5] T. Ogasawara, *Phys. Rev. B* 68, 180407(R) (2003).

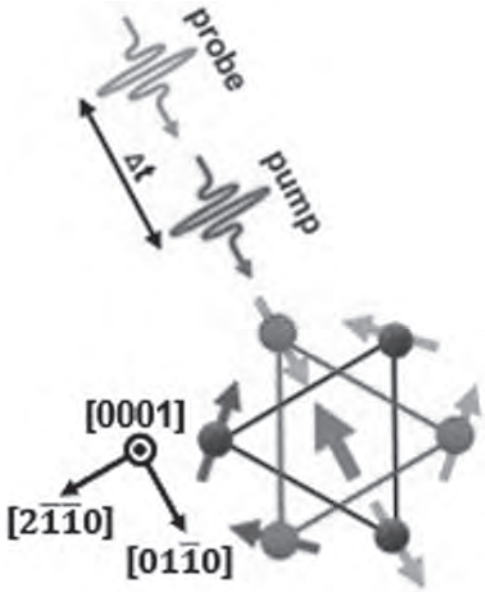

Fig.1: Schematic illustration of measurement configuration.

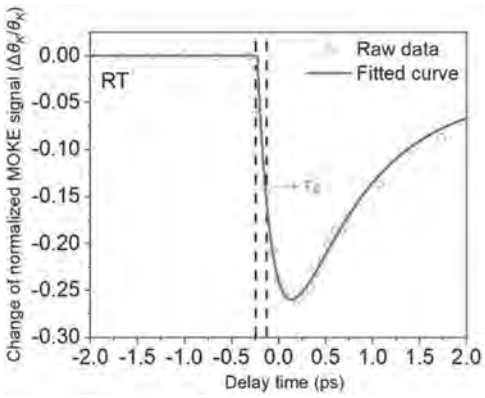

Fig.2: Typical TRMOKE signal obtained for the Mn_3Sn film at 0.7mJ/cm^2.

HF-04. Ultrafast spin-transport dynamics revealed by broadband terahertz spectroscopy. *L. Nadvornik*[1], J. Jechumtal[1], R. Rouzegar[2,3], O. Gueckstock[2,3], C. Denker[4], W. Hoppe[5], Q. Remy[2], T. Seifert[2,3], P. Kubascik[1], G. Woltersdorf[5], P. Brouwer[2], M. Münzenberg[4] and T. Kampfrath[2,3] *1. Faculty of Mathematics and Physics, Charles University, Prague, Czechia; 2. Department of Physics, Freie Universität Berlin, Berlin, Germany; 3. Department of Physical Chemistry, Fritz Haber Institute of the Max Planck Society, Berlin, Germany; 4. Institut für Physik, Universität Greifswald, Greifswald, Germany; 5. Institut für Physik, Martin-Luther-Universität, Halle, Germany*

The spin currents are fundamental building blocks of modern spintronic devices, such as giant magnetoresistance sensors or magnetic random-access memories. In light of the potential applications of terahertz (THz) and antiferromagnetic spintronics, there is a growing need to comprehend the spatial and temporal dynamics of THz spin currents (TSCs). For example, the TSCs has been recently employed to trigger ultrafast spin-torque [2], to reverse magnetization in antiferromagnets [3], or to generate broadband pulses of THz radiation [4]. Following the theoretical works on TSCs [5], a rising number of experimental studies appeared, reporting either on their temporal [6] or spatial dynamics [7] after traversing a spacer of a certain thickness. Nevertheless, to gain a comprehensive understanding of the intricate dynamics of TSCs, it is essential to detect the entire spatio-temporal evolution of the spin current pulse. In our contribution [8], we study such spatio-temporal evolution of subpicosecond TSCs by means of the time-domain THz emission spectroscopy with the high temporal resolution. By detecting and analysing THz pulses emitted by TSC after traversing a Cu spacer of variable thickness, we inferred the speed, broadening and attenuation of the TSC pulse. We observed that the propagation velocity of the leading edge of the pulse is approaching the ultimate Fermi velocity of electrons in copper and the duration of the pulse to increase by a factor of 1.5 over a distance of 8 nm. By matching a simple model based on the frequency-dependent diffusion with the measured dynamics of TSCs, we could infer their intrinsic spin-transport parameters, reveal the dispersion of propagation velocities due to the electron scattering as the leading mechanism behind the pulse broadening, and identify the diffusion as the dominant spin-transport mechanism for traveled distances above 2 nm.

[1] P. Němec, M. Fiebig, T. Kampfrath, and A. V. Kimel, Nat. Phys. 14, 229 (2018). [2] A. Melnikov, L. Brandt, N. Liebing et al., Phys. Rev. B 106, 104417 (2022). [3] Y. Behovits, A. L. Chekhov, S. Bodnar, O. Gueckstock et al., Nat. Commun. 14, 6038 (2023). [4] T. S. Seifert, L. Cheng, Z. Wei, T. Kampfrath, and J. Qi, Appl. Phys. Lett. 120, 180401 (2022). [5] Y.-H. Zhu, B. Hillebrands, and H. C. Schneider, Phys. Rev. B 78, 054429 (2008). [6] A. J. Schellekens, K. C. Kuiper, R. R. J. C. de Wit, and B. Koopmans, Nat. Commun. 5, 4333 (2014). [7] J. Gorchon, S. Mangin, and M. Hehn, Appl. Phys. Lett. 121, 012402 (2022). [8] J. Jechumtál, R. Rouzegar, O. Gueckstock, Ch. Denker et al., Phys. Rev. Lett. 132, 226703 (2024).

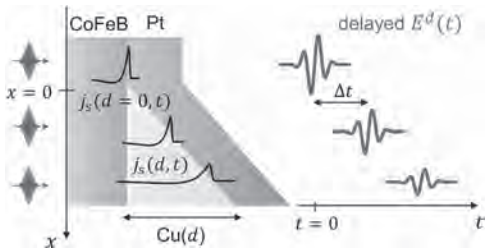

Fig. 1: A sketch of THz emission from a CoFeB/Cu(*d*)/Pt stack with a variable spacer thickness *d*. After the excitation by an ultrashort laser pulse, the emitted pulses are delayed by Δ*t* and spectrally modified dependening on *d*.

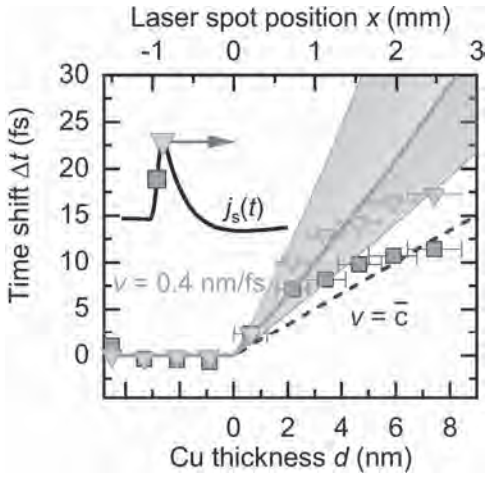

Fig. 2: Temporal shifts Δ*t* as a function of *d* for the leading edge (squares) and the maximum (triangle) of the ultrafast spin-current pulse.

HF-05. Antiferromagnetic Quantum Spin and Anomalous Hall Insulator: Dissipationless Neel Spin-orbit Torque. *J. Tang*[1], H. Zhang[2] and R. Cheng[1,2,3] *1. Department of Physics and Astronomy, University of California, Riverside, CA, United States; 2. Department of Electrical and Computer Engineering, University of California, Riverside, CA, United States; 3. Department of Materials Science and Engineering, University of California, Riverside, CA, United States*

Interplay between magnetic ordering and topological electrons not only enables new topological phases but also underpins electrical control of magnetism. Here we extend the Kane-Mele model to include the exchange coupling to a background antiferromagnetic (AFM) order, which can describe a number of transition metal trichalcogenides. Owing to the intrinsic and Rashba spin-orbit coupling, the system could exhibit the quantum anomalous Hall and quantum spin Hall effects in the absence of a net magnetization. Besides edge states protection, these topological phases support a staggered Edelstein effect through which an electric field can generate opposite non-equilibrium spin polarizations on the two AFM sublattices, realizing the Néel-type spin-orbit torque (NSOT). Contrary to known NSOTs in AFM metals driven by conduction currents, the NSOT here arises from pure adiabatic currents not accompanied by Joule heating. By virtue of the NSOT, the microwave absorption rate of the AFM resonance can be enhanced by over an order of magnitude as the power conversion process is dominated by the electric field component of the microwave rather than the magnetic component, opening an incredible way of generating ultrafast spin dynamics with extremely low dissipation.

[1] D. N. Sheng, Z. Y. Weng, L. Sheng, and F. D. M. Haldane, Quantum spin-hall effect and topologically invariant chern numbers, Phys. Rev. Lett. 97, 036808 (2006). [2] L. Sheng, D. Sheng, C. Ting, and F. Haldane, Nondissipative spin hall effect via quantized edge transport, Physical review letters 95, 136602 (2005) [3] J.-Y. Tang and R. Cheng, Voltage-driven exchange resonance achieving 100% mechanical efficiency, Physical Review B 106, 054418 (2022).

HF-06. Helicity-dependent THz emission induced by circularly-polarized light in platinum-thin films. *K. Ishibashi*[1,2], K. Nukui[1,2], S. Iihama[3], H. Morishita[4,2] and S. Mizukami[2,4] *1. Dept. of Appl. Phys., Tohoku University, Sendai, Japan; 2. WPI-AIMR, Tohoku University, Sendai, Japan; 3. Dept. of Mater. Phys., Nagoya University, Nagoya, Japan; 4. CSIS, Tohoku University, Sendai, Japan*

Recently, the effects of circularly-polarized light on spin transport and dynamics attract enormous attention. Hirai et al.reported the helicity-dependent (HD) THz emission in a Bi film induced by circularly-polarized light, which was due tothe conversion of spin current created by circularly-polarized light into charge current via the inverse spin Hall effect (ISHE) in the Bi film [1]. This study indicates that helicity-dependent THz emission induced by circularly-polarized lightshould be observed in various heavy metal films exhibiting a large efficiency of photonic-to-electronic spin conversion as well as spin-to-charge current conversion; however, no experimental investigations have yet been reported. Here, we investigated laser-induced HD-THz emission in a Pt film with a large spin-Hall angle to deepen the underlying physics in the light-helicity effect. Pt thin films with various thicknesses were deposited on glass substrates using ultrahigh vacuum magnetron sputtering. HD-THz emission was measured via THz time-domain spectroscopy (THz-TDS) with Ti: Sapphire fs laser [2,3]. A pump laser pulse was circularly polarized and emitted THz was detected via electro-optic sampling with a ZnTe crystal. We clearly observed THz emissions (Fig. 1) and confirmed the THz signal polarity was flipped with light helicities, *i.e.* HD-THz emission was observed when the pump laser was obliquely incident to the Pt films (Fig. 1). Those THz signal polarities were also dependent on the angle of the incident, which was also similarly observed in Bi films [1,2]. The HD-THz emission observed in Pt films is considered to be due to a large efficiency of photonic-to-electronic spin conversion [4-6] as well as ISHE in Pt [7]. This work is partially supported by KAKENHI(21H05000, 24K21234) and X-NICS(JPJ011438). K. I. acknowledges Grant-in-Aid for JSPS Fellow (22J22178). K.I. and K.N. thank to GP-Spin at Tohoku Univ. S. I. thanks to JST PRESTO (JPMJPR22B2). H. M. and S.M. thank to CSRN in CSIS at Tohoku Univ.

[1]Y. Hirai, N. Yoshikawa, H. Hirose, M. Kawaguchi, M. Hayashi, and R. Shimano, Phys. Rev. Appl. 14, 064015 (2020). [2]K. Ishibashi, S. Iihama, and S. Mizukami, Phys. Rev. B 107, 144413(2023). [3]R. Mandal, R. Momma, K. Ishibashi, S. Iihama, K. Suzuki, and S. Mizukami, NPG Asia Mater. 16, 1 (2024). [4]G. M. Choi, J. H. Oh, D. K. Lee, S. W. Lee, K. W. Kim, M. Lim, B. C. Min, K. J. Lee, and H. W. Lee, Nat. Commun. 11, 1482 (2020). [5]S. Iihama, K. Ishibashi, and S. Mizukami, Nanophotonics 10, 1169 (2021). [6]S. Iihama, K. Ishibashi, and S. Mizukami, J. Appl. Phys. 131, 023901 (2022). [7]E. Saitoh, M. Ueda, H. Miyajima, and G. Tatara, Appl. Phys. Lett. 88, 182509 (2006).

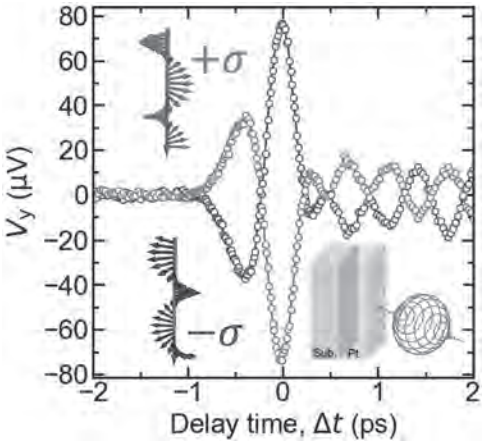

Fig. 1: Blue and red show the THz emissions in the Pt thin film (2.5 nm) induced by right- and left-handed circularly polarized laser pulses with oblique incidence, respectively.

HF-07. Magnon-mediated terahertz spin transport in metallic Gd|Pt thin-films. *O. Gueckstock*[1], T. Amrhein[1], B. Andres[1], P. Jimenez Cavero[2], C. Gahl[1], T. Seifert[1], M. Rouzegar[1], I. Radu[1], I. Lucas[2], L. Morellon[2], M. Weinelt[1], T. Kampfrath[1] and N. Thielemann-Kühn[1] *1. Freie Universität Berlin, Berlin, Germany; 2. Universidad de Zaragoza, Zaragoza, Spain*

Transport of spin angular momentum is a fundamental operation required for future spin-electronic devices. To be competitive with other information carriers, it is required to push spin transport to ultrafast time scales [1]. Here, we use femtosecond laser pulses to trigger ultrafast spin transport in prototypical F|Pt bilayers from a ferromagnetic layer F into a heavy metal layer of Pt [2]. Following absorption of the pump, a spin current from F to Pt is launched and converted into a transverse charge current in Pt, where it gives rise to the emission of a THz electromagnetic pulse [2]. Two driving forces can occur: (i) a difference in temperature gradient (Seebeck-like effect) [3] and (ii) spin voltage between F and Pt [4]. In metallic F, (ii) dominates and relies on conduction electrons, while (i) is found for insulating F and mediated by magnons [3,4]. Remarkably, however, in the fully metallic ferromagnet Gd, we find Seebeck-type dynamics and, thus, magnon-mediated spin transport into Pt. The surprising absence of a conduction-electron mediated spin current in a metallic ferromagnet is supported by time- and spin-resolved photoemission that shows equal populations and lifetimes for majority- and minority-spin electrons close to the Fermi energy. These findings highlight the importance of magnon-mediated spin transport in certain metallic systems.

[1] Vedmedenko et al., J. Phys. D: Appl. Phys. 53, 453001 (2020) [2] T. Seifert et al., Nat. Phot. 10, 483 (2016) [3] T. Seifert et al., Nat. Comm. 9, 2899 (2018) [4] R. Rouzegar et al., Phys. Rev. B 105, 184408 (2022).

Session HG
ENERGY AND POWER APPLICATIONS

Mariappan Parans Paranthaman, Chair
Oak Ridge National Laboratory, Oak Ridge, TN, United States

INVITED PAPER

HG-01. Enhancing Thermoelectric Effects with Magnetism and Topology. *S. Watzman*[1], E.F. Scott[1] and K.A. Schlaak[1] *1. Department of Mechanical and Materials Engineering, University of Cincinnati, Cincinnati, OH, United States*

While conventional thermoelectric materials have been widely studied for waste-heat recovery and use in niche applications, their commercial efficiency has not increased in recent years. Here, magnetism is used to not only enhance thermal-to-electrical energy conversion, but it is also used to decouple the direction of the applied heat flux from the resultant electric field, offering an engineering design degree of freedom via the Nernst effect. In this talk, magneto-thermoelectric transport will be explored in conjunction with topological band structures, which offer unique transport signatures in topological materials such as Weyl and Dirac semimetals. Previous work in the Type I, inversion symmetry-breaking Weyl semimetal NbP demonstrated the simultaneous presence of both a large Nernst (transverse) and magneto-Seebeck (longitudinal) effect, which is rarely seen in a singular material, and how doping strongly alters both thermopowers [1]. The theory underlying transport in NbP is now applied to the Dirac semimetal Cd_3As_2 in order to predict the carrier concentrations at which the combined Nernst and Seebeck thermopowers are maximized under various temperature and field conditions. To achieve the very precise doping necessary for these predictions, thin films of Te-doped Cd_3As_2 were grown via molecular-beam epitaxy (MBE) at the predicted carrier density levels. The magneto-thermoelectric transport of these samples is characterized to determine the predictive power of the model and the viability of the MBE growth method for tuning the material to the specific operating conditions (i.e. temperature and magnetic field). This work is then extended to WTe_2, a Type II Weyl semimetal that breaks inversion symmetry. While Type I Weyl semimetals like NbP have symmetric Dirac bands, Type II Weyl semimetals have tilted Dirac bands. Through experimental results of magneto-thermoelectric transport in conjunction with theoretical modeling and comparison to previous results in NbP [1], we determine that when Dirac bands are tilted, their signature contributions to transport are washed out by parabolic bands. Therefore, we offer this comparison between Type I and Type II Weyl semimetals as evidence supporting the use of Type I Weyl semimetals for future applications of topological materials in solid state energy conversion devices. While non-magnetic topological materials do exhibit a large Nernst effect in externally applied magnetic fields, magnetic Weyl semimetals offer the potential to substantially decrease, or even eliminate, the need for the external field. $YbMnSb_2$, an antiferromagnetic Weyl semimetal that breaks time-reversal symmetry, has a highly anisotropic band structure in addition to a net Berry curvature. In this work, the relationship between the anisotropic band structure, the orientation of the net Berry curvature, and the geometry of the fluxes associated with the Nernst effect is explored. This will elucidate a crystallographic orientation in which the Nernst effect is maximized, offering insight for energy generation applications of topological materials. This work is supported by the U.S. Department of Energy, Office of Science, Office of Basic Energy Sciences Early Career Research Program under Award No. DE-SC0020154.

[1] E. F. Scott et al. *Phys. Rev. B* 107, 115108 (2023).

CONTRIBUTED PAPERS

HG-02. Crossover from mono to multi-stable coupled non-linearity in a wideband electromagnetic vibrational energy harvester for self-powering wireless sensor nodes. *S. Roy*[1], A. Amann[2] and K. Roy[1] *1. School of Physics, Tyndall National Institute, Cork, Ireland; 2. School of Mathematical Science, University College Cork, Cork, Ireland*

Non-linearity in any oscillatory system can be classified as either monostable or bistable, depending on the potential energy profile. Introducing monostable non-linearity into miniaturized vibrational energy harvesters significantly enhances operational bandwidth, often achieved by stretching fixed-guided spring arms[1] of the designed oscillators. Whereas, the bistable non-linearity can be incorporated into the system using magnetic levitation[2]. With increased operational bandwidth, non-linear electromagnetic vibration energy harvester(EM-VEH) can capture untapped energy sources(mechanical vibrations) to power highly miniaturized autonomous wireless sensor nodes[4-7]. This work presents the design and characterization of a cascaded tapered spring topology in an EM-VEH further combined with magnetic levitation to demonstrate a crossover from mono to multi-stable coupled non-linearity for achieving higher figure of merit. The designed prototypes have springs tapered and arranged in a cascaded configuration(Figure 1). The taper ratio[8], which measures the degree of tapering of the spring arms has been optimized to 0.5. The prototypes are fabricated on FR4 sheets via laser micromachining, with the sheet thickness optimized to 0.25mm. The device includes electromagnetic transducer constituted of moving sets of oppositely polarized NdFeB magnets(8mmx4.2mmx2mm) along with soft magnetic cuboids(8mmx4.2mmx1.6mm) around a fixed Cu-coil(2,500 turns; resistance of 1016Ω). Additionally, a pair of magnets(2mmx2mmx2mm) are positioned in a way to induce magnetic levitation into the system. This design enhances power output and allows tuning of non-linearity by leveraging stretching of the spring arms and modifying the potential further by magnetic levitation. The combination of cubic stiffness(due to cascading) and double-well potentials(due to magnetic levitation) results in lowering the height of the potential barrier which triggers the large amplitude inter-well motion for generating higher output power even at relatively lower frequency and acceleration.

[1] D. Mallick et al, Smart Mater. Struct., 24, 015013 (2015). [2] P Podder et al, Sens. Actuators A: Phys., 227, 39 (2015). [3] F. Cottone et al, Phys. Rev. Lett., 102, 080601 (2009). [4] A. Hosseinkhani et al, Energy Reports 7, 852 (2021). [5] M. Gao et al, Energy Environ. Sci., 14, 2114 (2021). [6] Soliman et al, J. Micromech. Microeng., 22(12), 115021 (2008) [7] Polo et al, Sensors, 20, 1873 (2020). [8] K. Paul et al, Appl. Energy, 283, 116267 (2021).

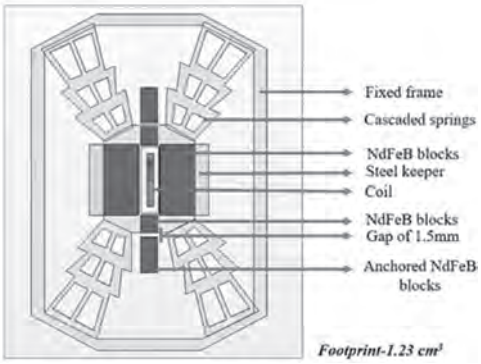

Fig. 1: Cascaded spring EM-VEH with pairs of repulsive magnets showing multi-stabile non-linearity.

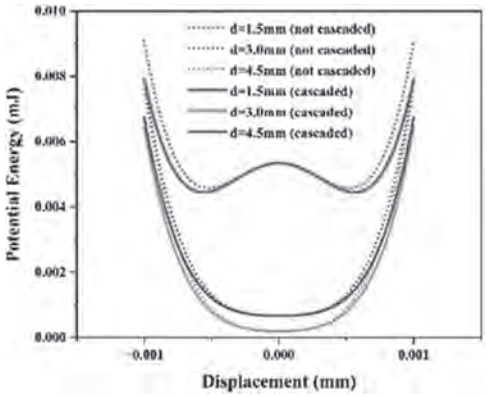

Fig. 2: Potential energy vs Displacement for cascaded and not cascaded prototypes.

HG-03. High-bandwidth Current Shunt with Extremely Low Stray Magnetic Field for Accurate Magnetic Loss Measurement in Non-sinusoidal Power Converters. L. Yi[1], W. Lee[2] and *J. Moon*[1]
1. Florida State University, Tallahassee, FL, United States; 2. Michigan State University, East Lansing, MI, United States

With wide bandgap devices, there is a growing demand for high bandwidth current shunts in power electronics. For instance, in the case of hard-switched non-sinusoidal power conversion, a common 10 ns rise time corresponds to an equivalent bandwidth of 35MHz (BW = 0.35/trise). Considering the ringing during/after the transition at a higher frequency (e.g., 50 MHz), precise capturing of the edge details requires a high measurement bandwidth. The suggested bandwidth is at least 5 or 10 times the maximum frequency of interest for adequate magnitude or phase fidelity. Thus, a bandwidth beyond 500MHz is preferable to get reliable measurement in power electronics. Voltage probes with a bandwidth of 1 GHz are readily available commercially. In contrast, a current probe is severely limited in signal bandwidth among commercially available products, mostly limited below 200 MHz [1-6]. A resistive current sensor, often called a current shunt, converts magnetic field measurement into electric potential measurement, enabling us to use well-established GHz-level voltage probes. The overall structure must have an extremely low level of stray magnetic field to minimize parasitic inductance and hence to increase the measurement bandwidth. In this abstract, we propose a new magnetic structure for a high-bandwidth (GHz+) current shunt to be used in emerging in-situ magnetic loss measurement techniques [7-9] in general, non-sinusoidal power electronic converters. The structure aims to cancel magnetic fields in various axes such that stray magnetic fields are nearly nonexistent outside the structure. This will in turn lead to an extremely low parasitic inductance. As illustrated in Figure 1, thirty 0402 surface mount resistors are paralleled in a coaxial manner in our structure, providing overall flux cancellation in a radial manner. Two adjacent resistors in this structure also have opposite current directions as shown in Fig. 2. The magnetic fields generated by incoming and outgoing current in the printed circuit boards are layered such that magnetic fields are mostly cancelled. In simulation, we confirmed 2 GHz 3dB bandwidth. In the final manuscript, we will add detailed analysis and experimental validation.

[1] I. A. Metwally, "Self-integrating rogowski coil for high-impulse current measurement," IEEE Transactions on Instrumentation and Measurement, vol. 59, no. 2, pp. 353–360, 2010. [2] J. Wang, M. H. Hedayati, D. Liu, S.-E. Adami, H. C. P. Dymond, J. J. O. Dalton, and B. H. Stark, "Infinity sensor: Temperature sensing in gan power devices using peak di/dt," in 2018 IEEE Energy Conversion Congress and Exposition (ECCE), 2018, pp. 884–890. [3] F. Naseri, E. Farjah, and T. Ghanbari, "Application of an efficient rogowski coil sensor for online estimation of turn-off energy loss of power diodes," IEEE Sensors Journal, vol. 19, no. 16, pp. 6675–6683, 2019. [4] V. Dubickas and H. Edin, "High-frequency model of the rogowski coil with a small number of turns," IEEE Transactions on Instrumentation and Measurement, vol. 56, no. 6, pp. 2284–2288, 2007. [5] M. H. Samimi, A. Mahari, M. A. Farahnakian, and H. Mohseni, "The rogowski coil principles and applications: A review," IEEE Sensors Journal, vol. 15, no. 2, pp. 651–658, 2015. [6] P. Electronics, "PEARSON TM CURRENT MONITOR MODEL 2877," https://www.pearsonelectronics.com/pdf/2877.pdf, accessed: 2023-09-18. [7] L. Yi and J. Moon, "Direct in-situ measurement of magnetic loss in power electronic circuits," IEEE Trans. Power Electron., vol. 36, no. 3, pp. 3247–3257, Mar. 2021. [8] L. Yi and J. Moon, "In situ direct magnetic loss measurement with improved accuracy for lossier magnetics," IEEE Trans. Instrum. Meas., vol. 71, pp. 1–14, 2022. [9] L. Yi, M. McTigue, D. Gines, B. Doerr, and J. Moon, "Minimally invasive direct in-situ magnetic loss measurement in power electronic circuits," IEEE Trans. Power Electron., vol. 38, no. 11, 783, pp. 14334–14344, Nov. 2023.

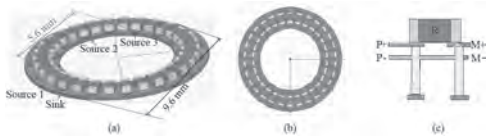

Fig. 1

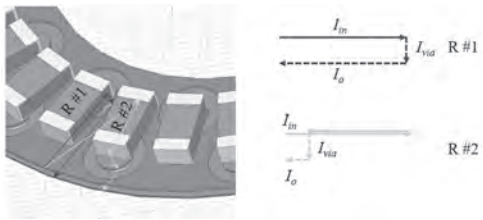

Fig. 2.

HG-04. Additional Degree of Freedom in the Design of Shifted Inductances Axes Synchronous Motors. H.N. Nasser[1], Y. Amara[1], F. Chabour[1], *J.J. Paulides*[2] and M. Ghandour[3] *1. GREAH, Université Le Havre Normandie, Le Havre, France; 2. Advanced Electromagnetics Group, Waalwijk, Netherlands; 3. Faculty of Engineering, Lebanese University, Beirut, Lebanon*

Shifted inductances axes synchronous motors (SIASMs), also known as asymmetrical rotor structure motors, have recently gained significant attention within the electric machine designers' community [1]. This contribution presents a new tool for designing SIASMs, building on previous works primarily focused on synchronous machines [2,3]. The previous tools feature a structure with two rotors within a shared stator (Fig. 1): a non-salient permanent magnet (PM) rotor and a variable reluctance rotor, respectively defined by their electrical park reference frames (d_{PM}, q_{PM}) and $(d_{Reluc.}, q_{Reluc.})$ shifted by an angle β (Fig. 2). The $d_{PM.}$ axis is defined as the axis of maximum flux linkage and the $d_{Reluc.}$ axis can be the axis of minimum or maximum inductance. The concept aims to align the peak torque from

the permanent magnets with the torque generated by the rotor's variable reluctance, enhancing overall torque capability. Additionally, the inclusion of wound field excitation, combined with the PM excitation to form a hybrid excited machine, allows for control of the air-gap excitation flux, further improving torque controllability. In this work, the previously non-salient PM rotor is now replaced by a non-salient one, and the angle β, which was previously fixed to maximize rated speed torque, is now changeable during operation [4], thereby adding another degree of freedom to the structure. Similar to reference [3], the new tool accounts for electromagnetic losses (joule and iron losses) while excluding mechanical losses. Permanent magnet machines, wound field machines, and hybrid excited synchronous machines are treated as specific cases within the newly developed tool. Furthermore, since that power capability and efficiency maps are essential for assessing the viability and sustainability of electric machines and providing a comprehensive view of their operation, investigations into the potential benefits of the design optimization in terms of β for maximizing torque at low speeds or maximizing efficiency at most solicited operating area are conducted.

[1] Z.Q. Zhu, Y. Xiao, "Novel magnetic-field-shifting techniques in asymmetric rotor pole interior PM machines with enhanced torque density," IEEE Trans. Magn, vol. 58, no. 2, pp. 1–10, February 2022. [2] Y. Amara, S. Hlioui, M. Gabsi, "Overview of Degrees of Freedom in the Design of PM Synchronous Machines," Energies, vol. 14, 3990, July 2021. [3] H. Nasser, Y. Amara, F. Chabour, M. Ghandour, "Efficiency Maps of Shifted Inductances Axes Permanent Magnet Synchronous Motors," World Electr. Veh. J, vol. 14, 174, June 2023. [4] B. Kraber, F. Rattei, " Mechanical Field Weakening with Actuation by the Stator Currents," In Proceedings of International Conference on Electrical Machines, Helsinki, Finland, vol. 4, pp. 1956-1960, August 2000.

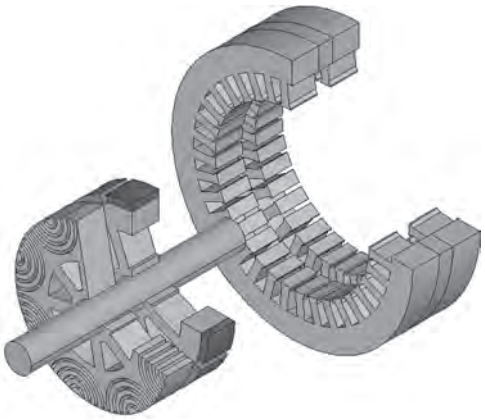

Fig. 1: Example of two separate rotors structure for a SIASM.

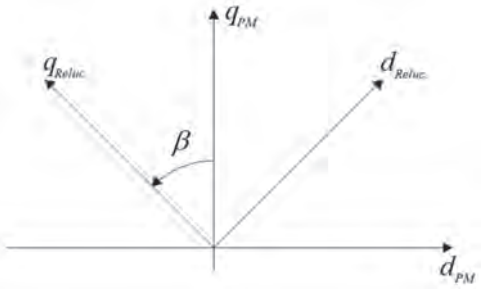

Fig. 2: Park's referential frames related to each rotor (PM rotor and variable reluctance rotor).

HG-05. Force Wave and Vibration Analysis of Different Rotor Slot Combinations in Induction Motors. *D. Kong*[1], B. Jia[1] and Y. Xiang[1]
1. Guangdong Ocean University, Zhanjiang, China

The squirrel-cage three-phase induction motor has many advantages, such as high efficiency, simple structure, and reliable operation, making it widely used in various fields. The selection of the stator and rotor slot numbers in induction motors has a decisive impact on the motor's performance, primarily affecting losses, torque, and vibration noise. To achieve lower vibration and noise, the appropriate slot combinations are mainly considered based on asynchronous torque, synchronous torque, and force-wave orders. To explore stator and rotor slot combinations that can reduce vibration, this paper establishes finite element models with different slot combinations. The analysis focuses on typical slot combination parameters where the stator has 36 slots, and the rotor has 28, 36, and 44 slots, respectively. It is determined that when the stator and rotor slots are in a fractional slot combination, the larger the difference between the two, the higher the force wave orders of the motor. However, when the rotor slot number exceeds the stator slot number, it leads to a reduction in torque. Therefore, under the condition of satisfying performance requirements, it is preferable to choose a rotor slot number less than the stator slot number. When the stator and rotor have the same slot number, the main vibration order is the 0th order, requiring the stator to have good stiffness to effectively suppress vibration.

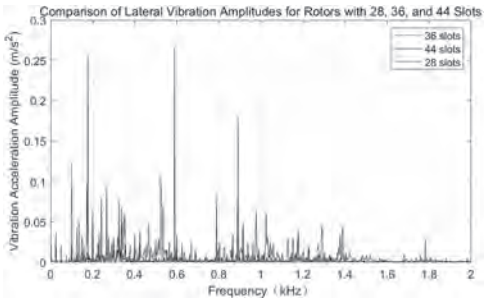

Fig. 1: Comparison of Lateral Vibration Amplitudes for Rotors with 28, 36, and 44 Slots

HG-06. Dynamic Analysis and Validation of Superconducting Rotor with a Spoke Suspension Torque Tube. *J. Xiao*[1], S. Sirimanna[2], H. Rautela[1], T. Balachandran[2] and K. Haran[1] *1. University of Illinois Urbana Champaign, Champaign, IL, United States; 2. Hinetics LLC, Champaign, IL, United States*

A superconducting rotor with a spoke suspension system can achieve a high specific power of 40kW/kg [1]. The spokes act as a torque tube with strong thermal insulation, virtually eliminating the conductive heat transfer between the ambient-temperature drive shaft and the cryogenic rotor shell, where superconducting coils are mounted [2]. An example of the spoke suspension system is shown in Fig. 1. However, since the spoke geometries differ from a solid torque tube, existing rotordynamic analytical models cannot be applied directly[3] [4]. This paper aims to model the dynamics of the rotor spoke system with experimental validation and propose a design for a specific superconducting rotor. The study is conducted through three aspects: analytical derivation of the spoke system resonant frequencies, 3-D finite element modal verification using Comsol, and experimental validation through a ping test. Analytical derivation treats the shaft and the shell as rigid bodies; each spoke as a mass-spring system. The analytical model traces the relative movement between the shaft and shell and derives the spoke system's stiffness and the fundamental resonant frequencies in each of the six degrees of freedom (DOF). The finite element analysis (FEA) confirms the fundamental frequencies from the analytical model and reveals modes within the rings and shells by including the finite modulus of the rotor shaft and the shell. Fig. 2 shows the preliminary resulting Campell diagram. The red line indicates rotor rotation speed. The solid, dashed, and dotted lines correspond to axial, forward, and backward modes. A rapid change in eigenfrequencies is

also discovered after passing a certain rotation speed due to spoke preload. Then, a full-scale rotor is built to validate the FEA analysis. A ping test reveals the free free mode of the rotor. The experimental modal shapes and frequencies are compared with the FEA results. After the analytical calculation, FEA, and experimental validation, the study concludes by proposing a spoke suspension design with the calibrated dynamic model for a 10MW, 3000 RPM superconducting rotor.

[1] J. Xiao and K. S. Haran, U.S. Patent (Pending) US20220302816A1 (2021) [2] J. Xiao, T. Balachandran and A. J. Samarakoon, IEEE Transactions on Magnetics, vol. 58, no. 8, pp. 1-5 (2022) [3] B. Silwal, P. Rasilo and L. Perkkiö, IEEE Transactions on Magnetics, vol. 52, no. 3, pp. 1-4 (2016) [4] D. -K. Hong, B. -C. Woo and D. -H. Koo, IEEE Transactions on Magnetics, vol. 45, no. 6, pp. 2831-2834 (2009)

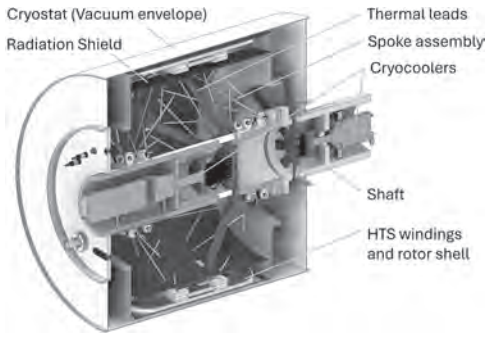

Fig. 1: Superconducting Rotor with a Spoke Torque Tube

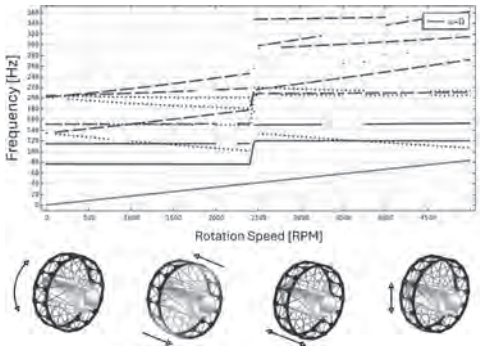

Fig. 2: Campbell Diagram and First Four Mode Shapes

HG-07. Optically Excited Brushless High-Speed Wound Field Synchronous Generator. *K. Lee*[1], G. Gardner[2], R. Atkinson[2] and W. Lee[1]
1. Purdue University, West Lafayette, IN, United States; 2. Michigan State University, East Lansing, MI, United States

I. Introduction Electrical power demands in transportation have been growing due to an increased number of electrical loads [1]. The generators with rare-earth permanent magnets opened a door for the increasing power density of the propulsion system, but their magnetic fields cannot be turned off at will, posing challenges in case of prime mover failure [2]-[3]. Therefore, wound-field synchronous generators (WFSGs) are promising to mitigate the limitation. However, mechanical brushes carrying power from the inverter to the rotor in WFSGs are a crucial disadvantage because they are worn out [4]. Therefore, wireless power transfer systems have been proposed as capacitive or inductive (CPT or IPT), but the bulky capacitors or inductors increase the overall system volume [5]-[6]. This paper proposes an optically powered ultra-high-speed (OPUS) WFSG to maximize its power density. II. Advantage of Ultra-High-Speed for OPUS An OPT system provides brushless field winding excitation through a rotating solar cell directly connected to the rotor's field winding, as shown in Fig. 1. The OPT system enables ultra-high-speed generator operation, which significantly reduces the power required for the field winding, as well as the thickness of the stator and rotor yokes. A comparative study is conducted between a conventional WFSG operating at 8,000 rpm and the proposed OPUS WFSG designed to operate at 40,000 rpm. Both generators are designed to produce 40 kW under specified operating conditions, maintaining a consistent back-EMF of 330 V_{rms}. Notably, as the operational speed of the generator increases, the thickness of both the rotor and stator outer yokes proportionally decreases, leading to a weight reduction of more than half (i.e., Estimated total weight: 19.5 kg (conventional) and 9.3 kg (OPUS WFSG)). III. Conclusion and Future Work This paper introduces OPUS WFSG and verifies that its power density is expected to achieve twice the performance of traditional WFSGs with mechanical brushes. In the final paper, additional advantages of OPUS WFSG, including cost, EMI noise, and efficiency, will be addressed with the test setup, as shown in Fig. 2.

[1] S. Gnanavendan, S. Selvaraj, S. Dev, K. Mahato, R. Swathish, G. Sundaramali, O. Accouche, and M. Azab, "Challenges, Solutions and Future Trends in EV-Technology: A Review," *IEEE Access*, vol. 12, pp. 17242-17260, 2024. [2] M. G. Pasquinelli, P. Bolognesi, A. Guiducci, S. Nuzzo, and M. Galea, "Design of a High-Speed Wound-Field Synchronous Generator for the More Electric Aircraft," *2021 IEEE Workshop on Electrical Machines Design, Control and Diagnosis (WEMDCD)*, Modena, Italy, 2021, pp. 64-69. [3] R. Parman, "An elemental issue". Available: https://www.army.mil/article/227715/an_elemental_issue. [4] H. Kim, D. Kim, J. Jeong, and J. Hong, "Proposition of structures for brushless hybrid-excitation synchronous motors with improved rotor," *IEEE Trans. Magn.*, vol. 52, no. 9, pp. 1-15, Sept. 2016. [5] J. Dai and D. C. Ludois, "A Survey of Wireless Power Transfer and a Critical Comparison of Inductive and Capacitive Coupling for Small Gap Applications," *IEEE Trans. Power Electron.*, vol. 30, no. 11, pp. 6017-6029, Nov. 2015. [6] D. C. Ludois, J. K. Reed, and K. Hanson, "Capacitive power transfer for rotor field current in synchronous machines," *IEEE Trans. Power Electron.*, vol. 27, no. 11, pp. 4638–4645, Nov. 2012.

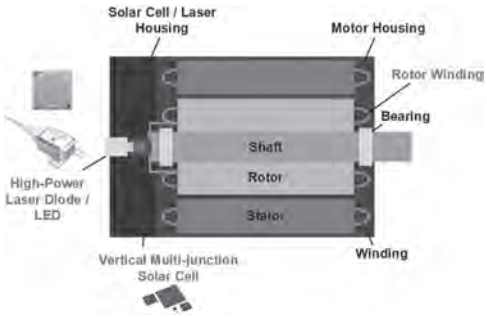

Fig. 1. <u>Proposed</u> OPUS system.

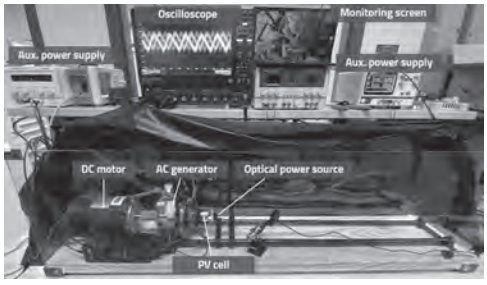

Fig. 2. Experimental setup with laser-based OPT system.

Session VP1
BIOMAGNETICS AND MICROFLUIDICS
(Poster Virtual Session)

Jenifer Gomez-Pastora, Co-Chair
Texas Tech University, Lubbock, TX, United States
Cristina González Fernández, Co-Chair
Universidad de Cantabria, Santander, Spain

VP1-03. Unlocking Preclinical Drug Screening Application with Magnetoimpedance Sensor. *J. Ma*[1], N. Ohta[1], T. Ozaki[1], S. Moribe[1], H. Kikuta[1], Y. Hirata[1] and M. Hirano[1] *1. Toyota Central R&D Labs., Inc., Nagakute, Japan*

In vitro cardiac function assays for drug screening have traditionally relied on electrophysiological techniques like the patch-clamp method and micro-electrode arrays (MEA), as well as fluorescent microscopy. However, these methods often induce cellular stress and damage, require skilled operators, and necessitate specialized culture dishes [1, 2]. To address these limitations, we have developed a non-invasive, real-time magnetic recording system utilizing Magneto-Impedance (MI) sensors. Our system improves the sensor detection methodologies, and incorporates noise reduction techniques to enhance sensitivity and simplify drug screening. It boasts high field detection sensitivity, excellent linearity, and a noise level of approximately 2 pT/Hz$^{1/2}$ at room temperature. As shown in Figure 1, we have successfully performed the first measurement and analysis of magnetophysiological signals from human induced pluripotent stem cell-derived cardiomyocytes (hiPSC-CMs) using MI sensors. We compared our results with those obtained from existing techniques such as MEA and fluorescence imaging. Our MI sensor detected signals featuring a sharp peak combined with low-frequency components (Fig. 1(c)). Our system effectively assesses the impact of drugs with positive chronotropic properties and those that may induce serious side effects, such as QT prolongation, at therapeutic blood concentration levels. Fig. 2 illustrates the beat rate of hiPSC-CMs measured by the MI sensor, both with and without treatment using positive and negative reagents. The observed trends matched those obtained with two other measurement methods [3]. Using our system, we propose the potential for high-throughput, preclinical drug screening assays with magnetic detection. This technique obviates the need for expensive, bulky equipment or specialized culturing instruments, thus overcoming previous challenges in the field.

[1] O. Scheel, S. Frech, B. Amuzescu, et al., ASSAY and Drug Development Technologies, 12, 457-469 (2014). [2] M.F. Peters, S.D. Lamore, L. Guo, et al., Cardiovasc Toxicol, 15 127-139 (2015). [3] L. Guo, R.M.C. Abrams, J.E. Babiarz, et al., TOXICOLOGICAL SCIENCES 123(1), 281–289 (2011)

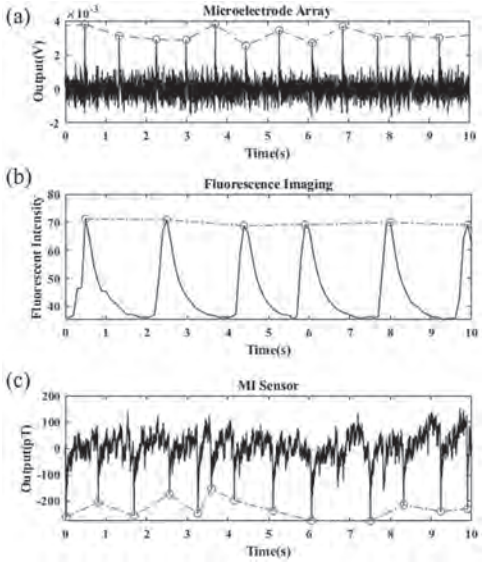

Fig 1. Measurements of the magnetophysiological signals of hiPSC-CMs via (a) MEA, (b) Fluorescence imaging, and (c) MI sensor.

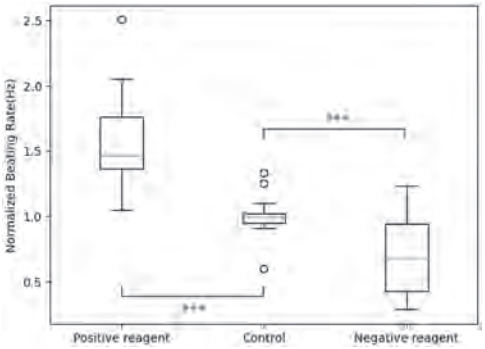

Fig 2. Box plots of the beating rate of hiPSC-CMs measured by the MI sensor, both with and without treatment using positive and negative reagents.

VP1-04. Magnetic analysis of magnetically controlled capsule endoscopes in curved intestines under a rotating magnetic field drive strategy. *Z. Teng*[1,2], J. Ren[3,4], H. Sun[3,4], J. Liu[3,4] and Q. Wang[3,4] *1. Department of Automation, University of Science and Technology of China, Hefei, China; 2. The Ganjiang Innovation Academy, Chinese Academy of Sciences, Ganzhou, China; 3. Institute of Electrical Engineering, Chinese Academy of Sciences, Beijing, China; 4. The University of Chinese Academy of Sciences, Beijing, China*

The magnetically controlled capsule endoscopy (MCCE) application in intestinal examinations has the potential to shorten examination time and reduce operator burden. Although many types of MCCE have been developed, the analysis of their position-magnetism relationship in geometrical space in curved intestines is still limited, which is a great challenge for controlling the flexible motion of the MCCE. In this paper, the rotating magnetic field of the external permanent magnet in space is modeled, a model based on the magnetic balance of a permanent magnet under a rotating magnetic field is proposed, and the magnetic force and torque applied to the MCCE under different geometrical actuation angles are analyzed by simulation, finally, into the effect of different actuation angles on the actuation ability of the MCCE in a curved intestine by experimental strategies. This work provides a new strategy for magnetic control of the MCCE in curved intestines, promoting the application of the MCCE in biomedical engineering.

VP1-05. Assessing the resolution of transcranial magnetic stimulation by measuring the magnetic flux density at the cortical surface. A. Sato[1] and *T. Torii*[1,2] *1. Department of Human Information Engineering, Tokai University, Kumamoto, Japan; 2. Graduate School of Science and Technology / Course of Science and Technology, Tokai University, Kumamoto, Japan*

Transcranial magnetic stimulation (TMS) is a non-invasive and localized stimulation technique. Local stimulation technologies play an important role in brain function research and treatment. Previously, the TMS resolution was found to be 5 mm when using a figure eight-shaped stimulus coil. The stimulus resolution has been evaluated using various measurement techniques. Here, we explored whether the stimulation area could be evaluated using a simple method and small dataset. In our experiment, a Rapid2 stimulator (Magstim Co.,) was set to deliver pulses at 75% magnetic intensity, and the distance from the scalp to the cortex was assumed to be 15 mm. The magnetic flux density was measured within ±30 mm on the x- and y-axis from the center of the stimulus coil. On a curved model of the surface of the head, this corresponded to a curve with a radius of 70 mm on the x-axis and 100 mm on the y-axis. We used a sensor coil and simple measurement circuit to measure the magnetic flux density. Our results showed that the stimulus resolution on a flat surface was within approximately 5 mm of the center position. In contrast, the stimulus resolution on the curved surface was extremely small, as indicated by a significant difference at each measurement point compared with the central magnetic flux density ($p < 0.01$, less than 2 mm in diameter). The stimulation area within which the magnetic flux density decreased by less than 1% compared with the full magnetic flux density at the center of the stimulation coil was approximately 37 mm^2 on a flat surface and 23 mm^2 on a curved surface. The Q (quality factor) value, which indicates the kurtosis of the measured value, was obtained by inputting the measured data into an approximate formula model. The Q value on the flat surface was approximately 0.68 on the x-axis and 0.56 on the y-axis, while the Q value on the curved surface was approximately 0.75 on the x-axis and 0.63 on the y-axis. Therefore, the Q value obtained by measuring of the magnetic flux density may be useful as an index of magnetic stimulation resolution.

S. Ueno, T. Matsuda et al., "Localized stimulation of the human brain and spinal cord by a pair of opposing pulsed magnetic fields," J Appl. Phys., vol. 67(9), pp. 5838-5840, 1990. T. Torii, H. Sakamoto, A. Sato, "Simplified Magnetic Flux Density Measurement for Local Resolution Analysis of Transcranial Magnetic Stimulation," 2023 IEEE International Magnetic Conference (INTERMAG), doi.org/10.1109/INTERMAG50591.2023.10265102, 2023.

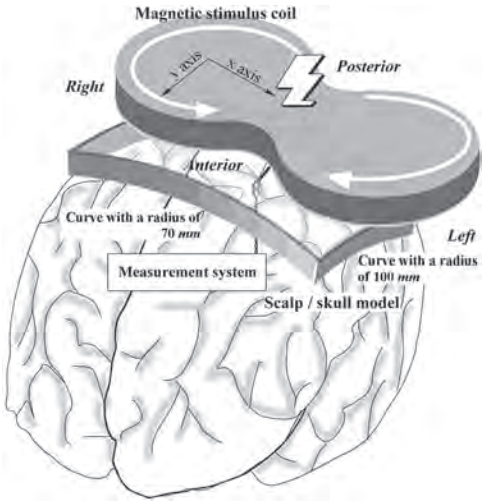

Fig. 1: Experimental setting image

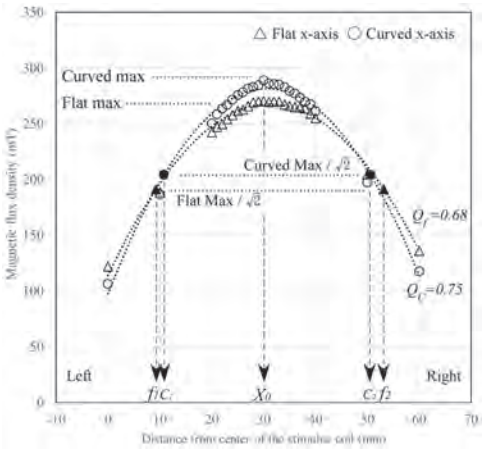

Fig. 2: Magnetic flux density distribution on the x-axis

VP1-06. Investigating the inclusion of anatomical variations in computer-assisted exploration of the induced electric field in transcranial magnetic stimulation. *X. Zhong*[1], D. Jiles[2] and H. Jiang[1,3] *1. Research Institute of Tsinghua University in Shenzhen, Shenzhen, China; 2. Department of Electrical and Computer Engineering, Iowa State University, Ames, IA, United States; 3. School of Integrated Circuits, Tsinghua University, Beijing, China*

Transcranial magnetic stimulation (TMS) is a promising tool in the diagnosis and treatment of neurological disorders non-invasively. Derived from the electromagnetic induction principle, it generates electric fields in the targeted areas in the brain by the alternating magnetic fields from the TMS coil. The brain structure is complicated and varies from person to person, which renders it difficult to predict and enhance the efficacy of TMS treatment for a specific subject. This work takes advantage of computational modeling and involves 50 realistic heterogeneous head models to explore how anatomical variations affect the induced electric field, from the perspective of intensity and focality. Six commercially available TMS coils were placed at two anatomical positions: the vertex and the dorsolateral prefrontal cortex. Finite element method was used to calculate the induced electric field in the brain. Two metrics, E-max and V-half were used to evaluate the induced electric field intensity and focality. The results were examined taking the fifty head models as a group or dividing them by their age or/and gender. It shows that age and gender have significant influence on the induced electric field. The effects of individual anatomical structure on induced electric field are also illustrated. This work will provide reference and support in explaining and determining TMS device configuration and treatment protocols for real-world clinical applications.

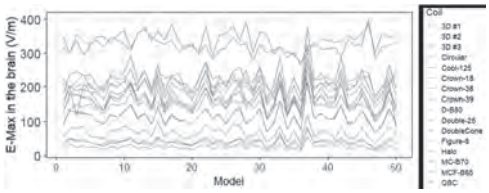

Fig. 1: E-max values for each head model with coils placed at the vertex

VP1-07. Investigation of transmitting coil with rotating magnetic field in real-time monitoring system for laboratory animals. *T. Omori*[1], F. Sato[1], Y. Furuya[2] and S. Sasaki[2] *1. Graduate School of Engineering, Tohoku Gakuin University, Sendai, Japan; 2. Hikaridenshi Co., Ltd., Osaki, Japan*

The purpose of animal experiments is to record changes in the biological information of experimental animals that occur during the course of the experiment, and this information is used to discuss the effects of drugs and technologies on the animals. There are a wide variety of types of biometric acquisition devices, but in recent years, the most commonly employed devices are those implanted in the body[1,2]. This is because they can accurately and continuously acquire biometric information such as body temperature, heart rate, activity level, and blood pressure. However, the means of supplying power to the device is a challenge. Currently, the mainstream method is to supply power from a battery embedded with the biometric data acquisition device[1,3,4]. Although this method can provide a stable power supply wirelessly, it does not have sufficient capacity for experiments. As a result, it is difficult to meet the greatest requirement in animal experiments, which is to monitor biological information in real time[5]. To solve this problem, we will construct a system in which power is constantly supplied to the biometric data acquisition device by electromagnetic induction between the power-receiving coil inside the experimental animal and the power-transmitting coil placed under the floor of the rearing cage. In addition, it is necessary to take into consideration that the coupling state of the coils changes as the position and posture of the animal changes during the construction process. Fig. 1 shows the appearance of the biometric data acquisition system to be constructed. Fig. 2 shows a graph of the magnetic flux density measured at the bottom of the power transmission coil. From this figure, it can be confirmed that the magnetic flux density in the planar direction is uniform.

[1]H. Mei, K. A. Thackston, R. A. Bercich, IEEE Trans. Biomed. Eng., vol. 64, no. 4, p. 775(2017) [2]P. Cong, N. Chaimanonart, W. H. Ko, IEEE J. Solid-State Circuits, vol. 44, no. 12, p.3631(2009) [3]S. T. Lee, P. A. Williams, C. E. Braine, IEEE Trans. Neural Syst. Rehabilitation Eng., vol. 23, no. 4, p.655(2015) [4]T. A. Szuts, V. Fadeyev, S. Kachiguine, Nat. Neurosci., vol. 14, no. 2, p. 263(2011) [5]B. D. Nelson, S. S. Karipott, Y. Wang, *Sensors*, vol. 20, p.4604(2020)

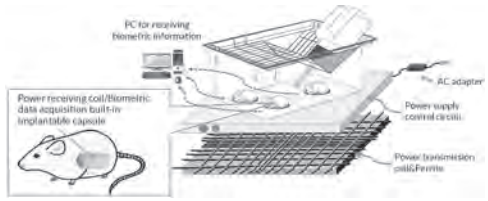

Fig. 1 Overview of the biometric acquisition device.

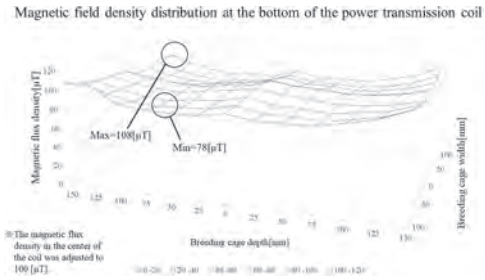

Fig. 2 Magnetic flux density distribution at the bottom of the power transmission coil.

VP1-08. A Study on Optimization of Power Receiving Coil for Real-Time Vital Signs Measurement in Small Laboratory Animals. *K. Hase*[1], T. Omori[1], F. Sato[1], Y. Furuya[2], K. Sagara[2], S. Sasaki[2] and T. Yoshikawa[3] *1. Tohoku Gakuin Univ., Sendai, Japan; 2. Hikaridenshi Co., Ltd., Osaki, Japan; 3. Hokkaido Univ., Sapporo, Japan*

Animal experiments are useful in drug discovery and medical technology development. In current animal experiments, activity meters are implanted in the bodies of small laboratory animals to measure their vital signs, and the most common method is to supply power to the meter via batteries or a wired connection to a power source. However, there are concerns that these methods may adversely affect the health of laboratory animals due to stress. Therefore, this study proposes a power supply method using wireless power transfer and examines the optimization of the power receiving coil. It is important that the power transmission system is not affected by the position and posture of the laboratory animals. To achieve this, the transmitting coil should be shaped to generate a rotating magnetic field, and the receiving coil should be shaped so that it is chained to the rotating magnetic field at any angle to efficiently receive the rotating magnetic field. Fig.1 shows a model of a power receiving coil based on this idea, in which two curved coils are attached to the upper and lower surfaces of a magnetic core with a circular cross-sectional shape. Since the angles of the upper and lower coils are offset by 90deg, both coils feed the power if the receiving coil is oriented vertically, and if it is oriented horizontally, the coil facing a different direction from the axis of rotation of the circular orbit of the rotating magnetic field feeds the power. Confirm that the devised receiving coil is capable of stable power supply without being affected by its angle or misalignment. The output voltage fluctuations at load release were measured when the receiving coil was fixed on the transmitting coil in the vertical and horizontal orientations, respectively, and rotated 360deg in 15deg increments. The experimental results for the vertical orientation are shown in Fig.2. The experimental results, including the horizontal orientation, confirmed that the output voltage was supplied without interruption, and thus it can be said that stable power supply is possible regardless of the orientation or angle of the receiving coil.

H. Mei, K. A. Thackston, R. A. Bercich, J. G. R. Jefferys, and P. P. Irazoqui, IEEE. Trans. Biomed. Eng. 64, 775 (2017). S. T. Lee, P. A. Williams, C. E. Braine, D.-T. Lin, S. W. M. John, and P. P. Irazoqui, IEEE Trans. Neural Syst. Rehabilitation Eng. 23, 655 (2015). F. Sato, H. Kotake, T. Takura, T. Sato, H. Matsuki, and S. Yamada, J. Magn. Soc. Jpn. 35, 404 (2011).

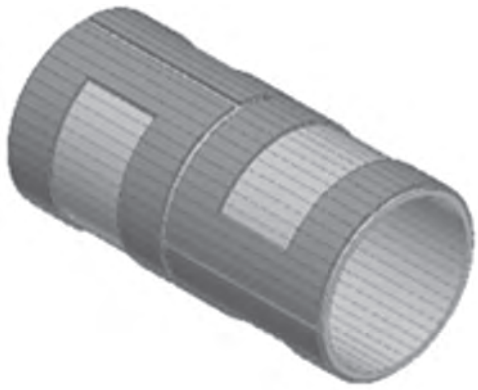

Fig. 1: Model of receiving coil

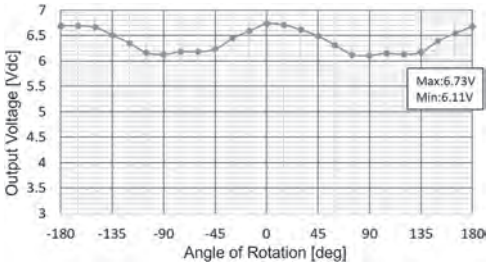

Fig. 2: Output Voltage Characteristics (Vertical orientation of receiving coil)

VP1-09. The behavior of magnetic emulsions in microchannels under the influence of an inhomogeneous magnetic field. *D. Kalyuzhnaya*[1], E. Sokolov[1] and P. Ryapolov[1] *1. Southwest State University, Kursk, Russian Federation*

Magnetic emulsions are a liquid composite medium, one of the phases of which is represented by a magnetic nanocolloid. A unique feature of these media is the presence of pronounced magnetic properties [1, 2]. Magnetic emulsions are a promising material for targeted drug delivery [3]. Their production can be carried out in various ways, for example, mechanical dispersion [4] or emulsification using microfluidic chips [5]. The production of magnetic emulsions is usually carried out by dispersing magnetic fluids based on hydrocarbons in water [2]. Emulsions in which the dispersed phase is formed by water and the dispersion medium by a hydrocarbon magnetic fluid are less common and have been studied to a much lesser extent. The most original variants are emulsions using water-based magnetic fluids [6], as well as emulsions obtained using other polar liquids. The theoretical and experimental formation of emulsions using a magnetic fluid in a vertical microchannel under the influence of an inhomogeneous magnetic field is considered in this paper. The magnetic field has a focusing effect and helps to control the size of the emulsion droplets and their dynamics. The source of the magnetic field is represented as a combination of a solenoid, on top of which there is an annular permanent magnet. An experiment was conducted and a simulation of the system was carried out in the femm software package. Modeling of a water drop in a kerosene-based magnetic fluid under the influence of a combined magnetic field source is shown in Fig. 1. The effect of the ponderomotor force is described in detail. The forces acting on both non-magnetic droplets floating in a magnetic fluid and drops of magnetic fluid floating in a non-magnetic liquid medium are determined. The results contribute to the further development of detailed mechanisms for the formation of emulsions based on magnetic fluid, and their size control in real time.

1. X. Huang, M. Saadat, M. A. Bijarchi, Chemical Engineering Science., Vol. 270, p. 118519 (2023) 2. S. A. Suslov, ASME Journal of Heat and Mass Transfer., Vol. 145, p. 030801 (2023) 3. E. Elkalla, S. Khizar, Z. Ait-Touchente, Emergent Materials., Vol. 6, p. 2027-2039 (2023) 4. A. R. Zakinyan, A. A. Zakinyan, Sensors and Actuators A: Physical., Vol. 314, p. 112347 (2020) 5. S. Kahkeshani, D. Di Carlo, Lab on a Chip., Vol. 16, p. 2474-2480 (2016) 6. D. Kalyuzhnaya, E. Sokolov, A. Vasilyeva, Fluids., Vol. 8, p. 42 (2023)

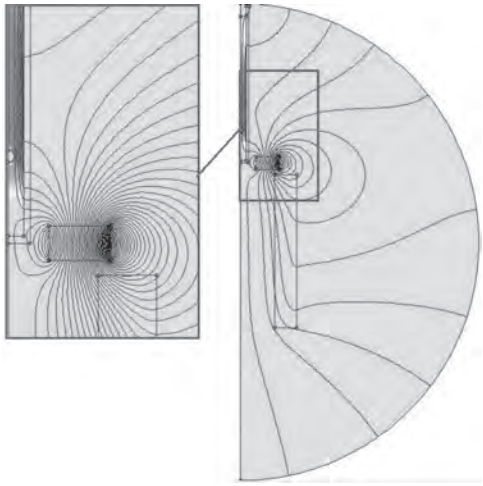

Fig. 1. Simulation results in the femm software package

VP1-10. EMI Shielding Effectiveness of Ferrofluid Layer in the Presence of Oscillating Magnetic Field. H. Hsieh[1], H. Kuan[1], *Y. Li*[1] and Y. Cheng[1] *1. Mechanical and Aerospace, Chung-Cheng Institute of Technology, National Defense University, Taoyuan, Taiwan*

This work investigates the impact of dynamic magnetic fields on ferrofluid instability and electromagnetic interference (EMI) shielding effectiveness (SE) of a flexible ferromagnetic material. The ferrofluid crests varies with magnetic field strengths and oscillating frequencies. Fig. 1 shows the periodical instability of a ferrofluid layer subjected to an oscillating magnetic field with a frequency of 1 Hz within one period. The ferrofluid exhibits pulsating instability, with crests periodically appearing and disappearing. At a frequency of 5 Hz, due to the phase lag between the ferrofluid oscillation and the magnetic field, the number of crests decreases and their height varies, resulting in oscillatory instability. However, excessively high frequencies cause static instability, preventing the ferrofluid crests from synchronizing with the magnetic field oscillations, and eventually returning to a stable state. Fig. 2 shows the comparison of EMI SEs of a ferrofluid layer with pulsating, oscillatory, and statistic instability, respectively. Experimental results indicate that when the crests exhibit pulsating (magnetic field frequency at 1 Hz) or oscillatory states (magnetic field frequency at 5 Hz), the SE also changes correspondingly with the pulsating or oscillatory state of the crests. Without the influence of a magnetic field, the ferrofluid remains in a horizontal state with no crest formation, providing SE of nearly 19 dB at EMW frequencies of 13 GHz and 16 GHz. When a magnetic field strength of 40.5 mT without oscillation (f=0 Hz) is applied to the ferrofluid, the SE is slightly declined due to the reduction of the layer thickness. As an oscillation field with a frequency of 1 Hz is applied, the pulsating instability of the ferrofluid crests enhances the highest of the SE to nearly 40 dB at EMW frequency of 15 GHz. When the oscillating frequency increases to 5 Hz, the oscillatory instability of the ferrofluid crests causes the highest SE of 37.7 dB at EMW frequency of 17.5 GHz. The results indicate dynamic crests significantly improve the SE of the EMI for the flexible ferrofluid layer.

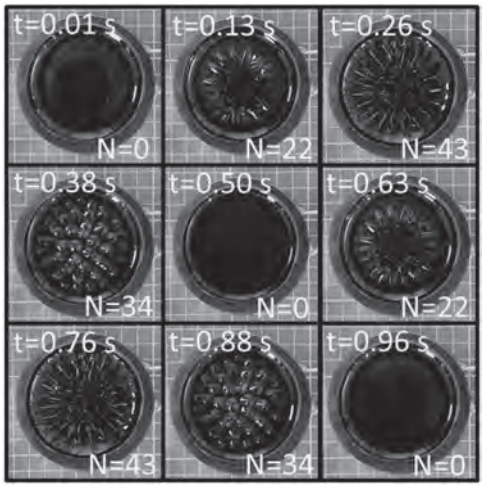

Fig.1 Sequential images of dynamic ferrofluid crests

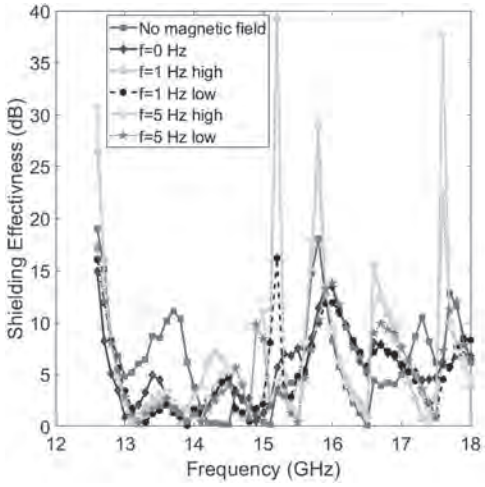

Fig. 2 EMI SEs of ferrofluid layer at various oscillating field

VP1-11. Rheological properties of magnetorheological fluids using magnetic spherical nickel particles with different surface roughness.
G. Stoian[1], G. Balusescu[1], M. Grigoras[1], H. Chiriac[1] and N. Lupu[1]
1. National Institute of Research and Development for Technical Physics, Iasi, Romania

Magnetorheological fluids (MRFs) are fluids suspension composed by micron magnetic particles dispersed in non-magnetic carrier fluid [1]. These intelligent materials respond to applied magnetic fields by changing the rheological behaviour, developing a yield stress that increases with the applied magnetic field [2]. MRFs are visible in a variety of applications in science and engineering [3]. The rheological properties of MRFs are determined by concentration of magnetic particles, their size, shape and magnetic properties [4]. This study investigates the influence of the surface characteristics of the magnetic nickel particles on the performances of MR fluids. Micrometric Ni powders, with spherical and similar size particles, with different surface roughness (smooth-MRF1 vs. high surface roughness-MRF2) were used for the preparation of the MRFs. Engine oil was used as carrier fluid for the dispersed phase. The particles were characterized by SEM and VSM, while the magnetorheological properties have been studied using a magneto-rheometer. Ni particles (Fig.1) have similar sizes, same saturation magnetization and soft magnetic properties but they differ on the surface. The share stress vs. share rate curves were plotted with the magnetic field as a parameter. From these flow curves the yield stress corresponding to different values of the magnetic field were calculated according to the Bingham model. Fig. 2 shows that MRF1 based on smooth surface particles exhibits much higher yield stresses. To explain this behaviour, we performed oscillation tests to investigate the internal structure of MRFs. Although the surface roughness is expected to increase the friction forces between particles and create stronger particle chains, it seems that the roughness of the particles negatively impacts the formation of the chains. In conclusion, the surface has a significant influence on the performance of MRFs. A higher roughness negatively impacts the flow behaviour in magnetic field. Acknowledgements. Financial support from NUCLEU Programme - Contract No. 18N/01.01.2023, project PN 23 11 01 01 is highly acknowledged.

1. Sun, Y., Wang, Y., Deng, H., Sang, M., Gong, X., (2022), Effect of MXene nanosheets attached to carbonyl iron microspheres on the performance and stability of magnetorheological fluid, *Journal of Industrial and Engineering Chemistry*, 114, 508–517. 2. Zhang, L., Luo, Y., Ren, H., Wang, Y., Gu, Z., (2023), Microscopic modeling of magnetorheological fluids containing spherical and ellipsoidal ferromagnetic particles, *Journal of Magnetism and Magnetic Materials*, 586, 171204. 3. Ashtiani, M., Hashemabadi, S.H., Ghaffari, A., (2015), A review on the magnetorheological fluid preparation and stabilization, *Journal of Magnetism and Magnetic Materials*, 374, 716–730. 4. Kariganaur, A.K., Kumar, H., Arun, M., (2022), Effect of temperature on sedimentation stability and flow characteristics of magnetorheological fluids with damper as the performance analyser, *Journal of Magnetism and Magnetic Materials*, 555, 169342.

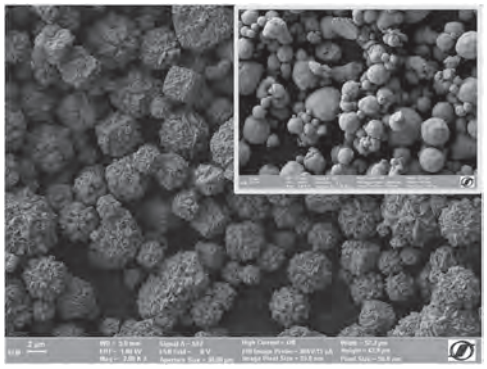

Fig. 1. SEM image of Ni magnetic particles

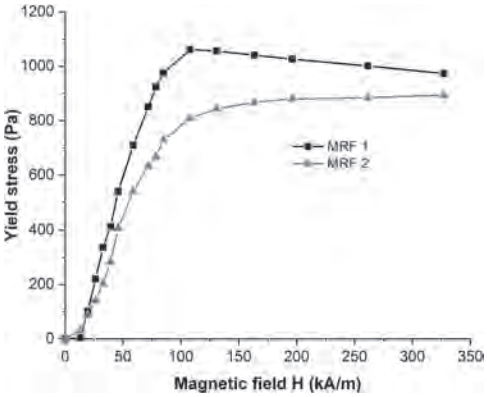

Fig. 2. Yield stress under different magnetic fields

VP1-12. Machine learning-based prediction model for magnetic hyperthermia.
D. Chu[1] and *A. Tomitaka*[1] *1. University of Houston-Victoria, Victoria, TX, United States*

Magnetic hyperthermia has great potential as a non-invasive cancer treatment. However, the limited success in clinical translation stems from a lack of systematic nanoparticle optimization. To bridge this gap, machine learning models that predict the heating efficiency of magnetic nanoparticles (MNPs) have been developed in a few studies [1][2]. Even though deep learning that uses artificial neural networks (ANNs) outperform traditional machine learning models in many cases, the ANNs trained on experimental data have

not been studied for magnetic hyperthermia. In this study, the ANN models with different architectures were explored to predict the heating efficiencies of MNPs. The dataset containing physical and magnetic properties of MNPs and external magnetic field conditions as input features and specific absorption rate (SAR) representing the heat generation efficiency of MNPs as a target variable was collected through the literature search and the existing database [2]. As the performance of the ANN model largely depends on the architecture, the optimal architecture was explored by varying the number of neurons and hidden layers. The R^2 values of the ANN models improved from 0.790 to 0.883 by increasing the number of neurons from 10 to 500 in a hidden layer. Figures 1 and 2 show the scatter plots of actual vs predicted SARs of the ANN models with 2 hidden layers of 500 neurons and 4 hidden layers of 500 neurons, respectively. The diagonal line represents the ideal fit where predicted SAR is always equal to actual SAR. The model performance was further improved by adding the second hidden layer of 500 neurons. However, a deeper architecture having more than 3 hidden layers reduced their prediction performances with higher errors. These results indicate that a shallow ANN is suitable to capture the patterns in this dataset and the optimized ANN model could be a great tool to design optimal MNPs.

[1] M. Coïsson, G. Barrera, F. Celegato, et al., APL Materials, 2022, 10, 081108. [2] P. Kim, N. Serov, A. Falchevskaya, *et al.*, Small 2023, 19, 2303522.

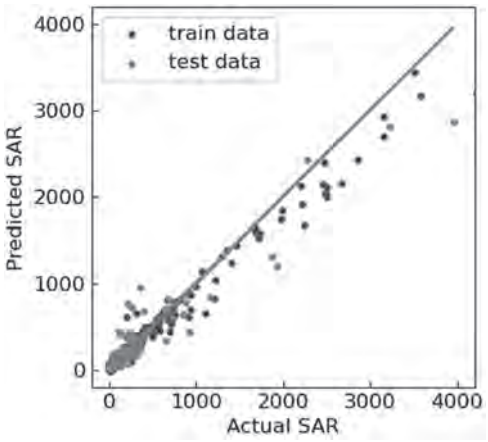

Fig. 1. Actual vs predicted SARs of ANN models with 2 hidden layers of 500 neurons.

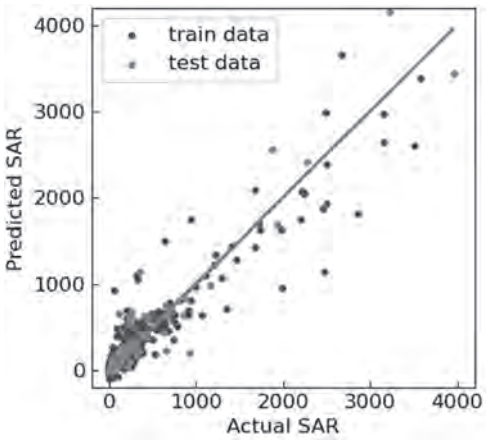

Fig. 2. Actual vs predicted SARs of ANN models with 4 hidden layers of 500 neurons.

Session VP2
ELECTRICAL MACHINES AND POWER ELECTRONICS I
(Poster Virtual Session)

Amanda de Oliveira Barros, Co-Chair
University of Texas at El Paso, El Paso, TX, United States
Ahmed Hemeida, Co-Chair
Aalto University, Helsinki, Finland
Anh Thanh Huynh, Co-Chair
University of Nottingham, Nottingham, United Kingdom

VP2-01. An Improved Equivalent Magnetic Network for Performance Prediction of Yokeless and Segmented Armature Axial Flux Permanent Magnet Motor. *C. Wang*[1] and B. Peng[1] *1. Shenyang University of Technology, Shenyang, China*

The existing quasi-3D equivalent magnetic network (EMN) all prioritize the YASA-AFPM's magnetic field in the air gap but ignore that in the slot [1-3], which may result in errors in predicting synchronous inductance L_s and related performance, such as power factor and maximum torque. An improved quasi-3D EMN, based on [4], is proposed for the YASA-AFPM, whose main novelty is that both magnetic field in the air gap and slot can be accurately predicted. The improved EMN is composed of rectangular permeance element, magnetomotive force (MMF) source and boundary condition, as shown in Fig. 1. There are four crossing permeances per element, and there are multiple elements covering all regions of the motor, especially the air gap and slot region. The PM MMF sources are located in elements at PM region. The winding MMF sources, generated by a single coil, are located both in elements at stator tooth, where the coil is wound, and the slot region, where the coil is occupied. The values of winding MMF sources are calculated by Ampere's law. The MMF at stator tooth is generated by the whole coil, while that at slot region is generated by the portion of coil surrounding the element. Moreover, the periodic or anti-periodic, and symmetry boundary conditions are employed here to reduce computation time. The nodal analysis, based on Kirchhoff's law, is employed to solve the EMN, thereby obtaining the distributions of magnetic density, which, in turn, are used to calculate the flux linkage and magnetic energy. The no-load back-EMF is the derivative of no-load flux linkage with respect to time. The inductance can be obtained by utilizing its relationship with current and the stored magnetic energy in the air gap and slot. With i_d=0, the torque and phase voltage of a 167 r/min YASA-AFPM are shown in Fig. 2. When the phase voltage reaches its maximum, the phase current is 35.2A, and the torque predicted by the EMN is 728.09 Nm, which is 3.75% smaller than 756.43 Nm obtained by the 3D-FEA. Moreover, the influence of L_s on maximum torque cannot be ignored. Ignoring L_s, the calculated phase voltage with 35.2A is 164.4V, which is 21.71% smaller than the actual 210V.

[1] Y. Huang, T. Zhou, J. Dong, et al., IEEE Trans. Magn., vol. 50, pp. 1-4(2014). [2] X. Sun, L. Wang, X. Fan, et al., Proc. IEEE Trans. Electrific. Conf. Expo, pp. 1-6 (2022). [3] A. Hemeida,A. Lehikoinen, P. Rasilo, et al., IEEE Trans. Ind. Electron., vol. 66, pp. 8318-8333 (2019). [4] S. Yang, S. Asfirane, S. Hlioui, et al., CES Trans. Elect. Machines Syst., vol. 5, pp. 152-162(2021).

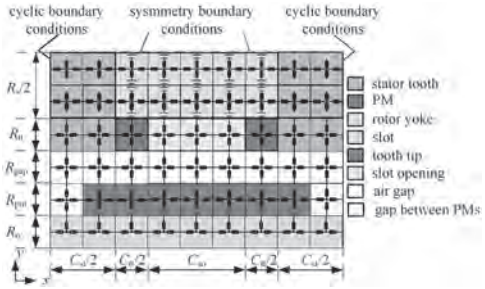

Fig. 1 EMN within one slot pitch

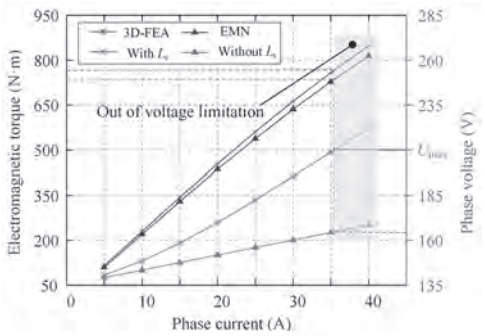

Fig. 2 Torque and phase voltage

VP2-02. Analysis of Air-Gap Field Modulation Effect in Multi-Unit Distributed Permanent Magnet Arc Motor. *Z. Pan*[1], J. Zhao[1], S. Fang[2] and Z. Yu[1] *1. School of Electrical Engineering and Automation, Hefei University of Technology, Hefei, China; 2. School of Electrical Engineering, Southeast University, Nanjing, China*

I. INTRODUCTION Permanent magnet arc motor (PMAM) is widely used in the large scanning equipment such as large telescope and servo turntable [1]-[2]. According to the different position of the PM, the PMAMs are summarized as rotor-PM type PMAMs (RPM-PMAMs) and stator-SPM type PMAMs (SPM-PMAMs). However, the past works mainly focus on the design, optimization and performance analysis of PMAMs, the quantification of the torque contributions of the air-gap field harmonics in the FR-PMAM remain unreported. Therefore, the field modulation effect of the FR-PMAM is investigated to provide an in-depth understanding of the field harmonics torque production mechanism in this paper. II. MOTOR TOPOLOGY As shown in Fig. 1, the motor structure of the FR-PMAM is made up of three stator segments and one rotor structure. Each stator segment and the rotor form a unit motor with 6/11-stator slot/rotor pole (SSRP) combination. The design idea of unit motor is introduced to design and analysis the FR-PMAM. As shown in Fig. 1(c), the FR-PM motor can be seen as the combination of five unit motors having 6/11 SSRP combination. III. FIELD MODULATION EFFECT The Maxwell stress tensor method is

used to quantify the torque contributions of various working harmonics. The torque contribution of the air-gap field harmonics having pole-pairs of iNs/2 and |iNs/2± nNr| is given in Fig. 2 and Table I. Apart from the torque generation of the air-gap field harmonics having the pole-pairs of iNs/2, various modulated field harmonics with pole-pairs of |iNs/2± nNr| also engage in the torque generation, In addition, the analytical results agree well with the FE results, which confirm the field modulation effect in the FR-PM motor and FR-PMAM. IV. EXPERIMENTAL VALIDATION Fig. 1(e)-(f) show the prototype of FR-PMAM. The FE-predicted and experimental test results are given in Fig. 3. It can be seen that the measured back-EMF and torque are slightly lower than the FE predictions, which is mainly due to the fact that the end-winding effect and mechanical tolerance are not considered in FE analysis. More FE simulation results and experimental results will be presented in the full paper.

[1] J. J. Chang, W. L. Ma, et al. "Design and optimization of arc permanent magnet synchronous motor used on large telescope," IEEE Trans. Magn., vol. 48, no. 5, pp. 1943-1947, May 2012. [2] Z. Pan, and S. Fang, "Torque performance improvement of permanent magnet arc motor based on two-step strategy," IEEE Trans. Ind. Infomat., vol. 17, no. 11, pp. 7523-7534, Nov. 2021.

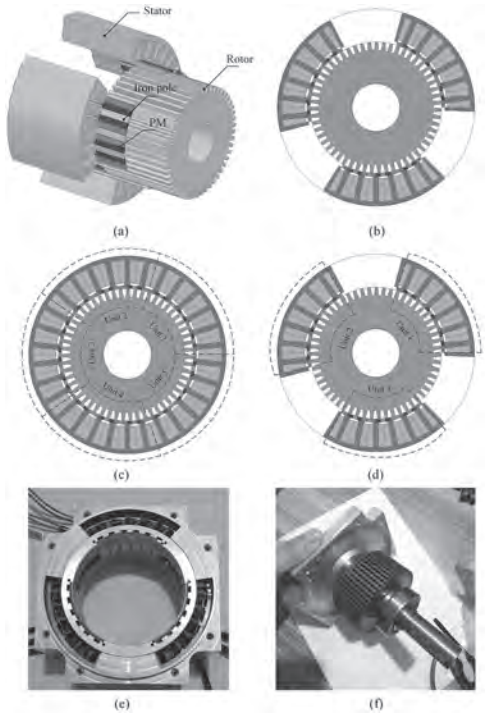

Fig. 1. Motor Topologies.

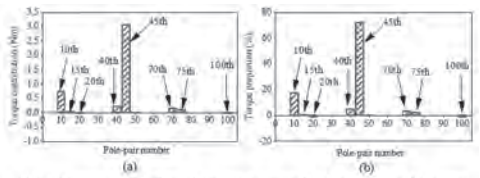

Fig. 2. Torque contribution of the main air-gap field harmonics. (a) Torque contribution. (b) Torque proportion.

TABLE I
TORQUE CONTRIBUTION OF MAIN AIR-GAP FIELD HARMONICS

Harmonic order	FR- PM motor				
	B_{sk} (T)	B_{rk} (T)	$\cos(\theta_{sk}-\theta_{rk})$	T_{mk} (Nm)	λ_{mk} (%)
10th	0.174	0.032	0.842	0.745	17.5
15th	0.430	0.104	0.004	0.026	0.66
20th	0.019	0.011	-0.971	-0.04	-0.75
40th	0.081	0.052	0.317	0.217	5.09
45th	0.498	0.261	0.146	3.069	72.2
70th	0.086	0.057	0.184	0.146	3.44
75th	0.128	0.124	0.042	0.109	2.56
100th	0.058	0.069	-0.049	-0.032	-0.75
Average torque of FR PM motor(Analytical)				4.24	99.95
Average torque of FR-PM motor(FE)				4.32	100%
Average torque of FR PMAM (Analytical)				2.54	99.95
Average torque of the FR-PMAM (FE)				2.52	100%

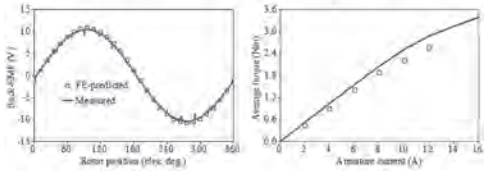

Fig. 3. Measured and FE-predicted results. (a) Back-EMF. (b) Average torque.

VP2-09. AC Loss Analysis of Flat Wire Motor based on Hybrid Winding Structure of Litz Wire and Flat Wire. *Y. Li*[1], J. Li[1], Y. Li[1], S. Wang[1], L. Zhang[1], L. Zeng[2] and R. Pei[1,2] *1. Shenyang University of Technology, Shenyang, China; 2. Suzhou Inn-Mag New Energy Ltd, Suzhou, China*

In recent years, electric vehicles have become an important way to respond to the global demand for green mobility. Flat wire motors are widely used in electric vehicle drive motors due to their high slot fullness and high power density, but the skin effect and proximity effect are more pronounced due to the flat wire is thicker than the round wire, resulting in a significant increase in AC loss at high frequency. Researchers have proposed different ways to suppress the AC loss, some scholars have used radial and axial layering to reduce the loss of the motor winding [1,2], and the most effective way to reduce the proximity effect and skin effect of the bundled layer is to use litz wire to reduce the cross-sectional area of the wire so as to reduce the internal circulating current [3]. In this paper, a hybrid connection of flat wire and litz wire is proposed, as shown in Fig. 1, a high-speed flat wire motor with 48 slots and 8 poles, as a reference model. Since the proximity effect and skin effect are obvious at the slot opening of the flat wire motor, the litz wire is used at the slot opening and the flat wire is used at other positions. Comparing the effects of different stranding methods and different diameters of litz wire hybrid topology on the performance of the motor, a 2-row and 6-column litz wire stranding method with a wire diameter of 0.3 mm is finally determined. Based on the field-circuit-coupled finite element method, a more uniform current density distribution of flat wire winding with hybrid topology are calculated and obtained as shown in Fig. 2. In this paper, by mixing the connection of litz wire and flat wire, the effect of skin effect on the AC loss of the motor is reduced on the basis of ensuring the slot fullness, and the effect of the application of litz wire on the efficiency of the motor is verified. This paper summarizes the impact of the wire diameter and stranding method of the litz wire on the slot fullness, establishes the copper loss analysis model of the litz wire hybrid topology, and provides guidance for the application of the litz wire in the electric vehicle drive motor.

[1] G. Du, W. Xu and J. Zhu, "Power Loss and Thermal Analysis for High-Power High-Speed Permanent Magnet Machines," in *IEEE Transactions on Industrial Electronics*, Vol. 67, pp. 2722-2733(2020). [2] F. Momen, K. Rahman, and Y. Son, "Electrical propulsion system design

of chevrolet bolt battery electric vehicle," IEEE Trans. Ind. Appl., Vol. 55, pp. 376–384(2019). [3]Z. Liu, J. Zhu and L. Zhu, "Accurate Calculation of Eddy Current Loss in Litz-Wired High-Frequency Transformer Windings," in *IEEE Transactions on Magnetics*, Vol. 54, pp. 1-5(2018).

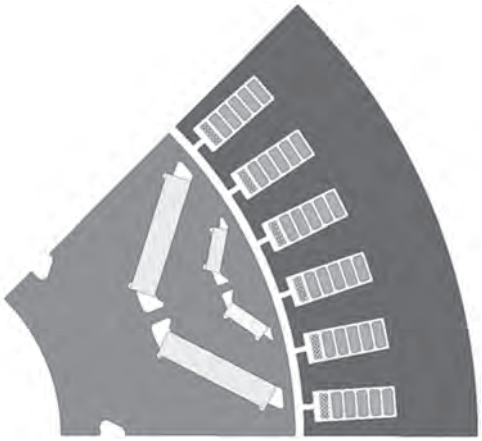

Fig.1 The high-speed flat wire motor model

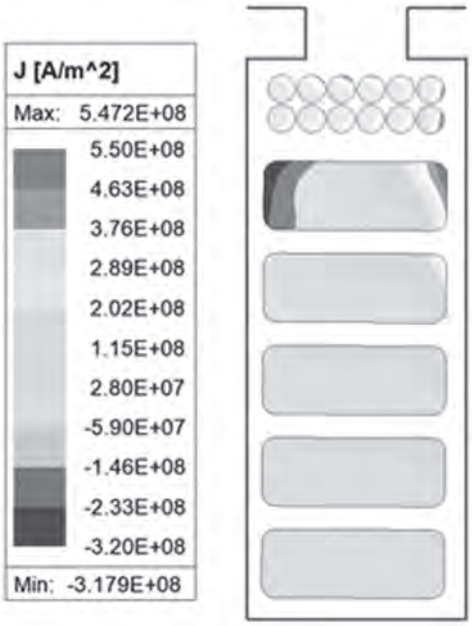

Fig.2 The current density of winding with hybrid topology

VP2-10. Advanced Study of Lateral Inter-Laminar Faults in Laminated Magnetic Cores with Homogenization Method. *S. Gao*[1,2], Y. Gao[2], X. Zhao[1], H. Hamzehbahmani[3], W. Guan[4] and K. Muramatsu[5]
1. North China Electric Power University, Baoding, China; 2. Oita University, Oita, Japan; 3. Durham University, Durham, United Kingdom; 4. Wuhan University, Wuhan, China; 5. Saga University, Saga, Japan

1. Introduction Electrical steel laminations stacked by a set of grain-oriented (GO) silicon steels is generally implemented in magnetic cores of electromagnetic devices. During the manufacturing process, edge burrs can be generated when cutting the lamination. This will introduce the inter-laminar eddy currents on the lateral side of steels known as lateral inter-laminar faults [1, 2]. When the lateral inter-laminar faults occur, the simulation of the silicon laminated core with conventional finite element method could be time consuming considering the specific structure of model. Thus, we proposed a homogenization method with equivalent electrical conductivity considering the inter-laminar eddy currents on the lateral side for saving the computing costs. For the experimental verification, the edge burrs are represented by the artificial faults with lead-free solder on the lateral side of lamination. The simulated results are compared to the measured results for validation. 2. Analysis model and method The analyzed and experimental laminated core model with solder on the lateral side is shown in Fig. 1. The laminated core is stacked with GO silicon steel M105-30P with the thickness of 0.3 mm, the electrical conductivity of 2.169×10^6 S/m, and the nominal lamination factor of 0.983. Sinusoidal excitation is imposed on *y*-direction. The proposed homogenization method considers the inter-laminar eddy currents by introducing the equivalent electrical conductivity. As the parameter of the equivalent electrical conductivity in the model is identified for a peak induction of 1.1 T and 50 Hz, it can be applied for the cases under other excitations. 3. Results The comparison results of the measured and the calculated classical eddy current losses by the homogenization model under different excitations are shown in Fig. 2. More investigations will be given in the full paper.

[1] H. Hamzehbahmani, P. Anderson, J. Hall, and D. Fox, "Eddy current loss estimation of edge burr-affected magnetic laminations based on equivalent electrical network—Part II: analytical modeling and experimental results," *IEEE Trans. Power Delivery*, vol. 29, no. 2, pp. 651-659, Apr. 2014. [2] H. Hamzehbahmani, "An enhanced analysis of inter-laminar faults in magnetic cores with grain oriented electrical steels for fault diagnosis and condition monitoring: theoretical background and experimental verification," *IEEE Trans. Instrumentation and Measurement*, vol. 72, pp. 1-10, 2023, art no. 6002610.

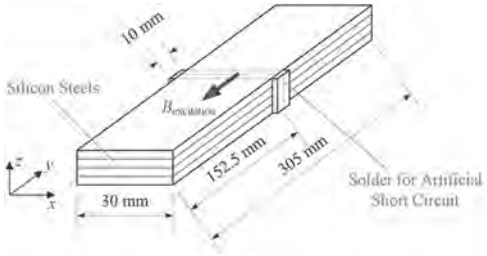

Fig. 1. Lamination model with artificial faults.

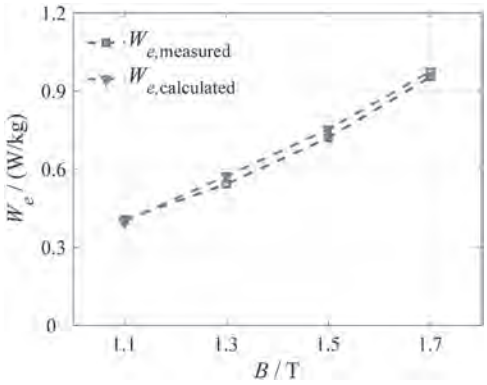

Fig. 2. Comparison of classical eddy current losses with artificial faults (f = 50Hz).

VP2-11. Calculation of Core and PM Losses Considering Current Harmonics and Saturation Effects Based on Exact Analytical Model. *D. Hoang*[1], M. Nguyen[1], K. Shin[2], Y. Kim[1], A. Phung[3] and J. Choi[1]
1. Chungnam National University, Daejeon, The Republic of Korea;
2. Changwon National University, Changwon, The Republic of Korea;
3. Hanoi University of Science and Technology, Hanoi, Vietnam

Due to their high performance, permanent magnet synchronous machines (PMSMs) are crucial for various applications such as traction applications and aerospace. Accurate calculation of core and Permanent Magnet (PM) losses is vital for optimizing machine design and improving efficiency.

Although these losses are often predicted accurately by finite element analysis (FEA), analytical models (AM) are preferred for initial design stages due to their greater insights and reduced computation time. However, the models without coupling FEA typically overlook saturation effects, assuming the core has infinite or constant permeability [1]-[3]. To deal with this problem, this paper anatically predicts the core and PM losses in Surface Permanent Magnet (SPM) machines using harmonic modeling, as developed in [4] combined with an iterative process to find nonlinear solutions. The solution is utilized to extract the magnetic quantities necessary for loss calculations. Additionally, the effects of current harmonics on core loss are further introduced, providing a more realistic assessment of machine performance under varying operational conditions. The accuracy of the proposed method is validated through FEA and experimental tests, demonstrating high precision and reliability making it a valuable tool for the initial design stage.

[1] D. Ishak, Z. Q. Zhu, and D. Howe, IEEE Trans Magn, vol. 41, no. 9 (2005). [2] L. J. Wu, Z. Q. Zhu, and D. Hawkins, IEEE Trans Magn, vol. 48, no. 1 (2012). [3] Z. Djelloul-Khedda, K. Boughrara, and A. Tikellaline, IEEE Trans Magn, vol. 55, no. 1 (2019). [4] Z. Djelloul-Khedda, K. Boughrara, and B. Souleyman, IEEE Trans Magn, vol. 54, no. 7 (2018).

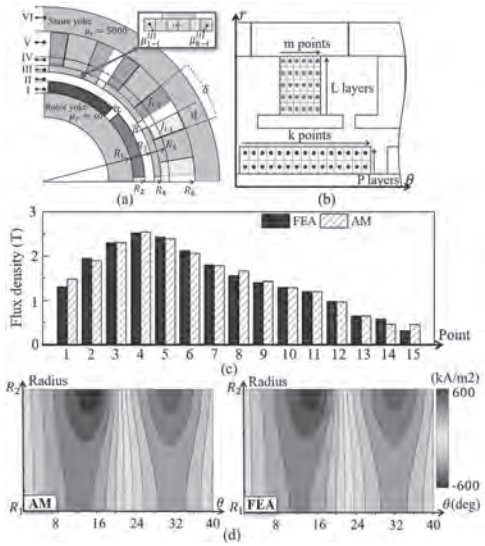

Fig. 1. (a) Analytical model. (b) Definition of divisions for PM and iron parts in calculations. (c) Comparison of first-harmonic flux densities at a tooth tip. (d) Comparison of the current density distribution on a magnet.

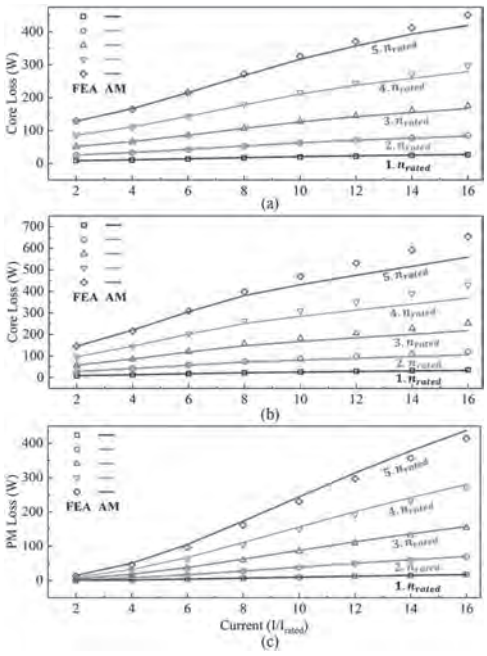

Fig. 2. Comparison of results: (a) total core loss with pure sinusoidal currents, (b) total core loss with currents including 5th and 10th harmonics, and (c) total PM loss with pure sinusoidal currents.

Session VP3
ELECTRICAL MACHINES AND POWER ELECTRONICS II
(Poster Virtual Session)

Amanda de Oliveira Barros, Chair
University of Texas at El Paso, El Paso, TX, United States

VP3-01. A Novel Optimization Method of Topology for Improving Torque Quality in Permanent Magnet Synchronous Machine.

X. Liang[1], M. Wang[1], Y. Liu[1], P. Zheng[1] and W. Li[1] *1. Harbin Institute of Technology, Harbin, China*

High performance machines are the guarantee for the development of industry and economy. The demand for machine performance and design efficiency drives the continuous improvement of machine design and optimization. Many scholars have proposed or improved methods to further improve these processes. Structural optimization is mainly divided into parameter optimization (PO) and topology optimization (TO) [1]. TOs allow the boundaries of each material to be randomly generated. TOs are being attempted to be applied in the topology design to explore performance boundaries [2]. Many machines with better performance that may have never been considered in traditional methods are discovered by TOs. However, the high-degree freedom topology generation based on TOs also brings disorder and inefficiency, and the final result also needs to be obtained after extensive manual screening. Existing research mainly focuses on the algorithm, with little study on how to combine expert experience in conventional method with topology generation without strong constraints in TOs. By this, the design efficiency and performance of machine can be further enhanced. The previous result of TOs can also be better transferred to the research of new structures. The proposed method combining the above professional knowledge and TO is shown in Fig. 1. Compared with the existing method, the improved algorithm assumes several optimization paths based on professional knowledge firstly, multi-objective penalty functions are used to improve the generation direction after each round of result, and the adjustment region sequence is determined quickly by the analytic model. Taking the Permanent Magnet Synchronous Machine as an example, the schematic diagram of structure optimization is shown in Fig. 2. The minimum unit of random generation is determined based on the grid. Guided by the expert experience, the data-driven iterative algorithm optimizes the topology automatically, and extracts the optimal substructure to provide prior data for future design.

[1] H. Sato and H. Igarashi, "Automatic Design of PM Motor Using Monte Carlo Tree Search in Conjunction With Topology Optimization," IEEE Transactions on Magnetics, vol. 58, no. 9: 7200504 (2022) [2] N. Takahashi, S. Nakazaki and D. Miyagi, "Optimization of Electromagnetic and Magnetic Shielding Using ON/OFF Method," IEEE Transactions on Magnetics, vol. 46, no. 8, pp. 3153-3156 (2010)

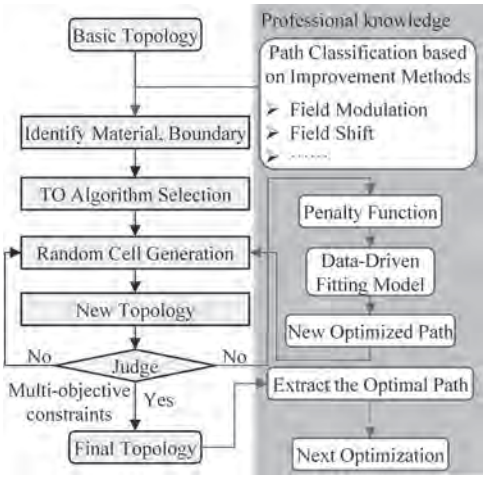

Fig. 1. The proposed structural optimization method and improvement.

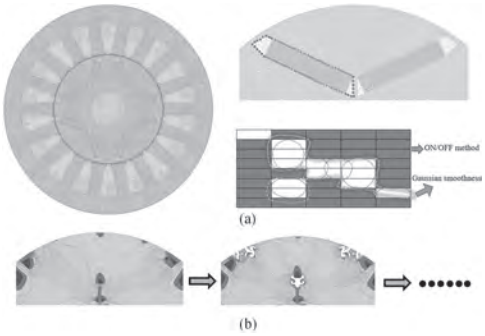

Fig. 2. Structural optimization. (a)Solution domain discretization and various material elements generation (b)Topology iteration.

VP3-02. Generalized Newton-Raphson Iteration Algorithm for Solving Nonlinear Magnetic Field Problems Considering Vector Hysteresis Models.

J. Yin[1], Y. Li[1], S. Yue[1], Y. Dou[2] and Z. Li[3] *1. Key Laboratory of Reliability and Intelligence of Electrical Equipment, Hebei University of Technology, Tianjin, China; 2. Zhejiang University–University of Illinois at Urbana-Champaign Institute, Zhejiang University, Haining, China; 3. Key Laboratory of Smart Grid of Ministry of Education, Tianjin University, Tianjin, China*

Accurate modeling of magnetic properties for iron core materials is of great significance for loss prediction and high-quality design of electrical machines and transformers, where the hysteresis models are commonly incorporated in the numerical calculation of electromagnetic fields [1]. However, due to the limitations of stability and computational efficiency of the built-in nonlinear solvers, customized material models with high complexity remain difficult to be generally encapsulated in commercial software. In this paper, a new approach for implementing the Newton-Raphson (NR) iteration technique is proposed, where a numerical method of evaluating the differential reluctivity is adopted to free the magnetic characterization from analytical expressions,

supported by a localized algorithm of assembling Jacobian matrix according to the convergence condition during each iteration, shortening the calculation time drastically. Three typical Preisach-type models of characterizing hysteresis are established based on measured 2-D magnetic property data of a non-oriented electrical steel sheet, and further employed by in-house finite-element (FE) codes to investigate the performance improvement of the introduced algorithm. A permanent magnet synchronous motor (PMSM) shown in Fig. 1 is analyzed and the computational costs of time-stepping solution for one electrical period are depicted in Fig. 2. Remarkable superiorities of the new method in terms of the total CPU time are observed with almost the same total iteration numbers compared with the traditional way. Note that the iron regions in Fig. 1 of the studied PMSM are all treated as two-axis anisotropy in this digest [2]. More comparative analysis and detailed procedure of the proposed method involving different hysteresis models will be illustrated in the full paper. The adaptability, stability and efficiency of traditional NR iteration technique are comprehensively enhanced by this work, which offers effective instructions for the development of more universal solvers accommodating material models with distinct mathematical characteristics.

J. Chen, S. Wang and H. Shang, IEEE Transactions on Energy Conversion, vol. 37, no. 4, pp. 2472-248 (2022) S. Hussain and D. A. Lowther, IEEE Transactions on Magnetics, vol. 54, no. 3, pp. 1-4 (2018)

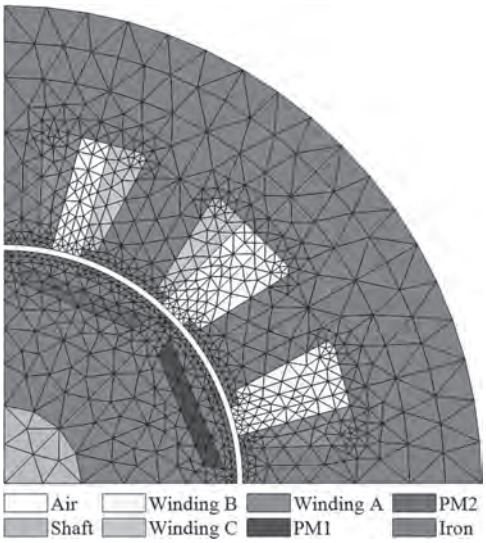

Fig. 1. Geometry of the analyzed PMSM.

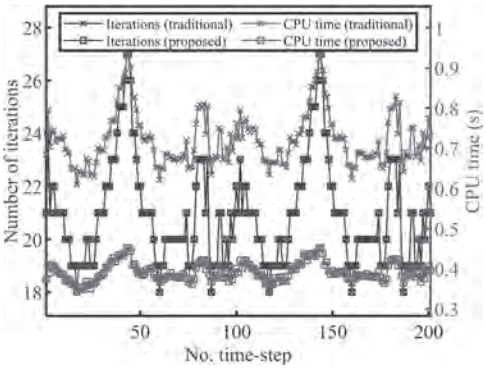

Fig. 2. Computaional costs of the traditinal and the proposed method.

VP3-03. Torque Performance Improvement of CP-PMSM Based on Decision Tree and Bayesian Optimization Algorithm. Z. Pan[1], *J. Zhao*[1] and K. Wei[1] *1. School of Electrical Engineering and Automation, Hefei University of Technology, Hefei, China*

I. INTRODUCTION Consequent-pole permanent magnet motor (CP-PMSM) is recognized as a promising candidate for traction systems [1]. The multi-objective optimization design plays an important role in the motor performance improvement [2]. In this paper, a new multi-objective optimization design method combining the decision tree (DT) and the Bayesian optimization algorithm (BOA) is proposed to achieve performance improvement for the CP-PMSM. This work presents the first application of the DT in the field of the CP-PMSM optimization design. The intelligent optimization algorithm BOA is adopted to optimize the structural parameters and achieve the optimal optimization objectives of the studied CP-PMSM. II. OPTIMIZATION DESIGN The motor topology of the CP-PMSM is shown in Fig. 1. In this motor, the radially magnetized CP-PMs are pasted on the rotor. The fractional slot concentrated windings are located in the stator slot. In order to achieve performance improvement for the CP-PMSM, a new multi-objective optimization design method based on DT and BOA is proposed, which mainly contains the following four steps: (1) First, the structural parameters, objectives and their constraints are confirmed. (2) Second, the FE software is used to obtain adequate training and test dataset for next-step regression modeling. (3) Third, the DT is introduced to build surrogate model between output objectives and input parameters. (4) Finally, the BOA is used to obtain the optimal structural parameters, thereby achieving the motor performances improvement. III. PERFORMANCES COMPARISON Figs. 2(a)-(b) compare the regression accuracy of the DT and KNN. Compared with KNN, DT can better fit the FE data. Therefore, the DT can provide an accurate surrogate model for the multi-objective optimization design. The back-EMF and output torque of the initial and optimized CP-PMSM are compared in Figs. 2(c)-(d). It can be seen that compared with the initial motor, the optimized CP-PMSM has a higher back-EMF and average torque, and lower torque ripple. The results well verifies the effectiveness of the proposed method. More design considerations and comparative results will be given in the full paper.

[1] H. Yang, H. Lin, Z. Q. Zhu, S. Fang, and Y. Huang, "A winding-switching concept for flux weakening in consequent magnet pole switched flux memory machine," IEEE Trans. Magn., vol. 51, no. 11, Article No. 8108004, May 2015. [2] G. Lei, C. Liu, J. Zhu, and Y. Guo, "Techniques for multilevel design optimization of permanent magnet motors," IEEE Trans. Energy Convers., vol. 30, no. 4, pp. 1574-1584, Dec. 2015.

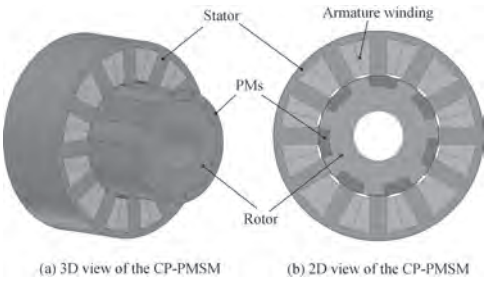

Fig. 1. Motor topology.

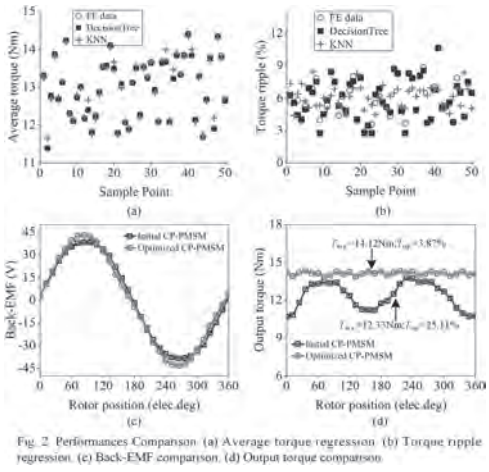

Fig. 2. Performances Comparison. (a) Average torque regression. (b) Torque ripple regression. (c) Back-EMF comparison. (d) Output torque comparison.

Fig. 2. Performances comparison.

VP3-04. The Structure Improvement Method and Analysis Based on the Characteristics of Motor Magnetic Field. *X. Liang*[1], M. Wang[1], Y. Liu[1], P. Zheng[1] and J. Gao[1] *1. Harbin Institute of Technology, Harbin, China*

With high-power, high-torque density, permanent magnet (PM) synchronous motor (PMSM) is widely used as torque motor and drive motor. The higher energy-density motor can save more space for other structures in these fields. Many scholars have proposed different structural improvement schemes from the aspects of Pole-Slot combination and PM form for this [1, 2]. In the closed magnetic field inside the motor, it can be divided into the airgap magnetic field for direct electromechanical energy conversion, which is intersected by the windings; the "connecting" magnetic field, which ensures magnetic field closure, is mainly located in the yoke. If a stronger airgap magnetic field can be achieved with less flux connection structure, the energy density will be improved. Different types of motors have different magnetic field characteristics, which determine how to improve the original structure. The magnetic field distribution of the integer slot distributed winding (ISDW, such as 24S4P) and fractional slot concentrated winding (FSCW, such as 24S20P) motor under no load are shown in Fig. 1 as example. The number of parallel magnetic circuits of 24S20P motor is larger, and the required yoke is narrower, however there are more fractional harmonics and zigzag magnetic leakage of tooth. The 24S4P motor requires a wider structure of 'flux connection' with lower harmonic content. The above problems limit the further improvement of their performance. The magnetic field distribution of them under load are shown in Fig. 2. The synthetic magnetic field of 24S4P motor is stronger than that of 24S20P motor, and the magnetic field especially at rotor is shift due to the larger armature inductance and other factors. Based on the analysis, the flux connection structure of the FSCW motor can be harmonic-oriented designed to suppress invalid harmonics and ensure fundamental harmonic. The ISDW motor can shift PM and armature magnetic field, and change their superposition relationship to reduce saturation.

[1] H. Chen, N. A. O. Demerdash, and A. M. EL-Refaie, "Investigation of a 3D-Magnetic Flux PMSM With High Torque Density for Electric Vehicles," IEEE Transactions on Energy Conversion, vol. 37, no. 2, pp. 1442-1454 (2022) [2] Y. Du, Chen Xu, and Feng Xiao, "Low Harmonics Design for Modular Permanent Magnet Synchronous Machine Using Partitioned Winding," IEEE Transactions on Industrial Electronics, vol. 69, no. 9, pp. 9268-9278 (2022)

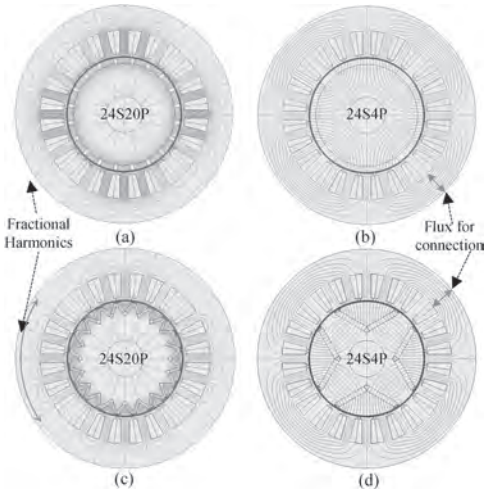

Fig. 1. Magnetic field distribution under no load. (a)24S20P Surface PMSM (SPMSM) (b)24S4P SPMSM (c)24S20P interior PMSM (IPMSM) (d)24S4P IPMSM.

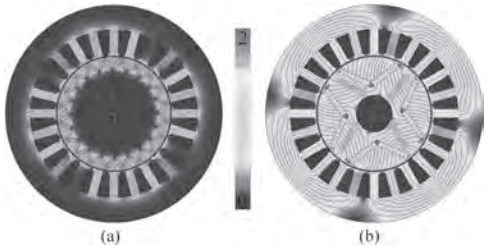

Fig. 2. The difference in synthetic magnetic field. (a)24S20P IPMSM (b)24S4P IPMSM.

VP3-05. Analysis of Stator Iron Loss in Permanent Magnet Synchronous Motor Under Rotating Magnetization Based on Field-Oriented Control. *H. Shi*[1,2], Y. Li[1,2], J. Yin[1,2] and S. Yue[1,2] *1. Hebei University of Technology, State Key Laboratory of Reliability and Intelligence of Electrical Equipment, Tianjin, China; 2. Hebei University of Technology, Hebei Key Laboratory of Equipment and Technology Demonstration of Flexible DC Transmission, Tianjin, China*

The electric drive systems of modern new energy vehicles predominantly rely on vector control technology (FOC). Hence, investigating the impact of different modulation parameters under FOC control on the magnetic flux density distribution in the stator core of PMSMs is of significant importance for enhancing motor efficiency and analyzing losses. The paper outlines the design of an 8-pole 12-slot interior permanent magnet synchronous motor, where both the stator core and rotor are constructed using non-oriented electrical steel strip B25AV1300, with a laminated core thickness of 40mm. Simultaneously, this study measures and calculates the hysteresis losses of the non-oriented electrical steel strip B25AV1300 under alternating and rotating magnetization. Therefore, to investigate the effect of magnetic flux density distribution in the stator core on the iron losses of PMSM, four characteristic positions on the stator core were selected. Holes were drilled and windings were applied at the teeth, yoke, and between the teeth and yoke, each with a diameter of 1mm and a single turn of winding. Additionally, one slot was chosen for teeth winding and yoke winding, with sensor wires drawn out and subsequently connected to the acquisition device.[1] The two-dimensional planar view of the motor after drilling is depicted in Figure 1. Upon establishing the finite element simulation platform and the experimental apparatus, various modulation parameters of the PMSM excitation are altered to analyze the variations in magnetic flux density at four typical characteristic positions of the PMSM under different modulation conditions. A meticulous analysis of the rotating magnetization process is conducted, followed by the testing and calculation of stator core iron losses[2]-[3].

This research establishes a connection between modulation parameters, rotating magnetization, and stator iron losses. The overall framework of the experimental platform is illustrated in Figure 2.

[1] Okamoto S, Denis N, Kato Y, et al. Core loss reduction of an interior permanent-magnet synchronous motor using amorphous stator core[J]. IEEE Transactions on Industry Applications, 2016, 52(3): 2261-2268. [2] Liu G, Liu M, Zhang Y, et al. High-speed permanent magnet synchronous motor iron loss calculation method considering multiphysics factors[J]. IEEE Transactions on Industrial Electronics, 2019, 67(7): 5360-5368. [3]Fan X, Li W, Sun Y, et al. Iron Loss Evaluation of Permanent Magnet Synchronous Motor using FEM and hysteresis model combined method[C]//2022 IEEE 3rd China International Youth Conference on Electrical Engineering (CIYCEE). IEEE, 2022: 1-5.

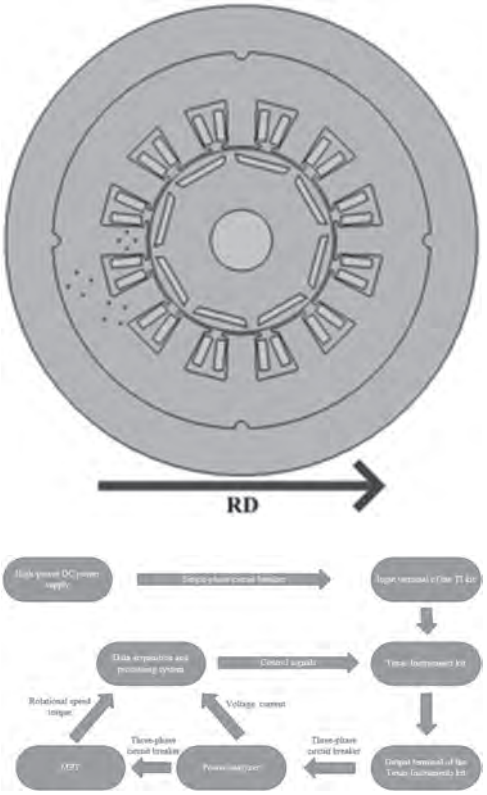

VP3-06. Optimization of the Magnetic Field of the Main and Auxiliary Poles of a Disc Motor by Analytical Method. *J. Wang*[1], Z. Xu[1], Y. Liu[1], Z. Xing[1] and W. Ji[1] *1. School of Electrical Engineering, Shenyang University of Technology, Shenyang, China*

The amplitude of the air gap flux density will directly affect the back electromotive force waveform of the motor winding, and indirectly affect the output torque and efficiency. In order to increase the amplitude of the air gap flux density and reduce the harmonic distortion rate at the same time, this paper takes the main and auxiliary permanent magnet pole arc ratio as a variable and uses the vector magnetic potential for analytical optimization. The magnetic field formed by the fan-shaped main and auxiliary poles can be equivalent to the magnetic field generated by N linear motors along the radial direction. Assume that the permanent magnet is uniformly magnetized. The relationship between the magnetic induction intensity and the magnetic field intensity in area I as shown in Figure 1 can be obtained. Considering the relative magnetic permeability of the permanent magnet and the additional magnetization vector. The relationship between the magnetic induction intensity and the magnetic field intensity in area II can also be obtained. The magnetization direction of the permanent magnet of the disc motor is different from that of the radial motor. When the external magnetic field is removed, the residual magnetization intensity is still in the axial direction. At this time, the axial residual magnetization intensity can be calculated. Combined with the arc occupied by the main pole permanent magnet and the arc occupied by the auxiliary pole permanent magnet at this time. The vector magnetic potential equation group of areas I and II can be obtained from the Poisson equation. The boundary conditions of regions I and II are introduced to obtain the general solution, and then the axial air gap flux density of region 1 is obtained. The same method can be used to obtain the expression of the air gap flux density on the other side. Finally, finite element verification is performed using Ansys software. The results show that the analytical method is consistent with the finite element method. As shown in Figure 2, the optimal main and auxiliary pole arc ratio increases the air gap flux density of the motor by 9.63% compared with the traditional motor, and the waveform harmonic distortion rate is improved by 13.39%.

[1] Z. Yue, Z. Sun and Z. Liu, "Design and Magnetic Field Simulation of 3.0T MRI Superconducting Magnet," *IEEE Trans. Appl. Supercon*., vol. 29, no. 2, pp. 1-6, March 2019. [2] Y. Lu, Y. Yang, M. Zhang, R. Wang, L. Jiang and B. Qin, "Improved Square-Coil Configurations for Homogeneous Magnetic Field Generation," *IEEE Trans. Ind. Electron.*, vol. 69, no. 6, pp. 6350-6360, June 2022.

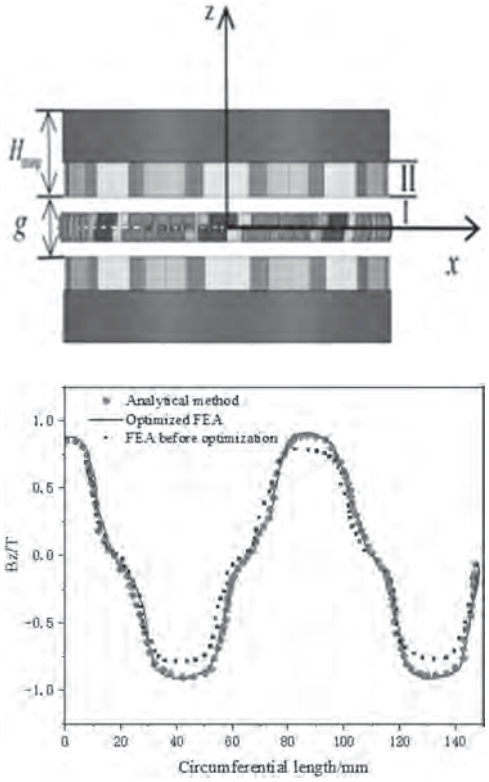

VP3-07. Fast Quasi-Three-Dimensional Modeling of Double-Sided Axial Flux Permanent Magnet Machines Considering End Effect. L. Dai[1], S. Niu[1], *J. Wen*[1], L. Xiao[1] and M. Hu[1] *1. Department of Electrical and Electronic Engineering, The Hong Kong Polytechnic University, Hong Kong, Hong Kong*

I. Introduction Double-sided axial flux permanent magnet synchronous machines (DAFPMSMs) are characterized by their symmetrical structure with two-layer airgaps and axial flux direction, as depicted in Fig. 1. This design allows for larger and more stable torque, making DAFPMSMs well-suited for applications with high torque density requirements, such as in-wheel motors and electric propulsion systems. Accurate modeling is crucial for the reliable design of DAFPMSMs. The commonly used three-dimensional finite element method (3D FEM) provides good accuracy [1]. However, the computational demands associated with 3D FEM, which requires millions of meshes per operating case, make it impractical for large-scale design

optimization. To overcome this limitation, this paper proposes a simplified quasi-3D modeling approach for DAFPMSMs, offering both high-fidelity prediction and fast solving speed. II. Proposed Model Conventional simplified models often struggle to account for end effects in the inner and outer circumferential surfaces, leading to reduced prediction fidelity [2]. To address this challenge, this paper presents a quasi-3D model, illustrated in Fig. 2. The 3D field calculation is divided into a multi-slice circumferential 2D model and a radial 2D model. The circumferential model accurately captures the flux distribution throughout the machine, excluding the end regions. On the other hand, the radial model effectively considers the end effects. By combining these two modeling approaches, the proposed quasi-3D model comprehensively accounts for flux leakage and accurately predicts the machine's performance, resulting in high-fidelity predictions.

[1] J. Si, M. Huang, R. Nie, C. Gan and Y. Han, "Inductance Calculation and Analysis of Axial-Flux Slotless Surface-mounted Permanent Magnet Machine with Equidirectional Toroidal Winding," in IEEE Transactions on Energy Conversion, Early Access, doi: 10.1109/TEC.2024.3380808. [2] A. Daghigh, H. Javadi and A. Javadi, "Improved Analytical Modeling of Permanent Magnet Leakage Flux in Design of the Coreless Axial Flux Permanent Magnet Generatorx," in Canadian Journal of Electrical and Computer Engineering, vol. 40, no. 1, pp. 3-11, winter 2017, doi: 10.1109/CJECE.2016.2550667.

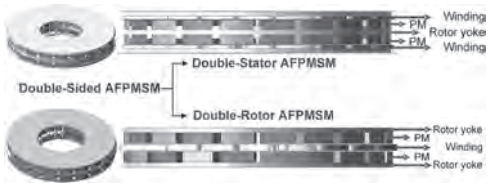

Fig. 1. Classification of double-sided AFPMSMs.

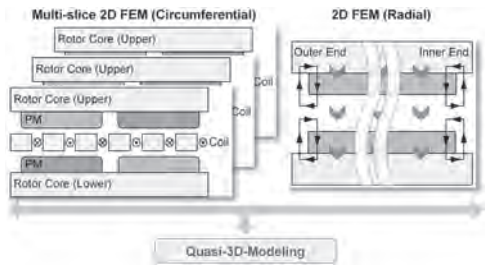

Fig. 2. Illustration of the proposed simplified quasi-3D-modeling.

VP3-08. Advanced Harmonic Interaction Modeling for Fast and Accurate Cogging Torque Calculation in Permanent Magnet Machines. L. Dai[1], S. Niu[1], *J. Gao*[2] and S. Huang[2] *1. Department of Electrical and Electronic Engineering, The Hong Kong Polytechnic University, Hong Kong, Hong Kong; 2. Hunan University, Changsha, China*

I. Introduction Cogging torque is an inherent but undesirable characteristic of permanent magnet machines (PMMs). It introduces torque pulsations that can negatively impact control accuracy and smoothness. Accurately predicting cogging torque is essential for analyzing its characteristics and implementing targeted reduction methods [1]. Existing accurate cogging torque calculation models rely on numerical methods [2], which lack a direct correlation between field harmonics and cogging torque, making it challenging to directly reduce the cogging torque by design optimization. To overcome this limitation, this paper proposes an advanced cogging torque model based on the rules of field harmonic interaction in PMMs. This model offers significant advantages in terms of speed, accuracy, and a deeper understanding of the fundamental principles governing cogging torque. II. Results The proposed method involves analyzing individual field harmonics and directly calculating the results of harmonic interaction based on the cogging torque's action law. This approach eliminates the need for computing multiple transient fields and establishes a direct relationship between field harmonics and cogging torque. Figs. 1 and 2 depict a comparison of the prediction results between the harmonic interaction modeling (HIM) method and the finite element method (FEM) for two PMMs. The results demonstrate that the HIM method achieves excellent accuracy while significantly reducing the computation time required.

[1] L. Dai, S. Niu, W. Zhang, J. Gao and S. Huang, "Harmonic Modeling and Ripple Suppression of Electromagnetic Torque in IPMSMs," in IEEE Transactions on Industrial Electronics, Early Access, doi: 10.1109/TIE.2024.3384614. [2] S. A. Saied, K. Abbaszadeh, A. Tenconi and S. Vaschetto, "New Approach to Cogging Torque Simulation Using Numerical Functions," *IEEE Trans. Ind. Appl.*, vol. 50, no. 4, pp. 2420-2426, July-Aug. 2014, doi: 10.1109/TIA.2013.2293814.

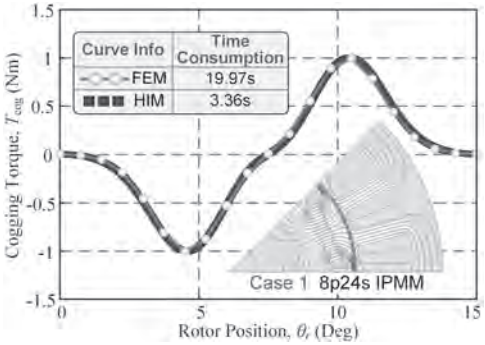

Fig. 1. Cogging torque prediction results of the FEM and the proposed HIM for Case 1.

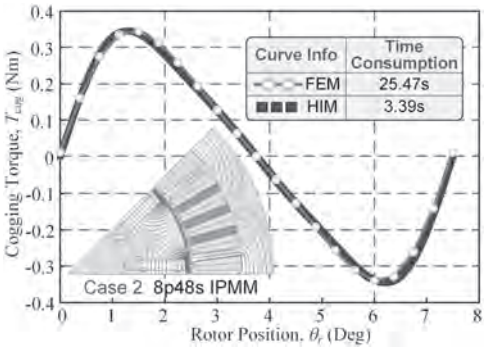

Fig. 2. Cogging torque prediction results of the FEM and the proposed HIM for Case 2.

VP3-09. Three phase transmitting coil for leakage magnetic field reduction in wireless power transfer. *D. Kim*[1], J. Cheon[1], H. Park[1] and D. Kim[1] *1. Yeungnam University, Gyeungsan-si, The Republic of Korea*

Wireless power transfer technology has been widely used based on convenience and safety. Specifically, various technologies for transmitting power in a situation that the receiving (Rx) coil moves along the transmitting (Tx) coil has been actively studied. In these systems, a long Tx coil is embedded to the road and high power is transmitted to the Rx coil. Consequently, a large amount of leakage magnetic field is generated around the Tx coil due to strong electromagnetic field [1]. Reducing the leakage magnetic field is very important because it can significantly affect not only human body but also surrounding electronic devices [2], [3]. In this paper, a three phase Tx coil structure is proposed to reduce the leakage magnetic field as illustrated in Fig. 1. Through the simulation, the leakage magnetic field is compared for the conventional and proposed Tx coil structures at the observation assuming the center of Tx coil as the origin, and magnetic field distribution is compared at the center of Tx coil. Also, a certain Rx coil is added to compare the induced voltage when the Rx coil is in the -900 mm to 900 mm position respect to the center of Tx coil. Simulation results represent that the proposed type B has the smallest leakage magnetic field as depicted in

Fig. 2(a). Compared to the single phase coil, magnetic field decreased by about 82.5% at the observation point. In addition, the magnetic field distribution has decreased compared to the rest of the structures as illustrated in Fig. 2(b). The average induced voltage generated in Rx coil is 2.297 V, 0.391 V, 1.160 V, and 1.079 V in single phase, meander type, proposed type A, and proposed type B, respectively. The proposed type B has average induced voltage value of about 46.9% for the single phase, and it is verified that this value is appropriate compared to the amount of leakage magnetic field reduction.

[1] M. Kim et al., "A Three Phase Wireless Power Transfer System for Online Electric Vehicles with Reduction of Leakage Magnetic Fields," IEEE Transactions on Microwave Theory and Techniques, Vol. 63, No. 11, Nov., 2015. [2] S. Kim et al., "Design and Analysis of a Resonant Reactive Shield for a Wireless Power Electric Vehicle," IEEE Transactions on Microwave Theory and Techniques, Vol. 62, No. 4, Apr., 2014. [3] H. Moon et al., "Design of a Resonant Reactive Shield With Double Coils and a Phase Shifter for Wireless Charging of Electric Vehicles," IEEE Transactions on Magnetics, Vol. 51, No. 3, Mar., 2015.

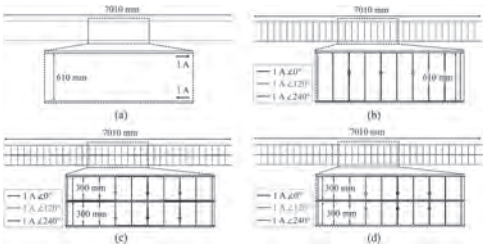

Fig. 1. Conventional and proposed three phase Tx coil structure. (a) Single phase, (b) Meander type, (c) Proposed type A, (d) Proposed type B.

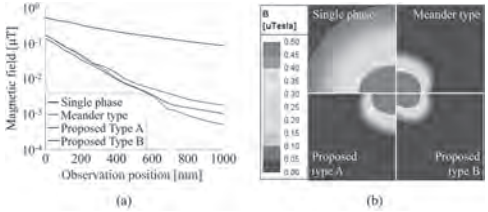

Fig. 2. The simulation results demonstrate (a) The magnetic field values at the observation point according to various Tx coil structures, (b) The magnetic field distribution at the center of Tx coil.

VP3-10. Magnetic Field and Torque Analysis of Coaxial Magnetic Gear Considering Permeability Nonlinear in Harmonic Modeling Method. *M. Nguyen*[1], D. Hoang[1], K. Shin[2], Y. Kim[3], A. Phung[4] and J. Choi[1] *1. Electrical Engineering, Chungnam National University, Daejeon, The Republic of Korea; 2. Electrical Engineering, Changwon National University, Changwon, The Republic of Korea; 3. Biosystem Machinery Engineering, Chungnam National University, Daejeon, The Republic of Korea; 4. Electrical Engineering, Hanoi University of Science and Technology, Hanoi, Vietnam*

Magnetic gears (MGs) transfer power between high-torque, low-speed, and low-torque, high-speed rotations by leveraging magnetic field interactions rather than the physical interlocking of teeth found in traditional mechanical gears. The concept of coaxial magnetic gears was first introduced in [1]. To obtain MGs characteristic, the analytical method provides faster processing times to compare with FEM simulations. Two main analytical methods are commonly explored. The first, subdomain modeling, involves directly solving Maxwell's equations and boundary/interface conditions using Fourier series expansion. This method was applied to magnetically geared machines in [2]. The second method, harmonic modeling, solves permeability issues using the complex Fourier series and Cauchy product, which enables the consideration of nonlinear core characteristics. Harmonic modeling was initially introduced in a straightforward configuration with a single stator and one air gap [3]. A convergence algorithm is proposed to consider the nonlinear aspect of the iron used in the machine's stator [4]. The prototype is illustrated in the 2-D polar coordinate system and divided into eight regions, as shown in Fig. 1. Each area is described by a vector potential which will be derived in the following section. The authors separated the steel material regions (I, IV, VII) into sub-regions that have corresponding permeability. A 3/16/19 specification given in Fig.1 was simulated in 2-D FEM. Fig. 2 depicts a good agreement between harmonic modeling and FEM simulation not only in linear analysis but also in saturation cases. It can be seen that flux densities are generally diminished due to saturation in the outer rotor yoke. It leads to an output torque decrease. A prototype shown in Fig.1(a-d) was validated for torque measurement. Further results will be presented in a full paper.

[1] T. Martin, Magnetic transmission., U.S. Patent 3 378 710, Apr. 16, 1968. [2] Manh-Dung Nguyen, Su-Min Kim, Hyo-Seob, AIP Advances., 1 February 2024; 14 (2). [3] R. L. J. Sprangers, J. J. H. Paulides, B. L. J. Gysen, IEEE Trans. Magn., vol. 52, no. 2, pp. 1-10, Feb. 2016. [4] D. C. Teles, C. Chillet, L. Garbuio, 2022 International Conference on Electrical Machines (ICEM), Valencia, Spain, 2022, pp. 178-184.

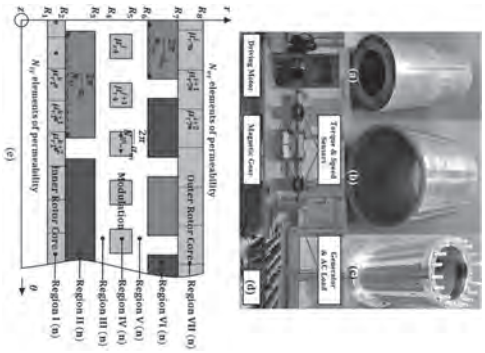

Fig. 1. Magnetic gear prototype with (a) inner rotor, (b) outer rotor, (c) modulation, (d) test bench, and (e) a simplified model.

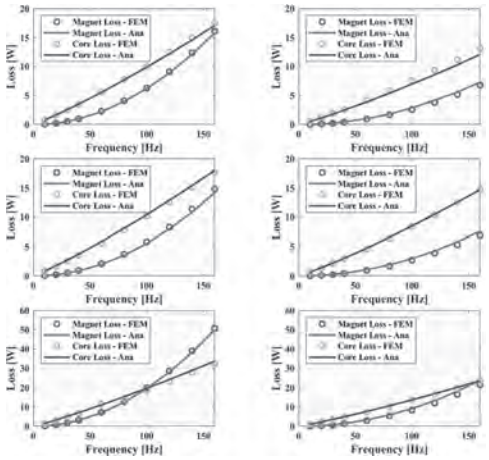

Fig. 2. FEM-Analytical comparison of flux density at (a) inner air gap, (b) modulation, (c) outer air gap of non-saturation case, (d) inner air gap, (e) modulation, and (f) outer air gap of full-outer-yoke-saturation case.

Session VP4
ELECTRICAL MACHINES AND POWER ELECTRONICS III
(Poster Virtual Session)

Ahmed Hemeida, Chair
Aalto University, Helsinki, Finland

VP4-01. Core Loss Separation Model Based on Static Hysteresis Loops. *J. Li*[1], L. Zeng[2] and R. Pei[1,2] *1. School of Electrical Engineering, Shenyang University of Technology, Shenyang, China; 2. Suzhou Inn-Mag New Energy Ltd., Suzhou 215000, China, Suzhou, China*

The study of core loss modeling has been an active research topic in recent decades [1]-[2], and many scholars have targeted to propose the actual required core loss model. Aiming at the shortcomings of the existing core loss model with complicated calculation process and low prediction accuracy, this paper through the multi-physical field test conditions, study the effects of frequency, temperature, stress, harmonic magnetic field and thickness of soft magnetic material on the static hysteresis loss and dynamic eddy current loss, and analyses the functional expressions of the degree of influence of different influencing factors on the static hysteresis loop area and dynamic eddy current loss coefficient, proposes a separation model of core loss that includes static hysteresis loss and dynamic eddy current loss. So as to realize the accurate prediction of the core loss. The dynamic hysteresis loop area is proportional to the core loss, and the area of the dynamic hysteresis loop is equal to the sum of the area of the static hysteresis loop and the area corresponding to the dynamic eddy current loss, while the hysteresis loss is proportional to the area of the static hysteresis loop, and the dynamic eddy current loss is derived by using Faraday's Law of Electromagnetic Induction and Ohm's Law, and considering the influence of multi-physical factors to get the separation model of the core loss: as shown in Fig.1. Where f is the frequency, S_m is the area of the static hysteresis loop, ρ is density of soft magnetic materials, k_e(T, f) is dynamic eddy current loss coefficient, T is temperature, B_{mk} is amplitude of the kth harmonic magnetic field. The area of the static hysteresis loop is almost unaffected by temperature, therefore the static hysteresis loss is not affected by temperature, as shown in Fig.2. But the area of static hysteresis loop is affected by the frequency, and with the increase of the magnetic field frequency the area of static hysteresis loop will increase. The dynamic eddy current loss coefficient decreases with increasing temperature and decreases significantly with increasing magnetic field frequency.

[1] A. Hilal, M.-A. Raulet and C. Martin, "Power loss prediction and precise modeling of magnetic powder components in DC–DC power converter application," IEEE Trans. Power Electron., vol. 30, no. 4,pp. 2232–2238, Apr. 2015. [2] S. Yue, Y. Li and Q. Yang, "Comparative analysis of core loss calculation methods for magnetic materials under nonsinusoidal excitations," IEEE Trans. Magn., vol. 54, no. 11, Nov. 2018, Art. no. 6300605.

The separation model of the core loss:

$$P_{Fe} = \frac{f \cdot S_m}{\rho} + k_e(T, f)\sum_{k=1}^{n}(kf)^2 B_{mk}^2$$

Fig.1 The separation model of the core loss

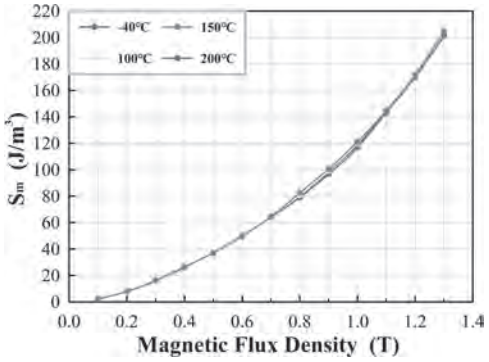

Fig.2 Area of static hysteresis loop at frequency 400 Hz

VP4-02. A Multi-Topology and Multi-Objective Optimization System for PMSM Using AutoML-Based Surrogate Models. *J. Luo*[1], X. Zhu[1] and J. Wu[1] *1. School of Electrical and Information Engineering, Jiangsu University, Zhenjiang 212013, Zhenjiang, China*

In recent years, Permanent Magnet Synchronous Motors (PMSMs) have been widely utilized across various fields due to their high torque density and high efficiency[1]. However, the diversity of design schemes necessitates extensive Finite Element Analysis (FEA) during the motor design phase to evaluate performance[2], [3]. To address this issue, this study proposes a multi-topology design system based on Automated Machine Learning (AutoML)[4]. This system can accurately predict the performance of motors with different topologies and adaptively optimize designs to meet specific requirements. Compared to traditional FEA methods, this system significantly enhances design efficiency, reducing the overall simulation time to less than 1/8000 of the time required by conventional FEA, and it enables parallel optimization of multi-topology motor designs. The system provides a unified representation of various rotor topologies and uses FEA to generate structured data for calculating torque and loss, as shown in Fig. 1. Initially, the structural parameters of different motor rotors are used as data inputs, and the motor characteristics obtained from FEA are used as data outputs. These multi-topology motor data are then combined into a dataset to train the automated machine learning model, resulting in a multi-dimensional motor model matrix. The predictive accuracy of the proposed automated machine learning model compared to other common machine learning models is shown in Fig. 2(1). Subsequently, this model replaces FEA for multi-objective optimization, ultimately producing optimized motor design schemes. A comparison of the pre- and post-optimization designs for the double V+1 topology is shown in Fig. 2(2). Overall, the system uses a unified dataset to describe multi-topology motors, employs an automated machine learning model to accurately predict their performance, and implements a rotor optimization design system that can achieve parallel optimization of multi-topology motors within 19 minutes.

[1] J. Gu, W. Hua and W. Yu, "Surrogate Model-Based Multiobjective Optimization of High-Speed PM Synchronous Machine: Construction and Comparison," IEEE Transactions on Transportation Electrification, vol. 9, no. 1, pp. 678-688 (2023). [2] Z. Qian, T. Huang and Q. Wang, "Torque Ripple Reduction of PMSM Based on Modified DBN-DNN Surrogate Model," IEEE Transactions on Transportation Electrification, vol. 9,

no. 2, pp. 2820-2829 (2023). [3] A. Khan, C. Midha and D. Lowther, "Reinforcement Learning for Topology Optimization of a Synchronous Reluctance Motor," IEEE Transactions on Magnetics, vol. 58, no. 9, pp. 1-4 (2022). [4] E. LeDell and S. Poirier, "H2O AutoML: Scalable Automatic Machine Learning," 7th ICML Workshop on Automated Machine Learning (AutoML) (2020). [Online]. Available:https://www.automl.org/wp-content/uploads/2020/07/AutoML_2020_paper_61.pdf.

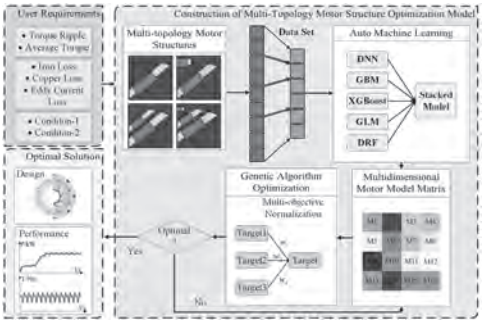

Figure 1

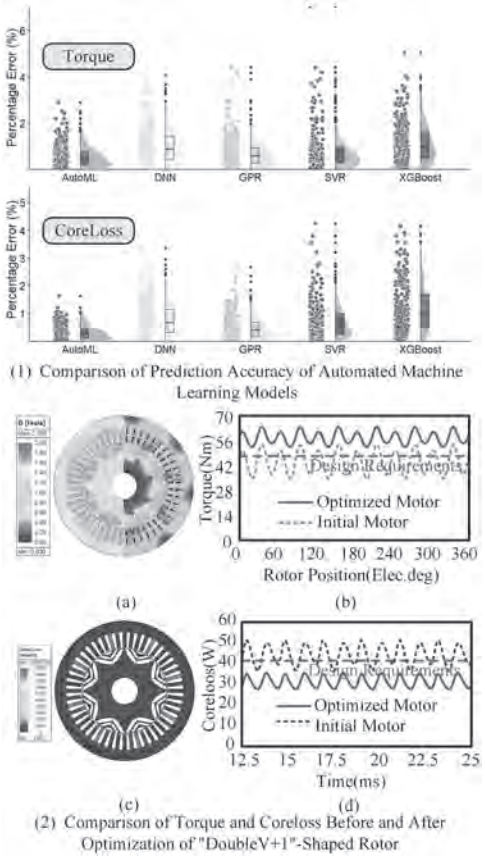

Figure 2

VP4-03. Effect of Different Winding Layers and Connection Method on the Electromagnetic Performance of Dual Three-Phase HSPMSG.

Q. Fan[1], X. Zhang[1], L. Zeng[2] and R. Pei[1,2] *1. School of Electrical Engineering, Shenyang University of Technology, Shenyang, China; 2. Suzhou Inn-Mag New Energy Ltd, Suzhou, China*

In recent years, dual three-phase(DTP) high-speed permanent magnet synchronous generators(PMSG) have been widely used in the aerospace field due to their high reliability. However, it tends to generate abundant harmonics when the generator is loaded. Researchers have proposed the use of dual multiphase winding to reduce the low harmonics of fractional slot winding[1],[2], but the use of multilayer and star-delta connection winding has a more significant impact in reducing the harmonic of the MMF. In this paper, five different winding configuration are investigated: three-phase double-layer short-pitch winding, DTP star-star connection double-layer winding(DLW), DTP star-delta connection DLW, DTP star-star connection four-layer winding(FLW), and DTP star-delta connection FLW. Firstly, 24-plot/4-pole finite element analysis(FEA) model is established to study the performance of these five winding configurations in terms of winding coefficient, harmonic distribution of armature MMF, radial air-gap magnetic flux density, electromagnetic torque, torque ripple, and inductance between different winding. The results show that when the number of winding layers is the same, the motor with star-delta connection can significantly reduce the low harmonics of the radial armature magnetic flux density and increase the amplitude of the armature fundamental MMF, thus improving the electromagnetic torque. When the number of winding layers is increased from two to four, the torque ripple, iron and copper loss are reduced. The armature fundamental MMF and average torque are slightly lower as shown in Fig.1, which is acceptable for the generator. Furthermore, the multi-objective optimization strategy is used to optimize and analyze the DTP star-delta connection FLW motor, and the torque ripple is reduced to 0.15%. Finally, a 24-plot/4-pole prototype is developed based on the optimized design scheme of the DTP star-delta connection FLW motor as shown in Fig. 2.

[1] A. S. Abdel-Khalik, S. Ahmed, and A. M. Massoud, "Low Space Harmonics Cancelation in Double-Layer Fractional Slot Winding Using Dual Multiphase Winding," *IEEE Trans. Magn.*, vol. 51, no. 5, pp. 1–10, May 2015. [2] V. I. Patel, J. Wang, W. Wang, and X. Chen, "Six-Phase Fractional-Slot-per-Pole-per-Phase Permanent-Magnet Machines With Low Space Harmonics for Electric Vehicle Application," *IEEE Trans. Ind. Appl.*, vol. 50, no. 4, pp. 2554–2563, Jul. 2014.

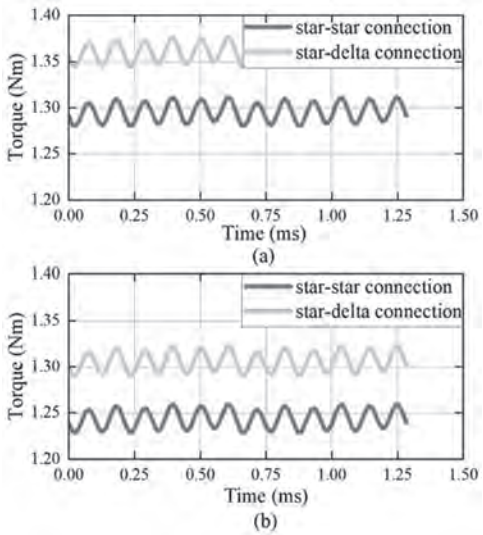

Fig. 1. Electromagnetic torque with different winding layers and connection (a) Two layers. (b) Four layers

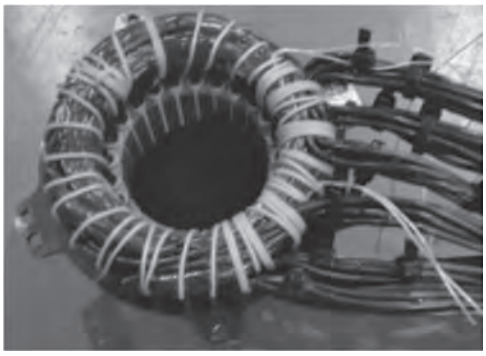

Fig.2. the armature of FLW star-delta connection

VP4-04. Multi-objective Optimization Design of Built-in High-speed Permanent Magnet Synchronous Motor Based on High Silicon Steel.
P. Meng[1], D. Ma[1], Q. Fan[1], L. Zeng[2] and R. Pei[1,2] *1. Shenyang University of Technology, Shenyang, China; 2. Suzhou Inn-Mag New Energy Ltd, Suzhou, China*

With the continuous improvement of motor performance requirements in new energy vehicles and other fields, it is difficult to further improve the performance of motors by simply optimizing the motor topology [1]. Currently, scholars have taken the optimization of motor structure design and material combination as a means of motor performance improvement [2], but there are few studies on the multi-objective optimal design of motors combining the characteristics of high-silicon steel (6.5%Si) and optimization algorithms. This is crucial for the design and application of high silicon steel motors, so this paper carries out the following research. In the second part of this paper, two materials, 6.5% silicon steel and ST100 alloy, are tested and comparatively analyzed, as shown in Fig. 1. In the third part, based on the experimental data, a multi-objective optimization strategy based on particle swarm optimization algorithm is proposed for the first time to address the characteristics of 6.5% silicon steel by taking an 8-pole, 48-slot "V" built-in permanent magnet synchronous motor as the object of study. The key parameters affecting the performance of the motor are identified through sensitivity analysis, and multi-objective optimization is carried out by taking the rotor structure parameters as the design variables and the torque and motor efficiency as the optimization objectives. In the fourth part, the finite element simulation software is used to establish the motor model with two material characteristics. And the operating performance of the motor before and after optimization under different working conditions is analyzed and compared, and the comparison before and after optimization of 6.5% silicon material is shown in Figure 2. The results show that the new material motor designed by multi-objective optimization performs better in improving torque and efficiency. Ultimately, through the scheme proposed in this paper, it is possible to achieve an increase in motor optimization rate while improving the motor torque and efficiency, which provides a reference for the optimization design of high silicon steel motors.

[1] S. Li, M. Hou, and R. Tang, "Analytical Model for No-Load Electromagnetic Performance Prediction of V-Shape IPM Motors Considering Nonlinearity of Magnetic Bridges," in IEEE Transactions on Energy Conversion, vol. 37, no. 2, pp. 901-911, (2022). [2] G. Li, X. Guan and B. Wang, "Influence of Silicon Steel Materials on Performance of PMSM with V-Shape PMs," 2021 IEEE 4th International Electrical and Energy Conference (CIEEC), Wuhan, China, pp. 1-6.,(2021).

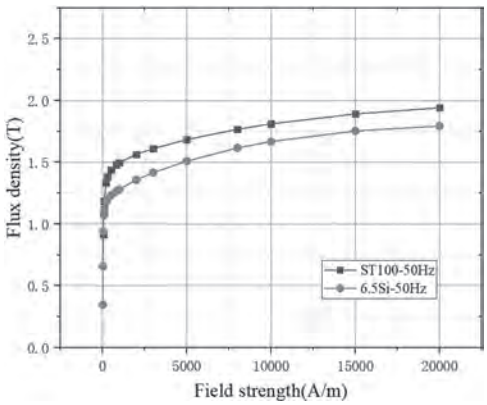

Fig.1 Magnetization curve

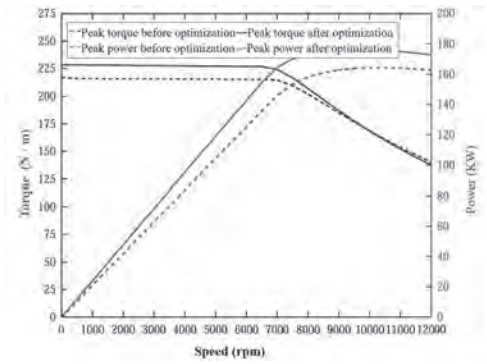

Fig. 2 External characteristic curve before and after optimization

VP4-06. Air-gap Region Topology Optimization of a Hair-pin PM Motor for Electromagnetic Vibration Reduction.
P. Zhao[1] and X. Zhu[1] *1. School of Electrical and Information Engineering, Jiangsu University, Zhenjiang, China*

In recent years, Hair-pin Permanent Magnet (PM) motors, which utilize hair-pin windings in the stator and embedded permanent magnets in the rotor, have become a popular choice among electric vehicle manufacturers due to their high torque density and efficiency [1]. However, the dual-layer permanent magnet structure of these motors increases the complexity of the magnetic circuit and results in inadequate rotor rigidity at high speeds, leading to prominent vibration and noise issues [2]. This paper proposes a new method for the refined design of the regions on both sides of the air gap, aimed at improving the electromagnetic vibration characteristics of PM Hair-pin motors and enhancing motor quality. The method adaptively reshapes the air gap areas without altering the basic structure of the stator and rotor, thus reducing radial electromagnetic forces and torque fluctuations without sacrificing torque and efficiency. A 48-slot/8-pole Hair-pin PM motor with an 8-layer winding was selected as an example. Under the NGnet topology optimization algorithm, the stator tooth boot area and the rotor edge area, located on both sides of the air gap, were effectively reshaped. Fig. 1 illustrates the structure of the motor. Due to the Hair-pin windings being inserted from the end of the core, the stator slot openings are relatively small. The rotor features a double-layer V-shaped design, with strategically placed rectangular magnetic barriers between the second-layer V-shaped permanent magnets. This enhances the motor's overload capacity and improves its speed extension capability. Fig. 2(a) displays the air gap design area, which includes the stator tooth boot, the initial uniform air gap, and the rotor edge side. Fig. 2(b) shows multiple Gaussian functions uniformly arranged in the design area, with the grid materials within the area dependent on the weights of the Gaussian basis functions. Fig. 2(c) presents the optimization results of the design area. Fig. 3 illustrates the visualization process of the topological evolution of the air gap design area. Fig. 4 demonstrates that the optimization significantly reduces torque ripple and vibration acceleration. More details will be presented in the full text.

[1] G. Bramerdorfer, J. Tapia, J. Pyrhonen and A. Cavagnino, "Modern Electrical Machine Design Optimization: Techniques, Trends, and Best Practices, " *IEEE Trans. Ind. Electron*, vol. 65, no. 10, pp. 7672-7684, Oct. 2018. [2] C. Peng, D. Wang, B. Wang, J. Li, C. Wang and X. Wang, "Different rotor segmented approaches for electromagnetic vibration and acoustic noise mitigation in permanent magnet drive motor: A comparative study," *IEEE Trans. Ind. Electron*, vol. 71, no. 2, pp. 1223-1233, Feb. 2024.

Fig.1. The three-dimensional structure and planar diagram of Hairpin PM motor

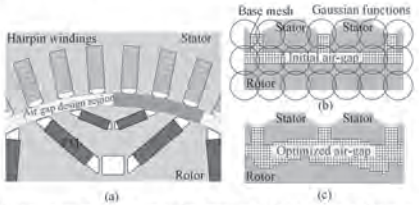

Fig.2. Air-gap region local design. (a)Design region. (b)Initial air-gap. (c)Optimized air-gap

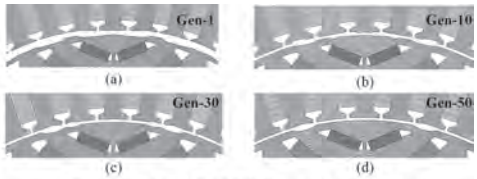

Fig.3. Evolution of air gap topology during the optimization.

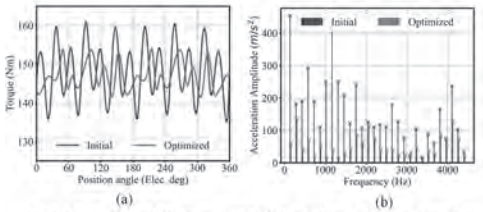

Fig.4. Comparison of vibration characteristics before and after optimization.
(a) Torque ripple. (b) Surface vibration acceleration of the shell.

VP4-07. A Sensitivity-Region-Extended Robust Optimization Approach for Spoke-type Permanent Magnet Synchronous Motor.
J. Wu[1], X. Zhu[1] and P. Zhao[1] *1. School of Electrical and Information Engineering, Jiangsu University, Zhenjiang, China*

Numerous uncertainties exist in the manufacturing and assembly of permanent magnet synchronous motors (PMSMs). Robust optimization can enhance the consistency between prototypes and designs, but it typically requires predefined information about parameter fluctuations, which is often lacking during the design phase. Therefore, this paper proposes a sensitivity-region-extended robust optimization method, using acceptable performance degradation as a criterion to quantify the robustness of design solutions. By expanding the size of the sensitivity region (SR) through optimization, the robustness of the design is enhanced. Additionally, the SR size can guide the determination of manufacturing tolerances. This method has been validated in a small batch of ten motors. Fig. 1 contrasts robust optimization with traditional approaches, showing that traditional designs (red points) are more susceptible to performance degradation due to slight parameter deviations compared to robust designs (blue points). Existing robust optimization methods focus on motor performance variations under parameter fluctuations or finding optimal worst-case designs considering parameter deviations [2], [3]. Fig. 2 illustrates the concept of the SR for PMSM. Fig. 2(a) defines the acceptable performance variation region (APVR), showing performance limits, while Fig. 2(b) depicts the SR, indicating the design parameter variation range within the APVR. Due to varying parameter sensitivities, the SR shape is irregular. Points A and B are within the SR, meeting performance requirements, while point C exceeds the SR, failing to meet the APVR. The design goal is to expand the SR through optimization, enhancing robustness and reducing machining precision demands. Fig. 3(a) shows the motor's structure with a closed-slot design for enhanced torque and efficiency. To simplify manufacturing and reduce costs, a split yoke design is used, requiring only two stamping processes. Fig. 3(b) presents the motor's specific design parameters. Fig. 4(a) shows the prototype's structure. Ten prototypes with identical specifications, shown in Fig. 4(b), were manufactured and tested to validate the proposed method. The full manuscript will detail the complete process.

[1] Z. Qian, T. Huang, Q. Wang, W. Deng, Q. Chen, Z. Sun, and Q. Ye, "Torque Ripple Reduction of PMSM Based on Modified DBN-DNN Surrogate Model," in *IEEE Transactions on Transportation Electrification*, vol. 9, no. 2, pp. 2820-2829, 2023, doi:10.1109/TTE.2022.3219092. [2] B. Yan, Y. Yang, and X. Wang, "Design of a Large Capacity Line-Start Permanent Magnet Synchronous Motor Equipped With Hybrid Salient Rotor," in *IEEE Transactions on Industrial Electronics*, vol. 68, no. 8, pp. 6662-6671, 2021, doi:10.1109/TIE.2020.3008360. [3] A. Khan, C. Midha, and D. Lowther, "Reinforcement Learning for Topology Optimization of a Synchronous Reluctance Motor," in *IEEE Transactions on Magnetics*, vol. 58, no. 9, pp. 1-4, 2022, doi:10.1109/TMAG.2022.3184246.

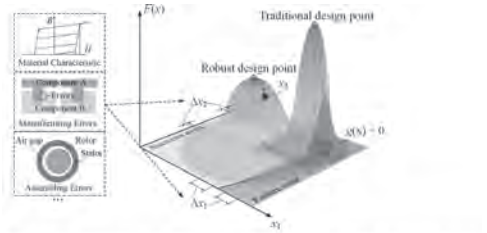

Fig. 1. PMSM manufacturing deviations and the conceptual diagram of robust optimization design.

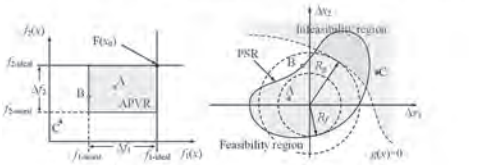

Fig. 2. Conceptual diagram of APVR and PSR.
(a) Acceptable performance variation region (APVR).(b) Parameter sensitivity region (PSR).

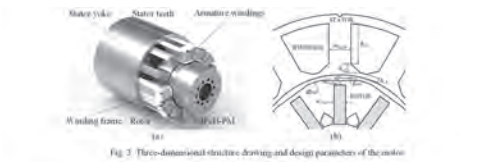

Fig. 3. Three-dimensional structure drawing and design parameters of the motor.

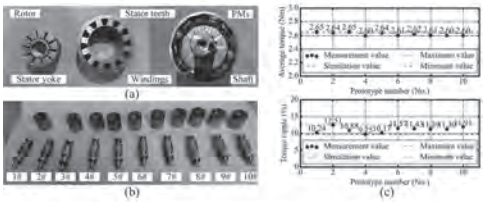

Fig. 4. Demonstration of processing prototype and experimental results.

VP4-08. Automatic Design Method for Motor Topology Based on Data-Driven. *Q. Xu*[1], S. Fang[1], X. Lin[1] and Y. Wang[1] *1. Southeast University, Nanjing, China*

In response to the critical need for diminished carbon emissions [1], the aviation industry has accelerated the development of multi-electric aircraft (MEA) technologies [2], [3]. The performance of these aircraft depends on the design of electric motors which is predicated on the accuracy of electromagnetic simulations in finite element method (FEM) [4], [5]. Despite the sophisticated analyses provided by simulation software like ANSYS and JMAG, there is an ongoing quest for streamlined design methodologies [6], [7]. This article introduces a Python-based JMAG enhancement, automating simulation workflows and laying the groundwork for AI-augmented motor design optimization, thereby enhancing efficiency and pioneering innovative avenues in motor design. Capitalizing on Python's scripting prowess, this article enhances JMAG via COM interface integration, automating motor design. The flowchart and specific execution process is shown in Fig. 1. By inputting detailed initial structural parameters, the encapsulation of the automated topology design method can be achieved, exemplified by the prevalent surface-mounted PMSM in MEA. A refined input schema ensures methodical topological accuracy. The integrative program is weighted by application criteria, quantitatively assesses motor performance, computes an evaluative composite score, and streamlines design optimization. After the motor topology design is completed, electromagnetic parameters are automatically assigned to various parts of the topology, and the secondary development program automatically performs meshing and finite element analysis on the designed topology. The final motor topology and electromagnetic performance designed through data-driven automated design methods are shown in Fig. 2. The detailed description of the data-driven automated motor topology design method, encompassing its methodological exposition, evaluative metrics, and experimental verification, will be addressed in the full paper.

[1] X. Li, D. Shi, Y. Li and X. Zhen, *IEEE Trans. Syst. Man Cybern.: Syst.*, vol. 49, no. 6, pp. 1218-1227. [2] J. Ebersberger, M. Hagedorn, M. Lorenz et al., *IEEE J. Emerging Sel. Top. Power Electron.*, vol. 10, no. 5, pp. 5264-5279. [3] B. Sarlioglu and C. T. Morris, *IEEE Trans. Transport. Electrific.*, vol. 1, no. 1, pp. 54-64. [4] T. Kosaka, Y. Miyama, H. Ukaji et al., *IPEC-Himeji 2022- ECCE Asia*, Himeji, Japan, 2022, pp. 1990-1996. [5] Y. Hidaka, T. Sato and H. Igarashi, *IEEE Trans. Magn.*, vol. 50, no. 2, pp. 617-620. [6] L. Yu et al., *Proceedings - 2017 Chinese Automation Congress* (*CAC*), Jinan, China, 2017, pp. 4484-4488. [7] Y. Wu, T. Huang and H. Yu, *IMCEC*, Xi'an, China, 2018, pp. 197-201.

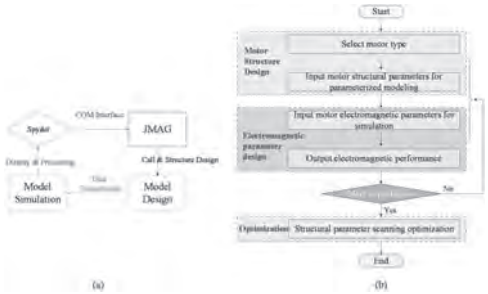

Fig. 1. The development concept. (a) Flowchart, (b) execution process.

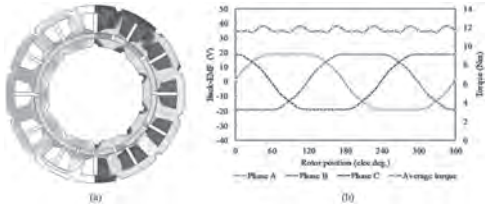

Fig. 2. The motor topology and its electromagnetic performance. (a) Flux line and Flux density distributions, (b) back-EMFs and average torque.

VP4-09. A Novel Modular Consequent-Pole PMSM with Low Rotor Losses and High-Power Factor. X. Zheng[1], H. Lin[1] and *X. Zeng*[1] *1. School of Electrical Engineering, Southeast University, Nanjing, China*

Large-scale permanent magnet synchronous machines (PMSMs) with high performance and low cost are urgently required in ship propulsion, power generation and other fields. Consequent-pole PMSMs (CP-PMSMs) with fractional slot concentrated winding (FSCW) have drawn increasingly more attention [1-3]. However, rich non-working harmonics in their armature reaction magnetic field will lead to plenty of problems, such as high rotor losses and low power factor, affecting the machine performance [4,5]. This paper presents a novel modular CP-PMSM equipped with two slot-pitches overlapping windings, which has the advantages of low rotor losses, modularization, and high-power factor. The proposed machine topology is shown in Fig. 1(a). For the stator, the stator shifting technique is employed to offset the non-working harmonics of armature reaction MMF, as shown in Fig. 1(b). For the rotor, the appropriate flux barriers are designed in the rotor yoke, as shown in Fig. 1(c), thereby reducing the flux densities of low order non-working harmonics. In addition, the machine has six stator teeth not covered by the winding ends, so that the stator can be modularized by cutting these teeth. The armature reaction magnetic field distributions of the conventional CP-PMSM with FSCW and the proposed machine are shown in Fig. 2(a). It can be seen that the periodicity of the armature reaction fields of the latter is more apparent. This is attributed to the lower non-working content of armature reaction flux density in the proposed machine, as shown in Fig. 2(b). Moreover, the torque ripple of the proposed machine is 43.51% lower than that of conventional one, as shown in Fig. 2(c). The PM eddy losses, rotor core losses, and stator core losses of the proposed machine are reduced by 73.28W, 17.55W and 25.89W respectively compared with the conventional machine, as shown in Fig. 2(d). According to the angle between the fundamental harmonics of the induced voltage and the input current, as shown in Fig. 2(e), the power factor of proposed machine can be calculated to be 0.89, which is 34.85% higher than that 0.66 of conventional one.

[1] K. Wang, H. Lin, and H. Yang, "A novel modular 18-slot 10-pole pmsm with 9-phase unequal-coil-pitch fractional-slot winding," in 2018 21st International Conference on Electrical Machines and Systems (ICEMS), 2018, pp. 132-136. [2] Z. Q. Zhu, Z. Azar, and G. Ombach, "Influence of additional air gaps between stator segments on cogging torque of permanent-magnet machines having modular stators," in IEEE Transactions on Magnetics, vol. 48, no. 6, pp. 2049-2055, 2012. [3] S. Cai, Z. Q. Zhu, and C. Wang, et al., "A novel fractional slot non-overlapping winding hybrid excited machine with consequent-pole PM rotor," in IEEE Transactions on Energy Conversion, vol. 35, no. 3, pp. 1628-1637, 2020. [4] Y. Li, H. Yang, and H. Lin, et al., "Investigation of double-side field modulation mechanism in consequent-pole pm machines with concentrated windings," in IEEE Transactions on Energy Conversion, vol. 36, no. 3, pp. 1635-1648, 2021. [5] H. Yang, Y. Li, and H. Lin, et al., "Principle investigation and performance comparison of consequent-pole switched flux pm machines," in IEEE Transactions on Transportation Electrification, vol. 7, no. 2, pp. 766-778, 2021.

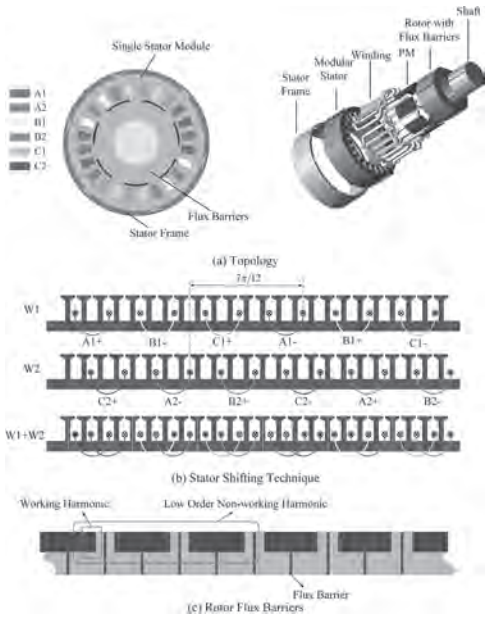

Fig. 1. Topology and operating principles of the proposed machine

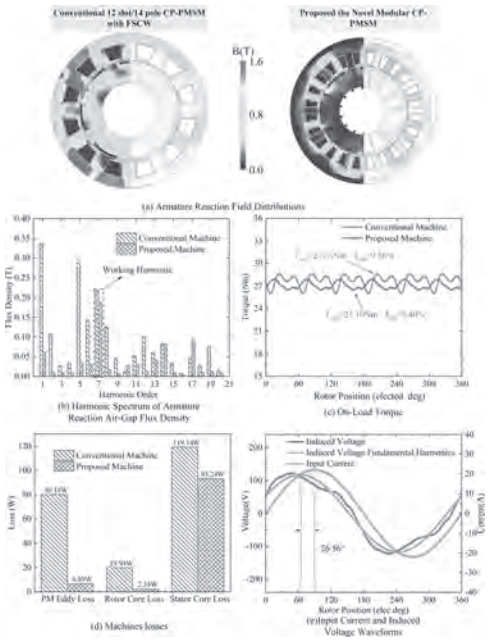

Fig. 2. Electromagnetic characteristics

Session VP5
ELECTRICAL MACHINES AND POWER ELECTRONICS IV
(Poster Virtual Session)

Anh Thanh Huynh, Chair
University of Nottingham, Nottingham, United Kingdom

VP5-01. Design and Investigation of Combinatorial-Magnetic-Source Topology for a High Torque Performance Field-Modulated Permanent Magnet In-Wheel Motor. *Y. Xie*[1], Z. Xiang[1] and Y. Zhou[1]
1. Jiangsu University, Zhen Jiang, China

In-wheel motor, as the core component of distributed-drive systems, has been a research hotspot [1]. Magnetic field-modulated motors are considered promising options for in-wheel motors due to their potential for high torque and low speed, attributed to the magnetic gear effect [2]. The energy conversion process of the magnetic field-modulated motor predominantly relies on its airgap harmonics for energy transfer, which is a crucial factor contributing to its high torque density. Yet, the presence of a large number of harmonics inevitably impacts the torque ripple characteristics of the motor. Hence, the concept of working harmonics and non-working harmonics in the airgap magnetic field is emerged, thereby offering a valuable research avenue to enhance motor performances. The unified field modulation theory reveals that airgap harmonics are created when airgap permeability is modulated in relation to the MMF source [3]. So, improving the harmonic characteristics from the MMF source can increase working harmonics and decrease non-working harmonics, providing a valuable way for improving in-wheel motor performances. Based on this, a combinatorial-magnetic-source field-modulated permanent magnet in-wheel (CMS-FMPMIW) motor is proposed in this paper, where the motor configuration can be seen in Fig. 1 (a). The innovation of this research lies in the integration of the design concept of a combined magnetic source into the PM MMF design, resulting in a combinatorial-magnetic-source topology. Furthermore, by utilizing harmonic characteristics as guidance, the CMS-FMPMIW motor is designed and investigated to effectively enhance torque performances. The modulation process of PM MMF is presented in Fig. 1 (b). It can be seen that, from the perspective of theoretical analysis, the introduction of an additional magnetic source contributes to improving PM MMF characteristics of the CMS-FMPMIW motor. Then, Fig. 2 (a) and (b) shows the analysis of PM MMF and its harmonic spectrum. As expected, the torque performance analysis depicted in Fig. 2 (c) and (d) illustrates this phenomenon. More detailed analysis and experimental verification will be presented in the full paper.

[1] Y. Tang, F. Chai, Y. Xie, W. Cai, "Design of a modular in-wheel motor with high fault-tolerant performance and low MMF space harmonic," *IEEE Trans. Ind. Electron.*, vol. 70, no. 7, pp. 6574-6584, Jul. 2023. [2] Z. Xiang, J. Wei and X. Zhu, "Torque ripple suppression of a PM vernier machine from perspective of time and space harmonic magnetic field," *IEEE Trans. Ind. Electron.*, vol. 71, no. 9, pp. 10150-10161, Sep. 2024. [3] Z. Xiang, Y. Zhou, X. Zhu, L. Quan, D. Fan and Q. Liu, "Research on characteristic airgap harmonics of a double rotor flux-modulated PM motor based on harmonic dimensionality reduction," *IEEE Trans. Transport Electrific.*, doi: 10.1109/TTE.2023.3318648.

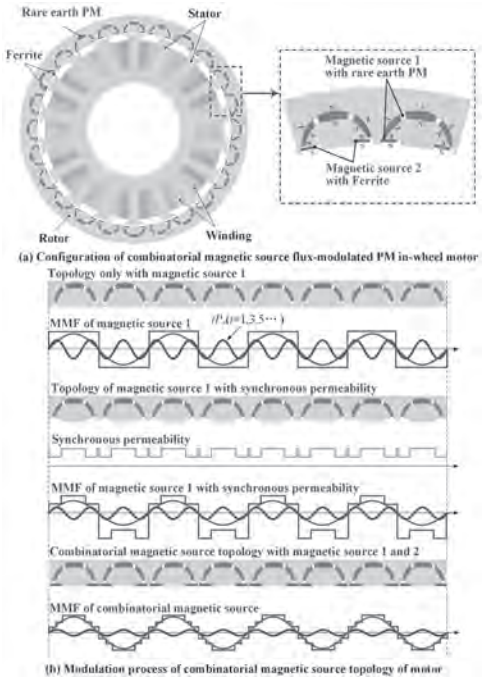

Fig. 1. Motor and its MMF.

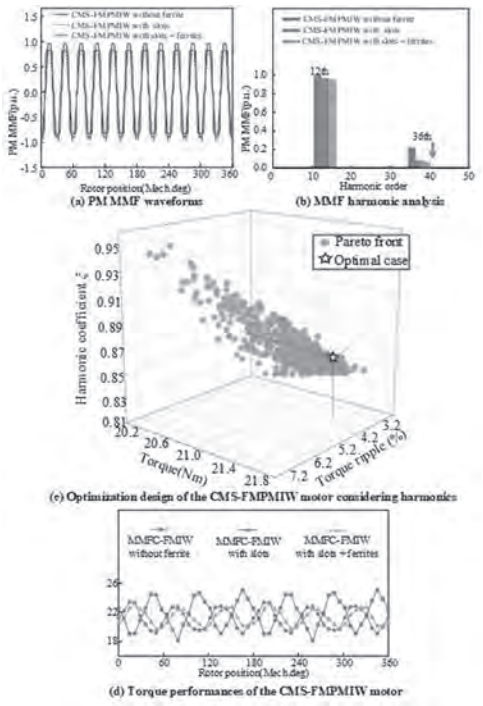

Fig. 2. Analysis results.

VP5-02. Field-Collaborative-Modulated Design and Investigation for a High Torque Performance Permanent Magnet Vernier Machine. *X. Wang*[1], Z. Xiang[1], Y. Zhou[1] and Y. Xie[1] *1. Jiangsu University, Zhen Jiang, China*

Permanent magnet Vernier (PMV) machines possess remarkable advantages in terms of their capability for low-speed and high-torque operations, thereby demonstrating significant potential for direct-drive applications [1]. Due to the phenomenon of magnetic gear effect, this particular type of motor showcases a wide array of harmonic components within its airgap magnetic field, which predominantly facilitates energy transfer through these harmonics. Consequently, the torque capability of such motors is prominently evident. However, it should be duly noted that the presence of these magnetic field harmonics also impacts certain performance aspects including torque pulsation, losses and so on [2]. Actually, the harmonics of airgap magnetic field in the PMV machines are engendered by the process of permeability modulating the MMF of both the armature and PM, which is comprehensively elucidated by the emergence, continuous refinement, and ongoing development of the unified theory of magnetic field modulation [3]. In other words, the modulation behavior of the magnetic field is the pivotal factor in determining the harmonic characteristics of the airgap. Mastering the process of exploring and guiding this modulation behavior is crucial for effectively enhancing the airgap harmonic characteristics of permanent magnet motors, thereby achieving performance improvement. This paper proposes a novel field-collaborative-modulated design for permanent magnet vernier machines, wherein the key lies in considering the magnetic field modulation behavior as both synchronous and asynchronous modulation behaviors. Based on this, a harmonic-oriented design approach is further investigated for improving the torque performances. Fig. 1 shows the motor topology and the synchronous and asynchronous modulation process. The flux density characteristics and torque performances are also analyzed, as shown in Fig. 2. It can be seen that the torque performances are improved effectively by utilizing the field-collaborative-modulated design. Building on this foundation, the full paper will provide more detailed analysis and experimental verification.

[1] Z. Xiang, J. Wei and X. Zhu, "Torque ripple suppression of a pm vernier machine from perspective of time and space harmonic magnetic field," *IEEE Trans. Ind. Electron.*, vol. 71, no. 9, pp. 10150-10161, Sept. 2024. [2] L. Xu, Z. Sun and W. Zhao, "Stator core loss analysis and suppression of permanent magnet vernier machines," *IEEE Trans. Ind Electron.*, vol. 70, no. 12, pp. 12155-12167, Dec. 2023. [3] M. Cheng, H. Wen, P. Han and X. Zhu, "Analysis of airgap field modulation principle of simple salient poles," *IEEE Trans. Ind. Electron.*, vol. 66, no. 4, pp. 2628-2638, Apr. 2019.

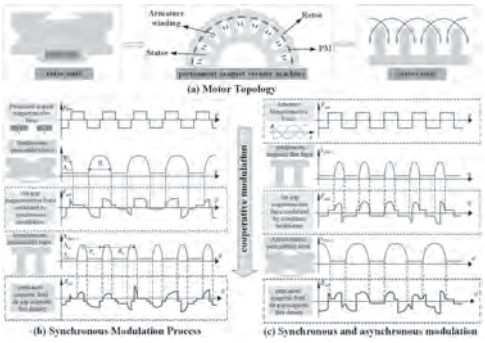

Fig. 1. Motor topology and modulation process.

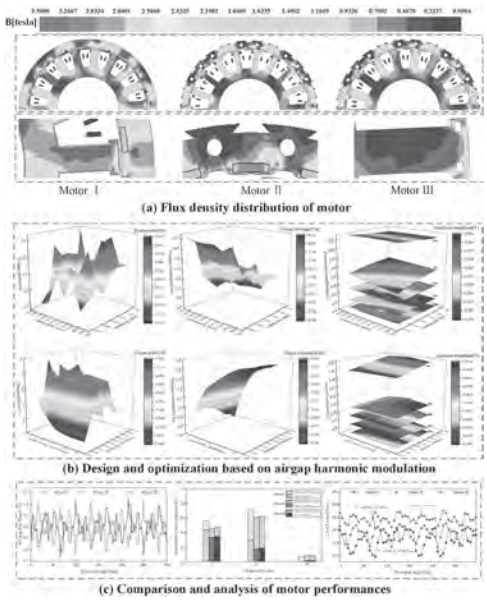

Fig. 2. Performance analysis.

VP5-03. Investigation of Flux Barrier Design on Flux Weakening Capability of Consequent Pole Reverse Salient PM Machines. *Q. Zhou*[1], Y. Li[1], S. Ding[1] and J. Hang[1] *1. School of Electrical Engineering and Automation, Anhui University, Hefei, China*

Introduction Permanent magnet (PM) synchronous machines (PMSMs) are widely used in electric vehicles due to their high efficiency, high power density, and compact size. Due to the use of PM material, it is difficult to regulate the air gap flux density directly. Negative *d*-axis current is adopted to achieve field-weakening operation in vector control method, which results a potential irreversible demagnetization risk of PMs [1]. Different from the traditional PMSMs with relatively higher *q*-axis inductance, the reverse salient PM (RSPM) machines show a larger *d*-axis inductance and lead to reduced negative *d*-axis current [2]. When using maximum torque per ampere (MTPA) control strategy, the *d*-axis current of RSPM changes from positive to negative, which means it has a flux intensifying region [3][4]. This feature endows the PM with a strong resistance to demagnetization [5], making it feasible to reduce requirements for PM [6]. Consequent pole machines can reduce the number of PMs used and has a larger *d*-axis inductance [7]. This paper proposed consequent pole RSPMs with different *q*-axis flux barriers and investigates the flux weakening capability under different structures. Machine Topologies The consequent pole machines with different *q*-axis barriers are shown in Fig. 1. Preliminary Electromagnetic Performance In vector control method, MTPA is used when the operation speed is lower than base speed. The smaller copper loss leads to higher efficiency. Because of the relatively higher base speed, the high-efficiency (≥90%) region of the machines with central barrier are shifted to the higher speed region, as shown in Fig. 2. Conclusions This paper investigates six consequent pole machines with different *q*-axis flux barriers, including one layer, two-layer, three-layer arc flux barriers, and trapezoid central barriers. The basic electromagnetic performances show that multi-layer structure can achieve the reverse salient characteristic and improve the flux weakening capability. Due to the extended base speed, topologies with trapezoid central barrier have higher efficiency in high-speed region.

Y. Liu, K. Ma, H. Gao and Z. Zhang, *IEEE Trans. Ind. Electron.*, vol. 71, no. 8, pp. 8503–8513 (2024) R. H. Moncada, J. A. Tapia and T. M. Jahns, *2009 IEEE Energy Conversion Congress and Exposition*, pp. 2368-2373(2009) Bianchi N, Bolognani S and Jang J H., *IEEE Trans. Power Elec.*, 22(06): 2466-2475 (2007) Kan A, Minoru A, Shinji W., *IEEE Trans. Ind. Appl.*, 126(07): 827-834(2006) M. Kashif and B. Singh, *2021 IEEE International Power and Renewable Energy Conference (IPRECON)*, Kollam, India, pp. 1-4(2021) T. Kato, N. Limsuwan and C.-Y. Yu, K., *IEEE Trans. Ind. Appl.*, vol. 50, no. 3, pp. 1748–1756(2014) Y. Li, H. Yang, and H. Lin, *IEEE T. Transp. Electr.*, vol. 9, no. 1, pp. 819–832(2023)

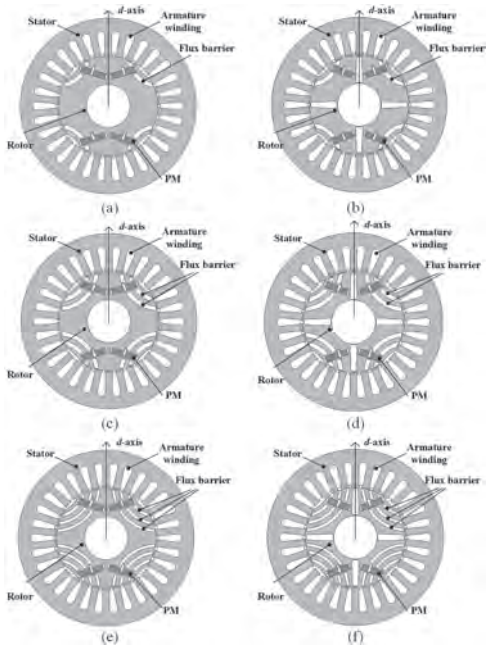

Fig. 1. Machine topologies.

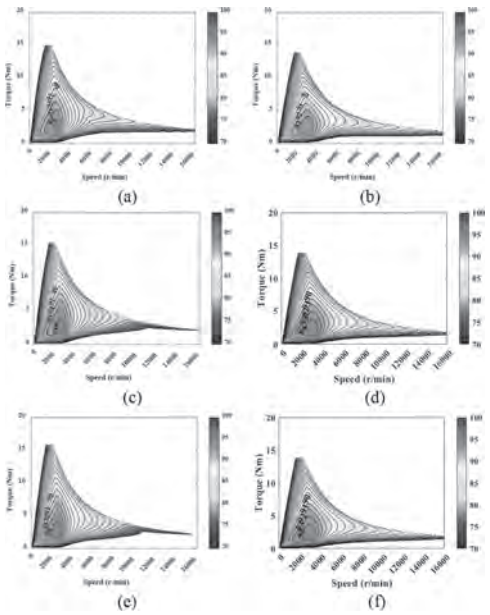

Fig. 2. Efficiency maps.

VP5-04. Design of Winding Connections of Permanent Magnet Synchronous Motor for Widening Speed. Y. Du[1], *H. Yuan*[1] and F. Xiao[1]
1. Jiangsu University, Zhenjiang, China

Permanent magnet synchronous motor (PMSM) is one of the most competitive candidates for applications, such as electric vehicles and electric tractors due to the merits of high torque density and high efficiency. However, the speed range is limited because of the constant PM field. By selecting the connections of coils to form different winding types, namely the star, the delta and the star-delta connections, different torque-speed output capacities can be obtained, which is absent in literatures for speed widening of PMSM. In this paper, the coil connection-changing design is proposed, and the output performances are analyzed based on a 12/10-pole surface mounted PMSM. As shown in Fig. 1, there are 12 coils in the PMSM. When different switches turn on, the star-, the delta-, and hybrid star-delta-connections can be realized, which is similar with the situation of star-delta start of induction motors, in which the numbers of 1 to 12 represent the slot numbers. Because there are 4 coils per phase distributed in the stator slots, the phase angle between the star connected winding and the delta connected winding can be 0°, 30° and 60° by selecting different coils into the star connected winding and the delta connected winding, which decides the winding factor, so as to the output performance of the motor. The results show when the phase angle is 0°, the equivalent winding factor of the hybrid star-delta connected winding and the torque density is the highest. Fig. 2 shows the back-EMF waveforms of different coil-connections. It can be seen that the back-EMF amplitudes per phase are 20.7V, 15.2V and 12.1V, respectively. So, the speed regulation range can be adjusted by changing the coil connections. Furthermore, because the winding contains the delta connection part, the reduction of the third harmonics in back-EMF is considered in the winding design to reduce the circulation in delta part. More theoretical analysis and simulation analysis will be included in the full paper.

[1] A. M. El-Refaie and T. M. Jahns, "Optimal flux weakening in surface PM machines using concentrated windings," Conference Record of the 2004 IEEE Industry Applications Conference, 2004. 39th IAS Annual Meeting., Seattle, WA, USA, 2004. [2] M. V. Cistelecan, F. J. T. E. Ferreira and M. Popescu, "Adjustable Flux Three-Phase AC Machines With Combined Multiple-Step Star-Delta Winding Windings," in IEEE Transactions on Energy Conversion, vol. 25, no. 2, pp. 348-355, June 2010.

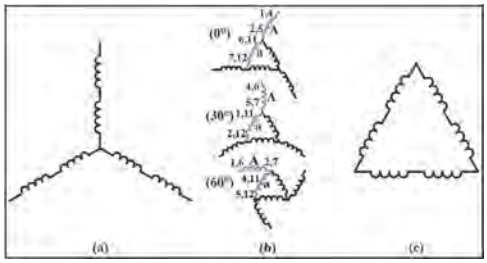

Fig.1. Connection of armature winding (a)Star winding(b)Star-delta winding(c)Delta winding

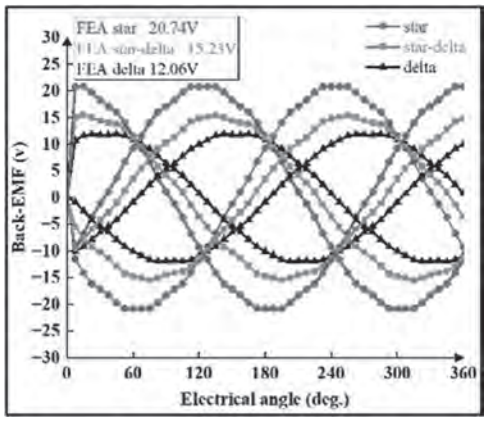

Fig.2. No-load back electromotive force

VP5-05. Low Electromagnetic Vibration Design and Investigation of Hair-pin Dual-V-type Motor Considering Winding Magnetomotive Force. *H. Qu*[1], L. Quan[1] and D. Fan[1] *1. School of Electrical and Information Engineering, Jiangsu University, Zhenjiang 212013, China, Zhenjiang, China*

In recent years, hair-pin permanent magnet motors have attracted more and more attention because of advantages such as high slot-filling rate, and high power density[1]. Electromagnetic vibration, as one of the main indicators for evaluating the performance of motors, is receiving more and more attention from academia and industry. Many scholars have proposed methods to reduce motor electromagnetic vibration, including stator slot skewing, rotor segment, permanent magnet modification, and so on[2][3]. The above

methods are used to suppress motor vibration from the perspectives of motor permanent magnet topology and stator/rotor structure, but the inherent structural characteristics of the windings of hair-pin motors limit the design of stator slot skewing. At the same time, the high-speed and even ultra-high-speed operating characteristics of the motor impose severe requirements on the stress characteristics of the motor stator/rotor. Therefore, it is difficult for the methods to solve the vibration suppression of traditional PMSM to solve the actual vibration suppression of hair-pin motor. In fact, the armature winding magnetomotive force harmonics is one of the internal causes of the radial electromagnetic force harmonics, so how to research a low vibration motor design method from the perspective of winding magnetomotive force has become a valuable research direction. In this paper, a low-vibration design method considering motor windings is proposed, so that reduced motor vibration and competitive output torque can be realized. Fig. 1 shows the three stator topological structures of the flat wire motor. Fig. 2 shows the low vibration design method of flat wire motor. Fig. 3 shows flux density distributions of three motors. The harmonic analysis of the electromagnetic force is shown in Fig. 4, and the torque and vibration acceleration changes of the three motors are compared in Fig. 5. Fig. 6 shows the winding structure under different layers and shapes. In summary, it can be seen that compared with other pole/slot ratio, 8-pole, 48-slot has the lowest electromagnetic vibration and the highest torque. More detailed analysis and test verification will be presented in the full paper.

[1] M. Popescu, L. Di Leonardo and G. Fabri. "Design of Induction Motors With Flat Wires and Copper Rotor for E-Vehicles Traction System," in *IEEE Transactions on Industry Applications*, vol. 59, no. 3, pp. 3889-3900, May-June 2023. [2] C. Peng, D. Wang and B. Wang. "Different Rotor Segmented Approaches for Electromagnetic Vibration and Acoustic Noise Mitigation in Permanent Magnet Drive Motor: A Comparative Study," in *IEEE Transactions on Industrial Electronics,* vol. 71, no. 2, pp. 1223-1233, Feb. 2024. [3] M. S. Islam, R. Islam and T. Sebastian. "Noise and vibration characteristics of permanent-magnet synchronous motors using electromagnetic and structural analyses," *IEEE Transactions on Industry Applications*, vol. 50, no. 5, pp. 3214-3222, Sept.-Oct. 2014.

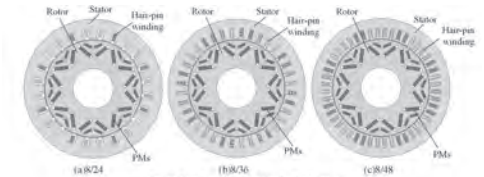

Fig. 1 Topological structure and pole slot ratio

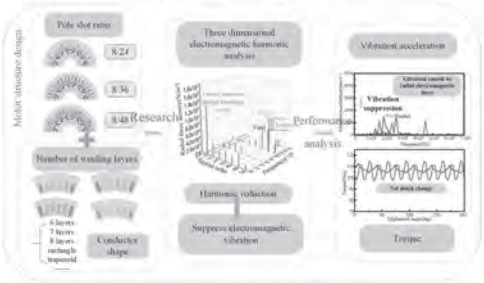

Fig. 2. Process of electromagnetic vibration suppression

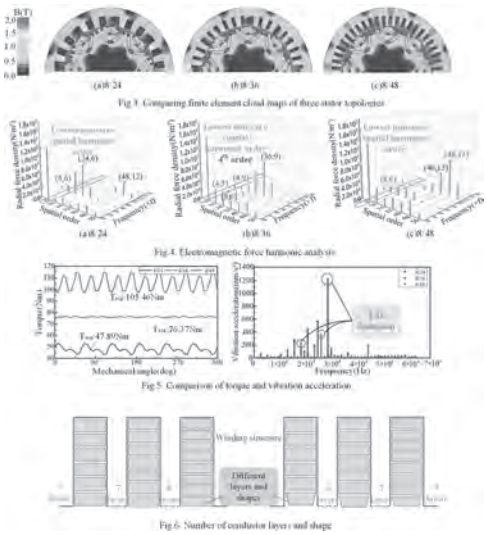

Fig. 3. Comparing finite element cloud maps of three motor topologies

Fig. 4. Electromagnetic force harmonic analysis

Fig. 5. Comparison of torque and vibration acceleration

Fig. 6. Number of conductor layers and shape

VP5-06. An Interior Permanent Magnet Synchronous Machine with Asymmetric Structure for Improving Torque Density. *X. Liang*[1], M. Wang[1], Y. Liu[1], P. Zheng[1] and W. Li[1] *1. Harbin Institute of Technology, Harbin, China*

Permanent magnets (PMs) and armature windings generate electromagnetic fields with different harmonic characteristics and spatial distribution in permanent magnet synchronous machine (PMSM). With the needs of industry development, more and more design and combination methods of them are being adopted to improve the efficiency of energy conversion and energy density in PMSM. In conventional interior PMSM (IPMSM), the reluctance torque (T_R) and PM torque (T_P) cannot reach the maximum at the same time (current angle), limiting the above performance. The design based on magnetic-field-shifting (MFS) can place the PM and armature magnetic field in a specific spatial angle relationship in the IPMSM according to their characteristics. Based on this, the current angle difference of the peak of T_R and T_P can be reduced, and thus the electromagnetic torque (T_E) can be increased to improve the efficiency of energy conversion [1, 2]. Although this method achieves the improvement of T_E, the asymmetric structure adopted by this process may have a negative impact on each magnetic field and torque component. The study of IPMSM topology helps to reduce the negative effects and achieve better MFS. The effect and principle of MFS machine are shown in Fig. 1. Through a specific asymmetric structure, the angle between the two torque components (T_R and T_P) is reduced to improve the combined torque (T_E) significantly by theoretical analysis. It can be seen that MFS causes changes in physical quantities such as current in *d*- /*q*-axis coordinates in the phasor diagram. The torque characteristics of the conventional and proposed machine with asymmetric structure are shown in Fig. 2. The proposed machine achieves the torque-current angle characteristics in the theoretical analysis. The torque output and overload capacity of the proposed are improved. By studying the topology of the MFS IPMSM, the torque density and torque characteristics can be improved to increase the energy conversion efficiency.

[1] Z. Q. Zhu and Y. Xiao, "Novel Magnetic-Field-Shifting Techniques in Asymmetric Rotor Pole Interior PM Machines With Enhanced Torque Density," IEEE Transactions on Magnetics, vol. 58, no. 2: 8100610 (2022) [2] X. Zhu, Sipeng Li, and Shiyue Zheng, "Torque Component Redistribution and Enhancement for Hybrid Permanent Magnet Motor With Permanent Magnet Offset Placement," IEEE Transactions on Transportation Electrification, vol. 9, no. 1, pp. 631-641 (2023)

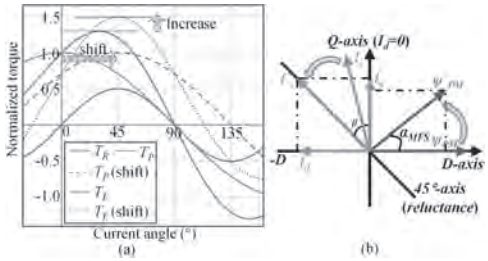

Fig. 1. Effect and principle of MFS machine. (a)Torque-Current angle characteristics (b)Phasor relation.

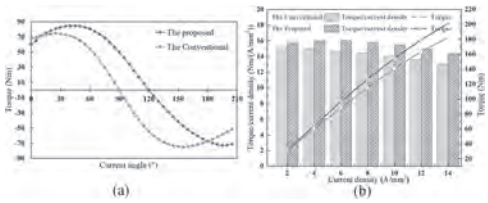

Fig. 2. Torque characteristics of the proposed and conventional machine. (a)Torque-Current angle (b)Torque-Current density.

VP5-07. A New Hybrid-excited Permanent Magnet Arc Motor with Different Permanent Magnet Arrays Exhibiting Flux-reversal Effect in Dual Stators. *N. Chen*[1], S. Fang[1], X. Lin[1] and Z. Chen[1] *1. School of Electrical Engineering, Southeast University, Nanjing, China*

The rapid development of permanent magnet (PM) materials, especially rare earth permanent magnets has brought out the further performance improvement of PM motors. Due to the significant advantages as simple structure, small loss, high efficiency and high power-density, the PM motors have gradually attracted the attention of researchers [1] [2]. To make full use of the inner cavity space of the motor, and thus improve the power density and torque density of the motor, two-stator structure have been adopted [3]. Aiming at achieving the flux regulation function, the dc-biased sinusoidal current is injected, which is beneficial for improving the electromagnetic performance of the proposed hybrid-excited doubly salient dual-PM machine [4]. Arc motors with low torque ripple and high torque density are researched [5]. This paper proposes an innovative hybrid-excited PM arc motor (HE-PMAM) with different PM arrays displaying flux-reversal effect in dual stators. The topology and working principle of HE-PMAM are briefly introduced. Then, the flux regulation of the HE-PMAM is analyzed. The HE-PMAM is composed of three module motors, and each module motor is composed of a construction of 11 rotor-poles and 6 stator-slots of inner and outer stators respectively. The PMs in the dual stators exhibit the flux-reversal effect. With the adoption of dual-stator structure, the robust rotor modulates the magnetomotive force produced by PMs on both sides to enhance the flux modulation effect and generate abundant air-gap flux density harmonics. The HE-PMAM operates mainly based on the flux modulation. The direct-current (dc) biased armature windings are beneficial to achieving flux regulation through adjusting the dc without additional field windings. As shown in Fig. 2, the average output torque of the HE-PMAM increases from 446mNm to 539mNm as the dc changes from -1.6A to 0.8A while the alternating current (ac) remains 2.3A (RMS value), which is the rated current value. It can be concluded from Fig. 2 that the HE-PMAM has a good flux-regulation capability.

[1] B. Kim and T. A. Lipo, *IEEE Trans. Ind. Appl.*, vol. 52, no. 1, pp. 217-225, Jan.-Feb. 2016. [2] M. Onsal, Y. Demir and M. Aydin, *IEEE Trans. Magn*., vol. 58, no. 2, pp. 1-5, Feb. 2022. [3] H. Wang, H. Zhu and S. Ding, *IEEE Trans. Magn.*, vol. 58, no. 8, pp. 1-6, Aug. 2022. [4] Y. Meng, S. Fang and Z. Pan, *IEEE Trans. Appl. Supercond.*, vol. 31, no. 8, pp. 1-5, Nov. 2021. [5] Z. Pan and S. Fang, *IEEE Trans. Ind. Inform.*, vol. 17, no. 11, pp. 7523-7534, Nov. 2021.

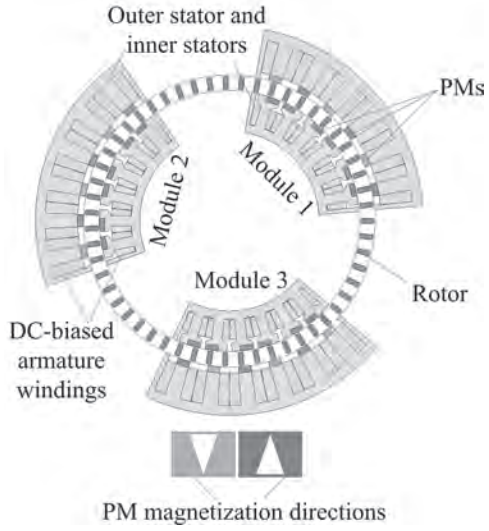

Fig. 1. Topology of the HE-PMAM.

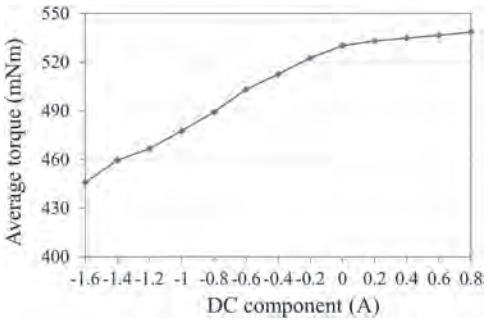

Fig. 2. The average torque variation with the dc section at the rated ac section.

VP5-08. High-Order-Harmonic Suppression Design Method with Halbach Magnetic Field Based on Multi-Objective Genetic Algorithm. L. Yin[1], *Y. Wang*[1], R. Sun[1], L. Wu[1] and X. Xu[2] *1. State Grid Lianyungang Power Supply Company, Lianyungang, China; 2. College of Automation Nanjing University of Posts and Telecommunications, Nanjing, China*

The price of rare earth is rising, which lead to the rare earth crisis and restricted the development of permanent magnet (PM) motors [1]. To solve the problem. domestic and foreign scholars pay attention to the research on consequence pole permanent magnet (CP-PM) motors. But, the application of the consequence poles makes adjacent magnetic poles asymmetric, and inevitably introduces even harmonics, leading to the larger cogging torque and higher torque ripple. In [2], the PMs are designed into the shape of sine, anti-cosine, and other functions to reduce the harmonics of the airgap flux density, which contributes to the suppression of the cogging torque and torque ripple. However, the output torque of the motor is inevitably reduced. For the PM eccentricity technology, the eccentricity distance limited the reduction effect of the cogging torque and torque ripple [3]. In this paper, to improve the utilization rate of PMs and output torque, and reduce the torque ripple, a CPM motor applied the Halbach permanent magnet array, and a highly adaptive Halbach magnetic field optimization method based on the genetic algorithm is proposed. Fig.1(a) shows the conventional and proposed CP-PM motor with the Halbach PM array (HCP-PM) motor., The key parameters of the HPM-PM motor are optimized in Fig. 1(b). The motor performance can achieve convergence under four magnetizing angles and the Pareto front at each angle has been marked. For better presentation, the related performance of SPM motor, CP-PM motor and the optimized HCP-PM motor are analyzed and compared in Fig. 2(a). The flux linkage waveform and corresponding spectrum analysis of the three motors shows

that the SPM motor maybe has the lowest torque ripple, which is determined by its own structure. The analysis is confirmed by the output torque in Fig.2(b), where the HCP-PM motor has higher torque ripple and the SPM motor has lower torque output capacity. This proves the correctness of the basic theory and effectiveness of the magnetic field sine method based on genetic algorithm proposed in this paper. More detailed theoretical analysis and experimental results will be given in full paper.

[1] X. Liu, H. Chen, J. Zhao, and et al, "Research on the Performances and Parameters of Interior PMSM Used for Electric Vehicles*," IEEE Transactions on Industrial Electronics*, vol. 61, no.06, pp. 5696-5711(2016). [2] Y. Li, J. Zou, Y, Lu, "Optimum design of magnet shape in permanent-magnet synchronous motors*," IEEE Transactions on Magnetics*, vol.39, no.06, pp. 3523-3526(2013). [3] X. Liu, H. Chen, J. Zhao, and et al, "Modeling and analyzing of surface-mounted permanent-magnet synchronous machines with optimized magnetic pole shape*," IEEE Transactions on Magnetics*, vol. 50, no.11, pp.1-4(2014).

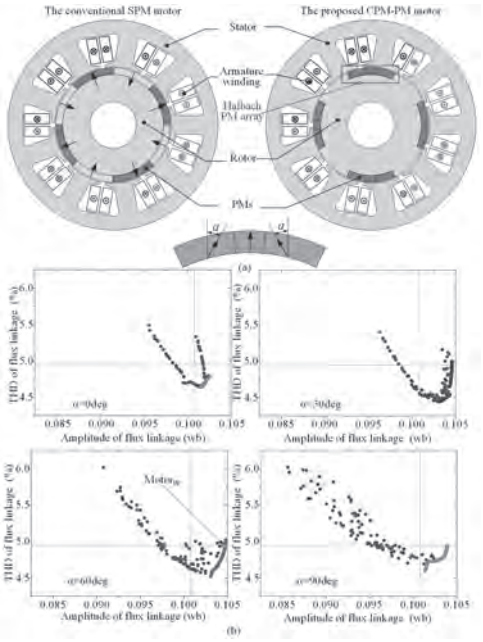

Figure 1

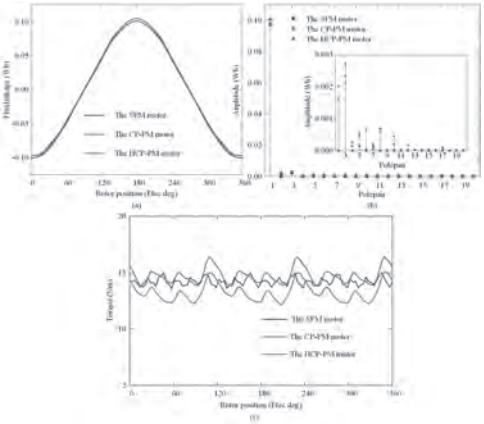

Figure 2

VP5-09. Motor Performance Analysis Considering the Effects of Carbon Fiber Preload Force and Rotor Centrifugal Force on Silicon Steel Characteristics. *B. Yang*[1], Y. Li[1], C. Yan[1], L. Zeng[2] and R. Pei[1,2] *1. Shenyang University of Technology, Shenyang, China; 2. Suzhou Inn-Mag New Energy Ltd, Suzhou, China*

High-speed Interior permanent magnet synchronous machine (IPMSMs), due to their high efficiency, high power density and high stability, play an important role in many fields and applications [1-2]. However, the huge centrifugal force generated by the high speed and the preload force of the sleeve can cause deterioration of the magnetic properties of the rotor material and lead to a reduction in the performance of the motor. In the past, when studying the effect of high rotational speed on the performance of motors, more often than not, only the single effect of rotor centrifugal force or sleeve preload force was considered, rather than a comprehensive consideration of the effect of both on the magnetic properties of the motor material. In order to investigate this effect, theoretical and simulation analyses are carried out on a high-speed IPMSM (maximum speed: 20,000 rpm) with a carbon fiber sleeve [3]. Firstly, the magnetic induction strength, magnetic field strength and iron loss of the motor rotor silicon steel material under multi-physical field (variable stress-variable frequency) conditions are tested. Meanwhile, the preload force of the carbon fiber sleeve and the rotor centrifugal force are determined by using theoretical analysis, and then the changes in motor performance after considering the rotor centrifugal force and the preload force of the sleeve at different rotational speeds are derived by simulation [4]. Finally, through theoretical analysis, finite element simulation and prototype test, it is verified that both rotor centrifugal force and sleeve preload force will affect the magnetic properties of the motor material, which in turn affects the performance of the motor, and it is also summarized that the rotational speed affects the rotor material and the performance of the motor under the comprehensive consideration of the two kinds of force, which puts forward a more accurate idea for the design of high-speed motors and the selection of the sleeve.

[1] Guanghui Du et al., "Multiphysics comparative study of high speed PM machines for ring PM rotor and solid PM rotor," IEEE Trans. Energy Conver, vol. 38, pp. 1421–1432(2023) [2] M. E. Gerlach, M. Zajonc, "Mechanical stress and deformation in the rotors of a high-speed PMSM and IM," e & I Elektrotechnik und Informations technik, vol. 138, pp. 96–109(2021) [3] D. Gerada, A. Mebarki and N. L. Brown, "High-speed electrical machines: Technologies, trends, and deveop-ments," IEEETrans. Ind. Electron., vol. 61, pp. 2946–2959(2014) [4] Jianxin Shen, Xuefei Qin, and Yao Lei, "Rotor strength analysis and retaining sleeve for high-speed permanent magnet machines," Proc. CSEE, vol. 42, pp. 2334-2346(2022)

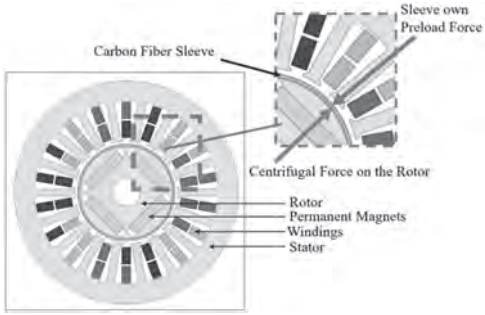

Fig. 1. Cross-section of the IPMSM.

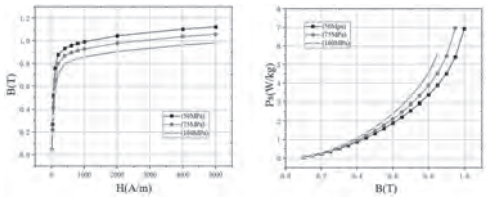

Fig. 2. B-H, B-P curves under compressive stress test of rotor. (The compressive stresses measured by the aids are almost equivalent to the centrifugal force on the rotor at high speeds)

VP5-10. Investigation of Different Pole Configurations in New Asymmetric Permanent Magnet Synchronous Reluctance Machines.
A. Mohammadi Ajamloo[1,2], A. Ghaheri[3], M. Ibrahim[1,2,4] and P. Sergeant[1,2]
1. Electromechanical, Systems and Metal Engineering, Ghent University, Gent, Belgium; 2. Core Lab MIRO, FlandersMake@UGent, Leuven, Belgium; 3. Department of Electrical Engineering, Shahid Beheshti University, Tehran, The Islamic Republic of Iran; 4. Department of Electrical Engineering, Kafrelshiekh University, Kafr el-Sheikh, Egypt

Permanent Magnet (PM) machines have been widely used in various applications due to their high torque density and efficiency. However, high price of rare-earth PMs and their market instability have raised concern regarding wide-spread usage of PM machines [1]. PM-assisted Synchronous Reluctance Machines (PMaSynRMs) emerge as a good solution in reducing the PM usage due to high contribution of the reluctance torque in the total torque [2]. However, two limitations prevent more efficient utilization of PMs: 1) the theoretical displacement between the reluctance and magnet torque components by 45 electrical degrees (E.D) [3], 2) the coupled design of the PM and flux barrier shapes [4]. This study presents and compares different configurations of a new family of Asymmetric PMSynRM (APMSynRM) with the conventional topology, all shown in Fig. 1, categorized based on the number of poles (p). In the proposed APMSynRM designs, two types of poles are utilized: interior PM (IPM) poles and SynRM poles. This allows for the independent design of flux barriers and PMs, facilitating optimal design of rotor geometry. Additionally, the d-q axes of the SynRM poles (d_r-q_r) are strategically displaced by β degrees relative to the d-q axes of the IPM poles (d_m-q_m). This ensures peak electromagnetic torque from each pole aligns at the same current angle, maximizing the utilization of rotor pole capacity. A comparative study is conducted between the proposed and conventional topologies, as presented in Table I, while keeping the copper loss, outer diameter, length, and PM volume fixed. The rotor configurations have been optimized to achieve maximum torque. Among the designs with the highest torque, the design with the lowest torque ripple is selected as the optimal design. The results show that the proposed APMSynRM designs achieve higher maximum torque (T_{max}) compared to conventional PMaSynRMs. Additionally, most asymmetric designs demonstrate relatively lower torque ripple. However, some asymmetric configurations exhibit unbalanced magnetic pull (UMP), which requires consideration.

[1]. B. Poudel, E. Amiri, P. Rastgoufard, IEEE Transactions on Magnetics., Vol. 57, p.1-19 (2021) [2]. K. Tawfiq, E. El-Kholy, M. Ibrahim, IEEE Transactions on Magnetics., Vol. 57, p.1-11 (2021) [3]. Z. Zhu, Y. Xiao, IEEE Transactions on Magnetics., Vol. 58, p.1-10 (2021) [4]. A. Nobahari, A. Vahedi, R. Nasiri-Zarandi, IEEE Transactions on Energy Conversion., Vol. 37, p. 989-998 (2021)

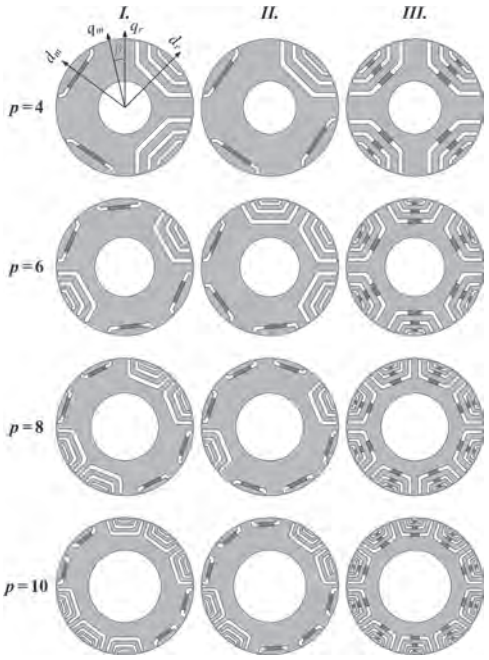

Fig. 1. Topologies of asymmetric (*I*, *II*) and conventional (*III*) PMSynRMs.

Design		T_{max} [N.m]	UMP	T_{ripple} [%]	β [E.D]
$p=4$	*I.*	8.5	Yes	13	7.6
	II.	8.2	Yes	22	5.9
	III.	8.1	No	16	—
$p=6$	*I.*	8.6	No	14	10.2
	II.	8.8	Yes	12	12.5
	III.	8.0	No	18	—
$p=8$	*I.*	8.9	No	8	16.0
	II.	8.3	No	14	10.2
	III.	7.8	No	10	—
$p=10$	*I.*	8.7	No	9	18.0
	II.	8.3	No	8	14.4
	III.	7.7	No	8	—

TABLE I Comparison of Characteristics of Various Asymmetric PMSynRM Topologies

VP5-11. Comparative study of electromagnetic and mechanical characteristics of permanent magnet synchronous generator according to magnet mounting method.
J. Park[1], W. Jung[1], H. Ban[1], K. Shin[2], K. Kim[3], K. Kim[3] and J. Choi[1] *1. Chungnam National University, Daejeon, The Republic of Korea; 2. Changwon National University, Changwon, The Republic of Korea; 3. Korea Research Institute of Ships and Ocean Engineering, Daejeon, The Republic of Korea*

In a wave energy conversion system, a Permanent Magnet Synchronous Generator (PMSG) is characterized by its ability to operate over a wide range of variable speeds [1]. Therefore, a structure is necessary to support the magnets and prevent them from dispersing during the PMSG operation. In this study, bolted fastening and clamp methods were adopted to secure permanent magnets, and a comparative study of their electromagnetic and mechanical properties was conducted using finite element analysis. Fig. 1(a) and (b) show the basic model and the magnet mounting methods. To prevent the permanent magnets from scattering, four magnet mounting methods were adopted, including the bolting method used in previous research. Fig. 1(c) and (d) show the actual manufactured models [2]. The results of different magnet mounting methods were compared and studied using actual experimental data. Fig. 2(a) and (b) present experimental data values. Based on the 2D analysis results and experimental data from the bolting mounting method, the characteristics of the magnet mounting method applied to other models are

analyzed using an electromagnetic analysis program. Fig. 2(c) and (d) display the stress analysis results corresponding to the magnet mounting method [3]. Lower stress applied to the rotor enhances the stability and performance of the electrical device. This study, the electromagnetic and mechanical properties of a Permanent Magnet Synchronous Generator (PMSG) were compared and analyzed according to the magnet mounting method. The full paper analyzes the electromagnetic characteristics of the clamp method from an electromagnetic perspective and the stress results applied to the rotor from a mechanical perspective to propose the optimal model.

[1] Y. J. Oh, J. S. Park, B. J. Hyon, and J. Lee, "Novel control strategy of wave energy converter using linear permanent magnet synchronous generator," IEEE Trans. Appl. Supercond., vol. 28, no. 3, pp. 1-5, 2018. [2] K. -H. Shin, T. -K. Bang, H. -W. Cho, K. -H. Kim, K. Hong and J. -Y. Choi, "Characteristic Analysis of Wave Power Generator Considering Bolting to Fix Permanent Magnet Based on Analytical Method," in IEEE Trans. Magn., vol. 55, no. 10, pp. 1-5, Oct. 2019. [3] J. -W. Jung et al., "Mechanical Stress Reduction of Rotor Core of Interior Permanent Magnet Synchronous Motor," in IEEE Trans. Magn., vol. 48, no. 2, pp. 911-914, Feb. 2012.

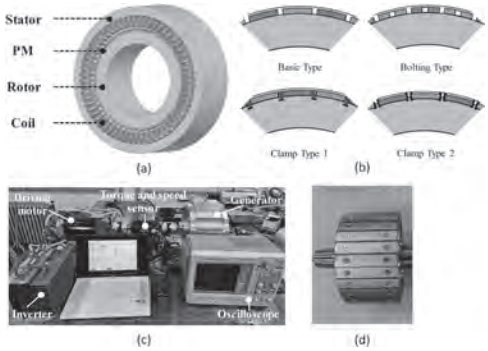

Fig. 1. Basic Model, Magnet mounting method and Manufactured Model: (a) Basic Model, (b) Magnet mounting method, (c) Manufactured Model, (d) Rotor with bolting.

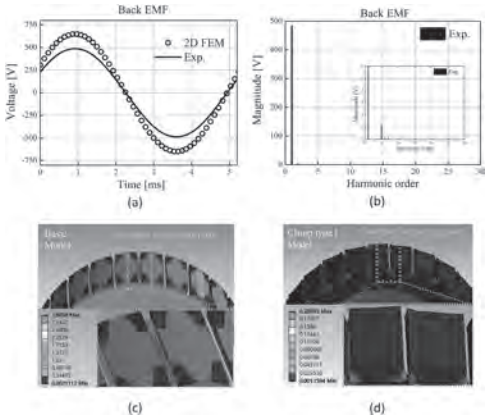

Fig. 2. Electromagnetic and mechanical analysis results according to magnet mounting method: (a) Line to line back-EMF under no-load, (b) FFT results for no-load back-EMF, (c) Rotor stress analysis with Basic Model, (d) Rotor stress analysis with Clamp type 1 Model.

VP5-12. Electromagnetic Field Analysis for Axial Flux Permanent Magnet Motor Based on 3-D Analytical Method. *M. Koo*[1] and H. Shin[2]
1. Purpose Built Mobility Group, Korea Institute of Industrial Technology, Gwangju, The Republic of Korea; 2. Specialized Machinery and Robotics Group, Korea Institute of Industrial Technology, Gimje, The Republic of Korea

An axial flux permanent magnet motor (AFPM) has been widely used in various industrial applications such as industries, in-wheel motor, drone propulsion motor, and related studies are being actively pursued [1]. Owing to its structural features and leakage flux in air-gap, the AFPM requires three-dimensional (3D) analysis methods. Various approaches for electromagnetic field analysis were addressed in previous studies including [2] and [3]. In this paper, we proposed the 3-D analytical approach that improves the computational burden of the existing analytical approach and enables the analysis to consider the end effects and slotting effect of the AFPM motor. In the θ-z plane of the AFPM motor, the slotting effect was considered using the subdomain method. To consider the end effects in the r-direction, the correction function Gr was derived using analytical modeling in the r-z plane. Finally, the results of the electromagnetic field analysis of the proposed 3-D analytical approach, such as 3-D magnetic flux density, back-EMF and cogging torque, are analyzed and compared with the results of the FEM and the experimental result in no-load condition. Fig. 1 shows the analytic model and experimental setup. Fig. 2 shows Electromagnetic analysis results and flux density using the 3-D analytical method. More detailed results, discussions, and desired effects will presented in the full paper.

[1] J. F. Gieras, R, -J, Wang, and M. J. Kamper, Axial Flux Permanent Magnet Brushless Machines. Dordrecht, The Netherlands: Kluwer, 2004. [2] F. Nishanth, J. V. Verdeghem, and E. L. Severson, "A review of axial flux permanent magnet machine technology," IEEE Trans. Ind. Appl., vol. 59, no. 4, pp. 3920-3933, Jul./Aug. 2023. [3] W. Zhao, T. A. Lipo, and B. I. Kwon, "Comparative study on novel dual stator radial flux and axial flux permanent magnet motors with ferrite magnets for traction application," IEEE Trans. Magn., vol. 50, no. 11, 8104404, Nov. 2014.

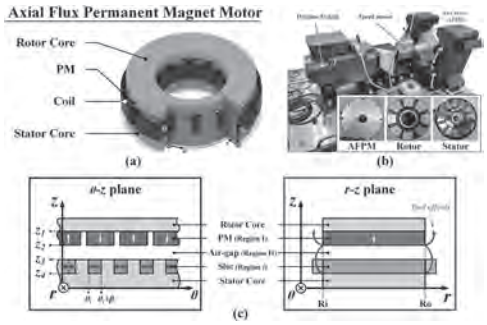

Fig. 1. (a) AFPM motor with FSCW stator, (b) experimental setup and parts of AFPM motor and (c) simplified analytical model.

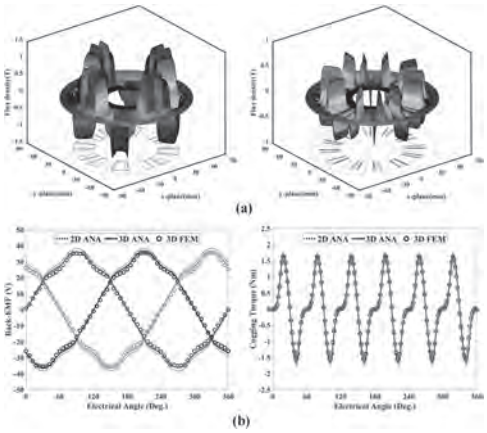

Fig. 2. (a) Results of flux density using the 3-D analytical method in air gap and (b) electromagnetic field analysis results of back-EMF and cogging torque.

VP5-13. Topology Optimization for a Magnetic Actuator Using Different Gradient-Based Solvers. *M. Mahmoud*[1,2,3], M. Ibrahim[1,2,4] and P. Sergeant[1,2] *1. Department of Electromechanical, Systems, and Metal Engineering, Ghent University, Gent, Belgium; 2. FlandersMake@UGent, Core Lab MIRO, Leuven, Belgium; 3. Electrical Engineering Department, Faculty of Engineering, Minia University, Minia, Egypt; 4. Department of Electrical Engineering, Kafrelshiekh University, Kafrelshiekh 33511, Egypt*

This paper presents a comparative study on density based topology optimization for a magnetic actuator using different gradient-based solvers. The applied solvers are method of moving asymptotes (MMA), interior point optimizer (IPOPT), and sparse nonlinear optimizer (SNOPT). The objective is to enhance the performance of the magnetic actuator in terms of maximizing the electromagnetic force by optimizing material distribution. The objective function is formulated using Maxwell stress tensor to calculate the force exerted on the armature. Density based method is implemented based on Solid Isotropic Material with Penalization (SIMP) as material interpolating scheme, Helmholtz filtering and hyperbolic tangent projection method. This study investigates the convergence behaviour, computational time, solution quality, and sensitivity for filtering and projection schemes of each solver. The results provide valuable insights into the strengths and limitations of MMA, IPOPT, and SNOPT in solving complex topology optimization problems, and offering guidance for selecting appropriate solvers. The results proved that applying topology optimization enhanced the performance of the magnetic actuator by increasing the force and reducing the amount of the material of optimal designs comparing to the initial c-core actuator. The obtained results proved that SNOPT is suitable for large scale problem as it has a robust convergence. However, it needs both filtering and projection to avoid the mechanical strength problems. MMA performance is robust gradient solver with low computational time and efficient solution. Efficient solutions can be achieved using IPOPT without high sensitivity for filtering and projection but not suitable for large-scale problems due to high computation time.

[1] S. i. Park, S. Min, S. Yamasaki, S. Nishiwaki, and J. Yoo, "Magnetic Actuator Design Using Level Set Based Topology Optimization," *IEEE Transactions on Magnetics,* vol. 44, no. 11, pp. 4037-4040, 2008. [2] S. Lim, T. Yamada, S. Min, and S. Nishiwaki, "Topology Optimization of a Magnetic Actuator Based on a Level Set and Phase-Field Approach," *IEEE Transactions on Magnetics,* vol. 47, no. 5, pp. 1318-1321, 2011. [3] C. Midha, M. H. Mohammadi, R. C. P. Silva, and D. A. Lowther, "Selection of Spatial Filters for ON/OFF Based Topology Optimization of a C-Core Electromagnetic Actuator," *IEEE Transactions on Magnetics,* vol. 55, no. 10, pp. 1-4, 2019.

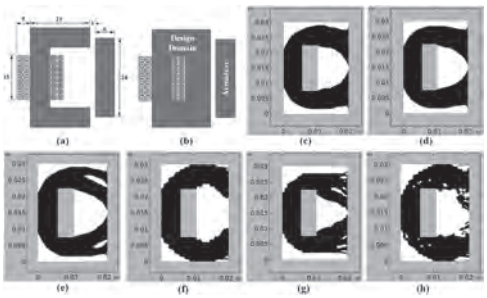

Fig. 1. Initial and optimal designs: (a) Initial design (unit: mm) (b) Design domain (c) MMA with filtering and projecting (d) IPOPT with filtering and projecting (e) SNOPT with filtering and projecting(f) MMA without filtering and projecting (g) IPOPT without filtering and projecting (h) SNOPT without filtering and projecting.

Initial Design			
Electromagnetic Force (N)	1.10		
Initial C-Core Area (mm^2)	360		
Topology Optimization with Filtering and Projection			
	MMA	IPOPT	SNOPT
Electromagnetic Force (N)	2.808	2.8103	2.807
Number of Iterations	200	200	111
Optimal Area (mm^2)	322.31	322.76	314.22
Computation Time	17 min 47s	24 min 41s	20 min 51s
Topology Optimization without Filtering and Projection			
	MMA	IPOPT	SNOPT
Electromagnetic Force (N)	2.1832	2.7914	2.0861
Number of Iterations	58	176	45
Optimal Area (mm^2)	342.62	342.98	341.14
Computation Time	3 min 56s	12 min 51s	3 min 26s

Table 1, Comparison between different gradient based solvers.

Session VP6
ELECTRICAL MACHINES AND POWER ELECTRONICS V
(Poster Virtual Session)

Duc-Kien Ngo, Chair
University of Technology and Education - The University of Danang, Vinh, Vietnam

VP6-01. A Phase-Decoupled Dual Three-phase Permanent Magnet Synchronous Motor Using Auxiliary Teeth. *Q. Wu*[1], W. Li[1], L. Wang[1], L. Li[1], F. Xu[2] and J. Zhu[1] *1. Nanjing University of Science and Technology, Nanjing, China; 2. Nanjing Chenguang Group Co., Ltd., Nanjing, China*

Dual three-phase permanent magnet synchronous motors (PMSMs) are widely preferred in industrial and commercial applications due to their ability to deliver smoother and more efficient power output. However, practical implementation reveals the presence of magnetic coupling among the phases of dual three-phase PMSMs. This magnetic coupling implies that electrical faults occurring in one phase can disrupt the operation of healthy phases, leading to a significant impact on reliability and safety [1]. Furthermore, PMSMs commonly display substantial torque ripple as a result of cogging torque, thereby presenting challenges to achieving precise control and stability [2]. To address these issues, this paper proposes a 40-poles, 36-slots dual three-phase PMSM, comprising six stator modules and one rotor. Each stator module forms phases A, B, C, U, V, and W respectively, as illustrated in Fig. 1. When only one phase is in normal operation, as shown in Figs 2(a) and 2(b), the presence of auxiliary teeth physically isolates each phase winding, making the self-inductance of each phase significantly higher than the mutual inductance, reducing the influence of the faulty phase on the healthy ones. As indicated in Fig. 2(c), by decoupling the cogging torque generated by intermediate slots and auxiliary slots, it is observed that adjusting the width of the auxiliary teeth can effectively regulate the magnitude and phase of the cogging torque produced by the stator modules, thus realizing the effective suppression of the effect of the cogging torque. As depicted in Fig. 2(d), through enhancements to the width of the auxiliary teeth of the proposed motor, the motor demonstrates a torque ripple of 59.7 mNm and an average torque of 12.75 Nm, thereby achieving a torque ripple rate of under 1%. The full paper will provide specific modeling details and experimental data.

[1] R. Li, H. Fang, D. Li, R et al. "A Search Coil Design Method of PMSM for Detection of Inter-Turn Short-Circuit Fault," IEEE Transactions on Industrial Electronics, Article vol. 71, no. 4, pp. 3964-3974, Apr 2024. [2] Q. Lu, B. Wu, Y. Yao, Y. Shen, and Q. Jiang, "Analytical Model of Permanent Magnet Linear Synchronous Machines Considering End Effect and Slotting Effect," IEEE Transactions on Energy Conversion, vol. 35, no. 1, pp. 139-148, Mar 2020.

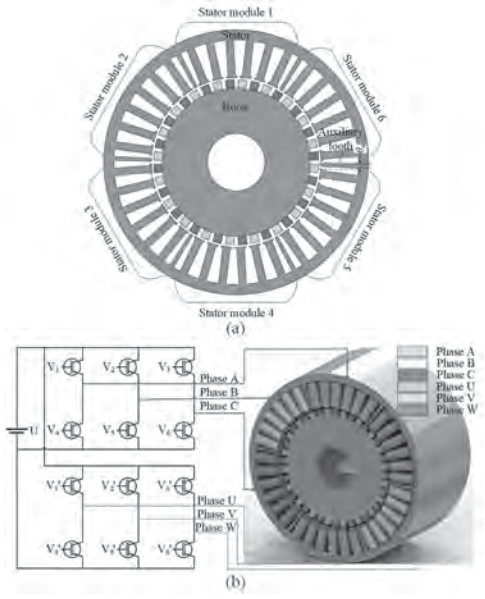

Fig. 1 Proposed motor structure. (a) Main components of the motor. (b) Winding arrangement and drive circuit.

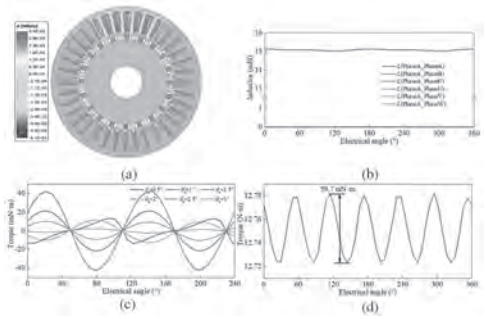

Fig. 2 Operational performance. (a) Magnetic field distribution during normal single-phase operation. (b) Self-inductance and mutual inductance between phases. (c) Cogging torque at different auxiliary tooth widths. (d) Rated torque.

VP6-02. Flux Regulation Capability and Torque Performance Enhancement Design of a New Hybrid-Rotor-Pole Controllable Flux PM Motor. *W. Fan*[1], X. Zhu[2], L. Xu[2] and L. Quan[2] *1. Nantong University, Nantong, China; 2. Jiangsu University, Zhenjiang, China*

Recently, due to the constant PM magnetic field, the conflict between the wide speed range and high torque density has been a hot issue for PM motors used in electric vehicles (EVs) [1]-[2]. How to broaden the speed range without deteriorating output torque capability has been a research difficulty [3]. To solve the problems, a type of variable flux (VF) PM motors has attracted the attention of scholars, where the PM effective flux can be varied by controlling the PM leakage flux according to the magnitude of the

armature reaction [4]. However, due to the increased saturation of the magnetic bridge, the output torque capability of such motors is aggravated and the cogging torque under load is accordingly increased, resulting in a significant increase in the torque ripple compared to traditional PM motors. In this paper, a new hybrid-rotor-pole controllable flux (HRPCF) PM motor is proposed, where the rotor is constituted by two pole units for the objective of realizing the synchronous improvement of the flux-weakening capability and output torque. Meanwhile, through the special notch design of the rotor surface, the torque ripple of such motors can be also effectively reduced. Fig. 1(a) shows the topology of the motor, which is separated into the variable flux pole (VFP) unit and non-variable flux pole (NVFP) unit in Fig. 1(b), the VFP unit realizes the flux regulation while NVFP unit ensures the output torque. Fig. 1(c) shows the ideal air gap flux density, due to the notch design, the resulting position and angle of the saturation region are both varied. In Fig. 2(a), the variation of the *d*-axis flux linkage is compared with a traditional VF-PM motor with the same PM consumption. It shows the proposed motor not only exhibits a higher value of flux linkage at a rated current but also a wider flux variation range. The torque performance in Fig. 2(b) verifies that the notch design can significantly suppress the torque ripple. Finally, the prototyped motor is manufactured, the no-load back-EMF is tested and agreed with the simulated results in Fig. 2(d). In addition, the transient response indicates that the motor possesses a quick response and can satisfy the multiple operating conditions for EV applications.

[1] Y. Tang, F. Chai and et. al., *IEEE Transactions on Industrial Electronics*, Vol. 70, no. 7, pp. 6574-6584 (2023) [2] X. Zhao, S. Niu and et. al., *IEEE Transactions on Industrial Electronics*, Vol. 68, no. 7, pp. 6075-6086 (2021) [3] Y. Du, Y. Mao and et. al., *IEEE Transactions on Transportation Electrification*, Vol. 8, no. 2, pp. 2479-2489 (2022) [4] L. Xu, X. Zhu and et. al., *IEEE Transactions on Industrial Electronics*, Vol. 69, no. 9, pp. 8862-8874 (2022)

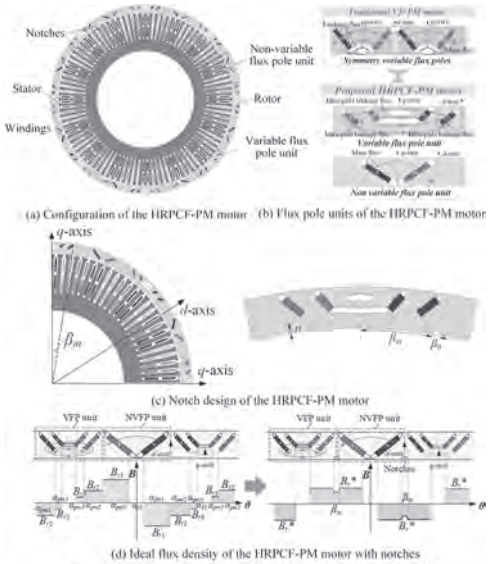

Fig. 1 Configuration of the proposed HRPCF-PM motor and notch design

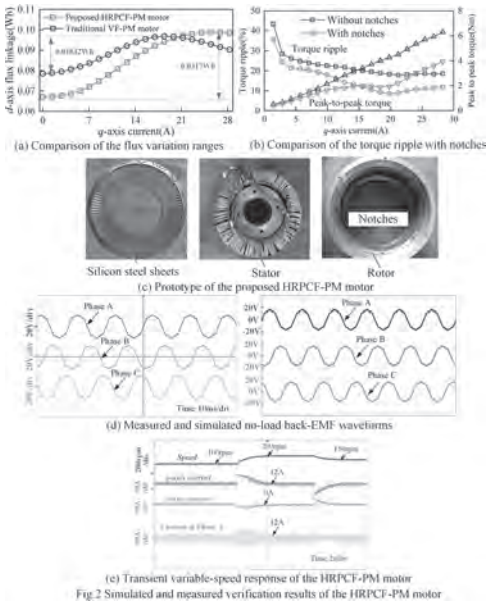

Fig.2 Simulated and measured verification results of the HRPCF-PM motor

VP6-03. Withdrawn

VP6-04. Open-Phase Fault-Tolerant Control for Dual Three-Phase PMSMs Using PIR Controller. Q. Wu[1], W. Li[1], *H. Li*[1] and B. Ji[1]
1. Nanjing University of Science and Technology, Nanjing, China

Due to the high-power density, efficiency, and fault-tolerant capability, dual three-phase permanent magnet synchronous motors (DTP-PMSMs) attract increasing attention in industrial applications [1-3]. Open-phase faults are common and can lead to the generation of negative sequence currents in the stator winding, thereby degrading overall drive performance. To facilitate post-fault operation, both positive and negative sequence currents should be appropriately regulated [4]. The use of a conventional proportional-integral (PI) controller with a low-pass filter has limitations when operating over a wide speed range. A novel fault-tolerant control approach using a proportional-integral-resonant (PIR) controller is proposed to directly regulate the AC reference signals for open-phase fault-tolerant control of DTP-PMSMs. Unlike the existing methods, the PIR controller reduces the number of regulators required and enhances dynamic performance across a wide speed range. Fig. 1 shows the proposed PIR-controller based fault-tolerant control scheme for DTP-PMSMs under open-phase fault. The PIR current controller comprises a conventional PI controller and a resonance controller, which incorporates a notch filter with a resonant gain. The resonant frequency is determined based on motor speed to appropriately regulate the double-frequency AC signals in the *dq* reference frame. Fig. 2 presents the performance of the PIR-based current controllers. As depicted in Fig. 2(a), the current error of the PIR controller converges to zero, highlighting the efficacy of the PIR controller. Frequency changes in the PIR regulator are governed by a hysteresis loop to ensure smooth transitions. In Fig. 2(b), the current waveform under the PIR controller demonstrates its ability to track AC frequency changes from 100 Hz to 150 Hz at 0.5 seconds, showcasing rapid and approximate speed tracking capabilities that enhance dynamic performance across a wide speed range. The detailed modeling and experimental verification will be presented in the full paper.

[1] Z. Zhang, J. Zhang, R. Han, Y. Wu, Y. Gong, and S. Chang, "Computation-efficient current harmonic mitigation for dual three-phase permanent magnet synchronous motors," IEEE Trans. Magn., 2024. [2] J. Paredes, S. Ademi, and R. McMahon, "Performance of a dual three-phase permanent magnet machine for a steer-by-wire system under healthy and faulty conditions," IEEE Trans. Energy Convers., pp. 1-10, 2024. [3] P. Song, W. Li, Z. Li, and N. C. Kar, "Comparative analysis of noise and vibration for dual

three-phase IPMSM under healthy and multi-phase open-circuit fault operations," IEEE Trans. Magn., vol. 59, no. 11, pp. 1-7, Nov. 2023. [4] W. Li, P. Song, Q. Li, Z. Li, and N. C. Kar, "Open-phase fault modeling for dual three-phase pmsm using vector space decomposition and negative sequence components," IEEE Trans. Magn., vol. 58, no. 8, pp. 1-6, Aug. 2022.

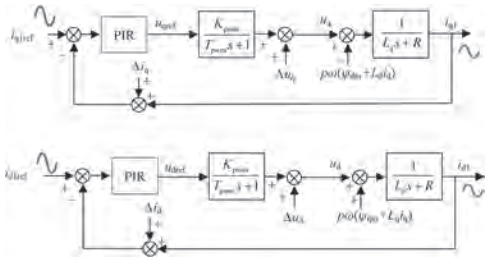

Fig. 1. Proposed fault-tolerant control for DTP-PMSMs using PIR controllers.

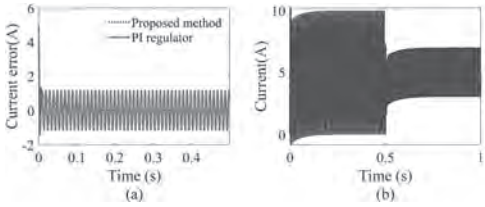

Fig. 2. Performance of PIR based current controllers. (a) Current error waveforms. (b) *q*-axis current waveform.

VP6-05. Inter-Turn Short-Circuit Fault Detection Method for DTPPMSM Based on Voltages Demodulation. S. Li[1] and *C. Liu*[1]
1. Harbin Institute of Technology, Harbin, China

I. Introduction Dual three-phase permanent magnet synchronous motor (DTPPMSM) has been widely used in transportation fields such as electric vehicles, hybrid vehicles and more electric aircraft because of the advantages of high reliability, high efficiency and fault tolerant capability. The timely and online detection of inter-turn short-circuit (ITSC) fault is crucial for ensuring the healthy and stable operation of the motor, thus drawing increasingly attentions. II. Voltage Analysis Assuming that the ITSC fault occurs in phase a1, and the ITSC faulty part occupies a proportion of *k* of the entire phase, then the ITSC fault leads to a voltage remainder Ur in phase voltage equations. When transferring the phase voltage into *d*- and q-axis voltage, Ur leads to a 2nd voltage fluctuations. Then, the demodulation matrix is employed to transfer the 2nd *d*- and *q*-axis voltage fluctuations into DC component, and the low pass filter is employed to obtain the pure DC signal. The fault indicator *F*i can be obtained from the sum of square of DC signals. The whole process of the fault indicator *F*i establishment can be seen from Fig.1. And the fault indicator can be checked without extra sensors, and it can achieve online ITSC fault detection. III. Experimental validation. A 22-pole 24-slot DTPMSM prototype is manufactured to experimentally validate the proposed ITSC fault detection method. The k is given as 0.05 and 0.2 separately, and the corresponding results are shown in Fig.2. The k calculated from *F*i are 0.0507 and 0.1962 correspondingly, which are similar to the given k of 0.05 and 0.2. So the proposed method can achieve accurate ITSC fault detection. IV Conclusion This paper proposed an inter-turn short-circuit (ITSC) fault detection method for dual three-phase permanent magnet synchronous motor (DTPPMSM) based on voltages demodulation. The paper investigated the influence of ITSC fault on voltage, based on the demodulation and filtering of voltage fluctuations caused by ITSC fault, realizing the online ITSC fault detection without extra sensors. The effectiveness and correctness of the proposed method are validated by prototype experiment.

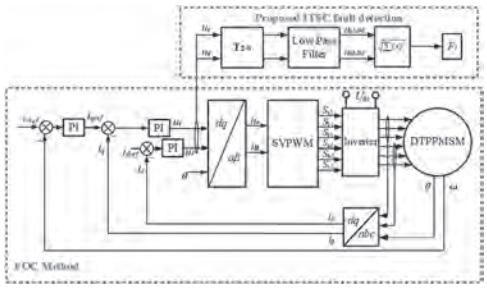

Fig.1. Construction of fault indicator Fi

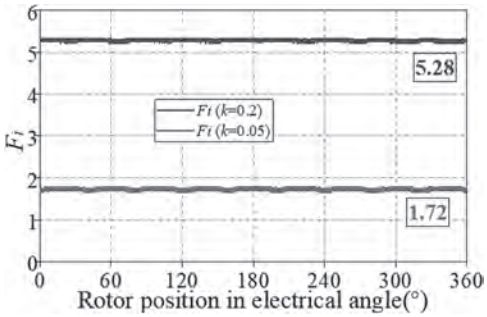

Fig.2. Measurd Fi of different fault severity

VP6-06. Analysis of a New Consequent-Pole Hybrid Excited Machine with Drum Winding. G. Qu[1], *J. Yu*[1], Z. Li[1], Y. Liu[1] and Y. Jiang[2]
1. College of Nuclear Technology and Automation Engineering, Chengdu University of Technology, Chengdu, China; 2. College of Automation & College of Artificial Intelligence, Nanjing University of Posts and Telecommunications, Nanjing, China

I. INTRODUCTION Owing to the merits of high torque density, low permanent magnet (PM) usage and large speed range, hybrid excited (HE) machines have drawn much attention in electric vehicles [1-3]. However, due to the series magnetic circuits, slip rings and brushes can't be avoided in HE machines with the rotor-PM structures [4]. To achieve the brushless hybrid excitation, both PMs and field coils are placed in stators, which may lead to crowed stators [5]. In this paper, a new consequent-pole HE machine with drum winding (CPHE-DW machine) are proposed, which can achieve both the brushless hybrid excitation and the excellent flux-regulating ability. II. MACHINE TOPOLOGY As shown in Fig. 1(a), The U-type PM-pole, which consists of three PMs, is housed in the consequent-pole rotor. In addition, all the PM-poles are magnetized in the same direction. To simplify the winding structure, the three-phase drum winding is adopted on the stator. The stator teeth are subdivided into the main teeth and the auxiliary teeth. The inverter circuit is illustrated in Fig. 1(b). The currents input into the winding are divided into two types: the DC component and the AC component. According to the DC current directions, the coils in each phase winding are divided into two sub-types. The DC currents and the PMs can be regarded as two excitations. According to the particular slot/pole combination, an electromagnetic coupling effect between these two excitations can be achieved. The flux paths generated by these two excitations are exhibited in Fig. 1(c). III. ELECTROMAGNETIC ANALYSIS The back electromotive forces (back-EMFs) are simulated as shown in Fig. 2(a). The output torque waves under no DC current are shown in Fig. 2(b). The average torques under different DC currents are exhibited in Fig. 2(c). Hence, it can be found that the excellent flux-regulating ability can be achieved. IV. CONCLUSION In this paper, a new CPHE-DW machine with drum winding is exhibited, in which the rotor-PM brushless hybrid excitation can be achieved.

[1] J. Jiang and S. Niu, "A novel high-order-harmonic winding design in hybrid-excited reluctance machine for electric vehicle application," *IEEE Trans. Magn.*, vol. 59, no. 11, pp. 1-7, Nov. 2023 [2] L. Cinti, N. Bianchi and M. Bertoluzzo, "Performance and short-circuit fault analysis in hybrid excited and interior PM motors," *IEEE Trans. Energy Convers.*, vol. 39, no. 2, pp. 1412-1422, Jun. 2024. [3] C. Xia, Y. Feng, M. Jia, Y. Gao and S. Huang, "A novel counter-rotating axial-flux hybrid-excitation permanent magnet machine with dual-rotor," *IEEE Trans. Magn.*, vol. 59, no. 11, pp. 1-5, Nov. 2023. [4] Q. Chen, J. Liao, Z. Sang, W. Qian, G. Xu and Z. Liu, "Design and analysis of a novel hybrid rotor PM machine considering negative torque ripple contribution," *IEEE Trans. Ind. Electron.*, vol. 71, no. 7, pp. 6775-6786, Jul. 2024. [5] G. Qu and Y. Fan, "Design of a new consequent-pole segmented dual-stator permanent magnet machine," *IEEE Trans. Magn.*, vol. 58, no. 2, pp. 1-5, Feb. 2022.

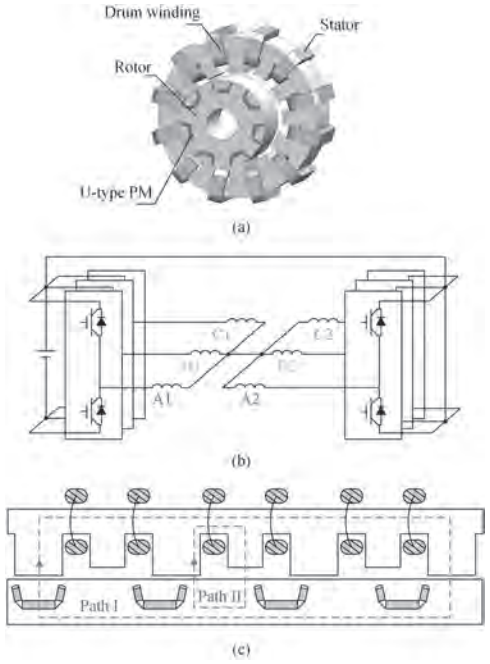

Fig. 1. Machine topologies. (a) CPHE-DW machine. (b) Inverter. (c) Flux paths.

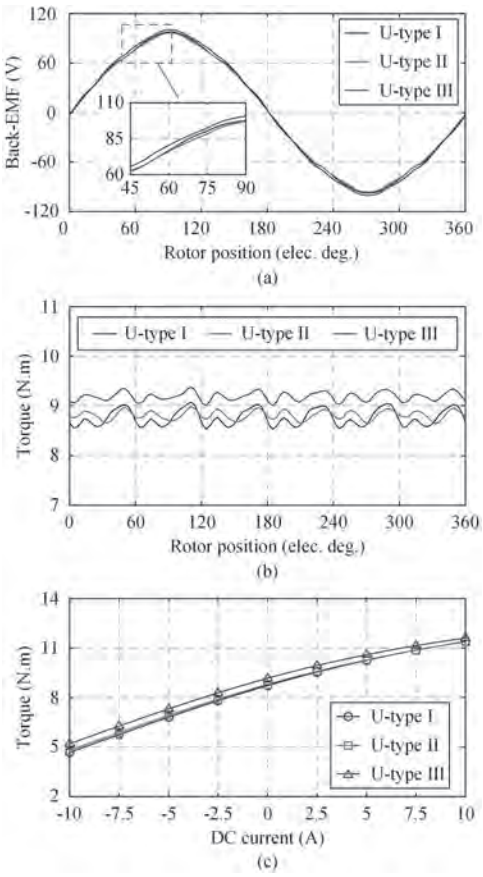

Fig. 2. Electromagnetic characteristics. (a) Back-EMFs. (b) Torque waves. (c) Average torques under different DC currents.

VP6-07. A High-power Density Permanent Magnet Machine Featuring a Novel Lightweight Rotor with A Fin Reuse Structure. *J. Yu*[1], J. Yang[1], Y. Jiang[1] and S. Huang[1] *1. Hunan University, Changsha, China*

High-power density permanent magnet machine (HDPMM) has been widely concerned in aerospace propulsion, vehicle drive, industrial automation and so on, because of its excellent performance [1]. Due to the high temperature rise of permanent magnet (PM) of HDPMM, PM is extremely sensitive to temperature rise, it shows that it is extremely important to carry out thermal management on the PM [2]. Currently, enhancing the heat dissipation capacity of PMs is an effective method to suppress the temperature rise[3]. For surface HDPMM, materials with poor thermal conductivity are usually used to bind the PMs, making heat dissipation more difficult [4]. And the wind cooling of the rotor requires additional fans or blades, which increases the complexity of the system. In this paper, a novel lightweight rotor of HDPMM with fin reuse structure (FRS) is proposed. It can improve the thermal management of the PMs without external devices. As shown in Fig. 1, FRS includes the fin on the inside of lightweight rotor frame, which are inclined at a certain angle to realize fluid self-driving. The flow field and temperature distribution are shown in Fig. 2. It can be seen that FRS can provide enough driving force for flow field, and form an axial flow velocity greater than 10m/s on the fin surface. From Figs. 2(b) and (c), it can be seen that FRS can reduce the temperature of PMs from 256.97 °C to 148.5 °C, a decrease of 42.25%. To show the excellent heat dissipation performance of FRS, the heat dissipation effects of FRS are further compared with those of traditional fin heat dissipation structure, ventilation heat dissipation structure, fin and ventilation heat dissipation mixed structure. To explore the influence mechanism of key parameters of FRS on its cooling effect, this paper also investigates different designs of heat dissipation fins, investigating the impact of the number, length, width, and inclination angle of the fins on the fluid flow characteristics, machine power characteristics, and

temperature rise of the PMs. Finally, the heat dissipation performance of the structure is tested by experiments. More research contents will be shown in the full text.

[1] Wang X. *et al.*, "A critical review on thermal management technologies for motors in electric cars," *Appl. Therm. Eng.*, vol. 201, p. 117758, Jan. 2022. [2] A. S. Fawzal, R. M. Cirstea, K. N. Gyftakis, T. J. Woolmer, M. Dickison, and M. Blundell, "Fan Performance Analysis for Rotor Cooling of Axial Flux Permanent Magnet Machines," *IEEE Trans. Ind. Appl.*, vol. 53, no. 4, pp. 3295–3304, Jul. 2017. [3] B. B. St-Jacques, R. Shi, and P. Pillay, "An Enhanced PMSM Cooling Design for Traction of an Electric Vehicle," *IEEE Trans. Transport. Electrific.*, pp. 1–1, 2023. [4] H. Fang, R. Qu, J. Li, P. Zheng, and X. Fan, "Rotor Design for High-Speed High-Power Permanent-Magnet Synchronous Machines," *IEEE Trans. Ind. Appl.*, vol. 53, no. 4, pp. 3411–3419, Jul. 2017.

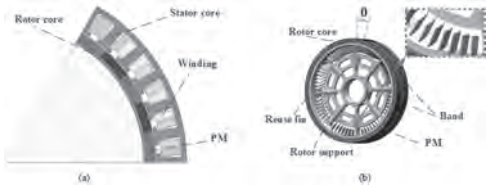

Fig. 1 Electromagnetic structure and FRS schematic diagram. (a) Electromagnetic structure. (b) FRS

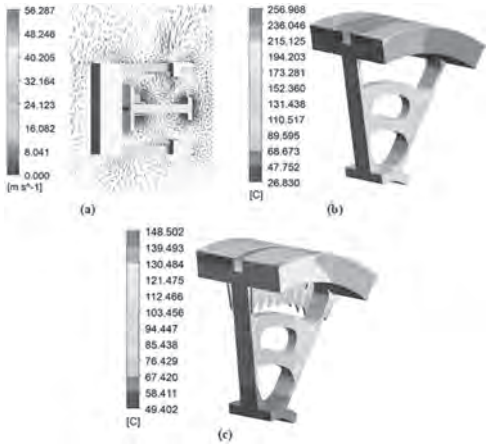

Fig. 2 Flow field and temperature distribution of HDPMM. (a) Flow field of FRS. (b) Temperature distribution of no FRS. (c) Temperature distribution of FRS

VP6-08. Analytical analysis and experimental verification of electromagnetic performance of slotless permanent magnet brushless motor. *H. Li*[1], J. Yang[1], Y. Jiang[1] and S. Huang[1] *1. College of Electrical and Information Engineering, Hunan University, Changsha, China*

This paper introduces an analytical approach for assessing the electromagnetic performance of sectoral windings in slotless permanent magnet brushless motors. Initially, the methodology involves the electromagnetic torque of a single coil, which is subsequently analyzed in a categorical manner, yielding analytical expressions that capture the electromagnetic performance for scenarios where p≠2, as well as the specific case of p=2. Subsequently, to validate the practicality of this analytical method, finite element simulations and analytical computations are conducted on a range of sectoral winding motors, encompassing diverse pole-slot configurations. Ultimately, a prototype of a 6-slot 4-pole motor is fabricated, serving as a testbed to verify the precision of the proposed analytical framework. While the electromagnetic parameters of slotless permanent magnet motors have been analyzed in [2], it does not take into account the specific case of p = 2. In light of this, this paper proposes a more comprehensive analytical model to derive more precise analytical results. From the Fig. 1 equation, it is evident that a discrepancy arises in the fundamental analytical formula of the slotless permanent magnet motor when the number of pole pairs is different (p ≠ 1). Specifically, there is a distinction between the cases where the number of pole pairs is equal to two (p = 2) and when it is not (p ≠ 2). In the particular instance where p is specifically equal to 2, a separate calculation is required. A comparative analysis is undertaken between the specific instance of P = 2 and the broader case of P ≠ 2, utilizing finite elements and analytical methods accordingly. Fig. 2(a)(b) presents the torque comparison outcomes for 6S2P and 6S4P brushless motors. Notably, the deviation between these two methodologies is negligible, thus preliminarily validating the accuracy of the analytical approach. To validate the accuracy of this analytical method, a 6-slot 4-pole motor, as shown in Fig. 2(c), has been designed and tested through rigorous experimental procedures.

[1] Yang J, Dai S, Wang Z, et al. IEEE Transactions on Transportation Electrification, 2023: 1–1. Doi: 10.1109/TTE. 2023.3306458 [2] Min S G, Sarlioglu B. IEEE Transactions on Transportation Electrification, 2018, 4(2): 517–524. [3] Z. Q. Zhu, D. Howe, and C. C. Chan, IEEE Trans. Magn., vol. 38, no. 1, pp. 229–238, Jan. 2002. [4] Markovic M, Perriard Y. IEEE Transactions on Magnetics, 2006, 42(12): 3842–3846.

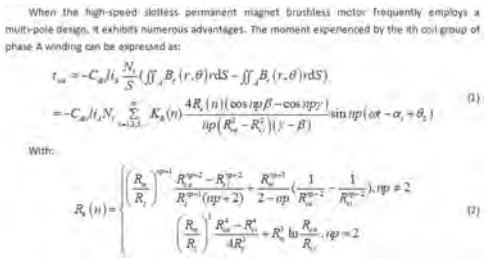

Fig. 1. The main formula to distinguish p=2 and p≠2.

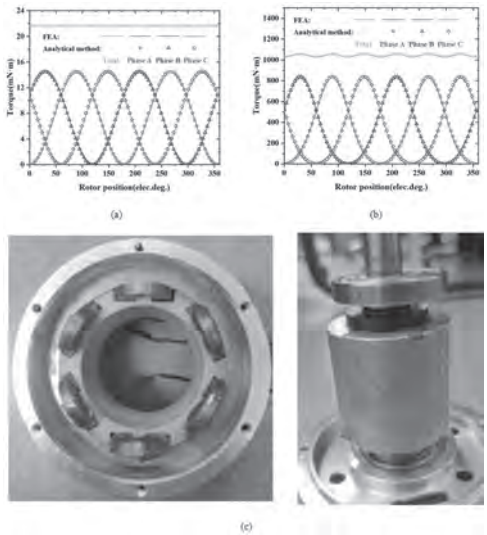

Fig. 2. Experimental motor and torque comparison results. (a) 6S2P. (b) 6S4P. (c) Prototype stator and rotor.

VP6-09. Design of Pole-changing Flux Reversal PM Motor Based on PM Magnetomotive-Force Period. *H. Chen*[1], Y. Du[1], F. Xiao[1], X. Zhu[1], Z. He[1] and Z. Chen[1] *1. School of Electrical and Information Engineering, Jiangsu University, Zhenjiang, China*

Flux reversal permanent magnet (FRPM) motor owns an inherent advantage of simpler stator structure over other stator permanent magnet (PM) motors [1]. However, the speed range of the FRPM motor is limited due to the constant PM field. As a method to widen speed range, pole-changing (PC) has been investigated widely and has been introduced into the FRPM motor recently to obtain a PC-FRPM motor. But how to make the FRPM

motor possess the ability of PC operation was absent. In this paper, the PM flux density in airgap of conventional FRPM motors with the commonly used "NSNS" and "NSSN" PM structures is analyzed. The results show that these motors cannot realize PC operation. Then, according to the operation principle analysis of PC motors, a design method based on the variation of the PM magnetomotive-force (MMF) period is deduced. Consequently, a PC-FRPM motor with the "NNSS" PM pattern is proposed, of which the performance is analyzed and compared. Three FRPM motors with different PM patterns are shown in Fig. 1, where the PM MMF period of "NNSS" structure is half of those of "NSNS" and "NSSN" ones. Therefore, the distribution and spectrum of modulated PM field are changed. The pole-pair numbers of airgap flux density harmonics using "NSNS" and "NSSN" structures can be expressed as $|kN_s\text{-}N_r|$ and $|(2k\text{-}1)N_s/2\text{-}N_r|$, respectively, where k is a positive integer, N_s and N_r are the numbers of stator teeth and rotor teeth, respectively. But it is changed as $|(2k\text{-}1)N_s/4\text{-}N_r|$ in "NNSS" one, which can be used for realizing PC operation [2]. Moreover, a novel design process focused on the PC operation of FRPM motors is further proposed and will be included in the full paper. The three motors have been optimized and compared. The efficiency maps in Fig. 2 show that the proposed motor can obtain high torque and wide speed range, respectively, in two operation modes by PC, named Mode I and Mode II. Thus, high efficiency can be obtained in the whole work region. More details about the theoretical analysis, simulation and experimental results will be included in the full paper.

[1] H. Hua, Z. Q. Zhu, *IEEE Trans. Energy Convers.*, vol. 37, no. 3, pp. 1815–1824 (2022)

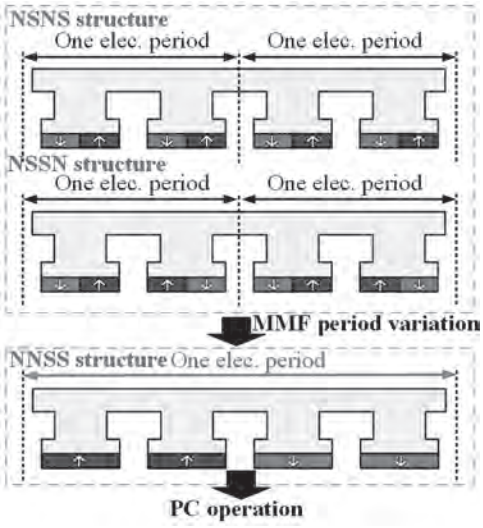

Fig. 1. Stator PM topology evolution for PC operation.

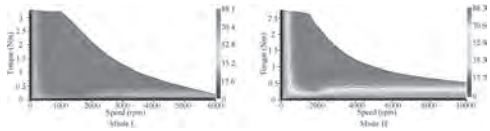

Fig. 2. Efficiency maps of PC-FRPM motor using "NNSS" structures in different operation modes.

VP6-10. Experimental Verification of Electromagnetic Characteristic Analysis of Outer-Rotor-Type BLDC Motor Using Subdomain Method and Optimal Design Using Genetic Algorithm. *T. Kim*[1], J. Yang[1], K. Shin[2] and J. Choi[1] *1. Chungnam National University, Daejeon, The Republic of Korea; 2. Changwon National University, Changwon, The Republic of Korea*

Outer-rotor-type BLDC motors generally have a PM overhang structure, as shown in Fig. 1(a) and (c). The 3D analysis required by this structure is very time-consuming. Therefore, a 2D equivalent analysis method using PM operating point conversion is performed[1]. Electromagnetic analysis is essential for understanding the characteristics of outer-rotor-type BLDC motors. Among electromagnetic analysis methods, the analytical method using spatial harmonics divides the machine into areas, as shown in Fig. 1(b) and solves the governing equations for each area directly using Maxwell's equations[2]. Efficiency and power density are important variables that indicate the performance of electric motors; however, they are inversely proportional and are only appropriate as multi-objective functions. Thus, a genetic algorithm(GA) can be used to optimize these objective functions for an optimal design[3]. Figures 2(a) and (b) are diagrams comparing the results derived by an analytical method with the finite element analysis(FEA) results. In particular, Fig. 2(b) shows experimental results with values similar to the derived values. The analysis results were performed by applying the 2D equivalent method, and were confirmed to be similar compared to FEA. The Pareto front in Fig. 2(c) was derived from 10,000 design candidates selected based on the GA. In observing the Pareto boundary of the graph, the relationship between output density and efficiency is observed to be inversely proportional to each other. In this study, a point with relatively high efficiency was selected as the optimal point. As shown in Fig. 2(d), the efficiency increases by 0.51% and the power density increases by 9.9kW/m3, indicating that the optimal design was successfully achieved. Detailed results will be provided in the full paper.

[1] T. Y. Lee, M. K. Seo, Y. J. Kim, and S. Y. Jung, "Motor Design and Characteristics Comparison of Outer-Rotor-Type BLDC Motor and BLAC Motor Based on Numerical Analysis," IEEE Trans. Appl. Supercond., vol. 26, no. 4, June. 2016, ID 5205506. [2] K. Shin, K. Jung, H. Cho and J. Choi, "Analytical Modeling and Experimental Verification for Electromagnetic Analysis of Tubular Linear Synchronous Machines with Axially Magnetized Permanent Magnets and Flux-Passing Iron Poles," IEEE Trans. Magn., vol. 54, no. 11, Nov. 2018, ID 8204006. [3] J. Gao, L. Dai, and W. Zhang, "Improved genetic optimization algorithm with subdomain model for multi-objective optimal design of SPMSM," CES Trans. on Electrical Machines and Systems., vol. 2, no. 1, March. 2018.

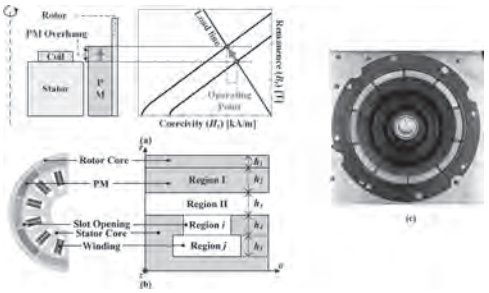

Fig. 1. Outer-rotor-type BLDC motors: (a) 2D equivalent method of 3D structure through operating point conversion and (b) simplified analytical model (c) rotor of manufactured model.

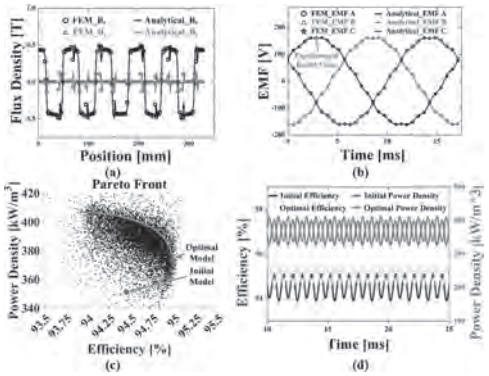

Fig. 2. Electromagnetic performance comparing analytical method, FEA results, and experimental results: (a) magnetic flux densities at the airgap and (b) back-EMF (c) Pareto front derived by GA (d) comparison of initial design and optimal design.

Session VP7
ELECTRICAL MACHINES AND POWER ELECTRONICS VI
(Poster Virtual Session)

Christopher H. T. Lee, Chair
Nanyang Technological University, Singapore

VP7-01. Mechanical Flux-Weakening Design of the Bidirectional Flux-Modulated Radial Permanent Magnet Generator for Wind Power Generation. *Z. Dong*[1], M. Jiang[1] and S. Niu[1] *1. Department of Electrical and Electronic Engineering, The Hong Kong Polytechnic University, Hung Hom, Hong Kong*

I. Introduction Nearly one-fifth of the world's population still lacks access to the grid, with many of these populations residing in remote areas where expanding the grid may not be feasible. Therefore, stand-alone wind power generation systems are highly applicable in such scenarios. Permanent magnet synchronous motor (PMSM) is widely used because of its excellent performance, but usually requires two sets of windings. In addition, in order to achieve weak magnetic and speed up, previous motors usually use electrical method, but electrical method will cause PM demagnetization and additional current consumption. This paper proposes a bidirectional flux-modulated radial permanent magnet synchronous generator (PMSG) based mechanical flux-weakening design. By implementing the flux modulation principle to achieve a mechanical flux-weakening, the risk of demagnetization of the PMs is avoided. By selecting the working harmonic, ensuring that the pole pair number of the outer rotor matches the number of stator slots, the adjustment of total back electromotive force (EMF) output can be achieved with only one set of windings, greatly reducing the manufacturing complexity of the motor. II. Proposed Motor Structure The generator topology is shown in the Fig. 1, consisting of the stator, rotor, and adjustable modulation ring. The angle of the adjustable modulation ring is controlled by an additional servo motor to achieve the purpose of controlling the magnetic flux. Both the rotor and adjustable modulation ring contain radial PMs. The number of pole pair on the adjustable modulation ring matching the number of stator slot, in order to use one set of winding to produce total back EMF. III. Performance After optimization and finite element analysis, the performance of the motor is shown. Fig. 2 shows the voltage regulation curve as the modulation ring angle changes, the voltage regulation ratio can up to 93%, which indicates a large regulation range and also indicates that the system is very suitable for the stand-alone wind power generation system

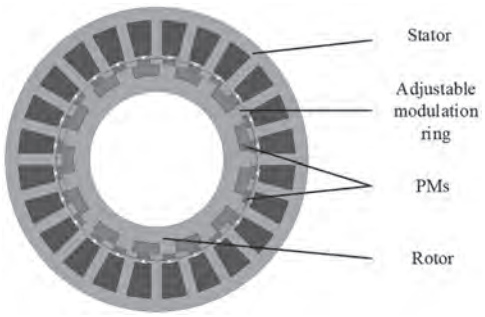

Fig. 1 The topology of generator

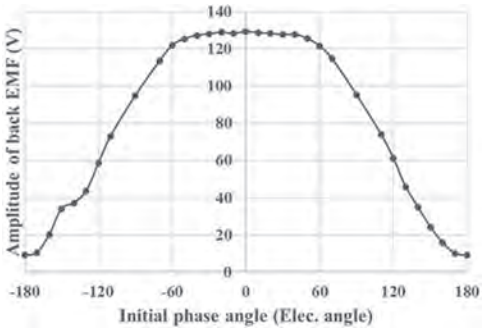

Fig. 2 The curves of back EMF amplitude vs. the initial phase angle

VP7-02. Withdrawn

VP7-03. High-Efficiency-Region Broadening Design and Analysis of A Variable-Leakage-Flux Permanent Magnet Motor from the Perspective of Losses Replacement. *M. Jiang*[1], X. Zhu[2] and Z. Xiang[2] *1. Jiangsu Ocean University, Lianyungang, China; 2. Jiangsu University, Zhenjiang, China*

With the increasing complexity of traffic conditions around the world, the driving cycle of EVs has attracted more and more attention in the field of drive motor research. The high-efficiency driving of the drive motor under multiple operation conditions cannot be satisfied by the improvement of single-operation-point efficiency. Thus, in [1], the efficiencies under different flux leakage states of a flux-leakage controllable permanent magnet are improved. Yet, the ignorance of the driving cycle brings poor adaptability to the working conditions of EVs. Meanwhile, the efficiencies of representative points, picked out according to the distribution of actual operation points, are improved in [2], emphasizing the driving cycle and ignoring the characteristics of the motor itself, affecting the fit between the motor and the drive cycle. In this paper, according to the distribution of actual operating points of EVs, the high-efficiency region of the drive motor is broadened directionally, improving the operation quality of the drive motor. Fig. 1(a) shows the topology and efficiency map of the research variable leakage flux permanent magnet (VLF-PM) motor, and the distribution of high-energy operating points of the typical New European Driving Cycle (NEDC). To orientally broaden the high-efficiency region of the VLF-PM motor, the key operation points are selected as the key operating points and marked in Fig. 1(a). The derivative of core loss and copper loss on output torque under the 6 key operation points are calculated and presented in Fig. 1(b) and (c). Then, the rated performances of the initial motor and improved motor are compared and shown in Fig. 2. It can be seen that based on the directional losses replacement, the efficiencies of the 6 key operation points are all improved. As a result, with similar speed-torque and speed-power characteristics, the high-efficiency region is directionally broadened, improving the efficiency of the operation points in NEDC. More detailed theoretical analysis and experimental results will be given in full paper.

[1] X. Zhou, X. Zhu, W. Wu, Z. X and et al, "Multi-objective optimization design of variable-saliency-ratio pm motor considering driving cycles," *IEEE Trans. Ind. Electron.*, vol. 68, no. 8, pp. 6516-6526(2021). [2] X. Sun, Z. Shi, Y. Cai, and et al, "Driving-Cycle-Oriented Design Optimization of a Permanent Magnet Hub Motor Drive System for a Four-Wheel-Drive Electric Vehicle", *IEEE Trans. Transport. Electrific.*, vol. 6, no. 3, pp. 1115-1125(2019).

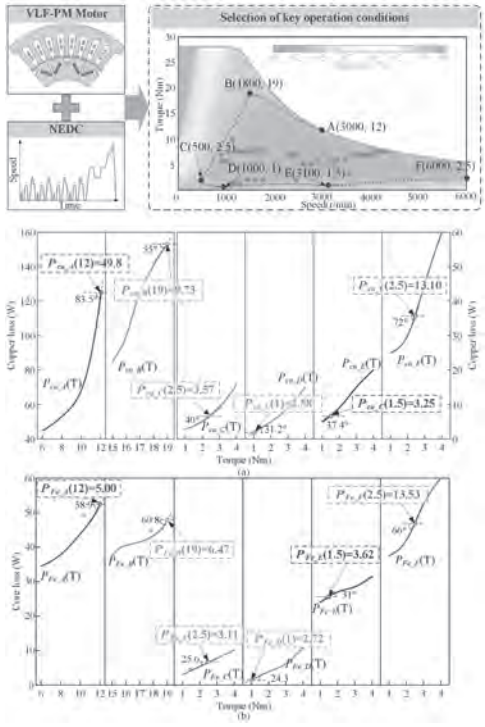

Figure 1

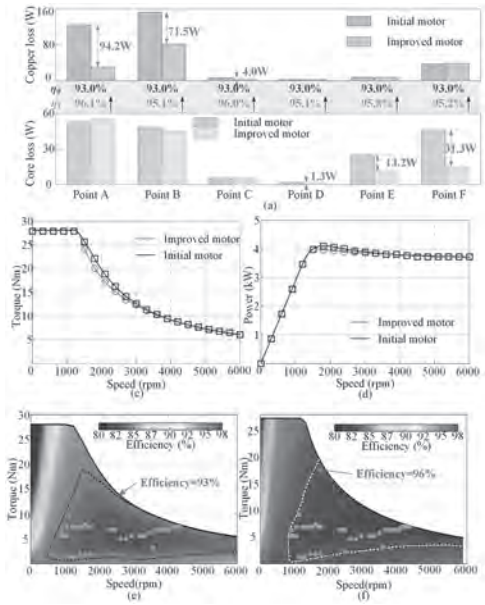

Figure 2

VP7-04. Investigation on Influence of Varying Design Dimensions of AFSRM on Output Performance. *Q. Guo*[1] and W. Zhang[1] *1. College of Electrical Engineering, Zhejiang University, Hangzhou, China*

During the 3D design process of axial flux switch reluctance motors (AFSRMs), certain design dimensions such as pole arc and yoke height are difficult to obtain through direct calculations. Additionally, when designing rotor teeth, it is typical to make the rotor tooth edge extensions intersect at the center of the motor. However, the unique structure of axial flux motors allows for significant optimization of the rotor tooth shape. Taking a 12/8 poles three-phase AFSRM as a case study, this research establishes a motor model utilizing the equivalent magnetic circuit method, analyzes the impact of the above factors on inductance and torque. Utilizing the optimal switching angles of various dimension conditions obtained from genetic algorithm (GA), finite element analysis was employed to explore the influence of these factors on both the average torque output and the torque ripple of the motor. The results suggest that increasing the stator and rotor yoke height helps improve the average torque and reduce torque ripple, but the benefits diminish with increasing yoke height. Moderately increasing the rotor pole arc helps enhance average torque but also increases torque ripple. The stator pole arc has the greatest impact on output performance, and appropriately increasing it helps improve average torque and reduce torque ripple. Adjusting the rotor pole arc by increasing it on the inner circle and reducing it on the outer circle, so that the intersection of the rotor tooth edge extension line is appropriately positioned away from the center of the motor, helps to improve the average torque and reduce torque ripple. During assembly, there can be deviations such as rotor eccentricity and non-uniform air gaps in axial flux motors, which may influence the motor's output performance. This paper explores the effects of these assembly deviations on motor performance, revealing that eccentricity of the rotor can lead to a reduction in average torque and an increase in torque ripple while minor irregularities in the air gap have negligible effects on motor performance.

[1] H. Goto, S. Murakami and O. Ichinokura, IECON 2015 - 41st Annual Conference of the IEEE Industrial Electronics Society, Yokohama, Japan, pp. 005191-005196 (2015) [2] M. Sepehrinour, A. Kalantarikhalilabad and A. Rezaei-Zare, 2023 IEEE International Electric Machines & Drives Conference (IEMDC), San Francisco, CA, USA, pp. 1-7 (2023) [3] D. Gong and J. Chen, Journal of ACTA ELECTRONICA SINICA, vol. 42, no. 8, pp. 1538-15244 (2014)

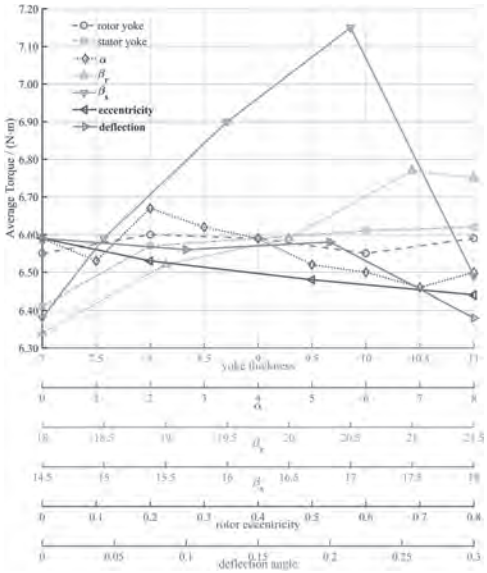

Fig. 1 Influence of varying design dimensions on output average torque

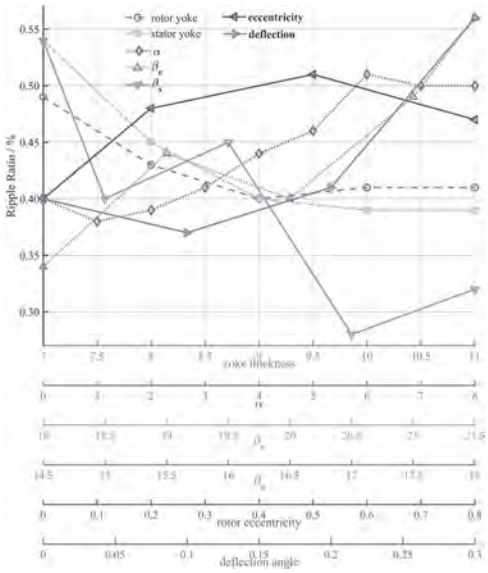

Fig. 2 Influence of varying design dimensions on output torque ripple ratio

VP7-05. Torque Ripple Reduction Design Approach of Permanent Magnet Machines Based on Circumferential Pole Pair Shift. *L. Dai*[1], S. Niu[1], J. Gao[2] and S. Huang[2] *1. Department of Electrical and Electronic Engineering, The Hong Kong Polytechnic University, Hong Kong, Hong Kong; 2. Hunan University, Changsha, China*

I. Introduction Electromagnetic torque is the fundamental property of permanent magnet machines (PMMs). Achieving minimal torque ripple is highly desirable for high-performance PMMs. Various methods have been explored to reduce torque ripple in PMMs. However, the existing approaches often come with drawbacks. For instance, some methods result in reduced torque density due to an increased effective airgap volume [1], while others lead to decreased winding utilization [2]. Moreover, the associated rise in manufacturing costs poses a significant concern. To overcome these limitations, this paper proposes a novel method for suppressing torque ripple in PMMs. The approach proposes a circumferential shift strategy of the rotor pole-pair, accompanied by two shifting approaches. II. Verification This paper presents two design paths, namely reverse shifting and gradual shifting of pole pairs, for reducing torque ripple in PMMs. Fig. 1 illustrates these design paths, while Fig. 2 showcases the torque waveforms over one electrical cycle obtained of a motor case study under both shifting methods. Notably, the results show a significant reduction in torque ripple, with method-1 achieving a reduction from 30.26% to 4.82% and method-2 achieving a reduction to 1.93%. These findings demonstrate the effectiveness of the two approaches in suppressing torque ripple to varying degrees. Furthermore, it is essential to highlight that implementing these methods does not result in additional manufacturing costs.

[1] Y. Yokoi and T. Higuchi, "Stator Design of Alternate Slot Winding for Reducing Torque Pulsation With Magnet Designs in Surface-Mounted Permanent Magnet Motors," IEEE Transactions on Magnetics, vol. 51, no. 6, pp. 1-11, June 2015, Art no. 8202911. [2] M. S. Islam, R. Mikail, M. A. Kabir and I. Husain, "Torque Ripple and Radial Force Minimization of Fractional-Slot Permanent Magnet Machines Through Stator Harmonic Elimination," IEEE Transactions on Transportation Electrification, vol. 8, no. 1, pp. 1072-1084, March 2022.

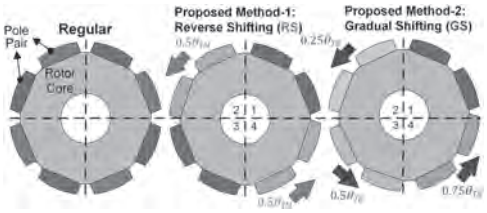

Fig. 1. Illustration of the proposed method.

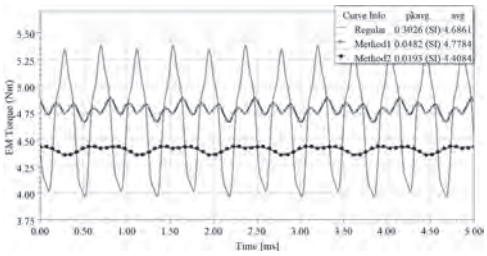

Fig. 2. Torque waveforms using the proposed design approaches.

VP7-06. Design and Optimization of Torque and Loss Characteristics for a Permanent Magnet In-Wheel Motor Considering Dominant Airgap Harmonic. *J. Ren*[1], L. Quan[1] and Z. Xiang[1] *1. School of Electrical and Information Engineering, Jiangsu University, Zhenjiang, China*

In-wheel motor system is the core moving part of hub-driven electric vehicles, which usually integrates drive motor, electronic control component transmission and braking device into the wheel, forming an integrated design of power, transmission and braking [1], [2]. The vehicle power system equipped with in-wheel motor can effectively eliminate the mechanical transmission structure and present the characteristics of distributed drive, which makes the hub-driven electric vehicle have outstanding performance advantages such as flexible spatial layout and efficient power transmission [3]. To sum up, this paper introduces "flux modulation" into the design of permanent magnet in-wheel motor and proposes a spoke-type permanent magnet in-wheel (SPM-IW) motor. The key of this study is to evaluate the contributions of harmonics on torque and loss, and further determines the harmonics related to them. Then based on these harmonics, the motor is designed and optimized in layers. Fig. 1 shows the motor structure of regular and proposed SPM-IW motor. Fig. 2 shows the additional modulation effect generated by new modulation structure. Fig. 3 gives the analysis of air gap harmonic, in which modulated wave (5th and 19th harmonics) and fundamental wave (7th harmonic) are considered as main harmonics. The analysis of torque and iron loss characteristics based on air gap harmonic are shown in Fig. 4 and 5. torque enhancement factor Ξ_T and loss suppression factor $\Xi_{T/L}$ are introduced for motor design and optimization, and specific flow chart of the optimization process is proposed in Fig. 7. Fig. 8 and Fig. 9 show the result of the first and second level optimization. Fig. 10 compares the iron loss distribution diagram of the motor before and after optimization. The torque performance and rotor iron loss before and after optimization are shown in Fig. 11.

[1] Z. Q. Zhu and J. T. Chen, "Advanced Flux-Switching Permanent Magnet Brushless Machines," IEEE Trans. Magn., vol. 46, no. 6, pp. 1447-1453, June 2010. [2] Z. Li, L. Zheng, W. Gao, and Z. Zhan, "Electromechanical Coupling Mechanism and Control Strategy for In-Wheel-Motor-Driven Electric Vehicles," IEEE Trans. Ind. Electron., vol. 66, no. 6, pp. 4524-4533, June 2019. [3] X. Zhu, Z. Shu, L. Quan, Z. Xiang, and X. Pan, "Design and Multicondition Comparison of Two Outer-Rotor Flux-Switching Permanent-Magnet Motors for In-Wheel Traction Applications," IEEE Trans. Ind. Electron., vol. 64, no. 8, pp. 6137-6148, Aug. 2017.

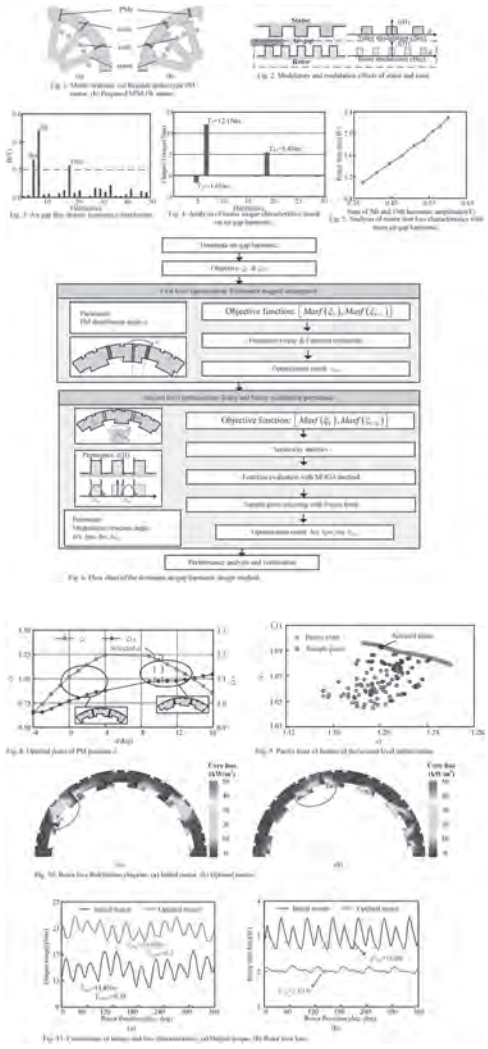

VP7-07. A Flywheel Energy Storage System with Double High-Strength Steel Rotors. *P. Zhang*[1], J. Yang[1], Y. Jiang[1] and S. Huang[1] *1. College of Electrical and Information Engineering, Hunan university, Changsha, China*

Flywheel energy storage (FES) has attracted much attention due to its merits of no environmental pollution, fast response time, high power density, and high reliability [1]. However, the idling loss caused by the stator core loss would reduce the energy conversion efficiency, especially for the long idling operation state. Addressing this issue, this paper proposes a novel FES system (FESS) with double high-strength steel rotors, as shown in Figs. 1(a) and 1(b). The inner and outer rotors are connected to each other and rotate synchronously. The inner surface of the outer rotor is equipped with halbach array permanent magnets. The armature windings are placed on the stator processed from nylon material. Meanwhile, the rotors are supported by magnetic bearing. It has the merits of low idling loss, high charge/discharge efficiency, and high energy storage density. The key structure parameters of the electrical machine are optimized and electromagnetic performance is analyzed. Due to the ironless structure of stator, the air-gap length of the proposed machine is larger than of the electrical machine with the iron core structure [2][3]. The amplitude of the air-gap flux density is unequal along the radial direction. To accurately calculate the electromagnetic performance of the electrical machine, an analysis is proposed and analyzed. Figs. 1(c) and 1(d) give the back electromotive force (Back-EMF) and electromagnetic torque obtained by analytical and finite analysis methods. The amplitudes of the Back-EMF are 228V and 226V, and the average torques are 7.75 Nm and 7.62 Nm. It can be found that the results obtained by the analytical calculations are well coincide with those obtained by the finite analysis method. The magnetic bearing is designed and the magnetic force is analytically calculated using the Maxwell tensor method. The magnetic bearing provides the magnetic force that counteracts the gravity of the rotors to reduce friction loss in mechanical bearings. Finally, a prototype of the proposed FESS with a 24-slot and 8-pole electrical machine is being manufactured. The machined outer rotor with halbach array permanent magnets is shown in Fig. 2. The tested results will be presented in full paper.

[1] Z. Zhang, C. Wang and W. Geng, "Design and Optimization of Halbach-Array PM Rotor for High-Speed Axial-Flux Permanent Magnet Machine With Ironless Stator," in *IEEE Transactions on Industrial Electronics*, vol. 67, no. 9, pp. 7269-7279, Sept. 2020, doi: 10.1109/TIE.2019.2944033. [2] Z. Wang, J. Yang, H. Chen, C. Ye and S. Huang, "Electromagnetic Performance Analysis of a Dual-rotor Ironless Stator PM Machine," *2022 International Conference on Electrical Machines (ICEM)*, Valencia, Spain, 2022, pp. 874-879, doi: 10.1109/ICEM51905.2022.9910693. [3] Z. Q. Zhu, D. Howe, and C. C. Chan, "Improved analytical model for predicting the magnetic field distribution in brushless permanent-magnet machines," IEEE Trans. Magn., vol. 38, no. 1, pp. 229–238, Jan. 2002.

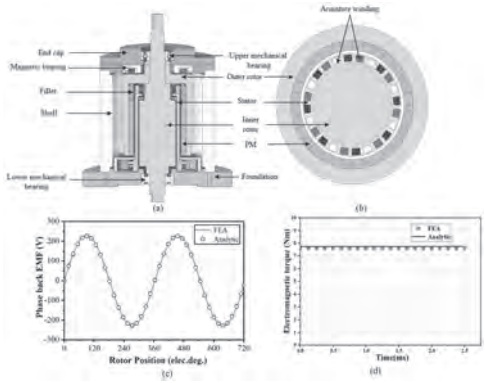

Fig 1 Topology and electromagnetic performance of the FESS. (a) 3D model of the flywheel energy storage system. (b) 2D model of the flywheel energy storage system. (c) Back-EMF. (d) Torque

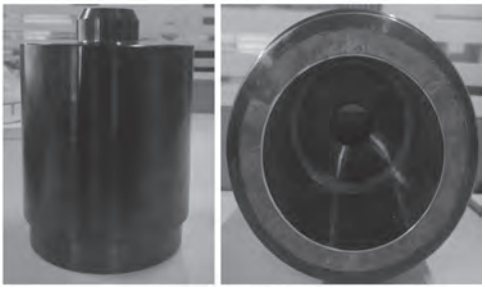

Fig.2. Manufacture of outer rotors

VP7-08. Study on AC Copper Loss Suppression of Permanent Magnet Flat Wire Motor Based on Flux Density Harmonic Suppression. *X. Wang*[1], L. Quan[1] and Z. Xiang[1] *1. School of Electrical and Information Engineering, Jiangsu University, Zhenjiang 212013, Zhenjiang, China*

Permanent magnet (PM) flat wire motors offer a number of advantages, including a high slot fill factor, high power density, high efficiency, and good heat dissipation, [1] are well suited to the needs of electric vehicle operation. Consequently, these motors have become the dominant type of electric vehicle drive motor. However, due to the larger cross-sectional area of flat wire windings in comparison to round wire windings, they are subject to more prominent eddy current effects. The AC copper loss of the motor is primarily attributable to the armature magnetic field (AMF) and the permanent magnetic magnet field (PMMF) in conjunction [2]. The AC copper loss of the motor can be classified into DC loss, AMF eddy current loss, and

PMMF eddy current loss. This paper concentrates on the impact of motor topology on AC copper loss, with the objective of reducing motor copper loss and enhancing motor efficiency. Fig. 1(a) shows the different rotor structures of the motor and its stator structure. Fig. 1(b) illustrates the composition of copper loss in the linear part of the motor under different operating conditions. The motor operates at medium and high speeds, resulting in an increase in the share of eddy copper loss. At deep flux-weakening, the eddy current losses caused by the PMMF are mitigated. Fig. 2(a) reflects the effect of some of the stator parameters on copper loss. The lowest AC copper loss is observed when the winding aspect ratio is close to 1. In addition, increasing the stator slot height and decreasing the stator slot width can reduce the eddy current loss. Fig. 2(b) illustrates that the utilization of multilayer PMs can mitigate the impact of leakage flux generated by the conductor subjected to the PMMF. It is noteworthy that the PMs employ the ∇+v structure, which effectively minimizes both the magnitude of the flux density and the distortion rate of the flux density in the conductor, resulting in lower copper loss. Fig. 2(c) illustrates the copper loss and the torque performance of different motors.

[1] S. Nuzzo, D. Barater, C. Gerada and P. Vai, "Hairpin Windings: An Opportunity for Next-Generation E-Motors in Transportation," in IEEE Industrial Electronics Magazine., vol. 16, no. 4, pp. 52-59, Dec. 2022. [2] X. Ju, Y. Cheng, B. Du and M. Yan, "AC Loss Analysis and Measurement of a Hybrid Transposed Hairpin Winding for EV Traction Machines," IEEE Trans. Ind. Electron., vol. 70, no. 4, pp. 3525-3536, Apr 2023.

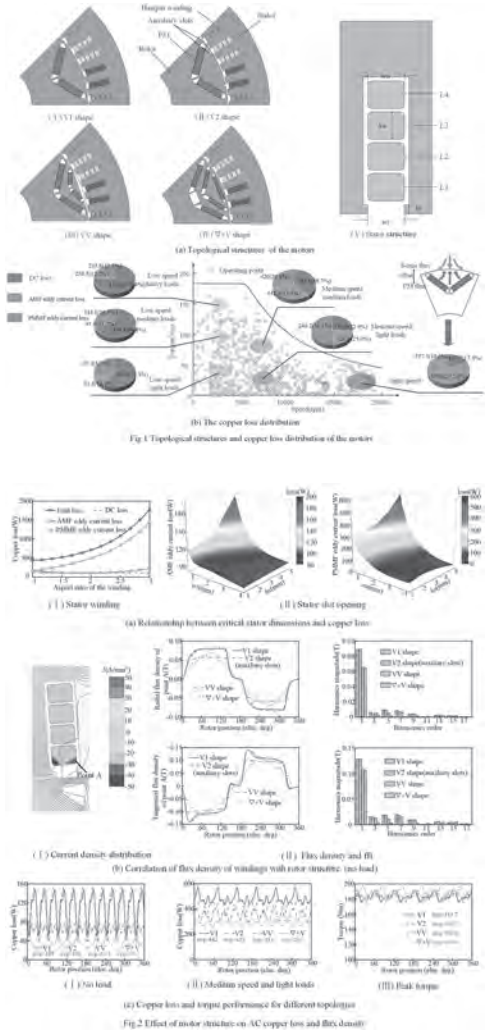

VP7-09. A Pole-Changing Double-sided Permanent Magnet Vernier Motor. H. Chen[1], Y. Du[1], F. Xiao[1], X. Zhu[1] and *Z. He*[1] *1. School of Electrical and Information Engineering, Jiangsu University, Zhenjiang, China*

Permanent magnet vernier (PMV) motor has the merits of low torque ripple and high torque density due to the magnetic gear effect [1]. However, in some variable-speed applications, such as electric vehicles, not only high torque density but also a wide speed range is required [2]. Thus, numerous novel motor topologies, such as hybrid excitation motors, pole-changing (PC) motors, and memory motors have been proposed. Among them, PC motors combine the advantages of high efficiency in the high-speed region and ease of speed regulation. In [1], a PC-PMV motor was proposed. The results show that this motor possesses both advantages of high torque and wide speed range due to the PC operation. However, the stator space utilization ratio has been reduced since the adoption of split stator tooth structure, as shown in Fig. 1. In this paper, a PC-PMV motor with double-sided PM (PC-DPMV) motor is proposed. As shown in Fig. 1, a consequent-pole PM structure is employed on the rotor, and one PM is inserted in each slot between the split stator teeth. Thus, the total PM consumption of PC-DPMV motor is a little lower than that of the existing PC-PMV motor with a single-sided PM structure (PC-SPMV). By employing an unevenly split modulation tooth, two groups of PM flux density harmonics with different slot pitch angles can be generated and coupled with the PC winding. Thus, two operating modes before and after PC called M1 and M2 can be obtained by reconnecting the windings for both motors. Then, different output performances can be obtained to achieve high torque in M1 and good speed-widening capability in M2. The corresponding torque-speed curves by FEA and tests are shown in Fig. 2, in which the FEA results agree well with experimental results. Meanwhile, the proposed PC-DPMV motor shows a higher average torque in M1 and a larger operation region in M2 than its counterpart motor. More details will be presented in the full paper.

[1] Y. Du, Z. F. He, et al., *IEEE Trans. Ind. Electron.*, vol. 70, no. 6, pp. 6110–6120 (2023) [2] X. Zhao, and S. X. Niu, *IEEE Trans. Ind. Electron.*, vol. 64, no. 12, pp. 9943–9952 (2017)

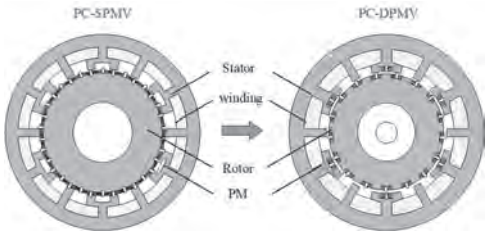

Fig.1. PC-PMV topologies.

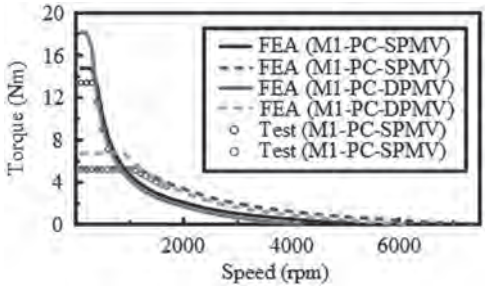

Fig.2. Torque-speed curves of the PMV motors by FEA and experiment.

VP7-12. Design and Optimization of Wireless Power Transfer Module for Electrically Excited Axial Flux Motor. *Y. Xin*[1], W. Geng[1], J. Liu[1], Y. Fu[1] and Y. Gu[1] *1. Nanjing University of Science and Technology, Nanjing, China*

I. Introduction Due to the advantages of rare-earth free composition and controllable excitation, the electrically excited synchronous motor (EESM) meets the requirements of electric drive system for low cost and wide speed regulation range [1] [2]. However, the traditional excitation system of EESM requires brush and collector ring to supply power to the excitation windings, which leads to the difficulty of compact structure design and problems such as wear and spark [3] [4]. In this paper, the brushless excitation on wound rotor is realized by the combination of the electrically excited axial flux motor (EEAFM) and the wireless power transfer (WPT). Through the design and optimization of the WPT module, the compact structure and low loss of brushless excitation are implemented. II. The working principle of WPT module in brushless excitation system of EEAFM The wireless excitation structure of the two-rotor single-stator EEAFM is shown in Fig. 1 (a). The WPT module acts as a rotating transformer, supplying power to the wound rotor. The magnetically coupled inductive WPT system adopts S-S compensation network structure, as shown in Fig. 1 (b). III. Design and optimization of WPT module Power level and volume should be considered in the design of coupler, which requires a complex multi-objective optimization. The 3-D model of the WPT module can be equivalent to the 2-D model shown in Fig. 2 (a). By changing the core thickness, air gap height and inner and outer diameter parameters of the core, the data are sorted out to obtain the calculation formula of inductance value, coupling coefficient and loss. The optimized WPT module is shown in Fig. 2 (b), and the specific design parameters are shown in Table 1. Under the requirements of the inductance value of 14 uH and coupling coefficient of 0.8, the inner and outer diameters of the WPT module are reduced to 42 mm and 77.4 mm, and the litz wire loss is reduced to 116.54 W. IV. Conclusion In this paper, by optimizing the key parameters of WPT module, a brushless EEAFM with low loss and compact size is designed.

[1] I. Boldea, L. N. Tutelea, and D. Dorrell, "Automotive Electric Propulsion Systems With Reduced or No Permanent Magnets: An Overview," IEEE Transactions on Industrial Electronics., Vol. 61, pp. 5696-5711, (2014) [2] W. Q. Chu, Z. Q. Zhu, and M. P. Foster, "Investigation on Operational Envelops and Efficiency Maps of Electrically Excited Machines for Electrical Vehicle Applications," IEEE Transactions on Magnetics., Vol. 51, pp. 1-10, (2015) [3] S. Müller, D. Maier, and N. Parspour, "Inductive electrically excited synchronous machine for electrical vehicles—design, optimization and measurement," Energies., Vol. 16, pp. 1657, (2023) [4] T. Raminosoa, R. H. Wiles and J. Wilkins, "Novel Rotary Transformer Topology With Improved Power Transfer Capability for High-Speed Applications," IEEE Transactions on Industry Applications., Vol. 56, pp. 277-286, (2020)

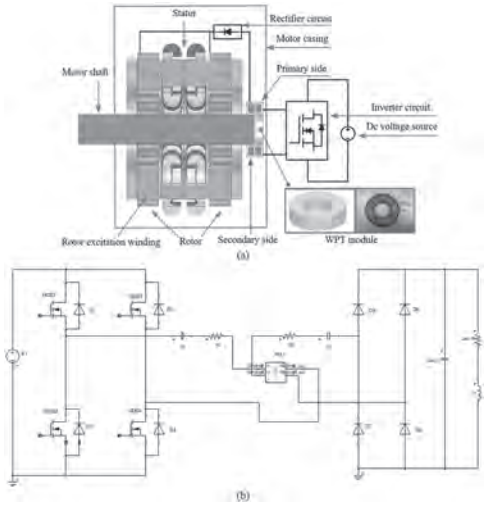

Fig.1. (a) The wireless excitation structure of the EEAFM. (b) Circuit model of WPT system.

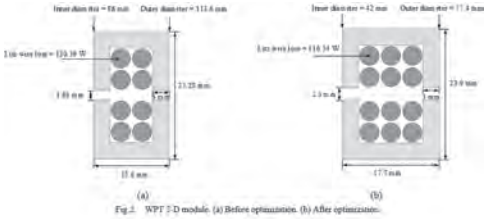

Fig.2. WPT 2-D module. (a) Before optimization. (b) After optimization.

TABLE I
Parameters of the WPT

Items	
Self-inductance value/uH	14
Coupling coefficient	0.8
Coil turns	6
Wire type	Litz wire
Wire diameter/mm	0.1
Strand number	575
Core material	TDK_PC90
Core thickness/mm	3
Inner diameter/mm	42
Outer diameter/mm	77.4
Axial height/mm	23.9
Air-gap height/mm	2.3
Litz wire loss/W	116.54
Core loss/W	1.41

Fig.2. WPT 2-D module. (a) Before optimization. (b) After optimization.

Session VP8
EMERGING COMPUTING SYSTEMS & MAGNETIC RECORDING
(Poster Virtual Session)

Sara Majetich, Chair
Carnegie Mellon University, Pittsburgh, PA, United States

VP8-01. Exploring the energy efficiency of MRAM-based Computing-in-Memory for DNN training. *S. Zhou*[1] and Y. Jiang[1]
1. Jiangnan University, Wuxi, China

As Deep Neural Networks (DNNs) are widely used in various AI applications, there is an increasing demand for energy efficiency and computational speed. Computing-in-Memory (CIM), as a potential solution, can significantly reduce the energy consumption and latency associated with data transmission by performing computation in memory. In this paper, the application of spintronics-based in-store computing methods in training DNNs is explored. Firstly, the fundamentals of spintronic devices and their potential application in nonvolatile storage are introduced. Subsequently, an architecture for in-store computation using spintronic devices is proposed, as shown in Fig. 1. This architecture is capable of efficiently performing computational tasks of neural networks at the storage level. The architecture can be used to accelerate the DNN training process and reduce the energy consumption for training by utilizing the parallel computing power and low energy consumption characteristics of spintronic devices. Based on the designed architecture, the effectiveness and the performance of the proposed in-store computation scheme are verified based on NeuroSim simulation platform. By conducting the standard DNN training task, it shows that the spintronic device-based in-store computation method is able to significantly reduce the energy consumption compared to SRAM- and PCM-based training with the same accuracy, as shown in Fig. 2. Finally, the challenges and future research directions for in-store computational methods based on spintronic devices are discussed. These challenges include aspects of device fabrication and consistency, architecture scalability, and algorithm optimization. In conclusion, the potential and advantages of in-store computing methods based on spintronic devices in training deep neural networks are demonstrated by the theoretical analysis and the experimental validation. This research provides valuable reference and guidance for future efficient AI hardware design and development.

Doevenspeck J, Garello K, Verhoef B, et al. "SOT-MRAM based analog in-memory computing for DNN inference." IEEE Symposium on VLSI Technology. IEEE, 2020. Yu Pan, Peng Ouyang, Yinglin Zhao. et al. "A multilevel cell STT-MRAM-based computing inmemory accelerator for binary convolutional neural network." IEEE Transactions on Magnetics, vol. 54, no. 11, pp. 1-5, 2018. Q. Dong, Mahmut E. Sinangil, Burak Erbagci. et al., "A 351TOPS/W and 372.4 GOPS compute-in-memory SRAM macro in 7nm FinFET CMOS for machine-learning applications." IEEE International Solid-State Circuits Conference (ISSCC), 2020. Peng X, Huang S, Luo Y, et al. "DNN+ NeuroSim: An end-to-end benchmarking framework for compute-in-memory accelerators with versatile device technologies." IEEE international electron devices meeting (IEDM), 2019.

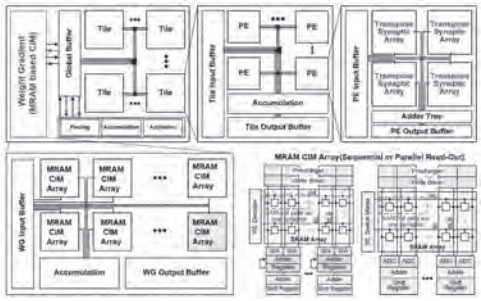

Fig. 1: MRAM-based Computing-in-Memory architecture scheme

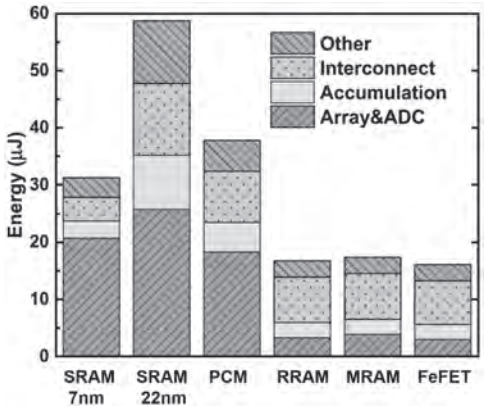

Fig. 2: Energy consumption of Computing-in-Memory based on various types of memories in the training of DNNs

VP8-03. Experimental Demonstration of Reliable Probabilistic Switching in SOT-MRAM. *C. Fu*[1], Z. Liu[1], J. Liu[1], S. Lu[1], H. Zhang[1], W. Li[1], J. Lu[1] and S. Peng[1] *1. Fert Beijing Institute School of Integrated Circuit Science and Engineering, Beihang University, Beijing, China*

Magnetic Random-Access Memory (MRAM) represents a promising candidate for the next generation of memory devices due to its high speed, non-volatility, and impressive storage density. Within the MRAM family, spin-orbit torque MRAM (SOT-MRAM) offers several key features, including the separation of read and write channels, non-destructive read and write operations, and endurance of up to 10^{15} cycles [1-4]. Notably, SOT-MRAM exhibits robust probabilistic switching characteristics, allowing precise control of the writing probability based on the magnitude of the writing SOT current. Consequently, SOT-MRAM holds significant potential across probability-related fields, including applications in probabilistic binary neural networks (PBNNs) and true random number generators [5-7]. In this paper, we fabricate elliptical magnetic tunnel junctions based on W/CoFeB/MgO/CoFeB on an 8-inch wafer (Fig. 1a). Remarkably, our SOT-MRAM devices achieve reliable switching even with pulses as short as 2ns (Fig. 1b). Furthermore, we measure the tunnel magnetoresistance ratio (TMR) in over 100 randomly selected devices, observing an approximately normal distribution. Notably, the minimum TMR exceeded 69%. To assess endurance, after over 10^{11} read-write cycles we find that resistance fluctuations remain below 3%.

We also perform curve fitting for probabilistic switching, yielding a thermal stability factor of 68.5 ± 5.6 (Fig. 2a). Subsequently, we analyze the probabilistic switching performance by testing 8 randomly selected devices from the wafer (Fig. 2b). These devices consistently exhibit excellent and stable probabilistic switching behavior, with minimal differences among multiple devices. These findings demonstrate the strong performance and consistent probabilistic characteristics of the SOT-MRAM devices fabricated in our study, highlighting their potential for large-scale applications.

[1]L. Liu, C. Pai and Y. Li, Science., Vol. 336, p.555-558(2012) [2]J. Lu, W. Li and J. Liu, Appl. Phys. Lett., Vol. 122, no.1, Art. no.012402(2023) [3]W. Li, Z. Liu and S. Peng, IEEE Electron Device Lett., Vol. 45, no.5, p.921–924(2024). [4]S. Peng, D. Zhu and W. Li, Nat. Electron., Vol. 3, p.757–764(2020) [5]R. Zhang, X. Li and M. Zhao, Adv. Sci., Vol. 11, no.23, p.2402182(2024) [6]H. Zhang, Y. Sun and K. Hu, J. Semicond., Vol. 43, no.10, p.102501(2022) [7]J. Yin, Y. Liu and B. Zhang, in Proc. IEEE Int. Electron Devices Meeting., p.36.1.1-36.1.4(2022)

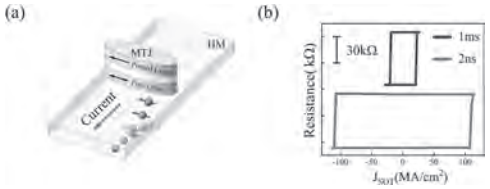

Fig.1 (a)Schematic of SOT-MRAM. (b)SOT-driven switching curve with 1ms and 2ns pulse width.

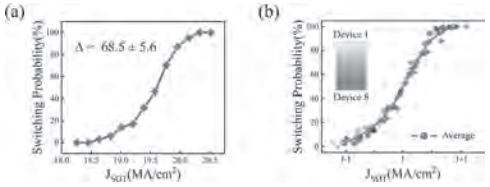

Fig.2 (a)Switching probability under various write voltages. (b)Probabilistic switching curves from 8 randomly selected devices on the wafer.

VP8-04. Magnetization Transition in Dual-Layer Heat-Assisted Magnetic Recording. *Y. Jian*[1], V. Lomakin[2], K. Luo[1] and J. Chen[1] *1. Huazhong University of Science and Technology, Wuhan, China; 2. University of California San Diego, La Jolla, CA, United States*

Three-dimensional magnetic recording (3DMR) has recently been introduced as a novel solution that promises to far exceed the capacity of existing hard disk drive (HDD) products [1,2]. The multi-layer recording medium of 3DMR presents various new challenges, one of which will be more complex magnetization transitions. In this work, the magnetization transitions and their associated noise in a dual-layer heat-assisted magnetic recording (HAMR) system are investigated and discussed via micromagnetic simulation. Dual-layer FePt-based nanogranular films [3] are modeled and the two-pass writing process under HAMR is simulated by solving the Landau-Lifshitz-Bloch (LLB) equation on MARS [4]. At the first pass, both layers are heated beyond their Curie temperatures. Their magnetization polarities are all aligned with the direction of the applied field. At the second pass, the peak temperature of the thermal field is higher than the Curie temperature of the top layer but lower than that of the bottom layer. Only the magnetization state of the top layer will be changed. Fig. 1 shows the variation of each layer's magnetization distribution between the two passes when writing the transition pattern that is denoted as [01,10] (in terms of adjacent bit-pairs [B_x^{top} B_x^{bottom}, B_y^{top} B_y^{bottom}]). The medium signal-to-noise ratio (SNR) is calculated from the obtained magnetization of 6 possible transition patterns, as shown in Fig. 2. The results indicate that, in addition to grain distribution and thermal fluctuation, the final SNR seems to depend on the number of times and the sequence in which the magnetization states are switched during the two-pass writing, explaining why the opposite transitions in the dual layers bring the most severe noise.

[1] E. Roddick, M. Kief, and A. Takeo, in 2022 IEEE 33rd Magnetic Recording Conference (TMRC), pp. 1–2 (2022). [2] S. Greaves, J. Magn. Magn. Mater., vol. 588, p. 171343 (2023). [3] P. Tozman, S. Isogami, I. Suzuki et al, Acta Mater., vol. 271, p. 119869 (2024). [4] S.E. Rannala, A. Meo, S. Ruta et al, Comput. Phys. Commun., vol. 279, p. 108462 (2022).

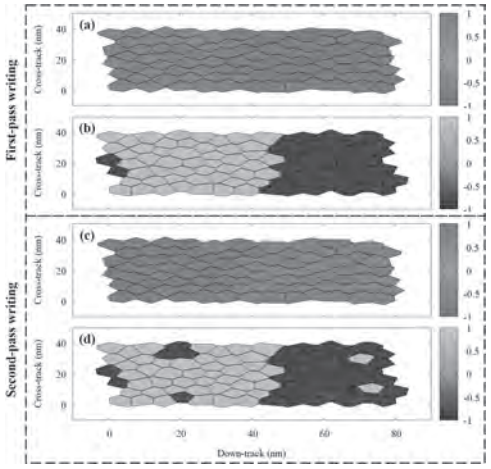

Fig. 1. In-plane magnetization distribution of the dual-layer recording medium after the first-pass writing (a,b) and the second-pass writing (c,d) when the transition pattern is [01,10]. Red/blue legends (a,c) and yellow/purple legends (b,d) represent the top and bottom layers, respectively.

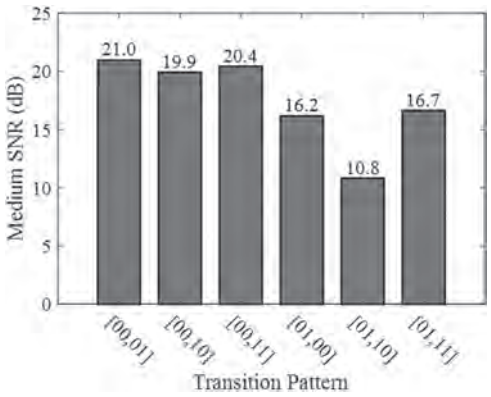

Fig. 2. Medium SNR corresponding to various transition patterns written in the double-layer recording medium.

VP8-05. A Study on Applying GA for Performance Improvement of SP Decoder in SMR. *M. Nishikawa*[1], Y. Nakamura[1], Y. Kanai[2] and Y. Okamoto[1] *1. Matsuyama, Japan; 2. Niigata Institute of Technology, Kashiwazaki, Japan*

We previously investigated low-density parity-check (LDPC) coding and iterative decoding methods for shingled magnetic recording (SMR) in hard disk drives (HDDs). In sum-product (SP) decoding, we evaluate the log-likelihood (LLR) for check nodes and external information using parity check information [1], and realize that performance could be improved by multiplying the LLR by a weight based on the results. Furthermore, we explore the weights by applying the genetic algorithm (GA) to improve the decoding performance. We use the same read/write system except for the SP decoder shown in [2] in the study and assume an areal recording density of 4 Tbits/inch^2. We use the LLR related to message node calculation in the SP decoding [2]. The neural network inputs the LLRs for the target and its adjacent bits to consider the influence of noise depending on the recording pattern. Also, the reliable LLR chosen based on the result of the neural network is updated to realize effective iterative decoding. In the study, we explore the weight based on the parity check information "0", "1", "2", and "3" [1] to be multiplied by the LLR for the check nodes and external

information by applying the GA shown in Figure 1. Here, the fitness of the *l*th individual in the δth generation is defined by $f_{\delta l} = -\log_{10}\mathrm{BER}_{SP}$ [2]. BER_{SP} (bit error rate) is calculated by comparing the recorded sequence with the hard decision sequence after turbo equalization. We arrange the weights in one dimension as one chromosome and perform the selection, crossover, and mutation [3]. However, the individuals with the highest fitness are left by applying the elitist preserving selection [3]. Figure 2 shows the BER performance for SNR_S (signal-to-noise ratio), where $x_h = 0.4$, $N_t = 15$, $i_{sp} = 6$, and $i_{global} = 23$ [2]. When we do not apply GA to explore the weights, we refer to the cases with and without the neural network in [2] as conventional methods 1 and 2, respectively. We clarified by Fig. 2 that the proposed method achieved error-free at $\mathrm{SNR}_S = 21.0$ dB, and improved the required SNR for error-free decoding by 0.5 and 2.5 dB compared with conventional methods 1 and 2, respectively.

[1] M. Nishikawa, Y. Nakamura, H. Osawa, Y. Okamoto, Y. Kanai, and H. Muraoka, "A study on iterative decoding with LLR modulator by parity check information in SMR system," *IEEE Trans. Magn.*, vol.54, no.11, 3001304, Nov. 2018. [2] M. Nishikawa, Y. Nakamura, Y. Kanai, and Y. Okamoto, "Improvement of SP decoding considering the influence of recording patterns by neural network in SMR," *IEEE Trans. Magn.*, 2024 (to be published). [3] David E. Goldberg, *Genetic algorithms in search, optimization, and machine learning*, Addison-Wesley, Boston, pp.59–87.

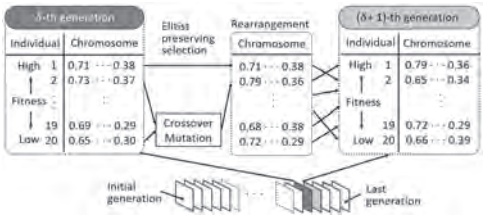

Fig. 1: Concept of GA to explore the weights.

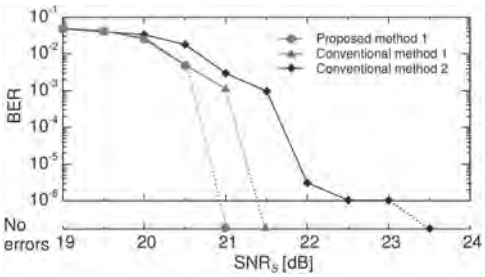

Fig. 2: BER performance for SNR_S.

VP8-06. Time dependence of signal-to-noise ratio for recording media designed for microwave-assisted magnetic recording. *T. Tanaka*[1], S. Onaka[1], S. Kashiwagi[1], X. Ya[2] and Y. Kanai[3] *1. ISEE, Kyushu University, Fukuoka, Japan; 2. Artificial Intelligence and Big Data College, Chongqing College of Electronic Engineering, Chongqing, China; 3. Department of Engineering, Niigata Institute of Technology, Kashiwazaki, Japan*

Microwave-assisted magnetic recording (MAMR) [1] has attracted as one of the promising next-generation ultra-high-density recording technologies of hard disk drives. Layer anisotropy structured media, such as notched type structures have been proposed [2] for improving MAMR writability. Magnetization switching of notched structured media follows incoherent process, so the nudged elastic band calculations are necessary to evaluate magnetization thermal stability of the magnetizations of the magnetic grains. This study employed 12-nm-thick 4-layered-stacked-media (4-2-2-4 nm) designed for MAMR. Averaged medium H_k and M_s were 26 kOe and 800 emu/cc, respectively. Average grain size $\langle D\rangle$ was 5 nm. The corresponding K_uV/k_BT@ 300K was 58. 16 dB of SNR without wide writing was obtained for MAMR simulations with the 30-nm-track-wide SPT head and 22 GHz [3] of microwave field generated by 30×30×10 nm^3 of a spin torque oscillator. Figure 1 and 2 indicate time dependence of SNRs in terms of standard deviations of the grain size, $\sigma(D)$. Here, ideal recorded bit patterns were artificially defined to evaluate magnetization thermal stability and the thermal stability indexes $\Delta E/k_BT$@300K were estimated using the nudged elastic band calculations. Time dependences of magnetization switching probability for magnetic grains were estimated using the Arrhenius-Néel law and the resultant SNRs were plotted as a function of storage time. In the case of $\sigma(D)/\langle D\rangle = 0.15$, SNRs just after recording tend to be slightly higher than those for $\sigma(D)/\langle D\rangle = 0.10$, but SNRs decrease faster for all the linear density signals. On the other hand, high SNRs retained relatively long period of time for high linear density signals for $\sigma(D)/\langle D\rangle = 0.10$, and the SNRs abruptly decrease at the specific time. The reductions of the SNR at 5 years are significant, which imply that magnetizations of the grains need to be thermally much stable.

[1] J.-G. Zhu, X. Zhu, Y. Tang, IEEE Trans. Magn. 44 (2008) 125-131. [2] X. Bai, J. Zhu, IEEE Magn. Lett. 7 (2016) 4507904. [3] Y. Kanai, R. Itagaki, S.J. Greaves, H. Muraoka, IEEE Trans. Magn. 55 (2019) 300061

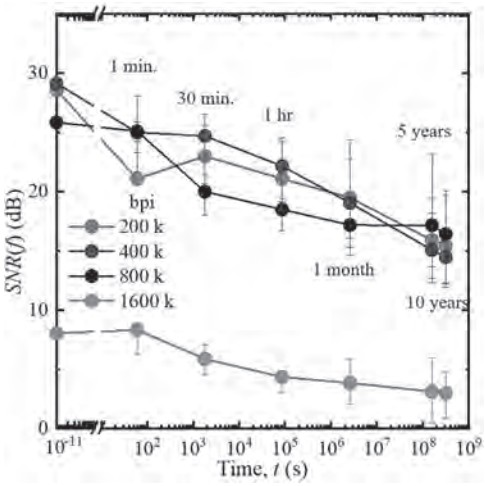

Fig. 1: Time dependence of SNRs for the media with $\sigma(D)/\langle D\rangle$=0.15.

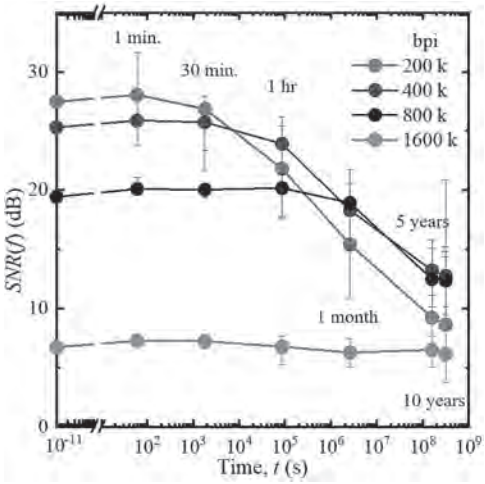

Fig. 2: Time dependence of SNRs for the media with $\sigma(D)/\langle D\rangle$=0.10.

VP8-07. Reynolds Number in Electrodynamics. *Y. Lunin*[1] *1. retired, retired, Kherson, Ukraine*

ABSTRACT In this work: - the electric charge definition is formulated; - the refined formula of the electric charge non-invariance is given; - the concept of "the charged particle spin" is clarified; - the electric charge momentum conservation law is obtained; - the angular momentum conservation law for electric charge is obtained; - the formula for the kinetic energy of the translational motion of an electric charge is constructed; - Steiner's theorem

for electrodynamics is formulated; - the rotational motion dynamics equation is constructed for electric charge; - the formula for the kinetic energy of the rotational motion of an electric charge is constructed; - a Planck's formula analog for the magnetic field was obtained; - another kind of uncertainty relation was obtained; - formula for the interval between two events is constructed in the electric charge space; - a Reynolds number analog for electromagnetism is obtained; - the experiments results on finding the Reynolds number in electrodynamics are given. Key words: *the electric charge non-invariance, the angular momentum of electric charge, the kinetic energy of the rotational motion of an electric charge, a Planck's formula for the magnetic field, a Reynolds number in electrodynamics.*

VP8-08. Binary neural networks with giant conductance changes in $Co_2MnSi/MgO/Co_2MnSi$ magnetic tunnel junctions. R. Kusunose[1], *T. Marukame*[1] and T. Uemura[1] *1. Hokkaido University, Sapporo, Japan*

With the growth of generative AI such as large-scale language models (LLMs), there is a global concern about their environmental impact due to high energy consumption [1, 2]. Recently, LLM models have been investigated for efficient computation using vector matrix multiplications (VMMs) of neural networks (NNs) represented as binary -1/+1 weights [1, 2]. However, binary hardware with realistic memory cells has yet to be implemented in LSI. In this study, we focus on $Co_2MnSi/MgO/Co_2MnSi$ magnetic tunnel junctions (MTJs) [3], whose conductance corresponds to binary weights, and analyze binary NN computation. Conventional VMMs have used resistance change devices, such as ferroelectric tunnel junctions, due to their multilevel resistances [4]. In contrast, MTJs are generally stabilized at two values. A pair of the resistance change devices can be used to represent binary values in analog circuits [5]. To use binary (-1/+1) signals in the circuits, the rate of the conductance change should be high. Figure 1 shows conductance-voltage characteristics of our $Co_2MnSi/MgO/Co_2MnSi$ MTJ, indicating huge conductance changes for binary states. The tunnel magnetoresistance ratio was 362% at room temperature, which is due to a halfmetallic property of Co_2MnSi and a coherent MgO tunnel barrier, along with linear regions. In NN learning, connection weights between neurons are iteratively updated during learning and then used for inference. We assume the MTJs (Fig. 1) as binary connections with weights of -1/+1 when used in NN. The NN simulation with MNIST handwritten digits results show the inference accuracy of binary NN during and after learning (Fig. 2). We further propose the learning protocol using binary values in the early epochs and continuous values after that. Thus, we confirmed that the accuracy is improved due to the unique weight distribution, suggesting the feasibility of the MTJs with giant conductance changes for VMM applications.

[1] H. Wang, et al., arXiv:2310.11453 (2023) [2] S. Ma, et al., arXiv:2402.17764 (2024) [3] H-x, Liu, et al., Appl. Phys. Lett. 101(13), 132418 (2012) [4] R. Berdan, T. Marukame, et al., Nature Electronics 3, 259 (2020) [5] T. Marukame, et al., Jpn. J. Appl. Phys. 59, 040606 (2020)

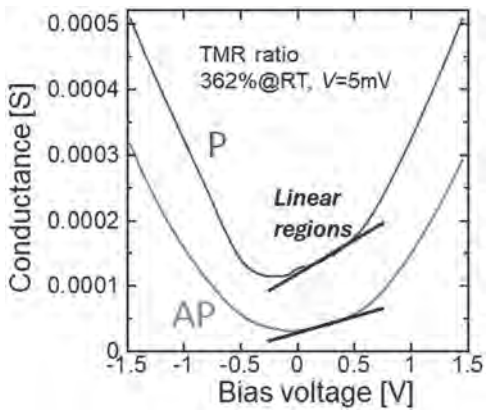

Fig. 1 Conductance curves in a $Co_2MnSi/MgO/Co_2MnSi$ MTJ. P/AP: parallel/antiparallel magnetization configurations. Solid black lines show fitted linear regions.

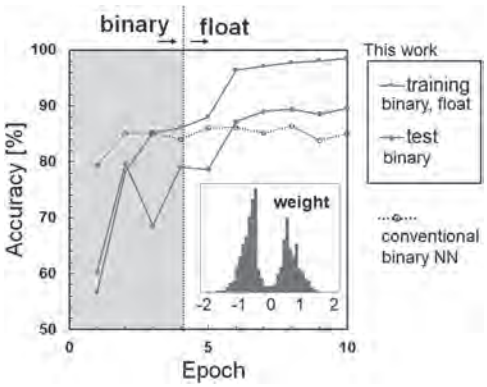

Fig. 2 Simulations of neural networks with binary and floating-point weights. The inset shows the weight distribution after training.

VP8-09. Transient Magnetic Field Optimization for Stable Entanglement in Spin Dimers. *J. Wang*[1] and J. Krause[2] *1. University of Michigan, Northville, MI, United States; 2. Northville High School, Northville, MI, United States*

Quantum entanglement, a core element of quantum information and computation, involves particles sharing a collective wave function and influencing each other even over great distances. This paper introduces optimized time-varying magnetic field functions designed to stabilize and enhance entanglement in a decoherence-free Heisenberg spin dimer. It explores how magnetic field affects coherence and population terms in the density matrix, showing that optimized transient magnetic fields can eliminate natural oscillations in entanglement and thus maximize its stability. These findings offer valuable insights into the nature of the magnetic field solutions and the system's progression toward a stable entangled state. Understanding how time-varying magnetic field can sustain a nearly perfect entangled state in Heisenberg spin chains is essential for advancing potential quantum computing applications.

[1] Ren. Ground-to-satellite quantum teleportation. Nature. 2017;549: 70–73. [2] Groisman B, Strelchuk S. Optimal amount of entanglement to distinguish quantum states instantaneously. Phys RevA. 2015;92:052337. doi:10.1103/PhysRevA.92.052337 [3] ArnesenMC, Bose S, Vedral V. Natural thermal and magnetic entanglement in the 1D Heisenberg model. Phys Rev Lett. 2001;87:017901. doi:10.1103/PhysRevLett.87.017901 [4] Wang J, Landman M, Sutter T, et al. Entanglement evolution in a Heisenberg spin dimer. IEEE Trans Magn. 2019;55(12):1–3. [5] Hill S, Wootters WK. Entanglement of a pair of quantum bits. Phys Rev Lett. 1997;78: 5022–5025. doi:10.1103/PhysRevLett.78.5022

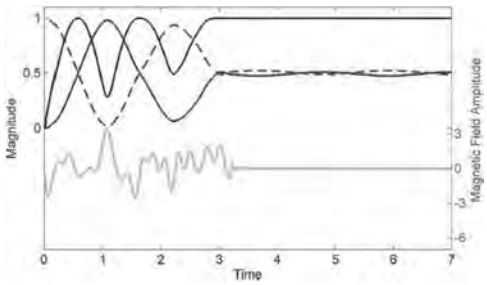

Fig. 1: The excited state is represented as a sinusoidal solid (blue) line while the ground state is a dashed (blue) line. The entanglement is represented by the rectified sinusoidal solid (black) line. The bottom solid (green) line varies according to the time-varying magnetic field from the first trial solution. The horizontal axis represents the passage of time. The spin dimer system starts out initially in the ground state.

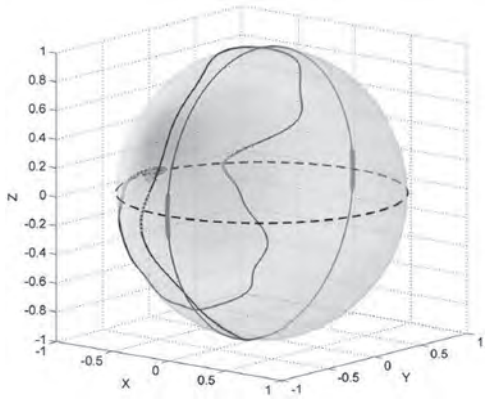

Fig. 2: The Bloch Sphere diagram shows the spin dimer's state evolution under time-invariant and time-varying magnetic fields. For the constant field, the green circle shows oscillation between states, with purple markers indicating maximum entanglement. For the time-varying field, the irregular blue line traces the state evolution, with bright green segments showing near-maximal entanglement. The red cross marks the transition to a constant field, and the small green circle represents the stabilized entangled state.

Session VP9
HARD MAGNETS
(Poster Virtual Session)

H. Sepehri-Amin, Chair
National Institute for Materials Science (NIMS), Tsukuba, Japan

VP9-01. Composition Design of Sintered Sm_2Co_{17}-type Magnets with High Magnetic Properties and Remanence Temperature Stability. *Z. Long*[1], C. Zhang[2], Y. Teng[3], C. Ling[1], Y. Kang[1], B. Zhang[2], H. Zhang[1], Y. Li[1] and M. Yue[1] *1. College of Materials Science and Engineering, Beijing University of Technology, Beijing, China; 2. Hangzhou Kede Magnetic Components Co., Ltd, Hangzhou, China; 3. Guangdong Ocean University, Yangjiang, China*

The Sm_2Co_{17}-type permanent magnets exhibit exceptionally high coercivity and excellent temperature stability, thus widespread applications in critical fields such as microwave communication, precision instruments, and high-temperature motors. The advancement in corresponding application fields has imposed greater demands on the temperature stability and magnetic properties. In this study, the composition design were carried out to prepare $(Sm,Er)(Co,Fe,Cu,Zr)_z$ magnets with high magnetic properties and remanence temperature stability. Also, the impact of Er substitution for Sm on the magnetic properties and microstructure of 2:17-type magnets and the associated mechanisms were investigated. Experimental results indicate that with increasing Er substitution, the magnetic properties of the magnets gradually decline, accompanied by a significant increase in the remanence temperature coefficient. When the Er substitution reaches 60%, the comprehensive performance is optimal, with remanence of 8.81 kG, coerocvity of 30.01 kOe, while maintaining a near zero temperature coefficient of remanence within the range of 20-150 °C. X-ray diffraction refinement and first-principles calculations reveal that Er initially substitutes for Sm at the 2b crystallographic site in 2:17H phase, thereby increasing the resistance to basal plane slip and atomic diffusion. Consequently, raising the energy barrier for the transformation from the 2:17H phase to the 2:17R phase, resulting in an increase in the 2:17H phase content. TEM results disclose that as the Er substitution increases, the cellular structure morphology was gradually deteriorated, and the Cu-enrichment and continuity of the 1:5 phase was weakened, and ordering-degree of intracellular phase also decreased, thereby reducing the coercivity. Our findings can provide reliable references for the development of SmCo magnets with high remanence temperature stability.

VP9-02. Adjusting initial mixing and calcination processes to prepare high-performance strontium ferrite magnets. H. Muhammad[1], *Y. Li*[1], H. Zhang[1], L. Rongming[2] and M. Yue[1] *1. Beijing University of Technology, Beijing, China; 2. BGRIMM Technology Group Co Ltd, Beijing, China*

In the preparation technology of permanent magnet ferrite, initial mixing and calcination are crucial for achieving high magnetic properties. This work investigated the effects of different initial mixing methods and calcination temperatures on the magnetic properties and microstructure of ferrite. Results show that dry mixing at 1260 °C produces the largest magnetic energy product (35.4 kJ/m^3) when sintered at 1225 °C, with a maximum remanence of 437 mT and coercivity of 384 kA/m. Conversely, wet mixing at 1230 °C produces the optimal magnetic performance as a coercivity of (415 kA/m), remanence of (435 mT) and $(BH)_{max}$ of 33.4 kJm^{-3} at a sintering temperature of 1215 °C. Wet mixing is better for low-temperature calcination due to reduced particle size, greater specific surface area, and lower energy needs. The dry mixing technique at 1260 °C and the wet mixing process at 1230 °C yield good magnetic characteristics for La-Ca-Co doped strontium ferrite. While dry mixing produces a higher total energy product, wet mixing is superior when operating at lower sintering temperatures.

Wang, Siyuan, et al. "High coercivity in Sm-doped SrFe12O19 powders with spherical morphology prepared by ultrasonic spray pyrolysis." *Ceramics International* 50.6 (2024): 9510-9519. Lee, Jimin, et al. "Anisotropic characteristics and improved magnetic performance of Ca–La–Co-substituted strontium hexaferrite nanomagnets." *Scientific reports* 10.1 (2020): 15929.

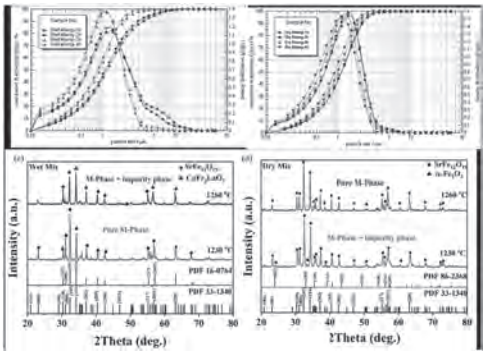

Fig. 1. Laser particle size graphs of a) wet and b) dry mixed samples a) XRD pattern of the ball milled powder calcined at 1230°C and 1260°C a) wet mixed b) dry mixed, both for 4h mixing time

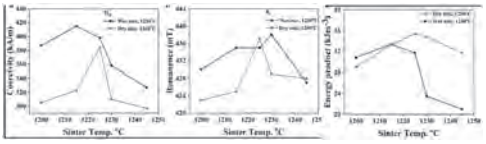

Fig. 2. Coercivity, remanence and energy product comparison graphs of dry and wet mixed samples calcined at1230°C and 1260°C

VP9-03. Magnetic properties, interaction and magnetic hardening of nanocrystalline $PrCo_5$/NdFeB hybrid magnets. J. Zuo[1], *W. Lu*[1], Y. Bo[1], C. Li[1], M. Zhang[1], Y. Liu[1], S. Bai[1], F. Liu[1] and Y. Li[2] *1. School of Science, Inner Mongolia University of Science and Technology, Baotou, China; 2. Instrumental Analysis Center, Inner Mongolia University of Science and Technology, Baotou, China*

The magnetic properties, interaction and magnetic hardening of nanocrystalline $PrCo_5$/NdFeB hybrid magnets were investigated. Mixtures of $PrCo_5$ and $Nd_xFe_{14}B$ (x=1.8, 2.0, 2.2) were prepared with $PrCo_5$/NdFeB wt. ratio ranging from 1:0.06 to 1:0.15, and then were ball milled for 5 h in a high-energy ball mill. The as-milled powders were hot compacted at 973 K under 500 MPa using spark plasma sintering. The crystal structure of the magnets was examined by XRD; the magnetic hysteresis loops were measured by VSM with a maximum magnetic field of 3 T. The optimal wt. ratio of $PrCo_5$/NdFeB was determined as follows: $9\%PrCo_5/Nd_{2.2}Fe_{14}B$,$9\%PrCo_5/Nd_2Fe_{14}B$ and $15\%PrCo_5/Nd_{1.8}Fe_{14}B$. The XRD Bragg peaks were identified as belonging to the 2:14:1 phase, 1:5 phase and Fe phase. The recoil loops tests showed all these three hybrid magnets had closed loops, indicating complete reversible behavior; the recoil loops were open and the openness indicated there was an irreversible magnetization during the measurement process. The normalized ratio $\Delta M_{rc}(H)=[M_{up}(H)-M_{dw}(H)]/Ms$ was used to quantitatively characterize the openness of recoil loops (Fig. 1), it was found that $\Delta M_{rc}(H)$

increased with increasing amount of Nd content, therefore, one can conclude that the recoil loop openness was related to composition of nanocomposite hybrid magnets. Therefore 9%$PrCo_5$/$Nd_{2.2}Fe_{14}B$ was dominated by exchange coupling interactions; 9%$PrCo_5$/$Nd_2Fe_{14}B$ and 15%$PrCo_5$/$Nd_{1.8}Fe_{14}B$ intergranular interactions were dominated by long-range static magnetic interactions. The δm plots showed the exchange coupling in 9%$PrCo_5$/$Nd_{2.2}Fe_{14}B$ was very strong, the positive part of δm(H) was far higher that of negative part; δm of 15%$PrCo_5$/$Nd_{1.8}Fe_{14}B$ drop to negative values indicating that magnetostatic interactions become dominant. To verify the coercivity mechanism, minor loops were tested and normalized coercivity and remanence on different applied fields in the minor loops were studied. Asymmetric were observed when the applied field was lower than the intrinsic coercivity; the normalized coercivity increases faster than remanence, which is the evidence for the dominant role of pinning mechanism on the coercivity of three hybrid magnets.

[1]Rong C, Liu Y, Liu J P. Do thermal fluctuations influence the recoil loops of nanocomposite magnets? [J]. Applied Physics Letters, 2008, 93(4): 042508. [2]Rong C, Liu J P. Grain boundary contribution to recoil loop openness of exchange-coupled nanocrystalline magnets [J]. Applied Physics Letters, 2009, 94(17): 172510. [3]Minmin Li, Jianhua Zuo, Yongjie Hou, Bo Yu, et al. Interaction and Magnetic Properties of NdCeFeB Melt-spun Ribbons [J]. Rare Metal Materials and Engineering. 2023.

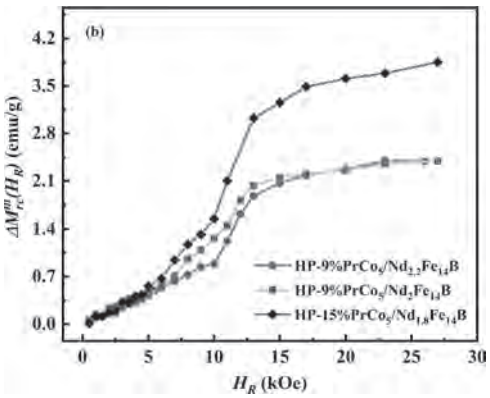

VP9-04. Magnetic properties in bulk nanocrystalline $Nd_{1.8}Fe_{14}B/PrCo_5$ magnet prepared by hot deformation. *J. Zuo*[1], W. Lu[1], Y. Bo[1], C. Li[1], M. Zhang[1] and Y. Li[1] *1. School of Science, Inner Mongolia University of Science and Technology, Baotou, China*

Bulk anisotropic nanocrystalline $Nd_{1.8}Fe_{14}B/PrCo_5$ magnet had been prepared by hot deformation method. The $Nd_{1.8}Fe_{14}B$ and $PrCo_5$ melt-spun ribbons were uniformly mixed at a mass ratio of 1:0.15 and then were subjected to high energy ball milling for 5 hours. The as-milled powders were hot pressed and hot deformed with height reduction of 70–90%. The crystal structure was studied by XRD; magnetic measurement of the hot compacted and hot deformed magnets were carried out in a VSM with a maximum magnetic field of 3T. For the hot deformed magnets, the intensity of *(00l)* diffraction peaks become stronger compared to the hot pressed sample and the bigger the height reduction of the magnets the stronger of the intensity of (00l) peaks in the patterns. The coercivity of the hot compacted and hot deformed magnets decreased with increase the height reduction; the remanence increased first, then decreased, peaked at 70% height reduction. The normalized ratio $\Delta M_{rc}(H)=[M_{up}(H)-M_{dw}(H)]/Ms$ was used to quantitatively characterize the openness of recoil loops (Fig. 1). The maximum $\Delta M_{rc}(H)$ in each recoil loop was defined as$\Delta Mm\ rc(H)$. Peaks of $\Delta Mm\ rc(H)$ were observed for the magnet with 80% height reduction, while there were no peaks for the hot pressed and the other height reduction magnets. The appearance of the peak and the applied fields at which the peak appeared may be related to the magnetization behavior. The δm plots showed the hot deformed magnets had large negative δm peaks, indicateing that for the hot deformed magnets magnetostatic interactions dominated the intergranular interaction. Minor loops were tested and normalized coercivity and remanence on different applied fields in the minor loops were studied. Asymmetric were observed when the applied field was lower than the intrinsic coercivity; with the increase of the applied field, the asymmetry phenomenon gradually disappeared, indicating that the coercivity mechanism of the hot-deformed magnets was the pinning mechanism; the normalized coercivity increased faster than remanence, which was the evidence for the dominant role of pinning mechanism on the coercivity.

[1] M. Yue, J. H. Zuo, W. Q. Liu. Magnetic anisotropy in bulk nanocrystalline SmCo5 permanent magnet prepared by hot deformation. JOURNAL OF APPLIED PHYSICS 109, 07A711 (2011) [2] Rong C, Liu Y, Liu J P. Do thermal fluctuations influence the recoil loops of nanocomposite magnets?. Applied Physics Letters, 2008, 93(4): 042508.

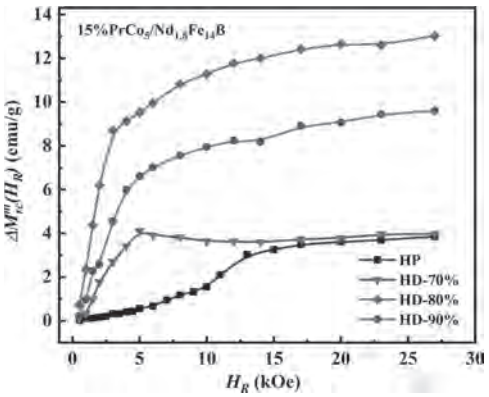

Fig. 1: Dependence of $\Delta mrc(H_R)$ on the maximum applied field H_R

VP9-05. Magnetic properties of Fe-Pt/Pr-Fe-B/Fe-Pt tri-layered thin sheet magnets. *K. Okamura*[1], A. Yamashita[1], T. Yanai[1], C. Qi[2], K. Nagai[2], T. Shinshi[2], H. Fukunaga[1] and M. Nakano[1] *1. Nagasaki university, Nagasaki, Japan; 2. Tokyo Institute of Technology, Yokohama, Japan*

The miniaturization of Fe-Pt magnets with excellent biocompatibility is required to develop the performance of a medical devices [1]. Several researchers studied Fe-Pt bulk magnets via a cold rolling and a rapidly quenching method [2][3][4]. We recently reported Fe-Pt thin sheets prepared by taking advantage of the exfoliation behavior after depositing Fe-Pt films on Si substrates using a laser ablation technique [5]. This contribution reports the preparation of Fe-Pt/Pr-Fe-B/Fe-Pt tri-layered thin sheet magnets to explore an advanced magnetic material. Fe-Pt and Pr-Fe-B magnets were fabricated using a Nd-YAG laser (wavelength: 355 nm, frequency: 30 Hz) in a vacuum atmosphere of approximately 1×10^{-4} Pa. After depositing a three-layer structure of Fe-Pt/Pr-Fe-B/Fe-Pt in-situ, the sample was peeled off from a Si substrate. An as=deposited sample was annealed by using two method of CA (Conventional annealing) and PA (Pulse annealing) to transform a disordered A1 (fcc) structure of Fe-Pt crystalline phase to an ordered L10 (fct) one and crystallize an amorphous phase of a Pr-Fe-B layer. Figure shows J-H loops of two tri-layered samples annealed by each method of CA and PA. Here, the film thicknesses of each sample were fixed at approximately 50 μm. Coercivity exceeding 300 kA/m could be obtained in the two thin sheet magnets and a PA method (solid line) was effective to obtain higher values of coercivity and remanence. In the present stage, the coercivity values of a single layer Fe-Pt sheet and an Fe-Pt/Pr-Fe-B/Fe-Pt tri-layered sheet (PA method) were almost the same, therefore further investigation such as optimization of annealing condition is required to improve magnetic properties in the tri-layered sample.

[1] A. Yamazaki, et al., J. Magn. Magn. Mater., Vol. e1741, p. 272(2004). [2] K. Watanabe et al., J. Japan Inst. Metals, Vol. 47, p. 699(1983). [3] N. H. Hai et al., J. Magn. Magn. Mater. Vol. 262, p. 353(2003). [4] T. Bitoh et al., Scripta Materialia Vol. 53, p. 429 (2005). [5] M. Nakano et al., AIP Advances Vol. 12, p. 035232 (2022).

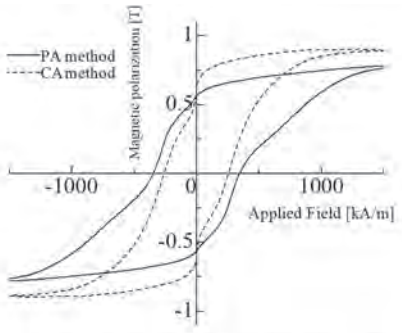

Figure J-H loops of Fe-Pt/Pr-Fe-B/Fe-Pt tri-layered thin sheet magnets annealed by CA and PA methods, respectively.

Fig. 1

VP9-06. Ba-substituted Sr hexaferrites for microwave absorber application: Structural & magnetic properties. *S. Kaushik*[1], M. Dabla[1], M. Sharma[1,2] and B.K. Kuanr[1] *1. Special Centre for Nanoscience, Jawaharlal Nehru University, New Delhi, India; 2. Department of Physics, Deshbandhu College, New Delhi, India*

We report the microwave absorption properties of $Ba_xSr_{1-x}Fe_{12}O_{19}$ hexaferrites nanoparticles (x=0.0,0.1,0.5,1.0) synthesized via auto-combustion sol-gel method for K_u band (12 GHz - 18 GHz). Prepared nanoparticles were characterized by techniques such as XRD, SEM-EDX, VSM and microwave measurements using vector network analyzer (VNA). XRD pattern matched with the space group $P6_3/mmc$ of magneto-plumbite hexagonal crystal structure [Fig. 1(A)]. The lattice parameters and crystallite size were observed to increase initially with Ba substitution and decreased for Ba-hexaferrite. This is due to large ionic radius of Ba^{2+} (1.35 Å) as compared to Sr^{2+}(1.18 Å). From the SEM images, the particles showed uniform hexagonal crystal structure. Saturation magnetization increased with increase of Ba doping which is due to lattice distortion enhancing the super-exchange interaction whereas coercivity decreased substantially (2.2 kOe to 1.6 kOe) [Fig. 1(B)]. The EM parameters were measured using a VNA in K_u band with 50% wax as binder. The effect of thickness with matching frequency have been studied for different compositions. The λ/4 mechanism governs the appearance of reflection loss minima (RL_{min}) at a specific frequency. Fig. 2(A) shows the RL vs. frequency for Sr hexaferrite at different thicknesses. The RL_{min} values increases for different thicknesses of 0.5, 2 and, 3mm to -20, -35 and, -41 dB observed at 15.7, 14, and 13.03 GHz for Sr hexaferrite. These are in close proximity with theoretical frequencies (15.9, 14.6 and, 13.02GHz). Fig. 2(B) displays variation of RL vs. frequency for 2 mm thick Ba-doped Sr hexaferrites indicating Ba incorporation reduces the RL which can be due to large value of loss tangets [1]. The effective absorption bandwidth observed at -10dB were determined to be 1.80, 0.92, 0.80, and 1.36 GHz for Ba-Sr hexaferrites. Hence, the synthesized composite samples have demonstrated great potential as EMI absorbers for use in radar and stealth technologies [2-3].

[1] Singh, J. et al. (2021). Journal of Alloys and Compounds, 855, 157242. [2] Kaur, H et al. (2019). Journal of Alloys and Compounds, 806, 1220-1229. [3] Thanh, T. D. et al. (2024). *Journal of Alloys and Compounds*, *970*, 172421.

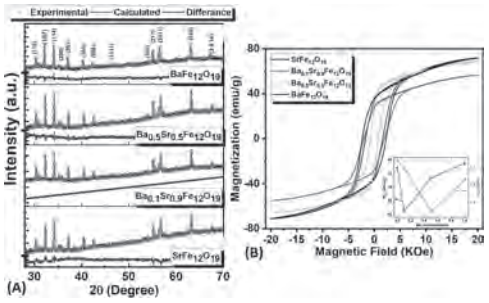

Fig. 1: (A) XRD spectra (B) M-H loop Ba-Sr nanoparticles (inset: M_s and H_c for Ba-concentration).

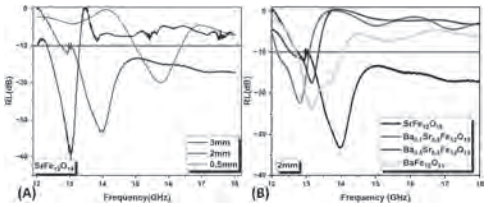

Fig. 2: (A) RL vs. frequency for different thicknesses (B) RL vs. frequency for different Ba-doped samples at 2 mm thickness.

VP9-07. Fe-Pt films prepared from plating baths containing glycine as a complexing agent. *Y. Yamaguchi*[1], N. Ogushi[1], A. Hamakawa[1], D. Fukushima[1], T. Yanai[1], A. Yamashita[1], M. Nakano[1] and H. Fukunaga[1] *1. Nagasaki University, Nagasaki, Japan*

Pt-based magnets are expected to be used in medical applications due to high crystalline magnetic anisotropy and excellent corrosion resistance. We have already reported electroplating Fe-Pt and Co-Pt films using plating baths with citric acid (pH = 2) [1,2]. Recently, we investigated the effect of Cl ions in the plating baths on the hard magnetic properties of the Fe-Pt films and reported that the Cl ions decrease the coercivity [3]. In the present study, we focused on glycine instead of citric acid as a complexing agent, to investigate the effect of the complex agent on the reduction of coercivity by the Cl ions. Firstly, we developed an electroplating process of Fe-Pt films using glycine-based baths and then investigated the effect of Cl ions on the coercivity. We electroplated Fe-Pt films on Cu substrates. The plating bath consisted of $FeSO_4{\cdot}7H_2O$ (2 g/L), $Pt(NO_2)_2(NH_3)_2$ (10 g/L), $NH_4NH_2SO_3$ (30 g/L), and glycine. The plating conditions were (j = 1 A/mm^2, t = 10 min, T_{bath} = 70°C), and pH = approximately 2.0. The plated Fe-Pt films were annealed at 700°C to transform the fcc structure to the fct one. Figure 1 shows the Fe composition and the coercivity of the annealed Fe-Pt films as a function of the amount of glycine in the plating bath. As shown in Fig.1, the Fe composition slightly increased with the increase in glycine. The coercivity showed almost the same value in the glycine amount from 10 to 40 g/L. In our experimental conditions, a high coercivity of 1,000 kA/m was obtained at 20 g/L, and this value was the same as that for the citric acid-based bath, as shown in the inset of Fig.1. Figure 2 shows the coercivity of the annealed Fe-Pt films as a function of the amount of $FeCl_2$ in the plating bath. We added Cl ions to the plating bath by partially replacing $FeSO_4$ with $FeCl_2$. As shown in Fig.2, the coercivity decreased with increasing the $FeCl_2$, indicating that a large amount of Cl ions in the plating baths is unsuitable for obtaining high coercivity. From Fig.2 and our previous studies for the citric-acid-based baths [3], we found that complex agents are not a factor in the reduction of coercivity by existing Cl ions in the baths.

[1]T. Yanai, K. Furutani, T. Ohgai, M. Nakano, K. Suzuki, H. Fukunaga, "Fe-Pt thick-film magnets prepared by electroplating method", *Journal of Applied Physics*. Vol.117, (2015) #17A744. [2]T. Yanai, R. Hamamura, J. Honda, A. Tomita, H. Yamada, N. Fujita, K. Takashima, M. Nakano, H. Fukunaga, "Electroplated Co-Pt thick-film-magnets prepared in citric-acid-based plating baths", *IEEE Transactions on Magnetics*, Vol.53 (2017) #2101803. [3]T. Yanai, D. Fukushima, R. Narabayashi, N. Ogushi,

Y. Yamaguchi, A. Yamashita, M. Nakano, and H. Fukunaga, “Reduction effect of coercivity of electroplated Fe-Pt film magnets by chloride ion in plating baths”, AIP Advances, Vol. 14, (2024) #015032.

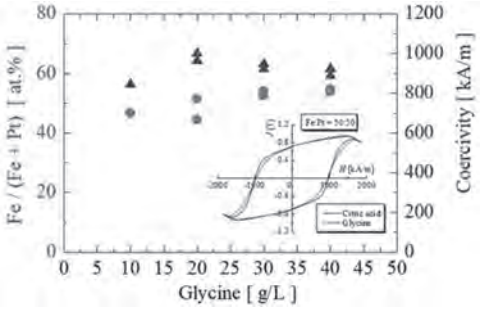

Fig. 1: Fe composition and coercivity.

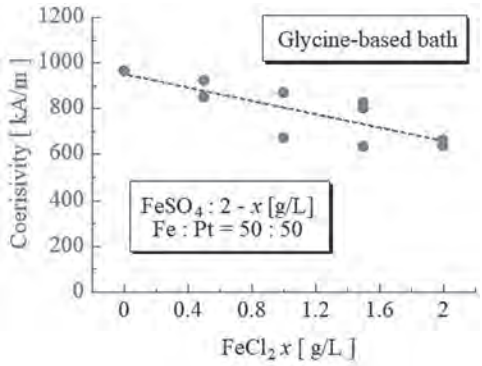

Fig. 2: Relationship between the amount of FeCl2.

VP9-08. Magnetic properties of Sm(Fe,Ga)$_7$C melt-spun ribbons.

T. Saito[1] and D. Nishio-Hamane[2] *1. Chiba Institute of Technology, Narashino, Japan; 2. The University of Tokyo, Kashiwa, Japan*

The $Sm_2Fe_{17}N_3$ phase possesses a high saturation magnetization with a large anisotropy field and a high Curie temperature [1]. Many fundamental investigations have been carried out on the $Sm_2Fe_{17}N_3$ phase [2-5]. $Sm_2Fe_{17}N_3$ has been prepared in powder form by the nitrogenation of Sm_2Fe_{17} alloy powder. It would be desirable if the magnetic properties of the Sm_2Fe_{17} phase could be increased without the need for nitrogenation. Thus, we seek to produce high-coercivity Sm-Fe alloys without nitrogenation. This study discusses the structures and magnetic properties of Sm-Fe-Ga-C alloys produced by melt-spinning. Sm(Fe,Ga)$_7$C alloy ingots were prepared by induction melting under an argon atmosphere. The molten alloy ingots were then ejected through an orifice with argon onto a copper wheel rotating at a surface velocity of 40 ms^{-1}. The melt-spun ribbons obtained through this process were annealed under an argon atmosphere at 873–1073 K for 0–1 h. The specimens were examined by an X-ray diffraction (XRD) system, transmission electron microscope (TEM), and vibrating sample magnetometer (VSM). The Sm(Fe,Ga)$_7$C melt-spun ribbons consisted of either amorphous or the $TbCu_7$-type phase. These ribbons showed low coercivity of less than 1 kOe. The coercivity of the Sm(Fe,Ga)$_7$C melt-spun ribbons increased as the annealing temperature increased. The highest coercivity of 12.6 kOe was achieved in the Sm(Fe,Ga)$_7$C melt-spun ribbon annealed at 1073 K (Fig.1).

[1] J. M. D. Coey and H. Sun, J. Magn. Magn. Mater. 87, L251 (1990). [2] K. Schnitzke, L. Schultz, J. Wecker, and M. Katter, Appl. Phys. Lett. 57, 2853 (1990). [3] J. P. Liu, K. Bakker, P. R. de Boer, T. H. Jacobs, D. B. de Mooij, and K. H. J. Buschow, J. Less-Common Met. 170,109 (1991). [4] S. Miraglia, J. L. Soubeyroux, C. Kolbeck, O. Isnard, and D. Fruchrat, J. Less-Common Met. 171, 51 (1991). [5] T. Iriyama, K. Kobayashi, and H. Imai, IEEE Trans. Magn. 28, 2326 (1992).

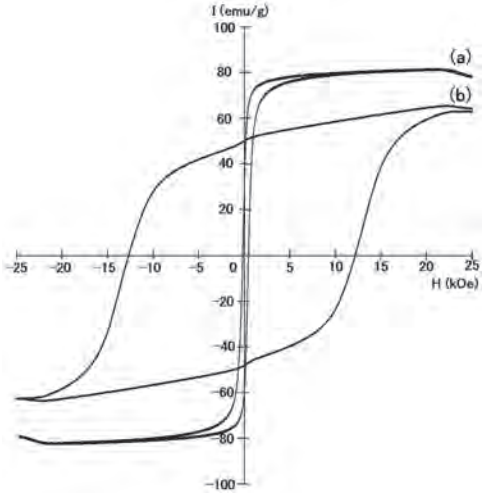

Fig.1 Hysteresis loops of Sm(Fe,Ga)$_7$C melt-spun ribbon: (a) as-quenched and (b) annealed at 1073 K.

Session VP10
HIGH SPEED MACHINES
(Poster Virtual Session)

Kenji Nakamura, Chair
Tohoku University, Sendai, Japan

VP10-01. Hybrid Surrogate Model-Based Multidisciplinary Optimization on High Speed Permanent Magnet Synchronous Motor Facilitating Rotor Design. *Y. Liu*[1], F. Zhang[1] and X. Luo[1] *1. School of Electrical Engineering, Shenyang University of Technology, Shenyang, China*

High-speed permanent magnet synchronous motor (HSPMSM) is electromechanical energy conversion device with deep multi-physics field coupling, featuring small volume and high power density. During high-speed rotation, predicting critical speed is essential to prevent rotor bending resonance. Permanent magnet material necessitates the carbon fiber sleeve due to tensile stress limits. Multi-objective collaborative optimization is required to achieve near-limit material application. Traditional serial design of finite element models isolates dynamic constraints between various physical fields and neglects the dynamic cross-influences of nonlinear changes [1]. Surrogate model enables efficient multidisciplinary parallel optimization by predicting data from sample sets, crucial for multi-objective optimization [2]. However, multiple optimization objectives and large nonlinear search space of HSPMSM reduce model accuracy. This paper proposes an improved hybrid surrogate model composed of sub-models with the highest fitting accuracy for each variable, resulting in high global surrogate accuracy and wide range. Multidisciplinary optimization design is for a 100 kW, 20000 r/min HSPMSM, as shown in Fig.1(a) and (b). The objective variables include maximizing sleeve tangential stress and magnet radial stress within constraints, and minimizing core loss, copper loss, and torque ripple. Constraints include no-load back electromotive force and critical speed. The mathematical model is built. Sensitivity analysis using the LTSM-SOBOL model identifies six structural parameters for optimization. Optimal Latin Hypercube Sampling generates a highly space-filling sample set. Various surrogate models are trained using the sample set to establish a hybrid surrogate model, shown as Fig.1(c). NSGA-II is used for multidisciplinary optimization [3]. This approach effectively decreases the sleeve thickness and reduces losses, verified through finite element analysis, yielding a high-reliability and high-efficiency motor optimization solution, as shown in Fig.2(a) and (b). This method is applicable to multidisciplinary optimization of various types of PMSM.

[1] G. Bramerdorfer, J. A. Tapia, J. J. Pyrhonen, et al, IEEE Transactions on Industrial Electronics., Vol. 65, p. 7672–7684 (2018) [2] B. Xie, Y. Zhang, Z. Xu, et al, IEEE Transactions on Energy Conversion., Vol. 38, p. 859–868 (2023) [3] K. Deb, A. Pratap, S. Agarwal, et al, IEEE Transactions on Evolutionary Computation., Vol. 6, p. 182-197 (2002)

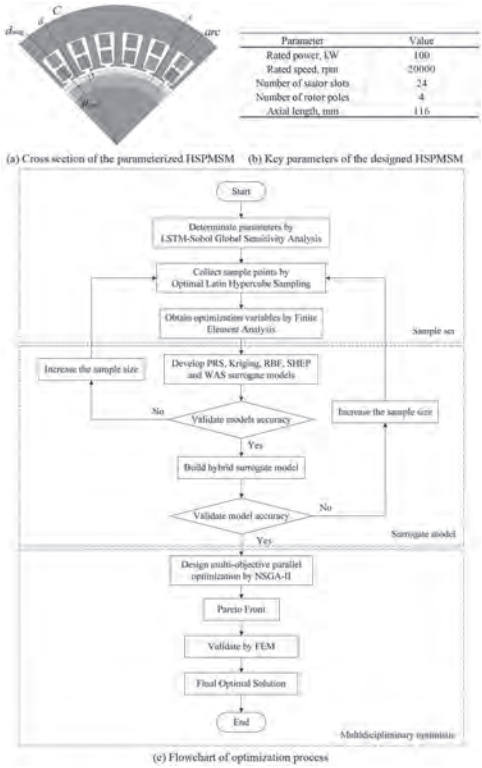

Fig. 1. HSPMSM configuration and optimised process.

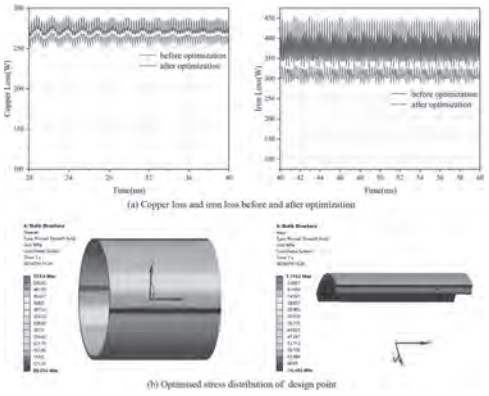

Fig. 2. The design point.

VP10-02. Electromagnetic Heat Flow Coupling Optimization of High Speed Permanent Magnet Motor Based on Deep Neural Network.
X. Luo[1] and F. Zhang[1] *1. Shenyang University of Technology, ShenYang, China*

Optimizating of electromagnetic thermal fluid couplings is commonly used in design of high-speed permanent magnet synchronous motors[1-2]. However, a clear disadvantage of conventional design methods is their time-cost issue when applied throughout the optimization process. Less computing is an advantage of the agent model, which can result in significant optimization time savings. However, common agent models with large construction costs and low global agent precision are the response surface model, radial basis function, and kriging model[3]. Deep learning can be built at a minimal cost and offers excellent global prediction and agent accuracy[4]. In order to lower the computational cost of the electromagnetic heat flow coupling optimization of high speed permanent magnet motors, this article using deep learning. In this paper, the optimization of high speed permanent magnet motor is 24 slot 4 pole. The Fig.1(a) shows the optimization variables of high speed permanent magnet motor. And the electromagnetic heat flow coupling process as Fig.1(b) show. Then through the deep neural network is used to estimate the loss, torque, efficiency, maximum winding temperature and maximum rotor permanent magnet temperature of the high-speed motor. Aiming at the neural network's accuracy of global predictions, this paper propose optimizing the number of layers and nodes. Aiming at the problem of sample size of training neural network, a method of increasing sample points based on local sensitivity analysis is proposed in this paper. Through this method the global proxy precision of the deep network is improved, and reduce computation. The Figure.2 shows the comparison between the predicted value of neural network and the calculated value of finite element for different design objectives.Next,NSGA-2 is used to optimize efficiency and torque by using deep neural network prediction model to maximize efficiency and torque. The Figure.2(i) shows the preliminary optimization result, the torque is 44.72 N●m, the efficiency is 96.89%. At last, an optimization procedure was verified through the creation and testing of a prototype. The full paper will present the detailed calculation procedure and analysis.

○ N. Uzhegov, E. Kurvinen and J. Nerg, J. Pyrhönen, IEEE Transactions on Industrial Electronics., vol. 63, pp. 784-795(2016). ○ M. K. Islam, K. N. Tasnim and S. Choi, IEEE Access., vol. 10, pp. 106305-106323(2022). ○ H. Sasaki,K. Yamamura, IEEE Transactions on Magnetics., vol. 60,pp. 1-4(2024). ○ M. N. Al-Andoli, K. S. Sim, S. C. Tan and P. Y. Goh, IEEE Access., vol. 11, pp. 76330-76346(2023).

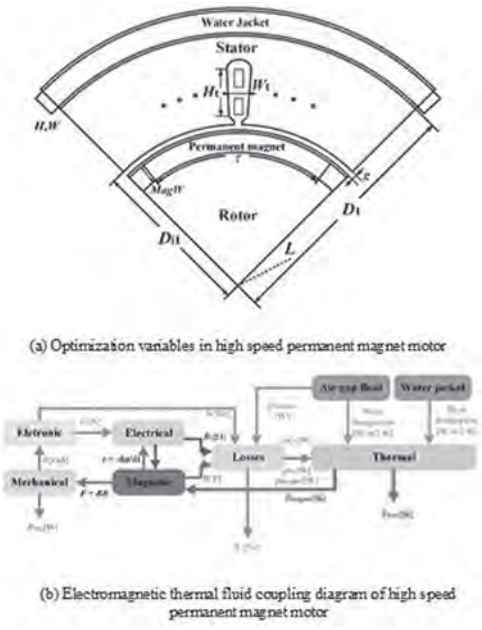

(a) Optimization variables in high speed permanent magnet motor

(b) Electromagnetic thermal fluid coupling diagram of high speed permanent magnet motor

Fig. 1

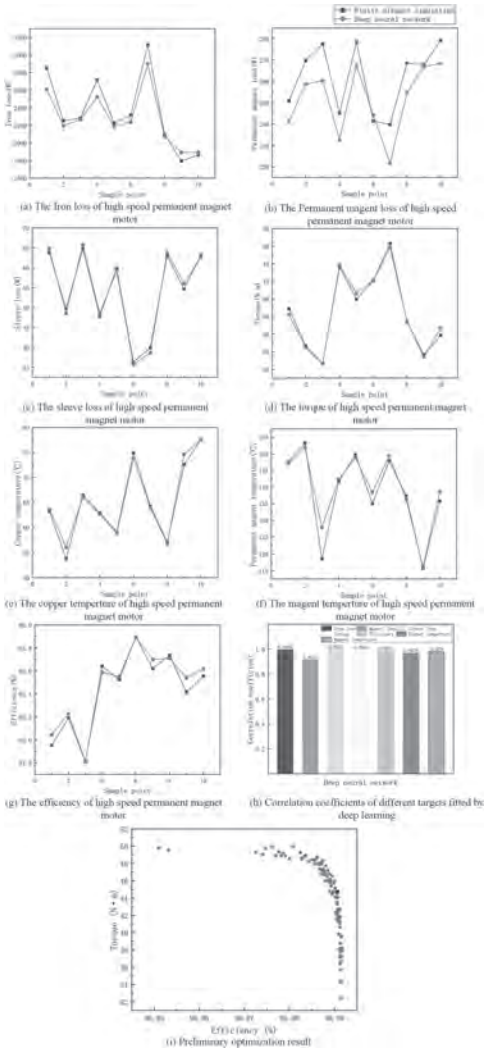

(a) The iron loss of high speed permanent magnet motor
(b) The Permanent magnet loss of high speed permanent magnet motor
(c) The sleeve loss of high speed permanent magnet motor
(d) The torque of high speed permanent magnet motor
(e) The copper temperture of high speed permanent magnet motor
(f) The magent temperture of high speed permanent magnet motor
(g) The efficency of high speed permanent magnet motor
(h) Correlation coefficients of different targets fitted by deep learning
(i) Preliminary optimization result

Fig. 2

VP10-03. Rotor Stress Analysis of High-Speed Permanent Magnet Machines Considering Adhesive Debonding.
Y. Pan[1], J. Yang[1], Y. Jiang[1] and S. Huang[1] *1. College of Electrical and Information Engineering, Hunan University, Changsha, China*

The high-speed permanent magnet (PM) machines are widely used due to the merits of high efficiency and high power density. In practice, the gaps between the segmented PMs and between the PMs and shaft are filled with adhesive. However, the adhesive layer faces the risk of debonding under high speed and high temperature conditions, which has a crucial effect on the stress of PMs. For the design of high-speed PM machines, it is important to accurately evaluate the rotor strength to ensure the reliable operation of rotor at high speeds [1], [2]. However, the previous studies of rotor stress ignore the effect of adhesive debonding on rotor stress. In this paper, the rotor stress of segmented PMs is analyzed considering adhesive debonding to evaluate the rotor stress more accurately in the design stage. Firstly, based on bilinear traction separation, the cohesive zone model (CZM) is established to describe the failure behavior of the adhesive layer. The stress of segmented PMs is calculated using the CZM. Then, in the case of considering the adhesive debonding, the influence of PM segments number and temperature on the rotor stress is determined. The results show that the maximum principal stress of the segmented PMs appears at the contact position with the shaft considering adhesive debonding. In addition, with the increase of segments number, the stress concentration of the PMs is relieved. Fig. 1 illustrates the schematic structural diagram of a 48-slot 4-pole high-speed PM machine retained by a carbon-fiber sleeve. The PMs and shaft are assembled by

bonding, which is same as the assembly method of segmented PMs. Fig. 2 presents the tangential stress distribution of the PMs with and without considering the debonding of adhesive. It is obvious that there is a difference in stress distribution between the two. The stress concentration is more severe when the debonding of adhesive is considered. Thus, it is crucial to evaluate the rotor stress considering the adhesive debonding in the design stage to ensure the reliable operation of rotor. More detailed analysis and results will be presented in the full paper.

[1] G. Du, W. Xu, J. Zhu, and N. Huang, "Rotor Stress Analysis for High-Speed Permanent Magnet Machines Considering Assembly Gap and Temperature Gradient," *IEEE Trans. Energy Convers.*, vol. 34, no. 4, pp. 2276–2285, Dec. 2019. [2] Y. Wang, Z.-Q. Zhu, J. Feng, S. Guo, Y. Li, and Y. Wang, "Rotor Stress Analysis of High-Speed Permanent Magnet Machines With Segmented Magnets Retained by Carbon-Fibre Sleeve," *IEEE Trans. Energy Convers.*, vol. 36, no. 2, pp. 971–983, Jun. 2021.

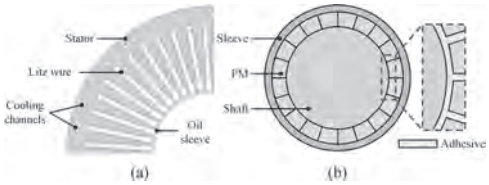

Fig. 1. Cross-section of a 48-slot 4-pole high-speed PM machine. (a) Stator. (b) Rotor with segmented PMs

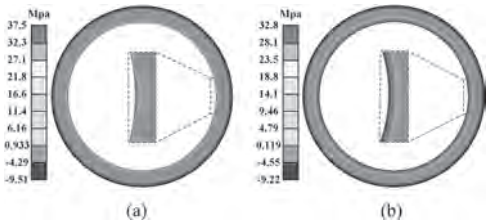

Fig. 2. Tangential stress distribution of PMs. (a) Considering the adhesive debonding. (b) Without considering the adhesive debonding

VP10-04. Analysis and Verification of Motor Performance Based on Local Carburizing of Rotor. *Y. Li*[1], C. Sun[2], C. Yan[1], W. Li[1], L. Zeng[3] and R. Pei[1,3] *1. Shenyang University of Technology, Shenyang, China; 2. Technology Center of Angang Steel Company Limited, Anshan, China; 3. Suzhou Inn-Mag New Energy Ltd., Suzhou, China*

In the future, high speed and high efficiency are the development trends of electric vehicle drive motors [1]-[2]. At present, most of the core materials of the drive motor are non-grain-oriented (NGO) silicon steel, and its performance determines the characteristics of the drive motor. For meeting the high speed, high efficiency and reliability of the drive motor, NGO silicon steel must not only have excellent magnetic properties, but also have higher yield strength, so that the rotor can resist the huge centrifugal force generated during high-speed rotation [3]. Carburizing is a heat treatment process to increase the carbon content of the alloy surface and improve its strength. Carburizing process is generally applied to the preparation process of alloy or grain-oriented silicon steel, and there are few cases in literature describing the application of NGO silicon steel to motors after carburizing. In this study, NGO silicon steel was carburized and innovatively used in the rotor, and its magnetic and mechanical properties were further investigated. Based on vacuum carburizing furnace and Thurckon PAC for stop-off paints, the local carburizing of flux barrier and rib in rotor was completed. As a result, the strength of the rotor is increased, thereby increasing the maximum speed of the motor. The purpose of this research is to improve the maximum speed and torque of motor based on carburized silicon steel, which is finally applied to the vehicle drive motor. The magnetic permeability of the silicon steel decreases after carburizing, which can reduce the magnetic leakage of the motor. In addition, the flux barrier can achieve a higher yield strength after carburizing, which can make the motor reach a higher speed. The finite element simulation analysis shows that the rotor can withstand greater stress after local carburizing. The maximum speed has been increased by 2,000 r/min or even more. On the other hand, the maximum efficiency of the motor is reduced from 97.3% to 96.85%, which is acceptable. From the test results of the motor, this research has been verified to be reasonable and it has the engineering feasibility.

[1] Aldo Boglietti, Chris Gerada, Andrea Cavagnino. High-speed electrical machines and drives [J]. IEEE Transactions on Industrial Electronics, 2014, vol.61(6):2943-2945. [2] Gerada D, Mebarki A, Brown N L, et al. High-speed electrical machines: Technologies, trends, and developments[J]. IEEE Transactions on Industrial Electronics, 2014, 61(6): 2946-2959. [3] Tenconi A, Vaschetto S, Vigliani A. Electrical machines for high-speed applications: Design considerations and tradeoffs[J]. IEEE Transactions on Industrial Electronics, 2014, 61(6): 3022-3029.

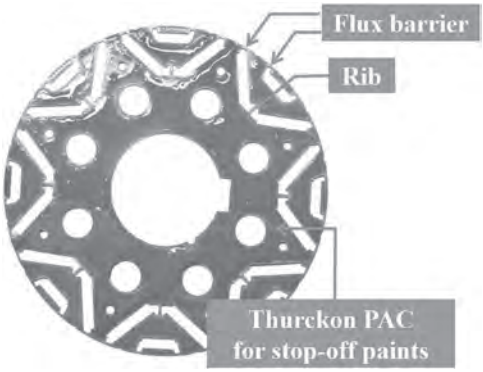

Fig. 1. Treatment of rotor before carburizing

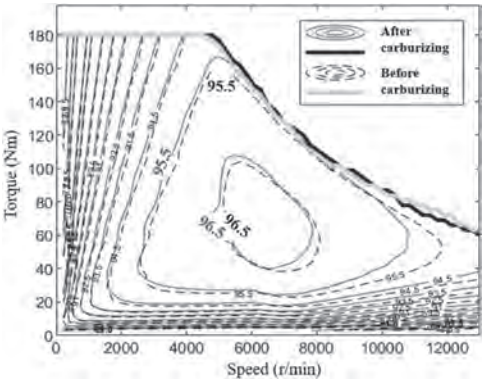

Fig. 2. Comparison of efficiency.

VP10-05. Performance Study of High-Speed Motors Based on the Forming Transposition Winding Method. *S. Wang*[1], L. Zhang[1], J. Li[1], Y. Li[1], Z. Li[1], R. Pei[1,2] and L. Zeng[2] *1. Shenyang University of Technology, Shenyang, China; 2. Suzhou Inn-Mag New Energy Ltd, Suzhou, China*

The magnetic field distribution in the radial direction of the stator core of the flat wire motor is not uniform, and the induced electromotive force generated by the conductors cutting the magnetic inductance at different locations is different, so there is a circulating current between the conductors[1]. In addition when the motor is running, there is a current passing through the winding, and the magnetic field in the slot interacts with the current in the conductor to generate electromagnetic force, which affects the winding conductor to offset, winding structure deformation and other phenomena[2,3]. In order to attenuate this effect, this paper takes the high-speed flat wire motor with 48 slots and 8 poles as a model, and explores the effects of different conductor numbers and different angles of winding transposition. In this paper, the single-turn winding is axially and radially divided into different numbers of strands based on five strands of wire for 360° complete transposition and incomplete transposition of various angles, and

a schematic diagram of the partial transposition is shown in Fig.1, and the cross-section of the motor stator is shown in Fig.2. Secondly, finite element simulation is used to verify the reasonableness and feasibility of the forming transposition winding technology in the application of high-speed flat wire motor. Following that, the AC copper loss of the motor stator winding under different transposition cases is compared. Then, the article explores the distribution of electromagnetic force in the forming transposition winding of high-speed flat wire motor, and analyzes the magnitude of electromagnetic force in the conductor of stator winding according to the Lorentz force calculation method. Finally, the article found by comparison, transposition winding to each turn of the winding into five strands, the angle of 324°, the motor stator winding between the best suppression of circulating current, and radial electromagnetic force is the smallest, the results of this paper for the forming transposition winding processing to provide a theoretical basis.

[1] D. Wang, Y. Liang and L. Gao, "A New Global Transposition Method of Stator Winding and Its Loss Calculation in AC Machines," in IEEE Transactions on Energy Conversion, vol. 35, no. 1, pp. 149-156(March 2020) [2] Y. Liang, F. Zhao and K. Xu, "Analysis of Copper Loss of Permanent Magnet Synchronous Motor With Formed Transposition Winding," in IEEE Access, vol. 9, pp. 101105-101114(2021) [3] D. Wang, Y. Liang and L. Gao, "Research on Transposition Method and Loss of Multi-Turn Coil in an Induction Motor," in IEEE Transactions on Magnetics, vol. 55, no. 10, pp. 1-4(Oct. 2019)

Fig.1 A schematic diagram of the partial transposition

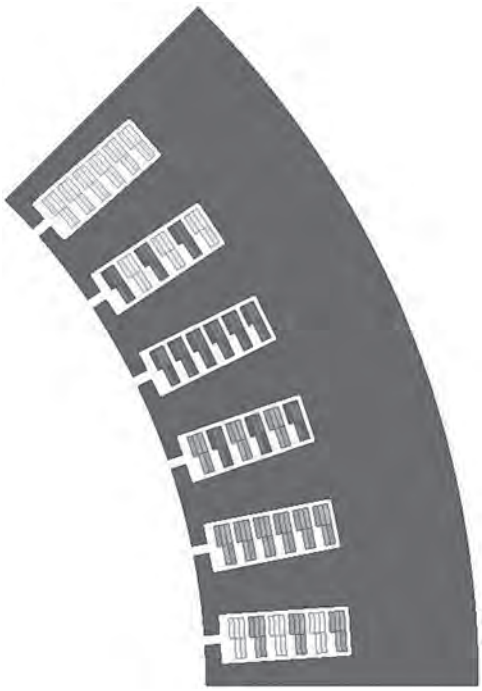

Fig.2 The cross-section of the motor stator

VP10-06. Design of a High-Speed Solid-Rotor Induction Motor with Resonant Winding. *L. Xiao*[1], S. Niu[1] and M. Jiang[1] *1. Department of Electrical and Electronic Engineering, The Hong Kong Polytechnic University, Hong Kong, China*

I.Introduction Solid rotor induction machine (SRIM) is a promising solution for high-speed operations due to its unique characteristics and advantages including excellent mechanical stability, high thermal properties, as well as great rotor dynamics [1]. However, a major drawback of the SRIM is its lower torque density and the occurrence of maximum torque at relatively lower speed regions, significantly limiting its industrial applications. To address these limitations and enhance the performance of the SRIM, this paper proposes a resonant solid rotor induction motor (RSRIM) that incorporates capacitors in the stator windings. By utilizing the principle of resonance, the RSRIM demonstrates significantly improved electromagnetic performance compared to the conventional SRIM design. II. Proposed Motor Structure Fig. 1 illustrates the configuration of RSRIM, where the stator is constructed using general silicon steel sheets and the rotor is composed of materials exhibiting both magnetic permeability and electrical conductivity, such as grey cast iron and EN24T [2]. The RSRIM's performance is significantly influenced by resonant capacitors within the stator winding sets, which necessitate analysis and calculation using a T-type equivalent circuit and 2D-Finite Element Method (FEM). III.Verification To validate the proposed model, a comprehensive assessment is performed on a 6-pole 36-slot structure by conducting FEM simulations and analytical modeling. This validation process enables a detailed comparison of the operating characteristics between SRIM and RSRIM, as demonstrated in Fig. 2. Under the identical voltage supply, the maximum torque of RSRIM is enhanced, nearing the optimal efficiency point as well.

[1] E. Kurvinen *et al*., "Design and Manufacturing of a Modular Low-Voltage Multimegawatt High-Speed Solid-Rotor Induction Motor," in *IEEE Transactions on Industry Applications*, vol. 57, no. 6, pp. 6903-6912, Nov.-Dec. 2021. [2] L. Papini and C. Gerada, "Sensitivity analysis of magnetizing inductance in solid rotor induction machine," *2016 19th International Conference on Electrical Machines and Systems (ICEMS)*, Chiba, Japan, 2016, pp. 1-6.

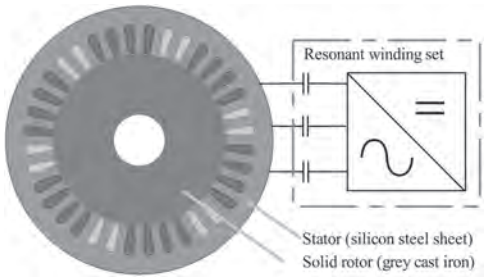

Fig.1 Topology of RSRIM.

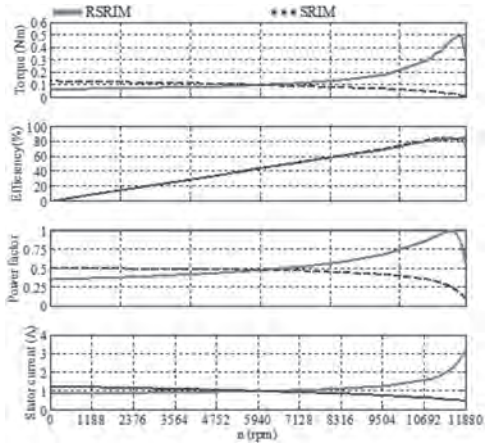

Fig. 2 FEM comparison of SRIM and RSRIM under the same voltage supply

VP10-07. Exploring the Application of High Conductivity Graphene-copper Composites for High Speed Motors. *J. Li*[1], Y. Li[1], S. Wang[1], R. Pei[1,2] and Y. An[1] *1. Shenyang University of Technology, Shenyang, China; 2. Suzhou Inn-Mag New Energy Ltd, Suzhou, China*

In recent years, the booming electric vehicle market has put forward higher requirements for the efficiency and temperature rise of drive motors. Flat wire motors have significant advantages in efficiency, power density, heat dissipation, etc., but its larger conductor cross-section is accompanied by the skin effect, high-frequency operating conditions of AC loss is twice as much as DC, inhibiting the development of flat wire motors to high-speed[1-3]. How to inhibit high-frequency AC copper loss to ensure motor efficiency and thermal safety has become an urgent problem. In this paper, a high conductivity graphene-copper composite material is proposed as a motor winding to reduce AC copper loss in high-speed motors, and its applicability and reliability are demonstrated. In this case, the graphene-copper composite material is shown in Fig. 1. On the basis of material preparation, the mechanical properties and electrical conductivity of the material are explored for different tension conditions and frequency conditions. Copper graphene is found to have good electrical conductivity and is suitable as a motor winding material. Based on the reference motor topology with 48 slots and 8 poles, the ordinary copper material and graphene-copper composite material are used as the motor windings, and the copper loss of the motor is calculated to compare and analyze the changes of the AC loss and efficiency under different working conditions, and to analyze the suppression of the skin effect of graphene-copper composite material under high frequency, The current density distribution of the graphene-copper composite material is shown in Fig. 2. It is found that the conductivity of graphene copper composite material is 18.6% higher than that of ordinary copper material under 1000Hz condition, and the AC copper loss is reduced by 40% under the condition of maximal torque.

[1] M. Aoyama and J. Deng, "Visualization and quantitative evaluation of eddy current loss in bar-wound type permanent magnet synchronous motor for mild-hybrid vehicles," in *CES Transactions on Electrical Machines and Systems*, Vol. 3, pp. 269-278(2019) [2] C. Du-Bar and O. Wallmark, "Eddy Current Losses in a Hairpin Winding for an Automotive Application," *2018 XIII International Conference on Electrical Machines (ICEM)*, Alexandroupoli, Greece, pp. 710-716(2018). [3] G. Berardi and N. Bianchi, "Design Guideline of an AC Hairpin Winding," *2018 XIII International Conference on Electrical Machines (ICEM)*, Alexandroupoli, Greece, pp. 2444-2450(2018).

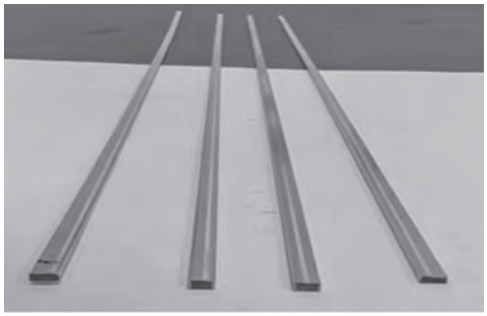

Fig.1 The graphene-copper composite material

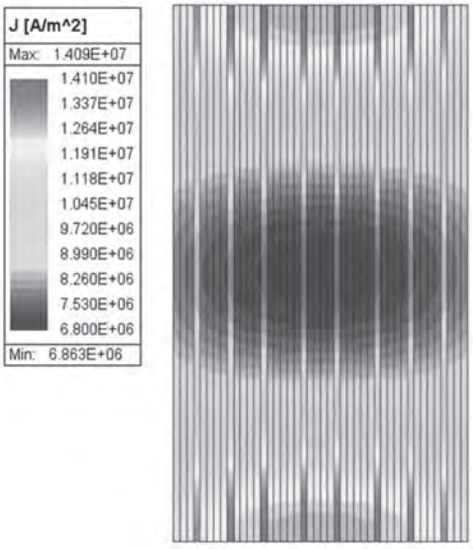

Fig.2 The current density distribution of the graphene-copper composite material

VP10-08. Optimal Design of Rotor Bar in Squirrel-Cage Induction Motor according to Rotor Bar Angle. *H. Ban*[1], S. Eom[1], K. Yu[1], J. Park[1], J. Jang[1], K. Shin[2] and J. Choi[1] *1. Electrical Engineering, Chungnam National University, Daejeon, The Republic of Korea; 2. Electrical Engineering, Changwon National University, Changwon, The Republic of Korea*

The shape of a rotor bar in squirrel-cage induction motors is closely related to the starting torque and efficiency, which significantly affect the performance of the motor. To improve the low starting torque and efficiency of squirrel-cage induction motors, studies have focused on optimizing rotor bar shapes. Generally, deep-bar and double-cage rotor bar shapes have been proposed as alternatives to enhance performance [1]. However, designs aimed at starting torque enhancements may lead to reduced efficiency; moreover, certain optimally designed double-cage rotor-bar geometries are difficult to manufacture [2]. Therefore, an appropriate shape that improves the starting torque and efficiency using the angle of the rotor bars has been proposed [3]. This study presents an optimal design that enhances the starting torque and efficiency by adjusting the rotor bar parameters and angles of aluminum rotor bars. Fig. 1(a) shows analysis models for the deep-bar and double-cage rotors. Fig. 1(b) presents tilted analysis models with the angle in clockwise directions. Fig. 1(c) and (d) show the magnetic flux lines according to the rotor bar angles. As the angle increases, the magnetic flux lines become distorted, elongating the magnetic rotor path and increasing the resistance. Figs. 2(a) and (b) show the efficiency and rated torque of the analysis models based on rotor bar angles. Figs. 2(c) and (d) show the efficiency according to the rotor bar height and angle, respectively. Efficiency could be increased while maintaining the characteristics of deep-bar and double-cage shapes. This study provides a comparison of results based on various rotor bar parameter, optimization using genetic algorithms (GA), and equivalent circuit parameter evaluations according to rotor bar shapes.

[1] D.-H. Kim, J.-H. Choi and W.-H. Kim, "Design process of working bar of double-cage induction motor," *IEEE Trans. Appl. Supercond.*, vol. 30, no. 4, pp. 1-5, 2020. [2] M. Di Nardo, A. Marfoli and C. Gerada, "Rotor slot design of squirrel cage induction motors with improved rated efficiency and starting capability," *IEEE Trans. Ind. Appl.*, vol. 58, no. 3, pp. 3383-3393, 2022. [3] C. G. Heo, H. M. Kim and G. S. Park, "A Design of Rotor Bar Inclination in Squirrel Cage Induction Motor," *IEEE Trans. Magn.*, vol. 53, no. 53, pp. 1-4, 2017.

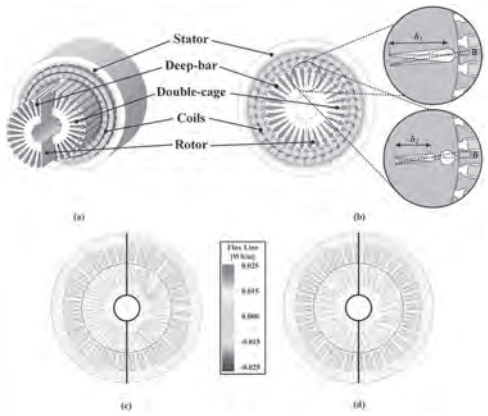

Fig. 1. Induction machine: (a) analysis model, (b) inclined rotor bar, magnetic flux line according to rotor bar angle (c) deep-bar and (d) double-cage.

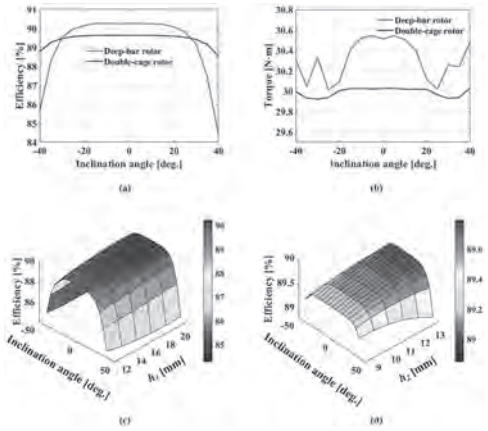

Fig. 2. Results according to rotor bar angle (a) efficiency, (b) torque, efficiency according to rotor bar height (c) deep-bar and (d) double-cage.

VP10-11. Quarter Sub-Harmonic-Based Self-Excited Brushless Wound Field Synchronous Machine Using Three-Layer Winding Configuration. *S. Bukhari*[1] and P. Rasilo[1] *1. Electrical Engineering, Tampere University, Tampere, Finland*

Wound field synchronous machines (WFSMs) have gained significant attention in recent years due to their lower manufacturing costs compared to permanent magnet machines [1]-[2]. However, these machines face a major drawback due to the use of brushes, slip rings, exciters, and pilot exciters for rotor field excitation. This paper introduces a novel quarter sub-harmonic-based self-excited brushless topology for WFSMs, utilizing a three-layer armature winding configuration. The armature winding in this design includes an 8-pole, double-layer main armature winding (*ABC*) and a 2-pole single-layer exciter winding (*X*) connected in series through a diode rectifier. When the inverter supplies three-phase currents (Iabc) to the main armature winding, it energizes the 2-pole exciter winding after rectification, simultaneously creating an 8-pole rotating magnetic field and a 2-pole pulsating magnetic field in the machine's air gap. The rotor of the machine features an 8-pole rotor field winding (F) and a 2-pole harmonic winding (H), both connected in series through a full-bridge diode rectifier. As the rotor rotates, the harmonic winding intercepts the pulsating 2-pole magnetic field, inducing harmonic current in it. This current is rectified to energize the rotor field winding, generating the rotor field. The electromagnetic interaction between the main stator and rotor fields produces torque. The proposed self-excited brushless WFSM topology is illustrated in Fig. 1(a). To validate the operation of the proposed topology, finite element analysis (FEA) is conducted in JMAG-Designer for an 8-pole, 48-slot machine model, as shown in Fig. 1(b). The machine is supplied with a current of 4A (peak) and analyzed at the rated speed of 900 rpm. The induced harmonic current and the rectified rotor field winding currents are presented in Fig. 2(a). Fig. 2(b) shows the output torque of the machine using the proposed brushless WFSM topology. These results demonstrate that an average torque of 8.55 Nm with a ripple of 25.59% is achieved. A detailed perfromance analysis of the proposed topology will be presented in the final paper.

[1] S. S. H. Bukhari, J. Ikram, F. Wang, X. Yu, J. Imtiaz, J. Rodas, and J. -S. Ro, "Novel Self-Excited Brush-less Wound Field Vernier Machine Topology", in *IEEE Access*, vol. 10, pp. 97868-97878, 2022. [2] S. S. H. Bukhari, J. Yu, M. A. Shah, J. Rodas, M. Bajaj, and J. -S. Ro, "Novel Sub-Harmonic-Based Self-Excited Brushless Wound Rotor Synchronous Machine", *IEEE Canadian Journal of Electrical and Computer Engineering*, vol. 45, no. 4, pp. 365-374, Fall 2022.

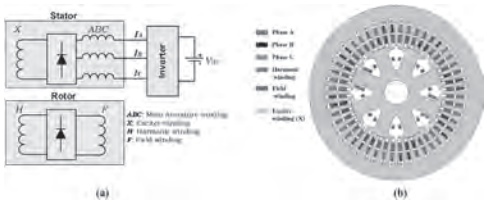

Fig. 1. (a) Proposed topology, and (b) machine model

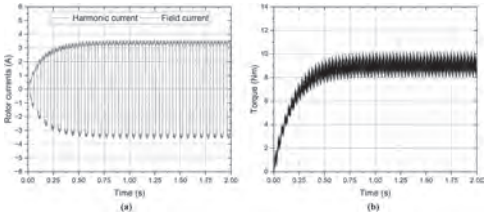

Fig. 2. (a) Rotor currents, and (b) torque

VP10-12. Quarter Sub-Harmonic-Based Self-Excited Brushless Wound Rotor Synchronous Machine Topology. *S. Bukhari*[1] and P. Rasilo[1] *1. Electrical Engineering, Tampere University, Tampere, Finland*

In literature, various brushless topologies of wound rotor synchronous machines (WRSMs) have been proposed. These topologies are based on either the third-harmonic field excitation or the sub-harmonic field excitation methods. With the third-harmonic field excitation method, the rotor harmonic winding requires three times the number of poles as the field winding. In contrast, the sub-harmonic-based field excitation method requires half the number of poles as the field winding, reducing the usage of copper and simplifying the rotor structure (as it depends on the number of harmonic winding poles) [1]-[2]. To achieve simplified and self-excited brushless operation of WRSMs, this paper proposes a brushless WRSM based on the quarter sub-harmonic field excitation method. In this topology, a magnetic field at 1/4th of the fundamental frequency is generated in the machine's airgap using a unique armature winding configuration, which combines single and double-layer winding patterns. This arrangement generates both fundamental and quarter sub-harmonic MMF components in the airgap when supplied with current from an inverter and requires 1/4th the harmonic winding poles compared to the rotor field winding to achieve brushless operation. To validate the operation of the proposed topology, finite element analysis (FEA) is performed in JMAG for an 8-pole, 48-slot machine model. The proposed topology, along with the machine model and

its winding configuration, are presented in Fig. 1(a)-(c). In the proposed armature winding configuration [shown in Fig. 1(b) and (c)], 6-slots are used for a single-layer winding, and 42-slots are used for a double-layer winding pattern to achieve 8-pole and 2-pole fields in the airgap. The 2-pole quarter sub-harmonic field is used to induce harmonic current in the harmonic winding of the rotor, which is rectified to excite the rotor field winding for brushless operation. The rotor currents and output torque of the machine are presented in Fig. 2(a) and (b). Detailed analysis and optimization of the proposed topology will be presented in the final paper.

[1] S. S. H. Bukhari, J. Ikram, F. Wang, X. Yu, J. Imtiaz, J. Rodas, and J. -S. Ro, "Novel Self-Excited Brush-less Wound Field Vernier Machine Topology", in *IEEE Access*, vol. 10, pp. 97868-97878, 2022. [2] S. S. H. Bukhari, J. Yu, M. A. Shah, J. Rodas, M. Bajaj, and J. -S. Ro, "Novel Sub-Harmonic-Based Self-Excited Brushless Wound Rotor Synchronous Machine", *IEEE Canadian Journal of Electrical and Computer Engineering*, vol. 45, no. 4, pp. 365-374, Fall 2022.

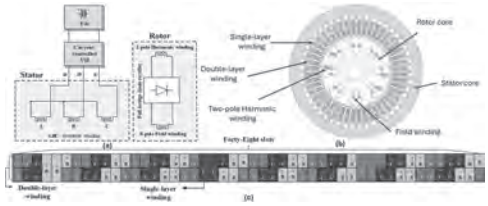

Fig. 1. Proposed (a) topology, (b) machine model, and (c) armature winding.

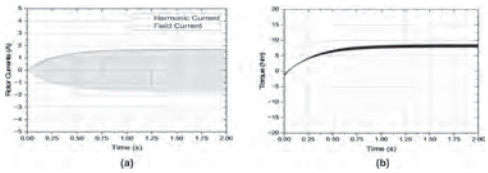

Fig. 2. (a) Rotor currents, and (b) torque.

VP10-13. High-Efficient Self-Excited Brushless Wound Rotor Synchronous Machine Topology. *S. Bukhari*[1] and P. Rasilo[1] *1. Electrical Engineering, Tampere University, Tampere, Finland*

In recent years, brushless wound rotor synchronous machines (BL-WRSMs) have gained significant attention over permanent magnet machines due to the rising costs of permanent magnets [1]. A simplified BL-WRSM topology with a dual armature winding is proposed in [2], where both the main armature and exciter windings are connected in series. The exciter winding has half the number of poles compared to the main armature winding, developing a sub-harmonic MMF in the airgap for brushless operation. This topology is termed the conventional topology in this paper. This paper proposes a highly efficient, self-excited BL-WRSM topology with a single armature winding to reduce copper losses and enhance efficiency. The proposed armature winding combines single and double-layer patterns to generate fundamental and sub-harmonic MMF components in the airgap. The rotor of the machine houses harmonic and field windings connected through a diode rectifier. The sub-harmonic MMF induces a harmonic current in the rotor's harmonic winding, which is rectified to excite the rotor field winding for brushless operation. FEA validates the operation of the proposed topology and compares it with the conventional BL-WRSM for its performance. For the conventional topology, the 8-pole main armature winding has 30 and 4-pole exciter winding has 10 turns per phase. In the proposed topology, the armature winding has 30 turns per phase, with 12 slots having a single-layer and 36 slots wound with a double-layer pattern. The structural parameters of the machines are presented in Fig. 1(c). The output torque of both machines is shown in Fig. 2(a), while losses and efficiency are depicted in Fig. 2(b). These results indicate that the proposed topology achieves brushless operation at an efficiency of 91.10%, which is 1.15% higher than the conventional BL-WRSM. The performance comparison of the conventional and proposed topologies is presented in Fig. 2(c). An optimized number of turns for single and double-layer winding for the proposed BL-WRSM will be presented in final paper

[1] S. Tariq, J. Ikram, S. S. H. Bukhari, Q. Ali, A. Hussain and J. Ro, *IEEE Access*, vol. 10, pp. 101609-101621, 2022 [2] M. Ayub, S. Atiq, Q. Ali, A. Hussain and B. -I. Kwon, *IEEE Access*, vol. 8, pp. 115812-115822, 2020

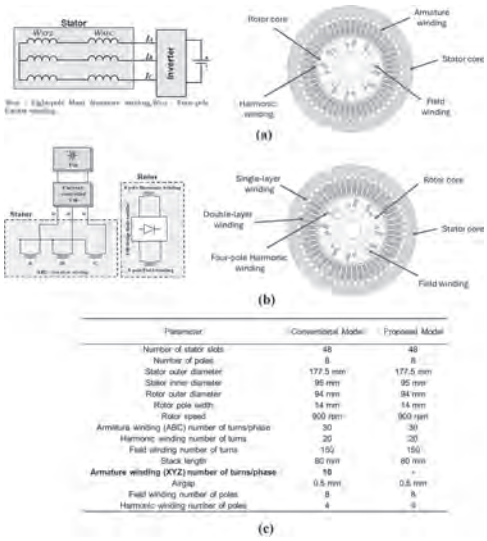

Fig. 1. (a) Conventional and, (b) proposed topologies, and (c) machine parameters

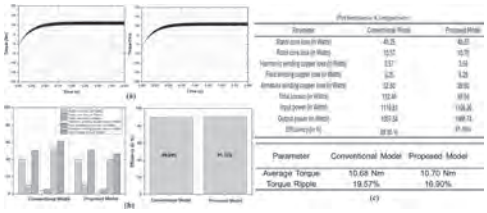

Fig. 2. (a) Torque, (b) losses and efficiency, and (c) performance comparison

Session VP11
MAGNETIC ASPECTS RELATED TO ELECTROMECHANICAL CONVERSION, TRANSFORMERS AND INDUCTORS (Poster Virtual Session)

Yacine Amara, Chair
Université Le Havre Normandie, Le Havre, France

VP11-01. A novel method for eliminating residual flux in transformers using composite voltage. *Y. Ren*[1], Y. Wang[1] and C. Liu[1] *1. Hebei University of Technology, Tianjin, China*

I Introduction After the transformer is cut out for operation and DC resistance test, the residual flux (RF) can be generated in the transformer core. To date, there is no effective means to distinguish between internal faults of transformers and RF, which can interfere with transformer diagnostic results [1]. In addition, serious inrush current may occur as a result of RF. Therefore, it is necessary to eliminate the RF. The existing demagnetization methods are mainly divided into DC demagnetization method and AC demagnetization method. According to IEEE Std C57.152-2013, the DC demagnetization method is widely used due to its low power requirements and good demagnetization effect. However, reference [2] indicates that there are still non-negligible currents after the last excitation, which may increase the magnetic flux to 10% of the knee point flux after the discharge process, leading to demagnetization failure. This paper aims to study an efficient method for eliminating RF. II Proposed method This paper proposes a demagnetization method using a composite voltage combining DC and AC signals. The applied voltage waveform is shown in Figure 1. The first applied is a DC voltage with periodic polarity changes. Due to the large inherent time constant of transformers, series resistors are used to reduce the demagnetization period. The initial voltage V_1 is determined based on the rated current and resistors. A suitable voltage decay rate will be studied for various RF. Once the flux is reduced to a lower level, the applied voltage is changed to a sine signal. When the voltage amplitude is less than the threshold, the demagnetization ends and RF is completely eliminated. III Experimental results and conclusions Experimental tests are conducted on a 20 kVA transformer, as shown in Figure 2. The RF is weakened to within 1% of the knee point flux using the proposed method. By connecting resistors in series, the entire demagnetization process is controlled within 2 s. The maximum power of the proposed method is only 20 W, which is much less than the AC demagnetization method. The experimental results show that the proposed method is more efficient than existing methods.

[1] S. Zhang *et al.*, "Improved Flux-Controlled VFCV Strategy for Eliminating and Measuring the Residual Flux of Three-Phase Transformers," *IEEE Transactions on Power Delivery*, vol. 35, no. 3, pp. 1237–1248, Jun. 2020, doi: https://doi.org/10.1109/TPWRD.2019.2937900. [2] Yasin Zabihinia Gerdroodbari, Mahdi Davarpanah, and Shahrokh Farhangi, "Remanent Flux Negative Effects on Transformer Diagnostic Test Results and a Novel Approach for Its Elimination," *IEEE Transactions on Power Delivery*, vol. 33, no. 6, pp. 2938–2945, Dec. 2018, doi: https://doi.org/10.1109/tpwrd.2018.2827179.

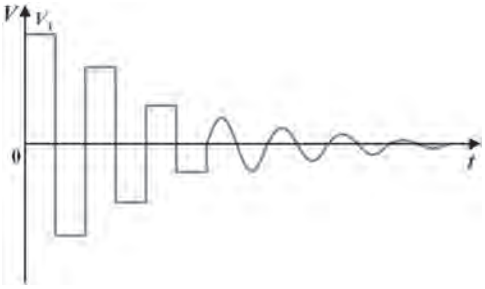

Fig. 1: The applied voltage waveform

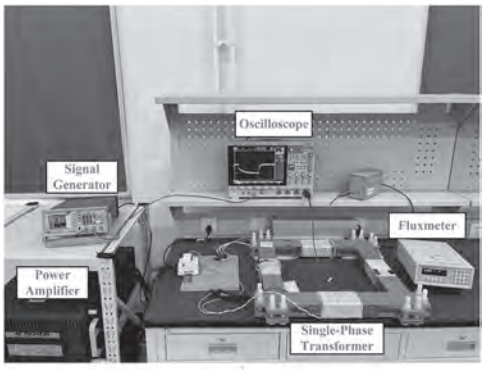

Fig. 2: The experimental platform

VP11-02. Using Solenoid Coils to Enhance the Anti-offset Capability of the Bipolar Coil in Wireless Power Transfer Systems. *R. Xie*[1], W. Pan[1], X. Chen[1], X. Mao[1] and Y. Zhang[1] *1. Fuzhou University, Fuzhou, China*

The wireless power transfer (WPT) technology is becoming increasingly popular due to its convenience and efficiency. The wireless charging systems consist of various components, including converters, compensation networks, and coupling structures. When the coupling structures are perfectly aligned, it allows for maximum energy transfer between the transmitting (TX) and receiving (RX) coils. This alignment results in a high coupling coefficient, which directly impacts the operating efficiency of the system. With a high coupling coefficient, more power can be efficiently transferred from the TX coil to the RX coil. However, the misalignment of the coupling structure can degrade the performance of wireless charging systems. The magnetic field generated by one coil does not fully intersect with it generated by another coil, leading to reduced magnetic flux linkage and decreased energy transfer efficiency. To enhance the anti-offset ability of the bipolar coil, solenoid coils are utilized to expand the effective charging range of the bipolar coil. The solenoid coils have a simple structure wound around the ferrite. It can greatly extend the zero crossing of the conventional bipolar coil, and effectively increase the charging range of the system. In addition, the solenoid coils can make the mutual inductance change smoothly in the middle region and reduce the influence caused by the misalignment of the coupling structure. The use of the proposed solenoid coils does not require any change to the original coil, which can better reduce the volume and cost of the system.

[1] Y. Zhang, et al., "Current balancing of a multiphase inverter for LCC-S compensated wireless power transfer system based on mutually negatively coupled inductors," *IEEE Trans. Power Electron.,* vol. 10, no. 38, pp. 12411-12415, Oct. 2023. [2] R. Xie, et al., "An interoperable wireless power transmitter for unipolar and bipolar receiving coils based on three-switch dual-output inverter," *IEEE Trans. Power Electron.,* vol. pp. 1-5, Feb. 2024. [3] Y. Wu, et al., "An antioffset electric vehicle wireless charging system based on dual coupled antiparallel coils," *IEEE Trans. Power Electron.,* vol. 5, no. 38, pp. 5634-5637, May. 2023. [4] Y. Zhang, et al., "Passive paralleling of multi-phase diode rectifier for wireless power transfer systems," *IEEE Trans. Circuits Syst. II-Express Briefs,* vol. 2, no. 70, pp. 646-649, Feb. 2023. [5] J. Mai, et al., "High-misalignment-tolerant IPT systems with solenoid and double D pads," *IEEE Trans. Ind. Electron.,* vol. 4, no. 69, pp. 3527-3535, Apr. 2022.

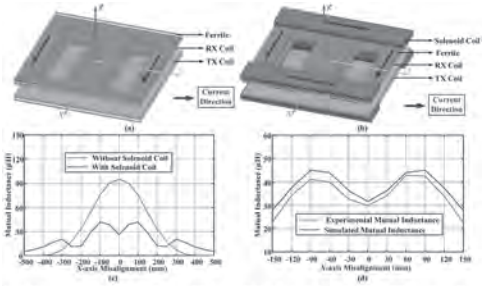

Fig. 1. Magnetic couplers and mutual inductance. (a) Bipolar coil without solenoid coils. (b) Bipolar coil with solenoid coils. (c) The mutual inductance with X-axis misalignment. (d) The simulated and experimental mutual inductance.

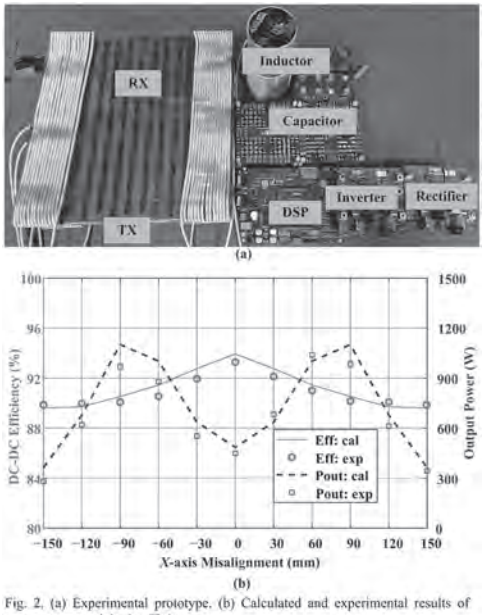

Fig. 2. (a) Experimental prototype. (b) Calculated and experimental results of output power and dc-dc efficiency.

VP11-03. The Analytical Calculation Model for Litz Wire Winding Loss in High-Power High-Frequency Transformers. *X. Li*[1,2] and Y. Li[1]
1. Hebei University of Technology, Tianjin, China; 2. The State Key Lab of Reliability and Intelligence of Electrical Equipment, Tianjin, China

High-power HFT, as key electromagnetic energy conversion components in high-power power electronic converters, account for approximately 30% of the total equipment loss. The calculation of winding loss is one of the primary focuses in the loss calculation of high-power HFT. Currently, Litz wire, composed of multiple smaller diameter strands intertwined, is selected as the winding material for high-power HFT due to its reduced high-frequency skin effect[1-2]. For the calculation of Litz wire winding loss, a theoretical analytical calculation model was proposed by Tourkhani in 2001[3], which has been widely applied in the efficient calculation of high-frequency transformer winding losses. However, as HFTs are increasingly applied in high-power scenarios, Litz wire windings are required to carry larger currents. Larger currents necessitate an increase in the cross-sectional area and the number of strands of each Litz wire, thereby imposing stricter requirements on the calculation of Litz wire winding loss. Through experimental measurements, it has been observed that the calculation error of the Tourkhani model increases as the number of Litz wire strands increases[4]. To address this drawback, an analytical calculation model suitable for high-current conditions is proposed in this paper. The analytical calculation model presented in this paper incorporates Ferreira's two-dimensional loss calculation model for round conductors. The fine strands within the Litz wire are thoroughly decomposed into magnetic field influences, specifically the internal magnetic field influence of other strands within the Litz wire (H_{int}) and the external magnetic field influence of other turns of Litz wire in the winding (H_{ext}). In the traditional Tourkhani model, due to excessive simplifications during the magnetic field decomposition and derivation process, accurate winding loss calculations are achieved for Litz wire windings with fewer strands. However, as the number of strands increases to hundreds or thousands, the calculation accuracy significantly decreases. The significance of the proposed analytical model lies in the accurate calculation of the AC resistance coefficient for Litz wire windings with a larger number of strands.

[1] Wojda R P, Kazimierczuk M K. Winding resistance and power loss of inductors with Litz and solid-round wires[J]. IEEE Transactions on Industry Applications, 2018, 54(4): 3548-3557. [2] Niyomsatian K, Gyselinck J J C, Sabariego R V. Experimental extraction of winding resistance in Litz-wire transformers—influence of winding mutual resistance[J]. IEEE Transactions on Power Electronics, 2019, 34(7): 6736-6746. [3] F. Tourkhani and P. Viarouge, "Accurate analytical model of winding losses in round Litz wire windings," IEEE Trans. Magn., vol. 37, no. 1, pp. 538–543, Jan. 2001. [4] C. Peng, G. Chen, B. Wang, and J. Song, "Semi-Analytical AC Resistance Prediction Model for Litz Wire Winding in High-Frequency Transformer," IEEE Trans. Power Electron., vol. 38, no. 10, pp. 12730–12742, Oct. 2023.

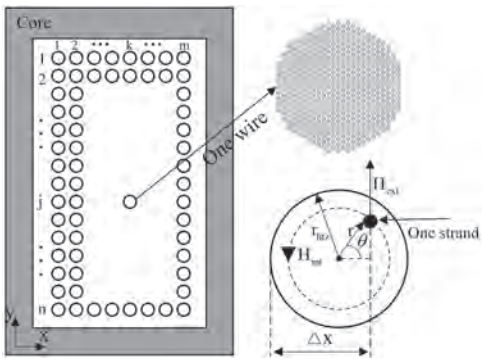

Fig. 1

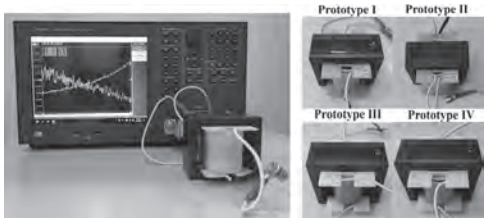

Fig. 2

VP11-04. The Influence of Different Slot Permanent Magnet Magnetization Directions on the Power Density Enhancement of Transverse Flux Linear Generator. *M. Chen*[1,2], L. Huang[2], G. Meng[1], T. Xia[1] and Y. Li[2] *1. Smart Grid Research Institute, Nanjing Institute of Technology, Nanjing, China; 2. School of Electrical Engineering, Southeast University, Nanjing, China*

I.Introduction In the past decades, low speed high power density machines have been widely used in direct drive wind power generation, direct drive wave energy conversion and ship propulsion system. Longitudinal flux linear generators are difficult to further improve their power density due to the mutual restraint of electromagnetic loads. In transverse flux linear generator (TFLG), the plane where the main magnetic flux path is located is perpendicular to the direction of secondary motion, thus the electrical and magnetic loads are decoupled and the problem of mutual constraints of electromagnetic loads is solved. Therefore, TFLG can achieve higher power density [1]. Placing permanent magnets (PMs) in the slot is a feasible method to further improve the power density and back electromotive force (EMF) quality [2]. In-depth research should be conducted on the shape and magnetization direction of the slot PMs, and adjustments should be made when considering actual prototype manufacturing and PM placement problems to obtain a better machine topology design solution. In this paper, a TFLG for direct drive wave energy conversion is proposed. Analysis is made on the shape and magnetization direction of the slot PMs. The simulation results prove that tangential magnetization can achieve higher power density than radial magnetization. II. Machine Configuration As shown in Fig. 1, the proposed TFLG consists of two primaries and a secondary. The slot PMs are inserted between the outer primary shoes and their magnetization directions are indicated in the figure. The secondary is composed of magnetic bars and nonmagnetic bars and it moves back and forth in a straight line along the *z*-axis. Fig. 1. III.Results As shown in Fig. 2, the average thrust and power density of tangential magnetized and radial magnetized slot PM types are 247.01N, 8.518kN/m^3 and 196.02N, 6.759kN/m^3, respectively. Fig. 2. IV.Conclusion Simulation results show that the outer primary slot PMs can help enhance thrust/power density and tangential magnetized slot PM type can achieve higher power density than radial magnetized one.

[1]M. Chen, L. Huang, Y. Li, J. Zhang, P. Tan and G. Ahmad, "Design and Analysis of a Field Modulated Transverse Flux Linear Generator Used in Direct Drive Wave Energy Converter," *IECON 2023- 49th Annual Conference of the IEEE Industrial Electronics Society*, Singapore, Singapore, 2023, pp. 1-6. [2]X. Zhao and S. Niu, "Design and Optimization of a Novel Slot-PM-Assisted Variable Flux Reluctance Generator for Hybrid Electric Vehicles," in *IEEE Transactions on Energy Conversion*, vol. 33, no. 4, pp. 2102-2111, Dec. 2018.

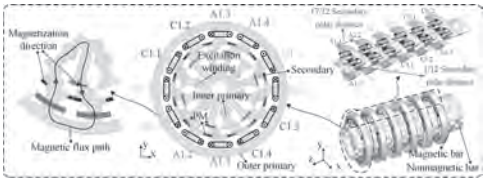

Fig. 1. Configuration of the proposed TFLG.

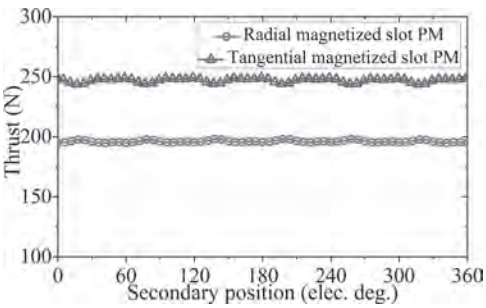

Fig. 2. Thrust waveforms of tangential magnetized and radial magnetized slot PM types.

VP11-05. Design and Analysis of a Dual-PM Excited Permanent Magnet Arc Motor With Staggered Rotor Configuration. *K. Wei*[1], Z. Pan[1], J. Zhao[1] and J. Cai[1] *1. School of Electrical Engineering and Automation, Hefei University of Technology, Hefei, China*

I. INTRODUCTION As a special linear motor, permanent magnet arc motor (PMAM) is widely used in some low-speed, high-torque applications [1]-[2]. However, the traditional PMAMs show the relatively high torque ripple. To address this issue, this paper proposes a new PMAM with parallel complementary (PC) configuration (PC-PMAM). The proposed PC-PMAM features a staggered rotor, which shows high average torque and low torque ripple. II. MOTOR TOPOLOGY AND OPERATION PRINCIPLE Fig. 1 shows the topologies of three different PMAMs. All the PMAMs consist of three stator units and a rotor. Each stator unit and the rotor forms a unit motor with 6 stator-slots/14 rotor-teeth combination. In Figs. 1(a)-(b), the proposed PC-PMAM is made up of two stacked axially sub-PMAMs. Moreover, the two sub-PMAMs share the common three-phase winding. More importantly, the two sub-PMAMs have the staggered rotors with the mechanical angle of 180°/70. And the staggered rotors have the opposite magnetized PMs. The PC-PMAM utilizes two staggered rotor to eliminate the even-order harmonics of the back-EMF, thereby reducing the cogging torque and torque ripple. The two comparative PMAMs shown in Figs. 1(c) and (d) are named as DPM-PMAM and SPM-PMAM, respectively. The DPM-PMAM has the indentical rotor and PMs. The SPM-PMAM has the staggered rotors having the opposite magnetized PMs. III. PERFORMANCE EVALUATION Fig. 2 compares the motor performances of three different PMAMs. As shown in Fig. 2(a), compared with the SPM-PMAM and DPM-PMAM, the proposed PC-PMAM has higher and more symmetrical flux linkage. In addition, compared with the SPM-PMAM, the proposed PC-PMAM and DPM-PMAM have higher back-EMF, as shown in Fig. 2(b). Figs. 2(c) and 2(d) show the torque performances of three PMAMs. Compared with the SPM-PMAM and DPM-PMAM, the proposed PC-PMAM has the highest average torque. Moreover, the PC-PMAM has lower torque ripple than the DPM-PMAM. Therefore, it can be concluded that the proposed PC-PMAM significantly reduces the torque ripple of the PMAM without reducing the average torque. More detailed design considerations and analysis of the comparative results will be presented in the full paper.

[1] Z. Pan, S. Fang, H. Lin, H. Yang, and S. Xue, "A new double-sided flux reversal arc permanent magnet machine with enhanced torque density capability," IEEE Trans. Magn., vol. 55, no. 6, pp. 1-6, Jun. 2019. [2] Y. Meng, S. Fang, Y. Zhu, Y. Yu, L. Qin, "Investigation of new dual-stator consequent-pole flux reversal permanent magnet arc machines," IEEE Trans. Appl. Supercon., vol. 34, no. 8, Nov. 2024, Art. no. 5204105.

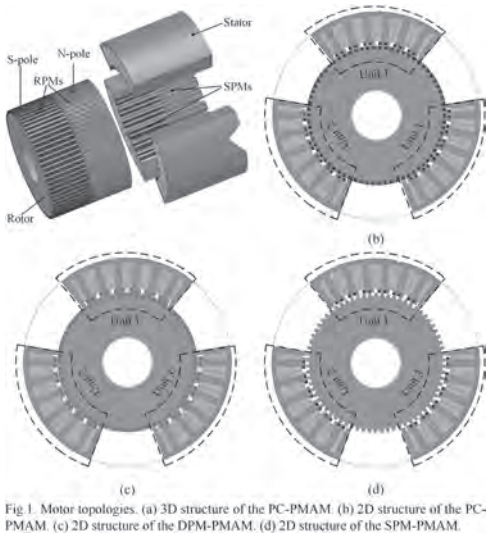

Fig 1. Motor topologies. (a) 3D structure of the PC-PMAM. (b) 2D structure of the PC-PMAM. (c) 2D structure of the DPM-PMAM. (d) 2D structure of the SPM-PMAM.

Fig. 1. Motor topologies.

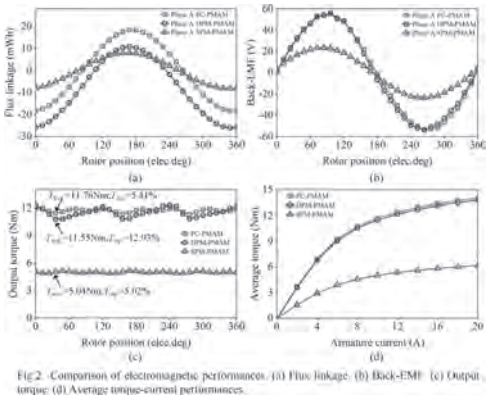

Fig. 2. Performances comparison.

VP11-06. Analysis of Receiving Coil Turns and Simplified Receiving Coil Configuration Effects on Inductive Angular Position Sensor Performance. *D. Xu*[1], Y. Zhao[1], X. Wang[1], F. Zeng[2] and S. Hwang[3]
1. School of Mechatronic Engineering and Automation, Shanghai University, Shanghai, China; 2. Shanghai Zenidrive Technology Co., Shanghai, China; 3. School of Mechanical Engineering, Pusan National University, Busan, The Republic of Korea

Inductive sensors are extensively utilized in automotive, motor, and industrial automation applications because of their high accuracy, reliability, and robust anti-interference capabilities [1]. Current researches on inductive angular position sensors aims to enhance measurement precision and reduce manufacturing costs. The sensor examined in this research features a rotor with four-phase pole pairs and a stator that includes excitation coils, receiving coils, and an integrated chip, all embedded on a PCB. The receiving coils shuttled back and forth as a sine shape or a cosine shape between the layers of excitation coil and connected by copper pillars as shown in Fig.1 (a) was named as one turn in this research. This study investigated the effects of the number of turns in the stator's receiving coils, as shown in Fig.1 the coil turns increasing from one turn in Type A to three turns in Type C, and the effects of simplified receiving coil design as Type D compared with Type A in Fig.1 in an inductive angular position sensor. In order to analyze the magnetic flux density, eddy current and induced voltage, four types were modeled and simulated by finite element method in transient electromagnetic field as shown in Fig.2 (a). The simulated induced voltages could be obtained in receiving coils, as shown in Fig.2 (b), and the simulated angular error could be processed in details following our previous work [2]. The detailed working principle and the effects of receiving coil turns and simplified receiving coil on inductive angular position sensor performance will be illustrated in the full manuscript. Four prototypes with different receiving coils will be manufactured and tested to verify the simulation results. This research contributes to the development of high-precision, cost-effective inductive angular position sensors by highlighting key considerations for the design of receiving coils.

[1] Gao, W., H. Shi, and Q. Tang, A Contactless Planar Inductive Sensor for Absolute Angular Displacement Measurement. *IEEE Access*, 2021. 9: p. 160878-160886. [2] Dan-Ping Xu, Guochao Ma, Silong Fang, Fanlin Zeng, Sang-Moon Hwang "A Contactless Inductive Position Sensor with Four-Phase Rotor for Angular Displacement Detection." *IEEE transactions on magnetics,* 60.2 (2024): 1–5.

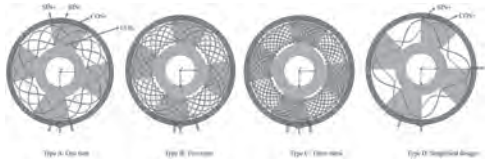

Fig.1 Different turns and simplified design of receiving coils

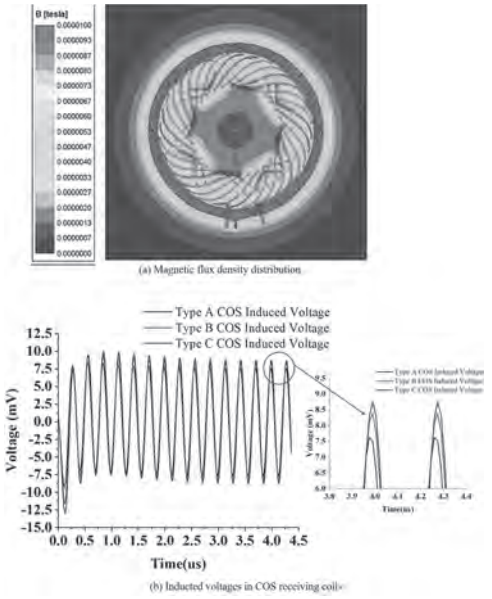

Fig.2 Distribution of magnetic flux density and inducted voltages.

VP11-08. Research on Radial Electromagnetic Force of FESS Hybrid Maglev Bearing. A. Zhongliang[1], *Y. Haoze*[1], G. Jun[1], Z. Ting[1] and L. Xiaojie[1] *1. Shenyang University of Technology, Shen Yang, China*

1 Intro There are some advantages by comparing hybrid magnetic bearings(HMB) with mechanical bearings. It has been applied in many applications such as high-speed compressors, FESS with HMB[1]. 2 Analysis of EMF in HMB Under ideal conditions, the HMB air gap is symmetrical. However, the geometric axis of the rotor in actual assembly may be offset. The rotor attitude diagram is shown in Figure 1. The air gap calculation is shown in formula(1) as $\delta_{min}=\delta_0-t\sin\theta-e$ (1) In the formula, δ_{min} is defined as the minimum air gap length, the air gap length at the equilibrium position is defined as δ_0, the length of the rotor deflection radius is defined as t, the deviation angle of the rotor geometric centerline is defined as θ, and the eccentricity is defined as e. The EMF calculation formula for HMB is shown in formula(2) as $F_{rad}=B^2(r,t)/2\mu_0$(2) In the equation, the EMF of HMB is defined as F_{rad}, the air gap magnetic density is defined as B(r, t), and the relative magnetic permeability in vacuum is defined as μ_0 The amplitude of magnetic density is affected by the size of the air gap, according to equations (1) and (2). Therefore, the magnitude of EMF is related to θ and e.A 6-pole HMB with a stator outer diameter of 135mm and an axial length of 23mm was selected as the research object. In this paper, the influence of the EMF magnitude of HMB on the rotor posture was explored. If the rotor is deflected around the x-axis and moves in the negative y-axis direction, the maximum EMF values and response surfaces of the two parameters mentioned above are calculated during the rotation period, as shown in Fig. 2. F_{rad} has been increased by 117.02% due to the expansion of θ and e. 3 Conclusion The conventional electromagnetic turbine mechanical EMF calculation formula is referenced, and the analytical model of EMF is established while considering the rotor deflection attitude. The correctness of the derived model was verified through finite element method, and the relationship between EMF and rotor attitude was summarized. The maximum value of EMF was positively correlated with θ and e.

[1] T. Du, H. Geng, Y. Zhang, H. Lin, Y. Li and L. Yu, "Exact Analytical Method for Active Magnetic Bearings With Rotor Eccentricity," *IEEE Trans. Magn.*, vol. 55, no. 12, pp. 1-12, Dec. 2019, Art no. 8301112.

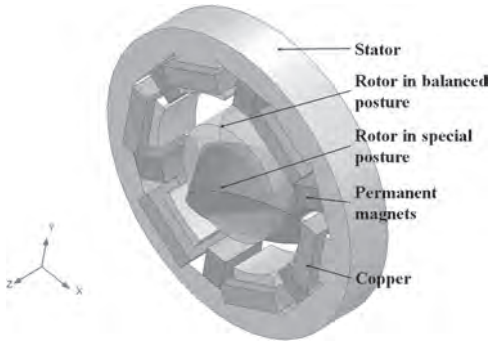

Fig. 1 Schematic diagram of rotor posture (enlarged air gap)

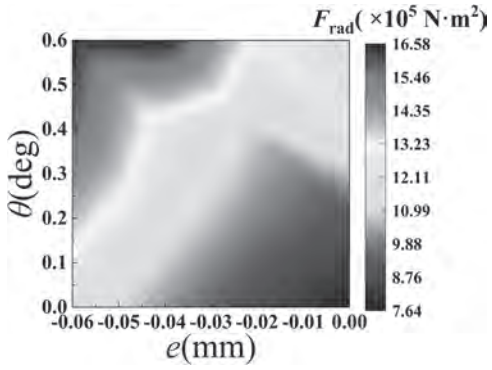

Fig. 2 Max of EMF response surface

VP11-09. Space-Time Simulation of Fault Current Limiters Involving Cores Exhibiting Hysteresis. *A.A. Adly[1,2] 1. Egypt-Japan University of Science and Technology (E-JUST), Alexandria, Egypt; 2. Elect. Power Engineering, Cairo University, Giza, Egypt*

Power systems are becoming more complex due to the recent trends of integration of different non-traditional sources as well as monitoring and protection components. While circuit breakers represent the main power systems protection components, inclusion of fault current limiters in specific network zones can enhance the protection level in addition to downscaling specifications requirements of those circuit breakers. In recent years, considerable efforts have been directed towards the development of fault current limiters. In these efforts, limiters comprised of conventional conducting coils have emerged as practical and low-cost alternatives (see [1]-[3]). For most fault current limiters laminated cores are utilized. However, the operation mechanism of such limiters offers the possibility of employing low-cost solid cores. In such cases, their design methodologies become more complicated since pronounced hysteresis and eddy currents and their effects on the limiters transient current limitation performance would have to be taken into consideration. The purpose of this paper is to present a space-time finite difference simulation approach for fault current limiters involving solid conducting cores exhibiting hysteresis as shown in Fig. 1. According to this approach, Maxwell's equations for each of the cylindrical cores may be expressed as [4]: $\nabla X \nabla XH=-\sigma(\partial B/\partial H)(\partial H/\partial t)$ (1) H_core1=H_DC+H_AC (2) H_core2=H_DC-H_AC (3) where, σ is the core conductivity, B is the flux density and H is the field resulting from the superposition of the applied bias DC current and the AC load current. An important feature of this approach is its ability to highlight the limiter surge current limitation as a function of its conductivity and complex magnetic properties thus facilitating its accurate design actions. Sample correlation between the limiter flux of its dual cores and the load current before and after a short circuit fault instant is shown in Fig. 2. Details of the approach, its computational approach and more simulation results are presented in the full paper.

[1] J.W. Moscrop, IEEE Transactions on Magnetics, Vol. 49, pp. 874-882 (2013). [2] J. Yuan et. al., Jiaxin, High Voltage, Vol. 5, pp. 416-424 (2020). [3] J.C. Knott and J.W. Moscrop. IEEE Transactions on Magnetics, Vol. 49, pp. 4132-4136 (2013). [4] A.A. Adly, Journal of Applied Physics, Vol. 79, pp. 4675-4677 (1996).

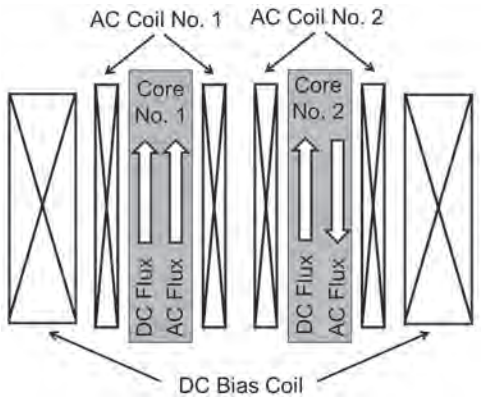

Fig. 1. Configuration of the solid core fault current limiter.

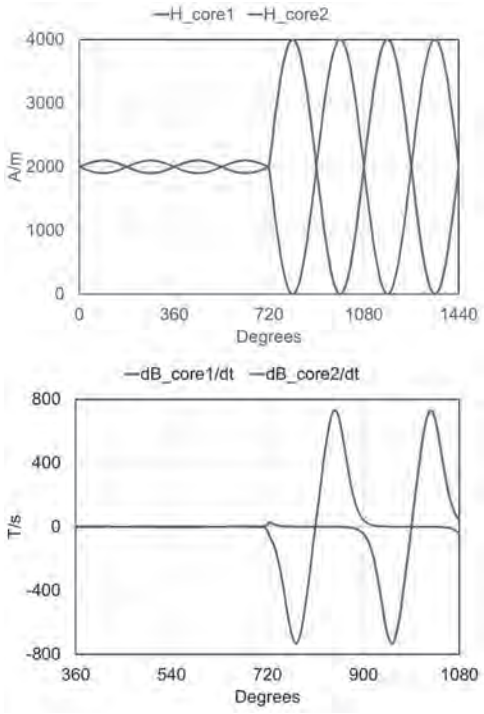

Fig. 2. Sample total field and voltage drop per turn and unit core coross sectional area.

VP11-10. Performance of Oriented Si-steel and Fe-Based Amorphous Alloy Core Transformers under DC Bias. *M. Zou*[1], M. Yang[1], T. Tang[1], L. Wu[1] and J. Si[1] *1. Chongqing University of Posts and Telecommunications, Chongqing, China*

Oriented silicon steel and Fe-based amorphous alloys are both widely used as iron core materials in power transformers. Silicon steel transformers (ST) offer good magnetic and electrical properties at a low cost. The amorphous transformer (AT) reduces 60% to 70% in no-load losses under sinusoidal excitation conditions compared to Si-steel core [1]. However, the performance of AT under DC bias remains less understood, despite the increasing occurrence of DC bias [2]. Existing literature primarily focuses on the magnetic and electrical properties of ST under DC bias [3]. Magnetic property research includes the frequency-dependent reluctance-based model [4],

Preisach hysteresis modeling [5], and anisotropic magnetostriction measurements [6]. Conversely, the electrical properties have been explored through studies on transformer protection [7], mitigation strategies [8], and transformer modeling [9]. However, the AT has lower saturation flux density, iron loss and higher electrical resistance than the ST. These inherent differences significantly impact their performances under DC bias conditions. This paper analyzes the influencing factors of primary side currents in transformers under DC bias using analytical methods. DC bias experiments are conducted on AT and ST. The primary side currents under loaded and unloaded conditions are measured, and changes in harmonic amplitudes under DC bias are analyzed (Fig. 1). Reactive power variations among different transformers are also examined. Finally, finite element models (FEM) are implemented in ANSYS to compare differences in iron core losses under DC bias (Fig. 2). The results show the amplitude of the primary current in ST is 11.3% higher than in AT. The increase in harmonic amplitudes is more pronounced in ST compared to AT. Peak iron core losses in AT decrease by 85.4% compared to ST. DC bias exacerbates the disparity in iron core losses between AT and ST. Due to abstract length limitations, additional experimental and FEM results will be presented in the full paper.

[1] Alexandrov N, Schulz R, Roberge R. Amorphous alloys for distribution transformers: design considerations and economic impact[J]. IEEE transactions on power delivery, 1987, 2(2): 420-424. [2] Harrison C W, Anderson P I. Characterization of grain-oriented electrical steels under high DC biased conditions[J]. IEEE Transactions on Magnetics, 2016, 52(5): 1-4. [3] Chen J, Wang D, Cheng S, et al. Influence of DC-biased magnetic induction on magnetic property of silicon steel[J]. IEEE Transactions on Magnetics, 2019, 55(5): 1-7. [4] Canturk S, Balci M E, Hocaoglu M H, et al. Investigation of the effects of DC bias on single-phase shell type transformers using frequency-dependent reluctance-based model[J]. IEEE Transactions on Magnetics, 2021, 57(9): 1-9. [5] Li Y, Zou J, Li Y, et al. Prediction of Core Loss in Transformer Laminated Core under DC Bias Based on Generalized Preisach Model[J]. IEEE Transactions on Magnetics, 2023. [6] Zhang Y, Wang J, Sun X, et al. Measurement and modeling of anisotropic magnetostriction characteristic of grain-oriented silicon steel sheet under DC bias[J]. IEEE transactions on magnetics, 2014, 50(2): 361-364. [7] Ahmadzadeh-Shooshtari B, Rezaei-Zare A. Advanced transformer differential protection under GIC conditions[J]. IEEE Transactions on Power Delivery, 2021, 37(3): 1433-1444. [8] Yang M, Deswal D, de Leon F. Mitigation of half-cycle saturation of adjacent transformers during HVDC monopolar operation—Part II: Detecting zero-sequence fault currents[J]. IEEE Transactions on Power Delivery, 2019, 35(1): 16-24. [9] Fuchs E F, You Y, Roesler D J. Modeling and simulation, and their validation of three-phase transformers with three legs under DC bias[J]. IEEE Transactions on Power Delivery, 1999, 14(2): 443-449.

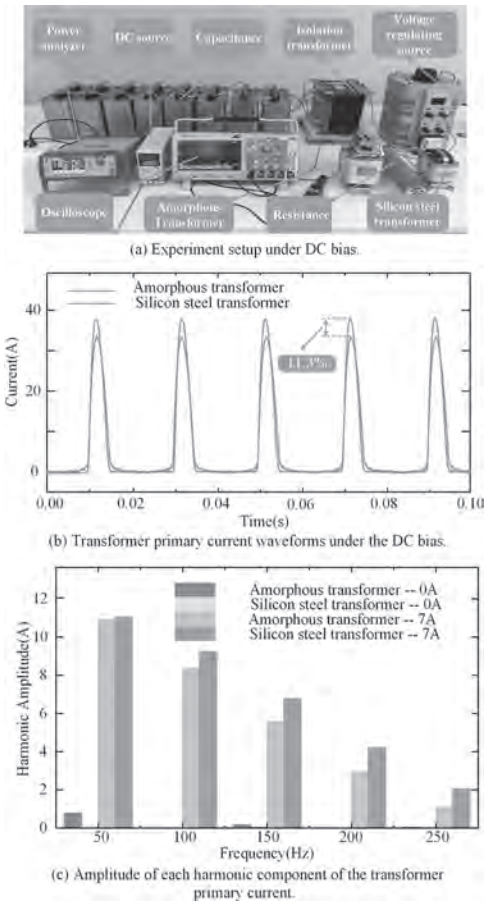

Fig.1 Experiment and results under DC bias.

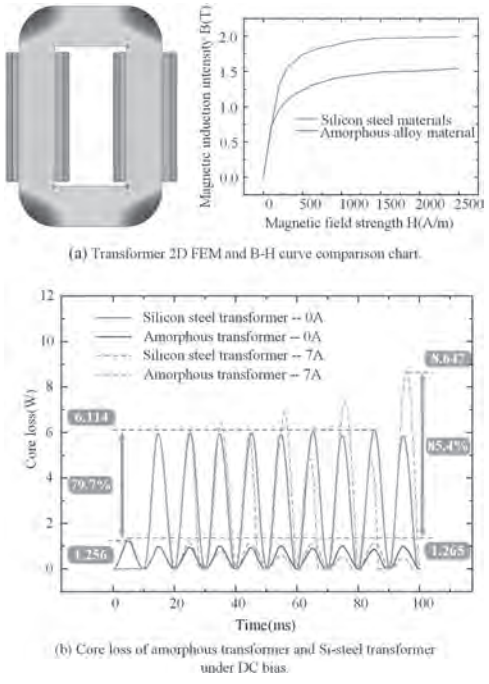

Fig.2 Transformer 2D finite element model and iron core loss waveform.

Now GV-01

VP11-11. A novel composite soft magnetic material based three-phase saturated core fault current limiter. *J.L. Liu*[1,2], J. Yuan[1,2] and J. Wu[3]
1. School of Electrical Engineering and Automation, Wuhan Univerisity, Wuhan City, China; 2. State Key Laboratory of Power Grid Environmental Protection, Wuhan University, Wuhan City, China; 3. Central China Branch of State Grid Corporation of China, Wuhan City, China

The traditional three-phase saturated core fault current limiter (TFCL) uses silicon steel sheet as the its body core. And the core is alternately desaturated when the short circuit fault occurs. However, the silicon steel sheet has a high saturation point (1.9T~2.0T), which causes the excitation source to need a larger magnetomotive force to bias the silicon steel sheet to the saturation state during normal operation, which increases the overall cost. In addition, the dynamic performance of the silicon steel sheet is insufficient, the transient change speed of the permeability is not good at the moment when the fault occurs, and the current limiting effect of the transient short circuit current is poor, which is difficult to meet the requirements of the rapid protection of the system. Therefore, the study of new magnetic materials has become a new direction to solve the above problems. This paper proposes a novel composite soft magnetic material based three-phase saturated core fault current limiter (NTPFCL). The four transient short-circuit fault currents of three-phase HVAC systems can be limited. Through the finite element simulation, it can be seen that the current limiting effect of NTPFCL body can be significantly improved compared with the TFCL current limiting result of external reactor. For example, in the case of single-phase short circuit fault, NTPFCL current limiting effect is improved by 16%. Compared with TFCL of external reactor, the current limiting effect is close to that of external reactor. Therefore, NTPFCL can not only further improve the transient current limiting effect of short circuit current, but also eliminate TFCL external current limiting reactor, which has higher economy and application prospects. The simulation results show that the structure and function of NTPFCL are effective.

J. Yuan et al., "A novel concept of fault current limiter based on saturable core in high voltage DC transmission system," AIP Adv. 8 (2018).

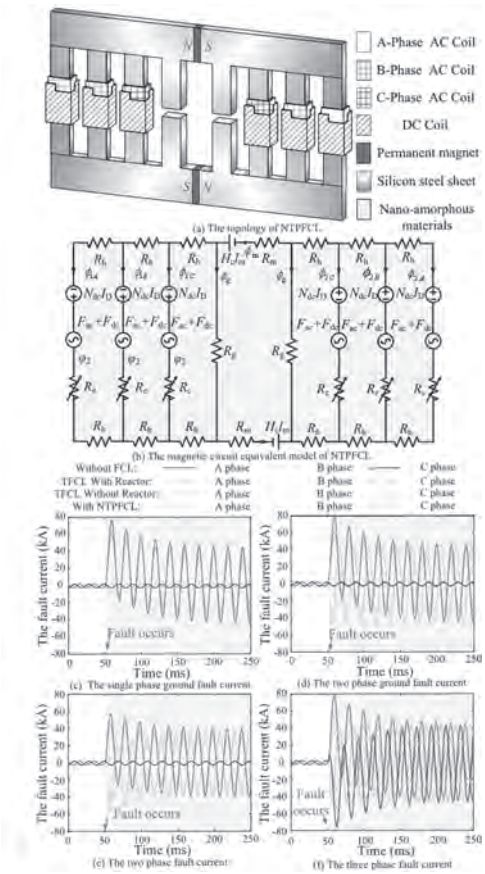

Figure 1

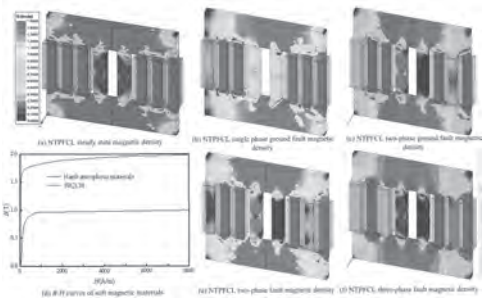

Figure 2

VP11-12. Design and Implementation of Fixed-bias Flux 3-Phase Magnetic Bearing. *S. Noh*[1], J. Park[1], D. Lee[2] and H. Cho[1,2] *1. Convergence System Engineering, Chungnam National University, Daejeon, The Republic of Korea; 2. Electrical, Electronics, and Communication Engineering Education, Chungnam National University, Daejeon, The Republic of Korea*

This paper presents the design and experimental results of a magnetic bearing system that employs permanent magnets part as a fixed-bias flux and incorporates a three-phase electromagnet part to maintain the rotor's central position. Magnetic bearings (MB) offer numerous advantages over traditional contact bearings, including lubrication-free operation, no wear, and extended lifespan due to their contactless nature [1-4]. Conventional hybrid magnetic bearings typically control the rotor position through differential control of bias flux generated by permanent magnets and control current from electromagnets. However, this approach does not fully utilize the force of the permanent magnets. To address this limitation, the proposed design maximizes the utilization of permanent magnet force. Additionally, magnetic bearings that use a three-phase winding system require fewer circuit

components compared to those operating with a single-phase full-bridge converter. Therefore, a 12-pole heteropolar magnetic bearing connected in a three-phase arrangement is placed at the top and bottom to enable radial position control. The electromagnetic characteristics of the proposed model were analyzed using an equivalent magnetic circuit modeling approach. Specifically, the study examined the relationship between the rotor's eccentricity. Fig. 1. shows the magnetic flux density in the permanent magnet region for rotor eccentricities of 0.1 mm, 0.3 mm, and 0.5 mm along the x-axis. Precise force calculations were performed based on the calculated magnetic flux density, and the results were compared and validated with three-dimensional(3-D) finite element analysis (FEA). Based on this analysis, comprehensive system force modeling was conducted. Subsequently, a 3-D mechanical design was performed to develop manufacturing plans and the experimental setup. Fig. 2. shows the fabricated electromagnet part of the system. Using a digital signal processing (DSP) microcontroller and other low-cost electronic components, experimental tests were conducted.

[1] N. R. Hemenway and E. L. Severson, "Three-Pole Magnetic Bearing Design and Actuation," *IEEE Trans. Ind. Appl.,* vol. 56, no. 6, pp. 6348-6359, Nov.-Dec. 2020. [2] X. Sun, L. Chen and Z. Yang, "Overview of Bearingless Permanent-Magnet Synchronous Motors," *IEEE Trans. Ind. Electron.*, vol. 60, no. 12, pp. 5528-5538, Dec. 2013. [3] H. Sugimoto, Y. Uemura, A. Chiba and M. A. Rahman, "Design of Homopolar Consequent-Pole Bearingless Motor With Wide Magnetic Gap," *IEEE Trans. Magn.,* vol. 49, no. 5, pp. 2315-2318, May 2013. [4] W. Zhao and L. Mei, "Reseach on Modular Permanent Magnet Bias Magnetic Bearing," *J. Electr. Eng. Technol.*, vol. 17, pp. 3283-3296, Aug. 2022.

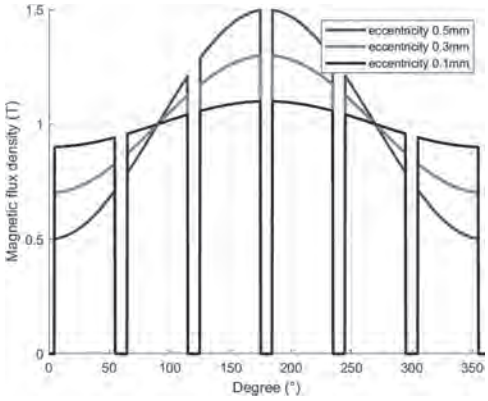

Fig.1. Magnetic flux density in the permanent magnet region for rotor eccentricities of 0.1 mm, 0.3 mm, and 0.5 mm along the x-axis.

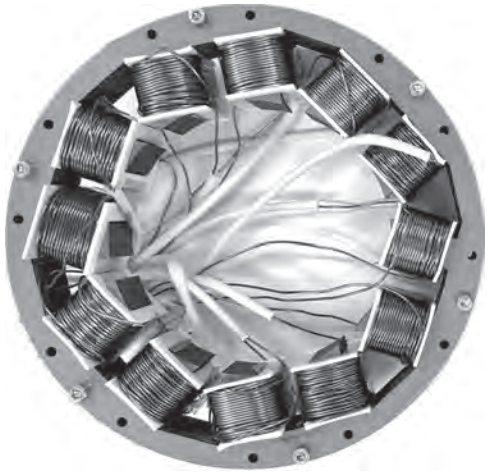

Fig.2. Fabricated electromagnet part of the system.

VP11-13. Study on the performance regulation characteristics of orthogonal controllable reactors considering different magnetic materials. J. Yuan[1,2], *J. Hou*[1,2], H. Zhou[1,2], X. Li[1,2] and G. Ma[1,2,3]
1. State Key Laboratory of Power Grid Environmental Protection, Wuhan University, Wuhan, China; 2. School of Electrical Engineering and Automation, Wuhan University, Wuhan, China; 3. Department of Electrical and Electronic Engineering, The Hong Kong Polytechnic University, Hong Kong, China

The orthogonal controllable reactors(OCRs) operate based on the magnetron principle, whereby the degree of magnetic saturation in the orthogonal region is controlled by superimposing a regulated DC flux. This process alters the permeability of the region and consequently adjusts the reactor's inductance [1]. The device is characterized by linear and smooth regulation of inductance, making it highly suitable for resonant applications such as filtering[2]. Theoretical analysis underscores that the core material's properties in the OCR are pivotal in determining its inductance regulation range and losses. Therefore, selecting appropriate materials is critical to optimizing device performance. This study focuses on three types of silicon steel sheet materials: ordinary thickness oriented silicon steel sheet, ultra-thin oriented silicon steel sheet, and ultra-thin non-oriented silicon steel sheet. Specifically, we evaluate 30Q130, GT100, and 10JNEX900 to compare their effects on the inductance adjustment range and losses of OCR through simulation. The topology of the OCR is depicted in Fig. 1(a), where the AC core adopts a closed core configuration, and the DC core consists of two identical 'C-type' cores orthogonal to the AC core. The windings include two AC windings (W_{ac1}, W_{ac2}) and two DC windings (W_{dc1}, W_{dc2}), with each winding placed on the side columns of their respective cores and connected in series. Fig. 1(b)(c) displays the BH and BP curves for the three materials. Fig. 2 presents the inductance regulation characteristics and losses of the OCR utilizing these materials. Notably, 30Q130 exhibits the widest inductance regulation range, while GT100 demonstrates the highest inductance value in the absence of DC current. Conversely, 10JNEX900 saturates first due to its higher initial permeability and lower saturation point when unsaturated. Furthermore, the OCR using 30Q130 material exhibits the lowest losses, aligning with its lower iron loss curve. Therefore, for applications at 50 Hz, 30Q130 emerges as the superior material.

[1]Y. Li *et al*., "A Controllably Inductive Filtering Method With Transformer-Integrated Linear Reactor for Power Quality Improvement of Shipboard Power System," *IEEE Transactions on Power Delivery*, vol. 32, no. 4, pp. 1817-1827(2017) [2]J. Yuan, X. Zheng and F. Chen, "Analysis and Optimized Design of a Novel Compact Orthogonal Controllable Reactor,", IEEE Transactions on Power Delivery, vol. 37, no. 6, pp. 4527-4538(2022)

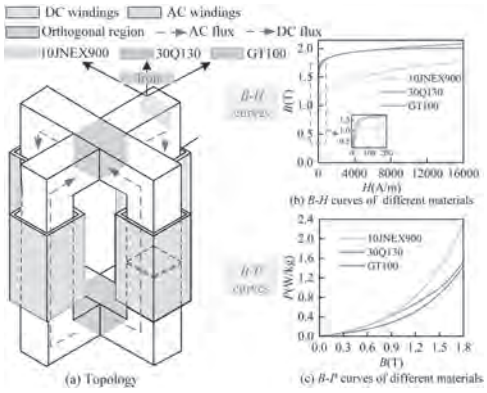

Fig. 1: Topology of OCR and B-H and B-P curves for the core materials used

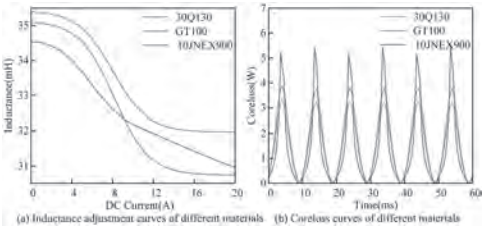

Fig. 2: Inductance regulation characteristic curves and loss curves of OCR using three materials.

Session VP12
MAGNETIC TEXTURES AND DYNAMICS: EXPERIMENTAL DETECTION AND MODELING (Poster Virtual Session)

Jonathan Leliaert, Co-Chair
Ghent University, Ghent, Belgium
Lucas Perez, Co-Chair
Universidad Complutense de Madrid, Madrid, Spain

VP12-01. In-plane magnetic field dependence of torque exerted on a domain wall in Pd/Co_2MnGa. *T. Koyama*[1], Y. Nishioka[1], T. Uemura[1] and M. Yamanouchi[1] *1. Graduate School of Information Science and Technology, Hokkaido University, Sapporo City, Japan*

A heavy metal/a Weyl ferromagnet bilayers are promising for efficient current-induced domain wall (DW) motion because one can use both topological Hall torque (THT) induced by Weyl electrons in the Weyl ferromagnet [1] and spin-orbit torque (SOT) originating from the spin Hall effect in the heavy metal to move DWs. In this work, we investigated the in-plane magnetic field dependence of torque exerted on the DW to clarify the mechanism of current-induced DW motion in a perpendicularly magnetized bilayer composed of heavy metal Pd and Weyl ferromagnet Co_2MnGa (CMG). Pd (3.0 nm) / CMG (1.8 nm) was deposited on an MgO (001) substrate. The stack was processed into a Hall-bar structure with a 2-μm wide channel and a pair of Hall probes. After preparing a DW in the channel, the DW position was monitored by measuring the transverse resistance while sweeping a perpendicular magnetic field under a constant current and in-plane magnetic field (H_x) along the channel direction. The coercive field required to propagate the DW through the probes varied almost linearly with current under H_x, which indicates an effective perpendicular magnetic field (H_{eff}) was exerted on the DW by current. From the linear slope, efficiency (η_J) of H_{eff} generation per unit current density was evaluated. The value of η_J showed the local maximum at $\mu_0 H_x$ = 10 mT and decreased monotonically at large | $\mu_0 H_x$|, where μ_0 is the permeability of the vacuum. On the other hand, η_J originating from SOT, which is derived by measuring the hysteresis loop shift, varied almost linearly with respect to H_x at low $|H_x|$ and saturated at large $|H_x|$ in a heavy metal/a conventional ferromagnet bilayers, as reported previously [2]. These results indicate that the observed current-induced DW motion cannot be explained only by the contribution of SOT and the other torque such as the THT can be exerted on DW in Pd/CMG. This work was supported in part by JSPS KAKENHI (22K18961), MEXT X-NICS (JPJ011438), MEXT ARIM (JPMXP1224HK0020), and JST CREST (JPMJCR22C2).

[1] Y. Araki and J. Ieda, Phys. Rev. Lett. 127, 277205 (2021). [2] C. Pai, *et al*., Phys. Rev. B 93, 14409 (2016).

VP12-02. Thermal stability of skyrmions in polycrystalline thin film. *S. Onaka*[1], T. Tanaka[1], S. Kashiwagi[1] and X. Ya[2] *1. ISEE, Kyushu University, Fukuoka, Japan; 2. Artificial Intelligence and Big Data College, Chongqing College of Electronic Engineering, Chongqing, China*

In recent years, there has been a great deal of research on skyrmions that can be used as magnetic memories [1-2]. LLG and the nudged elastic band (NEB) calculations estimated magnetic energy for skyrmion configured in magnetic thin film pattern consisted of fine grains where the magnetizations of the neighboring grains coupled through weak inter-gain exchange interactions in the present study. A magnetic thin film pattern was modeled by 0.5-nm-thick and laterally 256 nm square. The averaged values of the perpendicular anisotropy field, the saturation magnetization and Voronoi grain size were 14 kOe, 800 emu/cc and 8 nm, respectively. DMI constant was 1.5 erg/cm^2. Figure 1 shows diameters of the skyrmion for relax state as a function of the inter-grain exchange constant, where large area (16% of the film pattern size) initial reverse domain was artificially introduced before the magnetization relaxations. Theoretical diameter of skyrmion for single crystal film is 26 nm[3]. The figure indicates that skyrmion diameter increases with decreasing the inter-grain exchange constant due to non-flat energy landscapes, causing domain wall pinning at grain boundaries in relaxation process. Energy barrier height ΔE was derived using NEB calculations. There are two typical cases need to be considered. One is skyrmion collapse, where magnetizations of the center of the skyrmion switch, and the other is boundary annihilations. Magnetic structure of the skyrmion is topologically stable, so resultant $\Delta E/k_B T$ were high in the case of the skyrmion collapse. On the other hand, $\Delta E/k_B T$ for the boundary annihilation case are low especially for the film with large inter-grain exchange constant. Figure 2 shows the thermal stability indexes ($\Delta E/k_B T$) for the two typical cases as a function of the diameters of the skyrmions. The figure indicates that ΔE/kBT are proportional to the diameter of skyrmions. Probable reason is that magnetostatic energies are lower when the diameter of skyrmions are larger.

[1] R. Tomasello, E. Martinez, R. Zivieri, L. Torres, M. Carpentieri, G. Finocchio, Scientific Reports 4, 6784 (2014). [2] J. Ding, X. Yang, and T. Zhu, J.Phys.D:Appl. Phys. 48(11), 115004 (2015). [3] X. S. Wang, H. Y. Yuan, X. R. Wang, Nat. Commun. Phys. 1, 31 (2018).

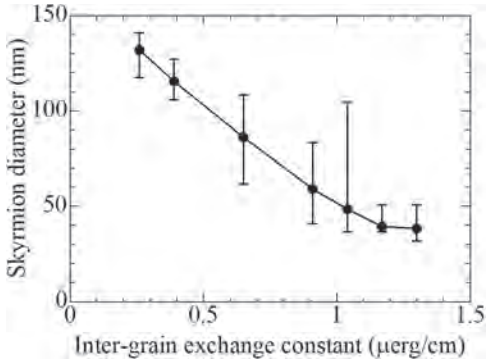

Fig. 1: Diameters of skyrmions.

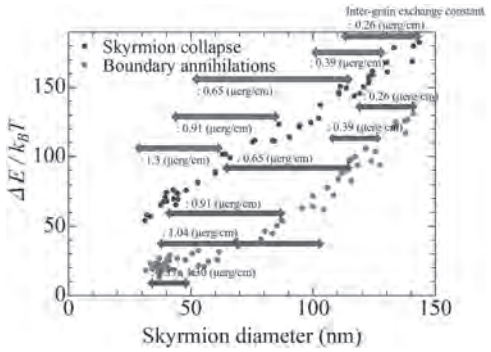

Fig. 2: Thermal stability indexes for skyrmions collapse and boundary annihilation.

VP12-03. Excitation Modes for Spin Waves in a Two-dimensional Magnetic Vortex Lattice. *P. Bhattacharjee*[1] and S. Barman[1,2] *1. Department of Basic Sciences and Humanities, Institute of Engineering & Management, Kolkata, India; 2. University of Engineering & Management, Kolkata, India*

In the flux-closure vortex state, nano- and micron-sized magnetic platelets exhibit in-plane curling magnetization and nanometer-sized perpendicularly magnetized vortex cores. Possessing the simplest nontrivial configuration, these objects are of wide interest to micromagnetics and may provide novel paths for spintronics applications. Spin wave eigen modes resulting from the magnetostatic interaction are present in vortex state structures at frequencies more than an order of magnitude higher. Using micromagnetic simulations, we looked at the spin wave modes of a two-dimensional square magnetic vortex lattice in six different lattice configurations using a sinc-function field applied in-plane and perpendicular to the disk plane. This study, therefore, provides an in-depth understanding of the collective azimuthal and radial spin-wave eigen frequencies in a two-dimensional lattice of magnetic vortices and may provide a new approach for creating a new type of magnonic crystal employing magnetic vortices arranged in a lattice.

[1] M.-W. Yoo, J. Lee, and S.-K. Kim, *Appl. Phys. Lett.* 100, 172413 (2012). [2] M. Helsen, A. Gangwar, J. De Clercq, A. Vansteenkiste, M. Weigand, C. Back, B. Van Waeyenberge, *Appl. Phys. Lett.* 106, 032405 (2015). [3] M. Noske, H. Stoll, M. Fahnle, R. Hertel, G. Schutz, *Phys. Rev. B* 91, 014414 (2015).

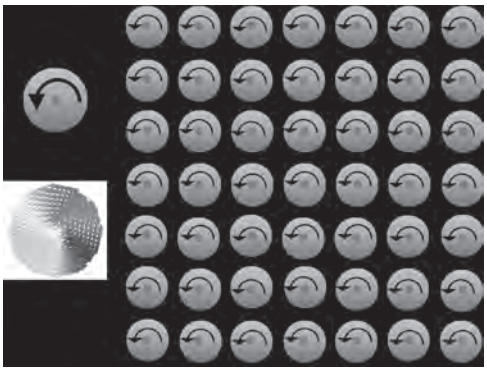

Fig. 1: A diagrammatic representation of the two-dimensional lattice of magnetic vortices under consideration. The zoomed image to the left displays the micromagnetic structure of the isolated magnetic vortex, which has a diameter of 100 nm and a thickness of 30 nm

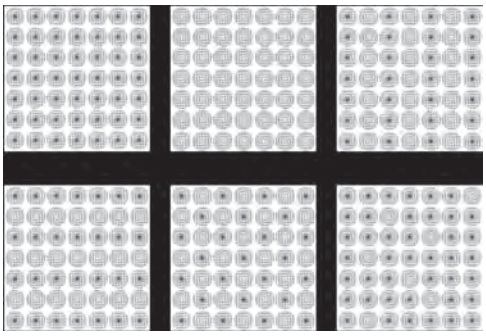

Fig. 2: The ground state spin configuration of the two-dimensional magnonic vortex lattice: (I) Ferromagnet (F+1), (II) Ferromagnet (F-1), (III) Vertical Stripe Antiferromagnet (VSA) (IV) Horizontal Stripe Antiferromagnet (HSA) (V) Chessboard Antiferromagnetic (CA), and (VI) Random Point Defects (RPD). The magnetic vortices have CCW (c = +1) chirality, and the black and white dots depict the vortex cores with polarizations of p = +1 and p = -1, respectively.

VP12-04. Constriction Effects on Magnetic Skyrmion Behavior in Magnetic Nanowires. *W.Z. Al Saidi*[1] and R. Sbiaa[1] *1. Physics, Sultan Qaboos University, Muscat, Oman*

Artificial intelligence (AI) has recently advanced beyond conventional boundaries and found applications in varied scientific domains, including physics. One area of particular interest is the intersection of AI with magnetic skyrmions, which are chiral nanoscale spin structures known for their topological protection [1]. Skyrmions show promises for high-density, low-power spintronic devices [2], and as such, they are a focus of research aimed at revolutionizing memory technologies and computational paradigms. Skyrmions have the potential for applications requiring precise manipulation at the nanoscale because of their small size, stability, and controllability [3]. Recent research has demonstrated the generation, manipulation, and annihilation of skyrmions by different mechanisms, such as spin-orbit torque, magnetic fields, spin transfer torque (STT), and ultrafast heating pulses [4]–[6]. Furthermore, a path toward applying multistate memory devices is provided by studying skyrmion dynamics in multi-stepped nano-tracks [7]. The behavior of skyrmions under various situations is crucial in the search to develop efficient memory systems. The impact of material characteristics, current pulses, and nano-constriction dimensions on skyrmion dynamics has been investigated. The possibilities for large-capacity memory systems that can store several states per cell were achieved. The notable repulsive forces between skyrmions and the edges of nanostructures highlight the complex interplay of forces controlling skyrmion motion. Researchers can accomplish accurate positioning and stable confinement within individual steps of the nanostructure by taking advantage of the repulsive forces between skyrmions. This work not only opens the door for multistate memory devices but also has potential applications in artificial intelligence (AI) and neuromorphic computing, fields where effective information processing and storage are critical. In conclusion, the convergence of memory technology, artificial intelligence, and skyrmion research presents extensively unheard-of chances for creativity.

[1] O. Boulle et al., Nature Nanotech. 11, 449 (2016). [2] H. Y. Kwon et al., NPG Asia Materials 12, 86 (2020). [3] A. Casiraghi et al., Communications Physics 2, 145 (2019). [4] J. Masell et al., Phys. Rev. B 101, 214428 (2020). [5] S. Woo et al., Nature comm. 8, 15573 (2017). [6] S. G. Je et al., Nano letters 18, 7362-7371 (2018). [7] W. Al Saidi et al., Sci. Rep. 12, 10141 (2022).

VP12-05. Simulation on Spin-Orbit Torque Switching with Stray Field Assistance. *J. Chen*[1], J. Liu[1], Z. Liu[1], W. Li[1], J. Lu[1] and S. Peng[1] *1. Fert Beijing Institute, School of Integrated Circuit Science and Engineering, BeihangUniversity, Beijing, China*

Spin-orbit torque (SOT) is a key writing technology for magnetic random access memory (MARM) due to fast speed, high reliability, and separation of read and write paths [1-2]. Voltage-controlled magnetic anisotropy (VCMA) lowers the energy barrier during magnetization switching by applying a voltage across the magnetic tunnel junction (MTJ) [3-5]. Integrating multiple MTJs on a shared write line can improve the storage density by using the VCMA effect as a selective mechanism and the SOT effect as a write mechanism. However, SOT-induced switching of deterministic perpendicular magnetization necessitates an in-plane external field, which limits its practical application. Utilizing the in-plane stray field from a magnet under the heavy metal layer is promising to realize field free SOT switching [6-8], while further study is needed in MTJ arrays. In this paper, we simulate spin-orbit torque switching with stray field assistance in a single MTJ and MTJ arrays. First, the stray field of an in-plane magnet with the size of 120nm×60nm×3nm is calculated to be 12.6mT (Fig. 1a). Through Mumax simulation, the single MTJ with the diameter of 60nm can be switched under the cirtical current of 12MA/cm^2 with pulse width of 2ns (Fig. 1b). Moreover, in the array of two MTJs, both MTJs can be switched with a critical current of 13MA/cm^2. However, the in-plane component of stray field in the MTJ2 is only 0.9 mT in the array of three MTJs (Fig. 2a). The perpendicular component of the magnetic moment oscillates slowly, which takes 10ns to switch with a critical current of 14MA/cm^2 (Fig. 2b). Furthermore, in

an array of four MTJs, the MTJ2 and MTJ3 cannot be switched due to the small stray field. In conclution, this work demonstrates feasibility of SOT switching with stray filed assistance in a single MTJ and the array with two MTJs, but the arrays with more than three MTJs cannot perform well.

[1] M. Cubukcu, O. Boulle, M. Drouard, Appl. Phys. Lett., Vol. 104, no. 4, Art. no. 042406(2014) [2] M. Wang, W. Cai, D. Zhu, Nat. Electron., Vol. 1, no. 11, p.582-588(2018) [3] S. Peng, J. Lu, W. Li, in Proc. IEEE Int. Electron Devices Meeting, p.28.6.1-28.6.4(2019) [4] W. Li, Z. Liu, S. Peng, IEEE Electron Device Lett., Vol. 45, no. 5, p.921-924(2024) [5] J. Lu, W. Li, J. Liu, Appl. Phys. Lett., Vol. 122, no. 1, Art. no. 012402(2023) [6] K. Cai, G. Talmelli, K. Fan, in Proc. IEEE Int. Electron Devices Meeting, p.36.2.1-36.2.4(2022) [7] K. Garello, F. Yasin, H. Hody, in Proc. Symp. VLSI Circuits, p.T194-T195(2019) [8] M. Gupta, Y. Xiangt, F. García-Redondo, in Proc. IEEE Int. Electron Devices Meeting, p.1-4(2023).

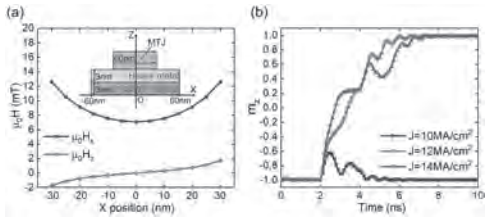

Fig. 1 (a)Distribution of the stray field. Inset: Schematic of a single MTJ stack. (b)Perpendicular component of magnetization (m_z) under different SOT currents.

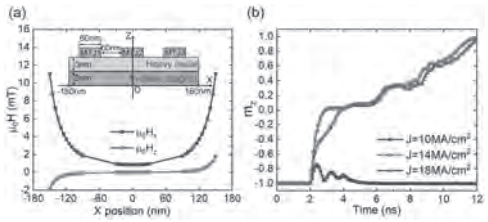

Fig. 2 (a)Distribution of the stray field. Inset: Schematic of three MTJs array. (b)Perpendicular component of magnetization (m_z) under different SOT currents.

VP12-06. Incorporation of Anisotropic Vector Hysteresis Model into FEA Based on TEAM Problem 32. *R. Chen*[1], F. Martin[2], S. Yue[3], Y. Li[3] and Y. Li[3] *1. Department of Electrical Engineering, Tsinghua University, Beijing, China; 2. Department of Electrical Engineering and Automation, Aalto University, Espoo, Finland; 3. Hebei University of Technology, Tianjin, China*

The precise electromagnetic simulation of electrical equipment requires an accurate magnetic properties model of the core material. General finite element analysis (FEA) software can not consider the hysteresis effect and magnetic anisotropy of material at the same time and only uses simple models such as isotropic or orthotropic models to characterize the magnetic properties, inevitably resulting in inaccurate magnetic field distribution and loss calculations. The Newton method is widely used in FEA software as a solving method. However, most hysteresis models are numerically discrete, making it difficult to effectively define the Jacobian matrix, which affects the convergence of Newton method. Besides, when a complex anisotropy model is incorporated, the differential magnetic permeability matrix is asymmetric, reducing the efficiency of Newton method. An anisotropic vector hysteresis model is proposed in our previous work [1], which can reproduce and forecast the anisotropic properties and the losses of electrical steel sheets over a wide range of rotational and alternating excitations. This paper studies the incorporation of the proposed model into FEA. First, the magnetic field equations based on scalar magnetic potential are selected according to the features of the proposed model and the corresponding solving process of the magnetic field is derived. Second, the positive definiteness of the partial derivative matrix of the proposed model is checked to ensure the convergence stability of its application. Then, the calculation program is written in Freefem++ software [2] and the calculation process is introduced in detail. Finally, experiments and simulations are conducted on the TEAM32 problem [3-4], as shown in Fig.1. In the simulation, the average number of iterations is 30 and the overall computation time is relatively short, demonstrating the high computational efficiency of the proposed method. By comparing the simulation results of magnetic flux density at different positions with the experimental results, the accuracy of the proposed method is verified, as shown in Fig.2.

[1] R. Chen, F. Martin, Y. Li, IEEE Transactions on Industrial Electronics., Vol. 71, No. 6, pp. 6084-6094 (2024). [2] F. Hecht, Journal of numerical mathematics., Vol. 20, No. 3-4, pp. 251-266 (2012). [3] O. Bottauscio, M. Chiampi, C. Ragusa, IEEE Transactions on Magnetics., Vol. 38, No. 2, pp. 893-896 (2002). [4] S. Yue, P. I. Anderson, Y. Li, IEEE Transactions on Energy Conversion., Vol. 36, No. 4, pp. 3251-3260 (2021).

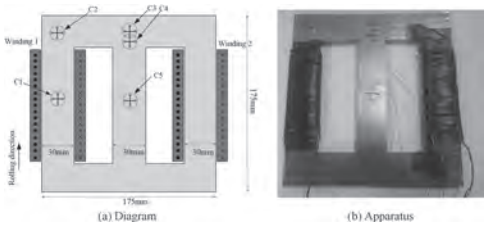

Fig.1 TEAM32 problem.

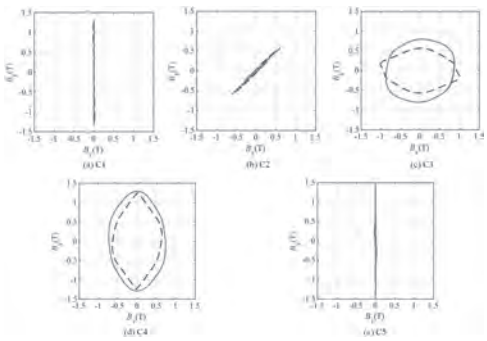

Fig.2 Comparison of measured (dashed line) and simulated (solid line) magnetic flux density loci.

VP12-07. Data-Driven Neural Network Prediction of Hysteresis Behavior of Soft Magnetic Materials under Physical Constraints. *Y. Qin*[1], Z. Li[1], Y. Li[1], R. Pei[1,2] and L. Zeng[2] *1. Department of Electric Engineering, Shenyang University of Technology, Shenyang, China; 2. Suzhou Inn-Mag New Energy Ltd., Suzhou, China*

Soft magnetic materials (e.g. electrical steel) are widely used in electrical equipment for electric motors, transformers and reactors due to excellent magnetic properties. However, rotation of magnetic domains during the magnetization process results in a nonlinear hysteresis of the magnetic properties, which has an important impact on the magnetic field, excitation source, and energy loss of electrical equipment. Relying on tests to obtain hysteresis characteristics under various conditions is expensive in terms of time and cost, so it is important to accurately and quickly calculate and predict the hysteresis behavior of soft magnetic materials. In this paper, a physically constrained neural network is proposed to predict the hysteresis behavior of soft magnetic materials based on the preisach analytic positive hysteresis model. The Preisach model reflects the physical mechanism of the magnetization process in a certain sense and is superior in simulating the hysteresis properties of magnetic materials. Based on the method proposed, not only the hysteresis behavior of soft magnetic materials at a single frequency can be predicted, but also the hysteresis behavior at different frequencies can be predicted, and the six parameters of the preisach analytical model can be identified based on the measured data. In order to verify

the validity of the method, tests were carried out using oriented electrical steel (GOES), and non-oriented electrical steel (NGOES). The results show that based on the method proposed in this paper, the predicting of hysteresis behavior of soft magnetic materials has the characteristics of high accuracy and fast convergence speed, which can better judge the hysteresis behavior of soft magnetic materials, and is of great significance for the calculation of hysteresis loss and the optimal design of electrical equipment.

[1] Grech C, Buzio M, and Pentella M, "Dynamic ferromagnetic hysteresis modelling using a Preisach-recurrent neural network model", Materials., Vol.13, No. 11, p.2561(2020). [2] Semenov M E, Borzunov S V, and Meleshenko P A, "The Preisach model of hysteresis: fundamentals and applications", Physica Scripta, Vol.99, No.6, p.062008(2024). [3] R Liu, Y Du, and L Li, "Derivation and modification of analytical forward Preisach hysteresis model", Proc.CSEE, Vol.43, p.2070-2079(2023).

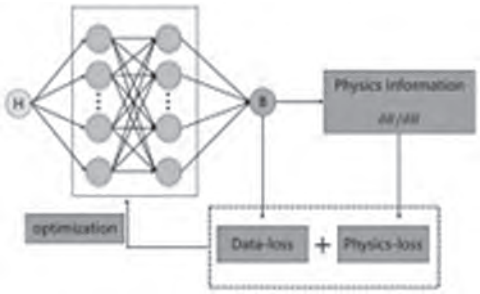

Fig.1 Data-driven neural network calculation flow

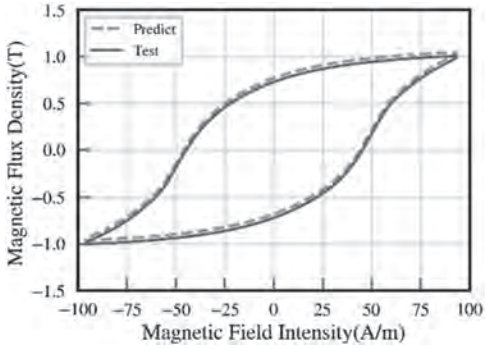

Fig.2 Comparison of test results and predicted results

VP12-08. Simulation of ultrafast magnetization dynamics in ferromagnetic nanoparticles. P. Steblinski[1], T. Blachowicz[1,2] and *A. Ehrmann*[1,3] *1. Virtual Institute of Applied Research on Advanced Materials (VIARAM), Bobolin, Poland; 2. Institute of Physics—Center for Science and Education, Silesian University of Technology, Gliwice, Poland; 3. Faculty of Engineering and Mathematics, Bielefeld University of Applied Sciences and Arts, Bielefeld, Germany*

Ultrafast magnetization dynamics of thin-film magnetic samples can be investigated by pump-probe experiments, i.e. a strong pump laser induces a heat pulse which leads to a reduction of the magnetic anisotropies in the sample and thus a change in the direction of the superposition of external magnetic field and internal anisotropies. The resulting magnetization vector change leads to a damped precession which can be measured by the weak probe laser [1-3]. Experimental investigations by pump-probe measurements pose challenges regarding the overlap of both laser spots and the delay between both measurements. Modeling this process can thus be supportive to understand ultrafast magnetization dynamics of thin film samples or magnetic nanostructures [4]. Here we report a new model based on micromagnetic simulations, using the finite element method, which we applied to investigate ultrafast magnetization dynamics in Fe nanoparticles, embedded in an MgO layer to ensure adequate thermal conditions (Fig. 1). Heat transport was calculated by the two-temperature model. The simulations are based on solving the Landau-Lifshitz-Bloch (LLB) equation. As an example, Fig. 2 shows the y-component of the spin precession in the Fe nanoparticle depicted in Fig. 1, applying an external magnetic field of 35.8 kA/m at an angle of 30° to reach saturation. Angle-dependent simulations of the precession frequencies (Fig. 2b) reveal a clear difference between such nanoparticles and the values calculated by the Kittel equation [5] for demagnetization factors representing a large thin film [6]; instead they show angle-dependent anisotropies strongly dependent on the sample orientation (Fig. 2b-d). Such simulations thus allow for estimating the ultrafast magnetization dynamics of diverse samples and optimizing samples for ultrafast magnetization reversal.

[1] E. Carpene, E. Mancini, D. Dazzi, C. Dallera, E. Puppin, S. De Silvestri, Ultrafast three-dimensional magnetization precession and magnetic anisotropy of a photoexcited thin film of iron, Phys. Rev. B 81, 060415(R) (2010) [2] E. Carpene, E. Mancini, C. Dallera, E. Puppin, S. De Silvestri, Femtosecond laser spectroscopy of spins: Magnetization dynamics in thin magnetic films with spatio-temporal resolution, Thin Solid Films 519, 1642-1648 (2010) [3] S. Monda, A. Barman, Laser Controlled Spin Dynamics of Ferromagnetic Thin Film from Femtosecond to Nanosecond Timescale, Phys. Rev. Appl. 10, 054037 (2018) [4] T. Korn, F. Giesen, J. Podbielski, D. Ravlic, C. Schueller, D. Grundler, Time-resolved study of the increased magnetization precession frequency in Fe wires, J. Magn. Magn. Mater. 285, 240-244 (2005) [5] C. Kittel, Introduction to Solid State Physics 4th Edition, John Wiley and Sons (New York, London, Sydney, Toronto) (1971) [6] M. Bauer, Grundlagen und Strategien für schnelles Schalten der Magnetisierung, PhD thesis, Kaiserslautern University (2000)

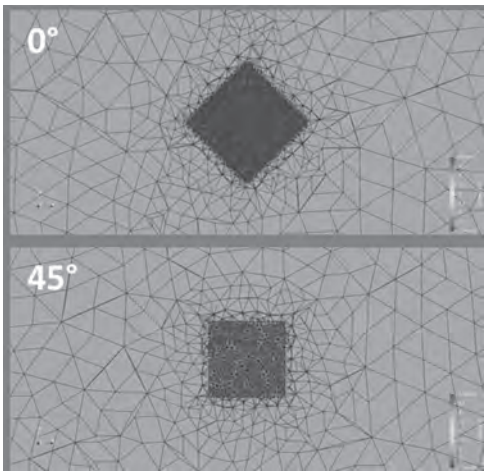

Fig. 1: Meshing of an Fe nanoparticle embedded in a larger MgO film.

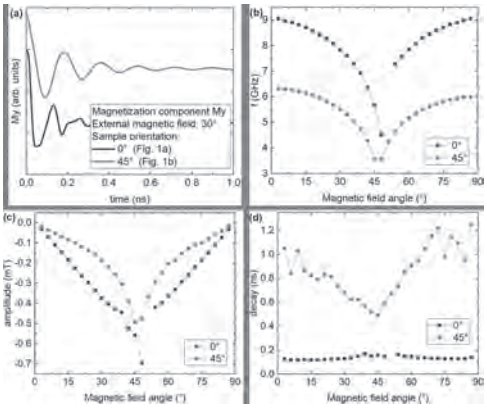

Fig. 2: (a) Spin precession (y-component) after applying a pump-pulse on a square Fe nanoparticle (50 nm x 50 nm x 5 nm) at an external magnetic field orientation of 30°; fits of (b) precession frequency, (c) precession amplitude, and (d) decay of the precession for the sample orientations shown in Fig. 1.

Session VP13
MAGNETOELECTRIC MATERIALS AND PHENOMENA & ENERGY HARVESTING AND VIBRATION ANALYSIS (Poster Virtual Session)

Raghav Sharma, Chair
Indian Institute of Technology Ropar, Delhi, India

VP13-01. Voltage-controlled magnetic anisotropy gradient-driven skyrmion-based half-adder and full-adder. *S. Sara*[1], C. Murapaka[1] and A. Haldar[2] *1. Physics, IITH, Hyderabad, India; 2. MSME, IITH, Hyderabad, India*

Spintronic devices have revolutionized the way we process or store information compared to dissipative charge-based electronics [1]. Among various spin-based technologies, skyrmions – topologically protected nano-size spin textures have emerged as the most promising alternative for future data processing [2]. We have proposed and demonstrated a skyrmion-based novel nanomagnetic device that executes Half-Adder and Full-Adder logic operations by driving the skyrmions through voltage-controlled magnetic anisotropy gradient (VCMA). VCMA is a more desirable method of driving the skyrmions as it avoids Joule heating to a greater extent, suppressing skyrmion and device instability issues. The proposed method of moving the skyrmions is energy efficient as it consumes much less energy than the skyrmion motion driven by electric currents[3]. This research presents a robust and scalable design for skyrmion-based logic devices, paving the way for advanced, energy-efficient data processing technologies.

1 S. A. Wolf, D. D. Awschalom, and R. A. Buhrman, *Science* 294(5546):1488-95 (2001). 2 Fert, A., Reyren, N. & Cros, V. *Nat Rev Mater* 2, 17031 (2017) 3 W. Kang, Y. Ran, and W. Zhao, *IEEE Trans Nanotechnol*,16, 387–395(2017).

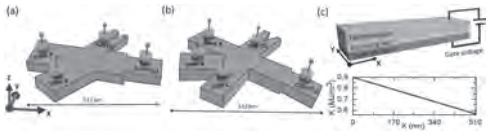

Fig. 1. Schematic of skyrmion-based logic device: (a) Half-adder with two inputs (A, B) and two outputs (S, C_0) (b) Full-adder with three inputs (A, B, C) and two outputs (S, C_0). (c) Sketch of voltage-controlled magnetic anisotropy device, where the voltage-controlled magnetic anisotropy *K* linearly decreases along the spatial coordinate *x* with a graph showing the decrease of magnetic anisotropy *K* with increasing the distance along the *x*-direction.

VP13-02. Strain induced multiferroicity in $Co_{3-x}Sb_xO_4$ (x=0, 0.1 and 0.2) thin films. *J. Rahman*[1], V. Gowtham[2], S. Murugan[2], N. Rajeevan[1] and R. Ramadurai[2] *1. Department of Physics, Farook Autonomous College, University of Calicut, Calicut, India; 2. Material Science and Metallurgical Engineering, IIT, Hyderabad, Hyderabad, India*

Cobalt oxide (Co_3O_4) with spinel structure is extensively studied for its magnetic properties and its multifunctional applications. The doping of stereo chemically active elements is expected to reduce the symmetry and in effect alter the electric and magnetic properties of Co_3O_4 spinel oxides. In this study, the effect of doping of Sb, a stereo chemically active element in Co_3O_4 powder prepared by solid state method and thin films grown by pulsed laser ablation was carried out. The thin films were deposited on Al_2O_3 (0001) single crystal substrates. The effect of substitution in the structure of the parent compound was analyzed using x-ray diffraction and Raman studies. The magnetic measurements performed at room temperature confirmed the presence of ferrimagnetic ordering in these powder samples as well as in thin films. The symmetry reduction due to the lone pair effect of Sb doping was studied and the effect of it was observed in the ferroelectric properties of the thin film studied under Piezoresponse Force Microscopy and in magneto-optic Kerr studies. The stereo chemically active Sb is expected to have induced a symmetry reduction in these thin films and give rise to ferroelectric behavior and magneto-optic effects at room temperature. The study confirms the simultaneous presence of electric and magnetic ordering in thin films thus showing potential multiferroic character.

1. B. Antic, G.F. Goya, H.R. Rechenberg, V. Kusigerski, N. Jovic, M. Mitric, J. Phys.: Condens. Matter 16 (2004) 651. 2. S. Kumar, Alimuddin, R. Kumar, A. Dogra, V.R. Reddy, A. Banerjee, J. Appl. Phys. 99 (2006) 08M910. 3. N. Fujiwara, H. Yasuoka, Y. Ueda, Phys. Rev. B 57 (1981) 3539. 4. J. L. Dormann, M. Nogues, J. Phys.; Condens. Matter 2 (1990) 1223. 5. G. Srinivasan, E.T. Rasmussen, R. Hayes, Phys. Rev. B 67 (2003) 014418. 6. D. Joung, A. Chunder, L. Zhai, S.I. Khondaker, Appl. Phys. Lett. 97 (2010) 093105. 7. Y. Ikedo, J. Sugiyama, H. Nozaki, H. Itahara, J. Brewer, E. J. Ansaldo, G.D. Morris, D. Andreica, A. Amato, Phys. Rev. B 75 (2007) 054424. 8. W.L. Smith, A.D. Hobson, Acta Cryst. B 29 (1973), 362. 9. N. E. Rajeevan, P. P. Pradyumnan, Appl. Phys. 92 (2008) 102910. 10. N.E. Rajeevan, K. Ravi, D. K. Shukla, P.P. Pradyumnan, S.K. Arora, I.V. Shvets, Mater. Sci. Eng. B 163 (2009) 48. 11. N. E. Rajeevan, R. Kumar, D. K. Shukla, P. Thakur, N. B. Brookes, K. H. Chae, W. K. Choi, S. Gautam, S. K. Arora, I. V. Shvets, P. P. Pradyumnan, J. Phys.: Condens. Matter 21 (2009) 406006. 12. S.R. Gawali, A. C. Gandhi, S.S. Gaikwad, J. Pant, T-S. Chan, C-L. Cheng, Y-R. Ma, S. Y. Wu, Sci. Rep. 8(1) (2018) 249.

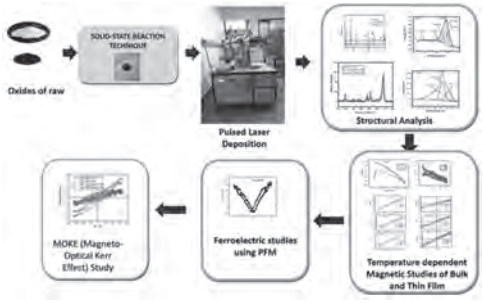

Fig. 1: Graphical Abstract of the work

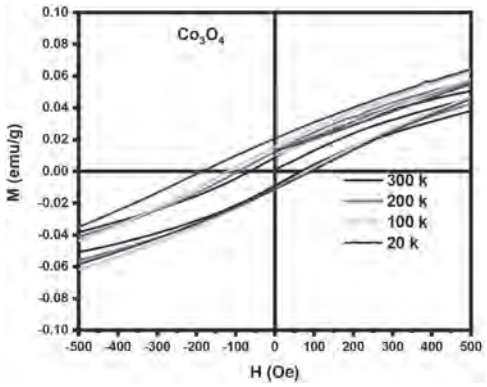

Fig. 2: M-H loop of Co3O4

VP13-03. Investigation of structural and magnetic properties of $MnTa_2O_6$. *M. Anas*[1] and P. Kharel[1] *1. Chemistry, Biochemistry and Physics, South Dakota State University, Brookings, SD, United States*

The XY_2O_6 (X = Cr, Mn, Fe, and Co and Y = Ta/Nb) class of compounds have several applications in communications, high-performance capacitors, etc. Depending on the X and Y cations, the crystal structure can be either tetragonal, orthorhombic, or monoclinic. In the present work, the magnetic properties of $MnTa_2O_6$ have been investigated. The compound is found to have an orthorhombic (space group *Pbcn*) crystal structure, with the unit cell parameters a = 14.4421(14)Å, b = 5.7649(4) Å, and c = 5.0910(4) Å, obtained from Rietveld refinement of the x-ray diffraction data, shown in the figure below. The magnetic properties have been studied by measuring dc magnetization of the compound. A magnetic transition is found to occur at 6K in the magnetization vs temperature curve due to the antiferromagnetic ordering of the Mn moments. The presence of short-range correlations is also observed in the temperature variation of magnetization measurement. The analysis of dc magnetization has been done using the Curie-Weiss law in the paramagnetic regime. The effective magnetic moment is calculated to be 6 μ_B/f.u., in accordance with the theoretically expected value for manganese at Mn^{2+} state. In addition, the value of Curie-Weiss temperature is found to be negative, confirming the presence of antiferromagnetic interactions in the system. From the analysis of dc magnetization data, the values of exchange constants in the mean-field approximation have also been determined. In the isothermal magnetization measurements at 2K, a spin-flop transition from one antiferromagnetic state to another is observed in the system near 2.4T. The effect of temperature on the spin-flop transition is studied systematically. In, addition, the impact of substitution on the magnetic properties and the spin-flop transition will also be discussed. This work is supported by the U.S. Department of Energy (DOE) Established Program to Stimulate Competitive Research (EPSCoR) grant no. DE-SC0024284

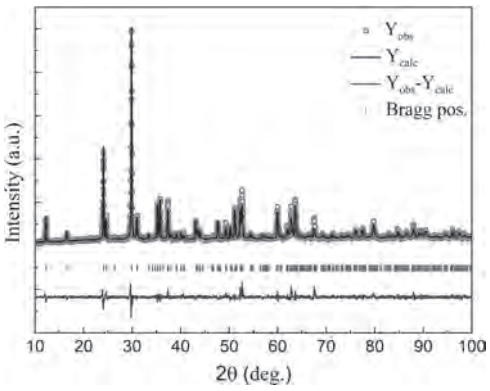

Fig. 1: Room temperature XRD pattern and fit for $MnTa_2O_6$.

VP13-04. Calculation of Vibration in Transformer Laminated Cores under DC Bias Based on Electric-magnetic-mechanical Coupling Model. *H. Li*[1], X. Zhao[1], Y. Yu[1], R. Li[1], L. Liu[2] and Z. Du[2] *1. Department of Electrical Engineering, North China Electric Power University, Baoding, China; 2. Hebei Provincial Key Laboratory of Electromagnetic and Structural Performance of Power Transmission and Transformation Equipment, Baoding, China*

1. Introduction Direct current (DC) bias is an abnormal working state of power transformers. The vibration and the noise of the laminated cores increase significantly, which affects the stable operation of the Power grid [1]. Conventionally, core vibration is calculated based on the finite element method. Although the calculation accuracy is guaranteed, the calculation speed is not satisfactory. In this article, a new modeling method is proposed to calculate the flux density and the vibration displacement. Moreover, its input parameter only requires the voltage and the direct current as the input data, making it more suitable for practical engineering applications. The accuracy of calculation results under varying DC biased excitations is evaluated and validated experimentally using the laminated core model of a single-phase three-column transformer. 2. Electric-magnetic-mechanical coupling Model To accurately analyze the vibration characters of the laminated core, the magnetic field distribution characteristics of the cores are calculated first. Due to the inner and outer magnetic circuit length and effective magnetic permeability area of the core are different, the magnetic reluctance distribution on the magnetic flux path of the core is not uniform. Based on the laminated core structure characteristics, the magnetic circuit model of the laminated core is presented. The structure of the laminated core is shown in Fig.1. The coupling between the electric circuit and the magnetic circuit is realized by harmonic balance method. The vibration equation of the laminated core under magnetostriction can be obtained by D 'Alembert's principle. Based on the vibration equation, the equivalent vibration two-port networks of the core is presented using the electro-mechanical analogy method [2]. 3. Results and analysis The comparison results of the measured and the calculated vibration displacement under DC magnetic field H_{dc}=6A/m and 12A/m are shown by Fig.2. Due to the DC bias, the vibration displacement waveform of the core is distorted. More details about modeling and calculation will be presented in the extended full paper.

Y. Li, J. Zou and Y. Li, IEEE Transactions on Magnetics., Vol. 60, p.1-5 (2024) X. Zhao, Li Lin and Cheng Zhiguang, Proceedings of the CSEE., Vol.30, p.103-108 (2010) L. Butler J, H. Sherman C, Transducers and Arrays for Underwater Sound., p.91-115 (2016)

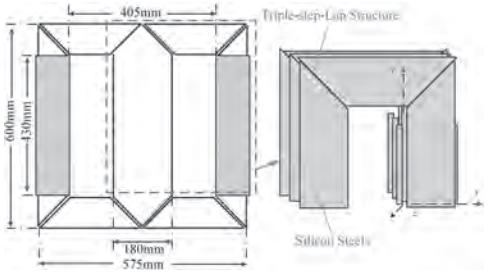

Fig. 1: The structure of the laminated core model

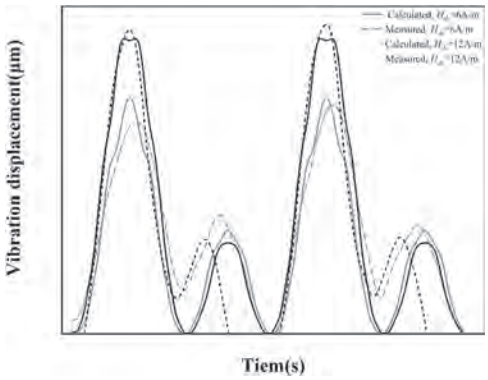

Fig. 2: Comparison of calculated and measured results under DC bias

VP13-05. Vibration and Noise Measurement of High-frequency Transformer Cores with Different Shapes Under Non-Sinusoidal Excitation. Y. Li[1], *X. Liu*[1], Y. Dou[2], T. Chen[1] and Z. Dong[1] *1. State Key Laboratory of Reliability and Intelligence of Electrical Equipment, Tianjin, China; 2. Zhejiang University–University of Illinois at Urbana-Champaign Institute, Zhejiang University, Haining, China*

With the rapid development of power electronic technology and the widespread use of new magnetic materials, the application of high-frequency transformers is becoming increasingly widespread. Compared to traditional transformers, high-frequency transformers have more diminutive size, higher power density, and environmental friendliness. Therefore, they are widely used in smart grids, photovoltaic power generation, wind power, electric vehicles, and other fields, making them indispensable core equipment in power electronic transformers [1-3]. This study chooses the widely used magnetic material nanocrystalline 1K107 to fabricate four different shapes of transformer cores: rectangular, square, ring, and oval, as shown in Fig.1. The vibration and noise characteristics of these different geometric core shapes were measured under sinusoidal and square wave excitations. The study includes analyses of the vibration velocity and noise of cores with different geometric shapes, exploring the impact of excitation waveforms and geometric shapes on the vibration and noise of high-frequency transformers. Experimental results indicate that the amplitude of vibration velocity and noise increases with increased excitation frequency and magnetic flux density. Vibration and noise under square wave excitation are more significant than under sinusoidal excitation. Under square wave excitation, vibration contains more even-order high-frequency harmonics, leading to more severe waveform distortion. Fig.2 shows that the vibration of rectangular core is the largest, followed by oval and square ones, while the vibration and noise of ring core is the smallest. A more symmetrical geometric structure can effectively reduce the vibration and noise of the core.

[1] P. C. Sarker, M. R. Islam and Y. Guo, State-of-the-art technologies for development of high frequency transformers with advanced magnetic materials, IEEE Trans. Appl. Supercond., vol. 29, no. 2, pp. 1-11(2019). [2] M. Mogorovic, and D. Dujic, Sensitivity analysis of medium-frequency transformer designs for solid-state transformers, IEEE Trans. Power Electron., vol. 34, no. 9, pp. 8356-8367(2019). [3] Y. Li, Z. Yang and C. Zhang, vibration and noise measurement of medium-high frequency transformer cores under non-sinusoidal excitation, IEEE Trans. Magn., vol. 58, no. 8, pp. 1-5(2022).

Fig. 1. Nanocrystalline cores and their sizes.

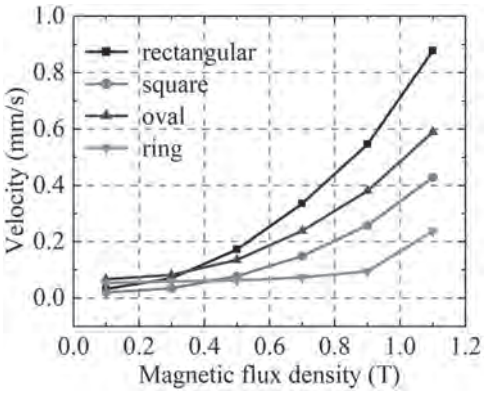

Fig. 2. Average vibration velocity of cores with different shapes under square wave excitation(5kHz)

VP13-06. Optimizing Wave-Driven Electromagnetic Energy Harvesters: An Evaluation of Magnetic Configurations. *J. Park*[1], T. Martinez[1], S. Jordon[1], Y. Choi[1], N. Wereley[1] and A. Flatau[1] *1. University of Maryland, College Park, MD, United States*

With increasing concerns about global climate change, there is a growing emphasis on renewable energy sources. Wave energy, with a global potential of 2 terawatts, presents a significant opportunity for sustainable power generation [1], [2]. This research aims to design and fabricate a wave-driven electromagnetic energy harvester to capture low-frequency ocean waves (0.03 - 0.3 Hz), with a particular emphasis on optimizing performance through various magnetic configurations. The system harnesses wave energy through repulsive magnetic levitation, generating electricity using a levitating permanent magnet and a copper coil. External transferring magnets, influenced by the vertical motion of the waves, cause the levitating magnet to move [Fig. 1]. When the transferring magnets move the levitating magnet downward, it is repelled by the base magnet, causing the levitating magnet to rapidly ascend and generate electricity. As the waves move upward, the combined effects of gravity and magnetic repulsion lead to higher acceleration of the magnet, producing greater electricity. Experimental trials with a sine wave of 0.2 Hz demonstrated successfully induced voltage peaks at regular intervals [Fig. 2(a)]. The observed maximum output voltage was 2.4 V. The relative force between the transferring magnets and the levitating magnet is crucial, as it determines the repelling force between the levitating magnet and the base magnet. Four different configurations of the transferring magnets were tested, showing a correlation between the number of transferring magnets and power [Fig. 2(b)]. The tests with different wave frequencies produced varying average power outputs (0.08 - 0.12 W), indicating that the wave speed influences the levitating motion [Fig. 2(c)]. This research explores various magnetic configurations to optimize the harvester, including the strength of the transferring, levitating, and base magnets.

[1] L. Buttel, "America's electricity generation capacity," American Public Power Association, (2023) [2] T. Thorpe, "A brief review of wave energy, technical report. no. r120," Energy Technology Support Unit (ETSU), A report produced for the UK, Department of Trade and Industry, (1999)

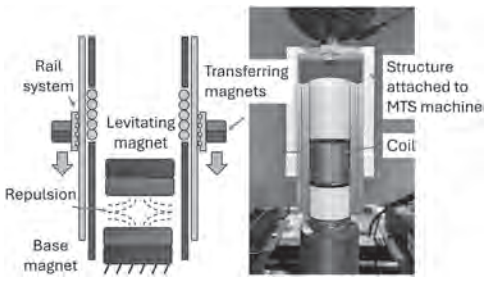

Fig. 1 (Left) Schematic illustration of the energy harvester. (right) energy harvester in the uniaxial testing setup.

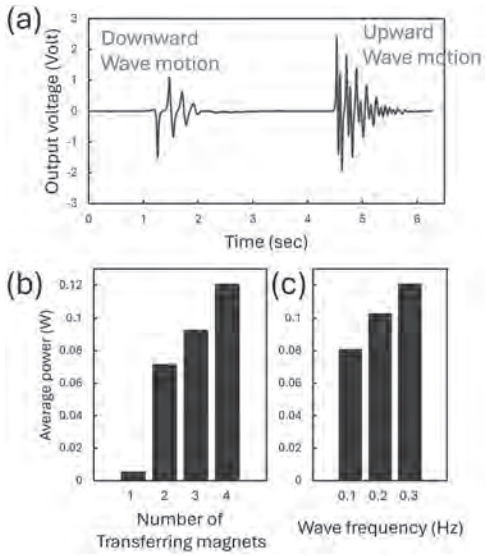

Fig. 2 (a) Voltage generated during sine wave excitation at 0.2. Hz. (b) average output power plotted as a function of the number of transferring magnets and (c) excitation wave frequency (Hz).

VP13-07. Analyzing Electrical Transport Phenomena in $NdMn_{0.3}Co_{0.7}O_3$. *F.H. Bhat*[1], G. Anjum[2] and A. Jan[1] *1. Physics, IUST, Kashmir, Awantipora, India; 2. Physics, SAM Degree College, Budgam, J&K, Budgam, India*

The effect of Co doping on the conduction mechanism of polycrystalline $NdMn_{0.3}Co_{0.7}O_3$ (NMCO7) sample, is studied by measuring the temperature-dependent dc resistivity ρ(T) in the temperature range of 150 K to 400 K. The temperature dependence of electrical resistivity indicates a typical semiconducting behaviour of NMCO7. Because of the interaction of various degrees of freedom exhibited by mixed valence manganites, the latter displays a complex transport mechanism described by multiple models like the bandgap model, SPH, and VRH. Some perovskites exhibit all three mechanisms in different temperature ranges [1-2]. To understand the mechanism behind the electrical transport properties in the NMCO7 sample, the electrical resistivity data as a function of temperature is fitted using models such as the Arrhenius law, small polaron hopping (SPH), Mott-variable range hopping (VRH), and Effros-Shklovskii (ES)-VRH. It is observed that in the high-temperature region, the data follows the Arrhenius law of activation and the SPH model, which account for electron-phonon interaction. In contrast, at lower temperatures, the VRH model and Mott-VRH yield better results. Hence, in the NMCO7 system, the charge transport properties are governed by a complex interplay among thermal activation, localized electronic states, and Coulomb interactions. Acknowledgements We are thankful to Dr. Dinesh K. Shukla, UGC –DAE CSR, Indore, India for the measurements done.

References 1. A. Bhogra, A. Masarrat, R. Meena, et al. Scientific Reports 9 (2019) 14486. 2. J. P. Palakkal, P. N. Lekshmi, S. Thomas, M. Valant, K. G. Suresh and M. R. Varma, Mater. Res. Bull., 2016, 76, 161.

VP13-08. Magneto-elastic Properties of Samarium Doped Cobalt-Nickel Ferrite Ceramics Obtained by Spark Plasma Sintering. *M. Ibuado*[1], C. Santillan[1], J. Saenz[1], M. Grijalva-Castillo[1] and J. Matutes[1] *1. Materials physics, CIMAV, Chihuahua, Mexico*

Cobalt ferrite nanoparticles belong in the smart materials that exhibit large magnetostriction, which makes them good candidates to replace Rare-Earth based alloys like Terfenol-D in technological applications. Proper chose of substituents in either octahedral or tetrahedral sites, and a fine control of their microstructure result in the capability of tunning their magnetic properties. For instance, the substitution of Ni^{2+} for Co^{2+} will result in an increase in the magnetic susceptibility, with a detriment in magneto-crystalline anisotropy and, therefore, in saturation magnetization and magnetostriction [1]. The objective of this study is to increase the magnetostriction and magnetic susceptibility with the addition of Sm^{3+} as a substituent in Fe^{3+} site. Bulk ceramics were obtained from nanoparticles of $Co_{0.8}Ni_{0.2}Fe_{2-x}Sm_xO_4$ (x = 0-0.02) by spark plasma sintering. Nanoparticles of the compound were synthesized using the sol-gel method from high purity nitrate precursors. Their composition, structure and microstructure were characterized by X-ray diffraction, Raman spectroscopy, transmission electron microscopy and dispersive energy spectroscopy. Room temperature hystesis loops and magnetostriction were measured in a Quantum Design Physical Properties Measurement System equipped with a Vibrating Sample Magnetization and Dilatometric Probes. The observed particle size was between 18 and 25 nm. Rietveld refinement was performed using the Fullprof Suite program, confirming the cubic phase, Fd-3m, space group 227. The change in lattice parameter and crystallite size with Ni and Sm content is showed in Table 1, as well as the changes in magneto-elastic properties. From the approximation to saturation calculations, the decrease in saturation magnetization is explained in terms of the reduction of the magneto-crystalline anisotropy coefficient (K1). An increment in magnetic susceptibility and in magnetostriction was observed in the Cobalt-Nickel ferrites doped with 1 at% Sm, attributed to the decrease in microstrains. In addition, the magnetic field required to bring the doped samples to saturation (H_S) was lower in samples doped with 2 at% Sm.

[1] S. Bhame, A. Bhapkar, M. Shirolkar and P. Joy, Journal of the Indian Chemical Society, 99 (8), 100599 (2022).

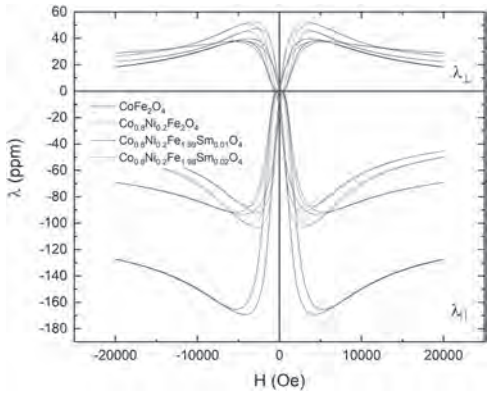

Fig. 1: Magnetostrictive hysteresis loops

Sample	a (Å)	Crystallite size (nm)	Microstrain (10^{-4})	M_s (emu/g)	K_1 (KJ/m^3)	χ	λ_s (10^{-6})	H_s (Oe)
$CoFe_2O_4$	8.396(1)	16.0	70.0	66.8	358.7	0.01499	-169	4274
$Co_{0.8}Ni_{0.2}Fe_2O_4$	8.395(1)	15.3	73.4	60.3	288.6	0.01694	-100	2844
$Co_{0.8}Ni_{0.2}Fe_{1.99}Sm_{0.01}O_4$	8.371 (1)	18.9	57.8	62.7	334.6	0.01744	-109	4595
$Co_{0.8}Ni_{0.2}Fe_{1.98}Sm_{0.02}O_4$	8.375 (1)	21.9	49.5	46.2	218.8	0.01751	-86	2775

Fig. 2: Structural and magnetoelastic properties

Session VP14
MATERIALS FOR SPINTRONICS & MAGNETIZATION DYNAMICS
(Poster Virtual Session)

Kevin Garello, Chair
SPINTEC, Grenoble, France

VP14-01. $L1_0$ FeAu perpendicular magnetic tunnel junction: A DFT + NEGF study. *R.R. Sheikh*[1] and R.K. Ghosh[1,2] *1. Electronics and Communication Engineering, Indraprastha Institute of Information Technology Delhi, New Delhi, India; 2. Center for Quantum Technologies, Indraprastha Institute of Information Technology Delhi, New Delhi, India*

This work examines the spin dynamic and transport properties of transition metal intermetallic alloy, $L1_0$ FeAu, using density functional theory (DFT) combined with the nonequilibrium Green's function (NEGF) technique. The motivation behind this work is driven by the potential application of this ferromagnet in spintronic devices, where it can act as a magnetic electrode material for MgO-based perpendicular magnetic tunnel junction (p-MTJ) for spin transfer torque magnetic random-access memory (STT-MRAM). Our analyses show several advantages of $L1_0$ FeAu, like large bulk magnetic anisotropy energy (1.20meV/f.u.), which contributes to higher thermal stability, relatively low Gilbert damping (0.0035), that helps to reduce the switching current and also has spin-polarized Δ_1 bands on Fermi surface that can effectively provide higher tunneling magnetoresistance (TMR) for better read-operation. In our analysis, we find that the TMR of FeAu-based MTJs (having 0.9nm thick MgO barrier) is around 34000%, which is 8 times higher than that of our calculated conventional Fe-based p-MTJ with similar barrier thickness. It was also found that the RA product of FeAu MTJ is one order higher than that of Fe-based MTJs, which helps in improving switching efficiency; however, the switching voltage can also increase. Overall, the collective computations demonstrate the importance of $L1_0$ FeAu ferromagnetic material for future STT-MRAMs.

1. Gilmore, K., Idzerda, Y. U. & Stiles, M. D. *Phys. Rev. Lett.* 99, 027204 (2007). 2. Takanashi, K. *et al.. Appl. Phys. Lett.* 67, 1016 (1995). 3. Zhang, X. *et al., Appl. Phys. Lett.* 110, (2017). 4. Daalderop, G. H. O., Kelly, P. J. & Schuurmans, M. F. H. *Phys. Rev. B* 41, 11919–11937 (1990). 5. Galanakis, I., Alouani, M, H. *Phys. Rev. B - Condens. Matter Mater. Phys.* 62, 6475–6484 (2000). 6. Mahfouzi, F. & Kioussis,. *Phys. Rev. B* 98, (2018). 7. G. Hu et al., 2021 IEEE IEDM, San Francisco, CA, USA, 2021, pp. 2.5.1-2.5.4 8. C. Park *et al*., *2018 IEEE Symposium on VLSI Technology*, Honolulu, HI, USA, 2018, pp. 185-186

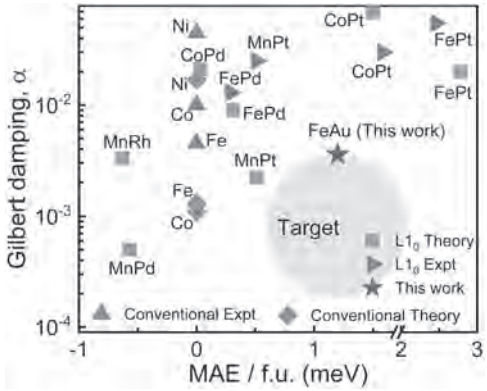

Fig.1 Comparison of magnetocrystalline anisotropy energy (MAE) and Gilbert damping (α) of FeAu with different classes of materials.

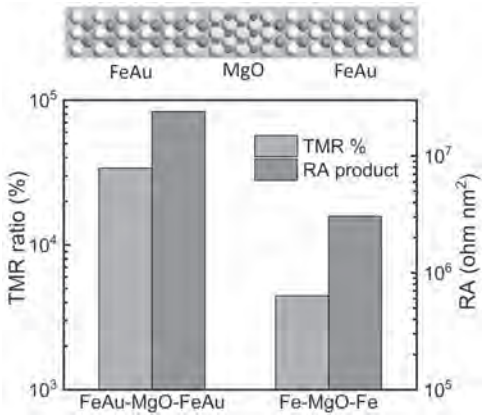

Fig.2 Comparision of TMR ratio and RA product of FeAu/MgO/FeAu with Fe/MgO/Fe MTJ having 0.9nm thick MgO barrier.

VP14-02. Electric Field Control of Spin in Monolayer WS_2/WTe_2 Field Effect Transistors:- A DFT+NEGF Study. A. Shah[1] and *A. Kashyap*[2] *1. SCEE, IIT Mandi, Mandi, India; 2. SPS, IIT Mandi, Mandi, India*

Two-dimensional transition metal dichalcogenides(TMDC) like MoS2 and WSe2 have garnered significant interest for spintronic applications. However, monolayer WS2, despite its intriguing electronic properties, remains relatively unexplored for such purposes. This study presents a first-principles theoretical investigation of quantum transport in a monolayer WS2/WTe2 field-effect transistor, focusing on the electric control of spin. Leveraging the strong spin-orbit interaction inherent to WS2 and its unique electronic structure, we demonstrate the potential for spin manipulation via an external gate electric field. Our calculations, based on density functional theory and the non-equilibrium Green's function formalism, reveal that the gate voltage can induce a significant shift in the spin texture of the WS_2 channel, transitioning from a Zeeman-like to a Rashbha-like spin texture with increasing field strength. This electric field-induced spin control leads to a substantial modulation of the conductance, with variations observed within experimentally accessible gate voltage ranges. We analyse the interplay between the intrinsic spin orbit interaction(SOI) of WS2 and the Rashbha spin-orbit coupling generated by the applied gate voltage and discuss its implications for potential spintronic applications of monolayer WS_2/WTe_2 FETs. Our findings provide a theoretical foundation for the development of novel spin-based devices leveraging the unique properties of this promising two-dimensional material. Key Words :- Spintronics, monolayer, spin-FET, Rashbha Spin orbit, conductance, electronic transport, TMDC.

1.Gong, K., Zhang, L., Liu, D., Liu, L., Zhu, Y., Zhao, Y. and Guo, H., 2014. Electric control of spin in monolayer WSe2 field effect transistors. *Nanotechnology*, *25*(43), p.435201. 2.Semenov, Y.G., Kim, K.W. and Zavada, J.M., 2007. Spin field effect transistor with a graphene channel. *Applied Physics Letters*, *91*(15). 3.Chuan, M.W., Wong, K.L., Hamzah, A., Rusli, S., Alias, N.E., Lim, C.S. and Tan, M.L., 2020. 2D honeycomb silicon: A review on theoretical advances for silicene field-effect transistors. *Current Nanoscience*, *16*(4), pp.595-607.

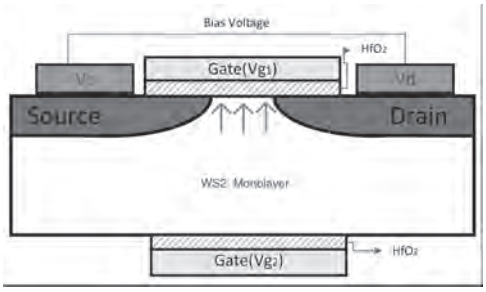

Figure 1

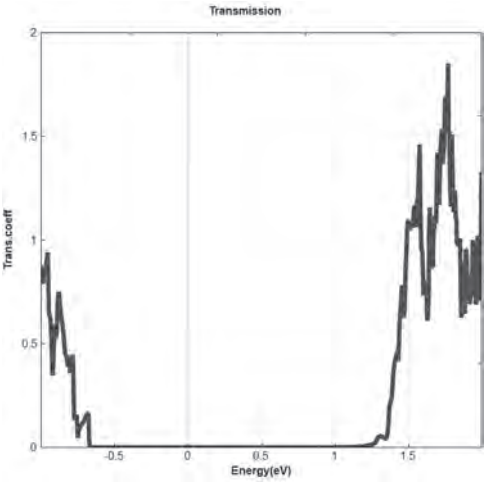

Figure 2

VP14-03. Magnetic and electrical transport properties of a prospective altermagnet NdB_2C_2. M. Anas[1] and *P. Kharel*[1] *1. Chemistry, Biochemistry and Physics, South Dakota State University, Brookings, SD, United States*

The RB_2C_2 compounds have tetragonal crystal structure, can exhibit antiferroquadrupolar ordering, in addition to the antiferromagnetic ordering, depending on the type of rare-earth elements. The rare-earth ions are present in between the covalent-bonded boron and carbon layers. Recently, this material has also been suggested to be a potential candidate for altermagnetism [1]. We have studied the structural, magnetic, and electrical transport properties of the polycrystalline NdB_2C_2 material prepared by arc-melting and annealing. It has a tetragonal crystal structure with space group *P4/mbm*. The lattice parameters are found to be $a = b = 5.3561(23)$ Å and $c = 3.8080(22)$ Å. The as-prepared sample shows significant texturing/preferred orientation which can be reduced by appropriate heat treatment. The magnetization measurements (M vs. T) on the annealed polycrystalline sample reveal its paramagnetic nature at room temperature and the antiferromagnetic ordering of the Nd-moments near 9 K. The magnetic moment due to Nd from the analysis of the magnetization data using the Curie-Weiss law has been found to be $3.7\mu_B$/f.u. This value is in agreement with the theoretically expected value for Nd^{3+} moments. In addition to the antiferromagnetic transition at 9K, we found the signature of additional field-dependent transitions in the magnetization isotherm measured at 2K. The resistivity (ρ) vs temperature (T) measurements shown in figure 1 corroborate the magnetic transition seen in the *M-T* data, and also revealing the metallic nature of the material. This work is supported by the U.S. Department of Energy (DOE) Established Program to Stimulate Competitive Research (EPSCoR) grant no. DE-SC0024284.

[1] L. Bai et al., Altermagnetism: Exploring New Frontiers in Magnetism and Spintronics, (2024) 1–49. http://arxiv.org/abs/2406.02123.

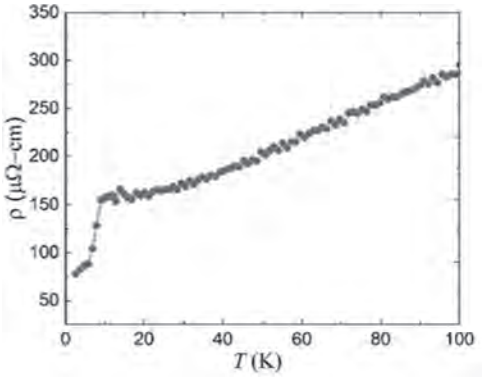

Variation of resistivity with temperature in NdB_2C_2.

VP14-04. High temperature ferrimagnetic semiconductors by spin-dependent doping in high temperature antiferromagnets. *J. Li*[1], G. Su[1] and B. Gu[1] *1. University of Chinese Academy of Sciences, Beijing, China*

To realize room temperature ferromagnetic (FM) semiconductors is still a challenge in spintronics. Many antiferromagnetic (AFM) insulators and semiconductors with high Neel temperature TN are obtained in experiments, such as LaFeO3, BiFeO3, etc. High concentrations of magnetic impurities can be doped into these materials, but AFM state with very tiny net magnetic moments was obtained in experiments, because the magnetic impurities were equally doped into the spin up and down sublattices. Here, we propose that the effective magnetic field from FM substrate could guarantee the spin-dependent doping in AFM materials, where the doped magnetic impurities prefer one sublattice of spins, and the ferrimagnetic (FIM) materials are obtained. We study the doped AFM insulator LaFeO3 with FM substrate of Fe metal by the density functional theory DFT calculations. The results show dopants prefer one spin sublattices, and introduce large magnetic moments. With 1/8 and 1/4 doping concentrations, many room temperature FIM semiconductors are predicted in doped LaFeO3, BiFeO3, SrTcO3 and CaTcO3. Our theoretical results propose a way to obtain high TC FIM semiconductors by spin-dependent doping in high TN AFM insulators and semiconductors.

ResearchGate:10.13140/RG.2.2.32127.83361

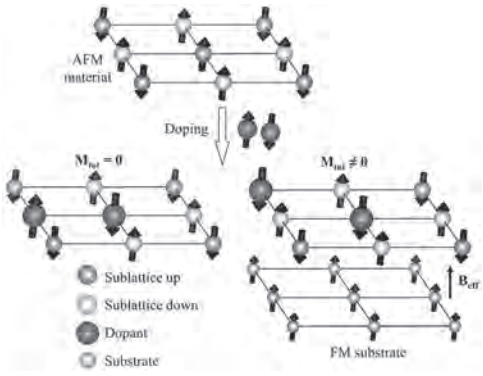

Fig. 1: Schematic diagram of spin-independent doping (left) with zero net magnetic moment and spin-dependent doping (right) with non-zero net magnetic moment, for the AFM materials doped with magnetic impurities.

VP14-05. Néel-order spin-orbit torques in CuMnAs from first principles ballistic transport. *M.T. Stamenova*[1] and A. Droghetti[2]
1. School of Physics and CRANN, Trinity College Dublin, Dublin, Ireland; 2. CNR-SPIN Research unit, d'Annunzio University, Chieti, Chieti, Italy

The tetragonal metallic antiferromagnet CuMnAs has been proposed for devices relying on electrical Néel vector switching [1] or electrical/optical heat-assisted toggling into a nano-fragmented domain state with a GMR-like level of resistance change [2]. CuMnAs in its tetragonal phase, belongs to a special class of non-centrosymmetric lattice AFMs, in which the two magnetic sublattices form inversion partners (see Figure 1). Inversion symmetry breaking in magnetic crystals, combined with relativistic effects, gives rise to key spintronic effects like the inverse spin-galvanic effect, in which the electron flow induces local spin-polarisations on the two sublattices. These give rise to atomically-staggered local fields, generating opposite torques, so called Néel-order spin-orbit torques (SOTs), on the two sublattices [3]. As the AFMs are immune to external magnetic field, this mechanism is essential for the manipulation of their order parameter in novel AFM-spintronic devices. The Néel-order SOTs' mechanism has been demonstrated theoretically and first principle results based on Kubo linear response formalism provide quantitative insights – staggered fields of about $3x10^{-3}$ T per 10^7 A/cm^2 locally at each sublattice [1]. We have set out to instead investigate this effect from the other theoretical extreme – ballistic transport from first principles (DFT+NEGF) [4,5] close to the linear response regime in wide slabs of CuMnAs. Our calculated atomically-resolved Néel-order SOTs (Fig. 1) reproduce the desired staggered (switching-friendly) behaviour of the SOTs shown in Ref. [1]. Quantitatively, however, for ballistic conductivity of the slab of $3.4x10^{14}$ A/(V.m^2), we find average SOT fields of about 70 T/V, suggesting a substantially larger ballistic SOT effect. We investigate further the role of disorder in suppressing the ballistic SOT effect.

[1] P. Wadley, et al., Science 351, 587 (2016). [2] Z. Kaspar, et al., Nature Electronics 4, 30 (2022). [3] J. Železný, et al., Phys. Rev. Lett. 113, 157201 (2014). [4] A. R. Rocha, et al., Phys. Rev. B 73, 085414 (2006); J.M. Soler, et al, J. Phys. Condens. Matter 14, 2745 (2002). [5] I. Rungger, et al, (2020). Non-equilibrium Green's Function Methods for Spin Transport and Dynamics. In: Andreoni, W., Yip, S. (eds) Handbook of Materials Modeling. Springer, Cham.

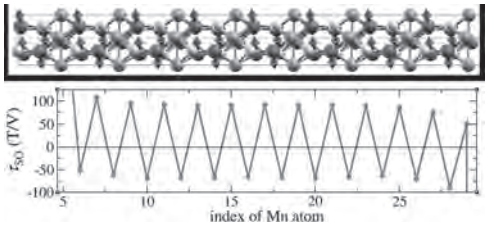

Fig. 1: A schematic of the slab of CuMnAs used in the open-boundary (finite bias) ballistic transport simulations (with periodic boundary conditions in the transverse plane). In the bottom panel are the calculated atom-resolved Néel-order SOTs (linear response) as function of the position (index, sorted by z-coordinate) of each Mn atom in the stack.

VP14-06. Tailoring $LaMn_{1-x}Co_xO_3$ Thin Film Properties Using Swift Heavy Ion Irradiation. *A. Jan*[1] *1. Physics, Islamic University of Science and Technology, Kashmir, Pulwama, India*

Manganite perovskites are highly regarded for their diverse electrical and magnetic properties, such as mixed valence, ferromagnetism/antiferromagnetism [1-2], metal-insulator transition, and colossal magnetoresistance (CMR) [3], in addition to spin, orbital, and charge ordering properties [4]. These characteristics make them suitable for applications in read heads, storage media, and magnetic sensors [5]. In this study, we have synthesized $LaMn_{1-x}Co_xO_3$ (LMCO) thin films using Pulsed Laser Deposition technique onto a single crystalline $LaAlO_3$ substrate. Structural analysis was conducted using X- ray diffraction and transport properties were studied using standard four probe technique. The as-prepared samples exhibit semiconducting properties and magnetic measurements indicate paramagnetic to ferromagnetic transition, along with the presence of an anti-ferromagnetic component. To explore the effects of swift heavy ion irradiation, these thin films were subjected to 100 MeV Ag ion irradiation at a fluence of $5X10^{12}$ ions/cm^2. This study presents a comparative analysis of the structural, electrical, and magnetic properties of the un-irradiated and irradiated thin films. The results demonstrate significant modifications in the properties due to ion irradiation, providing insights into the underlying mechanisms governing the phase transitions and magnetic interactions in LMCO thin films with potential implications for the development of advanced materials in spintronics and magnetic applications.

[1] S. Chauhan, S. Kumari, and P. K. Siwach, Physica E: Low-dimensional sys. and Nanost. 128, 114573 (2021). [2] F. H. Bhat, G. Anjum, and R. Kumar, Ceramics International 47 (5), 6753-6763 (2021). [3] R.M. Kusters, J. Singleton, and D.A. Keen, Physica B 155, 362 (1989). [4] C. N. R. Rao, A. Arulraj, and A. K. Cheetham, J. Phys. Condens. Matter 12, R83 (2000). [5] N. Adeela, U. Khan, and S. Naz, Applied Surface Science, 422, 184-191 (2017).

VP14-07. Spin dynamics of room temperature van der Waals (vdW) ferromagnets $Fe_{4.8}Ni_{0.2}GeTe_2$. *P. Kumar*[1,2], S. Patnaik[1] and B.K. Kuanr[2]
1. School of Physical Sciences, Jawaharlal Nehru University, New Delhi, India; 2. Special Centre for Nanoscience, Jawaharlal Nehru University, New Delhi, India

The emergence of quasi-two-dimensional (2D) van der Waals (vdW) ferromagnets are notable as they exhibit unique spintronic functionalities, like magnetic tunnel junctions and giant magnetoresistance, hence making them promising for quantum computing, data storage, etc. However, the practicality of these ferromagnet is limited by their stability above room temperature, hindering their use in next-generation spintronic devices. Fe_5GeTe_2, a 2D itinerant ferromagnet, shows stability close to room temperature (Tc ~ 220 K), which can be tuned to above room temperature by doping [1]. Here, we have investigated the spin dynamics of single crystalline $Fe_{4.8}Ni_{0.2}GeTe_2$ having T_c nearly 400 K prepared by self-flux method. The X-ray diffraction and EDX spectroscopy confirms rhombohedral lattice structure of synthesized flakes with the space group (No. 166). Ferromagnetic resonance (FMR) measurements reveal that the effective magnetization of $Fe_{4.8}Ni_{0.2}GeTe_2$ is approximately 6.2 kOe. It exhibits broad linewidths of 0.32 kOe. It may be due to inhomogeneous line broadening mediated by two-magnon scattering. Additionally, the effective Gilbert damping constant (α) obtained is approximately 0.033, which is comparable to other ferromagnets such as $Cr_2Ge_2Te_6$ and permalloy(NiFe) [2,3]. For application of vdW in magnonics, we have used dual-coupled microstrip lines where spinwaves can propagate through 2D-ferromagnet [4]. We have demonstrated nonreciprocal ($S_{12} \neq S_{21}$) magnetostatic surface wave (MSSW) propagation through $Fe_{4.8}Ni_{0.2}GeTe_2$. Hence determination group velocity (v_g), relaxation time (ς) and decay length (l_d) from spin-wave dispersion relation. v_g, ς and l_d are observed to be highly sensitive to external magnetic field. This work provides an avenue to promote the practical applications of 2D-vdW-integrated spintronic devices at room-temperature.

[1] Chunli Tang et.al., Physics Reports 1032 (2023) 1–36 [2] Zhang T, Chen Y, Li Y, Guo Z, Wang Z, Han Z, He W and Zhang Appl. Phys. Lett. 116 223103 (2020) [3] Zhao Y, Song Q, Yang S-H, Su T, Yuan W, Parkin S S P, Shi J and Han W, Sci. Rep. 6 22890 (2016) [4] Yi Li, et.al., Appl. Phys. Lett. 123, 022406 (2023)

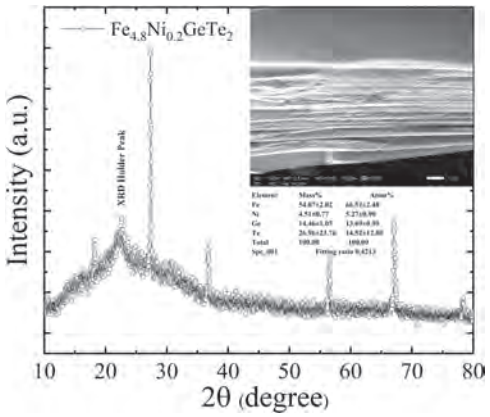

Fig. 1 XRD pattern of single-crystal $Fe_{4.8}Ni_{0.2}GeTe_2$. Inset: SEM image depicting layered morphology of single crystal $Fe_{4.8}Ni_{0.2}GeTe_2$ and EDX composition

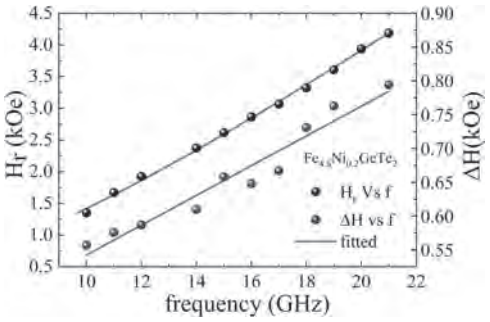

Fig. 2 Resonance field (H_r) and line-width (ΔH) versus frequency. Inset shows absorption spectrum at 11 GHz.

VP14-08. A study of spin wave properties of YIG based microstrip coupled line geometry. *S. Kumar*[1] and B.K. Kuanr[1] *1. SCNS JNU, Jawaharlal Nehru University, New Delhi, India*

An yttrium iron garnet (YIG) based coupled microstrip line with high band rejection and miniaturized size is effective technology for modern communication system like radars, meteorology and wireless communication [1]. For effective application of YIG for magnonics applications, it is required to find coupled line geometries in which spin wave propagates over long distances. A mm thick YIG has extremely low Gilbert damping of $\alpha \approx 3 \times 10^{-5}$ at GHz frequencies [2]. In spin-wave propagation experiments, the properties of Damon-Eshbach spin waves [5], [6] with a wave vector (k) perpendicular to the in-plane magnetization direction are frequently examined. The unique characteristics of magnetostatic surface waves (MSSW) in microwave ferrites like YIG facilitate the creation of advanced nonreciprocal devices. The issue with straight edge microstrip geometry can cause spurious resonances, leading to the generation of both forward and backward waves, which in turn results in standing wave modes [4]. MSSW being nonreciprocal wave an isolation of 12-15 dB is obtained in the present investigation [Fig:1]. Thick YIG pallets were used to characterize spin wave with wave vector up to 135 cm^{-1}. A tapered curved fillet design coupled line geometry is chosen to reduce spurious mode and the gap variation from d_1 =0.65 mm and d_2=1mm are used to study the spin wave propagation. This allows for the determination of critical spin wave parameters such as group velocity (V_g), the relaxation time (ζ), the spin decay length(l_d) and the Gilbert damping constant (α) from spin-wave dispersion relation. For 400mm YIG slab, Gilbert damping of $\alpha \approx 2.4 \times 10^{-5}$ and maximum decay length of 1.16 mm at maximum group velocity 1.062 km/s is obtained using above geometry as shown in fig:2. A strong spin wave interaction for 135 cm^{-1} at 3kOe fields is obtained.

[1] J. Wu, X. Yang, S. Beguhn, J. Lou, and N. X. Sun, "Nonreciprocal tunable low-loss bandpass filters with ultra-wideband isolation based on magnetostatic surface wave," *IEEE Trans Microw Theory Tech*, vol. 60, no. 12, pp. 3959–3968, 2012. [2] H. Qin, S. J. Hämäläinen, K. Arjas, J. Witteveen, and S. van Dijken, "Propagating spin waves in nanometer-thick yttrium iron garnet films: Dependence on wave vector, magnetic field strength, and angle," *Phys Rev B*, vol. 98, no. 22, p. 224422, Dec. 2018, doi: 10.1103/PhysRevB.98.224422. [3] J. D. Adam, "An MSW Tunable Bandpass Filter," in *IEEE 1985 Ultrasonics Symposium*, IEEE, 1985, pp. 157–162. doi: 10.1109/ULTSYM.1985.198496. [4] K. W. Chang and W. Ishak, "Magnetostatic surface wave straight-edge resonators," *Circuits Syst Signal Process*, vol. 4, pp. 201–209, 1985. [5] Y. V. Khivintsev, Y. A. Filimonov, and S. A. Nikitov, "Spin wave excitation in yttrium iron garnet films with micron-sized antennas," *Appl Phys Lett*, vol. 106, no. 5, Feb. 2015, doi: 10.1063/1.4907626. [6] H. Yu *et al.*, "Magnetic thin-film insulator with ultra-low spin wave damping for coherent nanomagnonics," *Sci Rep*, vol. 4, no. 1, p. 6848, 2014.

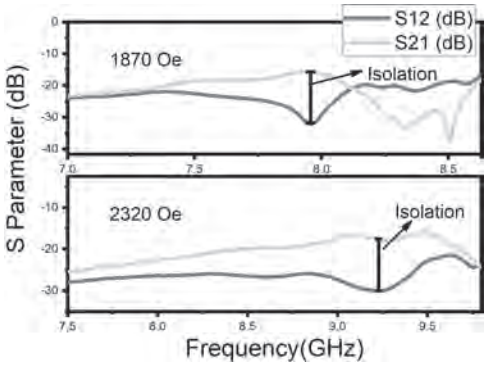

Fig.1: MSSW Spin wave isolation spectra. An isolation of 12-15 dB is obtained in the above spectra.

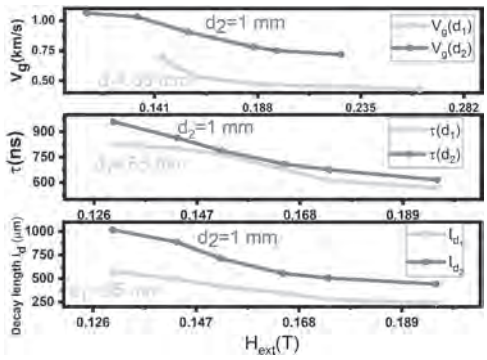

Fig.2: Experimentally obtained values of spin wave group velocity (V_g) (top), spin wave relaxation time (ζ) (middle) and spin decay length(l_d) (bottom) Vs. external magnetic bias.

VP14-09. Reversible Sign Change in the Anomalous Hall Effect Induced by Strain. *T. Morita*[1], T. Koyama[1,2,4] and D. Chiba[1,2,3] *1. SANKEN, Osaka University, Ibaraki, Japan; 2. CSRN, Osaka University, Toyonaka, Japan; 3. SRIS, Tohoku University, Sendai, Japan; 4. PRESTO, JST, Kawaguchi, Japan*

The anomalous Hall effect (AHE) is a fundamental physics related to spin-dependent transport. It is reported that a sign change of the AHE depending on the temperature and the layer structure [1,2]. The origin of the sign change of the AHE is attributed to band filling effect [3]. Recently, flexible spintronics utilizing the inverse magnetostriction effect has attracted attention [4]. The magnetostriction effect is a well-known phenomenon that combines strain and magnetism, but the modulation of magnetism by strain is still not fully understood. In this study, we observed reversible sign change of the AHE induced by strain in Co/Ni multilayered film. We deposited a

$[Co/Ni]_n$ multilayer on a flexible substrate by magnetron sputtering. Hall measurement was conducted without (w/o) and with (w/) application of a uniaxial strain in various temperatures. The small tensile jig was used to apply a strain. The results of Hall measurement at 260 K are shown in Figure 1. Blue and red plots represent the results w/o and w/ strain, respectively. In w/o strain, the sign of the AHE is positive; saturation value of Hall resistance (R^s_H) is positive under positive magnetic field. In contrast, in w/ strain, the sign of the AHE reverses to negative. When the strain is removed, the sign of the AHE returns to positive (dashed blue plot). Figure 2 shows the temperature dependence of R^s_H w/o and w/ strain. The temperature at which the sign of the AHE changes is around 210 K w/o strain. When strain is applied, the sign of the AHE changes around 270 K. The datas suggest that band filling can be reversibly controlled by strain. We will discuss in more detail the effect of strain on the sign change in the AHE. The authors thank S. Ota for technical support. This work is supported by Program for Leading Graduate School: "Interactive Materials Science Cadet Program", JSPS KAKENHI (Grant No. 24KJ1613 and 23H00183), JST A-Step (Grant No. JPMJTR233A), JST CREST (Grant No. JPMJCR20C6), MEXT X-NICS, and the Spintronics Research Network of Japan.

[1] Z.B. Guo, W.B. Mi and R.O. Aboljadayel *et al*., Phys. Rev, B Vol. 86, p.104433 (2012). [2] V. Keskin, B. Aktas and J. Schmalhorst *et al*., Appl. Phys. Lett. Vol. 102, p.022416 (2013). [3] I. Turek J. Kudrnovský and V. Drchal Phys. Rev. B Vol. 86, p.014405 (2012). [4] S. Ota, A. Ando and D. Chiba Nat. Electron. Vol. 1, p.124 (2018).

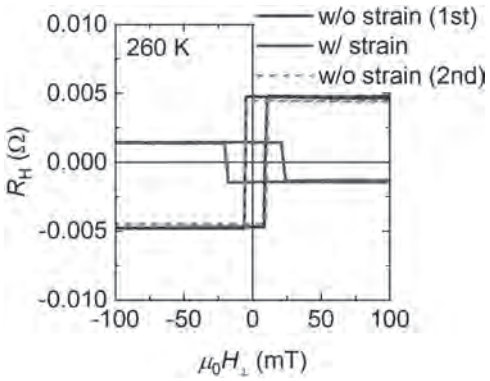

Figure 1: The results of Hall measurement w/o and w/ strain at 260 K.

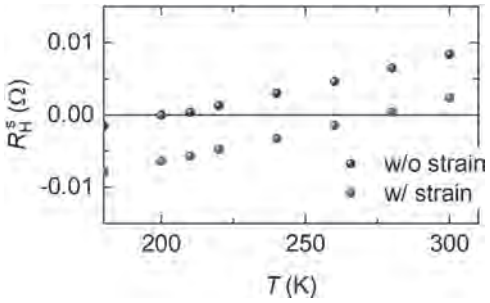

Figure 2: Temperature dependence of the saturation value for the AHE under positive magnetic field.

Session VP15
MICROSCOPY, IMAGING, AND MAGNETIC CHARACTERIZATION & STRUCTURED MATERIALS (Poster Virtual Session)

Robert Hicken, Chair
University of Exeter, Exeter, United Kingdom

VP15-01. Shortening of Pre-data Acquisition Time in Magnetic Particle Imaging Using AC Susceptometry. *T. Sasayama*[1], N. Futagawa[1] and T. Yoshida[1] *1. Kyushu University, Fukuoka, Japan*

Magnetic particle imaging (MPI) that employs magnetic nanoparticles (MNPs) to detect tumors, has attracted attention in recent years. Previously, we proposed MPI using a detection coil array that estimates the position of MNPs by obtaining a harmonic magnetic field from nonlinear magnetic responses and solving the inverse problem using a system matrix [1]. The time-consuming acquisition of the system matrix, for example, pre-data, affects the accuracy of the inverse problem analysis, mainly owing to temperature fluctuations in the excitation coils and electric circuits. In this study, we propose to reduce the acquisition time by fitting the system matrix computed using AC susceptometry (ACS) to the measured system matrix [2] and reducing the number of measurement points. Fig. 1 shows MPI using the detection coil array. A sinusoidal current with an amplitude of 1, 2, ..., 20 A_{peak} and a frequency of 5400 Hz was applied to the excitation coil to generate a magnetic field. Sixteen detection coils detected the third harmonic magnetic field from an MNP sample (Resovist, 100 μgFe), and a system matrix was constructed from the measured values. The spatial resolution was set to 5 mm × 5 mm, and the number of pixels was 39 × 25. Subsequently, the spatial resolution of the system matrix was reduced to 1/*d* times (*d*: natural number) in the *x*- and *y*-axis directions and fitted with a numerically computed system matrix. The results of the inverse problem analysis using nonnegative least squares were compared with the system matrices before and after reduction. Fig. 2 shows the results of the inverse problem before and after reduction. The results demonstrated that the position estimation performance of the MNPs was nearly maintained even after reduction. ACKNOWLEDGEMENTS This study was supported by the Japan Society for the Promotion of Science (JSPS) KAKENHI Grant Numbers JP23K20939 and JP20H05652.

[1] T. Sasayama, T. Yoshida, and K. Enpuku, "Two-dimensional magnetic nanoparticle imaging using multiple magnetic sensors based on amplitude modulation," *J. Magn. Magn. Mater.*, vol. 505, Jul. 2020, Art. no. 166765.
[2] N. Futagawa, M. Fujimoto, K. Higashino, T. Sasayama, and T. Yoshida, "Imaging of magnetic nanoparticles using AC susceptibility data," *IEEE Trans. Magn.*, vol. 59, no. 11, Nov. 2023, Art. no. 5101205.

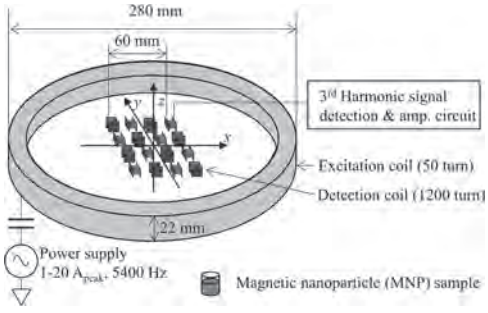

Fig. 1 MPI using detection coil array.

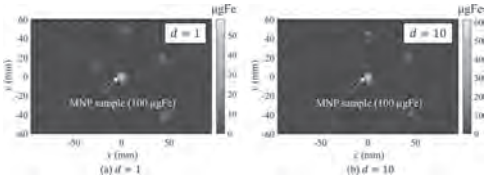

Fig. 2 Results of the inverse problem before and after the reduction.

VP15-03. Direct Magnetic Field Compensation with Multichannel Digital-to-Analog (D/A) Converter in Magnetic Particle Imaging. *T. Matsushita*[1], T. Sasayama[1] and T. Yoshida[1] *1. Department of Electrical and Electronic Engineering, Kyushu University, Fukuoka, Japan*

Magnetic particle imaging (MPI), which displays the concentration distribution of magnetic nanoparticles (MNPs), has gained attention as a new diagnostic imaging technology [1]. One problem with MPI is that it requires a strong gradient field, that causes peripheral nerve stimulation. In this study, the concentration distribution was obtained by arranging the detection coils in an array without a gradient field [2]. The voltage from the detection coil also contained a fundamental component derived from the external magnetic field, that interfered with the measurement. To solve this problem, a single-channel D/A converter and variable resistors were used to compensate for the fundamental component [3]. However, this compensation method is inaccurate. In this study, we propose a new compensation circuit that uses a multichannel digital-to-analog (D/A) converter. Fig. 1 shows the experimental setup. The excitation coil generated an oscillating field of 5400 Hz, that magnetized the Resovist MNP sample (500 μg-Fe / 150 μg). The voltage signal from a detection coil contained the third harmonic and fundamental components, that were the effects of the non-linear magnetization of the sample and oscillating field, respectively. The fundamental components were compensated for using a 5400 Hz voltage supply from a multichannel D/A converter and subtracting it with an instrumentation amplifier. The sample was moved in the *x*–*y* plane, and the harmonic signal amplified by an operational amplifier was detected at each point. Fig. 2 shows the two-dimensional distribution of the third harmonic signal from the sample at depths of 25 and 50 mm. The image at 50 mm was blurred compared with that at 25 mm because the magnetic flux derived from the oscillating magnetic field coupled to the sample was reduced. The fact that the image was acquired at 50 mm demonstrates the feasibility of MPI using the proposed method. This study was supported by the Japan Society for the Promotion of Science (JSPS) KAKENHI Grant Numbers JP23K20939 and JP20H05652.

[1] T. Knopp and T. M. Buzug, "Magnetic Particle Imaging—An Introduction to Imaging Principles and Scanner Instrumentation," Springer, 2012.
[2] T. Sasayama, T. Yoshida, and K. Enpuku, "Two-dimensional magnetic nanoparticle imaging using multiple magnetic sensors based on amplitude modulation," *J. Magn. Magn. Mater.*, vol. 505, Jul. 2020, Art. no. 166765.
[3] T. Sasayama, N. Okamura, and T. Yoshida, "Sensitivity improvement of magnetic nanoparticle imaging by compensation with digital-to-analog converter" *IEEE Trans. Magn.,* vol. 57*,* no. 2*,* Feb. 2021, Art. no. 5300605.

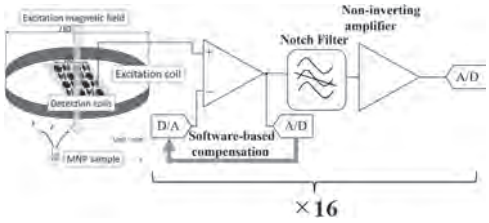

Fig. 1. Experimental set up.

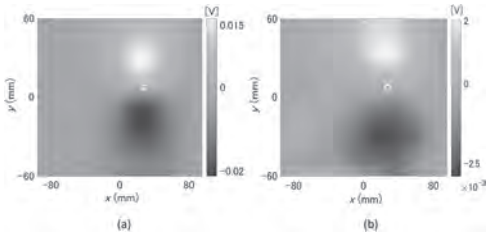

Fig. 2. Third harmonic signal distributions of the sample captured at depths of (a) 25 mm and (b) 50 mm. The white circle indicates the position of a detection coil.

VP15-04. A novel EUV x-ray polarimeter for single-pulse experiments at MagneDyn@FERMI. A. Caretta[1], S. Laterza[1] and *M. Malvestuto*[1]
1. elettra-sincrotrone trieste, Trieste, Italy

We developed a polarimeter, resembling the Wollaston balanced-photodetection scheme in the visible range, capable of single-pulse linear polarization angle detection in the EUV energy range. The Wollaston polarimeter for x-ray FEL sources (TONIX) is currently installed at the MagneDyn beamline at the FERMI FEL in Trieste, Italy, and is available for users. Here, we describe first the conceptual design and the mechanical realisation of the TONIX, secondly we test the instrument by performing time-resolved magnetization dynamic studies on a $Ni_{80}Fe_{20}$ permalloy.

Caretta A., et al. *A Novel free-electron laser single-pulse Wollaston polarimeter for magneto dynamical studies* Structural Dynamics 8, 034304 (2021); https://doi.org/10.1063/4.0000104

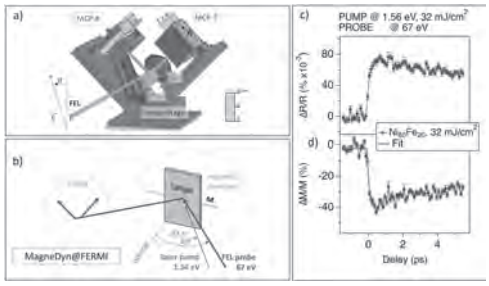

Figure 1

VP15-05. Magnetic structure of rare earth intermetallic compound Er_6MnTe_2: neutron diffraction and magnetization study. *R. Nirmala*[1], G. Jangam[2], T. A[2], A.V. Knotko[3,4], V. Yapaskurt[5] and A. Morozkin[3]
1. Physics, Indian Institute of Technology Madras, Chennai, India; 2. Tata Institute of Fundamental Research, Mumbai, India; 3. Department of Chemistry, Moscow State University, Moscow, Russian Federation; 4. Faculty of Materials Science, Moscow State University, Moscow, Russian Federation; 5. Department of Petrology, Moscow State University, Moscow, Russian Federation

Ternary rare earth intermetallic compounds R_6TX_2 where R = Rare earth, T = transition metal and X = Sb, Te and Bi, have hexagonal Fe_2P-type structure (space group P-62m, no. 189, $hP9$) with tunable magnetic properties [1, 2]. From crystal structural point of view, the rare earth sublattice of the R_6TX_2 can be considered as distorted Mg-type rare-earth lattice because of the insertion of transition metal elements and p-elements and this leads to corresponding change in magnetic ordering as compared to the magnetic properties of the individual rare earth elements. The compound Er_6MnTe_2 is particularly interesting in the family of R_6TX_2 because magnetic ordering temperatures of Mn-containing samples are higher than the counterparts with T = Fe, Co, Ni and Ru. For instance, Er_6FeBi_2 has a ferromagnetic Curie temperature (T_C) of 15 K, whereas Er_6MnBi_2 exhibits a higher T_C of 115 K, while in the elemental Mg-type Er, the antiferromagnetic ordering temperature T_N is 85 K and T_C is 20 K. This has stimulated us to study the magnetic properties of Er_6MnTe_2 by dc magnetization and neutron diffraction experiments. From the temperature dependent magnetization, it is found that Er_6MnTe_2 compound orders ferromagnetically at 76 K and shows a low temperature peak at 10 K (T_m) [Fig. 1]. Saturation magnetization value at 2 K is about 6.7 μ_B/Er^{3+}. From powder neutron diffraction study carried out in zero applied magnetic field, it is found that Er_6MnTe_2 is paramagnet from 300 K to 76 K [Fig. 2a]. From 68 K to 48 K, a set of commensurate magnetic reflections appear indicating a-axis collinear ferromagnetic ordering of Er sublattice with propagation vector (K_0 = [0, 0, 0] [Fig. 2a]. Meanwhile from 38 K to 8 K, variation of intensity of magnetic reflections suggests non-collinear ab-plane ferromagnetic ordering of Er_6MnTe_2 [Fig. 2b]. At T_C, the moments at two Er sites (3f and 3g) are different whereas at 8 K (i.e. below T_m), these reach the theoretical Er moment of 9 μ_B.

1. A. Herrero, I. R. Aseguinolaza, A. Oleaga, A. J. Garcia-Adeva, E. Apiñaniz, A. V. Garshev, V. O. Yapaskurt and A. V. Morozkin, Dalton Trans. 52 (2023) 5780 and references therein. 2. Meng Zhao, Jinlei Yao, A. Oleaga, A.V. Knotko, V.O. Yapaskurt and A.V. Morozkin, J. Solid State Chem. 323 (2023) 124058

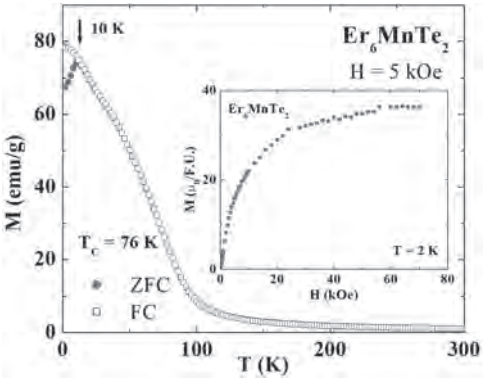

Figure 1 Magnetization vs temperature of Er_6MnTe_2 in applied field of 5 kOe. Inset: Magnetization vs field at 2 K.

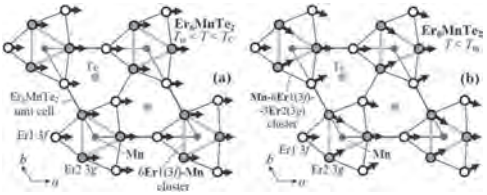

Figure 2 Magnetic structure of Er_6MnTe_2 (a) below T_C and (b) below T_m.

VP15-06. Improving Reciprocating SQUID Magnetometry by Explicit Response Linearization. *P.S. Stamenov*[1] *1. School of Physics and CRANN, Trinity College, Dublin, Ireland*

Contemporary magnetometry is widely used by physicists, chemists and material scientists as a routine technique for sample characterization of both bulk and thin film materials. Its most popular modality: the SQUID-based, superconducting second-order gradiometer magnetometry has become the de facto standard. A decade ago, the go-to systems were primarily extraction-style, operating at low frequencies (~ 1 Hz), e.g. the popular by QD MPMS system. Lately, higher frequency (many 10ns of Hz), shorter linear drives,

such as the one of the MPMS3 SQUID-VSM, by the same vendor, are gaining popularity. An overall higher sample throughput demands different design solutions and the benefits must be paid by compromises elsewhere: e. g. shorter maximal translation span and narrower gradiometers, yielding increased sample geometry- and position-dependent systematic errors. Here, we focus on the analysis of the temporal spectral components produced by the rather non-linear Point Spread Function (PTF) [1] and formulate a strategy for the minimization of the same for any particular choice of sample geometry restrictions. While at frequencies over few 10ns of Hz the main source of interference is mains-power induction, a typical large amplitude oscillation of the sample is generating primarily even harmonics of the drive frequency, whose low-frequency spectrum is overlapping with typical digital communication interference as shown on the figure. Following drive waveform modification, only the second harmonic survives, significantly enhancing the filtering possibilities and thus diminishing the noise and interference pickup. This methodology is applicable to both small-amplitude VSM-type oscillations and large-amplitude, low frequency sample reciprocation, necessitated by the mass of certain custom probe types, such as FMR rods [2] and liquid sample mounts.

[1] P. Stamenov and J.M.D. Coey, Rev. Sci. Instr. 77, 015106 (2006) [2] J. M. O'Reilly and P. Stamenov, Rev. Sci. Instr. 89, 044701 (2018)

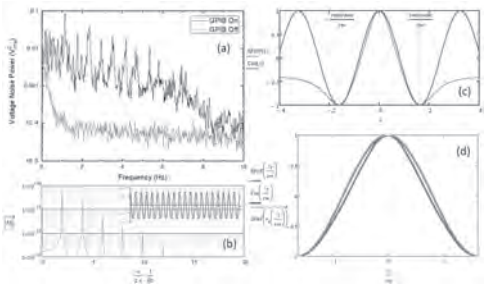

Fig. 1: (a) Typical low-frequency noise spectra of a commercial magnetometer, showing the dominant 1/*f* technical noise below about 1 Hz and the digital communications interference. (b) Real time and frequency spectrum of the response at large amplitude of sample oscillation. (c) Region of the PSF best utilized for linearization. (d) Sample drive waveform before and after correction.

VP15-07. Wide temperature range magnetocaloric effect with $Gd_{1-x}Pr_xNi_{2-y}Co_y$ alloys. R. Duarte de Melo[1], C.L. Rodrigues[1], D.M. Garcia[1] and *A. Gomes*[1] *1. Universidade Federal do Rio de Janeiro, Rio de Janeiro, Brazil*

The magnetocaloric effect (MCE) has significant interest for its potential applications in magnetic refrigeration technology [1]. Binary compounds $R_{1-x}R'_xTM_2$, where TM represents Al or Ni, and R,R′ denote rare earth elements [2, 3], have been identified as promising candidates for use in different temperature range. Alho et al. have studied $Gd_{1-x}Pr_xNi_2$ which showed a wide and interesting MCE properties for hydrogen liquefaction, while Ermolenko et al.[4] demonstrated that the substitution of Ni for Co in $PrNi_2$ alloys induces the magnetism and increase the Curie temperature. These alloys exhibit a noteworthy temperature range (T_c), particularly interesting for hydrogen liquefaction. The present study aims to consolidate both works in the $Gd_{1-x}Pr_xNi_{2-y}Co_y$ alloys, in order to verify the MCE as well as its temperature range. Using computational methods, we developed a mean field Hamiltonian to describe the magnetic system, calculated eigenvalues and eigenstates for use in the partition function, and determined magnetization curves, Gibbs free energy, and entropy variation under applied magnetic fields. The self-consistent algorithm provided valuable insights into the T_c value. To validate the results of the calculations, we synthesized some of these alloys and compared the experimental results to theorectical ones.

[1] Gschneidner Jr. et al. Recent Developments in Magnetic Refrigeration. Materials Science Forum, 315-317, 69–76 (1999). [2] Alho, B. P. et al. Magnetic and magnetocaloric properties in $Gd_{1-y}Pr_yNi_2$ compounds. Journal of Magnetism and Magnetic Materials, 449, 308–312 (2018). [3] Ribeiro, P. O. et al. Theoretical investigations on the magnetocaloric and barocaloric effects in $Tb_yGd_{(1-y)}Al_2$ series. Journal of Alloys and Compounds, 563, 242–248 (2013). [4] Ermolenko, A. S. et al. Compositional genesis of ferromagnetism in alloys $PrNi_{2-x}Co_x$. Journal of Magnetism and Magnetic Materials, 490, 165489 (2019).

VP15-08. Magnetocaloric effect for pyramid and flower-shaped CoO nanoparticles. Y. Hotta[1], T. Tachibana[1] and *S. Kobayashi*[1] *1. Iwate University, Morioka, Japan*

Magnetic refrigeration systems based on the magnetocaloric effect (MCE) have received much attention due to possible higher energy efficiency and environmentally friendly features. In particular, magnetic nanoparticles have a possibility of including the MCE materials into electric devices and better heat exchange with a surrounding matrix owing to their large surface area. So far, many kinds of magnetic nanoparticles have been surveyed [1], with varying particle size, chemical compositions, etc., the effect of particle shape on MCE was less studied though MCE-related magnetic properties such as effective anisotropy, surface effect, can be tuned. In this study, we focused on the effect of particle morphology on MCE for pyramid and flower CoO nanoparticles (insets in Fig.1). We examined four CoO samples: hexagonal pyramid CoO with size of 26 nm (P26) and 32 nm (P32), face-centered-cubic flower CoO with size of 24 nm (F24) and 29 nm (F29). A flower nanoparticle for F24 and F29 consists of randomly oriented small grains with size of 5.2 and 8.5 nm, respectively, whereas a pyramid nanoparticle is typically a single crystal. Magnetization under magnetic fields was measured in the temperature range of 2-300 K to evaluate a magnetic entropy change, which is the measure of MCE. Whereas CoO is antiferromagnetic in nature, all the samples exhibit ferromagnetism, which develops at low temperatures. Magnetic entropy changes calculated from magnetization curves exhibit a maximum at low temperatures below 10 K (Fig. 1). Although the maximum value is weakly dependent on particle size for pyramid nanoparticles, it drastically increases with decreasing particle size for flower nanoparticles and attains 0.49 J/K/kg at T=3 K for F24. These results indicate that the surface spin freezing dominates MCE for CoO nanoparticles, but magnetic coupling between small grains can give an additional effect on MCE for flower-shaped nanoparticles.

[1] V. Franco, J.S. Blazquez, J.J. Ipus, L.M. Moreno-Ramirez, A. Conde, Prog. Mater. Sci. vol. 93, 112 (2018).

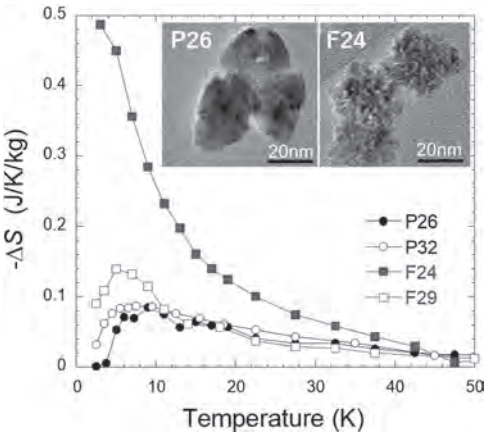

Fig.1: Magnetic entropy changes as a function of temperature for a field change of 50 kOe. The insets show transmission electron microscopy images for P26 and F24.

VP15-09. Enhanced High-Energy Products in Core@Shell Nanoparticles of Hard@Soft Magnetic Materials. l.F. Silva[1], *L.L. Oliveira*[1], M.S. Nunes[2], A.L. Dantas[1,2] and A.S. Carriço[3] *1. Department of Science and Technology, State University of Rio Grande do Norte, Natal, Brazil; 2. Department of Physics, State University of Rio Grande do Norte, Mossoro, Brazil; 3. Department of Physics, Federal University of Rio Grande do Norte, Natal, Brazil*

Combining hard and soft magnetic materials in core@shell nanoparticles (hard@soft) can potentially enhance their technological applications [1]. This study investigates how core@shell nanoparticles made of high coercivity core materials (such as $Nd_2Fe_{14}B$ or CoPt) and high saturation magnetization shell materials (such as Fe or $CoFe_2$) may be tailored to optimize their high-energy product (BH_{max}) [2]. Alongside anisotropy and saturation magnetization, this improvement can also be credited to the exchange stiffness constant (A). The exchange stiffness is a key parameter that governs magnetization reversal, stabilizes the magnetization, and reduces demagnetization effects. For instance, although CoPt has higher anisotropy than $Nd_2Fe_{14}B$, the BH_{max} of $Nd_2Fe_{14}B$ (515 kJ/m^3) is greater than that of CoPt (199 kJ/m^3). Our findings suggest that using shell materials with larger values of A may lead to a more effective enhancement of the BH_{max}. Fig.1 shows BH_{max} values as a function of the shell thickness δ for $Nd_2Fe_{14}B$(9 nm)@Fe(δ), $Nd_2Fe_{14}B$(9 nm)@$CoFe_2$(δ), CoPt(9 nm)@Fe(δ), and CoPt(9 nm)@$CoFe_2$(δ). The optimized value of the BH_{max} of $Nd_2Fe_{14}B$(9 nm)@Fe(δ) nanoparticles is 813 kJ/m^3, and occurs for δ = 3nm, and is higher than the optimized BH_{max} of $Nd_2Fe_{14}B$(9 nm)@$CoFe_2$(δ) nanoparticles, which is 731 kJ/m^3, and occurs for δ = 1nm. Table I displays the highest BH_{max} in core-shell nanoparticles with a 3 nm Fe shell, and 1 nm $CoFe_2$ shell thickness. Our results show a significant increase in the BH_{max} relative to the single-phase materials values. Table I shows that the BH_{max} efficiency increases as the core diameter decreases. These findings highlight the potential of core-shell nanoparticles as promising candidates for advanced magnetic applications requiring high-performance magnets.

[1] A. Lopez-Ortega, M. Estarder, G. Salazar-Alvarez, A. G. Roca, andJ. Nogues, *Phys. Rep.,* 553, 1, 2015. [2] L. L. Oliveira, A. L. Dantas, S. S. Pedrosa, G. O. Rebouças, R. B. Silva, J. M. Araújo, and A. S. Carriço, *Phys. Rev. B,* 97, 134413, 2018.

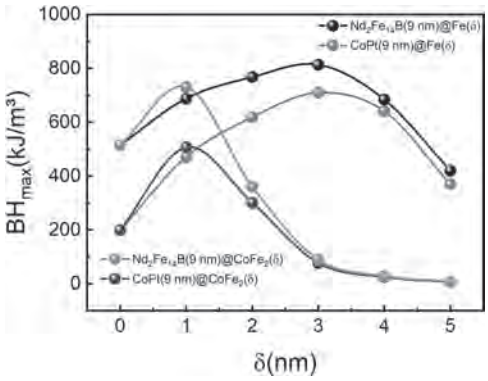

Fig. 1: BH_{max} values as a function of the shell thickness δ for $Nd_2Fe_{14}B$@Fe, $Nd_2Fe_{14}B$@$CoFe_2$, CoPt@Fe, CoPt@$CoFe_2$.

Core	Shell – Fe(3 nm)	Shell – $CoFe_2$(1 nm)
$Nd_2Fe_{14}B$(9 nm)	813 kJ/m³	731 kJ/m³
$Nd_2Fe_{14}B$(15 nm)	750 kJ/m³	649 kJ/m³
$Nd_2Fe_{14}B$(21 nm)	707 kJ/m³	615 kJ/m³
CoPt(9 nm)	709 kJ/m³	507 kJ/m³
CoPt(15 nm)	589 kJ/m³	380 kJ/m³
CoPt(21 nm)	501 kJ/m³	330 kJ/m³

Table I - BH_{max} values for core@shell nanoparticles of $Nd_2Fe_{14}B$@Fe(3 nm), $Nd_2Fe_{14}B$@$CoFe_2$(1 nm), CoPt@Fe(3 nm), CoPt@$CoFe_2$(1 nm), with core sizes of 9 nm, 15 nm, and 21 nm.

VP15-10. Experimental Investigation of Core-Shell Tungsten Nanoclusters for Radiation Protection. *X. Tao*[1,2], X. Sun[1], F. Liu[2], B. Wang[1] and S. Peng[1] *1. Fert Beijing Institute, School of Integrated Circuit Science and Engineering, Beihang University, Beijing, China; 2. Hefei Innovation Research Institute of Beihang University, Anhui Hefei, China*

With the advancement of thin films and nanomaterials, it has been discovered that nanomaterials hold promising applications in radiation protection. In 2010, Bai et al. theoretically unveiled the mechanism of self-healing of radiation damage in nanomaterials [1]. In the same year, Ackland highlighted the potential of nanomaterials as a highly promising material in the realm of radiation resistance [2]. The synthesis of materials with a significant number of grain boundaries and interfaces is crucial for achieving outstanding radiation resistance. Several studies have indicated that materials with nanocrystalline structures exhibit superior radiation resistance [3]. In recent years, researchers have discovered that film layer with special structures have prospects for radiation protection[4][5]. Nanoclusters have received extensive attention within the realm of nanomaterials due to their multitude of interfaces, making them a highly promising material for radiation protection. In this paper, we first synthesized W-WOx core-shell nanoclusters using a combination of magnetron sputtering and gas aggregation methods [6][7]. The core-shell tungsten nanoclusters were characterized by a variety of devices. As illustrated in Figure 1, transmission electron microscope (TEM) analysis confirms the distinct core-shell morphology of the tungsten nanoclusters. Then, we fabricated core-shell tungsten nanocluster films with a thickness of 200 nm on 50μm silicon substrates. To evaluate the radiation shielding performance, we encapsulated the nanocluster films on static random-access memory (SRAM) and assessed the number of single event upset (SEU) errors under 1.3GeV tantalum ion irradiation. As detailed in Figure 2, the results indicate that SRAM remains error-free under irradiation when it is packaged with nanocluster films, signifying that the nanocluster films can substantially mitigate the energy of radiation particles.

[1] X. M. Bai, A. F. Voter,R. G. Hoagland, Science., Vol.327, no.5973, p.1631-1634 (2010). [2] G. Ackland, Science., Vol.327, no.5973, p.1587-1588(2010) [3] T.D. Shen, S. Feng, M. Tang, Appl. Phys. Lett., Vol.90, no.26 (2007) [4] R. Laptev, A. Lomygin,D. Krotkevich, Metals., Vol.10, no.4, p.535(2020). [5] K.K. Kadyrzhanov, D.I. Shlimas, A.L. Kozlovskiy, Journal of Materials Science: Materials in Electronics., Vol.31, p.11729–11740 (2020). [6] H. Haberland, M. Karrais, Y. Thurner, Journal of Vacuum Science & Technology A: Vacuum, Surfaces, and Films, Vol.10, no.5, p.3266-3271(1992). [7] Y. Qiang, Y. Thurner, H. Haberland, Surface and Coatings Technology, Vol.100, p. 27-32(1998).

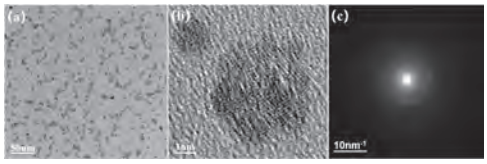

Fig.1 Transmission electron microscopy (TEM) image of core-shell tungsten nanoclusters(a)TEM image(b)TEM images illustrating the nanocrystalline architecture(c)Electron diffraction pattern from a single nanocluster.

SRAM number	Package type	Fluence rate (/cm²·s)	Total fluence (n/cm²)	SEU error count
#1	No package	1.00×10^4	7.80×10^8	110
#2	200nm cluster film package	1.70×10^4	1.00×10^7	0

Fig.2 Single event upset (SEU) test results induced by 1.3 GeV tantalum particle irradiation

VP15-11. Size Dependence of Magneto-Optical Scattering by Superparamagnetic Nanoparticles and its Connection to Aggregation.

M. Syed[1], S. Reza[1], H. Lu[1] and W. Amory[1] *1. Physics & Optical Engineering, Rose-Hulman Institute of Technology, Terre Haute, IN, United States*

Superparamagnetic nanoparticles (SNPs) are increasingly deployed in biomedical applications like imaging, magnetic hyperthermia, drug delivery, etc. [1]. We present a continuation of our previous studies that examine the scattering properties of dilute aqueous suspensions of single-domain iron oxide nanoparticles using an AC Faraday rotation setup [2-4]. Our experimental approach captures both even and odd harmonics of the magneto-optical response. In this work we focus on the even harmonics that arise due to scattering. We have measured the scattering response of SNPs that vary in size from 10 to 30 nm for the longitudinal standard geometry where the applied magnetic field is along the direction of light propagation. In addition, we also discuss data that is acquired in a transverse geometry where the direction of the applied field and that of light propagation are perpendicular to each other. Our results provide important insight into the role of nanoparticle size (core and hydrodynamic) and particle concentration in the formation dynamics of clusters. While our previous work utilized the second harmonic (2*f*) of the received irradiance signal to analyze light scattering by SNPs subjected to an AC magnetic field, here we continue to further investigate even harmonics (primarily 2*f* and 4*f*) signal to analyze scattering but with added emphasis on the size of the SNPs. This approach allows us to investigate how scattering can be used as a useful probe for the formation of SNP aggregates. Scattering results from three different SNP sizes (samples of diameters of 10 nm, 20 nm, and 30 nm) are presented. Differences in scattering responses are then related to the structural details of the aggregates. While the main emphasis is on the SNP size as a key parameter, we have extended the measurements to different concentrations of SNPs to better investigate our framework regarding the sample properties that help (nearest-neighbor distance, effective magnetic moment) in aggregate formation.

[1] Y. Xiao and J. Du, "Superparamagnetic nanoparticles for biomedical applications," J. Mater. Chem. B, vol. 8, 3, 354–367, (2020). [2] S. Vandendriessche, W. Brullot, D. Slavov, V. Valev, and T. Verbiest, "Magneto-optical harmonic susceptometry of superparamagnetic materials," Appl. Phys. Lett., vol. 102, (2013). [3] C. Patterson, M. Syed, Y. Takemaura, "Harmonic decomposition of magneto-optical signal from suspensions of superparamagnetic nanoparticles," JMMM, 451, 248-253 (2018). [4] M. Syed, W. Li, N. Fried, and C. Patterson, "Magneto-optical investigation of scattering by superparamagnetic nanoparticles using multi-harmonic analysis," AIP Advances 11, 015328 (2021).

Session VP16
SENSORS AND APPLICATIONS
(Poster Virtual Session)

Prasanth Velvaluri, Chair
Northeastern University, Boston, MA, United States

VP16-01. Magnetotransport Properties of Tunneling Magnetoresistance Devices with CoFeBSi, CoFeB/CoFeBSi and CoFeB/Ru/CoFeBSi Free Layers. *P. Las*[1], F. Matos[2], R. Macedo[2], S. Cardoso de Freitas[2], P. Freitas[2] and P. Wisniowski[1] *1. Institute of Electronics, AGH University of Krakow, Krakow, Poland; 2. INESC-MN, Lisbon, Portugal*

The ongoing development of TMR devices for detecting ultralow magnetic fields at low frequencies focuses on increasing sensitivity and lowering noise. Sensitivity improvement research aims to find free layer materials and structures with a low saturation field (anisotropy) and a high tunneling magnetoresistance ratio. Several studies [1,2.3] showed that the most promising free layer is based on CoFeB coupled to CoFeBSI. The devices with that free layer showed up to 50% Oe sensitivity and a hysteresis of 4 Oe [3]. However, the devices' field detection depends on both sensitivity and noise. The noise is typically of magnetic origin, resulting from magnetization fluctuations in the free (sensing) layer. Noise is strongly dependent on the free layer's magnetization process and correlates with sensitivity. Thus, investigating the free layer response to magnetic field for the devices is equally important as improving sensitivity. We studied the response to magnetic field of devices with CoFeBSi, CoFeB/CoFeBSi, and CoFeB/Ru/CoFeBSi free layers. We evaluated the sensitivity, saturation (switch) field, coercivity, and coupling field for the devices. We use a two-step annealing process to induce cross anisotropy between the reference and free layer in order to linearize device responses to magnetic fields (transfer curves). Shape anisotropy was also used on some devices to influence their magnetization process. The device without shape anisotropy demonstrated a switching of magnetization for all free layers and high sensitivity (Fig. 1). While the device with shape anisotropy showed rotation of the magnetization and lower sensitivity. These results demonstrated that a two-step annealing process alone is insufficient to achieve linear response in the device. Furthermore, using high aspect ratio devices does not eliminate hysteresis in devices with those types of free layers.

[1] M. Kato et al., Fabrication of Magnetic Tunnel Junctions with Amorphous CoFeSiB Ferromagnetic Electrode for Magnetic Field Sensor Devices Appl. Phys. Express 6, 103004 (2013). [2] R. Rasly, et al. Magnetic, magnetoresistive and low-frequency noise properties of tunnelmagnetoresistance sensor devices with amorphous CoFeBTa soft magnetic layersJ. Phys. D.Appl. Phys. 54, 095002 (2021) [3] M. Nakano Enhanced sensitivity and thermal tolerance in tunnel magnetoresistance sensor using Ta-doped CoFeSiB soft magnetic layer Appl. Phys. Lett. 123, 072404 (2023).

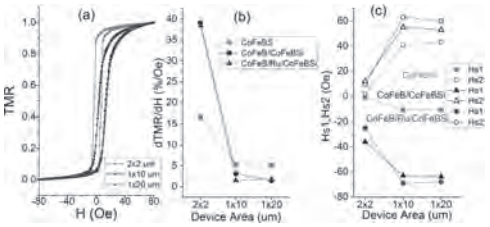

Fig. 1. Transfer curve of devices with and without shape anisotropy for CoFeBSi free layer (a). Sensitivity (b) and switching (saturation) field (c) of the devices with different free layers.

VP16-02. Analysis of Inductive Angular Position Sensor with the Characteristic of Annular Sector Coils. *D. Xu*[1], S. Fang[1], F. Zeng[2] and S. Hwang[3] *1. School of Mechatronic Engineering and Automation, Shanghai University, Shanghai, China; 2. Shanghai Zenidrive Technology Co., Shanghai, China; 3. School of Mechanical Engineering, Pusan National University, Busan, The Republic of Korea*

More interests and attentions were taken into the inductive angular position sensor because of their high accuracy and low price in the electric drive system. As showed in Fig.1 (a), three models with different annular sector coil structures were designed to study the effect of characteristic of coils to the performance and accuracy of an Inductive Angular Position Sensor (IAPS). The structure of an IAPS was divided into two parts: a PCB stator and a rotor [1]. The coils were manufactured into a PCB and were composed of three parts: one set of excitation coil and two sets of receiving coils. The receiving coils shuttled back and forth as a sine shape or a cosine shape between the layers of excitation coil and connected by copper pillars. A chip also placed on the PCB to process the voltage signals induced from the receiving coils [2]. The metal rotor was assembled on the shaft and sealed in the motor enclosure with 4 blades related with the pole number of motor was employed in this study. Compared with the Type A, three time turns of receiving coils were structured in Type B. And Type C had a doubled length of both excitation coil and receiving coils compared with Type B. The parameters and dimensions of three structures were detailed in Table I. The magnetic analyses were simulated by using finite element method. The detailed working principle and the effect of characteristic of annular sector coils of the IAPS would be illustrated in the manuscript [3]. The distributions of magnetic flux density were obtained as shown in Fig.1 (b). The simulated three type induced voltages obtained in the receiving coils could be used to signal processing and derived the simulated angular errors. Three prototypes as in Fig.1 (a) were manufactured. The experimental induced voltages would verify the simulation results, and the experimental accuracies would be compared with the simulated accuracies after voltage signals processing. The data processing and the detailed effect of coil characteristic would be presented in the full manuscript.

[1] Q. Tang, D. Peng, L. Wu and X. Chen, "An Inductive Angular Displace-ment Sensor Based on Planar Coil and Contrate Rotor," in *IEEE Sensors Journal*, vol. 15, no. 7, pp. 3947-3954, July 2015, doi: 10.1109/JSEN.2015.2404349. [2] W. Gao, H. Shi and Q. Tang, "A Contactless Planar Inductive Sensor for Absolute Angular Displacement Measurement," in *IEEE Access*, vol. 9, pp. 160878-160886, 2021, doi: 10.1109/ACCESS.2021.3131344. [3] Dan-Ping Xu, Guochao Ma, Silong Fang, Fanlin Zeng, Sang-Moon Hwang "A Contactless Inductive Position Sensor with Four-Phase Rotor for Angular Displacement Detection." *IEEE transactions on magnetics* 60.2 (2024): 1–5.

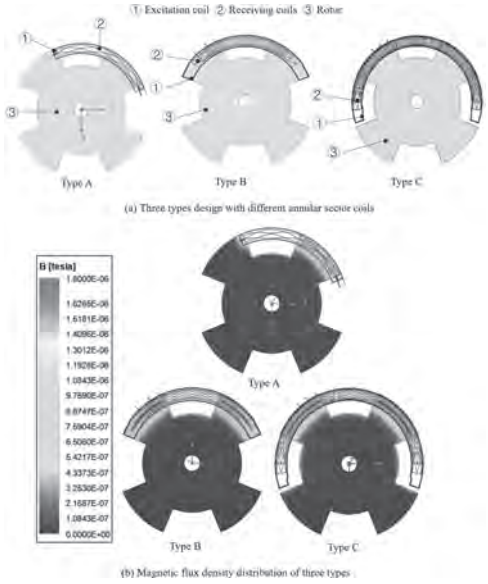

Fig. 1. Three types design with different annular sector coils and their magnetic flux density distributions.

Parameter	Symbolic meaning	Type A (mm)	Type B (mm)	Type C (mm)
D_{R1}	Rotor outer diameter	115	140	140
D_{B1}	Rotor blade outer diameter	115	120	120
D_{B2}	Rotor blade inner diameter	74	70	80
D_{R2}	Rotor inner diameter	53	53	53
H_R	Rotor thickness	5	7	7
H_B	Rotor blade thickness	5	8.5	8.5
W_C	Coil width	0.2	0.1	0.1
H_C	Coil thickness	0.035	0.035	0.035
N_E	Number of turns per layer of excitation coil	2	3	3
N_{R1}	Number of total turns of SIN receiving coil	1	3	3
N_{R2}	Number of total turns of COS receiving coil	1	3	3
L_E	Number of layers of excitation coil	3	2	2

Table 1: Parameters and Dimensions of different three types design.

VP16-03. Research on magnetic interference compensation based on improved ellipsoidal fitting method. *B. Fan*[1], J. Qiu[1], C. Cao[1], S. Huang[1] and X. Zeng[1] *1. College of Optoelectronic Engineering, Chongqing University, Chongqing, China*

Magnetic anomaly detection technology has shown a wide range of application value in many fields such as underwater target detection and identification, mineral resource development, etc. As the carrier of the magnetic measurement system, the magnetic compensation technology can effectively eliminate the interference magnetic field of the platform, which is the core point of the magnetic anomaly detection technology, which directly affects the detection accuracy [1]. In this paper, the magnetic sensor interference, the maneuvering interference field and the geomagnetic gradient interference are improved on the original basis, and the research content includes the following three aspects: firstly, the magnetic interference mechanism of the magnetic measurement motion platform is analyzed, and the corresponding interference model is established. The interference mechanism of geomagnetic field, magnetic sensor and mobile interference field is studied, and the corresponding interference magnetic field model is established. Secondly, based on the method of improved ellipsoid fitting, the ellipsoid compensation parameters are obtained by using the least squares method, and the interference compensation algorithm of the ellipsoidal fitting magnetic sensor with the "optimal random selection" mechanism is proposed, which further improves the compensation accuracy of the magnetic sensor [2]. Finally, based on the improved Tolles-Lawson model, the influence of noise on the compensation is analyzed, the compensation parameters are solved by the fixed-point change measurement attitude experiment, and the geomagnetic gradient correction is integrated into the compensation process in the maneuvering experiment of the moving platform, so as to verify the compensation effect of the proposed method on the magnetic interference of the moving platform [3]. It provides reliable technical support for further research on magnetic field detection.

[1]Alken P, Thébault E, Beggan C D, et al. International geomagnetic reference field: the thirteenth generation. Earth, Planets and Space, 2021, 73: 1-25. [2]Lee H, Lee C, Jeon H, et al. Interference-compensating magnetometer calibration with estimated measurement noise covariance for application to small-sized UAVs. IEEE Transactions on Industrial Electronics, 2019, 67(10): 8829-8840. [3]Li Y, Han Q, Li Q, et al. On the correction of the positional error caused by the coordinate origin in Tolley–Lawson model. IEEE Geoscience and Remote Sensing Letters, 2022, 19: 1-5.

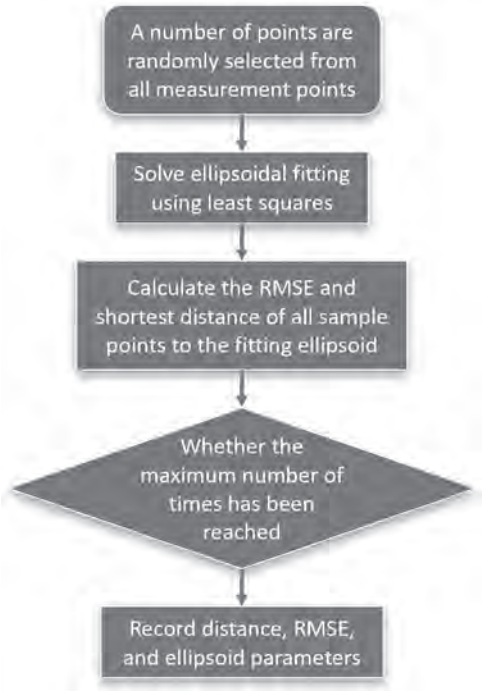

Fig. 1 Flowchart of improved ellipsoidal fitting algorithm

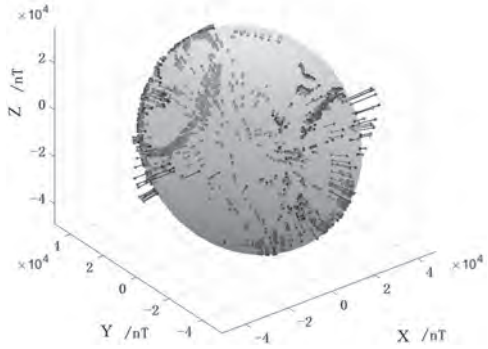

Fig. 2 Schematic diagram of the distance from a point to an ellipsoidal surface

VP16-04. Analysis of Radial Eccentricity and Axial Misalignment Effects on Inductive Angular Position Sensor Performance. *D. Xu*[1], Y. Zhao[1], X. Wang[1], F. Zeng[2] and S. Hwang[3] *1. School of Mechatronic Engineering and Automation, Shanghai University, Shanghai, China; 2. Shanghai Zenidrive Technology Co., Shanghai, China; 3. School of Mechanical Engineering, Pusan National University, Busan, The Republic of Korea*

The precise measurement capabilities and robustness of inductive sensors make them indispensable in automotive, motor control, and industrial automation [1]. The assembling error, mechanical robustness, insensitivity to electrical or magnetic fields as well as its mechanical tolerances makes the sensor suitable for harsh environment [2]. Despite their established reliability and accuracy, maintaining high performance under varying mechanical conditions remains challenging. The effects assembling accuracy, specifically radial eccentricity and axial misalignment, on the performance of an IAPS were investigated in this research. The sensor used in this study features a rotor with four-phase pole pairs and a stator embedded with excitation and receiving coils, along with an integrated chip, all mounted on a PCB, as shown in Fig.1 (a). The modeling of the radial eccentricity was shown in Fig.1, the Fig.1 (a) was assembled without radial eccentricity, and the Fig.1 (b) and (c) were with different radial eccentricity. The axial misalignment of the IAPS during assembling was shown in Fig.2. The finite element method was adopted in the electromagnetic simulation [3], and were employed to assess the sensor's performance under radial eccentricity up to 0.5 mm and axial misalignment up to 1°, as shown in Fig.2. The induced voltage, angle error, and magnetic flux density are analyzed to find the impact of radial displacement and tilt angle variations on inductive angular position sensor performance. The prototype will be manufactured and tested in these two different situations. The simulation results will be verified experimentally and be shown in the full manuscript. These insights highlight the necessity of careful mechanical design and calibration to maintain sensor performance. This research contributes to developing more robust and precise inductive angular position sensors, offering strategies for optimizing performance in variable mechanical environments.

[1] Tang, Q., et al., An Inductive Angular Displacement Sensor Based on Planar Coil and Contrate Rotor. *IEEE Sensors Journal*, 2015. 15(7): p. 3947-3954. [2] Li, L., M. Yang, and L. Ye, Design of inductive contactless angular sensor electromagnetic coupling system. *Transducer and Microsystem Technology*, 2011. 30(10): p. 130. [3] Dan-Ping Xu, Guochao Ma, Silong Fang, Fanlin Zeng, Sang-Moon Hwang "A Contactless Inductive Position Sensor with Four-Phase Rotor for Angular Displacement Detection." IEEE transactions on magnetics 60.2 (2024): 1–5.

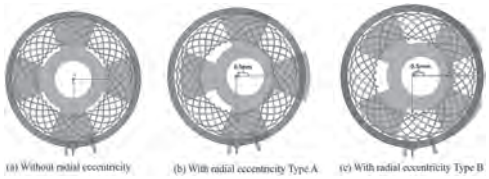

Fig.1The modeling of radial eccentricities.

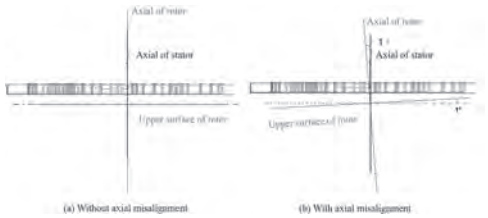

Fig.2 The axial misalignment of the IAPS during assembling.

VP16-05. Implementation of ENG Metasurfaces for 5G Antenna Systems. A. Eroglu[1] and *T. Islam*[2] *1. ECE, University of Massachusetts Boston, Boston, MA, United States; 2. ECE, North Carolina A&T State U, Greensboro, NC, United States*

In this paper, Epsilon-negative (ENG) metasurfaces and their application in enhancing antenna performance for 5G applications are presented. A unit cell designed to operate at 26GHz has been presented and validated using the 3D electromagnetic simulator, CST. This unit cell is then utilized to construct a metasurface with a circularly polarized radiating patch antenna. Through the analysis of the S-parameters and permittivity of the ENG metasurface, improvements in gain and beamforming capabilities have been realized. It is shown that the proposed design also enhances the wide-bandwidth capabilities of the antenna by employing a single metasurface layer. Additionally, the design offers a low profile and circular polarization, making it ideal for 5G millimeter-wave systems and MIMO applications. ENG metasurfaces are a category of materials that manipulate electromagnetic waves in innovative ways, leading to significant advancements in antenna design and functionality. Their use relies on their ability to exhibit negative permittivity, a feature that is exploited to improve antenna gain, directivity, bandwidth, and other performance parameters [1-2]. This property has been applied in this paper to design a unit ENG cell as shown in Fig.1a, with a radiating patch to enhance the antenna performance. The simulation results showing S_{11} and S_{21} of the antenna are given in Fig. 1b. Fig. 1c displays the antenna performance improvement in gain, bandwidth and radiation efficiency.

1. E. Ozbay, K. Guven, and K. Aydin, "Metamaterials with negative permeability and negative refractive index: Experiments and simulations," Journal of Optics A: Pure and Applied Optics, vol. 9, no. 9, Aug. 2007. doi:10.1088/1464-4258/9/9/s04 2. R. A. Shelby, D. R. Smith, S. C. Nemat-Nasser, and S. Schultz, "Microwave transmission through a two-dimensional, isotropic, left-handed metamaterial," Applied Physics Letters, vol. 78, no. 4, pp. 489–491, Jan. 2001. doi:10.1063/1.1343489 S. Abeywickrama, R. Zhang, and C. Yuen, "Intelligent reflecting surface: Practical phase shift model and beamforming optimization," ICC 2020 - 2020 IEEE International Conference on Communications (ICC), Jun. 2020. doi:10.1109/icc40277.2020.9148961

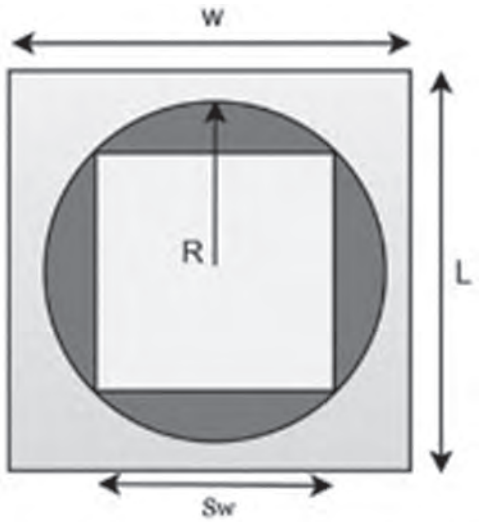

Fig. 1: Single element unit cell

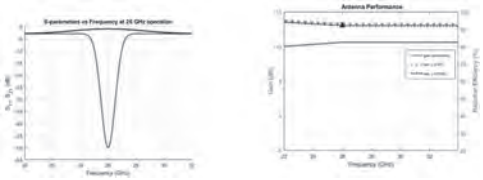

Fig. 2: (b) Simulation results for S11 and S21 (c) Performance improvement of the antenna

VP16-06. Modeling Non-Linear and Non-Stationary Magnetic Signals: An Enhanced Signal Processing Strategy for Wind Time Series Analysis. *A. Swain*[1], I. Hossain[1], C. Liu[2] and P. Pong[1] *1. Electrical and Computer Engineering, New Jersey Institute of Technology, Newark, NJ, United States; 2. School of Energy and Environment, City University of Hong Kong, Kowloon Tong, Hong Kong*

Magnetic-flux-based condition monitoring techniques are becoming increasingly popular due to their advantages such as non-invasiveness, low-costs, and ease of sensor installation. However, developing diagnostic- and prognostic-based condition monitoring sytems become challenging as magnetic signals based wind time series exhibit nonlinear and non-stationary characteristics due to being subjected to diverse combination of dynamic system behavior [1]. Present data-driven-based feature extraction techniques and knowledge and parameter estimator models are successful in detecting and quantifying the nonlinear and nonstationary behaviour in wind speed time series and wind vibration time series [2],[3]. Further, short-time Fourier transform and discrete wavelet transform have proven suboptimal for analyzing nonlinear magnetic flux signals [4]. This research bridges the gap by investigating a new methodology of feature extraction to adeplty process the nonlinear and nonstationary behaviour in magnetic signals based wind time series. This methodology is unique in nature since it utilizes magnetic signature-based condition indicators derived from distributed TMR sensors placed on a model that accounts for the electromagnetic nature of the drive train coupling as shown in Fig. 1. Further, the signal processing technique employed here takes into account various non-linearities that arises from magnetic saturation, hysteresis and eddy currents in the generator's magnetic circuit and the non-stationarity that arises from variations in wind speed, mechanical vibrations and environmental factors such as changes in temperature. Next, these bivatiate features are decomposed into its first, second, and higher order of moments in time frequency domain to efficiently extract the underlying fault features. Finally, faults on both mechanical and electrical components of the drive train are identified and successfully classified using a machine learning based multi class classification algorithm. The proposed methodology is validated using distributed sensors on a drive train emulator.

[1] M. S. Kan, A. C. C. Tan, and J. Mathew, "A review on prognostic techniques for non-stationary and non-linear rotating systems," *Mechanical Systems and Signal Processing,* vol. 62-63, pp. 1-20, 2015. [2] S. Solari and M. Á. Losada, "Simulation of non-stationary wind speed and direction time series," *Journal of Wind Engineering and Industrial Aerodynamics,* vol. 149, pp. 48-58, 2016. [3] R. Uma Maheswari and R. Umamaheswari, "Trends in non-stationary signal processing techniques applied to vibration analysis of wind turbine drive train – A contemporary survey," *Mechanical Systems and Signal Processing,* vol. 85, pp. 296-311, 2017. [4] I. Zamudio-Ramirez, R. A. Osornio-Rios and J. A. Antonino-Daviu, "Magnetic Flux Analysis for the Condition Monitoring of Electric Machines: A Review," *IEEE Transactions on Industrial Informatics,* vol. 18, no. 5, pp. 2895-2908, 2022.

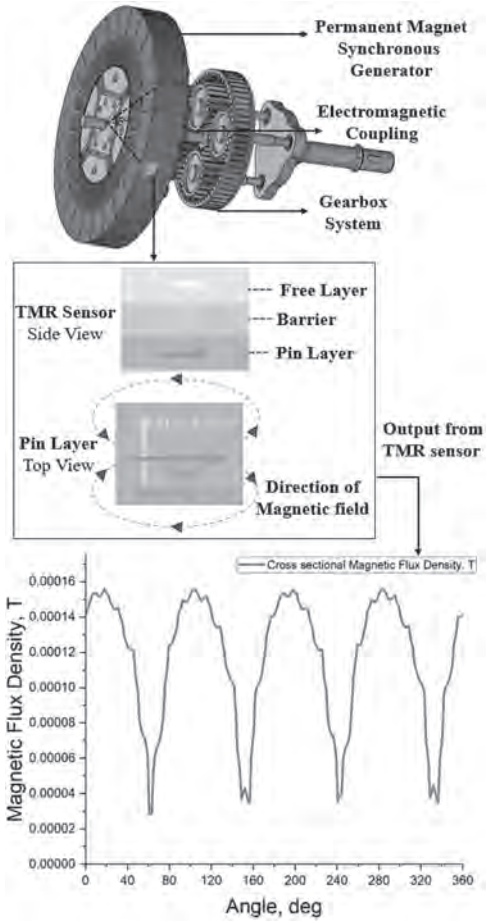

Fig 1. Wind turbine drive train geometry and TMR sensor placement

VP16-07. Magnetic Anomaly Target Motion State Detection Based on 3D Convolutional Neural Network. *H. Sun*[1], J. Qiu[1], S. Huang[1], C. Cao[1] and X. Zeng[1] *1. Chongqing University, Chongqing, China*

Magnetic anomaly detection, as a new detection technology with excellent environmental adaptability and concealment, can be used to detect and track ferromagnetic targets in invisible environments. However, it is extremely challenging to calculate the target's motion state information based on the passively detected magnetic field signals. To address this problem, we propose a magnetic anomaly target motion state detection method based on 3D convolutional neural network(3D CNN). 3D CNN is an advanced technology that can extract and analyze temporal and spatial features in image sequences, to achieve classification and action recognition. A magnetic field sensor array is used to collect a group of magnetic field signals with relative position information, which are converted into time-related images after preprocessing. These images are then input into a 3D CNN, which uses the target mobility and the detection correlation of the sensor array to detect the interested motions from the continuous motion stream, and then classifies the interested motions to complete the target motion state recognition. Simulation experiments show that the proposed method can effectively identify the motion state of ferromagnetic targets, improve the efficiency and accuracy of the identification of the motion state of magnetic anomaly targets, and provide theoretical basis and empirical reference for the further application of magnetic anomaly data such as the identification, tracking and positioning of ferromagnetic targets.

1. Y. J. Xu, Z. Wang and S. C. Liu, Ieee Geosci Remote S 19 (2022). 2. Y. LeCun, Y. Bengio and G. Hinton, Nature 521 (7553), 436-444 (2015). 3. Z. Y. Wang, Z. L. Kong and S. Chandra, Proc Int Conf Data, 1418-1429 (2019).

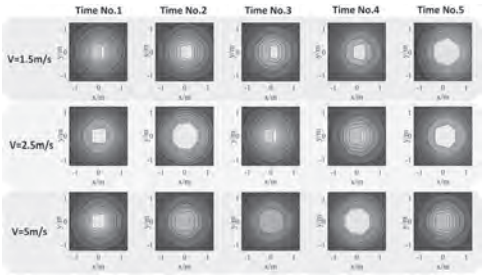

Fig. 1 Comparison of magnetic anomaly image flow of moving targets at different speeds

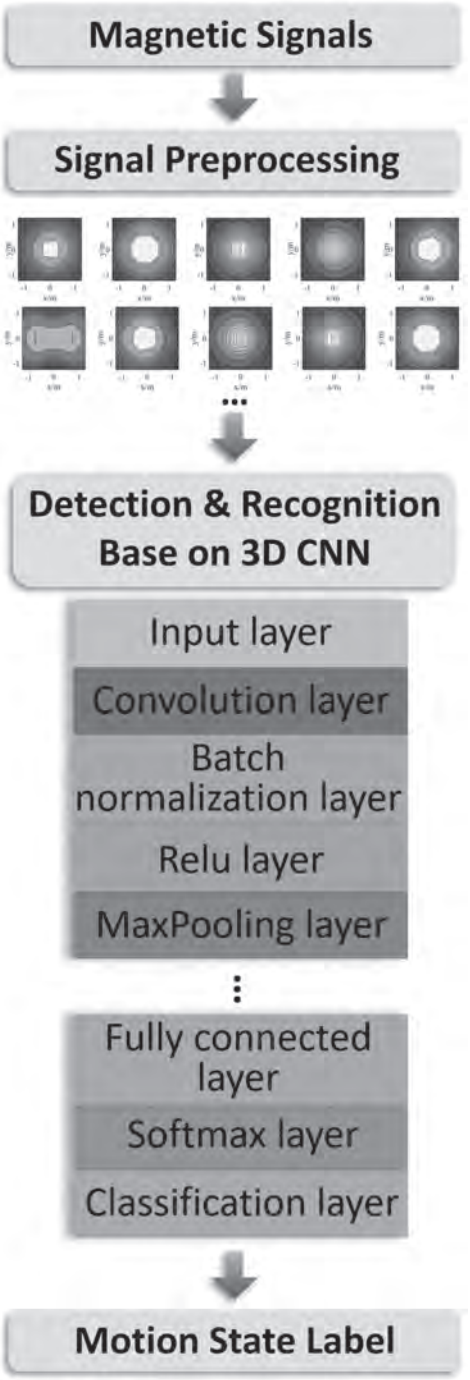

Fig. 2 Method flow chart

VP16-08. Multi-Axial Magnetic Sensing Using Co/Pt Double-Hall Superlattice SOT Structure: Experimental and Simulation. Y. Huang[1], A. Fathy[1], L. Chang[2] and *Y. Tseng*[1] *1. National Yang Ming Chiao Tung University, Hsinchu, Taiwan; 2. Industrial Technology Research Institute, Hsinchu, Taiwan*

We demonstrate a superlattice Co/Pt spin-orbit torque (SOT) double-Hall device featuring multi-axial magnetic field sensing ability. The Co/Pt superlattice with perpendicular magnetic anisotropy enabled *z*-directional sensing with the anomalous Hall effect. Conversely, the double-Hall configuration achieved x and *y* directional sensing based on the SOT effect. A magnetic field sensing range of ~±80 Oe can be obtained for the three axes. We explored how current density affects multi-axial sensitivity, linearity, SOT effects, and magnetization dynamics from experimental and theoretical approaches (OOMMF). Our findings highlight the critical role of current density in optimizing multi-axial sensing performance and elucidate how Dzyaloshinskii-Moriya interactions (DMI) and superlattice thickness could stabilize the magnetic structure with exchange coupling strength (Jex). This stability ensures predictable sensing responses along the three axes, crucial for the sensor's reliability and linearity. The simulation suggests that domain wall motion rather than abrupt nucleation events determine the SOT switching, and DMI is critical in developing the chiral spin structure, which influences domain wall motion and thus determines the sensing linearity. This design offers three-dimensional sensing with good scalability.

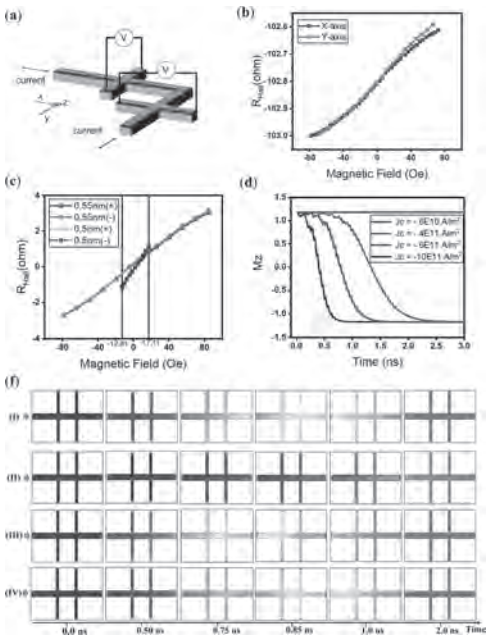

Fig. 1: (a) Schematic of the double-Hall configuration for three-axial magnetic field detection. Current can be injected via either the x or y channel; (b) Hall resistance (R_{Hall}) as a function of the magnetic field along the x (Hx) and y (Hy) axis. (c) R_{Hall} with layer thicknesses along the z-axis (Hz) showing tunable linearity. (d) Time evolution of the average z-component magnetization under different current densities (Jc). (f) Evolution of magnetization during the switching process with different interlayer exchange coupling (Jex) values, under a fixed Jc of -6x10^{11} A/m^2: (I) Jex = 0 J/m^2, (II) Jex = 10^{-3} J/m^2, (III) Jex = 10^{-4} J/m^2, (IV) Jex = 10^{-5} J/m^2.

VP16-09. High-Sensitivity Magnetoresistive Sensor with Optimized Orthogonal Exchange Bias for Low-Field Measurement. Y. Yang[1], *S. Lamichhane*[1], C. Chen[2], A. Sokolov[3], X. Yin[1,3], Y. Liu[1,3], J. Hong[4], L. Chang[5] and S. Liou[1,3] *1. Department of Physics and Astronomy, University of Nebraska-Lincoln, Lincoln, NE, United States; 2. Department of Physics, National Central University, Taoyuan City, Taiwan; 3. Nebraska Center for Materials and Nanoscience, University of Nebraska-Lincoln, Lincoln, NE, United States; 4. Department of Physics, Tamkang University, New Taipei City, Taiwan; 5. Industrial Technology Research Institute, Hsinchu County, Taiwan*

Magnetoresistive sensors based on magnetic tunnel junction (MTJ), among different types of magnetic sensors, have exhibited extraordinary performance, especially high achievable sensitivity at room temperature [1,2,3]. Other than high sensitivity, in some applications where low magnetic fields are measured, improved reversibility and linearity of the response of magnetoresistive sensors to external magnetic fields are also needed. To achieve good reversibility and linearity, as studied in some other experiments [4], a potentially effective technique is setting exchange bias that is perpendicular to the sensing direction. In this paper, a high-sensitivity magnetoresistive sensor that combines optimized orthogonal exchange bias with the novel magnetic flux guiding structure that was discussed in our previous papers [2,3] is studied for improved overall performance. The MTJ stack is shown in Fig. 1, where a $Co_{70.5}Fe_{4.5}Si_{15}B_{10}$ layer that is about 50 nm thick is coupled to the free layer (3.4-nm $Co_{20}Fe_{60}B_{20}$) through a 0.5-nm Ru layer to reduce the magnetic hysteresis of the free layer and guide magnetic flux, where the $Co_{70.5}Fe_{4.5}Si_{15}B_{10}$ compound is an amorphous soft magnetic material [5]. This $Co_{70.5}Fe_{4.5}Si_{15}B_{10}$ layer is adjacent to an antiferromagnetic $Ir_{20}Mn_{80}$ layer, so the $Co_{70.5}Fe_{4.5}Si_{15}B_{10}$ layer and free layer are expected to be pinned by the antiferromagnetic layer after field annealing. The MTJ devices were annealed multiple times in different conditions to set orthogonal exchange bias for the reference layer and free layer. With external magnetic flux concentrators added to the sensor to form double staged magnetic flux concentrators, the output voltage was measured in the field range from about -0.043 Oe to about +0.043 Oe, as shown in Fig. 2. With double staged magnetic flux concentrators, the sensor exhibits a sensitivity of 3.82×10^3 %/Oe (3.82×10^4 %/mT). The studied magnetoresistive sensor has great potential for application in low-field measurement at room temperature.

[1] C. Zheng et al., IEEE Transactions on Magnetics, vol. 55, no. 4, pp. 1-30 (2019) [2] Y. Yang, A. Sokolov, X. Yin, J. Hua, Y.-F. Liu, S. Lamichhane, and S.-H. Liou, IEEE Transactions on Magnetics, vol. 59, no. 1, pp. 1-7 (2023) [3] S. Lamichhane, Y. Yang, A. Sokolov, X. Yin, Y.-F. Liu, and S.-H. Liou, Appl. Phys. Lett. 124, 212401 (2024) [4] R. Ferreira, E. Paz, P. P. Freitas, J. Wang, and S. Xue, IEEE Transactions on Magnetics, vol. 48, no. 11, pp. 3719-3722 (2012) [5] D. Kato, M. Oogane, K. Fujiwara, T. Nishikawa, H. Naganuma, and Y. Ando, Appl. Phys. Express 6, 103004 (2013)

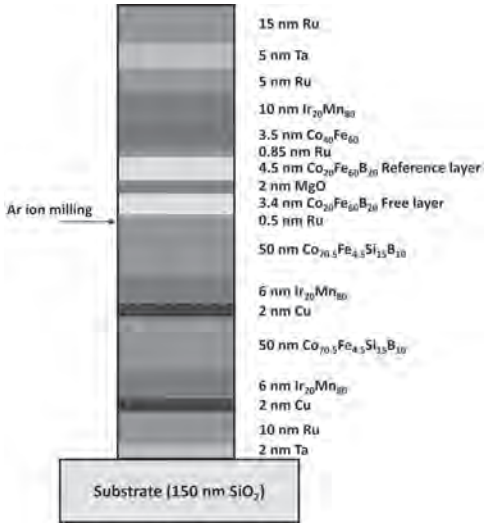

Fig. 1. Layer structure of the MTJ stack used in this study.

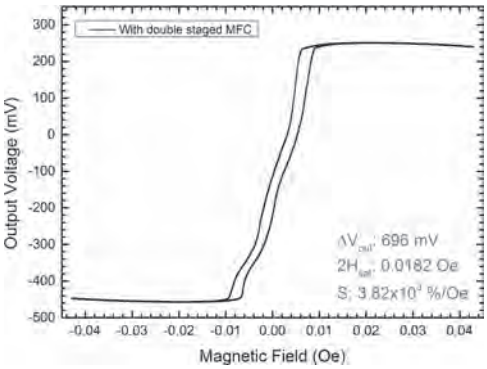

Fig. 2. Output voltage of the sensor with double staged magnetic flux concentrators.

VP16-10. Temperature-Dependent Performance of Magnetic Tunnel Junction Sensors with Linear Response Across a Wide Field Range. *S. Lamichhane*[1], C. Chen[2], A. Sokolov[3], X. Yin[1], Y. Liu[1], J. Hong[4], *L. Chang*[5] and S. Liou[1,3] *1. Physics & Astronomy, University of Nebraska-Lincoln, Lincoln, NE, United States; 2. Physics & Astronomy, National Central University, Taoyuan City, Taiwan; 3. Nebraska Center for Materials and Nanoscience, University of Nebraska-Lincoln, Lincoln, NE, United States; 4. Department of Physics, Tamkang University, New Taipei City, Taiwan; 5. Department Mechanical and Mechatronics Systems Research Labs, Industrial Technology Research Institute (ITRI), Hsinchu County, Taiwan*

Magnetic Tunnel Junctions (MTJ) sensors with a linear response over a wide field range are applicable in current sensing in electric vehicles, transmission grid lines and failure testing.[1] This study investigates the wide field sensor and its temperature dependence response of a magnetoresistance (MR), highlighting its performance across a wide temperature and field range. The magnetoresistance and sensor measurements were performed on a magnetic tunnel junction stack consisting of the following layered structure: Si/SiO2 (150 nm) / Ta (1.5 nm) / Ru (25 nm) / $Ir_{20}Mn_{80}$ (7 nm) / $Co_{30}Fe_{70}$ (2.2 nm) / Ru (0.85 nm) / $Co_{40}Fe_{40}B_{20}$ (2.8 nm) / MgO (2 nm) / $Co_{40}Fe_{40}B_{20}$ (1.3 nm) / Ta (2 nm) / Ru (15 nm).[2] Sensor devices based on this stack were fabricated which demonstrated a change in magnetoresistance, decreasing from 60% at 60 K to 50% at 380 K. Sensor devices based on this stack were fabricated, and sensor measurements revealed a linear response over a wide field range from -800 Oe to 800 Oe at room temperature, and maintained linearity from 77 K within the -900 Oe to 900 Oe range. The coercivity of the layer varied with temperature, from 21.7 Oe at 77 K to 3.8 Oe at 380 K. This consistent linearity and reversibility make the sensor particularly suitable

for applications requiring reliable performance across diverse thermal conditions. The sensor's robust sensitivity, along with its linear response over a wide field range, underscores its potential for integration into systems requiring high-precision current sensing. [1,2]

[1] Y. Rezaeiyan, N. Madsen, T. Böhnert, *IEEE Nordic Circuits and Systems Conference (NorCAS) Aalborg, Denmark, pp. 1-4 (2023)* [2] S. Lamichhane, Y. Yang, A. Sokolov, *Appl. Phys. Lett.* 124, 212401 (2024)

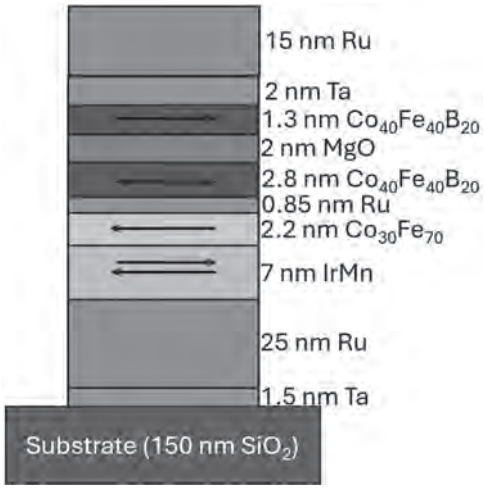

Fig1: Layered structure of the MTJ stack displaying the thickness of the free layer and the pinned layer.

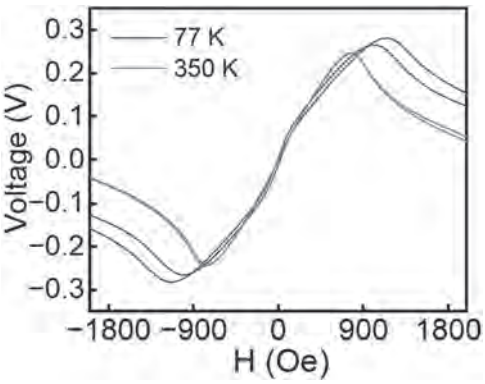

Fig2: Sensor response at 77 K and 350 K.

VP16-11. Microstructural Considerations on the Magnetostriction Enhancement in Dy Doped $Fe_{81}Al_{19}$ Alloys. J. Uribe-Chavira[1], C. Santillan[1], J. Saenz[1], M. Ibuado[1], J. Matutes[1] and *M. Grijalva-Castillo*[2] *1. Centro de Investigación en Materiales Avanzados, S.C., Chihuahua, Mexico; 2. Conahcyt-Centro de Investigación en Materiales Avanzados, S.C., Chihuahua, Mexico*

Polycrystalline alloys with a nominal composition $(Fe_{81}Al_{19})_{100-x}Dy_x$ were arc melted using high purity elements (99.99%), in a water-cooled copper crucible under an argon atmosphere. Each alloy was melted four times to obtain a better homogeneity of the elements. Composition of the alloys was verified by energy dispersive spectroscopy and optical microscopy was used to observe the microstructure. Structural characterization was carried out by X-ray diffraction and Rietveld refinement using the Fullprof Suit software [1]. Peak profile analysis was performed using the Thompson-Cox-Hastings pseudo-Voigt function in the Rietveld method, which are useful to determinate the microstrains and volume-average apparent crystallite size contribution on the peaks broadening. Room temperature hysteresis loops were measured in a Physical Properties Measurement System from Quantum Design up to 1 T. The standard straing gauge method was used to measure room temperature magnetostriction parallel and perpendicular to an applied magnetic field up to 0.5 T. All the results are summarized in Table 1. All samples were indexed to the A2 disordered cubic structure (space group 229, Im-3m). A lattice parameter increase is noticed, asserting the introduction of Dy into the cubic structure. This can also be noticed in a decrease in the observed saturation magnetization (Ms) from 187 to 183 emu/g with the increase in Dy content. On the other hand, all doped samples show an increase in total magnetostriction ($\lambda_{\parallel}$-$\lambda_{\perp}$), rising from 28 ppm in the undoped alloy to 92 ppm in the x=0.1 alloy. Adding more Dy to the samples does not make them magnetostrictically stronger, which means that the solubility limit has been reached. This behavior has been explained by two factors: 1) the increase of the (100) peak intensity ratio (preferential orientation), whith Dy content [2] and 2) the decrease of the average maximum strain calculated from Rietveld refinement [3, 4]. In summary, the alloy with x=0.1 has a good preferential orientation (57.42 %) but the lowest average maximum strain 55.36 x 10^{-4}, which results in the maximum magnetostriction found in these alloys.

[1] J. Rodríguez-Carvajal. Phys. B Condens. Matter. 192:55 (1993). [2] H. Chang, S. Jen, Y. Liao, D. Tseng, H. Hsieh, W. Chang, and I. Golovin. Journal of Alloys and Compounds, 893, 162262 (2022). [3] J. Uribe, G. Herrera, C. Santillán, R. Sáenz, J. Matutes and M. Grijalva. Journal of Rare Earths, 41(8), 1217-1224, (2023). [4] V. Palacheva, A. Mochugovskiy, D. Chubov, A. Koshmin, V. Cheverikin and J. Cifre. Materials Letters, 310, 131521 (2022).

Table 1. Structural and magnetoelastic properties of Dy doped $Fe_{81}Al_{19}$ alloys.

$(Fe_{81}Al_{19})_{100-x}Dy_x$	x			
	0	0.05	0.10	0.15
Lattice parameter a (Å)	2.9028(7)	2.9034(4)	2.9035(5)	2.9044(6)
(100) Peak intensity ratio (%)	50.07	54.31	57.42	61:33
Volume-average apparent crystallite size (nm)	14.02	14.32	14.73	14.15
Average maximum strain (10^{-4})	60.60	56.14	55.36	57.51
$\lambda_{\parallel} - \lambda_{\perp}$ (10^{-6})	28	85	92	78
Saturation Magnetization M_s (emu/g)	187.5	187	185.1	183.4

Table 1. Structural and magnetoelastic properties of Dy doped $Fe_{81}Al_{19}$ alloys.

VP16-12. Indirect Current Feedback of Low-Frequency Signals in Rectangular Wave Eddy Current Testing of a Tunnel Magnetoresistive Sensor. *Z. Guo*[1] and T. Sasayama[1] *1. Department of Electrical and Electronic Engineering, Kyushu University, Fukuoka, Japan*

The rectangular wave eddy current testing method can be used to detect conductor metal defects and simultaneously obtain multiple signals to distinguish defect information. In a previous study, we proposed a method for improving the sensitivity of deep defect detection using a magnetoresistive (MR) sensor [1]. However, signal-to-noise ratios at low frequencies were low because the MR sensor was affected by excitation fields. Therefore, we developed a method to eliminate the effect of the excitation field by using an external coil. Moreover, a digital-to-analog converter (DAC) compensation method proposed in a previous study could not be applied to the MR sensor because of the differential output of the MR sensor [2]. Therefore, we developed a method to apply a DAC compensation to MR sensors using an indirect current feedback (ICF) circuit. The experimental setup is illustrated in Fig. 1. A rectangular current flowed in an excitation coil. A cancellation coil generated a proximity field to counteract the excitation field. A tunnel magnetoresistive (TMR) sensor was placed at the center of the cancellation coil to receive the magnetic field generated by the eddy currents and convert it into differential voltage signals. Then, an ICF circuit was constructed using an instrumentation amplifier, and a 1 μF capacitor was connected in parallel to form an integration circuit to minimize the effects of harmonics. Moreover, the voltage signals were compensated for by generating a compensation waveform via the DAC to decrease the harmonic noise generated. The processed voltage signal was captured using an analog-to-digital converter (ADC). A 12-mm-thick aluminum plate specimen with three artificial circular defects (φ3 mm × 2, 4, and 6 mm) on the specimen surface or back surface was used. Fig. 2 shows the contour maps of the voltage signals of the third harmonic. The results show that the proposed method can improve the detection of surface and back-surface defects with low-frequency signals. This work was supported by JST SPRING, Japan (grant number: JPMJSP2136).

[1] Z. Guo and T. Sasayama, *IEEE Trans. Magn.*, Vol. 59, No. 11, Art. No. 6200505 (2023) [2] T. Sasayama and Z. Guo, *Int. J. Appl. Electromagn. Mech.*, Vol. 71, No. S1, pp. S39–S46 (2023)

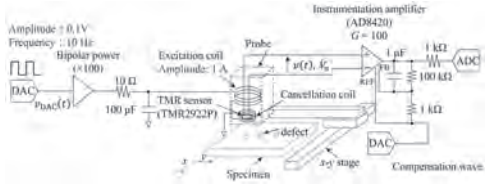

Fig. 1. Experimental setup.

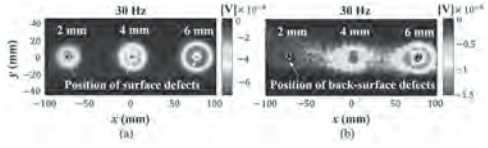

Fig. 2. Contour maps of the voltage signals of the third harmonic, i.e., 30 Hz. Defects are on the (a) surface and (b) back surface.

VP16-13. Dynamic Magnetization Measurement System for Soft Magnetic Materials. Y. Chang[1], V. Doan[2], L. Bui[1,3], T. Nguyen[1] and *J. Jeng*[1] *1. Department of Mechanical Engineering, National Kaohsiung University of Science and Technology, Kaohsiung City, Taiwan; 2. Faculty of Electrical and Electronic Engineering, University of Technology and Education, The University of Da Nang, Da Nang, Vietnam; 3. Faculty of Mechanical Engineering, Hung Yen University of Technology and Education, Hung Yen, Vietnam*

Evaluating the dynamic magnetization characteristics of the soft magnetic materials is essential for modeling the output response of a fluxgate sensor for which the demagnetizing effect of the core is generally non-negligible [1]. In this work, the dynamic magnetization measurement system for characterizing the soft magnetic core materials of a fluxgate sensor is investigated. The alternating magnetizing field is generated by a solenoid with an inductance of 27.5 mH. The pickup coil, which consists of inversely cascaded sensing and reference solenoids, is mounted inside the magnetizing coil. The reduction in field strength caused by the inductive reactance is overcome by cascading a proper metal film capacitor to the magnetizing coil to form a tank circuit. The distortion of the voltage waveform detected by the pickup coil is minimized by tuning the parameters of the integrator circuit, which converts the voltage waveform into the magnetization signal of the test sample inserted into the sensing coil. It is found that the magnetizing curve of a short ferrite rod shows the frequency-independent magnetizing curve with negligible hysteresis, which can be chosen as the standard sample for calibrating the conversion factor of magnetization measurement. The built system is capable of characterizing the dynamic magnetization cycle of the amorphous soft magnetic materials for use in fluxgate sensors, as shown in Fig. 1. Experimental results show that the material with higher demagnetizing effect exhibits a more consistent susceptibility and saturation field under various amplitudes of magnetizing field up to kilohertz frequencies. The proposed system is valuable for exploring the dynamic magnetic properties of miscellaneous soft magnetic materials to construct the numerical model.

[1] F. Primdahl et. al, "The fluxgate ring-core internal field," Measurement Science and Technology, Vol. 13, p. 1248 (2002)

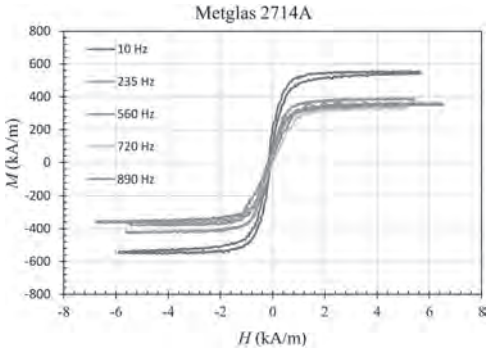

Fig. 1. Dynamic magnetization curve of Metglas 2714A amorphous film at frequencies from 10 to 890 Hz.

VP16-14. Advanced TMR Sensor-Based Magnetrodes for High-Sensitivity Biomagnetic Field Detection. *J. Chen*[1,2,3] *1. State Key Laboratory of Transducer Technology, Aerospace Information Research Institute, Chinese Academy of Sciences, Beijing, China; 2. School of Electronic, Electrical and Communication Engineering, University of Chinese Academy of Sciences, Beijing, China; 3. College of Materials Sciences and Opto-Electronic Technology, University of Chinese Academy of Sciences, Beijing, China*

The neural network of the human brain generates both electrical and magnetic signals. The magnetic fields produced by neuronal activity offer non-invasive, undistorted, and reference-free advantages for brain research. Traditional methods like Magnetoencephalography (MEG) using SQUIDs[1] and nitrogen-vacancy centers[2] have limitations in size, cost, and complexity. Spintronics-based magnetoresistance (MR) sensors, integrated into needle-shaped silicon-based substrates called "magnetrodes"[3], present a promising alternative due to their high sensitivity and compact size. Traditional magnetoresistance (MR) sensors have shown promising potential, but TMR sensors offer significantly enhanced sensitivity, making them ideal candidates for neural magnetic field measurements. This research introduces innovative TMR sensor-based magnetrodes designed for high-sensitivity biomagnetic field detection, particularly in neurological applications. Key advancements include the fabrication of magnetrodes with varying aspect ratios of the free layer, different junction shapes, and configurations to enhance the magnetic detectivity. Utilizing a custom-built magnetotransport and noise measurement system, these magnetrodes achieved a sensitivity of 22.29%/mT and an impressive limit of detection (LOD) of 300 pT/√Hz at 1 kHz. In vitro simulation experiments validate the ability of these magnetrodes to detect magnetic signals from neuronal action potentials, with firing rates matching the corresponding electrical signals. These results highlight the potential of TMR-based magnetrodes for high-resolution biomagnetic field detection, advancing our understanding of neuronal function and offering promising applications in neuroscience and biomedical engineering.

[1] R. Hari, R. Salmelin, Magnetoencephalography: From SQUIDs to neuroscience: Neuroimage 20th Anniversary Special Edition, NeuroImage, 61 (2012) 386-396. [2] J.F. Barry, M.J. Turner, J.M. Schloss, Optical magnetic detection of single-neuron action potentials using quantum defects in diamond, Proceedings of the National Academy of Sciences, 113 (2016) 14133-14138. [3] L. Caruso, T. Wunderle, C.M. Lewis, In Vivo Magnetic Recording of Neuronal Activity, Neuron, 95 (2017) 1283-1291.e1284.

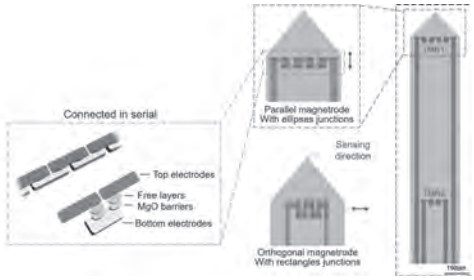

Figure 1. Schematic view of the magnetrodes, highlighting the structure connected in serial and detailing two distinct configurations.

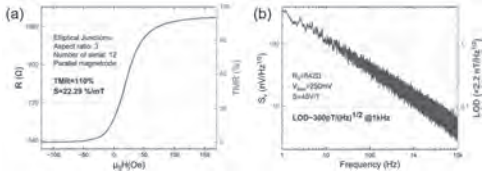

Figure 2. (a) R-H curves of the optimally performing magnetrode featuring elliptical junctions. (b) Noise PSD (left) and LOD (right) as a function of frequency for magnetrode with elliptical junctions.

Session VP17
SOFT MAGNETIC MATERIALS I
(Poster Virtual Session)

Vinay Sharma, Chair
University of Maryland, College Park, MD, United States

VP17-01. Influence of Crushing Process on the Magnetic Properties of Configurable Nanocrystalline Flake Ribbons. *Y. Wang*[1], C. Jiang[1], J. Xiang[1], L. Mo[1], X. Wang[1] and W. Guo[1] *1. City University of Hong Kong, Kowloon, Hong Kong*

This paper analyzes the configurable nanocrystalline flake ribbon (NFR) material with different crushing processes. The NFR soft magnetic material has gained significant attention in power electronics applications such as inductive power transfer (IPT), power transformers, inductors, and filters. The material originates from the Fe-based nanocrystalline alloy and undergoes further crushing process to exhibit lower conductivity, compromising the permeability and high-frequency performance. Different crushing processes can result in various performances even with the same achieved permeability. This study compares sample cores with dot and square crushing from the perspective of permeability variations against frequency and core loss characteristics. The two sample cores under evaluation have the same initial permeability at 10 kHz. However, the permeability of dot crushing drops nearly 37% from 10 kHz to 1 MHz, while the decrease in the square crushing core is only 25%. Moreover, core loss measurements are conducted with sinusoidal excitation, revealing that the square crushing core exhibits less core loss compared to the dot crushing core. These findings highlight the critical role of the crushing process in determining the magnetic performance of the material.

[1] D. Wang *et al.*, "Modern Advances in Magnetic Materials of Wireless Power Transfer Systems: A Review and New Perspectives," *Nanomaterials*, vol. 12, no. 20, Art. no. 20, Jan. 2022. [2] Z. Li, W. Han, Z. Xin, Q. Liu, J. Chen, and P. C. Loh, "A Review of Magnetic Core Materials, Core Loss Modeling and Measurements in High-Power High-Frequency Transformers," *CPSS Transactions on Power Electronics and Applications*, vol. 7, no. 4, pp. 359–373, Dec. 2022. [3] A. Ahmad, M. S. Alam, and R. Chabaan, "A Comprehensive Review of Wireless Charging Technologies for Electric Vehicles," *IEEE Transactions on Transportation Electrification*, vol. 4, no. 1, pp. 38–63, Mar. 2018. [4] P. Thakur, D. Chahar, S. Taneja, N. Bhalla, and A. Thakur, "A review on MnZn ferrites: Synthesis, characterization and applications," *Ceramics International*, vol. 46, no. 10, Part B, pp. 15740–15763, Jul. 2020. [5] P. Thakur, S. Taneja, D. Chahar, B. Ravelo, and A. Thakur, "Recent advances on synthesis, characterization and high frequency applications of Ni-Zn ferrite nanoparticles," *Journal of Magnetism and Magnetic Materials*, vol. 530, p. 167925, Jul. 2021. [6] X. Qi *et al.*, "A Review of Fe-Based Amorphous and Nanocrystalline Alloys: Preparations, Applications, and Effects of Alloying Elements," *physica status solidi (a)*, vol. 220, no. 14, p. 2300079, 2023. [7] Y. Wang, C. Q. Jiang, C. Chen, T. Ma, X. Li and T. Long, "Hybrid Nanocrystalline Ribbon Core and Flake Ribbon For High-Power Inductive Power Transfer Applications," *IEEE Transactions on Power Electronics*, vol. 39, no. 1, pp. 1898-1911, Jan. 2024 [8] Z. Luo, X. Li, C. Jiang, and T. Long, "Characterization of Nanocrystalline Flake Ribbon for High Frequency Magnetic Cores," *IEEE Transactions on Power Electronics*, vol. 37, no. 12, pp. 14011–14016, Dec. 2022. [9] Wang Y, Jiang C Q, Mo L, et al. "Magnetic analysis of permeability configurable nanocrystalline flake ribbons for medium frequency energy conversion applications." *Materials Today Sustainability*, 2024, 27: 100795.

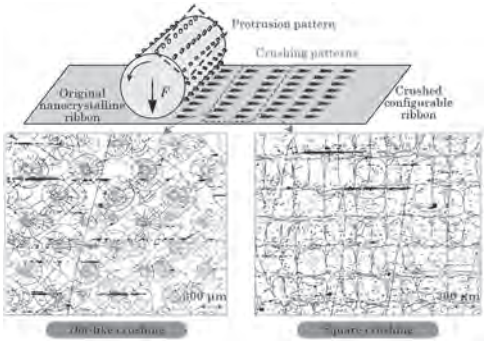

Fig. 1: Magnified view on the surface of the sample nanocrystalline flake ribbon with dot and square crushing patterns.

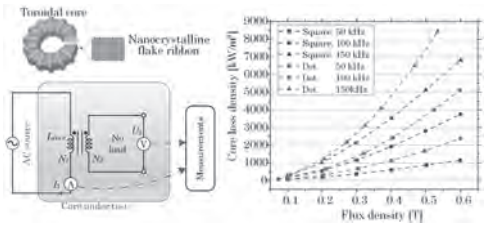

Fig. 2: Core loss measurement for dot-like crushing and square crushing cores. (a) measurement setup. (b) core loss density results from 0.1 T to 0.6 T in 50 kHz, 100 kHz and 150 kHz.

VP17-02. Effects of compressive stress in thickness direction on the magnetic properties of grain-oriented electrical steel sheet. *S. Yue*[1], C. Zhang[1], R. Chen[2], X. Li[1] and Y. Li[1] *1. Hebei University of Technology, Tianjin, China; 2. Tsinghua University, Beijing, China*

Grain oriented (GO) electrical steel is extensively utilized as the core material in power transformers. During the manufacturing of power transformer cores, clamps or bolts are commonly employed to secure the oriented electrical steel sheets. This process inevitably induces compressive stress in the thickness direction of the electrical steel, as depicted in Figure 1, thereby impacting its magnetic properties. However, existing research on stress-dependent magnetic properties primarily concentrates on in-plane tensile or compressive stress [1-2]. Further investigation is warranted into the effects of normal stress on the magnetic properties of the GO steel. In this paper, a magnetic property measurement setup for electrical steel sheet under normal stress loading is established based on a single-chip tester. The system applies a maximum stress of 40 MPa. The influence of normal stress on the hysteresis loop, permeability, and core loss of three grades of GO electrical steels. Figure 2 illustrates the hysteresis loops of a 0.3 mm thick GO steel in the rolling direction under different normal stresses. It is observed that with increasing normal stress, the hysteresis loop gradually shifts rightward, indicating a progressive deterioration in the magnetic property. Further experimental results and analysis will be presented in the full article. This research aims to provide insights for optimizing the clamping force applied to iron cores during the fabrication of power transformers.

[1] Pulnikov A, Permiakov V, De Wulf M, et al. Measuring setup for the investigation of the influence of mechanical stresses on magnetic properties of electrical steel[J]. Journal of Magnetism and Magnetic Materials, 2003, 254: 47-49. [2] Mailhé B J, Bernard L D, Daniel L, et al. Modified-SST for uniaxial characterization of electrical steel sheets under controlled induced voltage and constant stress[J]. IEEE Transactions on Instrumentation and Measurement, 2020, 69(12): 9756-9765.

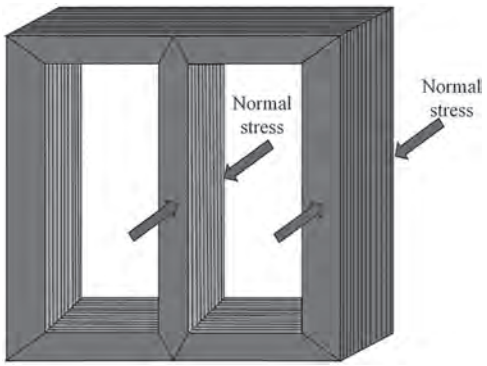

Fig.1 Normal stress in transformer iron core in thickness direction

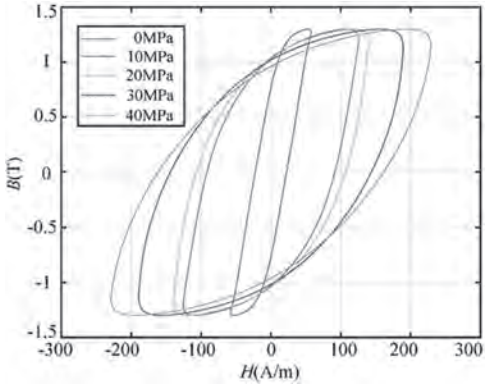

Fig.2 Measured hysteresis loops of GO steel at varying normal stress

VP17-04. Structure Design and Magnetic-Vibration Characteristics Analysis of Hybrid Core for High Efficiency Distribution Transformer. Y. Li[1], *G. Han*[1], S. Yue[1], Z. Wan[1] and J. Yin[1] *1. State Key Laboratory of Reliability and Intelligence of Electrical Equipment, Hebei University of Technology, Tianjin, China*

Amorphous alloy and oriented silicon steel are two commonly used materials for making distribution transformer cores, each of which has its own advantages[1]. The hybrid core structure formed by the two materials can synthesize their respecive advantages. The proper allocation of amorphous alloy and oriented silicon steel is crucial for reducing core loss and minimizing vibration in distribution transformer cores[2]. Therefore, it is necessary to investigate the structural design methodologies and magnetic properties of hybrid cores. This paper proposes a hybrid core design method based on magnetomotive force for the double-layer hybrid wound core structure of amorphous alloy wound core and oriented silicon steel wound core. Firstly, an experimental setup for core loss and vibration measurement is built. This setup can provide real-time voltage waveforms adjustment, data visualization and automatic post-processing, which makes the measurement more rapid and accurate. Then, based on the structural characteristics of the hybrid core, an equivalent magnetic circuit model is established. By comparing the magnitude of the magnetomotive force of the two parts of the hybrid core, the magnetic flux density for each part of the hybrid core can be obtained. A hybrid core is made according to the designed size, and then two cores of the same size are made, one made entirely of amorphous alloy and the other entirely made of oriented silicon steel. The loss characteristic and vibration acceleration of the three cores under power frequency sinusoidal voltage excitation are measured.

[1] L. Gang etal, IEEE Transactions on Magnetics, vol. 56, p. 1-4, (2020) [2] H. Chen etal, Journal of Magnetism and Magnetic Materials, vol. 590, p. 171689, (2024)

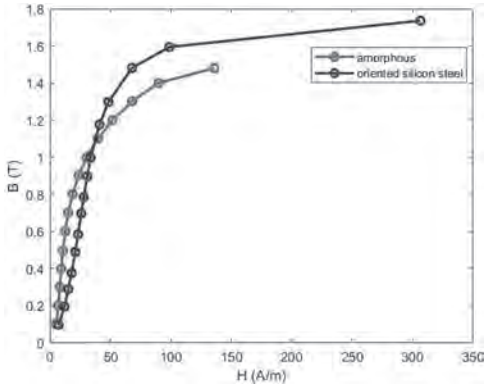

Fig.1 B-H curves

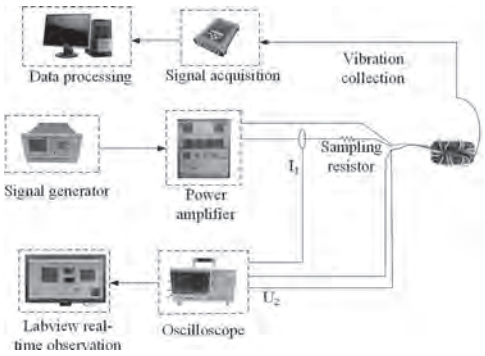

Fig.2. Real-time measurement platform

VP17-05. Analysis of Magnetic Domains Motion and Magnetic Properties of the Amorphous Sheet under the Uniaxial Stress. Y. Li[1], *J. Li*[1], Y. Dou[2], S. Yue[1] and J. Zhou[1] *1. State Key Laboratory of Reliability and Intelligence of Electrical Equipment, Hebei University of Technology, Tianjin, China; 2. Zhejiang University–University of Illinois at Urbana-Champaign Institute, Zhejiang University, Haining 314400, Haining, China*

The macroscopic magnetic properties of amorphous and other magnetic materials are intricately linked to their magnetic domain structure and dynamics[1]. Establishing a clear understanding of this relationship is crucial for accurately characterizing the magnetization behavior[2]. For now, the micro-macro magnetic property testing systems in magnetic materials are often conducted using separate devices. This discrepancy prevents the consistency between the regions tested for macroscopic magnetic properties and those observed for mesoscopic magnetic domains, leading to incorrect interpretations of the relationship between magnetic domain movement and changes in macroscopic magnetic properties under stress conditions[3]. To address this issue, a comprehensive micro-macro magnetic property testing system including a stress loading mechanism is designed and constructed, as shown in Fig.1. The study investigates the effects of uniaxial stress loading on magnetic domain movement and magnetization characteristics of amorphous material. The amorphous samples are with dimensions of 240 mm × 30 mm × 0.26 mm. The magnetic domain images of the samples were observed under various stress and magnetic field intensities, and the magnetic properties of the imaging area were simultaneously captured. It was found that under the action of tensile stress, the magnetic domain structure gradually transitions from an irregular strip domain to a parallel strip domain structure, with the orientation of the strip domains gradually rotating towards the direction of the tensile stress, leading to a lower coercivity. Conversely, when subjected to compressive stress, the orientation of the parallel strip domains gradually turns towards a direction perpendicular to

the compressive stress, leading to a higher coercivity, making magnetization more difficult. More details will be shown in the full text.

[1] Y. Dou, Y. Li, C. Zhang, IEEE TRANSACTIONS ON MAGNETICS, Vol. 56, p. 1-4 (2022) [2]T. Meydan, N. Derebasi, A. Honda, JOURNAL OF MAGNETISM AND MAGNETIC MATERIALS, Vol. 112, p. 23-25 (1992) [3] J. Zhou, Y. Li, C. Zhang, AIP Advances, Vol 14, p. 1-5(2024)

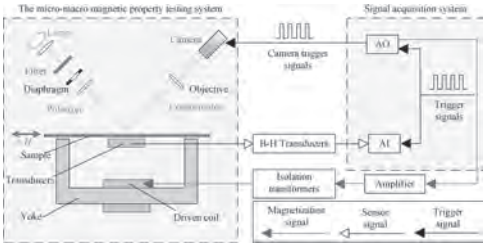

Fig.1 Diagram of micro-macro magnetic measurement system

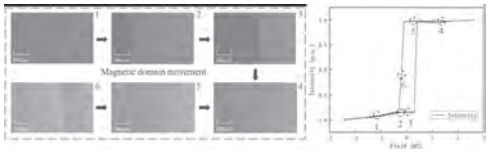

Fig.2 Synchronous observation results of domains in amorphous sheet

VP17-06. Comprehensive investigation on high-frequency rotational magnetic properties of core materials for high-speed motors.

M. Yang[1,2], Y. Li[3,4], Z. Hu[1,2], S. Yue[3,4], J. Li[1,2], Q. Yang[5] and M. Ouyang[1,2]
1. State Key Laboratory of Automotive Safety and Energy, Tsinghua University, Beijing, China; 2. School of Vehicle and Mobility, Tsinghua University, Beijing, China; 3. State Key Laboratory of Reliability and Intelligence of Electrical Equipment, Hebei University of Technology, Tianjin, China; 4. Hebei Key Laboratory of Equipment and Technology Demonstration of Flexible DC Transmission, Hebei University of Technology, Tianjin, China; 5. School of Electrical Engineering and Automation, Tianjin University of Technology, Tianjin, China

The development of electric vehicles requires the permanent magnet synchronous motors to be miniaturized and used at high speed. As a key component in motors, soft magnetic materials can directly affect the overall performance of the motor. Ultra-thin silicon steel and nanocrystalline alloys have thin strip sizes and high resistivity, which makes them have low eddy current losses at high frequencies. Meanwhile, both materials have great magnetic properties, and can better meet the design requirements of high-speed motors. However, there are usually different rotational magnetic fields in the stator yoke of the motor [1-2]. The magnetic properties and loss of core material are greatly different from those under alternating magnetization. To improve the reliability of the motor, the variation of material magnetic properties at high frequency from alternating to circular magnetization should be further studied [3]. In this paper, the rotational magnetic properties of non-oriented ultra-thin silicon steel ST100 (200Hz - 5kHz) and nanocrystalline alloy 1K107B (1kHz - 20kHz) under high-frequency conditions are measured by the novel two-dimensional magnetic properties tester shown in Fig.1. Based on the experimental results, the anisotropy of the above materials under different flux densities is analyzed. The anisotropy change of the material under circular magnetization is explained by analyzing the *B-H* phase difference at different flux densities and frequencies. Taking the elliptical magnetization of ST100 at 1 kHz as an example, the magnetic properties of ST100 with different levels of rotational magnetization are studied, as shown in Fig.2. The unidirectional magnetic properties of ST100 under rotational magnetization are systematically analyzed. By comparing the *B-H* phase difference and the *H* harmonic content at different conditions, the factors affecting the nonlinearity of the rotational magnetization are analyzed, and the variation of core loss under rotational conditions is investigated. It can provide theoretical and data support for the magnetic design and loss evaluation of the motor.

[1] O. de la Barriere, C. Appino, C. Ragusa, F. Fiorillo, M. LoBue, F. Mazaleyrat, IEEE Transactions on Magnetics., Vol. 54, p.2001415 (2018). [2] S. Yue, Y. Li, Q. Yang, K. Zhang, C. Zhang, IEEE Transactions on Magnetics., Vol. 55, p.6100705 (2019). [3] L. Chen, T. Ben, H. Zhao, C. Fang, Y. Wang, AIP Advances., Vol. 9, p.035316 (2019).

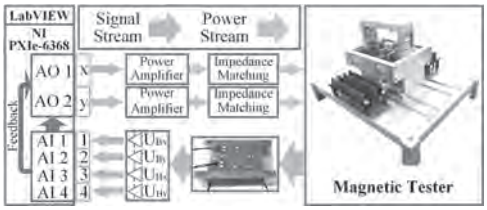

Fig.1 Measurement system of 2-D magnetic properties

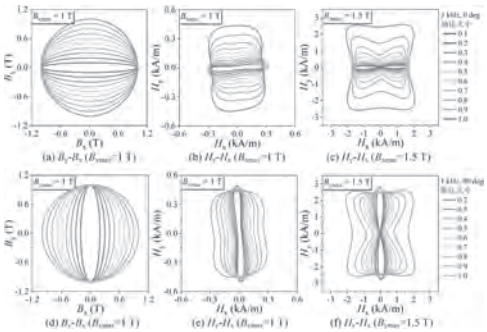

Fig.2 *B* and *H* trajectory under elliptical excitation

VP17-07. Research on the characteristics and suppression techniques for vibration and noise in amorphous three-dimensional wound core transformer.

Z. Dong[1], Y. Li[1], S. Yue[1] and X. Liu[1] *1. State Key Laboratory of Reliability and Intelligence of Electrical Equipment, Hebei University of Technology, Tianjin, China*

Amorphous materials have excellent magnetic properties, such as high permeability, low iron loss and high coercivity[1]. The three-dimensional wound transformer made of amorphous strip has strong short-circuit resistance because of its completely symmetrical magnetic circuit structure, so amorphous three-dimensional wound transformer is widely used in distribution network[2]. However, due to the obvious magnetostrictive effect of amorphous strip[3], the noise problem is serious. The vibration and noise reduction of amorphous three-dimensional winding transformer needs to be improved. In this paper, a three-dimensional coiled amorphous core transformer is modeled by finite element method considering the magnetostrictive effect and anisotropy of amorphous materials. The study conducts a magnetic-mechanical-acoustic coupling analysis of the transformer, evaluating magnetic field distribution, stress patterns, and sound field characteristics in depth. Based on these findings, the article proposes a method to mitigate vibration noise by applying stress to the iron core, given the sensitivity of amorphous materials to mechanical stress. Subsequently, a multiphysics test platform is established to measure the vibration and noise from different parts such as the core column and yoke of the amorphous three-dimensional wound core transformer. The noise levels around the iron core are measured and analyzed. Comparisons of vibration amplitudes and noise levels before and after applying stress confirm the effectiveness of the proposed vibration and noise suppression method.

[1]Liu Y, Yi Y, Shao W, et al., Journal of magnetism and magnetic materials, 330: 119-133(2013). [2]Song W, Han Y, Yang F, et al., IEEE Access, 12: 43958-43967(2024). [3]Liu D, Li J, Noubissi R K, et al., IET Electric Power Applications, 13(10): 1589-1597(2019).

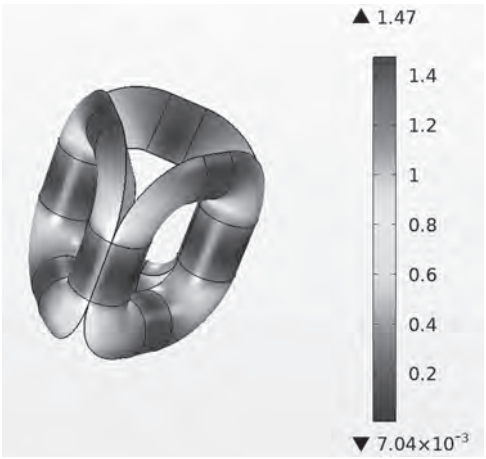

Fig. 1: Flux distribution map of the core

Fig. 2: Distribution of vibration displacement on core surface

VP17-08. Phase transition and magnetic properties of $LaMnO_3$- Mn_3O_4 composites. *A. Dhakal*[1], S. Mishra[1], J. Mohapatra[2] and P. Joshi[2] *1. Physics and Materials Science, The University of Memphis, Memphis, TN, United States; 2. The University of Texas at Arlington, Arlington, TX, United States*

Magnetocaloric materials have garnered significant global interest for their potential application as solid-state refrigerants in magnetic cooling devices. Research into magnetic refrigeration technology, driven by the magnetocaloric effect (MCE), is promising due to its high efficiency and potential to replace conventional vapor-compression cooling systems [[1]]. Magnetic refrigeration capitalizes on the isothermal magnetic entropy change or the adiabatic temperature change in magnetic materials when a magnetic field is applied. Recent research has focused on identifying magnetic refrigerants suitable for higher temperature operation, including those near room temperature. Nanocomposites of $LaMnO_3$(LMO)-Mn_3O_4(MO) (100%: 0%, 90:10%,70:30%, and 50:50% by weight) were synthesized by using the autocombustion method to study the impact of MO phase on structural, magnetic, and magnetocaloric properties of LMO. The structural properties of LMO- MO composites were investigated by using X-ray powder diffraction (XRD), confirming the presence of individual compounds in the proper ratio. The 5K saturation magnetization of LMO is recorded at 41.3 emu/g, LMO-MO (90%: 10%) at 91.1 emu/g, LMO-MO (70%: 30%) at 80.9 emu/g, at LMO-MO (50%: 50%) at 65.2 emu/g. Coercivity in the composites is observed except for LMO-MO (90%: 10%) composites. As indicated by temperature-dependent field-cooled magnetization curves, the transition from paramagnetic to ferromagnetic phases shows a second-order phase transition at different temperatures. The maximum entropy change ($-\Delta S_m$) peaks at approximately 7 J/kg/K at 253 K, with relative cooling power (RCP) values around 203 J/kg for LMO-MO (90%: 10%) composites, calculated from magnetic isotherms. These values are higher than those reported for $LaMnO_{3+\delta}$ (ΔS_m ~ 0.45 J/kg/K and RCP ~ 54.29 J/kg) [[2]]. The enhanced phase transition temperature and magnetocaloric effect are attributed to the interfacial effect between LMO and MO. The presence of Mn_3O_4 at the intervening grain boundaries between LMO phase altered the double exchange interaction between Mn^{3+} and Mn^{4+} ions. Authors: A. Dhakal, P. Joshi, Dr. J. Mohapatra, Dr. S R Mishra.

[1]. Giauque, W. F., and MacDougall, D. P. (1933). *Physical Review*, *43*, 768. [2]. Iqbal, M., Khan, M. N., and Khan, A. A. (2018). *Journal of Magnetism and Magnetic Materials*, *465*, 670-677.

VP17-09. Measurement and Analysis of Magnetostriction of Nanocrystalline Alloy Laminations under Medium-frequency Excitation. *C. Zhang*[1], H. Zhang[1], Y. Li[1] and T. Chen[1] *1. State Key Laboratory of Reliability and Intelligence of Electrical Equipment, Hebei University of Technology, Tianjin, China*

The medium-frequency transformer is a vital component of high-voltage and large-capacity DC/DC converters, in which the vibration and acoustic noise of the transformer will be intensified at high frequencies and high-power densities. Nanocrystalline alloys, widely used as core materials of medium-frequency transformers, require accurate measurement of their magnetostrictive properties to calculate core vibration and noise during the transformer design phase[1]. Currently, the magnetostriction of soft magnetic material sheets is typically measured using laser methods, which require the sheets to maintain a fixed shape and be easy to handle[2]. However, due to the softness, brittleness, and small magnetostriction coefficient of the annealed nanocrystalline alloy sheets, measuring their magnetostriction requires bonding the sheets and utilizing high-precision laser sensors[3]. In this paper, a measuring system consisting of NI PXIe-6368 DAQ, two magnetic yokes, a laser vibrometer with an optical reflector, and a PC is constructed to measure the in-plane magnetostriction of nanocrystalline alloy laminations under alternating magnetic field within medium-frequency excitation. The magnetic properties and magnetostriction of nanocrystalline alloy laminations are measured and the variations with magnetic flux density and magnetization frequency are investigated. The results indicate that the magnetostriction of nanocrystalline alloy laminations gradually increases with the rise in magnetic flux density, with a more pronounced increase in the saturation region, which aligns with the vibration patterns of nanocrystalline cores. At different magnetization frequencies, the results indicate distinct elongation or contraction characteristics. An elongation appears and the amplitude of magnetostriction increases with the increase of frequency within 5 kHz. A contraction characteristic is evident and the amplitude of magnetostriction decreases as the frequency increases at higher frequencies.

[1]Chen B, Wan N, Wang, S, COMPEL-The international journal for computation and mathematics in electrical and electronic engineering., Vol. 42(3), p.718-739(2023) [2]Siebert S, Kajiwara C, Fujiwara K, Journal of Magnetism and Magnetic Materials., Vol. 565, p.170295(2023) [3]LI Y, ZHU J, LI Y, Journal of Magnetism and Magnetic Materials., Vol. 529, p.167854(2021)

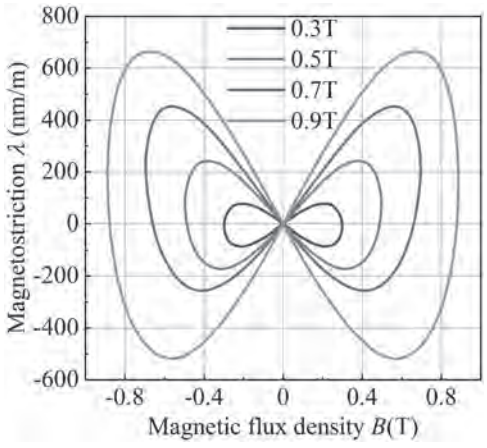

Fig.1 Magnetostriction loops corresponding to different magnetic flux densities at 5kHz

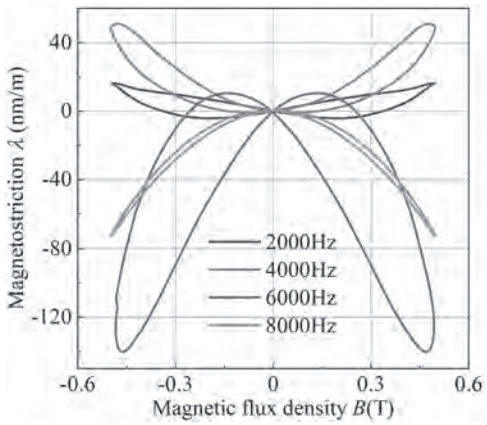

Fig.2 Magnetostriction loops at 0.5T corresponding to different magnetization frequencies

Session VP18
SOFT MAGNETIC MATERIALS II
(Poster Virtual Session)

Ju-Young Yoon, Chair
Tohoku University, Sendai, Japan

VP18-01. Modelling of loss in amorphous ribbons with longitudinal-induced anisotropy: theory and experiments.
O. de la Barrière[1], C. Ragusa[2], E. Ferrara[3], A. Magni[3], F. Mazaleyrat[1] and F. Fiorillo[3] *1. CNRS, Gif-sur-Yvette, France; 2. Politecnico di Torino, Torino, Italy; 3. INRIM, Torino, Italy*

The amorphous (AM) and nanocrystalline (NC) ribbons are endowed with thickness in the 10–20um range, relatively high resistivity, and weak dependence of properties on temperature, and appear as excellent alternatives to soft ferrites in power electronic applications. Their high saturation polarization allows for a significant volume reduction, while the loss remains generally lower at all frequencies [1]. Among different annealing treatments, transverse-induced anisotropy (TA) samples have received considerable interest [2][3], because, due to the predominance of magnetization rotations, the permeability cutoff can be shifted towards the MHz range, with the loss figure strongly reduced with respect to zero-field or longitudinal field-annealed (LA) samples [1]. The magnetisation process in TA ribbons is linked to spin rotations at high frequencies and, therefore, can be addressed via the Landau–Lifshitz–Gilbert equation [1]. LA, however, exhibit higher permeability than their TA counterpart at frequencies and induction values useful for a number of applications, e.g. in transformers and power electronics [4][5]. There is, however, limited understanding of the broadband frequency dependence of the magnetic loss in AM/NC LA ribbons, which compounds with the lack of direct observations of the related domain wall (dw) dynamics. In this communication, we discuss loss measurements carried out in 17 - 22 μm thick LA Co-based AM and NC ribbons, tested either as single strip samples or tapewound rings up to a few MHz, in parallel with stroboscopic Kerr effect imaging [6] of the evolving longitudinal domain pattern up to about 1 MHz. Under conditions of constant domain wall spacing (much larger than the ribbon thickness), less-than-linear increase of the dynamic energy loss Wdyn(f) with frequency is observed beyond a few kHz. Both deterministic and statistical models are worked out, to connect the observed dw dynamics to the broadband W(f) behavior. The former is based, in particular, on a numerical model, dwelling on the concept of dw bowing [7] applied to small and fast oscillations of domain walls. An example of calculated Wdyn(f) is shown, compared with the experimental data, in Fig. 1.

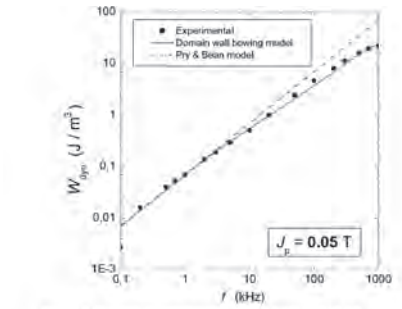

Figure 1: Dynamic loss behaviour up to 1 MHz and 50 mT. Dots: experiments; Red line: domain wall bowing model; dotted line: Pry & Bean model

[1] C. Beatrice, et al., «Broadband magnetic losses of nanocrystalline ribbons and powder cores,» *JMMM,* vol. 420, pp. 317-323, 2016. [2] A. Magni, et al., «Domain wall processes, rotations, and high-frequency losses in thin laminations,» *IEEE Trans. Magn.,* vol. 48, n°111, pp. 3796-3799, 2012. [3] A. Magni, et al., «Spin precession by pulsed inductive magnetometry in thin amorphous plates,» *JAP,* vol. 115, n°117, p. 14A338, 2014. [4] H. Cui, B. Dong, Y. Xing, L. Wang et S. Zhou, *Journal of Materials Science: Materials in Electronics,* vol. 35, n°1393, 2024. [5] R. Hasegawa, «Applications of amorphous magnetic alloys,» *Materials Science and Engineering: A,* vol. 375, pp. 90-97, 2004. [6] A. Magni, *International Journal of Applied Electromagnetics and Mechanics,* vol. 48, n°12-3, pp. 295-300, 2015. [7] J. E. L. Bishop, «Modelling domain wall motion in soft magnetic alloys,» *JMMM,* vol. 41, n°11-3, pp. 261-271, 1984.

VP18-02. Investigation of magnetic properties of high permeability materials at 77.15K temperature. *J. Ge*[1], J. Li[1] and R. Pei[1] *1. Shenyang University of Technology, Shenyang, China*

With the development of the times, there is an increasing demand for low-temperature high-speed motors in aerospace and aviation fields [1]. The main method to enhance the performance of traditional high-speed motors is by changing the topology of the rotor [2]. In this paper, a new core material, FeNi (1J50), is proposed to utilize the material's low magnetic field and high permeability characteristics to make the motor with low losses, which is very suitable for high-speed motors. However, extremely low temperatures can have an effect on the material properties and thus the motor. Currently, there have been few studies on the changes in magnetic properties of 1J50 at low temperatures. In the second part of this paper, low-temperature experiments on 1J50 were conducted by building a magnetic-thermal coupling experimental setup, as shown in Fig. 1. The magnetic properties of 1J50 material are tested under variable temperature (77K-223.15K), and some experimental results are shown in Fig. 2. The iron loss change rule of 1J50 under the influence of low temperature is revealed. The third part of this paper utilizes the above experimental data to reconstruct the loss model for 1J50. On the basis of the existing classical loss model of silicon steel, the influence of low temperature is added, the correlation analysis of the influence of low temperature on the eddy current loss and hysteresis loss of 1J50 is carried out, and the loss coefficients are corrected. In the fourth part of this paper, the proposed loss model is validated using the finite element method to verify the accuracy of the model.

[1] Wolnik, Tomasz, Tomasz Jarek. "Improvement Studies of High Power Density Motor for Aviation and Marine Application." In 2023 23rd International Scientific Conference on Electric Power Engineering (EPE), pp. 1-6. IEEE, 2023. [2] A. Credo, G. Fabri, M. Villani, "Adopting the Topology Optimization in the Design of High-Speed Synchronous Reluctance Motors for Electric Vehicles," in IEEE Transactions on Industry Applications, vol. 56, no. 5, pp. 5429-5438, Sept.-Oct. 2020.

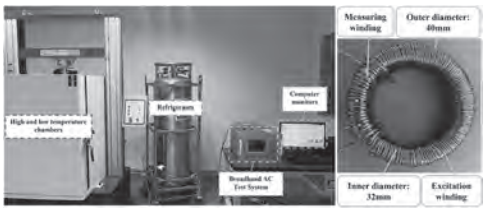

Fig.1 Magneto-thermal coupling experimental setup and test samples.

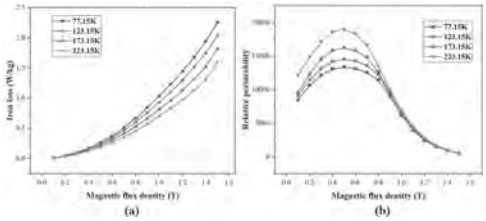

Fig.2 Effect of low temperature on the magnetic properties of the high permeability material 1J50. (a)Iron loss curves at different temperatures. (b)Variation of magnetic permeability with temperature.

VP18-03. Magnetic Anisotropy Investigation of Grain-Oriented Electrical Steels for a Wide Range of Temperatures. *Z. Li*[1], Y. Qin[1], X. Liu[1], Y. Li[1], R. Pei[1,2] and L. Zeng[2] *1. Department of Electric Engineering, Shenyang University of Technology, Shenyang, China; 2. Suzhou Inn-Mag New Energy Ltd., Suzhou, China*

Grain oriented electrical steel (GOES) has the advantages of high permeability, low iron loss and high saturation flux density in the rolling direction (RD), so it is popular with electrical equipment such as transformers and electric motors. Whether transformers with 1D magnetic circuits or electric motors with 2D magnetic circuits, the magnetic field is not ideally in the direction of RD when the GOES is really operating. Therefore a comprehensive insight into the magnetic anisotropy of GOES can help researchers to better utilize GOES. In addition, energy losses in electrical equipment and ambient temperatures can cause GOES to operate over a wide temperature range. In order to design high quality electrical devices, it is necessary to investigate the effect of temperature on the magnetic anisotropy of GOES. In this paper, the magnetic properties of GOES such as magnetic flux density, specific core loss, permeability, etc. are investigated at different temperatures and magnetization angles. The results show that the temperature has a significant effect on the magnetic anisotropy of GOES. Similar to the properties of non-grain oriented electrical steel, an increase in temperature causes a decrease in permeability and iron loss, and their pattern of change is minor in relation to the magnetic anisotropy. Interestingly, however, the anisotropy of the magnetic flux density responds in different ways to an increase in temperature. When the magnetization angle is below 40°, the increasing temperature decreases the magnetic flux density, in contrast to the increasing flux density when the magnetization angle is above 40°.The effect of temperature and anisotropy on the magnetic properties of GOES is well demonstrated in this paper, which has important implications for the design and performance prediction of electrical equipment.

[1] W. Zhang, Q. Yang, Y. Li, "Temperature dependence of powder cores magnetic properties for medium-frequency applications" in IEEE Transactions on Magnetics, Vol.58, No.2, p.1-5(2022). [2] M. L. Ababsa, O. Ninet, G. Velu, "High-Temperature Magnetic Characterization Using an Adapted Epstein Frame" in IEEE Transactions on Magnetics, Vol.54, No.6, p.1-6(2018). [3] X. Pei, A. C. Smith, L. Vandenbossche, "Magnetic Characterization of Soft Magnetic Cores at Cryogenic Temperatures," in *IEEE Transactions on Applied Superconductivity*, vol. 29, No. 5, p. 1-6(2019). [4] K. Kume, R. Inoue, H. Ueda, "Study on the Magnetic Properties of Metal Substrates at Low Temperature by Fabricated Compact SST," in *IEEE Transactions on Applied Superconductivity*, Vol. 32, No. 6, p. 1-4(2022).

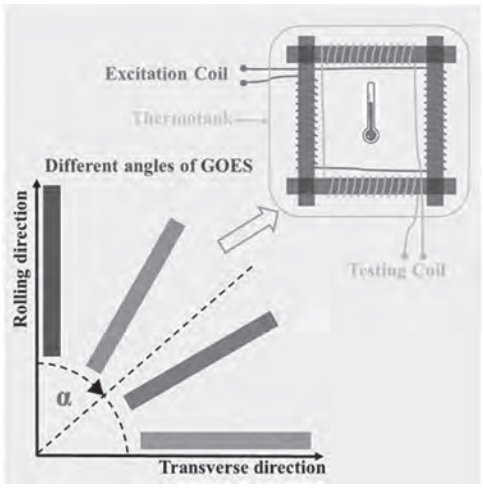

Fig.1 Experimental method for magnetic anisotropy of GOES under magneto-thermal coupling conditions

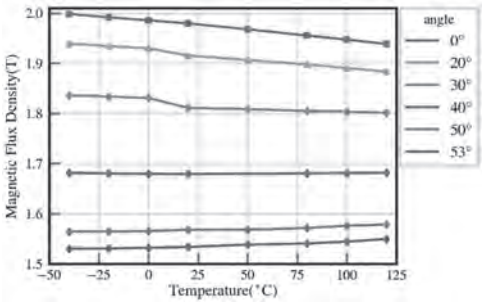

Fig.2 Sensitivity of GOES to temperature at different magnetization angles

VP18-04. Magnetic Characteristics and Losses of High-Silicon Steel Core for High-Speed Motors in Ultra-low Temperature Environment. *D. Ma*[1], J. Ge[1] and R. Pei[1] *1. Shenyang University of Technology, Shenyang, China*

In recent years, there has been an increasing demand for extremely low-temperature, high-speed permanent magnet motors in aerospace, aviation, and deep-sea fields [1]. High-silicon steel (6.5% Si) is considered to be extremely suitable for use as high-speed motor cores due to its excellent soft magnetic properties. However, very low temperatures affect the magnetic properties and losses of high Si steel, which in turn affects the motor. It has been reported that 6.5%Si losses increase with increasing temperature, a change that is opposite to conventional silicon steel [2]. At present, the changes in magnetic properties and losses of high Si steels at low temperatures have rarely been reported so far. In the second part of this paper, the magnetic properties of high silicon steel are tested at low temperature, as shown in Fig 1. The experiment reveals the magnetic properties and iron loss change rule of high silicon steel and conventional silicon steel under the influence of low temperature, and the results are shown in Fig 2. And from the internal microstructure of the material to explain the reason for this phenomenon. The third part of this paper uses the above experimental data to reconstruct the loss model for the low temperature characteristics of high silicon steel. On the basis of the existing classical loss model, low-temperature influencing factors are added, and the correlation analysis of the influence of temperature on the eddy current loss and hysteresis loss of high-silicon steel is carried out, and the coefficients affected by temperature are introduced into the loss model. The fourth part of this paper compares the experimental test data of high-silicon steel loss, the calculation data of traditional loss model and the calculation data of loss model in this paper to analyze the error accuracy, and finally verifies that the iron loss model proposed in this paper is more accurate than the traditional calculation model.

[1] Hou, Hucan, et al. “Numerical analysis of entropy production on a LNG cryogenic submerged pump.” Journal of Natural Gas Science and Engineering 36 (2016): 87-96. [2] Ou, Jing, et al. “Experimental characterization and feasibility study on high mechanical strength electrical steels for high-speed motors application.” IEEE Transactions on Industry Applications 57.1 (2020): 284-293.

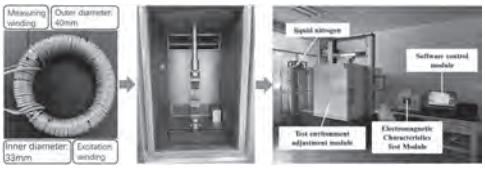

Fig. 1 Flow of silicon steel performance testing in extremely low temperature environment.

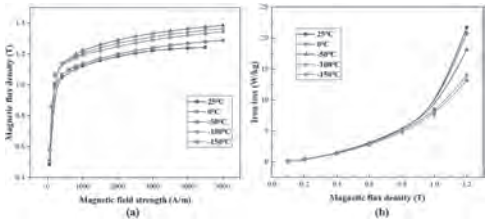

Fig. 2 Effect of extremely low temperatures on the magnetic properties of high-silicon steel. (a) Magnetization curve. (b) Loss curve.

VP18-05. Giant Magnetoimpedance and Susceptibility by Magneto-optical Kerr Effect in Amorphous CoFeSiB Ribbons. F.A. Albuquerque[1], V. Bellintani[1], J.H. Severo[2], A.D. Santos[2] and *C.S. MARTINS*[1] *1. Physics Laboratory, Faculty of Technology of São Paulo, São Paulo, Brazil; 2. Institute of Physics, University of São Paulo, São Paulo, Brazil*

Giant Magnetoimpedance (GMI) is a large variation in the impedance Z (H) of magnetic materials when subjected to an external magnetic field[1,2]. The objective of this work is to analyze samples of amorphous magnetic materials, in the case of CoFeSiB ribbons, which were produced by melt-spinning. The Giant Magnetoimpedance measurements that will be presented were carried out in low and moderate frequency regimes. It was observed that the increase in the impedance value with frequency is related to the increase in the imaginary contribution. The peak value of magnetoimpedance is completely frequency dependent. In figure 01 it is possible to observe that there is a variation in impedance according to the applied field, with a peak at 10 Oe. At 1 MHz, representing a variation of 75% and a sensitivity of 7.5%/Oe. Furthermore, it was observed that the susceptibility measured by the magneto-optical Kerr effect presents a behavior similar to that of magnetoimpedance[3].

[1] F. L. A. Machado, B. L. da Silva, S. M. Rezende, C.S. Martins.“Giant ac magnetoresistance in the soft ferromagnet $Co_{70.4}Fe_{4.6}Si_{15}B_{10}$” *J. Appl. Phys*, Vol.75, p.6563 (1994). [2] R.S. Beach, A.E. Berkowitz, “Sensitive field and frequency dependent impedance spectra of amorphous FeCoSiB wire and ribbon (invited)”, J. Appl Phys. Vol 76, p. 6209(1994). [3] P. Corte-Leon *et al*. “Giant magnetoimpedance and magneto-optical Kerr effects in $(Co_{63}Ni_{37})_{75}Si_{15}B_{10}$ amorphous ribbon”, Intermetallics, Vol.125, p.106925(2020).

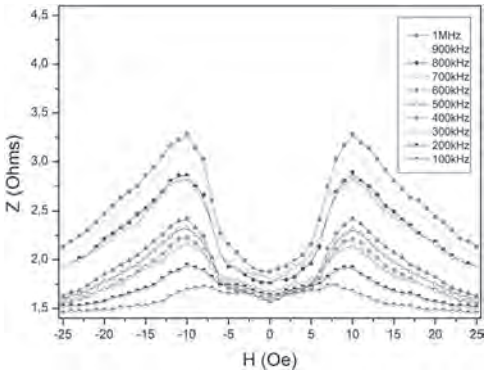

Figure 01 – Value of the impedance (Z) as a function of the field for frequencies from 100 kHz to 1 MHz

VP18-06. Temperature dependent structural, magnetic and microwave properties of hexagonal $BaFe_{12}O_{19}/Ba_2Co_2Fe_{12}O_{22}$ composite. *S. Singh*[1], P. Sharma[2] and B. Chudasama[1,3] *1. Department of Physics & Material Sciences, Thapar Institute of Engineering & Technology, Patiala, India; 2. IILM University, Greater Noida, India; 3. TIET-VT Centre for Excellence in Emerging Materials, Thapar Institute of Engineering and Technology, Patiala, India*

In recent past, exchange coupled composites of hard and soft ferrites have gained attention for their applications in microwave absorbers. Among the choices for the hard ferrites, M-type hexaferrites are prominent for their c-axis anisotropy, high magnetocrystalline anisotropy (H_a ~17 kOe) and high ferromagnetic resonance (FMR) frequency (~36 GHz). Extensive work has been reported on composites with M-type hexaferrite as the hard phase and cubic spinel/garnet ferrites as the soft phase. However, composites with a hexagonal soft magnetic phase are still unexplored. Y-type hexaferrites, which exhibit c-plane anisotropy and FMR frequencies up to 14 GHz, have distinct magnetic properties from M-type ferrites. As evident, one type of hexaferrite has limited frequency range, therefore focus has been shifted on development of composite ferrites with contrast magnetic and microwave properties. In the present work, composite of $BaFe_{12}O_{19}$ (BaM)/$Ba_2Co_2Fe_{12}O_{22}$ (Co_2Y) in 70/30 weight ratio were prepared by one-pot method. Effect of different annealing temperatures (1000 °C-1200 °C) on structural, magnetic and microwave properties have been investigated. XRD patterns confirmed the co-existence of M-type and Y-type phases without any secondary phase till 1050 °C temperature (Fig.1). With further increase in temperature to 1100 °C, along with M and Y phases secondary Z-type phase start appearing. Magnetic studies revealed that composite exhibit stepped *M-H* loop till 1100 °C, referring to non-exchange coupled system (Fig.2). Notably, at 1150 °C and 1200 °C smooth demagnetization curve has been observed, indicating coherent rotation of M and Y magnetic spins suggesting that phases are coupled. Saturation magnetization (M_s) increased from 48.6 emu/g to 56.88 emu/g with drastic decrease in coercivity (H_c). The observed variations in M_s and H_c indicated that annealing temperature has strong influence on exchange coupling. Microwave studies in K_u–band indicated that the exchange coupling significantly influences the microwave absorption losses which can be suitably tuned with annealing temperature.

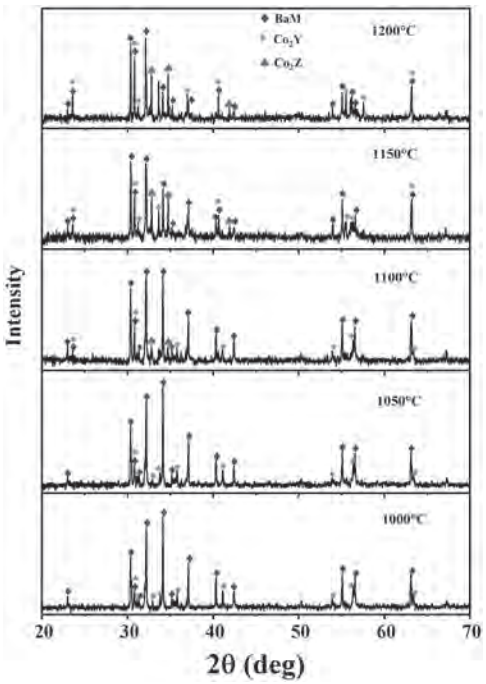

Fig.1 XRD patterns of BaM/Co_2Y composite annealed at 1000-1200°C

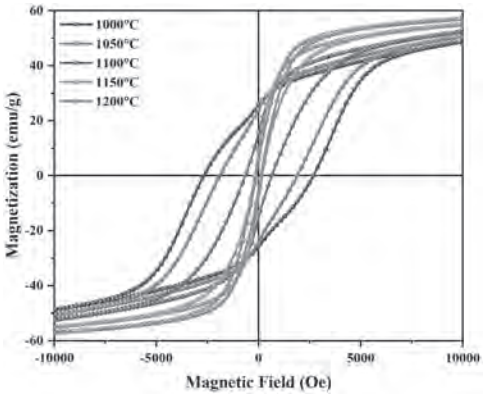

Fig.2 *M-H* loops of BaM/Co_2Y composite annealed at 1000-1200°C

VP18-07. Studies of The Magnetic Properties of FeSiBCCr Amorphous Alloys Fabricated by Spark Plasma Sintering. *X. Wang*[1], Z. Lin[1,2], S. Yue[1], Q. Chi[2], X. Guo[2] and Y. Li[1] *1. State Key Laboratory of Reliability and Intelligence of Electrical Equipment, Hebei University of Technology, Tianjin, China; 2. Ningbo Magnetic Materials Application Technology Innovation Center Co., Ltd, Ningbo, China*

Fe-based amorphous soft magnetic alloys exhibit superior properties, such as high resistivity, high permeability, and saturation magnetization, compared to traditional materials like silicon steel and ferrite. FeSiBCCr powders are ideal candidates for integrated inductors used in high frequencies up to 200 KHz. However, fabricating techniques need to be innovated to optimize the characteristics of the inductors[1]. Normally, cold or hot pressing is used in sintering soft magnetic composites (SMCs). Spark plasma sintering (SPS), due to its low temperature, fast heating rate, and high densification capability, is an advanced technique to sinter binder-free amorphous SMC showing superior soft magnetic properties. While many studies have explored the static magnetization properties of bulk Fe-based amorphous alloys fabricated via SPS[2], a few studies investigate dynamic magnetization properties. This study uses custom-made measurement equipment to investigate the influence of the SPS process on static and dynamic magnetic properties of amorphous FeSiBCCr samples in real application conditions, for example, excited by non-sinusoidal waveforms. In addition, the impact of various annealing processes on magnetic properties is also investigated. The results show that sintering temperature significantly affects magnetic and mechanical properties. The elevated sintering temperature is of benefit to mechanical properties, but some crystallites which degrade the magnetic properties are formed at a certain temperature, which depends on the heating rate, sintering temperature and pressure. The detailed results will be presented in the full paper.

[1]Jiaqi Liu, Yuan Gao and Pu Wang, Journal of Non-Crystalline Solids, Volume 622,122651(2023) [2]Dong Y, Liu J and Wang P, Materials, 15, 1106(2022)

VP18-08. Crystallographic and Magnetic Properties of Manganese Ferrites Prepared by Liquid-Nitrogen Quenching. *S. Yoon*[1] *1. Department of Physics, Gunsan National University, Gunsan, The Republic of Korea*

Structural and magnetic properties of $Mn_{3-x}Fe_xO_4$ (0£x£2) has been studied by using X-ray diffraction (XRD), vibrating sample magnetometer (VSM) and Mössbauer spectroscopy. Polycrystalline $Mn_{3-x}Fe_xO_4$ (0£x£2) samples were prepared by solid-state reaction method followed by sudden liquid nitrogen quenching. Room temperature XRD indicated a tetragonal to cubic structural transition across x=1 with the increase of x. Diffraction patterns showed a very dynamic shifts of peak positions as shown in Fig. 1; 2 or 3 peaks in the tetragonal realm have merged into single peak, and (105) and (312) diffraction peaks have even crossed each other. The lattice distortion can be explained by the Jahn-Teller effect of Mn^{3+} ions in the octahedral (B) site. Right of Fig. 1 shows the variations of the lattice constants and the tetragonality (c/a) with Fe substitution x. It is notable from GSAS refinement that tetragonal and cubic (~17 %) phases coexisted when x=1, which means $FeMn_2O_4$ is the marginal composition between cubic and tetragonal structures. Room-temperature M-H curves of the $Mn_{3-x}Fe_xO_4$ (0x£2) are shown in Fig. 2. M_S increases with Fe substitution x indicative of the occupancy of Fe^{3+} ions on the B site. When x=0.5 in the right of Fig. 2, paramagnetism and ferrimagnetism with M_S»0.08 emu/g superimposed in the hysteresis curve and finally became paramagnetic when x=0. All the samples showed soft magnetic nature. Coercivity H_C above x=0.5 were about 100 Oe, independent of composition. Mössbauer spectra showed asymmetric paramagnetic doublet below x=0.5 at room temperature. Since the room-temperature spectra for x≥1 also had overlap of thermally broadened magnetic sextets, we used the spectra taken at T=20 K in order to analyze the Fe cation distribution in the samples. All the cubic samples (x≥1) showed comparable absorption areas of the tetrahedral (A) and the B sites. Isomer shift of the sub-spectra indicated that all Fe ions were in ferric stare. Quadrupole splitting of the octahedral site increased as Fe ion content x decreased down below x=1. Spectral area ratio analysis reveals that there is significant amount of Fe^{3+} in the A site, which is in contrast to many reports that all the Mn^{2+} preferentially occupy the A site.

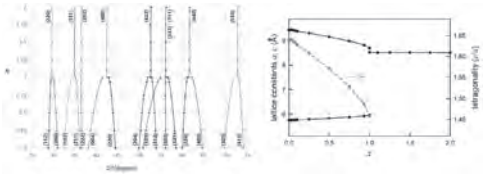

Figure 1

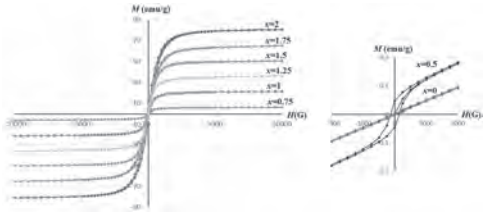

Figure 2

Session VP19
SOFT MAGNETIC MATERIALS III
(Poster Virtual Session)

Keita Nakagawara, Chair
Tohoku University, Sendai, Japan

VP19-01. Room temperature magnetodielectric studies of $Sr_{3-x}La_xCo_2Fe_{24}O_{41}$ hexaferrite. *A. Choudhary*[1], P. Sharma[2] and B. Chudasama[1,3]
1. DPMS, Thapar Institute of Engineering & Technology, Patiala, India; 2. IILM University, Greater Noida, India; 3. TIET-VT Centre for Excellence in Emerging Materials, Thapar Institute of Engineering & Technology, Patiala, India

Strontium Z-type hexaferrites ($Sr_3Co_2Fe_{24}O_{41}$) have received significant interest owing to their high permeability (μ) and permittivity (ε) making them suitable candidates for use in antenna miniaturization, multilayer chip inductors and other electronic devices for telecommunication applications. Recently, Z-type hexaferrites have attracted much attention for magnetodielectric (*MD*) effect at room temperature (*RT*), which is ascribed to transverse conical spin structure and spin-phonon coupling. Any disorder at regular Sr or Fe/Co sites may affect them. In the present study, La^{3+} ions were substituted for Sr^{2+} ions to induce two-fold effect, i.e different ionic radii and ion valency may disturb the conical spin structure and spin-phonon coupling. In the present work, La^{3+} substituted $Sr_{3-x}La_xCo_2Fe_{24}O_{41}$ (x = 0.0 and 0.20) hexaferrite were prepared by solid-state reaction method and their magnetodielectric properties were investigated. Z-type hexaferrite was formed as major phase with some minor impurity phases of M and W phases (Fig 1). Both saturation magnetization (M_s) and coercivity (H_c) increases with La content. The increase in M_s was attributed to the reduction of Fe^{3+} to Fe^{2+} at antiparallel 2a sites, whereas grain size reduction led to slight increase in H_c. FESEM micrographs showed densely packed hexagonal platelet-like structures with smaller grain size (~ 1.74 μm). The highest *MD* of 4.5% was observed at low frequency (100 Hz), which decrease with increase in frequency followed by a rapid increase at higher frequency (Fig 2). The large MD effect at low frequency is due to Maxwell-Wagner type Magnetoresistance (*MR*) effect whereas inverse Dzyaloshinskii–Moriya (DM) interaction induced spin phonon coupling is the dominant mechanism at high frequencies.

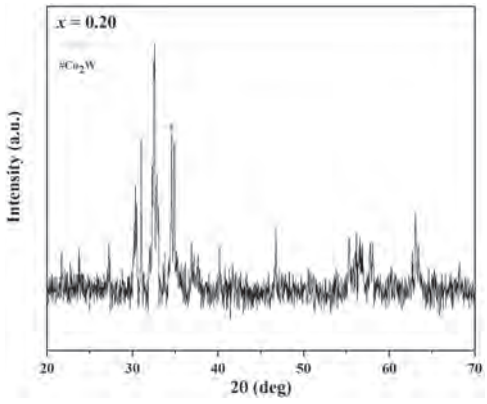

Fig1. XRD pattern of $Sr_{3-x}La_xCo_2Fe_{24}O_{41}$ hexaferrite

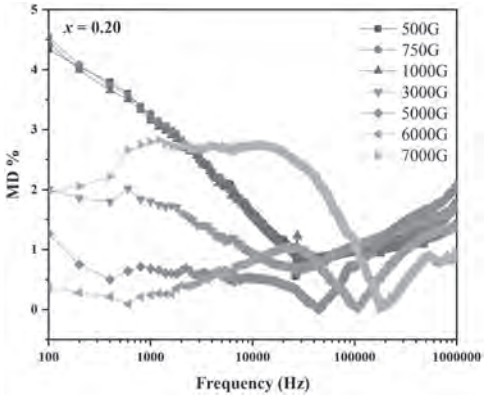

Fig2. Frequency dependent magnetodielectric (*MD*) property of $Sr_{3-x}La_xCo_2Fe_{24}O_{41}$ hexaferrite.

VP19-04. Magnetic Properties of High Permeability Alloys Considering Stress Factors. *J. Li*[1], J. Ge[1] and R. Pei[1] *1. Shenyang University of Technology, Shenyang, China*

With the development of the motor industry, various new soft magnetic materials have been continuously applied. Among them, high permeability alloys (ferronickel alloy/1J50) are more suitable for synchronous reluctance motors, because 1J50 can increase the difference between the inductance of q-axis and d-axis of the motor by using the high permeability to improve the reluctance torque of the motor. However, during the application of the material, it was found that the magnetic properties of the core material are easily affected by the coupling of stress field and electromagnetic field [1], and the compressive stress tends to deteriorate the loss of the core material [2-3]. However, there is no study on the magnetic properties of 1J50 under stress-magnetic field coupling conditions. In this manuscript, the magnetic characteristics of 1J50 were tested under stress conditions by setting up a stress field-magnetic field coupling test setup (shown in Fig. 1), and some of the results are shown in Fig. 2. As the compressive stress increases, the flux saturation density and loss of 1J50 decrease. However, the tensile stress is opposite, which indicates that the performance of the motor under the influence of the stress field will have a large error from the predicted performance. In addition, this paper also explains the reasons for the changes in the magnetic properties of 1J50 by observing the microstructure. Finally, the performance of the 1J50 motor under different stresses is accurately simulated by the finite element method, which provides a basis for subsequent motor manufacturing.

[1] Tani, Y., A. Daikoku, M. Nakano, "Magnetic power loss characteristics of non-oriented electrical steel sheets under stress." *JOURNAL-MAGNETICS SOCIETY OF JAPAN* 30, no. 2 (2006): 196. [2] K. Fujisaki, R. Hirayama and T. Kawachi, "Motor core iron loss analysis evaluating shrink fitting and stamping by finite-element method," IEEE Trans. Magn., Vol. 43, no. 5, pp. May 2007. [3] D. Miyagi, N. Maeda, and N. Takahashi, "Estimation of iron loss in motor core with shrink fitting using FEM analysis," IEEE Trans. Magn., Vol. 45, no. 3, pp. 1704-1707, March 2009.

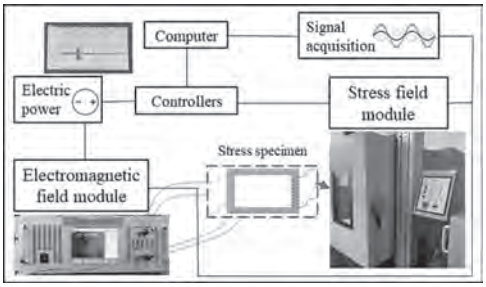

Fig.1 Experimental platforms

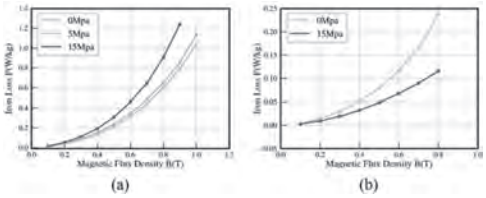

Fig.2 Magnetic properties of 1J50 under stress, (a)loss curves under compressive stress. (b)loss curves under tensile stress.

VP19-05. Loss analysis of amorphous high-speed PMSMs considering the effect of cutting damage. *X. Lu*[1], L. Zhang[1] and R. Pei[1] *1. Shenyang University of Technology, Shenyang, China*

The weight share of soft magnetic materials in permanent magnet synchronous machines (PMSMs) is usually around 70%, and the proportion of iron loss in the total loss is also large [1]. Currently, researchers have begun to study the use of high permeability, low iron loss amorphous materials(AM) for high-speed PMSM to reduce iron loss, but the measured iron loss performance of AM in motors has a large difference with the simulation results [2]. The reason may be that AM core generates stress and crystallization occurs at the cutting edges during processing, which leads to an increase in losses [3]. Therefore, the analysis of AM losses considering the effect of cutting is crucial for the design and application of AM HS PMSM, and there are fewer researches in this area. In the second part of this paper, in order to investigate the effect of cutting on the magnetic performance of AM, the core is cut into four rings with the same outer diameter and different inner diameters using wire cutting, as shown in Fig. 1(a). Using the self-developed variable temperature magnetic performance test system, the iron loss value of AM at different temperatures (298.15K ~423.15K) was measured to reveal the change rule of the magnetic performance of AM under the coupling of variable temperature and cutting method. In the third part, the part affected by cutting is explored, and the equivalent depth of the performance degradation part is calculated, schematically shown in Fig. 1(b). The unit weight loss of the degraded part is further separated from that of the normal AM to optimize the iron loss model. In the fourth part, a AM HS PMSM prototype is fabricated, and the measured iron loss values of the motor are compared with the optimization model data of this paper and the traditional iron loss model data to verify the correctness of the optimization analysis. This will provide more accurate guidance for the design and application of AM HS PMSMs.

[1] T. Li, Y. Zhang, Y. Liang, "Multiphysics Analysis of an Axial-Flux In-Wheel Motor With an Amorphous Alloy Stator," *IEEE Access*, vol. 8, pp. 27414-27425, 2020. [2] Z. Wang, Y Enomoto, M Ito, "Development of a Permanent Magnet Motor Utilizing Amorphous Wound Cores," IEEE Transactions on Magnetics, vol. 46, no. 2, pp. 570-573, Feb. 2010. [3] F. Chai, Z. Li, L. Chen, "Effect of Cutting and Slot Opening on Amorphous Alloy Core for High-Speed Switched Reluctance Motor," *IEEE Transactions on Magnetics*, vol. 57, no. 2, pp. 1-5, Feb. 2021.

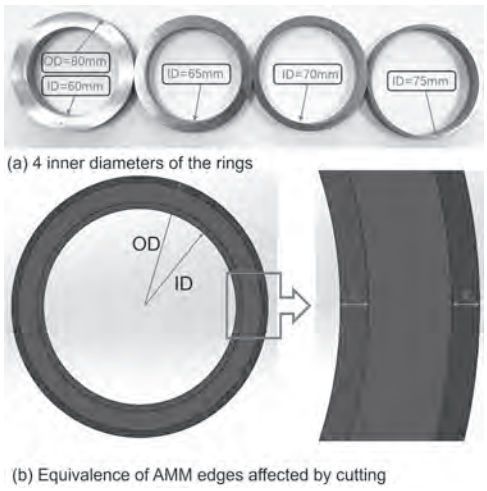

Fig.1 Method of prototyping and iron loss equivalence considering the effect of cutting.

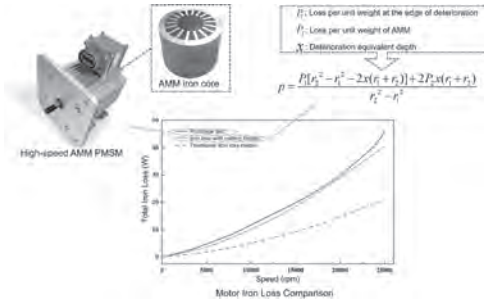

Fig.2 Validation of iron loss model considering cutting factors.

VP19-06. Microwave absorption properties of graphene oxide/Zn-substituted Cobalt ferrites composites. *M. Dabla*[1], S. Kaushik[1], M. Sharma[1,2] and B.K. Kuanr[1] *1. Special Centre for Nanoscience, Jawaharlal Nehru University, New Delhi, India; 2. Department of Physics, Deshbandhu College, New Delhi, India*

We report microwave absorption properties of graphene oxide(GO wt.%=0.0,2.5,5,7.5)/$Zn_xCo_{1-x}Fe_2O_4$(x=0.0,0.1,0.2,0.3) ferrite-composites (FCs) synthesized via ball-milling method. The prepared nanoparticles were characterized by various techniques such as XRD, SEM embedded with EDX, VSM and microwave measurements using vector network analyzer (VNA). XRD pattern of FCs matched with space group:Fd-3m [Fig. 1(A)]. The crystallite size was observed to increase with Zn substitution. The saturation magnetization and coercivity gradually increases with the increase of Zn doping in cobalt ferrites [Fig. 1(B)]. It is due to the replacement of Co^{2+} by Zn^{2+} ions at A-site, decreasing the antiferromagnetic interaction between A and B sites which results in enhancement of net magnetic moment [1]. The EM parameters are measured using VNA in Ku band (12–18 GHz) for FCs with 50% wax as binder. The effect of thickness with matching frequency (f_m) have been studied. The $\lambda/4$ mechanism governs the appearance of reflection loss (RL) minima at a specific frequency. Fig. 2(A) shows the RL vs. frequency for GO(7.5 wt.%)/$Zn_{0.3}Co_{0.7}Fe_2O_4$ FCs at different thicknesses. It is interesting to note that ferrite exhibits a RL_{min} dip of -40 dB at a frequency of 13.95 GHz (with f_m=13.71 GHz) and effective absorption bandwidth@-10 dB (EAB) is 0.75 GHz. Fig. 2(B) shows the variation of RL vs. frequency with different wt.% of GO at a fixed thickness of 2.5 mm. The graph indicates that increase of GO increases the RL_{min} value and EAB width of the FCs. The increase of GO wt.% from zero to 7.5% results in increase of RL_{min} from -11.2 dB to -40 dB and EAB from 0.22 GHz to 0.75 GHz, respectively. RL_{min} frequency shifted from 13.95 GHz to 13.69 GHz with increasing GO. When carbon is added to FCs, it increases dielectric loss, aspect ratio and reduce weight, improve impedance matching, and broaden

EAB[2]. Hence, the synthesized composite samples have demonstrated great potential as EMI absorbers for use in radar and stealth technologies [3].

[1] Muscas, G. et al. (2019). Journal of Alloys and Compounds, 796, 203-209. [2] Xu, J. et al. (2023). Journal of Materials Science & Technology, 132, 193-200. [3] Abbas, N., et al. (2024). Results in Physics, 59, 107576.

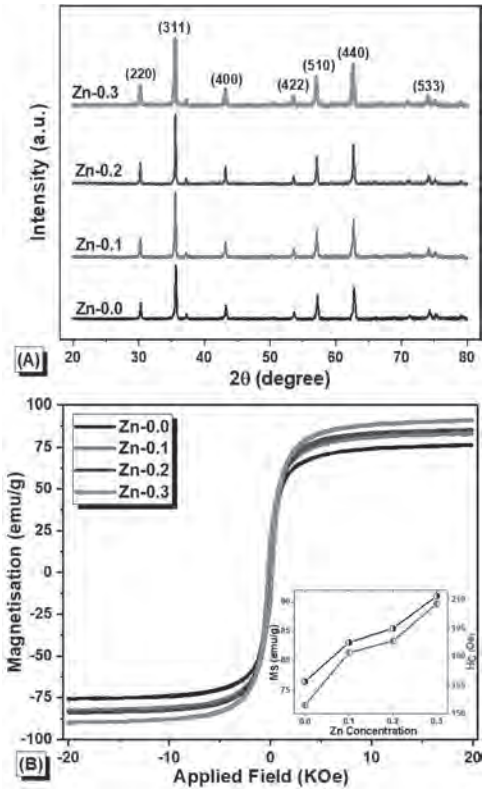

Fig. 1: (A) XRD spectra (B) M-H loop of FCs (inset: M_s and H_c for Zn doping).

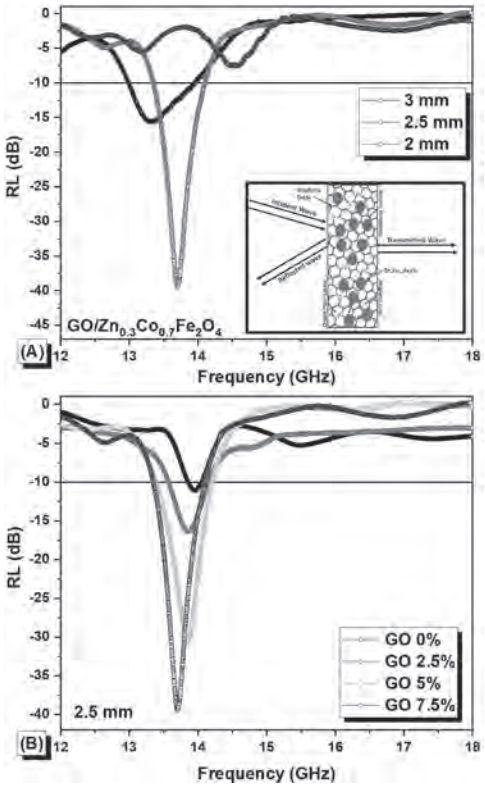

Fig. 2: (A) RL with frequency for different thicknesses (inset: Schematic of microwave absorber mechanism) (B) RL vs. frequency for different wt% of *GO*.

VP19-07. First-principles calculations of electronic and magnetic properties of Co-Ni-Fe ternary alloy. *G.D. Demin*[1], R.D. Tikhonov[2] and N.A. Djuzhev[1] *1. R&D Center "MEMSEC", National Research University of Electronic Technology (MIET), Moscow, Russian Federation; 2. Scientific-Manufacturing Complex "Technological Centre", Moscow, Russian Federation*

One of the main tasks in the formation of electrodeposited soft magnetic Co-Ni-Fe films used in magnetic field amplifiers and giant magnetoimpedance (GMI) sensors is to achieve their high magnetic permeability and low coercive force [1]. The magnetic properties of the Co-Ni-Fe ternary alloy are primarily determined by its crystal structure, which depends on the composition of elements (atomic fractions of Co, Fe and Ni) that control the ratio δ of bcc (100) phase to fcc (111) phase in the crystal lattice [2, 3]. Based on density functional theory, we estimated the change in saturation magnetization M_S and magnetic anisotropy field H_A of the Co-Ni-Fe alloy as a function of the percentage of Co and Fe (at the fixed atomic fraction of Ni at the level of about 27%). It was shown that an increase in the atomic fraction of Co leads to a change in the ratio δ towards the predominance of the fcc phase in the crystal and corresponding decrease in both M_S and H_C values. In turn, it provides high magnetic permeability μ of Co-Ni-Fe film, which is characteristic of Co-rich soft magnetic alloys, as it was previously confirmed by micromagnetic calculations of GMI structures [4]. The variation of the coercive force H_C and the maximum magnetic permeability $\mu=\mu_{max}$ of electrodeposited Co-Ni-Fe films depending on their elemental composition was also experimentally studied, where the best magnetic parameters were achieved for the $Co_{58.5}Ni_{27.4}Fe_{14.1}$ ternary alloy: μ_{max} = 12320 and H_C=1.64 Oe. Using glancing incidence X-ray diffraction (GI-XRD) method, it was found that the $Co_{58.5}Ni_{27.4}Fe_{14.1}$ film has a polycrystalline fcc phase with space group Fm-3m (No. 225) and the lattice parameter a=3.52 Å. This is in a good agreement with the results of our theoretical calculations of the diffraction pattern for the $Co_{58.5}Ni_{27.4}Fe_{14.1}$ crystal, which gives a predominant reflection in fcc (111) direction and the parameter a≈3.55 Å (Figure 1). The results obtained

can be useful for developing the technology for electrodeposition of soft magnetic Co-Ni-Fe films with improved magnetic properties. This work was supported by State Assignment No. FSMR-2023-0003.

[1] R.D. Tikhonov, et al., Russ. Microelectron., Vol. 51, pp. 273-281 (2022) [2] H.-S. Nam, et al., Thin Solid Films, Vol. 384, pp. 288-293 (2001) [3] M.A. Milyaev, et al., Journal of Alloys and Compounds, Vol. 854, p. 157171 (2021) [4] G.D. Demin, et al., Proc. of the 2024 IEEE International Magnetic Conference (INTERMAG), Rio de Janeiro, Brazil, 5–10 May 2024, pp.1-2 (2024)

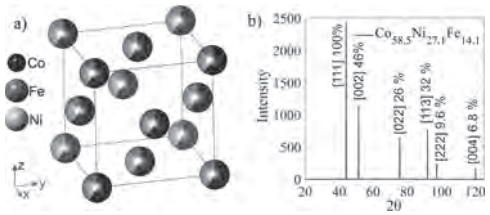

Figure 1. (a) Crystal structure and (b) radiation pattern of $Co_{58.5}Ni_{27.4}Fe_{14.1}$ alloy.

VP19-08. Effect of Swift Heavy Ion (SHI) Irradiation on Magnetic Properties of Soft Magnetic FeGaB Thin Film. *B. Arun*[1], J. Rahman[2] and K. James Raju[1] *1. School of Physics, University of Hyderabad, Hyderabad, India; 2. Department of Physics, Farook Autonomous College, University of Calicut, Calicut, India*

FeGaB is an exceptionally soft magnetic and microwave-friendly material. These attributes render them valuable for tunable microwave magnetoelectric devices. The Swift Heavy Ion (SHI) Irradiation technique effectively tunes the magnetic characteristics of thin films by deliberately inducing controlled defects. This research examines the impact of fast heavy ion irradiation on the structural and magnetic characteristics of FeGaB thin films that were deposited on an Al2O3 (0001) single crystal substrate using RF magnetron sputtering. The FeGaB samples were irradiated with 120 MeV Ag8+ ions at three fluences: 1×10^{11}, 1×10^{12}, and 1×10^{13} ions/cm^2. The structural change was examined by X-ray Photoelectron Spectroscopy (XPS). An Atomic Force Microscope (AFM) was used to analyze the surface image of both pristine and irradiated samples. Magnetic measurements were conducted at 5K and room temperature to observe the alteration of magnetic characteristics caused by fast heavy ion irradiation. When Swift Heavy Ions traverse through the material, they deposit energy into the material and produce localized structural and surface modifications, including ion tracks. These can affect the magnetic properties of the material.

1. J. Lou, R. E. Insignares, Z. Cai,*Appl. Phys. Lett.* 91, 182504 (2007), https://doi.org/10.1063/1.2804123 2. S.N. Dolia, P.K. Sharma, M.S. Dhawan, February 2012, Applied Surface Science 258 (2012): 4207– 4211, DOI:10.1016/j.apsusc.2011.06.011 3. Pawanpreet Kaur, K. K. Sharma, Rabia Pandit, Journal of Magnetism and Magnetic Materials, Volume 398, 2016, DOI:10.1016/j.jmmm.2015.09.006

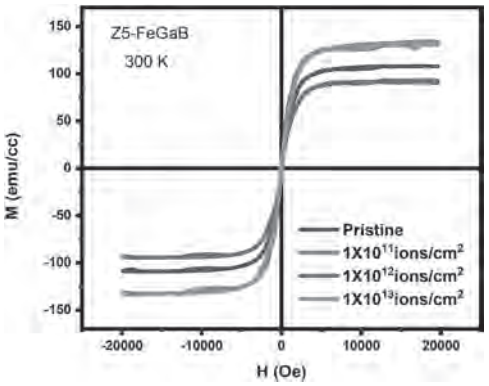

Fig 1. Show magnetization vs emu/cc graph for FeGaB sample irradiated at various fluences.

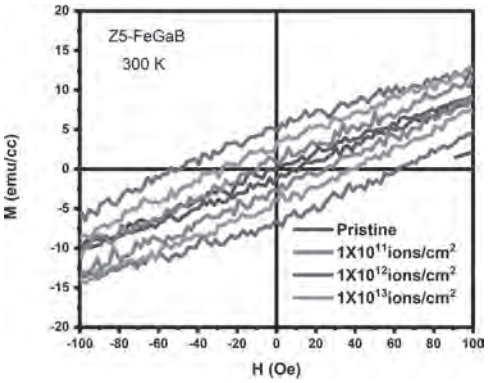

Fig 2. Show variation in the coercivity values for FeGaB samples irradiated at various fluences

VP19-09. Improvement in magnetic properties of soft magnetic films prepared from gel electrolyte. *K. Shiraki*[1], Y. Matsumoto[1], M. Tashiro[1], T. Yanai[1], A. Yamashita[1], M. Nakano[1] and H. Fukunaga[1] *1. Nagasaki University, Nagasaki, Japan*

Recently, we reported soft magnetic Ni films prepared from gel electrolytes and showed the potential of the gel-plating process [1]. In our previous study, we confirmed that the saturation magnetization, M_s, of the Ni films was smaller than that of bulk Ni, indicating that we need to improve the soft magnetic properties for gel-plating. In the present study, we, therefore, focused on the improvement in the current efficiency (C.E.) of the plating process, which is the ratio of the electroplated film's weight to the theoretical one obtained by Faraday's law, and investigated the effects of the current density, j, during the electroplating on the C.E. and M_s of Ni and Co films. The films were electroplated using a DC power supply. Metal (Ni or Fe) and Cu plates were used as an anode and a substrate, respectively. The gel electrolyte was filled between the electrodes. In our previous study, we employed $j = 15 – 45$ mA/mm^2, and the results suggested that low current density is effective in obtaining a high deposition rate. In the present study, j was changed from 5 to 60 mA/cm^2. Figure 1 shows the current efficiency of the plating processes as a function of the current densities As shown in Fig.1, since the decrease in the current density improves the C.E., we confirmed that increase in the deposition rate in our previous study [1] was attributed to the increase in the C.E. Figure 2 shows the hysteresis loops of the Co films. As shown in Fig. 2, the improvement in the C.E. increased the M_s. When the C.E. is low, the decomposition of H_2O occurs on the cathode surface, generating H_2 gases and $(OH)^-$ ions. Since it is considered that the $(OH)^-$ ions easily combine the metal ions M^{2+} (Ni^{2+} and Co^{2+}), we considered that low M_s is affected by the oxidation of the Ni and Co. In other words, a gel-plating process with high C.E. is preferable to obtain good soft magnetic properties, and we found that the low current density is one of effective conditions in obtaining high C.E. and high M_s.

[1] T. Yanai et al., *AIP advances*, Vol. 14, #025331 (2024).

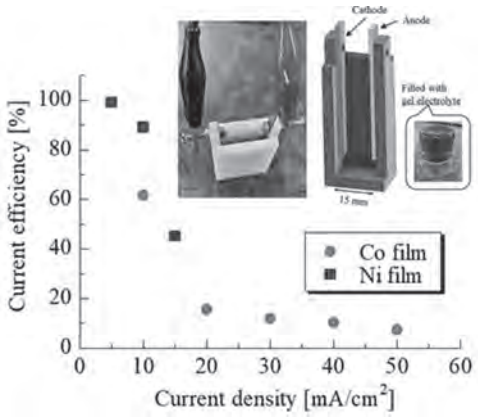

Fig. 1: Current efficiency as a function of current density. The inset indicates a jig for gel-plating.

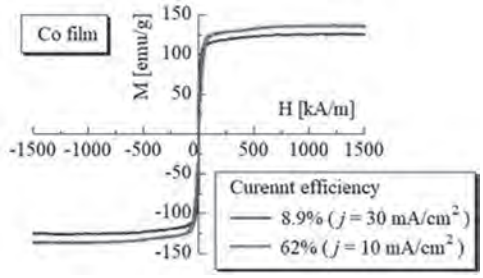

Fig. 2: Hysteresis loops of the Co films prepared from the gel electrolytes.

Session VP20
SPECIAL MACHINES AND GEARED MACHINES I
(Poster Virtual Session)

Doğa Ceylan, Chair
Eindhoven University of Technology, Eindhoven, Netherlands

VP20-01. Investigation of Dual-stator Flux Modulated Machines With Multiple-PM Excitation. *Y. Meng*[1], X. Yang[1], H. Chen[1] and S. Fang[2]
1. College of Electrical Engineering and Automation, Shandong University of Science and Technology, Qingdao, China; 2. School of Electrical Engineering, Southeast University, Nanjing, China

I.Introduction Due to the merits of high power factor, improved space utilization, and high torque density, the dual-stator flux modulated machine (DSFMM) with multiple-PM excitation (DS-FMMPMM) has attracted considerable attention[1] [2]. In this paper, two typical DS-FMMPMMs, i.e. a DSFMM with dual-PM (DS-FMDPMM) and a DSFMM with triple-PM excitation (DS-FMMTPMM) are comprehensively analyzed and compared. The topologies and operation principles of two machines are described. The electromagnetic performances of machines are compared by finite element analysis. II. Machine Topology and Operation Principle Fig. 1 shows the topologies of two DS-FMMPMMs. It can be seen that both machines have two stators and a sandwiched rotor. The three-phase concentrated windings are wound on both inner and outer stator teeth. The consequent pole PM arrays are employed in both the stator and rotor side. All of PMs in the rotor and stator are magnetized with the same radially directions. The DS-FMTPMM differs from the DS-FMDPMM in that CP PM arrays are mounted on both the inner and outer stators. The operation principles of DS-FMDPMM and DS-FMTPMM are based on the bidirectional flux modulation effect. The stator and rotor PM magnetomotive force (MMF) are modulated by the rotor iron poles and stator teeth, respectively, which contribute to abundant harmonic components in the air-gap flux densities, which contribute to the torque generation. III. Electromagnetic Performance Comprasion Fig.2 (a), (b), (c) and (d) compare the inner and outer air-gap flux densities of two machines at no-load condition, respectively. It can be observed that the DS-FMTPMM has a higher amplitude due to the stronger PM MMF. Hence, the higher back-EMF amplitude will be induced and larger torque delivered in DS-FMTPMM, as shown in Fig.2 (e) and (h). Besides, Fig.2 (h) illustrates the variation of average torque along with phase current. It is clear that the overload capability of both machines is similar, but the DS-FMTPMM always has a higher torque under various load conditions. More detailed design considerations and electromagnetic performance comparison results will be presented in the full paper.

[1] C. Liu, K. T. Chau, and Z. Zhang, "Novel design of double-stator single rotor magnetic-geared machines," *IEEE Trans. Magn.*, vol. 48, no. 11, pp. 4180–4183, Nov. 2012. [2] Y. Meng, S. Fang, Y. Li, Y. Zhong, and L. Qin, "Design and analysis of new dual-stator flux modulated machines with dual-PM excitation," *IEEE Trans. Ind. Appl.*, vol. 59, no. 2, pp. 1383-1393, March-April 2023.

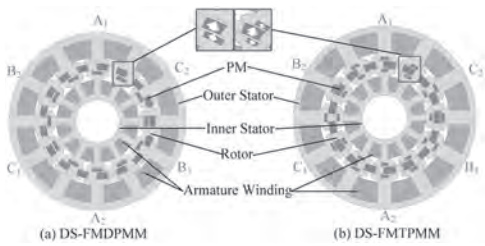

Fig. 1

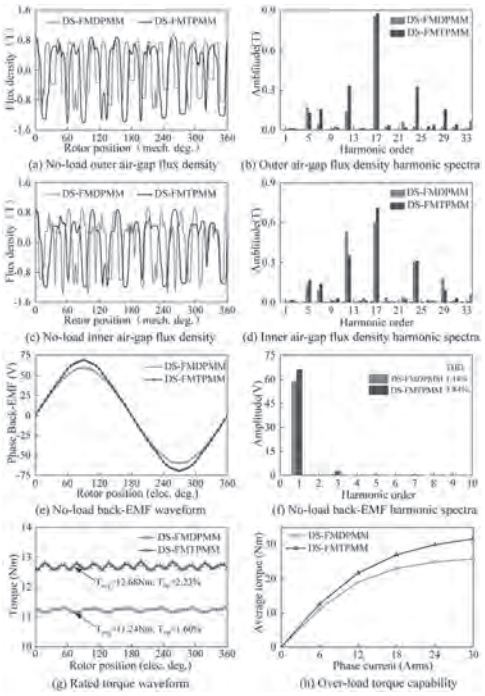

Fig. 2

VP20-02. Investigation of Vernier Arc Machines with IPM Rotor Structures. Y. Meng[1], M. Yang[1], S. Fang[2], *H. Chen*[1] and N. Wu[1]
1. College of Electrical Engineering and Automation, Shandong University of Science and Technology, Qingdao, China; 2. School of Electrical Engineering, Southeast University, Nanjing, China

I. Introduction Due to the merits of simple structure and high torque density, vernier permanent magnet arc machine (VPMAM) has been an appealing choice in large telescope drive[1]. In this paper, four VPMAMs with different rotor topologies are designed and comprehensively compared to provide a basic design reference of designing VPMAM. Meanwhile, a preferable candidate can also be selected based on the analysis results. II. Machine Topology and Operation Principle As an example of the investigation, the 12 stator-slot /17 rotor-pole-pair VPMAMs were considered. In Fig.1, four VPMAMs with different rotor topologies are presented, including a conventional surface-mounted PM rotor, a consequent-pole PM rotor, a spoke array PM rotor and a V-shaped PM rotor, which are named as Type I, Type II, Type III, and Type IV, respectively. To make a fair comparison, all the design parameters of each machine are identical except for the PM arrangements. For all four VPMAMs, the magnetomotive force produced by PMs is modulated by the stator slot to produce rich working harmonics. Because of the different arrangement of PMs, the PM magnetomotive forces are different, so the harmonic type and amplitude are also affected, which will be discussed in the full paper. III. Electromagnetic Performance Comparison The no-load air-gap flux densities of the four topologies are compared in Fig. 2(a) and(b). It can be found that the air-gap flux density harmonics of Type III are more abundant, in which the 5th and 17th have the higher amplitudes.

Fig. 2(c) shows the open-circuit phase flux linkages. It shows that Type IV has a larger peak-to-peak value than other machines. The back EMFs of four machines are compared in Fig.2(d). It can be seen that Type III can achieve the maximum back EMF. The cogging torques of four machines are compared in Fig. 2(e), where the peak values of cogging torque in Type II is maximum and the Type IV is the minimum. The steady-state average torque under the same electrical load is compared in Fig.2(f). It can be observed that the torque capability of Type III is much better than others. More detailed design considerations and electromagnetic performance comparison results will be presented in the full paper.

[1] P. M. Tlali, R. J. Wang, S. Gerber, IEEE Trans. Ind. Appl., vol. 56, no. 3, pp. 2570–2579(2020).

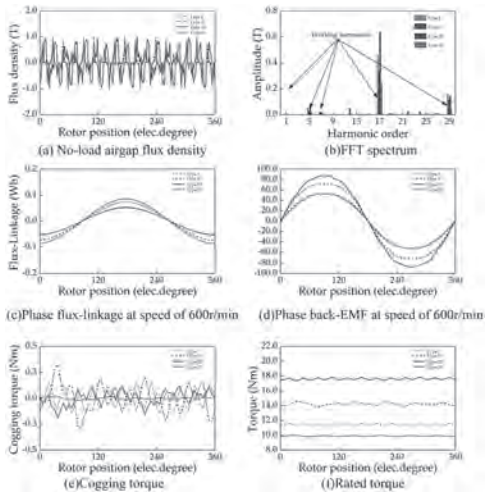

Figure 1

VP20-03. A New Asymmetric Permanent Magnet Variable Flux Memory Machine with Magnetic-Field-Shifting Effect. W. Liu[1], C. Zhang[1], J. Chen[1], Y. Fu[1] and *J. Zhang*[1] *1. Ningbo Institute of Materials Technology and Engineering, Chinese Academy of Science, Ningbo, China*

I. Introduction Variable flux memory machines (VFMMs) [1]-[2] employ the low-coercive-force (LCF) PMs to achieve precise adjustment of air-gap flux density, which are considered promising solutions for electric vehicles. Nevertheless, current VFMMs normally suffer from limitations such as narrow flux regulation range and reduced torque under low MS [3]. Therefore, this paper proposes a novel asymmetric PM VFMM (APM-VFMM), which utilizes the magnetic-field-shifting (MFS) effect [4] to adjust the peak angular difference between the PM torque and the reluctance torque, thus contributing to the improvement of torque. Additionally, the multi-parallel magnetic circuit design further enhances the flux regulation range of the VFMM. II. Machine Topology The operation principle and topology of the APM-VFMM are plotted in Fig. 1. It can be seen that only LCF PMs are employed on one side of each pole while the other side has only high-coercive-force (HCF) PMs, thus forming an asymmetric PM design. Moreover, the first layer has two PMs spliced together, with the second layer employing two spoke PM structures. Each layer can form an independent parallel magnetic circuit, which significantly enhances the flux regulation range of the VFMM. Additionally, when the machine is shifted from high MS to low MS, its PM *d*-axis will be shifted, which will affect the total torque of the APM-VFMM. III. Electromagnetic Performance The electromagnetic characteristics of the APM-VFMM are shown in Fig. 2. The proposed machine exhibits a shift of the PM *d*-axis at the low MS compared to the high MS due to the presence of the MFS effect. Additionally, this machine achieves more than three times the flux regulation range by magnetization operation. Benefiting from the MFS effect, the torque drop at the low MS can be mitigated. Most importantly, the APM-VFMM can shift the high-efficiency region to the high-speed region at the low MS, implying that the overall high-efficiency characteristics can be achieved by combining different MSs.

[1] A. N. Charamba, L. Masisi, and M. Ibrahim, "Variable flux machines: A review," in *2024 32nd Southern African Universities Power Engineering Conference (SAUPEC),* Jan. 2024. [2] M. A. Darmani et al., "AFPM machines equipped with multilayer magnets," *IEEE Trans. Energy Convers.*, early access, 2024. [3] R. Tsunata, M et al., "Variable flux memory motor employing double-layer delta-type PM arrangement and large flux barrier for traction applications," *IEEE Trans. on Ind. Appl.*, vol. 57, no. 4, pp. 3545–3561, Jul. 2021. [4] Z. Q. Zhu and Y. Xiao, "Novel magnetic-field-shifting techniques in asymmetric rotor pole interior PM machines with enhanced torque density," *IEEE Trans. Magn.*, vol. 58, no. 2, pp. 1–10, Feb. 2022.

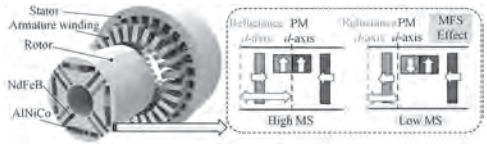

Fig. 1. Operation principle and topology of the APM-VFMM.

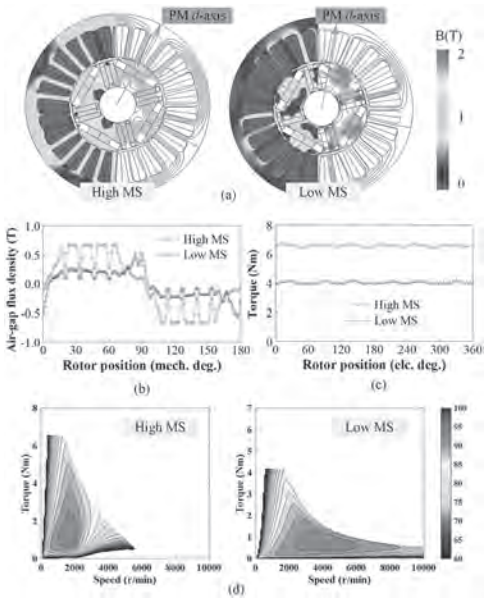

Fig. 2. Electromagnetic characteristics. (a) No-load magnetic field distribution. (b) No-load air-gap flux density. (c) Torque waveforms. (d) Efficiency maps.

VP20-04. Power Factor Improvement Mechanism of Dual-PM Excited Vernier Machines. H. Chen[1], Y. Meng[1], D. Li[2], R. Qu[2] and *X. Yang*[1] *1. Shandong University of Science and Technology, Qingdao, China; 2. Huazhong University of Science and Technology, Wuhan, China*

I.Introduction Taking advantage of the flux modulation effect, permanent magnet vernier machines (PMVMs) exhibit significantly high torque density with multiple working harmonics. However, the conventional PMVMs with only rotor-PMs suffer from a low power factor [1]. This paper comparatively investigates the power factor improvement mechanism of a novel dual-side PMVM (DPMVM) with two-slot-pitch coils featuring high power factor and torque density. The performances are verified by finite element analysis and prototype testing. II. Machine Topology and Operation Principle Fig. 1 (a) and (b) illustrate the proposed DPMVM and its counterpart, which are named topology I and topology II, respectively. For the two DPMVMs, both the stator and rotor have consequent-pole PM arrangement forming doubly salient structures, and the stator slot number and rotor pole number are the same. Due to the different stator-PM arrangements of the two topologies, the modulating tooth number is different, which brings about the differences in the winding pole pair numbers and winding configurations. The operation principles of both DPMVMs are based on the flux modulation effect.

The different stator-PM arrangements and winding configurations of the two DPMVMs result in a large difference in the harmonic components of the modulated airgap flux fields, contributing to different inductance and power factor performances of the two DPMVMs. III. Power Factor Evaluation Fig. 2 (a) and (b) compare the phase flux linkages produced by PMs and armatures of the two DPMVMs, respectively. It can be observed that topology I has higher PM flux linkage and lower armature flux linkage than that of topology II. According to Fig.2 (c) and (d), it can be deduced that the power factor of topology I is higher than that of topology II. To verify the forgoing analyses, the power factors of the two topologies are calculated based on FEA and comparatively investigated in Fig.2(e) and (f). The power factor of topology I is much higher than that of topology II. More detailed design considerations and electromagnetic performance comparison results will be presented in the full paper.

[1]Y. Gao, M. Doppelbauer, R. Qu, etc., *IEEE Trans. Ind. Appl.*, vol. 57, pp. 294(2021).

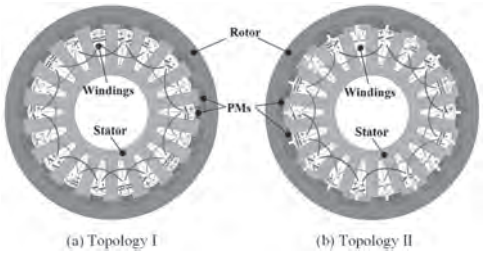

Fig.1

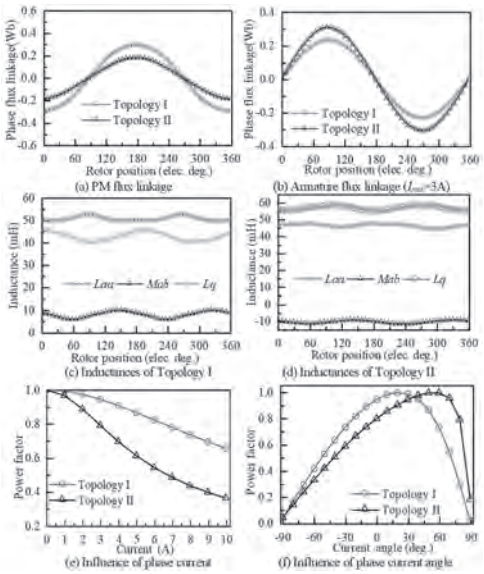

Fig.2

VP20-05. Topology Design and Performance Analysis of a New Arch-shaped Magnet Variable Flux Memory Machine. *W. Liu*[1], C. Zhang[1], J. Chen[1] and Y. Fu[1] *1. Ningbo Institute of Materials Technology and Engineering, Chinese Academy of Sciences, Ningbo, China*

I. Introduction Variable flux memory machines (VFMMs) [1]-[2] equipped with low-coercive-force (LCF) PMs are competent for automotive applications. The magnetization states (MSs) of the LCF PMs can be flexibly varied by a current pulse, which can achieve excellent flux adjustability with negligible additional copper loss [3]-[4]. However, existing VFMMs face the challenges of a narrow flux regulation range and significant difficulties in magnetization operation. Thus, this paper proposes a novel arch-shaped magnet VFMM (ASM-VFMM), which can significantly enhance the flux short-circuit effect in the low magnetization state (MS), thereby remarkably improving its flux regulation capability and efficiency in the high-speed region. II. Machine Topology The proposed ASM-VFMM configuration is illustrated in Fig. 1, which features a dual-layer PM arrangement forming an arched structure. An inverted V-shaped PM design is adopted for the first layer, which is closer to the air gap to reduce the difficulty of magnetization operation. The second layer employs a spoke-type PM structure, with an asymmetric PM design increasing the usage of LCF PMs, thus contributing to the enhancement of the flux regulation capability. Furthermore, the high-coercive-force (HCF) PMs in the second layer can form a series magnetic circuit with adjacent or slightly distant LCF PMs, ensuring the on-load MS stability of the VFMM. III. Electromagnetic Performance The electromagnetic characteristics of the ASM-VFMM are shown in Fig. 2. The proposed machine exhibits a substantial decrease in the magnetic field at the low MS compared with that at the high MS. Besides, this machine can achieve over three times the flux regulation range and wide torque variation range through the magnetization operation. Most notably, when shifting from the high MS to the low MS, the high-efficiency region can be shifted from the low-speed region to the high-speed region, indicating that the proposed ASM-VFMM features overall high-efficiency characteristics.

[1] V. Ostovic, "Memory motors," *IEEE Ind. Appl. Mag.*, vol. 9, no. 1, pp. 52–61, Jan. 2003. [2] M. A. Darmani et al., "AFPM machines equipped with multilayer magnets," *IEEE Trans. Energy Convers.*, early access, 2024. [3] R. Tsunata, M et al., "Variable flux memory motor employing double-layer delta-type PM arrangement and large flux barrier for traction applications," *IEEE Trans. on Ind. Appl*., vol. 57, no. 4, pp. 3545–3561, Jul. 2021. [4] A. Athavale et al., "Enabling driving cycle loss reduction in variable flux PMSMs via closed-loop magnetization state control," *IEEE Trans. on Ind. Appl*., vol. 54, no. 4, pp. 3350–3359, Jul. 2018.

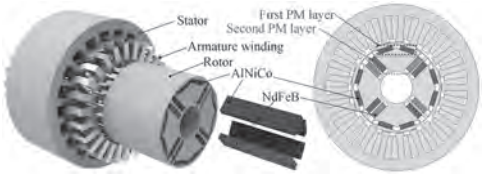

Fig. 1. Configuration of the proposed ASM-VFMM.

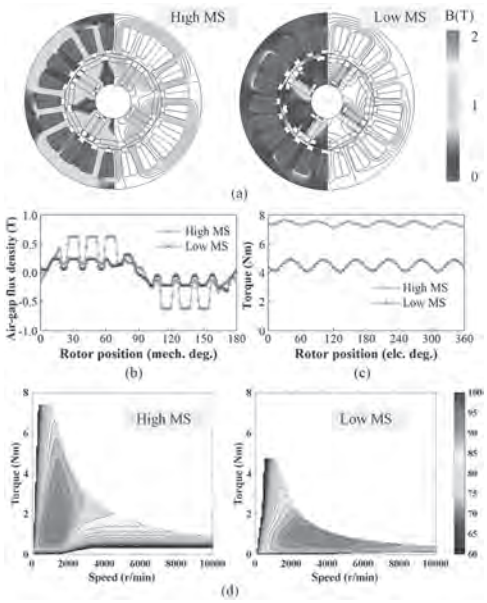

Fig. 2. Electromagnetic characteristics. (a) No-load magnetic field distribution. (b) No-load air-gap flux density. (c) Torque waveforms. (d) Efficiency maps.

VP20-06. A Novel Dual Magnetically Geared Halbach Array Based Tubular Linear Permanent Magnet Generator for Wave Energy Conversion. *N. Shrivastava*[1], S. Sampathirao[1] and B. Subudhi[1] *1. School of Electrical Sciences, Indian Institute of Technology Goa, Ponda, India*

With oceans covering nearly 70% of Earth, harnessing marine energy offers a promising alternative for sustainable power. Among the various types, wave energy is notable for its high power density, but faces challenges in direct-drive wave energy conversion (DD-WEC) due to the low generated voltage and power density, attributed to the slow wave speeds. Enhancing magnetic field density and increasing the translator speed are key to addressing these issues. In an attempt to maximize energy extraction, a dual magnetically geared tubular linear permanent magnet generator with dual armature and dual Halbach array (DMG-TLPMG) is proposed in this paper. This paper presents the novel integration of two tubular linear permanent magnet generators (TLPMG) and two tubular linear magnetic gear (TLMG) machines into a single machine. The proposed design features dual armatures, identified as the inner and outer armatures, which are positioned to convert the kinetic energy of waves into electrical power. This design is shown in Fig.1. The translator is hollow and cylindrical which has embedded ring magnets on both the inner and outer circumferences. It induces voltage in both the armatures with a single stroke. This design has an additional advantage of fault tolerance, as each armature is electrically isolated. Further, the magnetic gearing effect enhances the rate of change of the magnetic field, thereby increasing the generated voltage as the translator's stroke is constrained to the motion of the wave. The permanent magnets (PMs) are systematically arranged as a Halbach array as shown in Fig. 1. It achieves two primary objectives, segregates the magnetic fields of the inner and outer PMs resulting in distinct magnetic fields for the outer and inner armatures, and it enhances the magnetic field density in both the armatures. For the design, wave data from the cities Varsova and Karwar in India are considered. The analytical analysis is carried out for the proposed generator and the findings are correlated with the 3-D finite element analysis.

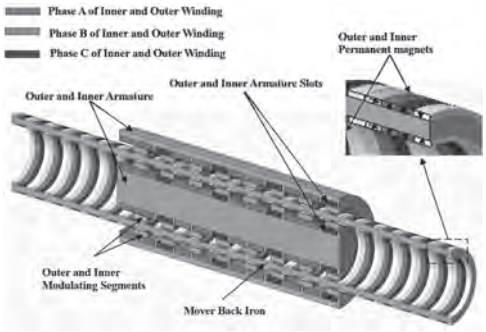

Fig. 1: 3-D half model of the proposed DMG-TLPMG.

VP20-07. Design of a Novel Carbon Nanotube Based Coreless Axial Flux Motor with Heat Pipes. *V. Basam*[1] and S. Sampathirao[1] *1. School of Electrical Sciences, Indian Institute of Technology Goa, Ponda, India*

This article presents the advancements and challenges in carbon nanotube (CNT) based axial flux motor topologies, focusing on coreless configurations. Despite the manufacturing ease of coreless axial motors, their limitations in high-power applications persist. To overcome this drawback, a novel customized carbon nanotube composite-based coreless motor configuration is proposed as shown in Fig. 1. This design aims to integrate the benefits of recently existing coreless configurations while addressing their drawbacks. Existing research indicates that heat pipes are becoming more popular for the thermal management of power-dense electric motors. However, the interaction of heat pipes with ohmic losses poses significant challenges, especially in coreless motors. Further, this article investigates the impact of heat pipe losses on the thermal management of CNT-based coreless motors. It highlights the necessity of addressing the interaction between heat pipes and electromagnetic fields. To mitigate these issues, a flux blanking method is presented to minimize ohmic losses associated with heat pipes. The effectiveness of this method is made evident by initial assessments, and further optimization is also discussed. Here, the flux blanking method has the potential to enhance thermal management in coreless motors, thereby facilitating the development of more efficient high-power applications.

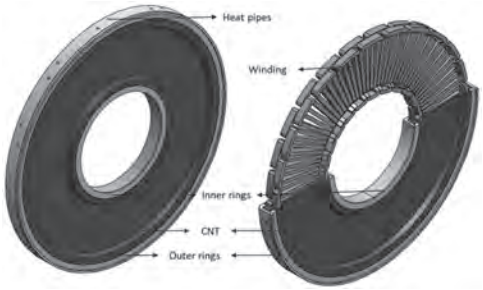

Fig. 1: Proposed carbon nanotube (CNT) based coreless axial flux motor windings.

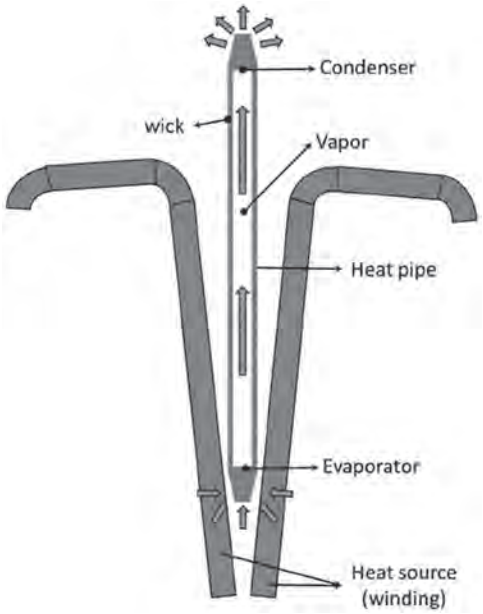

Fig. 2: Cross-section of heat pipe place between windings.

VP20-08. A High Torque Density Axial-Flux Permanent Magnet Machine with Yokeless and Segmented Armature. *L. Dai*[1], S. Niu[1], M. Jiang[1] and W. Wenjie[1] *1. Department of Electrical and Electronic Engineering, The Hong Kong Polytechnic University, Hong Kong, Hong Kong*

I.Introduction High torque density has been a long-standing pursuit in the field of electric machines, particularly in areas such as electric vehicle and aircraft where smaller sizes and weights are crucial [1]. Axial flux permanent magnet synchronous machines (AFPMSMs) offer higher torque capability compared to radial flux PMSMs due to their larger airgap area within the unit volume. Therefore, AFPMSMs are well-suited for high-torque density applications. To further enhance the torque capability of AFPMSMs with yokeless and segmented armature (YASA), this paper presents a novel skew-spoke YASA AFPMSM. The improved torque capability is attributed to the axial-tilt-placed magnets, which generate a larger rotor flux compared to conventional spoke-type AFPMSM [2]. Consequently, this leads to higher airgap flux density and output torque. II. Proposed Motor Structure Fig. 1 provides a clear visual comparison between the conventional spoke YASA AFPMSM and the proposed skew configuration. Furthermore, Fig. 1 presents a 2D view of the two types of rotors. It is evident that the proposed structure exhibits an increased PM flux. III. Verification Fig. 2 illustrates the electromagnetic torques of the two motors, clearly demonstrating a substantial increase in torque output resulting from using the skew-spoke design.

Specifically, the average torque is enhanced from 2.36 Nm to 3.64 Nm through the adoption of a 45-degree skew angle for the PMs. Furthermore, the complete paper will extensively investigate the proposed design method across various skew angles and pole-slot combinations.

[1] M. Polat, A. Yildiz and R. Akinci, "Performance Analysis and Reduction of Torque Ripple of Axial Flux Permanent Magnet Synchronous Motor Manufactured for Electric Vehicles," in IEEE Transactions on Magnetics, vol. 57, no. 7, pp. 1-9, July 2021, Art no. 8106809, doi: 10.1109/TMAG.2021.3078648. [2] Z. Shi et al., "Design Optimization of a Spoke-Type Axial-Flux PM Machine for In-Wheel Drive Operation," in IEEE Transactions on Transportation Electrification, vol. 10, no. 2, pp. 3770-3781, June 2024, doi: 10.1109/TTE.2023.3310738.

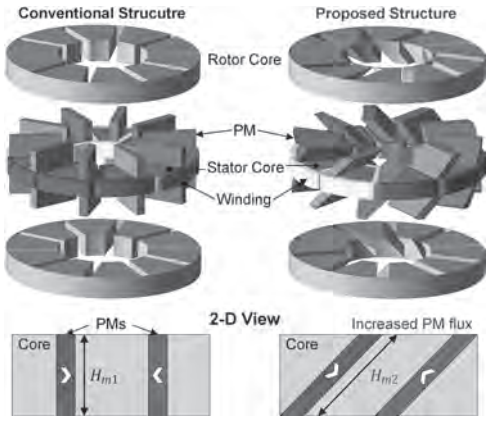

Fig. 1. Structure comparison between the conventional spoke YASA AFPMSM and the proposed skew-spoke AFPMSM.

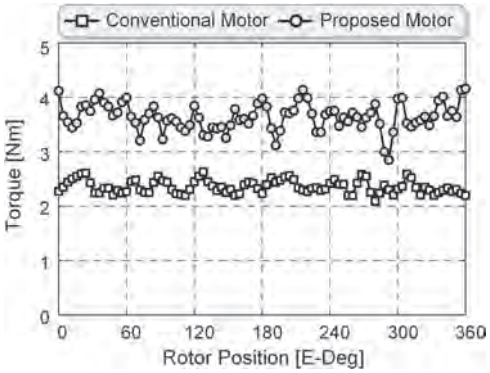

Fig. 2. Torque comparison between the conventional and the proposed AFPMSMs.

VP20-09. Design and Analysis of a Brushless Power Feedback PM Adjustable Speed Drive with Bilayer Wound Rotor. *X. Zheng*[1], H. Lin[1] and Y. Li[2,3] *1. School of Electrical Engineering, Southeast University, Nanjing, China; 2. Industrial Center, Nanjing Institute of Technology, Nanjing, China; 3. Jiangsu Provincial Engineering Research Center for Bionics Control Technology and Equipment, Nanjing, China*

With the improvement of performance of PM materials, PM adjustable speed drive (PMASD) technology for energy-saving has aroused extensive interests of researchers [1,2]. However, in mainstream PMASDs, the slip power is dissipated into the environment in the form of conductor heating so that the energy-saving efficiency is not very satisfactory [3,4]. In this paper, a brushless power feedback PMASD (BLPF-PMASD) with a double-layer wound rotor is proposed. The BLPF-PMASD can convert slip power into electrical power and mechanical power, without brushes and slip rings, resulting in higher efficiency and stability. Fig. 1(a) shows the topology of the proposed BLPF-PMASD, which mainly consists of a PM rotor, a bilayer wound rotor, and a stator. As shown in Fig. 1(b), the PM rotor is connected to a high-power induction motor rotating at an approximately constant speed. The bilayer wound rotor is connected to a mechanical load and can adjust its output speed as needed. The stator winding is connected to a slip power control unit (SPCU) adjusting the output speed and torque of the wound rotor by controlling the stator current. Moreover, in order to avoid direct coupling between the inner and outer magnetic fields, a non-magnetic layer is set between the inner and outer windings. Fig. 2(a) shows the flux field distributions of the proposed BLPF-PMASD under working points of 1050rpm and 850rpm. No extreme saturation in the iron core implies that the flux density designs of the drive is reasonable. As shown in Fig. 2(b), assuming that the drive is operating at working point A, and then it can be adjusted to working point B by adjusting the stator current. As shown in Fig. 2(b), the output torque ripples under the two working points are both below 10%, which can meet operational requirements of almost all kinds of fan and pump loads. It can be seen that the efficiency of the proposed BLPF-PMASD is higher than that of the traditional PMASD. Fig. 2 (e) shows the input powers of the two compared drives. The result confirms that the proposal can achieve the goal of energy conservation through adjusting the speed of load with a higher efficiency.

[1] J. Wang, H. Lin, and S. Fang, et al., "A general analytical model of permanent magnet eddy current couplings," in IEEE Transactions on Magnetics, vol. 50, no. 1, pp. 1-9, 2014. [2] S. Alshammari, P. Lazari, and K. Atallah, "Comparison of eddy current coupling topologies for high efficiency mechanical power transmission," in IEEE Transactions on Energy Conversion, vol. 38, no. 2, pp. 982-992, 2023. [3] Y. Li, H. Lin and H. Yang, "A novel squirrel-cage rotor permanent magnet adjustable speed drive with a non-rotary mechanical flux adjuster," in IEEE Transactions on Energy Conversion, vol. 36, no. 2, pp. 1036-1044, June 2021. [4] Y. Li, H. Lin, and Q. Tao, et al., "Analytical analysis of an adjustable-speed permanent magnet eddy-current coupling with a non-rotary mechanical flux adjuster," in IEEE Transactions on Magnetics, vol. 55, no. 6, pp. 1-5, June 2019.

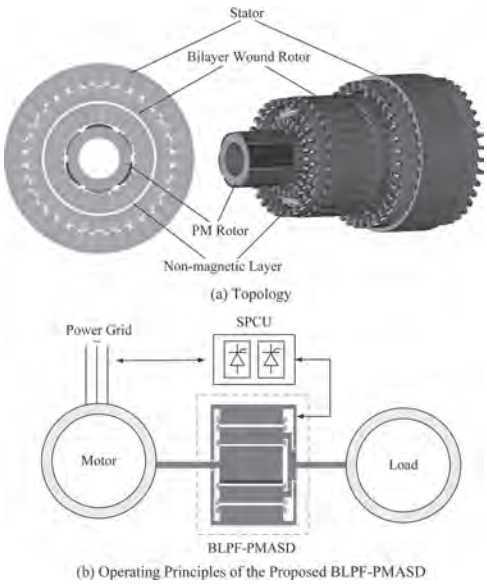

Fig. 1. Topology of the proposed BLPF-PMASD

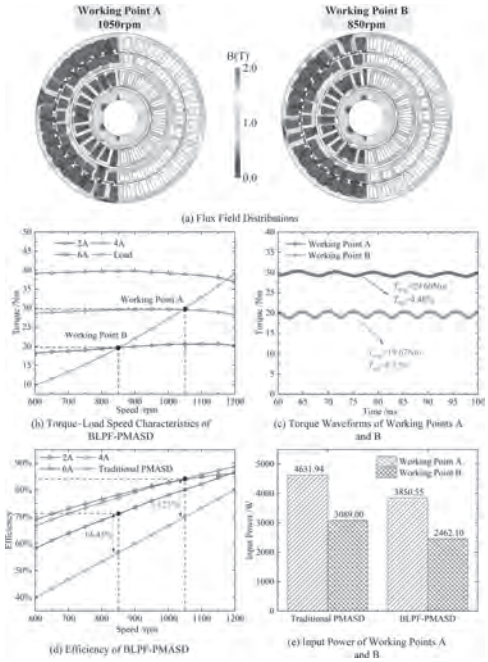

Fig. 2. Electromagnetic characteristics

VP20-10. Experimental Verification of Eddy Current Loss Reduction in Magnets of Flux-Modulated-type Magnetic Gears. *E. Asahina*[1] and K. Nakamura[1] *1. Tohoku University, Sendai, Japan*

Next-generation mobilities, such as advanced air mobility and electric aircraft, have attracted great attention. Their drive trains require an extremely high power-to-weight ratio of over 20 kW/kg [1]. Although their electric motors need to be driven at 50,000 rpm or more, no mechanical gearboxes are feasible. Magnetic gears can be a candidate for overcoming this problem because they have no mechanical contact. However, eddy current loss in magnets must be addressed under such ultra-high-speed operation [2] [3]. Ref. [3] discusses magnet division in permanent magnet motors to suppress eddy current loss and clarifies that a circumferential division can reduce the eddy current loss more effectively than an axial division. This paper experimentally investigates whether the above results are also effective in flux-modulated-type magnetic gears. Fig. 1(a) shows the specifications of a flux-modulated-type magnetic gear used in this study. Fig. 1(b) compares the calculated eddy current losses in magnets when the number of magnet divisions in the axial and circumferential directions is varied. It is understood that the circumferential division can reduce eddy current losses in magnets more effectively than the axial division. Fig. 2(a) depicts the outer stators with different magnet divisions and the experimental setup for measuring the magnet temperature of the outer stator of the prototype magnetic gear (MG). Fig. 2(b) shows the measured temperature changes in different magnet divisions when the inner rotor rotates at 18,669 rpm. The temperature is the average value measured at four different points using thermocouples, as shown in Fig. 2(a). The figure reveals that the no-division exhibits the most significant temperature rise, while the circumferential division has a smaller temperature rise than the axial division. At the conference, the measured temperature changes at higher speeds and the relationship between the eddy current loss distribution in magnets and the temperature distribution will be discussed.

[1] J. Z. Bird, *IEEE Trans. Magn.*, vol. 58, no. 2, 8201108, 2022. [2] J. J. Scheidler, V.M. Asnani, and T. F. Tallerico, Proc. AIAA/IEEE Electric Aircr. Technol. Symp., pp. 1–12, 2018 [3] K. Yamazaki and Y. Fukushima, pp. 1-6 2009 International Conference on Electrical Machines and Systems, 2009.

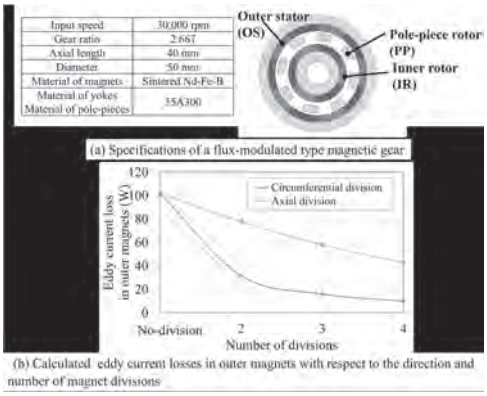

Fig. 1. Specifications of a flux-modulated-type magnetic gear and calculated eddy current losses in magnet.

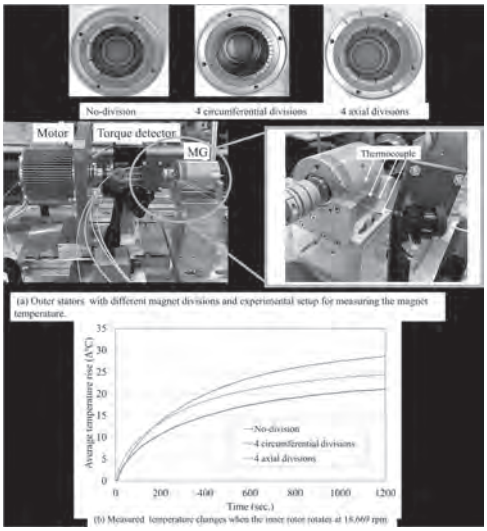

Fig. 2. Experimental setup and measured temperature changes in magnets.

Session VP21
SPECIAL MACHINES AND GEARED MACHINES II
(Poster Virtual Session)

Chuanbing Rong, Chair
Ford Motor Company, Dearborn, MI, United States

VP21-01. A Novel Double-sided PM Flux Modulated Machine with Hybrid Magnet Arrangement. H. Chen[1], Y. Meng[1], D. Li[2], R. Qu[2] and *Y. Zhang*[1] *1. Shandong University of Science and Technology, Qingdao, China; 2. Huazhong University of Science and Technology, Wuhan, China*

I. Introduction Permanent magnet vernier machines (PMVMs) exhibit significantly high torque density taking advantage of the multiple working harmonics. To further improve the magnet utilization and torque density, the dual-side PMs vernier machine with magnets placed in both stator and rotor sides has been a research spot in recent years [1]. This paper proposes a novel dual-side PM vernier machine (DPMVM) with hybrid excitation, in which the radial and tangential excited PMs are adopted. The torque generation mechanism and performance evaluation of the proposed DPMV machine are investigated by finite element analysis (FEA). II. Machine Topology and Operation Principle The topology of the proposed DPMVM is illustrated in Fig.1. It can be found that both the stator and rotor of the proposed DPMVM have consequent-pole radial-excited-PM arrangements forming doubly salient structures. In addition, two tangential excited PMs with opposite magnetization directions are placed on the sides of each split-tooth. The operation principle of the DPMVM is based on the flux modulation effect, and several low-order harmonic components in the modulated airgap flux field are produced, contributing to multiple torque contents to enlarge the torque density of the DPMVM. III. Performance Evaluation The flux density and flux line distributions of the proposed DPMVM are analyzed in Fig. (a) and (b), respectively. It can be seen that the saturation effect is slight, and the modulated 2nd-order harmonic is produced. Fig. 2 (c) and (d) investigate the no-load airgap flux densities produced by the stator-PMs, rotor-PMs, and dual-PMs. It can be observed that the working harmonics consist of modulated components and conventional component. Fig.2(e) investigates the phase back-EMF waveforms produced by the stator-PMs, rotor-PMs, and dual-PMs excitations. The RMS values of the corresponding back-EMFs are 10.2V, 12.0V and 18.1V. Furthermore, Fig. (f) analyzes the rated torques. It can be calculated that the average torques produced by the stator-PMs, rotor-PMs, and dual-PMs excitations are 14.2Nm, 15.5Nm, and 26.6Nm. The full paper will present more detailed design considerations and electromagnetic performance investigation results.

[1] Y. Li, H. Yang, H. Lin,W. Liu, and X. Zhao, "Torque generation mechanism and performance evaluation of a dual-sided PM machine with stator U-Shaped magnets," IEEE Trans. Ind. Appl., vol. 58, no. 1, pp. 250–260, Jan./Feb. 2022.

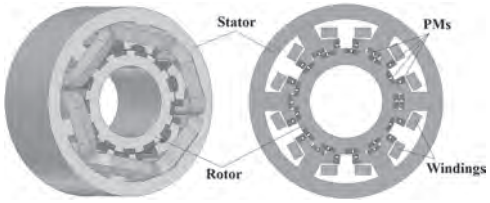

Fig.1

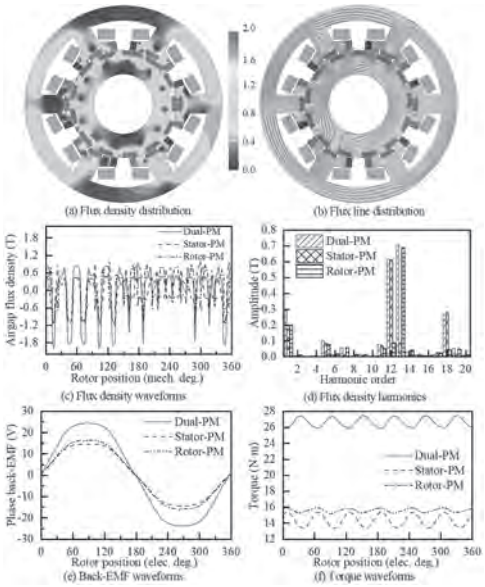

Fig.2

VP21-02. Bagging-GA-Driven Multi-Objective Optimization of MR Fluid Brake-Integrated PMSM Considering Brake Torque Constraint. Y. Hu[1], *H. Lu*[1] and W. Xu[1] *1. School of Electrical Engineering, Southeast University, Nanjing, China*

1. Introduction Magnetorheological (MR) fluid is a smart fluid capable of reversibly converting between liquid and semi-solid states within milliseconds, controlled by a magnetic field[1]. This effect makes MR fluid medium-based brakes have adjustable torque, fast response, and compact volume[2]. MR fluid brake-integrated PMSM (MRFB-I-PMSM) is a novel machine topology[3] used to improve the compactness and lightweight of robot joints. However, the integrated topology augments dimensionality and structural complexity, posing challenges for optimization including brake torque, electromagnetic (EM) torque, and EM torque ripple. Thus, this paper proposes a multi-objective optimization method for MRFB-I-PMSM driven by Bagging-GA considering brake torque constraint. 2. Methodology Fig. 1(a) to (c) show the machine topology and the proposed optimization methodology, respectively. This article opts not to directly optimize brake torque T_b but rather to constrain it as a passive variable within a certain range related to average EM torque T_{avg}. It is reflected by introducing the constraint ratio $R_T=T_b/T_{avg}$. Then, this paper sets expected R_T at the rated braking current as the range of [0.9, 1.0]. Thus, the objective function in genetic algorithm (GA) can be simplified as shown in Fig1. (d). 3. Optimization design Bagging is an ensemble machine learning method, which can effectively reduce the risk of overfitting and improve the efficiency of surrogate models[4]. Fig. 2(a) shows that trained Bagging-based surrogate models exhibit almost the same accuracy as finite element analysis (FEA). In the brake constrained GA optimization process, R_T began to converge within [0.9, 1.0]. Finally, It can be observed in Fig. 2(b) that the points within the expected range of $0.9 \le R_T \le 1.0$ have formed a Pareto front. To verify the validity of the proposed method, the torque performances of MRFB-I-PMSM in two modes with and

without optimization are compared based on FEA. Fig. 2(c) shows torque performances of the initial and optimal models of the MRFB-I-PMSM. It can be observed after optimization, T_{avg} has increased by 9.89 %, T_{rip} has decreased by 60.34 %, and T_b has increased by 18.46 %.

[1] C. Rossa, A. Jaegy, J. Lozada, *et al*., "Design considerations for magnetorheological brakes," IEEE/ASME Trans. Mechatronics., vol. 19, no. 5, pp. 1669-1680, Oct. 2014. [2] I. Bahiuddin, *et al*., "A new constitutive model of a magneto-rheological fluid actuator using an extreme learning machine method," Sens. Actuators A. Phys., vol. 281, pp. 209-221, Oct. 2018. [3] Y. Hu and W. Xu, "A Built-in Integrated Magnetorheological Fluid Brake Permanent Magnet Synchronous Motor", IEEE Trans. Magn., vol. 59, no. 11, pp. 1-6, Nov. 2023. [4] K. Chen, Y. Peng, S. Lu, B. Lin and X. Li, "Bagging based ensemble learning approaches for modeling the emission of PCDD/Fs from municipal solid waste incinerators," Chemosphere, vol. 287, no. 4, pp. 1-11, Jan. 2022.

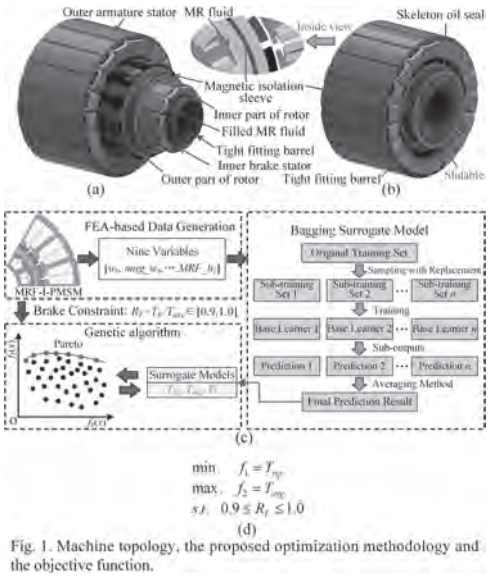

Fig. 1: Machine topology and methodology

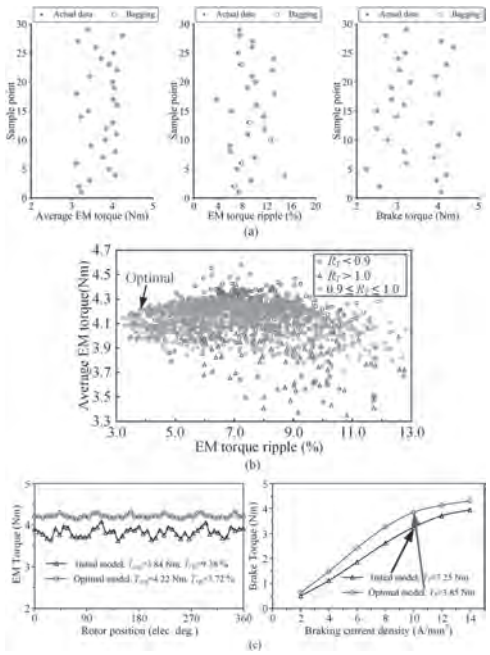

Fig. 2: Optimization process

VP21-03. A New Asymmetric Consequent Pole Flux-Reversal Permanent Magnet Machine With DC-biased Sinusoidal Current.

Y. Meng[1], *M. Yang*[1], H. Chen[1], X. Bai[1] and S. Fang[2] *1. College of Electrical Engineering and Automation, Shandong University of Science and Technology, Qingdao, China; 2. School of Electrical Engineering, Southeast University, Nanjing, China*

I.Introduction Hybrid-excited flux reversal permanent magnet machine has the merits of good flux regulation ability and high torque density, which is widely used in many applications. In this paper, a new asymmetric consequent-pole flux reversal permanent magnet machine with dc-biased sinusoidal current (DC-biased ACPFRPMM) is proposed and studied[1][2]. The topology and operation principle of the proposed machine are described. The electromagnetic performances of machine are evaluated using finite element analysis. II. Machine Topology and Operation Principle Fig. 1 shows the topology of the proposed DC-biased ACPFRPMM. It can be seen that the main teeth and auxiliary teeth are alternately distributed on the stator to compose an asymmetric consequent pole arrangement, and the rotor adopts salient pole structure. In addition, the armature windings of DC-biased ACPFRPMM are injected with dc-biased sinusoidal current to regulate the air-gap flux density. The proposed DC-biased ACPFRPMM can be regarded as a flux modulated machine and the principle can be explained by the flux modulation principle. In addition, a good flux regulation ablity can be obtained by using dc-biased sinusoidal current. III. Electromagnetic Performance Evaluation Fig. 2(a) and (b) shows the no-load air-gap flux densities of machine under different dc excitations. It can be found that when the dc current is injected into windings, the amplitudes of working harmonics can be effectively regulated. The no-load back EMFs of AT-CPFRPMM under different dc currents are compared in Fig. 2(c) and (d). It can be seen that the fundamental component can be regulated with the injected dc current, which illustrates a flexible field adjustment ability. The torque waveforms of machine under different dc current are compared and shown in Fig. 2(e), which suggests the torque can be well regulated with the participation of dc currents. As shown in Fig. 2(f), the over-load torque does not change significantly with the injection of dc currents. More detailed design considerations and electromagnetic performance comparison results will be presented in the full paper.

[1] Y. Gao, D. Li, R. Qu, X. Fan, J. Li, and H. Ding, "A novel hybrid excitation flux reversal machine for electric vehicle propulsion," *IEEE Trans. Veh. Technol*., vol. 67, no. 1, pp. 171–182, Jan. 2018. [2] L. Xu et al., "Design and analysis of a new linear hybrid excited flux reversal motor with inset permanent magnets," *IEEE Trans. Magn.*, vol. 50, no. 11, pp. 1–4, Nov. 2014.

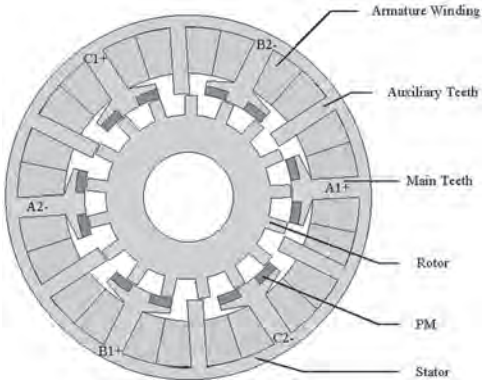

Fig.1

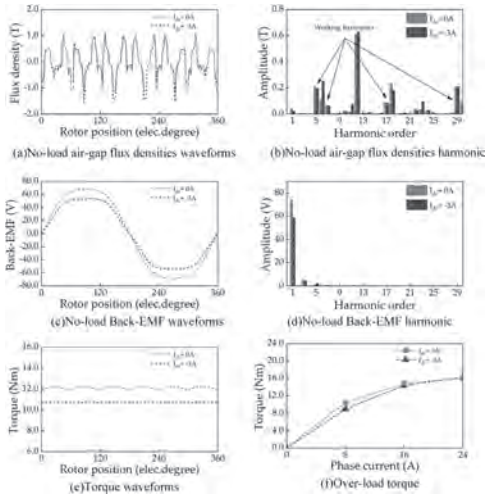

Fig. 2

VP21-04. A New Double-Sided Flux Modulated Permanent Magnet Arc Motor Having Parallel Complementary Effect. *J. Cai*[1], Z. Pan[1], J. Zhao[1], K. Wei[1] and Z. Yu[1] *1. School of Electrical Engineering and Automation, Hefei University of Technology, Hefei, China*

I. INTRODUCTION Permanent magnet (PM) arc motor(PMAM) has the merits of simple structure and high torque. It is widely used in the some low-speed high-torque direct drive applications [1]. The traditional single-sided flux modulated PMAM (SS-FMPMAM) has the limited average torque and high torque ripple. Hence, a double sided FMPMAM (DS-FMPMAM) is studied to improve the output torque and PM utilization rate [2]. In order to further reduce the torque ripple, this paper proposes a new parallel complementary DS-FMPMAM (PCDS-FMPMAM) based on the parallel complementation and bidirectional flux modulation effect. II. MOTOR TOPOLOGY AND WORKING PRINCIPLE Figs. 1 (a) and (b) show the topologies of the SS-FMPMAM and DS-FMPMAM, respectively. Figs. 1 (c) and (d) show the 2D and 3D view of the PCDS-FMPMAM, respectively. They are composed of three stator modules and one rotor. Each stator module and the rotor forms a unit motor. Three PMAMs adopt the consequent-pole PM (CPM) design. Besides, the PM arrangement of stator is the N-Iron-N. As shown in Fig. 1, both the SS-FMPMAM and DS-FMPMAM have the same PM magnetized direction. However, the PCDS-FMPMAM is formed by the front DS-FMPMAM and the rear DS-FMPMAM in parallel. The PMs of front motor and the rear motor in PCDS-FMPMAM are radially outward and inward magnetized, respectively. The rotor difference between the front motor and rear motor is 180° electrical angle. The stator has no mechanical displacement, and the front motor and rear motor share the common armature winding. III. ELECTROMAGNETIC PERFORMANCE ANALYSIS Figs. 2 (a) and (b) show the flux linkage and back-EMF of the three PMAMs, respectively. Compared with SS-FMPMAM, both DS-FMPMAM and PCDS-FMPMAM can provide twice the flux linkage and back-EMF. Figs. 2 (c) and (d) compare the torque characteristics of the three motors. The results show that the DS-FMPMAM and PCDS-FMPMAM has 50% higher torque than the SS-FMPMAM. Compared with DS-FMPMAM, the torque ripple of PCDS-FMPMAM has also been reduced by about 50%. Therefore, the PCDS-FMPMAM has the best motor performances in the three PMAMs. More design considerations and results analysis will be given in the full paper.

[1] C. J. Jian, M. W. Li, and H. J. Long, "Design and optimization of arc permanent magnet synchronous motor used on large telescope," IEEE Trans. Magn., vol. 48, no. 5, pp. 1943-1947, May 2012. [2] Y. Meng, S. Fang, Y. Zhu, Y. Yu, L. Qin, "Investigation of new dual-stator consequent-pole flux reversal permanent magnet arc machines," IEEE Trans. Appl. Supercon., vol. 34, no. 8, Nov. 2024, Art. no. 5204105.

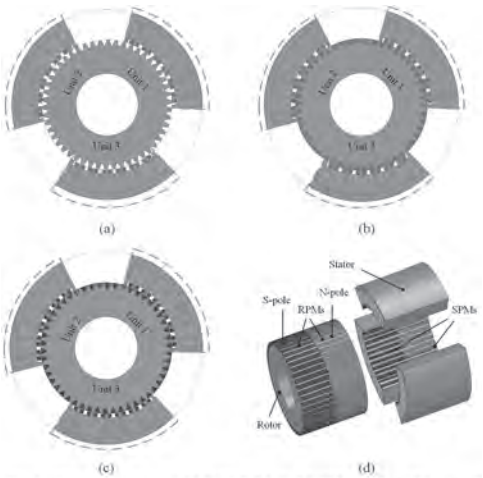

Fig. 1. Motor topologies. (a) SS-FMPMAM. (b) DS-FMPMAM. (c) 2D view of PCDS-FMPMAM. (d) 3D view of the PCDS-FMPMAM.

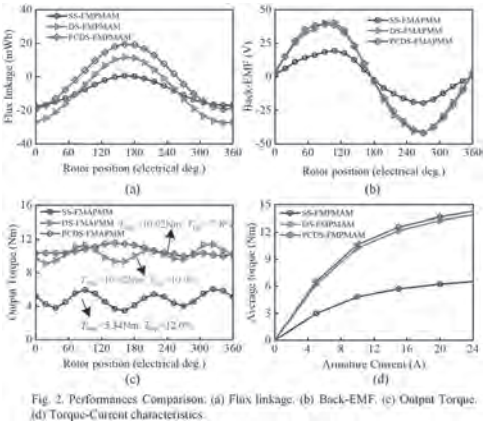

Fig. 2. Performances Comparison. (a) Flux linkage. (b) Back-EMF. (c) Output Torque. (d) Torque-Current characteristics.

VP21-05. Research of Asymmetric Interior Permanent Magnet Synchronous Machine Considering the Characteristics of Different Excitation Sources. *X. Liang*[1], M. Wang[1], P. Zheng[1], Y. Liu[1] and J. Gao[1] *1. Harbin Institute of Technology, Harbin, China*

Permanent Magnet synchronous machine (PMSM) are widely used in fields such as new energy vehicles due to their high power and torque density. But the presence of permanent magnet (PM) field leads to a high back electromotive force at high speed. Many control strategies of flux-weakening (FW) have been proposed to further expand the speed under the inverter capacity. In the conventional machine, even the salient interior PMSM (IPMSM), its d-axis inductance is small for increasing reluctance torque [1]. For solving the above problem to improve FW ability, Flux-intensifying IPMSM (FI-IPMSM) has been proposed with higher d-axis inductance, speed and power [2]. However, the PM on d-axis and magnetic barrier on q-axis limit the further improvement of the power and FW ability. Based on the analysis of the characteristics of different excitation sources, it is necessary to research a novel FI-IPMSM that encompasses the above requirements. By changing their amplitude and phase relationship of excitation sources, the performance such as speed range and power can be improved based on the different excitation source interaction. The proposed novel asymmetric FI-IPMSM and its excitation source are shown in Fig. 1, where the d-axis flux path without low-permeability material greatly improves the inductance and FW ability. The shifting angle of PM can be adjusted to achieve the optimal design. The combined PM poles can achieve higher and more sinusoidal magnetic field of rotor, while the discrete armature magnetic field can better solve the power and speed limitation and uneven saturation through theoretical deduction. The schematic diagram of the torque and speed characteristics of the machine are shown in Fig. 2. Based on the research of

excitation source superposition relationship, the machine can achieve higher speed and power. The more reasonable excitation and topology make the torque quality better than the conventional machine.

[1] X. Zhu, J. Huang, and L. Quan, "Comprehensive Sensitivity Analysis and Multi-objective Optimization Research of Permanent Magnet Flux-Intensifying Motors," IEEE Transactions on Indus-trial Electronics, vol. 66, no. 4, pp. 2613-2627 (2019) [2] X. Zhao, B. Kou and C. Huang, "A Reverse-Salient Permanent Magnet Synchronous Motor and Its dq-Axis Current Distribution Laws," IEEE Transactions on Industrial Electronics, vol. 70, no. 4, pp. 3337-3347 (2023)

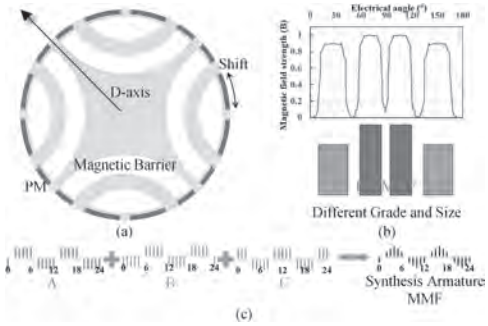

Fig. 1. The proposed topology and its excitation sources (a)The proposed novel asymmetric FI-IPMSM (b)Characteristics of combined PM (c) Synthesis of discrete armature magnetomotive force (MMF).

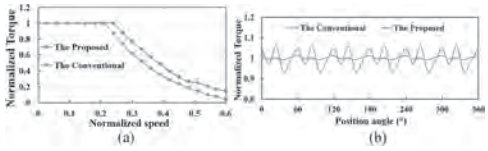

Fig. 2. The performance schematic diagram (a)The torque-speed characteristics (b) Torque quality.

VP21-06. Integration Design of MR Fluid Brake-Based External Rotor PMSM For Robotic Arm Application. *Y. Hu*[1], W. Xu[1] and W. Zhang[1]
1. School of Electrical Engineering, Southeast University, Nanjing, China

1.Introduction Due to the high efficiency, high torque density, and fast dynamic response, the external rotor permanent magnet synchronous motor (PMSM) is prone in robotic arms [1]-[2]. With the increasing use of robotic arms in human-robotic interaction, it is desirable to minimize the risk of impulsive force injury when an unexpected impact occurs. Faced with this demand, magnetorheological (MR) fluid-based brakes are a novel passive way of compliance that has been widely applied in robotic interaction tasks to provide adjustable brake torque [3]. In [4], the design of MR fluid-based human-friendly manipulator is proposed to balance safety and performance. The common connection type between the MR fluid brake and PMSM is cascaded through an additional transmission unit, resulting in a low integration and space utilization. This article proposes an integration design of MR fluid brake-based external rotor PMSM (MRFB-B-ERPMSM) for robotic arm application. By adding the inner braking teeth to the stator with outer armature teeth, the MR fluid brake is integrated into the interior of the external rotor PMSM. The multimode stator design can allow the proposed machine to operate in both rotation and brake modes while improving space utilization in a relatively simple structure. 2. Machine topology and FE analysis Fig.1(a) shows the detailed integration topology of the proposed machine. The detailed design parameters of the proposed MRFB-B-ERPMSM are shown in Fig.1(b). Fig. 2(a) shows the flux density and magnetic field distribution in the open-circuit field. A small amount of magnetic leakage enters the inner braking tooth area of the stator under the open circuit field. Fig. 2(b) further illustrates the impact of this magnetic leakage on the back electromotive force (EMF) of the proposed machine under 1200 rpm. Fig.2(c) shows the flux density of the MR fluid in the inner air-gap under two operation states. Fig.2(d) compares the torque versus different current densities under rotation state and brake state. It can be observed that the built-in integration of the MRFB does not have a significant impact on the performances of the ERPMSM.

[1] C. Ma et al., "Analytical calculation of no-load magnetic field of external rotor permanent magnet brushless direct current motor used as in-wheel motor of electric vehicle," IEEE Trans. Magn., vol. 54, no. 4, pp. 1-6, Apr. 2018. [2] S. Zuo, F. Lin, and X. Wu, "Noise analysis, calculation, and reduction of external rotor permanent-magnet synchronous motor," IEEE Trans. Ind. Electron., vol. 62, no. 10, pp. 6204-6212, Oct. 2015. [3] P. Fauteux, M. Lauria, M. A. Legault, B. Heintz, and F. Michaud, "Dual differential rheological actuator for robotic interaction tasks," IEEE/ASME Int. Conf. Adv. Intell. Mechatronics, AIM, pp. 47-52, 2009. [4] A. S. Shafer and M. R. Kermani, "On the feasibility and suitability of MR fluid clutches in human-friendly manipulators," IEEE/ASME Trans. Mechatronics, vol. 16, no. 6, pp. 1073-1082, Dec. 2011.

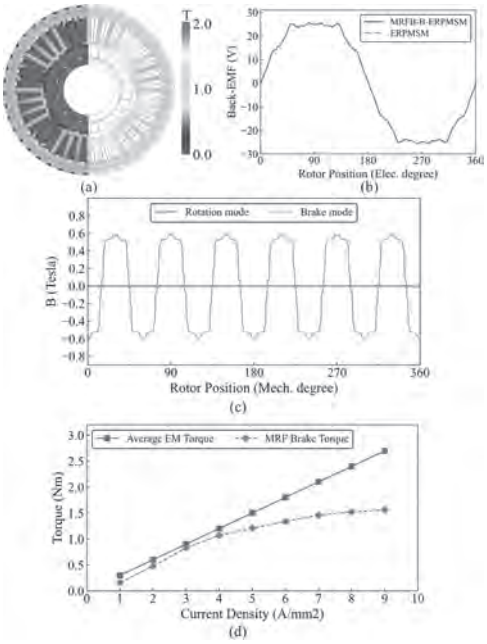

Fig. 1: Results of finite element analysis

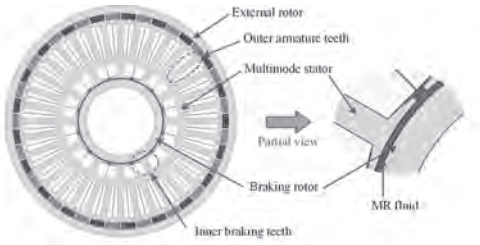

DESIGN PARAMETERS OF MACHINE TOPOLOGY

Parameters	Value	Parameters	Value
Outer radius [mm]	45.5	Number of slots	36/12
Inner radius [mm]	11	Number of poles	40
Axial length [mm]	25/35	Parallel branches	2/1
Air-gap [mm]	1/1	Current density [A/mm²]	7/10
PM thickness	3	Number of turns	20/10

*ERPMSM / MRFB

(b)

Fig. 2: Machine topology and design parameters

VP21-07. A Novel Twelve-Phase Variable Magnetic Circuit Memory Machine for Rim Thrusters. *Y. Fu*[1,2], W. Liu[1], C. Zhang[1] and J. Chen[1]
1. Ningbo Institute of Materials Technology and Engineering, Chinese Academy of Science, Ningbo, China; 2. University of the Chinese Academy of Sciences, Beijing, China

I.Introduction Shaftless rim thrusters are widely employed in underwater propulsion systems due to the advantages of compact structure and high transmission efficiency [1]. Nevertheless, traditional shaftless rim thrusters mostly use surface-mounted permanent magnet (PM) machines, which suffer from the narrow high-speed efficiency region and operation range. To address the above issues, this paper proposes a novel variable magnetic circuit memory machine (VMCMM) employing the low coercive force (LCF) PMs [2]. The magnetization states (MSs) of the LCF PMs can be adjusted through the imposition of the *d*-axis pulse current, which can improve the efficiency [3]. Besides, the proposed VMCMM utilize twelve-phase winding to reduce the torque ripple under different MSs [4]. II. Machine Topology The structure of the proposed VMCMM is shown in Fig. 1(a). When the machine is under flux-enhanced state, half part of high coercive force (HCF) PMs close to the inner side of the rotor and LCF PMs form series magnetic circuits, while the half part of HCF PMs close to the air-gap and LCF PMs form parallel magnetic circuits. When the VMCMM is switched to the flux-weakened state, the magnetic circuit of the rotor varies as the magnetization direction of the LCF PMs is reversed, with the LCF and HCF PMs forming parallel magnetic circuit. Fig. 1(b) shows the electromotive force distribution of the winding, which uses a twelve-phase winding consisting of four sets of star-connected three-phase windings for π/12 multiplex offset. III. Electromagnetic Performance The electromagnetic performance is plotted in Fig. 2. Figs. 2 (a)-(b) reveal the excellent flux changeable performance. Besides, the twelve-phase winding enables the machine to have excellent output torque and low torque ripple. Moreover, the efficiency maps exhibit that the machine can expand the high-speed efficiency region through flux adjustment. It is confirmed that the proposed VMCMM can effectively solve the cruising anxiety of the rim thrusters and the problem of high torque ripple.

[1] X. Yan, X. Liang, W. Ouyang, Z. Liu, B. Liu, and J. Lan, "A review of progress and applications of ship shaft-less rim-driven thrusters," *Ocean Engineering*, vol. 144, pp. 142–156, Nov. 2017. [2] V. Ostovic, "Memory motors," *IEEE Ind. Appl. Mag.*, vol. 9, no. 1, pp. 52–61, Jan. 2003. [3] H. Hua, Z. Q. Zhu, A. Pride, R. Deodhar, and T. Sasaki, "Comparative study on variable flux memory machines with parallel or series hybrid magnets," *IEEE Trans. Ind. Appl.*, vol. 55, no. 2, pp. 1408–1419, Mar/Apr. 2019. [4] C. Liu, "Emerging electric machines and drives — An overview," *IEEE Trans. Energy Convers*., vol. 33, no. 4, pp. 2270–2280, Dec. 2018.

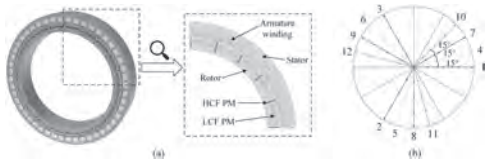

Fig. 1. (a) Topology. (b) Winding electromotive force distribution.

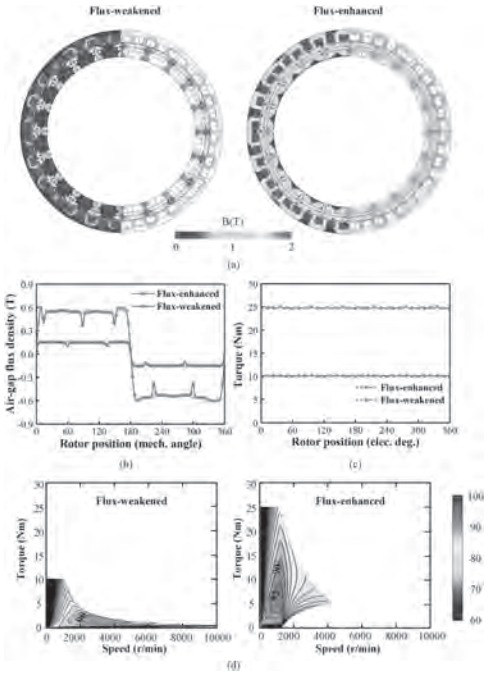

Fig. 2. (a) Open-circuit field distributions. (b) No-load radial flux densities. (c) Torque waveforms. (d) Efficiency maps.

VP21-08. Design and Analysis of a Pole-changing Machine with Multi-auxiliary-teeth Structure. *W. Wenjie*[1], S. Niu[1] and M. Jiang[1]
1. EEE, Hong Kong Polytechnic University, Hong Kong, Hong Kong

I. Introduction With the increasing demand for high-speed and high torque density machines in electric vehicles application fields, the pole-changing machine has attracted more and more attention because of its superior effects in speed range expansion. At present, many different pole-changing machine structures such as [1],[2] are designed to improve the flux-weakening ability, while pay little attention to the torque density. In order to realize the high torque density and improved flux-weakening ability simultaneously, the multi-auxiliary teeth structure is applied in a pole-changing machine. Besides, the number of the auxiliary teeth is the key factor to influence the torque and flux-weakening ability of this proposed machine. Therefore, the performances with the different auxiliary teeth are simulated and compared which helps to select the optimal design based on different design requirements. II. Proposed design and simulated result Fig. 1 illustrates the proposed topological structure and the different auxiliary teeth distribution. It can be observed that the number of the auxiliary teeth mainly affect the pole-pair number of the excitation source. Therefore, when the number of auxiliary teeth changes, the flux density and flux linkage of the proposed machine have the variation, which affects the torque density and flux-weakening ability. The specific relationship between them will be deduced in detail in subsequent paper. Fig. 2 illustrates the comparison results of the torque and flux-weakening ability based on the different auxiliary teeth structures. With the increase of the auxiliary teeth number, the torque performance of the proposed machine is improved while the flux weakening ability is decreased.

[1] M. Tian, X. Wang, D. Wang, W. Zhao and C. Li, "A Novel Line-Start Permanent Magnet Synchronous Motor With 6/8 Pole Changing Stator Winding," *IEEE Trans. Energy Convers.*, vol. 33, no. 3, pp. 1164-1174, Sept. 2018. [2] C. Contà and N. Bianchi, "Pole-Changing in Synchronous Machines: A Reluctance-Permanent Magnet Hybrid Motor," *IEEE Trans. Ind. Appl.*, 2023, doi: 10.1109/TIA.2023.3338194.

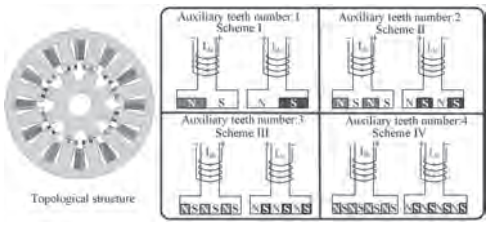

Fig. 1. Topological structure and the different auxiliary teeth distribution.

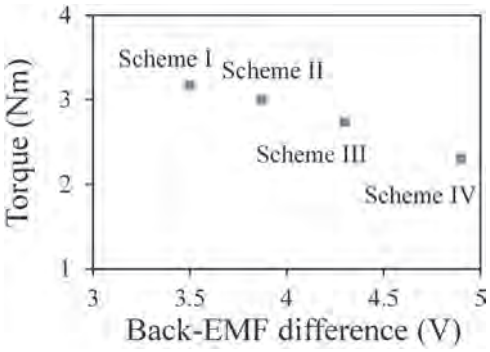

Fig. 2. Torque and flux-weakening ability comparison based on the different auxiliary teeth.

VP21-09. Improved Flux Observer Sensorless Control of Permanent Magnet Assisted Synchronous Reluctance Motor. *T. Tang*[1], X. Liu[1], M. Lu[1], D. Lu[2] and P. Lin[1] *1. College of Electrical and Information Engineering, Hunan University, Changsha, China; 2. Nanjing Nari-Relays Electric Co., Ltd, Nanjing, China*

For the magnetic saturation and cross coupling effect, the dq axis inductance parameters of the PMaSynRM are unstable. In sensorless control of PMaSynRM, traditional EMF observers have low control accuracy due to low signal-to-noise ratio during low-speed operation. Unlike the electromagnetic field, the rotor flux remains constant during low-speed operation, so the flux observer has better performance during low-speed operation[1]. In [2], the author points out that there is a DC offset problem using the conventional flux observer method and proposes the use of a non-ideal PR controller in a flux observer based machine current model to suppress this problem and experimentally verifies the scheme. And unlike the traditional flux observer, the nonlinear flux observer makes a difference between the magnitude of the estimated flux and the actual flux as the compensation of the estimated flux component, which solves the problem of poor tracking accuracy from start to low-speed operation more efficiently, and the system reliability is improved. In [3], it combines the nonlinear flux observer with the gradient descent method to propose an improved nonlinear flux observer for PMSM, which greatly reduces the angular error. So in order to accommodate inductive instability and improve the performance of the system at start and low-speed operation, we propose a variable gain nonlinear flux observer by researching the relationship between observer gain and load. Meanwhile, in order to adapt to the influence of PMaSynRM dq-axis inductance variation on the observer, online parameter identification is introduced to improve the system reliability. In simulation, the maximum angular error when the PMaSynRM start is 0.138rad, and the angular error is stable at 0.054rad after the given speed is reached in 0.5s, which basically achieves effective and reliable tracking. The simulation results (Fig.1 and Fig.2) verify the effectiveness and feasibility of the method.

[1] W. Xu, Y. Jiang, C. Mu and F. Blaabjerg, "Improved Nonlinear Flux Observer-Based Second-Order SOIFO for PMSM Sen-sorless Control," in IEEE Transactions on Power Electronics, vol. 34, no. 1, pp. 565-579, Jan. 2019. [2] D. Wang, K. Lu and P. O. Rasmussen, "Improved Closed-Loop Flux Observer Based Sensorless Control Against System Oscillation for Synchronous Reluctance Machine Drives," in IEEE Transactions on Power Electronics, vol. 34, no. 5, pp. 4593-4602, May 2019. [3] J. Liu and Y. Zhang, "Performance Improvement of Nonlinear Flux Observer for Sensorless Control of PMSM," in IEEE Transactions on Industrial Electronics, vol. 70, no. 12, pp. 12014-12023, Dec. 2023.

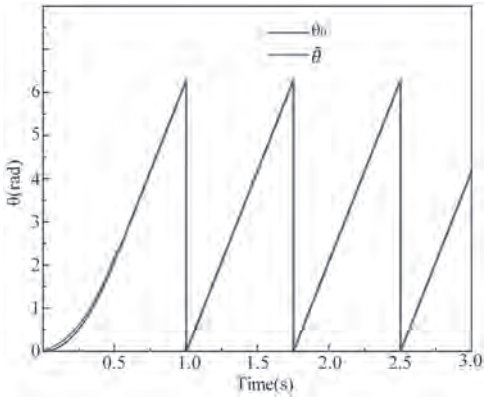

Fig.1 Motor position tracking under start and low-speed operation

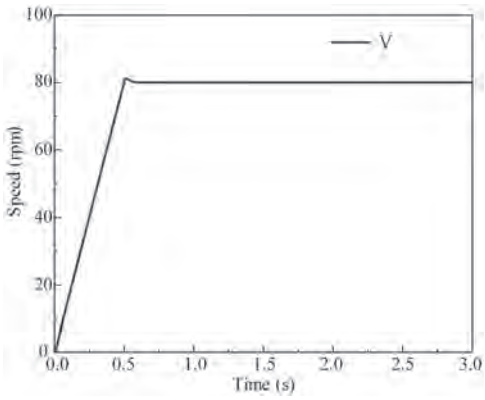

Fig.2 Motor speed under start and low-speed operation

Session VP22
SPECIAL MACHINES AND GEARED MACHINES III
(Poster Virtual Session)

Kinjal Gandha, Chair
MP Materials, Fort worth, TX, United States

VP22-01. A High-Performance Flux Modulated Arc Motors with Dual-PM Excitation. *X. Yang*[1], S. Fang[1], X. Lin[1] and Q. Xu[1] *1. Southeast University, Nanjing, China*

Flux modulated permanent magnet (PM) arc motors (FMPMAM) are widely used in tanks and astronomical telescopes due to the properties of high torque at low speed [1], [2]. Dual stator FMPMAM with single PMs (SPM-FMDSAM) is proposed to improve torque density by taking fully use of the internal space [3], [4]. To further improve the output torque, multi-PMs excited FMPMAM is proposed [5], [6]. However, it suffers from the low PM utilization and high cost with complex structure. To overcome the above limitations, a novel FMPMAM with dual PMs excitation (DPM-FMDSAM) is proposed and compared with a SPM-FMDSAM as shown in Figs. 1(a) and (b). By adopting dual PMs on the inner and outer stators with reversely magnetized PMs at corresponding positions, a superimposed flux is achieved as shown in Figs. 1(c) and (d), resulting in the increases of flux density and output torque. To validate the advantages of the proposed DPM-FMDSAM, the two motors with same sizes and turns in series per phase are optimized. The finite element analysis results at the rated current of 8 A are shown in Fig. 2. The back-electromotive force (EMF) of the proposed motor is obviously higher than that of SPM-FMDSAM leading to the higher average torque. Although the torque ripple of the proposal is larger compared with that of SPM-FMDSAM due to the structure of dual PMs excitation, it is low enough to be accepted. Moreover, the torque/PM ratio of the proposed motor (0.189Nm/cm^3) is more than twice than that of SPM-FMDSAM (0.089Nm/cm^3), which enhances PM utilization and reduces cost. Therefore, the proposed DPM-FMDSAM exhibits the properties of high torque, low ripple and high torque/PM ratio, making it an ideal choice for direct drive applications. More detailed analysis and results will be introduced in the full paper.

[1] N. Tong, H. Liu, Y. Chen, et al, 2021 24th International Conference on Electrical Machines and Systems (ICEMS), Gyeongju, Korea, Republic of, 2021, pp. 1630-1635. [2] Z. Pan, S. Fang, H. Lin, et al, in IEEE Transactions on Magnetics, vol. 55, no. 7, pp. 1-10, July 2019, Art no. 8105610. [3] Z. Pan, J. Zhao, S. Fang et al, in IEEE Transactions on Transportation Electrification, vol. 9, no. 2, pp. 2509-2523, June 2023. [4] Y. Meng, S. Fang, Y. Zhu, et al, in IEEE Transactions on Applied Superconductivity, vol. 34, no. 8, pp. 1-5, Nov. 2024, Art no. 5204105. [5] N. Chen and S. Fang, 2023 IEEE International Conference on Applied Superconductivity and Electromagnetic Devices (ASEMD), Tianjin, China, 2023, pp. 1-2. [6] K. Wei, Z. Pan, J. Zhao, et al, 2023 26th International Conference on Electrical Machines and Systems (ICEMS), Zhuhai, China, 2023, pp. 1400-1403.

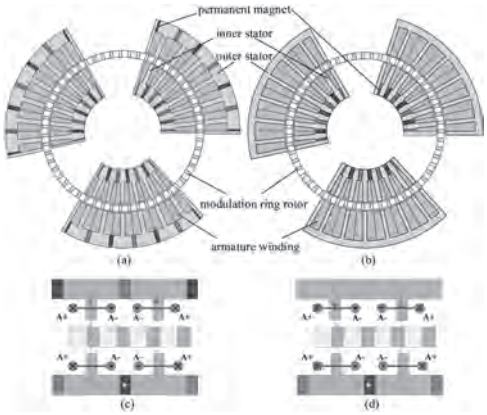

Fig. 1. Topologies and effective flux path of the motors. (a) Topologies of DPM-FMDSAM. (b) Topologies of SPM-FMDSAM. (c) Effective flux path of DPM-FMDSAM. (d) Effective flux path of SPM-FMDSAM

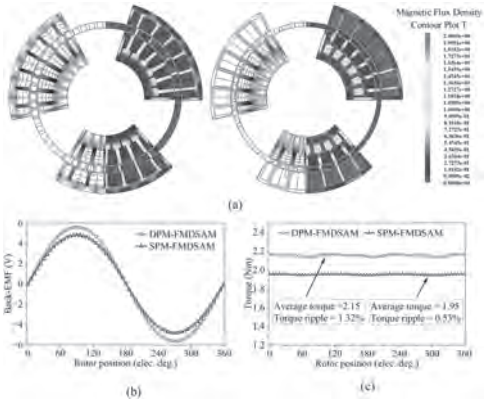

Fig. 2. The finite element analysis results of the motors. (a) Open-circuit magnetic field distribution of DPM-FMDSAM (left) and SPM-FMDSAM (right). (b) Open-circuit back-EMFs of the motors. (c) Output torque of the motors.

VP22-02. Performance Analysis and Optimization of a New Torque Enhanced Permanent Magnet Arc Machine. *X. Lin*[1], S. Fang[1] and Q. Xu[1] *1. School of Electrical Engineering, Southeast University, Nanjing, China*

The permanent magnet (PM) arc machines (PMAM) are widely used in large direct-drive scanning system like tanks and large telescopes due to the merits of high reliability and high efficiency [1], [2]. To further improve the torque density of PMAM, some concepts of dual-stator and hybrid-excited PMAM are proposed [3]. However, the structures of these machines are complex and not suitable for large scanning devices. A torque enhanced method by embedding multiple PMs in the machine has been proposed in recent years [4]. But it leads to the increase of PM usage and torque ripple. To address these problems, this paper proposes a new torque enhanced PMAM with flux-reversal and flux-switching PMs. After optimization, the proposal exhibits good electromagnetic performance of high torque with

low PM usages. The topology of the proposed PMAM is shown in Fig. 1(a). The flux-reversal and the flux-switching PMs are embedded on the stator teeth. The MFF waveforms are superimposed on each other resulting in larger working harmonics of flux density in air-gap and higher output torque as shown in Fig. 1(a). The proposed machine is comprehensively optimized and analyzed by finite element analysis (FEA) as shown in Fig. 2. The optimization results and the selected point are shown in Fig. 2(a). The back electromotive force (EMF) waveforms are symmetric with a total harmonic distortion of 0.2% at a rated speed of 600 rpm. The cogging torque is 17.6 mNm and the period is. The total average torque is 5.25 Nm at the rated current amplitude of 12 A, which is larger than the sum of the torques excited by flux-reversal (T_{PM2}) and flux-switching (T_{PM1}) PMs because the combination of two types of PMs produces a higher main working harmonics of air-gap flux density. More details about optimization and performance analysis will be addressed in the full paper.

[1] H. Hu, J. Zhao, X. Liu, et al, *IEEE Trans. Magn.*, vol. 50, no. 11, pp. 1-4, Nov. 2014. [2] Q. Xu, S. Fang, P. Wan, et al, *IEEE J. Emerg. Sel. Top. Power Electron.*, vol. 11, no. 6, pp. 6016-6027, Dec. 2023. [3] Z. Pan, J. Zhao, S. Fang, et al, *IEEE Trans Transp. Electrif.*, vol. 9, no. 2, pp. 2509-2523, June 2023. [4] Y. Meng, S. Fang, Y. Zhu, et al, *IEEE Trans Transp. Electrif.*, early access, doi: 10.1109/TTE.2024.3358392.

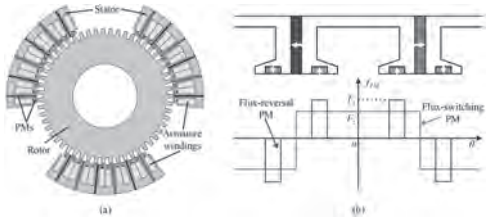

Fig. 1. Operation principle of the proposed APMM. (a) Machine topology. (b) MMF waveforms generated by two types of PMs.

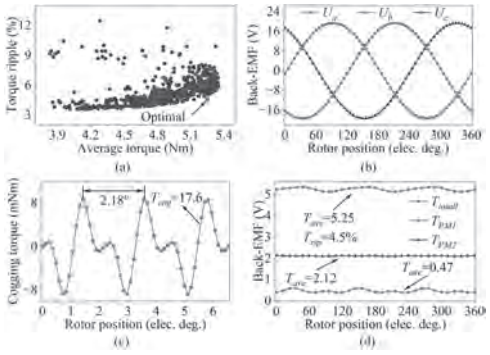

Fig. 2. FEA results. (a) Optimization results and selected point. (b) Back-EMF waveforms. (c) Cogging torque waveform. (d) Torque waveforms excited by different PMs.

VP22-03. Modeling and Suppression of Torque Ripple of Direct-Drive V-Shape Permanent Magnet Motor Considering Effects of Stator Teeth and PM Shape. D. Fan[1] and *X. Chen*[1] *1. School of Electrical and Information Engineering, Jiangsu University, Zhenjiang, China*

Recently, vernier permanent magnet motors have become competitive candidates for low-speed, high-torque direct-drive applications. In this kind of motor, by the design of three elements (PMs, flux modulators, and windings), not only fundamental airgap magnetic field harmonics would contribute to the production of motor output torque, so motor torque density can be effectively increased. However, such airgap flux harmonics would also inevitably produce additional torque pulsations, which limits the further applications of permanent magnet vernier motors. Recently, many torque ripple reduction methods have been proposed, including segmented rotor, rotor notching, and slot skewing [1], [2]. However, current publications often try to suppress torque ripple only from the perspective of flux modulators, while the influence of other elements of magnetic field modulation theory is often ignored. In this paper, torque ripple generation mechanism is analyzed analytically and a novel motor torque ripple reduction approach is proposed, in which both shapes of PMs and rotor are considered comprehensively. Fig. 1 (a) and (b) show the motor structure of the original and proposed direct-drive delta-shaped PM (DS-PM) motor respectively, and the corresponding detailed rotor topologies are presented in Fig. 1(c) and (d). As can be seen, additional harmonics are injected in the rotor and PM shape simultaneously. Fig. 2 shows the comparison of the magnetic field modulation process of two DS-PM motors. Furthermore, Fig. 3 illustrates the configuration of the shaped rotor and PM. Fig. 4 and Table I show the electromagnetic performance comparison between the original and proposed DS-PM motor. As can be seen, with the assistance of the shaped rotor and PM, while the motor average torque is almost the same, motor cogging torque and torque ripple have reduced by 81.4% and 73.7% respectively. It is indicated that, by the artful introduction of shaped rotor and PM, reduced torque ripple can be realized effectively, which provides a new research path for the design of low-torque ripple PM motors. More simulation, optimization, and experimental results will be presented in the full paper.

[1]M.Jiang,X.Zhu,Z.Xiang,S.Zheng,D.Fan,andW.Chen,"Dual-Sub-Region Rotor Design of a Permanent Magnet Hub Motor with Enhanced Speed Regulation and Output Torque for Electric Vehicles," *IEEE Transactions on Industrial Electronics*, doi: 10.1109/TIE.2024.3370946. [2] L. Fang, D. Li, X. Ren, and R. Qu, "A Novel Permanent Magnet Vernier Machine with Coding-Shaped Tooth," *IEEE Transactions on Industrial Electronics*, vol. 69, no. 6, pp. 6058-6068, June 2022, doi: 10.1109/TIE.2021.3088331.

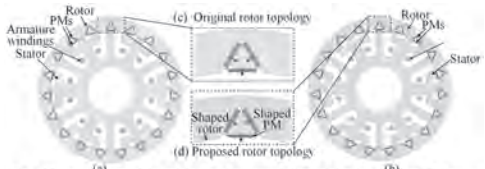

Fig. 1 Motor topology of the original and proposed direct-drive delta-shaped PM motor

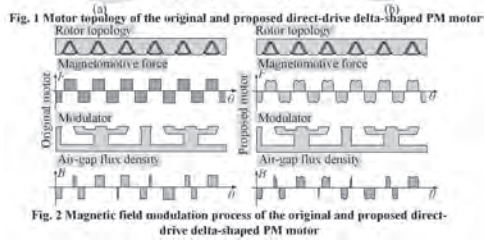

Fig. 2 Magnetic field modulation process of the original and proposed direct-drive delta-shaped PM motor

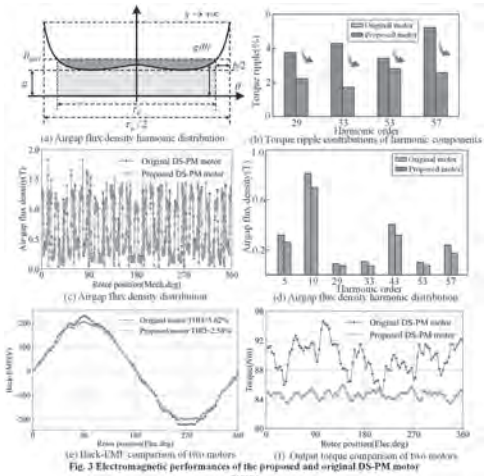

Fig. 3 Electromagnetic performances of the proposed and original DS-PM motor

TABLE I
ELECTROMAGNETIC PERFORMANCE COMPARISON BETWEEN THE ORIGINAL AND PROPOSED DS-PM MOTORS

Items	Original motor	Proposed motor
THD of back-EMF	5.62%	2.58%
Amplitude of back-EMF	213.2V	193.9V
Cogging torque	7.80Nm	1.455Nm
Average output torque	89.71Nm	84.625Nm
Torque ripple	16.25%	2.95%
Iron loss	282.6W	268.8W

VP22-05. Low-Torque-Ripple Bi-Directional Magnetic Field Modulation PM Motor considering Magnetic Motive Force Distribution Perspective.
D. Fan[1], H. Tian[1] and W. Shan[1] *1. School of Electrical and Information Engineering, Jiangsu University, Zhenjiang, China*

In recent years, bi-directional magnetic field modulation (BD-MFM) motors have attracted considerable attention, due to their inherent advantage of high torque density. However, the bi-directional magnetic field modulation structure often leads to unavoidable high torque ripple and flux leakage[1]-[2]. Therefore, it has been a challenge issue on how to further reduce the torque ripple of BD-MFM motors while maintaining the high torque. In this paper, a novel trapezoidal-shaped PM BD-MFM motor is proposed, the contribution of the proposed motor is presented as follows. Firstly, the relationship among the cogging torque harmonics, airgap flux harmonics, and torque harmonics is investigated. Then, the magneto-motive force of the stator permanent magnets is investigated in detail considering stator PM topology. Finally, to minimize magnetic leakage and cogging torque, the trapezoidal PM structure and rotor magnetic barrier are designed. It provides an effective research path to realize the low-torque-ripple design of BD-MFM motors. Fig. 1(a) illustrates the structures of the proposed trapezoidal PM BD-MFM motor, the reference BD-MFM motor I, and the reference BD-MFM motor II. The reference motor and the proposed motor have the same structure size and permanent magnet dosage. Fig. 1(b) shows the modulation process of the stator-PM MMF and rotor-PM MMF respectively. Fig. 2(a) shows the comparison of the magnetic field distribution and leakage analysis between the proposed trapezoidal PM BD-MFM motor and the reference BD-MFM motor II, and it can be found that the magnetic flux leakage at the airgap is significantly reduced. Fig. 2(b)-(d) shows the comparison results of electromagnetic performances of three motors, including cogging torque, airgap flux density, and output torque. It is noted that the proposed trapezoidal PM BD-MFM motor torque is increased by 4.9 Nm and the torque ripple is reduced by more than 70% which verifies the reasonability and effectiveness of the proposed trapezoidal PM BD-MFM motor. More detailed analysis and experimental verification will be presented in the full paper.

[1] W. Zhao, Q. Hu, J. Ji, Z. Ling, and Z. Li, "Torque Generation Mechanism of Dual-Permanent-Magnet-Excited Vernier Machine by Air-Gap Field Modulation Theory," *IEEE Transactions on Industrial Electronics*, vol. 70, no. 10, pp. 9799-9810, Oct. 2023. [2] H. Huang, D. Li, X. Ren, and R. Qu, "Analysis and Reduction Methods of Cogging Torque in Dual PM Vernier Machines with Unevenly Distributed Split Teeth," *IEEE Transactions on Industry Applications*, vol. 58, no. 4, pp. 4637-4647, July-Aug. 2022.

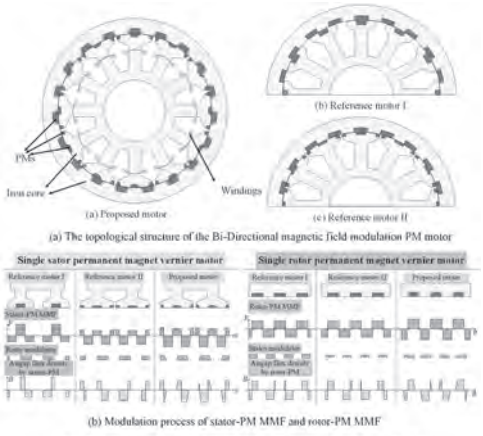

Fig. 1. Motor structure, modulation process of permanent magnet MMF

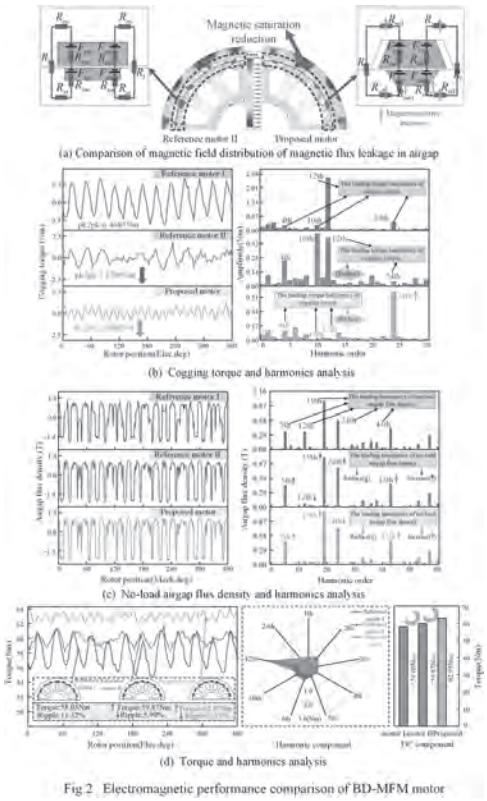

Fig.2 Electromagnetic performance comparison of BD-MFM motor

VP22-06. A Novel Cylindrical Laminated Rotor for High-Speed Homopolar Inductor Machine.
Q. Li[1], J. Yang[1], Y. Jiang[1] and S. Huang[1] *1. College of Electrical and Information Engineering, Hunan University, Changsha, China*

Affected by the unipolar air gap flux density, the power density of the homopolar inductor machine (HIM) is lower than the traditional permanent magnet synchronous machine [1]. The 3-D topology of HIM and its excitation magnetic circuit are as shown in Fig. 1. The main components of HIM include the shell, segmented stator, AC winding, DC field winding and a solid rotor. Under the action of the magnetic field generated by the field winding, the no-load excitation magnetic circuit of the HIM is shown in Fig. 1(b), and its unilateral air-gap flux density has the characteristics of unipolarity. The rotation of the rotor causes the excitation flux to cut the armature windings, which in turn generates a symmetrically distributed back-EMF. The integrated solid rotor of HIM can be rotated at very high speed, which often used as an effective way to improve the power density [2]. However, severe high-frequency eddy current losses and windage losses during high-speed operation would be produced due to the integrated salient-pole rotor of HIM, seriously affecting the operating efficiency. Aiming at this problem, a novel cylindrical laminated rotor for HIM is proposed by this paper to suppress the high-frequency eddy current loss and windage loss generated by the integrated rotor at high speed, as shown in Fig. 2(a) and (b). To verify the loss suppression performance of the rotor proposed in this paper, the influence of the parameters of the cylindrical laminated rotor on the HIM output performance is studied based on FEA. Finally, a 30kW-30,000rpm HIM with cylindrical laminated rotor is manufactured, as shown in Fig. 2(c), and the rationality of FEA is demonstrated by experiments. After the cylindrical rotor is axially segmented, the high-frequency eddy current loss on the rotor can be suppressed by 88.37%. By introducing the rotor bridge, the windage loss can be suppressed by 87.14%, as shown in Fig. 2(d). The suppression of eddy current loss and high-speed windage loss can effectively promote the application of HIM in fields such as flywheel energy storage.

[1] J. Yang, C. Ye, G. Liu, X. Liang, W. Xu and X. Wang, "Research on the No-Load Rotor Eddy Loss of a High-Speed Pulsed Alternator," in IEEE Transactions on Plasma Science, vol. 45, no. 7, pp. 1213-1219, July 2017. [2] Q. Li, J. Yang, J. Yu, P. Zhang, X. Zhao and S. Huang, "Investigation and Suppression of Electromagnetic Vibration of Permanent Magnet Homopolar Inductor Machine," in IEEE Transactions on Industrial Electronics, doi: 10.1109/TIE.2024.3404120.

Fig. 1

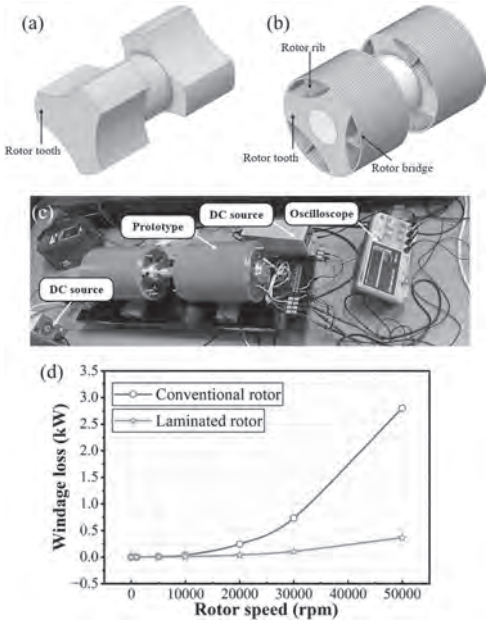

Fig. 2

VP22-07. An Axial Parallel Memory Machine with DC Bias Adjustment Flux Capability. *L. Qin*[1], H. Yang[2] and S. Fang[2] *1. Tongji University, Shanghai, China; 2. Southeast University, Nanjing, China*

I.Introduction The traditional stator PM memory machines (MM) are basically geometrically characterized by a re/demagnetization winding surrounded by the low coercive force (LCF) PM [1-3]. This type of winding is applied the pulse current to adjust the magnetization state of LCF PM. However, these windings can only be used in the re/demagnetization operation, but do not have other functions in normal working condition. In order to improve the space utilization, the MM with DC bias adjustment flux capability is proposed [4]. However, the working point of LCF PM is still easily affected by high CF (HCF) PM, leading to low overload capability. Herein, a new axial parallel MM with DC bias adjustment flux capability (DCB-AXMM) is proposed. The DCB-AXMM utilizes an integrated winding to generate DC bias magnetizing current pulse to change the MS of the LCF PMs. II. Topology and Electromagnetic Performances Fig. 1 shows the topology of the DCB-AXMM. The proposed machine consists of three sub-machines, i.e., Part I, Part II and Part III, respectively. They share the same stator/rotor combinations. The PMs in the Parts I and III sub-machines utilize the N42SH (HCF PM), which are magnetized in the opposite direction. The PMs in the Parts II and III sub-machines are magnetized in the same direction and the PM in Part II are AlNiCo9 (LCF PM). The rotors of Parts II and III sub-machines have no offset, while the rotor of Part I sub-machine is shifted 45° mechanical angle compared to that of the Part II and Part III sub-machines. The integrated windings are wrapped around the stator poles. Fig. 2(a) shows the no-load back-EMF at flux-enhanced(FM) and zero-magnetization (ZM) levels. The total harmonic distortion (THD) of back-EMF in different magnetization levels are 12.4% and 8.9%, respectively. Fig. 2(b) shows the steady-state torque under different magnetization levels. As shown in Fig. 2(b), the torque profiles under different MSs experience a clear vibration which indicates that the output torque can be flexibly adjusted by applying different magnitudes of zero-sequence magnetization current pulse. The details will be addressed in the full paper.

[1]W. Li, K. T. Chau, Y. Gong, J. Z. Jiang and F. Li. A new flux-mnemonic dual-magnet brushless machine. *IEEE Trans. Magn.,* vol. 47, no.10, pp:4223-4226, 2011. [2]F. Li, K. T. Chau, C. Liu and C. Qiu. "New approach for pole-changing with dual-memory machine". *IEEE Trans. Appl. Supercon.*, 2014, 24(3):1-4, Art no. 0501504. [3]H. Yang, H. Lin, S. Fang, Z. Q. Zhu and Y. Huang. "Flux-regulatable characteristics analysis of a novel switched-flux surface-mounted PM memory machine". *IEEE Trans. Magn.*, vol. 50, no.11, Nov. 2014. [4]L. Qin, H. Yang, S. Fang, H. Lin, Z. Pan and Y. Meng, "Design and Investigation of a hybrid stator pole memory machine with DC bias magnetization capability". *IEEE Trans. Appl. Supercon.*, vol. 31, no. 8, pp. 1-5, Nov. 2021, Art no. 5205005.

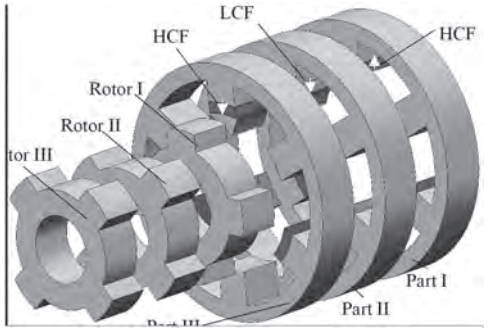

Fig.1. DCB-AXMM topology

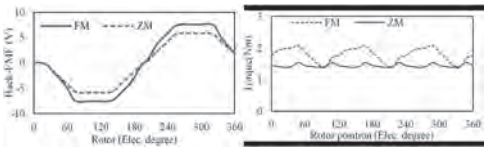

Fig.2. Electromagntic performances

VP22-08. Design and Optimization of a High Torque Density Dual Permanent Magnet Excited Vernier Machine with Non-Uniformly Distributed Stator Tooth. *A. Chen*[1], L. Quan[1], Z. Xiang[1] and D. Fan[1] *1. School of Electrical and Information Engineering, Jiangsu University, Zhenjiang, China*

In recent years, permanent magnet vernier machines (PMVMs) have been studied by researchers because of their high torque density, benficial from their so-called flux modulation effect [1]. The dual permanent magnet excited (DPME) machine, with PMs in both the stator and rotor often exhibits a higher torque density than conventional single-side PMVMs [2]. Due to the additional auxiliary permanent magnets on both sides, the torque ripple is also relatively high. And the variation relationships between the leading working harmonics and key parameters are diverse, which exists a certain extent of design conflicts in the process of optimization design. Consequently, it has been a hot but challenging issue on how to further motor torqe density and maintain relatively low torque ripple. In this paper, in order to improve motor output torque and reduce torque ripple simultaneously, a split-tooth DPME machine with non-uniformly distributed stator tooth is proposed and designed purposefully. Fig. 1 shows the proposed DPME machine and geometry parameters. The modulation generation process with SPM or RPM is exhibited in Fig. 2. The airgap flux density waveform and spectra for the RPM-DPME and SPM-DPME are shown in Fig.3. Fig.4 shows the influence of dual-PM pole arc factor on back EMF and flux linkage. The leading working harmonics variation trend are shown in Fig. 5. Fig. 6

shows the optimized machine magnetic field distributions. Fig. 7 shows the no-load back-EMF waveforms of the initial and optimal model. It can be seen that based on the optimization design, the fundamental is increased from 125.5 to 145.7 V. Fig.8 shows the torque performances of initial and optimal models. The peak-to-peak value of the cogging torque in optimal model is reduced 46.1%, and the average output torque is improved by around 28.1% as compared with the initial model. It is noted that, with the assistance of the proposed non-uniformly distributed stator tooth, increased output torque and reduced torque ripple can be realized effectively. More detailed analysis and experimental verification will be presented in the full paper.

[1] M. Cheng, P. Han, and W. Hua, "A general airgap field modulation theory for electrical machines," IEEE Trans. Ind. Electron., vol. 64, no. 8, pp. 6063–6074, Aug. 2017. [2] Y. Gao and M. Doppelbauer, "Comparative analysis of double flux modulation flux reversal machines with PMs on both stator and rotor," in Proc. IEEE Int. Conf. Elect. Mach., 2020, pp. 1964–1970.

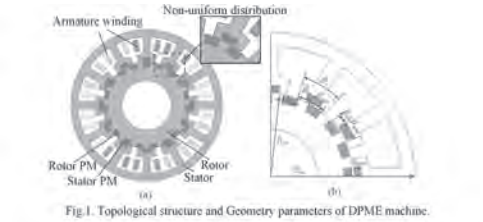

Fig.1. Topological structure and Geometry parameters of DPME machine.

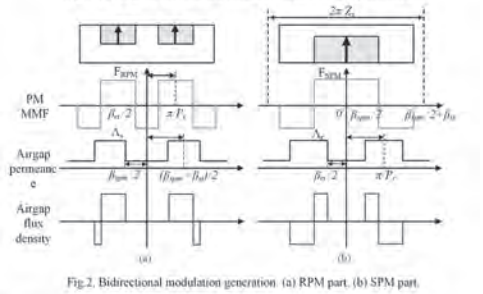

Fig.2. Bidirectional modulation generation. (a) RPM part. (b) SPM part.

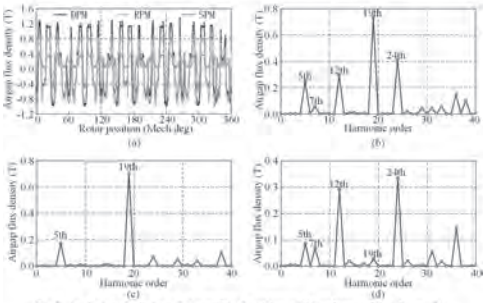

Fig.3. Analysis calculation of airgap flux densities.(a) Waveforms of the airgap. (b) Harmonic characteristics of the DPM airgap (c) Harmonic characteristics of the RPM airgap. (d) Harmonic characteristics of the SPM airgap.

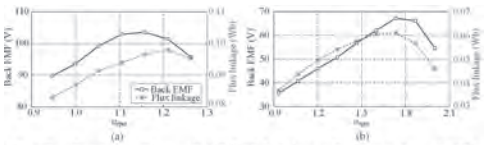

Fig.4. The influence of α_{rpm} and α_{spm} on back EMF and flux linkage. (a)The influence of α_{rpm} under RPM excited. (b)The influence of α_{spm} under SPM excited.

Fig.5. The influence of α_{rpm} and α_{spm} on airgap harmonic. (a)The influence of α_{rpm} under RPM excited. (b)The influence of α_{spm} under RPM excited.

Fig.6. Magnetic field distributions.

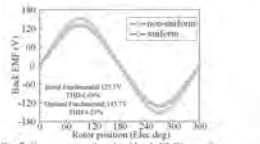

Fig. 7. Comparison of no-load back-EMF waveforms.

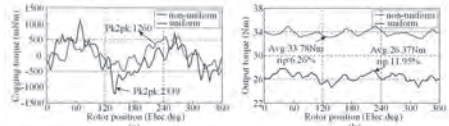

Fig.8. Torque performances of initial and optimal models. (a) Cogging torque of initial and optimal models. (b) Output torque of initial and optimal models.

VP22-09. Power Factor Enhancement Design and Optimization of Variable Leakage Flux Permanent Magnet Motor Considering Driving Cycles. *X. Zhou*[1] and Z. Xiang[1] *1. School of Electrical and Information Engineering, Jiangsu University, Zhenjiang, China*

I. Introduction Recently, variable leakage flux permanent magnet (VLF-PM) motors have attracted more and more attention in electrical vehicles field due to their merits of high efficiency and high reliability [1]. And yet, due to the uncontrollable leakage flux, the VLF-PM motors suffer from the relatively low power factor at diverse operation conditions, especially at heavy load condition. Hence, how to improve power factor of VLF-PM motors under the complicated operation conditions has become a hot issue. Recently, the spoke-type PM and consequent-pole PM structure are employed to improve air-gap flux density, so as to improve power factor [2]. Yet, the high torque ripple is inevitable. Besides, the current angle of the motor can be increased by designing magnetic reluctance, so as to improve power factor. Yet, the torque reduction is inevitable. In this paper, the design concept of variable-saliency-ratio enhancement is proposed in VLF-PM motor to improve power factor. Moreover, to further improve power factor, the multi-conditions optimization method is employed. II. Power factor enhancement at multiple operation conditions Fig. 1 shows the principle of power factor enhancement of VLF-PM motor considering driving cycles. Obviously, Fig. 1(c) exhibits the relationship between power factor and saliency ratio of VLF-PM motor at various driving conditions. It can be noted that, at low-speed condition, if the positive-saliency-ratio inverse degree K_{DL+} is lager, the PM flux, the power factor, and output torque can be increased. At high-speed condition, if the negative-saliency-ratio inverse degree K_{DL-} is slightly larger, the current angle and power factor can be increased. III. Motor design and results Fig.2 shows the VLF-PM motor design, optimization and performances validation. Obviously, Fig. 2(a) shows the flux path oriented design of VLF-PM motor for power factor enhancement. It can be seen that, by adding multilayer flux barriers along q-axis, the larger K_{DL+} and larger K_{DL-} can be realized to improve power factor. Besides, the measured power factor map is shown in Fig. 2(d), and the distribution meets the design demands. More theoretical analysis and experimental results will be presented in the full paper.

[1] L. Xu et al., "Flux-leakage design principle and multiple-operating conditions modeling of flux leakage controllable PM machine considering driving cycles," *IEEE Trans. Ind. Electron*., vol. 69, no. 9, pp. 8862-8874, Sept. 2022. [2] S. Stipetic, D. Zarko and N. Cavar, "Adjustment of rated current and power factor in a synchronous reluctance motor optimally designed for maximum saliency ratio," *IEEE Trans. Ind. Appl*., vol. 56, no. 3, pp. 2481-2490, May-Jun. 2020.

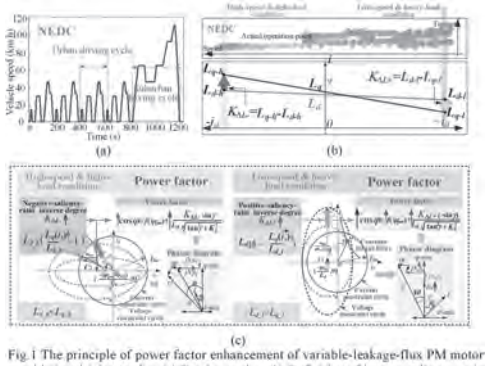

Fig. 1 The principle of power factor enhancement of variable-leakage-flux PM motor considering driving cycles. (a) Driving cycles. (b) Definition of inverse-saliency-ratio degree. (c) The relationship between saliency ratio characteristic and power factor at different operation conditions.

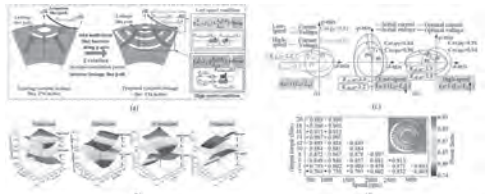

Fig. 2 Motor design and optimization. (a) The flux path oriented design under different operation conditions for power factor improvement. (b) The IRSs under different operation conditions. (c) The relationship between inverse-saliency-ratio degree and power factor at different operation conditions. (d) The measured power factor map under different operation conditions.

Session VP23
SPIN-ORBITRONICS: DMI, SOT MRAM AND ENERGY EFFICIENT SWITCHING (Poster Virtual Session)

Yufan Li, Chair
The Chinese University of Hong Kong, Sha Tin, Hong Kong

VP23-01. Orbitronics for Energy-Efficient Magnetization Switching.
Y. Yao[1], D. Zhu[1] and W. Zhao[1] *1. School of Integrated Circuit Science and Engineering, Beihang Univerisity, Beijing, China*

Spin-orbit torque (SOT), as a promising writing method for magnetic random-access memory (MRAM), has garnered widespread interest for over a decade [1,2]. Heavy metals, such as β-W, have been broadly adopted as spin current sources, but suffer from a drastic drop of charge-to-spin conversion efficiency at a limited thickness [3]. This poses challenges for simultaneously satisfying SOT efficiency, etching-stop margins, and back-end-of-line (BEOL) compatibility. Orbitronics brings new opportunities for addressing these issues by bringing novel material options [4,5]. Here, we systematically investigate the charge-to-spin conversion efficiency θ_H in X/Pt/CoFeB/MgO multilayers (X = Ta, Cr, W, Ru are chosen due to their predicted large orbital Hall conductivity [6]). We report an enhanced θ_H of 0.168 in Ta/Pt/CoFeB and θ_H of 0.1 in Ru/Pt/CoFeB compared to the Pt, attributed to the large orbital Hall effect (OHE). The quantified θ_H for Cr/Pt and W/Pt SOT bilayers is smaller than that of Pt(10) when the thickness of X and Pt layers are fixed to 8 nm/2 nm, as shown in Fig. 1, because of the orbital current may not saturate in the limited thickness [7,8]. We also show that the Ta/Pt bilayer can achieve efficient current-induced magnetization switching in Ta(8-12 nm)z/Pt(2 nm)/Co(0.65 nm) heterostructures with perpendicular magnetic anisotropy. The switching current density J_c for the device with t_{Ta} = 11.7 nm is only ~1.3×10^{11} A/m^2, as shown in Fig. 2. For the switching current I_c, it firstly increases with t_{Ta} because the SOT channel becomes thicker, and then decreases because of the increased θ_H. Consequently, the I_c for Ta(8)/Pt(2) and Ta(12)/Pt(2) remains nearly the same, thus helping solve the etching-stop issue. Further, the Hall-bar devices were post-annealed at 400°C for 30 minutes. The SOT-induced switching remains robust, and the J_c is just slightly increased though the anisotropic field is substantially enhanced to over 0.9 T, which is of practical interest for BEOL-compatible SOT-MRAM. Our results shed light on the development of high-performance SOT-MRAM leveraging the freedom of orbital angular momentum.

1. Z. Guo, et al., Proceedings of the IEEE, Vol. 109, p. 1398-1417 (2021) 2. Y. Yao, et al., Materials Futures, Vol. 2, p. 032302 (2023) 3. C. Pai, et al., Applied Physics Letters, Vol. 101, p. 122404 (2012) 4. D. Lee, et al., Nature Communications, Vol. 12, p. 6710 (2021) 5. Y. Choi, et al., Nature, Vol. 619, p. 52-56 (2023) 6. L. Salemi, P. Oppeneer, Physical Review Materials, Vol. 6, p. 095001 (2022) 7. H. Hayashi, et al., Communications Physics, Vol. 6, p. 32 (2023) 8. S. Lee, et al., Communications Physics, Vol. 4, p. 234 (2021)

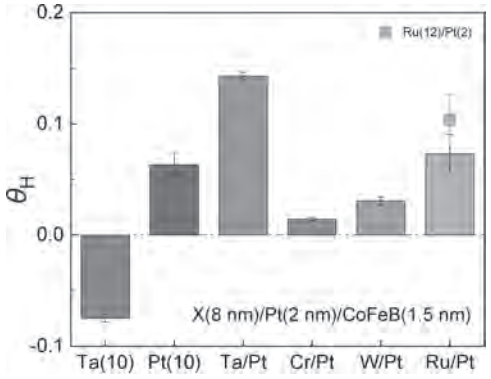

Figure 1. Comparison of θ_H of different X/Pt bilayers.

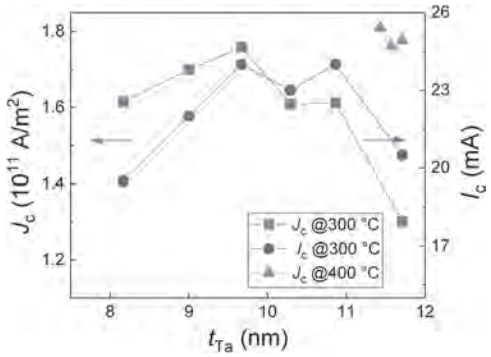

Figure 2. J_c and I_c for Ta/Pt bilayer SOT channels.

VP23-03. Design of memory compiler for non-volatile embedded SOT-MRAM.
H. Lin[1] and Y. Jiang[1] *1. Jiangnan University, Wuxi, China*

Spin-Orbit Torque Magnetic Random Access Memory (SOT-MRAM) shows outstanding durability and switching speed, with the merits of non-volatile and low power consumption. The separation of the read and the write paths enables it to have excellent read and write accuracy rates, attracting many attentions from both academic and industrial communities[1-2]. However, the design of SOT-MRAM is still not included in EDA tools. It would take a lot of time to meet specific requirements in the system design. In order to improve the efficiency of memory research and shorten the memory design cycle, memory compilers are widely used in various fields of integrated circuit design, mainly relying on the regular array structure of memory[3-4]. The corresponding memory circuit design and layout can be automatically generated by the memory compiler according to user-defined specifications and parameters, such as word length and operating voltage. Personalized memory designs can be provided rapidly. The design efficiency can be greatly improved, and various performance indicators of the memory can also be effectively assisted by researchers for optimization. While common memory compilers are very mature in dealing with SRAMs, the support for the technology of non-volatile memories is insufficient, especially for SOT-MRAM. A memory compiler for SOT-MRAM is designed in the paper. With specific constraints, the random access memories with a

maximum word line length of 8 and their peripheral circuits can be generated with the designed compiler. Also, the detailed design documents and reports are provided, including layout information, performance parameters, power consumption information, etc., which are helpful for users to understand and evaluate the generated MRAM memory design. The information is very helpful to explore the next-generation memory architectures and optimization techniques. Fig. 1 is the cell circuit and layout of SOT-MRAM. Fig. 2 shows the structure of SOT-MRAM.

[1] K. Garello, F. Yasin and G. S. Kar, 2019 IEEE 11th International Memory Workshop (IMW),Vol. 1-4(2019). [2] M. Baumgartner, K. Garello, J. Mendil, C. O. Avci, E. Grimaldi, C. Murer, J. Feng, M. Gabureac, C. Stamm, Y. Acremann, S. Finizio, S. [3] Wintz, J. Raabe and P. Gambardella, Nature Nanotechnology, Vol. 12, p.980-986(2017). [4] Y. Xu, Z. Gao and X. He, 2007 IEEE International Symposium on Circuits and Systems (ISCAS),Vol. 3756-3759(2007). [5] S. Wu, X. Zheng, Z. Gao and X. He, 13th IEEE Symposium on Design and Diagnostics of Electronic Circuits and Systems, Vol. 123-124(2010).

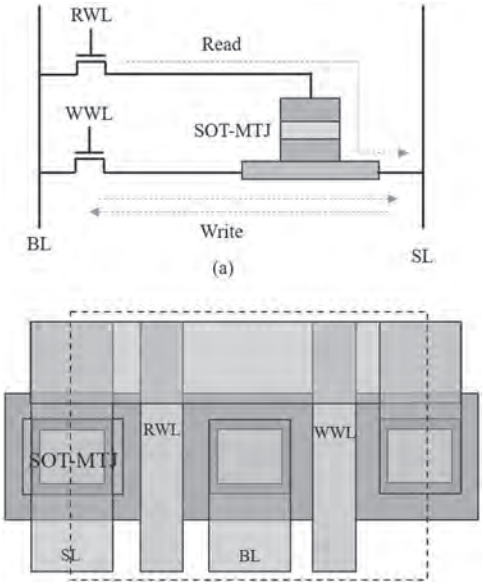

Figure 1. (a)SOT-MRAM cell circuit. (b)cell layout.

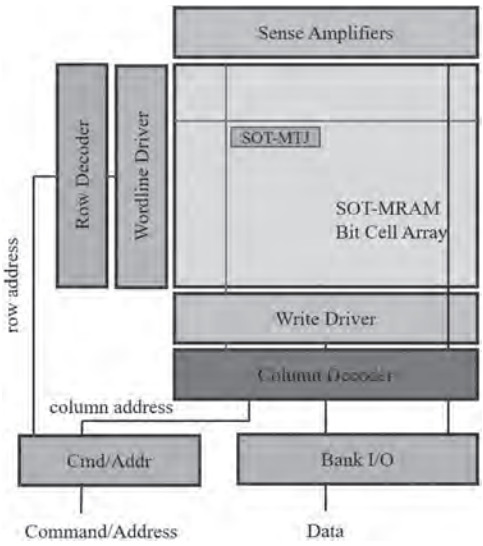

Figure 2. Schematic structure of SOT-MRAM.

VP23-04. 3-D MRAM memory compiler for high density memory design with TSVs interconnection. H. Lin[1] and *Y. Jiang*[1] *1. Jiangnan University, Wuxi, China*

Spin-transfer torque (STT) magnetic random access memory (MRAM) has entered into the consumer market, and is regarded as a promising candidate for applications such as artificial intelligence (AI) and Internet of Things (IoTs). Embedded STT-MRAM has been mass-produced by several semiconductor foundries to replace the embedded NOR flash at specific technology nodes[1]. To keep the pace of Moore's Law in the field of circuit scaling, through-silicon via (TSV) is introduced into vertical integrated circuits. In this way, 3-D stacking ICs with high density can be prepared [2]. This 3-D stacking structure can save the chip area, reduce the power consumption, and increase the speed. To improve the performance of STT-MRAM, 3-D architecture is a promising solution for the practical application in SoC system. In the paper, 3-D STT-MRAM compiler is proposed and fulfilled. At present, several memory compilers for static random access memory (SRAM) are reported, which are very helpful to expedite the design process and shorten the design time. Even the 3-D stacking function is already supplemented in SRAM compiler[3]. However, no report on 3-D memory compiler is published until now. In this paper, the 3-D STT-MRAM compiler is designed and reported. In the designed compiler, the TSV structure is added in the MRAM compiler. The generated structure based on the compiler shows the stacked layers, in which TSVs are included to act as the interconnections among the different layers. With the designed structure, the impact of the stacking on the performance such as the area and power consumption of 3-D STT-MRAM is analyzed. Fig.1 shows the workflow diagram of the memory compiler. Fig.2 shows the schematic of 3-D stacking SOT-MRAM.

[1] S. Salahuddin, K. Ni and S. Datta, Nature Electronics, Vol. 1, p.519-519(2018). [2] K. Flamm, Ewing Marion Kauffman Foundation Research Paper Series, (2018). [3] D. Kim, E. Lee, J. Seo, J. Kim, S. K. Lim and S. Mukhopadhyay, IEEE Journal on Exploratory Solid-State Computational Devices and Circuits, Vol. 7, p.106-114(2021).

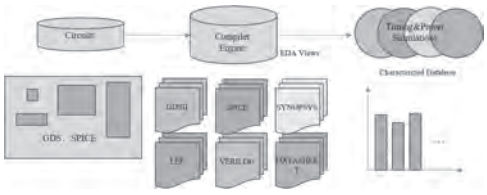

Figure 1. Workflow diagram of the memory compiler.

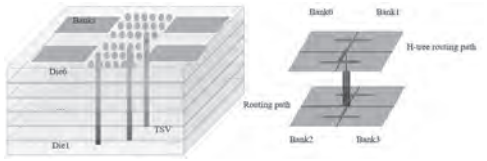

Figure 2. Schematic of 3-D stacking SOT-MRAM.

VP23-05. Research and Design of Hierarchical Cache with Mixed SOT- and STT-MRAM in Multi-core CPU Environments. *Y. Dai*[1] and Y. Jiang[1] *1. Jiangnan University, Wuxi, China*

In modern CPU system, the number of computational cores is increased, which can effectively enhance the computing capability. However, the performance gained from on-chip caches in single-core versus multi-core scenarios is not always linearly increased. Substituting static random-access memory (SRAM) with magnetic random-access memory (MRAM) in computational systems can improve cache performance since MRAM shows the merits of low power, non-volatile and high density, etc.. In this paper, based on the Reduced Instruction Set Computer-Five (RISC-V) instruction set framework, a novel simulation strategy is employed to evaluate the performance of a multi-core hybrid cache system (L1, L2, and L3

caches). By comparing the performance of Spin-Transfer Torque MRAM (STT-MRAM), Spin-Orbit Torque MRAM (SOT-MRAM), and SRAM in a multi-core environment, an octa-core CPU system with a three-tier cache structure is proposed, in which SOT-MRAM and STT-MRAM are used to replace L2 and L3 caches, respectively. Additionally, the cache coherence protocol of the optimized architecture is tailored for magnetic memory components in an eight-core CPU system. Simulation results demonstrate that this hybrid cache system achieves 54.96% leakage power savings and 22.53% overall power savings compared to SRAM. The evaluation of the hybrid cache system aligns closely with real-world requirements and exhibits scalability.

[1]Saha, Rajesh, Yogendra Pratap Pundir, and Pankaj Kumar Pal. "Comparative analysis of STT and SOT based MRAMs for last level caches." Journal of Magnetism and Magnetic Materials 551 (2022): 169161. [2]F. Hameed and J. Castrillon, "A novel hybrid DRAM/STT-RAM last-level-cache architecture for performance, energy, and endurance enhancement," IEEE Trans. Very Large Scale Integr. (VLSI) Syst., vol. 27, no. 10, pp. 2375–2386, Oct. 2019. [3]E. Cheshmikhani, H. Farbeh and H. Asadi, "A System-Level Framework for Analytical and Empirical Reliability Exploration of STT-MRAM Caches," in IEEE Transactions on Reliability, vol. 69, no. 2, pp. 594-610, June 2020, doi: 10.1109/TR.2019.2923258. [4]Gao, L., Wang, R., Xu, Y. et al. SRAM- and STT-RAM-based hybrid, shared last-level cache for on-chip CPU–GPU heterogeneous architectures. J Supercomput 74, 3388–3414 (2018).

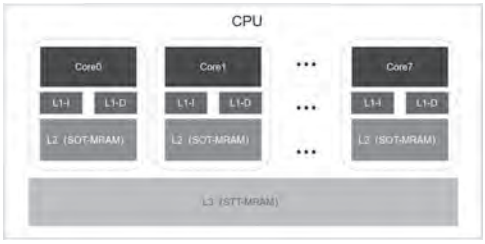

Fig. 1: Structure block diagram of hybrid-MRAM hierarchical cache.

Fig. 2: SOT-MRAM and STT-MRAM

VP23-06. Stable Data Store Operation in Magnetic Nanowire Memory with Stepped Structures Observed by Magneto-optical Kerr Effect Microscopy. *D. Kato*[1], K. Ogura[1], N. Kinoshita[1] and Y. Miyamoto[1]
1. Science & Technology Research Labs., NHK, Setagaya, Japan

We have been studying the magnetic nanowire (NW) memory, which uses current-driven domain wall motion to shift the written magnetic domains, to achieve ultra-high data transfer rate for future "immersive media" storages. In our previous work[1], we tried to install periodic ratchet trap sites along NW for the constant domain shift. However, since these ratchets induced the Bloch domain wall mode and their trapping energy was too high, the uniform shift of domains was obstructed. While the NW with stepped structures exhibited the chiral domain wall mode and offered the prospect of achieving a constant domain shift length[2]. In this study, we report the successful memory operation in the stepped NW observed by magneto-optical Kerr effect microscopy (MOKE). Fig.1 shows a microscopic image of the fabricated NW memory device. To define the unit shift length, periodic SiN(4) steps with a width of 3 μm and a pitch of 6 μm were formed under the NW consisting of Pt(3)/$[Co(0.35)/Tb(0.85)]_4$ (units in nm). The width of the NW was 3 μm. A writer for forming domains was placed orthogonally to the NW with the insertion of an insulating layer. The experimental procedure is as follows: 0. initialize (the magnetic direction in NW is set downward by an external field of 1kOe), 1. write (a bidirectional field is generated by a current applied to a writer, which forms domains in NW), 2. drive (the written domains are shifted along NW by a drive current) By repeating write and drive, sequential binary data is stored in NW. The current density for write and drive was set to 4.1 and 9.0 MA/cm^2, respectively. We tried to store 7-bits consisting of "1101110" data queue in the NW as illustrated in Fig.2(a). Fig.2(b) shows the MOKE image of the data-stored NW, where the dark and bright regions correspond to "0" and "1", respectively, and that 7-bits of data could be regularly stored by defining the domain length and shift length at intervals of the stepped structures under the NW. These results suggest that binary information can be stored in this memory structure in a first-in-first-out manner.

[1]M. Takahashi *et al*.: MMM2022, IPA-05 (2022) [2]D. Kato *et al*.: MMM2023, DG-06 (2023)

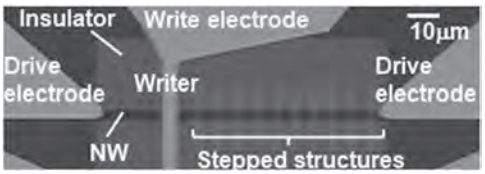

Fig.1 Fabricated magnetic NW memory with stepped structures

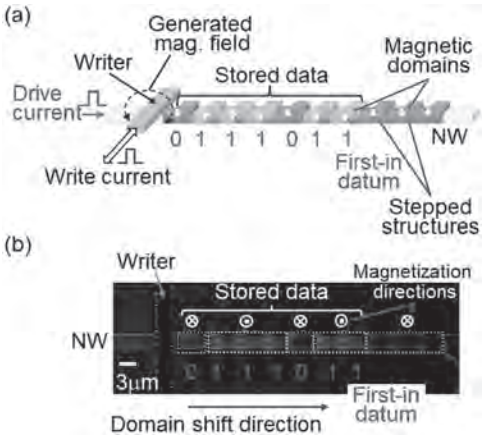

Fig.2 (a)Schematic illustration and (b)MOKE image of stored 7-bits in NW memory

VP23-07. Monte Carlo Simulation on Spinterface's Atomic Migration in SOT-MTJ Device. *Y. Yuan*[1] and Y. Jiang[1] *1. Jiangnan University, Wuxi, China*

In recent years, as one of the most representative MTJ devices, spin orbit torque (SOT) MTJ is regarded as a key direction for the development of MRAM[1]. However, atomic diffusion and migration behaviors commonly occur at the heterojunction spinterfaces, which show obvious impact on the device and should be included in the characterizations of the device. In this study, an innovative computational approach that includes the migration of oxygen and metal atoms at the spinterfaces within SOT-MTJ is proposed. Here, the spinterfaces include the interface between the free layer (FL) and the oxide layer, as well as that between the FL and the heavy metal (HM) layer[2]. Utilizing Monte Carlo simulation, a simulation tool that models atomic migration at these heterojunctions is constructed. This tool innovatively applies the backward propagation of variance (BPV) technique[3] to both corner and statistical models, which is effective to link the electrical characteristics of SOT-MTJ device with the manufacturing process variations. Based on the simulation tool, it reveals the effect of the atomic migration on the electrical performance of the MTJ device. More specifically, the atomic mechanisms related to the substantial variability observed in Tunnel Magnetoresistance (TMR) values[4] of SOT-MTJ is discussed based on the simulation results, offering detailed insights at the atomic level into this pivotal phenomenon. This comprehensive understanding paves the way for improvements in SOT device reliability and performance.

[1] Y. Wang, Y. Zhang, E. Y. Deng, J. O. Klein, L. A. B. Naviner, and W. S. Zhao, "Compact model of magnetic tunnel junction with stochastic spin transfer torque switching for reliability analyses," Microelectron. Reliab., vol. 54, no. 9–10, pp. 1774–1778, Sep. 2014, doi: 10.1016/j.microrel.2014.07.019. [2] Z. Wang et al., "Atomic-Scale Structure and Local Chemistry of CoFeB–MgO Magnetic Tunnel Junctions," Nano Lett., vol. 16, no. 3, pp. 1530–1536, Mar. 2016, doi: 10.1021/acs.nanolett.5b03627. [3] C. He, J. Victory, Y. Xiao, H. D. Vleeschouwer, E. Zheng, and Z. Hu, "SiC MOSFET Corner and Statistical SPICE Model Generation," in 2020 32nd International Symposium on Power Semiconductor Devices and ICs (ISPSD), Vienna, Austria: IEEE, Sep. 2020, pp. 154–157. doi: 10.1109/ISPSD46842.2020.9170091. [4] Y. Ke, K. Xia, and H. Guo, "Oxygen-Vacancy-Induced Diffusive Scattering in Fe / MgO / Fe Magnetic Tunnel Junctions," Phys. Rev. Lett., vol. 105, no. 23, p. 236801, Nov. 2010, doi: 10.1103/PhysRevLett.105.236801.

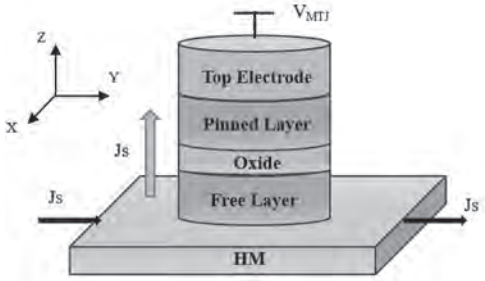

Fig. 1

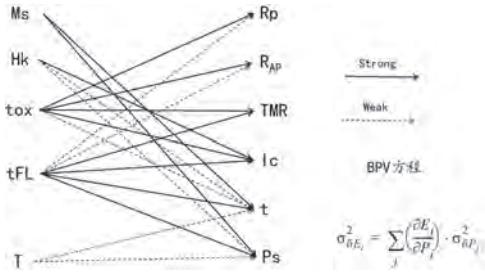

Fig. 2

VP23-08. Electronic and Magnetic Properties of a New Pnictide ($EuMn_2Bi_2$). *D. Sagar*[1], Y. Khatri[1] and A. Kashyap[1] *1. School of Physical Science, Indian Institute of Technology Mandi, Mandi, India*

Pnictides are an interesting class of materials with the chemical formula AB_2X_2 (A = rare earth, B = transition metal, and X = pnictogen); they crystallize in tetragonal $ThCr_2Si_2$-type[1], [2] and trigonal $CaAl_2Si_2$-type[3] structures. In the $ThCr_2Si_2$-type structure, the most common and widely studied property is the high-Tc superconductivity[4]. These compounds also exhibit antiferromagnetic (AFM) behaviour[5]. The $CaAl_2Si_2$-type structure is driven mainly by its thermoelectric and topological properties. In the prototype material $CaAl_2Si_2$, for example, both electrons and holes are involved in its electrical transport properties[6]. Further, pnictides involving Europium (Eu) and Manganese (Mn) have attracted significant attention due to their intriguing electronic and magnetic properties arising as a result of complex magnetic interactions between $4f^7$ (with Spin 7/2) and $3d^5$ (with Spin 5/2) electrons of Eu and Mn, respectively. Herein, using Density Functional Theory (DFT) we report the electronic and magnetic properties of a new pnictide, $EuMn_2Bi_2$, as predicted stable using the machine learning by Khatri *et al.*[7]. Our findings indicate that the compound $EuMn_2Bi_2$ exhibits a C-type anti-ferromagnetic (C-AFM) ground state with band gap of 0.258 eV and inclusion of spin orbit coupling shows the topological nature of this compound and this material can be used in spintronics. Fig. 1 shows the DOS, and Fig. 2 show the band structures for the C-AFM electronic ground states within GGA+U.

[1] M. Tegel, M. Rotter, V. Wei, F. M. Schappacher, R. Pöttgen, and D. Johrendt, "Structural and magnetic phase transitions in the ternary iron arsenides SrFe2As2 and EuFe2As2," *J. Phys. Condens. Matter*, vol. 20, no. 45, 2008, doi: 10.1088/0953-8984/20/45/452201. [2] G. R. Stewart, "Superconductivity in iron compounds," *Rev. Mod. Phys.*, vol. 83, no. 4, 2011, doi: 10.1103/RevModPhys.83.1589. [3] R. Rhhl and W. Jeitschko, "NEW PNICTIDES WITH Ce202S-TYPE STRUCTURE," 1979. [4] P. L. Alireza *et al.*, "Superconductivity up to 29 K in SrFe2As2 and BaFe2As2 at high pressures," *J. Phys. Condens. Matter*, vol. 21, no. 1, 2009, doi: 10.1088/0953-8984/21/1/012208. [5] K. A. Filsinger *et al.*, "Antiferromagnetic structure and electronic properties of BaCr2As2 and BaCrFeAs2," *Phys. Rev. B*, vol. 95, no. 18, pp. 1–13, 2017, doi: 10.1103/PhysRevB.95.184414. [6] M. Imai, H. Abe, and K. Yamada, " Electrical Properties of Single Crystalline CaAl 2 Si 2., " *ChemInform*, vol. 35, no. 42, pp. 1–2, 2004, doi: 10.1002/chin.200442010. [7] Y. Khatri and A. Kashyap, "Advancing magnetic material discovery through machine learning: Unveiling new manganese-based materials," *APL Mach. Learn.*, vol. 1, no. 4, Dec. 2023, doi: 10.1063/5.0171320.

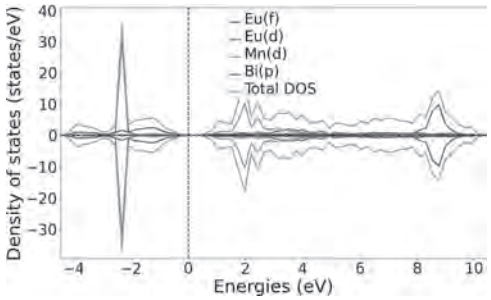

Fig. 1: Density of state in GGA+U

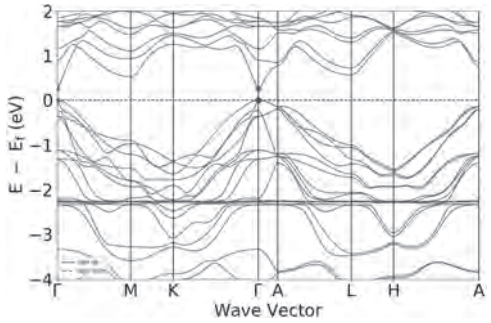

Fig. 2: Band structure in GGA+U

VP23-09. Magnetic Control of Electromagnetically Induced Transparency in Slow Light Experiments. *J. Wang*[1] and J. Krause[2] *1. University of Michigan, Dearborn, MI, United States; 2. Northville High School, Northville, MI, United States*

This study investigates the influence of magnetic fields on electromagnetically induced transparency (EIT) and slow light phenomena in rubidium vapor experiments. Magnetic fields significantly impact system dynamics, influencing critical parameters including Faraday rotation, susceptibility, transmission, population distributions, and coherence. The research explores various effects of magnetic fields on coherence properties and the efficiency of EIT-based light storage mechanisms, aiming to minimize decoherence losses and enhance quantum memory device performance. Key findings highlight the necessity of comprehending magnetic effects for controlling EIT and slow light phenomena while mitigating decoherence. The study provides insights into atomic state dynamics influenced by magnetic fields, particularly in relation to interactions with control and signal fields. This research aims to develop a comprehensive model that quantifies these effects, focusing specifically on maintaining prolonged quantum coherence. These advancements are crucial for practical applications in

quantum information and optical technologies, ensuring robust performance in essential domains such as quantum communication and computation.

H. Gao, M. Rosenberry, J. Wang, and H. Batelaan, J. Phys. B, 38, 1857 (2005). G. Lindblad, Commun. Math. Phys. 48, 119 (1976). M. Fleischhauer and M. D. Lukin, Phys. Rev. Lett. 84, 5094 (2000). M. Fleischhauer and M. D. Lukin, Phys. Rev. A 65, 022314 (2002).

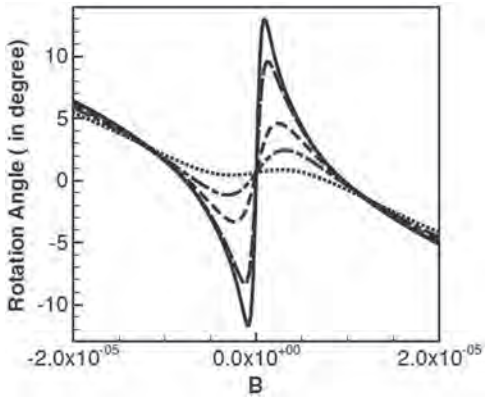

Fig. 1: Plot of the Faraday rotation angle versus the applied magnetic field in teslas for different combined dephasing rates.

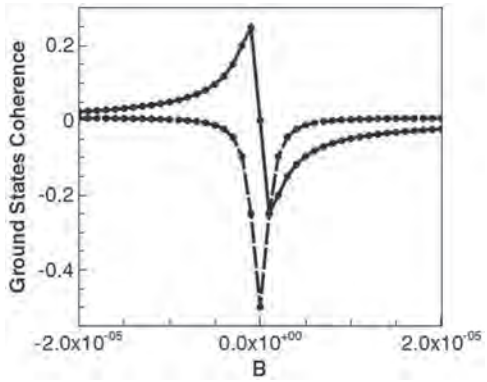

Fig. 2: Plot of the coherence between the two ground states versus an applied B field around the EIT condition. The absorption is represented by the solid curve and the dispersion is shown as a dashed curve.

- A -

*Best student presentation award finalist

- B -

*Best student presentation award finalist

- C -

*Best student presentation award finalist

*Best student presentation award finalist

- D -

*Best student presentation award finalist

- E -

- F -

*Best student presentation award finalist

- G -

*Best student presentation award finalist

*Best student presentation award finalist

- H -

*Best student presentation award finalist

- I -

*Best student presentation award finalist

- J -

- K -

*Best student presentation award finalist

*Best student presentation award finalist

*Best student presentation award finalist

- L -

*Best student presentation award finalist

*Best student presentation award finalist

*Best student presentation award finalist

- M -

*Best student presentation award finalist

*Best student presentation award finalist

- N -

- O -

*Best student presentation award finalist

- P -

*Best student presentation award finalist

- Q -

- R -

*Best student presentation award finalist

- S -

*Best student presentation award finalist

*Best student presentation award finalist

*Best student presentation award finalist

- T -

*Best student presentation award finalist

*Best student presentation award finalist

- U -

- V -

- W -

*Best student presentation award finalist

- X -

*Best student presentation award finalist

- Y -

*Best student presentation award finalist

- Z -

*Best student presentation award finalist

*Best student presentation award finalist